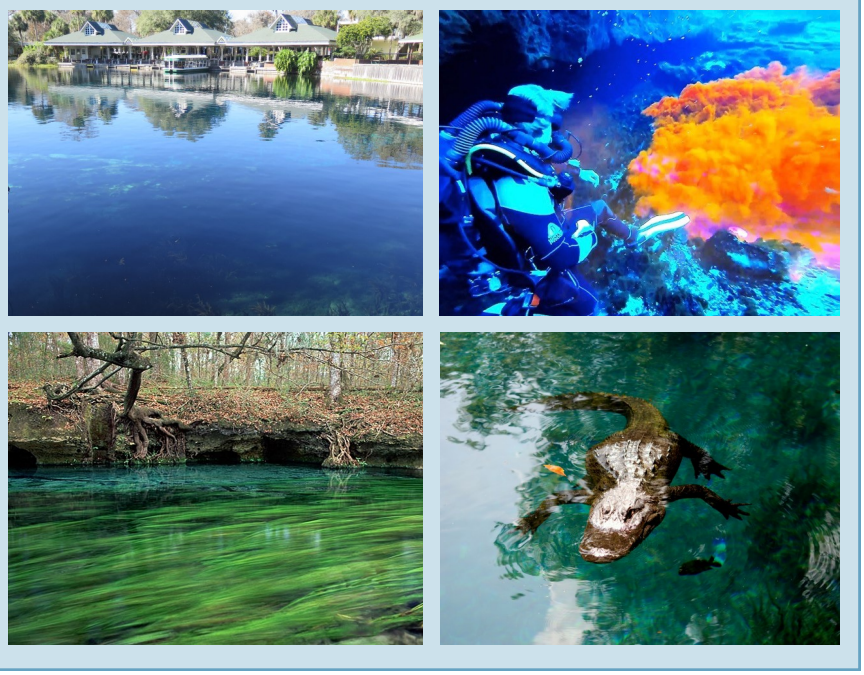

Collaborative Research Initiative on Sustainability and Protection of Springs

CRISPS

FINAL REPORT

2014 - 2017

submitted to:

St. Johns River Water Management District
Springs Protection Initiative [SPI], UF Contract # 27789

UF | UNIVERSITY of FLORIDA
Water Institute

C R I S P S

COLLABORATIVE RESEARCH INITIATIVE ON SPRINGS PROTECTION AND SUSTAINABILITY [CRISPS]

Final Report
December 2017

Principal Investigators

K. Ramesh Reddy, University of Florida
Dean Dobberfuhl and Casey Fitzgerald, St. Johns River Water Management District

University of Florida Investigators
Matt Cohen, Tom Frazer, Wendy Graham, James Jawitz,
David Kaplan, Patrick Inglett, Jon Martin, and Todd Osborne

St. Johns River Water Management District Investigators
Patrick Burger, Andy Canion, Mike Coveney, Ed Lowe,
Rob Mattson, Jodi Slater, and Peter Sucsy

This is the Final report of a 3-year project in compliance with Agreement between University of Florida (UF) and St. Johns River Water Management District (SJRWMD), UF Contract #27789.

ACKNOWLEDGEMENTS

This document reports work conducted as a part of three-year project in compliance with an Agreement between University of Florida (UF) and St. Johns River Water Management District (SJRWMD) (UF Contract #27789). It is part of the UF *Collaborative Research Initiative on Springs Protection and Sustainability* and supports the science component of the SJRWMD's Springs Protection Initiative. We especially thank Ms. Lisette Staal, UF Water Institute and Ms. Mary Braham, SJRWMD for their superb project management during the life of this project. We also recognize the exceptional cooperation of Ms. Sally Lieb and her staff at Silver Springs State Park in accommodating extensive fieldwork; and Mr. Clay Coates and Ocala National Forest staff for fieldwork facilitation at Alexander Springs. Finally, many thanks to Ms. Jennifer Hornsby, UF Soil and Water Sciences Department for her editing and compiling of the annual and final project reports.

TABLE OF CONTENTS

Page

ACKNOWLEDGEMENTS ii

LIST OF TABLES xvii

LIST OF FIGURES xxv

EXECUTIVE SUMMARY ES-1

ES.1 INTRODUCTION ES-1
ES.2 GENERAL CONCLUSIONS ES-3
ES.3 SPRINGSHED PROCESSES ES-6
ES.3.1 Groundwater Hydrology: Conduit and Fracture Flow Modeling ES-6
ES.3.2 Springshed Hydrology: Nitrogen Transport and Loss ES-7
ES.3.3 Springshed Biogeochemistry: Nitrogen Transformations ES-8
ES.4 SPRINGS ECOSYSTEM PROCESSES ES-9
ES.4.1 Hydraulics and Hydrodynamics ES-9
ES.4.2 Springs Ecosystem Physicochemistry ES-10
ES.4.2.1 Nitrogen Dynamics and Metabolism ES-10
ES.4.2.2 Nitrate Inhibition of Submerged Aquatic Vegetation ES-11
ES.4.2.3 Benthic Sources and Sinks of Nutrients ES-12
ES.4.3 Springs System Biology - Trophic Interactions ES-13

INTRODUCTION

1 OVERVIEW OF THE COLLABORATOVE RESEARCH INITIATIVE ON SUSTAINABILITY AND PROTECTION OF SPRINGS, CRISPS 1-1

1.1 INTRODUCTION 1-2
1.2 BACKGROUND 1-3
1.2.1 The Floridan Aquifer 1-3
1.2.2 Silver Springs 1-4
1.2.3 Alexander Springs 1-6
1.2.4 Responses to Declining Spring Health 1-8
1.2.5 The C ollaborative R esearch In itiative on Springs Protection and Sustainability (CRISPS) 1-9
1.3 SPRINGSHED SUPERGROUP 1-10
1.3.1 Groundwater Hydrology: Conduit and Fracture Flow Modeling 1-10
1.3.2 Springshed Hydrology: Nitrogen Transport and Loss 1-11
1.3.3 Springshed Biogeochemistry: Nitrogen Transformations 1-11
1.3.4 Springs Ecosystem Workgroup 1-11
1.3.5 Hydraulics and Hydrodynamics 1-12
1.3.6 Nitrogen Dynamics and Metabolism 1-12
1.3.7 NO_3 Inhibition of Submersed Aquatic Vegetation (SAV) 1-12
1.3.8 Potential Hypoxia Effects on Invertebrate Herbivores 1-12
1.3.9 Benthic Sources and Sinks of Nutrients 1-12
1.3.10 Trophic Interactions within the Spring Ecosystem 1-13

Page

1.4 REFERENCES 1-13

GROUNDWATER HYDROLOGY

2 CONDUIT AND FRACTURE FLOW MODELING 2-1

2.1.1 ABSTRACT…,,,..... 2-2
2.1.2 BACKGROUND 2-2
2.1.2.1 Conduit Evolution Algorithms..... 2-3
2.1.2.2 Global Sensitivity Analyses..... 2-4
2.1.2.3 Report Outline..... 2-5
2.1.3 CONDUIT GENERATION ALGORITHM..... 2-5
2.1.3.1 Flow and Reactive Solute Transport 2-8
2.1.3.2 CALCITE DISSOLUTION 2-9
2.1.4 MODEL DESIGN..... 2-12
2.1.4.1 THE QUASI-STEADY STATE APPROXIMATION..... 2-12
2.1.4.2 NUMERICAL SOLUTION OF FLOW 2-13
2.1.4.3 NUMERICAL SOLUTION OF TRANSPORT 2-13
2.1.5 INITIAL PALEOKARST NETWORK..... 2-14
2.1.5.1 Horizontal Preferential Flowpaths 2-14
2.1.5.2 Vertical Preferential Flowpaths 2-15
2.1.5.3 Boundary Conditions for Regional Scale Modeling 2-16
2.1.6 MODEL APPLICATION TO THE SILVER SPRINGSHED 2-17
2.1.6.1 Boundary Conditions 2-17
2.1.6.2 Paleokarst Template Generation..... 2-18
2.1.6.3 Morris Method Global Sensitivity Analyses..... 2-19
2.1.6.4 Simulation Response Metrics 2-20
2.1.6.4.1 Dissolution Response Metrics 2-20
2.1.6.4.2 Hydrograph Response Metrics..... 2-21
2.1.6.4.3 Transport Response Metrics 2-22
2.1.7 RESULTS AND DISCUSSION..... 2-22
2.1.7.1 Dissolution Behaviors and Sensitivity..... 2-22
2.1.7.2 Steady-State and Hydraulic Pulse Response Behaviors and Sensitivity 2-26
2.1.7.3 Transport Pulse Response Behaviors and Sensitivity..... 2-29
2.1.7.4 Investigation of Individual Behavioral and Non-Behavioral Conduit Networks..... 2-31
2.1.8 SUMMARY AND CONCLUSIONS 2-34

2.2 MONTE CARLO SIMULATION FLOW AND TRANSPORT IN AN IDEALIZED SILVER SPRINGSHED..... 2-36

2.2.1 BACKGROUND 2-36
2.2.2 METHOD..…… 2-37
2.2.3 RESULTS AND DISCUSSION..... 2-39

Page
2.2.3.1 Hydrologic and Forward Transport Response 2-39
2.2.3.2 Backward Transport Pulse 2-44
2.2.3.3 Investigation of Individual Behavioral Replicates 2-47
2.2.4 SUMMARY AND CONCLUSIONS 2-51

2.3 REFERENCES 2-52

3 TRANSPORT AND LOSS OF NITROGEN WITHIN THE UPPER FLORIDAN AQUIFER IN THE SILVER SPRINGS SPRINGSHED 3-1

3.1 ABSTRACT 3-2
3.2 INTRODUCTION 3-2
3.3 SITE DESCRIPTION 3-3
3.4 METHODS 3-3
3.4.1 Groundwater Velocity and Nitrate Flux Measurements 3-3
3.4.2 Soil N Flux 3-11
3.5 RESULTS 3-15
3.5.1 Groundwater Velocity and Nitrate Flux Measurements 3-15
3.5.2 Soil N Flux 3-31
3.6 DISCUSSION 3-34
3.7 CONCLUSIONS AND RECOMMENDATIONS 3-37
3.8 FUTURE RESEARCH NEEDS 3-37
3.9 REFERENCES 3-38

NITROGEN BIOGEOCHEMISTRY

4 SOURCES, TRANSFORMATIONS AND LOSS OF NITROGEN FROM LAND SURFACE TO SPRINGS 4-1

4-i PROLOGUE 4-2

4.1 SURFACE ATTENUATION PROCESSES OF NITROGEN ACROSS VARIOUS LAND USES IN THE SILVER SPRINGS SPRINGSHED 4-2

4.1.1 ABSTRACT 4-2
4.1.2 INTRODUCTION 4-3
4.1.3 MATERIALS AND METHODS 4-4
4.1.3.1 Site Description and Sampling 4-4
4.1.3.2 Redox and Nutrient Parameters 4-5
4.1.3.3 Denitrification Enzyme Activity 4-5
4.1.3.4 Stable Isotope Analysis 4-5
4.1.3.5 DNA Extraction and Gene Quantification 4-6
4.1.3.6 Statistical Analysis 4-7
4.1.4 RESULTS AND DISCUSSION 4-7
4.1.4.1 Profile Lithographic Characteristics 4-7

Page

4.1.4.2 Extractable N and Denitrification Enzyme Activities 4-18
4.1.4.3 Surface/Groundwater Relationships 4-24
4.1.4.4 Microbial Indicators of Denitrification in Soil Profiles 4-28
4.1.5 CONCLUSIONS AND RECOMMENDATIONS 4-37
4.1.6 FUTURE RESEARCH NEEDS 4-39
4.1.7 REFERENCES 4-39

4.2 ASSESSING VARIABILITY AND CONTROLS OF DENITRIFICATION IN SANDY SOIL FROM DIFFERENT LAND USES IN THE SILVER SPRINGS SPRINGSHED 4-43

4.2.1 ABSTRACT 4-43
4.2.2 INTRODUCTION 4-43
4.2.3 MATERIALS AND METHODS 4-44
4.2.3.1 Site Description 4-44
4.2.3.2 Sample Collection 4-45
4.2.3.3 Experimental Design 4-45
4.2.3.4 Pre- and Post-Incubation Analysis 4-47
4.2.3.5 Statistical Analysis 4-48
4.2.4 RESULTS AND DISCUSSION 4-48
4.2.4.1 Post- Incubation Soil Nutrient Characterization 4-48
4.2.4.2 Factors Affecting N_2O Respiration 4-49
4.2.4.3 Factors affecting temperature sensitivity 4-55
4.2.5 CONCLUSIONS AND RECOMMENDATIONS 4-56
4.2.6 LIMITATIONS AND FUTURE RESEARCH 4-57
4.2.7 REFERENCES 4-57

4.3 IDENTIFYING AND TRACING NITROGEN SOURCES IN THE SILVER SPRINGS SPRINGSHED 4-63

4.3.1 ABSTRACT 4-63
4.3.2 INTRODUCTION 4-64
4.3.3 MATERIALS AND METHODS 4-65
4.3.3.1 Site Description 4-65
4.3.3.2 Sampling 4-66
4.3.3.3 Sample Analysis 4-66
4.3.3.4 Estimation of Excess Air, Recharge Temperature, and Excess N_2 4-67
4.3.3.5 DNA extraction and gene quantification 4-69
4.3.3.6 Statistical Analysis 4-69
4.3.4 RESULTS AND DISCUSSION 4-70
4.3.4.1 Categorization of the Wells and Spring Vents based on Land Use 4-70
4.3.4.2 Geochemistry of Ground Water and Springs Vents 4-70
4.3.4.3 Spatial and Seasonal Pattern of Dissolved Gases in Ground Water and Spring Vents 4-76

Page

4.3.4.4 Stable Isotopic values ($\delta^{15}N\text{-}NO_3$ and $\delta^{18}O\text{-}NO_3$) of Ground Water....4-83
4.3.4.5 Denitrification Progression....4-92
4.3.4.6 Microbial Evidence of Denitrification in Groundwater....4-93
4.3.5 CONCLUSIONS AND RECOMMENDATIONS....4-95
4.3.6 FUTURE RESEARCH NEEDS....4-96
4.3.6 REFERENCES....4-97

HYDRAULICS AND HYDRODYNAMICS

5 HYDRAULICS AND HYDRODYNAMICS....5-1

5.0 EXECUTIVE SUMMARY....5-2

5.1 VELOCITY AND RESIDENCE TIME DISTRIBUTIONS AND TRANSIENT STORAGE....5-5

5.1.1 INTRODCUTION....5-5
5.1.1.1 Site Description....5-6
5.1.2 MATERIALS AND METHODS....5-7
5.1.2.1 Dye Tracer Experiments....5-7
5.1.2.1.1 Field and Laboratory Methods....5-7
5.1.2.1.2 Tracer Data Analysis....5-17
5.1.2.1.2.1 Solute Transport Model....5-17
5.1.2.1.2.2 Model Fitting Approaches....5-18
5.1.2.1.2.3 Moment Analysis of Breakthrough Curves....5-21
5.1.2.2 Raz-Rru Experiments....5-22
5.1.2.2.1 Raz-Rru Detection Wavelengths....5-22
5.1.2.2.2 Field Sites....5-23
5.1.2.2.3 Batch Experiments....5-23
5.1.2.2.4 Kinetics and Advection-Dispersion Modeling....5-23
5.1.3 RESULTS AND DISCUSSION....5-24
5.1.3.1 Dye Tracer Experiments....5-24
5.1.3.1.1 Breakthrough Curve Data....5-24
5.1.3.1.2 Model Fitting and Experiments Comparisons....5-34
5.1.3.1.3 Moment Analysis....5-41
5.1.3.1.4 Alexander Springs Dye Trace....5-43
5.1.3.1.5 Breakthrough Curve Data versus EFDC Model....5-44
5.1.3.2 Raz-Rru Experiments....5-45
5.1.3.2.1 Raz and Rru Transformation versus Time....5-45
5.1.3.2.2 Kinetic Parameters....5-46
5.1.3.2.3 Advection-Dispersion Modeling....5-47
5.1.3.2.4 Raz and Rru Discussion....5-48
5.1.4 CONCLUSIONS, RECOMMENDATIONS, AND FUTURE RESEARCH NEEDS....5-49

Page
5.1.5 REFERENCES 5-50

5.2 CRITICAL VELOCITY/SHEAR STRESS....5-52

5.2.1 INTRODUCTION 5-52
5.2.2 MATERIALS AND METHODS....5-52
5.2.2.1 Flow-ways....5-53
5.2.2.2 Critical Velocity Estimation from Observational Data....5-63
5.2.2.3 Optical Methods....5-68
5.2.3 RESULTS AND DISCUSSION....5-70
5.2.3.1 Flow-ways....5-70
5.2.3.2 Critical Velocity Estimation from Observational Data....5-77
5.2.3.3 Optical Methods....5-89
5.2.4 CONCLUSIONS, RECOMMENDATIONS, AND FUTURE RESEARCH NEEDS....5-90
5.2.5 REFERENCES 5-90

5.3 VELOCITY VALIDATION TRANSECTS....5-91

5.3.1 INTRODUCTION 5-91
5.3.2 MATERIALS AND METHODS....5-91
5.3.3 RESULTS AND DISCUSSION....5-93
5.3.4 CONCLUSIONS, RECOMMENDATIONS, AND FUTURE RESEARCH NEEDS....5-95

5.4 HYDRODYNAMIC EFFECTS OF VEGETATION ON VELOCITY AND STAGE IN SILVER RIVER....5-96

5.4.1 INTRODUCTION 5-96
5.4.2 REVIEW OF VEGETATIVE FLOW RESISTANCE 5-98
5.4.3 DESCRIPTION OF STUDY AREA 5-100
5.4.4 MATERIALS AND METHODS....5-100
5.4.4.1 Defining the Shoreline 5-100
5.4.4.2 Defining Bottom Type 5-103
5.4.4.3 Model Grid Development 5-103
5.4.4.4 Formulation of the Governing Equations for EFDC With Vegetation 5-106
5.4.5 RESULTS AND DISCUSSION....5-107
5.4.5.1 Bottom Type 5-107
5.4.5.2 Hydrodynamic Model Tests....5-108
5.4.5.3 Cause of Altered Stage/Discharge Relationship of Silver River 5-112
5.4.6 CONCLUSIONS AND RECOMMENDATIONS 5-114
5.4.7 REFERENCES 5-115

Page

5.5 REDUCED COMPLEXITY MODELING OF HYDRODYNAMIC EFFECTS OF VEGETATION ON VELOCITY AND STAGE IN SILVER RIVER....5-117

5.5.1 INTRODUCTION....5-117
5.5.2 MATERIALS AND METHODS....5-118
5.5.2.1 Stage/Discharge Data Analysis....5-118
5.5.2.2 Velocity Impacts of Stage/Discharge Shift....5-118
5.5.2.3 Statistical Change Point Analysis....5-118
5.5.2.4 Modeling Stage/Discharge Shift and Alternative Stable States....5-120
5.5.2.5 Coupled Aquifer, Spring, and Spring Run Conceptual Model....5-122
5.5.3 RESULTS AND DISCUSSION....5-123
5.5.3.1 Stage/Discharge Data Analysis....5-123
5.5.3.2 Velocity Impacts of Stage/Discharge Shift....5-125
5.5.3.3 Statistical Change Point Analysis....5-126
5.5.3.4 Modeling Stage/Discharge Shift and Alternative Stable States....5-128
5.5.3.5 Coupled Aquifer, Spring, and Spring Run Conceptual Model....5-129
5.5.4 CONCLUSIONS, RECOMMENDATIONS AND FUTURE RESEARCH NEEDS....5-130
5.5.5 REFERENCES....5-130

PHYSICOCHEMISTRY

6 NITROGEN DYNAMICS AND METABOLISM....6-1

6.1 ABSTRACT....6-2
6.2 INTRODUCTION....6-5
6.3 ECOSYSTEM METABOLISM....6-5
6.3.1 Data Availability and Methods....6-6
6.3.2 Metabolism Results....6-10
6.3.3 Benthic Light and Predicting GPP and ER....6-26
6.3.4 Nitrate Dynamics....6-43
6.4 SILVER RIVER BENTHIC SURVEY....6-57
6.4.1 Field Methodology....6-57
6.4.2 Laboratory Analyses....6-58
6.4.3 Physical Controls....6-61
6.4.4 Vegetation Inventory....6-61
6.4.5 Vegetation Chemistry....6-66
6.4.6 Water Chemistry....6-67
6.4.7 Soil Chemistry....6-73
6.4.8 Soil Particle Size Distribution....6-77
6.4.9 Physical and Chemical Controls on SAV and Algal Abundance....6-79
6.4.9.1 Physical Controls....6-79
6.4.9.2 Water Chemistry Controls....6-80
6.4.9.3 Soil Chemistry and Texture Controls....6-83

Page

6.5 NUTRIENT LIMITATION ASSAYS – METABOLISM AND ALGAL GROWTH RESPONSES....6-84
6.5.1 Control Chamber Metabolism....6-88
6.5.1.1 Substrate Type....6-90
6.5.1.2 Light....6-91
6.5.1.3 Time of Year....6-93
6.5.1.4 Canopy Cover....6-94
6.5.1.5 Water Depth....6-94
6.5.1.6 Vegetation Biomass....6-94
6.5.1.7 Nutrient Effects on Chamber Metabolism....6-98
6.5.1.8 Algal Growth on Substrates....6-106
6.6 BENTHIC CHAMBERS – NUTRIENT DYNAMICS AND DEPLETION RESPONSES....6-112
6.6.1 Methods....6-114
6.6.1.1 Data Collection....6-114
6.6.1.2 Modeling....6-115
6.6.2 Results....6-117
6.6.3 Discussion....6-122
6.6.3.1 Model Limitations and Future Improvement....6-122
6.6.3.1.1 Fine-scale Profile Geometry....6-124
6.6.3.1.2 Uptake Kinetics and Nutrient Limitation....6-124
6.6.4 Conclusion....6-127
6.7 *IN SITU* VEGETATION GROWTH EXPERIMENTS....6-127
6.7.1 Background....6-127
6.7.1.1 Light....6-128
6.7.1.2 Nutrients....6-129
6.7.1.3 Algae....6-130
6.7.1.4 Dissolved Oxygen and Grazers....6-130
6.7.1.5 Hydrodynamics....6-131
6.7.1.6 Sediment Texture and Redox Potential....6-131
6.7.1.7 Research Motivation....6-132
6.7.1.8 Hypothesis....6-132
6.7.2 Methods....6-132
6.7.2.1 Overview....6-132
6.7.2.2 Site Description....6-133
6.7.2.3 Species....6-133
6.7.2.4 Clipping Technique....6-134
6.7.2.5 Site Selection....6-134
6.7.2.6 Field and Laboratory Methods....6-134
6.7.2.7 Statistical Analysis....6-139
6.7.3 Results....6-140
6.7.3.1 River Characteristics....6-140
6.7.3.2 Sampling Effects....6-140
6.7.3.3 Measured Growth and Standing Stock....6-141
6.7.3.4 Pairwise Controls on SAV Productivity....6-146

Page

6.7.3.5 Multivariate Controls on SAV Productivity 6-146
6.7.4 Discussion 6-152
6.7.4.1 Spatial and Temporal Heterogeneity in SAV Growth 6-152
6.7.4.2 Multivariate Controls on SAV Productivity 6-153
6.7.4.3 Redox Potential 6-154
6.7.4.4 Nitrate Effects 6-154
6.7.4.5 Gross Primary Production 6-155
6.7.5 Conclusion 6-157
6.8 SUMMARY AND MANAGEMENT IMPLICATIONS 6-157
6.9 REFERENCES 6-162

7 NITRATE INHIBITION OF SUBMERGED AQUATIC VEGETATION: INVESTIGATION OFTHE NITROGEN OVERLOAD HYPOTHESIS 7-1

7.1 Direct EFFECTS OF ELEVATED NO_3-N IN THE GROWTH OF *Vallisneria americana* AND *Sagittaria kurziana* IN SPRING ECOSYSTEMS 7-2

7.1.1 ABSTRACT 7-2
7.1.2 INTRODUCTION 7-2
7.1.2.1 Competing Hypotheses 7-3
7.1.2.2 Evidence of Direct Effects of Nitrate on SAV 7-5
7.1.2.3 Potential Mechanisms of Inhibition 7-7
7.1.2.4 Assimilatory Nitrate Reduction 7-7
7.1.2.5 Ammonium Toxicity 7-11
7.1.2.6 Amino-Acid Synthesis 7-11
7.1.2.7 Summary of Mechanisms of Inhibition 7-12
7.1.2.8 Ecological Implications 7-12
7.1.2.9 Objectives 7-12
7.1.3 MATERIALS AND METHODS 7-13
7.1.3.1 Field Collection Methods 7-13
7.1.3.2 Mesocosm Description 7-13
7.1.3.3 Laboratory Methods 7-16
7.1.3.3.1 Nutrient Analysis of SAV 7-16
7.1.3.3.2 Nitrate Reductase Activity (NRA) 7-16
7.1.3.3.3 Quantification of SAV Growth 7-16
7.1.3.3.4 Anatomical Responses 7-17
7.1.3.3.4.1 Starch and Amino Acid Assays 7-17
7.1.3.3.4.2 Leaf Anatomical Structure Analysis 7-17
7.1.3.3.5 Effects of Oxygen on SAV Growth 7-17
7.1.3.3.6 Effects of Sulfide on SAV Growth 7-18
7.1.3.3.7 Epiphytic Algae Quantification 7-18
7.1.3.3.8 Statistical Analyses 7-18
7.1.4 RESULTS AND DISCUSSION 7-18

Page
7.1.4.1 Root : Shoot Ratios 7-18
7.1.4.2 Nitrate Reductase Activity 7-22
7.1.4.3 Tissue Elemental Analysis 7-25
7.1.4.4 Cellular Level Responses 7-26
7.1.4.5 Structural Responses to Hypoxia 7-31
7.1.4.6 Structural Responses to Sulfide Toxicity 7-32
7.1.4.7 Additional Observations 7-37
7.1.5 CONCLUSIONS AND RECOMMENDATIONS 7-38
7.1.5.1 Management Implications 7-39
7.1.6 REFERENCES….. 7-40
7.1.7 PUBLICATIONS AND PRODUCTS 7-47
7.1.7.1 Theses…….. 7-47
7.1.7.2 Presentations 7-47

7.2 DECLINING OXYGEN AS A MECHANISM FOR EXTIRPATION OF INVERTEBRATE HERBIVORES IN SILVER SPRINGS- A RESPIROMETRY STUDY OF *Viviparus georgianus*, *Elimia floridensis*, *Micromenteus floridensis* and *Palaemonetes paludosus* 7-48

7.2.1 ABSTRACT…. 7-48
7.2.2 INTRODUCTION 7-48
7.2.2.1 Bottom Up Control of Algal Productivity 7-49
7.2.2.2 Top Down Control of Algal Biomass 7-50
7.2.2.3 Controls on Grazers 7-51
7.2.2.4 Gastropoda…… 7-53
7.2.2.5 Decapoda……. 7-54
7.2.2.6 Hypotheses……. 7-54
7.2.2.7 Objectives…… 7-55
7.2.3 MATERIALS AND METHODS 7-55
7.2.3.1 Field Collection 7-55
7.2.3.2 Laboratory Analyses 7-56
7.2.3.3 Settling Period 7-56
7.2.3.4 Hypoxia Treatment 7-57
7.2.3.5 Nitrate Effects on Hypoxia Resistance 7-58
7.2.4 RESULTS AND DISCUSSION 7-59
7.2.4.1 Chronic and Episodic Hypoxia 7-66
7.2.5 CONCLUSIONS AND RECOMMENDATIONS 7-67
7.2.6 REFERENCES.. 7-67
7.2.7 PUBLICATIONS AND PRODUCTS 7-78
7.2.7.1 Theses…….. 7-78
7.2.7.2 Presentations 7-78

7.3 EFFECTS OF FLOW VELOCITY ON GROWTH AND PROLIFERATION OF EPIPHYTIC ALGAE ON SAV IN SPRING ECOSYSTEMS 7-79

		Page
7.3.1	ABSTRACT….	7-79
7.3.2	INTRODUCTION	7-79
7.3.3	METHODS……	7-80
7.3.4	RESULTS AND DISCUSSION	7-86
7.3.5	CONCLUSIONS	7-88
7.3.6	REFERENCES..	7-89
8	BENTHIC SOURCES AND SINKS OF NUTRIENTS	8-1
8.1	ABSTRACT	8-2
8.2	INTRODUCTION	8-3
8.2.1	Project Objectives	8-5
8.3	SITE DESCRIPTION	8-6
8.4	MATERIALS AND METHODS	8-6
8.4.1	Sediment Mapping, Core Collection and Analysis	8-8
8.4.2	Sediment Accumulation Rate	8-10
8.4.3	Hydraulic Gradients and Groundwater Flow	8-11
8.4.4	Pore Water Chemistry	8-15
8.4.5	Benthic Flux Calculation	8-16
8.5	RESULTS	8-17
8.5.1	Sediment Stratigraphy	8-17
8.5.2	Chemical Compositions of the Sediment	8-19
8.5.3	C and N Isotopic Composition of the Sediment	8-23
8.5.4	^{210}Pb and Sedimentation	8-24
8.5.5	Hydrological Variables	8-24
8.5.6	Pore Water Chemistry	8-26
8.6	DISCUSSION	8-28
8.6.1	Distributions, Compositions, and Possible Origins of Benthic Sediments	8-28
8.6.2	Sources of Organic Carbon in Riverbed Sediments	8-31
8.6.3	Groundwater Flow to the River	8-33
8.6.4	Controls on Pore Water Chemistry	8-35
8.6.5	Benthic Fluxes of Solutes	8-36
8.7	CONCLUSIONS	8-40
8.7.1	Specific Colnclusions	8-41
8.7.2	Management Implications	8-41
8.7.3	Future Research Needs	8-42
8.8	REFERENCES	8-43

BIOLOGY

9	TROPHIC INTERACTIONS	9-1
9.i	ABSTRACT	9-2

Page

9.1 DETERMINING FOOD WEB STRUCTURE AND ELUCIDATING TROPHIC LINKS....9-4

9.1.1 INTRODUCTION....9-4
9.1.2 STUDY SITES....9-7
9.1.3 METHODS....9-12
9.1.3.1 Sampling Design....9-12
9.1.3.2 Primary Producers....9-12
9.1.3.3 Consumers....9-13
9.1.3.4 Stable Isotope and Elemental Analyses....9-14
9.1.3.5 Isotopic Mixing Model Analysis and Isotopic Niche Metrics....9-14
9.1.35.1 Bayesian Isotopic Mixing Model (SIAR)....9-14
9.1.3.5.2 Measuring Dietary Specialization....9-14
9.1.3.5.3 Estimating the Isotopic Niche Area....9-15
9.1.3.6 Stomach Content Analysis....9-15
9.1.3.7 Turtles, Gastropods, and Herbivorous/Omnivorous Fish....9-16
9.1.3.8 Statistical Methods....9-16
9.1.4 RESULTS....9-17
9.1.4.1 Stable Isotope Ratios and Elemental Composition of Primary Producers....9-17
9.1.4.2 Stable Isotope Composition of Less Common and Unique Autotroph....9-23
9.1.4.3 Stable Isotope Composition of Consumers....9-23
9.1.4.4 Stable Isotope Compostion of Primary Consumers (Herbivores) and Omnivores....9-25
9.1.4.5 Stable Isotope Composition of Secondary Consumers....9-33
9.1.4.6 Comments on Parasitic Organisms....9-36
9.1.4.7 Stable Isotope Composition of Top and Apex Predators....9-36
9.1.4.8 Isotopic Niche Area (SEA_B) Herbivores and Omnivores....9-39
9.1.4.9 Isotopic Mixing Model Analysis and Niche Specialization Index (ε)....9-45
9.1.4.10 Analysis of Stomach Content and Scat....9-51
9.1.5 DISCUSSION....9-57
9.1.5.1 What is the fate of nutrients and energy sequestered by nuisance algae?....9-57
9.1.5.2 Which consumers forage on nuisance algae and to what degree?....9-58
9.1.5.3 Which predator taxa are major consumers of grazers?....9-60
9.1.5.4 Future Research Directions....9-60
9.1.6 CONCLUSIONS AND RECOMMENDATIONS....9-61
9.1.7 REFERENCES....9-62

9.2 GRAZING RATES FOR HERBIVORES FEEDING ON MACROPHYTES AND MACROALGAE....9-68

9.2.1 INTRODUCTION....9-68

Page
9.2.2 DESIGNOF THE EXPERIMENTS 9-69
9.2.2.1 Laboratory Enclosures and Flow –through Systems 9-69
9.2.2.2 Collection, Breeding and Housing of Organisms 9-69
9.2.3 METHODS AND MATERIALS 9-70
9.2.3.1 Sourcing, Cleaning and Processing Macrophytes and Macroalgae 9-70
9.2.3.2 Grazing Experiments 9-71
9.2.3.3 Statistical Methods....9-72
9.2.4 RESULTS 9-72
9.2.4.1 Macroalgae Trials 9-72
9.2.4.2 Macrophyte Trails....9-78
9.2.5 DISCUSSION....9-83
9.2.5.1 What grazers have the capacity to eat macroalgae?....9-83
9.2.5.2 What grazers have the capacity to eat macrophytes?....9-85
9.2.5.3 Future Research Directions....9-86
9.2.6 CONCLUSIONS AND RECOMMENDATIONS 9-86
9.2.7 REFERENCES 9-87

9.3 ASSESSING TOP-DOWN (CONSUMER) CONTROL OF KEY GRAZERS 9-89

9.3.1 INTRODUCTION 9-89
9.3.2 EXPERIMENTAL DESIGN 9-90
9.3.3 MATERIALS AND METHODS....9-91
9.3.3.1 Exclusion Cages....9-91
9.3.3.2 Aboveground Growth of Macrophytes 9-91
9.3.3.3 Biomass and Leaf Areas of Macrophytes 9-92
9.3.3.4 Biomass of Epiphytic Algae 9-92
9.3.3.5 Abundance, Biomass, and Community Composition for Macroinvertebrates 9-93
9.3.3.6 Statistical Analyses 9-93
9.3.4 RESULTS 9-94
9.3.4.1 Aboveground Growth of Macrophytes 9-94
9.3.4.2 Aboveground Biomass of Macrophytes....9-99
9.3.4.3 Biomass of Epiphytic Algae 9-100
9.3.4.4 Abundance, Biomass, and Community Composition for Macroinvertebrates 9-103
9.3.5 DISCUSSION....9-122
9.3.6 CONCLUSIONS AND RECOMMENDATIONS 9-123
9.3.7 REFERENCES 9-123

APPENDICES A-1
Appendix 5.1.1....A-2
Appendix 5.3.1....A-176
Appendix 6.1....A-185
Appendix 6.2....A-186

Page
Appendix 8.1 ..... A-190
Appendix 8.2 ..... A-195
Appendix 8.3 ..... A-201
Appendix 8.4 ..... A-203
Appendix 9.1.1 ..... A-205
Appendix 9.1.2 ..... A-208
Appendix 9.1.3 ..... A-210
Appendix 9.1.4 ..... A-214

LIST OF TABLES

		Page
Table 2.1.1.	Horizontal and vertical preferential flowpath (HPF and VPF) and matrix properties for Morris Method Global Sensitivity Analysis.	2-21
Table 2.1.2.	Comparison of flows and radii statistics at steady flow dissolution time and 1.5 times the steady flow dissolution time (statistics calculated over all 90 replicates).	2-24
Table 2.1.3.	Behavioral and non-behavioral group statistics for dissolution metrics.	2-25
Table 2.1.4.	Behavioral and non-behavioral group statistics for hydraulic pulse metrics.	2-27
Table 2.1.5.	Behavioral and non-behavioral group statistics for flow fractions through concentric control planes located 2, 8 and 12 km from the spring at steady-state and peak flow.	2-28
Table 2.1.6.	Behavioral and non-behavioral group statistics for solute transport pulse metrics.	2-30
Table 2.2.1.	Hydrologic and transport pulse metrics for MM-GSA replicates meeting the springflow and head behavioral criteria for Silver Springs.	2-38
Table 2.2.2.	Morris Method parameters for MM-GSA replicates meeting the springflow and head behavioral criteria for Silver Springs and parameters used in the Monte Carlo experiment.	2-38
Table 2.2.3.	Output statistic convergence results for Monte Carlo simulations.	2-39
Table 2.2.4.	Head Transect output statistic convergence results for Monte Carlo Simulations.	2-39
Table 2.2.5.	Complete ensemble mean and standard deviation for hydrologic and forward transport metrics.	2-40
Table 2.2.6.	Behavioral ensemble mean and standard deviation for hydrologic and transport metrics.	2-42
Table 3.1.	Parameters used for of soil moisture profile prediction in HYDRUS-1D.	3-13
Table 3.2.	Borehole dilution test results from Sharpes Ferry wells. Insufficient data were collected from this method for definitive conclusions, but the measured water fluxes were reasonably consistent with values determined from passive flux meters.	3-16
Table 3.3.	Summary of BHD results at six depths in well M0789.	3-16
Table 4.1.1.	Land use description, and well depth for the project wells in the Silver Springs springshed..	4-9
Table 4.1.2.	Denitrification enzyme activities (DEA, nmols N_2O g^{-1} dw h^{-1}) with and without the addition of glucose for the 0-0.6 m and 0.6-1.2 m soil profiles in the 12 wells.	4-20
Table 4.2.1.	Soil land use type, suborder, dominant textural class, vegetation, and nutrient characteristics for each site sampled.	4-46

Page

Table 4.2.2. Treatments for denitrification incubations. Moisture Content (MC) × N Rate or cattle stocking density for each land use, including 3 replicate jars. The number of total jars for each land use is denoted in parentheses. 4-47
Table 4.2.3 Differences in nutrient contents for un-amended (control) soils after denitrification incubation (Mean ± s.d.) and the One-way ANOVA analysis of those nutrients between pre-and post-incubation. Lowercase letters after the values represent significant difference between different land uses. 4-49
Table 4.3.1. Percentage of area for each of the eight land use categories (1-urban and built-up, 2-agriculture, 3-rangeland, 4-upland forest, 5-water, 6-wetlands, 7-barren land, 8-transportation, communication and utilities waste water treatment facility (WWTF)), results of cluster analysis, and the final assignment of the land use....4-71
Table 4.3.2. Statistical summary of selected water chemical data for the 61 wells sampled in this study. 4-73
Table 4.3.3. The eigenvectors of the principal component analysis for the first and second principal components (PC1 and PC2). 4-75
Table 4.3.4 Comparison of N_2O concentrations for subsurface waters from aquifers and agricultural drainage (adopted from Hiscock et al. 2003). 4-78
Table 4.3.5 Significant correlation of dissolved CH_4 and N_2O with selected properties of groundwater sampled in the study wells....4-79
Table 4.3.6 Values of $\delta^{18}O$ and $\delta^{15}N$ of nitrate, excess N_2 and the fraction of remaining nitrate (f $[NO_3]_R$) in groundwater in the Silver Spring springshed in the dry season. 4-87
Table 5.1.1. Estimated proportion of NO_3-N removal via denitrification versus autotrophic uptake....5-6
Table 5.1.2. Fitted OTIS model parameters for the downstream reach of the Silver River. 5-39
Table 5.1.3. Fitted OTIS model parameters for the whole length of the Silver River....5-40
Table 5.1.4. Comparison of OTIS and moment for downstream reach. 5-41
Table 5.1.5. Comparison of OTIS and moment for whole river....5-41
Table 5.1.6. Comparison of Alexander Springs hydraulic properties for the 2009 and 2017 dye trace experiments....5-44
Table 5.1.7. Relative sediment sorption capacities. 5-46
Table 5.1.8. Fitted reaction and sorption rates. 5-47
Table 5.1.9. Fitted reaction and sorption rates. 5-47

Page

Table 5.2.1. Results of the bootstrapping version of the Kolmogorov-Smirnov test to check for hysteresis. Significant differences ($p<0.05$) in algal abundance distributions before installation and after removal of the Shadow structure are noted in bold. Only two of the treatments had statistically differences before installation and after removal (one with less algae after the removal and one with more). Note: Deployment 3 had the shortest observation interval following Shadow removal, so higher post-removal algal coverage in Deployment 3, Site 4 may be due to experimental error. 5-77

Table 6.1. Summary of metabolism variables, their associated symbols, and units. 6-6

Table 6.2. Predicting GPP - Upper Silver River (Mammoth to SILGOLD). 6-39

Table 6.3. Predicting GPP – Upper Half of Silver River (Mammoth to S5).. 6-40

Table 6.4. Predicting GPP – Middle Reach of Silver River (SILGOLD to S5) 6-41

Table 6.5. Predicting GPP - Lower Silver River (S5 to S1). 6-42

Table 6.6A. Predicting GPP – Alexander Springs Creek. 6-43

Table 6.6B. Summary of characteristics, sample sizem and preservative by stream sample area.. 6-59

Table 6.7. Summary of porewater, soil and water chemistry across the Silver River. Note that concentrations for Fe and Mn were consistently below detection limits. 6-68

Table 6.8. Correlation (Pearson's r) matrix for physical controls on autotroph cover. Bolded correlations are significant at $p < 0.05$. 6-80

Table 6.9. Summary of correlation coefficients between water chemistry[B] and both SAV and algal cover. Shown are correlations[C] for both water column chemistry and porewater chemistry. 6-82

Table 6.10. Summary of correlation coefficients between soil chemistry and both SAV and algal cover. Bolded correlations are significant at $p < 0.05$.. 6-83

Table 6.11. Distance downstream was negatively and significantly correlated to control chamber GPP whereas surface light and water depth were positively and significantly correlated to GPP. Significant correlations ($p < 0.05$) are shown in bold, negative correlations in red. 6-96

Table 6.12. Results of general linear model predictions of control box a) GPP and b) ER based on physical site attributes and timing.. 6-97

Table 6.13. Results of general linear model predictions of GPP_t:GPP_c for Silver River based on nutrient enrichment and distance. 6-101

Table 6.14. Results of general linear model predictions of GPP_t:GPP_c for Alexander Springs Creek based on nutrient enrichment only (distance was not considered). 6-102

Page

Table 6.15. Summary of R^2 values for various models (Equations. 6.4 – 6.8) fitted to benthic chamber nitrate concentrations over time (e.g., Figure 6.105). Each deployment represents a different location in the listed river (Silver, Gum, Rainbow, Alexander).. 6-121

Table 6.16. Summary of optimized model parameters. . n_A – assimilatory uptake kinetic exponent, τ – assimilatory offset from solar noon (hrs), n_D – dissimilatory uptake kinetic exponent. Each deployment was in a different geographic location in each river. 6-123

Table 6.17. Summary of river characteristics (mean ± standard deviation) for sixteen sites measured from May 2015 – December 2016 in Silver River and January – December 2016 in Alexander Springs Creek. A summary of the individual site characteristics in each river is included in Appendix 6.2. 6-142

Table 6.18. Summary of significant main effects at Silver River including mean-centered standardized slope, standard error, and t-value (Deviance = 260.04, Marginal $R^2 = 0.31$ Conditional $R^2 = 0.45$). 6-147

Table 6.19. Summary of significant main effects at Alexander Springs Creek including mean-centered standardized slope, standard error, and t-value (Deviance = 238.77, Marginal $R^2 = 0.23$, Conditional $R^2 = 0.35$). 6-147

Table 7.3.1. Results of velocity and algal biomass measures for four flow rates investigated. 7-87

Table 8.1. Location and information of the CTDs deployment. 8-12

Table 8.2. Sediment diffusion coefficient, D_s ($cm^2\ s^{-1}$) for solutes.....8-17

Table 8.3. Concentration of chemical variables in deep pore waters collected by vapor probe. 8-18

Table 8.4. Benthic fluxes of solutes across the sediment - water interface in the Silver River. 8-40

Table 9.1.1. Summary of water quality characteristics of the Silver Springs group. Summary statistics are for the period-of-record, which varied by analyte. Source: SJRWMD unpublished and Munch et al. (2006). 9-8

Table 9.1.2. Stable isotope composition ($\delta^{15}N$ and $\delta^{13}C$) and elemental ratios (C:N) of broadly characterized primary producer groups from Silver River as a function of river region. For each group the bold numbers are overall values averaged across river regions, i.e. upper, mid and lower. 9-18

Table 9.1.3. Stable isotope composition ($\delta^{15}N$ and $\delta^{13}C$) and elemental ratios (C:N) of algal growth forms from Silver River. 9-20

Table 9.1.4. Stable isotope composition ($\delta^{15}N$ and $\delta^{13}C$) of gastropods. 9-25

Table 9.1.5. Stable carbon and nitrogen isotope ratios and statistics for SEA_B estimates for herbivorous and omnivorous taxa from Silver River. 9-40

Table 9.1.6. Summary of posterior distributions from four end-member SIAR mixing model simulations and niche specialization index (ε) calculated for herbivore and omnivore taxa.....9-47

Page

Table 9.1.7. Percent Index of Relative Importance (%IRI) values for nine prey categories determined for *Alligator mississippiensis* size classes. 9-51
Table 9.1.8. Number of individuals examined for stomach content analysis of fish species. 9-53
Table 9.1.9. Number of individual turtles that have been analyzed for composition of scat. 9-56
Table 9.2.1. Concentrations of macronutrients and micronutrients in concentrated solution (stock) used to provide nutritional support to algae colonies (1 mL dose) and the expected nutrient concentrations (end) in 10 L colony tanks 9-70
Table 9.2.2. Log-likelihood, number of parameters (*k*), Akaike's second-order information criterion (AICc), ΔAICc, and Akaike weight (*w*) for candidate generalized linear models of per capita consumption rate (g algae g grazer^{-1} d^{-1}) of macroalgae during 3-day trials.....9-73
Table 9.2.3 Predicted β coefficient estimates and 95% Confidence Intervals based on our best fit GLM for per capita consumption rate of macroalgae as affected by grazer taxa. 9-73
Table 9.2.4 Predicted β coefficient estimates and 95 % Confidence Intervals based on our best fit GLM for per capita consumption rate of macroalgae as affected by macroalgae taxa. 9-75
Table 9.2.5 Predicted β coefficient estimates and 95 % Confidence Intervals based on our best fit GLM for per capita consumption rate (g algae g grazer^{-1} d^{-1}) of macroalgae as affected by the interaction of grazer and macroalgae taxon. (–) denotes the grazer taxon is unchanged from row above. 9-76
Table 9.2.6 Log-likelihood, number of parameters (*k*), Akaike's second-order information criterion (AICc), ΔAICc, and Akaike weight (*w*), for candidate generalized linear models of per capita consumption rate (g macrophyte g grazer^{-1} d^{-1}) of macrophytes during 3-day trials. 9-79
Table 9.2.7 Predicted β coefficient estimates and 95 % Confidence Intervals based on our best fit GLM for per capita consumption rate of macrophytes as affected by grazer taxa. 9-79
Table 9.2.8 Predicted β coefficient estimates and 95 % Confidence Intervals based on our best fit GLM for per capita consumption rate of macrophytes as affected by macrophyte taxa. 9-80
Table 9.2.9 Predicted β coefficient estimates and 95 % Confidence Intervals based on our best fit GLM for per capita consumption rate (g macrophyte g grazer^{-1} d^{-1}) of macrophytes as affected by the interaction of grazer and macrophyte taxon. (–) denotes the grazer taxon is unchanged from row above. 9-81
Table 9.3.1 Prevalence of macrophyte taxa randomly selected to perform growth assays in each river region. 9-94

Page

Table 9.3.2 Model structure, number of parameters (*k*), log-likelihood, Akaike's second-order information criterion (AICc), ΔAICc, and Akaike weight (*w*), for candidate generalized linear models explaining variation in aboveground growth rates (g d^{-1}).....9-95

Table 9.3.3 Model averaged β coefficient estimates and 95 % CI's based on our top performing candidate models explaining variation in aboveground macrophyte growth rates.....9-95

Table 9.3.4 Model structure, Model structure, number of parameters (*k*), log-likelihood, Akaike's second-order information criterion (AICc), ΔAICc, and Akaike weight (*w*), for all candidate GLMs explaining variation in aboveground macrophyte biomass. 9-99

Table 9.3.5 Model structure, number of parameters (*k*), log-likelihood, Akaike's second-order information criterion (AICc), ΔAICc, and Akaike weight (*w*), for top performing candidate GLMs explaining variation in epiphytic algae biomass.....9-101

Table 9.3.6 Model averaged β coefficient estimates and 95 % CIs based on our top performing candidate GLMs explaining variation in epiphytic algae biomass.....9-101

Table 9.3.7 Model structure, number of parameters (*k*), log-likelihood, Akaike's second-order information criterion (AICc), ΔAICc, and Akaike weight (*w*), for all candidate generalized linear models explaining variation in total macroinvertebrate biomass. 9-103

Table 9.3.8 Model averaged β coefficient estimates and 95 % CIs based on our top performing candidate models explaining variation in total macroinvertebrate biomass. 9-103

Table 9.3.9 Model structure, number of parameters (*k*), log-likelihood, Akaike's second-order information criterion (AICc), ΔAICc, and Akaike weight (*w*), for top performing candidate GLMs explaining variation in macroinvertebrate grazer biomass. 9-105

Table 9.3.10 Model averaged β coefficient estimates and 95 % CIs based on our top performing candidate GLMs explaining variation in macroinvertebrate grazer biomass. 9-105

Table 9.3.11 Model structure, number of parameters (*k*), log-likelihood, Akaike's second-order information criterion (AICc), ΔAICc, and Akaike weight (*w*), for all candidate generalized linear models explaining variation in macroinvertebrate omnivore biomass.....9-106

Table 9.3.12 Model averaged β coefficient estimates and 95 % CIs based on our top performing candidate models explaining variation in macroinvertebrate omnivore biomass.....9-107

Table 9.3.13 Model structure, number of parameters (*k*), log-likelihood, Akaike's second-order information criterion (AICc), ΔAICc, and Akaike weight (*w*), for top performing candidate GLMs explaining variation in macroinvertebrate predator biomass.....9-108

Page

Table 9.3.14 Model averaged β coefficient estimates and 95 % CIs based on our top performing candidate models explaining variation in macroinvertebrate predator biomass 9-108
Table 9.3.15 Model structure, number of parameters (*k*), log-likelihood, Akaike's second-order information criterion (AICc), ΔAICc, and Akaike weight (*w*), for top performing candidate GLMs explaining variation in macroinvertebrate parasite biomass..... 9-109
Table 9.3.16 Model averaged β coefficient estimates and 95 % CIs based on our top performing candidate models explaining variation in macroinvertebrate parasite biomass. 9-109
Table 9.3.17 Model structure, number of parameters (*k*), log-likelihood, Akaike's second-order information criterion (AICc), ΔAICc, and Akaike weight (*w*), for top performing candidate GLMs explaining variation in macroinvertebrate abundance. 9-110
Table 9.3.18 Model averaged β coefficient estimates and 95 % CIs based on our top performing candidate models explaining variation in macroinvertebrate abundance. Coefficient estimates are not transformed. 9-111
Table 9.3.19 Model structure, number of parameters (*k*), log-likelihood, Akaike's second-order information criterion (AICc), ΔAICc, and Akaike weight (*w*), for top performing candidate GLMs explaining variation in macroinvertebrate grazer abundance. 9-112
Table 9.3.20 Model averaged β coefficient estimates and 95 % CIs based on our top performing candidate models explaining variation in macroinvertebrate grazer abundance. Coefficient estimates are not transformed. 9-112
Table 9.3.21 Model structure, number of parameters (*k*), log-likelihood, Akaike's second-order information criterion (AICc), ΔAICc, and Akaike weight (*w*), for the top performing GLM explaining variation in macroinvertebrate omnivore abundance. 9-114
Table 9.3.22 Model averaged β coefficient estimates and 95 % CIs based on our top performing candidate models explaining variation in macroinvertebrate omnivore abundance. Coefficient estimates are not transformed. 9-114
Table 9.3.23 Model structure, number of parameters (*k*), log-likelihood, Akaike's second-order information criterion (AICc), ΔAICc, and Akaike weight (*w*), for all candidate GLMs explaining variation in macroinvertebrate predator abundance. 9-115
Table 9.3.24 Model averaged β coefficient estimates and 95 % CIs based on our top performing candidate models explaining variation in macroinvertebrate predator abundance. Coefficient estimates are not transformed. 9-116

Page

Table 9.3.25 Model structure, number of parameters (*k*), log-likelihood, Akaike's second-order information criterion (AICc), ΔAICc, and Akaike weight (*w*), for top performing candidate GLMs explaining variation in macroinvertebrate parasite abundance. 9-117

Table 9.3.26 Model averaged β coefficient estimates and 95 % CIs based on our top performing candidate models explaining variation in macroinvertebrate parasite abundance. Coefficient estimates are not transformed. 9-117

Table 9.3.27 Community composition (% abundance and % mass) of macroinvertebrates as a function of experimental treatments based on empirical data. 9-118

Table 9.3.28 Community composition (% abundance and % mass) of macroinvertebrates as a function of river region based on empirical data. 9-119

LIST OF FIGURES

		Page
Figure ES.1.	List of work orders of the CRISPS project	ES-15
Figure 2.1.1.	Conduit Evolution Algorithm, adapted from Borghi et al. (2012).	2-6
Figure 2.1.2.	Silver Springshed site map showing A) location in Florida and B) Silver Springs (filled blue circle), 1,000-year spring groundwater capture zone (black outline), photolineament defined regional fracture sets, extensive sinks (black dots) and NDM –V4 model domain (red outline).	2-7
Figure 2.1.3.	Reaction rate according to equation 2.1.22.	2-14
Figure 2.1.4.	Swamee and Swamee (2007) pipe flow equation with r = 0.005 m and ε = 0.001 m showing smooth transition between laminar and turbulent flow as hydraulic gradient in pipe increases (solid line). Poiseuille equation for laminar flow (dotted line) and Darcy-Weisbach equation for turbulent flow (dashed line) are also shown for comparison.	2-15
Figure 2.1.5.	Silver Spring model domain showing model grid and model surface topography elevations.	2-18
Figure 2.1.6.	Example lnQ versus t plot showing hydrograph (black), log transformed flow (blue) and computed inflection point separating early and late hydrograph recession periods.	2-22
Figure 2.1.7.	Simulated springflow during dissolution for A) steady state flow dissolution time and B) 1.5 times the steady state flow dissolution time.	2-23
Figure 2.1.8.	Conduit flow during evolution showing A) flow rates through conduit network at 15,000 years (steady state), B) network at 20,000 years (1.33*steady state , and C) network at 25,000 years (1.66*steady state).	2-24
Figure 2.1.9.	Morris Method Global Sensitivity Analysis dissolution statistic plots showing A) dissolved HPF density, B) median radii, and C) max radii. $\mu = \sigma$ (blue lines) and $\mu = 2\sigma/\sqrt{r} = 0.63\ \sigma$ (red lines) are shown to aid in interpretation of parameter interactivity.	2-26
Figure 2.1.10.	Ensemble hydrograph (A) and behavioral ensemble hydrograph () showing mean (black line) and standard deviation (gray shaded region).	2-27
Figure 2.1.11.	Morris Method Global Sensitivity Analysis hydrologic pulse response metrics, showing A) steady-state flow, B) peak flow, C) early recession coefficients, and D) late recession coefficients.	2-29
Figure 2.1.12.	Ensemble breakthough curve (A) and behavioral ensemble breakthrough curve (B) showing mean (black line) and standard deviation (gray shaded region).	2-30

Page

Figure 2.1.13. Morris Method Global Sensitivity Analysis transport pulse response metrics, showing A) peak solute mass flux B) peak transport time, C) normalized first moment (mean travel time), and D) square root of normalized second central temporal moment (travel time standard deviation). 2-31
Figure 2.1.14. Two non-behavioral conduit networks, showing development of localized flow systems. 2-32
Figure 2.1.15. Three behavioral conduit networks with the same transport peak time but increasing steady-state flux from left to right. Steady state flux for A) is 10 $m^3 s^{-1}$, B) is 18 $m^3 s^{-1}$, and C) is 24 $m^3 s^{-1}$. 2-32
Figure 2.1.16. Lower behavioral end member with spring flow approximately equal to total 9.93 $m^3 s^{-1}$. 2-33
Figure 2.1.17. Upper behavioral end member with spring flow approximately equal to total 28 $m^3 s^{-1}$. 2-34
Figure 2.2.1. Potentiometric surface maps for Silver Springs showing contoured potentiometric surface in ft. above mean sea level for 2010 (1 m=3.28 ft). 2-37
Figure 2.2.2. Complete ensemble hydrograph showing mean (black line) and standard deviation (gray shaded region). 2-40
Figure 2.2.3. Complete ensemble head transects showing mean (black line) and standard deviation (gray shaded region). Spring is at zero on x-axis and distances are in the direction away from the spring. A) north transect, B) west transect, C) south transect, and D) east transect. 2-41
Figure 2.2.4. Complete ensemble forward breakthough curve showing mean (black line) and standard deviation (gray shaded region). 2-41
Figure 2.2.5. Behavioral ensemble hydrograph showing mean (black line) and standard deviation (gray shaded region). 2-42
Figure 2.2.6. Behavioral ensemble head transects showing mean (black line) and standard deviation (gray shaded region). Spring is at zero on x-axis and distances are in the direction away from the spring. A) north transect, B) west transect, C) south transect, and D) east transect. 2-43
Figure 2.2.7. Behavioral ensemble forward breakthough curve showing mean (black line) and standard deviation (gray shaded region). 2-44
Figure 2.2.8. Mean of behavioral ensemble head, 0th moment (mass arriving at surface), peak arrival time and median arrival time for backward pulse experiment. 2-45
Figure 2.2.9. Standard Deviation of behavioral ensemble head, 0th moment (mass arriving at surface), peak arrival time and median arrival time for backward pulse experiment. 2-46
Figure 2.2.10. Behavioral case 79 showing A) initial HPF network, B) steady-state hydraulic heads, and C) developed conduit network. 2-47
Figure 2.2.11. Backwards transport pulse for case 79 showing A) mass recovery (0th moment) B) peak arrival time, and C) median arrival at the land surface. Black lines represent evolved conduits. Black dots represent VPFs. 2-48

Page

Figure 2.2.12. Behavioral case 83 showing A) initial HPF network, B) steady-state hydraulic heads, and C) developed conduit network. 2-48
Figure 2.2.13. Backwards transport pulse for case 83 showing A) mass recovery (0th moment) B) peak arrival time, and C) median arrival at the land surface. Black lines represent evolved conduits. Black dots represent VPFs. 2-49
Figure 2.2.14. Head, 0th moment (mass arriving at surface), peak arrival time and median arrival time for equivalent porous media model. 2-50

Figure 3.1. (a) Passive flux meter (PFM) schematic diagram, and (b) photograph of PFM deployment in a well. 3-4
Figure 3.2. Karstic borehole device (KBHD) during retrieval from a monitoring well following a borehole dilution test. 3-6
Figure 3.3. Kevlar packer being attached to the karstic borehole device. 3-7
Figure 3.4. Watertight fittings. 3-7
Figure 3.5. View of the down-hole lines during injection of a tracer pulse. 3-8
Figure 3.6. Cable eyelet welded to the top cap of the pump shroud. 3-8
Figure 3.7. Pump being installed in shroud (left), pump installation above the bottom packer (middle), shroud being capped with the bottom of the water tight line (right). 3-9
Figure 3.8. Conductivity meter and flourometer used during a borehole dilution test. 3-9
Figure 3.9. KBHD assembled to test 10' intervals (left) and KBHD in vertical position in preparation for downhole deployment (right). 3-10
Figure 3.10. Several 10-foot sections of pipe with downhole lines through them and in preparation for down-hole deployment. 3-10
Figure 3.11. KBHD being deployed in well M0789. 3-11
Figure 3.12. Above-ground equipment during a borehole dilution test. 3-11
Figure 3.13. Schematic of the soil column constructed for the soil moisture profile measurements. 3-14
Figure 3.14. Darcy flux profile from BHD tests performed in well M0789. 3-17
Figure 3.15. Electrical conductivity timeseries from test 1. 3-17
Figure 3.16. Electrical conductivity timeseries from test 2. 3-18
Figure 3.17. Electrical conductivity timeseries from test 3. 3-18
Figure 3.18. Electrical conductivity timeseries from test 4. 3-18
Figure 3.19. Electrical conductivity timeseries from test 5. 3-19
Figure 3.20. Electrical conductivity timeseries from test 6-1. 3-19
Figure 3.21. Electrical conductivity timeseries from test 6-2. 3-19
Figure 3.22. Electrical conductivity timeseries from test 6-3. 3-20
Figure 3.23. Log-transformed C/C_0 data from test 1 used for Darcy flux estimation. 3-20
Figure 3.24. Log-transformed C/C_0 data from test 2 used for Darcy flux estimation. 3-20
Figure 3.25. Log-transformed C/C_0 data from test 3 used for Darcy flux estimation. 3-21

Page

Figure 3.26. Log-transformed C/C_0 data from test 4 used for Darcy flux estimation. 3-21
Figure 3.27. Log-transformed C/C_0 data from test 5 used for Darcy flux estimation. 3-21
Figure 3.28. Log-transformed C/C_0 data from test 6-1 used for Darcy flux estimation. 3-22
Figure 3.29. Log-transformed C/C_0 data from test 6-2 used for Darcy flux estimation. 3-22
Figure 3.30. Log-transformed C/C_0 data from test 6-3 used for Darcy flux estimation. 3-22
Figure 3.31. Comparison of rhodamine and KCl log transformed data from conduit test 6-1. 3-23
Figure 3.32. Comparison of rhodamine and KCl log transformed data from conduit test 6-2. 3-23
Figure 3.33. Comparison of rhodamine and KCl log transformed data from conduit test 6-3. 3-23
Figure 3.34. Summary of Darcy fluxes measured by PFMs, and location map of well locations in relation to 14 and 28 km diameter circles around Silver Springs. 3-24
Figure 3.35. (left) Well M0789 push-pull test apparatus. (right) Background nitrate concentrations measured as a function of depth in M0789. Samples were collected using the KBHD device. 3-25
Figure 3.36. (left) Sprayfield well push-pull test apparatus. (right) Background nitrate concentrations measured as a function of depth at the Sprayfield well. Samples were collected using the KBHD device. 3-25
Figure 3.37. Well M0789 (top) Measured relative concentrations of rhodamine and KNO_3 tracers during injection (push). Right side graph shows that the integrated measured mass equals the expected value. (bottom) Measured relative concentrations of rhodamine and KNO_3 tracers during extraction (pull). Right side graph shows that both tracers recovered similar mass. 3-26
Figure 3.38. Sprayfield well (top) Measured relative concentrations of rhodamine and KNO_3 tracers during injection (push). Right side graph shows that the integrated measured mass equals the expected value. (bottom) Measured relative concentrations of rhodamine and KNO3 tracers during extraction (pull). Right side graph shows that both tracers recovered similar mass. 3-27
Figure 3.39. Expected mass loss from zero- and first-order degradation as a function of residence time. (left) Longer residence times with relatively lower rate constants and (right) Shorter residence times with relatively higher rate constants. Measurable mass loss (~ 10 % or more) within just a few hours requires relatively high rate constants ($k \sim 0.1\ h^{-1}$ or higher). 3-28

Page

Figure 3.40. Top and bottom are two replicated push-pull tests at M779 134-145 ft. (left) Measured relative concentrations of rhodamine and KNO_3 tracers during extraction. (right) Integrated measured mass recovery. NO_3 recovery was only approximately 60% of the rhodamine recovery. 3-29

Figure 3.41. Well M0780 59-69 ft (top) Measured relative concentrations of rhodamine and KNO_3 tracers during injection (push). Right side graph shows that the integrated measured mass equals the expected value. (bottom) Measured relative concentrations of rhodamine and KNO3 tracers during extraction (pull). NO_3 recovery was only approximately 60% of the rhodamine recovery. 3-30

Figure 3.42. Well M0781 25-35 ft (top) Measured relative concentrations of rhodamine and KNO_3 tracers during injection (push). Right side graph shows that the integrated measured mass equals the expected value. (bottom) Measured relative concentrations of rhodamine and KNO_3 tracers during extraction (pull). Right side graph shows that both tracers recovered similar mass. 3-31

Figure 3.43. Steady-state soil moisture profile of macroporous anion exchange resin layered between Arredondo fine sand, with a constant water flux of 2 cm d^{-1} 3-32

Figure 3.44. HYDRUS-1D simulation of the steady-state soil moisture profile of a macroporous anion exchange resin/Arredondo fine sand mixture layered between Arredondo fine sand, with a constant water flux of 23 cm d^{-1} 3-32

Figure 3.45. Measured and predicted soil moisture profile (left) and comparison of measured soil moisture data points and soil moisture modeled in HYDRUS-1D (right). 3-33

Figure 3.46. HYDRUS-1D simulation of the steady-state soil moisture profile of a macroporous anion exchange resin/Arredondo fine sand mixture layered between Arredondo fine sand with a constant water flux of 23 cm d^{-1} (solid) and 2 cm d^{-1} (dashed). 3-33

Figure 3.47. Nitrate recovery in soil column (± SE). 3-34

Figure. 3.48. (left) Schematic diagram of a hypothetical cylinder through the Upper Floridan aquifer, with thickness B and radius r. (right) Average Darcy flux, qavg (m d^{-1}), and recharge, QR (m^3 s^{-1}), as a function of radius from spring outlet. 3-35

Figure. 3.49. Measured Darcy fluxes from PFMs, BHD tests, and dye tracer test (DTT) estimates from previous studies conducted within the 14 km radius of Silver Springs, (see Figure 3.33 for locations). 3-36

Figure. 3.50. Non-matrix fraction of the total flow and total cross-sectional area, based on mean matrix and non-matrix fluxes qm = 0.06 m d^{-1} and qc = 30.1 m d^{-1}. 3-36

Figure. 3.51. Measured head profile with distance from the spring. (left) A homogeneous porous medium would have a convex head profile. (right) Decreasing conduit density with distance. 3-37

Page

Figure 4.1.1. Locations and IDs of the wells installed for the project and used for collection of soil and vadose zone profile materials. Sites with wells at multiple depths are indicated by multiple IDs. 4-8

Figure 4.1.2. Vertical cross section of lithographic units encountered in the study area crossing Alachua, Marion, and Lake Counties (from Scott 1988). 4-10

Figure 4.1.3. Vertical patterns of soil and vadose zone materials encountered during installation of study wells in the Silver Spring springshed. 4-11

Figure 4.1.4. Vertical profiles of redox potential (mV) in soil and vadose zone profiles for the 12 study wells. The gray areas and the dash lines represent the clay layers and the water table, respectively. 4-12

Figure 4.1.5. Vertical profiles of loss on ignition (LOI) in soil and vadose zone profiles for the 12 study wells. The gray areas and the dash lines represent the clay layers and the water table, respectively. 4-14

Figure 4.1.6. Vertical profiles of total carbon (TC) (TC, g kg^{-1}), extractable total organic carbon (Ext. TOC, mg kg^{-1}), and total nitrogen (TN, 0.01 g kg^{-1}) in soil and vadose zone profiles for the 12 study wells. The gray areas and the dash lines represent the clay layers and the water table, respectively. 4-16

Figure 4.1.7. Vertical profiles of water extractable nitrate and ammonium (Ext. NO_3/NH_4) in soil and vadose zone profiles for the 12 study wells. The gray areas and the dash lines represent the clay layers and the water table, respectively. 4-21

Figure 4.1.8. Vertical profiles of denitrfication enzyme activity (DEA) in soil and vadose zone profiles for the 12 study wells. The gray areas and the dash lines represent the clay layers and the water table, respectively. 4-23

Figure 4.1.9. Comparison of denitrfication enzyme activity (as production of N_2O) with and without added glucose in soil and vadose zone profiles for the 12 study wells. 4-24

Figure 4.1.10. Regressions of denitrfication enzyme activity (DEA) with with total and extractable carbon and nitrogen parameters in soil and vadose zone profiles for the 12 study wells. 4-25

Figure 4.1. 11. Vertical profiles of $\delta^{18}O$ and $\delta^{15}N$ of soil extractable nitrate (Ext. NO_3-N), $\delta^{18}O$ and $\delta^{15}N$ of nitrate for groundwater in the well, and $\delta^{15}N$ of total bulk N in soil profiles for the sites M-0774, M-0776, M-0786, and M-0782. The dash blue lines represent the water table. 4-27

Figure 4.1.12. Isotopic biplot of adjusted $^{15}N/^{18}O$ of water extractable NO_3^- from surface (<4 m) soils in this study. The solid line represents actual correlation and dotted line represents the hypothetical 1:1 ratio. 4-28

Figure 4.1.13. Abundances of 16S rRNA gene and nosZ gene copies normalized to per gram soil arranged by land use type with depth and standard errors (A-E). Ratio of nosZ to 16S rRNA gene copy numbers along the depth profiles (F-H). 4-29

Page

Figure 4.1.14. Principal component analysis (PCA) of the quantitative PCR data and sediment chemical parameters. Samples that did not have detectable 16S rRNA gene or nosZ gene copies were discarded.....4-31
Figure 4.1.15. Margalef's richness, Pielou's evenness (J') and Shannon diversity (H') of the aquifer sediment bacterial communities according to depth (Shallow=0-3 m, Medium=3.6-11.6 m, Deep=>12 m) (A-C) and by well (D-F).....4-32
Figure 4.1.16. Similarity Percentage Analysis (SIMPER) identifying bacterial phyla that contributed most to the Bray-Curtis dissimilarity among depth groups. (A) Shallow-Medium, (B) Shallow-Deep, (C) Medium-Deep. Percentages indicate the SIMPER-derived percent contribution to the total dissimilarity between comparisons. 4-33
Figure 4.1.17. Relative abundances of the top phyla by (A) well and (B) depth category. Percent abundances were calculated using the sum of sequences identified within each well or depth category.....4-34
Figure 4.1.18. Non-metric multi-dimensional scaling (NMDS) of the 16S rRNA gene-derived bacterial communities based on the Hellinger-transformed relative abundance based Bray-Curtis dissimilarity matrix showing grouping according to depth. Group similarities are illustrated by green (15 %) and blue (25 %) dashed ellipses. Well ID's are illustrated by each point. 4-37
Figure 4.2.1. Aerial view of PSREU located in Marion County, FL; red points represent the sampling locations for HD and LD pasture, crop, and turf soils. 4-45
Figure 4.2.2. Relationship between denitrification enzyme activity (N_2O nmol g^{-1} dw^{-1} hr^{-1}) to WFPS (A) and Temperature (B) for LD. pasture soil. 4-52
Figure 4.2.3. Relationship between denitrification enzyme activity (N_2O nmol g^{-1} dw^{-1} hr^{-1}) to WFPS (A) and Temperature (B) for HD pasture soil.....4-52
Figure 4.2.4. Temperature effects on denitrification (N_2O nmol g^{-1} dw^{-1} hr^{-1}) by WFPS for Crop soil. A= <2 kg ha^{-1} NO_3^-., B= 35 kg ha^{-1} NO_3^-., and C= 50 kg ha^{-1} NO_3^-.....4-53
Figure 4.2.5. WFPS effects on denitrification (N_2O nmol g^{-1} dw^{-1} hr^{-1}) by Temperature for Crop soil. A= <2 kg ha^{-1} NO_3^-, B= 35 kg ha^{-1} NO_3^-, and C= 50 kg ha^{-1} NO_3^-.....4-53
Figure 4.2.6. Temperature effects on denitrification (N_2O nmol g^{-1} dw^{-1} hr^{-1}) by WFPS for Turf soil. A= <2 kg ha^{-1} NO_3^-, B= 35 kg ha^{-1} NO_3^-, and C= 50 kg ha^{-1} NO_3^-.....4-54
Figure 4.2.7. WFPS effects on denitrification (N_2O nmol g^{-1} dw^{-1} hr^{-1}) by Temperature for Turf soil. A= <2 kg ha-1 NO_3^-, B= 35 kg ha^{-1} NO_3^-, and C= 50 kg ha^{-1} NO3-.....4-54
Figure 4.2.8. Q10 values by WFPS, soil type, and NO_3^- concentrations (kg NO_3–N ha^{-1}). 4-56

Page

Figure 4.3.1. Schematic of typical ranges of $\delta^{18}O$ and $\delta^{15}N$ of nitrate from various sources as well as the isotopic effect of denitrification. (Adapted from http://wwwrcamnl.wr.usgs.gov/isoig/isopubs/Fig16-9.jpg) 4-65
Figure 4.3.2. Piper diagram showing the hydrogeochemical characteristics of sampled groundwater (n= 61) and spring vents for wet and dry season based on land use (a,b). 4-74
Figure 4.3.3. Principal component analysis based on selected water physical and chemical properties for the 61 wells in the wet season, the centroids were the average principal component values for each land use. 4-75
Figure 4.3.4. Dissolved CH_4 and N_2O in the 61 wells in the wet season. 4-77
Figure 4.3.5 Concentrations of dissolved N_2 and Ar observed in the east, west vent of the Silver Spring mammoth head spring, other five vent and in the 61 wells in the Silver Spring springshed catergorized by land use in the wet season. 4-80
Figure 4.3.6. Measured concentrations of dissolved gases (CH_4 and N_2O) in groundwater samples collected from the 15 study wells in dry and wet seasons.* denotes significant difference between wet and dry season. 4-81
Figure 4.3.7. Seasonal patterns of dissolved N_2O and CH_4 from July 2014 through April 2015 in the east and west vents of the Silver Spring mammoth head spring. 4-82
Figure 4.3.8. Seasonal patterns of dissolved N_2 and N_2:Ar observed from July 2014 through October 2015 in the east and west vents of the Silver Spring mammoth head spring. 4-83
Figure 4.3.9. Spatial distribution of nitrate concentration in the Silver Spring springshed (dry season) in relation to land use distributions. 4-84
Figure 4.3.10. Spatial distribution of nitrate concentration in the Silver Spring springshed (dry season) in relation to depth to the Upper Floridan Aquifer (UFA). 4-85
Figure 4.3.11. Correlation between NO_x-N and dissolved oxygen (DO) in the groundwater in wet and dry season. 4-86
Figure 4.3.12. The $\delta^{18}O$ and $\delta^{15}N$ of nitrate from the 61 wells in the silver springs springshed. Solid and dotted lines represent theoretical upper and lower bounds for enrichment due to denitrification based on the $\delta^{18}O$-NO_3: $\delta^{15}N$-NO_3 fractionation ratio of 1:1 and 1:2, respectively. 4-89
Figure 4.3.13. Correlation between principal component 1 and 2 and concentration and isotopic composition of nitrate categorized by land use. 4-90
Figure 4.3.14. Boxplot of (a) excess N_2 and (b) fraction of NO_3 remaining for different land uses in the dry and wet season. 4-91
Figure 4.3.15 Relationship between ln([NO_3]R) and $\delta^{15}N$-/ $\delta^{18}O$ [NO3]R for different land use. 4-92

Page

Figure 4.3.16. Variation of $\delta^{15}N$ and $\delta^{18}O$ of remaining nitrate with the fraction of NO3- remaining. 4-93

Figure 4.3.17. 16S rRNA gene and nosZ gene copy numbers obtained from filtering 20 L of water with standard errors (top). Average ratios of nosZ to 16S rRNA gene copy numbers in the identical wells. Wells with no data indicate that no detectable amplification of either gene was present across multiple runs....4-94

Figure 4.3.18. Principal components plot of the filter 16S rRNA and nosZ data with measured water chemistry data showing the loading of each vector and position of each well. Samples were excluded if they did not have detectable gene copies. 4-95

Figure 5.1.1 4 March 2015 dye trace. Clockwise from top left: diver just after releasing injection vessel cap, research vessels in main spring bowl after dye release, underwater view of diver after dye release, injection vessel suspended from research vessel with dye release. 5-10

Figure 5.1.2. Fixed-location dye sampling sites on the Silver River for 4 Match 2015 injection....5-10

Figure 5.1.3. Clockwise from top: hand pump device, sampling tube and weight deployed for sample collection, "rover" boat sample collection. 5-11

Figure 5.1.4. Locations of "rover" grab samples taken for the 4 March 2015 dye trace. 5-11

Figure 5.1.5. October 2, 2015 dye trace. Clockwise from top left: diver holding injection pump hose in from of Mammoth vent during initial moments of the dye release, diver illuminated by research vessels while situated in front of Mammoth vent prior to dye injection, the main spring bowl looking downstream following dye injection, snorkeler assisting divers with illumination during the dye injection....5-12

Figure 5.1.6. Locations of "rover" grab samples taken for the 2 October 2015 dye trace 5-13

Figure 5.1.7. Aerial imagery. Clockwise from top left: the main spring bowl following dye injection, dye pulse has left the spring vent and is tracing initial flow partitioning in the spring bowl, main spring bowl after most of the dye has cleared, upper 1,200 meters of the river showing dye pulse tracing main flow path while clear water input from side springs is visible. 5-13

Figure 5.1.8. Images from the August 24, 2016 dye trace. Left Panel: Divers resurfacing after releasing Rhodamine WT dye in Mammoth Vent. Top Right: Researchers on the surface illuminate the divers with spot lights just prior to the dye release. Bottom Right: The Mammoth Vent spring pool immediately after the release of the dye. Photos by Jenny Adler (https://walkingonwaterfl.org/) 5-14

Figure 5.1.9. Fixed-location dye sampling sites on the Silver River for the August 24, 2016 injection. 5-14

Page

Figure 5.1.10. Images from the December 8, 2016 dye trace. Right Panel: SAV near the Mammoth Vent spring pool shortly after Rhodamine WT was released. Top Left: Nathan Reaver dives to inspect dye plume shortly after dye release in the Mammoth Vent spring pool. Bottom Left: Reaver inspects the dye mixing interface within the Mammoth Vent spring pool. Photos by Jenny Adler (https://walkingonwaterfl.org/) 5-15
Figure 5.1.11. Summary of the seasonal and hydrologic conditions for the four Silver River dye traces conducted in this study, as well as an earlier dye trace conducted in 2009. 5-16
Figure 5.1.12. Images from the January 19, 2017 dye trace at Alexander Springs. Clockwise from top left: Dye being released by pouring into spring boil from canoe on the surface, Alexander Spring pool just after dye release, dye release team sampling following the dye release, UF volunteers collecting roving grab samples..... 5-16
Figure 5.1.13. Fixed-location dye sampling sites on Alexander Springs Creek for the January 19, 2017 dye trace..... 5-17
Figure 5.1.14. Example fitted parameter distribution (solid black line) and 95 % credible interval resulting from Bayesian model fitting versus a single parameter value derived from traditional techniques (black dashed line). 5-19
Figure 5.1.15. Visual interpretation of dye flows after March 2015 dye injection. Figure by Ed Carter..... 5-25
Figure 5.1.16. Aerial photograph from the October 2015 dye trace showing the three primary flow paths that the spring flow takes after leaving the vent. The first flow path leaves the spring pool and heads downstream. The second flow path leads to the Fort King waterway back channel. The third flow path circles back around to fill the spring pool. 5-26
Figure 5.1.17. August 2015 BTC at the 1,200 m station measured continuously (blue dots) and with ISCO grab samples (orange squares), which agree closely. Note three distinct concentration peaks. See Figure 5.1.2 for measurement locations.. 5-26
Figure 5.1.18. August 2015 BTCs at the midpoint and downstream stations measured continuously (red and green dots) and with ISCO grab samples (black and orange squares). See Figure 5.1.2 for measurement locations. 5-27
Figure 5.1.19. August 2015 BTCs at four ISCO monitoring stations. See Figure 5.1.2 for measurement locations. 5-27
Figure 5.1.20. October 2015 BTCs at the 1,200 m station in the main channel (black dots) and at the USGS station (blue dots). See Figure 5.1.2 for measurement locations. 5-29
Figure 5.1.21. October 2015 BTCs at the midpoint (red dots) and downstream (green dots) stations measured continuously. See Figure 5.1.2 for measurement locations. 5-29

Page

Figure 5.1.22. 1,200 m USGS Station and fluorometer from a watercraft. The water passing over the USGS station is only partially dyed, suggesting most of that water is not from the main channel, but rather has taken the back channel flow path.. 5-30
Figure 5.1.23. ,200 m USGS Station and fluorometer from the air. The water passing over the USGS station is only partially dyed, suggesting water passing that location is not from the main channel, but from the back channel flow path. 5-31
Figure 5.1.24. Aerial image of the Fort King waterway back channel viewed from the spring bowl facing SW. The dye bifurcates into two distinct flow paths, with faster "Flow Path 1" eventually becoming the 2nd peak in the 1,200 m BTC and the slower "Flow Path 2" becoming the 3rd peak. 5-32
Figure 5.1.25. Aerial image of the Fort King waterway back channel, main spring bowl, and main channel, facing NE. The dye bifurcates into two distinct flow paths, with the faster "Flow Path 1" eventually becoming the 2nd peak in the 1,200 m BTC and the slower "Flow Path 2" becoming the 3rd peak. In this image, Flow Path 2 is still clear of dye. 5-32
Figure 5.1.26. August 2016 BTC for Reach 1. See Figure 5.1.9 for measurement locations 5-33
Figure 5.1.27. August 2016 BTCs at the midpoint (red dots) and downstream (green dots) stations. See Figure 5.1.9 for measurement locations. 5-33
Figure 5.1.28. December 2016 BTCs at the midpoint (red dots) and downstream (green dots) stations. See Figure 5.1.9 for measurement locations. 5-34
Figure 5.1.29. OTIS model (red line) fitted to March 2015 BTC data (black circles) from the midpoint station (upper left). Parameter estimates from standard model fitting (black dashed lines) are compared with Bayesian parameter distributions (solid black line) and the mean/95 % credible parameter intervals (blue/red lines, respectively). 5-35
Figure 5.1.30. OTIS model (red line) fitted to March 2015 BTC data (black circles) from the downstream station (upper left). Parameter estimates from standard model fitting (black dashed lines) are compared with Bayesian parameter distributions (solid black line) and the mean/95 % credible parameter intervals (blue/red lines, respectively). 5-36
Figure 5.1.31. Relationships between parameter pairs across the entire population of Bayesian model fits for the March 2015 experiment. 5-37
Figure 5.1.32. Comparison of observed midpoint and downstream BTCs for the October 2009 (a), March 2015 (b), October 2015 (c), August 2016 (d), and December 2016 (e) tracer experiments on the Silver River. 5-38
Figure 5.1.33. Comparison of fitted BTCs for the October 2009, March 2015, October 2015, August 2016, and December 2016 experiments for the downstream portion of the Silver River. 5-38

Page

Figure 5.1.34. Comparison of fitted BTCs for the October 2009, March 2015, October 2015, August 2016, and December 2016 experiments for the entire Silver River. 5-39
Figure 5.1.35. Fitted reach-scale, advective zone velocities (u) for the whole river and downstream reaches of the Silver River over the five dye trace experiments relative to literature-derived algal velocity thresholds (see Section 5.2). 5-41
Figure 5.1.36. Reach-scale mean velocities calculated using moment analysis for upstream and downstream reaches of the Silver River over the five dye trace experiments relative to literature-derived algal velocity thresholds (see Section 5.2). 5-42
Figure 5.1.37. Reach-scale mean velocities as a function of discharge (left) and surface water elevation drop from the spring pool to the Silver-Ocklawaha River confluence (right). Upstream velocity is poorly predicted by flow, while downstream velocity is negatively correlated. Elevation drop is a positive predictor reach-scale velocity. 5-42
Figure 5.1.38. Breakthrough curves from the Alexander Springs Creek Dye trace. 5-43
Figure 5.1.39. Comparison of observed Reach 1 and Reach 2 for the July 2009 (a) and January 2017 (b) tracer experiments on Alexander Springs Creek. 5-43
Figure 5.1.40. Comparison between observed (red lines, blue dots) and modeled (green lines) BTCs at five locations on the Silver River for the March 2015 dye release. See Figure 5.1.2 for measurement locations. Figures by Yanfeng Zhang. 5-45
Figure 5.1.41. Adsorption to inactive sediment. 5-46
Figure 5.1.42. Combined effects of microbial activity and adsorption to sediment. 5-46
Figure 5.1.43. Raz and Rru breakthrough curves using kinetic and transport parameters for Jennings Creek (A) and Silver River (B). 5-48
Figure 5.2.1. Algal cover is hypothesized to be controlled by velocity, which has decreased markedly in the Silver River in recent years. Lower figure from Lowe (2014); red line represents initially identified velocity threshold of 0.35 m s^{-1} from King (2012), which was later updated to 0.22 m s^{-1} in King (2014). 5-52
Figure 5.2.2. Original proposed flow-way design. 5-53
Figure 5.2.3. Reimagined flow-way design (v2). This design was constructed and deployed in the Silver River (see Figures 5.2.4 and 5.2.6). 5-54
Figure 5.2.4. Modified flow-way (v2) deployed in the Silver River. 5-54
Figure 5.2.5. Modified flow-way (v3) deployed in the Silver River. 5-54
Figure 5.2.6. Flow-way (v2) deployed in the Silver River undergoing performance testing. 5-55
Figure 5.2.7. Flow-way (v3) deployed in the Silver River undergoing performance testing. 5-55

Page

Figure 5.2.8. Schematic of the "Shadow" deployment concept. See text for description. 5-56
Figure 5.2.9. The "Shadow" structure in the lab. Blue arrow indicates flow direction. 5-57
Figure 5.2.10. "Shadow" structure deployed in the Silver River. 5-57
Figure 5.2.11A. Example of flow suppression by the Shadow structure. Shown are velocity profiles at a location in the Silver River both before (blue) and after (red) the deployment of a Shadow structure. Velocity profiles consist of the average velocity (solid colored line) and plus and minus one standard deviation (dotted colored lines). The black line indicates the height of the top of the Shadow structure. 5-58
Figure 5.2.11B. Example of a beta distribution. The dotted vertical line shows the location of the average value of the distribution. 5-59
Figure 5.2.12. *Example of a logistic model for algal abundance.* 5-60
Figure 5.2.13. The time points in which algal abundance value distributions were compared for hysteresis effects in relation to Shadow installation and removal 5-64
Figure 5.2.14. Schematic of the critical algal removal hypothesis testing framework. The distribution of algal abundances observed below the critical velocity (black) should be different from and larger than the distribution of velocities observed above the critical velocity (red). 5-65
Figure 5.2.15. Schematic of the critical algal removal hypothesis testing framework. The left panel is equivalent to Fig. 5.2.15 rotated 90 degrees. The right panel illustrates the algal distributions as they would be observed as a function of velocity (if a velocity threshold exists). 5-65
Figure 5.2.16. Schematic of red-green-blue color separation (a), standard SAV-algae image used to test optical methods (b), and chromaticity distribution of various algal covers (c). 5-69
Figure 5.2.17. Optical algal cover image collection via GoPro camera mounted to research vessel. Images captured at night using an artificial light source to standardize lighting. 5-70
Figure 5.2.18. Vertical velocity profiles during flow-way (v2) testing. 5-71
Figure 5.2.19. Vertical velocity profiles during flow-way (v3) testing. 5-72
Figure 5.2.20. Algal colonization and growth in treatment versus control sites during "Shadow" deployment. 5-72
Figure 5.2.21. One week of algal growth in the velocity shadow of the "Shadow" structure 5-73
Figure 5.2.22. Progression of algal colonization and growth in treatment sites with ~0 flow velocity (left) and associated controls (right) over one-week deployment. 5-74

Page

Figure 5.2.23. Results of the Bayesian logistic fit to the categorical algal abundance values from an example treatment site (one of 20), shown with credible intervals (CI) on observed algal abundances (red-mean; orange-40 % CI; blue-60 % CI; gray-80 % CI, black-95 % CI). Black horizontal lines are fitted categorical algal cover classes. 5-75

Figure 5.2.24. Results of the Bayesian logistic fit to the categorical algal abundance values from an example treatment site (one of 20). Probability distributions are shown for the logistic model parameters K (carrying capacity), $\boldsymbol{P_0}$ (initial algal cover), and r (intrinsic algal growth rate). Red, blue, and green lines represent the 95 % credible interval, mean, and median, respectively. 5-75

Figure 5.2.25. Summary of algal colonization/growth rate results from all treatment sites. Black intervals represent a specific deployment. Center dots represent the means of the probability distributions, and end points represent the 95 % credible interval (CI). The top red interval is the distribution of the central tendencies of all treatment sites, suggesting an intrinsic algal colonization/growth rate in the absence of velocity of 1.14 1 day^{-1} (95 % CI: 0.70 day^{-1} to 1.60 day^{-1}). 5-76

Figure 5.2.26. Zoom-in of Figure 5.2.25 to highlight variance around the overall central tendencies. 5-76

Figure 5.2.27. Algae cover versus velocity for 14 springs (across 26 transects) from the Florida Springs Synoptic Study. 5-78

Figure 5.2.28. Algae cover category versus velocity from diver-collected data on the Silver River. 5-78

Figure 5.2.29. Probability distribution of the critical algal velocity based on data from the Springs Synoptic Study. Red, blue, and green lines represent the 95 % credible interval, mean, and median, respectively. 5-79

Figure 5.2.30. Probability distribution of the critical algal velocity based on data from Silver River. Red, blue, and green lines represent the 95 % credible interval, mean, and median, respectively. 5-80

Figure 5.2.31. Probability distribution of the critical algal velocity based on data from Gum Slough. Red, blue, and green lines represent the 95 % credible interval, mean, and median, respectively. We focus on the non-zero critical algal velocity. 5-80

Figure 5.2.32. Probability distribution of the critical algal velocity based on data from the Shadow experiment in the Silver River. Red, blue, and green lines represent the 95 % credible interval, mean, and median, respectively. 5-81

Figure 5.2.33. Probability distribution of the critical algal velocity based on data from the rivers, Weeki Wachee, Homosassa, and Chassahowitzka. Red, blue, and green lines represent the 95 % credible interval, mean, and median, respectively. 5-81

Page

Figure 5.2.34. Summary of critical velocity threshold estimates from the five observational datasets. The distribution of the central tendencies of all datasets suggests a critical algal removal rate of 0.215 m s^{-1} with 95 % CI (0.160 m s^{-1}, 0.270 m s^{-1}).....5-82

Figure 5.2.35. Data (open circles) and modeled algal abundance as a function of velocity for the Springs Synoptic Study, shown with credible intervals (CI) on observed algal abundances (red-mean; orange-40 % CI; blue-60 % CI; gray-80 % CI). Black horizontal lines are fitted categorical algal cover classes.....5-83

Figure 5.2.36. Data (open circles) and modeled algal abundance as a function of velocity for Silver River diver data, shown with credible intervals on observed algal abundances (red-mean; orange-40 % CI; blue-60 % CI; gray-80 % CI). Black horizontal lines are fitted categorical algal cover classes.....5-83

Figure 5.2.37. Data (open circles) and modeled algal abundance as a function of velocity for Gum Slough, shown with credible intervals on observed algal abundances (red-mean; orange-40 % CI; blue-60 % CI; gray-80 % CI). Black horizontal lines are fitted categorical algal cover classes.....5-84

Figure 5.2.38. Data (open circles) and modeled algal abundance as a function of velocity for the Shadow experiment in the Silver River, shown with credible intervals on observed algal abundances (red-mean; orange-40 % CI; blue-60 % CI; gray-80 % CI). Black horizontal lines are fitted categorical algal cover classes. 5-84

Figure 5.2.39. Data (open circles) and modeled algal abundance as a function of velocity for the Weeki Wachee, Homosassa, and Chassahowitzka Rivers, shown with credible intervals on observed algal abundances (red-mean; orange-40 % CI; blue-60 % CI; gray-80 % CI) 5-85

Figure 5.2.40. Algae cover category versus shear stress from diver-collected data on the Silver River. 5-85

Figure 5.2.41. Probability distribution of the critical algal shear stress based on data from Silver River. Red, blue, and green lines represent the 95 % credible interval, mean, and median, respectively.....5-86

Figure 5.2.42. Modeled algal abundance as a function of shear stress for the Silver River, shown with credible intervals on observed algal abundances (red-mean; orange-40 % CI; blue-60 % CI; gray-80 % CI). 5-86

Figure 5.2.43. Probability distribution of the critical SAV velocity based on cover data from the rivers, Weeki Wachee, Homosassa, and Chassahowitzka. Red, blue, and green lines represent the 95 % credible interval, mean, and median, respectively. 5-87

Page

Figure 5.2.44. Probability distribution of the critical SAV velocity based on mass data from the rivers, Weeki Wachee, Homosassa, and Chassahowitzka. Red, blue, and green lines represent the 95 % credible interval, mean, and median, respectively. We focus on the non-zero critical algal velocity.....5-87
Figure 5.2.45. Data (open circles) and modeled SAV abundance as a function of velocity for the rivers, Weeki Wachee, Homosassa, and Chassahowitzka, shown with credible intervals on observed algal abundances (red-mean; orange-40 % CI; blue-60 % CI; gray-80 % CI). Black horizontal lines are SAV cover classes. 5-88
Figure 5.2.46. Data (open circles) and modeled SAV abundance as a function of velocity for the rivers, Weeki Wachee, Homosassa, and Chassahowitzka, shown with credible intervals on observed algal abundances (red-mean; orange-40 % CI; blue-60 % CI; gray-80 % CI). 5-88
Figure 5.2.47. Summary of critical velocity threshold estimates for SAV from two observational datasets. The overall average value is 0.33 m s^{-1} and the credible intervals overlap between 0.24 m s^{-1} and 0.44 m s^{-1}. 5-89
Figure 5.2.48. Relationships between integrated images colors (B-G and G-R) and algal cover determined using visual and automated techniques. 5-89
Figure 5.3.1. Velocity validation transect locations. 5-91
Figure 5.1.2. A) Wading rod construction showing full-length extension. B) Taking velocity readings on T3. Note transect line for horizontal spacing and boat line (red) for stability. 5-92
Figure 5.3.3. Velocity transects at T3 (top) and T7 (bottom). Velocity is indicated by a shared color scale, illustrating slower velocities at T7. Point velocity measurement locations are indicated by crosses. X and Y scales are proportional (i.e., 1:1). 5-93
Figure 5.3.4. Rescaled velocity transect at T7. Color scale illustrates full range of measured velocity on T7. The Y scale is exaggerated 3x to make velocity variation with depth more visible.....5-93
Figure 5.3.5. Comparison of kriged point-based velocity EFM velocity measurements (top) and ADCP velocity measurements (bottom) on T3 (co-located transect). Note different color scales in top and bottom figures. 5-94
Figure 5.3.6. Comparison of kriged point-based velocity EFM velocity measurements (top) and ADCP velocity measurements (bottom) on T7 (transects NOT co-located). Note different color scales. 5-94
Figure 5.3.7. Comparison of measured velocity profiles at 16 (of >100) locations with velocities simulated by EFDC and modeled with a 1-D turbulence closure model. Figures by Yanfeng Zhang. 5-95
Figure 5.4.1. Monthly mean water level, 1970 to 2010, at the Silver Spring pool (USGS 02239500).....5-97

Page

Figure 5.4.2. Study area for the hydrodynamic analysis of Silver River comprising the main river channel, back-channel, and boat basin. SJRWMD collects water surface elevation at ten stations in Silver River (stations S1 through S10). USGS collects water surface elevation at four additional locations denoted "Pool Stage", "1,200 m station", "Lower Silver Stage", and Ocklawaha Stage, Discharge" in the figure. 5-101
Figure 5.4.3. Hardened shoreline in Silver River just downstream of the head pool. 5-102
Figure 5.4.4. Gradual shoreline adjacent to forested wetland. 5-102
Figure 5.4.5. Model grid detail with open edge boundary and shoreline ("flow boundary") used to guide the gridded area. 5-104
Figure 5.4.6. Final hydrodynamic model grid in head pool (upper plot, Map A) and lower river (lower plot, Map B). 5-105
Figure 5.4.7. Bottom type of Silver River assigned to each hydrodynamic model cell. 5-109
Figure 5.4.8. Fraction of bottom vegetation (green) compared with open water above the canopy (blue) at four transects. Transect T3 is in the Ocklawaha River just downstream of the Silver river mouth. Transects S-3, S-7, and S-10 are in the lower, middle, and upper portions of the Silver River, respectively. 5-110
Figure 5.4.9. Comparison of simulated and observed water elevation along Silver River for a discharge of 605 cfs (17.13 $m^3 s^{-1}$). Green circles are observed water level, dashed red line is simulated water level without submersed vegetation, and the solid black line is with submersed vegetation. 5-111
Figure 5.4.10. Sensitivity of simulated water elevation along Silver River to ±30 % changes in effective vegetative height, vegetative density and river discharge in comparison to a base test case. 5-112
Figure 5.5.1. Silver River main spring pool stage vs. discharge from 1947 to 2015. Historically, a discharge of 20 $m^3 s^{-1}$ (706 cfs) would produce a stage 0.6 m (2 ft) lower the stage the current river will produce at the same discharge. 5-118
Figure 5.5.2. SAV being uprooted by high flow velocities in the Silver River in 2016. 5-121
Figure 5.5.3. Reduced complexity modeling summary for the simulate river. 5-121
Figure 5.5.4. Conceptual coupled aquifer, spring, and spring run model. P is the recharge into the aquifer, h_A is the aquifer elevation, h_P is the spring pool elevation, h_r is the river depth, Q_s is the spring vent discharge, and Q_r is the river discharge. 5-122

Page

Figure 5.5.5. Stage and discharge data from the Silver River main spring pool from 1947-2015. Clockwise from top left: scatter plot of all data (blue), scatter plot of all data (blue) with data from 1947-1999 highlighted (yellow), scatter plot of all data (blue) with data from 2004-2015 highlighted (yellow), scatter plot of all data (blue) with data from 2000-2003 highlighted (yellow). 5-124

Figure 5.5.6. Stage and discharge data from the Silver River 1,200 m station. Data in blue covers the period from 7 February 1967 to 30 June 1972. Data in orange covers 21 November 2003 to 30 June 2015. 5-124

Figure 5.5.7. Stage and discharge data from the Ocklawaha River Conner station (just downstream of the Ocklawaha and Silver River confluence from the period 1932-1946, 1977-2015. Clockwise from top left: scatter plot of all data (blue), scatter plot of all data (blue) with data from 1932 to 1946, 1977 to 1999 highlighted (orange), scatter plot of all data (blue) with data from 2004 to 2015 highlighted (yellow), scatter plot of all data (blue) with data from 2000 to 2003 highlighted (yellow). 5-125

Figure 5.5.8. Stage and discharge data from the Silver River main spring pool from 1947 to 2015. Left: Illustrates historically (1999 or earlier) the expected state, given a discharge of 20 m^3 s^{-1} (706 cfs). The velocity in the main channel would be expected to be 0.244 m s^{-1} (8.62 cfs). Right: Illustrates currently (2004 or later) the expected state, given a discharge of 20 m^3 s^{-1}. The velocity in the main channel would be expected to be 0.159 m s^{-1} (5.62 cfs). 5-126

Figure 5.5.9. Stage and discharge data from the Silver River main spring pool from 1947 to 2015 (black circles), with the most statistically probable stage/discharge relationships found with the Bayesian change point analysis (red lines). 5-127

Figure 5.5.10. Probability distribution of the date of the change point (the most probable date where the stage/discharge shift can be said to have occurred). The black line signifies the probability density, the blue line give the location of the mean of the distribution, while the red lines give the locations of the 95 % credible interval. It should be noted that the dates shown in the probability distribution are not the exact dates where the stage/discharge shift in the Silver River occurred, but rather the date where it is most probable to split the dataset for the two stage/discharge relationships shown in Figure 5.5.8. 5-127

Figure 5.5.11. Simulated stage and discharge data from the reduced complexity modeling of SAV hydraulic interactions. This model allows for a shift from one stage discharge curve (one with little SAV) to another (dominated with SAV) and back again, driven by changes in river discharge. Each state is stable until discharge falls below or rises above a certain threshold, after which the system changes to the alternative state. 5-128

Page

Figure 5.5.12. Simulated SAV abundance time series from the reduced complexity modeling of SAV hydraulic interactions. 5-129
Figure 5.5.13. Simulated aquifer elevation (a) and spring run depth (b) time series for the low (red) and high (black) Manning's n simulations. 5-129
Figure 6.1. Locations of sensors at Silver River, from near the head spring (Mammoth; no sensors) to the confluence with the Ocklawaha (SILVERRIVERS1).....6-7
Figure 6.2. Breakthrough curves of dye at the 1200 m station (SILBIRD) illustrating the slower velocity and multi-model arrival. Dye breakthrough at a nearby location (less than 50 m away from SILBIRD, but in the advective zone of the river) are commensurate with expectations. 6-8
Figure 6.3. Map of the Alexander Springs Creek system showing the headspring sensor suite near the main boil, and the Tracy Canal site approximately 10 km downstream. 6-9
Figure 6.4. Schematic of metabolism inference from diel dissolved oxygen variation, showing calculation of primary production (GPP; stippled area) and ecosystem respiration (ER; grey area). Both GPP and ER are sensitive to reaeration estimates (k; hr^{-1}). 6-9
Figure 6.5. Time series of Silver River discharge (orange line) and estimated velocities at three sampling locations based on channel cross-sections (light and dark blue dots). Measured velocities from the dye injections (squares and diamonds) agree with mean velocity, but not time variation. To estimate both travel time and reaeration on each day, we used velocity estimates from channel cross sectional areas. 6-11
Figure 6.6. Reach mean water velocity (numbers at right in the upper panel) significantly impacts inference of GPP (25% variation or more). The lower panel shows dye trace velocities in upper and lower Silver River and propagates that range through the observed DO data (upper panel). To reduce uncertainty, we estimated daily velocity from discharge and cross-sectional area information.. 6-12
Figure 6.7. Diel variation in water temperature, pH, specific conductance and dissolved oxygen for SILGOLD (yellow), S5 (light blue), and S1 (dark blue) stations on Silver River. 6-13
Figure 6.8. Diel variation in turbidity, fluorescent DOM (fDOM), nitrate and phosphate for the three stations on Silver River. Note that no phosphate sensor was deployed at site S1.....6-13
Figure 6.9. Summary of period of record data for Alexander Springs Creek at Tracy Canal. No nutrient data were available for downstream sites in this river. 6-14
Figure 6.10. Time series of fDOM and chlorophyll a at Tracy Canal in Alexander Springs Creek.. 6-15

Page

Figure 6.11. Fine scale variation in solute chemistry in Silver River over two-weeks starting in late August 2016. This period was selected because it shows all three sensor stations, and also the influence of a significant rain event at the beginning of September on the various signals. 6-16

Figure 6.12. Two-week period of record showing diel variation in fDOM, nitrate and phosphate. Note that the timing of diel P variation is out of phase with diel N variation. 6-16

Figure 6.13. Two week period in Alexander Springs Creek containing a significant rain event (Hurricane Matthew) and the subsequent solute recovery as surface sources from swamps along the spring run cease to contribute significant water. 6-17

Figure 6.14. Two week period containing Hurricane Matthew during which fDOM increases, as expected, but also chlorophyll a increases. 6-18

Figure 6.15. Respiration (ER), gross primary production (GPP) and net ecosystem production (NEP) in Silver River over the period of record for S5 (upper half of Silver River; top) and S1 (lower half of Silver River; bottom). Both reaches are slightly net heterotrophic (NEP<0). 6-20

Figure 6.16. Comparison of GPP, ER and NEP for all three reaches in Silver River (upper, middle, lower) for the available period of overlap for all three stations (SILGOLD, S5 and S1). GPP and NEP are clearly higher for the upper reach (open, wide) than for the two lower reaches (narrower, more shaded). 6-21

Figure 6.17. Summary of gross primary production (GPP), ecosystem respiration (ER), and net ecosystem production (NEP) for the period of record at Alexander Springs Creek. The excursion in October 2016 is the result of Hurricane Matthew. 6-22

Figure 6.18. Seasonal and longitudinal variation in P:R in Silver River. 6-23

Figure 6.19. Summary of the three reaches of Silver River. Showing the marked drop in GPP, and marked increase in ER with distance downstream. 6-23

Figure 6.20. Summary of annual average GPP and ER for the S5 reach for 2015 and 2016. Note the considerable inter-annual variation (6.8 versus 8.2 g O_2 m^{-2} d^{-1}) between years. P:R values below 1 are conserved between years, with similar ratios (0.63 for 2015, 0.66 for 2016). 6-24

Figure 6.21. Comparison of GPP and ER between Silver River (high NO_3-N) and Alexander Springs Creek (low NO_3-N). GPP rates are not statistically different ($p = 0.19$). Respiration rates are significantly higher in Silver River ($p < 0.001$), sufficiently so to make the entire S5 reach (~5,500 m) net heterotrophic while the longer Alexander reach (~9,800 m) remains net autotrophic. 6-24

Page

Figure 6.22. Summary of GPP over a year of available data at the SILGOLD site, which corresponds approximately to the reach measured by Odum (1957) and Knight (1980) and again by Munch et al. (2006). The marked decline in GPP between Knight (1980) and Munch et al. (2006) measurements has not been sustained; GPP measured during 2016-2017 are as high or higher as those observed during the two earliest studies. 6-26

Figure 6.23. Logic of modeling benthic light attenuation. Measured incident open sky irradiance on each day is modified by the transmittance of the canopy given attributes of river width, canopy height, river azimuth, solar angles, and FPAR. The light that reaches the water surface is further modified by fDOM. 6-27

Figure 6.24. (top panel) Our canopy transmission model was based on earlier stream shade models (Davies-Colley and Rutherford 2005). In peninsular Florida, bank angle is negligible. (lower panel) a) Solar azimuth and solar zenith defined. Both solar azimuth (b and c) and solar zenith (d and e) vary greatly over the course of a day (b and d, for 1 January 2017) and a year (c and e, at 12pm) and impacts the length of the canopy shadow across the river. The canopy transmission model incorporated this temporal variation.. 6-28

Figure 6.25. (top) Segments used for canopy transmission model to capture the winding nature of Silver River. (second) Canopy transmittance over 2+ years for the middle reach of Silver River. (third) Comparison of canopy transmittance fraction. (bottom) Actual light reaching Silver River. 6-29

Figure 6.26. Covariance between GPP and ER in Silver River. Note, ER is positive (not negative as in previous plots) for this regression analysis. The slope indicates how important *in situ* primary production in controlling variation in respiration. The intercept indicates how other sources of organic matter are respired in the river. With distance downstream, the slope decreases, indicating reduced dependence of ER on GPP, and the intercept increases, indicating allocthonous C strongly influences the ecosystem energy budget. 6-30

Figure 6.27. Relationship between primary production and respiration in Alexander Springs Creek. The positive intercept suggests some persistent respiration predicted, even at zero GPP but the slope (near 1) suggests that the dominant control on respiration is the availability of fixed carbon from submerged autotrophs. The baseline respiration (1.5 g O_2 m^{-2} d^{-1}) may be respiration of organic matter sourced from emergent or riparian vegetation. 6-31

Figure 6.28. Temperature sensitivity of ER across the reaches of Silver River..... 6-32

Page

Figure 6.29. Comparison of light attenuation with depth in Silver River at S5 (left) and the Santa Fe River at the USGS 2500 station (right). The latter tannin-rich water column conforms with expected behaviors, exhibiting marked light attenuation with depth. In Silver River reflected light from the banks and bottom of the water column create conditions where estimates of light attenuation could not be made with equipment available. We thus focused on statistical links between light occluding factors in the water (fDOM, turbidity) rather fitting a physical model. 6-33

Figure 6.30. Time series of fluorescent DOM (top) and turbidity (bottom) at three stations in Silver River. Note the low fDOM values in the upper reach (SILGOLD, yellow dots), the higher values at lower stations (S5 (light blue) and S1 (dark blue)), and the time variation in response to inputs from Half-Mile Creek. The fDOM time series provided a third variable (with open sky irradiance and canopy % reduction) to predict GPP. Turbidity variation is less coherent, with a strong influence by very short term anomalies. These are not diel signals, but rather apparently random noise, the influence of which difficult to discern. Because of this, and because values are generally low and poorly predictive of GPP, we omitted turbidity from further analysis of metabolism. 6-34

Figure 6.31. Time series of daily total open-sky irradiance from the FAWN-Ocklawaha Station. This was used as the base input for our GPP prediction models. 6-35

Figure 6.32. Summary of bivariate relationships between incident open-sky radiation (obtained from the nearby Florida Automated Weather Network Ocklawaha station). Note that the slopes (power-function exponents) differ between river reaches, largely aligned with river width and thus canopy occlusion. The power function fit is the theoretical model best fit to light saturation occurring across a variety of benthic light conditions. 6-36

Figure 6.33. Bivariate relation between open sky irradiance and GPP in Alexander Springs Creek.. 6-36

Figure 6.34. fDOM (in Quinone Sulphate Equivalents) versus GPP for the 4 Silver River Reaches. The only compelling association is for the longest data record at S5 (lower left). Note that the upper (upper left) and middle (upper right) reaches had uniformly low fDOM values. 6-37

Figure 6.35. In Alexander Springs Creek the relationship between GPP and fDOM is strong, far stronger than with light, or between fDOM and GPP in Silver River. 6-37

Page

Figure 6.36. Schematic of methods to extract N assimilation and denitrification from the high resolution time series of nitrate concentrations (left) or nitrate retention (right; i.e., concentration change between stations multiplied by discharge and divided by benthic area). In both cases, diel variation is attributed to assimilation, while the remainder of the mass loss is attributed to heterotrophic processes. We refer to this remainder as U_{den} since denitrification is often a dominant fraction but note that this also includes nitrification and is thus more accurately interpreted as net denitrification (i.e., denitrification minus nitrification). 6-44

Figure 6.37. Schematic of methods to extract P assimilation and calcite sortion from the high resolution time series of phosphate concentrations (left) or phosphate retention (right; i.e., concentration change between stations multiplied by discharge and divided by benthic area). In both cases, diel variation is attributed to assimilation, while the remainder of the mass loss is attributed to geochemical processes. We refer to this remainder as U_d since dissimilatory processes are one component of this flux but note that this includes a complex array of desorption and mineralization processes; we do not interpret the magnitude of this flux in detail. 6-45

Figure 6.38. Nitrate metabolism calculated for the same time period using two different upstream boundaries: a, b, c uses SILHEAD as the upstream boundary while d, e, f uses the Oct 2015 Mammoth grab sample nitrate concentration as the upstream boundary. 6-46

Figure 6.39. Period of record nitrate concentrations for SILGOLD, Silver River S1 and Silver River S5. Also shown is the flow record over the same period. 6-47

Figure 6.40. Two week period with nitrate at both SILGOLD and S5. Shown with variation in dissolved oxygen. Note that the input concentration from the head springs is roughly 1.33 mg N L^{-1}, indicating net nitrate retention from the head springs to SILGOLD, and further from SILGOLD to S5. 6-48

Figure 6.41. Period of record phosphate measurements at S5 and SILGOLD, along with river flow. 6-49

Figure 6.42A. Two week period of record showing SRP concentration variation at SILGOLD (red) and S5 (black). Also show are attendant DO signals at S5.. 6-49

Figure 6.42B. Timing of DO production compared to solar forcing (left) and then lags of N (center) and P (right) uptake with respect to peak DO production. 6-50

Figure 6.43. Time series of N uptake ($U_{a,N}$) by autotrophs at the S5 station, along with DO. A moving average (red dots) is provided to better visualize the association to GPP. 6-51

Page

Figure 6.44. Time series of P uptake ($U_{a,P}$) by autotrophs at the S5 station, along with DO. A moving average (red dots) is provided to better visualize the association to GPP, which is relatively weak. 6-51

Figure 6.45. Covariance between GPP and (top) $U_{a,N}$ for both S5 and SILGOLD, and for (bottom) $U_{a,P}$, also for both stations. All regressions were significant at $p<0.001$, but were much stronger for N than for P. 6-52

Figure 6.46. Reach mean rates of (top) N retention due to both autotrophic assimilation ($U_{a,N}$), and denitrification (U_{den}) over the period of record for both S5 and SILGOLD reaches. Reach mean rates for P uptake ($U_{a,P}$, bottom panel) are for both reaches as well. 6-53

Figure 6.47. Ecosystem metabolism stoichiometry for N (upper) and P (lower) autotroph assimilation. The inset tables show measured tissue stoichiometry for the dominant autotrophs from Nifong et al. (2014). 6-55

Figure 6.48. Time series of N demand (top) and P demand (bottom) as a fraction of total mass loading from the spring vent. The mean value (red line) over the period of record is also shown. 6-56

Figure 6.49. Locations of twenty (20) lateral transects along the length of the Silver River at which channel morphology, vegetation, water chemistry and sediment properties were measured. Each transect consisted of 5 locations spanning the width of the river. 6-57

Figure 6.50. Deployment of quadrat for cover and composition measurements, and porewater sampler for collecting water samples. After benthic characterization, a sediment sample was obtained using a modified Ekman sampler, along with a water sample from the river. 6-58

Figure 6.51. Ambient conditions, including percent canopy cover, surface water velocity (m s^{-1}), and water depth (m), were measured during the comprehensive survey. Shown are values for each of 5 locations (randomly spaced) on each of the 20 transects along the river. 6-60

Figure 6.52. Individual water depths (m) and surface water velocity (m s^{-1}) for each location on each transect were measured as part of the comprehensive survey. Water depth explained little variation in surface water velocity. 6-61

Figure 6.53. Summary of overall river benthic cover of a) SAV and b) algae using the Braun-Blaunquet scale. The survey suggests that most (over 75 %) of the river retains dense SAV beds. Algal cover is variable, suggesting important controls on spatial heterogeneity that are the subject of our subsequent work. 6-62

Page

Figure 6.54. Association between benthic algae and SAV cover from individual locations on 20 transects along the Silver River suggests SAV and algae co-exist. However, while the river exhibits uniformly high SAV when algae cover is low, at high algal cover, SAV cover is spatial heterogeneous, consistent with potential smothering effects. Random variance has been added to these categorical cover class data to assist visualization of the association; regression results are for unmodified data. 6-63

Figure 6.55. Summary of SAV morphologic characterization with distance downstream for each of 5 locations location along each of 20 transects. Locations with no data were where that taxa was not found. 6-64

Figure 6.56. Longitudinal patterns in the mean cover of a) algae and b) SAV from each transect from the headspring (at left) to the confluence with the Ocklawaha River (at right). The decline in mean algal cover is statistically significant ($p < 0.001$), as is the increase in SAV cover ($p = 0.02$). 6-65

Figure 6.57. Across transects, mean SAV cover was highest in the center of the channel and declined towards the channel margins, while algae was highest at the south edge. Data are pooled across transect for each sampling location perpendicular to river flow. 6-66

Figure 6.58. No significant difference was found between average % carbon and nitrogen content in two dominant species found in Silver River, *Sagittaria kurziana* and *Vallisneria americana*. 6-66

Figure 6.59. Spatial patterns in tissue C:N (molar basis) across the Silver River. We noted a substantial increase in C:N in the lower river, though subsequent measurements (Figure 6.52) do not replicate finding. 6-67

Figure 6.60. Concentrations of key analytes in the thalweg sample along the length of the Silver River. All fitted lines are significant at $p < 0.001$. The nitrate trend was not significant despite repeated measures (Hensley et al. 2014) showing strong depletion trends along the length of the river. 6-69

Figure 6.61. Ratios of concentrations for key analytes in the thalweg sample versus the channel margin samples along the length of the Silver River. Values greater than 1 indicate a solute that is enriched in the thalweg compared with the channel margins, while values less than 1 indicate solutes that are depleted in the thalweg. Mean values for the entire river are shown in each graph, suggesting NO_3-N is slightly enriched in the thalweg vis-à-vis the channel margins, while all other solutes are depleted in the thalweg. 6-70

Page

Figure 6.62. Ratios of concentrations for key analytes in the thalweg sample versus the porewater samples along the length of the Silver River (later. Values greater than 1 indicate a solute that is enriched in the thalweg compared with the porewaters, while values less than 1 indicate solutes that are depleted in the thalweg. Mean values for the entire river are shown in each graph, suggesting NO_3-N is dramatically enriched in the thalweg vis-à-vis the porewaters, while all other solutes are depleted in the thalweg, some greatly so (e.g., NH_4-N and SRP). 6-71

Figure 6.63. A) Water column and B) porewater concentrations of ammonium-N (NH_4-N) and orthophosphate (SRP) showing the range of concentrations, and the covariance patterns, suggestive of regions of significant benthic porewater influences on river water. High concentrations are samples obtained near channel margins. 6-72

Figure 6.64. Summary of relative water concentrations across each transect, illustrating strong spatial heterogeneity driven by advection rates (high in the center, low at the edges). 6-73

Figure 6.65. . Soil samples collected across one transect prior to drying as well as dried samples from four transects (oriented by column) prior to LOI determination of organic matter content. 6-73

Figure 6.66. Average soil content by analyte by transect. Error bars are standard deviations. 6-74

Figure 6.67. Percent (%) soil organic matter was greatest along the upper and middle transects. 6-75

Figure 6.68. Variation in soil calcium content (Ca; g kg^{-1}) was explained by both a) porewater Ca concentrations (mg L^{-1}) and b) water column Ca concentrations (mg L^{-1}). 6-75

Figure 6.69. Soil %C and %N were significantly correlated to each other. This association was strongly significant ($p < 0.001$). 6-76

Figure 6.70. Soil Ca and P content were significantly correlated to each other. 6-76

Figure 6.71. Particle size analysis was completed on the upstream transects at Silver and mean values within transects showed an initial decrease in % sand, initial increase in % silt and clay, and stabilization in the last few transects. 6-77

Figure 6.72. Percent clay and percent organic matter were found to have a weak but significant negative relationship (p-value = 0.0249). 6-78

Figure 6.73. Percent clay explained approximately 19 % of the variation in soil phosphorus content (g kg^{-1}) over the first 14 transects surveyed at Silver River. 6-78

Figure 6.74. Percent clay explained approximately 12 % of the variation in soil calcium content (g kg^{-1}) over the first 14 transects surveyed at Silver River. 6-79

Page

Figure 6.75. Surface water velocity (m s^{-1}) explained some of the variation seen in algae cover (Braun-Blanquet values). The relationship is statistically significant ($p < 0.001$), but suggests that over 80 % of the variation in algal cover is not explained by surface velocity variation. 6-80

Figure 6.76. . Summary of patterns of covariance between solutes in the water column, porewater and some of the soil attributes and algal cover (above) or SAV cover (below). Correlations (y-axis) that are statistically significant are darker bars. 6-81

Figure 6.77. A clustered nutrient bioassay design was utilized to assess effects of nutrient additions (i.e., nutrient limitation) using seven combinations of N, P, and/or Fe. 6-86

Figure 6.78. Metabolism was measured simultaneously in one control chamber and three treatment chambers at 30 locations along Silver River between August 2015 and May 2016. 6-87

Figure 6.79. Metabolism was measured simultaneously in one control chamber and three treatment chambers at nine locations along Alexander Springs Creek between September and November 2016. Transport and sampling logistics constrained site selection to locations in close proximity to the bridge canoe access points 6-88

Figure 6.80. Comparison of dissolved oxygen curves in the control chambers showed high variation across locations at Silver River. 6-89

Figure 6.81. Comparison of dissolved oxygen curves in the control chambers showed less variation across locations at Alexander Springs Creek than at Silver River... 6-89

Figure 6.82. Summary of box GPP measurements between the two study rivers. Results are shown pooling across all box deployments and days. There was no difference between rivers in mean box GPP ($p = 0.96$). 6-90

Figure 6.83. Average control gross primary production (GPP) ranged from 1.0 to 13.0 g O_2 m^{-2} d^{-1} and was negatively correlated with distance downstream from the main spring vent. Over the short range of distances in Alexander Springs Creek (1,600 – 2,050 m below the spring vent) there was a strong and significant positive correlation between distance and both GPP and ER ($r^2 = 0.53$). The causes of this association are not clear, but are likely principally because the lower sites were sampled earlier in the year (longer day length). of sixteen selected experimental sites in Silver River. 6-91

Figure 6.84 Control gross primary production (GPP) in Silver River varied by substrate type and on average estimates were largest in flocculent, deep sediments and smallest in sandy substrates 6-91

Figure 6.85. Average control gross primary production was significantly correlated to mean surface light in Silver River.. 6-92

Figure 6.86. Average control gross primary production was significantly correlated to mean surface light in Alexander Springs Creek. 6-93

Page

Figure 6.87. Average gross primary production in control boxes was greatest in April, lowest in December. Note: deployments did not occur in all months (e.g., January and June). Deployments in Alexander River were all in September, October and November.. 6-93

Figure 6.88. Variation in control gross primary production estimates were not significantly correlated to percent canopy cover in Silver River. 6-94

Figure 6.89. In (A) Silver River, mean primary production and respiration were both significantly correlated to water depth (p-value = 0.014 and 0.003, respectively) with 19.7% and 28.2% of variation explained. Similar behavior, but with different slopes, was observed in (B) Alexander Springs Creek. 6-95

Figure 6.90. High variation in vegetation biomass (AFDM; ash-free dry mass) was observed within the control chambers. 6-96

Figure 6.91. A strong relationship between GPP and ER in the boxes at Alexander Springs Creek suggests that most of the system respiration is autotrophic, and that variation in respiration in time and space is principally governed by those factors (e.g., light) that control primary production. Within deployments, GPP and ER were less well correlated (mean $R^2 = 0.53$). 6-98

Figure 6.92. Large variation in nutrient effects (i.e., average GPP in treatment chamber divided by that in the control) were seen by treatment type and by distance downstream (i.e., location). Black bar represents 1:1, representative of control value. These data are shown with a log-scaled y-axis. All subsequent results will be for the log-transformed value of GPPt:GPPc, such that values less than 0 indicate GPP inhibition, while values greater than 1 indicate stimulation.....6-99

Figure 6.93. A) No significant nutrient effects for GPP response (measured as GPP_t:GPP_c) when averaged across all deployments in Silver River. B) In Alexander Springs Creek, there was evidence of weak P and Fe inhibition, and stimulation when all three nutrients were added. Error bars represent 95% confidence intervals. 6-100

Figure 6.94. Main effects of nutrient enrichment for A) Silver and B) Alexander. The only significant effect was weak stimulation of GPP by Fe in Silver River.....6-103

Figure 6.95. Summary of nutrient enrichment effects on GPP in A) Silver River, and B) Alexander Springs Creek, showing the relative response of GPP indexed to standing stock of biomass between treatment and control boxes (i.e., Log[$GPP_{B,t}$:$GPP_{B,c}$]). For Silver River, the only significant effect was apparent GPP_B inhibition with the addition of P and Fe. For Alexander Spring Creek, the only significant effect was P inhibition. 6-104

Figure 6.96. Photographs of two tiles which were suspended within chambers to measure algal growth given nutrient additions of phosphorus and iron (left) and iron alone (right). 6-106

Page

Figure 6.97. Large variation in algal biomass accumulation estimates were observed across the 13 deployments at Silver River with the largest growth found in upstream (~1,000 m) and downstream (>7,000 m) sections of the reach; note that each dot is algal biomass on tiles after one week in boxes (control or nutrient enrichment). 6-107

Figure 6.98. Summary of daily growth rates on tiles in deployed control boxes in the two rivers. The difference was not statically significant ($p = 0.34$), but may be biologically meaningful. 6-107

Figure 6.99. Mean algal biomass estimates per treatment type aggregated across locations in (A) Silver River and (B) Alexander Springs Creek showed greater stimulation in N, Fe, N+Fe, and P+Fe treatments although larger standard errors (bars) were also observed. 6-108

Figure 6.100. Total algal biomass accumulation on tiles was not significantly correlated to total GPP in Silver River ($R^2 = 0.01$, $p = 0.97$), but was weakly positively correlated in Alexander Springs Creek ($p = 0.06$). GPP explained 13 % of variation in algal growth, suggesting that controls on algal accumulation are distinct from factors influencing ecosystem metabolism. 6-109

Figure 6.101. Average relative algal biomass response for A) Silver River, and B) Alexander Springs Creek was compared between treatment and control chambers and averaged for each treatment type. Error bars denote 95 % confidence intervals for the mean value. 6-110

Figure 6.102. Main effects of nutrient addition showing the mean relative algal response to N, P and Fe additions in A) Silver River and B) Alexander Springs Creek. Only the Fe response was statistically significant (error bars denote 95 % confidence intervals) for Silver River. No nutrient additions were significant in Alexander Springs Creek.. 6-111

Figure 6.103. Benthic chamber NO_3-N profiles for Silver River (a), Rainbow River (b) and Gum Slough (c) all exhibit hyperbolic declines and diel variation. Uptake rates derived from profile slopes (d, e and f respectively) decline with time and exhibit diel peaks consistent with solar forcing of autotrophic assimilation. 6-117

Figure 6.104. Benthic chamber NO_3-N profiles for Alexander Creek for un-enriched deployments (a) and enriched deployments (b). Timing of diel variation in U_{NET} for un-enriched deployments (c), and after NO_3-N depletion back to ambient in enriched deployments (d), is opposite observed in the other sites, with net daytime NO_3-N production, indicating temporal decoupling of U_A from GPP in this low- NO_3-N site, and potentially daytime DO stimulation of nitrification. 6-118

Figure 6.105. Silver River 15-22 October 2015 deployment showing various configurations of models (dashed black lines) fit to the observed U_{NET} profile (gray). 6-119

Page

Figure 6.106. Distribution of n_A (a) and n_D (b) suggests U_A and U_D both follow efficiency loss (EL) kinetics however U_D is more concentration dependent. Distribution of τ (c) suggests in general U_A lags GPP, with a potential study site effect. 6-120

Figure 6.107. GPP (a) did not respond to NO_3-N depletion over the deployments. U_A (c) and U_D (d) both declined with NO_3-N depletion, with a larger effect on the latter. Inferred autotrophic uptake C:N (b) was often greater than the range observed in tissue (dashed lines) even under ambient conditions, and increased with NO_3-N depletion, suggesting a decoupling of U_A from GPP and/or reliance on an alternative N source. 6-122

Figure 6.108. NO_3-N profile (a) and U_{NET} (b) from 20 day Silver River deployment. Note following rapid NO_3-N depletion, concentration stabilizes around 0.1 mg N L^{-1} at which net NO_3-N removal and production pathways are roughly balanced over 24 h. 6-125

Figure 6.109. Geographic location of the sixteen selected study sites in each spring-fed river, Silver River (A) and Alexander Springs Creek (B). 6-136

Figure 6.110. Aboveground biomass in the upstream portion of the quadrat was clipped at one month and three-month intervals, and downstream biomass was clipped biannually to examine growth rate and aboveground production variability. 6-137

Figure 6.111. Shoots within 1 m^2 vegetation quadrats were clipped 2 cm above the basal sheath to enable regrowth from the basal meristem. Portions of the quadrats at each site were clipped at one-month, three-month, and six-month intervals over an annual cycle. 6-137

Figure 6.112. For each plot, electrodes were fastened to two PVC pipes attached to a central stand to minimize the effects of sediment disturbance. Electrode stands were configured with nine electrodes at each of three depths in the sediment (1.5 cm, 4.5 cm, and 7.5 cm). Electrodes were fastened to two PVC pipes (Photos from Joelle Laing). 6-138

Figure 6.113. (a) Mean aboveground biomass accrual for three growth periods shown with 95 % confidence intervals. (b) Aboveground biomass recovery time normalized to standing stock with 95 % confidence intervals. (c) Histogram of distribution and frequency of the slopes across all monthly measurements of mean site productivity. 6-143

Figure 6.114. Mean one-month shoot elongation rates shown with 95 % confidence intervals for *S. kurziana* and *V. americana* in Silver River and Alexander Springs Creek. Only *V. americana* was present in Alexander Springs Creek. 6-144

Figure 6.115. Log-normalized daily aboveground productivity shown with 95 % confidence intervals in Silver River from Jan – Dec 2016. 6-144

Page

Figure 6.116. (a) Mean aboveground biomass accrual ranked in site order from high to low productivity. Different lowercase letters indicate significant differences between sites at $p < 0.05$. (b) Annual frequency of biomass turnover across all sites. (c) Relationship between initial standing stock and productivity at each site. 6-145

Figure 6.117. Plots of the four best individual predictors of SAV aboveground biomass accrual at each site in Silver River and Alexander Springs Creek. 6-148

Figure 6.118. (A) Regression tree of controls on SAV productivity (g dry weight m^{-2} d^{-1}) at Silver River. (B) Plot of the goodness-of-fit between the observed and predicted values from the model. 6-149

Figure 6.119. (A) Regression tree of controls on aboveground SAV productivity (g dry weight m^{-2} d^{-1}) at Alexander Springs Creek. (B) Plot of the goodness-of-fit between the observed and predicted values from the model. 6-150

Figure 6.120. Plot of the goodness-of-fit between observed and GLM-predicted productivity in Silver River. 6-151

Figure 6.121. Plot of the goodness-of-fit between observed and GLM-predicted productivity in Alexander Springs Creek. 6-151

Figure 6.122. Comparison of river, upstream, and downstream GPP_{SAV} calculations in Silver River and Alexander Springs Creek shown with 95 % confidence intervals. Estimates account for the aboveground and belowground SAV component of ecosystem GPP 6-156

Figure 7.1.1. Average blade length of *V. americana* along a transect down the Wekiva River (Osborne and Mattson unpublished data). NO_3-N concentration declines downstream from site 1-3 which spans a distance of approximately 9 miles. These findings support the observation of increased vigor in *V. americana* as NO_3-N concentrations decrease. 7-6

Figure 7.1.2. Conceptual model of nitrate overload hypothesis. Uptake of nitrate is unregulated at the cellular level and presence of nitrate induces nitrate reduction to ammonia. Buildup of ammonia should be a negative feedback[-] for nitrate reduction enzymes; however this process appears not to function in some species. Ammonia can be toxic to plants and therefore is alleviated via protein synthesis, which requires energetic inputs from plant carbohydrate stores. Buildup of free amino acids and depletion of root carbohydrate stores are potential diagnostics of nitrate overload in SAV. 7-9

Figure 7.1.3. Assimilatory nitrate reduction in [A] SAV shoot and [B] cyanobacterial cell. Note cyanobacteria cannot utilize NAD(P)H as an electron donor in the reduction of nitrate to nitrite and thus rely solely upon ferrodoxin. Also note a slight energetic advantage [$\Delta G'$] exists for cyanobacteria in the reduction of nitrate to nitrite. 7-10

Page

Figure 7.1.4. Growth chamber arrays located in temperature and light controlled laboratory at the University of Florida Whitney Laboratory for Marine Bioscience in St. Augustine, FL. 7-14

Figure 7.1.5A. Schematic of mesocosm facility (top) and picture of constructed facility (bottom). 7-15

Figure 7.1.5B. Mesocosm vegetation (*V. americana* under variable water NO_3-N concentrations). 7-19

Figure 7.1.6. Mean root:shoot biomass ratios of *V. americana* and *S. kurziana* grown on sand at control (0.1 mg NO_3-N L^{-1}), Low (0.5 mg NO_3-N L^{-1}), Medium (1.0 mg NO_3-N L^{-1}) and High (5.0 mg NO_3-N L^{-1}) concentrations. A and B denote statistically significant difference between means. 7-20

Figure 7.1.7. Root:shoot ratios for *S. kurziana* grown on organic media at control (0.1 mg NO_3-N L^{-1}), Low (0.5 mg NO_3-N L^{-1}), Medium (1.0 mg NO_3-N L^{-1}) and High (5.0 mg NO_3-N L^{-1}) concentrations. A and B denote statistically significant difference between means. 7-21

Figure 7.1.8. Average number of ramets per pot after the growth trial of *S. kurziana*. Note: all pots were originally planted with a single ramet at the beginning of the experiment. A and B denote statistically significant difference between means. 7-21

Figure 7.1.9. Mean number of ramets produced by *V. americana* (dark gray) and *S. kurziana* (light gray) at control (0.1 mg NO_3-N L^{-1}), Low (0.5 mg NO_3-N L^{-1}), Medium (1.0 mg NO_3-N L^{-1}) and High (5.0 mg NO_3-N L^{-1}) concentrations. A, B, C denote statistically significant difference between means. 7-22

Figure 7.1.10. Two week shoot nitrate reductase activity (µmol h^{-1}) from mesocosm vegetation (*V. americana* under variable water NO_3-N N concentrations. A, B, C denote statistically significant difference between means. 7-23

Figure 7.1.11. Root (R) and shoot (S) nitrate reductase activity in *V. americana* and *S. kurziana* at control (0.1 mg NO_3-N L^{-1}), Low (0.5 NO_3-N L^{-1}), Medium (1.0 mg NO_3-N L^{-1}) and High (5.0 mg NO_3-N L^{-1}) concentrations. 7-23

Figure 7.1.12. Nitrate reductase activity (µmol g dw h^{-1}) from fine roots, roots, mid shoots, and shoot tips of *Vallisneria americana* from Silver River. 7-24

Figure 7.1.13. Nitrate reductase activity from roots, shoot bases, and shoot tips of *Vallisneria americana* from Silver River versus Wekiwa River, where NO3-N is twice the concentration. 7-25

Figure 7.1.14. Mean C:N ratios of root (red) and shoot (blue) tissue material at control (0.1 mg NO_3-N L^{-1}), Low (0.5 mg NO_3-N L^{-1}), Medium (1.0 mg NO_3-N L^{-1}) and High (5.0 mg NO_3-N L^{-1}) concentrations. 7-26

Figure 7.1.15. Arenchyma cells and vascular bundles in a microtome sliced thin section of *V. Americana*. Breakdown of arenchyma cells was a noted effect of NO_3-N stress reported by (Wang et al. 2012). 7-27

Page

Figure 7.1.16. Mean arenchyma cell diameter of *V. americana* shoots at control (0.1 mg NO_3-N L^{-1}), Low (0.5 mg NO_3-N L^{-1}), Medium (1.0 mg NO_3-N L^{-1}) and High (5.0 mg NO_3-N L^{-1}) concentrations. 7-28

Figure 7.1.17. Mean arenchyma cell diameter of *S. kurziana* shoots at control (0.1 mg NO_3-N L^{-1}), Low (0.5 mg NO_3-N L^{-1}), Medium (1.0 mg NO_3-N L^{-1}) and High (5.0 mg NO_3-N L^{-1}) concentrations.....7-28

Figure 7.1.18. Example of starch grain content (small black dots within plant cells) in the control (0.1 mg NO_3-N L^{-1}1)[A], and High (5.0 mg NO_3-N L^{-1}) concentrations[B].....7-29

Figure 7.1.19. Mean starch content of *V. Americana* (top) and *S. kurziana* (bottom) roots (red bars) and shoots (blue bars) at control (0.1 mg NO_3-N L^{-1}), Low (0.5 mg NO_3-N L^{-1}), Medium (1.0 mg NO_3-N L^{-1}) and High (5.0 mg NO_3-N L^{-1}) concentrations. 7-30

Figure 7.1.20. Mean amino acid concentration in tissue of *V. americana* and *S. kurziana* at control (0.1 mg NO_3-N L^{-1}), Low (0.5 mg NO_3-N L^{-1}), Medium (1.0 mg NO_3-N L^{-1}) and High (5.0 mg NO_3-N L^{-1}) concentrations. 7-31

Figure 7.1.21. Mean root:shoot ratios (top) and leaf elongation rates (bottom) of *V. americana* (blue) and *S. kurziana* (orange) under oxygenated and hypoxic conditions. 7-33

Figure 7.1.22. Mean leaf elongation of *V. americana* and *S. kurziana* under control (0 mM H_2S), Low (0.01 mM H_2S), Medium (0.1 mM H_2S), and High (0.75 mM H_2S), concentrations.....7-34

Figure 7.1.23. (Clockwise from top left) Photos of *V. americana* under control (0 mM H_2S), Low (0.01 mM H_2S), Medium (0.1 mM H_2S), and High (0.75 mM H_2S), concentrations. Note necrosis of tissues and blackening of roots as H_2S increases. 7-35

Figure 7.1.24. (Clockwise from top left) Photos of *S. kurziana* grown under control (0 mM H_2S), Low (0.01 mM H_2S), Medium (0.1 mM H_2S), and High (0.75 mM H_2S), concentrations.....7-36

Figure 7.1.25. Tissue necrosis of shoots (top) and roots (bottom) of *V. americana* under Medium (0.1 mM H_2S), concentrations.....7-37

Figure 7.1.26. Chlorophyll a production (top) and algal AFDM (bottom) in mesocosm tanks at control (0.1 mg NO_3-N L^{-1}), Low (0.5 mg NO_3-N L^{-1}), Medium (1.0 mg NO_3-N L^{-1}) and High (5.0 mg NO_3-N L^{-1}) concentrations. 7-38

Figure 7.2.1. Conceptual model of top down versus bottom up control of primary production in Florida Springs. Note bottom up control mechanisms limit production while top down control mechanisms limit standing biomass. Solid lines indicate direct influence of drivers and dotted lines represent feedbacks. Figure adapted from Osborne et al. (2013).....7-49

Page

Figure 7.2.2. Conceptual model of drivers of grazer population. The unknown stressor could be any compound or condition that negatively impacts grazer population leading to population decline or episodic extirpation. 7-51

Figure 7.2.3. Proportion of invertebrate herbivore biomass in Silver Springs. The micro-fauna category consists of several sub-groups each representing a very small portion of overall herbivore biomass including Hydrobiidae (mud snails), Oligochetes, gammarids (amphipods), midges, copepods, ostracods, flatworms, *Hydroptera* (caddisflies), Elophila (moths) and *Arcella* (testate amoebae). Pomacea (Apple snails), *Oxytrema* (spiral stream snails), and *Viviparus* (river snail) are all gastropods. *Palaemonetes* is a freshwater decapod (grass shrimp). (Adapted from Odum 1957). 7-52

Figure 7.2.4. Algal grazers utilized in respirometry experiments (clockwise from top left), *Palaemonetes paludosus* (decapoda); *Elimia floridensis* (gastropoda); *Viviparus georgianus* (gastropoda); *Micromenteus floridensis* (gastropoda). 7-56

Figure 7.2.5. Photograph of respirometry experimental array with 20 L holding tank fitted with test cells, timer switch, multi-plexer, and computer in foreground and 100 L sump in background. Four test cells were run in parallel allowing for testing of four individual animals during each iteration. 7-58

Figure 7.2.6: Raw data trace for one snail (*E. floridensis*) showing oxygen consumption in mg O_2 kg^{-1} snail per hour (MO_2) as a function of time. 7-59

Figure 7.2.7. Metabolic rate of *E. floridensis* relative to oxygen saturation. Metabolic rate (MO_2) is described in mg O_2 per kg^{-1} of snail h^{-1}. Oxygen saturation is in mg O_2 L^{-1} of water. 7-61

Figure 7.2.8. Oxygen consumption (mg O_2 kg^{-1} h^{-1}) by *Micromenetus floridensis* over a range of percent oxygen saturation at standard temperature and pressure. 7-62

Figure 7.2.9. Oxygen consumption (mg O_2 kg^{-1} h^{-1}) by *V. georgianus* over a range of percent oxygen saturation at standard temperature and pressure. 7-63

Figure 7.2.10. Oxygen consumption (mg O2 kg^{-1} h^{-1}) by *Palaemonetes paludosus* over a range of percent oxygen saturation at standard temperature and pressure. 7-64

Figure 7.2.11. Oxygen consumption (mg O_2 kg^{-1} h^{-1}) by *E. floridensis* (top) and *T. granifera* (bottom) exposed to high nitrate versus no nitrate exposure (control) over a range of percent oxygen saturation at standard temperature and pressure. 7-65

Figure 7.3.1. Initial flume construction in 10 m tank with electric motor creating constant velocity. 7-81

Figure 7.3.2. Top view of flowway mesocosms for shear stress experiments. 7-82

Page

Figure 7.3.3. View of four replicate flow way tanks for velocity study. Cinder blocks maintained smaller internal tanks in place during the experiment.....7-83
Figure 7.3.4. Close up view of flow way tank for current velocity study. Note pump locations at both ends of the highest velocity tank. Red circle indicates example of scouring from abrasive interaction between artificial blade and tank surface. 7-84
Figure 7.3.5. Close up view of artificial SAV in flow way (top) and an individual artificial SAV replicate with algal growth after 1 week (bottom).....7-85
Figure 7.3.6. Artificial SAV algal sampling post exposure to shear stress to monitor shearing effectiveness of established algal communities. 7-86
Figure 7.3.7. Algal biomass accumulation on synthetic leaf surface under variable velocity in mesocosms. 7-87
Figure 7.3.8. Algal biomass loss from artificial leaf surface during water velocity experiment. Note hysteresis of productivity and removal processes. 7-88
Figure 8.1. Redox reactions catalyzed by microbes in benthic sediments (Adapted after Gao et al. 2003).....8-4
Figure 8.2. DEM of the St. John River Water Management District area showing the location of Silver Springs and other major springs (not labeled on figure). The red line indicates the Silver Spring ground water basin from Knowles et al. (2010). Yellow box outlines the area shown in Figure 8.3A. 8-7
Figure 8.3. A) LIDAR image of area surrounding Silver Springs. Image provided by Harley Means, FGS and B) Cross-section along A-B with conceptualized groundwater flow patterns to the Silver Spring group (Knowles et al. 2010). The confining sediments could be either Hawthorn Gp rocks or material redeposited from the Hawthorn Gp.....8-8
Figure 8.4. Google earth view of the Silver River with the location of sediment transects showing the spatial distribution of sediment thickness and water depth. The red stars indicate the six transects where detailed sampling and observations were carried out. 8-9
Figure 8.5. Four transects selected for core collection, pore water sampling and CTDs installation. The transects show the location and depth of cores relative to the sediment thickness. 8-10
Figure 8.6. Sediment core image and distribution of bulk sediment density with depth. The dark colors indicate finer grained and higher organic carbon contents and the light colors indicate greater amounts of sandy and shelly layers. Stars indicate depth of slug tests and locations of CTDs. The yellow points represent the depth of pore water samples collected using the vapor probe for which concentrations are shown in Table 8.3.....8-18

		Page
Figure 8.7.	Sediment stratigraphy showing the distribution of different sediment types based in visible core inspections.	8-19
Figure 8.8.	Correlation between sediment bulk density and sediment porosity.	8-20
Figure 8.9.	Variation in the composition of the five cores (by weight) collected from Silver River including TOC (left), TN (middle) and TP (right).	8-21
Figure 8.10.	Correlation between total organic carbon (TOC) and total nitrogen (TN) in weight percent. Linear regressions are shown for each core.	8-22
Figure 8.11.	Correlation between total organic carbon (TOC) and total phosphorous (TP) in the Silver River bottom sediments. Linear regressions are shown for each core.	8-22
Figure 8.12.	Vertical and lateral variations in isotopic composition ($\delta^{13}C$ and $\delta^{15}N$) of sediment organic matter and molar ratio of C and N in the river sediments.	8-23
Figure 8.13.	^{210}Pb and ^{226}Ra activity in the river sediments in Silver River	8-25
Figure 8.14.	Plot showing ln of excess Pb-210 versus sediment depth in the Silver River. Slope of the line was used to estimate sedimentation rate based on equation 8.1	8-25
Figure 8.15.	A) ^{210}Pb profile with sediment depth, B) ln ^{210}Pb activities plotted against sediment depth to estimate the sedimentation rate at MFL 6	8-26
Figure 8.16.	Horizontal and vertical hydraulic conductivities of river bed sediments in the Silver River.	8-27
Figure 8.17.	10 days moving average of hydraulic head differences and total daily rainfall	8-27
Figure 8.18.	Pore water chemical profiles of NO_3-N (A), NH_4-N (B), SRP (C), Fe (D), Mn (E) and HS^- (F). River water samples, collected at each site, are plotted at 0 cm depth.	8-29
Figure 8.19.	$\delta^{13}C$ and C:N values of organic matter in river sediments with typical value range of terrestrial plants and freshwater algae.	8-32
Figure 8.20.	$\delta^{13}C$ and $\delta^{13}C$ of organic matter in riverbed sediments with end-members values. NUS = benthic filamentous algae, FREE = unattached algae, SAV/EPI = submersed aquatic veg and epiphytic algae, EMG = emergent vegetation.	8-33
Figure 8.21.	Groundwater flow to the Silver River through benthic sediments.	8-34
Figure 8.22.	PCA biplot of pore water chemistry data from the Silver River.	8-36
Figure 8.23.	A) Solute diffusion fluxes to the Silver River, B) Expanded scale for Fe and Mn fluxes.	8-38
Figure 8.24.	A) solute advection fluxes to the Silver River, B) expanded scale for Fe and Mn fluxes.	8-39
Figure 8.25.	Total benthic fluxes of solutes across the sediment – water interface in the Silver River.	8-40
Figure 9.1.1.	Aerial imagery of the Silver River system.	9-9

Page

Figure 9.1.2. Temporal trend in Nitrate-Nitrite N (NO_3-N) concentration in Silver Springs. 9-10
Figure 9.1.3. Aerial imagery of Alexander Springs Creek. 9-11
Figure 9.1.4. Map of Silver River with stable isotope sampling areas identified for the upper, mid and lower river reaches. Symbols denote center of 200 m sampling segment. 9-12
Figure 9.1.5. Stable carbon and nitrogen isotope composition of broad autotroph groups from Silver River. Points are means and error bars are ± 1 standard deviation (SD). 9-17
Figure 9.1.6. I nteraction plots of the combined effects of group and river region on $\delta^{13}C$ (top panel) and $\delta^{15}N$ (bottom panel) values of dominant autotrophs. Symbols represent mean values. 9-18
Figure 9.1.7. Carbon and nitrogen isotope composition of dominant autotroph groups and algal growth forms. Points are means and error bars are ± 1 standard deviation (SD). 9-20
Figure 9.1.8. Interaction plots of the combined effects of growth form and river region on $\delta^{13}C$ (top panel) and $\delta^{15}N$ (bottom panel) values of algal taxa. Symbols represent mean values. Note the interaction of algal growth form and river region was not significant for $\delta^{15}N$. 9-21
Figure 9.1.9. Box plot of $\delta^{13}C$ values measured in submerged macrophyte taxa. Center bars denote the median, box constrains the first and third quartiles, whiskers extend to data extremes, and points are individual sample values. 9-22
Figure 9.1.10. Scatter plot of $\delta^{13}C$ and $\delta^{15}N$ values measured in all food web constituents. Symbols represent means and error bars are ± Standard Error (SE). Resource group and consumer taxon are labeled under each symbol. 9-24
Figure 9.1.11. Interaction plot of the combined effects of taxon and river region on $\delta^{13}C$ values of gastropod taxa. Symbols represent mean values. 9-26
Figure 9.1.12. Box plot of $\delta^{15}N$ values measured for gastropods. Center bars denote the median, box constrains the first and third quartiles, whiskers extend to data extremes, and points are individual sample values. 9-26
Figure 9.1.13. Box plot of $\delta^{15}N$ values measured for gastropods from different river regions. Center bars denote the median, box constrains the first and third quartiles, whiskers extend to data extremes, and points are individual sample values. 9-27
Figure 9.1.14. Interaction plot of the combined effects of taxon and river region on $\delta^{13}C$ values of aquatic herbivorous insects. Symbols represent mean values. 9-28
Figure 9.1.15. Interaction plot of the combined effects of taxon and river region on $\delta^{15}N$ values of aquatic herbivorous insect taxa. Symbols represent mean values. 9-28

Page

Figure 9.1.16. Boxplot of $\delta^{13}C$ values measured in omnivorous crustaceans. Center bars denote the median, box constrains the first and third quartiles, whiskers extend to data extremes, and points are individual sample values. 9-29
Figure 9.1.17. Boxplot of $\delta^{13}C$ values measured in families of herbivorous and omnivorous fish. Center bars denote the median, box constrains the first and third quartiles, whiskers extend to data extremes, and points are individual sample values. 9-30
Figure 9.1.18. Boxplot of $\delta^{15}N$ values measured in families of herbivorous and omnivorous fish. Center bars denote the median, box constrains the first and third quartiles, whiskers extend to data extremes, and points are individual sample values. 9-30
Figure 9.1.19. Interaction plot $\delta^{15}N$ values measured in omnivorous fish taxa across river regions. Symbols are mean values. 9-31
Figure 9.1.20. Boxplot of $\delta^{13}C$ values measured for omnivorous turtle species. Center bars denote the median, box constrains the first and third quartiles, whiskers extend to data extremes, and points are individual sample values. 9-32
Figure 9.1.21. Boxplot of $\delta^{15}N$ values measured for omnivorous turtle species. Center bars denote the median, box constrains the first and third quartiles, whiskers extend to data extremes, and points are individual sample values 9-32
Figure 9.1.22. Boxplot of $\delta^{13}C$ values measured in families of predatory fish. Center bars denote the median, box constrains the first and third quartiles, whiskers extend to data extremes, and points are individual sample values. 9-33
Figure 9.1.23. Boxplot of $\delta^{15}N$ values measured in families of predatory fish. Center bars denote the median, box constrains the first and third quartiles, whiskers extend to data extremes, and points are individual sample values 9-34
Figure 9.1.24. Interaction plot of the combined effects of taxon and river region on predatory fish isotopic composition. Top panel $\delta^{13}C$ values and bottom panel $\delta^{15}N$ values. Symbols represent mean values. 9-35
Figure 9.1.25. Scatterplots of predatory fish $\delta^{13}C$ (top) and $\delta^{15}N$ (bottom) values as a function of total length (cm). Correlation coefficient (r) and p-value for Pearson's Correlation Test are displayed on the plot. 9-36
Figure 9.1.26. Boxplots of top predator fish taxa $\delta^{13}C$ (top) and $\delta^{15}N$ (bottom) values. Center bars denote the median, box constrains the first and third quartiles, whiskers extend to data extremes, and points are individual sample values 9-37
Figure 9.1.27. Map of American alligator capture locations along Silver River, Florida. Symbols are individual capture locations. 9-38

Page

Figure 9.1.28. Boxplot of $\delta^{15}N$ values measured in American alligator sexes (left) and size classes (right). Center bars denote the median, box constrains the first and third quartiles, whiskers extend to data extremes, and points are individual sample values. 9-39

Figure 9.1.29. Isotopic bi-plot of SEA's (Standard Ellipse Areas) calculated for gastropod taxa. Filled symbols are mean values. Open symbols are individual data points. Autotroph data added for reference. Error bars are ± 1 SD. 9-41

Figure 9.1.30. Isotopic bi-plot of SEA's (Standard Ellipse Areas) calculated for herbivorous insect taxa. Filled symbols are mean values. Open symbols are individual data points. Autotroph data added for reference. Error bars are ± 1 SD. 9-42

Figure 9.1.31. Isotopic bi-plot of SEA's (Standard Ellipse Areas) calculated for omnivorous crustaceans. Filled symbols are mean values. Open symbols are individual data points. Autotroph data added for reference. Error bars are ± 1 SD 9-43

Figure 9.1.32. Isotopic bi-plot of SEA's (Standard Ellipse Areas) calculated for herbivorous omnivorous fish taxa. Filled symbols are mean values. Open symbols are individual data points. Autotroph data added for reference. Error bars are ± 1 SD. 9-44

Figure 9.1.33. Isotopic bi-plot of SEA's (Standard Ellipse Areas) calculated for herbivorous omnivorous turtle taxa. Filled symbols are mean values. Open symbols are individual data points. Autotroph data added for reference. Error bars are ± 1 SD. 9-45

Figure 9.1.34. Boxplot of SIAR posterior distributions for the proportional contribution of resource groups to the diet of trichopterans using four end-member model. The outer light gray boxes enclose the 95% BCI, the slightly larger and darker boxes enclose the 75 % BCI, and the center box encloses the 50 % BCI. Points are median estimates. Source labels are as follows: EMG-emergent macrophytes, FREE-unattached algae, NUS-nuisance algae, SAV/EPI-submerged macrophytes + epiphytic algae.. 9-49

Figure 9.1.35. Boxplots of SIAR posterior distributions for the proportional contribution of resource groups to the diet of turtles using four end-member model. The outer light gray boxes enclose the 95 % BCI, the slightly larger and darker boxes enclose the 75% BCI, and the center box encloses the 50 % BCI. Points are median estimates. Source labels are as follows: EMG-emergent macrophytes, FREE-unattached algae, NUS-nuisance algae, SAV/EPI-submerged macrophytes + epiphytic algae 9-50

Figure 9.1.36. Bar charts of %IRI calculated for *Alligator mississippiensis* size classes. Color designation for prey categories are listed in the legend. 9-52

Page

Figure 9.1.37. Bar charts of %IRI calculated for herbivorous and omnivorous fish taxa. The species abbreviation is the first three letters of the genus and first two letters of the species epithet, for example the abbreviation for *Amia calva* (bowfin) is AMICA (refer to Table 9.1.8 for list of species). If the five letter species codes matched for any two species than a third letter from the species epithet was added. 9-54

Figure 9.1.38. Bar charts of %IRI calculated for predatory fish taxa. The species abbreviation is the first three letters of the genus and first two letters of the species epithet, for example the abbreviation for *Amia calva* (bowfin) is AMICA (refer to Table 9.1.8 for list of species names). If the five letter species codes matched for any two species than a third letter from the species epithet was added (e.g., LEPMAR and LEPMA). 9-55

Figure 9.1.39. Percent Index of Relative Importance (%IRI) calculated for turtle taxa. The species abbreviation is the first three letters of the genus and first two letters of the species epithet (see Table 9.1.9 for species information). 9-57

Figure 9.2.1. Photographs (left-all three systems and right-single system) of the laboratory flow-through systems used to house study organisms during grazing trials. 9-69

Figure 9.2.2. Photograph of microscope slides used to offer vegetation cuttings to grazers during experimental trials. 9-71

Figure 9.2.3. Predicted effects of grazer taxon on per capita consumption rate. Filled circles are mean values and error bars delineate the 95 % CI. The red dashed line represents zero change in macroalgae biomass during trials 9-74

Figure 9.2.4. Predicted effects of macroalgae taxon on per capita consumption rate. Filled circles are mean values and error bars delineate the 95 % CI. The red dashed line represents zero change in macroalgae biomass during trials 9-74

Figure 9.2.5. Interaction plot of per capita consumption rate as a function of grazer and macroalgae taxon. Symbols are predicted mean values. Error bars are not included for simplicity 9-75

Figure 9.2.6. Scatterplot of per capita macroalgae consumption rate as a function of grazer biomass (data combined for all taxa), left-simple linear model ($y = ax + b$) and right-logarithmic model ($y = \ln(x)$). Points are raw data. Solid red line is the regression line and dashed red lines enclose the 95 % CI. Note x-axis on the right graph is in log form. 9-76

Figure 9.2.7. Scatterplot of per capita consumption rate as a function of grazer biomass. Points are raw data from taxa reported above the plot. Solid red line is the regression line and dashed red lines enclose the 95 % CI. 9-78

Page

Figure 9.2.8. Predicted effects of grazer taxon on per capita consumption rate. Filled circles are mean values and error bars delineate the 95 % CI. The red dashed line represents zero change in macroalgae biomass during trials. 9-80

Figure 9.2.9. Interaction plot of estimated per capita consumption rate as a function of grazer and macrophyte taxon. Symbols are predicted mean values. Error bars are not included for simplicity. 9-82

Figure 9.2.10. Scatterplot of per capita consumption rate of macrophyte material as a function of grazer biomass. Points are raw data from taxa reported above the plot.. Solid red line is the regression line and dashed red lines enclose the 95 % CI.....9-83

Figure 9.3.1. Map of study area and location of experimental arrays. Green circles denote locations of Mammoth Spring (head spring) and the downstream 1,200 m station 9-90

Figure 9.3.2. Photographs of experimental cages in situ. Cage tops fully exposed (right) and fully submerged cage (left). 9-91

Figure 9.3.3. Predicted effects of river region (left) and macrophyte taxon (right) on macrophyte aboveground growth rates. Filled red circles are mean values and error bars delineate the 95 % CI. 9-96

Figure 9.3.4 Predicted effects of experimental treatments on macrophyte aboveground growth rates. 9-97

Figure 9.3.5. Interaction plot of mean aboveground growth rates as a function of the interaction between river region and macrophyte taxon. Error bars are not plotted for simplicity 9-97

Figure 9.3.6 Interaction plot of mean aboveground growth rates as a function of the interaction between river region and treatment type. Error bars are not plotted for simplicity....9-98

Figure 9.3.7. Predicted mean aboveground biomass across river regions. Large red circles are mean values and error bars are ± standard error (SE). Small black circles are empirical data. 9-100

Figure 9.3.8 Macrophyte aboveground biomass measured in treatment plots. Large red circles are mean values and error bars are ± standard error (SE). Small black circles are empirical data 9-100

Figure 9.3.9. Predicted epiphytic biomass as a function of treatment type based on model averaged coefficients. Large red circles are mean values and error bars are ± standard error (SE). Small black circles are empirical data. 9-102

Figure 9.3.10 Predicted effects of river region on epiphytic algae biomass. Large Red circles are estimated means and error bars are ± standard error (SE). Small black circles are empirical data. 9-102

Figure 9.3.11. Predicted effects of region on total macroinvertebrate biomass. Large red circles are mean values and error bars are ± standard error (SE). Small black circles are empirical data 9-104

Page

Figure 9.3.12 Predicted effects of treatment type on total macroinvertebrate biomass. Large red circles are mean values and error bars are ± standard error (SE). Small black circles are empirical data. 9-104

Figure 9.3.13. Predicted effects of river region (left) and treatment type (right) on macroinvertebrate grazer biomass. Large red circles are mean values and error bars are ± standard error (SE). Small black circles are empirical data. 9-106

Figure 9.3.14 Predicted effects of river region (left) and treatment type (right) on macroinvertebrate omnivore biomass. Large red circles are mean values and error bars are ± standard error (SE). Small black circles are empirical data. 9-107

Figure 9.3.15. Predicted effects of river region (left) and treatment type (right) on macroinvertebrate predator biomass. Large red circles are mean values and error bars are ± standard error (SE). Small black circles are empirical data. 9-108

Figure 9.3.16 Predicted effects of river region on macroinvertebrate parasite biomass. Large red circles are mean values and error bars are ± standard error (SE). Small black circles are empirical data. 9-110

Figure 9.3.17. Predicted effects of river region (left) and treatment type (right) on macroinvertebrate abundance. Large red circles are mean values and error bars are ± standard error (SE). Small black circles are empirical data. 9-111

Figure 9.3.18 Predicted effects of river region (left) and treatment type (right) on macroinvertebrate grazer abundance. Large red circles are mean values and error bars are ± standard error (SE). Small black circles are empirical data. 9-113

Figure 9.3.19. Predicted effects of river region (left) and treatment type (right) on macroinvertebrate omnivore abundance. Large red circles are mean values and error bars are ± standard error (SE). Small black circles are empirical data. Single extreme data point (see text) is removed to retain appropriate scale for presentation 9-115

Figure 9.3.20 Predicted effects of river region (left) and treatment type (right) on macroinvertebrate predator abundance. Large red circles are mean values and error bars are ± standard error (SE). Small black circles are empirical data. 9-116

Figure 9.3.21. Predicted effects of river region (left) and treatment type (right) on macroinvertebrate parasite abundance. Large red circles are mean values and error bars are ± standard error (SE). Small black circles are empirical data 9-117

Page

Figure 9.3.22 Shepard (left) and ordination plots of the first and second axes (right) resulting from nMDS analysis of macroinvertebrate community composition based on abundance data. Location of each plot within ordination space is labeled by site code, which denotes river region (mid [M] and upper [U] river), site number (1–5), and experimental treatment (control [C], cage control [CC], and exclusion [E]). 9-120

Figure 9.3.23. Ordination plots of the first and second axes from nMDS analysis of macroinvertebrate community composition, grouping site scores by treatment type (left) and river region (right) based on abundance data. Ellipses delineate the minimum bounds of the standard deviation for all ordination scores for communities within each corresponding group (color of ellipse contours matches the text color of communities within each group). Location of each plot within ordination space is labeled by site code, which denotes river region (mid [M] and upper [U] river), site number (1–5), and experimental treatment (control [C], cage control [CC], and exclusion [E]). 9-120

Figure 9.3.24 Shepard (left) and ordination plots of the first and second axes (right) resulting from nMDS analysis of macroinvertebrate community composition based on biomass data. Location of each plot within ordination space is labeled by site code, which denotes river region (mid [M] and upper [U] river), site number (1–5), and experimental treatment (control [C], cage control [CC], and exclusion [E]). 9-121

Figure 9.3.25. Ordination plots of the first and second axes from nMDS analysis of macroinvertebrate community composition, grouping site scores by treatment type (left) and river region (right) based on biomass data. Ellipses delineate the minimum bounds of the standard deviation for all ordination scores for communities within each corresponding group (color of ellipse contours matches the text color of communities within each group). Location of each plot within ordination space is labeled by site code, which denotes river region (mid [M] and upper [U] river), site number (1–5), and experimental treatment (control [C], cage control [CC], and exclusion [E]). 9-121

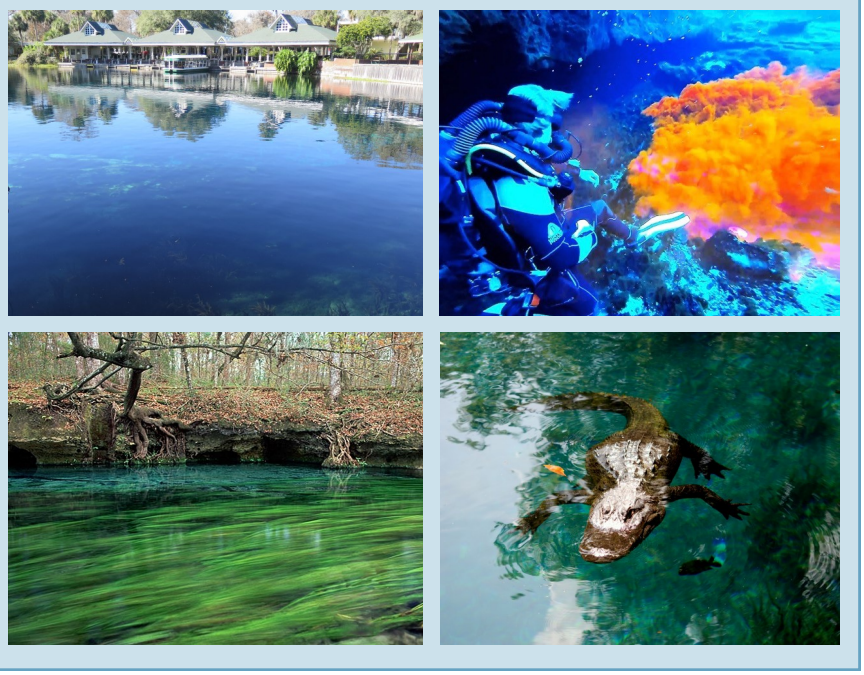

Collaborative Research Initiative on
Sustainability and Protection of Springs [**CRISPS]**

Executive Summary

FINAL REPORT

2014 - 2017

submitted to:

St. Johns River Water Management District
Springs Protection Initiative [SPI], UF Contract # 27789

UF | UNIVERSITY of FLORIDA
Water Institute

C R I S P S

EXECUTIVE SUMMARY

ES.1 INTRODUCTION

The Floridan aquifer is Florida's most significant water resource. Two of the best indicators of aquifer health are the quantity and quality of water emanating from the ground as spring discharge. Florida's springs not only reflect the status of the aquifer, but they also influence the ecological health and integrity of many of the State's most significant surface water ecosystems. The springs themselves are outstanding aquatic resources with aesthetic qualities, geological attributes, and biological characteristics that render them magnets for tourism and sanctuaries for renewal of the human spirit.

Over the last five decades or more, many springs have experienced a reduction in discharge, increased nitrate concentrations, increased occurrence of nuisance algae and invasive aquatic plants, decreased abundance of native vascular plants, and concomitant alterations of fish and invertebrate communities. These changes threaten the ecologic and socioeconomic values of the springs and their downstream receiving waters.

In recognition of the ecological and economic significance of the Floridan aquifer and its associated springs, the St. Johns River Water Management District (SJRWMD) developed a Springs Protection Initiative (SPI) in 2013, with three major programs: projects, regulation, and scientific research. In support of the initiative's scientific research program, the University of Florida (UF) and the SJRWMD implemented the Collaborative Research Initiative on Springs Protection and Sustainability (CRISPS) in 2014. The overarching goal of CRISPS was to understand the relative influence of natural and anthropogenic factors that affect a key indicator of healthy spring ecosystems – the relative abundances of native vascular plants and nuisance algae. An improved understanding of manageable factors promoting the growth of nuisance algae can inform effective management of the Floridan aquifer and its associated springs.

A major spring vent is part of a much larger and more complex system than is apparent from casual observation. Its origins extend over large areas and its functioning connects the depths of the unseen and extensive Floridan aquifer to the land's surface. A complete spring ecosystem comprises a terrestrial subsystem that generates aquifer recharge, a groundwater subsystem that conveys that water, and a surficial aquatic subsystem (hereafter, a spring) where that water reemerges at the land surface. Effective management of springs and their downstream waters will require an understanding of all subsystems and their interactions. This understanding entails tracing the sources of water and dissolved constituents from the land's surface to the groundwater subsystem, tracking the transport and transformations that occur in the aquifer, and examining the myriad factors and processes that affect the biological structure and function of the surficial aquatic ecosystem. Of special interest to those engaged in CRISPS, and to scientists and managers more broadly, is an improved understanding of what controls the relative abundance and interactions of nuisance algae (including mat forming taxa and epiphytic species) and other submersed aquatic vegetation (SAV), native vascular plants in particular, which make up the primary producer community structure (PPCS) in springs.

The complex system represented by springs is affected by land use, soil characteristics, geology, hydrologic characteristics of the aquifer, surface water hydrology, nutrient transformations and transport in both groundwater and surface water systems, as well as trophic interactions in the springs. Therefore, a highly integrated research effort is required to understand the linkages among these characteristics and processes, controls on the natural system, causes for changes to the system, and support efforts to ameliorate undesirable anthropogenic effects. CRISPS is inherently interdisciplinary, and provides the integrated framework required to significantly advance our understanding of the Silver Springs system and spring systems more generally. This work focused on the Silver Springs ecosystem for several reasons. Compared to most other major springs in Florida, it has a long history of in-depth ecological study and a substantive database for some key ecological drivers. It has experienced an increase in abundance of nuisance algae and changes in fish populations. Finally, it is one of Florida's most prominent springs in terms of discharge, biological and economic significance.

CRISPS concentrated on three major objectives:

1. Improve the scientific foundation for management of nitrate loading to springs. Through observations, experiments and modeling, CRISPS extended our understanding of the: a) sources, nature, and patterns of nitrogen loading to the groundwater subsystem; b) spatial variation in the hydrologic conveyance rates within the Silver Springs springshed; and c) the transformation and loss via denitrification, for example, of nitrate moving through the groundwater subsystem to the springs.

2. Evaluate whether a reduction in nitrate concentrations/loads alone will be sufficient to restore the balance between filamentous algae and submersed vascular plants. CRISPS expanded scientific understanding of the influence of nitrate as a driver of primary producers through observation and experimentation.

3. Assess the relative influence and manageability of non-nitrate drivers controlling primary producers. CRISPS examined the influence of other potential drivers of primary production including physical drivers such as light, temperature, and current velocity, as well as nutrients other than nitrate and grazing by aquatic herbivores.

The CRISPS research team was organized into two major groups: the Springshed Supergroup and the Springs Ecosystem Supergroup. The Springshed Supergroup focused experiments and modeling on identifying sources of nutrients, particularly nitrogen, conveyed from the land's surface to groundwater, as well as transformation, loss, and transport of nitrogen through soils and groundwater to the spring vents. Nitrogen loading in springsheds varies in response to rainfall, temperature, season, rates and forms of nitrogen inputs, soil types, land use, and land cover. Transport of inorganic and organic forms of nitrogen to the spring depends on aquifer properties, the geometry of conduits and fractures, and transformation and loss in the groundwater system.

Similarly, the Springs Ecosystem Supergroup used both experiments and modeling to explore hydrodynamic, biogeochemical, biological, and ecological processes in the Silver Springs ecosystem. Inputs from the groundwater and watershed models are critical for predicting

attributes of the physical-chemical environment that affect the functioning of the spring ecosystem (e.g., discharge and current velocities, depths, and nutrient concentrations). These inputs, along with other environmental characteristics such as light availability and dissolved oxygen concentrations, provide the template for biological responses, which can be described using mechanistic, empirical, or mixed models. Furthermore, internal controls arising from variation in biological drivers, such as grazing pressure on algae, also were considered. Based on the independent and interactive influences of physicochemical and biological processes, this group sought to assess the relative importance of these drivers in determining PPCS.

Key findings of this multi-disciplinary effort are summarized below. For details, the reader is referred to the nine, comprehensive, individual reports that comprise the complete study (Box ES.1).

ES.2 GENERAL CONCLUSIONS

The CRISPS research effort increased our understanding of the Silver Springs ecosystem specifically, and of Florida's springs in general. Many major and minor findings provide guidance for future management efforts. The salient conclusions relevant to each of the major research objectives listed below:

Objective 1. Improve the scientific foundation for management of nitrate loading to springs.

- **Land use patterns influence nitrate concentrations in soils.** Agricultural lands exhibit higher nitrate concentrations in their soils than urban landscapes, which, in turn, exhibit higher nitrate concentrations than either forests or wetlands. Agricultural and urban Best Management Practices (BMPs) that reduce the amount of nitrogen applied to the land's surface and improve the efficiency of assimilation by plants should reduce nitrate loading to springs.

- **Observations and modeling indicate that flow in conduits and fractures, rather than in porous media, dominates the delivery of water and solutes including nitrate within several kilometers of the springs**. Flows in conduits and fractures generate spatial heterogeneity in travel times for nitrate within the springshed. *In situ* measurements in the Floridan aquifer suggest that within a few kilometers of the springs, flows in conduits and fractures account for the vast majority of water movement, but only a very small portion of the volume of water in the aquifer. Although equivalent porous media matrix models may adequately simulate spring discharge, CRISPS modeling experiments highlight the value of including conduit networks when mapping vulnerability and targeting management interventions that will most quickly reduce nitrate concentrations in springs. A new calibrated Silver Springs model containing plausible conduit networks should enhance efforts to identify vulnerable areas of the Silver Springshed. Additional field measurements and modeling experiments would be needed to develop such a model.

- **Denitrification has the potential to remove a substantial fraction of the nitrate nitrogen load in the soils, vadose zone, and aquifer before it reaches the springs**. Rates and

timescales for removal of nitrogen due to denitrification vary across the springshed. Efforts to reduce nitrogen loads from the springshed could focus on enhancing the necessary conditions in areas where the nature of the soils and subsurface strata (sands or limestone containing little organic matter) limit denitrification rates or areas in close proximity to spring vents. These areas are typical of the western, unconfined portions of the springshed, including the city of Ocala and surrounding urban areas.

Objective 2. Evaluate whether a reduction in nitrate concentrations/loads alone will be sufficient to reduce the occurrence of nuisance algae and restore the balance between benthic filamentous algae and submersed vascular plants.

- **Ecosystem primary production does not currently appear to be nitrogen limited in either Silver River (1.38 mg N L^{-1}) or Alexander Springs Creek (0.05 mg N L^{-1})**. Three lines of evidence support this conclusion: 1) present day rates of primary production are similar to rates observed at earlier times when nutrient concentrations, nitrate specifically, were lower (i.e., 1955 and 1980), and rates are slightly higher in Alexander Springs Creek than in Silver River despite far lower nitrate concentrations; 2) uptake rates for nitrogen that would support current primary production (growth of plants and algae) in Silver River are less than 1.5 % of the nitrogen load delivered to the system, and 3) experimental nitrogen enrichment did not stimulate gross primary production (GPP) or increased algal accrual in either Silver River or Alexander Springs Creek, and nitrate depletion in benthic chambers created concentrations near background levels, but had no effect on GPP in Silver River.

- **High concentrations of nitrate do not appear to inhibit SAV growth**. High nitrate concentrations have been hypothesized to influence PPCS by inhibiting growth of SAV. Results from both field measurements and experimental manipulations do not support this hypothesis.

- **These observations indicate that nitrate reduction alone is unlikely to restore PPCS**.

Objective 3. Assess the relative influence and manageability of non-nitrate drivers of primary producer community structure.

- **The velocity of water movement strongly influences PPCS.** A velocity of approximately 0.22 m s^{-1} represents an important threshold for epiphytic algal cover, although algae may be present above and below this threshold. Before 2000, velocities often exceeded this threshold in Silver River. Between 2000-2003 the stage-discharge relationship changed to yield higher stage and lower velocity for a given discharge. For example, at a discharge of 20 m^3 s^{-1} (~700 cfs), the existing regime yields mean channel velocities of approximately 0.16 m s^{-1} in the stream run just below the main spring, whereas the previous regime gave velocities of about 0.24 m s^{-1} at this location. This hydrologic transition and concomitant velocity change may have reduced sloughing of epiphytic algae, leading to higher algal biomass. It is important to note, however, that areas of the river with slower flow likely always contained epiphytic algae, even when mean channel velocities were higher. Colonization and removal of epiphytic algae does not appear to be hysteretic, so restoring higher velocities should reduce epiphytic algal cover on SAV.

- **Light and temperature are the dominant controls on community-level primary production and respiration.** Most of the spatiotemporal variation in GPP is explained by corresponding variation in light and temperature alone, and patterns in these drivers have not changed substantially in recent history. The stability in production and respiration rates through time, and strong evidence for abiotic controls on PPCS, provide strong support for the view that increases in primary production do not underlie an increase in nuisance algal biomass. Other factors and processes, e.g., scouring and grazing, appear more relevant in accounting for changes in the PPCS; an increase in the prevalence of nuisance algae specifically.

- **Thick and mobile benthic sediments represent important sources of non-nitrate nutrients.** Unlike most Florida springs, which are punctuated by limestone outcroppings associated with the Floridan aquifer, the bottom of the Silver River is completely covered by sediment over 6 m deep. These sediments are deposited rapidly (~ 2 mm yr^{-1}), and at one site (RM 0.7) up to 50 cm were deposited sufficiently rapidly that ^{210}Pb decay ($t_{1/2}$ = 22.3 years) was unobservable. The sediments are a mix of autochthonous and allochthonous materials, and they contain large amounts of organic carbon; nearly 50 % by weight where sedimentation rate was most rapid. Mineralization of organic carbon drives rapid denitrification, but the loss of nitrate N from the water column is balanced by the flux of ammonium N from benthic sediments, which, in turn, is likely oxidized to other combined forms of nitrogen including nitrate. The sediments are also important sources of other nutrients, including phosphorus (P), iron (Fe), and sulfide. Flux across the sediment-water interface, in stagnant areas of the ecosystem, may represent a relatively more important source of solutes than delivery by flowing water.

- **Native macrophytes and their epiphytes provide much of the energy that is transferred to higher trophic levels.** Benthic filamentous algae (one form of nuisance algae) do not contribute substantially to production at higher levels in the aquatic food web. Herbivorous insect larvae, however, do appear to use these algae as food. Because nuisance algae are consumed primarily by these emergent insects, it is likely that much of this secondary productivity is exported to the surrounding terrestrial environment. In essence, nuisance algal mats in Silver River, and likely other spring systems, may be largely decoupled from the aquatic food web. Experimental work provided little evidence that predators mediate the impacts of grazing on plant and algal dynamics in Silver River, i.e., strong top-down influences were not apparent.

Based on findings, as summarized above, land use activities have a profound influence on soil nitrate concentrations and subsequent delivery of nitrate to the groundwater subsystem. Nitrate removal rates and hydrologic conveyance are, in turn, determined by soil properties and physical characteristics of the aquifer itself. Uncertainty remains regarding the precise location of conduit networks within the Silver River springshed. Empirical data and modeling efforts suggest, however, that such networks likely account for the vast majority of groundwater movement and solute transport and thus merit further investigation.

With regard to the surface water subsystem, a central question addressed as part of the CRISPS effort was whether nitrate reduction alone might be sufficient to affect a change in PPCS; specifically, a reduction in the abundance of nuisance algae. From an ecosystem-level perspective, it is unlikely that a reduction in nitrate alone will affect a change in the PPCS in the Silver River spring ecosystem. In fact, it appears that primary production in the Silver River spring ecosystem is currently relatively insensitive to large variations in nitrate concentrations because the availability of nitrate is primarily driven by the discharge and nitrate mass flux far exceeds the demands of primary producers. Water velocity, on the other hand, clearly influences PPCS in the Silver River and was identified as a primary determinant of epiphytic algal cover on native vascular plants. Algal abundance on vascular plants at any given location and time is a reflection of growth dynamics and losses. Sloughing of epiphytic algae represents a loss term due to physical processes associated with water movement, e.g., shear stress and turbulence. Grazing can also result in algal loss. Regarding the impacts of grazers on algal abundance, stable isotopic signatures clearly indicated that mat-forming, benthic filamentous algae in the Silver River is consumed primarily by emergent insects and not by other common grazers in the system. These other grazers, i.e., gastropods, turtles and some fishes, consume native macrophytes and/or their associated epiphytic algae (which, if left unchecked, can accrue to nuisance levels). The interactive effects of flow velocity, nutrient delivery and grazers on the composition and abundance of epiphytic algae merit additional study.

In general, management of a spring will involve each of the three major subsystems of the complete ecosystem: the terrestrial subsystem (the springshed), the groundwater subsystem (the shallow, intermediate, and Floridan aquifers), and the surficial aquatic subsystem (the springs). In support of a holistic view of spring ecosystems, summaries of the key findings and outcomes from all projects are provided below.

ES.3 SPRINGSHED PROCESSES

This element of the program elucidated the sources of nitrogen within the Silver Springs springshed, developed models of flow in conduits and fractures for the Upper Floridan aquifer within the springshed, and examined the transport and loss of nitrogen within the aquifer system. One of the salient difficulties in understanding and managing springs is that their source water flows through a concealed and complex system of porous limestone that includes fractures and conduits. The karst system of the Floridan aquifer typically has been modeled as an equivalent porous media. It is well known; however, that karst contains fractures and conduits that transmit water at rates much higher than those characteristic of the surrounding porous rock. These more direct connections to spring vents are distributed heterogeneously, creating regions where water and solute travel rapidly to the vents. These regions create “hot-spots” within the springshed where nitrate applied to the land is transported more rapidly to springs with little opportunity for removal, e.g., via denitrification.

ES.3.1 Groundwater Hydrology: Conduit and Fracture Flow Modeling

Modeling was used to examine how conduits might develop in the aquifer and how spatial variation in the network of conduits could affect delivery of water and nutrients to Silver Springs. The overall goals were to determine the significance of conduits in the transport of water and solutes (particularly nitrate) to Silver Springs and to estimate the uncertainty

associated with predictions about transport and flow resulting from uncertainty about the geometry of conduits. The results of Monte Carlo simulations indicate that incorporating plausible conduit networks within a calibrated Silver Springs model would help identify vulnerable areas in the springshed that could be targeted for management interventions leading to more rapid and effective reductions of nitrate in the springs. Specific results of this work (Section 2 of this report - Graham et al.) indicate that:

- Conduit networks that evolved from models based on physicochemical equations to produce first magnitude springs demonstrated a range of physical configurations. However, for the ensemble of networks that produced first magnitude springs, conduits tended to develop in topographic lows that drained nearby high regions. In general, these networks exhibited high connectivity and relatively rapid transport along a north-south axis within the springshed.
- For the ensemble of conduit networks that produced first magnitude springs, the uncertainty surrounding the magnitude of flow and concentration of solutes arriving at the spring vent after a unit pulse applied to the land's surface was relatively low, and the results were consistent with field observations. These outcomes suggest a high level of consistency regarding aggregated flow and transport of solutes across the variable conduit networks.
- Simulations of reverse transport across the ensemble of conduit networks that produced first magnitude springs predicted large, vulnerable regions in the springshed (i.e., areas with short travel times from the land surface to the spring) with relatively low uncertainty. Vulnerable regions tended to be topographic lows in the central part of the domain where conduits developed. The spatial distribution of these vulnerable regions was significantly different from the concentric ellipses which would be identified using an equivalent porous media model.
- Results of this modeling experiment highlight the value of including conduit networks when mapping vulnerability and planning management interventions that will reduce concentrations of contaminants in spring flows.
- Monte Carlo analysis of backwards tracer pulse experiments conducted on a new calibrated Silver Springs model containing plausible conduit networks should enhance efforts to identify vulnerable areas of the Silver Springshed that could be targeted for management interventions.

ES.3.2 Springshed Hydrology: Nitrogen Transport and Loss

The goal of this work was to gather hydrogeologic data in the field. Passive flux meters (PFMs) within wells that reached the Floridan aquifer measured flows of water and solutes in order to identify portions of the aquifer that deliver more significant quantities of water and solutes to the spring. These measurements were employed subsequently to examine the characteristics of flow and natural attenuation of solute loads, with special emphasis on nitrate (for additional details, see Section 3 of this report - Jawitz et al.). Key findings are:

- A wide distribution of groundwater velocities were measured *in situ* using PFMs in the Floridan aquifer, with the lowest velocities representative of matrix flow and the highest velocities likely representing contributions from fractures and conduits. Measured groundwater velocities ranged from 2.6 to 10.9 cm d^{-1} with a mean of 6.2 cm d^{-1}. These velocities are consistent with slow flow through the rock matrix.

- Nitrate-N fluxes in the rock matrix were below detection limit of the PFM technique. However, measured phosphate fluxes were in the range of 0 to 0.8 mg PO_4-P m^{-2} d^{-1} and sulfate fluxes ranged from 1.3 to 31 mg SO_4-S m^{-2} d^{-1}.
- A new karstic borehole device (KBHD) fabricated for this study measured groundwater and solute flux in fracture and conduit zones. The resultant fluxes were more than 50 times greater (mean = 3.1 m d^{-1}) than those previously measured with PFMs in the aquifer matrix.
- These data combined with velocities measured in tracer tests, the known flux from Silver Springs, and the aquifer dimensions suggest that within approximately 5 km of the spring vent, matrix flow contributes only approximately 10 % of the discharge from Silver Springs. Non-matrix flow, which includes fractures and conduits, is therefore surmised to contribute approximately 90 % of the water discharged from Silver Springs within this distance. The relative contribution of non-matrix flow diminishes slowly with distance from the spring vent.
- *In situ* nitrate attenuation also was evaluated in five wells with push-pull tests and the KBHD. In three of these wells, nitrate was not detected while two wells had mean mgNO_3-N L^{-1} concentrations of 0.77 and 2.2 mg L^{-1}, respectively. In the two wells with measurable nitrate, nitrate was not lost during the push-pull tests, with similar rates of recovery for both non-reactive (Rhodamine) and reactive (KNO_3) tracers indicating that denitrification at these locations was below the detection limit of this technique. However, in the wells where background nitrate and oxygen concentrations were low, recovery of nitrate in the push-pull tests was approximately 40 % less than the recovery of the non-reactive tracer. This loss of nitrate suggests redox conditions suitable for denitrification.

ES.3.3 Springshed Biogeochemistry: Nitrogen Transformations

In addition to the amount of nitrate carried in flowing water, biogeochemical transformations of nitrogen compounds in the soil, vadose zone and surficial aquifer determine how much nitrate enters the Floridan aquifer. The goal of this project was to trace nitrogen from sources within the springshed through the vadose zone and aquifer to discharge at the spring vent. Laboratory and field measurements were coupled in various ways to determine concentrations of nutrients, microbial composition, and denitrification rates in profiles through the soil and vadose zone, as well as concentrations of nutrients, ratios of stable isotopes for nitrate, and concentrations of dissolved gases in groundwater (for additional details, see Section 4 of this report - Inglett et al.). Key findings are:

- Nitrate concentrations in soils varied among land uses, and they ranked in the order of agriculture>urban>forest≥wetlands. Thus, patterns in land use point to patterns in surficial loading of nitrogen.
- Results suggest the potential for significant denitrification during transit through surface soils to groundwater as evidenced by changes in the isotopic composition of nitrate-N and oxygen, measured rates of denitrification, and abundance of denitrifying microorganisms in profiles through the soil and vadose zone. Surface soils containing more organic matter are the most significant sink for nitrate, however, layers of relic peat and deposits of marine groundwater demonstrate the potential for high rates of denitrification deeper in the system.
- Laboratory studies with the most abundant soil type in the springshed (sandy soils with little organic matter) showed that temperature exerted the strongest control on soil denitrification. Across all land uses, denitrification increased with increasing temperature regardless of

whether water filled pore spaces or concentrations of nitrate or organic carbon were high. These laboratory incubations also indicated that nitrate was converted to ammonium at higher temperatures, particularly below pastures amended with manure.

- Direct measurements confirm low rates of denitrification in samples of limestone from the aquifer, but estimates based on concentrations of dissolved gases from the east and west Mammoth vents indicate that approximately 17 to 43 % of the nitrate load to the aquifer was lost through denitrification. Much of this apparent denitrification could occur in isolated surficial aquifers (e.g., peat layers) and areas of mixing with deep, more marine-based groundwater.
- Stable isotope values for nitrate-N and oxygen from profiles of the soil and vadose zone indicate that caution is warranted when attributing the source of nitrate in groundwater to land uses. Nitrification and denitrification, as well as interactions of nitrate with soil particles, all affect the isotopic signature of leached nitrate. Isotopic signatures from at least one site indicated potential contributions from multiple sources within a single profile.
- The amount of excess N_2 and accompanying changes in isotopic ratios for nitrate nitrogen and oxygen in samples from wells and the Mammoth vent complex indicate that most of the nitrogen in the unconfined, western springshed originates from a common source, with $\delta^{15}N$ and $\delta^{18}O$ signatures of approximately 6-7 ‰. These signatures likely represent more organic sources, such as wastewater, manure, or soil N, but caution should be used until additional analyses can better establish this end member.

ES.4 SPRINGS ECOSYSTEM PROCESSES

ES.4.1 Hydraulics and Hydrodynamics

The objectives of the Spring System Hydrodynamics/Hydraulics work order were to: 1) yield a more thorough understanding of the distributions of velocities and residence times in the Silver River's channel , including quantifying the location and magnitude of transient storage and exchange; 2) identify critical shear stresses for the entrainment and detachment of epiphytic algae; and 3) link these findings to three-dimensional modeling with a focus on how SAV impacts velocities, residence times, and the stage-discharge relationship (for additional details, see Section 5 of this report - Kaplan et al.). Key findings are:

- Breakthrough curves (BTCs) fit to measured data delineated flow paths and estimated reach-scale hydraulic properties of the Silver River for five dates that had differing hydraulic conditions. These results also provided valuable data for calibrating and validating the Environmental Fluid Dynamics Code (EFDC) model.
- Reach-scale velocities and mixing parameters measured via dye releases were variable in time and space, illustrating how the flow regime of the Silver River changes with different boundary conditions (spring flow and downstream river stage), as well as with in-channel properties such as SAV cover and density. Such variation impacts in-channel hydrodynamics and likely affects biogeochemical transformations in the river's advective and transient storage zones.
- Mixing parameters also were variable across experiments, illustrating differential mixing mechanisms across seasons and boundary conditions. Dispersion and transient storage were generally greatest when mean velocity was low and downstream stage was high. Beyond

empirical modeling, comparison of measured BTCs in beds of vegetation and the adjacent main channel suggests that vegetation can serve as zones of transient storage.

- Experimental approaches identified thresholds for critical velocity and shear stress below which algal biomass accrual increased.
- Data from the Florida Springs Synoptic Study, the Silver River, Gum Slough, and several coastal springs yielded an overall mean critical threshold for algal sloughing of 0.22 m s^{-1}. Mean critical shear stress for algal sloughing in the Silver River was 0.35 N m^{-2}, and the mean critical velocity threshold estimated to disrupt SAV (*Vallisneria americana* and *Sagittaria kurziana*) was 0.33 m s^{-1}.
- Models that include the observed stage/discharge shift suggest that under historic conditions, the mean velocity in the main channel near the spring was approximately 0.24 m s^{-1}, greater than the critical threshold for algal sloughing. Under the current stage/discharge relationship, the mean velocity in this location is predicted to be < 0.16 m s^{-1}, significantly lower than historic velocities and the critical velocity. This finding could, in part, explain algal biomass proliferation in some areas of the spring run.

ES.4.2 Springs Ecosystem Physicochemistry

This portion of the project quantified benthic sources and sinks of nutrients and characterized nitrogen dynamics and metabolism. This was accomplished through three sub-projects:

ES.4.2.1 Nitrogen Dynamics and Metabolism

Elevated nitrate concentrations have been invoked to explain increasing algal abundance and declining SAV health across springs. In this research element, four lines of inquiry evaluated this hypothesis, emphasizing spatial heterogeneity within spring systems and contrasting patterns across two springs with dramatically different nitrate concentrations (Silver River and Alexander Springs Creek) (for additional details, see Section 6 of this report - Cohen et al.). Key findings are:

- High resolution time series data for pH, dissolved oxygen (DO), nitrate, and phosphate were used to estimate ecosystem metabolism in the open channel as well as uptake of nutrients by autotrophs in 3 reaches along the Silver River and 1 reach along Alexander Springs Creek.
- Significant diel variation was observed for nearly all solutes in the Silver River, consistent with strong temporal forcing from solar insolation. Time series of solute concentrations were used to estimate GPP and ecosystem aerobic respiration (ER). Observed rates of primary production were consistent with historical rates recorded in the 1950s and 1980s, with net autotrophy in the upper river (GPP > ER), net heterotrophy in the lower river (GPP < ER), and similar temporal variation for both GPP and ER. In Alexander Springs Creek, where nitrate-N concentrations remain near background levels (0.05 mg NO_3-N L^{-1}), and below those measured in the Silver River in the 1950s, GPP was slightly but not significantly higher and ER was slightly but not significantly lower than in Silver River.
- Using high resolution nitrate-N measurements, we determined that denitrification is the dominant N mechanism leading to loss of nitrate-N, with mean rates of 0.22 g N m^{-2} d^{-1} Autotrophic uptake (i.e., assimilation by plants) accounted for 0.06 g N m^{-2} d^{-1} or about 20 % of the gross loss. The assimilation flux of N equals 1.4 % of N delivered from the spring vents.

- Data on algal and SAV cover along the entire length of the Silver River showed that SAV cover was generally high (>75 % cover at nearly 90 % of 100 sites) while algal cover was more variable. Spatial variation in algal cover was best explained by negative correlations with SAV cover (which suggests inhibition), distance downstream, and surface water velocity.
- None of the parameters characterizing Silver River water chemistry provided significant explanatory power for algal cover, though algal cover was weakly and positively associated with some sediment properties (i.e., concentrations of Calcium (Ca), P, and magnesium). Cover of SAV declined with increasing concentrations of Ca in the water column, concentrations of chloride in the water column and porewater, and clay content of the sediment.
- Measurements of metabolism in benthic chambers confirmed that light availability was the dominant control on GPP. Nutrient enrichment (N, P, and Fe) yielded no significant effects on GPP in benthic chambers or algal growth rates on experimental tiles. Nitrate dynamics within the benthic chambers documented denitrification as the dominant process contributing to nitrate loss according to nearly 1^{st} order kinetics, with assimilation by plants and algae accounting for a smaller flux that more closely follows 0^{th} order kinetics (i.e., concentration independent). GPP was independent of (uncorrelated with) nitrate-N concentration.
- In Silver River, where *Vallisneria americana* and *Sagittaria kurziana* are both present, their growth rates were similar; Alexander Springs Creek only had *V. americana*, with mean growth rates nearly identical to plants in Silver River. Single variables yielded modest and inconsistent relationships with SAV growth, but multivariate models explained 60 % of variation in SAV growth, with key parameters being forest canopy cover, algal cover (for *Vallisneria* only), concentrations of soluble reactive phosphorus (SRP) in porewater, and redox conditions in the sediment.

ES.4.2.2 Nitrate Inhibition of Submerged Aquatic Vegetation

In response to observations of declines in SAV abundance and productivity in several Florida springs, an investigation was initiated to determine if high concentrations of nitrate-N (NO_x-N) can inhibit SAV growth. The potential for such inhibition follows from the hypothesis that two dominant SAV species, *Vallisneria americana* and *Sagittaria kurziana*, have not yet evolved a metabolic mechanism to turn off nitrate reductase, an enzyme that converts nitrate into ammonia. Because ammonia is phyto-toxic at elevated concentrations, it must be utilized rapidly, predominantly in protein synthesis. This process requires energy from metabolism of photosynthate, and under elevated nitrate availability, it could produce a significant energetic burden on SAV. In an effort to validate field observations by other researchers, mesocosms constructed for this work also were utilized to investigate the role of dissolved oxygen stress (hypoxia) on invertebrate grazers and the effects of flow velocity on the proliferation of epiphytic algae. Key findings of this study are presented below (for additional details, see Section 7 of this report - Osborne et al.).

- Results of this study do not support the hypothesis that elevated nitrate concentrations have a negative effect on the physiology of SAV in spring ecosystems.
- The two species responded differently to increased nitrate. The response of *V. americana* tended to be increased growth of both roots and shoots, while *S. kurziana* tended to show increased shoot production as nitrate increased.

- Nitrate reductase activity (NRA) in SAV tended to be greatest in roots for *V. americana* and in shoots for *S. kurziana,* further suggesting significant physiological differences between these species. Both species were proficient at nitrate uptake and incorporation into tissues, as indicated by decreased carbon to nitrogen ratios.
- Results suggest that four species of grazers experience hypoxic stress below 2 mg O_2 L^{-1}. The gastropod *Viviparus georgianus* was observed to be the most sensitive to low DO concentrations, with a threshold of 2.7 mg O_2 L^{-1}, while the grass shrimp *Palaemonetes paludosus* remained functional to 1.6 mg O_2 L^{-1}. Exposure to increased nitrate did not alter thresholds for hypoxic stress for *E. floridensis* and *T. granifera*. These findings suggest that the current frequency of hypoxic events (DO <2.0 mg O_2 L^{-1}) may reduce the abundance and activity of grazers.
- Shear stresses were observed to dramatically decrease algal growth and recruitment at velocities of 0.25 m s^{-1} and higher. While algal growth clearly was related to velocity, scouring of established epiphytic algal biomass did not exhibit any pattern potentially due to friction caused by SAV blades and steep velocity profiles.

ES.4.2.3 Benthic Sources and Sinks of Nutrients

Benthic sediments in streams act as biogeochemical reactors that change the chemical compositions of porewater relative to the overlying stream water. Biogeochemical reactions could thus provide an important source of solutes to stream water leading to effects on benthic and lotic ecosystems. However, impacts on stream water chemistry depend on the magnitude of fluxes of solutes to and from porewater, which is driven by the difference between concentrations of solutes in stream water and porewater and transport mechanisms, e.g., whether from advection of water and/or diffusion of solutes. Objectives of this study were to: 1) evaluate the distribution and chemical composition of sediments; 2) measure physical and hydraulic characteristics of the sediment; 3) assess the biogeochemical reactions in the sediment and their impacts on porewater compositions; and 4) estimate potential impacts of fluxes of solutes between bottom sediment and the river. Key findings from this study are presented below (for additional details, see Section 8 of this report - Martin et al.):

- Thick sedimentary deposits were found along the length of the Silver River. These sediments may have been deposited when the system was a quiescent lake and/or by flowing water. Excess ^{210}Pb in sediment cores indicated a high and constant rate of sedimentation that ranged from 1.6 to 2.2 mm yr^{-1}. This excess ^{210}Pb indicated that if sediments were originally deposited in a lake, they are being reworked by the river. Much of the inorganic sediment originated from erosion of the highlands to the west.
- The sediments comprise shell hash and sandy layers interbedded with fine grained layers rich in organic carbon. Some of the organic carbon was allochthonous, which represented a new source of nutrients to the river. The sediments were found to act as a barrier to flow into the river from the underlying Upper Floridan aquifer, except where water discharges from spring vents.
- Hydraulic conductivity of the sediments ranged from 5.5×10^{-7} to 6.2×10^{-3} m s^{-1}, similar to values expected from gravel beds. Horizontal hydraulic conductivities were higher than vertical hydraulic conductivities by factors from 1.1 to 25. Horizontal hydraulic conductivities were considered representative of the sandy shell layers, which may act as preferential flow paths to the channel if they are continuous. The distribution of such

continuous layers could not be determined with the limited distribution of sampling in this study. Head gradients were oriented from the sediment to the river through the entire 2-yr period of monitoring, which suggests groundwater flowed continuously to the river. Head gradients were low, which limited average horizontal and vertical flow rates to 1.4 and 0.4 cm d^{-1}, respectively.

- Biogeochemical reactions in the sediment are dominated by redox reactions, and porewater chemistry profiles that indicated that redox conditions extended to methanogenesis. However, each sampling site had unique chemical gradients. The biogeochemical reactions created concentration gradients in which maximum concentrations of solutes could be more than 100 times greater than concentrations in the river. Solutes produced by these reactions could be important inputs to the river, unless precipitated at the sediment-water interface, as would be expected as dissolved Fe(II) is oxidized to solid Fe-oxides.
- Concentration gradients created by the biogeochemical reactions drove diffusional fluxes of ecologically important solutes from the sediments to the river, including ammonium (NH_4), SRP, Fe, Mn and HS^-; whereas, nitrate was lost to the sediments from the water column. In addition, the hydraulic conductivities and head gradients indicated that flow also transported solutes to the river, although the estimated advective fluxes for all solutes were lower than diffusive fluxes. The total benthic flux (advection and diffusion) for NH_4-N, SRP, Fe, and Mn represented 12, 4, 12, and 5 % of the load from the spring. All sulfide originated from benthic fluxes. Depending on mixing with the overlying water column and residence time in stagnant zones, these fluxes may contribute more to macrophyte and algal growth than these percentages suggest.

ES.4.3 Springs System Biology - Trophic Interactions

Major objectives of this study were to: 1) identify the major algal grazers and their consumers; 2) determine algal growth relative to grazing rates of small grazers; and 3) assess the potential for top-down (consumer) control of key grazers that were identified as part of objectives 1 and 2. Natural abundances of stable carbon and nitrogen isotopes ($\delta^{13}C$ and $\delta^{15}N$) were employed as tracers to identify pathways of energy flow and material transport in Silver River. Manipulative field experiments assessed algal grazing and the influence of predators on those rates. Key findings are presented below (for additional details, see Section 9 of this report - Frazer et al.):

- In the Silver River, $\delta^{13}C$ and $\delta^{15}N$ values together with predictions from empirical models clearly indicate that native macrophytes and their associated epiphytes fuel much of the secondary production that, in turn, supports a diverse assemblage of organisms that occupy higher trophic levels.
- Nuisance filamentous algae do not contribute substantially to the diet of key consumers, such as gastropods, turtles and large herbivorous fish. Instead, it appears that a small number of insect larvae (i.e., trichopterans and chironomids), amphipods, and smaller omnivorous fish (i.e., shiners and darters) heavily exploit nuisance algae as a food source (contributions to diets $\geq$ 30 %). Because nuisance algal production is consumed predominantly by emergent insects, it is likely that much of this production is exported to the surrounding terrestrial environment upon emergence. In essence, nuisance algal mats in Silver River, and likely other spring systems, may be largely decoupled from the broader aquatic food web. This is a dynamic that merits further investigation as it may fundamentally impact energy flow and material transport at the watershed scale.

- Alligators in the Silver River rely heavily on gastropods and crustaceans to support metabolism and growth. This finding has profound implications for any effort to model the river's food web. Previous models have considered alligators to be top/apex predators that mainly consume fish and other vertebrates occupying intermediate trophic levels. In other ecosystems, alligators are known to both directly and indirectly affect key ecosystem processes through their interactions with prey and the environment. Integration of these novel data and insights into food webs will help to refine our understanding of how predation and top-down pressures influence community dynamics within these complex ecosystems.
- Field experiments provided little evidence of predator-mediated impacts on plant and algal dynamics in Silver River; i.e., strong top-down influences were not apparent. Thus, management activities focused on reducing abundances of higher-level organisms in the system are not likely to result in marked changes in the PPCS.

For detailed information, the reader is referred to final work order reports (2014 - 2017) presented in this report (Figure ES.1; see below).

CRISPS: Work Orders- 2014 - 2017

Springshed Supergroup

Work Order # 1: Nitrogen Biogeochemistry: Sources, transformations and loss of nitrogen from land surface to springs.
Patrick Inglett, pinglett@ufl.edu

Work Order #4: Groundwater Hydrology: Conduit and Fracture Flow Modeling.
Wendy Graham, wgraham@ufl.edu

Work Order #6: Springshed Hydrology: Transport and Loss of Nitrogen within the Upper Floridan Aquifer in the Silver Springs Springshed.
James Jawitz, jawitz@ufl.edu

Spring Ecosystem Supergroup

Work Order #2: Silver River Hydraulics and Hydrodynamics
David Kaplan, dkaplan@ufl.edu

Work Order #3: Physicochemistry: Benthic Sources and Sinks of Nutrients and Nitrogen Dynamics and Metabolism.
Matt Cohen, mjc@ufl.edu
Jon Martin, jmartin@geology.ufl.edu
Todd Osborne, osbornet@ufl.edu

Work Order #5: Biology: Trophic Interactions.
Tom Frazer, frazer@ufl.edu

Figure ES.1. List of work orders of the CRISPS project

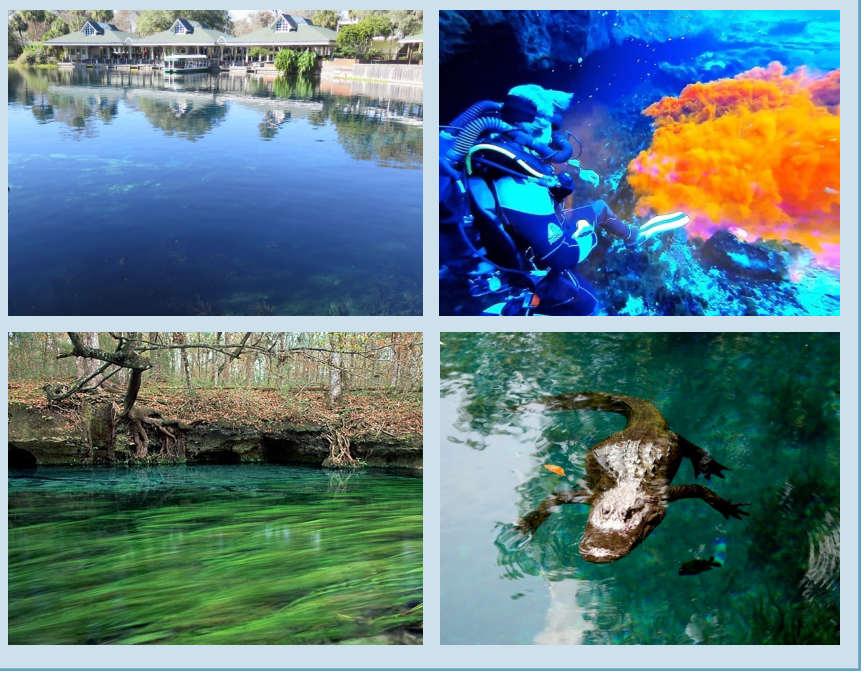

Collaborative Research Initiative on
Sustainability and Protection of Springs [**CRISPS]**

Section 1

[Work Order No: 7]

FINAL REPORT

2014 - 2017

submitted to:

St. Johns River Water Management District
Springs Protection Initiative [SPI], UF Contract # 27789

UF | UNIVERSITY of FLORIDA
Water Institute

C R I S P S

Section 1

INTRODUCTION

Overview of The Collaborative Research Initiative on Sustainability and Protection of Springs, CRISPS

Final Report 2017

Project Team:

St. Johns River Water Management District
Dean Dobberfuhl, Casey Fitzgerald, Steven J. Miller, Rob Mattson,
Chuck Jacoby, and Edgar F. Lowe

University of Florida
Matt Cohen, Tom Frazer, Wendy Graham,
Patrick Inglett, Jim Jawitz, David Kaplan, Jon Martin,
Todd Osborne and K. Ramesh Reddy

This document reports findings and results of a work order for a 3-year project in compliance with Agreement between University of Florida (UF) and St. Johns River Water Management District (SJRWMD) UF Contract #27789. It is part of the *UF Collaborative Research Initiative on Springs Protection and Sustainability (CRISPS)* and supports the science component of *the SJRWMD Springs Protection Initiative (SPI).*

1.1 INTRODUCTION

In the 1700s English naturalist William Bartram described Florida springs as "blue ether of another world" and in the mid 1900s Florida environmentalist Marjory Stoneman Douglas called them "bowls of liquid light." In response to their crystal-clear waters and natural beauty, Florida's springs have been a popular tourist destination for over 130 years and, to this day, continue to attract and awe visitors from around the nation and the world (FSTF 2000). Modern-day visitors to springs provide significant economic benefits to regional economies. In 2003 and 2004, direct annual consumer spending at only three of Florida's major springs (Silver, Ichetucknee and Wakulla) was estimated to exceed $130 million when converted to 2014 monetary values (Wynn et al. 2014). These three springs alone also supported over 1,700 jobs (Bonn and Bell 2003; Bonn 2004). Unfortunately, many of Florida's iconic springs are showing signs of anthropogenic stress in the form of undesirable ecological changes such as declines in the abundance and biomass of native submersed aquatic vegetation, increased cover of nuisance algae and algal mats, and changes in fish and invertebrate communities. Most of these undesirable changes have been attributed to declining spring discharges and increasing nutrient concentrations, particularly nitrogen (FSTF 2000; Scott et al. 2004; Munch et al. 2006; Stevenson et al. 2007; Brown et al. 2008; Harrington et al. 2008; Quinlan et al. 2008; Heffernan et al. 2010).

While natural springs play a vital role in Florida's ecotourism industry, they also provide a lens into the quantity and quality of the groundwater resources that feed them (Copeland et al. 2009). Of the 1,089 spring vents that have been identified in Florida, nearly all are fed by artesian flow from the Floridan Aquifer (Mattson and Means 2016). The Floridan Aquifer is the State of Florida's most significant underground freshwater resource, providing greater that 90% of the State's drinking water, and supporting daily water withdrawals of over three billion gallons (Marella and Berndt 2005; FDCA 2008). Two of the best indicators of the status and health of the Floridan Aquifer are the quantity and quality of water flowing from Florida's springs (Copeland et al. 2009). Declining spring flows raise concerns about the ability of the aquifer to support Florida's burgeoning growth while still providing sufficient water to protect valuable surface water resources. Increasing nitrogen concentrations in groundwater which have been implicated as causing undesirable ecological changes in the springs and downstream rivers and estuaries, and also raise public health concerns with regard to drinking water supplies from the aquifer (Lee et al. 1992; Wolfe and Patz 2002; Camargo and Alonso 2006).

Recognizing the economic and ecological significance of the Floridan Aquifer and its springs, the St. Johns River Water Management District (SJRWMD) developed the Springs Protection Initiative (SPI) in 2013. One of the primary SPI objectives was to provide a sound scientific foundation for the development of cost-effective approaches for the management of the primary factors influencing the hydrology, hydrodynamics, physical/chemistry, and biology of spring ecosystems. The initiative was comprised of two major components: science and projects. The science component of the initiative acknowledged that a more thorough understanding of the influences and manageability of the numerous natural and anthropogenic factors that effect the ecological health of springs was needed. In addition, enhanced understanding of the effects of the various factors simultaneously could only be achieved through integrated, interdisciplinary research (FDEP 2006). Research results will be useful to guide future District water supply planning and regulatory protection of the springs, springsheds and the aquifer. In addition,

research results will provide a sound scientific foundation that policy makers can use to help identify and rank the value of various projects being considered to protect water quantity and quality in the aquifer and restore important ecosystem functions in the springs and their associated spring runs.

In support of the SPI scientific research component, the St. Johns River Water Management District (SJRWMD) formed a partnership with the University of Florida (UF) in 2014 called the Collaborative Research Initiative on Springs Protection and Sustainability (CRISPS). The goal of CRISPS was to better understand how various natural and anthropogenic factors (both physical and chemical) affect the primary producer community (plants and algae), which are the critical indicators of spring ecosystem health. To meet this goal, studies focused on identifying those factors responsible for the loss of native submersed aquatic vegetation and the proliferation of attached algae and benthic algal mats (collectively referred to as nuisance algae). To apply multidisciplinary research to investigate complex physical, chemical and biological interactions, the Silver Springs ecosystem in Marion County was chosen as the primary study ecosystem. Alexander Springs in Lake County was also examined in a less comprehensive fashion to provide valuable context for the work conducted in Silver Springs.

1.2 BACKGROUND

1.2.1 The Floridan Aquifer

The Floridan Aquifer is one of the largest and most productive aquifers in the world (Miller 1990). Underlying much of the southeastern United States, including the entire state of Florida, the Floridan Aquifer covers an area of approximately 100,000 square miles and provides drinking water for over 10 million people (Marella and Berndt 2005). In addition to being a primary source of potable water, the Floridan Aquifer also supports agriculture, industry, tourism and natural ecosystems throughout the region (Miller 1990). The Floridan Aquifer is comprised of a thick sequence of carbonate rock that is generally divided into upper and lower units separated by a less permeable confining layer (Bush and Johnston 1988). Most of the aquifer is overlain by sedimentary rocks that varies in permeability which, in turn, influences recharge, discharge, and ground-water flow. The carbonate rocks of the Floridan Aquifer are readily dissolvable, especially in areas where the aquifer is unconfined or where the top confining layer of the aquifer is thin (Bush and Johnston 1988; Miller 1990). In these areas, recharge of water that is under-saturated with respect to calcite causes dissolution within the rock matrix and creates a series of underground conduits, caves, caverns, sinkholes and other types of openings. This type of topography caused by dissolution is commonly referred to as “karstic” (Miller 1990; Miller 1997). A prominent feature of the karstic landscape in areas where the Floridan Aquifer is unconfined or thinly confined is the occurrence of springs. Before development, about 88 % of the total Floridan Aquifer discharge occurred to springs, rivers, and lakes (Bush and Johnston 1988). Despite ground water withdrawals from the Floridan Aquifer by the early 1980’s exceeding 3 billion gallons per day, predevelopment flow characteristics have remained relatively unchanged and groundwater withdrawals still account for less than 20 % of the total aquifer discharge (Bush and Johnston 1988; Miller 1990). In general, groundwater withdrawals have reduced the overall Floridan Aquifer discharge to springs, lakes and rivers by less than 5 %, although effects can be more pronounced in localized areas (Bush and Johnston 1988). Copeland et al. (2009) documented declining flow trends between 1991-2003 in a number of Florida springs which they

attributed primarily to rainfall/recharge deficits with groundwater pumping a potential additional stressor.

Another potentially significant threat to the Floridan Aquifer, other than water withdrawals, is the degradation of water quality that has accompanied human development of the landscape (Katz 2004; Phelps 2004; Katz and Griffin 2008; Copeland et al. 2009). In particular, there has been widespread nitrate [NO_3-N] enrichment of the Floridan Aquifer in the last 30–50 years (Spechler and Halford 2001; Phelps 2004; Scott et al. 2004; Phelps et al. 2006; Copeland et al. 2009). Sources of the increased NO_3-N include animal and human waste, synthetic fertilizers used on lawns and golf courses, and agricultural activities (Copeland et al. 2009; Harrington et al. 2010). Reduced flows and increased NO_3-N concentrations have been implicated as causative factors in the substantial changes in the ecological character of many of Florida's most significant springs. These changes include increased biomass and cover of algae and invasive aquatic plants, decreased abundance of native submersed aquatic vegetation, and changes in fish and invertebrate communities (Scott et al. 2004; Munch et al. 2006; Stevenson et al. 2007; Brown et al. 2008; Quinlan et al. 2008). These changes threaten the ecologic and economic values of the springs and of the surface water ecosystems to which they flow. Increasing nitrogen concentrations in groundwater also lead to public health concerns (Lee et al. 1992; Wolfe and Patz 2002; Camargo and Alonso 2006).

1.2.2 Silver Springs

Silver Springs is a composite of 30+ contributing spring vents, collectively known as the Silver Springs Group (SSG), that form the headwaters of the Silver River (Scott et al. 2002; Scott et al. 2004), a major tributary of the Ocklawaha River. In this section, "Silver Springs", is used synonymously with SSG. Silver Springs is located about 9 km east of Ocala in Marion County, Florida and is the largest of Florida's 33 first-magnitude springs (Scott et al. 2002). Silver Springs is also home of a major tourist attraction that has been a popular visitor destination for over a century (Crum 1954; Martin 1966). In 2004 alone, visitors to Silver Springs were estimated to annually spend about $65 million (Bonn 2004) which equates to more than $73 million in current dollar values (Wynn et al. 2014). In 1971, Silver Springs was listed by the National Park Service as a National Natural Landmark. This designation recognizes sites requiring preservation because of their geological and biological resources. In 1987, the Silver River was given the designation of an Outstanding Florida Water (OFW). This designation is meant to prevent future water quality degradation (FDEP 2017). Recent amendments to Florida Statutes designated Silver Springs as an Outstanding Florida Spring and required the adoption of minimum flows and levels for Silver Springs and the Silver River by July 1, 2017 (Sutherland et al. 2017) .

The Silver Springs springshed covers an area of 3,100 km^2 (1,200 square miles). From 1946-2010 the mean annual discharge of Silver Springs was estimated to be 19.8 $m^3 s^{-1}$ (699 cfs) (Sutherland et al. 2017). Maximum and minimum discharge ranged from 34.5 $m^3 s^{-1}$ to 4.0 $m^3 s^{-1}$ (1,218 to 141 cfs). The 30+ spring vents of Silver Springs can be divided into three to five subgroups based on similar water chemistry (Butt and Ally 2006; Munch et al. 2006; Knowles et al. 2010). The two uppermost headwater springs (Mammoth East and West) contribute slightly greater than 50 % of the total Silver Springs discharge (Munch et al. 2006; Knowles et al. 2010). These two spring vents discharge relatively young water estimated to be, on average, 6-7 years

of age (Knowles et al. 2010). Downstream vents discharge water estimated to be, on average, 26-35 years of age. Age differences in water discharges between the vents reflect the complexity of flow systems in the karstic aquifer that result in a mixing of groundwater from the porous matrix with conduit flows from both shallow and deep zones in the aquifer. More complete descriptions of the Silver Springs watershed, the underlying geologic formations, runoff, infiltration, and historical flows can be found in Munch (2006) and Sutherland et al. (2017).

Discharge from Silver Springs has declined approximately 32 % since the 1930s (Sutherland et al. 2017). This is based on a decline in the mean flow from 21.9 $m^3 s^{-1}$ (773 cfs) over the years 1930-1939 to a mean flow of 14.9 $m^3 s^{-1}$ (526 cfs) over the years 2005-2015. This variability in spring discharge has been attributed primarily to temporal patterns in rainfall, with groundwater withdrawals estimated to only be responsible for 3.5 % of the decline in flow from Silver Springs since 1970. Flow suppression due to increased densities of submersed aquatic vegetation in the lower Silver River is also hypothesized to be an important factor over this period (Sutherland et al. 2017).

In addition to declining flows, Silver Springs has also experienced a dramatic increase in NO_3-N over the past 50+ years (Munch et al. 2006; Knowles et al. 2010; Hicks and Holland 2012). In water samples taken from the Mammoth Springs vents, NO_3-N has increased from 0.4 mg L^{-1} in 1964 to 1.28 mg L^{-1} in 2016 (Sutherland et al. 2017). This increase has been linked to anthropogenic nitrogen sources, primarily agricultural and urban runoff (Munch et al. 2006; Harrington et al. 2010; Knowles et al. 2010). The Florida Impaired Waters Rule sets 0.35 mg L^{-1} NO_3-N as a limit for listing Florida springs as impaired for nitrogen (Harrington et al. 2010). From 1964 to 2016 only two observed water samples collected had NO_3-N concentration less than 0.35 mg L^{-1} (Sutherland et al. 2017). Recent NO_3-N concentrations measured at Silver Springs (> 1.2 mg L^{-1}) are approaching levels found to be toxic to some aquatic invertebrates (Mattson et al. 2007).

Aside from increasing NO_3-N, other water quality parameters in Silver Springs have remained relatively stable over the past 50+ years. For example, phosphorous concentrations, another nutrient associated with increasing eutrophication, have remained relatively stable and current concentrations are similar to those observed in the 1950s (Hicks and Holland 2012). Two exceptions, however, are temporal trends in water clarity and dissolved oxygen (DO), particularly at night (Munch et al. 2006). Horizontal secchi depth measurements in 2004 were approximately 9 % lower than measurements taken in the 1950s while light attenuation coefficients increased from 166 % – 466 % (Munch et al. 2006). Although these results suggest a decrease in overall water clarity in Silver Springs, they should be viewed cautiously given the few data points collected during the 1950s. Nighttime DO concentrations in Silver Springs declined from 3.1 mg L^{-1} during the 1950s to 2.8 mg L^{-1} in the 1970s to 2.5 mg L^{-1} in 2004 (Munch et al. 2006). Hypothesized causes for the observed declines in DO over this period include reduced DO concentrations in the artesian inflow to the springs and/or increased community respiration in the spring boil and spring run (Munch et al. 2006). A possible explanation for lower DO concentrations in the artesian inflow may be that the percentage of inflow contributed to the spring discharge of the older lower Floridan Aquifer water has been increasing (Toth and Katz 2006).

Silver Springs has also been a focal point of numerous studies on springs ecology. In the 1950's H. T. Odum studied water quality, productivity, ecosystem structure and energy flows in Silver Springs over a period of 5 years (Odum 1957b). A second ecological study was conducted approximately 25 years later by Robert L. Knight using many of the methods originally employed by Odum (Knight 1980; Knight 1983). In addition, Knight also conducted mesocosm experiments testing the importance of consumers for ecosystem control and maintenance. From 2003-2005, a repeat of Odom's 1957 study of the ecology of Silver Springs was conducted by the St. Johns River Water Management District and the University of Florida to assess land use and water quality changes in Silver Springs and develop possible cause-and-effect relationships to explain changes in the springs ecology (Munch et al. 2006). Results of this retrospective study compared to the earlier studies are summarized below.

- Strap-leaf Sagittaria (*Sagittaria kurziana*) was the dominant submersed aquatic plant in Silver Springs over the 1955-2005 50-year study period and remains a main ecological component of the ecosystem today.
- While biomass estimates for submersed aquatic plants in the summer remained stable, winter biomass estimates in 2004–2005 were 31 % lower than in the 1950s.
- Summer epiphyte community biomass increased approximately 300 % between the 1950s and the early 2000s. The largest change in estimates of primary producer biomass were due to an increase in benthic algal mat biomass. Benthic algal mats were dominated by the blue-green algae *Lyngbya wollei* (Quinlan et al. 2008). The xanophyte *Vaucheria* was also found in mats in certain regions of the springs. While Odum discounted the contribution of benthic algal mats to the primary producer community, Munch (2006) and Quinlan et al. (2008) reported biomass estimates of the benthic algal mats were similar to biomass estimates for epiphytes and submersed aquatic plants. However, due the considerable spatial variation observed in the primary producer communities, long-term comparisons of system-wide primary producer biomass should be viewed cautiously (Quinlan et al. 2008).
- The dominant species and species richness of birds, fish, and reptiles in Silver Springs remained similar over the 50-year study period. However, estimated total fish biomass in 2004–2005 declined 96 % since the 1950s and 61 % since the 1970s. These declines were due to large reductions in the biomass of Channel Catfish (*Ictaluras punctatus)*, Striped Mullet (*Mugil cephalus*), and Gizzard Shad (*Dorosoma cepedianum*). Likely, construction of Kirkpatrick Dam on the Ocklawaha River downstream of Silver Springs had a significant impact of the species changes observed by preventing upstream migration of fishes from the St. Johns River to Silver Springs.
- Measured daily emergence rates of aquatic insects declined about 72 % over the 50-year study period.
- Over the 50-year study period annual gross primary productivity declined around 27 % while community respiration declined around 26 %. Resulting net community primary productivity declined about 59 %.

1.2.3 Alexander Springs

Alexander Springs is a 1st magnitude spring located approximately 59 km east of Ocala Florida, or approximately 50 km east of Silver Springs (Scott et al. 2002; Scott et al. 2004). Alexander Springs discharges from a conical depression in a large spring pool; its spring run, Alexander

Springs Creek, then flows east about 13 km before reaching the St. Johns River. Because of Alexander Springs' relatively unimpacted conditions, and many natural attributes, the spring boil and the spring run are both regionally important destinations for swimming, canoeing, kayaking and other recreation. In addition, Alexander Springs is the only 1st magnitude spring in Florida in the federal parks system (Scott et al. 2004). From 1998–2002 the number of annual visitors to the springs ranged between 70,000 to 80,000 and its estimated economic value to the local economy was around $ 4.5 million annually (Bonn 2004). Alexander Springs has been designated by the state as both an OFW and Outstanding Florida Spring. Florida Statute requires the adoption of minimum flows and levels for Outstanding Florida Springs by 1 July 2017 (Freese and Sutherland 2017).

The Alexander Springs watershed covers an area of approximately 260 km^{-2} (100 square miles) (Shoemaker et al. 2004). Most of the springshed is forested (Freese and Sutherland 2017). From 1931–2016 the average discharge from Alexander Springs was 2.9 $m^3 s^{-1}$ (102 cfs) and ranged from 1.7–5.7 $m^3 s^{-1}$ (60-202 cfs) (Freese and Sutherland 2017). Trend analyses indicate that Alexander Springs flows have remained relatively stable over at least the last 30 years lacking the negative temporal trend that has been observed for other spring systems (Walsh et al. 2009; Freese and Sutherland 2017).

Alexander Springs discharge is high in sodium chloride, likely because it originates from vertical upconing of water from the Lower Floridan Aquifer (Toth and Katz 2006; Walsh et al. 2009). Water samples collected in 2001 from Alexander Springs represented a mixture containing about 30% water from the Lower Floridan Aquifer and 70% water from the Upper Floridan aquifer that had a mean age of about 15 years (Toth and Katz 2006).

Nutrient concentrations in Alexander Springs discharge are low. Over the past 30 years the mean NO_3-N concentration has been < 0.05 mg L^{-1}, whereas total phosphorous concentrations averaged < 0.06 mg L^{-1} (Walsh et al. 2009; Freese and Sutherland 2017). Since 1990, calcium, magnesium and potassium concentrations have exhibited slightly increasing trends in Alexander Springs, indicating longer water contact time with the rock matrix of the Upper Floridan Aquifer and potentially older water (Freese and Sutherland 2017). The median DO concentrations in Alexander Springs discharge was around 2.1 mg L^{-1} (Walsh et al. 2009).

Few studies on the flora and fauna of Alexander Springs have been conducted. Walsh et al. (2009) provides information on macroinvertebrates and fishes from surveys conducted in 2007. Mattson and Lehmensiek (2010) reported on vegetation and algal mapping and monitoring efforts conducted on Alexander Springs run from 2007 to 2010. They estimated that overall, about 57% of the Alexanders Springs run was covered by submersed aquatic vegetation. Dominant plant taxa were eelgrass (*Vallisneria Americana*) and southern naiad (*Najas guadalupensis*). Southern naiad was generally found only in the upper portion of the spring run. Algal cover was also dense in in the upper reaches of Alexander Springs. Dominant genera were the filamentous green algae *Oedogonium* and *Spirogyra* and the diatom *Pleurosira laevis*. The most abundant cyanobacteria genera present were *Lyngbya* and *Oscillatoria* spp.

1.2.4 Responses to Declining Spring Health

In 1999, in response to public concern over the declining health of Florida Springs, the Florida Department of Environmental Protection (FDEP) formed a Springs Task Force consisting of 16 scientist, planners, and citizens, to investigate causes of springs degradation and outline potential policy and management responses to facilitate springs protection and restoration. In 2000, this task force published a guiding document that identified a wide variety of strategies to protect springs encompassing outreach, information, management, regulation and funding approaches (FSTF 2000). In 2001, Governor Jeb Bush established the Florida Springs Initiative which has provided over 15 million dollars in funding for research, monitoring, education, and landowner assistance to improve spring water quality and flows (FDEP 2006). In addition, using the principles and strategies developed in the task force report the Florida Department of Community Affairs (FDCA) and DEP developed a guidebook to provide technical assistance to local governments to help them protect springs that fell within their jurisdiction (FDCA 2008). This guide provided information local governments could use to protect springs through amending their comprehensive plan and land development regulations.

In 2016, the Florida legislature passed the Florida Springs and Aquifer Protection Act (FSAPA), which provides a framework for restoring and protecting Florida springs and the Floridan aquifer. The legislature also passed the Legacy Florida Act that earmarked a minimum of one billion dollars to be spent on springs protection and restoration over a 20-year period. This increase in state funding will leverage regional and local dollars to fund a multitude of in-ground projects that will benefit both the aquifer and the springs.

FSAPA designated thirty-nine Outstanding Florida Springs (OFS) and established specific deadlines for establishing Minimum Flows and Levels (MFLs) for these springs. MFLs establish minimum flows and/or water levels for a spring below which further reductions would significantly harm the water resources or ecology of the area. Per FSAPA, FDEP or the Water Management Districts (WMDs) were required to establish MFLs for these designated springs by 1 July 2017. In addition, if at any time over the next 20 years an OFS is not expected to meet its MFLs, then a recovery or prevention strategy must be judiciously enacted by FDEP or the appropriate WMD to ensure the MFL is met. The FDEP and the WMDs must also establish 5-, 10-, and 15-year milestones for meeting the adopted MFLs. Each individual WMD's consolidated annual report must also include a 5-year comprehensive work plan listing upcoming projects aimed at protecting springs. This will allow timely disclosure of future funding needs. (Abrahams and Fitzgerald 2016).

FSAPA also re-addressed regulatory measures intended to protect OFS and their watersheds from nutrient pollution. Examples include: Basin Management Action Plans (BMAPs) designed to ensure that necessary nutrient load reductions to impaired OFS must in place by 1 July 2018; in areas where septic tanks are a significant contributor to nutrient loading, BMAPs must also include a detailed septic tank remediation strategy; and local governments within an OFS springshed were required to adopt the Florida model fertilizer ordinance by 1 July 2017 (Abrahams and Fitzgerald 2016).

FSAPA further mandates that FDEP delineate a Priority Focus Area (PFA) for each impaired OFS. PFAs are the areas where the aquifer is more vulnerable to inputs of nutrients and other

pollutants and there is a groundwater connection to the spring. Under FSAPA, certain activities are forbidden within these PFAs. Examples include: wastewater treatment facilities with permitted capacities exceeding 100,000 gallons per day must meet advanced wastewater treatment standards; new septic tanks on lots smaller than one acre are prohibited if they conflict with an established BMAP remediation strategy; all new agricultural operations must implement best management practices (BMPs); hazardous waste disposal sites are prohibited; and land application of biosolids and partially treated wastewater must minimize pollutant discharge (Abrahams and Fitzgerald 2016).

Since the release of the Florida Springs Task Force report in 2000, there have been numerous plans developed and projects proposed and implemented to reduce NO_3 loading to Florida springsheds (Loper et al. 2005; FDEP 2006; FDCA 2008; SWFWMD 2008; SWFWMD 2015; Brown 2016; Chaisson et al. 2016; Fitzgerald and Dobberfuhl 2016). The focus of these efforts was driven in large part by the assumption that increased NO_3-N has been responsible for the increase in algae and loss of submersed aquatic vegetation that has been observed in many Florida springs (Cowell and Dawes 2004; Stevenson et al. 2007; Albertin 2008; Harrington et al. 2010). In general, literature on stream and lake eutrophication supports this assumption (Dodds et al. 2002; Dodds 2006; Schindler 2006; Smith 2006; Dodds 2007). However, other studies have reported results that are inconsistent with this NO_3-N enrichment hypothesis (Odum 1957a; Canfield and Hoyer 1988; Duarte and Canfield Jr. 1990; Cowell and Botts 1994; Heffernan et al. 2010). In addition, an extensive review of existing literature on Florida springs concluded that attempting to link nutrient enrichment of springs directly to algal proliferation was tentative at best (Brown et al. 2008). More recent research suggests complex feedback mechanisms likely influence the eutrophication process and algal growth and proliferation (Heffernan et al. 2010). These mechanisms include direct physical effects of flow (Odum 1957a; Quinlan et al. 2008; King 2014), light limitation (Odum 1957a; Duarte and Canfield Jr. 1990), competitive interactions with vascular plants (Doyle and Smart 1998; Chen et al. 2007), abundance of grazers (Dormsjo 2008; Liebowitz et al. 2014), dissolved oxygen (Duarte and Canfield Jr. 1990; Munch et al. 2006; Dormsjo 2008; Heffernan et al. 2010), episodic flow reversals (Hensley and Cohen 2017), recreational use (Mumma et al. 1996), and invasive plant management (Evans 2008). While anthropogenic nitrogen enrichment is widely accepted to be a cause of algal proliferation in springs and reductions in nitrogen into the aquifer are certainly warranted, alternative hypotheses other than nitrogen enrichment alone need to be more thoroughly evaluated (Heffernan et al. 2010).

1.2.5 The Collaborative Research Initiative on Springs Protection and Sustainability (CRISPS)

The physical, chemical, and biological status of springs is affected by surface water hydrology, groundwater hydrology, land use, soils, geology, nutrient transformations and transport in the groundwater system, and biological interactions. Therefore, CRISPS included applied and foundational science, spanning various environmental drivers that influence spring hydrology, hydrodynamics, biogeochemical cycling of elements, water quality, and primary producer community structure and function.

There were three primary research objectives addressed by the CRISPS:

1. **To improve the scientific foundation for management of nitrate [NO_3] loading to the Silver Springs system.**

Research associated with this objective was needed to enhance our current understanding of: 1) the spatial variation in hydrologic conveyance to the spring system; 2) to identify the important sources of nitrogen to the springs (both rates and forms); and 3) to better understand nitrogen transformations and loss rates in soils and shallow aquifers.

2. **To evaluate whether reduction of NO_3 alone will be sufficient to restore the balance between benthic filamentous algae and native aquatic plants.**

Research associated with this objective is needed to better understand relationships between NO_3 and benthic algal abundance and other ecological attributes of the springs ecosystem.

3. **To assess the relative influence and manageability of factors other than NO_3 as drivers controlling primary producers.** NO_3

Research associated with this objective is needed to better understand other physicochemical and physical factors that affect the abundance of both native aquatic plants and benthic filamentous algae.

To address the complexity of the research objectives, the research team was organized into (1) Springshed and (2) Springs Ecosystem Supergroups that worked together cooperatively. The Springshed Supergroup consisted of smaller separate workgroups addressing groundwater hydrology, nitrogen transport and nitrogen transformations. The Springs Ecosystem Supergroup consisted of smaller workgroups addressing spring system hydrodynamics/hydraulics, nitrogen dynamics and metabolism, NO_3 inhibition of submersed aquatic vegetation, potential effects of hypoxia on invertebrate herbivores, benthic sources and sinks of nutrients, and trophic interactions within the springs ecosystem.

1.3 SPRINGSHED SUPERGROUP

The Springshed Supergroup focused on loads of nutrients, especially nitrogen, in surface water and groundwater and nitrogen biogeochemistry (input rates and forms, transformations, losses, and transport). Outputs constitute spatial and temporal variation in hydrologic and nutrient loads to the Floridan Aquifer and springs. Springshed hydrologic and nutrient outputs were expected to be related to variation in rainfall, temperature, season, nitrogen input rates and forms, soil types, and land use and land cover. Importantly, the significance of flows in conduits/fractures and transformation, loss, and transport of nitrogen through the groundwater system was investigated to improve groundwater modeling.

1.3.1 Groundwater Hydrology: Conduit and Fracture Flow Modeling

The purpose of this project is to incorporate representative realizations of conduits and fractures into the local-scale Silver Springshed equivalent porous media model to systematically explore the relative importance of conduit/fracture geometry and porous matrix properties on predicting the sources, fluxes, travel paths and travel times of water and solutes to Silver Springs. (Graham

et al., this volume). Results of this effort will help determine whether it is important for the S JRWMD to incorporate conduits into their models of the Silver Springshed to make management decisions.

1.3.2 Springshed Hydrology: Nitrogen Transport and Loss

In this project, field measurements from wells within the springshed were collected to identify portions of the aquifer that contribute most significantly to water flow and solute flux to Silver Springs (Jawitz et al. this volume). The goals of this work will provide field-measured hydrogeologic data that can be used for active resource management in the Silver Springs springshed. *In situ* measurements were also conducted to identify portions of the aquifer that contribute most significantly to water flow and solute flux to the spring. These measurements were used to determine flow characteristics and natural attenuation of solute loads with special emphasis on NO_3-N.

1.3.3 Springshed Biogeochemistry: Nitrogen Transformations

In addition to water delivery, biogeochemical transformations of N species in soils and shallow aquifers determine how much nitrate enters the Floridan Aquifer. The goal of this project was to trace nitrogen from sources within the springshed through the vadose zone and aquifer to discharge at the spring vent (Inglett et al., this volume). Three main approaches were used. First, nitrogen sources and attenuation in the surface system were assessed through analysis of nutrient composition and rates of denitrification in soil and vadose zone profiles. Second, composition of nutrients in groundwater, ratios of stable isotopes for nitrate, and dissolved gases were monitored in wells throughout the springshed to assess large-scale patterns of denitrification within the aquifer and determine the potential pathways involved. Lastly, ratios of stable isotopes for nitrate and dissolved gases were monitored seasonally at the spring vents to determine the over-all potential for denitrification within the aquifer as well as any seasonal variation which may be taking place. Statistical analysis of dissolved gases and denitrification indicators with groundwater geochemistry will identify specific zones in the springshed with high potential for denitrification. Additional soil-based work will derive a relationship for surface nitrogen attenuation through denitrification based on nitrogen loading level, moisture content, and temperature. Measurements of boron isotopes will be applied to help identify and disentangle nitrate isotopic signatures in groundwater where manure and sewage inputs are likely. Age dating of ground waters will facilitate our understanding of hydrologic flow path for calculation of nitrate transport in the aquifer and identification of denitrification hotspots, particularly those involving mixing of deep, older groundwater.

1.3.4 Springs Ecosystem Workgroup

The Springs Ecosystem Supergroup worked to develop a set of related hydrodynamic, biogeochemical, and biological models of the Silver Springs ecosystem. These models can simulate the effects of inputs from the groundwater and watershed models on various attributes of the physiochemistry of the springs such as flow rate and velocities, depths, nutrient concentrations, photosynthetically active radiation, and dissolved oxygen concentrations. Spatial and temporal variation in physicochemical attributes are used in mechanistic, empirical, or mixed models to evaluate their effects on primary producers. Potential effects of biological drivers, such as density of benthic algal grazers, on primary producers were also considered. Based on

physicochemical and biological forcings, the relative potential influences of the various drivers on primary producers was assessed.

1.3.5 Hydraulics and Hydrodynamics

The purpose of this project was to: 1) develop a more thorough understanding of water velocity and residence time distributions in the channel of Silver River and to quantify the location and magnitude of transient storage and exchange, 2) identify critical shear stresses for the entrainment and detachment of algae; and 3) link study findings to ongoing 3-D modeling to elucidate potential impacts of submerged aquatic vegetation on water velocities, residence times, and stage-discharge relationships (Kaplan et al , this volume).

1.3.6 Nitrogen Dynamics and Metabolism

In this project, the hypotheses that elevated NO_3-N explains increasing algal abundance and declining health across springs was evaluated (Cohen et al., this volume). First, high resolution time series data for pH, dissolved oxygen, nitrate, and phosphate were collected to estimate open-channel ecosystem metabolism and autotrophic nutrient uptake along the Silver River and along Alexander Springs Creek. This allowed direct comparisons between two springs with dramatically different nitrate concentrations (high and low concentration springs, respectively). Second, algal and SAV cover, along with a suite of hydraulic, edaphic and ecological variables, were sampled along the entire length of the Silver River to examine causes for variations in primary producer community structure. Third, benthic chambers were deployed in both spring run streams to measure ecosystem metabolism (from continuous DO measurements) in response to factorial nutrient additions (N, P, Fe). Control chambers were further instrumented with continuous nitrate sensors to explore nitrogen uptake kinetics below ambient concentrations. Finally, SAV growth was evaluated in both the Silver River and Alexander Springs Creek at 16 sites that spanned a broad range of benthic conditions relating to algal cover, sediment properties, and physical factors such as light and velocity.

1.3.7 NO_3 Inhibition of Submersed Aquatic Vegetation (SAV)

The primary purpose of this project was to evaluate the potential for NO_3-N concentration to inhibit the growth of SAV (Osborne et al., this volume). Mesocosm studies were conducted to evaluate changes in the root to shoot ratios, leaf blade elongation rates, tissue protein, enzyme activity, and abundance of starch storage in tissues of the two dominant species of SAV, *Vallisneria americana* and *Sagittaria kurziana* subjected to varying NO_3 concentrations. In addition, field assessment of nitrate reductase activity (NRA) across several springs was initiated to determine the naturally occurring range of this enzyme in SAV tissue and its relationship to concentrations of NO_3-N.

1.3.8 Potential Hypoxia Effects on Invertebrate Herbivores

In this project, respirometry studies were conducted to investigate the potential role of hypoxia in extirpating invertebrate herbivores in the Silver River (Osborne et al., this volume).

1.3.9 Benthic Sources and Sinks of Nutrients

Bottom sediments of streams act as biogeochemical reactors that change the chemical compositions of pore water and cause them to differ from the overlying stream water. Biogeochemical reactions could thus provide an important source of solutes to stream water and

affect benthic and lotic ecosystems of the Silver River. The goals of this project were to: 1) evaluate bottom sediment distributions and chemical compositions in the Silver River, 2) measure physical and hydraulic characteristics of the sediment, 3) assess the biogeochemical reactions in the sediment and their impacts on pore water compositions, and 4) estimate potential impacts of fluxes of solutes between bottom sediment and the river (Martin et al., this volume).

1.3.10 Trophic Interactions within the Spring Ecosystem

Ratios of stable carbon and nitrogen isotopes ($\delta^{13}C$ and $\delta^{15}N$) were used as natural tracers to identify pathways of energy flow and material transport within the Silver Springs and Silver River ecosystem (Frazer et al, this volume). Of interest was the use of stable isotope signatures to discriminate among primary producers supporting the Silver River food web and to determine the fate of benthic filamentous algae. Insights into spring food webs help to refine our understanding of predation and top-down pressures on community dynamics within spring ecosystems. This work element also included laboratory mesocosm work to study algal growth rates and grazing rates of selected small grazers, and including a field enclosure survey to evaluate potential for grazer control of algae.

The purpose of this final report is to present the research methods, data analyses, and conclusions of the CRISPS effort. Following this introductory chapter, individual chapters are presented for each of the workgroups beginning with groundwater hydrology and ending with biotic interactions. The FDEP and SJRWMD have multiple regulatory and programmatic tools that can be applied to aid in improving impaired springs. The use of these tools depends on acquiring the best available science to make the most informed cost-effective management decisions and determine those management activities that have the greatest chance for success. Results from the CRISPS research will facilitate implementing these future management and regulatory actions.

1.4 REFERENCES

Abrahams, N., and Fitzgerald, C. 2016. Florida Spring Restoration: The Time is Now! 2016 Legislative and Funding Advances. Water Resources Impact 18(6):10-11.

Albertin, A. R. 2008. Nutrtient dynamics in Florida springs and relationships to algal blooms. Ph.D. Dissertation. University of Florida, Gainesville, FL. 156 pp.

Bonn, M. A. 2004. Visitor profiles, economic impacts and recreational aesthetic values associated with eight priority Florida springs loacted within the St. Johns River Water Management District. St. Johns River Water Management District. Special Publication SJ2004-SP35, Palatka, FL.

Bonn, M. A., and Bell, F. W. 2003. Economic impact of selected Florida springs and surrounding local areas Florida Department of Environmental Protection Florida Springs Task Force Special Report, Tallahassee, FL. .

Brown, A. 2016. Springs of the Suwannee: working together for water solutions. Water Resources Impact 18(6):27-29.

Brown, M. T., and coauthors. 2008. Summary and syntheses of the available literature on the effects of nutrients on spring organisms and systems. University of Florida Water Institute, Gainesville, FL.

Bush, P. W., and Johnston, R. H. 1988. Ground-water hydraulics, regional flow, and ground-water development of the Floridan aquifer system in Florida and in parts of Georgia, South Carolina, and Alabama. U. S. Geological Survey Professional Paper 1403 80 pp. <https://pubs.er.usgs.gov/publication/pp1403C > (Accessed 03/20/2017).

Butt, P., and Ally, A. 2006. Silver Springs vent documentation and geocehmical characterization St. Johns River Water Management District Special Publication SJ2008-SP6. Palatka, FL.

Camargo, J. A., and Alonso, A. 2006. Ecological and toxicological effects of inorganic nitrogen pollution in aquatic ecosystems: a global assessment. Environment International 32(2006):831-849.

Canfield, D. E., and Hoyer, M. V. 1988. Influence of nutrient enrichment and light availability on the abundance of aquatic macrophytes in Florida streams. Canadian Journal of Fisheries and Aquatic Sciences. 45:1467-1472.

Chaisson, L., Chelette, A., and Thorpe, P. 2016. Spring restoration and protection in urban and rural landscapes. Water Resources Impact 18(6):18-21.

Chen, C., Yin, D. Q., Yu, B. and Zhu, H. K. 2007. Effect of epiphytic algae on photosynthetic function of Potamogeton crispus. Journal of Freshwater Ecology 22(3):411-420.

Copeland, R., Doran, N. A., White, A. J., and Upchurch, S. B. 2009. Regional and Statewide Trends in Florida's Spring and Well Groundwater Quality (1991-2003). Florida Geological Survey Bulletin Number 69., Tallahassee, FL.

Cowell, C. B., and Botts, P. S. 1994. Factors infleuncing the distribution, abundance and growth of *Lyngbia wollei* in central Florida. Aquatic Botany 49:1-17.

Cowell, C. B., and Dawes, C. J. 2004. Growth and nitrate-nitrogen uptake by the cyanobacterium *Lyngbia xollei*. Journal of Aquatic Plant Management 42:69-71.

Crum, L. J. 1954. The Ocklawaha River. MS Thesis. Florida State University, Tallahassee, Fl. .

Dodds, W. K. 2006. Eutrophication and trophic state in rivers and streams. Limnology and Oceanography 51(1):671-680.

Dodds, W. K. 2007. Trophic state, eutrophication and nutrient criteria in streams. Trends in Ecology & Evolution 22(12):669-676.

Dodds, W. K., Smith, V. H., and Lohman, K. 2002. Nitrogen and phosphorus relationships to benthic algal biomass in temperate streams. Canadian Journal of Fisheries and Aquatic Sciences 59(5):865-874.

Dormsjo, K. 2008. Oxygen Mediated Grazing Impacts in Florida Springs. University of Florida, Gainesville, FL. 69 pp.

Doyle, R. D., and Smart, R. M. 1998. Competetive reduction of noxious *Lyngbia wollei* mats by rooted aquatic plants. Aquatic Botany 61:17-32.

Duarte, C. M., and Canfield Jr., D. E. 1990. Macrophyte standing crop and primary productivity in some Florida spring runs. Water Resources Bulletin 26(6):927-934.

Evans, J. 2008. Ecosystem implications of invasive aquatic plants and aquatic plant control in Florida springs. Pages 249-270 *in* M. T. Brown, editor. Summary and syntheses of available literature on the effects of nutrients on springs organisms and systems. Florida Department of Environmental Protection, Tallahassee, FL. .

FDCA (Florida Department of Community Affairs). 2008. Protecting Florida's springs: an implementation guidebook. Florida Department of Community Affairs, Tallahassee, FL.

FDEP (Florida Department of Environmental Protection). 2006. Florida springs initiative achievements. Available: <http://www.dep.state.fl.us/springs/initiative.htm> (Accessed 5/17/2017).

FDEP (Florida Department on Environmental Protection). 2017. Outstanding Florida waters. Available: <http://www.dep.state.fl.us/WATER/wqssp/ofw.htm.> (Accessed 04/20/2017).

Fitzgerald, C., and Dobberfuhl, D. 2016. Springs Protection Initiative: Solving scientific mysteries and developing effective solutions. Water Resources Impact 18(6):12-15.

Freese, R., and Sutherland, A. B. 2017. Minimum flow determination for Alexander Springs Lake County, Florida. St. Johns River Water Management District Technical Publication SJ2017-XX DRAFT, Palatka, FL.

FSTF (Florida Springs Task Force). 2000. Florida's springs strategies for restoration and protection. Florida Department of Environmental Protection, Tallahassee, FL.

Harrington, D., Maddox, G., and Hicks, R. 2008. Florida springs initiative monitoring network report 2008. Florida Department of Environmental Protection, Tallahassee, FL.

Harrington, D., Maddox, G., and Hicks, R. 2010. Florida springs initiative monitoring network report and recognized sources of nitrate. Florida Department of Environmental Protection, Tallahassee, Fl.

Heffernan, J. B., Liebowitz, D. M., Frazer, T. K., Evans, J. M., and Cohen, M. J. 2010. Algal blooms and the nitrogen-enrichment hypothesis in Florida springs: evidence, alternatives, and adaptive management. Ecological Applications 20(3):816-829.

Hensley, R. T., and Cohen, M. J. 2017. Flow reversals as a driver of ecosystem transition in Florida's springs. Freshwater Science 36(1):14-25.

Hicks, R., and Holland, K. 2012. Nutrient TMDL for Silver Springs, Silver Springs Group, and Upper Silver River (WBIDs 2772A, 2772C, and 2772E). November 2012. . Florida Department of Environmental Protection, Tallahassee, FL.

Katz, B. G. 2004. Sources of nitrate contamination and age of water in large karstic springs of Florida. Environmental geology 46:689-706.

Katz, B. G., and Griffin, D. W. 2008. Using chemical and microbiological indicators to track the impacts from the land application of treated municipal wastewater and other sources on groundwater quality in a karstic springs basin. Environmental geology 55(4):801-821.

King, S. A. 2014. Hydrodynamic control of filamentous macroalgae in a sub-tropical spring-fed river in Florida, USA. Hydrobiologia 2014(734):27-37.

Knight, R. L. 1983. Energy basis of ecosystem control at Silver Springs, Florida. Pages 161-79 *in* T. D. Fontaine, and S. M. Bartell, editors. Dynamics of Lotic Systems. Ann Arbor Science Publishers, Ann Arbor, MI.

Knight, R. L. 1980. Energy basis of control in aquatic ecosystems. Ph. D. Dissertation. University of Florida, Gainesville, FL.

Knowles, L., Katz, B. G., and Toth, D. J. 2010. Using multiple chemical indicators to characterize and determine the age of groundwater from selected vents of the Silver Springs Group, central Florida, USA. Hydrogeology Journal 18(8):1825-1838.

Lee, Y. W., Dahab, M. F., and Bogardi, I. 1992. Nitrate Risk Management under Uncertainty. Journal of Water Resources Planning and Management-Asce 118(2):151-165.

Liebowitz, D. M., Cohen, M. J., Heffernan, J. B., Korhnak, L. V., and Frazer, T. K. 2014. Environmentally-mediated consumer control of algal proliferation in Florida springs. Freshwater Biology 59(10):2009-2023.

Loper, D. W., Landing, W., Pollman, C., and Hilton, A. C. 2005. Degradation of water quality at Wakulla Springs, Florida: assessment and recomendations. Florida Department of Environmental Protection, Tallahassee, FL.

Marella, R. L., and Berndt, M. P. 2005. Water withdrawals and trends from the Floridan aquifer system in the southeastern United States, 1950-2000, U. S. Geological Survey Circular 1278 20 pp. <http://pubs.er.usgs.gov/publication/cir1278 > (Accessed 03/07/2017).

Martin, R. A. 1966. Eternal Spring: Man's 10,000 Years of History at Florida's Silver Springs. Greta Outdoors Press Incorporated, St. Petersburg, FL.

Mattson, R. A., and Lehmensiek, M. 2010. Mapping and monitoring of submersed aquatic vegetation and macroalgae in spring run streams of the middle St. Johns River and Lake George Basins. St. Johns River Water Management District, Unpublished Report, Palatka, FL.

Mattson, R. A., and Means, G. H. 2016. A Florida springs primer. Water Resources Impact 18(6):6-8.

Mattson, R. A., Lehmensiek, M., and Lowe, E. F. 2007. Nitrate toxicity in Florida springs and spring-run streams: A review of the literature and its implications. St. Johns River Water Management District Professional Paper SJ2007-PP1, Palatka, FL.

Miller, J. A. 1990. Ground Water Atlas of the United States Alabama, Florida, Georgia, and South Carolina. U. S. Geologica Survey Hydrologic Investigation Atlas HA 730-G <https://pubs.usgs.gov/ha/ha730/ch_g/G-text6.html> (Accessed 3/21/2017).

Miller, J. A. 1997. Hydrogeology of Florida. Pages 69-88 *in* A. F. Randazzo, and D. S. Jones, editors. The Geology of Florida. University of Florida Press, Gainesville, FL.

Mumma, M. T., Cichra, C. E., and Sowards, J. T. 1996. Effects of recreation on the submersed on the submersed aquatic plant community of the Rainbow River, Florida. Journal of Aquatic Plant Management 34:53-56.

Munch, D. A., and coauthors. 2006. Fifty-year retrospective study of the ecology of Silver Springs, Florida. St. Johns River Water Management District Special Publication SJ2007-SP4, Palatka, FL.

Odum, H. T. 1957a. Primary production measurements in eleven Florida springs and a marine turtle-grass community. Limnology and Oceanography 2(2):85-97.

Odum, H. T. 1957b. Trophic Structure and Productivity of Silver Springs, Florida. Ecological Monographs 27(1):55-112.

Phelps, G. G. 2004. Chemistry of groundwater in the Silver Springs basin, Florida, with an emphasis on nitrate. U. S. Geologic Survey Scientific Investigations Report 2004-5144, 54 pp.

Phelps, G. G., Walsh, S. J., Gerwig, R. M., and Tate, W. B. 2006. Characterization of the hydrology,water chemistry, and aquatic communities of selected springs in the St. Johns River Water Management District, Florida, 2004. U. S. Geologic Survey Scientific Investigations Report 2006-1107, 51 pp.

Quinlan, E. L., and coauthors. 2008. Primary producers and nutrient loading in Silver Springs, FL, USA. Aquatic Botany 88(3):247-255.

Schindler, D. W. 2006. Recent advances in the understanding and management of eutrophication. Limnology and Oceanography 51(1):356-363.

Scott, T. M., Means, G. H., Means, R. C., and Meegan, R. P. 2002. First magnitude springs of Florida. Florida Geological Survey Open File Report No. 85., Tallahassee, Florida.

Scott, T. M., Means, G. H., Meegan, R. P., Means, R. C., Upchurch, S., Copeland. R. E., Jones, J., Roberts, T. and Willet, A.. 2004. Springs of Florida. Florida Geological Survey. Bulletin No. 66., Tallahassee, FL.

Shoemaker, W. B., and coauthors. 2004. Comparison of estimated areas contributing recharge to selected springs in north-central Florida by using multiple ground-water flow models. US Geological Survey. Open File Report 03-448.

Smith, V. H. 2006. Responses of estuarine and coastal marine phytoplankton to nitrogen and phosphorus enrichment. Limnology and Oceanography 51(1):377-384.

Spechler, R. M., and Halford, K. J. 2001. Hydrogeology, water quality, and simulated effects of ground-water withdrawals from the Floridan Aquifer System, Seminole County and vicinity, Florida. U. S. Geological Survey Water-Resources Investigations Report -1-4182, 166 pages.

Stevenson, R. J., Pinowska, A., Albertin, A., and Sickman, J. O. 2007. Ecological conditions of algae and nutrients in Florida springs: the synthesis report. Department of Zoology, Michigan State University, East Lansing Michigan. Report prepared for the Florida Department of Environmental Protection, Tallahassee, FL.

Sutherland, A. B., and coauthors. 2017. Minimum flow determination for Silver Springs Marion County, Florida. St. Johns River Water Management District Technical Publication SJ2017-2, Palatka, FL.

SWFWMD (South West Florida Water Management District). 2015. 2015-2019 Springs Management Plan. Available: http://www.swfwmd.state.fl.us/publications/files/Springs_Management_Plan.pdf (Accessed 05/15/2017).

SWFWMD (Southwest Florida Water Management District). 2008. Rainbow River technical summary. Report by the Southwest Florida Water Management District, Brooksville, Florida.

Toth, D. J., and Katz, B. G. 2006. Mixing of shallow and deep groundwater as indicated by the chemistry and age of karstic springs (vol 14, pg 827, 2006). Hydrogeology Journal 14(6):1060-1080.

Walsh, S. J., Knowles Jr., L., Katx, B. G., and Strom, D. G. 2009. Hydrology, Water Quality, and Aquatic Communities of Selected Springs in the St. Johns River Water Management District, Florida. U. S. Geological Survey Scientific Investigations Report 2009-5046, Gainesville, FL.

Wolfe, A. H., and Patz, J. A. 2002. Reactive nitrogen and human health: Acute and long-term implications. Ambio 31(2):120-125.

Wynn, S., Borisova, T., and Hodges, A. 2014. Economic value of the services provided by Florida springs and other water bodies: a summary of existing studies. University of Florida Institute of Food and Agricultural Sciences Publication FE959, Gainesville, FL.

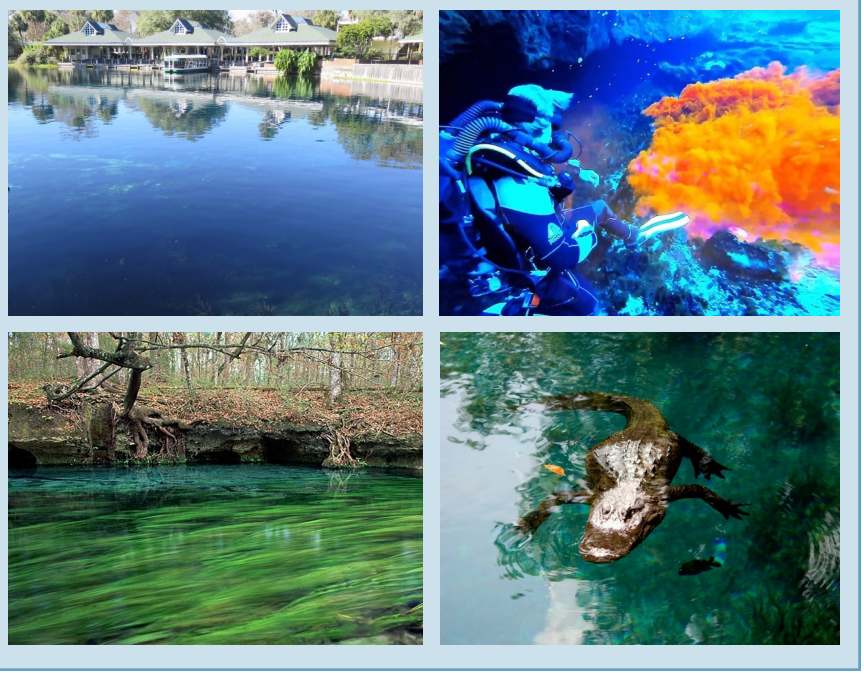

Collaborative Research Initiative on
Sustainability and Protection of Springs [**CRISPS]**

Section 2

[Work Order No: 4]

FINAL REPORT

2014 - 2017

submitted to:

St. Johns River Water Management District
Springs Protection Initiative [SPI], UF Contract # 27789

UF | UNIVERSITY of FLORIDA
Water Institute

C R I S P S

Section 2

GROUNDWATER HYDROLOGY

Conduit and Fracture Flow Modeling

Final Report 2017
Work Order No.4

Principal Investigators:

Wendy Graham, University of Florida
Patrick Burger, St. Johns River Water Management District

Project Team

Wendy Graham
Rob de Rooij
Wesley Henson
Agricultural and Biological Engineering
Water Institute,
University of Florida,

Patrick Burger
Douglas Hearn
St. Johns River Water Management District

This document reports findings and results of a work order for a 3-year project in compliance with Agreement between University of Florida (UF) and St. Johns River Water Management District (SJRWMD) UF Contract #27789. It is part of the *UF Collaborative Research Initiative on Springs Protection and Sustainability (CRISPS)* and supports the science component of *the SJRWMD Springs Protection Initiative (SPI).*

2.1.1 ABSTRACT

Physics-based distributed models for simulating flow and solute transport in karst aquifers are generally based on the discrete-continuum approach in which flow in the three-dimensional porous limestone matrix is coupled with flow in discrete one-dimensional conduits. In general, however, little is known about the geometry of conduit networks. To quantify and analyze the reliability of discrete-continuum models it is important to explore flow and transport behavior over an ensemble of possible karst conduit networks within a stochastic framework. This report documents a new methodology to generate a stochastic ensemble of possible karst conduit networks that honor what is known about the topography, geology, hydrology and climate of the system under study. The resulting hydrogeochemical model was used to simulate the widening of conduits over geological timescales, and subsequently to simulate flow and solute transport within an evolved karst aquifer representative of the Silver Springshed.

Morris Method Global Sensitivity Analysis showed that a limited combination of porous matrix properties and horizontal and vertical preferential flowpath (HPF and VPF) statistics produced karst conduit networks that generated first magnitude springflow rates (i.e., > 2.8 $m^3 s^{-1}$). Monte Carlo simulations of conduit generation, groundwater flow and conservative solute transport for conditions representative of the Silver Springshed showed that in addition to the statistics governing the distribution of VPFs and HPFs, the actual locations of VPFs and HPFs in relation to each other and the spring outlet determines whether a spring will develop. However, if a network developed, the uncertainty in the hydraulic and solute pulse response at the spring vent, and the locations of vulnerable regions within the springshed due to unknown locations of VPFs and HPFs, was minimal. The Monte Carlo simulation predicted large vulnerable regions of the idealized Silver Springshed (i.e., areas with peak solute travel times to the spring of less than 30 years) with low uncertainty. The spatial distribution of these vulnerable regions was quite different from that which would be identified using an equivalent porous media model. These results indicate that incorporating conduit flow processes that honor what is known about the topography, geology, hydrology and climate into the model is important, but that exact knowledge of conduit locations and orientations may be less important, for understanding springshed behavior. Further work to calibrate a Silver Springshed model that includes the ensemble of conduit geometries identified in this study is recommended.

2.1.2 BACKGROUND

Karst aquifers are highly heterogeneous due to the presence of conduits that have a higher permeability than the surrounding porous limestone matrix. Most models applied to the Floridan Aquifer are based on an equivalent porous medium formulation (Kuniansky 2016). Typically, these models simulate reasonable average values for spring flows and head contours by assigning relatively high hydraulic conductivities to certain model cells. Cells with a relatively high hydraulic conductivity may be placed along well-known conduits as illustrated by Kuniansky, (2016). Alternatively, if the conduit locations cannot be mapped, it is common to calibrate hydraulic conductivities to measured head values and spring flows. Typically this results in zones with elevated hydraulic conductivities. However, although such models can yield reasonable head contours and spring flows, the maximum flow velocities in the conduits will be underestimated. As such, these models may not accurately simulate solute transport.

Models based on the discrete-continuum approach may yield more accurate flow velocity fields for simulating solute transport. In such models conduits are explicitly represented as discrete one-dimensional features embedded in a porous limestone continuum (Kiraly 1984,1998; de Rooij et al. 2013; Shoemaker et al. 2008). However, the applicability and validity of discrete-continuum models is limited because, in general, little is known about the geometry of conduit networks. As a result, discrete-continuum modeling studies are often restricted to hypothetical karst systems Kiraly 1998; de Rooij et al. 2013). Modeling studies of hypothetical karst systems have proven to be useful for gaining insights into the hydrodynamic functioning of karst systems (Kiraly et al. 1995; Eisenlohr et al. 1997a) and for testing classical methods for spring hydrograph analysis (Eisenlohr et al. 1997a, 1997b).

2.1.2.1 Conduit Evolution Algorithms

A rigorous analysis of model uncertainty, originating from lack of knowledge about conduit network geometry, requires multiple model runs using an ensemble of possible karst conduit networks. Thus, there is a need for methodologies to generate realistic karst conduit networks. These methodologies may be based on process-imitating or structure-imitating approaches (Pardo-Iguzquiza et al. 2012). Process-imitating or speleogenetic approaches are based on models that simulate the evolution of conduits due to dissolution kinetics. To date, the main objective of speleogenetic models has been to study the evolution of the conduits (Kaufmann et al. 2010; Kaufmann 2003a, 2003b, 2009; Dreybrodt et al. 2010; Gabrovsek et al. 2010) and not to generate an ensemble of possible conduit networks. Structure-imitating approaches aim to reproduce the structure of the conduit network by empirical means without accounting for physical and chemical processes. For example, the structure-imitating approach proposed by Pardo-Iguzquiza et al. (2012) is based on re-sampling from templates to generate individual conduit sections, and a diffusion-limited aggregation method to join the conduit segments and generate the network topology. Ronayne (2013) used a non-looping invasion percolation model, proposed by Stark (1991), to generate conduit networks.

Structure-imitating approaches have the disadvantage that the empirical models require statistical information about the conduit network geometry that is often unavailable. Moreover, a drawback of many empirical models is that it is difficult to predict, a priori, overall topology of the resulting conduit network in terms of connectivity. For example, Pardo-Iguzquiza et al. (2012) simulate connectivity using a diffusion-limited aggregation method and information about the resulting network connectivity is only available after the simulation.

Pseudo-genetic approaches, that mimic speleogenetic processes without simulating actual dissolution processes, have been developed to generate conduit networks more efficiently by avoiding computations needed to simulate dissolution kinetics Borghi et al. (2012). Pseudo-genetic approaches define a heuristic erosion potential along preferential flow paths and an iterative process over which conduits are progressively widened. The pseudo-genetic approach proposed by Jaquet et al. (2004) is based on a modified lattice-gas automaton in which walkers with a certain erosion potential travel through the medium. Borghi et al. (2012), use a pseudo-genetic approach in which conduits are eroded iteratively along minimum effort pathways computed by a fast-marching algorithm. The methodology of Lafare (2012) generates conduits using a heuristic erosion potential function depending on the flow velocities and mean water ages.

Pseudo-genetic and pure speleogenetic approaches have a disadvantage in that they depend on boundary conditions that govern the evolution process. These boundary conditions ideally require the reconstruction of geological conditions during the formation of conduits, which is not always feasible. A related problem is that it is not clear when to stop the conduit generation process. Moreover, many pseudo-genetic and genetic models are not be capable of reproducing actual locations of known geologic features. However, considering that the topology of a conduit network is the result of dissolution processes, pseudo-genetic and genetic approaches are well-suited to reproduce realistic conduit networks in terms of connectivity. In particular, these approaches account for the positive feedbacks between flow and dissolution (Siemers and Dreybrodt 1998; Worthington and Ford 2009) as the conduits are being generated.

2.1.2.2 Global Sensitivity Analyses

Sensitivity analysis (SA) provides a mechanism to identify and prioritize influential model inputs, identify non-influential parameters so that they can be fixed to representative values, and calibrate model inputs to achieve desired model behaviors (Saltelli et al. 2004, Pappenberger et al. 2008). SA methods are highly useful for understanding models of complex non-linear systems, such as the coupled dissolution, transport and discrete continuum hydrological model used in this study. Robust SA techniques have been widely applied to hydrological models (van Griensven et al. 2006; Muñoz-Carpena et al. 2007; Pappenberger et al. 2008; Srivastava et al. 2014) and contaminant transport models (James and Oldenburg 1997; Pan et al. 2011).

Much research has documented the benefits and limitations of SA methods (Foglia et al. 2009, Nossent and Bauwens 2012, Herman et al. 2013, Li et al. 2013, Shin et al. 2013. The complexity of SA analyses ranges from one at a time sensitivity analysis (OAT-SA) to global sensitivity analysis (GSA). In OAT-SA, only one variable is changed and a response metric is evaluated relative to that change. The main difference between OAT-SA and GSA methods is that GSA methods account for non-linear interactions among parameters. This increased information from GSA methods comes at a computational cost, often requiring thousands of model executions.

An alternative to OAT-SA and full variance-based GSA are a subset of GSA methods called global screening methods (e.g., the Morris method, [Morris 1991; Campolongo et al. 2007]). The Morris method provides a more rigorous evaluation of model parameter importance than single variable OAT-SA methods. Global screening methods provide qualitative information about the effective parameters and interactions with significantly fewer model executions. While variance decomposition GSA methods like the method of Sobol (Sobol 2001) and the extended Fourier Amplitude Sensitivity Test (FAST) (Saltelli et al. 1999) provide detailed quantitative information about parameter contributions to uncertainty, recent studies have illustrated that the Morris method accurately identifies the non-influential and most sensitive model parameters with significantly fewer model executions (Confalonieri et al. 2010; Herman et al. 2013; Li et al. 2013; Srivastava et al. 2014).

To date, SA methods employed in most karst hydrologic and dissolution studies have focused on OAT-SA (Király and Morel 1976; Kaufmann and Braun 2000; Birk 2003; Scanlon et al. 2003; Kovács et al. 2005; Perrin et al. 2007; Doummar et al. 2012) and local sensitivity measures (Dafny et al. 2010; Mazzilli et al. 2012). Karst modeling using OAT-SA has been used to

evaluate the effect of properties of the porous matrix (e.g., hydraulic conductivity) and properties of well-defined conduit geometries (e.g., roughness, exchange parameters) on spring hydrograph baseflow recession (Király and Morel 1976; Eisenlohr 1996; Eisenlohr et al. 1997a; Cornaton 1999). Recently, OAT-SA of conduit conductivity and frequency was used to define two end members of karst domains: a conduit influenced flow regime (CIFR) where recession is controlled by the conductive capacity of the conduit system, and matrix restricted flow domain (MRFD) where recession is controlled by the low permeability porous matrix (Kovács et al. 2005). While previous studies have provided significant contributions to our understanding of how hydrograph baseflow recession relates to the geometric and permeability properties of karst aquifers, these studies employed simple 2-D models that did not consider turbulent flow within the networks.

2.1.2.3 Report Outline

In sections 2.1.3 through 2.1.5 of this this report, we present an efficient and versatile process-imitating speleogenetic methodology to generate conduit networks, adapted from the pseudo-genetic procedure presented by Borghi et al (2012). In section 2.1.6-2.1.8 we apply the model to an idealized Silver Springshed and present a Morris Method Global Sensitivity Analysis (MM-GSA) that investigates the most important parameters that influence how stochastically generated vertical preferential flowpaths (VPFs) and horizontal preferential flowpaths (HPFs) (i.e., paleokarst templates) evolve into karst conduit networks that create first magnitude springs (flow > 2.8 m^3 s^{-1}), and assesses hydrologic and transport pulse responses in the resulting evolved networks. In section 2.2, we present a Monte Carlo analysis to gain insight into the impact of conduit network uncertainty on flow and transport prediction uncertainty in the idealized Silver Springshed. Although conduit evolution and flow and transport responses are simulated in an idealized system, interpretation of flow and transport phenomena in the idealized system provides new information about the importance of incorporating vertical and horizontaly preferential flow path and the resulting conduit network uncertainty into hydrologic decision models.

2.1.3 CONDUIT GENERATION ALGORITHM

A schematic describing the process-imitating speliogenetic conduit generation framework is shown in Figure 2.1.1. Contrary to existing models that simulate karst genesis, our hydrogeochemical model is not intended primarily to study karst genesis. Instead we aim to generate conduit networks, with minimal computational effort on a relatively large regional scale, that honor known field conditions such as springs, sinkholes, fracture planes and bedding planes. Our ultimate goal is to use the model in a Monte Carlo framework to generate an ensemble of realistic conduit networks and evaluate the uncertainty of discrete-continuum model predictions of flow and solute transport in real-world systems when conduit geometries are imperfectly known.

The proposed methodology is sufficiently general to be applied to different hydrogeological settings. In this study, we apply the model to the Silver Springshed in North Central Florida (Figure 2.1.2). Silver Springs is a first-order magnitude spring that discharges from the Upper Floridian Aquifer. Previous efforts have modeled groundwater flow in the Silver Springshed using the equivalent porous medium MODFLOW model (HydroGeoLogic 2013). While these

equivalent porous media models reproduce reliable steady-state springflow rates and regional hydraulic head contours, they likely underestimate maximum flow velocities and may not accurately reproduce water and solute flowpaths because they do not account for the presence of conduits.

We assume that karst aquifers can be represented by one-dimensional conduits with a circular cross-section embedded in a porous limestone matrix. We consider physical and chemical processes within the conduits and the matrix. Some previous studies karst evolution studies have represented conduits as ducts having a rectangular cross-section. In these studies, the conduits are often referred to as fractures even when the fractures are represented by one-dimensional discrete features. Other studies have considered karst dissolution in a single two-dimensional fracture (Hanna and Rajaram 1998; Szymczak and Ladd 2009, 2011; Detwiler and Rajaram 2007; Pandey et al. 2014; Chaudhuri et al. 2013; Andre and Rajaram 2005).

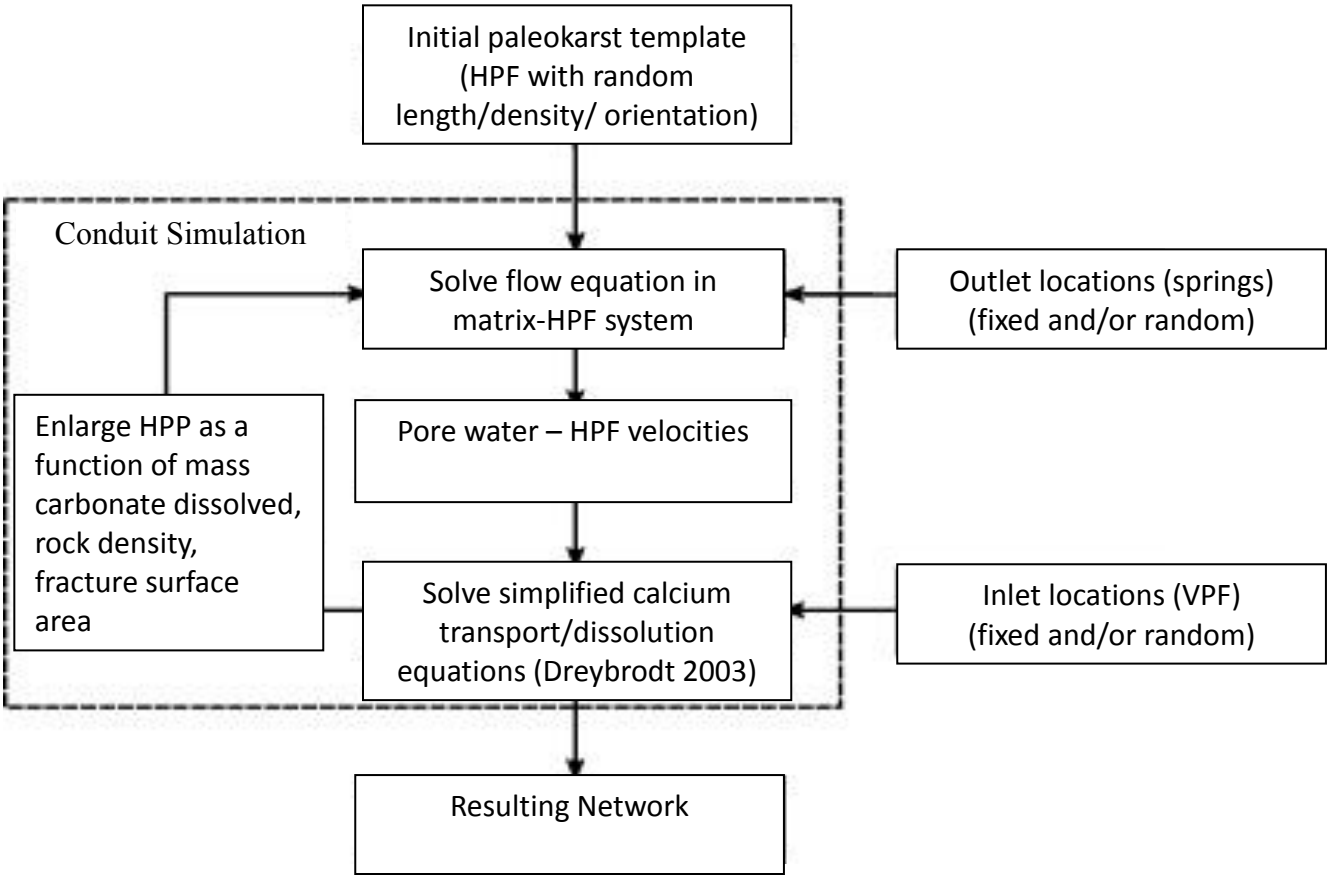

Figure 2.1.1. Conduit Evolution Algorithm, adapted from Borghi et al. (2012).

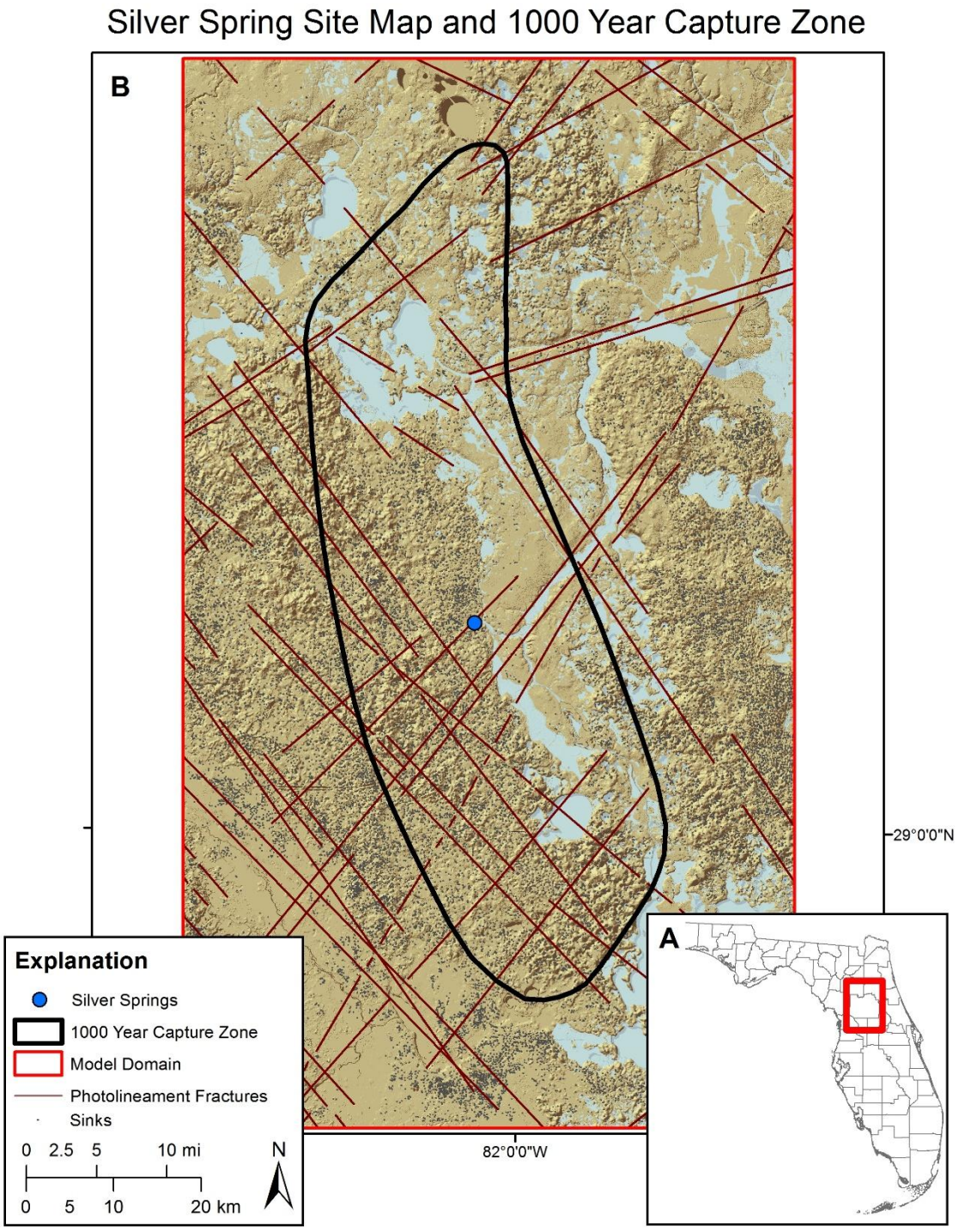

Figure 2.1.2. Silver Springshed site map showing A) location in Florida and B) Silver Springs (filled blue circle), 1,000-year spring groundwater capture zone (black outline), photolineament defined regional fracture sets, extensive sinks (black dots) and NDM –V4 model domain (red outline).

2.1.3.1 Flow and Reactive Solute Transport

Conduit flow is governed by the following mass-balance equation:

$$C_c \frac{\partial p}{\partial t} + \frac{\partial (vA)}{\partial s} + q_{c,O} - q_{c,I} + q_{c \to m} = 0 \tag{2.1.1}$$

where C_c is the capacity term for conduit flow [m], p the pressure head [m], v the velocity [m s^{-1}], A the cross-sectional area of flow [m^2], s the spatial coordinate in the direction parallel to the conduit [m], $q_{c \to m}$ a sink term associated with exchange from the conduit to the matrix [m^2 s^{-1}] and $q_{c,O}$ and $q_{c,I}$ are conduit sink and source terms [m^2 s^{-1}], respectively. The flow velocity v in the conduit equals Q/A.

Assuming laminar flow the conduit volumetric flux rate is given by the Poisseuille equation:

$$Q = -\frac{g \pi d^4 S_f}{128 \upsilon} \tag{2.1.2}$$

where d is the conduit diameter [m], g the gravitational acceleration constant [m s^{-2}], S_f is the friction slope [-]and υ the kinematic viscosity [m^2 s^{-1}]. In this study g = 9.81 m s^{-2} and $\upsilon = 10^{-6}$ m^2 s^{-1} were assumed. Turbulent flow in the conduits is often described by the Darcy-Weisbach equation. Using the friction factor from the Colebrook-White equation, the conduit volumetric flux rate can be expressed as:

$$Q = -0.965 d^2 \sqrt{g d S_f} \ln\left(\frac{\varepsilon}{3.7d} + \frac{1.78\upsilon}{d\sqrt{g d S_f}} \right) \tag{2.1.3}$$

where ε the rugosity [m] of the conduit surface, assumed in this study to be 10% of the conduit radius. Using the full-range pipe-flow equation as proposed by Swamee and Swamee (2007), laminar and turbulent conduit flow can be expressed by a single equation (Figure 2.1.4):

$$Q = d^2 \sqrt{g d S_f} \left\{ \left(\frac{128\upsilon}{\pi d \sqrt{g d S_f}} \right)^4 + 1.153 \left[\left(\frac{415\upsilon}{d\sqrt{g d S_f}} \right)^8 - \ln\left(\frac{\varepsilon}{3.7d} + \frac{1.775\upsilon}{d\sqrt{g d S_f}} \right) \right]^{-4} \right\}^{-1/4} \tag{2.1.4}$$

The mass balance equation for matrix flow is given by:

$$C \frac{\partial p}{\partial t} - \nabla \cdot \mathbf{q} + q_{m,O} - q_{m,I} + q_{m \to c} = 0 \tag{2.1.5}$$

where C is a capacity term for matrix flow [L^{-1}], p the pressure head, $\mathbf{q}$ the darcy flux [m s^{-1}], $q_{m \to c}$ a sink term associated with exchange from the matrix to the conduit [s^{-1}] and $q_{m,O}$ and $q_{m,I}$ are matrix sink and source terms, respectively [s^{-1}]. The Darcy flux is determined by $\mathbf{q} = \mathbf{K} \nabla h$, where $\mathbf{K}$ is the hydraulic conductivity tensor, and h is the hydraulic head.

Reactive solute transport of calcium in the conduits is governed by the following advection-dispersion-reaction equation:

$$\frac{\partial(Ac)}{\partial t}+\frac{\partial(vAc)}{\partial s}-\frac{\partial}{\partial s}\left(DA\frac{\partial c}{\partial s}\right)+cq_{\mathrm{c,O}}-c_I q_{\mathrm{c,I}}+cq_{\mathrm{c}\to m}-P_c=0 \qquad (2.1.6)$$

where c is the concentration [mol m^{-3}], D is the hydrodynamic dispersion coefficient for conduit flow [m^2 s^{-1}], c_I is the concentration at inflow boundaries and P_c is a calcium production term [mol m^{-1} s^{-1}]. Reactive transport in the matrix is governed by the following advection-dispersion-reaction equation:

$$\frac{\partial(\theta c)}{\partial t}+\nabla(\mathbf{q}c)-\nabla(\theta\mathbf{D}\nabla c)+cq_{\mathrm{m,O}}-c_I q_{\mathrm{m,I}}+cq_{m\to c}-P_m=0 \qquad (2.1.7)$$

where θ is the water content [-], **D** is the hydrodynamic dispersion tensor [m s^{-1}] for matrix flow and P_m is a calcium production term [mol m^{-3} s^{-1}]. Equations (2.1.6) and (2.1.7) are based on the assumption that solute transport between the conduits and the matrix is solely governed by advection.

2.1.3.2 CALCITE DISSOLUTION

The change in conduit radius r [m] due to a dissolution rate R [mol m^{-2} s^{-1}] follows from a mass balance at the conduit wall:

$$\frac{\partial r}{\partial t}=\frac{R}{\omega\rho} \qquad (2.1.8)$$

where ω is the number of moles of calcite per unit mass of calcite [mol kg^{-1}] and ρ the density of calcite [kg m^{-3}]. In this study, ω was assumed to be 9.99 mol kg^{-1} and ρ was assumed to be 2,700 kg m^{-3} (Kaufmann 2003). Similarly, within the porous matrix, change of porosity φ [–] due to a dissolution rate R [mol m^{-2} s^{-1}] is given by:

$$\frac{\partial\varphi}{\partial t}=\frac{\theta RS}{\omega\rho} \qquad (2.1.9)$$

where S is the specific reaction surface [m] of porous limestone. Typically, the reaction surface per unit volume of porous material is very large and water entering the porous matrix that is under-saturated with respect to calcite quickly becomes saturated. As a result, dissolution of the porous matrix is effectively limited to a small region with a sharp reaction front where the under-saturated water is introduced. Within the bulk of the matrix continuum, the calcium concentration simply equals the saturation equilibrium concentration for calcium c_eq:

$$c=c_{\mathrm{eq}} \qquad (2.1.10)$$

The dissolution of limestone at the conduit-matrix interface is governed by surface-controlled and transport controlled-reaction rates. The first-order surface-controlled dissolution rate R_s [mol m^{-2} s^{-1}] is given by Dreybrodt (1988):

$$R_s = \alpha_s \left(c_{eq} - c_s \right) \tag{2.1.11}$$

where α_s is the surface-controlled rate coefficient [ms^{-1}]. c_s the calcium concentration at the interface [mol m^{-3}] and c_{eq} the calcium saturation equilibrium concentration [mol m^{-3}]. The transport-controlled dissolution rate accounts for transport through the diffusion boundary layer and is given by:

$$R_t = \alpha_t \left(c_s - c \right) \tag{2.1.12}$$

where α_t is the transport-controlled rate coefficient and c the bulk calcium concentration within the water. Equating equation (2.1.11) and equation (2.1.12) gives an expression for c_s which can be inserted in either one of these two equations to find the following expression for the effective first-order dissolution rate R (Szymczak and Ladd 2009; Perne at al. 2014):

$$R_1 = k_1 \left(1 - c / c_{eq} \right) \tag{2.1.13}$$

with:

$$k_1 = \frac{k_t k_s}{k_t + k_s} \tag{2.1.14}$$

where $k_s = \alpha_s / c_{eq}$ and $k_t = \alpha_t / c_{eq}$ and k_1 the effective rate coefficient [mol m^{-3}]. In this study, c_{eq} was assumed to be 2.0 mol m^{-3} and k_s was assumed to be $4E^{-7}$ mol m^{-2} s^{-1} (Kaufmann 2003). The transport-controlled rate coefficient k_t is given by:

$$k_t = \frac{D_m}{\delta c_{eq}} \tag{2.1.15}$$

where D_m is the diffusion coefficient [m^2 s^{-1}] and δ the thickness of the boundary layer [m]. In this study D_m was assumed to be $1E^{-10}$ m^2 s^{-1} (Kaufmann 2003) The thickness of the boundary layer is defined by the Sherwood number:

$$N_{Sh} = \frac{d}{\delta} \tag{2.1.16}$$

where $d = 2r$ is the diameter of the conduit. The Sherwood number for laminar conduit flow is 3.66 (Beek and Muttzall 1975). For turbulent flow, the Sherwood number is derived using (Beek and Muttzall 1975):

$$N_{\mathrm{Sh}} = 0.027 N_{\mathrm{Re}}^{4/5} N_{\mathrm{Sc}}^{1/3} \tag{2.1.17}$$

where N_{Re} and N_{sc} are the Reynolds number and the Schmidt number, respectively. The Reynolds number is given by:

$$N_{\mathrm{Re}} = \frac{vd}{\upsilon} \tag{2.1.18}$$

with v the velocity [m s^{-1}] and and υ the kinematic viscosity [$m^2 s^{-1}$]. The Schmidt number is given by:

$$N_{\mathrm{Sc}} = \frac{\upsilon}{D_{\mathrm{m}}} \tag{2.1.19}$$

It has been observed that as calcium concentrations approach saturation the reaction rate decreases due to impurities within the limestone which inhibit dissolution (Svensson and Dreybrodt 1992). This phenomenon is known as the kinetic trigger effect (White 1977) and has been modeled by switching dissolution from first-order to higher order kinetics when the calcium concentration exceeds a certain value c^*. The higher order effective rate is typically given by (Palmer 1991):

$$R_n = k_n \left(1 - c/c_{\mathrm{eq}}\right)^n \tag{2.1.20}$$

with k_n defined as:

$$k_n = k_1 \left(1 - c^*/c_{\mathrm{eq}}\right)^{1-n} \tag{2.1.21}$$

such that $R_1 = R_n$ at $c = c^*$. A general expression for the reaction rate be written as:

$$R = \begin{cases} R_1 & \text{if} \quad c \le c^* \\ R_n & \text{if} \quad c > c^* \end{cases} \tag{2.1.22}$$

In this study n was assumed to be 4 (Liedl et al. 2003) and $c^* = 0.8 c_{\mathrm{eq}}$. Figure 2.1.3 illustrates the effect of the kinetic trigger on reaction rate R. The decrease in dissolution rates close to saturation allows water, under-saturated with respect to calcite, to penetrate further into the aquifer than would otherwise be possible.

2.1.4 MODEL DESIGN

2.1.4.1 THE QUASI-STEADY STATE APPROXIMATION

Combining equation (2.1.6) and (2.1.8) and using $P_c = 2\pi rR$ results in the following reactive transport equation:

$$\frac{\partial(Ac)}{\partial t} + \frac{\partial(vAc)}{\partial s} - \frac{\partial}{\partial s}\left(DA\frac{\partial c}{\partial s}\right) + cq_{c,O} - c_I q_{c,I} + cq_{c\to m} = 2\pi r\omega\rho\frac{\partial r}{\partial t} \quad (2.1.23)$$

Hanna and Rajaram (1998) and Lichtner (1988) have shown that because the density of the limestone rock is much larger than the maximum calcium concentration, the rate of change in conduit radius is much slower than the rate of change in concentration and the rate of change in the flow field. Thus, the flow and reactive transport equations in the conduits can be simplified with a "quasi-stationary state approximation" using the steady-state equations:

$$\begin{aligned} \frac{\partial(vA)}{\partial s} + q_{c,O} - q_{c,I} + q_{c\to m} &= 0 \\ \frac{\partial(vAc)}{\partial s} - \frac{\partial}{\partial s}\left(DA\frac{\partial c}{\partial s}\right) + cq_{c,O} - c_I q_{c,I} + cq_{c\to m} &= 2\pi rR \end{aligned} \quad (2.1.24)$$

Within the matrix, we assume that the porosity remains constant and that the concentration of calcium equals the equilibrium concentration. Therefore, the flow and reactive transport equations in the matrix are simplified:

$$\begin{aligned} \nabla\cdot\mathbf{q} + q_{m,O} - q_{m,I} + q_{m\to c} &= 0 \\ c &= c_{eq} \end{aligned} \quad (2.1.25)$$

Equations (2.1.24) and (2.1.25) allow simulation of conduit generation processes through a sequence of steady states (Hanna and Rajaram 1998; Lichtner 1988). To begin, steady state flow and concentrations fields and corresponding dissolution rates are computed based on initial conduit diameters. The dissolution rate, in turn, determines the rate of conduit radius enlargement. The quasi-steady rate of conduit radius enlargement is applied over a "dissolution time step" to modify the conduit diameters, where the size of the dissolution time step is selected to maximize solution accuracy while minimizing computation time. The process is then repeated using the modified conduit diameters. A sequence of these dissolution time steps can be applied to simulate the dissolution process over the desired geologic timescale.

Equations (2.1.24) and (2.1.25) constitute a speleogenesis model that solves advective-dispersive-reactive transport within the conduits. This is different from many other speleogenesis models in which advective-reactive transport is solved within the conduits and fractures (Kaufmann and Braun 2000; Siemers and Dreybrodt 1998; Perne et al. 2014). The advection-reaction equation is independent of downstream conditions and may be solved from upstream to

downstream. Equations are solved for each conduit cell separately with complete mixing assumed at conduit junctions. The strength of our scheme lies in the fact that it can be easily implemented in any model code capable of handling advective-dispersive transport.

2.1.4.2 NUMERICAL SOLUTION OF FLOW

The numerical solution of flow in the conduits and the porous limestone matrix follows the approach described by De Rooij et al. (2013). This solution is based on a discrete-continuum approach and a finite difference scheme. The coupling of conduit-matrix flow is governed by a Peaceman well-index (Peaceman 1978, 1983). The projection well-index is used to handle conduits that are not aligned with the model grid orientation (Schlumberger 2008). The Peaceman well-index is a function of the hydraulic conductivity and size of the surrounding matrix cell and the conduit radius. As discussed by De Rooij et al. (2013), these indices decrease the dependency of the computed exchange fluxes with respect to the size of the matrix blocks surrounding the conduits. After each dissolution timestep, the Peaceman well-indices are updated.

To permit efficient steady-state flow computations for large regional domains, instead of using Richards equation to simulate variably saturated flow in the porous matrix, the option to solve for flow using the 3-D saturated flow equation was selected. In this option the height of the model domain is adjusted in accordance with the change in height of the water table at each time step, using an approach similar to that used in MODFLOW. Contrary to MODFLOW. However, net recharge is applied to the topmost model cells (i.e., land surface) even if the water table drops below those cells. The hydraulic conductivity in the cells above the water table is assumed to remain constant, at its saturated value, to transmit recharge to the water table.

Within the conduits the pipe flow equation proposed by Swamee and Swamee (2007) is implemented, assuming the conduits always remain full. This equation provides for a smooth transition between laminar and turbulent flow. For laminar flow the equation approximates the Poiseuille equation. For turbulent flow, the equation approximates the Darcy-Weisbach equation. The Swamee and Swamee (2007) equation allows conduit flow to automatically switch from laminar to turbulent conditions during conduit evolution (Figure 2.1.4). The system of non-linear flow equations is solved using a Newton-Raphson procedure and the adaptive under-relaxation scheme of Cooley (1983).

2.1.4.3 NUMERICAL SOLUTION OF TRANSPORT

Transient solute transport and steady state reactive solute transport are also simulated using finite differences. To avoid small space and time discretization that would result in extremely long computation times for large regional models, an upwinding approach is used to approximate the mass fluxes and an implicit time-marching is used to approximate the changes in mass with time Upwinding and implicit time-marching introduce numerical dispersion (Noorishad et al. 1992). It is noted that the numerical dispersion associated with implicit time-marching only affects transient simulations. Upwinding results in a numerical dispersion $D_{up} = v\Delta s/2$, where v is the pore water velocity and Δs is the grid spacing. Implicit time-marching introduces numerical dispersion $D_{time} = v^2\Delta t/2$ where Δt is the time step. In essence, if transient solute transport is simulated then our scheme behaves identical to a Crank-Nickolson scheme without upwinding (i.e., a scheme without numerical dispersion) if the physical dispersion would equal $D_{up}+D_{imp}$. It

is known that this scheme without numerical dispersion is only stable if PeCr ≤ 2 where Pe is the Péclet number (v$\Delta s/D$) and Cr the Courant number ($v\Delta t/\Delta s$) (Noorishad et al. 1992). In our scheme this requirement is always fulfilled by means of the numerical dispersion terms. It can be shown that if $D = D_{up}+D_{imp}$ then PeCr ≤ 2 is satisfied. In terms of efficiency this means that the scheme remains stable even for large Courant numbers, since an increase in velocity results in an increase in numerical dispersion. For steady state solute transport problems upwinding assures that Pe≤ 2. Because of the introduction numerical dispersion, no physical hydrodynamic dispersion terms were included in the model.

Due to the reaction terms, the reactive-transport equations are non-linear. Like the flow equations the reactive-transport equations are solved using a Newton-Raphson procedure and the adaptive under-relaxation scheme of Cooley (1983). Note that that for simulating dissolution time-marching is not applied as it involves steady-state computations.

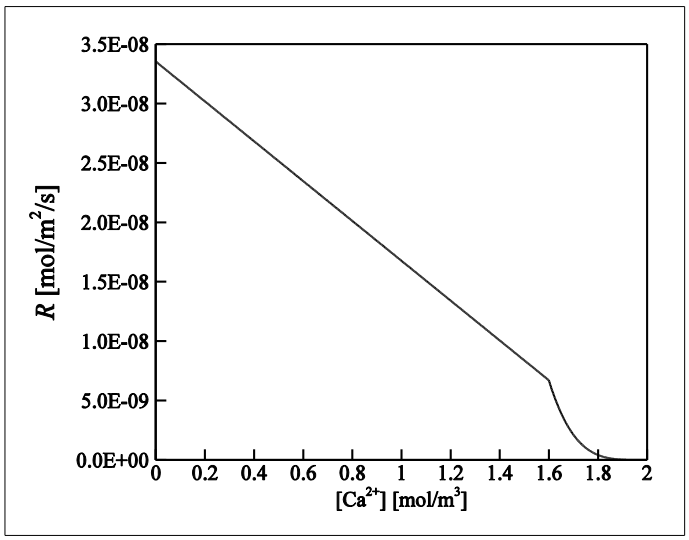

Figure 2.1.3. Reaction rate according to equation 2.1.22.

2.1.5 INITIAL PALEOKARST NETWORK

2.1.5.1 Horizontal Preferential Flowpaths

The simulation of conduit evolution requires an initial paleokarst network in order for dissolution to begin. This requirement constrains conduits to only evolve within a predefined network, which is a limitation of the methodology. However, specification of the initial paleokarst work does provide a means to force the generation of conduits in certain locations (i.e., known inception horizons, Filipponi et al. 2009).

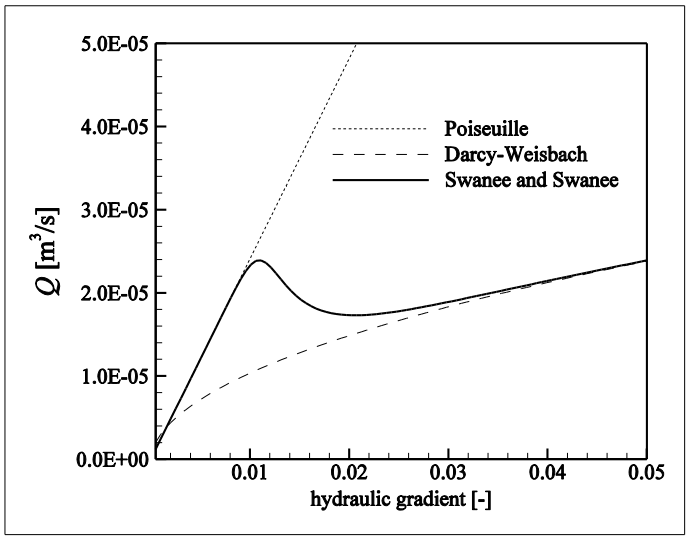

Figure 2.1.4. Swamee and Swamee (2007) pipe flow equation with r = 0.005 m and ε = 0.001 m showing smooth transition between laminar and turbulent flow as hydraulic gradient in pipe increases (solid line). Poiseuille equation for laminar flow (dotted line) and Darcy-Weisbach equation for turbulent flow (dashed line) are also shown for comparison.

In our work, the initial paleokarst network is generated using an approach similar to that typically used to generate stochastic fracture networks (Xu and Dowd 2010). The main difference is that we generate line segments (horizontal preferential flow paths, HPFs) instead of planes. From a conceptual point of view, the HPFs may be viewed as the intersections of fracture planes with a bedding plane or inception horizon. To reflect that sets of HPFs may exist in various orientations, the HPFs are subdivided into a number of subsets, each with a different orientation. For each subset, a number of HPFs and probability distribution functions for the location, length and orientation of HPFs within the subset must be specified and an initial radius must be assumed. If necessary geometrical restrictions may be imposed on the HPF generator. For example, a minimum distance between HPFs in the same subset can be specified to avoid multiple HPFs with similar orientations within a small region. Between two intersecting HPFs a minimum distance between the intersection point and the end points of the HPFs may be provided to avoid very small conduit cells in the final spatial discretization.

2.1.5.2 Vertical Preferential Flowpaths

As discussed by Bauer et al. (2005) and Clemens et al. (1999) the epikarst, a zone of enhanced weathering near the surface, plays a significant role in speleogenesis by distributing the effective rainfall within the subsurface. In the absence of an evolved conduit network, this distribution will generally be diffuse. Once a conduit network starts to form and the first sinkholes appear the epikarst layer will focus flow towards the sinkholes. This flow focusing mechanism enhances dissolution in the conduit network. As the conduit network evolves, the water table may be lowered below the epikarst layer causing sinkholes at higher elevations to become inactive.

To account for the flow focusing mechanism of vertical fractures, root networks and sinkholes we place a number of vertical preferential flowpaths (VPFs) randomly along the initial conduit network. These VPFs are connected to the conduit layer by a vertical stack of matrix cells with a

relatively high hydraulic conductivity. A column of high hydraulic conductivity porous media is used, rather than a vertical conduit, in order to avoid computational difficulties associated with variably saturated vertical conduits in the vadose zone. The topmost matrix cells are assigned the same high hydraulic conductivity throughout the domain. Using this set up, as conduits begin to form and lower the local water table the high conductivity cells focus flow from the top layer toward the VPFs and conduit, mimicking the natural process. Although this is a highly simplified representation of VPFs, flow into the VPF is computed implicitly. Thus, the method does not require specification of additional boundary conditions at sinkhole locations as is the case in other methods (Bauer et al. 2005). This methodology proposed here is reasonable if the main interest is to generate a conduit network of large lateral extent.

2.1.5.3 Boundary Conditions for Regional Scale Modeling

The flow boundary conditions during the conduit evolution process are generally unknown and may be varied to obtain different conduit configurations. Nevertheless, the land surface boundary condition must be handled carefully to avoid unrealistic flow scenarios. For example, if the presence of surface water is not accounted for, then the effective rainfall rate (precipitation – evapotranspiration) into the subsurface may be overestimated, resulting in unrealistically high hydraulic heads (i.e., above the land surface). Moreover, forcing all effective rainfall to be transmitted by the subsurface can result in unrealistically steep hydraulic gradients. Simulating surface water flow using rigorous mass balance and flux equations over large regional domains can be computationally demanding, therefore an alternative computationally efficient methodology was developed. This methodology limits the hydraulic heads in the topmost matrix cells to a spill elevation by applying drains to these cells. The flux rate associated with these drains is:

$$q = \begin{cases} \gamma\left(h_c - z_s\right) & \text{if } h_c > h_s \\ 0 & \text{if } h_c \le z_s \end{cases} \tag{2.1.26}$$

where h_c is the hydraulic head in a topmost cell, z_s the spill elevation associated with the drain and γ the drain conductance term [L s^{-1}]. In this study γ was set to $2K_z\Delta x\Delta y/\Delta z$ where K_z is the vertical hydraulic conductivity of the top cell, $\Delta x\Delta y$ is the area of the top cell, and Δz is the thickness of the top cell. Spill elevations were computed from topography using a procedure adapted from Wang and Liu (2006). The original purpose of the Wang and Liu (2006) procedure was to increase the topography in digital elevation models to the spill elevation such that local depressions were removed. Here the spill elevation was used to approximate the maximum depth of water that can be stored in local depressions. Thus, within local depressions the spill height is above the land surface and water can pond on the surface up to the spill height. Outside local depressions the spill elevation equals land surface elevation. Water drained from the land surface using this method is permanently removed from the domain. As the conduit network evolves through time heads throughout the domain are lowered and flow is captured from the surface boundaries and routed to the spring.

2.1.6 MODEL APPLICATION TO THE SILVER SPRINGSHED

The conduit generation algorithm described above was applied to the Silver Springshed in North Central Florida, with the long term goal of generating an ensemble of realistic conduit networks that can be incorporated into the existing regional MODFLOW model (HydroGeoLogic 2013) using MODFLOW-CLN or MODLFOW-USG. The conceptual model for the Silver Springshed was derived from the Northern District Model (NDM-V4) (HydroGeoLogic 2013) clipped to the 1,000 year capture zone (Figure 2.1.2). All surface topography, layering, and total Floridan Aquifer depths were taken from the NDM but porous media properties were homogenized and boundary conditions were simplified to facilitate analysis of complex heterogeneity induced by variations in paleokarst templates. The model contained 7 layers, 161 rows and 92 columns with 762 m square model cells (Figure 2.1.5). Model layer 1 represents the surficial aquifer and epikarst, which collects and conveys recharge to the karst aquifer through both focused (VPF) and diffuse recharge. Layers 2 through 7 represent the limestone aquifer.

Silver Springs is primarily sourced from Ocala Limestone (Faulkner 1970) which is represented by layer 4 in the original NDM. Most reported cave systems in the UFA form at the contacts between shallow stratigraphic units (e.g., Ocala and Avon Park formation contact) (Beck 1986). The interface between the Ocala Limestone and Avon Park Formation is presumed to be the location of extensive karst development because of the lower relative permeability of the Avon Park Formation (Phelps and Survey 2004). Prior studies in the UFA in north Florida (Langston et al. 2012a) suggest that conduits are located 10-15m below sea level, the top and bottom median elevation values for model layer 4 are -4.23 and -37.61, respectively. Accordingly, HPFs were placed throughout layer 4 to generate paleokarst templates.

To generate conduits for the Silver Springshed an initial random paleokarst network, consisting of sets of intersecting HPFs within a horizontal plane, was generated and mapped to the middle of layer 4. Subsequently, a specified number of VPFs was located randomly at the land surface overlying the initial conduit network. As described above, these VPFs are represented by a stack of relatively high permeability cells that occupy layers 1-4. In the original equivalent porous media MODFLOW model, the calibrated effective hydraulic conductivity for the Upper Floridan aquifer was relatively high, reflecting the influence of karstification. It is reasonable to assume a significantly lower Upper Floridan matrix hydraulic conductivity in the conduit evolution model, since the conduits are represented as discrete features. For the examples presented here the hydraulic conductivity for the matrix blocks in layers that make up the Floridian Aquifer was approximated to be $1E^{-4}$ m s^{-1}, a value representative of karst limestone rock (Freeze and Cherry 1979). The top epikarst layer and VPFs were assigned a higher hydraulic conductivity of $1E^{-3}$ m $s^{-1,}$ a value representative of sand.

2.1.6.1 Boundary Conditions

Lateral no flux boundaries were placed along the springshed boundaries (1,000 year capture zone), resulting in 4,179 active cells in each layer. The spring was represented as a fixed-head boundary with the spring pool elevation set to 12.2 m above mean sea level (HydroGeoLogic 2013). Steady-state surface recharge of $1.18E^{-8}$ m s^{-1}, which is based upon the mean areal recharge for the NDM model within the Silver Spring subdomain, was simulated using a specified flux boundary at the land surface. The resulting total areal steady-state recharge flux is

28.7 $m^3 s^{-1}$, somewhat larger than long term average springflow of 20.9 $m^3 s^{-1}$ estimated Silver Springs observations from 1935 to 2015 (USGS 2014). The surface boundary condition described above was used to remove excess recharge (surface water) from the model domain. Water entering the conduit network via the VPFs was assumed to be completely under-saturated with respect to calcite, (i.e., c = 0.0 mol m^{-3}). This concentration was set on matrix cells where the VPFs were connected to the conduits using a Dirichlet boundary condition. The concentration of water entering the conduits from porous matrix cells without VPFs was assumed to be saturated with respect to calcite, and was set using a Dirichlet boundary condition with $c = c_{eq}$.

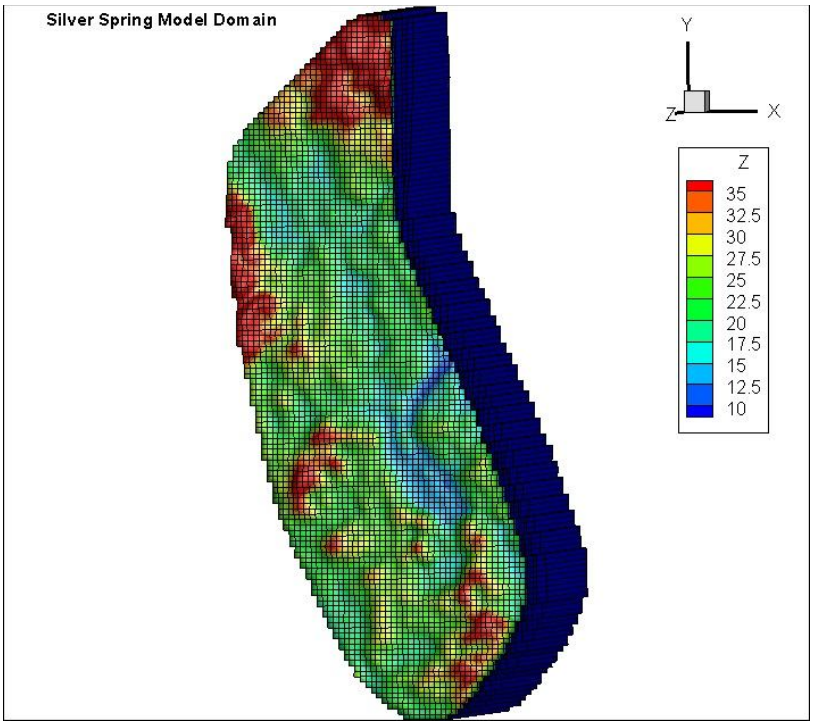

Figure 2.1.5. Silver Spring model domain showing model grid and model surface topography elevations.

2.1.6.2 Paleokarst Template Generation

As discussed above the karst evolution model requires the specification of a set of HPFs and VPFs (referred to here as the paleokarst template) to facilitate calcite dissolution. The conceptual geologic model for HPFs in this study is based on northwest and northeast trending fractures and joints observed in a prior photolineament study (Vernon 1951) (Figure 2.1.2). The random length distribution of HPFs was assumed to follow a gamma distribution with two parameters, K and theta. For the gamma distribution; K values less than 1 approach power law behavior, K values equal to 1 approach exponential behavior and K values greater than one represent distributions approaching more symmetrical behavior. The theta parameter is a scale value. The expected mean HPF length for each distribution is equal to K*theta.

Sinks and other VPFs have been observed near photolinear features, common in valley floors (Littlefield et al. 1984), and are often associated with the oldest karst depressions (Upchurch and

Littlefield 1988). In a previous UFA study near the Suwannee River, mean sinkhole densities were approximately 6 per km^2 (Denizman 1998), and have been reported to range between 3.5 to 19.9 per km^2 in other temperate subtropical settings (Ford and Williams 2013). Figure 2.1.2 illustrate the locations of sinkholes based upon a geographic analysis of surface topography obtained from the Florida Geological Survey. However, it is unknown how many of the mapped sinks or depressions extend as active VPFs into the Ocala limestone layer of the UFA. Due to the uncertainty in the locations and spatial density of HPFs and VPFs in the Silver Springshed, various densities and configurations were evaluated for the paleokarst template algorithm using Morris Method Global Sensitivity Analyses.

2.1.6.3 Morris Method Global Sensitivity Analyses

Morris Method Global Sensitivity Analysis (MM-GSA) was used to sample a wide range of possible VPF, HPF and porous matrix properties that influence spring network genesis and hydrologic and transport response. Furthermore, insights from the MM-GSA were used to evaluate properties driving network development, observed flow and transport behaviors, and sensitivity to input parameters.

Each paleokarst template used in the MM-GSA contained a specified number of stochastically generated gamma distributed HPFs, randomly located VPFs with a specified density, and random spatially homogeneous matrix porosity, hydraulic conductivity, and specific storage coefficient values. Values for the parameters of the gamma distribution, HPF and VPF densities, HPF orientation and porous media properties varied across the MM-GSA replicates using ranges taken from the literature and previous studies in the Silver Springshed (Table 2.1.1). Across the ensemble, HPF fracture sets had mean orientations of 45° and 315°, northeast and northwest, following orientations of a prior photolineament study; however, a random spread of 0° to 60° was implemented, to allow a gradient from ordered orthogonal HPFs to more randomly oriented HPFs. The location of each HPF and VPF was randomly selected from a uniform distribution of x and y coordinates in the model domain. All HPFs were set to an initial diameter of 2 mm and one HPF was deterministically placed at the location of Silver Springs.

The Morris method is an elementary effects method where the domain of experimental inputs, Ω is a k dimensional p-level grid (Campolongo et al. 2007); where k is the number of independent model input parameters (i.e., input parameter space is a vector θ_i with i=1,2,…,k) and p is the number of levels which span the specified value range for each parameter. For each model run, a change in a single parameter is generated and its effect on the output (x) is examined. The change in x in response to a change in the i^{th} parameter (θ) is the elementary effect (EE) of the i^{th} input on output x calculated as:

$$EE_i = \frac{[x(\theta_1, \theta_2 \dots, \theta_i + \Delta_i, \dots, \theta_k) - x(\theta_1, \dots, \theta_k)]}{\Delta} \quad (2.1.27)$$

where Δ represents a non-dimensional step change of parameter θ within the specified range, i.e., $i/(p\text{-}1)$ where i=1, 2,…, p-2. For this study, p=4 was selected (Khare and Muñoz-Carpena 2014). Different θ from Ω are randomly sampled to create a finite sample of EE_i. These effects are used to derive sensitivity indices based upon the mean (μ) and the standard deviation (σ) of the EE_i over the ensemble. Large μ values indicate a large influence of the corresponding parameter on

model output. Large values of σ indicate that the corresponding input parameter exerts a non-linear effect on model output or has non-linear interactions among other input parameters. Parameters with larger values of σ but μ values near zero are indicative of parameters with non-monotonic sensitivities, i.e., some of the sensitivities are positive and others negative so they cancel out in μ.

The number of simulations in the Morris analysis (N) is:

$$N = r(k + 1) \tag{2.1.28}$$

where r is the sampling size for each trajectory and k is the number of parameters being investigated. Parameters were sampled using the eSU method (Khare and Muñoz-Carpena 2014). A value of r =10 was selected based on previous research (Saltelli et al. 2004, Muñoz-Carpena et al. 2007) and k = 8 for the MM-GSA analysis (Table 2.1.1) resulting in N = 90 simulations.

Morris results were analyzed using the Elementary Measures and Plots Matlab software (Khare and Muñoz-Carpena 2014). The red lines on the plots represent μ equal to two times the standard error of the mean estimate, i.e., $\mu = 2\sigma/\sqrt{r}$ or $\mu = 0.68\sigma$ for r =10, the trajectory sampling size used in this study. The blue line on the μ versus σ plot reflects μ = σ, i.e., a coefficient of variation equal to 1. Parameters close to the origin in both plots are considered unimportant. Parameters that plot far from the origin outside the red lines (i.e., have μ values greater than 2 times the standard error of the mean estimate) can be interpreted as having a significant (non-zero) influence on the model output. Parameters that plot far from the origin outside the blue line have significant influence on the model output and negligible non-linear effects or interactions with other parameters. Parameters that plot far from the origin between the blue and red lines have significant influence on the model output and moderate non-linear effects or interactions with other parameters. Parameters that plot far from the origin within the red lines have large non-linear effects or interactions with other parameters.

2.1.6.4 Simulation Response Metrics

2.1.6.4.1 Dissolution Response Metrics

Springflow as a function of dissolution time was used to determine when the conduit network reached a stable configuration. Hydraulic and transport pulse experiments were evaluated on the stable network. Differences in conduit radii statistics (median, mean, maximum), and network plots were used to compare conduit networks. Effective porosity for the evolved karst aquifer in layer 4 of the model was computed as:

$$\frac{V_\mathrm{c} + n(V_\mathrm{m} - V_\mathrm{c})}{V_\mathrm{m}} \tag{2.1.29}$$

where V_c is the conduit volume, V_{vm} is the matrix volume in layer 4, and n is the porosity. The HPF density [km^{-1}] was defined as:

$$\frac{L_\mathrm{t}}{A_\mathrm{t}} \tag{2.1.30}$$

Table 2.1.1. Horizontal and vertical preferential flowpath (HPF and VPF) and matrix properties for Morris Method Global Sensitivity Analysis.

Parameter	Units	Probability Distribution*	Source
HPF Number	Count	U(2500, 4000)	(Vernon 1951)
Northeast HPF Set 1 Orientation	Degrees	Fixed 45°	(Vernon 1951)
Northwest HPF Set 2 Orientation	Degrees	Fixed 315°	(Vernon 1951)
HPF Spread	Degrees	U(0°, 60°)	Estimated
HPF k	Unitless	U(0.75, 2.00)	Estimated
HPF theta	M	U(4000, 6000)	Estimated
VPF Number	count	U(200, 500)	(Denizman 1998; Ford and Williams 2013)
Matrix Porosity	unitless	U(0.25, 0.40)	(Langston et al. 2012b)
Matrix Hydraulic Cond.	m s^{-1}	LU($1E^{-4}$, $1E^{-8}$)	(Heath 1983)
Matrix Specific Storage	m^{-1}	U($1E^{-4}$, $1E^{-6}$)	(Batu 1998)
Epikarst Hydraulic Cond.	m s^{-1}	Fixed $1E^{-3}$	(Heath 1983)
Epikarst Porosity	unitless	Fixed 0.3	(Langston et al. 2012b)
Epikarst Specific Storage	m^{-1}	Fixed $1E^{-4}$	(Batu 1998)

*U (minimum, maximum) uniform distribution probability range for GSA
LU (minimum, maximum) is log uniform distribution probability range for GSA

where L_t is the total length of HPFs and A_t is the springshed area. Dissolved HPF density was used to evaluate magnitude of dissolution across replicates. For that metric, L_t is the total HPF length for HPFs with radii greater than 0.5 m was used in equation 2.1.30.

2.1.6.4.2 Hydrograph Response Metrics

Replicates were classified as behavioral if they evolved to generate a first order magnitude spring (i.e., steady state springflow greater than 2.8 $m^3 s^{-1}$). Hydrograph response metrics were derived from simulated spring hydrograph storm pulse responses for both the entire ensemble and the ensemble of behavioral replicates. Metrics included steady-state flow magnitude, timing and magnitude of peak flow, and hydrograph recession coefficients. Hydrograph recession is often separated into two periods, an early period which is controlled by rapid drainage of water in the conduit network and epikarst, and a later period that is controlled by slow draining of storage in the lower permeability porous matrix often referred to as baseflow recession (Atkinson 1977; Padilla et al. 1994; Kiraly 2002; Kovács et al. 2005; Geyer et al. 2008b). Early hydrograph behavior tends to be dominated by focused recharge into the conduit systems while late recession tends to be dominated by diffuse recharge into the porous matrix (Covington et al. 2009). Recession coefficients and inflection points were calculated based upon linear regression of the natural logarithm of springflow with time (lnQ versus t plots). Defining inflection points is subjective; however, the point where the hydrograph recession becomes linear on the lnQ versus

t plot (i.e., exponential decay defined by a change in slope less than $1E^{-4}$ between successive time steps) has been widely used to separate early and late recession behavior (Baedke and Krothe 2001; Dewandel et al. 2003; Kovács and Perrochet 2008; Chang et al. 2015). This was the approach used to separate early and late recession behavior in this study (Figure 2.1.6).

To evaluate the relative influence of conduit versus matrix flow, the fraction of flow being carried by conduits through 3 concentric cylindrical control surfaces located within the aquifer located 2, 8, and 12 km away from the spring were calculated for both steady-state and peak flow.

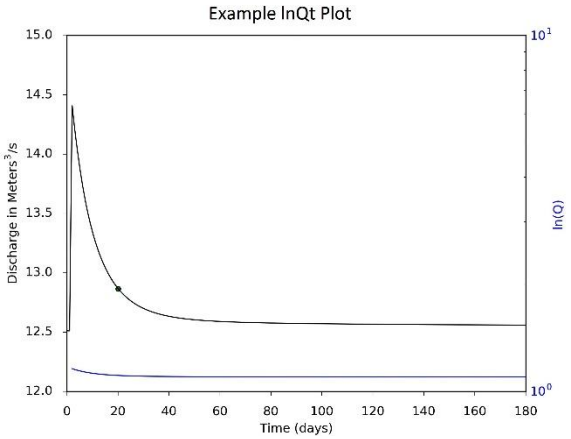

Figure 2.1.6. Example lnQ versus t plot showing hydrograph (black), log transformed flow (blue) and computed inflection point separating early and late hydrograph recession periods.

2.1.6.4.3 Transport Response Metrics

Transport response metrics were derived from surface tracer pulse breakthrough curves (BTC) at the spring. A uniform instantaneous pulse of 1 kg m^{-2}, was applied to the model land surface and transported to the spring using the steady flow field. Surface boundary and spring BTC analyses included evaluation of peak solute mass flux magnitude and arrival time, and BTC moment analysis including total mass (0^{th} moment), mean travel time (normalized 1^{st} moment), and travel time standard deviation (square root of normalized 2^{nd} central moment). Since the experiments allowed two boundaries for tracer mass to exit, the fraction of mass delivered to the spring or to the surface boundary varied among replicates. Combined tracer mass recovery from the surface and spring boundary conditions was required to be at least 90% before moments were calculated.

2.1.7 RESULTS AND DISCUSSION

2.1.7.1 Dissolution Behaviors and Sensitivity

As dissolution occurred and conduit networks evolved they began to capture more of the surface recharge, and consequently spring flows increased through time. Networks reached a steady spring flow over varying timescales (Figure 2.1.7A); however, every conduit system produced a maxima after which steady state flow did not change significantly (< 0.01% change in springflow).

Of the 90 simulations in the MM-GSA, only 58 were behavioral (i.e., generated springs with steady state flows >2.8 $m^3 s^{-1}$). To test whether non-behavioral networks continued to be non-behavioral with longer dissolution, dissolution was allowed to proceed for a duration of 1.5 times the point at which solution steady state flow was observed for each replicate. Results confirmed that non-behavioral networks continued to be non-behavioral (Figure 2.1.7B).

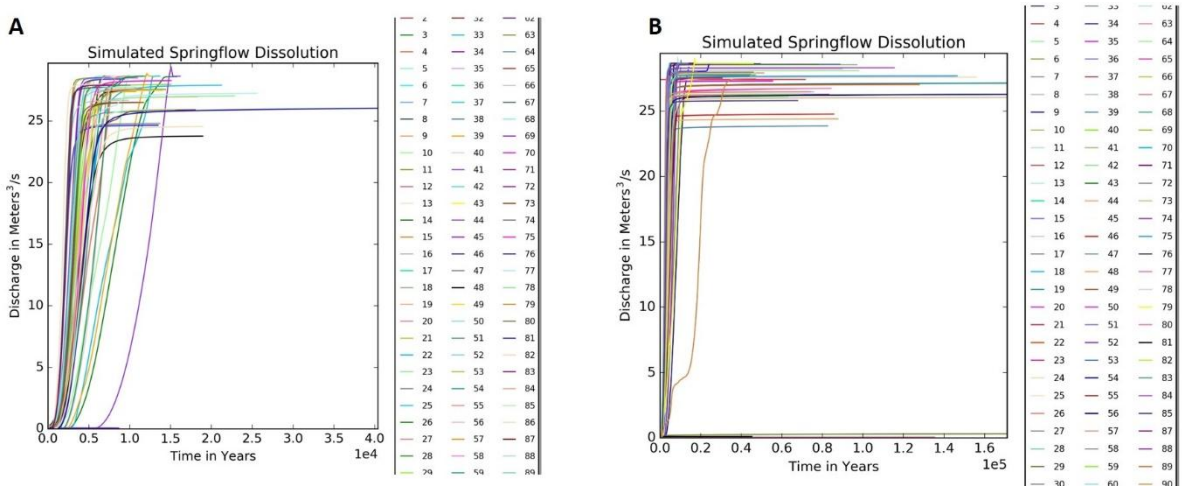

Figure 2.1.7. Simulated springflow during dissolution for A) steady state flow dissolution time and B) 1.5 times the steady state flow dissolution time.

To test whether steady-flow behavior represents karst system maturity, i.e., that the majority of flow paths that will connect to the network have become stable when steady flow is achieved, plots of conduit flow at steady-state (15,000 years), 20,000 years, and 25,000 years were examined during network development for behavioral cases (Figure 2.1.8). While some very small conduits continued to develop near the distal edges of the network over time, the majority of the network stayed the same. These results support the hypothesis that when the steady flow is obtained the configuration of the network has become stable; a state that could be described as self-organized. Thus, the time that steady state flow was achieved was selected as an appropriate time to compare flow and solute transport behaviors across different conduit networks.

Although steady spring flow was achieved at a certain point during dissolution, the HPFs continued to dissolve and radii continued to increase after this time. While this had minimal effect on steady-state spring fluxes, peak flow response to the hydraulic pulse increased (Table 2.1.2). As the conduit diameters in the network increased, resistance to flow in the conduits decreased, the head gradient across the conduits dropped. Thus, the conduits began to behave like fixed head boundaries, equal to the springhead, distributed throughout the domain. This allowed the hydraulic pulse to be transmitted more quickly to the spring through the conduit network producing higher peak flows.

Table 2.1.3 summarizes difference between behavioral and non-behavioral groups for dissolution metrics. Minimum, maximum, mean and standard deviation in paleokarst template HPF density is similar between the groups, while dissolved HPF densities are larger for behavioral cases. This

indicates th at the sta tistical pa rameters dict ating the p robability d istribution of paleokar st template param eters specified in the MM-GSA (Table 2.2.1) m ay not be the only im portant driver of behavioral networks; the actual ra ndom placement and connectivity of HPFs and VPFs within the dom ain m ay asse rt sig nificant con trol over pa tterns in co nnectivity a nd eventu al network development. As expected, radii were more developed in the behavioral replicates with higher ensemble m edian and m aximum radii. However, conduits volum es are a negligible portion of total aquifer volum e in both behavi oral and non-behavioral cases, m aking up a maximum of 2% of the tota l volu me of the Ocala lim estone laye r (model layer 4) in th e behavioral networks. This small influence of conduit networks on effective porosity is consistent with prior karst modeling studies, (Bonacci 1987; Worthington 1999; Ford and Williams 2013).

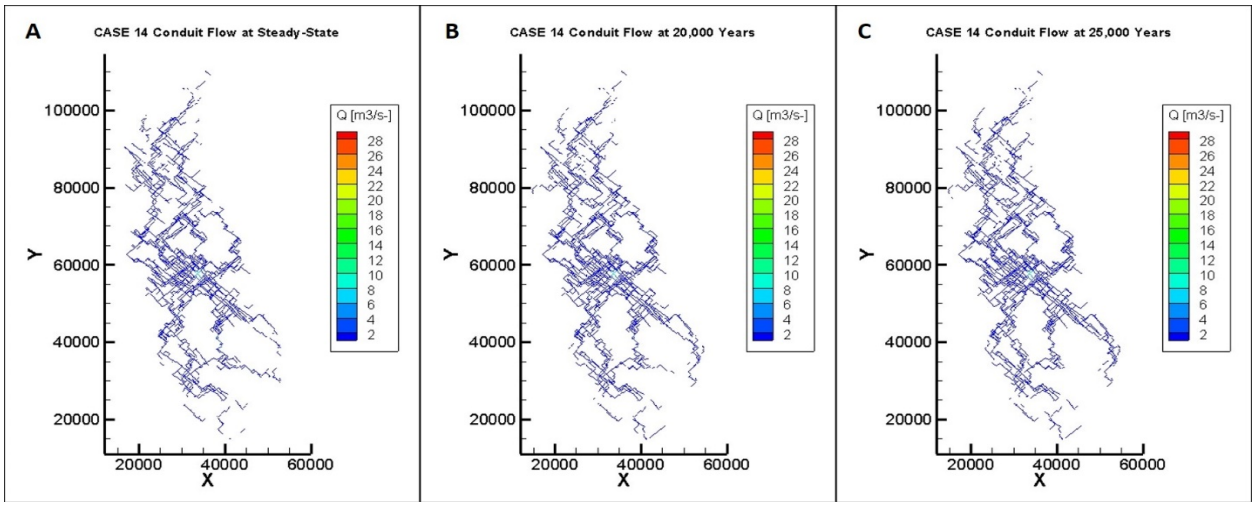

Figure 2.1.8. Conduit flow during evolution showi ng A) flow rates through conduit network at 15,000 years (steady state), B) netw ork at 20,000 years (1.33*steady state , and C) network at 25,000 years (1.66*steady state).

Table 2.1.2. Com parison of flows and radii statis tics at steady flow dissolution tim e and 1.5 times the steady flow dissolution time (statistics calculated over all 90 replicates).

	Steady-state flow ($m^3 s^{-1}$)	**Peak flow ($m^3 s^{-1}$)**	**Max radii (m)**	**Mean radii (m)**	**Median radii (m)**
Steady-flux dissolution time					
Minimum	0.00 0.00	0.04	0.01	0.01	
Maximum	28.13 28.9	3 31.5	9	1.90	2.57
Mean	2.58 2.86	3.36	0.36	0.11	
Standard Deviation	6.33 6.92	5.03	0.52	0.38	
1.5 steady-flux dissolution time					
Minimum	0.00 0.00	0.05	0.01	0.01	
Maximum	28.46 30.3	4 38.2	1	2.56	3.52
Mean	2.61 3.02	4.39	0.47	0.14	
Standard Deviation	6.39 7.33	6.26	0.69	0.50	

Table 2.1.3. Behavioral and non-behavioral group statistics for dissolution metrics.

Metric	All HPF Density (km^{-1})	Dissolved HPF Density (km^{-1})	Steady State Dissolution Time (years)	Median Radii (m)	Max Radii (m)	Effective Porosity	Conduit Volume Fraction (model layer 4)
Behavioral (58 replicates)							
Minimum 1.57		0.83	12,557	0.01	5.13	0.25	0.00
Maximum 6.11		5.26	114,155	6.28	53.06	0.40	0.02
Mean 3.82		2.29	52,361	2.28	14.22	0.32	0.00
Standard Deviation	1.13 0.89		29,401	2.07	6.76	0.06	0.00
Coefficient of variation	0.30 0.39		0.56	0.91	0.48	0.19	0.00
Non-Behavioral (32 replicates)							
Minimum 1.53		0.00	684	0.01	0.32	0.25	0.00
Maximum 6.71		2.57	114,155	3.81	25.49	0.40	0.00
Mean 3.91		0.49	10,609	0.18	2.76	0.32	0.00
Standard Deviation	1.31 0.77		27,476	0.66	5.49	0.06	0.00
Coefficient of variation	0.34 1.57		2.59	3.67	1.99	0.19	0.00

The MM-GSA results for the entire ensem ble (Figure 2.1.9) showed th at hydraulic conductivity was the most sensitive parameter for the dissolution metrics and it had relatively low interactions (see green circles which fall on or outside of blue lines). Higher values of hydraulic conductivity contributed to lower dissolved H PF density (i.e., density of HPFs that have radii greater than 0.5 m) (Figure 2.1.9A), and lower m edian and m aximum radii (Figures 2.1.9B and 2.1.9C). In this experiment, distributed recharge was applied across the top surface of the m odel dom ain and flow focusing through the VPFs to the conduits occurred if conduit heads decreased and, as a result, gradients between the epikarst and conduits increa sed. Higher hydraulic conductivity values allowed distributed recharge to be distri buted easily within the porous m atrix, producing lower head gradien ts between the m atrix and co nduits, reducing flow focusing in V PFs and less impetus for conduits to develop. Thus, higher h ydraulic conductivity wa s observed to im pede network development.

Network develop m ent was also sensitiv e to p arameters th at specified the connectivity of the paleokarst network (see red circles on Figure 2.1.9) . Dissolved HPF density was sen sitive to th e HPF length distribution gamma di stribution param eters K and th eta, and HPF spread. Median radii was sensitiv e to th e num ber of VPFs, whic h deliver under-saturated water to the network . Thus, higher connectivity in the paleokarst template due to longer HPFs (higher K*theta), higher variation in HPF orienta tion a nd m ore VPFs led to m ore ne twork develop m ent. The sensitive network connectivity parameters showed more interactions with other parameters than hydraulic conductivity, i.e., tended to fall within the blue and red lines.

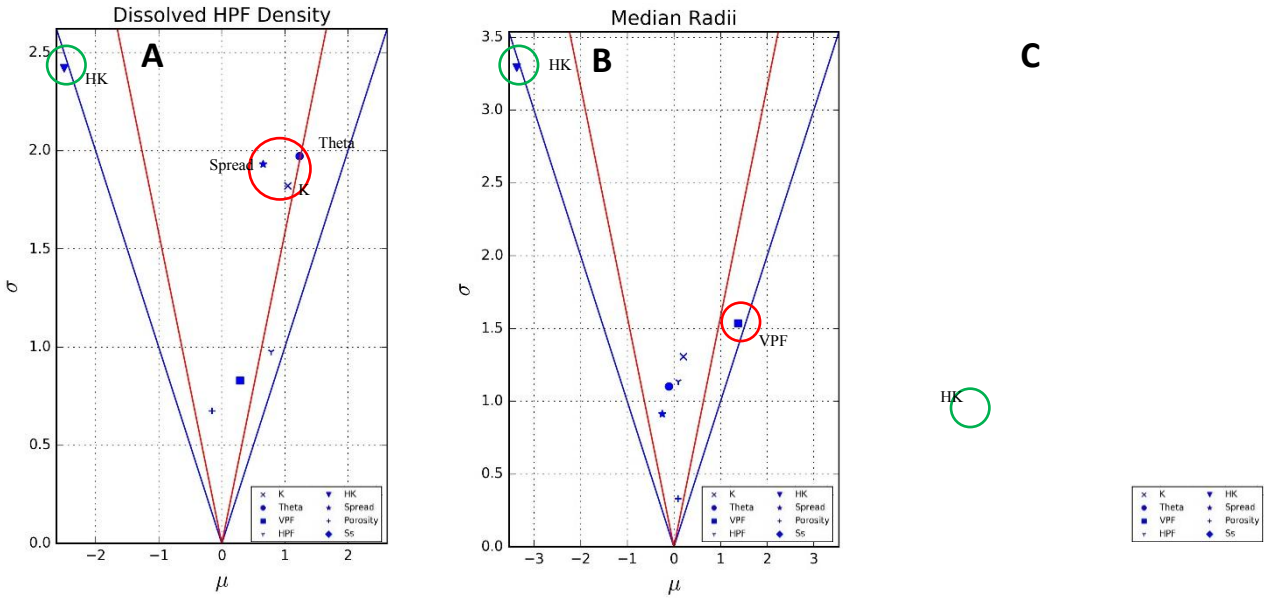

Figure 2.1.9. Morris Method Global Sensitivity Analysis dissolution statistic plots showing A) dissolved HPF density, B) median radii, and C) max radii. $\mu = \sigma$ (blue lines) and $\mu = \frac{2\sigma}{\sqrt{r}} = 0.63\,\sigma$ (red lines) are shown to aid in interpretation of parameter interactivity.

2.1.7.2 Steady-State and Hydraulic Pulse Response Behaviors and Sensitivity

Ensemble hydrograph plots illustrate the variability in spring flow over the entire Morris Method ensemble and behavioral replicates (Figure 2.1.10). Behavioral replicate spring flows ranged from approximately 40% to 100% of total areal recharge. The mean steady-state springflow was 20.21 $m^3\ s^{-1}$ and the standard deviation around this mean was 6.72 $m^3\ s^{-1}$. Hydrograph metrics for behavioral and non-behavioral replicates (Table 2.1.4) illustrate expected behaviors, with steady state and peak flow is substantially higher in behavioral cases.

Hydrograph recession values for the behavioral cases (Table 2.1.4) are in the range of values estimated from the observed Silver Springs flow data, where the best fit of exponential recession coefficients ranged from 0.22 to 0.67 $year^{-1}$ (i.e., hydraulic response time of 1.5-4.5 years, Jim Jawitz, personal communication, September 1, 2015). In this study, early recession coefficients for behavioral cases ranged from 0.36 to 6.7 $year^{-1}$ with a mean of 1.86 $year^{-1}$; late baseflow recession coefficients from less than 0.01 $year^{-1}$ to 0.09 $year^{-1}$. The smaller values suggest that storage release during baseflow recession can extend for long periods of time in some systems.

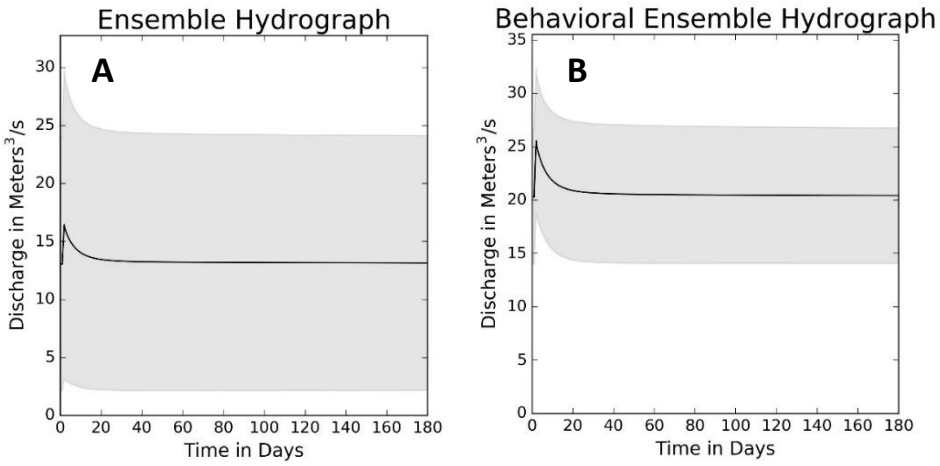

Figure 2.1.10. Ensemble hydrograph (A) and behavioral ensemble hydrograph () showing mean (black line) and standard deviation (gray shaded region).

Table 2.1.4. Behavioral and non-behavioral group statistics for hydraulic pulse metrics.

Metric	Steady-State Flow ($m^3 s^{-1}$)	Peak Flow ($m^3 s^{-1}$)	Alpha Early Recession Coefficient ($year^{-1}$)	Inflection Time (days)	Alpha Late Recession Coefficient ($year^{-1}$)
Behavioral (58 replicates)					
Minimum	3.50	3.80	0.36	2.61	0.00
Maximum	29.45	34.97	6.70	27.15	0.09
Mean	20.21	25.27	1.86	20.03	0.01
Standard Deviation	6.72	7.27	0.94	7.42	0.02
Coefficient of variation	0.33	0.29	0.51	0.37	2.00
Non-Behavioral (32 replicates)					
Minimum	0.00	0.00	-	-	-
Maximum	0.63	0.63	-	-	-
Mean	0.05	0.05	-	-	-
Standard Deviation	0.11	0.11	-	-	-
Coefficient of variation	2.20	2.20	-	-	-

Flow through concentric control planes toward the spring provides further insight into differences in behavioral and non-behavioral groups (Table 2.1.5). In behavioral cases, flow through the control planes was dominated by conduit flow with nearly all of the flow occurring in the conduits and small decreases in percentage of conduit flow with distance from the spring. Note that this is in spite of the fact that conduits have a negligible impact on effective porosity. In contrast, non-behavioral case mean behavior shows small flow fractions near the spring and increasing flow fractions as distance from the spring increases. This suggests that in these non–

behavioral cases local conduit systems developed away from the spring and routed water to the surface boundary instead of the spring.

Table 2.1.5. Behavioral and non-behavioral group statistics for flow fractions through concentric control planes located 2, 8 and 12 km from the spring at steady-state and peak flow.

Metric	2 km Steady-State Flow Fraction	2 km Peak Flow Fraction	8 km Steady-State Flow Fraction	8 km Peak Flow Fraction	12 km Steady-State Flow Fraction	12 km Peak Flow Fraction
Behavioral (58 replicates)						
Minimum	0.99	1.00	0.99	0.99	0.98	0.97
Maximum	1.00	1.00	1.00	1.00	1.00	1.00
Mean	1.00	1.00	1.00	1.00	1.00	1.00
Standard Deviation	0.00	0.00	0.00	0.00	0.00	0.00
Coefficient of variation	0.00	0.00	0.00	0.00	0.00	0.00
Non-Behavioral (32 replicates)						
Minimum	0.00	0.00	0.01	0.01	0.04	0.04
Maximum	0.99	0.99	1.00	1.00	1.00	1.00
Mean	0.39	0.39	0.49	0.49	0.59	0.59
Standard Deviation	0.38	0.38	0.37	0.37	0.35	0.35
Coefficient of variation	0.97	0.97	0.76	0.76	0.59	0.59

The MM-GSA results over the entire ensemble (Figure 2.1.11) showed that for all flow metrics hydraulic conductivity (green circles) was a highly sensitive, moderately interactive parameter. Increased hydraulic conductivity was associated with lower steady-state spring flows, lower peak flows, and slower recession which is somewhat counter-intuitive. However, as discussed above, increased hydraulic conductivity led to less conduit development. Thus, the observed sensitivity of these flow metrics to hydraulic conductivity is dominated by its indirect influence on conduit development rather than its direct influence on porous media flow. In fact, that highest values of hydraulic conductivity ($1E^{-4}$ m s^{-1}) often resulted in non-behavioral systems. Of the 20 simulations in the MM-GSA with the highest hydraulic conductivity values, only 4 generated a first magnitude spring.

Increased HPF length scales (theta) led to higher steady and peak flows, while increased HPF length scale and increased numbers of VPFs led to faster recession (red circles). These results are expected because, as discussed above, increases in these parameters tended to produce more conduit development, which produces higher steady and peak flows and more rapid recession of hydraulic pulses. In general HPF length scale theta and number of VPFs showed large non-linear or interactive behavior for all flow metrics (i.e., fell on or within red lines). The number of HPFs and the HPF spread parameter showed near zero mean sensitivities to steady state and peak flow but high interactions, indicating non-monotonic behavior (i.e., large positive and negative sensitivities that tended to cancel each other when averaged).

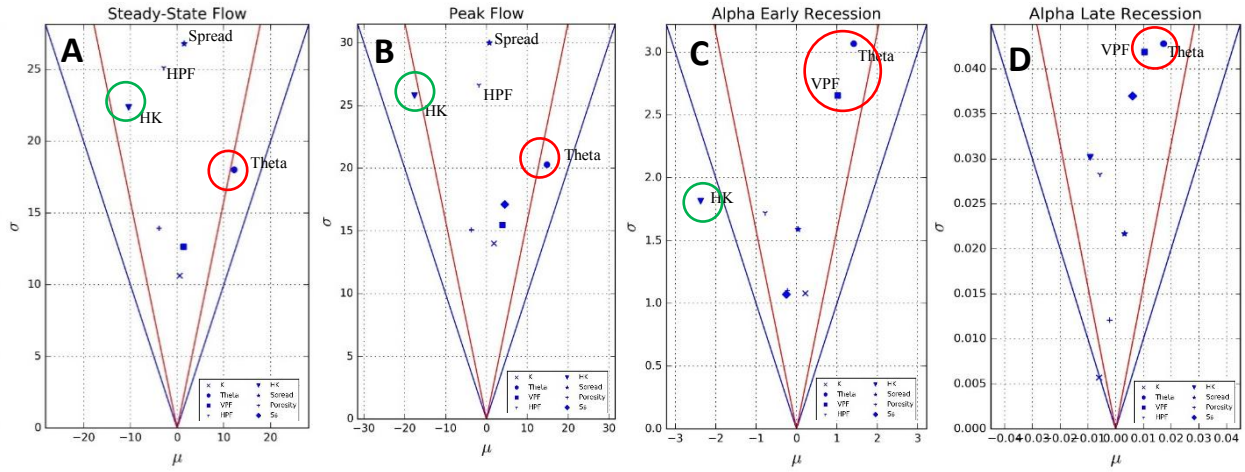

Figure 2.1.11. Morris Method Global Sensitivity Analysis hydrologic pulse response metrics, showing A) steady-state flow, B) peak flow, C) early recession coefficients, and D) late recession coefficients.

It is possible that differences in individual network connectivity that are not accounted for in the Morris methodology (i.e., actual locations and connections among VPFs and HPFs with the same densities, spread and/or gamma distribution parameters) are responsible for some of observed interactive behavior. In other words, these parameters may be experiencing significant interactions with actual network geometry rather than the specific Morris method parameters summarized in Table 2.1.1.

2.1.7.3 Transport Pulse Response Behaviors and Sensitivity

The entire ensemble of solute breakthough curves showed substantial variation in transport pulse response due to low spring mass flux for non-behavioral cases; however, the behavioral group breakthough curves were less variable (Figure 2.1.12). The behavioral breakthrough curves were highly skewed with an average peak travel time of approximately 10 years, but an average mean travel time (normalized first moment) of approximately 40 years (Table 2.1.6). Peak travel time statistics for the behavioral replicates are in good agreement with prior estimates of apparent groundwater age at Silver Springs that range from 9.9 to 27.5 years (Phelps and Survey 2004).

Overall mass recovery was good with a minimum of approximately 88% and mean of 93% mass recovery through both the surface and spring boundary for non-behavioral cases and a minimum of 89% with a mean of 98% for behavioral cases (Table 2.1.6). Unrecovered likely mass remains in the domain at the end of the 1,250 simulation, although model precision could account for up

to 4% error at each boundary over the simulation. In general behavioral cases showed faster tracer travel times and less tracer spread than non-behavioral cases.

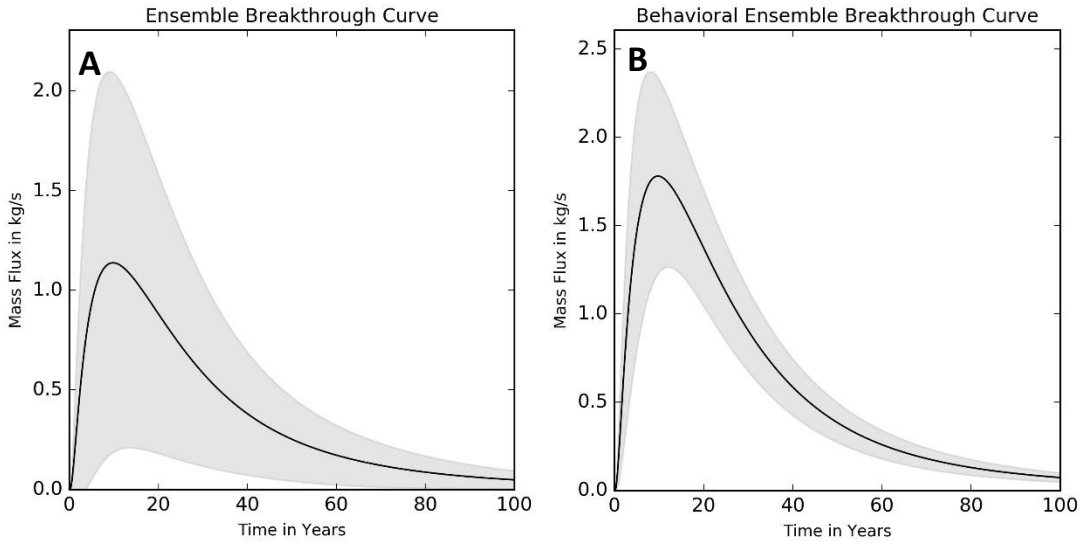

Figure 2.1.12. Ensemble breakthough curve (A) and behavioral ensemble breakthrough curve (B) showing mean (black line) and standard deviation (gray shaded region).

Table 2.1.6. Behavioral and non-behavioral group statistics for solute transport pulse metrics.

Metric	**Percent Tracer Mass Recovery**	**Percent Tracer Infiltrated**	**Peak Travel Time (years)**	**Peak Solute Mass Flux (kg s^{-1})**	**Mean Travel Time (years)**	**Travel Time Standard Deviation (years)**
Behavioral (58 replicates)						
Minimum	89%	43%	1.98	0.38	26.70	39.27
Maximum	100%	99%	20.63	2.86	68.46	101.39
Mean	98%	82%	10.49	1.79	39.31	51.89
Standard Deviation	22%	26%	4.43	0.68	18.47	20.74
Coefficient of variation	0.22	0.32	0.42	0.38	0.47	0.40
Non-Behavioral (32 replicates)						
Minimum	88%	0%	6.62	0.00	40.02	41.72
Maximum	100%	21%	418.43	0.89	309.51	151.14
Mean	93%	4%	50.25	0.05	107.31	98.43
Standard Deviation	3%	17%	80.06	0.18	56.52	29.01
Coefficient of variation	0.03	4.25	1.59	3.60	0.53	0.29

The MM-GSA results for the entire ensemble of transport pulses again showed that hydraulic conductivity was a highly sensitive parameter with moderate interactions (Figure 2.1.13, green circles). Higher hydraulic conductivity decreased the magnitude of peak solute mass flux and increased the mean and standard deviation of the travel time. Again, this result may be attributed to the fact that high hydraulic conductivities promote more flow through the matrix and inhibit development of the conduit network. Thus, more solute is transported more slowly through the porous media. Interestingly, peak transport time was insensitive to hydraulic conductivity.

Peak solute mass flux, peak transport time, and the mean travel time (first normalized moment) were also sensitive to the HPF length scale parameter, theta, and this parameter showed relatively high interactions (Figure 2.1.13, red circles). In general longer HPFs increased the magnitude of peak solute mass flux, and reduced the peak, mean and standard deviation of travel time. The HPF gamma distribution parameter K, HPF spread, number HPFs and number of VPFs showed near zero mean sensitivities to solute transport metrics but high interactions, indicating non-monotonic behavior.

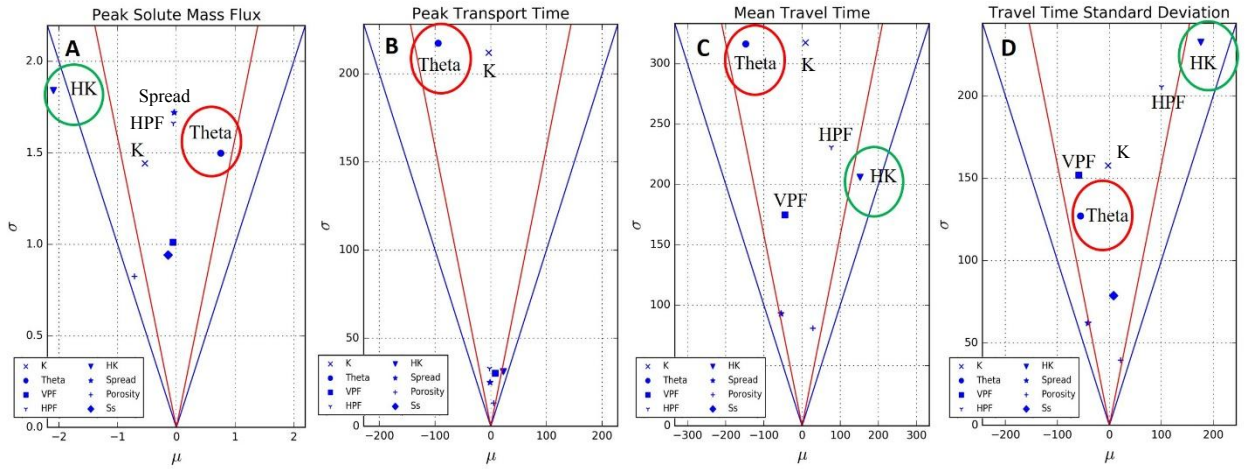

Figure 2.1.13. Morris Method Global Sensitivity Analysis transport pulse response metrics, showing A) peak solute mass flux B) peak transport time, C) normalized first moment (mean travel time), and D) square root of normalized second central temporal moment (travel time standard deviation).

2.1.7.4 Investigation of Individual Behavioral and Non-Behavioral Conduit Networks

Network plots for a few non-behavioral (Figure 2.1.14) and behavioral replicates (Figure 2.1.15) were examined to further investigate causes of non-behavioral replicates. Behavioral replicates showed more extensive conduit networks with much more connectivity to the spring. On the other hand non-behavioral replicates tended to develop localized networks, some of which discharged to the surface boundary. Figure 2.1.15 shows three behavioral conduit networks with similar peak solute travel times (8.18, 8.37, and 8.71 years) but increasing steady-state flux from left to right. These figures illustrate important characteristics of behavioral networks: intense development of conduits near the spring, and spring fluxes which increase with network extent and number of HPFs oriented along the dominant north-south springshed head gradients. These networks also illustrate that in behavioral cases conduits tend to develop in the lower lying areas of the model domain (compare networks to model topography in Figure 2.1.5).

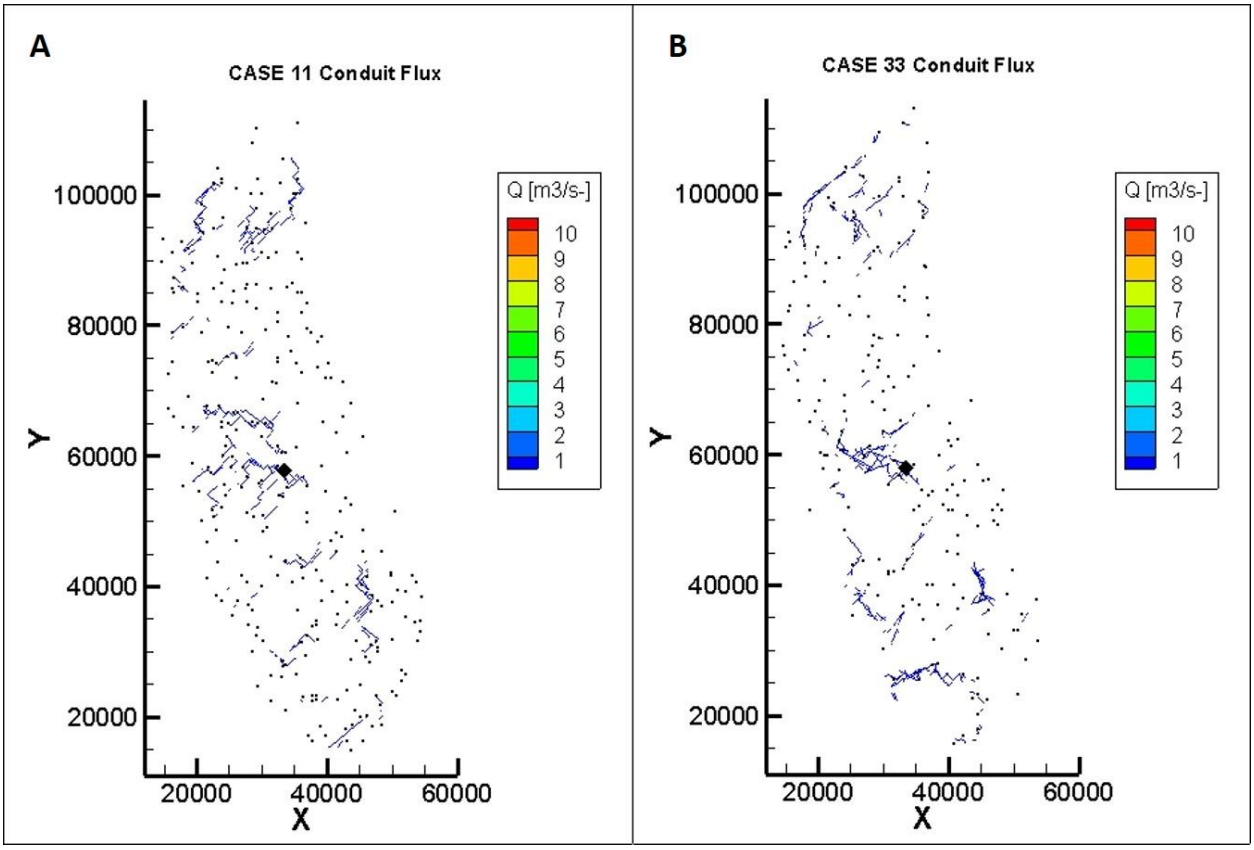

Figure 2.1.14. Two non-behavioral conduit networks, showing development of localized flow systems.

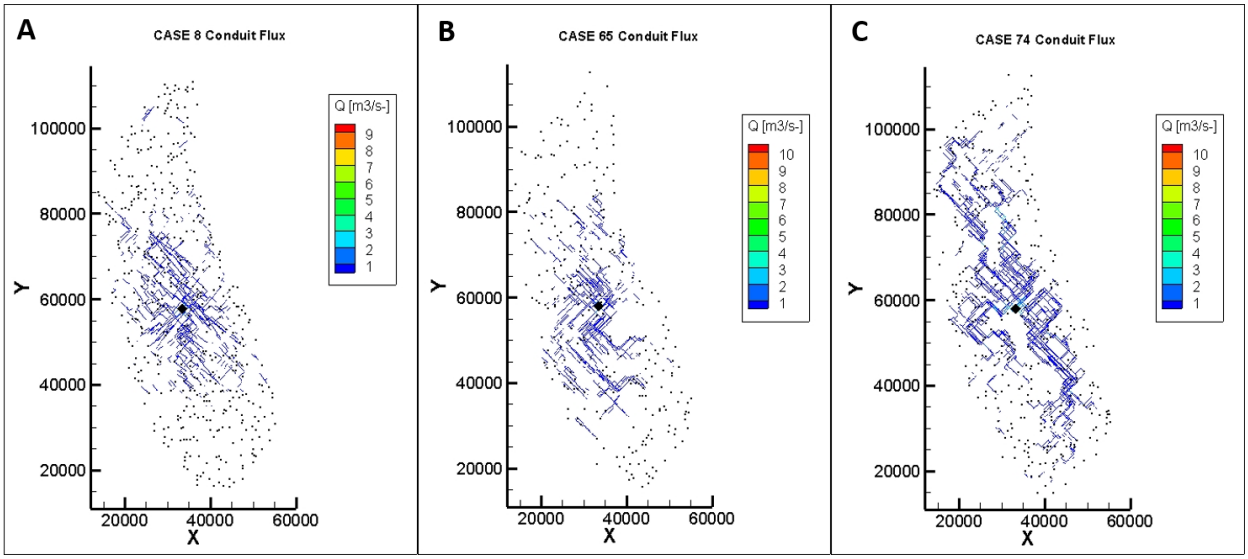

Figure 2.1.15. Three behavioral conduit networks with the same transport peak time but increasing steady-state flux from left to right. Steady state flux for A) is 10 $m^3 s^{-1}$, B) is 18 $m^3 s^{-1}$, and C) is 24 $m^3 s^{-1}$.

Figures 2.1.16 and 2.1.17 show the steady-state hydraulic heads and conduit networks for two behavioral replicates. Case 86 (Figure 2.1.16) has low matrix hydraulic conductivity ($1E^{-8}$ m s^{-1})

and a less dense network which produce a steady state spring flow of 9.93 $m^3 s^{-1}$, and peak solute travel time of 15 years. Case 14 (Figure 2.1.17) has high matrix hydraulic conductivity ($1E^{-4}$ m s^{-1}) and a more dense paleokarst network which produce steady-state spring flow equal to total areal recharge 28.65 $m^3 s^{-1}$, and a peak solute travel time of 14 years.

Hydraulic heads in Figure 2.1.16 are significantly higher than observed in the Silver Springshed (Figure 2.2.1) due to the low matrix hydraulic conductivity. Areas of lower hydraulic head correspond quite closely to regions with significant conduit development. The dark circular features represent local low head regions around VPFs that are well-connected to the spring through the conduit network. Lower hydraulic conductivity results in more pronounced differences between conduit-influenced porous matrix cells and porous matrix cells more distant form conduits. In contrast the hydraulic head values, pattern, and smooth potentiometric surface in the higher hydraulic conductivity case 14 (Figure 2.1.17A) correspond better with observations from the Silver Springshed (Figure 2.2.1) and illustrate the smoothing influence of high porous matrix hydraulic conductivity on the potentiometric surface.

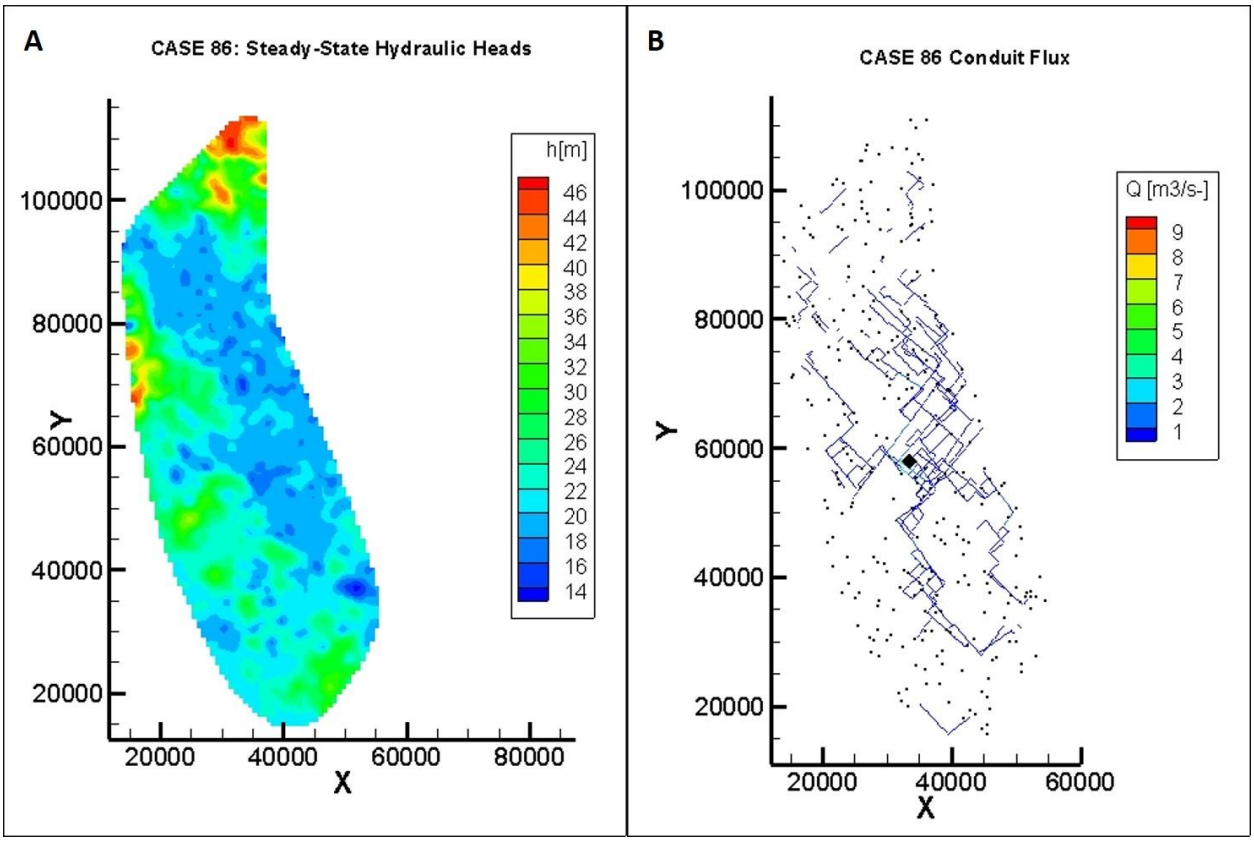

Figure 2.1.16. Lower behavioral end member with spring flow approximately equal to total 9.93 $m^3 s^{-1}$.

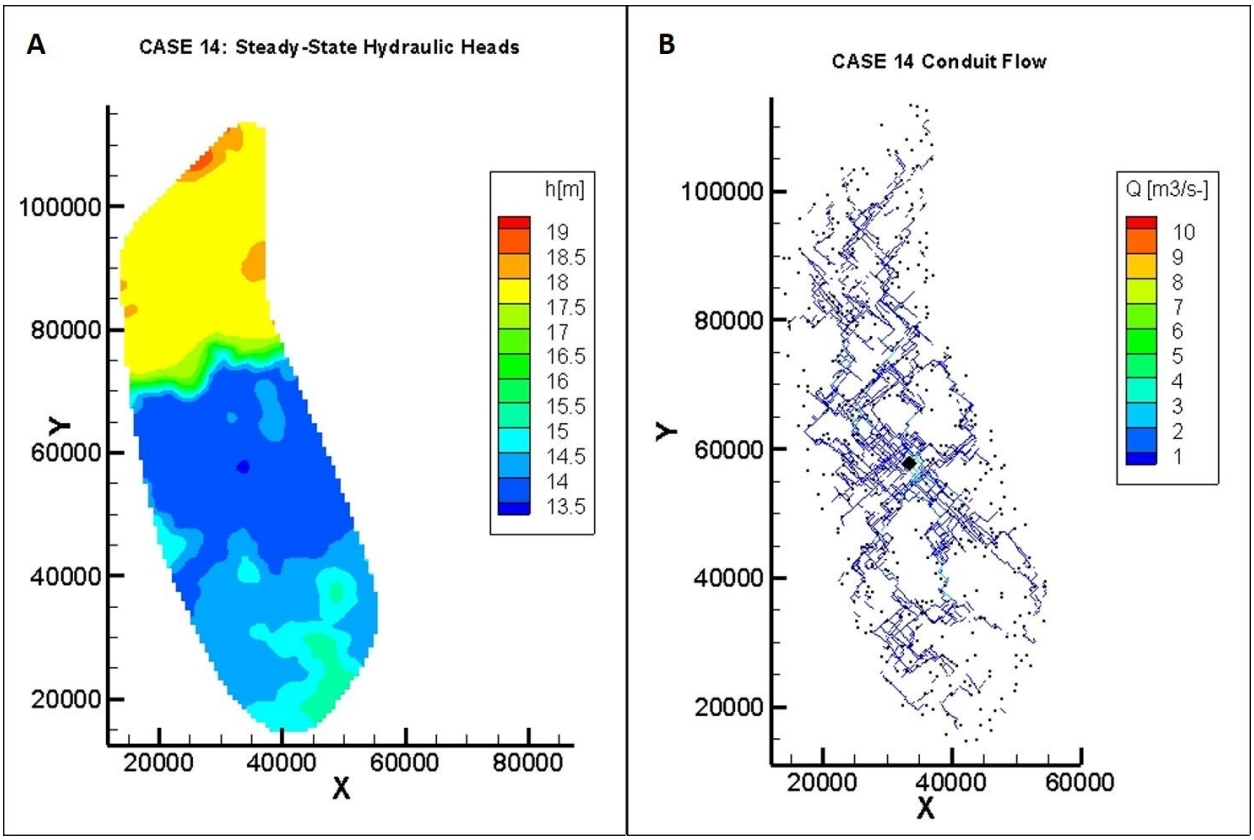

Figure 2.1.17. Upper behavioral end member with spring flow approximately equal to total 28 $m^3 s^{-1}$.

2.1.8 SUMMARY AND CONCLUSIONS

This study presented a stochastic framework for evolving conduit networks in karst aquifer systems. The framework is comprised of a preferential flowpath generation algorithm to create paleokarst templates and a 3-D hydrogeochemical model to simulate dissolution of the paleokarst templates by spatially distributed recharge that is under-saturated with respect to calcite. A generalized geologic model for karst properties and boundary conditions representative of the Silver Springshed was created using available literature, geologic reports, and insights from meetings with local hydrogeologists. This information was used to identify parameter ranges for simulation of conduit evolution and subsequent flow and transport in an idealized Silver Springshed model.

Morris Method Global Sensitivity Analyses was used to identify the porous media and paleokarst parameters that have the strongest influence on conduit development and hydrologic and solute transport metrics. Hydrologic and transport response across the ensemble of parameter ranges was used to evaluate how variability in conduit geometry and porous media properties contribute to variability in hydrographs and solute breakthrough curves.

This analysis resulted in the following insights:

- Limited combinations of porous media and paleokarst template parameters resulted in the evolution of a conduit network that generated a first magnitude spring in the idealized Silver Springshed. Parameters that increased paleokarst connectivity and decreased porous matrix conductivity were the most influential in producing first magnitude springs.
- Conduits tended to develop in topographic lows that drained nearby high regions. Steady-springflow occurred when the conduit network reached a stable configuration and the springshed contributing area stabilized.
- The Horizontal Preferential Flowpath (HPF) length scale (theta) and hydraulic conductivity were the most sensitive parameters for both hydrologic and transport pulse response metrics. Lower hydraulic conductivity and longer HPF length scales tended to produce more developed conduit networks with higher springflows and faster solute travel times. However, behavioral replicates (i.e., those that generated first magnitude springs) occurred across all hydraulic conductivity and length scale ranges suggesting that paleokarst connectivity resulting from the actual random VPF and HPF placement within the domain was a limiting factor.
- Hydrologic response for behavioral networks resulted in mean steady-state flow values of 20.48 $m^3 s^{-1}$ with a standard deviation of 6.38 $m^3 s^{-1}$, close to the long-term average Silver Springs flow of 20.9 $m^3 s^{-1}$. Peak spring flows had a mean of 25.58 $m^3 s^{-1}$ with a similar standard deviation of 6.73 $m^3 s^{-1}$.
- Solute transport breakthough curves were highly skewed. Behavioral networks resulted in peak travel times with a mean of 10 years and standard deviation of 4 years, and mean travel times with a mean of 60 years and a standard deviation of 40 years. Peak travel time results are close to previously estimated mean groundwater age measurements reported in the literature (Phelps and Survey 2004).
- Although spring hydraulic and transport pulse response variability was relatively low among behavioral replicates, distributed head fields were more highly variable and dependent on conduit configuration and hydraulic conductivity.
- Behavioral and non-behavioral networks often had similar paleokarst template Morris Method input parameters. This suggests that in addition to the sensitive parameters identified by the Morris Method, the actual random VPF and HPF placements and their resulting connectivity may exert a large influence on the evolution of conduit networks that produce first magnitude springs. High interactions among input several parameters with low mean sensitivities further supports this premise.

2.2 MONTE CARLO SIMULATION FLOW AND TRANSPORT IN AN IDEALIZED SILVER SPRINGSHED

2.2.1 BACKGROUND

Locations of karst conduits and conduit properties are unknown and poorly constrained. Furthermore the impact of uncertainty in conduit location, density, network geometry and connectivity on hydrologic and solute transport response is not well quantified. As a result the use of models that incorporate conduit networks for regulatory or decision making purposes is limited.

As mentioned previously most models applied to the Floridan Aquifer are based on an equivalent porous medium formulation with relatively high hydraulic conductivities assigned were conduits are known or assumed to exist (Kuniansky 2016).. While this approach can provide reasonable water balances for calibrated models, hydrologic flowpath heterogeneity, which is particularly important for predicting solute transport, is neglected. Furthermore, as shown in the MM-GSA presented in the previous section, and by (Bonacci 1987), the majority of the flow in karst aquifers can occur in the conduit system. Therefore, it is important to evaluate the uncertainty of conduit location, orientation and connectivity on flow and transport in karst aquifers.

The MM-GSA presented in the previous section examined the influence of parameters governing the gamma distribution function for horizontal preferential flowpath (HPF) length, HPF density, HPF angle of orientation, vertical preferential flow path (VPF) density and properties of the porous matrix. Results indicated that the HPF gamma distribution length scale factor (theta) and hydraulic conductivity were highly influential in determining conduit network development and first order magnitude spring generation. However, the mechanisms explaining highly interactive parameters with near-zero mean sensitivity, and differences between non-behavioral and behavioral replicates, were not fully uncovered. Results suggested that variations in network connectivity imposed by the specific random placement and orientation of HPFs and VPFs, even for the same Morris Method paleokarst parameters, may have led to differences that contributed to differences in conduit network evolution.

This section presents a Monte Carlo experiment that addresses two questions 1) for specified statistical properties of the paleokarst template (HPF length pdf parameters theta and K, HPF number, HPF orientation and spread, VPF number) and fixed porous media properties that are representative of the Silver Springshed, does random placement of individual HPFs and VPFs create differences in connectivity among replicates that drive significant differences in resulting conduit networks and the tendency to create first magnitude springs; and 2) what is the uncertainty in head fields, and hydraulic and transport pulse response contributed by randomly placed VPFs and HPFs that honor paleokarst template and porous media properties representative of the Silver Springshed? To answer these questions, the statistical properties of the paleokarst network and the porous media properties were fixed in a Monte Carlo experiment, so the only random variations among replicates were the locations and orientation of individual HPFs and the locations of individual VPFs.

2.2.2 METHODS

Results of the MM-GSA showed that the ensemble mean of behavioral replicates (i.e., those that generated a first magnitude spring) reproduced observed Silver Springs flows and groundwater ages fairly well, with relatively small coefficients of variation. However, distributed head fields were more highly variable among these replicates, with some showing significant differences from observed heads in the Silver Springshed. Thus, in addition to the behavioral criteria for springflow, a second behavioral criteria for hydraulic head was defined. North-South and East-West head transects from Silver Springs to the model domain boundaries were examined and MM-GSA replicates with hydraulic head values within 2 m of the 2010 observed potentiometric surface values (Figure 2.2.1) at each springshed boundary were considered behavioral. Combined use of the first magnitude springflow and head criteria to the screen the MM-GSA replicates resulted in only two behavioral replicates: 14 and 81. These networks had similar flow and transport metrics (Table 2.2.1) and similar paleokarst and porous media parameters (Table 2.2.2). In particular, both replicates had the highest hydraulic conductivity values included in the MM-GSA (i.e., $1E^{-4}$). Paleokarst and porous media properties near the mean of the two behavioral replicates were selected and fixed (Table 2.2.2), allowing only the individual placement and orientation of HPFs and the individual location of VPFs to be random in the Monte Carlo experiment.

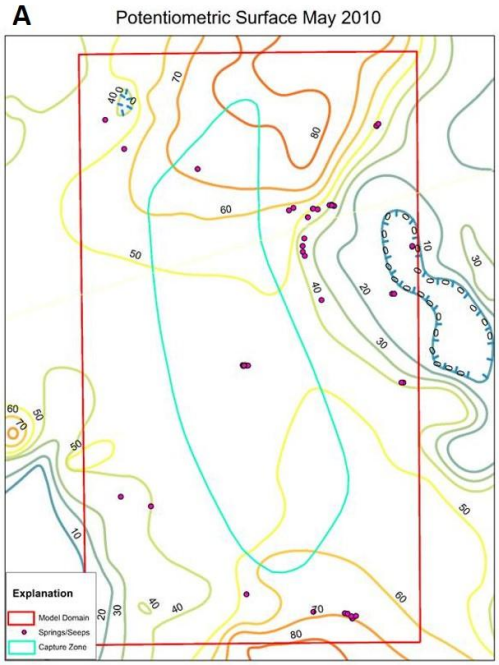

Figure 2.2.1. Potentiometric surface maps for Silver Springs showing contoured potentiometric surface in ft. above mean sea level for 2010 (1 m=3.28 ft).

Table 2.2.1. Hydrologic and transport pulse metrics for MM-GSA replicates meeting the springflow and head behavioral criteria for Silver Springs.

	Peak Flow ($m^3 s^{-1}$)	Steady-State Flow ($m^3 s^{-1}$)	Transport Peak Time (years)	Peak Solute Mass Flux ($kg s^{-1}$)
Case 14	30.00	28.90	14	1.72
Case 81	34.97	28.94	15	1.30

Table 2.2.2. Morris Method parameters for MM-GSA replicates meeting the springflow and head behavioral criteria for Silver Springs and parameters used in the Monte Carlo experiment.

	K	Theta	Number VPF	Number of HPF	Hydraulic Conductivity ($m s^{-1}$)	Spread (°)	Porosity	Specific Storage (m^{-1})
Case 14	1.17	6,000	500	3,000	$1E^{-4}$	20	0.25	$3.4E^{-5}$
Case 81	1.58	4,000	200	3,500	$1E^{-4}$	40	0.35	$6.7E^{-5}$
Average	1.375	5,000	350	3,250	$1E^{-4}$	30	0.3	$5.1E^{-5}$
Monte Carlo Parameters	1.5	5,000	350	3,250	$1E^{-4}$	30	0.3	$1E^{-5}$

Springs integrate springshed behaviors through converging flowpaths. As a result spring solute breakthough curves from instantaneous surface solute pulses are typically smooth and cannot reveal vulnerable areas of the springshed that contribute to early arrival of solute at the spring. Therefore, in addition to the forward hydraulic and solute pulse experiments conducted for the MM-GSA, a backward solute pulse experiment from the spring outlet was conducted for this Monte Carlo simulation. A backwards pulse equal to the 1 kg m^{-2} over the entire springshed area was applied at the spring. The velocity field was reversed, the simulation was run for 1,250 years, and the breakthrough of solute at the model land surface was observed. Distributed spatial plots of the mean and standard deviation of the head field, 0^{th} solute moment (total mass arriving at the land surface), peak travel time to the land surface and median travel time to the surface were produced to investigate vulnerable locations within the springshed. Median travel times (i.e., tome at which 50% of the solute has arrived) were evaluated rather than mean travel times due to the large tailing behavior of the solute breakthrough at the land surface.

Monte Carlo replicates were generated and run through the dissolution, hydraulic pulse and solute pulse experiments until the ensemble mean values for the flow and transport outputs of interest converged for the entire ensemble. Mean convergence was tested using the T test to test the null hypothesis that the ensemble means were equal among successive sets of 100 replicates.

2.2.3 RESULTS AND DISCUSSION

Convergence of ensemble output means occurred after 400 replicates. All p values for the hydraulic and forward transport pulse output metrics (Table 2.2.3) and head transects in the cardinal directions (Table 2.2.4) were greater than 0.7, allowing the acceptance of the null hypothesis that the means were equal. For the head transects only the means of the individual head values along the transect and their t-statistics are provided in the table; however, each location along each transect met the above criteria.

Table 2.2.3. Output statistic convergence results for Monte Carlo simulations.

Output Statistic	Mean 300 Replicates	Mean 400 Replicates	T statistic	p-value
Steady-State Flow (m^3 s^{-1})	5.71	5.39	-0.14	0.89
Peak Flow (m^3 s^{-1})	5.94	5.62	0.36	0.72
Transport Peak Time (years)	20.26	20.30	0.200	0.75
Peak Solute Mass Flux (kg s^{-1})	0.29	0.31	0.25	0.71
Mean Travel Time (years)	70.95	71.01	-0.17	0.89
Travel Time Standard Deviation (years)	95.97	96.11	0.41	0.71

Table 2.2.4. Head Transect output statistic convergence results for Monte Carlo Simulations.

Output Statistic	Mean 300 Replicates	Mean 400 Replicates	Mean T statistic	Mean p-value
East transect	18.94	18.87	-0.35	0.73
North transect	20.95	24.08	-0.41	0.68
South transect	19.74	19.39	-0.35	0.73
West transect	19.48	19.45	-0.34	0.73

As mentioned in the previous section, in the MM-GSA only four of the 20 replicates with the highest hydraulic conductivity (i.e., $1E^{-4}$) produced first magnitude springs. As a result, the number of behavioral Monte Carlo replicates was also expected to be low. In fact, only 88 out of the 400 Monte Carlo replicates were behavioral for the first magnitude spring criterion, and only 37 of these were behavioral for the additional hydraulic head criterion. This shows that, particularly for the case of high hydraulic conductivity, the random placement of individual HPF and VPF elements within the domain exerts significant control on behavioral conduit network development, even when the HPFs and VPFs have the same statistical properties.

2.2.3.1 Hydrologic and Forward Transport Response

Hydrologic and transport metrics (Table 2.2.5), hydrographs (Figure 2.2.2), head transects (Figure 2.2.3), and forward solute pulse breakthrough curves (Figure 2.2.4) for the full Monte Carlo ensemble showed substantial variability in dissolution, hydrologic, and transport behavior.

For example, the coefficient of variation for steady-state flow was 2.1, peak flow was 2.1, peak forward solute travel time 3.1, and mean forward solute travel time was 0.3.

Table 2.2.5. Complete ensemble mean and standard deviation for hydrologic and forward transport metrics.

Statistic	Steady-State Flow ($m^3 s^{-1}$)	Peak Flow ($m^3 s^{-1}$)	Transport Peak Time (years)	Peak Solute Mass Flux ($kg s^{-1}$)	Mean Travel Time (years)	Travel Time Standard Deviation (years)
Min	0.0	0.0	0.0	0.0	0.0	0.0
Max	28.7	35.8	67	1.5	300	147
Mean	5.4	5.6	20	0.3	71	96
Standard Deviation	11.3	11.7	62	0.6	24	23
Coefficient of variation	2.1	2.1	3.1	2.0	0.3	0.2

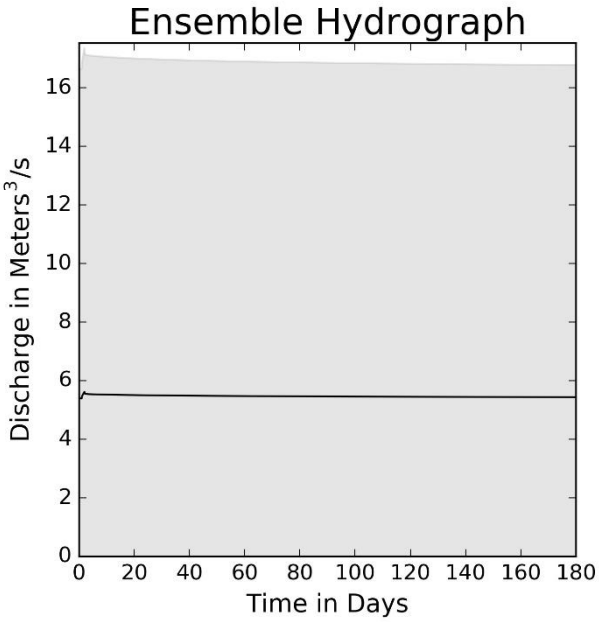

Figure 2.2.2. Complete ensemble hydrograph showing mean (black line) and standard deviation (gray shaded region).

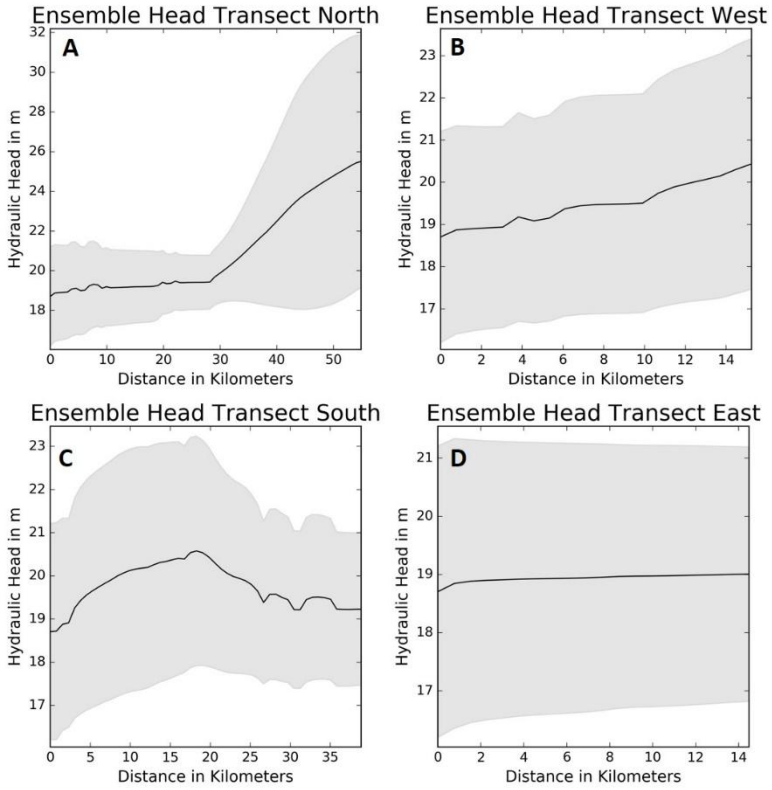

Figure 2.2.3. Complete ensemble head transects showing mean (black line) and standard deviation (gray shaded region). Spring is at zero on x-axis and distances are in the direction away from the spring. A) north transect, B) west transect, C) south transect, and D) east transect.

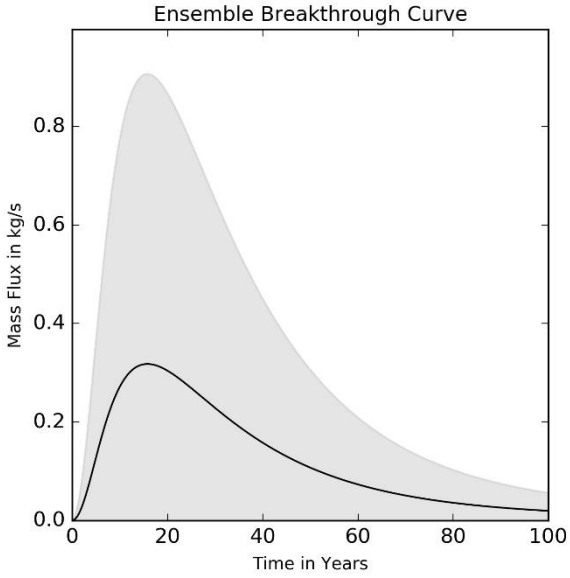

Figure 2.2.4. Complete ensemble forward breakthough curve showing mean (black line) and standard deviation (gray shaded region).

Hydraulic pulse response statistics and hydrographs for the 37 behavioral replicates (Table 2.2.6 and Figure 2.2.5) showed that variation among behavioral networks was very small. If a first magnitude spring developed in a particular replicate, it tended to capture all of the applied recharge and springflows tended to the value of the really integrated recharge, with a mean value of 29.2 $m^3 s^{-1}$, low standard deviation (0.15 $m^3 s^{-1}$), and extremely low CV (0.01). Similarly, mean peak flow for behavioral replicates was 30.4 $m^3 s^{-1}$ with a CV of 0.03.

Table 2.2.6. Behavioral ensemble mean and standard deviation for hydrologic and transport metrics.

Statistic	Steady-State Flow ($m^3 s^{-1}$)	Peak Flow ($m^3 s^{-1}$)	Transport Peak Time (years)	Peak Solute Mass Flux ($kg s^{-1}$)	Mean Travel Time (years)	Travel Time Standard Deviation (years)
Min	28.9	29.6	13.3	1.30	54.7	74.8
Max	29.7	35.8	18.7	1.54	67.1	94.9
Mean	29.2	30.4	15.8	1.42	59.4	84.1
Standard Deviation	0.15	1.0	1.1	0.05	2.6	3.9
Coefficient of variation	0.01	0.03	0.07	0.03	0.04	0.05

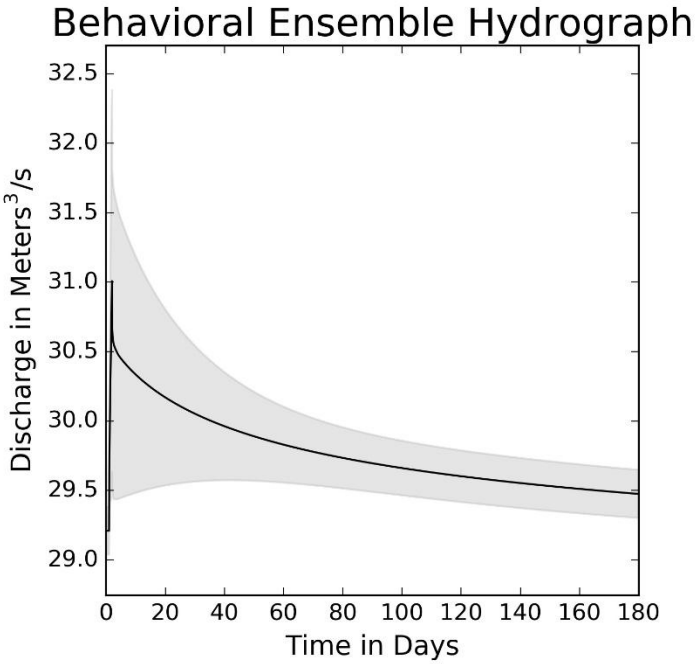

Figure 2.2.5. Behavioral ensemble hydrograph showing mean (black line) and standard deviation (gray shaded region).

Mean head transects for behavioral replicates also showed fairly small standard deviation with values of approximately less than approximately 1m in each cardinal direction near the spring and approximately 2 m by the boundary (Figure 2.2.6).

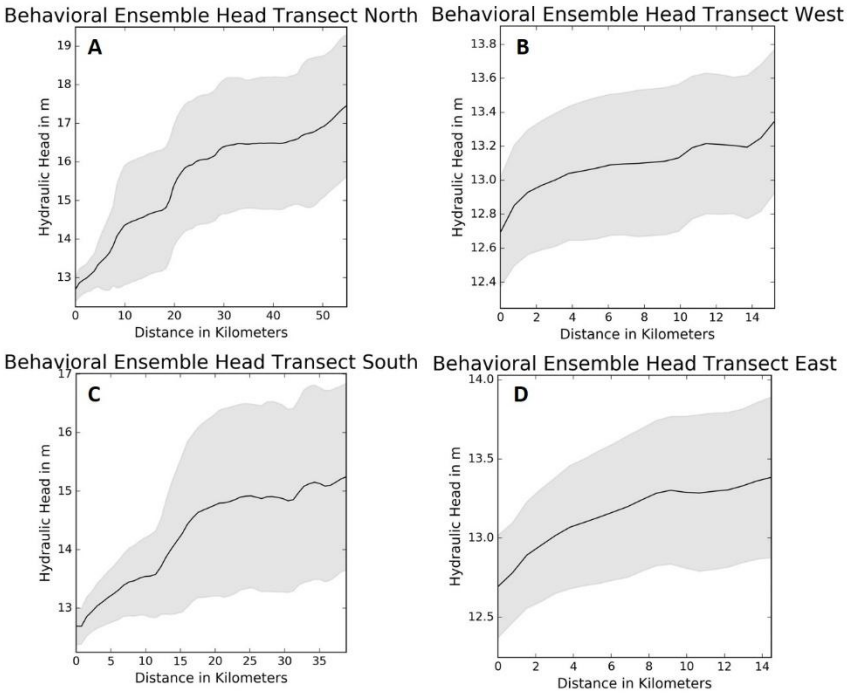

Figure 2.2.6. Behavioral ensemble head transects showing mean (black line) and standard deviation (gray shaded region). Spring is at zero on x-axis and distances are in the direction away from the spring. A) north transect, B) west transect, C) south transect, and D) east transect.

Forward breakthrough curves (Figure 2.2.7) for the behavioral ensemble showed limited variability. Ensemble mean peak forward travel times for the behavioral replicates were 15.8 years (Table 2.2.6), similar to previously measured mean groundwater ages of approximately 10 to 30 years (Phelps and Survey 2004). The mean forward travel time (first normalized temporal moment) for behavioral replicates was approximately 60 years, and the mean forward travel time standard deviation (square root of second centralized moment) was approximately 84 years, indicative of the highly skewed mean solute breakthrough curve with long tailing behavior. Coefficients of variation of transport solute metrics were very small; the CV of the peak solute mass flux was 0.03 peak solute arrival time was 0.07, mean travel time was 0.04, and travel time standard deviation was 0.05. This low variability in steady flow, heads, hydraulic pulse breakthrough curves and forward solute pulse breakthrough curves across behavioral replicates suggests that knowing the actual spatial configuration of the conduit network may not be important to accurately predicting integrated spring measures within the set of behavioral replicates, as long as conduits that honor what is known about the topography, geology, hydrology and climate are represented in the model.

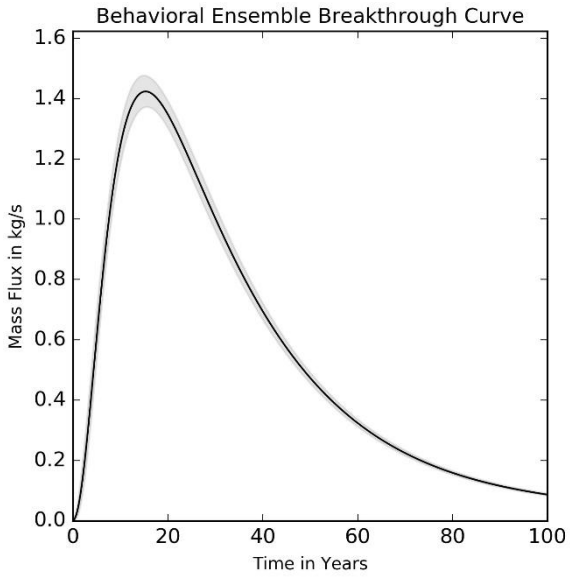

Figure 2.2.7. Behavioral ensemble forward breakthough curve showing mean (black line) and standard deviation (gray shaded region).

2.2.3.2 Backward Transport Pulse

A backwards transport pulse experiment at the spring outlet was conducted on the behavioral replicates and maps of the spatial distribution of the mean (Figure 2.2.8) and standard deviation (Figure 2.2.9) of the hydraulic head, 0^{th} solute moment (total mass arriving at the land surface) peak travel time to the land surface, and median travel time to the land surface within the springshed were produced. Mean hydraulic heads (Figure 2.2.8A) reasonably reproduce the 2010 Silver Springshed potentiometric surface (Figure 2.2.1). The mean 0^{th} solute moment map (Figure 2.2.8B) shows that the mass exits the domain evenly over the entire springshed surface; however, the mean peak arrival time at the land surface (Figure 2.2.8C) shows significant spatial variability. Mean peak arrival times between 10 and 20 years occur in regions to the west and northwest of the spring, and mean peak arrival times less than 30 years occur in an elongated region stretching north and south of the spring. The shape of mean median arrival time contours (Figure 2.2.8D) are similar to the mean peak travel time contours but more clearly show lower values in topographic lows in the central part of the domain where conduits tended to develop. The standard deviation maps (Figure 2.2.9) indicate there is relatively little variability among the behavioral replicates for either hydraulic head or the backward transport parameters. In particular there is no uncertainty in the 0^{th} solute moment map (Figure 2.2.9B), and in areas of the domain where mean arrival times are more rapid the standard deviations around the mean estimates are quite low (Figures 2.2.9CD). The dark blue region of the peak arrival time standard deviation map (Figure 2.2.9C) indicates a large vulnerable region stretching north and south of the spring where peak travel times of less than 30 years are predicted for the behavioral replicates with low uncertainty.

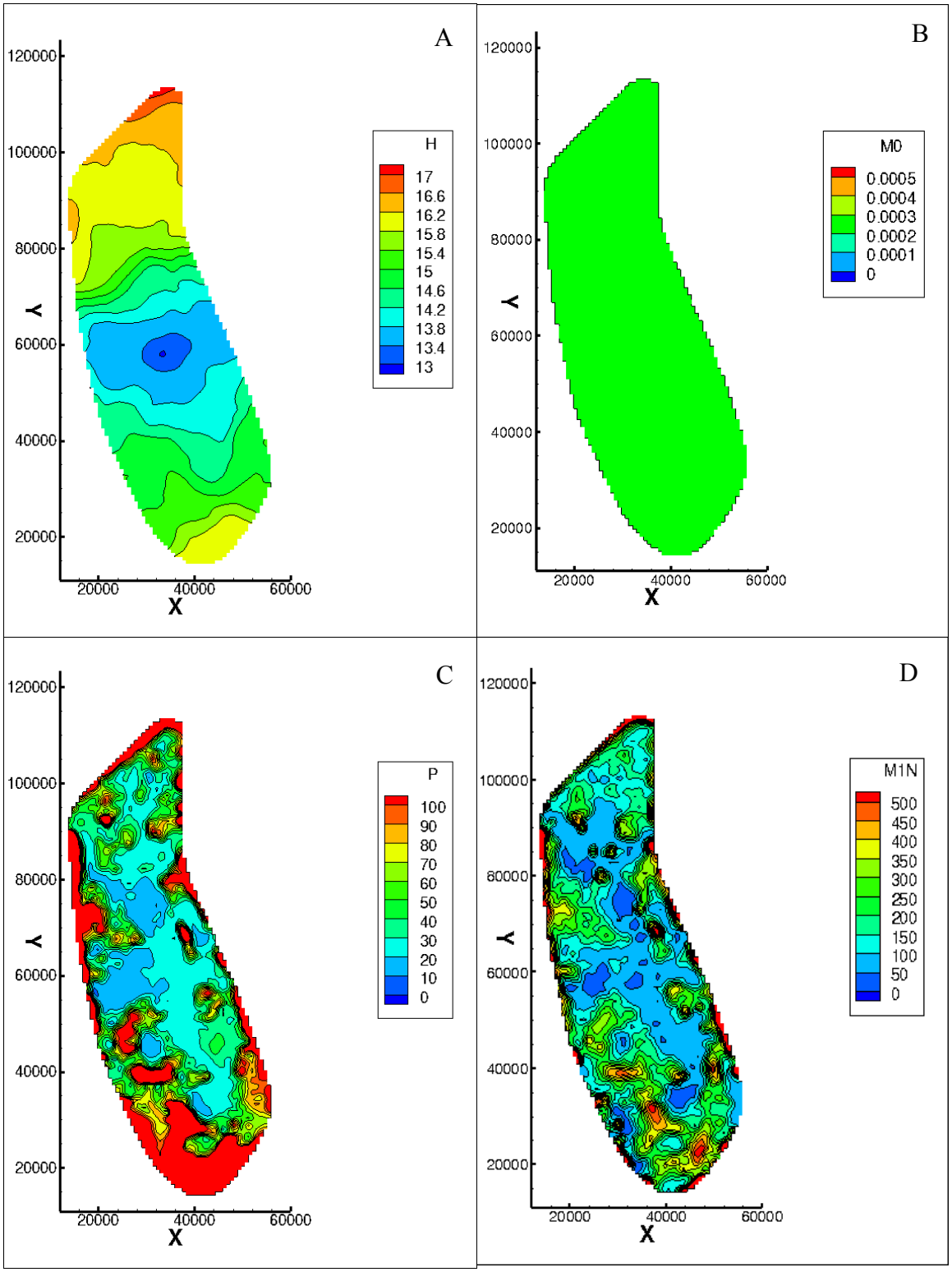

Figure 2.2.8. Mean of behavioral ensemble head, 0^{th} moment (mass arriving at surface), peak arrival time and median arrival time for backward pulse experiment.

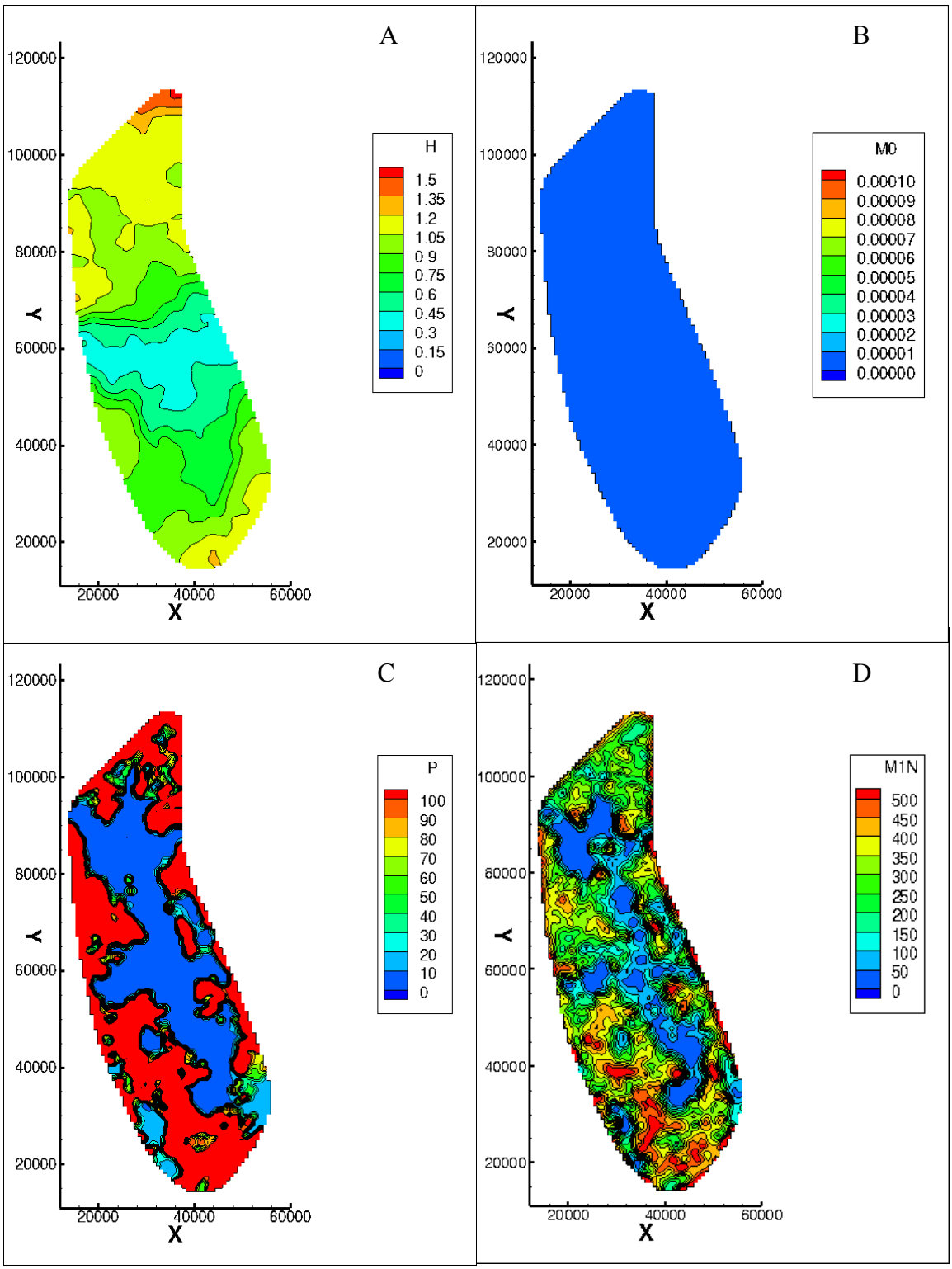

Figure 2.2.9. Standard Deviation of behavioral ensemble head, 0^{th} moment (mass arriving at surface), peak arrival time and median arrival time for backward pulse experiment.

2.2.3.3 Investigation of Individual Behavioral Replicates

To further understand the variability in behavioral replicates, two example behavioral replicates were compared, cases 79 and 83. The density of the paleokarst network for the chosen replicates was representative of both non-behavioral and behavioral networks (Figures 2.2.10A and 2.2.12A). The hydraulic heads in behavioral replicates 79 and 83 differed, but showed similar spatial patterns with a low, flat area in the center of the domain near the spring and high head areas in the northern and southern portions of the domain (Figures 2.2.10B and 2.2.12B). The conduit networks after dissolution were different but have similar characteristics as previously observed behavioral replicates; extensive development of networks near the spring and long branches that extend up through lower topographic regions to the northern and southern boundaries (Figure 2.2.10C and 2.2.12C).

Figures 2.2.11 and 2.2.13 show results of the backward pulse responses for case 79 and 83 respectively. Both replicates confirm that mass exits uniformly throughout the domain (Figures 2.2.11A and 2.2.13A). Peak solute travel times to the surface as a result of the backward pulse (Figures 2.2.11B and 2.2.13B) illustrate the importance of VPFs and the conduit network configuration to determining vulnerable areas of the springshed that quickly contribute solute to the spring outlet. For both replicates a region northwest of the spring on the western boundary in a relatively high topographic area not directly adjacent to the spring (Figure 2.1.5), showed the fastest peak pulse arrival times (i.e., less than 10 years). The mean travel times maps (Figures 2.2.11C and 2.2.13C) show regions with exit times less than 50 years occurring in very close proximity to the developed conduit networks.

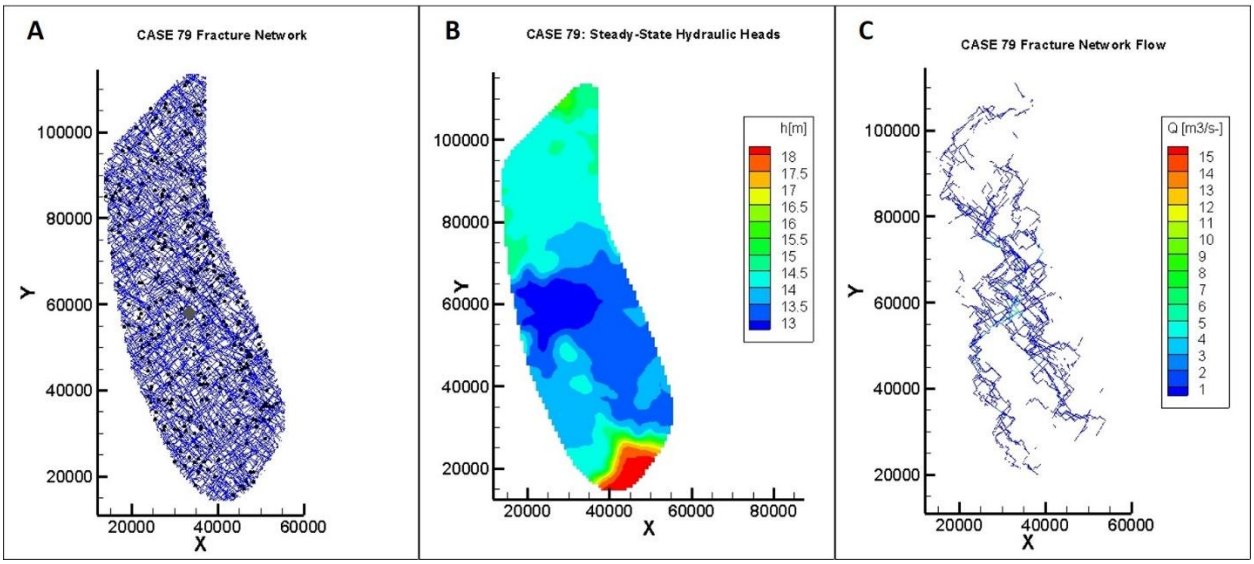

Figure 2.2.10. Behavioral case 79 showing A) initial HPF network, B) steady-state hydraulic heads, and C) developed conduit network.

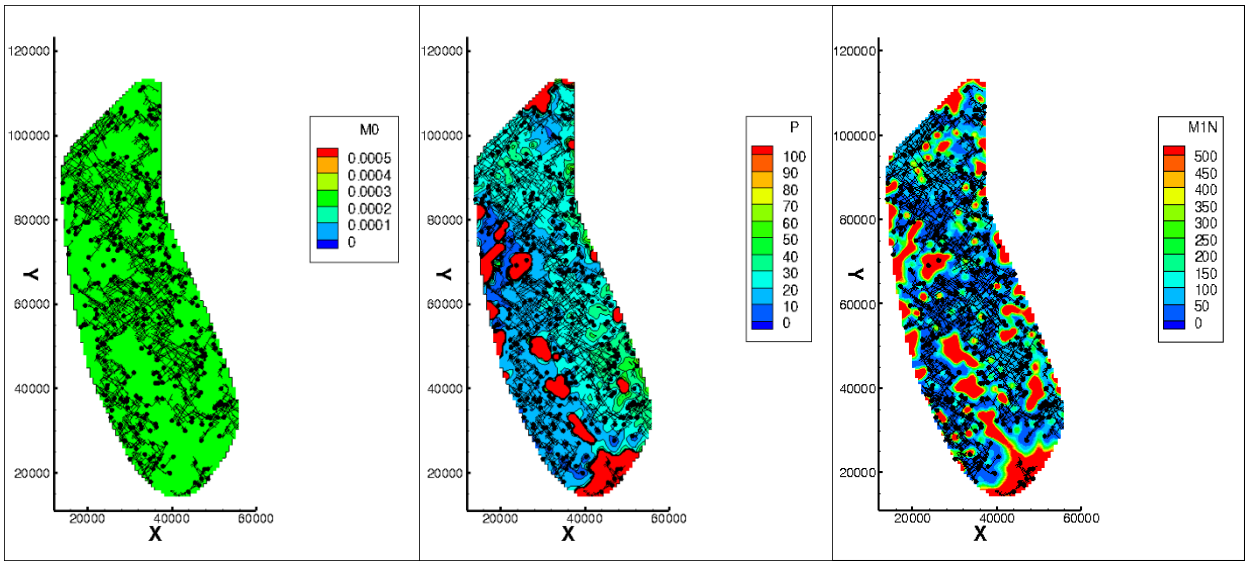

Figure 2.2.11. Backwards transport pulse for case 79 showing A) mass recovery (0th moment) B) peak arrival time, and C) median arrival at the land surface. Black lines represent evolved conduits. Black dots represent VPFs.

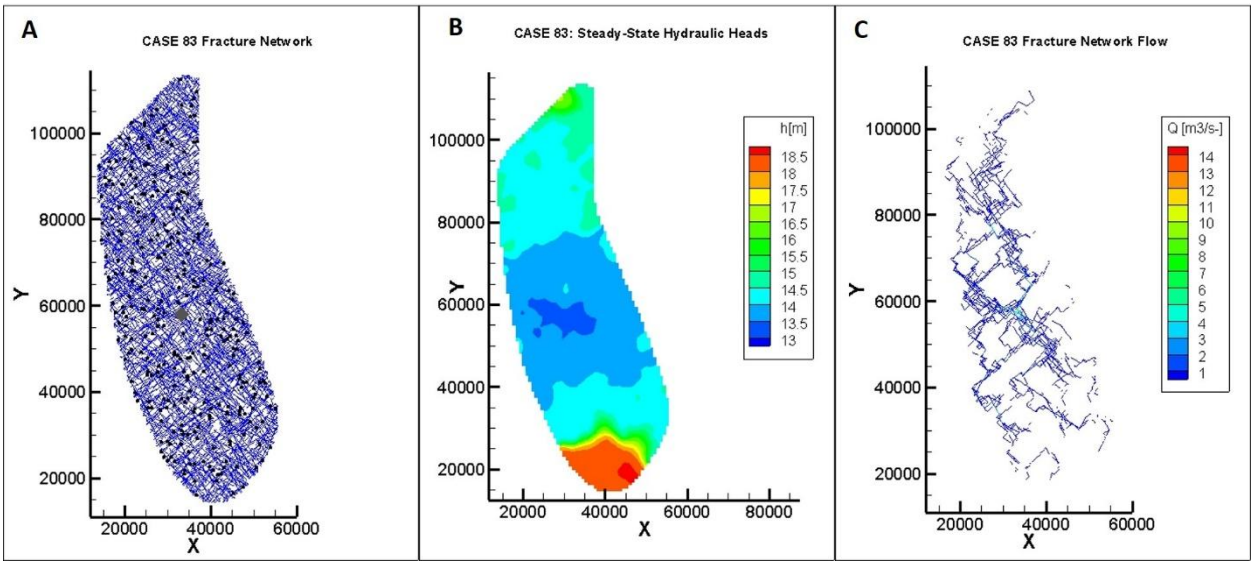

Figure 2.2.12. Behavioral case 83 showing A) initial HPF network, B) steady-state hydraulic heads, and C) developed conduit network.

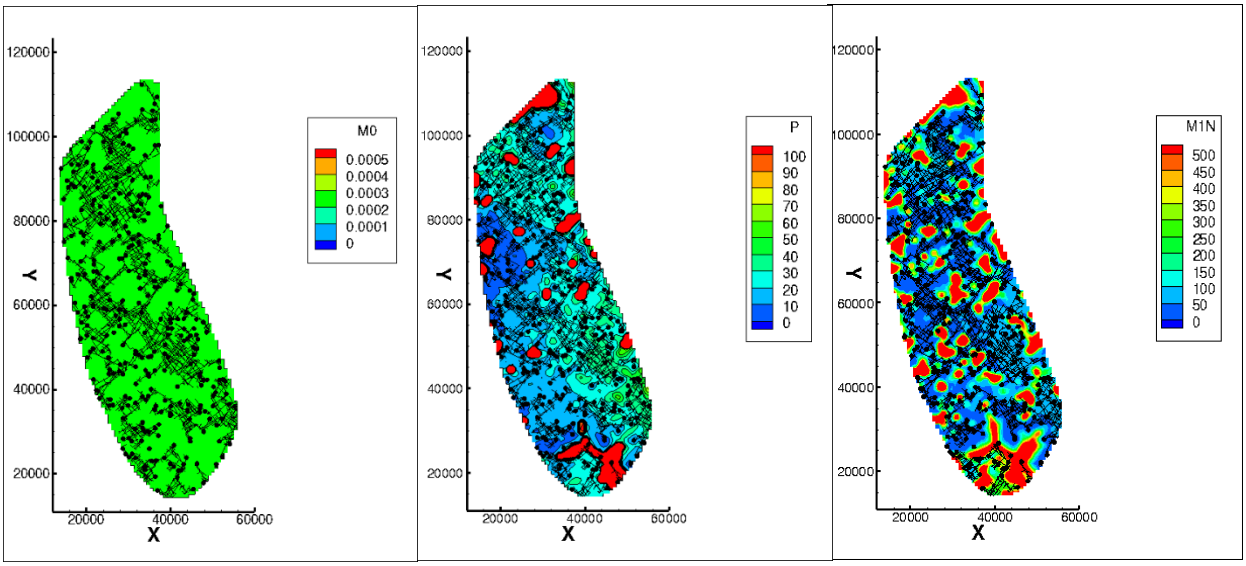

Figure 2.2.13. Backwards transport pulse for case 83 showing A) mass recovery (0th moment) B) peak arrival time, and C) median arrival at the land surface. Black lines represent evolved conduits. Black dots represent VPFs.

Finally, for comparison purposes Figure 2.2.14 shows the head fields and backward transport moments for a hypothetical equivalent porous media model with layer 1-4 hydraulic conductivity equal to $5E^{-2}$ m s^{-1} and layer 5-7 hydraulic conductivity equal to $1E^{-3}$ m s^{-1}. As expected the head field is smooth (Figure 2.2.14A) and mass exits the domain uniformly over the entire land surface (Figure 2.2.14B). Peak arrival time and median arrival time maps (Figure 2.2.14C and 2.2.14D, respectively) show smooth concentric contours with very different spatial patterns for travel times to the land surface than either of the behavioral replicates or the ensemble mean of the behavioral replicates.

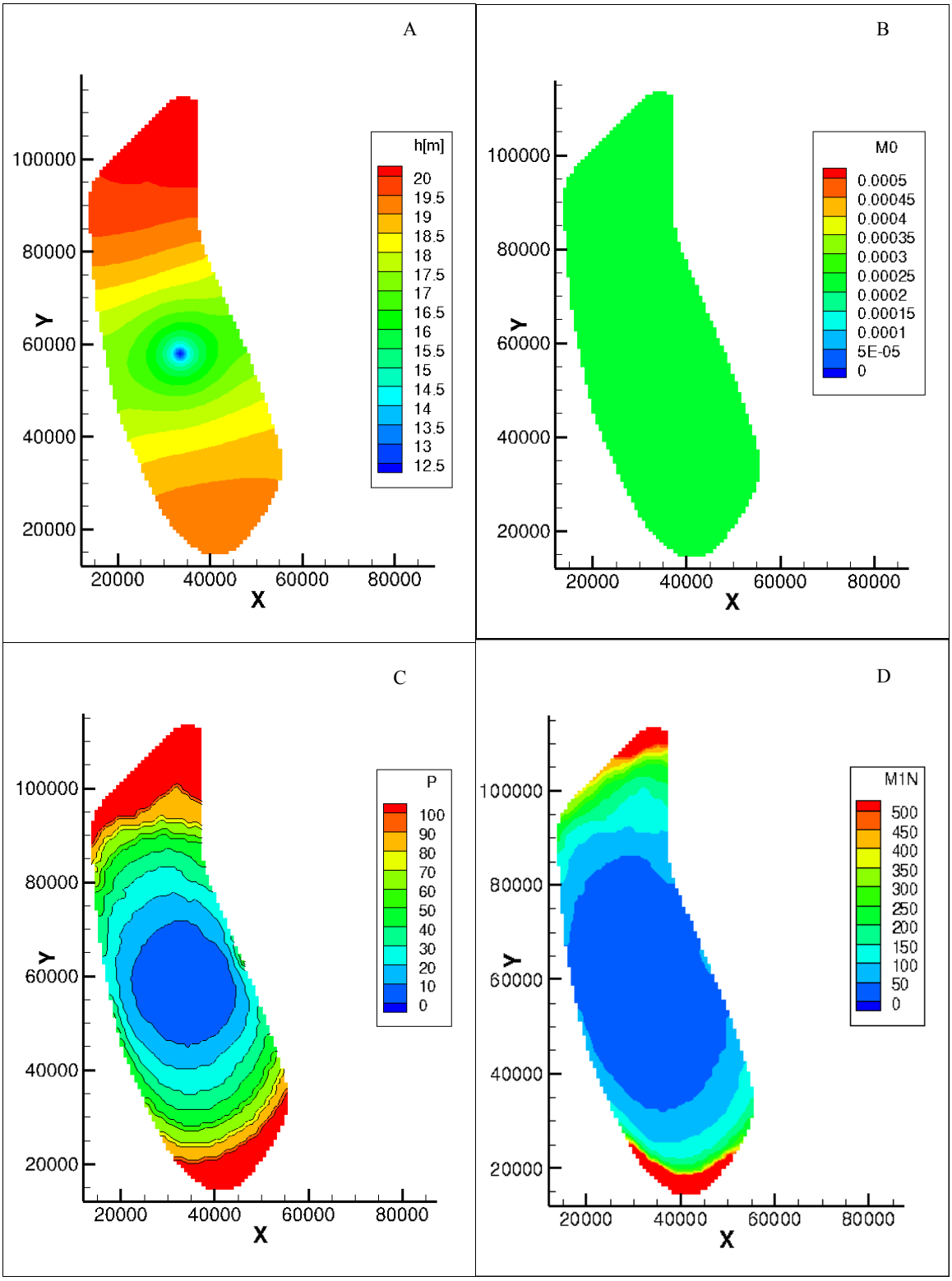

Figure 2.2.14. Head, 0th moment (mass arriving at surface), peak arrival time and median arrival time for equivalent porous media model.

2.2.4 SUMMARY AND CONCLUSIONS

Differences in mean behaviors between the entire Monte Carlo ensemble and the behavioral ensemble indicated that individual connectivity of horizontal and vertical preferential flow paths within a particular replicate of the Monte Carlo experiment exerted important control on conduit evolution and resulting springflows. Although the ensemble statistical paleokarst properties underlying each replicate were the same, variations in the resulting connectivity of the paleokarst elements resulted in a small number of behavioral systems (30 out of 400) that generated a first order magnitude spring and had head fields similar to those observed in the Silver Springshed. The small number of behavioral samples indicates that the statistical parameters of the VPF and HPF distributions and the hydraulic conductivity of the porous matrix are not the only drivers, and perhaps not the most significant drivers, of first magnitude spring development in the idealized Silver Springshed studied here.

Consistent springflows among behavioral replicates (i.e., small standard deviation and coefficient of variations of spring flows) indicates that spring development was "all or nothing" for the parameter values explored here. Recharge was either lost completely to the surface boundary (resulting in steady-state spring flow of < 0.1 m^3 s^{-1} for non-behavioral replicates) or it was directed completely to the spring outlet (resulting in spring flow equal to total areal recharge for behavioral replicates). Low standard deviations for flow and transport metrics among behavioral replicate indicate that, for the cases investigated here, paleokarst connectivity is extremely important in determining whether a spring will form, but once it is formed knowledge of the actual location of preferential paths may not be important for accurately predicting hydraulic and solute pulse response at the spring vent or vulnerable regions in the watershed.

The backwards tracer pulse experiments illustrated that spatially variable differences vulnerability across the springshed exist. For the boundary conditions and parameters assumed for this Monte Carlo simulation vulnerable regions (where mean peak arrival times were estimated to be between 10 and 20 years) were identified to the west and northwest of the spring. The mean median arrival time contours clearly showed lower mean travel times in topographic low regions in the central part of the domain where conduits tended to develop. In general, topography and conduit network geometry interacted to impact springshed vulnerability. This emphasizes the importance of including conduit networks in vulnerability mapping exercises, and suggests that simulating transport using equivalent porous media flow and transport models is insufficient to characterize springshed vulnerability or plan cost-effective land management strategies for reducing contaminant concentrations in spring flows.

Hydrologic models used for springshed management typically neglect the influence of preferential flow pathways on hydrologic and transport response due to lack of information about the location and properties of preferential flow pathways. This study developed a new methodology to generate a stochastic ensemble of possible karst conduit networks that honor what is known about the topography, geology, hydrology and climate of the system under study. The resulting hydrogeochemical model was used in a Monte Carlo framework to simulate the widening of conduits over geological timescales, and subsequently to simulate flow and solute transport within an evolved karst aquifer representative of the Silver Springshed. Results of the Monte Carlo experiment indicates that incorporating preferential flow processes into the

hydrologic model is important, but that once incorporated spatiotemporally integrated flow and transport behavior at springs can be predicted with relatively low uncertainty. Furthermore Monte Carlo results confirmed that conduit networks lead to spatially heterogeneous vulnerable regions in the aquifer; however, vulnerable regions in the idealized Silver Springshed were identified with relatively low uncertainty. Combining Monte Carlo analysis of behavioral networks and backwards tracer pulse experiments on a calibrated Silver Springs model would enhance current efforts to identify vulnerable areas of the Silver Springshed that could be targeted for management interventions.

2.3 REFERENCES

Andersson, J., Shapiro, A. M. and Bear, J. 1984. A stochastic model of a fractured rock conditioned by measured information. Water Resources Research 20 (1): 79–88.

Andre, B. J. and Rajaram, H. 2005. Dissolution of limestone fractures by cooling waters: Early development of hypogene karst systems. Water Resources Research. 41(1).

Atkinson, T. C. 1977. Diffuse flow and conduit flow in limestone terrain in the Mendip Hills, Somerset (Great Britain). Journal of Hydrology 35 (1-2): 93–110 DOI: 10.1016/0022-1694(77)90079-8.

Baedke, S., and Krothe, N. C. 2001. Derivation of effective hydraulic parameters of a karst aquifer from discharge hydrograph analysis. Water Resour. Res. 37 (1): 13–19.

Batu, V. 1998. Aquifer hydraulics: a comprehensive guide to hydrogeologic data analysis. John Wiley & Sons.

Bauer, S., Liedl, R., and Sauter, M. 2005. Modeling the influence of epikarst evolution on karst aquifer genesis: A time-variant recharge boundary condition for joint karst-epikarst development. Water Resources Research 41 (9): 1–12 DOI: 10.1029/2004WR003321.

Beck, B. F. 1986. A generalized genetic framework for the development of sinkholes and karst in Florida, USA. Environmental Geology and Water Sciences 8 (1-2): 5–18.

Beek, W. and Muttzall, K. Transport Phenomena, 1975, J. Wiley & Sons, XP009060252.

Birk, S. 2003. Hydraulic boundary conditions as a controlling factor in karst genesis: A numerical modeling study on artesian conduit development in gypsum. Water Resources Research 39 (1): 1–14 DOI: 10.1029/2002WR001308.

Birk, S., Liedl, R., and Sauter, M. 2004. Identification of localised recharge and conduit flow by combined analysis of hydraulic and physico-chemical spring responses (Urenbrunnen, SW-Germany). Journal of hydrology 286 (1): 179–193.

Bonacci, O. 1987. Karst Hydrology. Herdelberg, Germany.

Bonacci, O. 1993. Karst springs hydrographs as indicators of karst aquifers. Hydrological Sciences Journal 38 (August): 51–62 DOI: 10.1080/02626669309492639.

Borghi, A., Renard, P., and Cornaton, F. 2016. Can one identify karst conduit networks geometry and properties from hydraulic and tracer test data? Advances in Water Resources 90: 99–115.

Borghi, A., Renard, P., and Jenni, S. 2010. How to Model Realistic 3D Karst Reservoirs Using a Pseudo-Genetic Methodology–Example of Two Case Studies. In Advances in Research in Karst MediaSpringer; 251–255.

Borghi, A., Renard, P., and Jenni, S. 2012. A pseudo-genetic stochastic model to generate karstic networks. Journal of Hydrology 414-415: 516–529 DOI: 10.1016/j.jhydrol.2011.11.032.

Cacas, M. C., Ledoux, E., Marsily, G. de, Barbreau, A,, Calmels, P., Gaillard, B., and Margritta, R. 1990. Modeling fracture flow with a stochastic discrete fracture network: Calibration and validation: 2. The transport model. Water Resources Research 26 (3): 491–500.

Campolongo, F., Cariboni, J., and Saltelli, A. 2007. An effective screening design for sensitivity analysis of large models. Environmental Modelling and Software 22 (10): 1509–1518 DOI: 10.1016/j.envsoft.2006.10.004.

Ceryak, R., Knapp, M. S., and Burnson, T. 1983. The geology and water resources of the upper Suwannee River basin, Florida. Published for the Bureau of Geology, Division of Resource Management, Florida Department of Natural Resources.

Chang, Y., Wu, J., and Liu, L. 2015. Effects of the conduit network on the spring hydrograph of the karst aquifer. Journal of Hydrology 527: 517–530 DOI: 10.1016/j.jhydrol.2015.05.006.

Chaudhuri, A., Rajaram, H. and Viswanathan, H. 2013. Early-stage hypogene karstification in a mountain hydrologic system: A coupled thermohydrochemical model incorporating buoyant convection. Water Resources Research.49(9):5880-99.

Clemens, T., Huckinghaus, D., Liedl, R. and Sauter, M. 1999. Simulation of the development of karst aquifers: role of the epikarst. International Journal of Earth Sciences. 1999;88(1):157-62.

Confalonieri, R., Bellocchi, G., Bregaglio, S., Donatelli, M., and Acutis, M. 2010. Comparison of sensitivity analysis techniques: A case study with the rice model WARM. Ecological Modelling 221 (16): 1897–1906 DOI: 10.1016/j.ecolmodel.2010.04.021.

Cooley, R. L. 1983. Some new procedures for numerical-solution of variably saturated flow problems. Water Resources Research.19(5):1271-85.

Cornaton, F. 1999. Utilisation des modeles continu discret et a double continuum pour l'analyse des reponses globales de l'aquifere karstique.Universite de Neuchatel.

Covington, M. D., Wicks, C. M. and, Saar, M. O. 2009. A dimensionless number describing the effects of recharge and geometry on discharge from simple karstic aquifers. Water Resources Research 45 (11): 1–16 DOI: 10.1029/2009WR008004.

Dafny, E., Burg, A., and Gvirtzman, H. 2010. Effects of Karst and geological structure on groundwater flow: The case of Yarqon-Taninim Aquifer, Israel. Journal of Hydrology 389 (3-4): 260–275 DOI: 10.1016/j.jhydrol.2010.05.038.

Denizman, C. 1998. EVOLUTION OF KARST IN THE LOWER SUWANNEE RIVER BASIN, FLORIDA.University of Florida. DOI: 10.16953/deusbed.74839.

Detwiler, R. L. and Rajaram, H. 2007. Predicting dissolution patterns in variable aperture fractures: Evaluation of an enhanced depth-averaged computational model. Water Resources Research. 43(4).

Dewandel, B., Lachassagne, P., Bakalowicz, M., Weng, P., and Al-Malki, A. 2003. Evaluation of aquifer thickness by analysing recession hydrographs. Application to the Oman ophiolite hard-rock aquifer. Journal of Hydrology 274 (1-4): 248–269 DOI: 10.1016/S0022-1694(02)00418-3.

Diersch, H. J. G. 2005. FEFLOW finite element subsurface flow and transport simulation system. Inst. for Water Resources Planning and System Res., Berlin.

Doummar, J., Sauter, M., and Geyer, T. 2012. Simulation of flow processes in a large scale karst system with an integrated catchment model (Mike She) - Identification of relevant parameters influencing spring discharge. Journal of Hydrology 426-427: 112–123 DOI: 10.1016/j.jhydrol.2012.01.021.

Dreybrodt, W. 1988. Processes in karst systems, physics, chemistry and geology.: Springer-Verlag, New York.

Dreybrodt, W. 1990. The role of dissolution kinetics in the development of karst aquifers in limestone: a model simulation of karst evolution. The Journal of Geology: 639–655.

Dreybrodt, W. 1996. Principles of early development of karst conduits under natural and man-made conditions revealed by mathematical analysis of numerical models. Water Resources Research 32 (9): 2923–2935 DOI: 10.1029/96WR01332.

Dreybrodt, W., Romanov, D. and Kaufmann, G.2010. Evolution of caves in porous limestone by mixing corrosion: A model approach. Geologia Croatica. 63(2):129-35.

Eisenlohr, L. 1996. Eisenlohr, L., 1996. Variabilite des reponses naturelles des aquiferes karstiques.Universite de Neuchatel.

Eisenlohr, L., Bouzelboudjen, M., Király, L., and Yvan Rossier, Y. 1997a. Numerical versus statistical modelling of natural response of a karst hydrogeological system. Journal of Hydrology 202 (1-4): 244–262 DOI: 10.1016/S0022-1694(97)00069-3.

Eisenlohr, L., Király, L., Bouzelboudjen, M., and Rossier, Y. 1997b. Numerical simulation as a tool for checking the interpretation of karst spring hydrographs. Journal of Hydrology 193 (1-4): 306–315 DOI: 10.1016/S0022-1694(96)03140-X.

Ewers, R. O. 2006. Karst aquifers and the role of assumptions and authority in science. Geological Society of America Special Papers 404 (19): 235–242 DOI: 10.1130/2006.2404(19).

Faulkner, G. L. 1970. Geohydrology of the Cross-Florida Barge Canal Area: With Special Reference to the Ocala Vicinity. DIANE Publishing.

Fiorillo, F. 2014. The Recession of Spring Hydrographs, Focused on Karst Aquifers. Water Resources Management 28 (7): 1781–1805 DOI: 10.1007/s11269-014-0597-z.

Foglia, L., Hill, M. C., Mehl, S. W., and Burlando. P. 2009. Sensitivity analysis, calibration, and testing of a distributed hydrological model using error-based weighting and one objective function. Water Resources Research 45 (6): 1–18 DOI: 10.1029/2008WR007255.

Ford, D.and, Williams, P. D. 2013. Karst hydrogeology and geomorphology. John Wiley & Sons.

Fournillon, F., Viseur, S., Arfib, B., and Borgomano, J. 2010. Insights of 3D geological modelling in distributed hydrogeological models of karstic carbonate aquifers. In Advances in Research in Karst MediaSpringer; 257–262.

Gabrovsek, F. and Dreybrodt, W. 2010. Karstification in unconfined limestone aquifers by mixing of phreatic water with surface water from a local input: A model. Journal of Hydrology. 386(1-4):130-41.

Gallegos, J. J., Hu, B, X,, and Davis, H. 2013. Simulating flow in karst aquifers at laboratory and sub-regional scales using MODFLOW-CFP. Hydrogeology Journal 21 (8): 1749–1760 DOI: 10.1007/s10040-013-1046-4.

Geyer, T., Birk, S., Liedl, R., and Sauter, M. 2008a. Quantification of temporal distribution of recharge in karst systems from spring hydrographs. Journal of hydrology 348 (3): 452–463.

Geyer, T., Birk, S., Liedl, R., and Sauter, M. 2008b. Quantification of temporal distribution of recharge in karst systems from spring hydrographs. Journal of Hydrology 348 (3-4): 452–463 DOI: 10.1016/j.jhydrol.2007.10.015.

van Griensven, A,, Meixner, T., Grunwald, S., Bishop, T., Diluzio, M., and Srinivasan, R. 2006. A global sensitivity analysis tool for the parameters of multi-variable catchment models. Journal of Hydrology 324 (1-4): 10–23 DOI: 10.1016/j.jhydrol.2005.09.008.

Groves, C. G., and Howard, A. D. 1994. Early development of karst systems: 1. Preferential flow path enlargement under laminar flow. Water Resources Research 30 (10): 2837–2846 DOI: 10.1029/94WR01303.

Hanna, R. B. and Rajaram, H. 1998. Influence of aperture variability on dissolutional growth of fissures in karst formations. Water Resources Research. 34(11):2843-53.

Hanshaw, B. B., and Back, W. 1979. Major geochemical processes in the evolution of carbonate—aquifer systems. Journal of Hydrology 43 (1): 287–312.

Heath, R. C. 1983. Basic Ground-Water Hydrology.

Herman, J. D., Kollat, J. B., Reed, P. M., and Wagener, T. 2013. Technical Note: Method of Morris effectively reduces the computational demands of global sensitivity analysis for distributed watershed models. Hydrology and Earth System Sciences 17 (7): 2893–2903 DOI: 10.5194/hess-17-2893-2013.

Howard, A. D., and Groves, C. G. 1995. Early Development of Karst Systems: 2. Turbulent Flow. Water Resources Research 31 (1): 19 DOI: 10.1029/94WR01964.

Hunn, J. D., and Slack, L. J. 1983. Water Resources of the Santa Fe River Basin, Florida. U.S. Geological Survey.

HydroGeoLogic. 2013. Northern District Groundwater Flow Model Version 4.0.

Iooss, B., and Lemaître, P. 2014. A review on global sensitivity analysis methods. arXiv:1404.2405 [math, stat] Available at: http://arxiv.org/abs/1404.2405.

James, A. L., and Oldenburg, C. M. 1997. Linear and Monte Carlo uncertainty analysis for subsurface contaminant transport simulation. Water Resources Research 33 (11): 2495 DOI: 10.1029/97WR01925.

Jaquet, O., and Jeannin, P. Y. 1994. Modelling the karstic medium: a geostatistical approach. In Geostatistical SimulationsSpringer; 185–195.

Jaquet, O., Siegel, P., Klubertanz, G., and Benabderrhamane, H. 2004. Stochastic discrete model of karstic networks. Advances in Water Resources 27 (7): 751–760 DOI: 10.1016/j.advwatres.2004.03.007.

Katsanou, K., Lambrakis, N., Tayfur, G., and Baba, A. 2015. Describing the Karst Evolution by the Exploitation of Hydrologic Time-Series Data. Water Resources Management 29 (9): 3131–3147 DOI: 10.1007/s11269-015-0987-x.

Kaufmann, G. 2003. A model comparison of karst aquifer evolution for different matrix-flow formulations. Journal of Hydrology 283 (1-4): 281–289 DOI: 10.1016/S0022-1694(03)00270-1.

Kaufmann, G. 2003. Numerical models for mixing corrosion in natural and artificial karst environments. Water Resources Research. 39(6).

Kaufmann, G. 2003. A model comparison of karst aquifer evolution for different matrix-flow formulations. Journal of Hydrology. 283(1-4):281-9.

Kaufmann, G. 2009. Modelling karst geomorphology on different time scales. Geomorphology 106 (1): 62–77.

Kaufmann, G., and Braun, J. 2000. Karst aquifer evolution in fractured, porous rocks. Water Resources Research 36 (6): 1381–1391 DOI: 10.1029/1999WR900356.

Kaufmann, G., Romanov, D., and Hiller, T. 2010. Modeling three-dimensional karst aquifer evolution using different matrix-flow contributions. Journal of Hydrology 388 (3-4): 241–250 DOI: 10.1016/j.jhydrol.2010.05.001.

Khare, Y. ,and Muñoz-carpena, R. 2014. Global Sensitivity Analysis : Elementary Effects Screening Method of Morris using Sampling Uniformity (SU) MatLab code manual. 0570 (352).

Kiraly, L. 1985. FEM 301-a three dimensional model for groundwater flow simulation. Nationale Genossenschaft fuer die Lagerung Radioaktiver Abfaelle (NAGRA).

Kiraly, L. 1998. Modelling karst aquifers by the combined discrete channel and continuum approach. Bulletin du Centre d'Hydrogéologie. 1998;16:77-98.

Kiraly, L. 2002. Karstification and groundwater flow. Evolution of Karst: Prekarst to Cessation: Postojna-Ljubljana, Zalozba ZRC: 155–190.

Király, L., and Morel, G. 1976. Remarques sur l'hydrogramme des sources karstiques simulé par modèles mathématiques. Bulletin du Centre d'Hydrogéologie 1: 37–60.

Kiraly, L., Perrochet, P. and Rossier, Y. 1995. Effect of epikarst on the hydrograph of karst springs: a numerical approach. Bulletin du Centre d'Hydrogéologie. 14:199-220.

Kovács, A. 2003. Geometry and hydraulic parameters of karst aquifers: a hydrodynamic modeling approach. These de Doctorat, CHYN, Univ de Neuchaˆ tel: 1–131 Available at: http://en.scientificcommons.org/833403.

Kovács, A., and Perrochet, P. 2008. A quantitative approach to spring hydrograph decomposition. Journal of Hydrology 352 (1-2): 16–29 DOI: 10.1016/j.jhydrol.2007.12.009.

Kovács, A., Perrochet, P., Király, L., and Jeannin, P. Y. 2005. A quantitative method for the characterisation of karst aquifers based on spring hydrograph analysis. Journal of Hydrology 303 (1-4): 152–164 DOI: 10.1016/j.jhydrol.2004.08.023.

Kuniansky, E.L. 2016. Simulating groundwater flow in karst aquifers with distributed parameter models – Comparison of porous-equivalent media and hybrid flow approaches. US Geological Survey Scientific Investigations Report 2016-5116 14 p.

Lafare, A. 2011. Modélisation mathématique de la spéléogenèse: une approche hybride à partir de réseaux de fractures discrets et de simulations hydrogéologiques Sciences de la Terre Université Montpellier II – Sciences et Techniques du Languedoc.

Langston, A. L., Screaton, E.,J., Martin, J. B. and, Bailly-Comte, V. 2012a. Interactions of diffuse and focused allogenic recharge in an eogenetic karst aquifer (Florida, USA). Hydrogeology Journal 20 (4): 767–781 DOI: 10.1007/s10040-012-0845-3.

Langston, A. L., Screaton, E. J., Martin, J. B., and Bailly-Comte, V. 2012b. Interactions of diffuse and focused allogenic recharge in an eogenetic karst aquifer (Florida, USA). Hydrogeology Journal 20 (4): 767–781.

Lauritzen, S. -E., Odling, N., and Petersen, J. 1992. Modeling the evolution of channel networks in carbonate rocks. In ISRM Symposium: Eurock57–62.

Li, J., Duan, Q. Y., Gong, W., Ye, A., Dai, Y., Miao, C., Di, Z., Tong, C., and Sun, Y. 2013. Assessing parameter importance of the Common Land Model based on qualitative and quantitative sensitivity analysis. Hydrology and Earth System Sciences 17 (8): 3279–3293 DOI: 10.5194/hess-17-3279-2013.

Lichtner, P. C. 1988. The quasi-stationary state approximation to coupled mass-transport and fluid-rock interaction in a porous medium. Geochimica Et Cosmochimica Acta. 52(1):143-65.

Liedl, R. 2003. Simulation of the development of karst aquifers using a coupled continuum pipe flow model. Water Resources Research 39 (3): 1–11 DOI: 10.1029/2001WR001206.

Littlefield, J. R,, Culbreth, M. A,, Upchurch, S. B,, and Stewart, M. T. 1984. Relationship of modern sinkhole development to large scale-photolinear features. In Proceedings of First Multidisciplinary Conference on Sinkholes, Orlando, Florida189–195.

Maramathas, A. J., and Boudouvis, A. G. 2006. Manifestation and measurement of the fractal characteristics of karst hydrogeological formations. Advances in water resources 29 (1): 112–116.

Mazzilli, N., Guinot, V., and Jourde, H. 2012. Sensitivity analysis of conceptual model calibration to initialisation bias. Application to karst spring discharge models. Advances in Water Resources 42: 1–16 DOI: 10.1016/j.advwatres.2012.03.020.

Morris, M. D. 1991. Factorial Sampling Plans for Preliminary Computational Experiments. Technometrics 33 (2): 161–174 DOI: 10.2307/1269043.

Munch, D.A. , Toth, D. J., Huang, C., Davis, J. B., Fortich, C. M., Osburn, W. L., Phlips, E. J., Quinlan, E. L., Allen, M. S. and, Woods, M. J. 2006. Fifty-year retrospective study of the ecology of Silver Springs, Florida. Publication Number: SJ2007-SP4. St. Johns River Water Management District, Palatka, FL.

Muñoz-Carpena, R., Zajac, Z., and Kuo, Y. M. 2007. GLOBAL SENSITIVITY AND UNCERTAINTY ANALYSES OF THE WATER QUALITY MODEL VFSMOD-W. 50 (5): 1719–1732.

Noorishad, J., Tsang, C. F., Perrochet, P. and Musy, A. 1992. A perspective on the numerical solution of convection-dominated transport problems: A price to pay for the easy way out. Water Resources Research. Feb 1;28(2):551-61.

Nossent, J., and Bauwens, W. 2012. Multi-variable sensitivity and identifiability analysis for a complex environmental model in view of integrated water quantity and water quality modeling. Water Science and Technology 65 (3): 539–549 DOI: 10.2166/wst.2012.884.

Padilla, A., Pulido-Bosch, A., and Mangin, A. 1994. Relative Importance of Baseflow and Quickflow from Hydrographs of Karst Spring. Ground Water 32 (2): 267–277 DOI: 10.1111/j.1745-6584.1994.tb00641.x.

Palmer, A. N. 1991. Origin and development of limestone caves. Geological Society of America Bulletin 103 (2): 1–21 DOI: 10.1177/030913338100500204.

Palmer, A. N. 2003. Speleogenesis in carbonate rocks. Speleogenesis and Evolution of Karst Aquifers 1 (1): 1–11.

Palmer, A. N. 2006. Digital modeling of karst aquifers—successes, failures, and promises. Geological Society of America Special Papers 404: 243–250.

Pan, F., Zhu, J., Ye, M., Pachepsky, Y. A. and, Wu, Y. -S. 2011. Sensitivity analysis of unsaturated flow and contaminant transport with correlated parameters. Journal of Hydrology 397 (3): 238–249.

Pandey, S. N., Chaudhuri, A., Kelkar, S., Sandeep, V. R. and Rajaram, H. 2014. Investigation of permeability alteration of fractured limestone reservoir due to geothermal heat extraction using three-dimensional thermo-hydro-chemical (THC) model. Geothermics. 51:46-62.

Pappenberger, F., Beven, K. J., Ratto, M. and, Matgen, P. 2008. Multi-method global sensitivity analysis of flood inundation models. Advances in Water Resources 31 (1): 1–14 DOI: 10.1016/j.advwatres.2007.04.009.

Pardo-Igúzquiza, E., Dowd, P. A., Xu, C., and Durán-Valsero, J. J. 2012. Stochastic simulation of karst conduit networks. Advances in Water Resources 35: 141–150 DOI: 10.1016/j.advwatres.2011.09.014.

Peaceman, D. W. 1978. Interpretation of well-block pressures in numerical reservoir simulation (includes associated paper 6988). Society of Petroleum Engineers Journal 18 (03): 183–194.

Peaceman, D. W. 1983. Interpretation of well-block pressures in numerical reservoir simulation with nonsquare grid blocks and anisotropic permeability. Society of Petroleum Engineers Journal 23 (03): 531–543.

Phelps, B. G. G., Survey USG. 2004. Chemistry of Ground Water in the Silver Springs Basin, Florida , with an U. S. Department of the Interior. Ground Water.

Perne, M., Covington, M. and Gabrovsek, F. 2014. Evolution of karst conduit networks in transition from pressurized flow to free-surface flow. Hydrology and Earth System Sciences. 18(11):4617-33.

Perrin, J., Jeannin, P. Y., and Cornaton, F. 2007. The role of tributary mixing in chemical variations at a karst spring, Milandre, Switzerland. Journal of Hydrology 332 (1-2): 158–173 DOI: 10.1016/j.jhydrol.2006.06.027.

Raeisi, E., Groves, C., and Meiman, J. 2007. Effects of partial and full pipe flow on hydrochemographs of Logsdon river, Mammoth Cave Kentucky USA. Journal of Hydrology 337 (1): 1–10.

Randazzo, A. F. 1997. The sedimentary platform of Florida: Mesozoic to Cenozoic. The Geology of Florida. University Press of Florida, Gainesville: 39–56.

Randazzo, A. F. ,and Bloom, J. I. 1985. Mineralogical changes along the freshwater/saltwater interface of a modern aquifer. Sedimentary geology 43 (1): 219–239.

Reeves, D. M., Benson, D. A., Meerschaert, M. M., and Scheffler, H. P. 2008. Transport of conservative solutes in simulated fracture networks: 2. Ensemble solute transport and the correspondence to operator-stable limit distributions. Water Resources Research 44 (5): 1–20 DOI: 10.1029/2008WR006858.

~~Reimann, T., Geyer, T., Shoemaker, W. B., Liedl, R., and Sauter, M. 2011a. Effects of dynamically variable saturation and matrix-conduit coupling of flow in karst aquifers. Water Resources Research 47 (11): 1–19 DOI: 10.1029/2011WR010446.~~

~~Reimann, T., Rehrl, C., Shoemaker, W. B., Geyer, T., and Birk, S. 2011b. The significance of turbulent flow representation in single-continuum models. Water Resources Research 47 (9): 1–15 DOI: 10.1029/2010WR010133.~~

de Rooij, R., Perrochet, P., and Graham, W. 2013. From rainfall to spring discharge: Coupling conduit flow, subsurface matrix flow and surface flow in karst systems using a discrete-continuum model. Advances in Water Resources 61: 29–41 DOI: 10.1016/j.advwatres.2013.08.009.

Ronayne, M. J. 2013. Influence of conduit network geometry on solute transport in karst aquifers with a permeable matrix. Advances in Water Resources. 56:27-34.

Saller, S. P., Ronayne, M. J., and Long. A. J. 2013. Comparison of a karst groundwater model with and without discrete conduit flow. Hydrogeology Journal 21 (7): 1555–1566 DOI: 10.1007/s10040-013-1036-6.

Saltelli, A., Tarantola, S., Campolongo, F., and Ratto, M. 2004. Sensitivity analysis in practice: a guide to assessing scientific models. John Wiley & Sons.

Saltelli, A., Tarantola, S., and Chan, K-. S. 1999. A quantitative model-independent method for global sensitivity analysis of model output. Technometrics 41 (1): 39–56.

Scanlon, B. R., Mace, R. E., Barrett, M. E., and Smith, B. 2003. Can we simulate regional groundwater flow in a karst system using equivalent porous media models? Case study, Barton Springs Edwards aquifer, USA. Journal of Hydrology 276 (1-4): 137–158 DOI: 10.1016/S0022-1694(03)00064-7.

Schlumberger. 2008.Schedule user guide.

Scott, T. M., Means, G. H., Meegan, R. P., Means, R. C., Upchurch, S., Copeland. R. E., Jones, J., Roberts, T. and Willet, A.. 2004. Springs of Florida.

Shin, M. J., Guillaume, J. H. A., Croke, B. F.W. and Jakeman, A. J. 2013. Addressing ten questions about conceptual rainfall-runoff models with global sensitivity analyses in R. Journal of Hydrology 503: 135–152 DOI: 10.1016/j.jhydrol.2013.08.047.

Shoemaker, W. B., Cunningham, K. J., Kuniansky, E. L. and Dixon, J. 2008. Effects of turbulence on hydraulic heads and parameter sensitivities in preferential groundwater flow layers. Water Resources Research 44 (3): 1–11 DOI: 10.1029/2007WR006601.

Shoemaker, W. B., Kuniansky, E. L., Birk, S., Bauer, S.and Swain, E. D. 2005. Documentation of a Conduit Flow Process (CFP) for MODFLOW-2005. U.S. Geological Survey Techniques and Methods, book 6, chapter A24: 50.

Shoemaker, W. B., Kuniansky, E. L., Birk, S., Bauer, S. and Swain, E. D. 2008. Documentation of a Conduit Flow Process (CFP) for MODFLOW-2005.Techniques and Methods, Book 6, Chapter A24.

Siemers, J. and Dreybrodt, W. 1998. Early development of karst aquifers on percolation networks of fractures in limestone. Water Resources Research. 34(3):409-19.

Sobol, I. M. 2001. Global sensitivity indices for nonlinear mathematical models and their Monte Carlo estimates. Mathematics and computers in simulation 55 (1): 271–280.

Srivastava, V., Graham, W., Muñoz-Carpena, R. and Maxwell, R. M. 2014. Insights on geologic and vegetative controls over hydrologic behavior of a large complex basin - Global Sensitivity Analysis of an integrated parallel hydrologic model. Journal of Hydrology 519 (PB): 2238–2257 DOI: 10.1016/j.jhydrol.2014.10.020.

Stark, C. P. 1991. An invasion percolation model of drainage network evolutioN. Nature. 352(6334):423-5.

Svensson, U. and Dreybrodt, W. 1992. Dissolution kinetics of naturalcalcite minerals in CO_2-water systems approaching calcite equilibrium. Chemical Geology. 100(1-2):129-45.

Swamee, P. K. and Swamee, N. 2007. Full-range pipe-flow equations. Journal of Hydraulic Research. 45(6):841-3.

Szymczak, P. and Ladd, A. J. C. 2011. The initial stages of cave formation: Beyond the one-dimensional paradigm. Earth and Planetary Science Letters. 301(3-4):424-32.

Szymczak, P. and Ladd, A. J. C. 2009. Wormhole formation in dissolving fractures. Journal of Geophysical Research-Solid Earth. 114.

Taylor, C. J. and Greene, E. A. 2005. Hydrogeologic Characterization and Methods Used in the Investigation of Karst Hydrology. Field Techniques for Estimating Water Fluxes Between Surface Water and Ground Water: 75–114 DOI: PNR61.

Teutsch, G. and Sauter, M. 1991. Groundwater modeling in karst terranes: Scale effects, data acquisition and field validation. Proc. Third Conf. Hydrogeology, Ecology, Monitoring, and Management of Ground Water in Karst Terranes, Nashville, TN: 17–35 DOI: PNR61.

U.S. Geological Survey (USGS). 2014. National Water Information System data available on the World Wide Web (Water Data for the Nation), accessed [June 10, 2014], at URL [http://waterdata.usgs.gov/nwis/].

Upchurch, S. B. and Littlefield Jr., J. R. 1988. Evaluation of data for sinkhole-development risk models. Environmental Geology and Water Sciences 12 (2): 135–140.

Vernon, R. O. 1951. Geology of Citrus and Levy Counties, Florida. Tallahassee, Fl.

Wang, L. and Liu, H. 2006. An efficient method for identifying and filling surface depressions in digital elevation models for hydrologic analysis and modelling. International Journal of Geographical Information Science 20 (2): 193–213.

White, W. B. 1993. Analysis of karst aquifers. Van Nostrand Reinhold.

Worthington, S. R. H. 1999. A comprehensive strategy for understanding flow in carbonate aquifers. Karst modeling: special publication 5: 30–37.

Worthington, S. R.H. and Ford, D. C. 2009. Self-organized permeability in carbonate aquifers. Ground Water 47 (3): 326–336 DOI: 10.1111/j.1745-6584.2009.00551.x.

Xu, C. S. and Dowd, P. 2010. A new computer code for discrete fracture network modelling. Computers & Geosciences. 36(3):292-301.

Xu, Z., Hu ,B. X., Davis, H. and Kish, S. 2015. Numerical study of groundwater flow cycling controlled by seawater/freshwater interaction in a coastal karst aquifer through conduit network using CFPv2. Journal of Contaminant Hydrology 182: 131–145 DOI: 10.1016/j.jconhyd.2015.09.003.

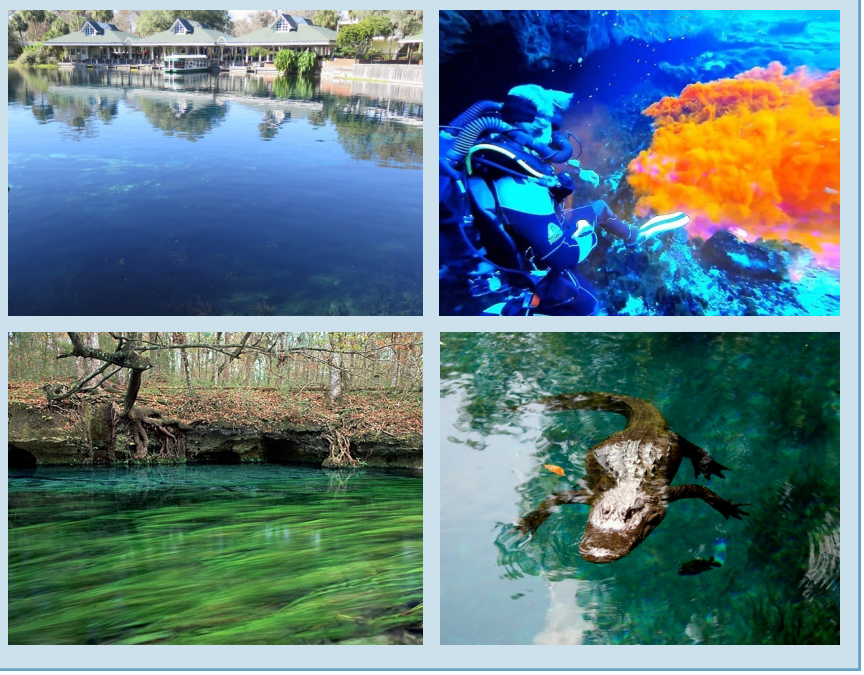

Collaborative Research Initiative on
Sustainability and Protection of Springs [**CRISPS]**

Section 3

[Work Order No: 6]

FINAL REPORT

2014 - 2017

submitted to:

St. Johns River Water Management District
Springs Protection Initiative [SPI], UF Contract # 27789

UF | UNIVERSITY of FLORIDA
Water Institute

C R I S P S

Section 3

GROUNDWATER HYDROLOGY

Transport and Loss of Nitrogen within the Upper Floridan Aquifer in the Silver Springs Springshed

Final Report 2017
Work Order No. 6

Principal Investigators:

James W. Jawitz, University of Florida
Patrick Burger, St. Johns River Water Management District

Project Team

Michael D. Annable, Engineering School of Sustainable Infrastructure and Environment
Minjune Yang, Soil and Water Sciences Department
Antonio Yaquian, Soil and Water Sciences Department
Amanda Desormeaux, School of Natural Resources and the Environment

This document reports findings and results of a work order for a 3-year project in compliance with Agreement between University of Florida (UF) and St. Johns River Water Management District (SJRWMD) UF Contract #27789. It is part of the *UF Collaborative Research Initiative on Springs Protection and Sustainability (CRISPS)* and supports the science component of *the SJRWMD Springs Protection Initiative (SPI).*

3.1 ABSTRACT

The goals of this work are to provide field-measured hydrogeologic data that can be used for active resource management in the Silver Springs springshed. *In situ* measurements were conducted to identify portions of the aquifer that contribute most significantly to water and solute flow to the spring and to identify relationships between land use practices and vadose zone nitrate fluxes. In the first phase of this project, we measured groundwater velocities and solute fluxes *in situ* using passive flux meters (PFMs). Instruments were deployed for approximately 2 months at a time in 16 locations. Groundwater fluxes measured using this technique ranged from 1.8 to 10.7 cm d^{-1} with mean 6.03 cm d^{-1}. These velocities are consistent with slow flow through the rock matrix. In the second phase of this project, we designed and fabricated a new karstic borehole device (KBHD) to measure groundwater and solute flux in karst fracture and conduit zones. Improvements in site selection based on borehole videos and the incorporation of borehole dilution tests enabled us to measure fluxes in fractures zones and conduits. These fluxes were more than 50 times greater (mean 3.05 m d^{-1}) than those previously measured with PFMs in the aquifer matrix. These data combined with velocities measured in tracer tests, the known flux from Silver Springs, and the aquifer dimensions suggest that matrix flow contributes only approximately 20% of the discharge for a transect of radius 14 km from Silver Springs. Non-matrix flux is therefore surmised to contribute more than 80% of the water discharged from Silver Springs. However, no direct *in situ* measurements of conduit flux have previously been available. *In situ* nitrate attenuation was also evaluated in five wells with push-pull tests and our new karstic borehole device. At two wells where the mean nitrate concentration was 0.77 and 2.2 mg/L, no nitrate degradation was observed with similar mass recovery for both non-reactive (Rhodamine) and reactive (KNO_3) tracers. This result may be constrained by the short tracer residence times, which were much shorter than average aquifer residence times. Significant nitrate degradation was observed at two wells where no background nitrate was detected. Even during relatively the short experiment, nitrate mass recovery at both wells was approximately 60% of non-reactive tracer recovery. The results suggest that the nitrate concentrations in groundwater samples provide direct evidence for denitrifying conditions. Finally, ion-exchange soil resin columns were installed at sites representing the dominant land uses across the springshed to measure *in situ* vadose zone nitrate fluxes across a range of nitrogen application rates.

3.2 INTRODUCTION

This document provides a compilation of our activities investigating the movement of water and solutes through the Silver Springs groundwater system. The goals of this work were to provide field-measured hydrogeologic data that can be used for active resource management in the Silver Springs springshed. Specific management questions to be addressed included: What portions of the springshed are most directly linked to the spring outlet? Which portions of the springshed have the shortest-circuit connections of water flow and solute pathways from the land surface to the spring outlet? Which areas are more likely to have little connection to the spring outlet? If management interventions are desired, such as land use modification or restriction, then which portions of the springshed should be targeted? The types of information needed to answer these questions are as follows:

- Recharge of water and solutes (such as nitrate) within the springshed,

- Attenuation of solute leaching through soil and vadose zones, and
- Aquifer flow path lengths, velocities, and solute attenuation through the aquifer.

Each of these processes is heterogeneous and thus must be understood in terms of the spatial distribution throughout the springshed. This work was intended to provide new data about these processes within the Silver Springs springshed to be integrated within a management-decision framework.

The goal of this project is to determine groundwater flow characteristics and natural attenuation rates of nitrogen (N) loads in the upper Floridan Aquifer System (FAS). Groundwater velocities, nitrate fluxes, and denitrification rates were measured at a network of wells using a suite of monitoring techniques. The data from this project may be used directly in springshed models.

3.3 SITE DESCRIPTION

Silver Springs with an approximate discharge of 25 m^3 s^{-1} is one of Florida's first magnitude springs and among the largest springs worldwide. Its 2,500 km^2 springshed overlies the mostly unconfined Upper Floridan Aquifer. The aquifer is approximately 100 m thick and predominantly consists of porous, fractured and cavernous limestone, which leads to excellent surface drainage properties (no major stream network other than Silver Springs run) and complex groundwater flow patterns through both rock matrix and fast conduits. Over the past few decades, discharge from Silver Springs has been observed to slowly but continuously decline, while nitrate concentrations in the spring water have enormously increased from a background level of 0.05 mg L^{-1} to over 1 mg L^{-1}. In combination with concurrent increases in algae growth and turbidity, and despite an otherwise relatively stable water quality, this has given rise to concerns about the ecological equilibrium in and near the spring run.

Among the largest remaining uncertainties are the largely unknown geometry and properties of the karst conduit network. In the case of the karstified Silver Springs aquifer, the interplay of slow matrix flow and fast fracture / conduit flow creates highly complex flow and transport conditions.

Groundwater travel times to a stream network are usually exponentially distributed, independent of size, shape and conductivity of the watershed and independent of the stream network geometry. This assumption for karst appears reasonable, since the conduits are so much more conductive as the matrix and travel time along them are so much shorter (as reported from tracer tests). Overall, tracer results (directly injected into fast flow zones) give travel times on the order of months, while the porous media models range over several decades. The groundwater age analyses are in the middle, which may again be indicative of the importance of mixing between fast conduit and slow matrix water. So travel time may be exponential in the porous matrix and then something else, but much quicker, in the conduits, which in total would give a bimodal (dual domain) travel time distribution (Padilla and Pulidobosch 1995).

3.4 METHODS

3.4.1 Groundwater Velocity and Nitrate Flux Measurements

In the case of the karstified Silver Springs aquifer, the interplay of slow matrix flow and fast fracture / conduit flow creates highly complex flow and transport conditions. Borehole dilution

tests and passive flux meters (PFMs) were used in conjunction to characterize the groundwater velocity distribution vertically in selected wells,

Passive Flux Meters. The passive flux meter (Hatfield et al. 2004) simultaneously measures time-averaged water flux, q, and solute mass flux, J, with depth in a flow field in a porous medium. The interior composition consists of a permeable sorbent that can intercept and retain nutrients (or contaminants) from up-gradient groundwater flow (Figure 3.1). An appropriate sorbent (e.g., activated carbon, activated alumina, anionic/cationic resin, etc.) can be selected according to the target solute. The sorbent is pre-loaded with known amounts of water-soluble tracers. When the PFM is exposed to groundwater flow, the resident tracers are desorbed and eluted from the sorbent matrix at rates proportional to groundwater flow through the PFM. Since the magnitude of groundwater flow is unknown in the actual application, multiple resident tracers, which have different elution rates, are used. The degree of tracer elution is related to the retardation factor, which can be measured by laboratory column elution or batch sorption/desorption tests (Hatfield et al. 2004). After sufficient exposure to groundwater flow, the PFM is removed from the well and the sorbent is extracted to quantify the nutrients (or contaminants) intercepted and resident tracers remaining. The extracted nutrients and residual tracer mass are used to estimate time-averaged nutrient and water flux, respectively.

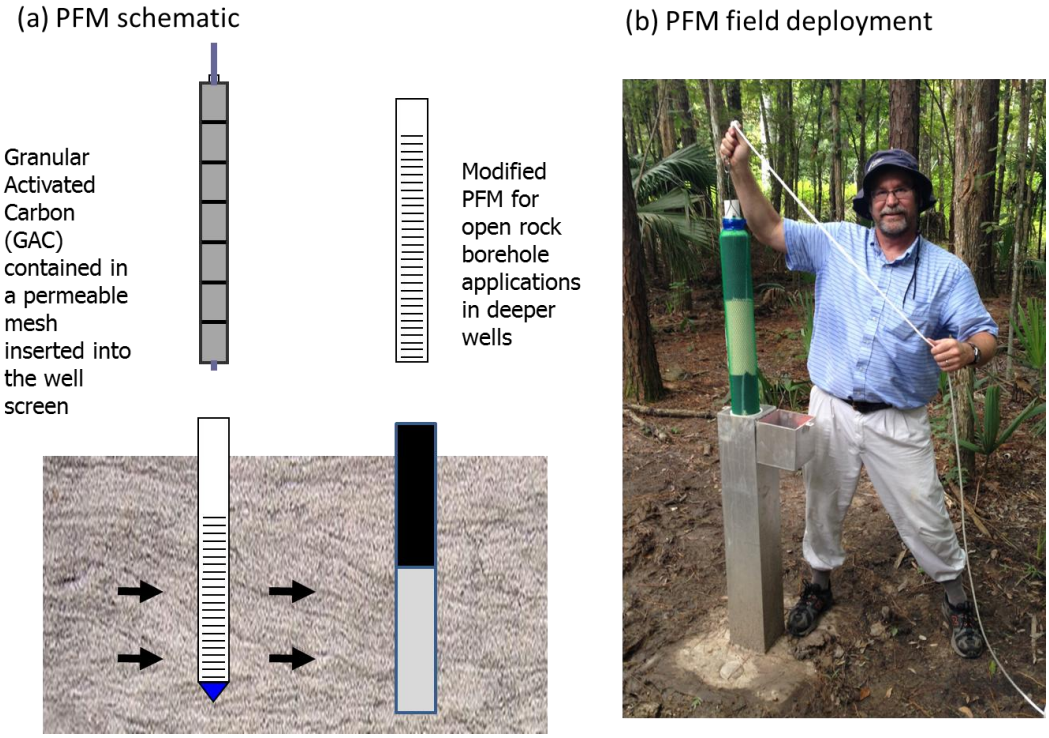

Figure 3.1. (a) Passive flux meter (PFM) schematic diagram, and (b) photograph of PFM deployment in a well.

Using PFMs, karst flux data becomes available as depth profiles along monitoring wells, which allows a characterization several important features: (1) Vertical heterogeneity of flow and transport as produced by spatial heterogeneity in input sources and aquifer characteristics. This

type of information is fundamental for assessing the internal dispersion and mixing behavior of the aquifer as well as for the interpretation of any kind of point measurements. (2) Vertical trends in flow and transport as produced by the large scale boundary conditions of the aquifer. This may help delimiting the hydraulically active upper portion of the aquifer from a possibly stagnant lower part. The size of the active aquifer is directly related to the mean nitrate travel time towards the spring and stagnant parts of the aquifer may act as additional nitrate reservoirs, with nitrate uptake and release by diffusion from / into the active aquifer. (3) The spatial distribution of well averaged groundwater and nitrate fluxes may contribute to identifying larger scale flow, transport and reaction patterns between recharge locations and the spring. Comparing depth averaged fluxes of nitrate and its degradation products, for example, at different distances from the spring allows conclusions about nitrate reaction behavior at the transport scale. (4) Temporal variations in measured fluxes (e.g., between rainy and dry seasons) indicates the temporal variability of aquifer behavior.

A modified PFM enclosed in PVC screened pipe was developed and laboratory experiments were conducted for feasibility testing for *in situ* velocity measurement in down-well cavities and conduits. The results of these experiments indicated that groundwater bypasses the device at high velocities, which are expected in the fractured regions, suggesting the modified PFM will not work in conduit segments of the borehole.

Borehole Dilution. Borehole dilution is a common well monitoring technique used to estimate groundwater Darcy flux. The method relies on isolation of a section of the borehole using inflatable packers, followed by the injection and recirculation of a tracer pulse within the zone between the packers. Aquifer velocity can be inferred from the dilution of the injected tracer, which is attributed to advective losses (Pitrak et al. 2007). This method is subject to considerable constraints in open-rock boreholes, as the sharp edges characteristic of conduit/cavernous regions greatly increase the risk of rupturing the rubber packers commonly used to isolate sections of the borehole. Additionally, the karstic nature of the UFA makes placement and retrieval of testing equipment much more intricate. Thus, a modified karstic borehole device (KBHD) was designed and constructed to aid in the deployment and retrieval of borehole dilution instruments in karstic environments (Figure 3.2).

Like other packer-based aquifer testing devices (Shapiro 2007), the KBHD has the capability to isolate sections of the borehole through inflatable packers in the top and bottom of the targeted volume. However, unlike most such devices which use rubber packers, the KBHD packers are made of Kevlar to reduce the risk of rupturing (Figure 3.3). The Kevlar is covered by a rubber membrane that improves the seal between the packers and the borehole when inflated and compresses the fabric when deflated for deployment through the borehole.

This method has been used for a single fracture or a short interval of multiple fractures, assuming water flow is dominated horizontally during the test (Quinn et al. 2012). In densely fractured rock with vertically connected fractures, vertical resolution of the measurements may decrease due to preferential flow from above and below the packer interval (Quinn et al. 2016).

Figure 3.2**.** Karstic borehole device (KBHD) during retrieval from a monitoring well following a borehole dilution test.

Both packers are inflated through a 1/4" diameter airline connected to a compressor. The inflation pressure, P_{inf}, is calculated as the local water pressure (ρgh) plus 20 PSI to achieve pneumatic seal and volume isolation. The diameter of the deflated packers was decreased from previous designs to 3.5" OD, giving a ¼" ring between the packer and a 4" borehole. In addition to the use of Kevlar packers, other differences between the KBHD and other aquifer testing devices are the method of deployment into the borehole and its modular design. The KBHD is attached to a 1 ¼" PVC pipeline, which is used both as a placement rod and also containment for the tubing and wiring used in the test. These design modifications reduce the opportunity for lines or packers to catch on rough edges of the borehole and enhance the maneuverability of the device during deployment, placement and retrieval. All new features were designed to ensure the successful retrieval of the device after deployment.

The KBHD has five lines that run through the interior of the placement pipe and attach to fittings that allow watertight transition into the open borehole (Figure 3.4). These custom fittings are 6" long and have a 1 ¼" in diameter. Both ends have NPT thread with interior compression fittings. This design ensures that there is no contact between waters from the tested volume of borehole and the inside of the conduction pipe. The five lines are electrical, water in and out, air, and an emergency cable. The electrical line powers the submersible pump (MP1, Grundfos). A 3/8" polyethylene tube conducts water out from the Groundfos pump to the ground surface, and a similar tube returns the water down to the borehole after passing through a flourometer and conductivity meter at the ground surface. A ¼" polyethylene tube conducts air for packer inflation from a compressor (Figure 3.2). As a safety measure, a stranded cable gage is attached to the bottom cap of the watertight line.

Figure 3.3. Kevlar packer being attached to the karstic borehole device.

A submersible pump (Grunfos MP1) was used to recirculate water from the tested borehole to the ground surface. The pump inlet has a mesh of 1” in length and 2” in diameter and is housed in a steel shroud. The pump shroud was made with 3/8” thick perforated stainless steel; the ¼” perforations resulted in a 45% open area.

Figure 3.4. Watertight fittings.

Figure 3.5. View of the down-hole lines during injection of a tracer pulse.

Figure 3.6**.** Cable eyelet welded to the top cap of the pump shroud.

Figure 3.7. Pump being installed in shroud (left), pump installation above the bottom packer (middle), shroud being capped with the bottom of the water tight line (right).

Initial borehole dilution tests utilized a dual-tracer approach with a saline solution (KCl) and dye (rhodamine), to validate pilot measurements. Electrical conductivity was measured at 15 second intervals using a conductivity datalogger (REED, SD-4307) and rhodamine concentrations were measured at 60 second intervals using a flourometer (Figure 3.8).

Figure 3.8. Conductivity meter and flourometer used during a borehole dilution test.

The modular design of the KHBD is advantageous as it can be modified to test different borehole lengths, with a minimum of 48 inches, as the pump shroud is 24 inches and each line fitting is 6". Figures 3.9 through 3.12 show how the KBHD was assembled to test a 10-foot section of the borehole.

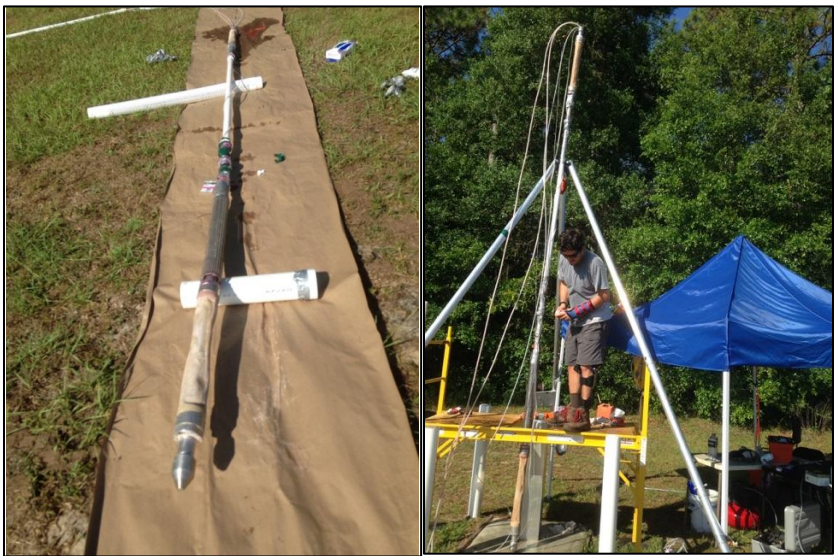

Figure 3.9. KBHD assembled to test 10' intervals (left) and KBHD in vertical position in preparation for downhole deployment (right).

After insertion into the well, all downhole lines were introduced into 10-foot sections of 1 ¼" PVC placement pipes that were threaded together and lowered into the borehole until the target depth was reached. The lines were lowered into the borehole using drop pipe elevators and pipe holders (Figure 3.10), which allowed for maneuvering of the KBHD.

Figure 3.10. Several 10-foot sections of pipe with downhole lines through them and in preparation for down-hole deployment.

Figure 3.11**.** KBHD being deployed in well M0789.

Figure 3.12**.** Above-ground equipment during a borehole dilution test.

Push-pull Tracer Tests. The modified KBHD was designed for coupled field tests of borehole dilution and push-pull tracer tests. Push-pull tracer tests are used to assess reaction rates of microbial activities in an aquifer. A solution containing a tracer and reactant specific to a microbial process of interest are injected into a well, followed by a resting/reaction phase, and finally an extraction phase, where water is extracted from the well until the entire tracer mass is recovered (Kim et al. 2005). Injecting nitrate as a reactant allows quantification of reactant rates for nitrate degradation processes, with nitrate loss attributed to denitrification.

3.4.2 Soil N Flux

The dominant land uses within the springshed are subject to a wide range of anthropogenic N inputs, which vary based on land use type and management intensity. The karst topography is inherently vulnerable to nitrate loading, as nitrate can be rapidly transported to the aquifer in

unconfined regions of the springshed. While surface loading can be estimated from fertilizer sales or recommended fertilizer application rates for different land uses, only a fraction of the surface loading reaches the groundwater. Direct measurements of soil nitrate fluxes below the root zone are critical for quantifying actual nitrate leaching and attenuation.

There are a variety of methods commonly used to measure soil nitrate, including soil cores, suction lysimeters, and drainage lysimeters; however, each of these methods has significant limitations (Weihermüller et al. 2007). A low-cost alternative to these methods that overcomes the limitation of frequent sampling is ion-exchange resin, which enables temporal integration. The resin adsorbs and accumulates ions from the soil solution and allows for cumulative nitrate flux measurements. Resin bags are commonly used to measure nitrate leaching (Kramer et al. 2006) and storing the resin in a rigid column allows for flux calculations (Ventura et al. 2013).

The heterogeneity of land use practices and environmental factors at the springshed scale make modeling N transformations even more complex, emphasizing the importance of adequate replication of measurement devices. The replication necessary to accurately estimate N fluxes are highly dependent on the surface area of the measurement device, with smaller surface areas requiring greater replication (Lilburne et al. 2012). Construction of resin columns and analysis of resin-adsorbed nitrate is inexpensive, making the replication necessary to capture the landscape heterogeneity economically viable.

While ion-exchange resin columns avoid many of the pitfalls associated with alternative methods to measure nitrate flux, differences in hydraulic conductivity between the resin and surrounding soil can alter water flux dynamics (Roth 2006). Slight differences in resin column construction have led to wide range of reported solute recovery efficiencies (Siemens and Kaupenjohann 2004; Predotova et al. 2011), emphasizing the importance of resin column design. The textural discontinuity between the resin and surrounding soil can also lead to an artificially saturated layer, creating the anoxic conditions necessary for denitrification.

Numerical modeling was used to simulate steady-state soil moisture dynamics of resin placed between two layers of native soil (Arredondo fine sand, Loamy, siliceous, semiactive, hyperthermic Grossarenic Paleudults) to help inform resin column design. The aim of the modeling efforts was to design a column that avoids the buildup of artificially saturated zones above the resin layer, while still containing a volume of resin that accommodates nitrate loads well above those expected within the springshed. Resin columns were then installed at sites representing the dominant land uses within the Silver Springs springshed.

Resin Column Design. Soil moisture release data were used to calculate Van Genuchten parameters from an anion-exchange resin and three soil samples from an agricultural field within the Silver Springs springshed. This data was input into HYDRUS-1D (Simunek et al. 2005) along with other measured soil and resin properties (e.g., Ksat, θr, θs) to evaluate soil moisture distribution in the column.

A lab column study was designed to transition from HYRDUS-1D simulations to development of a specific resin-column design for field application; the aim of the experiment was to confirm the design of a resin column that encourages soil water through flow, avoiding both flow

diversion around the resin column and the development of a saturated layer at the resin/soil boundary. A field tracer study was designed following the lab column study to validate resin column performance in the field (Lang and Kaupenjohann et al. 2004). Finally, a sensitivity analysis was performed in HYDRUS-2D to evaluate convergence/divergence factors for a range of soil properties and resin mixtures.

Lab Column Study. A soil column was constructed from 10 cm x 10 cm acrylic columns stacked together, sealed with silicone, and enclosed in a mesh liner (Figure 3.13). Arredondo fine sand (Loamy, siliceous, semiactive, hyperthermic Grossarenic Paleudult), a soil characteristic of 18% of the springshed, was taken from the field and wet packed into the bottom 30 cm of the soil column, a mesh liner was placed above the 30 cm soil layer and another 20 cm of soil was wet packed above the liner. A mixture of nitrate specific anion-exchange resin (Purolite A520-E) and native soil from the 30-40 cm soil profile at a 1:1 ratio was placed above this layer, followed by the top 30-cm of the excavated field soil.

On 25 October 2016, water application to the column was initiated at the rate of 22.75 cm d^{-1} (1.79 L d^{-1}). This rate is within the range of the maximum precipitation rates for the springshed, which can be as high as 300 cm d^{-1} for short durations (calculated from FAWN rain gauge in Citra, FL between 2011-2016 found at fawn.ifas.ufl.edu). Once steady state was reached, irrigation was suspended for one hour and 12 g of NO_3-N from KNO_3 was applied to the surface of the column as a single application of a 149 mL solution of 131.5 g L^{-1} KNO_3 (80.5 g L^{-1} NO_3-N). A final two days of water application followed NO_3-N application, resulting in a total time of 9 days. The soil column was dissected in 5 cm increments and volumetric water content was measured gravimetrically for each section. After drying for water content measurements, 5 g aliquots (n=3) from all sections were eluted using 50 mL of 2 *M* KCl and samples were sent to the University of Florida Analytical Research Lab (Gainesville, FL) for NO_3^- analysis (EPA method 353.2) to determine resin recovery.

Neural-network predictions for Van Genuchten parameters were calculated in HYDRUS-1D, using soil texture and moisture release curve data for the soil and texture and saturated water content for the resin. Saturated hydraulic conductivity was 792 and 6,307 cm d^{-1} for the soil and resin, respectively. Geotextile data from Nahlawi et al. (2007) was used to estimate hydraulic parameters for the mesh liner.

Table 3.1. Parameters used for of soil moisture profile prediction in HYDRUS-1D.

	K_{sat} (cm d^{-1})	α (1 cm^{-1})	*n* *(-)*
Tavares fine sand (0-10 cm)	792	0.032	3.23
Tavares fine sand (11-90 cm)	792	0.068	1.28
Resin/sand mixture	3,122	0.053	2.35
Mesh liner	34,560	0.855	6.51

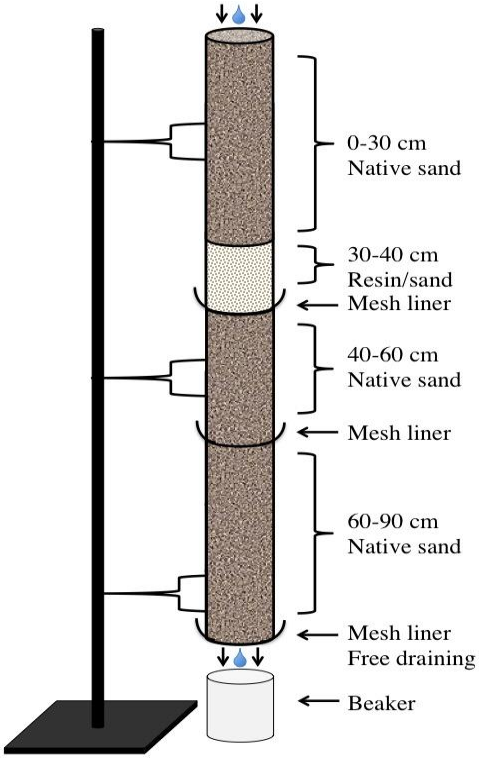

Figure 3.13. Schematic of the soil column constructed for the soil moisture profile measurements.

Field Tracer Test. A field tracer test was performed at the University of Florida Agricultural Teaching Farm to determine the efficiency of soil porewater flow through the column and to measure NO_3^- degradation between fertilizer application and resin adsorption, to give final verification of soil water through flow and nitrate retention under field conditions. To prepare the resin before column installation, 150 g of dried Purolite A520-E anion exchange resin was rinsed with DI water, decanted three times, and stored moist in labeled bags. Four 5 g aliquots of the resin were taken for background analysis.

Four resin columns were installed in 1 m^2 plot at a depth of 30-50 cm. An intact 20 cm x 20 cm soil core was excavated from the surface using a drain spade and placed on a plastic tarp, with soil below this depth excavated in 10 cm increments using a soil auger and placed on the tarp in the order of excavation. Soil from the 40-50 cm depth was mixed with 150 g of Purolite A520-E anion exchange resin at a 1:1 ratio and placed into the bottom half of the resin column. Soil from the 30-40 cm depth was placed in the soil column over the resin/soil layer and the soil column was placed into the excavated hole ensuring the bottom of the drain cloth was in contact with the soil. The remaining soil was replaced over the column in the original order and the intact soil core was placed on the surface. Following column installation, the fertilizer/tracer solution was applied to the soil surface using a tank sprayer. The fertilizer/tracer solution was applied at the rate of 100 kg ha^{-1} NO_3-N from KNO_3 and 148 kg ha^{-1} Br^- from KBr, resulting in an expected 81

mg NO_3-N and 24 mg Br^- adsorbed to the resin and extractant concentrations of 20 mg L^{-1} NO_3-N and 6 mg L^{-1} Br^- for 5 g aliquots extracted with 40 mL of 2 *M* KCl.

After the columns were installed, the plot was irrigated at the rate of 5 cm d^{-1} for two days prior to the fertilizer/tracer application. After the application of the fertilizer/tracer solution, plots were irrigated 10 cm d^{-1} for 3 days, resulting in a total of 30 cm (2 pore volumes) of irrigation. The columns were left to drain for one additional day and were excavated 9 days after installation. Soil samples were taken from the 0-30 cm depth as the columns were being excavated. All soil and resin samples were dried prior to extraction. After being dried, 5 g aliquots of soil and resin were extracted using 2 *M* KCl. Samples were submitted to the UF ARL during March 2017. The recovery data were used to calculate a convergence/divergence factor (α) for the resin columns. Values greater than 1 represent convergence of soil water through the column, while values less than 1 represent divergence around the column.

Nitrate Flux Measurements. Soil resin columns were deployed during June 2017 to quantify below root zone N fluxes in representative land uses across the Silver Springs Springshed, including agriculture (corn and hay; fertilizer N), urban lawns and golf courses (fertilizer N), fertilized horse farms (fertilizer N + manure N), fertilized cattle pastures (fertilizer N + manure N), unfertilized horse farms (manure N), and unfertilized cattle pastures (manure N) in close proximity to monitoring wells. The sites were instrumented with 5 columns per site in June 2017 and retrievals will be retrieved from each site in September 2017 to capture wet season (Jun-Sep) fluxes. An additional 5 resin columns will be installed in new locations at each site, which will be retrieved in May 2018 to measure cumulative and dry season (Oct-May) fluxes (cumulative fluxes – wet season fluxes = dry season fluxes).

Soil columns were constructed using 20 cm x 10 cm PVC, with drain cloth stretched over the bottom and secured with a pipe clamp. Resin was be prepared by rinsing with DI water and was be stored in labeled bags prior to field installation. Representative soil samples were taken and analyzed for soil organic carbon (SOC). During installation, the top 30 cm of soil was excavated using a drain spade and placed intact on a tarp. Soil from the 30 to 40 cm depth was removed using a 10 cm soil auger and mixed with ion-exchange resin at a 1:1 ratio in the field. The bottom 10 cm of the soil column was packed with the resin/soil mixture and the top 10 cm was packed with 100% native soil. The soil column was then installed at the 30 to 50 cm depth; ensuring close contact between the mesh liner and the native soil at 50 cm. Resin columns will be retrieved after 3 months, brought back to the lab, and immediately extracted with 2 *M* KCl and analyzed for NO_3-N. Nitrate flux will be calculated using the surface area of the column and the mass of eluted NO_3^-.

3.5 RESULTS

3.5.1 Groundwater Velocity and Nitrate Flux Measurements

Borehole Dilution. Initial borehole dilution tests were performed in three locations using a preliminary design (dates and locations are described in Table 3.1). The data collected from these initial tests are incomplete, but in general they showed velocities that were relatively low in the confined aquifer (< 20 cm d^{-1}, Table 3.2). The preliminary BHD device was lost in M-0762 at 173 feet (52.73 m).

Table 3.2. Borehole dilution test results from Sharpes Ferry wells. Insufficient data were collected from this method for definitive conclusions, but the measured water fluxes were reasonably consistent with values determined from passive flux meters.

Well Name	Date	Depth	Data collection	Collected data points	Data points used in calculations	q (cm d^{-1})
M-0764	20-Aug	48-52	Manual	12	7	29.8
M-0762	20-Aug	122-126	Manual	4	2	18.6
M-0762	12-Sep	148-152	Logged	749	413	13.6

The new karst borehole dilution device, KBHD, was deployed in June 2016 in well M-0789. This well was chosen due to visual evidence of large fractures in the 120-140 ft (36.56-42.67 M) depth interval from a down-borehole video recorded by SJRWMD staff. Additionally, this well is located only 2.4 km from the Silver Springs main boil. Five BHD tests were performed at different 10 ft intervals in the matrix region of the well. An obstruction in the well prevented the installation of the KBHD beyond 130 ft below the surface, so the KBHD was extracted from the borehole and the bottom packer was removed. The KBHD was re-deployed and a second series of tests was performed. The interval was tested three times, using both KCl and rhodamine as tracers.

The results for the matrix region of the well (Table 3.3, tests 1 to 5) are generally consistent with the previous matrix flux measurements performed in other wells using PFMs; however, fluxes observed in the first two matrix test are considerably higher than any recorded PFM results. Importantly, the tests performed in the conduit showed fluxes orders of magnitude larger than in the matrix region. These three tests were performed at the same depth and thus can be considered replicates.

Table 3.3. Summary of BHD results at six depths in well M0789.

			KCl			Rhodamine		
Test Number	Depth (ft bls)	Predominant porosity	Slope ln(C/C0)	q (cm/day)	q (m/day)	Slope ln(C/	q (cm/day)	q (m/day)
1	69-79	Matrix	-0.002714	31.9			0.0	
2	79-89	Matrix	-0.004838	56.8			0.0	
3	89-99	Matrix	-0.000440	5.2			0.0	
4	99-109	Matrix	-0.000170	2.0			0.0	
5	107-117	Matrix	-0.000209	2.5			0.0	
6-1	119-160	Conduit	-0.175199	2057.1	20.6	-0.131800	1547.6	15.5
6-2	119-160	Conduit	-0.125032	1468.1	14.7	-0.1725	2025.4	20.3
6-3	119-160	Conduit	-0.150638	1768.7	17.7	-0.1769	2077.1	20.8
		Average Conduit	-0.150290	1764.7	17.6	-0.160400	1883.4	18.8

The vertical profile of Darcy flux estimaes from the KBHD for M0789 are illustrated in Figure 3.14 (note the log scale for the x-xis). Measured time series of electrical conducitivty used to obtain these estimates are shown in Fiugres 3.15 to 3.22. Linear regression fits to the log-transformed relative concentration time series are shown in Figures 3.23 to 3.30. Rhodamine and

KCl-based data are compared in Figures 3.31 to 3.33, indicating close agreement between the two methods.

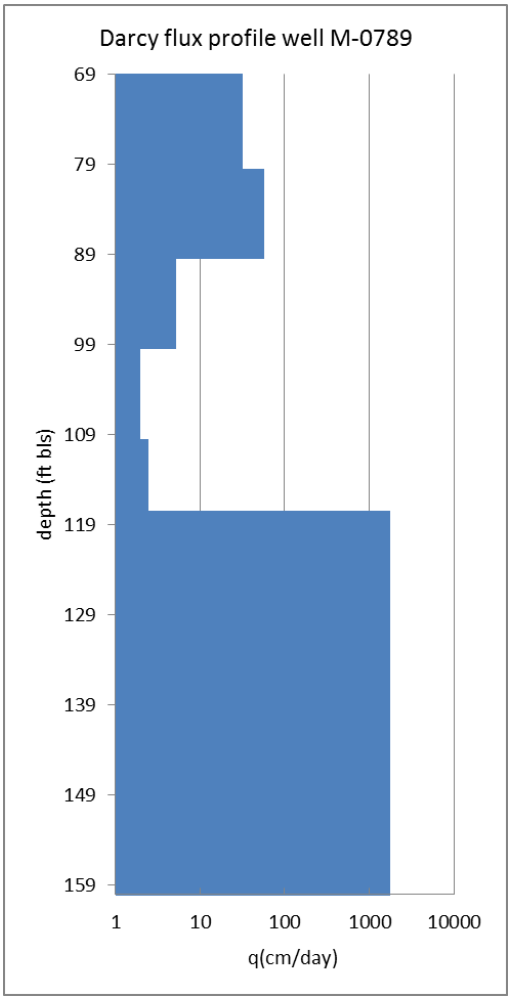

Figure 3.14. Darcy flux profile from BHD tests performed in well M0789.

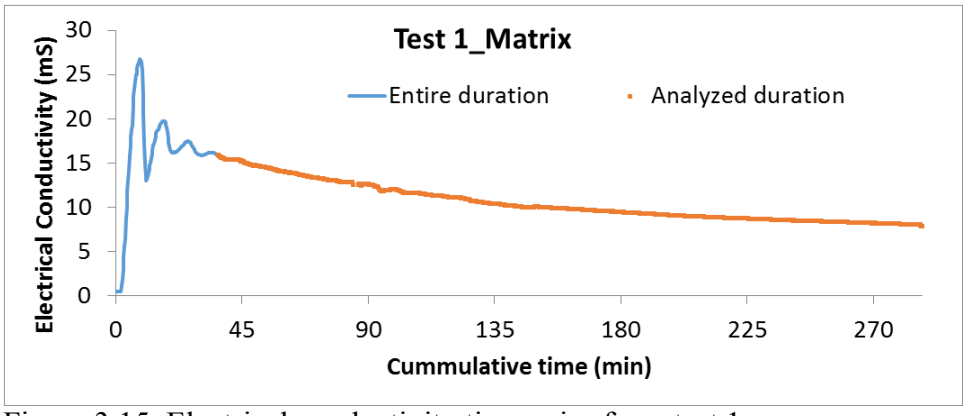

Figure 3.15. Electrical conductivity timeseries from test 1.

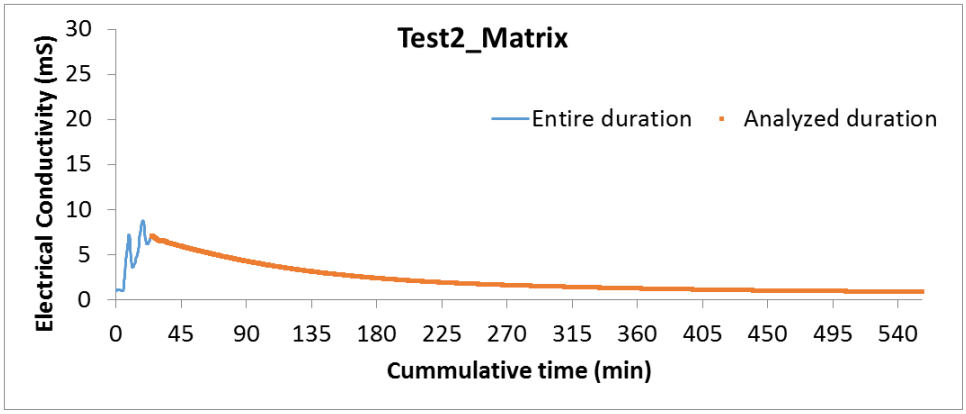

Figure 3.16. Electrical conductivity timeseries from test 2.

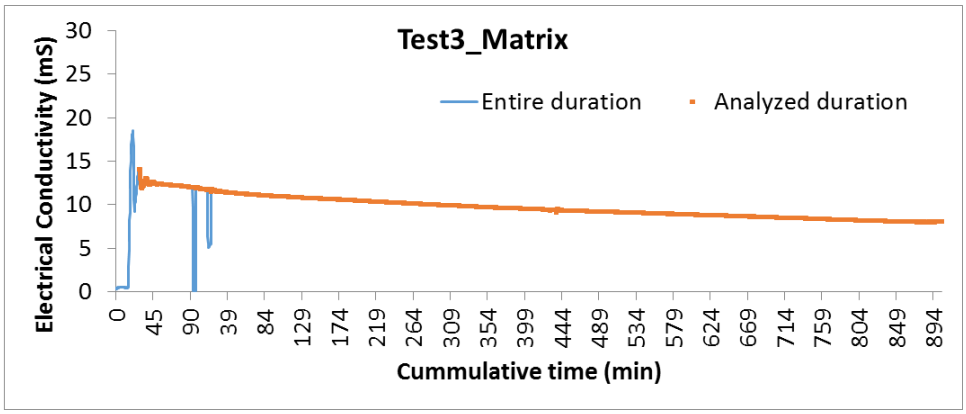

Figure 3.17. Electrical conductivity timeseries from test 3.

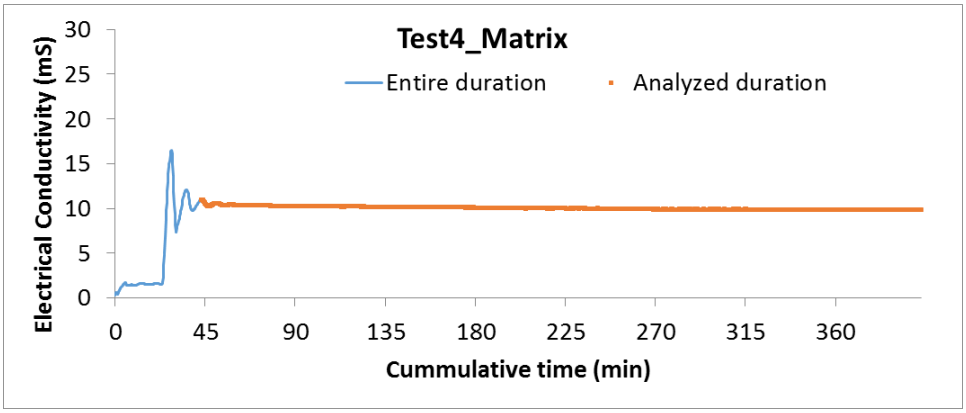

Figure 3.18. Electrical conductivity timeseries from test 4.

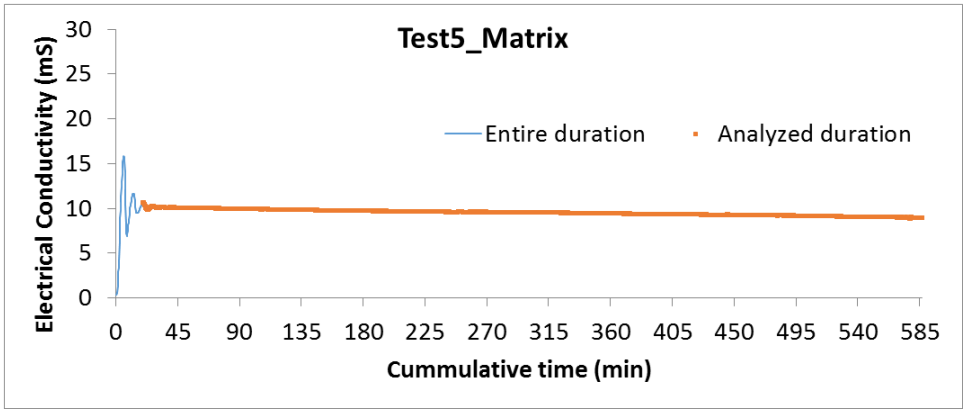

Figure 3.19. Electrical conductivity timeseries from test 5.

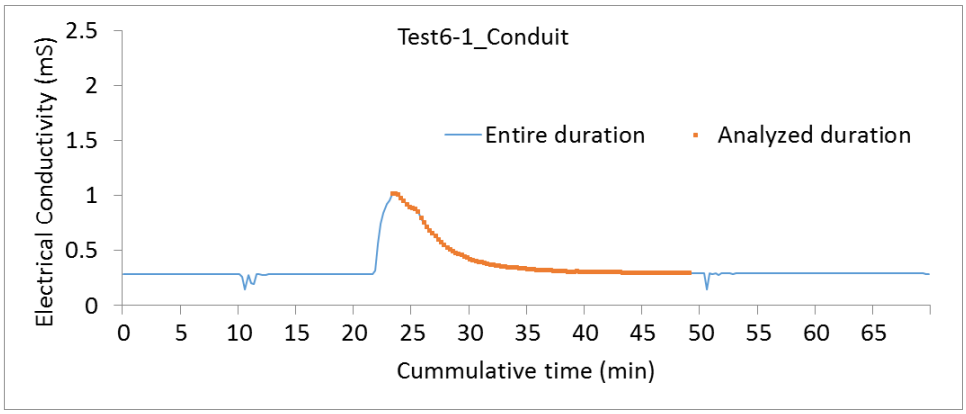

Figure 3.20. Electrical conductivity timeseries from test 6-1.

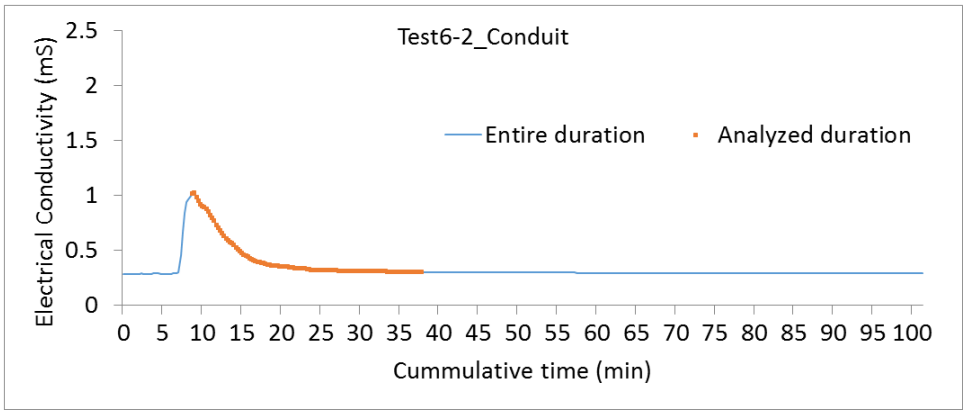

Figure 3.21. Electrical conductivity timeseries from test 6-2.

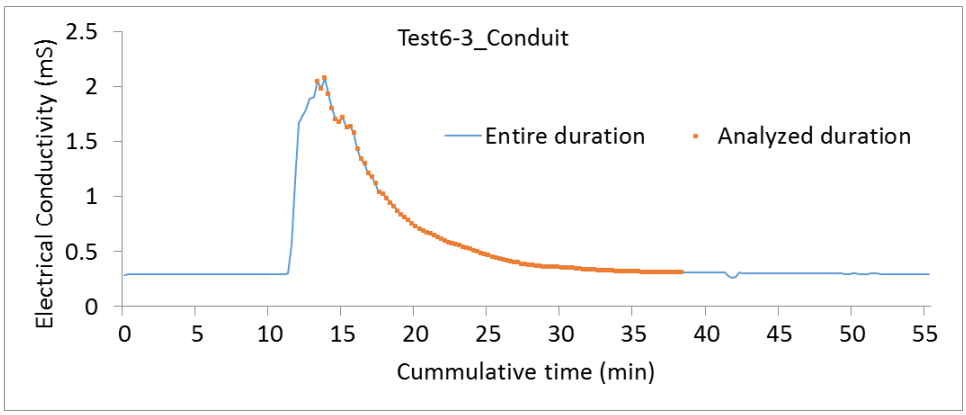

Figure 3.22. Electrical conductivity timeseries from test 6-3.

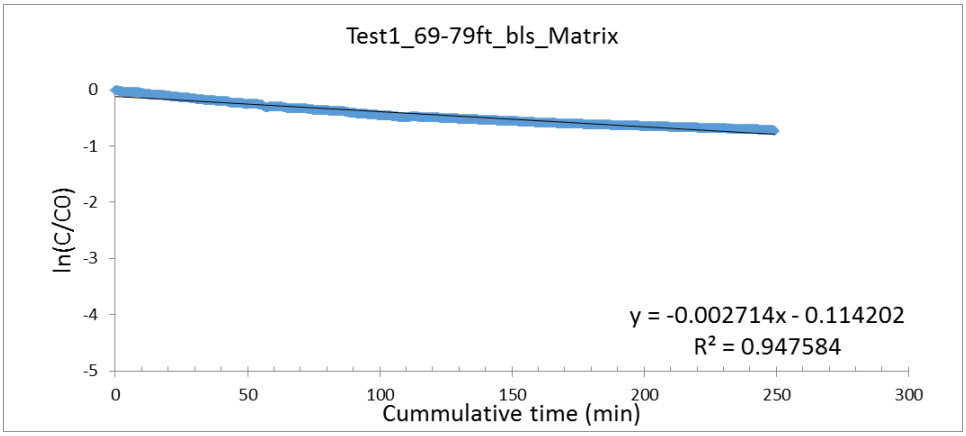

Figure 3.23. Log-transformed C/C_0 data from test 1 used for Darcy flux estimation.

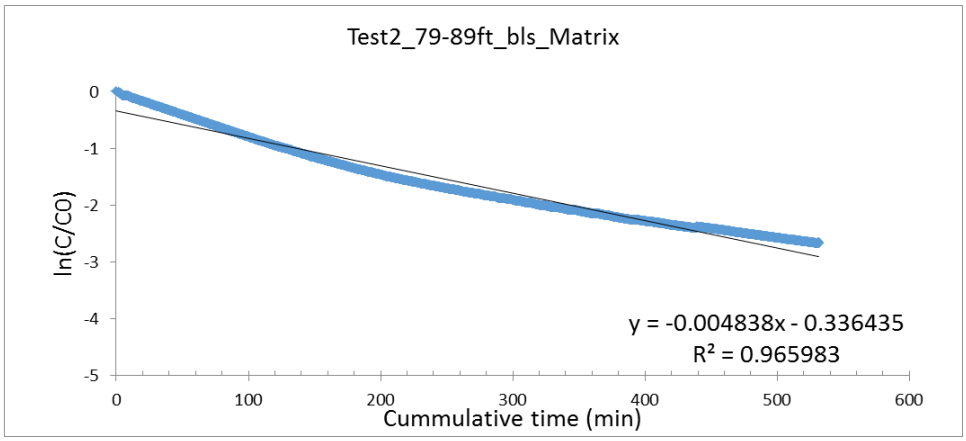

Figure 3.24. Log-transformed C/C_0 data from test 2 used for Darcy flux estimation.

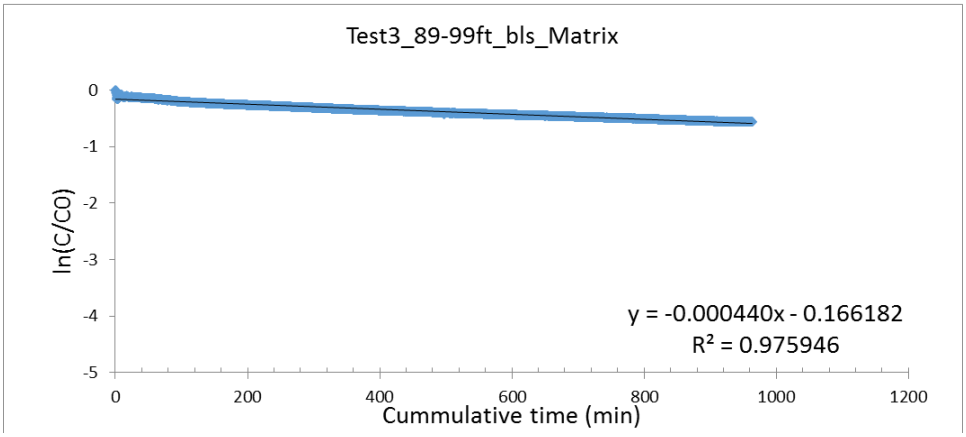

Figure 3.25. Log-transformed C/C_0 data from test 3 used for Darcy flux estimation.

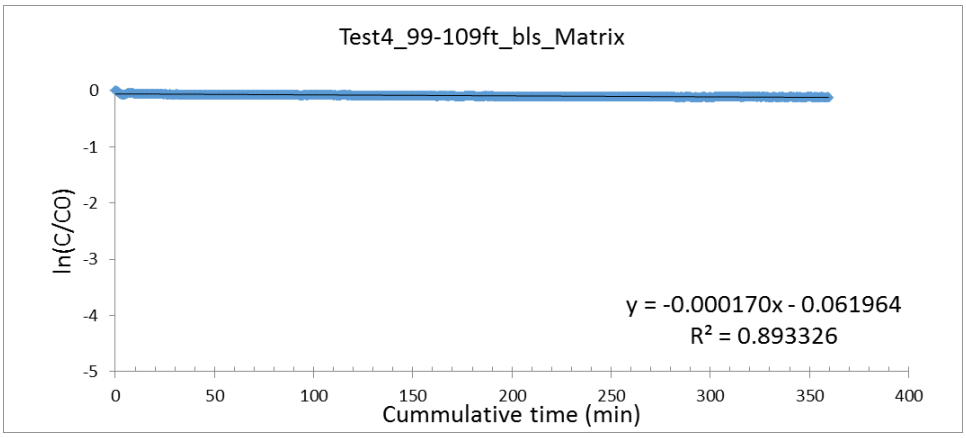

Figure 3.26. Log-transformed C/C_0 data from test 4 used for Darcy flux estimation.

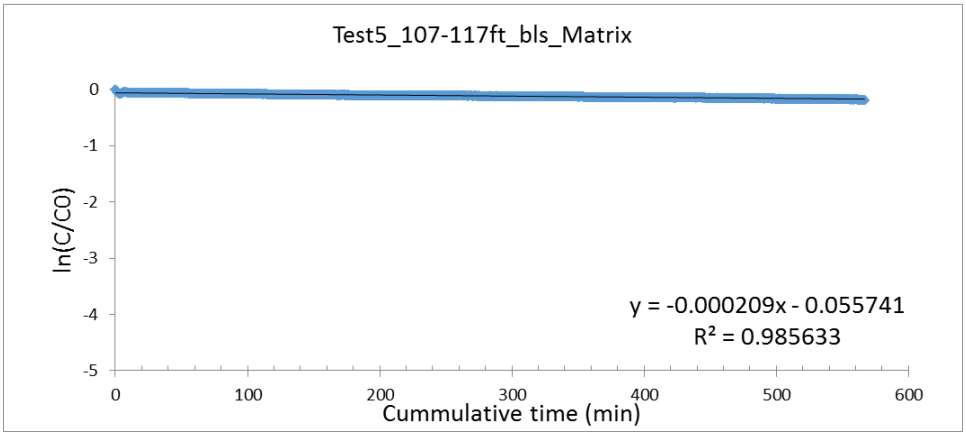

Figure 3.27**.** Log-transformed C/C_0 data from test 5 used for Darcy flux estimation.

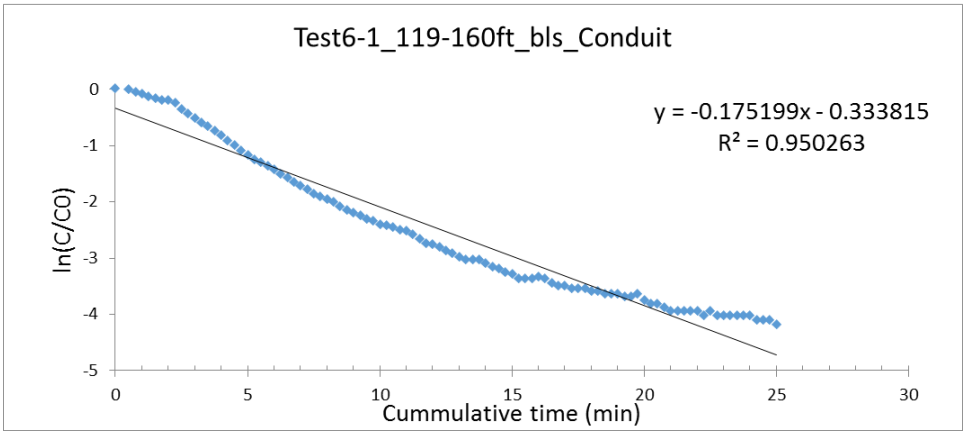

Figure 3.28**.** Log-transformed C/C_0 data from test 6-1 used for Darcy flux estimation.

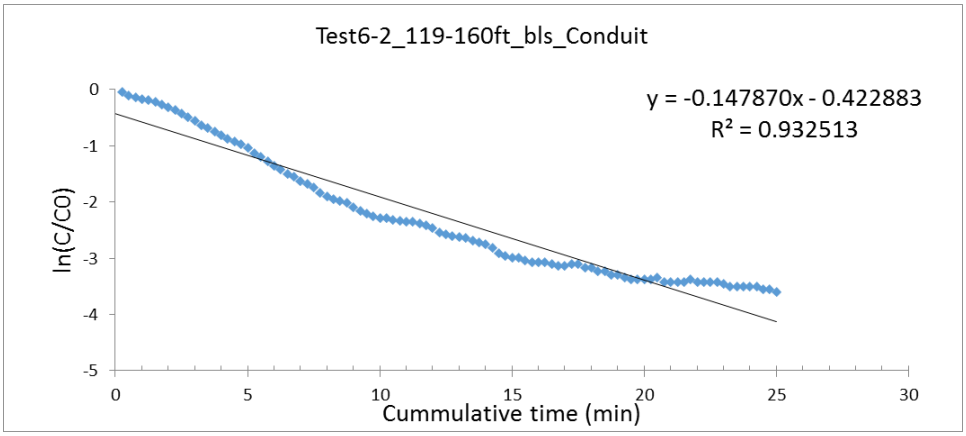

Figure 3.29. Log-transformed C/C_0 data from test 6-2 used for Darcy flux estimation.

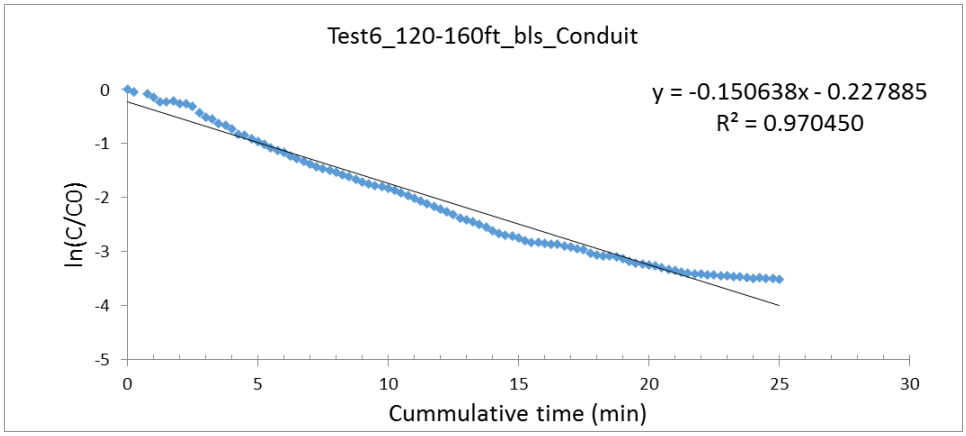

Figure 3.30. Log-transformed C/C_0 data from test 6-3 used for Darcy flux estimation.

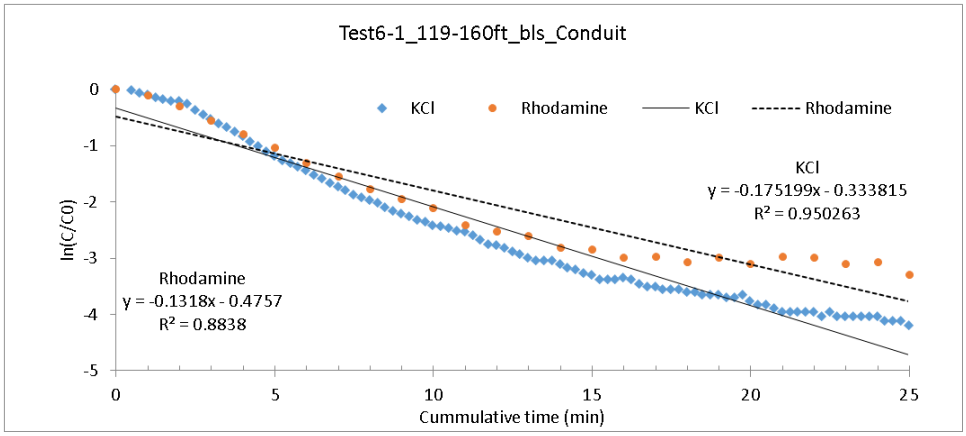

Figure 3.31**.** Comparison of rhodamine and KCl log transformed data from conduit test 6-1.

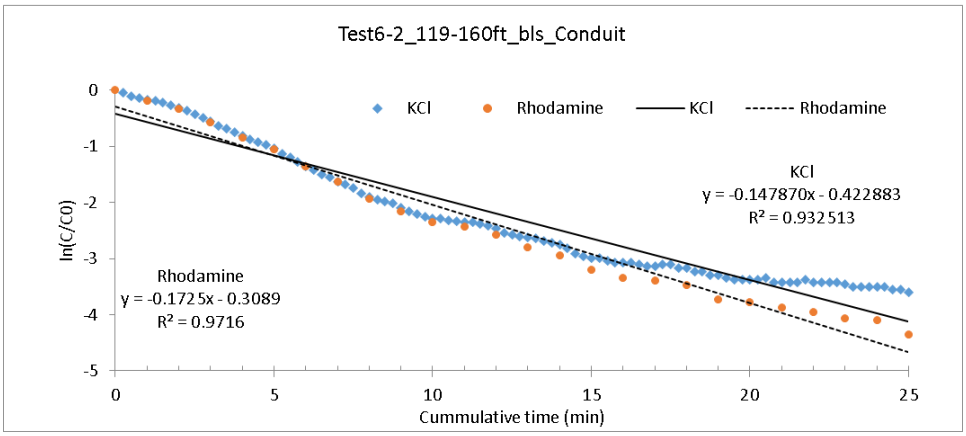

Figure 3.32**.** Comparison of rhodamine and KCl log transformed data from conduit test 6-2.

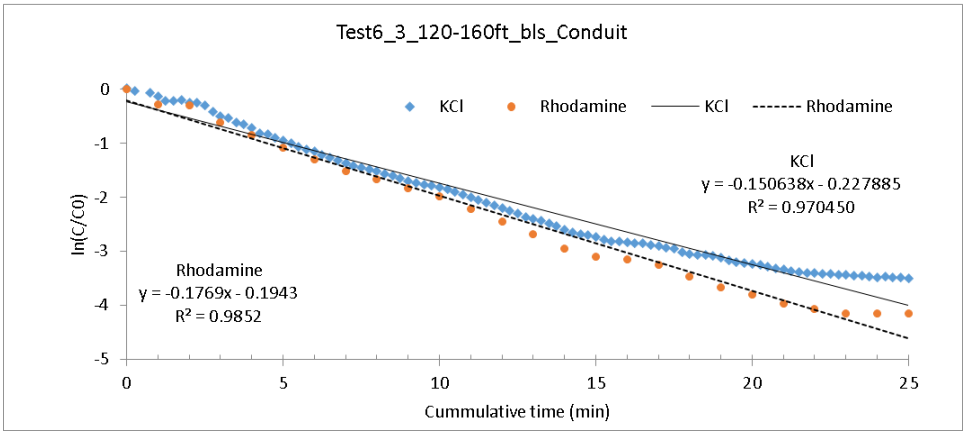

Figure 3.33. Comparison of rhodamine and KCl log transformed data from conduit test 6-3.

Flux Meters. Darcy flux results from the PFM deployments, and the locations of these wells in relation to 14 and 28 km transects centered around Silver Springs are shown in Figure 3.34. Note that the PFM deployment depths were also variable. Despite the wide distribution of deployment locations and depths, very low variability was found in PFM-measured water fluxes.

Well Number	Darcy Flux (cm/day)
M-0625	6.6
M-0762	5.4
M-0764	7.0
M-0771	4.8
M-0772	5.5
M-0773	5.4
M-0774	7.5
M-0775	4.4
M-0776	3.9
M-0777	9.1
M-0778	9.5
M-0780	2.7
M-0781	3.7
M-0785	6.8
M-0786	6.2
M-0787	8.1
Mean	6.03
Std	1.93
Variation Coeff	0.32

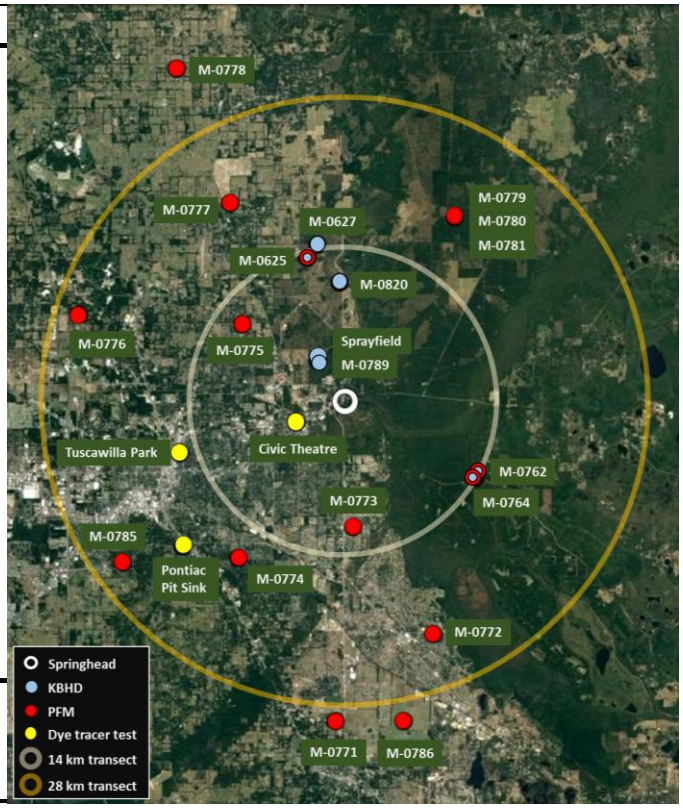

Figure 3.34. Summary of Darcy fluxes measured by PFMs, and location map of well locations in relation to 14 and 28 km diameter circles around Silver Springs.

Push-pull Tracer Tests. Push-pull tracer tests were conducted in five wells: M0789, Sprayfield, M779, M780, and M781. Water samples were collected at different depths in the wells using the KBHD device to vertically isolate sections of the aquifer. At well M0789, the push-pull test was conducted at depths 89-99 ft bgs, where the mean nitrate concentration was 0.77 mg L^{-1} (Figure 3.35). At the Sprayfield well, the push-pull test was conducted at depths 59-69 ft bgs, where the mean nitrate concentration was approximately 2.2 mg L^{-1} (Figure 3.36).

At well M0789, approximately 73% of both rhodamine (non-reactive) and KNO_3 (reactive) tracers were recovered (Figure 3.37). The similar mass recovery indicates that no degradation of NO_3 was observed at this well. At the Sprayfield well, approximately 85% of both tracers were recovered (Figure 3.38). Again, similar mass recovery indicates that no degradation of NO_3 was observed at this well.

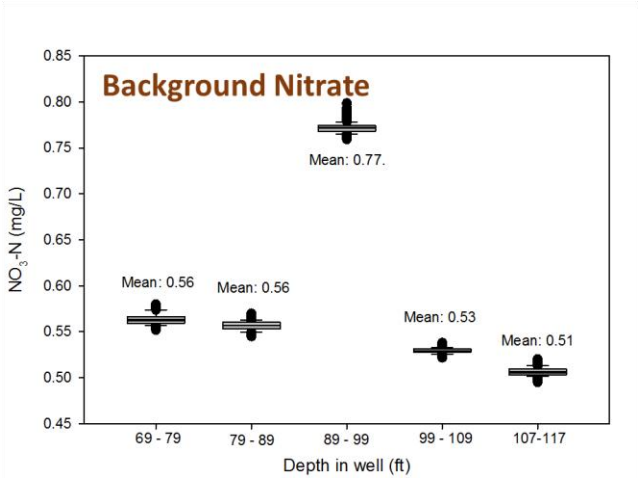

Figure 3.35. (left) Well M0789 push-pull test apparatus. (right) Background nitrate concentrations measured as a function of depth in M0789. Samples were collected using the KBHD device.

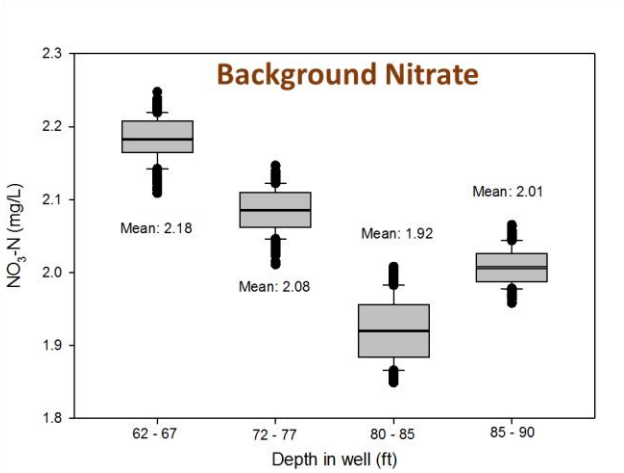

Figure 3.36. (left) Sprayfield well push-pull test apparatus. (right) Background nitrate concentrations measured as a function of depth at the Sprayfield well. Samples were collected using the KBHD device.

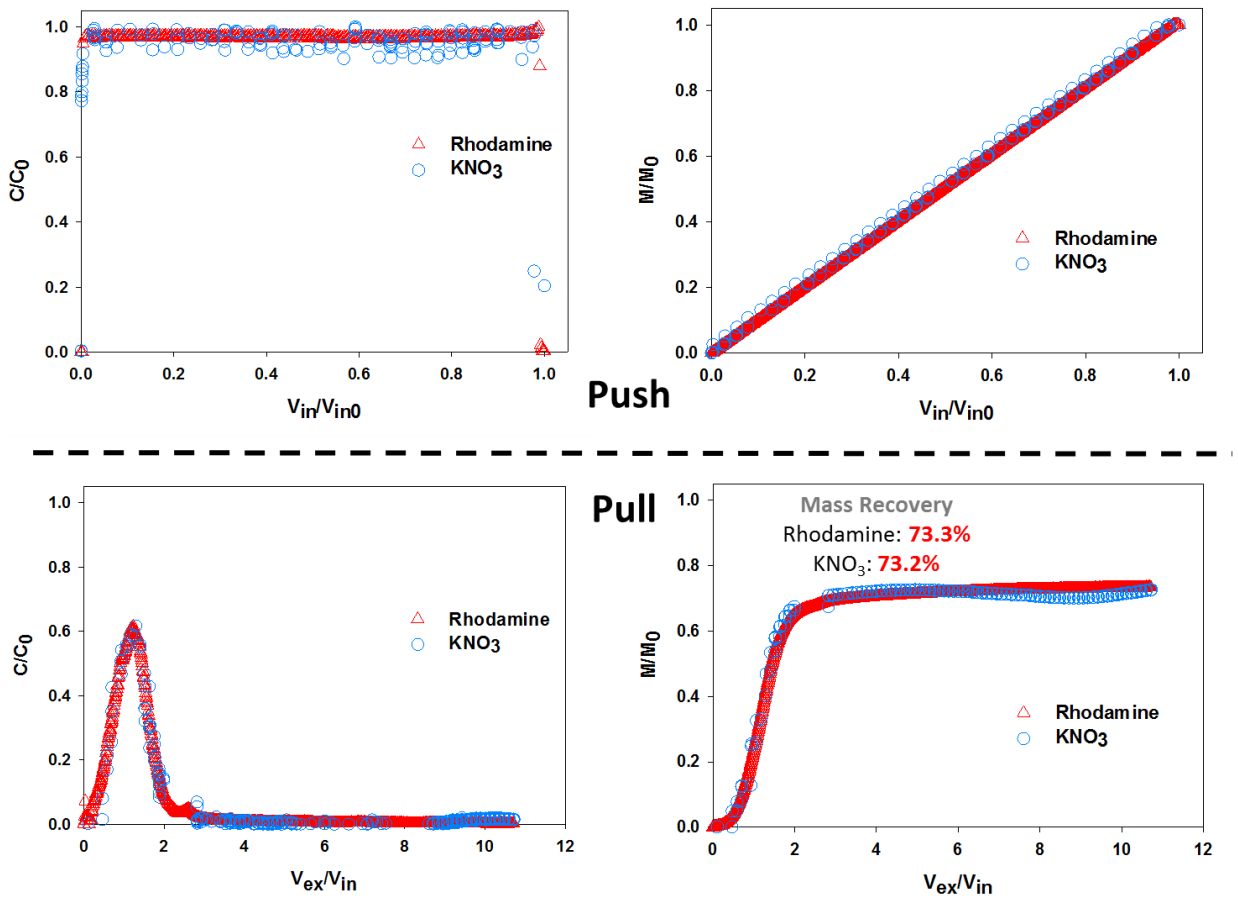

Figure 3.37. Well M0789 (top) Measured relative concentrations of rhodamine and KNO_3 tracers during injection (push). Right side graph shows that the integrated measured mass equals the expected value. (bottom) Measured relative concentrations of rhodamine and KNO_3 tracers during extraction (pull). Right side graph shows that both tracers recovered similar mass.

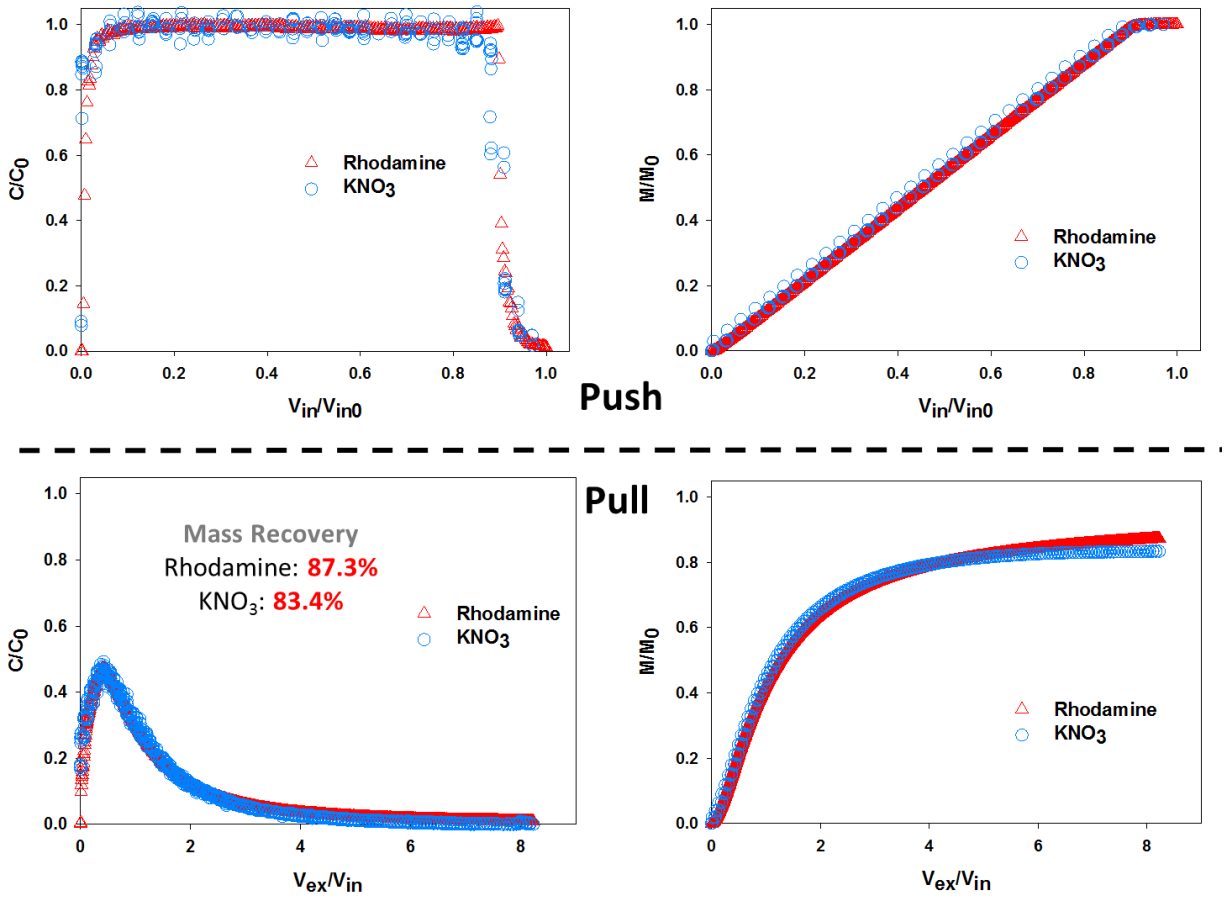

Figure 3.38. Sprayfield well (top) Measured relative concentrations of rhodamine and KNO_3 tracers during injection (push). Right side graph shows that the integrated measured mass equals the expected value. (bottom) Measured relative concentrations of rhodamine and KNO_3 tracers during extraction (pull). Right side graph shows that both tracers recovered similar mass.

However, degradation potential is a function of degradation rate and residence time. The residence times in these push-pull tests are much shorter than average aquifer residence times. The expected mass loss from first-order degradation is illustrated as a function of residence time in Figure 3.39. These data show that measurable mass loss (~ 10% or more) within just a few hours requires relatively high rate constants (k and B ~ 0.1 h^{-1} or higher).

Significant NO_3 degradation was observed at wells M779 (135-145 ft) and M780 (59-69 ft). Mass recovery of KNO_3 at both wells was only approximately 60% of the rhodamine recovery (Figures 3.40 and 3.41), indicating substantial degradation (k = 0.42 h^{-1} and B = 0.75 h^{-1}), even during this relatively short experiment. Thus, these locations show evidence of a denitrification hot-spot. Note that at a shallow well at the same location (M781, 25-35 ft), both tracers showed similar recovery (Figure 3.42), once again indicating no degradation. This result is expected at the shallow well with relatively higher oxygen levels (0.2 mg L^{-1}) than the others (0.08 mg L^{-1}). Importantly, at all three wells no background nitrate was detected. These results suggest that

measurable nitrate concentrations (as detected at M0789 and Sprayfield) indicate a lack of strongly denitrifying conditions.

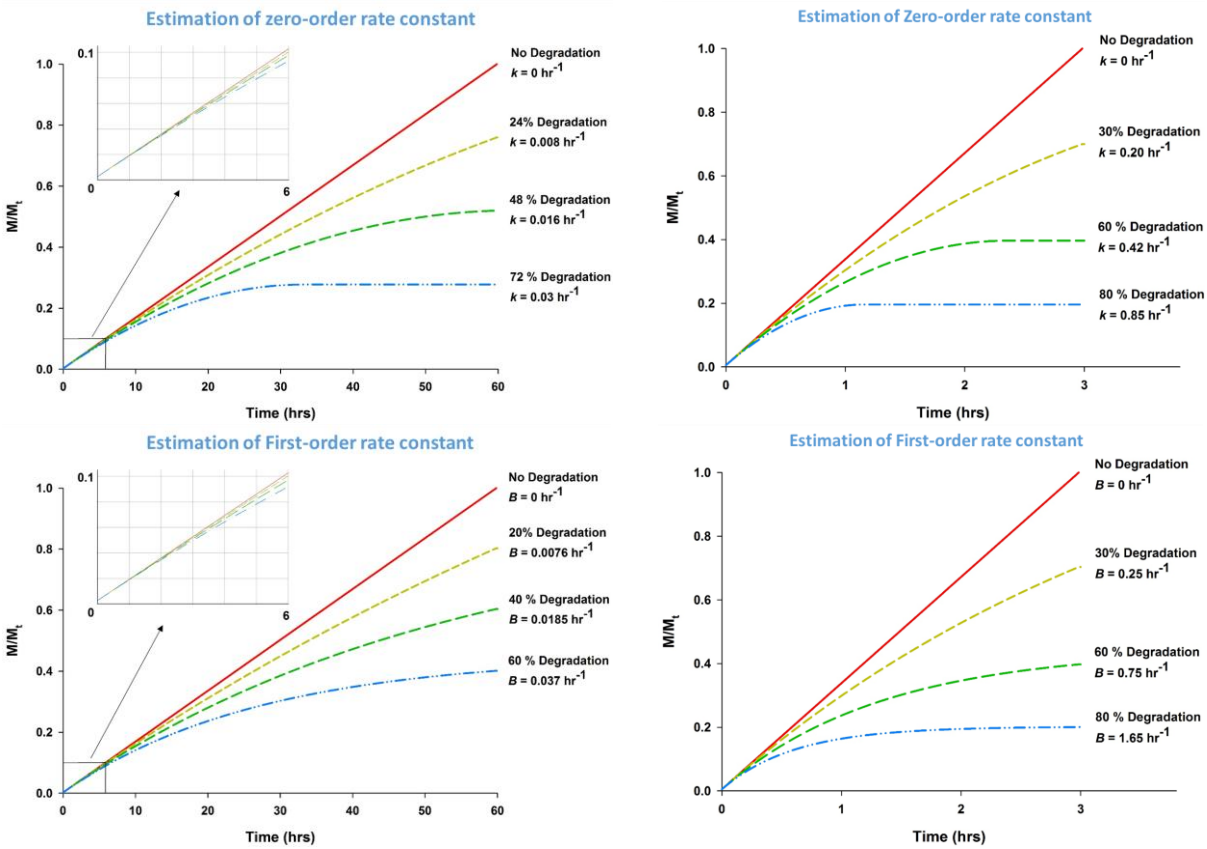

Figure 3.39. Expected mass loss from zero- and first-order degradation as a function of residence time. (left) Longer residence times with relatively lower rate constants and (right) Shorter residence times with relatively higher rate constants. Measurable mass loss (~ 10% or more) within just a few hours requires relatively high rate constants (k ~ 0.1 h^{-1} or higher).

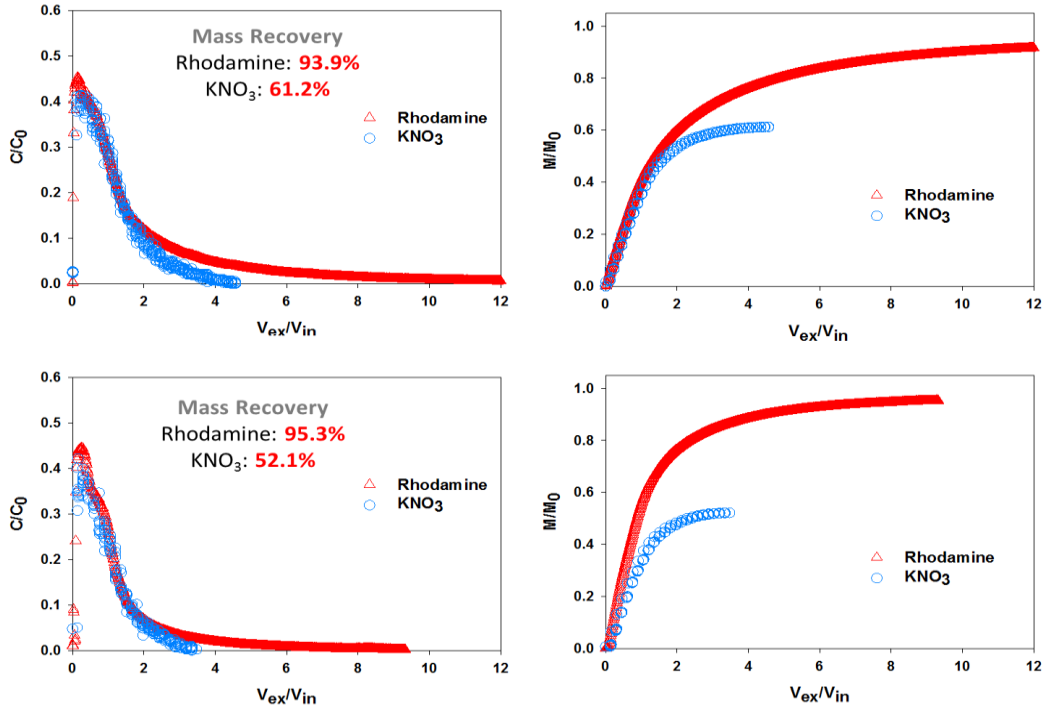

Figure 3.40. Top and bottom are two replicated push-pull tests at M779 134-145 ft. (left) Measured relative concentrations of rhodamine and KNO_3 tracers during extraction. (right) Integrated measured mass recovery. NO_3 recovery was only approximately 60% of the rhodamine recovery.

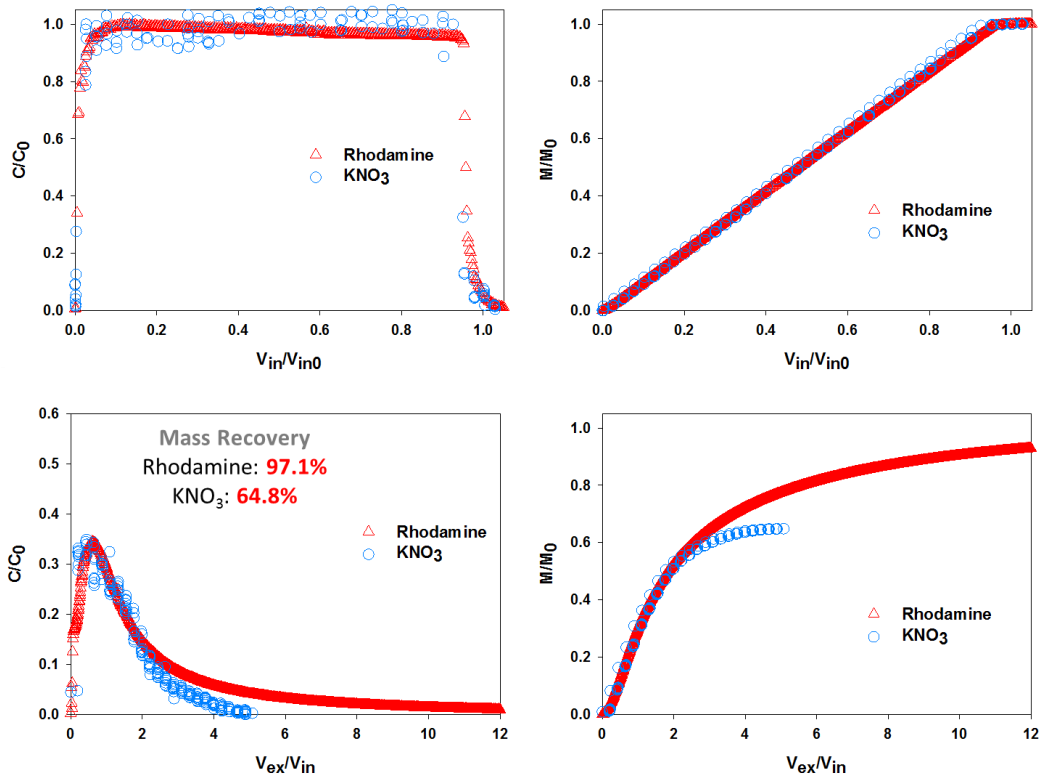

Figure 3.41. Well M0780 59-69 ft (top) Measured relative concentrations of rhodamine and KNO_3 tracers during injection (push). Right side graph shows that the integrated measured mass equals the expected value. (bottom) Measured relative concentrations of rhodamine and KNO_3 tracers during extraction (pull). NO_3 recovery was only approximately 60% of the rhodamine recovery.

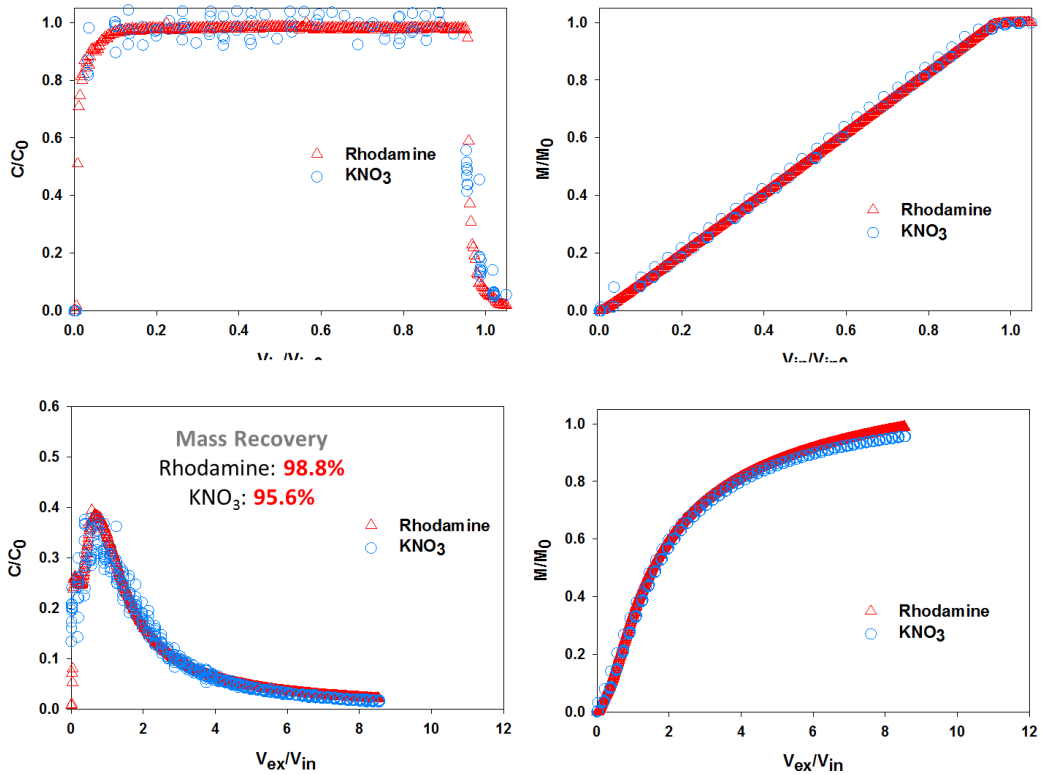

Figure 3.42. Well M0781 25-35 ft (top) Measured relative concentrations of rhodamine and KNO_3 tracers during injection (push). Right side graph shows that the integrated measured mass equals the expected value. (bottom) Measured relative concentrations of rhodamine and KNO_3 tracers during extraction (pull). Right side graph shows that both tracers recovered similar mass.

3.5.2 Soil N Flux

Resin Column Design. HYDRUS-1D simulations supported the hypothesis that installing resin columns with a 100% resin layer between two layers of native soil would result in the build-up of a saturated layer above the column (Figure 3.43). Figure 3.44 shows the build-up of a saturated layer within the resin column when the resin is mixed with native soil at a 1:1 ratio, but avoids the overlying saturated layer that occurs when 100% resin is placed at the bottom of the column.

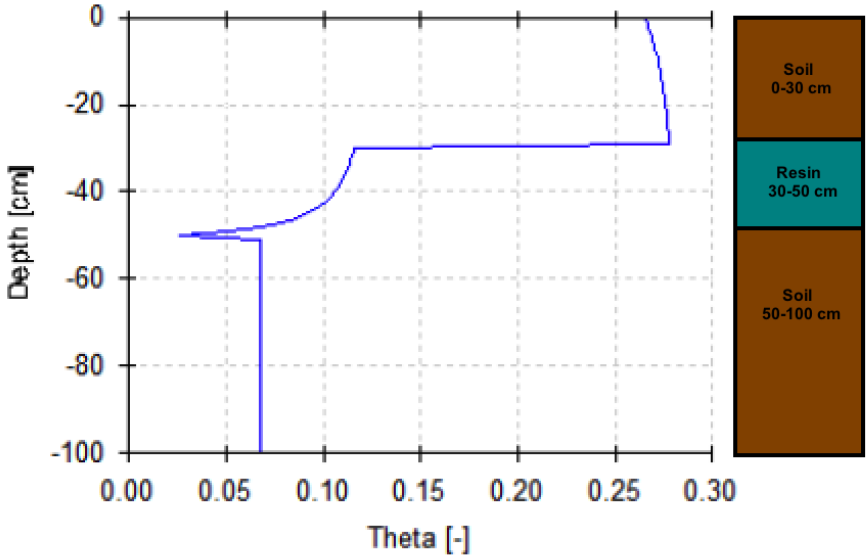

Figure 3.43. Steady-state soil moisture profile of macroporous anion exchange resin layered between Arredondo fine sand, with a constant water flux of 2 cm d^{-1}.

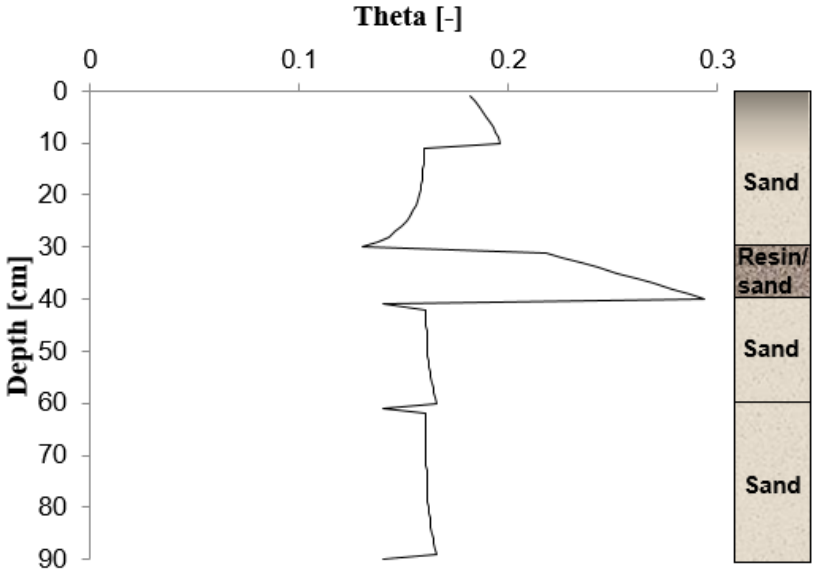

Figure 3.44. HYDRUS-1D simulation of the steady-state soil moisture profile of a macroporous anion exchange resin/Arredondo fine sand mixture layered between Arredondo fine sand, with a constant water flux of 23 cm d^{-1}.

Measured soil moisture was compared with soil moisture modeled in HYDRUS-1D, as shown in Figure 3.45. Measured data was in good agreement with modeled soil moisture (R^2=0.94), suggesting that soil, resin, and mesh parameters used in the model are appropriate for the materials used. As hypothesized, the resin/soil mixture avoided the build-up of a saturated zone above the resin at high water fluxes. Additional modeling in HYDRUS-1D showed a mirror-image pattern of soil moisture distribution when water was supplied at a steady rate of 2 cm d^{-1}

(Figure 3.46), which is closer to the 10 year average daily precipitation rate of 1 cm d^{-1} for rainy days in the springshed. While the water content of the soil layer is greater than the underlying soil/resin layer, the overlying soil layer does not approach saturation. Additionally, the 20 cm soil column contains 10 cm of the soil/resin mix and 10 cm of the overlying soil. This ensures that the first half of the column is at the same moisture content of the surrounding soil, which should prevent convergence or divergence of soil water around the resin column.

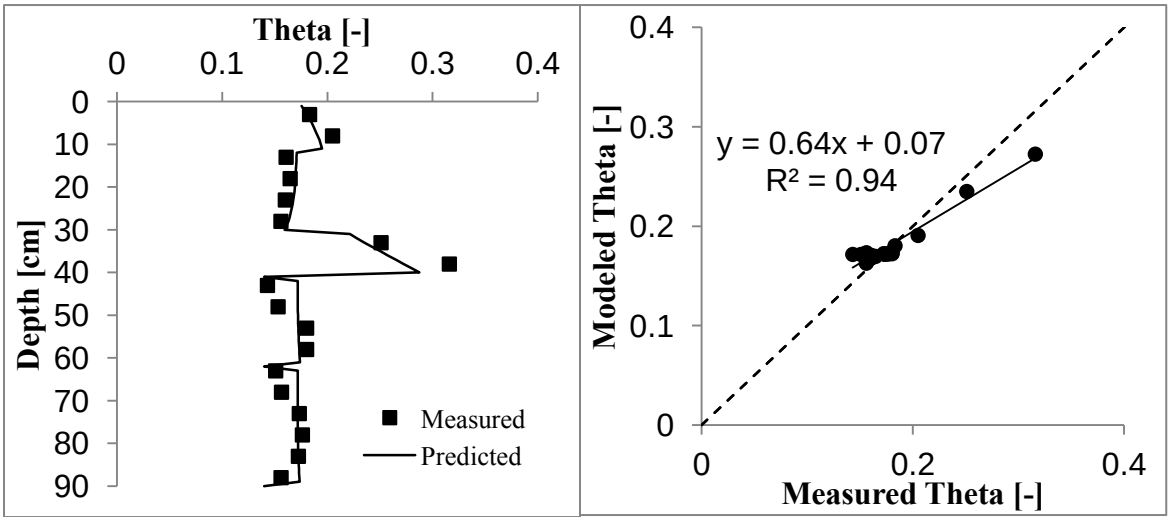

Figure 3.45. Measured and predicted soil moisture profile (left) and comparison of measured soil moisture data points and soil moisture modeled in HYDRUS-1D (right).

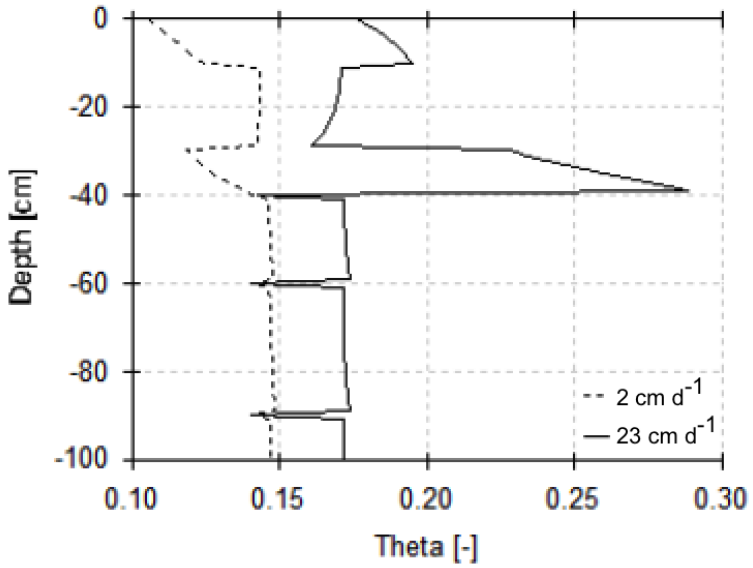

Figure 3.46. HYDRUS-1D simulation of the steady-state soil moisture profile of a macroporous anion exchange resin/Arredondo fine sand mixture layered between Arredondo fine sand with a constant water flux of 23 cm d^{-1} (solid) and 2 cm d^{-1} (dashed).

All applied nitrate was recovered and no nitrate was found below the resin layer (Figure 3.47); the extraction efficiency for the initial elution was 63%, consistent with initial elution extraction efficiencies in previous experiments (see previous annual report). The nitrate adsorbed to the resin corresponds to a nitrate flux rate of 2,100 kg NO_3-N ha^{-1}, suggesting that the capacity of the resin is high enough to accommodate nitrate loads an order of magnitude greater than the highest expected loads in the springshed without nitrate breakthrough.

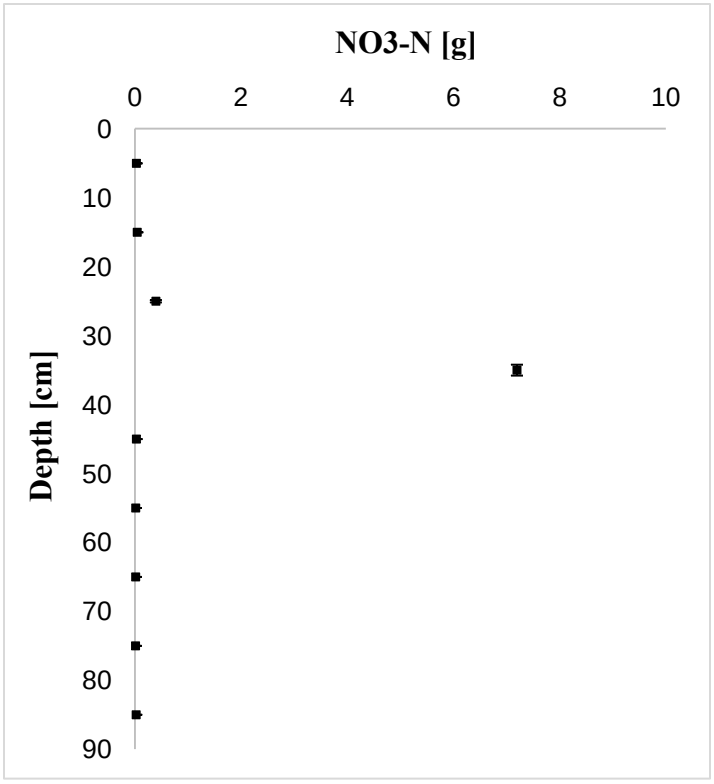

Figure 3.47. Nitrate recovery in soil column (± SE).

Field Tracer Test. Bromide recovery was 129% ± 37% (**α=**1.29 ± 3.7) and nitrate recovery was 134% ± 17% (**α=**1.29 ± 1.7), suggesting that slight convergence of soil water occurred. This was potentially due to the nature of the installation of the columns, as simulations in HYDRUS-2D result in **α** close to 1 for a range of soil properties when resin is mixed with the native soil. Therefore, bromide tracer solution was applied to the surface above all *in situ* soil columns to calculate **α** and reduce error due to changes in **α** from installation procedures.

Nitrate Flux Measurements. At the time of project completion, columns are still in the field and columns deployed during the first measurement period will be collected during Fall 2017.

3.6 DISCUSSION

The water fluxes measured above can be compared to estimated average fluxes in the aquifer to gain insights into the relative contributions of matrix and non-matrix flow to the total spring discharge. The schematic diagram in Figure 3.48 is used to illustrate the computation of the average Darcy flux. Within the springshed, all of the groundwater flow through the thickness, *B*,

of the Upper Floridan aquifer is considered to exit as discharge from Silver Springs, Q_{ss}. The total discharge is then the product of the average Darcy flux, q, and the aquifer cross-sectional area, A, for a cylinder in the aquifer at radius r. For B = 50 m and r = 14 km, the average flux q = 0.4 m d^{-1}. The average Darcy flux decreases exponentially with distance from the spring outlet (Figure 3.48).

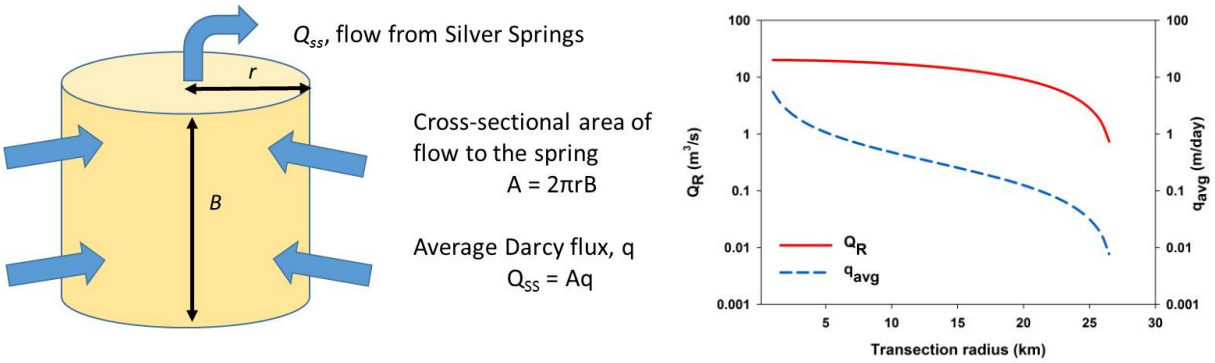

Figure. 3.48. (left) Schematic diagram of a hypothetical cylinder through the Upper Floridan aquifer, with thickness B and radius r. (right) Average Darcy flux, q_{avg} (m d^{-1}), and recharge, Q_R (m^3 s^{-1}), as a function of radius from spring outlet.

The PFM-measured Darcy fluxes within this 14 km radius were much lower than 0.4 m d^{-1} (mean 0.06 m d^{-1}, Figure 3.49). These low fluxes indicate that these values are likely representative of the rock matrix and other portions of the aquifer (e.g., conduits) are responsible for the remainder of the flux. We estimated matrix fluxes to be below 0.1 m d^{-1} while fluxes above this are representative of non-matrix including fractures, faults, and conduits. Our measured fluxes from PFMs and BHD tests are shown in Figure 3.49 together with dye tracer test (DTT) estimates from previous studies conducted within the 14 km radius of Silver Springs, (see Figure 3.34 for locations). The means of our matrix and non-matrix measurements are q_m = 0.06 m d^{-1} and q_c = 30.1 m d^{-1}.

The non-matrix fraction of the total flow and total cross-sectional area (based on the mean matrix and non-matrix flux values q_m = 0.06 m d^{-1} and q_c = 30.1 m d^{-1}) are shown in Figure 3.50. For a transect of radius 14 km, the non-matrix represents approximately 1% of the cross-sectional area, but deliver nearly 80% of the flow through the UFA. This ratio is a function of the distance from the spring (Figure 3.50).

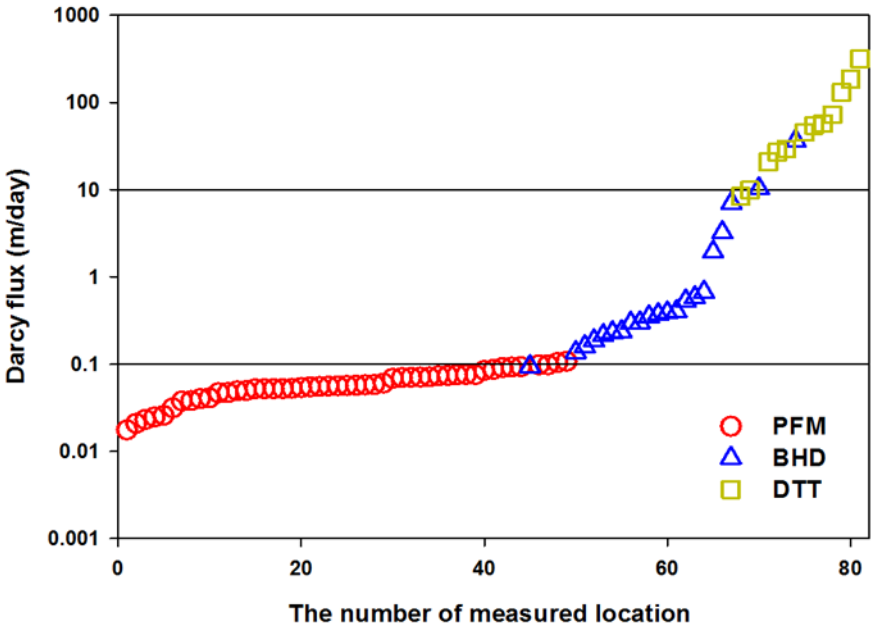

Figure. 3.49. Measured Darcy fluxes from PFMs, BHD tests, and dye tracer test (DTT) estimates from previous studies conducted within the 14 km radius of Silver Springs, (see Figure 3.33 for locations).

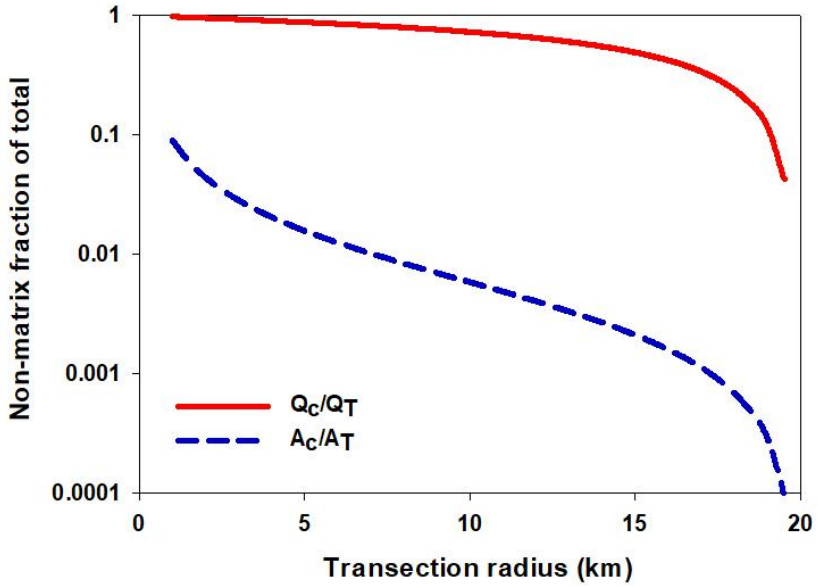

Figure. 3.50. Non-matrix fraction of the total flow and total cross-sectional area, based on mean matrix and non-matrix fluxes q_m = 0.06 m d^{-1} and q_c = 30.1 m d^{-1}.

Other evidence of the conduit contribution comes from the measured head profile with distance from the spring (Figure 3.51) (Worthington, 2009). Based on Darcy's Law, a homogeneous porous medium would have a convex head profile, with a head difference of approximately 5 m

at a distance of 10 km from the spring. However, the measured head difference is less than 1 m at this distance, indicating a system with very high hydraulic conductivity (conduits) near the spring, and decreasing in density with distance from the spring, as illustrated in Figure 3.51 (decreasing area fraction with distance).

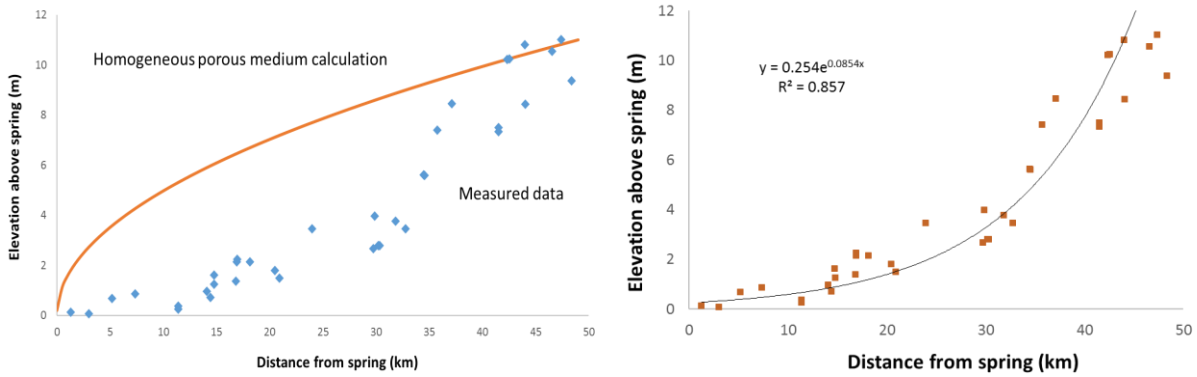

Figure. 3.51. Measured head profile with distance from the spring. (left) A homogeneous porous medium would have a convex head profile. (right) Decreasing conduit density with distance.

3.7 CONCLUSIONS AND RECOMMENDATIONS

Measured values of groundwater flux (Darcy velocity) from PFMs were relatively low, indicative of matrix flow through the limestone. By specifically targeting portions of the aquifer that were suggestive (from down-hole videos) of fractures and conduits, we found much higher velocities using the KBHD. The relative contribution of conduit flow to the spring discharge is not known with certainty, but these results suggest that within a few kilometers of the spring conduit flows is the dominant contributor. These are the first *in situ* measurements of conduit flow.

In situ denitrification was assessed using push-pull test. This technique was able to identify zones of high denitrification potential (hot spots). However, other evidence (e.g., very low NO_3 concentrations, presence of H_2S) may provide similar information.

3.8 FUTURE RESEARCH NEEDS

A priority is to locate high-flux zones for both water and nitrate. *In situ* measurement of water and solute flux in conduits flowing towards Silver Springs from different directions will provide insight into the spatial distribution of nitrate sources and denitrification. Another priority is field evaluation of *in situ* denitrification in the soil zone.

3.9 REFERENCES

Annable, M. D., et al., 2005. Field-scale evaluation of the passive flux meter for simultaneous measurement of groundwater and contaminant fluxes. *Environmental science and technology*, 39(18): 7194-7201.

Hatfield, K., Annable, M., Cho, J., Rao, P. S. C. and Klammler, H., 2004. A direct passive method for measuring water and contaminant fluxes in porous media. *Journal of Contaminant Hydrology*, 75(3): 155-181.

Kim, Y., Kim, J. H., Son, B. H., Oa, S. W. 2005. A single well push-pull test method for *in situ* determination of denitrification rates in a nitrate-contaminated groundwater aquifer. *Water Science and Technology*, 52(8), 77-86.

Klammler, H., Newman, M. A., Szilágyi, E., Padowski, J. C., Hatfield, K., Jawitz, J. W., and Annable, M.D. 2007. Initial Test Results for a Passive Surface Water Fluxmeter to Measure Cumulative Water and Solute Mass Fluxes. *Environmental Science & Technology*, 41:2485-2490.

Kramer, S. B., Reganold, J. P., Glover, J. D., Bohannan, B. J. M., and Mooney, H. A. 2006. Reduced nitrate leaching and enhanced denitrifier activity and efficiency in organically fertilized soils. *Proceedings of the National Academy of Sciences of the United States of America,* 103(12), 4522-4527.

Lilburne, L., Carrick, S., Webb, T., and Moir, J. 2012. Computer based evaluation of methods to sample nitrate leached from grazed pasture. *Soil Use and management,* 28(1), 19-26.

Minet, E., Coxon, C. E., Goodhue, R., Richards, K. G., Kalin, R. M., and Meier-Augenstein, W. 2012. Evaluating the utility of ^{15}N and ^{18}O isotope abundance analyses to identify nitrate sources: a soil zone study. *Water research*, 46(12), 3723-3736.

Nahlawi, H., A. Bouazza, and J. Kodikara. "Characterisation of geotextiles water retention using a modified capillary pressure cell." Geotextiles and Geomembranes 25, no. 3 (2007): 186-193.

Padilla, A. and Pulidobosch, A. 1995. Study of Hydrographs of Karstic Aquifers by Means of Correlation and Cross-Spectral Analysis. *Journal of Hydrology*, 168(1–4), 73–89. https://doi.org/Doi 10.1016/0022-1694(94)02648-U

Padowski, J. C., Rothfus, E. A., Jawitz, J. W., Klammler, H., Hatfield, K., and Annable, M. D. 2009. Effect of Passive Surface Water Flux Meter Design on Water and Solute Mass Flux Estimates. *Journal of Hydrologic Engineering*, 14(12), 1334-1342.

Pitrak, M., Mares, S., and Kobr, M. 2007. A simple borehole dilution technique in measuring horizontal ground water flow. *Ground Water*, *45*(1), 89-92.

Predotova, M., Bischoff, W. A., and Buerkert, A. 2011. Mineral nitrogen and phosphorus leaching from vegetable gardens in Niamey, Niger. *Journal of Plant Nutrition and Soil Science,* 174(1), 47-55.

Quinn, P. M., Cherry, J. A., and Parker, B. L. 2012 Hydraulic testing using a versatile straddle packer system for improved transmissivity estimation in fractured rock boreholes. *Hydrogeology Journal*, 20(8), 1529-1547.

Quinn P. M., Parker, B. L., and Cherry, J. A. 2016 Blended head analyses to reduce uncertainty in packer testing in fractured-rock boreholes. *Hydrogeology Journal*, 24, 59-77

Siemens, J., and Kaupenjohann, M. 2004. Comparison of three methods for field measurement of solute leaching in a sandy soil. *Soil Science Society of America Journal*, 68(4), 1191-1196.

Simunek, J., Th Van Genuchten, M., and Sejna, M.. "The HYDRUS-1D software package for simulating the one-dimensional movement of water, heat, and multiple solutes in variably-saturated media." University of California-Riverside Research Reports 3 (2005): 1-240.

SJRWMD, 2006. Fifty-Year Retrospective Study of the Ecology of Silver Springs, Florida. Special Publication SJ2007-SP4, SJRWMD.

SJRWMD, 2011. Silver Springs Nutrient Pathway Characterization Project. Final Report, Florida Department of Environmental Protection.

Ventura, M., Sorrenti, G., Panzacchi, P., George, E., and Tonon, G. 2013. Biochar reduces short-term nitrate leaching from a horizon in an apple orchard. *Journal of environmental quality*, 42(1), 76-82.

Weihermüller, L., Siemens, J., Deurer, M., Knoblauch, S., Rupp, H., Göttlein, A.and Pütz, T. 2007. *In situ* soil water extraction: A review. *Journal of Environmental Quality*, 36(6), 1735-1748.

Worthington, S. R. H. 2009, hydrogeologic characteristics of a karst aquifer (Kentucky, USA). *Hydrogeology Journal*, 17, 1665-1678.

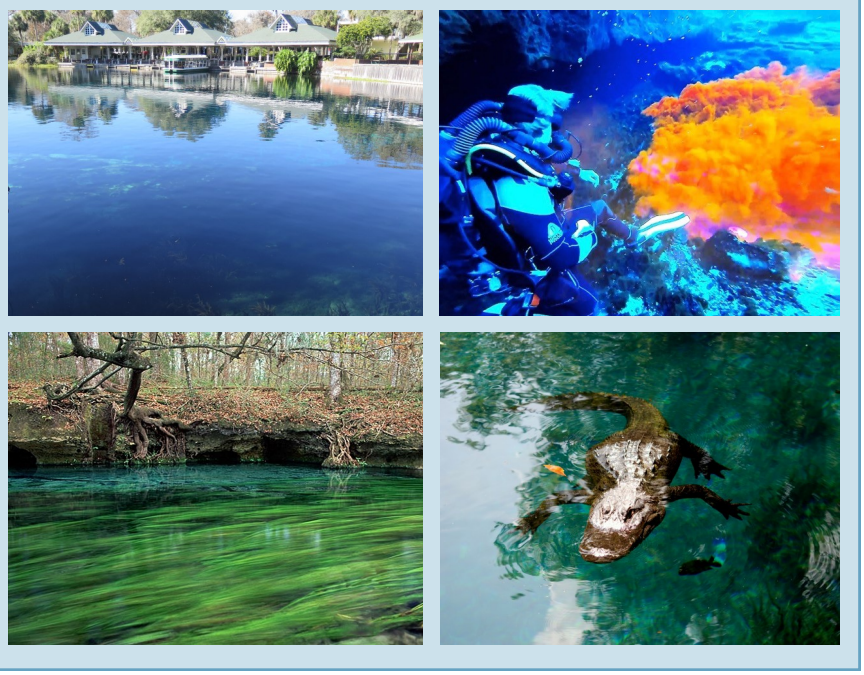

Collaborative Research Initiative on
Sustainability and Protection of Springs [**CRISPS]**

Section 4

[Work Order No: 1]

FINAL REPORT

2014 - 2017

submitted to:

St. Johns River Water Management District
Springs Protection Initiative [SPI], UF Contract # 27789

UF | UNIVERSITY of FLORIDA
Water Institute

C R I S P S

Section 4

NITROGEN BIOGEOCHEMISTRY

Sources, Transformations and Loss of Nitrogen from Land Surface to Springs

Final Report 2017
Work Order No. 1

Principal Investigators:

Patrick W. Inglett, University of Florida
Dean Dobberfuhl, St. Johns River Water Management District

Project Team:
Patrick Inglett
Xiaolin Liao
Katelyn Foster
Soil and Water Science Department
University of Florida

C. Ryan Penton
Arizona State University

Dean Dobberfuhl
Andy Canion
St. Johns River Water Management District

This document reports findings and results of a work order for a 3-year project in compliance with Agreement between University of Florida (UF) and St. Johns River Water Management District (SJRWMD) UF Contract #27789. It is part of the *UF Collaborative Research Initiative on Springs Protection and Sustainability (CRISPS)* and supports the science component of *the SJRWMD Springs Protection Initiative (SPI).*

4.i PROLOGUE

This portion of the project was tasked with tracing nitrogen (N) from sources within the springshed through the vadose zone and aquifer to discharge at the spring vent. The extent to which nitrogen sources are attenuated between land surface and the aquifer depends on the nitrogen source, transit time to the groundwater, and soil and aquifer processes. Attenuation is often estimated as a simple coefficient from literature values for similar nitrogen sources. However, spatial variability in groundwater recharge, soil processes, and geologic features (e.g., presence of a confining unit) are not accounted for using this approach and may exert a stronger control on nitrogen transport than the original source of nitrogen.

In support of the St. John's River Water Management District's efforts in springs protection, the overall goal of this project was to determine the capacity for natural attenuation of land surface N loads in the soil, vadose zone, and upper FAS and identify potential sources of other nutrient/geochemical constituents which may influence biota in springs. The approach of this work was to characterize patterns of N forms and other nutrients in relation to microbial composition and denitrification activity.

Three main studies were used to reach this objective. First, nitrogen sources and attenuation in the surface system were assessed through analysis of nitrate isotopic composition and rates of denitrification in soil and vadose zone profiles. Second, groundwater composition, stable isotopes of nitrate, and dissolved gases were monitored in wells throughout the springshed to assess large-scale patterns of N sources and denitrification within the aquifer and determine the potential pathways involved. Lastly, stable isotopes of nitrate and dissolved gases were monitored seasonally at the main spring vents to determine the overall potential for denitrification within the aquifer as well as any seasonality (e.g., in water sources, N sources, or temperatures) which may be taking place.

4.1 SURFACE ATTENUATION PROCESSES OF NITROGEN ACROSS VARIOUS LAND USES IN THE SILVER SPRINGS SPRINGSHED

4.1.1 ABSTRACT

Profiles of the soil/subsoil of key land uses were obtained at 12 locations while drilling experimental wells in the Silver Spring springshed. The samples were characterized using a range of parameters including total and extractable nutrients (carbon, organic matter, nitrogen, phosphorus, and selected metals), reduction/oxidation potential, stable isotopic ratios of bulk soil ($\delta^{15}N$) and nitrate ($\delta^{18}O/\delta^{15}N$) and potential denitrification activity (DEA). Groundwater samples from these and additional wells were also sampled for physicochemical, nutrients, dissolved gases and nitrate stable isotopes to derive patterns and interactions of aquifer and land use throughout the springshed. Quantitative PCR (qPCR) analysis of denitrification genes was also performed on profile samples and well water particulates to describe and confirm the relative abundance of denitrifying organisms.

For most of the profiles obtained, there were three main layers, including a surface sand overlying clays (sometimes mixed with sand and potentially calcareous and mottled with iron)

which is then over the bedrock limestone. Surficial aquifers (occurring where the water table is above the clay confining unit) were observed at two locations, and at one location buried peat and relic marine horizons were observed.

Significant denitrification enzyme activity was only observed in the surface 0 to 3 m and very low rates were observed in deeper profile layers. One notable exception to this rule was the site with buried peat and relic marine horizons which exhibited strong denitrification potential at depths of over 12 m. Denitrification activity was occasionally limited by carbon (C), but most often was limited by nitrate (NO_3-N). Correlations were observed primarily with nitrogen parameters, and the most variability was explained by total extractable nitrogen. Quantitative PCR (qPCR) analysis confirmed the presence of denitrifying microbes in the soil profiles, again, with higher abundances and diversity in the upper soil profile.

Stable isotopic profiles in the vadose zone support the patterns of denitrification and indicate a potential for using isotopic ratios to track nitrogen sources in the springshed. However, in many cases, surface isotopic ratios were not reflected in the groundwater, indicating transport of other nitrogen sources or physical processes affecting nitrate transport through the profile. Dissolved N_2 indicated that significant denitrification occurred at some locations within the aquifer, which limits the use of stable isotope ratios to determine N sources without also simultaneously measuring N_2 concentrations. Differences in N_2 concentrations were observed between the two main spring vents (Mammoth East and West) as well as with sampling date, with higher concentrations of N_2 gas being found in the West vent. Spatial variability coincided with similar variability in nitrate stable isotopic ratios indicating differences in denitrification potential on the basis of groundwater ages or biogeochemical conditions.

4.1.2 INTRODUCTION

Characteristics of watersheds including geology, biota, and land use activities are known to control water quality and parameters in surface and ground waters. Slow percolation rates and long residence times allow groundwaters to acquire much of their character from the mineral composition and makeup from the soils and rocks through which they pass. Similarly, nutrients and other trace elements added to the system through anthropogenic activities can also be passed along to surface and ground waters.

Silver Spring has a demonstrated trend of increasing concentrations of nitrate over the past 50 years, and much of this change is directly attributed to changes in land use within the springshed (Munch et al. 2007). Despite this correlation, it is difficult to determine the contribution of various nitrogen sources within the landscape because of the karst geology, which consists of the carbonate Floridan aquifer with overlying sands and clays. This diversity in lithology may be further complicated by the existence of relict marine deposits and mixing between the surficial, intermediate and deep aquifers.

Denitrification is an important microbial-facilitated process for nitrate attenuation in the soil, and is most efficient in the presence of carbon and nitrate, and under anaerobic conditions. In a soil, aerobic conditions coincide with high saturation, or with depth (natural soil compaction, a water table, and distance from surface oxygen diffusion). Carbon and nitrate sources are most likely to

be found at the surface of a soil where sources of each are both naturally and anthropogenically applied, but there are some exceptions. There are formations of humus-dominated horizons, known as Spodosols; buried peat marine sediments; dominantly sandy soils that allow for rapid infiltration of the mobile anion nitrate. All three of these conditions exist within the Silver Spring springshed. Based on these pre-existing conditions and our measurements of redox potential, extractable nutrients and stable isotopes of nitrogen and oxygen in nitrate, we were able to estimate the possible location of denitrification within the soil and vadose zone profiles.

4.1.3 MATERIALS AND METHODS

4.1.3.1 Site Description and Sampling

The Silver Springs springshed covers more than 230,000 ha (2,300 km²) in north-central Florida, occurring primarily in the counties of Alachua and Marion (Phelps 2004). The climate of the region (measured at Ocala, FL) is humid sub-tropical with a warm wet season (June-October) and a cool dry season (November-May). Approximately 51 inches (1,295 mm) of rainfall occurs annually and the mean annual temperature is approximately 22 °C (http://www.usclimatedata.com/).

Twelve sites were selected representing the major land uses within the springshed (Table 4.1.1, Figure 4.1.1). Soils and vadose zone materials were sampled from each of these locations during the installation of water sampling wells during the period of September and October 2014. Well drilling was conducted using a standard geotechnical rig by Huss Drilling, Inc. (Dade City, FL). The approach utilized a 6-inch auger to develop the main borehole with subsequent sampling at defined intervals using a 2-inch diameter, 2-feet in length split-spoon core sampler. Photographs were recorded for each spoon section, and as unique soils materials or geologic features were encountered (based on color and textural discontinuities), samples were collected from the split spoon sampler for further analysis of nutrients and microbial activity.

Samples for analysis of extractable and total nutrients were collected into polyethylene bags and stored on ice, while separate samples for microbial community analysis were collected into sterile whirl-Pak sampling bags using sterile techniques (sterilizing with ethanol between samples and collecting sample from only the central portion of the core) and placed on dry ice. Samples for nutrients were stored inside airtight containers at 4 °C until analyzed while frozen samples for molecular analysis were stored on dry ice until they could be shipped for analysis.

Fresh soils were used to measure redox potential and water extractable nutrients. A portion of soil samples was oven dried at 105 °C for 3 days to determine moisture content and ground using a mortar and pestle and total nutrient determinations. Another subsample of sieved soil was air-dried and ground using a mortar and pestle for Mehlich-3 extractable P, Fe, Al, Ca, and Mg.

Once established, these wells were sampled quarterly for water quality by the District. In addition to these wells, the District routinely samples a suite of groundwater wells in the area. Water samples were collected from these wells during the dry season (January to April of 2015) and wet season (July to November of 2015). Well water samples were collected using a Grundfos Redi-flo II submersible well pump. Water samples for the analysis of nutrients and

metals were collected into rinsed polyethylene bottles and stored at 4 °C, for stable isotopes ($\delta^{15}N$ and $\delta^{18}O$) analysis, water samples were frozen until the analysis.

4.1.3.2 Redox and Nutrient Parameters

Redox potential was measured using a commercial platinum wire redox electrode (Thermo Fisher Scientific #1363982) referenced to a Calomel standard electrode (Thermo Fisher Scientific accumet #13620258) both electrodes were calibrated using standardized solution (Ricca Chemical, R5464500-550C) and results expressed as millivolts (mV) relative to standard hydrogen electrode. Field moist materials were extracted with DI water (1:10, soil: water ratio) for determination of water extractable NO_3^-, NH_4^+, TN, and TOC.

Loss on ignition (LOI) was obtained by combusting 0.2 g dry soil at 550 °C for 4 h. Soil total C and N (TC and TN) content were measured using Thermo Flash EA 1112 elemental analyzer (CE Elantech, Inc.). Soil total P (TP) was measured colorimetrically using a Shimadzu UV-160 spectrometer (method 365.1 U.S. EPA 1993) following ashing and dissolution in 6 **N** HCl (Anderson 1976). Extractable ammonium (Ext. NH_4-N) and nitrate (Ext. NO_3-N) were determined in distilled de-Ionized water (DDI) extracts using methods 350.1 and 353.2, respectively (USEPA 1993) by a discrete analyzer (AQ2, Seal Analytical, Mequon, WI, USA). Soil extracts were also measured for soluble reactive P directly and for total dissolved P following autoclave persulfate digestion using Shimadzu UV-160 spectrophotometer (method 365.1 U.S. EPA 1993). The water quality for the ground water were analyzed in the SJRWMD laboratory.

4.1.3.3 Denitrification Enzyme Activity

Soil profile materials covering the range of depths and textures were selected to measure denitrification enzyme activities in profiles. The method was modified from Smith and Tiedje (1979), using the acetylene block technique. Samples were amended with NO_3-N, chloramphenicol, and acetylene, and were incubated under anaerobic conditions at room temperature (~23°C), with and without glucose added. Headspace gas was collected at 6, 24, 48, and 72 hours. The potential denitrification rate was calculated from the steepest portion of curve produced when cumulative N_2O evolution was plotted against time.

Concentration of N_2O in the headspace gas was determined with a Shimadzu GC-14A gas chromatograph equipped with an electron capture detector (ECD) and Porapak Q column. The operation temperatures for the column, injection port, and detector were 70, 120, and 230°C, respectively. A 10 ppm standard N_2O gas (Scott Specialty Gases, Inc., Plumsteadville, PA) was used to calibrate the measurement, and results were reported as nmols N_2O per gram dry weight per hour (nmols $N_2O\ g^{-1}\ dw\ h^{-1}$).

4.1.3.4 Stable Isotope Analysis

Bulk soils $\delta^{15}N$ were determined using a Costech Model 4010 Elemental Analyzer (Costech Analytical Industries, Inc., Valencia, CA) coupled to a Finnigan MAT DeltaPlus^{XL} Mass Spectrometer (CF-IRMS, Thermo Finnigan) via a Finnigan Conflo II interface. Stable isotope results are expressed in standard delta notation, with samples measured relative to the atmospheric N_2 for N. Water extractable nitrate in soil and vadose zone materials was analyzxed for dual isotopes of $\delta^{15}N$ and $\delta^{18}O$ using the bacterial reduction to N_2O method and continuous-

flow isotope-ratio mass spectrometry at the Facility for Isotope Ratio Mass Spectrometry (CFIRMS) at the University of California, Riverside (Riverside, CA, USA).

4.1.3.5 DNA Extraction and Gene Quantification

Genomic DNA from 0.5 g of sediment was extracted using the MoBio Powerlyzer PowerSoil DNA Isolation kit (MoBio Laboratories, Carlsbad, CA, USA). To improve desorption of DNA from sediment, 200 µL of Tris buffer (0.5*M* Tris-HCL pH 9) and 200 µL of phosphate buffer (0.2*M* Na_2HPO_4 pH 8) was added to bead tubes loaded with sediment and bead solution, mixed and 60 µL of solution C1 was added, incubated at 70ºC for 10 minutes and frozen at -80ºC for 5 minutes. Following pre-treatment, DNA extraction was carried out according to the manufacturer's manual. Extracts were quantified using the Qubit dsDNA high sensitivity assay kit (Life Technologies, Carlsbad, CA, USA) and stored at -20ºC until amplification.

Genomic DNA from *E. coli* K-12 (ATCC 10798-D) and *Pseudomonas stutzeri* (ATCC 11607) were used as standards for the *16s rRNA* and *nosZ* genes, respectively. Primer set 341F (5'-CCT ACG GGA GGC AGCAG-3') (Muyer et al., 1993)/ 797R (5'- GGA CTA CCA GGG TAT CTA ATC CTG TT-3') (Nadkarni et al. 2002) was used to target the *16s rRNA* gene and primer set nosZ2F (5'- CGC RAC GGC AAS AAG GTS MSS GT -3')/ nosZ2R (5'- CAK RTG CAK SGC RTG GCA GAA-3') (Henry et al., 2006) was used for the *nosZ* gene. PCR products were cloned into plasmids using the TOPO TA Cloning Kit (Invitrogen, Carlsbad, CA, USA) and the extraction of plasmids was carried out using the PureLink™ Quick Plasmid Miniprep kit (Invitrogen, Carlsbad, CA, USA) according to the manufacturer's manual. Ten-fold dilution series from 10^8 - 10^2 gene copies for both *16S rRNA* and *nosZ* were used as standards in each qPCR run to generate a standard curve. Amplification of qPCR was carried out on the QuantStudio 3 Real-Time PCR system (ThermoFisher Scientific, Waltham, MA, USA) in a reaction mixture of 0.2 *µM* of each primer for the selected target gene, 10 µL 2X PowerUp SYBR Green Master mix (ThermoFisher Scientific, Waltham, MA, USA), 1 µL of DNA, and PCR-grade water to yield a total volume of 20 µL. Three replicate qPCR amplifications were performed for each sample. The qPCR procedure for 16s rRNA included an initial denaturation step at 95 ºC for 3 minutes, 40 cycles of amplification (95 ºC for 45 sec, 60 ºC for 45 sec, 72 ºC for 1 minutes) and a final elongation step at 72 ºC for 7 minutes. The thermocycle conditions for nosZ included an initial denaturation step at 95 ºC for 1.5 minutes, 40 cycles of amplification (95 ºC for 24 sec, 56 ºC for 24 sec, 58 ºC for 24 sec, 72 ºC for 24 sec) and a final elongation step at 72 ºC for 7 minutes. Fluorescent quenching due was determined to be less than 1 % by the addition of 10^6 copies of the standard to representative samples and comparing the quantification with that of the sample alone. Standard deviations among technical replicates averaged 0.16± 0.15 % for *16S rRNA* and 0.14±0.09 % for *nosZ*.

Illumina Sequencing: Amplicon libraries for the 16s rRNA gene V4 region were generated for sediment samples using a previous protocol (Kozich et al. 2013). For library preparation, a single PCR was performed per sample on a 96-well plate, product size was confirmed on a 2 % agarose gel in 1X TAE buffer. PCR product was purified and normalized using the SequalPrep Normalization Plate kit (Invitrogen, Carlsbad, CA, USA). Pooled amplicon libraries were sequenced on Illumina MiSeq instrument using the 250-base paired-ends kit at the genomic core facilities, Arizona State University. The 16s rRNA gene sequence paired-end reads were demultiplexed on the MiSeq instrument at the time of sequencing. Sequences were processed

using the QIIME software (Caproraso et al. 2010). Chimeric sequences were filtered using UCHIME and clustered using open reference OTU picking against the Greengenes database. Sequences that failed to hit the reference database were subsequently clustered in de-novo mode using UCLUST. Samples were rarified to 104,100 sequences per sample; operational taxonomic units were defined at 3 % dissimilarity.

4.1.3.6 Statistical Analysis

Data were analyzed with JMP v.11© (SAS Institute Inc., Cary, NC). The differences between east and west vent, and between different seasons were tested using the Student's t test. Nonparametric correlation were performed between different properties. All results are reported as significance when $P < 0.05$. Quantitative PCR data were log-transformed for normality and correlations to soil chemistry were performed in R using the vegan package (Dixon 2003). Principal component analysis was performed using the HSAUR library in R with varimax rotation and the percentage of variance accounted by each variable was assessed using vegan in R. or the sequencing data, Statistical analysis of community composition was performed using PRIMER-6 software (Clarke and Gorley 2006). Raw OTU abundances were normalized by Hellinger transformation to construct a Bray-Curtis dissimilarity matrix. Significant differences between sample site and depth was treated with PERMANOVA (Anderson 2001) and ANOSIM (Clarke 1993), SIMPER (Warwick et al. 1990) was used to identify significant taxa that contributed to differences between sample depths. The BEST function was used to investigate the main environmental drivers between differences in sediment depth. Alpha diversity was indices and qPCR results were subject to a one-way ANOVA performed using R version 3.3.2. in R studio (version 1.0.136, RStudio Team, 2015), $p < 0.05$ was considered significant. Tukey's multiple comparisons were computed using the agricolae package in R.

4.1.4 RESULTS AND DISCUSSION

4.1.4.1 Profile Lithographic Characteristics

Table 4.1.1 shows the descriptive land use for the well sites used in the study. The collection of samples during installation of the wells in these land uses revealed a wide diversity of soil and geologic materials in the vadose zone of the springshed. The layers were typical of the widely established geologic profiles of the region with sands overlying various thicknesses of undifferentiated sediments and units of the Hawthorn layer overlying Ocala limestone (Scott 1988; Scott et al. 2001).

Where present, clay layers were generally thin (2-3 m) with one exception being the almost continuous clay layer (> 40 m) encountered at the site of M-0782/0787 (Figure 4.1.2 and Appendix 4.1.4). These clay layers most likely belong to the Hawthorn group, as several of these heavy clay samples exhibited greenish or pale gray colors commonly attributed to this unit (Scott 1988). Apart from texture (clay versus sand), the most prominent feature of the samples was a reddish color indicating the presence of extensive amounts of oxidized iron (Appendix Figures 4.1.4a-l).

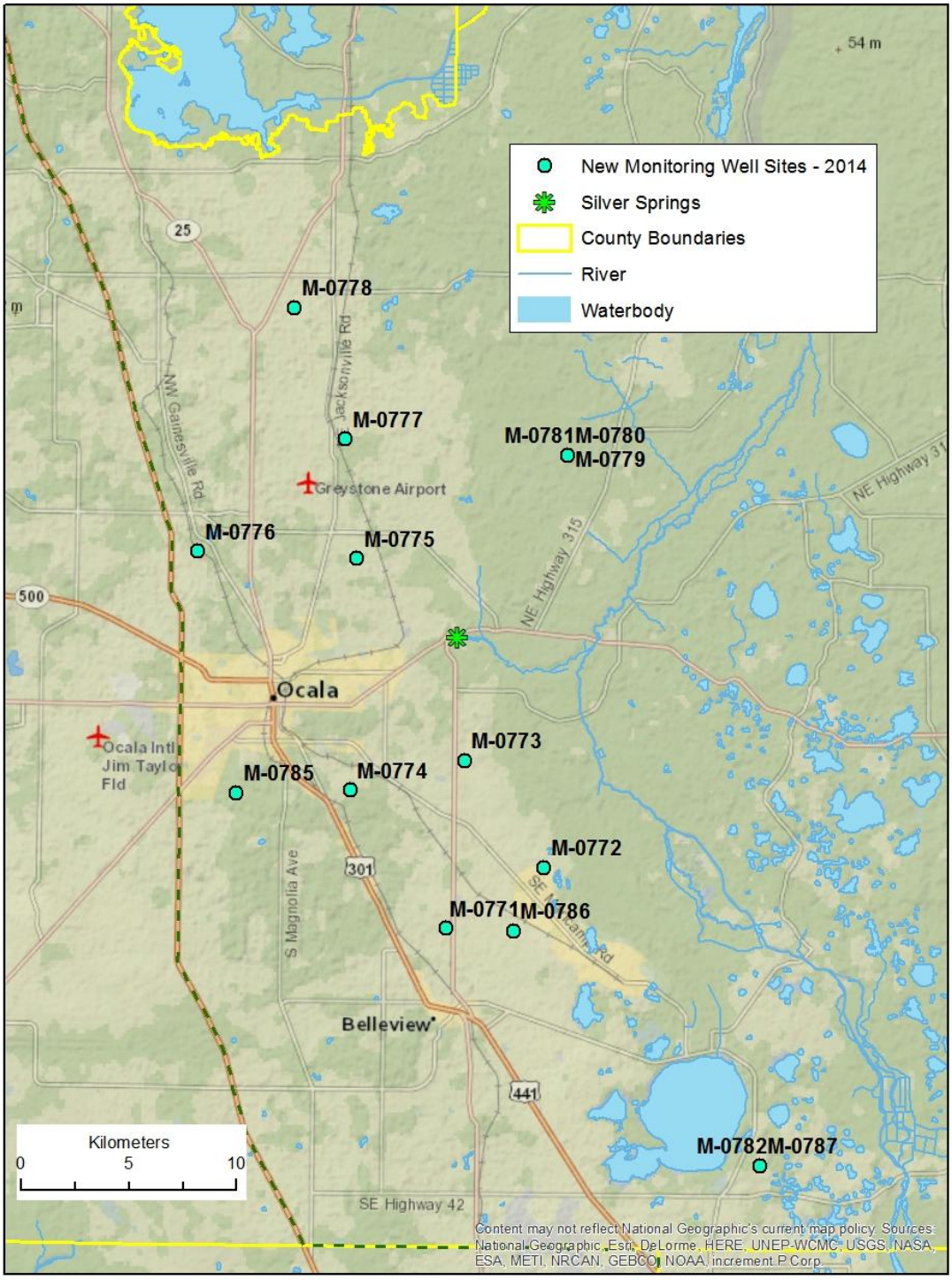

Figure 4.1.1. Locations and IDs of the wells installed for the project and used for collection of soil and vadose zone profile materials. Sites with wells at multiple depths are indicated by multiple IDs.

Table 4.1.1. Land use description, and well depth for the project wells in the Silver Springs springshed.

Well ID	Depth (feet)	Depth (m)	Major Land use
M-0771	56	17	Urban, low density residential
M-0772	35	11	Urban, medium density residential
M-0773	42	13	Urban, medium density residential
M-0774	95	29	Urban, medium density residential
M-0775	52	16	Urban, mixed low density residential, field crops, and pastures
M-0776	50	15	Agriculture, horse farm
M-0777	60	18	Agriculture, field crops and pastures
M-0778	60	18	Agriculture, horse farm
M-0779	145	44	Pine plantation
M-0780	69	21	Pine plantation
M-0781	35	11	Pine plantation
M-0785	90	27	Urban, mixed Low Density Residential, Horse Farms
M-0786	42	13	Agriculture, spray field
M-0782	195	59	Agriculture, mixed pastures and citrus groves
M-0787	102	31	Agriculture, mixed pastures and citrus groves

In general, the lowest redox potentials were encountered in the surface soils (0-1.8 m) or deep in the profile, while the highest redox potentials were measured in intermediate layers with high clay content (Figure 4.1.4). For the site M-0779/0780/0781, the redox potential reached as low as -186 mV at the depth of 9.1 to 9.8 m (Figure 4.1.4). For most of the soil profile, the redox potential should indicate the dominant electron acceptor being used by microbial respiration, where highly positive values (+400-700 mV) are indicative of aerobic respiration. For most of the profile samples, the redox potential was positive, but within ranges favorable to denitrification (e.g., < 250 mV) (Feast et al. 1998; Wlodarczyk et al. 2003).

Loss on ignition (LOI) also showed higher values in the clay layer, and then decreased with the soil depth (Figure 4.1.6). For most of the sites, LOI fell in the range of 0-10 %, however, in the site M-0779/0780/0781 it reached as high as 53.1 % at the depth of 10.4 to11.0 m (Figure 4.1.5). Typically, LOI is used to infer organic matter content. This is likely true in the surface soil layers, however the high porosity in the tight clays may have resulted in weight changes due to loss of tightly held interstitial water.

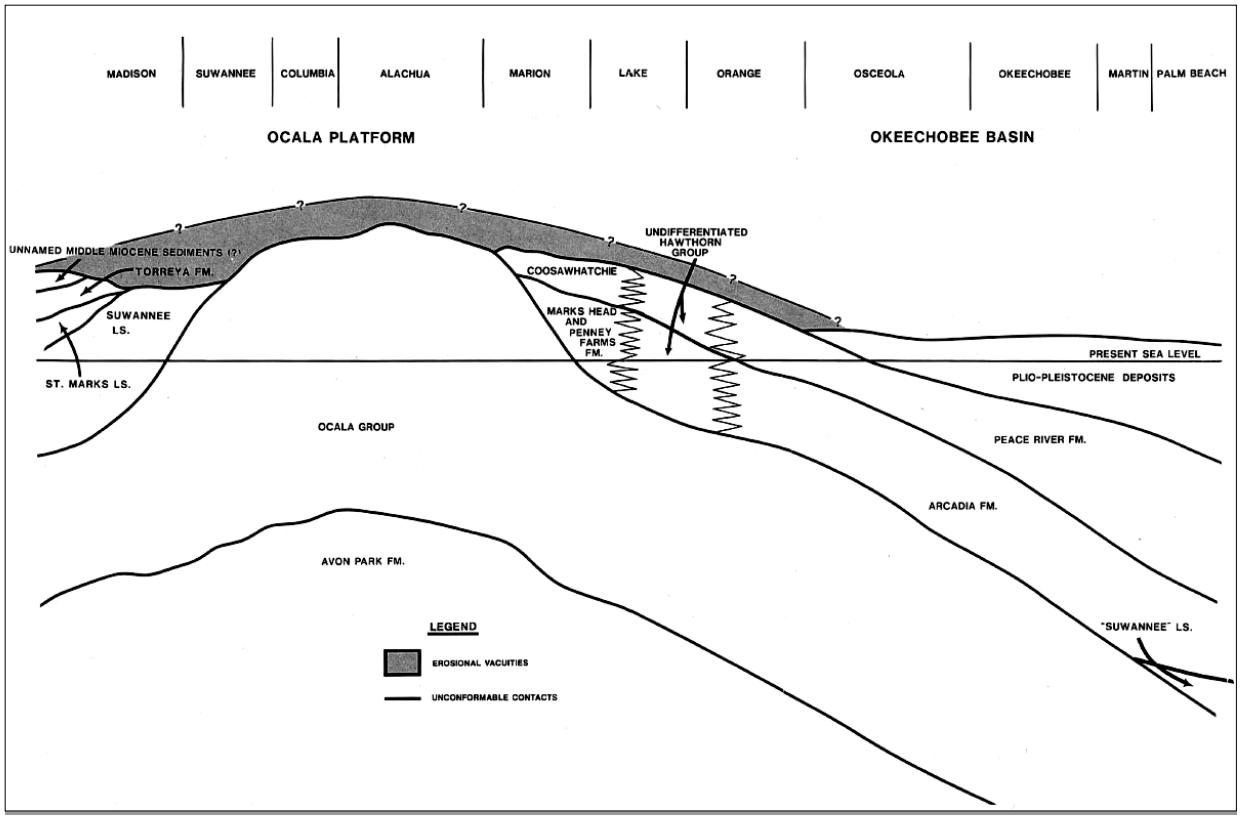

Figure 4.1.2. Vertical cross section of lithographic units encountered in the study area crossing Alachua, Marion, and Lake Counties (from Scott 1988).

More indicative of organic matter content in the surface layers, total carbon (TC) contents were below 10 % in the sand and clay layers, and exceeded 10 % in the deep limestone layers which reflected C as $CaCO_3$ and $MgCO_3$ (12 % -14 % TC content) (Figure 4.1.6). Above the limestone, TC content likely reflected organic matter with accumulations only in the surface soils zone. This was not the case for the 10-12 m depth at the site M-0779/0780/0781, where a buried layer of peat was encountered with TC contents reaching > 30 % (Figure 4.1.6).

As a confirmation of suspected patterns of organic matter, water extractable total organic carbon (Ext. TOC) immediately decreased below the top 1.2 m soil profiles for most of the sites (Figure 4.1.6). For wells M-0779/0780/0781, however, Ext. TOC has a sharp increase in the 9.1 to 9.8 m and 10.4 to 11.0 m clay layers with the values of 186 and 165 mg kg^{-1}, respectively.

Generally, the TN showed a decreasing tread with increasing soil depth, and sometimes had a peak in the clay layers. For most of sites, the total nitrogen contents (TN) were very low (<1 %) compared to other terrestrial soils (Figure 4.1.6). The TN in the site M-0779/0780/0781was higher and reached a peak of approximately 1.4 % in the buried peat layers.

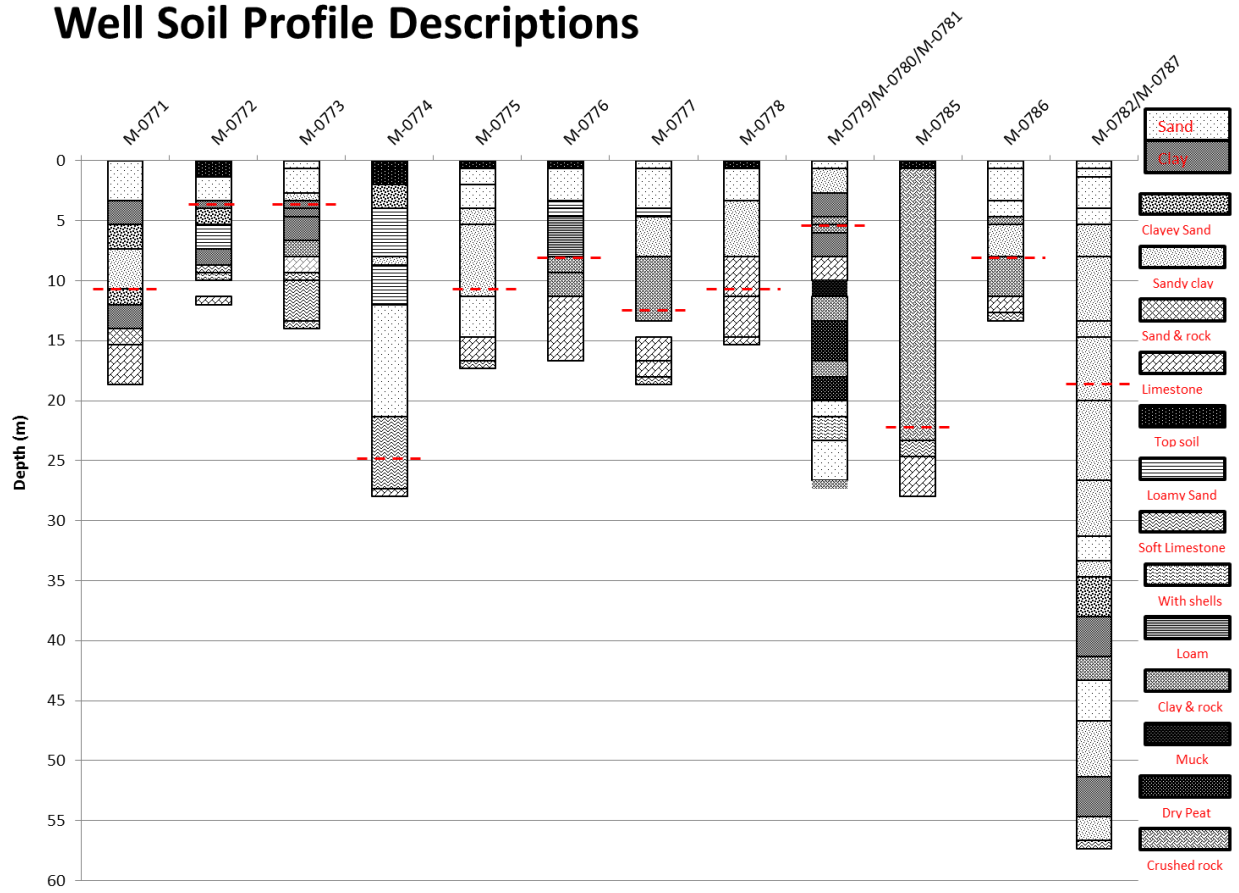

Figure 4.1.3. Vertical patterns of soil and vadose zone materials encountered during installation of study wells in the Silver Spring springshed.

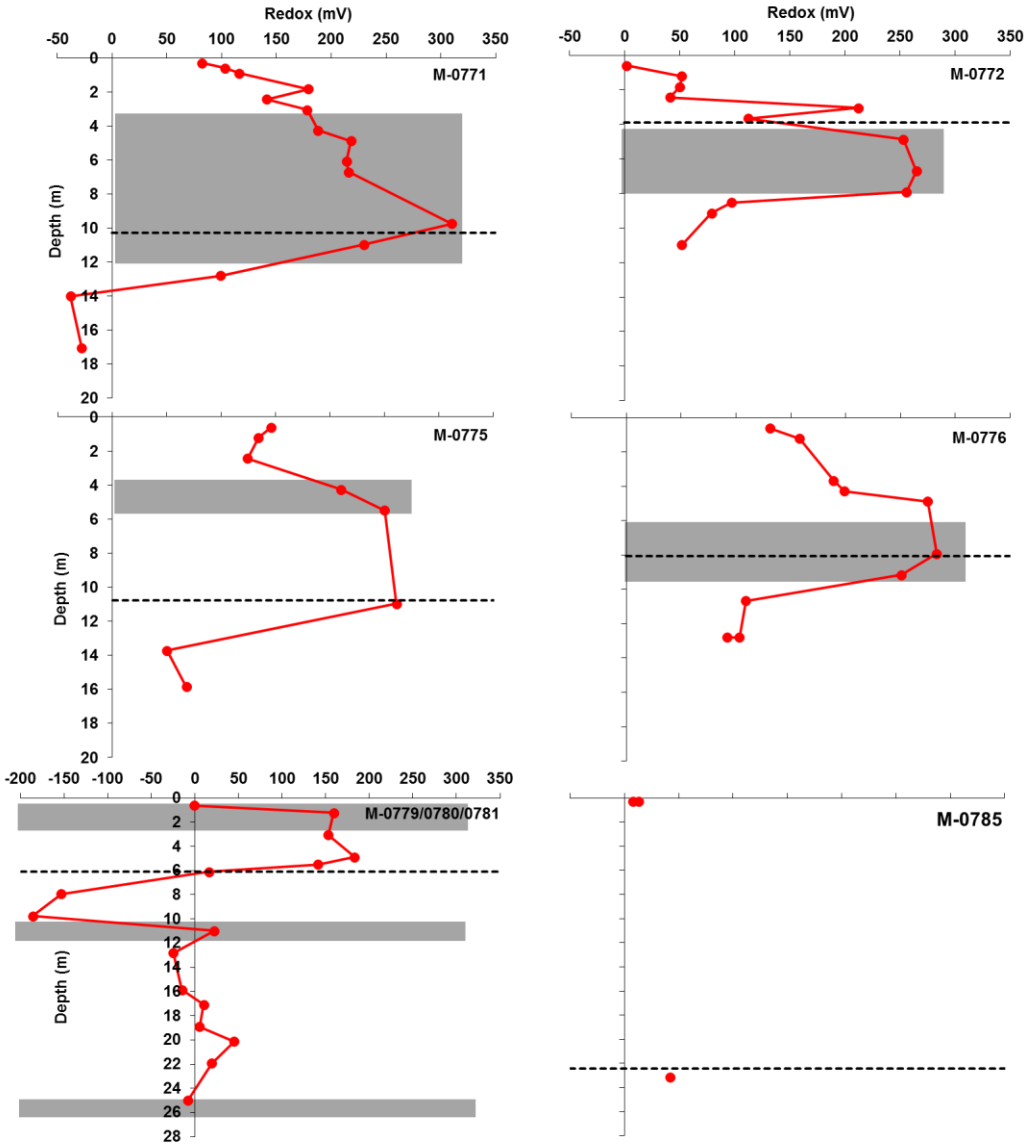

Figure 4.1.4. Vertical profiles of redox potential (mV) in soil and vadose zone profiles for the 12 study wells. The gray areas and the dash lines represent the clay layers and the water table, respectively.

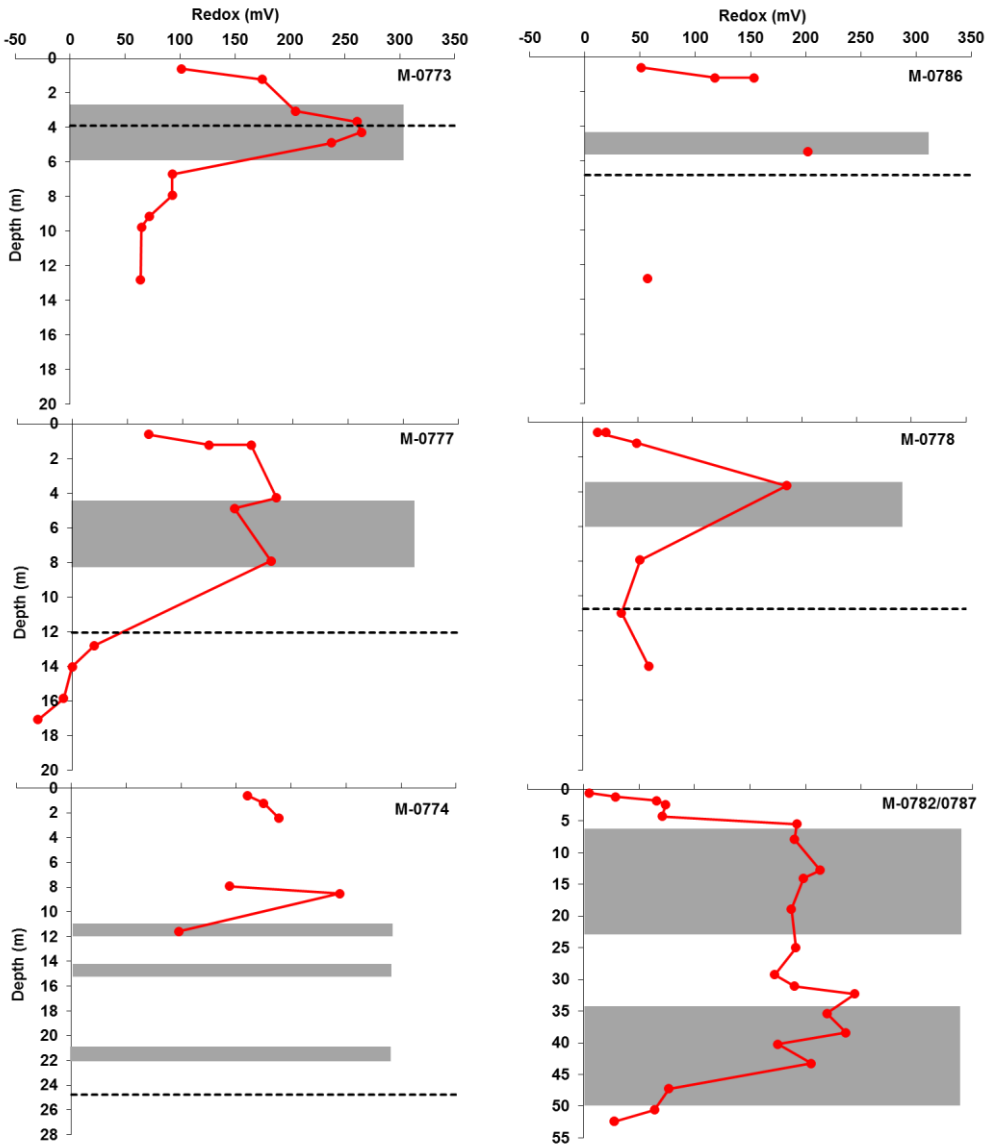

Figure 4.1.4 (cont.). Vertical profiles of redox potential (mV) in soil and vadose zone profiles for the 12 study wells. The gray areas and the dash lines represent the clay layers and the water table, respectively.

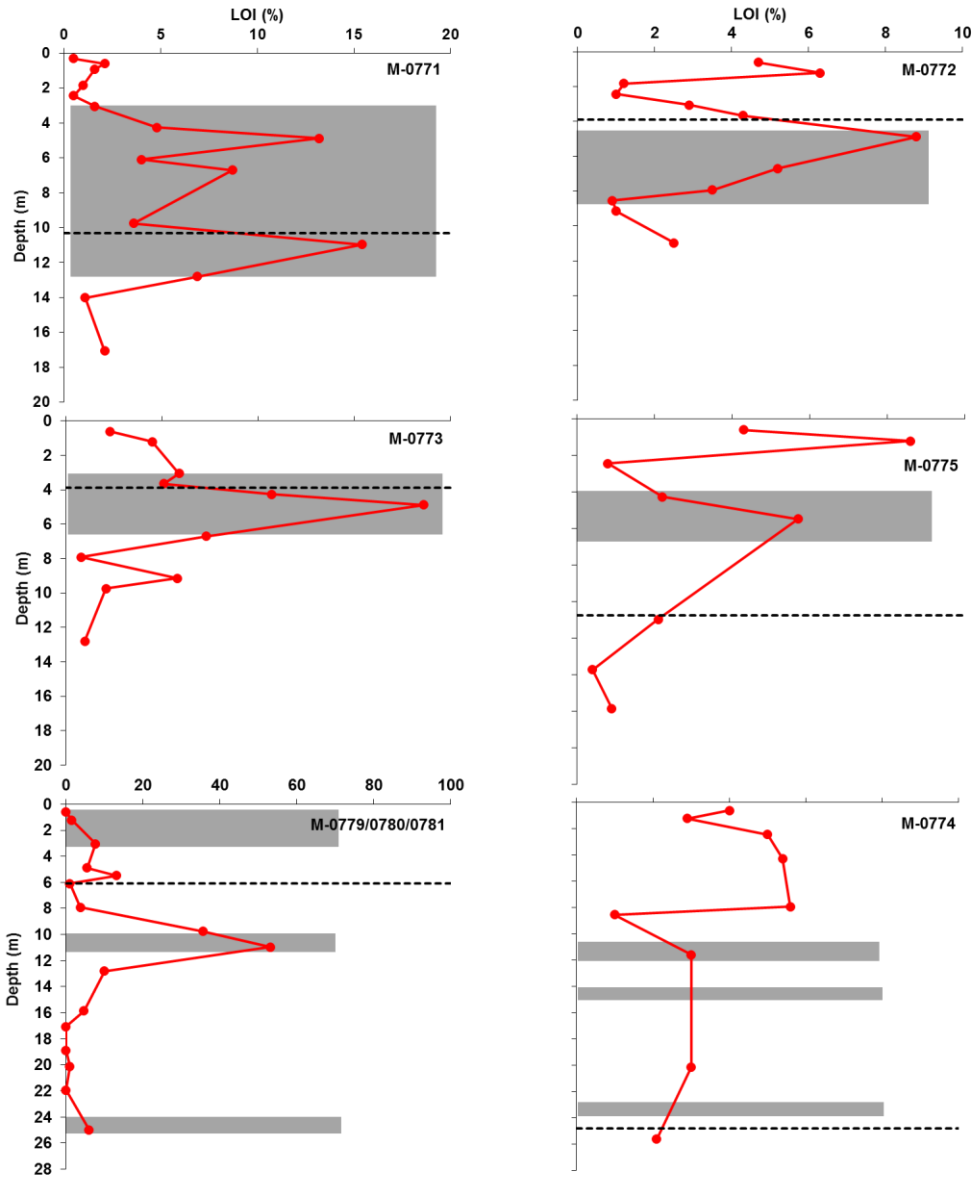

Figure 4.1.5. Vertical profiles of loss on ignition (LOI) in soil and vadose zone profiles for the 12 study wells. The gray areas and the dash lines represent the clay layers and the water table, respectively.

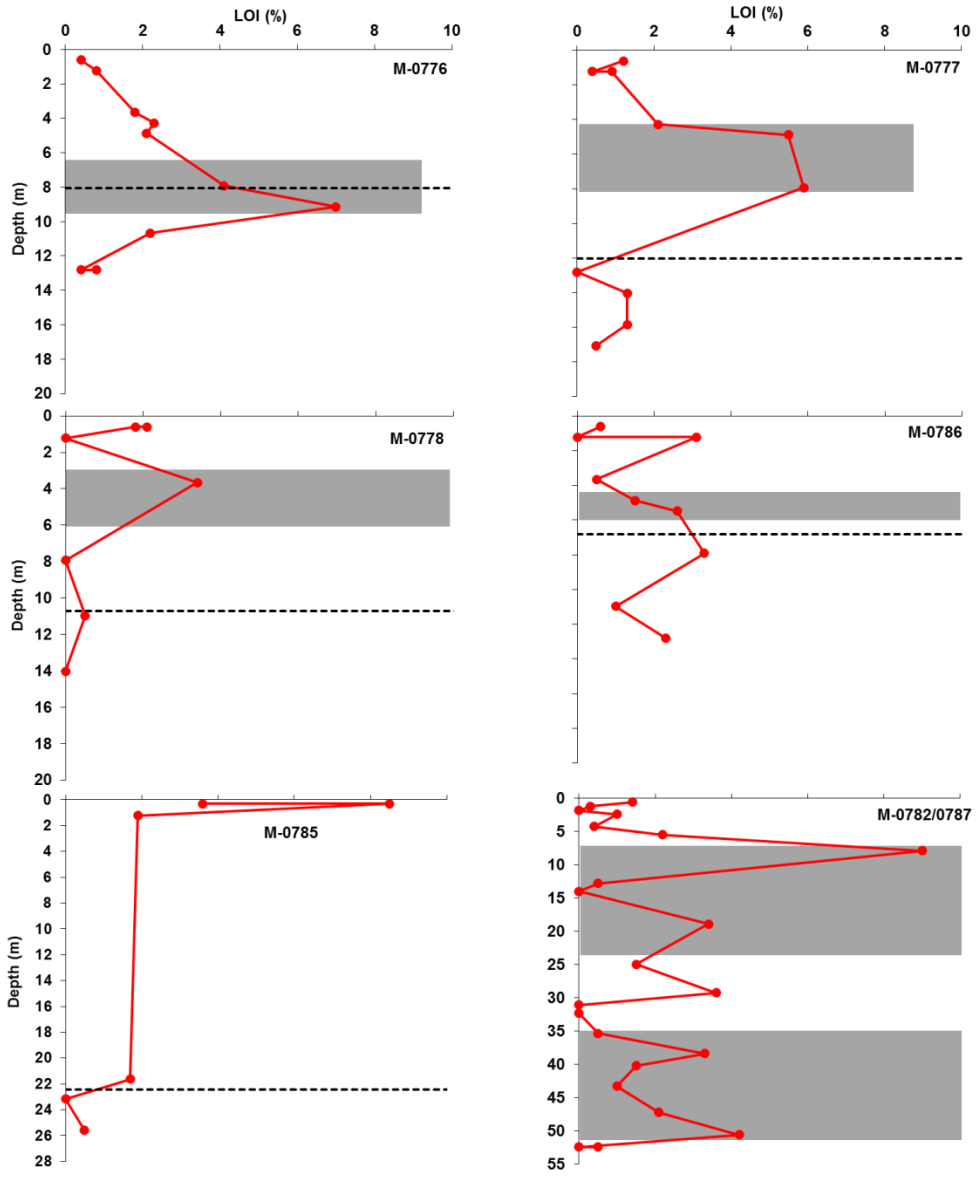

Figure 4.1.5 (cont.). Vertical profiles of loss on ignition (LOI) in soil and vadose zone profiles for the 12 study wells. The gray areas and the dash lines represent the clay layers and the water table, respectively.

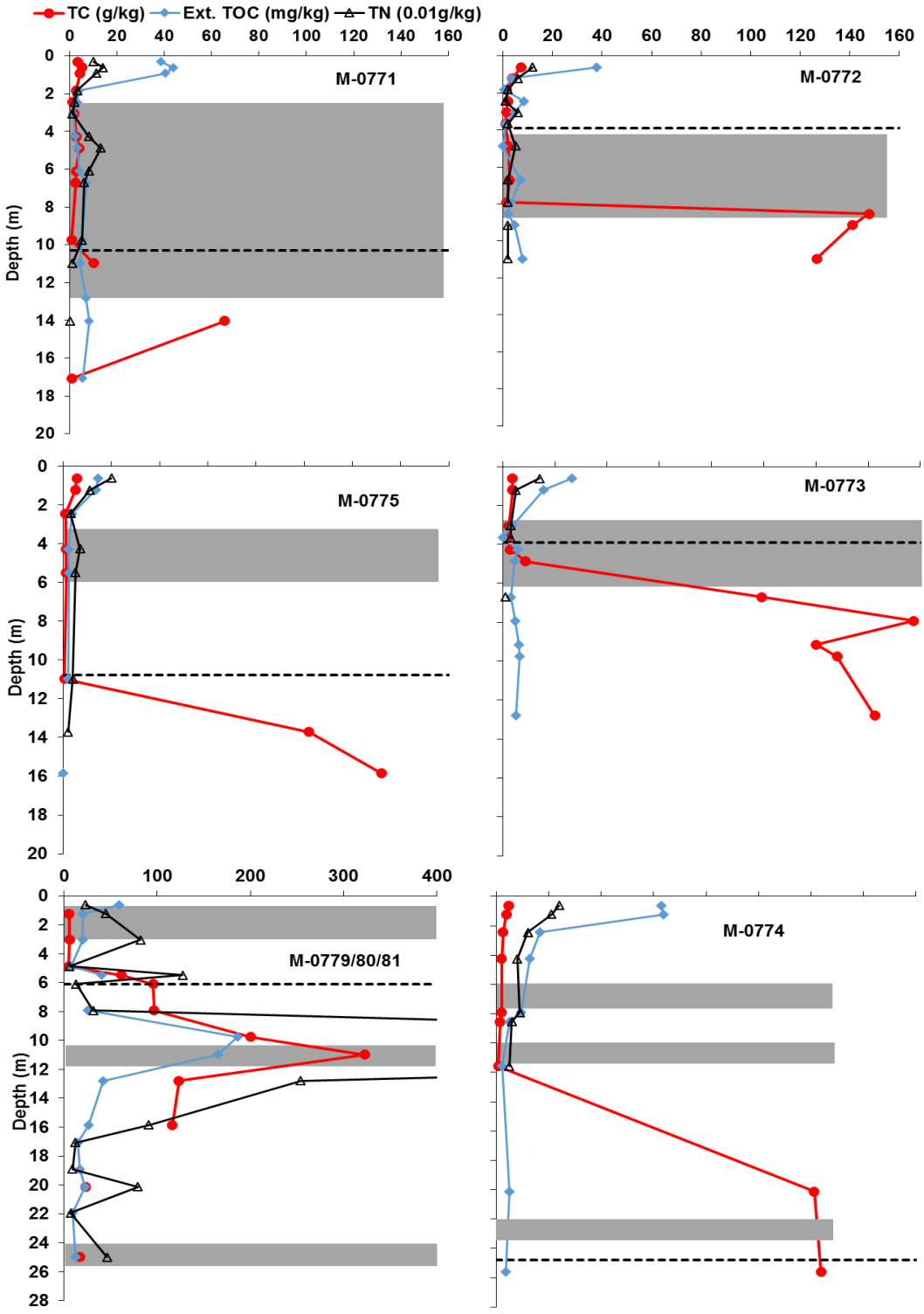

Figure 4.1.6. Vertical profiles of total carbon (TC) (TC, g kg^{-1}), extractable total organic carbon (Ext. TOC, mg kg^{-1}), and total nitrogen (TN, 0.01 g kg^{-1}) in soil and vadose zone profiles for the 12 study wells. The gray areas and the dash lines represent the clay layers and the water table, respectively.

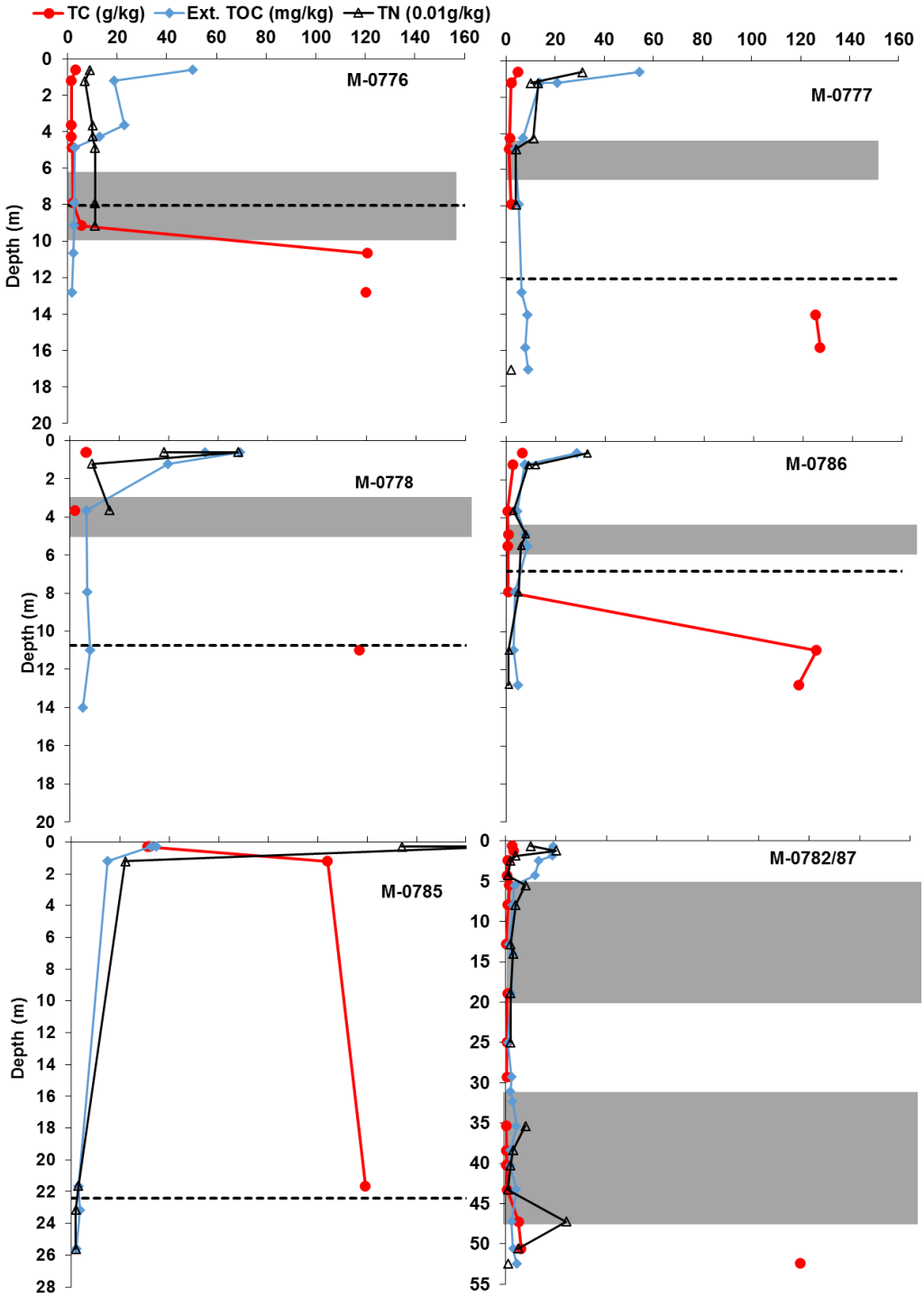

Figure 4.1.6 (cont.). Vertical profiles of total carbon (TC) (TC, g kg^{-1}), extractable total organic carbon (Ext. TOC, mg kg^{-1}), and total nitrogen (TN, 0.01 g kg^{-1}) in soil and vadose zone profiles for the 12 study wells. The gray areas and the dash lines represent the clay layers and the water table, respectively.

4.1.4.2 Extractable N and Denitrification Enzyme Activities

The patterns of water extractable ammonia and nitrate (Ext. NH_4-N and Ext. NO_3-N) varied between different sites (Figure 4.1.7). In the sites of M-0777, M-0778, M-0775, and M-0785, there was a decreasing trend of Ext. NH_4-N and Ext. NO_3-N with soil depth though the values did not change significantly. High Ext. NH_4-/NO_3-N values were observed in the clay layers for other sites. In the sites of M-0771, M-0772, and M-0776, the soil Ext. NH_4-N values were similar with or higher than the Ext. NO_3-N values above the water level, but below the water table, the Ext. NO_3-N levels exceeded the Ext. NH_4-N. In the sites of M-0773, M-0786, M-0774, and M-0782/0787, the dominant inorganic nitrogen form was Ext. NO_3-N which were much higher than the concentration of Ext. NH_4-N. In contrast, Ext. NH_4-N was the dominant inorganic nitrogen form throughout the profile at the sites of M-0779/0780/0781.

Denitrification enzyme activities (DEA) with the addition of glucose and nitrate showed a decreasing trend with the soil depth in all the sites (Table 4.1.2, Figure 4.1.8). Significant DEA activities were observed only in the top 1.2 m soils. For the top 0-0.6 m, soils in the wells of M-0786 (1.1 ± 0.004 nmols N-N_2O g^{-1} dw h^{-1}), M-0779/0780/0781 (0.94 ± 0.30 nmols N-N_2O g^{-1} dw h^{-1}), M-0785 (0.98 ± 0.36 nmols N-N_2O g^{-1} dw h^{-1}), and M-0774 (0.96 ± 0.08 nmols N-N_2O g^{-1} dw h^{-1}) had the highest DEA values, followed with M-0773 (0.64 ± 0. 42 nmols N-N_2O g^{-1} dw h^{-1}), and M-0778 (0.48 ± 0.12 nmols N-N_2O g^{-1} dw h^{-1}). The 0.6 to 1.2 m deep soil in the well of M-0779/0780/0781 still showed high DEA values with the average of 0.36 ± 0.10 nmols N-N_2O g^{-1} dw h^{-1}.

These results document the potential of surface soils in this region to denitrify, however the observed rates were very low compared with agricultural soils, or manure loaded systems (Barton et al. 1999). Only in one case did we observe significant DEA activity at depth in the profile (Figure 4.1.8), with that being the 20 m layer at the M-0779/0780/0781 site. The high detected presence of sulfide at this site may indicate the potential for autotrophic denitrification with H_2S as an electron donor.

Sulfur-based autotrophic denitrification is of special interest due to its simultaneous removal of nitrate and reduced sulfur (Shao et al. 2010). This process is mostly found in hydrothermal vents, marine sediments, oil field, and wastewater treatment plants (Jannasch and Mott 1985; Brettar 1991; Vaiopoulou et al. 2005; Manconi et al. 2007), but its importance in freshwater systems has also been indicated (Burgin and Hamilton 2007). For example, Böttcher et al. (1990) found that much of the nitrate uptake in a groundwater aquifer was ascribed to *Thiobacillus denitrificans* which is one of the most commonly reported autotrophic denitrifiers.

The observation of higher NH_4-N than NO_3-N concentrations at 20 m in the M-0779/0780/0781 site indicates there is also a potential for either anaerobic mineralization of buried peat N or dissimilatory nitrate reduction to ammonium (DNRA). Though most studies on the pathway of DNRA have been done in marine ecosystems, evidence has also been found in aquifers and systems with high amounts of chemically-reduced sulfur (Burgin and Hamilton 2007). The presence of ammonium in the layers for some other sites in this study also indicates the potential for anaerobic ammonia oxidation (Anammox). Burgin and Hamilton (2007) hypothesized that Anammox would be expected to be limited to areas that relatively low in labile carbon. Apart from the M-0779/0780/0781 site, we saw the coexistence of both NO_3^- and NH_4^+ (Figure 4.1.7), and the decreasing ext. TOC (Figure 4.1.6) in the deep soil.

Additionally, iron can be used as an energy source/electron donor by iron-oxidizing bacteria to reduce nitrate lithotrophically in reduced iron environments (Lowrance and Pionke 1989; Straub et al. 1996; Hauck et al. 2001). We did see iron-rich layers in some wells (e.g., M-0772, M-0773, M-0774, M-0777, M-0779/0780/0781, and M-0786). Though we did not measure any significant DEA rates, it is possible that other nitrate removal pathways could happen.

Comparison of the DEA rates with and without the addition of glucose tests whether carbon is a limiting factor for denitrification (Figure 4.1.9). This analysis showed that only the soils in the sites of M-0773 and M-0774 would be limited by carbon for denitrification. We did not find a highly significant correlation between any of the measured nutrient parameters and rates of DEA, but the DEA rates were more likely to be controlled by extractable nitrate and carbon (Figure 4.1.10). For this reason, we constructed the following stepwise multiple regression model as a potential predictor of DEA in soils of the springshed.

$$DEA=-0.06-0.03*MC+0.0002*TP+0.99*TN+0.21*Ext.\ NO_3\text{-}N-0.004*Ext.\ TOC,\ R^2 = 0.67$$

In this analysis, total nitrogen (TN) was the most influential variable followed by extractable nitrate, with minimal contributions from extractable organic carbon, phosphorus or moisture content. TN values were highest within the top 2 m of soil and decreased overall with depth, with the exception of slight increases at or just above suspected clay layers, and due to the occurrence of peat at 10 m at site M0779/0780/0781.

When TN was compared to the Ext. NO_3-N and Ext. NH_4-N measurements, within the top 2m both forms of nitrogen contribute to TN. Decreases in both could suggest the simultaneous formation and removal of nitrate at the surface in a process known as simultaneous nitrification/denitrification (7 of 12 sites). At sites where Ext. NO_3-N is decreasing relative to the increase of Ext. NH_4-N, nitrate is either being denitrified or leached faster than nitrification process can occur (2 of 12 sites). Where Ext. NO_3-N is increasing relative to the decrease in Ext. NH_4-N, nitrification is occurring faster than denitrification or leaching (2 of 12 sites).

Table 4.1.2 Denitrification enzyme activities (DEA, nmols N_2O g^{-1} dw h^{-1}) with and without the addition of glucose for the 0-0.6 m and 0.6-1.2 m soil profiles in the 12 wells.

	Without the addition of glucose		With the addition of glucose	
Well ID	0-0.6 m	0.6-1.2 m	0-0.6 m	0.6-1.2 m
M-0771	0.03 ± 0.01	0.02 ± 0.01	0.02 ± 0.01	0.01 ± 0
M-0772	0.06 ± 0.02	0.06 ± 0	0.01 ± 0.01	0 ± 0
M-0773	0.09 ± 0	0.65 ± 0.42	0.02 ± 0.01	0.14 ± 0.18
M-0774	0.37 ± 0.06	0.96 ± 0.08	0.09 ± 0	0.17 ± 0.04
M-0775	0.03 ± 0	0.03 ± 0.01	0.01 ± 0	0.01 ± 0
M-0776	0.03 ± 0	0.04 ± 0.01	0.01 ± 0.01	0.01 ± 0
M-0777	0.03 ± 0.01	0.03 ± 0	0 ± 0	0.01 ± 0
M-0778	0.32 ± 0.02	0.48 ± 0.13	0.09 ± 0	0.1 ± 0.03
M-0779	0.91 ± 0.13	0.95 ± 0.3	0.28 ± 0.03	0.36 ± 0.11
M-0785	1.02 ± 0.13	0.97 ± 0.37		
M-0786	1.02 ± 0.06	1.11 ± 0	0.09 ± 0.01	0.11 ± 0.01
M-0782/87	0.05 ± 0.02	0.09 ± 0.01	0.07 ± 0.01	0.11 ± 0.03

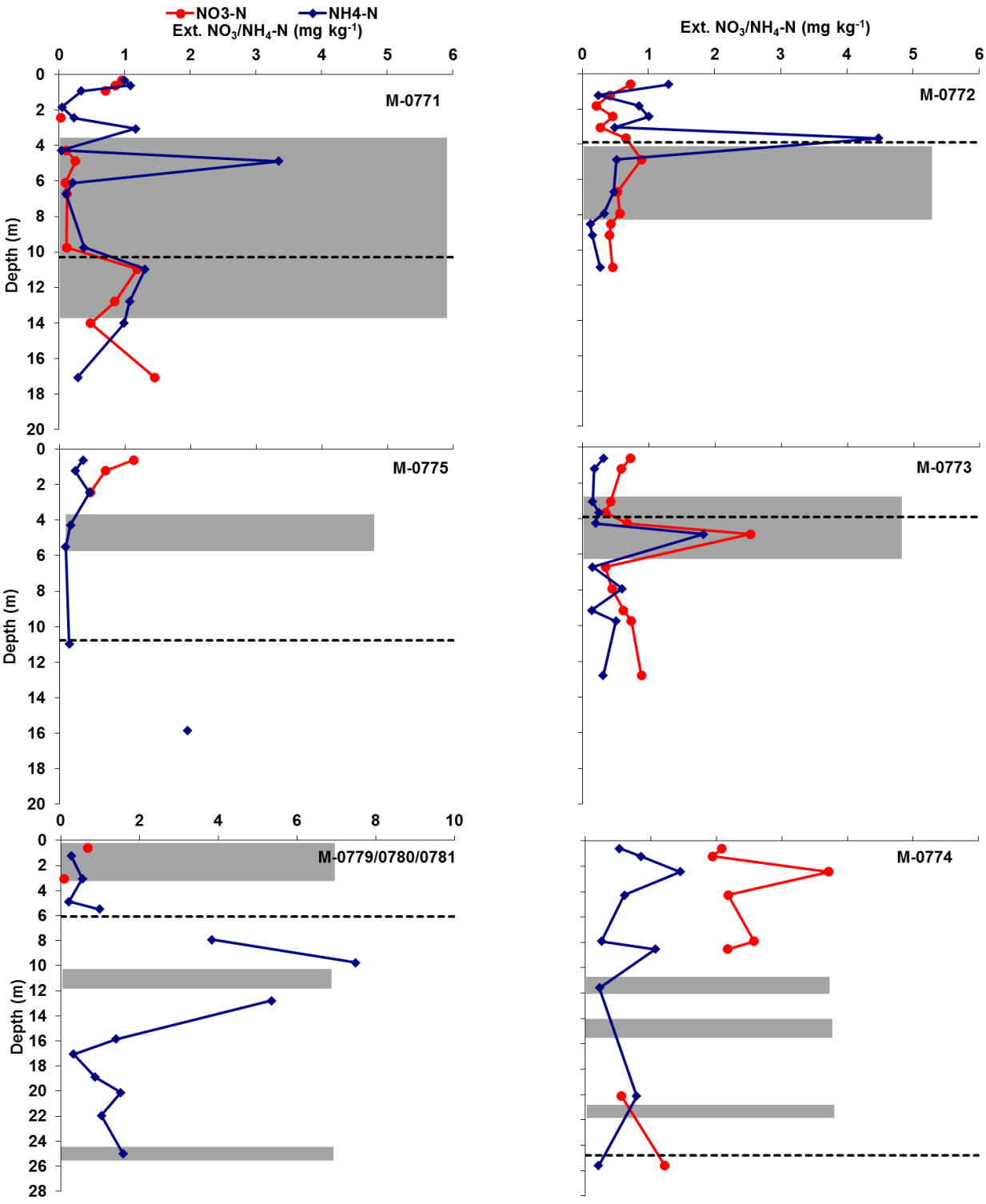

Figure 4.1.7. Vertical profiles of water extractable nitrate and ammonium (Ext. NO_3/NH_4) in soil and vadose zone profiles for the 12 study wells. The gray areas and the dash lines represent the clay layers and the water table, respectively.

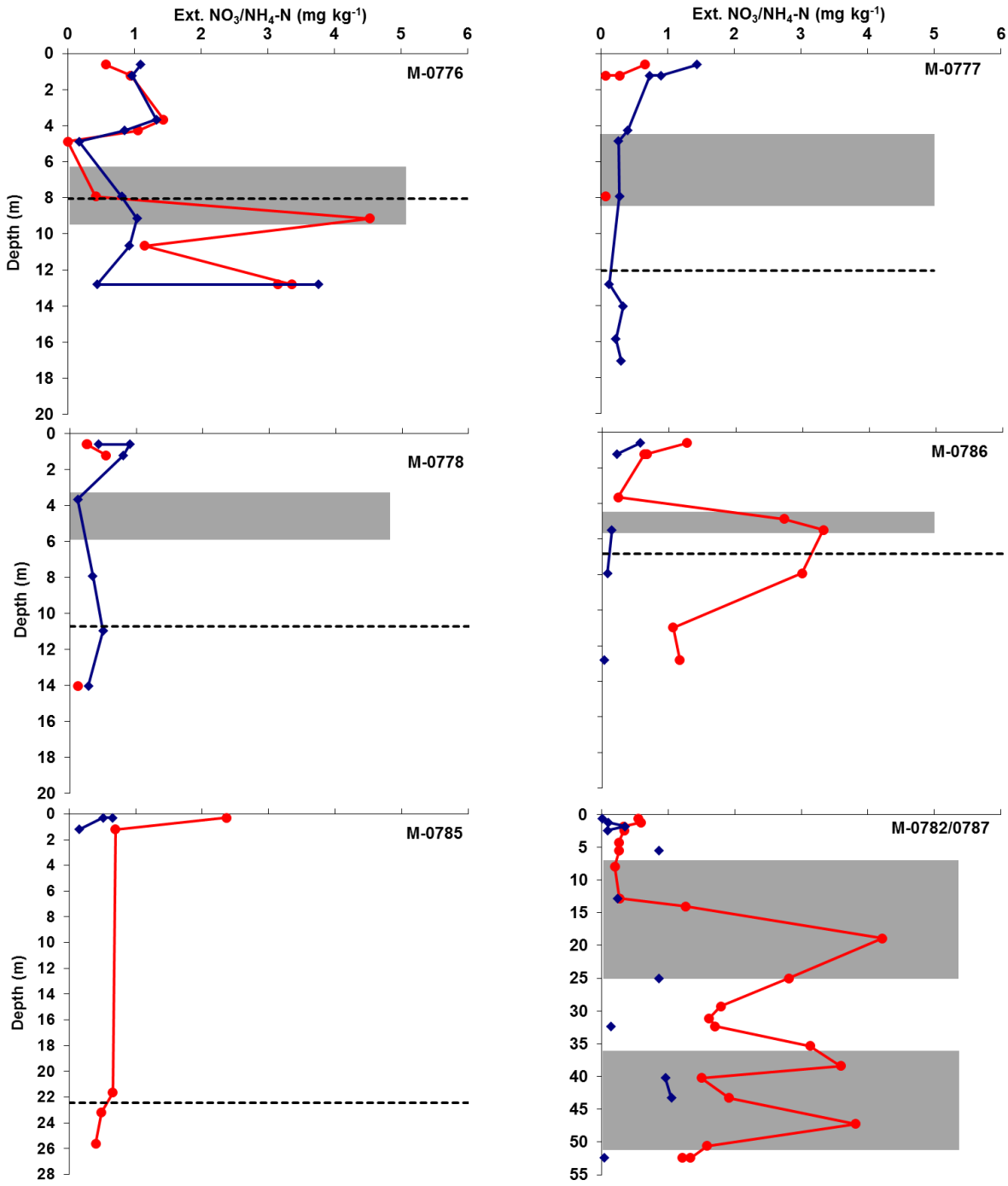

Figure 4.1.7 (cont.). Vertical profiles of water extractable nitrate and ammonium (Ext.NO_3/NH_4) in soil and vadose zone profiles for the 12 study wells. The gray areas and the dash lines represent the clay layers and the water table, respectively.

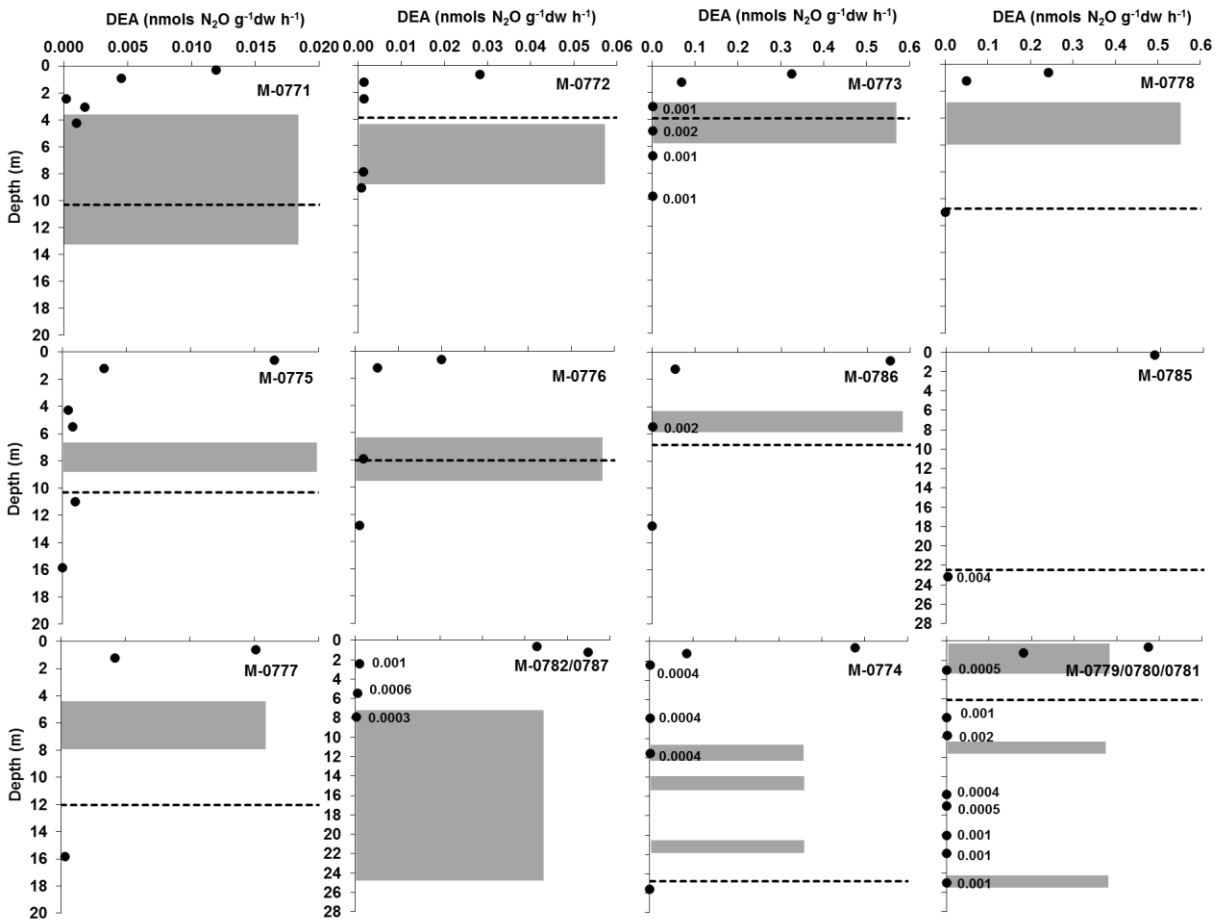

Figure 4.1.8. Vertical profiles of denitrfication enzyme activity (DEA) in soil and vadose zone profiles for the 12 study wells. The gray areas and the dash lines represent the clay layers and the water table, respectively.

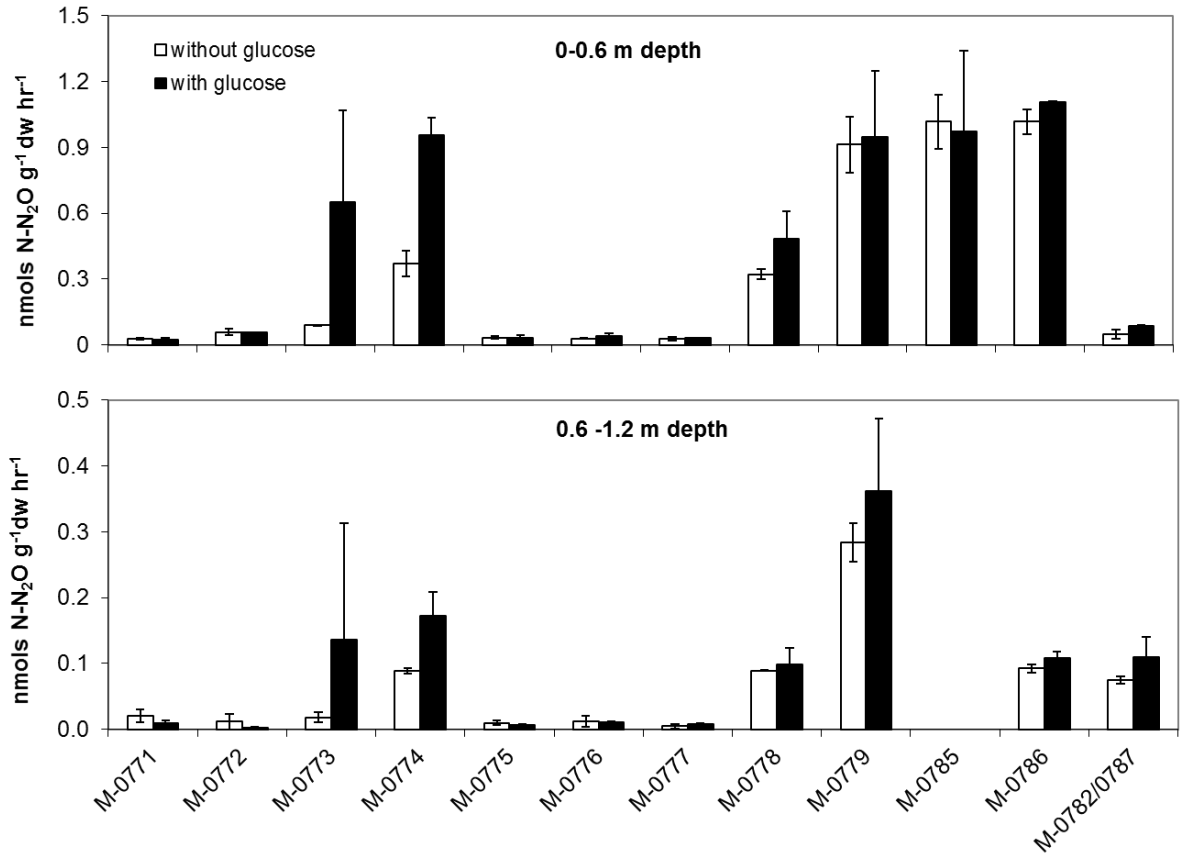

Figure 4.1.9. Comparison of denitrfication enzyme activity (as production of N_2O) with and without added glucose in soil and vadose zone profiles for the 12 study wells.

One factor missing in the regression equation is the redox potential, which is the potential for a reduction-oxidation reaction is likely to occur and is highly variable depending on the presence of oxygen. At low redox potentials, there is little to no oxygen present which creates reducing conditions, and more optimal conditions for denitrification. The redox potentials measured at all 12 sites was comparatively lowest in the top 2 m. Exceptions include layers with saturated limestone, and site M0779/0780/0781, where at 10 m redox was measured at its lowest potential for that site.

4.1.4.3 Surface/Groundwater Relationships

We measured the $\delta^{15}N$ and $\delta^{18}O$ of water extractable NO_3^- across the soil profiles at four of the well sites. The $\delta^{15}N$ values were measured for the bulk soil along the soil profiles for the 12 new sites. Patterns of stable isotopes of nitrate ($\delta^{15}N$, $\delta^{18}O$) in these profiles indicate a potential movement of nitrate throughout profiles as well as location of major biological activity, primarily at the surface (Figure 4.1.11). The lowest isotopic values of both nitrogen and oxygen were observed at M-0774 indicating the predominance of other ammonium fertilizer or soil

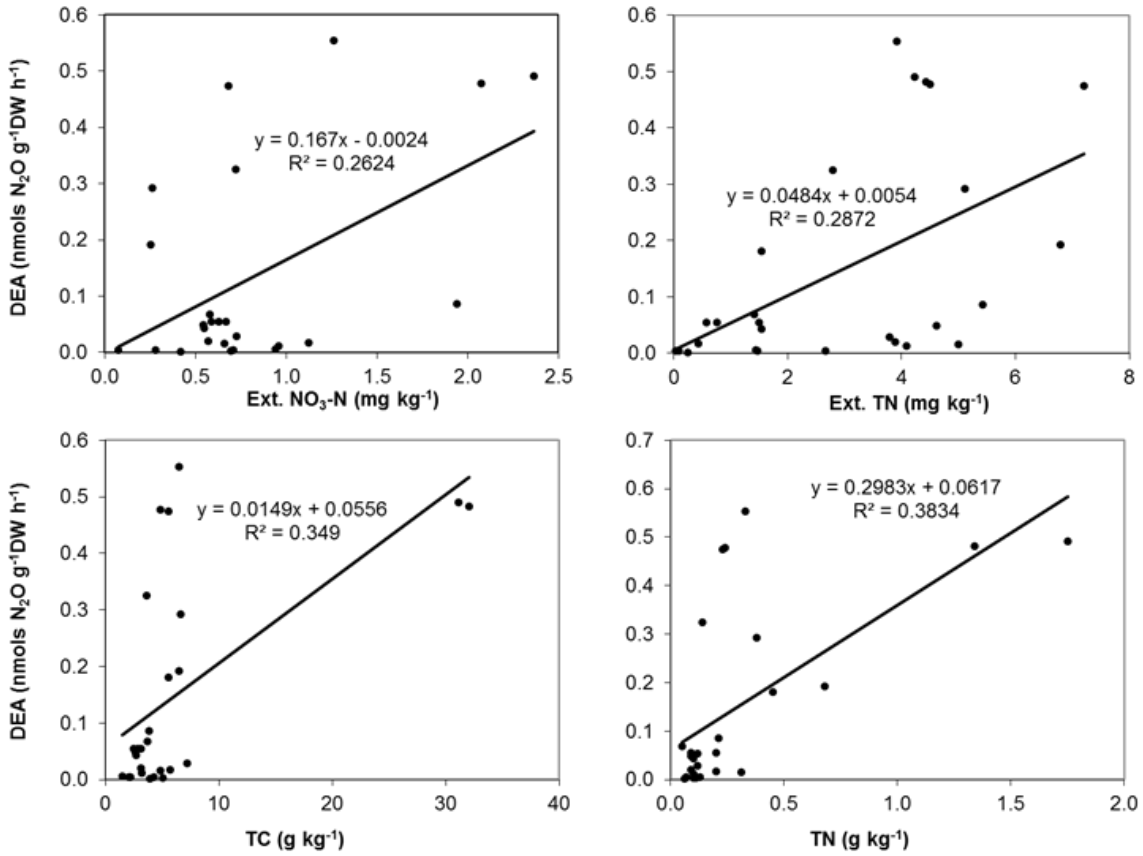

Figure 4.1.10. Regressions of denitrfication enzyme activity (DEA) with with total and extractable carbon and nitrogen parameters in soil and vadose zone profiles for the 12 study wells.

organic N sources. In contrast, much higher $\delta^{18}O$ values indicate an increased source of nitrate fertilizer at both M-0776 and M-0782/0787 sites (Figure 4.1.11). The patterns observed at the M-0786 are puzzling as they tend to indicate a significant nitrification effect (e.g., lower $\delta^{15}N$ of nitrate than soil total nitrogen and low $\delta^{18}O$) and do not exhibit the high $\delta^{15}N$ characteristic of wastewater which is the suspected dominant matter to source at this site (Figure 4.1.11). Complicating the interpretation of these isotopic patterns is the fact that in most cases the observed signature likely represents a mixture of nitrogen sources which may vary seasonally.

At all sites, isotopic values for extractable nitrate in the surface appeared decoupled from those observed in groundwater. Because this study assessed extractable nitrate, our measured values could represent on the nitrate being adsorbed onto soil particles (i.e. the nitrate left behind after leaching). This type of isotopic interaction could appear as an enrichment in our measured value with our extractant removing nitrate which is preferentially held by the soil particles (Ledgard et al. 1984; Jones et al. 2015). As the extractant in this study was water, however, this effect should be minimal, and the observed isotopic signatures should reflect the "leachable" nitrate. Further, in the sandy soils of this region, interaction between nitrate and the soil should be minimal;

however, iron oxide coatings observed in these profiles have shown potential to interact with nitrogen forms (Huang et al. 2003).

Two main observations were noted in the isotopic profiles. First, in all cases $\delta^{15}N$ was more depleted than the bulk TN in the surface 1-2 meters (Fig. 4.1.11). The isotopic signature of bulk TN primarily represents that of the soil organic components. As this organic N mineralizes to ammonium and then is nitrified, the resulting nitrate becomes progressively lighter than the source N. Thus, the lighter than bulk values of $\delta^{15}N$ in the surface likely reflects the creation of nitrate (nitrification) within the soil, not the presence of fertilizer or added nitrate.

The second observation is that all soils displayed an enrichment in $\delta^{15}N/^{18}O - NO_3^-$ with depth in the upper 4 m of the profile, and in M-0774, enrichment continued with depth in the vadose zone. Denitrification is suspected to have caused this type of enrichment evident from the approximate 1:1 ratio of adjusted $\delta^{15}N/^{18}O - NO_3^-$ ratio (Figure 4.1.11). But denitrification is not the only soil process affecting enrichment or depletion of NO_3 stable isotopes, and the slope of the adjusted $\delta^{15}N/^{18}O - NO_3^-$ falls 30 % short of the expected slope of 1. Studies by Spoelstra et al. (2007) and Mayer et al. (2001) showed both enrichment and depletion of the $\delta^{15}N - NO_3^-$ and the $\delta^{18}O - NO_3^-$ during denitrification or nitrification in forest soils. Patterns in this study may thus exhibit simultaneous nitrification and denitrification causing the pattern of lower $\delta^{18}O - NO_3^-$ for a given $\delta^{15}N - NO_3^-$.

In addition to isotopic fractionation through particle interaction and biological processes, other potential factors could hinder attribution of groundwater N sources based on isotopic ratios. For example, at the M-0782/0787 site there appeared to be three regions of isotopic composition including the surface extending down to the first clay layer at 7 m, a second intermediate region from the water table at 18 m down to 35 m, and a third distinct isotopic signal from the clay layer encountered at 35 m to the bottom of the profile (Figure 4.1.11). It is unclear what is driving these observed differences; However, these observations (particularly the reversals in $\delta^{18}O$) do not reflect a pattern that would be observed through infiltration from the surface alone. The isotopic transitions and reversals may indicate lateral water movement and/or contrasting water and N sources for the surficial and confined aquifers at the site.

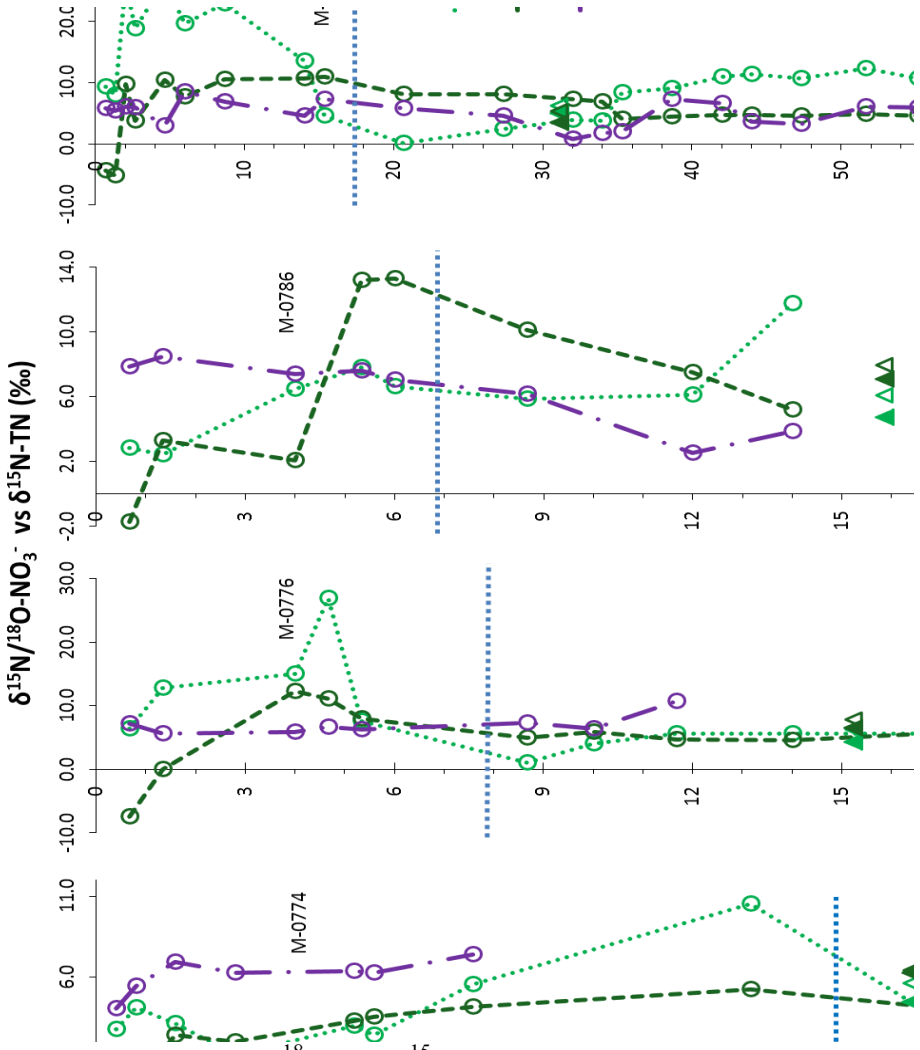

Figure 4.1. 11. Vertical profiles of $\delta^{18}O$ and $\delta^{15}N$ of soil extractable nitrate (Ext. NO_3-N), $\delta^{18}O$ and $\delta^{15}N$ of nitrate for groundwater in the well, and $\delta^{15}N$ of total bulk N in soil profiles for the sites M-0774, M-0776, M-0786, and M-0782. The dash blue lines represent the water table.

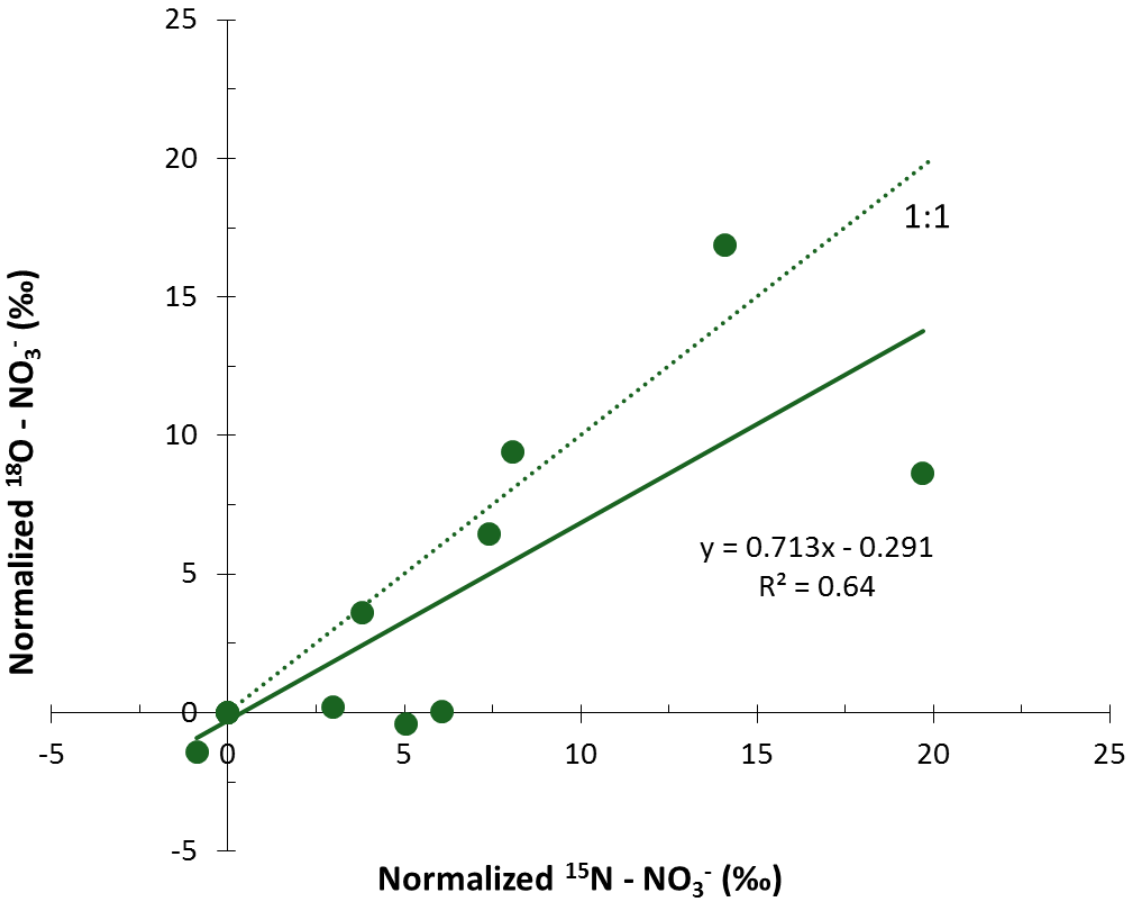

Figure 4.1.12. Isotopic biplot of adjusted $^{15}N/^{18}O$ of water extractable NO_3^- from surface (<4 m) soils in this study. The solid line represents actual correlation and dotted line represents the hypothetical 1:1 ratio.

4.1.4.4 Microbial Indicators of Denitrification in Soil Profiles

Q-PCR Results: Within the aquifer sediment samples, *16S rRNA* gene abundances generally decreased with depth though overall abundances generally remained quite high (Figure 4.1.13). Overall, *nosZ* harboring bacteria generally accounted for between 0 to 4 % of the total bacterial community. The highest ratio occurred in the surface 0 to 1 m of M-0777 in the agricultural land use with a sub-surface peak in the 3 to 4 m sediments from the urban land use well M0782. This peak corresponds with a large observed decrease in NH_4^++NO_3^- in the same well. The majority of other urban land use wells (M-0772, M-0773, M-0774, M-0782) exhibited the lowest overall *nosZ* ratio along the depth profile. Well M-0779 of the forest land use showed a sub-surface decrease to 0 % abundance from the 2.5 to 10 m depth, followed by a peak at ~25 m. This corresponds roughly to the lowest redox observed in any well from ~6 to 10 m (Figure 4.1.4) and to the only significant DEA activity in the sub-surface at 20 m. Despite high DEA and the highest TN in M-0779, *nosZ* abundance remained constrained in this depth range, despite fairly stable bacterial abundance between 10^6 and 10^8 *16S rRNA* gene copies g^{-1} sediment. All well

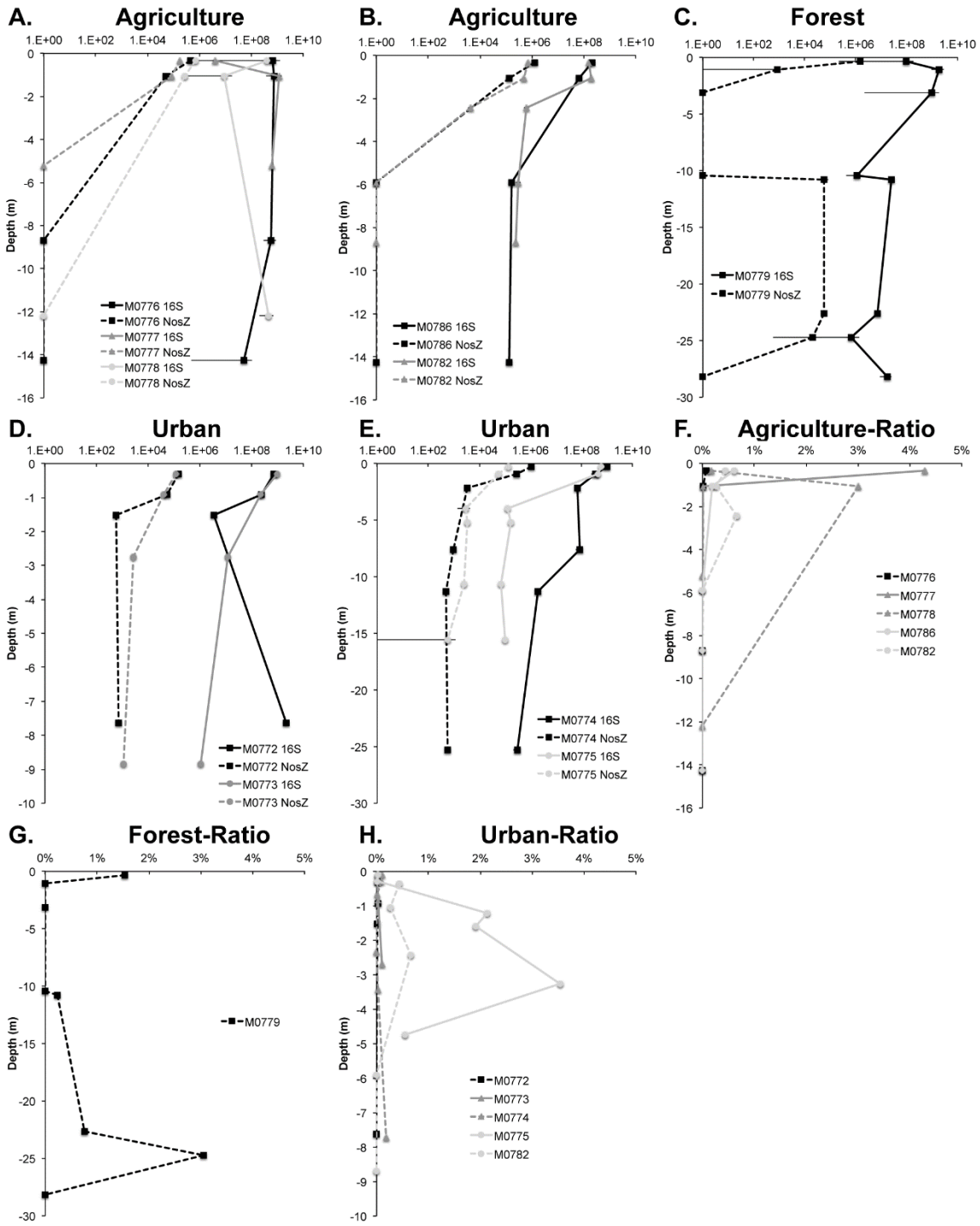

Figure 4.1.13. Abundances of *16S rRNA* gene and *nosZ* gene copies normalized to per gram soil arranged by land use type with depth and standard errors (A-E). Ratio of *nosZ* to *16S rRNA* gene copy numbers along the depth profiles (F-H).

sediment profiles in the agricultural land use category (M-0776. M-0777, M-0778, M-0782, M-0786) contained *nosZ*-harboring bacteria at higher abundances in the shallower sediment (<6 m) followed by a decrease with depth without substantial sub-surface peaks identified in the other

sediments. Indeed, most sediments showed un-detectable *nosZ* abundances below ~8 m (Figure 4.1.13). This corresponds to near-surface peaks in both TN and TOC in these samples, compared to the sub-surface peaks observed in M-0779 and, with the exception of M-0782, resides at the depth at which redox potential begin to decrease after a peak at ~4 m. Wells within the urban land use category (M-0772, M-0773, M-0774, M-0775) exhibited the most consistent *nosZ* gene abundance with depth and a high *nosZ* ratio as well in M-0775 that peaked at ~3.5 m.

When all samples were combined the only significant correlation identified was between *16S rRNA* gene abundance and total phosphorus (TP) ($r=-0.548$, $p=0.006$). Parsing samples according to land use type showed that among the agricultural samples, *16S rRNA* gene abundance was negatively correlated to TP ($r=-0.701$, $p=0.016$) while *nosZ* abundance was negatively correlated to both TN ($r=-0.722$, $p=0.012$) and TP ($r=-0.856$, $p<0.001$). The ratio of *nosZ* to *16S rRNA* abundance was positively correlated to soil moisture content (MC) ($r=0.666$, $p=0.025$) and loss on ignition (LOI) ($r=0.781$, $p=0.005$). Within the urban samples *16S rRNA* abundance was negatively correlated to MC ($r=-0.695$, $p=0.038$) and TP ($r=-0.742$, $p=0.022$), *nosZ* negatively with TP ($r=-0.877$, $p=0.002$) and positively with TC ($r=0.702$, $p=0.035$) while the *nosZ* to *16S rRNA* gene abundance ratio was also positively correlated with TC ($r=0.678$, $p=0.045$). These urban land use wells are shown to contain a high concentration of TP in the aquifer water.

Principal component analysis (PCA) of the gene abundance data and chemical properties revealed no clear grouping based on either land use category (Figure 4.1.14). Well M-0779-1, representing the shallowest sample at this site, was distinctively separated from other sites, reflecting the general pattern of differentiation of this well from others. There was a general pattern of shallower samples being located at PC1 values of <-0.1 correlating most with TOC, TN, NH_4^+ and DEA. Deeper samples were mostly partitioned to the lower right quadrant, positively correlated with TP, ^{15}N measurements, redox values and, to a lesser extent, moisture content.

These results demonstrate that populations of *nosZ*-harboring putative denitrifiers are generally more abundant in the surface soils. These populations tend to drop off most rapidly in the wells located within the agricultural land use category while the urban wells contain denitrifying populations, while in lower abundance, more consistently with depth. This indicates a potential for higher depth-integrated denitrification within these wells. Well M-0779 (forest land use) was the most unique with a significant sub-surface peak of putative denitrifiers corresponding to the only significant sub-surface DEA activity. DEA with added C measurements suggested that M-0773 and M-0774 may be C limited for denitrification. *nosZ* abundance profiles show fairly high abundances throughout the depth profile, potentially supporting this hypothesis, though interactive effects with other soil edaphic properties likely play a role.

Bacterial Community Composition: A total of 14,573,314 raw *16S rRNA* gene sequences were obtained from 43 sediment samples of varying depths (M-0569, M-0773-M-0777, M-0778-M-0779). After paired-end assembly and quality filtering, 12,970,621 sequences remained. Chimeric sequences constituted 1.20 % of all reads, resulting in 12,389,807 sequences that were rarified to 102,800 sequences per sample. A total of 22,040 OTUs were obtained after clustering at 3 % nucleotide dissimilarity and the removal of 3,189 OTUs (4,654 sequences) that were singletons and doubletons.

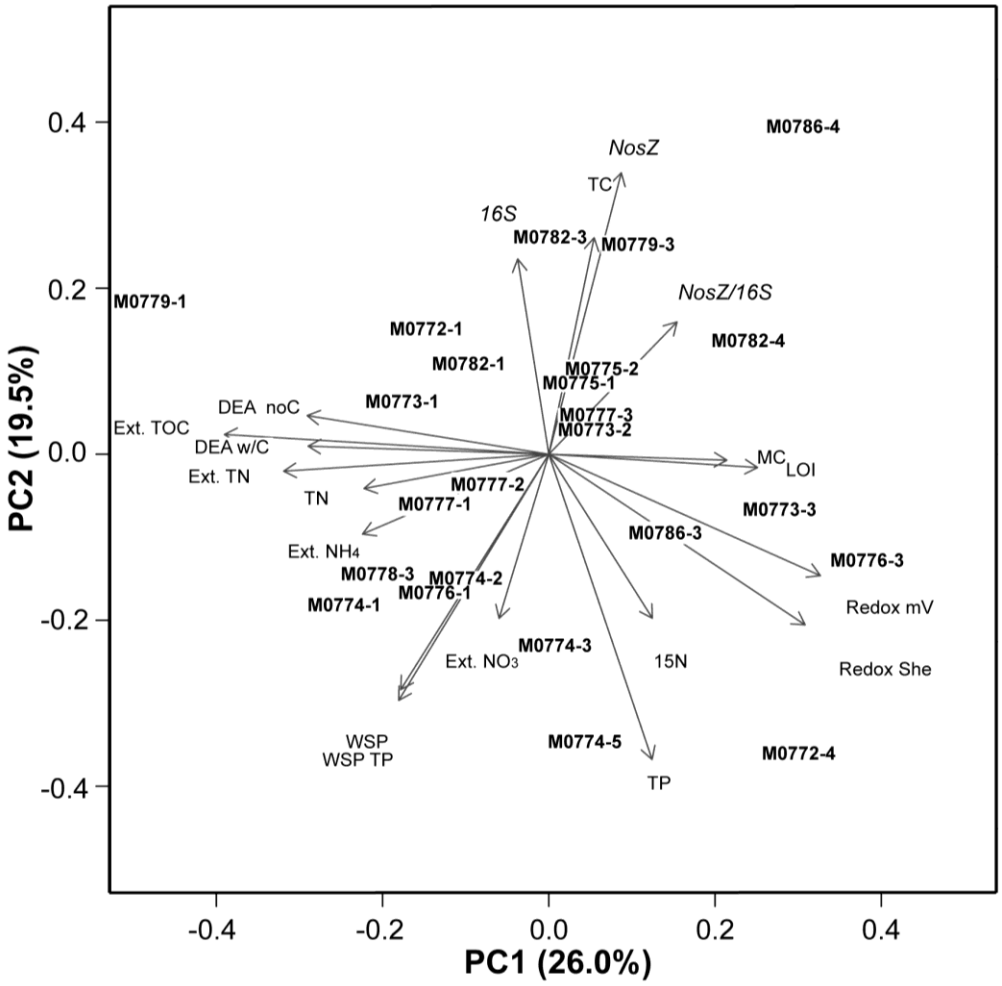

Figure 4.1.14. Principal component analysis (PCA) of the quantitative PCR data and sediment chemical parameters. Samples that did not have detectable *16S rRNA* gene or *nosZ* gene copies were discarded.

Overall, bacterial community composition did not vary significantly among wells with all depths included (PERMANOVA; F=1.330, P=0.065). However, depth was a significant factor (PERMANOVA; F=7.453, P=0.001; ANOSIM; R=0.666,P=0.001) as was the interaction between well and depth (PERMANOVA; F=2.403, P=0.001; ANOSIM; R=0.635, P=0.001). Differences in bacterial community composition among depths was best explained by a combination of TP, TC, extractable NO_3^-, extractable total organic carbon and denitrifying enzyme activity (DEA) without glucose addition (BEST: ρ=0.29, p=0.04). With significant variation with depth, soil and vadose zone materials were placed into three groups: shallow (0-3 m), intermediate (3.6-11.6 m) and deep (>12 m). Both bacterial richness (ANOVA; F=22.02, p<0.001) and diversity (F=16.89, p<0.001) were significantly higher in the shallow materials compared to the medium and deep while there was no significant variation in evenness (F=0.834, p=0.44) (Figure 4.1.15). This pattern of deceasing diversity has also been identified in comparing

182 m, 290 m and 455 m deep aquifer water samples (Hubalek et al. 2016), though evenness was found to be higher in deeper samples.

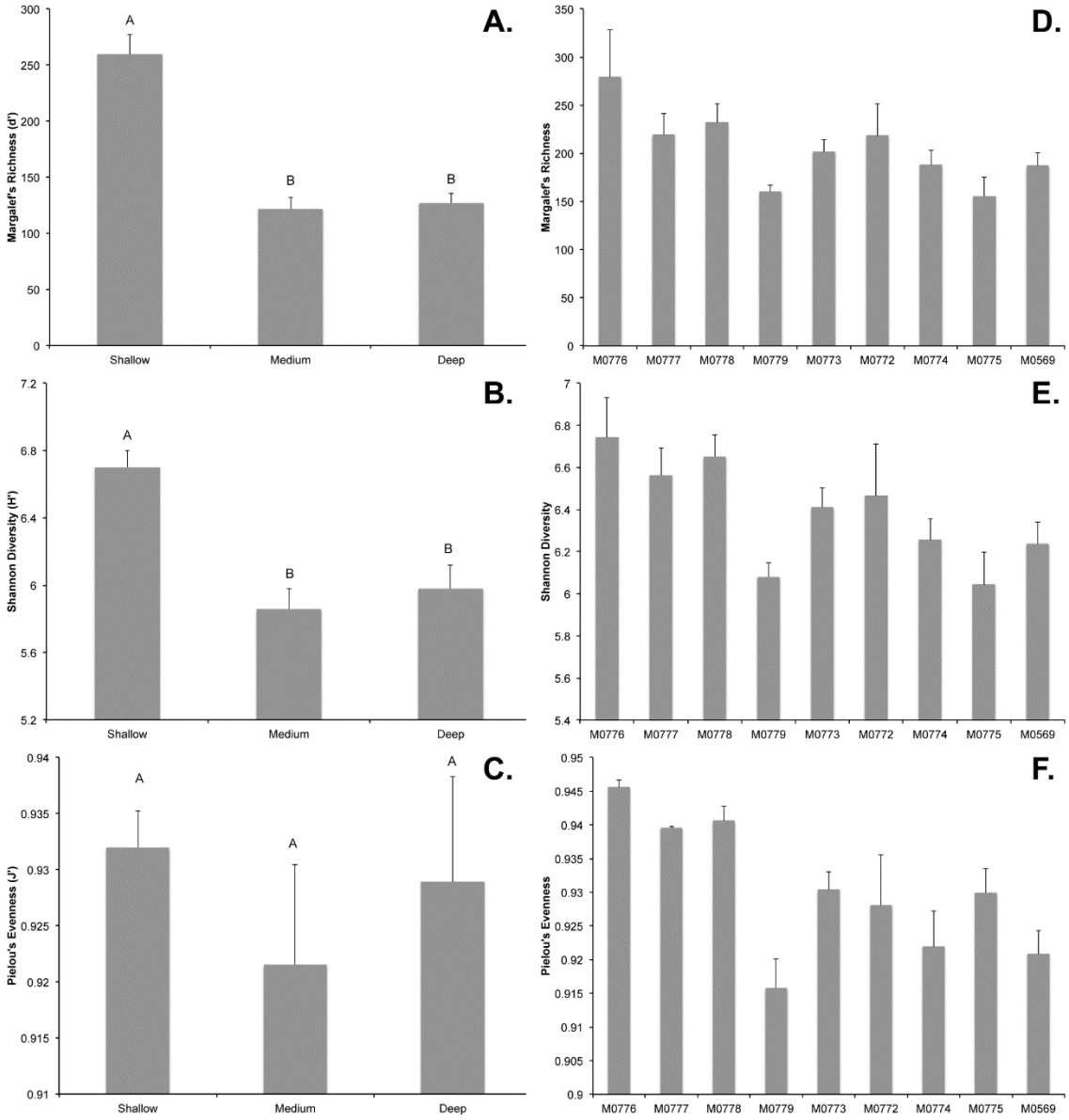

Figure 4.1.15. Margalef's richness, Pielou's evenness (J') and Shannon diversity (H') of the aquifer sediment bacterial communities according to depth (Shallow=0-3 m, Medium=3.6-11.6 m, Deep=>12 m) (A-C) and by well (D-F).

Bacterial community richness, diversity and evenness were also examined across all sampled sites where no significant difference was identified according to site, regardless of depth (ANOVA, Margalef; F=0.75, P=0.65; Pielou F=0.97, P=0.47; Shannon F=0.79, P=0.62). However, there was a general trend of higher diversity, richness and evenness in the agricultural wells (M0776-M0778), compared to the urban and forest samples.

As depth was a significant factor, Similarity Percentage Analysis (SIMPER) was used to identify the bacterial phyla that contributed most to the Bray-Curtis dissimilarity between the shallow, medium and deep groupings (Figure 4.1.16). *Proteobacteria*, largely beta- and gamma-*Proteobacteria*, contributed to the majority of the dissimilarity among all depth groupings. This was followed by changes in the contributions by *Actinobacteria*, *Firmicutes* and *Acidobacteria* (GP6). The majority of the *Acidobacteria* are difficult to isolate, leaving their general ecology and physiology unknown (Liles et al. 2010). Plots of relative abundances for each site indicated that differences in the abundances of *Proteobacteria*, *Acidobacteria* and *Actinobacteria* were also large drivers of the changes in community composition among wells (Figure 4.1.17).

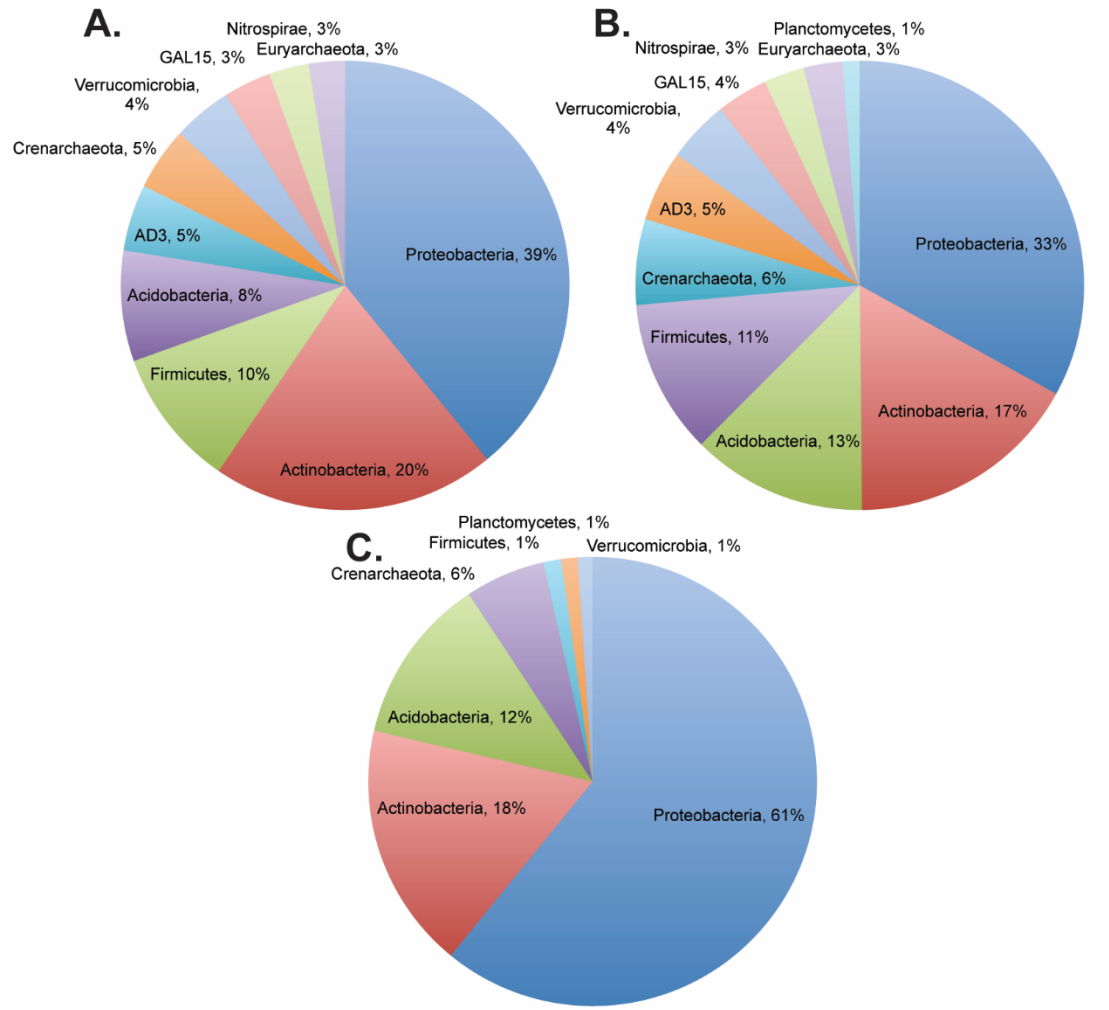

Figure 4.1.16. Similarity Percentage Analysis (SIMPER) identifying bacterial phyla that contributed most to the Bray-Curtis dissimilarity among depth groups. (A) Shallow-Medium, (B) Shallow-Deep, (C) Medium-Deep. Percentages indicate the SIMPER-derived percent contribution to the total dissimilarity between comparisons.

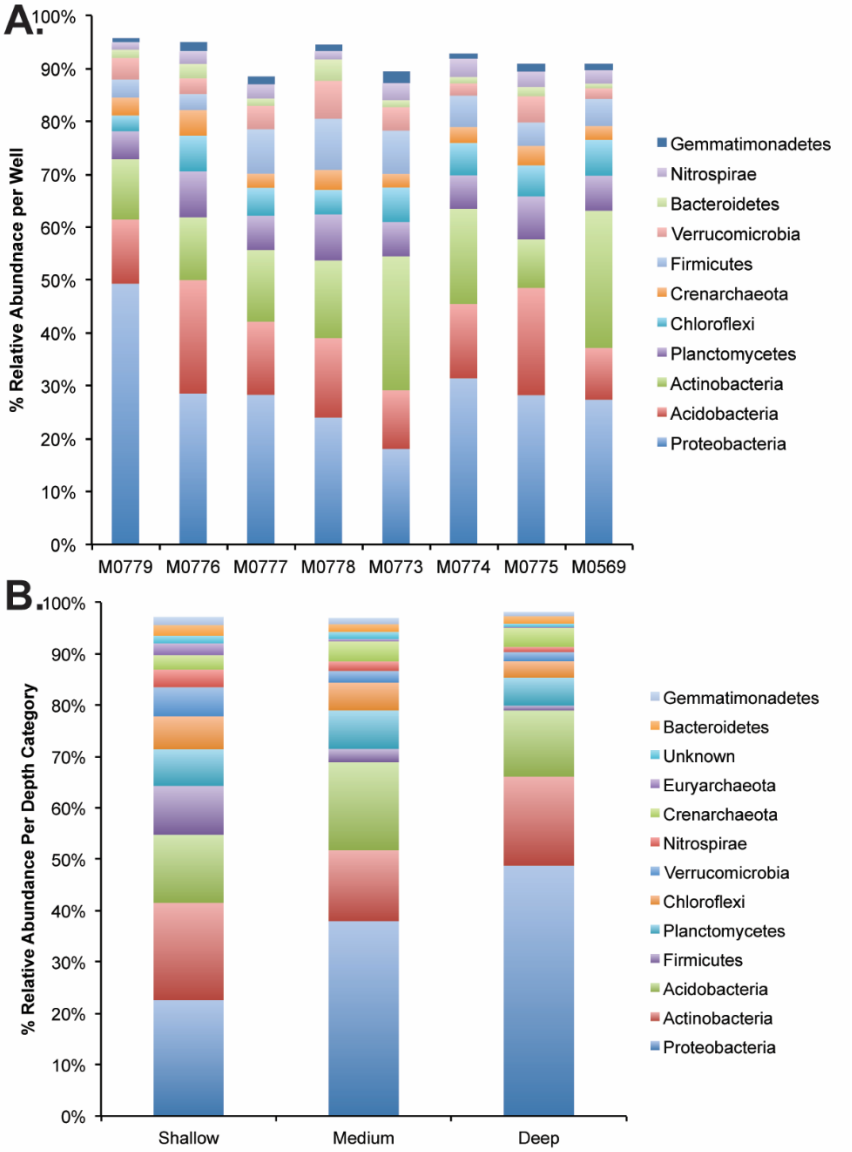

Figure 4.1.17. Relative abundances of the top phyla by (A) well and (B) depth category. Percent abundances were calculated using the sum of sequences identified within each well or depth category.

Interestingly, the abundance of *Firmicutes* decreased substantially from the surficial soils (~9.5 % abundance) to the medium depth (2.5 %) to the deep materials (0.9 %) while, among land use categories, the lowest *Firmicutes* abundance occurred in the forest (3.0 %), followed by agricultural (5.5 %) and urban wells (6.3 %). Prominent genera in the *Firmicutes-Bacilli* include the *Paenibacillus* (2.54 % in shallow, 1.70 % in intermediate and 0.19 % in deep subsoils) associated with a variety of natural and clinical habitats and identified in other aquifers (Lehman et al. 2001a; Jiang et al. 2014), the ubiquitous *Bacillus*, *Alicyclobacilli*, the halo-alkalitolerant methylotrophic *Ammoniphilus* and fecal associated *Enterococcus*. The finding of the moderately thermophilic, acidophilic *Alicyclobacilli* as well as thermophilic *Rubrobacter* in this environment

is interesting, similar to an earlier finding of *Alicyclobacilli* in another aquifer borehole (Lehman et al. 2001b).

The *Clostridia* were present in a low abundance in these samples, constituting 0.37 % of the community with the fecal associated *Coprococcus* and *Clostridium* accounting for only 0.4 %. The *Nitrospira-Nitrosporales*, characterized as nitrite-oxidizing chemolithoautotrophs (Ehrich et al. 1995; Luecker et al. 2010), were a relatively abundant group at 2.5 % of all sequences and decreased with depth from 3.4 % to 2.3 % (medium) to 1.0 % in the deep sediments. Forest well soil/subsoils harbored the smallest population (1.3 %), followed by agricultural wells (2.2 %) and urban wells (2.8 %).

Proteobacterial abundance increased from 22.6 % to 38.0 % to 48.8 % from the shallow to the deep sediments and was markedly more abundant in the forest (M-0779) versus urban and agricultural samples. Indeed, the lower richness in the M-0779-forest well sediments was likely due to the higher abundance of *Proteobacteria* (49.3 %), compared to other samples. Among the *Proteobacteria*, alpha-*Proteobacteria* comprised 6.3 % of the total microbial community with the orders *Rhizobiales* encompassing 2.9 %, the *Sphingomonadales* that contains putative bioremediation species (1.8 %), *Rhodospirilalles* comprised of acetic acid and purple non-sulfur bacteria (0.8 %) and *Caulobacterales* 0.3 %. Within the *Sphingomonadales* were *Sphingomonas* (0.3 %), strict aerobic heterotrophs that can survive in low nutrient concentrations (Stolz, 2009; Krieg, 2010). The organic-rich environment dependent *Hyphomicrobiaceae* and *Rhodospirillaceae* comprised 2.35 %, 1.72 % and 0.62 % of the shallow, intermediate and deep soils, respectively. Their reduction in the deeper vadose zone materials reflects a decrease in total organic carbon with depth.

Beta-*Proteobacteria* comprised 14.5 % of the entire vadose/aquifer community but only 6.0 % of the total OTUs, indicating highly abundant clustering with few singletons/doubletons. Of these, the order *Burkholderiales* comprised an astonishing 13.5 %. Within this order were the genus *Burkholderia* and the family *Oxalobacteraceae* (11.5 % of all sequences). Delta-*Proteobacteria* were present at an abundance of 2.3 % with the genera *Bdellovibrio*, *Geobacter* and the sulfate-reducing *Syntrophobacteraceae* family the most prevalent. *Bdellovibrio* species have been shown to be obligate predators (Keya and Alexander 1975; Jurkevitch et al. 2000) of plankton in aqueous environments and have been identified in a groundwater-fed cave (Hutchens et al. 2004). The iron-reducing *Geobacter* (Lonergan et al. 1996) have been found widely dispersed in iron-reducing sandy aquifer sediments (Snoeyenbos-West et al. 2000; Röling et al. 2001) with some species identified as nitrate reducers, as well (Kashima and Regan, 2015). Lastly, the gamma-*Proteobacteria* contained 7.5 % of all sequences with the potentially pathogenic *Enterobacteriaceae* with many unresolved genera (1.0 %) and *Xanthomonadales* (1.5 %), including some potentially pathogenic genera, the most prevalent.

Interestingly we did not find sequences related to the nitrate-reducing sulfur oxidizing *Sulfurimonas* or *Sulfurovum* found in high abundance in another aquifer (Hubalek et al. 2016), suggesting that reduced sulfur is not generally in high concentrations in the Silver Springs aquifer. DA101, a *Chthoniobacteraceae* was prevalent at a very high abundance in the shallow soils (4.13 %), followed by the intermediate (1.0 %) and deep (0.9 %). First identified in 1998 as an abundant sequences from Netherlands grassland soils (Felske and Akkermans 1998), the

DA101 phylotype has since been found to be within the top ten most abundant bacteria in >1,000 soils where it is suggested to be passively correlated with higher labile C inputs (Brewer et al., 2016). This appears to be the first report of this bacteria in aquifer samples or water. Remarkably, it is also a rare example of a reduced genome size that dominates bacterial communities, where the inverse is usually the rule (Brewer et al., 2016). Again, here it appears that organic carbon availability (and likely lability, though not measured in this study) serves to shape the occurrence of this abundant organism along the soil/vadose zone profile.

Denitrifiers are a broad polyphyletic group of bacteria with a large proportion of members within the alpha-, beta- and gamma-*Proteobacteria* (among others) and are difficult to identify unless genus level resolution is achieved (23.2 % of all sequences were identified to the genus level). *Azoarcus*, a dentrifying *Actinobacteria* (Zhou et al. 1995) was observed in low abundance (<0.01 %) and have also been identified in a landfill leachate polluted aquifer (Röling et al. 2001). Members of the genus *Pseudomonas* are known denitrifiers that can also exhibit aromatic hydrocarbon degradation (Mikesell et al. 1993). These were found at 0.59 %, 5.74 % and 2.88 % abundance in the shallow, intermediate and deep soils, respectively. Other denitrifiers include *Paracoccus* (S=0.001 %, I=0.1 %, D=0.42 %) and *Acinetobacter* (S=0.44 %, I=4.56 %, D=2.86 %) that contains species capable of heterotrophic nitrification and aerobic denitrification (Huang et al. 2013; Yao et al. 2013; Ren et al. 2014). These putative denitrifiers all show a consistent peak in the intermediate subsoil depth that generally corresponds to subsurface water saturated conditions where redox values tended to decrease.

Another set of putative denitrifiers was more associated with the shallow soils. The *Actinobacteria* genus *Streptomyces*, often associated in high abundance in sewage sludge and contains species known to be incomplete denitrifiers, exhibited a large peak in the surface soils (5.10 %) that drastically reduced in the intermediate (0.96 %) followed by the deep vadose materials (0.32 %). Other genera that contain denitrifying species include the *Burkholderia* (S=1.78 %, I=0.36 %, D=0.07 %), *Rhodoplanes* (S=1.19 %, I=0.73 %, D=0.49 %) that contains species capable of complete denitrification (Hiraishi and Ueda 1994).

The *Crenarchaeota* were solely comprised of the family *Nitrososphaeraceae-Candidatus Nitrososphaera*, a group of archaeal ammonia oxidizers (Kerou and Schleper 2016). These *Archaea* remained largely consistent with depth at 2.8 %, 3.9 % and 3.7 % in the shallow, medium and deep depths, respectively. The *Euryarchaeota*, present at 2.2 % in the surficial soils but <0.05 % in the medium and deep sediments consisted largely of methanogens in the genera *Methanocella*, *Methanobacterium* and *Methanosarcina* and thermophilic acidophiles of the class *Thermoplasmata*. Of these, *Methanocella* and *Methanosarcina* were the most abundant. The higher abundance in the surface soils indicate they are surviving in more aerobic conditions, a capability due to the presence of oxygen detoxifying enzymes (Angel et al. 2011; Erkel et al. 2006). Indeed these genera have been identified in freshwater (Bogard et al. 2014) and oxic terrestrial soils (Angel et al. 2012). Of the methanogens, the O_2-sensitive *Methanobacterium* was in the lowest abundance. Surprisingly, we captured 20,130 *Cyanobacteria* sequences (0.4 % of all reads), corresponding to 0.4 % of reads identified in a shallow aquifer compared to 16 % of all reads in a deep aquifer (Hubalek et al. 2016).

Non-metric multi-dimensional scaling (NMDS) was utilized to visualize the distribution of wells and depths according to the bacterial community composition (Figure 4.1.18). As shown by the PERMANOVA results, the most prominent grouping occurred according to depth categories with the shallow sediments clustering separately from the medium and deep. Shallow samples clustered significantly more tightly than the medium and deep samples (PERMDISP, F=4.92, P=0.04), indicating community variation increases with depth. Conversely, there was no significant difference in community dispersion within each well (PERMDIPS, F=1.77, P=0.31). Overall, land use category had no significant impact on bacterial community composition. Instead, depth was the significant factor indicating that large-scale changes to community composition are due to depth as an encompassing factor of changes in sediment chemistry, redox and electron acceptor abundance.

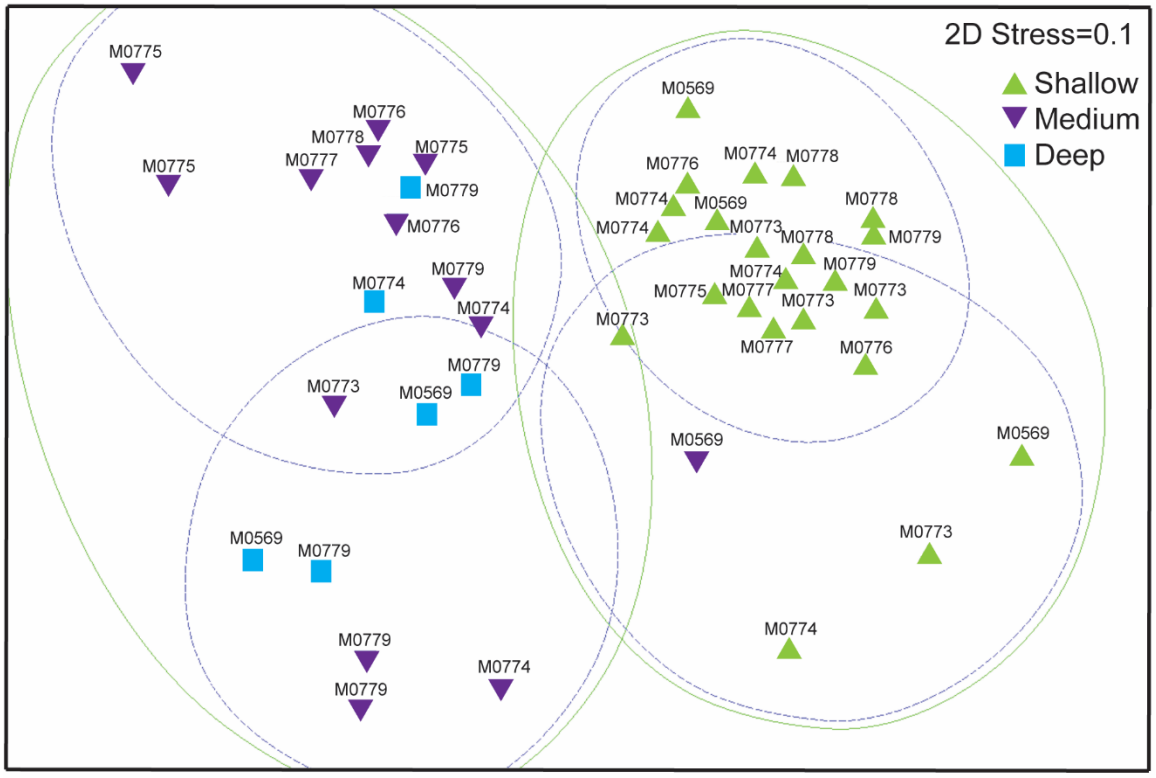

Figure 4.1.18. Non-metric multi-dimensional scaling (NMDS) of the *16S rRNA* gene-derived bacterial communities based on the Hellinger-transformed relative abundance based Bray-Curtis dissimilarity matrix showing grouping according to depth. Group similarities are illustrated by green (15 %) and blue (25 %) dashed ellipses. Well ID's are illustrated by each point.

4.1.5 CONCLUSIONS AND RECOMMENDATIONS

Profiles of soil and vadose zone materials indicate a diversity of conditions for denitrification potential and N transformation pathways within the Silver Spring springshed. In general, soils and vadose zone materials were dominated by sands with low organic composition and clays with low transmissivity. These types of materials should not promote high rates of denitrification. Most denitrification in the profiles sampled occurs in the topsoil and down to a

depth of 3 m. However, certain profiles in the Silver Spring springshed do contain lithologies with iron, sulfur as well as buried organic horizons which may promote enhanced or alternate pathways of nitrogen transformations such as denitrification. Redox conditions above and below clay layers further indicate the potential for denitrification. This highlights the importance of other indirect measures of denitrification, such as dissolved gases and stable isotope measurements.

We know, based on our potential denitrification measurements, that denitrification occurred predominately at the surface in all of our soils at all 12 sites. However, we do not know if this is actually an effect of land use (type and amount of nitrate applied). Stable isotopic patterns in the soil/vadose zone profiles indicated that isotopes could potentially be used for tracing (unique surface source characteristics). However, alteration of these signals by nitrification, denitrification, lateral mixing of soil groundwater, and possible physical interaction with clays or other reactive surfaces warrant the exploration of more tracers to improve the interpretation of groundwater signatures as indications of land use and loading.

From the perspective of microbial communities, depth profiles indicated that surficial soils harbored the most abundant populations of putative denitrifiers and total bacterial communities. Wells located within the agricultural land use category exhibit the most rapid decrease of denitrifiers with depth while those located in the urban land use harbor populations that continue into the deeper soils. Putative denitrifier and total bacterial community abundances were most related to total phosphorus, likely due to spatial competition with R-strategists, moisture content that limits N species diffusion rates as well as impacts niche differentiation due to redox state, total nitrogen and total carbon that directly impact denitrification rates and thus population growth responses.

The soil/vadose zone bacterial community was most shaped by profile depth with higher diversity and richness in the surface sediments. Nitrifying bacteria were most prevalent near the surface comprising up to 3.4 % of the total community with the largest populations associated with the urban wells. Ammonia oxidizing Archaea were also present at relatively high abundances, up to 3.9 % of the community, though their populations remained consistent through the depth profile. Genera that are known to contain denitrifiers were divided into two groups, one at more than 10 % relative abundance in the intermediate depth sediments, corresponding roughly to the water table depth. The second group contained >8 % of sequences in the shallow sediments, likely more associated with C input.

Proteobacterial relative abundance increased with depth, driven by increases in putative sulfate reducing and methylotrophic bacteria. Conversely, the abundance of methanogens was highest in the shallow soils. Potentially pathogenic or fecal-related bacteria were detectable in low abundance, accounting for ~3 % of the community, though more refined taxonomic identification is needed to confirm this. As such, land use category exhibited a minor impact on microbial community composition. Rather, depth-related edaphic properties imparted the most significant role in shaping aquifer sediment microbial community composition.

4.1.6 FUTURE RESEARCH NEEDS

Limitations in the analysis based on limited wells may be alleviated with inclusion of more well locations. The wells used in this study were in many cases considered adjacent to the actual land use with surface soils not reflective of the typical N loads or inputs. For this reason, additional soil work should utilize samples collected directly from the are of land use activity (i.e., within the field not on the edge). The understanding of wet season and dry season differences may also be explained through more long-term (climate-related wet/dry cycles) as well as more high resolution (within a season) sampling. Age dating of well samples would also help to more accurately identify potential mixing between surficial and deep aquifers.

Because of the limitations of isotopes in soil profiles, future studies should focus on the denitrification process in surface soils taken directly from specific land uses. Understanding how denitrification is affected in these land uses by nitrate concentration, type (depending on land use), moisture content, and temperature is critical for developing attenuation models. This may also help predict the fate of nitrate from its source to the groundwater and potentially identify to what extent the isotopic value may have changed based on soil temperature and moisture content.

4.1.7 REFERENCES

Anderson, J. M. 1976. An ignition method for determination of total phosphorus in lake sediments. Water Research, 10: 329–331.

Anderson, M. J. 2001. A new method for non-parametric multivariate analysis of variance. Austral Ecol 26:32-46.

Andersson, H., Bergström, L., Djodjic, F., Ulén, B., and Kirchmann, H. 2013. Topsoil and subsoil properties influence phosphorus leaching from four agricultural soils. Journal of Environmental Quality, 42: 455-463.

Angel, R., Matthies, D., and Conrad, R. 2011. Activation of methanogenesis in arid biological soil crusts despite the presence of oxygen. PLoS One 6 (5).

Angel, R., Claus, P., and Conrad, R. 2012. Methanogenic archaea are globally ubiquitous in aerated soils and become active under wet anoxic conditions. ISME J. 6 (4), 847e862.

Bogard, M. J., del Giorgio, P. A., Boutet, L., Chaves, M. C. G., Prairie, Y. T., Merante, A., and Derry, A. M. 2014. Oxic water column methanogenesis as a major component of aquatic CH4 fluxes. Nat. Commun. 5.

Böttcher, J., Strebel, O., Voerkelius, S., and Schmidt, H. L. 1990. Using isotope fractionation of nitrate nitrogen and nitrate oxygen for evaluation of microbial denitrification in a sandy aquifer. Journal of Hydrology, 114: 413–24.

Brewer, T. E., Handley, K. M., Carini, P., Gilbert, J. A., and Fierer, N. 2016. Genome reduction in an abundant and ubiquitous soil bacterium 'Candidatus Udaeobacter copiosus'. Nat. Microbiol. 2 doi:10.1038/nmicrobiol.2016.198.

Clarke, K. R. 1993. Non-parametric multivariate analysis of changes in community structure. Aust J Ecol 18:117-143.

Clarke, K. R., Gorley, R. N. 2006. PRIMER v6: User Manual-Tutorial. Plymouth Marine Laboratory: Plymouth.

Dixon, P., 2003. VEGAN, a package of R functions for community ecology. Journal of Vegetation Science, 14(6), pp.927-930.

Djodjic, F., Börling, K., and Bergström, L. 2004. Phosphorus leaching in relation to soil type and soil phosphorus content. Journal of Environmental Quality, 33:678–684. doi:10.2134/jeq2004.0678.

Ehrich, S., Behrens D., Lebedeva, E., Ludwig, W., and Bock ,E. 1995. A new obligately chemolithoautotrophic, nitrite-oxidizing bacterium,Nitrospira moscoviensis sp. nov. and its phylogenetic relationship. Arch. Microbiol. 164 (1), 16e23.

Erkel, C., Kube, M., Reinhardt, R., and Liesack, W. 2006. Genome of Rice Cluster I archaea e the key methane producers in the rice rhizosphere. Science 313 (5785), 370e372.

Faulkner, G. L. 1973, Geohydrology of the cross-Florida barge canal area with special reference to the Ocala vicinity: U.S. Geological Survey Water-Resources Investigations Report 1-73, 117 p.

Feast, N. A., Hiscock, K. M., Dennis, P. F., and Andrews, J. N. 1998. Nitrogen isotope hydrochemistry and denitrification within the chalk aquifer system of north Norfolk, UK. Journal of Hydrology, 211(1-4): 233-252.

Felske, A. and Akkermans, A. D. L. 1998. Prominent occurrence of ribosomes from an uncultured bacterium of the Verrucomicrobiales cluster in grass soils. Lett. Appl. Microbiol. 26:219-233.

Fogg, G. E., Rolston, D. E., Decker, D. L., Louie, D. T., and Grismer, M. E. 1998. Spatial variation in nitrogen isotope values beneath nitrate contamination sources. Groundwater, 36(3): 418-426.

Hem, J. D. 1985, Study and interpretation of the chemical characteristics of natural water: U.S. Geological Survey Water-Supply Paper 2254 (3rd. ed.), 263 p.

Hiraishi, A. and Ueda Y. 1994. Rhodoplanes gen. nov., a New Genus of Phototrophic Bacteria Including Rhodopseudomonas rosea as Rhodoplanes roseus comb. nov. and Rhodoplanes elegans sp. nov. Int. J. Syst. Evol. Microbiol. 44(4):665-673.

Huang, X., Li W., Zhang D., and Qin, W. 2013. Ammonium removal by a novel oligotrophic Acinetobacter sp. Y16 capable of heterotrophic nitrification–aerobic denitrification at low temperature. Biores. Tech. 146:44-50.

Hubalek V., Wu X., Eiler A., Buck M., Heim C., Dopson M., Bertilsson S., and Ionescu, D. 2016. Connectivity to the surface determines diversity patterns in subsurface aquifers of the Fennoscandian shield. ISME J. 10(10):2447-2458.

Hutchens, E., Radajewski, S., Dumont, M. G., McDonald, I. R., and Murrell, J. C. 2004. Analysis of methanotrophic bacteria in Movile Cave by stable isotope probing. Environ. Microbiol. 6:111-120.

Jiang Z., Li P., Wang Y., Li B., Deng Y., and Wang Y. 2014. Vertical distribution of bacterial populations associated with arsenic mobilization in aquifer sediments from the Hetao plain, Inner Mongolia. Environ. Earth Sci. 71: 311-318.

Jurkevitch E., Minz D., Ramati B., and Barel G. 2000. Prey range characterization, ribotyping, and diversity of soil and rhizosphere Bdellovibrio spp. isolated on phytopathogenic bacteria. Appl. Environ. Microb. 66:2365-2371.

Kashima H. and Regan J.M. 2015. Facultative nitrate reduction by electrode-respiring Geobacter metallireducens biofilms as a competitive reaction to electrode reduction in a bioelectrochemical system. Environ. Sci. Technol. 49:3195-3202.

Katz, B. G., Hornsby, H. D., Bohlke, J. K., and Mokray, M. F. 1999, Sources and chronology of nitrate contamination in spring waters, Suwannee River basin, Florida: U.S. Geological Survey Water-Resources Investigation Report 99-4252, 54 p.

Kendall, C., and McDonnell, J. J., eds. 1999. Isotope tracers in catchment hydrology. Elsevier.

Kerou M. and Schleper C. 2016. Nitrososphaera. Bergey's Manual of Systematics of Archaea and Bacteria. 1-10.

Keya S. O. and Alexander M. 1975. Regulation of paratism by host density: the Bdellovibrio-Rhizobium interrelationship. Soil Biol. Biochem. 7:231-237.

Krieg N. R. 2010. Bergey's Manual of Systematic Bacteriology. Springer, New York.

Lehman R. M., Colwell F. S., and Bala G. A. 2001a. Attached and unattached microbial communities in a simulated basalt aquifer under fracture-and porous-flow conditions. Appl. Environ. Microbiol. 67(6):2799-2809.

Lehman R. M., Roberto F. F., Earley D., Bruhn D. F., Brink S. E., O'Connell S. P., Delwiche M. E., and Colwell, F. S. 2001b. Attached and unattached bacterial communities in a 120-meter corehole in an acidic, crystalline rock aquifer. Appl. Environ. Microbiol, 67(5): 2095-2106.

Liles, M. R., Turkmen O., Manske B. F., Zhang M., Rouillard J. M., George I., Balser T., Billor N., and Goodman R. M., 2010. A phylogenetic microarray targeting 16S rRNA genes from the bacterial division Acidobacteria reveals a lineage-specific distribution in a soil clay fraction. Soil Biol. Biochem. 42 (5), 739e747.

Lonergan, D. J., Jenter H. L., Coates J. D., Phillips E. J. P., Schmidt T. M., and Lovley D. R. 1996. Phylogenetic analysis of dissimilatory Fe(III)-reducing bacteria. J. Bacteriol. 178:2402-2408.

Luecker, S., Wagner M., Maixner F., Pelletier E., Koch H., Vacherie B., Rattei T., Damste J. S. S., Spieck E., Le Paslier D., and Daims H., 2010. A Nitrospira metagenome illuminates the physiology and evolution of globally important nitrite- oxidizing bacteria. Proc. Natl. Acad. Sci. U. S. A. 107 (30), 13479e13484.

Mikesell, M. D., Kukor, J. J., and Olsen, R. J. 1993. Diversity of aromatic hydrocarbon-degrading bacteria from a petroleum contaminated aquifer. Biodegradation 4:249-259.

Munch, D. A., Toth, D. J., Huang, C., Davis, J. B., Fortich, C. M., Osburn, W. L., Phlips, E. J., Quinlan, E. L., Allen, M. S., Woods, M. J., Cooney, P. Knight, R. L., Clarke, R. A., and Knight, S. L. 2007. *Fifty-year retrospective study of the ecology of Silver Springs, Florida*. *Special Publication SJ2007-SP4*. Palatka: St. Johns River Water Management District.

Nair, V. D. and Harris, W. G. 2014. Soil phosphorus storage capacity for environmental risk assessment. Adv. Agri. 2014:723064. doi: 10.1155/2014/723064

Peltovuori, T., 2007. Sorption of phosphorus in fi eld-moist and air-dried samples from four weakly developed cultivated soil profi les. Eur. J. Soil Sci. 58:8– 17. doi:10.1111/j.1365-2389.2006.00789.x.

Phelps, G. G. 2004. Chemistry of ground water in the Silver Springs basin, Florida, with an emphasis on nitrate. U.S. Geological Survey Scientific Investigations Report 2004-5144, 54 p.

Pizzeghello, D., Berti, A., Nardi, S., and Morari, F. 2014. Phosphorus-related properties in the profiles of three Italian soils after long-term mineral and manure applications. Agriculture, Ecosystems & Environment, 189: 216-228.

Röling, W. F. M., van Breukelen, B. M., Braster, M., Lin B., and van Verseveld, H. W. 2001. Relationships between microbial community structure and hydrochemistry in a landfill leachate-polluted aquifer. Appl. Env. Microbio. 67:4619-4629.

RStudio Team (2015). RStudio: Integrated Development for R. Rstudio, Inc. Boston, MA.

Sacks, L. A. 1996, Geochemical and isotopic composition of ground water with emphasis on sources of sulfate in the Upper Floridan aquifer in parts of Marion, Sumter, and Citrus Counties, Florida: U.S. Geological Survey Water-Resources Investigations Report 95-4251, 47 p.

Scott, T. M. 1988. The lithostratigraphy of the Hawthorn Group (Miocene) of Florida: Florida Geological Survey Bulletin 59, 148 p.

Scott, T. M., Campbell, K. M., Rupert, F. R., Arthur, J. D., Missimer, T. M., Lloyd, J. M., Yon, J. W., and Duncan, J. G. 2001. Geologic map of the State of Florida: Florida Geological Survey Map Series 146, 1 map sheet, [accessed 12/16/2003] http://www.dep.state.fl.us/geology/gisdatamaps/index.htm.

Smith, M. S., and Tiedje, J. M. 1979. Phases of denitrification following oxygen depletion in soil. Soil Biology and Biochemistry, 11(3): 261-267.

Snoeyenbos-West O. L., Nevin K. P., Anderson R. T., and Lovley D. R. 2000. Enrichment of Geobacter species in response to stimulation of Fe(III) reduction in sandy aquifer sediments. Microb Ecol 39:153-167.

Sokal, R. R., and Rohlf, F. J. 1995. Biometry. W.H. Freeman, New York.

Stolz A. 2009. Molecular characteristics of xenobiotic-degrading sphingomonads. Appl. Microbiol. Biotechnol. 81 (5), 793e811.

Warwick, R. M., Clarke, K. R., and Suharnso. 1990. A statistical analysis of coral community responses to the 1982-1983 El Nino in the Thousand Islands, Indonesia. Coral Reefs 8:171–179.

Wlodarczyk, T., Stepniewska, Z., and Brzezinska, M. 2003. Denitrification, organic matter, and re- dox potential transformations in Cambisols. International Agrophysics, 17: 219-227.

van Beek, C. L., van der Salm, C., Plette, A. C. C, and van de Weerd, H., 2009. Nutrient loss pathways from grazed grasslands and the effect of decreasing inputs: Experimental results for three soil types. Nutrient Cycling Agroecosystem, 83:99–110. doi:10.1007/s10705-008-9205-z.

Xue, D., Botte, J., De Baets, B., Accoe, F., Nestler, A., Taylor,P., Van Cleemput, O., Berglund, M., and Boeckx, P., 2009. Present limitations and future prospects of stable isotope methods for nitrate source identification in surface-and groundwater. Water research 43(5): 1159-1170.

Yao S., Ni J., Ma T., and Li C. 2013. Heterotrophic nitrification and aerobic denitrification at low temperature by a newly isolated bacterium, Acinetobacter sp. HA2. Biores. Tech., 139:80-86.

Zhou J. Z., Fries, M. R., Cheesanford, J. C., and Tiedje, J. M. 1995. Phylogenetic analyses of a new group of denitrifiers capable of anaerobic growth on toluene and description of Azoarcus tolulyticus sp. nov. Int. J. Syst. Bacteriol. 45:500–506

4.2 ASSESSING VARIABILITY AND CONTROLS OF DENITRIFICATION IN SANDY SOIL FROM DIFFERENT LAND USES IN THE SILVER SPRINGS SPRINGSHED

4.2.1 ABSTRACT

Because most studies on terrestrial denitrification are in temperate climates with soils of higher water filled pore space (WFPS) (clayey, silty, loamy soils), the majority of denitrification models used for assessing nitrogen impacts in watersheds have been developed and tested under ideal denitrification conditions. Thus, there is limited research on denitrification controls in terrestrial systems where *in situ* WFPS is naturally less than 50 %. Addressing terrestrial denitrification in sandy soils of humid subtropical systems can augment current data sets that are used to develop and test models that inform N budgets for impacted watersheds like the Silver Springs springshed.

Land use in the Silver Springs springshed has changed from predominantly natural to urban/agricultural over the past 50 years (SJRWMD 2007). Agriculture has historically been the predominant land use within the Silver Springs basin in Marion County. However, the city continues to experience rapid population growth and urbanization, and the surrounding rural areas have become increasingly attractive for development as retirement communities. These communities often include golf courses with turf that require fertilization. In addition, in 1990, only about 35 % of dwellings in Marion County were served by public sewage treatment facilities; the remainder presumably use onsite sewage disposal systems, commonly known as septic tanks (Phelps 2004).

In this study, a series of denitrification incubations over a range of temperatures were performed in sandy soils collected from established land uses (crop, turf, high and low density pastures, and septic leach field) representative of those in Silver Springs springshed. Intact cores were amended to create a range of WFPS representative of *in situ* conditions for sandy soils in a humid subtropical climate, and nitrate (NO_3^-) was added at representative concentrations for fertilized (turf and crop) land uses. Denitrification rates between treatments were compared and statistically analyzed to determine which parameter had the strongest control over denitrification. We found that the strongest control on denitrification in sandy soils collected from a humid subtropical system was temperature. Across all land uses, denitrification increased with increasing temperature regardless of WFPS or NO_3^- or organic carbon concentrations.

4.2.2 INTRODUCTION

An important step towards remediating nitrate (NO_3-N) impacted watersheds is not only to identify where NO_3 can be removed, but to predict the extent of its removal. The conditions that facilitate denitrification in soils include soils have high clay or organic matter content, and with high WFPS such as those formed above a perched water table. Maintaining a high WFPS (usually above 60 % saturation) is difficult in sandy soils because the large pores spaces allow rapid infiltration of water, which can affect the distribution of soil nutrients as well as microbial activity (Hu et al. 2011; Ghafoor et al. 2013; Ma et al. 2016). For example, often the highest WFPS attainable in sandy soils is 50 % before gravimetric infiltration takes effect.

Denitrification is particularly sensitive to the amount of available C or nitrate which varies with land use, for example, different fertilizer types and application rate vary between agriculture and turf management. The variability in WFPS and nutrient concentrations within different land uses can create variable denitrification rates (Xu et al. 2013, Christensen et al. 1990). Although there are many studies on denitrification response to WFPS, nutrient concentration, and temperature (Klemedtsson et al. 1988; Christensen et al. 1990; Weier et al. 1992; Maag and Vinther 1996, Abbasi and Adams 2000), there is limited information on the denitrification response in sandy soils with a WFPS at or below field capacity (Ciarlo et al. 2006; Pihlatie et al. 2004).

To address the need for data concerning drivers of terrestrial denitrification in sandy soils at field conditions expected for sub-tropical climates, a laboratory incubation was conducted with the following objectives: 1) measure actual (rather than potential) denitrification at different temperatures and NO_3^- concentrations in sandy soils that are un-saturated (<50 % WFPS) and 2) determine how land use (soil characteristics) may affect which of these two factors exert the strongest control over denitrification rates.

4.2.3 MATERIALS AND METHODS

4.2.3.1 Site Description

Soil samples for this study were collected from a septic drain field in a private, residential home in Apopka FL (28°41'20.0"N 081°28'26.3"W), and the Plant Science Research and Education Unit (PSREU) located in Citra, FL (Figure 4.2.1). Citra is in north central Florida and 20 miles northwest of Silver Springs (Ocala, FL). The climate is sub-tropical with a warm, wet season from June- October and a cool, dry season from November-May. The PSREU is a dedicated research station, chosen for this study because of the similarity of its soil types to Silver Springs springshed and its well-maintained land use stations. Soil types within PSREU include Psamments, Udults, and Aqualfs, all sand-dominant soils within the top 20 cm. Sampling locations were chosen based on land use type, i.e., low and high density pasture, crop, and turf grass. Documentation on each station ensured that land use where soil samples were collected had been established for at least a year.

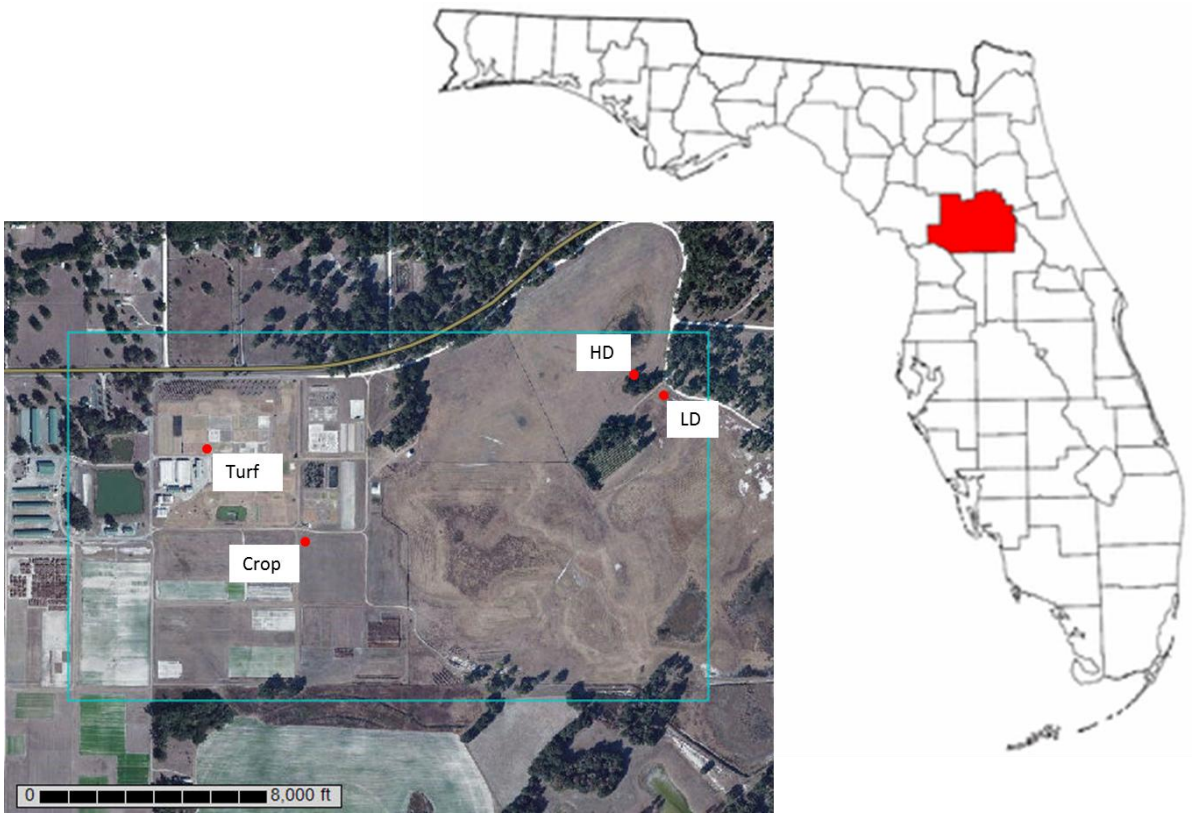

Figure 4.2.1. Aerial view of PSREU located in Marion County, FL; red points represent the sampling locations for HD and LD pasture, crop, and turf soils.

4.2.3.2 Sample Collection

Samples for denitrification analysis were collected from PSREU using a push-core and extrusion method that ensured soil cores remained intact. Aluminum foil was rolled into cylinders with the dimensions of 4 cm x 12 cm (diameter x length). A hollow, open-ended, metal coring tool was inserted into the soil down to 10 cm, removed, and an aluminum tube was slipped over the bottom of the coring tool. The core was extruded into the aluminum tube, resulting in an intact core wrapped in aluminum foil. Bulk soil samples for pre-denitrification analysis were collected from the surface in replicates of 3 for each land use type, and stored separately in re-sealable plastic bags. All samples were stored at 4 °C until nutrient analysis and denitrification incubation.

Samples for denitrification analysis and pre-denitrification analysis were collected from the residential home in bulk from a septic drain field approximately 3 m below the soils surface using a posthole digger. Before analysis, homogenized soil was packed into aluminum cores to approximate the bulk density of intact cores collected from PSREU. Samples were stored in self-sealing 5 gallon buckets at 4°C until nutrient analysis and denitrification incubation.

4.2.3.3 Experimental Design

For denitrification rate determination, a series of incubations were performed in 1 L glass jars, the set-up modeled after Ryden et al. (1987) and De Klein and Logtestijn (1996). Each jar contained 3 replicates, aluminum wrapped cores, with holes punched into the length of the foil to

allow gas diffusion. To replicate field conditions in a laboratory setting, physical controls and land use were used to determine nitrate application rate and WFPS alteration. Cores were amended with double deionized water to adjust the WFPS to 22, 35 or 50 % and to add 35 or 50 kg ha^{-1} of KNO_3^- depending on land use and treatment (Tables 4.2.1 and 4.2.2). Rate of application "<2 kg ha^{-1}" is indicative of a typical field N fertilizer application of NO_3^-.

Table 4.2.1. Soil land use type, suborder, dominant textural class, vegetation, and nutrient characteristics for each site sampled.

Land Use	Soil type	Texture	Vegetation	Ext. NO_3^- (mg l^{-1})	Ext. TOC (mg l^{-1})	Ext. TN (mg l^{-1})	Ext. NH_4^+ (mg l^{-1})
Septic		Sand	None				
Pasture (LD)	Aquept	Sand	Grass	0.81	7.19	0.59	0.00
Pasture (HD)	Aquept	Sand	Grass	2.86	7.14	1.92	0.14
Crop	Psamment	Sand	None	1.61	3.18	0.55	0.14
Turf	Psamment	Sand	Grass	1.16	2.48	0.24	0.14

Once cores were amended, jars were sealed using plastisol-lined metal lids outfitted with septa for acetylene injection and gas sample collection. Sealed jars were placed in incubators and temperatures raised sequentially from 15 °C, 20 °C, and 25 °C every 72 hours. For each temperature, headspace gas was collected using glass syringes at 0, 12, 24, 48, and 72 hour mark. Gas samples were analyzed for N_2O using a Hewlett Packard 5890 Series II Gas Chromatograph equipped with an electron capture detector (Porapak Q 80-100, detector 325 °C, injection port 30 °C, column 30 °C) and a Hewlett Packard 3396 Series II integrator. After denitrification analysis was complete, jars were deconstructed, homogenized and stored in individual, plastic specimen containers at 4 °C for post- incubation nutrient analysis.

The Q_{10} value was calculated for each jar by plotting the N_2O rate (nmol $g^{-1}dw^{-1}hr^{-1}$) with temperature, and fitted exponentially. The reaction rate constant "k" was derived from the equation of the exponential line of fit and used to calculate individual Q_{10} values as:

$$Q_{10} = 10^{(k)}$$

The mean of Q_{10} values from replicate jars were taken to represent the Q_{10} of that soil type, WFPS, and NO_3^- treatment.

Table 4.2.2. Treatments for denitrification incubations. Moisture Content (MC) × N Rate or cattle stocking density for each land use, including 3 replicate jars. The number of total jars for each land use is denoted in parentheses.

Land use (75)	MC (%)	N Rate (kg ha^{-1})
Septic (3)	FC	<2
Pasture (18)	FC	Low density
		High density
	35	Low density
		High density
	50	Low density
		High density
Crop (27)	FC	<2
		35
		50
	35	<2
		35
		50
	50	<2
		35
		50
Turf	FC	<2
		35
		50
	35	<2
		35
		50
	50	<2
		35
		50

FC= field capacity; MC= ~22 %

4.2.3.4 Pre- and Post-Incubation Analysis

Pre- and post-incubation bulk soil and replicates from all land uses (LD manure, HD manure, crop, turf, and septic) were sub sampled for analysis of moisture content (MC), pH, TN/TC, %LOI, and water Ext. NO_3^-, TN/TOC, NH_4^+, $\delta^{15}N/\delta^{18}O$- NO_3^-. Bulk density of pre-incubation soil was calculated using the weight and volume of soil cores from each land use and using the average as the representative value. The pH was measured using an AR50 dual channel pH/ion/conductivity meter (Fisher Scientific, Hampton, NH, USA). MC was recovered by oven drying approximately 10 g of sample at 70°C for 96 hours. %LOI was determined by ashing 0.2 g of sample in a muffle furnace at 550°C for 4 hours. TN/TC was analyzed on a Thermo Flash EA 1112 elemental analyzer. Ext. TN/TOC was analyzed on a Shimadzu combined TOC-L analyzer and TNM-L module (Wetland Biogeochemistry Core Lab, University of Florida, Gainesville, FL, USA).

The stable isotope ratios ($\delta^{15}N$ and $\delta^{18}O$) of Ext. NO_3^- were analyzed using a bacterial reduction to N_2O method and continuous-flow isotope-ratio mass spectrometry (CF-IRMS) at the Facility for Isotope Ratio Mass Spectrometry at the University of California, Riverside (Riverside, CA, USA). Water Ext. NH_4^+ was analyzed on an air-segmented continuous autoflow analyzer (ANSERV Labs, University of Florida, Gainesville, FL, USA) following EPA method 350.1 (modified). Ext. NO_3^- was analyzed on a UV-1800 spectrophotometer (Shimadzu Corp., Kyoto, Kyoto Prefecture, Japan) using a modified method of cadmium reduction of NO_3^- to NO_2^- (EPA 353.2; Jones 1984).

4.2.3.5 Statistical Analyses

Linear regression analysis was used to calculate the N_2O respiration rate by taking the slope of the fitted line for N_2O respiration over time (hours) for each treatment and replicate. Linear regression was also used to assess the relationship of N_2O respiration rate with temperature and WFPS, and for $\delta^{15}N/^{18}O$- NO_3^- analysis. Two-way and One-way ANOVAs and Tukey HSD analyses were used to compare means in post- incubation nutrient concentrations, soil types and treatments, Q10 values, and $\delta^{15}N/^{18}O$- NO_3^-. Linear regression was used to correlate model predicted denitrification rates values against actual denitrification rates. Data was log transformed or standardized when necessary, and checked for normality using normal distribution curve and a Chi-square test. All statistical analyses were performed using SAS JMP Pro ® 12.0.0 software.

4.2.4 RESULTS AND DISCUSSION

4.2.4.1 Post- Incubation Soil Nutrient Characterization

Pre- and post- incubations nutrient concentrations were compared to assess the changes in nutrient concentrations for each soil type. Ext. NO_3^- concentrations decreased for all soil types except for septic soil, and Ext. TN concentrations increased for all soil types. Ext. TOC concentrations increased for pasture and turf soils and decreased for crop soils. Ext. NH_4^+ concentrations increased in pasture and turf soils, and showed little change in crop soils.

A One-way ANOVA and Tukey HSD were calculated for post- incubation nutrient concentrations by soil type to compare the change in nutrients among sites (Table 4.2.3). The ANOVA for Ext. NO_3^- was significant ($P < 0.0001$) and explained 59 % ($R^2 = 0.59$) of the variance. The Tukey HSD showed significant difference between septic and crop ($P = 0.0024$) and between pasture and crop ($P < 0.0001$). There was no significant difference between turf and crop and septic and pasture ($P > 0.05$). The ANOVA for Ext. TN was significant ($P < 0.0001$) and explained 73 % ($R^2 = 0.73$) of the variance. The Tukey HSD showed that septic was significantly different from turf, pasture and crop ($P < 0.0001$) and crop was significantly different from turf and pasture ($P < 0.0001$). Turf and pasture were not significantly different from each other ($P > 0.05$). The ANOVA for Ext. TOC was significant ($P < 0.0001$) and explained 37 % ($R^2 = 0.37$) of the variance. The Tukey HSD showed that all soil types were significantly different from each other ($P < 0.05$). The ANOVA for Ext. NH_4^+ was significantly different ($P < 0.0001$) and explained 71 % ($R^2 = 0.71$) of the variance. The Tukey HSD showed that each soil type was significantly different from the other ($P < 0.05$).

Table 4.2.3. Differences in nutrient contents for un-amended (control) soils after denitrification incubation (Mean ± s.d.) and the One-way ANOVA analysis of those nutrients between pre-and post-incubation. Lowercase letters after the values represent significant difference between different land uses.

Nutrient	Septic	Pasture	Crop	Turf	*df*	*F*	*P*
	----------Difference (Pre-Post)----------						
Ext. NO_3^-	-0.24±0.52a	-0.35±0.21a	-2.41±0.21b	-1.39±0.9ab	3	17.2	<0.0001
Ext. TN	1.93±0.20a	0.36±0.08b	-0.44±0.07b	0.47±0.07b	3	63.8	<0.0001
Ext. TOC	ND	1.98±0.12a	0.98±0.1c	1.47±0.1b	2	19.8	<0.0001
Ext. NH_4^+	-4.06±0.45d	-0.98±0.15b	-2.00±0.12c	-0.04±0.12a	3	56.7	<0.0001

4.2.4.2 Factors Affecting N_2O Respiration

Mean N_2O respiration rates (nmol g^{-1}dw hr^{-1}) were calculated from three replicate samples and reported for each land use/soil type and its corresponding NO_3^- concentration (LD, HD, <2, 35, and 50 kg ha^{-1}). N_2O respiration rates varied across all soil types ranging from 0.000097-0.00027 nmol g^{-1}dw h^{-1} for septic, 0.0004 to 0.0076 nmol g^{-1}dw h^{-1} for LD pasture, 0.001 to 0.1667 nmol g^{-1}dw h^{-1} for HD pasture, 0.0007 to 0.0065 nmol g^{-1}dw h^{-1} for Crop, and 0.0013 to 0.9378 nmol g^{-1}dw h^{-1} for Turf. A Two-way ANOVA identified Temp, Soil Type, Rate [Soil Type], and WFPS had significant effects ($P < 0.0001$) on N_2O respiration rates, but there was a confounding effect between factors of WFPS, Soil Type, Temp, and Rate.

For Soil Type, soils collected from Turf showed the highest N_2O rate, followed by soil from Pasture, Crop, and Septic. For nitrate application Rate, N_2O rate from soils of HD pasture was significantly different from that of LD pasture ($P = 0.0034$) and Field ($P < 0.0001$), N_2O rates from soils of 50, 35, and <2 kg ha^{-1} N were significantly different from Field ($P < 0.0001$, $P = 0.0001$, $P = 0.0002$, respectively). For WFPS, no significant difference was found between treatments of 35 % and 50 % MC ($P > 0.05$), but soils under 22 % MC showed significantly lower N_2O rates than soils under 50 % MC ($P = 0.0023$). For Temp, soils under 25 °C showed the highest N_2O rates followed by soils under 20 °C and 15 °C.

A linear regression of N_2O rate with temperature showed that all soil types exhibited the same general response to temperature, where as temperature increased, the rate of N_2O respiration also increased. For LD pasture soil, N_2O increased exponentially with increasing temperature for all WFPS (Figure 4.2.2B). For HD pasture soil, N_2O increased linearly at 50 % WFPS and exponentially at 22 and 25 % WFPS (Figure 4.2.3B). For Crop soil, N_2O increased exponentially for all rates and WFPS except for 22 % WFPS at <2 kg ha^{-1} NO_3^- (Figure 4.2.4A). For Turf soil, N_2O rates increased exponentially for 35 and 50 % WFPS at 35 and 50 kg ha^{-1} NO_3^-, and increased linearly for 50 % WFPS at <2 kg ha^{-1} NO_3^- and at 22 % WFPS for all rates of NO_3^- (Figure 4.2.6A-C).

A linear regression of WFPS with N_2O rate showed a non-uniform by soil types, varying by temperature or rate of NO_3^- or response type (linear or exponential). For LD soil N_2O increased exponentially with increasing WFPS for all temperatures (Figure 4.2.2A). For HD soil N_2O decreased with increasing WFPS. At 20 and 25 °C the decrease in N_2O rates were exponential and for 15 °C the decrease in N_2O rates was linear (Figure 4.2.3A). For Crop soil, exponential increase of N_2O to WFPS only occurred for <2 kg ha^{-1} NO_3^- at 25°C and 50 kg ha^{-1} NO_3^-. N_2O increased linearly to WFPS for all NO_3^- rates and temperatures except for <2 kg ha^{-1} at 15 and 20 °C where N_2O decreased linearly (Figure 4.2.5A-C). For Turf soil N_2O increased exponentially at 20 and 25°C for <2 and 50 kg ha^{-1} NO_3^-. N_2O rate increased linearly for all other rates and temperatures except for <2 kg ha^{-1} NO_3^- where it decreased linearly at 15 °C.

The pasture soils exhibited less variability in denitrification response to WFPS than the crop or turf soils (Figure 4.2.2A, 4.2.3A). Although it is unclear why the pasture soils denitrification response was less variable with WFPS, especially since the *in situ* NO_3^- concentrations were comparable to the lowest NO_3^- application rate for turf and crop, it could potentially be tied to the initial soil C concentrations. Both pasture soils had approximately double the amount of pre-incubation TOC than turf and crop soils. The N_2O respiration increased with increasing WFPS for low density pasture soils as we expected. However, high density pasture soils exhibited an inverse response to WFPS, with denitrification rates decreasing with increasing WFPS. This is suspected to be due to competition between denitrification and the alternative nitrate reduction process, dissimilatory nitrate reduction to ammonium (DNRA).

During the pasture soil incubations, N_2O respiration rates increased with simultaneous increases in Ext. TOC and Ext. NH_4^+ and decreases in Ext. NO_3^- concentrations. This response to NO_3^- is expected because denitrification requires NO_3^- as an electron acceptor. However, the increase in Ext. TOC in the HD pasture soils is unexpected because traditionally denitrification involves the utilization of C as an electron donor. The increase in soil organic C during denitrification incubations could be the result of increased temperature solubility of C, making C more readily available, and increasing the C:N ratio of the soil supporting DNRA (Rutting et al. 2011). The only differentiating factors between LD and HD pasture preincubation was HD had a higher Ext. NO_3^- and Ext. TN concentrations than LD. The lower C:N ratio in HD pasture in pre- incubation soil likely lead to faster NO_3^- reduction and build-up up C (high C:N), which facilitated DNRA. The Two-way ANOVA that compared the effects of WFPS, rate, and temperature had on soil extractable nutrients found the models significant for Ext. TOC (P <0.0001) and Ext. NH_4^+ (P = 0.0003). Both nutrients were positively affected in HD pastures, and WFPS also had a positive effect on Ext. TOC (P = 0.0193). This shows that DNRA activity can occur in a pasture system, and can compete with denitrification for nutrients at C:N ratio greater than 15.

Studies have shown that DNRA in terrestrial systems can occur under a variety of redox conditions and has been positively and negatively correlated with C:N ratios. Yin et al. (199) concluded that C:N greater than 12 was sufficient for DNRA activity. The C:N ratios from 6 of the 9 incubations for the HD pasture soils ranged from 15- 46, well above the ratio cited by in et al. (199). R tt ing et al. (2011) also demonstrated that terrestrial DNRA was dependent upon soil C content and increased when available C increased and nitrate was limiting (high C:N), and concluded that low redox was not a requirement for DNRA. Minick et al. (2016) came to the same conclusion concerning redox conditions, but found that redox exerted more control over

DNRA than C:N ratio, where C:N was negatively correlated with DNRA activity, but positively correlated with N_2O respiration.

Soil texture affects denitrification rates by its control on water transport. Soils that have increasing amounts of finer textures (silt and clay) are able to maintain high water contents (Groffman and Tiedje, 1989). This allows for less diffusion of O_2 into soil pore spaces which creates a more anaerobic environment. More water in pore spaces also allows for a more equal dispersion of C and NO_3^- throughout the soil (Christensen et al. 1990) and buffers internal change in temperature against increasing external temperatures. Often in fine textured soils the soil water content (or water filled pore space (%WFPS)) is the major driver of denitrification followed by temperature (De Klein and Logtestijn 1995; Maag and Vinther 1996), but both can cause positive response in N_2O emissions (Schindlbacher and Zechmeister-Boltenstern 2004). In sand-dominated soils these influences can be reversed because of the larger pore spaces between sand grains, however these effects are highly variable.

A study by Grant and Pattey (2008) found that N_2O emissions were sensitive to increasing temperature when WFPS decreased but the effects of one over the other could not be determined because the parameters were confounding, and tied to soil C content. Kamp et al. (1998) found variable results between field and laboratory experiments, where laboratory experiments showed an increasing microbial response with increased temperature, but low WFPS at high temperatures caused a negative response (lower N_2O emissions). In contrast, field studies showed both negative and positive effects of temperature on N_2O emissions. Because of the variability in denitrification response to temperature and WFPS in literature, the results from this study support the conclusions drawn in literature, and merely represent another scenario that makes predicting terrestrial hotspots of denitrification difficult. Both Grant and Pattey (2008) and Kamp et al. (1998) studies were done in forested soils of predominantly fine-particle textures.

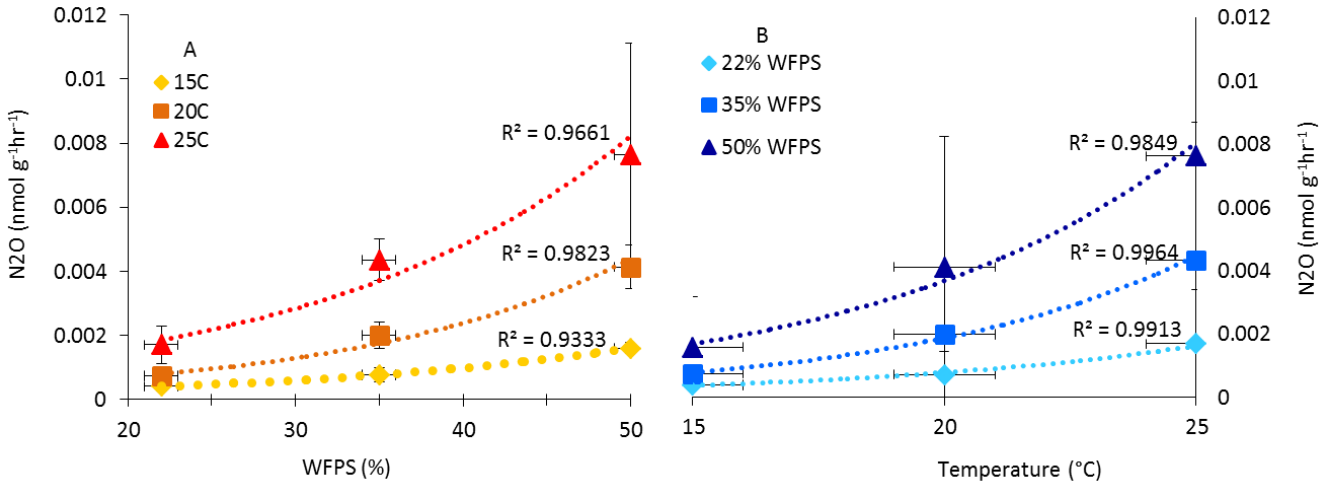

Figure 4.2.2. Relationship between denitrification enzyme activity (N_2O nmol g^{-1} dw^{-1} hr^{-1}) to WFPS (A) and Temperature (B) for LD. pasture soil.

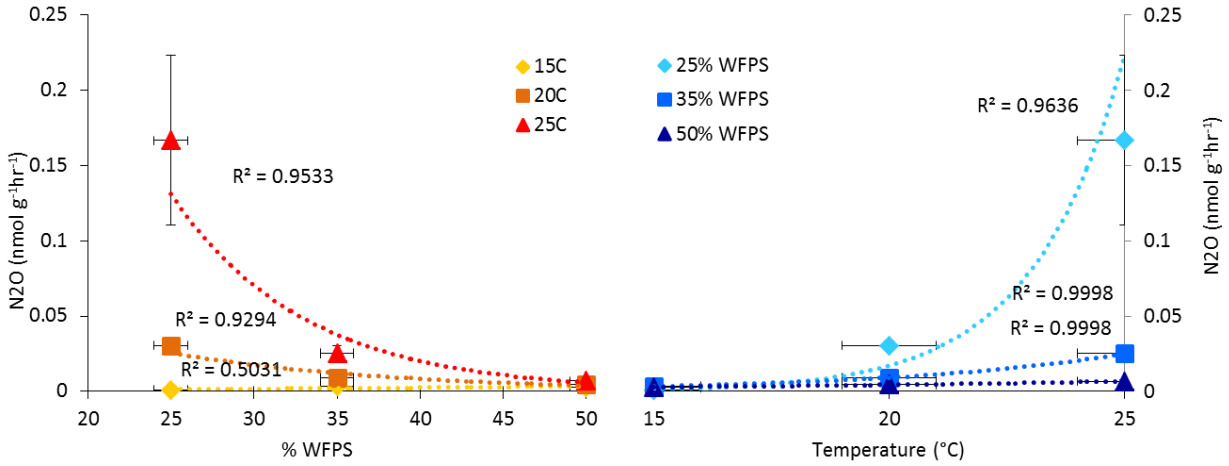

Figure 4.2.3. Relationship between denitrification enzyme activity (N_2O nmol g^{-1} dw^{-1} hr^{-1}) to WFPS (A) and Temperature (B) for HD pasture soil.

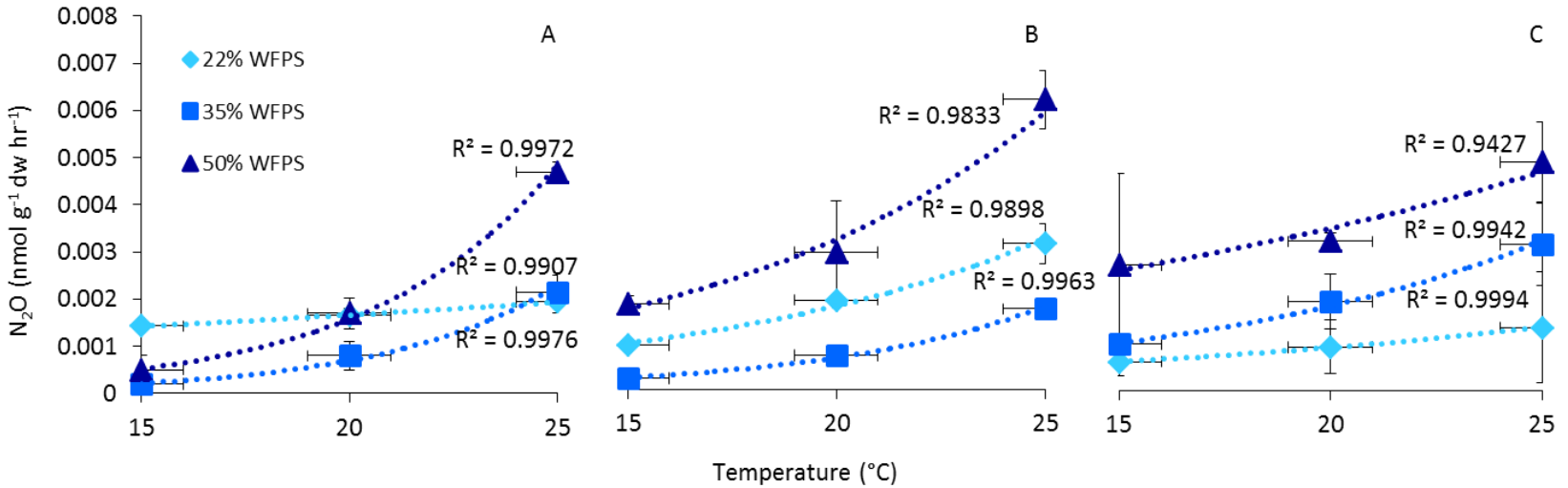

Figure 4.2.4. Temperature effects on denitrification (N_2O nmol g^{-1} dw^{-1} hr^{-1}) by WFPS for Crop soil. A= <2 kg ha^{-1} NO_3^-, B= 35 kg ha^{-1} NO_3^-, and C= 50 kg ha^{-1} NO_3^-.

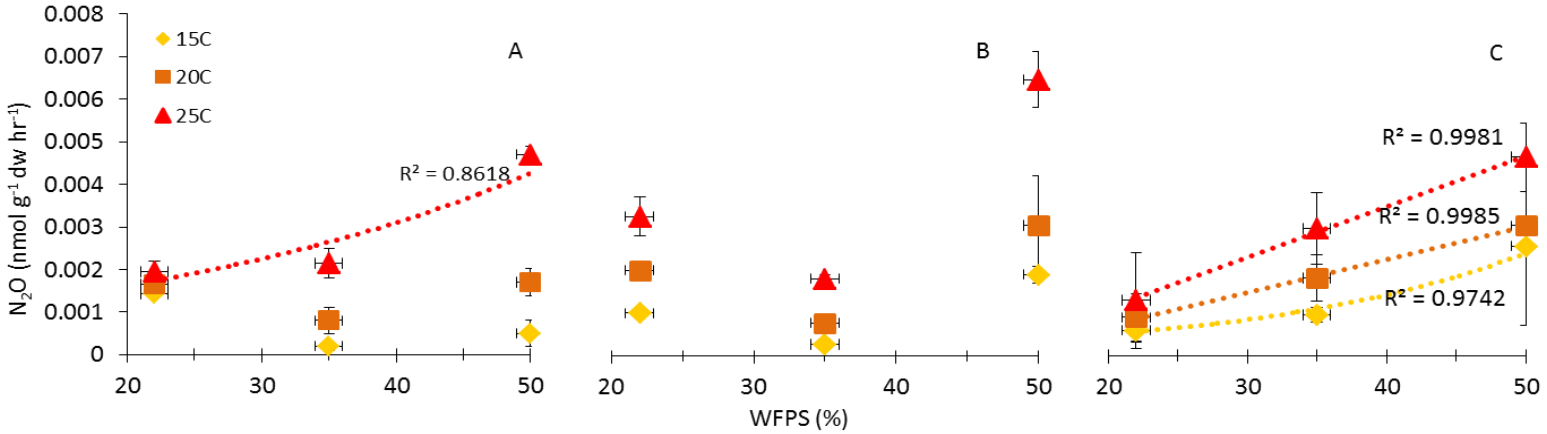

Figure 4.2.5. WFPS effects on denitrification (N_2O nmol g^{-1} dw^{-1} hr^{-1}) by Temperature for Crop soil. A= <2 kg ha^{-1} NO_3^-, B= 35 kg ha^{-1} NO_3^-, and C= 50 kg ha^{-1} NO_3^-.

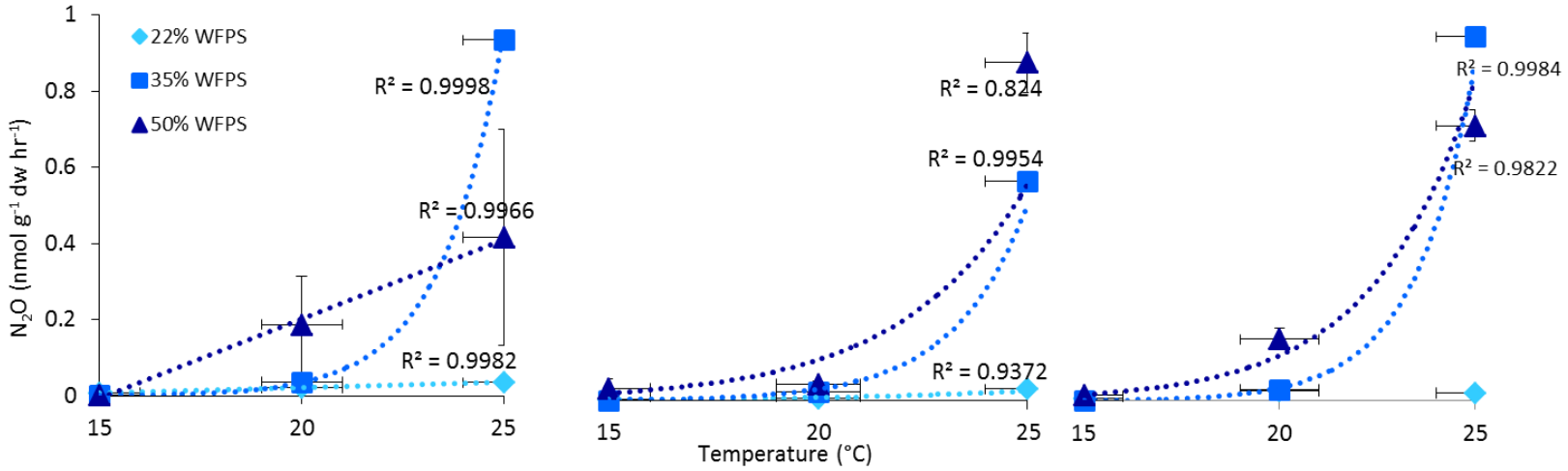

Figure 4.2.6. Temperature effects on denitrification (N_2O nmol g^{-1} dw^{-1} hr^{-1}) by WFPS for Turf soil. A= <2 kg ha^{-1} NO_3^-, B= 35 kg ha^{-1} NO_3^-, and C= 50 kg ha^{-1} NO_3^-.

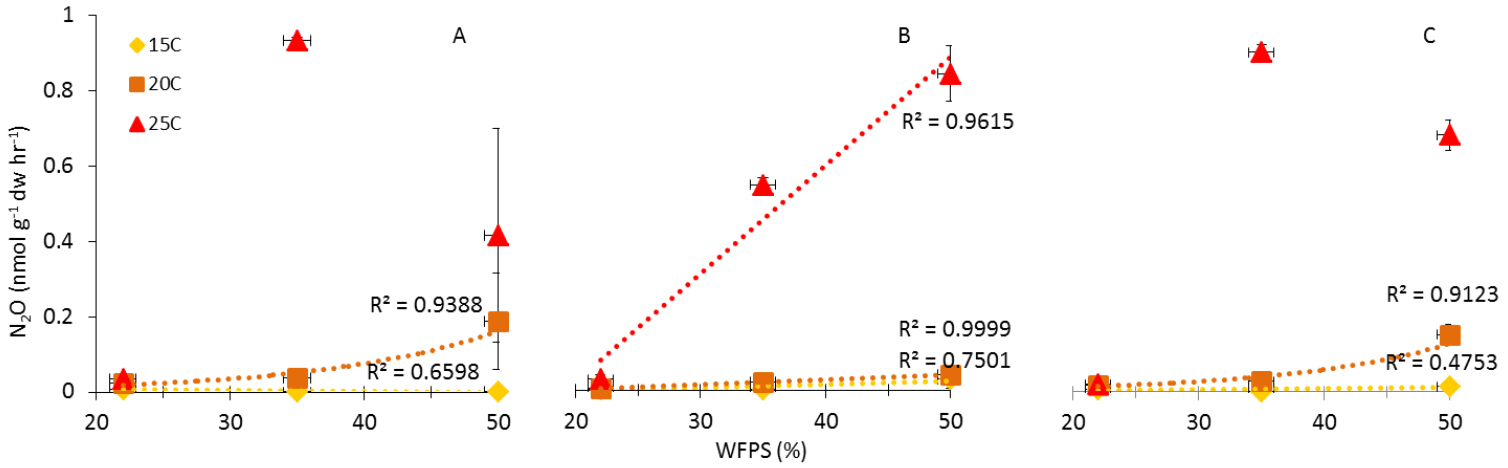

Figure 4.2.7. WFPS effects on denitrification (N_2O nmol g^{-1} dw^{-1} hr^{-1}) by Temperature for Turf soil. A= <2 kg ha^{-1} NO_3^-, B= 35 kg ha^{-1} NO_3^-, and C= 50 kg ha^{-1} NO_3^-.

4.2.4.3 Factors affecting temperature sensitivity

The $Q10_x$ value is a temperature coefficient used in modeling to represent temperature effects on the enzyme reaction during denitrification, where every 10 degree increase in temperature causes rates to change by a factor of 'x'. Because denitrification is an enzyme driven process, its response to temperature is expected to follow a first-order reaction, where denitrification activity increases exponentially with temperature to an optimum after which declines are observed as proteins become denatured. Because of this assumption, most denitrification models use a Q10 value of 2, when estimating actual denitrification rates.

The factors of WFPS, Soil Type, and Rate [Soil Type] had significant effects on Q10 values ($P < 0.0001$). At 22 % WFPS Q10 values for all land uses were affected by the NO_3^- concentrations, where Q10 increased with increasing NO_3^-application rate in turf and crop soils, and increased from LD to HD soils (Figure 4.2.8). At 35 % WFPS the trend still holds for pasture soils but the difference in Q10 values decreased for HD pastures. Q10 values for crop soils increased for <2 and 35 kg ha^{-1} and decreased for 50 kg ha^{-1}, and for turf soils, Q10 value variable by NO_3^- rate and ranged from 305-579, with the lowest Q10 calculated in 35 kg ha^{-1}. At 50 % WFPS, Q10 values for HD pasture dropped below LD and crop Q10 values decreased for all NO_3^- rate applications. In turf soils Q10 values decreased for <2 and 50 kg ha^{-1} and increased for 35 kg ha^{-1}. A One-way ANOVA and Tukey HSD were calculated to compare the effects of Soil Type and WFPS levels on Q10 values. The Soil Type significantly affected Q10 ($P < 0.0001$), specifically, "Turf" soil was significantly different from Pasture ($P < 0.0001$), "Crop" ($P < 0.0001$), and "Septic" ($P = 0.0118$). Septic, Crop, and Pasture were not significantly different from each other ($P > 0.05$). The WFPS significantly affected Q10 ($P < 0.0001$), for example, the Q10 for WFPS 35 was significantly different from WFPS 22 ($P < 0.0001$) and WFPS 50 ($P = 0.0005$).

Overall, the values for Q10 observed in these sandy soils are high compared to typical Q10 responses for biological systems often assumed to be approximately 2 (Fig. 4.2.8). Such high values (Q10>10), are explainable based on system changes in oxygen diffusion and anaerobic soil volume which decrease and increase, respectively with warming (Smith 1997). As a result, the combination of greater anaerobic soil volume and enhanced biological activity can exponentially increase overall system rates (Smith et al. 1995).

Novak (1974) found an interaction between temperature and substrate types on denitrification in an effluent stream. Q10 depended on substrate concentrations in the medium, increasing with higher concentrations. This same trend can be seen in our study when comparing Q10 values by land use, WFPS and NO_3^- application rate. At 22 % WFPS all land uses increased with increasing NO_3^- concentration. With increasing WFPS this trend was more variable, but overall increased WFPS appears to have a negative effect on Q10 value within a land use. Davidson et al. (1998) found variability in Q10 values with changes in soil water content finding a negative correlation between soil temperature and water content, which is partially supported by the results from this study, where each land use showed a decrease in Q10 values with increasing WFPS but these changes were variable with NO_3^- application rate.

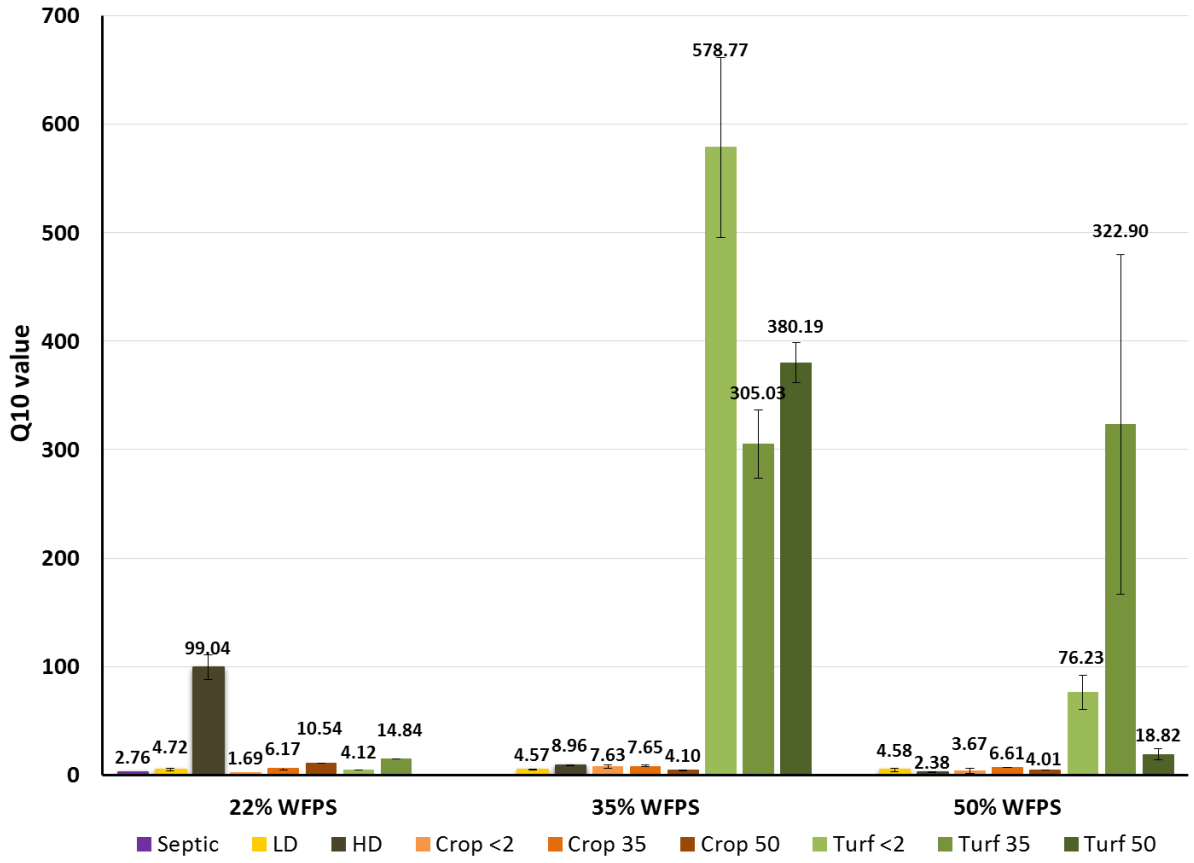

Figure 4.2.8. Q10 values by WFPS, soil type, and NO_3^- concentrations (kg NO_3^- N ha^{-1}).

4.2.5 CONCLUSIONS AND RECOMMENDATIONS

The purpose of this study was to assess the effects of temperature, water filled pore space (WFPS), and NO_3^- concentrations (nitrate application rates) on denitrification enzyme activities in sandy soils collected from land uses typifying those within the Silver Springs Springshed. Based on the results, it is possible the measured rates can be incorporated into surface N attenuation models or denitrification models from literature.

Soil nutrients, WFPS, and temperature all exhibited control over denitrification rates. Of these, denitrification responded more positively to increased temperature regardless of soil type (with the exception of septic soil), WFPS, or nutrient concentrations. Denitrification response to WFPS varied with soil type and soil nutrients, indicating that WFPS and nutrients are likely confounding factors. At high WFPS, soils with high C:NO_3^- ratios showed an apparent competition between denitrification and DNRA for NO_3^-, causing a decrease in denitrification rate (as produced N_2O) at high WFPS in HD pastures and turf soils. In contrast, Crop and LD pasture soils were not visibly affected by this apparent DNRA competition at high WFPS. In these sandy soils, available C content exerts a significant control on denitrification activity, but this is tied to the percent WFPS.

Q10 values varied with soil types, WFPS, and NO_3^- application rates. Soils under 22 % WFPS showed an increase in Q10 value with increasing NO_3^- concentrations for each land use, but as WFPS increased, Q10 values, overall, decreased within a given land use. In HD pasture specifically, Q10 values decreased with increasing WFPS reflecting the trend also seen in HD pasture N_2O rates with increasing WFPS. This indicates that calculated Q10 values representing temperature sensitivity of denitrification are highly influenced by various soil characteristics including NO_3^- availability or C content.

4.2.6 LIMITATIONS AND FUTURE RESEARCH

Although the results of this study can contribute to current knowledge on what controls the heterogeneity of terrestrial denitrification, there are a few limitations to the study that should be addressed with future research. Although the experiment was modeled after successful incubation studies by Ryden et al. (1987) and De Klein and Logtestijn (1996), opening the jars and aerating them between each step increase in temperature would have made headspace conditions more similar to what would maintained in the field. In this way, oxygen drawdown during the experiment may have been artificially enhancing the observed temperature response.

In addition to aeration, sampling soil or having extra incubation chambers for destructive sampling between temperature changes may have given a clearer picture as to how nutrient concentrations were changing in the soil with temperature and WFPS over time. Collection of gas samples for CO_2 or O_2 analysis would also have been beneficial to this study so that aerobic conditions could be monitored throughout the study.

Future research is needed to expand on information pertaining to terrestrial denitrification controls in sandy soils from humid subtropical systems and how the variability in these systems can be represented by models. The results from this study represent only one location, and the addition of more denitrifications studies in similar systems can help improve current denitrification models, allowing them to be applied at larger spatial and temporal scales (McClain et al. 2003).

4.2.7 REFERENCES

Abbasi, M. K., and Adams, W. A. 2000. Gaseous N emission during simultaneous nitrification–denitrification associated with mineral N fertilization to a grassland soil under field conditions. Soil Biology and Biochemistry, 32(8), 1251-1259.

Albertin, A. R., Sickman, J. O., Pinowska, A., and Stevenson, R. J. 2012. Identification of nitrogen sources and transformations within karst springs using isotope tracers of nitrogen. Biogeochemistry, 108(1-3), 219-232.

Andrews, R. J., Lloyd, J. W., and Lerner, D. N. 1997. Modelling of nitrate leaching from arable land into unsaturated soil and chalk 1. Development of a management model for applications of sewage sludge and fertilizer. Journal of Hydrology, 200(1-4), 179-197.

Barton, L., McLay, C. D. A., Schipper, L. A., and Smith, C. T. 1999. Annual denitrification rates in agricultural and forest soils: a review. Soil Research, 37(6), 1073-1094

Blackmer, A. M., and Bremner, J. M. 1977. Nitrogen isotope discrimination in denitrification of nitrate in soils.

Bowman, R. A., and Focht, D. D. 1974. The influence of glucose and nitrate concentrations upon denitrification rates in sandy soils. Soil Biology and Biochemistry, 6(5), 297-301.

Bril, J., Van Faassen, H. G., and Gunnewiek, H. K. 1994. Modeling N_2O emission from grazed grassland (No. 24). AB-DLO.

Cameron, K. C., Di, H. J., and Moir, J. L. 2013. Nitrogen losses from the soil/plant system: a review. Annals of Applied Biology, 162(2), 145-173.

Christensen, S., Simkins, S., and Tiedje, J. M. 1990. Spatial variation in denitrification: dependency of activity centers on the soil environment. Soil Science society of America journal, 54(6), 1608-1613.

Ciarlo, E., Conti, M., Bartoloni, N., and Rubio, G. 2007. The effect of moisture on nitrous oxide emissions from soil and the N2O/(N2O+ N2) ratio under laboratory conditions. Biology and Fertility of Soils, 43(6), 675-681.

Clément, J. C., Pinay, G., and Marmonier, P. 2002. Seasonal dynamics of denitrification along topohydrosequences in three different riparian wetlands. Journal of Environmental Quality, 31(3), 1025-1037.

Davidsson, T. E., and Ståhl, M. 2000. The influence of organic carbon on nitrogen transformations in five wetland soils. Soil Science Society of America Journal,64(3),1129-1136.

Davidson, E., Belk, E., and Boone, R. D. 1998. Soil water content and temperature as independent or confounded factors controlling soil respiration in a temperate mixed hardwood forest. Global change biology, 4(2), 217-227.

De Klein, C. A. M., and Van Logtestijn, R. S. P. 1996. Denitrification in grassland soils in the Netherlands in relation to irrigation, N-application rate, soil water content and soil temperature. Soil Biology and Biochemistry, 28(2), 231-237.

Delwiche, C. C., and Steyn, P. L. 1970. Nitrogen isotope fractionation in soils and microbial reactions. Environmental Science and Technology, 4(11), 929-935.

Densmore, J. N., and Bohlke, J. K. 2000. Use of nitrogen isotopes to determine sources of nitrate contamination in two desert basins in California. IAHS Publication(International Association of Hydrological Sciences), (260), 63-73.

Einsiedl, F., Maloszewski, P., and Stichler, W. 2005. Estimation of denitrification potential in a karst aquifer using the ^{15}N and ^{18}O isotopes of NO_3^-. Biogeochemistry, 72(1), 67-86.

Fitts, C. R. (2002). Groundwater science. Academic press.

Fogg, G. E., Rolston, D. E., Decker, D. L., Louie, D. T., and Grismer, M. E. 1998. Spatial variation in nitrogen isotope values beneath nitrate contamination sources. Ground water, 36(3), 418-426.

Ghafoor, A., Koestel, J., Larsbo, M., Moeys, J., and Jarvis, N. 2013. Soil properties and susceptibility to preferential solute transport in tilled topsoil at the catchment scale. Journal of Hydrology, 492, 190-199.

Girard, P., and Hillaire-Marcel, C. 1997. Determining the source of nitrate pollution in the Niger discontinuous aquifers using the natural ^{15}N:^{14}N ratios. Journal of Hydrology, 199(3-4), 239-251.

Granger, J., Sigman, D. M., Lehmann, M. F., and Tortell, P. D. 2008. Nitrogen and oxygen isotope fractionation during dissimilatory nitrate reduction by denitrifying bacteria. Limnology and Oceanography, 53(6), 2533-2545.

Grant, R. F., and Pattey, E. 2008. Temperature sensitivity of N_2O emissions from fertilized agricultural soils: mathematical modeling in ecosys. Global Biogeochemical Cycles, 22(4).

Griffiths, N. A., Jackson, C. R., McDonnell, J. J., Klaus, J., Du, E., and Bitew, M. M. 2016. Dual nitrate isotopes clarify the role of biological processing and hydrologic flow paths on nitrogen cycling in subtropical low‐gradient watersheds. Journal of Geophysical Research: Biogeosciences.

Groffman, P. M. 2012. Terrestrial denitrification: challenges and opportunities. Ecological Processes, 1(1), 11.

Groffman, P. M., Butterbach-Bahl, K., Fulweiler, R. W., Gold, A. J., Morse, J. L., Stander, E. K., and Vidon, P. 2009. Challenges to incorporating spatially and temporally explicit phenomena (hotspots and hot moments) in denitrification models. Biogeochemistry, 93(1-2), 49-77.

Groffman, P. M., and Tiedje, J. M. 1989. Denitrification in north temperate forest soils: spatial and temporal patterns at the landscape and seasonal scales. Soil Biology and Biochemistry, 21(5), 613-620.

Gupta, S., and Larson, W. E. 1979. Estimating soil water retention characteristics from particle size distribution, organic matter percent, and bulk density. Water resources research, 15(6), 1633-1635.

Hall, S. J., Weintraub, S. R., and Bowling, D. R. 2016. Scale-dependent linkages between nitrate isotopes and denitrification in surface soils: implications for isotope measurements and models. Oecologia, 181(4), 1221-1231.

Heffernan, J. B., Albertin, A. R., Fork, M. L., Katz, B. G., and Cohen, M. J. 2012. Denitrification and inference of nitrogen sources in the karstic Floridan Aquifer. Biogeosciences, 9(5), 1671-1690.

Heinen, M. 2006. Simplified denitrification models: overview and properties. Geoderma, 133(3), 444-463.

Hénault, C., and Germon, J. C. 2000. NEMIS, a predictive model of denitrification on the field scale. European Journal of Soil Science, 51(2), 257-270.

Hu, H., Tian, F., and Hu, H. 2011. Soil particle size distribution and its relationship with soil water and salt under mulched drip irrigation in Xinjiang of China. Science China Technological Sciences, 54(6), 1568-1574.

Jahangir, M. M., Johnston, P., Barrett, M., Khalil, M. I., Groffman, P. M., Boeckx, P., and Richards, K. G. 2013. Denitrification and indirect N_2O emissions in groundwater: hydrologic and biogeochemical influences. Journal of contaminant hydrology, 152, 70-81.

Kamewada, K. 2007. Vertical distribution of denitrification activity in an Andisol upland field and its relationship with dissolved organic carbon: effect of long-term organic matter application. Soil Science and Plant Nutrition, 53(4), 401-412.

Kamp, T., Steindl, H., Hantschel, R. E., Beese, F., and Munch, J. C. 1998. Nitrous oxide emissions from a fallow and wheat field as affected by increased soil temperatures. Biology and Fertility of Soils, 27(3), 307-314.

Katz, B. G., Chelette, A. R., and Pratt, T. R. 2004. Use of chemical and isotopic tracers to assess nitrate contamination and ground-water age, Woodville Karst Plain, USA. Journal of Hydrology, 289(1), 36-61.

Kendall, C., and McDonnell, J. J. (Eds.). 2012. Isotope tracers in catchment hydrology. Elsevier.

Klemedtsson, L., Svensson, B. H., and Rosswall, T. 1988. Relationships between soil moisture content and nitrous oxide production during nitrification and denitrification. Biology and Fertility of Soils, 6(2), 106-111.

Krapac, I. G., Dey, W. S., Roy, W. R., Smyth, C. A., Storment, E., Sargent, S. L., and Steele, J. D. 2002. Impacts of swine manure pits on groundwater quality. Environmental Pollution, 120(2), 475-492.

Lane, E., and Hoestine, R. W. 1991. Environmental geology and hydrogeology of the Ocala area, Florida. Spec. publ. Florida. Geol. survey.

Lin, S., Iqbal, J., Hu, R., and Feng, M. 2010. N_2O emissions from different land uses in mid-subtropical China. Agriculture, ecosystems & environment, 136(1), 40-48.

Liu, R., Suter, H., He, J., Hayden, H., and Chen, D. 2015. Influence of temperature and moisture on the relative contributions of heterotrophic and autotrophic nitrification to gross nitrification in an acid cropping soil. Journal of Soils and Sediments, 15(11), 2304-2309.

Lorenz, K., and Lal, R. 2005. The depth distribution of soil organic carbon in relation to land use and management and the potential of carbon sequestration in subsoil horizons. Advances in agronomy, 88, 35-66.

Luo, J., Tillman, R. W., White, R. E., and Ball, P. R. 1998. Variation in denitrification activity with soil depth under pasture. Soil Biology and Biochemistry, 30(7), 897-903.

Ma, Z., Lian, X., Jiang, Y., Meng, F., Xi, B., Yang, Y., and Xu, X. 2016. Nitrogen transport and transformation in the saturated-unsaturated zone under recharge, runoff, and discharge conditions. Environmental Science and Pollution Research, 23(9), 8741-8748.

Maag, M., and Vinther, F. P. 1996. Nitrous oxide emission by nitrification and denitrification in different soil types and at different soil moisture contents and temperatures. Applied Soil Ecology, 4(1), 5-14.

Majumdar, D., and Gupta, N. 2000. Nitrate pollution of groundwater and associated human health disorders. Indian Journal of Environmental Health, 42(1), 28-39.

Mariotti, A., Germon, J. C., Hubert, P., Kaiser, P., Letolle, R., Tardieux, A., and Tardieux, P. 1981. Experimental determination of nitrogen kinetic isotope fractionation: some principles; illustration for the denitrification and nitrification processes. Plant and soil, 62(3), 413-430.

Mariotti, A., Leclerc, A., and Germon, J. C. 1982. Nitrogen isotope fractionation associated with the $NO_2^- \rightarrow N_2O$ step of denitrification in soils. Canadian journal of soil science, 62(2), 227-241.

Mayer, B., Bollwerk, S. M., Mansfeldt, T., Hütter, B., and Veizer, J. 2001. The oxygen isotope composition of nitrate generated by nitrification in acid forest floors. Geochimica et Cosmochimica Acta, 65(16), 2743-2756.

McClain, M. E., Boyer, E. W., Dent, C. L., Gergel, S. E., Grimm, N. B., Groffman, P. M., and McDowell, W. H. 2003. Biogeochemical hot spots and hot moments at the interface of terrestrial and aquatic ecosystems. Ecosystems, 6(4), 301-312.

McLay, C. D. A., Dragten, R., Sparling, G., and Selvarajah, N. 2001. Predicting groundwater nitrate concentrations in a region of mixed agricultural land use: a comparison of three approaches. Environmental Pollution, 115(2), 191-204.

Mingzhu, L., Seyf-Laye, A. S. M., Ibrahim, T., Gbandi, D. B., and Honghan, C. 2014. Tracking sources of groundwater nitrate contamination using nitrogen and oxygen stable isotopes at Beijing area, China. Environmental earth sciences, 72(3), 707-715.

Minick, K. J., Pandey, C. B., Fox, T. R., and Subedi, S. 2016. Dissimilatory nitrate reduction to ammonium and N_2O flux: effect of soil redox potential and N fertilization in loblolly pine forests. Biology and Fertility of Soils, 1-14.

Munch, D. A., Toth, D. J., Huang, C., Davis, J. B., Fortich, C. M., Osburn, W. L., Phlips, E. J., Quinlan, E. L., Allen, M. S., Woods, M. J., Cooney, P. Knight, R. L., Clarke, R. A., and Knight, S. L. 2007. *Fifty-year retrospective study of the ecology of Silver Springs, Florida*. *Special Publication SJ2007-SP4*. Palatka: St. Johns River Water Management District.

Novak, J. T. 1974. Temperature-substrate interactions in biological treatment. Journal (Water Pollution Control Federation), 1984-1994.

O'Reilly, A. M., Chang, N. B., and Wanielista, M. P. 2012. Cyclic biogeochemical processes and nitrogen fate beneath a subtropical stormwater infiltration basin. Journal of contaminant hydrology, 133, 53-75.

Panno, S. V., Hackley, K. C., Hwang, H. H., and Kelly, W. R. 2001. Determination of the sources of nitrate contamination in karst springs using isotopic and chemical indicators. Chemical Geology, 179(1), 113-128.

Pihlatie, M., Syväsalo, E., Simojoki, A., Esala, M., and Regina, K. 2004. Contribution of nitrification and denitrification to N_2O production in peat, clay and loamy sand soils under different soil moisture conditions. Nutrient Cycling in Agroecosystems, 70(2), 135-141.

Rütting, T., Boeckx, P., Müller, C., and Klemedtsson, L. 2011. Assessment of the importance of dissimilatory nitrate reduction to ammonium for the terrestrial nitrogen cycle. Biogeosciences, 8(7), 1779-1791.

Ryden, J. C., Skinner, J. H., and Nixon, D. J. 1987. Soil core incubation system for the field measurement of denitrification using acetylene-inhibition. Soil Biology and Biochemistry, 19(6), 753-757.

Saghravani, S. R., Yusoff, I., Tahir, W. Z. W. M., and Othman, Z. 2016. Estimating groundwater recharge based on mass balance evaluation of unsaturated zone in a coastal catchment characterized by tropical rainforest weather conditions. Environmental Earth Sciences, 75(8), 1-16

Saxton, K. E., Rawls, W., Romberger, J. S., and Papendick, R. I. 1986. Estimating generalized soil-water characteristics from texture. Soil Science Society of America Journal, 50(4), 1031-1036.

Salazar, O., Vargas, J., Nájera, F., Seguel, O., and Casanova, M. 2014. Monitoring of nitrate leaching during flush flooding events in a coarse-textured floodplain soil. Agricultural water management, 146, 218-227.

Schindlbacher, A., Zechmeister‐Boltenstern, S., and Butterbach‐Bahl, K. 2004. Effects of soil moisture and temperature on NO, NO_2, and N_2O emissions from European forest soils. Journal of Geophysical Research: Atmospheres, 109(D17).

Scott, T. M. 1988. The lithostratigraphy of the Hawthorn Group (Miocene) of Florida, Florida Geological Survey bulletin 59. Florida Geological Survey, Tallahassee.

Scott, T. M. 1992. A geological overview of Florida.

Scott, T. M. 1997. Miocene to Holocene history of Florida. The geology of Florida: Gainesville, University Press of Florida, 57-68.

Sigman, D. M., Casciotti, K. L., Andreani, M., Barford, C., Galanter, M. B. J. K., and Böhlke, J. K. 2001. A bacterial method for the nitrogen isotopic analysis of nitrate in seawater and freshwater. Analytical chemistry, 73(17), 4145-4153.

Smith, K. A., Clayton, H., McTaggart, I. P., Thomson, P. E., Arah, J. R. M., Scott, A., Goulding, K. W. T., Monteith, J. L. and Phillips, V. R., 1995. The measurement of nitrous oxide emissions from soil by using chambers. *Philosophical Transactions of the Royal Society of London A: Mathematical, Physical and Engineering Sciences*, *351*(1696), pp.327-338.

Smith, K., 1997. The potential for feedback effects induced by global warming on emissions of nitrous oxide by soils. *Global Change Biology*, *3*(4), pp.327-338.

Soil Survey Staff, Natural Resources Conservation Service, United States Department of Agriculture. Web Soil Survey. Available online at https://websoilsurvey.sc.egov.usda.gov/. Accessed [2016].

Spoelstra, J., Schiff, S. L., Hazlett, P. W., Jeffries, D. S., and Semkin, R. G. 2007. The isotopic composition of nitrate produced from nitrification in a hardwood forest floor. Geochimica et Cosmochimica Acta, 71(15), 3757-3771.

Tiedje, J. M. 1982. Denitrification. Methods of Soil Analysis. Part 2. Chemical and Microbiological Properties, (methodsofsoilan2), 1011-1026.

Ullah, S., and Faulkner, S. P. 2006. Denitrification potential of different land-use types in an agricultural watershed, lower Mississippi valley. Ecological Engineering, 28(2), 131-140.

Watts, F. C., and Collins, M. E. 2008. Soils of Florida. ASA-CSSA-SSSA.

Weier, K. L., Doran, J. W., Power, J. F., and Walters, D. T. 1993. Denitrification and the dinitrogen/nitrous oxide ratio as affected by soil water, available carbon, and nitrate. Soil Science Society of America Journal, 57(1), 66-72.

White, W. B. 2002. Karst hydrology: recent developments and open questions. Engineering geology, 65(2), 85-105.

Xu, Y., Xu, Z., Cai, Z., and Reverchon, F. 2013. Review of denitrification in tropical and subtropical soils of terrestrial ecosystems. Journal of Soils and Sediments, 13(4), 699-710.

Xue, D., Botte, J., De Baets, B., Accoe, F., Nestler, A., Taylor, P., and Boeckx, P. 2009. Present limitations and future prospects of stable isotope methods for nitrate source identification in surface-and groundwater. Water Research, 43(5), 1159-1170.

Yeomans, C., Bremner, M., and McCarty, W. 1992. Denitrification capacity and denitrification potential of subsurface soils. Communications in Soil Science and Plant Analysis, 23(9-10), 919–927. https://doi.org/10.1080/00103629209368639

Yin, S. X., Shen, Q., Tang, Y., and Cheng, L. 1998. Reduction of nitrate to ammonium in selected paddy soils of China. Pedosphere, 8(3), 221-228.

Zhang, J., Tian, P., Tang, J., Yuan, L., Ke, Y., Cai, Z., and Müller, C. 2016. The characteristics of soil N transformations regulate the composition of hydrologic N export from terrestrial ecosystem. Journal of Geophysical Research: Biogeosciences, 121(6), 1409-14.

4.3 IDENTIFYING AND TRACING NITROGEN SOURCES IN THE SILVER SPRINGS SPRINGSHED

4.3.1 ABSTRACT

In addition to understanding nitrogen (N) attenuation in the soil and vadose zone, denitrification within the Floridan Aquifer System (FAS) may also remove nitrate after it has passed through the unsaturated zone. This loss of N in the aquifer may be underestimated in groundwater models, which generally assume negligible denitrification rates in the FAS. Further, the ability to trace N sources within the Silver Springs springshed is complicated by the variety of land uses, geologic and karst conditions, and aquifer types. In this study, groundwater characteristics (dissolved nutrients/metals, physicochemical parameters, dissolved gases, and isotopes of nitrate) were assessed on samples from 61 wells throughout the springshed as well as samples from the Mammoth East and West vents. The results were used to characterize N sources and denitrification in the aquifer system and potentially identify hotspots of attenuation.

Based on the geochemical properties of the groundwater from 61 wells throughout the springshed, most of the groundwater samples belong to a $CaHCO_3$ water type, several samples from a surficial aquifer belong to either Na-K water type, Cl-NO_3, or SO_4 water type. Using a principal component analysis, the watershed wells were separated into two groups of which one closer in composition to the West Mammoth vent and featured the primary land uses of forest and wetlands. The second group identified contained the East Mammoth vent, featured mostly agriculture and urban land uses.

Nitrogen attenuation in the aquifer was estimated by analyzing dissolved gases (e.g., dissolved N_2, Ar, N_2O, CH_4) in the springshed wells and vents. Dissolved nitrous oxide (N_2O) has potential to indicate the process of nitrification or denitrification. In our study, significant positive correlation between N_2O with dissolved oxygen (DO) and nitrate, negative correlation with total organic carbon and ammonia, indicates most N_2O came from nitrification process. Based on the presence of dissolved methane and nitrous oxide, we infer the East vent to be more anaerobic and favorable for denitrification. Despite this observation, however, there is apparently more denitrification (excess N_2) present in the West Mammoth vent. Based on the current data set, no seasonal patterns were observed, except that significantly higher dissolved N_2O and methane (CH_4) were observed in the dry and wet season, respectively.

We also attempted to trace sources of nitrogen in the Silver Spring watershed back to particular land uses or springshed regions using dissolved gases and isotopic composition of nitrate. Patterns of stable isotopic ratios of nitrate in well samples indicated the potential contribution of fertilizer, wastewater/septic, and manure/organic-derived nitrate sources and potential alteration due to denitrification. Dissolved gas composition allowed the back calculation of the proportion of original nitrate remaining in a given sample, as well as an estimate of the isotopic identity of the presumed average original nitrogen source (isotopic mass balance).

This preliminary analysis based on a limited number of wells and vent samples suggests two main isotopic signatures of nitrate in the groundwater. One source is characterized by lighter $\delta^{15}N$ and $\delta^{18}O$ (< 0 ‰) and could represent soil N, atmospheric N, or fertilizer. The second

presumed source has $\delta^{15}N$ and $\delta^{18}O$ signatures of approximately 6-7‰ and likely represents more organic N sources such as wastewater, manure, or soil N. The second source includes most of the study wells and the Mammoth East and West vents, but overlap in the isotopic signatures still prevents a clear interpretation.

4.3.2 INTRODUCTION

There is a wide variety and combination of N sources that give rise to the nitrogen load in a watershed. Land use dependent sources can come through a variety of activities, most notably, agriculture (fertilizers, livestock/manure and soil amendments) and urban and residential (wastewater and fertilizers). Most natural sources exist at low levels and thus are not a major concern, but the combination of these sources with anthropogenic sources make it difficult to identify nitrogen sources based solely on concentration, especially given the complexity of transport and biogeochemical processes in various geologic and aquifer settings.

Apart from concentration, sources of nitrogen in groundwater systems are frequently inferred based on the isotopic composition of nitrate (Fogg et al. 1998) where various N sources have distinct isotopic composition ranging in $\delta^{15}N$ and $\delta^{18}O$ values (Figure 4.3.1, Kendall and McDonnel 1999). Based on changes in groundwater nitrate isotopic composition, it is also possible to infer and calculate denitrification and other N loss processes, but with the caveat that isotopic composition of nitrate sources is known (Xue et al. 2009). For this reason, accurate spatial measurements of nitrate isotopic composition within the watershed are required to adequately separate transformation and mixing processes of nitrogen in groundwater systems. Heffernan et al. (2012) demonstrated that analysis of dissolved gases and stable isotopic composition of nitrate can be used to indicate the percentage of nitrogen present in samples of spring water that has been removed by the process of denitrification during transit to the spring vent.

It has been demonstrated that the different vents of the Silver Springs group represent a variety of potentially different groundwaters from the springshed (Osmond et al. 1974; Phelps 2004). Likewise, there is also high potential for these different groundwaters to reflect different N sources and potential for attenuation of N loading to the Silver River. Previous studies have indicated that denitrification may occur in the FAS in North and Central Florida (Knowles et al. 2010; Heffernan et al. 2012). Measurements of excess N_2 (the end product of denitrification) and stable isotopes of nitrate ($\delta^{15}N$ and $\delta^{18}O$) from the Silver Springs main vent has not provided clear evidence for denitrification within the FAS (Phelps 2004). However, multiple sources of nitrate and a varying contribution of young and old groundwater may obscure any denitrification signal at the spring vent. The sources and attenuation processes are also likely to be seasonal in nature varying with both intensity of groundwater discharge and changes in land use activities. Thus, seasonal changes in these indicators of denitrification could serve as a powerful tool to identify covarying springshed or climate-related processes which contribute to the observed nitrogen attenuation within the FAS.

This work focused on determining the spatial and temporal patterns of N transformations in the Silver Spring main vents (Mammoth East and Mammoth West) and the Upper Floridan aquifer across different land uses within the springshed. In addition to estimating the fraction of

denitrified nitrogen, we sought to identify of the sources of N through the use of stable isotopes and to estimate of the degree of isotopic modification of the source signature through denitrification. We also analyzed particulates collected from groundwater samples for diversity and abundance of microorganisms involved in N cycling.

4.3.3 MATERIALS AND METHODS

4.3.3.1 Site Description

Silver Springs, the largest of Florida's first magnitude springs, (Scott et al.2004; Rosenau et al. 1977) discharges approximately 500 million gallons per day [mgd]) from the Floridan Aquifer (Osburn et al. 2002) and is also likely the largest limestone spring in the United States (Rosenau et al. 1977). Silver 'head' spring consists of two primary vents (East and West) which represent on average, about 45 % of flow in the Silver River is from Silver Main Spring.

The Silver Springs springshed covers more than 230,000 ha in north-central Florida, occurring primarily in the counties of Alachua and Marion (Phelps 2004). The climate of the region (measured at Ocala, FL) is humid sub-tropical with a warm wet season (June-October) and a cool dry season (November-May). Approximately 51 inches of rainfall occurs annually and the mean annual temperature is approximately 22 °C (http://www.usclimatedata.com/).

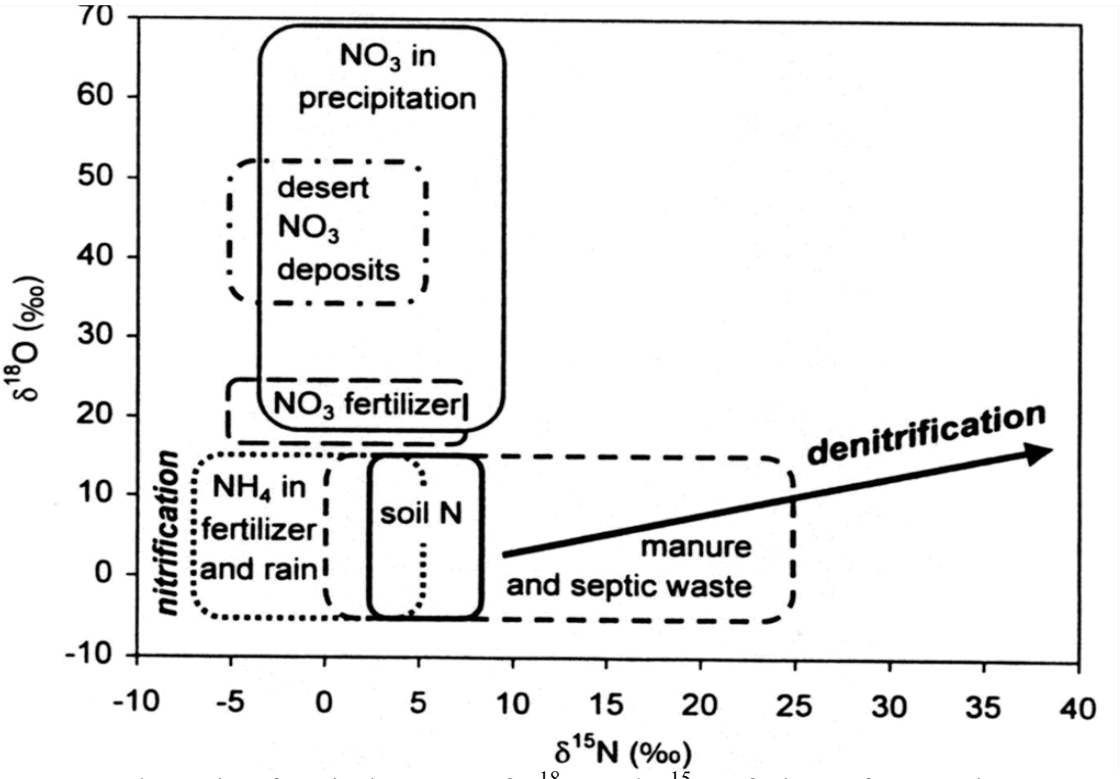

Figure 4.3.1. Schematic of typical ranges of $\delta^{18}O$ and $\delta^{15}N$ of nitrate from various sources as well as the isotopic effect of denitrification. (Adapted from http://wwwrcamnl.wr.usgs.gov/isoig/isopubs/Fig16-9.jpg)

4.3.3.2 Sampling

Water samples were collected from the 15 recently-built wells during the dry season (January to April of 2015) and wet season (July to November of 2015) for determination of dissolved gas composition (N_2, Ar, CH_4, and N_2O), and stable isotopic composition of nitrate. In addition to these wells, the Water Management District routinely sampled an additional 46 groundwater wells in the springshed to support Basin Management Action Plan (BMAP) development. Water samples were collected from these additional wells for chemical analyses and determination of isotopic composition of nitrate.

Well water samples were collected using a Grundfos Redi-flo II submersible well pump. Water samples for nitrate stable isotopes were collected into rinsed polyethylene bottles and stored frozen. Water samples for dissolved gases were collected by adjusting be pump flow rate to approximately 4 L per minute and eliminating bubbles from all tubing. Samples were collected underwater with no gaseous headspace into either 160 mL serum bottle (dissolved CH_4, N_2O) or 22 mL glass tubes with polyseal caps (N_2/Ar).

Water samples were collected from the Silver Spring vents (East and West) quarterly in 2014 and every other month beginning in January 2015. Samples for nutrients, metals, and stable isotopes of nitrate were collected by the water management district in their routine sampling. Samples for dissolved gases (CH_4, N_2O, N_2, and Ar by MIMS) were collected inside the vents by divers using double ended glass tubes sealed at both ends with septa caps.

Dissolved noble gas samples were collected from selected wells and spring vents using standard techniques of the Dissolved and Noble Gas Lab at the University of Utah (http://www.noblegaslab.utah.edu/dissolved_gas.html). Briefly, diffusion gas samplers consisting of two segments of 3/” copper tubing joined by a gas-permeable silicone tube (Aesbach-Hertig and Solomon 2013). One end of each tube had been sealed while the ends with silicone tubing were left open such that each tube shared a common airspace. The samplers were submerged to a specific depth in the wells for at least 24 hours. Upon retrieval, the open ends of the two copper segments were quickly sealed by crimping before gas exchange occurs at the silicone tubing surface. The sealed copper tubes were sent to Utah for the analysis of noble gases.

Additionally, during February and March in 2016, 3 L water from the 15 recently-built wells were pumped and filtered through 5µm TSTP (Millipore) pre-filter and subsequently filtered on 0.22µm PES filter (Millipore). Filters were stored frozen with dry ice in the field and transformed to -80^{o}C freezer when back to the lab until DNA extraction.

4.3.3.3 Sample Analysis

To characterize the land use of the whole watershed, we used the land use map generated most recently by SJRWMD in 2009 using the Florida Land Use and Cover Classification System (FLUCCS). In this study, we only used the first level classification (i.e., 1-Urban, 2-Agriculture, 3-Rangeland, 4-Forest, 5-Water, 6-Wetlands, 7-Barren land, 6-Transportation, community, and facility). In order to represent the land uses of the well site, a 500 m buffer (1,000 m diameter circle, USGS) were created, and the acreage of each land use in that buffer zone was

summarized. Based on the percentage of each land use, Cluster Analysis was performed to further classify the 61 wells.

Analyses for nutrients and metals were conducted by the St. John's River Water Management District certified analytical laboratory while the samples for stable isotopic composition of nitrate were shipped on ice to the Facility for Isotope Ratio Mass Spectrometry at the University of California, Riverside. The N and O isotopic composition of nitrate was determined by bacterial reduction to N_2O and continuous-flow isotope-ratio mass spectrometry (CFIRMS) (Sigman et al. 2001).

The determination of dissolved methane and nitrous oxide followed the EPA method (Kampbell and Vandegrift 1998). Briefly, a headspace was prepared by displacing 10 % of the water with high purity helium (He). The bottles were shaken for five minutes and specific volumes of headspace samples were injected onto gas chromatographic (GC) columns. For our purposes, 1,000 μL headspace gas samples were measured for methane (CH_4) on a Shimadzu GC-14-A gas chromatograph equipped with a flame ionized detector (FID) with column and detector/injector port temperatures of 110^{o}C and 160^{o}C, respectively. Similarly, 500 μL from the bottle headspace was analyzed for nitrous oxide (N_2O) using a GC-ECD with column, injection port, and detector temperatures of 70, 120, and 230°C, respectively.

Analysis of dissolved N_2 and Ar was conducted using a membrane inlet mass spectrometer (MIMS, Bay Instruments, Easton, MD) based on a QMG 422 quadrupole mass spectrometer (Pfeiffer Vacuum GmbH, Asslar, Germany)(Kana et al. 1994). All samples were analyzed in duplicate using water standards at 20.0 and 30.0°C to calibrate the measurement (Inglett et al. 2013). The analysis of dissolved noble gases was performed at the Dissolved and Noble Gas Lab at the University of Utah using a Stanford Research SRS – Model RGA 300 quadrupole mass spectrometer. In lieu of a total dissolved gas pressure measurement, total concentrations of noble gases in the diffusion samplers were derived by normalizing the Ar signal measured in Utah to the dissolved Ar concentration measured by UF using MIMS.

4.3.3.4 Estimation of Excess Air, Recharge Temperature, and Excess N_2

Dissolved N_2 and Ar concentrations were used to estimate the quantities in ground water of dissolved gases originating from atmospheric and biological sources (Vogel et al. 1981). In ground water, dissolved gases may originate from equilibrium exchange with the atmosphere at the water table, dissolution of entrapped air bubbles, and production by reactions such as denitrification. Typically, dissolved gases include some fraction from bubbles of air that become trapped under recharging water and entrained in the saturated zone. As long as the hydrostatic pressure remains greater than the total pressure of gases in solution, degassing is unlikely (Blicher-Mathiesen et al. 1998). Similarly, denitrification produces N_2 that remains in solution in recharging ground water. Recent literature has used the terms “excess air” to refer to atmospheric gases originating from entrained bubbles, and “excess N_2” to refer to N_2 originating from denitrification (Green et al. 2006).

Excess air and excess N_2 concentrations in ground water were estimated using the concentrations of N_2 and Ar, their solubility in water (Weiss 1970), the atmospheric pressure, and the recharge

temperature. The recharge temperature was estimated by the noble gas modeling of a suite of noble gas (He, Ar, Ne, Kr, and Xe) (Cey 2008; Aesbach-Hertig and Solomon 2013).

The excess air concentration in each sample was calculated with

$$[air_{bub}] = ([Ar_{meas}]-[Ar_{equil}](T,elev))\times 0.417 \quad (4.2.1)$$

where $[air_{bub}]$ is the concentration of excess air from entrained bubbles ($cm^3\ L^{-1}$), $[Ar_{meas}]$ is the measured concentration of Ar in the sample ($\mu mol\ L^{-1}$), $[Ar_{equil}](T,elev)$ is the concentration of Ar in humid, air-saturated water ($\mu mol\ L^{-1}$) at the temperature, T, and elevation, elev, of the water table, and 0.417 is the conversion factor for the quantity of Ar per volume of air ($\mu mol\ cm^{-3}$) at standard temperature and pressure of 1 atm and 0 °C. The temperature was the groundwater temperature measured by the St. John's River Water Management District when collecting water samples. The excess N_2 derived from denitrification was then calculated using

$$[N_{2,bub}] = [air_{bub}] \times 34.8 \quad (4.2.2)$$

$$[N_{2,excess}] = [N_{2,meas}] - [N_{2,equil}](T,elev) - [N_{2,bub}] \quad (4.2.3)$$

where $[N_{2,bub}]$ is the N_2 from entrained bubbles ($\mu mol\ L^{-1}$), 34.8 is the conversion factor for the quantity of N_2 per volume of air ($\mu mol\ cm^{-3}$) at standard temperature and pressure, $[N_{2,excess}]$ is the N_2 from denitrification ($\mu mol\ L^{-1}$), $[N_{2,meas}]$ is the measured concentration of N_2 in the sample ($\mu mol\ L^{-1}$), and $[N_{2,equil}](T,elev)$ is the concentration of N_2 in air-saturated water as a function of T and elev.

The reconstructed (initial) concentration of NO_3^- ($[NO_3^-]_{initi}$) before denitrification allows determination of the progression of denitrification. For each observation, we calculated the proportion of nitrate remaining from the original pool $[NO_3^-]_R$ as

$$[NO_3^-]_{init} = [NO_3^-]_{meas} + 2\times[N_{2,\ excess}] \quad (4.3.4)$$

$$[NO_3^-]_R = [NO_3^-]_{meas}/[NO_3^-]_{init} \quad (4.3.5)$$

Where $[NO_3^-]_{meas}$ is measured concentration. Uncertainties in the reaction progress estimate were caused mainly by uncertainties in the assumed recharge conditions affecting the calculation of $[N_{2,excess}]$. Isotope fractionation effects were evaluated with respect to hypothetical Rayleigh distillation kinetics

$$\delta^{15}N\text{-}[NO_3]_{init} = \delta^{15}N\text{-}[NO_3]_R + \ln([NO_3^-]_R \times \varepsilon \quad (4.3.6)$$

Where $\delta^{15}N_0$ and $\delta^{15}N_{meas}$ are the $\delta^{15}N$ of the source (initial) and observed NO_3-N, respectively. ε is the isotopic enrichment factor for $\delta^{15}N$ of NO_3-N. We used linear regression to determine ε as the slope of the relationship between $\delta^{15}N\text{-}[NO_3]_R$ and $\ln([NO_3^-]_R$.

4.3.3.5 DNA extraction and gene quantification

DNA extraction from filtered water samples was initially tested by comparing DNA extraction kits and whether a 2.7 µm GF/D pre-filter (Whatman, UK) altered bacterial abundances and DNA concentration. For this, Sterivax-GP 0.22 µm polyethersulfone gamma irradiated filters were broken open and the filter column removed from the casing. A quarter of the filter was pealed from the column and loaded into the PowerLyzer PowerSoil bead tube (Carlsbad, CA, USA) and Qiagen DNeasy Blood and Tissue kit (Hilden, Germany). To improve desorption of DNA, 200 µL of Tris buffer (0.5 *M* Tris-HCL pH 9) and 200 µL of phosphate buffer (0.2 M Na_2HPO_4 pH 8) was added to bead tubes loaded with filter and bead solution, mixed and 60ul of solution C1 was added, incubated at 70ºC for 10 minutes and frozen at -80ºC for 5 minutes. Based on the results we decided to not pre-filter as q-PCR based bacterial abundances were higher and to use the PowerLyzer PowerSoil kit, as it resulted in lower replicate dispersion compared to the Qiagen kit. Following pre-treatment, DNA extraction was carried out according to the manufacturer's manual. Extracts were quantified using the Qubit dsDNA high sensitivity assay kit (Life Technologies, Carlsbad, CA, USA) and stored at -20ºC until amplification.

Genomic DNA from *E. coli* K-12 (ATCC 10798-D) and *Pseudomonas stutzeri* (ATCC 11607) were used as standards for the *16s rRNA* and *nosZ* genes, respectively. Primer set 341F (5'-CCT ACG GGA GGC AGCAG-3') (Muyer et al. 1993)/ 797R (5'- GGA CTA CCA GGG TAT CTA ATC CTG TT-3') (Nadkarni et al. 2002) was used to target the *16s rRNA* gene and primer set nosZ2F (5'- CGC RAC GGC AAS AAG GTS MSS GT -3')/ nosZ2R (5'- CAK RTG CAK SGC RTG GCA GAA-3') (Henry et al. 2006) was used for the *nosZ* gene. PCR products were cloned into plasmids using the TOPO TA Cloning Kit (Invitrogen, Carlsbad, CA, USA) and the extraction of plasmids was carried out using the PureLink™ Quick Plasmid Miniprep kit (Invitrogen, Carlsbad, CA, USA) according to the manufacturer's manual. Ten-fold dilution series from 10^8 - 10^2 gene copies for both *16S rRNA* and *nosZ* were used as standards in each qPCR run to generate a standard curve. Amplification of qPCR was carried out on the QuantStudio 3 Real-Time PCR system (ThermoFisher Scientific, Waltham, MA, USA) in a reaction mixture of 0.2 *µM* of each primer for the selected target gene, 10 µL 2X PowerUp SYBR Green Master mix (ThermoFisher Scientific, Waltham, MA, USA), 1 µL of DNA, and PCR-grade water to yield a total volume of 20 µL. Three replicate qPCR amplifications were performed for each sample. The qPCR procedure for 16s rRNA included an initial denaturation step at 95ºC for 3 minutes, 40 cycles of amplification (95 ºC for 45 sec, 60 ºC for 45 sec, 72 ºC for 1 min) and a final elongation step at 72 ºC for 7 minutes. The thermocycle conditions for nosZ included an initial denaturation step at 95 ºC for 1.5 minutes, 40 cycles of amplification (95 ºC for 24 sec, 56 ºC for 24 sec, 58 ºC for 24 sec, 72 ºC for 24 sec) and a final elongation step at 72 ºC for 7min. Fluorescent quenching due was determined to be less than 1 % by the addition of 10^6 copies of the standard to representative samples and comparing the quantification with that of the sample alone. Standard deviations among technical replicates averaged 0.16±0.15 % for *16S rRNA* and 0.14±0.09 % for *nosZ*.

4.3.3.6 Statistical Analysis

Data were analyzed with JMP v.11© (SAS Institute Inc., Cary, NC). Cluster analysis, and principal component analysis were applied to geochemical and land use classification data. Principal component analysis (PCA) was performed using relevant chemical parameters of groundwater and vents, and we further calculated the average PC values for each land use. Piper

plots were made by the software of GW-chart (Winston 2000) to show the hydrogeochemical characteristics of sampled groundwater for wet and dry season. The differences between east and west vent, and between different seasons were tested with Student's t test. Nonparametric correlation were performed between different properties. All results are reported as significance when $P < 0.05$.

4.3.4 RESULTS AND DISCUSSION

4.3.4.1 Categorization of the Wells and Spring Vents based on Land Use

The land use that is indicated for a particular well site may be significantly different from adjacent land use. Also, land use categorization can be somewhat subjective and may not accurately reflect the actual activities at the site. Furthermore, in an area with rapid growth, such as Marion County, land use coverages rapidly become out-of-date (Phelps 2004).

In an effort to reduce the subjectivity of land use classification, we used Cluster Analysis to classify the 61 wells into six groups (C1-C5) based on the combination of mixed land use types. The dominant land use for C1 to C4 were Urban (C1), Agriculture (C2), Forests (C3), and Wetlands (C4). The Cluster 5 (C5) was separated because of a high percentage of transportation and utilities, but it also featured with high Forest coverage (> 25 %), and most of our sites were in the wastewater treatment facility (WWTF) (Table 4.3.1).

4.3.4.2 Geochemistry of Ground Water and Springs Vents

The concentration of calcium, sulfate, and chloride are important in ground water because they can give implications for the treatment needed for water supply (Phelps 2004). Sulfate and chloride did not show much change in wet and dry seasons (Table 4.3.2). Calcium showed the highest value of 460.9 mg L^{-1} (in the well M-0774) in the dry season but showed the highest value of 296.9 mg L^{-1} (in the well M-0778) in the wet season. The highest sulfate values occurred in M-0771 and M-0026 with the value of 221.8 and 179.8 mg L^{-1} respectively in the dry season, and 215.1 and 183 mg L^{-1}, respectively in the wet season. These are typical ranges for water in the Upper Floridan aquifer (Phelps 2004). Sulfate concentrations can range widely due to the presence or absence of sulfate minerals such as gypsum in the aquifer (Sacks 1996). Sulfate concentrations generally increase with depth in the Upper Floridan aquifer (Faulkner 1973).

In this study, there was no significant correlation either between calcium and sulfate or between sulfate and well depth. However, the two highest sulfate concentrations did accompany high calcium values in M-0771 and M-0026, and also the well M-0026 was one of the deepest wells (192 feet [58.5 m]) sampled in this study. We would suggest the presence of sulfate minerals such as gypsum in the aquifer of M-0026. We are not sure of the cause of high sulfate concentration in the well M-0771, which could be anthropogenic or derived from mixing with a deep aquifer source. Significant correlation were found between chloride (Cl^-) concentration and sodium (Na^+) concentration ($R^2 = 0.67$, $P < 0.05$), indicating a source of seawater.

Table 4.3.1. Percentage of area for each of the eight land use categories (1-urban and built-up, 2-agriculture, 3-rangeland, 4-upland forest, 5-water, 6-wetlands, 7-barren land, 8-transportation, communication and utilities waste water treatment facility (WWTF)), results of cluster analysis, and the final assignment of the land use.

	Land use category									
Well ID	1	2	3	4	5	6	7	8	Assigned Cluster	Land use description
	----------%----------									
M-0771	91	9	0	0	1	0	0	0	C1	Urban
M-0772	84	0	1	14	0	1	0	0	C1	Urban
M-0773	98	0	2	0	0	0	0	0	C1	Urban
M-0774	97	0	0	2	0	0	0	1	C1	Urban
M-0775	54	42	0	3	0	0	0	1	C1	Urban
M-0776	26	42	3	22	7	0	0	0	C2	Agriculture
M-0777	21	66	0	13	0	0	0	0	C2	Agriculture
M-0778	25	75	0	0	0	0	0	0	C2	Agriculture
M-0779	11	0	2	85	0	2	0	0	C3	Forest
M-0780	11	0	2	85	0	2	0	0	C3	Forest
M-0781	11	0	2	85	0	2	0	0	C3	Forest
M-0785	47	28	0	19	1	0	0	6	C1	Urban
M-0786	0	73	0	0	0	0	0	27	C2	Agriculture
M-0782	15	63	0	22	0	0	0	0	C2	Agriculture
M-0787	15	63	0	22	0	0	0	0	C2	Agriculture
A-0421	5	6	1	64	0	15	0	10	C3	Forest
M-0419	53	34	0	7	0	0	0	6	C1	Urban
M-0205	71	0	2	21	0	0	0	7	C1	Urban
A-0725	0	0	0	29	0	71	0	0	C4	Wetlands
M-0443	3	36	0	21	0	41	0	0	C4	Wetlands
M-0036	10	0	0	62	15	12	0	0	C3	Forest
M-0045	0	0	0	61	0	39	0	0	C3	Forest
M-0044	0	0	0	61	0	39	0	0	C3	Forest
M-0239	97	0	0	1	1	0	0	1	C1	Urban
A-0436	51	0	0	45	0	3	0	0	C1	Urban
A-0071	51	0	0	45	0	3	0	0	C1	Urban
A-0420	0	0	28	51	0	21	0	0	C4	Forest
M-0527	34	46	0	20	0	0	0	0	C2	Agriculture
M-0063	76	22	0	3	0	0	0	0	C1	Urban
M-0052	9	0	0	89	0	2	0	0	C3	Forest
M-0040	90	0	0	0	2	0	0	8	C1	Urban
M-0026	31	0	6	11	0	52	0	0	C4	Forest
M-0764	10	0	0	27	7	56	0	0	C4	Forest
M-0762	10	0	0	27	7	56	0	0	C4	Forest
M-0445	5	15	4	58	0	15	0	3	C3	Forest

Table 4.3.1. continued.

Well ID	Land use category 1	2	3	4	5	6	7	8	Assigned Cluster	Land use description
	----------%----------									
M-0467	77	6	0	12	4	2	0	0	C1	Urban
M-0465	66	0	0	18	0	0	0	16	C1	Urban
M-0031	23	77	0	0	0	0	0	0	C2	Agriculture
M-0041	18	62	0	19	0	0	0	0	C2	Agriculture
M-0528	56	18	0	20	0	0	0	6	C1	Urban
M-0039	63	6	2	24	0	1	0	4	C1	Urban
M-0209	97	0	0	0	0	0	0	3	C1	Urban
M-0242	55	0	8	21	0	0	0	15	C1	Urban
M-0211	92	0	0	0	6	0	0	2	C1	Urban
M-0212	92	0	0	0	6	0	0	2	C1	Urban
M-0213	94	0	3	2	1	1	0	0	C1	Urban
M-0481	16	9	12	22	6	35	1	0	C4	Wetlands
M-0483	16	9	12	22	6	35	1	0	C4	Wetlands
M-0013	3	13	0	33	6	30	4	11	C6	Forest
L-0095	22	40	0	28	5	4	0	0	C3	Forest
L-0926	23	0	0	13	3	56	0	4	C4	Wetlands
L-0927	23	0	0	13	3	56	0	4	C4	Wetlands
L-0883	19	18	0	49	4	4	0	7	C3	Urban
L-0884	19	18	0	49	4	4	0	7	C3	Urban
L-0902	19	18	0	49	4	4	0	7	C3	Urban
L-0874	0	10	6	29	0	23	0	32	C5	Transport/WWTF
L-0924	0	12	6	29	0	21	0	32	C5	Transport/WWTF
L-1050	0	13	6	28	0	21	0	32	C5	Transport/WWTF
L-1049	0	13	6	28	0	21	0	32	C5	Transport/WWTF

The trace constituent manganese (Mn) was analyzed in ground-water samples because it may reflect the application of synthetic fertilizers or the source of wastewater (Phelps 2004). The high Mn values in those wells with the land use of improved pasture/nursery (i.e., M-0778 and M-0787) and retention pond/septic (e.g., M-0774) would suggest the effect of fertilizer.

Dissolved oxygen (DO) measured in the field can be an indicator of recently recharged ground water because there generally are no sources of oxygen in the aquifer and the longer the water is contained in an aquifer, the lower the DO becomes (Katz et al. 1999). Low DO concentrations mostly occurred with the land use of forest, for which most sites were also included in the confined aquifer portions of the eastern springshed. The water from well M-0779/80 had a hydrogen sulfide odor, indicating that it probably came from marine origin or deep in the aquifer. In general, areas with high levels of DO in the ground water could be more vulnerable to rapid infiltration of N loads from the land surface (Phelps 2004).

Table 4.3.2. Statistical summary of selected water chemical data for the 61 wells sampled in this study.

	Ca-T mg L^{-1}	Fe-T µg L^{-1}	Mn-T µg L^{-1}	Na-T µg L^{-1}	Cl mg L^{-1}	SO_4-T mg L^{-1}	NO_3-T mg L^{-1}	DO mg L^{-1}	PO_4-P mg L^{-1}	TP mg L^{-1}
dry season										
Min.	0.40	1.19	0.05	1.31	2.00	0.45	0.00	0.03	0.01	0.01
Max.	460.9	2135	83.57	30.03	54.50	221.8	13.85	7.25	1.21	2.32
Median	51.57	119.1	4.67	6.66	9.85	4.43	0.31	1.77	0.06	0.08
average	65.99	316.9	11.66	8.66	12.51	16.81	1.19	2.24	0.14	0.25
wet season										
Min.	bd	bd	bd	bd	4.16	0.02	bd	0	0.0051	0.0057
Max.	296.9	3110	97.93	28.34	50.6	215.1	12.19	7	1.49	2.64
Median	54.14	58.26	4.01	6.07	11.56	4.6	0.24	1.63	0.05	0.06
average	64.54	429.6	12.14	7.97	13.42	17.00	1.14	2.11	0.16	0.27

*bd: below detection limit.

Concentrations of phosphorus (P) were analyzed as total phosphorus (TP) and total orthophosphate (PO_4-P). Phosphorus is not as mobile as nitrogen and because of the ability of phosphate to sorb onto metal oxides and carbonate minerals. High concentration of TP (> 1 mg L^{-1}) in the ground water occurred mostly in the surficial aquifer and in sites with urban land use (e.g., M-0771, M-0774, M-0778, M-0209, M-0211/12/13, A-0436). Hem (1985) reported that P is present in animal metabolic waste and that domestic and industrial sewage effluents probably are sources of P in surface water. In the study area, where wastewater is disposed by land application instead of to surface water, effluent could thus be a source of P to the ground water. Hawthorn Group sediments containing phosphate-bearing minerals such as apatite, could be another source but because those minerals have a low solubility, they probably are not a major source of phosphate in ground water (Phelps 2004).

The major geochemical characteristics measured in wet and dry season were shown in two Piper diagrams (Figure 4.3.2). The two seasons showed similar results. Most of the groundwater samples belong to the Ca-HCO_3 water type, some of them fell in the Cl-SO_4 water type. The Piper diagram is a conventional method of categorizing geochemistry of waters, particularly in aquifers, but is based on limited water chemical parameters. Land use is likely to be reflected in more diverse types of analytes including trace metals and nutrients. Principal components analysis (PCA) is a multivariate statistical technique that simplifies datasets through derivation of new 'component' variables. PCA also enables the ordination of samples on the basis of the multiple water chemical variables.

Using the nine selected parameters (Table 4.3.3), the first two principal components explained 52 % of the information with 30.2 % and 21.8 % for PC1 and PC2, respectively (Figure 4.3.3). The PC1 negatively correlated with dissolved CH_4, NH_4-N, and TOC, positively correlated with DO, water temperature, and Cu (Table 4.3.3), maybe indicating old and new water. The PC2 showed positive loadings for Cu, Fe, Cl, and SO_4, indicating a surficial source of these ions (rainwater, wastewater, fertilizer). The PC1 well separated the two vents with east vent being recharged with comparatively new water (high DO). When labeling with land uses, the west vent was grouped with the land uses of Forest and Wetlands whereas the east vent was with the land uses of

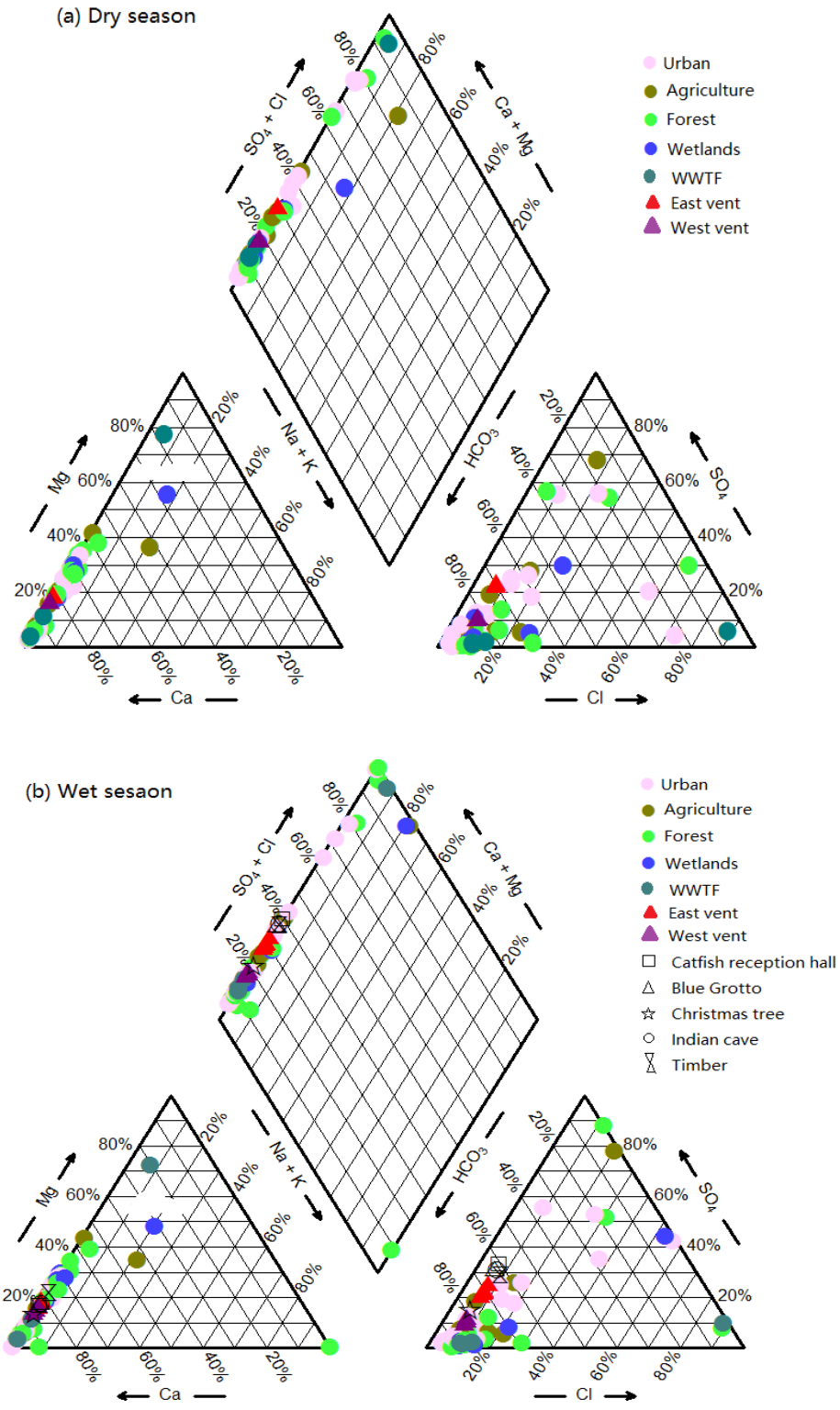

Figure 4.3.2. Piper diagram showing the hydrogeochemical characteristics of sampled groundwater (n= 61) and spring vents for wet and dry season based on land use (a,b).

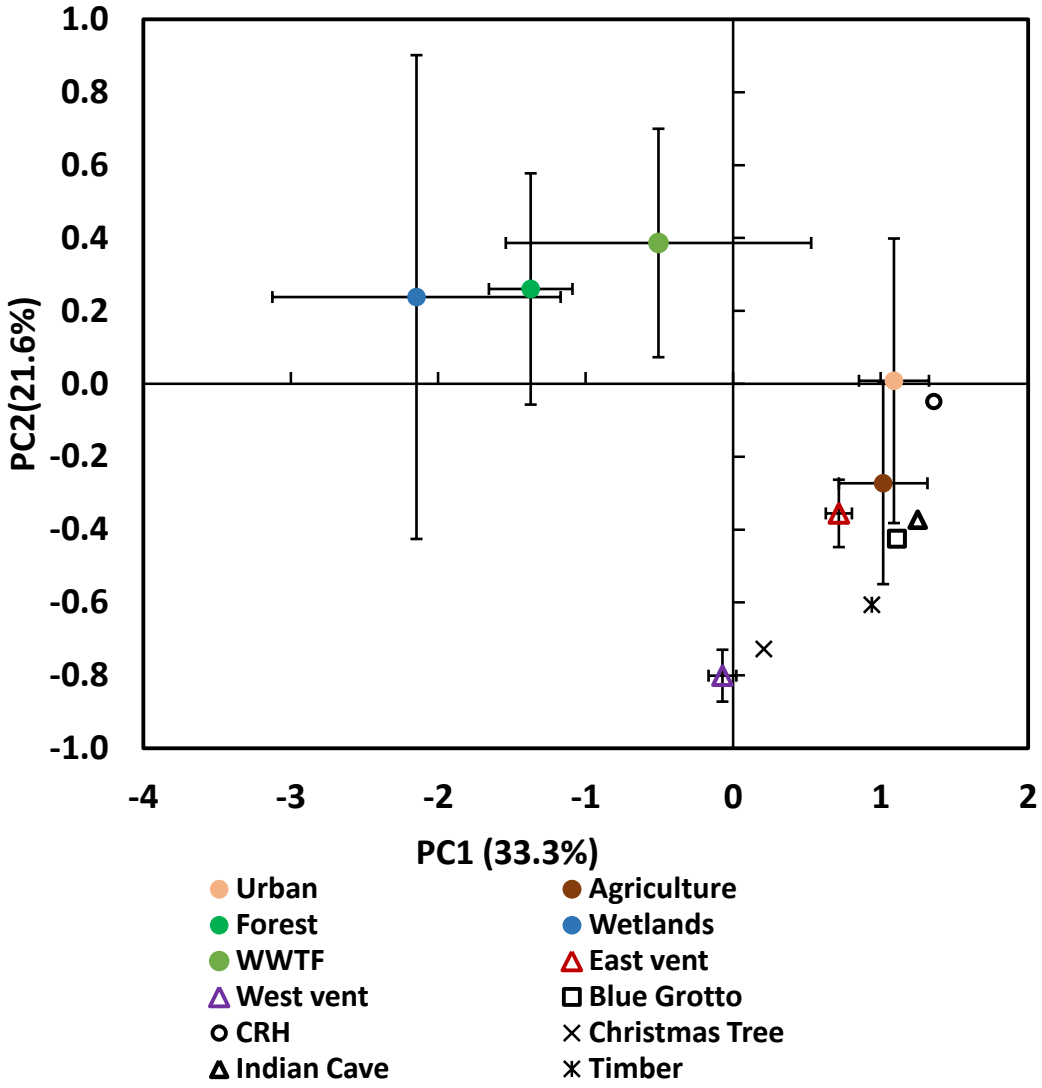

Figure 4.3.3. Principal component analysis based on selected water physical and chemical properties for the 61 wells in the wet season, the centroids were the average principal component values for each land use.

Table 4.3.3. The eigenvectors of the principal component analysis for the first and second principal components (PC1 and PC2)

	PC1	PC2
Dis.CH4	-0.419	0.039
DO	0.390	-0.22
Water Temp	0.389	0.101
Cu-T	0.309	0.484
Fe-T	-0.151	0.512
Cl	0.041	0.414
SO_4-T	0.276	0.447
NH_4-T	-0.439	0.167
TOC	-0.364	0.205

Agriculture and Urban (Figure 4.3.3). Similarly, these designations on the basis of land use also roughly correspond to separation between the East and West Mammoth vents on the basis of confined (eastern springshed, West vent) versus unconfined (western springshed, East vent) aquifer portions.

4.3.4.3 Spatial and Seasonal Pattern of Dissolved Gases in Ground Water and Spring Vents

For all the 61 wells, high concentrations of dissolved CH_4 mostly appeared in the land use of forest while high dissolved N_2O concentrations mostly appeared in the land use of urban and agriculture (Figure 4.3.4). Those values fell in the range of the same land use reported by others (Table 4.3.4, Hiscock et al. 2003). Again, the separation of wetland and forest systems can also represent the inclusion of most of these sites in the confined aquifer of the eastern springshed.

Formation of N_2O in the groundwater is predominately controlled by incomplete nitrification and denitrification reactions, and therefore could potentially be associated with various indicators of denitrification including low oxygen, or the presence of potential electron donors (e.g., organic C, sulfide, or CH_4) (Jahangir et al. 2013). If this is indeed the case, N_2O levels (which are stable under most groundwater conditions) could be used as a sensitive indicator of potential nitrification and denitrification within the groundwater system.

In the dry season with only 15 data points, we did not observe a significant correlation of N_2O levels in groundwater with any of these potential indicators of denitrification. We did observe a significant correlation between dissolved N_2O and water Cl^- (r = 0.82, P <0.01, Table 4.3.5), indicating a possible interaction (through denitrification or DNRA) of nitrate containing waters with a deeper anoxic, marine derived aquifer (Molofsky et al. 2013). Alternatively, correlation of N_2O with chloride could indicate dominance of nitrogen sources from wastewater treatment or septic systems which are also enriched in chloride (McQuillan 2004). In the wet season, dissolved N_2O significantly positively correlated with dissolved oxygen (r = 0.64, P < 0.001), water temperature (r = 0.52, P < 0.001), SO_4 (r = 0.48, P < 0.001), and NO_3-N (r = 0.82, P < 0.001), significantly negatively correlated with NH_4-N (r = -0.72, P < 0.001), TOC (r = -0.53, P < 0.001), TKN (r = -0.54, P < 0.001), and dissolved CH_4 (r = -0.66, P < 0.001).

Based on the dissolved oxygen levels in the groundwater, the N_2O in the wells of M-0779/0780/0781 was likely controlled by incomplete denitrification because of the low DO (<0.5 mg L^{-1}) and low nitrate (<0.01 mg L^{-1}). In contrast, for other wells, the N_2O may be more likely to correlate with nitrification because of the comparatively high DO (>1 mg L^{-1}) and nitrate (>0.1 mg L^{-1}). For example, Hiscock et al. (2013) observed a positive correlation between NO_3^- and N_2O for Chalk groundwater samples indicating that nitrification was the principal production mechanism for N_2O. McMahon et al. (2000) concluded that N_2O in the central High Plains aquifer was produced primarily by nitrification because large concentrations of O_2 and NO_3^- and small concentrations of NH_4^+ and dissolved organic carbon.

Heisig and Scott (2013), for example, reported that in south-central New York states, in the wells with methane concentration of 0.5 mg L^{-1} or greater, the concentration of dissolved oxygen was 0.2 mg L^{-1} or less and hydrogen sulfide was detected. We did not measure the hydrogen sulfide concentration but did see the significantly negative correlation between dissolved methane and DO (Table 4.3.5). The significant negative correlation between dissolved CH_4 and NO_3-N and

NH_4-N indicate the possibility of alternate nitrate reduction pathways coupled to anaerobic methane oxidation (Ettwig et al. 2010; Haroon et al. 2013).

$$CH_4 + 4NO_3^- \rightarrow CO_2 + 4NO_2^- + 2H_2O$$

$$3CH_4 + 8NO_2^- + 8H^+ \rightarrow 3CO_2 + 4N_2 + 10H_2O$$

$$CH_4 + NO_3^- + 2H^+ \rightarrow CO_2 + NH_4^+ + H_2O$$

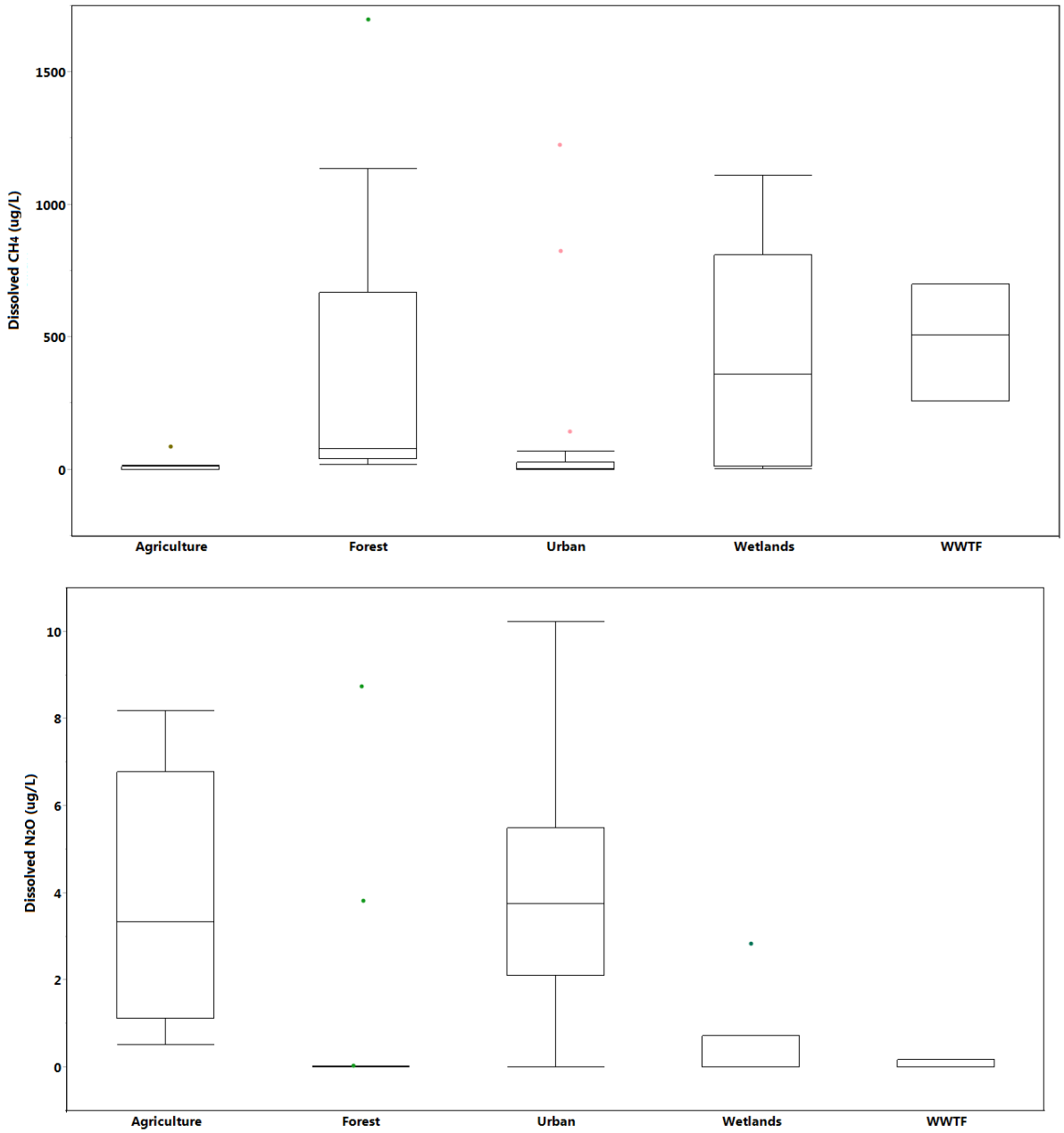

Figure 4.3.4. Dissolved CH_4 and N_2O in the 61 wells in the wet season.

Table 4.3.4. Comparison of N_2O concentrations for subsurface waters from aquifers and agricultural drainage (adopted from Hiscock et al. 2003).

aquifer (unconfined)	**land use**	**N_2O (µg L^{-1})**
Chalk, Cambs, and Norfolk	arable	6.6-84.8 (26.5)
Chalk, Cambridgeshire	arable	6.9-169.7 (52.3)
weathered bedrock, England and Scotland	uncultivated upland	0.5-2.1 (1.2)
poorly consolidated clay, silt, sand, and gravel	rangeland, arable and cattle	0.04-41.4 (1.3)
alluvium, sands, and gravels	urban, forest, and cropped field soils	0.7-310.6 (30.4)
Sand	woodland with manure disposal	11-22
karstic limestone	sewage effluent disposal	4.0-13.2
Sand	sewage effluent disposal	83.6-396
clay soils, agricultural drains	arable	0.5-15689 (96.8)
alluvial riparian zone underlain by clay aquiclude	maize, riparian forest	(756.8)
clay and loess soils, agricultural drains	grassland	<6.292
	mixed arable and grass	<94.3
hydromorphic silty clay loam soils, shallow water table	arable and pasture	9.4-957.9

Table 4.3.5. Significant correlation of dissolved CH_4 and N_2O with selected properties of groundwater sampled in the study wells.

Parameter, y	Season*	Parameter, x	Spearman ρ	Prob>|ρ|
Dissolved N_2O	dry	Cl^-	0.74	**
	wet	Dissolve oxygen (DO)	0.64	***
		Total organic carbon (TOC)	-0.53	**
		TKN	-0.54	**
		NH_4-T	-0.73	***
		NO_3-T	0.82	***
		SO_4	0.48	**
		Water temperature	0.52	**
		Dissolved CH_4	-0.66	***
Dissolved CH_4	dry	DO	-0.56	*
		TOC	0.73	**
		NH_4-T	0.83	***
		NO_3-T	-0.69	**
		Water Temperature	-0.67	**
		Alkalinity	0.52	*
	wet	DO	-0.68	***
		TOC	0.65	***
		TKN	0.76	***
		NH_4-T	0.84	***
		NO_3-T	-0.67	***
		SO_4	-0.52	***

***-$P < 0.001$; **-$P < 0.01$, *-$P < 0.05$

*Season: 15 wells in dry season and 61 wells in wet season, were used to run correlation.

Since denitrification results in the production of dissolved N_2, increase in N_2 concentration in the water has been used to estimate microbial denitrification (Blicher-Mathiesen et al. 1998). Due to the relatively high background concentration of dissolved N_2, its dependence on the recharge temperature, and degassing problems, dissolved Ar is measured in addition of N_2 to estimate the excess of N_2 produced by denitrification (Kendall 1998). Measurements of dissolved N_2 and Ar in the Silver Spring Mammoth vents are similar to, but slightly higher than those reported by Phelps (2004) (Figure 4.3.5).

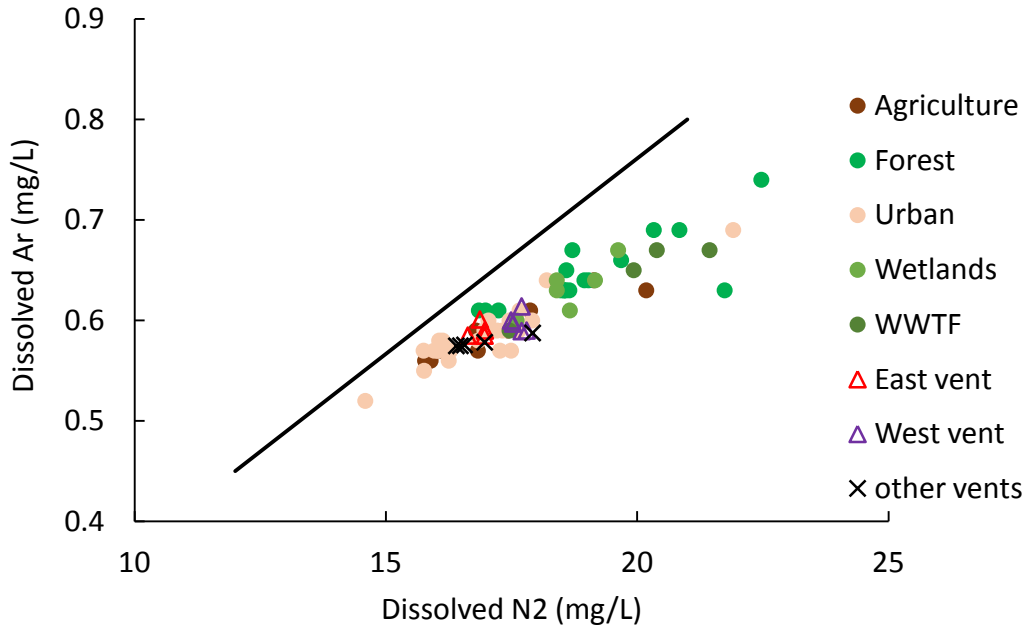

Figure 4.3.5 Concentrations of dissolved N_2 and Ar observed in the east, west vent of the Silver Spring mammoth head spring, other five vent and in the 61 wells in the Silver Spring springshed catergorized by land use in the wet season.

In general, for most of the 15 new wells, significantly higher dissolved N_2O and CH_4 were observed in dry and wet season, respectively ($P<0.05$, Figure 4.3.6). In both seasons, the underground water in the well M-0774, M-0771, and M-0776 had high dissolved N_2O with the values of 0.74 ± 0.01 and 0.51 ±0.0 μM, 0.48 ± 0.01 and 0.22 ± 0.0 μM, 0.53 ± 0.0 and 1.98 ± 0.0 μM, in the dry and wet season, respectively.

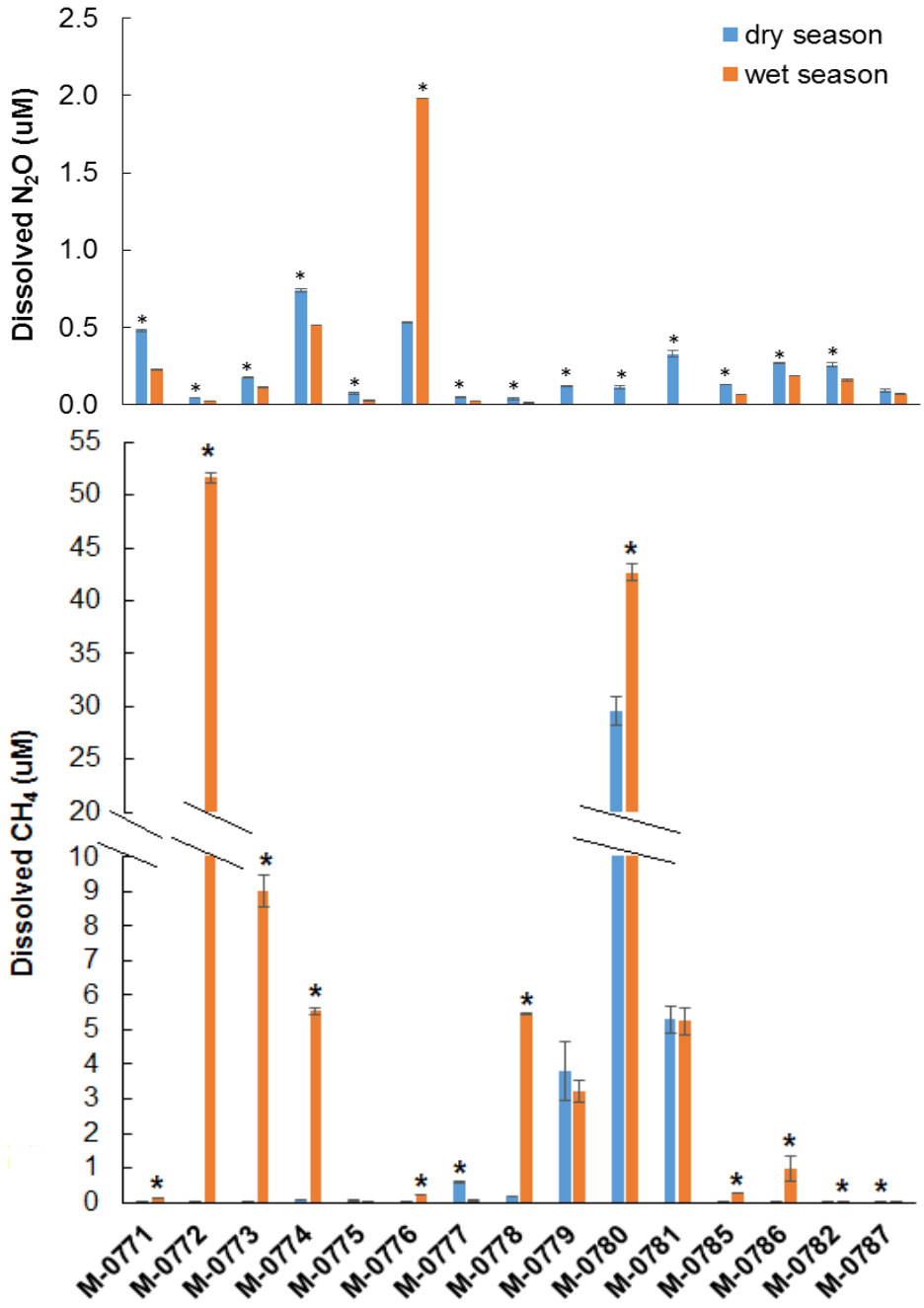

Figure 4.3.6. Measured concentrations of dissolved gases (CH_4 and N_2O) in groundwater samples collected from the 15 study wells in dry and wet seasons.* denotes significant difference between wet and dry season.

The concentrations of dissolved N_2O gas for the spring vents were in the range of 0.05 to 0.2 μM (Figure 4.3.7). Generally, the values in the East vent were significantly higher than those in the West vent, which would attribute to the higher NO_3-N concentration typically observed in the east vent (Butt and Aly 2008). The dissolved CH_4 in the spring vents fell in the range of 0.01-0.06 µM, with higher values in the east vents (Figure 4.3.7). Concentrations of both methane and

nitrous oxide were variable with sampling date, but it is difficult to draw any conclusions regarding a seasonal pattern with such a limited dataset.

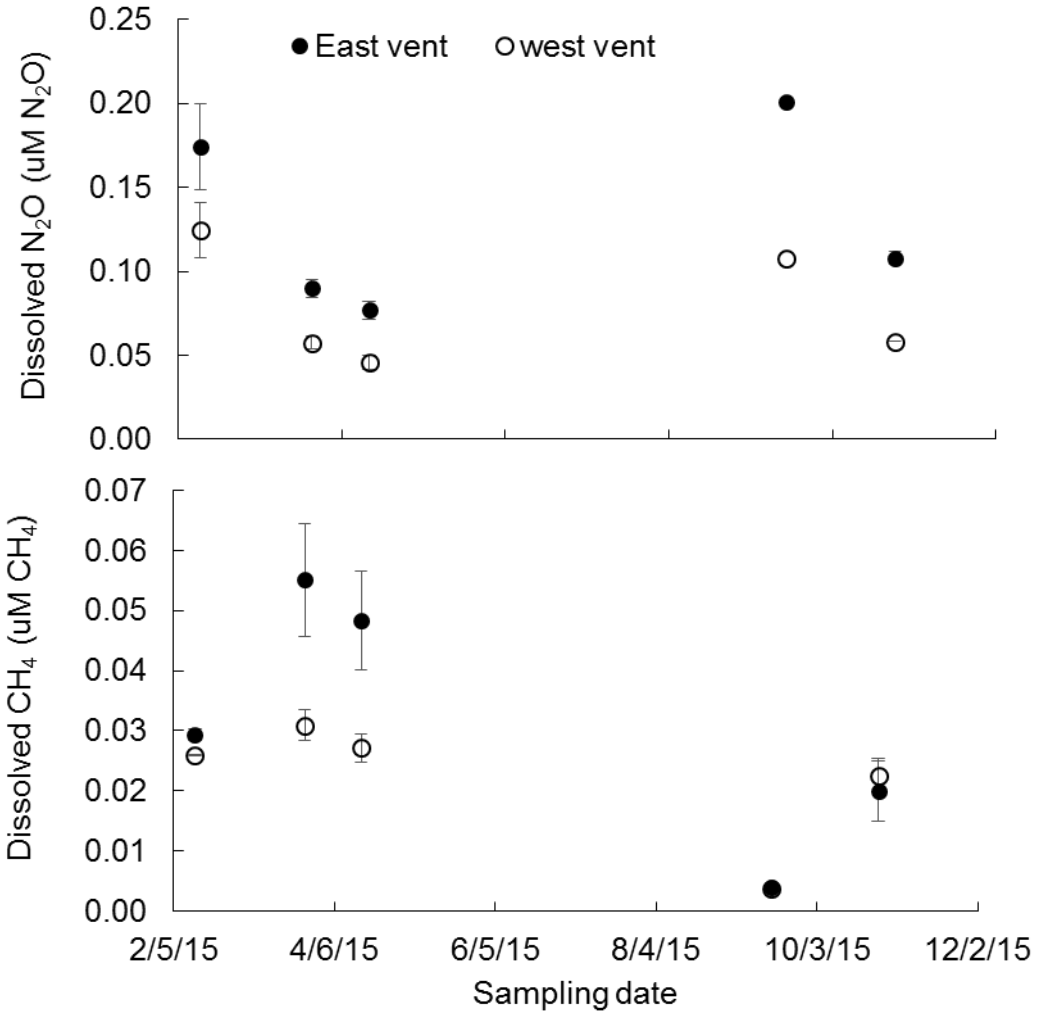

Figure 4.3.7. Seasonal patterns of dissolved N_2O and CH_4 from July 2014 through April 2015 in the east and west vents of the Silver Spring mammoth head spring.

Analysis of the patterns of dissolved N_2 and the N_2:Ar can be used to indicate the potential for seasonality in the amount of excess N_2 derived from denitrification (Figure 4.3.8). Small but measurable changes are present in these values in the water discharging in the Mammoth vents. There seemed to be a slight seasonal pattern with highest vales of N_2:Ar observed just following the wet season in late summer/early autumn. This pattern could indicate the potential for either temperature or high C inputs from surficial aquifers leading to higher amounts of denitrification and dissolved N_2 gas. With such a small dataset however, it is premature to infer seasonal trends or causes.

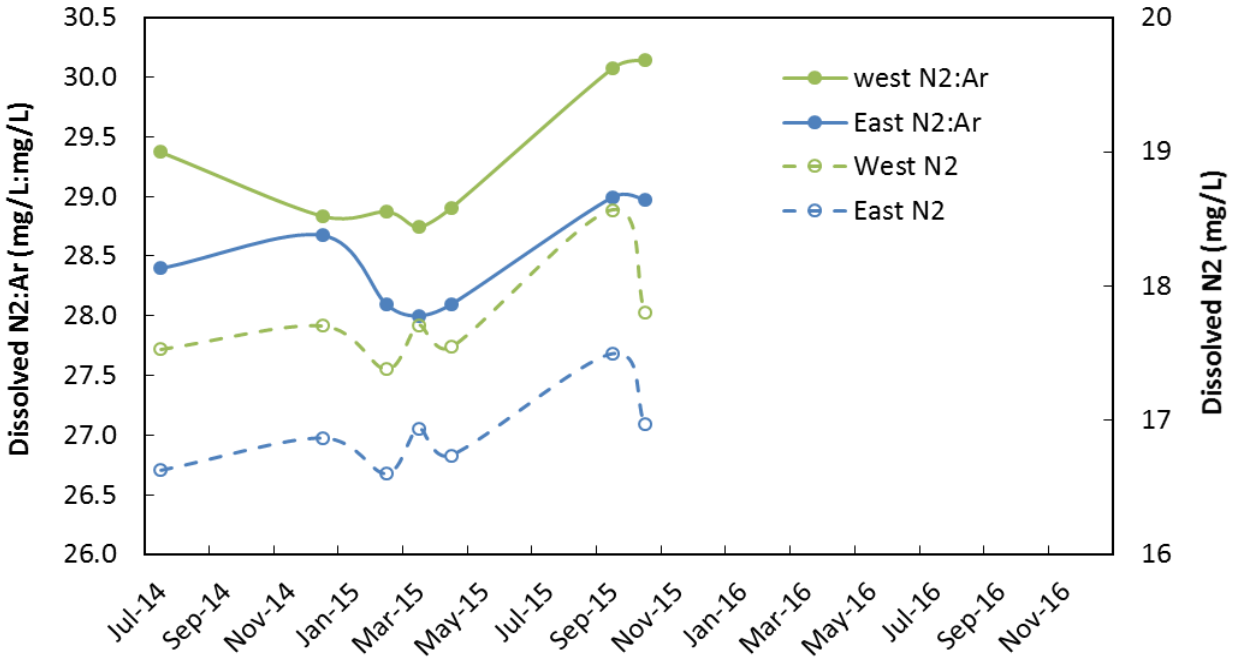

Figure 4.3.8. Seasonal patterns of dissolved N_2 and N_2:Ar observed from July 2014 through October 2015 in the east and west vents of the Silver Spring mammoth head spring.

4.3.4.4 Stable Isotopic values (δ^{15}N-NO_3 and δ^{18}O-NO_3) of Ground Water

Based on ranges described by Madison and Brunett (1985), the groupings of wells based on nitrate values would be as follows (Figures 4.3.9 and 4.3.10):

I. Less than 0.2 mg L^{-1}: assumed to represent background conditions (M-0779/80/81 with the land use of pine plantation, and M-0777 with the land use of agriculture/forest)
II. 0.2-3.0 mg L^{-1}: Transitional; concentrations may or may not represent influence from human activities (M-0772, M-0773, M-0774, M-0775, M-0778, M-0785, and M-0786)
III. 3.01-10 mg L^{-1}: May indicate elevated concentrations resulting from human activities (M-0771, M-0782/87, M-0527)
IV. More than 10 mg L^{-1}: Exceeds Maximum Contaminant Level (MCL) for nitrate-N (U.S. Environmental Protection Agency, 2003) (M-0776).

Overall the pattern of nitrate concentration showed highest values in the western springhsed with land uses of Agriculture and Urban (Figure 4.3.9). Coincidentally, these regions are also characterized as the unconfined portions of the springshed (Figure 4.3.10)The highest nitrate values were observed in M-0776 with the land use of horse farm (13.8 and 12.2 mg L^{-1} in the dry and wet season, respectively), M-0771 with the land use of golf course/septic tank (9.32 and 8.05 mg L^{-1} in the dry and wet season, respectively), and M-0782/87 with the land use of improved pasture/nursery (9.1 and 8.1 mg L^{-1}, respectively in the dry and wet season, respectively). After removing those high points, a significant linear relationship was observed between NO_x-N concentrations and DO values, and the equations were similar in dry and wet seasons (Figure 4.3.11).

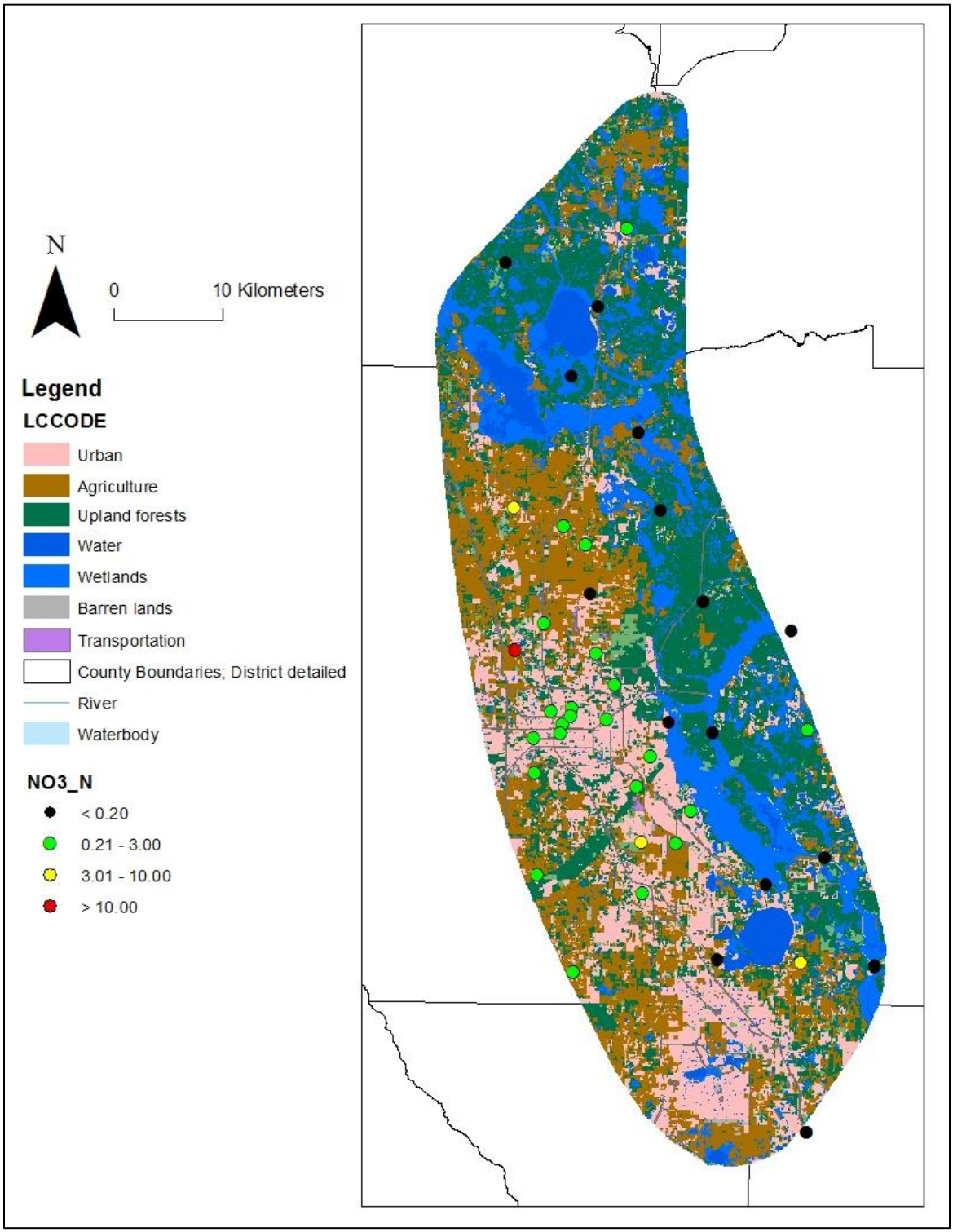

Figure 4.3.9. Spatial distribution of nitrate concentration in the Silver Spring springshed (dry season) in relation to land use distributions.

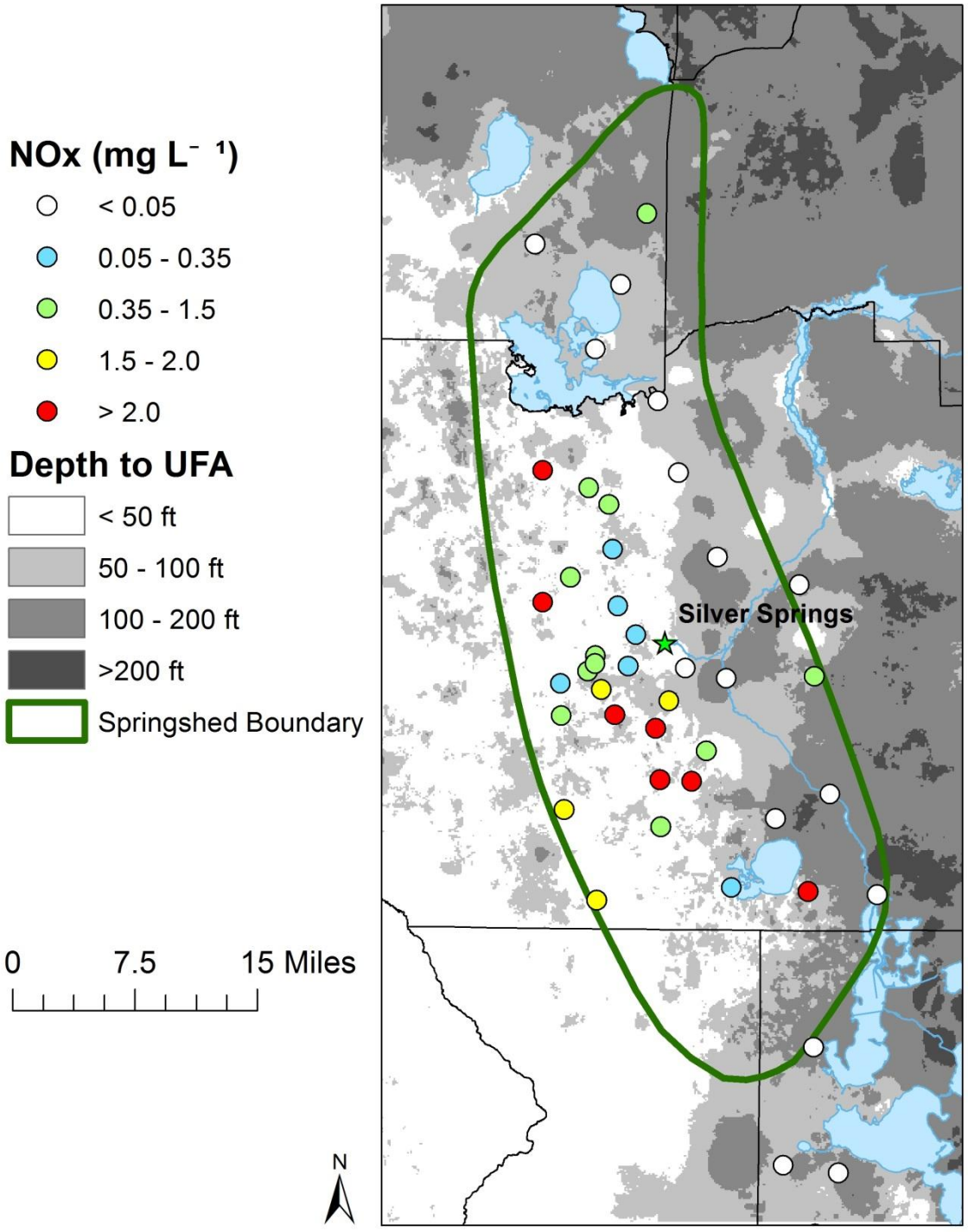

Figure 4.3.10. Spatial distribution of nitrate concentration in the Silver Spring springshed (dry season) in relation to depth to the Upper Floridan Aquifer (UFA).

According to traditional isotopic values of nitrogen sources, these ranges tend to indicate a predominance of ammonium fertilizer, manure and septic waste, and soil nitrogen in the wells of this study (Figure 4.3.12). With the assumption that denitrification proceeds in an approximate 1:1 (Granger et al. 2008) to 2:1 (Aravena and Robertson 1998; Lehmann et al. 2003) enrichment ratio, most of the isotopic values for nitrate in these aquifer samples may both directly reflect or be explained by denitrification of the original nitrogen sources indicated above (Figure 4.3.12).

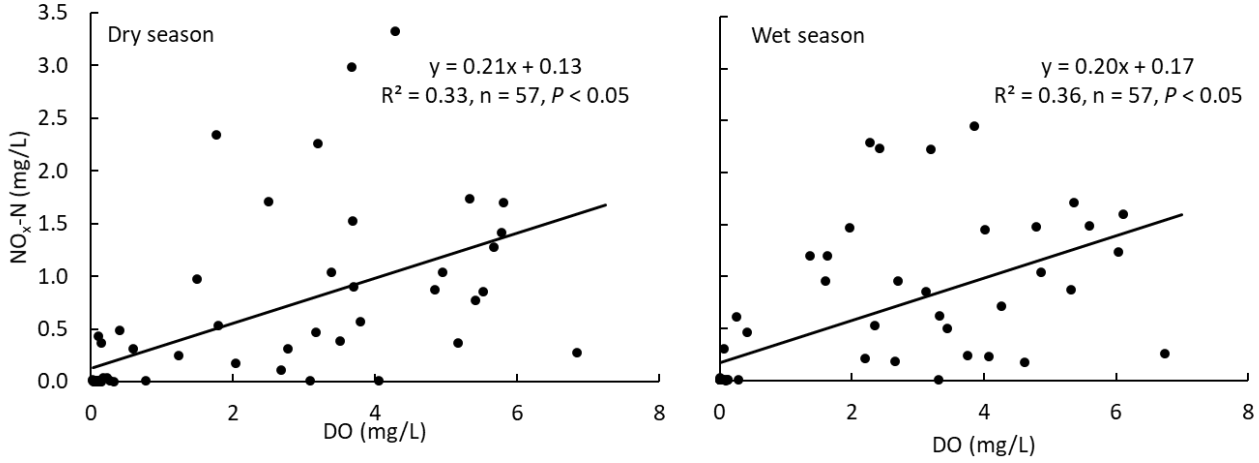

Figure 4.3.11. Correlation between NO_x-N and dissolved oxygen (DO) in the groundwater in wet and dry season.

Table 4.3.6. Values of $\delta^{18}O$ and $\delta^{15}N$ of nitrate, excess N_2 and the fraction of remaining nitrate (f $[NO_3]_R$) in groundwater in the Silver Spring springshed in the dry season.

Sample I.D.	Sampling date	Land use	Excess N2	Est. Initial NO3	f NO_3 remaining	$\delta^{18}O$-NO_3	$\delta^{15}N$-NO_3	NOx-T
			mg L^{-1}	mg L^{-1}		‰	‰	mg L^{-1}
Dry season								
M-0771	2/12/2015	Urban	0.79	10.11	0.92	5.75	6.03	9.32
M-0772	2/12/2015	Urban	neg	ND	ND	2.89	4.86	0.37
M-0773	2/12/2015	Urban	0.03	1.74	0.98	4.66	7.21	1.71
M-0774	3/19/2015	Urban	0.31	2.65	0.88	4.48	6.25	2.34
M-0775	3/19/2015	Urban	neg	ND	ND	3.03	1.27	0.27
M-0776	3/19/2015	Agriculture	0.22	14.08	0.98	4.25	6.48	13.85
M-0777	2/9/2015	Agriculture	0.02	0.12	0.87	0.86	3.66	0.11
M-0778	2/9/2015	Agriculture	0.71	1.08	0.34	15.09	17.06	0.37
M-0779	1/22/2015	Forest	1.10	1.11	0.01	14.74	7.39	0.01
M-0780	1/22/2015	Forest	0.68	0.68	0.01	14.35	7.69	0.00
M-0781	1/22/2015	Forest	neg	ND	ND	9.48	6.43	0.00
M-0782	3/17/2015	Agriculture	neg	ND	ND	11.49	2.26	9.14
M-0787	3/17/2015	Agriculture	neg	ND	ND	5.01	3.53	8.09
M-0785	2/9/2015	Urban	neg	0.85	1.03	6.09	6.59	0.87
M-0786	3/17/2015	Agriculture	0.02	3.01	0.99	4.72	7.09	2.99
East Vent	2/13/2015		0.46	1.85	0.75	5.50	6.20	1.39
West Vent	2/13/2015		0.79	1.85	0.57	6.87	7.62	1.06
East Vent	3/26/2015		0.34	1.78	0.81	5.39	6.29	1.44
West Vent	3/26/2015		0.82	1.91	0.57	7.30	7.84	1.09
Wet season								
M-0776	9/10/2015	Agriculture	1.66	13.85	0.88	6.26	7.80	12.19
M-0777	8/17/2015	Agriculture	0.68	0.85	0.20	7.12	4.54	0.17
M-0778	8/17/2015	Agriculture	2.28	2.58	0.12	19.91	19.43	0.30
M-0786	9/8/2015	Agriculture	1.12	3.35	0.66	6.08	7.95	2.23
M-0782	9/8/2015	Agriculture	1.05	10.85	0.90	14.36	4.59	9.80
M-0787	9/8/2015	Agriculture	0.40	7.91	0.95	6.21	5.31	7.51
M-0527	7/21/2015	Agriculture	1.25	4.55	0.73	6.81	6.97	3.30
M-0031	8/13/2015	Agriculture	0.52	2.23	0.77	7.02	5.24	1.71
M-0041	8/13/2015	Agriculture	0.47	1.92	0.75	6.77	5.88	1.45
M-0013	9/15/2015	Forest	1.37	1.38	0.00	5.67	7.64	0.01
M-0779	10/20/2015	Forest	0.25	0.26	0.04	12.26	-2.06	0.01
M-0780	10/20/2015	Forest	0.45	0.46	0.01	5.21	-3.55	0.01
M-0781	10/20/2015	Forest	0.48	0.49	0.02	2.54	-2.62	0.01

Table 4.3.6. continued.

Sample I.D.	Sampling date	Land use	Excess N2	Est. Initial NO3	f NO_3 remaining	$\delta^{18}O$-NO_3	$\delta^{15}N$-NO_3	NOx-T
			mg L^{-1}	mg L^{-1}		‰	‰	mg L^{-1}
M-0044	7/23/2015	Forest	1.72	1.72	0.00	4.10	-2.56	
M-0052	7/21/2015	Forest	0.90	0.95	0.05	6.68	6.48	0.05
M-0445	8/19/2015	Forest	1.12	1.12	0.00	8.51	9.69	0.00
M-0771	11/17/2015	Urban	1.84	9.89	0.81	5.94	5.19	8.05
M-0772	11/17/2015	Urban	0.40	0.58	0.31	0.63	4.09	0.18
M-0773	11/17/2015	Urban	1.96	3.16	0.38	5.16	7.10	1.20
M-0774	9/10/2015	Urban	0.88	3.17	0.72	5.63	6.42	2.29
M-0775	9/10/2015	Urban	0.62	0.88	0.30	5.00	1.70	0.26
M-0785	11/17/2015	Urban	0.61	1.32	0.54	15.22	-2.29	0.71
M-0419	7/23/2015	Urban	0.47	2.04	0.77	4.19	3.95	1.57
M-0063	7/21/2015	Urban	0.32	1.60	0.80	4.04	3.94	1.28
M-0040	8/26/2015	Urban	0.38	0.62	0.39	8.66	2.33	0.24
M-0467	8/19/2015	Urban	1.11	1.32	0.16	5.19	6.46	0.21
M-0465	8/19/2015	Urban	0.38	1.25	0.69	7.56	5.55	0.87
M-0528	8/13/2015	Urban	0.70	2.92	0.76	4.92	7.43	2.22
M-0039	8/11/2015	Urban	0.97	2.44	0.60	3.09	2.12	1.47
M-0211	8/11/2015	Urban	0.53	1.06	0.50	6.81	9.20	0.53
M-0212	8/11/2015	Urban	0.99	1.95	0.49	6.37	8.88	0.96
M-0026	8/26/2015	Forest	1.26	1.26	0.00	15.68	7.58	0.00
M-0481	9/15/2015	Wetlands	0.70	1.55	0.55	6.30	6.36	0.85
M-0483	9/15/2015	Wetlands	1.61	1.62	0.00	0.05	9.61	0.01
East Vent	10/26/2015		1.41	2.78	0.49	6.40	5.96	1.37
West Vent	10/26/2015		1.99	2.96	0.33	8.70	7.68	0.97
East Vent	6/27/2016	Vent	0.99	0.99	0.57	4.55	7.16	1.33
West Vent	6/27/2016	Vent	1.65	1.65	0.37	5.85	6.55	0.96
CRH	6/28/2016	Vent	0.90	0.90	0.64	8.60	8.32	1.62
Blue Grotto	6/28/2016	Vent	0.50	0.50	0.77	5.86	5.86	1.68
Christmas tree	6/28/2016	Vent	2.05	2.05	0.35	5.82	6.20	1.09
Indian cave	6/28/2016	Vent	0.83	0.83	0.68	9.32	8.72	1.76
Timber	6/28/2016		0.70	0.70	0.70	5.68	6.35	1.65

*UFA: Upper Floridan aquifer; IAS: Intermediate aquifer system; LFA: Low Floridan aquifer; WWTF: wastewater treatment facility. CRH: Catfish recreation hall.

To further understand the springshed patterns of denitrification, we performed the correlation of denitrification-related parameters (e.g., nitrate, $\delta^{15}N\text{-}NO_3$ and $\delta^{18}O\text{-}NO_3$) with the geochemical-based principal component (PC1 and PC2) scores obtained in section 4.3.4.2 (Figure 4.3.3). As mentioned in section 4.1.4.3, the PC1 negatively correlated with dissolved CH_4, NH_4, and TOC, positively correlated with dissolved oxygen and water temperature. It thus makes sense that PC1 correlated positively with nitrate in the ground water ($P < 0.05$, Figure 4.3.13). It is more likely that dissolved oxygen and nitrate which were significantly correlated with both PC1 and PC2, were the most important factors that affected denitrification process.

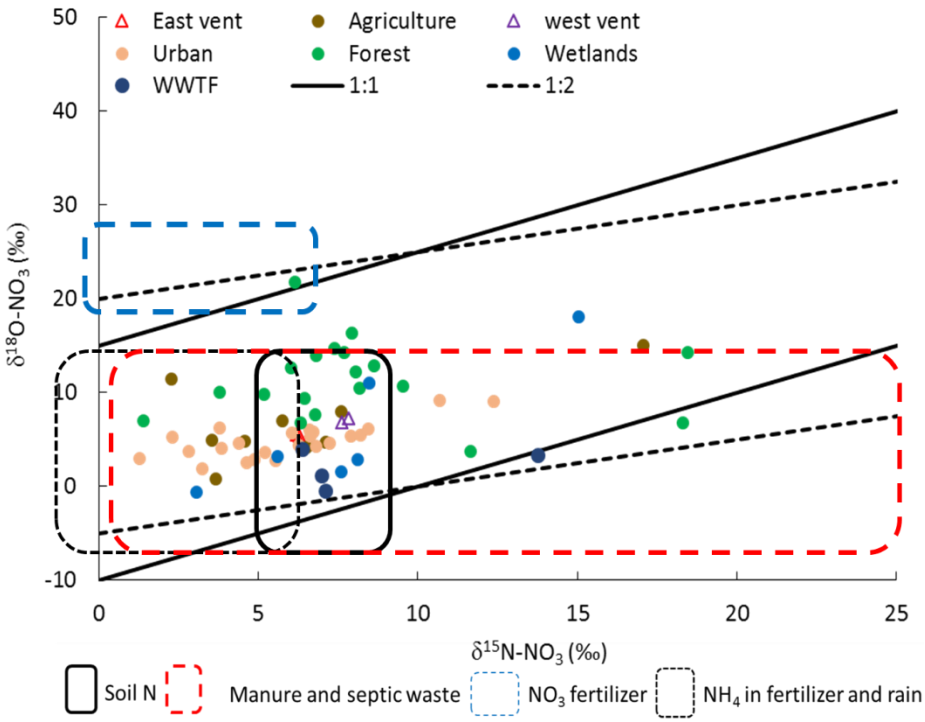

Figure 4.3.12. The $\delta^{18}O$ and $\delta^{15}N$ of nitrate from the 61 wells in the silver springs springshed. Solid and dotted lines represent theoretical upper and lower bounds for enrichment due to denitrification based on the $\delta^{18}O\text{-}NO_3$: $\delta^{15}N\text{-}NO_3$ fractionation ratio of 1:1 and 1:2, respectively.

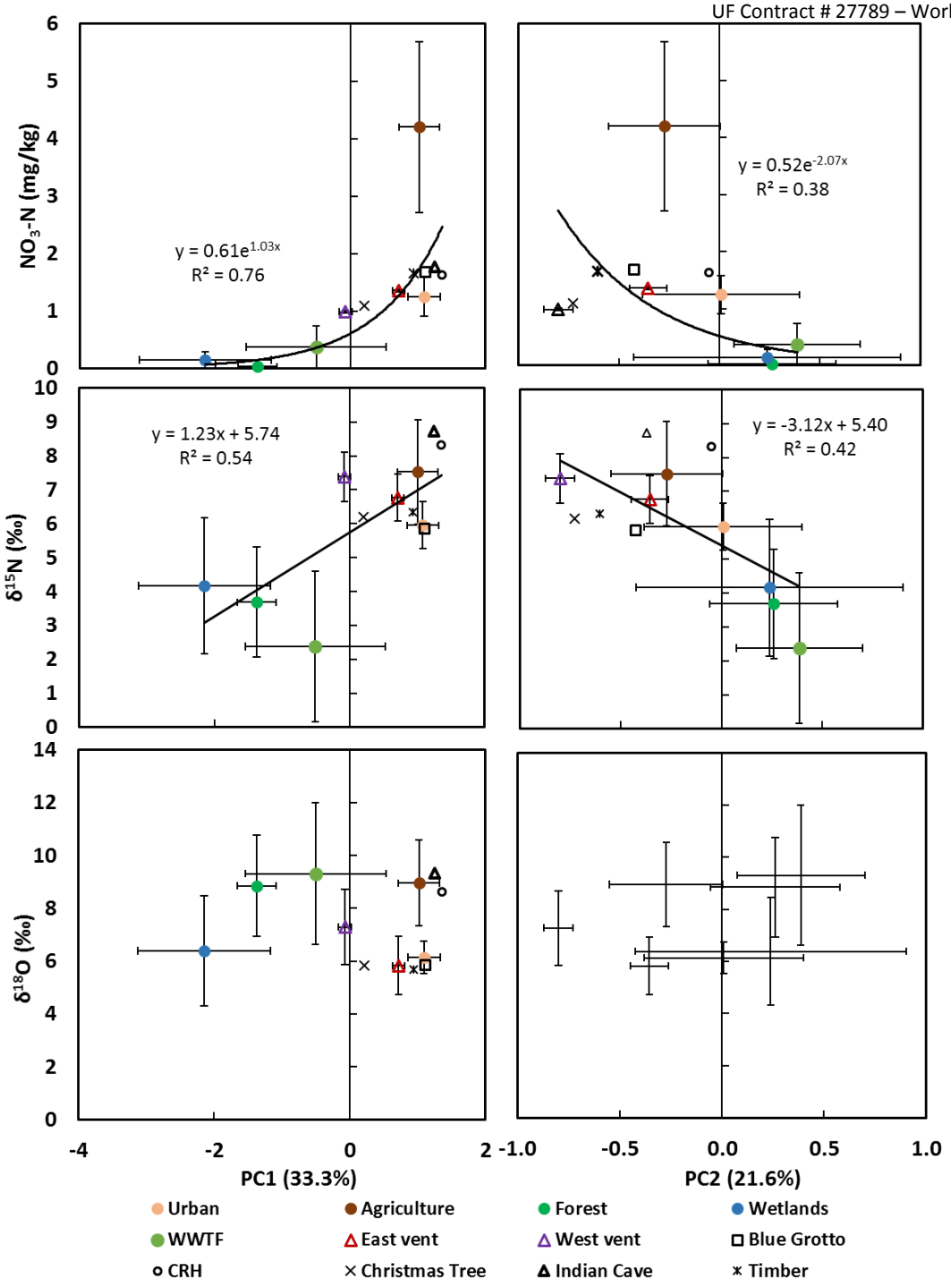

Figure 4.3.13. Correlation between principal component 1 and 2 and concentration and isotopic composition of nitrate categorized by land use.

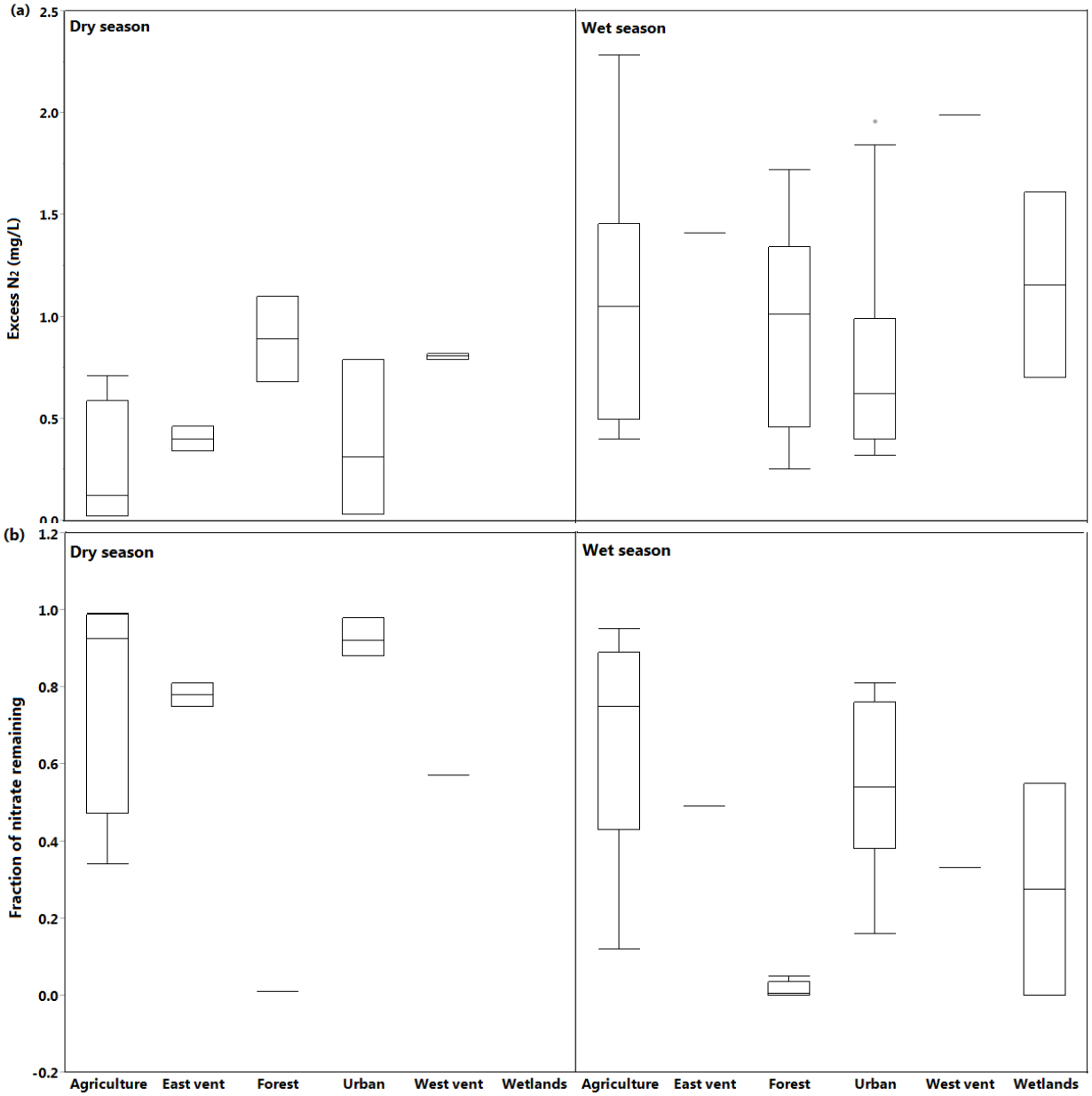

Figure 4.3.14. Boxplot of (a) excess N_2 and (b) fraction of NO_3 remaining for different land uses in the dry and wet season.

Based on the measured nitrate concentration and calculated excess N_2 derived from denitrification, we estimate that the nitrate concentration in the East and West Mammoth vents represents approximately 75-81 % and 57 %, respectively of the original nitrate contained in those waters (Table 4.3.6). The west vent showed higher excess N_2 and a lower fraction of remaining nitrate than east vent in both wet and dry season (Figure 4.3.13), indicating more N_2 removal at the west vent. Correspondingly, since the west vent grouped with land uses of Forest and Wetlands (largely in the confined aquifer of the Eastern springshed), a lower fraction of

remaining nitrate also occurred in groundwater with these land uses in both dry and wet seasons (Figure 4.3.13b). However, the groundwater in land uses of Forest and Wetlands did not show higher excess N_2 compared to that of urban and agriculture land uses in wet season (Figure 4.3.13a).

4.3.4.5 Denitrification Progression

The exact isotopic enrichment factor ε for $\delta^{15}N\text{-}NO_3$ can be derived using the relationship between $\delta^{15}N\text{-}[NO_3]_R$ and $\ln([NO_3]_R)$ (Böhlke et al. 2002; Green et al. 2008; Heffernan et al. 2012). For our study, we found for the two groups, $^{15}\varepsilon$ would be -5~ -7 ‰ (Figure 4.3.15), which fell in the range reported for denitrification in groundwater elsewhere (Mariotti et al. 1988; Böhlke et al. 2002; Green et al. 2008). Accordingly, there would be one source of nitrate with isotopic composition of $\delta^{15}N$=-21 and $\delta^{18}O$=-15 ‰ and, another with $\delta^{15}N$=5 and $\delta^{18}O$=5 ‰ (Figure 4.3.16). To our knowledge the very low isotopic signature of the first source is likely the result of poor isotopic measurement in these extremely low nitrate-containing samples. The second source is plausible and may be indicative of nitrate derived from soil N or organic sources such as manure, wastewater or septic N (Kendall 1998; Figure 4.3.1 and 4.3.12).

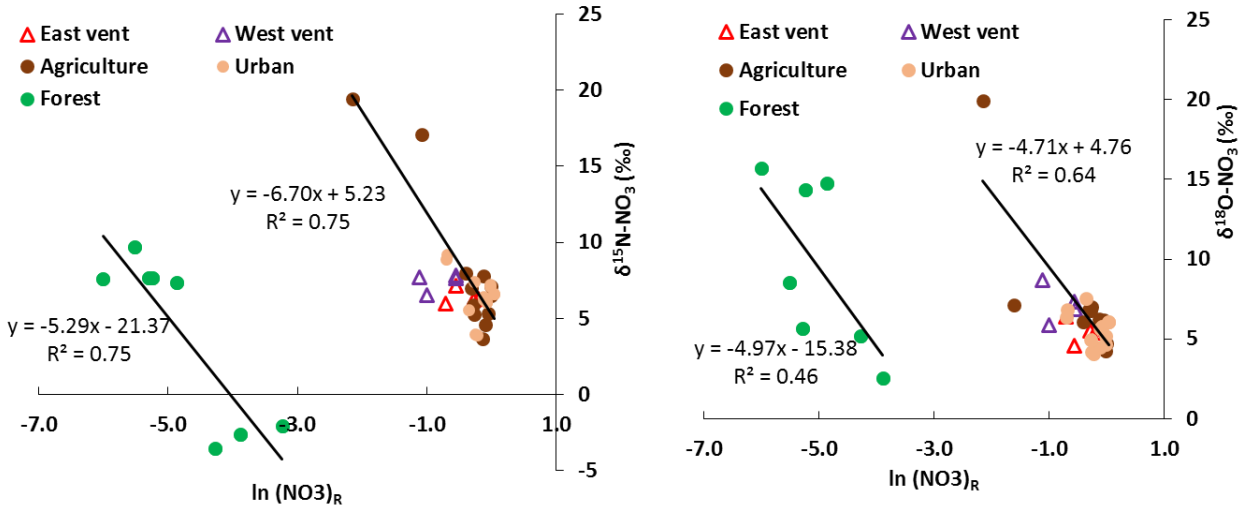

Figure 4.3.15 Relationship between $\ln([NO_3]_R)$ and $\delta^{15}N$-/ $\delta^{18}O$ $[NO_3]_R$ for different land use.

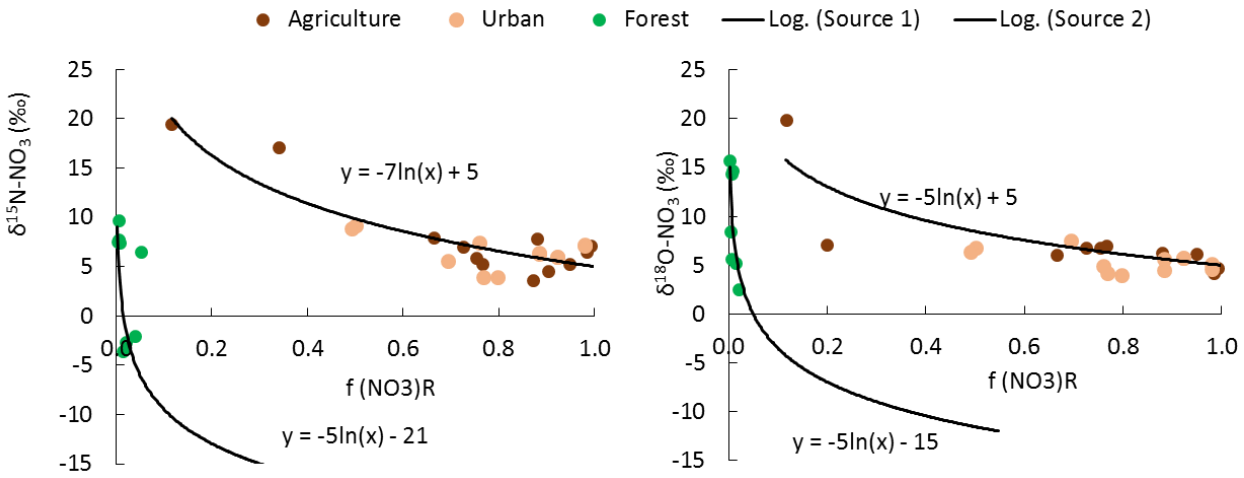

Figure 4.3.16. Variation of $\delta^{15}N$ and $\delta^{18}O$ of remaining nitrate with the fraction of NO_3^- remaining.

4.3.4.6 Microbial Evidence of Denitrification in Groundwater

Overall, in the aquifer water filter samples there **w**as no clear impact of land use on the relative abundance of *nosZ*-harboring putative denitrifying bacteria or *16S rRNA* gene based bacterial community abundances. Bacterial abundances generally varied between 10^5-10^8 bacteria L^{-1} water while *nosZ* gene abundances were between 10^4 and 10^6 L^{-1}, comprising between 0.8 and 7.3 % of the total bacterial community (Figure 4.3.17). N*osZ* ratios tended to decrease with increasing sample depth, though not significantly (r=0.551, p=0.079). Overall, the ratio of *nosZ* to *16S rRNA* gene abundance was markedly higher (1 to 3 magnitudes) than that found in the aquifer sediments associated with these wells, regardless of sediment depth, indicating a high potential for denitrification to occur in the water. The highest proportion of *nosZ* to the size of the total bacterial community occurred in M0785 a low density residential area with horse farms, followed by M0777 characterized by field crops and pasture land, M0771 in a low density residential area associated with golf courses and septic systems and M0775, a low density residential area with field crops and pasture land.

The pre-experimental finding that the use of a 2.7 um pre-filter did not consistently result in lower abundances (data not shown) suggests that bacterial communities are not associated with larger suspended particulate matter in the aquifer water. There was only one significant correlation between abundance data and 48 measured water parameters, *16S rRNA* gene abundance was significantly correlated with *nosZ* (r=0.73, p=0.01). No *16S rRNA* or *nosZ* genes were detected in the forest land use M-0779 and M-0780 filters, despite multiple extraction and amplification attempts. These wells correspond to very low DO values and the presence of H_2S, indicating highly anaerobic conditions. While this would be expected to depress the abundance of denitrifiers we have no reason to suspect that bacteria as a whole are absent from these wells. Likewise, amplification of both genes failed in well M0776 with no apparent explanation.

Principal component analysis (PCA) was performed to discern the grouping of sites and their relationship to abundance and water chemistry measures (Figure 4.3.18). Overall the water chemistry parameters imparted a much stronger shaping effect to the orientation of the wells in

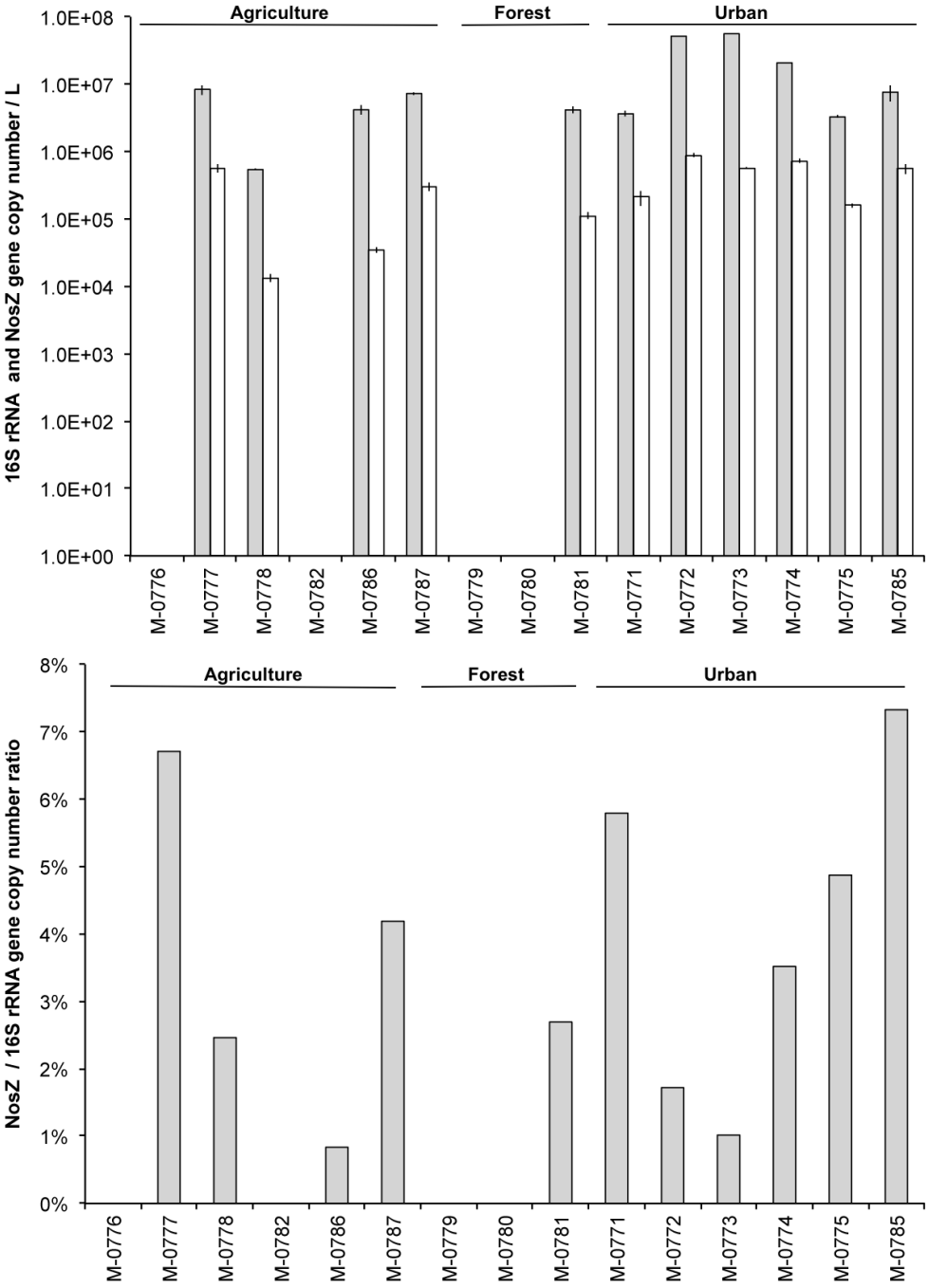

Figure 4.3.17. *16S rRNA* gene and *nosZ* gene copy numbers obtained from filtering 20 L of water with standard errors (top). Average ratios of *nosZ* to *16S rRNA* gene copy numbers in the identical wells. Wells with no data indicate that no detectable amplification of either gene was present across multiple runs.

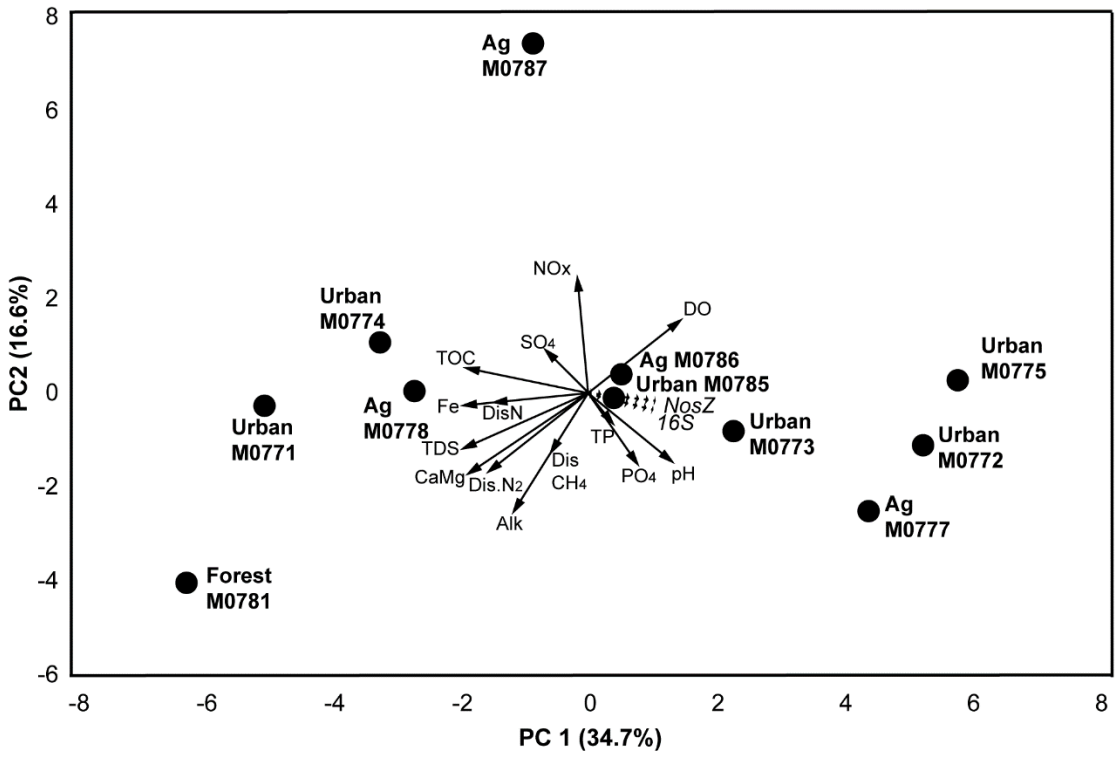

Figure 4.3.18. Principal components plot of the filter *16S rRNA* and *nosZ* data with measured water chemistry data showing the loading of each vector and position of each well. Samples were excluded if they did not have detectable gene copies.

the PCA plot, compared to the abundance data. The majority of site differentiation was due to PC1 while M0787, a mixed pasture and former citrus grove with a high concentration of NO_3^-, was separated by PC2 and the NO_x vector. Wells with the highest *nosZ* and *16S rRNA* gene abundance, with the exception of M0787, were partitioned to positive PC1 values with negative relationships to TOC, Fe and dissolved N.

In summary, unlike the aquifer sediment samples originating from many of the same wells, there was no impact of depth on the abundances of putative denitrifiers or the bacterial community as a whole. Both the aquifer water and sediment samples did not find significant grouping of wells according to land use type. The data shows that a high proportion of *nosZ*-harboring bacteria are present and thus, water chemistry such as TOC availability, DO, and presence of nitrate/nitrite likely influence denitrification activity.

4.3.5 CONCLUSIONS AND RECOMMENDATIONS

Geochemical approaches characterize the groundwater wells into two main categories where ~80 % of the springshed is of the Ca/HCO_3- type with various other wells being dominated by Na/Cl or SO_4. A better separation of water compositions was obtained using principal component analysis based on non-conservative geochemical variables, which better ordinated samples from

the well and vent locations according to land use. In this analysis, the East and West Mammoth vents were separated with the West vent being similar to wells in the confined aquifer portion of the springshed with the land uses of forest and wetland and the East vent being similar to the more unconfined western springhsed with more agricultural and urban land use.

This study targeted the spatial and temporal patterns of denitrification indicators in the Floridan Aquifer System of the Silver Spring springshed. The results thus far are inconclusive, but a number of important findings have been made. For example, estimates of aquifer denitrification based on dissolved gases indicate that up to 25 % and 43 % of nitrate in the groundwater is being denitrified within the aquifers of the east and west Mammoth vents, respectively,. Similar findings are also possible for other locations (based on a limited subset of wells) and are confirmed by the presence of denitrification genes and microorganisms in aquifer samples throughout the springshed.

Based on the spatial patterns of nitrate concentration with the land uses and combined with the results of the principle component analysis, the land uses of forest and wetlands are features with low nitrate compared to the land uses of agriculture and urban. The denitrification progression based on the calculation of dissolved N_2 and Ar also showed higher remaining proportion of nitrate in the agriculture and urban areas, indicating greater potential sources and more potential for denitrification in those areas. This finding is somewhat complicated by the fact that sites in this study were also segregated on the basis of confinement of the aquifer, with highest potential for denitrification (more anaerobic conditions) being observed on the eastern portion of the springhsed along with the predominance of forested and wetland land uses.

Back calculation of the isotopic composition of nitrate source stable isotopic ratios of nitrate seem to indicate two apparent nitrate sources with enrichments consistent with isotopic theory during denitrification. Considerable uncertainty remains in the exact identity of this groundwater nitrogen source as there is still considerable overlap of the isotopic sources in this region, particularly for organic N sources of wastewater and manure.

Dissolved concentrations of methane and nitrous oxide also show potential association with nitrogen cycling processes as they have in other systems. Although the relative contribution of the electron donors responsible for denitrification (e.g., organic carbon, iron, reduced sulfur) and the processes responsible for dissolved gases (CH_4 and N_2O) were not fully explored, the patterns of the correlations of these gases with other water quality parameters suggest a promising use of these to better identify zones of potential denitrification. Dissolved gas concentrations, gas ratios (N_2:Ar), and stable isotopic ratios of nitrate in the spring vents demonstrate there is potential for seasonal variability, and that this variability is likely related to recharge patterns, age of water exiting the vents, and patterns of denitrification in the aquifer.

4.3.6 FUTURE RESEARCH NEEDS

Estimates of aquifer denitrification have been made only at selected springshed locations. For this reason, a thorough spatial evaluation of hotspots of denitrification has not been attempted.

Based on the apparent utility of the dissolved gas and stable isotopic ratios of nitrate, there is a continued need for monitoring of seasonal patterns in dissolved gases and isotopes in vents and wells. More samples for excess N determination are needed to better establish the potential isotopic character of source N throughout the springshed, especially in areas with very low nitrate.

The uncertainties in isotopic signal, whether by soil processes or by outside source contribution, may be constrained by the addition of a third natural tracer, boron. Boron has been used to trace nitrate in groundwater because its mobility is very similar to that of nitrate, and boron stable isotopes, ^{11}B and ^{10}B, are unaffected by the soil processes that affect the fractionation of nitrate stable isotopes (Bassett et al. 1995). Boron stable isotope values are also specific enough to organic sources that they can help distinguish between possible manure and septic sources of nitrate, or could indicate when fractionation is occurring (Seiler 2005; Widory et al. 2003).

4.3.7 REFERENCES

Aeschbach-Hertig, W. and Solomon, D. K. 2013. Noble gas thermometry in groundwater hydrology, in: Burnard, P. (Ed.), The noble gases as geochemical tracers. Advances in Isotope Geochemistry. Springer Verlag, pp. 81-122

Aravena, R. and Robertson, W. D. 1998. Use of multiple isotope tracers to evaluate denitrification in ground water: study of nitrate from a large-flux septic system plume. Groundwater, 36(6): 975-982.

Blicher-Mathiesen, G., McCarty, G. W. and Nielsen, L. P. 1998. Denitrification and degassing in groundwater estimated from dissolved dinitrogen and argon. Journal of Hydrology, 208: 16-24.

Böhlke, J. K., Wanty, R., Tuttle, M., Delin, G. and Landon, M. 2002. Denitrification in the recharge area and discharge area of a transient agricultural nitrate plume in a glacial outwash sand aquifer, Minnesota. Water Resources Research, 38(7): 1-26

Cey, B. D. 2008. Dissolved Noble gases in ground water. Dissertation, the University of Texas at Austin.

Christopher, T. Green, L. J., Puckett, Böhlke, J. K., Bekins, B. A., Phillips, S. P., Kauffman, L. J., Denver, J. M. and Johnson, H. M. 2006. Limited Occurrence of Denitrification in Four Shallow Aquifers in Agricultural Areas of the United States. Journal of Environmental Quality, 37 (3): 994-1009

Delwiche, C. C. and Steyn, P. L., 1970. Nitrogen isotope fractionation in soils and microbial reactions. Environmental Science & Technology, 4(11), 929-935.

Fogg, G. E., Rolston, D. E., Decker, D. L., Louie, D. T. and Grismer, M. E., 1998. Spatial variation in nitrogen isotope values beneath nitrate contamination sources. Ground water, 36(3), 418-426.

Granger, J., Sigman D. M., Lehmann, M. F. and Tortell, P. D. 2008. Nitrogen and oxygen isotope fractionation during dissimilatory nitrate reduction by denitrifying bacteria. Limnology and Oceanography, 53(6): 2533-2545.

Green, C. T., Puckett, L. J., Böhlke, J. K., Bekins, B. A., Phillips, S. P., Kauffman, L. J., Denver, J. M. and Johnson, H. M. 2006. Limited occurrence of denitrification in four shallow aquifers in agricultural areas of United States. J. Environ. Qual. 2006. 37(3): 994–1009.

Green, C. T., Puckett, L. J., Böhlke, J. K., Bekins, B. A., Phillips, S. P., Kauffman, L. J., Denver, J. M. and Johnson, H. M. Limited Occurrence of Denitrification in Four Shallow Aquifers in Agricultural Areas of the United States (2008). USGS Staff -- Published Research. Paper 24

Heffernan, J. B., Albertin, A. R., Fork, M. L., Katz, B. G. and Cohen, M. J. 2012. Denitrification and inference of nitrogen sources in the karstic Floridan Aquifer. Biogeosciences 9: 1671-1690.

Huang, Y. H., Zhang, T. C., Shea, P. J. and Comfort, S. D. 2003. Effects of Oxide Coating and Selected Cations on Nitrate Reduction by Iron Metal. Journal of Environmental Quality, 32(4): 1306-1315.

Inglett, P. W., Kana, T. and An, S. 2013. Membrane inlet mass spectrometry approaches for measuring denitrification. Chapter 27, pp. 503-518. In: DeLaune, Reddy, Richardson, and Megonigal, eds. Methods in Biogeochemistry of Wetlands, Soil Science Society of America. Madison, WI. 1024 pp.

Jones, L. C., Peters, B., Pacheco, J. S. L., Casciotti, K. L. and Fendorf, S. 2015. Stable Isotopes and Iron Oxide Mineral Products as Markers of Chemodenitrification. Environmental Science & Technology, 49(6): 3444-3452.

Kampbell, D. and Vandegrift, S. 1998. Analysis of dissolved methane, ethane, and ethylene in ground water by a standard gas chromatographic technique. Journal of Chromatography Science, 36: 253 - 256.

Knowles, L., Katz, B. G., and Toth, D. J. (2010). Using multiple chemical indicators to characterize and determine the age of groundwater from selected vents of the Silver Springs Group, central Florida, USA. *Hydrogeology Journal*, *18*(8), 1825–1838. https://doi.org/10.1007/s10040-010-0669-y

Ledgard, S. F., Freney, J. R. and Simpson, J. R. 1984. Variations in natural enrichment of ^{15}N in the profiles of some Australian pasture soils. Australian Journal of Soil Research, 22: 155-164.

Lehmann, M, F, Reichert. P., Bernasconi, S. M., Barbieri, A. and McKenzie, J. A. 2003. Modelling nitrogen and oxygen isotope fractionation during denitrification in a lacustrine redox-transition zone. Geochimica et Cosmochimica Acta, 67(14): 2529-2542.

Madison, R. J. and Brunett, J. O. 1985, Overview of the occurrence of nitrate in ground water in the United States, in National Water Summary 1984—Hydrologic events, selected water-quality trends, and ground-water resources: U.S. Geological Survey Water-Supply Paper 2275, p. 93-105.

Mariotti, A., Leclerc, A. and Germon, J. C. 1982. Nitrogen isotope fractionation associated with the $NO_2^- \rightarrow N_2O$ step of denitrification in soils. Canadian journal of soil science, 62(2), 227-241.

Mariotti, A. 1986: Denitrification in groundwaters, principles and methods for its identification: a review. Journal of Hydrology 88(1/2): 1-23.

Munch, D. A., Toth, D. J., Huang, C., Davis, J. B., Fortich, C. M., Osburn, W. L., Phlips, E. J., Quinlan, E. L., Allen, M. S., Woods, M. J., Cooney, P. Knight, R. L., Clarke, R. A., and Knight, S. L. 2007. *Fifty-year retrospective study of the ecology of Silver Springs, Florida*. *Special Publication SJ2007-SP4*. Palatka: St. Johns River Water Management District.

Osburn, W., Toth, D. J. and Boniol, D. 2002. Springs of the St. Johns River Water Management District. Technical Report SJ2002-5. Palatka, FL: St. Johns River Water Management District.

Osmond, J. K., Kaufman, M. I. and Cowart, J. B. 1974, Mixing volume calculations, sources, and aging trends of Floridian Aquifer water by Uranium isotopic methods: Geochimica et Cosmochimica Acta, v. 38, p.1083-1100.

Phelps, G. G. 2004. Chemistry of ground water in the Silver Springs Basin, Florida, with an emphasis on nitrate. Scientific Investigations Report 2004-5144. Denver, CO: USGS.

Rosenau, J. C., Faulkner,G. L., Hendry, Jr., C. W. and Hull, R. W. 1977. Springs of Florida. Geological Bulletin No. 31, revised. Tallahassee, FL: Florida Geological Survey.

Scott, T. M., Means, G. H., Meegan, R. P., Means, R. C., Upchurch, S. B., Copeland, R. E., Jones, J., Roberts, T. and Willet, A. 2004. Springs of Florida. Bulletin No. 66. Tallahassee, FL: Florida Geological Survey.

Sigman, D. M., Casciotti, K. L., Andreani, M. C., Barford, C., Galanter, M. and Böhlke, J. K. 2001. A bacterial method for the nitrogen isotopic analysis of nitrate in seawater and freshwater. Anal. Chem.,73: 4145–4153.

Seiler, R. L. 2005. Combined use of ^{15}N and ^{18}O of nitrate and 11 B to evaluate nitrate contamination in groundwater. Applied Geochemistry, 20(9), 1626-1636.

Bassett, R. L., Buszka, P. M., Davidson, G. R. and Chong-Diaz, D. 1995. Identification of groundwater solute sources using boron isotopic composition. Environmental science & technology, 29(12), 2915-2922.

Vogel, J. C., Talma, A. S. and Heaton, T. H. E. Gaseous nitrogen as evidence for denitrification in ground water. J. Hydrol. 1981. 50:191–200.

Widory, D., Kloppmann, W., Chery, L., Bonnin, J., Rochdi, H. and Guinamant, J. L. 2004. Nitrate in groundwater: an isotopic multi-tracer approach.Journal of Contaminant Hydrology, 72(1), 165-188.

Winston, R. B., 2000, Graphical User Interface for MODFLOW, Version 4: U.S. Geological Survey Open-File Report 00-315, 27 p.

Weiss, R. F. 1970. The solubility of nitrogen, oxygen, and argon in water and seawater. Deep Sea Res. 17: 721-735.

Xue, D., Botte, J., De Baets, B., Accoe, F., Nestler, A., Taylor, P., Van Cleemput, O., Berglund, M. and Boeckx, P. 2009. Present limitations and future prospects of stable isotope methods for nitrate source identification in surface-and groundwater. Water research 43(5): 1159-1170.

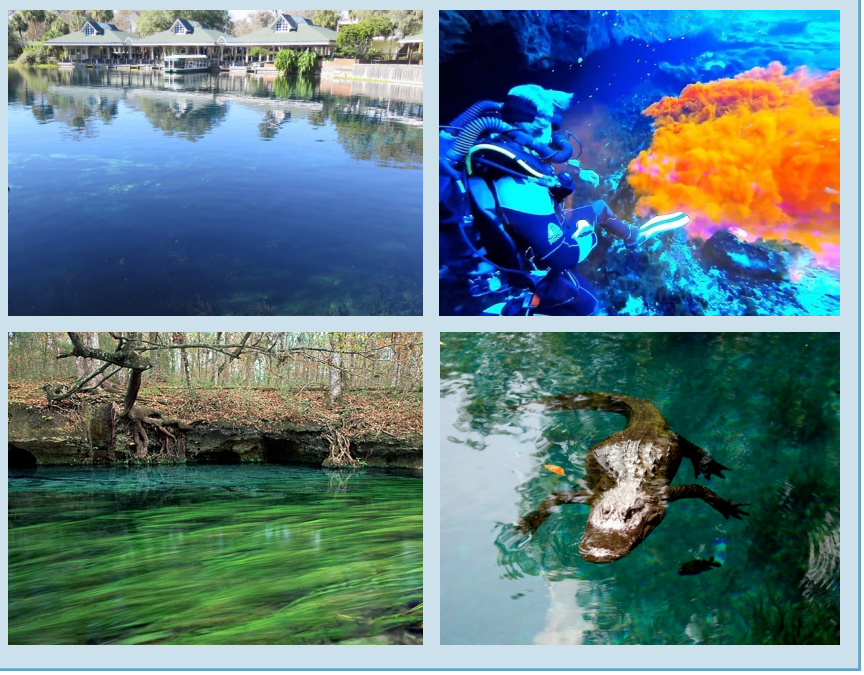

Collaborative Research Initiative on
Sustainability and Protection of Springs [**CRISPS]**

Section 5

[Work Order No: 2]

FINAL REPORT

2014 - 2017

submitted to:

St. Johns River Water Management District
Springs Protection Initiative [SPI], UF Contract # 27789

UF | UNIVERSITY of FLORIDA
Water Institute

C R I S P S

Section 5

HYDRAULICS AND HYDRODYNAMICS

Final Report 2017
Work Order No. 2

Principal Investigators:

David Kaplan, University of Florida
Pete Sucsy, St Johns River Water Management District

Project Team

David Kaplan
Nathan Reaver
Alexis Johnson
Engineering School of Sustainable Infrastructure and Environment
University of Florida

Pete Sucsy
Ed Carter
Joseph Stewart
Yanfeng Zhang
St Johns River Water Management District

This document reports findings and results of a work order for a 3-year project in compliance with Agreement between University of Florida (UF) and St. Johns River Water Management District (SJRWMD) UF Contract #27789. It is part of the *UF Collaborative Research Initiative on Springs Protection and Sustainability (CRISPS)* and supports the science component of *the SJRWMD Springs Protection Initiative (SPI).*

5.0 EXECUTIVE SUMMARY

The St. Johns River Water Management District (SJRWMD), in partnership with the University of Florida (UF), has initiated the SJRWMD-UF *Springs Protection Initiative-Science (SPIS)/Collaborative Research Initiative on Sustainability and Protection of Springs (CRISPS)* via RFQ 27789. A detailed background and set of major objectives and questions related to Silver River hydraulics and hydrodynamics are presented in Section 4 of that RFQ, with a primary goal of predicting unsteady water level profiles and velocity profiles using the Environmental Fluid Dynamics Code (EFDC) to determine whether velocity may be an important non-nitrate factor influencing the community structure and function of primary producers in the system. In support of that goal, the objectives of the University of Florida Spring System Hydrodynamics/Hydraulics work order are to: 1) yield a more thorough understanding of the velocity and residence time distributions in the channel of the Silver River and to quantify the location and magnitude of transient storage and exchange; 2) identify critical shear stresses for the entrainment and detachment of algae; and 3) link study findings to ongoing 3-D modeling with a focus on submerged aquatic vegetation (SAV) influence on velocity, residence times, and effects on stage-discharge relationship. In addition to reporting on these objectives, this chapter also summarizes progress to date on the SJRWMD's hydrodynamic modeling.

Regarding Objective 1, four dye tracer experiments using *in situ* fluorometry and grab samples (along with data from a previous study) allowed us to delineate flow paths and estimate reach-scale hydraulic properties of the Silver River across different seasons and hydraulic conditions by fitting observed breakthrough curves (BTCs) using 1-D transport and mixing models. Dye tracer results also provided valuable data for testing and calibration of the Environmental Fluid Dynamics Code (EFDC) model. BTC data indicated the presence of three upstream flowpaths: one via the main river channel and two through the "back channel" (i.e., Ft. King Waterway). Reach-scale velocities and mixing parameters measured via dye trace experiments were variable in time and space, illustrating how the flow regime of the Silver River changes with different boundary conditions (spring flow and downstream river stage), as well as with in-channel properties such as SAV coverage and density. This variation impacts in-channel hydrodynamics and likely affects biogeochemical transformations in the river's advective and transient storage zones.

Whole-river advective zone velocity varied from 0.17 to 0.22 m s^{-1} (near or below our best estimate of the critical velocity for algal presence; see below), while mean advective zone velocity for the downstream reach varied from 0.19 to 0.32 m s^{-1} (bounding our estimate of critical flow velocity). Higher spring discharge was not a good predictor of higher reach-scale velocity, illustrating the need to simultaneously consider changes in discharge, stage, and vegetative drag to understand reach-scale velocity. Upstream overall mean reach velocity was always lower than downstream, and the ratio of downstream to upstream velocities was highly variable, reinforcing the idea that the upstream and downstream river reach hydrodynamics act at least somewhat independently.

Mixing parameters were also variable across experiments, illustrating differential mixing mechanisms across seasons and boundary conditions; dispersion and transient storage were

generally greatest when mean velocity was low and downstream stage was high. Beyond model fitting, comparison of BTCs in vegetation beds relative to the adjacent main channel suggests that vegetation beds can serve as a partial barrier to mixing as well as zones of transient storage. Reactive tracer (Raz-Rru) results from our pilot study identified substantial Rru sorption to organic sediments that make reach-scale studies in large, highly organic spring systems impractical.

Regarding Objective 2, observational and experimental approaches were used to identify critical velocity and shear stress thresholds of algal presence to use as management targets. *In situ* flow modification devices were employed using a before/after control/impact (BACI) design to identify critical velocity and shear stress thresholds, quantify algal colonization and growth rates under reduced velocities, quantify algal clearing rates after flow restoration, and identify hysteretic behavior (if present). These experiments showed clear algal-colonization and growth effects from induced velocity reduction. While control sites only saw modest epiphytic algal growth, algal cover at treatment sites approached 100 % after one week. Fitted logistic models revealed an intrinsic algal growth rate (in the absence of velocity) near 1 day^{-1} with a 95 % credible interval (CI) of 0.70 day^{-1} to 1.60 day^{-1}, indicating a doubling of algal cover/abundance every day until reaching carrying capacity at or near 100 % cover. Hysteretic behavior was not observed.

Modeling and analysis of algal cover, SAV cover, and velocity datasets from several Florida springs were used to statistically identify critical velocities and shear stresses that predict algal/SAV presence and absence. Data from the FL Springs Synoptic Study, the Silver River, Gum Slough, and several coastal springs had an overall mean algal velocity threshold of 0.215 m s^{-1} with a 95 % CI of 0.160 to 0.270 m s^{-1}. These values are supported by data from other studies, which identify critical values from 0.22 to 0.25 m s^{-1}. Mean critical shear stress calculated using diver-collected data from the Silver River was 0.35 N m^{-2} with a 95 % CI of 0.02 to 0.70 N m^{-2}. Mean critical velocity threshold estimated for SAV was 0.33 m s^{-1}, with a 95 % CI between 0.24 m s^{-1} and 0.44 m s^{-1}. These experimental and observational results can be used together with EFDC modeling to predict the impact of alternate flow restoration and management scenarios on likely algal and SAV cover.

Regarding Objective 3, we analyzed changes in the stage/discharge relationships at the Silver River main spring pool, Silver River 1,200 m station, and Ocklawaha River Conner station. These results were used to calculate likely velocity changes due to observed stage/discharge shifts and assess their possible implications for algal proliferation. We also tested whether the visually apparent shift in stage/discharge relationship was statistically supported and explored a possible mechanism of SAV growth and uprooting to explain this shift. All stations showed a discernable shift in the stage/discharge relationship at roughly the same time (2000-2003), and all relationships shifted from a state of lower stage for a given discharge to a state of higher stage for the same discharge (0.6-0.8 meters increase in stage for all stations). This finding suggests either the phenomena causing the shift is present throughout the river or is only acting at the end of the river, with the influence propagating upstream through a backwater effect.

Modeled velocity impacts of the stage/discharge shift suggest that under historic conditions, velocity in the main channel leaving the spring bowl was > 0.24 m s^{-1}, close to the critical algal

velocity threshold. Under the current stage/discharge relationship, the expected velocity is < 0.16 m s^{-1} at the same discharge, significantly lower than historic velocities and the critical velocity. This finding could, in part, explain algal proliferation in areas of the spring run where there historically had been very little macroalgae; a shift in the stage/discharge relationship generally means a slower moving river, potentially facilitating algal colonization. Change point analysis identified July 2001 as the most probable time to split the dataset into two distinct stage/discharge relationships. Reduced-complexity numerical simulation demonstrated the potential for simple feedbacks among Manning's equation-based roughness, logistic growth of SAV, and a critical velocity for SAV removal can reproduce a stage/discharge shift with a transition period in between shifts and hysteretic properties. This model lends support to the idea that SAV may play a role in the stage/discharge shift observed in the Silver River, with subsequent effects on in-stream velocity and algal cover.

Additional reduced-complexity modeling of the coupled aquifer-spring pool-spring run system was applied to constrain the range of spring discharge and aquifer level changes that might be brought about though vegetative changes in the spring run. Results of this conceptual model showed that an increase in river resistance (due to SAV expansion or any other biophysical driver) can have substantial impacts on the surface hydrology (e.g., stage and velocity) of a spring-fed river. However, the impact of channel roughness changes on the level and discharge of the connected aquifer system depends on the relative size of the aquifer region feeding the spring. These results suggest that even large changes in channel roughness in the Silver River due to SAV expansion are not likely to have a substantial impact on aquifer level or spring discharge.

Finally, velocity validation transects confirmed that velocities measured using Acoustic Doppler Current Profilers (ADCP) and the Electromagnetic Flow Meter (EFM) were in the same range, with several noteworthy exceptions. The ADCP data was more highly resolved and identified small patches of high-velocity flow that were not captured by the point-based EFM technique. However, the point-based measurements captured velocity data near the benthic surface in some locations where the ADCP did not; this was also evident in the differences in inferred bathymetry between the approaches. These data also provided a set of reference velocity measurements for calibration and validation of modeled 1-D velocity profiles using EFDC algorithms and an analytical vegetation drag and turbulence closure model.

Regarding EFDC modeling, we completed calibration and confirmation of a three-dimensional hydrodynamic model of Silver River that includes vegetative drag and generation of turbulence by submersed aquatic vegetation (SAV). The hydrodynamic model is an application of the Environmental Fluid Dynamics Code (EFDC) with modifications to the momentum and turbulence closure equations. The model simulates water level, three-dimensional velocity, turbulence intensity and length scale, turbulent mixing, and dispersion given Silver River discharge and downstream tailwater of the Ocklawaha River at Connor.

The model grid consists of 13,439 horizontal cells and 8 vertical cells for a total of 107,512 cells. Cell area generally increases from upstream to downstream with an average cell area of 29.4 m2 in the upper third of the river, 30.2 m2 in the middle third, and 41.5m2 in the lower third. The average horizontal cell length is 5.8 m.

The EFDC hydrodynamic model was calibrated and confirmed for stage, velocity, and conservative transport using two dye tracer experiments conducted by University of Florida and 40 observed conditions of discharge and stage by the U.S. Geological Survey for both pre- and post- 2000 periods. The range of time periods represented a range of shifting stage-discharge relationships for Silver River that evidently result from reach-scale changes to SAV coverage and density. The EFDC model parameters represented SAV changes by altering the model parameters of SAV height and vegetative drag coefficient.

The calibrated EFDC hydrodynamic model is presently being used to (a) characterize velocity by river segment for both pre- and post-2000 conditions, (b) test the response of stage and velocity to SAV reduction within each river segment, (c) quantify the effect of altered stage-discharge relationships for the Ocklawaha River at Connor on stage and velocity in Silver River, and (d) test the effect on velocity in the upper Silver River on diversion of flow through the back-channel.

5.1 VELOCITY AND RESIDENCE TIME DISTRIBUTIONS AND TRANSIENT STORAGE

5.1.1 INTRODUCTION

Velocity and residence time distributions (RTDs) are sentinel hydraulic characteristics that describe solute transport in riverine systems and are critical for understanding the potential for biogeochemical transformations in the advective and transient storage pools. In particular, the primary in-stream controls on NO_3-N concentration in springs are uptake and storage by autotrophs (i.e., submerged aquatic vegetation [SAV] and benthic and epiphytic algae) and denitrification in biofilms and sediments. Several microcosm studies suggest that NO_3-N removal in a wetland system is accomplished primarily by macrophyte uptake rather than denitrification (Veraart et al. 2011), however a number of field studies show wide variation in the relative proportion of NO_3-N uptake via denitrification versus autotrophic uptake (Table 5.1.1).

Literature suggests the region beneath a stream bed where surface water and groundwater interact—known as the hyporheic zone—is a biogeochemical hotspot, however the hydraulic interactions between flow, velocity, hyporheic exchange, and water column autotrophic uptake of NO_3-N in springs are not well understood (Chapman et al. 1995; Heffernan and Cohen 2010). Given the importance of flow, velocity, and mixing in dictating spring chemistry and biology, the objectives of this effort are to use pulse injection of a conservative solute to perform in-stream tracer studies. Experimental results allow us to estimate reach-scale hydraulic properties of the Silver River by fitting observed breakthrough curves (BTCs) via non-linear regression fitting of 1-D transport and mixing models (e.g., OTIS [Runkel 2007]) and provide valuable data for Environmental Fluid Dynamics Code (EFDC) model testing and calibration. These results are also compared with the one previous tracer available for the Silver (Hensley 2010).

While the tracer injections described above allow us to estimate hyporheic exchange volumes by fitting hydraulic parameters to BTCs data, novel hydraulic tracer methods have recently been

introduced to directly quantify the role of microbial metabolism in nutrient processing. One such "smart tracer" (Haggerty et al. 2008) is the resazurin-resorufin system. Resazurin (Raz) is a redox-sensitive phenoxazine compound that reduces to resorufin (Rru) in the presence of metabolic activity by aerobes and facultative anaerobes; thus, the Raz-Rru system can be used to assess the relative proportion of spring vent discharge water that is directly affected by microbial metabolism (and is therefore likely to be undergoing denitrification). While unlikely to be feasible for reach-scale use on large rivers due to cost, we present initial results of lab studies using the Raz-Rru system with Silver River sediments that are useful for predicting Raz transformations under varying hydrologic conditions and may be useful for identifying the presence of transient storage zones with high rates of biogeochemical activity.

5.1.1.1 Site Description

Experiments described in this section were undertaken in the Silver River in Ocala, FL. Additional information about the Silver River can be found in the overall document introduction. Additionally, a single dye trace experiment was conducted in Alexander Springs Creek in the Ocala National Forest, FL. Alexander Springs Creek is fed by a 1st magnitude group of vents located in Lake County within the boundaries of the Ocala National Forest. The average discharge for this spring group from 1931-2010 was 105 cubic feet per second (cfs) or 68 million gallons per day (MGD). Nitrogen concentrations in this spring run are considerably lower than that of the Silver River, near the background levels of nitrate in the Floridan aquifer, approximately 0.044 mg L^{-1} (Scott et al. 2004).

Table 5.1.1. Estimated proportion of NO_3-N removal via denitrification versus autotrophic uptake.

Denitrification (%)	Autotrophic Uptake (%)	Notes	Source
16 ±10	-	NO_3-N removal, tracer study in Tennessee	Mulholland et al. 2004
16-43	-	Over 43 % in 25 % of streams studied (probably more because study disregarded time delay)	Mulholland et al. 2008
-	34-40	NH_4 and NO_3-N removal in wastewater treatment wetland, greater in submerged plants than cattails because of roots/leaves	Reddy 1983
6	77	77 % value based on Cedergreen and Madsen, 2002	Veraart et al. 2011
50-59	-	NO_3- removal with groundwater input	Hanson et al. 1994
72	-	Under N fertilization	Hamersley 2002 (thesis)
75	25	Seasonal discrepancy in percentages of root uptake	Caffrey and Kemp 1992
89-96	4-11	In microcosms with emergent and free floating plants	Lin et al. 2002
80	-	In spring and fall in the Ichetucknee Springs	Heffernan and Cohen 2010

5.1.2 MATERIALS AND METHODS

5.1.2.1 Dye Tracer Experiments

5.1.2.1.1 Field and Laboratory Methods

With the assistance of over 20 volunteers, UF implemented the first of four proposed dye tracer experiments on 4 March 2015 at approximately 18:00. Divers assisted in the release of 18.9 L (5 gallons) of 20 % Rhodamine WT directly in the flow stream of the Mammoth (Main) Spring vent (Figure 5.1.1). The flow of dye downstream was tracked at nine fixed stations (Figure 5.1.2). Three in-stream, submersible fluorometers (two Turner Designs CS3 and one Turner Designs SCUFA, Turner Designs, Inc., Sunnyvale, CA) were calibrated in the lab prior to deployment and collected data at 1-minute intervals. Six ISCO automated samplers collected 250-500 mL grab samples at one-hour intervals, with the exception of the unit in the main spring bowl, which collected samples every 30 minutes. Three ISCO samplers were located adjacent to in-stream fluorometers, but sampled within vegetation beds to explore the potential for differential mixing and transient storage in these zones.

Additionally, three boats ("rovers") collected 318 grab samples to characterize differential mixing (if present) along three gradients: 1) across the channel reach; 2) with depth; and 3) within five eco-geomorphological features (SAV beds, debris jams, emergent beds, and benthic depressions). Samples were collected using weighted tubing connected to a hand pump (Figure 5.1.3). Rover sampling continued overnight through the next morning. Rover samplers noted time, GPS location, sample depth, distance from bank, and eco-geomorphological feature. Samples were taken from as frequently as possible and from as many locations as possible to provide a good overall coverage of the river (Figure 5.1.4)

All ISCO and grab samples were refrigerated within 24 hours of collection and analyzed within one week. Rhodamine calibration curve development and concentration measurements used a 30 ppb stock solution of Rhodamine to produce the standard concentrations (30, 27, 21, 18, 15, 12, 9, 6, 3, 1.5, 0.3, 0.15, and 0 ppb, each with 7 replicates. Florescence of each of the 7 replicates was measured using an excitation filter of 530/25 nm and an emission filter of 590/35 nm with a detector sensitivity of 75. Replicate measurements for each concentration were averaged and a linear calibration model was fit to the averaged values (R^2 = 0.9972). The calibration equation was then used to calculate Rhodamine concentrations of collected samples based on their florescence measurements under the same excitation and emission settings.

The second of the four proposed dye tracer experiments was implemented on 2 October 2015 at approximately 07:11. The setup and methods for this dye trace were very similar to the March 2015 dye trace. Divers assisted in the release of 18.9 L (5 gallons) of 20 % Rhodamine WT directly in the flow stream of the Mammoth (Main) Spring vent (Figure 5.1.5). The injection method was considerably different from the March 2015 dye trace. Previously a container full of the dye was opened in the flow stream, while the October dye trace used a pump to quickly deliver the dye to the flow stream. Both of these methods approximate an instantaneous pulse injection; however, the pump assisted method proved to have less technical issues during deployment. The flow of dye downstream was tracked at five fixed stations. All five stations consisted of in-stream, submersible fluorometers (one Albillia Co. GGUN-FL30, Albillia Co., Neuchâtel, Switzerland; three Turner Designs CS3, Turner Designs, Inc., Sunnyvale, CA; and

one Turner Designs SCUFA, Turner Designs, Inc., Sunnyvale, CA) were calibrated in the lab prior to deployment and collected data at 1minute intervals. 3 of 5 of these stations were positioned in the same locations as the March 2015 dye trace. Referring to Figure 5.1.2, these three stations were the 1,200 m Fluorometer, the Midpoint Fluorometer, and the Lower Fluorometer. The remaining two fluorometers were deployed near the USGS 1,200 m station to help characterize possible transient storage and mixing hypothesized to occur in that location.

Three boats ("rovers") collected 377 grab samples along three gradients: 1) across the channel reach; 2) with depth; and 3) within five eco-geomorphological features (SAV beds, debris jams, emergent beds, and benthic depressions). Samples were collected using the same method and equipment at the March 2015 dye trace. Samples were taken from as frequently as possible and from as many locations as possible to provide a good overall coverage of the river (Figure 5.1.6). Rover sampling occurred through the day. Rover samplers noted time, GPS location, sample depth, distance from bank, and eco-geomorphological feature. The rhodamine concentrations of grab samples were determined using the same protocol as the March 2015 dye trace.

In addition to the fixed sampling stations and rover sampling, aerial video and images of the dye trace was captured using a remotely operated quadcopter (Figure 5.1.7). The aim of the aerial imagery was to gather information on bulk mixing patterns for the following events: The initial release and mixing of the dye in the main spring bowl, the heterogeneity of flow and dye mixing in the first 1,200 m of the river, flow division and dye movement in the back channel, and channel bank transient storage.

The third dye tracer experiment was implemented on 24 August 2016 at approximately 07:07. The methods and setup of this experiment were essentially identical to the 2 October 2015 dye trace. Divers assisted in the release of 18.9 L (5 gallons) of 20 % Rhodamine WT directly in the flow stream of the Mammoth (Main) Spring vent (Figure 5.1.8). Like the October dye trace, a pump was used to quickly deliver the dye to the flow stream. The flow of dye downstream was tracked at five fixed stations (Figure 5.1.9). All five stations consisted of in-stream, submersible fluorometers (one Albillia Co. GGUN-FL30, Albillia Co., Neuchâtel, Switzerland; three Turner Designs CS3, Turner Designs, Inc., Sunnyvale, CA; and one Turner Designs SCUFA, Turner Designs, Inc., Sunnyvale, CA). The fluorometers were calibrated in the lab prior to deployment and collected data at 1 minute intervals. Two of the five stations were positioned in the same locations as the March and October 2015 dye trace. Referring to Figure 5.1.2, these two stations were the Midpoint Fluorometer and the Lower Fluorometer.

Similar to the two previous dye traces, three boats ("rovers") collected a total of 401 grab samples along three gradients: 1) across the channel reach; 2) with depth; and 3) within five eco-geomorphological features (SAV beds, debris jams, emergent beds, and benthic depressions). Samples were collected using the same method and equipment as the March and October 2015 dye trace. Rover samplers noted time, GPS location, sample depth, distance from bank, and eco-geomorphological feature. The rhodamine concentrations of grab samples were determined using the same protocol as the March and October 2015 dye traces.

The last of the four proposed dye tracer experiments for the Silver River was implemented on 8 December 2016 at approximately 17:02. The methods and setup of this experiment were

essentially identical to the October 2015 and August 2016 dye traces. Divers assisted in the release of 18.9 L (5 gallons) of 20 % Rhodamine WT directly in the flow stream of the Mammoth (Main) Spring vent (Figure 5.1.10). Like the October dye trace, a pump was used to quickly deliver the dye to the flow stream. The flow of dye downstream was tracked at five fixed stations. All five stations consisted of in-stream, submersible fluorometers (one Albillia Co. GGUN-FL30, Albillia Co., Neuchâtel, Switzerland; three Turner Designs CS3, Turner Designs, Inc., Sunnyvale, CA; and one Turner Designs SCUFA, Turner Designs, Inc., Sunnyvale, CA). The fluorometers were calibrated in the lab prior to deployment and collected data at 1-minute intervals. The five stations were located in the same positions as the August 2016 dye trace (Figure 5.1.9). This dye trace differed from the previous three (i.e., March 2015, October 2015, and August 2016), in that no roving grab samples were taken.

The four dye traces experiments on the Silver River were conducted under different seasonal and hydrologic conditions. A dye trace was conducted for each of the four nominal seasons (i.e., spring, summer, fall, winter), allowing us to capture potential hydrologic changes induced from seasonal vegetation variation. The four dye traces also captured significant variation in spring run discharge, stage, and tail water conditions. Figure 5.1.11 lists the seasonal and hydrologic conditions for the four dye traces conducted in this study, and for one additional dye trace conducted in the Silver River in 2009 for which we have data.

An additional dye trace experiment was performed in Alexander Springs Creek. This dye trace was implemented on 19 January 2017 at approximately 18:15. The methods and setup of this experiment were similar to the March 2015 dye trace on the Silver River: 2.9 L (7 lbs) of 20 % Rhodamine WT dye were released directly into the spring boil of the main vent within the Alexander Springs group by pouring from a canoe (Figure 5.1.12). Like the other dye trace experiment discussed, the method of release approximates an instantaneous pulse injection. The flow of dye downstream was tracked at five fixed stations along the spring run (Figure 5.1.13). All five stations consisted of in-stream, submersible fluorometers (one Albillia Co. GGUN-FL30, Albillia Co., Neuchâtel, Switzerland; three Turner Designs CS3, Turner Designs, Inc., Sunnyvale, CA; and one Turner Designs SCUFA, Turner Designs, Inc., Sunnyvale, CA). The fluorometers were calibrated in the lab prior to deployment and collected data at 1-minute intervals.

In the same manner as the March 2015, October 2015, and August 2016 dye traces, three canoes ("rovers") collected 239 grab samples along three gradients: 1) across the channel reach; 2) with depth; and 3) within five eco-geomorphological features (SAV beds, debris jams, emergent beds, and benthic depressions). Samples were collected using the same method and equipment as the March 2015, October 2015, and August 2016 dye traces. Rover samplers noted time, GPS location, sample depth, distance from bank, and eco-geomorphological feature. The rhodamine concentrations of grab samples were determined using the same protocol as the March 2015, October 2015, and August 2016 dye traces.

Figure 5.1.1. March 4, 2015 dye trace. Clockwise from top left: diver just after releasing injection vessel cap, research vessels in main spring bowl after dye release, underwater view of diver after dye release, injection vessel suspended from research vessel with dye release.

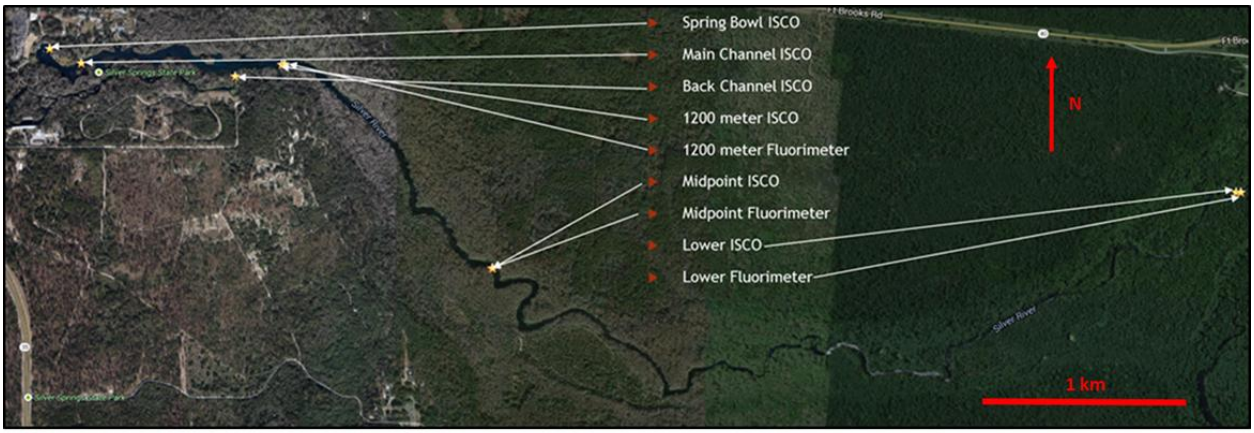

Figure 5.1.2. Fixed-location dye sampling sites on the Silver River for 4 March 2015 injection.

Figure 5.1.3. Clockwise from top: hand pump device, sampling tube and weight deployed for sample collection, "rover" boat sample collection.

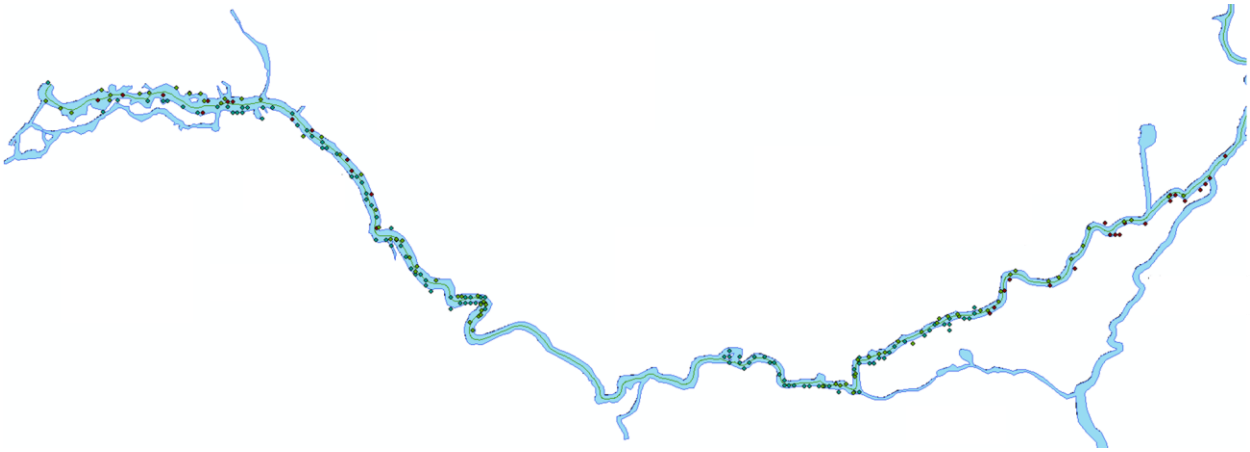

Figure 5.1.4. Locations of "rover" grab samples taken for the 4 March 2015 dye trace.

Figure 5.1.5. October 2, 2015 dye trace. Clockwise from top left: diver holding injection pump hose in from of Mammoth vent during initial moments of the dye release, diver illuminated by research vessels while situated in front of Mammoth vent prior to dye injection, the main spring bowl looking downstream following dye injection, snorkeler assisting divers with illumination during the dye injection.

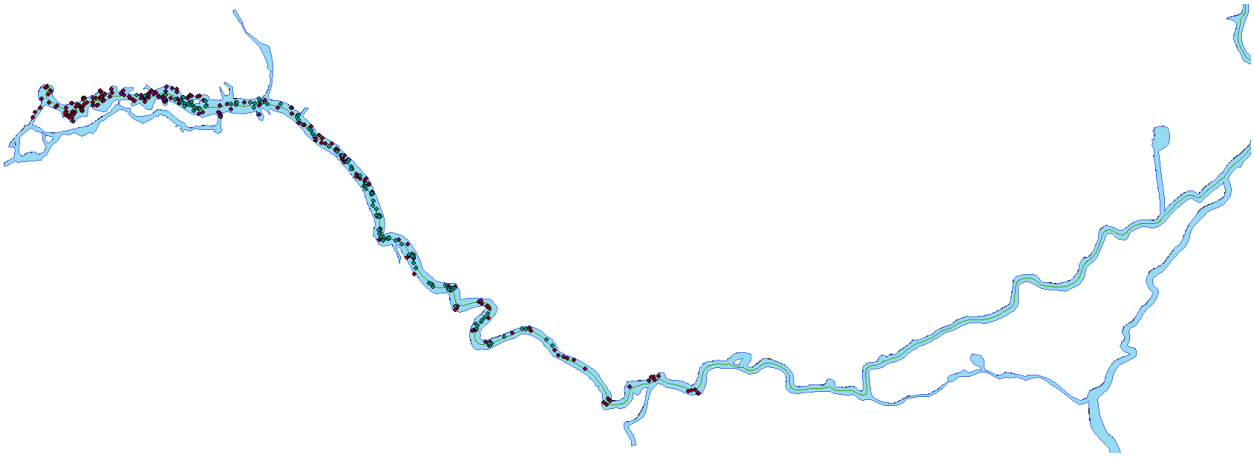

Figure 5.1.6. Locations of "rover" grab samples taken for the 2 October 2015 dye trace

Figure 5.1.7. Aerial imagery from the October 2, 2015 dye trace. Clockwise from top left: the main spring bowl following dye injection, dye pulse has left the spring vent and is tracing initial flow partitioning in the spring bowl, main spring bowl after most of the dye has cleared, upper 1,200 m of the river showing dye pulse tracing main flow path while clear water input from side springs is visible.

Figure 5.1.8. Images from the August 24, 2016 dye trace. Left Panel: Divers resurfacing after releasing Rhodamine WT dye in Mammoth Vent. Top Right: Researchers on the surface illuminate the divers with spot lights just prior to the dye release. Bottom Right: The Mammoth Vent spring pool immediately after the release of the dye. Photos by Jenny Adler (https://walkingonwaterfl.org/)

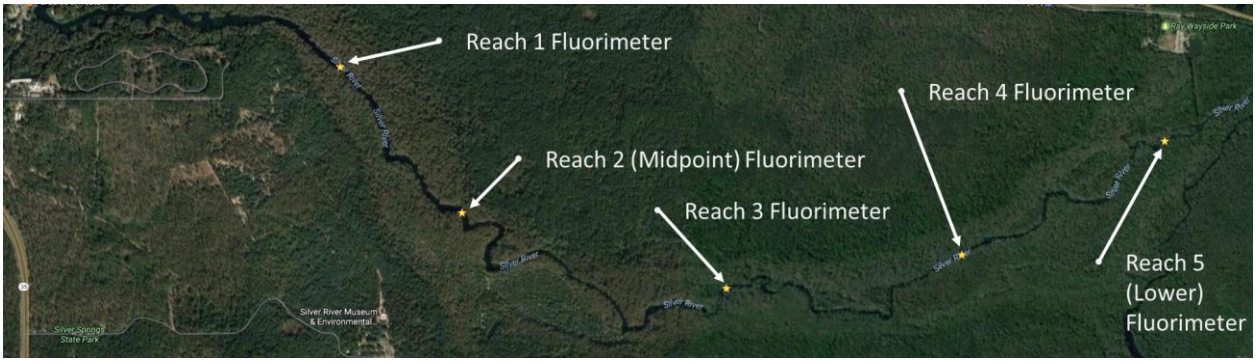

Figure 5.1.9. Fixed-location dye sampling sites on the Silver River for the August 24, 2016 injection.

Figure 5.1.10. Images from the December 8, 2016 dye trace. Right Panel: SAV near the Mammoth Vent spring pool shortly after Rhodamine WT was released. Top Left: Nathan Reaver dives to inspect dye plume shortly after dye release in the Mammoth Vent spring pool. Bottom Left: Reaver inspects the dye mixing interface within the Mammoth Vent spring pool. Photos by Jenny Adler (https://walkingonwaterfl.org/)

Silver River Dye Traces			
Date	Discharge (cfs)	Water Level Elevation NAVD 1988 at 1200m USGS Station (ft)	Water Level Elevation NAVD 1988 at Confluence (ft)
September 25 2009	549	39.65	34.14
March 4 2015	707	39.71	36.08
October 2 2015	672	40.2	37
August 24 2016	464	38.84	33.41
December 8 2016	441	38.211	33.59

Figure 5.1.11. Summary of the seasonal and hydrologic conditions for the four Silver River dye traces conducted in this study, as well as an earlier dye trace conducted in 2009.

Figure 5.1.12. Images from the January 19, 2017 dye trace at Alexander Springs. Clockwise from top left: Dye being released by pouring into spring boil from canoe on the surface, Alexander Spring pool just after dye release, dye release team sampling following the dye release, UF volunteers collecting roving grab samples.

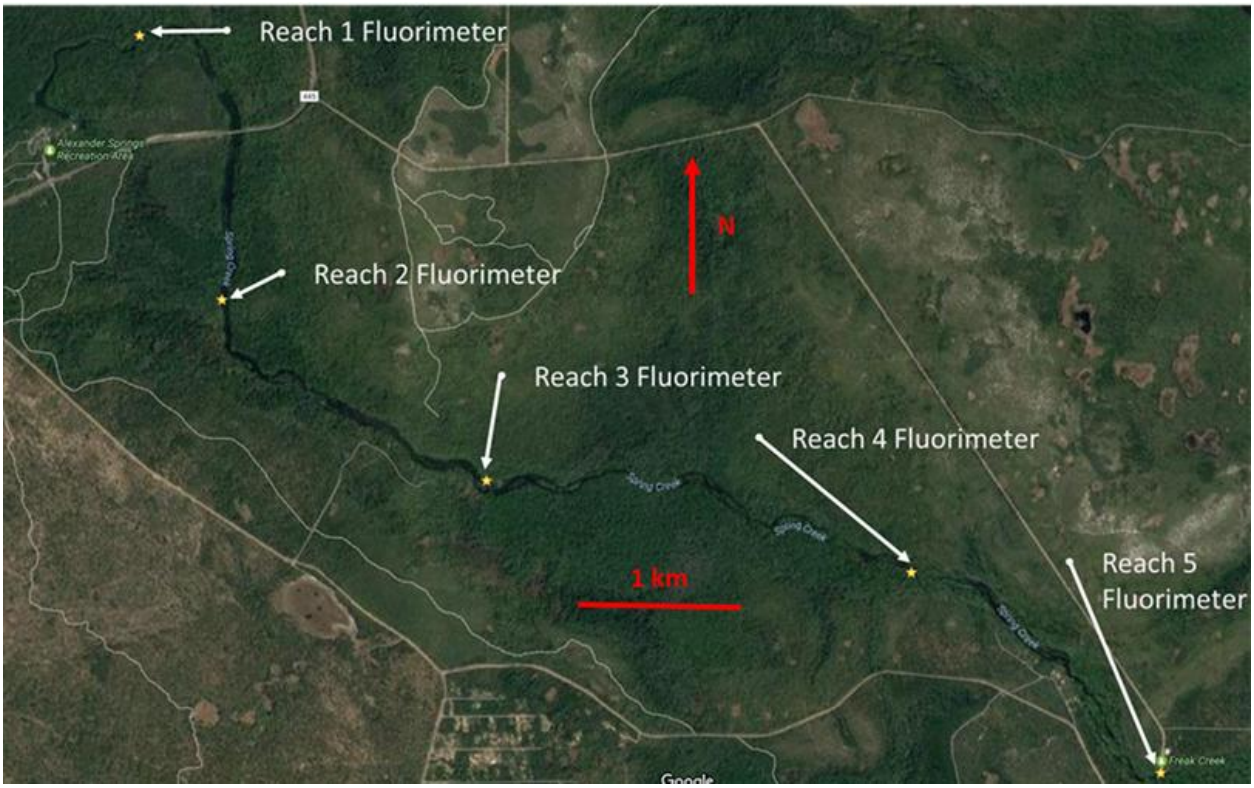

Figure 5.1.13. Fixed-location dye sampling sites on Alexander Springs Creek for the January 19, 2017 dye trace.

5.1.2.1.2 Tracer Data Analysis

5.1.2.1.2.1 Solute Transport Model

Hydraulic transport parameters were estimated from BTC data using the **O**ne-dimensional **T**ransport with **I**nflow and **S**torage (OTIS) model (Runkel 1998). OTIS is a solute transport model for streams and rivers that models one-dimensional flow and transport along river longitudinal distance, but assumes spatial homogeneity of solute concentration in other two dimensions (width and depth). The model is based on the advection-dispersion equation, which relates changes in solute concentration with respect to time and space to advection, dispersion, and transient storage in the stream system and is given by a set of coupled differential equations:

$$\frac{\partial C}{\partial t} = -\frac{Q}{A}\frac{\partial C}{\partial x} + D\frac{\partial^2 C}{\partial x^2} + \frac{q_{LIN}}{A}(C_L - C) + \alpha(C_s - C)$$

$$\frac{\partial C_s}{\partial t} = \alpha\frac{A}{A_s}(C - C_s)$$

where C is concentration (ppb), t is time (s), Q is discharge ($m^3\ s^{-1}$), A is channel cross-sectional area (m^2), D is the dispersion coefficient ($m^2\ s^{-1}$), q_{LIN} is the sum of inflows to the system ($m^3\ s^{-1}$), C_L is solute concentration in inflows (ppb), α is the storage exchange coefficient ($L\ s^{-1}$), and C_s is solute concentration in transient storage (ppb). The second equation describes the rate of concentration change in the transient storage zone as a function of the effective stream and storage zone areas and concentrations, where A_s is storage zone cross-sectional area (m^2) and C_s is storage zone concentration (ppb) (Stream Solute Workshop, 1990). OTIS is solved

numerically using various finite difference approaches (each with pros and cons regarding solution stability and accuracy, see below), but it also has an analytic solution for a pulse injection and no lateral inflow, which allows for numerical solution benchmarking:

$$C(x,t|A,As,D,\alpha,Q) = e^{-\alpha t}\left[\frac{\frac{M}{A}}{2\sqrt{\pi D t}}e^{\frac{-\left(x-\frac{Q}{A}t\right)^2}{4Dt}}\right] + \alpha\int_0^t\left[\frac{\tau I_1\left(\frac{2\alpha A}{As}\sqrt{\frac{As}{A}(t-\tau)\tau}\right)}{\sqrt{\frac{As}{A}(t-\tau)\tau}}e^{-\frac{\alpha A}{As}(t-\tau)-\alpha\tau}\frac{\frac{M}{A}}{2\sqrt{\pi D\tau}}e^{\frac{-\left(x-\frac{Q}{A}\tau\right)^2}{4D\tau}}\right]d\tau$$

5.1.2.1.2.2 Model Fitting Approaches

Conventional model fitting techniques seek the "best" fit of a model to observed data via optimization of an objective function (e.g., minimizing sum of square errors, maximizing R^2, etc.). While widely used, this approach has limitations for some applications. Optimization with an objective function requires a search procedure of parameter space. If the objective function has many features (i.e., local minima or maxima) in parameter space, it is possible for the searching algorithm to become trapped in a region that does not contain the "true" best fit parameters of the model to the data. In addition, the objective function may not be very sensitive to changes in certain parameters of the model. This could potentially cause certain parameters in the model to be non-identifiable, meaning that many different values of that parameter would give a similar value to the objective function.

Various methods have been proposed to address these issues, such as weighting data or using only portions of a dataset to fit models. However, these methods add a subjective component to the analysis that then has to be justified. In addition, it is more difficult to determine the uncertainty in the parameter estimates resulting from the optimization process. There has been discussion in the literature about whether all of the parameters in the OTIS model are identifiable when fitting to breakthrough curve data (Kelleher et al. 2013). Identifiability of model parameters is important when trying to understand reach-scale properties of streams, as each parameter has a physical interpretation.

To identify and address some of these issues of identifiability, we used a Bayesian method to estimate OTIS model parameters in addition to a standard objective function optimization using OTIS-P software, which uses non-linear regression routines from STARPAC (Donaldson and Tryon 1990). The Bayesian method does not depend on searching an objective function in parameter space; instead, it involves drawing samples from a parameter probability distribution defined by the model, data, and any prior knowledge about the parameters. The Bayesian method allows to us determine the most likely parameter values of the model for the data, much like the objective function optimization, but also provides a probability distribution for each parameter, giving a quantitative measure of the uncertainty for each parameter. Additionally, by sampling probability distributions of model parameters, the Bayesian approach allows us to develop parameter uncertainty estimates versus a single deterministic number for each parameter (Figure 5.1.14). We expect this method to allow us to better understand the uncertainty in OTIS model parameters estimated from our dye tracing experimental data.

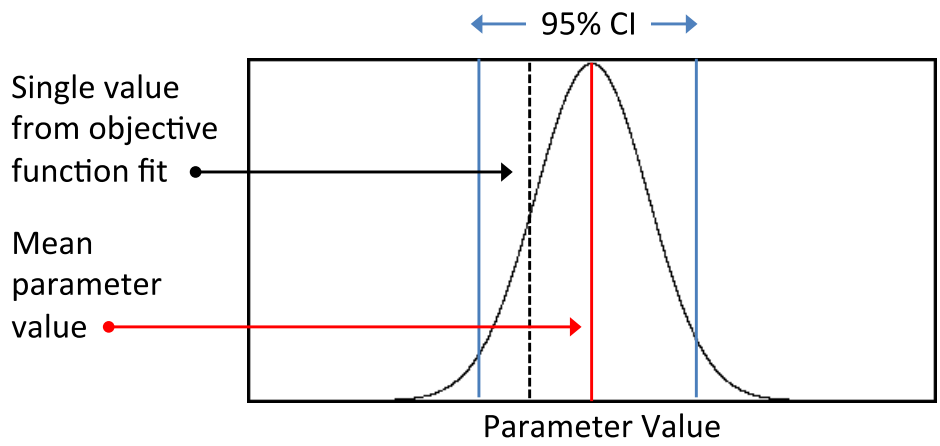

Figure 5.1.14. Example fitted parameter distribution (solid black line) and 95 % credible interval resulting from Bayesian model fitting versus a single parameter value derived from traditional techniques (black dashed line).

Bayesian model fitting is based on Bayes theorem:

$$p(Hypothesis|Data) = \frac{p(Data|Hypothesis)p(Hypothesis)}{p(Data)}$$

or the commonly used form:

$$p(Hypothesis|D) \propto p(Data|Hypothesis)p(Hypothesis)$$

The components of this proportionality are generally referred to in the following manner:

$$posterior\ distribution \propto likelihood\ distribution \times prior\ distribution$$

The prior distribution reflects the knowledge of the model parameters before including experimental data, the likelihood distribution is the distribution from which the data is thought to be generated (i.e., the model under consideration), and the posterior distribution reflects the knowledge of the model after including experimental data.

For our specific case, the data are the measured breakthrough curves, and the hypothesis is that the data is generated from the OTIS model. Since the OTIS model is solved numerically, rather than with an analytic expression, it can be represented with the following notation:

$$OTIS(A, As, D, \alpha, x, t)$$

where A is the channel cross sectional area, As storage zone cross section area, D is the aggregate dispersion coefficient, α is the exchange rate between the channel and storage zone, x is the longitudinal position from the dye release point, and t is the time elapsed since the dye release. The measured breakthrough curve data have three coordinates, concentration $\{C_i\}$, longitudinal position from the dye release point $\{x_i\}$, and time elapsed since the dye release $\{t_i\}$.

For our analysis, we are interested in the probability distribution of the parameters of the OTIS model given the measured breakthrough curves. For a single measured breakthrough curve observation, i, Bayes theorem can be written as:

$$p(A, As, D, \alpha | C_i, x_i, t_i) \propto Normal(C_i | mean = OTIS(A, As, D, \alpha, x_i, t_i), variance = \sigma^2) p(A) p(As) p(D) p(\alpha) p(\sigma^2)$$

where:

$$p(A) = Normal(A | mean = 0, variance = 100^2)$$
$$p(As) = Normal(As | mean = 0, variance = 100^2)$$
$$p(D) = Normal(D | mean = 0, variance = 100^2)$$
$$p(\alpha) = Normal(\alpha | mean = 0, variance = 100^2)$$
$$p(\sigma^2) = Gamma\left(\frac{1}{\sigma^2}, a = 0.001, b = 0.001\right)$$

In these expressions the observed concentration, C_i, is thought to come from a normal distribution (likelihood distribution) with a mean equal to the OTIS model evaluated at the corresponding longitudinal position and time, and variance representing deviations from the OTIS model due to experimental error. The remaining distributions are the prior distributions for the OTIS model parameters and variance parameter. These priors have been chosen to be very vague for all of the parameters, reflecting little knowledge about the value of the parameter before the experiment. This reflected in the choice of mean (0) and variance (100^2) for these distributions, giving a very wide, nearly flat distribution centered on zero. This effectively means before our experiment we think almost any parameter values are equally likely. These weakly informative priors allow the data to dominate the shape of the posterior distribution.

If we take into all of the experimental data Bayes theorem becomes:

$$p(A, As, D, \alpha | \{C_i\}, \{x_i\}, \{t_i\}) \propto \left[\prod_i Normal(C_i | mean = OTIS(A, As, D, \alpha, x_i, t_i), variance = \sigma^2)\right] p(A) p(As) p(D) p(\alpha) p(\sigma^2)$$

where:

$$p(A) = Normal(A | mean = 0, variance = 100^2)$$
$$p(As) = Normal(As | mean = 0, variance = 100^2)$$
$$p(D) = Normal(D | mean = 0, variance = 100^2)$$
$$p(\alpha) = Normal(\alpha | mean = 0, variance = 100^2)$$
$$p(\sigma^2) = Gamma\left(\frac{1}{\sigma^2}, a = 0.001, b = 0.001\right)$$

All observed data points are independent and therefore their likelihood functions are multiplied together. The posterior distribution for the model parameters given the data is explicitly expressed in the above proportionality. To find the most likely parameter values we can calculate the mean of each of the parameters from the posterior distribution. Since the posterior distribution does not have an easily obtained analytic expression we use a Monte Carlo approach to draw enough samples from the distribution to characterize it. This is the main difference between the optimization of objective functions and Bayesian inference: in Bayesian inference we sample from a "known" probability distribution, while in optimization we search a parameter

space. The method we use to sample from the posterior distribution is a Markov chain Monte Carlo (MCMC) random walk using the Metropolis-Hasting within a Gibbs sampling algorithm.

As stated previously, "conventional" model fitting techniques seek the "best" fit of a model to observed data via optimization of an objective function. The objective function that we used in this study was the sum of the squares of the error (SSE). This function can be expressed as:

$$SSE(A, As, D, \alpha) = \sum_i \left(C_i - OTIS(A, As, D, \alpha, x_i, t_i)\right)^2$$

The fitting process involves minimizing the objective function iteratively, by changing the model parameters (i.e., A, As, D, and α) slightly in each step. The magnitude and direction change of the parameter values for each iteration are determined from the negative gradient of the objective function,

$$-\nabla SSE(A, As, D, \alpha).$$

This process of changing parameters continues until the following condition is met:

$$-\nabla SSE(A, As, D, \alpha) \cong 0$$

When this occurs the objective function, SSE, has been minimized. The resulting parameter values are ones that when used in the OTIS model produce the least amount of error compared to the observed BTCs.

5.1.2.1.2.3 Moment Analysis of Breakthrough Curves

In addition to fitting a theoretical model, we also performed moment analysis on the dye trace breakthrough curve (BTC) data. Our previous analyses relied on a model (i.e., OTIS) to extract reach scale velocities for BTC data; however, a model imposes a theoretical mechanistic structure on how the data is generated. For example, the OTIS model treats a river as composed of averaged uniform flowing regions and stagnant regions, when in reality there exists a distribution of velocities. If we wish to directly estimate the overall average velocity of a reach, rather than just the average velocity of the advective zone (as is the case with OTIS), we can apply a "model-less" method. Moment analysis one such method that can give information about flow velocities by using the observed data (i.e., BTCs) directly.

This method involved finding the first and second moments of the BTCs. A BTC can be thought of as a distribution of arrival times of dye passing the measurement location. The first and second moment of a BTC correspond to the mean arrival time, and the variance of arrival time around that mean. Since the distance the dye has traveled is known, the distribution of arrival times can be converted into a distribution of flow velocities. The first moment of a BTC is computed using a weighted arithmetic mean:

$$Mean\ Arrival\ Time = \frac{\sum_i C_i t_i}{\sum_i C_i}$$

Here the dye concentrations, C_i, are the weighted values for the arrival times, t_i. The mean flow velocity is computed as:

$$Mean\ Flow\ Velocity = \frac{Distance\ from\ the\ dye\ release\ point}{Mean\ Arrival\ Time} = \frac{x \sum_i C_i}{\sum_i C_i t_i}$$

The second moment of a BTC is computed as:

$$Variance\ Around\ Mean\ Arrival\ Time = \frac{\sum_i \left[\left(t_i - \frac{\sum_i C_i t_i}{\sum_i C_i} \right)^2 C_i \right]}{\sum_i [C_i] - 1}$$

From the variance, the standard deviation can be calculated:

$$Standard\ Deviation\ Around\ Mean\ Arrival\ Time = \sqrt{\frac{\sum_i \left[\left(t_i - \frac{\sum_i C_i t_i}{\sum_i C_i} \right)^2 C_i \right]}{\sum_i [C_i] - 1}}$$

The standard deviation in the flow velocity can be computed as:

$$Standard\ Deviation\ of\ Flow\ Velocity = x \left(\frac{\sum_i C_i}{\sum_i C_i t_i} - \frac{1}{\frac{\sum_i C_i t_i}{\sum_i C_i} + \sqrt{\frac{\sum_i \left[\left(t_i - \frac{\sum_i C_i t_i}{\sum_i C_i} \right)^2 C_i \right]}{\sum_i [C_i] - 1}}} \right)$$

Mean velocities obtained directly from BTC using the modeless moment analysis will be slower than mean velocities obtained from the OTIS model. This is because OTIS is providing the mean velocity of the advective zone of the river, while the moment analysis is providing the overall effective mean velocity of all flow paths.

5.1.2.2 Raz-Rru Experiments

This section describes batch experiment methods used to determine kinetic transformation and sorption rates for Raz and Rru in sediments from the Silver River. These rates were compared with those derived using sediments from a sandy-bottom river in order to quantify the general effectiveness of Raz as an indicator of microbial metabolism and biogeochemical potential in Florida streams. These experiments were not contracted tasks in this Work Order, but we include our methods, results, and preliminary conclusions here as a resource for future researchers looking to apply this or other reactive tracer methodologies to understand transient storage.

5.1.2.2.1 Raz and Rru Detection Wavelengths

Standard solutions of Raz and Rru were prepared in concentrations ranging from 0 to 200 µg L^{-1} (ppb) and for each, fluorescence was measured for a range of excitation and emission wavelengths on a bench-top fluorometer. As Rru exhibits greater fluorescence than Raz, there is a degree of error introduced in separating mixed signals and signal saturation can be an issue above 150 ppb. For both compounds, the strongest fluorescence signals were produced with excitation at 530 nm and emission at 645 nm (530/645 nm) and 480/590 nm, respectively. The best fit calibration equations for each compound are shown below:

$$Raz_{590} = 3.8144Z + 136.31$$
$$Raz_{645} = 17.238Z + 88.833$$
$$Rru_{590} = 99.206U + 86.351$$
$$Rru_{645} = 134.41U + 36.564$$

where Z is the Raz concentration in ppb and U is the Rru concentration in ppb. The total signals for each wavelength were set equal to the sum of the Raz and Rru signals, and the resulting set of equations was solved for Z and U in all subsequent measurements:

$$S_{590} = Raz_{590} + Rru_{590}$$
$$S_{645} = Raz_{645} + Rru_{645}$$

5.1.2.2.2 Field Sites

Sediment was collected from two systems in Florida with significant differences in soil composition and hydrologic regime. The first was the Silver River near Ocala, FL, a well preserved state park area where the river is driven by first magnitude spring flows of approximately 650 cubic feet per second (cfs) (18.41 m^3 s^{-1}).. The collection point was located on a vegetated slope where hyporheic exchange was likely forced by the direction of flow. The sediment was highly organic with a high water content and loamy texture. For comparison purposes, sediment was also collected from Jennings Creek, a 1.41 cfs (0.04 m^3 s^{-1}) urban stream in Gainesville, FL that is impacted heavily by runoff from surrounding roadways. The sediment was characterized primarily by sand and small gravel. The sample site was located on a similarly sloped area of the reach downstream of a small riffle-pool sequence where hyporheic exchange may be expected.

5.1.2.2.3 Batch Experiments

Batch culture experiments were performed according to methods adapted from González-Pinzón et al. (2012). A total of 20 samples were prepared where 50 g of sediment from the Silver River were added to each of nine 200 mL sample bottles. Another nine were filled with sediment from Jennings Creek. The final two samples contained deionized water only. Sediment samples were filled to a final volume of 60 mL using collected stream water. The water samples and 6 sediment samples from each site were autoclaved at 121°C for 20 minutes to eliminate the presence of microbial activity. Half of the autoclaved samples were then filled with the requisite volume of Raz for a final concentration of 100 ppb and the other half were treated with Rru to a concentration of 100 ppb. The 6 live samples were treated with Raz only. The samples were then placed on a shaker table and incubated at room temperature for a period of 6 hours. 250 µL samples were taken from each bottle at approximately 30 minute intervals over the incubation period. Samples were buffered to a pH above 8 with 10 µL of 1 ***M*** NaOH to avoid the need for signal corrections and then centrifuged to remove residual sediment. 200 µL samples were pipetted to 96 well plates and total fluorescence was measured at 480/590 nm and 530/645 nm. Laboratory lights were kept off throughout the experiment to avoid photodegradation.

5.1.2.2.4 Kinetics and Advection-Dispersion Modeling

The rates of Raz and Rru transformation and adsorption to sediment particles were modeled by fitting measured concentrations from the batch experiments to the following equations:

$$\partial Raz = -k_{fRaz} \cdot Raz \cdot Bac + k_{rRaz} \cdot Bac_{total} - k_{rRaz} \cdot Bac - k_{fsRaz} \cdot Raz \cdot S + k_{rsRaz} \cdot S_{total} - k_{rsRaz} \cdot S$$

$$\partial Rru = k_U \cdot Bac_{total} - k_u \cdot Bac - k_{fsRru} \cdot Rru \cdot S_u + k_{rsRru} \cdot S_{utotal} - k_{rsRru} \cdot S_u$$

$$\partial Bac = -k_{fRaz} \cdot Raz \cdot Bac + k_{rRaz} \cdot Bac_{total} - k_{rRaz} \cdot Bac + k_u \cdot Bac_{total} - k_u \cdot Bac$$

$$\partial S = -k_{fsRaz} \cdot Raz \cdot S + k_{rsRaz} \cdot S_{total} - k_{rsRaz} \cdot S$$

$$\partial S_u = k_{fsRru} \cdot Rru \cdot S_u + k_{rsRru} \cdot S_{utotal} - k_{rsRru} \cdot S_u$$

where k_f represents forward absorption by bacteria, k_{fs} represents forward sorption to sediment, and k_r represents reverse reactions. Bac_{total} is the total microbial concentration, Bac is number of bacteria occupied by Raz, k_u is the conversion of Raz to Rru, and S is the number of sorption sites available for Raz, while S_u represents sorption sites for Rru, and S_{total} is the total sorption sites. The conversion of Raz to Rru is assumed to be irreversible; however, Raz absorption by microbial cells does not necessarily indicate transformation. Sorption of both compounds to sediment is reversible.

Hydraulic transport parameters were estimated for two hypothetical reaches with sediments exhibiting the sorption and decay parameters fitted for Jennings Creek and the Silver River and applied to a modified version of the OTIS model presented above that includes decay terms (Runkel 1998; Hensley and Cohen 2012):

$$\frac{\partial C}{\partial t} = -\frac{Q}{A}\frac{\partial C}{\partial x} + D\frac{\partial^2 C}{\partial x^2} + \frac{q_{LIN}}{A}(C_L - C) + \alpha(C_s - C) - kC$$

$$\frac{\partial C_s}{\partial t} = \alpha\frac{A}{A_s}(C - C_s) - kC$$

When reduction and adsorption of Raz (or Rru) is observed, a - kC term is included in the model to account for the combined predicted first order conversion of resazurin to resorufin in the hyporheic zone as well as adsorption to sediments (Lemke et al. 2013). In this equation, α is mathematically equivalent to the parameter q_{he} developed by Lemke et al. (2013), which quantifies the discharge subject to hyporheic exchange per volume of stream water. Breakthrough curves of Raz and Rru in the two simulated systems were compared from the standpoints of adsorption capacity and microbial activity.

5.1.3 RESULTS AND DISCUSSION

5.1.3.1 Dye Tracer Experiments

5.1.3.1.1 Breakthrough Curve Data

During the first tracer experiment, dye was released at approximately 18:00 on 4 March 2015 and was completely mixed into the flow stream within approximately 5 minutes, with the majority of dye injected within the first 90 seconds. For the second tracer experiment, dye was release at 07:11 on 2 October 2015 using a pump. This allowed for the majority of the dye to be mixed into the main vent flow stream within 90 seconds and to be completely mixed within 3

minutes. Visual inspection of the dye plume from the first (March 2015) tracer experiment suggested three primary flow paths after injection: downstream, towards the back channel, and recirculation into the spring bowl (Figure 5.1.15). These three flow paths were confirmed during the second tracer experiment (October 2015) with aerial imagery (Figure 5.1.16). Mixing times were similarly rapid for the third and fourth dye tracer experiments in August and December 2016.

Figure 5.1.15. Visual interpretation of dye flows after March 2015 dye injection. Figure by Ed Carter.

Figure 5.1.16. Aerial photograph from the October 2015 dye trace showing the three primary flow paths that the spring flow takes after leaving the vent. The first flow path leaves the spring pool and heads downstream. The second flow path leads to the Fort King waterway back channel. The third flow path circles back around to fill the spring pool.

The following three figures show BTCs measured through *in situ* fluorometry at three locations and via ISCO grab samples at six locations for the March 2015 dye trace.

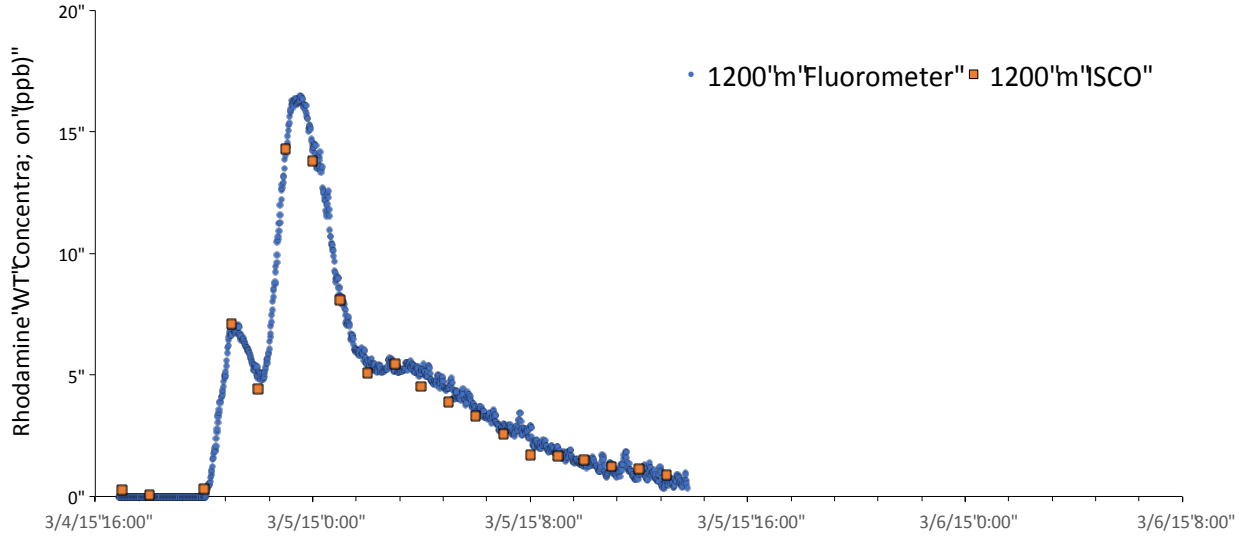

Figure 5.1.17. August 2015 BTC at the 1,200 m station measured continuously (blue dots) and with ISCO grab samples (orange squares), which agree closely. Note three

distinct concentration peaks. See Figure 5.1.2 for measurement locations.

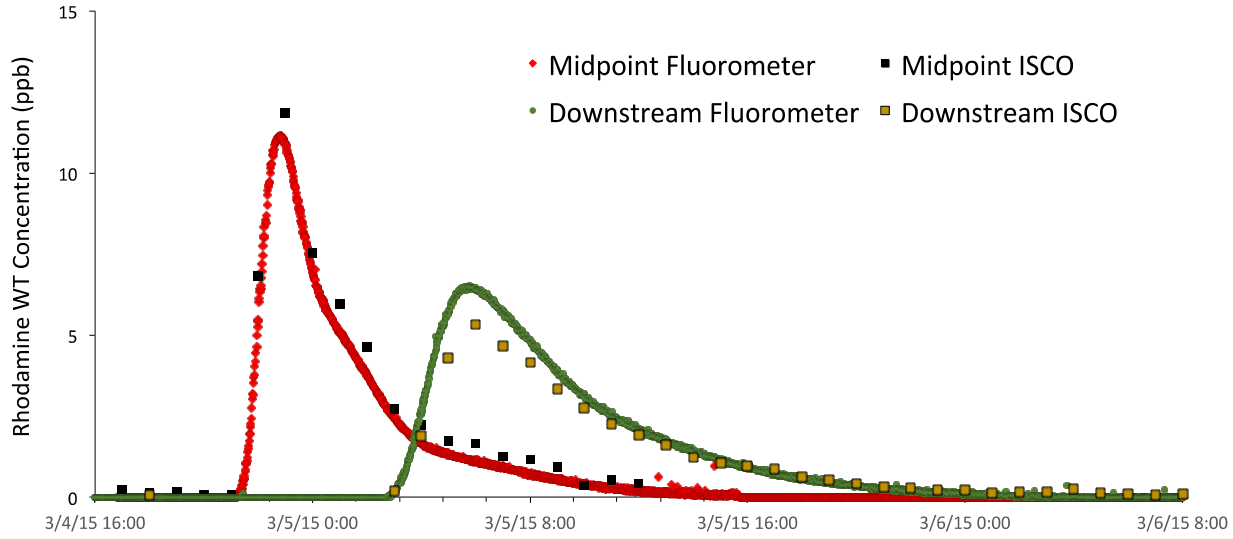

Figure 5.1.18. August 2015 BTCs at the midpoint and downstream stations measured continuously (red and green dots) and with ISCO grab samples (black and orange squares). See Figure 5.1.2 for measurement locations.

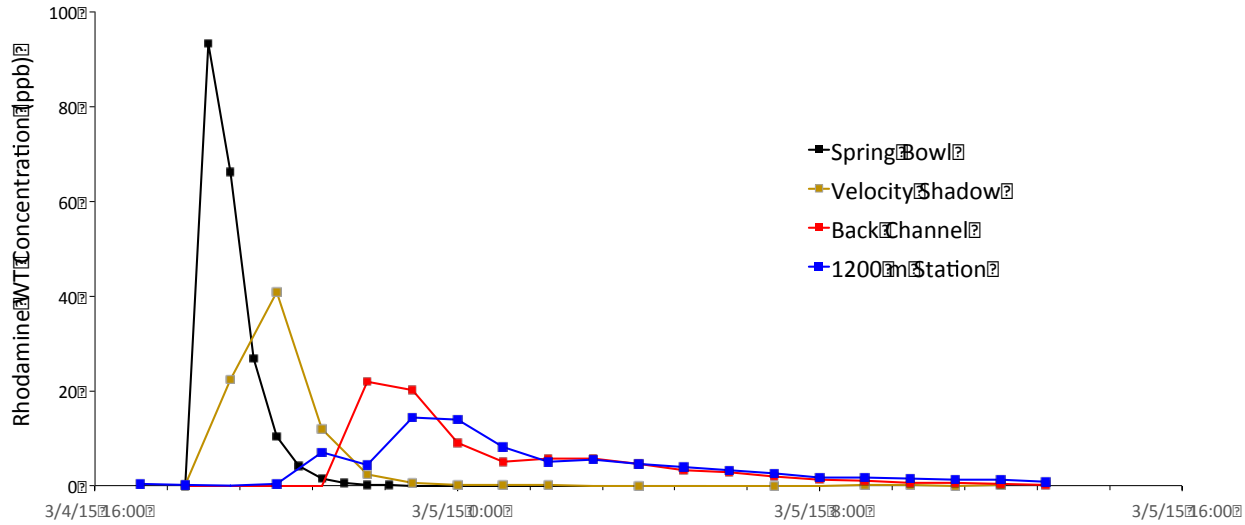

Figure 5.1.19. August 2015 BTCs at four ISCO monitoring stations. See Figure 5.1.2 for measurement locations.

After this first dye tracer, we were able to draw a number of preliminary conclusions about flow and transport in the Silver River, which were confirmed and refined in subsequent experiments. First, multiple peaks in the BTCs at the 1,200 m station (Figure 5.1.17) indicated the presence of three upstream flowpaths: one via the main river channel and two through the "back channel" (i.e., the Ft. King Waterway). While it is counterintuitive that the concentration of the first peak (characterizing main channel flow and the bulk of tracer mass) was lower than the second peak (characterizing the faster of the two back channel flow paths.), this occurred due to the

placement of both the fluorometer and ISCO sampler intake close to the right (southern) bank in this location (to take advantage of the 1,200 m USGS station as a mounting platform). Despite large flows out of the main spring bowl, complete transverse (and presumably vertical) mixing was not achieved within 1,200 m, resulting in the highest concentration dye plume bypassing the station in the channel center. Additional spring flows along the main channel also served to dilute concentrations relative to the pulse delivered from the spring bowl into the back channel. The higher-concentration second peak occured when that pulse arrived out of the back channel and "hugged" the right bank where it enters the main channel. These interpretations were well supported by EFDC modeling (see Section 5.4), providing support for that model and the utility of using tracer experiments to inform modeling efforts. However, due to incomplete mixing at this location, transport parameters could not be derived from the OTIS model for this BTC. During the second tracer experiment (October 2015), we were able to confirm the hypotheses about spring run flow paths drawn from the March 2015 data. These confirmations are discussed below.

BTCs at the midpoint and downstream stations (Figure 5.1.18) illustrated delayed arrival and attenuated peak concentration from advection, dispersion, and any transient storage. Triple peaks observed at the upstream station were smoothed out at both stations, allowing us to fit the OTIS model to estimate reach-scale advection and dispersion parameters (see below). At both stations, "fat" tails on the distribution of ISCO samples (i.e., slow concentration declines late in the BTC) suggest the potential for transient storage, which is also quantified via the model fitting process. In general, ISCO and fluorometer samples matched well at the midpoint station, but were divergent at the downstream station, where the Rhodamine concentration peak measured in the vegetation bed was lower than that in the main channel (and showed delayed attenuation), suggesting that vegetation beds can serve as a partial barrier to mixing.

Data from the four additional ISCOs (Figure 5.1.19) provide additional insight into flowpaths and residence times in the upper reach of the Silver River during the March 2015 experiment. In particular, data from the spring bowl ISCO suggest a complete flushing time of approximately 6 hours, and data from the back channel ISCO captures the two back-channel dye pulses, allowing us to qualitatively estimate mean travel times of water following those two paths (approximately 6 and 12 hours for the faster and slower flow paths, respectively). All BTCs data from this and subsequent experiments are included in Appendix 5.1.1. The following two figures shows BTCs measured through *in situ* fluorometry at four locations for the October 2015 dye trace.

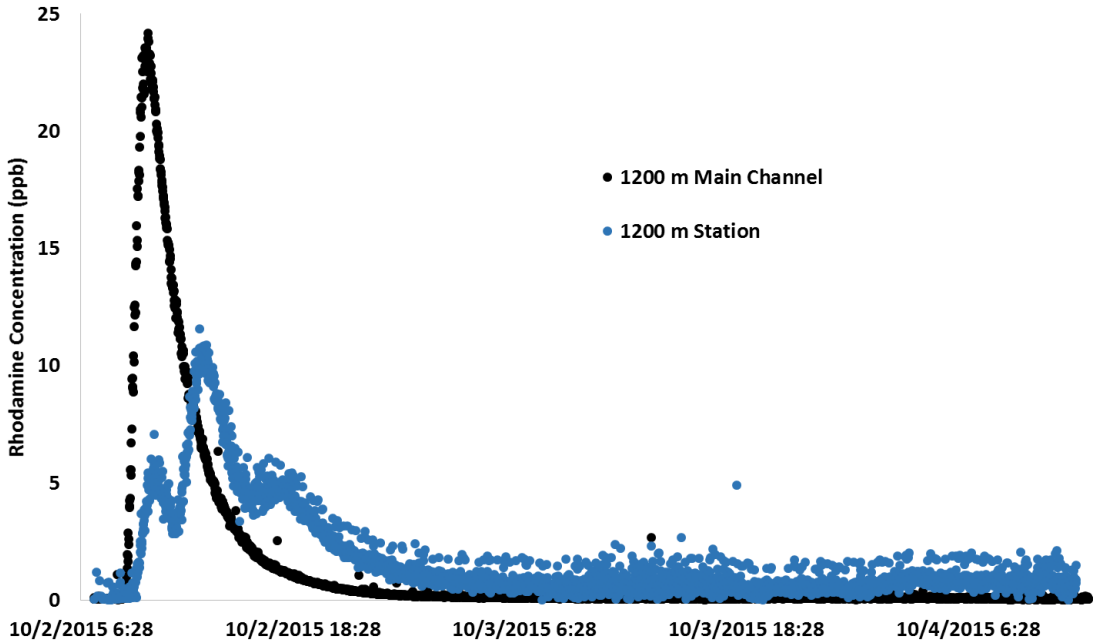

Figure 5.1.20. October 2015 BTCs at the 1,200 m station in the main channel (black dots) and at the USGS station (blue dots). See Figure 5.1.2 for measurement locations.

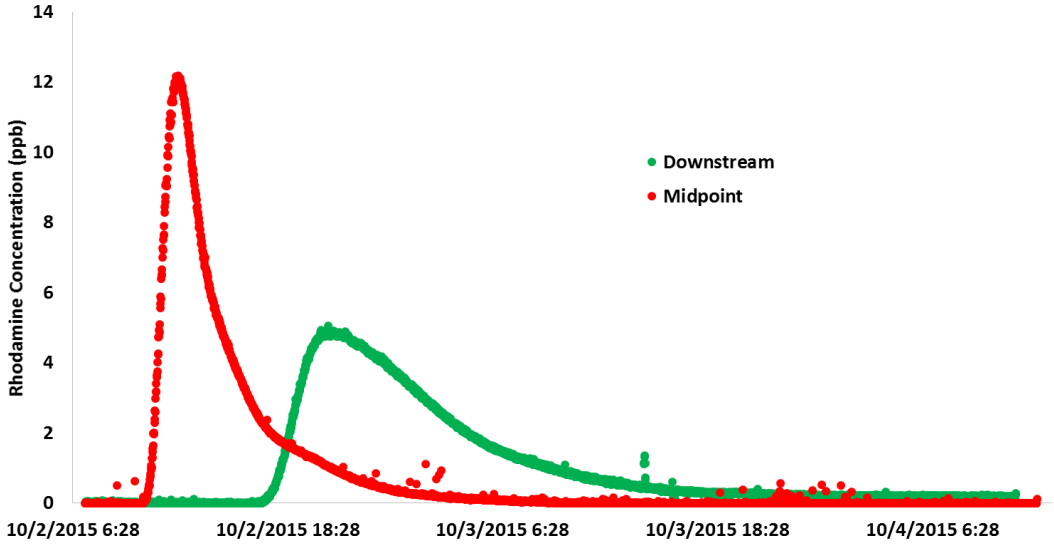

Figure 5.1.21. October 2015 BTCs at the midpoint (red dots) and downstream (green dots) stations measured continuously. See Figure 5.1.2 for measurement locations.

The October 2015 tracer experiment confirmed findings about flow paths drawn from the March 2015 experiment. For the October 2015 tracer test, two fluorometers were placed near the USGS 1,200 m station. One was placed adjacent to the station (i.e., near the bank of the river), while the other was placed in the center of the main channel. The data from these instruments (Figure 5.1.20) was consistent with that collected during the March 2015 tracer experiment and confirmed that there are indeed (at least) two primary flow paths. The BTC from the fluorometer

that was adjacent to the USGS station (closer to the river bank) had the three peaks observed during the March 2015 experiment, which suggests three flow paths is a consistent feature of the flow regime in the spring run. The main channel fluorometer BTC showed a single high-concentration peak that corresponded with the initial small peak in the BTC of the fluorometer mounted adjacent to the USGS station. This supports the previous hypothesis that the initial highest concentration dye plume bypasses the station in the channel center. This bypassing of the USGS station was also confirmed visually on the river (Figure 5.1.22) and with aerial images (Figure 5.1.23). Aerial images also confirmed the existence of two flow paths in the Fort King waterway back channel (Figures 5.1.24 and 5.1.25).

BTCs from the October 2015 tracer experiment at the midpoint and downstream stations (Figure 5.1.21) again illustrated delayed arrival and attenuated peak concentration from advection, dispersion, and any transient storage. As in the March 2015 data, triple peaks observed at the upstream station were smoothed at both stations, allowing us to fit the OTIS model to estimate reach-scale parameters advection and dispersion parameters (see below).

Figure 5.1.22. 1,200 m USGS Station and fluorometer from a watercraft. The water passing over the USGS station is only partially dyed, suggesting most of that water is not from the main channel, but rather has taken the back channel flow path.

Figure 5.1.23. 1,200 m USGS Station and fluorometer from the air. The water passing over the USGS station is only partially dyed, suggesting water passing that location is not from the main channel, but from the back channel flow path.

Figure 5.1.24. Aerial image of the Fort King waterway back channel viewed from the spring bowl facing SW. The dye bifurcates into two distinct flow paths, with faster "Flow Path 1" eventually becoming the 2nd peak in the 1,200 m BTC and the slower "Flow Path 2" becoming the 3rd peak.

Figure 5.1.25. Aerial image of the Fort King waterway back channel, main spring bowl, and main channel, facing NE. The dye bifurcates into two distinct flow paths, with the faster "Flow Path 1" eventually becoming the 2nd peak in the 1,200 m BTC and the slower "Flow Path 2" becoming the 3rd peak. In this image, Flow Path 2 is still clear of dye.

The following figures shows BTCs measured through *in situ* fluorometry at several locations for the August and December 2016 dye trace experiments.

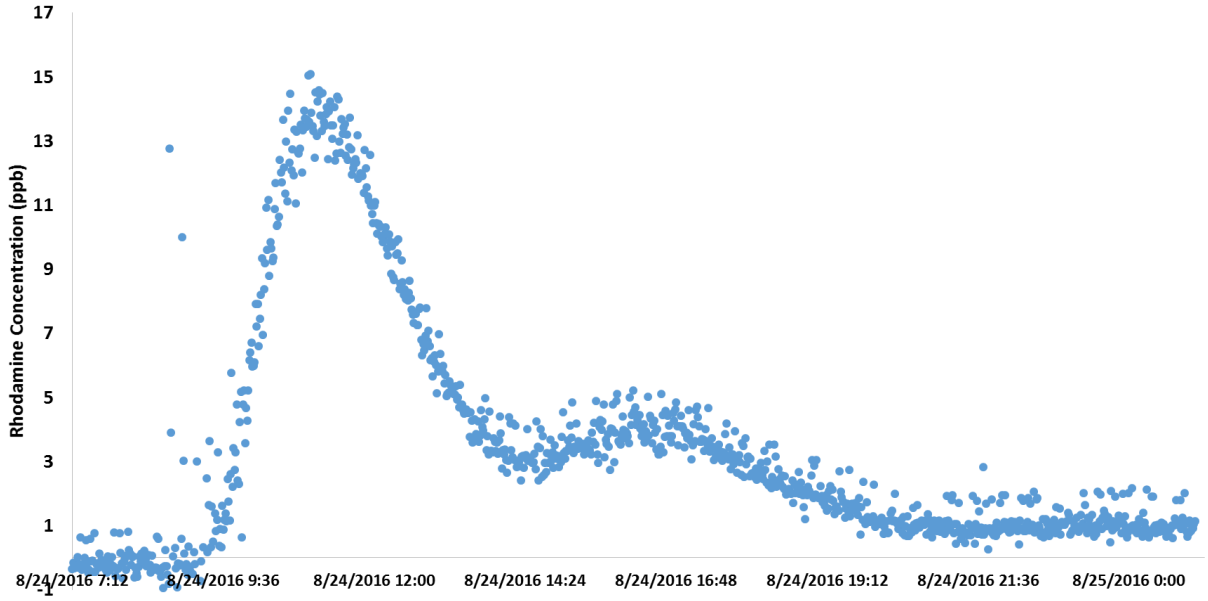

Figure 5.1.26. August 2016 BTC for Reach 1. See Figure 5.1.9 for measurement locations.

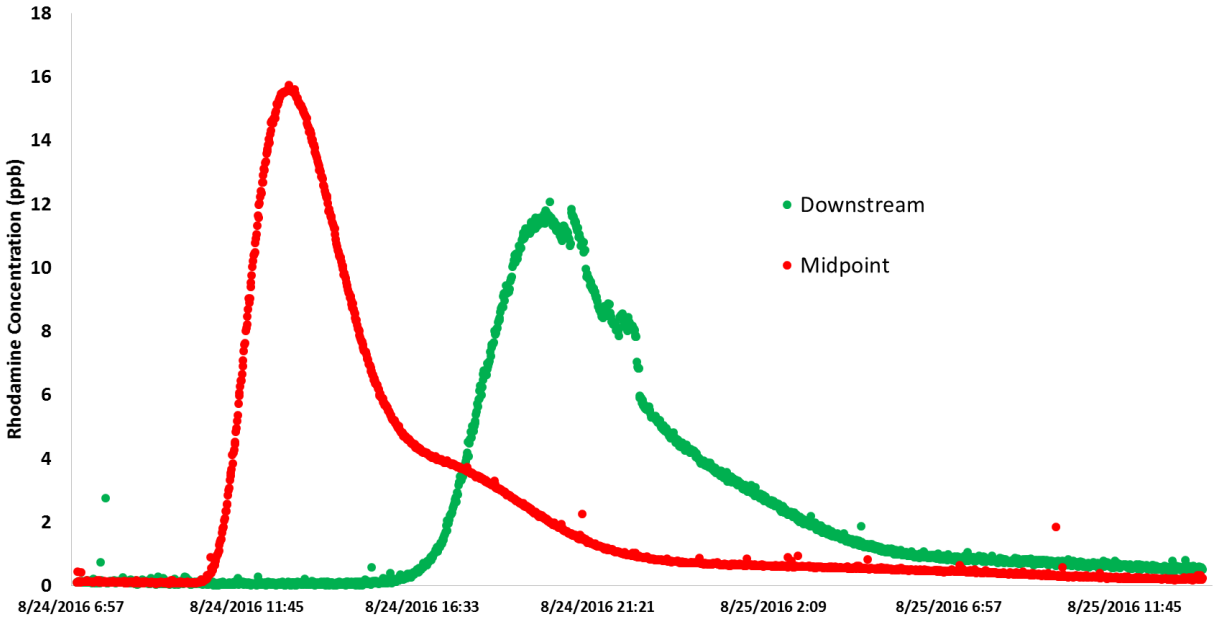

Figure 5.1.27. August 2016 BTCs at the midpoint (red dots) and downstream (green dots) stations. See Figure 5.1.9 for measurement locations.

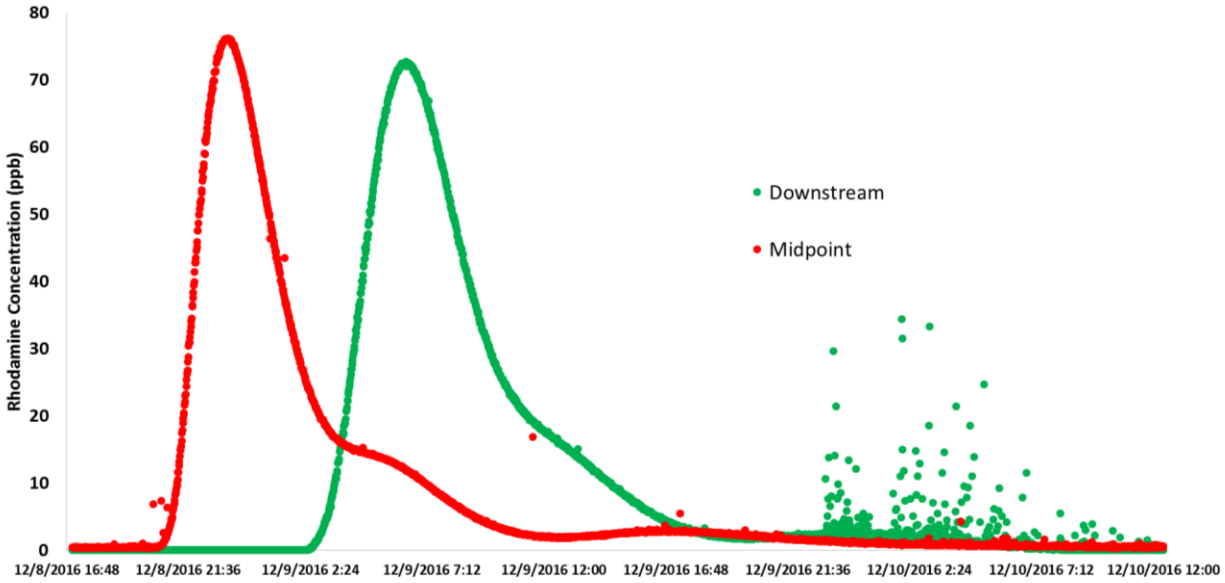

Figure 5.1.28. December 2016 BTCs at the midpoint (red dots) and downstream (green dots) stations. See Figure 5.1.9 for measurement locations.

BTCs from the August and December 2016 experiments followed the same overall pattern as those from 2015 (e.g., multiple upstream flowpaths leading to multiple peaks; Figure 5.1.26), but allowed us to measure reach-scale velocity and mixing parameters across different boundary conditions (i.e., discharge and stage; Figure 5.1.11).

5.1.3.1.2 Model Fitting and Experiment Comparisons

Observed BTC data from all dye traces were fitted to the OTIS model using both conventional and Bayesian techniques. While we continue to refine our numerical methods for Bayesian fitting (which was not a contracted task in this Work Order), results from both fitting procedures are shown for the March 2015 experiment as an example and to highlight the potential for future research into this topic. For all other experiments, we provide parameter estimates only using conventional fitting techniques, which we then use to compare flow and mixing across all four dye trace experiments. Fitting was applied for upstream and downstream reaches separately as well as for the entire river.

For the March 2015 experiment, Figure 5.1.29 characterizes the upper stream reach from the main vent to the midpoint station, Figure 5.1.30 characterizes the entire river to the downstream station, and a separate analysis of just the downstream reach (and comparison to a previous tracer injection experiment) appears below. Figures 5.1.29 and 5.1.30 illustrate the generally good agreement of fitted models with observed data, as well as between the parameter estimates from both fitting techniques. While BTC peaks are fitted fairly well in both locations, the models underestimate rhodamine concentration in the falling limb of the pulse, reflecting an underestimation of the role of transient storage. This finding has been noted by several authors, and is likely due to the assumption of exponentially distributed residence times (Gooseff et al. 2003), which may be better represented by a power-law distribution (Haggertey et al. 2002). Indeed, the magnitude of disagreement between the fitted OTIS and observed BTCs may be an indicator of longer and/or slower transient flowpaths (e.g., through the hyporheic zone or in vegetation beds). Also apparent in Figures 5.1.29 and 5.1.30 is the close agreement between

parameter estimates from conventional fitting and the mean parameter estimate using the Bayesian estimate (Table 5.1.2). While not unexpected, this gives us confidence in the Bayesian results, while the parameter estimate distributions provide a measure of relative parameter uncertainty.

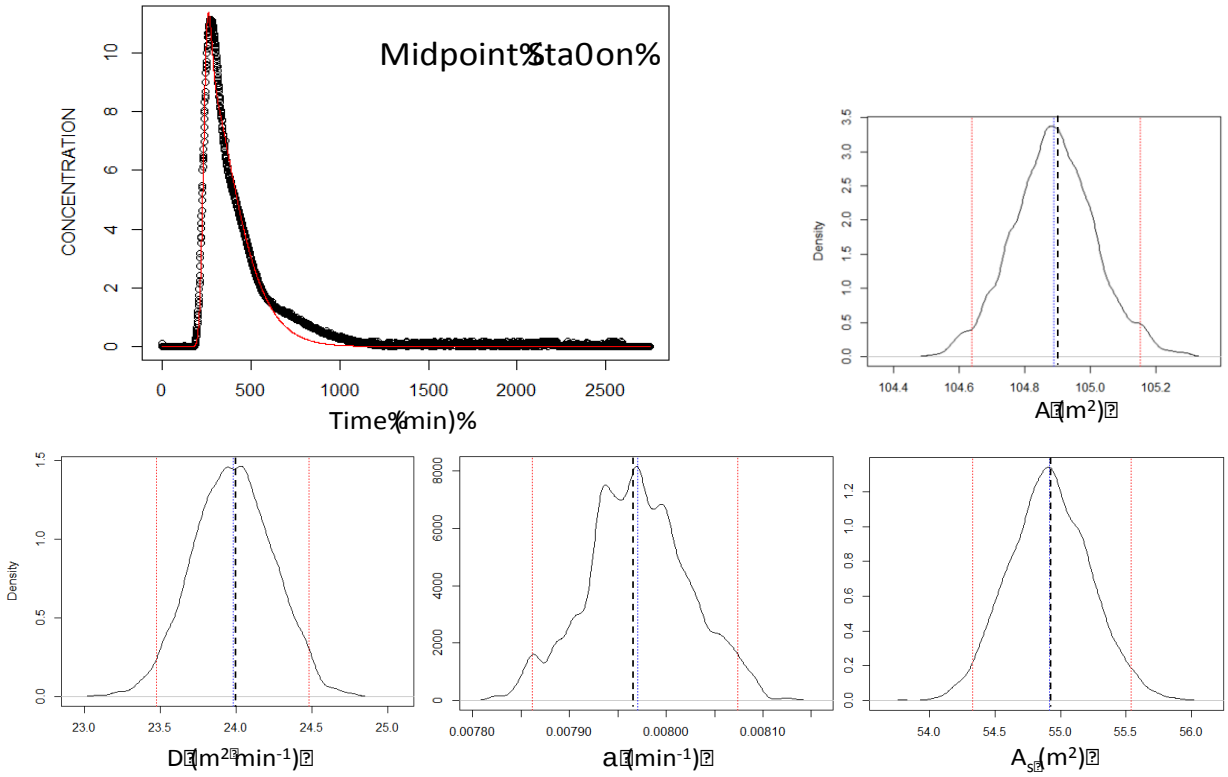

Figure 5.1.29. OTIS model (red line) fitted to March 2015 BTC data (black circles) from the midpoint station (upper left). Parameter estimates from standard model fitting (black dashed lines) are compared with Bayesian parameter distributions (solid black line) and the mean/95 % credible parameter intervals (blue/red lines, respectively).

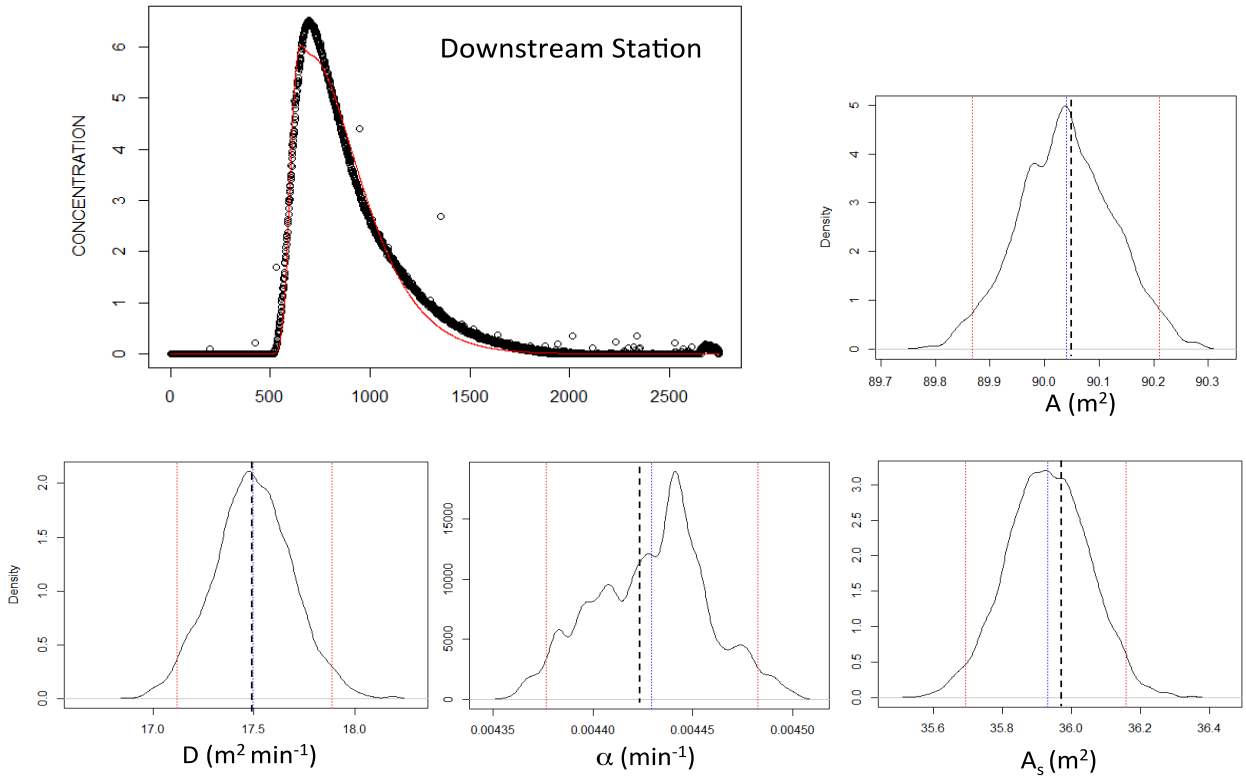

Figure 5.1.30. OTIS model (red line) fitted to March 2015 BTC data (black circles) from the downstream station (upper left). Parameter estimates from standard model fitting (black dashed lines) are compared with Bayesian parameter distributions (solid black line) and the mean/95 % credible parameter intervals (blue/red lines, respectively).

The population of model parameters derived with the Bayesian method can also be used to assess potential model identifiably issues by looking for relationships between model parameters. We would expect no correlation between truly unique model parameters, while parameters with interchangeable (i.e., non-unique) parameterizations might be expected to show strong correlation. Figure 5.1.31 presents these relationships based on our analyses, and a subset of model parameters (D and A_s, A and α; Figure 5.1.31) indicate parameter non-uniqueness, which can make interpretation and comparison of optimized model parameters difficult. Our lab will continue research to better quantify and, if possible, avoid issues of non-uniqueness using these data; however, we note that this is not a contracted Work Order task.

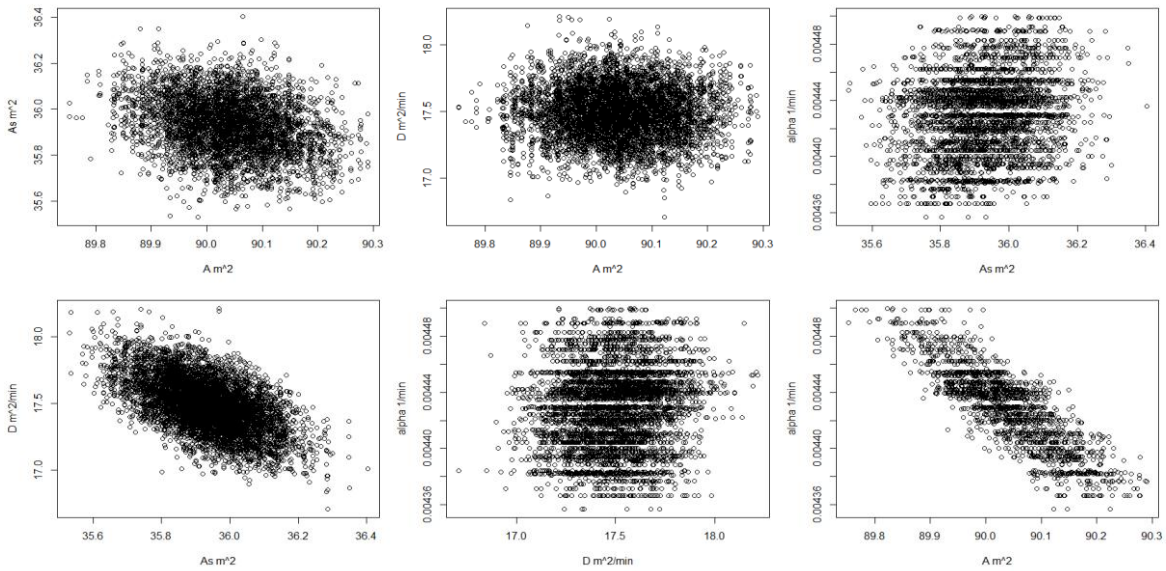

Figure 5.1.31. Relationships between parameter pairs across the entire population of Bayesian model fits for the March 2015 experiment.

For all dye trace experiments, several steps were required to estimate the hydraulic properties of the downstream reach (between the midpoint and downstream stations) and to compare these results to a previous experiment (Hensley 2010). While the midpoint and downstream measurement locations used in the two studies were identical, the 2009 study released the dye as a "line injection" at the 1,200 m station, and this study released the dye as a "point injection" in the main spring vent. To allow for comparisons across these studies we used the measured BTCs at the midstream reach as an upstream flow and concentration boundary condition and then fit the OTIS model to the BTCs at the downstream station. Fitted OTIS model parameters were then used to compare simulated October 2009, March 2015, October 2015, August 2016, and December 2016 BTCs at the downstream station based on the fitted hydraulic properties of each period.

Figure 5.1.32 presents measured BTCs at the midpoint and downstream locations for all five experiments. Fitted OTIS model parameters for these observed data were then used to simulate the BTCs for the downstream reach of the Silver River (Figure 5.1.33) and the whole Silver River (Figure 5.1.34), assuming an upstream dye injection based on Hensley (2010). Visual inspection of Figure 5.1.33 reveals substantial differences in the BTCs simulated for the five experiments. Notably, peak arrival times vary across experiments, indicating variations in reach-scale velocity in the downstream reach. For example, the peak arrives soonest for the March 2015 experiment and latest for the October 2015 experiment, indicating relatively high and low velocity "bookends", respectively, for this data set. Additionally, the BTC "tail" of the 2015 dye trace has much longer decay than all other traces, indicating increased dispersion and potential transient storage. Figure 5.1.34 reveals differences in the flow regime of the whole river that generally parallel those for the downstream reach: the peak arrives soonest for the March 2015 experiment and decays most slowly for the October 2015 conditions. Both the downstream and whole-river BTCs for the August and December 2016 experiments are similar in shape to the 2009 experiment (relatively symmetrical with rapid decay), but with slightly sooner arrival times

(higher velocity).

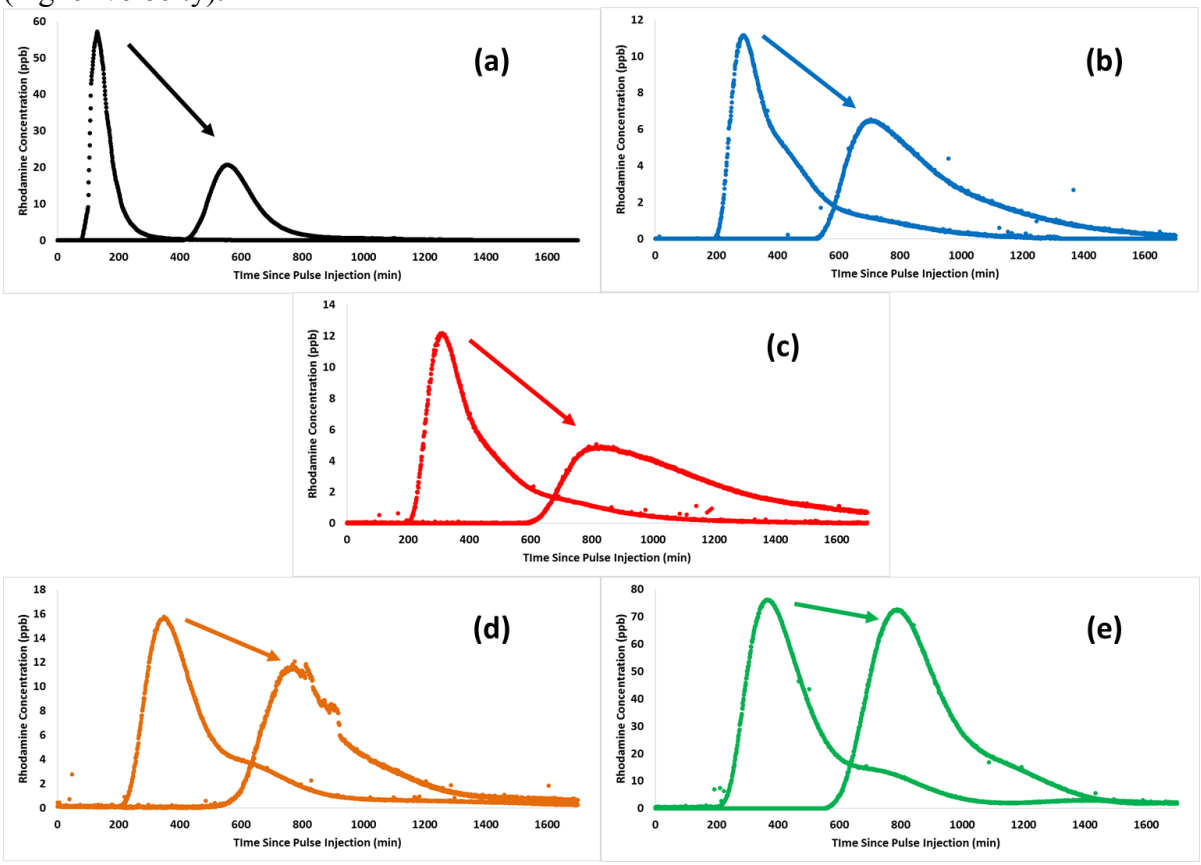

Figure 5.1.32. Comparison of observed midpoint and downstream BTCs for the October 2009 (a), March 2015 (b), October 2015 (c), August 2016 (d), and December 2016 (e) tracer experiments on the Silver River.

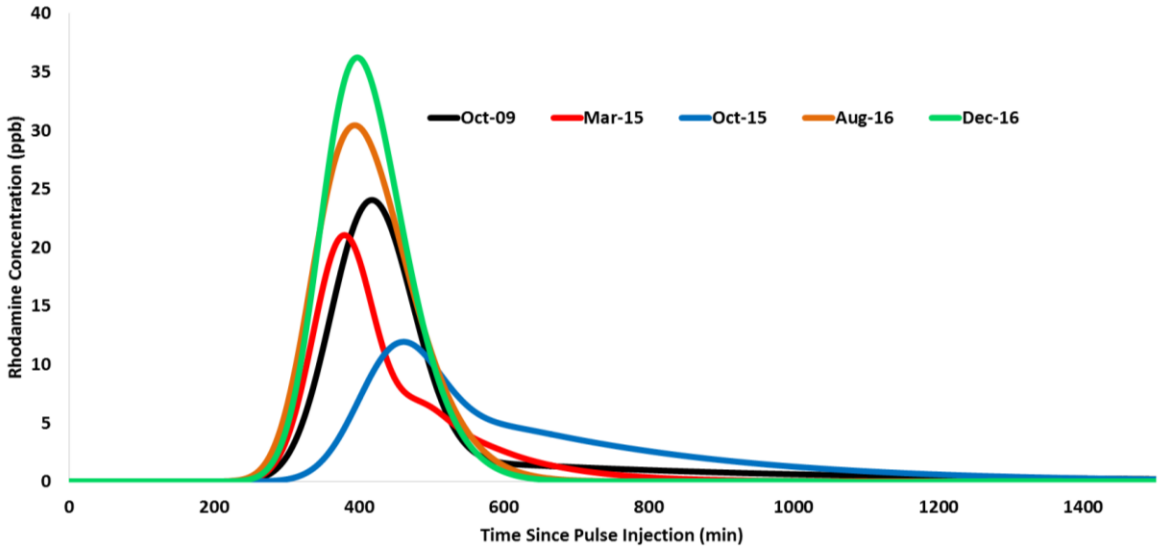

Figure 5.1.33. Comparison of fitted BTCs for the October 2009, March 2015, October 2015, August 2016, and December 2016 experiments for the downstream portion of the

Silver River.

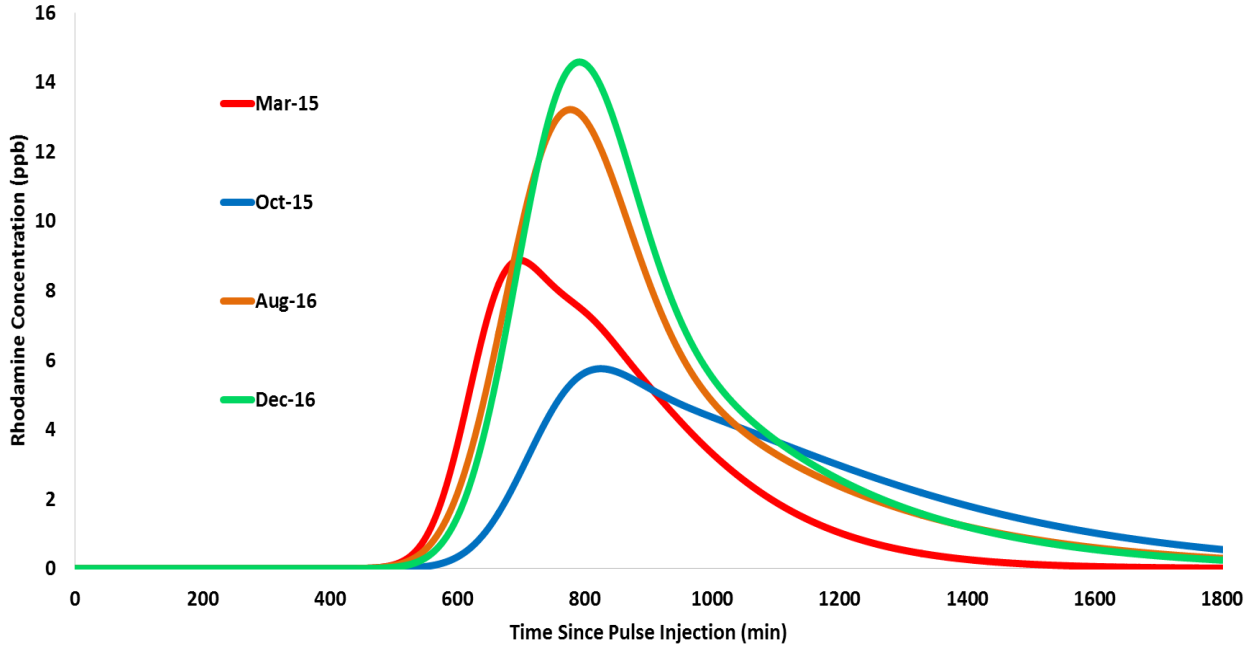

Figure 5.1.34. Comparison of fitted BTCs for the October 2009, March 2015, October 2015, August 2016, and December 2016 experiments for the entire Silver River.

These visual interpretations are supported by fitted OTIS model parameters for both the downstream reach and whole river, which are summarized in Tables 5.1.2 and 5.1.3. The differences in OTIS model parameter estimates among the different dye trace experiments suggest that the flow regime of the Silver River changes substantially with different boundary conditions (and in-channel properties such as SAV coverage and density), with likely impacts on in-channel hydrodynamics and biogeochemical transformations in the river's advective and transient storage zones. Note, comparisons of upstream versus downstream reach velocities (as opposed to downstream versus whole-river) are presented in Section 5.1.4.1.4 – Moment Analysis.

Table 5.1.2. Fitted OTIS model parameters for the downstream reach of the Silver River.

Parameter	2009 October	2015 March	2015 October	2016 August	2016 December	Units
Q	15.55	20.02	19.03	13.14	12.49	$m^3\ s^{-1}$
L	5,300	5,300	5,300	5,300	5,300	m
A	66.65	81.62	97.76	40.59	39.66	m^2
As	10.02	17.39	41.19	20.75	18.50	m^2
D	5.05	6.45	8.67	1.20	0.14	$m^2\ s^{-1}$
α	$6.66E^{-05}$	$4.89E^{-05}$	$3.90E^{-05}$	$4.95E^{-04}$	$5.05E^{-04}$	$1\ s^{-1}$
τ	378.64	360.07	453.76	272.87	280.51	min
u	0.23	0.25	0.19	0.32	0.31	$m\ s^{-1}$

Table 5.1.3. Fitted OTIS model parameters for the whole length of the Silver River.

Parameter	2015 March	2015 October	2016 August	2016 December	Units
Q	20.02	19.03	13.14	12.49	$m^3 s^{-1}$
L	8,150	8,150	8,150	8,150	$m^3 s^{-1}$
A	92.80	108.97	74.75	71.86	m^2
As	30.52	45.96	15.51	13.79	m^2
D	4.15	7.51	11.03	9.47	$m^2 s^{-1}$
α	$7.24E^{-05}$	$4.25E^{-05}$	$1.72E^{-05}$	$1.82E^{-05}$	$1 s^{-1}$
τ	629.56	777.77	772.70	781.53	min
u	0.22	0.17	0.18	0.17	$m s^{-1}$

Focusing first on the downstream reach (Table 5.1.2), reach-scale mean velocity for flow through the advective zone (u) varied from 0.19 m s^{-1} (October 2015) to 0.32 m s^{-1} (August 2016). Notably, these velocities bound our estimate of critical flow velocity for algal sloughing (see Section 5.2). The highest velocities were inversely correlated with advective zone cross-sectional area (A; $R^2 = 0.88$; not shown), indicating that the river flows fastest when confined within the channel and at lower stage. Crucially, higher discharge (Q) is not a good predictor of higher reach-scale velocity; in fact, over these five experiments, Q and u are inversely related (see Figure 5.1.37). Dispersion (D) was highest for the low-velocity October 2015 experiment, lowest in the fastest experiments (August and December 2016), and well predicted by u ($R^2 = 0.90$; not shown). Mirroring D, estimated transient storage area (A_s) was largest for the October 2016 experiment and lowest in 2016, but the association between u and As was weak ($R^2 = 0.21$; not shown).

Fitted parameters for the whole river (Table 5.1.3) were less variable across experiments than for the downstream reach only. This phenomenon is also apparent from visual comparison of the BTCs in Figure 5.1.34. Whole-river advective zone velocity varied from 0.17 to 0.22 m s^{-1} (below the estimated algal sloughing velocity) and was highest in March 2015 and lowest in October 2015 and December 2016. These results diverge from those for the lower reach, suggesting that reach-scale hydrodynamic patterns may be obscured by whole-river analysis. In particular, finding highest whole-river advective zone velocity in March 2015, but highest downstream advective zone velocity in August 2016, indicates that upstream and downstream reaches act somewhat independently, a finding supported by numerical modeling (Section 5.4).

Reach-scale advective zone velocities for the whole river and downstream reaches are summarized in Figure 5.1.35 and shown relative to algal velocity thresholds developed in King (2014) and Hoyer et al. (2004); algal velocity thresholds are discussed in Section 5.2.

5.1.3.1.3 Moment Analysis

As described above, moment analysis provides an alternative means to estimate mean reach-scale velocities (u) and residence times (τ) across experiments without imposing a specific transport model. Tables 5.1.4 and 5.1.5 compare values of u and τ estimated using moment analysis versus the OTIS model. Mean reach-scale velocities estimated using moment analysis are lower than those estimated using OTIS since they account for all transport, including transport through transient storage zones), but they are generally concordant.

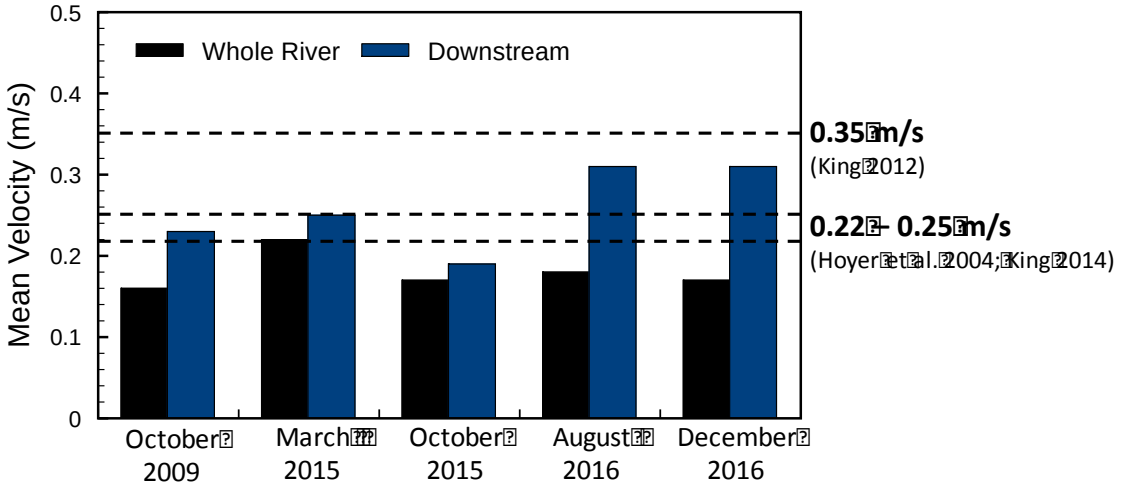

Figure 5.1.35. Fitted reach-scale, advective zone velocities (u) for the whole river and downstream reaches of the Silver River over the five dye trace experiments relative to literature-derived algal velocity thresholds (see Section 5.2).

Table 5.1.4. Comparison of OTIS and moment for downstream reach

Parameter	2009 October	2015 March	2015 October	2016 August	2016 December	Units
Q	15.55	20.02	19.03	13.14	12.49	$m^3 s^{-1}$
u OTIS	0.23	0.25	0.19	0.32	0.31	$m s^{-1}$
u moment	0.19	0.19	0.12	0.23	0.29	$m s^{-1}$
τ OTIS	378.6	360.1	453.8	272.9	280.5	min
τ moment	456.1	469.2	722.7	389.5	303.6	min

Table 5.1.5. Comparison of OTIS and moment for whole river

Parameter	2015 March	2015 October	2016 August	2016 December	Units
Q	20.02	19.03	13.14	12.49	$m^3 s^{-1}$
u OTIS	0.22	0.17	0.18	0.17	$m s^{-1}$
u moment	0.15	0.11	0.15	0.14	$m s^{-1}$
τ OTIS	629.6	777.8	772.7	781.5	min
τ moment	899.8	1,188.7	924.9	997.2	min

Moment analysis also allows us to make direct comparisons between mean reach-scale velocities in the upstream versus downstream reaches and compare these values to hydrologic boundary conditions. Figure 5.1.36 illustrates how Silver River mean velocities vary in time and space and

are often below identified thresholds for macro-algae presence. Upstream reach velocity is always lower than downstream, and the ratio of downstream to upstream velocities differences ranges from ~1 in October 2009 to >3 in December 2016 (increasing ratios also seen in OTIS-fitted advective-zone velocities; Figure 5.1.35), reinforcing the idea that the upstream and downstream river reach hydrodynamics are controlled, at least partially, by separate mechanisms. Figure 5.1.37 shows regressions among moment-derived reach-scale velocities, spring discharge, and surface water elevation change. Increased discharge does not equate to higher velocity, illustrating the need to simultaneously consider changes in Q, h, and vegetative drag (see Section 5.4).

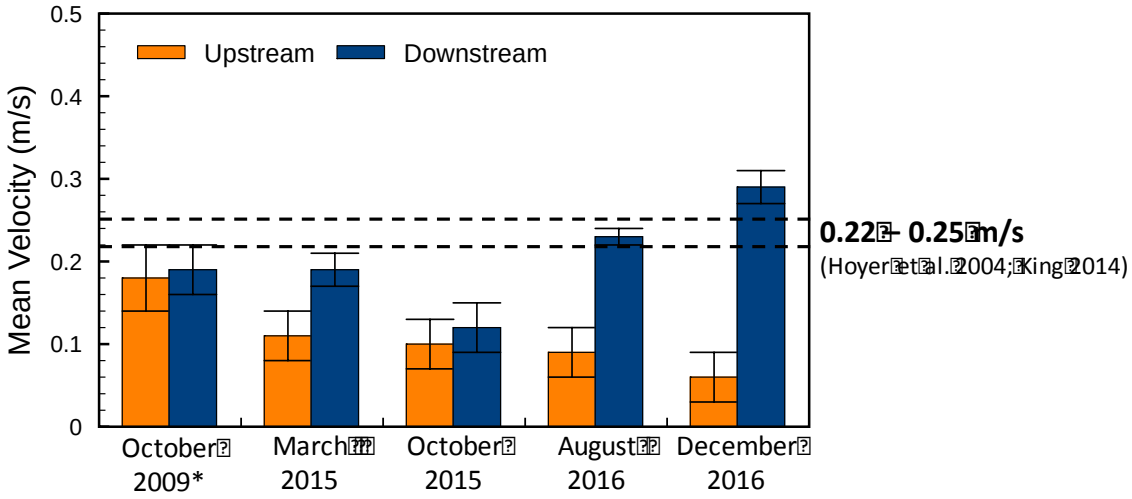

Figure 5.1.36. Reach-scale mean velocities calculated using moment analysis for upstream and downstream reaches of the Silver River over the five dye trace experiments relative to literature-derived algal velocity thresholds (see Section 5.2).

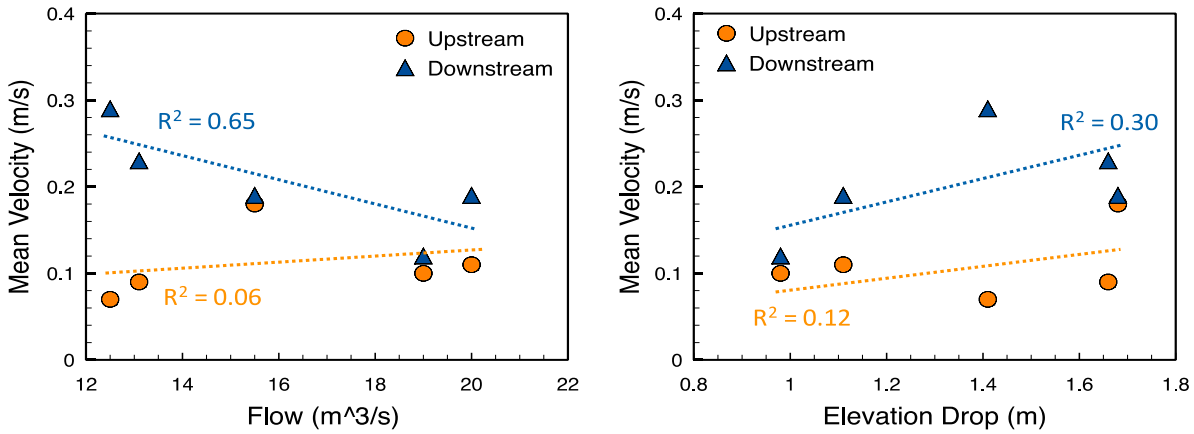

Figure 5.1.37. Reach-scale mean velocities as a function of discharge (left) and surface water elevation drop from the spring pool to the Silver-Ocklawaha River confluence (right). Upstream velocity is poorly predicted by flow, while downstream velocity is negatively correlated. Elevation drop is a positive predictor reach-scale velocity.

5.1.3.1.4 Alexander Springs Dye Trace

Breakthrough curves for the 19 January 2017 Alexander springs dye trace are shown in Fig. 5.1.38. Figure 5.1.39 and Table 5.1.6 compare the 2017 trace with results from a 2009 experiment, which characterized the first two spring reaches in the 2017 study. Mean velocities across these reaches were similar in 2009 and 2017 (0.080 and 0.079 m s^{-1}, respectively), despite 55 % higher flow in 2009. Velocity was higher in the downstream reach in 2009 during higher flows, but higher in the upstream reach in 2017 when flow was lower. While Alexander Springs is a substantially different system than the Silver River, this behavior mirrors the results observed on the Silver, where the upstream and downstream reaches respond somewhat independently to hydraulic drivers.

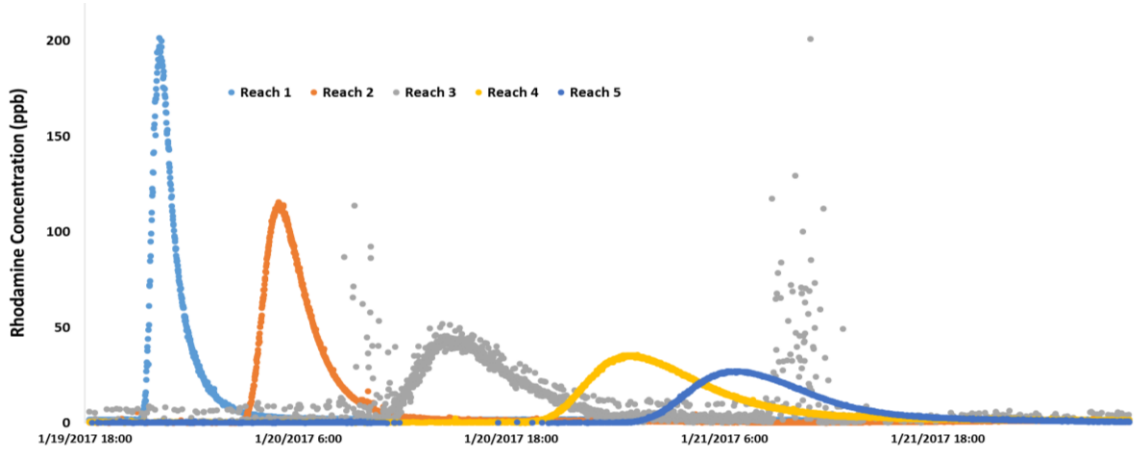

Figure 5.1.38. Breakthrough curves from the Alexander Springs Creek Dye trace.

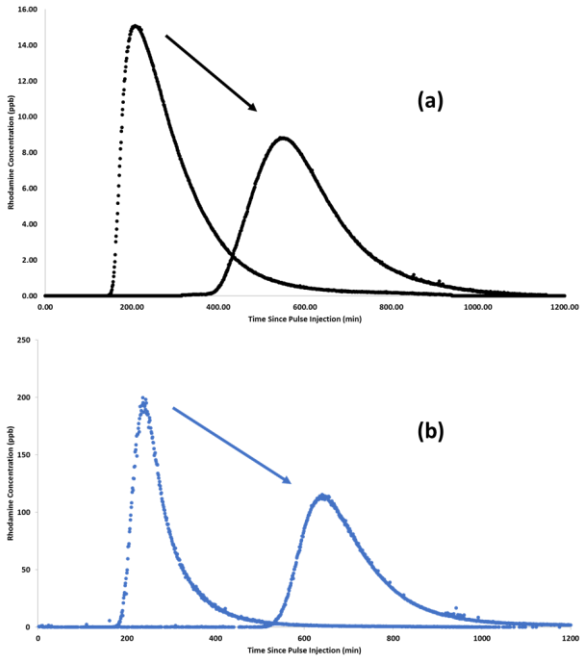

Figure 5.1.39. Comparison of observed Reach 1 and Reach 2 for the July 2009 (a) and January 2017 (b) tracer experiments on Alexander Springs Creek.

Table 5.1.6. Comparison of Alexander Springs hydraulic properties for the 2009 and 2017 dye trace experiments.

Parameter	2009 July Reach 1	2009 July Reach 2	2017 January Reach 1	2017 January Reach 2	Units
Q	3.80	3.80	2.46	2.46	$m^3 s^{-1}$
u moment	0.074	0.085	0.082	0.075	$m s^{-1}$
τ moment	293.7	607.3	283.6	707.4	min

5.1.3.1.5 Breakthrough Curve Data Versus EFDC Model

District scientists have been developing a hydrodynamic EFDC model for the Silver River with a primary goal of predicting non-uniform water level profiles and velocity profiles. The BTC data presented above provide an opportunity to calibrate and validate EFDC model performance using measured data. As an example, the EFDC model was used to simulate the March 2015 dye release for comparison with observed BTCs and aid in calibration (Figure 5.1.40). The model is able to capture some of the major features captured by the dye injection experiment and provides insight in locations where the match is poor. For example, the model recreates the three-peaked BTC observed at the 1,200 m station (Figure 5.1.40b) and two-peaked BTC at the back channel station (Figure 5.1.40c), corroborating our interpretation of flowpaths and incomplete channel mixing. On the other hand, measured data at these stations suggest longer residence times than those simulated in EFDC, which predicts rapid declines in concentration. Upriver in the main channel (Figure 5.1.40a), it is unclear whether EFDC overestimates the BTC peak or the 1-hr sampling resolution was insufficient to capture the peak concentration. The general time of arrival and mean residence times at the mid-point (Figure 5.1.38d) and downstream (Figure 5.1.40e) stations agree fairly well between modeled and measured data, though EFDC overestimates the peak at both stations.

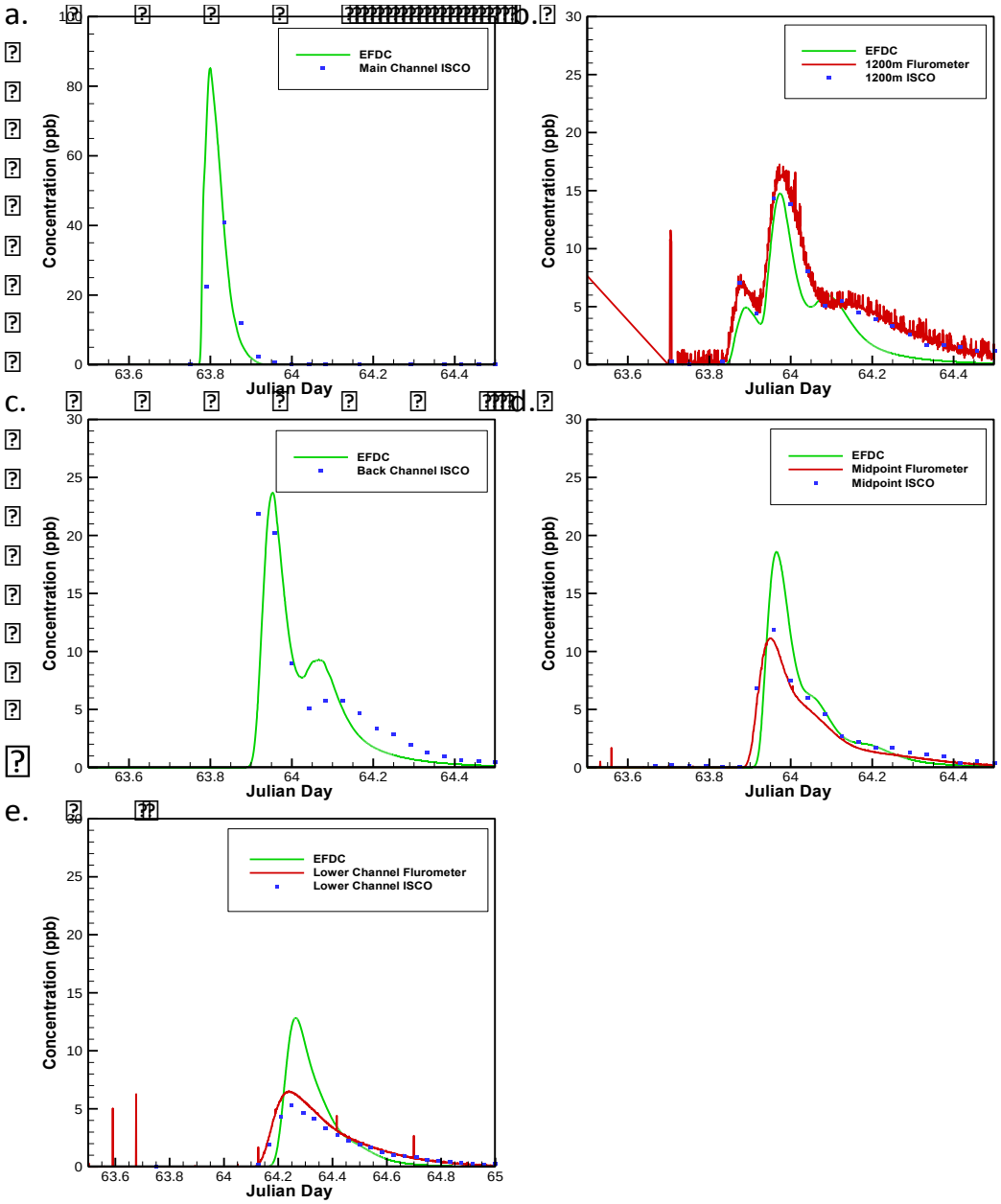

Figure 5.1.40. Comparison between observed (red lines, blue dots) and modeled (green lines) BTCs at five locations on the Silver River for the March 2015 dye release. See Figure 5.1.2 for measurement locations. Figures by Yanfeng Zhang.

5.1.3.2 Raz-Rru Experiments

5.1.3.2.1 Raz and Rru Transformation versus Time

For samples with autoclaved soils (Figure 5.1.41), the added tracer was the only compound assumed present throughout the experiment; concentrations over time were determined using a single calibration for the given tracer to avoid the introduction of error in solving the full set of equations. From the inactivated samples, the decrease of both Raz and Rru concentrations over the incubation period was more pronounced for the Silver River soils. As shown in Figure

5.1.42, this was also the case for live soils where the Raz concentration in Silver River soil decreased by more than 60 % over the first 40 minutes of incubation versus the initial 38 % change observed in the Jennings Creek sediment. However, the reported increasing Raz trend for the inactive Jennings Creek sediment is not possible and likely the product of signal separation error.

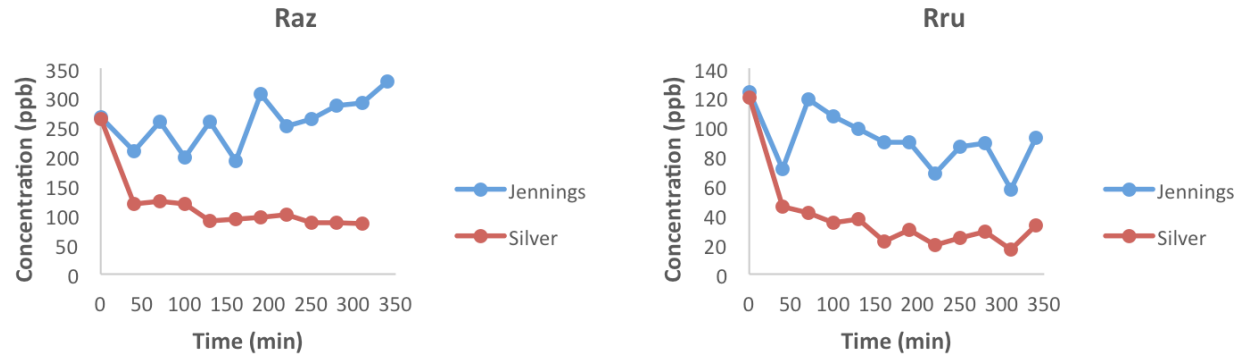

Figure 5.1.41. Adsorption to inactive sediment.

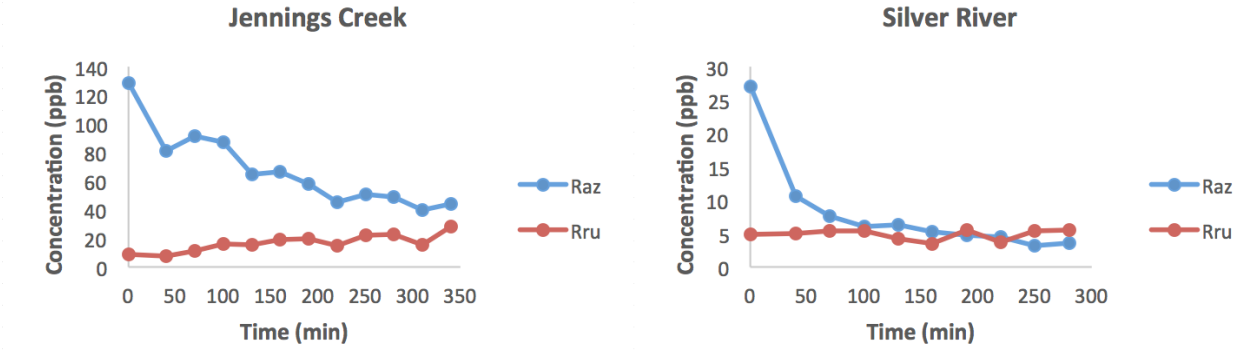

Figure 5.1.42. Combined effects of microbial activity and adsorption to sediment.

5.1.3.2.2 Kinetic Parameters

Tables 5.1.7 and 5.1.8 summarize the sorption and kinetic transformation rates for Raz and Rru determined by fitting the batch experiment data to the set of equations relating bacterial concentration, soil sorption, and overall conversion of Raz to Rru. For both tracers, the Silver River sediment was found to have a higher total adsorption capacity and in both sites, the adsorption capacity for Rru was twice that of Raz. The Silver River sediment was also more biologically active with a relative microbial concentration five times that of the Jennings Creek sediment. In terms of transformation and sorption rates, values were consistently greater for the Silver River, except for Raz conversion. In this organic sediment, adsorption may be the dominant removal mechanism for Raz. The results in Table 5.1.8 are also comparable to kinetic rates and sorption data in other studies (González-Pinzón et al. 2012; Lemke et al. 2013).

Table 5.1.7. Relative sediment sorption capacities.

System	Total Sorption Sites (M)	Total Microbes (M)
Jennings	1	2.2
Silver	5.8	11

Table 5.1.8. Fitted reaction and sorption rates.

Tracer	Kinetic rate (1/M*s)		Adsorption (1/M*s)	
	Jennings	*Silver*	*Jennings*	*Silver*
Raz	$2*10^{-5}$	$8.33*10^{-6}$	$1.67*10^{-6}$	$3.46*10^{-5}$
Rru	$3.33*10^{-5}$	$6.67*10^{-5}$	$1.67*10^{-5}$	$2.97*10^{-5}$

5.1.3.2.3 Advection-Dispersion Modeling

Kinetic transformation and sorption rates were combined as a single decay coefficient for each tracer and utilized in OTIS modeling of Raz and Rru breakthrough curves (BTCs) for simulated stream reaches containing the two sediment types. The Raz and Rru BTCs are presented alongside that of a conservative tracer for both reaches. Hydraulic parameters of the systems are summarized in Table 5.1.9.

Table 5.1.9. Fitted reaction and sorption rates.

Parameter	Modeled Value
Flow (m^3 min^{-1})	0.283
Effective Area (m^2)	0.5
Storage Area (mm^2)	1
Dispersion Coefficient (m^2 min^{-1})	0.003
Exchange Coefficient (L min^{-1})	0.12

As shown in Figure 5.1.43, a pulse injection of Raz and the conservative tracer fluorescein to a reach with Jennings Creek sediment would likely exhibit peak concentrations of 3.2 and 0.4 ppb Raz and Rru, respectively. This sums to the 3.6 ppb peak for fluorescein as expected. The Rru peak also occurs later due to retention in the transient storage zone. For the same reach with Silver River sediment, the same mean residence time of approximately 80 minutes is observed, however the Raz peak occurs sooner and the conversion of Raz to Rru is more pronounced as would be expected for more organic sediment. All three breakthrough curves also show longer tails than for the Jennings sediment which is likely a product of increased sorption and short-term tracer retention and release from hyporheic zones.

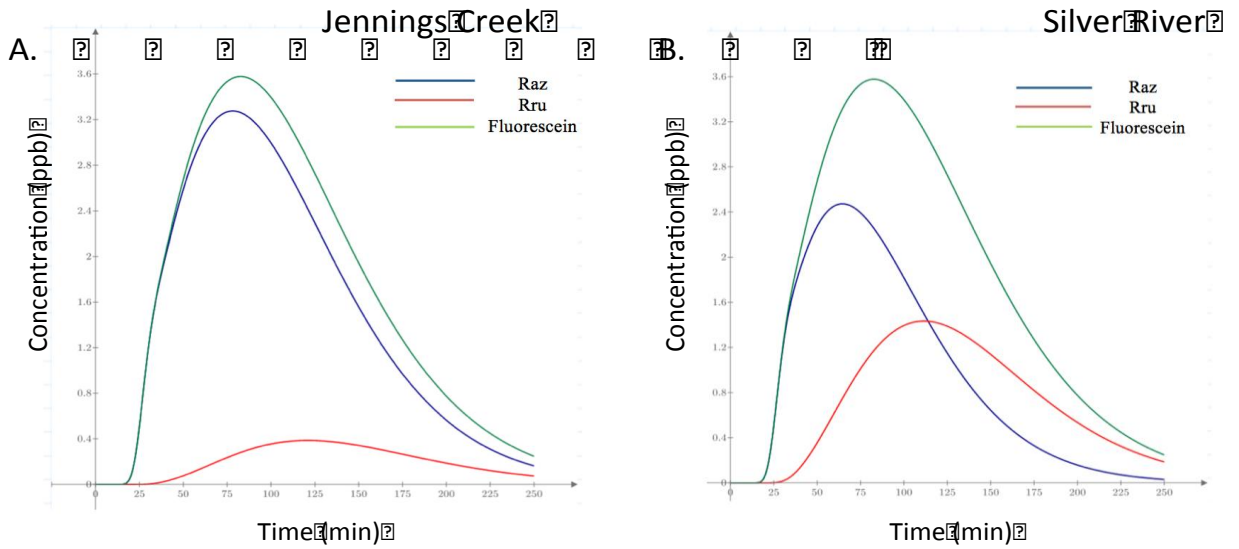

Figure 5.1.43. Raz and Rru breakthrough curves using kinetic and transport parameters for Jennings Creek (A) and Silver River (B).

5.1.3.2.4 Raz and Rru Discussion

As shown in Figures 5.1.41 and 5.1.42, measured Raz and Rru concentrations from the batch experiments contained a degree of uncertainty likely introduced by a combination of experimental and calibration error. Experimental issues could include pipetting and volume errors in sample preparation as well as slight photodegradation of the tracers. However, signal separation was likely dominant as preliminary tests of known Raz and Rru concentration mixes consistently produced overestimates of the Rru concentration. This is attributed to the fact that the fluorescence spectra for the two tracers overlap and that Rru is more fluorescent. Depending on the excitation and emission wavelengths employed, simultaneous measurements of both tracers below 1 ppb are not considered reliable (Lemke et al. 2013). In future laboratory work, calibrations will be performed with a set of wavelengths that will allow for more accurate Raz and Rru separation.

From the kinetic rate and sorption results summarized in Tables 5.1.7 and 5.1.8, the organic sediments of the Silver River were found to be orders of magnitude more active than those of Jennings Creek for some parameters. As Rru sorption was most significant in both systems, it is likely that this could be a major source of concentration detection error in reach scale studies and could make pulse injections infeasible even in small streams. The breakthrough curves shown in Figure 5.1.43 illustrates the predicted breakthrough curves for pulse injection tracer tests in reaches with Jennings Creek and Silver River sediment, respectively. As shown in Figure 5.1.43, Rru concentrations produced in Jennings Creek are below the 1 ppb detection limit for in-stream fluorometers which agrees with previous results in the actual stream (Lemke et al. 2013). For the same reach geometry with Silver River sediment, about 3 times more conversion of Raz to Rru can be expected with increased transient storage retention due to the higher sorption capacity and microbial activity of the system. Overall, fitted parameters from the batch experiments provide an accurate representation of the breakthrough curve trends that would be expected for sandy verusus organic sediments.

In terms of the effectiveness of the system in estimating microbial activity for a specific site, the model utilized in this study did predict a microbial concentration for the Silver River that was five times that of Jennings Creek as expected for a more productive system. While full reach scale studies in large, highly organic spring systems may be impractical, this may indicate that for studies of isolated areas within a reach, the Raz-Rru system could provide an estimate of the overall biogeochemical activity given varying hydraulic parameters. However, further work is needed to determine whether this estimate could provide proportions of various reactions (e.g., aerobic respiration versus denitrification).

5.1.4 CONCLUSIONS, RECOMMENDATIONS, AND FUTURE RESEARCH NEEDS

Four dye tracer experiments using *in situ* fluorometry and grab samples (along with data from a previous study) allowed us to delineate flow paths and estimate reach-scale hydraulic properties of the Silver River across different seasons and hydraulic conditions by fitting observed breakthrough curves (BTCs) using 1-D transport and mixing models. Dye tracer results also provided valuable data for testing and calibration of the Environmental Fluid Dynamics Code (EFDC) model. BTC data indicated the presence of three upstream flowpaths: one via the main river channel and two through the "back channel" (i.e., the Ft. King Waterway). Reach-scale velocities and mixing parameters measured via dye trace experiments were variable in time and space, illustrating how the flow regime of the Silver River changes with different boundary conditions (spring flow and river stage), as well as with in-channel properties such as SAV coverage and density. This variation impacts in-channel hydrodynamics and likely affects biogeochemical transformations in the river's advective and transient storage zones.

Whole-river advective zone velocity varied from 0.17 to 0.22 m s^{-1} (near or below our best estimate of the critical velocity for algal presence), while mean advective zone velocity for the downstream reach varied from 0.19 to 0.32 m s^{-1} (bounding our estimate of critical flow velocity). Higher spring discharge was not a good predictor of higher reach-scale velocity, illustrating the need to simultaneously consider changes in discharge, stage, and vegetative drag to understand reach-scale velocity. Upstream overall mean reach velocity was always lower than downstream, and the ratio of downstream to upstream velocities was highly variable, reinforcing the idea that the upstream and downstream river reach hydrodynamics act at least somewhat independently.

Mixing parameters were also variable across experiments, illustrating differential mixing mechanisms across seasons and boundary conditions; dispersion and transient storage were generally greatest when mean velocity was low and downstream stage was high. Beyond model fitting, comparison of BTCs in vegetation beds relative to the adjacent main channel suggest that vegetation beds serve as a partial barrier to mixing and zone of transient storage. Reactive tracer (Raz-Rru) results from our pilot study identified substantial Rru sorption to organic sediments that make reach-scale studies in large, highly organic spring systems impractical.

5.1.5 REFERENCES

Briggs, M. A., Lautz, L. K., Hare, D. K., and González-Pinzón, R. 2013. Relating hyporheic fluxes, residence times, and redox-sensitive biogeochemical processes upstream of beaver dams. *Freshwater Science, 32*(2).

Bristow, J. M., and Whitcombe, M. 1971. The role of roots in the nutrition of aquatic vascular plants. *Amer. J. Bot., 58*(1).

Caffrey, J. M., and Kemp W. M. 1992. Influence of the submersed plant, *potamogeton perfoliatus,* on nitrogen cycling in estuarine sediments. *Limnol.Oceanogr., 37*(7).

Carignan, R. 1982. An empirical model to estimate the relative importance of roots in phosphorus uptake by aquati macrophytes. *Can.J.Fish.Aquat.Sci, 39.*

Cedergreen, N., and Madsen, T. V. 2002. Nitrogen uptake by the floating macrophyte lemna minor. *New Phytologist, 155*(2), 285-292.

Chapman, R. S., and et al. 1995. *Investigation of wetlands hydraulic and hydrological processes, model development, and application.* (No. Wetlands Research Program Technical Report WRP-CP-6). Washington, D.C.: US Army Corps of Engineers.

González-Pinzón, R., Haggerty, R., and Myrold, D. D. 2012. Measuring aerobic respiration in stream ecosystems using the resazurin-resorufin system. *Journal of Geophysical Research: Biogeosciences, 117*(G3).

Haggerty, R., Argerich, A., and Martí, E. 2008. Development of a "smart" tracer for the assessment of microbiological activity and sediment-water interaction in natural waters: The resazurin-resorufin system.*Water Resources Research, 40.*

Haggerty, R., Marti, E., Argerich, A., von Schiller, D. and Grimm, N. B. 2009, Resazurin as a ‘‘smart’’ tracer for quantifying metabolically active transient storage in stream ecosystems, *Journal of Geophysical Research: Biogeosciences*, 114: G03014.

Hanson, G. C., Groffman, P. M., and Gold, A. J. 1994. Denitrification in riparian wetlands receiving high and low groundwater nitrate inputs. *Journal of Environmental Quality, 23*(5), 917-922.

Heffernan, J. B., and Cohen, M. J. 2010. Direct and indirect coupling of primary production and diel nitrate dynamics in a subtropical spring-fed river. *Limnology and Oceanography, 55*(2), 677.

Hensley, R. T., and Cohen, M. J. 2012. Controls on solute transport in large spring-fed karst rivers. *Limnology & Oceanography, 57*(4), 912.

Hinkle, S. R., and et al. 2001. Linking hyporheic flow and nitrogen cycling near the willamette river-a large river in Oregon, USA. *Journal of Hydrology, 244*(3-4).

Kelleher, C., et al. "Identifiability of transient storage model parameters along a mountain stream." *Water Resources Research* 49.9 (2013): 5290-5306.

Lemke, D., Liao, Z., Wohling, T., Osenbruck, K., and Cirpka, O. A. 2013. Concurrent conservative and reactive tracer tests in a stream undergoing hyporheic exchange. *Water Resources Research, 49,* 1-14.

Lemke, D., Schnegg, P. A., Schwientek, M., Osenbruck, K., and Cirpka, O. A. 2013. On-line fluorometry of multiple reactive and conservative tracers in streams. *Environmental Earth Science, 69,* 349-358.

Lin, Y., Jing, S., Wang, T., and Lee, D. 2002. Effects of macrophytes and external carbon sources on nitrate removal from groundwater in constructed wetlands. *Environmental Pollution, 119*(3).

Madsen, J. D., Chambers, P. A., James, W. F., Koch, E. W., and Westlake, D. F. 2002. The interaction between water movement, sediment dynamics and submersed macrophytes. *Hydrobiologia, 444*(1-3), 71-84. doi:10.1023/A:1017520800568.

Morris, E. P., and et al. 2008. Interaction between hydrodynamics and seagrass canopy structure: Spatially explicit effects on ammonium uptake rates. *Limnology and Oceanography, 53*(4), 1531–1539.

Mulholland, P., and et al. 2008. Stream denitrification across biomes and its response to anthropogenic nitrate loading. *Nature, 452.*

Mulholland, P.J., Valett, H. M., Webster, J. R., Thomas, S. A., Cooper, L. N., Hamilton, S. and Peterson. B. J. 2004. Stream denitrification and total nitrate uptake rates measured using a field ^{15}N tracer addition approach. Limnology and Oceanography 49:809-820.

Pusch, M., Fiebig, D., Brettar, I., Eisenmann, H., Ellis, B. K., Kaplan, L. A., and Traunspurger, W. 1998. The role of microorganisms in the ecological connectivity of running waters. *Freshwater Biology*, *40*(3), 453-495.

Reddy, K. R. 1983. *Fate of nitrogen and phosphorus in a waste-water retention reservoir containing aquatic Macrophytes1* Retrieved from https://www.agronomy.org/publications/jeq/abstracts/12/1/137

Runkel, R. L. 1998. *One-dimensional transport with inflow and storage (OTIS): A solute transport model for streams and rivers.* (No. 98-4018). Denver, CO: US Geological Survey.

Scott, T.M., et al. 2004. Springs of Florida. Florida Geological Survey Bulletin No. 66.

Stapel, J., and et al. 1996. Nutrient uptake by leaves and roots of the seagrass *thalassia hemprichii* in the spermonde archipelago, Indonesia. *Marine Ecology Progress Series, 134*

Stream Solute Workshop. 1990. Concepts and methods for assessing solute dynamics in stream ecosystems. *Journal of the North American Benthological Society, 9*(2), 95.

Veraart, A., Bruijne, W. J., Klein, J. M., Peeters, E. H. M., and Scheffer, M. 2011. Effects of aquatic vegetation type on denitrification. *Biogeochemistry, 104*(1-3), 267-274. doi:10.1007/s10533-010-9500-z.

Zarnetske, J. P. 2009. Resazurin as a "smart" tracer for investigating hyporheic biogeochemical processes. *Geological Society of America Abstracts with Programs, 41*(7), 470.

5.2 CRITICAL VELOCITY/SHEAR STRESS

5.2.1 INTRODUCTION

Section 4 of the RFQ identifies the identification of an upper velocity threshold or event (duration of exceedance) for the presence of filamentous algae or hydrilla as a major question, based on correlated observations of velocity declines and algal expansion. One previous study (King 2012) suggests that inhibitory effects may be present at low velocities (ca. 25 cm s^{-1}). Between 1933 and 1997, measured velocity in the Silver River exceeded this level approximately 50 % of the time, but in recent years this velocity is exceeded < 5 % of the time (Figure 5.2.1), providing correlative support for this hypothesis, however the presence of dense algal mats in areas where this velocity is frequently exceeded highlights a remaining gap in knowledge about the critical bed-shear for algal sloughing. Moreover, we expect that critical velocities or shear stresses for algal sloughing likely exhibit non-linear and density-dependent behavior whereby the clearing of dense algal mats (i.e., via flow increases) requires much greater velocity/shear stress than the prevention of algal accumulation in sparsely colonized reaches.

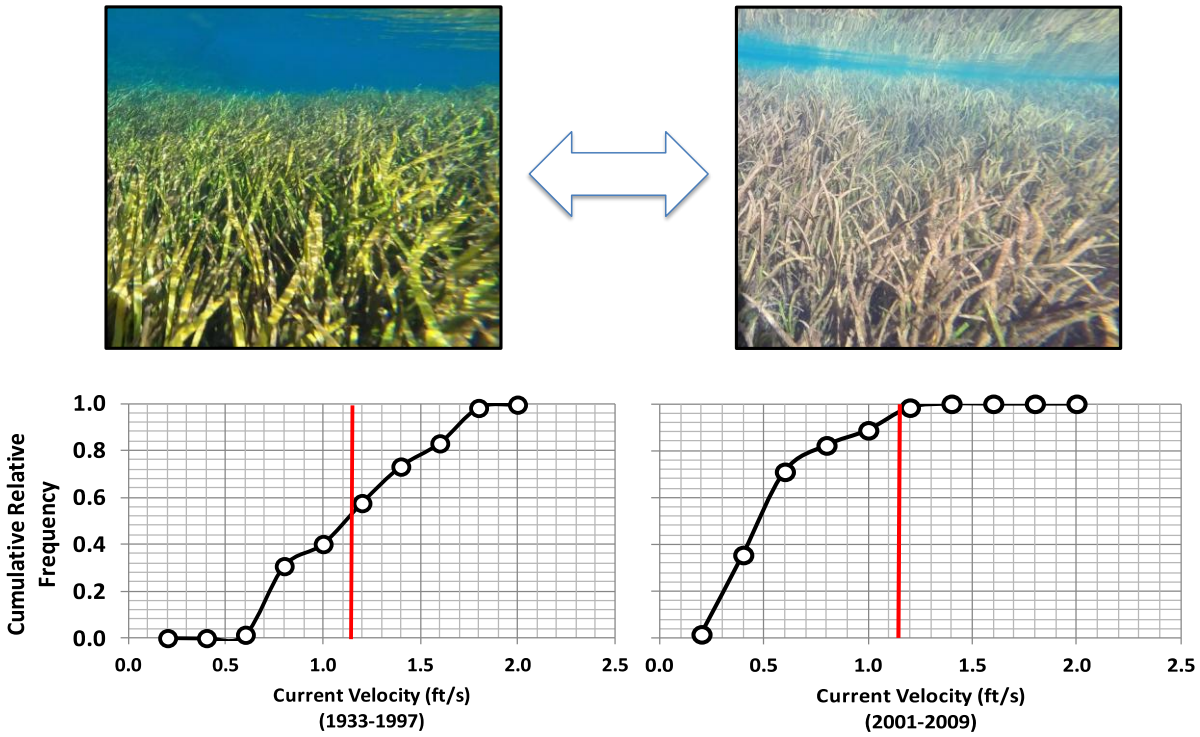

Figure 5.2.1. Algal cover is hypothesized to be controlled by velocity, which has decreased markedly in the Silver River in recent years. Lower figure from Lowe (2014); red line represents initially identified velocity threshold of 0.35 m s^{-1} from King (2012), which was later updated to 0.22 m s^{-1} in King (2014).

5.2.2 MATERIALS AND METHODS

Based on the knowledge gaps summarized above, we pursued two approaches to better test the velocity/shear stress-algal cover hypothesis and determine critical thresholds for algal entrainment that can be used as management targets. The first approach was experimental and

consisted of the deployment of field-based, *in situ* flow-ways to experimentally manipulate flow velocity and observe algal response. Several flow-way designs were developed over the course of the three-year project. The second approach was observational and leveraged algal cover and velocity data collected for the Silver River and other FL springs to statistically identify critical velocities and shear stresses that predict algal and SAV presence and absence. Finally, we pursued simultaneous optical algal and velocity measurements over large areas. While not a contracted task in this Work Order, we provide our prototype methodological approach and initial results as a template for future work.

5.2.2.1 Flow-ways

Our primary approach to addressing these knowledge gaps was to perform *in situ* experiments to elevate and/or exclude flow in order to determine critical shear stresses for the entrainment and sloughing of epiphytic and benthic algae. The application of *in situ* flow-ways deployed across a range of bottom types, vegetation covers, and algal densities provides a more robust estimation of critical hydraulic variables, which can be incorporated into models existing and proposed hydrodynamic models to predict the effect of management actions on attached algae. Adjustable experimental flow-ways may also be used in future experiments to test the effects of flow on other ecological components and processes (e.g., grazer density, grazing rate, productivity, autotrophic NO_3-N uptake, etc.).

Flow-ways were originally based on a modified design based on both the "Benthos Boxes" proposed for experimental work by the Nitrogen Effects/Dynamics and Trophic Interaction Groups and the experimental design used by King (2012). The initial design of the flow-ways was a rectangular (ca.1 x 2 m) enclosure that may extend out of the water column, open to flow on both ends, and screened to catch detached algae at the downstream end. An adjustable flange-type opening on the upstream end would allow for the focusing or exclusion of incoming flow to provide a range of flows, velocities, and shear stresses within a single experimental location (Figure 5.2.2). Due to challenges and physical restrictions in the field such as boat traffic, deep water, slow current velocities in shallow areas of the river, tall SAV, etc., flow-way design evolved over the course of the experiment (e.g., Figure 5.2.23), and prototypes were constructed and deployed in the field on multiple occasions (Figures 5.2.4 and 5.2.5). The performance of flow-ways was measured in the field (Figures 5.2.6 and 5.2.7) to determine if they would be able to sufficiently modulate velocity.

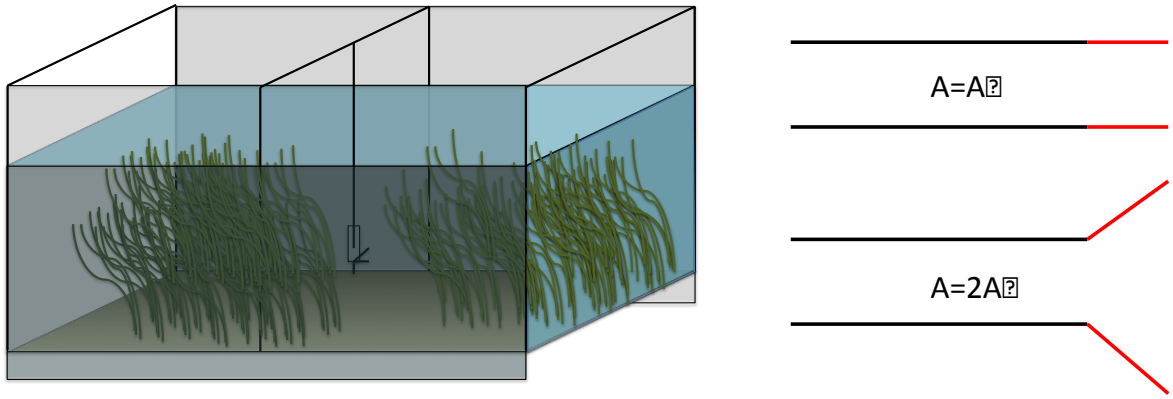

Figure 5.2.2. Originally proposed flow-way design (v1).

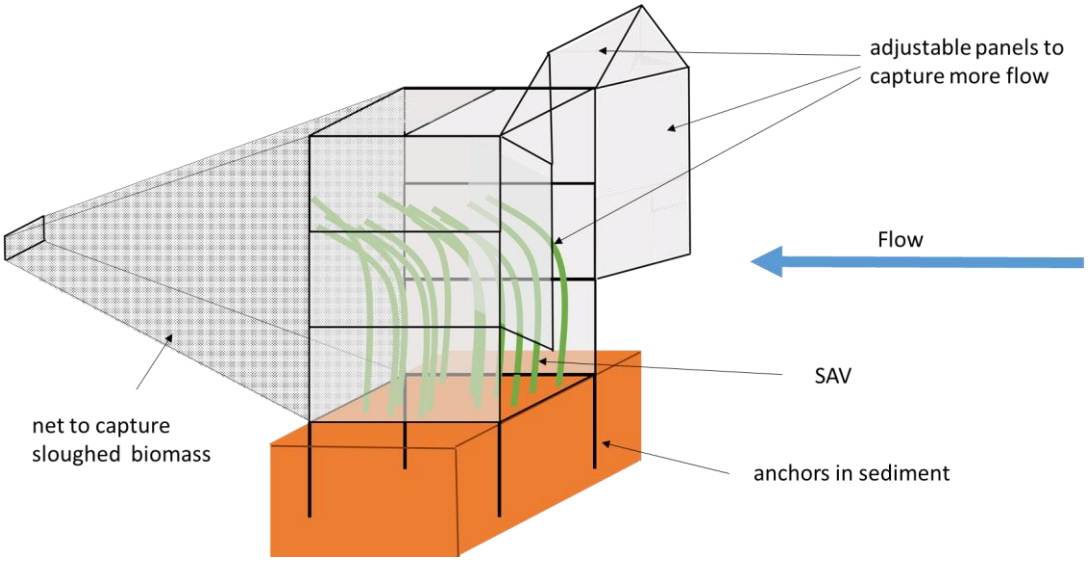

Figure 5.2.3. Reimagined flow-way design (v2). This design was constructed and deployed in the Silver River (see Figures 5.2.4 and 5.2.6).

Figure 5.2.4. Modified flow-way (v2) deployed in the Silver River.

Figure 5.2.5. Modified flow-way (v3) deployed in the Silver River.

Figure 5.2.6. Flow-way (v2) deployed in the Silver River undergoing performance testing.

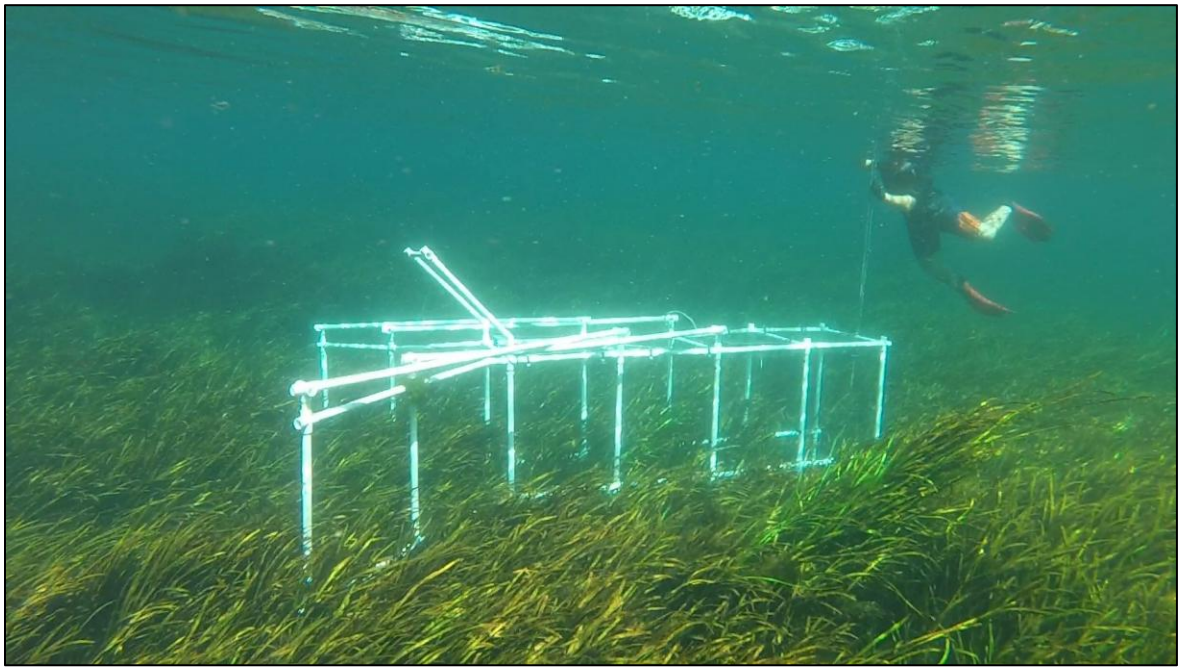

Figure 5.2.7. Flow-way (v3) deployed in the Silver River undergoing performance testing.

While the flow-way designs shown above were able to modify velocity in the fastest-flowing portions of the river (see Section 5.2.3.1), given other physical restrictions present in the Silver River (boat traffic, depth, slow flow in algal-dominated areas), the flange-type flow-way design was abandoned, and a new strategy was implemented. The concept for the new strategy consisted of blocking flow on the bottom of the river with a structure, observing the rate of algal colonization (if present) in these areas with artificially suppressed velocity, and then restoring the flow through the section of river bottom to measure algal removal rates (if present). This approach was then repeated along a gradient of flow velocities to quantify a critical algal removal velocity. This approach also allowed us to determine whether there is a hysteresis effect

of algal abundance after it has become established (i.e., are higher velocities required to clear dense algae relative to those required to maintain already clear SAV?). Finally, this experiment allowed us to quantify algal colonization and growth rates, by monitoring algal abundance after the flow had been suppressed.

This general concept is shown in Figure 5.2.8. We dubbed the flow-blocking structure "The Shadow" (Figures 5.2.9 and 5.2.10). The Shadow diverts flow above and around its footprint, effectively reducing flow velocity to zero directly behind the structure (Figure 5.2.11). The clear panels allow light through to the SAV. Shadow structures were deployed at 20 different locations in the Silver River, each for a duration of one week in spring 2017. During deployment, algal cover was measured behind the shadow structure and in an adjacent control site using digital photography). A minimum of six images were taken for each treatment site and control for every time point. These images were taken at slightly different heights, locations, and angles in order to capture and accurate representation of the algal distribution. After one week of algal growth, flow was restored and algal cover was measured for several days using the same imaging procedure. The full experiment consisted of four deployments of five treatments and controls each, resulting in a total of 20 paired treatment and control time series.

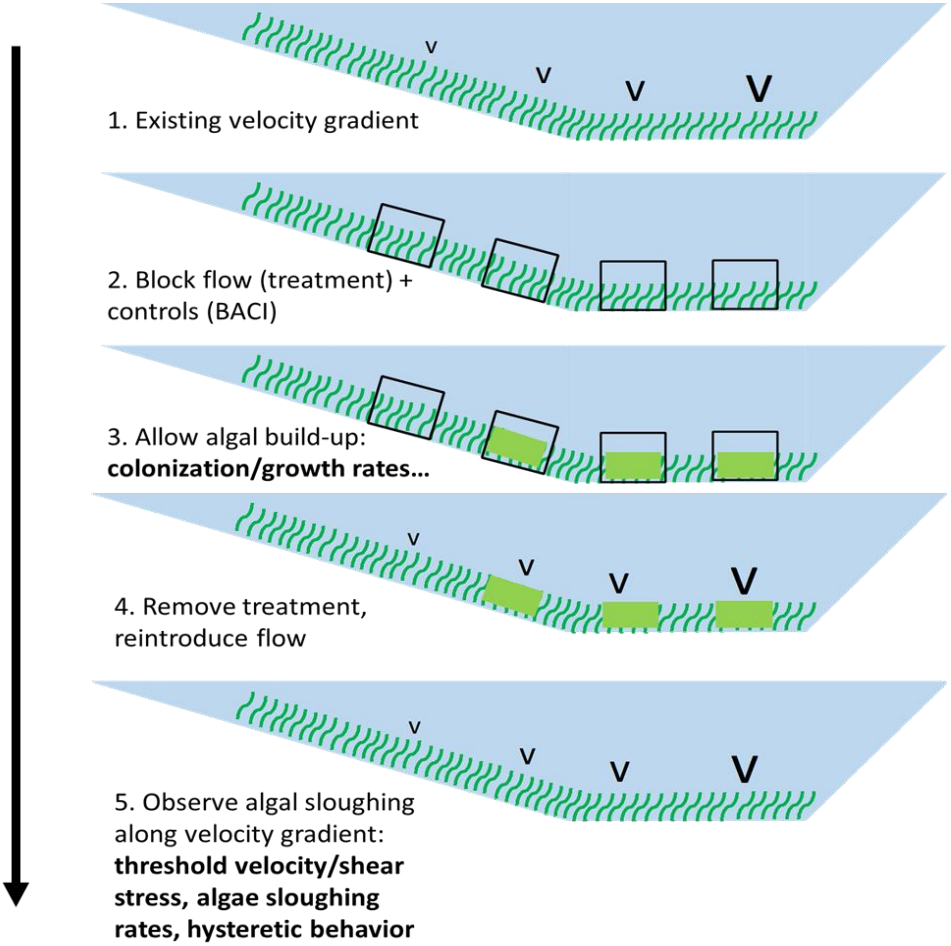

Figure 5.2.8. Schematic of the "Shadow" deployment concept. See text for description.

Figure 5.2.9. The “Shadow” structure in the lab. Blue arrow indicates flow direction.

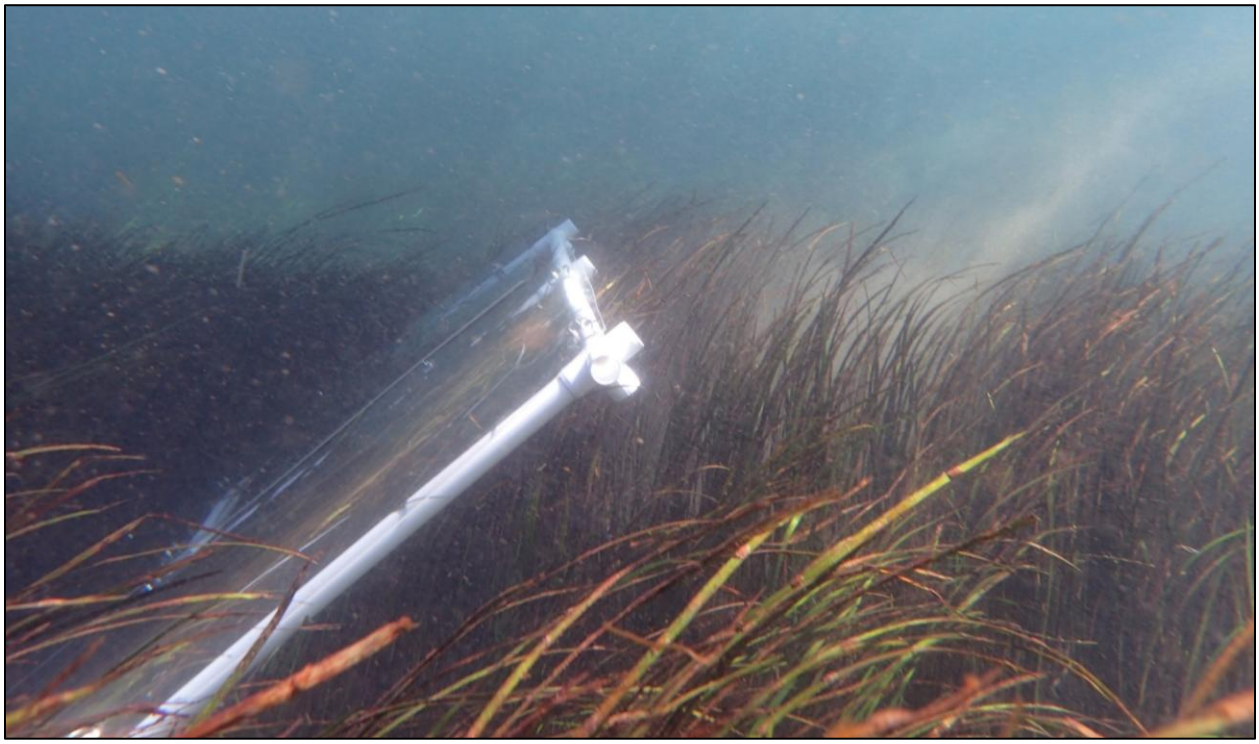

Figure 5.2.10. “Shadow” structure deployed in the Silver River.

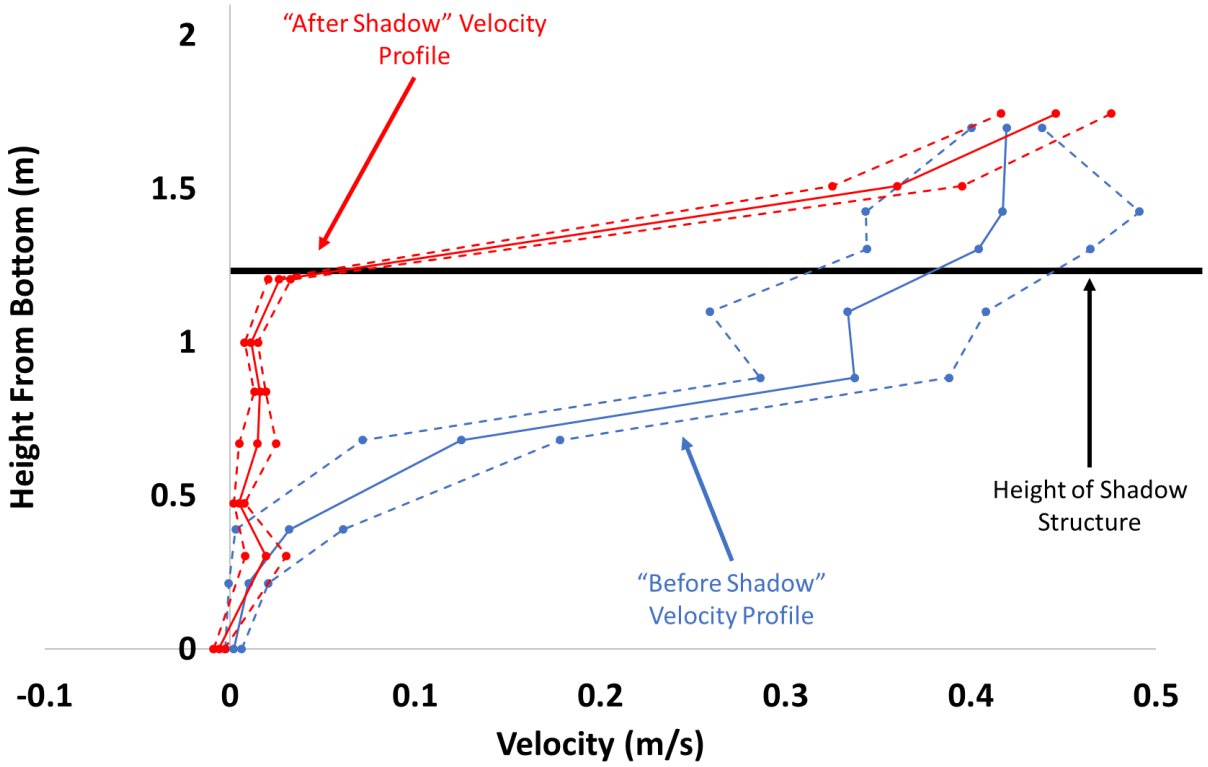

Figure 5.2.11A. Example of flow suppression by the Shadow structure. Shown are velocity profiles at a location in the Silver River both before (blue) and after (red) the deployment of a Shadow structure. Velocity profiles consist of the average velocity (solid colored line) and plus and minus one standard deviation (dotted colored lines). The black line indicates the height of the top of the Shadow structure.

Algal abundance was quantified visually from the images taken using classification categories. This process consisted of randomizing the order of the images then visually assigning each an algal abundance value of "very low", "low", "medium", "high", and "very high". This quantification scheme was selected to match observational data collected in passing by divers measuring SAV on the Silver River (see Section 5.2.2.2). These qualitative thresholds between categories are limited only by the constraint that they are sequential (i.e., very low < low < medium < high < very high). Given a classification scheme with undefined thresholds, we applied a quantitative model (see below) to determine the likely values of the unknown observer thresholds (i.e., what is the percent cover threshold between "very low" and "low"?) and estimate algal abundance estimates (in percent cover) that quantify the uncertainty associated with experimental and observer errors. This approach removes potential observer bias or error that is present when using a classification scheme that has defined thresholds, such as the Braun-Blanquet classification, or when estimating the cover directly, such as when assigning a percent cover. We applied this model both for the quantification of algal colonization/growth rate and critical algal removal velocity from the Shadow data as well as for critical velocities from diver-collected observational data. Here we present the model as applied for determining algal

colonization and growth rates; the model for determining the critical algal removal velocity will be discussed in Section 5.2.2.2.

Algal abundance can be quantified using percent cover. This quantification scheme is bounded between 0 % and 100 % cover. If we consider the algal coverage at a particular location as having a distribution of abundances/covers (i.e., there is some average algal cover over the location, with some areas of higher and lower coverage than that average), this distribution can be well described by the beta distribution. The beta distribution is a two-parameter distribution bounded between 0 and 1 (equivalent to 0 % and 100 %) and is described by the following equation:

$$Beta(\alpha,\beta) = \frac{x^{\alpha-1}(1-x)^{\beta-1}}{B(\alpha,\beta)}, where\ B(\alpha,\beta) = \frac{\Gamma(\alpha)\Gamma(\beta)}{\Gamma(\alpha+\beta)}$$

where $\Gamma(\ \ )$ is the Gamma function, α and β and the distributions parameters, and x is the distribution's random variable (algal cover % in this case). Using the beta distribution, we can set the range of values that algal cover can take (i.e., 0 % to 100 %) and estimate descriptive statistics of the distribution like the mean and variance (Figure 5.2.11B).

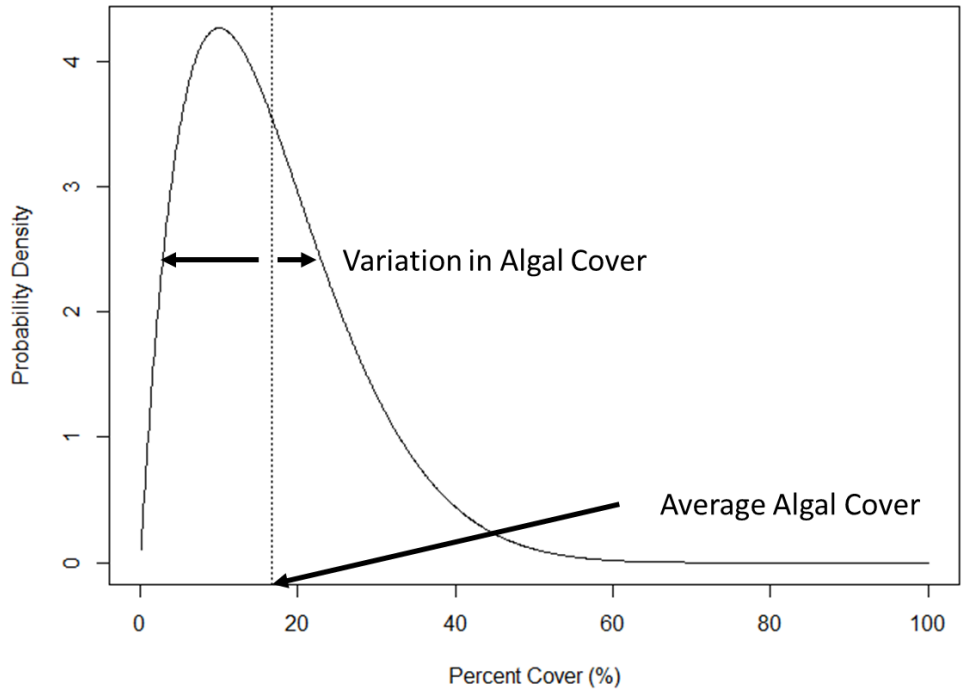

Figure 5.2.11B. Example of a beta distribution. The dotted vertical line shows the location of the average value of the distribution.

Next, we can couple this model of algal cover distribution to a model of our choosing that describes the dynamics of algal abundance. A commonly used model for population growth and dynamics is the logistic model. The logistic model is a sigmodal curve that describes population growth dynamics (see Figure 5.2.12.). A logistic model for algal abundance is as follows:

$$Algal\ Cover\ \%\ (t) = \frac{KP_0e^{rt}}{K + P_0(e^{rt} - 1)}$$

where K is the carrying capacity, P_0 is the starting algal cover, r is the intrinsic algal growth rate, and t is time. Both K and P_0 can range in value from 0 % and 100 %. K describes the maximum possible algal abundance and the parameter r describes how fast algae will proliferate if the population is freed from limitations.

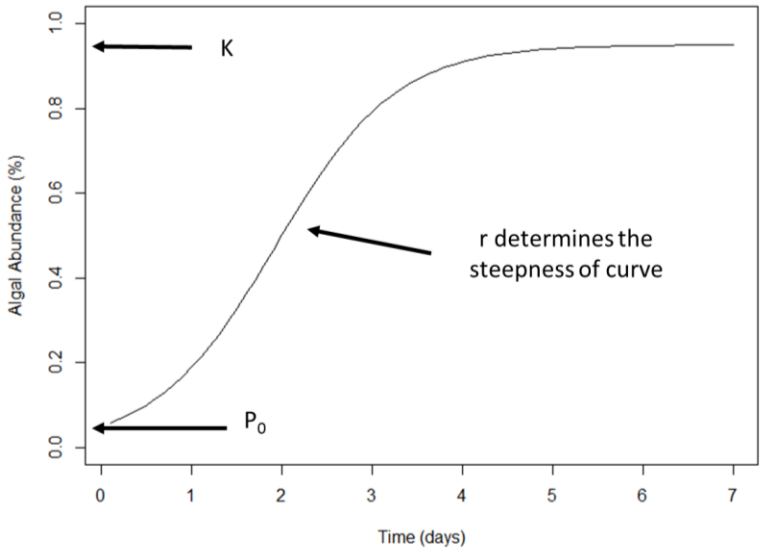

Figure 5.2.12. Example of a logistic model for algal abundance.

We set the logistic model equal to the average of the beta distribution to produce a statistical model of algal abundance as a function of time:

$$Algal\ Cover\ \%\ (t) \sim \frac{x^{\frac{L\beta}{1-L}-1}(1-x)^{\beta-1}}{B\left(\frac{L\beta}{1-L}, \beta\right)}\ , where\ L = \frac{KP_0e^{rt}}{K + P_0(e^{rt} - 1)}$$

This coupled model is at the core of our analysis of the Shadow experiment data to determine algal colonization/growth rates. We further adapt this model to use it with the algal abundance time series data generated in the Shadow experiment. The data from the Shadow experiment consists of a time series for each treatment and control site in the form:

$$(\{time\}_i, \{algal\ abundance\ value\}_i)$$

where *i* is the data index. While the categorical algal abundance data cannot be directly translated into a percent cover, each value corresponds to an actual algal percent cover that falls within two unknown observer thresholds. For example, take two algal cover percentages, 5 % and 30 %; if an observer classifies these cover percentages as "very low" and "low", respectively, we know that the observer's threshold to classify between "very low" and "low" occurs between 5 % and 30 %. The observer has six of these thresholds, 0 %, θ_1, θ_2, θ_3, θ_4, and 100 %. Four of these

thresholds are unknown (i.e., θ_1, θ_2, θ_3, and θ_4), but can be estimated from the data. An algal cover percentage that the observer classifies as "very low" must fall within the range of 0 % and θ_1. An algal cover percentage that the observer classifies as "low" must fall within the range of θ_1 and θ_2. An algal cover percentage that the observer classifies as "medium" must fall within the range of θ_2 and θ_3. An algal cover percentage that the observer classifies as "high" must fall within the range of θ_3 and θ_4. An algal cover percentage that the observer classifies as "very high" must fall within the range of θ_4 and 100 %. We can modify our statistical model for algal abundance as a function of time to produce a statistical model for each of the algal abundance values as a function of time:

$$\text{"very low"}\ (t) \sim \int_0^{\theta_1} \frac{x^{\frac{L\beta}{1-L}-1}(1-x)^{\beta-1}}{B\left(\frac{L\beta}{1-L},\beta\right)}dx\,,where\ L=\frac{KP_0e^{rt}}{K+P_0(e^{rt}-1)}$$

$$\text{"low"}\ (t) \sim \int_{\theta_1}^{\theta_2} \frac{x^{\frac{L\beta}{1-L}-1}(1-x)^{\beta-1}}{B\left(\frac{L\beta}{1-L},\beta\right)}dx\,,where\ L=\frac{KP_0e^{rt}}{K+P_0(e^{rt}-1)}$$

$$\text{"medium"}\ (t) \sim \int_{\theta_2}^{\theta_3} \frac{x^{\frac{L\beta}{1-L}-1}(1-x)^{\beta-1}}{B\left(\frac{L\beta}{1-L},\beta\right)}dx\,,where\ L=\frac{KP_0e^{rt}}{K+P_0(e^{rt}-1)}$$

$$\text{"high"}\ (t) \sim \int_{\theta_3}^{\theta_4} \frac{x^{\frac{L\beta}{1-L}-1}(1-x)^{\beta-1}}{B\left(\frac{L\beta}{1-L},\beta\right)}dx\,,where\ L=\frac{KP_0e^{rt}}{K+P_0(e^{rt}-1)}$$

$$\text{"very high"}\ (t) \sim \int_{\theta_4}^{1} \frac{x^{\frac{L\beta}{1-L}-1}(1-x)^{\beta-1}}{B\left(\frac{L\beta}{1-L},\beta\right)}dx\,,where\ L=\frac{KP_0e^{rt}}{K+P_0(e^{rt}-1)}$$

We use this statistical model in conjunction with Bayes theorem to determine the probability distributions for the algal colonization/growth rate for each of the treatment sites. It is important to note that the resulting estimates for the algal colonization/growth rate accounts for both the experimental and observer errors. As described in Section 5.1.2.1.2.2, the Bayesian model fitting is based on Bayes theorem:

$$p(Hypothesis|Data)=\frac{p(Data|Hypothesis)p(Hypothesis)}{p(Data)}$$

but typically we use the following form:

$$p(Hypothesis|D) \propto p(Data|Hypothesis)p(Hypothesis)$$

The components of this proportionality are generally referred to in the following manner:

$$posterior\ distribution \propto likelihood\ distribution \times prior\ distribution$$

The prior distribution reflects the knowledge of the model parameters before including experimental data, the likelihood distribution is the distribution from which the data is thought to be generated (i.e., the model under consideration), and the posterior distribution reflects the knowledge of the model after including experimental data. For our specific case, the data are the measured algal abundance values, and the hypothesis is that the data is generated from the algal abundance values statistical model described above. We embed the abundance values statistical model into Bayes theorem to obtain the equation below and used a Markov Chain Monte Carlo (MCMC) random walk with a Metropolis-Hasting Gibbs sampling algorithm to sample the distribution and obtain the algal colonization/growth rate (i.e., "r") probability distribution:

$$p\left(\theta_1, \theta_2, \theta_3, \theta_4, K, P_0, r, \beta \middle| N_1, \{t_i\}, N_2, \{t_j\}, N_3, \{t_k\}, N_4, \{t_q\}, N_5, \{t_w\}\right)$$

$$\propto \left[\prod_{i=1}^{N_1} \int_0^{\theta_1} \frac{x^{\frac{\frac{KP_0e^{rt_i}}{K+P_0\left(e^{rt_i}-1\right)}\beta}{1-\frac{KP_0e^{rt_i}}{K+P_0\left(e^{rt_i}-1\right)}}-1}(1-x)^{\beta-1}}{B\left(\frac{\frac{KP_0e^{rt_i}}{K+P_0\left(e^{rt_i}-1\right)}\beta}{1-\frac{KP_0e^{rt_i}}{K+P_0\left(e^{rt_i}-1\right)}}, \beta\right)} dx\right] \left[\prod_{j=1}^{N_2} \int_{\theta_1}^{\theta_2} \frac{x^{\frac{\frac{KP_0e^{rt_j}}{K+P_0\left(e^{rt_j}-1\right)}\beta}{1-\frac{KP_0e^{rt_j}}{K+P_0\left(e^{rt_j}-1\right)}}-1}(1-x)^{\beta-1}}{B\left(\frac{\frac{KP_0e^{rt_j}}{K+P_0\left(e^{rt_j}-1\right)}\beta}{1-\frac{KP_0e^{rt_j}}{K+P_0\left(e^{rt_j}-1\right)}}, \beta\right)} dx\right]$$

$$\left[\prod_{k=1}^{N_3} \int_{\theta_2}^{\theta_3} \frac{x^{\frac{\frac{KP_0e^{rt_k}}{K+P_0\left(e^{rt_k}-1\right)}\beta}{1-\frac{KP_0e^{rt_k}}{K+P_0\left(e^{rt_k}-1\right)}}-1}(1-x)^{\beta-1}}{B\left(\frac{\frac{KP_0e^{rt_k}}{K+P_0\left(e^{rt_k}-1\right)}\beta}{1-\frac{KP_0e^{rt_k}}{K+P_0\left(e^{rt_k}-1\right)}}, \beta\right)} dx\right] \left[\prod_{q=1}^{N_4} \int_{\theta_3}^{\theta_4} \frac{x^{\frac{\frac{KP_0e^{rt_q}}{K+P_0\left(e^{rt_q}-1\right)}\beta}{1-\frac{KP_0e^{rt_q}}{K+P_0\left(e^{rt_q}-1\right)}}-1}(1-x)^{\beta-1}}{B\left(\frac{\frac{KP_0e^{rt_q}}{K+P_0\left(e^{rt_q}-1\right)}\beta}{1-\frac{KP_0e^{rt_q}}{K+P_0\left(e^{rt_q}-1\right)}}, \beta\right)} dx\right]$$

$$\left[\prod_{w=1}^{N_5} \int_{\theta_4}^{1} \frac{x^{\frac{\frac{KP_0e^{rt_w}}{K+P_0\left(e^{rt_w}-1\right)}\beta}{1-\frac{KP_0e^{rt_w}}{K+P_0\left(e^{rt_w}-1\right)}}-1}(1-x)^{\beta-1}}{B\left(\frac{\frac{KP_0e^{rt_w}}{K+P_0\left(e^{rt_w}-1\right)}\beta}{1-\frac{KP_0e^{rt_w}}{K+P_0\left(e^{rt_w}-1\right)}}, \beta\right)} dx\right] \left[\frac{1}{\beta\sigma_\beta\sqrt{2\pi}} e^{-\frac{\left(ln(\beta)-\gamma_\beta\right)^2}{2\sigma_\beta{}^2}}\right]$$

where $N_1, N_2, N_3, N_4, and\ N_5$ are the number of observations in each of the algal abundance categories "very low, "low", "medium", "high", and "very high", respectively; $\{t_i\}, \{t_j\}, \{t_k\}, \{t_q\}, and\ \{t_w\}$ are the timing of the observations for each of the algal

abundance categories "very low, "low", "medium", "high", and "very high", respectively; β is one of the beta distribution parameters; and $K, P_0, and\ r$ are the logistic model parameters described previously.

Probability distributions of the algal colonization/growth rate (i.e., "r") were determined for each of the Shadow treatment sites. From these probability distributions, a measure of the distributions' central tendency (i.e., median or mean) were obtained. Median values were obtained from highly skewed distributions, otherwise mean values were selected. The average and standard deviation of these central tendency measures across treatments was used to determine the value and uncertainty of the algal colonization/growth rate. In addition to determining the algal colonization/growth rate, the Shadow experimental data was also used to determine a critical algal removal velocity (described in the next section) and to test for the presence of any hysteresis effect of algal abundance after it has become established.

To test for the presence of hysteresis, we compared the distribution of algal abundance values for each treatment site measured before the installation of the Shadow to the distribution of algal abundance values measured several days after flow was restored (Figure 5.2.13). We did this by testing the null hypothesis that algal abundance values (i.e., "very low", "low", etc.) were drawn from the same distribution before Shadow placement and after its removal. We used a version of the Kolmogorov-Smirnov (K-S) test, which is a distribution free test (meaning it makes no assumptions about the underlying probability distributions) that tests if two groups of samples are drawn from the same distribution. One assumption of the K-S test is that the distributions are continuous, and therefore cannot be used if the data contains ties (i.e., equal values). Since our algal abundance value data contains numerous ties, we applied a bootstrapping version of the test using randomly ordered and selected data. If we cannot reject that the null hypothesis that the measured algal abundance values are drawn from the same distribution (i.e., if the calculated p-value >0.05), it suggests that hysteresis is not occurring. However, if we can reject the null hypothesis (i.e., if the calculated p-value <0.05), it suggests that hysteresis may be occurring.

5.2.2.2 Critical Velocity Estimation from Observational Data

In the previous section, we described how algal abundance values generated from the Shadow experiment were used to determine algal colonization/growth rate and presence or absence of hysteresis. In this section, we use the Shadow experimental data, along with several other datasets, to determine a critical algal removal velocity. We also determine a critical velocity for SAV using the same method, which may have implications for understanding hydraulic and vegetation feedbacks. The observational datasets used for this analysis are all a form of algal abundance versus flow velocity data and include the following: 1) Shadow dataset from the Silver River; 2) Algal abundance versus flow velocity data for the Silver River (collected in passing by divers measuring SAV); 3) Gum Slough data (from King, 2014); 4) All of the springs studied in the Springs Synoptic Study; and 5) Data from the Weeki Wachee, Homosassa, and Chassahowitzka Rivers provided by Tom Frazer (UF).

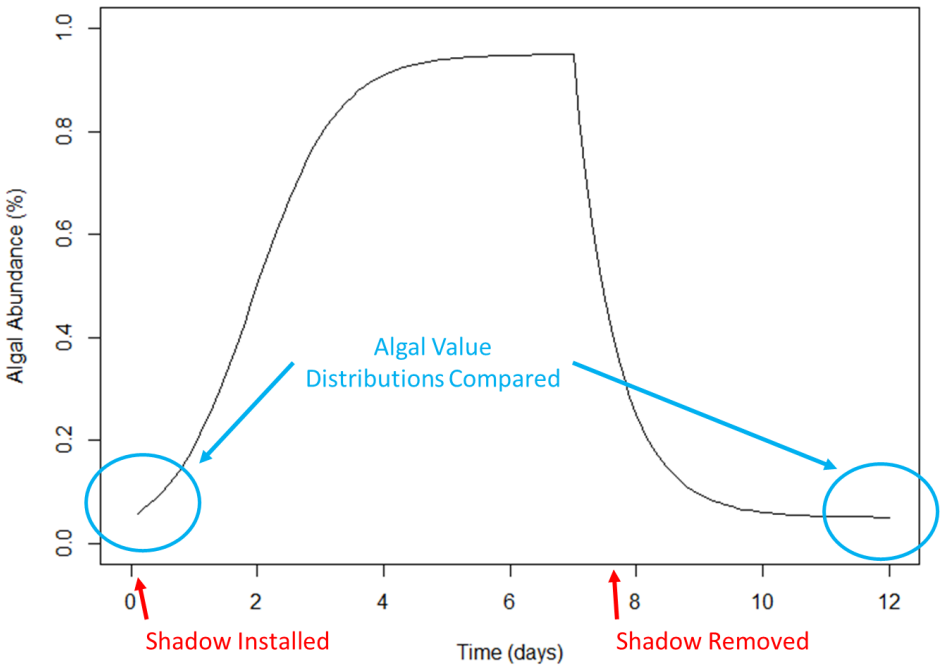

Figure 5.2.13. The time points in which algal abundance value distributions were compared for hysteresis effects in relation to Shadow installation and removal.

Each of these data sets were slightly different, requiring minor differences in their analysis, however the core concept and base model used in these analyses were common to all datasets. The primary hypothesis is that above a certain critical velocity, the amount of algae present should be substantially lower than below that critical velocity. Our approach tests this hypothesis and estimates the critical velocity, if present. In other words, if there is a critical algal removal velocity, we would expect to observe one distribution of algal coverage below this critical velocity and a different (lower) distribution of algal coverage above the critical velocity (Figs. 5.2.14 and 5.2.15).

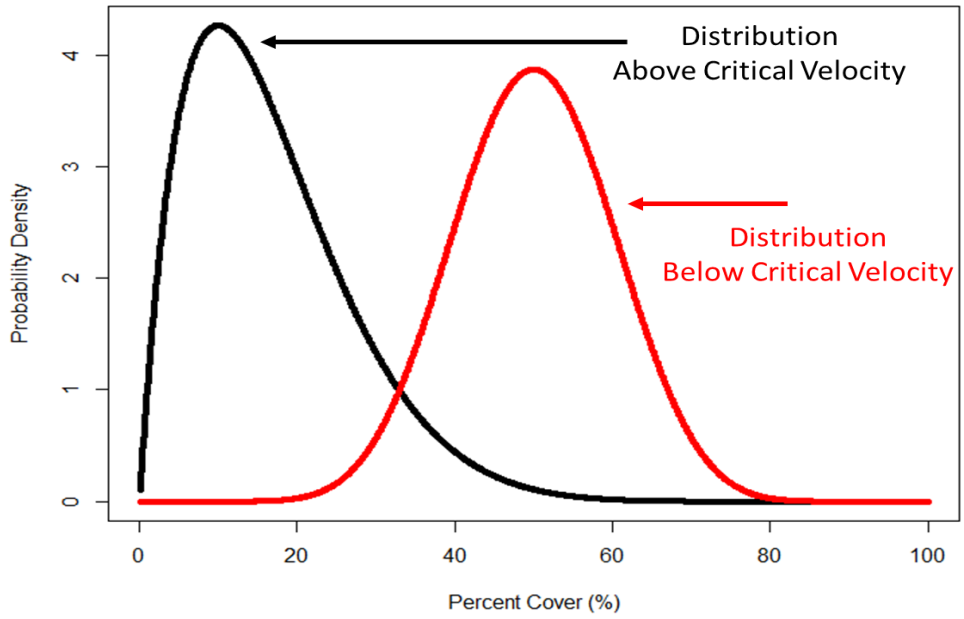

Figure 5.2.14. Schematic of the critical algal removal hypothesis testing framework. The distribution of algal abundances observed below the critical velocity (black) should be different from and larger than the distribution of velocities observed above the critical velocity (red).

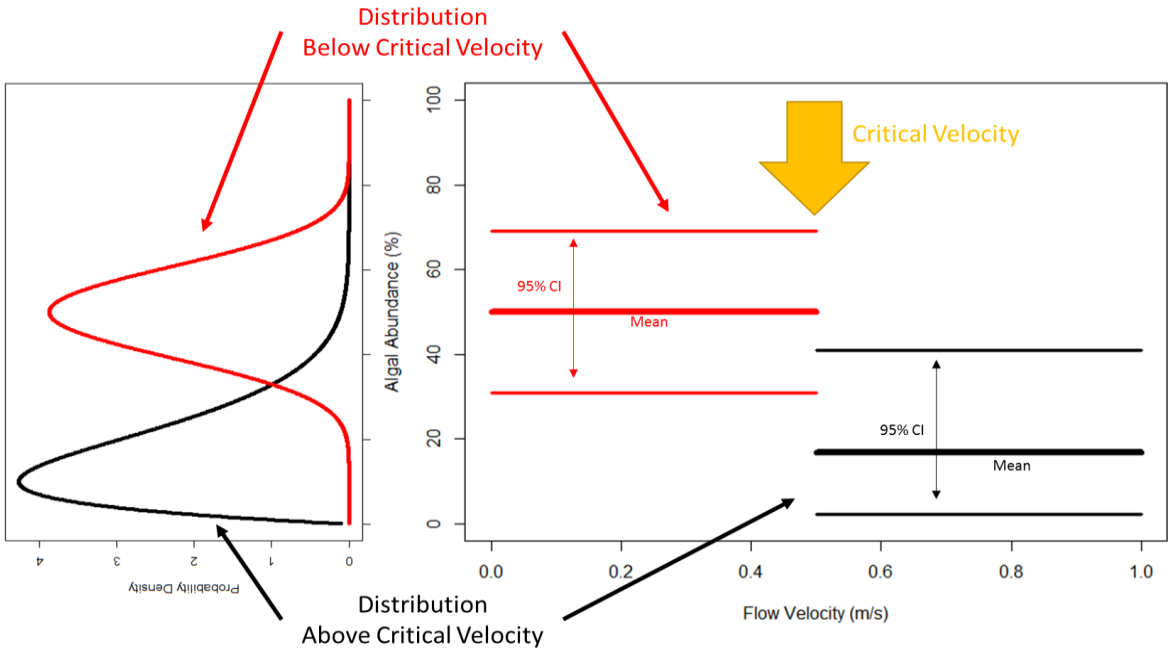

Figure 5.2.15. Schematic of the critical algal removal hypothesis testing framework. The left panel is equivalent to Fig. 5.2.15 rotated 90 degrees. The right panel illustrates the algal distributions as they would be observed as a function of velocity (if a velocity threshold exists).

We can express this hypothesis in a mathematical form suitable for model development using the Heaviside step function, $\Phi(\ \ )$. The Heaviside step function equals zero for all negative numbers and equals one for all positive numbers. This function allows us to "turn off" one distribution at the critical velocity and "turn on" another distribution. For example, if the average value of the algal cover distribution changes at a critical velocity, it can be represented as:

$$Average\ Algal\ Cover\ \%\ (v) = \mu_1\Phi(v) + \left(\mu_2 - \mu_1\right)\Phi(v - V_c)$$

Where v is the velocity, μ_1 is the average algal cover % below the critical velocity, μ_2 is the average algal cover % above the critical velocity, V_c is the critical velocity, and $\Phi(\ \ )$ is the Heaviside step function. This function's value is μ_1 for velocities below V_c and μ_2 for velocities above V_c. Using this approach, we developed models to analyze each of the datasets mentioned above. We used these statistical models in conjunction with Bayes theorem to determine the probability distributions for the critical algal removal velocity, critical algal removal shear stress, and critical SAV velocity. Each of these Bayesian analyses were performed as described in previous sections. Each dataset and corresponding model are described below. Critical velocity probability distributions were determined for each of the datasets. From these probability distributions, a measure of the distributions central tendency (i.e., median or mean) were obtained. Median values were obtained from highly skewed distributions, otherwise mean values were selected. The average and standard deviation of these central tendency measures was used to determine the value and uncertainty of the critical velocity.

<u>Shadow experiment</u>

Dataset: Flow velocities with corresponding categorical algal abundance values.

Model:

$$p\left(\theta_1,\theta_2,\theta_3,\theta_4,\mu_1,\mu_2,\beta_1,\beta_2,V_c\middle|N_1,\{v_i\},N_2,\{v_j\},N_3,\{v_k\},N_4,\{v_q\},N_5,\{v_w\}\right) \propto$$

$$\left[\prod_{i=1}^{N_1}\int_0^{\theta_1} x^{\frac{\mu_1\Phi(v_i)+(\mu_2-\mu_1)\Phi(v_i-V_c)}{1-\mu_1\Phi(v_i)-(\mu_2-\mu_1)\Phi(v_i-V_c)}\left(\beta_1\Phi(v_i)+(\beta_2-\beta_1)\Phi(v_i-V_c)\right)-1}(1-x)^{\beta_1\Phi(v_i)+(\beta_2-\beta_1)\Phi(v_i-V_c)-1}dx\right]$$

$$\left[\prod_{j=1}^{N_2}\int_{\theta_1}^{\theta_2} x^{\frac{\mu_1\Phi(v_j)+(\mu_2-\mu_1)\Phi(v_j-V_c)}{1-\mu_1\Phi(v_j)-(\mu_2-\mu_1)\Phi(v_j-V_c)}\left(\beta_1\Phi(v_j)+(\beta_2-\beta_1)\Phi(v_j-V_c)\right)-1}(1-x)^{\beta_1\Phi(v_j)+(\beta_2-\beta_1)\Phi(v_j-V_c)-1}dx\right]$$

$$\left[\prod_{k=1}^{N_3}\int_{\theta_2}^{\theta_3} x^{\frac{\mu_1\Phi(v_k)+(\mu_2-\mu_1)\Phi(v_k-V_c)}{1-\mu_1\Phi(v_k)-(\mu_2-\mu_1)\Phi(v_k-V_c)}\left(\beta_1\Phi(v_k)+(\beta_2-\beta_1)\Phi(v_k-V_c)\right)-1}(1-x)^{\beta_1\Phi(v_k)+(\beta_2-\beta_1)\Phi(v_k-V_c)-1}dx\right]$$

$$\left[\prod_{q=1}^{N_4}\int_{\theta_3}^{\theta_4} x^{\frac{\mu_1\Phi(v_q)+(\mu_2-\mu_1)\Phi(v_q-V_c)}{1-\mu_1\Phi(v_q)-(\mu_2-\mu_1)\Phi(v_q-V_c)}\left(\beta_1\Phi(v_q)+(\beta_2-\beta_1)\Phi(v_q-V_c)\right)-1}(1-x)^{\beta_1\Phi(v_q)+(\beta_2-\beta_1)\Phi(v_q-V_c)-1}dx\right]$$

$$\left[\prod_{w=1}^{N_5}\int_{\theta_4}^{1} x^{\frac{\mu_1\Phi(v_w)+(\mu_2-\mu_1)\Phi(v_w-V_c)}{1-\mu_1\Phi(v_w)-(\mu_2-\mu_1)\Phi(v_w-V_c)}\left(\beta_1\Phi(v_w)+(\beta_2-\beta_1)\Phi(v_w-V_c)\right)-1}(1-x)^{\beta_1\Phi(v_w)+(\beta_2-\beta_1)\Phi(v_w-V_c)-1}dx\right]$$

$$\left[\frac{1}{\beta_1\sigma_{\beta_1}\sqrt{2\pi}}e^{-\frac{\left(ln(\beta_1)-\gamma_{\beta_1}\right)^2}{2\sigma_{\beta_1}{}^2}}\right]\left[\frac{1}{\beta_2\sigma_{\beta_2}\sqrt{2\pi}}e^{-\frac{\left(ln(\beta_2)-\gamma_{\beta_2}\right)^2}{2\sigma_{\beta_2}{}^2}}\right]$$

Silver River Diver Data

Dataset: Flow velocities and shear stresses with corresponding categorical algal abundance values.

Model:

$$p\left(\theta_1,\theta_2,\theta_3,\mu_1,\mu_2,\beta_1,\beta_2,V_c\middle|N_1,\{v_i\},N_2,\{v_j\},N_3,\{v_k\},N_4,\{v_q\}\right)\propto$$

$$\left[\prod_{i=1}^{N_1}\int_0^{\theta_1} x^{\frac{\mu_1\Phi(v_i)+(\mu_2-\mu_1)\Phi(v_i-V_c)}{1-\mu_1\Phi(v_i)-(\mu_2-\mu_1)\Phi(v_i-V_c)}\left(\beta_1\Phi(v_i)+(\beta_2-\beta_1)\Phi(v_i-V_c)\right)-1}(1-x)^{\beta_1\Phi(v_i)+(\beta_2-\beta_1)\Phi(v_i-V_c)-1}dx\right]$$

$$\left[\prod_{j=1}^{N_2}\int_{\theta_1}^{\theta_2} x^{\frac{\mu_1\Phi(v_j)+(\mu_2-\mu_1)\Phi(v_j-V_c)}{1-\mu_1\Phi(v_j)-(\mu_2-\mu_1)\Phi(v_j-V_c)}\left(\beta_1\Phi(v_j)+(\beta_2-\beta_1)\Phi(v_j-V_c)\right)-1}(1-x)^{\beta_1\Phi(v_j)+(\beta_2-\beta_1)\Phi(v_j-V_c)-1}dx\right]$$

$$\left[\prod_{k=1}^{N_3}\int_{\theta_2}^{\theta_3} x^{\frac{\mu_1\Phi(v_k)+(\mu_2-\mu_1)\Phi(v_k-V_c)}{1-\mu_1\Phi(v_k)-(\mu_2-\mu_1)\Phi(v_k-V_c)}\left(\beta_1\Phi(v_k)+(\beta_2-\beta_1)\Phi(v_k-V_c)\right)-1}(1-x)^{\beta_1\Phi(v_k)+(\beta_2-\beta_1)\Phi(v_k-V_c)-1}dx\right]$$

$$\left[\prod_{q=1}^{N_4}\int_{\theta_3}^{1} x^{\frac{\mu_1\Phi(v_q)+(\mu_2-\mu_1)\Phi(v_q-V_c)}{1-\mu_1\Phi(v_q)-(\mu_2-\mu_1)\Phi(v_q-V_c)}\left(\beta_1\Phi(v_q)+(\beta_2-\beta_1)\Phi(v_q-V_c)\right)-1}(1-x)^{\beta_1\Phi(v_q)+(\beta_2-\beta_1)\Phi(v_q-V_c)-1}dx\right]$$

$$\left[\frac{1}{\beta_1\sigma_{\beta_1}\sqrt{2\pi}}e^{-\frac{\left(ln(\beta_1)-\gamma_{\beta_1}\right)^2}{2\sigma_{\beta_1}{}^2}}\right]\left[\frac{1}{\beta_2\sigma_{\beta_2}\sqrt{2\pi}}e^{-\frac{\left(ln(\beta_2)-\gamma_{\beta_2}\right)^2}{2\sigma_{\beta_2}{}^2}}\right]$$

Gum Slough, Spring Synoptic Study, and Frazer Macroalgae Data

Dataset: Flow velocities with corresponding Braun-Blanquet estimates

Model:

$$p\left(\mu_1,\mu_2,\beta_1,\beta_2,V_c\middle|N_0,\{v_z\},N_1,\{v_i\},N_2,\{v_j\},N_3,\{v_k\},N_4,\{v_q\},N_5,\{v_w\}\right)\propto$$

$$\left[\prod_{z=1}^{N_0}\int_0^{0.01} x^{\frac{\mu_1\Phi(v_z)+(\mu_2-\mu_1)\Phi(v_z-V_c)}{1-\mu_1\Phi(v_z)-(\mu_2-\mu_1)\Phi(v_z-V_c)}\left(\beta_1\Phi(v_z)+(\beta_2-\beta_1)\Phi(v_z-V_c)\right)-1}(1-x)^{\beta_1\Phi(v_z)+(\beta_2-\beta_1)\Phi(v_z-V_c)-1}dx\right]$$

$$\left[\prod_{i=1}^{N_1}\int_{0.01}^{0.05} x^{\frac{\mu_1\Phi(v_i)+(\mu_2-\mu_1)\Phi(v_i-V_c)}{1-\mu_1\Phi(v_i)-(\mu_2-\mu_1)\Phi(v_i-V_c)}\left(\beta_1\Phi(v_i)+(\beta_2-\beta_1)\Phi(v_i-V_c)\right)-1}(1-x)^{\beta_1\Phi(v_i)+(\beta_2-\beta_1)\Phi(v_i-V_c)-1}dx\right]$$

$$\left[\prod_{j=1}^{N_2}\int_{0.05}^{0.25} x^{\frac{\mu_1\Phi(v_j)+(\mu_2-\mu_1)\Phi(v_j-V_c)}{1-\mu_1\Phi(v_j)-(\mu_2-\mu_1)\Phi(v_j-V_c)}\left(\beta_1\Phi(v_j)+(\beta_2-\beta_1)\Phi(v_j-V_c)\right)-1}(1-x)^{\beta_1\Phi(v_j)+(\beta_2-\beta_1)\Phi(v_j-V_c)-1}dx\right]$$

$$\left[\prod_{k=1}^{N_3}\int_{0.25}^{0.5} x^{\frac{\mu_1\Phi(v_k)+(\mu_2-\mu_1)\Phi(v_k-V_c)}{1-\mu_1\Phi(v_k)-(\mu_2-\mu_1)\Phi(v_k-V_c)}\left(\beta_1\Phi(v_k)+(\beta_2-\beta_1)\Phi(v_k-V_c)\right)-1}(1-x)^{\beta_1\Phi(v_k)+(\beta_2-\beta_1)\Phi(v_k-V_c)-1}dx\right]$$

$$\left[\prod_{q=1}^{N_4}\int_{0.5}^{0.75} x^{\frac{\mu_1\Phi(v_q)+(\mu_2-\mu_1)\Phi(v_q-V_c)}{1-\mu_1\Phi(v_q)-(\mu_2-\mu_1)\Phi(v_q-V_c)}\left(\beta_1\Phi(v_q)+(\beta_2-\beta_1)\Phi(v_q-V_c)\right)-1}(1-x)^{\beta_1\Phi(v_q)+(\beta_2-\beta_1)\Phi(v_q-V_c)-1}dx\right]$$

$$\left[\prod_{w=1}^{N_5}\int_{0.75}^{1} x^{\frac{\mu_1\Phi(v_w)+(\mu_2-\mu_1)\Phi(v_w-V_c)}{1-\mu_1\Phi(v_w)-(\mu_2-\mu_1)\Phi(v_w-V_c)}\left(\beta_1\Phi(v_w)+(\beta_2-\beta_1)\Phi(v_w-V_c)\right)-1}(1-x)^{\beta_1\Phi(v_w)+(\beta_2-\beta_1)\Phi(v_w-V_c)-1}dx\right]$$

$$\left[\frac{1}{\beta_1\sigma_{\beta_1}\sqrt{2\pi}}e^{-\frac{\left(ln(\beta_1)-\gamma_{\beta_1}\right)^2}{2{\sigma_{\beta_1}}^2}}\right]\left[\frac{1}{\beta_2\sigma_{\beta_2}\sqrt{2\pi}}e^{-\frac{\left(ln(\beta_2)-\gamma_{\beta_2}\right)^2}{2{\sigma_{\beta_2}}^2}}\right]$$

Frazer Periphyton Data

Dataset: Flow velocities with corresponding normalized periphyton mass measurements

Model:

$$p(\mu_1,\mu_2,{\sigma^2}_1,{\sigma^2}_2,V_c|\{m_i\},\{v_i\}) \propto$$

$$\left[\prod_i \frac{1}{m_i\sqrt{ln\left(1+\frac{{\sigma^2}_1\Phi(v)+({\sigma^2}_2-{\sigma^2}_1)\Phi(v-V_c)}{\left(\mu_1\Phi(v)+(\mu_2-\mu_1)\Phi(v-V_c)\right)^2}\right)}\sqrt{2\pi}}e^{-\frac{\left(ln(m_i)-ln\left(\frac{\mu_1\Phi(v)+(\mu_2-\mu_1)\Phi(v-V_c)}{\sqrt{1+\frac{{\sigma^2}_1\Phi(v)+({\sigma^2}_2-{\sigma^2}_1)\Phi(v-V_c)}{\left(\mu_1\Phi(v)+(\mu_2-\mu_1)\Phi(v-V_c)\right)^2}}}\right)\right)^2}{2ln\left(1+\frac{{\sigma^2}_1\Phi(v)+({\sigma^2}_2-{\sigma^2}_1)\Phi(v-V_c)}{\left(\mu_1\Phi(v)+(\mu_2-\mu_1)\Phi(v-V_c)\right)^2}\right)}}\right]$$

$$\left[\frac{1}{\mu_1\sigma_{\mu_1}\sqrt{2\pi}}e^{-\frac{\left(ln(\mu_1)-\gamma_{\mu_1}\right)^2}{2{\sigma_{\mu_1}}^2}}\right]\left[\frac{1}{\mu_2\sigma_{\mu_2}\sqrt{2\pi}}e^{-\frac{\left(ln(\mu_2)-\gamma_{\mu_2}\right)^2}{2{\sigma_{\mu_2}}^2}}\right]$$

$$\left[\frac{{\beta_{\sigma^2}}_1^{\alpha_{\sigma^2_1}}}{\Gamma\left(\alpha_{\sigma^2_1}\right)}\frac{1}{{\sigma^2}_1}^{\alpha_{\sigma^2_1}-1}e^{-\beta_{\sigma^2_1}\frac{1}{\sigma^2_1}}\right]\left[\frac{{\beta_{\sigma^2}}_2^{\alpha_{\sigma^2_2}}}{\Gamma\left(\alpha_{\sigma^2_2}\right)}\frac{1}{{\sigma^2}_2}^{\alpha_{\sigma^2_2}-1}e^{-\beta_{\sigma^2_2}\frac{1}{\sigma^2_2}}\right]$$

5.2.2.3 Optical Methods

Finally, we explored the use of optical methods to collect algal cover and velocity data over wide areas to better explore the velocity-algal cover relationship and determine critical velocities more robustly. Current methods for algal cover characterization (i.e., visual estimation using quadrats) are impractical for acquiring high spatial resolution, spatially distributed data and relies on

human estimation, which introduces subjectivity. We sought a rapid, quantitative method to cover large areas using continuous image capture and processing coupled with continuous velocity measurement. We examined two optical techniques for algal cover estimation: average-image color shift and chromaticity (Figure 5.2.16).

Average-image color shift processes entire images by decomposing color into image-averaged values of the red, blue, and green bands (Figure 5.2.16a). Average image color was then calculated color according to:

$$Color = \log(Band\ 1) - \log(Band\ 2) = \log\left(\frac{Band\ 1}{Band\ 2}\right)$$

$$ColorBG = \log(B) - \log(G) = \log\left(\frac{B}{G}\right)$$

$$ColorGR = \log(G) - \log(R) = \log\left(\frac{G}{R}\right)$$

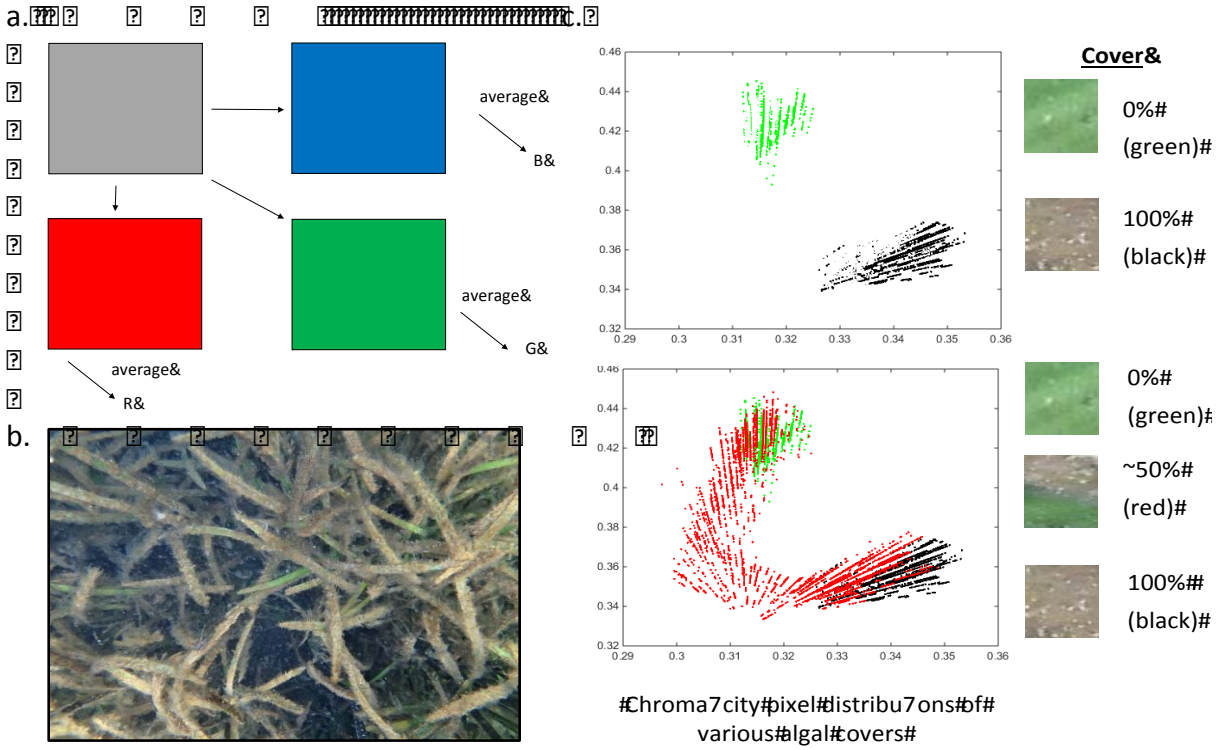

Figure 5.2.16. Schematic of red-green-blue color separation (a), standard SAV-algae image used to test optical methods (b), and chromaticity distribution of various algal covers (c).

The photometric color system was calibrated against field measurements of algal cover using a standard SAV image from the Silver River (Figure 5.2.16b) segmented into regions of varying algal cover using both a subjective (i.e., visual) and an objective K-clustering method. We present tests of the algal cover-velocity relationship using cover estimates derived with this method.

For field tests, still and video images were collected using a hand-held or boat mounted GoPro camera (Figure 5.2.17), and velocity was measured using an electromagnetic flow meter (EFM) (MF Pro Flow Meter, OTT Hydromet Inc., Loveland, CO). Additionally, depth measurements were taken with each image and used to correct image color for depth using a standard relationship developed using a color loss versus depth relationship.

For the chromaticity method, the image was analyzed pixel-by-pixel; since SAV and algae are visually distinct, they can potentially be identified based on their chromaticity, with total cover being calculated by summing cells the number of pixels that match a training image. While only preliminary test data are available for the chromaticity method (Figure 5.2.16c), the chromaticity pixel distribution of SAV (green points in Figure 5.2.16c) does not overlap with the periphytic algae distribution (black points). Moreover, the pixel distribution of 50 % algal cover is concentrated in the same locations as a pure SAV or algal image. While this approach is exploratory, and is not an explicitly contracted work order task, these initial findings show promise, we present these methods and preliminary results as a platform for future work.

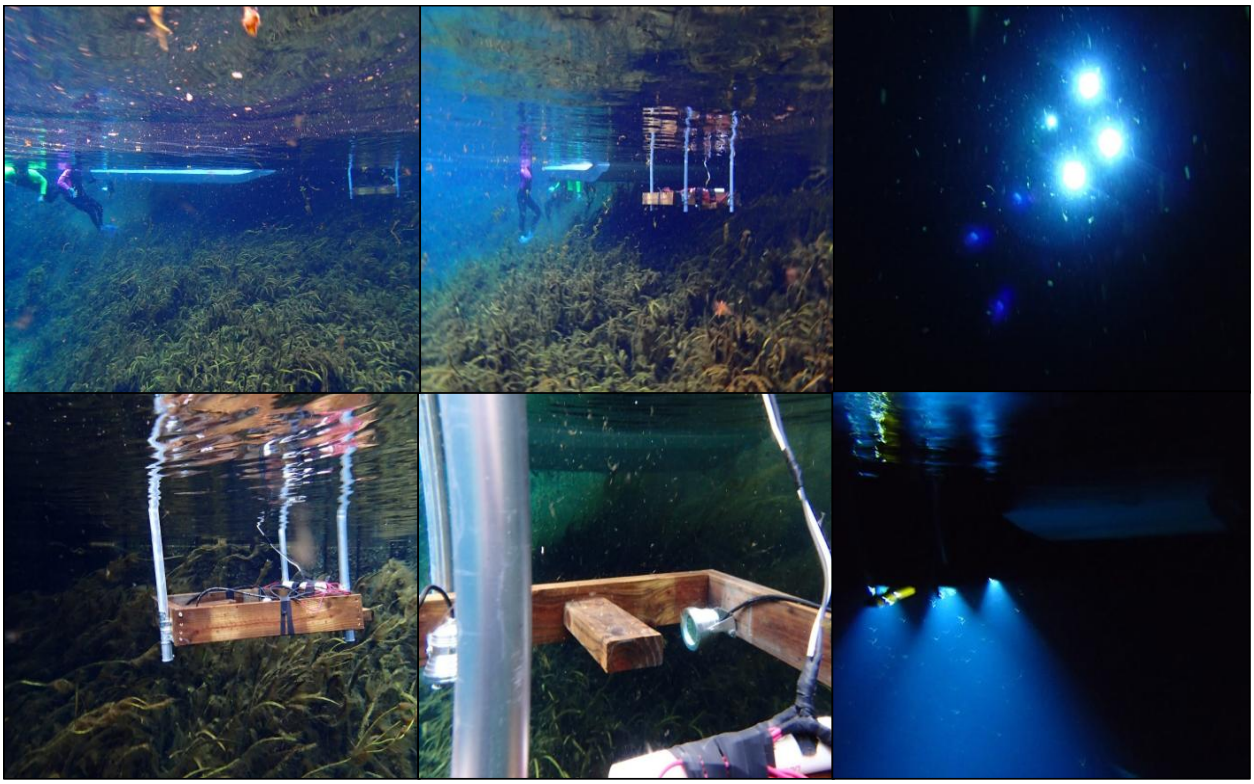

Figure 5.2.17. Optical algal cover image collection via GoPro camera mounted to research vessel. Images captured at night using an artificial light source to standardize lighting.

5.2.3 RESULTS AND DISCUSSION

5.2.3.1 Flow-ways

Results of the velocity-modulation performance testing for the field-deployed flow-way designs (versions 2 and 3) are shown in Figures 5.2.18 and 5.2.19. For flow-way v2, closing flow-way

doors (red lines in Figure 5.2.18) reduced flow across the profile relative to the background velocity profile (black lines), however opening flow-way doors only modestly increased velocity (blue lines), and these increases were mostly above the vegetation canopy height (green horizontal line). High-flow modulation was improved for flow-way v3 (Figure 5.2.19), particularly within the vegetation bed, where adding additional panels increased in-SAV velocities up to 10 times relative to background levels (red lines in Figure 5.2.19). Even with these modifications, however, it was difficult to increase velocity in the vegetation bed above 0.1 m s^{-1}. In general, this experimental structure (v3) may be useful for refining algal sloughing & colonization rates and SAV reconfiguration as a function of velocity, and the method may be applicable to other springs. However, while the flow-ways were able to reduce and increase flow velocity to some extent, their performance was not sufficient to justify the difficulties associated with transporting, deploying, and retrieving these devices, and no further experimental data were collected using these designs.

The "Shadow" experiment was successfully deployed 20 times (four deployments, each with five locations along a gradient of velocities; Table 5.1.5). Qualitative results showed clear (and rapid) algal-colonization and growth effects from the blocking of flow (Figures 5.2.20 to 5.2.22).

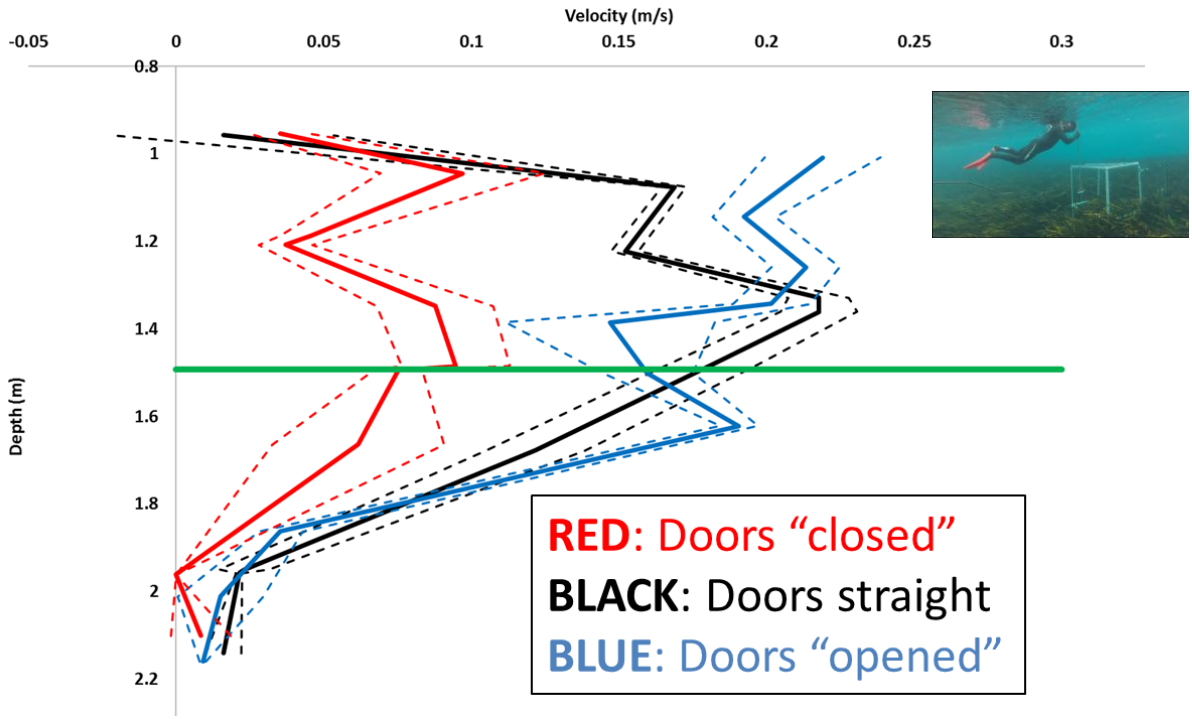

Figure 5.2.18. Vertical velocity profiles during flow-way (v2) testing.

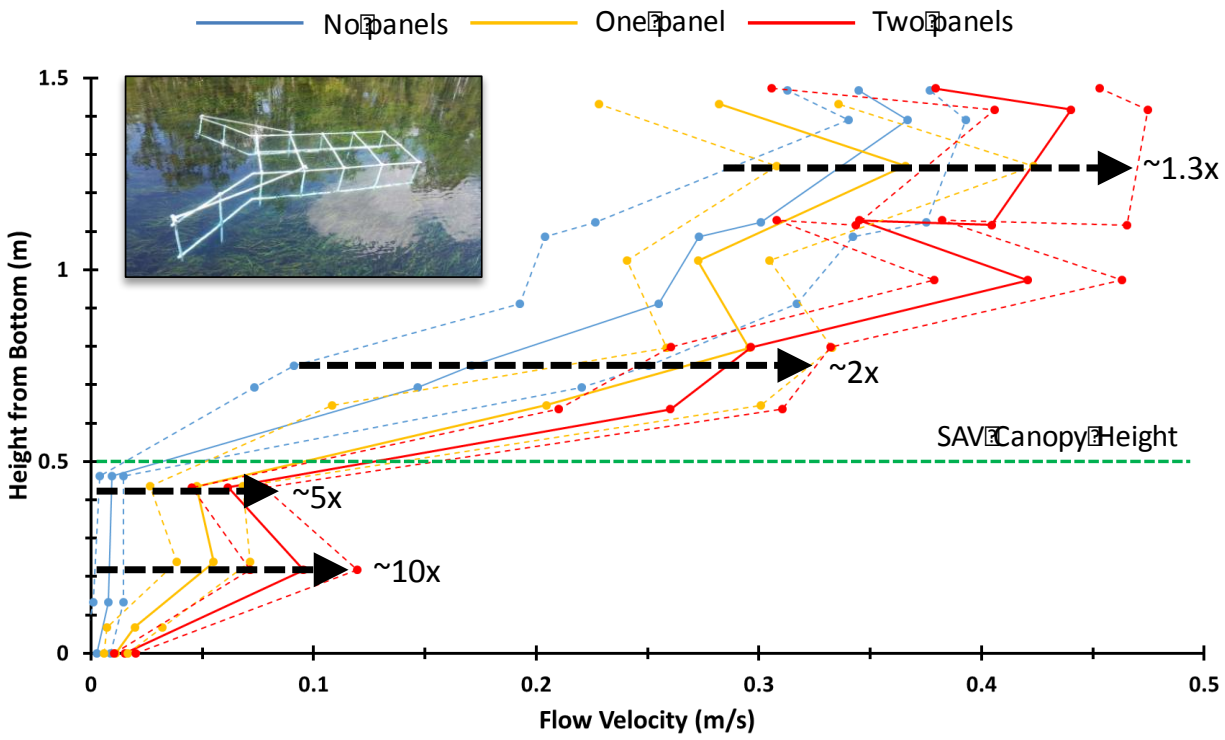

Figure 5.2.19. Vertical velocity profiles during flow-way (v3) testing.

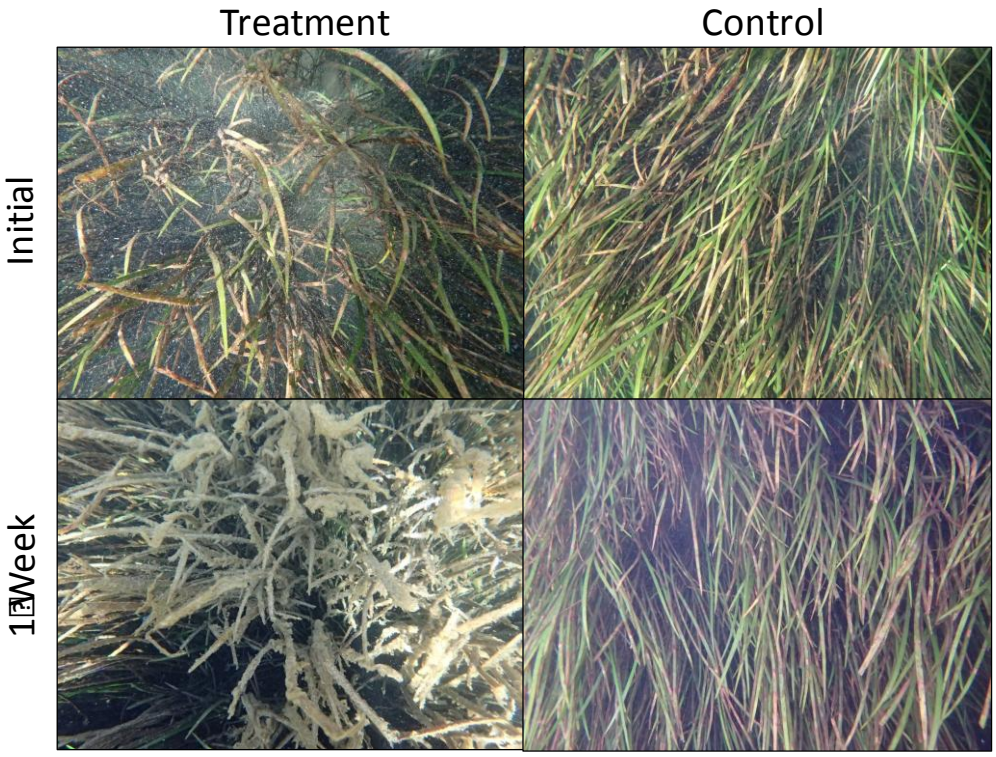

Figure 5.2.20. Algal colonization and growth in treatment versus control sites during "Shadow" deployment.

Figure 5.2.21. One week of algal growth in the velocity shadow of the “Shadow” structure.

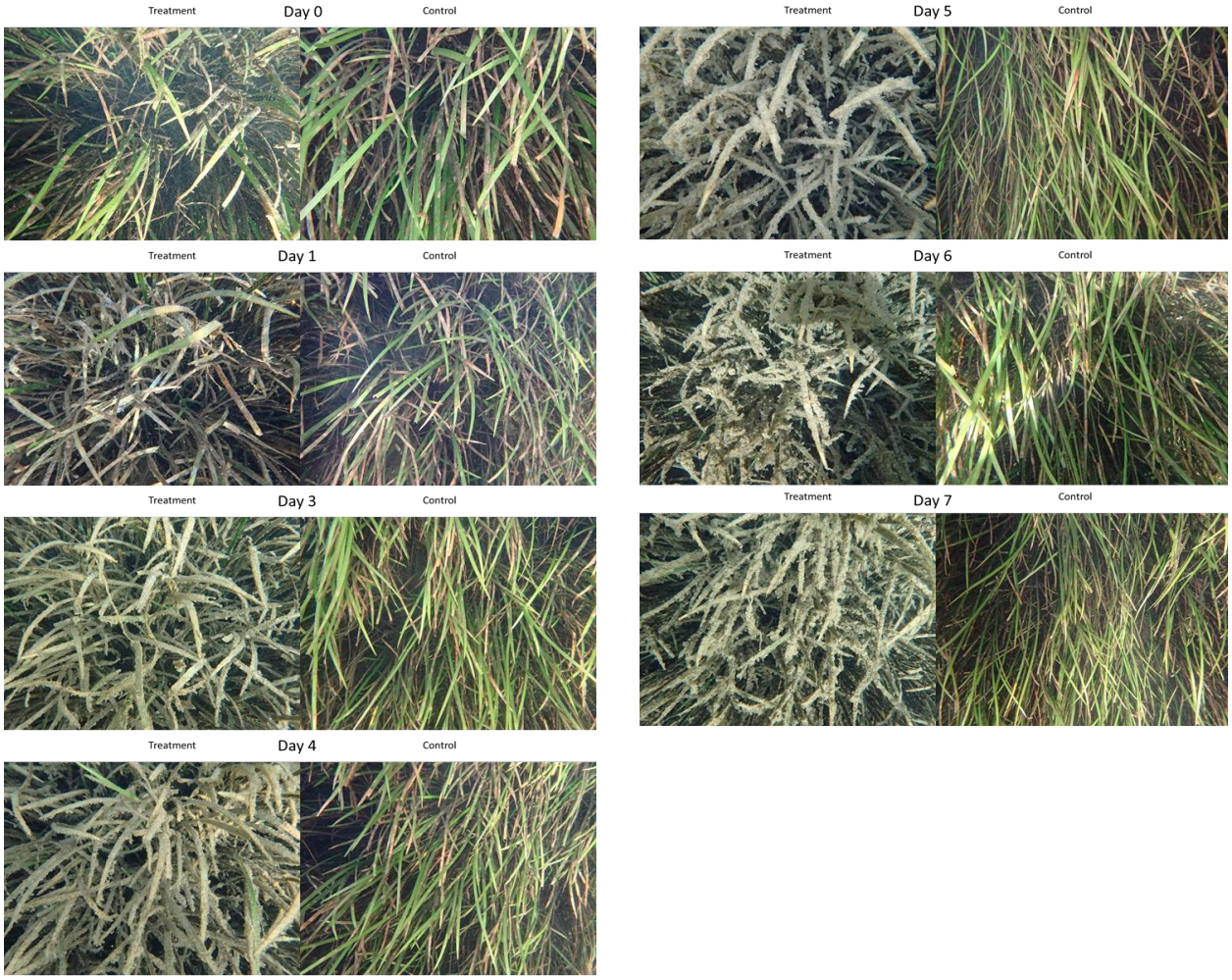

Figure 5.2.22. Progression of algal colonization and growth in treatment sites with ~0 flow velocity (left) and associated controls (right) over one-week deployment.

An example algal growth progression (i.e., one of 20 deployments) is shown in Figure 5.2.23, along with the fitted logistic model and its credible intervals (CI). Algal cover at this site was initially about 10 % and increased to approximately 90 % at the end of the one-week deployment. The mean logistic model (red line) does a good job representing the magnitude and shape of the observed growth curve, and the CI show how uncertainty in the model and the data map to the estimate of modeled growth at any time. Algal growth curves for all other deployments (not shown) mirrored this progression, with low initial algal cover, high final cover, and similar general shapes. From each of these 20 curves, we extracted the logistic curve parameters K (carrying capacity), P_0 (initial algal cover), and r (intrinsic algal growth rate). The distribution of these parameters for the curve shown in Figure 5.2.23 are illustrated in Figure 5.2.24.

Figures 5.2.25 and 5.2.26 summarize fitted algal growth rates across deployments. Mean/median growth rates were similar across sites, with an overall mean intrinsic algal colonization/growth of just over 1 day (CI: 0.70 day^{-1} to 1.60 day^{-1}). These results indicate that in the absence of flow,

algal cover/abundance doubles every day until it reaches carrying capacity (i.e., at or near 100 % cover).

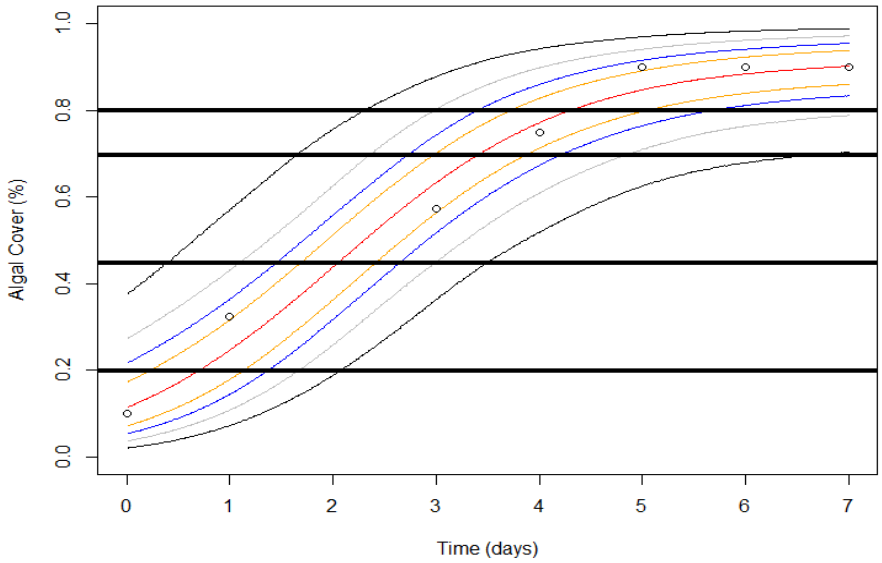

Figure 5.2.23. Results of the Bayesian logistic fit to the categorical algal abundance values from an example treatment site (one of 20), shown with credible intervals (CI) on observed algal abundances (red-mean; orange-40 % CI; blue-60 % CI; gray-80 % CI, black-95 % CI). Black horizontal lines are fitted categorical algal cover classes.

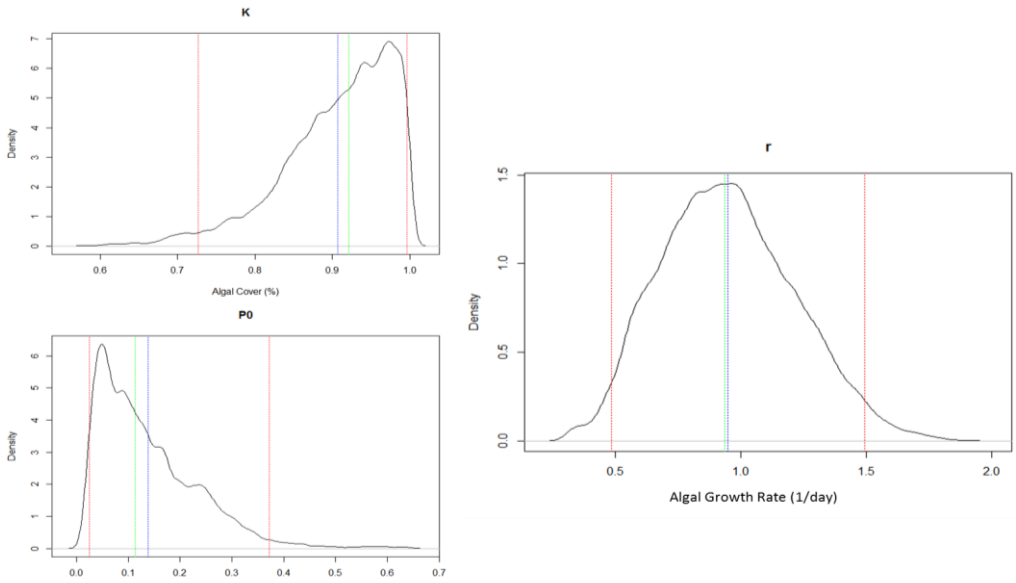

Figure 5.2.24. Results of the Bayesian logistic fit to the categorical algal abundance values from an example treatment site (one of 20). Probability distributions are shown for the logistic model parameters K (carrying capacity), $\boldsymbol{P_0}$ (initial algal cover), and r (intrinsic algal growth rate). Red, blue, and green lines represent the 95 % credible interval, mean, and median, respectively.

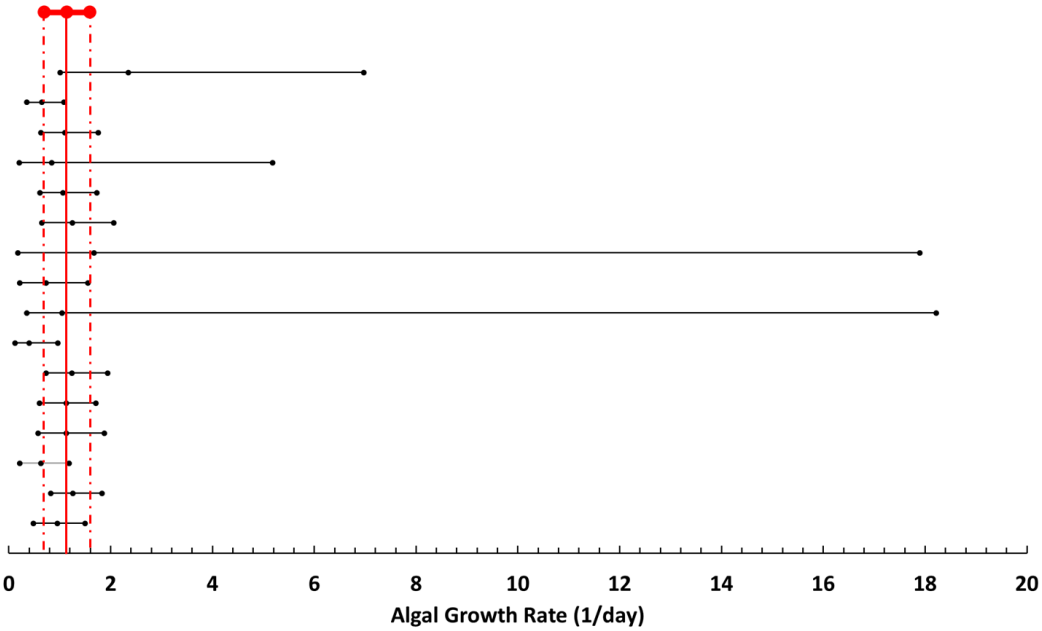

Figure 5.2.25. Summary of algal colonization/growth rate results from all treatment sites. Black intervals represent a specific deployment. Center dots represent the means of the probability distributions, and end points represent the 95 % credible interval (CI). The top red interval is the distribution of the central tendencies of all treatment sites, suggesting an intrinsic algal colonization/growth rate in the absence of velocity of 1.14 1 day^{-1} (95 % CI: 0.70 day^{-1} to 1.60 day^{-1}).

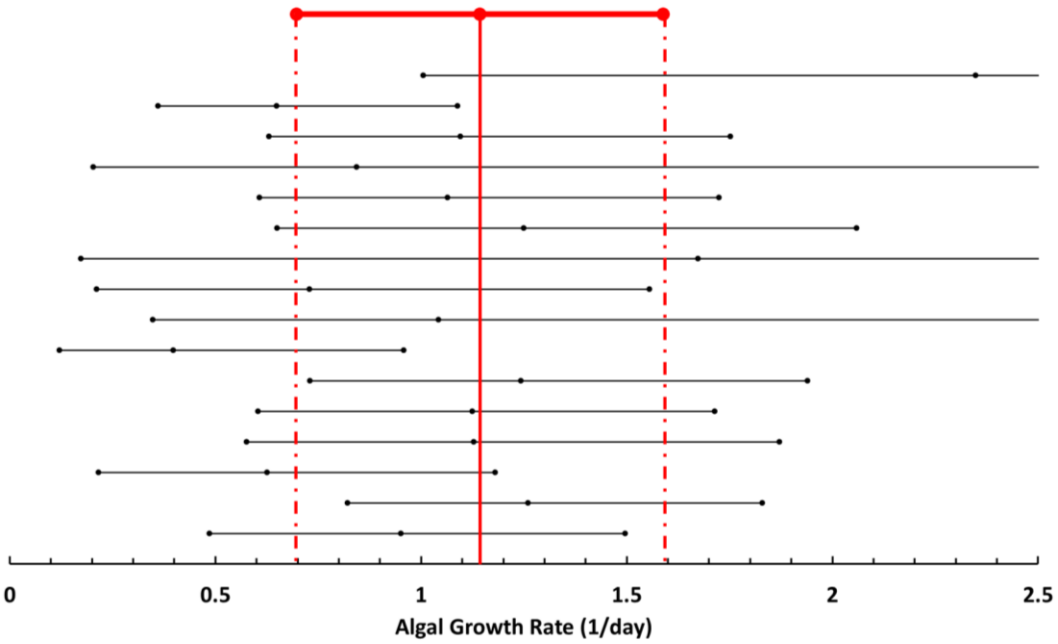

Figure 5.2.26. Zoom-in of Figure 5.2.25 to highlight variance around the overall central tendencies.

There was no consistent evidence (visual or statistical) of a hysteresis effect on algal abundance. In other words, algal growth during Shadow deployment was rapidly removed (within 1-2 days) once flow was reintroduced. Table 5.1.5 summarizes the results of the bootstrapped KS test to check for hysteresis. *P*-values >0.05 indicate that the algal abundance distributions for that site were the same before installation and after removal of the Shadow structure. Only two treatments had *p*-values <0.05; of these, one had less algae after the removal of the shadow than it did prior to deployment, while one had more algae. Two control sites (of 20) also had significantly different algal coverages before installation and after removal of the Shadow structure (both lower). Taken together, these results do not provide evidence for a hysteresis effect.

Table 5.2.1. Results of the bootstrapping version of the Kolmogorov-Smirnov test to check for hysteresis. Significant differences ($p<0.05$) in algal abundance distributions before installation and after removal of the Shadow structure are noted in bold. Only two of the treatments had statistically differences before installation and after removal (one with less algae after the removal and one with more). Note: Deployment 3 had the shortest observation interval following Shadow removal, so higher post-removal algal coverage in Deployment 3, Site 4 may be due to experimental error.

Deployment	Site	Treatment Site *p*-value	Control Site *p*-value	Notes
1	1	1	1	
1	2	1	1	
1	3	0.44231	**0.0053**	Less algae
1	4	0.07778	0.08936	
1	5	1	1	
2	1	1	1	
2	2	1	0.23082	
2	3	0.10209	0.9309	
2	4	1	1	
2	5	0.48489	0.53503	
3	1	0.89379	0.46355	
3	2	**0.02809**	0.14713	Less algae
3	3	0.46335	0.73486	
3	4	**0.00067**	0.14828	More algae
3	5	0.0527	**0.00596**	Less algae
4	1	1	1	
4	2	0.73516	1	
4	3	0.08915	0.53834	
4	4	0.5377	0.2297	
4	5	0.09009	0.14835	

5.2.3.2 Critical Velocity Estimation from Observational Data

Algal cover and velocity data from the Springs Synoptic study are shown in Figure 5.2.27. Across springs, the relationship is relatively noisy, but visual observation suggests a drop-off in algal coverage above 0.3 m s^{-1}. For Silver River (open squares), algal coverage is low above 0.26 m s^{-1}. These results are mirrored in the data collected by divers in the Silver River (Figure 5.2.28;

note, these are different data than those in the Synoptic Study). From these data, it appears that algal cover can range from very low to very high at velocities below 0.2 m s^{-1}, but are generally low above 0.25 m s^{-1}.

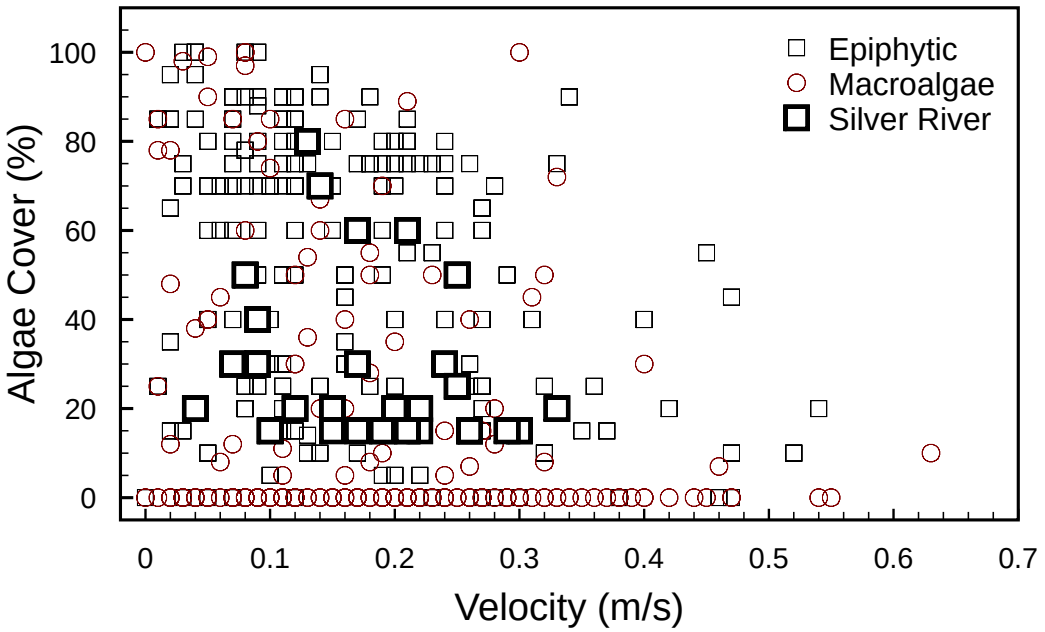

Figure 5.2.27. Algae cover versus velocity for 14 springs (across 26 transects) from the Florida Springs Synoptic Study.

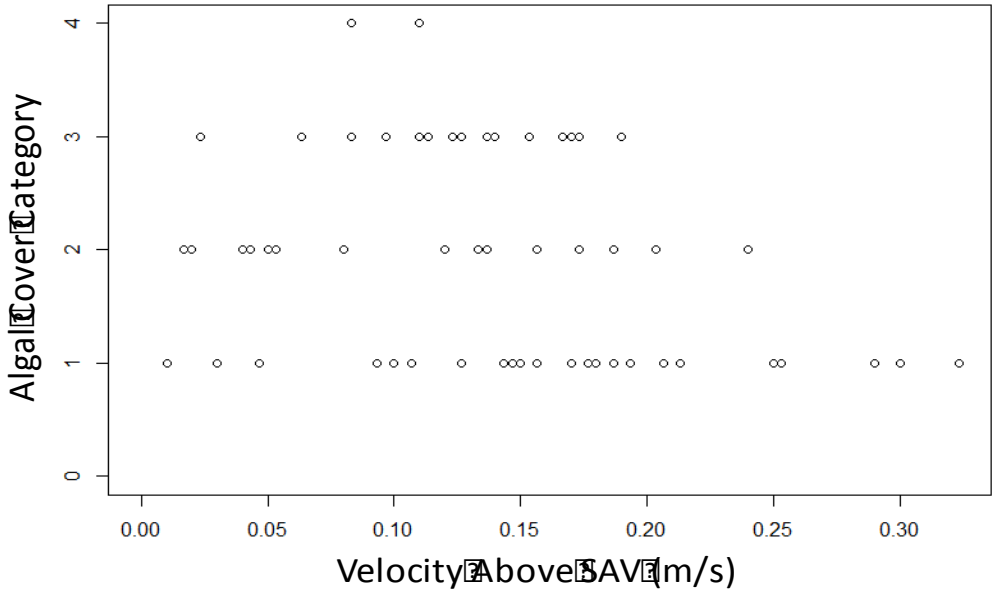

Figure 5.2.28. Algae cover category versus velocity from diver-collected data on the Silver River.

Results of the statistical critical velocity threshold analysis generally support this visual inspection. Figures 5.2.29 to 5.2.33 show probability distribution functions for critical velocity

thresholds identified from each of the five datasets analyzed: 1) Springs Synoptic Study data; 2) Silver River diver data; 3) Gum Slough data (King 2014); Shadow data (this report); and 5) coastal springs data (courtesy of Tom Frazer). Across the Springs Synoptic Study (Figure 5.2.27), the mean critical velocity threshold was 0.22 m s^{-1}, with a 95 % credible interval of 0.14 to 0.26 m s^{-1}. This relatively wide range follows from the range of algal cover measures across velocities (Figure 5.2.27) in this study. From the Silver River diver data (Figure 5.2.30), the mean critical velocity threshold was 0.24 m s^{-1}. The bi-modal distribution density surrounding this value is due to the absence of measurements between 0.22 and 0.24 m s^{-1} (see Figure 5.2.28), which reduces model confidence in this region. The wide confidence interval for Silver River is driven by the structure of the observed data, which show that algal coverage can vary from very low to very high at low velocities, as well as a paucity of data in high-velocity regions.

For the Gum Slough data (Figure 5.2.31), the low-velocity density peak represents the potential for these data to lack a critical threshold; here we focus on the non-zero critical algal velocity, which shows a mean critical velocity threshold of 0.20 m s^{-1}, with a 95 % credible interval of 0.16 to 0.25 m s^{-1}. These results agree with the findings of King (2014): "…macroalgal cover was minimal above 22 cm s^{-1}." For the Shadow data, a single, narrow peak suggests a critical velocity of 0.17 m s^{-1}, with a 95 % credible interval of 0.16 to 0.18 m s^{-1}. Finally, for the coastal springs data, the mean critical velocity is 0.21 m s^{-1}, with a 95 % credible interval of 0.18 to 0.26 m s^{-1}.

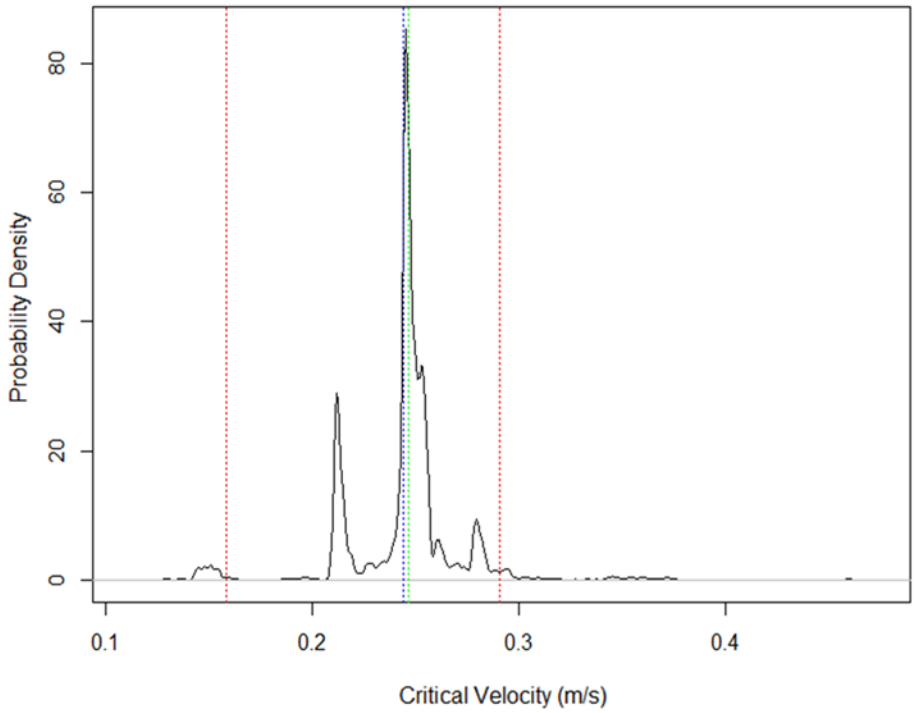

Figure 5.2.29. Probability distribution of the critical algal velocity based on data from the Springs Synoptic Study. Red, blue, and green lines represent the 95 % credible interval, mean, and median, respectively.

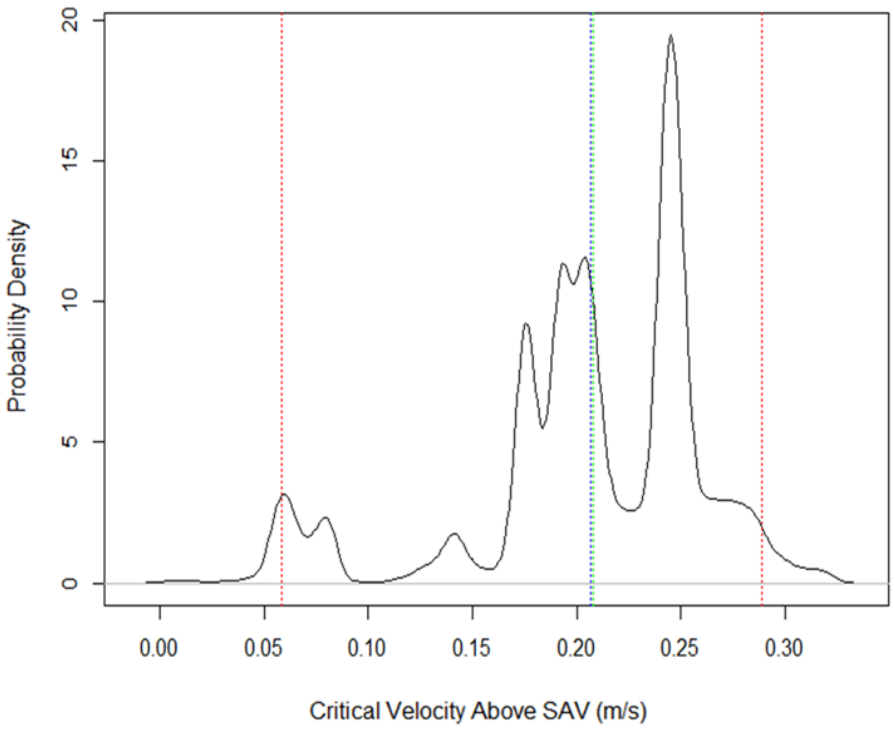

Figure 5.2.30. Probability distribution of the critical algal velocity based on data from Silver River. Red, blue, and green lines represent the 95 % credible interval, mean, and median, respectively.

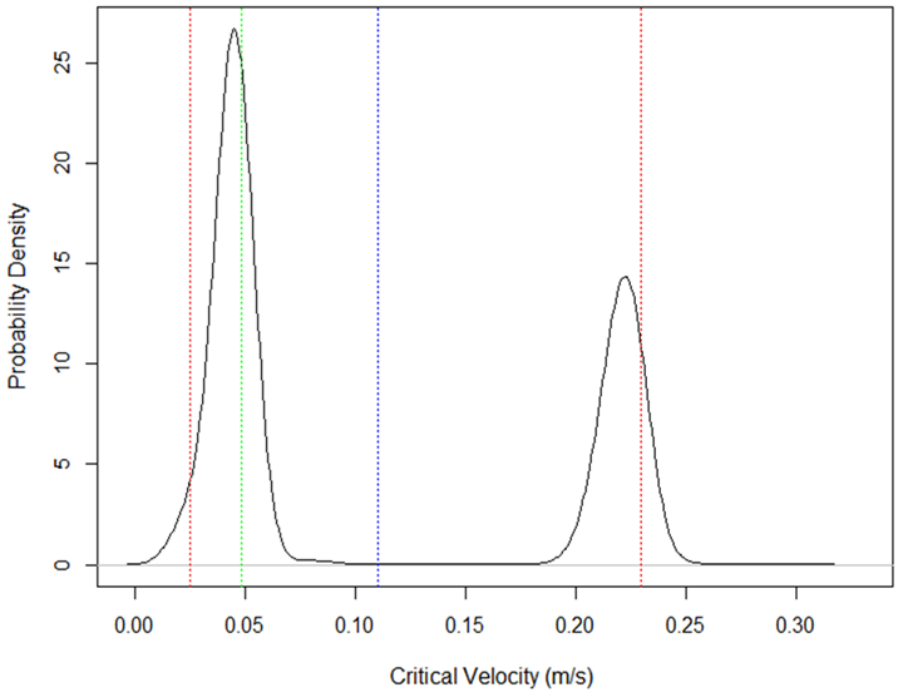

Figure 5.2.31. Probability distribution of the critical algal velocity based on data from Gum Slough. Red, blue, and green lines represent the 95 % credible interval, mean, and median, respectively. We focus on the non-zero critical algal velocity.

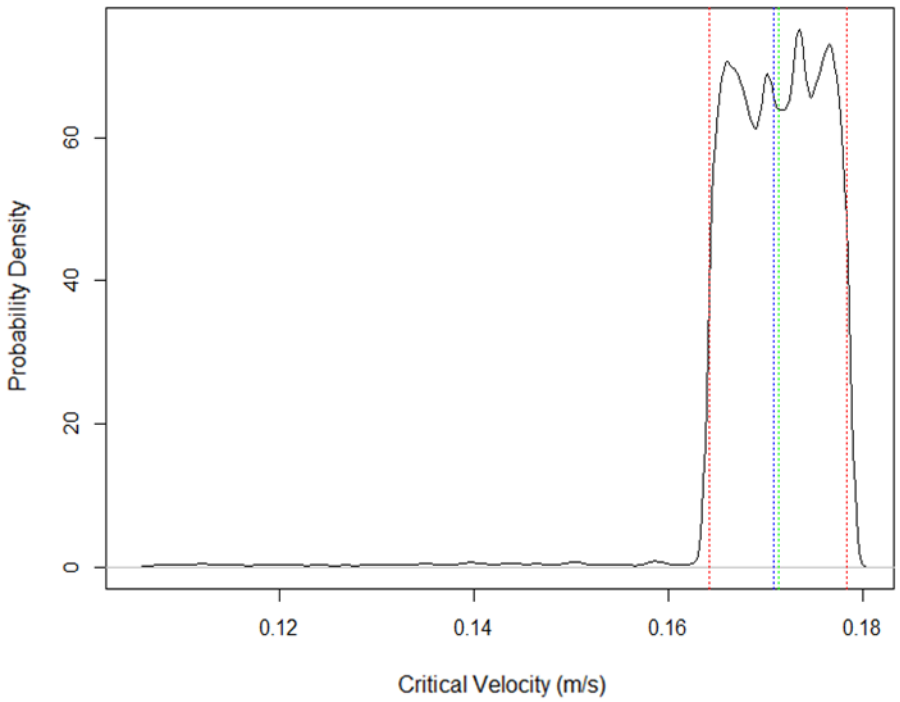

Figure 5.2.32. Probability distribution of the critical algal velocity based on data from the Shadow experiment in the Silver River. Red, blue, and green lines represent the 95 % credible interval, mean, and median, respectively.

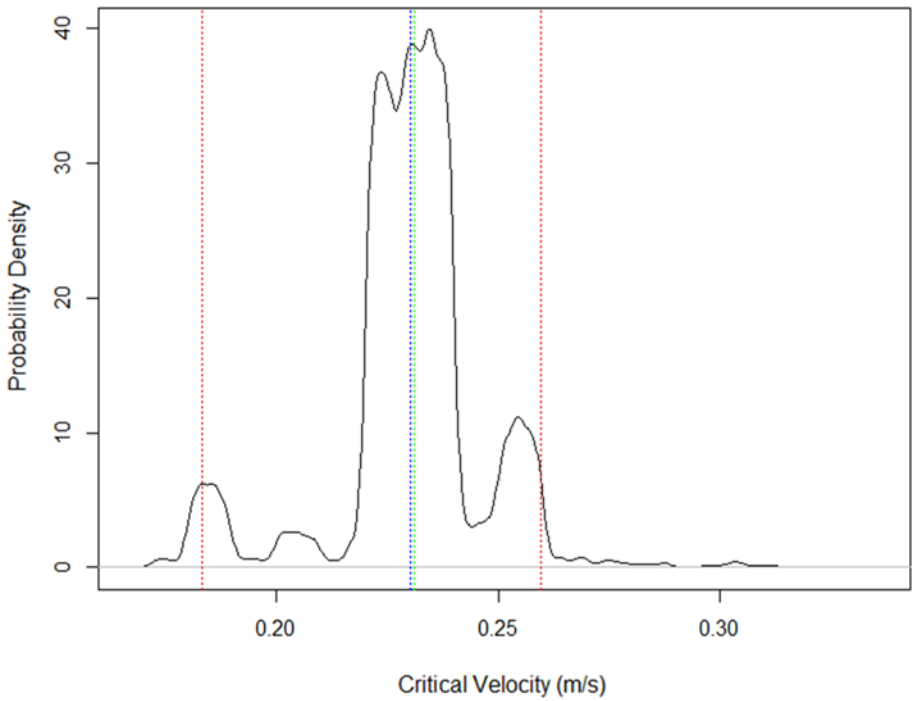

Figure 5.2.33. Probability distribution of the critical algal velocity based on data from the rivers, Weeki Wachee, Homosassa, and Chassahowitzka. Red, blue, and green lines represent the 95 % credible interval, mean, and median, respectively.

Critical velocity thresholds from all five datasets are summarized in Figure 5.2.34. Note that the 95 % CI ranges represents uncertainty that comes both from the model chosen (i.e., two separable distributions; Fig. 5.2.14), as well as the data, which have inherent differences in quantity and quality. Despite these differences, taking the distribution of the central tendencies of all datasets suggests a relatively tightly bounded critical algal removal rate of 0.215 m s^{-1} with a 95 % CI of 0.160 m s^{-1}, to 0.270 m s^{-1}.

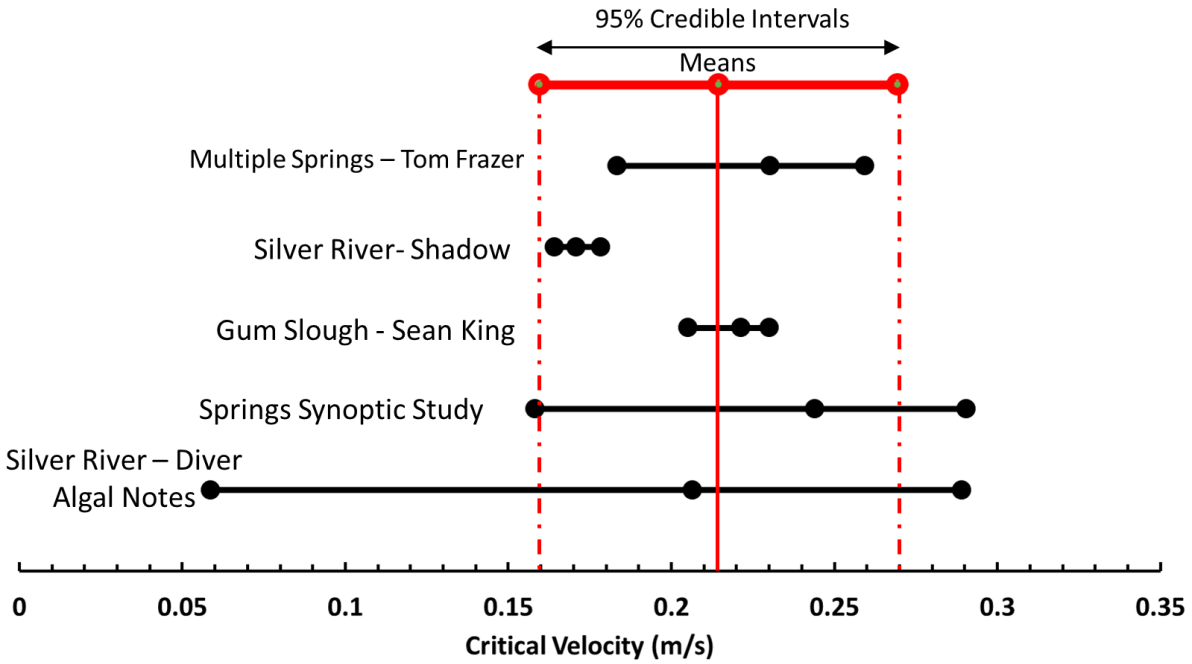

Figure 5.2.34. Summary of critical velocity threshold estimates from the five observational datasets. The distribution of the central tendencies of all datasets suggests a critical algal removal rate of 0.215 m s^{-1} with 95 % CI (0.160 m s^{-1}, 0.270 m s^{-1}).

The statistical model and sampling approach described in Section 5.2.2.2 also allowed us to visualize the relationship between observed velocity and the range of likely algal coverages. Figures 5.2.35 thru 5.2.39 show these relationships for the five compiled datasets. These results do not constitute a deterministic predictive model, but show how the range of likely algal coverage values change with velocity. The red line in each figure represents mean algal coverage as a function of velocity based on the data from each study, and the range of likely algal coverages are represented using credible intervals (orange, blue, and gray lines represent the 40, 60, and 80 % credible intervals [CI], respectively). Given the wide ranges of algal coverages observed across velocities, CI can be large, especially at low velocities and for studies with less data.

Despite these wide CIs, the method successfully identified a "break" between low and high algal coverage values across a particular velocity range for each dataset (Figures 5.2.35 to 5.2.39). The PDFs of the critical velocity thresholds shown in Figures 5.2.29 thru 5.2.33 are drawn from these relationships. The modeled breakpoint is particularly well defined (i.e., sharp declines across

CIs) for the data from the Synoptic Springs Study, Gum Slough, Shadow, and the coastal springs, but more gradual from the diver-collected data from Silver River, which is reflected in the wider 95 % credible interval for these data (see Figure 5.2.34).

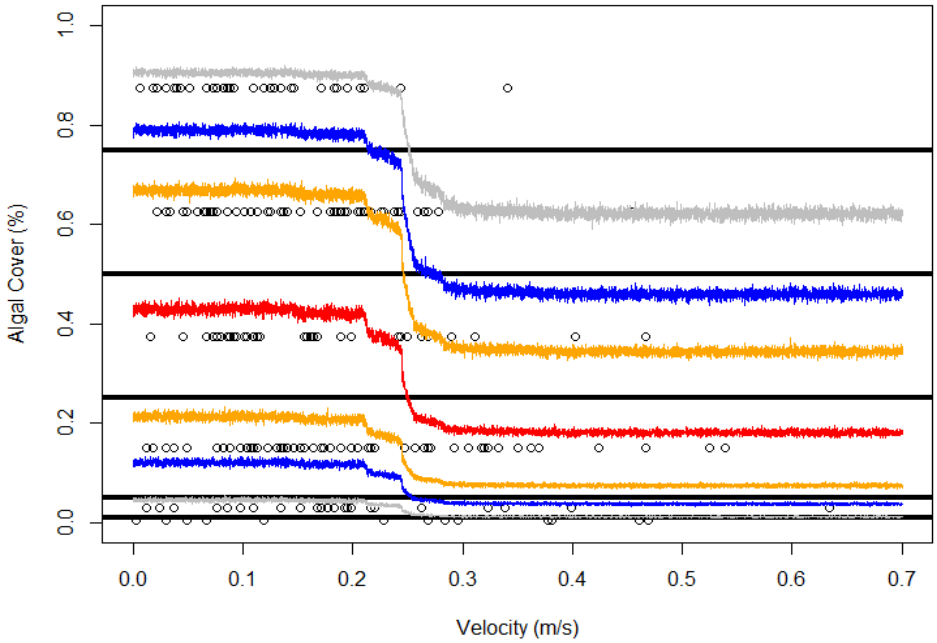

Figure 5.2.35. Data (open circles) and modeled algal abundance as a function of velocity for the Springs Synoptic Study, shown with credible intervals (CI) on observed algal abundances (red-mean; orange-40 % CI; blue-60 % CI; gray-80 % CI). Black horizontal lines are fitted categorical algal cover classes.

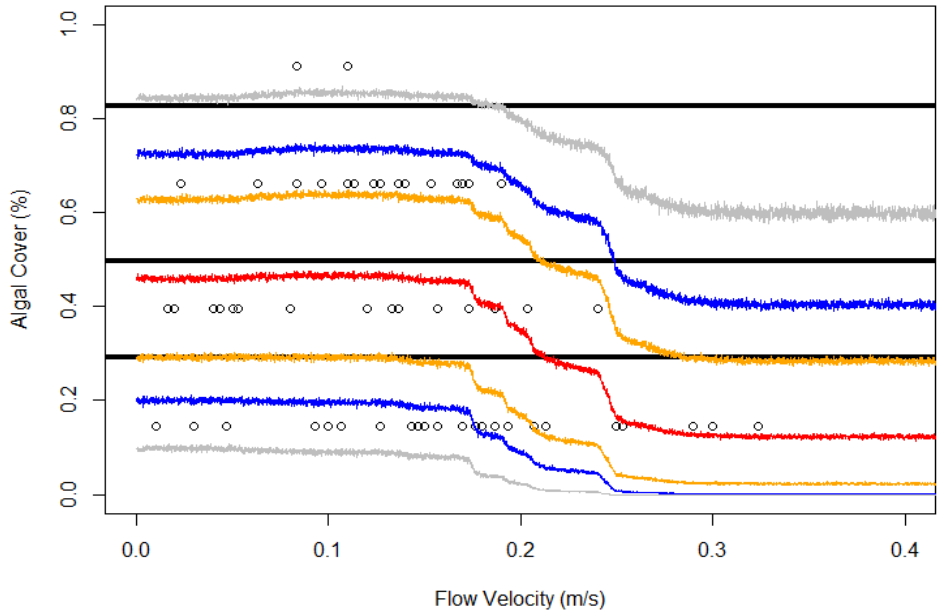

Figure 5.2.36. Data (open circles) and modeled algal abundance as a function of velocity for Silver River diver data, shown with credible intervals on observed algal abundances (red-mean; orange-40 % CI; blue-60 % CI; gray-80 % CI). Black horizontal lines are fitted categorical algal cover classes.

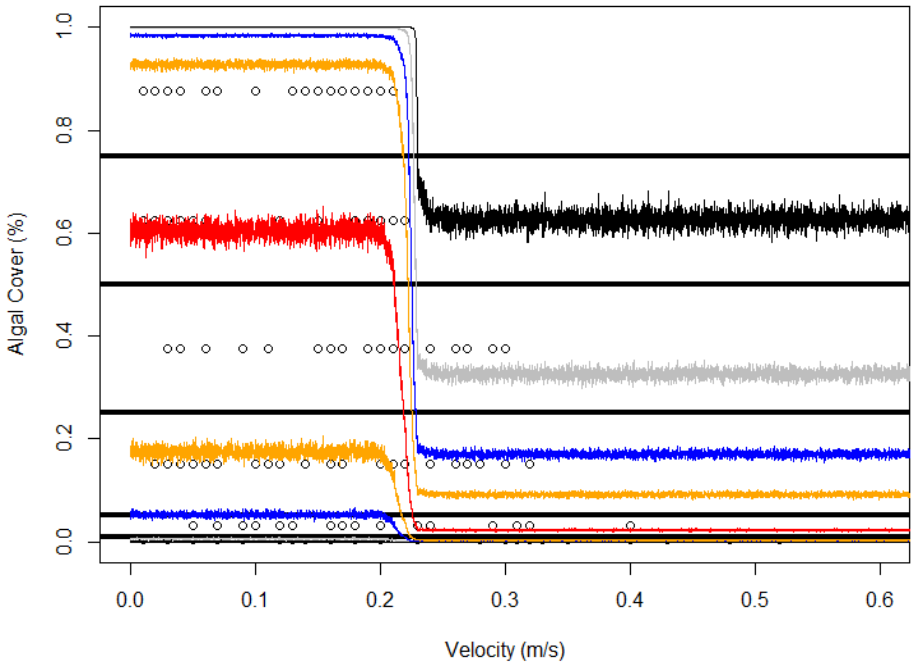

Figure 5.2.37. Data (open circles) and modeled algal abundance as a function of velocity for Gum Slough, shown with credible intervals on observed algal abundances (red-mean; orange-40 % CI; blue-60 % CI; gray-80 % CI). Black horizontal lines are fitted categorical algal cover classes.

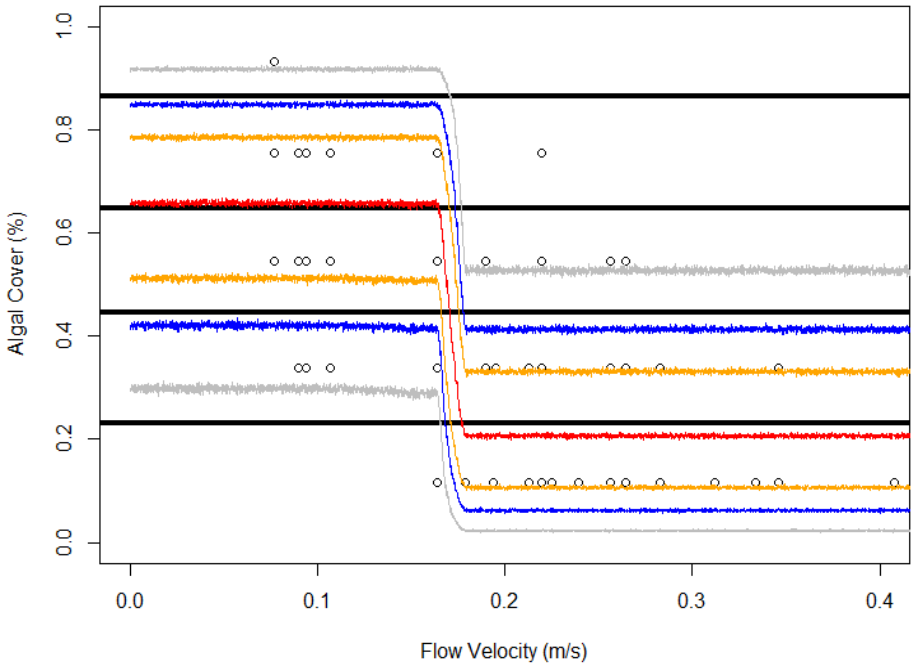

Figure 5.2.38. Data (open circles) and modeled algal abundance as a function of velocity for the Shadow experiment in the Silver River, shown with credible intervals on observed algal abundances (red-mean; orange-40 % CI; blue-60 % CI; gray-80 % CI). Black horizontal lines are fitted categorical algal cover classes.

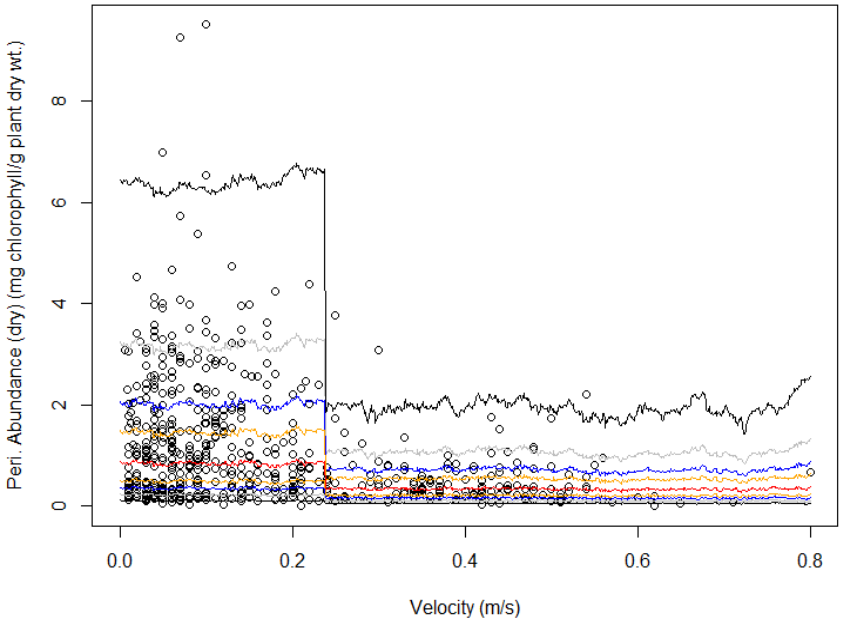

Figure 5.2.39. Data (open circles) and modeled algal abundance as a function of velocity for the Weeki Wachee, Homosassa, and Chassahowitzka Rivers, shown with credible intervals on observed algal abundances (red-mean; orange-40 % CI; blue-60 % CI; gray-80 % CI).

For the diver-collected data on the Silver River (which included both within-SAV and above-SAV velocity measurements), we applied the same analysis to identify critical shear stresses for algal presence. Observed algal-shear stress data, threshold PDFs, and model output are given in Figures 5.2.40 to 5.2.42. Finally, threshold PDFs, and model output of the critical SAV velocity based on cover and biomass data from the coastal springs dataset are given in Figures 5.2.43 to 5.2.46 and summarized in Figure 5.2.47.

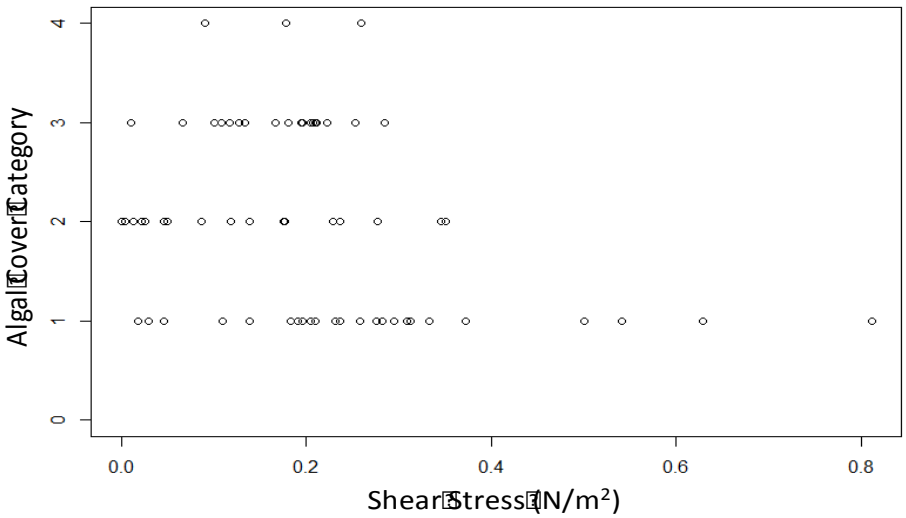

Figure 5.2.40. Algae cover category versus shear stress from diver-collected data on the Silver River.

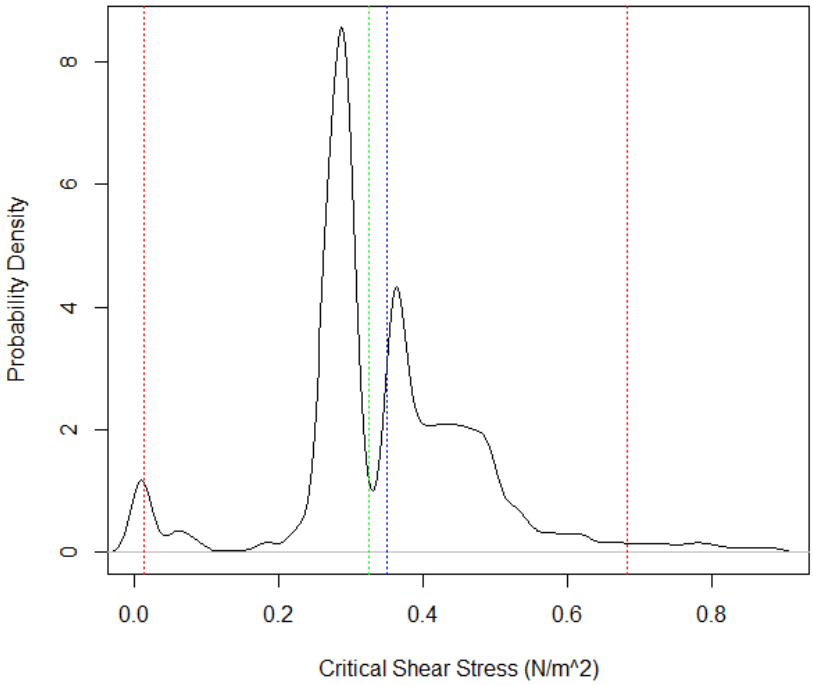

Figure 5.2.41. Probability distribution of the critical algal shear stress based on data from Silver River. Red, blue, and green lines represent the 95 % credible interval, mean, and median, respectively.

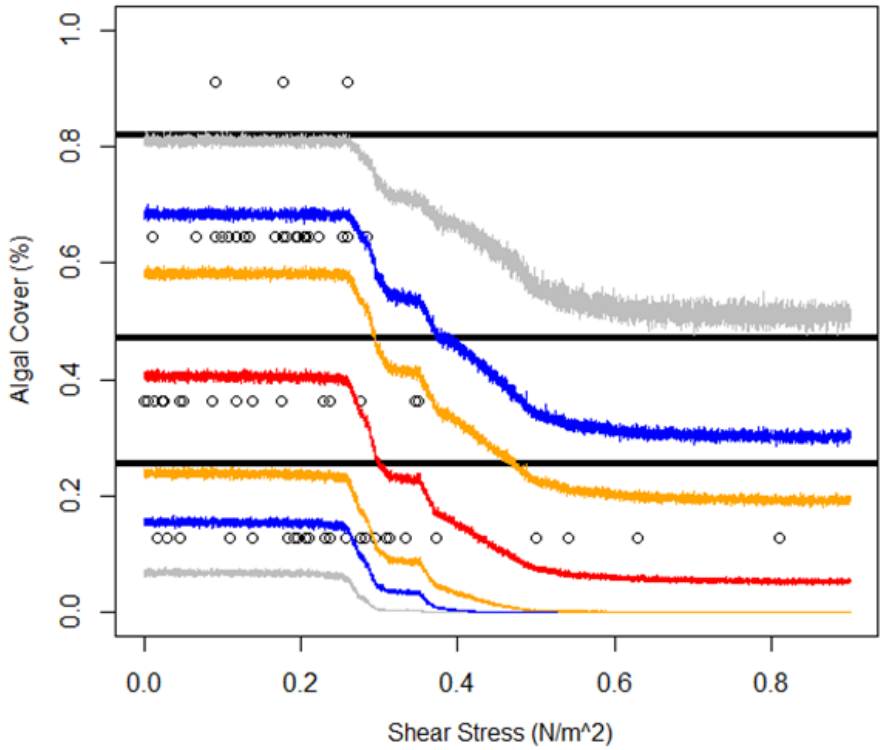

Figure 5.2.42. Modeled algal abundance as a function of shear stress for the Silver River, shown with credible intervals on observed algal abundances (red-mean; orange-40 % CI; blue-60 % CI; gray-80 % CI).

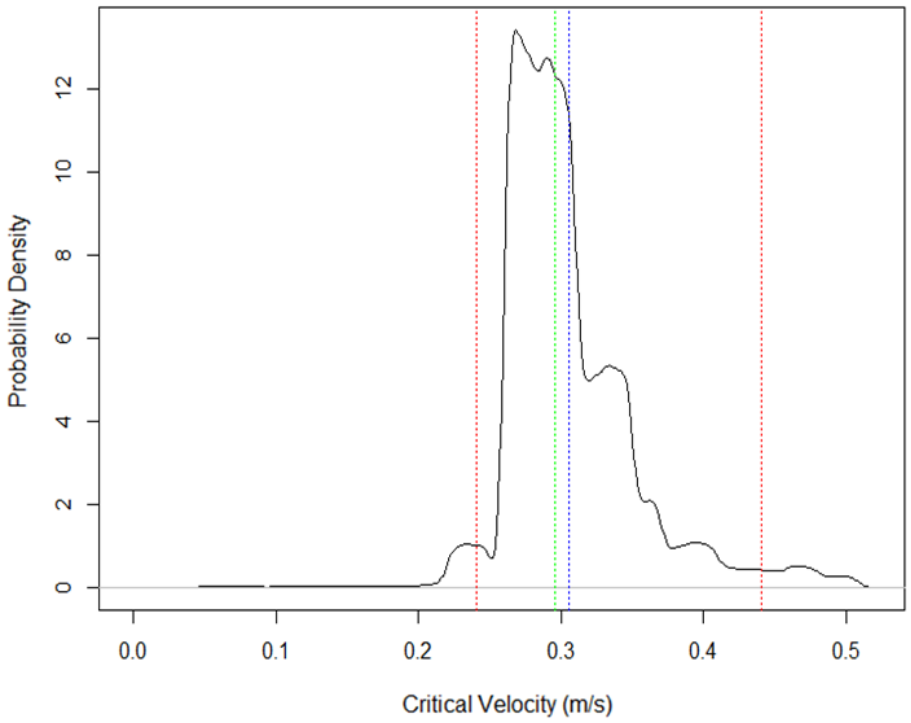

Figure 5.2.43. Probability distribution of the critical SAV velocity based on cover data from the rivers, Weeki Wachee, Homosassa, and Chassahowitzka. Red, blue, and green lines represent the 95 % credible interval, mean, and median, respectively.

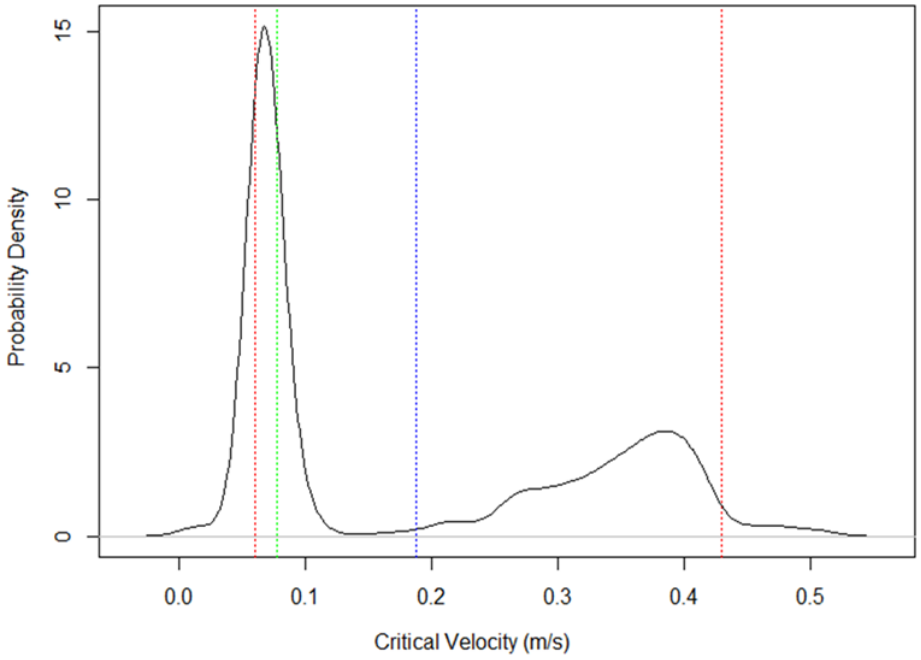

Figure 5.2.44. Probability distribution of the critical SAV velocity based on mass data from the rivers, Weeki Wachee, Homosassa, and Chassahowitzka. Red, blue, and green lines represent the 95 % credible interval, mean, and median, respectively. We focus on the non-zero critical algal velocity.

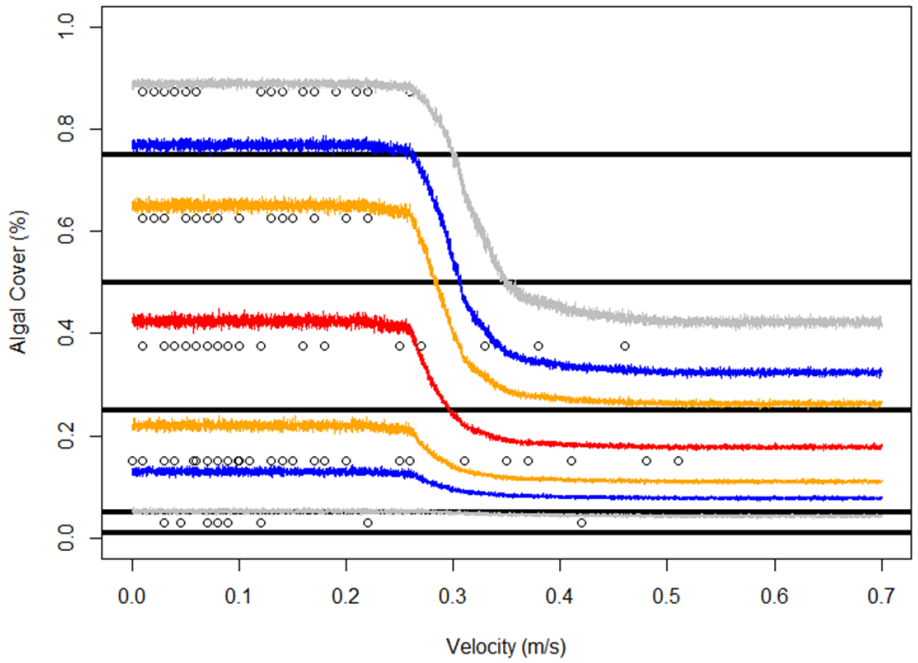

Figure 5.2.45. Data (open circles) and modeled SAV abundance as a function of velocity for the rivers, Weeki Wachee, Homosassa, and Chassahowitzka, shown with credible intervals on observed algal abundances (red-mean; orange-40 % CI; blue-60 % CI; gray-80 % CI). Black horizontal lines are SAV cover classes.

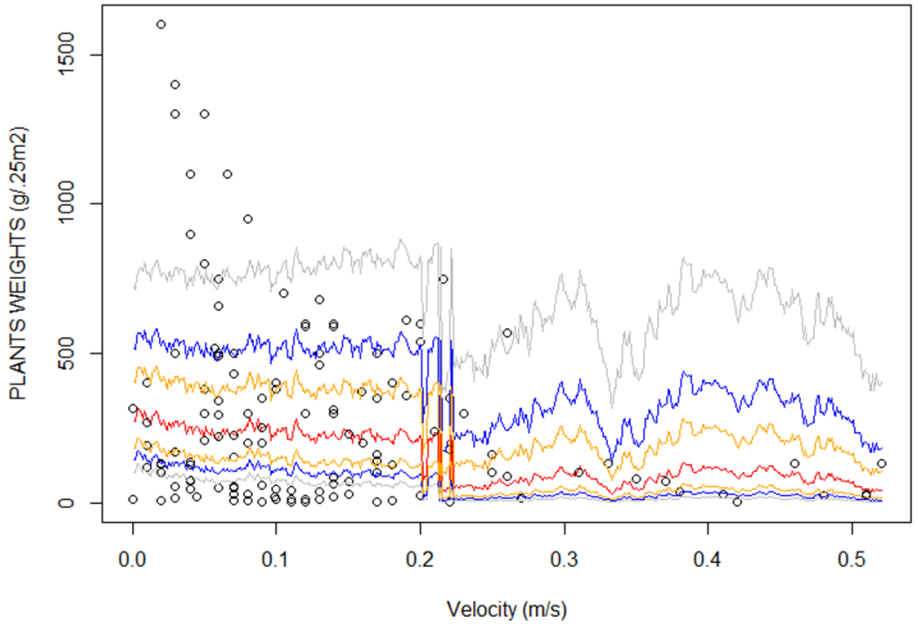

Figure 5.2.46. Data (open circles) and modeled SAV abundance as a function of velocity for the rivers, Weeki Wachee, Homosassa, and Chassahowitzka, shown with credible intervals on observed algal abundances (red-mean; orange-40 % CI; blue-60 % CI; gray-80 % CI).

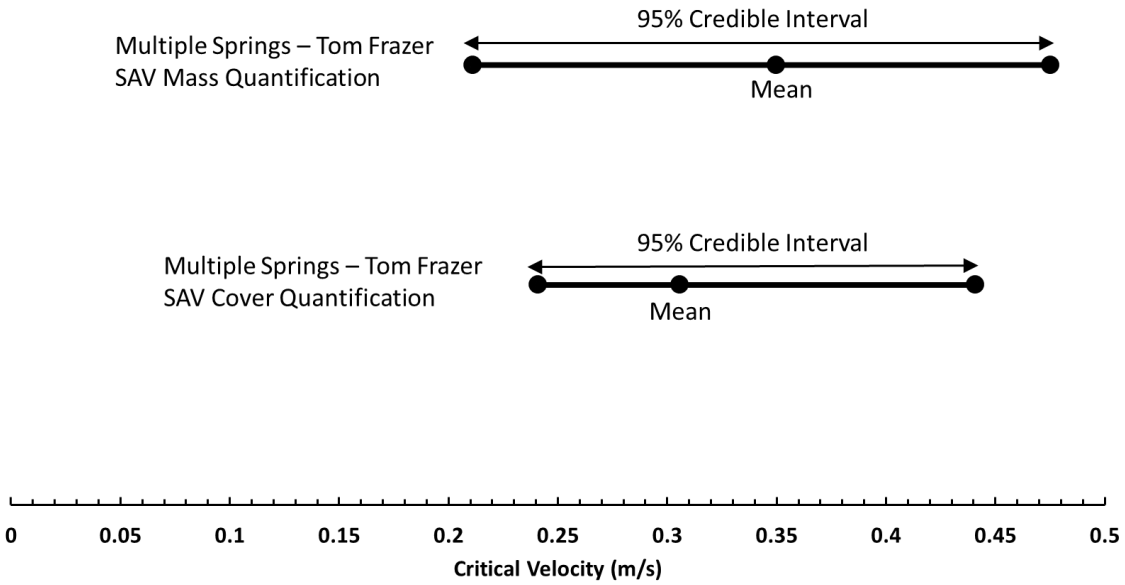

Figure 5.2.47. Summary of critical velocity threshold estimates for SAV from two observational datasets. The overall average value is 0.33 m s^{-1} and the credible intervals overlap between 0.24 m s^{-1} and 0.44 m s^{-1}.

5.2.3.3 Optical Methods

Initial results from the average-image color shift show substantial promise for high-resolution, spatially distributed mapping of algal cover (Figure 5.2.48). Both of the integrated images colors (B-G and G-R) are correlated to algal cover, and are more tightly correlated to cover determined by K-clustering method. Moreover, both B-G color and algal cover correlate with flow velocity, suggesting that the B-G color of an algal covered SAV bed can be used as a proxy for algal cover, perhaps providing a more accurate measure than quadrat methods. This process can be automated to map large areas of SAV beds and provides additional support for the hypothesis that velocity plays some level of control on epiphytic algal communities.

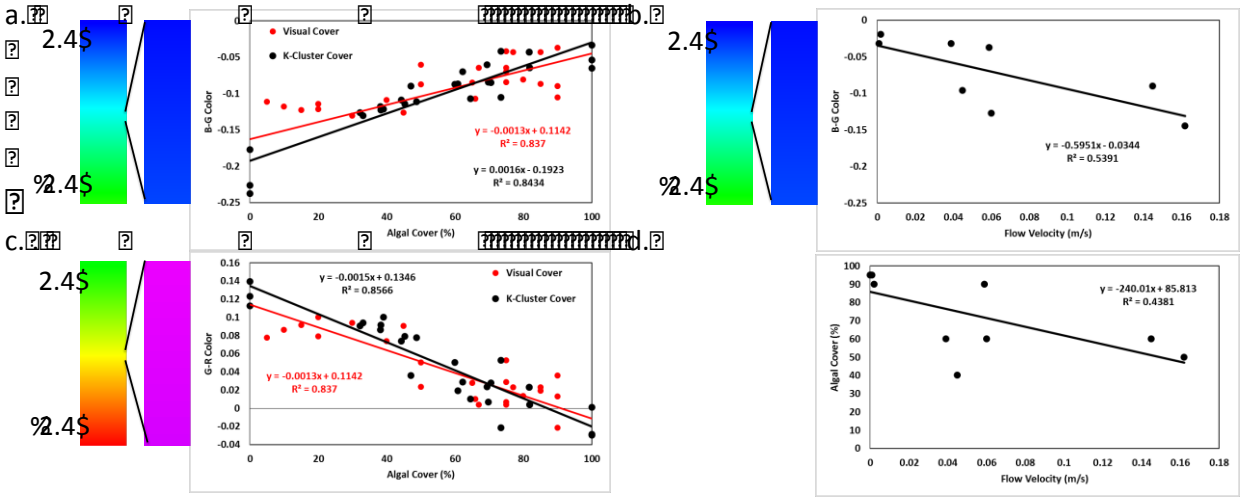

Figure 5.2.48. Relationships between integrated images colors (B-G and G-R) and algal cover determined using visual and automated techniques.

5.2.4 CONCLUSIONS, RECOMMENDATIONS, AND FUTURE RESEARCH NEEDS

We used observational and experimental approaches to identify critical velocity and shear stress thresholds for the algal presence to use as management targets. *In situ* flow modification devices were employed using a before/after control/impact (BACI) design to identify critical velocity and shear stress thresholds, quantify algal colonization and growth rates under reduced velocities, quantify algal clearing rates after flow restoration, and identify hysteretic behavior (if present). These experiments showed clear algal-colonization and growth effects from induced velocity reduction. While control sites only saw modest epiphytic algal growth, algal cover at treatment sites approached 100 % after one week. While control sites only saw modest epiphytic algal growth, algal cover at treatment sites approached 100 % after one week. Fitted logistic models revealed an intrinsic algal growth rate (in the absence of velocity) near 1 day^{-1} with a 95 % credible interval (CI) of 0.70 day^{-1} to 1.60 day^{-1}, indicating a doubling of algal cover/abundance every day until reaching carrying capacity at or near 100 % cover.

Modeling and analysis of existing algal cover, SAV cover, and velocity datasets from several Florida springs were used to statistically identify critical velocities and shear stresses that predict algal/SAV presence and absence. Data from the FL Springs Synoptic Study, the Silver River, Gum Slough, and several coastal springs had an overall mean algal velocity threshold of 0.215 m s^{-1} with a 95 % CI of 0.160 to 0.270 m s^{-1}. These values are supported by data from other studies, which identify critical values from 0.22 to 0.25 m s^{-1}. Mean critical shear stress calculated using diver-collected data from the Silver River was 0.35 N m^{-2} with a 95 % CI of 0.02 to 0.70 N m^{-2}. Mean critical velocity threshold estimated for SAV was 0.33 m s^{-1}, with a 95 % CI between 0.24 m $s^{-1}$and 0.44 m s^{-1}.

These experimental and observational results can be used together with EFDC modeling to predict the impact of alternate flow restoration and management scenarios on likely algal and SAV cover. Specifically, EFDC may be used to model current and historical hydrodynamic conditions and coupled with these relationships to predict where (and when) algae and SAV may be present. EFDC may also be used to model different restoration scenarios, including increased discharge, tailwater elevation management, closing of the Ft. King Waterway, or SAV grazing/removal to predict how coupled hydrodynamic-vegetation feedbacks will affect river-wide SAV and algal coverage. In general, applying these coupled models in an adaptive management framework (with ongoing hypothesis testing, model refinement, and data collection) will be important to understand if restoration efforts are successful and to respond quickly if they are not.

5.2.5 REFERENCES

Lowe, E. 2014. The Research Component of the Springs Protection Initiative of the St. Johns Water Management District. UF Water Institute Symposium, February 2014, Gainesville, FL.

King, S. A. 2014. Hydrodynamic control of filamentous macroalgae in a sub-tropical spring-fed river in Florida, USA. *Hydrobiologia*, *734*(1), 27-37.

5.3 VELOCITY VALIDATION TRANSECTS

5.3.1 INTRODUCTION

A major objective of EFDC modeling is to generate predictions of horizontal and vertical flow velocities under a variety of boundary conditions and bottom characteristics. In order to validate EFDC results, field measurements of velocity are required; however, the use of 4-beam acoustic Doppler current profilers (ADCP) provides limited information in reaches with dense submerged aquatic vegetation. The goals of the velocity validation effort are to provide discrete, point-based velocity data for use in model calibration and validation and to determine when and where ADCP measurements are sufficient to characterize discharge and velocity profiles.

5.3.2 MATERIALS AND METHODS

Velocity measurements are needed to validate the EFDC modeling to predict horizontal and vertical flow velocities under a variety of boundary conditions and bottom characteristics. The District deployed 4-beam acoustic Doppler current profilers (ADCP) for this purpose; however, ADCP profilers provide limited information in reaches with dense submerged aquatic vegetation. As such, UF collected discrete, point-based velocity data for use in model calibration and validation and to aid in determining when and where ADCP measurements are sufficient to characterize discharge and velocity profiles.

To meet this goal, UF worked with the District to develop a set of riverine transects where velocity measurements were made using both a floating ADCP (District-owned) and point-based electromagnetic flow meter (UF-owned). Transect locations were selected to characterize a variety of bottom conditions (bare, sparse and dense macrophyte coverage, benthic algae dominated, etc.). Selected transects corresponded to transects developed for development of the Silver River MFL and include T3, T7, and T10 (Figure 5.3.1).

Figure 5.3.1. Velocity validation transect locations.

At each transect, velocity was measured using an electromagnetic flow meter (EFM) (MF Pro Flow Meter, OTT Hydromet Inc., Loveland, CO). The EFM was found to provide reasonable velocity data even in dense vegetation, which the previously proposed acoustic Doppler velocimeter (ADV) was unable to do. The EFM was mounted to a custom-made wading rod (Figure 5.3.2) to allow discrete depth measurements to a depth of 19.7 ft (6 m).

Velocity profiles were made by traversing the river with a boat secured on both banks to keep the boat perpendicular to flow. A dedicated transect line marked with meters (Figure 5.3.2B) was used to determine distance across the transect. The wading rod was placed so that it rested on the sediment surface, and velocity readings were taken at a minimum of 8 depths at each measurement location. Horizontal spacing across the transect was every 3.28 ft (1 m) on T3 and every 6.56 ft (2 m). Velocity measurements were not collected on T10 due to glass-bottom boat traffic, which made the placement of transect and boat lines unfeasible.

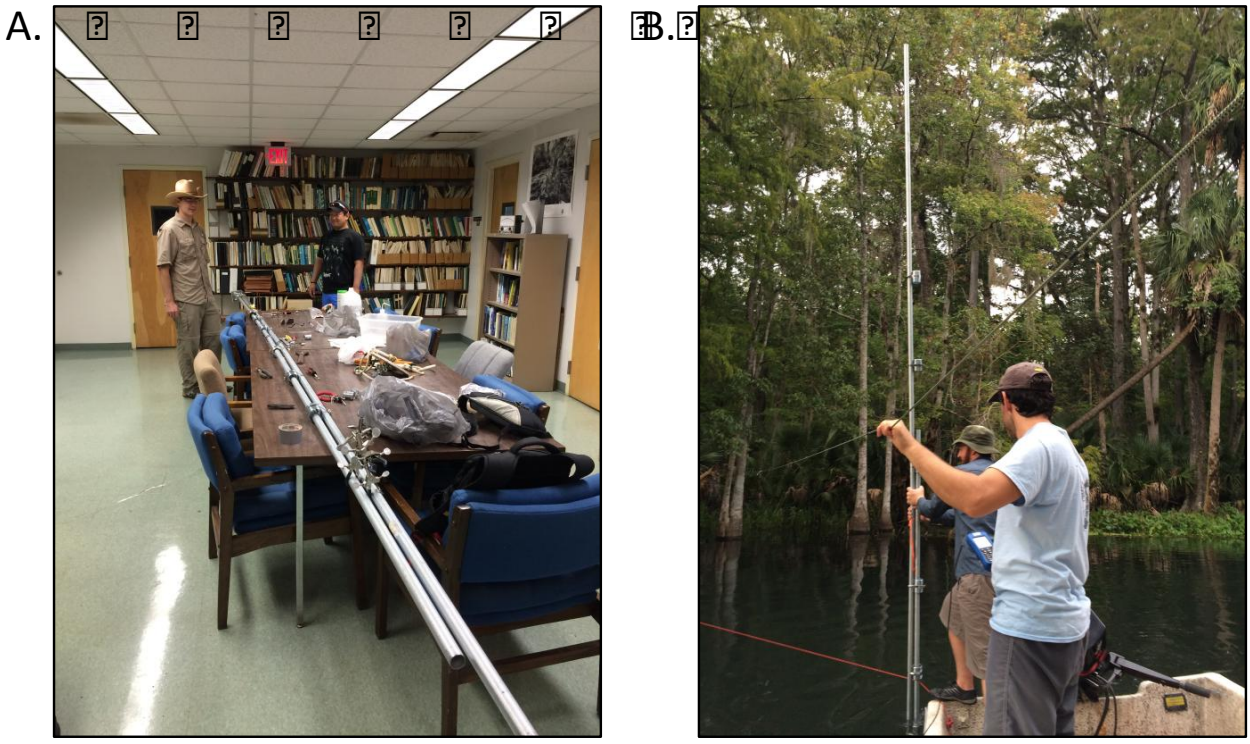

Figure 5.1.2. A) Wading rod construction showing full-length extension. B) Taking velocity readings on T3. Note transect line for horizontal spacing and boat line (red) for stability.

The EFM was programmed to output 10 second velocity averages based on 4 Hz data; a minimum of three 10-s average samples were taken for calculation of an average velocity value at each measurement point. Based on the horizontal and vertical spacing described above, a total of 1,131 discrete velocity measurements were taken on 3 October, 6 October, and 8 October 2014 (Appendix 5.3.1). Depth to vegetation was also noted at each distance across the transect where it was visible. Based on the average value at each measurement point, we created velocity contours and surfaces for each transect by ordinary kriging using statistical software (Surfer 11, Golden Software, Golden, CO).

5.3.3 RESULTS AND DISCUSSION

Velocity data are presented in Figures 5.3.3 and 5.3.4. These figures are useful for comparison with ADCP data collected at the same transects. We note that we were able to coordinate with District staff in the field to co-locate ADCP and EFM measurements on T3, but not on T7, so comparability of data collected by ADCP and EFM should be better on T3 (Figure 5.3.5). In general, velocities measured by each method are in the same range, but with several noteworthy exceptions. The ADCP data is clearly more highly resolved and identifies small patches of high-velocity flow that is not captured by the point-based EFM technique due to its lower spatial resolution. On the other hand, the point-based measurements capture velocity data near the benthic surface in some locations where the ADCP does not provide data. This is also evident in the differences in inferred bathymetry between the EFM and ADCP approaches. Additional analysis of these data and subsequent velocity measurements will quantify "missing" flows from the absence of velocity readings in shallow and vegetated regions.

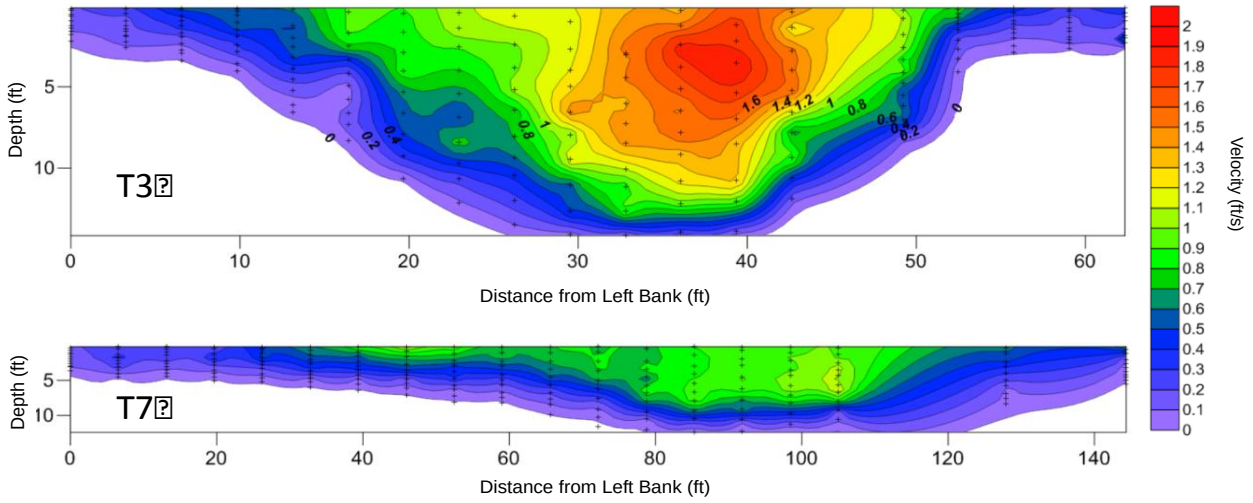

Figure 5.3.3. Velocity transects at T3 (top) and T7 (bottom). Velocity is indicated by a shared color scale, illustrating slower velocities at T7. Point velocity measurement locations are indicated by crosses. X and Y scales are proportional (i.e., 1:1).

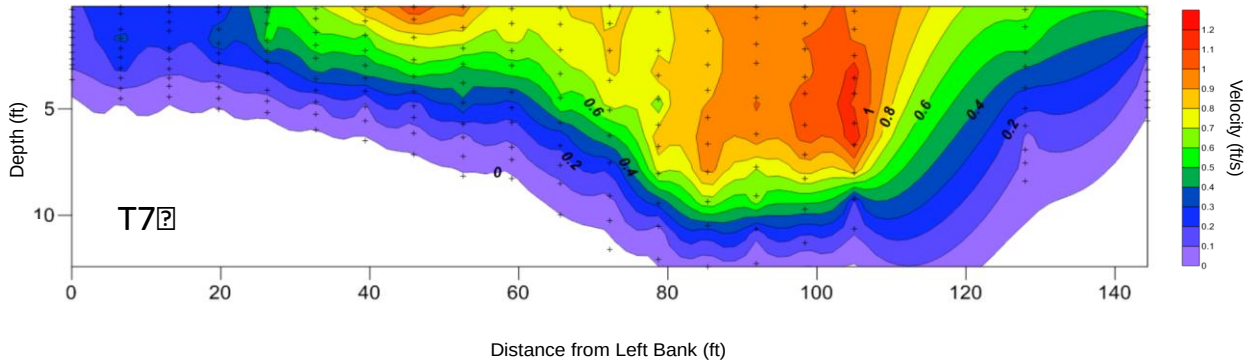

Figure 5.3.4. Rescaled velocity transect at T7. Color scale illustrates full range of measured velocity on T7. The Y scale is exaggerated 3x to make velocity variation with depth more visible.

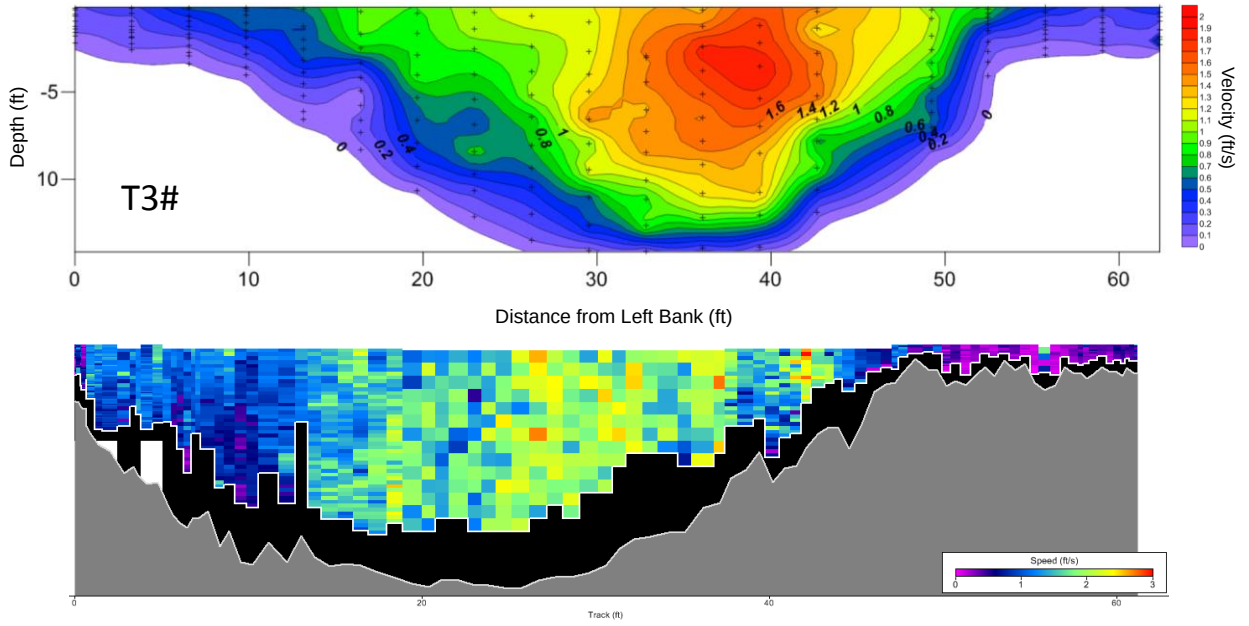

Figure 5.3.5. Comparison of kriged point-based velocity EFM velocity measurements (top) and ADCP velocity measurements (bottom) on T3 (co-located transect). Note different color scales in top and bottom figures.

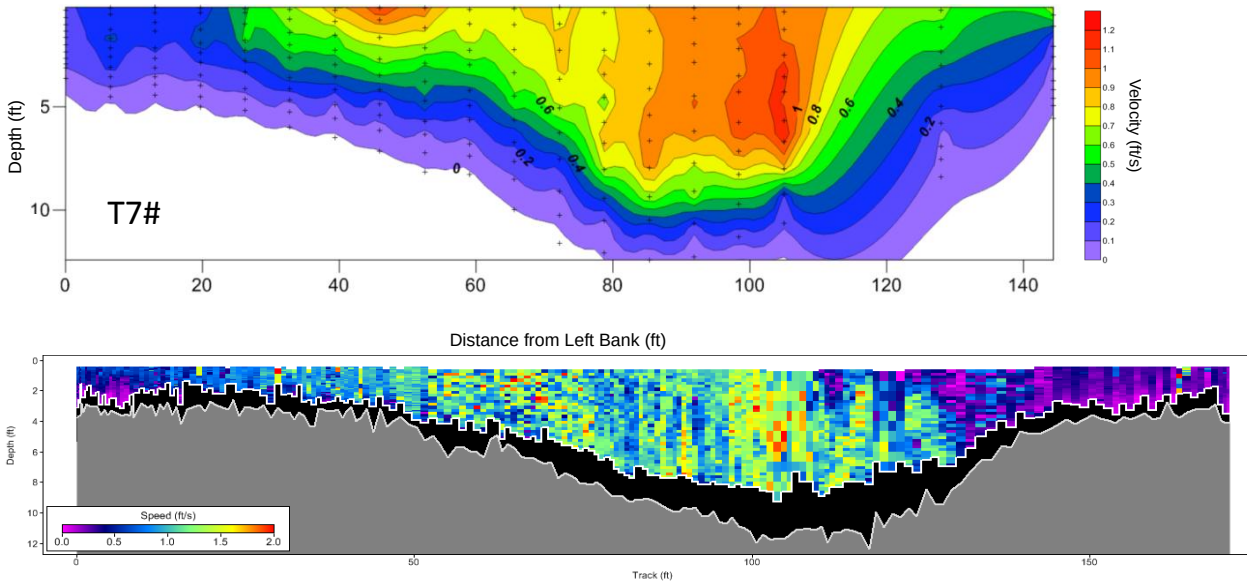

Figure 5.3.6. Comparison of kriged point-based velocity EFM velocity measurements (top) and ADCP velocity measurements (bottom) on T7 (transects NOT co-located). Note different color scales.

Critically, these data also provide a set of reference velocity measurements for calibration and validation of modeled 1-D velocity profiles using EFDC algorithms and an analytical vegetation drag and turbulence closure model (Figure 5.3.6). Initial parameterization of these 1-D velocity profiles showed general agreement with measured velocities on Transects 3 and 7 despite simplified assumptions about vegetation cover characteristics, providing support for their formulation.

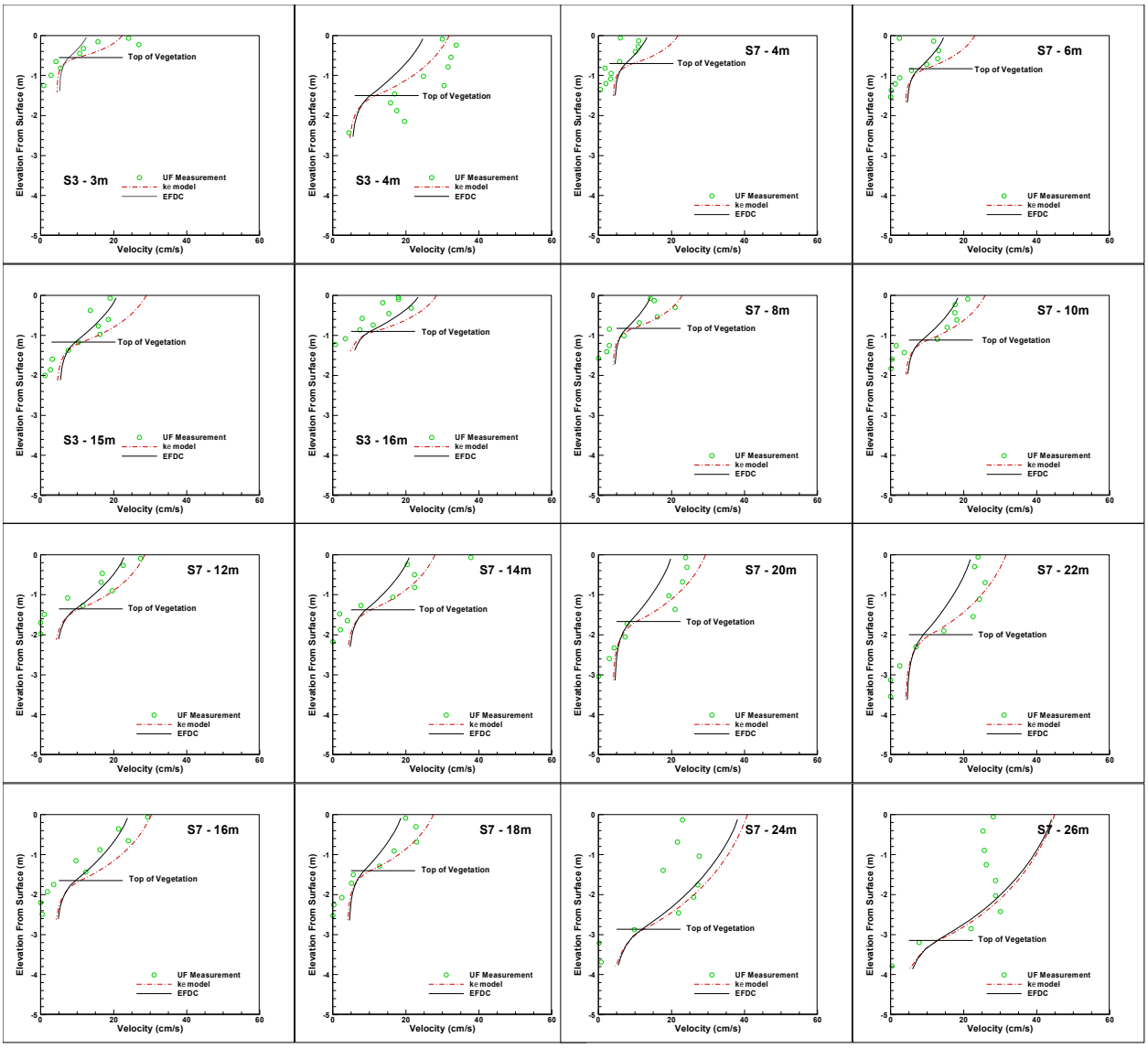

Figure 5.3.7. Comparison of measured velocity profiles at 16 (of >100) locations with velocities simulated by EFDC and modeled with a 1-D turbulence closure model. Figures by Yanfeng Zhang.

5.3.4 CONCLUSIONS, RECOMMENDATIONS, AND FUTURE RESEARCH NEEDS

Velocity validation transects confirmed that velocities measured using Acoustic Doppler Current Profilers (ADCP) and the Electromagnetic Flow Meter (EFM) were in the same range, with several noteworthy exceptions. The ADCP data was more highly resolved and identified small patches of high-velocity flow that were not captured by the point-based EFM technique. However, the point-based measurements captured velocity data near the benthic surface in some locations where the ADCP did not; this was also evident in the differences in inferred bathymetry between the approaches. These data also provided a set of reference velocity measurements for calibration and validation of modeled 1-D velocity profiles using EFDC algorithms and an analytical vegetation drag and turbulence closure model.

5.4 HYDRODYNAMIC EFFECTS OF VEGETATION ON VELOCITY AND STAGE IN SILVER RIVER

5.4.1 INTRODUCTION

A hydrodynamic analysis of velocity, discharge, and stage in Silver River is needed to meet the overall aim of the CRISPS study to determine whether velocity is an important non-nitrate factor influencing the community structure and function of primary producers in the system. King (2014) suggested that hydrodynamics could contribute to, or even dominate, the control of filamentous macroalgae on and attached to submersed aquatic vegetation in Florida spring runs. Section 5.2 of this report illustrated that much of Silver River falls within a zone of velocity close to King's target threshold for control of filamentous macroalgae.

The role of hydrodynamics in determining the dominant plant communities in streams is well-documented (Biggs 1996; Franklin 2008). Increases in velocity tend to increase growth rates of submersed aquatic vegetation (SAV) by thinning the diffusive boundary layer over the plant surface (Biggs 1996; Biggs et al. 1998). At too high a velocity, however, the plants suffer stress from excessive drag and are ultimately uprooted as velocity increases. In general, SAV in streams require low absolute velocity, low velocity variability and stable substrates (Biggs 1996). Velocity < 30 cm s^{-1} (0.98 ft s^{-1}) was reported by Biggs (1996) for macrophyte dominance. Hoyer et al. (2004) found unfavorable conditions for both macrophytes and macroalgae in three west Florida springs at velocities exceeding only 25 cm s^{-1} (0.82 ft s^{-1}), a threshold similarly reported by King (2014) for macroalgae. Franklin (2008) reported peak vegetative abundance in stable streams occurring in the range of 30 – 50 cm s^{-1} (0.98 – 1.64 ft s^{-1}. This optimal range is particularly interesting given that SAV generally is absent when inter-flood velocities exceed 70 cm s^{-1} (2.3 ft s^{-1}). An optimum velocity range for SAV in Silver River may be constrained, then, to a fairly narrow velocity range of 25 – 70 cm s^{-1} (0.8 – 2.3 ft s^{-1}), below which the macrophyte beds are subject to invasion by macroalgae, and above which the macrophyte beds cannot withstand the drag forces.

Flow resistance within the river channel, of course, directly effects velocity since greater flow resistance lowers velocity and increases stage and depth of the river for a given discharge. After the year 2000, Silver River experienced a distinct shift in its stage/discharge relationship (Figure 5.4.1) with increased stage for lower discharge. If flow resistance in Silver River was dominated by wall resistance alone, then stage would have decreased with lower discharge. Wall resistance could not, then, be the cause of the change to the stage/discharge relationship. The altered stage/discharge relationship must instead be a result of a change to vegetative drag.

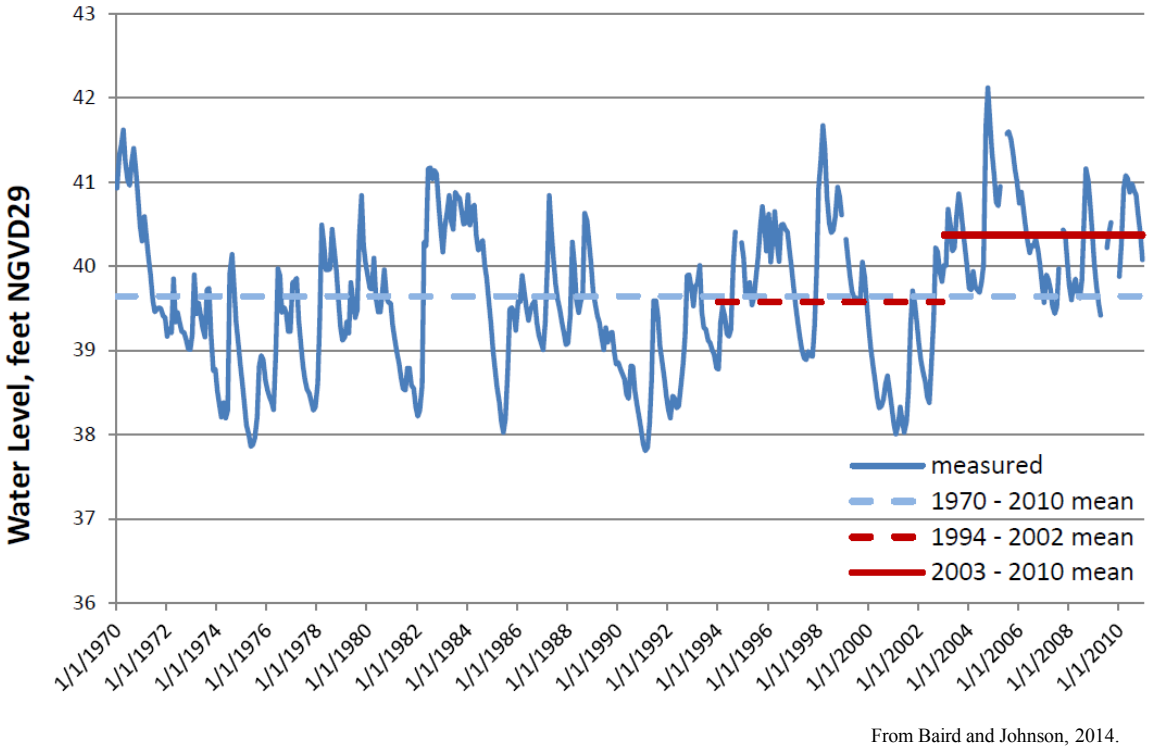

From Baird and Johnson, 2014.

Figure 5.4.1. Monthly mean water level, 1970 to 2010, at the Silver Spring pool (USGS 02239500).

The hydrodynamic analysis required to address the above issues must include mechanisms accounting for vegetative drag, spatial gradients of velocity, turbulent shear stress at the top of macrophyte beds, and turbulence intensity. The range of hydrodynamic mechanisms needed warrants the use of a three-dimensional hydrodynamic model. Numerical turbulence models were first developed to solve the turbulent flow field with incorporation of both form drag and vegetation effects on turbulence. Aquatic vegetation properties of density, height and stem diameter were used as model inputs. Drag coefficients were obtained by comparison with both laboratory experiments and field measurements. After testing, a final turbulence model was then adapted to a three-dimensional hydrodynamics model, Environmental Fluid Dynamics Code (EFDC; Hamrick 1992), to predict unsteady water level, velocity profiles and estimate turbulent shear stress within the heavily vegetated Silver River.

Numerical tests using EFDC illustrate the dominance of vegetative drag on flow resistance, consistent with the general hydrodynamic analysis of Luhar et al. (2008). Numerical tests also illustrate the relative sensitivity of model stage (and hence resistance) to vegetative bed height and the relative insensitivity to stem density. The sensitivity of Silver River stage to bed height points to reconfiguration of vegetation as a possible cause of the altered stage/discharge relationship after the year 2000. Reconfiguration refers to changes in the resistance of vegetation to flow as velocity increases because of greater streamlining at higher velocity (Vogel 1994).

Reconfiguration can result from either a change in frontal area exposed to the flow (caused by plant bending) or streamlining of plant blades allowed by the plant's flexible tissues (Luhar et al. 2013). Reconfiguration, then, is an alternative hypothesis to increased areal coverage and biomass for explaining the unusual shift of stage/discharge relationship as discharge dropped following the 1999–2000 droughts.

Our hydrodynamic analyses and hydrodynamic model development, then, are aimed at understanding the important factors dynamically influencing velocity in Silver River. This understanding will help us determine whether velocity is an important non-nitrate factor influencing the community structure and function of primary producers in Silver River, with an ultimate goal of improving our understanding and providing management recommendations on how velocity in this system affects the ecological health and ecosystem services of the river.

5.4.2 REVIEW OF VEGETATIVE FLOW RESISTANCE

Historically the primary purpose of engineering research on the effects of vegetation on flow has been limited to resistance estimation in streams and flood plains (Arcement and Schneider, 1990). These early studies generally assessed vegetation effects using bulk energy loss coefficients, such as Manning *n*, Darcy-Weisbach f or Chezy C, because of their ease of application and demonstrated validity. The effects of flow conditions and vegetation properties are normally incorporated in these coefficients from empirical formulations or other regression techniques. Of these energy loss coefficients, Manning *n* is most frequently used in the computation of open-channel and overland flows.

Guidance for selection of Manning *n* coefficients was provided by Arcement and Schneider (1990) with an emphasis on unsubmerged vegetation on flood plains. For floodplains with nonrigid and unsubmerged vegetation, Manning *n* increases proportionally to the square root of flow depth regardless of tree species, or foliage shape and distribution due to the increase of submerged momentum absorbing area with depth of flow (Fathi-Maghadam and Kouwen 1997). Density of vegetation is always a dominant parameter, then, under nonsubmerged conditions.

Flow resistance by submerged vegetation, in contrast, has a strong dependence on the height of the vegetative bed. For flexible vegetation, bed height is variable, depending on flow conditions, and is defined as the projection of the vegetation in the direction perpendicular to the water flow and often termed "*effective vegetative height*" (Kutija and Hong 1996). The dependence of flow resistance on effective vegetative height often leads to a lowering of friction coefficients at higher flow velocities. This phenomenon is long known from the classical use of empirical *n*-VR curves for estimating flow resistance in vegetated channels (Kouwen 1992) which relate Manning *n* to the product of cross-sectionally averaged velocity and hydraulic radius. Wu (1999) pointed out that, given relatively constant kinematic viscosity, VR is directly related to a Reynolds number with hydraulic radius (often channel depth) the characteristic length. Wu (1999) further noted that Manning *n* decreases with flow depth for flexible submerged vegetation but increases with flow depth for unsubmerged vegetation. Carollo et.al (2005) expanded on this research to develop a flow resistance law for channels with flexible submerged vegetation that depended on a shear Reynolds number, the depth-vegetation height ratio and the degree of

vegetation inflection. The shear Reynolds number is defined for inside the vegetated bed and uses the effective vegetative height as the characteristic length.

Although the Manning Equation with dynamic alteration of Manning *n* can be used to assess the bulk frictional resistance of a vegetated channel, it is difficult to apply as a predictive tool and it does not provide information about either flow structure or turbulence intensity (Nepf 1999) that directly affect transport processes for sediments and nutrients in the water. For this reason, numerous numerical modeling efforts have focused on understanding vegetative effects on velocity profiles and turbulent characteristics (Lopez and Garcia 2001; Choi and Kang 2003; Defina and Bixio 2005; Gao et al. 2011; Dimitris and Panayotis 2011). This modeling focus is a move away from lumped friction parameterizations to physically based laws describing each component contributing to the energy loss source term in the Navier-Stokes equations. Because of the complex nature of the interaction between vegetation and flow, some assumptions and parameterizations are normally made for these conceptual and mathematical models. In general, uniform flow conditions are assumed and vegetation spatial variations are not considered. As the wake turbulence generated by vegetation has a larger effect on vertical than on horizontal mixing, turbulence closure modeling is simplified to a one-dimensional, rather than a fully three-dimensional, model structure. Bottom friction from roughness is often neglected because near-bottom velocities are small in the presence of vegetation and drag force becomes the major contributor to total resistance (Luhar and Nepf 2013).

Two principal one-dimensional model types have been used to describe the flow and turbulence structure within and above a vegetated canopy: two-layer and modified turbulence κ-ε models. A two-layer model determines flow velocity profiles in two separate layers, the bottom vegetated layer and the upper layer above the vegetation. For this model type, the momentum equation is solved in the vegetated layer by mixing length turbulent theory and vegetation drag. In the upper layer, a logarithmic velocity profile is assumed (Defina and Bixio 2005). The parameters of the log law are determined by matching the continuity of velocity and shear stress at the interface. The characteristic length of turbulence is obtained from a semi empirical model (Klopstra et al. 1997; Meijer and van Velzen 1999; Righetti and Armanini 2002; Defina and Bixio 2005). The two-layer model can only be applied to steady state system with uniform vegetation distribution and constant drag coefficient.

A modified turbulence κ-ε model accounts for vegetative drag through both a momentum equation and turbulence equations for κ (turbulent kinetic energy) and ε (dissipation rate) (Lopez and Garcia 2001; Stoesser et al. 2004; Defina and Bixio 2005). The coefficients for drag-related source terms in κ and ε turbulence equations are determined empirically. For a one dimensional κ-ε model, both vegetation density and drag coefficient can vary vertically.

Both the two-layer model and one-dimensional κ-ε model were tested for Silver River as a progression towards a fully three-dimensional model. Both models reasonably reproduced vertical velocity profiles and shear stress obtained from laboratory experiments. (Figure 28 in Section 5.3 shows results from the κ-ε model). These one-dimensional models, however, are not practical for direct application to Silver River for two reasons. First, the pressure gradients required for boundary conditions are generally not available to solve for velocity profiles at a given location. Second, these models cannot account for varying flow patterns caused by

spatially varying shoreline, bathymetry and vegetation characteristics. The methodologies developed from these one-dimensional models were thus incorporated into a fully three-dimensional circulation model EFDC (Environmental Fluid Dynamics Code) to simulate flows and turbulence in the highly vegetated Silver River system.

5.4.3 DESCRIPTION OF STUDY AREA

The study area for the hydrodynamic analysis is the Silver River main-stem, the back channel and boat basin (Figure 5.4.2). Nearly all discharge enters Silver River through a complex of spring vents at the head. USGS monitors discharge just below this complex at the "3,900 ft stage" approximately 1,200 m from the head pool and immediately downstream of the back channel exit. The Silver River enters the Ocklawaha River about 8 km (4.97 miles) below the head pool. The Ocklawaha River water level at the confluence ranges over 2 m (6.5 ft) and backwater effects are observed in Silver River as far as the head pool.

SJRWMD has monitored water level at ten locations in Silver River (S1 through S10) since June 2007 (Figure 5.4.2). USGS monitors four additional locations with long-term monitoring near the head pool (1947 to present) and at the Hwy 40 Bridge at Conner (1963 to present). These locations are listed as "Pool Stage" and "Ocklawaha Stage, Discharge" in Figure 5.4.2. Silver River discharge at the 1,200 m station also has a long-term record with daily discharge available from 1933 to present.

5.4.4 MATERIALS AND METHODS

5.4.4.1 Defining the Shoreline

A critical component for a robust model is an accurate representation of the model domain, in this case the shoreline of the mainstem and back channel of the Silver River. Use of aerial imagery for discerning the shoreline suffered from spatial inaccuracies in this relatively small system. The forested canopy that overhangs the river also obscures a significant percentage of the open water surface further compounding the difficulty of using aerial imagery. The District's 1:24,000 GIS Hydrography layer was (likely) developed from 1984 aerials and is not sufficiently accurate for hydrodynamic analysis of the river. Thus, we developed an alternative shoreline for the study area specifically designed for the hydrodynamic analyses of the river.

The new shoreline coverage was created by first mapping the navigable "open edge" of flow and then using a horizontal offset based on shoreline type to estimate the location of the zero flow boundary (hereafter termed the *flow boundary*). Kayaks with mounted GPS units were used to trace the open edge during June 2014. Any areas too shallow or with too dense of vegetation for passage by kayak generally contribute minimally to total river discharge. A GPS antenna was mounted on a rod tall enough to clear the operator but low enough to avoid overhead obstructions. The GPS antenna was connected to a handheld Trimble Pathfinder. A Garmin 441s was used to collect additional waypoints of features of interest, and a description was noted for each waypoint in a field journal. A shape file was produced from the waypoints. Two kayaks were employed so that both north and south banks could be mapped simultaneously. The kayaks were maneuvered typically within half paddle length (ca.1 m) from the water edge or as far as could be reached along the shoreline to map the open edge of flow.

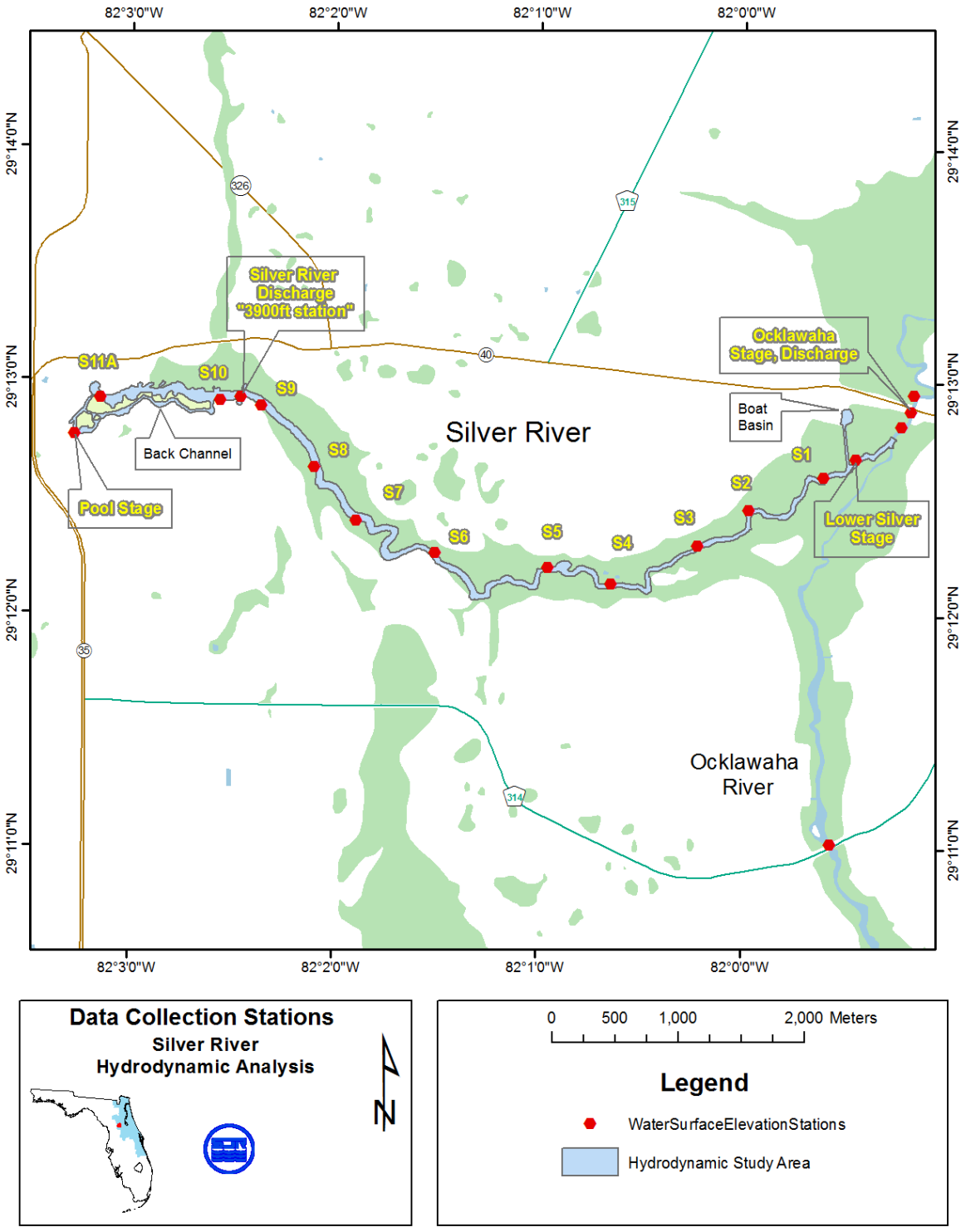

Figure 5.4.2. Study area for the hydrodynamic analysis of Silver River comprising the main river channel, back-channel, and boat basin. SJRWMD collects water surface elevation at ten stations in Silver River (stations S1 through S10). USGS collects water surface elevation at four additional locations denoted "Pool Stage", "1,200 m station", "Lower Silver Stage", and Ocklawaha Stage, Discharge" in the figure.

Shoreline types were categorized into three classes: hardened, abrupt, and gradual. Hardened shorelines with concrete headwalls are found in the head pool and the boat basin at the lower end (Figure 5.4.3). The remainder of the river shoreline is either an abrupt shift to uplands in excavated areas of canals, the back channel, and along the edge of Indian mounds or a gradual transition from open water to forested wetlands (Figure 5.4.4).

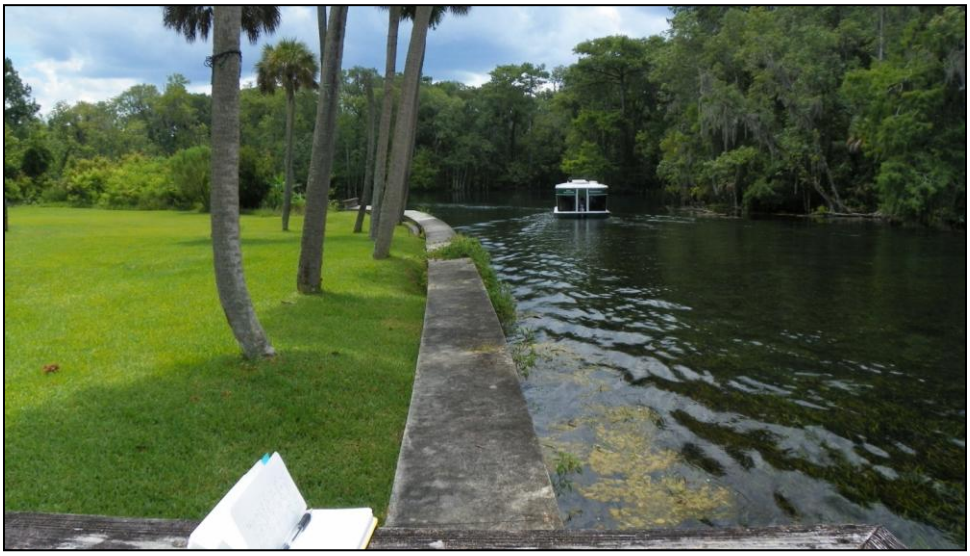

Figure 5.4.3. Hardened shoreline in Silver River just downstream of the head pool.

Figure 5.4.4. Gradual shoreline adjacent to forested wetland.

Tree canopy sometimes interfered with the GPS antennae and satellites requiring remapping of affected areas during times of more advantageous satellite geometries. In some areas, floating vegetation mats and logs blocked surface flow, but obviously allowed subsurface flow. For these areas the open edge was extrapolated across to the next good open edge location.

5.4.4.2 Defining Bottom Type

Bottom types were mapped at the spatial scale of the hydrodynamics model grid for two primary purposes: first, to guide the interpretation of remotely-sensed vegetative heights using Sonar, and second, to guide selection of stem density. We are presently collecting Sonar data using a Sontek M9 Acoustic Doppler Current Profiler. This device is assumed to measure depth to the top of vegetation in areas of high vegetative cover. In these areas, the measured depths must be corrected for vegetative bed height. In bare or sparsely vegetated areas no correction to depth is required. Areas with topped out vegetation cannot be measured using Sonar. Estimation of stem density will be based on an established relationship with Braun-Blanquet number (Munch et al. 2006). For this reason, bottom types were established to be consistent with the Braun-Blanquet classification, with allowances for horizontal scale.

Where water clarity was sufficient (primarily the upper half of the river above S-6) visual inspection was made by boat. In the lower river (below S-6), high turbidity obscured the bottom and inspection was made using a GoPro camera mounted on a 10-ft PVC pole.

Bottom types were classified into six categories: bare, patchy, vegetated, heavily vegetated, topped out, and with trees. General category definitions are as follows:

1. ***Bare*** Sandy, rocky, or muddy bottom with less than 5 % rooted vegetation. Logs may be present.

2. ***Patchy*** Clumped, thin, or widely spaced vegetation.

3. ***Vegetated*** Continuously vegetated with the bottom mostly obscured; open water above canopy deeper than 1 m.

4. ***Heavily Vegetated*** Continuously vegetated with the bottom mostly obscured; vegetation takes up the majority of the water column.

5. ***Topped Out*** Vegetation reaches completely to the surface; emergent vegetation may be present.

6. ***Trees*** Extensive roots and trunks of cypress and other trees.

5.4.4.3 Model Grid Development

A curvilinear, orthogonal boundary-fitted grid was developed jointly by Jones Edmunds Associates, Janicki Environmental, and SJRWMD. The grid encompassed the open edge and followed the flow boundary as much as was practical for maintaining orthogonality (Figure 5.4.5).

The model grid consists of 13,439 horizontal cells and 8 vertical cells for a total of 107,512 cells. The total surface area of the grid is 108.12 acres (437,546.12 m²), which includes 3.58 acres (14,487.75 m²) for the boat basin and 15.0 acres (60,702.8 m²) in the back channel. Cell area generally increases from upstream to downstream with an average cell area of 29.4 m^2 in the upper third of the river (Figure 5.4.6, Map A), 30.2 m^2 in the middle third (Figure 5.4.6, Map B), and 41.5m^2 in the lower third (not shown). The average horizontal cell length is 5.8 m.

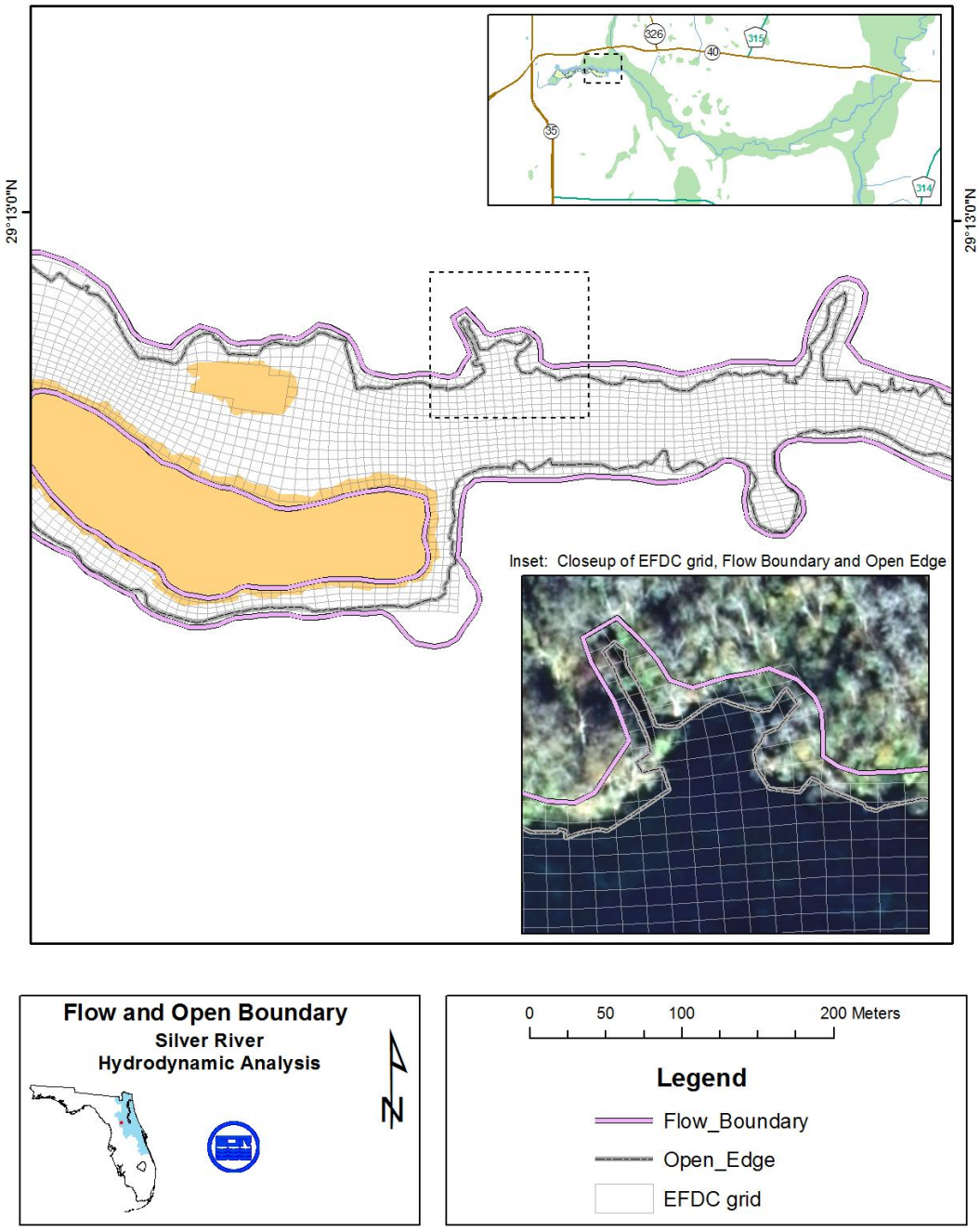

Figure 5.4.5. Model grid detail with open edge boundary and shoreline ("flow boundary") used to guide the gridded area.

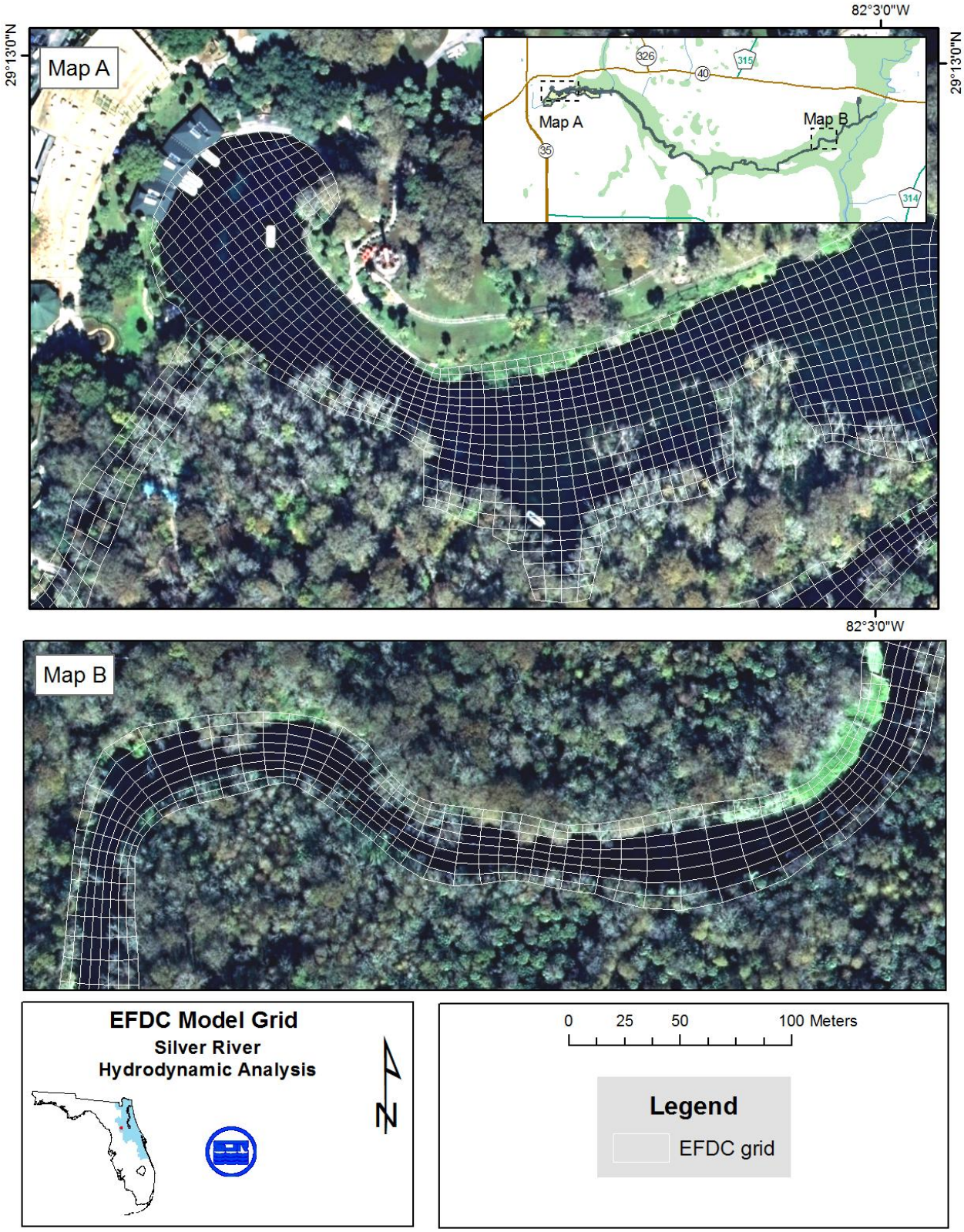

Figure 5.4.6. Final hydrodynamic model grid in head pool (upper plot, Map A) and lower river (lower plot, Map B).

5.4.4.4 Formulation of the Governing Equations for EFDC With Vegetation

The formulation of the governing equations of EFDC is developed for an incompressible, variable density fluid to account for the effects of submersed vegetation on drag and turbulence. In horizontal, the equations are formulated in curvilinear and orthogonal coordinates to accommodate realistic boundaries. In vertical, a time variable mapping or stretching transformation is used to provide uniform vertical resolution with changing depth.

The momentum and continuity equations from Hamrick (1986) are adjusted to incorporate the vegetation effect and can be written in the following form:

$$\partial_t(mHu) + \partial_x\left(m_y Huu\right) + \partial_y(m_x Hvu) + \partial_z(mwu) - \left(mf + v\partial_x m_y - u\partial_y m_x\right)Hv$$
$$= -m_y H\partial_x(g\zeta + p) - m_y(\partial_x h - z\partial_x H)\partial_z p + \partial_z(mH^{-1}A_V\partial_z u) + Q_u - c_t\sqrt{u^2+v^2}umH \qquad (5.4.1)$$

$$\partial_t(mHv) + \partial_x\left(m_y Huv\right) + \partial_y(m_x Hvv) + \partial_z(mwv) + \left(mf + v\partial_x m_y - u\partial_y m_x\right)Hu$$
$$= -m_x H\partial_y(g\zeta + p) - m_x(\partial_y h - z\partial_y H)\partial_z p + \partial_z(mH^{-1}A_V\partial_z v) + Q_v - c_t\sqrt{u^2+v^2}vmH \qquad (5.4.2)$$

$$\partial_z p = -gH(\rho - \rho_0)\rho_0^{-1} = -gHb \qquad (5.4.3)$$

$$\partial_t(m\zeta) + \partial_x\left(m_y Hu\right) + \partial_y(m_x Hv) + \partial_z(mw) = 0 \qquad (5.4.4)$$

$$\partial_t(m\zeta) + \partial_x\left(m_y H\int_0^1 udz\right) + \partial_y\left(m_x H\int_0^1 vdz\right) = 0 \qquad (5.4.5)$$

$$\rho = \rho(p, S, T) \qquad (5.4.6)$$

In these equations, u and v are the horizontal velocity components in the curvilinear, orthogonal coordinates x and y, m_x and m_y are the square roots of the diagonal components of the metric tensor, $m = m_x m_y$ is the Jacobian or square root of the metric tensor determinant. The vertical velocity, with physical units, in the stretched, dimensionless vertical coordinate z is w. H is total depth, ζ is surface elevation, f is the Coriolis parameter, p is the physical pressure in excess of the reference density hydrostatic pressure, $\rho_o gH(1- z)$, divided by the reference density, ρ_o, A_v is vertical eddy viscosity, and Q_u and Q_v are momentum source-sink terms which will be later modeled as subgrid scale horizontal diffusion. The density, ρ is in general a function of temperature, T, and salinity, S. The buoyancy, b, is defined as the normalized deviation of density from the reference value. The continuity equation has been integrated with respect to z over the interval (0, 1) to produce the depth-integrated continuity equation. The total drag coefficient from vegetation is defined as:

$$c_t = \begin{cases} \frac{1}{2}C_D A_z \lambda & z \le h_p \\ 0 & z > h_p \end{cases} \qquad (5.4.7)$$

Where C_D is form drag coefficient, A_z is frontal plant area per unit depth, λ is the number of stems per unit area, and h_p is plant height.

To provide the vertical turbulent viscosity and diffusivity, the second-moment turbulence closure model developed by Mellor and Yamada (1982) and modified by Galperin et al. (1988) is used. The model relates the vertical turbulent viscosity and diffusivity to the turbulent intensity, qq, a turbulent length scale, l, and a Richardson number R_q by:

$$A_v = \phi_v ql = 0.4\left(1 + 36R_q\right)^{-1}\left(1 + 6R_q\right)^{-1}\left(1 + 8R_q\right)ql \tag{5.4.8}$$

$$A_b = \phi_b ql = 0.5\left(1 + 36R_q\right)^{-1}ql \tag{5.4.9}$$

$$R_q = \frac{gH\,\partial_z b}{q^2}\frac{l^2}{H^2} \tag{5.4.10}$$

where the so-called stability functions ϕ_v and ϕ_b account for reduced and enhanced vertical mixing or transport in stable and unstable vertically density stratified environments, respectively. The turbulence intensity and the turbulence length scale are determined by a pair of transport equations:

$$\partial_t(mHq^2) + \partial_x\left(m_y Huq^2\right) + \partial_y(m_x Hvq^2) + \partial_z(mwq^2) = \partial_z\left(mH^{-1}A_q\partial_z q^2\right) + Q_q$$

$$+2mH^{-1}A_V((\partial_z u)^2 + (\partial_z v)^2) + 2mgA_b\partial_z b - 2mH(B_1 l)^{-1}q^3 + c_{fq}c_t(u^2 + v^2)umH \tag{5.4.11}$$

$$\partial_t(mHq^2 l) + \partial_x\left(m_y Huq^2 l\right) + \partial_y(m_x Hvq^2 l) + \partial_z(mwq^2 l) = \partial_z\left(mH^{-1}A_q\partial_z q^2 l\right) + Q_l$$
$$+mH^{-1}E_1 lA_V((\partial_z u)^2 + (\partial_z v)^2) + mgE_1E_3 lA_b\partial_z b - mHB_1^{-1}q^3(1 + E_2(\kappa L)^{-2}l^2) + c_{fl}c_t(u^2 + v^2)umHl \tag{5.4.12}$$

with,

$$L^{-1} = H^{-1}(z^{-1} + (1 - z)^{-1}) \tag{5.4.13}$$

and where B1, E1, E2, and E3 are empirical constants, and Q_q and Q_l are additional source-sink terms for subgrid scale horizontal diffusion. The vertical diffusivity, A_q, is in general taken equal to the vertical turbulent viscosity, A_v. The last term in equation (5.4.11) and (5.4.12) account for the presence of vegetation.

5.4.5 RESULTS AND DISCUSSION

5.4.5.1 Bottom Type

Bottom types associated with each hydrodynamic model grid cell are shown in Figure 5.4.7 for two representative areas. The percentage of each bottom type over the entire 108.1 acres (437,465.18 m²) contained within the hydrodynamic model grid is 8.5 % bare, 17.7 % patchy, 37.6 % vegetated, 8.7 % heavily vegetated, 14 % topped out, and 13.5 % trees. The river is highly vegetated; slightly more than 60 % of the model area is completely covered with vegetation and 78 % of the area contains at least some submersed aquatic vegetation.

Present day coverage in the upper 1,200 m (¾ mile) near the headspring is similar to that observed by Odum (1957) and Munch et al. (2006). The extensive vegetative cover in the lower river, however, is in stark contrast to the lack of SAV reported in the early 1950s by both Odum (1957) and Whitford (1956).

The large spatial coverage of present day Silver River by aquatic plants is confirmed also by vegetation surveys made along several transects perpendicular to the channel (Figure 5.4.8). Vegetation tends to be absent in deeper areas of the river. The deep thalweg in the lower river, for example, was often bare as were the deep holes near S-1. Odum (1957) noted that *Sagittaria kurtziana* was not found in depths greater than 15 feet (4.5 m). We similarly observed few macrophytes of any kind below 4.5 m (15 ft) and none deeper than 5.5 m (19 ft).

5.4.5.2 Hydrodynamic Model Tests

The EFDC model modified for vegetation effects was tested using observed conditions of 29 May 2014 when discharge was 17 $m^3 s^{-1}$ (605 cfs) and the downstream stage was 10.75 m (35.27 ft) NAVD88 at Conner. Water elevations were observed at ten stations along the river (S1 to S10). In addition to testing EFDC with the added vegetation algorithms, we simulated stage using the original EFDC model formulated with the Manning Equation. A Manning *n* of 0.5 was used to conservatively represent flow resistance by dense, extensive SAV coverage. Although this value of Manning *n* is extreme (five times greater than the largest value suggested by Arcement and Schneider 1990), the original EFDC model could not generate friction sufficient to explain the elevation drop of the river. The observed elevation drop of the river from head to mouth was 1.3 m and the simulated drop using Manning *n* was only 0.5 m. The EFDC model modified to include the effects of SAV drag significantly improved the simulated elevation drop (Figure 5.4.9, black line). The simulated elevation drop using the modified EFDC model was 1.2 m, in close agreement to observations. We note that this is at present an uncalibrated model that should be significantly improved when more realistic bathymetry and spatially varying vegetation characteristics are developed for the CRISPS project.

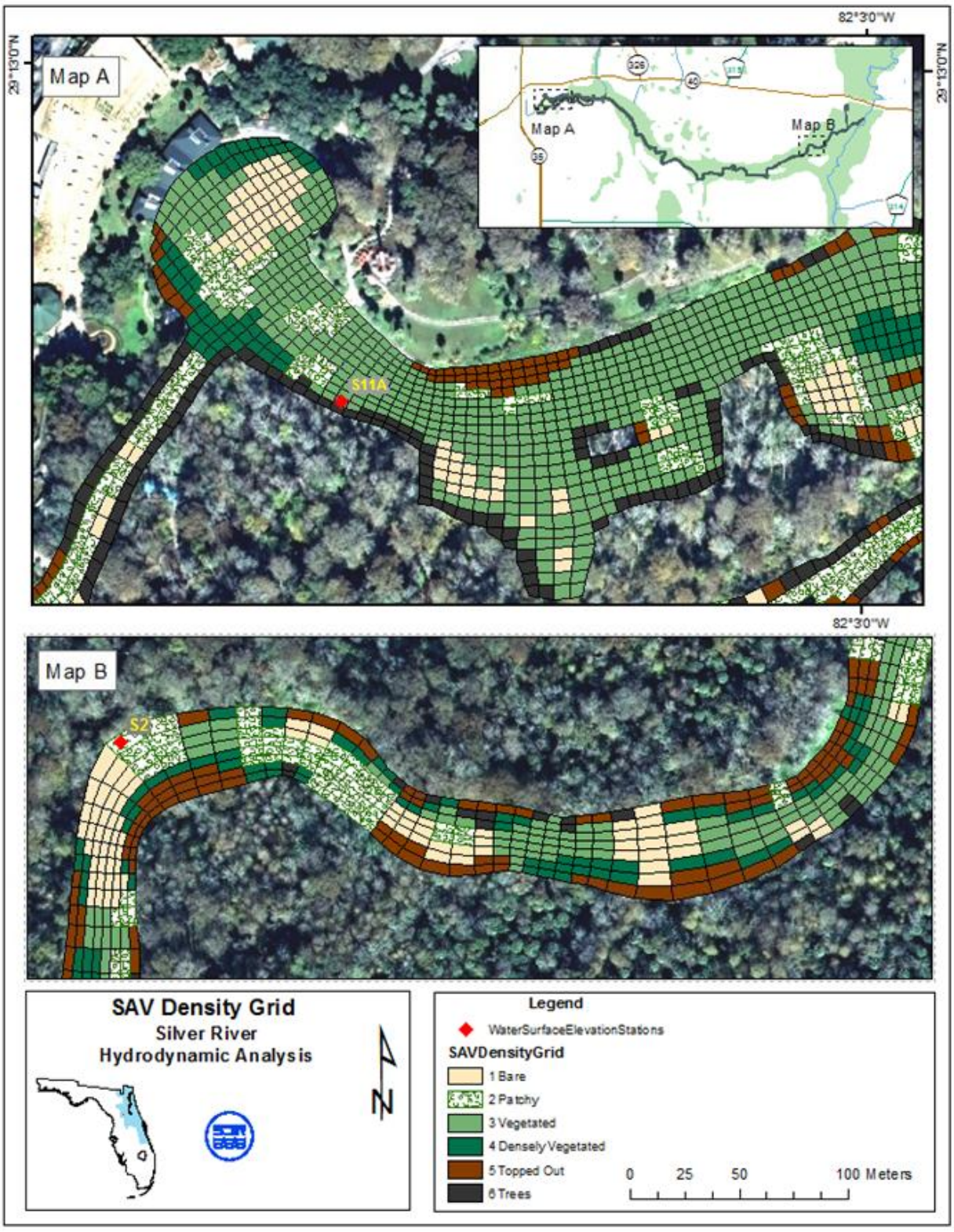

Figure 5.4.7. Bottom type of Silver River assigned to each hydrodynamic model cell.

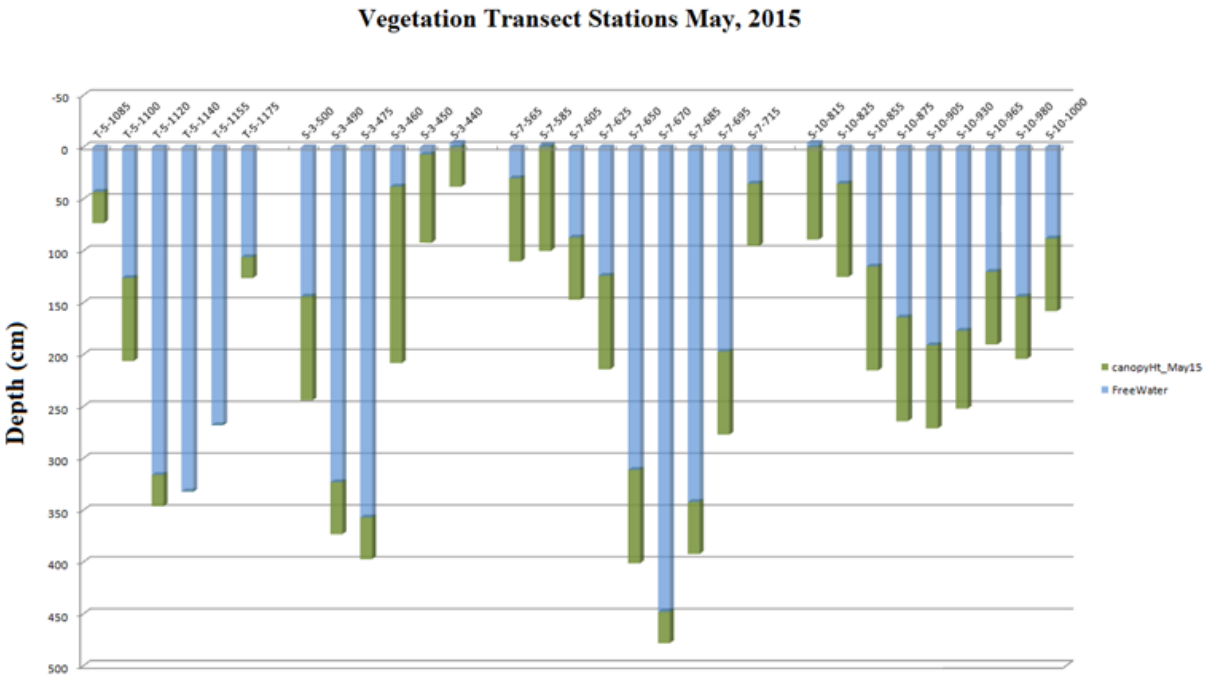

Figure 5.4.8. Fraction of bottom vegetation (green) compared with open water above the canopy (blue) at four transects. Transect T3 is in the Ocklawaha River just downstream of the Silver river mouth. Transects S-3, S-7, and S-10 are in the lower, middle, and upper portions of the Silver River, respectively.

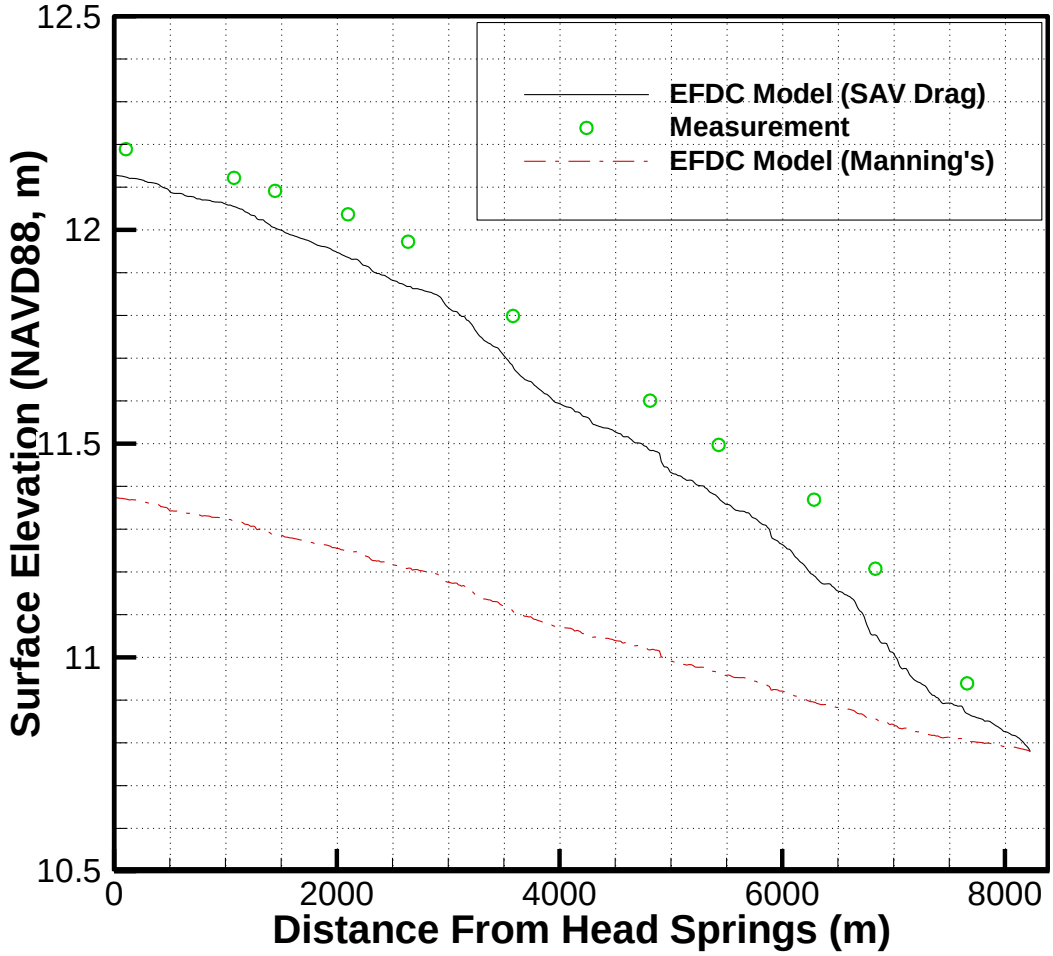

Figure 5.4.9. Comparison of simulated and observed water elevation along Silver River for a discharge of 605 cfs (17.13 m^3 s^{-1}). Green circles are observed water level, dashed red line is simulated water level without submersed vegetation, and the solid black line is with submersed vegetation.

Model sensitivity was tested for two vegetative parameters, effective vegetative height and vegetation density, on water elevation. For context, the sensitivity of water elevation to river discharge was also tested. Values for each of the two vegetative parameters and river discharge were varied ±30 %. The results (Figure 5.4.10) imply that for the same percentage change of parameter, the model is more sensitive to effective vegetative height than to vegetative density. Interestingly, altering effective vegetative height had nearly an equivalent effect on water elevation as altering river discharge. These results illustrate the possible importance of reconfiguration for prediction of water elevation in Silver River.

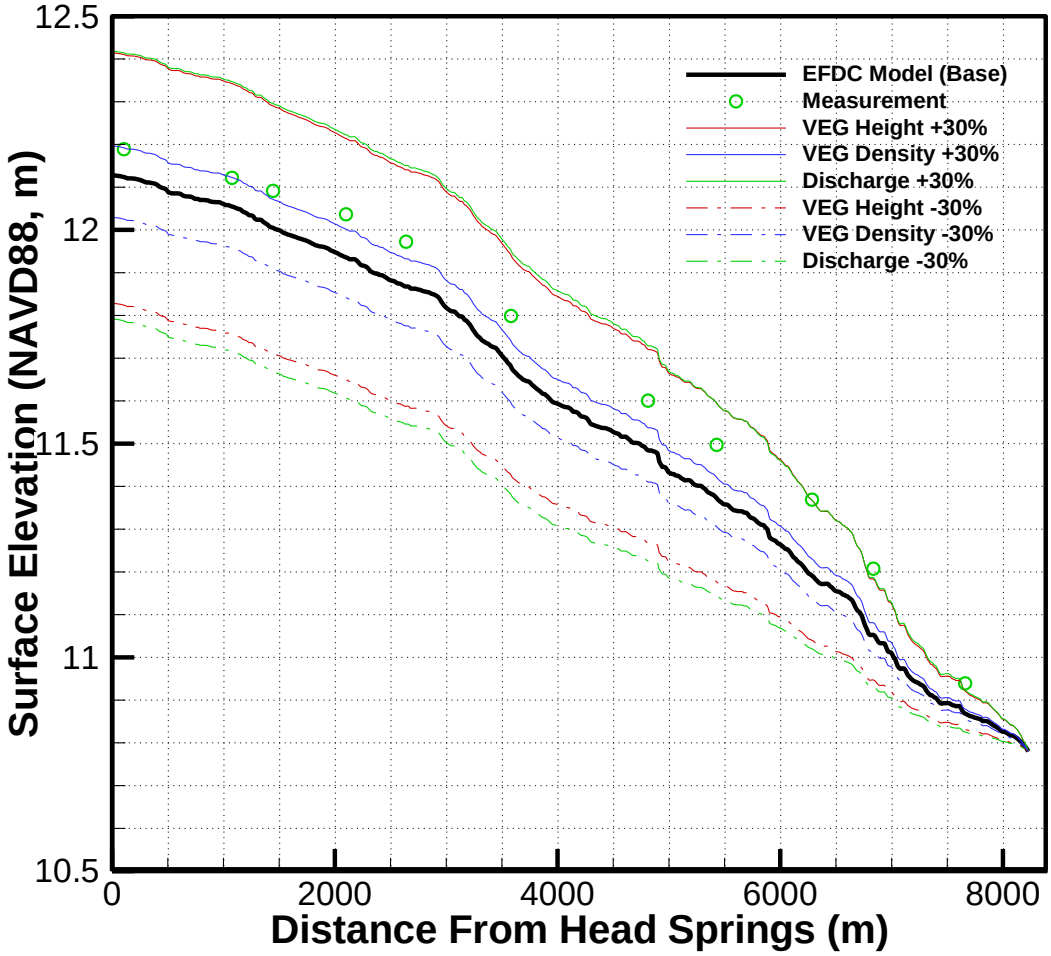

Figure 5.4.10. Sensitivity of simulated water elevation along Silver River to ±30 % changes in effective vegetative height, vegetative density and river discharge in comparison to a base test case.

5.4.5.3 Cause of Altered Stage/Discharge Relationship of Silver River

Determining the causes of the altered stage/discharge relationship of Silver River following the year 2000 has practical value since this understanding will allow us to understand how vegetation controls both stage and velocity throughout the river. At present, we have identified three possible causes: (a) expansion of vegetative coverage and/or density, (b) reconfiguration of vegetation under lower velocities, and (c) expansion of hydrilla in the lower Silver River and adjacent Ocklawaha River.

Historic observations of vegetative cover in the lower Silver River are sparse. Only recently have studies addressed the ecosystem structure of the lower Silver River (Wetlands Solutions 2012; Wetlands Solutions 2014). Little information exists, then, for the lower Silver River prior to 2012 regarding SAV abundance, community structure, vegetative cover presence or absence of

vegetation, or even the general structure of the river channel.

Two descriptions, provided verbatim, indicate a distinct absence of SAV in the early 1950s:
Whitford (1956):

> "After the first mile Silver Springs run becomes narrow and the banks heavily wooded. It also receives some brown water down run. Consequently *about 2 ½ miles from the boil flowering plants largely disappear* probably due to reduced light. Mats of Vaucheria with some filamentous blue-green algae, and a few of the usually dominant diatoms, are abundant in the shallows. The deeper channel has *relatively little plant life*."

Odum (1957):

> "Except for its thick bed of rich muck Silver River would be a rushing canal through a pipe of limestone rock. *Further downstream below the study area it is of this nature*"

Odum is describing the substrate underlying *Sagittaria* beds in the head pool region when the total river discharge was about 930 cfs (26.28 $m^3 s^{-1}$) with a velocity of 0.21 m s^{-1} (0.69 ft s^{-1}) and a cross-sectional area of 125.1 m^2. He concludes the sedimentation rate is balanced by organic matter decomposition and downstream transport. The net sedimentation balance observed by Odum is consistent with Hoyer et al. (2004) who found a gradient of bottom sediment from "mud, mud/sand, sand and rock substrates" over a velocity gradient of 0.08, 0.11, 0.16 and 0.22 m s^{-1} (0.26, 0.36, 0.52 and 0.72 ft s^{-1}), respectively.

Importantly, they found "little or no SAV" above a velocity of approximately 0.25 m s^{-1} (0.82 ft s^{-1}). Velocity in the lower river would easily have exceeded this threshold during the high discharges of the 1950s. Scaling the characteristic velocities shown for the lower river in Table 2 Ch 6.1, for example, results in a characteristic velocity of 0.32 m s^{-1} (1.05 ft s^{-1}) in the lower river. It seems possible, then, that velocity may play a role in determining vegetative structure and density in portions of Silver River, especially downstream where the typical stream cross-section is smaller producing higher velocity for a given discharge. The absence of vegetation observed by Odum (1957) and Whitford (1956) in the lower river may have been a result of higher stream velocities.

It is tempting, then, to explain the stage/discharge shift about the year 2000 as a sudden expansion of vegetative cover in the lower river as discharge and velocity decreased. Such a supposition is not supported by the limited available data, however. Over a decade prior to 2000, Duarte et al. (1990) observed SAV biomass at four locations throughout the length of Silver River and found macrophytes present throughout the lower river. Vegetation survey data by the Florida Fish and Wildlife Commission (FWC 2014) also indicate a continued presence of macrophytes in the lower river at least since 1990. Finally, it seems uncharacteristic of a river known for its remarkable stability (Odum 1957) to experience a rapid change in its SAV coverage.

A sudden expansion of SAV in the Silver River about the year 2000, then, seems unlikely to be the sole cause of the 2000 stage/discharge shift. There is some evidence that river stage in the Ocklawaha River has recently been elevated due to blockage by hydrilla, but FWC (2014) data

indicates that expansion of hydrilla in the Silver River is a recent phenomenon, perhaps only becoming appreciable since 2011. This observation does not discount the possibility of blockage by hydrilla in the Ocklawaha River. An analysis of stage/discharge at Conner is presently underway to examine this possibility. Preliminary results, however, seem to indicate that flow blockages by hydrilla in the Ocklawaha River are transient and blockages are removed during high discharge events. If this preliminary result holds, the blockage of the Ocklawaha River by hydrilla is unlikely to be more than a secondary factor influencing the stage/discharge of Silver River.

Finally, model results have demonstrated that reconfiguration can have an appreciable effect on stage under lowering discharge as occurred during the prolonged drought of 1999 through 2000. This correlation of events and subsequent continued decline in discharge supports the reconfiguration hypothesis. We expect, though, that each of the three factors may have played a role to some extent. Reconfiguration of vegetation as an important mechanism for predicting stage and velocity changes in Silver River has not been widely discussed, however, and we emphasize it here for the benefit of its proper consideration.

5.4.6 CONCLUSIONS AND RECOMMENDATIONS

Flow resistance in Silver River is dominated by vegetative drag. A three-dimensional hydrodynamic model that accounts for vegetative drag and turbulence was successfully implemented and tested for Silver River. The model provides a methodology for estimating velocity profiles, shear stresses, and dispersion throughout the river, especially for conditions outside of present day observations, and provides a means to test the efficacy of proposed management scenarios.

A distinct shift in discharge-stage relationship in Silver River that occurred about 2000 is likely a result of some alteration to vegetative characteristics. Preliminary analyses show three possible mechanisms, perhaps in combination, could account for this change. These three mechanisms are as follows:

- Increased spatial coverage of submersed aquatic vegetation
- Reconfiguration of vegetation under low discharge conditions
- Expansion of hydrilla in the lower Silver River and Ocklawaha River near Conner.

Work should continue to separate the relative importance of these mechanisms using available hydrologic data over as much of the historic flow record as practical. These results would inform management decisions concerning appropriate baselines, spring flow management, and conceptual project development. Finally, quantification of the relative importance of the highly altered Ocklawaha River flow regime on Silver River stages and velocities can guide potential development of a “designed hydrograph” for this managed system or at least determine the practical limitations to restoration targets or management goals.

5.4.7 REFERENCES

Arcement, G. J. and Schneider, V. R. 1990. *Guide for Selecting Manning's Roughness Coefficients for Natural Channels and Flood Plains*, United States Geological Survey Water-supply Paper 2339.

Baird, S. F. and Johnson, N. T. 2014. Guide to Silver River Hydrologic Data. St. Johns River Water Management District, Palatka, FL. May 2014. 59 pp.

Biggs, B. J. F. 1996. Hydraulic habitat of plants in stream. Regulated Rivers: Research and Management. Vol. 12: 131–144.

Biggs, B. J. F., Goring, D. G., and Nikora, V. I. 1998. Subsidy and stress responses of stream periphyton to gradients in water velocityas a function of community growth form. J. Phycol., 34: 598–607.

Carollo, F. G., Ferro, V., and Termini, D. 2005. Flow resistance law in channels with flexible submerged Vegetation". Journal of Hydraulic Engineering, Vol. 10: 554–564.

Choi, S. and Kang H. 2003. Reynolds stress modeling of vegetated open channels. J. Hydr. Res., Vol. 42(1): 3–11.

Defina, A. and Bixio, A. C. 2005. Mean flow and turbulence in vegetated open channel flow. Water Resources Res., 41: W07006, 12 pp.

Dimitris, S. and Panayotis, P. 2011. Macroscopic turbulence models and their application in turbulent vegetated flows. J. Hydraul. Eng., 137: 315–332.

Fathi-Maghadam, M., and Kouwen, N. 1997. Nonrigid, unsubmerged, vegetative roughness on floodplains". Journal of Hydraulic Engineering, Vol. 123(1): 51–57.

Florida Fish and Wildlife Conservation Commission. 2014. EXCEL spreadsheet containing results of vegetative surveys made within Ocklawaha River and Silver River. Obtained from Jodi Slater, SJRWMD.

Franklin, P., Dunbar, M., and Whitehead, P. 2008. Flow controls on lowland river macrophytes: A review. Science of the Total Environment, 400: 369–378.

Galperin, B., Kantha, L. H. Hassid, S. and Rosati, A.. 1988. A quasi-equilibrium turbulent energy model for geophysical flows. J. Atmos. Sci., 45: 55–62.

Gao, G., Falconer, R. A., and Lin, B. 2011. Modelling open channel flows with vegetation using a three-dimensional model. J. Water Res. Protection, 3: 114–119.

Hamrick, J. M. 1992. A Three-Dimensional Environmental Fluid Dynamics Computer Code: Theoretical and Computational Aspects. The College of William and Mary, Virginia Institute of Marine Science, 50 pp.

Hoyer, M. V., Frazer, T. K., Notestein, S. K., and Canfield, D. E. 2004. Vegetative characteristics of three low-lying Florida coastal rivers in relation to flow, light, salinity and nutrients. Hydrobiologia, 528: 31–43.

King, S. A. 2014. Hydrodynamic control of filamentous macroalgae in a sub-tropical spring-fed river in Florida, USA. Hydrobiologia, 734: 27–37.

Klopstra, D., Barneveld, H. J., Van Noortwijk, M., and Van Velzen, E. H. 1997. Analytical model for hydraulic roughness of submerged vegetation. In *Managing Water With Scarcity and Abundance, Proceddings IAHR*, pp. 775-780, ASCE, Reston, VA.

Kouwen, N. 1992. Modern approach to design of grassed channels. Journal of Irrigation and Drainage Engineering, 118 (5): 733–743.

Lopez, F. and Garcia, M. H. 2001. Mean flow and turbulence structure of open-channel flow through non-emergent vegetation. J. Hydraul. Eng., 127: 392–402.

Luhar, M., Rominger, J. and Nepf, H. 2008. Interaction between flow, transport and vegetation spatial structure. Eviron. Fluid. Mech., 8: 423–439.

Luhar, M., and Nepf, H. 2013. From the blade scale to the reach scale: A characterization of aquatic vegetative drag. Adv. Water Res., 51: 305–316.

Meijer, D. G. and Van Velzen, E. H. 1999. Prototype-scale flume experiment on hydraulic roughness of submerged vegetation, in Proceedings of XXVII IAHR Congess, Graz, Abstract 221, & pp., Int. Assoc. for Hydraul. Res., Madrid.

Mellor, G. L., and Yamada, T. 1982. Development of a turbulence closure model for geophysical fluid problems. Rev. Geophys. Space Phys., 20: 851–875.

Munch, D. A., Toth, D. J., Huang, C., Davis, J. B., Fortich, C. M.. Osburn, W. L., Phlips, E. J., Quinlan, E. L., Allen, M. S., Woods, M. J., Cooney, P., Knight, R. L., Clarke, R. A. and Knight, S. L. 2006. *Fifty-Year Retrospective Study of the Ecology of Silver Springs, Florida.* Special Publication SJ2007-SP4, SJRWMD, Palatka, FL. 314 pp.

Odum, H. T. 1957. Trophic structure and productivity of Silver Springs, Florida. Ecological Monographs. Vol. 27(1): 55–112.

Righetti, M. and Armanini, A. 2002. Flow resistance in open channel flows with sparsely distributed bushes. J. Hydrolog., 269: 55–64.

Stoesser, T, Neary, V., and Wilson, C.A.M.E. 2004. *Modeling Vegetated Channel Flows: Challenges & Opportunities*, WSEAS Conference, Corfu, August 2004.

Vogel, S. 1994. Life in Moving Fluids. Princeton University Press, Princeton, NJ.

Wetlands Solutions, Inc. 2012. Silver River Ecosystem Metabolism (2011-2012). Gainesville, FL. 46 pp.

Wetlands Solutions, Inc. 2014. Silver Springs Ecosystem Study (2012-2013). Gainesville, FL. 39 pp.

Whitford, L. A. 1956. The communities of algae in the springs and spring streams of Florida. Ecology. Vol. 37(3): 433-444.

Wu, F., Shen, W. H., and Chou, Y. 1999. Variation of roughness coefficients for unsubmerged and submerged vegetation". Journal of Hydraulic Engineering, Vol. 125(9): 934–942.

5.5 REDUCED COMPLEXITY MODELING OF HYDRODYNAMIC EFFECTS OF VEGETATION ON VELOCITY AND STAGE IN SILVER RIVER

5.5.1 INTRODUCTION

The role that hydrodynamics plays in controlling dominant plant communities in streams and the possible feedbacks of plants on the hydrodynamics were discussed in depth in the previous section. As a short recap, higher flow velocities tend to increase growth rates of submersed aquatic vegetation (SAV) by thinning the diffusive boundary layer over the plant surface (Biggs 1996; Biggs et al. 1998), or by excluding algae through sloughing and exportation (King 2014), but at sufficiently large velocities, plants suffer stress from excessive drag and can be uprooted. Therefore, there likely exists an optimal flow velocity range in which SAV in springs can thrive.

Submerged vegetation provides a substantial resistive drag force on stream or river flow. Greater flow resistance in a river channel lowers flow velocity, while at the same time increasing the stage and depth of the river for a given discharge. As stated in the previous section, the Silver River appears to have experienced a shift in its stage/discharge relationship in the late 1990s and early 2000s, with an increased stage for a given discharge (Figure 5.5.1). In its current high-stage state, the river will have lower average velocities than it had in past decades, which could influence algal abundance. If we use Manning's equation for open channel flow to approximate the river's stage/discharge relationship, then this apparent shift can only be explained through an increase of the resistance/friction parameter (n), or a decrease in the overall slop of the channel (S):

$$Q = \frac{k}{n}\left(\frac{A}{P}\right)^{\frac{2}{3}} (S)^{\frac{1}{2}} A$$

For the Silver River, the dominant feature that appears to contribute to flow resistance is SAV. Due to its importance to flow resistance, any changes in the SAV, whether coverage, density, or reconfiguration, could have a large impact on reach scale river properties, such as the stage/discharge relationship. There is some anecdotal evidence that vegetation coverage has changed over time the Silver River, suggesting the run had substantially less SAV in the past. This possible increase in SAV may at least partially explain why the stage discharge shift has occurred.

In this section, we analyze several stage/discharge relationships measured on the Silver and Ocklawaha Rivers, calculate likely impacts of the stage/discharge shift on stream flow velocity, statistically test if a shift has occurred in the stage discharge relationship, explore a possible mechanism for the observed stage/discharge shift, and use Manning's equation to statistically test what physical properties of the river have changed. Additionally, we describe a simple conceptual model of a coupled aquifer, spring, and spring run and use this model to explore feedbacks between the coupled systems. In particular, we seek to constrain the likely range of spring discharge and aquifer level changes that might be brought about though vegetative changes in the spring run.

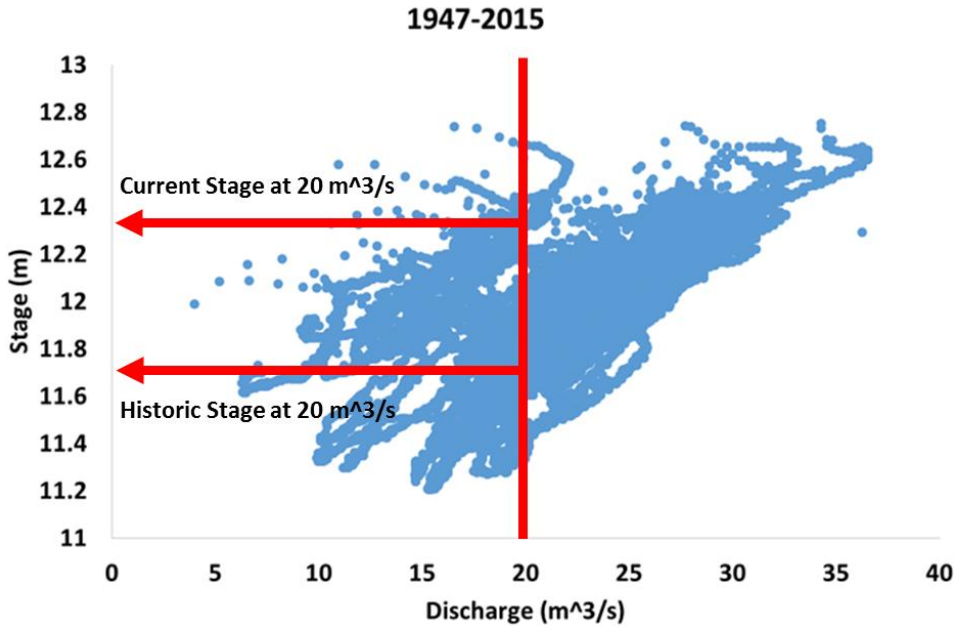

Figure 5.5.1. Silver River main spring pool stage versus discharge from 1947 to 2015. Historically, a discharge of 20 m^3 s^{-1} (706 cfs) would produce a stage that is 0.6 m (2 ft) lower than in the current river at the same discharge.

5.5.2 MATERIALS AND METHODS

5.5.2.1 Stage/Discharge Data Analysis

The full available record of stage and discharge data for the Silver River main spring pool, Silver River 1,200 m station, and Ocklawaha River Conner station (just downstream of the Ocklawaha and Silver River confluence) were obtained from the USGS database. The corresponding stage and discharge time series for each station were plotted against each other to give a scatterplot of the stage/discharge relationship. Several time windows were selected and tested from the whole record to determine visually when the stage/discharge relationship began to change.

5.5.2.2 Velocity Impacts of Stage/Discharge Shift

The stage/discharge scatter plot for the main spring pool of the Silver River was used to determine likely stages for both historic and current stage/discharge relationships for a given discharge of 20 m^3 s^{-1} (706 cfs). These stage values were used to calculate the expected average velocity in the main channel of Silver River leaving the main spring bowl (using measured stream bed morphology) for both current and historic stage/discharge relationships. The average velocities were compared with threshold values for the inhibition of macroalgae previously reported (Hoyer et al. 2004; King 2014).

5.5.2.3 Statistical Change Point Analysis

A Bayesian statistical change point analysis was performed on the stage/discharge data from the main spring pool of the Silver River. A change point analysis is able to determine, solely from the data, where or not a change has occurred in the data. When applied to stage/discharge data, the change point analysis "fits" two different stage/discharge relationships to the data and segments the data at the most probable time a change has occurred in the data. It is important to

note that this process is completely driven by the data (the algorithm has no prior knowledge of the location of a change point) and is not required to find a "change" in the data. A change is only found if the structure of the data suggests there is one.

The Bayesian statistical change point analysis is based on Bayes theorem, given as:

$$p(Hypothesis|Data) = \frac{p(Data|Hypothesis)p(Hypothesis)}{p(Data)}$$

or the commonly used form:

$$p(Hypothesis|D) \propto p(Data|Hypothesis)p(Hypothesis)$$

The components of this proportionality are generally referred to in the following manner:

$$posterior\ distribution \propto likelihood\ distribution \times prior\ distribution$$

The prior distribution reflects the knowledge of the model parameters before including experimental data, the likelihood distribution is the distribution from which the data is thought to be generated (i.e., the model under consideration), and the posterior distribution reflects the knowledge of the model after including experimental data.

For our specific case, the data are the stage/discharge data, and the hypothesis is that the data is generated from the one of two stage/discharge relationships. A general stage/discharge relationship can be written as:

$$Q = C_r(G - a)^{\beta}$$

where Q is the discharge, G is the stage, and C_r, a, and β are fitting parameters the control the shape of the stage/discharge curve. This relationship can be rearranged to the following:

$$G = \left(\frac{Q}{C_r}\right)^{\frac{1}{\beta}} + a$$

The stage/discharge data have two coordinates, discharge $\{Q_i\}$, and stage $\{G_i\}$. For the change point analysis, we are interested in the probability distribution of the parameters of the two stage/discharge relationships and the location of the change point, which separates these two relationship given the stage/discharge data. This probability distribution can be written using Bayes theorem as:

$$p(C_{r1}, \beta_1, a_1, B_1, C_{r2}, \beta_2, a_2, B_2, N|\{Q_i\}, \{G_i\})$$
$$\propto \left[\prod_{i=1}^{N} \frac{B_1 \left(\left(\frac{Q_i}{C_{r1}}\right)^{\frac{1}{\beta_1}} + a_1\right)^{B_1}}{\Gamma\left(\left(\left(\frac{Q_i}{C_{r1}}\right)^{\frac{1}{\beta_1}} + a_1\right) B_1\right)} G_i \left(\left(\frac{Q_i}{C_{r1}}\right)^{\frac{1}{\beta_1}} + a_1\right)^{B_1 - 1} e^{-B_1 G_i}\right]$$

$$\left[\prod_{i=N+1}^{n_{total}} \frac{B_2}{\Gamma\left(\left(\left(\frac{Q_i}{C_{r2}}\right)^{\frac{1}{\beta_2}}+a_2\right)B_2\right)} G_i^{\left(\left(\frac{Q_i}{C_{r2}}\right)^{\frac{1}{\beta_2}}+a_2\right)B_2-1} e^{-B_2 G_i}\right]$$
$$\left[\frac{B_{C_{r1}}{}^{A_{C_{r1}}}}{\Gamma\left(A_{C_{r1}}\right)} C_{r1}{}^{A_{C_{r1}}-1} e^{-B_{C_{r1}} C_{r1}}\right]\left[\frac{B_{\beta_1}{}^{A_{\beta_1}}}{\Gamma\left(A_{\beta_1}\right)} \beta_1{}^{A_{\beta_1}-1} e^{-B_{\beta_1}\beta_1}\right]\left[\frac{B_{a_1}{}^{A_{a_1}}}{\Gamma\left(A_{a_1}\right)} a_1{}^{A_{a_1}-1} e^{-B_{a_1} a_1}\right]$$
$$\left[\frac{B_{B_1}{}^{A_{B_1}}}{\Gamma\left(A_{B_1}\right)} B_1{}^{A_{B_1}-1} e^{-B_{B_1} B_1}\right]\left[\frac{B_{C_{r2}}{}^{A_{C_{r2}}}}{\Gamma\left(A_{C_{r2}}\right)} C_{r2}{}^{A_{C_{r2}}-1} e^{-B_{C_{r2}} C_{r2}}\right]\left[\frac{B_2{}^{A_{\beta_2}}}{\Gamma\left(A_{\beta_2}\right)} \beta_2{}^{A_{\beta_2}-1} e^{-B_{\beta_2}\beta_2}\right]$$
$$\left[\frac{B_{a_2}{}^{A_{a_2}}}{\Gamma\left(A_{a_2}\right)} a_2{}^{A_{a_2}-1} e^{-B_{a_2} a_2}\right]\left[\frac{B_{B_2}{}^{A_{B_2}}}{\Gamma\left(A_{B_2}\right)} B_2{}^{A_{B_2}-1} e^{-B_2 B_2}\right]\left[\frac{1}{n_{total}}\right]$$

The posterior distribution for the model parameters (i.e., $C_{r1}, \beta_1, a_1, B_1, C_{r2}, \beta_2, a_2, B_2, N$) given the data is explicitly expressed in the above proportionality. To find the most likely parameter values we can calculate the mean of each of the parameters from the posterior distribution. Since the posterior distribution does not have an easily obtained analytic expression we use a Monte Carlo approach to draw enough samples from the distribution to characterize it. The method we use to sample from the posterior distribution is a Markov chain Monte Carlo (MCMC) random walk using the Metropolis-Hasting within a Gibbs sampling algorithm.

5.5.2.4 Modeling Stage/Discharge Shift and Alternative Stable States

As stated in the introduction, submerged vegetation provides a substantial resistive drag force on stream or river flow, and at sufficiently large velocities, SAV experience excessive drag and can be uprooted. However, the drag produced by SAV reduces flow velocity in channel, and therefore dense SAV could possibly provide enough drag to slow flow enough to prevent itself from being uprooted. This is a situation where there are two different positive feedback loops that could dominate the system under different starting conditions, which allows for the possibility of alternative stable states.

The first positive feedback loop is the runaway removal of SAV which proceeds as follow: Flow velocity increases → SAV is uprooted due to increased flow velocity → less SAV reduces drag so flow velocity increases → more SAV is uprooted → higher flow velocity → etc. This feedback loop results in a situation with little or no SAV.

The second feedback loop is the runaway growth of SAV which proceeds as follow: Flow velocity decreases → SAV is able grow and expand → more SAV increase drag so flow velocity decreases → less SAV is uprooted → lower flow velocity → etc. This feedback loop results in a situation where SAV dominates.

The two final states (either no SAV or dominate SAV) are an example of a pair of alternative stable states. In addition, they also correspond to two different possible states in a river, which would have different stage/discharge relationships. An SAV dominated river would have a

higher stage for a given discharge than a river devoid of SAV. This is a possible explanation for the apparent stage discharge shift observed in the Silver River.

We have also observed SAV uprooting in the field due to high flow velocities (Figure 5.5.2), which suggests the two processes that can lead to alternative stable states (SAV uprooting and regrowth) do occur in the Silver River.

Figure 5.5.2. SAV being uprooted by high flow velocities in the Silver River in 2016.

We used a reduced complexity modeling approach to attempt to reproduce stage discharge shifts due to alternative stable SAV states in a simulated river (Figure 5.5.3). In this model, the flow velocity is assumed to follow Manning's equation. The simulated river is assumed to have a trapezoid cross sectional area. SAV is assumed to grow in a logistic manner, SAV uprooting occurs past a threshold flow velocity and increases linearly after the threshold is crossed. The channel friction (Manning's *n*) is determine by the amount of SAV in the channel and the flow velocity, as SAV can reduce its drag through reconfiguration during high flow velocity events.

$$Q = \frac{k}{n}\left(\frac{A}{P}\right)^{\frac{2}{3}}(S)^{\frac{1}{2}}A \qquad \longleftarrow h \longrightarrow$$

$$v = \frac{Q}{A}$$

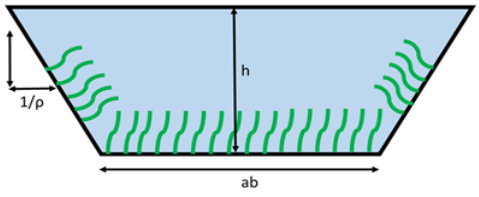

$$n = n_{no\ SAV} + \left(\frac{n_{SAV} - n_{no\ SAV}}{1-0} - [N_v V \Phi(V) + (n_{saturated} - N_v V)\Phi(V - V_{sat})]\right) SAV$$

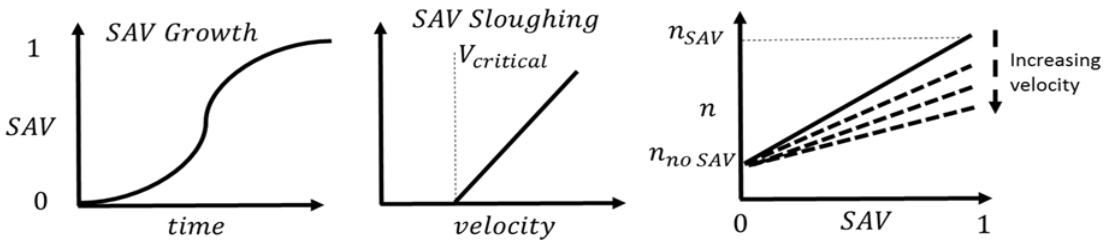

Figure 5.5.3. Reduced complexity modeling summary for the simulated river.

When all the components shown in Figure 5.5.3 are combined, the resulting model is a differential equation governing the growth rate of SAV in the river:

$$\frac{dSAV}{dt} = rSAV(1-SAV) - \theta[SAV]\left[\frac{Q}{\frac{ab+2\rho h}{2}h}\Phi\left(\frac{Q}{\frac{ab+2\rho h}{2}h} - V_{critical}\right)\right]$$

$$f_1(h) = 0 = \frac{k}{\left(n_{no\ SAV} + \left(n_{SAV} - N_v\frac{Q}{\frac{ab+2\rho h}{2}h} + \left(-n_{SAV} + n_{saturated} + N_v\frac{Q}{\frac{ab+2\rho h}{2}h}\right)\Phi\left(n_{SAV} - n_{saturated} - N_v\frac{Q}{\frac{ab+2\rho h}{2}h}\right) - n_{no\ SAV}\right)SAV\right)\left(\frac{\left(\frac{ab+2\rho h}{2}h\right)}{ab+2\sqrt{h^2+(\rho h)^2}}\right)^{\frac{2}{3}}\left(\frac{(el_1+h)-(el_2+h)}{L}\right)^{\frac{1}{2}}\left(\frac{ab+2\rho h}{2}h\right) - Q}$$

This model was numerically simulated to produce potential stage/discharge curves under variety of conditions.

5.5.2.5 Coupled Aquifer, Spring, and Spring Run Conceptual Model

We also developed a coupled, but highly simplified, aquifer-spring- spring run model to explore possible hydraulic feedbacks between the surface water and groundwater systems. This conceptual model is illustrated in Figure 5.5.4. The aquifer is considered to act as a large pool with a porosity less than one. The spring bowl is also considered a pool, and the two are connected with a cylindrical tube, which represents the spring vent. The spring pool is connected to a channel, which represents the spring run.

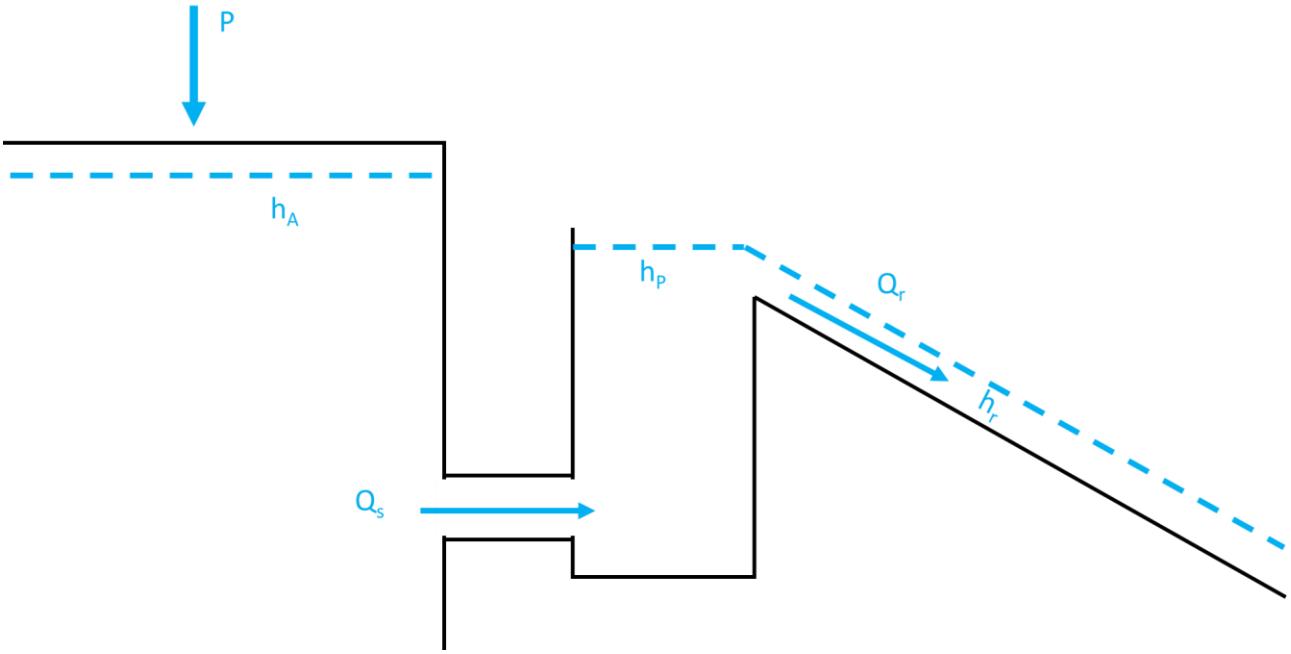

Figure 5.5.4. Conceptual coupled aquifer, spring, and spring run model. P is the recharge into the aquifer, h_A is the aquifer elevation, h_P is the spring pool elevation, h_r is the river depth, Q_s is the spring vent discharge, and Q_r is the river discharge.

To simulate the dynamics of this system, we can write two coupled differential equations, one for the aquifer elevation, h_A, and one for the spring pool elevation, h_P:

$$\frac{dh_A}{dt} = \frac{-Q_s}{A_A \varphi} + P(t)$$

$$\frac{dh_P}{dt} = \frac{Q_s - Q_R}{A_P}$$

where $P(t)$ is the rainfall time series, A_A is the area of the aquifer, φ is the porosity of the aquifer, A_P is the area of the spring pool, Q_s is the spring discharge, and Q_R is the spring run discharge. $P(t)$ is modeled as a marked Poisson process, Q_s is determined by a mechanical energy balance between the aquifer and spring pool (i.e., Bernoulli's Equation), and Q_R is modeled with Manning's Equation as in the previously described model.

To simulate system dynamics, we assigned actual or reasonable values for physical parameters (e.g. spring vent diameter, area of spring pool, area of aquifer, etc.). We then performed two simulations to understand the potential role that increased river resistance due to SAV could have on aquifer levels and spring run discharge. This was accomplished by running two identical simulations, with the exception of changing the value of Manning's *n* in the spring run. For the simulation of low SAV/low resistance, we used n=0.02, which is representative of a "clean" channel; for high SAV/high resistance, we used n=0.1, which is representative of a heavily vegetated channel (Maidment 1993).

5.5.3 RESULTS AND DISCUSSION

5.5.3.1 Stage/Discharge Data Analysis

Full record stage and discharge scatterplots for the Silver River main spring pool, Silver River 1,200 m station, and Ocklawaha River Conner station (just downstream of the Ocklawaha and Silver River confluence) are given in Figures 5.5.5, 5.5.6, and 5.5.7, respectively. All three periods of record show a visually discernible shift in the stage/discharge relationship at roughly the same time. All of these shifts go from a state of lower stage for a given discharge to a state of higher stage for the same discharge. The magnitude of the shift is approximately a 0.6-0.8 meters increase in stage for all of the stations. This suggests either the phenomena causing the shift is present throughout the river or is only acting at the end of the river with the influence is propagated upstream through a backwater effect. The timing of the shift is also consistent between all stations. The transition appears to occur during the years of 2000-2003.

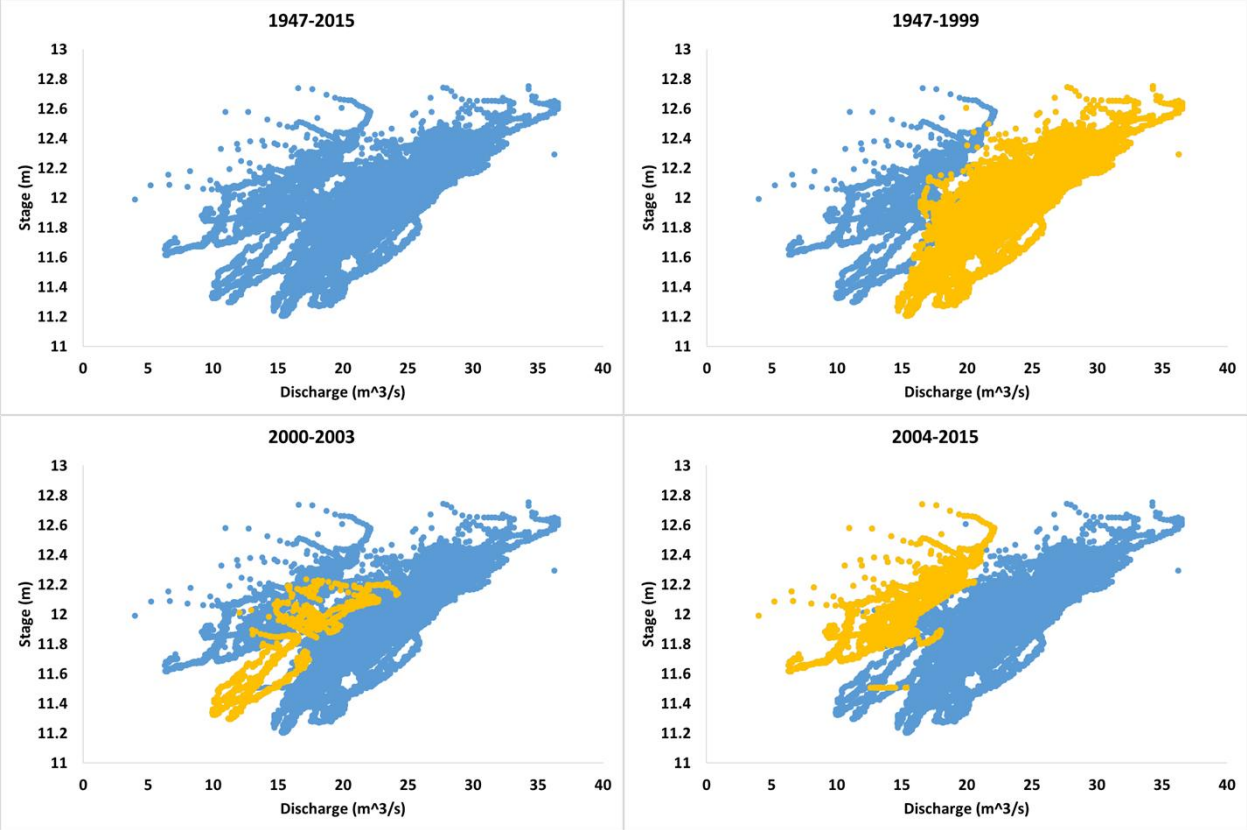

Figure 5.5.5. Stage and discharge data from the Silver River main spring pool from 1947-2015. Clockwise from top left: scatter plot of all data (blue), scatter plot of all data (blue) with data from 1947-1999 highlighted (yellow), scatter plot of all data (blue) with data from 2004-2015 highlighted (yellow), scatter plot of all data (blue) with data from 2000-2003 highlighted (yellow).

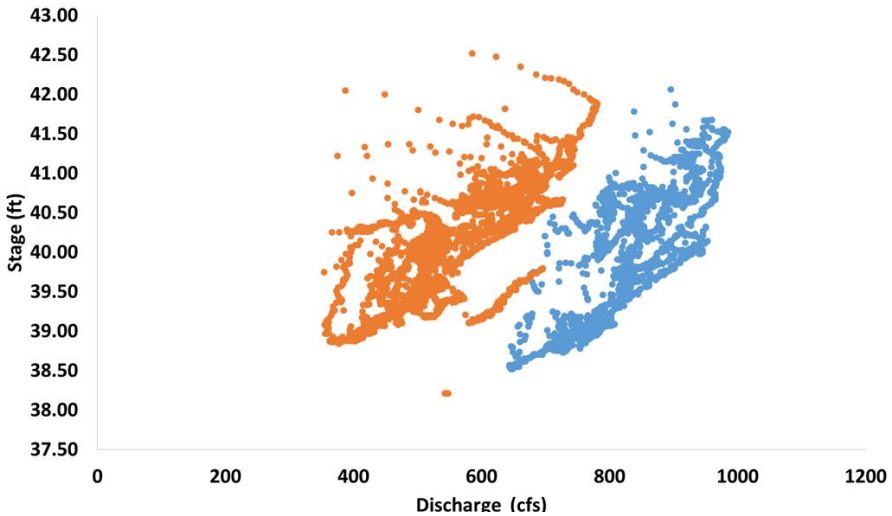

Figure 5.5.6. Stage and discharge data from the Silver River 1,200 m station. Data in blue covers the period from 7 February 1967 to 30 June 1972. Data in orange covers 21 November 2003 to 30 June 2015.

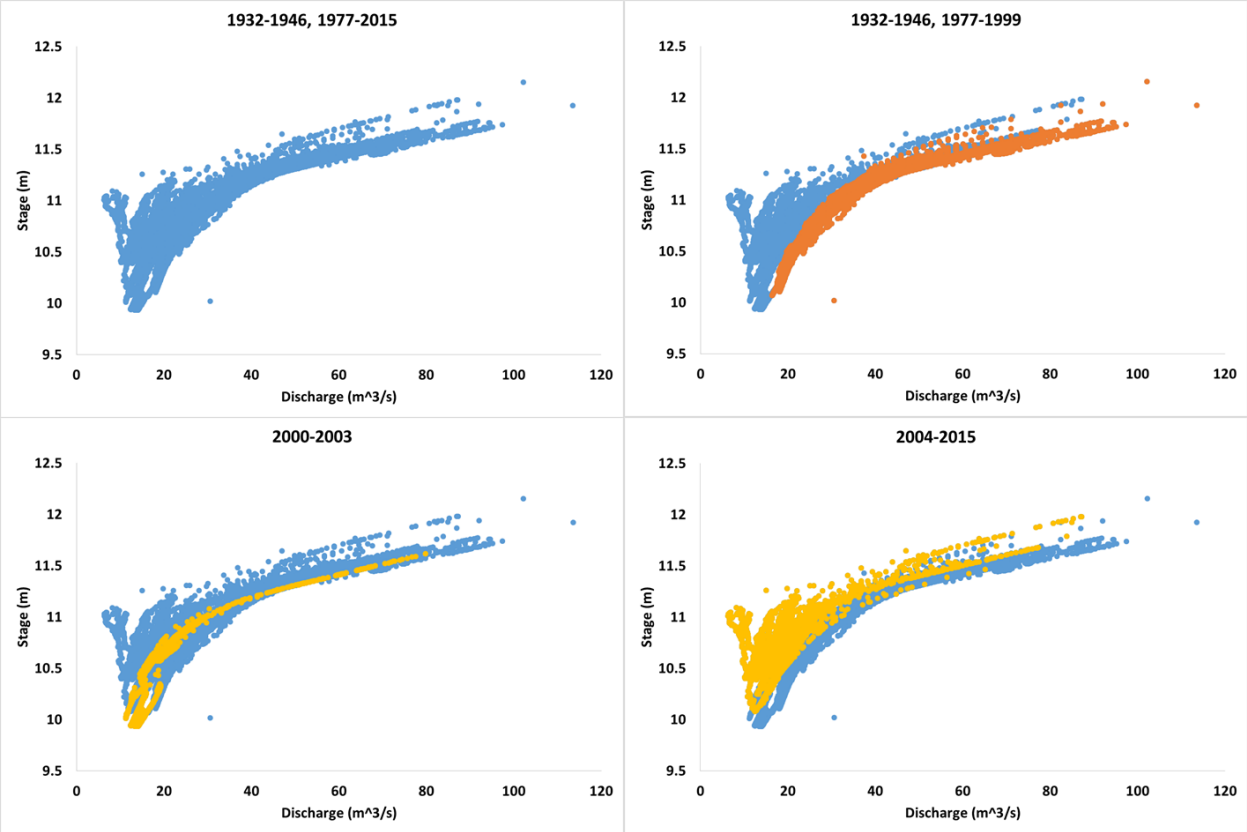

Figure 5.5.7. Stage and discharge data from the Ocklawaha River Conner station (just downstream of the Ocklawaha and Silver River confluence from the period 1932-1946, 1977-2015. Clockwise from top left: scatter plot of all data (blue), scatter plot of all data (blue) with data from 1932 to 1946, 1977 to 1999 highlighted (orange), scatter plot of all data (blue) with data from 2004 to 2015 highlighted (yellow), scatter plot of all data (blue) with data from 2000 to 2003 highlighted (yellow).

5.5.3.2 Velocity Impacts of Stage/Discharge Shift

Figure 5.5.8 summarizes the results from the calculation of the velocity impacts of the stage/discharge shift. Under the historic stage/discharge relationship, the expected velocity in the main channel leaving the spring bowl is 0.244 m s^{-1} (8.62 cfs). This value is very close to the 0.25 m s^{-1} (8.83 cfs) velocity that has been found to inhibit macroalgae colonization (King 2014). Under the current stage/discharge relationship, the expected velocity is 0.159 m s^{-1} (5.62 cfs) for the exact same spring discharge. This value is significantly lower than historic velocities, and lower than the macroalage inhibition velocity. This could be part of the explanation for algal proliferation in areas of the spring run where there historically had been very little macroalgae. The stage/discharge shift has resulted in a generally slower moving river, potentially opening up new areas of the spring and run for algae to colonize.

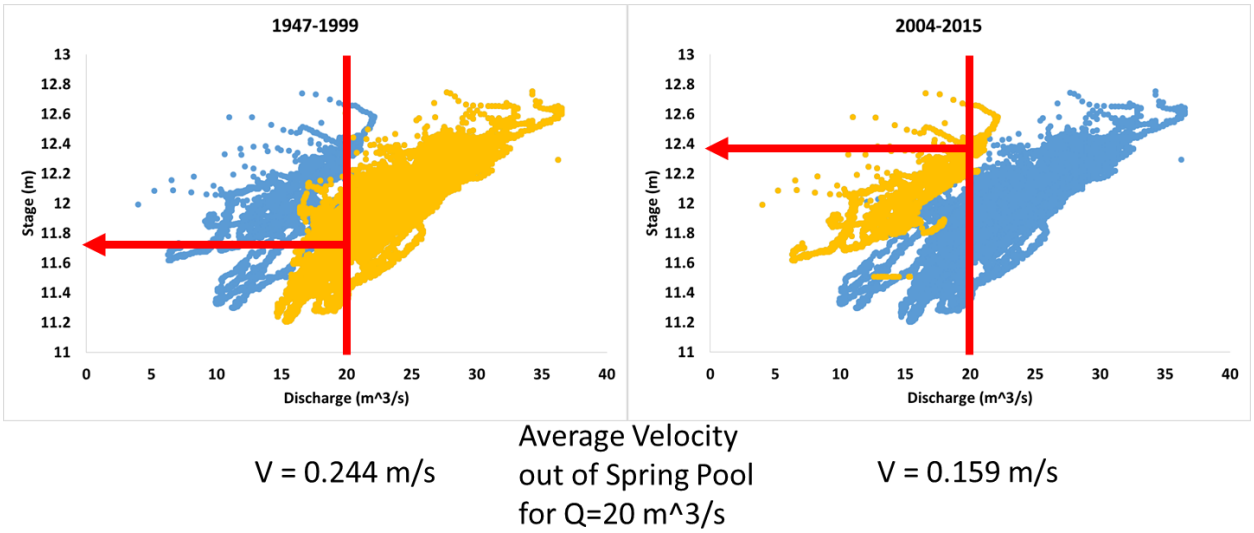

Figure 5.5.8. Stage and discharge data from the Silver River main spring pool from 1947 to 2015. Left: Illustrates historically (1999 or earlier) the expected state, given a discharge of 20 m^3 s^{-1} (706 cfs). The velocity in the main channel would be expected to be 0.244 m s^{-1} (8.62 cfs). Right: Illustrates currently (2004 or later) the expected state, given a discharge of 20 m^3 s^{-1}. The velocity in the main channel would be expected to be 0.159 m s^{-1} (5.62 cfs).

5.5.3.3 Statistical Change Point Analysis

Results of the Bayesian statistical change point analysis are given in Figures 5.5.9. Figure 5.5.9 displays the full data record of the Silver River main spring pool with the two statistically probable stage/discharge relationships found. These two relationships are statistically distinct with wide separation of 95 % credible intervals. This suggests that the existence of the pattern we observe visually in the data is statistically supported.

Figure 5.5.10 displays the probability distribution of the date of the change point. This distribution is very multi-modal, however the range of possible dates is essentially limited to a set of 20 days in the middle of 2001. It is important to note that these 20 days were selected in a completely automated manner as most probable from a data record of 24,930 days. The change point dates shown in the probability distribution are not the exact dates where the stage/discharge shift in the Silver River occurred, but rather the date where it is most probable to split the dataset for the two stage/discharge relationships shown in Figure 5.5.8.

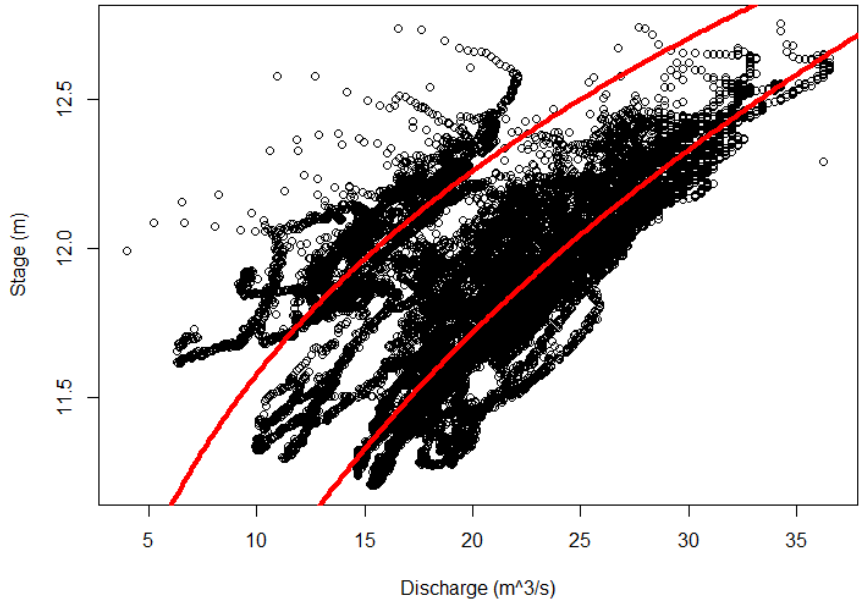

Figure 5.5.9. Stage and discharge data from the Silver River main spring pool from 1947 to 2015 (black circles), with the most statistically probable stage/discharge relationships found with the Bayesian change point analysis (red lines).

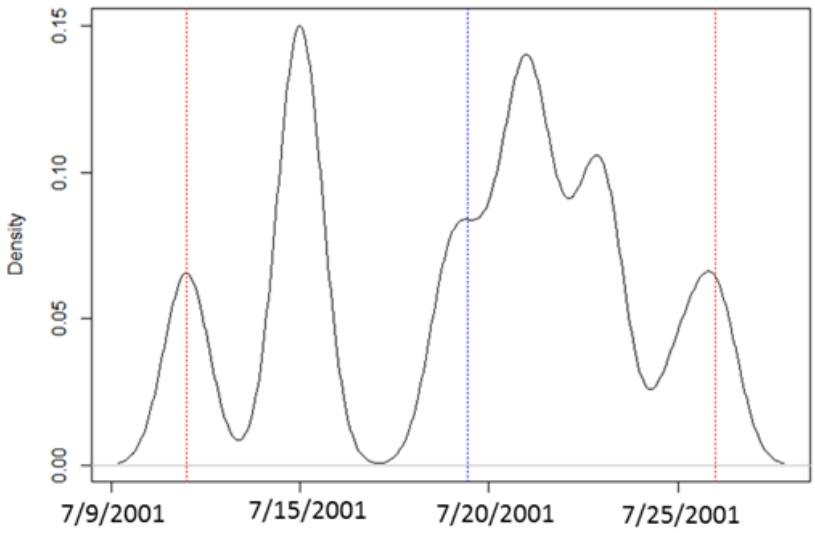

Figure 5.5.10. Probability distribution of the date of the change point (the most probable date where the stage/discharge shift can be said to have occurred). The black line signifies the probability density, the blue line give the location of the mean of the distribution, while the red lines give the locations of the 95 % credible interval. It should be noted that the dates shown in the probability distribution are not the exact dates where the stage/discharge shift in the Silver River occurred, but rather the date where it is most probable to split the dataset for the two stage/discharge relationships shown in Figure 5.5.8.

5.5.3.4 Modeling Stage/Discharge Shift and Alternative Stable States

Results of the numerical simulation of the reduced complexity model are given in Figures 5.5.11 and 5.5.12. Figure 5.5.11 is a simulated stage/discharge scatterplot. This scatterplot demonstrates that this very simple model based on Manning's equation and logistic growth of SAV can indeed reproduce a stage/discharge shift with a transition period in between shifts. This model lends support to the idea that SAV may play a role in the shift observed in the Silver River.

Figure 5.5.12 is a simulated SAV abundance time series that corresponds to the stage/discharge scatterplot in Figure 5.5.9. When discharge and flow velocity are high initially, SAV abundance decreases. Once discharge and flow velocity have decreased past the uprooting threshold, SAV quickly grows in, causing a shift in the stage discharge curve. The dense SAV bed now causes a large drag force on the river and hence slower velocity, which protects it from being uprooted. Discharge must increase to much higher levels before uprooting occurs and the system shifts back to the original stage/discharge curve. The river SAV system has the property of hysteresis.

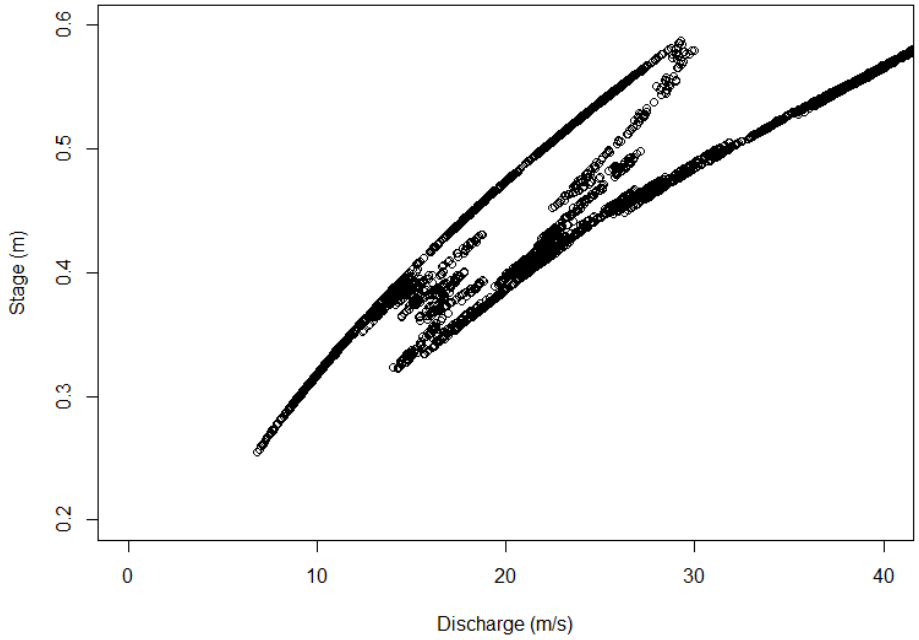

Figure 5.5.11. Simulated stage and discharge data from the reduced complexity modeling of SAV hydraulic interactions. This model allows for a shift from one stage discharge curve (one with little SAV) to another (dominated with SAV) and back again, driven by changes in river discharge. Each state is stable until discharge falls below or rises above a certain threshold, after which the system changes to the alternative state.

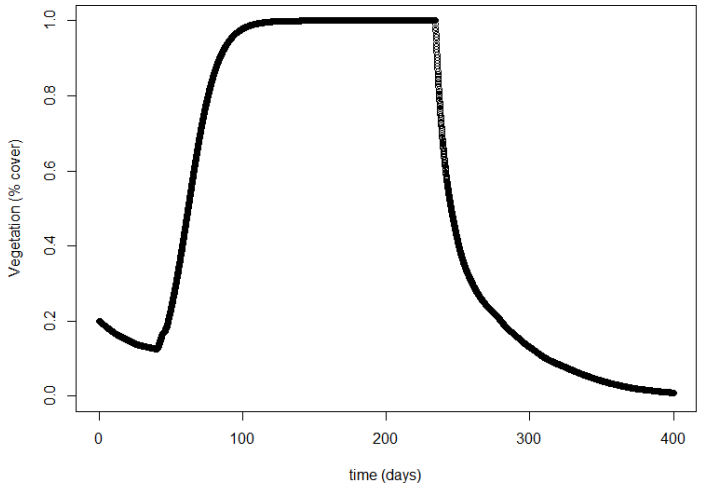

Figure 5.5.12. Simulated SAV abundance time series from the reduced complexity modeling of SAV hydraulic interactions.

5.5.3.5 Coupled Aquifer, Spring, and Spring Run Conceptual Model

Results of the numerical simulation of the simplified aquifer-spring- spring run model are summarized in Figure 5.5.13. Figure 5.5.13a is a simulated aquifer elevation time series for the low and high Manning's n simulations. Notably, the aquifer level is similar between the two simulations despite very different channel resistances. Figure 5.5.13b shows simulated river depth for both simulations. River depth in the simulation with the higher Manning's *n* value is substantially higher. Taken together, these two results suggest that increased river resistance can have large impacts on river hydrology and hydraulics, but these effects do not necessarily propagate substantial changes back into the aquifer. In other words, an increase in river resistance (due to SAV expansion or any other biophysical driver) can have substantial impacts on the surface hydrology of a spring-fed river, but the impact on the connected aquifer system feeding the spring, which depends on the relative size of the aquifer region feeding that spring, is likely very low for the Silver River.

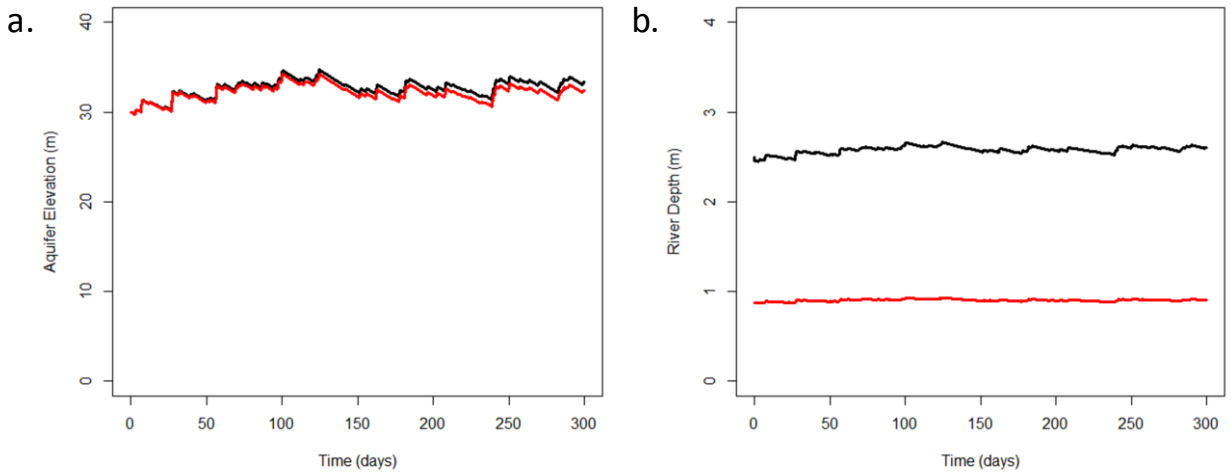

Figure 5.5.13. Simulated aquifer elevation (a) and spring run depth (b) time series for the low (red) and high (black) Manning's *n* simulations.

5.5.4 CONCLUSIONS, RECOMMENDATIONS, AND FUTURE RESEARCH NEEDS

We analyzed changes in the stage/discharge relationships Silver River main spring pool, Silver River 1,200 m station, and Ocklawaha River Conner station; calculated flow velocity decreases due to the stage/discharge shift and discussed their possible implications for algal proliferation; tested to determine if the shift was statistically supported, and explored a possible mechanism of SAV growth and uprooting for the observed stage/discharge shift. All stations showed a discernable shift in the stage/discharge relationship at roughly the same time (2000-2003), and all relationships shifted from a state of lower stage for a given discharge to a state of higher stage for the same discharge (0.6-0.8 meters increase in stage for all stations). This finding suggests either the phenomena causing the shift is present throughout the river or is only acting at the end of the river with the influence is propagated upstream through a backwater effect.

Modeled velocity impacts of the stage/discharge shift suggest that under historic conditions, velocity in the main channel leaving the spring bowl was > 0.24 m s^{-1}, close to the critical algal velocity threshold. Under the current stage/discharge relationship, the expected velocity is <0.16 m s^{-1} at the same discharge, significantly lower than historic velocities and the critical velocity. This finding could, in part, explain algal proliferation in areas of the spring run where there historically had been very little macroalgae; a shift in the stage/discharge relationship generally means a slower moving river, potentially facilitating algal colonization. Change point analysis identified July 2001 as the most probable time to split the stage/discharge relationships.

Reduced-complexity numerical simulation demonstrated the potential for simple feedbacks among Manning's equation-based roughness, logistic growth of SAV, and a critical velocity for SAV removal can reproduce a stage/discharge shift with a transition period in between shifts and hysteretic properties. This model lends support to the idea that SAV may play a role in the shift observed in the Silver River. Simplified modeling of the aquifer-spring pool-spring run system suggested that SAV expansion can affect spring run hydrology (e.g., stage and velocity), but is unlikely to affect aquifer level and spring discharge. In the future, both of these simplified models should be tested and refined using data and outputs of the analytical and numerical models developed elsewhere in the larger CRISPS study.

5.5.5 REFERENCES

Biggs, B. J. F. 1996. Hydraulic habitat of plants in stream. Regulated Rivers: Research and Management. Vol. 12: 131–144.

Biggs, B. J. F., Goring, D. G., and Nikora, V. I. 1998. Subsidy and stress responses of stream periphyton to gradients in water velocityas a function of community growth form. J. Phycol., 34: 598–607.

Hoyer, M. V., Frazer, T. K., Notestein, S. K., and Canfield, D. E. 2004. Vegetative characteristics of three low-lying Florida coastal rivers in relation to flow, light, salinity and nutrients. Hydrobiologia, 528: 31–43.

King, S. A. 2014. Hydrodynamic control of filamentous macroalgae in a sub-tropical spring-fed river in Florida, USA. Hydrobiologia, 734: 27–37.

Maidment, D. R. *Handbook of hydrology*. Vol. 1. New York: McGraw-Hill, 1993.

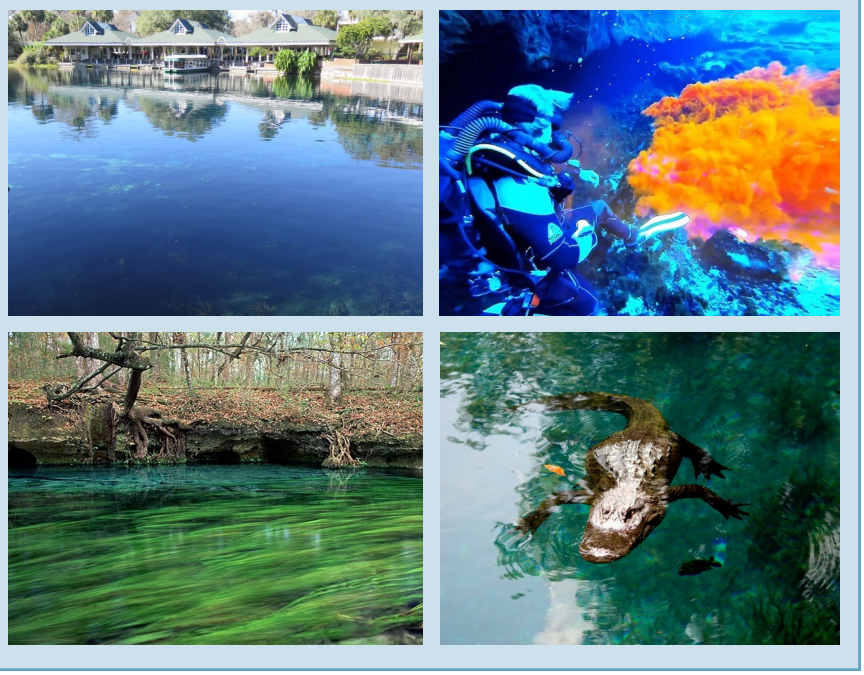

Collaborative Research Initiative on
Sustainability and Protection of Springs [**CRISPS]**

Section 6

[Work Order No: 3]

FINAL REPORT

2014 - 2017

submitted to:

St. Johns River Water Management District
Springs Protection Initiative [SPI], UF Contract # 27789

UF | UNIVERSITY of FLORIDA
Water Institute

C R I S P S

Section 6

PHYSICOCHEMISTRY

Nitrogen Dynamics and Metabolism

Final Report 2017
Work Order No.3: Part 1 of 3

Principal Investigators:

Matthew Cohen, University of Florida
Michael F. Coveney, St. Johns River Water Management District
Jodi Slater, St. Johns River Water Management District

Project Team

Matthew Cohen, University of Florida
Jennifer McBride, MS Student
Bobby Hensley, Post-Doctoral Researcher
Courtney Reijo, PhD Student
Larry Korhnak, Laboratory Manager
Chad Foster, Field Technician
Lily Kirk, PhD Student
Sarah Power, Undergraduate Assistant in SFRC
UF Ecohydrology Laboratory

School of Forest Resources and Conservation
University of Florida

Michael F. Coveney
Jodi Slater
St. Johns River Water Management District

This document reports findings and results of a work order for a 3-year project in compliance with Agreement between University of Florida (UF) and St. Johns River Water Management District (SJRWMD) UF Contract #27789. It is part of the *UF Collaborative Research Initiative on Springs Protection and Sustainability (CRISPS)* and supports the science component of *the SJRWMD Springs Protection Initiative (SPI).*

6.1 ABSTRACT

Understanding how spring ecosystems respond to various stressors is crucial for prioritizing restoration and protection activities. Contrasting two springs with different nitrate concentrations (Silver River and Alexander Springs Creek), we implemented four research elements on spring ecosystem processing of carbon and nutrients, and controls on autotroph composition, growth and structure. The four areas are 1) controls on river metabolism and nutrient cycling, 2) surveys of river ecosystem condition, 3) benthic chamber measurements of metabolism, nutrient limitation, and *in situ* nitrogen depletion, and 4) controls on submerged aquatic vegetation (SAV) growth.

We interpreted high resolution time series of flow, pH, dissolved oxygen, nitrate, and phosphate to estimate open-channel ecosystem metabolism and autotroph nutrient use. Clear diel solute variation in both rivers suggests light is the dominant ecosystem control. We observed:

- Silver River is generally net heterotrophic, with ecosystem respiration (ER) exceeding gross primary production (GPP) by roughly 20 %. However, the upper river is net autotrophic (GPP > ER). Alexander Springs Creek is net autotrophic.
- GPP declines with distance downstream in Silver River, largely due to changes in the light regime driven by river morphology. Extreme climate events (e.g., Hurricane Matthew) impacted GPP substantially, especially in Alexander Springs Creek. Year-to-year variation in Silver River GPP was high, with 2015 exhibiting 20-30 % lower GPP and ER than 2016.
- Primary production did not differ significantly between rivers, with mean GPP in the first 5 km of Silver River (headspring to S5) of 7.8 g O_2 m^{-2} d^{-1}, and 8.3 g O_2 m^{-2} d^{-1} in Alexander Springs Creek. ER was significantly higher in Silver River (11.1 g O_2 m^{-2} d^{-1}) than Alexander Springs Creek (6.9 g O_2 m^{-2} d^{-1}), suggesting external sources of organic matter are crucial to Silver River metabolism.
- Upper Silver River (headspring to SILGOLD), a reach that has been historically measured (e.g., Odum 1957; Knight 1980; Munch et al. 2006), exhibited mean GPP of 16 g O_2 m^{-2} d^{-1}, slightly in excess of the earliest measurements (Odum 1957; Knight 1980), and greater than more recent measurements (Munch et al. 2006).
- A benthic light availability model adjusts open-sky irradiance based on solar zenith angles, river azimuth, canopy cover (from MODIS leaf area index estimates) and canopy geometry (height, channel overhang); this model suggests roughly 30% of incident light reaches the river surface. Further light attenuation through the water column was estimated from continuous measurements of fDOM (colored organic matter) and turbidity. This model allowed us to explain 70-80 % of GPP variation.
- *In situ* nitrate (NO_3) and phosphate (PO_4) sensors revealed clear diel signals, implying autotrophs in Silver River induce ~70 µg N L^{-1} diel nitrate variation and ~8 µg P L^{-1} diel phosphate variation, yielding plants demands of 128 mg N m^{-2} d^{-1} and 13 mg P m^{-2} d^{-1}. Combining these with GPP yields C:N ratios for upper and lower Silver River, respectively, of 14 and 23, consistent with the expected stoichiometry of vascular plants (C:N ~ 20) dominating the lower river, and algae (C:N ~ 10) more dominant in the upper river. Molar C:P ratios in the lower river are ~500:1, consistent with algal and vascular plant stoichiometry; C:P in the upper river is implausibly low (~ 110:1) suggesting a strong geogenic P sink. N assimilation is contemporaneous with photosynthesis, but P

assimilation lags GPP by roughly 7 hours. N retention is dominated by heterotrophic processes, with net denitrification accounting for 75 % of the total, consistent with measurements in other springs.

- Assimilation of N and P in Silver River over the 5km reach between the headsprings and S5, and assuming no nutrient recycling, accounts for 1.2 % of N supply; similarly, P demand is 5.5 % of supply. Even at historical N concentrations (0.05 mg N L^{-1}) current assimilatory demand, assuming no N remineralization, represents 34 % of available supply, indicating N limitation of primary producers is, and historically was, unlikely. High rates of GPP in Alexander Springs Creek, where N is at background levels, further supports this inference.

We extensively sampled algal and SAV cover along the entire length of the Silver River, along with a suite of hydraulic, edaphic and ecological variables to explore patterns of, and controls on, variation in primary producer community structure.

- The river exhibited high SAV cover, with 75 % of sites exhibiting >75 % SAV cover, and only 10 % of sites exhibiting <50 % cover. Algal cover was lower, with 50% of sites exhibiting less than 50 % cover.
- A weak but significant negative association between SAV and algal cover suggests a competitive interaction. When SAV cover was low (<50 %), algal cover was high (> 50%), but high SAV cover exhibited algal cover across the entire range.
- There were no clear trends in SAV biomass, root:shoot allocation, stoichiometry or blade length. There was a strong longitudinal decline in algal cover.
- Water column ammonium and phosphate concentrations increase with distance downstream, while sediment Ca and organic matter concentrations decline.
- A weak but significant negative association between surface water velocity and algal cover supports scour impacts on biomass accrual. However, no clear threshold was evident in the association.
- Water chemistry controls on algal and SAV spatial variation were generally weak. Algal cover increased with soil Ca and P concentrations, and SAV declined with porewater and water column Cl, porewater Ca and % clay. The best predictor of SAV cover was algal cover, and vice versa.

We used benthic chambers to measure ecosystem metabolism in response to factorial nutrient additions (N, P, Fe). Control chambers were further instrumented with continuous nitrate sensors to explore N uptake kinetics below ambient concentrations.

- Control-box GPP was highly variable across sites, but highly predictable ($R^2 > 0.8$) based on incident light and water depth. In Silver River, GPP varied slightly with sediment type, and showed clear seasonality.
- No clear nutrient enrichment effect was observed for GPP in Silver River, either for raw GPP (i.e., GPP_{treat}:$GPP_{control}$) or when normalized by biomass standing stock. In Alexander Springs Creek, we observed a consistent inhibitory effect of P, but no effect of N or Fe despite low ambient levels of both. Pooled treatments suggested a weak but significant Fe enrichment effect in Silver River, and no effect in Alexander Springs Creek. These results suggest nutrient enrichment has limited impact on primary production in both rivers.

- Growth tiles in each chamber informed nutrient enrichment effects on algal growth. Control chamber growth rates were not significantly different between rivers, and algal accumulation on tiles was not strongly associated with GPP. Only Fe exhibited a significant growth response in Silver River, and none of the three nutrients impacted algal growth in Alexander Springs Creek.
- Nitrate sensors in control boxes yielded signals consonant with open channel measurements of both assimilation and denitrification. Rapid N depletion was typical, with concentrations at the end of deployments near 0.05 mg N L^{-1}. Stair-step depletion patterns suggest multiple retention processes. Model fitting enabled estimation of both process rates and kinetics. A 2-process model (assimilation proportional to sunlight + denitrification) best fit the time-series in 85 % of cases.
- Denitrification was a 1^{st} order process, with retention rates linearly dependent on concentration. Across deployments (n = 25) denitrification kinetic order varied between 0.75 and 1, consistent with literature observations. This is the first time *in situ* reactions have been enumerated over such a large concentration gradient.
- Assimilation was a 0^{th} order process (i.e., independent of concentration), with a mean kinetic exponent <0.2. Plant N uptake is not strongly influenced by concentration variation over the range of observed concentrations, suggesting N saturation, even at low levels. Exploring Monod kinetics (i.e., zero-order at high concentration, 1^{st} order at low concentration) is an area for further research; the Monod half-saturation parameter may be of regulatory interest.
- No association was observed between nitrate concentration and GPP, suggesting that even the kinetic response in nitrate assimilation is principally the autotrophs utilizing alternative N sources to support growth. Despite dramatic declines in N availability during chamber deployments, GPP increased, suggesting that efforts to reduce N concentrations in springs are unlikely to induce N limitation and thus may have limited impact on autotroph structure, composition, and biomass accrual.

We measured submersed aquatic vegetation (SAV) growth over 18 months at Silver River and 12 months at Alexander Springs Creek. The 16 sites in each river spanned the range of observed benthic conditions (algal cover, sediment properties, light, flow velocity). We focused site selection to measure the two dominant taxa (*Sagittaria kurziana and Vallisneria americana*).

- SAV growth was not significantly different between rivers, nor across species in Silver River (where both were present). Growth rates were correlated with standing biomass in Alexander Springs Creek, but not in Silver River. Sampling logistics precluded measurements in the deepest, most productive parts of Silver River.
- SAV growth was high spatially variable in both rivers, with site means ranging over an order of magnitude in both rivers (between 0.4 and 2 g dry mass m^{-2} d^{-1}). Spatial variation was much larger than temporal variation, though there was clear evidence of seasonality, with peak SAV growth in the summer.
- Multivariate models of SAV growth were successful (R^2 ~ 0.5) at predicting observed spatial and temporal variation. Two contrasting methods identified light as the dominant control, with porewater soluble reactive phosphorus (inhibiting SAV growth), and redox potential (enhancing SAV growth) also significant in both rivers. Model consonance across methods and rivers supports redox and light management as key factors for

ecosystem management and restoration. Inhibitory effects of porewater SRP are poorly understood and merit further research.

- In both river, SAV contributes approximately 25% of total primary production (measured using open channel metabolism, and adjusted to estimate net production). Primary production due to other autotrophs, or in unsampled locations, is critically important for riverine primary production.

6.2 INTRODUCTION

The St. Johns River Water Management District (SJRWMD), in partnership with the University of Florida (UF), has initiated the SJRWMD-UF Springs Protection Initiative – Collaborative Research Initiative on Sustainability and Protection of Springs (CRISPS). A detailed background and set of major objectives and questions related to Silver River nitrogen dynamics are presented elsewhere, with a primary goal of predicting how nitrogen enrichment impacts primary producer community structure and function, and whether N reductions alone (to meet the statewide springs numeric nutrient criterion of NO_3-N < 0.35 mg L^{-1}) will be sufficient to restore community structure. The purpose of this annual report is to describe four (4) research elements to address that primary goal, with links explicitly made to other elements of CRISPS: 1) quantify continuous river metabolism (C cycling) and nutrient dynamics (N and P cycling) using *in situ* sensor data collected by SJRWMD; 2) comprehensive survey of the benthic condition of Silver River, including vegetation composition and abundance, water column and pore water chemistry, and sediment characteristics; 3) *in situ* pathway-specific nitrogen depletion experiments with factorial investigation of sediment, vegetation and trace nutrient effects; and 4) *in situ* SAV growth experiments with factorial evaluation of sediment/porewater variation, algal cover, light regime and velocity.

Silver River has been the primary field site for these measurements, and most of the results presented in this report are from that system. However, we also sampled in Alexander Springs Creek for metabolism measurements, benthic chamber experiments, and SAV growth assessments to provide a low N site for comparison.

This report is divided into four sections, corresponding to the work elements outlined above. In each section, we describe the rationale, methods, and preliminary results from efforts to date. We close with a synthesis of findings across work elements, and recommended next steps.

6.3 ECOSYSTEM METABOLISM

Ecosystem metabolism is an integrative measure of autotroph and heterotroph activity. Using diel variation in dissolved oxygen concentrations (Odum 1957; Munch et al. 2005), it is possible to estimate C fluxes associated with aggregate gross primary production (GPP), and whole ecosystem respiration (ER). Based on published estimates of autotroph respiration, it is also possible to estimate respiration due to microbes and animals. Exploring temporal and spatial variation in ecosystem metabolism provides an important foundation for understanding specific ecological behaviors. For example, does an increase in biomass correspond to an increase the rate of primary production? Similarly, how does variation in flow, light (seasonal and day-to-day), and chemistry impact metabolic behavior at the ecosystem scale? Recently, sensor

advances have enabled an expansion of the logic behind the diel oxygen method to also include ecosystem N and P dynamics (Heffernan and Cohen 2010; Cohen et al. 2013), from which autotrophic ($U_{a,N}$, $U_{a,P}$), heterotrophic (U_{den}) and geochemical ($U_{geo,P}$) removal pathways can be determined; metabolism measurement nomenclature is summarized in Table 6.1. This advance allows coupling between C, N and P element cycles to be made explicit, and to ask questions about how changes in both time and space in metabolism or ecosystem structure affect the ecosystem's capacity to process nitrogen. Given the central role that N and P processing plays in the rationale for setting statewide water quality standards for springs (especially for N), this coupling is integral to understanding how and why springs change, and for interpreting the responses to ongoing restoration activities.

Table 6.1. Summary of metabolism variables, their associated symbols, and units.

Variable	Symbol	Units
Gross Primary Production	GPP	g O_2 m^{-2} d^{-1}
Net Primary Production	NPP = 0.1875 * GPP	mol C m^{-2} d^{-1}
Ecosystem Respiration	ER	g O_2 m^{-2} d^{-1}
Net Ecosystem Production	NEP = GPP - R_E	g O_2 m^{-2} d^{-1}
Production:Respiration	P:R	Unitless
Autotroph N assimilation	$U_{a,N}$	mg N m^{-2} d^{-1}
Denitrification	U_{den}	mg N m^{-2} d^{-1}
Autotrophic P assimilation	$U_{a,P}$	mg P m^{-2} d^{-1}
Abiotic P retention	$U_{geo,P}$	mg p m^{-2} d^{-1}
Ecosystem stoichiometry*	NPP:$U_{a,N}$:$U_{a,P}$	Unitless

* - Note that for ecosystem metabolism stoichiometry, autotroph P and N assimilation is on a molar basis.

Metabolism data are most informative when they are continuous and long term (e.g., Roberts and Mulholland 2007). As part of this project SJRWMD deployed and maintained dissolved oxygen, phosphate, and nitrate sensors, along with a suite of ancillary solute measurements (pH, temperature, specific conductance fluorescent dissolved organic matter or fDOM, turbidity) at multiple locations in the Silver River, providing estimates of metabolic behavior (GPP, R, $U_{a,N}$, $U_{a,P}$, U_{den}, $U_{geo,P}$) over extended periods of time. These measurements serve as a foundation for assessing changes in the river, and for interpreting the finer-scale results from other elements.

6.3.1 Data Availability and Methods

Sensors were initially deployed at four locations over the 10 km length Silver River before the confluence with the Ocklawaha River (Figure 6.1), and two in Alexander Springs Creek. At Silver River, the 4 sensor suites were initially installed at SILHEAD (near the bank 50 m from Mammoth Spring), SILBIRD (at the USGS gage structure 1.2 km downstream of the head spring, S5 (at a SJRWMD Minimum Flows and Levels (MFL) transect station 5900 m downstream of the head spring), and SILCONN (near the confluence with the Ocklawaha River). Initial data from these sites suggested challenges to their validity. Specifically, the SILHEAD site was a clear spring-vent signal when the vegetation near the sensor suite was removed, but reverted to a far stronger riverine signal as vegetation occluded flow. Because it is impossible to ascertain when the sensor was accurately reflecting the spring vent boundary condition, versus when it represents that signal plus significant benthic reactivity, we have omitted this station

from all subsequent analyses. The sensors at the SILBIRD site were found to be sampling water from the Ft. King Waterway (a man-made bypass channel that receives water from the headsprings, but has a much longer residence time). As such, interpretation of chemical changes as representative of the upper river ecosystems are problematic, and sensors were deployed instead at the SILGOLD site just upstream and demonstrably in the main river advective zone. Similarly, the SILCONN site was clearly not sampling the advective zone of the river, but rather a backwater area for which hydraulic exchange was slow. This was manifest as implausibly high diel DO variation, implausibly low nitrate concentrations compared to measured channel chemistry, and implausibly late DO peaks (suggesting low reaeration rates in that quiescent water). As such, we also have omitted this station from further analysis. In response to this feedback about sensor locations vis-à-vis the advective zone of the river, SJRWMD discontinued sensor measurements at SILCONN and enabled measurements at S1 (an MFL transect location 8,900 m downstream of the spring vent, but slightly upstream of SILCONN). Sensors at previous stations (SILCONN, SILBIRD) were outside the advective zone, and were moved to SILVERRIVERS1 and SILGOLD, respectively. The central lesson from these challenges is that riverine nutrient sampling for open channel metabolic and nutrient processing needs to done in the river thalweg where hydraulic exchange is maximum

Figure 6.1. Locations of sensors at Silver River, from near the head spring (Mammoth; no sensors) to the confluence with the Ocklawaha (SILVERRIVERS1).

despite the logistical challenges of deploying continuous monitoring equipment far from the river bank. A further challenge was identified following the first dye trace done as part of the larger CRISPS project. That dye, released at the Mammoth Head Spring identified that the water passing the USGS gage and thus the sensors at SILBIRD was mostly from the Ft. King Waterway, and not from the main stem of the river (Figure 6.2). This does not impact the flow measurements, but dramatically impacts measures of any solute variation and associated inference of metabolism. Again, these data were judged to be poorly informative of the Silver River and were thus omitted. In response to this concern, SJRWMD deployed the sensor suite at an alternative location (SILGOLD; a site 800 m downstream of the spring vent). Our analysis of these data suggests that time series from SILGOLD, S5 and S1 are valid representations of the river. As such, the remainder of this analysis works only with the available time series of oxygen

and nutrient data from these three locations (Figure 6.1). We note that only S5 has data prior to 2016.

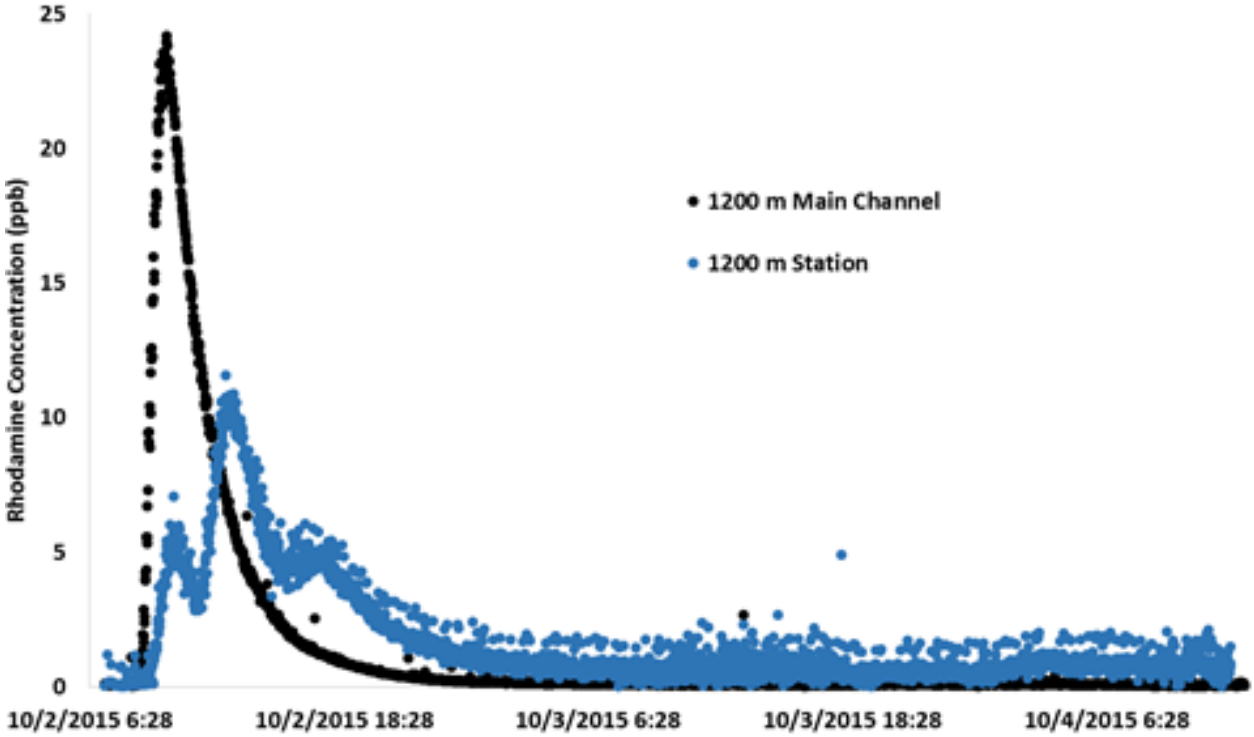

Figure 6.2. Breakthrough curves of dye at the 1200 m station (SILBIRD) illustrating the slower velocity and multi-model arrival. Dye breakthrough at a nearby location (less than 50 m away from SILBIRD, but in the advective zone of the river) are commensurate with expectations.

The sensor suite in Alexander Springs Creek has one station at the spring vent; because the second station is far downstream (ca. 10.5 km below the spring vent at the Tracy Canal site), whole-river metabolism can be effectively assessed using the one station method, obviating the need to use the upstream boundary condition (Figure 6.3). No nutrient data were available for the Tracy Canal site, so our analysis focuses on the metabolic behaviors of the river over the period of record.

Figure 6.3. Map of the Alexander Springs Creek system showing the headspring sensor suite near the main boil, and the Tracy Canal site approximately 10 km downstream.

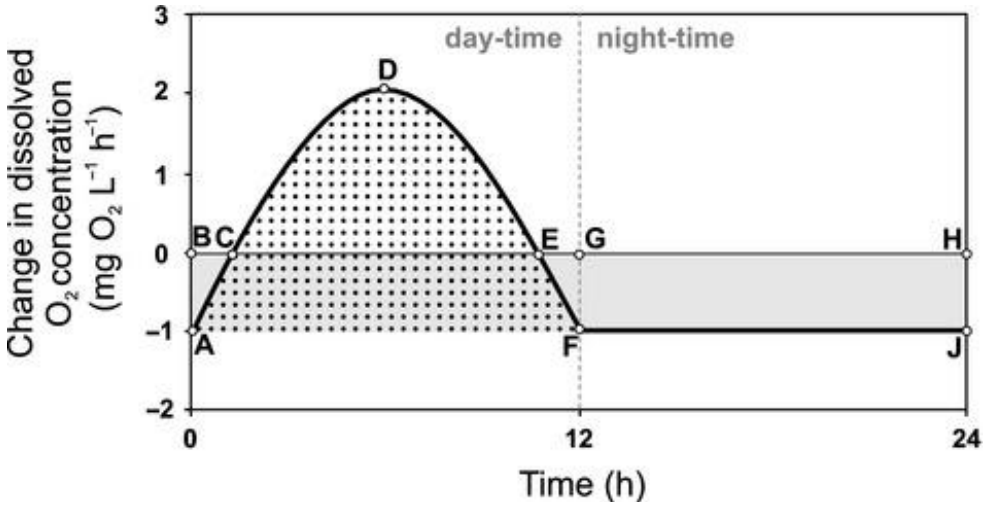

Figure 6.4. Schematic of metabolism inference from diel dissolved oxygen variation, showing calculation of primary production (GPP; stippled area) and ecosystem respiration (ER; grey area). Both GPP and ER are sensitive to reaeration estimates (k; hr^{-1}).

The conceptual model for the metabolism measurements is depicted in Figure 6.4, follows the logic originally described in Odum (1956), and is still widely used for lotic ecosystem primary production and respiration measurements today. In short, the daily excursion of oxygen production from a nighttime baseline is attributed to primary production. Respiration is inferred from the oxygen mass balance at night, during which gas concentrations represent the equilibration between respiration and the reaeration flux from atmospheric oxygen. Throughout,

except where stated specifically, we calculated metabolism using the two-station method due to the constant upstream boundary conditions typical in a spring-fed river. The two-station method requires DO signals at the upstream and downstream locations be temporally aligned based on the mean travel time between them. The change in DO between stations is attributed to net ecosystem production (NEP), which is net metabolism or GPP minus ER, and reaeration (E).

$$\Delta DO = NEP + E$$

Reaeration is maximum reaeration constant (k) times the instantaneous measured saturation deficit in dissolved oxygen, measured in % saturation. In this formulation, k has units g m^{-2} d^{-1} or hr^{-1}, and the reaeration flux into the water column from the air is estimated by:

$$E = k(1 - DO_{\%sat})$$

We estimated k using an equation obtained from floating dome measurements in Silver River and other spring-fed river sites (Munch et al 2006):

$$k = 0.0604u + 0.0929$$

where k is in g m^{-2} h^{-1} and u is mean velocity in cm s^{-1}. Note that the velocity is crucial information in two regards, both as the sole variable used to predict the reaeration constant and as the means to assess the signal offset between upstream and downstream signals.

ΔDO increases during the day due to photosynthesis, reaches a maximum, and then decreases at the end of the day. The daily excursion of dissolved oxygen is net ecosystem production (NEP). ER is calculated from the ΔDO minima of the night before and after each day. GPP is then estimated as the sum of ER and NEP:

$$GPP = NEP + ER$$

Metabolism in this way is on a volumetric basis, which can be converted to a rate per unit benthic area (i.e., g O_2 m^{-2} d^{-1}) by multiplying by daily discharge and dividing by benthic area between the sensors. Discharge was obtained from the USGS gage 02239501 (at SILBIRD), and we assumed it was constant along the entire length of the Silver River. For Alexander Springs Creek, we used the same assumption applied to gage data from SJRWMD (Station # 18553786). Our benthic area footprint in Silver River was based on the average river widths of MFL transects in each reach; in Alexander River, we processed aerial imagery to estimate river widths, and reach lengths.

Because mean velocity determines travel time between the upstream and downstream stations, metabolism estimates can differ appreciably depending on the velocity used (Figure 6.5). We originally used mean velocities from the four dye traces conducted by the Hydrodynamics Group, but discovered those velocities can vary greatly in time (Figure 6.5). Another tool to assess selected velocity measurements is lining up the DO peaks from the combination of the two stations. Simply choosing the velocity that created the smoothest NEP graph was too subjective: Figure 6.6 illustrates that 0.17 m s^{-1} or 0.19 m s^{-1} are nearly identical. Ultimately, we

decided that modeling the velocity time-series on Silver River was necessary for accurate metabolism estimates. To that end, we used the SJRWMD survey of MFL transects to create a stream elevation to cross-sectional area rating curve, and then used the time-series of stream elevation at each transect to infer daily cross-sectional areas. We then modeled velocity by dividing measured discharge (Q) by this daily cross-sectional area (A) at each MFL transect and averaging all transects within each reach. To estimate continuous stream elevation profiles, we used a linear relationship between velocity and discharge from the previous years to estimate velocity. Modeled velocities are shown in Figure 6.5. Generally, they mirror discharge. However, they clearly diverge from the dye trace velocities calculated from mean residence time of Rhodamine WT breakthrough curves. The divergence is especially notable in the lower river. One possible explanation is that the stage to discharge relationship is not as accurate at very low stage (24 August 2016 and 8 December 2016) or when the Ocklawaha River backs up (2 October 2016). It is important to note, however, that the upstream and downstream reaches of the dye traces are not the same reaches used to calculate metabolism.

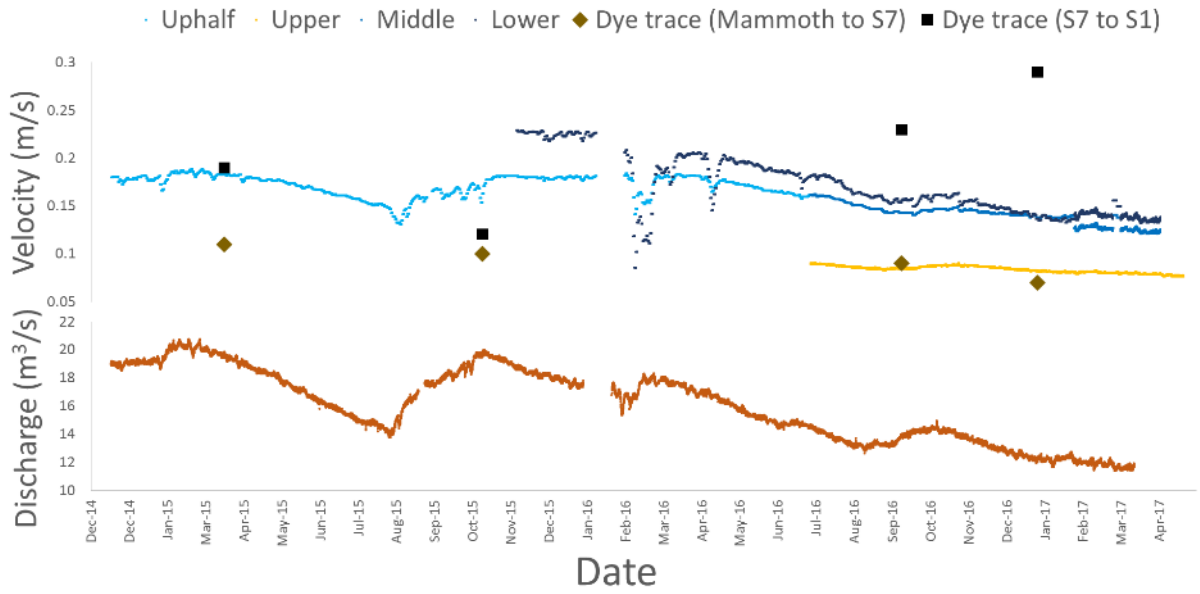

Figure 6.5. Time series of Silver River discharge (orange line) and estimated velocities at three sampling locations based on channel cross-sections (light and dark blue dots). Measured velocities from the dye injections (squares and diamonds) agree with mean velocity, but not time variation. To estimate both travel time and reaeration on each day, we used velocity estimates from channel cross sectional areas.

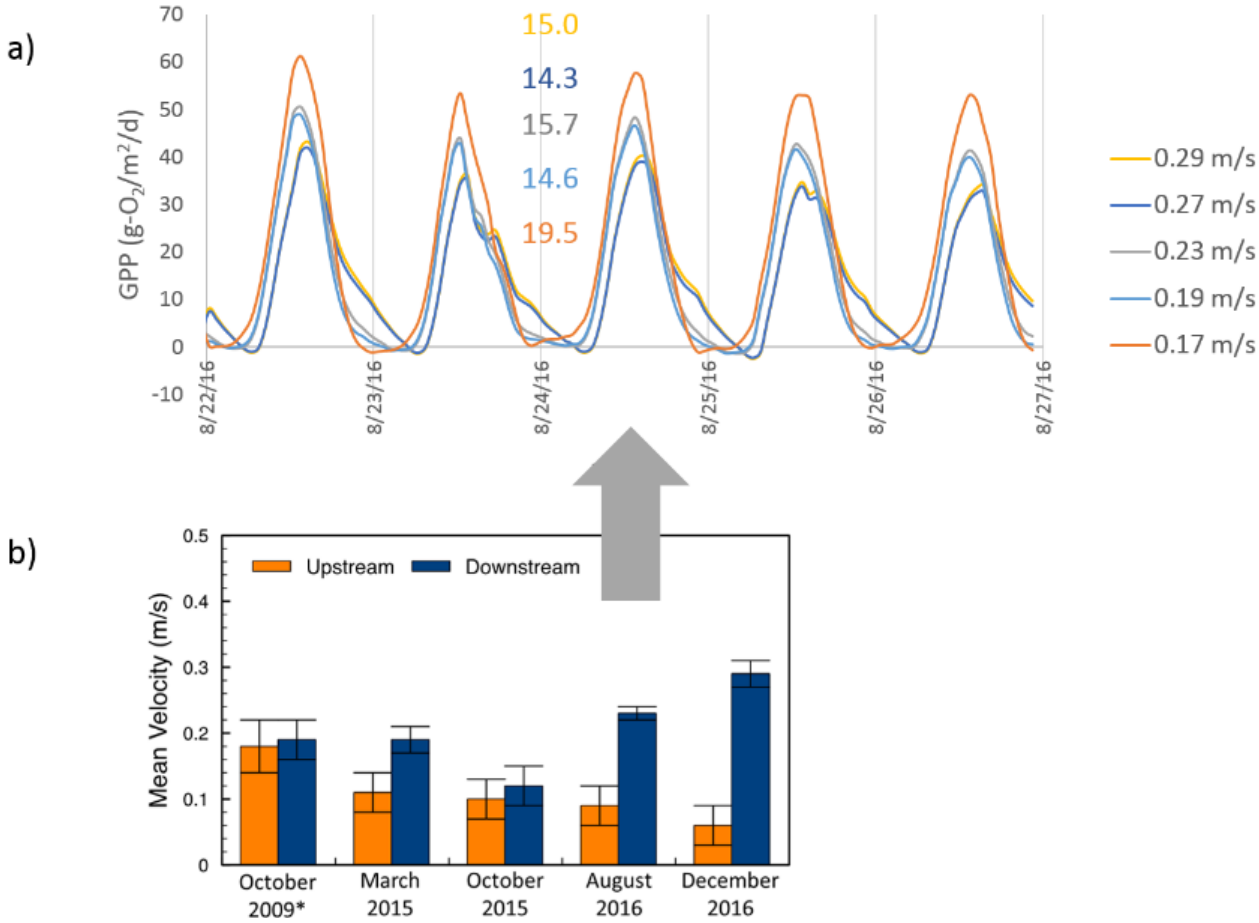

Figure 6.6. Reach mean water velocity (numbers at right in the upper panel) significantly impacts inference of GPP (25% variation or more). The lower panel shows dye trace velocities in upper and lower Silver River and propagates that range through the observed DO data (upper panel). To reduce uncertainty, we estimated daily velocity from discharge and cross-sectional area information.

Using continuous time series (e.g., 15 min sampling resolution) of DO and various environmental variables (Figure 6.7), and NO_3-N and SRP (Figure 6.2), as well as discharge information and travel times (see above), we constructed daily estimates of GPP, R, $U_{a,N}$, $U_{a,P}$, U_{den} and $U_{geo,P}$ using existing analytical templates developed by Cohen et al. (2013) for spring-fed rivers.

Among the notable features of the period of record data from Silver River (Figures 6.7 and 6.8) and Alexander Springs Creek (Figures 6.9 and 6.10) is that the field parameters are nearly continuous, and highly reliable. This includes dissolved oxygen, temperature, pH, and specific conductance. The availability of continuous nutrient data is less complete even though this data set represents perhaps the longest and most complete river nitrate records. In Alexander Springs Creek, SJRWMD nutrient data were available only for the headspring, and thus not useful for inferring river ecosystem nutrient processing rates; previous work (Cohen et al. 2010) explore reach-scale N processing in Alexander Springs Creek. This section of the report details primary production and respiration behavior for all reaches (upper, up-half, middle, lower on Silver; the

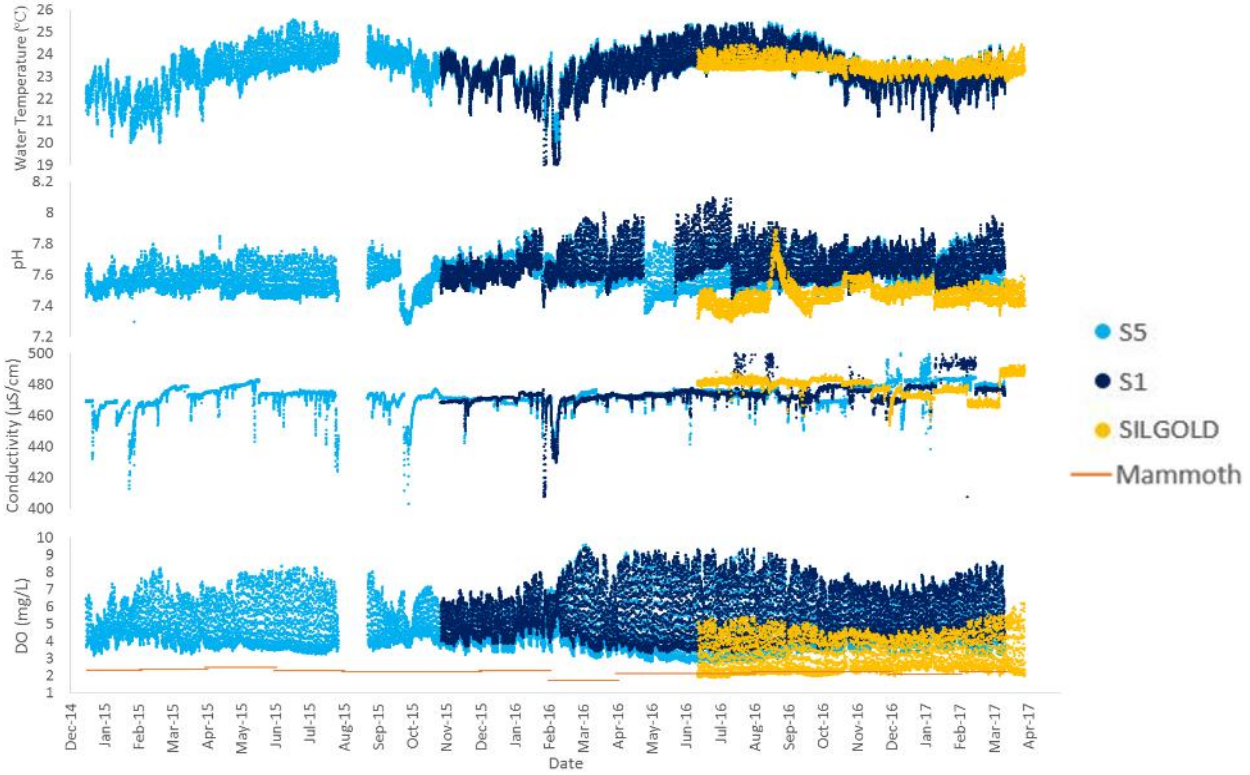

Figure 6.7. Diel variation in water temperature, pH, specific conductance and dissolved oxygen for SILGOLD (yellow), S5 (light blue), and S1 (dark blue) stations on Silver River.

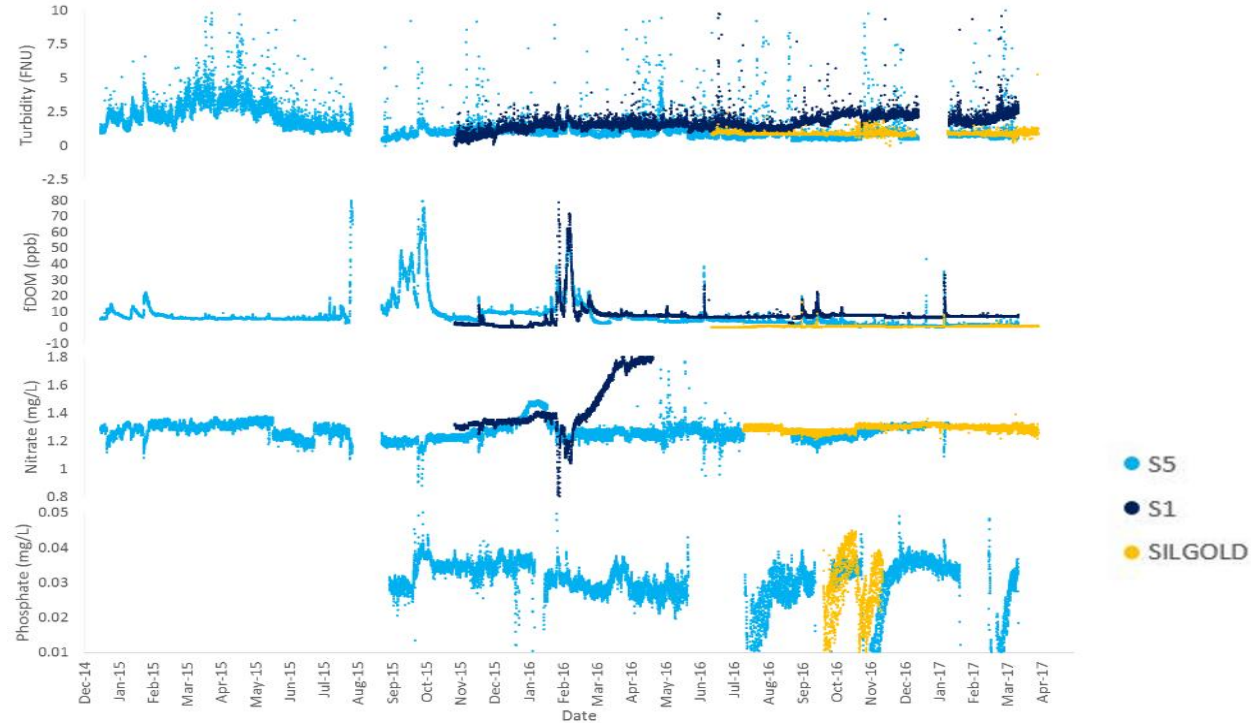

Figure 6.8. Diel variation in turbidity, fluorescent DOM (fDOM), nitrate and phosphate for the three stations on Silver River. Note that no phosphate sensor was deployed at site S1.

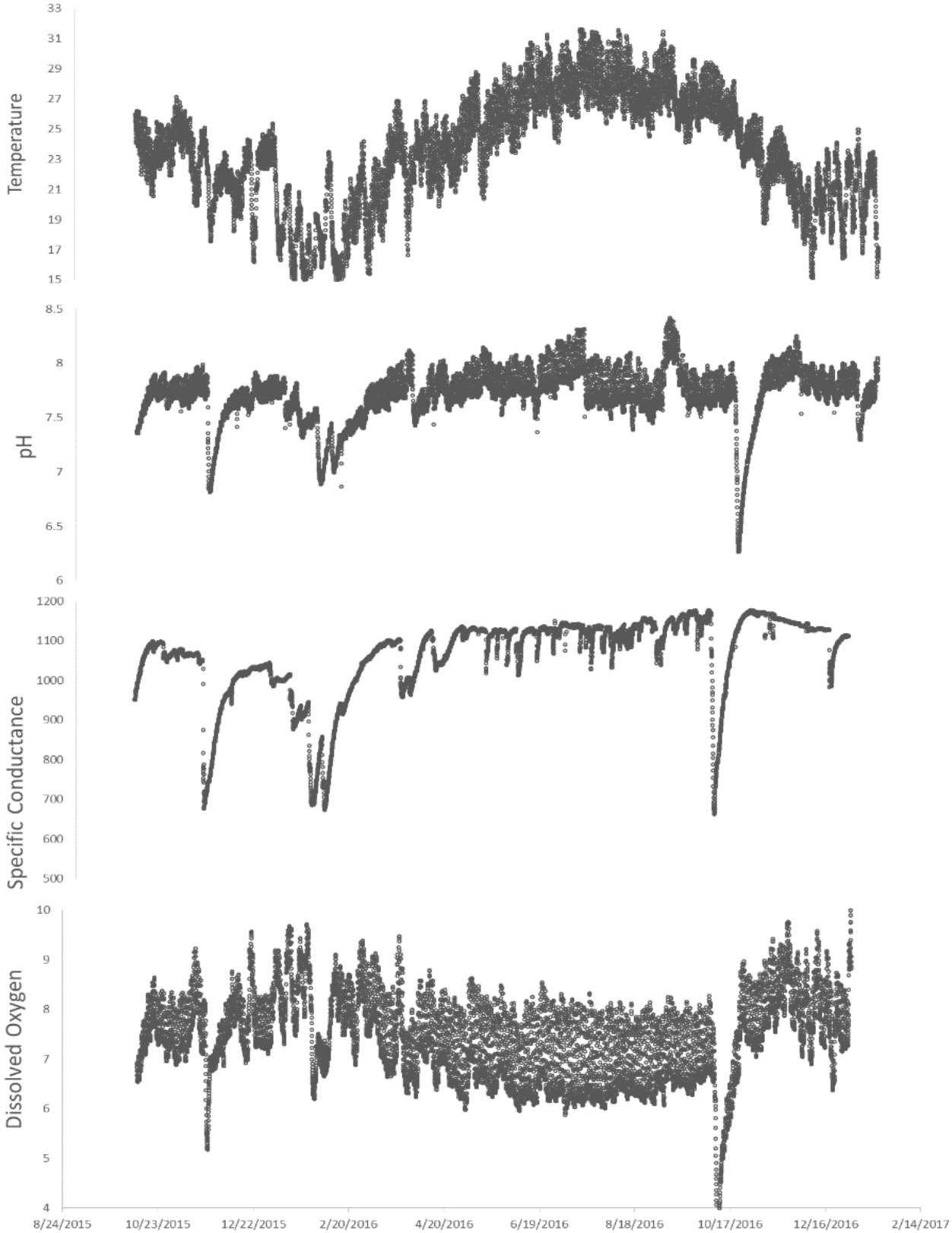

Figure 6.9. Summary of period of record data for Alexander Springs Creek at Tracy Canal. No nutrient data were available for downstream sites in this river.

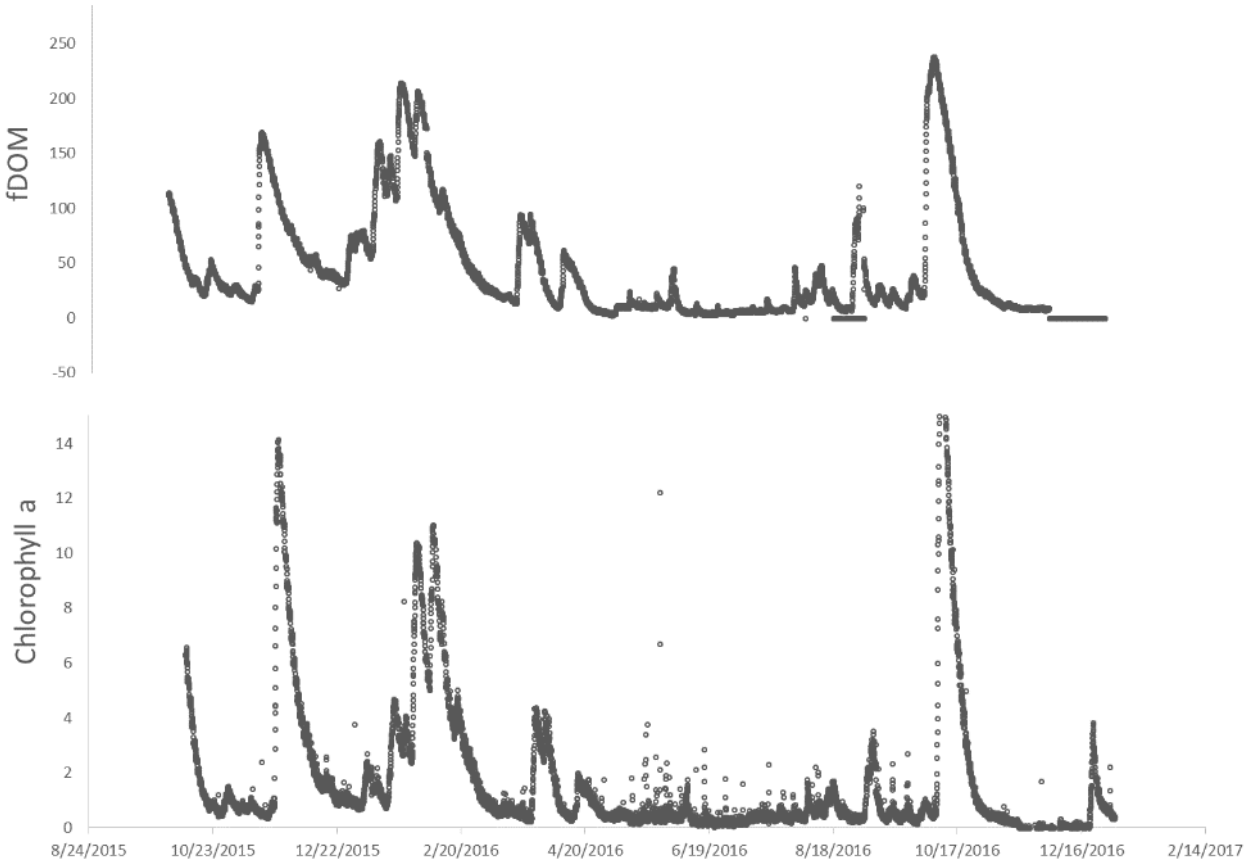

Figure 6.10. Time series of fDOM and chlorophyll a at Tracy Canal in Alexander Springs Creek.

entire river in Alexander), but provides estimates of nutrient dynamics principally at Silver River S5. Data were analyzed for SILGOLD for a short period of time, and not at all at S1. This latter limitation stems from the dramatic concentration enrichment anomaly observed at that station, the origins of which are unclear but have been observed elsewhere in response to biofouling, the fact that concentrations even before the onset of the anomaly are above the S5 levels (and the absence of deionized water blanks during routine maintenance), and that the diel signals are extremely hard to discern because of the digital truncation of the data employed to simplify data logging. Moreover, the covariate data for predicting primary production (i.e., fDOM and turbidity) have been substantially cleaned to present the data shown; field calibration corrections, zero-offsetting (to prevent negative values) and aligning time-series were data processing steps.

One aspect of quality control screening on data received was to examine the fine scale variation of the signal. These fine scale variations are the basis of the inferences about metabolism and nutrient assimilation and cycling, and are thus integral to our efforts.

Figures 6.11 and 6.12 show example data, zoomed in to indicate clear diel variation in almost all riverine measurements. This time period, starting in late August 2016, was selected because all three stations were online simultaneously for all solutes, and because there is a significant rain event in early September that helps illustrate the riverine response to daily variation in light forcing, and thus the integrated system that is stream metabolism. Similar data were obtained for

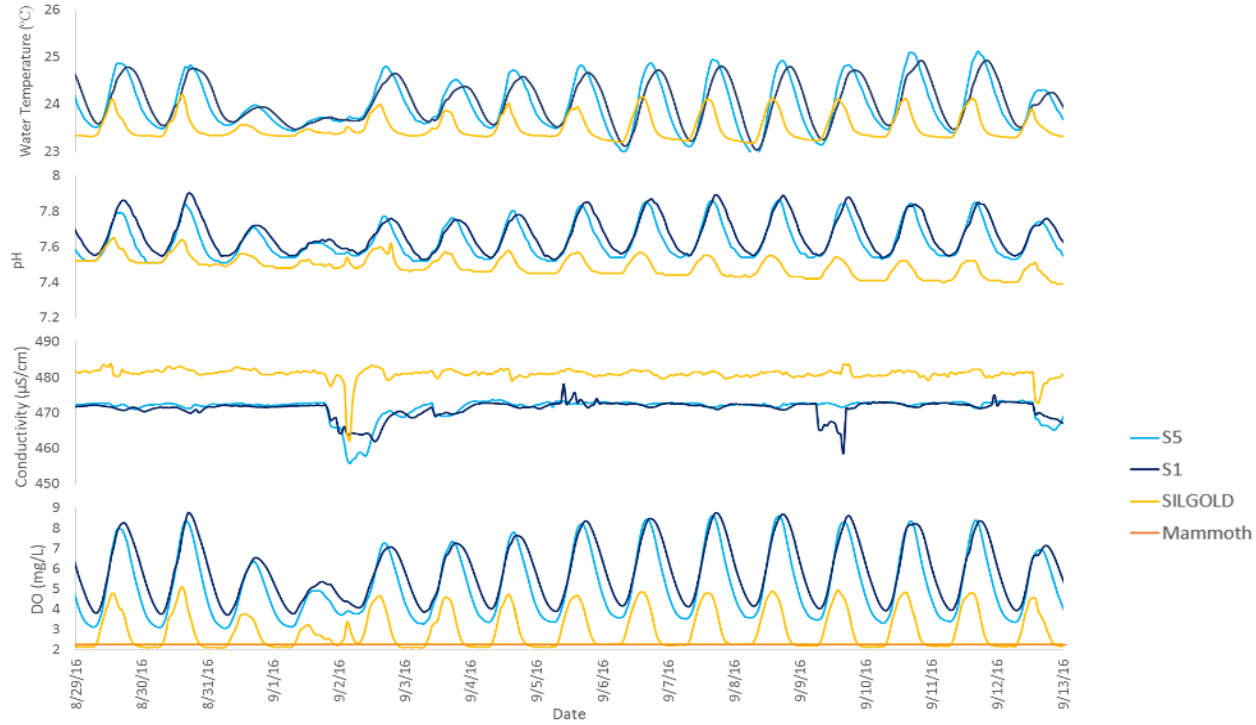

Figure 6.11. Fine scale variation in solute chemistry in Silver River over two-weeks starting in late August 2016. This period was selected because it shows all three sensor stations, and also the influence of a significant rain event at the beginning of September on the various signals.

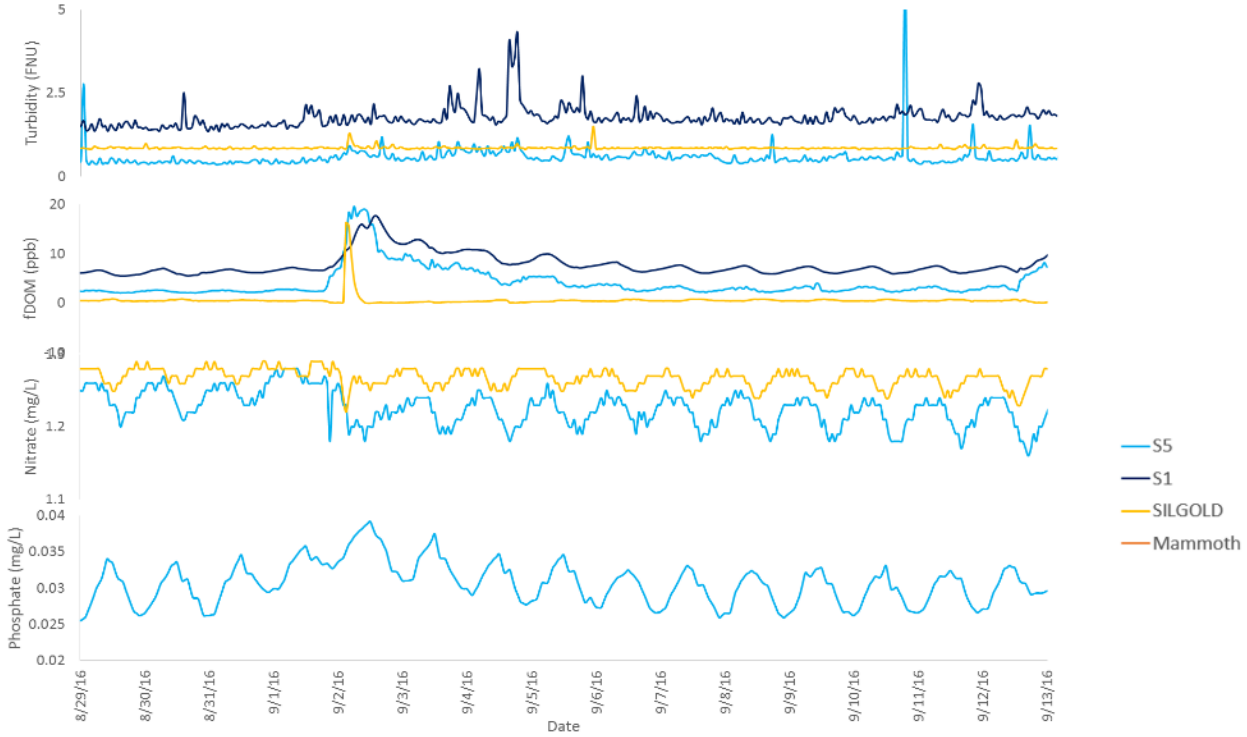

Figure 6.12. Two-week period of record showing diel variation in fDOM, nitrate and phosphate. Note that the timing of diel P variation is out of phase with diel N variation.

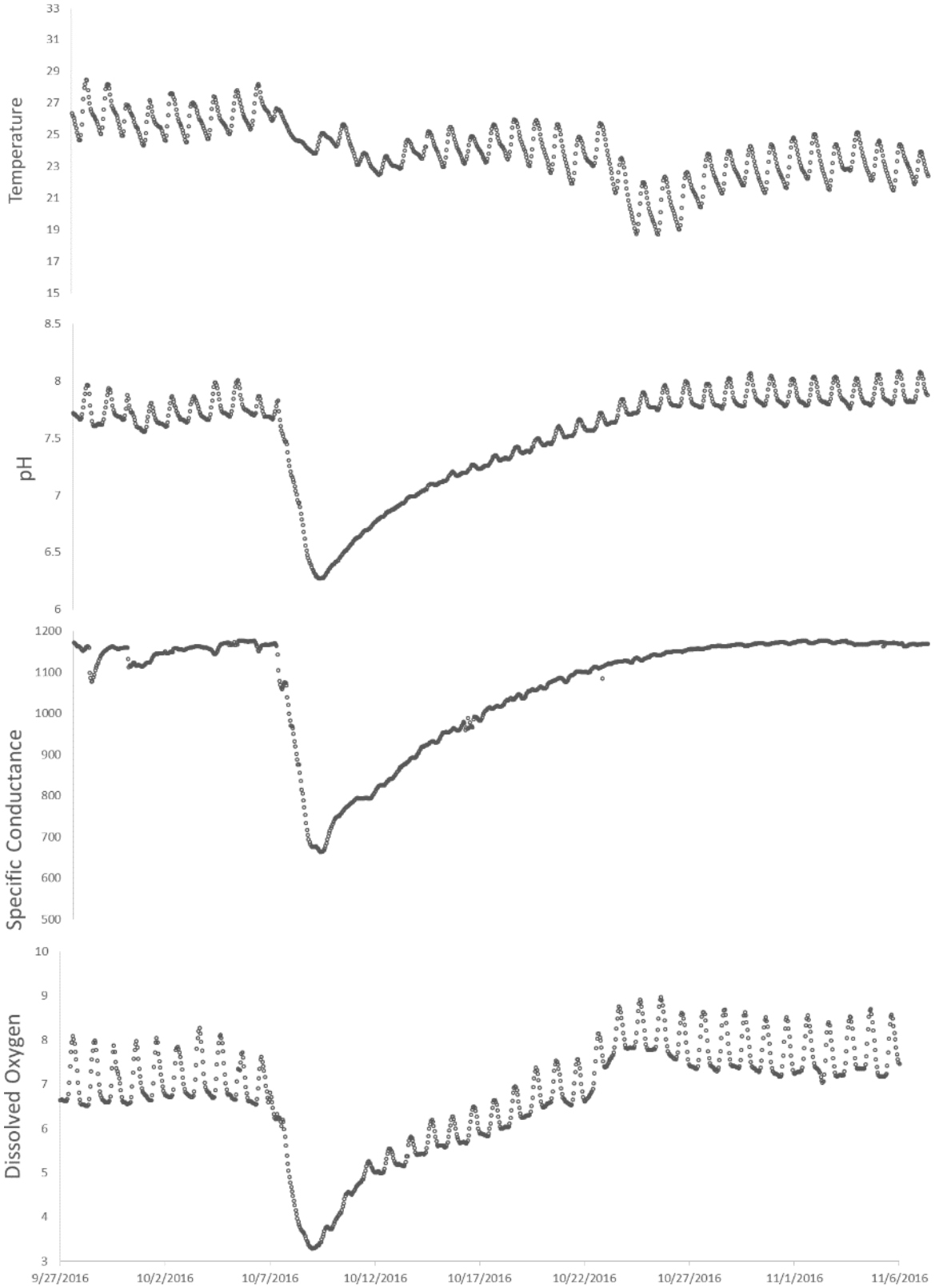

Figure 6.13. Two week period in Alexander Springs Creek containing a significant rain event (Hurricane Matthew) and the subsequent solute recovery as surface sources from swamps along the spring run cease to contribute significant water.

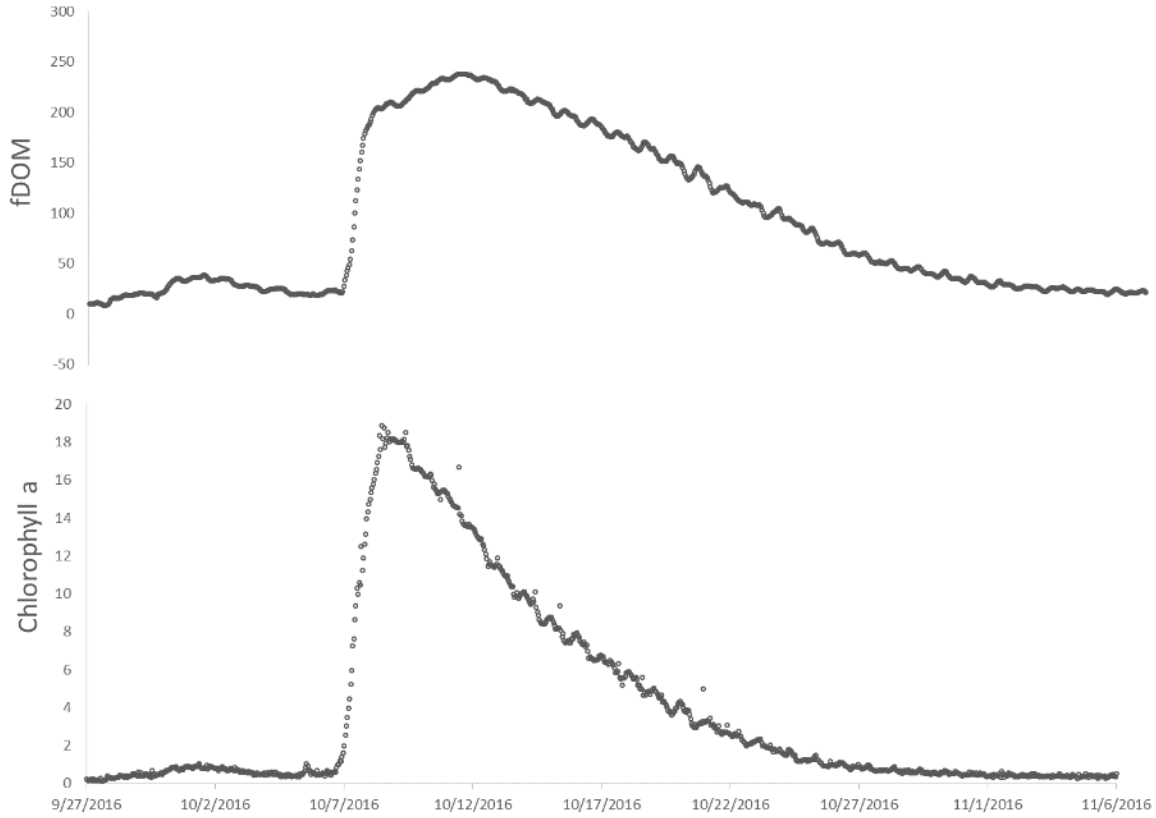

Figure 6.14. Two week period containing Hurricane Matthew during which fDOM increases, as expected, but also chlorophyll a increases.

Alexander Springs Creek (Figures 6.13 and 6.14), except for nutrient data, which were not collected. Diel variation in temperature and pH are related to thermal and metabolic impacts of solar forcing respectively (Figures 6.11 and 6.13 for Silver and Alexander, respectively). Commensurate variation in DO, nitrate and phosphate are also clear (Figures 6.11 and 12 for Silver, DO only in Figure 6.13 for Alexander); note that the phase of these diel signals is different. Notably, temperature, pH and DO are at their diel maximum in late afternoon, consistent with peak solar forcing and the time lags induced by water transport and (in the case of DO and pH) gas evasion. Nitrate peaks at night, with a diel minima consistently in the late afternoon, suggesting that the diel signal is mostly imposed by the action of autotrophs assimilating nitrate, and further that this process is confined to periods when photosynthesis is active. We note that nitrate data provided online are truncated to two significant digits despite evidence that the sensor can resolve nitrate concentrations in the third decimal place. Our analysis is performed on higher resolution data manually extracted from the sensor during regular maintenance visits, but not available from the SJRWMD web-portal. Diel variation is also evident for phosphate, but with a diel maxima at midday, and minima just after midnight; this divergence in the diel signals between nitrate and phosphate has been previously observed in spring-fed rivers (Cohen et al. 2013), and suggests that the timing of autotrophic assimilation is regulated by plant physiology to be out of phase with sunlight, and that N and P assimilation pathways at the ecosystem scale are temporally decoupled.

Diel variation is also evident in the time series of specific conductance (SpC), likely due to the effects of changing pH on mineral saturation state (leading to calcite precipitation, and the loss of ions from the water). The significant change in SpC in mid-March is associated with a storm, which lowered the nominal concentration, likely in response to direct rainfall. Note that the peak ionic retention (SpC trough) occurs slightly before peak pH. Evidence of consistent diel variation in turbidity and fDOM are also present, though we note that both are at very low levels; with raw data often containing negative values, especially in the case of fDOM. This indicates that these sensors are operating outside their optimal range. Despite this data caveat, the timing of diel turbidity increases and fDOM decreases is consistent with solar forcing and with event driven variation in water sources; sunlight induces pseudo-plankton generation and mineral sediment fluxes, leading to increased turbidity, and photolyzes chromophoric DOM, leading to lowered DOM. We note that chorophyll a and fDOM have similar but not identical time series in response to Hurricane Matthew, a significant rain event in early October 2016 (Figure 6.14). While the observed response may represent algal biomass mass mobilized by increased flows, it seems more likely that the fluorescent composition of tannic waters draining the fringing swamps yields dissolved organic matter that fluoresces in the same region a chlorophyll a. This represents one of the key limitations with optical DOM data. Diel variation in both chlorophyll and DOM is evident as concentrations return to normal with cessation of wetland flow.

6.3.2 Metabolism Results

Figures 6.15 and 6.16 show daily GPP, ER, and NEP over time for Silver River. Figure 6.15 compares the upper, middle, and lower reaches during the same time frame. Since the upper half and lower reaches have much longer periods of record, Figure 6.16 plots metabolism for their entire periods of record. There are gaps in the dataset where either discharge or DO data was not recorded. Figure 6.17 shows the period of record response in Alexander Springs Creek.

There is strong evidence of seasonality in both rivers, with far higher GPP and ER in the summer and autumn than in the winter. Notably, however, NEP does not exhibit marked seasonality. This suggests that respiration in these rivers is largely governed by autochthonous production, and not the delivery of organic materials from adjacent and remote sources (e.g., floodplain, emergent vegetation). We note, however, that diel DO dynamics can only capture aerobic respiratory pathways. In both rivers where the sediments are strongly anoxic and considerable evidence (e.g., benthic survey results presented later in this section and results from the Benthic Sources of Nutrients and Trace Elements section of the larger CRISPS report) exists for the utilization of alternative electron acceptors (e.g., nitrate, sulfate), the potential for significant anaerobic respiration is high.

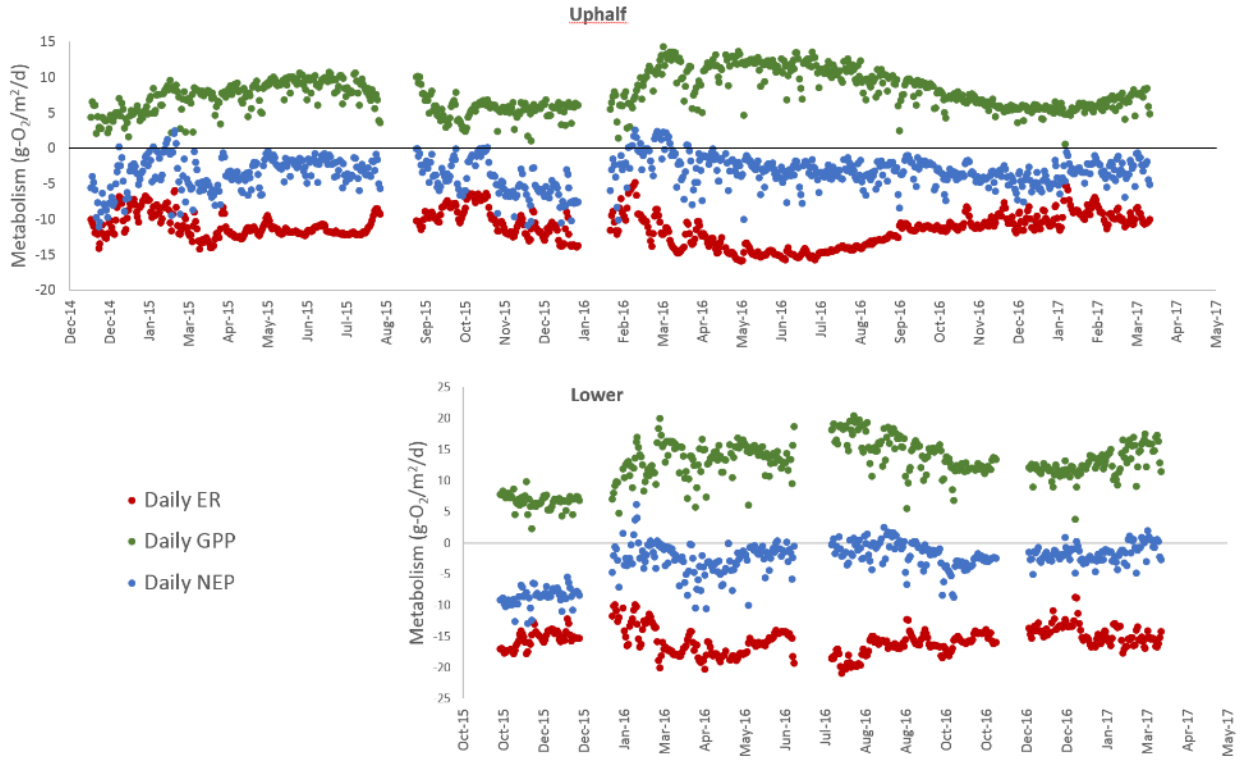

Figure 6.15. Respiration (ER), gross primary production (GPP) and net ecosystem production (NEP) in Silver River over the period of record for S5 (upper half of Silver River; top) and S1 (lower half of Silver River; bottom). Both reaches are slightly net heterotrophic (NEP<0).

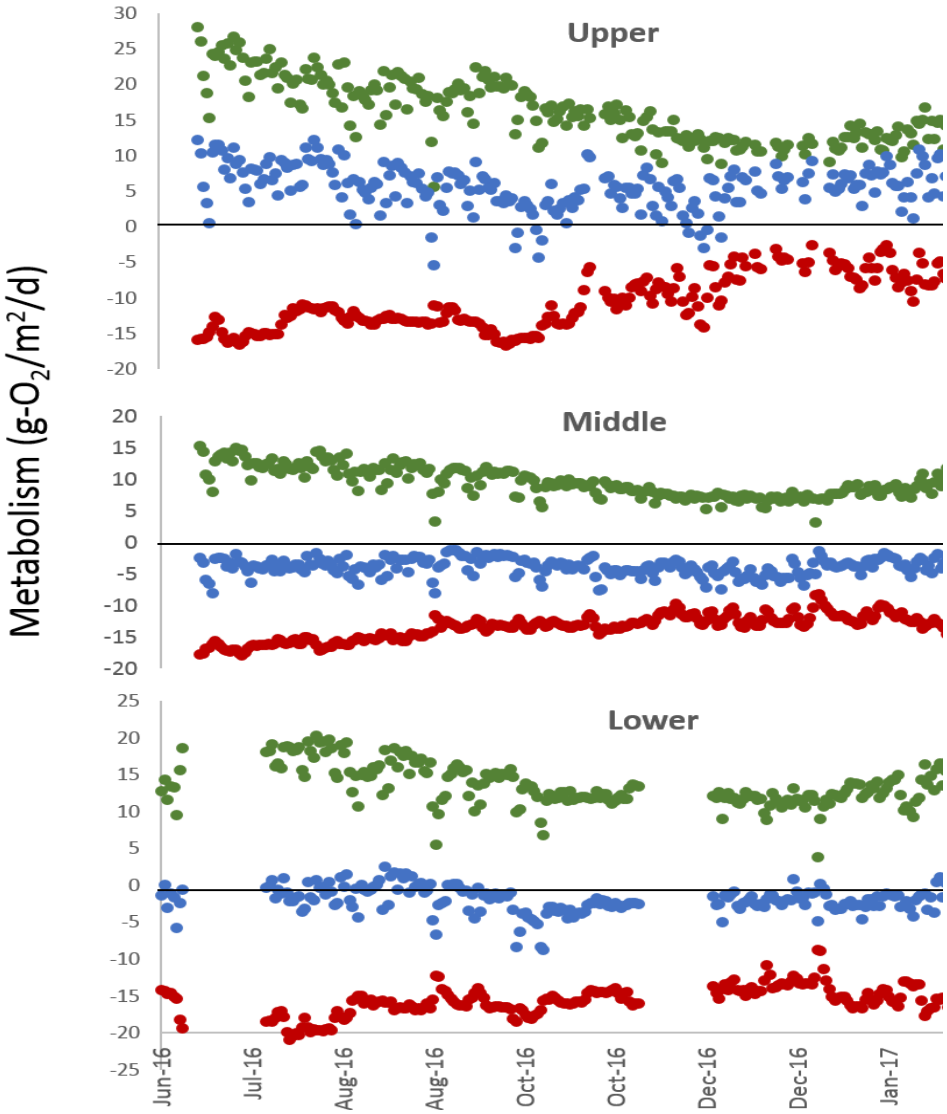

Figure 6.16. Comparison of GPP, ER and NEP for all three reaches in Silver River (upper, middle, lower) for the available period of overlap for all three stations (SILGOLD, S5 and S1). GPP and NEP are clearly higher for the upper reach (open, wide) than for the two lower reaches (narrower, more shaded).

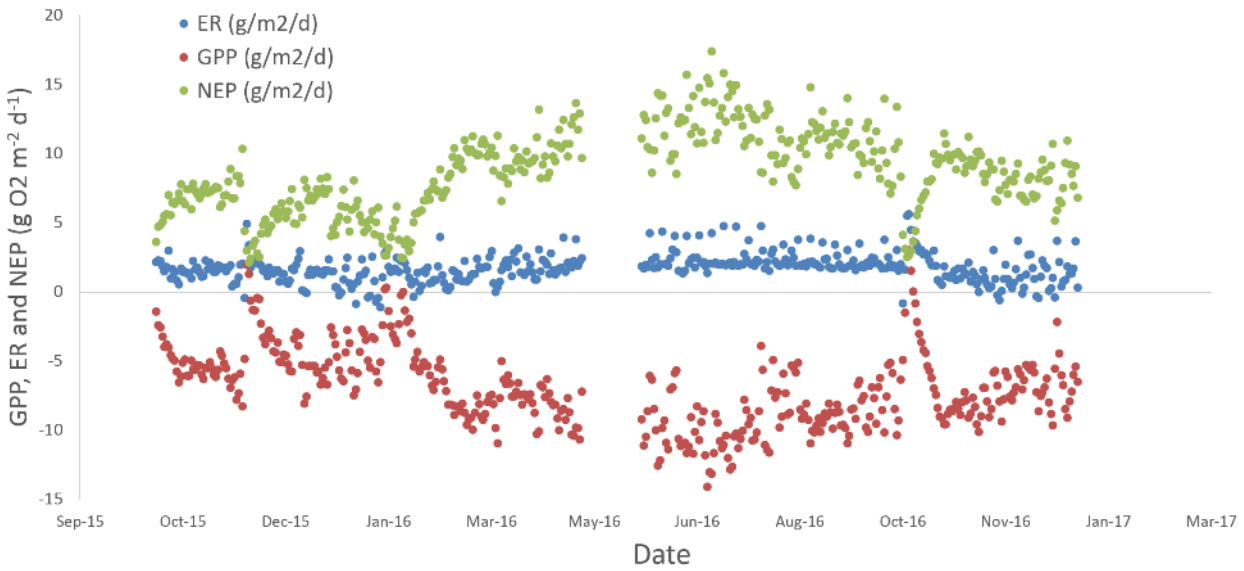

Figure 6.17. Summary of gross primary production (GPP), ecosystem respiration (ER), and net ecosystem production (NEP) for the period of record at Alexander Springs Creek. The excursion in October 2016 is the result of Hurricane Matthew.

P:R ratios also varied seasonally (Figure 6.18), but reach differences overshadow seasonal differences. Specifically, the upper half, middle, and lower reaches varied together and remained almost entirely below 1 or net heterotrophic (Figure 6.19). The upper reach remained mostly above 1 or net autotrophic. As such, metabolism in this river is characterized by two orthogonal modes of variation. Strong spatial variation, largely in response to canopy cover characteristics, but also water clarity, is coupled with seasonal variation induced by open sky irradiance variation at annual and inter-day time scales. The source of organic matter to sustain $P < R$ is likely both the net production from the upper river transported by flow and remineralized in the lower river, and increasing influence of emergent and riparian vegetation on organic matter supply in the lower river. Mean GPP values in Silver River can be compared with annual productivity averages for other ecosystems. Estimated biomass accrual for the three zones are 1,098, 548, and 821 g C m^{-2} yr^{-1}. The decline in GPP and increase in ER result in lower P:R in the lower river than the more open upper river.

The seasonality we observed in P:R ratios suggests higher values in two distinct seasons. In the summer months when GPP was highest due to high solar radiation, NEP was also especially high, likely suggesting lags between increased GPP and attendant respiration of the fixed organic matter. In late winter before leaf out when light reaching the river was not shaded, GPP is high but low temperatures and limited organic matter stocks likely kept ER low. In fact, for most of the river, the late winter was the only time the lower river became net autotrophic. P:R ratios are lowest in the late fall/early winter when solar radiation is low and the canopy still shades the river such that GPP is low, but water temperatures and organic matter stocks are still high keeping ER high.

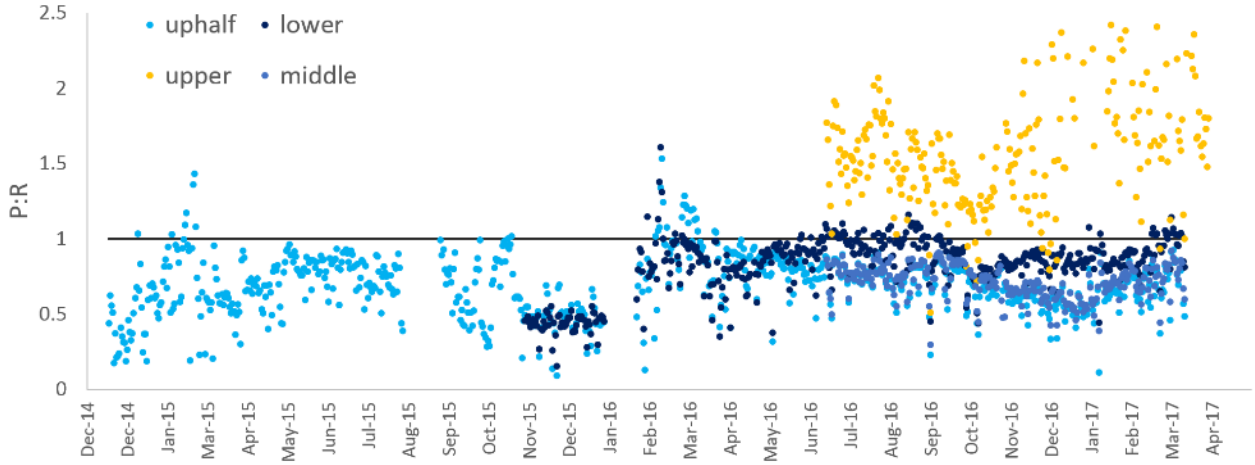

Figure 6.18. Seasonal and longitudinal variation in P:R in Silver River.

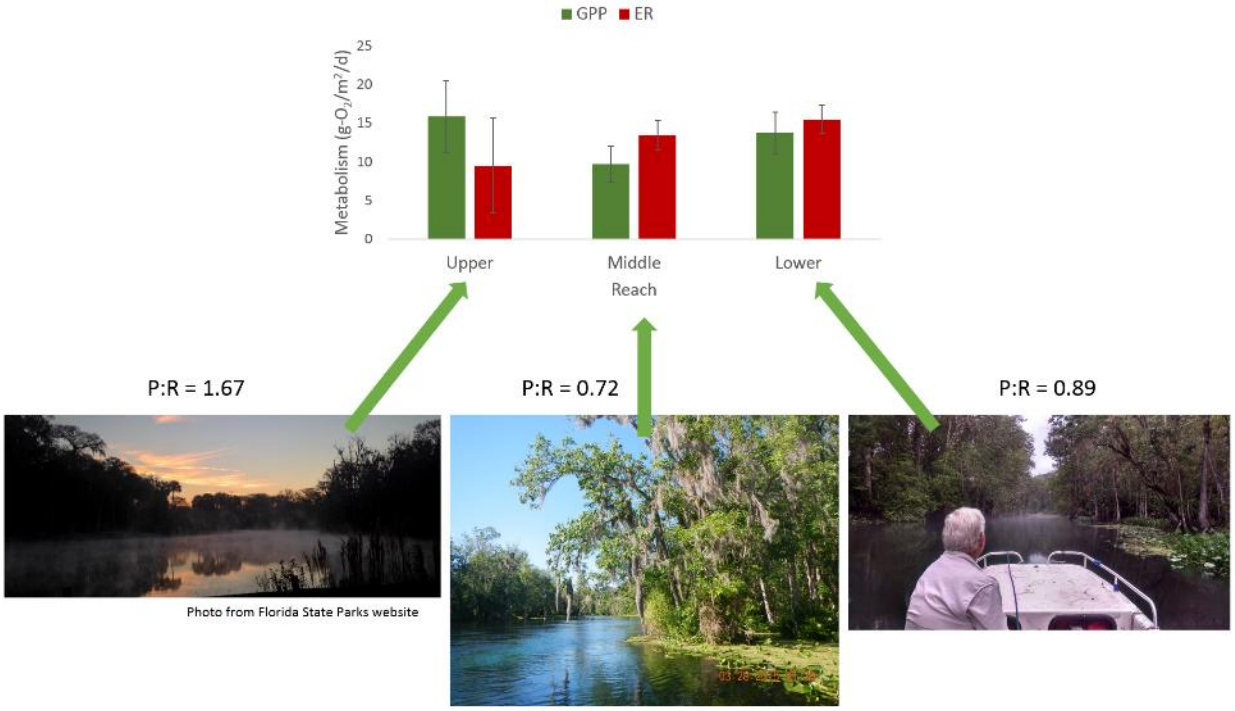

Figure 6.19. Summary of the three reaches of Silver River. Showing the marked drop in GPP, and marked increase in ER with distance downstream.

There is also marked inter-annual variation in metabolism. Figure 6.20 compares mean and standard deviations of daily GPP and ER for the upper reach between 2015 and 2016. In 2016, GPP was a third higher than the previous year, and ER was 15 % higher. The principal controls on GPP and ER, namely solar radiation and water temperature, remained relatively unchanged between the two years, so other factors such as fDOM or discharge must cause annual variation

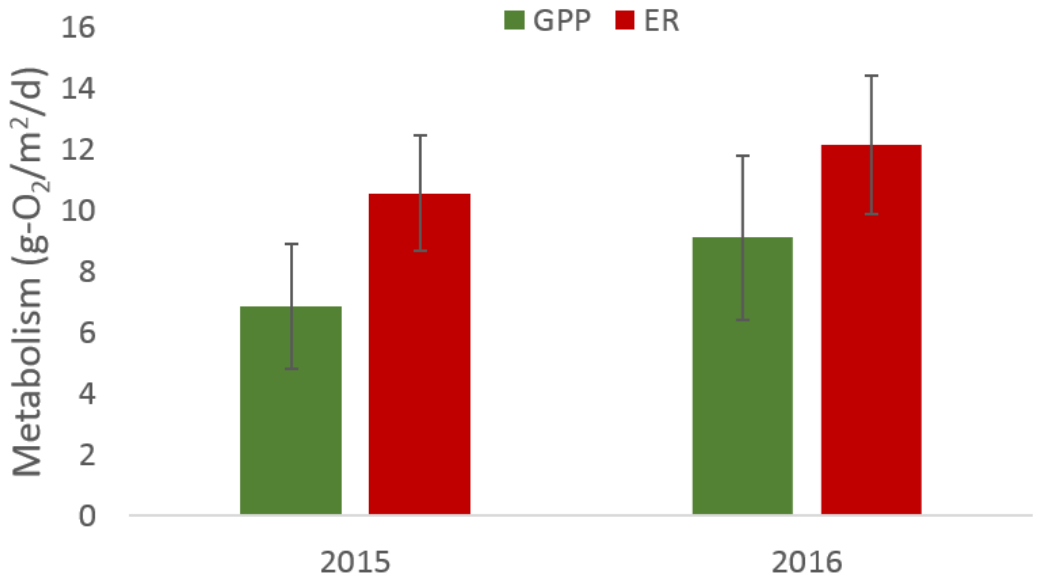

Figure 6.20. Summary of annual average GPP and ER for the S5 reach for 2015 and 2016. Note the considerable inter-annual variation (6.8 versus 8.2 g O_2 m^{-2} d^{-1}) between years. P:R values below 1 are conserved between years, with similar ratios (0.63 for 2015, 0.66 for 2016).

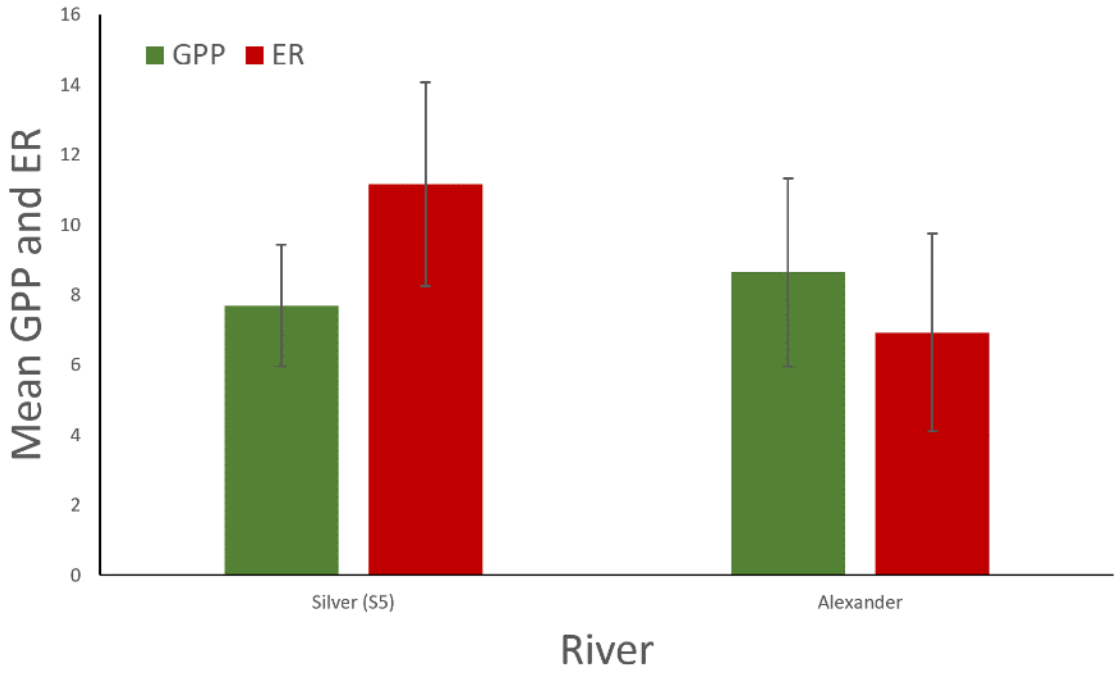

Figure 6.21. Comparison of GPP and ER between Silver River (high NO_3-N) and Alexander Springs Creek (low NO_3-N). GPP rates are not statistically different ($p = 0.19$). Respiration rates are significantly higher in Silver River ($p < 0.001$), sufficiently so to make the entire S5 reach (~5,500 m) net heterotrophic while the longer Alexander reach (~9,800 m) remains net autotrophic.

in metabolism. GPP is depressed whenever high fDOM blocks light through the water column. Higher discharge during 2015 resulted in higher velocities and shorter travel times between stations, which resulted in lower GPP calculated by the metabolism model.

One key reason for including GPP measurements in Alexander Springs Creek was to compare the two rivers, which differ in several key ways, but perhaps most notably in their dramatically different nitrate concentrations. A summary of the two long periods of record (S5 in Silver, Tracy Canal in Alexander) revealed no significant GPP differences between rivers (Figure 6.21) but significantly more respiration in Silver River than in Alexander Springs Creek. We are cautious in interpreting this because of the inherent uncertainty in the reaeration fluxes, but this may result from the much higher floodplain connectivity in Silver River than in Alexander. We note that while Alexander Springs Creek rarely stages up sufficiently to enable river interactions with the floodplain, there are significant lateral inputs of surface water (e.g., from Billies Bay and other surface water sources) that contribute DOM and solutes to the creek during periods of high flow. Such connectivity may be a source of organic matter to fuel detrital food webs in both Silver River and Alexander Springs Creek. Note, in comparing Figures 6.20 and 6.21 that inter-annual variation in GPP in Silver River is larger than the difference between Silver and Alexander. Understanding the temporal controls on metabolism, and what factors lead to inter-annual variation in primary production should be an important future goal. This may include more regular inventories of biomass standing stocks, and seasonal variation given observations made in the SAV growth element of this section report.

Silver River is uniquely positioned to inform metabolic changes over decades. Some of the earliest metabolism measurements were made in Silver River back in the 1950s, repeated in the 1980s and again in 2005. With this study, we can revisit one of the narratives that has emerged about Silver River metabolism, namely that over the last 15 years declining water quality and increased algal cover have led to declining primary production. Our estimates of GPP in the upper reach are commensurate with the values reported by Odum (1950's) and Knight (1980's) over approximately the same footprint (noting that our reach is slightly shorter because of the location of SILGOLD versus the USGS gage). Indeed, our estimates are consistently higher than either Odum (1957) or Knight (1980) (Figure 6.22). Two important notes: this is the first study to have continuous metabolism over multiple years, which is relevant because we have observed substantial GPP variation between years (Figure 6.20) depending on physical environmental factors. As such, it is plausible that metabolism is not declining, but rather that Munch et al (2006) study sampled during a low metabolism year. It is also possible that the location of sensors for the 2005 study were the same as those deemed unacceptable in this work because of the dominant influence of the Ft. King Waterway in the solute signal detected at the USGS gage. The temporal influence of that waterway (constructed during the 1960's and thus not likely to have influenced Odum's original 1957 metabolism measurements from this sampling site) on downstream solute signals should be considered when comparing early results with more recent results. However, the sensor suite at SILGOLD is well upstream of that confluence, values from that setting strongly support sustained high GPP despite the proliferation of algae and the high nitrate concentrations. It seems more likely from this evidence that primary production in the upper river remains near historical normal values and that the measurements in 2005 were anomalous.

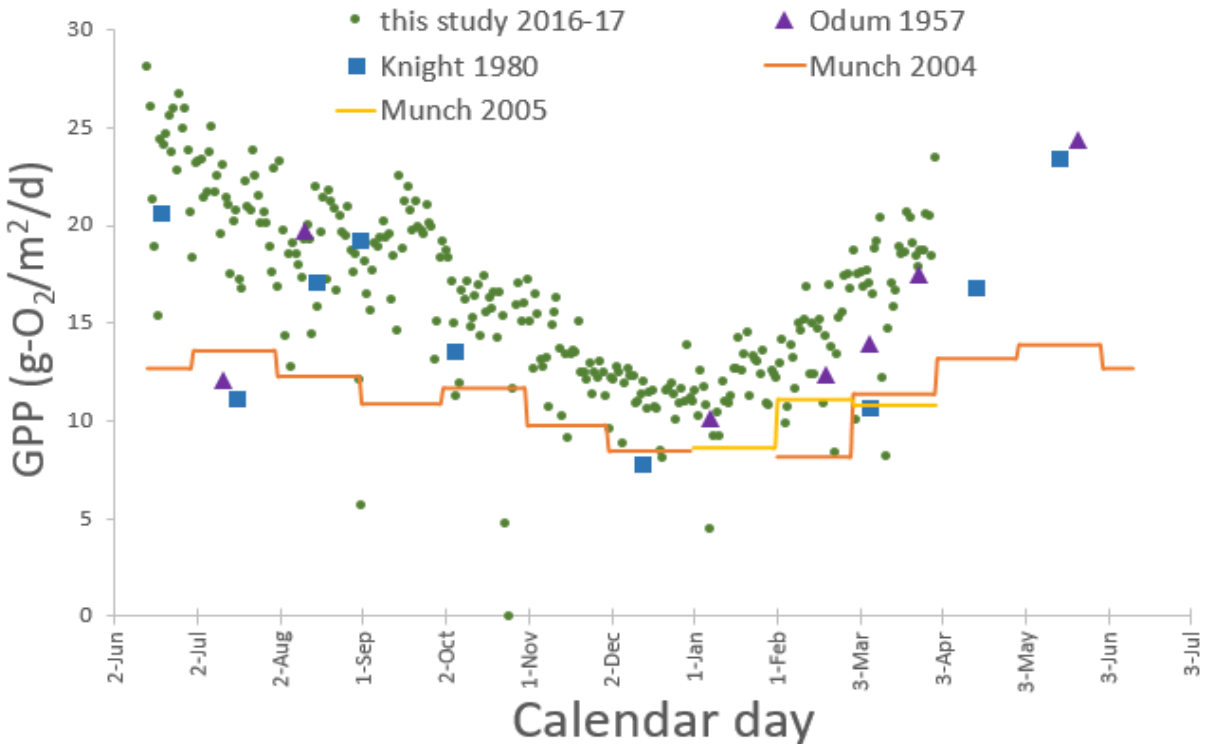

Figure 6.22. Summary of GPP over a year of available data at the SILGOLD site, which corresponds approximately to the reach measured by Odum (1957) and Knight (1980) and again by Munch et al. (2006). The marked decline in GPP between Knight (1980) and Munch et al. (2006) measurements has not been sustained; GPP measured during 2016-2017 are as high or higher as those observed during the two earliest studies.

6.3.3 Benthic Light and Predicting GPP and ER

Light availability directly controls primary production, but has received considerably less attention than nutrients as the dominant control on GPP in aquatic systems. Odum (1956) reported that spring ecosystems were light-limited, not in the sense of water column attention, because the water us uniquely clear, but rather that the incident photons hitting the water surface were the primary constraint on additional primary production. However, it is the light that reaches the bottom of the riverbed that matters, especially in macrophyte-dominated systems like Silver River and Alexander Springs Creek. As such, our effort here was to characterize both the ambient light environment (i.e., seasonal and day-to-day variation in open sky irradiance), the impact of tree canopy cover on light transmittance and finally characterizing the light that reaches the benthic surface through the water column (Figure 6.23). This is acutely relevant for both Silver River and Alexander Springs Creek because both are strongly influenced by surface drainage with high DOM concentrations (e.g., Half Mile Creek in Silver River). These sources deliver highly colored water for some period following intense rainfall, altering the light environment downstream. We sought to predict benthic light availability accurately on Silver River by using a model that refines the Benthic Light Availability Model (BLAM) developed by Julian et al. (2008). The physical model approach manipulates incident light (e.g., measured from open sky rediometers on site, or as in our case, obtained from the nearby Florida Automated

Weather Network site at Ocklawaha) with the phenology of the canopy occlusion of light (which is a function of leaf area index, height, solar angle, and canopy overhang across the channel), and then the timing of light-occluding substances in the water column. Because of uncertainties about the parameters that control the attenuation of light at each step, we elected to apply a statistical model to test the hypothesis that better accounting for benthic light availability, specifically by including canopy and water column attenuation, enable improved prediction of GPP. Linear models were run in R for three scenarios: 1) Open-sky irradiance only, 2) Open sky irradiance + Canopy occlusion, and 3) open sky irradiance + canopy occlusion + fDOM. We predicted improved fit with the additional parameters, and compared the models using the adjusted R^2 which penalizes model complexity.

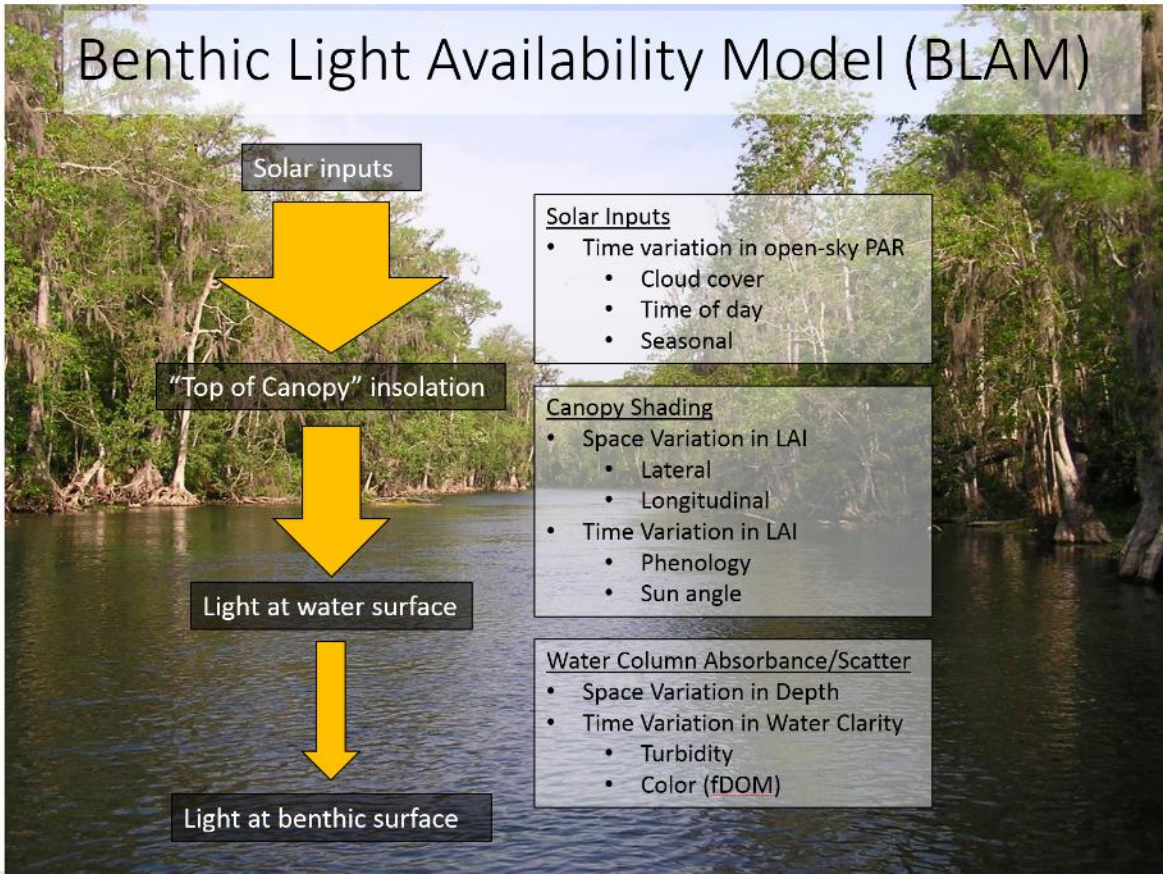

Figure 6.23. Logic of modeling benthic light attenuation. Measured incident open sky irradiance on each day is modified by the transmittance of the canopy given attributes of river width, canopy height, river azimuth, solar angles, and FPAR. The light that reaches the water surface is further modified by fDOM.

Open sky radiation data came from the Florida Automated Weather Network (FAWN) Ocklawaha station. For water column light attenuation, we explored fDOM and turbidity measurements made *in situ* at each station. Cursory analysis confirmed that while the fDOM signal was coherent, the turbidity levels were so low (near or below instrument detection) that temporal variation in values were unreliable. As a result, we only considered fDOM data in the GPP prediction models.

Canopy transmittance of light was based on NASA's MODIS (Moderate Resolution Imaging Spectroradiometer) leaf area index (LAI) and fraction of photosynthetically active radiation (FPAR) products that have a 1 km spatial resolution and 8 day temporal resolution. FPAR, or the fraction of incident photosynthetically active radiation absorbed by the green elements of a vegetation canopy, was extracted from the files. We then created a model that calculates canopy transmittance of light over time for any location when given FPAR, river azimuth, canopy height, and channel width (Figure 6.24, top panel). Riparian canopy was modeled as a translucent wall when in reality it has a 3D shape which overhangs the river. Hence, our model likely overestimates canopy transmission. Unlike other riparian shade models, however, our model takes a changing solar zenith and solar azimuth into account (Figures 6.24a-d), allowing river reach to be subdivided into segments to reflect the winding and heterogeneous nature of rivers (Figure 6.24), and calculates canopy transmittance (instead of percent shade).

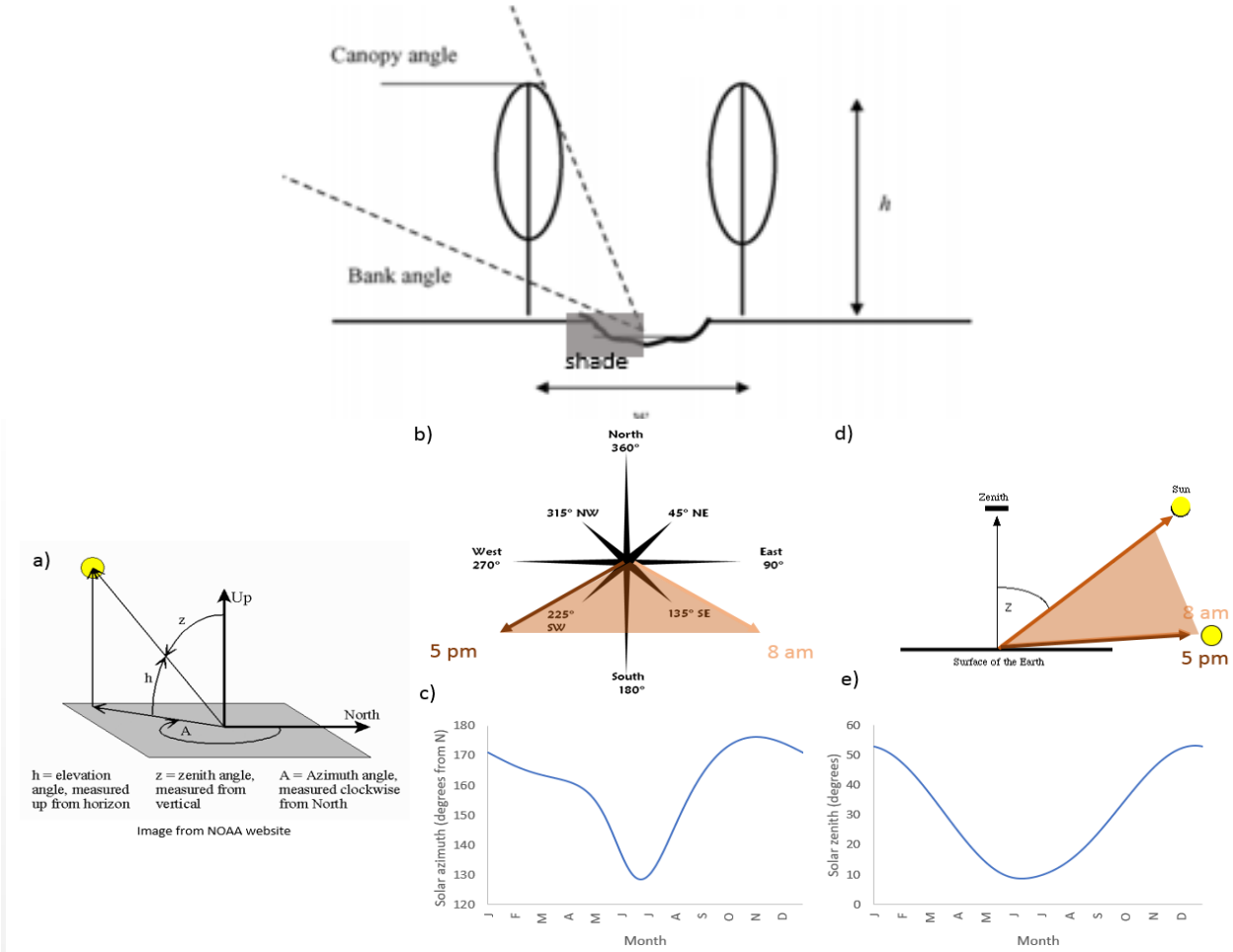

Figure 6.24. (top panel) Our canopy transmission model was based on earlier stream shade models (Davies-Colley and Rutherford 2005). In peninsular Florida, bank angle is negligible. (lower panel) a) Solar azimuth and solar zenith defined. Both solar azimuth (b and c) and solar zenith (d and e) vary greatly over the course of a day (b and d, for 1 January 2017) and a year (c and e, at 12pm) and impacts the length of the canopy shadow across the river. The canopy transmission model incorporated this temporal variation.

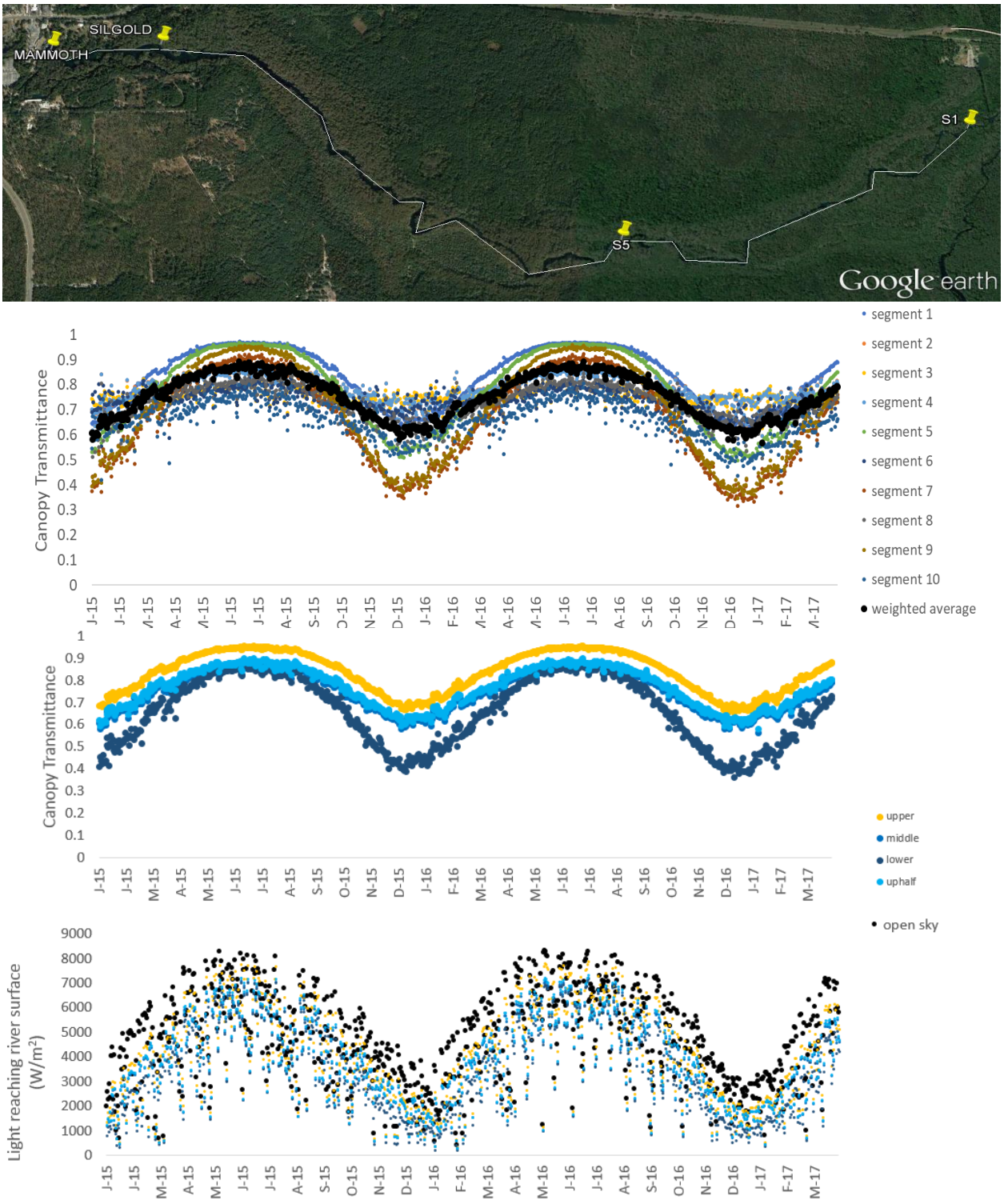

Figure 6.25. (top) Segments used for canopy transmission model to capture the winding nature of Silver River. (second) Canopy transmittance over 2+ years for the middle reach of Silver River. (third) Comparison of canopy transmittance fraction. (bottom) Actual light reaching Silver River.

The relationship between solar and river azimuths played a major role in determining riparian canopy transmittance of light. Figure 6.25 shows model results for the middle reach of Silver River broken into ten segments (6.25a) based on changing river azimuth. Canopy transmission only varied by 10 %, whereas it varied by 50 % in other river segments. We used the weighted average of all segments based on segment length in our statistical model of benthic light.

It may be surprising that the riparian canopy attenuates more light in the winter than the summer. While the lack of leaves in the winter does let more light through, the sun is much lower in the sky, thus casting more of the river in shade and letting less light through overall. The phenology of peak light availability is the reverse of peak open-sky irradiance which can result in seasonal metabolic patterns that diverge from the expected phenology for terrestrial systems; this divergence is most acute in narrow channels where canopy leaf area plays a dominant role in light availability. Our modeling efforts found that canopy transmittance of light depends more heavily on physical characteristics of the river than phenology.

As expected based on the longitudinal gradient in channel width, riparian canopy had the least impact on light transmission in the upper reach of Silver River and the greatest impact in the lower reach (Figure 6.25). (The canopy transmittance fraction in the uphalf reach did not differ appreciably from the middle reach because the uphalf reach is dominated by the middle reach.) Canopy transmittance of light was notably high in all reaches because Silver River is a relatively

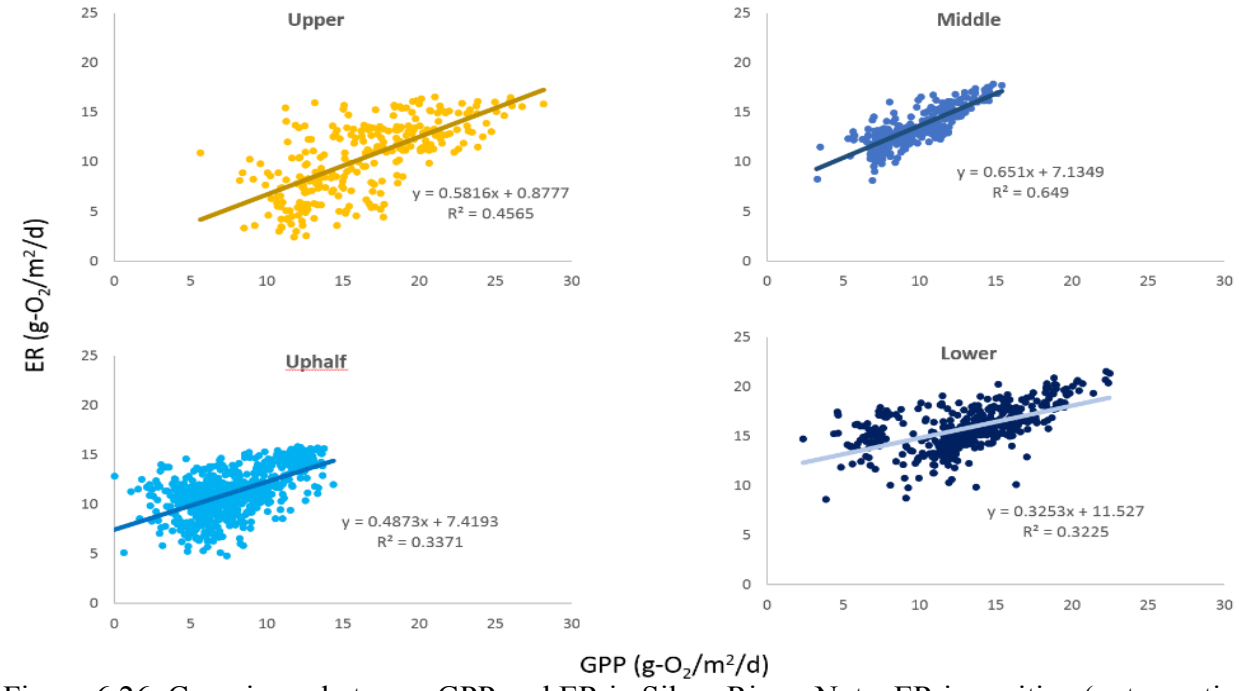

Figure 6.26. Covariance between GPP and ER in Silver River. Note, ER is positive (not negative as in previous plots) for this regression analysis. The slope indicates how important *in situ* primary production in controlling variation in respiration. The intercept indicates how other sources of organic matter are respired in the river. With distance downstream, the slope decreases, indicating reduced dependence of ER on GPP, and the intercept increases, indicating allocthonous C strongly influences the ecosystem energy budget.

large river. Because open sky irradiance is lowest during winter when the canopy transmittance fraction among reaches is most different, the mathematical effect of canopy attenuation is muted and light at the water surface mirrors open sky irradiance surprisingly well (Figure 6.25b).

One of the sentinel features in spring fed rivers is that there is limited supply of allochthonous organic matter; the spring vent contains nearly zero organic material, and the channel margins (from which direct emergent litterfall would be sourced), while ecologically productive, are a relatively small proportion of the total channel area because of the river size. As such, it is unsurprising that GPP and ER are strongly correlated in Silver River (Figure 6.26) and Alexander Springs Creek (Figure 6.27). The most striking feature of both graphs is the strong positive covariation between GPP and ER suggesting that *in situ* primary production is an important control on variation in respiration. We note that higher slopes for these relationships indicate stronger coupling between autochthonous primary production and respiration. That slope varies from a value of 1 in Alexander (Figure 6.27) to a low of 0.33 in the lower reach of Silver River. We interpret this to mean that respiration in Silver transitions from principally influenced by variation in primary production in the river, to allochthonous primary production delivered to the river from emergent, riparian, or more distant vegetation. Likewise, the intercept of these fitted lines indicates the baseline respiration predicted to occur in the absence of GPP. The intercept in Alexander Springs Creek (Figure 6.27) suggests small allochthonous or persistent respiration, paralleled by the behavior observed in the upper Silver River. In contrast, the lower Silver River exhibits much higher intercept values, consistent with the longitudinal transition from autochthonous to allochthonous sources as the basis for ecosystem respiration; note that some of the allochthonous organic matter must be fixed in the upper river and transported downstream with flow because P:R in the upper river exceeds 1.

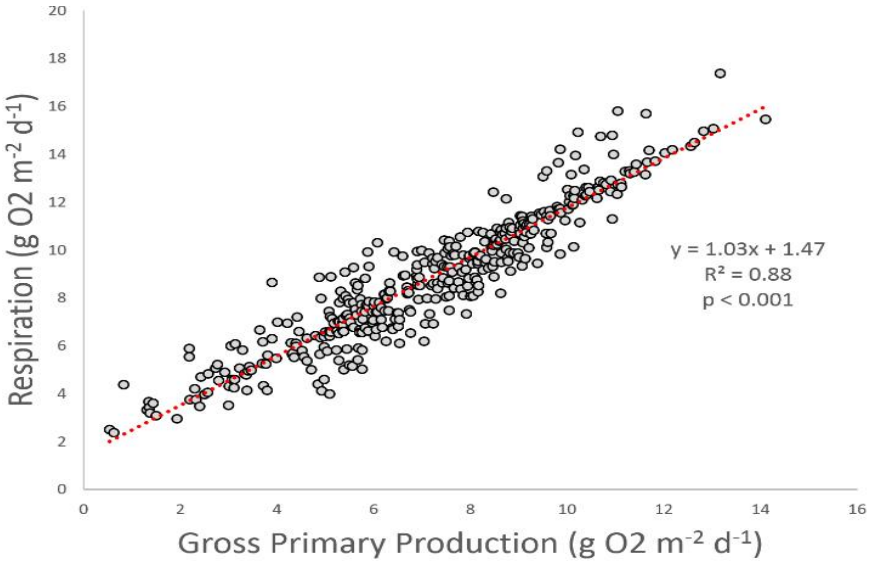

Figure 6.27. Relationship between primary production and respiration in Alexander Springs Creek. The positive intercept suggests some persistent respiration predicted, even at zero GPP but the slope (near 1) suggests that the dominant control on respiration is the availability of fixed carbon from submerged autotrophs. The baseline respiration (1.5 g O_2 m^{-2} d^{-1}) may be respiration of organic matter sourced from emergent or riparian vegetation.

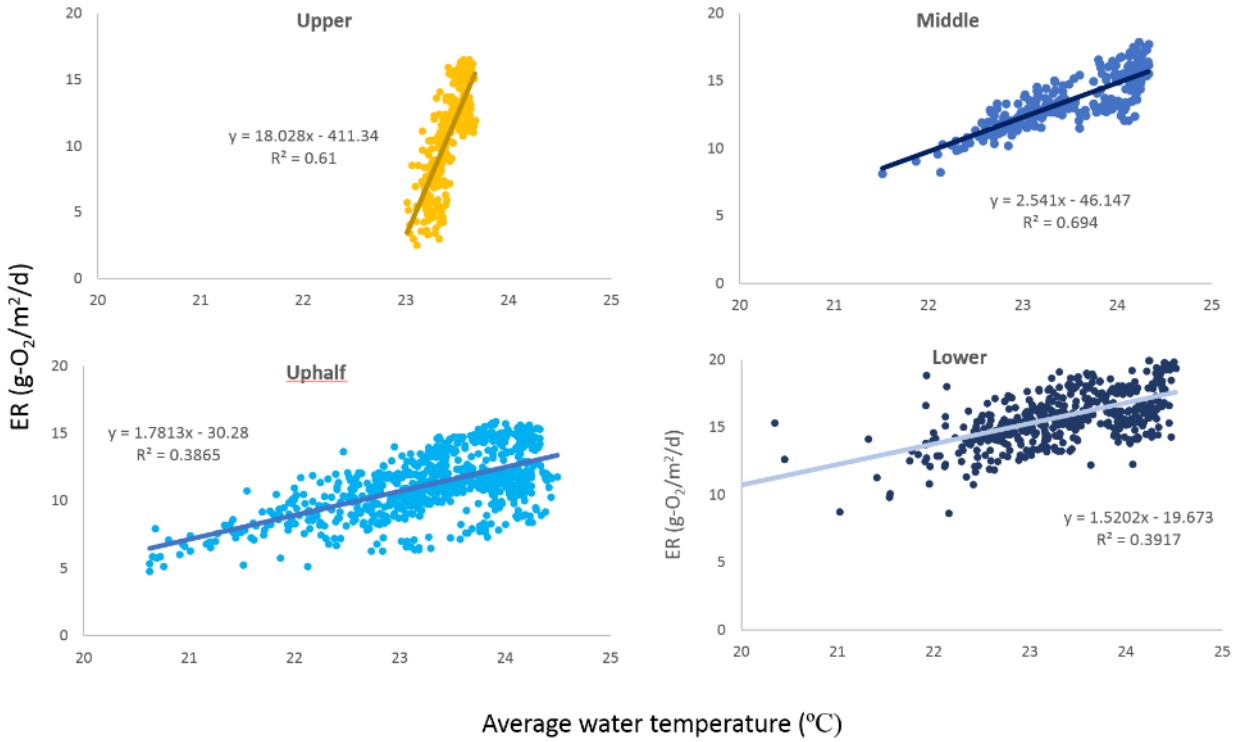

Figure 6.28**.** Temperature sensitivity of ER across the reaches of Silver River.

We further explored temperature controls on ER, noting our limited ability to disentangle temperature effects from GPP effects, which are expected to strongly covary. We observed very strong associations between temperature and respiration, as expected, but with different slopes in different parts of the river. Specifically, the slope in the upper river was very steep, and decreased with distance downstream. The temperature range in the upper river is much lower than downstream because of proximity to the spring vent, but respiration spans nearly the same range. For this reason, we interpret these relationships, at least in part, as indicating covariance between light and GPP. Light variation annually is strongly correlated with temperature, and Figure 6.26 illustrates that GPP and ER covary. Estimating direct temperature effect on system respiration would require additional modeling to control for light and GPP effects.

To measure light attenuation by the water column (k_{water}), we obtained underwater light profiles using HOBO pendant light meters. Based on the difference between light estimates just above and just below the water surface, we estimate that approximately 20 % of light is reflected by the water surface at midday. According to Lambert's Law, light passing through water column is absorbed exponentially by constituents (dissolved, colloidal, suspended); the magnitude of this decline in transmittance with depth informs a decay coefficient. Despite repeated measurements, significant noisiness of light intensity readings close to the water surface, have precluded establishing a reasonable exponential fit (Figure 6.11). Previous efforts to characterize water clarity in springs (Szafraniec 2015) reported significant reflective scattering by sediments and the water surface, creating anomalous lighting. We were unable to remedy this during the project, and focus instead on the statistical link between light occluding water column attributes (e.g.,

fDOM) and GPP rather than trying to create a physical model that enumerates the proportional light attenuation directly.

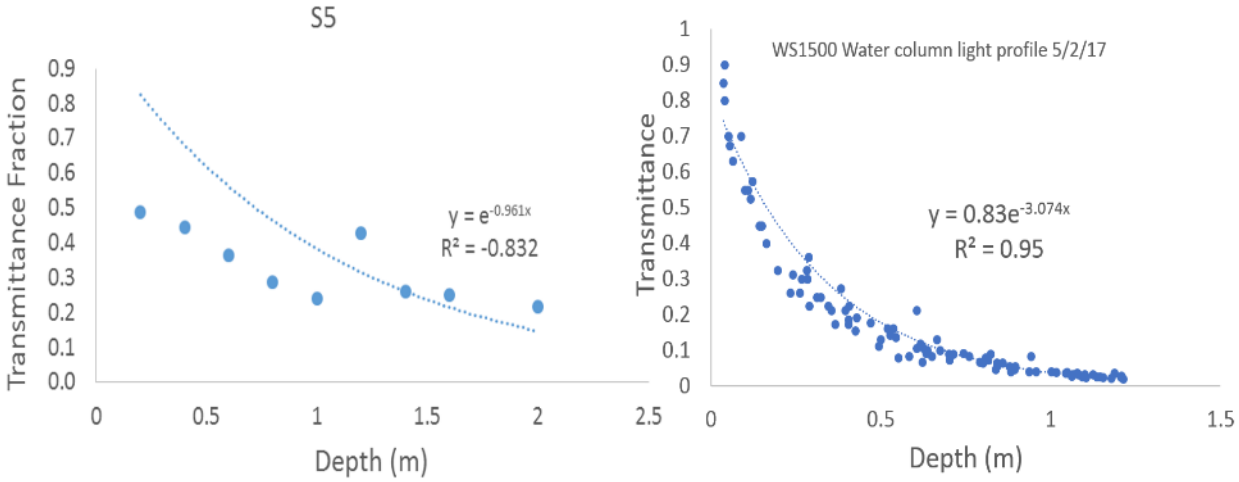

Figure 6.29. Comparison of light attenuation with depth in Silver River at S5 (left) and the Santa Fe River at the USGS 2500 station (right). The latter tannin-rich water column conforms with expected behaviors, exhibiting marked light attenuation with depth. In Silver River reflected light from the banks and bottom of the water column create conditions where estimates of light attenuation could not be made with equipment available. We thus focused on statistical links between light occluding factors in the water (fDOM, turbidity) rather fitting a physical model.

Two optical properties of water measured at high temporal resolution (e.g., color and turbidity) clearly vary with time and discharge. While we cannot establish a relationship directly linking fDOM and turbidity to light attenuation, we can use their temporal variation (Figure 6.30) to describe changing benthic light conditions. These two parameters do not covary (Figure 6.30), and while fDOM alone covaries with GPP, albeit weakly ($R^2 = 0.09$), there is no association with turbidity. As such, our statistical models uses only fDOM, and only as a statistical covariate, though the slope (sign, magnitude) of the fitted statistical effect is mechanistically informative.

To explore the factors that control primary production, we developed a series of statistical models based on open-sky light inputs (Figure 6.31), and chemical drivers of light attenuation (Figure 6.18c). We hypothesize that benthic light availability is the dominant driver of variation in GPP (and consequently ER), and seek a model to better characterize the controls on benthic light availability.

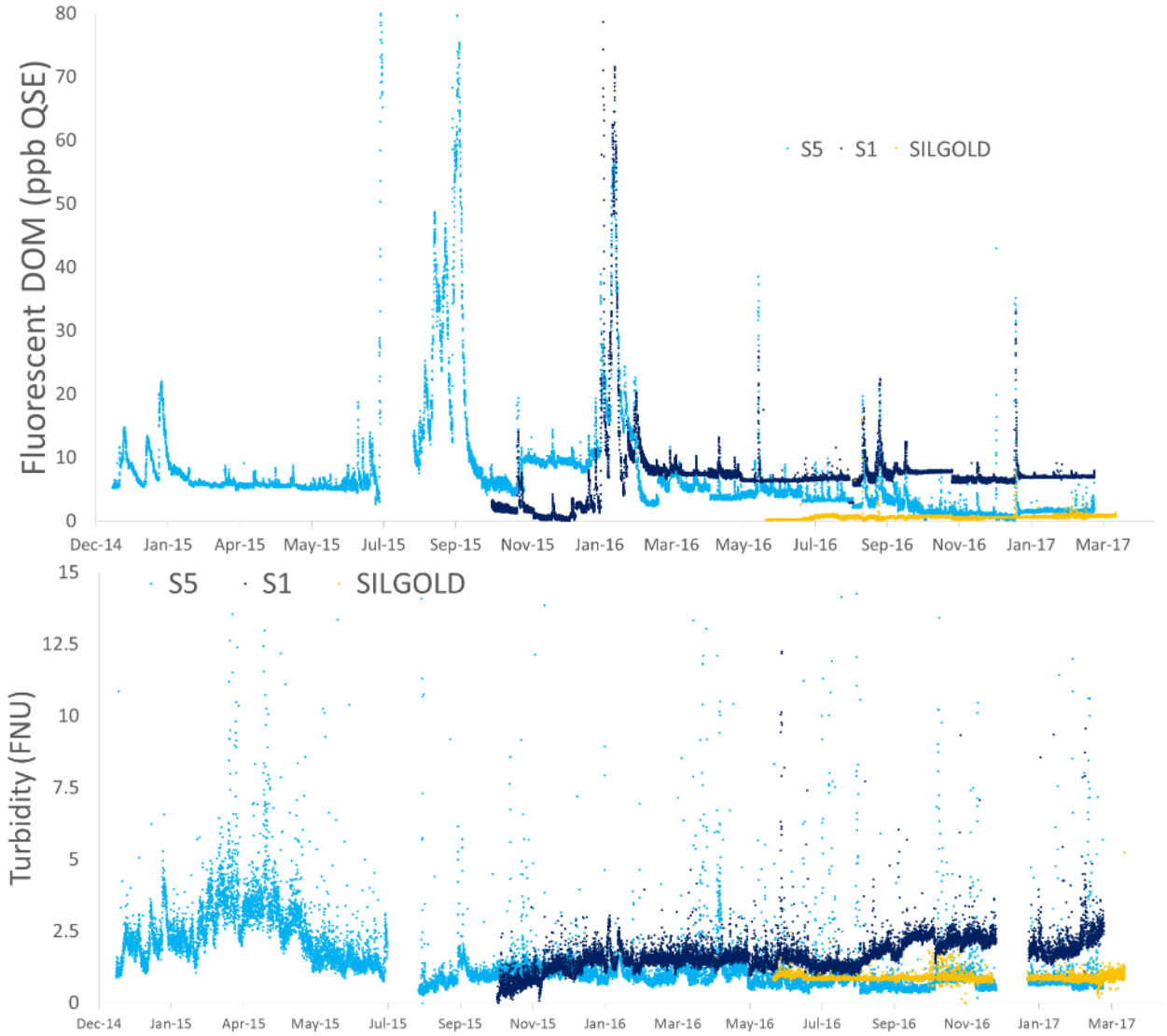

Figure 6.30**.** Time series of fluorescent DOM (top) and turbidity (bottom) at three stations in Silver River. Note the low fDOM values in the upper reach (SILGOLD, yellow dots), the higher values at lower stations (S5 (light blue) and S1 (dark blue)), and the time variation in response to inputs from Half-Mile Creek. The fDOM time series provided a third variable (with open sky irradiance and canopy % reduction) to predict GPP. Turbidity variation is less coherent, with a strong influence by very short term anomalies. These are not diel signals, but rather apparently random noise, the influence of which difficult to discern. Because of this, and because values are generally low and poorly predictive of GPP, we omitted turbidity from further analysis of metabolism.

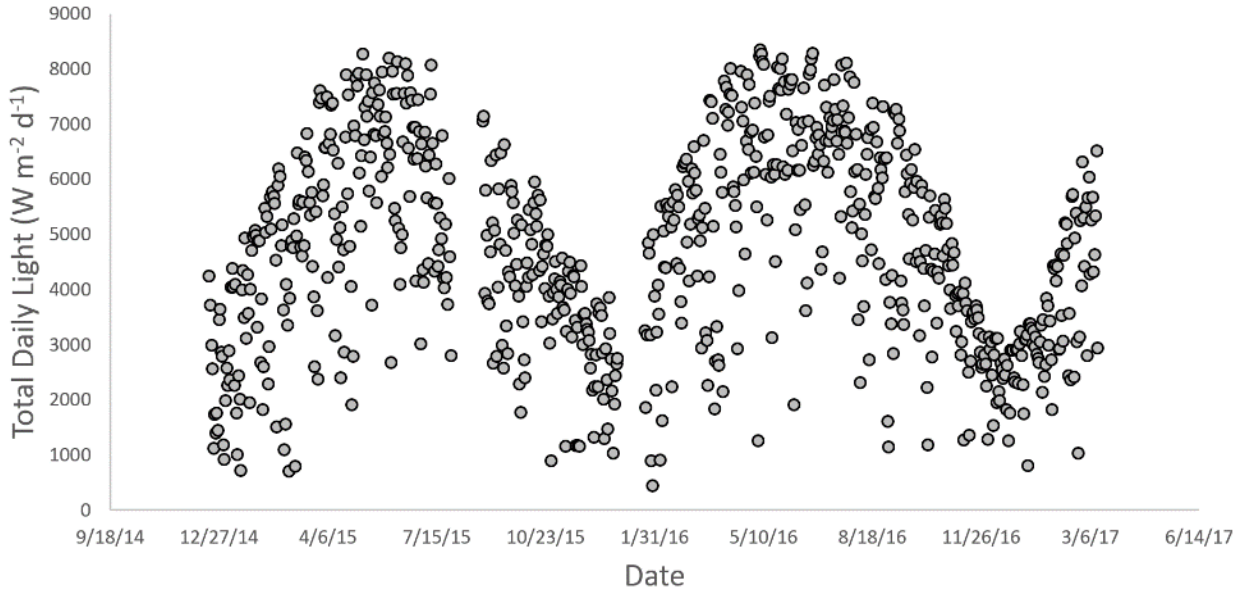

Figure 6.31. Time series of daily total open-sky irradiance from the FAWN-Ocklawaha Station. This was used as the base input for our GPP prediction models.

Our first step was to explore the pairwise associations between GPP at the various locations with Silver River, and in Alexander Springs Creek, and the physical controls on light regime. To that end, we evaluated the strength of the fit between open sky irradiance and GPP for all stations, and also between fDOM and turbidity and GPP for all stations where these data were available.

Figure 6.32 depicts the pairwise association between light and GPP for the 4 Silver River reaches and Figure 6.33 shows the same information for Alexander Springs Creek. The strength of the associations are unequivocal, with light explaining up to 75 % of the variation in GPP (in the upper reach), and uniformly explaining over 50 % of the variation throughout the river. In Alexander Springs Creek, the fit is substantially weaker, though still highly significant. Notably, the exponent is of similar magnitude.

The fit between fDOM and GPP is shown in Figure 6.34 for Silver River, and in Figure 6.35 for Alexander Springs Creek. While the fit is generally poor in Silver River, the temporal variation in fDOM in Alexander Springs Creek is extremely strong. We infer from this that fDOM occlusion of light, leading to lower GPP, is evident in Silver River, but dominant in Alexander Springs Creek.

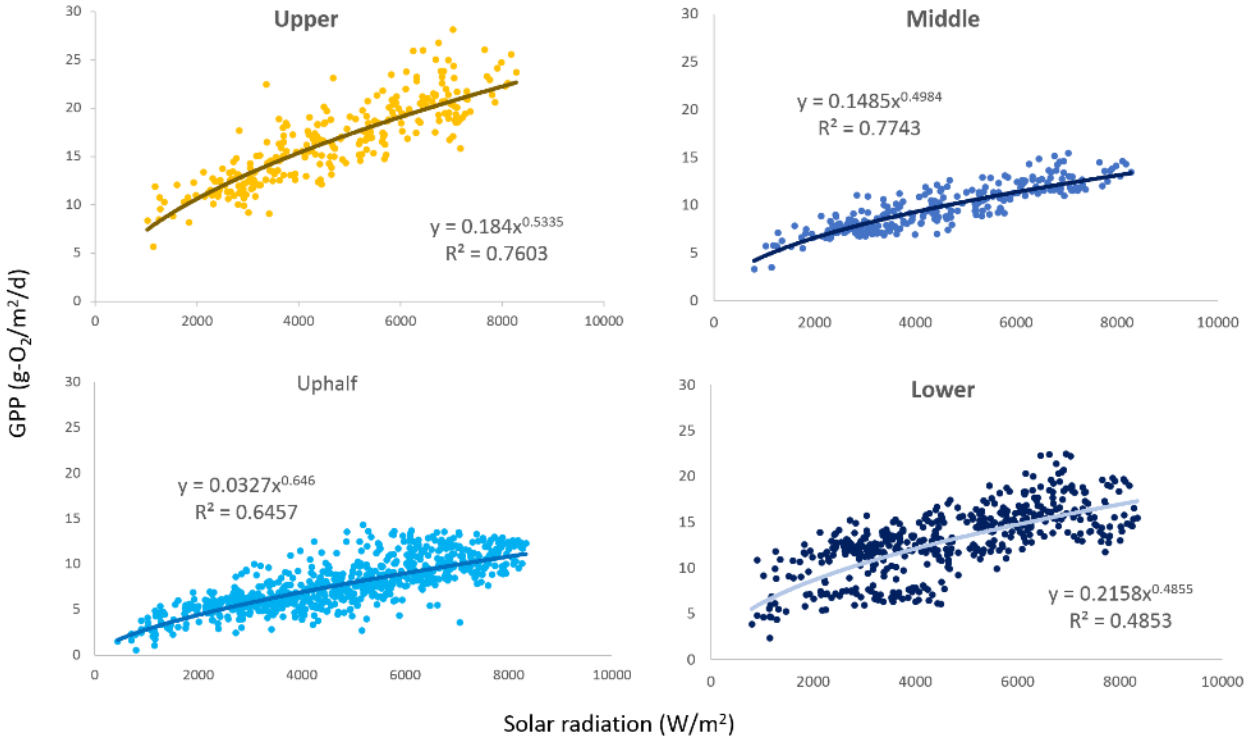

Figure 6.32. Summary of bivariate relationships between incident open-sky radiation (obtained from the nearby Florida Automated Weather Network Ocklawaha station). Note that the slopes (power-function exponents) differ between river reaches, largely aligned with river width and thus canopy occlusion. The power function fit is the theoretical model best fit to light saturation occurring across a variety of benthic light conditions

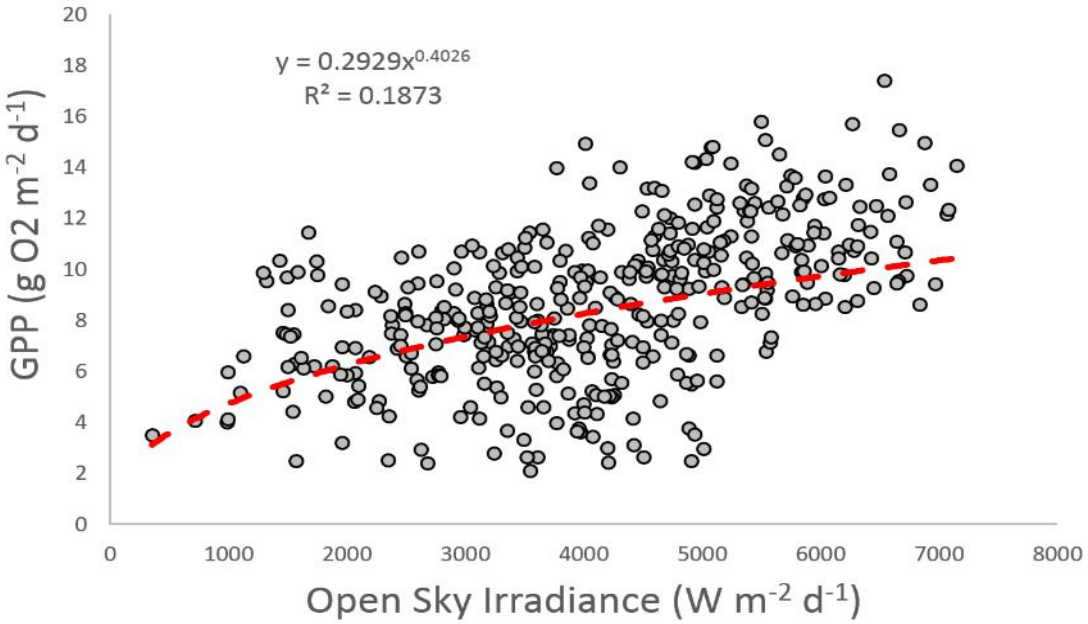

Figure 6.33. Bivariate relation between open sky irradiance and GPP in Alexander Springs Creek.

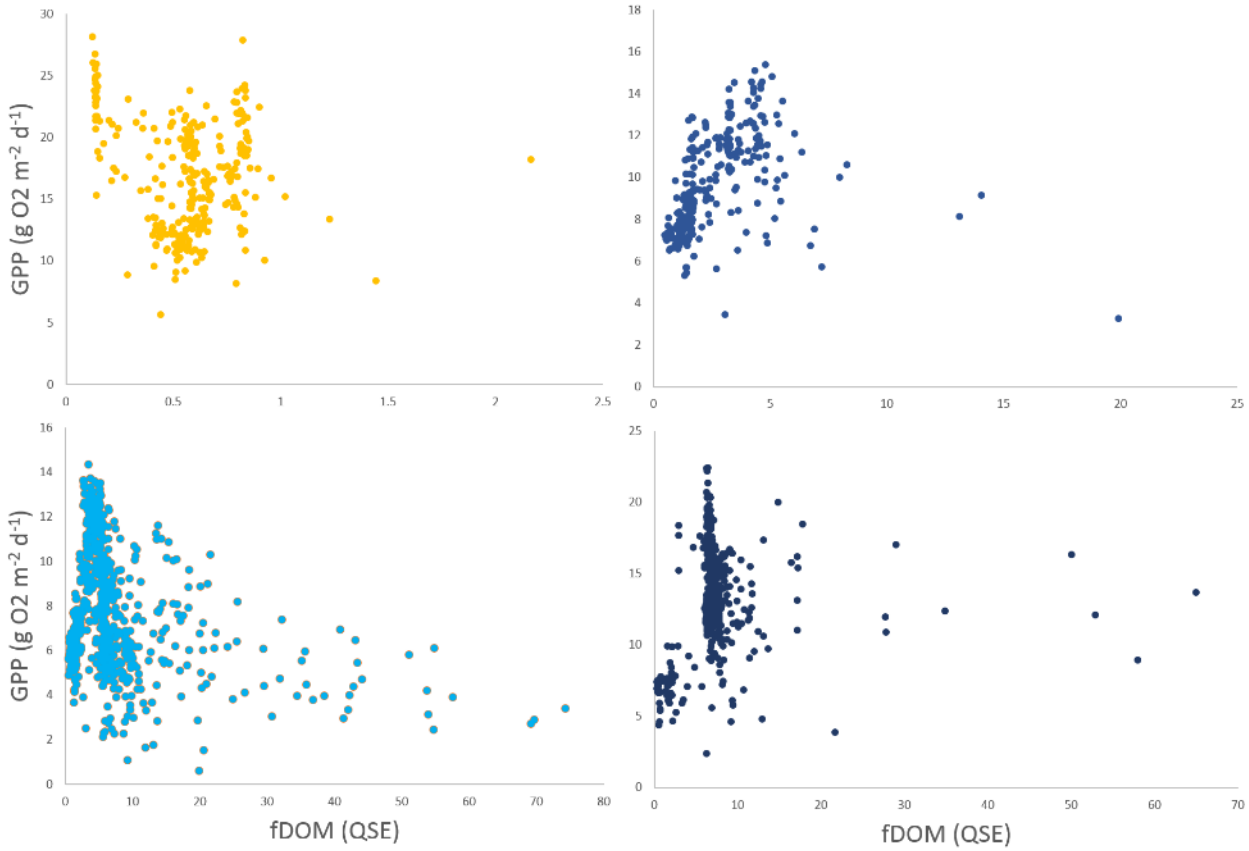

Figure 6.34. fDOM (in Quinone Sulphate Equivalents) versus GPP for the 4 Silver River Reaches. The only compelling association is for the longest data record at S5 (lower left). Note that the upper (upper left) and middle (upper right) reaches had uniformly low fDOM values.

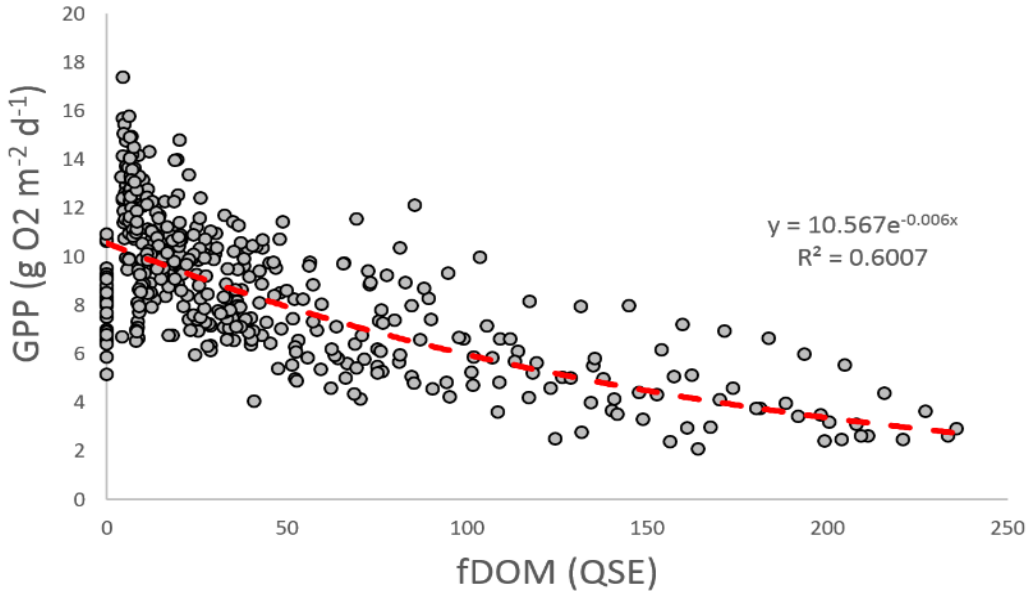

Figure 6.35. In Alexander Springs Creek the relationship between GPP and fDOM is strong, far stronger than with light, or between fDOM and GPP in Silver River.

Ultimately, we sought to predict GPP using all of the light related variables we had at our disposal. To that end, and to test the hypothesis that GPP prediction benefits from considering the ways in which the open sky irradiance is altered by the canopy and water column, we developed a series of models for each station that vary in complexity. The basic model always contains just light. We then explore the impacts of adjusting light by modeled canopy transmittance. Models were evaluated based on the resulting adjusted R^2 value (reported below as Model R^2) which penalizes models with more predictors. Finally, we explored models that further contained fDOM. Due to the right skewed distribution of fDOM values, we used the logarithm of fDOM in our linear models. Note that we do not have canopy cover data for Alexander Springs Creek, so are able to only supply the light only and light + fDOM models.

Tables 6.2 through 6.6 summarize the results. In all cases the model was improved by the addition of variables beyond just light, but in all cases except Alexander Springs Creek, this improvement was modest. In Silver River, the addition of canopy generally improved the model more than the addition of fDOM. The one exception was the uphalf reach which had a period of record twice as long as the other reaches and included many more large fDOM peaks (Figure 6.30a). The slopes of all variables were remarkably consistent across reaches, suggesting that the reaches were not as different from each other as we had hypothesized. The signs of the slopes were as expected: Positive for light, positive for canopy (higher canopy transmittance means more light for photosynthesis), and negative for fDOM (more color in the water means less light for photosynthesis).

In Alexander Springs Creek, the model improved markedly when both light and fDOM were included, suggesting that dark water from adjacent swamps and surface water runoff is a critically important factor controlling metabolism in this river. Since ER and GPP are nearly perfectly correlated in this river, this suggests that respiration is as sensitive to dark water inputs as GPP.

Overall, these models strongly support the inference that the overwhelmingly dominant control on GPP is light, and that enhancing beyond just open sky irradiance improves model performance. This improvement is less than we expected, except in Alexander Springs Creek, which we interpret as meaning that canopy cover and fDOM attenuation should be viewed as secondary controls on metabolism, and that light alone is the dominant factor controlling metabolism.

Table 6.2. Predicting GPP - Upper Silver River (Mammoth to SILGOLD).

	GPP ($g\ O2\ m^{-2}\ d^{-1}$)	Turbidity (FNU)	fDOM (QSE)	Light ($W\ m^{-2}$)	Canopy (% transmittance)
Mean	16.74	0.88	0.57	4,679	0.82
Std. Dev.	4.44	0.06	0.24	1,783	0.09

Model	**GPP ~ Light**			
Coefficients	Slope	SE	z-score	p-value
Intercept	6.61	0.38	17.62	$<2E^{-16}$
Light	0.0022	0.000075	28.91	$<2E^{-16}$
Model R2	0.7542			
F-statistic	835.8 on 1, 271 df; $p < 2E^{-16}$			

Model	**GPP ~ Light + Canopy**			
Coefficients	Slope	SE	z-score	p-value
Intercept	-3.75	1.27	-2.96	0.00334
Light	0.0015	$9.91E^{-05}$	15.58	$< 2E^{-16}$
Canopy	16.09	1.90	8.48	$1.45E^{-15}$
Model R2	0.8052			
F-statistic	563.3 on 2, 270 df; $p < 2E^{-16}$			

Model	**GPP ~ Light + Canopy + fDOM**			
Coefficients	Slope	SE	z-score	p-value
Intercept	-3.15	1.27	-2.48	0.0136
Light	0.0015	0.000098	15.74	$< 2E^{-16}$
Canopy	14.83	1.92	7.71	$2.44E^{-13}$
Log fDOM	-1.56	0.55	-2.83	0.0050
Model R2	0.8102			
F-statistic	388 on 3, 269 df; $p < 2E^{-16}$			

Table 6.3. Predicting GPP – Upper Half of Silver River (Mammoth to S5).

	GPP ($g\ O2\ m^{-2}\ d^{-1}$)	Turbidity (FNU)	fDOM (QSE)	Light ($W\ m^{-2}$)	Canopy (% transmittance)
Mean	7.77	1.82	7.34	4,735	0.67
Std. Dev.	2.65	3.37	8.77	1,850	0.09

Model	**GPP ~ Light**			
Coefficients	Slope	SE	z-score	p-value
Intercept	2.50	0.17	15.00	$<2E^{-16}$
Light	0.0011	0.000033	34.38	$<2E^{-16}$
Model R2	0.6123			
F-statistic	1182 on 1, 747 df; $p < 2E^{-16}$			

Model	**GPP ~ Light + Canopy**			
Coefficients	Slope	SE	z-score	p-value
Intercept	-1.74	0.56	-3.07	0.0022
Light	0.00088	$4.34E^{-05}$	20.35	$< 2E^{-16}$
Canopy	6.98	0.89	7.81	$1.91E^{-16}$
Model R2	0.6411			
F-statistic	669.1 on 2, 746 df; $p < 2E^{-16}$			

Model	**GPP ~ Light + Canopy + fDOM**			
Coefficients	Slope	SE	z-score	p-value
Intercept	-2.00	0.54	-3.73	0.00021
Light	0.00083	$4.15E^{-05}$	20.11	$< 2E^{-16}$
Canopy	8.87	0.87	10.18	$< 2E^{-16}$
Log fDOM	-1.38	0.15	-9.25	$< 2E^{-16}$
Model R2	0.6776			
F-statistic	525.1 on 3, 745 df; $p < 2E^{-16}$			

Table 6.4. Predicting GPP – Middle Reach of Silver River (SILGOLD to S5).

	GPP ($g\ O2\ m^{-2}\ d^{-1}$)	Turbidity (FNU)	fDOM (QSE)	Light ($W\ m^{-2}$)	Canopy (% transmittance)
Mean	9.68	1.13	2.72	4,485	0.73
Std. Dev.	2.33	2.18	2.06	1,765	0.09

Model	**GPP ~ Light**			
Coefficients	Slope	SE	z-score	p-value
Intercept	4.44	0.18	24.33	$<2E^{-16}$
Light	0.0012	0.000038	30.86	$<2E^{-16}$
Model R2	0.7782			
F-statistic	952.1 on 1, 270 df; $p < 2E^{-16}$			

Model	**GPP ~ Light + Canopy**			
Coefficients	Slope	SE	z-score	p-value
Intercept	-0.42	0.59	-0.71	0.48
Light	0.00082	0.000053	15.44	$< 2E^{-16}$
Canopy	8.77	1.03	8.55	$9.18E^{-16}$
Model R2	0.825			
F-statistic	639.9 on 2, 269 df; $p < 2E^{-16}$			

Model	**GPP ~ Light + Canopy + fDOM**			
Coefficients	Slope	SE	z-score	p-value
Intercept	-1.85	0.77	-2.39	0.018
Light	0.00079	0.000053	14.90	$< 2E^{-16}$
Canopy	11.33	1.36	8.33	$4.19E^{-15}$
Log fDOM	-0.95	0.34	-2.82	0.00518
Model R2	0.8294			
F-statistic	440.2 on 3, 268 df; $p < 2E^{-16}$			

Table 6.5. Predicting GPP - Lower Silver River (S5 to S1).

	GPP ($g\ O2\ m^{-2}\ d^{-1}$)	Turbidity (FNU)	fDOM (QSE)	Light ($W\ m^{-2}$)	Canopy (% transmittance)
Mean	13.0	1.6	6.3	4,618	0.63
Std. Dev.	3.7	0.6	5.5	1,861	0.16

Model	**GPP ~ Light**			
Coefficients	Slope	SE	z-score	p-value
Intercept	6.52	0.32	20.46	$<2E^{-16}$
Light	0.0014	0.0001	21.82	$<2E^{-16}$
Model R2	0.5017			
F-statistic	476.2 on 1, 471 df; $p < 2E^{-16}$			

Model	**GPP ~ Light + Canopy**			
Coefficients	Slope	SE	z-score	p-value
Intercept	4.68	0.47	9.88	$< 2E^{-16}$
Light	0.0010	0.00009	11.10	$< 2E^{-16}$
Canopy	5.57	1.08	5.16	$3.63E^{-07}$
Model R2	0.5274			
F-statistic	264.4 on 2, 470 df; $p < 2E^{-16}$			

Model	**GPP ~ Light + Canopy + fDOM**			
Coefficients	Slope	SE	z-score	p-value
Intercept	5.95	0.61	9.76	$< 2E^{-16}$
Light	0.0010	0.000093	10.88	$< 2E^{-16}$
Canopy	6.22	1.09	5.73	$1.84E^{-08}$
Log fDOM	-2.10	0.64	-3.27	0.00117
Model R2	0.5369			
F-statistic	183.4 on 3, 469 df; $p < 2E^{-16}$			

Table 6.6A. Predicting GPP – Alexander Springs Creek.

	GPP ($g\ O2\ m^{-2}\ d^{-1}$)	Turbidity (FNU)	fDOM (QSE)	Light ($W\ m^{-2}$)	Canopy (% transmittance)
Mean	8.64	1.690	44.62	4,208	N/A
Std. Dev.	2.91	1.12	51.89	1,462	N/A

Model	**GPP ~ Light**			
Coefficients	Slope	SE	z-score	p-value
Intercept	4.16	0.37	11.21	$<2E^{-16}$
Light	0.0011	0.00009	12.75	$<2E^{-16}$
Model R2	0.28			
F-statistic	162.5 on 1, 419 df; $p < 2E^{-16}$			

Model	**GPP ~ Light + fDOM**			
Coefficients	Slope	SE	z-score	p-value
Intercept	6.81	0.29	23.44	$< 2E^{-16}$
Light	0.009	0.00006	13.60	$< 2E^{-16}$
fDOM	-0.04	0.002	-20.74	$< 2E^{-16}$
Model R2	0.68			
F-statistic	379.6 on 2, 418 df; $p < 2E^{-16}$			

6.3.4 Nutrient Dynamics

Following the logic behind extracting primary production and respiration, high resolution time series of solute concentrations can be used to estimate ecosystem N and P demand (Heffernan and Cohen 2010; Cohen et al. 2013). The method is identical except that inference is simplified because neither nitrate nor phosphate has a gas phase. As such, the fine-scale mass balance need not account for reaeration estimates. This section describes inference of N retention due to assimilation by photoautotrophs ($U_{a,N}$) and denitrification (U_{den}) though we note the latter is better thought of as net denitrification because it includes all heterotrophic nitrate fluxes (removal due to denitrification and production due to nitrification). A schematic of the logic behind the nitrate method is shown in Figure 6.36. In short, all diel variation between nighttime baselines (red line) is attributed to autotroph uptake (green areas), and remaining mass retained vis-à-vis the upstream boundary input (black line; a constant for a spring-fed river, but not for a two-station deployment in other rivers) is attributed to net denitrification (blue areas). Repeating the mass balance calculation each day of the period of record yields N demand, total loss rates, ecosystem stoichiometry in combination with measured primary production, and the proportion of N supply from the spring vent that is used by the ecosystem, and more specifically by the autotrophs. These are informative for considering N demand, N saturation, and the drivers of assimilatory uptake.

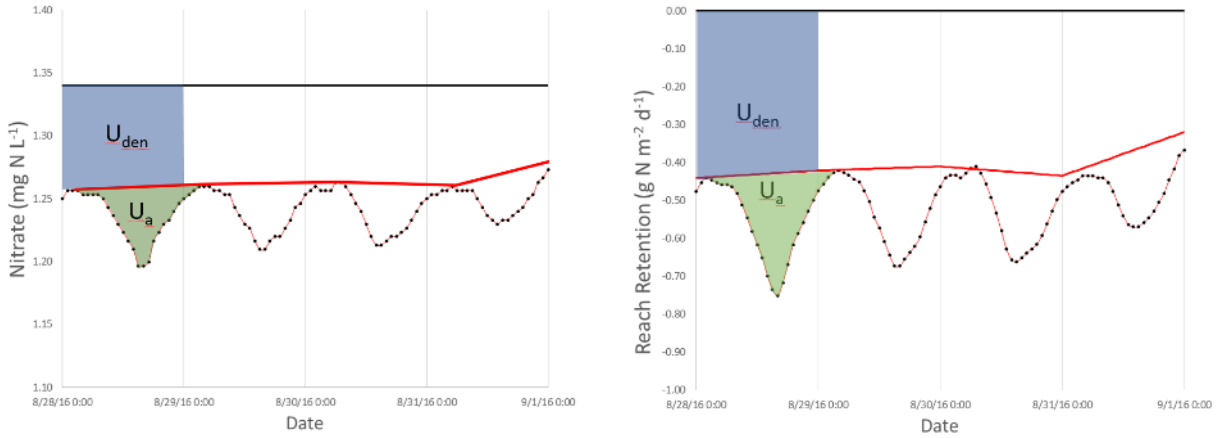

Figure 6.36. Schematic of methods to extract N assimilation and denitrification from the high resolution time series of nitrate concentrations (left) or nitrate retention (right; i.e., concentration change between stations multiplied by discharge and divided by benthic area). In both cases, diel variation is attributed to assimilation, while the remainder of the mass loss is attributed to heterotrophic processes. We refer to this remainder as U_{den} since denitrification is often a dominant fraction but note that this also includes nitrification and is thus more accurately interpreted as net denitrification (i.e., denitrification minus nitrification).

The same logic applies to inference of P use by autotrophs, but further requires adjusting the signal for impacts by P sorption to new carbonate minerals that occur in response to GPP-induced changes in pH. The entire method is detailed in Cohen et al. (2013). In short, the raw SRP signal measured at a given station is adjusted based on observations of specific conductance, diel variation in which is directly linked to carbonate mineral precipitation. Sorption of water column P to new carbonate minerals, precipitated only during the day, impacts concentrations. P assimilation can only be assessed after adjusting the raw signal for this sorption flux. Figure 6.37 illustrates the core method. The first step is to adjust the signal for $CaCO_3$ sorption, which effectively shifts the baseline (though the effect is more complex than this because it also changes the shape of the resulting concentration profile). The P assimilation flux (i.e., use by plants) is denoted by the green area. There is also a mass flux due to remineralization of organic matter but we do not interpret this flux further in this report, focusing our attention on the assimilation rate of P (i.e., $U_{a,P}$) and, by extension, system stoichiometry and total P use vis-à-vis supply.

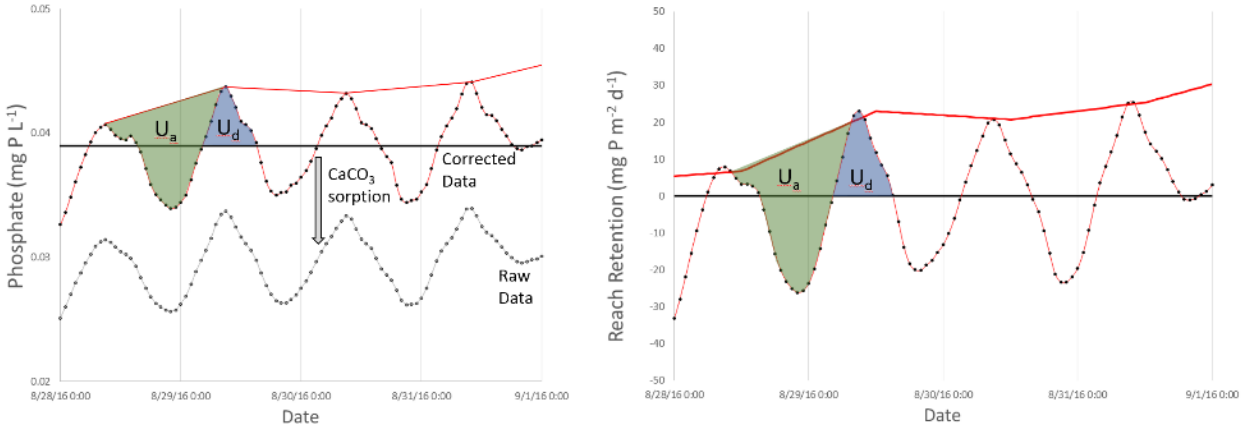

Figure 6.37. Schematic of methods to extract P assimilation and calcite sortion from the high resolution time series of phosphate concentrations (left) or phosphate retention (right; i.e., concentration change between stations multiplied by discharge and divided by benthic area). In both cases, diel variation is attributed to assimilation, while the remainder of the mass loss is attributed to geochemical processes. We refer to this remainder as U_d since dissimilatory processes are one component of this flux but note that this includes a complex array of desorption and mineralization processes; we do not interpret the magnitude of this flux in detail.

Nitrate retention estimates and pathway deconvolution using the diel method (Figure 6.36; Heffernan and Cohen 2010) require high resolution time series from sensors that have been intercalibrated and are sampling the advective zone of the river (precluding errors that arise because N concentrations can change more dramatically in the slow-moving parts of the river; Figure 6.38). It is striking that using SILHEAD as the upstream reference effectively removes denitrification from the signal, and dramatically alters the diel signal and thus the assimilatory flux. For this reason, and based on the magnitude of the diel signal at SILHEAD which is insufficiently constant to truly represent the upstream boundary condition, we used discrete sample measurements from the head spring as the upstream boundary, despite the lower temporal resolution. Results shown in Figure 6.38 are far more plausible.

Detailed investigation of final SJRWMD nitrate data revealed several limitations of the data time series, even though each signal was, by itself, strongly diel and suggestive of river N retention patterns that have been previously observed. First, nitrate concentrations at the Silver River S1 station diverged dramatically at the end of the monitoring period (Figure 6.39; grey line). One possibility for this discrepancy is that the Ocklawaha River was backed up, introducing colored water which interfered with the SUNA but not the laboratory analysis of grab samples (which diverged from the *in situ* sensor). However, continuous monitoring fDOM data (Figure 6.30) does not show sustained high levels of fDOM at S1. An alternative explanation is that the SUNAs

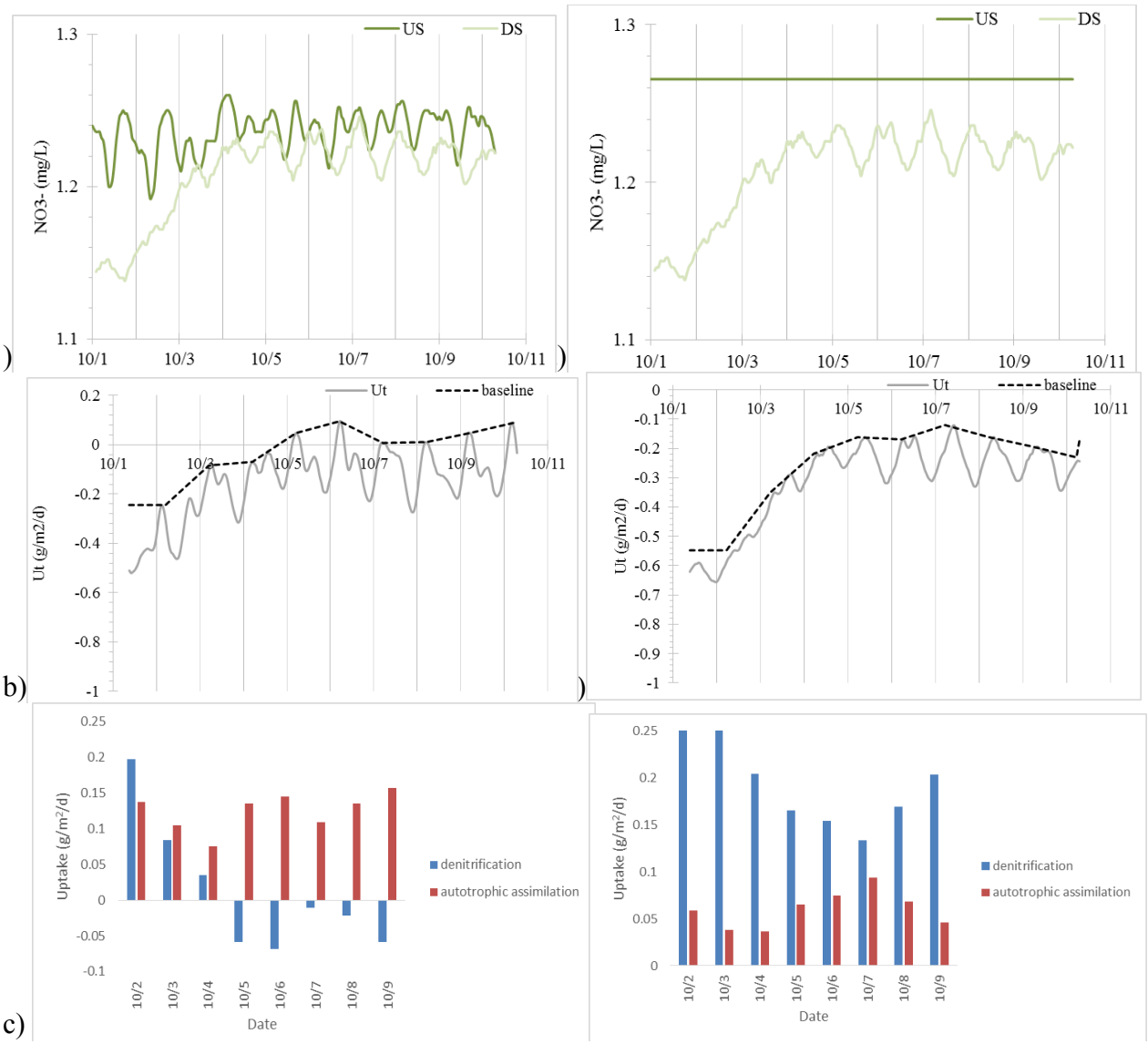

Figure 6.38. Nitrate metabolism calculated for the same time period using two different upstream boundaries: a, b, c uses SILHEAD as the upstream boundary while d, e, f uses the Oct 2015 Mammoth grab sample nitrate concentration as the upstream boundary.

required calibration and/or servicing, although in our experience, the SUNA readings do not drift markedly. Still another possibility is that complex riparian flowpaths dominate during periods of rising flow. Regardless of the mechanism for both this shift and for concentrations at S1 in excess of S5, when all longitudinal profiles suggest continued net N retention (Hensley et al. 2014), we decided that analysis of the S1 time series was not justified given the uncertainties. As previously described, measurements at SILHEAD, where vegetation growth creates a hydraulic environment that departs markedly from the open channel, and SILBIRD, where sensors are actually measuring water from the Ft. King waterway, were not considered for further analysis here. Finally, the nitrate data logged by SJRWMD is rounded to two decimal places to accommodate telemetry and data logging. Truncated NO_3-N concentrations produce

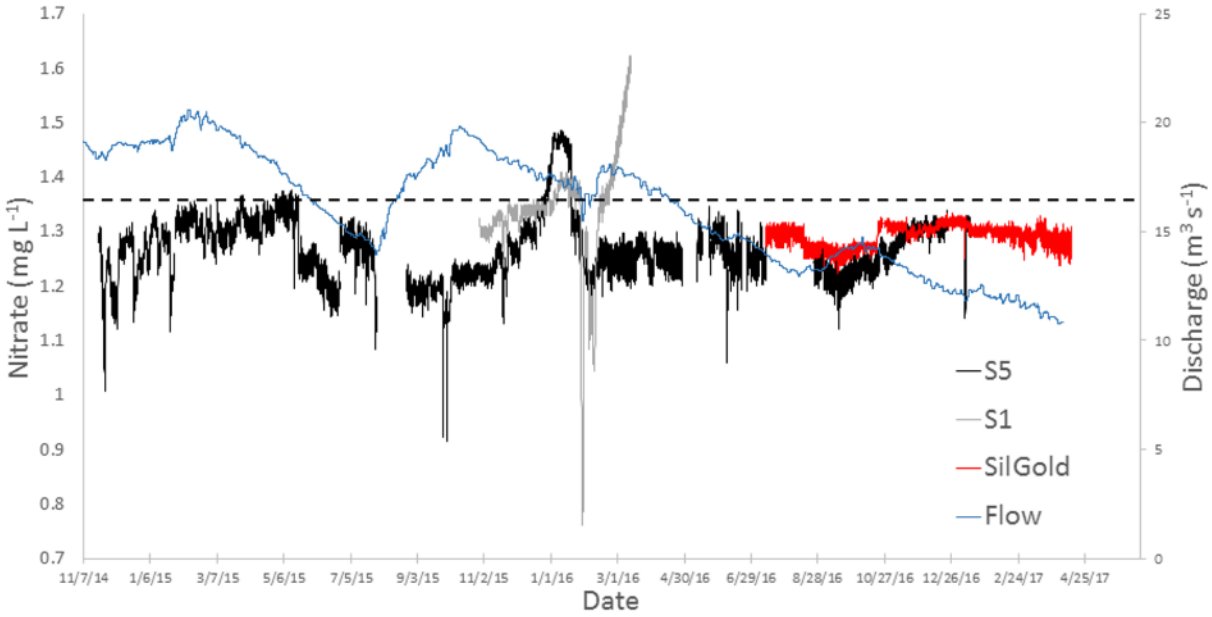

Figure 6.39. Period of record nitrate concentrations for SILGOLD, Silver River S1 and Silver River S5. Also shown is the flow record over the same period.

quantized data from which inference using the diel method is extremely challenging. We attempted various smoothing algorithms to retrieve a viable sensor signal, but were unable to do so satisfactorily, primarily because smoothing reduces the diel amplitude and lowers each daily baseline value. As such, we obtained and used nitrate data from a shadow data storage system. This was important to obtaining reasonable $U_{a,N}$ values.

Based on the experiences, we offer three recommendations for future riverine sensor deployments:

1) Ensure sensors are placed to sample the advective zone of the river, and not hydraulically distinct storage areas. The diel method (inference from solute time-series, described above) presumes a well-mixed water column, and a signal induced by the upstream benthic area. Where the advective zone is not sampled, these assumptions are violated.
2) Perform a DI blank measurement on the SUNA during each scheduled maintenance (preferably monthly). The allows any sensor drift to be corrected.
3) Maintain a shadow data storage system for SUNA data to contain both the non-truncated nitrate measurements and the actual UV absorbance values in each channel. The former will improve inference of N retention, and the latter will provide ancillary information about the chromophoric DOC concentrations in the water column to complement the fDOM measurements obtained here.

Screening the nitrate data for periods that are usable yielded 270 days at SILGOLD and 673 days at Silver River S5. Note that no nitrate data were available from Alexander Springs Creek, though the benthic chamber data (presented below) yields commensurate and important insights about N dynamics in that system. An example of typical nitrate data from Silver River, during a two week period in October 2016 is shown in Figure 6.40. Note that nitrate varies inversely to

DO, indicating that N uptake occurs at the same time as photosynthesis. For reference, the input nitrate concentration from the springs is 1.33 mg N L^{-1}, and varies very little over time.

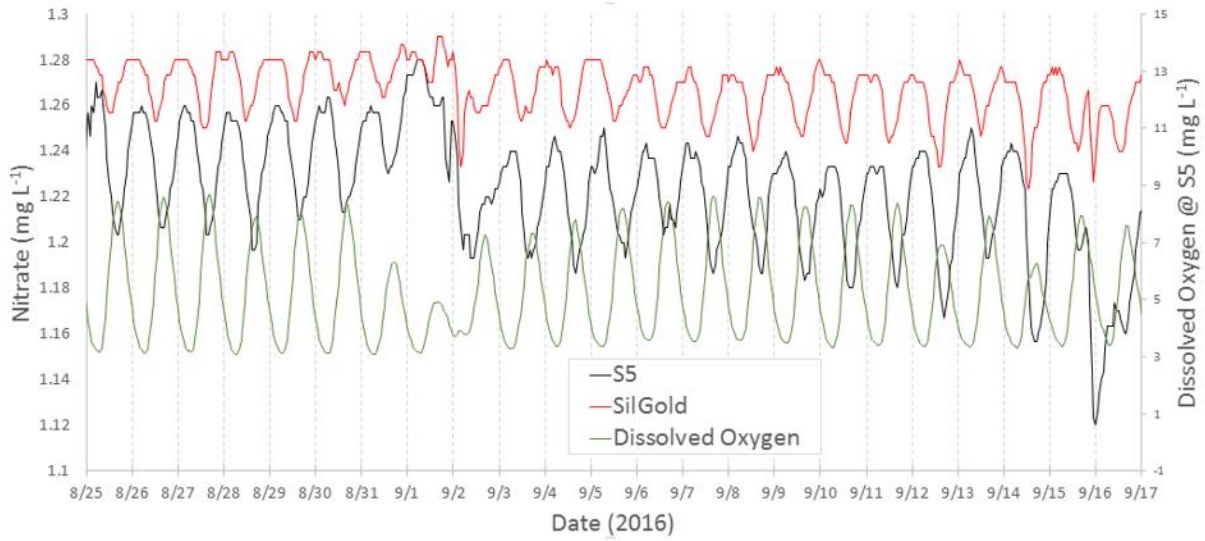

Figure 6.40. Two week period with nitrate at both SILGOLD and S5. Shown with variation in dissolved oxygen. Note that the input concentration from the head springs is roughly 1.33 mg N L^{-1}, indicating net nitrate retention from the head springs to SILGOLD, and further from SILGOLD to S5.

For phosphate, sensors were placed at SILHEAD and SILBIRD (which were not used for reasons previously described) and at S5; no sensor was deployed as S1 given SJRWMD prioritization of upper river sites for limited sensor utilization. The SILBIRD sensor was moved to SILGOLD. All data were viable after routine cleaning of the data to remove obvious outliers. Inference P assimilation rates were made on 185 days at SILGOLD, and 613 days at S5. Reduced numbers than for N were because of missing data, and sensor down time for routine maintenance. The entire period of record is shown in Figure 6.41. Several areas of notable anomalies are evident. In particular, the time series contains extended period of low SRP concentrations at both stations, but particularly at SILGOLD. The origin of these excursions is unknown, and may be associated with routine sensor maintenance since they are often evident after a period with no data. The diel signal still exists within these periods, and was analyzed as such. However, we note that setting the nighttime baseline value during these periods required careful attention.

A two-week window during which SRP measurements were available at both SILGOLD and S5 is shown in Figure 6.42A. Note that the SRP signal variation lags DO by roughly 8 hours, a finding consistent with observations in the Ichetucknee River (Cohen et al. 2013) and other spring fed rivers. However, in this case, the diel signal is much larger and much earlier at SILGOLD than at S5. Part of the difference in lags may be due to the shorter distance, though we note the lag is from DO, not solar input, the former of which is subject to the same distance effects. The difference in diel amplitude are very difficult to reconcile with biological differences because the imprinting of diel signals occurs in response to the aggregate mass retention from the water. This ultimately suggests far higher P assimilation in the upper river than elsewhere, a finding we explore in greater detail below. In short, the diel signal is likely too large to be

biological, and may represent particularly high rates of calcite mineral formation in the river (where CO_2 evasion rates are more rapid, and mineral saturation states are changing dramatically). Since we have applied the same mineral production and P sorption assumptions to both reaches of the river, it is plausible that our accounting for mineral sorption is dramatically underestimated in this upper region of the river.

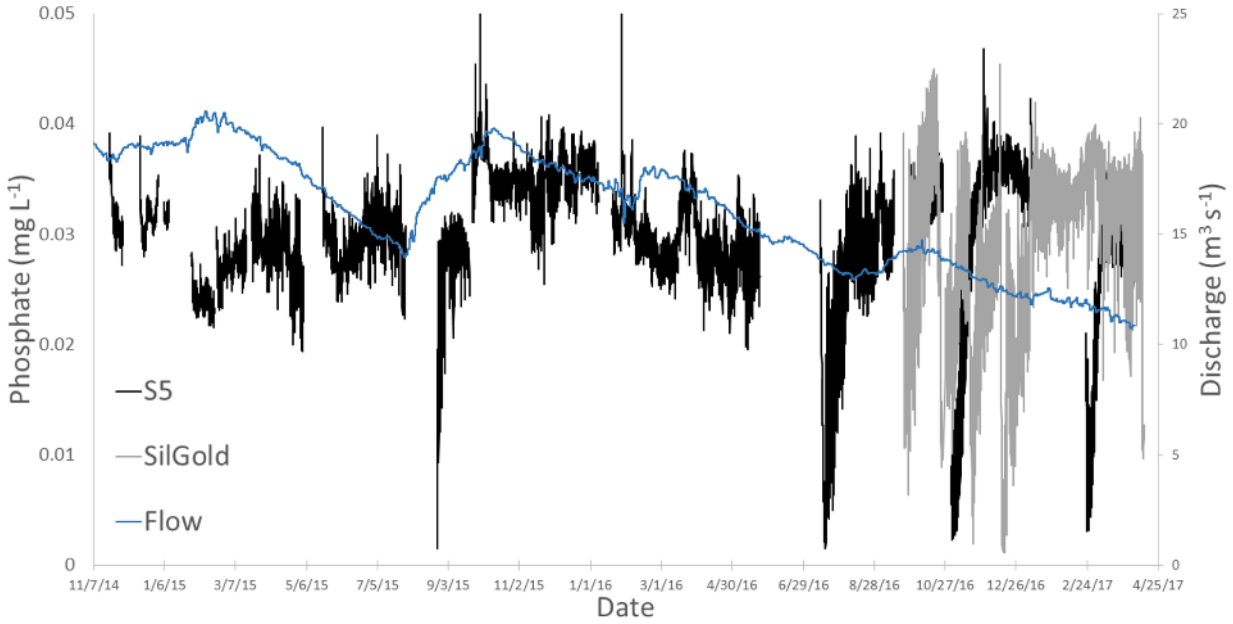

Figure 6.41. Period of record phosphate measurements at S5 and SILGOLD, along with river flow.

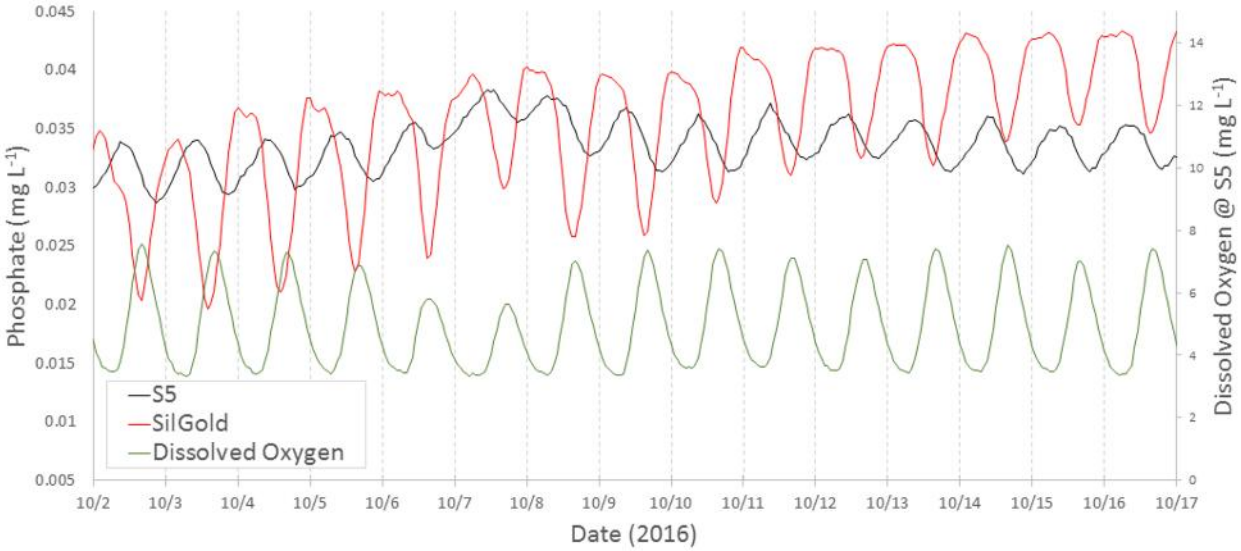

Figure 6.42A. Two week period of record showing SRP concentration variation at SILGOLD (red) and S5 (black). Also show are attendant DO signals at S5.

The time series can be summarized to visualize the inherent lags present in the solute signals. To start we show the diel pattern for dissolved oxygen with respect to solar forcing. This

demonstrates the 4-5 hour lag in DO from peak solar insolation at S5, a station roughly 5 km downstream of the headspring where constant DO conditions are present. This lag occurs because of hydraulic transport of water, and also reaeration. This lag creates counter-clockwise phase patterns when DO is plotted versus radiation. Similarly, we plot DO versus the two nutrient solutes to demonstrate strong phase alignment for nitrate (i.e., peak nitrate uptake lags peak DO production by less than an hour) and considerable lagging in P uptake, with peak SRP removal occurring 7-8 hours after peak DO production (Figure 6.42B). This timing suggests that N uptake is aligned with photosynthesis, and that P uptake occurs at the onset of darkness. This finding was extensively discussed in Cohen et al. (2013) for data from the Ichetucknee. In that work, the differential lag behavior was attributed to the fact that autotrophs require new P for ribosome construction during cell division, which occurs preferentially after dark. Gene regulation experiments from diatoms confirms that target organisms are capable of up and down regulating key uptake apparatus, and that they do so under nutrient replete conditions such that N uptake occurs during the daylight hours, and P uptake occurs at night. Confirmation of this gene-expression prediction at the ecosystem scale lends important support for the use of *in situ* sensors to detect nutrient uptake behaviors. Further work (Appling and Heffernan 2014) suggest that diel variation is itself diagnostic of nutrient saturation, suggesting that both N and P are supplied in excess of demand in Silver River at all times.

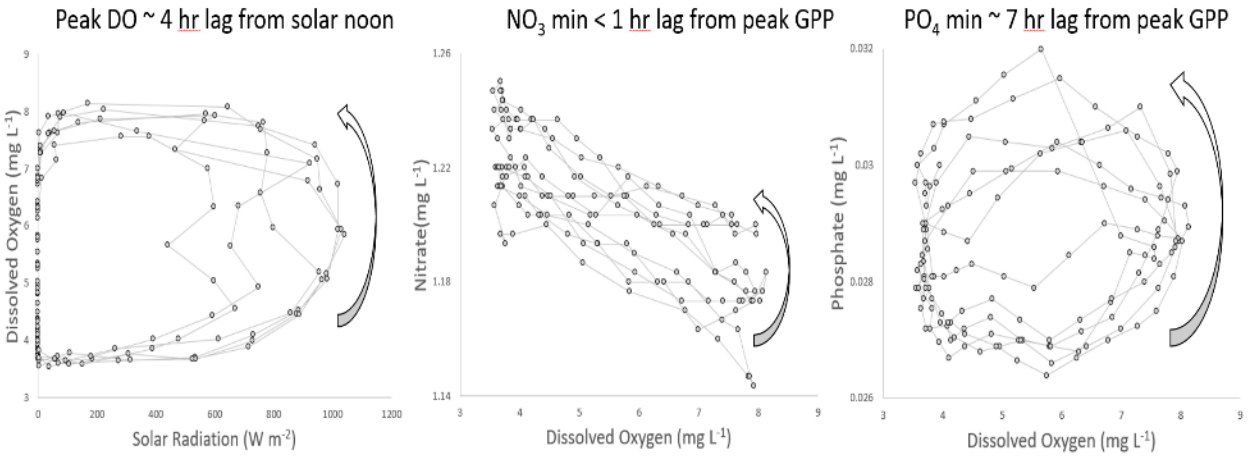

Figure 6.42B. Timing of DO production compared to solar forcing (left) and then lags of N (center) and P (right) uptake with respect to peak DO production.

As with metabolism, we can summarize the daily N and P uptake time series. Figure 6.43 shows N uptake and also gross primary production. The mean uptake rate across the period of record is 0.08 g N m^{-2} d^{-1}, a value broadly consistent with what has been observed in other spring fed rivers, and consistent also with the stoichiometric predictions of N uptake from primary production and tissue elemental composition. We also note that the short-term variation in N uptake appears correlated with attendant variation in GPP.

For phosphorus, the time series of $U_{a,P}$, shown in Figure 6.43, indicates modest variation around a mean of 10 mg m^{-2} d^{-1}, a value also consistent with previous observations. However, we note that the covariance between P uptake and GPP is clearly weaker.

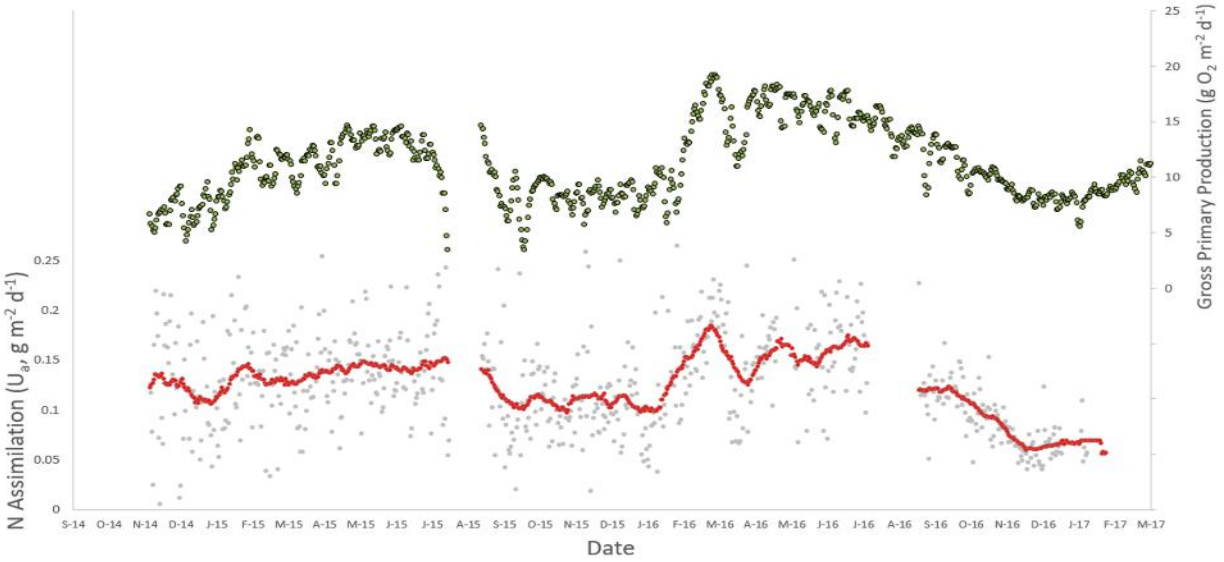

Figure 6.43. Time series of N uptake ($U_{a,N}$) by autotrophs at the S5 station, along with DO. A moving average (red dots) is provided to better visualize the association to GPP.

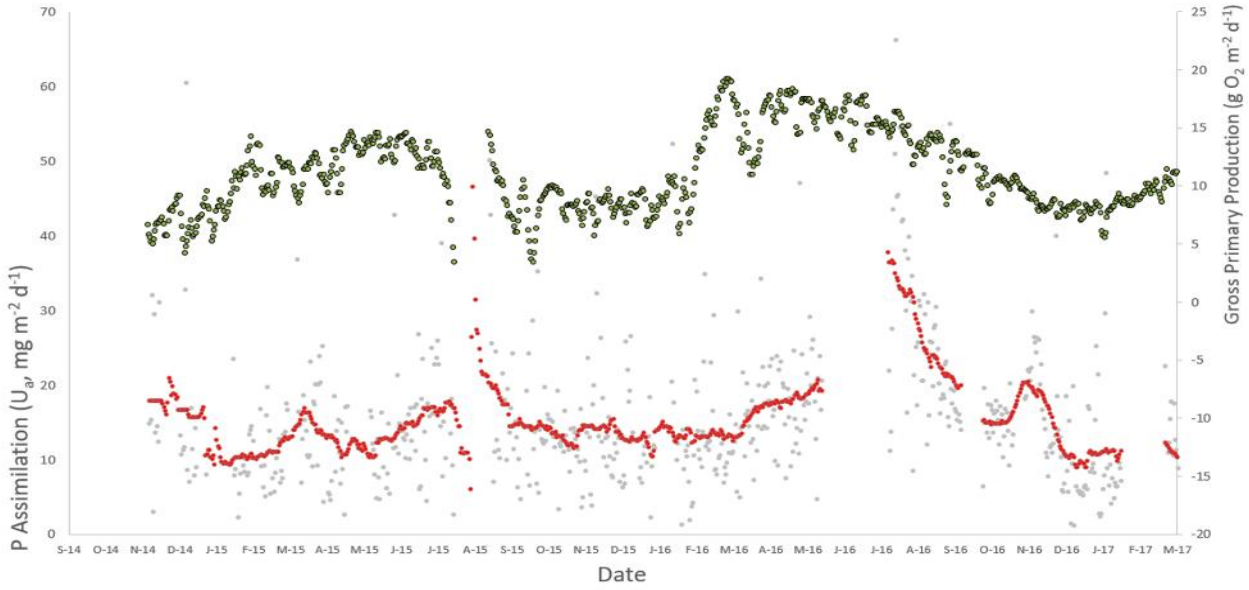

Figure 6.44. Time series of P uptake ($U_{a,P}$) by autotrophs at the S5 station, along with DO. A moving average (red dots) is provided to better visualize the association to GPP, which is relatively weak.

To better evaluate the covariance between GPP and nutrient assimilation, we plotted GPP versus $U_{a,N}$ and also versus $U_{a,P}$ (Figure 6.45). Both stations (SILGOLD and S5) are represented.

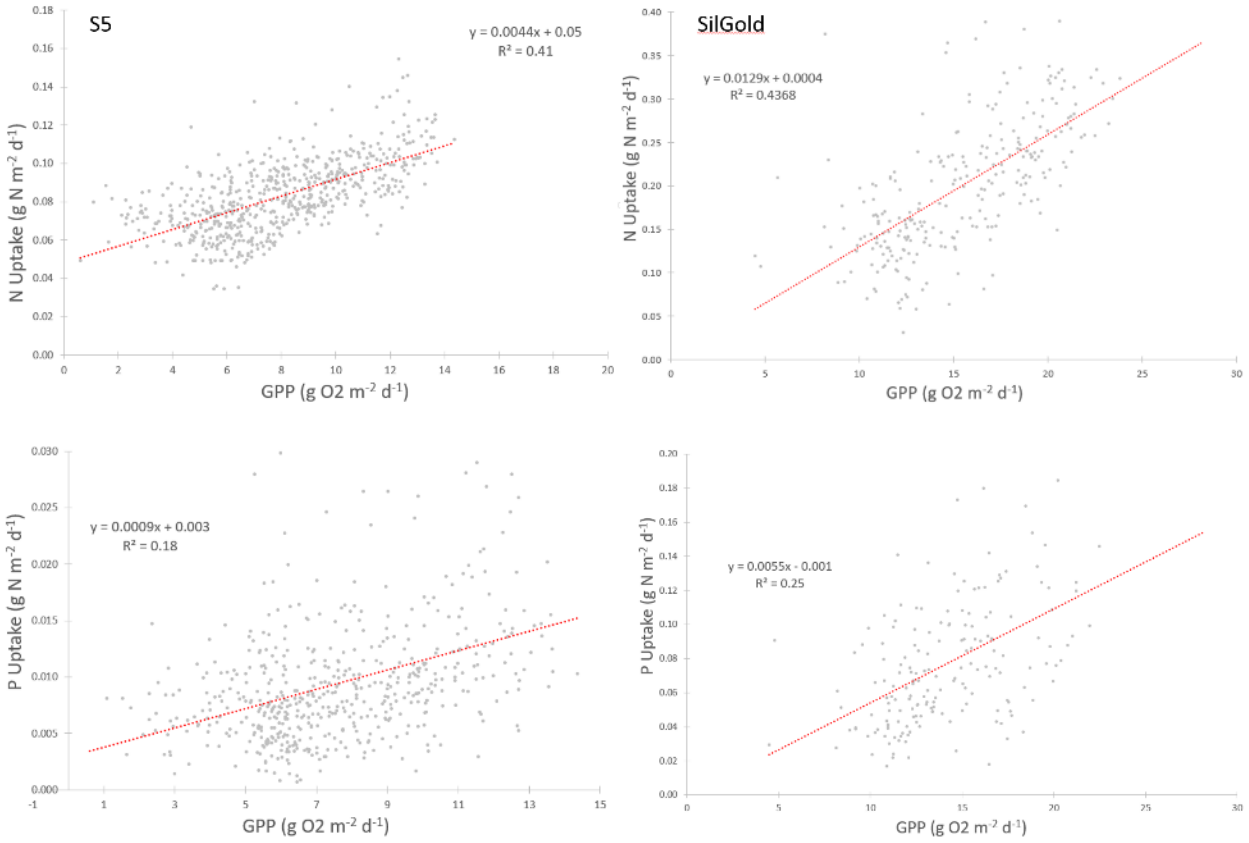

Figure 6.45. Covariance between GPP and (top) $U_{a,N}$ for both S5 and SILGOLD, and for (bottom) $U_{a,P}$, also for both stations. All regressions were significant at $p<0.001$, but were much stronger for N than for P.

Clearly, there is significant positive covariance for both uptake rates versus GPP at both stations, though we note that previous efforts with shorter deployments have generally yielded far stronger model fits. It is also notable that the slope of the fitted line at SILGOLD is consistently higher than at S5, particularly for P. Surveys of the Silver River done in 2015 suggest that most of the algal biomass is found in the upper river, and because algae generally have lower C:N ratios than rooted vascular plants, the difference in N uptake per GPP may be due to that. The increase in P uptake per unit GPP is less easily explained, since both algal taxa and SAV have similar C:P ratios (Nifong et al. 2014).

Reach mean assimilation rates are shown in Figure 6.46 for both the S5 and SILGOLD segments. As previously noted, the assimilation rate for N and P is higher in the SILGOLD reach, and in both cases this difference is statistically significant. For N dynamics, we also note here that denitrification is by far the larger flux, representing 73 % of retention in the S5 reach, and 78 % in the SILGOLD reach. This is broadly consistent with previous observations in other spring fed rivers, and supports the interpretation that the high productivity environments of spring ecosystems are capable of high rates of N removal. The absence of stronger longitudinal N removal gradients largely stems from the enormous mass of N available at the spring vent, not from low ecosystem biogeochemical reactivity.

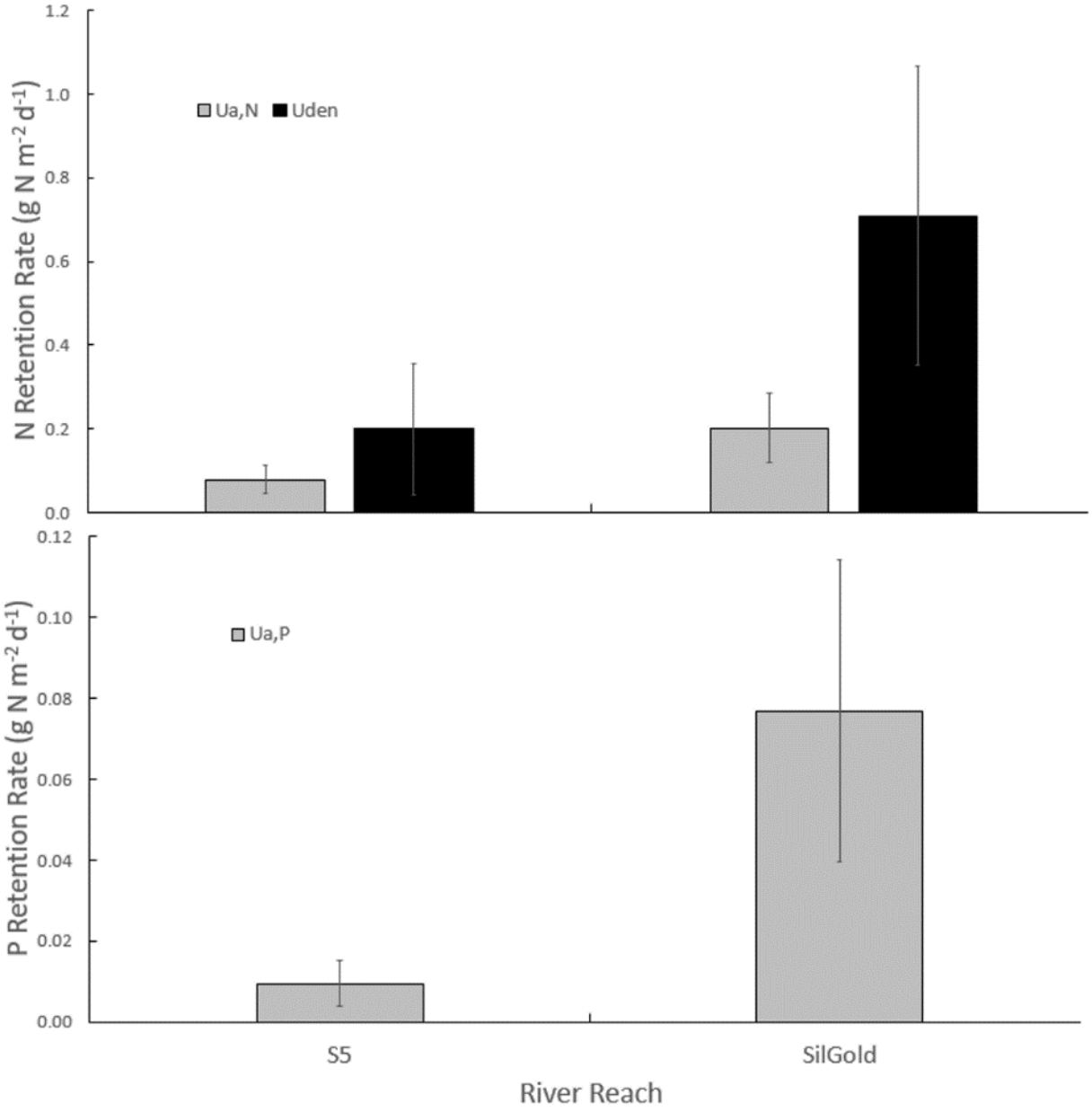

Figure 6.46. Reach mean rates of (top) N retention due to both autotrophic assimilation ($U_{a,N}$), and denitrification (U_{den}) over the period of record for both S5 and SILGOLD reaches. Reach mean rates for P uptake ($U_{a,P}$, bottom panel) are for both reaches as well.

For phosphorus, there is a similar difference between the S5 and SILGOLD reaches with much higher P assimilation rates in the upper river. While values for S5 are consistent with observations in other spring-fed rivers, the rates at SILGOLD are extremely high (nearly 5 times higher than the highest rates observed at the Ichetucknee River, and nearly 8 times higher than observed here for S5). Given the relatively homeostatic stoichiometry of the dominant autotrophs in all spring fed rivers (Nifong et al. 2014), this difference cannot be explained by compositional differences between the reaches. Indeed, we have summarized the stoichiometry implied by both

N and P uptake versus net primary production (i.e., GPP * 0.5; Heffernan and Cohen 2010), and adjusting for molecular weights. The resulting C:N and C:P behaviors is shown in Figure 6.47. Notably, the C:N ratio in the S5 reach is broadly consistent, albeit slightly higher than observed C:N ratios for the two dominant submerged vascular plants. This is consistent with most of this reach being dominated by dense meadows of these rooted plants. In contrast, in the upper river, where algal cover is generally highest, the ecosystem C:N ratio is considerably lower, more broadly consistent with a mix of autotrophs because algal species present in this area have much lower C:N ratios.

The stoichiometry of P uptake is reasonable for the S5 reach, well within the range of observed tissue concentrations. We note that failing to account for the geochemical attenuation of P yields C:P molar ratios that are far too high. We also note that while the S5 reach yields entirely plausible value, the C:P ratio observed in the SILGOLD reach are far too high to be entirely the result of P assimilation. Several explanations are possible, but all require additional measurements to resolve. One possibility is that the SILGOLD station is not entirely in the advective zone of the river. We generally discount this possibility because of the plausible values for N assimilation and GPP that were derived from sensors also at this location. It is also possible that the geochemical C flux via sorption is not confined to daytime hours only. Further work on the mineral saturation states of the water over time, and with distance downstream would be required to investigate this possibility. Finally, it is possible that some of the parameters used to model the P sorption process are incorrect. That model presumes features of the P sorption process that are difficult to empirically validate. For example, it assumes a P sorption rate per unit mineral area from the literature (Cohen et al. 2013) that may not be correct. For the time being, we simple urge caution when interpreting the C:P ratio in the SILGOLD reach as indicative only of assimilation.

The most important implication of the N stoichiometry is that the imputed N assimilation rate is entirely plausible. Given that we can reasonably assess N demand in the ecosystem, we can better understand the plausibility of N limitation in this river. Given nitrogen loading at the spring vent as a measure of total supply, we can use the measurements of N demand over the entire 5 km S5 reach with respect to that mass flux. When we multiply the observed N demand per unit area by the entire benthic area in this reach, and we divide this mass flux by the mass supplied from the river, we obtain an estimate of the fractional N use by the ecosystem (Figure 6.48). While that number varies considerably in response to metabolism variation, it averages 1.2 % of the total load. That is, by complement, 98.8 % of the N load that emerges from the spring vent is not assimilated; most passes by unaffected by the ecosystem, though roughly 7 % of the mass is denitrified over the same reach. It is extremely difficult to assert N limitation of ecosystem processes when so much of the flux is excess. A similar assessment can be made for P uptake, and indicates that autotrophs use ~ 5.5 % of the available load over the S5 reach.

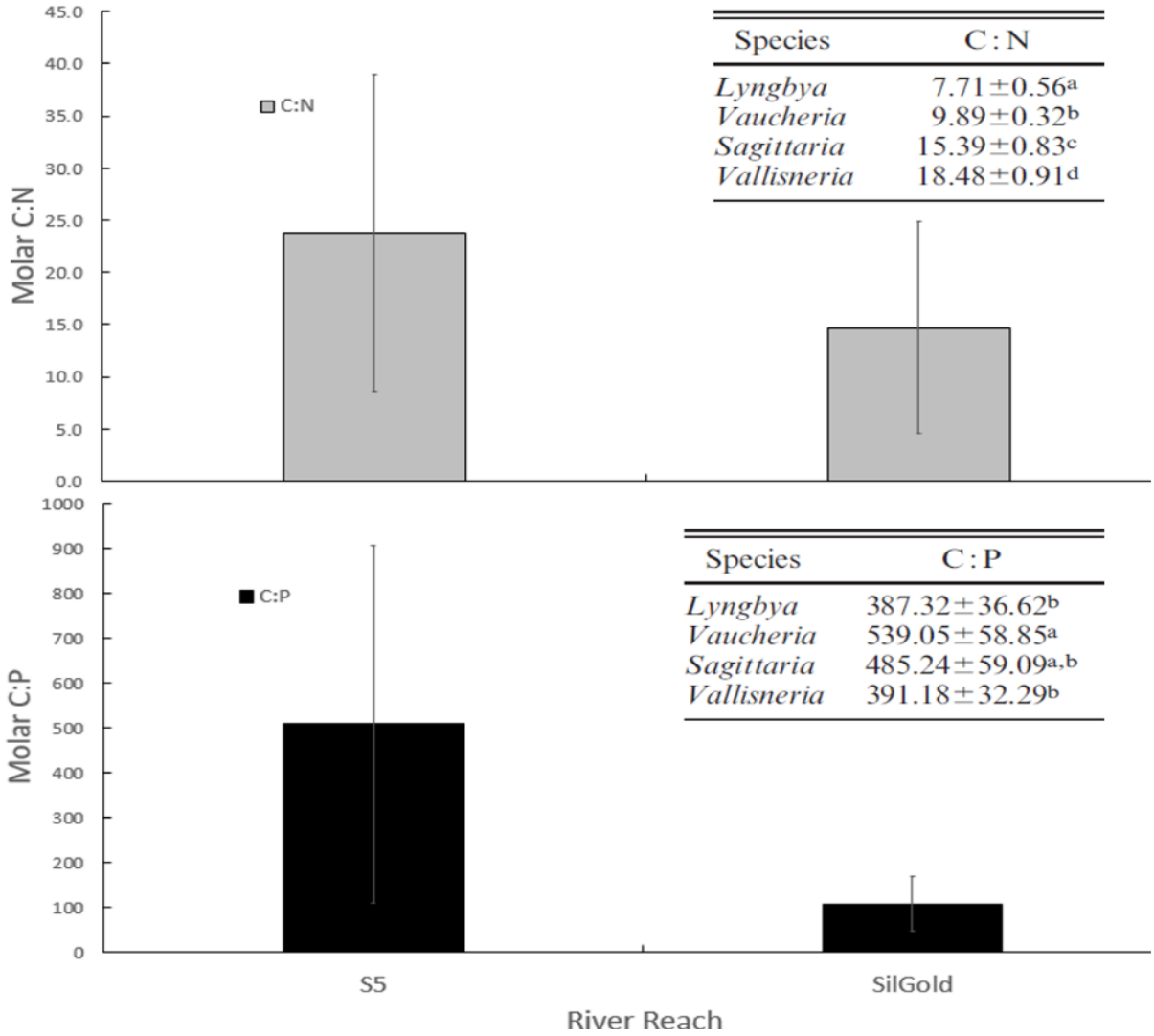

Figure 6.47. Ecosystem metabolism stoichiometry for N (upper) and P (lower) autotroph assimilation. The inset tables show measured tissue stoichiometry for the dominant autotrophs from Nifong et al. (2014).

A thought experiment can further put this in perspective. Silver River is currently significantly N enriched compared to historical background conditions near 0.05 mg N L^{-1}. Assuming that mass loading rate, but the same assimilation rate, the S5 reach would use 34 % of available N, assuming zero remineralization (which is untenable given benthic chamber observations, below). While the critical threshold at which N supply satisfies demand, and by complement when N limitation can be induced remains unclear, work by King et al. (2012) suggests that the ratio of flux to demand needs to substantially higher than was present in pre-development spring ecosystems to induce limitation. This is supported by the fact that GPP was as high or higher in Alexander Springs Creek despite nitrate levels at or near background concentrations. In short, while there is strong evidence of N use by the ecosystem (including SAV, algae, animals, and microorganisms), these data support previously derived measures of ecosystem N demand that call into question the plausibility of N limitation of aggregate ecosystems primary production that forms part of the rationale for dramatically lowering N concentrations.

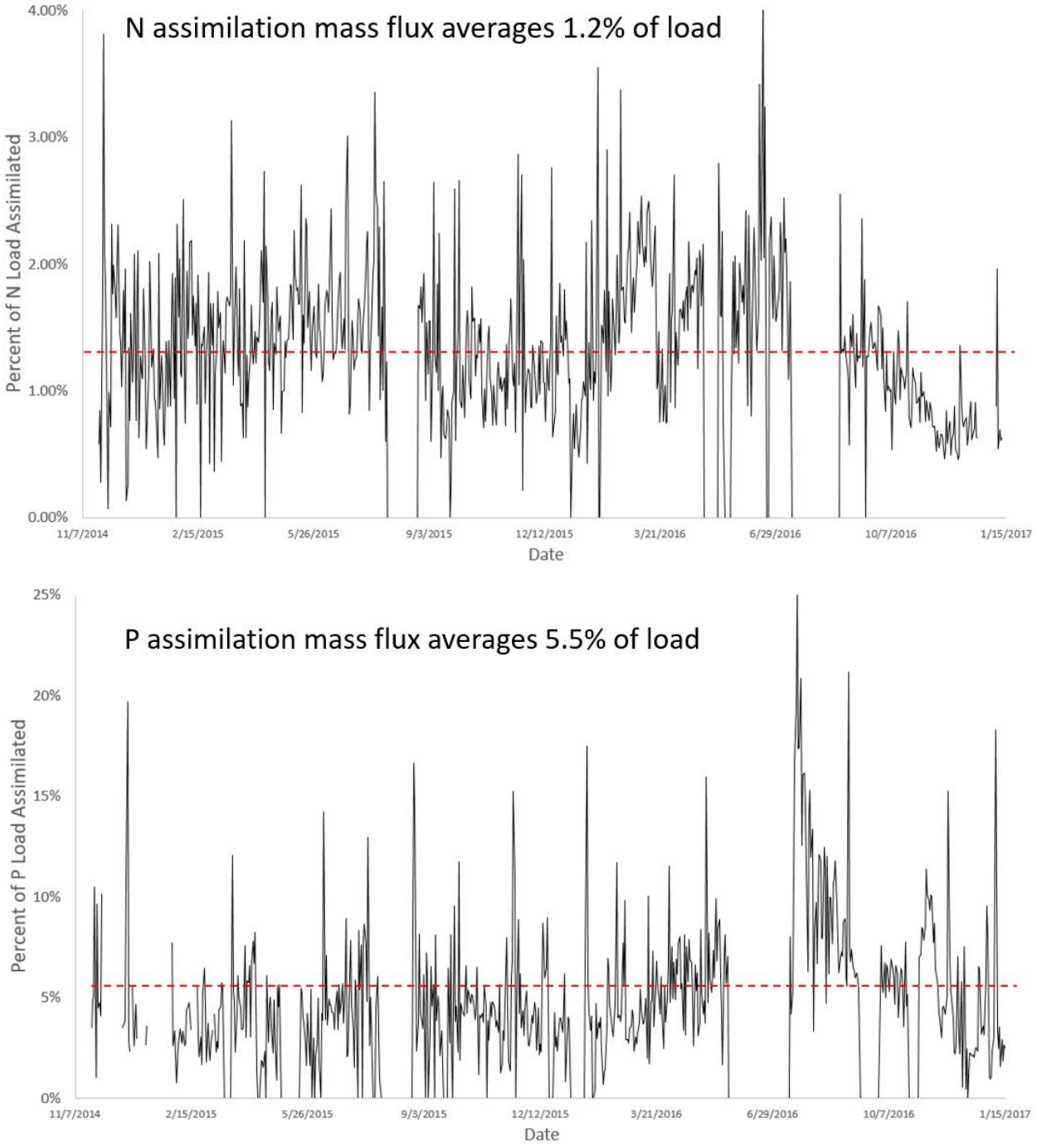

Figure 6.48. Time series of N demand (top) and P demand (bottom) as a fraction of total mass loading from the spring vent. The mean value (red line) over the period of record is also shown.

6.4 SILVER RIVER BENTHIC SURVEY

Beginning in August 2014 and ending in December 2014, a comprehensive linear survey was conducted to characterize the physical, chemical, and biological components of Silver Springs and Silver River. The survey was used to 1) determine how these characteristics co-vary across the Silver Springs system, and 2) inform site selection for vegetation growth and benthos box experiments. Twenty longitudinal transects were selected based on proximity to MFL locations, and overall water depth (Figure 6.49). Across each transect, five randomly selected quadrat locations with water less than 3-m deep were selected to allow free-diving for sample collection. In total, the survey included 100 sample locations (20 longitudinal transects with 5 latitudinal locations within each) where the biological, chemical, and physical components of the river were characterized (see Appendix 6.1 for geographic locations of transects and samples).

Figure 6.49. Locations of twenty (20) lateral transects along the length of the Silver River at which channel morphology, vegetation, water chemistry and sediment properties were measured. Each transect consisted of 5 locations spanning the width of the river.

6.4.1 Field Methodology

At each location, a 2'x2' vegetation quadrat was placed on the stream bottom (Figure 6.50) and the percent cover of submerged aquatic vegetation (SAV) and algae was characterized by species using the 5-point Braun-Blanquet classification system (described in 6.4.4). Percent cover of bare substrate was also recorded. The quadrat location was characterized by distance from channel bank and latitude/longitude coordinates. Water depth was taken within the quadrat and surface water velocity and canopy cover measurements were taken above the quadrat. Canopy

cover was determined by using a densiometer, determining percent open canopy in the four cardinal directions around the quadrat location, and converting to percent canopy cover. Porewater and water column samples were collected using a peristaltic pump, 0.45 micron filter, and acid preservative. Finally, two plant samples and a sediment grab sample were collected from within the quadrat. All water, sediment, and vegetation samples were placed on ice for transport. Analytes, sample sizes, and preservative per analysis are summarized in Table 6.6B.

6.4.2 Laboratory Analyses

Water samples were stored on ice and refrigerated until chemical analyses (Table 6.6B) were performed. All water analyte (NO_3-N, NH_4-N SRP, Ca, Cl, Fe, Mn) concentrations were analyzed at the University of Florida Analytical Research Laboratory (UF ARL) according to EPA standard methods. Specifically, NO_3-N, NH_4-N, SRP, and Cl were measured by automated colorimetry (EPA Method 353.2, 350.1, 365.1, and 325.2; respectively) and Ca, Fe, and Mn concentrations were determined through Inductively Coupled Mass Spectrometry (ICP-MS). Average, minimum, maximum, standard deviation, and variation in soil, water column, and porewater analyte concentrations were calculated.

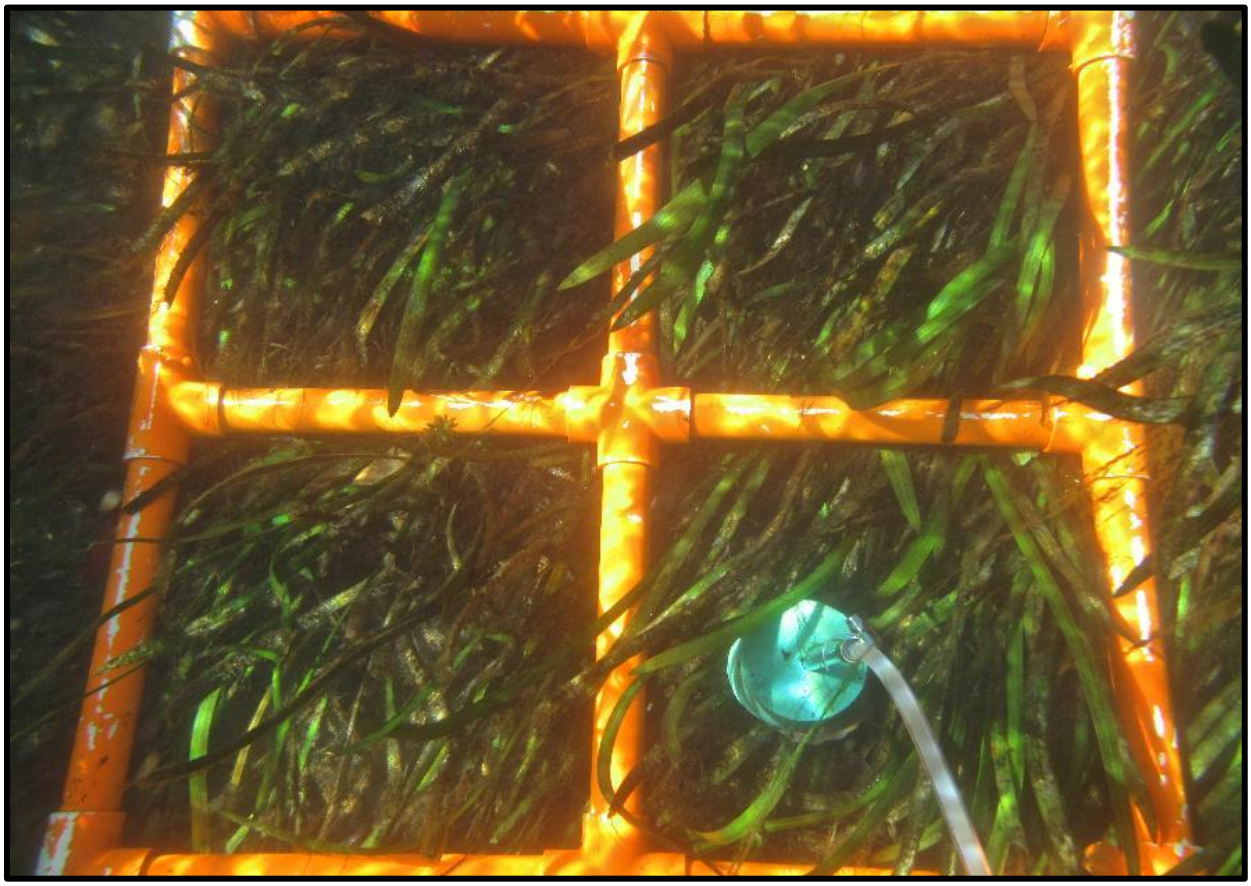

Figure 6.50. Deployment of quadrat for cover and composition measurements, and porewater sampler for collecting water samples. After benthic characterization, a sediment sample was obtained using a modified Ekman sampler, along with a water sample from the river.

Sediment samples were dried at 60 °C for 60-72 hours. After drying, the soils were homogenized through grinding by mortar and pestle and sieved with a 2 mm mesh (#10) sieve. Approximately 10 g of soil were analyzed for percent carbon, nitrogen, and sulfur (%C, %N, %S) by weight through Light Isotope Mass Spectrometry. The soil metals (P, K, Ca, Mg, Mn, and Fe) were extracted using 5 g of soil and 20 mL Mehlich-1 solution and analyzed on an Inductively Coupled Plasma Spectrometer at the UF ARL (EPA Method 200.7). The Loss on Ignition (LOI) Method was also used to analyze the soil for percent organic matter (% OM). Each sample (1-2 g of soil) was weighed, heated at 450 °C for 6 hours, and reweighed where percent organic matter is calculated as the difference between the dried (60 °C) and furnace (450 °C) weight. Lastly, soil particle size analysis was determined using the hydrometer method which is based on the rate of particle sedimentation when suspended in water (i.e., Stoke's Law).

Table 6.6B. Summary of characteristics, sample size, and preservative by stream sample area.

Sample Area	Analysis	Sample size	Preservative
Porewater and Water Column	NO_3-N, NH_4-N	20 mL scintillation	H_2SO_4; pH<2
	SRP, Ca, Cl	20 mL scintillation	No preservative
	Fe, Mn	20 mL scintillation	HNO_3 + HCl
	DOC	40 mL amber glass	HCl
	DIC	40 mL clear glass	$HgCl_2$
Sediment	%C, %N, %S	1-2 g dried soil	N/A
	Fe, Mn, Ca, P, Mg	5 g dried soil	
	%OM	10 g dried soil	
	Texture	50 g dried soil	
Vegetation	%C, %N, %P	Two plant samples measured, weighed, and dried	
	Aboveground biomass		
	Belowground biomass		
	Shoot and root length		
	Number of shoots		

Approximately 50 g of soil was treated with 100 mL of 5 % dispersing solution (hexametaphosphate), diluted to 1,000 mL with deionized water, and equilibrated to room temperature overnight. Prior to each reading, the water temperature and density of a blank sample (blank = 100 mL dispersing solution and 880 mL deionized water) was recorded. A plunger was then used to mix the soil sample for 30 seconds and a hydrometer was inserted into the suspension. Hydrometer readings were taken 40 seconds after mixing and 6 hours, 52 minutes after mixing. The difference in sample densities (corrected for temperature and the difference in blank readings) at both time intervals were used to determine % sand, % clay, and % silt distributions, where:

- % clay = corrected hydrometer reading at 6 hours, 52 minutes X 100/weight of sample
- % silt = corrected hydrometer reading at 40 seconds x 100/weight of sample
- % sand = 100% - % silt - % clay

Vegetation samples were stored on ice and triple washed in deionized water within 48 hours of collection to remove epiphytes. Submerged aquatic vegetation samples were separated into above- and belowground live biomass, and shoot and root lengths were measured. All samples

were dried at 60 ºC to constant weight, and above- and belowground biomass (g dry weight) was determined. Portions of leaf biomass were ground and homogenized for tissue analysis. Foliar carbon and nitrogen concentrations, in % C and % N, were measured using a Carlo Erba NA1500 CNHS elemental analyzer at the UF Light Stable Isotope Mass Spectrometry Laboratory. Total phosphorus was analyzed at the UF ARL according to EPA Method 365.1.

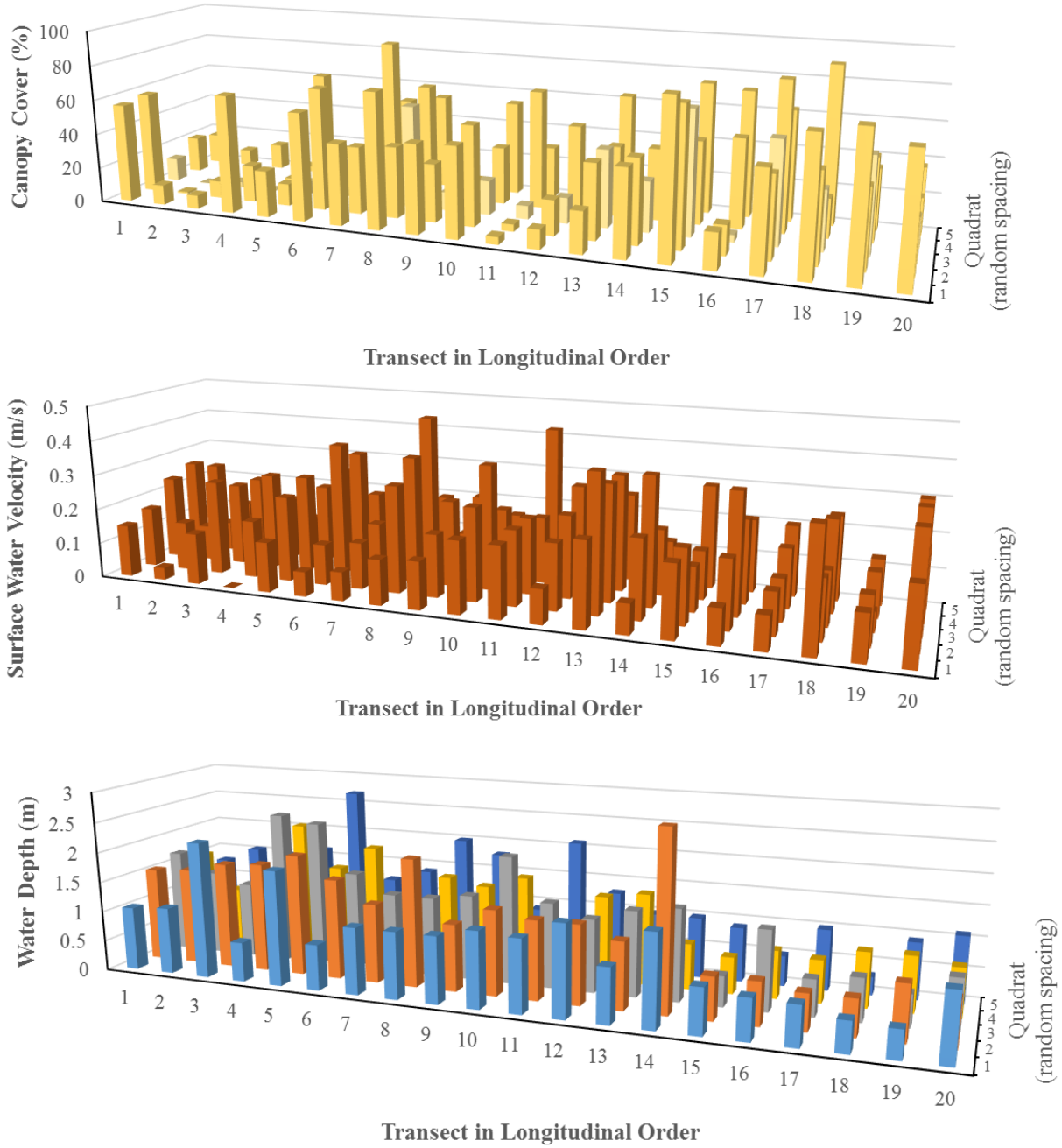

Figure 6.51. Ambient conditions, including percent canopy cover, surface water velocity (m s^{-1}), and water depth (m), were measured during the comprehensive survey. Shown are values for each of 5 locations (randomly spaced) on each of the 20 transects along the river.

6.4.3 Physical Controls

Physical and morphological conditions measured during the comprehensive survey were imported into ArcGIS and will be included in the Springs Initiative GIS database. In general, water depth was greater at the upstream transects, canopy cover increased downstream, and surface water velocity was variable across all transects (Figure 6.51). ANOVA between transects showed significant variation for all three characteristics (water depth, velocity, canopy cover) (p-value <0.001). Water depth explained little variation in surface water velocity ($R^2 = 0.08$; Figure 6.52), which may suggest future work should include measurements made within the water column.

6.4.4 Vegetation Inventory

In total, 207 vegetation samples were collected during the survey. *Sagittaria kurziana* and *Vallisneria americana* composed 80.2% and 17.4% of samples, respectively. Other species identified in the survey included *Ceratophyllum demersum* (Coontail), *Hydrilla verticillata*, *Lyngbya wollei*, *Spirogyra spp*., and *Vaucheria spp*. Our benthic inventory included cover estimates for each taxa, and as guilds (i.e., SAV versus algae). We used a modified Braun-Blanquet score for characterizing cover with:

- 0 = 0% cover
- 1 = 1 - 5% cover
- 2 = 6 - 25% cover
- 3 = 26 - 50% cover
- 4 = 51 - 75% cover
- 5 = 76 - 100% cover

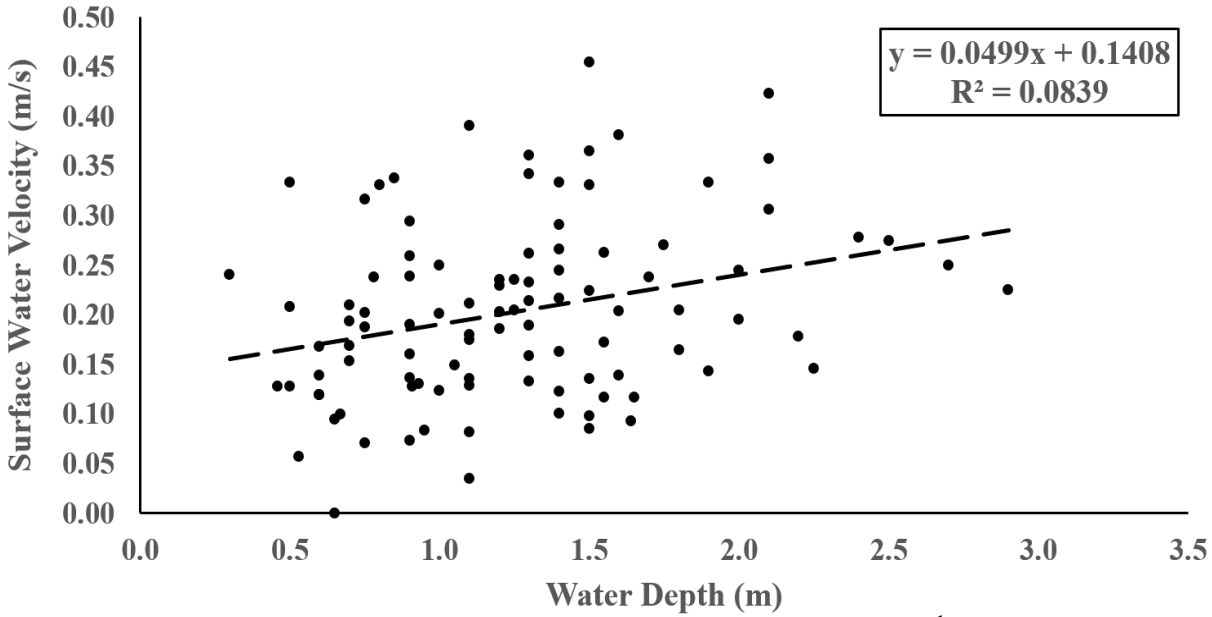

Figure 6.52. Individual water depths (m) and surface water velocity (m s^{-1}) for each location on each transect were measured as part of the comprehensive survey. Water depth explained little variation in surface water velocity.

While there is evidence of significant algal accumulation in the river (40 % of sites had algal cover > 50 %), the river remains dominated by dense SAV, with almost 75 % of sites having SAV cover in excess of 75 % (Figure 6.53).

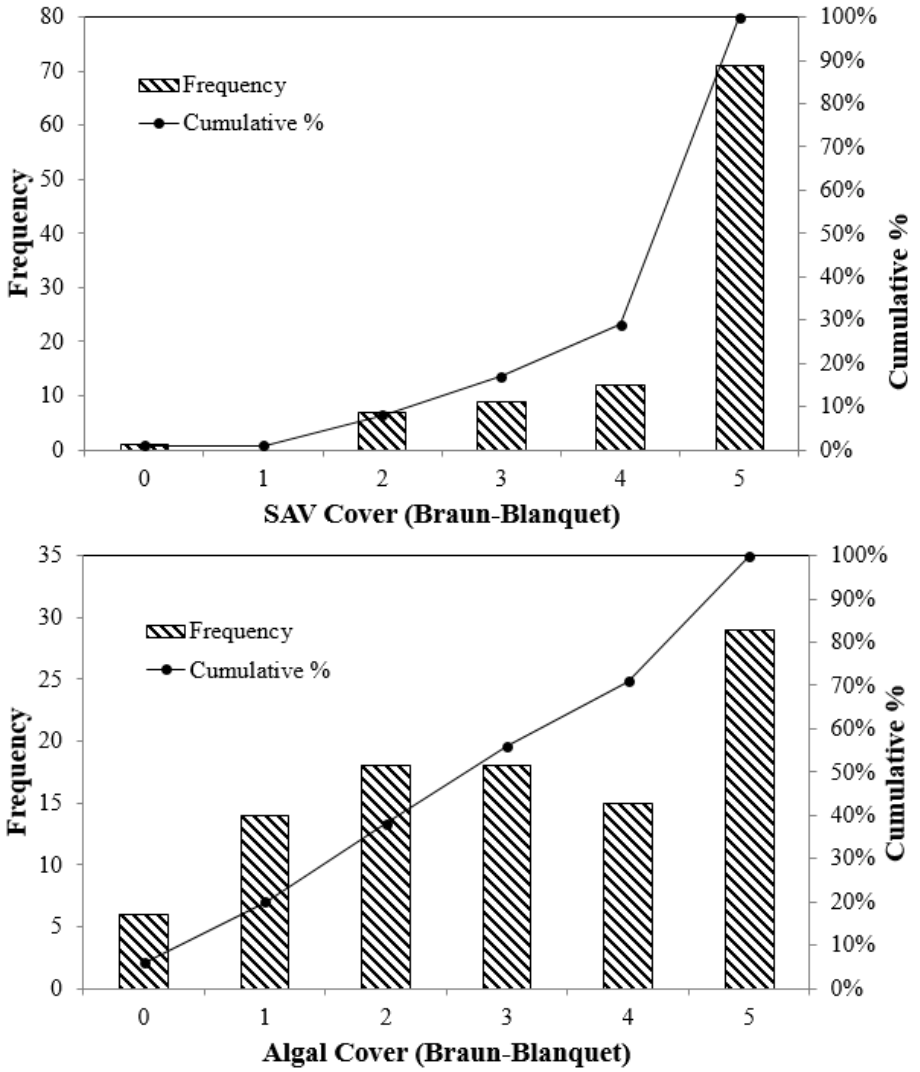

Figure 6.53. Summary of overall river benthic cover of a) SAV and b) algae using the Braun-Blaunquet scale. The survey suggests that most (over 75 %) of the river retains dense SAV beds. Algal cover is variable, suggesting important controls on spatial heterogeneity that are the subject of our subsequent work.

One of the key questions about the interaction between SAV and algae has to do with the shape of their competitive interaction. Plausible relationships include:

- Linear exclusion, wherein benthic cover for algae is the complement of benthic cover of SAV.
- Non-linear negative effects, wherein high algae is associated with low SAV (and vice versa), but the effect is not complementary.

- Positive effects, wherein SAV provide a venue for algal attachment, and therefore high algae are only found where there is high SAV.

We found evidence for a non-linear negative effect, with high algal cover associated with variation in SAV cover; that is, at high algal cover, SAV ranges from <5 % to over 75 % cover, but is always above 50 % when algal cover is low (Figure 6.54), potentially consistent with changing leaf-blade scouring under high flow velocity conditions.

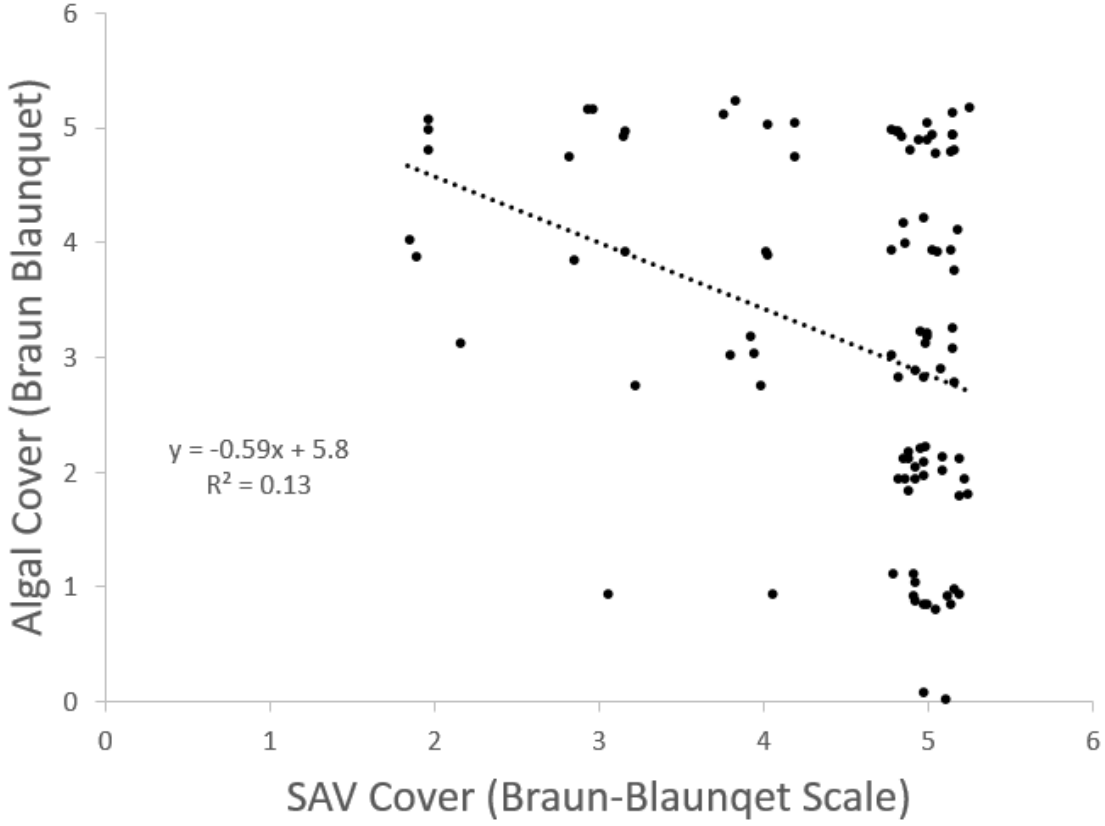

Figure 6.54. Association between benthic algae and SAV cover from individual locations on 20 transects along the Silver River suggests SAV and algae co-exist. However, while the river exhibits uniformly high SAV when algae cover is low, at high algal cover, SAV cover is spatial heterogeneous, consistent with potential smothering effects. Random variance has been added to these categorical cover class data to assist visualization of the association; regression results are for unmodified data.

Average shoot length of all *Vallisneria* samples (75.65 cm) exceeded that of *Sagittaria* (65.86 cm), while average *Sagittaria* root length (14.70 cm) was longer than *Vallisneria* root length (11.29 cm). However, despite significant variation in velocity, water depth, water clarity, and sediment properties, there were few systematic trends in any of the vegetation morphometric properties (Figure 6.55). Root:shoot biomass appeared to be highest through the middle part of the river (Transects 11-14), especially for *Sagittaria kurziana*, but that trend was less clear for root:shoot lengths, nor was it clear for *Vallisneria americana*.

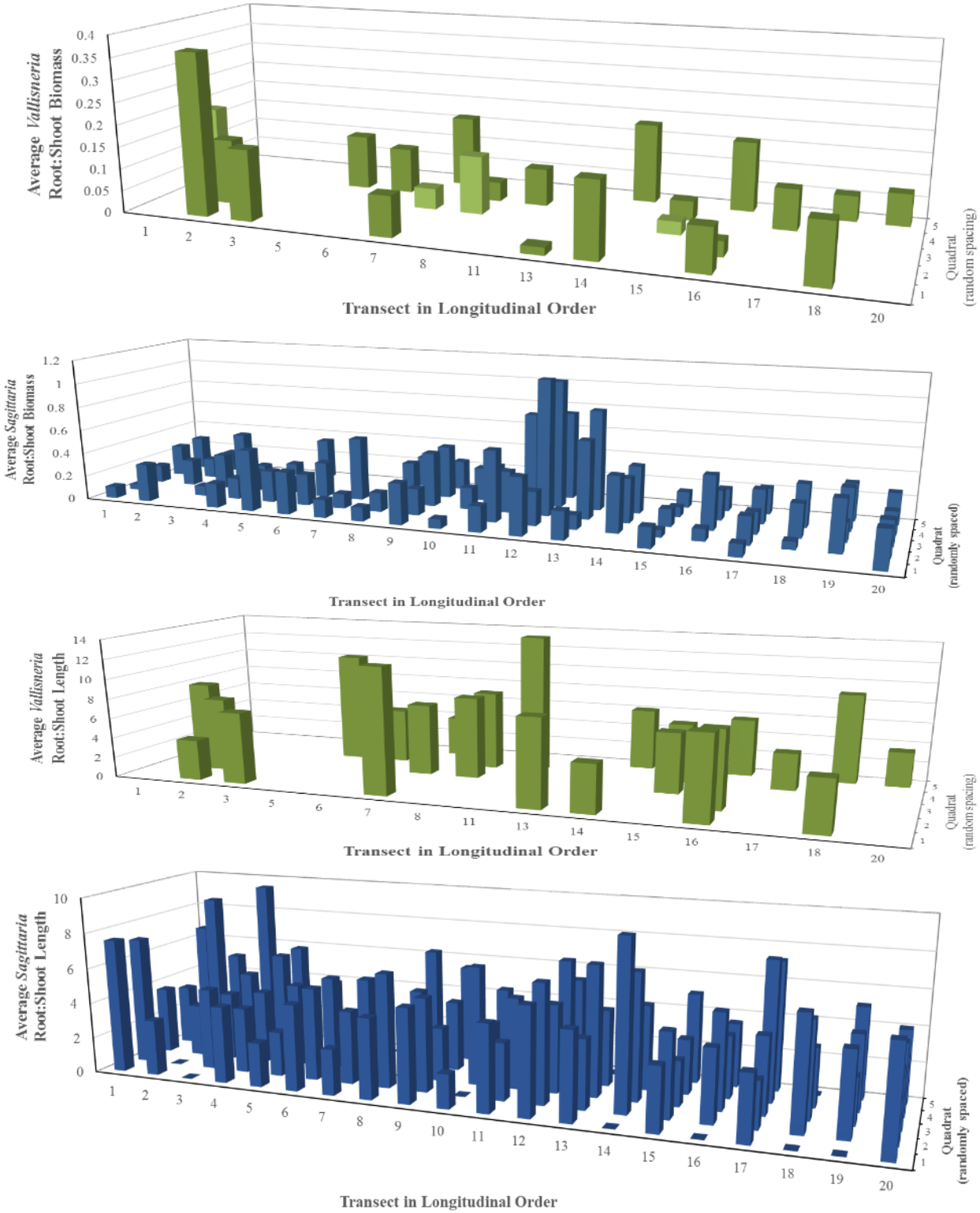

Figure 6.55. Summary of SAV morphologic characterization with distance downstream for each of 5 locations location along each of 20 transects. Locations with no data were where that taxa was not found.

Despite the absence of major vegetative morphologic variation, as would be expected if significant spatial heterogeneity in nutrient availability, or root porewater stresses exist, we did observe significant spatial patterns in benthic cover, both longitudinally (Figure 6.56) and laterally (Figure 6.57). We observed strong evidence for longitudinal declines in algae (to a predicted cover less than 25 % by the Ocklawaha confluence) and also evidence that algal cover is most pronounced on the south edge of the transects, suggesting some interaction with direct insolation.

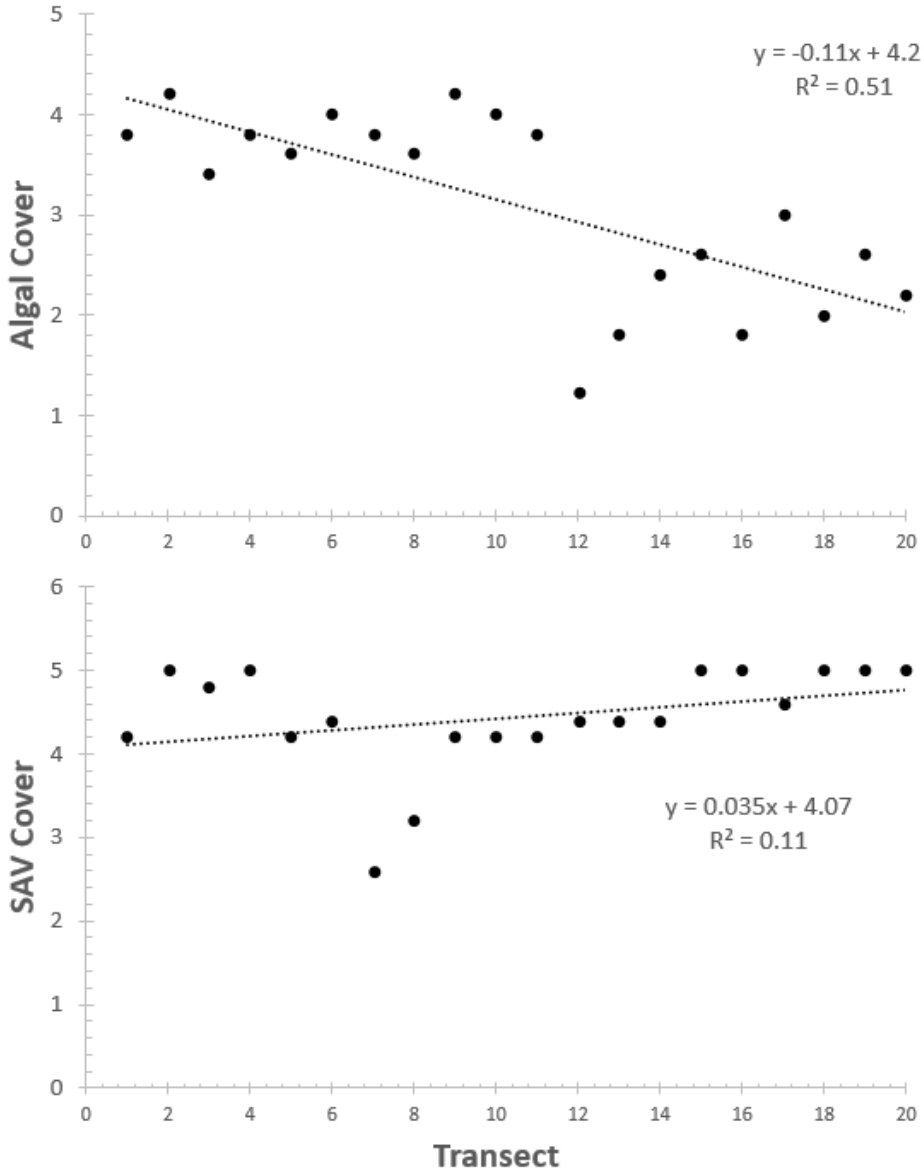

Figure 6.56. Longitudinal patterns in the mean cover of a) algae and b) SAV from each transect from the headspring (at left) to the confluence with the Ocklawaha River (at right). The decline in mean algal cover is statistically significant ($p < 0.001$), as is the increase in SAV cover ($p = 0.02$).

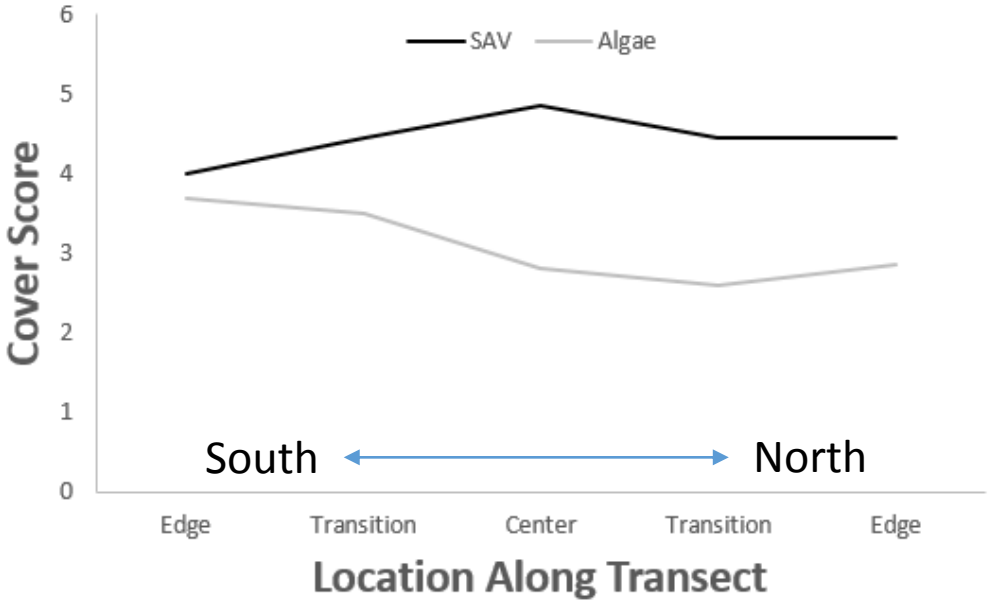

Figure 6.57. Across transects, mean SAV cover was highest in the center of the channel and declined towards the channel margins, while algae was highest at the south edge. Data are pooled across transect for each sampling location perpendicular to river flow.

6.4.5 Vegetation Chemistry

Student's t-tests showed no significant difference in average C (p-value = 0.30) and N (p-value = 0.50) tissue percent content between the two dominant SAV species (Figure 6.58).

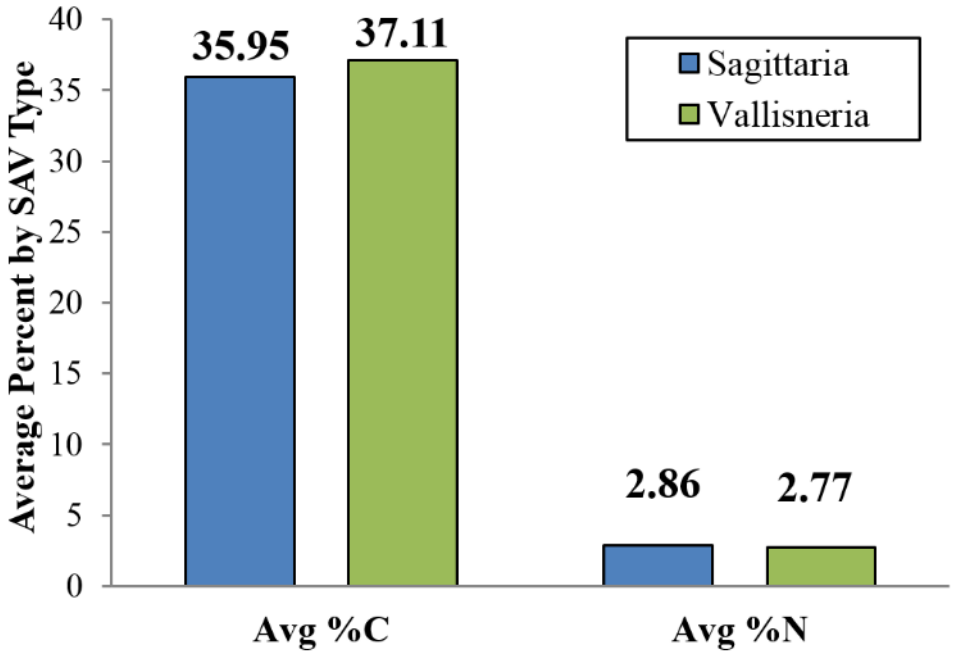

Figure 6.58. No significant difference was found between average % carbon and nitrogen content in two dominant species found in Silver River, *Sagittaria kurziana* and *Vallisneria americana*.

Average tissue C:N for all *Sagittaria* and *Vallisneria* samples was 12.97 and 12.84, respectively. We observed an increase in tissue C:N for both taxa near the confluence with the Ocklawaha River (Figure 6.59). This remains unexplained, and may indicate stoichiometric changes induced by backwater effects from Ocklawaha River flooding. The magnitude of the downstream increase is large compared to the variation along the rest of the river, or within and across other spring-fed rivers (Nifong et al. 2014).

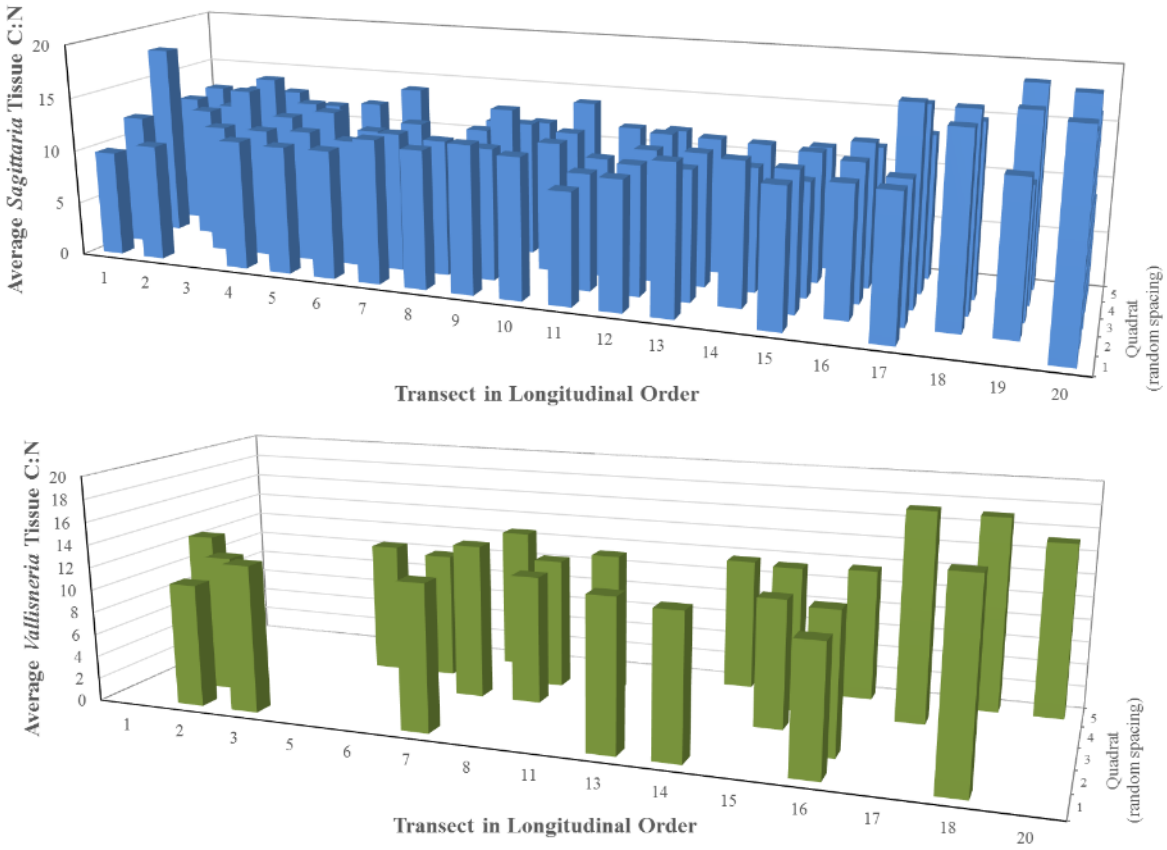

Figure 6.59. Spatial patterns in tissue C:N (molar basis) across the Silver River. We noted a substantial increase in C:N in the lower river, though subsequent measurements (Figure 6.52) do not replicate finding.

6.4.6 Water Chemistry

Concentrations in Fe and Mn were below detection limit for every sample collected from the water column and porewater (<0.001 mg L^{-1}); other sections of this CRISPS report (i.e., Benthic Sources of Nutrients and Trace Elements) used alternative methods but confirm extremely low levels of both elements, both in the water column and in the shallow porewaters. The other porewater and water column species (NO_3-N, NH_4-N, SRP, Ca, and Cl) were analyzed and exhibited interesting spatial variation. A summary of porewater and water column chemistry across all samples (i.e., pooled both laterally and longitudinally) are shown in Table 6.7. While mean and minima concentrations are as expected, we did obtain some samples that were extremely high concentrations, especially for NH_4-N and SRP.

Table 6.7. Summary of porewater, soil and water chemistry across the Silver River. Note that concentrations for Fe and Mn were consistently below detection limits.

Location	Parameter	Mean	Min	Max	SD
Soil	%OM	23.39	2.40	74.55	12.88
	%C	16.48	7.02	40.52	4.53
	%N	0.90	0.12	2.18	0.37
	C:N	21.79	12.12	91.58	11.96
	Mg (g kg^{-1})	0.31	0.00	1.30	0.18
	P (g kg^{-1})	0.04	0.00	0.28	0.05
	Ca (g kg^{-1})	10.91	2.36	35.96	4.40
Porewater	NO_3-N (mg L^{-1})	0.87	0.01	10.59	1.35
	NH_4-N (mg L^{-1})	4.86	0.06	25.23	6.09
	SRP (mg L^{-1})	0.47	0.00	3.26	0.73
	Ca (mg L^{-1})	88.88	37.54	162.82	27.90
	Cl (mg L^{-1})	12.12	5.71	31.10	4.14
Water Column	NO_3-N (mg L^{-1})	1.45	0.33	24.95	2.42
	NH_4-N (mg L^{-1})	0.84	0.06	19.92	2.71
	SRP (mg L^{-1})	0.09	0.00	3.48	0.37
	Ca (mg L^{-1})	71.73	30.65	132.99	23.29
	Cl (mg L^{-1})	11.17	4.28	27.39	3.36

We also observed interesting longitudinal trends in many of the analytes, which together suggest that the river is both processing solutes and likely mixing with both shallow groundwater and possibly also surface water from the Ocklawaha River in the lower reaches. Figure 6.60 shows the longitudinal trends in the thalweg concentrations (channel center), and fits a trendline where that line was statistically significant ($p < 0.05$). For all analytes except NO_3-N, the trend is significant, with NH_4-N increasing with distance downstream and SRP, Cl and Ca decreasing. The latter two analytes (Ca and Cl) may suggest that some of the water in the lower river near the Ocklawaha confluence represents a mixture of Silver River and Ocklawaha River water, but this would need to be further verified. Modest enrichment of NH_4-N and depletion of SRP with distance may indicate N cycling (i.e., assimilation of nitrate, conversion and export as NH_4-N), and P retention via both biotic and abiotic pathways.

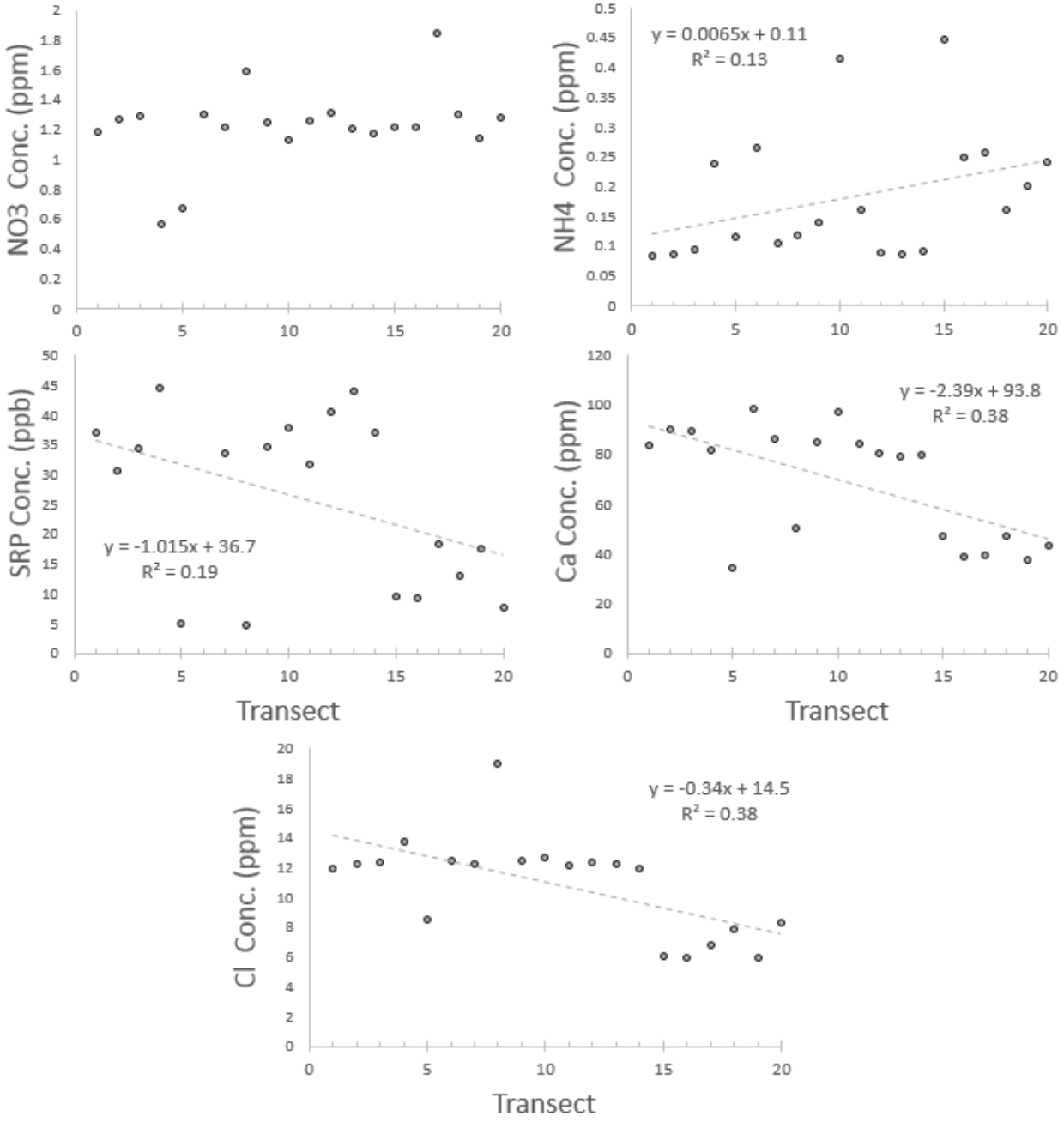

Figure 6.60. Concentrations of key analytes in the thalweg sample along the length of the Silver River. All fitted lines are significant at $p < 0.001$. The nitrate trend was not significant despite repeated measures (Hensley et al. 2014) showing strong depletion trends along the length of the river.

We also explored whether thalweg samples differed from channel margin samples. We defined the lateral ratio as the ratio of the thalweg samples mean to the channel margin samples mean; values above 1 indicate that thalweg samples are enriched compared to channel margin samples. Results suggest that the thalweg and the channel margin samples are very similar, with modest depletion of NO_3-N in channel margins, and modest enrichment of SRP, NH_4-N, Ca and Cl.

Despite significant spatial variation, there were no obvious longitudinal trends in this ratio (Figure 6.61).

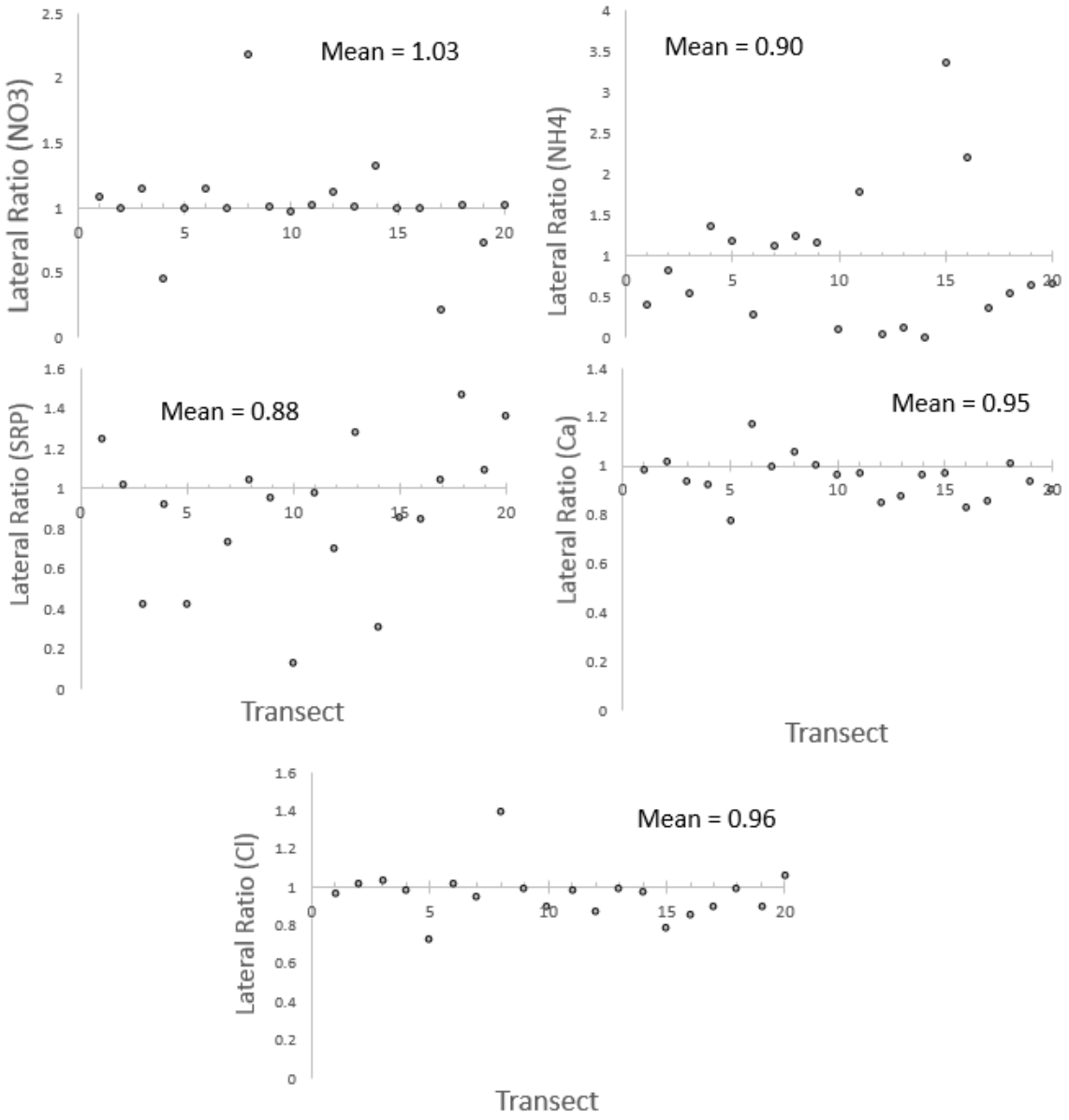

Figure 6.61. Ratios of concentrations for key analytes in the thalweg sample versus the channel margin samples along the length of the Silver River. Values greater than 1 indicate a solute that is enriched in the thalweg compared with the channel margins, while values less than 1 indicate solutes that are depleted in the thalweg. Mean values for the entire river are shown in each graph, suggesting NO_3-N is slightly enriched in the thalweg vis-à-vis the channel margins, while all other solutes are depleted in the thalweg.

Finally, we evaluate the same ratio, but this time comparing the thalweg samples (the actively mixed part of the river) with the porewater samples for each transect. These results (Figure 6.62) illustrated much more significant variation, with massive depletion of nitrate in the shallow

porewaters vis-à-vis the thalweg, and similarly significant enrichment of SRP and NH_4-N in the porewaters. Modest depletion of Ca and Cl in porewaters may suggest other sources of water.

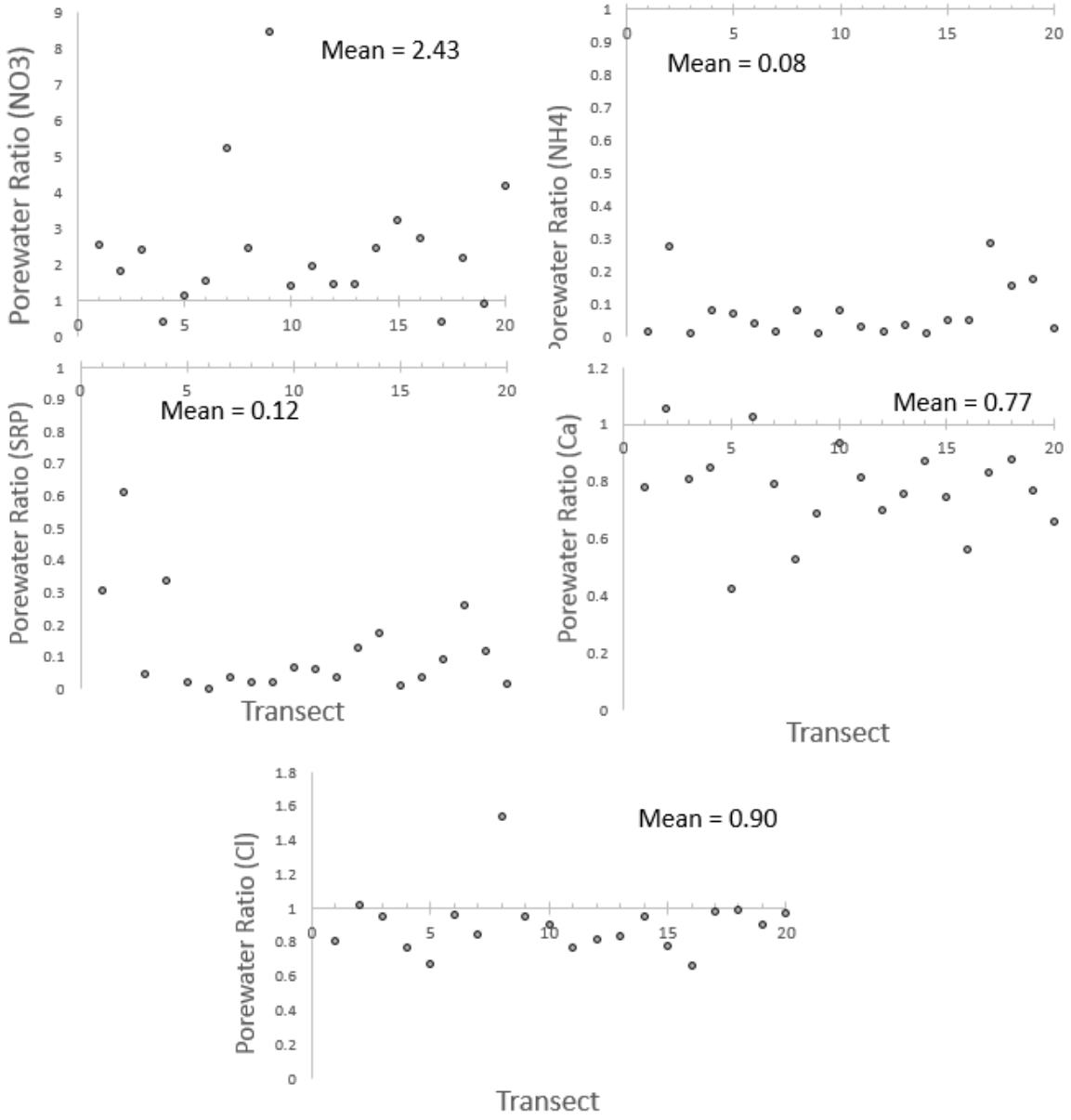

Figure 6.62. Ratios of concentrations for key analytes in the thalweg sample versus the porewater samples along the length of the Silver River (later. Values greater than 1 indicate a solute that is enriched in the thalweg compared with the porewaters, while values less than 1 indicate solutes that are depleted in the thalweg. Mean values for the entire river are shown in each graph, suggesting NO_3-N is dramatically enriched in the thalweg vis-à-vis the porewaters, while all other solutes are depleted in the thalweg, some greatly so (e.g., NH_4-N and SRP).

While NO_3-N and SRP concentrations were not significantly associated within the water column or porewater (p-value = 0.745 and 0.105, respectively), NH_4-N and SRP concentrations were

significantly associated (using a fitted power function). Specifically, the porewater SRP and NH_4-N concentrations were more significantly correlated to each other (R^2 = 0.532; p-value < 0.001) than in the water column (R^2 = 0.153; p-value = <0.001) (Figure 6.63).

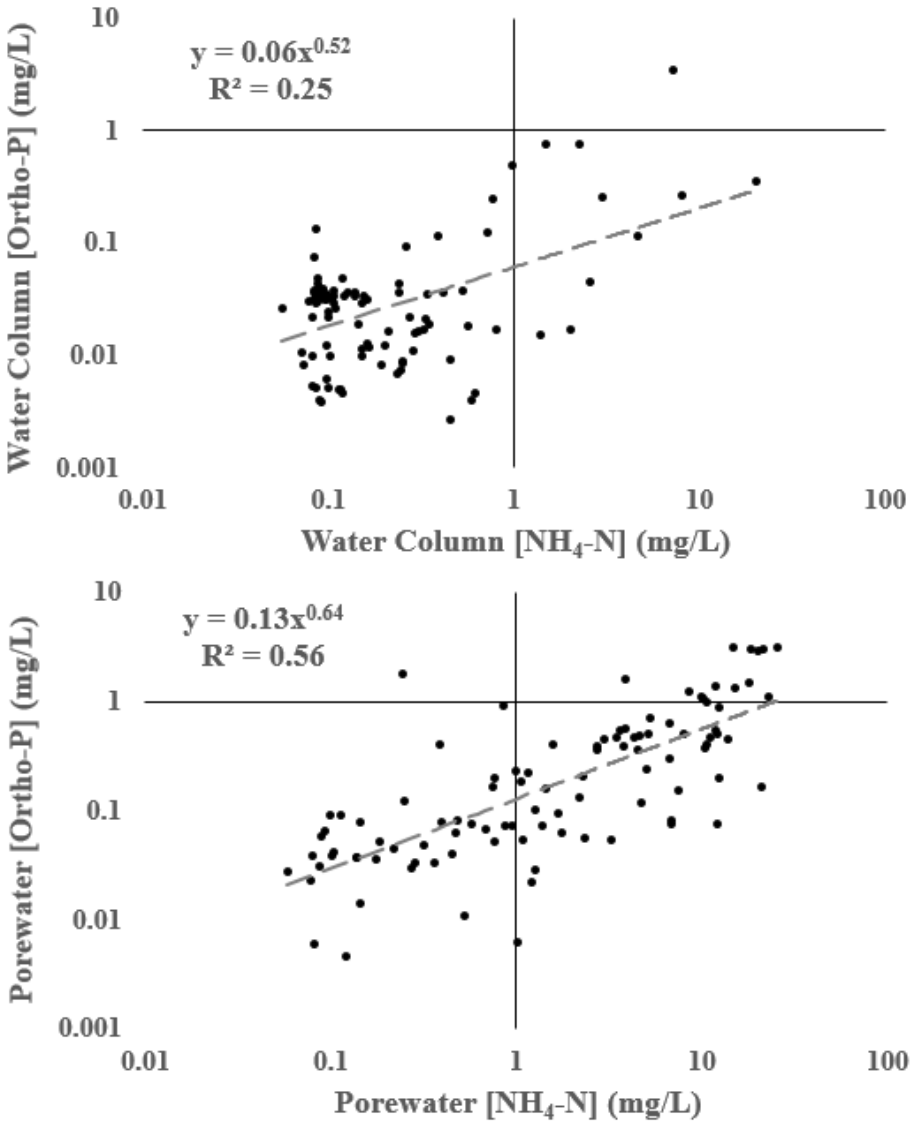

Figure 6.63. A) Water column and B) porewater concentrations of ammonium-N (NH_4-N) and orthophosphate (SRP) showing the range of concentrations, and the covariance patterns, suggestive of regions of significant benthic porewater influences on river water. High concentrations are samples obtained near channel margins.

Finally, we evaluated whether systematic trends existed for water chemistry across transects (Figure 6.64). We note no trend for chloride, a modest center sample enrichment of NO_3-N compared with the channel margins, and massive enrichment of PO_4 and NH_4-N in the channel margins compared with the center samples. The clear trends for SRP and NH_4-N indicate significant enrichment in the channel margins, presumably influenced by porewater seepage. In the channel center, these concentrations are markedly lower on average (ca. 4-8 times), while nitrate concentrations are slightly higher (consistent with spatial patterns in nitrate retention).

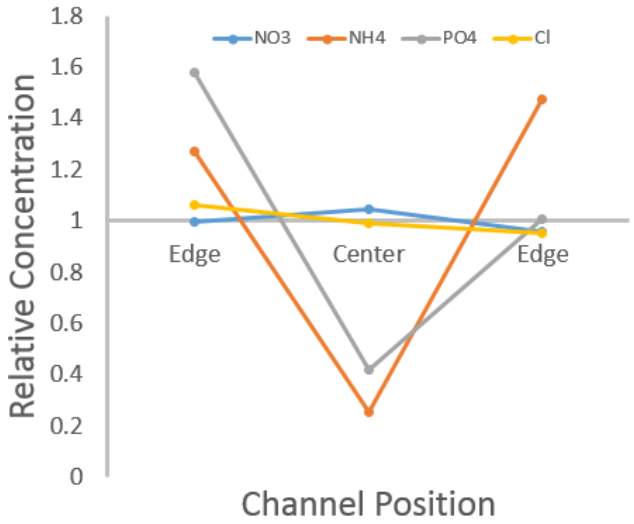

Figure 6.64. Summary of relative water concentrations across each transect, illustrating strong spatial heterogeneity driven by advection rates (high in the center, low at the edges).

6.4.7 Soil Chemistry

We measured a suite of informative analytes in the solid phase of the Silver River sediments, with samples from each location on each of the 20 transects. We observed significant variation in chroma (Figure 6.65) and field-based measures of texture, and these were confirmed with significant variation in soil chemical properties (Figure 6.66).

Figure 6.65. Soil samples collected across one transect prior to drying as well as dried samples from four transects (oriented by column) prior to LOI determination of organic matter content.

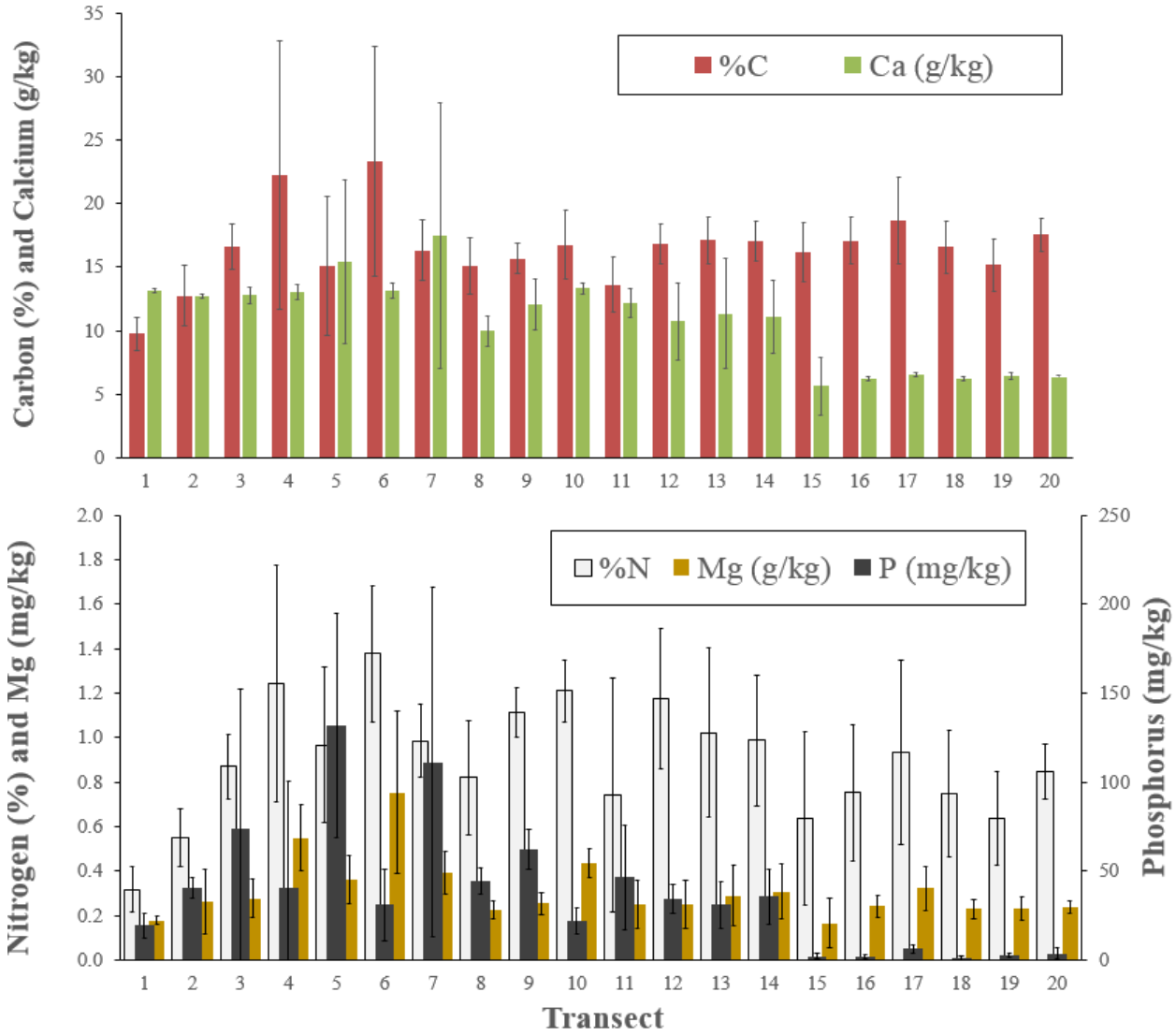

Figure 6.66. Average soil content by analyte by transect. Error bars are standard deviations.

Of particular note was the strong longitudinal enrichment of sediment C (roughly doubling along the length of the river), and the attendant decline in Ca (declining by 50 % along the length of the river). While longitudinal trends in N, Mg and P were less obvious, there were interesting spatial patterns, with the highest concentrations of P and Mg occurring from transect 5 to 7, and declining thereafter. This is coincident with the decline in water column P as well (Figure 6.63). While sediment N content was relatively constant after transect 4, the upper most river had very low N concentrations, likely indicating that fixed N is exported downstream rather than accumulating as sediment storage in the upper river.

Soil % organic matter (% loss on ignition) was explored as a potential explanatory factor in both vegetation and sediment and water chemistry variation. While the abundance of sediment organic matter was generally not a useful predictor of vegetation dynamics, there were interesting patterns present along the river. Specifically, OM was highest in the vicinity of the

confluence with Half Mile Creek, declining thereafter towards the Ocklawaha River (Figure 6.67).

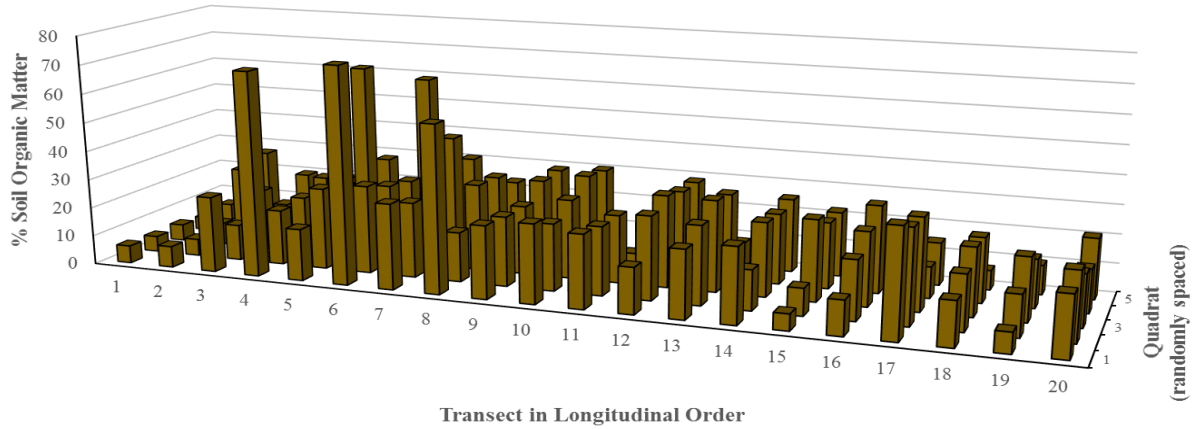

Figure 6.67. Percent (%) soil organic matter was greatest along the upper and middle transects.

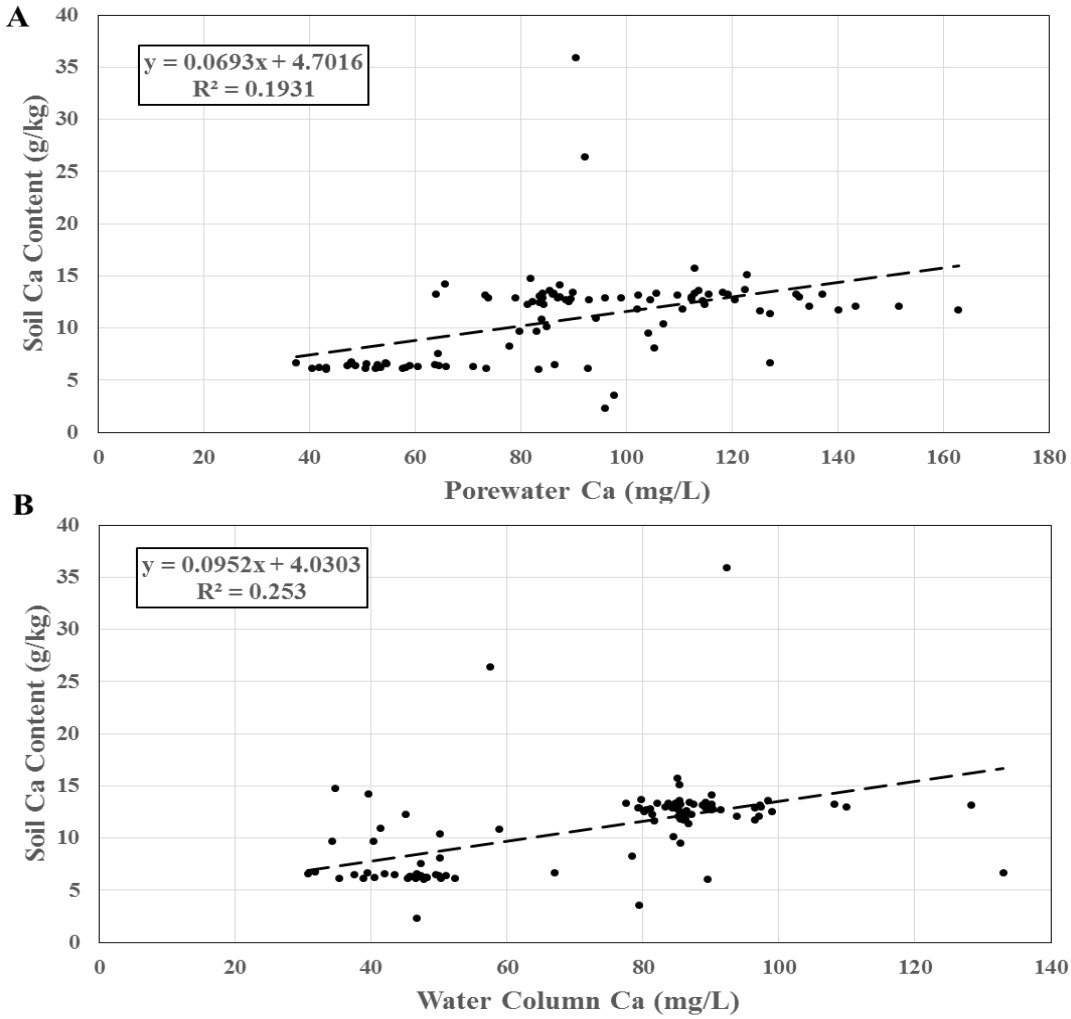

Figure 6.68. Variation in soil calcium content (Ca; g kg^{-1}) was explained by both a) porewater Ca concentrations (mg L^{-1}) and b) water column Ca concentrations (mg L^{-1}).

Some interesting covariance patterns were observed in the sediment chemistry and water chemistry. Most notably, there was a strong association between sediment Ca concentration and porewater Ca concentration (Figure 6.68), suggesting the sediment actively affects the porewater profile. There was an even stronger association between soil Ca and the water column, which, while slightly surprising, suggests that water exchange between the advective zone of the river and the porewaters and sediments is sufficient in magnitude to affect the water column chemical composition. Not unsurprisingly, soil C and soil N were strongly correlated (Figure 6.69), suggesting that the vast majority of sediment N is as stored organic matter, and not as mineral solutes. Finally, we observed a significant correlation found between soil Ca and P content (R^2 = 0.314; p-value < 0. 001) (Figure 6.70)

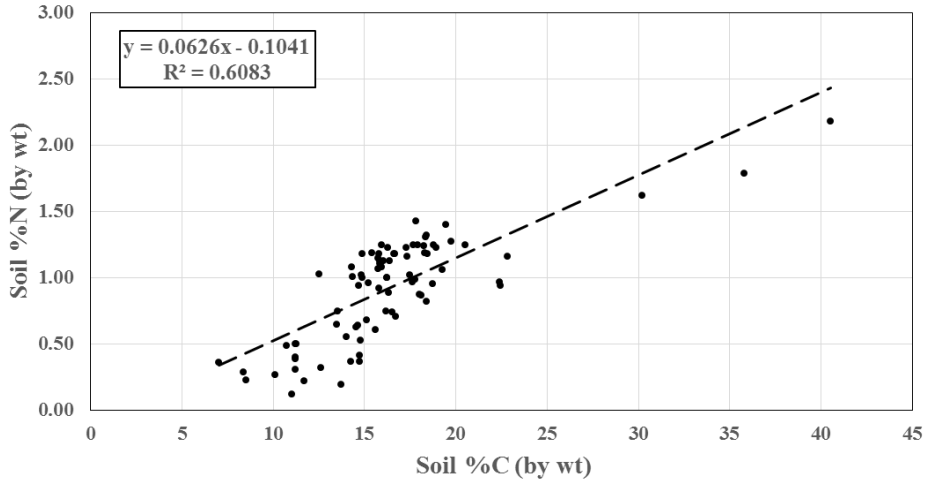

Figure 6.69. Soil %C and %N were significantly correlated to each other. This association was strongly significant (p < 0.001).

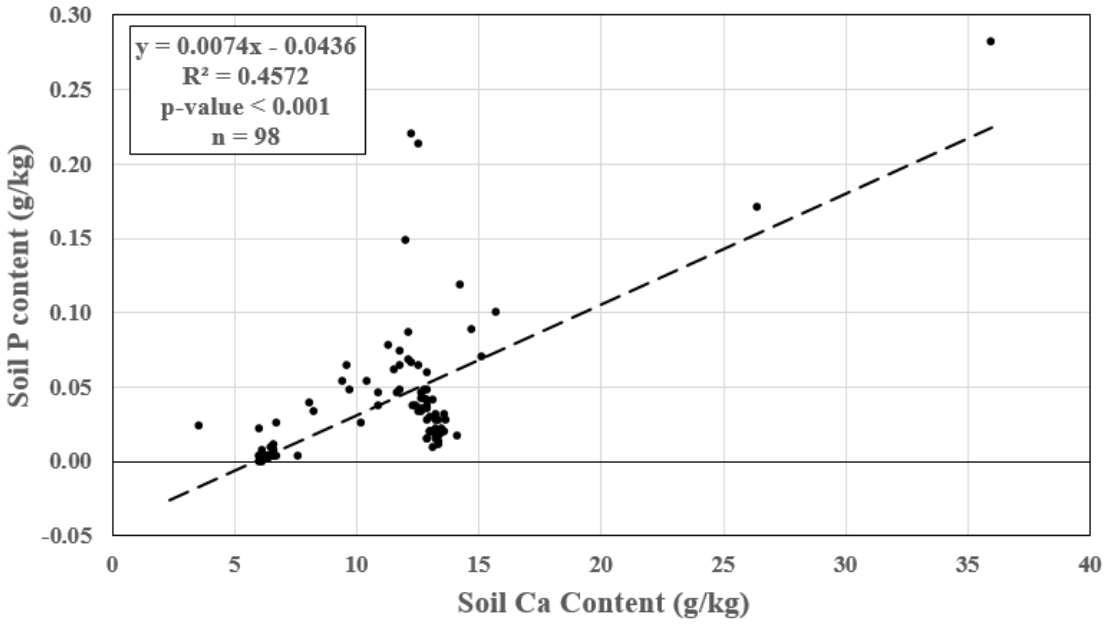

Figure 6.70. Soil Ca and P content were significantly correlated to each other.

6.4.8 Soil Particle Size Distribution

The distribution of soil particle sizes across the upstream transects at Silver showed an initial decrease in percent sand and increase in percent silt and clay (Figure 6.71). Percent clay was highest (15-25 %) in the middle transects (transects 5-9), located between the 0.7 Mile Mark and just below the county dock (i.e., between river km 1 and km 4). Particle size analysis in the lowest transects showed similarity in sand and silt distributions (40-50 %) and clay remained at ~ 10 %.

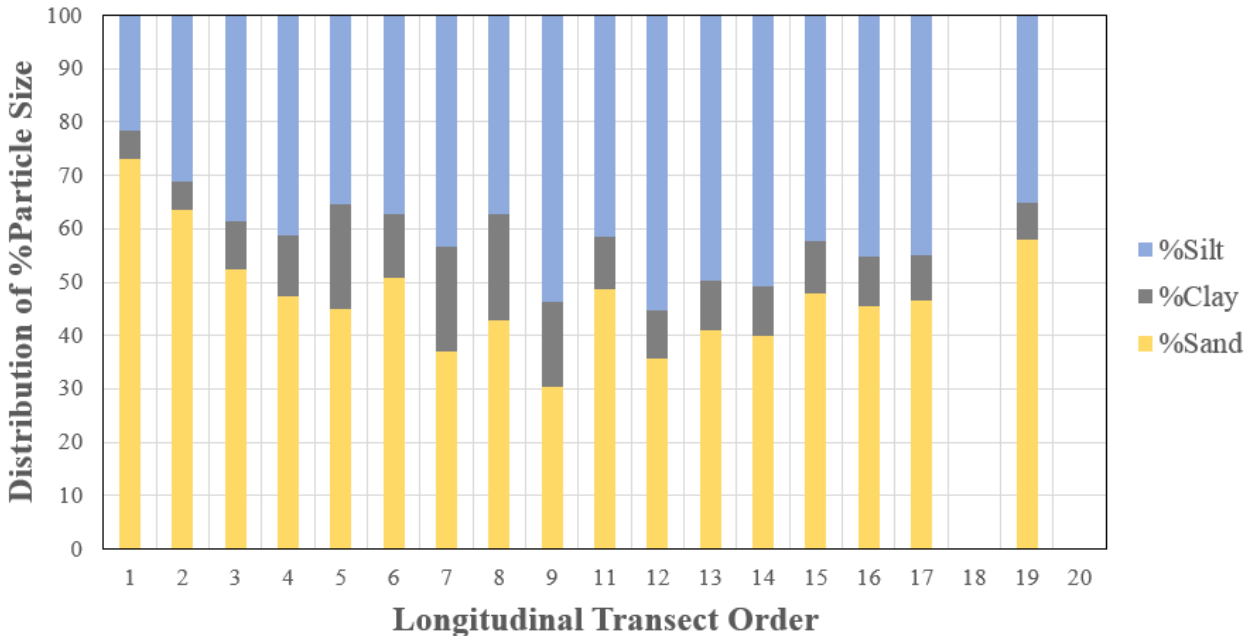

Figure 6.71. Particle size analysis was completed on the upstream transects at Silver and mean values within transects showed an initial decrease in % sand, initial increase in % silt and clay, and stabilization in the last few transects.

The relationships between the soil particle size distributions and other soil and water parameters were analyzed. No significant relationships were found between percent sand or silt and other water and soil parameters. A weak but significant negative relationship (p-value = 0.025, R^2 = 0.0823) was seen in percent clay and percent organic matter (Figure 6.72). Percent clay did explain approximately 19 % of the variation in soil phosphorus (p-value < 0.001, R^2 = 0.1937; Figure 6.73) and approximately 12 % of variation in soil calcium content (p-value = 0. 006, R^2 = 0.120; Figure 6.74). Together this suggests that the clay-sized particles in the river sediments are likely to be autogenic calcareous sediments to which significant P is sorbed.

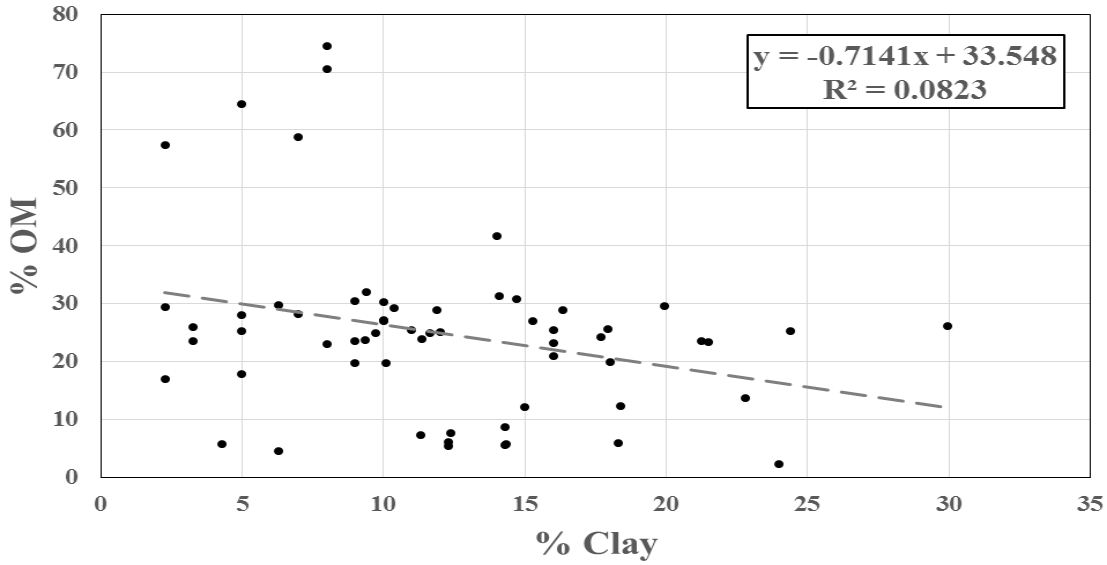

Figure 6.72. Percent clay and percent organic matter were found to have a weak but significant negative relationship (p-value = 0.0249).

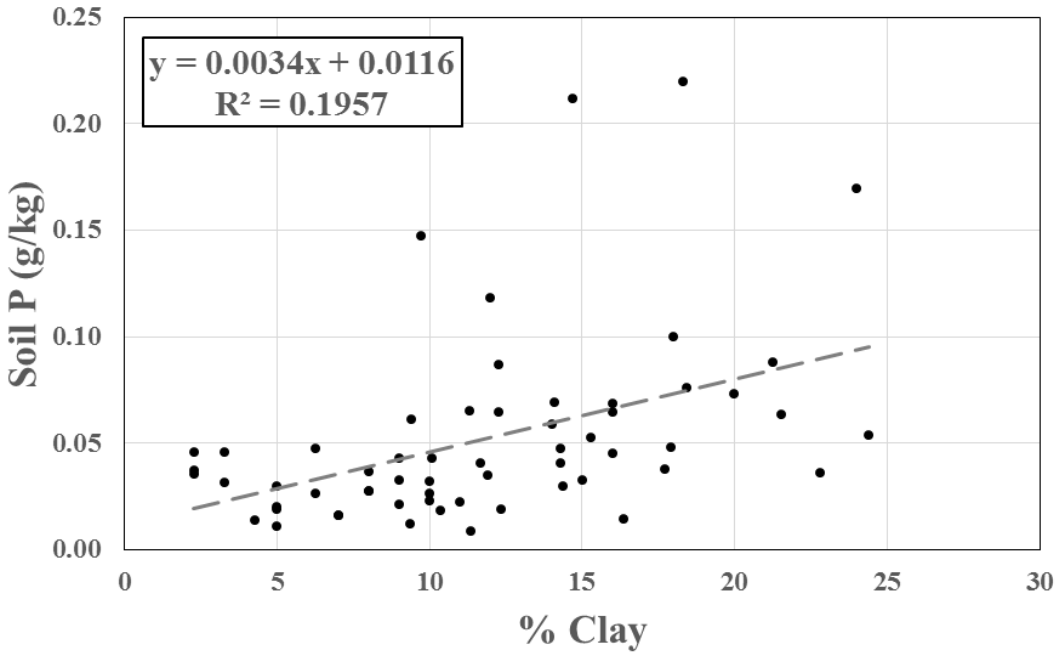

Figure 6.73. Percent clay explained approximately 19 % of the variation in soil phosphorus content (g kg^{-1}) over the first 14 transects surveyed at Silver River.

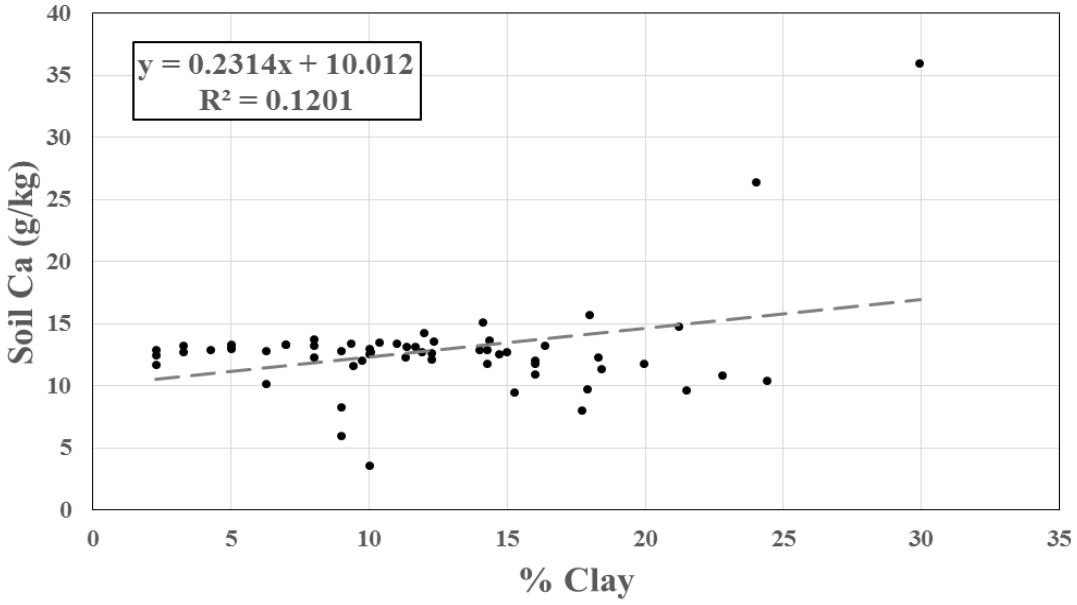

Figure 6.74. Percent clay explained approximately 12 % of the variation in soil calcium content (g kg^{-1}) over the first 14 transects surveyed at Silver River.

6.4.9 Physical and Chemical Controls on SAV and Algal Abundance

The inventory of benthic conditions on Silver River was principally done to explore spatial covariation patterns. Of particular interest was correlative evidence on the various controls on algal and SAV cover, ranging from physical controls (canopy cover, light) to chemical controls in the sediment, porewater and surface water. Below we summarize the preliminary results of that effort, focusing on both pairwise correlation analysis, and multivariate predictions.

6.4.9.1 Physical Controls

The physical controls on algal and SAV cover include canopy cover (%), water depth (m), flow velocity (m s^{-1}) and river position (longitudinal transect order). Table 6.8 summarizes the pairwise linear correlations between physical variables. The results suggest that SAV cover and canopy cover significantly increase with distance downstream, while algal cover and water depth significantly decrease. Significant physical controls on SAV cover also include canopy cover (significant negative association) and algal cover (significant negative association), while controls on algal cover also include velocity (significant negative association) and SAV.

The pairwise association between algal cover and velocity (Figure 6.75) indicates the limited explanatory power of that variable alone, but does indicate a promising covariate for more complex predictive models.

Table 6.8. Correlation (Pearson's r) matrix for physical controls on autotroph cover. Bolded correlations are significant at $p < 0.05$.

	Mean	SD	River Position (Transect)	% Canopy Cover	Water depth (m)	Velocity (m s^{-1})	SAV Cover
River Position (transect)	na	na					
Canopy Cover	37.02	24.96	**0.41**				
Water depth (m)	1.26	0.52	**-0.57**	**-0.49**			
Velocity (m s^{-1})	0.20	0.09	0.11	-0.09	**0.29**		
SAV Cover Class	4.44	1.03	**0.20**	**-0.21**	-0.04	0.16	
Algal Cover Class	3.09	1.61	**-0.40**	-0.17	0.09	**-0.38**	**-0.36**

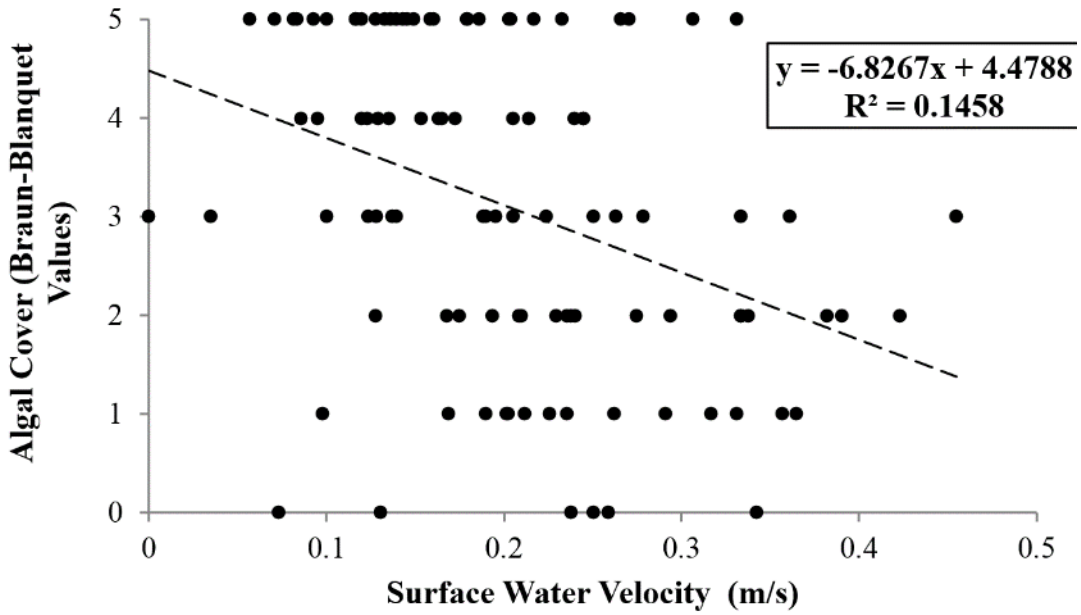

Figure 6.75. Surface water velocity (m s^{-1}) explained some of the variation seen in algae cover (Braun-Blanquet values). The relationship is statistically significant ($p < 0.001$), but suggests that over 80 % of the variation in algal cover is not explained by surface velocity variation.

A multivariate model of algal cover based on the 4 physical variables and SAV cover yielded a model with an R^2 of 0.28, and with only two significant predictors: river position (slope =0.36, $p = 0.003$) and velocity (slope = -0.31, $p = 0.001$). That is, the SAV-algal cover association was no longer significant when conditioned on other variables, suggesting that the association may arise from covariance with river position or velocity, and not a direct competitive interaction.

6.4.9.2 Water Chemistry Controls

Despite evidence for significant spatial variation in solutes, both in the porewater and the water column, we observed no significant associations between these chemical attributes and algal

cover (summarized in Figure 6.76). Indeed, the main water column drivers (SRP, NH_4-N, NO_3-N) all had linear correlation coefficients that suggest that these analytes explain less than 2 % of the variation in algal cover. Further evidence on Fe and Mn, which were uniformly below detection, and therefore sufficiently scarce to merit attention as limiting nutrients, is required.

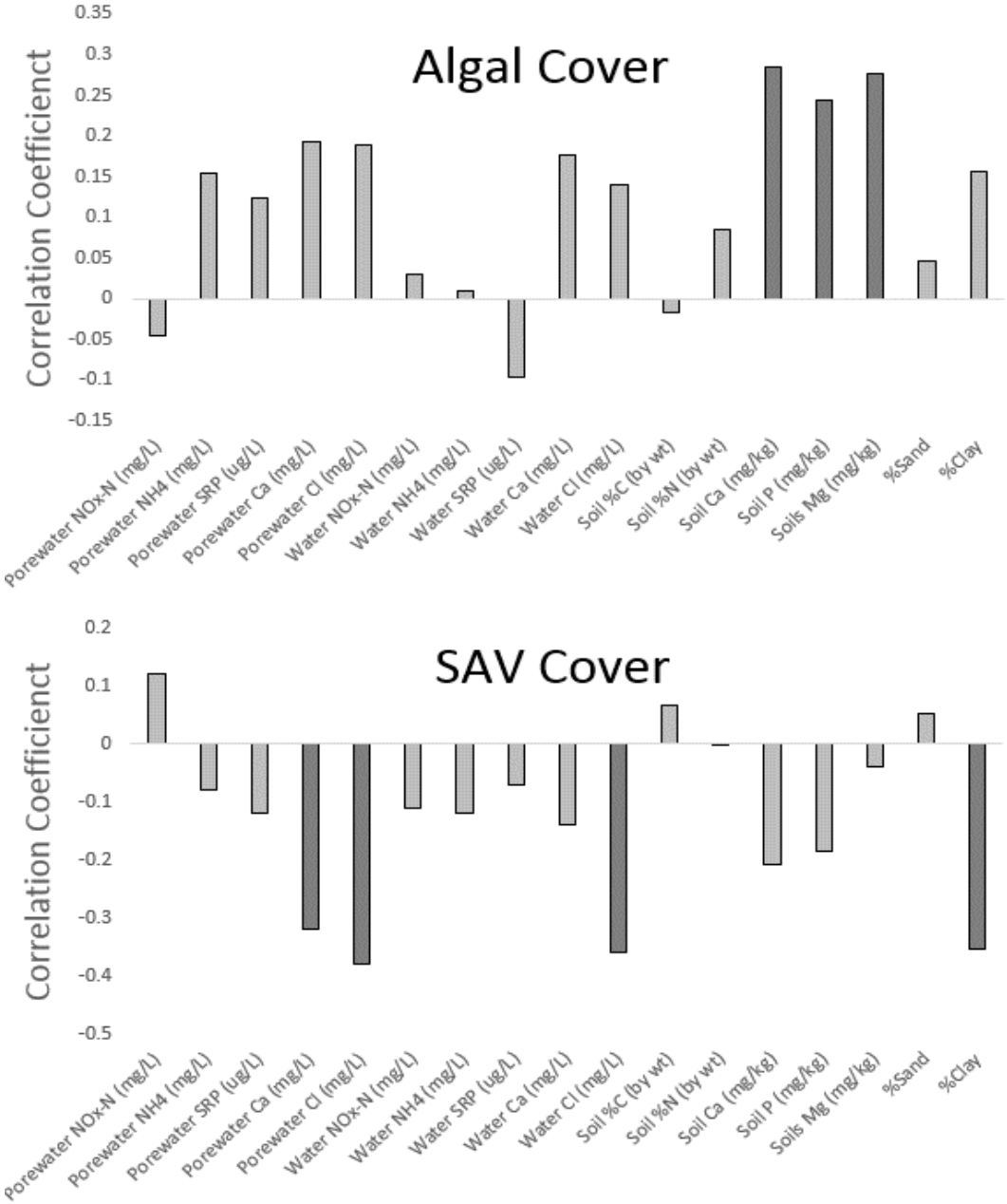

Figure 6.76. Summary of patterns of covariance between solutes in the water column, porewater and some of the soil attributes and algal cover (above) or SAV cover (below). Correlations (y-axis) that are statistically significant are darker bars.

The results from the pairwise correlation analysis (Table 6.9) suggest that no aspect of water chemistry in the porewater or water column can provide useful predictive power for algal cover. We further performed a multiple regression analysis using all of the water chemistry variables

(except Fe, which was below detection at all locations). That model removed all variables from analysis except SRP, which exerted a significant negative effect on algal cover (slope = -0.28, p = 0.04); notably, concentrations of NO_3-N in the porewater (p = 0.84) and water column (p = 0.69) were not significant predictors of algal cover. The overall model R^2 was 0.13, suggesting that the conjoined explanatory power of water chemistry on algal cover is low. Furthermore, we are aware of no mechanism via which P concentrations can inhibit algal cover.

Table 6.9. Summary of correlation coefficients between water chemistry[B] and both SAV and algal cover. Shown are correlations[C] for both water column chemistry and porewater chemistry.

	Mean	SD	Algal Cover	SAV Cover	Porewater NO_3-N (mg L^{-1})	Porewater NH_4-N (mg L^{-1})	Porewater SRP (ug L^{-1})	Porewater Ca (mg L^{-1})	Porewater Cl (mg L^{-1})	Water NO_3-N (mg L^{-1})	Water NH_4-N (mg L^{-1})	Water SRP (µg L^{-1})	Water Ca (mg L^{-1})
Algal Cover	3.09	1.61											
SAV Cover	4.40	1.03	**-0.36**										
Porewater NO_3-N (mg L^{-1})[A]	0.86	1.34	-0.04	0.12									
Porewater NH_4-N (mg L^{-1}) [A]	4.72	6.05	0.15	-0.08	**-0.25**								
Porewater SRP (µg L^{-1}) [A]	466	729	0.12	-0.12	-0.16	**0.73**							
Porewater Ca (mg L^{-1})	88.5	27.9	0.19	**-0.32**	**-0.21**	**0.47**	**0.57**						
Porewater Cl (mg L^{-1})	12.1	4.13	0.20	**-0.38**	-0.14	0.17	**0.24**	**0.78**					
Water NO_3-N (mg L^{-1}) [A]	1.45	2.40	0.03	-0.11	0.11	-0.07	-0.04	**-0.22**	-0.19				
Water NH_4-N (mg L^{-1}) [A]	0.70	2.28	0.01	-0.12	0.01	**0.30**	0.14	0.06	0.04	-0.05			
Water SRP (µg L^{-1}) [A]	93.5	364	-0.10	-0.07	-0.02	0.19	**0.41**	**0.22**	0.19	-0.03	**0.40**		
Water Ca (mg L^{-1})	71.5	23.3	0.18	-0.14	-0.14	0.18	**0.27**	**0.67**	**0.61**	-0.04	**0.22**	**0.42**	
Water Cl (mg L^{-1})	11.1	3.36	0.24	**-0.36**	-0.14	-0.01	0.13	**0.56**	**0.60**	-0.03	0.12	**0.20**	**0.64**

A – Variables log-transformed prior to correlation analysis
B - While Fe concentrations were analyzed in both water column and porewater samples, all were below detection limit.
C - Bolded correlations are significant at $p < 0.05$.

The pairwise correlations for SAV yielded more significant associations (Table 6.9), with porewater calcium and chloride, as well as water column chloride concentrations exerting significant pairwise effects (negative associations for all three variables). A multivariate model of SAV cover given the suite of chemical analytes yielded a relatively strong model (R^2= 0.29), but with two different significant predictors of cover than were expected from the pairwise analysis: water column nitrate (slope = -0.09, p = 0.02) and water column calcium (slope = 0.02, p = 0.004). These results suggest that SAV are inhibited by high nitrate, and enhanced by high Ca concentrations. It is particularly striking that chloride was not significant (though p = 0.05 for water column Cl) given the strong pairwise association. We note that none of the porewater chemical properties were significant predictors, providing limited support for the hypothesis that

SAV decline arises in response to porewater enrichment of ammonium. Indeed, while porewater NH_4-N and NO_3-N concentrations were not significant, their slopes were both positive.

6.4.9.3 Soil Chemistry and Texture Controls

Despite the absence of significant predictors of algal cover from porewater and water column chemical properties, we explored covariance patterns of SAV and algae with soil chemical properties, including texture distributions (i.e., %sand, %clay). The results of a pairwise correlation analysis (Table 6.10) are striking, in that two soil chemical variables apparently inhibit SAV cover (soil Ca and %clay), while three variables appear to enhance algal cover (soil Ca, soil P and soil Mg). Moreover, the correlations between variables suggests that there are numerous associations between sediment quality and texture (e.g., %clay impacts soil N, Ca, P and Mg). Since there are strong spatial gradients in soil texture (Figure 6.46), this merits consideration for inclusion in an overall model of SAV and algal abundance.

Table 6.10. Summary of correlation coefficients between soil chemistry and both SAV and algal cover. Bolded correlations are significant at $p < 0.05$.

	Mean	SD	SAV Cover	Algal Cover	Soil %C	Soil %N	Soil Ca (mg kg^{-1})	Soil P (mg kg^{-1})	Soils Mg (mg kg^{-1})	%Sand
SAV Cover	4.38	1.07								
Algal Cover	3.17	1.63	**-0.36**							
Soil %C	16.46	4.71	0.07	-0.02						
Soil %N	0.91	0.38	0.00	0.09	**0.77**					
Soil Ca (g kg^{-1})	11.36	4.29	**-0.21**	**0.29**	-0.09	0.08				
Soil P (mg kg^{-1})	41.08	48.47	-0.19	**0.24**	0.13	**0.22**	**0.66**			
Soils Mg (mg kg^{-1})	323.00	177.92	-0.04	**0.28**	**0.69**	**0.61**	**0.36**	**0.23**		
%Sand	46.68	15.32	0.05	0.05	-0.09	**-0.52**	-0.08	-0.03	-0.04	
%Clay	11.15	5.27	**-0.35**	0.16	0.08	**0.31**	**0.40**	**0.58**	**0.21**	**-0.52**

Some differences in mean SAV and algal cover values between this analysis and previous analyses arises because texture results were available for only 18 of 20 transects.

As with other controls, we performed a multivariate regression to assess conjoined explanatory power of soil properties. Overall, the explanatory power for SAV cover was modest ($R^2 = 0.18$), with only % clay (slope = -0.12, $p < 0.001$) emerging as a significant predictor, further suggesting that the correlation of SAV with Ca arises largely because Ca and % clay are correlated. The fact that dense sediments (i.e., high clay content) inhibits SAV comports with observations of SAV declines in other settings (e.g., Rainbow River) where clay content varies dramatically across the river. The model to predict algal cover yielded two significant predictors in a model that explained 21 % of the variation (i.e., $R^2 = 0.21$): soil % C was a significant negative predictor of algal cover (slope = -0.21, $p = 0.007$), while soil Mg was a positive predictor (slope = 0.005, $p = 0.009$). All other predictors were not significant. These results are striking in that they depart so dramatically from the pairwise correlations, especially with regard to soil C content. Further exploration of these associations is clearly warranted.

Finally, we combined all of the predictor variables into a stepwise regression analysis where variables were omitted where they failed to meet significance criteria. Starting with all of the physical, water chemical and soil chemical properties, we arrived at overall models of SAV and algal cover. The algal model explains over 30 % of the variation in algal cover ($R^2 = 0.30$) based on three selected variables: soil % C (slope = -0.15, $p < 0.001$), soil Mg (slope = 0.005, $p < 0.001$) and water velocity (slope = -0.69, $p < 0.001$). This suggests that the dominant spatial controls on algal density are sediment properties, the mechanisms of action for which are poorly understood, and water velocity. The SAV model has similar explanatory power ($R^2 = 0.32$), and also selected three variables: %clay (slope = -0.06, $p = 0.001$), % canopy cover (slope -0.014, $p < 0.001$) and porewater chloride concentrations (slope = -0.099, $p < 0.001$). The impacts of clay content and canopy cover would appear relatively clear (rooting inhibition for the former, light limitation for the latter). The mechanism of the strong inhibitory effect of chloride concentrations is less obvious. We note that chloride concentrations were generally relatively low (mean = 12.1 mg L^{-1}) and did not vary substantially across the river (SD = 4.13 mg L^{-1}). It may be that chloride concentrations act as a proxy for other variables, such as DO depletion or Fe concentrations, because direct effects seem unlikely given observed variation. It is also notable that there is a strong decline in chloride concentrations at the downstream end of the river (near the confluence with the Ocklawaha; (Figure 6.60), possibly suggesting mixing waters or diluted porewaters from interactions with the softer water Ocklawaha flow.

6.5 Nutrient Limitation Assays – Metabolism and Algal Growth Responses

Nutrient concentration is widely invoked as a dominant control on autotroph production in aquatic systems despite increasing evidence that enrichment effects in lotic systems differ from those in lakes (Biggs and Close 1999; Biggs 2000; Dodds et al. 2002; Hilton et al. 2006; King et al. 2014). In flowing water systems, nutrient resupply from upstream and turbulent mixing of the water column means that flux (concentration * discharge) may be more informative than concentration in describing nutrient availability to autotrophs (Newbold et al. 1982). Indeed, flux was a far better predictor of nutrient saturation and limitation when applied to *in situ* growth data (King et al. 2014). Understanding nutrient enrichment effects on primary producers, and specifically testing the hypothesis that nutrient availability limits primary production or biomass accrual, requires empirical tools that retain key system attributes (e.g., contact with sediments, natural vegetation, natural light regimes). As such, techniques like nutrient diffusing substrates and periphytometers, where nutrient concentrations can be modulated, fail to capture the composition and structure of the natural system, yielding results that are of debatable interpretive value regarding the ecosystem nutrient saturation status. However, adjusting nutrient supply at the ecosystem scale in flowing waters is challenging for two obvious reasons. First, water flow means that nutrient enrichment needs to be sustained for the duration of any experimental assessment period, which necessitates dosing pumps and large quantities of added solute. Second, enriching an entire river for long enough to assess a metabolic response precludes consideration of replication or factorial nutrient enrichment combinations. In this section, we describe a new method for *in situ* nutrient limitation assays that retain key elements of the system composition and structure, that enable replication and factorial enrichment experimental designs, and, perhaps most importantly, focus on primary production (i.e., GPP) as the aggregate metabolic response variable.

Methods for documenting stream responses to nutrient enrichment have been forced to either focus on very small streams and single nutrient (e.g., N) additions, or on the deployment of artificial substrates, variably enriched with nutrients, to which benthic biofilms can attach and grow. Our new method allows us to explore how metabolism (gross primary production and ecosystem respiration, GPP and ER) responds to nutrient enrichment. Metabolism is the integral of all ecological energy transformations and thus represents the gold standard for assessing nutrient limitation. Indeed, eutrophication as a concept is fundamentally defined as the amplification of the carbon cycle via elevated primary production, a process often linked to nutrient enrichment, but clearly not confined to that causal factor (e.g., light or grazer effects can impact stream metabolic behavior). Methods such as nutrient diffusing substrata and periphytometers are useful in this regard, but cannot evaluate the reaction of the actual ecosystem, focusing instead on an artificial subset of the attached algae, separated from sediment nutrient sources. To assess nutrient limitation (i.e., do nutrients limit primary production OR respiration), we utilized a chamber method to compare metabolic activity when dosed with nitrogen (N), phosphorus (P), and iron (Fe), added alone or in combination. A clustered nutrient bioassay design was used where one control chamber (no nutrient addition) was simultaneously paired with three nutrient treatment chambers per deployment (Figure 6.77). One of seven nutrient combinations were added to the treatment chamber, including nitrate (N), phosphate (P), iron (Fe), nitrate and phosphate (N+P), nitrate and iron (N+Fe), phosphate and iron (P+Fe), and nitrate, phosphate and iron (N+P+Fe). Ambient concentrations of the chambers were raised by 2, 0.05, and 0.05 mg L^{-1} for N, P, and Fe, respectively.

The method employed included benthic chambers (clear polycarbonate) sealed into the sediments to occlude flow and thus nutrient resupply. Chambers extended above the water column to allow normal gas exchange and light penetration, and were scaled (0.6 x 0.6 m) to allow representative benthic communities to be sampled. After installing each chamber, a HOBO Dissolved Oxygen sensor was deployed to measure DO at 15-minute intervals to determine metabolic rates from diel DO concentrations (Odum 1956). A HOBO Pendant Light Logger was deployed above the water surface, set at 15-minute intervals, to estimate the effect of light on GPP (i.e., GPP efficiency). Each of the four chambers received 20 mg L^{-1} of a conservative tracer, chloride (Cl), to test for hydrologic loss. Chambers with chloride losses greater than 5 mg L^{-1} or 10 % total chloride mass (by taking into account changes in water volume) were removed from further data analysis. Characterization of ambient, physical and chemical conditions accounted for any variation seen between each chamber location. Parameters measured included canopy cover, water depth, epiphytic algal cover, and vegetation percent cover as well as pre- and post-deployment water column sampling. Water samples were collected to determine overall change in nutrient (N, P, and Fe) and chloride concentrations over the deployment period.

Primary production was evaluated from the diel dissolved oxygen dynamics inside each benthic chamber. Reaeration estimates were obtained from dissolved propane declines following propane additions, adjusted for the relative molecular weight differences between oxygen and propane. Each deployment consisted of 6 days of primary production estimates; we did not include day 1 because boxes were deployed during the middle of the day, limiting our ability to estimate GPP, and because the installation process created substantial turbidity for several hours after deployment. For all analyses, we computed the mean GPP for the entire deployment, reasoning that instantaneous daily values are neither independent of each other, nor as reliable measures of

system behavior as a 6.day mean. We observed no decline in GPP over time in the chambers, supporting the assumption that box artifacts do not accrue over the deployment period. We do note that site visitation logistics precluded multiple solute injections during each deployment, and that solute utilization during the deployment may alter the water column concentrations substantially. If solute enrichment effects were present initially, and disappeared over the deployment as the solute is assimilated, we would expect GPP to initially increase and then decline over time. This was not the case. The mean slope relating GPP and deployment day was 0.23 (g O_2 m^{-2} d^{-2}), with the positive sign indicating no temporal trend towards lower GPP. In almost all cases, this slope was not statistically significant, which we interpret as evidence that box artifacts due to shading, algal colonization of the chamber surfaces, and depletion of internal solute mass are neither systematic nor substantial.

Figure 6.77. A clustered nutrient bioassay design was utilized to assess effects of nutrient additions (i.e., nutrient limitation) using seven combinations of N, P, and/or Fe.

Because of significant heterogeneity in environmental conditions, including incident light (the experiment spanned over 6 months), canopy cover, water depth, sediment conditions, and benthic cover conditions, our assessment of nutrient enrichment effects focused on the GPP response in each of the treatment chambers with respect to GPP observed in the adjacent control chamber. The relative response metric is defined as the logarithm of the ratio of the treatment chamber GPP (GPP_t) to the control chamber GPP (GPP_c). The log transformation creates symmetry between stimulatory and inhibition effects. As such, values larger than 0 indicate stimulatory effects of nutrient additions, while values below 0 indicate inhibitory effects. Each assessment was made on the mean across all days within all deployments receiving a given treatment. We also evaluated the capacity for environmental variables (light, depth, canopy cover, benthic biomass) to explain GPP observed in the control tanks. Strong consonance of predictions in the control tanks offers support for the mode of inference about nutrient effects because it suggests that metabolism is predicable.

In addition to measuring aggregate ecosystem responses to nutrient enrichment via metabolic behavior, we were also interested in the specific growth of algal taxa because of recent dramatic increases in algal cover in many springs. To measure algal biomass accrual in each experiment,

pre-scrubbed ceramic tiles were suspended within each chamber during all deployments. Algal biomass accrual was measured on tiles collected at the end of each deployment; tiles were transported on ice to the lab, and scraped in a known volume of deionized water. The water was homogenized and filtered onto dried and pre-weighed 0.45 µm filter papers. Algal biomass estimates were compared between the control and treatment chambers to determine the influence of nutrient additions on algal growth and compared to chamber GPP, and evaluated for nutrient enrichment effects.

At the end of each deployment, the vegetation within each chamber was harvested, dried, and weighed to yield specific growth rates (i.e., GPP per unit biomass). As with GPP alone, several vegetation subsets were further analyzed to determine the relationship between leaf area and biomass. We then analyzed the nutrient enrichment effects on GPP and algal growth using analysis of variance. Because our sample sizes for the seven nutrient treatments were relatively small, we also explored the main effects of nutrient enrichment by evaluating the relative response to a nutrient addition regardless of whether it was added alone or in combination with other nutrients. Overall, this study allowed us to: 1) determine how stream metabolism varies across the ambient physical, chemical, and vegetation gradients present in Silver River, 2) determine the effect of added N, P, and Fe on ecosystem metabolism dynamics, and 3) describe nitrate uptake kinetics across different ambient conditions. This method allowed us to compare metabolic activity and potential nutrient limitation under similar benthic and sunlight conditions. Through these objectives, this study evaluated the overarching and central question of ***nutrient limitation of primary production in springs***, using inference, in part, from comparisons of Silver River (high nitrate) and Alexander Springs Creek (low nitrate)

From August 2015 to May 2016, metabolism was measured for 72 total treatment replicates (i.e., each treatment was replicated ~10 times) at 31 locations that spanned Silver River, capturing variation in stream characteristics (Figure 6.78). Similarly, we measured at nine locations in Alexander Springs Creek (Figure 6.79) for a total of 34 treatment replicates (each treatment was replicated an average of 4 times, plus 9 controls).

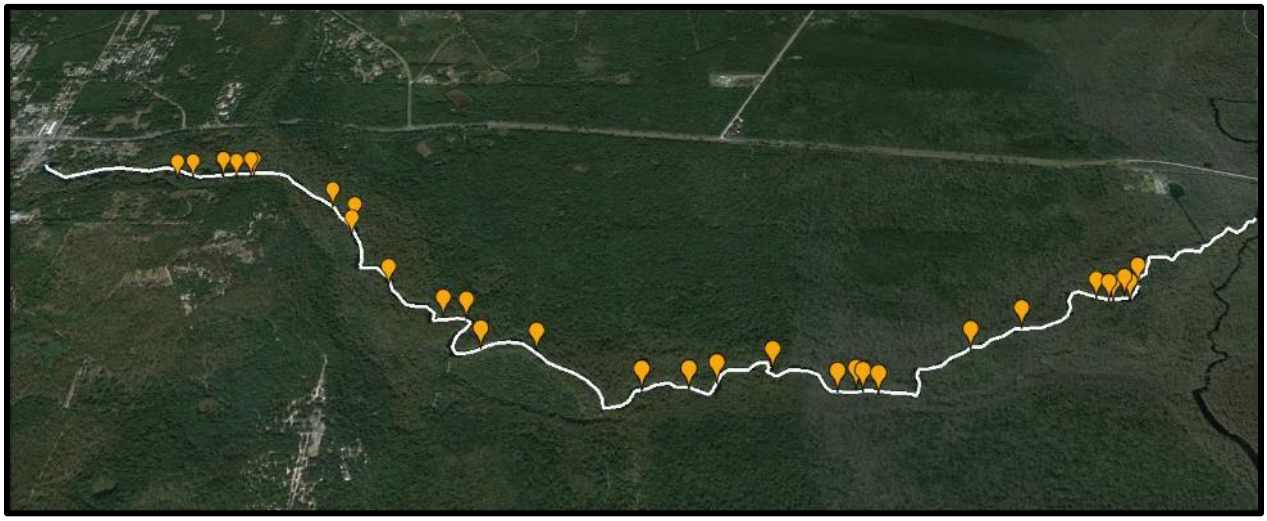

Figure 6.78. Metabolism was measured simultaneously in one control chamber and three treatment chambers at 30 locations along Silver River between August 2015 and May 2016.

Figure 6.79. Metabolism was measured simultaneously in one control chamber and three treatment chambers at nine locations along Alexander Springs Creek between September and November 2016. Transport and sampling logistics constrained site selection to locations in close proximity to the bridge canoe access points

6.5.1 Control Chamber Metabolism

Hydrologic losses, quantified by changes in chloride concentrations, were minimal across all but two deployments. For the two deployments that leaked, chloride loss exceeded 10% (38 and 45 %, respectively). For the remaining deployments, chloride loss averaged 7.59 %, with a minimum of 0.46 %, and a maximum of 9.75 %. None of the Alexander Springs Creek boxes leaked, with maximum chloride loss below 5 % for all deployments. The resulting 28 (Silver) and 9 (Alexander) control chamber datasets were analyzed for variation in DO and metabolism (GPP and ER), algal accrual rates, as well as correlation of these estimates with ancillary factors.

A large degree of variation was observed in DO and GPP estimates within the control boxes across all deployments. Large variation in DO amplitude, peak, and minimum values was observed through comparisons of the diel profiles in Silver River (Figure 6.80) and Alexander Springs Creek (Figure 6.81). Average GPP within control chambers varied from 1.0 to 13.0 g O_2 m^{-2} d^{-1} while average ER varied from 4.7 to 14.6 g O_2 m^{-2} d^{-1}. Respiration was generally greater than primary production with GPP:ER ratios varying from 0.12 to 2.4 with an average of 0.84.

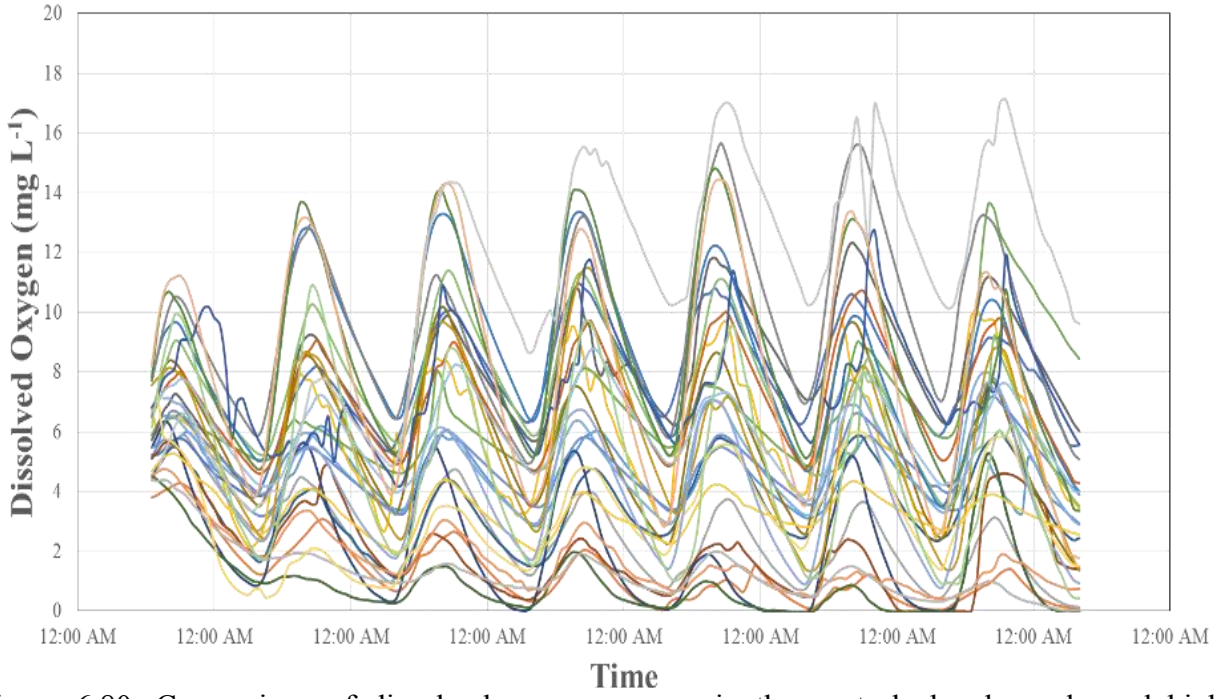

Figure 6.80. Comparison of dissolved oxygen curves in the control chambers showed high variation across locations at Silver River.

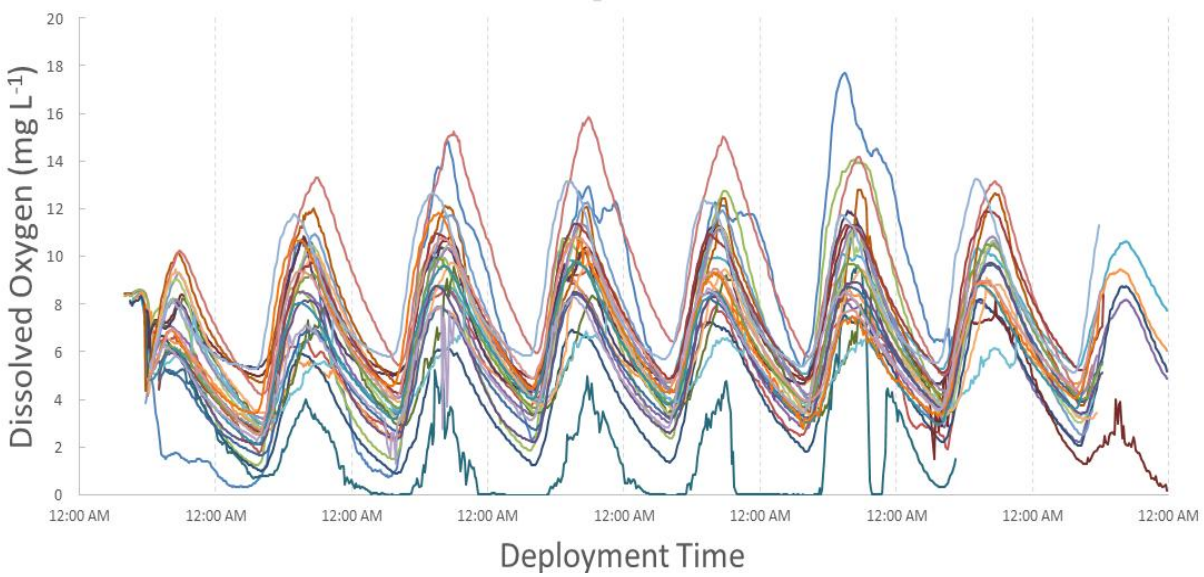

Figure 6.81. Comparison of dissolved oxygen curves in the control chambers showed less variation across locations at Alexander Springs Creek than at Silver River.

We compared control box GPP between rivers, and observed no differences. Figure 6.82 summarizes GPP across all deployments in both rivers, with nearly identical means (6.39 versus 6.3 g O_2 m^{-2} d^{-1}); we note far greater variation observed at Silver River, likely due to the longer experimental duration.

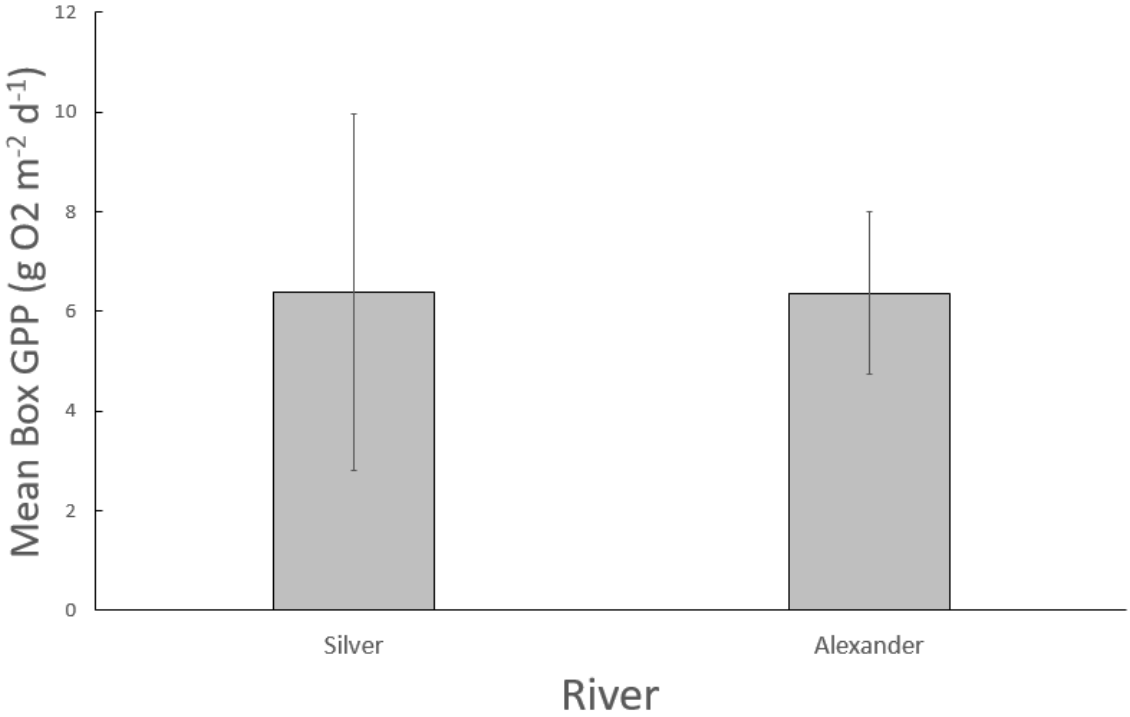

Figure 6.82. Summary of box GPP measurements between the two study rivers. Results are shown pooling across all box deployments and days. There was no difference between rivers in mean box GPP ($p = 0.96$).

Both GPP and ER significantly declined with distance downstream in Silver River (p-value < 0.001 and 0.024, respectively) (Figure 6.83). We urge caution interpreting this longitudinal signal as diagnostic of whole-river patterns because the box deployments were, due to geometry and logistics, confined to shallower river habitats (i.e., < 3.5 ft deep), at sites often associated with well-shaded channel margins. As such, the longitudinal declines may be a result of increased riparian shading or limited shallow-water settings for deployments. However, these results are broadly consistent with the trends observed in the open channel metabolism measurements, described in Section 6.3.

While primary production in the control chambers varied most clearly with longitudinal location, other potential controlling factors were explored, including: 1) dominant sediment type, 2) light, 3) time of year, 4) canopy cover, 5) water depth, and 6) biomass.

6.5.1.1 Substrate Type

Three general substrate types were observed at Silver River and were classified as either ***flocculent*** (i.e., thick organic matter on sediment surface), ***sand*** (i.e., little to no flocculent material and sand exposed), or ***mixed*** (i.e., shallow sediment with a mix of sand and organic matter). In general, lower average GPP values were observed in areas dominated by sandy substrates while the largest average GPP was observed in flocculent sediments (Figure 6.84). While differences in mean control GPP were small and not statistically significant ($p = 0.61$) across substrate types, these results correlated to areas of highest and lowest denitrification rates (described in later section). Similarly, while sand had lower ER, large variation meant that

differences with other substrates were not significant (p = 0.44). Sediment characteristics in Alexander Springs Creek were more uniform, and were not parsed in the same way.

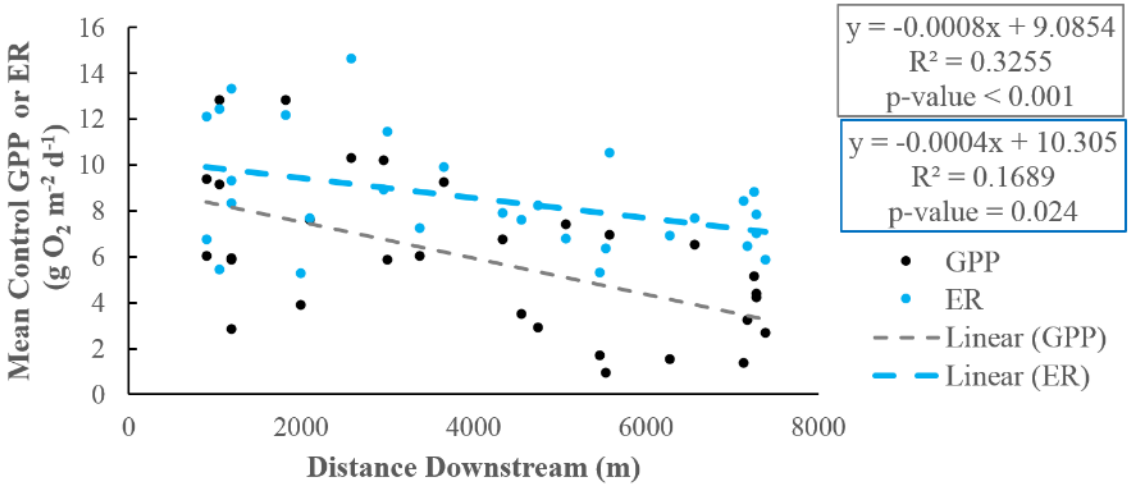

Figure 6.83. Average control gross primary production (GPP) ranged from 1.0 to 13.0 g O_2 m^{-2} d^{-1} and was negatively correlated with distance downstream from the main spring vent. Over the short range of distances in Alexander Springs Creek (1,600 – 2,050 m below the spring vent) there was a strong and significant positive correlation between distance and both GPP and ER (r^2 = 0.53). The causes of this association are not clear, but are likely principally because the lower sites were sampled earlier in the year (longer day length).

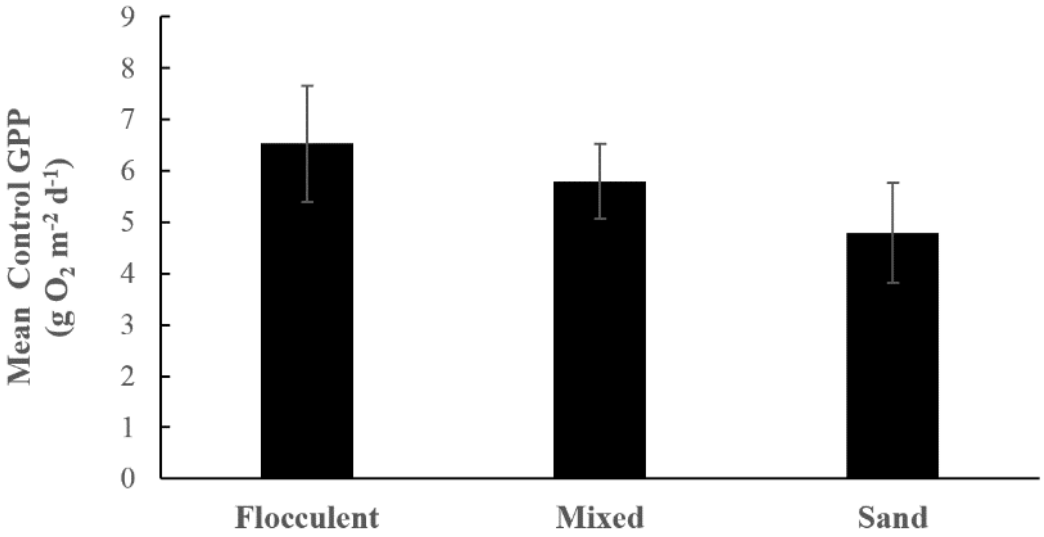

Figure 6.84. Control gross primary production (GPP) in Silver River varied by substrate type and on average estimates were largest in flocculent, deep sediments and smallest in sandy substrates

6.5.1.2 Light

While surface light (i.e., insolation above the water surface; w m^{-2}) was measured above each chamber over each deployment, water column light was also measured in 10 control chambers.

Surface light was significantly correlated to light measured in the water column but only explained 25 % of variation. During deployments, we observed significant particle deposition and algal growth on the Pendant light loggers which may explain this low correlation along with other factors (i.e., water clarity and turbidity, depth below and above surface, etc.). We therefore discount the veracity of the submerged sensors, and perform all subsequent analysis on the above water sensors.

In both rivers, average surface light within each deployment was significantly correlated to average deployment GPP within the control chambers (p-value < 0.001). Light explained 38.6 % of GPP variation in Silver River (Figure 6.85), and explained over 75 % of the variation in GPP in Alexander Springs Creek (Figure 6.86). This comports with previous experience in metabolic responsiveness, with measurements in the open channel of Silver River, and many other springs, principally controlled by the availability of light.

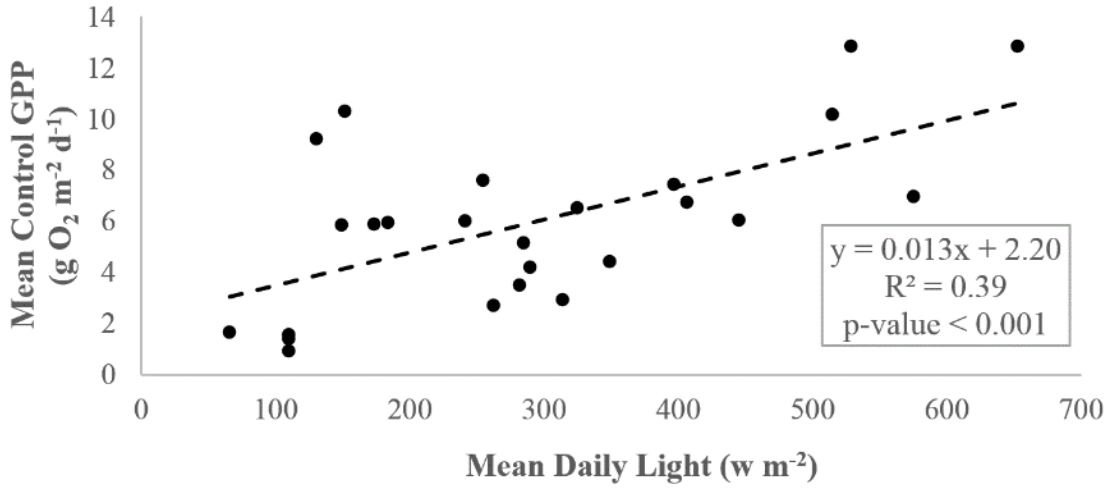

Figure 6.85. Average control gross primary production was significantly correlated to mean surface light in Silver River.

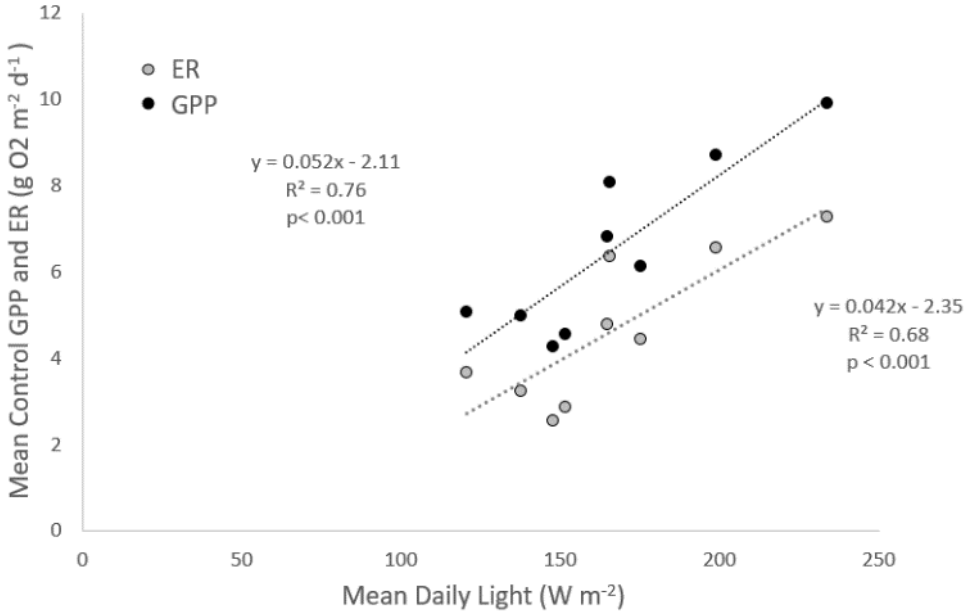

Figure 6.86. Average control gross primary production was significantly correlated to mean surface light in Alexander Springs Creek.

6.5.1.3 Time of Year

Estimates of average primary production in Silver River varied by time of year with the highest estimates in spring (April) and lowest estimates in winter (December) (Figure 6.87). Highest average light intensities were measured in the months of March (month 3), April (4), and October (10) which corresponded to times of year with largest mean GPP. Greater variation in GPP was observed in spring and summer months in Silver River. Deployments in Alexander Springs Creek spanned a shorter window (September to November). The strong light versus GPP association suggests a considerable seasonality to GPP, but this was not clearly observed, likely because the early deployments were at the most shaded sites.

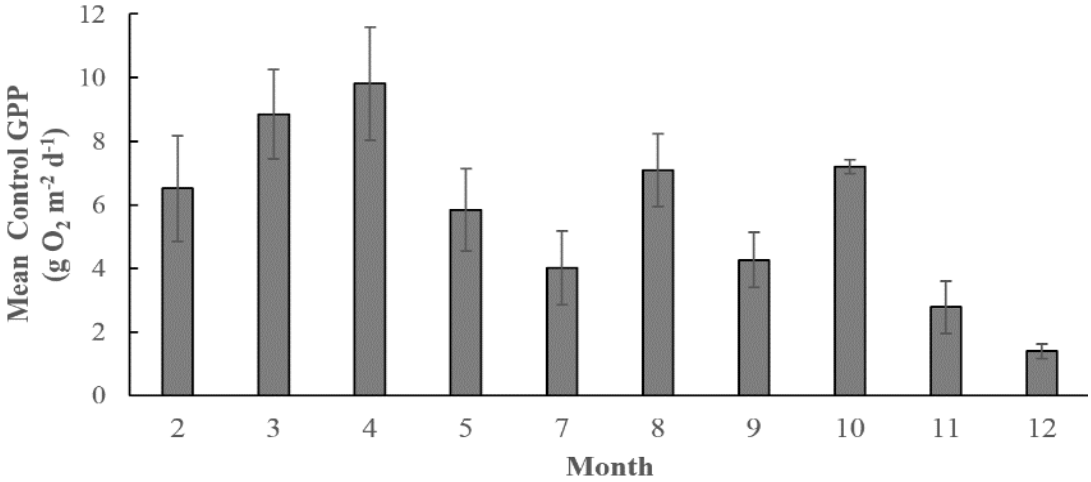

Figure 6.87. Average gross primary production in control boxes was greatest in April, lowest in December. Note: deployments did not occur in all months (e.g., January and June). Deployments in Alexander River were all in September, October and November.

6.5.1.4 Canopy Cover

Although all chamber deployments were restricted to shallower areas near the river margin, there was substantial variation in percent canopy cover. Estimates of percent cover varied from a minimum of 12.6 % to a maximum percent cover of 86.7 %. Notably, percent canopy cover did not vary significantly with longitudinal position, and was not significantly correlated to average surface light measurements, and did not, by itself, explain significant variation in primary production (Figure 6.88). One explanation for this is that canopy cover effects depend on solar zenith angle, particularly for an east-west azimuth river like Silver. However, given the strong link between GPP and light, this result was a surprise. Canopy cover was low for all Alexander Springs creek sites, and no association with GPP was observed.

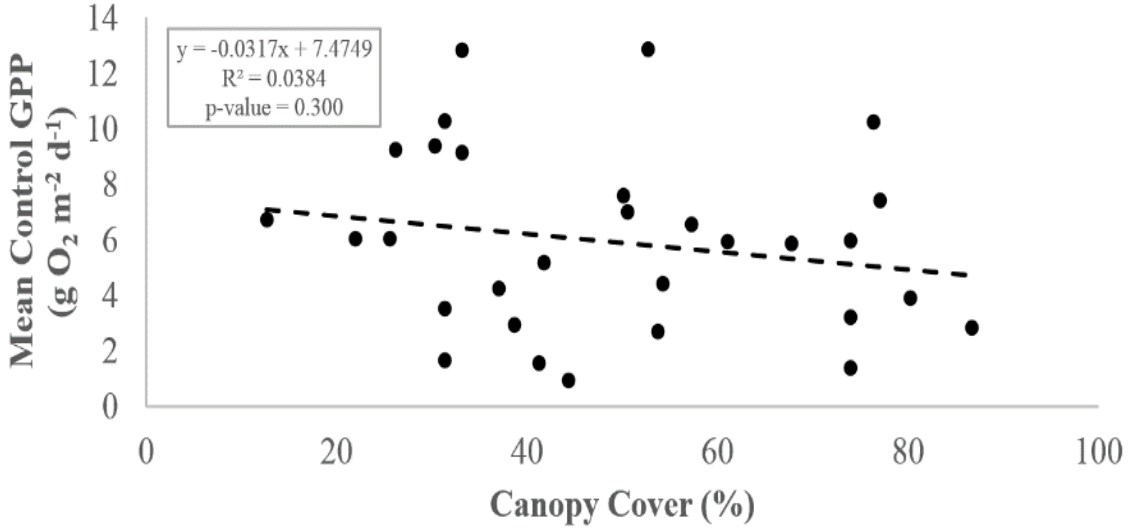

Figure 6.88. Variation in control gross primary production estimates were not significantly correlated to percent canopy cover in Silver River.

6.5.1.5 Water Depth

Water depth varied from 0.4 m to 1 m across deployments in Silver River. Average GPP and ER in Silver were both significantly correlated to water depth with depth explaining 28.2% of ER variation in respiration and 19.7% of GPP variation (Figure 6.64). Similar results were observed in Alexander Springs Creek where water depth explained 27% of the variation in ER, and 34% of the variation in GPP (Figure 6.89)

6.5.1.6 Vegetation Biomass

Vegetation dry biomass varied from 8.8 to 77.4 g within the control chambers. Total biomass was, surprisingly, not significantly correlated to control box GPP (p-value = 0.117; R^2=0.092) but was significantly correlated to ER (p-value = 0.003) (Figure 6.90). No association was observed between biomass and GPP or ER in Alexander Springs Creek.

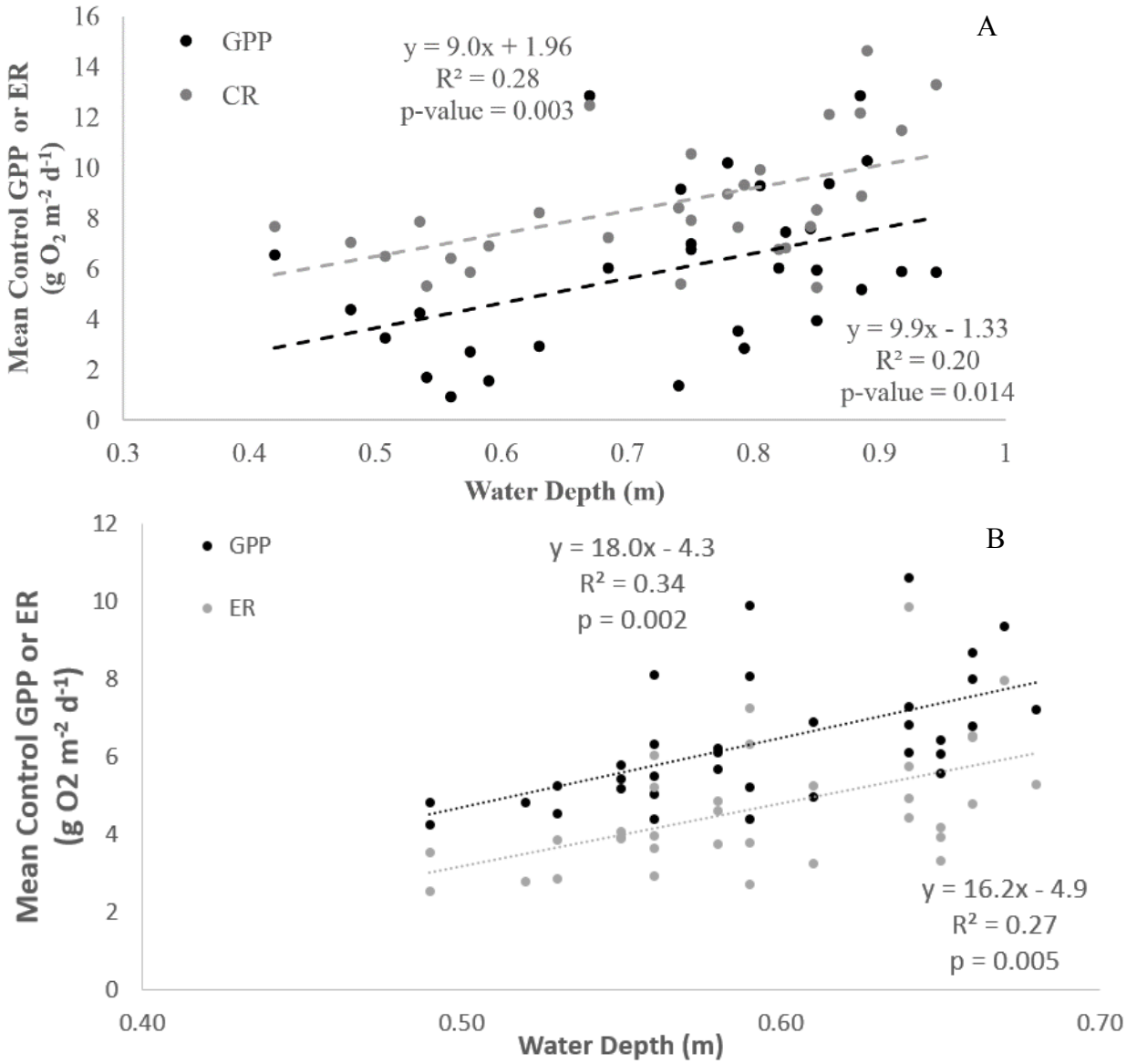

Figure 6.89. In (A) Silver River, mean primary production and respiration were both significantly correlated to water depth (p-value = 0.014 and 0.003, respectively) with 19.7% and 28.2% of variation explained. Similar behavior, but with different slopes, was observed in (B) Alexander Springs Creek.

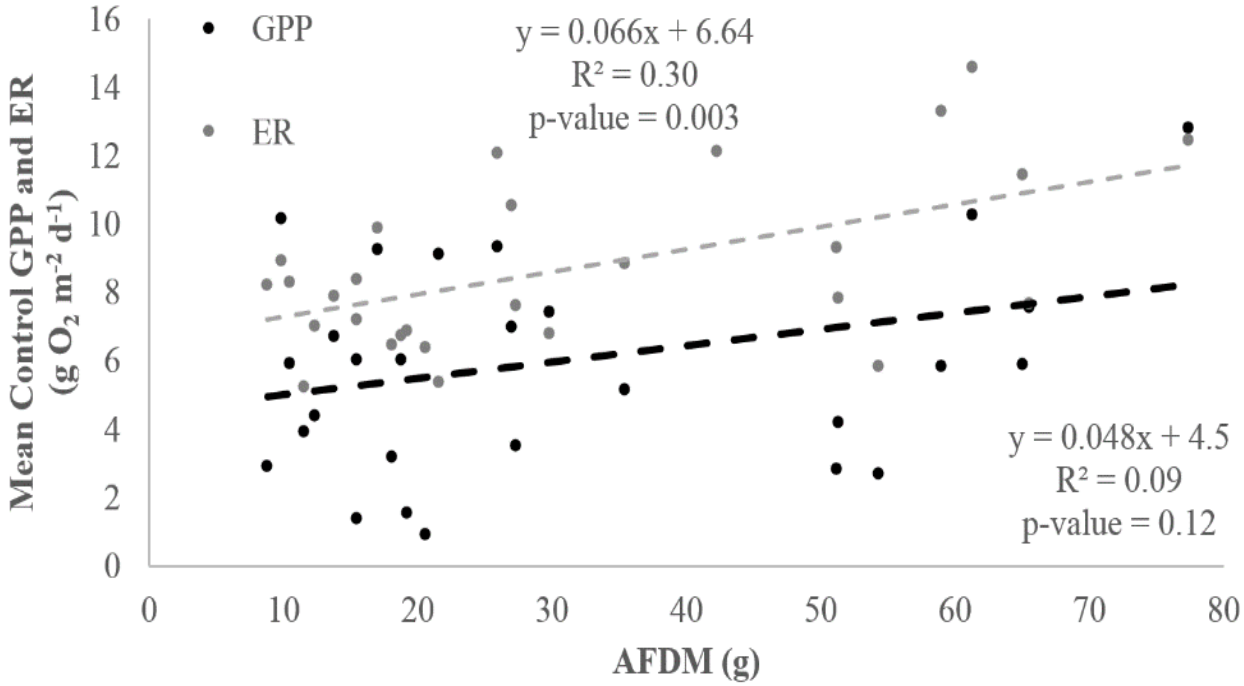

Figure 6.90. High variation in vegetation biomass (AFDM; ash-free dry mass) was observed within the control chambers.

In summary, statistical analysis of Silver River control box GPP with site characteristics showed downstream distance was negatively correlated with mean GPP while light and water depth were positively, significantly correlated to GPP (Table 6.11). For Alexander Springs Creek, correlations were significant only for light and distance downstream because of benthic sampling seasonality.

Table 6.11. Distance downstream was negatively and significantly correlated to control chamber GPP whereas surface light and water depth were positively and significantly correlated to GPP. Significant correlations ($p < 0.05$) are shown in bold, negative correlations in red.

SILVER RIVER	**Distance Downstream (m)**	**% Canopy Cover**	**Light (w m^{-2})**	**Biomass (g)**	**Water Depth (m)**
Correlation	-0.571	-0.250	0.621	0.303	0.610
P-value	**<0.001**	0.299	**<0.001**	0.117	**0.014**
ALEXANDER RIVER	**Distance Downstream (m)**	**% Canopy Cover**	**Light (w m^{-2})**	**Biomass (g)**	**Water Depth (m)**
Correlation	0.73	0.08	0.87	-0.03	0.58
P-value	**<0.001**	0.75	**<0.001**	0.94	0.002

A multivariate model (general linear model) using light, season, water depth and ash-free dry mass (AFDM), which pooled the effect of distance based on the Akaike Information Criterion (AIC), was able to explain over 80% of the variation in control box GPP in Silver River (Table

6.12), and over 60% of the variation in ER (Table 6.12). For Alexander Springs Creek, light was the only variable selected by the model, so the bivariate information in Figure 6.62 ($R^2 = 0.76$) summarizes the best fit model.

Table 6.12. Results of general linear model predictions of control box a) GPP and b) ER based on physical site attributes and timing.

A: GPP	Est.	SE	t-value	p-value
Intercept (Fall)	-7.83	2.37	-3.30	0.004
Light	0.01	0.00	4.38	0.000
Depth	10.83	3.09	3.51	0.003
AFDM	0.04	0.02	2.19	0.044
Spring	3.08	0.90	3.43	0.003
Summer	-0.66	1.28	-0.52	0.611
Winter	1.69	1.06	1.59	0.132
Null Deviance	245.40			
Resid. Deviance	45.60			

B: ER	Est.	SE	t-value	p-value
Intercept	3.34	2.30	1.45	0.164
MeanGPP	0.40	0.17	2.38	0.029
Light	0.00	0.00	-1.13	0.273
Depth	4.15	3.18	1.31	0.208
AFDM	0.03	0.02	1.75	0.098
Null Deviance	126.60			
Resid. Deviance	48.20			

Note that model effectiveness (r^2) can be obtained from (1 – residual deviance:null deviance); for GPP this is 0.83 and for ER this is 0.62

Table 6.12 suggests that GPP responds most strongly to light (+), a finding consistent with Alexander Springs Creek observations where light was the only significant predictor ($R^2 = 0.76$). Secondary conditional effects of depth (+) and season (particularly a large increase in spring, potentially associated with intrinsic autotroph phenology) were evident in Silver River. While these factors (depth and distance) were significant bivariate predictors in Alexander Springs Creek, they were omitted from the multivariate analysis, underscoring the importance of considering confounding effects of variables that are uncorrelated, often because of sampling logistical requirements or inherent location characteristics. The effect of biomass (AFDM, pooling across algae and SAV) was statistically significant (and positive), but weaker. For ER in Silver River, the strongest predictor of is GPP; while other factors were not significant, they were retained in the best-fit model, suggesting their omission reduces model effectiveness. The fitted slopes suggest a weak positive effect of depth and AFDM on ER; note that because of the model configuration, these effects are independent of the GPP effect. In Alexander Springs Creek, ER was nearly perfectly predicted by the combination of GPP and light ($R^2 = 0.98$, $p < 0.002$), with GPP increasing ER ($p << 0.001$) and light reducing ER ($p = 0.03$). The GPP versus ER relationship alone is shown in Figure 6.91; the small intercept suggests non-zero respiration in the absence of GPP. We note that while site mean GPP and ER (averaged across days within each deployment) were nearly perfectly correlated, the association within each deployment between GPP and ER was markedly weaker (mean $R^2 = 0.53$).

Critically, in both rivers we effectively constrain and predict GPP and ER variation in the control boxes, and are able to make robust predictions about GPP and ER at the point scale. We use this result as evidence that our nutrient enrichment dosing experiment is optimally interpreted when dosed boxes are conditioned on control box GPP (i.e., rather than interpreting raw GPP values).

Moreover, the fact that variation in GPP is so highly predictable means that signals of nutrient enrichment, if present, should be readily detectable, and interpretation of nutrient effect size can proceed without reservations related to our capacity to measure or predict GPP more broadly.

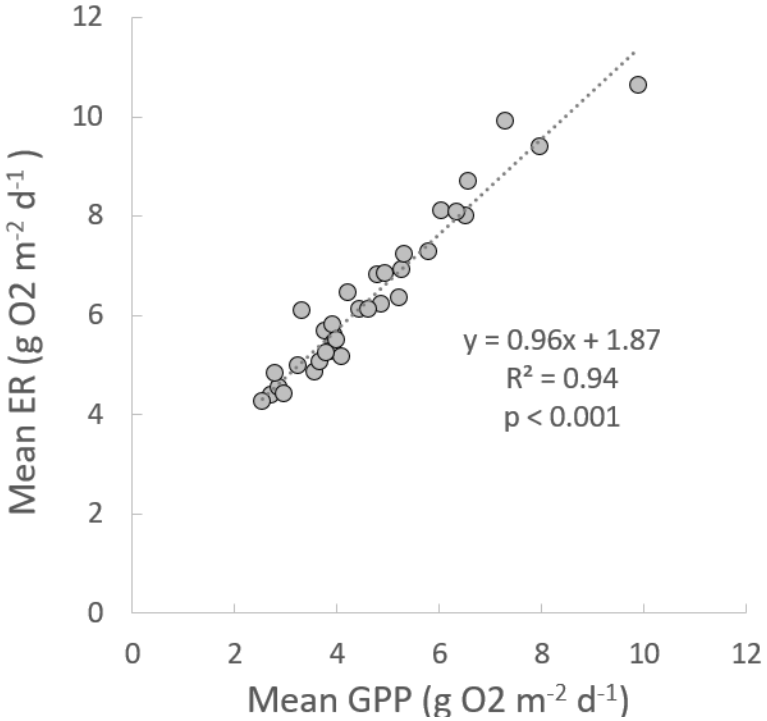

Figure 6.91. A strong relationship between GPP and ER in the boxes at Alexander Springs Creek suggests that most of the system respiration is autotrophic, and that variation in respiration in time and space is principally governed by those factors (e.g., light) that control primary production. Within deployments, GPP and ER were less well correlated (mean $R^2 = 0.53$).

6.5.1.7 Nutrient Effects on Chamber Metabolism

To assess the influence of nutrient additions on primary production, GPP in each treatment chamber was divided by that in the corresponding control chamber (GPP_t:GPP_c) and log-transformed such that values greater than 0 represent **stimulation** by nutrient additions (i.e., limitation present), values less than 0 represent potential **inhibition** by nutrient enrichment, and values approximating 1 represent no effect. The ratio of treatment and control GPP was averaged over each deployment and plotted by distance downstream (m), showing the large variation in potential nutrient effects (Figure 6.92).

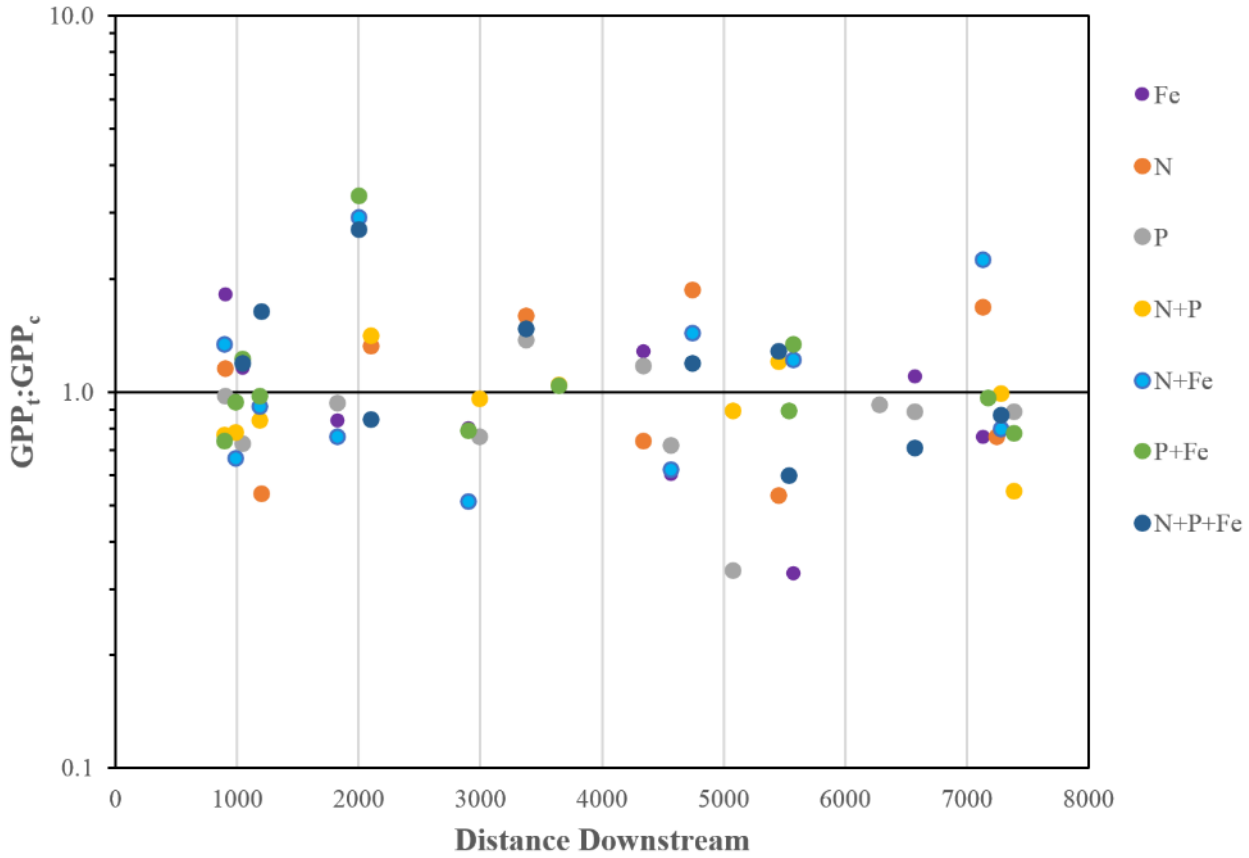

Figure 6.92. Large variation in nutrient effects (i.e., average GPP in treatment chamber divided by that in the control) were seen by treatment type and by distance downstream (i.e., location). Black bar represents 1:1, representative of control value. These data are shown with a log-scaled y-axis. All subsequent results will be for the log-transformed value of GPPt:GPPc, such that values less than 0 indicate GPP inhibition, while values greater than 1 indicate stimulation.

The mean Log[GPP_t:GPP_c] ratio showed no significant nutrient enrichment effects when averaged across all deployments in Silver River (Figure 6.93). In contrast, we observed weak but significant inhibition due to P and Fe addition, and weak stimulation of GPP when all three nutrients were added together.

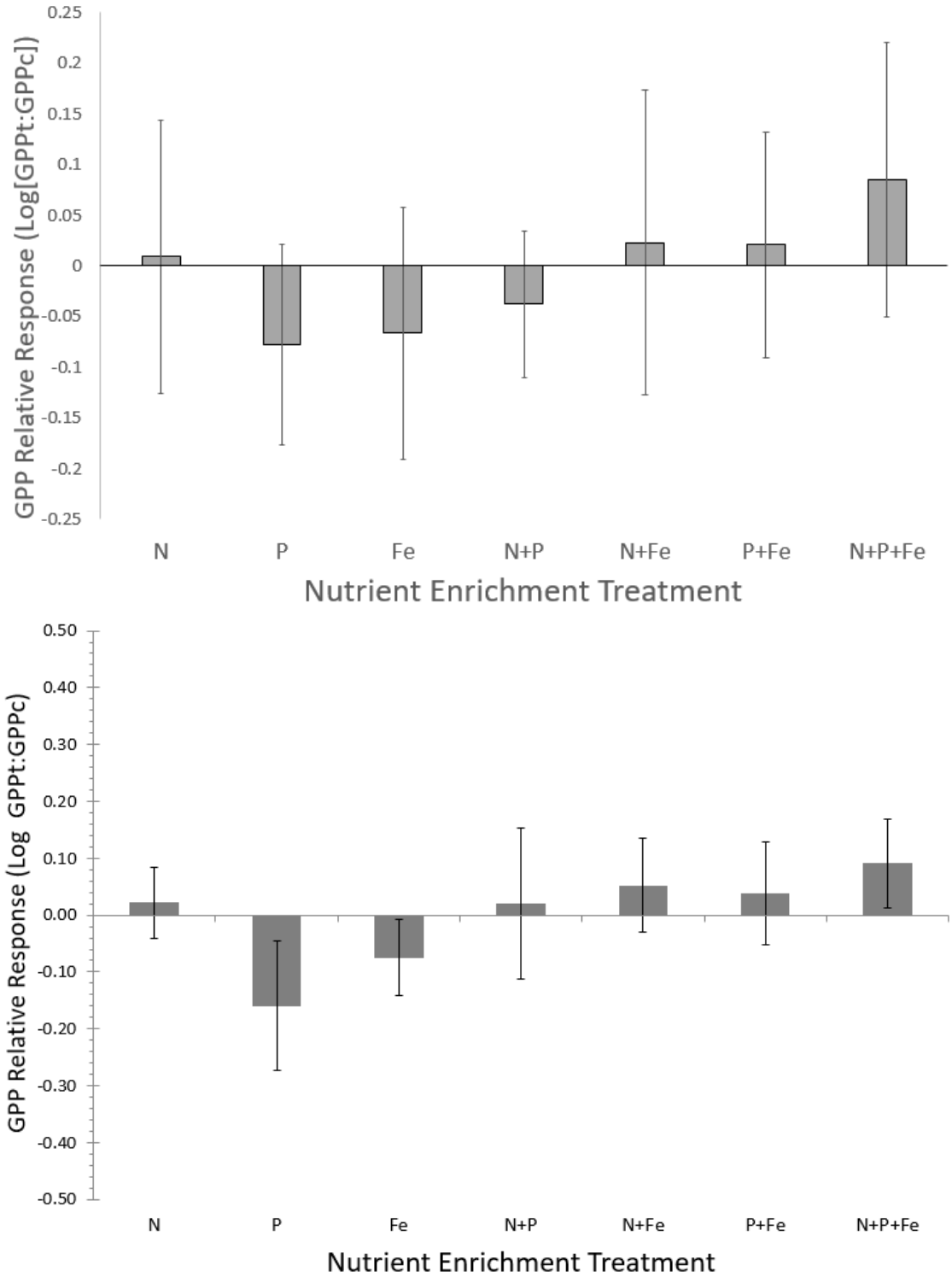

Figure 6.93. A) No significant nutrient effects for GPP response (measured as GPP_t:GPP_c) when averaged across all deployments in Silver River. B) In Alexander Springs Creek, there was evidence of weak P and Fe inhibition, and stimulation when all three nutrients were added. Error bars represent 95% confidence intervals.

Overall, this suggests that nutrient status in Silver River was not useful for predicting control versus treatment box primary production. From this result, the first-order inference is that nutrient concentrations do not meaningfully control metabolic response; as such, *enriching nutrients has no coherent effect on system level metabolic behavior*. In Alexander Springs Creek, there is weak evidence of inhibitory effects of P and Fe addition, but the modes of action are not well understood. It is important to note that the inhibitory effect averaged 30 % of GPP for P, and only 15 % for Fe, and that sample sizes for each treatment are small (n = 4). We further note that our range of concentrations is limited, and that this inference applies to enrichment effects (i.e., we were not able to experimentally reduce nutrient levels inside the boxes, though natural reductions in nitrate were observed and reported on in a later section of this report).

Analysis of variance results for treatment effects in Silver River enumerate that no significant differences among treatments were observed (pooling across distance; $p = 0.52$). Table 6.13 summarizes a more expansive model that considers the main effects of nutrient addition using general linear modeling to account for both treatment and distance effects. In summary, there is no significant nutrient effect at $p < 0.05$, but Fe exerts a significant positive effect on GPP for $p < 0.1$. Notably, there is no evidence of an N or P effect, nor any evidence of a distance*nutrient interaction for any of the nutrients. Further exploration of nutrient addition interactions (e.g., N + P) revealed no significant effects, and yielded models with AIC values higher than the main effects model, so these results are not shown. While the main effects model is the best fit, we note that the model explains only 14 % of the variation in GPP_t:GPP_c suggesting that other factors are substantially more influential.

A similar model (Table 6.14) for Alexander Springs Creek, focusing on the response ratio (GPP_t:GPP_c) yielded two important findings. First, there was no stimulatory effect of N in this low N system. There was, however, a significant inhibitory response to P additions and a weak stimulatory effect of all three nutrients added together.

Table 6.13. Results of general linear model predictions of GPP_t:GPP_c for Silver River based on nutrient enrichment and distance.

GPPt:GPPc	Estimate	Std. Error	t value	Pr(>|t|)
(Intercept)	0.62	0.34	1.81	0.075
N	0.19	0.26	0.73	0.466
Distant (km)	0.05	0.08	0.57	0.572
P	0.32	0.27	1.21	0.231
Fe	0.47	0.27	1.77	0.082
N:Dist	0.01	0.06	0.09	0.929
P:Dist	-0.06	0.06	-1.01	0.316
Fe:Dist	-0.07	0.03	-1.47	0.127
Null Deviance	21.66			
Residual Deviance	19.60			

Note that model effectiveness (r^2) obtained from (1 – residual deviance:null deviance) is 0.14. Only the main effect of Fe enrichment had a detectable effect.

Table 6.14. Results of general linear model predictions of GPP_t:GPP_c for Alexander Springs Creek based on nutrient enrichment only (distance was not considered).

GPPt:GPPc	Estimate	Std. Error	t value	Pr(>|t|)
TreatmentFe	**-0.075**	**0.036**	**-2.08**	**0.02**
TreatmentN	0.022	0.053	0.41	0.69
TreatmentP	**-0.160**	**0.053**	**-3.03**	**<0.001**
TreatmentN+Fe	0.052	0.040	1.27	0.22
TreatmentN+P	0.020	0.064	0.31	0.76
TreatmentP+Fe	0.039	0.041	0.95	0.36
TreatmentN+P+Fe	**0.091**	**0.046**	**2.01**	**0.06**
Null Deviance	0.30			
Residual Deviance	0.15			

Note that model effectiveness (r^2) obtained from (1 – residual deviance:null deviance) is 0.51. The only significant effects ($p < 0.1$) were for P (inhibition), Fe (inhibition) and all nutrients added together (stimulation).

The preceding analysis is predicated on the comparison between GPP in the treatment boxes (GPP_t) and in the unamended control boxes (GPP_c). The analysis was done for each of the treatment effects independently. The absence of significant enrichment effects is limited, in part, by the sample size, particularly in Alexander Springs Creek. However, because there is weak evidence of nutrient interaction effects, we can further explore the impacts of nutrient enrichment by examining only the main effects of each nutrient. That is, for all deployments where N was added, we assess whether there was a systematic increase or decrease in GPP compared to all deployments where N was not added. This ratio precludes the possibility of interaction effects, but also increases the statistical power with which to detect growth responses.

This analysis in Silver River revealed a modest Fe enrichment effect (Figure 6.94). Overall, GPP in deployments where N was added were slightly higher than deployments where N was not added, and the reverse was true for P (very slight inhibition), but neither effect was statistically significant. However, the deployments where Fe was added did respond with higher mean GPP than those deployments where Fe was not added. Together, we interpret this to mean that the P and Fe inhibition effects in Alexander Springs Creek are potentially artifacts of small sample size, though continued attention, particularly to P inhibition based on other lines of evidence presented in this report, is warranted. In Silver River, the evidence for Fe stimulatory effects is small, but coupled with the extremely low sediment and porewater Fe concentrations may support further scrutiny of Fe loading dynamics as a control on system metabolic response.

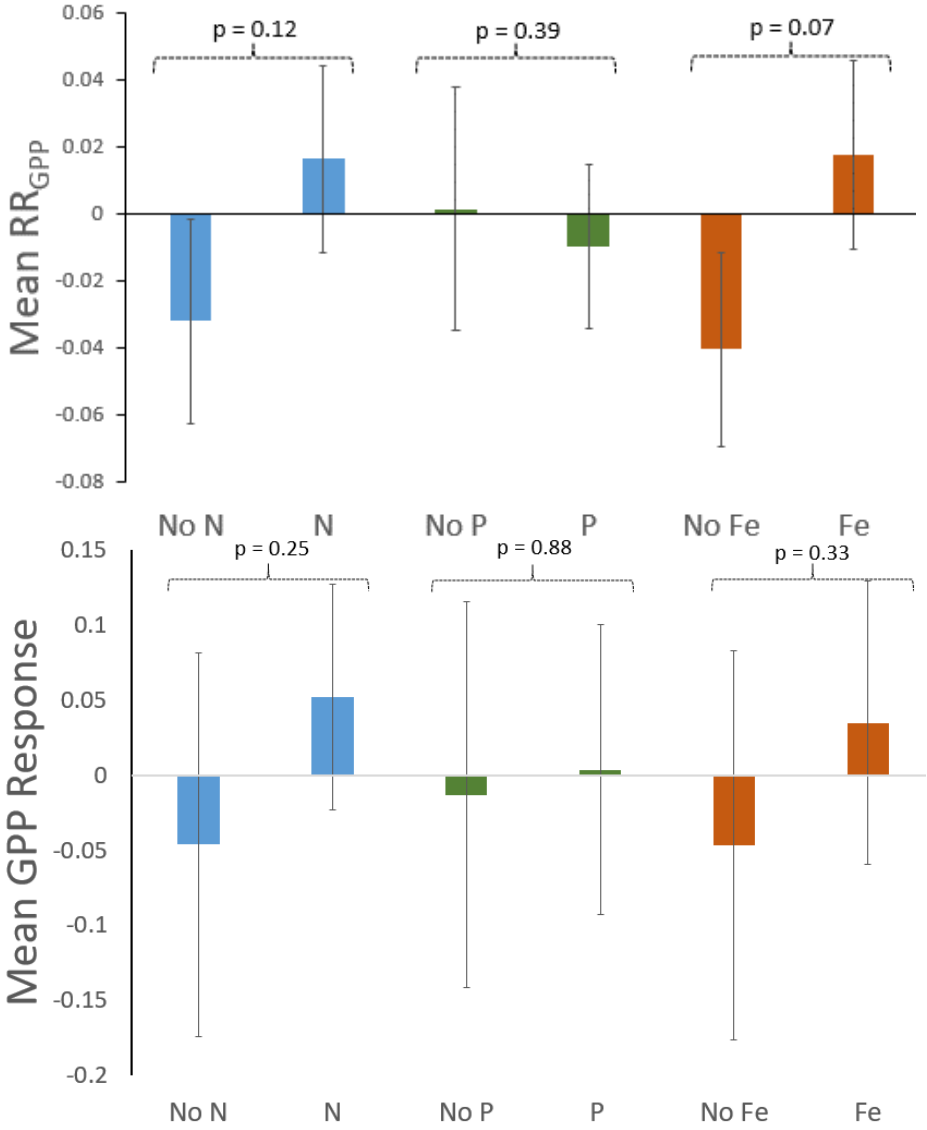

Figure 6.94. Main effects of nutrient enrichment for A) Silver and B) Alexander. The only significant effect was weak stimulation of GPP by Fe in Silver River.

Another important caveat to the analyses presented to this point is that they focus only on the GPP response. Primary production is biomass-specific, meaning that GPP is expected to vary with standing stocks of biomass. While we observed surprisingly weak covariation between GPP and biomass in the control boxes, with GPP overwhelmingly controlled by light, it still is instructive to index GPP to biomass when making comparisons between treatment and control boxes, principally to ensure that differences are not artifacts of contrasting benthic conditions. To that end, we further compared the effects of treatments by comparing the biomass indexed GPP (i.e., GPP_B = GPP/Biomass) between treatment and control boxes (i.e., $GPP_{B,t}$ versus $GPP_{B,c}$). Figure 6.95 summarizes the results of this analysis for both rivers.

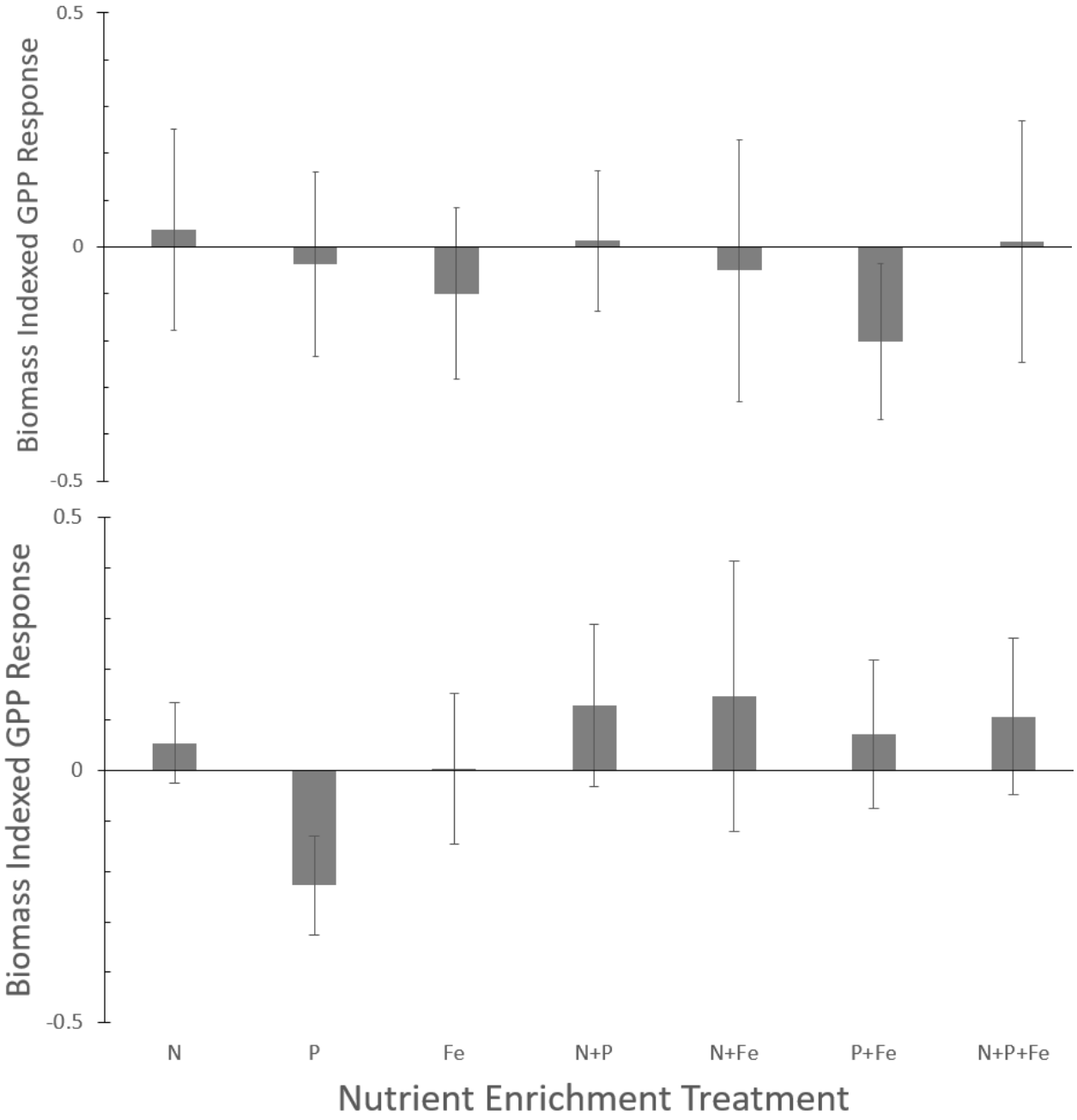

Figure 6.95. Summary of nutrient enrichment effects on GPP in A) Silver River, and B) Alexander Springs Creek, showing the relative response of GPP indexed to standing stock of biomass between treatment and control boxes (i.e., $Log[GPP_{B,t}:GPP_{B,c}]$). For Silver River, the only significant effect was apparent GPP_B inhibition with the addition of P and Fe. For Alexander Spring Creek, the only significant effect was P inhibition.

The combination of box responses to nutrient enrichment together suggest that changes in nutrient supply have negligible impacts on metabolism in both spring fed rivers. While there are

several modestly significant results, there is weak coherence among them between rivers, or between modes of analysis within rivers.

The single strongest finding that appears in both rivers is P inhibition of metabolism, a response without a clear mechanistic basis, but for which other lines of evidence provide support. Specifically, there is a strong cross-site trend in metabolism whereby primary production (GPP) is reduced with increased SRP concentrations (Cohen et al. 2013). Further, in this study, we observed SAV growth was significantly inhibited by P enrichment (see section below). Plausible direct mechanisms are limited, but may include shading effects from increased periphyton growth. These direct effects are rendered complex by the fact that the response is observed in both taxa-specific settings (i.e., SAV growth) and also in open-channel and box settings. If stimulation of periphyton and associated shading were the mechanism for reduced GPP, algal biomass would be far less efficient using light than SAV. More plausible is that the GPP effects are indirect, influenced by covariates such as sediment texture or redox that impair growth, and also enhance P availability. Experimental manipulations of P are necessary to elucidate among the competing explanations for this observed effect.

A second important finding is that despite very low Fe concentrations in Silver River sediments, the enrichment of Fe has a small effect, evident only when the main effect of Fe is evaluated on GPP responses alone (i.e., not indexed to biomass). There was some weak evidence of Fe stimulation of GPP, particularly when examining only the nutrient main effects, but this effect was small. It is plausible that the experimental design of a single injected dose of each nutrient at the outset of each deployment was not sufficient to ensure elevated concentrations throughout the deployment, rendering the enrichment effects transient and confounded. We note that in Alexander Springs Creek, where sediment Fe concentrations are much higher, there was actually weak evidence of Fe inhibition. Further investigation of Fe dynamics and growth impacts is clearly warranted, but direct management of Fe is not yet justified, particularly since it is not yet clear whether Fe concentrations have increased over time. Part of the rationale for including Fe in the study is that Fe availability is linked to oxygen levels via the differing solubilities of oxidized and reduced forms of Fe. Under low DO conditions, a state that has been linked to algal density in a broad survey of springs (Heffernan et al. 2010), the increased availability of Fe may stimulate growth, particularly for algal taxa that require roughly an order of magnitude higher Fe per unit biomass as the native SAV. Further work on Fe demand, and spatial and temporal heterogeneity in supply will be valuable avenues for future research.

Finally, we observed no evidence of N enrichment effects. This is to be expected in the already N-rich Silver River, but the absence of a stimulatory effect in Alexander Springs Creek, where N concentrations are at background levels supports the hypothesis that N supply does not limit growth in spring fed rivers. Along with N assimilation estimates presented earlier in this report, which suggest the ecosystem's autotrophs use less than 0.15 % of N available over the reach from the spring-vent to the S5 measuring station, this result does not support the hypothesis that alleviation of N limitation (i.e., eutrophication) is the reason for recent ecosystem change. This has important implications for N management and investment in correcting alternative mechanisms of spring ecosystem degradation.

6.5.1.8 Algal Growth on Substrates

Despite the absence of marked aggregate metabolic effects of nutrient enrichment, it remains plausible that individual components of the autotroph community may respond to nutrient enrichment differentially. That is, while SAV may not respond to enhanced supply, algal taxa that are far more constrained to water column nutrient sources than the rooted plants, may respond more vigorously. To test this possibility, we deployed bare ceramic tiles in each box deployment in both rivers. The accumulation of algal biomass on the tiles provides a measure of the algal growth conditions, and the contrast between the control and treatment boxes provides a direct measure of the capacity for nutrient enrichment to affect those growth conditions. Differences in short-term algal growth (i.e., biomass accumulated over one week deployments) were observed during retrieval of the suspended tiles post-deployment (Figure 6.96) in both rivers.

Figure 6.96. Photographs of two tiles which were suspended within chambers to measure algal growth given nutrient additions of phosphorus and iron (left) and iron alone (right).

In Silver River, there was marked variation in algal biomass estimates with the greatest algal colonization measurements observed in upstream and downstream locations (Figure 6.97). No such variation was observed in Alexander Springs Creek, likely because most of the box deployment locations were within 1,000 meters of each other, a necessity given complex deployment logistics in the absence of a motorized boat.

Mean algal accrual in the control boxes in Silver River was 0.56 g m^{-2} d^{-1}, and was unevenly distributed across treatments (Figure 6.98). Mean algal accrual was lower in Alexander Springs Creek (0.43 g m^{-2} d^{-1}), but this difference was not statistically significant ($p = 0.34$) because of relatively high spatial and temporal variation. One explanation for the modest difference in growth rates is differing environmental conditions between the rivers, but another is Alexander Springs Creek measurements were taken in the late autumn, with generally lower average light. In both rivers, there was considerable observed variation across nutrient enrichment treatments. We note that for all nutrient enrichment comparisons, we index the observed tile growth to observations from the control chambers, thereby obviating the light variation effects. Because differences in light intensity do impact how robust the comparison is between rivers, we truncated the Silver River data to the same period of the year as Alexander Springs Creek. Although modest differences were observed that may be biologicall significant, they did not meet statistical significance criterion ($p < 0.05$).

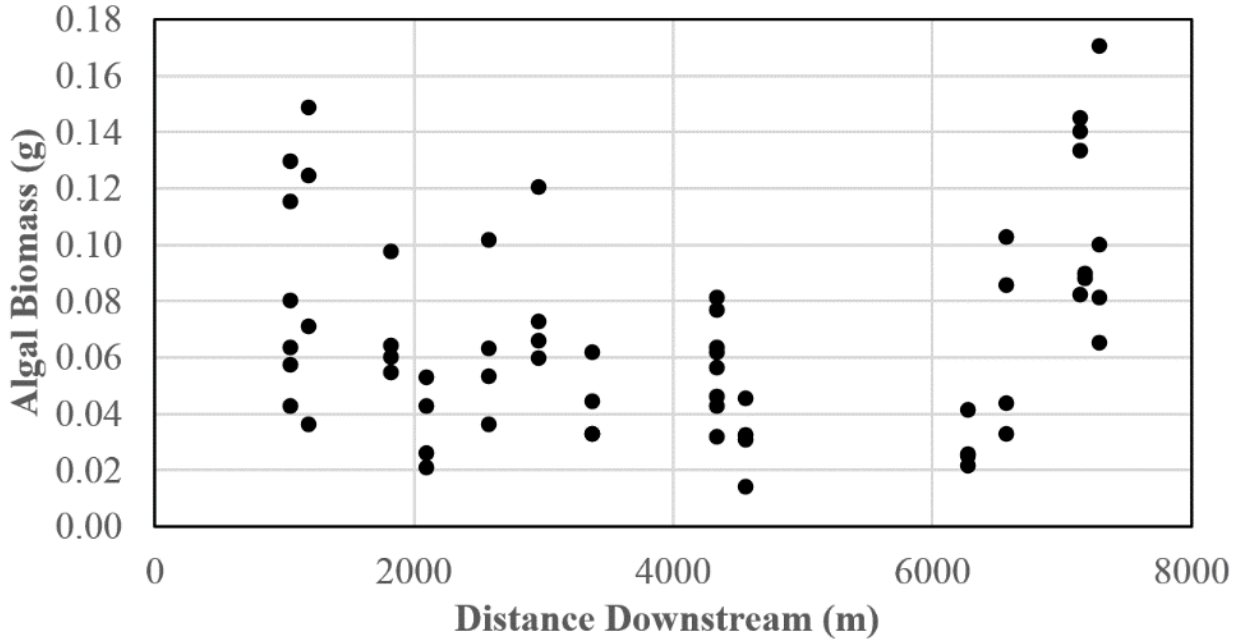

Figure 6.97. Large variation in algal biomass accumulation estimates were observed across the 13 deployments at Silver River with the largest growth found in upstream (~1,000 m) and downstream (>7,000 m) sections of the reach; note that each dot is algal biomass on tiles after one week in boxes (control or nutrient enrichment).

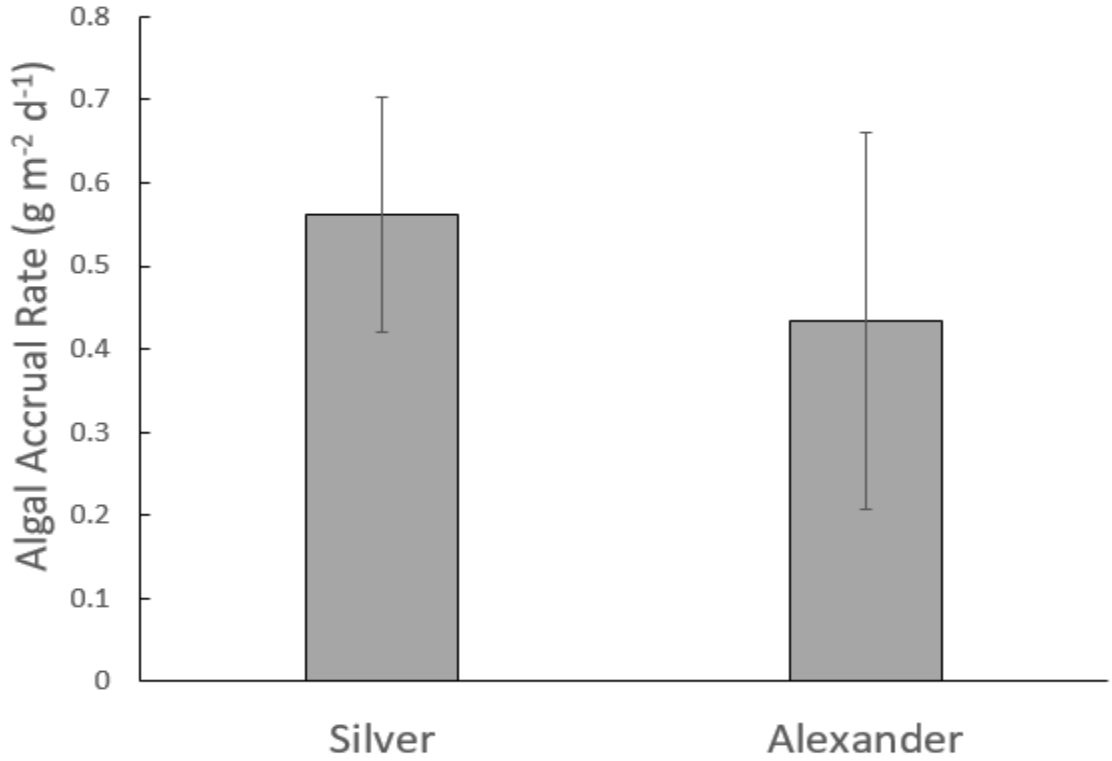

Figure 6.98. Summary of daily growth rates on tiles in deployed control boxes in the two rivers. The difference was not statically significant ($p = 0.34$), but may be biologically meaningful.

Average algal biomass accrual measurements were analyzed as a function of nutrient enrichment treatment. The highest biomass accrual rates (g m^{-2} d^{-1}) in Silver River were observed with N, Fe, N+Fe, and P+Fe enrichment; notably, nearly all nutrient enrichment treatment (except N+P) exhibited higher algal accrual than the controls (Figure 6.99). In Alexander Springs Creek, the highest accrual rates were for P and N+P treatments, but all treatments were similar to the control box algal accrual rates.

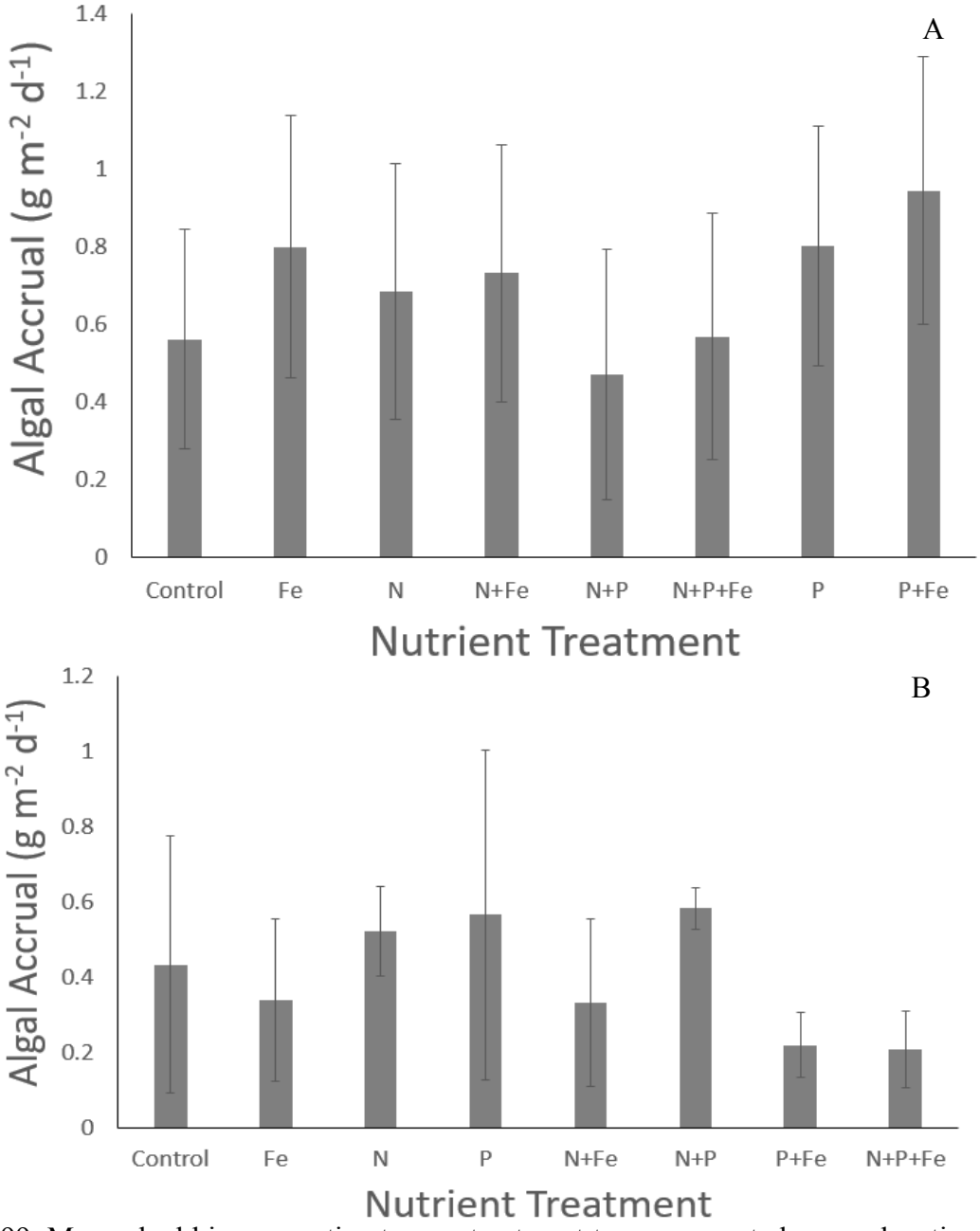

Figure 6.99. Mean algal biomass estimates per treatment type aggregated across locations in (A) Silver River and (B) Alexander Springs Creek showed greater stimulation in N, Fe, N+Fe, and P+Fe treatments although larger standard errors (bars) were also observed.

Algal biomass accrual was compared to GPP. No trend between algae and GPP was observed across all treatment types in Silver River, and only a weak positive association was observed in Alexander Springs Creek (Figure 6.100). This suggests that the controls on algal biomass accumulation are distinct from those that control GPP. This decoupling is surprising. Since by far the dominant control on GPP is incident light, this suggests that the light regime is not a good predictor of algal growth, despite nearly an order of magnitude variation in biomass accrual rates in both rivers. This reinforces anecdotal observations in both rivers that luxuriant algal mats can be supported in areas that are heavily shaded.

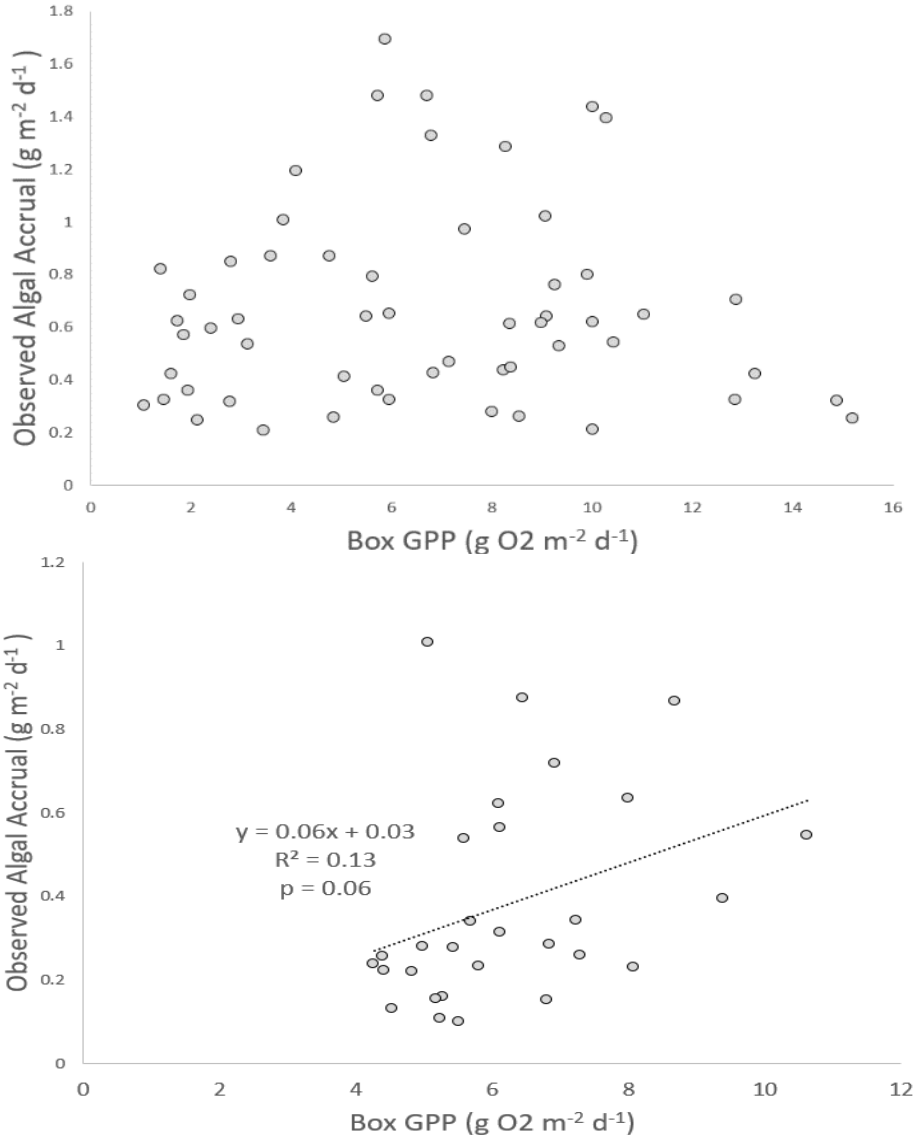

Figure 6.100. Total algal biomass accumulation on tiles was not significantly correlated to total GPP in Silver River ($R^2 = 0.01$, $p = 0.97$), but was weakly positively correlated in Alexander Springs Creek ($p = 0.06$). GPP explained 13 % of variation in algal growth, suggesting that controls on algal accumulation are distinct from factors influencing ecosystem metabolism.

When accounting for differences in ambient conditions by comparing treatment algal biomass to the corresponding control algal biomass (biomass treatment versus biomass control, Bt:Bc), no significant differences between treatments were observed; however, it was evident that on average the addition of nutrients increased the amount of algal colonization on the tile substrate with the largest effect magnitude seen with the addition of N, P and Fe, but only alone; when added in combination we observed no significant algal growth enhancement (Figure 6.101). As with all periphytometers, the selection of growth substrate (tile, wood, glass) can dramatically impact observed algal growth. We used the same substrate for all experiments, but cannot be sure that different substrates (e.g., organic materials) would exhibit similar behaviors. All single nutrient additions significantly stimulated algal growth in Silver River, and all other effects were not significant. In Alexander, none of the nutrient additions was significantly higher than the control.

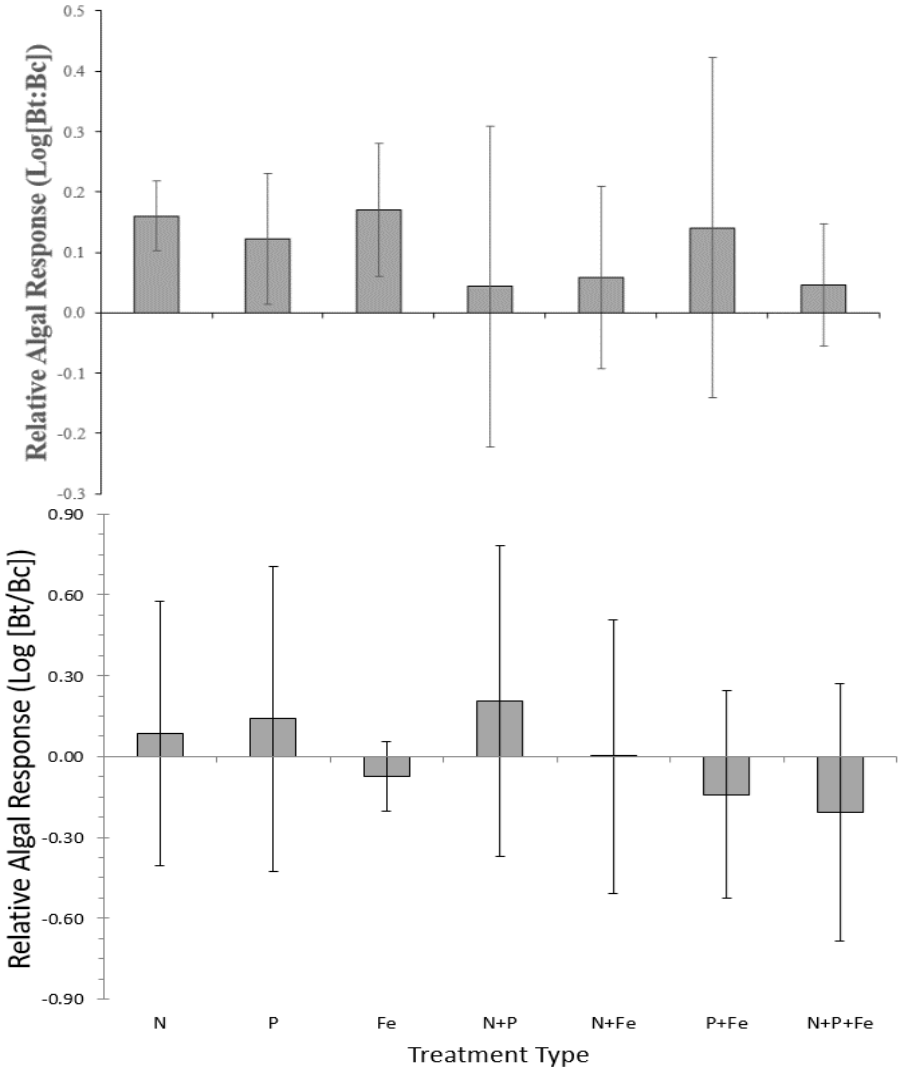

Figure 6.101. Average relative algal biomass response for A) Silver River, and B) Alexander Springs Creek was compared between treatment and control chambers and averaged for each treatment type. Error bars denote 95 % confidence intervals for the mean value.

As with GPP, we evaluated the main effects of nutrient enrichment to obviate low sample sizes available for analysis. As before, this meant analyzing the relative response for all treatments for which N, or P, of Fe was added, regardless of whether it was alone or in combination with other solutes. This precludes our ability to detect interaction effects, but yields more robust inferences of individual nutrient effects. The results (Figure 6.102) suggest all three nutrients stimulated algal growth in Silver River, but only Fe was statistically significant. We note the magnitude of the stimulatory effect is quite small (25 % increase in accrual), but potentially biologically significant.

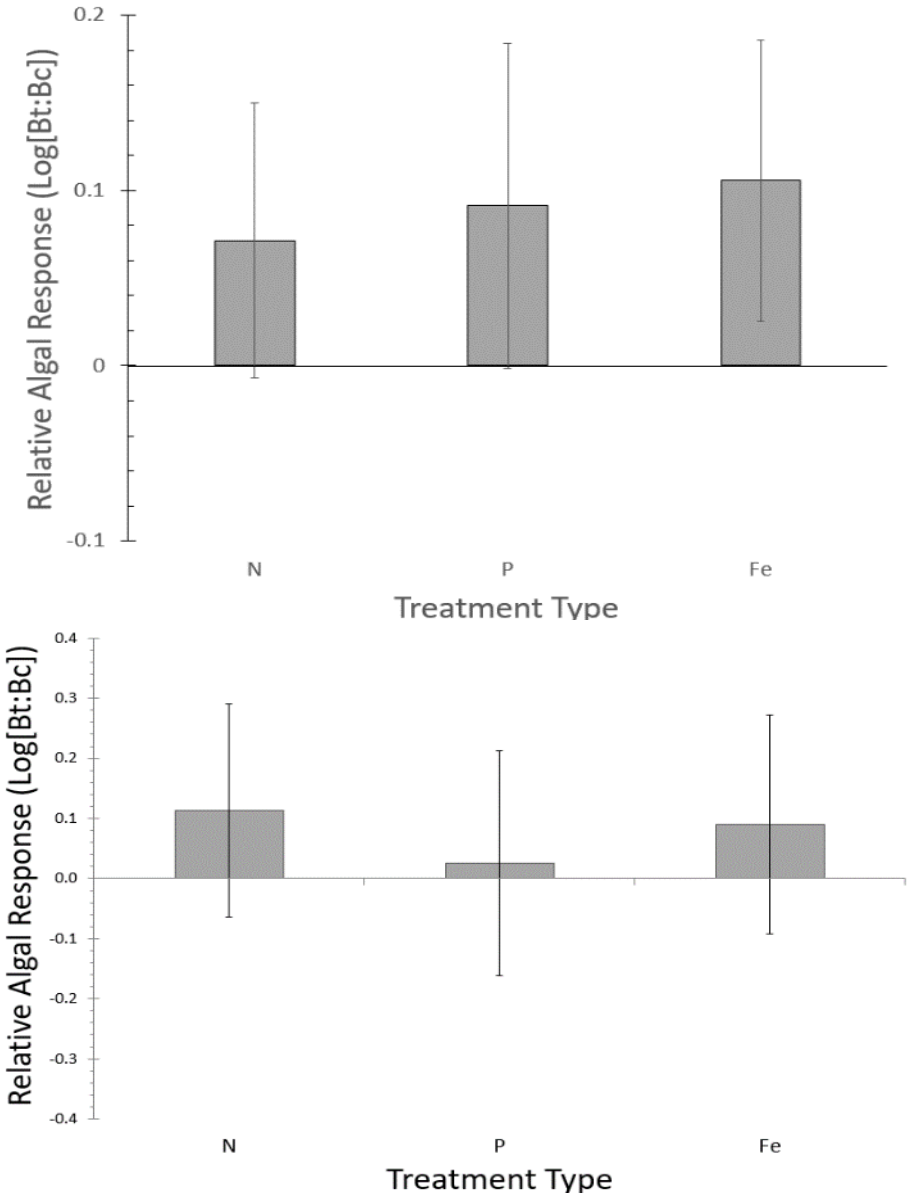

Figure 6.102. Main effects of nutrient addition showing the mean relative algal response to N, P and Fe additions in A) Silver River and B) Alexander Springs Creek. Only the Fe response was statistically significant (error bars denote 95 % confidence intervals) for Silver River. No nutrient additions were significant in Alexander Springs Creek.

In Alexander Springs Creek, the parallel analysis yielded no significant effects, though as before all three nutrients seemed to stimulate growth. The magnitude of the mean effects was the same, but the high variance precludes interpreting these stimulatory effects as meaningful. However, the general trends observed here warrant further investigation. Specifically, the potential for Fe limitation of algal growth in Silver River, and for N limitation of algal growth in Alexander Springs Creek (the only significant and largest in magnitude effects, respectively) may be broadly informative for algal management strategies if confirmed with further study.

In spite of the suggestive results presented, the clearest interpretation of the data is that nutrient enrichment effects are complex and, to the extent we can detect them, relatively weak. This does not support rejecting the hypothesis that nutrient enrichment should be part of a broader springs protection strategy. Indeed, nutrient availability is both globally supported as a major control on autotroph structure, growth, and composition, and locally supported as a modest factor in these results. However, it is also clear that whatever other variables control algal accrual they are of dominant influence. Specifically, a general linear model to predict the relative algal biomass response in Silver River yielded the same results as depicted in Figure 6.102 (with Fe the only significant predictor variable), but explained only 8 % of the variation in observed algal accrual (the same type of model in Alexander Springs Creek explained only 5 % of the variation). As such, our results can be interpreted as suggestive of a role for nutrients in controlling autotroph composition, but cannot support a singular focus on nutrient enrichment as the only or even primary causal pathway for recent ecosystem change.

6.6 BENTHIC CHAMBERS – NUTRIENT DYNAMICS AND DEPLETION RESPONSES

Stream solute signals reflect the convolution of multiple temporally varying delivery pathways, hydraulic transport and dispersion, and a multitude of biogeochemical processing pathways (Bormann and Likens 1967; McKnight and Bencala 1990; Mulholland and Hill 1997). Isolating processing signals is incredibly challenging, as for non-gaseous solutes such as nitrate (NO_3-N), delivery artifacts may persist over long distances (Hensley and Cohen 2016). Even when a two-station method is used to capture a delivery signal at the upstream boundary of a well-defined reach, uncertainty remains in how hydraulic transport (i.e., travel time and magnitude of dispersion) influences the downstream signal geometry (SSW 1990). By extension, this can create uncertainty in inferences regarding biogeochemical processing drawn from the timing and magnitude of differences between upstream and downstream signals (Hensley and Cohen 2016).

Biogeochemical signals are themselves a convolution of multiple processes. The aquatic nitrogen cycle is immensely complex, with a multitude of overlapping, intersecting and often poorly understood pathways (Burgin and Hamilton 2007, Jetten 2008), stoichiometrically coupled to other elemental cycles (Dodd et al. 2004; Gruber and Galloway 2008; Cohen et al. 2013). Focusing just on NO_3-N, there are removal pathways including autotrophic assimilation, heterotrophic assimilation, denitrification and dissimilatory reduction to ammonium (DNRA), as well as production pathways such as mineralization of organic matter or nitrification of ammonium (NH_4^+). All of these processes are potentially time varying, in response to concentration (i.e., reaction kinetics) and a host of other ancillary chemical and environmental factors such as sunlight, temperature, discharge and concentrations of other solutes.

The coupling of autotrophic assimilation of NO_3-N with primary productivity has been interpreted as the primary driver of the diel NO_3-N signals observed in many streams (Scholefield et al. 2005; Robert and Mulholland 2007; Rusjan and Mikos 2010; Heffernan and Cohen 2010; Pellerin et al. 2012; Cohen et al. 2013; Rode et al. 2016). However, de-coupling may occur under nutrient limitation (Appling and Heffernan, 2014) or in the presence of a more energetically favorable source of assimilatory nitrogen such as NH_4^+ (Peterson et al. 2001; Kemp and Dodds 2002). Denitrification has been observed to follow Efficiency-Loss (EL) kinetics (Dodds et al. 2002; Kemp and Dodds 2006; O'Brien et al. 2007; Mulholland et al. 2008; Mulholland et al. 2009), with rates increasing with NO_3-N concentration but with declining efficiency. In addition to varying in response to NO_3-N concentration, denitrification may be stimulated by temperature (Pfenning and McMahon 1997), inhibited by DO (Christensen et al. 1990; Pina-Ochoa and Alvarez-Cobelas 2006), and potentially limited by dissolved organic carbon (DOC) availability (Pfenning and McMahon 1997; Bernhardt and Likens 2002; Pina-Ochoa and Alvarez-Cobelas 2006; Heffernan and Cohen 2010). Nitrification rates vary in response to NH_4^+ concentrations (Webster et al. 2003; O'Brien et al. 2007) and may also be stimulated by higher daytime DO and temperature (Kemp and Dodds 2002; Gammons et al. 2010). Across sites nitrification rates also appear positively correlated with NO_3-N concentration (Bernhardt et al. 2002), explained as NO_3-N concentrations controlling the balance of NH_4^+ demand between heterotrophs and nitrifiers. DOC concentrations may influence nitrification in a similar way (Strauss and Lamberti 2000).

De-convolving these variable and overlapping biogeochemical processing signals, requires high-frequency, high-precision NO_3-N measurements. Recent advances of *in situ* sensors (Kirchner et al. 2004) have enabled this sort of analysis using open channel measurements (Pellerin et al. 2009; Heffernan and Cohen 2010; Pellerin et al. 2012; Cohen et al. 2013; Hensley et al. 2014; Rode et al. 2016). Here we present an alternative approach of placing high-frequency sensors within benthic chambers, which allows us to isolate biogeochemical processing within a well-defined benthic footprint (Reijo et al. in review). This ensures that the fine-scale structure NO_3-N signal we observe is solely the result of localized processing. This allows us to more accurately parse the overlapping constituent processing pathways. Equally important, by removing upstream resupply, we can induce natural concentration depletion over time, allowing us to examine the concentration dependence of processing pathways. Our understanding of reaction kinetics is primarily inferred from cross-site analysis (e.g., LINXII; Hall et al. 2009, Mulholland et al. 2009), however these analyses may be confounded by spatial heterogeneity in factors outside concentration which also influence uptake. Within-reach dynamics are difficult to ascertain, primarily because under natural conditions temporal concentration variation is typically limited. This constraint can be alleviated through artificial enrichment (Dodds et al. 2002; Payn et al. 2005), however this requires substantial time and effort and is impractical in certain settings, particularly larger rivers (Ensign and Doyle 2006; Tank et al. 2008). The concentration gradients we capture here (~2 orders of magnitude) are larger than can be produced through artificial dosing of streams of even moderate size, and more critically, we are able to examine kinetics at concentrations below ambient.

6.6.1 Methods

6.6.1.1 Data Collection

Benthic chambers were constructed from 2.54 cm thick transparent Lexan. Chambers were open on the top and bottom, with a footprint of 60 cm x 60 cm and a height of 120 cm. Sides were bolted together using steel angle bars, and edges were sealed using rubber cement. During deployment, the bottom of the chamber was inserted 10-20 cm into the sediments, with the top above the water surface exposed to the atmosphere. This isolated an approximately 0.30 m^3 volume of water within each chamber (average water depth inside chamber was 0.8 m). A conservative tracer (NaCl) was added at the beginning, and sampled at the conclusion of each deployment. A small amount of tracer loss (<10 %) due to expected leakage from diffusive exchange with hyporheic porewaters (Kurz et al. 2015) was acceptable; however, larger tracer loss likely indicated a broken seal and active exchange with the stream; these deployments were discarded. Deployments lasted one week, after which sensor data was downloaded, the chamber was scrubbed with a scouring pad to remove any accumulated algae which might occlude light, and then redeployed in a new location. Comparison of chamber metabolism and NO_3-N processing rates with those measured in the open channel (Reijo et al. in review) suggest chamber measurements strongly scale to the open channel, though chamber artifacts (speculated to be shading and reduced advective exchange) may result in slight underestimation of primary production and denitrification.

Within the chamber, we deployed a Submersible Ultra-violet Nitrate Analyzer (SUNA; Satlantic, Halifax NS). The SUNA is an *in situ* spectrophotometer which measures UV (190-370 nm) light attenuation over a 1 cm pathlength. The manufacturer reports an accuracy of 2 μM and precision of 0.5μM. The sensor was configured in "polled mode", with a burst of ten measurements taken every 15 minutes. The rate of change in NO_3-N concentration (i.e., the profile slope) was multiplied by the chamber water depth (d) to calculate the observed net NO_3-N uptake rate (U_{NET}) in units of mg N m^{-2} d^{-1}.

$$U_{NET} = \frac{\partial [NO_3^-]}{\partial t} \times d \times \frac{1000L}{m^3} \quad (6.1)$$

Using this connotation, negative values of U_{NET} indicate NO_3-N removal, while positive values indicate NO_3-N production. To account for sensor noise, we used a three-point running average of concentration to calculate the derivative.

Each chamber also contained a HOBO dissolved oxygen (DO) sensor (Onset, Bourne MA) and a small, battery powered aquarium pump to gently recirculate water and prevent stratification. The rate of change in DO concentration was corrected for aeration using a k value calculated daily from the slope of nighttime ΔDO versus saturation deficit and multiplied by d to calculate Net Ecosystem Production (NEP) in units g O_2 m^{-2} d^{-1}. The nighttime average value of NEP was assumed equal to Ecosystem Respiration (ER), and daytime increases over this value were ascribed to Gross Primary Production (GPP) (Odum 1956).

$$NEP = \left(\frac{\partial [DO]}{\partial t} - k(DO_{SAT} - [DO])\right) \times d \times \frac{1000L}{m^3} \quad (6.2)$$

$$GPP = \text{NEP} - \text{ER} \tag{6.3}$$

We chose four study sites located in north peninsular Florida; Silver River, Rainbow River, Gum Slough and Alexander Springs Creek. The upper Floridan aquifer which feeds these rivers has become contaminated by nitrogen loading from land uses on the springsheds, and thus they are heavily enriched in NO_3-N. The exception is Alexander Springs which is located in the Ocala National Forest, buffering it from anthropogenic loading. Within each river, we deployed benthic chambers at randomly chosen locations which spanned a gradient of substrate and vegetative cover. At Silver River, Rainbow River and Gum Slough we performed eight deployments each. At Alexander Springs Creek, we performed six deployments, four using ambient initial conditions, and two where we artificially enriched the chamber with NO_3-N.

6.6.1.2 Modeling

We developed a series of mechanistic models of net NO_3-N uptake with increasing levels of complexity. The simplest possible model would be a single parameter model where uptake is constant (zero-order kinetics). In a closed system such as a benthic chamber this would result in linearly declining concentration profiles which ultimately intersect zero producing "negative" concentrations, a physical impossibility. For our initial model, net NO_3-N uptake (U_{model}) was modeled as a single process which was a power function of concentration with a rate constant k and an exponent n.

$$U_{model} = -k[NO_3^-]^n \tag{6.4}$$

The value of the exponent n was allowed to freely vary. We hypothesized that it would converge on a value $0<n<1$ suggesting efficiency loss (EL) kinetics. We note a value $n>1$ is also a possibility, suggesting higher than first-order kinetics, however to our knowledge this has not been reported in the literature. We believe values $n<1$ would likely be the result of ancillary factors co-varying over time with concentration, rather than concentration directly; for example, inhibition of sunlight from algal accumulation on the Lexan or depletion of DOC within the chamber. Thus we constrained our model exponents to values less than or equal to one.

Our next model introduced diel variation by coupling NO_3-N uptake with GPP. In this model, the parameter k is a stoichiometric ratio of autotrophic assimilation. This model inherently assumes that U_{NET} is solely a function of autotrophic assimilation (or that remaining non-autotrophic pathways is always zero), resulting in net uptake rates of zero when GPP is not occurring.

$$U_{model} = -k\text{GPP} \tag{6.5}$$

We next partitioned net uptake into assimilatory (U_A) and dissimilatory (U_D) pathways (Heffernan and Cohen 2010). This model is a combination of the first two models, with assimilatory uptake modeled as a function of k_A and GPP, while dissimilatory uptake is a power function of NO_3-N concentration with coefficient k_D and exponent n_D. This model allows for a concentration-dependent dissimilatory uptake baseline (U_D) on top of which U_A creates diel variation.

$$U_{model} = U_A + U_D \tag{6.6}$$

$$U_{model} = -k_A GPP - k_D[NO_3^-]^{n_D} \quad (6.7)$$

Until this point, all models assume stoichiometric coupling of U_A with primary production. Effects on the magnitude of U_A as a result of NO_3-N concentration decline occur indirectly, vis-à-vis declining primary production (i.e., nutrient limitation). However, it is possible that U_A may decline with concentration depletion while GPP does not. This may occur because autotroph uptake stoichiometry is plastic, or may switch to an alternative source of N, for example NH_4^+. Thus, we modified the U_A term such that it was also concentration dependent. Additionally, U_A may not be temporally coupled with primary production. Hysteresis between U_A versus GPP, suggestive of a temporal lag has been observed in these systems (Heffernan and Cohen 2010, Kurz et al. 2014). Thus, the last model relaxes the assumption of stoichiometric and temporal coupling of U_A with GPP. U_A is modeled as a power function of NO_3-N concentration and a generic daily half sine wave *hsin(t,τ)*. This half sign wave has an amplitude of one, a frequency of 24 h and a phase offset τ (t and τ in hrs). A positive value of τ indicates a peak lagging noon, while a negative value indicates a peak preceding noon.

$$U_{model} = -k_A[NO_3^-]^{n_A} hsin(t,\tau) \ -k_D[NO_3^-]^{n_D} \quad (6.8)$$

$$hsin(t,\tau) = \begin{Bmatrix} 0 & if\ t-\tau < 6 \\ \sin\left(\left(\frac{2\pi}{24}\right)t - \tau - 6\right) & if\ 6 \le t-\tau \le 18 \\ 0 & if\ t-\tau > 18 \end{Bmatrix} \quad (6.9)$$

Note that all models contain only negative removal terms. Potential NO_3-N production pathways exist, namely nitrification. Our intent was to include a positive nitrification term; however, because of the dynamic between removal through U_D and production through nitrification, this class of model frequently converged on equi-final and/or implausible solutions (removal and production rates which were roughly balanced, but each exceeded maximum values reported in the literature by orders of magnitude). This model limitation, its effect on inferred process rates, and potential methods of overcoming it are important inferences.

By minimizing the sum of squared errors (SSE) between modeled and observed U_{NET} in the benthic chambers using a Generalized Reduced Gradient algorithm implemented using the Solver function in Microsoft Excel, we obtained the optimal values of unknown parameters for each model. We evaluated the Akaike Information Criterion (AIC) to determine the best model for each observed profile based on the number of observations, number of model parameters and SSE. Using the ratio of SSE to Total Sum of Squares (TSS), we also calculated the coefficient of determination (R^2) as a metric of the observed variance captured by each model.

After determining the most parsimonious model which satisfactorily described the observed behavior, we created histograms of the distributions of model parameters, specifically the model exponents, n_A and n_D. This allowed us to examine the reaction kinetics of assimilatory and dissimilatory uptake pathways. We also plotted daily GPP, U_A and U_D versus NO_3-N concentration for each deployment to better visualize how these reaction rates chance in response to concentration depletion. Finally, by converting GPP and U_A to molar units and assuming Net

Primary Production = ½GPP (Hall and Tank 2003; Hall and Beaulieu 2013) we estimated an ecosystem autotrophic uptake C:N ratio. We compared this with the tissue stoichiometry of the dominant autotrophs present in these streams, which on a mol-C:mol-N basis ranged from roughly 8:1 to 18:1 (Zimba et al. 1993; Nifong et al. 2014), and inferred how uptake C:N ratios changed in response to NO_3-N depletion over the course of the deployments.

6.6.2 Results

NO_3-N profiles from Silver River, Rainbow River and Gum Slough exhibited declining concentrations with time (Figure 6.103a-c), suggesting net removal of NO_3-N at all concentrations. While all of the profiles declined hyperbolically, the degree of inflection varied markedly; some profiles saw NO_3-N depleted by half in only a day or two, while others required an entire week. In addition to the global downward curvilinear trend, all profiles exhibited varying degrees of diel variation in profile slope, with daytime slopes generally steeper than nighttime slopes. The hyperbolic nature of the concentration profiles was clearly reflected in U_{NET} calculated from profile slopes (Figure 6.103e-h), which declined with time. Diel variation in U_{NET} was also readily apparent, with generally higher rates in the day relative to the night.

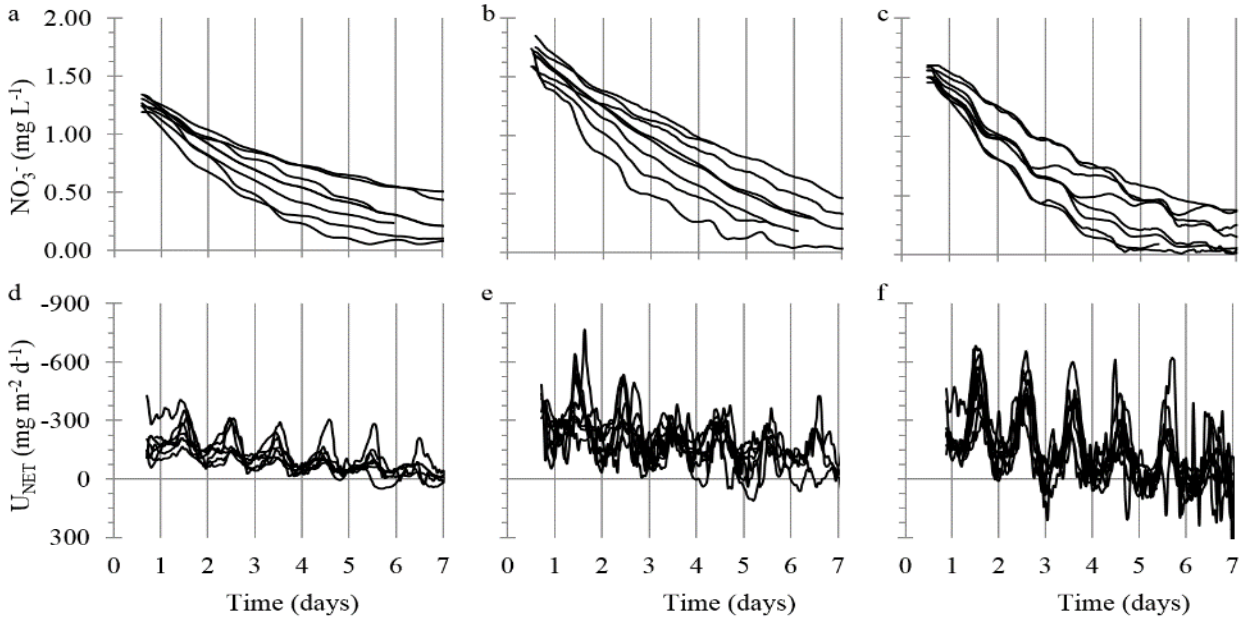

Figure 6.103. Benthic chamber NO_3-N profiles for Silver River (a), Rainbow River (b) and Gum Slough (c) all exhibit hyperbolic declines and diel variation. Uptake rates derived from profile slopes (d, e and f respectively) decline with time and exhibit diel peaks consistent with solar forcing of autotrophic assimilation.

The enriched Alexander Creek deployments exhibited NO_3-N profiles similar to those observed in the other study sites (Figure 6.104b), while the un-enriched deployments exhibited very little net change in NO_3-N over the deployments (Figure 6.104a). More interestingly, the diel variation in U_{NET} observed in Alexander Creek was markedly different than the other sites. In un-enriched deployments (Figure 6.104c), as well as after NO_3-N was depleted back to ambient concentrations in the enriched deployments (Figure 6.104d), daytime slopes were positive indicating net daytime production of NO_3-N. Because the models contain only negative terms,

they cannot fit positive U_{NET}. Secondly, the models ascribe diel variation solely to U_A and fitting the observed unenriched

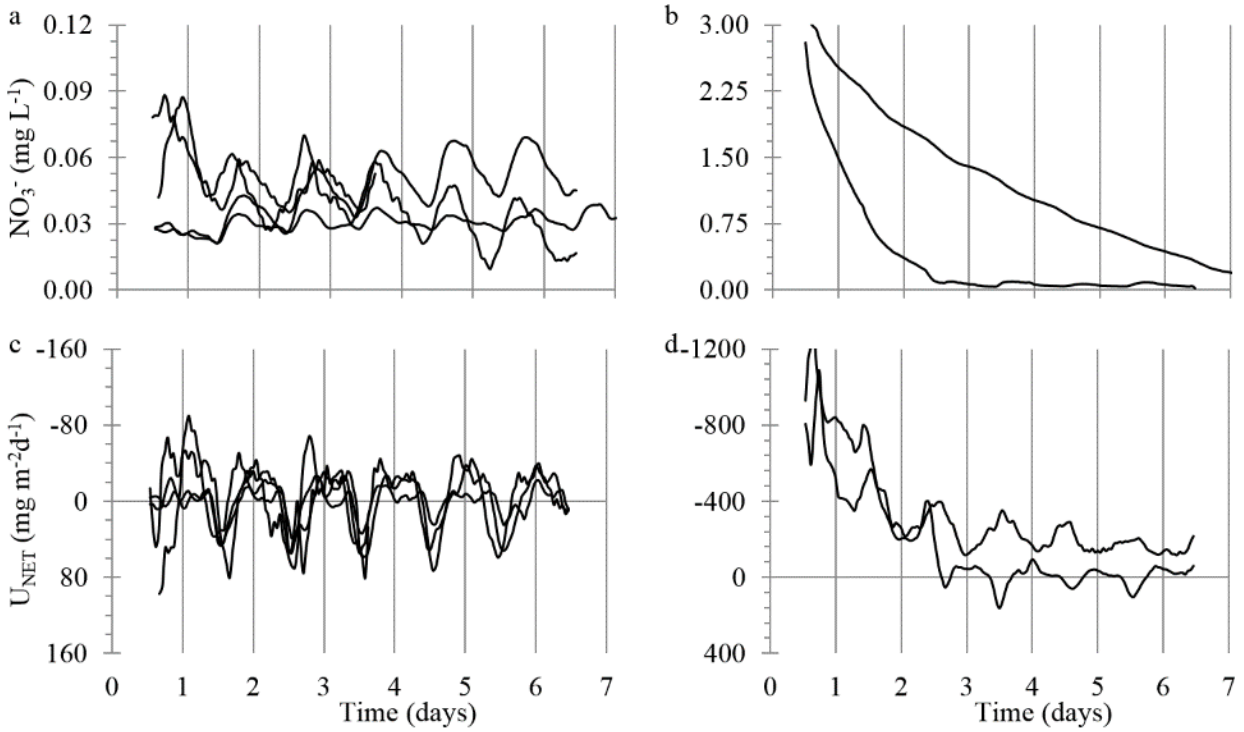

Figure 6.104. Benthic chamber NO_3-N profiles for Alexander Creek for un-enriched deployments (a) and enriched deployments (b). Timing of diel variation in U_{NET} for un-enriched deployments (c), and after NO_3-N depletion back to ambient in enriched deployments (d), is opposite observed in the other sites, with net daytime NO_3-N production, indicating temporal decoupling of U_A from GPP in this low- NO_3-N site, and potentially daytime DO stimulation of nitrification.

Alexander profiles would suggest autotrophic assimilation occurs during the night, something we find highly implausible. This inability to fit the observed profiles necessitated excluding the un-enriched Alexander Creek deployments from our subsequent analysis of reaction kinetics. While it would have been simpler and cleaner for us to not even present data from Alexander Creek in this manuscript, we believe the factors which resulted in the inability of the model to fit the observed profiles to be highly informative, and consistent with previous studies in this low N system (Cohen et al. 2013b).

Increasing model complexity almost universally resulted in a better model, with improved R^2 and AIC (Table 6.15). Models with a single processing pathway (Equations 6.4 and 6.5) were clearly insufficient to explain the structure of observed U_{NET} signals (Figure 6.105a and b). While partitioned pathway models with U_A coupled with GPP (Equation 6.7) had significant explanatory power (median $R^2 = 0.65$), temporally de-coupling U_A from GPP and allowing the magnitude to respond to NO_3-N concentration depletion (Equation 6.8) universally improves model fit (median $R^2 = 0.79$). Including additional parameters was always justified based on the AIC.

In nearly every model deployment $n_A < n_D$, suggesting U_D is more concentration dependent. For n_A the median was 0.43, while the median value of n_D was 0.93, substantially higher than the value (0.50) reported for denitrification in the LINXII experiment (Mulholland et al. 2009). Histograms reveal a roughly normal distribution of n_A, while n_D is heavily skewed to larger

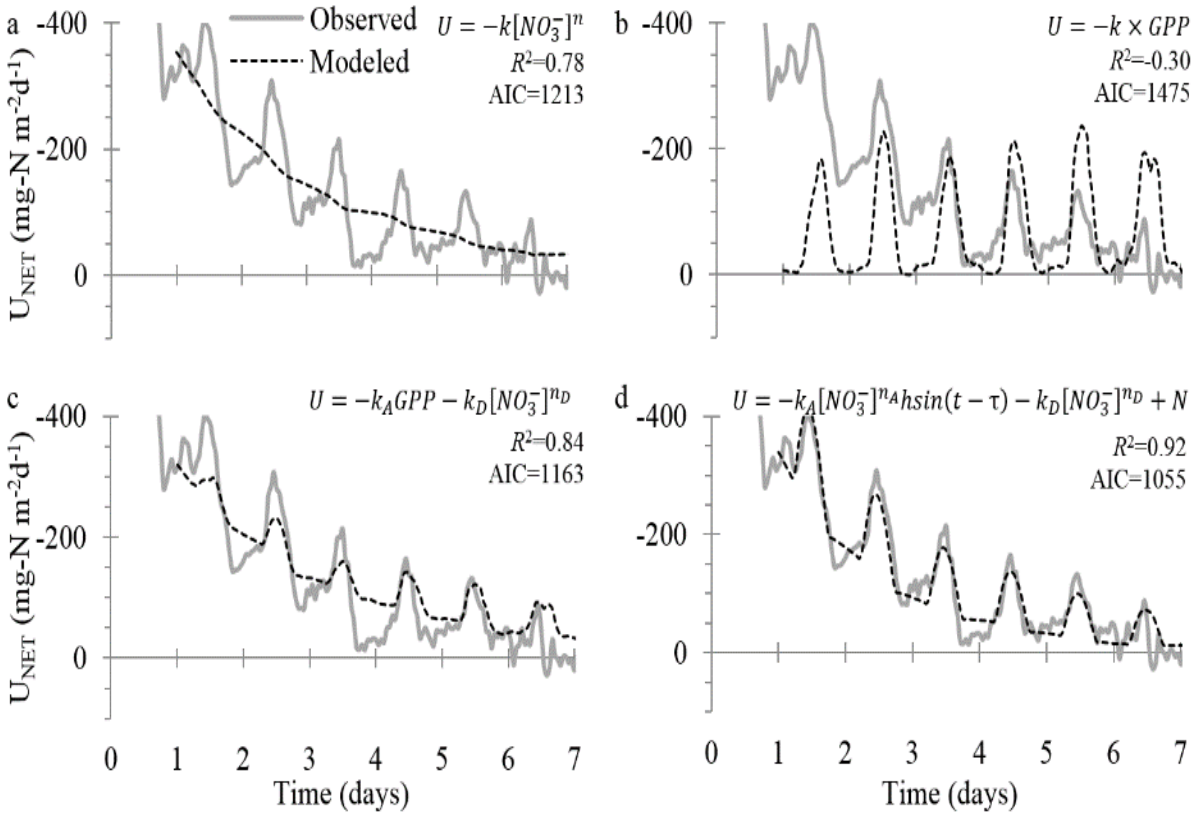

Figure 6.105. Silver River 15-22 October 2015 deployment showing various configurations of models (dashed black lines) fit to the observed U_{NET} profile (gray).

values (Figure 6.106a and b respectively). Overall, median τ (Figure 6.106c) was 1.2 h suggesting in general U_A may slightly lag GPP, though this appeared to consistently vary by site; Silver River leading, Gum Slough lagging, Rainbow River evenly distributed and Alexander Springs Creek with only two deployments assessed had too few samples to make any reasonable judgment.

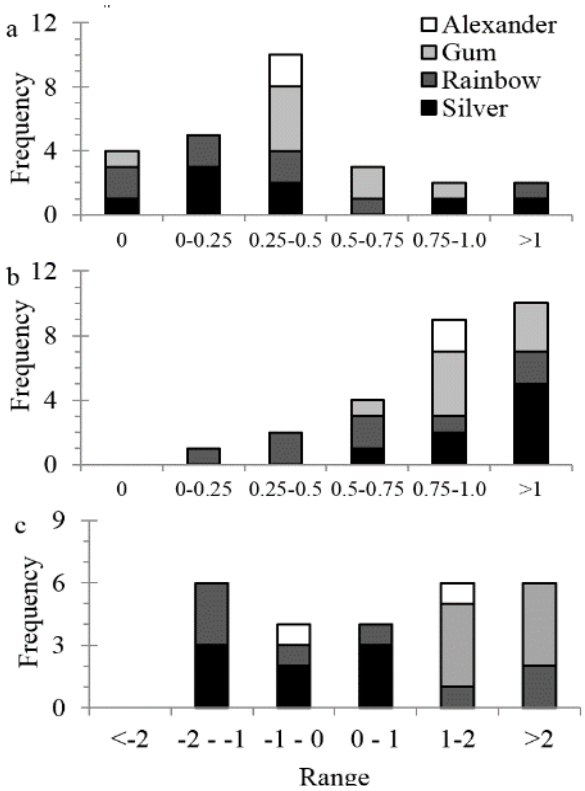

Figure 6.106. Distribution of n_A (a) and n_D (b) suggests U_A and U_D both follow efficiency loss (EL) kinetics however U_D is more concentration dependent. Distribution of τ (c) suggests in general U_A lags GPP, with a potential study site effect.

We observed no effect of NO_3-N depletion on rates of measured GPP (Figure 6.107a), consistent with previous applications of benthic chambers in these systems (Reijo et al. in review) and suggesting NO_3-N is not a limiting nutrient even at low concentrations. While U_A generally declined with concentration (Figures 6.107c), it was much less pronounced than U_D (Figures 6.107d) consistent with U_D being the more concentration dependent pathway (Reijo et al. in review). As GPP remained relatively constant and U_A declined, the inferred autotrophic uptake C:N ratios increased as NO_3-N became depleted over the course of the deployments (Figure 6.107b).

Table 6.15. Summary of R^2 values for various models (Equations. 6.4 – 6.8) fitted to benthic chamber nitrate concentrations over time (e.g., Figure 6.105). Each deployment represents a different location in the listed river (Silver, Gum, Rainbow, Alexander).

Deployment	Equ. 6.4	Equ. 6.5	Equ. 6.7	Equ. 6.8
Silver 1	0.83	-0.73	0.86	0.91
Silver 2	0.03	0.07	0.83	0.89
Silver 3	0.78	-0.30	0.84	0.92
Silver 4	0.62	-0.37	0.65	0.83
Silver 5	0.83	-2.18	0.88	0.91
Silver 6	0.85	-1.46	0.86	0.91
Silver 7	0.63	-0.14	0.76	0.80
Silver 8	0.21	-0.39	0.61	0.65
Rainbow 1	0.46	-2.70	0.62	0.78
Rainbow 2	0.70	-2.37	0.79	0.80
Rainbow 3	0.28	-8.86	0.50	0.58
Rainbow 4	0.36	-0.03	0.65	0.69
Rainbow 5	0.27	-0.10	0.44	0.79
Rainbow 6	0.12	-2.64	0.27	0.35
Rainbow 7	0.05	-0.46	0.43	0.45
Rainbow 8	0.28	-0.36	0.62	0.75
Gum 1	0.22	0.30	0.68	0.87
Gum 2	0.48	-0.09	0.57	0.70
Gum 3	0.04	0.36	0.54	0.71
Gum 4	0.16	0.31	0.63	0.67
Gum 5	0.28	0.45	0.72	0.90
Gum 6	0.11	0.25	0.39	0.39
Gum 7	0.23	0.49	0.58	0.66
Gum 8	0.33	0.46	0.74	0.92
Alexander 5*	0.92	-0.41	0.95	0.97
Alexander 6*	0.50	-1.74	0.74	0.85

* enriched deployments

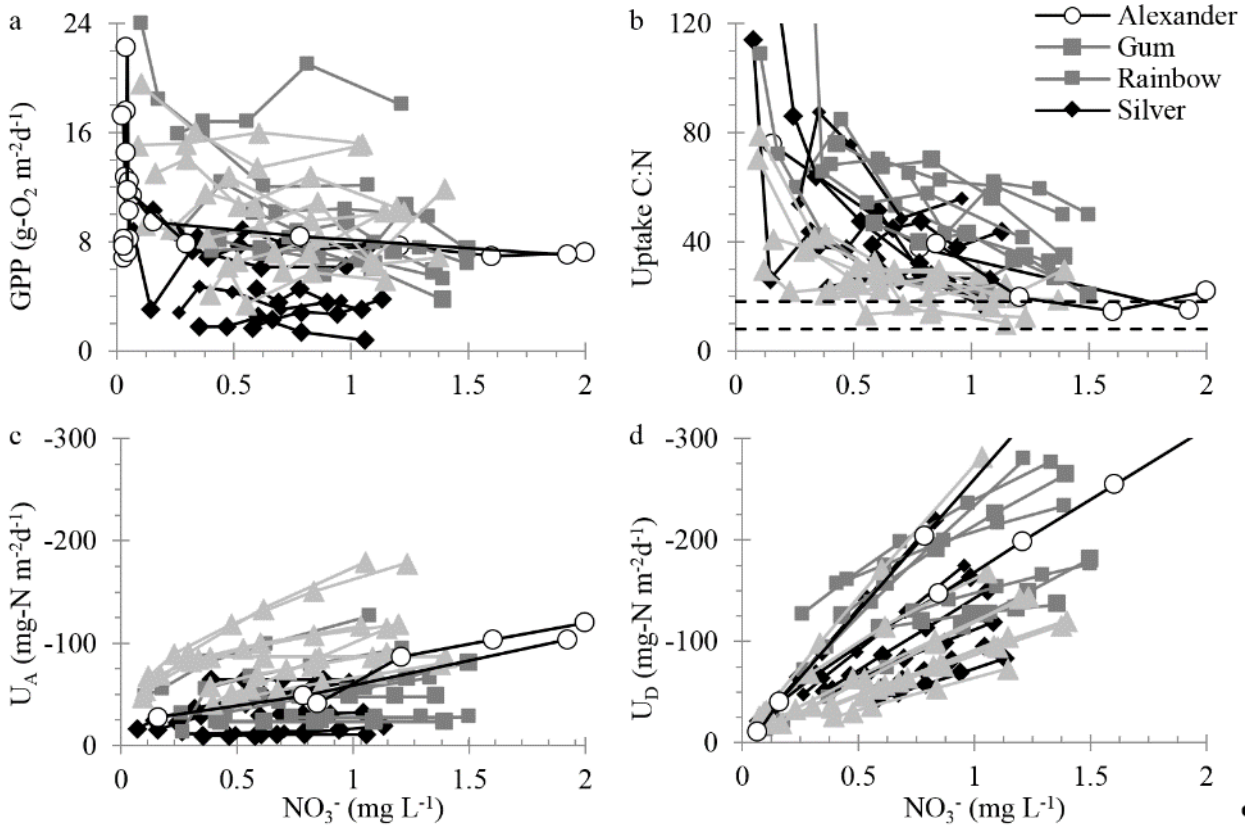

Figure 6.107. GPP (a) did not respond to NO_3-N depletion over the deployments. U_A (c) and U_D (d) both declined with NO_3-N depletion, with a larger effect on the latter. Inferred autotrophic uptake C:N (b) was often greater than the range observed in tissue (dashed lines) even under ambient conditions, and increased with NO_3-N depletion, suggesting a decoupling of U_A from GPP and/or reliance on an alternative N source.

6.6.3 Discussion

6.6.3.1 Model Limitations and Future Improvement

We acknowledge the shortcomings of our model and recognize it to be an oversimplification of the aquatic NO_3-N cycle. However even with this simple model we were able to explain a substantial fraction of observed variation (mean of 75 % and >90 % in many deployments). Furthermore, the inability of the model to fit all observed variation proved informative. It suggested that additional N processing pathways are likely to be occurring and the pathways we did model may be temporally varying in response to drivers other than NO_3-N concentration.

We spent considerable time experimenting with additional model terms, specifically those allowing NO_3-N production pathways, as well as temporal variation other than U_A. For example we experimented with fitting multiple overlapping diel sine and half-sine waves of unknown phase and amplitude. While doing so resulted in improved model fits, it also almost universally resulted in non-unique model solutions (i.e., several parameter values fit the observations equally well, making inferred rates poorly identified). Furthermore this mathematical versus mechanistic approach lacked clarity as to the physical processes represented. Thus, the models chosen were

best for parameter identifiability and meaningful inferences. As it was, our model fitting was based on only two solute signals: NO_3-N and DO (and the coupled approach resulted in a poorer fit).

Table 6.16. Summary of optimized model parameters. n_A – assimilatory uptake kinetic exponent, τ – assimilatory offset from solar noon (hrs), n_D – dissimilatory uptake kinetic exponent. Each deployment was in a different geographic location in each river.

Deployment	n_A	n_D	τ
Silver 1	0.22	1.00	-1.50
Silver 2	0.00	0.81	0.64
Silver 3	0.78	1.00	-0.49
Silver 4	0.46	0.79	-1.84
Silver 5	0.28	0.65	-0.71
Silver 6	0.07	1.00	-1.82
Silver 7	1.00	1.00	0.26
Silver 8	0.16	1.00	0.64
Rainbow 1	0.67	0.50	-1.76
Rainbow 2	0.00	0.64	-1.44
Rainbow 3	0.00	0.35	-1.41
Rainbow 4	0.43	0.91	2.75
Rainbow 5	0.43	1.00	-0.12
Rainbow 6	0.00	0.43	2.72
Rainbow 7	0.00	0.23	1.19
Rainbow 8	1.00	1.00	0.43
Gum 1	0.26	1.00	2.15
Gum 2	0.28	0.93	1.47
Gum 3	0.00	0.90	1.94
Gum 4	0.55	0.94	2.35
Gum 5	0.41	0.87	2.29
Gum 6	0.42	1.00	1.73
Gum 7	0.95	1.00	2.42
Gum 8	0.53	0.70	1.71
Alexander 5*	0.26	0.89	-0.94
Alexander 6*	0.49	0.88	1.63

* enriched deployments

We note that NO_3-N processing pathways are stoichiometrically coupled with other N species, for example production of N_2 through denitrification or consumption of NH_4^+ through nitrification. Furthermore, these pathways are likely to have different $^{15}N/^{14}N$ fractionation rates. At present, *in situ* sensors do not exist for these other species, however auto-samplers could be used to collect high-frequency grab samples (Cohen et al. 2012). Having signals of multiple N species to fit would likely address and improve parameter identifiability of more complex models.

6.6.3.1.1 Fine-scale Profile Geometry

The use of benthic chambers to isolate localized processing from hydraulic artifacts has the potential to reveal subtleties of processing signals which might otherwise be obscured by upstream delivery or hydraulic dispersion. For example, uptake rates inferred from open channel NO_3-N signals collected in similar settings using the same sensors (Heffernan and Cohen 2010) exhibit roughly sinusoidal diel variation. However, the chamber profiles reveal that generally the diel variation in uptake rates is better modeled using a half-sine function (Figure 6.108) evocative of solar insolation which is presumably driving assimilatory uptake vis-à-vis primary production. The more sinusoidal signals observed in the open channel are likely the result of hydraulic dispersion of this half-sine wave (Hensley and Cohen 2016).

The chambers also revealed slight offsets in the timing of maximum daily U_{NET} relative to maximum daily GPP circa solar noon. A slight lag had also been noted before (Heffernan and Cohen 2010; Kurz et al. 2014), but later interpreted to be potentially hydraulic (Hensley and Cohen 2016). Yet we still observe it in the chambers, where hydraulic transport effects have been removed. This may be a physiological offset between autotroph carbon fixation and nitrogen uptake, as has been observed for phosphorus (Cohen et al. 2013). However, another possibility is that diel variation in U_{NET} does not exclusively represent U_A. Variation in the amplitude and timing of other pathways relative to the timing and amplitude of U_A has the potential to shift the timing of the combined U_{NET} signal forward or backward in time. Afternoon accumulation of DO from primary production may stimulate nitrification (an aerobic process) while also potentially inhibiting denitrification (an anaerobic process). This decline in net dissimilatory removal (or potentially even net production) would offset U_A producing a U_{NET} signal which peaked earlier than solar noon. Alternatively, accumulation of DOC or increased temperatures may stimulate afternoon denitrification (or heterotrophic uptake), producing a U_{NET} signal which peaks later than solar noon.

Finally, nighttime U_{NET}, while sloping downwards night to night over the course of the deployment in response to NO_3-N depletion, often slopes upward over the course of individual nights (Figure 6.108). This raises several intriguing possibilities. One is that NO_3-N removal through U_D is becoming stimulated as the DO accumulated over the course of the day through primary production is consumed during the night through respiration (denitrification is an anaerobic process). Alternatively, production of NO_3-N through nitrification (an aerobic process) is inhibited via nighttime DO depletion. In either case, it further supports the conclusion that pathways other than U_A are also time varying.

6.6.3.1.2 Uptake Kinetics and Nutrient Limitation

The methodology presented here substantially advances our ability to assess NO_3-N uptake kinetics across a broad range of concentrations. It can be performed passively, using natural depletion to produce concentrations below ambient. Alternatively, chambers can also be dosed to observe uptake dynamics at enriched concentrations, and this can be performed infinitely easier than dosing an entire stream. The ability to assess uptake kinetics within a site is critical because it removes the influence of ancillary factors when comparing across sites. The method applies to even finer scales, allowing assessment of how within site variability in factors such as vegetative cover or substrate may influence uptake dynamics (Reijo et al. in review).

While generally following efficiency loss (EL) kinetics, we noted instances of U_A exhibiting zero-order kinetics, a situation in which NO_3-N would ultimately become completely depleted without some resupply mechanism such as nitrification. In many deployments, U_A remained high despite depletion to very low concentrations, and many NO_3-N profiles appeared to converge on decidedly non-zero asymptotes. This suggests some concentration at which removal through U_A and U_D are balanced by resupply via nitrification. A deployment from Silver River where the chamber was left in place with sensors recording for nearly three weeks is informative. We observe (Figure 6.108a) rapid depletion during the first week of the deployment, the NO_3-N profile remains relatively stable, diurnally varying around a concentration of 0.1 mg N L^{-1}. In fact, the magnitude of diel variation actually increases over the deployment. Net removal occurs during

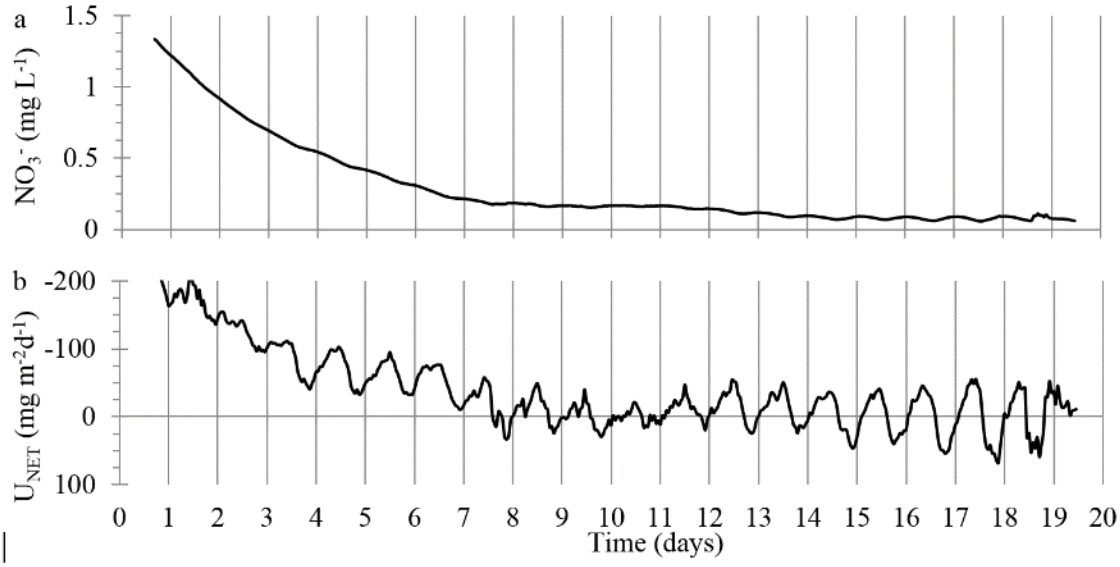

Figure 6.108. NO_3-N profile (a) and U_{NET} (b) from 20 day Silver River deployment. Note following rapid NO_3-N depletion, concentration stabilizes around 0.1 mg N L^{-1} at which net NO_3-N removal and production pathways are roughly balanced over 24 h.

the day, peaking around an hour before noon, and net production occurs during the night, peaking around an hour before midnight (Figure 6.108b), but these process are roughly balanced such that no net change in concentration occurs over 24 hours.

The un-enriched Alexander Creek profiles (Figure 6.108a) also exhibit no net change in concentration, suggesting removal and production pathways are roughly in balance. The phase of the U_{NET} signal has been shifted nearly 12 hours, with maximum U_{NET} occurring at night and net production occurring during the day, consistent with previous observations of nitrate dynamics in Alexander Springs Creek (Cohen et al. 2013b). At these low NO_3-N concentrations U_A may have become temporally de-coupled from primary production such that assimilation occurs continuously (Appling and Heffernan 2014), or an alternative N source such as NH_4^+ is being used (Peterson et al. 2001; Kemp and Dodds 2002). We believe the likely explanation for the observed diel U_{NET} variation, is daytime production of DO through photosynthesis stimulating NO_3-N production through nitrification (Kemp and Dodds 2002; Gammons et al. 2010), or

potentially inhibiting NO_3-N removal through denitrification (Christensen et al. 1990; Pina-Ochoa and Alvarez-Cobelas 2006). It is possible that increased daytime U_A is still occurring in these deployments while being counteracted by even larger daytime increases in nitrification. We reject this based on two lines of reasoning, the first being we have nothing to suggest diel variation in nitrification in Alexander Creek is any larger than in the other sites. Even more critical are the results of the enriched Alexander Creek deployments. If daytime U_A were already occurring, and nitrification rates are un-inhibited by NO_3-N enrichment (and literature suggest they may *increase* [Bernhardt et al. 2002]), then ascribing subsequent increases in daytime U_{NET} observed in the enriched deployments to addition U_A would result in far greater total U_A than could be explained by autotroph C:N.

Addition of NO_3-N to the chambers in Alexander Springs Creek stimulates both U_{NET} and U_A. Average daily U_{NET} and U_A on the initial days of the enriched deployments are comparable to respective rates observed in the other study sites which have similar ambient NO_3-N concentrations (Figures 6.107c and d). In addition to U_{NET} peaking concurrent with maximum GPP at solar noon, inferred assimilatory uptake C:N ratios at the initiation of the enriched deployments are concordant with autotroph tissue stoichiometry (Zimba et al. 1993; Nifong et al. 2014), suggesting a potential re-coupling of U_A with GPP. We note however that if diel variation in nitrification remains the same as in the control deployments, the magnitude of U_A inferred may actually be an underestimation of U_A (Hensley and Cohen 2016); additional assimilation is needed to balance increased daytime production of NO_3-N. This may explain why across previous studies (Heffernan and Cohen 2010; Cohen et al. 2014; Hensley et al. 2015), as well as here, we generally observe uptake C:N ratios which are slightly too high.

The observation that GPP remained constant over the course of the deployments while NO_3-N declined suggests that NO_3-N is not a limiting nutrient of autotrophic growth in these systems. At Alexander Springs Creek GPP both in the open channel and within the chambers is quite high despite it being a very low NO_3-N system. Enrichment by two orders of magnitude, while increasing NO_3-N uptake rates, had no effect on GPP. In Silver River, a system with high NO_3-N concentrations, we observed no reduction in GPP even over several weeks of depleted NO_3-N (Figure 6.108). Constant GPP and decreasing U_A may suggest autotrophic uptake C:N ratios must be increasing (Figure 6.107b). As NO_3-N becomes depleted, autotrophs may modify their C:N uptake stoichiometry by internal recycling of N and building lower N tissue. However, analysis suggests tissue stoichiometry to be largely homeostatic (Nifong et al. 2014). It's more plausible the actual stoichiometry of autotrophic uptake does not change, just our inference based on our assumptions. First, as water column NO_3-N becomes depleted, rooted macrophytes may obtain NO_3-N from hyporheic pore waters via their roots, which would not show up in the water column U_{NET} signal. We consider this possibility extremely unlikely as anoxic porewaters have likely been denitrified of NO_3-N (Kurz et al. 2015; Section 8 of this CRISPS report), and this source would not be available for non-rooted autotrophs such as benthic and water column algae, which may account for a substantial fraction of GPP in these systems [see in situ SAV growth: Section 6.7, this report]. Second, we are only measuring NO_3-N. As this source becomes depleted, autotrophs may switch to an alternative source of N, namely NH_4^+. In fact alternative N sources may potentially be in use at ambient concentrations, as evident by the higher than expected C:N ratios observed even at the beginning of many of the deployments (Figure 6.107b). While measured NH_4^+ in the water column is typically at detection limits in these systems

(Heffernan and Cohen 2010), this does not preclude and may even suggest it being rapidly assimilated. Finally, our estimates of U_A are based on diel variation. At low concentrations autotrophic assimilation may become decoupled from primary production such that N uptake is occurring continuously and not on a diel basis. Additionally, temporal variation in other processing pathways may influence the net amplitude of the diel signal.

6.6.4 Conclusion

Here we demonstrated a method of removing delivery and transport influence and isolating NO_3-N processing signals over a small, homogenous benthic footprint. The large concentration gradients achieved through natural depletion provide a passive method of assessing site-specific uptake kinetics. U_{NET}, as well as the constituent pathways U_D and U_A clearly followed E.L. kinetics. NO_3-N concentrations were clearly not a control on the magnitude of GPP. This potentially suggests a temporal de-coupling of assimilation from GPP (i.e., our method of using diel variation to measure U_A becomes inadequate), or a switch to an N source other than NO_3-N as concentrations become depleted. The results reinforced the idea that the aquatic nitrogen cycle is complex, composed of multiple overlapping and temporally varying removal and production pathways.

6.7 *IN SITU* VEGETATION GROWTH EXPERIMENTS

6.7.1 Background

Submerged aquatic vegetation (SAV) is an important biological, chemical, and physical component of many low relief lotic systems (Butcher 1933; Carpenter and Lodge 1986; Canfield and Hoyer 1988; Hoyer et al. 2004), providing refuge and habitat (Persson and Crowder 1998; Jeppesen et al. 1998), influencing water column chemistry (Carpenter 1980; Wetzel and Sondergaard 1998; Caraco and Cole 2002), and stabilizing sediments against resuspension and erosion (Barko and James 1998). The biotic integrity and health of aquatic ecosystems are often indicated by the spatial distribution and abundance of SAV (Dennison et al. 1993). SAV growth, composition, and density are controlled by a multitude of environmental factors, including light regime, nutrients, competition with algae, grazer interactions, hydraulics, and substrate characteristics. Understanding these controls is necessary to manage and restore healthy river ecosystems.

North Florida has the highest density of first-magnitude springs ($Q > 100$ ft^3 s^{-1}) in the world due to the highly transmissive karstic Floridan Aquifer (Scott et al. 2004). Low discharge variability, high water clarity, and chemical and thermal stability in North Florida's spring ecosystems result in dense and productive SAV communities (Odum 1957a; Canfield and Hoyer 1988; Duarte and Canfield 1990). In Florida's springs, as elsewhere, these SAV communities are the basis of the food-web, and variation in SAV health has important implications for the entire food web in aquatic ecosystems (Crowder and Cooper 1982; Camp et al. 2014).

Freshwater ecosystems are under increasing pressure from human development, including anthropogenic nutrient enrichment, recreation, pollutants, land use, and flow alterations within watersheds (Smith 2003; Dudgeon et al. 2006; Quinlan et al. 2008). As a result of increased landscape N loading (Katz et al. 2005), the groundwater emerging in many springs in Florida is significantly elevated in NO_3-N concentration (Jones et al. 1996; Katz 2004; Albertin et al.

2012). Filamentous macroalgal abundance has also increased in many of Florida's spring-fed rivers over recent decades (Stevenson et al. 2004). Corresponding declines in SAV growth and vigor in many of Florida's spring-fed rivers are an alarming development that remains poorly understood, and that has important and potentially long-lasting ecological implications. We note, however, that SAV beds in both Silver and Alexander remain relatively healthy, particularly downstream of the more impacted headspring areas. Indeed, increases in SAV density are putatively responsible for changing river bed hydraulic resistance and thus changing stage-discharge relationships.

Long-term data quantifying the relationship between SAV productivity and environmental conditions is inadequate, impeding the ability to recognize the predominant physical, chemical, and biological factors that control ecosystem structure and function. In particular, it remains unclear whether management efforts to reduce nitrogen concentrations are sufficient to restore SAV communities or whether other environmental drivers need to be explicitly considered. Indeed, it remains somewhat unclear whether SAV communities require restoration in Silver River or downstream of the headspring in Alexander Springs Creek; our survey measurements and observed growth data, along with measurements by other researchers, support the general conclusion that SAV beds are relatively healthy, at least in terms of abundance and density, vis-à-vis historical conditions wherein SAV beds were considerably less dense (e.g., Odum 1957).

6.7.1.1 Light

Light levels are an important factor in the distribution, abundance, and productivity of SAV (Duarte 1991; Dennison et al. 1993). Light requirements of submerged vascular plants for photosynthesis, growth, and reproduction are high (Dennison et al. 1993; Kirk 1994). While the upper limit of SAV growth can be regulated by physical conditions (turbulence, sediment, temperature, UV radiation), the maximum depth for SAV growth in marine and freshwater environments is controlled by light attenuation (Canfield et al. 1985; Duarte 1991; Dennison et al. 1993; Duarte 2002; Moore and Jarvis 2008). Light levels at the maximum depth of SAV survival range from 10-35% of stream surface irradiance (Batiuk et al. 2000; Kemp et al. 2004), suggesting that other factors attenuate light (e.g., forest canopy and water column clarity). In particular, submersed light in the blue wavelength is critical for SAV photosynthesis (Kirk 1994; Szafraniec 2014). Indeed, *Sagittaria kurziana* metabolism appears to be blue light limited in the lower Rainbow River and Weeki Wachee River (Szafraniec 2014), yielding a minimum blue light requirement of 38-45% of surface irradiance. Short-term temporal changes in productivity and global declines in SAV abundance (Kemp et al. 1983; Dennison et al. 1993; Stevenson et al. 1993; Quinlan et al. 2008) are associated with fluctuations in turbidity and light attenuation (Carter et al. 1994). Previous studies conducted in spring-fed rivers in Florida indicate light availability is more important than nutrient availability for SAV persistence and survival. This arises because continuous nutrient resupply from groundwater (Odum 1957b; Canfield and Hoyer 1988) is sufficient to satisfy autotroph demand (Nifong 2015). This is consistent with regional results suggesting light markedly influences SAV growth, while N and P did not (Hauxwell et al. 2007).

Dissolved substances, suspended particles, and epiphytic material in the water column intercept a large portion of incident light prior to reaching the SAV canopy (Kirk 1994; Short et al. 1995; Hauxwell et al. 2001; Hauxwell et al. 2003). Dissolved substances and particles absorb light,

increasing light attenuation through the water column (Kirk 1994; Gallegos 1994); particulate material can also scatter light, increasing path length and light attenuation. Particulate absorption and scattering were the overarching factors controlling light abundance in Rainbow and Weeki Wachee spring systems (Szafraniec 2014). In the Lower St. Johns River, colored dissolved organic matter, along with phytoplankton and suspended particulates, strongly contributed to water column light attenuation (Gallegos 2005).

The structure, biomass, and density of the SAV plant canopy can also influence the magnitude of light penetrating the photosynthetic biomass (Titus and Adams 1979; Zimmerman 2003). Canopy formation and leaf elongation are two shade-adaptation mechanisms observed for freshwater SAV species (Barko and Smart 1981; Barko et al. 1982; Vermaat et al. 1997; Middelboe and Markager 1997). Under low-light conditions, canopy-forming species exhibit stem elongation and retain only their uppermost leaves (Goldsborough and Kemp 1988; Maberly 1993). However, low light stress causes SAV to redirect resources away from other vital processes. *Vallisneria americana* allocates energy away from rosette and biomass production, leading to decreased reproduction and total leaf area, in order to promote vertical leaf growth and maximize light capture under reduced light conditions (Barko et al. 1982; Barko et al. 1991; French and Moore 2003). Overall, current literature convincingly suggests that SAV distribution, productivity, and other morphological attributes are highly dependent on light availability regardless of other environmental factors.

6.7.1.2 Nutrients

Understanding the role of nutrients in declining SAV abundance is critically important. Numerous studies suggest both N and P are central to growth regulation of algae and macrophytes (Barko et al. 1988; Maberly et al. 2002; James et al. 2005; Sagario et al. 2005; Dzialowski et al. 2005). Nitrogen enrichment is presumed to impact growth rates, indirectly leading to changes in autotroph composition, and is often implicated in the recent loss of SAV and simultaneous proliferation of filamentous algae in Florida springs (Stevenson et al. 2004). Total nitrogen (TN) flux in springs is dominated by NO_3-N (Cohen 2007), which historically ranged from 0.05 to 0.1 mg N L^{-1}. The current average NO_3-N concentration across all springs exceeds 1 mg N L^{-1} (Strong 2004). Soluble Reactive Phosphate (SRP) has remained relatively constant over time, ranging from 0.02 to 0.07 mg P L^{-1} (Scott et al. 2004). The presumed association between increased NO_3-N and SAV loss is reflected in management efforts and was part of the rationale for the establishment of numeric water quality standards. In Florida, the numeric nutrient criterion for springs is 0.35 mg L^{-1} of nitrate/nitrite-N ($NO_3 + NO_2$) to prevent an imbalance in natural populations of aquatic flora or fauna (Florida Department of Environmental Protection 2012). This imbalance is thought to arise from changes in growth enabled by alleviation of N limitation. While several studies from Florida springs do not support the nitrogen enrichment hypothesis (Heffernan et al. 2010a, Liebowitz et al. 2014, Nifong et al. 2015), nitrogen loading reductions often take precedence over other potential controls of ecosystem condition. Indeed, field studies evaluating the predictions that follow from the N enrichment hypothesis suggest weak or absent relationships between nutrient concentration, macroalgal abundance, and vegetative biomass across numerous spring systems (Canfield and Hoyer 1988; Stevenson et al. 2004; Stevenson et al. 2007). Additional studies highlight a discrepancy between the confinement of dense algal mats near headsprings (within 250 m) and the downstream persistence of elevated NO_3-N concentrations (Kurz et al. 2004; Mattson et al.

2006). The direct toxicity of water column nitrogen on SAV species has also been proposed as a potential cause of SAV stress (Burkholder et al. 1992; Boedeltje et al 2005). Additional evidence about the role of N enrichment on SAV growth or inhibition is important information to aid decision-making about the sufficiency of N reductions for ecological restoration.

6.7.1.3 Algae

Algae are an important component of aquatic ecosystems, influencing dissolved oxygen, nutrient dynamics, and energy transfer to higher trophic levels. Excessive levels of NO_3-N have been implicated in observed shifts in primary producer community structure via rapid utilization of excess nutrients by phytoplankton and epiphytic algae, thus stimulating growth (Duarte 1995; Borchardt 1996; Valiela et al. 1997), though the evidence for N effects of algal abundance and growth in springs are limited (Heffernan et al. 2010). The competitive interaction between SAV and algae was highlighted in several springs studies, identifying a negative correlation between SAV and algal abundance (Hauxwell et al. 2004; Jacoby et al. 2007). The enhancement of epiphytic algae may cause SAV to become light limited, and the decomposition of smothered SAV biomass may amplify nutrient concentrations (Borum 1985; Burkholder et al. 1992; Van den Berg et al. 1999). In high nitrogen estuaries, Hauxwell et al. (2004) demonstrated that eelgrass abundance declined substantially due to severe light limitation and biogeochemical alterations, specifically lowered redox and potentially toxic NH_4-N concentrations imposed by algal overgrowth. In addition to light attenuation by algae (Sand-Jensen and Borum 1984; Twilley et al. 1985; Dennison et al. 1993), the growth of epiphytes on the photosynthetic surface of SAV reduces gas exchange to the leaf surface (Sand-Jensen 1977), serves as a structure for the attachment of fouling materials (Kemp et al. 2004), and increases hydraulic drag on leaves (Dunn et al. 2008), potentially causing uprooting in higher flow conditions.

6.7.1.4 Dissolved Oxygen and Grazers

Where algal competition is an important control on SAV growth and composition, controls on algal growth and abundance become central factors in understanding SAV decline. While there is considerable evidence to link enhanced algal growth rates to nutrient enrichment across many aquatic systems, another general contributing factor is the decline of algal grazers. For springs in particular, Liebowitz et al. (2014) assert that dissolved oxygen has a significant indirect effect by controlling grazer abundance and/or activity. Dissolved oxygen has decreased in many Florida springs over recent decades (Heffernan et al. 2010), potentially limiting the ability of grazers to suppress algal overgrowth. The trophic structure of springs has been altered such that algal dominance is favored via top-down control by invertebrate grazers through indirect effects of dissolved oxygen (Liebowitz et al. 2014). Under similar nutrient enrichment and moderate to high flushing of water, herbivores have been observed to control epiphytic algal biomass (Neckles 1993). Under low velocity conditions, subsequent algal growth may outpace grazer pressure, resulting in severe light reductions that inhibit SAV growth (Harlin and Thorne-Miller 1981). In short, trophic interactions can exert indirect effects of SAV growth, even where the dominant herbivores are not consuming the vascular plant tissues directly. Recent evidence (Nifong, unpublished data) suggests that SAV is a major carbon source to the food web, suggesting a multitude of potential trophic interactions that may impact SAV growth.

6.7.1.5 Hydrodynamics

River hydrodynamics can be a primary contributor to aquatic plant community composition and structure (Butcher 1933; Heffernan et al. 2010b) and is recognized to be an important factor in determining whether conditions are suitable for SAV establishment (Madsen and Sondergaard 1983). At low to moderate flow velocities (0-0.10 m s^{-1}) in freshwater ecosystems, macrophyte abundance, photosynthetic rate, and diversity increase. Dense SAV beds reduce velocity, thus increasing sedimentation, decreasing turbidity, and augmenting light availability (Petticrew and Kalff 1992; Doyle 2000). Collectively, these factors further promote SAV productivity. Conversely, high flow can result in mechanical damage and changes in substrate type (Madsen et al. 2001). Hensley and Cohen (2012) identified a strong negative correlation between vegetation abundance and mean flow velocity in spring-fed rivers, resulting in reduced shear stress separation and dispersion. Several studies found that flow velocity influences sediment composition and particle size, subsequently impacting SAV colonization and productivity rates in lotic systems (Madsen et al. 2001; Hoyer et al. 2004).

Recent reductions in groundwater discharge from springs and related impacts on flow velocity (Copeland et al. 2009), possibly related to multidecadal rainfall patterns (Kelly and Gore 2008), created hydrodynamic conditions more favorable for epiphyte attachment on SAV and macroalgal expansion, as well as expansion of SAV cover. Hydrodynamic properties, such as flow velocity, shear stress, drag, and turbulence, strongly influence epiphyte abundance (Biggs 1996; Stevenson 1996; King 2014). Results from King (2014) suggest that hydrodynamic shear can influence filamentous algae in Florida spring-fed rivers, where cover significantly increased below and decreased above a flow velocity threshold (ca. 25 cm s^{-1}). It seems clear that flow velocity and hydrodynamic properties are likely to regulate the distribution and productivity of SAV.

6.7.1.6 Sediment Texture and Redox Potential

For rooted macrophytes, sediment can be a primary source for nitrogen, phosphorus, iron, manganese, and micronutrients (Barko et al. 1991). Sediment texture plays an important role in nutrient availability and by extension, SAV growth. Sandy sediments are typically characterized by low bulk density and low bioavailability of nutrients. In highly organic substrates characterized by low bulk density, macrophyte growth may be hindered by low nutrient availability due to complexation of nutrients with organic matter (Sikora and Keeney 1983; Barko and Smart 1986), potential production of toxins during anaerobic decomposition (Drew and Lynch 1980), and diminished water column clarity (Barko and Smart 1983, 1986). A fine-textured substrate with low to moderate organic content (10–20 %) is typically suitable for most SAV species. As a response to spatial and temporal gradients in sediment texture and nutrient availability, SAV adjusts root:shoot biomass ratios (Barko and Smart 1986). Fertile sediments maximize aboveground biomass (low root:shoot), while infertile sediments typically yield a high ratio of SAV root:shoot biomass (Aung 1974).

Submerged sediments are also characterized by spatial and temporal variation in redox potential. The availability of electron donors and acceptors depends on depth from sediment-water interface, substrate composition, water table fluctuations, and pore water flow (Santschi et al. 1990). Toxic compounds produced in low redox conditions, such as sulfide, reduced iron, and ammonium, can inhibit SAV growth at high concentrations (Van Der Welle et al. 2006; Sederias

and Colman 2009), making redox potential among the most likely controls on site-to-site variation in established SAV growth and vigor. Whether this translates to planted SAV success is unclear.

6.7.1.7 Research Motivation

Understanding the synergistic drivers contributing to primary producer community structure and function in Florida spring ecosystems is central to effectively managing and restoring spring ecosystems. An assessment of SAV growth under a natural gradient of ambient conditions will elucidate the role of nitrogen availability and a multitude of other environmental conditions in SAV growth. Improved understanding of the drivers contributing to growth will reveal sensitive and resilient aspects of primary producer communities in spring-fed rivers, specifically their ability to absorb natural or anthropogenic change (e.g., recreational impacts) and their capacity to withstand and respond to ecological disturbance (e.g., manatee grazing). This will enhance our ability to forecast autotroph response and mitigate any cumulative negative impacts from environmental stressors.

To address the knowledge gaps identified regarding the myriad of controls on SAV growth, we investigated the annual dynamics of SAV shoot elongation and aboveground productivity in two spring-fed rivers in north-central Florida with similar physical attributes but strongly contrasting nitrate concentrations. This comparison is integral to understanding growth response and determining future management activities given the questions related to the need for and effectiveness of controlling/reducing nitrogen levels in springs and groundwater.

6.7.1.8 Hypothesis

We tested the hypothesis that SAV growth is primarily controlled by physical attributes such as light and flow velocity rather than chemical (nutrient concentration) and biological conditions (algal cover). If SAV is primarily controlled by non-nutrient factors, we predict that the relative impacts of nitrate concentration on absolute growth rate will not be significant when compared between sites. The controls of SAV growth are expected to vary across taxa, providing important information about controls on SAV species geographic abundance.

6.7.2 Methods

6.7.2.1 Overview

To test the prediction that SAV growth is primarily controlled by physical rather than chemical and biological conditions, *in situ* measurements of leaf blade elongation and aboveground primary productivity were obtained over an annual cycle across several natural gradients within and across springs. Specifically, we investigated the impacts of ambient variation in epiphytic algal cover, light, flow velocity, substrate characteristics, redox potential, surface water and porewater chemistry. To test the particular prediction that nitrate concentrations influence SAV growth, we ompared measurements between a N enriched spring (Silver Springs at ~1.35 mg N-NO_3 L^{-1}) and one at background nitrate concentrations (Alexander Springs at ~0.05 mg N-NO_3 L^{-1}).

6.7.2.2 Site Description

Silver Springs is a first magnitude springs group in Marion County, Florida comprised of 30 springs with a combined mean discharge of 21.7 m^3 s^{-1} (514 million gallons per day) that combine to form the 12 km Silver River which flows into the Ocklawaha River (Osburn et al. 2002). Silver River is a chemostatic and thermostatic aquatic ecosystem with relatively stable hydrology (Odum 1957). Land use change in the watershed has led to nitrate concentration rising from 0.06 mg L^{-1} (Munch et al. 2006) to over 1.3 mg N L^{-1} (Phelps 2004; Munch et al. 2006; Quinlan et al. 2008). P concentrations are dominated by orthophosphate (SRP) and have remained unchanged near 0.05 mg P L^{-1} during that same period (Maddox et al. 2002; Scott et al. 2004).

Alexander Springs is a first magnitude spring located in Lake County, Florida in the Ocala National Forest with a mean discharge of 2.9 m^3 s^{-1} from 1956 to 2010 (USGS). The spring flows along Alexander Springs Creek for approximately 16 km until discharging to the St. Johns River. Average nitrate (0.05 mg N L^{-1}) and orthophosphate (0.04 mg P L^{-1}) have remained relatively constant over the last three decades. Specific conductance in Alexander Springs Creek (1,070 µS cm^{-1}) is considerably higher than Silver River (463 µS cm^{-1}) (SJRWMD, 1984-2010).

6.7.2.3 Species

While springs support several species of vascular submerged plants, two species dominate and were our focus. *Vallisneria americana,* a perennial, rooted macrophyte distributed in freshwater to mesohaline environments from Central America to Canada (Korschgen and Green 1988). Its ribbon-like leaves with rounded tips grow in excess of two meters from the basal meristem in individual ramets and extend via rhizomes and stolons (Korschgen and Green 1988). *Sagittaria kurziana*, a rooted submersed macrophyte found throughout central and northern Florida, but only at Silver River for this study (i.e., not at Alexander Springs). *S. kurziana* has dark green, ribbon-like leaves that can exceed one meter in length. The leaves have pointed tips and prominent ridges that run parallel along the length of the leaf (UF IFAS Center for Aquatic and Invasive Plants).

Odum (1957) observed that the high SAV turnover (i.e., growth per unit standing stock; units of yr^{-1}) in Silver River is controlled by strong colonization capabilities, rapid growth in clear water, and abundant nutrient supply (both from the water and sediments). Odum (1957) inferred this growth enables preservation of epiphyte-free photosynthetic leaves and quick recovery from grazing and disturbance. Submerged vascular plants have evolved unique adaptations to acquire nutrients. Root uptake (Chambers et al. 1989; Cedergreen and Madsen 2003) and foliar absorption from the water column (Madsen and Cedergreen 2002; Brabandere et al. 2007; Cohen et al. 2012) are both viable mechanisms to acquire nitrogen. The relative importance of root and foliar uptake is controlled by the nutrient status of the water and sediment. Ammonium (NH_4-N) is the preferred form of N used by macrophytes, but under conditions of low NH_4-N concentrations, nitrate can also be utilized (Nichols and Keeny 1976). Under some transient circumstances, shoot elongation and biomass production are supported by stored carbohydrates reallocated to new growth (Titus and Adams 1979). Hauxwell et al. (2007) demonstrated that stored energy reserves, obtained during non-limiting periods of growth, masked seasonality in *V. americana.*

6.7.2.4 Clipping Technique

SAV growth is often measured using leaf marking techniques (Odum 1957, Zieman and Wetzel 1980; Virnstein 1982; Hauxwell et al. 2007) that take advantage of typical SAV growth forms, where leaves emerge and lengthen from a basal meristem. Although individual leaf blades grow irregularly, with young blades growing fastest (Patriquin 1973; Tomlinson 1974; Jacobs 1979), an average growth rate for all blades exists since SAV biomass remains in steady state (Odum 1957). Preliminary field trials with multiple leaf tagging methods proved problematic for long-term repeated measurements due to SAV shoot fragility, as well as entanglement and tearing of leaf tags as a result of flowing water. To better capture spatial and temporal variation, my SAV growth experiments were conducted using a leaf clipping approach (Virnstein 1982). This method is frequently used for estimating shoot elongation and primary productivity (Dunton 1990; Lapointe et al. 1994). Some studies suggest that clip and reharvest techniques underestimate areal productivity and regrowth rates because while clipping may stimulate growth of new blades, loss of photosynthetic tissue mobilizes and depletes belowground reserves, and may prohibit individual shoots from reaching pre-disturbance levels of production (Morgan and Kitting 1984; Tomasko and Dunton 1995). Other studies suggest influence of clipping on regrowth may be overstated since blade regeneration is supported by rhizomes (Greenway 1974; Dawes and Lawrence 1979). Despite conflicting data about leaf clipping impacts to SAV regrowth, this approach is likely to be informative and robust when implemented uniformly across sites, particularly when clipping in adjacent plots is performed at different time intervals (e.g., 1, 3, 6 months) over an annual cycle.

6.7.2.5 Site Selection

Experimental sites were selected using data collected during spatial surveys of physical, chemical, and biological attributes completed prior to clip-plot installation (Cohen et al. 2015). Survey measurements (n = 100 plots across 20 transects) spanned longitudinal and lateral variation in Silver River, and included vegetation and algal cover classes by species (high and low SAV and algal cover), riparian forest canopy cover (high and low canopy cover), surface water velocity (high and low velocity), sediment texture, and chemistry of sediment porewater and river water. In Alexander Springs Creek, sampling locations were selected based on visual observations of SAV cover variation in the upper river (between the head spring and US445 bridge). The 16 selected sites (Figure 6.109A and B) in each river were relatively dense and homogenous SAV beds with water depth shallower than 1.5 m, which was necessary to allow clipping protocols to be implemented without the use of SCUBA equipment. This limits measurements to channel margin zones in Silver River, though all of Alexander Springs Creek could be sampled. The frequency and distribution of parameters in the survey were used to select sites. Sites were chosen to include high and low values for epiphytic algal cover (Braun-Blanquet high value ≥ 4 or low value ≤ 2), canopy cover (high > 60 % or low < 40 %), flow velocity (high > 0.15 m s^{-1} or low < 0.1 m s^{-1}), and sediment organic matter (high > 20 % or low < 10 % in Silver River and high >15 % or low < 5 % in Alexander Springs Creek), such that all gradient combinations were represented.

6.7.2.6 Field and Laboratory Methods

Growth attributes of the two dominant SAV species were evaluated over an annual cycle within and between sites across natural gradients in environmental drivers. Each of the 16 SAV plots per river consisted of a fixed 1 m^2 area divided into four 0.25 m^2 sections (Figure 6.110).

Vegetation surrounding each quadrat was regularly clipped to ensure light reaching the plot vegetation was not obstructed. At the outset of the experiment, the standing stock biomass was clipped 2 cm above the basal sheath across the entire fixed plot (Figure 6.111). To provide a baseline for productivity and biomass turnover and characterize variation in SAV morphology and tissue concentrations, biomass from a single 0.25 m^2 section was processed to estimate species-specific biomass, shoot width and length, and foliar C, N and P composition.

Leaf blade elongation and biomass production at each site were measured at one-, three-, and six-month intervals. SAV in the upstream quadrat sections was collected at one- and three-month intervals to examine seasonal variability and short-term growth, while the downstream quadrat portion was clipped every six months to assess long-term productivity. Comparisons of harvested biomass and accrual rates were used to evaluate the optimal sampling interval for SAV growth.

Water depth, flow velocity, epiphytic algal cover, canopy cover, benthic light attenuation, sediment organic matter, redox potential, water column and porewater chemistry were sampled at each site (Appendix 6.2). SAV density and epiphytic algal cover were characterized using a 5-point Braun-Blanquet scale (0 = 0 %, 1 = 1-5 %, 2 = 5-25 %, 3 = 25-50 %, 4 = 50-75 % and 5 = 75-100 % cover). Canopy cover was determined using a densiometer, determining percent open canopy in the four cardinal directions around the plot and converting to percent canopy cover. Light regime at each site was further characterized using a model to estimate incident light, which incorporates solar radiation from the Florida Automated Weather Network for a nearby station (Ocklawaha) and field measurements of seasonal canopy cover.

Porewater and water column samples were collected using a peristaltic pump to pass water through an inline 0.45 µm filter into acid-washed 20 mL scintillation vials. Water samples were stored cold until chemical analyses were performed. All water analytes (NO_3-N, NH_3-N SRP, Ca, Cl) concentrations were analyzed at the University of Florida Analytical Research Laboratory (UF ARL) using EPA standard methods. Specifically, NO_3-N, NH_3-N, SRP, and Cl were measured by automated colorimetry (EPA Method 353.2, 350.1, 365.1, and 325.2; respectively) and Ca concentration was determined through Inductively Coupled Mass Spectrometry (ICPMS).

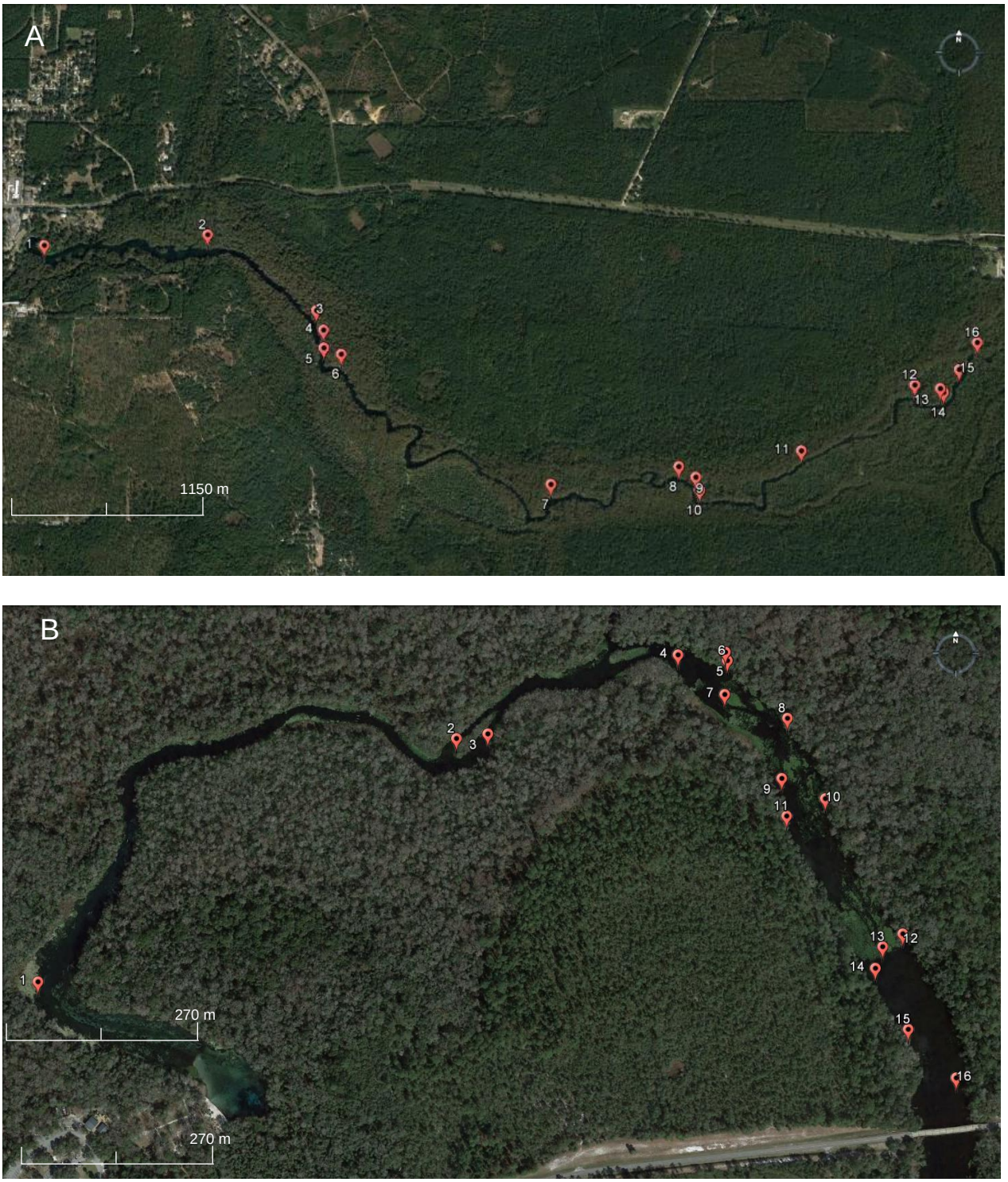

Figure 6.109. Geographic location of the sixteen selected study sites in each spring-fed river, Silver River (A) and Alexander Springs Creek (B).

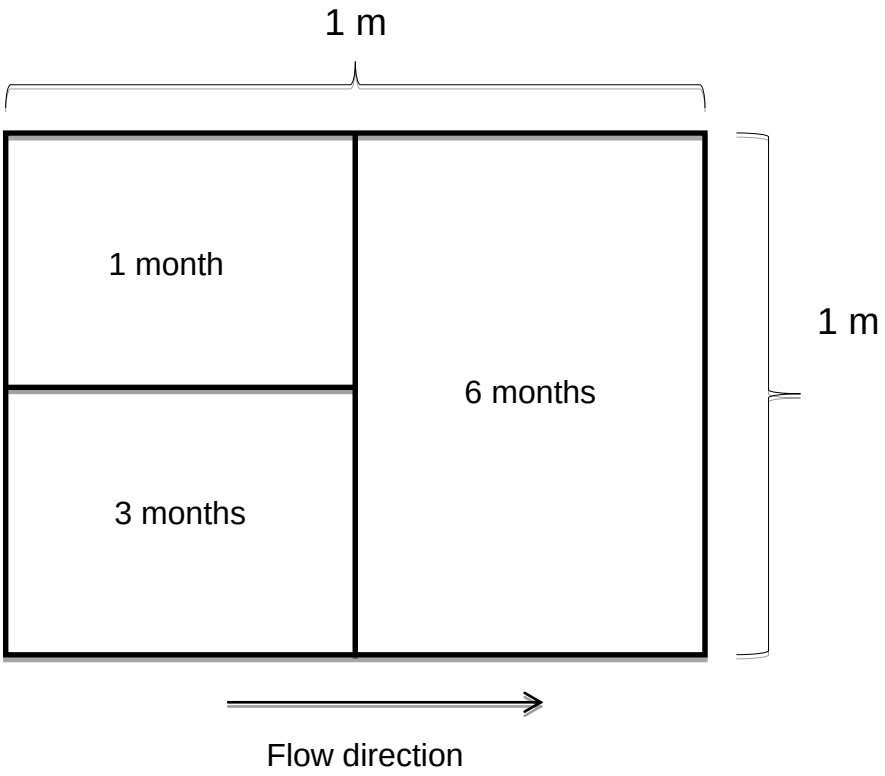

Figure 6.110. Aboveground biomass in the upstream portion of the quadrat was clipped at one month and three-month intervals, and downstream biomass was clipped biannually to examine growth rate and aboveground production variability.

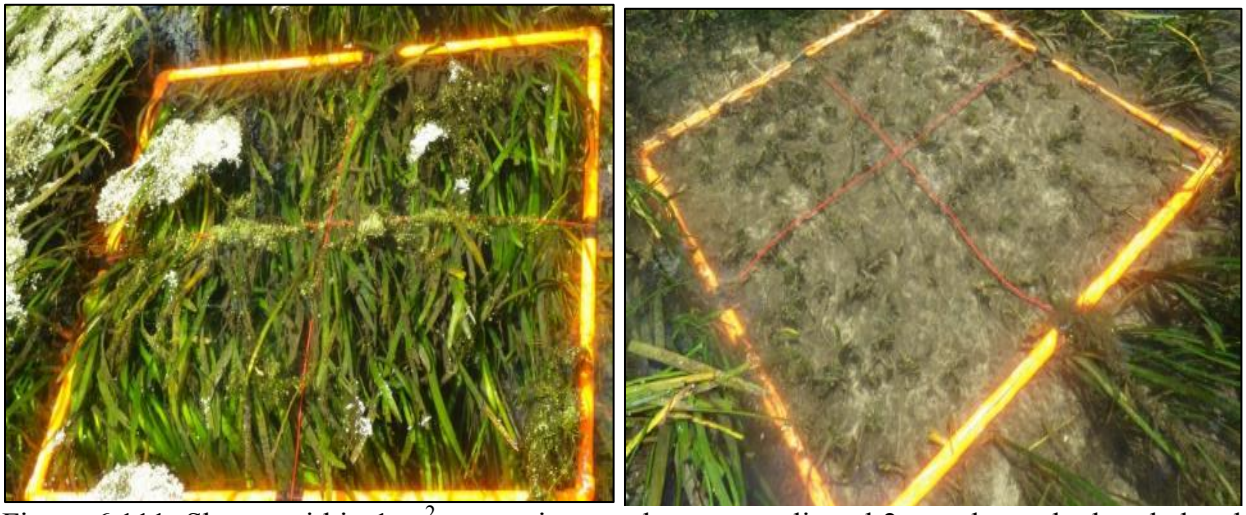

Figure 6.111. Shoots within 1 m^2 vegetation quadrats were clipped 2 cm above the basal sheath to enable regrowth from the basal meristem. Portions of the quadrats at each site were clipped at one-month, three-month, and six-month intervals over an annual cycle.

Sediment grab samples were collected at each site to assess substrate properties within the root zone. In the lab, sediment was dried at 60 °C for 60 to 72 hours. After drying, sediments were homogenized through grinding by mortar and pestle and sieved with a 2 mm mesh sieve, and analyzed for percent carbon, nitrogen, and sulfur (% C, % N, % S) using a Carlo Erba NA1500 CNHS elemental analyzer. Sediment metals (P, K, Ca, Mg, Mn, and Fe) were extracted using a Mehlich-1 solution analyzed on an Inductively Coupled Plasma Spectrometer (EPA Method 200.7). Loss on Ignition (LOI) was used to analyze for percent organic matter (% OM). Five grams of sample were weighed, heated at 450 °C for 6 hours, and reweighed with % OM calculated from the difference between dried (60 °C) and post-furnace (450 °C) weight.

To measure sediment redox potential, nine 8-mm submersible platinum redox electrodes (Paleo Terra, Amsterdam, Netherlands) were installed at each of three sediment depths within the root zone, 1.5 cm, 4.5 cm, and 7.5 cm (Figure 6.112). To capture heterogeneity, redox measurements were replicated at multiple sediment depths (Cogger et al. 1992,; Vepraskas and Faulkner 2001). To account for temporal variation and sediment disturbance during redox electrode installation, redox potential was only reported after full equilibration. Redox potential was measured at 15 minute intervals for a one-week duration at each site. Electrodes were fastened to PVC stands around each SAV growth plot to minimize sediment disturbance and maintain vertical electrode position (Figure 6.112). Initial stabilization was determined for each electrode using a three-hour moving window (12 readings) slope calculation across the time series beginning at t=0. Each electrode was considered stable at the first window where slope ≥ 0. Initial stabilization times were compiled and the start time for the analysis dataset was set to where all electrodes in the analysis period were considered stable. All data prior to stabilization were excluded, and values were normalized to uniform pH (6.8) and temperature (22°C).

Figure 6.112. For each plot, electrodes were fastened to two PVC pipes attached to a central stand to minimize the effects of sediment disturbance. Electrode stands were configured with nine electrodes at each of three depths in the sediment (1.5 cm, 4.5 cm, and 7.5 cm). Electrodes were fastened to two PVC pipes (Photos from Joelle Laing).

Harvested SAV biomass was stored on ice and washed to remove epiphytic algae, separated by species, and measured for shoot length. All samples were dried at 70 °C to constant weight to determine aboveground biomass (g dry weight per m^2). Aboveground biomass originally harvested from each site was ground and homogenized for tissue analysis. Foliar carbon and nitrogen concentrations, in % C and % N, were measured using a Carlo Erba NA1500 CNHS elemental analyzer at the UF Light Stable Isotope Mass Spectrometry Laboratory. Total phosphorus was analyzed at the UF ARL according to EPA Method 365.1.

6.7.2.7 Statistical Analysis

Shoot elongation rate was calculated from the average length of all clipped leaf blades, separated by species, for the specified time intervals (1, 3, and 6 months) at each site. Aboveground biomass accrual rates were assessed by weighing dried SAV biomass clipped from each 0.25 m^2 section at each time interval and converting the dry weight to daily aboveground biomass accrual rates (g dry weight m^{-2} d^{-1}).

Daily aboveground biomass accrual rates are more robust and informative than shoot elongation rates and will be preferentially used in analyses where appropriate. Individual shoot elongation is highly variable within sites, and daily biomass accrual is more representative of whole site productivity and replicable over time. In Silver River and Alexander Springs Creek, daily shoot elongation and biomass accrual rates are positively correlated for both *S. kurziana* ($R^2 = 0.44$, $p < 0.001$) and *V. americana* ($R^2 = 0.15$, $p < 0.001$).

To test the hypothesis that growth rate varies across taxa, we compared mean one-month shoot elongation rates for the two taxa of interest using a two-sample t-test.

Seasonality was assessed on a monthly basis across all sites over an annual cycle using log-normalized productivity rates.

Analysis of variance (ANOVA) was used to evaluate site-level differences among the sixteen sites in each river. A Tukey's honest significant difference (HSD) post-hoc comparison was applied in conjunction with the ANOVA to identify significant differences among site means. ANOVA ('aov' function) and post-hoc Tukey's HSD ('lsmeans' with 'cld' function) were performed in RStudio (R Core Team Version 1.0.136, 2016).

Turnover time was calculated for each site by dividing the initial SAV aboveground standing stock (g dry weight m^{-2}) collected at the outset of the experiment (May 2015 at Silver River and January 2016 at Alexander Springs Creek) by the average daily biomass accrual rate (g dry weight m^{-2} d^{-1}), yielding the number of days required to recover to standing stock and the annual frequency at which it occurs. We note that our measured growth rate and standing stock data suggest that while these measurements reference different times of the year, the standing stock values are not substantially different.

To evaluate the effect of NO_3-N on SAV productivity, we used a two-sample t-test and regression analysis to assess the correlation between NO_3-N (mg L^{-1}) and mean daily

aboveground biomass accrual between Silver River and Alexander Springs Creek, characterized as high- and low-N systems (~1.35 versus 0.05 mg N L^{-1}), respectively.

To test the hypothesis that SAV growth is primarily controlled by physical attributes rather than chemical and biological conditions, an evaluation of ecosystem interactions and the relationship between SAV growth and environmental conditions using pairwise comparisons, regression tree models, and a generalized linear mixed-effects model was conducted.

The regression tree is a predictive tree-based model that applies recursive partitioning of measured variables to predict a response variable. Regression tree models construct a set of decision rules for predictor variables and partition the data with binary splits using a single predictor variable, producing groups that maximize homogeneity of the response variable (Clark and Pregibon 1992). The 'rpart' function (Therneau et al. 2015) in RStudio (R Core Team Version 1.0.136, 2016) for the regression tree model using SAV biomass accrual rates as the response variable for each spring-fed river.

The generalized linear mixed-effects model (GLMM) assesses main effects and two-way interactions between covariates and allows for both fixed and random effects, with site designated as a random effect to control for associated variance. Specifically, the 'lmer' function was used with the 'lme4' package (Bates et al. 2016) in RStudio (R Core Team Version 1.0.136, 2016). It accounts for repeated measures at each site because SAV growth and field parameters were measured at various time intervals over an annual cycle. To limit the number of covariates and augment statistical power, variables that are not biologically relevant to SAV growth were selectively omitted from the model. The subset of covariates selected for the GLMM was informed via recursive model development and intercomparison. Model permutations and selection were also guided by the Akaike information criterion (AIC), which considers improvements in goodness-of-fit according to predictor variables and model complexity.

6.7.3 Results

6.7.3.1 River Characteristics

Variation between Silver River and Alexander Springs Creek was large for many field parameters. Whereas mean water depth, flow velocity, SRP, and sediment organic matter were relatively similar across sites in both spring-fed rivers, other river characteristics were distinctly different (Table 6.17). Notably, mean light availability, epiphytic algal cover, Cl, and sediment Fe are significantly higher in Alexander Springs Creek. Water column NO_3-N was consistently higher in Silver River (1.31 ± 0.23 mg L^{-1}) than Alexander Springs Creek (0.14 ± 0.11 mg L^{-1}).

6.7.3.2 Sampling Effects

Aboveground SAV biomass accrual (i.e., daily productivity) diminished across the three different growth periods (1, 3, and 6 month), indicating that longer than monthly intervals between clipping will underestimate growth as plots approach the initial standing stock (Figure 6.113). Aboveground biomass recovery time varied across rivers, with biomass recovering to 72% of initial standing stock within six months in Silver River but fully recovering over the same time frame in Alexander Springs Creek (Figure 6.113b). Seasonal variation in the standing

stock after 6 months of growth was surprisingly small. Variation across sites was also evident, suggesting that while initial standing stock varied, this is not a perfect proxy for growth.

The distribution and frequency of fitted slopes between time (across all measurements) and mean site productivity quantified the impact of repeated clipping on biomass recovery to test method reliability (Figure 6.113c). The mean slope across sites was 0.09 g m^{-2} d^{-1} per month (± 0.09) with predominantly positive slopes in both Silver River and Alexander Springs Creek. This strongly supports the assertion that repeated clipping did not inhibit growth, but rather may have resulted in modest growth stimulation at many sites.

6.7.3.3 Measured Growth and Standing Stock

Growth rates varied for both taxa of interest across sites, ranging from 0.10 – 1.50 and 0.12 – 1.92 cm d^{-1} for *S. kurziana* and *V. americana,* respectively. Mean shoot elongation was 0.49 cm d^{-1} for *S. kurziana* and 0.61 cm d^{-1} for *V. americana* in Silver River. In Alexander Springs Creek, mean shoot elongation for *V. americana*, the only SAV species, was 0.57 cm d^{-1} (Figure 6.114). Despite significant temporal and spatial variation in rates, a two-sample t-test showed significantly higher one-month shoot elongation rates for *V. americana* than *S. kurziana* (p = 0.03). A t-test of mean shoot elongation rates of *V. americana* between Silver River and Alexander Springs Creek revealed no significant differences (p = 0.42).

Seasonal growth trends were evaluated using log-normalized mean-centered monthly productivity rates. Mean daily aboveground biomass accrual across sites was 1.14 g dry mass m^{-2} d^{-1} from January – December 2016. *S. kurziana* and *V. americana* exhibited modest growth seasonality, with minimum values occurring in winter and maximum values occurring during the summer (Figure 6.115). However, no single month exhibited significantly higher or lower productivity than the annual mean, and monthly minimum (January = 0.83 dry weight m^{-2} d^{-1} which is 71% of mean) and maximum (August = 1.50 g dry weight m^{-2} d^{-1}, which is 131% of mean) values suggest surprisingly constant growth.

Spatial heterogeneity in aboveground SAV standing stock and productivity across sites was substantial. Initial standing stock ranged between 40.9 - 394.7 g dry weight m^{-2} in Silver River and 34.6 - 371.2 g dry weight m^{-2} in Alexander Springs Creek. In Alexander Springs Creek and Silver River, respectively, mean site productivity spanned from 0.39 – 1.89 and 0.11 – 2.31 g dry weight m^{-2} d^{-1}. ANOVA across sites along with Tukey's HSD for post-hoc comparison revealed significant differences among site means at $p < 0.05$ (Figure 6.116a). This suggests that these site differences are coherent over time, with some sites (e.g., sites 2 and 9 in Alexander Springs Creek, and sites 13 and 9 in Silver River) as much as 5-fold more productive on average than other sites (e.g., sites 8 and 5 in Alexander, and sites 3 and 8 in Silver River).

Annual turnover frequency (ratio of mean growth rate to initial standing stock; units per yr^{-1}) was positively correlated with site productivity (Alexander: R^2 = 0.33, p = 0.02; Silver: R^2= 0.48, p = 0.002). The time required for SAV to recover to initial standing stock varies broadly across sites, from 38 – 467 days (0.78 – 9.70 times per year) in Alexander Springs Creek and 74 – 410 days (0.89 – 4.94 times/year) in Silver River (Figure 6.116b). Average annual turnover in Alexander Springs Creek (88 days, 4.16 times per year) was nearly double Silver River (162 days, 2.25 times/year). Since growth rates were approximately the same across rivers, this must be due to

Table 6.17. Summary of river characteristics (mean ± standard deviation) for sixteen sites measured from May 2015 – December 2016 in Silver River and January – December 2016 in Alexander Springs Creek. A summary of the individual site characteristics in each river is included in Appendix 6.2.

	Silver	Alexander
Water depth (m)	0.64 ± 0.22	0.62 ± 0.13
Flow Velocity (m s^{-1})	0.16 ± 0.11	0.1 ± 0.07
Incident Light (W m^{-2})	90.21 ± 54.50	148.67 ± 65.32
Canopy Cover (%)	57.3 ± 23.4	34.9 ± 25.4
Algal Cover (Braun-Blanquet)	3 ± 2	4 ± 1
Water Column Ca (mg L^{-1})	80.8 ± 3.1	52.9 ± 15.0
Water Column Cl (mg L^{-1})	11.9 ± 0.9	305.4 ± 124.6
Water Column NH_3-N (mg L^{-1})	0.17 ± 0.24	0.04 ± 0.01
Water Column NO_3-N (mg L^{-1})	1.31 ± 0.23	0.14 ± 0.11
Water Column SRP (µg L^{-1})	37.7 ± 30.1	37.4 ± 6.7
Porewater Ca (mg L^{-1})	91.1 ± 21.7	63.9 ± 25.0
Porewater Cl (mg L^{-1})	14.2 ± 4.3	367.8 ± 186.3
Porewater NH_3-N (mg L^{-1})	0.27 ± 0.34	0.27 ± 0.52
Porewater NO_3-N (mg L^{-1})	0.81 ± 0.42	0.12 ± 0.08
Porewater SRP (µg L^{-1})	223.0 ± 414.4	101.7 ± 78.6
Sediment P (mg kg^{-1})	13.2 ± 10.4	226.1 ± 194.8
Sediment K (mg kg^{-1})	24.68 ± 14.4	62.0 ± 86.9
Sediment Ca (mg kg^{-1})	6338 ± 1168	4185 ± 1606
Sediment Mg (mg kg^{-1})	236.4 ± 121.9	707.0 ± 468.2
Sediment Mn (mg kg^{-1})	0.29 ± 0.3	0.48 ± 0.42
Sediment Fe (mg kg^{-1})	BDL	10.5 ± 11.2
Sediment %C	16.4 ± 6.2	8.5 ± 7.9
Sediment %N	0.6 ± 0.5	0.5 ± 0.5
Sediment %S	0.5 ± 0.5	0.3 ± 0.5
Sediment Organic Matter (%)	14.8 ± 11.7	13.5 ± 13.4
Shallow Redox Potential (mV)	-115.8 ± 170.4	-151.1 ± 56.6
Medium Redox Potential (mV)	-107.4 ±163.2	-155.6 ± 86.9
Deep Redox Potential (mV)	-175.5 ±139.8	-175.8 ± 55.5

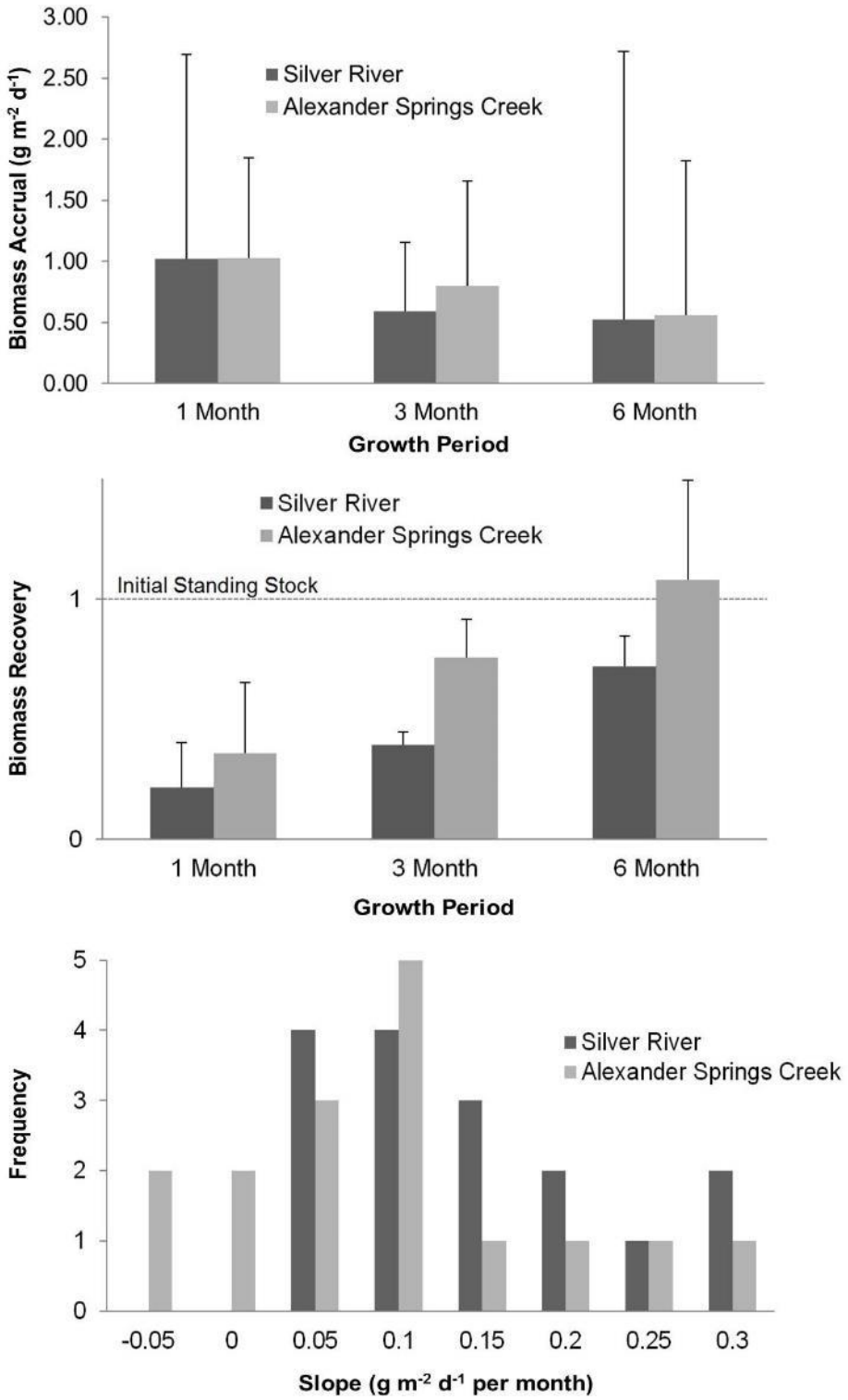

Figure 6.113. (a) Mean aboveground biomass accrual for three growth periods shown with 95 % confidence intervals. (b) Aboveground biomass recovery time normalized to standing stock with 95 % confidence intervals. (c) Histogram of distribution and frequency of the slopes across all monthly measurements of mean site productivity.

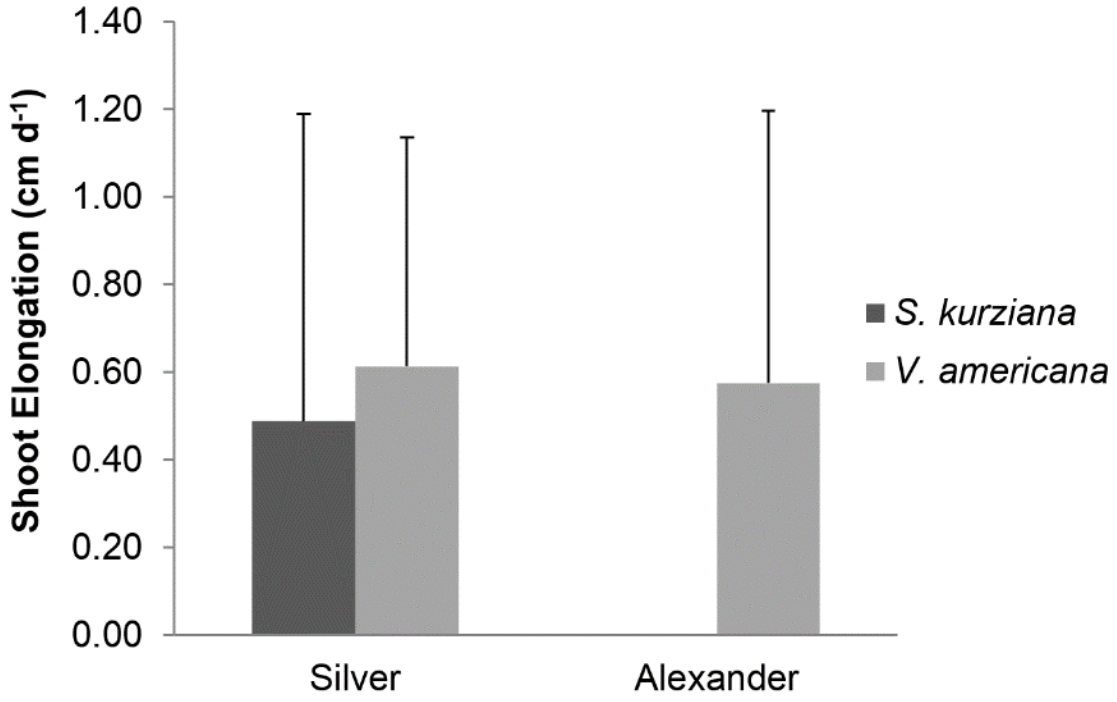

Figure 6.114 Mean one-month shoot elongation rates shown with 95 % confidence intervals for *S. kurziana* and *V. americana* in Silver River and Alexander Springs Creek. Only *V. americana* was present in Alexander Springs Creek.

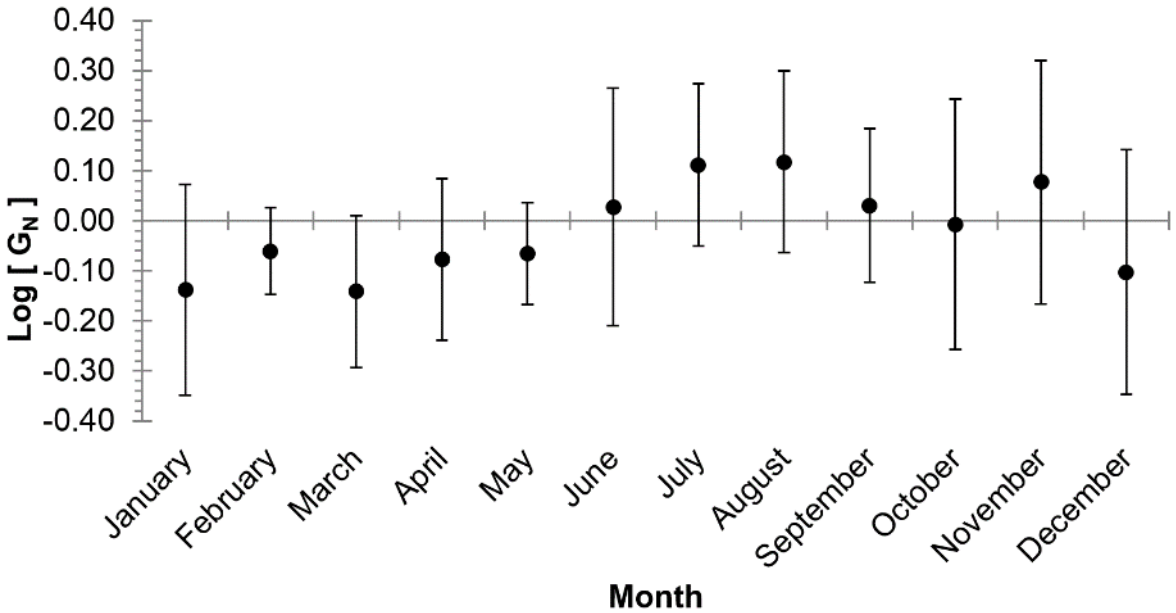

Figure 6.115. Log-normalized daily aboveground productivity shown with 95 % confidence intervals in Silver River from Jan – Dec 2016.

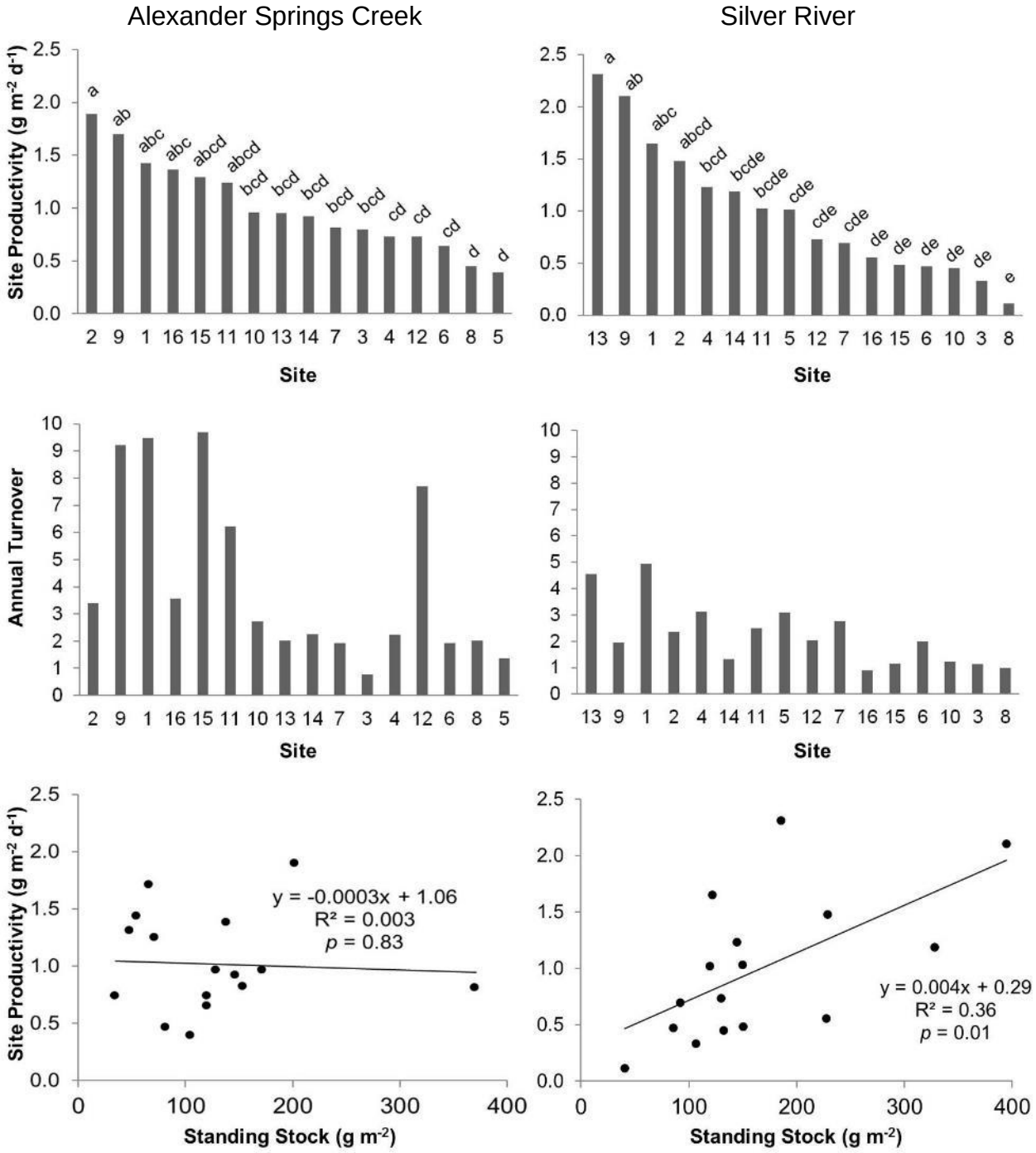

Figure 6.116. (a) Mean aboveground biomass accrual ranked in site order from high to low productivity. Different lowercase letters indicate significant differences between sites at $p < 0.05$. (b) Annual frequency of biomass turnover across all sites. (c) Relationship between initial standing stock and productivity at each site.

lower initial standing stocks in Alexander as a result of winter clipping. A two-sample t-test revealed significant differences in turnover times between rivers (p = 0.04). A comparison of upstream versus downstream SAV turnover time indicated no significant differences for either river (Alexander: p = 0.87, Silver: p = 0.14). Initial standing stock was weakly correlated to site productivity in Silver River (R^2 = 0.36, p = 0.01) and not correlated in Alexander Springs Creek (R^2 = 0, p = 0.83) (Figure 6.116c).

6.7.3.4 Pairwise Controls on SAV Productivity

To understand the pairwise controls on SAV growth, individual controls with the strongest correlation to SAV productivity were assessed (Figure 6.117). In Silver River, the four best single predictors of growth are sediment redox potential (R^2 = 0.40), canopy cover (R^2 = 0.39), porewater Cl (R^2 = 0.14), and epiphytic algal cover (R^2 = 0.13). In Alexander Springs Creek, the best predictor variables include sediment redox potential (R^2 = 0.24), sediment Fe (R^2 = 0.10), water column SRP (R^2 = 0.08), and porewater Cl (R^2 = 0.06). These pairwise comparisons are weak and are not conclusive for predicting SAV growth. Therefore, multivariate models are likely more informative and reliable for predicting SAV productivity.

6.7.3.5 Multivariate Controls on SAV Productivity

To evaluate control(s) on SAV growth, regression tree models were applied for each river using measured predictor variables and daily aboveground biomass accrual as the response variable. When all field parameters are included as predictor variables in the regression trees, the model output is difficult to interpret, incoherent for spring ecosystem management, and not informative for predicting SAV growth elsewhere. Therefore, sediment and water chemistry variables that are not central to SAV growth were selectively omitted while maximizing goodness-of-fit. Light, flow velocity, algal cover, water depth, sediment organic matter, redox potential, NO_3-N, and SRP were considered most relevant and applicable for management activities, and therefore were incorporated in the model. Cl was also included for Alexander Springs Creek, where water column concentrations varied broadly across sites (256.7 – 767.2 mg Cl L^{-1}) and high concentrations (mean ~ 370 mg Cl L^{-1} or ~0.75 ppt) may have implications for SAV growth. Water column and porewater NH_3-N were omitted from the model because the measured concentrations are below any published threshold for SAV toxicity, and results presented earlier in this report indicate no significant ammonium effect on SAV growth.

Regression trees can be unstable with minor perturbations in the dataset; thus, we considered predictor variables at the primary and secondary splits to be most valuable for assessing SAV growth controls. In Silver River, the combination of lower canopy cover (< 33.31 %) and sediment redox potential greater than or equal to -214 mV at 1.5 cm sediment depth yield the highest SAV productivity (2.34 g dry weight m^{-2} d^{-1}). Flow velocity and sediment organic matter are also important controls on SAV growth in Silver River (Figure 6.118). In Alexander Springs Creek, sediment redox potential above -141.3 mV at 4.5 cm depth and lower canopy cover (<42.15 %)

Table 6.18. Summary of significant main effects at Silver River including mean-centered standardized slope, standard error, and t-value (Deviance = 260.04, Marginal R^2 = 0.31 Conditional R^2 = 0.45).

Fixed Effect	Standardized Slope	Standard Error	t-value
Canopy Cover	-0.30	0.11	-2.65
Redox Potential at 1.5 cm	0.35	0.17	2.07
Porewater SRP	-0.65	0.19	-3.44

yield the highest SAV productivity (2.01 g dry weight m^{-2} d^{-1}). Water column Cl, water depth, algal cover, and porewater SRP also influence SAV growth rates at Alexander Springs Creek (Figure 6.119). To determine the variance explained by the model, a goodness-of-fit assessment revealed a positive correlation between observed and predicted SAV growth in Silver River (R^2 = 0.53) and Alexander Springs Creek (R^2 = 0.56).

The generalized linear mixed effects model selection was guided by AIC, recursive modeling, and goodness-of-fit. For this model, only the main effects, which ignore the effects of all other independent variables, were considered. Two-way interactions were deemed too complex for interpretation and management applications. Specifically, for two-way interactions at Silver River, the lowest AIC score required seven covariates. In Silver River, the significant main effects are canopy cover, sediment redox potential at 1.5 cm depth, and porewater SRP (Table 6.18). In Alexander Springs Creek, the significant main effects are canopy cover, sediment redox potential at 4.5 cm depth, and porewater SRP (Table 6.19) ; note that both models suggest and inhibitory effect of porewater SRP. Variance in SAV productivity was derived primarily from the residual at Silver River (0.68 ± 0.82) and Alexander Springs Creek (0.33 ± 0.58). Visualization of the overall model performance (Figure 6.120 for Silver River, Figure 6.121 for Alexander Springs Creek) suggest similar predictive power to the regression tree models.

Table 6.19. Summary of significant main effects at Alexander Springs Creek including mean-centered standardized slope, standard error, and t-value (Deviance = 238.77, Marginal R^2 = 0.23, Conditional R^2 = 0.35).

Fixed Effect	Standardized Slope	Standard Error	t-value
Porewater SRP	-0.30	0.10	-2.88
Canopy Cover	-0.19	0.08	-2.43
Redox Potential at 4.5 cm	0.47	0.11	4.16

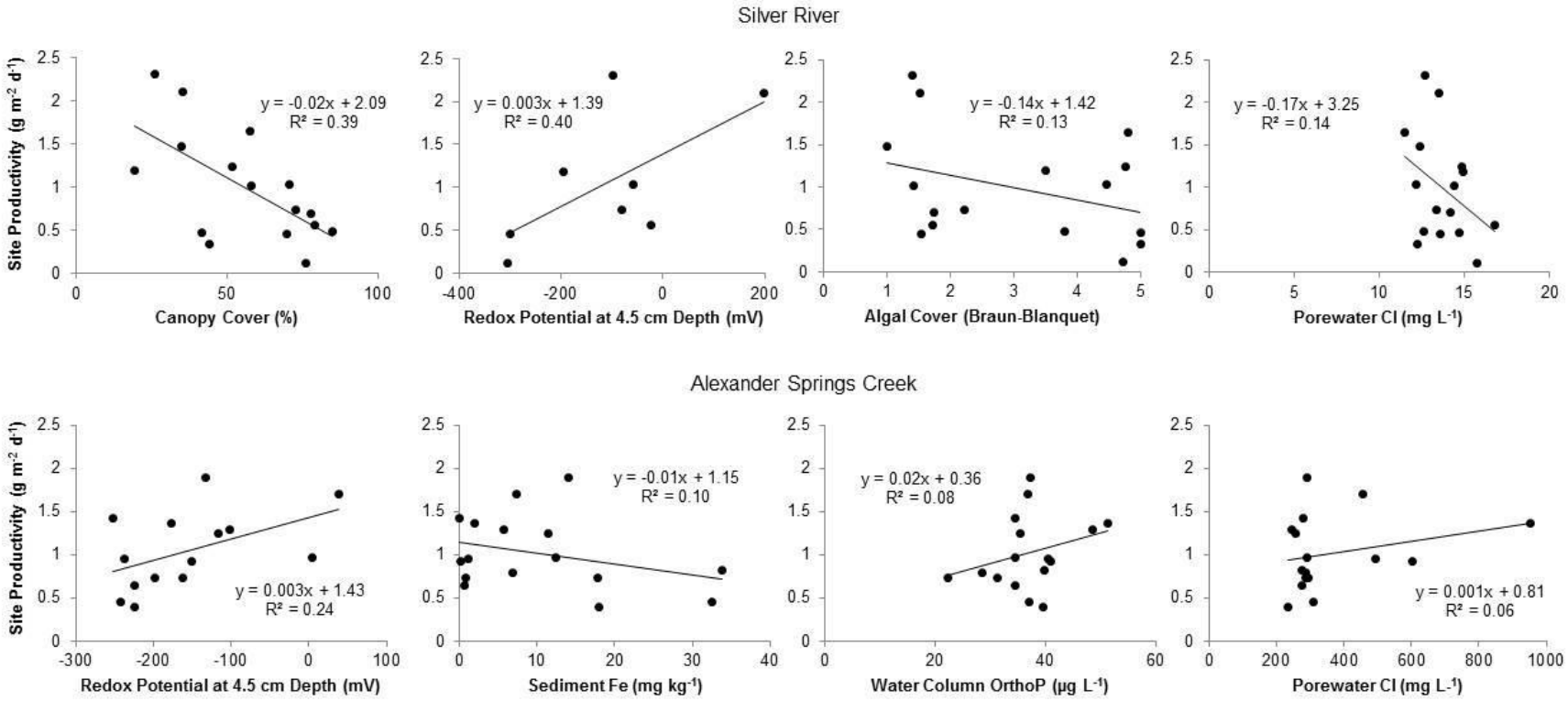

Figure 6.117. Plots of the four best individual predictors of SAV aboveground biomass accrual at each site in Silver River and Alexander Springs Creek.

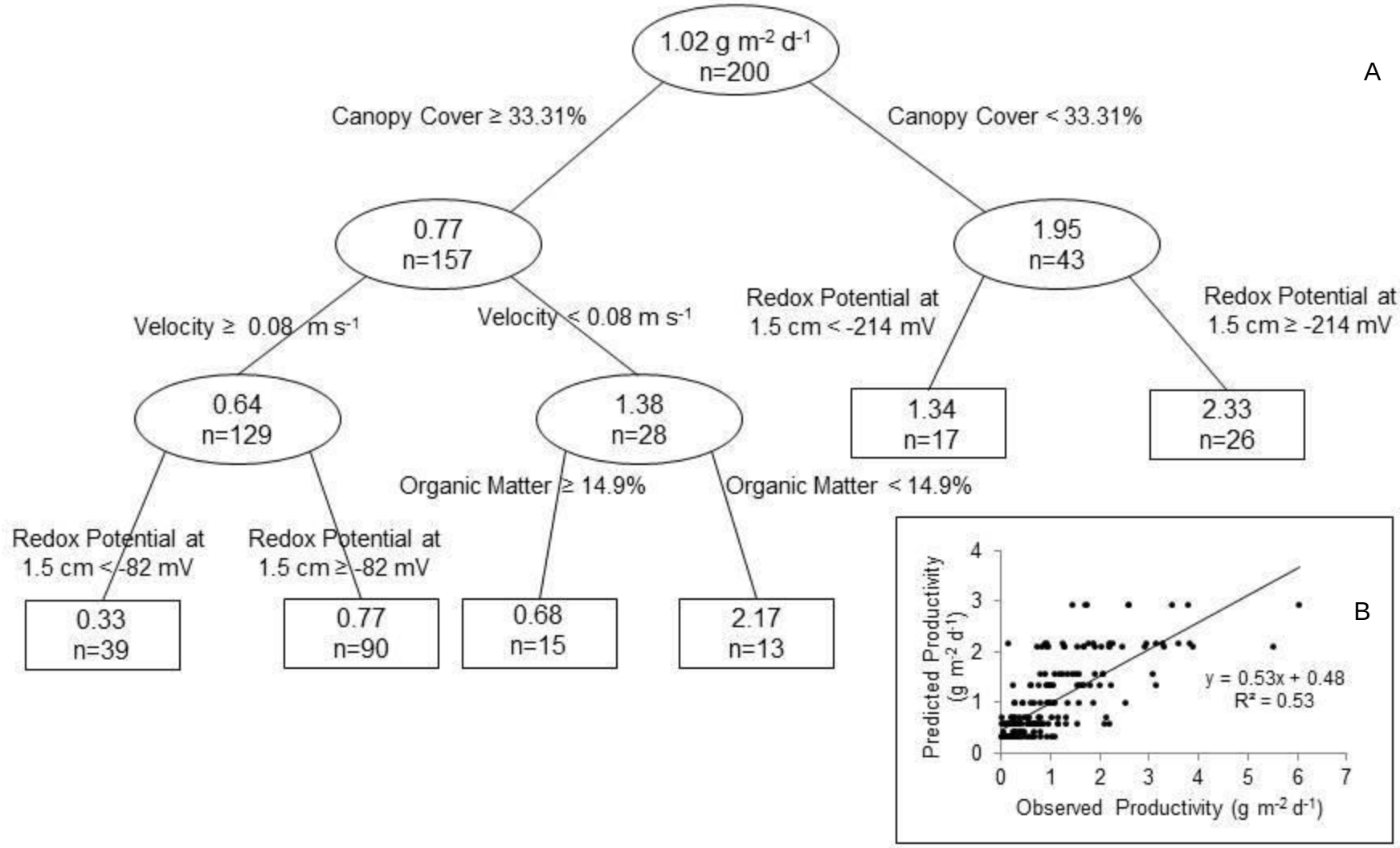

Figure 6.118. (A) Regression tree of controls on SAV productivity (g dry weight m^{-2} d^{-1}) at Silver River. (B) Plot of the goodness-of-fit between the observed and predicted values from the model.

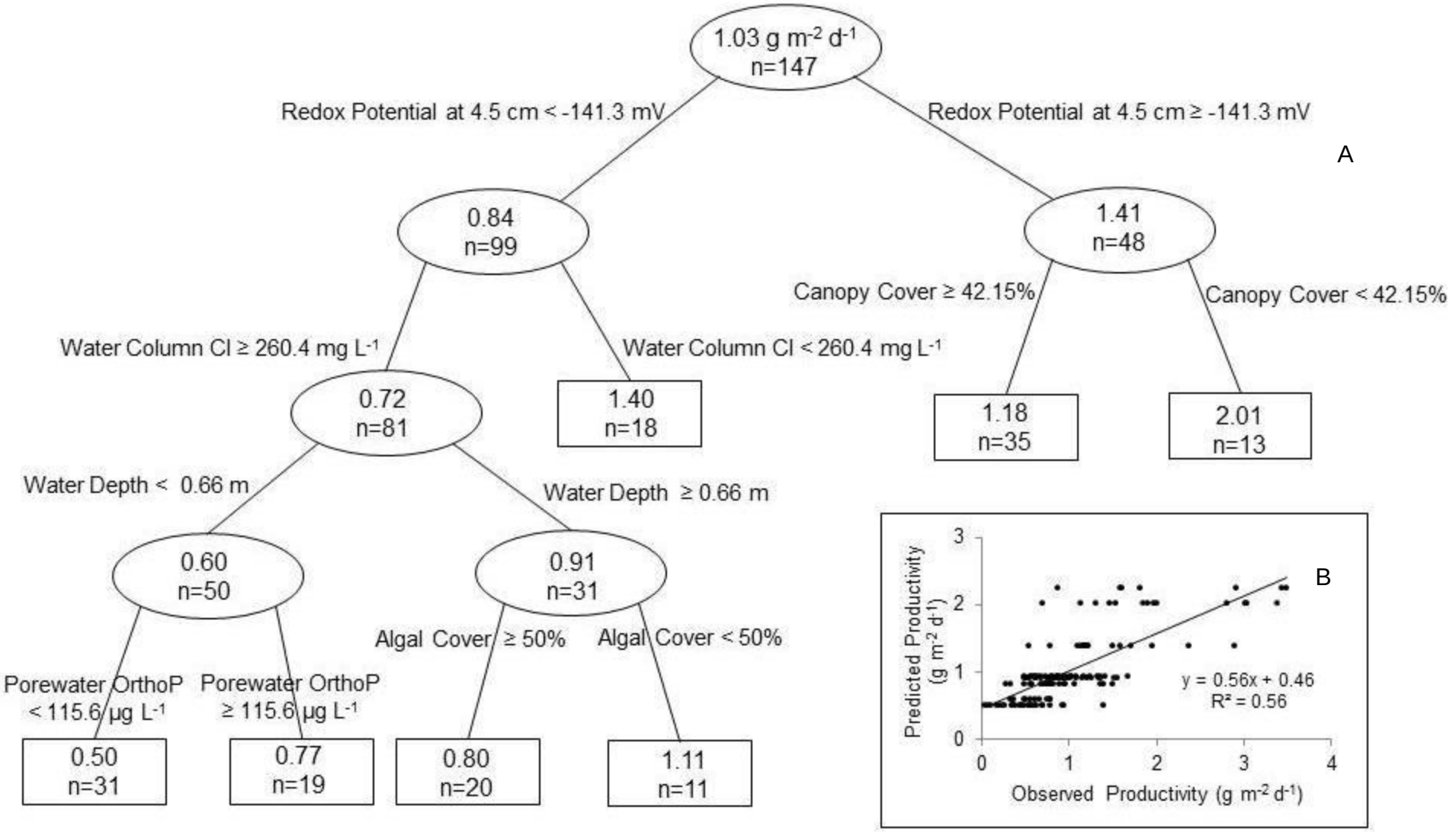

Figure 6.119. (A) Regression tree of controls on aboveground SAV productivity (g dry weight m^{-2} d^{-1}) at Alexander Springs Creek. (B) Plot of the goodness-of-fit between the observed and predicted values from the model.

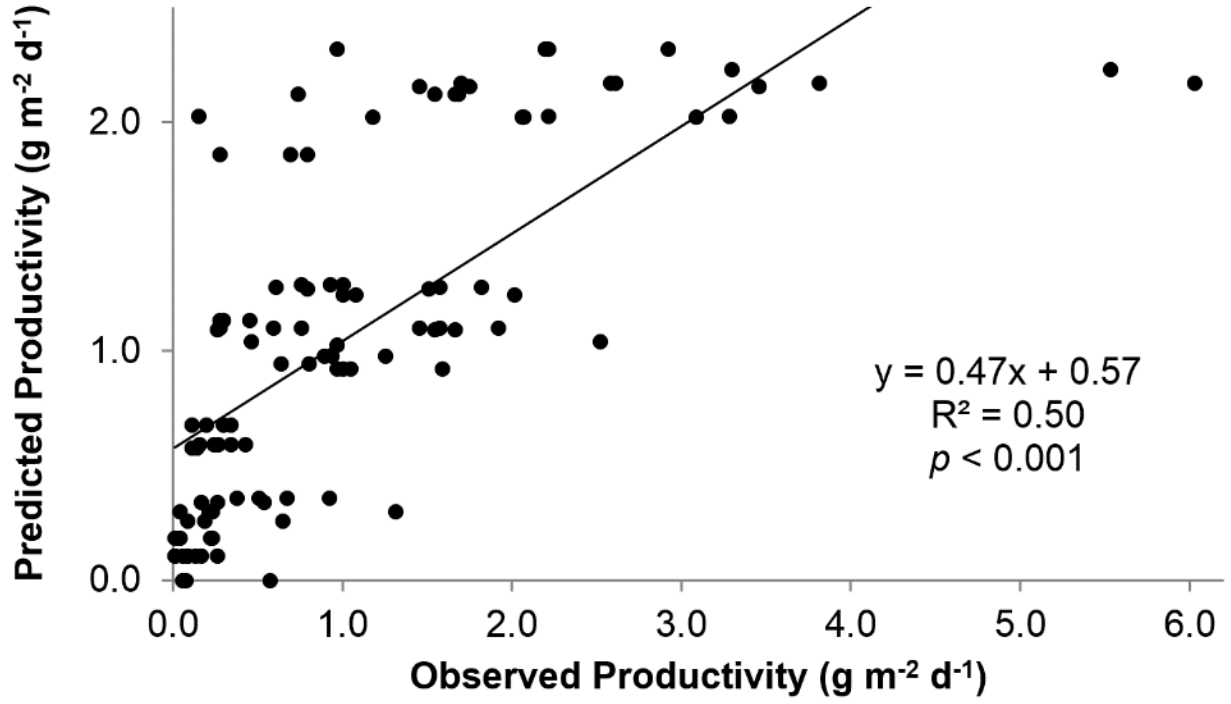

Figure 6.120. Plot of the goodness-of-fit between observed and GLM-predicted productivity in Silver River.

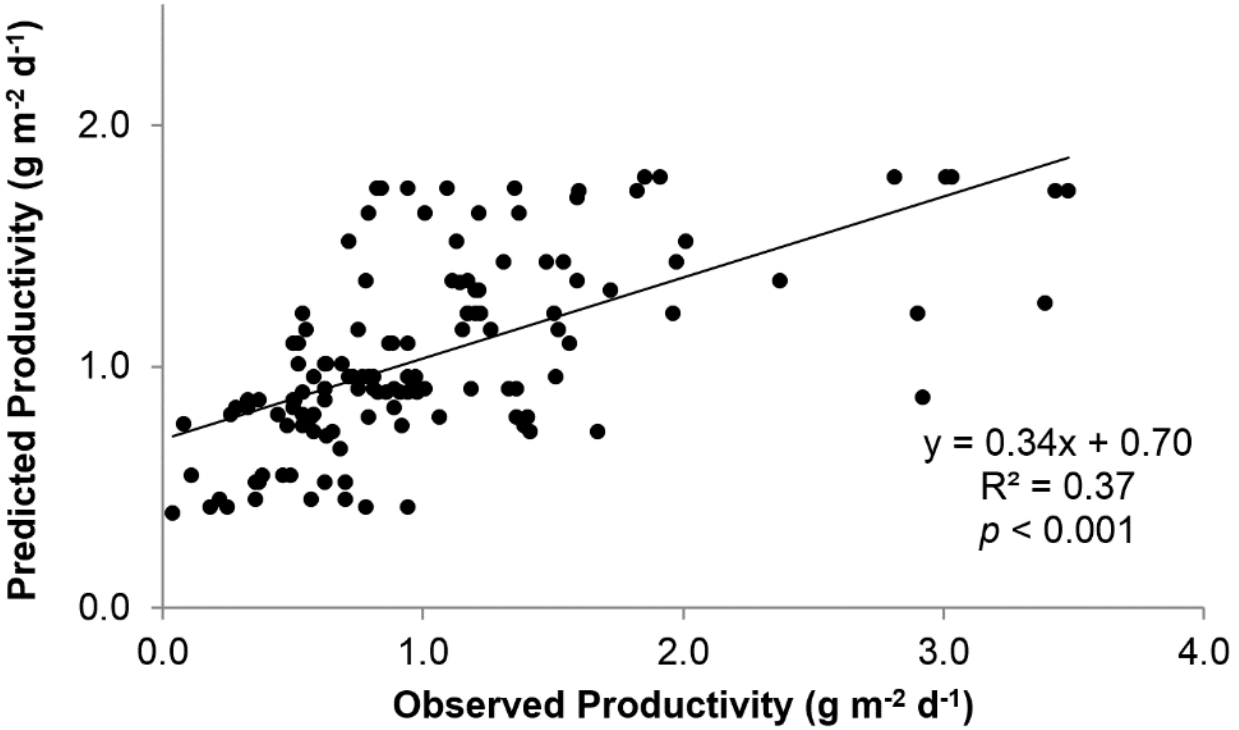

Figure 6.121. Plot of the goodness-of-fit between observed and GLM-predicted productivity in Alexander Springs Creek.

6.7.4 Discussion

6.7.4.1 Spatial and Temporal Heterogeneity in SAV Growth

The abundance and growth of SAV in Florida's spring-run ecosystems exhibit spatial and temporal heterogeneity. Initial standing stock ranged between 40.9 - 394.7 g dry weight m^{-2} (165.0 mean g dry weight m^{-2}) in Silver River and 34.6 - 371.2 g dry weight m^{-2} (126.5 mean g dry weight m^{-2}) in Alexander Springs Creek. In Silver River and Alexander Springs Creek, respectively, mean site productivity in this study spanned from 0.11 – 2.31 and 0.39 – 1.89 g dry weight m^{-2} d^{-1}. While spatial variation in SAV initial standing stock and productivity across sites was substantial in Silver River and Alexander Springs Creek, temporal variation in growth (i.e., seasonality) was modest and site differences were consistent over time, underscoring the chemical and thermal stability of spring ecosystems.

Similar studies in Florida's springs have also observed interannual stability and seasonal variation in SAV growth (Odum 1957; Quinlan et al. 2008). In Silver River, Quinlan et al. (2008) measured a mean aboveground biomass of 584 g dry weight m^{-2} (± 402) in the summer and 426 g dry weight m^{-2} (± 323) in the winter. Odum (1957) identified a mean annual SAV standing stock of 578 g m^{-2} in Silver River. Despite significant increases in nitrate loading over the past 50 years, the distribution and abundance of SAV communities in Silver River remained relatively unchanged (Quinlan et al. 2008). To compare our SAV biomass sampling with other studies, we measured a 10:1 conversion for wet-to-dry weight of SAV shoots, where a 2,580 g wet weight m^{-2} sample was processed and dried to 260 g m^{-2}. In Alexander Springs Creek, Canfield and Hoyer (1988) measured a mean biomass of 4,400 g wet weight m^{-2} (approximately 440 g dry weight m^{-2}) while Nifong (2015) found an average standing stock of 1,716 g wet weight m^{-2} (172 g dry weight m^{-2}). Hauxwell et al. (2007) measured total biomass of *V. americana* between 162 – 1,013 g dry weight m^{-2} in a spring-fed estuary in Florida where aboveground biomass comprised approximately 70% of total biomass, further highlighting the large spatial variation in SAV standing stock within and across springs. Productivity measurements in the St. Lawrence River, a shallow lotic system in Quebec, Canada, lie within our observed range of biomass accrual rates, where submerged macrophytes produced 0.08 g C m^{-2} d^{-1} (~0.24 g dry mass m^{-2} d^{-1} assuming similar foliar C content) (Vis et al. 2007).

Sampling bias in our site selection may have contributed to the low initial standing stocks relative to measurements from Odum (1957) and Quinlan et al. (2008). To employ the clipping method without SCUBA equipment required sites to be relatively shallow; these sites tend to be preferentially on the channel margins, particularly in Silver River, potentially selectively sampling sites with lower standing stocks and biomass accrual. These channel margin sites are also locations where light may be obstructed by canopy cover. Modest growth seasonality may be associated with consistent year round incident light levels resulting from canopy cover in the summer and canopy loss in the winter. Dampened seasonality may also arise from constant spring-water temperature. Temperature variation in spring-fed systems is low, and previous studies suggest temperature stability may limit growth variation (Hauxwell et al. 2007). Despite sampling bias, the uniform approach implemented across sites is informative for predicting SAV controls.

6.7.4.2 Multivariate Controls on SAV Productivity

Understanding the synergistic drivers contributing to primary producer community structure and function in Florida springs is central to effectively managing and restoring spring ecosystems. Multivariate approaches, including regression trees and general linear models, suggest complex and contingent controls on SAV growth. Crucially, pairwise predictions of SAV growth were of limited value, yielding models that explained only modest proportions of observed variation. In this work, it was found that SAV growth is highly conditional and contingent upon multiple environmental controls. Two comprehensive statistical analyses, regression trees and generalized linear models, strongly support the use of multivariate models to provide more informative and reliable predictions of SAV productivity.

Results from the multivariate models in this study indicate that the primary drivers of growth for both springs are light, sediment redox conditions, and porewater SRP. Regression tree models indicate water column Cl concentration, water depth, flow velocity, and sediment organic matter composition may also influence SAV growth. Notably, while we observed a tradeoff between SAV and algal abundance in our benthic surveys, algal cover was not linked to measured SAV growth. It is likely that this is because the clipping schedule limited the colonization and thus competitive control from dense epiphytic algal mats. These models were constructed independently for both rivers but yielded remarkably similar patterns, with light, sediment redox potential, and porewater SRP together providing robust predictions of growth. This uniformity of SAV growth controls in Silver River and Alexander Springs Creek is informative, convincing, and useful for management and restoration strategies across spring ecosystems.

While there is strong evidence that light markedly influences SAV distribution, abundance, and growth (Canfield and Hoyer 1988; Duarte and Canfield 1990; Hauxwell et al. 2007), multivariate models suggest that other environmental factors should also be considered. Canfield and Hoyer (1988) identified light availability as the central factor controlling SAV abundance in Florida streams, with substrate type, water depth, and flow velocity also governing growth. Butcher (1933) determined flow velocity, as well as substrate type and light availability, to be important factors driving SAV growth.

Though the effects of light and redox potential on SAV growth are well understood, the mechanism for phosphate growth inhibition (i.e., reduced growth at high SRP concentrations) is less clear. P is central to SAV growth regulation; however, the cause of the inhibitory SRP effect on SAV productivity is uncertain. It may be a proxy for another environmental condition that was not measured in this study or may result from interaction effects with redox potential where complexation and immobilization of phosphate with iron occurs in oxidized sediments (Moore and Reddy 1994). Diminished SAV productivity may also result from an indirect effect of increased periphyton from augmented P that causes shading and light reductions (Dierberg et al. 2002).

Improved understanding of growth controls enhances our ability to forecast autotroph response to environmental change and mitigate any negative impacts from environmental stressors in Florida springs.

6.7.4.3 Redox Potential

Within and across study sites, sediments were characterized by large spatial heterogeneity in redox conditions. Mean site redox potential varied considerably, ranging from -306.6 to +172.2 mV in Silver River and -235.2 to -72.2 mV in Alexander Springs Creek, underscoring the diversity of sediment redox conditions within the root zone. Overall, sediments were highly reducing (< -100 mV), potentially causing phytotoxic compounds such as hydrogen sulfide (H_2S) to accumulate in the root zone (Reddy and DeLaune 2008).

When assessed individually, redox potential is positively correlated to aboveground SAV productivity. In both multivariate models, redox potential was a strong predictor of SAV growth. Results from the GLM show that productivity increases by 1 g m^{-2} d^{-1} when redox potential increases 200 mV in Alexander Springs Creek (slope = 0.005) and 350 mV in Silver River (slope = 0.0028). These findings indicate that sediment redox conditions should be considered in spring ecosystem management and restoration, particularly for determining site suitability of SAV transplant efforts.

The results suggest that the chemical and physical properties of submerged sediments can both enhance and inhibit SAV growth. Sediment redox conditions appear to play an important role in regulating SAV growth, though the mechanisms of action are unclear. Redox potential controls nutrient availability and abundance of phytotoxic compounds in sediments of aquatic ecosystems (Reddy and DeLaune 2008); my results strongly support this mode of action, with higher redox potentials, at which phytotoxic compounds like H_2S and NH_4-N are less likely to accumulate, associated with higher growth rates. It is important to note that SAV can create sediment conditions favorable for growth and protect against phytotoxic compounds by lowering reduced ion concentrations and increasing redox potential via rhizosphere oxidation (Sand-Jensen et al.1982; Carpenter et al. 1983; Wigand et al. 1997). This aerated root zone creates high microscale heterogeneity of sediment redox conditions. Therefore, declines in SAV distribution and abundance, a trend occurring in some spring ecosystems (e.g., lower Rainbow River, Manatee Springs, Wakulla Springs) particularly in the areas near the head spring, may decrease redox heterogeneity and overall redox potential in river sediments, with implications for the growth and vigor of the remaining SAV and impacting efforts to restore SAV communities via replanting.

6.7.4.4 Nitrate Effects

Our results suggest nitrate has no effect on SAV growth in Florida's spring-fed rivers. Water column NO_3-N concentration was uncorrelated with aboveground SAV productivity in Silver River and Alexander Springs Creek (R^2 = 0, p = 0.94). A two-sample t-test revealed no significant difference (p = 0.88) in SAV biomass growth between high and low N systems. This supports the hypothesis that SAV growth is primarily controlled by factors other than nitrate concentrations.

These results contribute to a large and growing body of evidence that primary productivity and SAV growth are not limited by nutrient supply in spring ecosystems (Duarte and Canfield 1990; Heffernan et al. 2010; Nifong et al. 2014). Submerged vascular plants are stoichiometrically homeostatic regardless of ambient nutrient ratios, and autotrophic NO_3-N demand is saturated at

low concentrations (Nifong et al. 2014). Generally in lotic systems, nutrient flux via advection is often sufficient to satisfy biological demand, even at low concentration (King et al. 2014).

The presumed association between nitrate concentration and primary productivity, exemplified by the primary role of N in establishing statewide numeric nutrient standards for springs, often overshadows the importance of other potential controls. However, this evidence substantiates the assertion that nitrate plays an insignificant role in SAV growth. A broader systems-level view of the controls on SAV growth – one that explicitly includes considerations of light, redox potential, herbivory, velocity and micronutrients – may be necessary to enable effective spring ecosystem management.

6.7.4.5 Gross Primary Production

Primary production and respiration (i.e., metabolism) are the foundation of ecosystem energy and elemental processing. Gross Primary Production (GPP), the aggregate photoautotroph fixation of carbon, is central to understanding ecosystem function. While GPP is measured at the ecosystem scale using diel variation in dissolved oxygen, it is often difficult to disaggregate these reach scale estimates into contributions from different vegetation types. For this work, we estimated the SAV contribution to GPP based on measurements of aboveground SAV biomass accrual rates, which measures net primary production (NPP, defined as GPP less autotroph respiration, R):

$$GPP = NPP + R$$

Aboveground net primary production (ANPP) was converted to total net primary production (NPP; i.e., including belowground productivity) by multiplying by 1.33 to account for belowground SAV biomass. This value was obtained from the average SAV root-to-shoot biomass ratios measured during vegetation surveys on Silver River (Wigand et al. 1997; Van et al. 1999; Bailey and Inglett 2012, Cohen et al. 2015). NPP was converted to GPP by assuming autotrophic respiration was 50 % of GPP (Hall and Tank 2003). The resulting GPP estimate (g biomass m^{-2} d^{-1}) was converted to C fixed per unit area (g C m^{-2} d^{-1}) using mean foliar C content for *S. kurziana* and *V. americana* blades (36.8 % and 34.2 %, respectively), measured during a recent vegetation survey of Silver River (Cohen et al. 2015). Finally, to compare SAV growth rates to open channel metabolism measurements, GPP was converted from C to O_2 based on the ratio (32:12) of molecular weights.

Based on these assumptions and observed growth rates, it was estimated that SAV accounted for 2.43 g O_2 m^{-2} d^{-1} and 2.47 g O_2 m^{-2} d^{-1} of ecosystem GPP in Silver River and Alexander Springs Creek, respectively (Figure 6.121). In Silver River, GPP_{SAV} estimates range from 0.27 to 5.67 g O_2 m^{-2} d^{-1} across sites, with approximately equivalent upstream (2.41 g O_2 m^{-2} d^{-1}) and downstream (2.44 g O_2 m^{-2} d^{-1}) GPP. In Alexander Springs Creek, GPP_{SAV} estimates have a similar range from 0.95 – 4.57 g O_2 m^{-2} d^{-1}, but mean upstream GPP_{SAV} (3.32 g O_2 m^{-2} d^{-1}) exceeds downstream GPP_{SAV} (2.27 g O_2 m^{-2} d^{-1}). We note that we cannot estimate the contributions of other taxa (e.g., *Hydrilla, Potamegeton, Ceratophyllum*).

These GPP_{SAV} estimates are lower than open channel metabolism measurements made during the same time period. From May 2015 – December 2016, mean open-channel GPP was 8.76 g O_2 m^{-}

^{2} d^{-1} (± 2.79 g O_2 m^{-2} d^{-1}) in the upper Silver River and 10.62 g O_2 m^{-2} d^{-1} (± 3.28 g O_2 m^{-2} d^{-1}) in the lower Silver River (Kirk unpublished data), indicating that SAV accounts for 25% of ecosystem GPP and may not be the primary component of GPP in Florida springs.

The relative contribution of SAV to ecosystem GPP in Silver River and Alexander Springs Creek from this study is consistent with the St. Lawrence River, where SAV accounts for 27 % of the annual C budget (Vis et al. 2007). In the St. Lawrence River, total annual primary production is nearly equally distributed between submerged macrophytes, phytoplankton (34 %), epiphyton (16 %), and emergent macrophytes (23%; not accounted for in this study).

Two plausible explanations exist for the small fraction of open-channel GPP that can be attributed to these measured SAV growth rates. First, benthic and epiphytic algae may account for much of the GPP; their rapid turnover rate (Odum 1957b) and relative abundance in many of Florida's springs, even under historical conditions, may enable a disproportionate metabolic contribution. Second, systematic bias in site selection, discussed above in comparison with prior estimates in these and other spring-fed rivers, would lead to underestimates of the SAV contribution to GPP. Specifically, the densest SAV is typically in deep, well-lit regions of the channel, but our measurements were in shallower water, typically near the channel margins. Therefore, it is likely that this study undersampled SAV productivity and neglected potentially significant taxa (e.g., hydrilla), warranting further investigation into the role of SAV in ecosystem metabolism.

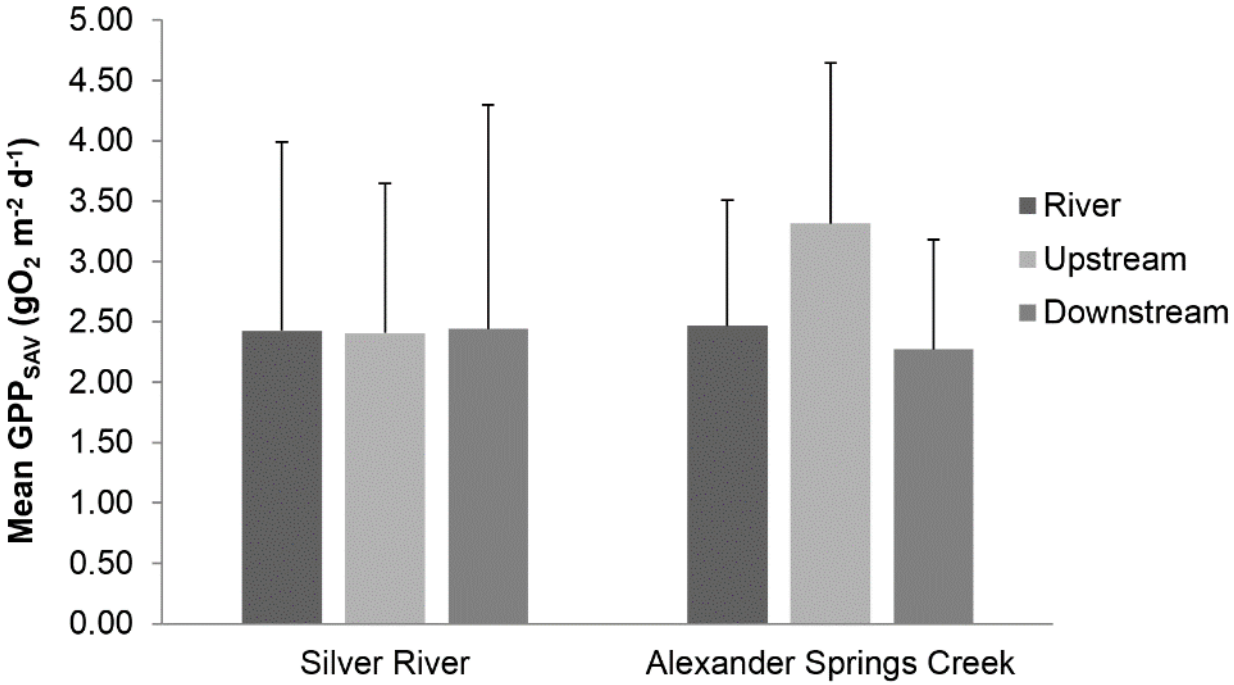

Figure 6.122. Comparison of river, upstream, and downstream GPP_{SAV} calculations in Silver River and Alexander Springs Creek shown with 95 % confidence intervals. Estimates account for the aboveground and belowground SAV component of ecosystem GPP.

6.7.5 Conclusions

Results from this study contribute to an improved understanding of the growth characteristics and controls on productivity of submerged aquatic vegetation in Florida's spring-fed rivers. It is clear that SAV productivity is highly conditional and controlled by a complex array of variables, primarily light, sediment redox conditions, and porewater SRP; however, growth appears to be relatively predictable and consonant across springs. These findings are critically important for SAV restoration and should be considered for effective spring ecosystem management.

6.8 SUMMARY AND MANAGEMENT IMPLICATIONS

We summarize the findings of this element of the CRISPS project in four areas, with key conclusions and management implications for each.

Our assessment of open-channel nutrient and oxygen dynamics lasted between 2015 and 2017 and revealed strong signals of metabolic imprinting (i.e., clear diel signals) on relatively constant spring-vent chemistry. Data of particular relevance were dissolved oxygen, from which we estimated primary production and respiration, nutrients (nitrate and phosphate) from which we inferred nutrient assimilation as well as retention due to heterotrophic pathways, and a suite of other solutes (fDOM, turbidity, specific conductance, pH) that were explored as possible controls on primary production as well as signals of water source shifts. Our results indicate several key findings:

- Silver River is, over most of its length, net heterotrophic, with ecosystem respiration (ER) exceeding gross primary production (GPP) by roughly 20 %. The exception is in the upper river, roughly consonant with the reach studied historically, over which the river is net autotrophic (GPP > ER). Significant allochthonous sources of organic matter from the floodplain allow the river to be net heterotrophic and still clearly export particulate and dissolved organic matter (OM). Alexander Springs Creek (spring to Tracy Canal) is net autotrophic. We note that these results depend strongly on models developed for flow velocity in the river, which impacts the reaeration fluxes and in turn strongly influences inference of respiration.
- There is a marked decline in GPP with distance downstream in Silver River (there was only one reach on Alexander). This appears largely due to changes in river morphology, with narrower channel width limiting light availability in the lower river. There is also clear signals in response to extreme climate events (e.g., Hurricane Matthew depressed metabolism in Alexander Springs Creek for nearly 3 weeks). There was also considerable year-to-year variation, with 2015 exhibiting 20-30 % lower GPP and ER than 2016 in the upper half of Silver River.
- In spite of dramatic differences between rivers with respect to nitrate concentrations, primary production did not differ significantly. Mean GPP in the upper half of Silver River (headspring to S5) was 7.8 g O_2 m^{-2} d^{-1}, and it was slightly higher (8.3 g O_2 m^{-2} d^{-1}) in Alexander Springs Creek. However, there was a significant difference in ER with Silver River much higher (11.1 g O_2 m^{-2} d^{-1}) than Alexander Springs Creek (6.9 g O_2 m^{-2} d^{-1}). We infer that floodplain or more distal sources of OM are greater in Silver River.

- In the upper river (headspring to SILGOLD), which roughly corresponds with the reach that has been historically measured (e.g., Odum 1957, Knight 1980, Munch et al. 2006), we observed GPP values (mean ~ 16 g O_2 m^{-2} d^{-1}) similar or slightly in excess of the earliest measurements (Odum 1957, Knight 1980), and greater than more recent measurements (Munch et al. 2006) that impled a systemic decline in primary production. The location of SILGOLD slightly upstream of the historical measurement site was necessary to sample Silver River water, not discharge emanating from the Ft. King Waterway.
- We developed a benthic light availability model that takes measured open-sky irradiance and adjusts this input based on the angles of solar inputs, canopy cover (from MODIS leaf area index estimates) as well as river (azimuth) and canopy geometry (height, channel overhang). This model suggests that a small fraction (ca. 30 %) of the incident light reaches the river surface. We further evaluated the attenuation of light through the water column based on continuous measurements of fDOM (colored organic matter) and turbidity. This model dramatically improved our ability to predict day-to-day and seasonal variation in GPP with the resulting models generally explaining 70-80 % of the GPP variation.
- *In situ* nutrient sensors for nitrate (NO_3) and phosphate (PO_4) revealed strong diel signals interpreted as autotrophic assimilation; these open-channel sensor measurements were available for Silver River only. The diel method for integrating these signals suggests that autotrophs in Silver River induce roughly 70 µg N L^{-1} diel nitrate concentration variation and 8 µg P L^{-1} diel phosphate variation. Given flow and benthic area, we estimate N assimilation to be 128 mg N m^{-2} d^{-1} and P assimilation to be 13 mg P m^{-2} d^{-1}. Given metabolic fluxes of C, we estimate C:N ratios for the upper and lower Silver River, respectively, of 14 and 23, consistent with the stoichiometry expected due to dominance by vascular plants in the lower river, and greater algal (i.e., lower C:N) contribution in the upper river. C:P ratios in the lower river are near 500, consistent with both algal and vascular plant tissue stoichiometry. In the upper Silver River, C:P ratios are implausibly low (~ 110) suggesting a geogenic sink for P. The diel signals suggest N assimilation is contemporaneous with photosynthesis, but that P assimilation lags GPP by roughly 7 hours. Most importantly, the mass flux of N is dominated by heterotrophic processes (e.g., net denitrification), representing nearly 75% of total N retention, not assimilation. This is consistent with similar measurements in other springs, and other modes of inference about N retention in Silver River.
- The total assimilatory flux of N and P in the river between the headsprings and S5 (ca. 5 km) assuming no nutrient recycling is small compared to river supply. We estimate that the ecosystem demand for N is roughly 1.22 % of N supply, and that P demand is 5.5 % of supply. Historical N concentrations (0.05 mg N L^{-1}) would still more than satisfy N demand, with current assimilatory demand representing 34 % of historical loading, even without N remineralization. GPP rates in Alexander Springs Creek, where nitrate concentrations are at background levels, are equal or greater than in Silver River, suggesting sufficient N supply to sustain demand even under pre-development conditions. These observations indicate that N limitation of primary producers is, and historically was, unlikely.

We conducted a benthic survey of Silver River in 2015 intended to provide a snapshot of river condition and chemical and biological heterogeneity from which to select subsequent sampling locations. The results of that survey yielded several important findings:

- Most of the river exhibited high SAV cover, with 75 % of random sites exhibiting greater than 75 % SAV cover, and only 10 % of sites exhibiting less than 50% cover. In contrast, algal cover was generally lower, with 50 % of sites exhibiting less than 50 % cover.
- There was a weak but significant negative association between observed SAV and algal cover, suggestive of a competitive interaction. Notably, when SAV cover was low (<50 %), algal cover was generally high (> 50 %), but sites with high SAV cover had algal cover spanning the entire range.
- There were no clear trends in SAV biomass, root:shoot allocation, stoichiometry or blade length. However, there was a strong longitudinal trend in algal cover, with prevalence declining dramatically in the lower river.
- We observed longitudinal variation in several water column, sediment, and porewater measurements. Most notably, water column ammonium and phosphate concentrations increase with distance downstream, and sediment Ca and organic matter concentrations decline in the lower river.
- We observed a weak but significant negative association between measurement surface water velocity and algal cover, suggesting scour impacts on biomass accrual. However, the 0.25 m s^{-1} threshold observed elsewhere was not clear from these measurements.
- We explored water chemistry controls on algal and SAV spatial variation, and observed several modest associations. Algal cover increased with soil Ca and P concentrations, and SAV appeared to decline significantly with porewater and water column Cl, porewater Ca and % clay. Overall, the best predictor of SAV cover was algal cover, and vice versa.

We developed and implemented a new chamber-based method for measuring nutrient limitation and examining nutrient dynamics for this project. The benthic boxes we developed were deployed in both Silver River and Alexander Springs Creek, with over 50 weeklong deployments of four boxes (1 control, 3 treatment chambers). Using this design, we investigated the controls on metabolism at the point scale (i.e., inside the control boxes based on DO variation), nutrient limitation of primary production (exploring N, P and Fe limitation), and used continuous nitrate sensors to understand N retention dynamics at below-ambient concentrations. We identified several important results:

- GPP inside the control boxes was highly variable across sites, and highly predictable (R^2 > 0.8) based on incident light and water depth. There was evidence of a modest sediment effect in Silver River (GPP in flocculent and mixed sediments was greater than in sandy sediments), and clear seasonality.
- Despite significant variation, there was no clear nutrient enrichment treatment effect on gross primary production in Silver River, either for the GPP response ratio (i.e., $GPP_{treatment}$:$GPP_{control}$) or when the response ration was further conditioned on biomass standing stock. In Alexander Springs Creek, we observed

a consistent inhibitory effect of added P, but no effect of N or Fe despite low ambient levels of both solutes. Notably, when we pooled treatments to reveal the effect of a single nutrient addition (added alone or in combination), we observed a weak but significant Fe enrichment effect, and no significant nutrient enrichment effect in Alexander Springs Creek. Given the robust nature of metabolism responses to light and depth variation, these results suggest that nutrient enrichment has limited impact on primary production.

- In each chamber, we also deployed algal growth tiles to isolate the effects of nutrient enrichment on algal growth. Tile growth rates in the control chambers were not significantly different between Silver River and Alexander Springs Creek despite the significant differences in ambient river water chemistry. Also notable was that algal growth on the tiles was not strongly associated with GPP, suggesting that the local controls on algal abundance are not the same as those that control ecosystem productivity. There was a statistically significant effect of single N, P and Fe additions in Silver River, but surprisingly no significant effect when nutrients were added in combination. When isolating a specific nutrient, only Fe exhibited a significant growth response in Silver River, and none of the three nutrients impacted algal growth in Alexander Springs Creek.
- Deploying *in situ* nitrate sensors in the control boxes yielded invaluable information about the N cycle in these systems. Of particular note is the consistency between the chamber measurements and open channel measurements with regard to the magnitude of assimilatory retention, and the dominance of heterotrophic N retention processes. Over each weeklong chamber deployment, there was clear evidence of N depletion, such that the terminal concentrations were near historical background levels despite starting at 1.3 mg N L^{-1} in Silver River. The stair-step dynamics illustrates the concatenation of multiple retention processes, and model fitting to these time series enabled estimation of both the rates and kinetics of the key processes. Of particular note is the finding that a simple 2-process model (assimilation in proportion to solar forcing and denitrification) was best able to adequately fit the time-series in 85% of cases. The inferred rates were remarkably consistent with measured open channel rates, but this approach allowed us to explore what happens when concentrations fall below ambient. In Alexander Springs Creek, we used this to explore what happens with nitrate enrichment as well.
- There is strong evidence to support modeling denitrification as a 1^{st} order process (i.e., retention rates strongly covarying with concentration). Most of the deployments (n = 25) had reaction kinetic orders between 0.75 and 1. This is consistent with literature observations, but is the first time that this has been demonstrated over such a large concentration gradient using *in situ* measurements.
- Even more importantly, the kinetics of nitrate assimilation are close to zero order (i.e., independent of concentration), with the mean kinetic exponent below 0.2. This means that N uptake is not strongly influenced by concentration. Clearly, extrapolating this logic to all concentrations is flawed, but over the large range of concentrations observed, the weak response to time-varying concentration is suggestive of N saturation. Evidence of Monod kinetics (with zero-order kinetics

at high concentrations and 1st order kinetics at low concentration) is an area for further research, particularly since the half-saturation constant specific to Monod kinetics could of considerable regulatory interest.

- Finally, there was no association between nitrate concentration and GPP. This zero-order association suggests that even where there is some kinetic response in nitrate assimilation to changing concentrations, the autotrophs are, at least for short deployment periods, fully capable of utilizing other external or internal sources of N to support growth. Indeed, despite dramatic declines in N availability over the week-long chamber deployments, GPP actually increased with time. This suggests that efforts to reduce N concentrations in springs may not induce N limitation and thus have limited impact of autotroph structure, biomass accrual, and composition.

In an effort to better understand the controls on SAV growth in springs, and predict the conditions that lead to decline or enhance restoration, we accomplished 18 months of SAV growth measurements at 16 sites in Silver River, and 12 months of growth at 16 sites in Alexander Springs Creek. From these measurements, we identified 4 key findings:

- SAV growth is high spatially variable in both rivers, with site means ranging over an order of magnitude in both rivers (between 0.4 and 2 g dry mass m^{-2} d^{-1}). Spatial variation was much larger than temporal variation, though there was clear evidence of seasonality, with peak SAV growth in the summer, and low growth between December and March.
- SAV growth rates were not significantly different between rivers, nor between taxa. Growth rates were strongly correlated with standing stock biomass in Alexander Springs Creek, but were, surprisingly, uncorrelated with biomass in Silver River. Sampling logistics precluded measurements in the deepest, most productive parts of Silver River, which may explain this result.
- Univariate controls on SAV growth were generally poor, but multivariate models were reasonably successful ($R^2 \sim 0.5$) at predicting the observed spatial variation. We used two multivariate methods, and both methods identified light as the dominant control, with porewater SRP uniformly inhibiting SAV growth, and redox potential uniformly positively associated with SAV growth. The consonance of models across methods and rivers lends strong support for the dominant control variables identified and points to redox and light management as key factors for both ecosystem management and restoration. The inhibitory effects of porewater SRP are poorly understood and merit further research.
- Despite significant SAV growth, our results suggest that in both rivers, SAV contributes approximately 25 % of primary production (measured using open channel metabolism, and adjusted to estimate net production). This suggests that primary production due to other autotrophs, or in locations that were unable to be sampled, are critically important for riverine primary production.

6.9 REFERENCES

Albertin, A. R., Sickman, J. O., Pinowska, A., and Stevenson, R. J. 2012. Identification of nitrogen sources and transformations within karst springs using isotope tracers of nitrogen. Biogeochemistry 108: 219-232.

Alexander Springs. St. Johns River Water Management District. Website. 12 January 2016. http://floridaswater.com/springs/alexander.html

Aung, L. H. 1974. Root-shoot relationships. The Plant Root and Its Environment, University Press of Virginia, Charlotte, pp. 29-61

Bailey, E., and Inglett, P. (2012). Effects of Sediments on the growth of *Vallisneria americana* in Lake Apopka.

Barko J. W., Smart, R. M., McFarland, D. G., and Chen, R. L. (1988) Interrelationships between the growth of *Hydrilla verticillata* (Lf) Royle and sediment nutrient availability. Aquatic Botany 32:205-216

Barko, J. W., Gunnison, D., and Carpenter, S. R. (1991). Sediment interactions with submersed macrophyte growth and community dynamics. Aquatic Botany, 41(1), 41-65.

Barko, J. W. and R. M. Smart. 1986. Sediment-related mechanisms of growth limitation in submersed macrophytes. Ecology 67: 1328-1340

Barko, J. W. and Smart, R. M. 1981. Comparative influences of light and temperature on the growth and metabolism of selected submersed freshwater macrophytes. Ecological Monographs, 51: 219-235.

Barko, J. W., Hardin, D. G., and Matthews, M. S. 1982. Growth and morphology of submersed freshwater macrophytes in relation to light and temperature. Canadian Journal of Botany, 60: 877-887.

Barko, J .W, and James, W. F., 1998. Effects of submerged aquatic macrophytes on nutrient dynamics, sedimentation, and resuspension. The Structuring Role of Submerged Macrophytes in Lakes. Springer, pp. 197-214.

Barko, J. W., Smart, R. M., and McFarland, D. G. 1991. Interactive effects of environmental conditions on the growth of submersed aquatic macrophytes. Journal of Freshwater Ecology, 6: 199-207.

Batiuk, R., Bergstrom, P., Kemp, M., Koch, E., Murray, L., Stevenson, C., Bartleson, R., Carter, V., Rybicki, N., Landwehr, J., Gallegos, C., Karrh, L., Naylor, M., Wilcox, D., Moore, K., Ailstock, S., and Teichberg, M. 2000. Chesapeake Bay submerged aquatic vegetation water quality and habitat-based requirements and restoration targets: A second technical synthesis. CBP/TRS 245/00. EPA 903-R-00-014, U.S. EPA, Chesapeake Bay Program.

Bernhardt, E. S., and Likens, G. E. (2002), Dissolved organic carbon enrichment alters nitrogen dynamics in a forest stream. Ecology, 83, 1689-1700 doi: 10.1890/0012-9658(2002)083[1689:DOCEAN]2.0.CO;2

Bernhardt, E. S., Hall Jr, R. O., and Likens, G. E. (2002), Whole-system estimates of nitrification and nitrate uptake in streams of the Hubbard Brook Experimental Forest. Ecosystems, 5, 419-430 doi: 10.1007/s10021-002-0179-4

Best, E. P. H. 1980. Effects of nitrogen on the growth and nitrogenous compounds of *Ceratophyllum demersum*. Aquatic Botany 8: 197-206.

Biggs, B. J. F., 1996. Hydraulic habitat of plants in streams. Regulated Rivers: Research & Management 12: 131-144.

Boedeltje, G., Alfons, A. J., Smolders, J. P., and. Roellofs, J. G. M. 2005. Combined effects of

water column nitrate enrichment, sediment type and irradiance on growth and foliar nutrient concentration of *Potamogeton alpines*. Freshwater Biology 50: 1537-1547.

Borchardt, M. A., 1996. Nutrients. In Stevenson, R.J., M.L. Bothwell & R.L. Lowe, Algal Ecology: Freshwater Benthic Ecosystems. Academic Press, San Diego, CA: 183-227.

Bormann, F. H., and Likens, G. E. 1967. Nutrient cycling. Science, 155, 424-429, doi: 10.1126/science.155.3761.424

Borum, J. 1985. Development of epiphytic communities on eelgrass (*Zostera marina*) along a nutrient gradient in a Danish estuary. Marine Biology 87: 211-218.

Brabandere, L. D., Frazer, T. K., and Montoya, J. P. (2007). Stable nitrogen isotope ratios of macrophytes and associated periphyton along a nitrate gradient in two subtropical, spring-fed streams. Freshwater Biology, 52(8), 1564-1575.

Bristow, J. M., and Whitcombe, M. 1971. The role of roots in the nutrition of aquatic vascular plants. American Journal of Botany 58(1).

Bulthuis, D. A., and W. J. Woelkerling. 1983. Biomass accumulation and shading effects of epiphytes on leaves of the seagrass, *Heterozostera tasmanica*, in Victoria, Australia. Aquatic Botany, 16: 137-148.

Burgin, A. J., and Hamilton, S. K. 2007. Have we overemphasized the role of denitrification in aquatic ecosystems? A review of nitrate removal pathways, Frontiers in Ecology and the Environment 5, 89-96 doi: 10.1890/1540-9295(2007)5[89:HWOTRO]2.0.CO;2

Burkholder, J. M., Mason, K. M., and Glasgow, Jr., H. B. 1992. Water column nitrate enrichment promotes decline of eelgrass *Zostera marina*: evidence from seasonal mesocosm experiments. Marine Ecological Progress Series 81: 163-178.

Burkholder, J. M., Mason, K. M., and Glasgow, Jr., H. B. 1992. Water column nitrate enrichment promotes decline of eelgrass *Zostera marina*: evidence from seasonal mesocosm experiments. Marine Ecological Progress Series 81: 163-178.

Butcher, R. W., 1927. A preliminary account of the vegetation of the River Itchen. Journal of Ecology 15:55-65

Butcher, R. W., 1933. Studies on the ecology of rivers: I. On the distribution of macrophytic vegetation in the rivers of Britain. Journal of Ecology 21: 58-91.

Caffrey, J. M., and Kemp, W. M. 1992. Influence of the submersed plant, *Potamogeton perfoliatus*, on nitrogen cycling in estuarine sediments. Limnology and Oceanography, 37(7).

Camp, E. V., Staudhammer, C. L., Pine, W. E., Tetzlaff, J. C., and Frazer, T. K. 2014. Replacement of rooted macrophytes by filamentous macroalgae: effects on small fishes and macroinvertebrates. Hydrobiologia, 722(1), 159-170.

Canfield, D. E. and Hoyer, M. V. 1988. Influence of nutrient enrichment and light availability on the abundance of aquatic macrophytes in Florida streams. Canadian Journal of Fisheries and Aquatic Sciences 45: 1467 -1472.

Canfield, D.E., Langeland, K. A., Lindea, S. B., and Haller, W. T. 1985. Relations between water transparency and maximum depth of macrophyte colonization in lakes. Journal of Aquatic Plant Management, 23: 25-28.

Caraco, N. F., and Cole, J. J., 2002. Contrasting impacts of a native and alien macrophyte on dissolved oxygen in a large river. Ecological Applications 12, 1496-1509.

Carignan, R. 1982. An empirical model to estimate the relative importance of roots in phosphorus uptake by aquatic macrophytes. Candian Journal of Fisheries and Aquatic Sciences 39.

Carpenter, S. R., Elser, J. J., and Olson, K. M. 1983. Effects of roots of *Myriophyllum verticillatum* L. on sediment redox conditions. Aquatic Botany, 17(3), 243-249.

Carpenter, S. R., 1980. Enrichment of Lake Wingra, Wisconsin, by submersed macrophyte decay. Ecology, 61, 588-602.

Carpenter, S. R., and Lodge, D. M. 1986. "Effects of submersed macrophytes on ecosystem processes." Aquatic botany 26: 341-370.

Cedergreen, N. and Madsen, T.V. 2003. Nitrate reductase activity in roots and shoots of aquatic macrophytes. Aquatic Botany 76: 203-212

Chambers, P. A., Prepas, E. E., Bothwell, M. L., and Hamilton, H. R. 1989. Roots versus shoots in nutrient uptake by aquatic macrophytes in flowing waters. Canadian Journal of Fisheries and Aquatic Sciences, 46(3), 435-439.

Chapra, S. C., and Di Toro, D. M. 1991. Delta method For estimating primary production, respiration, and reaeration in streams. Journal of Environmental Engineering 117: 640-655.

Christensen, P. B., Nielsen, L. P., Sorensan, J., and Revsbach, N. P. 1990. Denitrification in nitrate-rich stream: Diurnal and seasonal variation related to benthic oxygen metabolism. Limnology and Oceanography 35: 640–651, doi:10.4319/lo.1990.35.3.0640

Clark L. A., Pregibon D. 1992. Tree-based models. In: Chambers JM, Hastie TJ (eds) Statistical models S. Pacific Grove (CA): Wadsworth, p 377–419.

Clark, E. and Baldwin, H.A. 2002. Responses of wetland plants to ammonia and water level. Ecological Engineering 18: 257-264.

Cogger, C. G., Kennedy, P. E., and Carlson, D. 1992. Seasonally saturated soils in the Puget Lowland II. Measuring and interpreting redox potentials. Soil Science, 154(1), 50-58.

Cohen, M. J., Heffernan, J. B., Albertin, A., and Martin, J. B. 2012. Inference of riverine nitrogen processing from longitudinal and diel variation in dual nitrate isotopes. Journal of Geophysical Research: Biogeosciences, 117(G1).

Cohen, M. J., Kurz, M. J., Heffernan, J. B., Martin, J. B., Douglass, R. L., Foster, C. R., and Thomas, R. G. 2013. Diel phosphorus variation and the stoichiometry of ecosystem metabolism in a large spring-fed river. Ecological Monographs, 83, 155-176, doi: 10.1890/12-1497.1

Cohen, M., Lamsal, S. and Kohrnak, L. 2007. Sources, transport, and transformations of nitrate-N in the Florida environment. Special Publication 2007-10. St. Johns River Water Management District. Palatka, Florida, USA.

Cohen, M. J., Heffernan, J. B., Albertin, A., Hensley, R., Fork, M., Foster, C., and Korhnak, L. 2013b. Mechanisms of nitrate removal in spring-fed rivers. St. Johns River Water Management District Special Publication 2013-SP2. Palatka, Florida USA.

Cohen, M. J., Kurz, M. J., Heffernan, J. B., Martin, J. B., Douglass, R. L., Foster, C. R., and Thomas, R. G. 2013a. Diel phosphorus variation and the stoichiometry of ecosystem metabolism in a large spring-fed river. Ecological Monographs 83:155–176.

Copeland, R., Doran, N. A., White, A. J., and Upchurch, S. B. 2009. Regional and Statewide Trends in Florida's Spring and Well Groundwater Quality (1991-2003). Bulletin No. 69. Florida Geological Survey, Tallahassee, Florida.

Covino, T. P., McGlynn, B. L., and McNamara, R. A. 2010. Tracer Additions for Spiraling Curve Characterization (TASCC): Quantifying stream nutrient uptake kinetics from ambient to saturation. Limnology and Oceanography: Methods 8: 484–498, doi:10.4319/lom.2010.8.484

Crowder, L. B., and Cooper, W. E. 1982. Habitat structural complexity and the interaction between bluegills and their prey. Ecology, 63(6), 1802-1813.

Dawes, C. J., and Lawrence, J. M. (1979) Effects of blade removal on the proximate composition of the rhizome of the seagrass *Thalassia testundinum* Banks ex Konig. Aquatic Botany 7:255-266

Dennison, W. C., Orth, R. J., Moore, K. A., Stevenson, J. C., Carter, V., Kollar, S., Bergstrom, P.W., and Batiuk, R.A. 1993. Assessing water quality with submersed aquatic vegetation: Habitat requirements as barometers of Chesapeake Bay health. Bioscience, 43: 86-94.

Diehl, S., and Kornijow, R. 1998. Influence of submerged macrophytes on trophic interactions among fish and macroinvertebrates. The Structuring Role of Submerged Macrophytes in Lakes. Springer, pp. 24-46.

Dierberg, F. E., DeBusk, T. A., Jackson, S. D., Chimney, M. J., and Pietro, K. 2002. Submerged aquatic vegetation-based treatment wetlands for removing phosphorus from agricultural runoff: response to hydraulic and nutrient loading. Water Research 36:1408–1422

Dobberfuhl, D. R. 2007. Light limiting thresholds for submerged aquatic vegetation in a blackwater river. Aquatic Botany, 86: 346-352.

Dodds, W. K., Martí, E., Tank, J. L., Pontius, J., Hamilton, S. K., Grimm, N. B., Bowden, W. B., McDowell, W. H., Peterson, B. J., Valett, H. M., and Webster, J. R. 2004. Carbon and nitrogen stoichiometry and nitrogen cycling rates in streams. Oecologia, 140, 458-467 doi:10.1007/s00442-004-1599-y

Doyle, R. D. 2000. Effects of Navigation on Aquatic Plants: Effects of Sediment Resuspension and Deposition on Plant Growth and Reproduction. Upper Mississippi River - Illinois Waterway System Navigation Study, ENV Report.

Drew, M. C., and Lynch, J. 1980. Soil anaerobiosis, microorganisms, and root function. Annual Review of Phytopathology, 18(1), 37-66.

Duarte, C. M. 1991. Seagrass depth limits. Aquatic Botany, 27: 15-26.

Duarte, C. M. 2002. The future of seagrass meadows. Environmental Conservation, 29: 192-206.

Duarte, C. M., 1995. Submerged aquatic vegetation in relation to different nutrient regimes. Ophelia 41: 87-112.

Dudgeon, D., A.H. Arthington, M.O. Gessner and Z. Kawabata. 2006. Freshwater biodiversity: importance, threats, status and conservation challenges. Biological reviews 81: 163-182.

Dunn, A. E., Dobberfuhl, D. R., and Casamatta, D. A. 2008. A survey of algal epiphytes from *Vallisneria americana* Michx. (Hydrocharitaceae) in the Lower St. Johns River, Florida. Southeastern Naturalist, 7: 229-244.

Dunton, K. 1990. Production ecology of *Ruppia maritima* L. s.l. and *Halodule wrightii* Aschers. in two subtropical estuaries. Journal of Experimental Marine Biology and Ecology 143: 147-164.

Dzialowski, A. R., Wang,S. H., Lim, N. C., and Spotts, W. W. 2005. Nutrient limitation of phytoplankton growth in central plains reservoirs, USA. Journal of Plankton Research 27: 587-595.

Ensign, S. H., and Doyle, M. W. 2006. Nutrient spiraling in streams and river networks. Journal of Geophysical Research 111: G04009, doi:10.1029/2005JG000114

Fiedler, S., Vepraskas, M. J., and Richardson, J. L. 2007. Soil redox potential: importance, field measurements, and observations. Advances in Agronomy, 94, 1-54. Florida Department of Environmental Protection, 2012. Numeric Nutrient Criteria Paragraph 62-302.530(47)(b)

French, G. T. and Moore, K. A. 2003. Single and Interactive effects of light and salinity stress on the growth, reproduction and photosynthetic capabilities of *Vallisneria americana*. Estuaries, 26: 1255-1268.

Gallegos, C. L. 1994. Refining habitat requirements of submersed aquatic vegetation: role of optical models. Estuaries, 17: 198-219.

Gallegos, C. L. 2005. Optical water quality of a blackwater river estuary: the Lower St. Johns River, Florida, USA. Estuarine, Coastal and Shelf Science 63, 57-72.

Gammons, C. H., Babcock, J. N.,Parker, S. R., and Poulson, S. R. 2011. Diel cycling and stable isotopes of dissolved oxygen, dissolved inorganic carbon, and nitrogenous species in a stream receiving treated municipal sewage. Chemical Geology, 283, 44-55 doi:10.1016/j.chemgeo.2010.07.006

Goldsborough, W. J. and Kemp, W. M. 1988. Light responses of a submersed macrophyte: Implications for survival in turbid tidal waters. Ecology, 69: 1775-1786.

Greenway, M. 1974. The effects of cropping on the growth of the *Thalassia testudinum* (nig) in Jamaica. Aquaculture 4:199 – 206

Gruber, N., and Galloway, J. N. 2008. An Earth-system perspective of the global nitrogen cycle. Nature, 451, 293-296 doi:10.1038/nature06592

Hall, R. O., Tank, J. L., Sobota, D. J., Mulholland, P. J., O'Brien, J. M., Dodds, W. K., Webster, J. R., Valett, H. M., Poole, G. C., Peterson, B. J., Meyer, J. L., McDowell, W. H., Johnson, S. L., Hamilton, S. K., Grimm, N. B., Gregory, S. V., Dahm, C. N., Cooper, L. W., Ashkenas, L. R., Thomas, S. M., Sheibley, R. W., Potter, J. D., Niederlehner, B. R., Johnson, L. T., Helton, A. M., Crenshaw, C. M., Burgin, A. J., Bernot, M. J., Beaulieu, J. J., and Arango, C. P. 2009. Nitrate removal in stream ecosystems measured by 15N addition experiments: Total uptake. Limnology and Oceanography 54: 653–665, doi:10.4319/lo.2009.54.3.0653

Hall, R. O., and Tank, J. L. 2003. Ecosystem metabolism controls nitrogen uptake in streams in Grand Teton National Park, Wyoming, Limnology and Oceanography, 48, 1120–1128, doi:10.4319/lo.2003.48.3.1120

Hall, Jr., R. O., and Beaulieu, J. J. 2013. Estimating autotrophic respiration in streams using daily metabolism data, Freshwater Scence, 32, 507–516, doi:10.1899/12-147.1.

Harlin, M. M., and Thorne-Miller, B. 1981. Nutrient enrichment of seagrass beds in a Rhode Island coastal lagoon. Marine Biology. 65: 221-229.

Hauxwell, J., Cebrian, J. and Valiela, I. 2006. Light dependence of *Zostera marina* annual growth dynamics in estuaries subject to different degrees of eutrophication. Aquatic Botany 84: 17-25.

Hauxwell, J., Cebrian, J., Herrera-Silveira, J. A., Ramirez, J., Zaldivar, A., Gomez, N., Aranda- and Cirerol, N., 2001. Measuring production of *Halodule wrightii* Ascherson: additional evidence suggests clipping underestimates growth rate. Aquatic Botany 69: 41-54.

Hauxwell, J., Frazer, T. K., and Osenberg, C. W., 2003. Effects of herbivores and competing primary producers on *Vallisneria americana* in Kings Bay: implications for restoration and management. Final Report. Southwest Florida Water Management District, Surface Water Improvement and Management Program, Tampa, Florida. pp. 1-68.

Hauxwell, J., Frazer, T. K., and Osenberg, C. W., 2007. An annual cycle of biomass and productivty of *Vallisneria americana* in a subtropical spring-fed estuary. Aquatic Botany 87: 61-68.

Hauxwell, J., Osenberg, C. W., and Frazer, T. K. 2004. Conflicting management goals: manatees

and invasive competitors inhibit restoration of a native macrophyte. Ecological Applications 1: 571–586.

Heffernan, J. B., and Cohen, M. J. 2010. Direct and indirect coupling of primary production and diel nitrate dynamics in a subtropical spring-fed river. Limnology and Oceanography 55: 677–688, doi:10.4319/lo.2009.55.2.0677

Heffernan, J. B., Liebowitz, D. M., Frazer, T. K., Evans, J. M., and Cohen, M. J. 2010. Algal blooms and the nitrogen-enrichment hypothesis in Floria springs: evidence, alternatives, and adaptive management. Ecological Applications 20: 816-829.

Hensley, R. T., and Cohen, M. J. 2012. Controls on solute transport in large spring-fed karst rivers. Limnology and Oceanography, 57(4), 912-924.

Hensley, R. T., and Cohen, M. J. 2016. On the emergence of diel signals in flowing waters. Water Resources Research 52: 759–772, doi:10.1002/2015WR017895.

Hensley, R. T., Cohen, M. J., and Korhnak, L. V. 2014. Inferring nitrogen removal in large rivers from high resolution longitudinal profiling. Limnology and Oceanography 59: 1152–1170, doi:10.4319/lo.2014.59.4.1152.

Hensley, R. T., Cohen, M. J., and Korhnak, L. V. 2015. Hydraulic effects on nitrogen removal in a tidal springfed river. Water Resources Research 51: 1443–1456 doi:10.1002/2014WR016178

Hoyer, M., Frazer, T., and Notestein, S. 2004. "Vegetative characteristics of three low-lying Florida coastal rivers in relation to flow, light, salinity and nutrients."Hydrobiologia 528.1-3: 31-43.

Jacobs, R. P. W. M. 1979. Distribution and aspects of the production and biomass of eelgrass, Zostera marina L., at Roscoff, France. Aquatic Botany 7:151–172

Jacoby, C., Frazer. T., Swett, R., Keller, S., and Notestein, S. 2007. Kings Bay vegetation evaluation. Final report. Southwest Florida Water Management District. Brooksville, Florida. USA.

James, C., Fisher, J., and Moss, B. 2003. Nitrogen driven lakes: the Shropshire and Cheshire Meres. Archief fur Hydrobiologia 164: 249-266.

James, C., Fisher, J., Russell, V., Collings, S., and Moss, B. 2005. Nitrate availability and hydrophyte species richness in shallow lakes. Freshwater Biology 50: 1049-1063.

Jeppesen, E., Lauridsen, T. L., Kairesalo, T., and Perrow, M. R., 1998. Impact of submerged macrophytes on fish-zooplankton interactions in lakes. The Structuring Role of Submerged Macrophytes in Lakes. Springer, pp. 91-114.

Jetten, M. S. 2008. The microbial nitrogen cycle. Environmental Microbiology 10, 2903-2909 doi: 10.1111/j.1462-2920.2008.01786.x

Jones, G. W., Upchurch, S. B., and Champion, K. M.1996. Origin of nitrate in groundwater discharging from Rainbow Springs, Marion County, Florida. Southwest Florida Water Management District, Brooksville, FL.

Katz, B. G. 2004. Sources of nitrate contamination and age of water in large karstic springs in Florida. Environmental Geology 46: 689-706.

Kelly, M. H. and Gore, J. A. 2008. Florida river flow patterns and the Atlantic multidecadal oscillation. River Research and Applications 24: 598-616.

Kemp, M. J. and Dodds, W. K., 2002. The influence of ammonium, nitrate, and dissolved oxygen concentrations on uptake, nitrification, and denitrification rates associated with prairie stream substrata. Limnology and Oceanography, 47:1380-1393.

Kemp, W. M., Batiuk, R.,Bartleson, R., Bergstrom, P., Carter, V.,Gallegos, C.,Hunley,W.,

Karrh, L.,Koch, E. W., Landwehr, J., Moore, K., Murray, L., Naylor, M., Rybicki, N., Stevenson, J. C., and Wilcox, D. 2004. Habitat requirements for submerged aquatic vegetation in Chesapeake Bay: Water quality, light regime, and physical-chemical factors. Estuaries, 27: 363-377.

Kemp, W. M., Boynton, W. R., Twilley, R. R., Stevenson, J. C., and Means, J. C. 1983. The decline of submerged vascular plants in upper Chesapeake Bay: summary of results concerning possible causes. Marine Technology Society Journal, 17: 78-89.

Kenworthy, W. J. and Haunert, D. E. (eds.). 1991. The light requirements for seagrasses: proceedings from a workshop to examine the capability of water quality criteria, standards and monitoring programs to protect seagrasses. NOAA Technical Memorandum NMFS-SER C-287.

King, S. A. 2014. Hydrodynamic control of filamentous macroalgae in a sub-tropical spring-fed river in Florida, USA. Hydrobiologia 734: 27-37.

King, S. A., Heffernan, J. B., and Cohen, M. J. 2014. Nutrient flux, uptake, and autotrophic limitation in streams and rivers. Freshwater Science, 33(1), 85-98.

Kirchner, J. W., Feng, X., Neal, C., and Robson, A. J. 2004. The fine structure of water-quality dynamics: The (high-frequency) wave of the future, Hydrologic Processes, 18, 1353–1359, doi:10.1002/hyp.5537.

Kirk, J. T. O. 1994. Light and Photosynthesis in Aquatic Ecosystems. Cambridge University Press, Cambridge.

Korschgen, C. E. and Green, W. L. 1988. American wildcelery (Vallisneria americana): Ecological considerations for restoration. U.S. Fish and Wildlife Service, Fish and Wildlife Technical Report 19.

Kurz, M. J., Martin, J. B., Cohen. M. J., and Hensley, R. 2015. Diffusion and seepage-driven element fluxes from the hyporheic zone of a karst river. Freshwater Science 34: 206-221 doi: 10.1086/679654

Lapointe, B. E., Tomasko, D. A., and Matzie, W. R. 1994. Eutrophication and trophic state classification of seagrass communities in the Florida Keys. Bull Mar Sci 54:696–717

Liebig, J. (1840). Organic chemistry in its applications to agriculture and physiology. Friedrich Vieweg and Son Publishing, Braunschweig, Germany.

Liebowitz, D. M., Cohen, M. J., Heffernan, J. B., Frazer, T. K., and Korhnak, L. V. 2014. Environmentally-mediated consumer control of algae proliferation in Florida springs. Freshwater Biology, 59: 2009 - 2023

Maberly, S. C. 1993. Morphological and photosynthetic characteristics of Potamogeton obtusifolius from different depths. Journal of Aquatic Plant Management, 31: 34-39.

Maberly, S. C., King, L., Dent, M. M., Jones, R. I., and Gibson, C. E. 2002. Nutrient limitation of phytoplankton and periphyton growth in upland lakes. Freshwater Biology 47: 2136-2152.

Maddox, G. L., Lloyd, J. M., Scott, T. M., Upchurch, S. B., and Copeland, R. 1992. Florida's groundwater quality monitoring program, background geochemistry. Florida Geological Survey, Tallahassee, FL.

Madsen, J. D., Chambers, P. A., James, W. F., Kock, E. W., and Westlake, D. F. 2001. The interaction between water movement, sediment dynamics and submersed macrophytes. Hydrobiologia 444: 71–84.

Madsen, T. V., and Søndergaard, M. 1983. The effects of current velocity on the photosynthesis of *Callitriche stagnalis* Scop. Aquatic Botany, 15(2), 187-193.

Mattson, R. A., Lowe, E. F., Lippincott, C. L., Di, J., and Battoe, L. 2006. Wekiva River and Rock Springs Run Pollutant Load Reduction Goals. St. Johns River Water Management District, Palatka FL (1054 pp).

McKnight, D. M., and Bencala, K. E. 1990. The Chemistry of Iron, Aluminum, and Dissolved Organic Material in Three Acidic, Metal-Enriched, Mountain Streams, as Controlled by Watershed and in-Stream Processes, Water Resources Research, 26, 3087-3100, doi:10.1029/WR026i012p03087

Middelboe, A. L. and Markager, S. 1997. Depth limits and minimum light requirements of freshwater macrophytes. Freshwater Biology, 37: 553-568.

Mitchell, S. F., and Perrow, M. R. 1998. Interactions between grazing birds and macrophytes. The Structuring Role of Submerged Macrophytes in Lakes. Springer, pp. 3-23.

Moore, A., and Reddy, K. R. 1994. Role of Eh and pH on phosphorus geochemistry in sediments of Lake Okeechobee, Florida. Journal of Environmental Quality, 23(5), 955-964.

Moore, K. A. and Jarvis, J. C. 2008. Environmental factors affecting recent summertime eelgrass diebacks in the lower Chesapeake Bay: Implications for long-term persistence. Journal of Coastal Research, 55: 135-147.

Morgan, M. D. and Kitting, C. L. 1984. Productivity and utilization of the seagrass *Halodule wrightii* and its attached epiphytes. Limnology ad Oceanography 29: 1066-1076.

Morris, E. P., Morris, E. P., Peralta, G., Brun, F. G., van Duren, L., Bouma, T. J., and Perez-Llorens, J. L. 2008. Interaction between hydrodynamics and seagrass canopy structure: Spatially explicit effects on ammonium uptake rates. Limnology and Oceanography, 53(4), 1531–1539.

Mulholland, P. J., Hall, R. O., Sobota, D. J., Dodds, W. K., Findlay, S. E., Grimm, N. B., Hamilton, S. K., McDowell, W. H., O'Brien, J. M., Tank, J. L., Ashkenas, L. R., Cooper, L.W., Dahm, C. N., Gregory, S. V., Johnson, S. L., Meyer, J. L., Peterson, B. J., Poole, G. C., Valett, H. M., Webster, J. R., Arango, C. P., Beaulieu, J. J., Bernot, M. J., Burgin, A. J., Crenshaw, C. L., Helton, A. M., Johnson, L. T., Niederlehner, B. R., Potter, J. D., Sheibley, R. W., and Thomas, S. M. 2009. Nitrate removal in stream ecosystems measured by ^{15}N addition experiments: denitrification. Limnology and Oceanography 54: 666-680, doi: 10.4319/lo.2009.54.3.0666

Mulholland, P. J., and Hill, W. R. 1997. Seasonal patterns in streamwater nutrient and dissolved organic carbon concentrations: Separating catchment flow path and in-stream effects. Water Resources Research, 33, 1297-1306, doi:10.1029/97WR00490

Mulholland, P., Mulholland, P. J., Helton, A. M., Poole, G. C., Hall, Jr., R. O., Hamilton, S. K., Peterson, B. J.,Tank, J. L., Ashkenas, L. R., Cooper, L. W., Dahm, C. N., Dodds, W. K., Findlay, S. E. G., Gregory, S. V., Grimm, N. B., Johnson, S. L., McDowell, W. H., Meyer, J. L., Valett, H. M., Webster, J. R., Arango, C. P., Beaulieu, J. J., Bernot, M. J. ,Burgin, A. J., Crenshaw, C. L., Johnson, L. T., Niederlehner, B. R., O'Brien, J. M., Potter, J. D., Sheibley, R. W., Sobota, D. J., and Thomas, S. M. 2008. Stream denitrification across biomes and its response to anthropogenic nitrate loading. Nature, 452.

Mulholland, P. J., Valett, H. M., Webster, J. R., Thomas, S. A., Cooper, L. N., Hamilton, S., and Peterson, B. J. 2004. Stream denitrification and total nitrate uptake rates measured using a field ^{15}N tracer addition approach. Limnology and Oceanography 49:809-820.

Munch, D. A., Phlips, E. J., Allen, M. S., Knight, R. L., Toth, D. J., Huang, C., Davis, J. B., Fortich, C. M., Osburn, W. L., Quinlan, E. L., Woods, M. J., Cooney, P., Clarke, R. A.,

and Knight, S. L. 2006. Fifty-year retrospective study of the ecology of Silver Springs, Florida. SJ2007-SP4. St. Johns River Water Management District, Palatka, FL.

Neckles, H. A., Wetzel, R. L., amd Orth, R. J. 1993. Effects of nutrient enrichment and grazing on epiphyte-macrophyte (*Zostera marina* L.) dynamics. Oecologia 93: 285-295.

Nichols, D. S. and Keeney, D. R. 1976. Nitrogen nutrition of Microphyllum spicatum: uptake and translocation of 15N by ramets and roots. Freshwater Biology 6: 145-154.

Nifong, R. L. 2015. Linking autotrophic tissue stoichiometry in flowing waters to metabolism, structure, and nutrient limitation. Diss. University of Florida.

Nifong, R. L., Cohen, M. J., and Cropper, W. P. 2014. Homeostasis and nutrient limitation of benthic autotrophs in natural chemostats. Limnology and Oceanography, 59(6), 2101-2111.

Nimick, D. A., Gammons, C. H., and Parker, S. R. 2011. Diel biogeochemical processes and their effect on the aqueous chemistry of streams: A review, Chemical Geology, 283, 3–17, doi:10.1016/j.chemgeo.2010.08.017

Odum, H. T. 1956. Primary production in flowing waters. Limnology and Oceanography, 1, 102-117 doi: 10.4319/lo.1956.1.2.0102

Odum, H. T., 1957a. Primary production measurements in eleven Florida springs and a marine turtle-grass community. Limnology and Oceanography 2: 85-97.

Odum, H. T., 1957b. Trophic structure and productivity of Silver Springs, Florida. Ecological Monographs 27: 55-112.

Osburn, W., Toth, D., and Boniol, D. 2002. Springs of the St. Johns River Water Management District. Technical Report SJ2002-5. Palatka, FL: St. Johns River Water Management District.

Owens, M. 1974. Measurements on non-isolated natural communities in running waters, p. 111-119. In R. A. Vollenweider [ed.], A manual on methods for measuring primary production in aquatic environments. Blackwell Scientific Publications.

Patriquin, D., 1973. Estimation of growth rate, production and age of the marine angiosperm *Thalassia testudinum* Konig. Caribbean Journal of Science 13:111–123

Payn, R. A., Webster, J. R., Mulholland, P. J., Valett, H. M., and Dodds, W. K. 2005. Estimation of stream nutrient uptake from nutrient addition experiments. Limnology and Oceanography: Methods 3: 174–182, doi:10.4319/lom.2005.3.174

Pellerin, B. A., Downing,B. D., Kendall, C., Dahlgren, R. A., Krauss, T. E. C., Saraceno, J. F., Spencer, R. G. M., and Bergamaschi, B. A. 2009. Assessing the sources and magnitude of diurnal nitrage variability in the San Joaquin River (California) with an *in situ* optical nitrate sensor and dual nitrate isotopes, Freshwater Biology, 54, 376–387, doi:10.1111/j.1365-2427.2008.02111.x.

Pellerin, B. A., Saraceno, J. F., Shanley, J. B, Sebestyen, S. D., Aiken, G. R., Wollheim, W. M., and Bergamaschi, B. A.2012. Taking the pulse of snowmelt: *In situ* sensors reveal seasonal, event and diurnal patterns of nitrate and dissolved organic matter variability in an upland forest stream, Biogeochemistry, 108, 183–198, doi:10.1007/s10533-011-9589-8

Persson, L. and Crowder, L. B. 1998. Fish-habitat interactions mediated via ontogenetic niche shifts. The Structuring Role of Submerged Macrophytes in Lakes. Springer, pp. 3-23.

Petticrew, E. L. and Kalff, J. 1992. Water flow and clay retention in submerged macrophyte beds. Canadian Journal of Fisheries and Aquatic Sciences, 49(12), 2483-2489.

Pfenning, K. S. and McMahon, P. B. 1997. Effect of nitrate, organic carbon, and temperature on

potential denitrification rates in nitrate-rich riverbed sediments. Journal of Hydrology, 187, 283-295 doi:10.1016/S0022-1694(96)03052-1

Phelps, G. G. 2004. Chemistry of ground water in the Silver Springs basin, Florida, with an emphasis on nitrate. Scientific Investigations Report 2004-5144. USGS, Reston, VA.

Pina-Ochoa, E. and Alvarez-Cobelas, M, 2006. Denitrification in aquatic environments: a cross-system analysis. Biogeochemistry, 81:111–130 doi: 10.1007/s10533-006-9033-7

Quinlan, E. L., Phlips, E. J., Donnelly, K. A., Jett, C. H., Sleszynski, P., and Keller, S. 2008. Primary producers and nutrient loading in Silver Springs, FL, USA. Aquatic Botany 88: 247-255.

Reddy, K. R. 1983. Fate of nitrogen and phosphorus in a waste-water retention reservoir containing aquatic Macrophytes1 Retrieved from https://www.agronomy.org/publications/jeq/abstracts/12/1/137

Reddy, K. R. and DeLaune, R. D. 2008. Biogeochemistry of wetlands: science and applications. CRC press.

Reichert, P., Uehlinger,U., and Acuña, V. 2009. Estimating stream metabolism from oxygen concentrations: effect of spatial heterogeneity, Journal of Geophysical Research: Biogeosciences, 114(G3), doi:10.1029/2008JG000917

Roberts, B. J. and Mulholland, P. J. 2007. In-stream biotic control on nutrient biogeochemistry in a forested stream,West Fork of Walker Branch. Journal of Geophysical Research, 112: G04002, doi:10.1029/2007JG000422.

Rode, M., Halbedel, S., Anis, M. R., Borchardt, D., and Weitere, M. 2016. Continuous in-stream assimilatory nitrate uptake from high frequency sensor measurements. Environmental Science and Technology 50: 5685–5694, doi: 10.1021/acs.est.6b00943

Rusjan, S. and Mikos, M. 2010. Seasonal variability of diurnal in-stream nitrate concentration oscillations under hydrologically stable conditions, Biogeochemistry, 97, 123–140, doi:10.1007/s10533-009-9361-5.

Sagrario, M. A. G., Jeppesen, E., Goma, J., Sondergaard, M., Jensen, J. P., Lauridsen, T., and Landkildehus, F. 2005. Does high nitrogen loading prevent clear-water conditions in shallow lakes at moderately high phosphorus concentrations? Freshwater biology 50: 27-41.

Sand-Jensen, K. 1977. Effect of epiphytes on eelgrass photosynthesis. Aquatic Botany, 3: 55-63.

Sand-Jensen, K. and Borum, J. 1984. Epiphyte shading and its effect on photosynthesis and diel metabolism of *Lobelia dormanna* L. during the spring bloom in a Danish lake. Aquatic Botany, 20: 109-119.

Sand-Jensen, K., Prahl, C., and Stokholm, H. 1982. Oxygen release from roots of submerged aquatic macrophytes. Oikos, 349-354.

Santschi, P., Höhener, P., Benoit, G., and Buchholtz-ten Brink, M. 1990. Chemical processes at the sediment-water interface. Marine Chemistry, 30, 269-315.

Scott, T., Means, G., Meagan, R., Means, R., Upchurch, S., Copeland, R., Jones, R., and Willet, A. 2004. Springs of Florida. Bulletin No. 66 Florida Geological Survey, Tallahassee, FL.

Sederias, J., and Colman, B. 2009. Inhibition of *Chara vulgaris* oospore germination by sulfidic sediments. Aquatic Botany, 91(4), 273-278.

Short, F. T., Burdick, D. M., and Kaldy, J. E., 1995. Mesocosm experiments quantify the effects of eutrophication on eelgrass, *Zostera marina* L. Limnology and Oceanography 40: 740-749.

Sikora, L. J. and Keeney, D. R. 1983. Further aspects of soil chemistry under anaerobic

conditions. Mires: Swamp, Bog, Fen, and Moor, Elsevier, Amsterdam, The Netherlands, pp. 247-256.

Smith, V. H. 2003. "Eutrophication of freshwater and coastal marine ecosystems a global problem." Environmental Science and Pollution Research 10.2: 126-139.

Smolders, A.J., Hartog, C. D., Gestel, C. B., and Roelof, J. G.. 1996. The effects of ammonium on growth, accumulation of free amino acid and nutritional status of young phosphorus deficient *Stratiotes aloides* plants. Aquatic Botany 53: 85-96.

Smolders, A.J., van Reil, M. C., and Roelofs, J. G. M. 2000. Accumulation of free amino acids as an early indication for physiological stress (nitrogen overload) due to elevated ammonium levels in vital Stratiotes aloides L. stands. Archeif fur Hydrobiologie 150: 169-175.

Stapel, J., Stapel, J., Aarts, T. L., van Duynhoven, B. H. M., DeGroot, J. D., van den Hoogen, P. H. W., and Hemminga, M. A.1996. Nutrient uptake by leaves and roots of the seagrass *Thalassia hemprichii* in the Spermonde archipelago, Indonesia. Marine Ecology Progress Series, 134.

Stevenson, J. C., Staver. L. W., and Staver, K. 1993. Water quality associated with survival of submersed aquatic vegetation along an estuarine gradient. Estuaries, 16: 346-361.

Stevenson, R. J., 1996. The stimulation and drag of current. In Stevenson, R. J., M. L. Bothwell & R. L. Lowe (eds), Algal Ecology: Freshwater Benthic Ecosystems. Academic Press, San Diego, CA: 321-340.

Stevenson, R. J., Pinowska, A., Albertin, A., and Sickman, J. O. 2007. Ecological condition of algae and nutrients in Florida springs: the synthesis report S0291. Florida Department of Environmental Protection, Tallahassee, FL.

Strap-leaf Sagittaria. UF IFAS Center for Aquatic and Invasive Plants. Website. 13 Aug. 2015. http://plants.ifas.ufl.edu/node/387.

Strauss, E. A., and Lamberti, G. A. 2000. Regulation of nitrification in aquatic sediments by organic carbon. Limnology and Oceanography, 45, 1854-1859

Stream Solute Workshop (SSW). 1990. Concepts and methods for assessing solute dynamics in stream ecosystems. Journal of the North American Benthological Society 9: 95–119.

Strong, W. A. (2004). Temporal water chemistry trends within individual springs and within a population of Florida Springs (Doctoral dissertation, University of Florida).

Stross, R. G. 1979. Density and boundary regulations of the Nitella meadow in Lake George, New York. Aquatic Botany, 6: 285-300.

Tank, J. L., Rosi-Marshall, E.J., Baker, M.A., and Hall, R.O. 2008. Are rivers just big streams? A pulse method to quantify nitrogen demand in a large river. Ecology 89: 2935–2945.

Titus, J. E. and Adams, M. S. 1979. Coexistence and the comparative light relations of the submersed macrophytes *Myriophyllum spicatum* L. and *Vallisneria americana* Michx. Oecologia, 40: 273-286.

Tomasko, D. A. and Dunton, K. H. 1995. Primary productivity in *Halodule wrightii*: a comparison of technqiues based on daily carbon budgets. Estuaries, 18: 271-287.

Tomlinson, P. B. 1974. Vegetative morphology and meristem dependence. The foundation of productivity in seagrasses. Aquaculture 4: 107-130.

Turpin, D. H. 1991. Effects of inorganic N availability on algal photosynthesis and carbon metabolism. Journal of Phycology 27:14-20.

Twilley, R. R., Kemp, W. M., Staver, K. W., Stevenson, J. C., and Boynton, W. R. 1985. Nutrient enrichment of estuarine submersed vascular plant communities: I. Algal growth

and effects on production of plants and associated communities. Marine Ecology Progress Series, 23:179-191.

Valiela, I., MecClelland, J., Hauxwell, J., Behr, P. J., Hersh, D., and Foreman, K. 1997. Macroalgal blooms in shallow estuaries: controls and ecophysiological and ecosystem consequences. Limnology and Oceanography 42: 1105-1118.

Van den Berg, M. S., Sheffer, M., van Nes, E., and Coops, H. 1999. Dynamics and stability of *Chara* sp. and *Potamogeton pectinaus* in a shallow lake changing in eutrophication level. Hydrobiologia 408: 335-342.

van der Heide, T., van Nes, E. H., van Ktawijk, M. M., Scheffer, M., Hendriks, A. J., and Smolders, A. J. P. 2010. Alternative stable states driven by density-dependent toxicity. Ecosystems 13: 841-850.

van der Welle, M. E. W., Cuppens, M., Lamers, L. P. M., and Roelofs, J. G. M. 2006. Detoxifying toxicants: interactions between sulfide and iron toxicity in freshwater wetlands. Environmental Toxicology and Chemistry, 25(6), 1592-1597.

Van Dijk. H. F. G. and Roelofs, J. G. M. 1988: Effects of excessive ammonium deposition on the nutritional status and condition of pine needles. - Physiologia Plantarum 73: 494-501.

Vepraskas, M. J., and Faulkner, S. P. 2001. Redox chemistry of hydric soils. Wetland soils: Genesis, hydrology, landscapes, and classification, 85-105.

Veraart, A., Bruijne, W. J., Klein, J. M., Peeters, E. H. M., and Scheffer, M. 2011. Effects of aquatic vegetation type on denitrification. Biogeochemistry, 104(1-3), 267-274.

Vermaat, J. E, Agawin, N. S. R., Fortes, M. D., Uri, J. S., Duarte, C. M.,. Marba, N., Enriquez, and Van Vierssen, W.. 1997. The capacity of seagrasses to survive increased turbidity and siltation: The significance of growth form and light use. Ambio, 26: 499-504.

Virnstein, R. W. 1982. Leaf growth of the seagrass *Halodule wrightii* photographically measured *in situ*. Aquatic Botany 12: 209–218.

Vis, C., Hudon, C., Carignan, R., and Gagnon, P. 2007. Spatial analysis of production by macrophytes, phytoplankton and epiphyton in a large river system under different water-level conditions. Ecosystems, 10(2), 293-310.

Wang, Y., Gao, G., Qin, B., and Wang, X. 2012. Ecophysiological and anatomical responses of Vallisneria natans to nitrogen and phosphorus enrichment. Knowledge and Management of Aquatic Ecosystems 405, 05.

Webster, J. R., Mulholland, P. J., Tank, J. L., Valett, H. M., Dodds, W. K., Peterson, B. J., Bowden, W. B., Dahm, C. N., Findlay, S., Gregory, S. V., and Grimm, N. B. 2003. Factors affecting ammonium uptake in streams–an inter-biome perspective. Freshwater Biology, 48, 1329-1352 doi: 10.1046/j.1365-2427.2003.01094.x

Wetzel, R. G., and Sondergaard, M. 1998. Role of submerged macrophytes for the microbial community and dynamics of dissolved organic carbon in aquatic systems. The Structuring Role of Submerged Macrophytes in Lakes. Springer, pp. 133-148.

Wigand, C., Stevenson, J. C., and Cornwell, J. C. 1997. Effects of different submersed macrophytes on sediment biogeochemistry. Aquatic Botany, 56(3), 233-244.

Zieman, J. C. and Wetzel, R. G. 1980. Productivity in seagrasses: methods and rates. In: R. C. Phillips and C. P. McRoy (Editors), Handbook of Seagrass Biology, An Ecosystem Perspective. Garland STPM Press, New York, pp. 87-116

Zimba, P., Hopson, M. S., and Colle, D. E. 1993. Elemental composition of five submersed aquatic plants collected from Lake Okeechobee, Florida. Journal of Aquatic Plant Management 31: 137-140.

Zimmerman, R. C. 2003. A biooptical model of irradiance distribution and photosynthesis in seagrass canopies. Limnology and oceanography, 48(1)

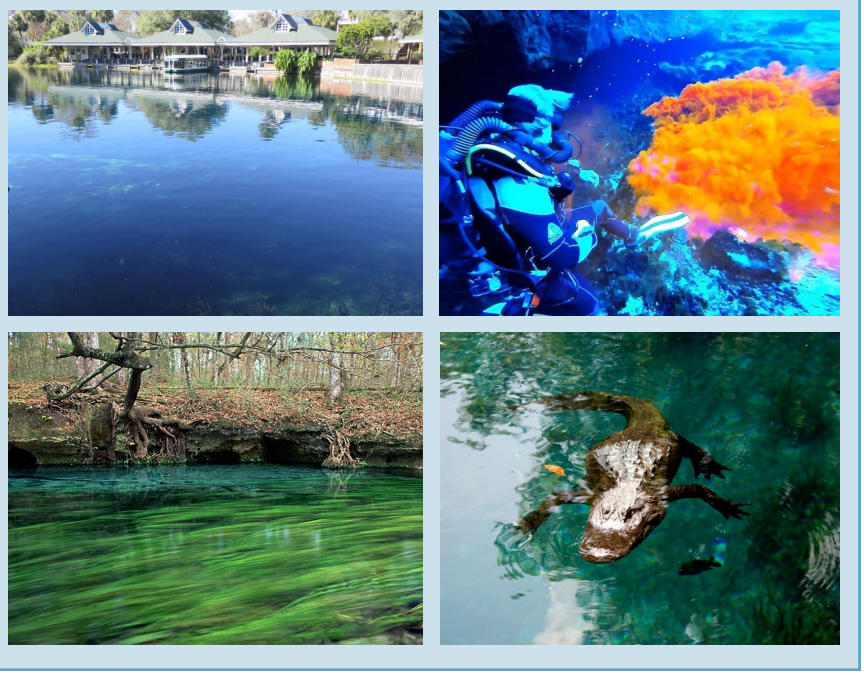

Collaborative Research Initiative on
Sustainability and Protection of Springs [**CRISPS]**

Section 7

[Work Order No: 3]

FINAL REPORT

2014 - 2017

submitted to:

St. Johns River Water Management District
Springs Protection Initiative [SPI], UF Contract # 27789

UF | UNIVERSITY of FLORIDA
Water Institute

C R I S P S

Section 7

PHYSICOCHEMISTRY

Nitrate Inhibition of Submerged Aquatic Vegetation: Investigation of the Nitrogen Overload Hypothesis

Final Report 2017
Work Order No. 3: Part 3 of 3

Principal Investigators:

Todd Z. Osborne, University of Florida

Jodi Slater, St. Johns River Water Management District

Project Team:
Todd Z. Osborne
Leah H. LaPlaca, MS Student
Tracey B. Schafer, MS Student
Jacob Johansen, Post Doctoral Associate
Whitney Laboratory of Marine for Marine Bioscience
Soil and Water Science Department
University of Florida

Jodi Slater
Michael F. Coveney
Robert A. Mattson
St. Johns River Water Management District

This document reports final results of a work order for a 3-year project in compliance with Agreement between University of Florida (UF) and St. Johns River Water Management District (SJRWMD) UF Contract #27789. It is part of the *UF Collaborative Research Initiative on Springs Protection and Sustainability (CRISPS)* and supports the science component of *the SJRWMD Springs Protection Initiative (SPI).*

7.1 DIRECT EFFECTS OF ELEVATED NO_3-N IN THE GROWTH OF *Vallisneria americana* AND *Sagittaria kurziana* IN SPRING ECOSYSTEMS.

7.1.1 ABSTRACT

Current observations of water quality in groundwater discharge from springs in Florida show anthropogenic enrichment of nitrate plus nitrite (NO_3-N), generally attributed to fertilizer application and/or wastewater or manure sources in individual springsheds. Excessive levels of NO_3-N have been implicated in eutrophication of, and observed changes in, submerged aquatic vegetation (SAV) communities in several spring runs (Mattson et al. 2007; Knight and Notestein 2008). While the indirect effects of nitrogen (N) enrichment on aquatic macrophytes are well-documented (i.e., algal productivity resulting in shading of macrophytes), there is considerably less information available concerning direct effects of NO_3-N, such as toxicity or inhibition of macrophyte growth.

This work explores the hypothesis that nitrate may have direct inhibitory effects on SAV growth in Florida springs via analysis of nitrate reductase activity (NRA), assimilatory nitrate reduction processes (ANR) and a variety of anatomical responses, including quantification of starch grains by assay and visualization and measurement of starch, arenchyma, epidermis and vascular bundles. Ratios of root to shoot biomass, measured at the end of the growing season, were also utilized to further help determine the direct effect of NO_3-N on SAV growth.

7.1.2 INTRODUCTION

Phosphorus (P) is often considered the limiting nutrient in freshwater ecosystems. Thus, when available in excess, it is implicated as a causative agent in anthropogenic eutrophication. Nitrogen (N), however, has been traditionally viewed by many as a lesser contributor to eutrophication of freshwaters, either because of the overshadowing nature of P issues or due to the ability of many cyanobacteria to fix atmospheric N, a process that significantly reduces perceived N limitation. This prevailing view stems from research conducted to elucidate the role of P in eutrophication (Schindler and Fee 1974; Schindler 1978) following the 1960s chemical industry claims of no effect of increased P in aquatic systems (Barker et al. 2008). More recently, several researchers have reasserted the view that N either alone or in concert with P, may exert ultimate control over algal productivity and subsequently macrophyte productivity in aquatic systems across the globe (Turpin 1991; Talling and Lemoalle 1998; Maberly et al. 2002; Clark and Baldwin 2002; James et al. 2003; James et al. 2005; Sagario et al. 2005; Dzialowski et al. 2005; Weyhenmeyer et al. 2007; Li et al. 2008). The extreme of this viewpoint suggests that N may have been the limiting nutrient in most northern hemisphere lakes and rivers prior to substantial N fertilizer utilization, which precipitated P limitation in enriched systems (Bergstrom and Jansson 2006). A recent meta-analysis of published nutrient limitation studies found the number of N limitation cases to equal those of P limitation (Elser et al. 2007) and a significant number of cases of co-limitation. Moss (1990) contends that co-limitation was the normal condition prior to anthropogenic nutrient enrichment of aquatic ecosystems. Recently, the

role of N enrichment in alteration of ecosystem health has received renewed attention in aquatic ecosystems (Porter et al. 2013; Baron et al. 2013).

Countless studies of eutrophication of freshwater ecosystems have observed a shift from macrophyte to phytoplankton dominance after anthropogenic increases in available P (Wetzel 2001; Lacoul and Freedman 2005; Reddy and DeLaune 2008). The process involves rapid utilization of excess nutrients by phytoplankton and epiphytic algae, which in turn enables explosive algal growth. The shift in primary productivity is also self-reinforcing; as turbidity increases with algal productivity, light becomes limiting to submerged aquatic vegetation (SAV) (Burkholder et al. 1992; Van den Berg et al. 1999). Death of SAV and decomposition of biomass only exacerbates excessive nutrient conditions.

Often, N and P have a positive synergistic effect on phytoplankton productivity. In a study by Sagarario et al. (2005) N and P additions alone did not show a significant effect, but when combined, the increase in phytoplankton and epiphytic algal biomass was statistically significant. In addition to light attenuation by phytoplankton proliferation, epiphyte biomass burden and subsequent shading can be a primary causal mechanism for SAV mortality under eutrophic conditions (Borum 1985). In many spring runs in Florida, proliferation of epiphytic algae, as well as benthic macroalgae, have been observed concomitantly with declines of SAV communities (Stevenson et al. 2004; Frazer et al. 2006; Pinowska et al. 2007; Stevenson et al. 2007; Quinlan et al. 2008; Brown et al. 2008). Water quality in groundwater discharged from many springs in Florida has shown significant increases in NO_3-N concentration, attributed predominantly to fertilizer application and/or wastewater or manure sources in individual springsheds (Jones et al. 1996; Katz 2004; Albertin et al. 2012). Odum (1957) reported mean NO_3-N concentration of 0.45 mg L^{-1} for Silver Springs in the 1950s which had risen to over 1 mg L^{-1} by 2005 (Munch et al. 2006; Quinlan et al. 2008). More dramatically, Rainbow River NO_3-N concentrations have increased from 0.08 to 1.22 mg L^{-1} (a 15 fold increase) over last 50 years (Cowell and Dawes 2008). Interestingly, during this period of increasing NO_3-N, P concentrations have remained constant (Maddox et al. 1992; Scott et al. 2004). These observations, while somewhat inconsistent with the common eutrophication paradigm, have prompted several hypotheses as to the role of increased nitrogen availability in the observed loss of SAV in spring systems statewide.

This report reviews these competing hypotheses concerning the relationship between elevated NO_3-N and observed ecological changes, specifically declines in SAV coverage and increases in epiphytic and benthic algae, in regional springs ecosystems. Significant attention is given to potential inhibitory effects of elevated NO_3-N on SAV growth in springs and possible mechanisms for this inhibition are addressed experimentally in mesocosm studies. The proposed mechanisms focus on the assimilative nitrate reduction (ANR) process, resulting buildup of toxic ammonia (NH_3), and energetic consequences of unregulated NO_3-N uptake on SAV.

7.1.2.1 Competing Hypotheses

The initial hypothesis posited by members of the scientific community, as well as the general public, was that the increase in N availability, observed as significant increases in NO_3-N concentration in spring waters, alleviated N limitation and therefore was responsible for a shift in

primary productivity from SAV to epiphytic algae and benthic macroalgae. While there have been studies to report N utilization by algal mats in Florida springs (Cowell and Botts 1994; Cowell and Dawes 2004; Albertin 2009; Sickman et al. 2009), there have been several observations that contradict the normal eutrophication paradigm, namely the lack of significant increase in other forms of N (Cohen et al. 2007) or P (Maddox et al. 1992; Scott et al. 2004) in spring waters. Brown et al. (2008) concluded that there was insufficient evidence to link nitrate enrichment to changes in algal cover. Heffernan et al. (2010) argue that studies by Canfield and Hoyer (1988) and Duarte and Canfield (1990) found no relationships between nutrients and total vegetative biomass in spring runs as would be expected under nutrient limitation scenarios, and that recent surveys of algal biomass have not found any significant linkage to N or P concentrations (Stevenson et al. 2004; Stevenson et al. 2007). Further, Heffernan et al. (2010) and Liebowitz (2013) report stronger relationships between dissolved oxygen (DO), grazer populations, and algal abundance than with nutrients.

Heffernan et al. (2010) suggests looking to other drivers of algal proliferation in spring systems, including DO control of invertebrate grazers, resulting in altered trophic structure in springs to favor algal dominance. Liebowitz (2013) reports a significant negative association between algal and gastropod biomass in Florida springs suggesting top down control of algae by invertebrate grazers, a finding supported by several studies of grazer control of algae in other systems (Hildebrand 2002; Heck and Valentine 2007; Gruner et al. 2008; Baum and Worm 2009; Estes et al. 2011). Further, Liebowitz (2013) also found a significant relationship between dissolved oxygen (DO) and gastropod biomass in a survey of 11 springs, suggesting DO has a significant indirect effect on algal biomass via controlling grazer abundance and/or activity. Under low flow or current velocity conditions, nutrient enrichment and subsequent algal growth may outpace grazer pressure resulting in severe light reductions (Harlin and Thorne-Miller 1981). Alternatively, under similar nutrient enrichment and moderate to high flushing or exchange of water (as in lotic or tidally influenced systems), herbivores have been observed to control epiphytic algal biomass (Neckles 1993). Liebowitz (2013) argues that hysteretic responses of grazer populations to disturbances could be responsible for the over-abundance of algae in springs where no clear grazer stress is present. For instance, invasive plant control measures utilizing herbicides and copper compounds are widely employed with known negative impacts on grazer populations (Evans 2008). Such a disturbance could enable algal populations to exceed thresholds for grazer control. This gives rise to a second hypothesis that grazer control of algae in springs has been altered by DO in some cases and by episodic or unknown exposures to other stressors.

The presence of herbicides or other agrochemicals that may be inhibitory to either algal grazers or macrophytes themselves supports a third hypothesis which states that a “nitrate cohort” (substance[s] associated with the same mechanisms involved in nitrate increases such as land use or waste disposal) has an inhibitory or toxic effect on SAV. The widespread use of agro-chemicals such as commercial pesticides, fungicides and herbicides increases potential for these compounds to impact spring ecosystems. Several anthropogenic organic compounds have been detected in springs: however, the concentrations of these observed were below levels considered toxic (Phelps et al. 2006; Phelps 2004). Recent increases in consumer use of compounds such as atrazine, a herbicidal fertilizer additive, (Ackerman 2007) and triclosan, an antimicrobial agent,

(Fulton et al. 2010) suggest these compounds may have deleterious effects on SAV (and/or grazer population dynamics).

A fourth hypothesis is that nitrate itself has an inhibitory (direct) effect on SAV growth resulting in a shift to algae dominated system. The accepted view of nitrate and ammonia combined with P to create conditions for algal dominance and subsequent shading out of macrophytes (Mulligan et al. 1976) is that of an indirect effect. However, a direct effect of nutrient enrichment has been suggested as a factor in macrophyte disappearance in aquatic systems undergoing enrichment (Genevieve et al. 1997; Farnsworth and Baker 2000). Several authors (Klotzli 1971; Schroder 1979; Boar et al. 1989) have reported correlation of reed bed disintegration and increases in nitrate loading to lakes in England. Decreases in *Phragmites australis* root and rhizome production was observed in concert with increased nitrate loading (Ulrich and Burton 1985). Ulrich and Burton (1985) also reported that nitrate stimulated growth and overall biomass increased with increased nitrate availability, however, below ground biomass production (roots and rhizomes) did not increase at concentrations up to 6 mg NO_3-N L^{-1}. These NO_3-N concentrations resulted in significant decreases in below ground to above ground biomass ratios and resulted in an overall decline in health of the reed stands. Nitrate to potassium ratios in surface waters and in tissues are correlated with highest degree of degradation of *Phragmites australis* beds (Boar et al. 1989); however, the causative mechanism is unknown, as is the potential for synergistic effects of increased availability of N and K. Because the aforementioned species is an emergent macrophyte, free of algal shading, it serves as a significant indicator of potential inhibitory effects of NO_3-N on plant growth. An in depth review of current literature suggests several authors have observed apparent direct inhibitory effects of NO_3-N on SAV in both marine and freshwater environments.

7.1.2.2 Evidence of Direct Effects of Nitrate on SAV

Opportunistic luxury consumption of nutrients is characteristic of SAV and thus accumulation in tissues is anticipated for macrophytes adapted to limited nutrient availability, such as seagrasses and some freshwater SAV (Wetzel 2001). The prevailing viewpoint is that most macrophytes acquire nitrogen via roots (Cedergreen and Madsen 2003), however, foliar absorption is also a viable mechanism when sediment sources are not available or abundant (Barko and Smart 1986). When ammonia nitrogen (NH_3-N) concentration exceeds 0.1 mg L^{-1}, macrophytes preferentially use NH_3-N (Nichols and Keeny 1976). Hence, the dominant form of N utilized by most SAV is NH_3-N, but under N limitation nitrate is also utilized, predominately from the water column. Due to the abundance of NO_3-N, this is the presumed mechanism for N uptake by SAV in Florida springs. Several researchers have made qualitative observations of SAV inhibition closest to spring vents where NO_3-N concentrations are highest (Munch et al. 2006; Osborne and Mattson unpublished data; Figure 7.1.1). Similarly, several authors suggest observed declines in macrophytes in other systems was a direct effect of increased NO_3-N (Burkholder et al. 1992; Burkholder et al. 1994; Wang et al. 2012), suggesting closer investigation of this phenomenon is warranted.

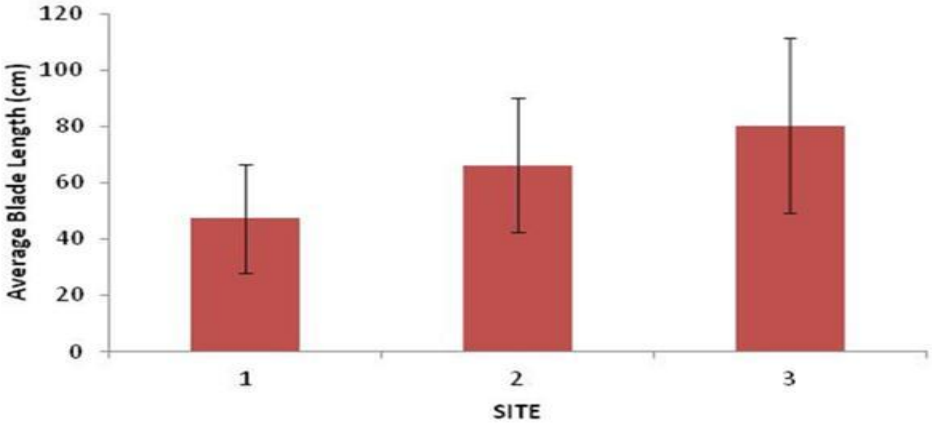

Figure 7.1.1. Average blade length of *V. americana* along a transect down the Wekiva River (Osborne and Mattson unpublished data). NO_3-N concentration declines downstream from site 1-3 which spans a distance of approximately 9 miles. These findings support the observation of increased vigor in *V. americana* as NO_3-N concentrations decrease.

Burkholder et al. (1992) report that *Zostera marina* (eelgrass) exhibited highly negative physiological effects (even death) when dosed with 0.05, 0.1 and 0.5 mg NO_3-N L^{-1}. Although a marine species, this plant shows extreme sensitivity to increased nitrate evidenced through loss of carbon storage in roots unrelated to shading by algae. The apparent lack of an inhibition or regulation mechanism of nitrate uptake by eelgrass (Roth and Pregnall 1988) was implicated in the observed disruption of internal nutrient ratios, presumably due to carbon expenditure in amino acid synthesis to reduce intracellular ammonia toxicity. Hierarchical partitioning analysis of water quality parameters found NO_3-N exerted the greatest detrimental effect on charophyte occurrence in wetlands of the UK (Lambert and Davy 2011). *In situ* studies of *Chara globularis* showed that it was extremely sensitive to nitrate with maximal relative growth rate observed at 0.5 mg NO_3-N L^{-1} and a linear decline in growth with higher concentrations. At 6 mg NO_3-N L^{-1}, growth was severely limited, similar to results of no NO_3-N treatment (Lambert and Davy 2011). Similarly, biomass accumulation was strongly inhibited by nutrient accumulation (N) in *Potamogeton maackianus* A. Been (Ni 2001). The most definitive observations of inhibition were in the form of shrinkage of arenchyma tissues and disappearance of starches and chloroplasts observed in increased NO_3-N and NH_4-N concentration treatments of *Vallisneria natans* (Wang et al. 2012.)

The paradigm of nitrogen effects on water clarity often overshadows potential direct effects of excess N on SAV. For instance, Sagrario et al. (2005) reported that high N is not directly inhibitory to *Potamogeton pectinatus* L., *Elodea canadensis* and *Nymphea sp*. at 10 mg L^{-1} of total N (TN) due to overpowering effects of increased algal shading. However, closer inspection of the results indicates moderate dosing of 4 mg TN L^{-1} resulted in decreased growth with respect to controls under equal or better water clarity, a noteworthy result that went unmentioned. Further, summer TN levels declined significantly in mesocosms truncating the duration of exposure for macrophytes, which likely confound interpretation of the results by the authors. In a study by Li et al. (2008), NO_3-N additions were noted to increase *Vallisneria*

spinulosa biomass over control at 2.5, 5.0, 7.5 mg L^{-1} concentrations in water column but at 10 mg L^{-1} growth was not significantly different from control (1 mg L^{-1}) suggesting some inhibition of growth. It is unclear why the authors did not conclude that a NO_3-N threshold had been exceeded between 7.5 and 10 mg L^{-1}. This lack of interpretation by some authors is likely due to a strong focus on algal production and subsequent shading, not direct effects of nitrate on SAV (Sturgis and Murray 1997). Further, variability among species with respect to effects of NO_3-N appears to be high (Burkholder et al. 1994). This is exemplified by conflicting reports on potential inhibition of macrophyte growth by excessive water column nitrate (Li et al 2005). Best (1980) reported no inhibition of *Ceratophyllum demersum* at concentrations of up to 105 mg NO_3-N L^{-1} but did observe ammonia toxicity at 45 mg NH_4-N L^{-1}. This finding suggests that *C. demersum* is well suited to luxury uptake of N. Conversely, Lambert and Davy (2011) assert a mean annual concentration limit of 2 mg NO_3-N L^{-1} is necessary to protect charophytes.

Our review of available literature did not find studies of N enrichment with SAV species common in Florida spring systems (*Vallisneria americana, Sagittaria kurziana, Najas* spp., *Potamogeton* spp.*)*. However, the potential mechanisms of inhibition, which likely vary among species, are discussed here in general terms for SAV and are viewed as potential mechanisms until tested on individual species of interest.

7.1.2.3 Potential Mechanisms of Inhibition

Nitrate toxicity has been well documented for vertebrate animals (including humans) (Kim-Shapiro et al. 2005) as well as invertebrates (Mattson et al. 2007). However, the potential of NO_3-N toxicity or inhibition of SAV is not well understood, nor is it intuitive given our understanding of mechanisms of toxicity for higher organisms. Observations coinciding with elevated inorganic N (NO_3-N and or NH_4-N) include stunted growth, iron deficiency, amino acid accumulation, oxidative stress and structural tissue damage (Burkholder et al 1992; Smolders et al. 1997; Smolders et al. 2000; van der Heide et al. 2005; Wang et al. 2012). To better determine potential inhibitory mechanism of NO_3-N, a closer look at the process of assimilation is necessary.

7.1.2.4 Assimilatory Nitrate Reduction

Most aquatic plants absorb nitrate, which is then sequentially converted to nitrite and then ammonium by the nitrate reductase system (Salisbury and Ross 1992). In SAV, before nitrate can be utilized by the plants, it must be converted to ammonium by a series of sequential enzyme mediated reactions (Figure 7.1.2) involving nitrate reductase and nitrite reductase (Guerrero et al. 1981). This process is termed assimilatory nitrate reduction (ANR) and results in ammonium being incorporated into amino acids. Genetic or environmental factors, such as light, temperature, depth, pH, and location within vegetated patch (edge versus center) (Roth and Pregnall 1988; van der Heide et al. 2008), can modulate this series of biochemical reactions resulting in a high level of variability among species with respect to nitrate reduction processes and rates (Pate 1980; Guerrero et al. 1981). Water temperature can be problematic for SAV by increasing respiration rates and impairing enzyme function (Zimmerman et al. 1989; Lacoul and Freedman 2006; Riis et al. 2012); however, SAV in spring runs generally do not experience thermal stress due to the thermal consistency of groundwater (unless exposed in shallow backwaters).

Uptake of NO_3-N is driven primarily by external nitrate concentrations (Marschner 1998) and in aquatic macrophytes, increased water column concentrations of NO_3-N results in significant increases in nitrate reductase activity (NRA) (Cedergreen and Madsen 2003). Studies of *Zostera marina* indicate newer leaves are more active with respect to NRA and rates between individual plants can be variable with a 2 to3 fold difference (Roth and Pregnall 1988). It has been suggested that differences between root and shoot NRA depends upon uptake rates of individual species (Gojon et al. 1994) and that location of nitrate reduction (root or shoot) is also species specific (Cedergreen and Madsen 2003). From an energetic standpoint, photosynthetic tissues would be a more advantageous location for NRA to occur (Raven 1985) and this appears to be the case for SAV (Roth and Pregnall 1988).

There is little intracellular space to store nitrate; therefore, rapid conversion to ammonia occurs before vacuolar storage. Increasing ammonia requires plants to avoid toxicity by allocating carbon and energy to protein (amino acid) synthesis to alleviate ammonia buildup (Salisbury and Ross 1992). Under normal exposure, ANR uses approximately 25 % of the reductant energy produced by photosynthesis and root/shoot respiration (Crawford 1995).

Closer inspection of the biochemical pathways for ANR reveals some significant differences between SAV and filamentous macroalgae, the two competing primary producers in many springs. Assimilatory nitrate reductase activity in green algae and higher plants is dependent upon NAD(P)H for reducing power (Figure 7.1.3A). This first reaction can be inhibited by p-HMB, cyanide, azide, and cyanate. Further, the negative feedback inhibitor of the nitrate reductase enzyme in some species is nitrite, which competitively binds with nitrate reductase. This is not the case for all species as reported by Roth and Pregnall (1988) who documented the inability of *Zostera marina* to "turn off" or regulate nitrate reductase, a very critical observation with respect to the potential for some SAV to moderate this enzyme. Cyanobacteria, on the other hand, cannot utilize reduced pyridine nucleotides as do green algae and higher plants. The alternative electron donor for algal nitrate reductase (Figure 7.1.3B) is ferredoxin (Guerrero et al. 1981). This reaction appears to give cyanobacteria a slight energetic advantage as the ΔG of the reaction is 4.6 Kcal greater per mole for ferredoxin mediated reduction versus NAD(P)H. The second reduction reaction, nitrite reduction to ammonium, is very similar in all photosynthetic organisms and utilizes ferredoxin as the electron donor specifically.

Ferredoxin requires iron in its structural complex, thus increased iron in springs may also give cyanobacteria a competitive advantage over green algae and SAV. This is due to the inability of the latter organisms to utilize ferredoxin in nitrate reduction. Smolders et al. (1997) report iron deficiency in SAV exposed to higher levels of NO_3-N, presumably due to the need for ferredoxin in nitrite reduction. Because NAD(P)H also serves as reducing power for many other metabolic reactions, utilization of NAD(P)H for nitrate reductase results in a decrease of other metabolic reactions and potential buildup of other metabolites within cells, which is another potential source of toxicity (Lea and Miflin 1979). Of greater concern, the accumulation of ammonia, the end product of ANR, can be extremely detrimental to photosynthetic organisms. Ammonia toxicity represents a primary potential source of toxicity for SAV due to the combined effect of

excess nitrate availability and the possibility of poorly regulated ANR, which can result in ammonia buildup in tissues.

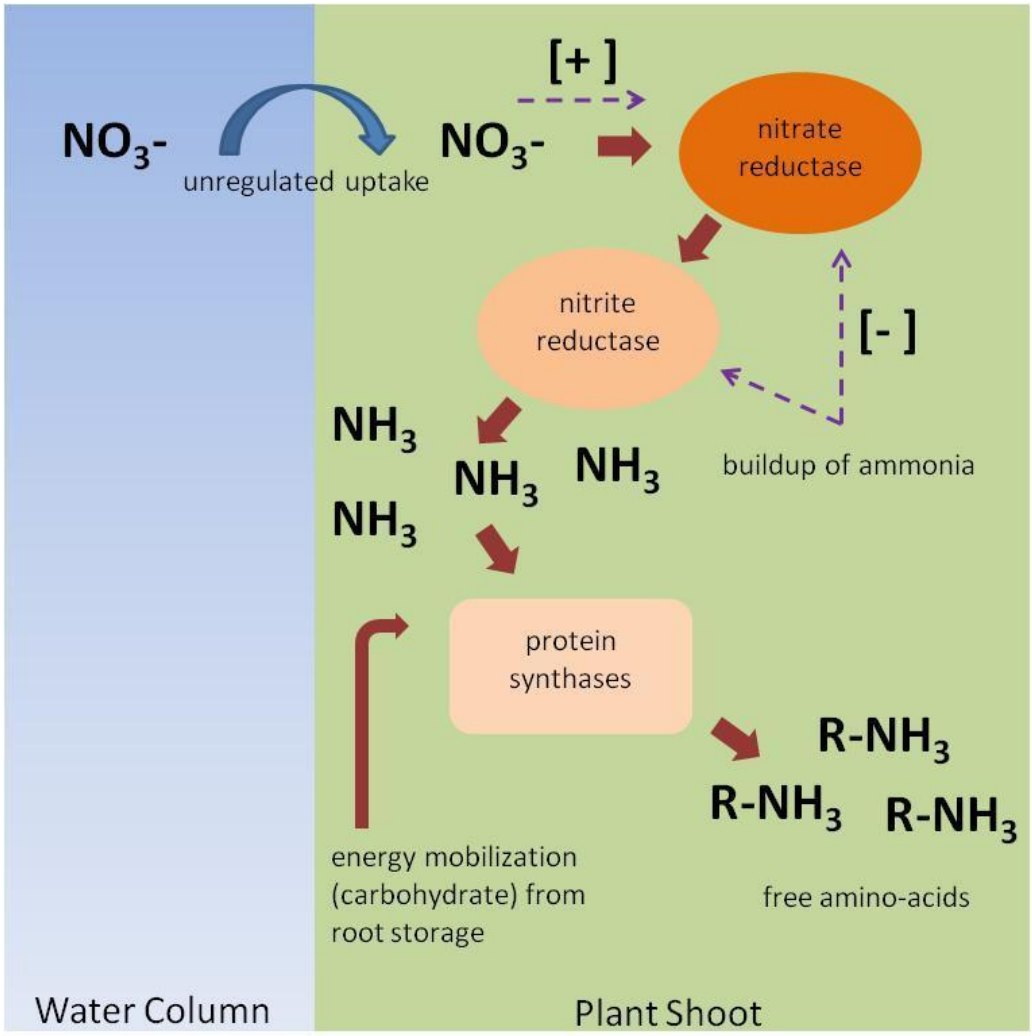

Figure 7.1.2. Conceptual model of nitrate overload hypothesis. Uptake of nitrate is unregulated at the cellular level and presence of nitrate induces nitrate reduction to ammonia. Buildup of ammonia should be a negative feedback[-] for nitrate reduction enzymes; however this process appears not to function in some species. Ammonia can be toxic to plants and therefore is alleviated via protein synthesis, which requires energetic inputs from plant carbohydrate stores. Buildup of free amino acids and depletion of root carbohydrate stores are potential diagnostics of nitrate overload in SAV.

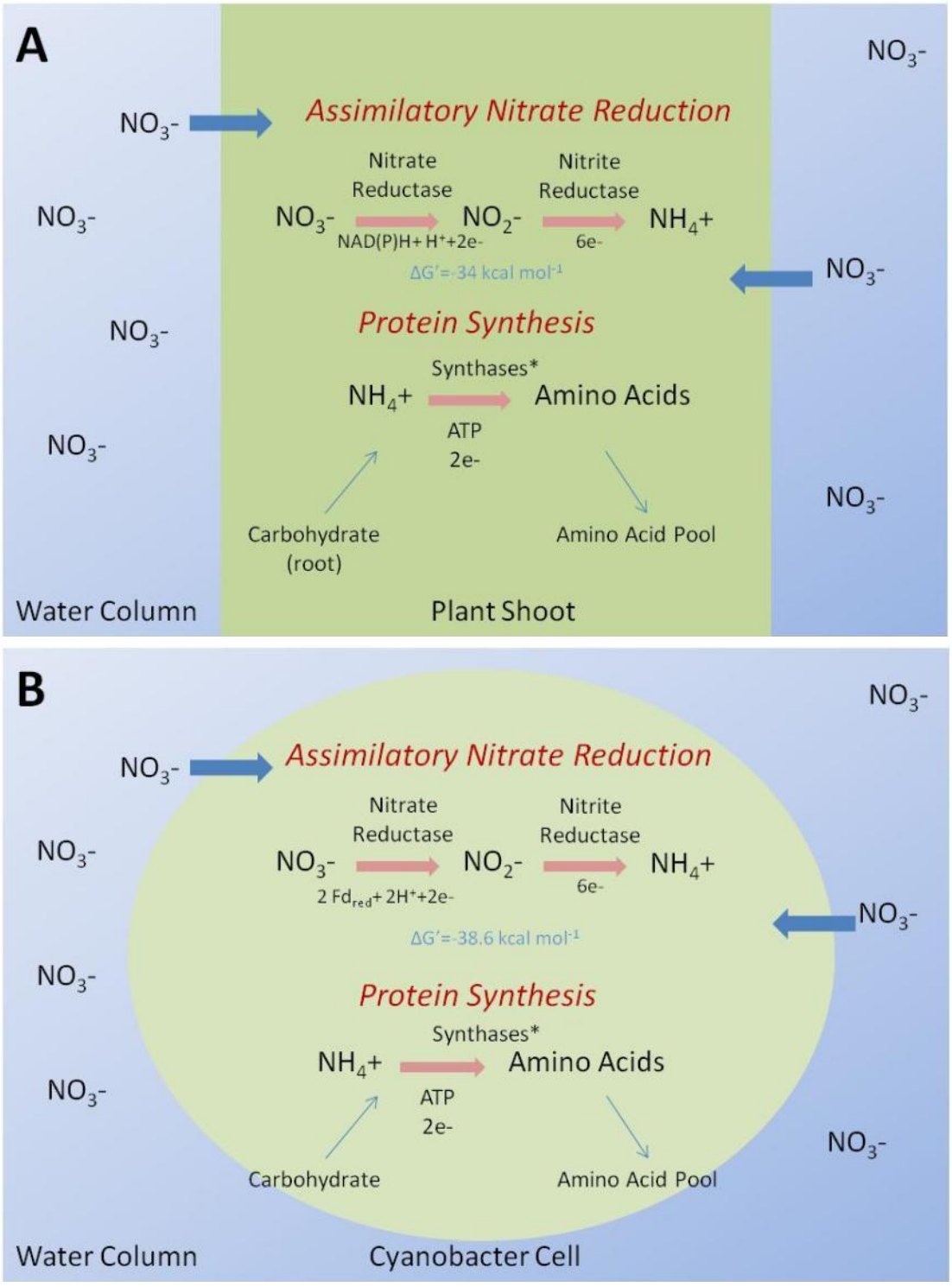

Figure 7.1.3. Assimilatory nitrate reduction in [A] SAV shoot and [B] cyanobacterial cell. Note cyanobacteria cannot utilize NAD(P)H as an electron donor in the reduction of nitrate to nitrite and thus rely solely upon ferrodoxin. Also note a slight energetic advantage [ΔG'] exists for cyanobacteria in the reduction of nitrate to nitrite.

7.1.2.5 Ammonia Toxicity

Ammonia toxicity is well documented in terrestrial plants (Salisbury and Ross 1992) as well as seagrasses (Katwijik et al. 1997; Hemminga and Duarte 2000). In most plants, ammonia toxicity is often associated with a decrease in soluble sugars in tissues due to ammonia assimilation and resulting need for protein synthesis (Cramer et al. 1993) or in excessive tissue concentrations that exceed the plants' ability to incorporate into amino acids (Meher and Mohr 1989). Inhibitory effects of high ammonia on SAV have been documented (Best 1980; Smolders et al. 1996) and implicated in succession of freshwater SAV communities (Schuurke et al. 1986; Brouwer et al. 1997; Clarke and Baldwin. 2002). Excessive ammonia can inhibit photosynthesis (Cao et al. 2004) resulting in diminished soluble sugar production and lead to necrosis in some macrophytes (Smolders et al. 1996). Water column ammonia concentrations >1 mg L^{-1} resulted in decreased soluble sugar content in *Potamogeton crispus* and increased soluble amino acids (Cao et al. 2004). Interestingly, in the study by Cao et al. (2004) responses of amino acids and soluble sugar indicators of ammonia stress were dependent upon duration of exposure. Further, activity of ascorbate peroxidase and superoxide dismutase (both anti-oxidant enzymes) were highest at 1 mg L^{-1} ammonia and decreased significantly as ammonia increased (Cao et al. 2004).

To alleviate NH_3-N stress, plants must convert the free ammonia to amino acids via synthesis (Figures 1 and 2). This process has an energetic cost, requiring carbon and energy inputs from the plant. Lambert and Davy (2011) invoke energetic expenditure in regulating ammonia internally as a likely cause of growth decline in *Chara* sp. exposed to NO_3-N in excess of 2 mg L^{-1}. The energetic demand of reducing ammonia toxicity, in concert with unregulated ANR, could represent a very significant stress on SAV (Smolders et al. 2000; Wang et al. 2012).

7.1.2.6 Amino-Acid Synthesis

Ammonia is incorporated into α-amino-acids by way of one or both known pathways (Figure 7.1.2), the glutamate dehydrogenase and the glutamate synthetase-glutamate synthase pathway (Guerrero et al. 1981). Buildup of free amino acids in tissues is considered an indication of "nitrogen overload" or impending toxicity due to excessive nitrogen availability (Smolders et al. 1996; Smolders et al. 2000; Wang et al. 2012). Specific types of amino acids that accumulate (for instance arginine, glutamine, asparginine) are dependent on the stresses involved (toxicity, mineral deficiency, grazer pressure) and the species of SAV (Rabe and Lovatt 1986; Rabe 1990; Marschner 1998; Smolders et al. 2000). Significant evidence of the nitrogen overload hypothesis is presented by Wang et al. (2012) who reported reduction of arenchyma tissue, chloroplasts and starch grains in tissues of *Vallisneria natans* exposed to increased nitrate and ammonia levels. The authors contend that loss of structures and starch content is related to photosynthate required to reduce nitrate to ammonia and further sequester toxic ammonia in amino acids, a process that requires significant energy expenditure by plants. Due to the high energetic demand, NO_3-N overload may perhaps lead to susceptibility to pathogens. For example, *Zostera marina*, as well as some other angiosperms, are known to decrease production of antimicrobial compounds such as phenolics during times of increased protein synthesis associated with N enrichment (Buchsbaum et al. 1990).

7.1.2.7 Summary of Mechanisms of Inhibition

Review of the current literature concerning NO_3-N effects on SAV is compelling in that the process of ANR is highly variable among species and the potential for unregulated uptake, an adaptation ostensibly stemming from luxury uptake, could induce the "nitrogen overload" condition (Smolders et al. 1996; Smolders et al 2000; Boedeltje et al. 2005; Wang et al. 2012). The resulting accumulation of ammonia, the end product of ANR, can itself be a significant stressor to plants or, by necessitating protein synthesis to alleviate ammonia stress, can cause depletion of SAV carbohydrate stores (Guerrero et al. 1981; Wang et al. 2012), resulting in reduced growth rates or biomass production. In other ecosystems, potential NO_3-N toxicity may be reduced based upon density of SAV (van der Heide et al. 2010); however, under the unique lotic conditions of springs (increasing nitrate concentrations and constant exposure), this effect is not anticipated. Determining the direct effects of NO_3-N on SAV native to Florida springs will be of primary importance to directing management effort with respect to springs restoration.

7.1.2.8 Ecological Implications

Globally, many aquatic ecosystems have been altered, some seemingly irrevocably, by the anthropogenic addition of excessive nutrients (N and P). For example, in both temperate and tropical lakes receiving nutrient enrichment, shifts from macrophyte to phytoplankton dominance have been observed with regularity in the last half century. In Florida, significant effort has been invested in ameliorating these shifts on large lakes such as Apopka (Dunne et al. 2012) and Okeechobee (James et al. 2011; Harwell and Sharfstein 2009). This shift in primary productivity has resounding effects throughout the food web. Further, habitat loss and susceptibility to altered environmental conditions (for example: hypoxia, shifts in pH) can have detrimental effects on established flora and fauna. In wetlands such as the Everglades, nutrient enrichment has resulted in marked shifts in the vegetation community from the native *Cladium jamaicense* dominated ridges and *Nymphaea odorata* and *Eleocharis interstincta* dominated sloughs to monotypic stands of *Typha latifolia* (Osborne et al. 2011). This shift in vegetation precipitated significant changes to ecosystem services such as carbon storage, biogeochemical cycling of nutrients, and habitat quality for fauna. Similarly, Florida's springs systems, which have immense ecological, cultural and economic value to the state, have undergone significant ecological degradation (e.g., proliferation of "nuisance" algae, loss of SAV, changes in fish communities) in recent decades. Therefore, concern exists for determining the relationship between these changes and the observed increase in NO_3-N in springs. Of primary concern is elucidating the role nitrate enrichment has had (whether direct or indirect via synergistic interactions with other stressors) in the observed decline of these systems.

7.1.2.9 Objectives

The objectives of this research were to investigate if SAV native to Florida springs are experiencing any inhibitory effects due to elevated NO_3-N concentrations by one or more of the proposed mechanisms: 1) unregulated NO_3-N uptake and reduction, 2) NH_3-N toxicity from excess accumulation in vivo, and 3) carbohydrate depletion from intercellular or root storages. The mechanisms were evaluated in SAV in controlled mesocosm experiments. Mesocosm results were corroborated by measurements of tissue samples collected from selected sites within Silver River, and Alexander Springs.

7.1.3 MATERIALS AND METHODS

7.1.3.1 Field Collection Methods

Collection of live plants (*Sagittaria kurziana* and *Vallisneria americana*) was conducted along the middle reach of the Silver River in June of 2015 and 2016 via motorized vessel under Florida Department of Agriculture and Consumer Services (FDACS) permit number 48016783. Suitable collection areas were identified in shallow (< 2 m depth) waters near the banks of the river and site GPS coordinates recorded; however, no site markers were installed. All precautions were taken to avoid other research plots or areas where SAV appeared sparse or stressed. Individual ramets of each species were collected by hand and placed in coolers in the river water and transported back to the laboratory. Care was taken to harvest smaller plants (< 20 cm in length) in a highly sustainable way with no more than 2-4 individuals being removed from a square meter. This method allowed harvest without observable denuding of vegetated areas.

Upon return to the laboratory, both species of SAV were planted in 15 cm square high density polyethylene (HDPE) pots with 500 µm sieved sand (referred to as "sand", no organic matter) or natural unsieved river sediment (referred to as "organic", with 5-7 % organic matter) as the growth media. Plants were then immediately introduced to mesocosms or growth chambers and allowed to acclimate for 2-3 weeks prior to initiation of growth measurements.

Collection of plant material for nitrate reductase activity (NRA) was conducted in several locations on Silver River and Alexander Springs (*S. kurziana* only) by hand and single blades of each species were removed and stored in a 3 L liquid nitrogen dewar (US Solid Cryogenics ®) and returned to the laboratory for analysis.

7.1.3.2 Mesocosm Description

All experiments were conducted in either controlled growth chambers in the laboratory or in an outdoor mesocosm facility constructed onsite at the University of Florida Whitney Laboratory for Marine Bioscience in St. Augustine, FL.

Growth chambers consisted of standard 45 L acrylic glass aquaria (25 cm W x 30 cm H x 50 cm L) on shelving banks (24 total aquaria) situated in front of growth spectrum (Ecolux 34W) light fixtures on a 14 h (per day) cycle. The room was kept at a constant 23 °C (figure 7.1.4). Both species of SAV were planted in 15 cm square high density polyethylene (HDPE) pots with 500 µm sieved sand or natural unsieved river sediment as the growth media.

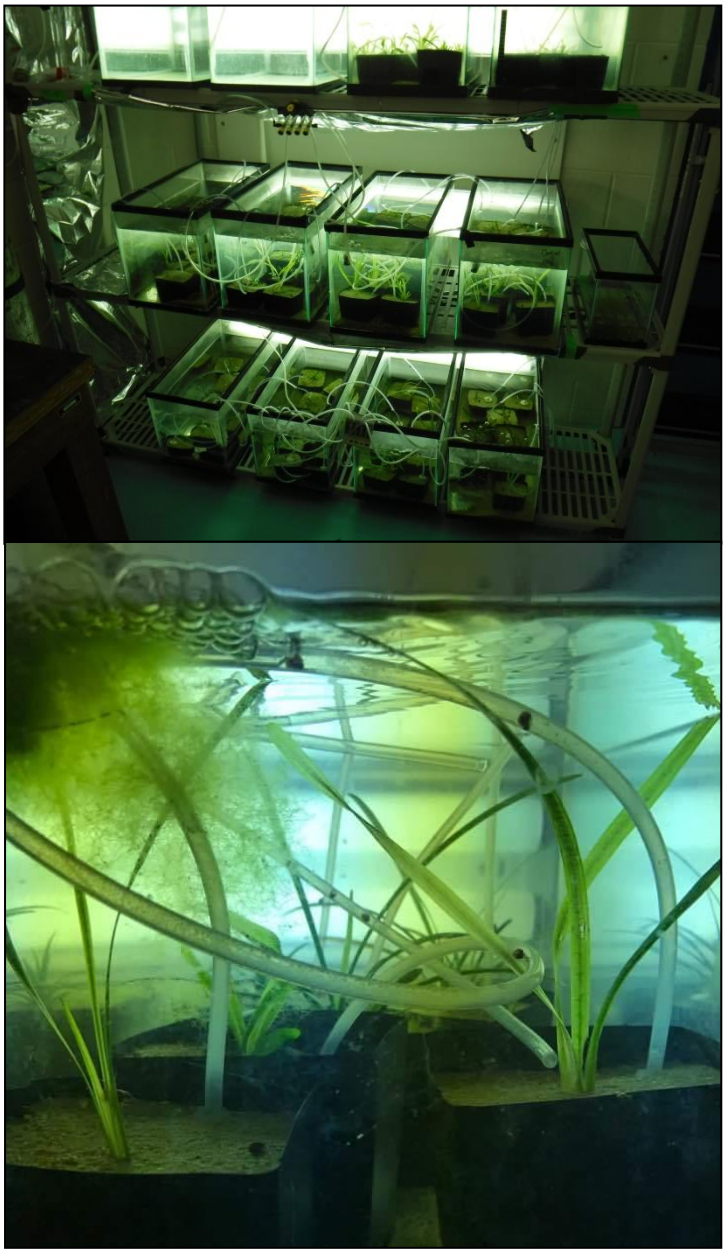

Figure 7.1.4. Growth chamber arrays located in temperature and light controlled laboratory at the University of Florida Whitney Laboratory for Marine Bioscience in St. Augustine, FL.

Mesocosms were constructed of high density polyethylene (HDPE) tanks of approximately 450 L volume (1.8 m L x 0.61 m W x 0.86 m H; Figure 7.1.5A). All tanks were plumbed with inert PVC and connected to opaque HDPE 1,000 L water reservoirs where flow was controlled via submersible pumps. The mesocosm facility is housed at the Whitney Laboratory in St. Augustine. Spring water was pumped from an onsite well at Silver Springs State Park and transported to the mesocosms via tanker truck (SJRWMD). Conductivity was monitored during mesocosm use to maintain proper water levels and regional well water was transported regularly to maintain water levels in experimental tanks in response to evaporation. Temperature control

was initiated in mid spring each year using large frozen water bottles and subsequently, electric chiller units deployed in the reservoir tanks.

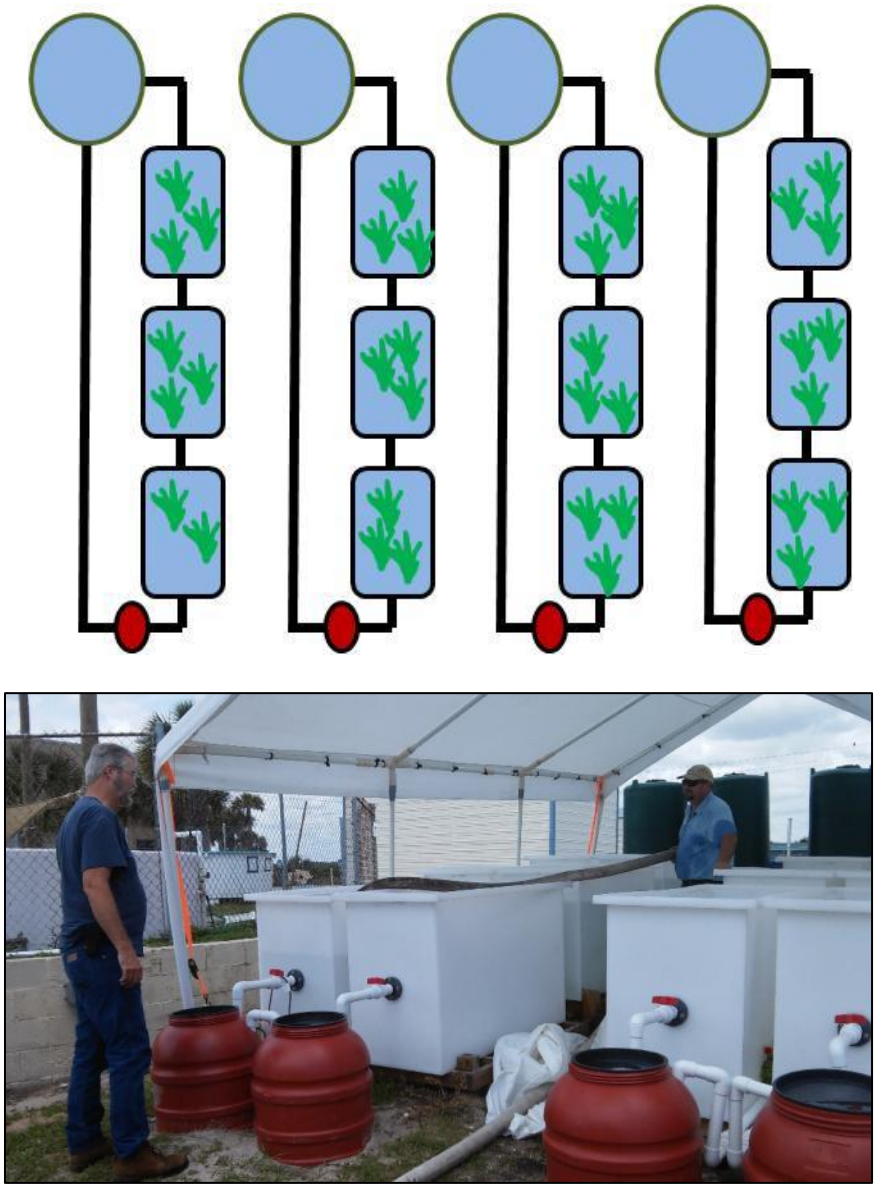

Figure 7.1.5A. Schematic of mesocosm facility (top) and picture of constructed facility (bottom).

Mesocosms were maintained at 4 relevant nutrient treatments of 0.1, 0.5, 1.0 and 5.0 mg NO_3-N L^{-1}. NO_3-N concentrations were artificially elevated from background with 1,000mg L^{-1} concentrated stock solution of KNO_3 and monitored every 2 to 3 days with an Orion® Nitrate Ion Selective Probe (Thermo Scientific model 9707BNWP) to determine when nutrient additions were necessary to maintain the appropriate concentration.

Algal biomass was controlled by addition of sock filters at each tank outfall and by manual cleaning of tanks on a weekly basis. Experimental trial (exposure period) duration varied per

iteration (range 12-14 weeks). At the cessation of the trial, plants from each pot were harvested and roots and shoots separated. Shoots were enumerated and measured (length and width) prior to analyses. Wet weight of both roots and shoots was measured prior to drying.

7.1.3.3 Laboratory Methods

All laboratory analyses were conducted at the University of Florida Whitney Laboratory for Marine Bioscience in St. Augustine FL and the Wetland Biogeochemistry Laboratory of the Soil and Water Sciences Department in Gainesville FL.

7.1.3.3.1 Nutrient Analysis of SAV

Upon returning to laboratory, SAV tissue samples were dried in drying ovens at 100°C for 72 hours then milled to <250 μm on a Spex 8000D ball mill. Approximately 10-15 mg of sample was wrapped in silver foil prior to combustion analysis for carbon and nitrogen. Total nitrogen (TN) and total carbon (TC) and ^{13}C and ^{15}N stable isotopes ratios were determined using a coupled Costech model 4010 Elemental Analyzer (Costech Analytical Industries, Valencia, CA) and Finnigan Mat Delta XL Isotope Ratio Mass Spectrometer (Thermo Finnigan, San Jose, CA). Total phosphorus (TP) was determined using acid digestion of tissue and digestate analyzed using colorimetric procedures (Method 365.4; USEPA, 1993) on a Hach DR 6000 dual beam spectrophotometer. Mass ratios of carbon to nitrogen were reported as C:N (g / g) and TP reported as mg kg^{-1}.

7.1.3.3.2 Nitrate Reductase Activity (NRA)

Nitrate reductase activity (NRA) was measured as maximal activity of the nitrate reductase enzyme in plant and algal tissues (MacKintosh et al. 1995) on fresh SAV, epiphytic and benthic algae tissues cultured in mesocosms and additional tissues of *S. kurziana* from Alexander Springs. The analysis was performed according to Cedergreen and Madsen (2003), Corzo and Niell (1991) and Scheible et al. (1997a) using an induction medium of 50 m*M* HEPES, 0.1 % 1-propanol, 30 m*M* KNO_3, 10 m*M* glucose, 1 m*M* EDTA and 0.1 *M* phosphate buffer. 5 mL of assay medium in 15 mL test tubes was then flushed with N_2 gas 2 minutes before and after the addition of 0.16 g of fresh tissue (roots, shoots, shoot tips seperated). Test tubes were then sealed with stoppers and incubated in the dark for 1 h in a water bath maintained at 30 °C. The NO_2^- produced is determined spectrophotometrically by adding 300 μL Sulfanilamide/ N-(1-Naphthyl) ethylenediamine Dihydrochloride solution (Ricca Chemical Company) to 700 μL of incubated assay and measuring OD at 540 nm after 20 minutes. NRA values were reported as activity per unit dry weight, which was determined by drying of subsamples of tissues as described previously.

7.1.3.3.3 Quantification of SAV Growth

At the end of each 16-week culture period, analysis of root and shoot biometrics was conducted. Digital images of the cultured SAV were taken and analyzed using the software programs RootFly and Easy Leaf Area. Assess 2.0: Image Analysis Software was used for measurement of leaf area and volume. The image analysis software program RootFly was used to determine root length, diameter, surface area and volume. RootFly and Easy Leaf Area uses the color ratios of each pixel to distinguish roots, leaves and calibration areas from their background and compares leaf pixel counts. Traditional measurements of leaf blade width, length, and root and shoot mass

were also made. Ratios of root:shoot biomass (dry) were calculated for comparison to Cohen et al. (2007).

7.1.3.3.4 Anatomical Responses

7.1.3.3.4.1 Starch and Amino Acid Assays

Undried samples of SAV roots and shoots were macerated with a tissue grinder (QUIGEN® TissueRuptor) to approximately 500 µm and subsamples weighed to 0.2 g. Samples were transferred to 150 mL flasks and stirred while adding 25 mL of deionized water (DI). The pH was adjusted to pH 7. The mixture was then boiled while continuing to gently stir for 3 minutes and then autoclaved for 1 hour at 135 °C, allowed to cool to 60 °C, then brought to a total volume of 100 mL with DI water. One ml of Starch Assay Reagent (Sigma Aldrich) and 1.0 mL of sample were transferred into test tubes to be incubated for 15 minutes at 60 °C in a shaking water bath. Next, 1.0 mL of glucose assay reagent (Sigma Aldrich) and 100 µL of starch assay reagent were added. Tubes were vortexed and incubated for 15 minutes at room temperature. The glucose produced was determined spectrophotometrically by measuring optical density (OD) at 340 nm.

For amino acid content, the same extraction method was employed as described above for starch analysis followed by the Ninhydrin Method for amino acid determination (Hwang and Ederer 1975, Wang et al. 2012). Then 10 mL of DI water was added to the wet, macerated tissue, which was then vortexed and centrifuged at 3,000 rpm for 3 minutes and the supernatant collected. One ml of Ninhydrin reagent (0.35 g of ninhydrin dissolved in 100 mL of ethanol) was added to the supernatant and heated to 100 °C for 5-7 minutes until color development occurred. After a short cooling period, the free amino acid content was determined spectrophotometrically by measuring OD at 570 nm.

7.1.3.3.4.2 Leaf Anatomical Structure Analysis

Microscopic visualization of SAV anatomical structure was made by fixation, dehydration, paraffin infiltration, sectioning (Institute of Molecular Development 2001) and staining of leaf and root tissue. Three cm sections of leaf tissue were fixed in formalin-acetic acid-alcohol (FAA) solution for 3 h. Tissue was then dehydrated in a series of increasing concentrations of t-butyl alcohol (TBA) and decreasing concentrations of ethanol and DI water. Leaf tissue was then infiltrated with paraffin overnight (changed with fresh paraffin every 4 h for 2-3 changes). Tissue was embedded in paraffin wax blocks and sectioned to 30 µm using a microtome (Microm model HM 325). Analysis of leaf and root anatomical structures by enumerating of stained starch grains, measurement of arenchyma cell diameter, and assessing condition of vascular bundles and epidermis) was made from bright/dark field microphotographs of structures at 100x magnification (similar to methods of Wang et al. 2012).

7.1.3.3.5 Effects of Oxygen on SAV Growth

To determine if reduced oxygen availability had any effect on SAV growth, both species were grown on sand media in 15 cm square pots under controlled condition in the laboratory in growth chambers. Two levels of oxygen availability (oxic and hypoxic) were compared for a period of 10 weeks. Using N_2 gas to sparge O_2 from the aquaria, water column oxygen was brought to 2

mg L^{-1} then aquaria water surfaces were covered with cellophane wrap to reduce oxygen diffusion into the chamber. Aquaria were sparged routinely (every 3-4 days to keep oxygen at or below 2 mg L^{-1}. The oxic treatment was left open to the atmosphere and oxygen levels were maintained at approximately 6-8 mg L^{-1}. At the cessation of the 10 week treatment, plants were harvested and growth metrics recorded (blade length, width, root:shoot mass).

7.1.3.3.6 Effects of Sulfide on SAV Growth

To determine effects of sulfide in the root zone on both SAV species, a 10 week experiment was conducted in growth chambers with plants in sand media in 15cm square pots. To induce sulfide production, sediment was spiked with 0.01, .1 and 0.75 *M* with potassium sulfate (a non-spiked treatment served as control). Glucose was added to promote the reduction of sulfate to H_2S (Koch et al., 2008). To confirm sulfate reduction, porewater samples were taken with in situ porewater sippers and analyzed for H_2S colormetrically. The analysis of H_2S was conducted on a Hach DR 6000 dual beam spectrophotomer using the USEPA Methylene Blue method (EPA Method 376.2).

7.1.3.3.7 Epiphytic Algae Quantification

Periphytometers were utilized to measure epiphytic algal production in mesocosms under four nitrate treatments (0.1, 0.5, 1.0 and 5.0 mg NO_3-N L^{-1}). Acid washed (10 % HCl bath) glass microscope slides were deployed for 1 month to quantify algal growth. Upon collection, slides were scraped with a razor blade and the algal biomass measured for both chlorophyll a and ash free dry mass (AFDM) via combustion in a muffle furnace. Chlorophyll a was determined using the alkaline acetone extraction method (Rice et al. 2012) in which algal biomass is sonicated in 20ml of 90% alkaline ($CaCO_3$ saturated) acetone. The resulting solution is centrifuged at 3000 rpm for 1 minute then the supernatant is measured for OD at 663 nm.

7.1.3.3.8 Statistical Analyses

Statistical analyses were performed using XLStat V14.0, a commercially available software package, or in R, a freely available statistical modelling software platform.

7.1.4 RESULTS AND DISCUSSION

7.1.4.1 Root : Shoot Ratios

Mesocosm growth experiments (Figure 7.1.5B) indicated nitrate induced responses by both SAV species and epiphytic algae from the four treatments (0.1, 0.5, 1.0 and 5.0 mg NO_3-N L^{-1}) (Figure 7.1.6). In *V. americana*, control NO_3-N levels were significantly higher than the low NO_3-N treatment (ANOVA $p<0.01$, Tukey's post hoc) but not statistically different from the medium and high treatments, although visual inspection of the data suggests an increasing trend in root:shoot with increasing NO_3-N availability. The nitrate overload hypothesis would predict a linear decrease in this ratio if NO_3-N was inducing excessive use of starch storage in roots to accommodate protein synthesis.

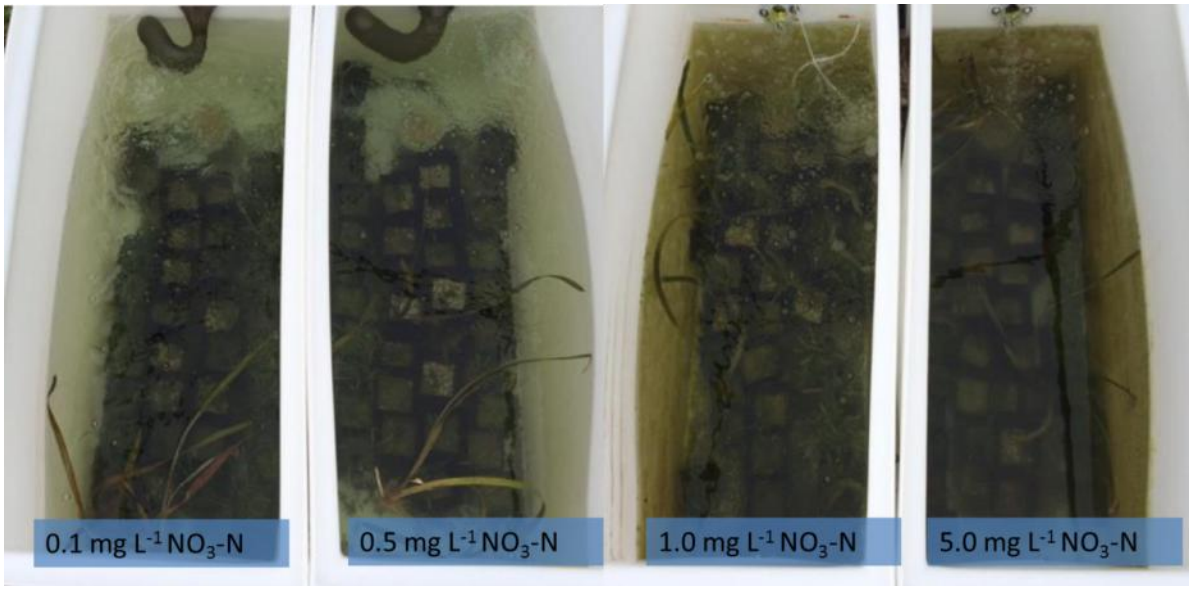

Figure 7.1.5B. Mesocosm vegetation (*V. americana* under variable water NO_3-N concentrations).

In *S. kurziana*, the control root:shoot was significantly higher than the treatments (ANOVA $p<0.01$). A visual downward trend in root:shoot with increasing NO_3-N is evident in the results, however, this trend is not statistically significant (Figure 7.1.6). Unlike *V. Americana,* these results suggest that perhaps S. kurziana is less efficient at regulating the use of available NO_3-N. Because there is no statistical difference between the NO_3-N treatments, results suggest that any increase in NO_3-N catalyzes a growth response which is concentration independent. These results also suggest that compared to *V. americana, S. kurziana* may respond to increased NO_3-N with more rapid blade growth. When grown on organic sediment, *S. kurziana* responded similarly to the sand media experiment, with one significant difference. The low NO_3-N treatment did not differ from the control. This result suggests that the organic sediment may have provided other limiting nutrients that would allow *S. kurziana* to match root growth and shoot growth without taxing root storages for ANR. This assertion is supported by the observation of more excessive growth of ramets grown on organic media versus clean sand (Figure 7.1.8). Direct comparison of growth responses between both species (Figure 7.1.9) suggests that

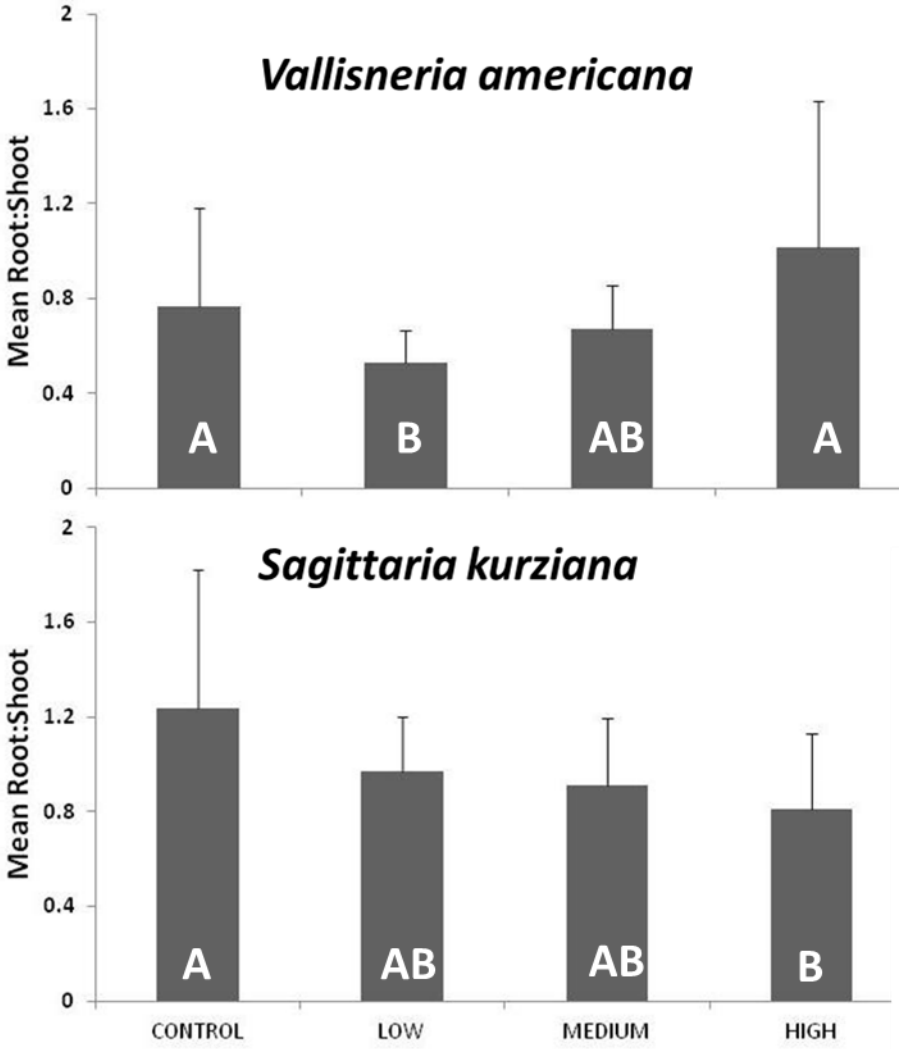

Figure 7.1.6. Mean root:shoot biomass ratios of *V. americana* and *S. kurziana* grown on sand at control (0.1 mg NO_3-N L^{-1}), Low (0.5 mg NO_3-N L^{-1}), Medium (1.0 mg NO_3-N L^{-1}) and High (5.0 mg NO_3-N L^{-1}) concentrations. A and B denote statistically significant difference between means.

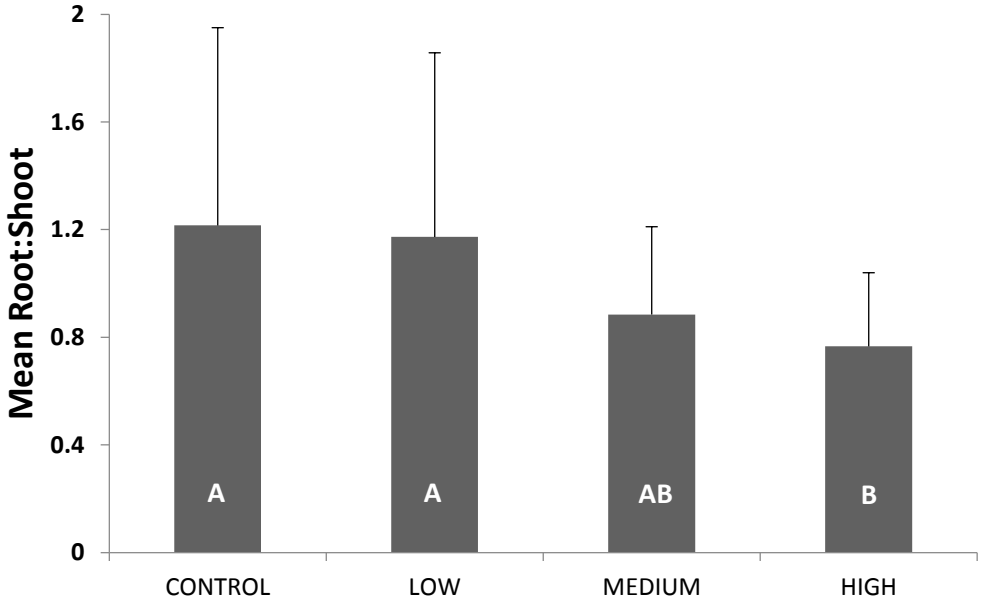

Figure 7.1.7. Root:shoot ratios for S. kurziana grown on organic media at control (0.1 mg NO_3-N L^{-1}), Low (0.5 mg NO_3-N L^{-1}), Medium (1.0 mg NO_3-N L^{-1}) and High (5.0 mg NO_3-N L^{-1}) concentrations. A and B denote statistically significant difference between means.

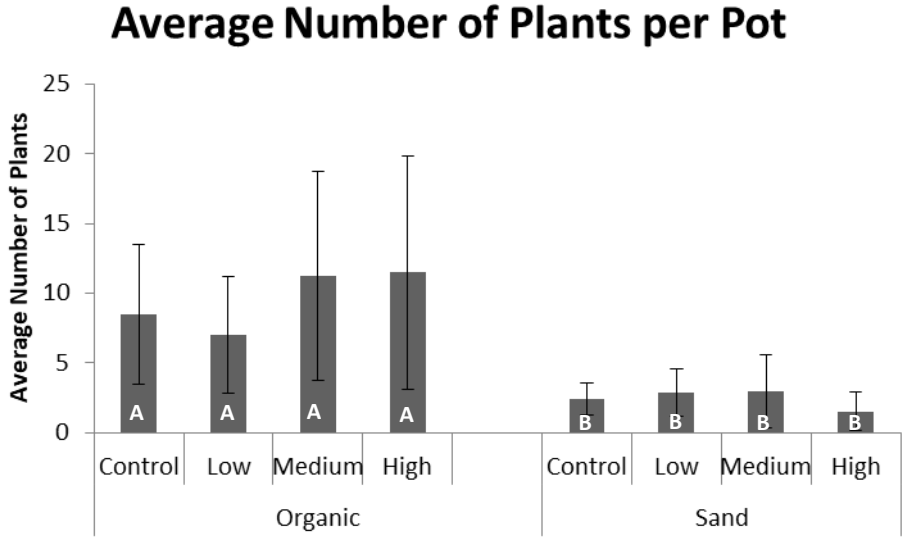

Figure 7.1.8. Average number of ramets per pot after the growth trial of *S. kurziana*. Note: all pots were originally planted with a single ramet at the beginning of the experiment. A and B denote statistically significant difference between means.

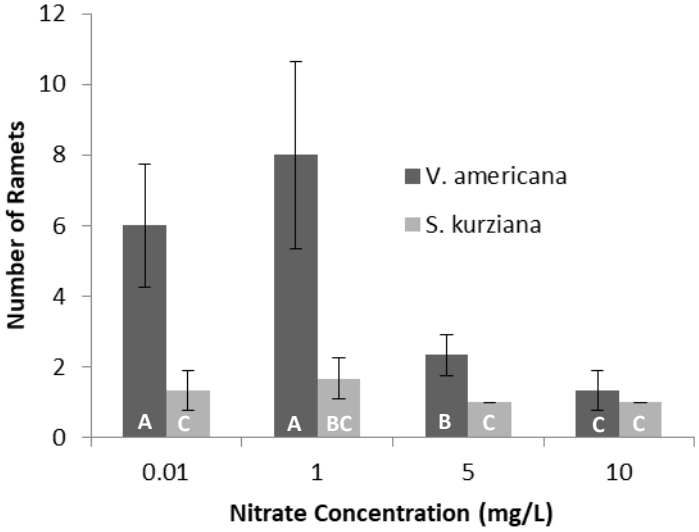

Figure 7.1.9. Mean number of ramets produced by *V. americana* (dark gray) and *S. kurziana* (light gray) at control (0.1 mg NO_3-N L^{-1}), Low (0.5 mg NO_3-N L^{-1}), Medium (1.0 mg NO_3-N L^{-1}) and High (5.0 mg NO_3-N L^{-1}) concentrations. A, B, C denote statistically significant difference between means.

7.1.4.2 Nitrate Reductase Activity

Nitrate reductase activity (NRA) is an enzymatic indicator of nitrate reduction in vivo in SAV tissues. Two weeks after the initial dosing of the mesocosms, *V. americana* tissues were sampled from each mesocosm NO_3-N treatment and analyzed for NRA. Results indicate active uptake of NO_3-N by SAV in mesocosms (Figure 7.1.10).

After 16 weeks of acclimation to mesocosms and nitrate concentration treatments, both species were sampled again for NRA. Results (Figure 7.1.11) suggest that NRA activity is reduced after the acclimation phase when compared to the initial sampling at two weeks of exposure to elevated nitrate. NRA production and molecular structure is different among species and thus regulation of NRA is also likely species specific. We observed variability among species in NRA activity in roots and shoots. In *V. americana,* the highest levels of NRA were observed at 0.5 mg NO_3-N L^{-1} and below, with highest levels being in shoots at 0.5 mg NO_3-N L^{-1}. With respect to *S. kurziana*, the highest levels of NRA were also observed at the control concentration of 0.1 mg NO_3-N L^{-1}, and no partitioning was observed between root or shoots. These findings suggest that in presence of nitrate, both species have the ability to regulate NRA. Between the two species investigated, *S. kurziana* appears to be the most able to control NRA suggesting that S. Kurziana has tighter molecular control over the NRA process and thus can better utilize NO_x when available (and conversely NOT over expend energy when NO_x is available in excess).

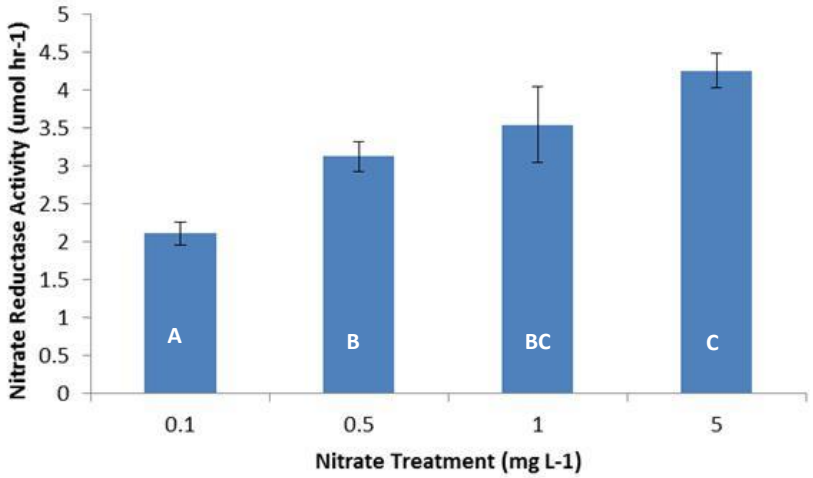

Figure 7.1.10. Two week shoot nitrate reductase activity (µmol h^{-1}) from mesocosm vegetation (*V. americana* under variable water NO_3-N concentrations. A, B, C denote statistically significant difference between means.

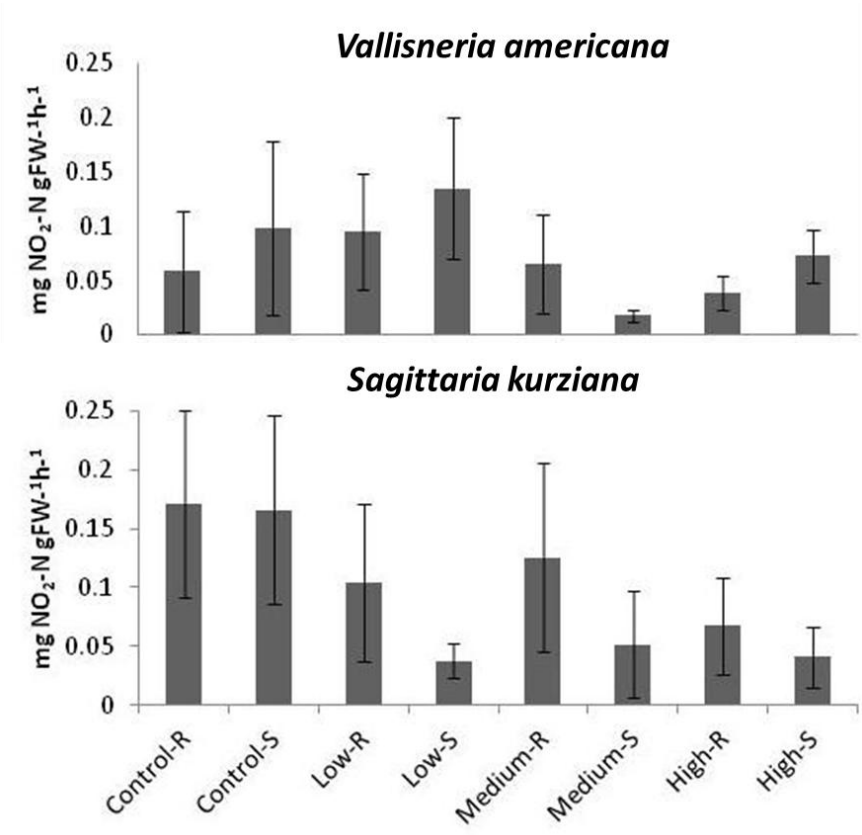

Figure 7.1.11. Root (R) and shoot (S) nitrate reductase activity in *V. americana* and *S. kurziana* at control (0.1 mg NO_3-N L^{-1}), Low (0.5 mg NO_3-N L^{-1}), Medium (1.0 mg NO_3-N L^{-1}) and High (5.0 mg NO_3-N L^{-1}) concentrations.

Opportunistic sampling of SAV in Silver River was conducted to collect tissue samples for NRA assays. Fine roots, rhizomes, shoots and shoot tips were investigated with NRA assays using whole tissue samples. Results of assays suggests significant partitioning of NRA activity in the fine roots (Figure 7.1.12). However, when viewed upon a tissue mass basis, this finding supports the assertion that most NO_3-N is derived from the water column via foliar adsorption versus root uptake from sediments as blade biomass is significantly higher than root. Another opportunistic comparison was made between *V. americana* from Wekiwa River and Silver River as to NRA (Figure 7.1.13). *In situ* results support observations made in mesocosms where higher rates of NRA were found in roots over shoots. However, the higher NRA in Wekiwa River samples does not match the observations from the mesocosms in that NRA was significantly higher in Wekiwa River samples where NO_3-N concentrations are higher. This observation suggests there are other potential drivers of NRA *in situ*, such as sediment chemistry or light availability. The assertion that sediment chemistry is a factor is supported by observations during the mesocosm study.

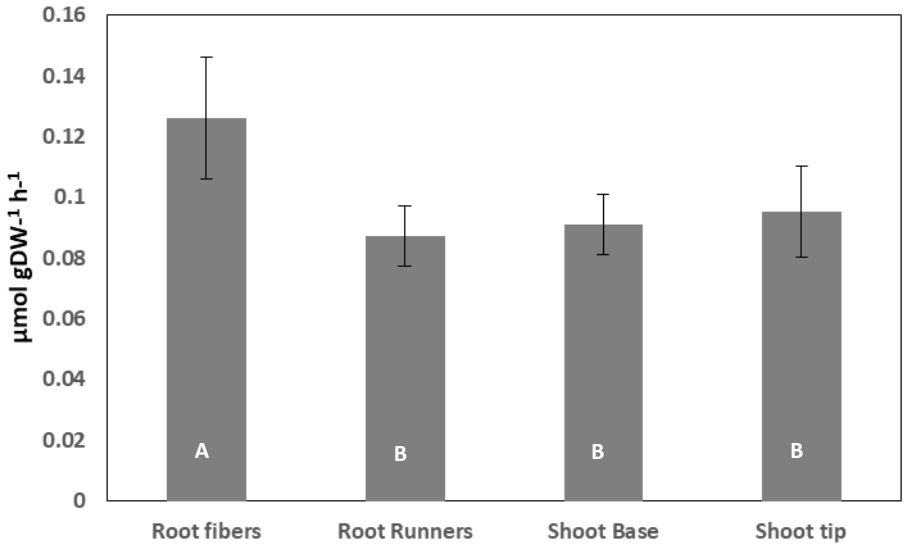

Figure 7.1.12. Nitrate reductase activity (µmol g dw h^{-1}) from fine roots, roots, mid shoots, and shoot tips of *Vallisneria americana* from Silver River.

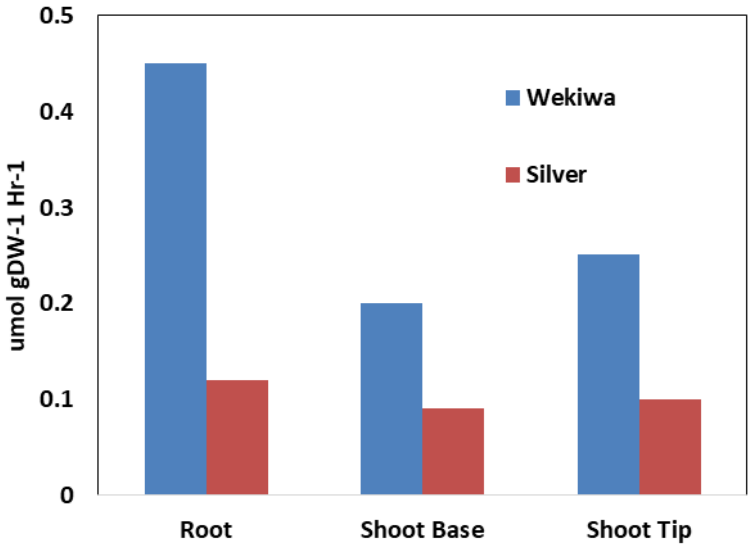

Figure 7.1.13. Nitrate reductase activity from roots, shoot bases, and shoot tips of *Vallisneria americana* from Silver River versus Wekiwa River, where NO_3-N is twice the concentration.

7.1.4.3 Tissue Elemental Analysis

Partitioning of N within tissues was investigated in an effort to better understand where plants were putting excess N (Figure 7.1.14). *S. kurziana* was observed to maintain statistically similar C:N ratios across the range of treatments with the exception of the Low (0.5 mg NO_3-N L^{-1}) treatment (ANOVA $p<0.001$). This observation suggests that *S. kurziana* may initiate substantial growth when low levels of NO_3-N are available. The ratios continue to decline as NO_3-N increases suggesting efficient assimilation of NO_3-N. At low nitrate concentration, *V. americana*, clearly partitioned N more in roots than shoots (ANOVA $p<0.001$). This trend appears to hold through all treatments, however, statistically relevant separation is lost as nitrate concentration increases. These findings suggest N (as protein) is used similarly in plant shoots and roots over a range of nitrate concentrations, or that NO_3-N processing in roots (as observed previously) concentrates N there and thus overcomes natural portioning differences between starch storage in root versus protein storage in shoots. C:N ratios of plant shoots and roots decline significantly from the control (0.1 mg NO_3-N L^{-1}) to the Low (0.5 mg NO_3-N L^{-1}) treatment (ANOVA $p<0.01$) and between control and the Medium (1.0 mg NO_3-N L^{-1})($p<0.001$) and High (5.0 mg NO_3-N L^{-1}) ($p<0.001$) concentrations. There was no statistical difference observed between the Medium and High NO_3-N treatments.

Results suggest that both species of SAV are incorporating NO_3-N as indicated by declining C:N ratio. The C:N of *S. kurziana* at the low treatment is somewhat unexpected as it suggests N limitation above 40. Perhaps growth in this species may be non-linear when growth is induced at low level nutrient additions. Similarly, the C:N of the control treatment of *V. americana* is also surprising as ratios above 40 can be indicative of N limitation.

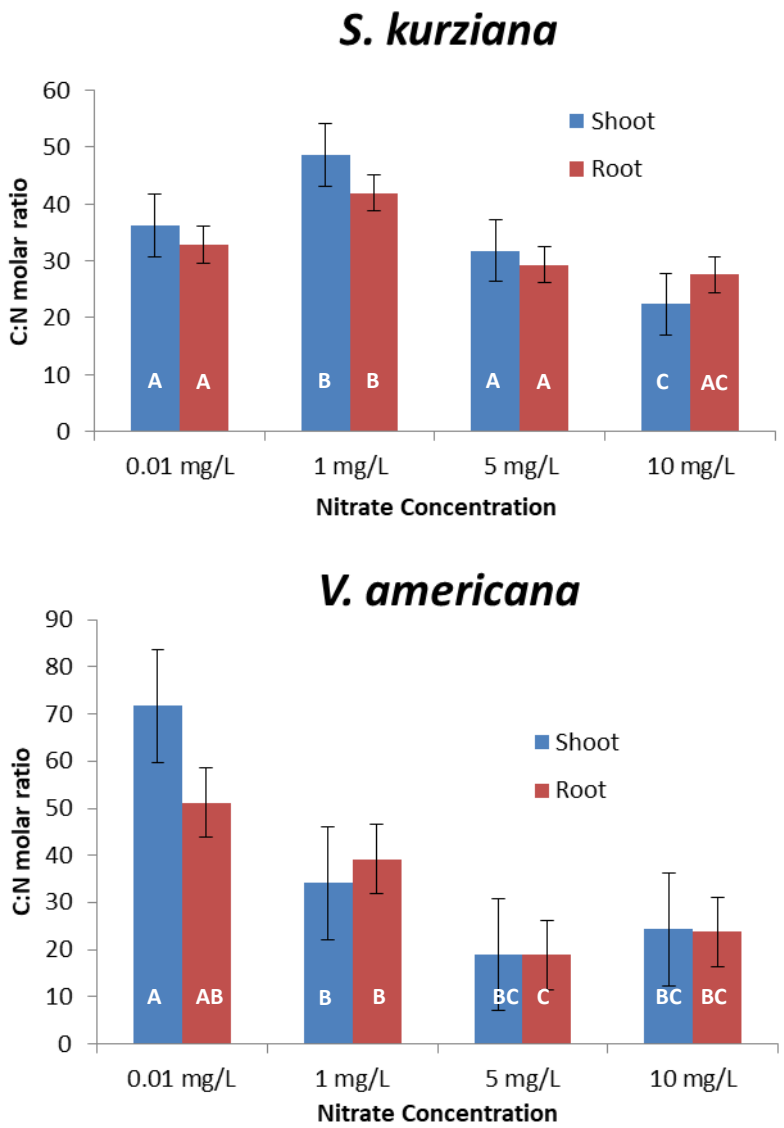

Figure 7.1.14. Mean C:N ratios of root (red) and shoot (blue) tissue material at control (0.1 mg NO_3-N L^{-1}), Low (0.5 mg NO_3-N L^{-1}), Medium (1.0 mg NO_3-N L^{-1}) and High (5.0 mg NO_3-N L^{-1}) concentrations.

7.1.4.4 Cellular Level Responses

Reduced arenchyma cell diameter and damaged cellular structure (Figure 7.1.15) was an indicator of nitrate stress in SAV reported by Wang et al. (2012). When investigated in *V. Americana* (Figure 7.1.16) and *S. kurziana* (Figure 7.1.17) by thin section microscopy, arenchyma diameter appeared to increase at concentrations of 0.5 mg NO_3-N L^{-1} then decrease with higher nitrate concentrations. No statistical difference was observed between the measurement populations and thus we conclude that there is no negative effect of nitrate concentration on the arenchyma cell diameter or integrity.

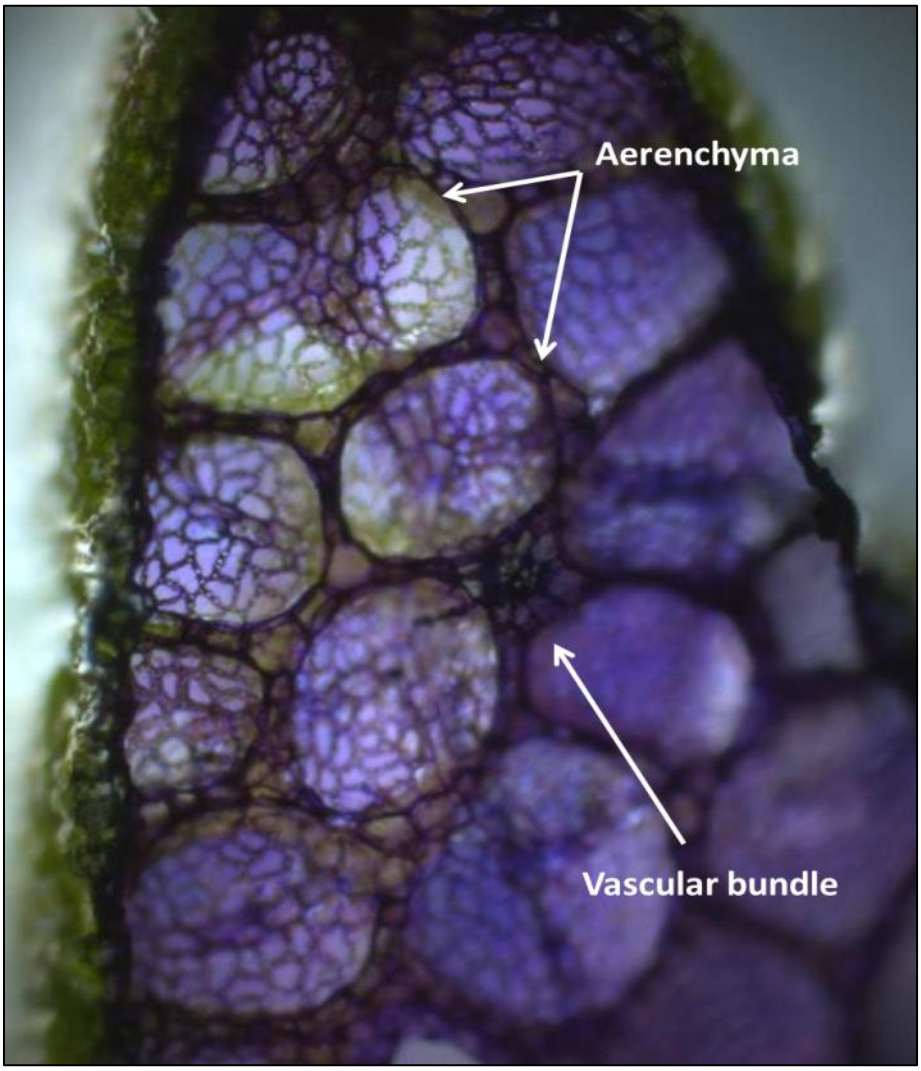

Figure 7.1.15. Arenchyma cells and vascular bundles in a microtome sliced thin section of *V. Americana*. Breakdown of arenchyma cells was a noted effect of NO_3-N stress reported by (Wang et al. 2012).

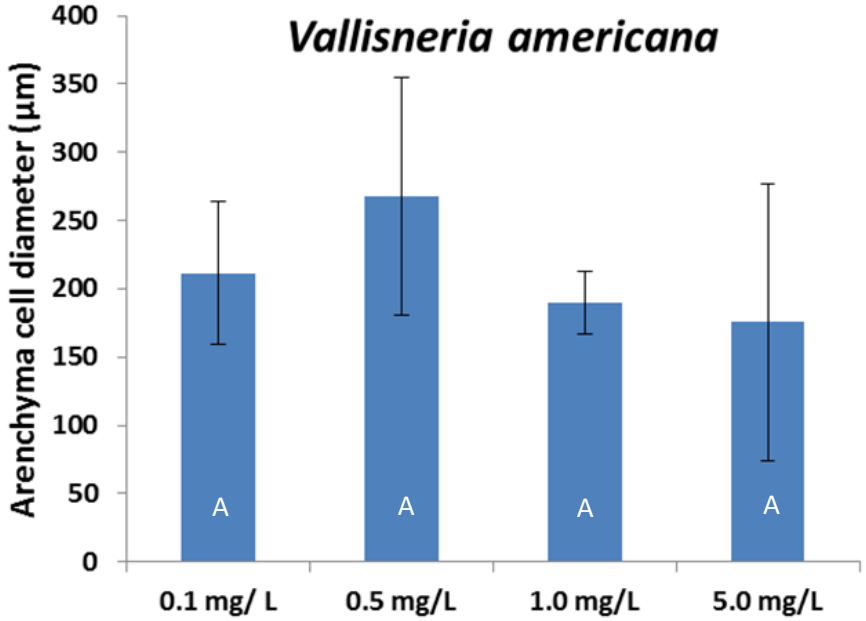

Figure 7.1.16. Mean arenchyma cell diameter of *V. americana* shoots at control (0.1 mg NO_3-N L^{-1}), Low (0.5 mg NO_3-N L^{-1}), Medium (1.0 mg NO_3-N L^{-1}) and High (5.0 mg NO_3-N L^{-1}) concentrations.

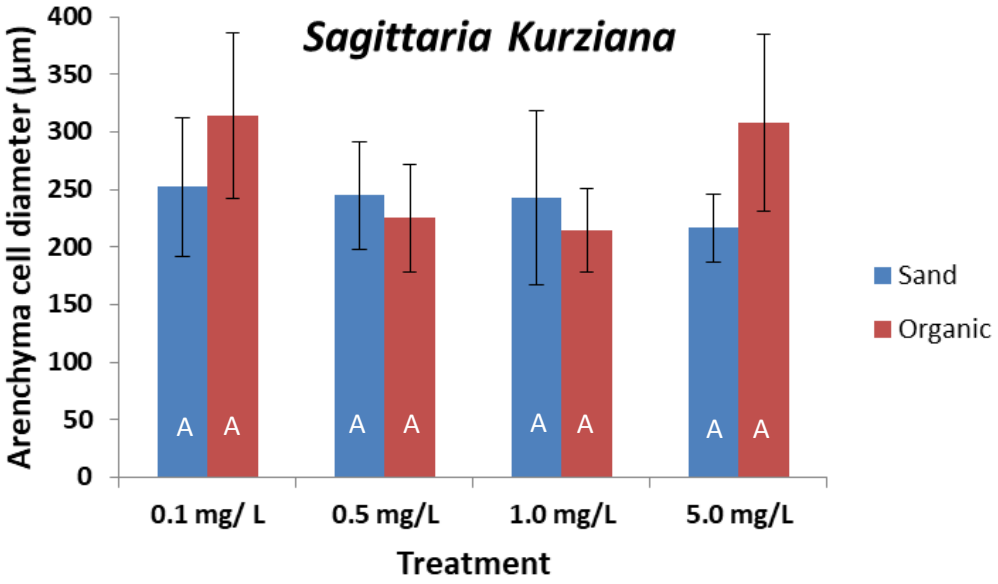

Figure 7.1.17. Mean arenchyma cell diameter of *S. kurziana* shoots at control (0.1 mg NO_3-N L^{-1}), Low (0.5 mg NO_3-N L^{-1}), Medium (1.0 mg NO_3-N L^{-1}) and High (5.0 mg NO_3-N L^{-1}) concentrations.

The NO_3-N overload hypothesis reasons that excessive NO_3-N will require SAV to utilize stored starch to fuel the energetic requirements of ANR and protein synthesis. If there is no biochemical

regulation of the process, starch stores in SAV roots could be exhausted resulting in diminished growth and/or health. We anticipated observing reduced starch storage in the form of starch grains and glucose content in tissues. The results of the starch grain enumeration using microscope views of tissues (Figure 7.1.18) found that at the control (0.1 mg NO_3-N L^{-1}) level, mean starch grain content per cell (17.8 ±2.8) was significantly higher ($t=1.78$, $p<=0.01$, $n=12$) than the High (5.0 mg NO_3-N L^{-1}) treatment (11.0 ±2.5). This result suggests lower storage of starch in the higher NO_3-N treatments.

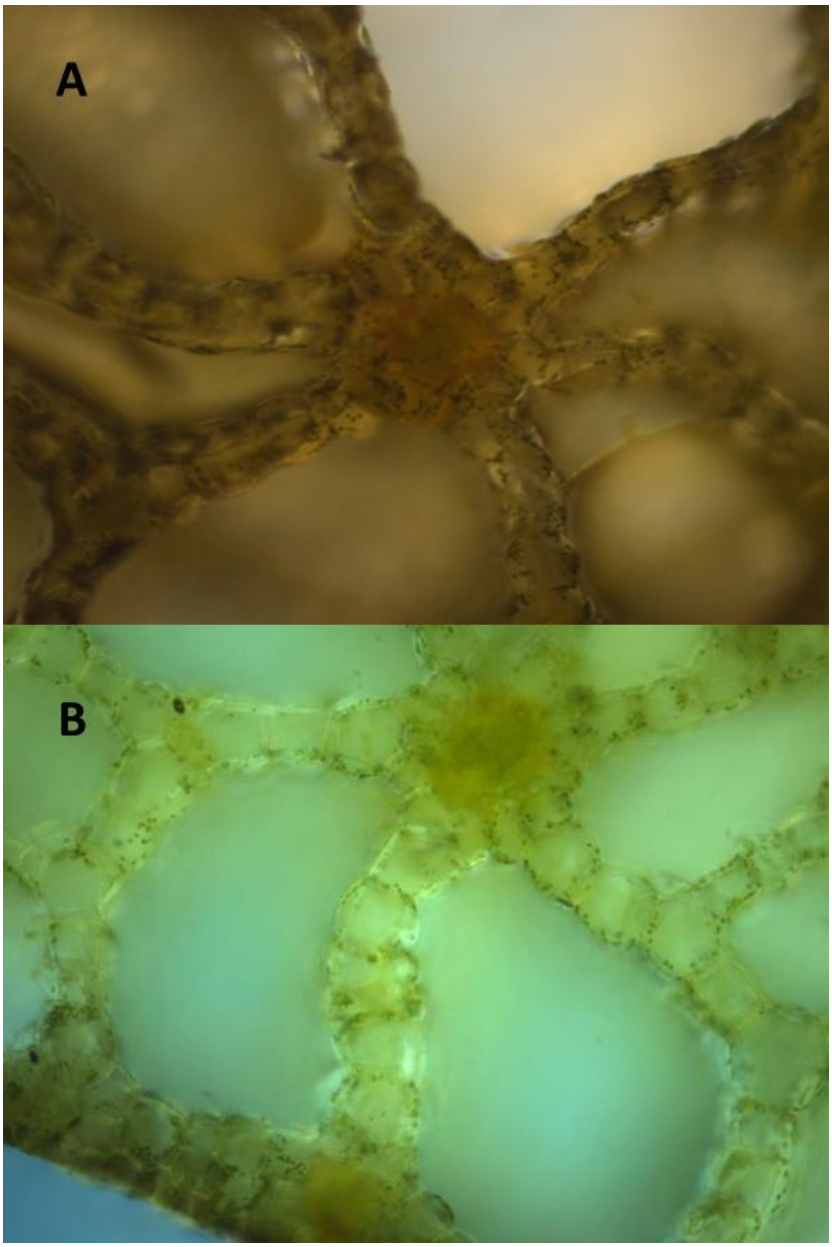

Figure 7.1.18. Example of starch grain content (small black dots within plant cells) in the control (0.1 mg NO_3-N L^{-1})[A], and High (5.0 mg NO_3-N L^{-1}) concentrations[B].

Due to excessive time and difficulty required for this analysis, we turned to total tissue glucose content analysis to further investigate this finding (Figure 7.1.19). Starch content in *V. americana* trended upward in higher NO_3-N treatments, however the only statistically significant difference was observed between the High NO_3-N treatment and the control and low NO_3-N treatments (ANOVA $p<0.01$). There was no significant difference observed between the control, low and medium treatments. In *S. kurziana* there were no significant differences observed between any treatment.

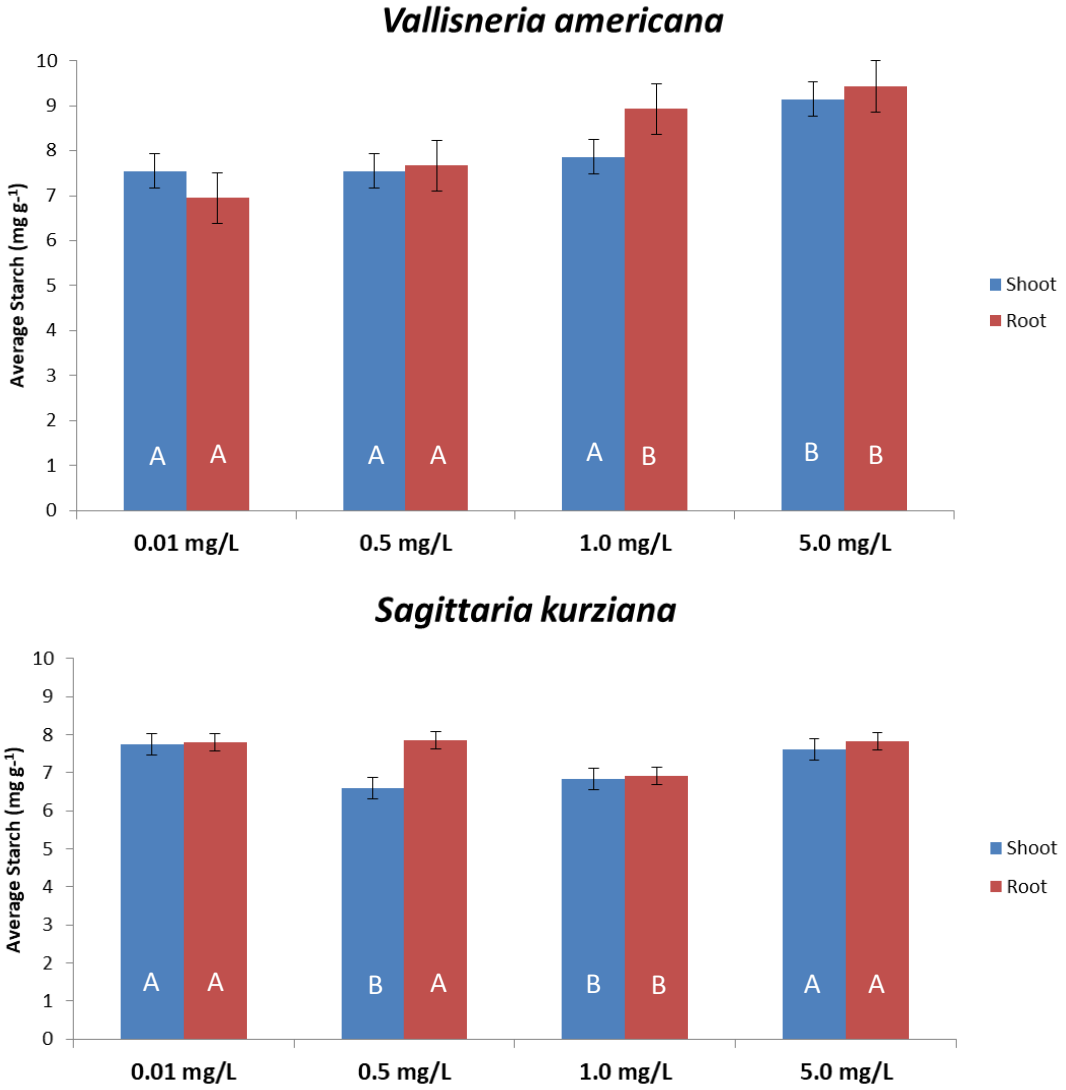

Figure 7.1.19. Mean starch content of *V. Americana* (top) and *S. kurziana* (bottom) roots (red bars) and shoots (blue bars) at control (0.1 mg NO_3-N L^{-1}), Low (0.5 mg NO_3-N L^{-1}), Medium (1.0 mg NO_3-N L^{-1}) and High (5.0 mg NO_3-N L^{-1}) concentrations.

We anticipated an increase in free amino acids in plant tissues with increased nitrate concentration, and a concomitant decline in starch content which would indicate uncontrolled

energy utilization for protein synthesis. When starch content was measured in *V. americana*, the opposite response was observed indicating no loss of free sugars to NRA in the presence of elevated nitrate concentrations (Figure 7.1.20). This finding does not support the N overload hypothesis and suggest that SAV in springs are able to assimilate nitrate without detrimental effects. Investigation of amino acid (AA) content supports the above assertion as both species appeared to have a steady or declining trend between the control and high NO_3-N treatments. Interestingly, both species exhibited significantly lower AA in the low versus control treatments (*V. americana* ANOVA p=0.02, *S. kurziana* p=0.01). Although the dip in response at the low treatment remains unexplained, these observations still do not support the NO_3-N overload hypothesis.

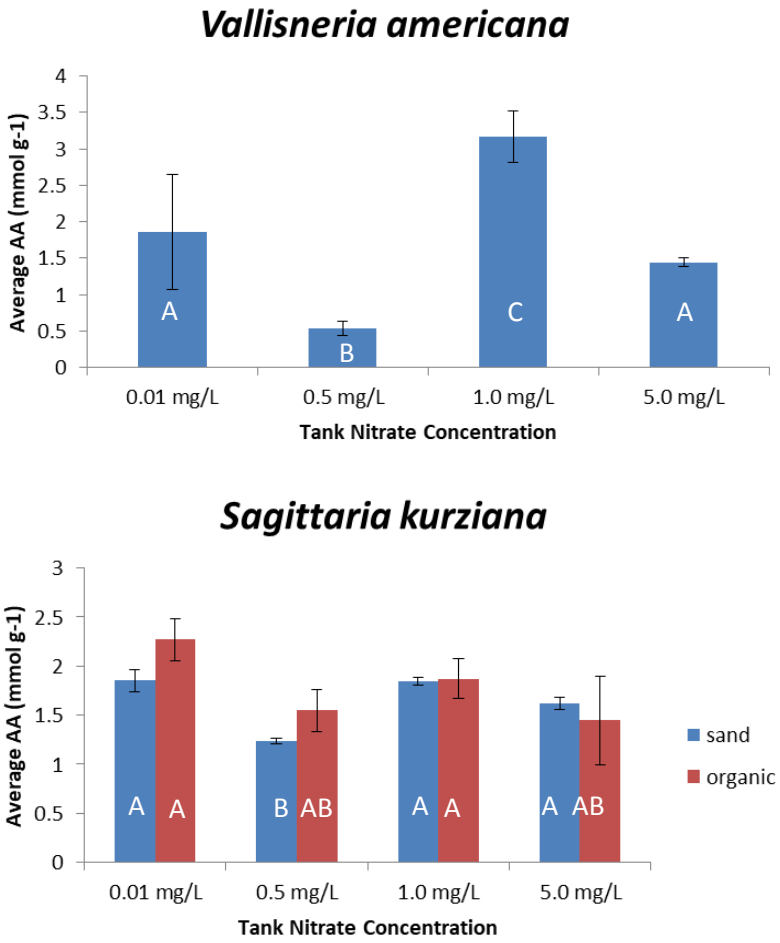

Figure 7.1.20. Mean amino acid concentration in tissue of *V. americana* and *S. kurziana* at control (0.1 mg NO_3-N L^{-1}), Low (0.5 mg NO_3-N L^{-1}), Medium (1.0 mg NO_3-N L^{-1}) and High (5.0 mg NO_3-N L^{-1}) concentrations.

7.1.4.5 Structural Responses to Hypoxia

As NO_3-N levels have increased across several springs in Florida, there have also been observations of diminished dissolved oxygen (DO) (Munch et al. 2006; Cohen et al. 2007) in

several springs. This decline in DO is also a potential driver of SAV growth as well as a significant factor in other ecologically relevant processes, such as invertebrate and fish community structure. Oxygen's role in SAV growth and proliferation was monitored in growth chambers during the study period to determine if low DO (hypoxic- DO <2 mg L^{-1}) conditions would alter SAV growth over a 10 week period. Root:shoot were significantly higher ($t=2.12$ $p<0.001$) under hypoxic conditions for *V. americana* suggesting that this species may respond to hypoxia by initiating increased root growth to increase oxygen transport to the roots (Figure 7.1.21). This assertion is supported by the observation that leaf elongation does not change under oxic versus anoxic condition and thus the change in ratio is not due to a reduction of shoot biomass. Root:shoot was not different between treatments for *S. kurziana*, however, leaf elongation was reduced in this species ($t=1.12$, $p=0.04$) which suggests this species experiences more physiological stress under hypoxia and thus shoot growth is diminished. It is important to note that although leaf growth is diminished, it is not suggestive of extirpation of SAV. An unreplicated experiment was conducted in which *S. kurziana* (whole plant) survived sealed in a gallon jar for 1.5 months with no oxygen additions. We contend that oxygen is a factor in SAV growth, but due to diel fluctuations in which hypoxia (when present) is alleviated, the relative influence of DO is likely low compared to other drivers.

7.1.4.6 Structural Responses to Sulfide Toxicity

Martin et al. (Chapter 8 this report) reported early in the research phase that sediment sulfide levels along Silver River could reach 34.2 mg L^{-1}, which is in excess of levels known to negatively affect SAV. In response to this observation, we took advantage of the mesocosms to test the effects of sulfide on SAV growth.

Mean leaf elongation of *V. americana* declined significantly as H_2S increased from the control to high (0.75 m*M* H_2S), concentrations (ANOVA $p<0.0001$)(Figure 7.1.22). Although the Low (0.01 m*M* H_2S) was not significantly different from the control (ANOVA $p=0.09$) or the Medium (0.1 m*M* H_2S) treatment, there was a significant difference between the control and Medium treatments (ANOVA $p<0.01$). This downward trend suggest strongly that sulfide has a negative growth effect at all treatment levels, however, inhibition of growth occurs above 0.1 m*M* H_2S.

S. kurziana appears to exhibit a positive reaction to low levels of H_2S (Figure 7.1.22). Leaf elongation of the control (0 m*M* H_2S) was significantly lower than the Low (0.01 m*M* H_2S) treatment (ANOVA $p=0.05$). The medium (0.1 m*M* H_2S) and Low treatments were also significantly higher than the High (0.75 m*M* H_2S) concentration treatments (ANOVA $p<0.01$ and $p=0.02$ respectively). These results indicate that even at high treatment levels of H_2S, *S. kurziana* is still in positive growth phase, a very unexpected result based upon literature studies that suggest toxicity of many SAV species at 0.1mM (Lamers et al. 2013). Inspection of post experiment photos of both species enable further interpretation of these responses.

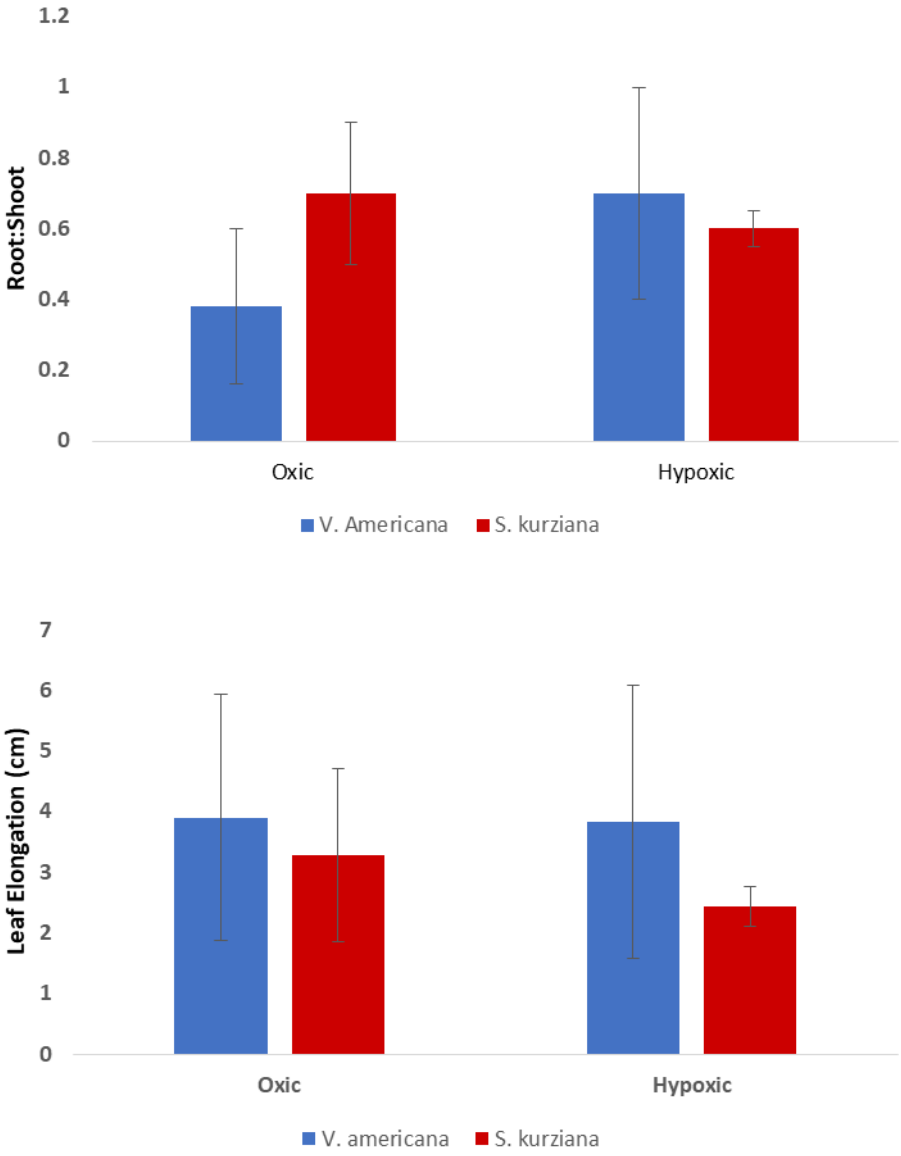

Figure 7.1.21. Mean root:shoot ratios (top) and leaf elongation rates (bottom) of *V. americana* (blue) and *S. kurziana* (orange) under oxygenated and hypoxic conditions.

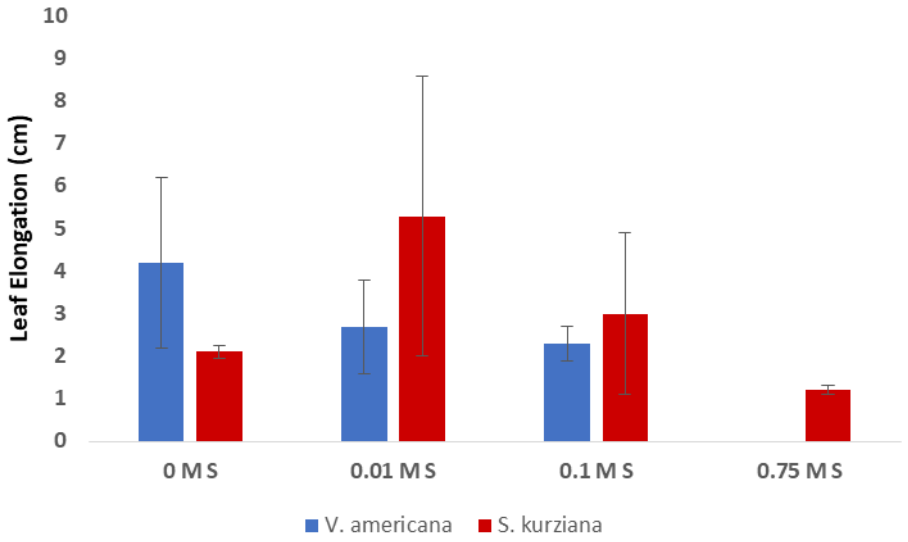

Figure 7.1.22. Mean leaf elongation of *V. americana* and *S. kurziana* under control (0 m*M* H_2S), Low (0.01 m*M* H_2S), Medium (0.1 m*M* H_2S), and High (0.75 m*M* H_2S), concentrations.

Visual inspection of *V. americana* from the four treatment levels of H_2S indicate substantial necrosis of plant tissue (a sign of toxicity) as H_2S levels increase (Figure 7.1.23). Unlike *V. americana, S. kurziana* appeared to react positively to lower levels of H_2S, a reaction recently observed in terrestrial plants but at uM concentrations (Figure 7.1.24). While *V. americana* showed distinct necrosis in all exposures (Figure 7.1.25), this was not evident in *S. kurziana* except in the High treatment. Even at the Highest tested level of H_2S, *S. kurziana* still continued positive growth. We assert that this species likely relies on arenchyma tissue (more extensive than *V. americana*) to overcome H_2S toxicity and may induce cell elongation and thus express growth in these exposure trials. In any case, it is clear that *V. americana* is much more sensitive to H_2S than *S. kurziana*, and it has been suggested that H_2S may be responsible for the patterning of these two species in Florida springs.

Figure 7.1.23. (Clockwise from top left) Photos of *V. americana* under control (0 m*M* H_2S), Low (0.01 m*M* H_2S), Medium (0.1 m*M* H_2S), and High (0.75 m*M* H_2S), concentrations. Note necrosis of tissues and blackening of roots as H_2S increases.

Figure 7.1.24. (Clockwise from top left) Photos of *S. kurziana* grown under control (0 m*M* H_2S), Low (0.01 m*M* H_2S), Medium (0.1 m*M* H_2S), and High (0.75 m*M* H_2S), concentrations.

Figure 7.1.25. Tissue necrosis of shoots (top) and roots (bottom) of *V. americana* under Medium (0.1 m*M* H_2S), concentrations.

7.1.4.7 Additional Observations

A significant observation beyond those reported previously is the response of algal communities to the variable nitrate dosing levels in mesocosms used for these experiments. While algal responses have not been well correlated with increases in nitrate in Florida springs (Cohen et al. 2011), glass slide periphytometers placed in spring water mesocosm tanks resulted in a clear increase in algal biomass in all treatments above the control (Figure 7.1.26). This observation supports a direct linkage between elevated nitrate and algal biomass on the Suwannee River reported by Mattson et al. (2007). This direct relationship between epiphytic algae and elevated nitrate, may have escaped more routine observation due to other confounding variables in other spring systems. In this experiment, chlorophyll a was observed to correlate with nitrate concentration, and when biomass was measured, the relationship became more clear. Community structure of algal species has not been determined.

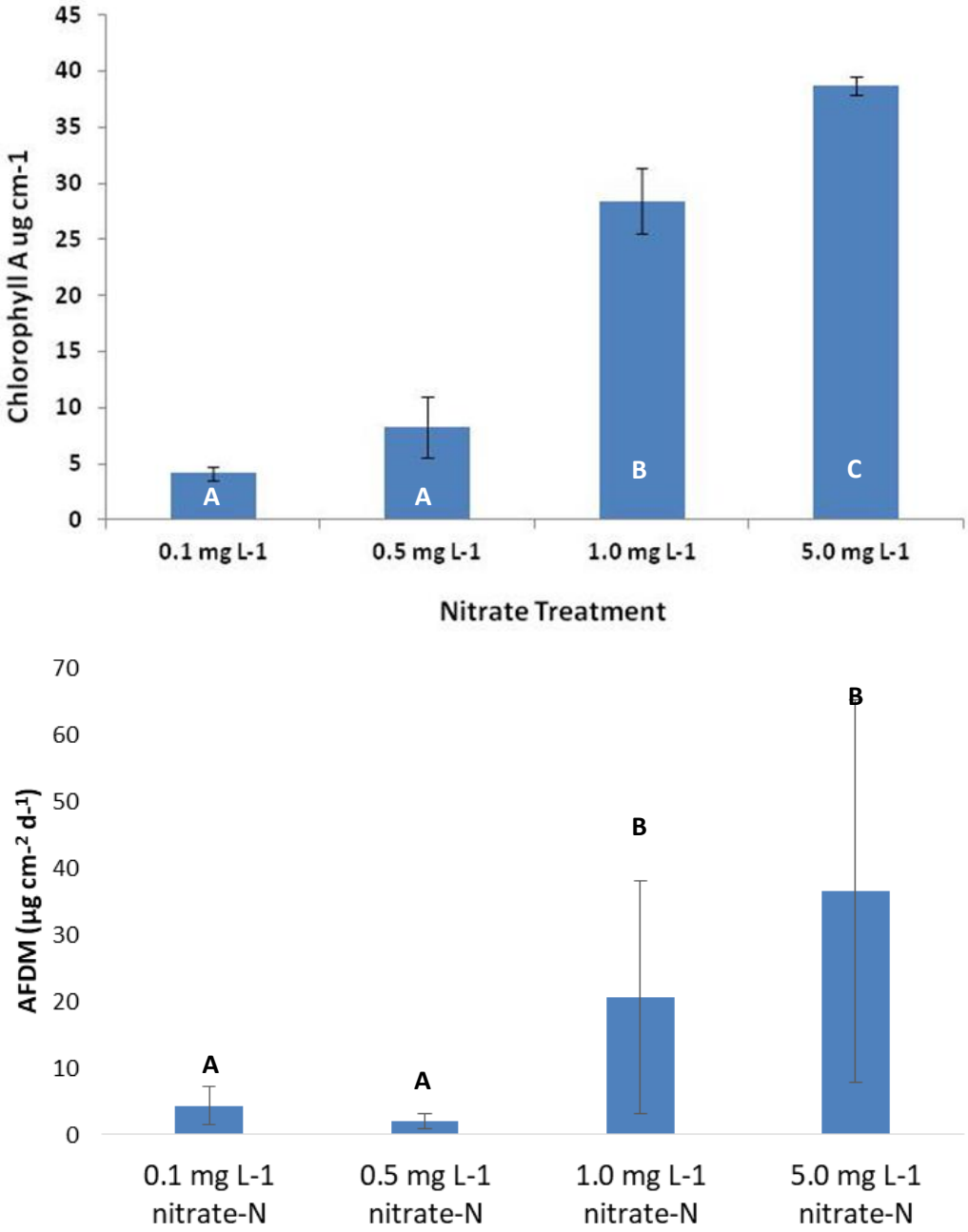

Figure 7.1.26. Chlorophyll a production (top) and algal AFDM (bottom) in mesocosm tanks at control (0.1 mg NO_3-N L^{-1}), Low (0.5 mg NO_3-N L^{-1}), Medium (1.0 mg NO_3-N L^{-1}) and High (5.0 mg NO_3-N L^{-1}) concentrations.

7.1.5 CONCLUSIONS AND RECOMMENDATIONS

The research presented here has several key findings relevant to the protection and management of spring ecosystems in Florida. The main objective of this work was to test the NO_3-N overload hypothesis which suggested that increased NO_3-N impairs SAV growth by causing excessive energy use to manage ANR and protein synthesis intercellularly. To test this hypothesis, several

experiments were conducted to document physical and biochemical responses of SAV to increased NO_3-N availability. First, mesocosm trials of SAV growth under elevated NO_3-N suggest that both species of SAV investigated here respond to increased nitrate differently. The primary response of *V. americana* tends to be distributed between root and shoot growth, while *S. kurziana* tends to be more productive in shoot production as NO_3-N increases. It was also noted that the sediment organic matter content increased productivity of *S. kurziana* under all treatment levels suggesting there may be other limiting factors (phosphorus, micro-nutrient limitation) to growth. Root: shoot ratio analysis did not support the hypothesis that this ratio would decline significantly under increased NO_3-N presence as plants utilized stored starch to fuel ANR and protein synthesis.

NRA rates were observed to be related to NO_3-N concentration after 2 weeks, but after 16 weeks of exposure, rates were not clearly linked to NO_3-N concentration with either species. Location of greatest NRA tends to be in roots for *V. americana* and shoots for *S. kurziana*. further suggesting significant physiological differences between these species and NRA. C:N ratios did suggest both species were proficient at NO_3-N uptake and incorporation into tissues.

Physiological changes such as starch storage in tissues was observed to decrease significantly in *V. americana* with nitrate concentration which does support the N overload hypothesis, however glucose content did not show a similar trend. In fact, no definitive trends were observed in glucose content. While not statistically significant, there appears to be a trend in glucose storage with higher concentrations being found in roots versus shoots in all treatments. Other physiological responses such as arenchyma diameter peaks at 0.5 mg NO_3-N L^{-1} indicating a possible low level catalyzation of growth at nitrate levels between 0.5-1.0 mg NO_3-N L^{-1} that alters cell diameter. It was expected that amino acid content would increase significantly if protein synthesis were elevated under the NO_3-N overload hypothesis, however, no definitive trends were observed with tissue amino acid content.

Additional investigations beyond elevated NO_3-N were conducted opportunistically. Differential responses were observed between species with respect to sulfide toxicity with *V. americana* being much more sensitive, and *S. kurziana* being exceptionally tolerant or potentially catalyzed cell elongation. With respect to hypoxia tolerance, *V. americana* responded with increased root growth and decreased shoot growth under hypoxic condition while *S. kurziana* did not have a significantly different response under either condition. We contend, however, that the exended hypoxia of the experimental trials is not realistic for springs and thus is not DO is not likely to be an inhibitor of SAV growth in springs under current conditions.

Another significant observation is that of a positive epiphytic algal response to nitrate concentration in the mesocosms utilized in this experiment. Both biomass and chlorophyll were observed to increase with increasing NO_3-N.

7.1.5.1 Management Implications

Results of the mesocosm studies conducted here do not support the assertion that elevated nitrate is having a negative effect on the physiology of SAV in spring ecosystems. However, we noted significant algal growth in mesocosm and microcosm trials that suggest nitrate can have an

influence on the proliferation of algae. A direct correlation between nitrate concentration and algal biomass production in springs has not been widely accepted (Brown et al. 2008; Heffernan et l. 2010). Stevenson et al. (2004) reported a positive correlation between nitrate and Vaucheria abundance in springs, and Mattson et al. (2007) reported a positive correlation between nitrate and periphyton biomass and chl a on the Suwannee River. Based upon this finding and the known detrimental effects of excessive periphytic algae on SAV, we assert that nitrate control in regional groundwater should be a priority for management of spring ecosystem integrity.

Results of growth chamber studies suggest that *V. americana* and *S. kurziana* are both tolerant of hypoxic conditions, however, both species are significantly affected by sulfide that is generated by reducing conditions in surface sediments. We assert that sulfur use in the watersheds may have implications for management with respect to SAV, however, sources of sulfur in particular watersheds is currently unknown and may be problematic to determine. We suggest that consideration of sulfide interactions be included when assessing spring ecosystem health and SAV condition.

7.1.6 REFERENCES

Ackerman, F. 2007. The economics of atrazine. International Journal of Occupational and Environmental Health. 13:437-445.

Albertin, A. R. 2009. Nutrient dynamics in Florida springs and relationships to algal blooms. Dissertation, University of Florida.

Albertin, A. R., Sickman, J. O., Pinowska, A., and Stevenson, R. J. 2012. Identification of nitrogen sources and transformations within karst springs using isotope tracers of nitrogen. Biogeochemistry 108: 219-232.

Barker, T., Hatton, K., O'Connor, M., Connor, L., and Moss, B. 2008. Effects of nitrate load on submergedplant biomass and species richness: results of a mesocosm experiment. Fundamental and Applied Limnology 173: 89-100.

Barko, J. W. and Smart, R. M. 1986. Sediment-related mechanisms of growth limitation in submersed macrophytes *Ecology* 67: 1328-1340.

Baron, J. S., Hall, E. K., Nolan, B. T., Finlay, J. C., Bernhardt, E. S., Harrison, J. A., Chan, F., and Boyer, E.W. 2013.Theinteractive effects of excess reactive nitrogen and climate change on aquatic ecosystems and water resources of the United States. Biogeochemistry 114: 71-92.

Baum, J. K. and Worm, B. 2009. Cascading top-down effects of changing oceanic predator abundances. Journal of Animal Ecology 78:699–714.

Bergstrom, A. K. and Jansson, M. 2006. Atmospheric nitrogen deposition has caused nitrogen enrichment and eutrophication of lakes in the northern hemisphere. Global Change Biology 12: 635-643.

van den Berg, M. S., Sheffer, M., van Nes, E., and Coops, H. 1999. Dynamics and stability of *Chara sp*. and *Potamogeton pectinaus* in a shallow lake changing in eutrophication level. Hydrobiologia 408: 335-342.

Best, E. P. H. 1980. Effects of nitrogen on the growth and nitrogenous compounds of *Ceratophyllum demersum*. Aquatic Botany 8: 197-206.

Boar, R. R., Crook, C. E., and Moss, B. 1989. Regression of *Phragmites ausitralis* reed swamps and recent changes if water chemistry in the Norfolk Broadland, England. Aquatic Botany 35: 41-55.

Boedeltje, G., Alfons, A. J., Smolders, J. P., and Roelofs, J. G. M. 2005. Combined effects of water column Nitrate enrichment, sediment type and irradiance on growth and foliar nutrient concentrations of *Potamogeton alpines*. Freshwater Biology 50: 1537-1547.

Borum, J. 1985. Development of epiphytic communities on eelgrass (*Zostera marina*) along a nutrient gradient in a Danish estuary. Marine Biology 87: 211-218.

Brouwer, E., Bobbink, R., Meeuwsen, F., and Roelofs, J. G. M. 1997. Recovery from acidification in aquatic mesocosms after reducing ammonium and sulfate deposition. Aquatic Botany 56: 119-130.

Brown, M. T., Chinner-Reiss, K., Cohen, M. J., Evans, J. M., Reddy, K. R., Inglett, P. W., Inglett, K. S., Frazer, T. K., Jacoby, C. A., Philips, E.J., Knight, R. L., Notestein, S. K., and McKee, K. A. 2008. Summary and synthesis of the available literature on the effectsof nutrients on springs organisms and systems. Final Report. Florida Department of Environmental Protection, Tallahassee, FL.

Buchsbaum, R. N., Short, F. T., and Cheney, D. P. 1990. Phenolic-nitrogen interactions in eelgrass (*Zostera marina* L.): possible implications of disease resistance. Aquatic Botany 37: 291-297.

Burkholder, J. M., Mason, K. M., and Glasgow, Jr., H. B. 1992. Water column nitrate enrichment promotes decline of eelgrass *Zostera marina*: evidence from seasonal mesocosm experiments. Marine Ecological Progress Series 81: 163-178.

Burkholder, J. M., Glasgow, H. B., and Cooke, J. E. 1994. Comparative effects of water column nitrate enrichment on eelgrass *Zostera marina*, shoal grass *Halodule wrightii* and widgeongrass *Ruppia maritime*. Marine Ecological Progress Series 105:121-138.

Canfield, H. E. and Hoyer, M. V. 1988. Influence of nutrient enrichment and light availability on the abundance of aquatic macrophytes in Florida streams. Canadian Journal of Fisheries and Aquatic Sciences 45: 1467-1472.

Cao, T., Ni, L., and Xie, P. 2004. Acute biochemical responses of a submersed macrophyte, *Potamogeton crispus L*., to high ammonium in an aquarium experiment. Journal of Freshwater Ecology 19: 279-284.

Cedergreen, N. and Madsen, T. V. 2003. Nitrate reductase activity in roots and shoots of aquatic macrophytes. Aquatic Botany 76: 203-212.

Clarke, E. and. Baldwin, H. A. 2002. Responses of wetland plants to ammonia and water level. Ecological Engineering 18: 257-264.

Cohen, M. J., Lamsal, S., and Korhnak, L. V. 2007. Sources, Transport and Transformations of Nitrate-N in the Florida Environment. St. Johns River Water Management District SJ2007-SP10. 125 pp. Palatka, FL.

Cowell, B. C. and Botts, P. S. 1994. Factors influncing the distribution, abundance, and growth of *Lyngbya wollei* in Central Florida. Aquatic Botany 49: 1-17.

Cowell, B. C. and Dawes, C. J. 2004. Growth and nitrate nitrogen uptake by the cyanobacterium *Lyngbya wollei.* Journal of Aquatic Plant Management. 42: 69-71.

Cowell, B. C. and Davis, C. J. 2008. Seasonal comparisons of the phytoplankton and decline in water transparency in spring-fed rainbow River, Florida. Journal of Freshwater Ecology 23: 169-177.

Cramer, M. D. and Lewis, O. A. M. 1993. The influence of NO_3 and NH_4 nutrition on carbon and nitrogen partitioning characteristics of wheat (*Triticum aestivum*) and maize (*Zea maize*) plants. Plant and Soil 154: 289-300.

Crawford, N. M. 1995. Nitrate: nutrient signal for plant growth. The Plant Cell 7:859-868.

De Brabandere, L., Frazer, T. K., and Montoya, J. P. 2007. Stable isotope ratios of macrophytes and associated periphyton along a nitrate gradient in two subtropical, spring fed streams. Freshwater Biology 52: 1564-1575.

Duarte, C. M. and Canfield, Jr., D. E. 1990. Macrophyte standing crop and primary productivityin some Florida spring-runs. Water Resources Bulletin 26(6): 927-934.

Dunne, E. J., Coveney, M. F., Marzolf, E. R., Hogue, V. R., Conrow, R., Naleway, R., Lowe, E. F., and Battoe, L. E. 2012. Efficacy of a large-scale constrcutied wetland to remove phosphorus and suspended solids from Lake Apopka, Florida. Ecological Engeineering 42: 90-100.

Dzialowski, A. R., Wang, S. H., Lim, N. C., and Spotts, W. W. 2005. Nutrient limitation of phytoplankton growth in central plains reservoirs, USA. Journal of Plankton Research 27: 587-595.

Elser, J. J., Bracken, M. E. S., Cleland, E. E., Gruner, D. S., Harpole, W. S., Hillebrand, H., Ngai, J. T., Seabloom, E. W., Shurin, J. B., and Smith, J. E. 2007. Global analysis of nitrogen and phosphorus limitation of primary producers in freshwater, marine , and terrestrial systems. Ecological Letters 10: 1135-1142.

Evans, J. 2008. Ecosystem implications of invasive aquatic plants and aquatic plant control in Florida Springs. P 249-270 In: M.T. Brown, Ed. Summary and synthesis of available literature on the effects of nutrients on springs organisms and systems. Florida Department of Environmental Protection. Tallahassee, FL.

Estes, J. A., Terborgh, J., Brashares, J. S., Power, M. E., Berger, J., Bond, W. J., Carpenter, S. R., Essington, T. E., Holt, R. D., Jackson, J. B. C., Marquis, R. J., Oksanen, L., Oksanen, T., Paine, R. T., Pikitch, E. K., Ripple, W. J., Sandin, S. A., Scheffer, M., Schoener, T. W., Shurin, J. B., Sinclair, A. R. E., Soulé, M. E., Virtanen, R., and Wardle, D. 2011. Trophic downgrading of planet Earth. Science 333:301–6.

Farnswoth, L. and Baker, L. A. 2000. Conceptual model of aquatic plant decay and ammonium toxicity for shallow lakes. Journal of Environmental Engineering. 126: 199-207.

Frazer, T. K., Notestein, S. K., and Pine, W. E. 2006. Changes in the physical, chemical and vegetative characteristics of the Homosassa, Chassahowitzka and Weeki Wachee rivers. Final Report. Southwest Florida Water Mangement District, Brooksville, FL.

Fulton, B. A., Brain, R. A., Usenko, S., Back, J. A., and Brooks, B. W. 2010. Exploring *Lemna gibba* thresholdsto nutrient and chemical stressors: differential effects of triclosan on internal stoichiometry and nitrate uptake across a nitrogen: phosphorus gradient. Environmental Toxicology and Chemistry 29:2363-2370.

Genevieve, M. C, Duthie, H. C., and Taylor, W. D. 1997. Models of aquatic plant productivity: a review of the factors that influence growth. Aquatic Botany 59: 195-215.

Gojon, A., Plassard, C., and Bussi, C. 1994. Root/shoot distribution of NO_3- assimilation in herbaceous and woody species. In: Roy, J. and E. Garnier (Eds.) A Whole Plant Perspective on Carbon – Nitrogen Interactions. SPB Academic Publishing, Hague, pp 131-148.

Gruner, D. S., Smith, J. E., Seabloom, E. W., Ngai, J. T., Sandin, S., Hillebrand, H., Harpole, W. S., Elser, J. J., Cleland, E. E., Bracken, M. E. S., Borer, E. T., and and Bolker, B. 2008. A cross system synthesis of consumer and nutrient resource control on producer biomass. Ecology Letters 11:740–755.

Guerrero, M. G., Vega, J. M., and Losada, M. 1981. The assimilatory nitrate reducing system and its regulation. Annual Reviews of Plant Physiology 32: 169-204.

Harlin, M. M. and Thorne-Miller, B. 1981. Nutrient enrichment of seagrass beds in a Rhode Island coastal lagoon. Marine Biology. 65: 221-229.

Harwell, M. C. and Sharfstein, B. 2009. Submerged aquatic vegetation and bulrush in Lake Okeechobee as indicators of greater Everglades ecosystem restoration. Ecological Indicators 9: S46-S55.

Heck, K. L. J. and Valentine, J. F. 2007. The primacy of top-down effects in shallow benthic ecosystems. Estuaries and Coasts 30:371–381.

Heffernan, J. B., Liebowitz, D. M., Frazer, T. K., Evans, J. M., and Cohen, M. J. 2010. Algal blooms and the nitrogen enrichment hypothesis in Florida springs: evidence, alternatives, and adaptive management. Ecological Applications 20:816–829.

van der Heide, T., van Nes, E. H., van Ktawijk, M. M., Scheffer, M.,. Hendriks, A. J., and Smolders, A. J. P. 2010. Alternative stable states driven by density-dependent toxicity. Ecosystems 13: 841-850.

Hemminga, M. A. and Duarte, C. M. 2000. Seagrass Ecology. Cambridge University Press, Cambridge UK. 298 pp.

Hillebrand, H. 2002. Top-down versus bottom-up control of autotrophic biomass—a meta analysis on experiments with periphyton. Journal of the North American Benthological Society 21:349–369.

Hwang, M. and Ederer, G. M. 1975. Rapid hippurate hydrolysis method for presumptive identification of group B streptococci, J. Clin. Microbiol., **1,** 114-121

James, C., Fisher, J., and Moss, B. 2003. Nitrogen driven lakes: the Shropshire and Cheshire Meres. Archif fur Hydrobiologia 164: 249-266.

James, C., Fisher, J., Russell, V., Collings, S., and Moss, B. 2005. Nitrate avilabliity and hydrophyte species richness in shallow lakes. Freshwater Biology 50:1049-1063.

James, R. T., Gardner, W. S., McCarthy, M. J., and Carini, S. A. 2011. Nitrogen dynamics in Lake Okeechobee: forms, functions, and changes. Hydrobiologia 669: 199-212.

Jones, G. W., Upchurch, S. B., and Champion, K. M. 1996. Origin of nitrate in ground water discharging from Rainbow Springs, Marion County, Florida. Southwest Florida Water Management District, Brooksville, FL.

Katwijik, M. M. V., Vergeer, L. H. T., Schmitz, G. H. W., and Reolofs, J. G. M. 1997. Ammonium toxicity in Eelgrass *Zostera marina*. Marine Ecology Progress Series 157: 159-173.

Katz, B. G. 2004. Sources of nitrate contamination and age of water in large karstic springs in Florida. Environmental Geology 46:689-706.

Kim-Shapiro, D. B., Gladwin, M. T., Patel, R. P., and Hogg, N. 2005. The reaction between nitrite and hemoglobin: the role of nitrite in hemoglobin mediated hypoxic vasodilation. Journal of Inorganic Biochemistry 99: 237-246.

Klotzli, F. 1971. Biogenous influence on aquatic macrophytes especially *Phragmites communus*. Hydrobiologia 12: 107-111.

Knight, R. L. and Notestein, S. K. 2008. Chapter 6 Effects of Nutrients on Spring Ecosystems. In: Summary and Synthesis of the Available Literature on the Effects of Nutrients on Spring Organisms and Systems. Final Report. Florida Department of Environmental Protection, Tallahassee FL 376p.

Lacoul, P. and Freedman, B. 2006. Environmental influences on aquatic plants in freshwater ecosystems. Environmental Reviews 14: 89-136.

Lambert, S. J. and Davy, A. J. 2011. Water quality as a threat to aquatic plants: discriminating between the effects of nitrate, phosphate, boron and heavy metals on Charophytes. New Phytologist 189: 1051-1059.

Lea, P. J. and Miflin, B. J. 1979. Photosyntheitc ammonia assimilation. *In:* Encyclopedia of Plant Physiology. Eds. M. Gibbs, E. Latzko. Springer, Berlin 578 pp.

Li, W., Zhang, Z., and Jeppesen, E. 2008. The response of *Vallisneria spinulosa* (Hydrocharitaceae) to different loadings of ammonia and nitrate at moderate phosphorus concentration: a mesocosm approach. Freshwater Biology 53: 2321-2330.

Liebowitz, D. M. 2013. Environmentally mediated consumer control of algae proliferation in Florida springs. Doctoral Dissertation, University of Florida, Gainesville, FL.

Liebowitz, D. M., Cohen, M. J., Heffernan, J. B., Frazer, T. K., and Korhnak, L.V. 2014 Environmentally mediated consumer control of algae proliferation in Florida springs. Freshwater Biology 59: 2009-2023

Maberly, S. C., King, L., Dent, M. M., Jones, R. I., and Gibson, C. E. 2002. Nutrient limitation of phytoplankton And periphyton growth in upland lakes. Freshwater Biology 47: 2136-2152.

Maddox, G. L., Lloyd, J. M., Scott, T. M., Upchurch, S. B., and Copeland, R. 1992. Florida's groundwater quality monitoring program, background geochemistry. Florida Geological Survey, Tallahassee, FL.

Marschner, H. 1998. Mineral Nutrition of Higher Plants. Academic Press, London, pp. 232-242.

Mattson, R. A. 2013. Personal Communication.

Mattson, R. A., Lehmensiek, M., and Lowe, E. F. 2007. Nitrate toxicity in Florida springs and spring-run streams: a review of the literature and its implications. Professional Paper SJ2007-PP1. St. Johns River Water Management District, Palatka, FL.

Mehrer, I. and Mohr, H. 1989. Ammonium toxicity: description of the syndrome in Sinapis alba and search for its causation. Physiologia Plantarum 77: 54554,

Moss, B. 1990. Engineering and biological approaches to restoration from eutrophication of shallow lakes in which aquatic plant communities are important components. Hydrobiologia 200: 367-377.

Mulligan, H. F., Baranowsky, A., and Johnson, R. 1976. Nitrogen and phosphorus fertilization of aquatic vascular plants and algae in replicated ponds. Initial responses to fertilization. Hydrobiologia 48: 109-116.

Munch, D. A., Toth, D. J., Huang, C., Davis, J. B., Fortich, C. M., Osburn, W. L., Phlips, E. J., Quinlan, E. L., Allen, M. S., Woods, M. J., Cooney, P., Knight, R. L., Clarke, R. A., and Knight, S. L. 2006. Fifty year retrospective study of the ecology of Silver springs, Florida. Special Publication SJ2007-SPA. St. John's River Water Management District, Palatka.

Neckles, H. A., Wetzel, R. L., and Orth, R. J. 1993. Effects of nutrient enrichment and grazing on epiphyte-macrophyte (Zostera marina L.) dynamics. Oecologia 93: 285-295.

Ni, L. 2001. Effects of water column nutrient enrichment on the growth of *Potamogeton maackianus* A. Been. Journal of Aquatic Plant Management 39: 83-87.

Nichols, D. S. and Keeney, D. R. 1976. Nitrogen nutrition of Microphyllum spicatum: uptake and translocation of ^{15}N by ramets and roots. Freshwater Biology 6: 145-154.

Odum, H. T. 1957. The Ecology of Silver Springs. Ecological Monographs.

Osborne, T. Z., Newman, S., Kalla, P., Scheidt, D. J., Bruland, G. L., Cohen, M. J., Scinto, L. J., and Ellis, L. R. 2011. Landscape patterns of significant soil nutrients and contaminants in the Greater Everglades Ecosystem: Past, Present, and Future. Crit. Rev. Environ. Sci. Technol. 41:6 121-148

Pate, J. S. 1980. Transport and partitioning of nitrogenous solutes. Annual Review of Plant Physiology 31: 313-340.

Phelps, G. G. 2004. Chemistry of Ground Water in the Silver Springs Basin, Florida, with an Emphasis on Nitrate. U.S. Geological Survey Scientific Investigations Report 2004-5144. vi, 54 pp.

Phelps, G. G., Walsh, S. J., Gerwig, R. M., and Tate, W. B. 2006. Characterization of the hydrology, water chemistry, and aquatic communities of selected springs in the St. Johns river Water Management District, Florida, 2004. Open-file report 2006-1107. USGS Reston, VA.

Pinowska, A., Stevenson, R. J., Sickman, J. O., and Anderson, M. 2007. Integrated interpretation of survey for determining nutrient thresholds for macroalgae in Floirda springs: macroalgal relationships to water, sediment, nutrients, diatom indicators, and land use. Florida Department of environmental Protection, Tallahassee, FL.

Porter, E. M., Bowman, W. D., Lark, C. M., Compton, J. E., Pardo, L. H., and Soong, J. L. 2013. Interactive effects Of anthropogenic nitrogen enrichment and climate change on terrestrial and aquatic biodiversity. Biogeochemistry 114: 93-12.

Quinlan, E. L., Phlips, E. J., Donnelly, K. A., Jett, C. H., Sleszynski, P., and Keller, S. 2008. Primary producers And nutrient loading in Silver Springs, FL, USA. Aquatic Botany 88: 247-255.

Rabe, E. 1990. Stress physiology: the functional significance of the accumulation of nitrogen containing compounds. Journal of Horticultural Science. 65: 231-243.

Rabe, E. and Lovatt, C. J. 1986. Increased arginine biosynthesis during P deficiency. Plant Physiology 81: 774-779.

Raven, J. A. 1985. Regulation of pH and generation of osmolarity in vascular plants: a cost-benefit analysis in relation to efficiency of use of energy, nitrogen, and water. New Phytologist 101: 25-77.

R Core Team (2013). **R**: A language and environment for statistical computing. Mar 28, 2013

Reddy, K. R and DeLaune, R. L. 2008. Biogeochemistry of Wetlands: Science and Applications. CRC Press Boca Raton. 774 pp.

Rice, E. W., Baird, R. B., Eaton, A. D., and Clesceri, L. S. 2012. Standard Methods for the examination of water and wastewater 22nd Ed. American Public Health Association. Washington DC.

Riis, T., Olesen, B., Clayton, J. S., Lambertini, C., Brix, H., and Sorrell, B. K. 2012. Growth and morphology in relation to temperature and light availability during the establishment of three invasive aquatic plant species. Aquatic Botany 102: 56-64.

Roth, N. C and Pregnall, A. M. 1988. Nitrate reductase activity in Zostera marina. Marine Biology 99: 457-463.

Sagrario, M. A. G., Jeppesen, E., Goma, J., Sondergaard, M., Jensen, J. P., Lauridsen, T., and Landkildehus, F. 2005. Does high nitrogen loading prevent clear-water conditions in shallow lakes at moderately high phosphorus concentrations? Freshwater Biology 50: 27-41.

Schindler, D. W. 1978. Factors regulating phytoplankton production and standing crop in the world's freshwaters. Limnology and Oceanography 23: 478-486.

Schindler, D. W. and Fee, E. J. 1974. Experimental lakes area: whole lake experiments in eutrophication. Journal of Fisheries Research Board Canada 32:937-953.

Schroder, R. 1979. Decline of reedswamps in Lake Constance. Symp. Biol. Hung. 19: 43-48.

Schuurkes, J. A., Kok, C. J., and Hartog, C. D. 1986. Ammonium and nitrate uptake by aqutic plants from poorly buffered and acidified waters. Aquatic botany 24: 131-146.

Scott, T., Means, G., Meagan, R., Means, R., Upchurch, S., Copeland, R. Jones, R., and Willet, A. 2004. Springs of Florida. Bulletin No. 66 Florida Geological Survey, Tallahassee, FL.

Sickman, J. O., Albertin, A. R., Anderson, M. W., Pinowska, A., and Stevenson, R. J. 2009. A comparison of internal and external supply of nutrients to algal mats in two first magnitude springs in Florida. Journal of Aquatic Plant Management. 47: 135-144.

Smolders, A. J., Hartog, C. D., Gestel, C. B., and Roelof, J. G. 1996. The effects of ammonium on growth, accumulation of free amino acid and nutritional status of young phosphorus deficient *Stratiotes aloides* plants. Aquatic Botany 53: 85-96.

Smolders, A. J., van Reil, M. C., and Roelofs, J. G. M. 2000. Accumulation of free amino acids as an early indication for physiological stress (nitrogen overload) due to elevated ammonium levels in vital *Stratiotes aloides* L. stands. Archeif fur Hydrobiologie 150: 169-175.

Smolders, A. J .P, Hendriks, R. J. J., Campschueur, H. M., and Roelofs, J. G. M. 1997. Nitrate induces iron deficiency chlorosis in J*uncus acutiflorus*. Plant and Soil 196: 37-45.

Stevenson, R. J., Pinowska, A., and Wang, Y. 2004. Ecological condition of algae and nutrients in Florida Springs. Florida Department of Environmental Protection, Tallahassee, FL.

Stevenson, R. J., Pinowska, A., Albertin, A. R., and Sickman, J. O. 2007. Ecological condition of algae and nutrients in Florida springs the synthesis report. Florida Department of Environmental Protection, Tallahassee, FL.

Sturgis, R. B. and Murray, L. 1997. Scaling of nutrient inputs to submersed plant communities: temporal and spatial variations. Marine Ecological Progress Series 152: 89-102.

Talling, J. F. and Lemoalle, J. 1998. Ecological Dynamics of Tropical Waters. Cambridge University Press. Cambridge UK 455 pp.

Ulrich, K. E. and Burton, T. M. 1985. The effect of nitrate, phosphate, and potassium fertilization on growth and nutrient uptake patterns of Phragmites australis (Cav.) Trin. Ex Steudel. Aquatic Botany 21:53-62.

Wang, Y., Gao, G, Qin, B., and Wang, X. 2012. Ecophysiological and anatomical responses of *Vallisneria natans* to nitrogen and phosphorus enrichment. Knowledge and Management of Aquatic Ecosystems 405, 05.

Wetzel, R. G. 2001. Limnology: Lake and River Ecosystems 3rd Ed. Academic Press, San Diego. 1006 pp.

Weyhenmeyer, G. A., Jeppesen, E., Adrian, R., Arvola, L., Blenckner, T., Jankowski, T., Jennings, E., and Straile, D. 2007. Nitrate depleted conditions on the increase in shallow northern European lakes. Limnology Oceanography 52: 13346-1353.

XLSTAT. 2017. Data Analysis and Statistical Solution for Microsoft Excel. Addinsoft, Paris, France

Zimmerman, R. C., Smith, R. D., and Alberte, R. S. 1989. Thermal acclimation and whole-plant carbon balance in *Zostera marina* L. (eelgrass). Journal of Experimental Marine Biology and Ecology 130: 93-109.

7.1.7 PUBLICATIONS AND PRODUCTS

Osborne, T. Z., Mattson, R. A., and Coveney, M. F. 2017. Potential for Direct Nitrate-Nitrite Inhibition of Submerged Aquatic Vegetation (SAV) in Florida Springs: A Review and Synthesis of Current Literature. *Water* 8: 30-46

7.1.7.1 Theses

LaPlaca, L. H. 2017. The role of NO_x in submerged aquatic vegetation growth and proliferation in spring ecosystems. MS Thesis, University of Florida. (Undefended to date)

7.1.7.2 Presentations

Osborne, T. Z. 2014. Freshwater springs: environmental and cultural treasures of Florida. REU lecture - Whitney Laboratory for Marine Bioscience, July 2014.

Osborne, T. Z. 2015. Evolution of Florida's aquatic ecosystems. REU lecture- Whitney Laboratory for Marine Bioscience, June 2015.

LaPlaca, L. H., Osborne, T. Z., Coveney, M. F., and Mattson, R. A. Direct inhibition of submerged aquatic vegetation (SAV) by nitrate-nitrite in Florida springs. 5th UF Water Institute Symposium. Gainesville, FL. Feb 16-17, 2016.

Osborne, T. Z. 2017. Florida's spring ecosystems under attack: drivers of spring ecosystem degradation. Seminar Series- Whitney Laboratory for Marine Bioscience, St. Augustine FL.

LaPlaca, L. H., R.A. Mattson, M. F. Coveney, J. Slater, T.Z. Osborne. Direct inhibition of submerged aquatic vegetation (SAV) by nitrate-nitrite in Florida springs. Seminar Series- Whitney Laboratory for Marine Bioscience, St. Augustine FL, Jan. 10, 2017.

LaPlaca, L. H., R.A. Mattson, M. F. Coveney, J. Slater, T.Z. Osborne. Direct inhibition of submerged aquatic vegetation (SAV) by nitrate-nitrite in Florida springs. Science by the Shore Symposium, Whitney laboratory for Marine Bioscience, St. Augustine, FL May 18, 2017.

7.2. DECLINING OXYGEN AS A MECHANISM FOR EXTIRPATION OF INVERTEBRATE HERBIVORES IN SILVER SPRINGS- A RESPIROMETRY STUDY OF *Viviparus georgianus*, *Elimia floridensis*, *Micromenteus floridensis* AND *Palaemonetes paludosus*

7.2.1 ABSTRACT

Dissolved oxygen stress has been suggested in recent studies to be a significant causal mechanism in population declines of aquatic herbivores in spring ecosystems. The decline of invertebrate grazers is suspected to have significant ecological effects (i.e., trophic cascade), such as a lapse of top-down control on the proliferation of algae in many springs across the state of Florida. This research was conducted to better our understanding of the relationships among water quality, grazers and algal community dynamics in spring ecosystems. Dissolved oxygen respiration requirements and survivorship thresholds for several key gastropod grazer species (*Viviparus georgianus*, *Elimia floridensis*, *Micromenteus floridensis)* and one decapod (*Palaemonetes paludosus*-Grass Shrimp) from Silver River were experimentally determined utilizing closed chamber respirometry methods in controlled laboratory conditions. Results suggest that all four species tested experiences hypoxic stress below 2 mg L^{-1} O_2. The gastropod *Viviparus georgianus* was observed to be the most sensitive to low DO with a threshold of 2.7 mg L^{-1} while the grass shrimp *Palaemonetes paludosus* was the most efficient at low DO with a measured threshold of 1.6 mg L^{-1}. The effect of nitrate exposure on respiration thresholds of *E. floridensis* and *T. granifera* were also investigated but no effect was observed. These findings suggest that hypoxia events (DO <2.0 mg L^{-1}), currently observed with some frequency in Florida springs, may contribute significantly to grazer population and activity.

7.2.2 INTRODUCTION

Hypoxia is emerging as one of the most significant stressors to biota in the estuarine and freshwater ecosystems worldwide due to the resulting impacts of mortality and food web alteration (Vaquer-Sunyer and Duarte 2008; Levin et al. 2009; Keeling et al. 2010). Recent reviews of the subject highlight the need for a multi-level approach to understanding the ecological consequences of consumer stressors, such as hypoxia, in aquatic systems (Diaz and Rosenberg 1995; Rabalais et al. 2002; Wu et al. 2002).

To better understand how stressors in the aquatic environment of Florida springs may result in the uncontrolled proliferation of algae, a review of the ecological drivers and controls of algal productivity is warranted. Aquatic communities and food web structure can be regulated by resource availability (bottom up forces) (Smith 2006; Carpenter et al. 2001; Rosemond et al. 1993) as well as, predation, herbivory, and physical characteristics of the environment such as flow velocity (top down forces) (King 2012; Liboriussen et al. 2005; Feminella and Hawkins 1995; Power 1992; Carpenter et al. 1987). In the case of Florida's spring ecosystems, resource availability refers to both water column nutrients (nitrogen and phosphorus) and sunlight. These resources directly affect the production of algal biomass and are thus considered bottom-up controls. Alternatively, herbivore (predation) by algal grazers and the sheer stress associated with

flow velocity acts to reduce or control the standing population of algae and is termed top-down control (Figure 7.2.1).

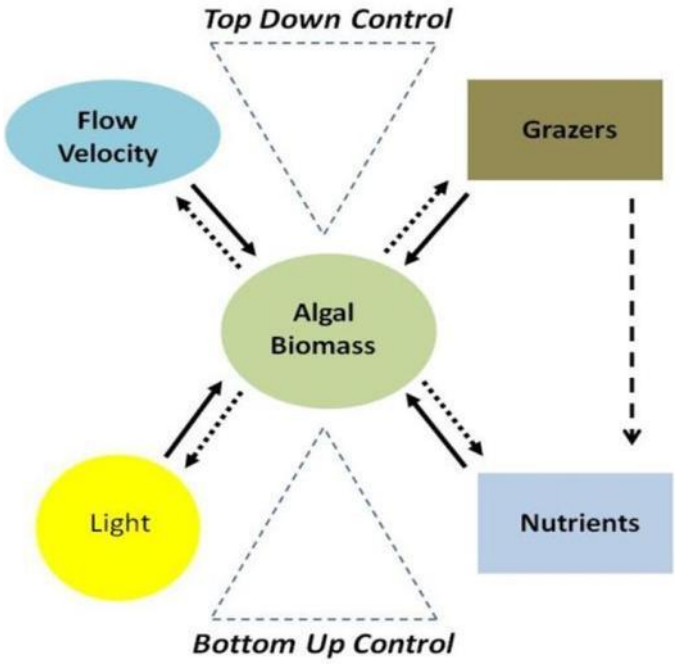

Figure 7.2.1. Conceptual model of top down versus bottom up control of primary production in Florida Springs. Note bottom up control mechanisms limit production while top down control mechanisms limit standing biomass. Solid lines indicate direct influence of drivers and dotted lines represent feedbacks. Figure adapted from Osborne et al. (2013).

7.2.2.1 Bottom Up Control of Algal Productivity

With respect to bottom up control mechanisms (those that exert control over the production of algal biomass), nutrients are by far the most well studied and therefore became the first priority in determining the drivers of algal proliferation in springs. Recent observations of increasing NO_3-N concentrations in Florida springs have garnered much attention by ecosystem managers (Munch et al. 2006; Quinlan et al. 2008; Heffernan et al. 2010). Contrary to expectation of a direct relationship between nutrients and algal biomass (Stevenson et al. 2004; Stevenson et al. 2007; Smith 2006; Smith 1982), the increase in nitrogen availability has not been shown to have a positive correlation with algal productivity (Canfield and Hoyer 1988; Duarte and Canfield 1990;; Brown et al. 2008; Heffernan et al. 2010). While there have been studies to report N utilization by algal mats in Florida springs (Cowell and Botts 1994; Cowell and Dawes 2004; Albertin 2009; Sickman et al. 2009), there have been several observations that contradict the normal eutrophication paradigm, namely the lack of significant increase in other forms of N (Cohen et al. 2007; Hensley and Cohen 2012) or P (Maddox et al. 1992; Scott et al. 2004) in spring waters. Therefore, focus on nutrient catalyzed algal proliferation may not lead to an

understanding of all the factors behind algal proliferation in (Brown et al. 2008; Heffernan et al. 2010).

A second bottom up control mechanism of algal populations, common to all aquatic ecosystems, is that of light availability (Biggs 1996; Wetzel 2001). Light availability in spring systems is directly related to vegetative canopy cover of the spring run and turbidity/clarity of water. Recent investigations by Szafraniec (2014) report preferential use of different portions of the red and blue spectra by SAV in spring runs. This has been documented in the seagrass literature (Dennison et al. 1993; Kirk 1994; Anastasiou 2009; Gallegos et al. 2009) but is a new finding with respect to spring ecosystem functions. Similarly, algae exhibit preferential usage of available light spectra, with nuisance algae such as *Lyngbya*, readily utilizing most spectra available (Szfraniec 2014). This additional finding suggests great adaptability of *Lyngbya* and other blue green algae to reduced light conditions. Recent work by Cohen et al. (chapter 6 this report) indicates that light availability is the most significant predictor of algal productivity (with covariates canopy coverage and dissolved organic matter adding little to the predictability model). Further, light attenuation measurements in Silver River do not suggest light limitation.

7.2.2.2 Top Down Control of Algal Biomass

A significant form of top down control of algal biomass is grazing by invertebrate herbivores (Figure 7.2.1). Top down control by grazers is a critical feedback to primary productivity (Altieri et al 2013) and is often termed density mediated control. Herbivory is an interactive process involving a primary producer that produces organic matter and a consumer that ingests this material (Mulholland et al. 1989). Capacity of primary producers to generate biomass may significantly influence herbivore interactions and vice-versa (Crawley 1983; Mulholland et al. 1989). Attached algae, also known as periphyton or epiphyton, is the main focus of invertebrate grazing in springs. Periphyton is a complex assemblage of algae and bacteria living on the surfaces of benthic substrata or macrophytes (Vermaat 2005; Burkholder and Wetzel 1989). A significant body of research reports periphyton abundance to be negatively correlated with grazer population (e.g. ciliates, metazoans, aquatic insects, gastropods) (Tarkowska-Kukuryk and Mieczan 2012; Mulholland 1991; Liboriussen et al. 2005; Wetzel 2001; Cuker 1983; Hill et al. 1992; Rosemond et al. 1993).

Grazers may show high specificity of forage by focusing on highly edible and nutritious algae (Jones et al. 1998; Jones and Sayer 2003). In a study conducted by Bronmark et al. (1992), snails preferred to feed on periphyton composed of filamentous algae and large stalked diatoms over filamentous blue-green algae (*Gloeotrichia*) and small adnate diatoms that came to dominate the highly grazed treatments. Grazing on inert substrate was observed to have greater effect on epiphytic algae than on macrophytes suggesting some nutrient source in aquatic macrophytes (Mulholland et al. 1991). In addition to location of periphyton, other physical characteristics of aquatic systems may influence grazing activity. In a recent study by Liboriussen et al. (2005), top down control by grazers was more pronounced in clear lakes and was dominated by snails while in turbid lakes, grazing was dominated by chironomids and ostracods. Mulholland et al. (1989) report that algal productivity outpaced consumer control (<15 % of biomass consumed) at high irradiance while >90% was consumed at low irradiance conditions in experimental streams. Rosemond (1993) found that light, nutrients, and grazer activity, simultaneously limited algal

productivity and community structure. Relationship between ciliates, metazoan and chironomid grazer activity was found to be significantly related to NO_3-N, temperature, Secchi and DO (Tarkowska-Kukuryk and Mieczan 2012).

Grazing on algae may be significant enough to offset the effects of increased algal productivity (Jacoby et al. 2008; Hauxwell et al. 1998; Duarte 1995), however, any perturbation to grazer populations could cause a shift in algal production. Recent work by Liebowitz et al. (2014) suggests an escape threshold exists at which point algal productivity outpaces grazer control. The mechanisms are not clear as to what causes algal production to reach that threshold, but the current view is that it may be due to several factors acting in concert similar to multiple drivers of algal growth.

7.2.2.3 Controls on Grazers

Established ecological theory predicts loss of top down controls of grazers could be an alternative explanation for algal dominance in spring systems when bottom up controls and the abiotic top down controls of algae growth appear to be unrestrictive (Liebowitz et al. 2014) (Figure 7.2.2). Top down control of invertebrate grazers by fish can alter grazer population dynamics, and indirectly promote algal proliferation by removing grazing pressure (Mazumder et al. 1989; Power 1990; Brönmark et al. 1992; Liboriussen et al 2005; Korpinen et al. 2007). A study by Beklioglu et al. (2003) supports top down control of fish to promote grazers and thus promote algae control.

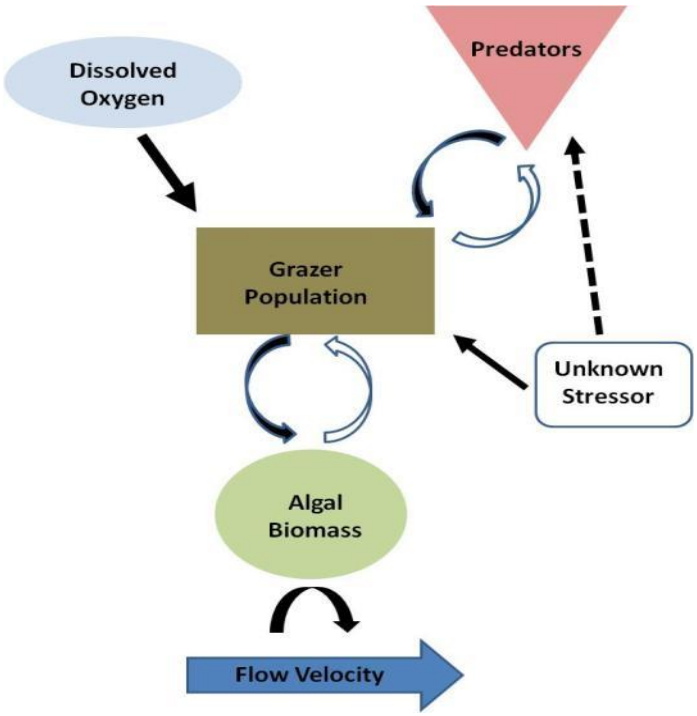

Figure 7.2.2. Conceptual model of drivers of grazer population. The unknown stressor could be any compound or condition that negatively impacts grazer population leading to population decline or episodic extirpation.

Changes in biotic populations often signal anthropogenic stress and impending ecosystem change (van Boclaer et al. 2012). Anecdotal evidence suggests a decline in grazer populations in many Florida springs, unfortunately, little biological data exists to support the assertion that grazer control of algae has lapsed. Many springs do not have any biological monitoring in place; hence, the few existing reports highly influence the current expectation on the grazer communities. Historic studies of Silver Springs by Odum (1957) lend some guidance in grazer community structure and populations. Review of that work indicates that approximately 44 % of the grazer biomass in Silver Springs was made up of grazing gastropods (*Pomacea, Oxytrema, and Viviparus*) (Figure 7.2.3). Grass shrimp (*Palaemonetes*) made up the next largest group of grazers by biomass (42 %). All other invertebrate grazers, including aquatic insects, made up the remaining 14 % of grazer biomass, hence the study of trophic interactions should rightfully focus on herbivorous snails and shrimp.

Because quantitative scientific observations of pristine spring ecosystem components are very rare. The work of Odum (1957) in Silver Springs provides a baseline from which change can be assessed in springs. Of significant interest for springs restoration is the type and distribution of algal grazers (snails and shrimp) in Florida springs prior to the shift in primary producers that is commonly observed today. The largest group of taxa by biomass was that of Gastropods.

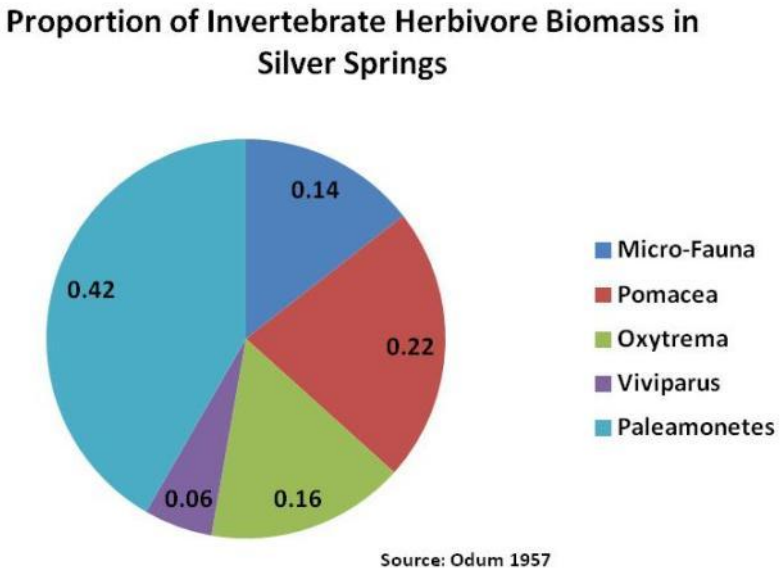

Figure 7.2.3. Proportion of invertebrate herbivore biomass in Silver Springs. The micro-fauna category consists of several sub-groups each representing a very small portion of overall herbivore biomass including Hydrobiidae (mud snails), Oligochetes, gammarids (amphipods), midges, copepods, ostracods, flatworms, *Hydroptera* (caddisflies), *Elophila* (moths) and *Arcella* (testate amoebae). *Pomacea* (Apple snails), *Oxytrema* (spiral stream snails), and *Viviparus* (river snail) are all gastropods. *Palaemonetes* is a freshwater decapod (grass shrimp). (Adapted from Odum 1957).

7.2.2.4 Gastropoda

The effect of snail herbivory on aquatic primary productivity has been supported in the literature. Mulholland et al. (1991) reported that nutrient reduction did not have a significant effect on algae in test streams, however, herbivory by snails reduced biomass, carbon fixation and reduced taxonomic diversity of periphyton. Sheldon (1987) found that macrophyte diversity increased with decreased snail population and increased snail grazing resulted in lowered macrophyte diversity by species least preferred by herbivorous snails. Bronmark (1990) however, discounted the simple association of snails and macrophytes citing several studies (among them his own) that show greater macrophyte herbivory by aquatic insects and decapods (crayfish) over aquatic snails. The relationship between snail abundance and macrophyte diversity, according to Bronmark (1990), is due to complex chemical and biological interactions, not simply snail herbivory. Studies of grazing activities of snails indicates they have a significant effect on epiphytic algal biomass, productivity and species composition (Marks and Lowe, 1989; Atalha et al. 2007; Li et al. 2008; Zhu et al. 2013). Grazing by snails has also been shown to have a significant indirect effect on macrophytes by reducing the adverse effects of epiphyton such as shading and nutrient competition (Bronmark 1989; Li et al. 2008). Wojdak and Mittelbach (2007) report that microcosms with multiple snail species had greater final biomass, less epiphytic algae, and less total organic matter at the end of experiment than did microcosms with a single species. This study strongly suggests that niche overlap among grazers has an additive effect on control of periphyton biomass.

Gastropods of the family Pleuroceridae have 12 genera found in North America but only one (*Elimia*) in the state of Florida (Thompson 2004). Several species of *Elimia* are common to regional springs. For instance, the Goblin Elimia (*Elimia vanhyningiana*) described by Goodrich (1921) is confined to springs and smaller streams of the St. Johns River basin in peninsular Florida and is named after O.C. Van Hyning the founder of the Florida Museum of Natural History. Another common species, *Elimia clavaeformis,* can reach 1,000 individuals m^{-2} under normal conditions (Mulholland et al. 1991) with 250 snails m^{-2} or 5 g m^{-2} (dry mass) considered a moderate consumer population (Lamberti et al. 1987; Steinman et al 1987; Mulholland et al. 1989). Dutoit (1979) reported densities of *E. floridensis,* a very common and widespread species, in the Ichetucknee River to approach 17,000 snails per m^{-2}. These populations sizes suggest potential for significant effects on physicochemical properties of water and on algal community structure. (Zhu et al. 2013; Rosemond 1993). Further, benthic snail feeding activity can enhance microbial growth and nutrient cycling via mixing of surface sediments and processing of detritus (Covich et al. 1999; Arango et al. 2009; Zheng et al. 2011).

Pulmonate snails (especially of the family Physidae) can tolerate low DO and are often observed in moderately to highly eutrophic systems receiving municipal wastewater (Giovanelli et al. 2005; Cui et al. 2008; Varnosfaderany et al. 2010; Cloherty and Rachlin 2011). Respiration of Pleuroceridae is strictly aquatic via internal gills (*ctenidium*) while several other families of gastropods utilize a pseudo “lung” or pulmonary cavity, an air-filled, highly vascualrized cavity portion of the mantle cavity that holds air and allows gas exchange. This method of respiration requires exchange with atmosphere for refreshing of oxygen supply. Some gilled snails such as *Amnicola limnosa* can tolerate DO below 3-4 mg L^{-1}, as can some species of Planorbidae, Physidae, Hydrobiidae, and Lymnaeidae (Cloherty and Rachlin 2011). This level of DO may not

be lethal to some species, however, chronic low DO may inhibit reproduction and encourage extirpation (Korpinen et al. 2006). Other environmental stressors such as pesticides, herbicides, and fungicides can have significant negative effect on grazers (snails) resulting in increased algal production (McMahon et al. 2012).

7.2.2.5 Decapoda

The genus *Palaemonetes*, commonly known as the grass shrimp, is a group of caridean shrimp consisting of over 35 species worldwide. This genus occupies freshwater, brackish (Tabb and Manning 1961; Rouse 1969) and salt waters (St. Amant and Hulquist 1969). Survival rates of grass shrimp in laboratory studies at 30 ppt suggests a large tolerance range for environmental conditions (Dobkin and Manning 1964). In Florida springs, *Palaemonetes paludosus* (Gibbes) predominately feed on algae, however, they are omnivorous and also ingest vascular plants, aquatic insects, and detritus (Beck and Cowell, 1976; Wessell et al. 2001). In Silver Springs, *P. paludosus* represented 42% of the grazer population by biomass (Odum 1957). Longevity of these shrimp is confined to 1 year, with post spawning mortality occurring from April-October in FL. Fecundity can be variable with 8-85 eggs per female (Beck and Cowell 1976). Grass shrimp have been observed in habitats with a range of DO tolerances from 2.8 to 6.0 mg L^{-1} (Wessell et al. 2001) suggesting significant tolerance of low DO. Brown-Peterson et al. (2008) report that *Palemonetes pugio*, an estuarine grass shrimp, exposed to cyclic hypoxia (3 days at 1.5 mg L^{-1} followed by 3 days of normal oxygen) showed reduced number of broods and eggs. Both cyclic and chronic (77 day) hypoxia resulted in decreased population growth indicative of population level impacts. These shrimp are especially abundant in central and South Florida marshes (Kushlan and Kushlan 1980) associated with vegetation communities providing cover and likely occupy a similar niche in spring systems.

7.2.2.6 Hypotheses

Nitrate reduction in the Upper Floridan Aquifer, the source of water for springs across the state, is linked to observations of reduced DO in spring vents and runs (Heffernan et al. 2012). Heffernan et al. (2010) suggests top down control of invertebrate grazers via altered DO has resulted in altered trophic structure in springs to favor algal dominance. Liebowitz (2013) reports a significant negative association between algal and gastropod biomass in Florida springs, suggesting top down control of algae by invertebrate grazers, a finding supported by several studies of grazer control of algae in other systems (Hildebrand 2002; Heck and Valentine 2007; Gruner et al. 2008; Baum and Worm 2009; Estes et al. 2011). Further, Liebowitz (2013) also found a significant relationship between dissolved oxygen (DO) and gastropod biomass in a survey of 11 springs, suggesting DO has a significant indirect effect on algal biomass via controlling grazer abundance and/or activity. Under low flow or current velocity conditions, nutrient enrichment and subsequent algal growth may outpace grazer pressure resulting in severe light reductions (Harlin and Thorne-Miller 1981). Alternatively, under similar nutrient enrichment and moderate to high flushing or exchange of water (as in lotic or tidally influenced systems), herbivores have been observed to control epiphytic algal biomass (Neckles 1993). Liebowitz (2013) argues that hysteretic responses of grazer populations to disturbances could be responsible for the over-abundance of algae in springs where no clear grazer stress is present. For instance, invasive plant control measures utilizing herbicides and copper compounds are widely

employed with known negative impacts on grazer populations (Evans 2008). Such a disturbance could enable algal populations to exceed thresholds for grazer control.

Based upon the available scientific literature, several hypotheses as to the causal mechanisms behind algal proliferation in springs are currently supported. The following hypotheses have foundations in the principles of top down control and trophic cascade theory. The commonality of all of these hypotheses is that alteration of top down control of grazers (be it predation or environmental stress) results in a cascading effect to the primary producer population, namely the epiphytic algal community in spring systems.

H_1- Declining DO levels have created chronic hypoxic stress on grazer communities resulting in lowered fecundity and grazing pressure (consumer stressor hypothesis 1)

H_2- Episodic hypoxia has extirpated invertebrate grazers resulting in loss of top down control of algal biomass (consumer stressor hypothesis 2)

H_3-Some combination of drivers/ stressors such as elevated NO_3 and hypoxia, working synergistically have caused dramatic declines in grazer communities (multiple stressor hypothesis)

7.2.2.7 Objectives

The objectives of this work are two-fold. First, we experimentally determined the necessary dissolved oxygen levels required for normal respiration, as well as, critical oxygen saturation thresholds for survival of hypoxic conditions. Secondly, we raised a second generation of test organisms under ambient, medium and high NO_3-N concentrations and tested for NO_3-N effects on both respiration and critical oxygen saturation requirements for these four organisms to determine any compound effect of NO_3-N on the already present oxygen stress.

7.2.3 MATERIALS AND METHODS

7.2.3.1 Field Collection

All test organisms were collected from Silver River and Alexander Springs Creek in March and April of 2015. The gastropods (*Viviparus georgianus*, *Elimia floridensis*, *Micromenteus floridensis*) and decapods (*Palaemonetes paludosus)* (Figure 7.2.4) were returned to the Whitney Laboratory at ambient temperatures where they were then cultured in aquaria utilizing algal pellets as a primary food source. Spawning of gastropods was induced by the temperature change, resulting in large populations of snails of each species. These populations were allowed to grow unhindered until the experimental phase began in which a majority of the population was moved to the mesocosm tanks to aid in algal control. The remaining specimens (approximately 25 of each species) were retained in the laboratory aquaria for testing.

Figure 7.2.4. Algal grazers utilized in respirometry experiments (clockwise from top left), *Palaemonetes paludosus* (decapoda); *Elimia floridensis* (gastropoda); *Viviparus georgianus* (gastropoda); *Micromenteus floridensis* (gastropoda).

7.2.3.2 Laboratory Analyses

The experimental respiration manipulations were conducted in a closed system consisting of an experimental aquarium (20 L aquarium) and a 100 L sump. Water in this closed system was circulated from the sump to the experimental aquarium using a brushless DC pump, before overflowing through a drain back into the sump. To minimize bacterial respiration, water was continuously circulated through a UV sterilization system (9 Watt Clarity +). The system was placed in a temperature controlled room which maintained the water temperature at 22.2 $\pm$ 0.1 °C, equivalent to the natural temperature experienced by this species in the wild.

Four identical 20 mL respirometry setups were placed in the aquarium side by side. Each respirometry set up consisted of a sealed 20 mL glass vial chamber connected to a recirculating pump (which mixed water inside the respirometer) and a flushing pump (which pumped water from the aquarium in and out of the chamber) (Steffensen 1989; Clark et al. 2013; Svendsen et al. 2015). Dissolved oxygen concentration in the chamber was measured and logged using a FireSting fibrer-optic oxygen meter (Pyroscience, Germany). The sensor was mounted in the recirculation loop, to ensure that flow was sufficient for the fast response time of the sensor. (Figure 7.2.5).

7.2.3.3 Settling Period

Snails were starved for a minimum of 16 hours prior to experimentation to ensure they were in a post-absorptive state (Niimi and Beamish 1974). Individual test subjects (*E. floridensis*, wet mass = 0.85 $\pm$ 0.05 g, wet volume = 0.32 $\pm$ 0.08 mL, mean $\pm$ SE; n = 12) were randomly selected and placed into one of the respirometry chambers 12-15 h prior to the experimental period in order to allow the test subjects to settle in and acclimate to the experimental setup. Oxygen

uptake rate (MO_2) was estimated using intermittent-flow respirometry, with a 180 s flush, 30 s wait and 690 s measurement period (controlled using a Titan Controls, Hades 2 ® timer). During the 690 s measurement period, the respirometry chamber was sealed to prevent water exchange between the chamber and surrounding aquarium. The length of the measuring period ensured that the animal reduced the oxygen saturation in the chamber by 3 to 5 % during each measurement period. After measurement phases were complete, snails were weighed whole in the shell and then without the shell.

7.2.3.4 Hypoxia Treatment

Following the overnight settling period, the oxygen saturation of the water in the system was systematically reduced by bubbling nitrogen through air stones into the experimental sump. The rate of nitrogen bubbling was manually controlled by monitoring the oxygen saturation in the sump using an YSI dissolved probe (oxygen EcoSense DO200A). This allowed MO_2 to be measured at 100, 70, 60, 50, 40, 30, 20 and 10 % oxygen saturation for each animal (for detailed methodology, see Domenici et al. 2000). Three MO_2 determinations were carried out at each oxygen saturation level. Time between the oxygen saturation levels ranged between 45 to 60 minutes, for a total experimental duration of approximately 8 hours.

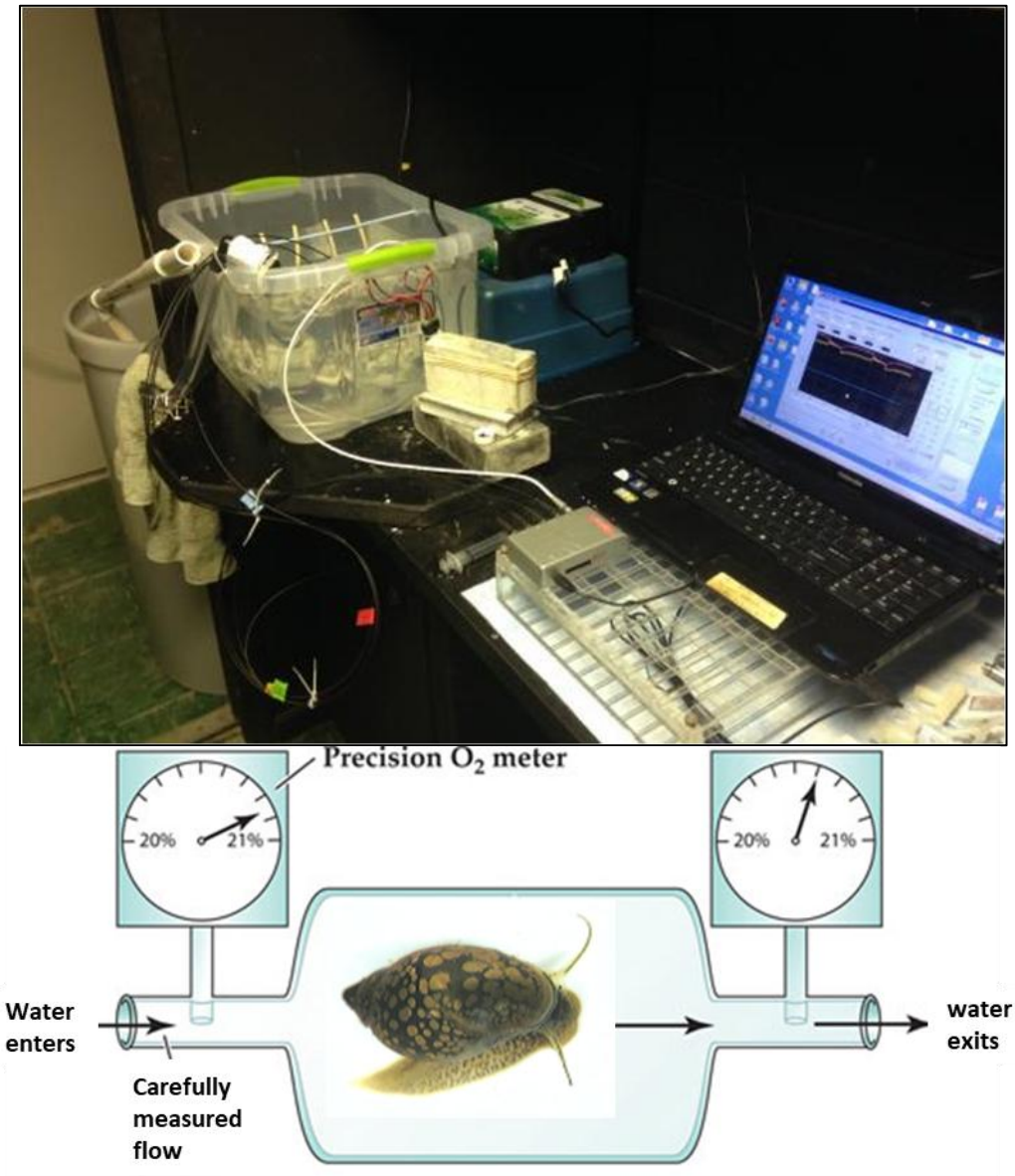

Figure 7.2.5. Photograph of respirometry experimental array with 20 L holding tank fitted with test cells, timer switch, multi-plexer, and computer in foreground and 100 L sump in background. Four test cells were run in parallel allowing for testing of four individual animals during each iteration.

7.2.3.5 Nitrate Effects on Hypoxia Resistance

Increased nitrate levels are of great interest in springs restoration efforts, and because nitrates are known to interfere with hemoglobin in humans and other higher animals, the effects of nitrate exposure on respiration was investigated. Identical methods of measuring metabolic and respiration rates were utilized with *E. floridensis* and *Teribia granifera* (an invasive species) that had been exposed to nitrate (control = 0.1 mg L^{-1} and trial =10 mg L^{-1}) in laboratory aquaria for 1 month prior to respirometry analysis.

7.2.4 RESULTS AND DISCUSSION

Data generated from respirometry requires extensive post processing (10-12 h for each run of 4 individuals) and is likely the reason why respiration investigations are lacking for most invertebrate species. The raw data trace depicted in Figure 7.2.6 shows a relatively stable MO_2 over time, until the end of the hypoxia experiment where oxygen saturation levels are experimentally reduced from 100 % to 70, 60, 50, 40, 30, 20 and finally 10 %. This decline in oxygen consumption at approximately 20% saturation indicates an inability of *E. floridensis* to adequately respire at its normal metabolic rate. Prolonged exposure to hypoxic conditions of 10% saturation (approximately 1.0 mg L^{-1}) for more than 6hrs results in mortality of organisms.

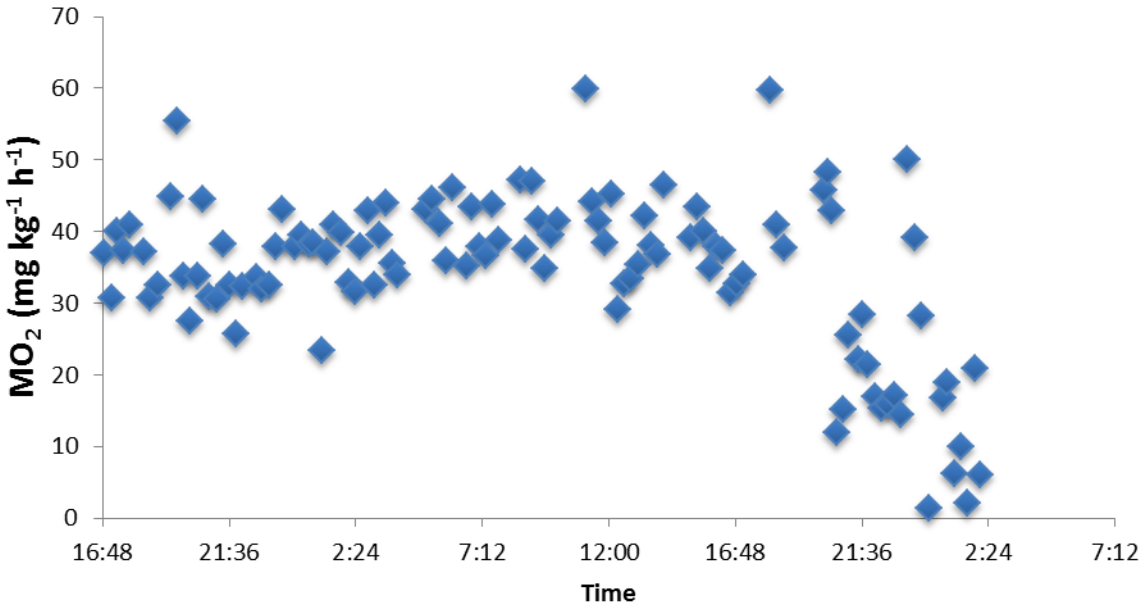

Figure 7.2.6: Raw data trace for one snail (*E. floridensis*) showing oxygen consumption in mg O_2 kg^{-1} snail per hour (MO_2) as a function of time.

While little work has been done in spring systems to determine the DO thresholds of algal grazers, current research on *Elimia floridensis* in Florida springs by Liebowitz et al. (2014) suggests a strong positive relationship between DO and snail grazing efficiency. Although hypoxic conditions were not tested in that investigation, other research suggests a wide range of tolerances similar to those observed in other invertebrate groups. For example, there was no observed negative effects of *Bellamya* sp. in high density algae experiments where DO averaged below 2 mg L^{-1} over 30 days (Zhu et al. 2013). Because several springs in Florida routinely drop below the hypoxia threshold (especially at night) we contend that DO is a significant driver of grazing activity. This assertion is supported by metabolic activity measurements for *E. floridensis* in experimental trials (Figure 7.2.7).

Graphical analysis using linear regression allows for the determination of critical DO thresholds from the respirometry results (Figure 7.2.7). The horizontal linear regression demonstrates the

standard metabolic rate (SMR) equivalent to 35.6 ± 0.7 mg O_2 kg^{-1} h^{-1} (mean ± S.E.). The linear regression intersecting with 0.0 shows the oxygen consumption of the snail under hypoxic conditions. The intersect between the two regression lines depicts the critical oxygen saturation level (O_2 crit), below which the snail can no longer extract adequate oxygen from the water to maintain its SMR. For these individuals (n=4) O_2 crit = 4.9 mg O_2 L^{-1}, which is well above observed low DO saturation in dark hours in both Silver River and Alexander Springs. This finding suggests that snails in both ecosystems are significantly stressed in the dark hours when DO often falls below 3 mg L^{-1} and perhaps remain in a low grade stressed condition at all times that DO falls below the O_2 crit.

Other species tested, such as *Micromenetus floridensis* and *Viviparus georgianus*, expressed variable physiological tolerances to low DO conditions (Figure 7.2.8 and 7.2.9), respectively. *M. floridensis* was observed to decline beyond recovery below 1.9 mg O_2 L^{-1} while *V. georgianus* was observed to have deleterious physiological effects at 2.7 mg O_2 L^{-1} (the highest DO threshold observed). These findings suggest that hypoxia, as commonly defined in the literature at 2.0 mg O_2 L^{-1}, is appropriate for gastropods common to springs that were investigated in this study. With respect to the *V. georgianus* snails, the risk of extirpation by low oxygen events is greater than that of *M. floridensis.*

The grass shrimp *Palaemonetes paludosus* was observed to have the lowest DO threshold (1.6 mg L^{-1}) in the trials conducted in this investigation. Of particular interest is the role of *P. paludosus* in Silver River. Odum (1957) identified grass shrimp as constituting approximately 42 % of the grazing invertebrate community biomass, and Frazer and Mattson (Chapter 9 this report) observed *P. paludosus* to have the highest consumption rate of nuisance algae in controlled feeding trials. Considering the importance of this species in algal grazing and their significant hypoxia tolerance, it appears that other factor influencing *P. paludosus* population dynamics may be responsible for reducing top down control of algae. At the time of this reporting, it is unknown if the population of *Palaemonetes paludosus* has been significantly reduced in recent years, a fact that would aid in interpretation significantly.

Effects of nitrate exposure (control = 0.1 mg L^{-1} and trial =10 mg L^{-1}) were determined after 1 month of exposure of *E. floridensis* and *T. granifera* to control and trial levels of nitrate (Figure 7.2.11). In the case of the native *E. floridensis*, critical oxygen levels were actually observed to be lower under high nitrate condition, but not significantly so (t=2.7, df=4, P= 0.40). Under identical tests, no significant difference (t=2.9, df=4, p=0.22) was observed in the response of the exotic species *T. granifera* to elevated nitrate versus control levels with respect to critical oxygen saturation.

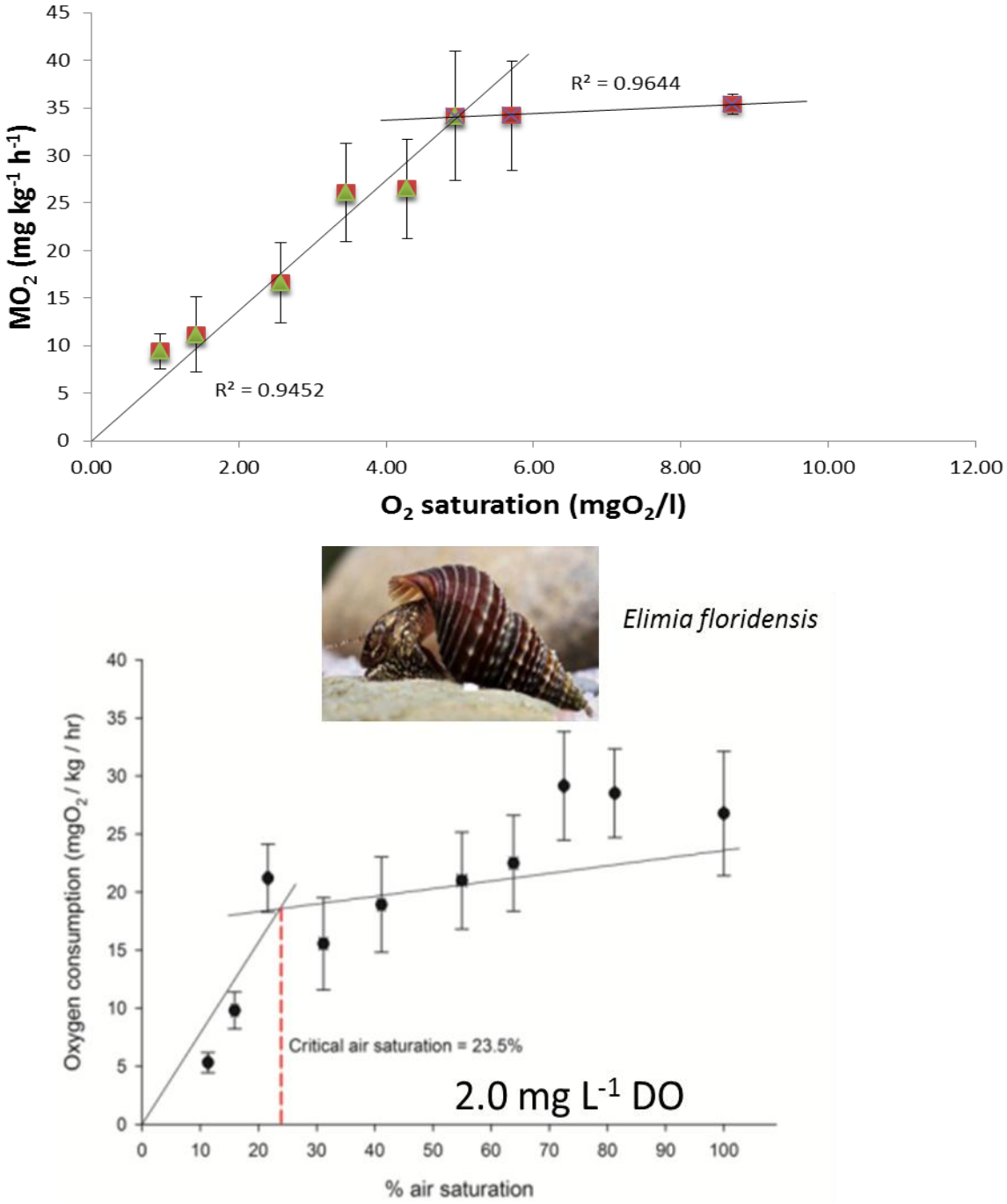

Figure 7.2.7. Metabolic rate of *E. floridensis* relative to oxygen saturation. Metabolic rate (MO_2) is described in mg O_2 per kg^{-1} of snail h^{-1}. Oxygen saturation is in mg O_2 L^{-1} of water.

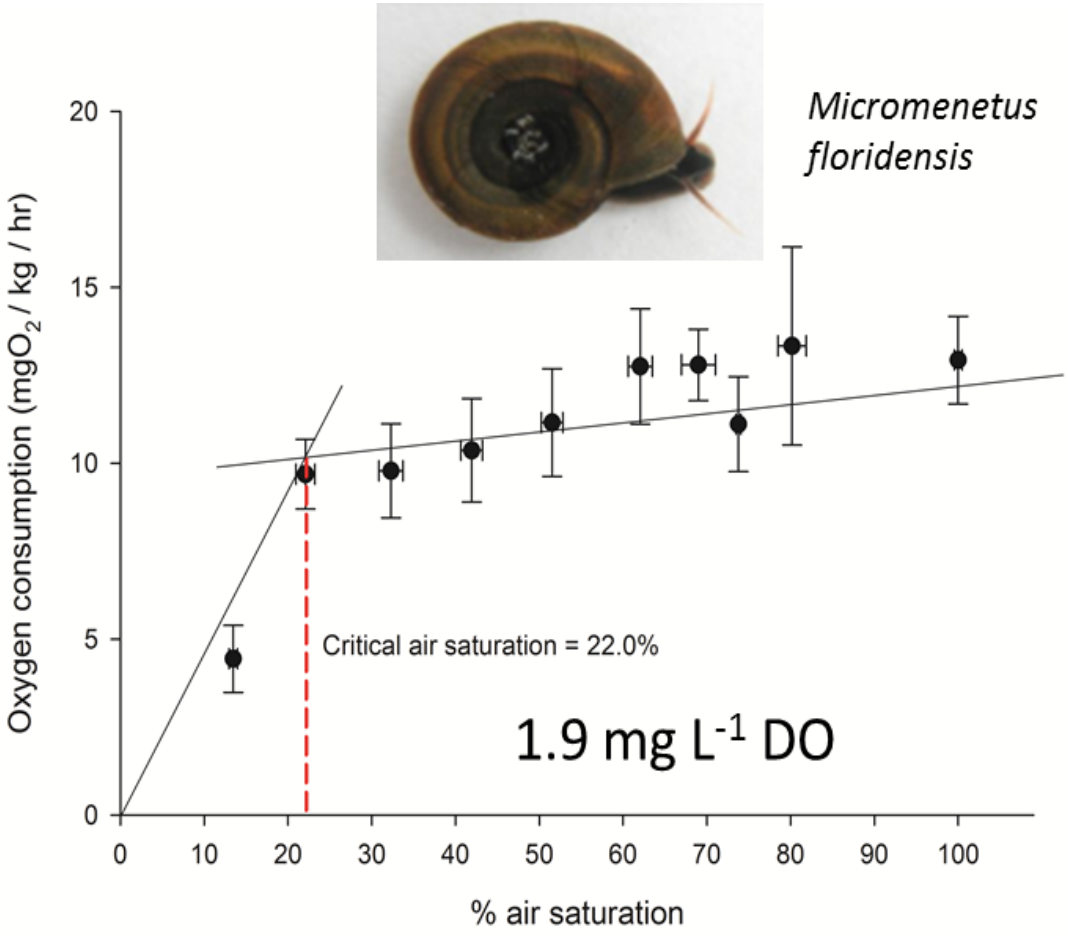

Figure 7.2.8. Oxygen consumption (mg O_2 kg^{-1} h^{-1}) by *Micromenetus floridensis* over a range of percent oxygen saturation at standard temperature and pressure.

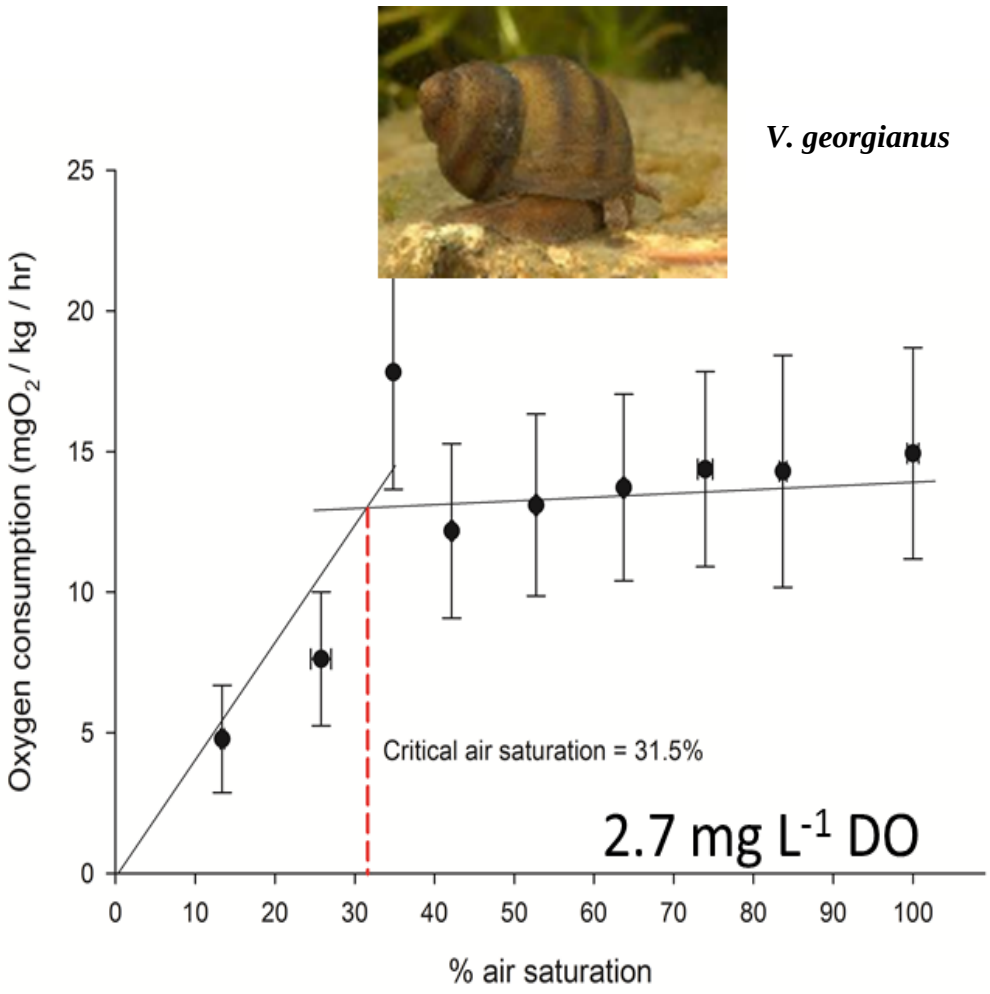

Figure 7.2.9. Oxygen consumption (mg O_2 kg^{-1} h^{-1}) by *V. georgianus* over a range of percent oxygen saturation at standard temperature and pressure.

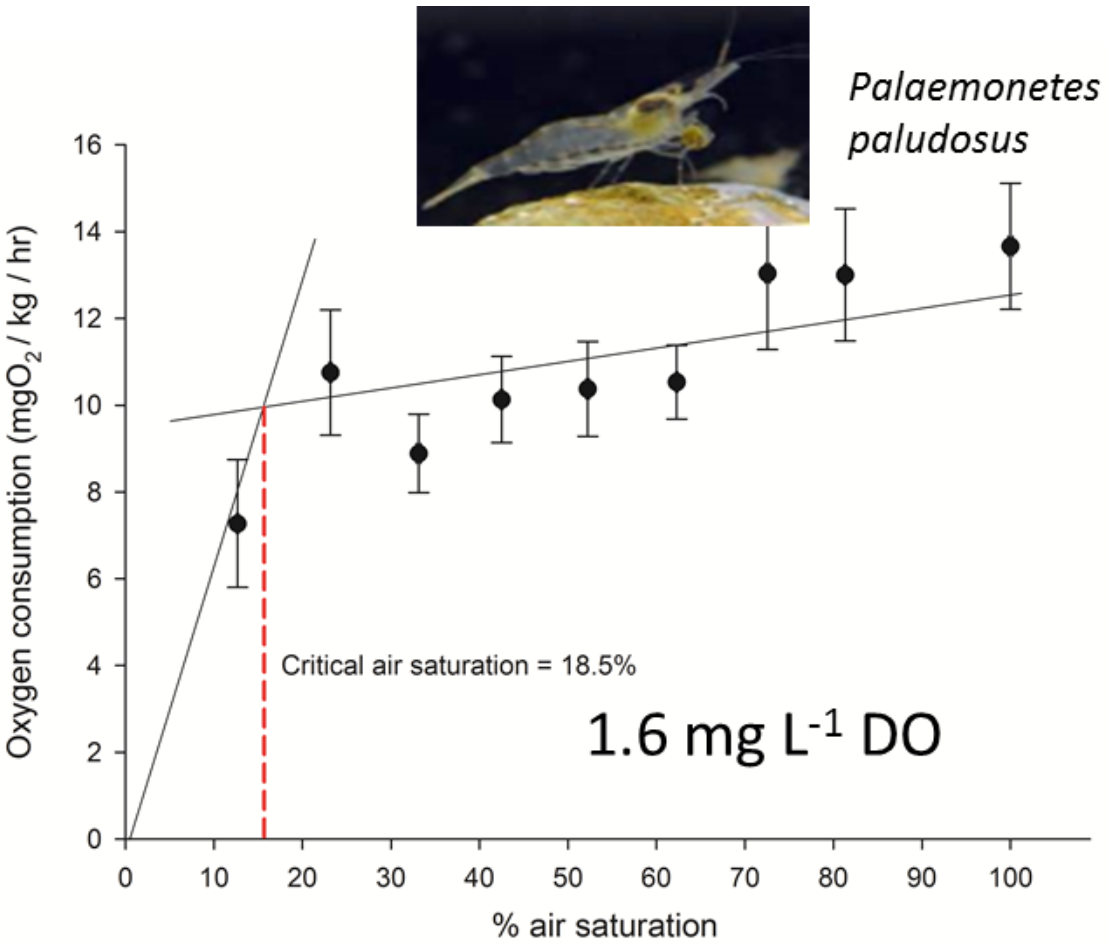

Figure 7.2.10. Oxygen consumption (mg O_2 kg^{-1} h^{-1}) by *Palaemonetes paludosus* over a range of percent oxygen saturation at standard temperature and pressure.

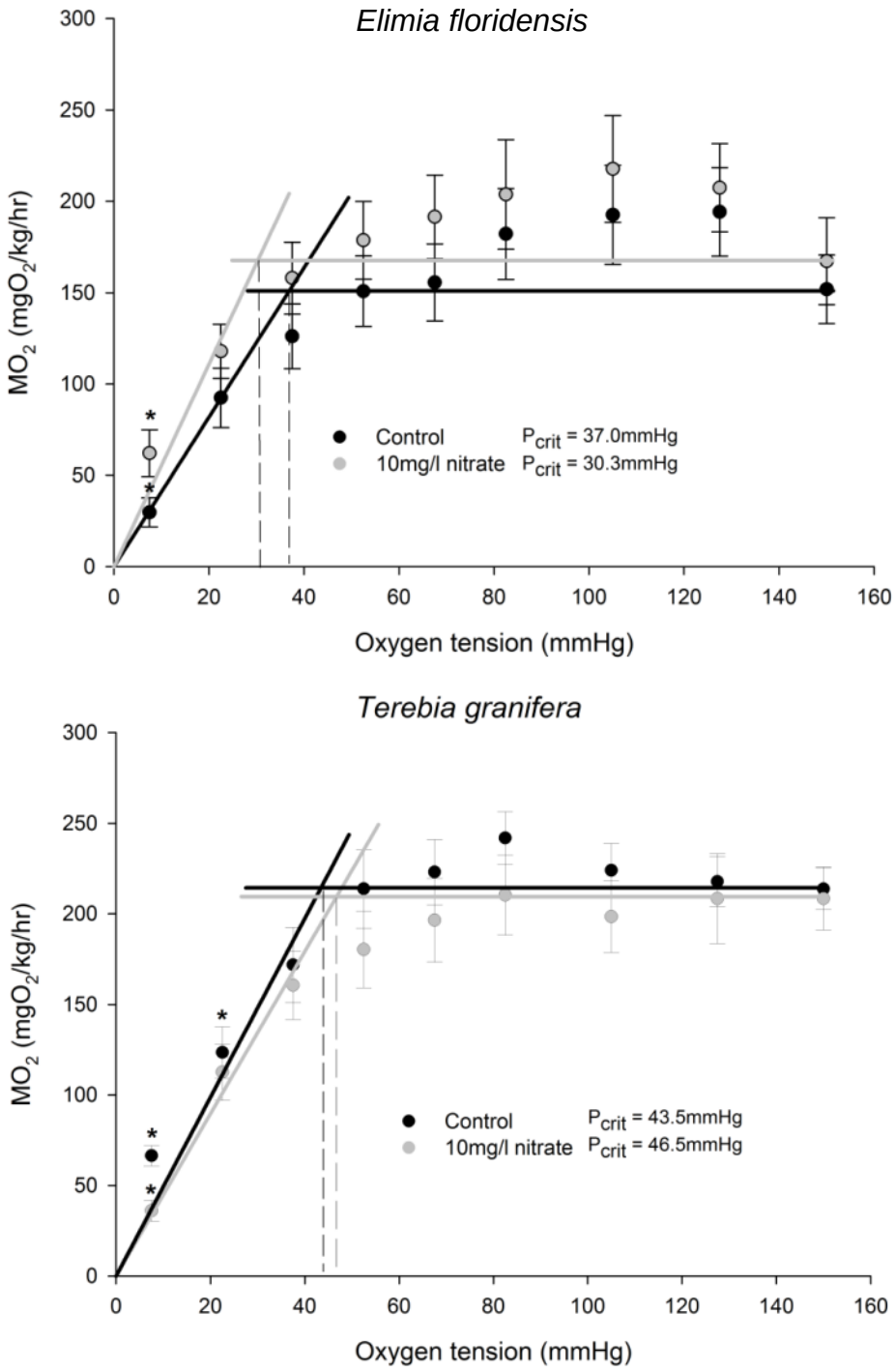

Figure 7.2.11. Oxygen consumption (mg O_2 kg^{-1} h^{-1}) by *E. floridensis* (top) and *T. granifera* (bottom) exposed to high nitrate versus no nitrate exposure (control) over a range of percent oxygen saturation at standard temperature and pressure.

7.2.4.1 Chronic and Episodic Hypoxia

Oxygen saturated, or normoxic, conditions are considered optimal for aquatic systems at DO concentration of 5 to 14 mg L^{-1} depending on water temperature and barometric pressure (Wetzel 2001). However, many organisms are adapted to tolerate much lower DO conditions. Hypoxia, or low oxygen stress, typically considered to be below 2.0 to 2.8 mg L^{-1}(Joyner-Matos et al. 2011). There have been significant efforts to study hypoxia in marine systems where many studies identify hypoxia at 2.0 mg L^{-1} with higher values (up to 4.0 mg L^{-1}) reported (Paerl 2006; Li et al. 2011). Ecological responses to hypoxia in marine systems include mass mortality, reduction of biomass and secondary production, and changes to community structure *sensu lato* elimination of sensitive species and proliferation of tolerant ones (Liu et al. 2011; Weisberg et al. 2008; Riedel et al. 2008; Wu 2002; Dauer 1993). Extinction or extirpation of local foundation species (species that have a strong role in structuring the community) by hypoxic events has been well documented in estuarine and freshwater literature as well with many reports of effects of high biological oxygen demand (BOD) effluents altering structure of biotic communities in receiving waters (Altieri and Witman 2006; Wu 1982).

In some cases, low DO is advantageous to some invertebrates as it can serve as refugia from predators such as fish (Chapman 2007; Chapman et al. 2004). Commonly, low DO forces invertebrates, especially insects, into areas with higher current and less cover, ostensibly to increase respiratory efficiency; however, this increases risk of predation by fish (Lowell et al. 2000). Perhaps more importantly, DO can be a stressor in itself or compound the affects of other stressors such as heavy metal toxicity (Irving et al. 2008). Oxygen availability can influence distribution of species of invertebrates and fishes alike (Parson 1991; Osborne et al. 2001; Chapman 2007). In many aquatic systems where hypoxia is prevalent, invertebrate communities are often dominated by physically small organisms (Chapman 2007). Too much oxygen can also be detrimental as organisms must repair damage from free radical exposure (Joyner-Matos et al. 2007).

Looking to the extensive aquatic insect (and other invertebrate) literature, interspecies variability in tolerances and responses to hypoxia by aquatic invertebrate grazers can be great (Merritt et al. 2008; Thorp and Covich 1991). For example, Munro Fox et al (1936) reported that for two species of Ephemoroptera (*Cloeon* and *Baetis*) responses to low oxygen were dramatically different with *Cloeon* reducing oxygen consumption only when levels reached 20 % saturation while *Baetis* reduced consumption linearly with decreases in O_2 availability. Similarly, DO below 5 mg L^{-1} reduced feeding by *Baetis tricaudatus* (Ephemeroptera) by 80 % and after two weeks of exposure, 60-90 % mortality was observed compared to high DO experimental streams (11 mg DO L^{-1}) (Lowell and Culp 1999). Further, similar species variability in oxygen consumption depends significantly on environmental conditions during growth (fast versus slow flowing water), a finding that suggests phenotypic plasticity in some aquatic insects with respect to adaptations to oxygen conditions. Invertebrates that utilize hemoglobin appear to have greater tolerances for hypoxia versus those that utilize hemocyanin. Most Florida gastropods use hemocyanin with the exception of the Planorbidae (Pennak 1989).

Many invertebrates can evade oxygen stress events with myriad adaptations for low oxygen survival. Some examples for highly mobile species includes drifting with current (downstream emigration; Connolly and Pearson 2007) to evade oxygen depleted waters or seeking surface films where oxygen diffusion is more rapid and thus DO more available (Apodaca and Chapman 2004). Estuarine fishes and crustaceans practice avoidance or escape behaviors when subjected to hypoxic conditions (Wannamaker and Rice 2000; Wu et al. 2002; Bell and Eggelston 2005) and may still suffer reductions in growth (Eby et al. 2005; Stierhoff et al. 2006). Physiological oxygen transport mechanisms have been documented in some organisms (McMahon 2001; Paul et al. 2004). Other avoidance mechanisms include decreasing activity, O_2 uptake capacity, or anaerobic metabolism (Grieshaber et al. 1994; Diaz and Rosenberg; Hochachka and Somero 2002; Wu et al. 2002). Eriksen (1963) describes respiratory adjustment as a phenomenon where aquatic insects reduce their oxygen consumption when oxygen availability is reduced (*Ephemera simulans* can survive oxygen concentrations down to 1.0 mg L^{-1} using this mechanism) however, not all species are capable of this.

Invertebrates show great adaptation in respiratory modes from atmospheric breathing to tracheal gill breathing allowing for dispersal in low DO habitats (Chapman et al. 2004; Chapman 2007). Some invertebrates have been documented to survive hypoxia and anoxia better if acclimated to cooler water temperatures (Nagell and Fagerstrom 1978). A study of stream invertebrates in tropical African aquatic systems with variable oxygen stress found low levels of gastropod grazers (<5 % relative abundance) in streams with DO averaging 7 mg L^{-1} while an adjacent swamp with average DO of 2 mg L^{-1} had a relative abundance of gastropods >25 % (Osborne et al. 2001). In the same study, insect grazers such as trichopterans and ephemeropterans were reported in greater abundance in streams with DO 5 mg L^{-1} than in high DO rivers or low DO swamps indicating adaptation and potential advantage of predator evasion under low DO.

7.2.5 CONCLUSIONS AND RECOMMENDATIONS

Four ecologically significant invertebrate grazer species (Odum 1957) have been tested for physiological thresholds, with gastropods exhibiting significant physiological stress from 2.7 mg DO L^{-1} and below. The grass shrimp (*Palaemonetes paludosus*), an active algal and detritus feeder, was the most resilient to hypoxia. Native species (*E. floridensis* and an invasive (*T. granifera* were tested under elevated nitrate conditions to determine if nitrate has an effect on respiration of invertebrates found in Florida spring ecosystems. Results suggested that nitrate did not significantly alter critical oxygen levels in these species.

The results of this work suggest that hypoxia may be a significant contributor to the reduction of grazer activity on algal biomass. Therefore, we recommend that hypoxia be considered a management issue to be further explored. While minor activities such as aeration may be useful in maintaining grazer communities in head springs, it is unknown if this approach is feasible.

7.2.6 REFERENCES

Albertin, A. R. 2009. Nutrient dynamics in Florida springs and relationships to algal blooms. Dissertation, University of Florida.

Altieri, A. H. and Witman, J. D. 2006. Local extinction of a foundation species in a hypoxic estuary: integrating individuals to ecosystems. Ecology 87: 717-730.

Altieri, A. H., Bertness, M. D., Coverdale, T. C., Axelman, E. E., Herrmann, N. C., and Szathmary, P. L. 2013.Feedbacks underlie the resilience of salt marshes and rapid reversal of consumer driven die-off. Ecology 94(7): 1647-1657.

Anastasiou, C. 2009. Characterization of the underwater light environment and its relevance to seagrass recovery and sustainability in Tampa Bay, Florida. PhD Dissertation. University of South Florida.

Apodaca, C. K. and Chapman, L. J. 2004. Larval damselflies in extreme environments: Behavioral and physiological response to hypoxic stress. Journal of Insect Phyisology 50:767-775.

Arango, C. P., Riley, L. A., Tank, J. L., and Hall, R. O. 2009. Herbivory by an invasive snail increases nitrogen fixation in a nitrogen-limited stream. Can. J. Fish. Aquat. Sci. 66: 1309-1317.

Atalah, J., Anderson, M. J., and Costello, M. J. 2007. Temporal variability and intensity of grazing: a mesocosm experiment. Marine Ecology Progress Series 341: 15-24.

Baum, J. K. and Worm, B. 2009. Cascading top-down effects of changing oceanic predator abundances. Journal of Animal Ecology 78:699–714.

Beck, J. T. and Cowell, B. C. 1976. Life history and ecology of the freshwater Caridean shrimp, *Palaemonetes paludosus* (Gibbes). Ameican Midland naturalist 96(1): 52-65.

Beklioglu, M., Ince, O., and Tuzun, I. 2003. Restoration of the eutrophic Lake Eymir, Turkey, by biomanipulation after a major external control. Hydrobiologia 489: 93-105.

Bell, G. W., Eggleston, D. B., and Wolcott, T. G. 2003. Behavioral responses of free-ranging blue crabs to episodic hypoxia. I. Movement. Marine Ecological Progress Series 259: 215-225.

Biggs, B. J. F. and Close, M. E. 1989. Periphyton biomass dynamics in gravel bed rivers: the relative effects of flows and nutrients. Freshwater Biology 22:209-231.

Biggs, B. J. F., Goring D. G., and Nikora, V. I. 1998. Subsidy and stress responses of stream periphyton togradients in water velocity as a function of community growth form. Journal of Phycology 34:598-607.

Bluzat, R. and Segue, J. 1983. Chronic intoxication by an herbicide 2,4,5-Trichlorophenoxyacetic acid in the pond snail Lymnaea stagnalis L. Environmental Research 31: 440-447.

van Boclaer, B., Shultheis, R., Plisnier, P., and Albrecht, C. 2012. Does the decline of gastropods in deep water herald ecosystem change in lakes Malawi and Tanganyika? Freshwater Biology: 57:1733-1744.

Bothwell, M. L. 1985. Phosphorus limitation of lotic periphyton growth rates: an intersite comparison using continuos flow troughs (Thompson River system, British Columbia). Limnology and Oceanography 30: 527-542.

Bronmark, C. 1989. Interactions between epiphytes, macrophytes, and freshwater snails: A review. Journal of Molluscan Studies 55: 299-311.

Bronmark, C. 1990. Do herbivorous freshwater snails affect macrophytes?- A comment. Ecology 71(3): 1212-1215.

Bronmark, C., Klosiewski, S. P., Stein. R. A. 1992. Indirect effects of predation in a freshwater, benthic food chain. Ecology 73(5): 1662-1674.

Brown, M. T., Chinner-Reiss, K., Cohen, M. J., Evans, J. M., Reddy, K. R., Inglett, P. W., Inglett, K. S., Frazer, T. K., Jacoby, C. A., Philips, E. J., Knight, R. L., Notestein, S. K., and McKee, K. A. 2008. Summary and synthesis of the available literature on the effects of nutrients on springs organisms and systems. Final Report. Florida Department of Environmental Protection, Tallahassee FL.

Brown-Peterson, N. J., Manning, C. S., Patel, V., Denslow, N., and Brouwer, M. 2008. Effects of cyclic hypoxia on gene expression and reproduction in a grass shrimp, *Palaemonetes pugio*. Biological Bulletin 214: 6-16.

Burkholder, J. M. and Wetzel, R. G. 1989. Epiphytic microalgae on natural substrata in a hardwater lake: Seasonal dynamics of community structure, biomass and ATP content. Archiv für Hydrobiologie, Suppl. 83: 1–56.

Canfield, H. E. and Hoyer, M. V. 1988. Influence of nutrient enrichment and light availability on the abundance of aquatic macrophytes in Florida streams. Canadian Journal of Fisheries and Aquatic Sciences 45: 1467-1472.

Carpetner, S. R., Kitchell, J. F., Jodgeson, J. R., Cochran, P. A., Elser, J. J., Elser, M. M., Lodge, D. M., Kretchmer, D., He, X., and Vonende, C. N. 1987. Regulation of lake primary productivity by food web structure. Ecology 68(6): 1863-1876.

Carpenter, S. R., Cole, J. J., Hodgeson, J. R., Kitchell, J. F., Pace, M. L., Blade, D., Cottingham, K. L., Essington, T. E., Houser, J. N., and Schlindler, D. E. 2001. Trophic cascades, nutrients, and lake productivity: whole lake experiments. Ecological Monographs 71(2): 163-186.

Carpenter, S. R. and Kitchell, J. F. 1988. Consumer control of lake productivity. Bioscience 38: 764-769.

Chapman, L. J., Schneider, K., Apodaca, C. K., and Chapman, C. A. 2004. Respiratory ecology of macroinvertebrates in a swamp-river system of East Africa. Biotropica 36: 572-585.

Chapman, L. J. 2007. Morpho-physiological divergence across oxygen gradients in fishes. Invited book chapter. pp. 14-29. In: M.N. Fernandes, F.T. Rantin, M.L. Glass, and B.G. Kapoor (editors). Fish Respiration and the Environment. Science Publisher, Inc., Enfield, NH.

Clark, T. D., Sandblom, E., and Fredrik, J. 2013. Aerobic scope measurements of fishes in an era of climate change: respirometry, relevance and recommendations. The Journal of Experimental Biology 216: 2771-2782.

Cloherty, T. M. and Rachlin, J. W. 2011. Physico-chemical and shoreline development factors affecting lake littoral benthic macroinvertebrates. Journal of Freshwater Ecology. 26: 517-525.

Cohen, M. J., Lamsal, S., and Korhnak, L. V. 2007. Sources, Transport and Transformations of Nitrate-N inthe Florida Environment. St. Johns River Water Management District SJ2007-SP10. 125 pp. Palatka, FL.

Cohen, M. J., Heffernan, J. B., Albertin, A., and Martin, J. B. 2012. Inference of riverine nitrogen processing from longitudinal and diel variation in dual nitrate isotopes. Journal of Geophysical Research 117: 1-17.

Connolly, N. M. and Pearson, R. G. 2007. The effect of fine sedimentation on tropical stream macroinvertebrate assemblages: a comparison using flow-through artificial stream channels and recirculating mesocosms. Hydrobiologia 592: 423-438.

Copeland, R. 2003. Florida spring classification system and spring glossary. Special Publication No. 52. Florida Geological Survey, Tallahassee, Florida, USA.

Copeland, R., Doran, N. A., White A. J., and Upchurch, S. B. 2009. Regional and statewide trends in Florida's spring and well groundwater quality (1991-2003). Bulletin No. 69. Florida Geological Survey, Tallahassee, Florida, USA.

Covich, A. P., Palmer, M. A., and Crowl, T. A. 1999. The role of benthic invertebrate species in freshwater ecosystems: zoobenthic species influence energy flows and nutrient cycling. BioScience 49: 119-127.

Cowell, B. C. and Botts, P. S. 1994. Factors influnceing the distribution, abundance, and growth of *Lyngbya wollei* in Central Florida. Aquatic Botany 49: 1-17.

Cowell, B. C. and Dawes, C. J. 2004. Growth and nitrate nitrogen uptake by the cyanobacterium *Lyngbya wollei.* Journal of Aquatic Plant Management. 42: 69-71.

Crawley, M. J. 1983. Herbivory: the dynamics of animal-plant interactions. University of California Press, Berkely CA USA.

Cui, Y., Liu, X., and Wang, H. 2008. Macrozoobenthic community of Fuxian Lake, the deepest lake of southwest China. Limnologica 38: 116-125.

Cuker, B. E. 1983. Competition and coexistence among the grazing snail Lymnaea, chironomidae, and microcrustacea in an arctic epilithic lacustrine community. Ecology 64_1_: 10–15.

Dauer, D. M. 1993. Biological criteria, environmental health and estuarine macrobenthic community structure. Marine Pollution Bulletin 26: 249-257.

Dennison, W. C., and others 1993. Assessing water quality with submersed aquatic vegetation. BioScience **43:** 86-94.

Diaz, R. J. and Rosenberg, R. 1995. Marine Benthic hypoxia: a review of its ecological effects and the behavioral responses of benthic macrofauna. Oceanography and Marine Biology Annual Review 33: 245-303.

Dobkin, S., and Manning, R. B. 1964. Osmoregulation in two species of *Palaemonetes monetes* (Crustacea: Decapoda) from Florida. Bull. Mar. Sci. Gulf. Caribb. 14: 149-157.

Domenici, P., Steffensen, J. F., and Batty, R. S. 2000. The effect of progressive hypoxia on swimming activity and schooling in Atlantic herring. Journal of Fish Biology 57: 6, 1526-1538.

DuToit, C.H. 1979. The carrying capacity of the Ichetucknee Springs and River. M.S. Thesis. University of Florida. Gainesville, FL. 176 pp

Duarte, C. M. 1995. Submerged aquatic vegetation in relation to different nutrient regimes. Ophelia 41: 87–112.

Duarte, C. M. and Canfield, Jr. D. E. 1990. Macrophyte standing crop and primary productivity in some Florida spring-runs. Water Resources Bulletin 26(6): 927-934.

Eby, L. A., Crowder, L. B., McClellan, C. M., Peterson, C. H., and Powers, M. J. 2005. Habitat degradation from intermittent hypoxia: impacts on demersal fishes. Marine Ecological Progress Series 291: 249-261.

Eriksen, C. H. 1963. Respiratory regulation in Ephemera simulans Walker and Hexagenia limbata (Serville) (Ephemeratopera). Journal of Experimental Biology 40: 455-467.

Estes, J. A, Terborgh, J., Brashares, J. S., Power, M. E., Berger, J., Bond, W. J., Carpenter, S. R., Essington, T. E., Holt, R. D., Jackson, J. B. C., Marquis, R. J., Oksanen, L., Oksanen, T., Paine, R. T., Pikitch, E. K., Ripple, W. J., Sandin, S. A., Scheffer, M., Schoener, T. W.,

Shurin, J. B., Sinclair, A. R. E., Soulé, M. E., Virtanen, R., and Wardle, D. 2011. Trophic downgrading ofplanet Earth. Science 333:301–306.

Farwick, F. and Schröder, A. T. 1909 Bericht über die botanischen und zoologischen Exkursionen nach dem Weißenstein bei Hohenlimburg und nach der Glörtalsperre am 25. -- S.-B. naturhist. Ver. preuß. Rheinl. Westf., E 1909: 94-101.

Feminella, J. W., Power. M. E., and Resh, V. H. (1989) Periphyton responses to invertebrate grazing and riparian canopy in three northern California coastal streams. Freshwater Biol 22:445-457.

Feminella, J. W. and Hawkins, C. P. 1995. Interactions between stream herbivores and periphyton: a quantitative analysis of past experiments. J. North American Benthological Society 14(4): 465-509.

Gallegos, C. L., Kenworthy, W. J., Biber, P. D., and Wolfe, B. S. 2009. Underwater spectral energy distribution and seagrass depth limits along an optical water quality gradient. Smithsonian Contributions to the Marine Sciences 38: 359-367.

Gilliom, R. J., Barbash, J. E., Crawford, C. G., Hamilton, P. A., Martin, J. D., and Nakagaki, N. 2007. Th equality of our nations waters: pesticides in the nations streams and ground water, 1992-2001. US Department of Interior, US Geological Survey, http://www.usgs.gov/pubprod. Accessed 8/7/2013.

Giovanelli, A., da Silva; C. L., Leal, G. B., and Baptista, D. F. 2005. Habitat preference of freshwater snails in relation to environmental factors and presence of the competitor snail Melanoides tuberculatus (Muller 1774). Memorias do Instituto Oswald Cruz, Rio de Janeiro 100: 169-176.

Giudice, B. D. and Young, T. M. 2010. The antimicrobial triclocarban stimulates embryo production in the freshwater mudsnail Potamopyrgus antipodarum. Environmental Toxicology and Chemistry 29(4): 966-970.

Goodrich, C. 1942. The Pleuroceridae of the Atlantic Coastal Plain. Occasional Papers of the Museum of Zoology, University of Michigan, (456): 1-6.

Grieshaber, M. K., Hartwig, I., Kreutzer, U., and Portner, H. O. 1994. Physiological and metabolic response to hypoxia in invertebrates. Reviews in Physiology, biochemistry, and Pharmacology 125: 43-147.

Gruner, D. S., J. E. Smith, E. W. Seabloom, J. T. Ngai, S. Sandin, H. Hillebrand, W. S. Harpole, J. J. Elser, E. E. Cleland, M. E. S. Bracken, E. T. Borer, and B. Bolker. 2008. A cross system synthesis of consumer and nutrient resource control on producer biomass. EcologyLetters 11:740–755.

Hart, D. D. and Robinson, C. T. 1990. Resource limitation in a stream community: phosphorus enrichment effects on periphyton and grazers. Ecology 71:1494-1502.

Hauxwell, J., McClelland, J., Behr, P. J., and Valiela, I. 1998. Relative importance of grazing and nutrient controls of macroalgal biomass in three temperate shallow estuaries. Estuaries 21: 347–360.

Heck, K. L. J. and Valentine, J. F. 2007. The primacy of top-down effects in shallow benthic ecosystems. Estuaries and Coasts 30:371–381.

Heffernan, J. B., Liebowitz, D. M., Frazer, T. K., Evans, J. M., and Cohen, M. J. 2010. Algal blooms and the nitrogen enrichment hypothesis in Florida springs: evidence, alternatives, and adaptive management. Ecological Applications 20:816–829.

Heffernan, J. B., Albertin, A. R., Fork, M. L., Katz, B. G., and Cohen, M. J. 2012. Denitrification and inference of nitrogen sources in the karstic Floridan Aquifer. Biogeosciences 9: 1671-1690

Hensley, R. T. and Cohen, M. J. 2012. Controls on solute transport in large spring fed karst rivers. Limnology and Oceanography 57(4): 912-924.

Hill, W. R. and Knight, A. W. 1987. Experimental analysis of the grazing interaction between a mayfly and stream algae. Ecology 68: 1955-1965.

Hill, W. R. and Harvey, B. C. 1990/ Periphyton responses to higher trophic levels and light in a shaded stream. Can J Fish Aquat Sci 47: 2307-2314.

Hill, W. R., Boston, H. L., and Steinman, A. D. 1992. Grazers and nutrients simultaneously limits lotic primary productivity. Canadian Journal of Fisheries and Aquatic Sciences 49: 504–512.

Hillebrand, H. 2002. Top-down versus bottom-up control of autotrophic biomass—a metaanalysis on experiments with periphyton. Journal of the North American BenthologicalSociety 21:349–369.

Hochachka, P. W. and Somero, G. N. 2002. Biochemical adaptation: mechanism and process in physiological evolution. Oxford University Press, New York.

Irving, E. C., Lowell, R. B., Culp, J. M., Liber, K., Xie, Q., and Kerrich, R.2008. Effects of arsenic speciation and low dissolved oxygen condition on the toxicity of arsenic to a lotic mayfly. Environmental Toxicology and Chemistry 27: 583-590.

Jacoby, C. A., Frazer, T. K., and Phlips, E. J. 2008. Nutrient effects on springs flora and fauna. Pgs 179-230. In Brown et al. Summary and Synthesis of the Available Literature on the Effects of Nutrients on Spring Organisms and Systems. Final Report to Florida Department of Environmental Protection Tallahassee, FL.

Jones, J. I., Moss, B., and Young, J. O. 1998. The interactions between periphyton, non-moluscan invertebrates and fish in standing freshwaters. P.69-90. In E. Jeppesen, M. Sondergaard, M. Sondergaard, K. Christophersen (Eds.) The structuring Role of Submerged Macrophytes in Lakes. Springer-Verlag, New York, USA.

Jones, J. I. and Sayer, C. D. 2003. Does the fish-invertebrate –periphyton cascade precipitate plant loss in shallow lakes? Ecology 84: 2155-2167.

Joyner-Matos, J., Chapman, L. J., Downs, C. A., Hofer, T., Leeuwenburgh, C., and Julian, D. 2007. Population distribution and stress response of a freshwater clam along a natural oxygen gradient. Functional Ecology 21:344-355.

Joyner-Matos, J., Richardson, H., Sammeli, T., and Chapman, L. J. 2011. A fingernail clam shows higher fitness in hypoxic waters. Canadian Journal of Zoology 89:161-168.

Joyner-Matos, J., Chapman, L. J., Downs, C. A., Hofer, T., Leeuwenburgh, C., and Julian, D. 2007. Stress response of a freshwater clam along an abiotic gradient: too much oxygen may limit distribution. Functional Ecology 21: 344-355.

Karevia, P. M., Kingsolver, J. G., and Huey, R. B. 1993. Biotic interaction and global change. Sinauer Associates, Sunderland, MA, USA.

Keeling, R. F., Kortzinger, A., and Gruber, N. 2010. Ocean deoxygenation in a warming world. Annual Review of Marine Science 2: 199-229.

King, S. A. 2012. Effects of flow on filamentous algae and nutrient limitation in lotic systems. Dissertation, University of Florida, Gainesville, FL.

Kirk, J. T. O. 1994. Light and photosynthesis in aquatic ecosystems, Second Edition Cambridge University Press.

Korpinen, S., Jormalainen, V., and Honkanen, T. 2007. Bottom-up and cascading top-down control of macroalgae along a depth gradient. Journal of Experimental Marine Biology and Ecology 343: 52-63.

Korpinen, S., Karjalainen, M., and Viitasalo, M. 2006. Effects of cyanobacteria on survival and repordcutionof the littoral crustacean Gammarus zaddachi (Amphopoda). Hydrobiologia 559: 285-295.

Lamberti, G. A. and Resh, V. H. 1983. Stream periphyton and insect herbivores: an experimental study of grazing by a caddis fly population. Ecology 64:1124-1135.

Lamberti, G. A., Feminella, J. W., and Resh, V. H. 1987. Herbivory and intraspecific competition in a stream caddisfly population. Oecologia 73: 75-81.

Lamberti, G. A., Gregory, S. V., Ashkenas, L. R., Steinman, A. D., McIntire, C. D. 1989. Prodcutive capacity of periphyton as a determinant of plant-herbivore interactions in streams. Ecology 70: 1840-1856.

Lawler, J. J., Aukema, J. E., Grant, J. B., Halpern, B. S., Kareiva, P., and Nelson, C. R. 2006. Conservation science: a 20 year report card. Frontiers in Ecology and the Environment 4: 473-480.

Lawton, J. H. 2000. Community ecology in a changing world. Ecology Institute, Oldendorf/ luhe, Germany.

Levin, L. A., Ekau, W., Gooday, A. J., Jorissen, F., Middleburg, J. J., Naqvi, S. W. A., Neira, C., Rabalais, N. N., and Zhang, J. 2009. Effects of natural and human induced hypoxia on coastal benthos. Biosciences 6(10): 2063-2098.

Li, K. Y., Liu, Z. W., and Gu, B. H. 2008. Persistence of clear water in a nutrient impacted region of Lake Taihu: the role of periphyton grazing by snails. Fundamental and Applied Limnology 173(1): 15-20.

Liboriussen, L., Jeppesen, E., Bramm, M. E., and Lassen, M. F. 2005. Periphyton-macroinvertebrate interactions in light and fish manipulated enclosures in a clear and a turbid shallow lake. Aquatic Ecology 39:23-39.

Liebowitz, D. M., Cohen, M. J., Heffernan, J. B., Frazer, T. K., and Korhnak, L. V. 2014. Environmentally mediated consumer control of algae proliferation in Florida springs. Freshwater Biology 59: 2009-2023

Liu, C. C., Chiu, J. M. Y., Li, L., Shin, P. K. S., and Cheung, S. G. 2011. Physiological response of two sublittoral nassariid gastropods to hypoxia. Marine Ecological Progress Series 429: 75-85.

Lowell, R. B. and Culp, J. M. 1999. Cumulative effects of multiple effluent and low dissolved oxygen stressors on mayflies at cold temperatures. Canadian Journal of Fisheries and Aquatic Sciences. 56: 1624-1630.

Lowell, R. B., Culp, J. M., and Dube, M. G. 2000. A weight-of-evidence approach for northern river risk assessment: Integrating the effects of multiple stressors. Environmental Toxicology and Chemistry 19: 1182-1190.

Maddox, G. L., Lloyd, J. M., Scott, T. M., Upchurch, S. B., and Copeland, R. 1992. Florida's groundwater quality monitoring program, background geochemistry. Florida Geological Survey, Tallahassee, FL.

Marks, J. C. and Lowe, R. L. 1989. The independent and interactive effects of snail grazing and nutrient enrichment on structuring periphyton communities. Hydrobiologia 185: 9-17.

McMahon, B. R. 2001. Respiratory and circulatory compensation to hypoxia in crustaceans. Respiration Physiology 128: 349-364.

McMahon, T. A., Halstead, N. T., Johnson, S., Raffel, T. R., Romansic, J. M., Crumrine, P. W., and Rohrm, J. R. 2012. Fungicide induced declines in freshwater biodiversity modify ecosystem functions and services. Ecology Letters 15: 714-722.

Merrit, R.W., Cummins, K. W., and Berg, M. B. 2008. An Introduction to the Aquatic Insects of North America 4th ed. Kendal Hunt Publishing Co. Dubuque IA USA. 1157 pp.

Mulholland, P. J., Steinman, A. D., Palumbo, A.V., Elwood, J. W. 1991. Role of nutrients cycling on herbivory in regulating periphyton communities in laboratory streams. Ecology 72: 966-982.

Munch, D. A., Toth, D. J., Huang, C., Davis, J. B., Fortich, C. M. ,Osburn, W. L., Phlips, E. J., Quinlan, E. L., Allen, M. S., Woods, M. J., Cooney, P., Knight, R. L., Clarke, R. A., and Knight, S. L. 2006. Fifty year retrospective study of the ecology of Silver springs, Florida. Special Publication SJ2007-SPA. St. John's River Water Management District, Palatka.

Munro-Fox, H., Wingfield, C. A., and Simmons, B. G. 1936. The oxygen Consumption of Ephemerid nymphs from flowing and from still waters in relation to the concentration of oxygen in the water. Journal of Experimental Biology 13: 210-218.

Munro-Fox, H., Wingfield, C. A., and Simmons, B. G. 1936. Oxygen consumption of mayfly nymphs in relation to oxygen availability. Nature 134: 1015.

Nagell, B. and Fagerstrom, T. 1978. Adaptations and resistance to anoxia in *Cloen dipterum* (Ephemeroptera) and *Nemoura cinera* (Plecoptera). Oikos 30: 95-99.

Newbold, J. D., Elwood, J. W., O'Neill, R. V., and Van Winkle, W.1981. Measuring nutrient spiralling in streams. Canadian Journal of Fisheries and Aquatic Sciences 38:860-863.

Newbold, J. D., O'Neill, R. V., Elwood, J. W., and Van Winkle, W. 1982. Nutrient spiralling in streams: implications for nutrient limitation and invertebrate activity. The American Naturalist 120:628-652.

Niimi, A. J. and Beamish, F. W. H. 1974. Bioenergetics and Growth of Largemouth Bass (*Micropterus- salmoides*) in Relation to Body-Weight and Temperature. Canadian Journal of Zoology 52: 4, 447-456.

Opsahl, R W., Wellnitz, T., and Poff, N. L. 2003. Current velocity and invertebrate grazing regulate stream algae: results of an *in situ* electrical exclusion. Hydrobiologia 499:135-145.

Osborne, T. Z., Chapman, L. J., Chapman, C. A., Crisman, T. L., Prenger, J., Nyguen, S., and Stecker, E. 2001. Invertebrate community structure and oxygen availability in an intermittent stream/wetland system of the Uganda uplands. Verhandlungen Internationale Vereinigung Limnologie 27:3599-3603.

Paerl, H. W. 2006. Assessing and managing nutrient-enhanced eutrophication in estuarine and coastal waters: interactive effects of human and climatic perturbations. Ecological Engineering 26: 40-54.

Parsons, P. A. 1991. Evolutionary rates: stress and species boundaries. *Annual Review of Ecology and Systematics* **22**, 1–18.

Paul, R. J., Zeis, B., Lamkemeyer, T., Seidl, M., and Pirow, R. 2004. Control of oxygen transport in the microcrustacean Daphnia: regulation of haemoglobin expression as central mechanism of adaptation to different oxygen and temperature conditions. Acta Physiol. Scand. 182: 259-275.

Pearson, R. G. and Connolly, N. M. 2000. Nutrient enhancement, food quality and community dynamics in a tropical rainforest stream. Freshwater Biology 43: 31-42.

Pennak, R. W. 1989. Fresh-water invertebrates of the United States, 3rd Ed. Protozoa to Mollusca. John Wiley and Sons. New York. 628 p.

Pimentel, D., C.A. Edwards. 1982. Pesticides and ecosystems. Bioscience 32(7): 595-600.

Poff, N. L. and Ward, J. V. 1995. Herbivory under different flow regimes: a field experiment and test of a model with a benthic stream insect. Oikos 72:179-188.

Power, M. E., Stewart, A. J., and Matthews, W. J. 1988. Grazer control of algae in an Ozark mountain stream: effects of short-term exclusion. Ecology 69:1894-1898.

Power, M. E. 1990. Effects of Fish in River Food Webs. Science 250: 811–814.

Power, M. 1992. Top-down and bottom-up forces in food webs: Do plants have primacy? Ecology 73_3_: 733–746.

Pringle, C. M. 1987. Effects of water and substratum nutrient supplies on lotic periphyton growth: an integrated bioassay. Can J Fish Aquati Sci 44:619-629.

Quinlan, E. L., Phlips, E. J., Donnelly, K. A., Jett, C. H., Sleszynski, P., and Keller, S. 2008. Primary producers and nutrient loading in Silver Springs, FL, USA. Aquatic Botany 88: 247-255.

Riedel, B., Zushin, M., Haselmair, A., and Stachowitsch, M. 2008. Oxygen depletion under glass: behavioral responses of benthic macrofauna to induced anoxia in the Northern Adriatic. Journal of experimental Marine Biology and Ecology 367: 17-27.

Rabalais, N. N., Turner, R. E., and Wiseman, W. J. 2002. Gulf of Mexico hypoxia, aka "the dead zone". Annual Review of Ecology and Systematics 33: 235-263.

Rosemond, A. D., Mulholland, P., and Elwood, J. W. 1993. Top-down and bottom-up control of stream periphyton: effects of nutrients and herbivores. Ecology 74: 1264-1280.

Rosemond, A. D. 1993. Interactions among irradiance, nutrients, and herbivores constrain a stream algal community. Oecologia 94: 585-596.

Rouse, W. L. 1969. Littoral crusatcea from southwest Florida. Q. J. Fla. Acad. Sci. 32: 127-152

Scott, T., Means, G., Meagan, R., Means, R., Upchurch, S., Copeland, R., Jones, R., and Willet, A. 2004. Springs of Florida. Bulletin No. 66 Florida Geological Survey, Tallahassee, FL.

Sheeb, N. H., Flores, T I., Kurobe, B., Franze, A., Ranganthan, B. D., and Hammock, S. J. 2011. The Bioconcentration, metabolism, and excretion of triclocarban in larval Qurt Medaka (Oryzias latipes). Aquatic Toxicology 105: 448-454.

Sheldon, S. P. 1987. The effects of herbivorous snails on submerged communities in Minnesota lakes. Ecology 68: 1920-1931.

Sickman, J. O., Albertin, A. R., Anderson, M. W., Pinowska, A., and Stevenson, R. J. 2009. A comparison of internal and external supply of nutrients to algal mats in two first magnitude springs in Florida. Journal of Aquatic Plant Management. 47: 135-144.

Smith, V. H. 2006. Response of estuarine and coastal marinephytoplankton to nitrogen and phosphorus enrichment. Limnology and Oceanography 51(1): 377-384.

Smith, V. H. 1982. The nitrogen and phosphorus dependence of algal biomass in lakes: an empirical and theoretical analysis. Limnology and Oceanography 27(6): 1101-1111.

St. Amant, J. A. and Hulquist, R. G. 1969. *Palaemonetes paludosus* collected in the Rio Hardy and Colorado River, Baja California. Calif. Fish game 55: 252.

Steinman, A. D., McIntire, C. D., Gregory, S. V., Lamberti, G. A., and Ashkenas, L. R. 1987. Effects of herbivore type and density on taxanomic structure and physiognomy of algal assemblages in laboratory streams. Journal of the North American Benthological Society 6: 175-188.

Steinman, A. D. 1992. Does an increase in irradiance influence periphyton in a heavily-grazed woodland stream? Oecologia 91: 163-170.

Steinman, A. D. and McIntire, C. D. 1987. Effects of irradiance on the community structure and biomass of algal assemblages in laboratory streams. Can J Fish Aquat Sci 44:1640 1648.

Steffensen, J. F. 1989. Some errors in respirometry of aquatic breathers: how to avoid and correct for them. Fish Physology and Biochemistry 6:1, 49-59.

Stevenson, R. J., Pinowska, A., and Wang, Y. 2004. Ecological condition of algae and nutrients in Florida Springs. Florida Department of Environmental Protection, Tallahassee, FL.

Stevenson, R.J., Pinowska, A., Albertin, A. R., and Sickman, J. O. 2007. Ecological condition of algae and nutrients in Florida springs: the synthesis report. Florida Department of Environmental Protection, Tallahassee, FL.

Stevenson, R. J. 1996. The stimulation and drag of current. Pages 321-340 in R. J. Stevenson, M. L. Bothwell and R. L. Lowe (editors). Algal ecology: freshwater benthic ecosystems. Academic Press, Inc., San Diego, CA, USA.

Stevenson, R. J. and Glover, R. 1993. Effects of algal density and current on ion transport through periphyton communities. Limnology and Oceanography 38:1276-1281.

Stierhoff, K. L., Targett, T. E., and Miller, K. 2006. Ecophsiological responses of juvenile summer and winter flounder to hypoxia: experimental and modeling analyses of effects on estuarine nursery quality. Marine Ecological Progress Series 325: 255-266.

Svendsen, J. C., Tirsgaard, B., Cordero, G. A., and Steffenson, J. E. 2015. Intraspecific variation in aerobic and anaerobic locomotion: gilthead sea bream (*Sparus aurata*) and Trinidadian guppy (*Poecilia reticulate*) do not exhibit a trade-off between maximum sustained swimming speed and minimum cost of transport. Frontiers in Physiology 6:43. DOI < 10.3389/fphys.2015.00043>.

Szafraniec, M. L. 2014. Spectral distribution of light in Florida spring ecosystems: the quantity and quality of light available for primary producers. Doctoral Dissertation, University of Florida, Gainesville, FL.

Tabb, D. and Manning, R. B. 1961. A checklist of the flora and fauna of northern Florida Bay and adjacent brackish waters of the Florida mainland collected during the period July a957 through September 1960. Bulletin Mar. Sci. Gulf. Caribbean 11: 554-649.

Tarkowska-Kukuryk, M. and Mieczan, T. 2012. Effect of substrate on periphyton communities and relationships among food web components in shallow hypertrophic lake. Journal of Limnology 71(2): 279-290.

Thompson, F. G. 2004. An identification manual for the freshwater snails of Florida. The Florida Museum of Natural History. http://www.flmnh.ufl.edu/malacology/fl-snail/snails1.htm Last accessed 7/31/2013.

Thorp, J. H. and Covich, A. P. 1991. Ecology and Classification of North American Freshwater Invertebrates. Academic Press, San Diego, CA, USA. 911 pp.

Varnosfaderany, M. N., Ebrahimi, E., Mirghaffary, N., and Safyanian, A. 2010. Biological assessment of Zayandeh Rud River, Iran, using benthic macroinvertebrates. Limnologica 40: 226-232.

Vermaat, J. E. 2005. Periphyton dynamics and influencing factors. P. 35-49 In: M.E. Azim, M. Verdegem, A. van Dam, M. Beveridge (Eds.) Periphyton: Ecology, Exploitation, and Management. CABI Publishing, London, UK.

Vitousek, P. M. 1994. Beyond global warming: ecology and global change. Ecology 75: 1861-1876.

Wannamaker, C. M. and Rice, J. A. 2000. Effects of hypoxia on movements and behavior of estuarine organisms from the southeastern United States. Journal of Experimental Marine Biology and Ecology 249: 145-163.

Warren, G. L., Hohlt, D. A., Cichra, C. E., and VanGenechten, D. 2000. Fish and Aquatic Invertebrate Communities of the Wekiva and Little Wekiva Rivers: A Baseline Evaluation in the Context of Florida's Minimum Flows and Levels Statutes. St. Johns River Water Management District Special Publication SJ2000-SP4. pp. variously numbered.

Weisberg, S. B., Thompson, B., Ranasinghe, J. A., and Montagne, D. E. 2008. The level of agreement among experts applying best professional judgment to assess the condition of benthic infaunal communities. Ecological Indicators 8: 389-394.

Werner, E. E. 1998. Ecological experiments and a research program in community ecology. Pages 3–26 *in* W. J. J. Resetarits and J. Bernardo, editors. Experimental ecology: issues and perspectives. Oxford University Press, Oxford, UK.

Wessell, K. J., Merritt, R. W., and Cummins, K. W. 2001. Distribution, diel movement, and growth of grass shrimp *Palaemonetes paludosus* in the Kissimmee River-floodplain ecosystem, Florida. Ann. Limnol. 37: 85-95.

Wetzel, R. G. 2001. 2001. Lake and River Ecosystems 3rd Ed. Academic Press, San Diego, CA, USA. 1006 pp.

Wilcove, D. S. and Master, L. L. 2005. How many endangered species are there in the United States? Frontiers of Ecology and Environment 3: 414-420.

Woin, P. and Bronmark, C. 1992. Effect of DDT and MCPA (4-Chloro-2-Methylphenoxyacetic acid) on reproduction of the pond snail, Lymnaea stagnalis L. Bulletin of Environmental Contamination and Toxicology 48: 7-13.

Wojdak, J. M. and Mittelbach, G. G. 2007. Consequences of niche overlap for ecosystem functioning: an experimental test with pond grazers. Ecology 88(8): 2072-2083.

Wu, R. S. S. 2002. Hypoxia: from molecular responses to ecosystem responses. Marine Pollution Bulletin 45:35-45.

Wu, R. S. S., Lam, P. K. S., and Wan, K. L. 2002. Tolerance to, and avoidance of, hypoxia by the peniad shrimp (*Metapenaeus ensis*). Environmental Pollution 118: 351-355.

Zheng, Z. M., Lv, J., Lu, K. H., Jin, C. H., Zhu, J. Y., and Liu. X. S. 2011. The impact of snail (Bellamya aeruginosa) bioturbation on sediment characteristics and organic carbon fluxes in an eutrophic pond. Clean Soil, Air, Water 39: 566-571.

Zhu, J., Lu, K., and Liu, X. 2013. Can the freshwater sanil Bellamya aeruginosa (Mollusca) affect phytoplankton community and water quality? Hydrobiologia 707: 147-157.

7.2.7 PUBLICATIONS AND PRODUCTS

Osborne, T. Z., Mattson, R. A., and Coveney, M. F. 201X. Macroinvertebrate grazers, dissolved oxygen, and the loss of top-down control of algae in Florida spring ecosystems: a review. Submitted to *WATER* (IN REVIEW)

Osborne, T. Z., Johanssen, J., and Schafer, T. 201X. Hypoxia tolerances of key herbivores in Florida spring ecosystems. Hydrobiologia (In prep)

7.2.7.1 Theses

N/A

7.2.7.2 Presentations

Osborne, T. Z., and LaPlaca, L. C. 2015. Florida's Imperiled Springs. UF Whitney Laboratory Docents Lecture. Marineland, FL. February 20, 2015.

7.3. EFFECTS OF FLOW VELOCITY ON GROWTH AND PROLIFERATION OF EPIPHYTIC ALGAE ON SAV IN SPRING ECOSYSTEMS

7.3.1. ABSTRACT

Mesocosms constructed at the UF Whitney Laboratory for Marine Bioscience were used to determine effects of shear stresses derived from velocity on the growth and proliferation of epiphytic algae on SAV in spring ecosystems. While much work has already been done *in situ* by others (King 2012; Cohen et al. this report), the opportunity to explore the effects of water velocity and associated shearing of algal biomass was valuable to inform algae growth models and support field observations by other researchers. Two methods of quantifying effects of shear on algal growth were investigated (motor driven flow way and pump driven flow way), however only the pump driven flow way was found to be viable and the results of that experiment are presented here. Shear stresses were observed to dramatically decrease algal growth and recruitment at velocities of 25cm s^{-1} and higher. While algal growth was predictable based upon velocity, shearing and scouring of established algal biomass did not exhibit any pattern. This is likely due to several factors, including blade friction and steep velocity profiles. We assert that these results suggest a need for maintaining velocity (and thus discharge rate) as a management strategy wherever possible.

7.3.2 INTRODUCTION

The effects of flow on attached algae in lotic systems (e.g., rivers, streams), are well known and include influencing nutrient availability and standing biomass. Increased velocity can reduce the diffusive boundary layer above algae and increase advective flux of nutrients through the water column, effectively increasing the exposure of algae to nutrients and aiding growth in situations where nutrients are at or near limiting concentrations (Stevenson and Glover 1993; Stevenson 1996; Biggs et al 1989). Alternatively, higher velocities can limit algal biomass by creating sheer stress on algal communities that scours algal biomass (an abiotic top down control mechanism). This observation can be confounded as velocities that limit algal biomass can also limit grazer accessibility to algae when velocity is high (Poff and Ward 1995; Opsahl et al. 2003). Spring runs, much like other lotic systems, experience a variety of flow rates and velocities due to the influence of rainfall and groundwater withdrawals on spring vent discharge (Copeland et al. 2009). Similarly, the positive relationship between velocity and nutrient availability observed in lotic systems (Stevenson 1996) would predict potential nutrient limitation if velocity were reduced significantly

More relevant to the discussion of velocity mediated control of algae in springs is the effect of velocity on algal biomass via sloughing/dislodgement of algae. For example, local velocities and the intensity and frequency of flood events have been shown to limit the amount of algal biomass in a given area (Biggs and Close 1989; Biggs 1996; Biggs et al. 1998) by physically scouring (via increased sheer stress) periphyton from surfaces. This sheer stress is directly proportional velocity and has been shown to have a negative effect on algal biomass at velocities from 5 to 35 cm s^{-1} with velocities above 25 cm s^{-1} dramatically decreasing filamentous algal biomass (King

2012). Decrease in discharge and thus velocity has the potential to contribute to proliferation of algae in several Florida springs.

The objective of this experiment was to test effects of velocity on epiphytic algal growth under controlled conditions.

7.3.3 METHODS

The first proposed method of quantifying effects of velocity on algal growth required the use of the tank mesocosms described earlier in this report (Section 7.2.1) and live potted SAV taken from previously conducted experiments. Unfortunately those mesocosms could not effectively simulate velocities and conditions needed and so the approach was abandoned. The next approach utilized live and artificial plants in a large tank (10 m diameter) in which a flume was constructed and an electric motor was employed to create velocity. The large pool allowed for an excess of water to maintain the flume (Figure 7.3.1) but after initial trials with live plants, this approach too was abandoned in favor of a smaller, more manageable system.

The final flow tank design consisted of four 150 cm diameter oblong water tank with a smaller tank inverted inside to create a 20 cm wide flow way (Figures 7.3.2 to 7.3.4). Tanks were painted white and allowed to cure for 2 weeks then leach with water for 2 weeks prior to use. Four ranges of velocity (quiescent, slow, moderate, and fast) were established using small electric fountain pumps submerged in the flow pathway. Pump speeds were 100, 200, 400, and 800 gal per hour and when installed each tank had a range of measured velocities due to flow dynamics of the tank (curves, straight ways, changes in width of flow way). This enabled us to populate a wide range of velocities which were determined at each location within each tank using a pygmy current meter.

To simulate plants in the flow way, we utilized 6mil plastic sheeting to make 2.5 cm x 20 cm artificial SAV leaf blades. These blades were anchored in a cup of fast-cure cement, the cup removed and the concrete allowed to cure for 5 days in the air then leached for 1 week in the dark in copious volumes of spring water. Artificial SAV was then placed in the raceways at a diversity of current velocities (Figure 7.3.5). Ten mL of concentrated nutrient solution (Hoaglands solution) was added to each flow way to promote algal growth. Experiments were run for two weeks and water levels were maintained at 30 cm depths with spring water. Each tank had 15 artificial plants and thus each plant was considered an independent observation (not replicates of a tank treatment).

Upon collection, artificial SAV strips were scraped with a razor blade and the algal biomass measured for both chlorophyll a and ash free dry mass (AFDM) via combustion in a muffle furnace (Figure 7.3.6). Chlorophyll a was determined using the alkaline acetone extraction method (Rice et al. 2012) in which algal biomass is sonicated in 20 mL of 90 % alkaline ($CaCO_3$ saturated) acetone. The resulting solution is centrifuged at 3,000 rpm for 1 minute then the supernatant is measured for OD at 663 nm.

Figure 7.3.1. Initial flume construction in 10 m tank with electric motor creating constant velocity.

Figure 7.3.2. Top view of flowway mesocosms for shear stress experiments.

Figure 7.3.3. View of four replicate flow way tanks for velocity study. Cinder blocks maintained smaller internal tanks in place during the experiment.

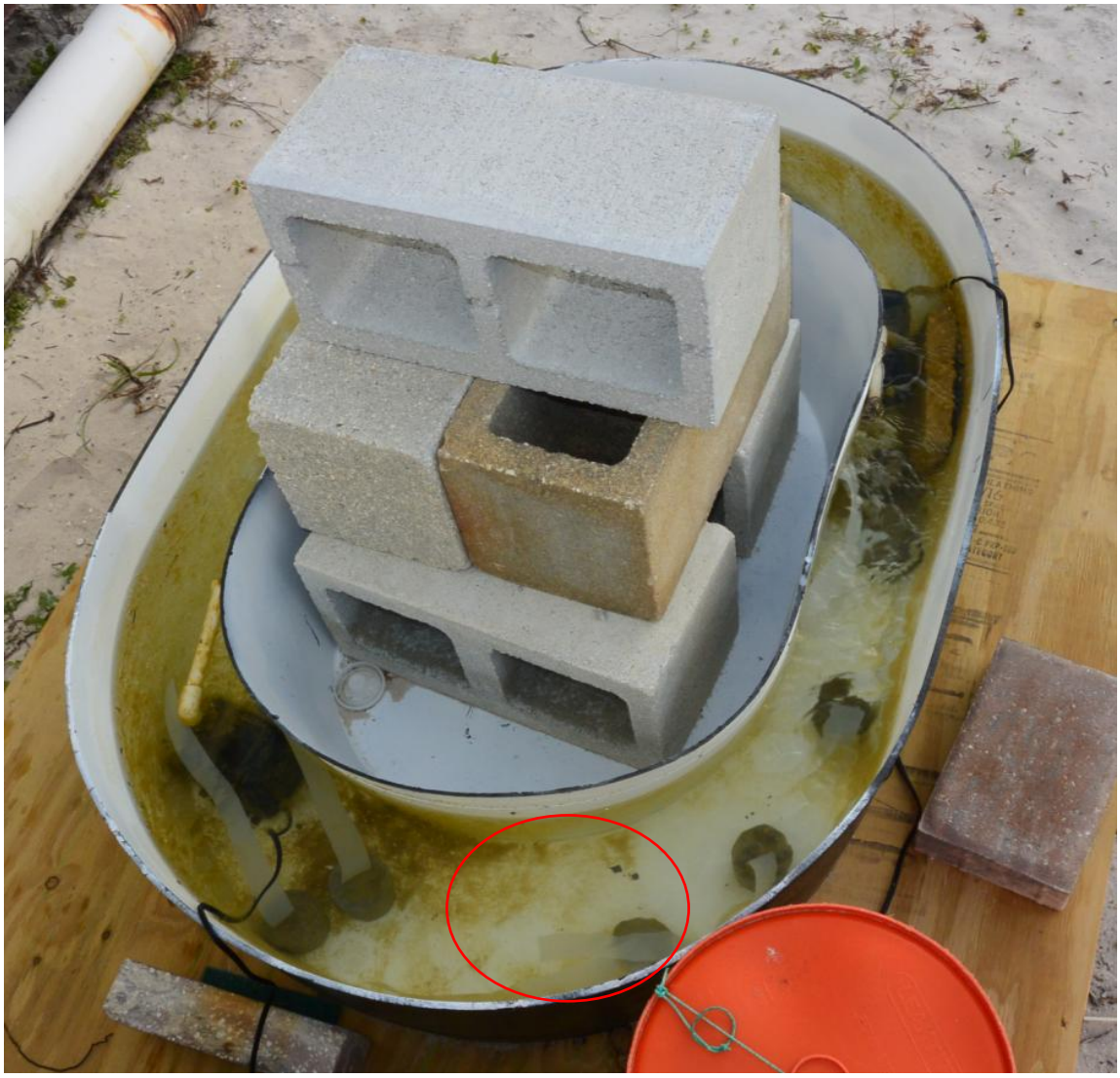

Figure 7.3.4. Close up view of flow way tank for current velocity study. Note pump locations at both ends of the highest velocity tank. Red circle indicates example of scouring from abrasive interaction between artificial blade and tank surface.

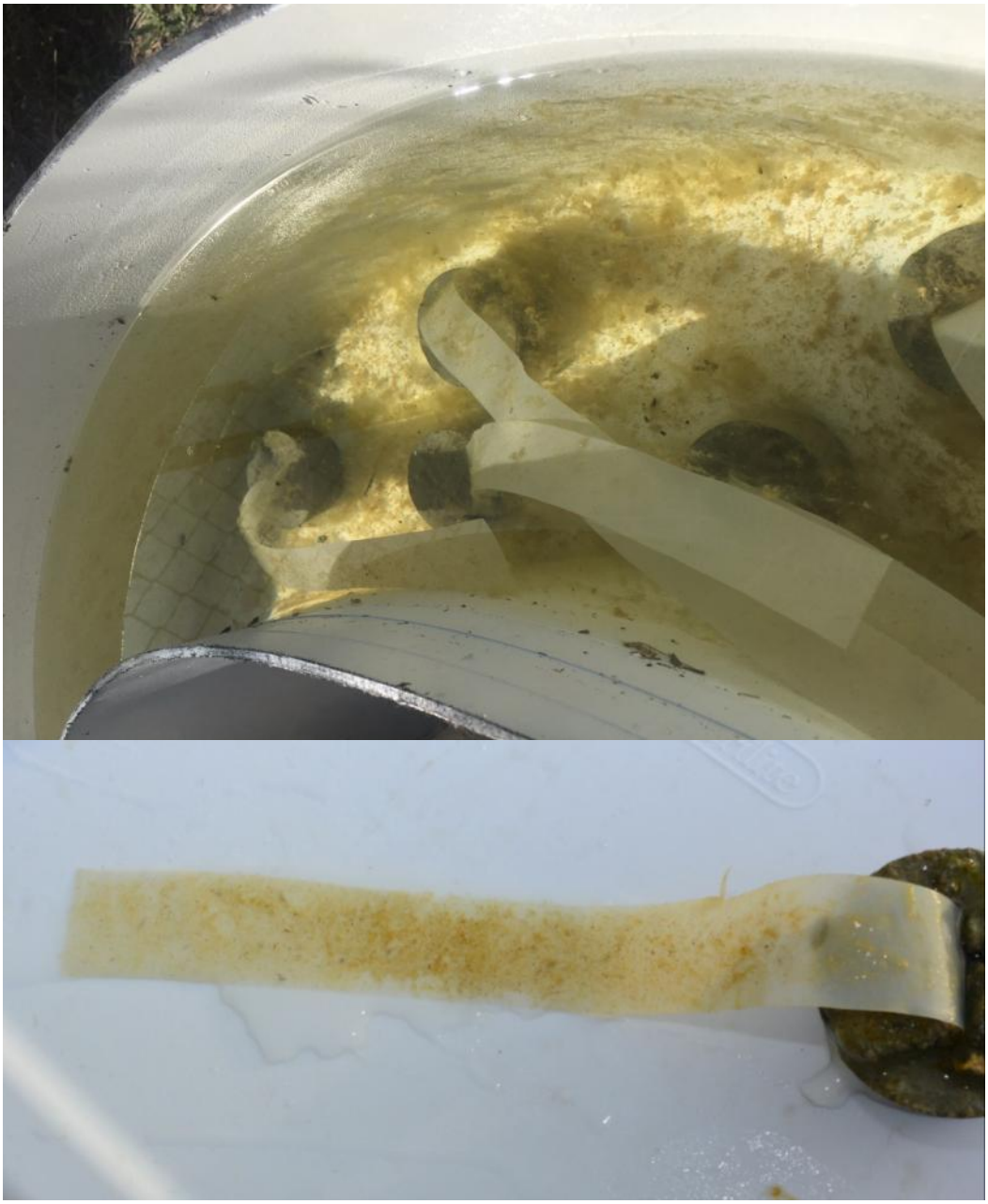

Figure 7.3.5. Close up view of artificial SAV in flow way (top) and an individual artificial SAV replicate with algal growth after 1 week (bottom)

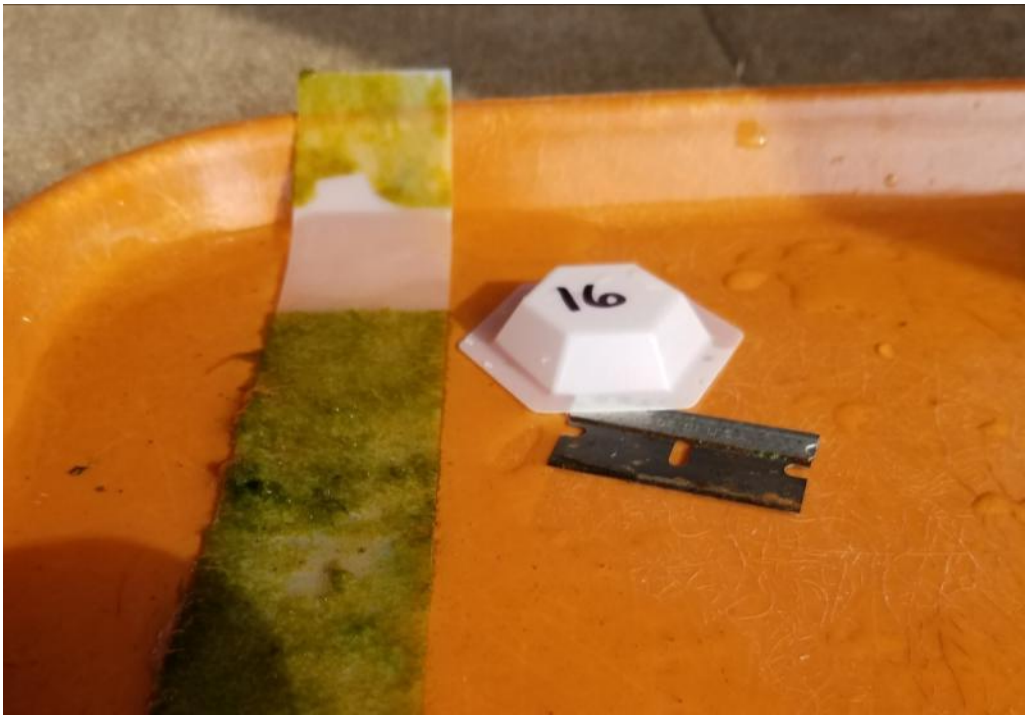

Figure 7.3.6. Artificial SAV algal sampling post exposure to shear stress to monitor shearing effectiveness of established algal communities.

After the growth versus current velocity trials were complete, 60 artificial SAV replicates were allowed to acquire a significant load of algae in slow moving tanks (compare Figure 7.3.6 to 7.3.5). A pre-test section of each of these replicates was scraped for algal biomass and Chl-a to establish the load on each individual replicate. Replicates were then redeployed randomly in flow ways with increased current velocities (created by doubling pumps in each tank). Again, a range of current velocities were created and measured via handheld current meter at the location of each replicate. After one week of exposure, replicates were removed and again sampled for algal biomass and Chl-a. The original scraped section was re-scraped to produce a correction factor for the one week of algal growth during the experimental shearing trial.

7.3.4 RESULTS AND DISCUSSION

Results of algal productivity on 60 replicate articifial plant leaves (Figure 7.3.7 and Table 7.3.1) suggest that approximately 70 % of the variability in experimental algal grwoth is explained by current velocity (R^2=0.71). A threshold for algal growth was observed at a current velocity of 25-30 cm s^{-1}. This observation is in agreement with that of King (2012) who found a similar threshold of shear stress at a current velocity of approximately 25 cm s^{-1}. Signficant observations include the scour interaction of blades with tank sides and with each other. These frictional stresses and subsequent algal removal were not quanitfyable in this experiment but were readily present and likely come into play in the natural environment where plant densities are much greater. These frictional interactions are also a likely the cause of variablility in the relationship observed here.

Table 7.3.1. Results of velocity and algal biomass measures for four flow rates investigated.

Flow Rate (gal hr^{-1})	N	Velocity (m s^{-1})	Algal Biomass (g dw m^{-2})
800	15	0.04-0.62	0.03-3.70
400	15	0.02-0.28	0.33-6.87
200	15	0.01-0.15	2.2-8.11
100	15	0.005-0.08	0.69-5.20

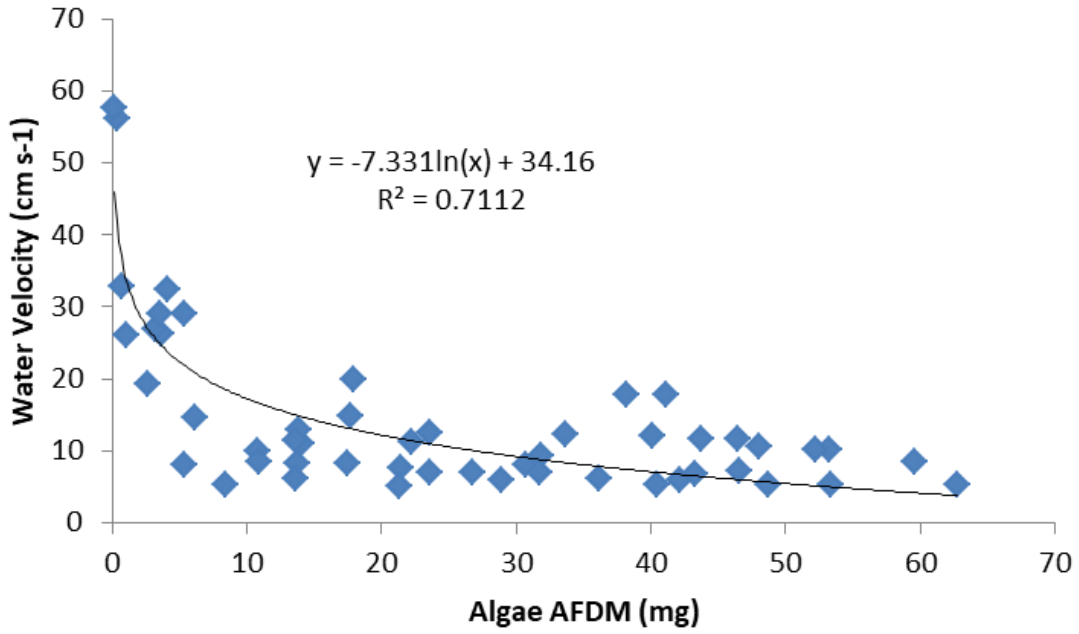

Figure 7.3.7. Algal biomass accumulation on synthetic leaf surface under variable velocity in mesocosms.

Results of shear stress removal of established algae from artificial leaves did not follow a predictable pattern (Figure 7.3.8). The clear hysteresis between colonization and removal suggests that anchoring processes enable algae to remain attached under variable conditions. We assert that algal diversity, community structure, and growth forms are all significant factors in the effectiveness of shear stress to remove established algae. These factors were not quantified in this experiment, however the variability of algal loss between velocities of 5 to 40 cm s^{-1} indicate several other factors regulate this process, including scouring due to interactions among blades and between blades and other surfaces. The implication of this finding is that once algal biomass has accumulated, increasing velocity will have unpredictable results on removal of algae.

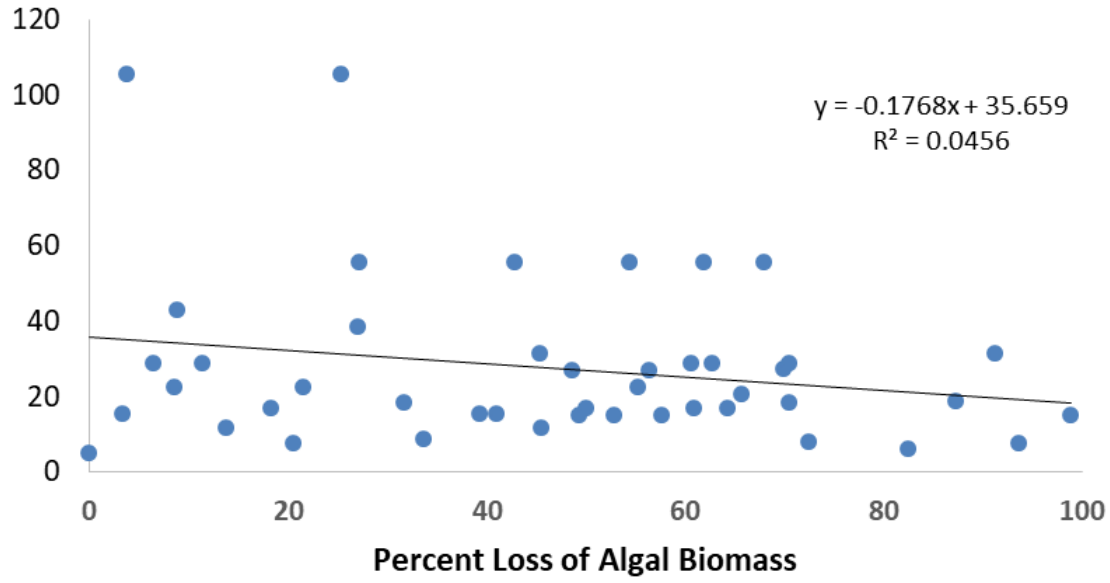

Figure 7.3.8. Algal biomass loss from artificial leaf surface during water velocity experiment. Note hysteresis of productivity and removal processes.

7.3.5 CONCLUSIONS

Current velocity above 25-30 cm s^{-1} (0.25-0.30 m s^{-1}) was observed to inhibit algal growth on SAV, corroborating previous studies conducted by King et al. (2012). Stresses induced by increasing current velocity do not remove algal biomass with the same level of predictability. These stresses are comprised of both shearing stresses from actual velocity of water passing over the algal biofilms and the abrasive interaction of SAV blades between themselves and other surfaces. Surface to surface interactions (i.e., blades rubbing together or against another surface) are extremely variable and were not held constant under our experimental design. Thus we cannot conclude that the observed responses are based solely on the shear stresses created by current velocity, rather the results indicate the combination of both shear-stresses and surface abrasion. As both forces are likely to act in concert in a natural setting, we contend that these observations indicate that reduced current velocities will have a significant effect on algal proliferation but a much more pronounced effect on algal sloughing once communities are established.

Management Implications

With respect to management of springs to deter algal proliferation, we assert that current velocity be maintained wherever possible as a management strategy to reduce algal colonization on SAV. In effect, this will require establishing minimum flows from which average current velocities remain at or above the required 25-30 cm s^{-1} to maintain control on algal proliferation. Because of natural and extensive variability associated with SAV beds, this may require site specific field investigation to determine flow conditions that result in the required mean velocity.

7.3.6 REFERENCES

Biggs, B. J. F. and Close, M. E. 1989. Periphyton biomass dynamics in gravel bed rivers: the relative effects of flows and nutrients. Freshwater Biology 22:209-231.

Biggs, B. J. F., Goring D. G., and Nikora, V. I. 1998. Subsidy and stress responses of stream periphyton togradients in water velocity as a function of community growth form. Journal of Phycology 34:598-607.

Copeland, R., Doran, N. A., White A. J., and Upchurch, S. B. 2009. Regional and statewide trends in Florida's spring and well groundwater quality (1991-2003). Bulletin No. 69. Florida Geological Survey, Tallahassee, Florida, USA

King, S. A. 2012. Effects of flow on filamentous algae and nutrient limitation in lotic systems. Dissertation, University of Florida, Gainesville, FL.

Opsahl, R W., Wellnitz, T., and Poff, N. L. 2003. Current velocity and invertebrate grazing regulate stream algae: results of an *in situ* electrical exclusion. Hydrobiologia 499:135-145.

Poff, N. L. and Ward, J. V. 1995. Herbivory under different flow regimes: a field experiment and test of a model with a benthic stream insect. Oikos 72:179-188.

Stevenson, R. J. 1996. The stimulation and drag of current. Pages 321-340 in R. J. Stevenson, M. L. Bothwell and R. L. Lowe (editors). Algal ecology: freshwater benthic ecosystems. Academic Press, Inc., San Diego, CA, USA.

Stevenson, R. J. and Glover, R. 1993. Effects of algal density and current on ion transport through periphyton communities. Limnology and Oceanography 38:1276-1281.

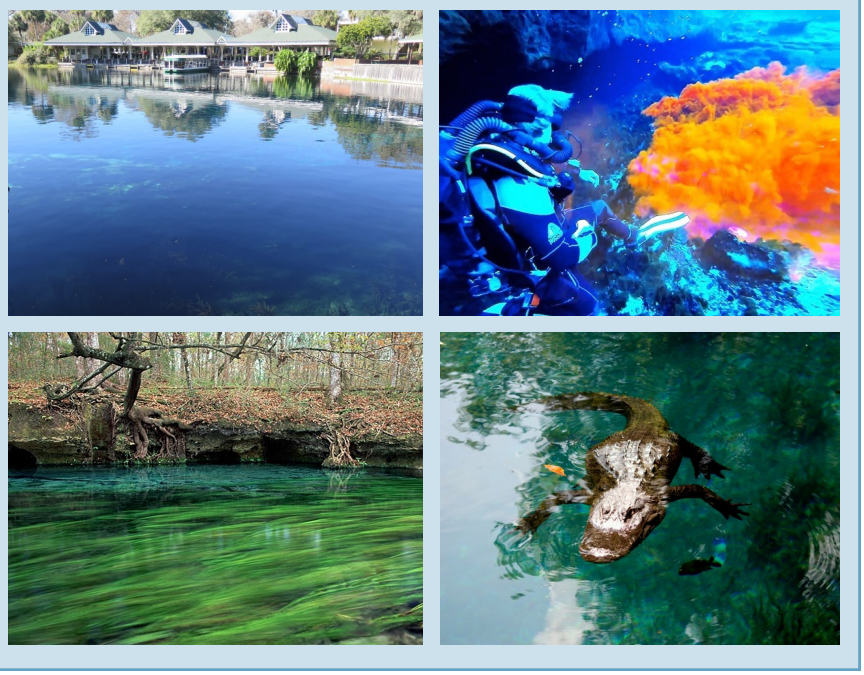

Collaborative Research Initiative on
Sustainability and Protection of Springs [**CRISPS]**

Section 8

[Work Order No: 3]

FINAL REPORT

2014 - 2017

submitted to:

St. Johns River Water Management District
Springs Protection Initiative [SPI], UF Contract # 27789

UF | UNIVERSITY of FLORIDA
Water Institute

C R I S P S

Section 8

PHYSICOCHEMISTRY

Benthic Sources and Sinks of Nutrients

Final Report 2017
Work Order 3: Part 3 of 3

Principal Investigators:

Jonathan B. Martin, University of Florida
Michael F. Coveney and Jodi Slater, St. Johns River Water Management District

Project Team
Jonathan B. Martin
Mitra B. Khadka,
Department of Geological Sciences, University of Florida
Michael F. Coveney
Jodi Slater
St. Johns River Water Management District

Other Collaborators
Junbing Pu, Robin Treilles, John Ezell
Department of Geological Sciences, University of Florida

This document reports findings and results of a work order for a 3-year project in compliance with Agreement between University of Florida (UF) and St. Johns River Water Management District (SJRWMD) UF Contract #27789. It is part of the *UF Collaborative Research Initiative on Springs Protection and Sustainability (CRISPS)* and supports the science component of *the SJRWMD Springs Protection Initiative (SPI).*

8.1 ABSTRACT

Bottom sediments of streams act as biogeochemical reactors that change the chemical compositions of pore water from the overlying stream water. Biogeochemical reactions could thus provide an important source of solutes to stream water and affect benthic and lotic ecosystems. However, the impact on stream water chemistry depends on the magnitude of solute fluxes to and from pore water and the difference between stream water and pore water solute concentrations. In support of the primary objective of the CRISP project (prediction of impacts of nitrogen enrichment on Silver River ecosystem and efficacy of N reduction for remediation), the goals of this work are to (1) evaluate bottom sediment distributions and chemical compositions, (2) measure physical and hydraulic characteristics of the sediment, (3) assess the biogeochemical reactions in the sediment and their impacts on pore water compositions, and (4) estimate potential impacts of fluxes of solutes between bottom sediment and the river. Our results indicate that bottom sediments are ubiquitous and in places greater than 6 m thick. The sediments contain interbedded shell hash layers and organic carbon-rich fine grained deposits. At the upstream site RM0.7, sedimentation rate estimates were poorly constrained because little ^{210}Pb decay had occurred by 30 cm burial depth which suggests rapid sedimentation. Sedimentation rates are 1.6 and 1.7 mm yr^{-1} at the midstream sites MFL7 and MFL6, respectively, while the rate at downstream site MFL3, was slightly faster at around 2.2 mm yr^{-1}. These rates suggest the upper 30 cm of sediment have been deposited within the past 150 years. The Silver River flows across flat topography that appears to be an ancient lake bed, although no lake existed at the site during the time of sediment deposition. This apparently contradictory observation suggests ancient lake sediments are being reworked, for example, as river meander bends migrate downstream. The sediments preferentially retain N over C based on smaller C:N ratios than expected from terrestrial organic matter, and have mineral sources of P (apatite and metal oxides) in addition to organic P. The riverbed sediments contain high organic carbon, preserved due to rapid sediment deposits. This organic carbon may act as a labile substrate and accelerate microbial decomposition releasing nutrients and metals to the water column. Based on the $\delta^{13}C$ and $\delta^{15}N$ values of the sediment organic matter and C:N molar ratios, terrestrial C3 plants appear to be the dominant sources of sediment organic carbon at the upstream site, while both terrestrial C3 plants and freshwater algae source the OC at the downstream sites.

Gradients of increasing Fe, Mn, soluble reactive phosphorous (SRP), NH_4-N, and H_2S concentrations in sediment pore water relative to the river water indicate these solutes diffuse from sediments to the overlying river water. However, NO_3-N concentrations decrease with depth in the pore water, which suggests that river bottom sediments are a sink for riverine NO_3-N. Highly permeable river bottom sediments with hydraulic conductivities ranging from 5.0×10^{-3} to 6.2×10^{-2} cm s^{-1} and orientation of hydraulic gradients towards the river suggest advection also provides an additional mechanism to transport solutes to the river., Results show that solute fluxes from diffusion are greater than fluxes from advection except of NO_3-N. More NO_3-N diffuses into than advects from the sediment indicating a net loss of the NO_3-N from the Silver River system. This NO_3-N loss is small and represents only 0.02 % of the daily NO_3-N load from the spring. However, total benthic fluxes of NH_4-N, SRP, Fe, Mn and HS^- could be important to benthic ecosystems and contribute about 12 %, 47 %, 12 %, 5 % and 100 % of the daily spring loads, respectively. Their importance would be enhancing because they are delivered

directly to low flow systems controlled by subaquatic vegetation. These findings indicate that management of the Silver River system should consider small scale delivery of nutrients to SAV meadows, the point discharge of Floridan aquifer water from high hydraulic conductivity pathways, and external loading of organic matter from the surrounding landscape.

8.2 INTRODUCTION

Assessment of transport and cycling of reactive solutes to and within streams is critical for understanding the controls of water quality, ecological health and ecosystem services of stream systems (Stream Solute Workshop 1990; Jones and Mulholland 2000; Harvey and Gooseff 2015). The fate of reactive solutes in streams is determined by several distinct physical and biogeochemical processes including sorption/desorption on particulate matter, biological uptake, and exchange of stream water with pore water of the benthic sediment (Runkel and Bencala 1995; Worman et al. 2002). The exchange between surface and pore waters, which occurs in a region of bed sediments known as the hyporheic zone as well as throughout the river corridor in a region that includes the hyporheic zone (e.g., see recent review by Cardenas 2015; Harvey and Gooseff 2015), is characterized by steep gradients in physical, chemical and biological characteristics. As a result, the exchange processes of stream water with hyporheic zone water and groundwater regulate fluxes of ecologically relevant substances including nutrients, carbon, and trace metals across the sediment-water interface (Kurz et al. 2015). These exchange processes are responsible for transporting dissolved oxygen, nutrients and organic matter into the stream sediments, where active biofilms carry out microbial-mediated transformation of pore water compositions and influence the biogeochemical characteristics of both surface and subsurface waters (Jones and Mulholland 2000; Packman and Salehin 2003; Boulton and Hancock 2006). Exchange between the stream and pore water may thus alter the stream water chemistry as water travels downstream (Findlay 1995; Boulton et al. 1998; Kurz et al. 2015). The presence and rate of each biogeochemical process depend on the rate of water exchange, solute content and residence time in contact with benthic sediments.

In aquatic environments, bottom sediments play an important role in cycling and fluxes of nutrients and metals across the sediment-water interface. Benthic sediments can filter fluxes of dissolved solutes by transforming, storing, and removing/suppling nutrients from/to overlying water column (Grenz et al. 2000; McGlathery et al. 2007). These processes are driven by microbial-mediated transformations and chemical sorption and dissolution processes in the sediments. Release of nutrients and metals from the sediments is primarily controlled by organic matter content and oxygen availability. Specifically, the amount and type of the organic substrate affect the bacterial community composition and can controls the rates and pathways of solutes cycling and fluxes across the sediment-water interface (Findlay et al. 2003; Torres et al. 2011). Sediments with elevated organic matter content can be a source of nutrients (e.g., N and P) as the organic matter decomposes. Elevated sedimentary organic matter content can be positively associated with elevated sedimentation rate because of less organic matter decomposition by organisms at the sediment-water interface prior to the burial (Berner 1980). Sediment-water coupling works in both ways, as the release of solutes from the benthic sediments enhances primary productivity in the water column, and the organic matter produced during primary productivity in the water column deposits organic matter to the sediments, providing labile

substrate to be regenerated (Grenz et al. 2000). Benthic sediments can thus act as both a source and sink of nutrients, becoming an important factor in controlling aquatic ecosystems.

Remineralization of OC drives a sequence of oxidation-reduction reactions along the well-known "redox ladder" of elements (Figure 8.1), including in order of energy yield (Froelich et al. 1979): oxygen, NO_3-N and Mn-oxides, Fe-oxides, SO_4, and CO_2 (i.e., methanogenesis). Reduction of NO_3–N acts as a sink for reactive N as it converts to N_2O or N_2 gas and volatizes from the system. Reduction of Fe-Mn oxides acts as sources of these elements to pore water as they are transformed from the solid Fe(III) and Mn(IV) oxidation states to dissolved Fe(II) and Mn(II). Reduction of SO_4 to H_2S or HS^-, which depends on the pH of the system, may provide toxic environments for rhizomes of benthic SAV (Terrados et al. 1999). Remineralization of organic carbon also releases NH_4-N and SRP, which may develop concentrations elevated by many times over their concentrations in the overlying water column (Cohen et al. 2013; Kurz et al. 2015). Assessments of fluxes of these solutes from bottom sediment to the river and their effects on riverine ecosystems require measurements of the redox conditions and changes in solute concentrations in the pore water of the sediment, as well as the transport mechanisms for the solutes.

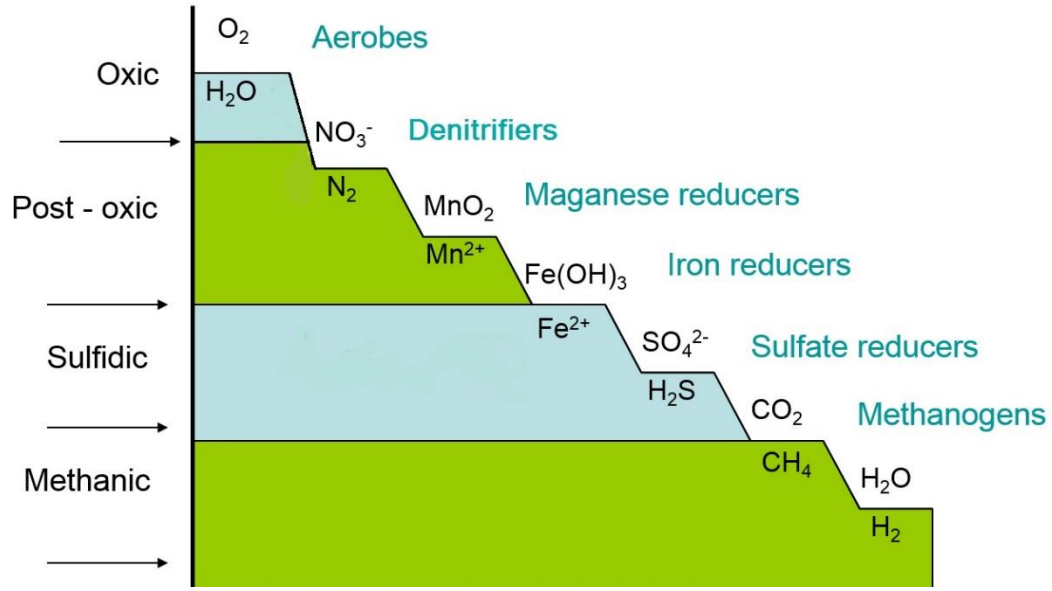

Figure 8.1. Redox reactions catalyzed by microbes in benthic sediments (Adapted after Gao et al. 2003).

Establishing the magnitude of benthic exchanges of nutrients and metals across sediment-water interface is critical to define the functionality of aquatic ecosystems and to provide measures for protecting and improving the ecological health of the systems. Pore water solutes may be delivered from bottom sediment to the overlying water column by two physical transportation mechanisms: diffusion and advection. Advection can dominate solute exchange across the sediment-water interface in sediments with elevated permeability (Harvey and Bencala 1993; Packman and Brooks 2001; Worman et al. 2002). Advective fluxes may include bi-directional exchange of water between the hyporheic zone and water column or by flow from or to

underlying aquifers if the aquifer hydraulic head is greater or smaller than the stream surface elevation. Hyporheic exchange results from pressure differences as water flow across bedforms, meander bends, and other perturbations in the stream channel. Exchange with aquifers may change through time depending on the river water elevation, for example from flooding or drought and the amount of recharge to the aquifer at seasonal and storm frequencies.

Diffusive fluxes of solutes depend on the concentration gradients between the sediment pore water and the overlying water column and these concentration gradients may be oriented into or out of the sediment. For example, NO_3-N, which is expected to be lost in the sediment through denitrification, should have concentration gradients oriented into the sediment, but NH_4-N and soluble reactive phosphorous (SRP), which may be sourced from remineralization of organic matter and mineral phases, is expected to have gradients oriented toward the river. Diffusive fluxes could be particularly significant in streams, where fine-grained sediments, low turbulence, and planar bedforms minimize hyporheic exchange or discharge from aquifers, which could allow development of steep concentration gradients between pore water and the overlying stream water (Kasahara and Wondzell 2003; Cardenas et al. 2004; O'Conner and Harvey 2008; Kurz et al. 2015). Separating and quantifying diffusive and advective transportation mechanisms, the primary objective of this project, is critical for understanding solute supplies to streams, particularly for redox-sensitive nutrients and trace metals.

8.2.1 Project Objectives

A primary goal of the CRISP project is to predict how nitrogen enrichment impacts primary producer community structure and function, and whether N reduction alone will be sufficient to restore community structure in Silver River. Our portion of this goal is to assess potential solute fluxes between Silver River and the benthic pore water, including nutrients and toxic substances such as H_2S, through reactions in its bottom sediment. These assessments are designed to contribute to models to be developed by District personnel of environmental controls on primary producers. To meet this goal, we worked on four research objectives that address the exchange of solutes, particularly nutrients, between river water, ecosystems and the river-bottom sediments. These objectives include:

1) map distribution and thickness of bottom sediment within the Silver River channel,

2) assess the physical properties of the sediment to estimate potential for flow through the sediment and from the sediment to the river,

3) identify biogeochemical transformations of pore water compositions with particular emphasis on N dynamics, alteration of SRP, and reductive dissolution of Fe-Mn oxide mineral phases, and

4) estimate the potential for and magnitudes of diffusive and advective fluxes of these solutes from the sediment to the overlying water column.

8.3 SITE DESCRIPTION

Silver River is a 9.7 km spring-fed river in central Florida. Its head water is the Silver Spring group, which is sourced from the Upper Floridan aquifer (FAS), a thick sequence of carbonate rocks of Eocene to early Miocene age (Faulkner 1973). The river flows east from the springs with an annual mean discharge of 21.7 m^3 s^{-1} (Knowles et al. 2010) before discharging to the Ocklawaha River (Figure 8.2).

The Silver Springs ground water basin (i.e., springshed), as delineated on the basis of the potentiometric surfaces of the Upper Floridan aquifer, covers about 3,100 km^2 in north-central Florida (Figure 8.2). Land surface altitude in the basin ranges from about 65 to 180 ft (19.8 to 54.9 m) above mean sea level and decreases in elevation from west to east. Faulkner (1973) has suggested that the area to the east of the springshed is controlled by faulting that structurally lowered the land surface. However, Knowles et al. (2010) suggested that the highly karstic nature of the top of the limestone can give the appearance of displacement and that an erosional unconformity has lowered the area east of the springshed (Figure 8.3). Regardless of the mechanism, low-permeability sediments overlie the limestone aquifer east of the river; the source of these sediments is erosion of older rocks from the west, including the Miocene Hawthorn Group (Gp). The Hawthorn Gp is composed primarily of fine-grained sedimentary rocks with common phosphate-bearing minerals and carbonate stringers of the Intermediate aquifer. Where present, the Hawthorn Gp serves as a confining unit to the Upper Floridan aquifer. Erosional processes of the strata west of the springs placed low-permeability beds in position to block eastward flow in the Upper Floridan aquifer and exposed the Ocala Limestone (Ls) rocks, thus maintaining a high enough potentiometric surface to cause discharge from open limestone caverns and sinkholes that source the Silver Spring group (Figure 8.3B, Knowles et al. 2010).

8.4 MATERIALS AND METHODS

To accomplish our goals for this project, field sampling at the Silver River and laboratory analyses were undertaken to assess physical properties and to determine chemical compositions and biogeochemical reactions occurring in the bottom sediment of the Silver River. The specific tasks include measuring sediment thicknesses, distributions, chemical compositions, and hydraulic conductivity, measuring river elevations relative to the groundwater head, sampling of pore water at various spatial scales, and measuring the chemical compositions of the pore water. Rainfall data were downloaded from St. Johns River Water Management District (SJRWMD) (http://www.sjrwmd.com/) at its Pine Oaks Ocala station located approximately 10 km west of Silver Springs. The measurements were used to assess potential origins and fluxes of solutes to and from the river with an emphasis on nutrients.

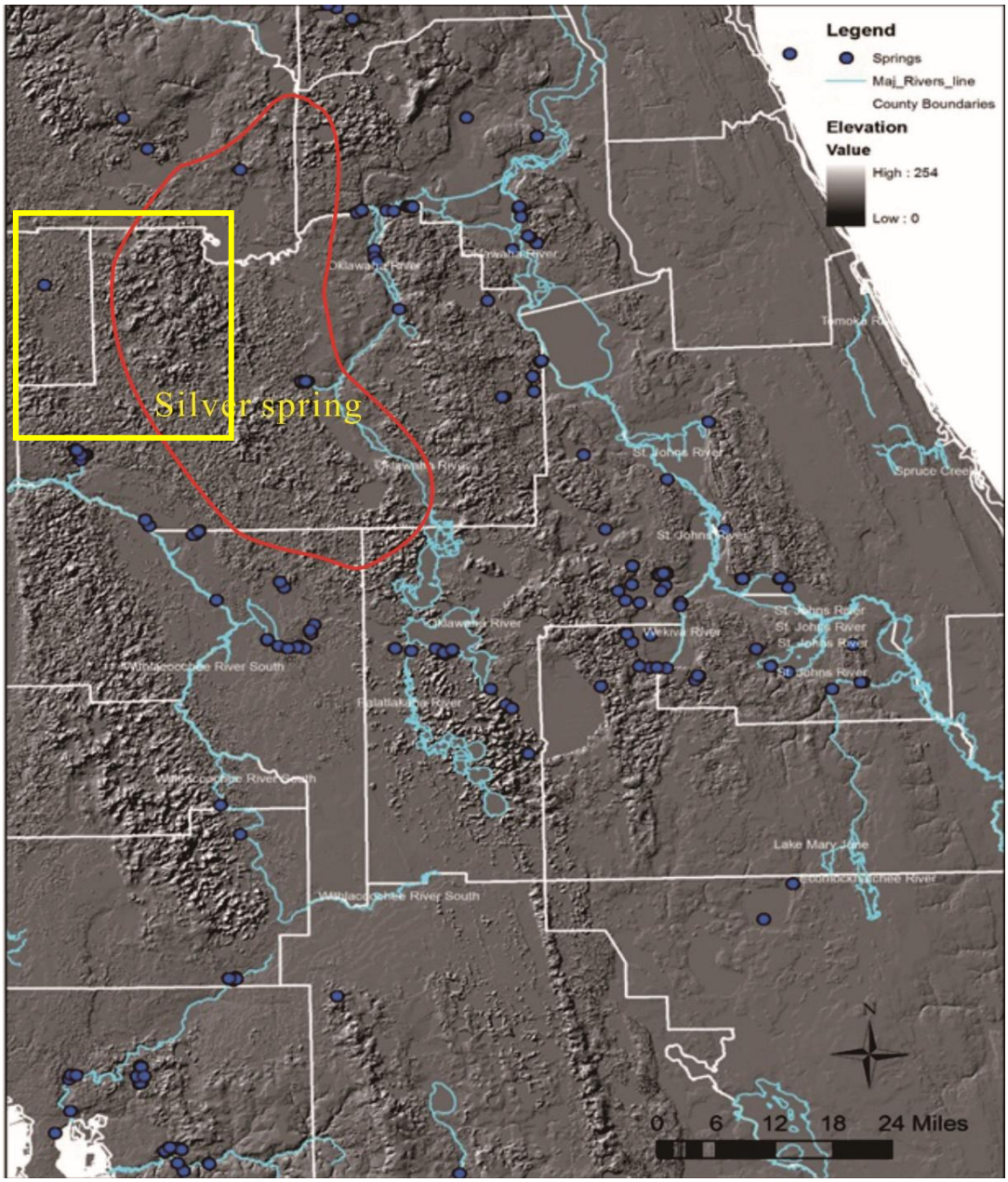

Figure 8.2. DEM of the St. John River Water Management District area showing the location of Silver Springs and other major springs (not labeled on figure). The red line indicates the Silver Spring ground water basin from Knowles et al. (2010). Yellow box outlines the area shown in Figure 8.3A.

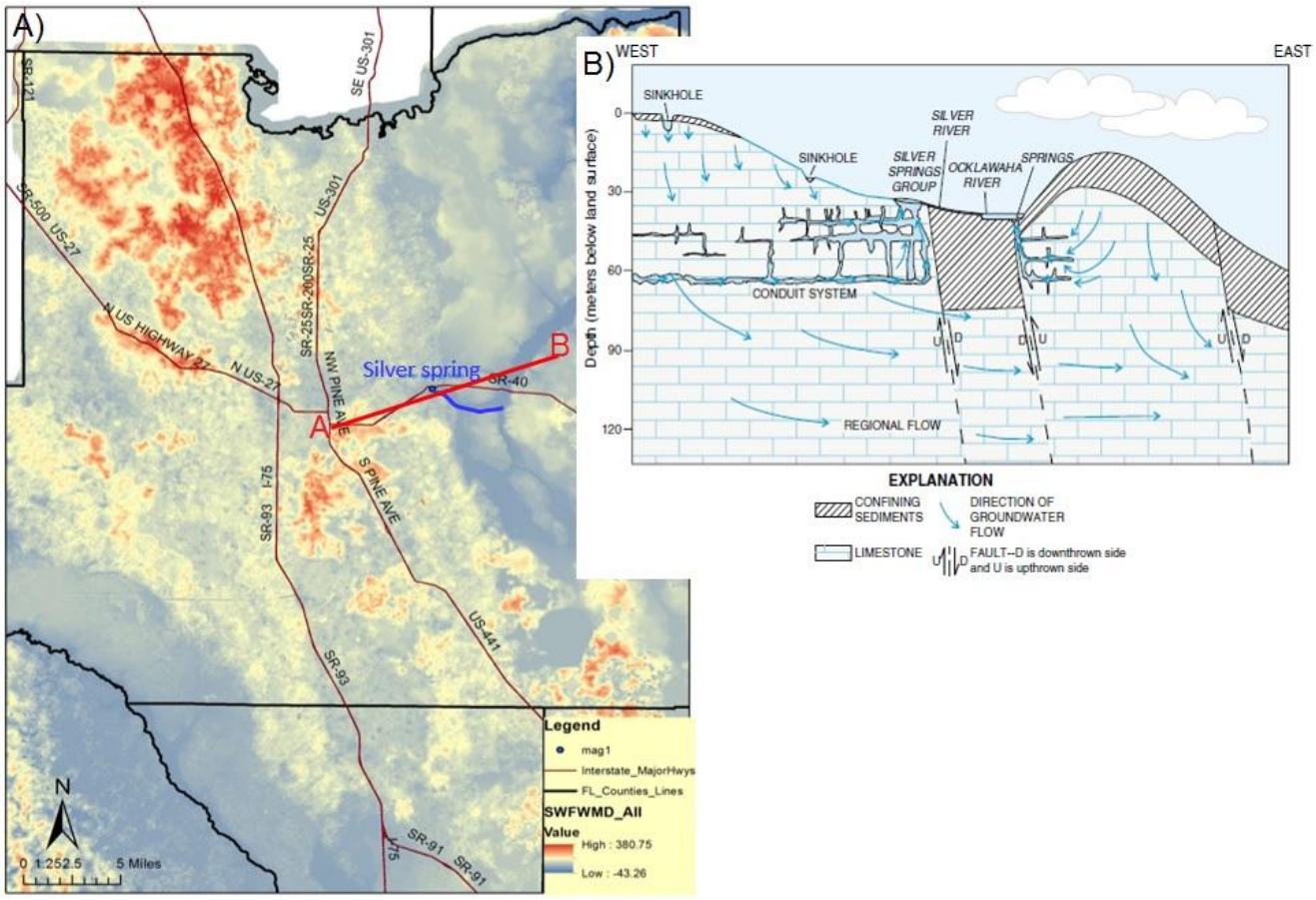

Figure 8.3. A) LIDAR image of area surrounding Silver Springs. Image provided by Harley Means, FGS and B) Cross-section along A-B with conceptualized groundwater flow patterns to the Silver Spring group (Knowles et al. 2010). The confining sediments could be either Hawthorn Gp rocks or material redeposited from the Hawthorn Gp.

8.4.1 Sediment Mapping, Core Collection and Analyses

Fifteen transects of water depths and sediment thicknesses were measured by inserting a tile probe (6 m long, thin diameter metal rod) to refusal or to the maximum length of the rod (6 m) at five stations at each transect (Figure 8.4). Water depth was measured at each sediment probe site using a hand-held depth sounder and their locations were recorded using hand-held Garmin GPS. Where water plus sediment thickness is greater than 6 m, the measured depth is a minimum value for the thickness of the sediments. Our transects are co-located with transects developed for minimum flows and level (MFL) studies, as well as at the USGS gauging station near the headwaters (USGS station 02239501 at river mile 0.7). Based on the distribution and thickness of the sediment, four transects were selected for more detailed observations and analyses along the length of the river (Figure 8.4). These transects are named for other studies occurring at the locations; three are co-located at the MFL transects (MFL3, MFL6, MFL7) and the fourth at the USGS gauging station (RM0.7). The results from four initial study locations included in the scope of work indicated wide range of sediment types and pore water compositions. To better

determine the heterogeneity of pore water compositions, pore water samples were collected at three additional sites, which are co-located with the sites described by the Physicochemistry Nitrogen Dynamics and Metabolism group (Section 6). These sites are designated CL5, CL10 and CL12 (CL = Cohen Lab) for consistency with their numbering scheme.

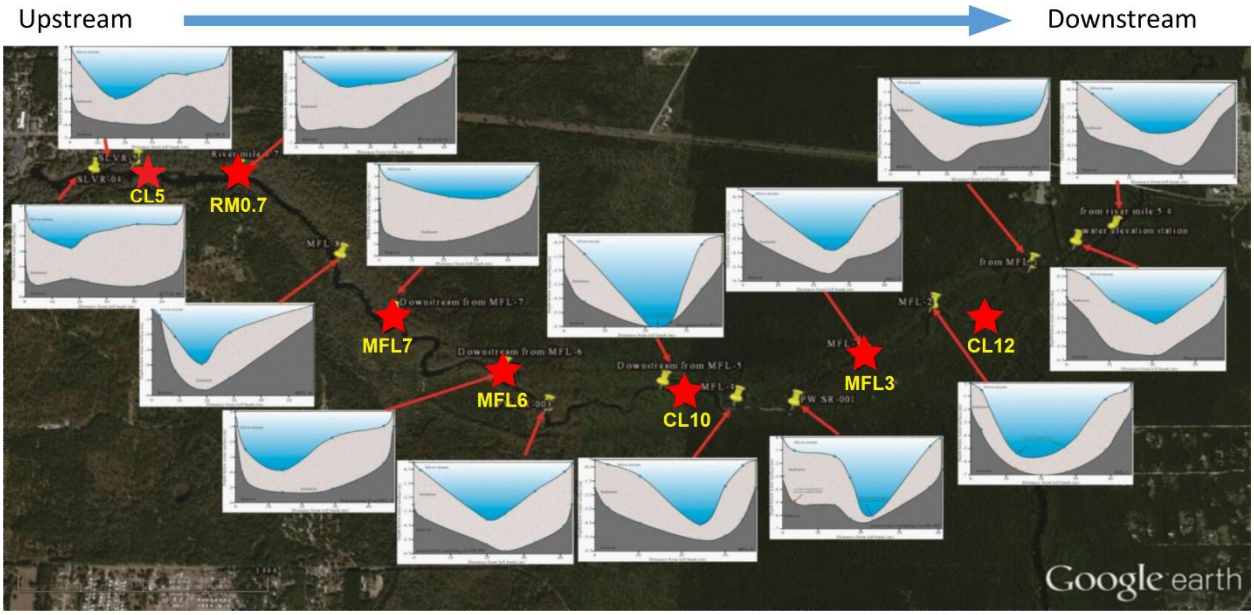

Figure 8.4. Google earth view of the Silver River with the location of sediment transects showing the spatial distribution of sediment thickness and water depth. The red stars indicate the seven transects where detailed sampling and observations were carried out.

The initial sampling included collection of five piston cores at the four original transects, one each at RM0.7, MFL6 and MFL7 and two on opposite banks of the river at MFL3 (Figure 8.5). Two cores were collected from MFL3 because the core could not penetrate beyond about 0.5 m below the sediment-water interface on the right bank. All of the other cores penetrated to depths that include all or most of the sediment column, i.e., to the depth of refusal by the tile probe (Figure 8.5). Except for the short core at MFL3, the other cores ranged in length from 2.1 to 4.2 m. All cores were returned to laboratory intact and were stored at 4ºC in a refrigerated cold room until further analysis.

Bulk densities of the whole-round cores were measured with a Geotek Multi-sensor core logger at a resolution of 1 cm. The core logger also recorded digital images of the fresh core surface after the cores were split vertically (Figure 8.6). The cores were divided into a working half for sampling and an archived half. The working half of the cores were subsampled at 5 cm intervals in the upper 50 cm and at 10 cm intervals at depths below 50 cm for analysis of porosity, inorganic and organic carbon content, total nitrogen (TN), total phosphorous (TP), and trace metal content. Weighed samples were freeze dried for a week and reweighed after drying to determine the water content, from which sediment porosity was calculated. The freeze dried samples were then crushed and homogenized for further analysis. Total carbon (TC) and TN contents were measured using a Carlo-Erba NA1500 CNS elemental analyzer. The total inorganic carbon (TIC) contents were measured using an automated UIC (Coulometrics) 5011

CO_2 coulometer. Total organic carbon (TOC) contents were estimated by subtracting TIC from TC. The TP contents of sediment were determined on a Seal Auto-Analyzer III after potassium persulfate digestion method (Schelske et al. 1986). Reproducibility of replicate measurements was better than 5 %. Trace metal contents were measured with XRF. Stable isotopes ($\delta^{13}C$ and $\delta^{15}N$) of bulk OM in sediments for cores RM0.7, MFL 7 and MFL3 were determined using a Carlo-Erba NA1500 CNS analyzer interfaced with a PRISM Series II mass spectrometer. Isotope ratios are reported in standard delta notation (‰), relative to the VPDB for $\delta^{13}C$ and air for $\delta^{15}N$.

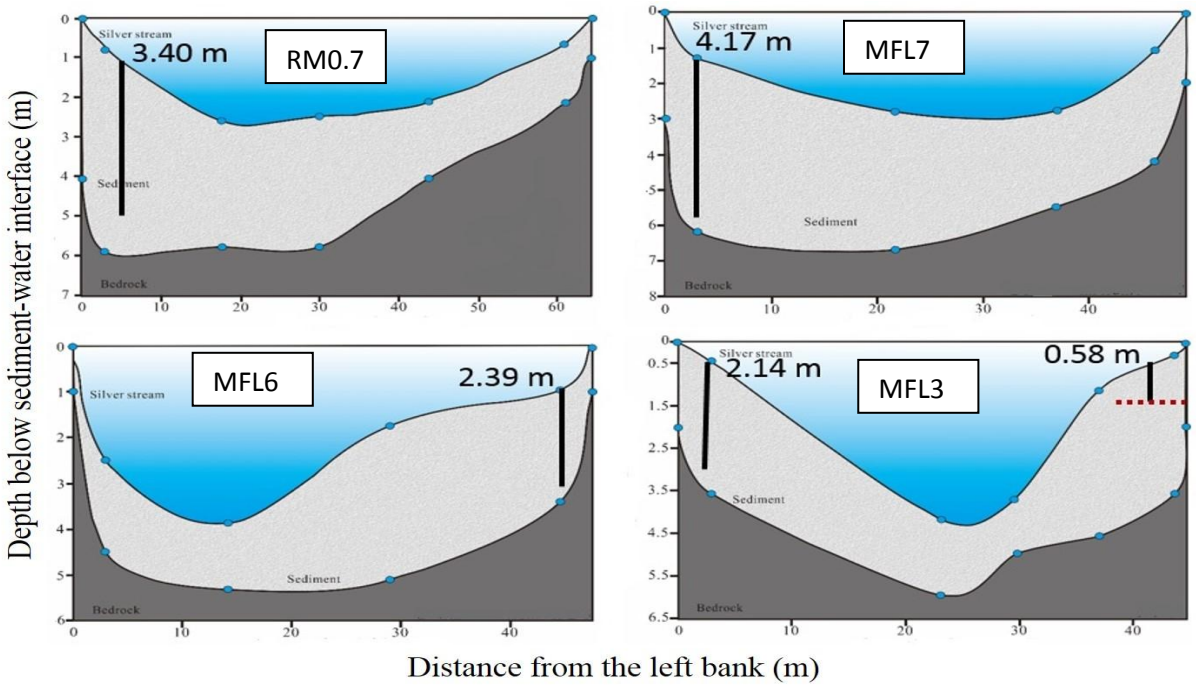

Figure 8.5. Four transects selected for initial core collection, pore water sampling and CTDs installation. The transects show the location and depth of cores relative to the sediment thickness.

8.4.2 Sediment Accumulation Rate

Four short (30 cm long), sediment-water interface cores (one each at RM0.7, MFL7, MFL6 and MFL3) were collected with a piston corer on 8 January 2016 to determine sediment age and sediment accumulation rates. The cores were extruded vertically and sectioned at 3 cm intervals in the field. Sediment samples were frozen, freeze-dried for a week and ground to fine powder in the laboratory. About 7 to 10 g from each dried homogenized sample was packed into an airtight cup and left for 30 days to allow the intermediate daughter product, radon (^{222}Rn), to reach equilibrium with radium (^{226}Ra). Gamma-emitting radionuclides, lead (^{210}Pb), ^{226}Ra and cesium-137 (^{137}Cs), were measured using a planar-style high-purity, low-energy, germanium gamma-ray spectrometer (Canberra Inc) at the U.S. Geological Survey St. Petersburg Coastal and Marine Science Center.

Unsupported (excess) ^{210}Pb was determined by subtracting the activity of ^{226}Ra from the total ^{210}Pb activity, based on the assumption that ^{222}Rn is in secular equilibrium with ^{226}Ra and the

excess ^{210}Pb represent atmospheric deposition. The sediment accumulation rate was calculated using the CFCS model which assumes a constant supply of ^{210}Pb and constant mass accumulation rate. The model is characterized by the basic exponential decay equation:

$$A(z) = A(0)\,e^{-\lambda * z / S} \quad (8.1)$$

where A(z) is excess ^{210}Pb activity at depth z, A(0) is excess ^{210}Pb activity at depth 0, λ is the ^{210}Pb decay constant (0.0311 yr^{-1}) and S is sedimentation rate.

Further, we collected three additional sediment cores from sites RM0.7, MFL6 and MFL7 in November 2016 for ^{210}Pb analyses by alpha counting to complement the previous analyses done by gamma counting. The samples were collected at high vertical resolution (1 cm) to improve the resolution of the prior sedimentation rates that used gamma counting techniques, which require larger volumes of sample than the alpha counting. Although the gamma counting technique provides a low resolution record of ^{210}Pb, it is required to determine the background ^{226}Ra activities that supply the unsupported ^{210}Pb. Alpha counting technique assumes ^{210}Po, an alpha-emitting radioisotope, to be in secular equilibrium with its parent isotope ^{210}Pb, thus allowing for determination of total ^{210}Pb activity in sediments. The ^{210}Po in our samples was measured by alpha spectroscopy, based on Flynn (1968) as modified by Martin and Rice (1981).

8.4.3 Hydraulic Gradients and Groundwater Flow

Conductivity, temperature, depth (CTD) loggers were mounted in piezometers at all four transects on February 2015 and left in the piezometers to collect data through December 2016. The piezometers were installed by pushing, or pounding, 1.25 in diameter PVC piezometers into the sediment, with 13 to 37 cm long screened (125 μm slot) intervals at the bottom of the piezometers (Table 8.1). The screened interval was installed at the depth where coarse-grained sediment were found in the cores (Figure 8.6) on the assumption these horizons would conduct most flow. After the piezometers were installed, they were developed by jetting water into the screened interval. The CTDs were set to log at 15 minute intervals and hung at a known depth from the top of the piezometers using non-stretch nylon line. As planned in the scope of work, only one site, MFL6 had a second stilling well installed next to the piezometers. This stilling well had a screened interval in the river water column. The stilling well was instrumented with two additional CTDs, one above the water surface that monitored barometric pressure, and one below the water surface to measure the river elevation at that location. In the original project scope, data for river elevations at the other sites were to be obtained from other sources, including the USGS (RM0.7) or the District (MFL7 and MFL3). However, data from these sources had spatial and temporal resolutions that were insufficient to compare with our pore water data. Consequently, additional stilling wells were installed in the river water column and equipped with CTDs on 6 August 2015 to compare with river water level. Published sensor accuracy and resolution are ±0.5 cm H_2O and 0.2 % cm H_2O for pressure, ±0.1 °C and 0.01 °C for temperature, and ±1 % and 0.1 % for conductivity, respectively. CTDs data were downloaded every 2-3 months at which time water surface elevations inside and outside of the piezometers were measured with a sounding tape. The river CTD at RM0.7 failed

Table 8.1. Location and information of the CTDs deployment.

Site	GPS Location		Serial no.	Measured Parameters	Screen Length (cm)	Top of screen (cm below S-W interface)	CTD depth (cm below S-W interface)	CTD cable length (cm)
	Latitude	Longitude						
RM0.7	N29°12.946'	W82°02.487'	R6313	GW level,temp, SpC,	37	125	160	369
			K1072	River stage, temp, SpC				
MFL7	N29°12.429'	W82°01.902'	R6318	GW level,temp, SpC,	31	160	160	332
			K1047	River stage, temp, SpC				
MFL6	N29°12.257'	W82°01.526'	R6288	GW level,temp, SpC,	13	53	60	229
			P4461	River stage, temp, SpC				219
			K0868	Atmospheric pressure				
MFL3	N29°12.296'	W82°00.227'	R7702	GW level,temp, SpC,	30	105	110	245
			K1088	River stage, temp, SpC				

on 22 October 2015, resulting in a curtailed record there. The measured hydraulic head difference data were used to calibrate the head difference data obtained from CTDs.

We carried out slug tests to calculate the horizontal hydraulic conductivity of sediment at each of the piezometers in which CTDs were installed. The falling-head method as described by Hvorslev (1951) was used by filling the piezometers with river water and measuring the drop in the water elevation through time with the CTDs set to measure pressure at a rate of 1 Hz. At least four slug tests were run on each piezometer and the hydraulic conductivity was calculated from these data using four applications of two methods. The first method is based on Hvorslev (1951) in which horizontal hydraulic conductivity, K_{hf}, is estimated from

$$K_{hf} = -\frac{A*S}{C} \tag{8.2}$$

Where A is the natural log of the slope of the change in water height, i.e., A = $\ln\left(\frac{H(t)}{H_0}\right)$, S is the cross sectional area of the piezometer, and C is the shape factor given by

$$\frac{C}{D} = \frac{2\pi*(L/D)}{ln(L/D+\sqrt{(L/D)^2+1})} \tag{8.3}$$

where L is the length of the screened interval and D is the diameter of the piezometer. The second method, referred to as the time ratio lag method, uses:

$$-\frac{C*K}{S} * t = \ln\left(\frac{H(t)}{H_0}\right) \tag{8.4}$$

from which a new variable T, the basic time lag, is defined:

$$T = \frac{S}{C*K} \tag{8.5}$$

Substituting T (eq. 8.5) into equation 8.4 gives

$$-\frac{t}{T} = \ln\left(\frac{H(t)}{H_0}\right) \leftrightarrow \quad \frac{H(t)}{H_0} = e^{\frac{-t}{T}} \tag{8.6}$$

where $\frac{t}{T}$ is called the time ratio lag. When t=T, equation 8.6 can be rewritten to be

$$\frac{H(T)}{H_0} = e^{\frac{-T}{T}} = \frac{1}{e} \approx 0.37 \tag{8.7}$$

The basic time lag T can be estimated by plotting and measuring the time required for $\frac{H(T)}{H_0}$ to equal 0.37. Hydraulic conductivity can then be estimated from T and the dimensions of the piezometer by:

$$K_{hf} = \frac{R^2 * \ln(L/R)}{2 * L * T} \quad (8.8)$$

(Freeze and Cherry 1979) where R is the radius of the piezometer. The value of T is found by fitting curves to plots of $H(t)/H_0$ versus t using

$$\frac{H(t)}{H_0} = A * e^{-B*t} \quad (8.9)$$

where A and B are fitted coefficients. We use three possible scenarios to fit the data where: (1) A and B are free parameters, (2) A = 1 and only B is fitted, and (3) A and B are fit to satisfy equation 8.9.

The falling-head method injects water into the aquifer and tends to displace aquifer sediments resulting in artificially high hydraulic conductivity values. Therefore, we also measured hydraulic conductivity using the rising head method at each piezometer to avoid sediment mobilization during the slug test. The test was conducted by pumping all water from the piezometer and allowing water to flow from the aquifer into the piezometer. As water flowed into the piezometer, the rising water head was recorded by using a CTD measuring at 1 Hz for at least 10 minutes. The processes were repeated 4 times at each site. Based on the head recovery in the piezometer, horizontal hydraulic conductivity (K_{hr}) of streambed sediments can be estimated using Hvorslev's (1951) equation:

$$K_{hr} = \frac{r^2 \ln(\frac{L}{R})}{2LT_o} \quad (8.10)$$

Where, r is the radius of piezometer, L is the screen length, R is radius of screen plus packing (=r in this case), and T_o is the time to reach 37 % of the initial water depth. H_t/H_o is the ratio of water depth at time t to the water depth at time zero. H_t/H_o was plotted along the y-axis in log scale, and time was plotted arithmetically along the x-axis. The plot was then used to identify the parameter (T_o).

Vertical hydraulic conductivity of the riverbed sediments were estimated from the standpipe technique as described by Chen (2000). The technique involves inserting a pipe vertically into streambed, filling the pipe with water, measuring the rate of decline of the water level, and then calculating the vertical hydraulic conductivity based on the rate of water level decline. We used a PVC pipe of inner diameter 5 cm and length 200 cm. The pipe, which extended above the rivers surface, was inserted into the streambed sediments to the sediment column depth of approximately 50 cm. The pipe was filled with river water and initial water head was recorded. At every 5 to 10 minutes interval, water level in the pipe was recorded until we obtained at least 5 to 6 measurements. The vertical hydraulic conductivity (K_v) can be calculated using Hvorslev (1951) equation:

$$K_v = \frac{\left(\frac{\Pi D}{11m}\right) + Lv}{t_2 - t_1} \ln\left(\frac{h_1}{h_2}\right) \quad (8.11)$$

Where D is the inner diameter of the pipe, m is the square root of the ratio of the horizontal conductivity (K_h) to the vertical conductivity (K_v), L_v is the length of the measured sediment column, t_1 and t_2 are the starting and ending times, respectively, and h_1 and h_2 are the corresponding starting and ending water heads, respectively.

Considering that K_h is normally larger than K_v, Chen (2000) has suggested a modified Hvorslev solution to estimate the K_v :

$$K_v = \frac{Lv}{t_2 - t_1} \ln\left(\frac{h_1}{h_2}\right) \quad (8.12)$$

When L_v is much larger than D with L_v/D >5; results obtained from the modified equation is within the 5 % of Hvorslev calculation. In our calculation, L_v /D was much higher than 5 at all the sites.

Vertical hydraulic head gradient at each piezometer were calculated by dividing the head difference between the piezometer and river by the piezometer depth (top of the screen to the sediment– water interface). We used vertical gradients in combination with measured hydraulic conductivities to estimate groundwater inflow to the river (q) based on Darcy's Law:

$$q = -K\left(\frac{dh}{dl}\right) \quad (8.13)$$

where K is hydraulic conductivity (m d^{-1}) and dh/dl is the hydraulic gradient based on the CTD data.

8.4.4 Pore Water Chemistry

We collected sediment pore water samples from each transect for the analysis of nutrients (NO_3-N, SRP, NH_4-N), carbon (DIC, DOC), sulfide, trace metals (Fe, Mn), major ion concentrations, and $\delta^{13}C_{DIC}$ values. We used two methods for pore water sampling, which included the vapor probe method (Charette and Allen 2006) for deep pore waters, but only at RM0.7, MFL7, MFL6 and MFL3 and a whole core squeezing method (Jahnke 1988) for high resolution sampling of pore waters to depths <35 cm below the sediment-water interface at all six sites. The vapor probe technique was able to extract water only from the shell hash layers (Figure 8.6) and therefore this technique provides a low vertical resolution. The whole core squeezer produces samples from fine grained sediment and thus has higher resolution than the vapor probe, but is limited in the depth of collection. For the whole-core squeezer, pore water was sampled every 2 cm in the upper 15 cm and every 3 cm below that depth. At the time of pore water sampling, we also collected river water samples at the core sites.

Prior to collecting deep pore water and river water samples, dissolved oxygen (DO), specific conductivity, temperature and pH were monitored constantly using a calibrated YSI ProPlus multiparameter meter until these parameters stabilized to ensure collection of pristine samples. All samples were filtered through 0.45 μm pore size in-line, trace-metal grade, canister filters and collected in HDPE plastic bottles for NO_3-N,' NH_4-N and SRP measurement. Samples collected for cation and metal concentrations were preserved with concentrated trace metal-grade

HNO_3, samples for sulfide measurements were preserved with zinc acetate, and no preservative was added to the samples collected for alkalinity and anions. Samples for DIC concentrations and $\delta^{13}C$ values were collected in glass vials and preserved with a saturated $HgCl_2$ solution to prevent microbial activity. Samples for DOC concentrations were collected in 40 mL amber glass vials with septa caps and preserved with HCl to a pH ~3. Samples were kept on ice until returned to the lab. The nutrient samples were kept frozen and all other samples were kept chilled at 4 °C while stored in the lab prior to analyses.

Alkalinity was measured by titration within 24 h of the sampling using the Gran method (Drever 1997). Concentrations of major cations (Ca, Na, K, Mg) were measured using an automated Dionex model ICS1600 ion chromatograph and concentrations of anions (Cl, F, SO_4) were measured using an automated Dionex model ICS2100 ion chromatograph. The relative standard deviation of internal standards measured along with the samples had a precision of <3 %. DIC concentrations were measured on CO_2 extracted by acidifying samples using an AutoMate Prep Device coupled with a UIC (Coulometrics) 5011 carbon coulometer. The method was standardized with dissolved $KHCO_3$. Data accuracy was better than ±0.04 μg L^{-1} for all runs. The $\delta^{13}C$ values of DIC were analyzed using a Thermo Finnigan GasBench II coupled with Thermo Finnigan DeltaPlus XL isotope ratio mass spectrometer and reported in standard delta notation relative to Vienna Peedee Belemnite (VPDB) with analytical precision of ±0.09 ‰. We measured total dissolved Mn and Fe concentrations with an HR ICP-MS Element 2 (Thermo-Finnigan, Bremen, Germany). We measured sulfide following the methylene blue method (Cline 1969). Nitrate, NH_4-N and SRP concentrations in water were measured with a Seal Analytical Auto-analyzer III (AA3). Precision of all analyses was <5 %, based on replicate analysis of internal standards.

8.4.5 Benthic Flux Calculation

We estimate the flux of a dissolve constituent across the sediment-water interface by the sum of two terms, one representing diffusion and the other advection:

$$J_{tot} = {}^{\varphi}D_s\left(\frac{dC}{dz}\right) + {}^{\varphi}v_o C_o \qquad (8.14)$$

where J is the solute flux (mass cm^{-2} s^{-1}), D_s is the sediment diffusion coefficient (cm^2 s^{-1}), dC/dz is the concentration gradient between the river and pore waters (mass cm^{-4}), φ is sediment porosity, v_o is groundwater flow (equal to the Darcy's flow, q, from Eq. 8.13) and C_o is the solute concentration at the sediment-water interface. The first term to the right side of the equation represents diffusion and second term represents advection. We calculated dC/dz at each site using the concentrations providing the steepest gradient. Ds was calculated for measured average porosity for each sediment core after correcting for sediment tortuosity ($Ds = D_m/\text{tortuosity}^2$) (Table 8.2). The molecular diffusion coefficient (D_m) for each solute was estimated by linearly interpolating at 23°C from values given in Li and Gregory (1974). To estimate the total diffusive flux, we multiplied flux rate (J) by the benthic surface area of the river (A= 0.23 km^2). We estimate the benthic area based on the river surface area determined based on Google Maps and assuming the two areas are equivalent. This estimate is a minimum value because bathymetric variations in the bottom will increase the true area of the sediment-water contact and if overhanging trees obscure the bank edge.

Table 8.2. Sediment diffusion coefficient, D_s ($cm^2\ s^{-1}$) for solutes.

Solute	Site						
	CL5	**RM0.7**	**MFL7**	**CL10**	**MFL6**	**MFL3**	**CL12**
NO_3-N	$9.19E^{-06}$	$9.19E^{-06}$	$8.74E^{-06}$	$8.46E^{-06}$	$8.18E^{-06}$	$8.46E^{-06}$	$8.46E^{-06}$
NH_4-N	$9.19E^{-06}$	$9.19E^{-06}$	$8.74E^{-06}$	$8.46E^{-06}$	$8.18E^{-06}$	$8.46E^{-06}$	$8.46E^{-06}$
PO_4	$3.42E^{-06}$	$3.42E^{-06}$	$3.26E^{-06}$	$3.15E^{-06}$	$3.05E^{-06}$	$3.15E^{-06}$	$3.15E^{-06}$
Fe	$2.54E^{-06}$	$2.54E^{-06}$	$2.41E^{-06}$	$2.34E^{-06}$	$2.26E^{-06}$	$2.34E^{-06}$	$2.34E^{-06}$
Mn	$3.64E^{-06}$	$3.64E^{-06}$	$3.46E^{-06}$	$3.35E^{-06}$	$3.24E^{-06}$	$3.35E^{-06}$	$3.35E^{-06}$
H_2S	$8.09E^{-06}$	$8.09E^{-06}$	$7.70E^{-06}$	$7.45E^{-06}$	$7.20E^{-06}$	$7.45E^{-06}$	$7.45E^{-06}$

8.5 RESULTS

8.5.1 Sediment Stratigraphy

The Silver River contains thick layers of sediments ranging up to >5 m that are present in each of the probe locations (Figure 8.4). We did not find bare rock exposed anywhere at the bottom of the river channel that we sampled using the tile probe (Figure 8.4). Spatial distribution of the sediments appears to be homogeneous with no systematic variations in thickness with distance downstream or across the channel. In general, sediments near the sediment-water interface are mostly black, organic carbon rich mud (Figure 8.6). All core sediments, except at RM0.7, gradually become coarser and lighter in color with depth as a result of increasing carbonate sand content with sporadic stringers of coarse shell hash (Figure 8.7). The RM0.7 core has muddy sediments at the top as well as near the bottom. The shell hash layers consist of course grained carbonate minerals, with occasional intact fossils. The abundance of course grained layers decreases downstream, with sediments containing more uniform sandy sediments and fewer fine-grained organic carbon-rich layers than at the upstream sites. The bulk density of the sediment ranges from 1.1 to 2.0 g cm^{-3} with course grained layers having elevated bulk density (Figure 8.6). Porosity of the sediments ranges from 26 to 63 % and decreases with depth. Porosity exhibits a strong negative correlation with the sediment bulk density (Figure 8.8). Although all four cores overlap in their bulk density and porosity characteristics, MFL7 and MFL6 cores have the lowest porosity and highest bulk density, while RM0.7 has the highest porosity and lowest bulk density. These differences in sediment characteristics reflect an increase in the number and thickness of the sandy layers.

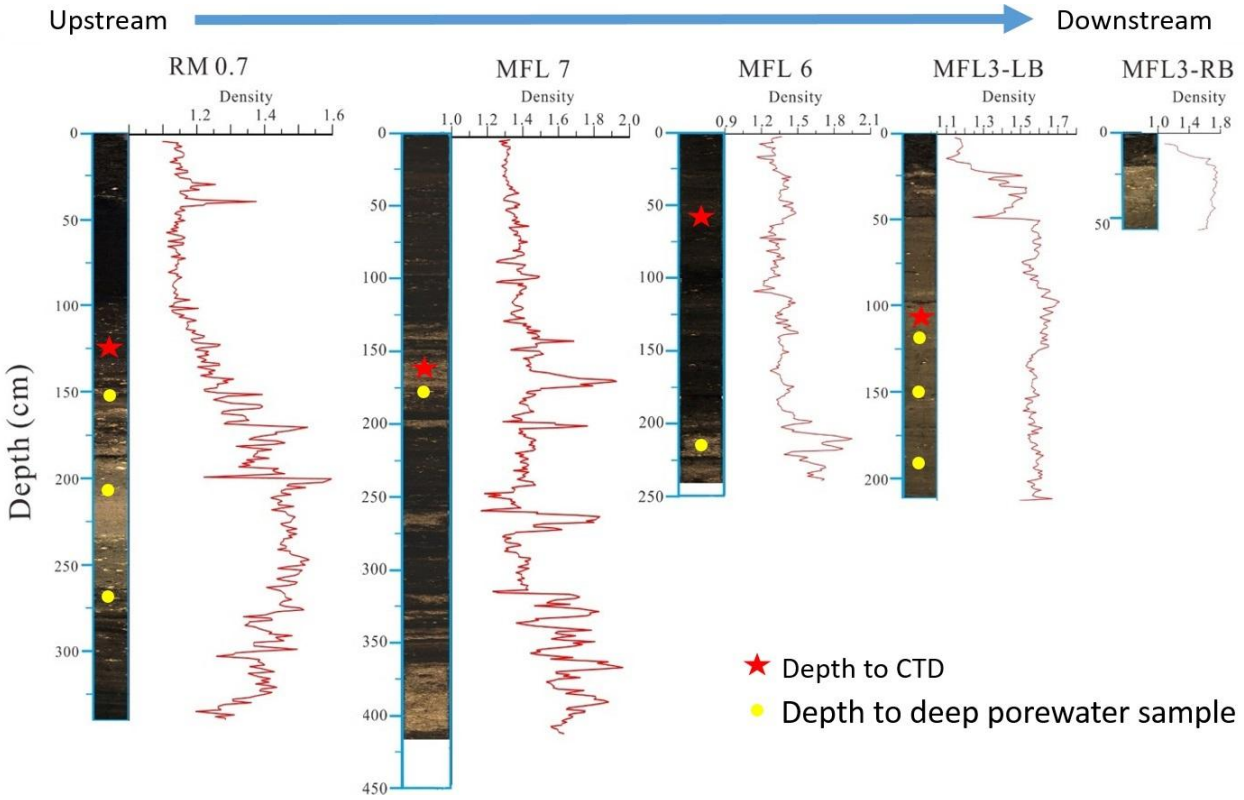

Figure 8.6. Sediment core image and distribution of bulk sediment density with depth. The dark colors indicate finer grained and higher organic carbon contents and the light colors indicate greater amounts of sandy and shelly layers. Stars indicate depth of slug tests and locations of CTDs. The yellow points represent the depth of pore water samples collected using the vapor probe for which concentrations are shown in table 8.3.

Table 8.3. Concentration of chemical variables in deep pore waters collected by vapor probe.

Site	Sample Depth (cm)	pH	Sp.C. ($\mu S\ cm^{-1}$)	ORP (mV)	NO_3-N ($\mu g\ L^{-1}$)	NH_4-N ($\mu g\ L^{-1}$)	SRP ($\mu g\ L^{-1}$)	Fe (ppb)	Mn (ppb)	HS^- ($mg\ L^{-1}$)
RM0.7	155	7.21	440	-197	78	1,833	17	8.2	9.0	16
	210	7.25	403	-234	78	2,396	34	3.2	2.1	14
	272	7.26	410	-210	14	1,466	18	7.2	10.5	16
MFL7	180	6.70	1,034	-253	22	12,861	137	53.4	152	34
MFL6	215	6.70	787	-262	26	6,440	280	15.8	15.5	32
MFL3	120	6.39	855	-257	0	333	30	14.8	29.0	na
	150	6.50	798	-266	0	296	33	26.3	26.7	na
	190	6.73	717	-288	0	482	44	7.6	16.4	na

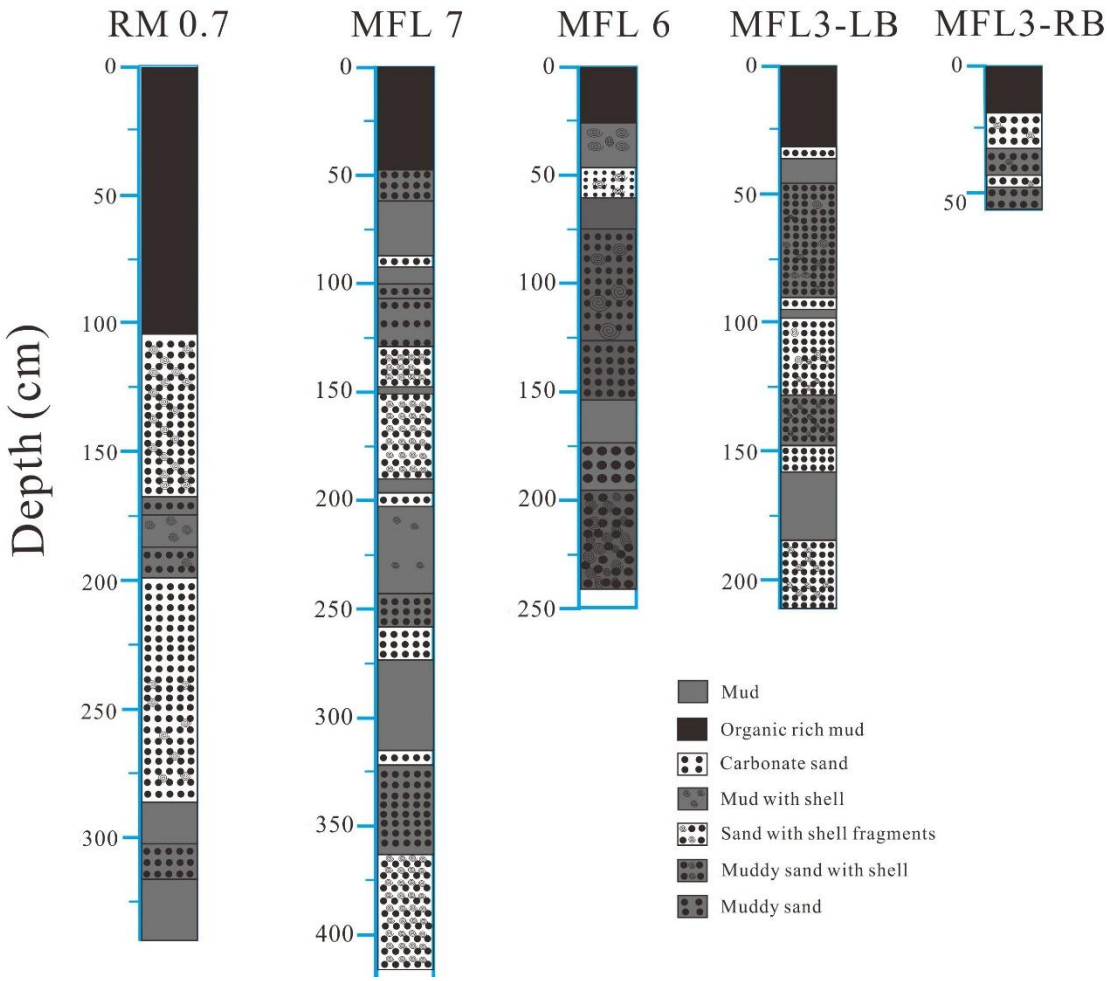

Figure 8.7. Sediment stratigraphy showing the distribution of different sediment types based in visible core inspections.

8.5.2 Chemical Compositions of the Sediment

The chemical compositions of the Silver River sediments vary widely between cores and with depth in individual cores (Figure 8.9). In the upper reaches of the channel, the sediment tends toward higher organic carbon (OC) contents than the lower reaches, with sediment containing nearly 50 % (by weight) organic carbon between about 50 and 100 cm below the sediment-water interface at RM0.7. The higher organic carbon content is reflected in lower inorganic carbon mineral phases (assumed to be calcite). In contrast, the farthest downstream core (MFL3) contains less organic carbon, with a maximum of around 20 wt % at the sediment-water interface that decreases in the upper 25 cm to $\leq$ 5 wt %. Variations with depth in total nitrogen (TN) in individual cores and with distance downstream are similar to the organic carbon concentrations, resulting in good positive correlations for each core ($0.87 < r^2 < 0.99$) between these two variables (Figure 8.10). The slope of the correlations for MFL3, MFL6 and MFL7 are similar, ranging from 12.7 to 14.4. RM0.7, which has the greatest scatter and thus the lowest r^2 value, has a steeper slope than the other cores of around 17. These slope values represent the average C:N

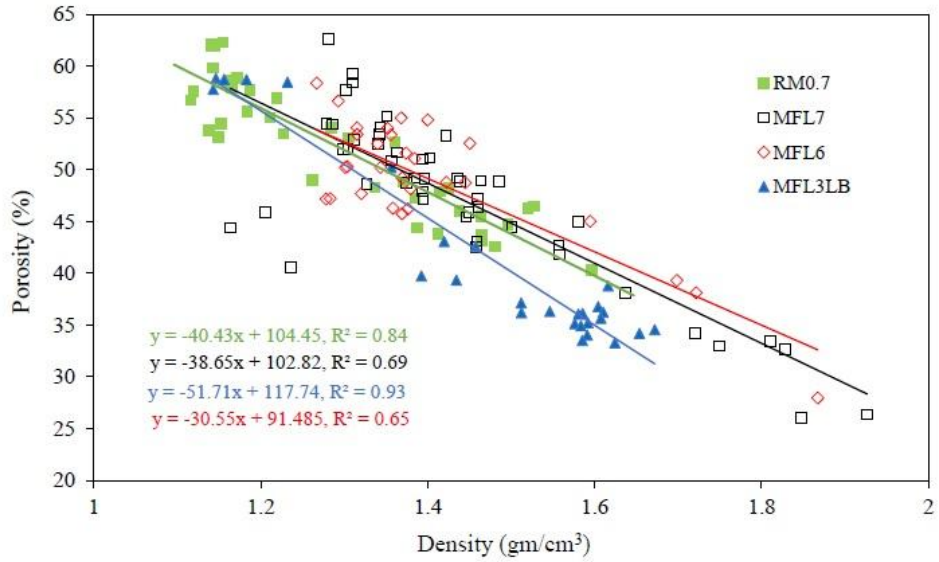

Figure 8.8. Correlation between sediment bulk density and sediment porosity.

weight ratios for each core, which show the average C:N molar ratio of the RM0.7 to be around 20 and for all other cores to be around 15 to 17.

Total phosphorous (TP) contents in the sediments are more variable with depth and distances downstream than the TOC and TN contents. The TP content ranges from about 0 to 1 % (by weight) (Figure 8.9). The lowest content occurs in core RM0.7 and the highest content in MFL7. At MFL3, the top 25 cm contains elevated TP and below this depth, the values are almost constant. However, at other sites, TP concentrations are highly variable with no clear trend with depth. Because of the variable TP contents in the cores, the correlations between TOC and TP are poor and the relationships are variable between the cores (Figure 8.11). Core RM0.7 has the highest TOC relative to TP content, while core MFL7 has the lowest TOC relative to TP content of all the cores.

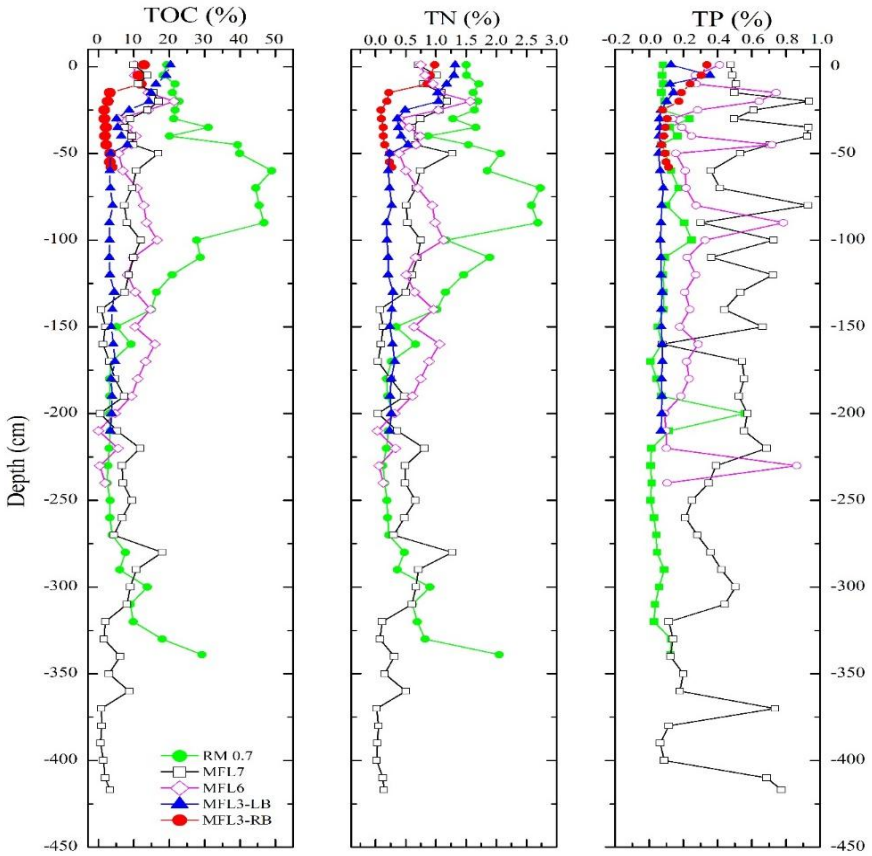

Figure 8.9. Variation in the composition of the five cores (by weight) collected from Silver River including TOC (left), TN (middle) and TP (right).

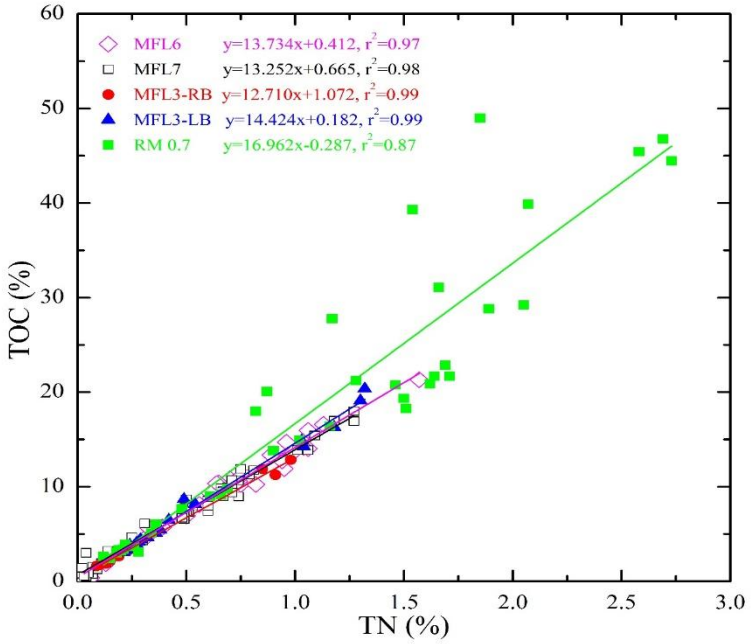

Figure 8.10. Correlation between total organic carbon (TOC) and total nitrogen (TN) in weight percent. Linear regressions are shown for each core.

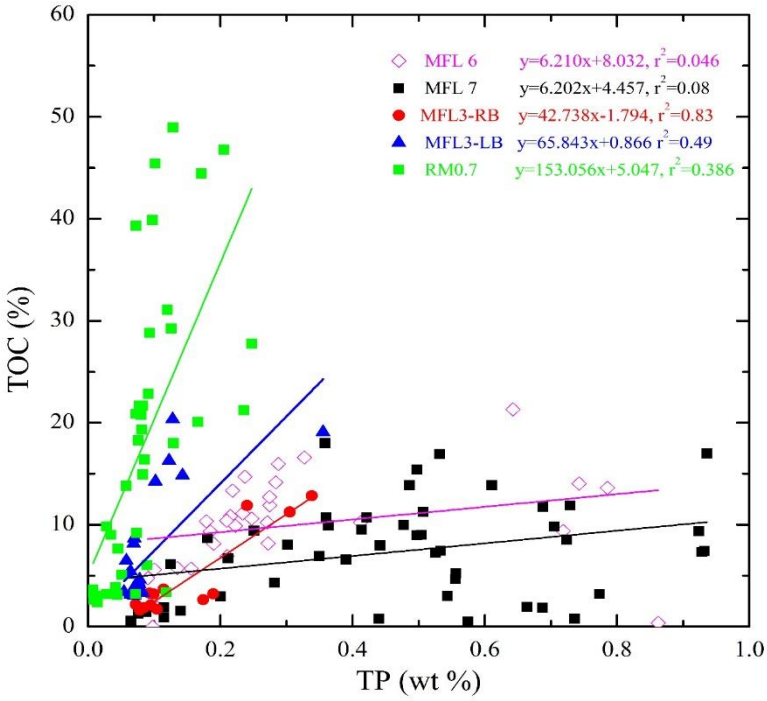

Figure 8.11. Correlation between total organic carbon (TOC) and total phosphorous (TP) in the Silver River bottom sediments. Linear regressions are shown for each core.

8.5.3 C and N Isotopic Composition of the Sediment

We analyzed three sediment cores (RM0.7, MFL7 and MFL3) for $\delta^{13}C$ and $\delta^{15}N$ values of sediment organic matter to assess potential sources of organic carbon to the Silver River sediments. The $\delta^{13}C$ values range from -34.9 ‰ to -23.0 ‰ among three cores, with each core having a distinct range (Figure 8.12). The smallest down-core variation of $\delta^{13}C$ values, ranging from -29.7 ‰ to -27.9 ‰ occurs in core MFL3, which is the farthest downstream core. Core RM0.7, near the head springs, shows highly variable $\delta^{13}C$ values, which includes the greatest range of all cores, from -34.9 ‰ to -23.0 ‰. There is negative C shift and corresponding positive N shift at 50-75 and 275-310 cm depth. The $\delta^{13}C$ values in MFL7 range from -33.9 ‰ to -28.9 ‰ with gradual decrease in isotope values until 300 cm below sediment-water interface where the isotope ratios increase to around -28 ‰. Therefore, the $\delta^{13}C$ values become less variable and more uniform with sediment depth downstream from the head spring. The $\delta^{15}N$ values show variations with sediment depth similar to those of $\delta^{13}C$ but with opposite depth patterns, reflecting an inverse correlation of these two isotopes. The $\delta^{15}N$ values range from 0.2 ‰ to 4.9 ‰ (Figure 8.12). The molar ratios of C and N of the river sediments vary from 12.9 to 30.8 and differ significantly with sediment depth and distance downstream.

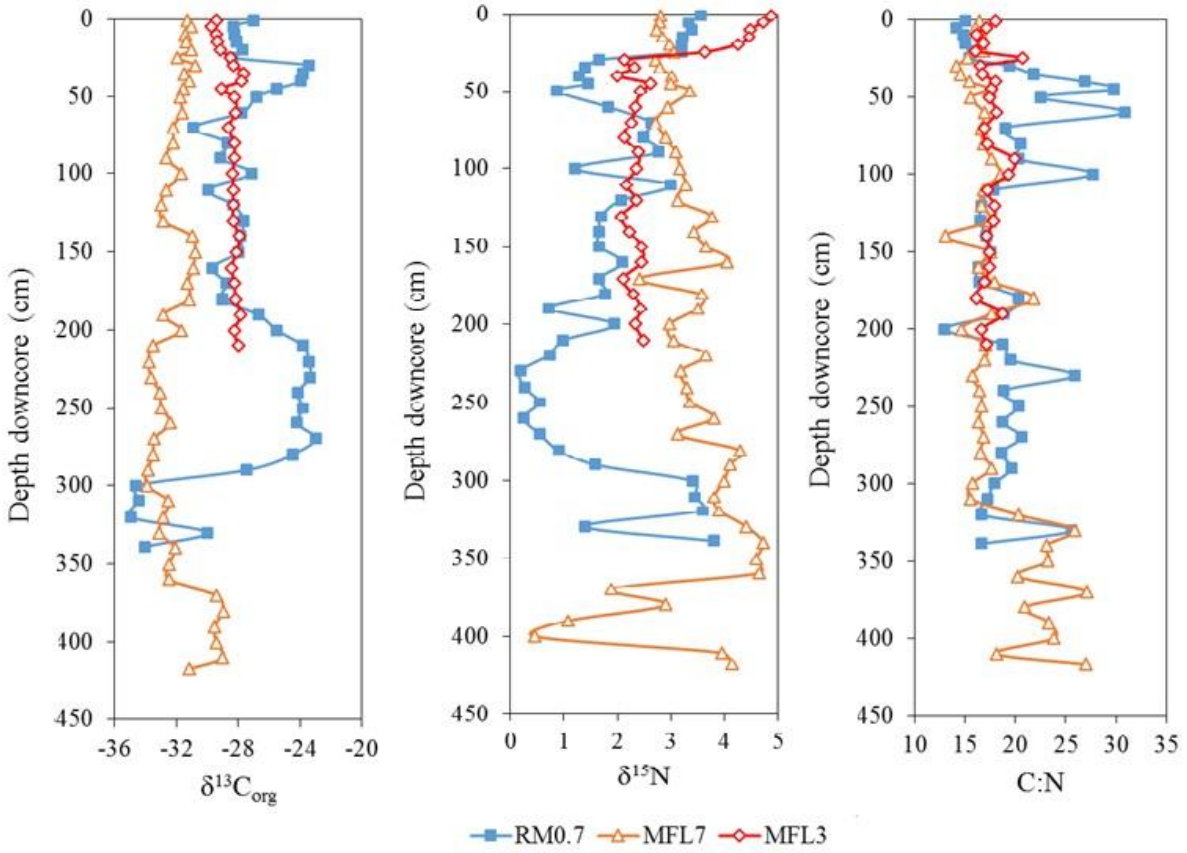

Figure 8.12. Vertical and lateral variations in isotopic composition ($\delta^{13}C$ and $\delta^{15}N$) of sediment organic matter and molar ratio of C and N in the river sediments.

8.5.4 ^{210}Pb and Sedimentation

We measured radioactive nuclides (^{210}Pb, ^{226}Ra and ^{137}Cs) to determine the age and accumulation rates of the river sediments. No measureable ^{137}Cs activity was detected in the river sediments. The ^{210}Pb profiles (Figure 8.13) shows spatial variation along the river. Limited ^{210}Pb decay over the depth interval measured prevented quantitative sedimentation rate estimates at the most upstream site, RM0.7. This lack of decay suggests rapid sedimentation at least over the upper 30 cm of the core. At midstream sites, MFL7 and MFL6, the ^{210}Pb profiles show similar decay trend with depth with excess ^{210}Pb gone at a depth of ~9 cm at both sites (Figure 8.13). This decay in ^{210}Pb activities yields an estimated sedimentation rates at MFL7 and MFL6 of around 1.6 and 1.7 mm yr^{-1}, respectively. These sedimentation rate estimates are based on three data points because of the relatively course sampling interval.

At the most downstream site, MFL3, excess ^{210}Pb activity decreased with depth from 20 to 1.9 dpm g^{-1} and the ^{210}Pb background values (i.e., ^{226}Ra) are nearly constant with depth. The ^{210}Pb activity profiles exhibit near-surface excess ^{210}Pb maxima, indicating active sedimentation. Decrease in ^{210}Pb activities with depth indicates that sedimentation rate is around 2.2 mm yr^{-1} based on CFCS model (Figure 8.14).

We collected three additional sediments cores from RM0.7, MFL7 and MFL3 for alpha counting of ^{210}Pb activities, to improve the sampling resolution (1 cm interval) over that obtained with the gamma counting method. Each core from MFL7 and MFL6 were 30 cm long, and the core from RM0.7 was 60 cm long to extend the ^{210}Pb profile deeper than original core. The ^{210}Pb profile at MFL6 shows steady decay of the ^{210}Pb to the depth of 18 cm (Figure 8.15A). Below this depth, ^{210}Pb is relatively constant. Plots of ^{210}Pb activities versus depth result in two slopes (Figure 8.15B), indicating variations in sedimentation rate with depth. The estimated sedimentation rates, are 1.8 cm yr^{-1} in the top 11 cm and 2.3 cm yr^{-1} in the top 19 cm of sediment depth, based on CFCS model (Figure 8.15B). These rates are slightly higher than the rate estimated from the original core as determined by gamma counting.

8.5.5 Hydrological Variables

The estimated hydraulic conductivities at all sites indicate that both the horizontal and vertical hydraulic conductivities of the Silver River bottom sediments are highly heterogeneous and variable (Figure 8.16). These values do not show any particular spatial patterns. The falling head method resulted in the highest hydraulic conductivity values, ranging from 5.0×10^{-3} to 6.2×10^{-2} cm s^{-1}. These values are 3 to 21 times higher than horizontal conductivity values obtained from rising head method. Hydraulic conductivities from the rising head method range from 1.3×10^{-3} to 3.0×10^{-3} cm s^{-1}. Vertical hydraulic conductivity values are the lowest at all sites, ranging from 5.5×10^{-5} to 1.2×10^{-3} cm s^{-1} (Figure 8.16). Horizontal hydraulic conductivity values are high as would be expected from the sandy layers in which the CTDs are installed, but are unlikely to reflect the range of hydraulic conductivities possible in these sediments. The vertical hydraulic conductivity values are representative of fine grained sediments in the top 50 cm.

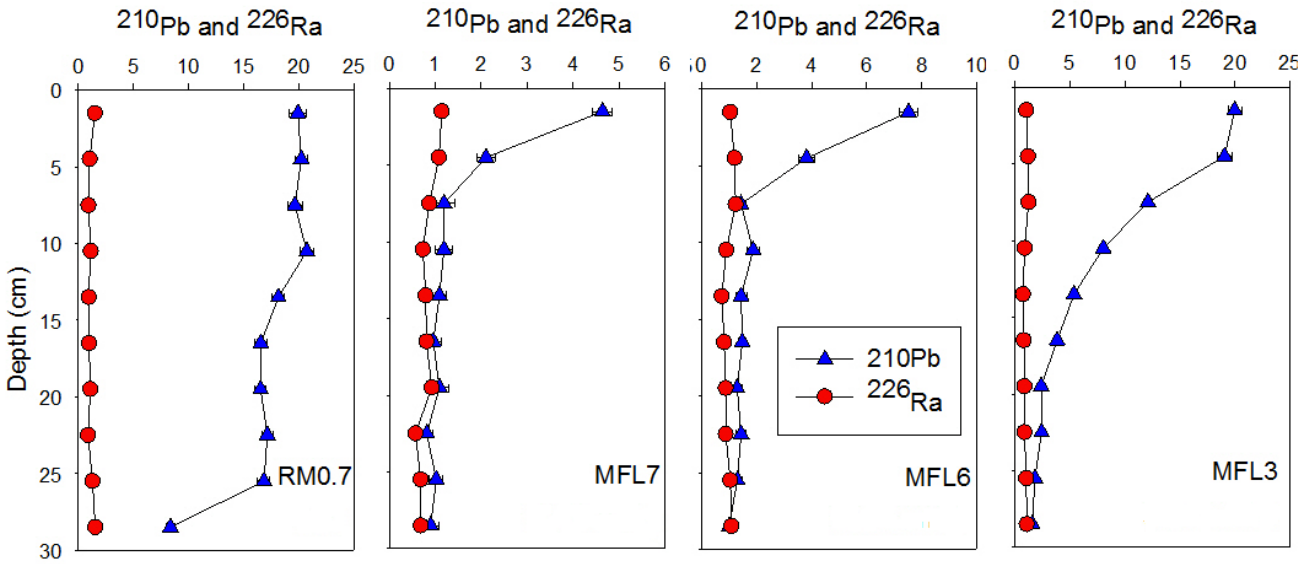

Figure 8.13. ^{210}Pb and ^{226}Ra activity in the river sediments in Silver River

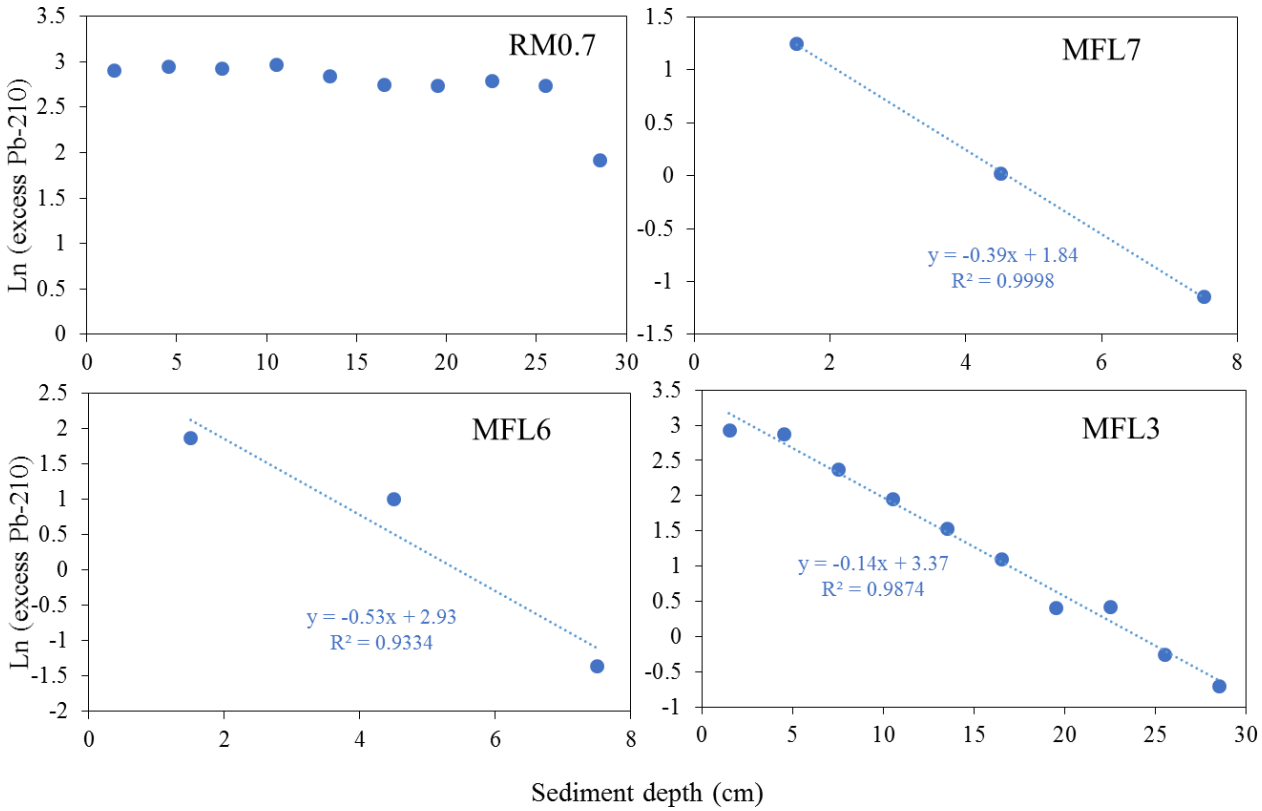

Figure 8.14. Plot showing ln of excess Pb-210 versus sediment depth in the Silver River. Slope of the line was used to estimate sedimentation rate based on equation 8.1.

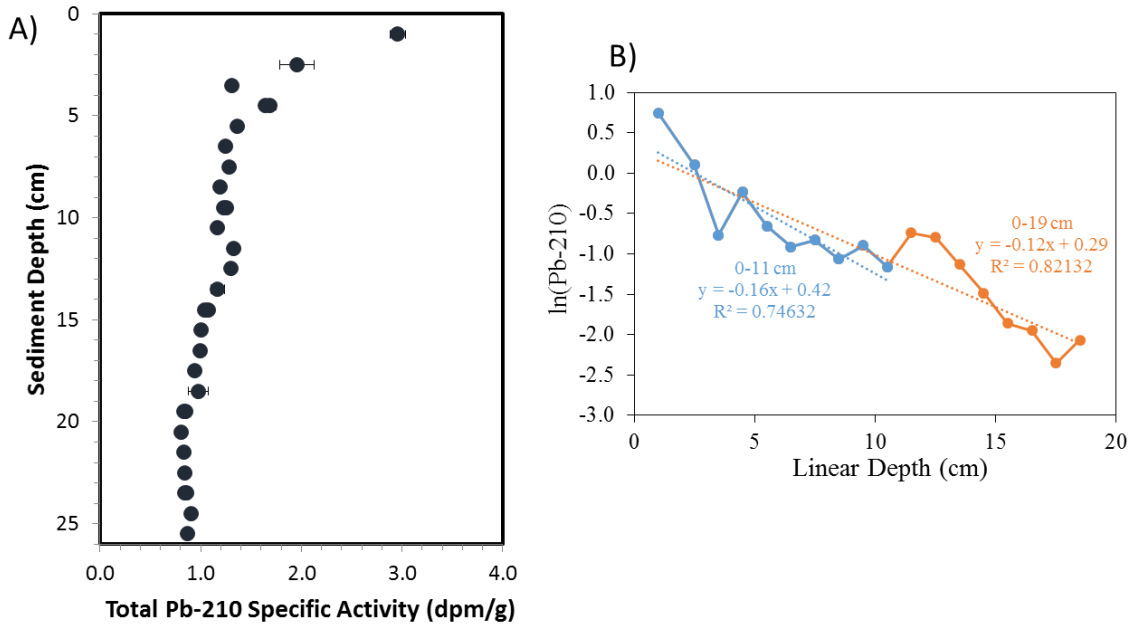

Figure 8.15. A) ^{210}Pb profile with sediment depth, B) ln ^{210}Pb activities plotted against sediment depth to estimate the sedimentation rate at MFL 6.

CTD data from all sites (from February 2015 to November 2016 at MFL6, from August 2015 to November 2016 at RM0.7, MFL3 and MFL7) showed that the ground water level was always higher than river water level, but each site differs in the time-series of head differences (Figure 8.17). The head differences at MFL3 and MFL6, the two downstream sites exhibit small temporal variations, ranging between 0.2 and 0.8 cm. The head differences at RM0.7 and MFL7, the upstream sites, have highest temporal variations with values ranging from 0.2 to 1.3 cm. The head difference at RM0.7 dropped during the summer rainy season; however, more data could not be collected at this site until August 2016 due to logger failure. At MFL7, the head difference climbed to its highest level during the fall and summer dry season.

8.5.6 Pore Water Chemistry

Sediment pore water chemistry in the Silver River showed steep chemical gradients (Figure 8.18). For most reactive solutes, the maximum difference between pore water chemistry and the river occurred in the upper 10 to 15 cm indicating a shallow, chemically reactive zone. NO_3-N concentrations decrease with depth from river values of 730 to 1,312 µg L^{-1} to values below the detection limit at depths 15 cm below the sediment-water interface (Figure 8.18A), creating a diffusional gradient from the river into the sediments. All other measured solutes, including NH_4-N, SRP, Fe, Mn and HS^- have chemical gradients oriented towards the river, creating diffusional gradients from the sediments into the river. The NH_4-N concentrations increase to maxima at depths around 10 to 15 cm below the sediment-water interface, with the greatest concentrations around 9,000 to 22,000 µg L^{-1} at RM0.7, MFL3, and MFL7 (Figure 8.18B). The NH_4-N concentrations were the lowest at CL5 with a maximum concentration of 1,500 µg L^{-1}. The SRP concentrations reach maxima at shallower depths than NH_4-N occurring around 3 to 9

cm below sediment water interface (Figure 8.18C). The highest concentrations of SRP occurred at MFL7 with the maximum value reaching up to 5,000 μg L^{-1} at the sediment depth of 9 cm. The most upstream site (CL5) and the most downstream site (CL12) exhibited the lowest SRP concentrations with the maximum values of < 300 μg L^{-1}.

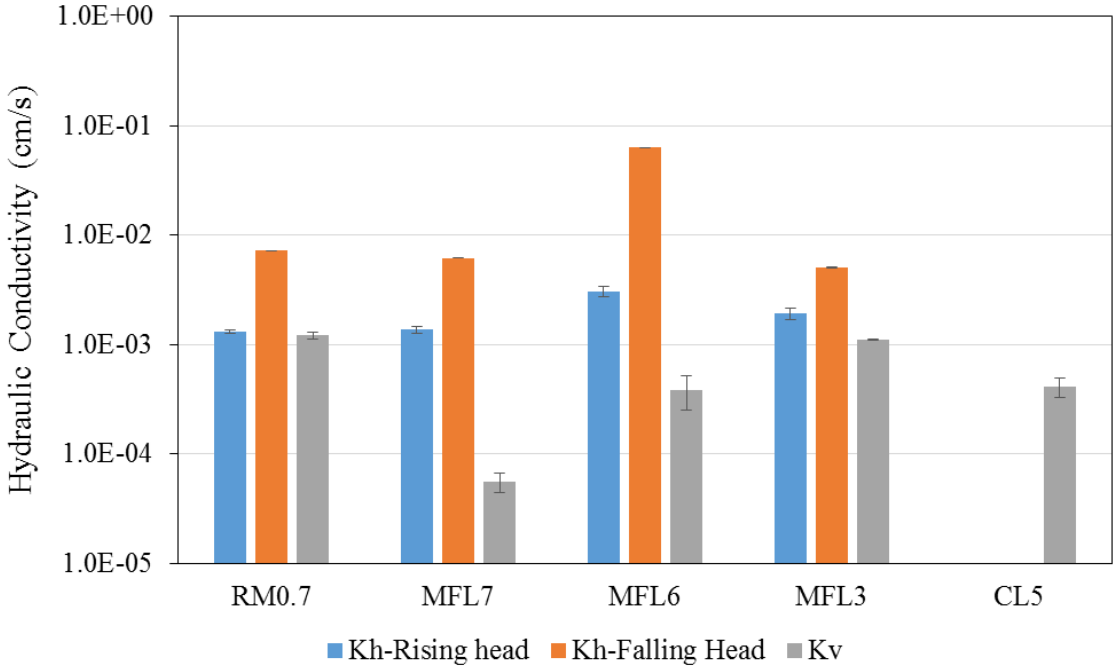

Figure 8.16. Horizontal and vertical hydraulic conductivities of river bed sediments in the Silver River.

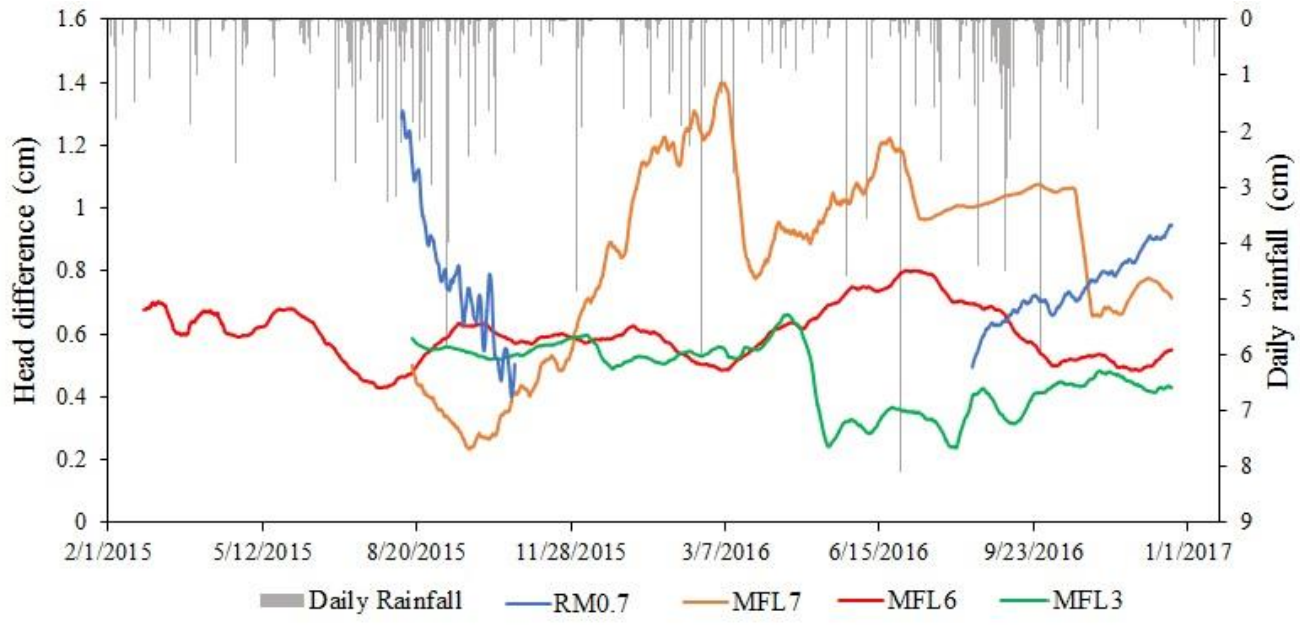

Figure 8.17. 10 days moving average of hydraulic head differences and total daily rainfall.

The Fe and Mn concentrations show similar profiles, reaching maxima at depths < 10 cm below the sediment-water interface from river values < 2 μg L^{-1} (Figures 8.18D and 8.18E). The clearest maximum occurs at RM0.7 where the Fe maximum (55 μg L^{-1}) occurs at 8 cm below the sediment-water interface, while the Mn maximum (67 μg L^{-1}) is shallower at 4 cm below sediment-water interface, as would be expected based on the energetics of the redox ladder shown in figure 8.1. The HS^- concentrations in pore water increase steadily with depth from river values of 0 mg L^{-1} to a maximum value of 29.5 mg L^{-1} (Figure 8.18F). The HS^- concentrations differ between sites with the highest concentrations at the farthest upstream site RM0.7 decreasing to CL12, the farthest downstream site. Although considerable spatial heterogeneity occurs in the composition of the pore waters at these sites, in general, pore waters in the upstream sites (CL5 for NO_3-N, RM0.7 for Fe, Mn and HS^-, and MFL7 for NH_4-N and SRP) contained the highest solute concentrations.

8.6 DISCUSSION

We present analyses of our results below. The analyses provided below are divided into three areas including (1) the characteristics of the bottom sediments, (2) groundwater flow through the sediments, and (3) changes from river water chemical compositions in the pore water caused by biogeochemical reactions to constrain models of diffusive and advective solute fluxes to the river.

8.6.1 Distributions, Compositions, and Possible Origins of Benthic Sediments

The physiography of the Silver Springs springshed and surrounding area support inferences from Phelps (1994, 2004) and Knowles et al. (2010) that the Silver River flows across a region which has been lowered relative to highlands to the west and east of the springshed (Figure 8.3). Regions to the east and south of Silver Spring are exceptionally flat with elevations similar to extant lakes in the region (Figure 8.3). These physiographic characteristics suggest that Silver River may flow across an old lakebed (Harley Means, FGS, email communication) and the uniform thickness and widespread sediments within the river basin support this inference. However, historical records indicate no lake existed at the site over the past 150 years when the sediments were being deposited. The rapid deposition of sediment and the presence of unsupported ^{210}Pb at all the four primary sampling sites (Figures 8.13 and 8.14) indicate the upper 30 cm of sediment have been deposited within the past 150 years. The physiographic evidence for deposition in a paleo-lake bed, but rapid recent deposition could result from fluvial reworking of previously deposited sediments. Such reworking is likely as river meander bends migrate downstream and the reworking could contribute additional nutrients to the benthic ecosystems by sediment resuspension. Ecological management of the Silver River system should thus consider channel and floodplain sediment dynamics along with their potential sources for recycled nutrients.

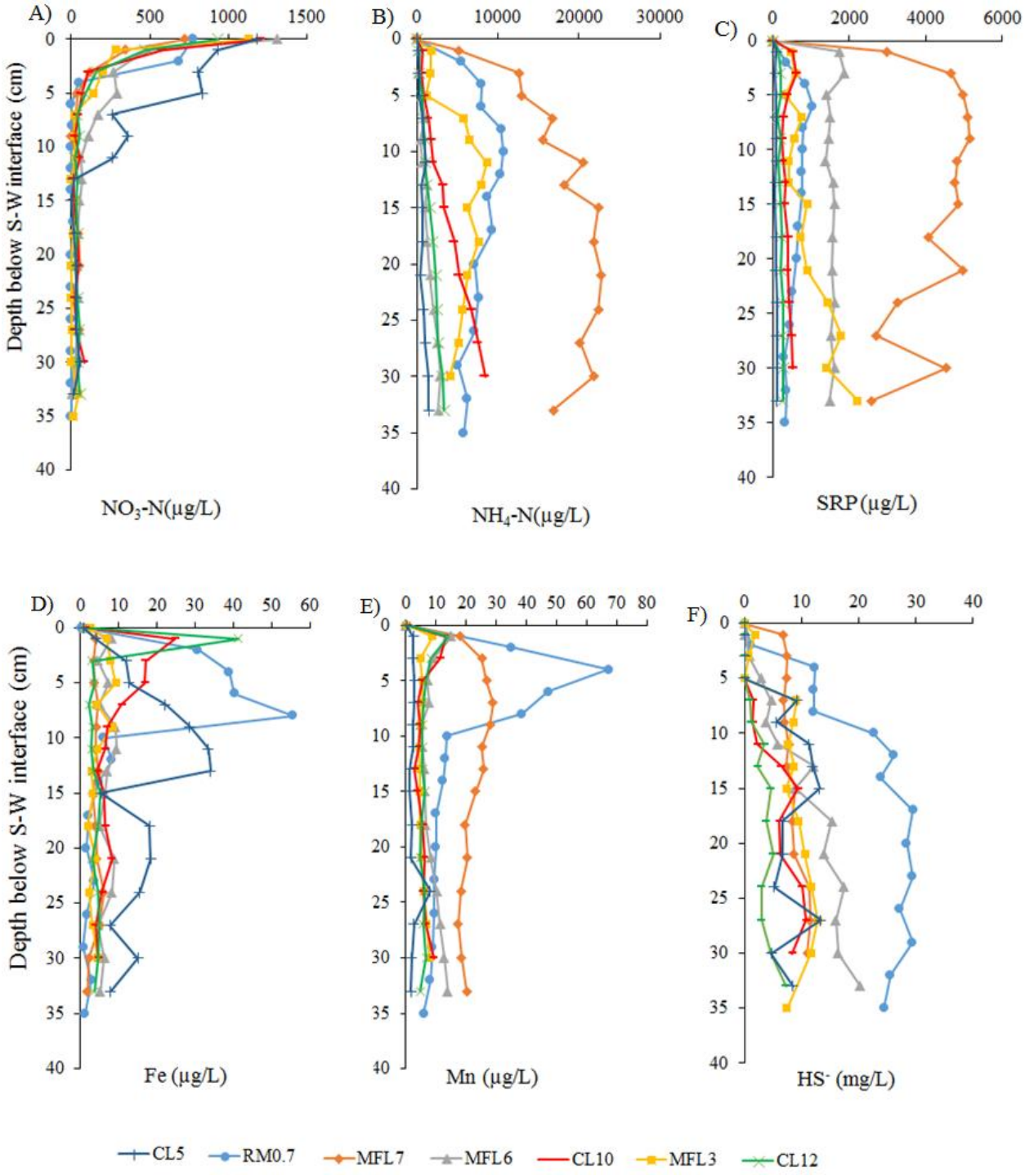

Figure 8.18. Pore water chemical profiles of NO_3-N (A), NH_4-N (B), SRP (C), Fe (D), Mn (E) and HS^- (F). River water samples, collected at each site, are plotted at 0 cm depth.

The interlayering of fine grained, organic carbon-rich sediment and coarse-grained carbonate sediments (Figures 8.6 and 8.7) suggest these sediments could have been deposited in alternatingly quiescent and flowing water, for example as the river thalweg meandered and eroded and redeposited flood plain sediments. Although less likely, the course grained shell hash layers could also reflect localized deposition of carbonate-producing organisms within a lake. Regardless of the origin of interlayered course and fine-grained material, their continuity (i.e., either isolated lenses or as broadly deposited strata) should control locations of flow paths for pore water. The distribution of the course shell layers could be determined by additional coring that would allow stratigraphic correlations between the layers. These lenses of course grained material will be important for estimated groundwater fluxes to the river.

The deepest sediments (>100-150 cm) at all sites show low TOC contents, low C:N ratios and elevated calcite contents within the shell hash layers. These deposits may reflect times when the channel shifted toward those banks and the increased flow within the channel winnowed fine-grained material including organic carbon. Shallower sediments (30-100 cm) contain elevated TOC contents, high C:N ratios and a shift to less negative $\delta^{13}C_{OC}$ values near the headwaters (Figures 8.9 and 8.12). These deposits suggest slow flow, possibly in shallow water characterized by dense subaqueous vegetation. Relatively high $\delta^{15}N$ values and low C:N ratios in the top 30 cm sediments indicate increased algal input with little or no input of terrestrial organic matter and sediments. The deposited sediments could possibly be organic carbon derived from sub-aquatic vegetation. A shift from macrophyte to phytoplankton dominated sediments around 65 years ago was observed in cores takes from lakes located around the upper Ocklawaha River basin south of Silver River (lakes Beauclair, Harris, Weir and Yale), corresponding to increased anthropogenic P loading (Kenney et al. 2010). Although the Silver River sediments appear to originate from old lakebed, they were deposited within the last 150 years and therefore also may contain elevated P from anthropogenic loading.

The good correlations between TOC and TN contents at MFL3, MFL6, and MFL 7 suggest that most N is contained within the sedimentary organic matter (Figure 8.10). At these sites, the molar C:N ratios between 15 and 17 could result from at least two processes. One process is if the OC represents a uniform mixture of algal and terrestrial sources. Alternatively, terrestrial organic matter with a C:N molar ratio > 20 may have been preferentially enriched in N relative to the C, either though diagenetic removal of C from the sediments or retention of the N within the sediments. Nitrogen could be enriched if organic-derived NH_4-N is sequestered into clay interlayer sites, while the CO_2 derived from oxidation of organic matter is flushed from the sediments.

In contrast with good C-N correlations, the poor correlation between TOC and TP in the sediment suggests several sources of P exist in the sediments (Figure 8.11). P is contained in sedimentary organic matter. P may also be contained within apatite ($Ca_5(PO_4)(OH,F,Cl)$), a mineral that is common to the Hawthorn Gp. Because erosion of Hawthorn Gp rocks to the west of Silver Spring provides sediments to the Silver River basin (Figure 8.3), a source of P from redeposited sediments should provide a variable amount of P to the bottom sediments. P can also be sequestered in solid Fe and Mn-oxide phases, and the precipitation and reductive dissolution of these phases as the sediments are buried through variable redox zones, could cause co-

precipitation and release of P to the pore water. Regardless of its source, the elevated P contents in the sediments indicate they could be an important source of P to the river, similar to results found in the Ichetucknee River (Kurz et al. 2015).

8.6.2 Sources of Organic Carbon in Riverbed Sediments

The origin of the benthic sediments influences the sources of OC buried in the sediments and thus their potential for generating nutrients through biogeochemical reactions. Typically, terrestrial C3 plants have C:N molar ratio >20 and $\delta^{13}C$ values of around -34 to -24 ‰ (Figure 8.19). Freshwater algae have C:N molar ratios between 4 and 10 and $\delta^{13}C$ values usually > -20 ‰ (Meyers and Teranes 2001). At the upstream sites RM0.7 and MFL7, some samples show high molar C:N ratios and less negative $\delta^{13}C_{OC}$ values that fall within the field for terrestrial C3 vegetation, while all but three of the samples from MFL3 and the remainder of the samples from RM0.7 and MFL7 fall between the field for C3 plants and freshwater algae (Figure 8.19). These data indicate that the primary source of organic matter during deposition of some of the sediment was terrestrial C3 plants with little algal input, but at other time, algal input mixed with the C3 source. The greatest variations of mixtures with C3 plants and algae occurred at RM0.7. This site also has higher OC contents than the other sites (Figure 8.9), with the highest contents between about 50 and 100 cm below sediment water interface. These elevated OC sediments also show $\delta^{13}C_{OC}$ values and C:N ratio that fall within the field for C3 plants, reflecting an allocthonous source for the elevated OC (Figure 8.12).

Variations in C and N isotopic composition of sediments with depth, specifically at RM0.7 (Figure 8.12), suggest the source of organic matter changes over the time. Less negative values of $\delta^{13}C_{OC}$ and less positive values of $\delta^{15}N$ at depths of around 25 to 50 cm and 200 to 300 cm, in the sediments indicate terrestrial C3 plant contribute more organic matter to the sediments. In contrast, lighter $\delta^{13}C_{OC}$ and heavier $\delta^{15}N$ values below 300 cm suggest more algal and planktonic contributions to the sediments.

Comparison of the C and N isotopic composition of the sediment with extant in-stream end-members may help discriminate between autochthonous and allochthonous sources of OC in the benthic sediments. We compared $\delta^{13}C$ and $\delta^{15}N$ values of sediments from three sites (RM0.7, MFL7 and MFL3) with end-member values provided by the Trophic Interactions Group, Section 9 (Figure 8.20). This plot shows that most of the OC from MFL7 falls between SAV/EPI and EMG, while the OC from MFL3 lies solely within the range of EMG end-member. These results indicate much of the organic matter is derived from autochthonous sources in midstream and downstream sites, with a minor amount of allochthonous plants. However, at the most upstream site RM0.7, the majority of data points fall outside the end-members mixing zone. Similar to the C and N isotope values, this pattern suggests an allochthonous origin of the organic matter near the headwaters with isotopic compositions that are not included in the end-member values for Silver Spring. Specifically, this OM may have been derived from surrounding terrestrial C3 plants as suggested by their relatively heavier $\delta^{13}C$ and lighter $\delta^{15}N$ values. Alternatively, sediments at RM0.7 may have undergone diagenetic alteration or remineralization, although the lack of similar changes in isotopic ratios at the other sites suggest the isotope signal is primary. Assuming a primary signal, the shift in isotopic compositions downstream indicates increased contributions of epiphytic algae and subaquatic vegetation.

Regardless of the sources of OC, it is obvious that Silver River sediments contain high concentration of OC (up to nearly 50 % by weight). High OC in aquatic sediments is associated with high primary productivity and rapid burial of organic matters (Berner et al. 1980). High sedimentation rates in the Silver River as estimated from ^{210}Pb activity, may have enhanced organic matter preservation in sediments with low decomposition by organisms prior to burial. High organic carbon content in the sediments would provide labile substrate allowing the delivery of nutrients and metals to the Silver River water column through microbial-mediated biogeochemical processes. At least some of these nutrients would represent a new source to the river, considering that the isotope ratios indicate much of upstream sediments is allochthonous.

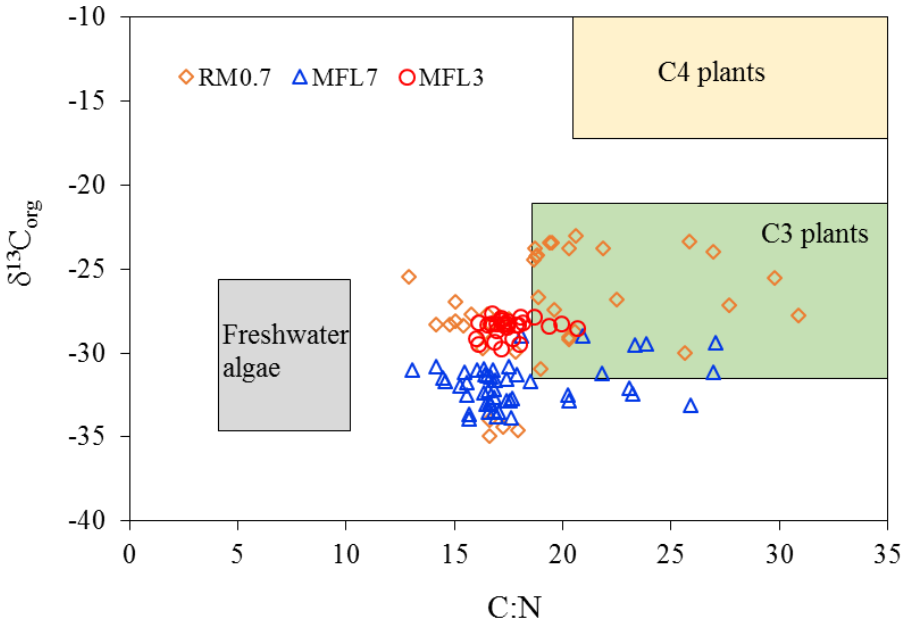

Figure 8.19. δ^{13}C and C:N values of organic matter in river sediments with typical value range of terrestrial plants and freshwater algae.

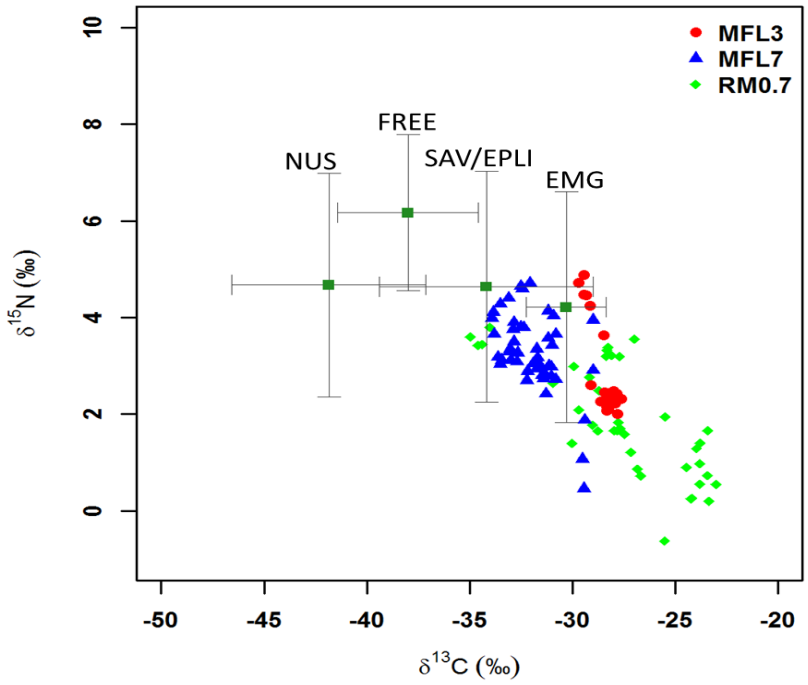

Figure 8.20. $\delta^{13}C$ and $\delta^{13}C$ of organic matter in riverbed sediments with end-members values. NUS = benthic filamentous algae, FREE = unattached algae, SAV/EPI = submersed aquatic veg and epiphytic algae, EMG = emergent vegetation.

8.6.3 Groundwater Flow to the River

Although hydraulic conductivity values measured at each of the transects vary by about three orders of magnitude, this variation is small compared with the range of hydraulic conductivity in sediments, which can vary from 8×10^{-13} to 3×10^{-2} m s^{-1} (Schwartz and Zhang 2003). The values we measured in the Silver River sediments (Figure 8.16) are at the upper end of this range and are similar to values for gravel and sandy sediments, which vary between around 5.5×10^{-7} to 6.2×10^{-3} m s^{-1}. One cause for these high hydraulic conductivity values could be an artifact resulting from the high porosity and water content of the sediment (Figure 8.8), which may allow the sediment to be mobilized during falling-head slug tests because of the elevated pressure during the tests. The rising-head method showed horizontal hydraulic conductivity to be 3-21 times lower than the values estimated using the falling-head method and considering potential sediment, remobilization could be closer to the *in situ* hydraulic conductivity. Regardless of the method used, the values are not unreasonable considering that the piezometer screens were located in coarse-grained sand layers that include large shell fragments (Figure 8.7), which could have hydraulic conductivity values similar to those of gravel aquifers (Schwartz and Zhang 2003). However, to be more confident and to avoid potential artifact caused by falling-head test, we use horizontal hydraulic conductivity data estimated by rising-head method for further calculation and discussion.

Interbedded sediment layers result in differences between vertical and horizontal hydraulic conductivity and at all sites, the estimated vertical hydraulic conductivity was lower than horizontal hydraulic conductivity with horizontal to vertical conductivity ratio of 1.1 to 25. Vertical hydraulic conductivity was estimated only for the upper layer, which is composed of fine, organic rich sediments, and horizontal hydraulic conductivity was estimated for the lower layer composed of course carbonate sand, and shell hash. Thus, horizontal hydraulic conductivity is expected to be higher than vertical hydraulic conductivity. Further, lower vertical hydraulic conductivity than horizontal hydraulic conductivity is also expected due to compaction of aquifer materials (Chen 2000).

The positive head differences between groundwater and river water through time (Figure 8.17) indicate that water flows from bottom sediments to the river. Based on Darcy's law calculations (Eq. 8.13), using the vertical hydraulic conductivity estimates, vertical groundwater flow to the river ranges from 0.03 to 0.64 cm d^{-1} with an average value of 0.4 cm d^{-1} (Figure 8.21). The lowest flow rate occurred at MFL7, which has an estimated hydraulic conductivity about an order of magnitude lower than other sites. Despite the high hydraulic conductivity values, head gradients are small (Figure 8.17) resulting in the slow flow rates. We also estimated lateral groundwater flow by combing horizontal hydraulic conductivity and head gradients, assuming continuous horizontal course layers that crop out at the sides of the deep central channel. The estimated lateral flow rates range from 0.7 to 3.4 cm d^{-1} with an average rate of 1.4 cm d^{-1} (Figure 8.21). However, horizontal flow would deliver solutes to the river only if they are well connected (Figure 8.4).

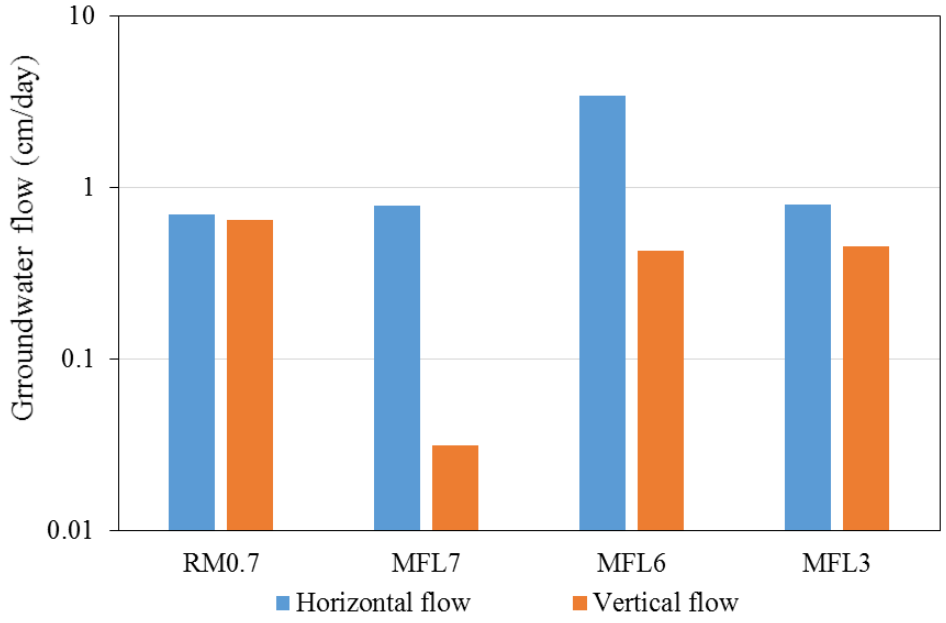

Figure 8.21. Groundwater flow to the Silver River through benthic sediments.

8.6.4 Controls on Pore Water Chemistry

Pore water compositions are controlled largely by changes in redox state caused by the oxidation of organic matter and reduction of various electron acceptors at least through sulfate and probably to methanogenesis (Figure 8.1). Decreasing NO_3-N concentrations with depth reflect denitrification and are consistent with high system-scale N removal observed in the Ichetucknee River system (Heffernan et al. 2010; Kurz et al. 2015). Organic carbon remineralization is reflected in the steep NH_4-N and SRP concentrations gradients in the shallow sediments (Figures 8.18B and 8.18C). If these two solutes were sourced solely from organic matter, then they should reflect the N:P ratio of the organic matter. Terrestrial organic matter exhibits N:P molar ratios that can vary from around 5 to as high as 30 in tropical forests, but tend to concentrate around 5 to 15 (Güsewell 2004; McGoddy et al. 2004). If N and P originated solely from organic carbon remineralization with a N:P ratio of 5 to 15, the ratio of NH_4-N and SRP concentrations should reflect the ratio in the OC. Average NH_4-N:SRP weight ratio in the pore water at RM0.7, MFL7, MFL6 and MFL3 are 14, 2, 3, and 9, respectively, reflecting a molar ratio of around 73, 10, 16, and 47, respectively. Molar N:P ratios at RM0.7 and MFL3 are higher than expected for pristine terrestrial organic matter (Güsewell 2004; McGoddy et al. 2004). These high ratios are somewhat of a surprise considering the elevated P contents in the sediment relative to the TOC contents (Figure 8.11). Although elevated sedimentary P may originate from the re-deposition of apatite from Hawthorn Gp rocks, it appears that this sedimentary source does not contribute much to the pore water SRP concentrations. The NH_4-N:SRP ratios in the pore water could also increase if N is concentrated through exchange of NH_4-N with the sediment, as indicated by the lower sedimentary C:N ratios than expected from terrestrial organic matter (Figure 8.10). The apparent lack of mobilization of mineral P suggests that the primary source of P to the river would be through organic matter oxidation. If some of the organic matter is allochothonous as suggested by the C:N ratios and C and N isotopic compositions, the oxidation of organic matter would represent a flux of new mineral P to the river. The question of origin of the P in the sediment could be addressed through separation of P sources in the sediment through sequential leaching experiments (Ruttenberg 1992).

Pore water chemistry profiles indicate that the redox conditions vary both with depth in the sediment as well as spatially along the river. At the upstream sites (RM0.7), NO_3-N is present to a depth of <5 cm below sediment water interface, while NO_3-N is present to a depth of >5 cm below the sediment-water interface at all other sites with NO_3-N present to the greatest depth of 13 cm at CL5 (Figure 8.18A). Such rapid reduction would be expected at RM0.7 because of the elevated TOC contents there (Figure 8.9) and because the organic matter has the highest C:N ratios expected from less altered, and potentially more labile, organic matter (Figure 8.10). Considering the energetics of the redox reactions (Figure 8.1), the depletion of NO_3-N concentrations would result first in Mn followed by Fe reduction. Mn concentrations were elevated at RM0.7 and MFL7, reflecting Mn-reduction. At RM0.7, Fe concentrations also pass through a maximum at a greater depth then the Mn maximum, reflecting its lower energy yield (Figure 8.1). The elevated Mn concentrations at MFL7 are not reflected in elevated Fe concentrations, however, which suggests a potential Fe sink. Both RM0.7 and MFL7 have elevated HS^- concentrations below 10 cm depth, and the increase in the HS^- concentration at RM0.7 corresponds to the decrease in the depth of the base of the Fe maximum, reflecting a loss of Fe to FeS precipitation. Considering the elevated sulfide concentration in the pore water

(Figure 8.18F), Fe loss to FeS precipitation is likely to be a common process throughout these sediments.

We performed principal component analysis (PCA) on the correlation matrix of variables describing the pore water chemistry of seven sites. The first two eigenvalues explain 75 % of the original data variance. Results from this PCA indicate that the redox sensitive solutes and nutrients (SO_4, NO_3-N, H_2S, NH_4-N, PO_4, Si) are controlled by the 1st component, but that the oxidized and reduced species are not completely inversely related, suggesting factors other than organic carbon oxidation may impact their concentrations (Figure 8.22). Carbonate mineral dissolution appears to be more important than gypsum dissolution given the lack of correlation between SO_4 and Ca. Close association between sulfide, NH_4-N and soluble reactive phosphorous (SRP) indicate that increased NH_4-N and SRP concentrations with sediment depth result from organic carbon oxidation via sulfate reduction. Fe concentrations show no relationship with the other components suggesting it is controlled by a complex set of processes including Fe-oxide reduction, Fe-sulfide precipitation, and potentially assimilation if Fe is consumed during primary productivity. As indicated by the inverse correlation in the PCA, SO_4 is reduced to enough H_2S to convert reactive iron to FeS_2.

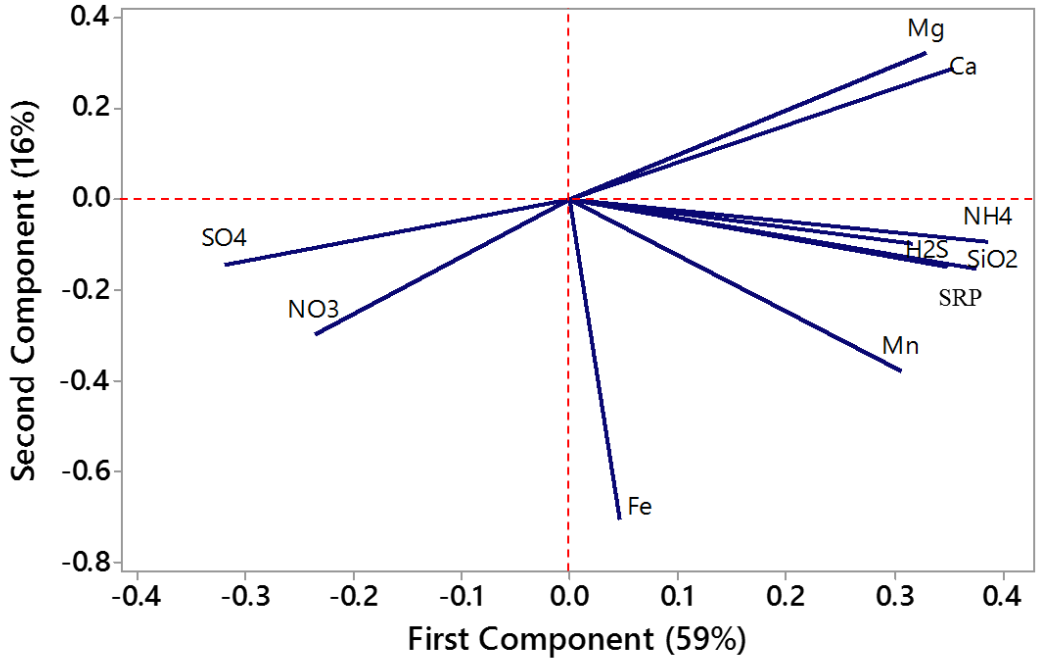

Figure 8.22. PCA biplot of pore water chemistry data from the Silver River.

8.6.5 Benthic Fluxes of Solutes

In the following discussion, we separate delivery mechanisms into diffusive and advective fluxes (equation 8.14) and evaluate the importance of each. We then calculate each separately and sum the two processes to estimate total solute fluxes to the river. All measured solutes except for NO_3-N show both diffusive and advective fluxes from the sediment to the river. In contrast,

NO_3-N has an advective flux to the river from the pore water and a diffusive flux from the pore water to the river.

The shallow pore water chemistry profiles suggest NH_4-N and SRP have strong diffusive fluxes from sediment to the river water column (Figures 8.18B and 8.18C). Similarly, the decrease in the NO_3–N concentration in the sediment indicates that NO_3-N diffuses from the river to the sediment. The maxima in Fe and Mn concentrations reflect reductive dissolution of the metal oxides and indicate these metals diffuse both upward and downward from the maxima. Similar gradients have been observed in Ichetucknee River pore waters (Kurz et al. 2015) but the ultimate fluxes of each solute to the river will depend on its reactivity as it passes through the sediment-water interface. The Fe fluxes are limited by re-precipitation of Fe-oxides as Fe diffuses from the sediment to the oxic river, but P does not have redox chemical reactions similar to Fe, although it may be sequestered in Fe-oxides as they precipitate. Consequently, elevated P concentrations in pore water has been found to be an important source of P to Ichetucknee River (Kurz et al. 2015). In addition to these nutrient fluxes, the increase in sulfide concentrations within the pore water could also be an important factor for the benthic ecosystems of the river depending on the toxic effects of the sulfide on the rhizomes of the subaquatic vegetation. Reducing environments have been shown to limit growth in some seagrasses (Terrados et al. 1999), and similar effects may occur in the Silver River.

Diffusive fluxes of the reactive solutes, based on equation 8.14, show solute fluxes are heterogeneously distributed along the river (Figure 8.23; Table 8.4). This heterogeneous distribution could be caused by many factors including sources and types of organic matter, sedimentation rate and redox potential. The largest diffusive fluxes of solutes to the river usually occur at sites RM0.7 and MFL7, which contain sediment organic carbon content preserved through rapid sedimentation. Kurz et al. (2015) estimated Fe, Mn and SRP flux rate to the Ichetucknee River to be 29.8, 0.4 and 3.7 mg m^{-2} d^{-1}, respectively. Our estimated SRP flux to the Silver River is similar to those found by Kurz et al. (2015); however, the Fe and Mn fluxes are two and one order of magnitude lower than that of the Ichetucknee River. Lower diffusive fluxes of Fe and Mn to the Silver River suggest either smaller sources of these elements from the sediment or that they may be trapped through re-precipitation once they have been mobilized. Trapping could result as Fe and Mn is adsorbed to the surface of the organic carbon. Iron could also be trapped in Silver River through precipitation as Fe-sulfide phases. The sulfide concentrations in Ichetucknee River sediments are unknown so comparisons cannot be made between the two rivers.

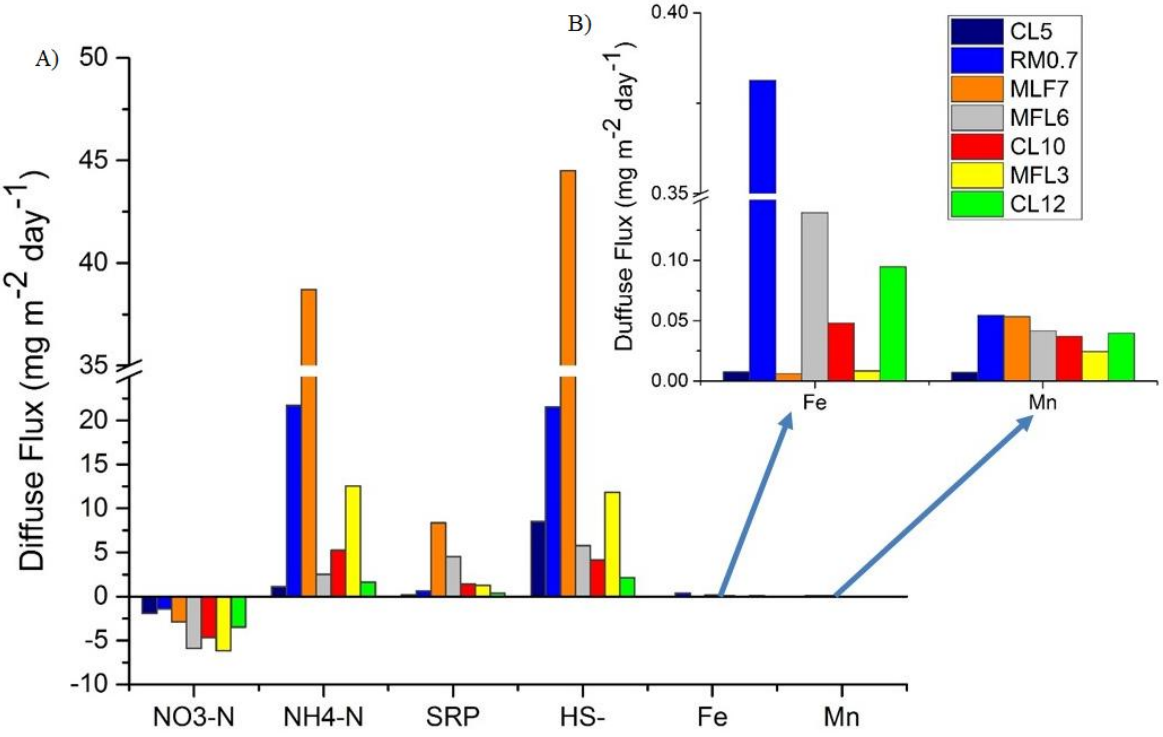

Figure 8.23. A) Solute diffusion fluxes to the Silver River, B) Expanded scale for Fe and Mn fluxes.

In addition to diffusive fluxes, the elevated concentrations of redox sensitive solutes flow to the river along with groundwater, providing solute fluxes that depend both on the rate of groundwater flow, and groundwater solute concentrations relative to the river water concentrations. Advective flux rates of solutes were estimated by combining average vertical groundwater flow (0.4 cm d^{-1}) to the river with solute concentration at the shallowest depth (i.e., 1 cm). For these estimates, we made two assumption: (1) groundwater flow rates measured at the sites were representative of groundwater flow in the entire river, and (2) no further change in solute concentrations occurs between the sediment-water interface and the concentration at 1 cm depth in the sediment. Similar to the diffusive flux rates, the estimated advective flux rates have a heterogeneous distribution throughout the river (Figure 8.24). Advective flux rates for all the solutes at all sites are lower than the diffusive flux rates (Figures 8.23 and 8.24), and Fe and Mn have the lowest advective flux rates, suggesting that diffusion is more important process in delivering solutes to the river than uni-directional advective fluxes. However, hyporheic exchange resulting from flow over bedforms on the river bottom could also provide an additional flux of water into and out of the sediment (e.g., Harvey and Gooseff, 2015). Such bi-directional exchange across the sediment-water interface cannot be evaluated based on the data collected as part of this project. The importance of diffusion controlled delivery of solutes results from the thick blanket of OC-rich and thus bio-reactive, sediment that covers the entire river bottom.

We upscaled diffusive and advective flux rates across the benthic surface area (0.23 km^2) to estimate the total benthic fluxes of the solutes to the water column (Figure 8.25 and Table 8.4).

Since the rates are highly variable with space along the river, we made the benthic flux estimates by dividing the river into 8 segments, each bounded by upstream and downstream sampling sites, and extrapolating the average solute concentrations of these two sites across the segment. Diffusive fluxes of all solutes are higher than the advective fluxes by a factor of 1 to 7. Higher diffusive flux of NO_3-N to the sediment than advective flux to the water column suggests the benthic sediment represents a net loss of the NO_3-N from the Silver River system. However, this loss of NO_3-N from the river to the sediment accounts for only 0.02 % of the daily NO_3-N load from the spring (Table 8.4). Fluxes of NH_4-N to the river water from bottom sediments exceed loss of NO_3-N to the sediments by a factor of about 6, indicating benthic sediments are a net source of N to the river. In addition to N, benthic sediments also provide 3.7 %, 12 %, 4.5 % and 100 % of the daily spring load of SRP, Fe, Mn and HS^- to the river, respectively (Table 8.4). Even though benthic fluxes of nutrients and trace metals to the water column appear to be small relative to the spring loads, these fluxes occur at the sediment-water interface which may enhance the impact to the benthic communities.

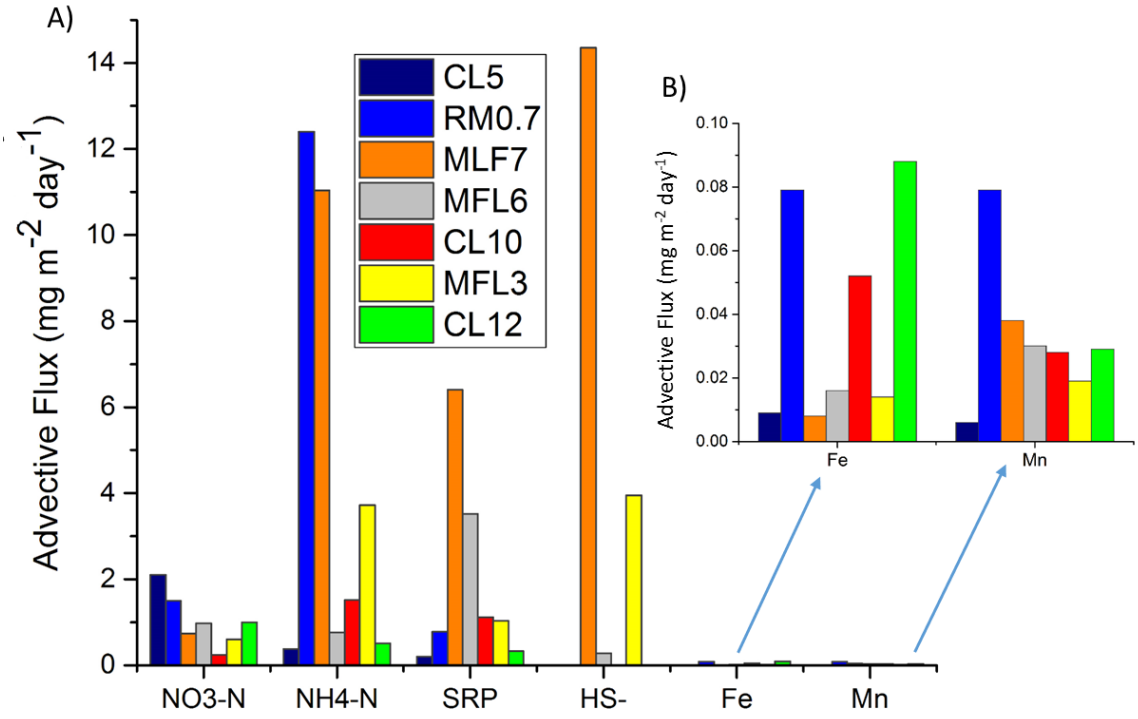

Figure 8. 24. A) solute advection fluxes to the Silver River, B) expanded scale for Fe and Mn fluxes.

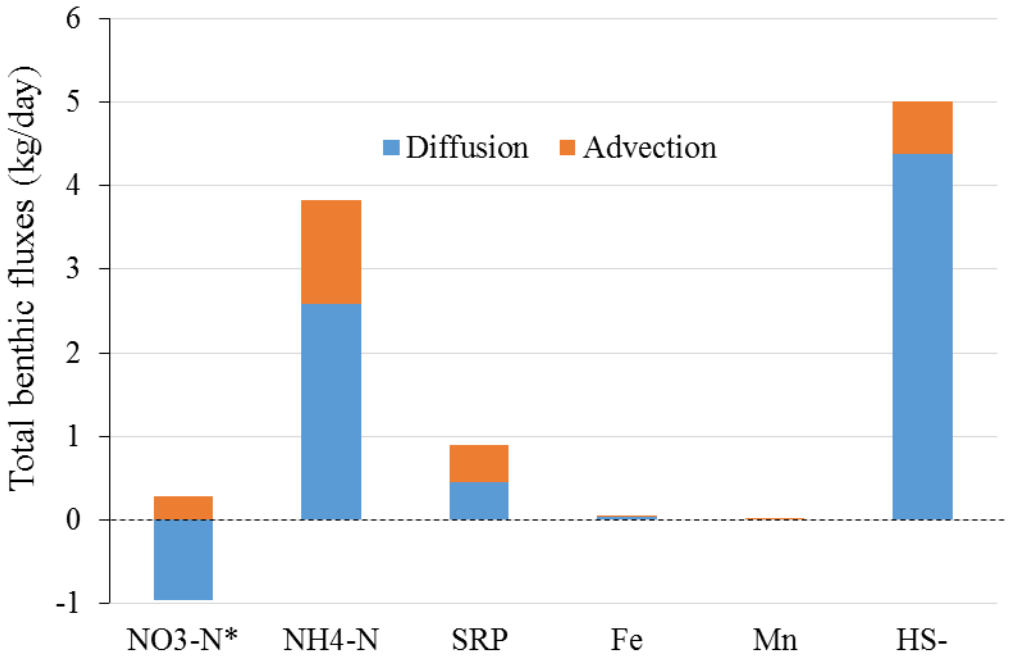

Figure 8.25. Total benthic fluxes of solutes across the sediment – water interface in the Silver River.

Table 8.4. Benthic fluxes of solutes across the sediment - water interface in the Silver River

Solute	Spring Load (kg d^{-1})	Diffusive flux (kg d^{-1})	Advective flux (kg d^{-1})	Total benthic flux (kg d^{-1})	Total benthic flux relative to the spring load (%)
NO_3-N*	4,087	0.95	0.28	0.68	0.02
NH_4-N	30.94	2.58	1.24	3.83	12.37
SRP	24	0.46	0.44	0.90	3.75
Fe	0.41	0.04	0.01	0.05	12.03
Mn	0.41	0.01	0.01	0.02	4.51
HS^-	0	4.38	0.62	5.01	100.00

*Diffusion is sink and advection is source to the water column. Since diffusion flux is higher than advection, the estimated total benthic flux for NO_3-N represents the net sink to the benthic sediments.

8.7 CONCLUSIONS

Based on results from this study, we find the following conclusions, which address the primary goals of the project. These conclusions have implications for management of Silver River, and potentially other spring systems across the state, which are also enumerated below. We end this

section with additional questions that have been raised based on our findings and potential methods for addressing those questions.

8.7.1 Specific Conclusions

(1) Thick sedimentary deposits underlie all of the Silver River and may have been deposited in quiescent lake settings and/or by flowing water. The excess ^{210}Pb measured in sediment cores indicate high and constant sedimentation rate that ranges from 1.6 to 2.2 mm yr^{-1}. The presence of excess ^{210}Pb indicates that if the sediment were originally deposited in a lake, they are being reworked by the river. Sediments originate from erosion of highlands to the west. The sediments are composed of interbedded shell hash and sandy layers with fine grained and organic carbon-rich layers. Some sedimentary organic carbon content is allochthonous, which represents a new source of nutrients to the river. The sediments exhibit C:N ratios that reflect an organic N source enriched in the sediment relative to the C contents. These sediments also have variable C:P ratios that suggest the presence of mineral P in apatite and Fe-Mn oxides in addition to organic P. The sediments act as a barrier to flow from the underlying Upper Floridan aquifer to the river, except where discharging from spring vents.

(2) Hydraulic conductivity of the sediments range from 5.5×10^{-7} to 6.2×10^{-3} m s^{-1}, similar to values expected from gravel beds. Horizontal hydraulic conductivity values are higher than vertical hydraulic conductivity by a factor of 1.1 to 25. Horizontal hydraulic conductivity values are representative of the sandy shell layers. These layers may act as preferential flow paths to the channel, but only if they are continuous, a characteristic which cannot be determined with the distribution of sampling. Head gradients are oriented from the sediment to the river, suggesting groundwater flows to the river. Head gradients are low, limiting the flow rates which we estimate to average between 1.4 and 0.4 cm d^{-1} for horizontal and vertical groundwater flow, respectively.

(3) Biogeochemical reactions in the sediment are dominated by redox reactions and pore water chemistry profiles and indicate that the redox state extends to methanogenesis. Each sampling site has unique chemical gradients. These reactions create concentration gradients to maximum concentrations of solutes that can be more than 100 times greater than the concentrations in the river. Solutes produced by these reactions could be important sources to the river, depending on reactions at the sediment-water interface as they discharge from the sediment to the river.

(4) Concentration gradients created by the biogeochemical reactions drive diffusional fluxes of ecologically important solutes including NH_4-N, SRP, Fe, Mn and HS^- from the sediments to the river, while NO_3-N is lost to the sediments from the water column. In addition, the measured hydraulic conductivity and head gradients indicate that flow also provides an additional mechanism to transport solutes to the river although the estimated advective fluxes of all solutes are lower than diffusion fluxes.

8.7.2 Management Implications

Our conclusions provide information that could contribute to development of management plans for the Silver River. Perhaps most important for the overall goal of this project – the reduction of NO_3-N in the Silver River - our studies indicate that benthic sediments are of limited importance to this goal. Although the sediment are an overall source of N, through diffusion and advection

of NH_4-N, the N fluxes are minor compared to those from the spring. However, benthic sediments are important sources of other solutes that could act as nutrients, including Fe and P. Even though the benthic fluxes are small relative to the spring loads, these nutrients are delivered directly to the benthic ecosystems and thus gradients in the stagnant zone within the SAV meadows could be important. Similarly, toxic effects of dissolved sulfide could also be an important effect to consider in management plans.

Management plans that include nutrient contributions from benthic sediments should consider the distribution of the sediment types and physical properties. The most important physical property to consider is the distribution of hydraulic conductivity, specifically high permeability shell hash layers that could act as conduits from the underlying Floridan aquifer to the river. Management plans should also consider that the distribution of benthic sediments is not static and that as the river channel meanders, sediment will be redistributed and resuspended, which will provide an additional mechanism to deliver all nutrients to the water column.

Finally, management of the delivery of solutes from benthic sediments to the stream should consider the source of the nutrients. The element and isotopic ratios of the extant organic matter indicates both internal and external loading to the river. The internally loaded organic matter would represent recycling of nutrients from the water column through the sediment back to the water column. However, externally loaded organic matter would represent a new source of nutrients to the water column. Prior to anthropogenic impacts to the surrounding landscape, this external source would have represented a natural source of nutrients to the river. However, as the surrounding landscape and land use are modified by human activities, the external loading could be modified, which stresses the importance of management of land use activities.

8.7.3 Future Research Needs

Results from this study have raised additional questions concerning linkages between Silver River and pore water of its bottom sediment that could not be developed until we understood more about the sediment characteristics. Consequently, some further work could improve understanding of the importance of benthic nutrient fluxes to the river and controls on those fluxes. Specifically:

(1) Additional coring would allow stratigraphic mapping of the course shell layers that would assess the three dimensional nature of these high permeability flow paths. This coring should occur at least as transects from the banks of river to the thalweg. Additional coring/drilling may be required from the uplands and wetlands surrounding the river. This three dimensional mapping would reflect potential drainage paths for interflow from the wetlands to the river.

(2) Our results indicate that Silver River bottom sediments are widespread and thick, covering the entire river bottom. Given the high heterogeneity in sediment pore water chemistry, additional sites for expanded detailed measurements of sediment pore water compositions would provide a refined assessment of the true heterogeneity of the sediment, biogeochemical reactions within the sediment, and the total loading of nutrients and other solutes from the pore waters.

(3) Methane concentrations and isotope ratios would further refine the redox states of the sediments to estimate the magnitude of organic carbon remineralization and the amount of nutrients provided by these reactions. In addition elevated methane concentrations could provide a natural tracer for flow of solutes from the sediments to the river (Cable et al. 1996a). These methane concentrations could be coupled with measurements of ^{222}Rn activities, which also may provide natural tracers for seepage (Cable et al. 1996b).

(4) The multiple potential sources of P available within the bottom sediments (Figure 8.11) could be determined through sequential leaching experiments on the sediments (Ruttenberg 1992). These experiments would be able to separate the P content of loosely sorbed P; Fe-bound P, apatite-bearing P (although both authigenic and detrital apatite can be separated, in Silver River most apatite is likely to be detrital), and organic P. Separating these different P-bearing components would allow a better assessment of the potential magnitudes of P fluxes from sediments to the river, a source that is critical for P dynamics in Ichetucknee River (Kurz et al. 2015).

8.8 REFERENCES

Berner, R. A. 1980. Early diagenesis: A theoretical approach. Princeton University Press.

Boulton, A. J. and Hancock, P. J. 2006. Rivers as groundwater-dependent ecosystems: a review of degrees of dependency, riverine processes and management implications. *Australian Journal of Botany*, 54(2), 133-144.

Boulton, A. J., Findlay, S., Marmonier, P., Stanley, E. H., and Valett, H. M. 1998. The functional significance of the hyporheic zone in streams and rivers. *Annual Review of Ecology and Systematics*, 59-81.

Cable, J. E., Bugna, G. C., Burnett, W. C., and Chanton, J. P. 1996a. Application of ^{222}Rn and CH_4 for assessment of ground water discharge to the coastal ocean. *Limnology and Oceanography*, 41(6), 1347-1353.

Cable, J. E., Burnett, W. C., Chanton, J. P., and Weatherly, G. L. 1996b. Estimating groundwater discharge into the northeastern Gulf of Mexico using radon-222. *Earth Planet. Sci. Lett.*, 144, 591-604.

Cardenas, M. B., Wilson, J. L., and Zlotnik, V. A. 2004. Impact of heterogeneity, bed forms, and stream curvature on subchannel hyporheic exchange. *Water Resources Research*, 40(8).

Cardenas, M. B. 2015. Hyporheic zone hydrologic science: A historical account of its emergence and a prospectus. *Water Resources Research*, 51(5), 3601-3616.

Charette, M. A. and Allen, M. C. 2006. Precision ground water sampling in coastal aquifers using a direct-push, shielded-screen well-point system. *Ground Water Monitoring and Remediation*, 26, 87-93.

Chen, X. 2000. Measurement of streambed hydraulic conductivity and its anisotropy. *Environmental Geology*, 39(12), 1317-1324.

Cline, J. D. 1969. Spectrophotometric determination of hydrogen sulfide in natural waters. *Limnology and Oceanography*, 14(3), 454-458.

Cohen, M. J., Kurz, M. J., Heffernan, J. B., Martin, J. B., Douglass, R. L., Foster, C. R., and Thomas, R. G. 2013. Diel phosphorus variation and the stoichiometry of ecosystem metabolism in a large spring-fed river. *Ecological Monographs*, 83(2), 155-176.

Drever, J. I. 1997. The Geochemistry of Natural Waters: Surface and Groundwater Environments, third ed. Prentice Hall, Englewood Cliffs, New Jersey, pp. 436.

Faulkner, G. L. 1973. Geohydrology of the cross-Florida barge canal area with special reference to the Ocala vicinity. US Geol. Surv. Water-Resour. Inves. Rep. 1-73, 117 pp.

Freeze, R. A. and Cherry, J. A. 1977. Groundwater, Prentice-Hall.

Findlay, S. 1995. Importance of surface-subsurface exchange in stream ecosystems: The hyporheic zone. *Limnology and oceanography*, 40(1), 159-164.

Findlay, S. E. G., Sinsabaugh, R. L., Sobczak, W., and Hoostal. M. 2003. Metabolic and structural response of hyporheic microbial communities to variations in supply of dissolved organic matter. Limnology and Oceanography, 48, 1608-1617.

Flynn, W. W. 1968. The determination of low levels of polonium-210 in environmental materials. *Analytica Chimica Acta*, 43, 221-227.

Froelich, P., Klinkhammer, G. P., Bender, M. A. A., Luedtke, N. A., Heath, G. R., Cullen, D., and Maynard, V. 1979. Early oxidation of organic matter in pelagic sediments of the eastern equatorial Atlantic: suboxic diagenesis. *Geochimica et Cosmochimica Acta*, 43(7), 1075-1090.

Gao, S., Tanji, K. K., and Scardaci, S. C. 2003. Incorporating straw may induce sulfide toxicity in paddy rice. *California Agriculture*, 57(2), 55-59.

Güsewell, S. 2004. N: P ratios in terrestrial plants: variation and functional significance. *New phytologist,* 164 (2), 243-266.

Grenz, C., Cloern, J. E., Hager, S. W., and Cole, B. E. 2000. Dynamics of nutrient cycling and related benthic nutrient and oxygen fluxes during a spring phytoplankton bloom in South San Francisco Bay (USA). *Marine Ecology Progress Series*, 67-80.

Harvey, J. W. and Bencala, K. E. 1993. The effect of streambed topography on surface-subsurface water exchange in mountain catchments. *Water Resources Research*, 29(1), 89-98.

Harvey, J. and Gooseff, M. 2015. River corridor science: Hydrologic exchange and ecological consequences from bedforms to basins. Water Resources Research, 51(9): 6893-6922.

Heffernan, J. B., Cohen, M. J., Frazer, T. K., Thomas, R. G., Rayfield, T. J., Gulley, J., Martin, J. B., Delfino, J. J., and Graham, W. D. 2010. Hydrologic and biotic influences on nitrate removal in a subtropical spring-fed river. *Limnology and Oceanography*, 55(1), 249-263.

Hvorslev, M. J. 1951. Bulletin 36. U.S. Waterways Experimental Station, US Army Corps of Engineers, Vicksburg, Mississippi.

Jahnke, R. A. 1988. A simple, reliable, and inexpensive pore-water sampler. *Limnology and Oceanography*, 33(3), 483-487.

Jones, J. B. and Mulholland, P. J. 1999. Streams and ground waters. Academic Press.

Kasahara, T. and Wondzell, S. M. 2003. Geomorphic controls on hyporheic exchange flow in mountain streams. *Water Resources Research*, 39(1).

Kenney, W. F., Brenner, M., Curtis, J. H., and Schelske, C. L. 2010. Identifying sources of organic matter in sediments of shallow lakes using multiple geochemical variables. *Journal of Paleolimnology*, 44(4), 1039-1052.

Knowles Jr., L., Katz, B. G., and Toth, D. J. 2010. Using multiple chemical indicators to characterize and determine the age of groundwater from selected vents of the Silver Springs Group, central Florida, USA. *Hydrogeology journal*, 18(8), 1825-1838.

Kurz, M. J., Martin, J. B., Cohen, M. J., and Hensley, R. T. 2015. Diffusion and seepage-driven element fluxes from the hyporheic zone of a karst river. *Freshwater Science*, 34(1), 206-221.

Li, Y. H. and Gregory, S. 1974. Diffusion of ions in sea water and in deep-sea sediments. *Geochimica et cosmochimica acta*, 38(5), 703-714.

Martin E. A. and Rice, C. A. 1981. Sampling and analyzing sediment cores for ^{210}Pb geochronology: U.S. Geological Survey Open-file Report 81-983, 31 p.

McGlathery, K. J., Sundbäck, K., and Anderson, I. C. 2007. Eutrophication in shallow coastal bays and lagoons: the role of plants in the coastal filter. *Marine Ecology Progress Series*, 348, 1-18.

McGroddy, M. E., et al. 2004. Scaling of C:N:P stoichiometry in forests worldwide: Implication of terrestrial Redfield-type ratios. *Ecology*, 85(9), 2390-2401.

Meyers, P. A. and Teranes, J. L. 2001. Sediment organic matter. In: Last, W.M., Smol, J.P. (Eds.), Tracking Environmental Changes Using Lake Sediments - Volume II: Physical and Chemical Techniques. Kluwer, Dordrecht, pp. 239–269.

O'Connor, B. L. and Harvey, J. W. 2008. Scaling hyporheic exchange and its influence on biogeochemical reactions in aquatic ecosystems. *Water Resources Research*, 44(12).

Packman, A. I. and Brooks, N. H. 2001. Hyporheic exchange of solutes and colloids with moving bed forms. *Water Resources Research*, 37(10), 2591-2605.

Packman, A. I. and Salehin, M. 2003. Relative roles of stream flow and sedimentary conditions in controlling hyporheic exchange. In The Interactions between Sediments and Water (pp. 291-297). Springer Netherlands.

Phelps, G. G. 1994. Hydrogeology, water quality, and potential for contamination of the Upper Floridan aquifer in the Silver Springs ground-water basin, central Marion County, Florida. 92-4159.

Phelps, G. G. 2004. Chemistry of Ground Water in the Silver springs Basin, Florida, with an Emphasis on Nitrate, US Geological Survey Scientific investigations Report 2004-5144, 54 p.

Runkel, R. L. and Bencala, K. E. 1995. Transport of reacting solutes in rivers and streams. In Environmental hydrology (pp. 137-164). Springer Netherlands.

Ruttenberg, K. C., 1992. Development of a sequential extraction method for different forms of phosphorus in marine sediments. *Limnology and Oceanography*, 37(7): 1460-1482.

Schelske, C. L., Conley, D. J., Stoermer, E. F., Newberry, T. L., and Campbell, C. D. 1986. Biogenic silica and phosphorus accumulation in sediments as indices of eutrophication in the Laurentian Great Lakes. *Hydrobiologia*, 143, 79–86.

Schwartz, F. W. and Zhang, H. 2003. Fundamentals of ground water. Wiley New York.

Stream Solute Workshop. 1990. Concepts and methods for assessing solute dynamics in stream ecosystems. *Journal of the North American Benthological Society*, 95-119.

Terrados, J., Duarte, C. M., Kamp-Nielsen, L., Agawin, N. S. R., Gacia, E., Lacap, D., Fortes, M. D., Borum, J., Lubanski, M., and Greve, T. 1999. Are seagrass growth and survival constrained by the reducing conditions of the sediment? *Aquatic Botany*, 65(1), 175-197.

Torres, I. C., Inglett, K. S., and Reddy, K. R 2011. Heterotrophic microbial activity in lake sediments: effects of organic electron donors. *Biogeochemistry*, 104,165–18.

Wörman, A., Packman, A. I., Johansson, H., and Jonsson, K. 2002. Effect of flow-induced exchange in hyporheic zones on longitudinal transport of solutes in streams and rivers. *Water Resources Research*, 38(1), 2-1.

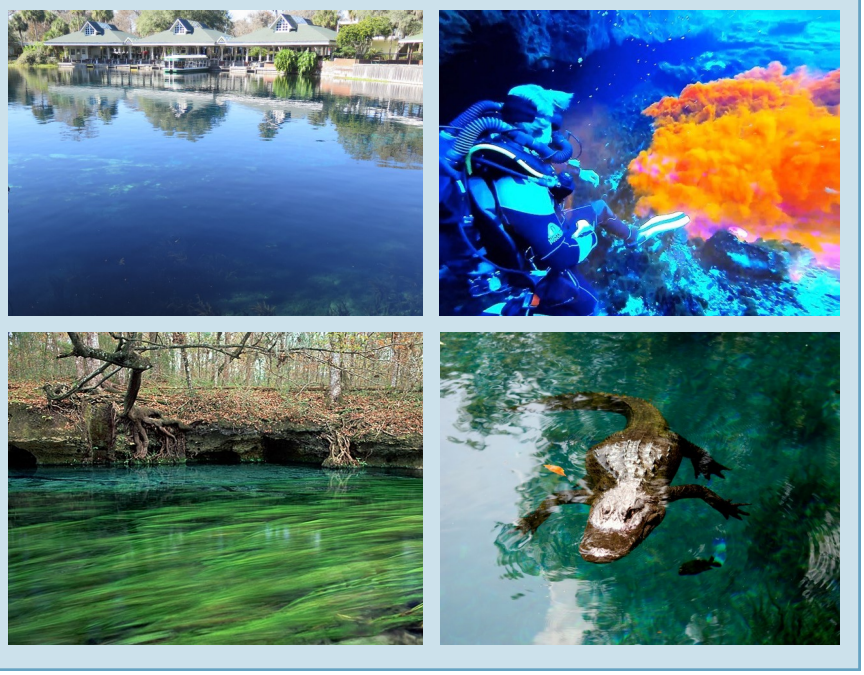

Collaborative Research Initiative on
Sustainability and Protection of Springs [**CRISPS]**

Section 9

[Work Order No: 5]

FINAL REPORT

2014 - 2017

submitted to:

St. Johns River Water Management District
Springs Protection Initiative [SPI], UF Contract # 27789

UF | UNIVERSITY of FLORIDA
Water Institute

C R I S P S

Section 9

BIOLOGY

Trophic Interactions

Final Report 2017
Work Order No. 5

Principal Investigators:

Thomas K. Frazer, University of Florida
Robert A. Mattson, St. Johns River Water Management District

Project Team:

Thomas K. Frazer, School of Natural Resources and Environment
and School of Forest Resources and Conservation
James Nifong, School of Forest Resources and Conservation
University of Florida

Robert A. Mattson
St. Johns River Water Management District

This document reports findings and results of a work order for a 3-year project in compliance with Agreement between University of Florida (UF) and St. Johns River Water Management District (SJRWMD) UF Contract #27789. It is part of the *UF Collaborative Research Initiative on Springs Protection and Sustainability (CRISPS)* and supports the science component of *the SJRWMD Springs Protection Initiative (SPI).*

9.i ABSTRACT

In this study, we focused on trophic interactions as influences on the structure and function of spring-fed systems. We identified primary producers, grazers and consumers; analyzed stable isotopes in the collected material to delineate food webs; assessed grazing rates relative to growth rates in laboratory experiments, and evaluated the potential for top-down (consumer) control of key grazers in a manipulative field experiment.

In Section 9.1, we employed stable isotopes of carbon and nitrogen ($\delta^{13}C$ and $\delta^{15}N$) as tracers to identify pathways of energy flow and material transport in Silver River. Of importance was the potential use of stable isotope values to discriminate among primary producers supporting the Silver River food web and to determine the fate of benthic filamentous algae that are considered nuisance in this system as well as many other spring-fed systems throughout the state. Data generated to date indicate clearly that macrophytes (emergent and SAV) and their epiphytes fuel much of the secondary production that, in turn, supports a diverse assemblage of organisms that occupy higher trophic levels. A key finding thus far is that benthic filamentous algae (hereafter nuisance algae) do not appear to contribute substantially to the production of higher-level organisms in the aquatic food web. Herbivorous insect larvae, however, do appear to use these algae as food. Because nuisance algae are consumed primarily by emergent insects, it is likely that much of this productivity is exported to the surrounding terrestrial environment. In essence, nuisance algal mats in Silver River, and likely other spring systems, may be largely decoupled from the broader aquatic food web. With regard to secondary consumers in the Silver River, stable isotope analysis coupled with other diet information clearly indicates that redear sunfish and kinosternid turtles (musk turtles) are primary predators on gastropods that have been reported to have the potential to exert control on nuisance algae production. These predator prey interactions to date have received little attention, but merit further study to understand more fully the strength of the relationships as they are likely to have a profound influence on ecosystem function. Finally, we note that alligators in the Silver River rely heavily on gastropods and crustaceans to support metabolism and growth. This finding has profound implications for any effort to model the Silver River food web. Previous food web models have considered alligators to be top/apex predators which mainly consume fish and other vertebrates occupying higher trophic levels. In other ecosystems alligators are known to both directly and indirectly affect key ecosystem processes through their interactions with prey and the environment. Integration of these novel data and insights into spring food webs will help to refine our understanding of predation and top-down pressures in influencing community dynamics within these complex ecosystems.

In Section 9.2, we used laboratory feeding trials to assess the capacity of common gastropod and decapod taxa to consume a macroalgal and macrophytic taxa. We assessed assess the capacity of six abundant grazers in the Silver River ecosystem (*E. floridensis*, *Viviparus georgianus*, *P. paludosa*, *Planorbella scalaris*-rams horn snail, *Palaemonetes paludosus*, and *Procambarus fallax*) to consume five macroalgal taxa (*Lyngbya*, *Vaucheria*, *Spirogyra*, *Rhizoclonium*, and *Cladophora*) and five submerged macrophytes (*Hydrilla verticillata*, *Ceratophyllum demersum*, *Sagittaria kurziana*, *Vallisneria americana*, and *Najas guadalupensis*). Consumption was assessed by measuring total mass of vegetative material lost or gained relative to control treatments containing no grazers. In terms of macroalgal consumption, we found *Palaemonetes*

paludosus has both the greatest consumption rate (up to 105 times greater than the consumption rates of other grazers) and the least restricted preferences. Overall, consumption rates for macroalgae were lowest for the nuisance algae *Lyngbya* and interestingly, rates were highest for the nuisance algae *Vaucheria*. In terms of macrophytes, consumption rates of decapod grazers far exceed those of gastropods. Moreover, we found the capacity of *Procambarus fallax* to consume various macrophytes was greater than consumption rates for other grazers.

In Section 9.3, we assessed the potential for top-down (predator) control of key grazers in the Silver River ecosystem using an exclusion approach. The direct (consumptive) and indirect (non-consumptive) effects of predators within food webs are known in many systems to have strong impacts on grazer populations and their behavior, often limiting the degree to which grazers can consume primary producers. In Florida spring-run stream ecosystems, it has been postulated that grazing or lack thereof by macroinvertebrates may play a key role in the regulation of nuisance and epiphytic algal growth and persistence. However, what is not well understood is the role predation may have in regulating grazer abundance and intensity of algal grazing. To begin to develop our understanding of the role of predation in regulating grazer abundance and dynamics of algae within Florida spring-run streams, we employed a predator exclusion approach. Wherein, we excluded small- to large-body predators (i.e., fish, turtles, alligators, etc.) from macrophyte beds and measured the response of macrophytes, epiphytic algae, and the macroinvertebrate community. Experiments were conducted for six months, and they were replicated in the upper and mid regions of Silver River. When predators were excluded, we found only qualitative evidence that macrophyte growth rates increased and epiphytic algal biomass decreased. Interestingly, abundances and biomasses of trichopterans, chironomids and other invertebrate grazers were higher in control treatments (predators present), which may be due to the availability of more food in the form of higher epiphytic loads. These findings, overall, provide little evidence of predator mediated impacts on plant and algal dynamics in Silver River; i.e., strong top-down influences were not apparent.

9.1 DETERMINING FOOD WEB STRUCTURE AND ELUCIDATING TROPHIC LINKS

9.1.1 INTRODUCTION

Freshwater rivers are important ecosystems, providing many essential ecosystem services including clean drinking water, nutrient cycling/sequestration, secondary production, and sediment transport (Wilson and Carpenter 1999; Duraiappah et al. 2005). Worldwide, aquatic ecosystems, including rivers, are experiencing dramatic alterations in vegetative community structure due to the combined effects of eutrophication, other anthropogenic stressors, and global climate change (Stevenson et al. 2010; Carpenter et al. 2011). Frequently, alterations in the identity and abundance of vegetation can have devastating impacts on the functionality of food webs, biodiversity, and greatly diminish the ecological services these systems provide, as well as consequences for human and wildlife health (Ansari et al. 2010a; Paerl and Otten 2013; Hudon et al. 2014). Typical changes in vegetative community structure along the eutrophication progression scheme include an initial shift from vascular submersed aquatic vegetation (SAV) to species of benthic filamentous algae (collectively termed nuisance algae) and within lakes and large rivers, a final progression to phytoplankton blooms and anoxia (Dodds 2006; Ansari et al. 2010b). Unlike the eutrophication sequence of lakes and large rivers, the autotroph community in fast-flowing spring-rivers rarely progresses to phytoplankton blooms, likely due to high discharge rates and short residence times within these systems (Brown et al. 2008).

Florida's underlying karst geology gives rise to the highest density of artesian springs in the world, with over 1,000 recognized springs that produce an extensive network of freshwater streams and rivers. Florida's springs range in discharge (Q) from numerous small seeps ($Q < 8$ mL s^{-1}) to 191 second magnitude springs ($Q = 10$ to 100 cfs or 0.28 to 2.8 m^3 s^{-1}) and 33 first magnitude springs ($Q > 100$ cfs or 2.8 m^3 s^{-1}). Collectively, first and second magnitude springs are responsible for nearly 80 % of the total water discharge from all Florida springs (Scott et al. 2004). Renowned for their exquisite water clarity and the remarkable temporal stability of abiotic conditions (i.e., water chemistry, temperature, discharge rate). Florida springs are also highly productive (range of gross primary productivity or GPP = 0.6 to 64.0 g O_2 m^{-2} d^{-1}, Odum 1957a, 1957b; Duarte and Canfield 1990; Wetland Solutions Inc. 2010), exceeding some of the most productive aquatic ecosystems in the world, such as coastal estuaries (range mean GPP = 2.3 to 28.1 g O_2 m^{-2} d^{-1}, Caffrey 2004) and salt marshes (range GPP = 3.7 to 16.3 g O_2 m^{-2} d^{-1}, Duarte and Agusti 1998). High rates of primary production, in turn, support diverse assemblages and robust populations of higher order consumers ranging from small invertebrates (e.g., bivalves, gastropods, amphipods, and shrimp) to large vertebrates (e.g., American alligator, turtle, fish, and birds), including many endemic and threatened species (Odum 1957a, 1957b; Woodruff 1993; Mattson et al. 1995; Scott et al. 2004; Stevenson et al. 2007). For these reasons Florida's springs and spring-fed rivers are highly important locations for nutrient sequestration, secondary production, sediment accrual, and many other integral ecological services (Brown et al. 2008). In addition, springs and their associated rivers are major destinations for ecotourism and outdoor recreation, bringing in more than five million visitors and $130 million annually, in addition to providing thousands of jobs for Florida residents (Bonn and Bell 2003; Wynn et al. 2014; Borisova et al. 2014).

Over the past 50 years, the combined effects of increased nutrient inputs, reduced discharge, and other environmental stressors (i.e., exotic species, habitat disturbance, etc.) have degraded the ecological health of Florida springs and spring-run streams (Hartnett and Stevenson 2000; Stevenson et al. 2004, 2007; Brown et al. 2008; Heffernan et al. 2010). Historically, dense stands of submersed aquatic vegetation (SAV), chiefly *Sagittaria kurziana* (strap-leaf sagittaria) and *Vallisneria americana* (eel grass), blanketed the benthic substrate of springs and spring-rivers, creating a structurally complex vegetative matrix for epiphytes and consumers to exploit (Odum 1957a, 1957b; Carpenter and Lodge 1986; Duarte and Canfield 1990; Mattson et al. 1995; Brown et al. 2008). More recently, reminiscent of a typical eutrophication scheme, multiple species of benthic filamentous algae (predominantly the cyanobacterium *Lyngbya wollei* and the xanthophyte *Vaucheria* spp., collectively termed nuisance algae), and exotic macrophytes (e.g., *Hydrilla*) have replaced native SAV as the dominant vegetation in many Florida spring-run streams (Munch et al. 2006; Stevenson et al. 2007; Brown et al. 2008). The proliferation of nuisance algae in Florida springs, in particular, has a strong potential to negatively impact the ecological services and economic returns these systems provide (Hartnett and Stevenson 2000; Brown et al. 2008; Hudon et al. 2014). Other aquatic systems that have undergone transition of their primary producer assemblages from SAV-dominated to nuisance algae-dominated have experienced a variety of ecological disturbances including shifts in trophic structure, reduced dissolved oxygen concentrations, decreased GPP, and altered nutrient cycling to name a few (reviews in Duarte 1995; Dodds et al. 2009; Ansari et al. 2010a; Hudon et al. 2014).

In Florida springs, there is some evidence for dramatic reductions in GPP and alterations in trophic structure resulting from reduced SAV abundance and nuisance algae proliferation (Munch et al. 2006; Brown et al. 2008; Quinlan et al. 2008; Camp et al. 2012, 2014). Beyond the ecological consequences of reduced SAV abundance and increased nuisance algal cover, algal mats negatively impact spring aesthetics and recreational activities, and they generate concerns over human and wildlife health due to toxic compounds produced by the cyanobacteria *L. wollei* (Brown et al. 2008; Paerl and Otten 2013; Quiblier et al. 2013; Hudon et al. 2014).

Rising concerns over the imperiled state of Florida's spring ecosystems has stimulated researchers and various state agencies to examine the potential causes for the proliferation and persistence of nuisance algae and exotic macrophytes and to identify prospective restoration techniques that could be employed to restore these ecosystems to their historic condition (Knight 1980; Canfield and Hoyer 1988; Duarte and Canfield 1990; Cowell and Botts 1994; Mumma et al. 1996; McKinsey and Chapman 1998; Hartnett and Stevenson 2000; Katz et al. 2001; Notestein et al. 2003; Stevenson et al. 2004, 2007; Strong 2004; Munch et al. 2006; Evans 2007; Brown et al. 2008; Cowell and Dawes 2008; Quinlan et al. 2008; Albertin 2009; Sickman et al. 2009; Heffernan et al. 2010; Albertin et al. 2012; Hensley and Cohen 2012; Liebowitz 2013; King et al. 2014; Liebowitz et al. 2014).

To date, however, the majority of studies have concentrated on the role of bottom-up factors such as nutrient concentrations (chiefly nitrogen, N, and phosphorus, P), discharge, physical disturbance, and other abiotic factors (e.g., pH, conductivity, light availability, etc.) in driving patterns of nuisance algae abundance and growth, while relatively few have examined the potential for consumer-driven processes (top-down mechanisms) to influence nuisance algal population dynamics in Florida springs (Knight 1980; Brown et al. 2008; Heffernan et al. 2010;

Jiang et al. 2010; Liebowitz et al. 2014; Nifong *In review*). Given that previous studies have failed to demonstrate strong correlations between many bottom-up factors and nuisance algae abundance and growth (Brown et al. 2008; Heffernan et al. 2010) and the mounting evidence that high advection rates in springs minimizes autotrophic nutrient limitation (King et al. 2014; Nifong et al. 2014), alternative causative mechanisms and restoration strategies such as top-down regulation by consumers (i.e., grazing, trophic cascades) should be considered (Heffernan et al. 2010; Hughes et al. 2013; Silliman et al. 2013; Liebowitz et al. 2014; Nifong 2017).

In other aquatic ecosystems (e.g., lakes, streams, sea grass meadows, and coral reefs) grazing has been demonstrated to be a highly important force influencing algal production (Carpenter et al. 1985; Power and Matthews 1985; Duffy et al. 2003; O'Leary and McClanahan 2010), and while understudied in Florida spring ecosystems, grazing could be an important factor in determining the prevalence and persistence of nuisance algae blooms (Liebowitz et al. 2014; Nifong 2017). The few studies conducted in Florida springs thus far have demonstrated certain gastropod species (in particular *Elimia floridensis* [rasp elimia]) have the potential to control growth of periphyton (Knight 1980) and young colonies of nuisance algae (Liebowitz et al. 2014; Nifong 2017). Florida springs are home to numerous herbivorous and omnivorous invertebrates, fish, turtles, and mammals that are capable of exploiting nuisance algae production (Odum 1957a; Mattson et al 1995). However, due to the paucity of data regarding the foraging preferences of herbivorous and omnivorous taxa in Florida spring ecosystems, the relative importance of grazer identify and grazing pressure in driving patterns of nuisance algae prevalence and proliferation remains unknown.

Increasingly ecologists employ measurements of the abundance of naturally occurring stable isotopes of elements ubiquitous to biological tissues (i.e., C, N, S, O, H) to elucidate food web structure and tracer energy flow within complex ecosystems (Peterson and Fry 1987; Fry 2006; Layman et al. 2012). The utility of stable isotope analysis (SIA) for food web studies hinges on the fact that the isotopic composition of a consumer's tissues closely resembles the isotopic composition of the available resource pool (Deniro and Epstein 1978, 1981). Furthermore, recent advances in our understanding of variation in isotopic discrimination (i.e., the difference between consumer tissues and resource isotope values) have extended the applicability of SIA to a wide range of organisms and tissues (McCutchan et al. 2003; Caut et al. 2009). Commonly, a dual isotope tracer approach using stable isotopes of carbon and nitrogen ($\delta^{13}C$ and $\delta^{15}N$) is employed when studying food web structure, since $\delta^{15}N$ provides information on a consumer's trophic position while $\delta^{13}C$ provides insight into the contribution of basal resources pools to consumer diets and use of specific habitats (Layman et al. 2007; Newsome et al. 2007).

To examine food web structure using SIA, various isotopic mixing models have been developed that generate estimates for the relative contribution of particular resources to the diet of consumers and even entire food webs (Oulhote et al. 2011; Kadoya et al. 2012; Phillips et al. 2014). However, the amount of uncertainty and resolution of isotopic mixing model predictions, and thus their usefulness to ecologists in investigating food web structure, are strongly dependent on the separation of source isotope values, variation and accuracy of isotopic discrimination factors used in model simulations, and sufficient characterization of the spatiotemporal variation in source isotope values (Vander Zanden and Rasmussen 2001; Caut et al. 2009; Oulhote et al. 2011; Phillips et al. 2014).

Here we employ SIA of dominant primary producers (i.e., SAV, nuisance algae, epiphytes, and emergent vegetation) and higher order consumers (i.e., herbivores, omnivores, predators) to address the following questions regarding food webs operating Florida's spring ecosystems: 1) What is the fate of nutrients and energy sequestered by nuisance algae? 2) Which consumers forage on nuisance algae and to what degree? 3) Which predator taxa are major consumers of algal grazers?

9.1.2 STUDY SITES

The main CRISPS study area is the Silver River, including its headsprings, which are located in central Marion County, just east of the City of Ocala (Figure 9.1.1). The Silver River system (defined as the river itself and its associated headsprings) is located in the Ocklawaha River sub-basin of the St. Johns River drainage. Silver River is a tributary of the Ocklawaha River, and it runs 5.2 miles (8.4 km), from the headspring to the confluence with the Ocklawaha. Silver Springs is defined as a "spring group" (Copeland 2003), consisting of 30 known springs with numerous spring vents, all located in the upper 1,200 m of the river system. It is the largest spring system in the St. Johns River drainage (in terms of mean annual discharge), and historically was the largest inland freshwater spring in Florida. Silver Springs has been a destination for tourists/site seers for over a century; steamboats from Palatka began ferrying tourists to the spring in the late 1800s. The headspring and surrounding land were leased by W.M. Ray and W.C. Davidson in the 1920s and developed into a tourist attraction, with glass-bottom boats, a reptile show, and other exhibits and amenities. At one point Silver Springs was the premier tourist destination in Florida. The headsprings and river are now part of Silver Springs State Park and managed accordingly by the Florida Park Service.

The Silver River originates at a main headspring, known as Mammoth Spring or Silver Spring. An additional 29 springs (many named, such as Catfish Reception Hall Spring, Blue Grotto Spring, Ladies Parlor Spring, etc.) contribute groundwater discharge to the river system. The water source for the Silver Springs group is the Floridan Aquifer. The Silver Springs group is a first magnitude spring system (defined as >100 cfs [or 2.8 $m^3 s^{-1}$] mean annual discharge), one of four in the St. Johns River Drainage. Historically, the combined flow of the spring group was listed as 820 cfs [23.22 $m^3 s^{-1}$] (Rosenau et al. 1977). Based on current period-of-record, the mean annual flow of the spring group is currently listed at 704 cfs [19.94 $m^3 s^{-1}$] (U.S. Geological Survey gauging station 02239501: access at http://waterdata.usgs.gov/fl/nwis/current/?type=flow& group_ key= basin_cd).

Silver Springs is characterized as a "calcium bicarbonate" system based on the composition of dissolved solids in the discharging groundwater (Woodruff 1993). Basic water quality characteristics are summarized in Table 9.1.1. The principal water quality issue now affecting Silver Springs is a significant increase in concentrations of nitrate (measured as Nitrate-Nitrite N or NO_x-N) over the past several decades (Figure 9.1.2). Natural background concentrations of NO_x-N in the Floridan Aquifer are circa 0.05 mg L^{-1} (Scott et al. 2004), and Silver Springs/Mammoth Springs was at this level in the early 1900s (Collins and Howard 1928; Munch et al. 2006). The Florida Department of Environmental Protection has adopted a Total

Maximum Daily Load for nitrate for Silver Springs/upper Silver River based on the recently adopted NO_x-N criterion of 0.35 mg L^{-1} for springs (Hicks and Holland 2012).

Table 9.1.1. Summary of water quality characteristics of the Silver Springs group. Summary statistics are for the period-of-record, which varied by analyte. Source: SJRWMD unpublished and Munch et al. (2006).

Analyte	Mean	Min	Max	Stand. Dev.
Basic Physical				
Alkalinity (mg L^{-1} as $CaCO_3$)	177.3	140	214	17.6
Conductivity (μmhos cm^{-1})	430.7	350	499	32.0
Total dissolved solids (mg L^{-1})	270.8	229	318	16.3
pH (units)	7.4	5.7	8.1	0.4
Dissolved oxygen (mg L^{-1})	1.9	1.0	5.7	0.9
Transparency				
Color (PCU)	3.0	0	5	1.7
Turbidity (NTU)	0.2	0.1	0.5	0.1
Horizontal Secchi length (m)	73	24	96	---
Nutrients				
Total ammonia (mg L^{-1}; dissolved)	0.01	0	0.04	0.01
Nitrate-Nitrite N (mg L^{-1}; dissolved)	0.92	0.07	1.28	0.27
Total Kjeldahl N (mg L^{-1}; total)	0.10	0.02	0.90	0.15
Total Phosphorus (mg L^{-1}; total)	0.04	0.01	0.07	0.01
Orthophosphate (mg L^{-1}; dissolved)	0.04	0.02	0.07	0.01

Figure 9.1.1. Aerial imagery showing the Silver River system.

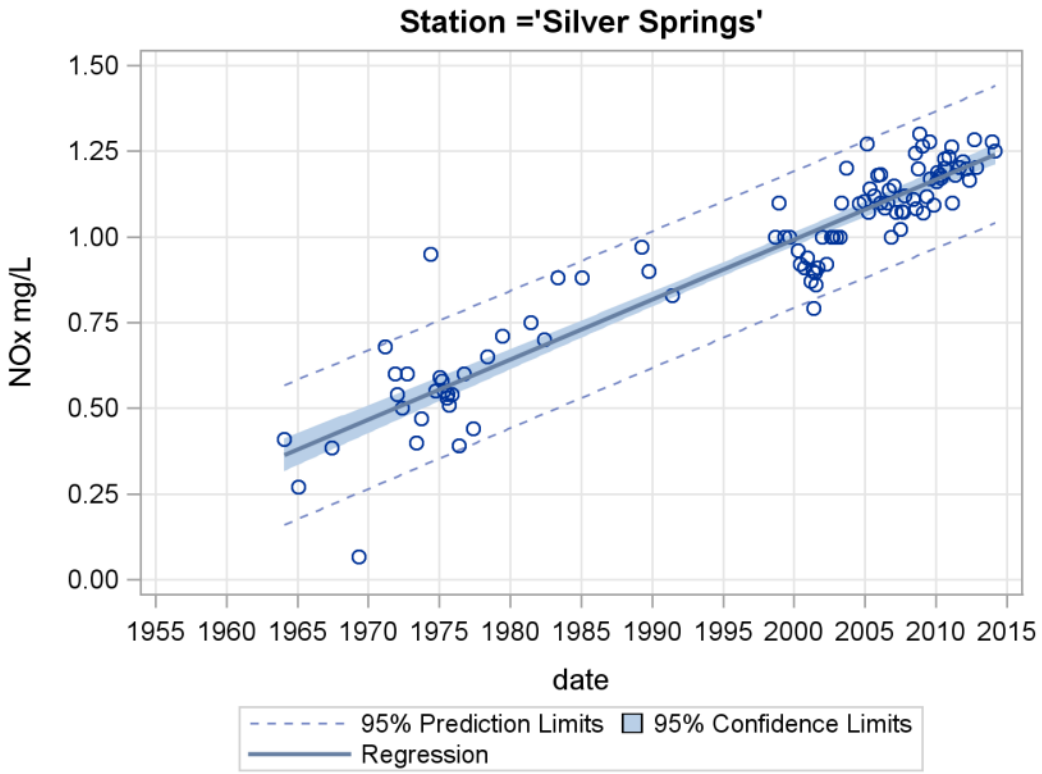

Figure 9.1.2. Temporal trend in Nitrate-Nitrite N (NO_x-N) concentration in Silver Springs.

As with many spring-run streams, Silver River supports extensive beds of SAV. Dominant macrophytes include spring-tape (*Sagittaria kurziana*), eelgrass (*Vallisneria americana*), southern naiad (*Najas guadalupensis*), coontail (*Ceratophyllum demersum*) and water thyme (*Hydrilla verticillata*). Total SAV cover in many areas of the riverbed is on the order of 75–100 % (SJRWMD unpublished data). The assemblage of benthic macroinvertebrates appears to be typical of the benthic communities in other stream ecosystems in north-central Florida; i.e., dominated by various larval and adult aquatic insects (Ephemeroptera, Odonata, Chironomidae and other Diptera, Coleoptera, Trichoptera, and Hemiptera). Other major freshwater benthic invertebrate groups are mollusks (gastropods and bivalves), oligochaetes, and crustaceans (amphipods, isopods, grass shrimp, and crayfish). The river is known to harbor 47 species of fish. Dominant groups (by taxa richness and abundance) are Centrarchidae (sunfish and bass), Cyprinidae (minnows and shiners), and Ictaluridae (catfish and madtoms). Marine species such as striped mullet and Atlantic needlefish are also common, along with gizzard shad.

A second study area in the CRISPS effort is Alexander Springs Creek, located in Lake County (Figure 9.1.3). The creek begins at Alexander Spring, located in a public recreation area in the Ocala National Forest. Alexander Spring is a first magnitude spring with a mean annual flow of 118 cfs (3.34 m^3 s^{-1}; Scott et al. 2002). The spring-run stream runs 11.9 miles (19.1 km) from the headspring to a confluence with the St. Johns River in lakes Dexter and Woodruff. Alexander Spring is classified as a “mixed” spring in terms of its dissolved solids composition (Woodruff 1993), primarily due to higher sodium and chloride levels. Thus, it is a “saltier” spring than the Silver Springs group. However, nitrate concentrations (as NO_x-N) in the spring approximate

background, generally running less than 0.1 mg L^{-1} NO_x-N. Therefore, we sampled this system as a "reference" stream in terms of water quality.

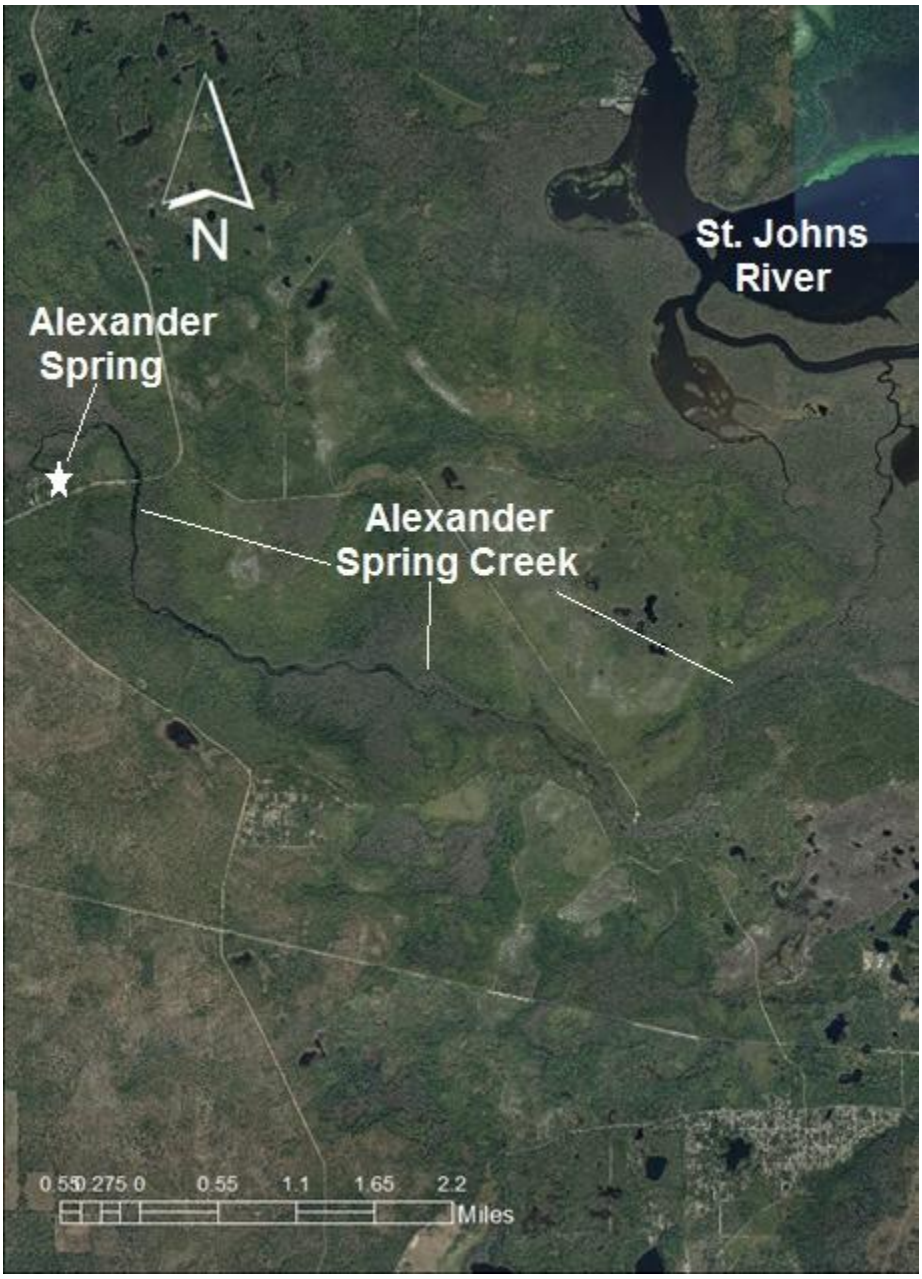

Figure 9.1.3. Aerial imagery of Alexander Springs Creek.

Like the Silver River, Alexander Springs Creek supports extensive beds of SAV. A mapping effort conducted in the creek in 2008 identified 113.35 total acres [458,711.175 m²] (Dial, Cordy and Assoc. 2008). Dominant taxa are, in general, similar to those observed in Silver River: eelgrass (dominant), southern naiad, and coontail. Spring-tape was not found in this system. SAV cover is slightly more variable, ranging from 50–100 % in much of the stream channel, but 75–100 % along many reaches (SJRWMD unpublished data). The benthic invertebrate community of Alexander Springs Creek has received little attention. Sampling of the fish

assemblage yielded 40 species. Fish community composition appears similar to that of Silver River, and it is dominated by centrarchids and cyprinids. Mullet, needlefish and possibly other marine taxa also occupy Alexander Springs Creek.

9.1.3 METHODS

9.1.3.1 Sampling Design

In July 2014, we established six sampling segments (200 m long) in three reaches (upper, mid, lower) in the main channel of the Silver River at different distances from the main spring boil (Figure 9.1.4). All sampling segments were near established SJRWMD vegetation monitoring stations. During initial sampling, we collected a broad suite of plants and animals to capture the full range of isotopic variation present in the food web. Targeted sampling of particular taxa provided additional insights into the observed isotopic variation. We opportunistically sampled larger-bodied consumers such as *Alligator mississippiensis* (American alligator), snakes, turtles, and highly mobile fish throughout the study area, recording capture locations using handheld GPS (Model 60 CSx, Garmin International, Inc., Olathe, Kansas). We assigned data from opportunistically captured taxa to nearest river reach for subsequent analyses.

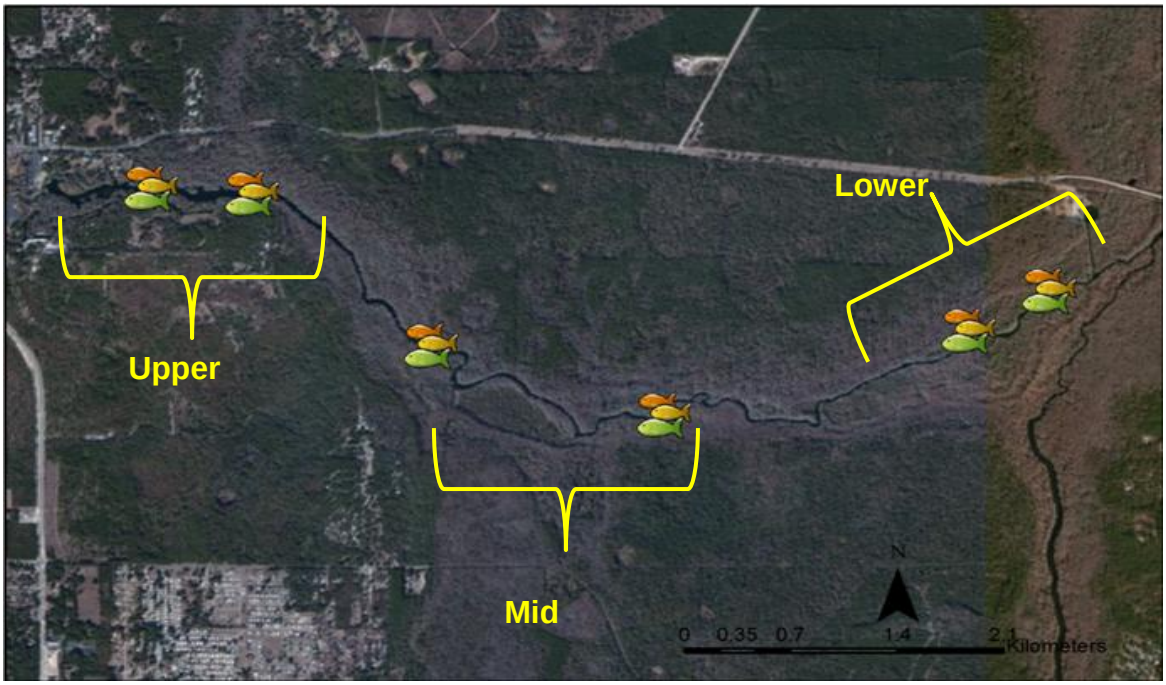

Figure 9.1.4. Map of Silver River with stable isotope sampling areas identified for the upper, mid and lower river reaches. Symbols denote center of 200 m sampling segment.

9.1.3.2 Primary Producers

We hand-collected vascular plant and algae samples either from a boat, by snorkeling, or using SCUBA. Along sampling transects within each river segment, we collected live healthy leaf material from 10 to 15 macrophytes and pooled like samples for subsequent analysis. Composite samples of epiphytic macroalgae and diatoms consisted of epiphyton removed from 10 to 15 macrophyte leaves. Similarly, we pooled samples of benthic algae from 5 to 10 locations within and among individual mats (depending on abundance), and we combined samples of unattached

filamentous algae from 5 to 10 individual algal patches. We stored all of the aforementioned samples in clean Ziploc bags, placed samples on ice at the time of collection, and transferred to -10 °C freezer until further processing.

In the laboratory, we thawed and then washed samples with deionized water. Macrophytes were thoroughly scraped and rubbed free of all epiphytic material using a sterile razor blade (material retained for subsampling of epiphytic algae), and macroalgae were examined with the aid of a dissecting microscope and/or compound microscope (10–45X) to identify them to the lowest possible taxonomic level and remove macroinvertebrates and debris (i.e., minerals, detritus, etc.). Following cleaning, we dried samples to a consistent mass at 60 °C and homogenized to fine powder with scissors and/or mortar and pestle.

9.1.3.3 Consumers

We collected consumers using a variety of gear types depending on microhabitat conditions and size of the target species. We collected macroinvertebrates and small fish (total length-TL < 5 cm) from submerged and emergent macrophytes using dip-nets or removed them from macrophytes and macroalgae during cleaning and processing. We collected larger fish using electrofishing. We collected turtles, snakes, and alligators using standard capture techniques (i.e., by hand, tongs, snare, or snag hook). For the majority of macroinvertebrate taxa (i.e., larval and adult insects), composite samples comprised 10–20 whole individuals. For larger specimens (i.e., grass shrimp and crayfish) and those with calcareous shells (i.e., gastropods, bivalves) bulk muscle tissue was removed from 1-5 individuals of similar size and combined into one composite sample. We obtained fish tissues for isotopic analysis through a combination of non-invasive fin clipping and dorsal muscle sampling. For small fish, we collected and euthanized individuals then clipped the entire dorsal portion of the caudal fin and removed a small section of dorsal muscle using sterile dissection scissors and/or scalpel. We then combined tissues from 10-15 individuals to yield one composite sample for each tissue type. In the case of larger fish, we sampled single live individuals by removing approximately 1 cm^2 of caudal fin tissue using sterile dissection scissors. A subset of larger fish were sacrificed for stomach content analysis; from these specimens we additionally removed 1 cm^3 of dorsal muscle tissue to compare isotopic values of fin and dorsal muscle tissue (Sanderson et al. 2009). From turtles, we collected a 6-mm diameter section of keratinized scute tissue from the plastron using a sterile biopsy punch. Alligators were subject to collection of blood and keratinized skin tissue from the caudal scute whirls. Excluding blood collected from alligators we stored all tissue samples in sterile containers/bags, immediately placed samples on ice at the time of collection, and froze at -10 °C until further processing. Before freezing, we centrifuged samples of alligator blood at 3,000 rpm for 5 minutes to separate red blood cell and plasma fractions.

Prior to stable isotope analysis we thawed whole specimens and sampled tissues, thoroughly cleaned samples to remove debris (i.e., epiphytic algae, detritus, and other foreign materials) using deionized water, dried samples at 60 °C to consistent mass, and homogenized into a fine powder. In the case of alligator scute tissue, we cleaned thawed samples and separated the keratinous epidermal layer of the alligator scute from dermal collagen layer by digesting in 0.1 *M* NaOH for 12–24 hours prior to drying and homogenizing (Radloff et al. 2012).

9.1.3.4 Stable Isotope and Elemental Analyses

We analyzed all tissue samples for composition of stable carbon and nitrogen isotopes ($\delta^{13}C$ and $\delta^{15}N$). In addition, we measured elemental ratios (C:N) for all primary producer samples and certain consumer samples (e.g., macroinvertebrates) with variable elemental composition that could potentially influence the interpretation of stable isotope data and require adjustment/normalization of isotopic values (i.e., lipid content, Post et al. 2007). We loaded approximately 500 to 800 µg of homogenized consumer tissues or 1 to 3 mg of primary producer tissues into 9 mm × 5 mm tin capsules for stable isotope analysis at the University of Florida Geology Stable Isotope Laboratory, Gainesville, Florida. We conducted sample analyses using one of two systems: either a Finnigan DeltaPlus XL isotope mass spectrometer with ConFlo III interface linked to a Costech ECS 4010 Elemental Combustion System (elemental analyzer) or Finnigan-MAT 252 isotope ratio mass spectrometer coupled with a ConFlo II interface linked to a Carlo Erba NA 1500 CNS Elemental Analyzer. Stable isotope values are expressed in standard per mil notation δX (‰): δX (‰) = [Rsample⁄Rstandard -1]×1,000, where X is the element of interest and R is the ratio of heavy to light isotopes ($^{13}C/^{12}C$ or $^{15}N/^{14}N$) of the sample and standard (Vienna Pee Dee Belemnite used for $\delta^{13}C$ and Atmospheric Nitrogen-AIR for $\delta^{15}N$). We measured machine accuracy during each sample run (max 42 samples per run), using four to seven measures of in-lab standard USGS-40 (L-glutamic acid, $\delta^{13}C$ = -26.39 and $\delta^{15}N$ = −4.52) and adjusted data accordingly. Across all runs, analytical machine error for USGS-40 was 0.16‰ ± 0.05 for $\delta^{15}N$ and 0.14‰ ± 0.07 $\delta^{13}C$ (n = 21).

9.1.3.5 Isotopic Mixing Model Analysis and Isotopic Niche Metrics

9.1.3.5.1 Bayesian Isotopic Mixing Model (SIAR)

To estimate the relative proportional contributions of basal resource groups to the diet of consumers, we applied the Bayesian based isotopic mixing model (SIAR, version 4.2) formulated by Parnell et al. (2010). The SIAR framework incorporates variation in end-member (resource) and consumer isotope values, as well as trophic discrimination factors (i.e., change in isotope value from diet to tissue; Parnell and Jackson 2013). Thus, SIAR provides robust approximations of the relative proportional contributions of resources to the diet of consumers while incorporating multiple sources of uncertainty (Parnell et al. 2010, Phillips et al. 2014). When available, we used experimentally determined taxon-specific trophic discrimination factors and for other cases, we calculated diet-dependent trophic discrimination factors using equations developed by Caut et al. (2009) based on consumer taxon, habitat type, and isotope values of potential food sources. In addition, for herbivorous consumers and certain omnivorous taxa we incorporated concentration dependence into the SIAR model framework using mean % C and % N data for each resource category (currently, SIAR does not allow for variation in elemental compositions to be incorporated into the model framework). Each SIAR simulation consisted of 500,000 iterations, a burn-in interval of 50,000 iterations, and thin-by interval of 15, producing marginal posterior distributions (contribution-to-diet vectors) containing 30,000 estimates for each potential resource group (end-member).

9.1.3.5.2 Measuring Dietary Specialization

To examine patterns in resource use specialization we used the posterior distributions (contribution-to-diet vectors) produced by SIAR mixing model analyses to calculated ε, the degree of dietary specialization at the population-level (Newsome et al. 2012). Values of ε range

from 0 to 1, where a value approaching 0 represents a population of ultra-generalist consumers (individuals forage on all resources in equal proportions) and a value of 1 denotes an ultra-specialist consumer population (consume a single resource).

9.1.3.5.3 Estimating the Isotopic Niche Area

As a proxy for trophic niche width (i.e., the breadth or diversity of resources a consumer uses), we calculated the standard ellipse area using Bayesian inference (SEA_B) based on bivariate $\delta^{13}C$ and $\delta^{15}N$ data from each consumer species or group (Jackson et al. 2011). SEA_B is the bivariate equivalent of the univariate standard deviation and encompasses the core isotopic niche area occupied by a population or sub-population. The Bayesian framework used to estimate SEA_B incorporates uncertainty in the calculation of the covariance matrix used to estimate the standard ellipse area, and it is unbiased with respect to sample size (Jackson et al. 2011). Larger values of SEA_B represent species/groups that demonstrate a broader range of trophic interactions, a proxy for trophic niche width (Newsome et al. 2007). Similar to SIAR simulations, each SEA_B simulation consisted of 500,000 iterations, a burn-in interval of 50,000 iterations, and thin-by interval of 15, producing marginal posterior distributions containing 30,000 estimates of SEA_B ($‰^2$) for each taxa of interest.

9.1.3.6 Stomach Content Analysis

For the majority of fish species, we collected stomach contents from live individuals by gastric lavage following momentary immobilization by electrofishing. Smaller fish (TL<10 cm) and those species whose anatomy limits the success of gastric lavage (e.g., striped mullet, gizzard shad, and gar) were sacrificed and the entire stomach removed. Similar to large fish, stomach contents were collected from alligators using a modified form of gastric lavage known as the hose-Heimlich technique developed for crocodilians (Fitzgerald 1989). Once removed, stomach contents were sieved using 300 μm mesh, preserved in 10 % formalin, and transferred to 70 % ethanol for storage. Contents were visually inspected under a dissecting and/or compound microscope to separate prey and non-prey items; prey items were identified to lowest possible taxonomic level (family in most cases) and identifiable individuals enumerated. For fish, stomach content fractions (i.e., prey and non-prey material) were dehydrated at 60 °C and dry mass measured to the nearest 0.0001 g using a digital scale (XS204DR, Mettler Toledo, Columbus, Ohio). Due to the large size of some prey remains in alligator stomach contents, wet mass was measured to the nearest 0.01 g using a digital scale (PGL 2002, Adam Equipment Inc., Oxford, Connecticut) after gently blotting material with paper towels to remove excess water and preservative.

We quantified diets of consumer species or subgroupings by calculating percent numerical abundance (%N), percent gravimetric abundance (%W), percent frequency of occurrence (%FO), and percent Index of Relative Importance (%IRI) for each prey category using as follows (Cortés 1997, Liao et al. 2001):

$$\%N = \frac{100N_i}{\sum_{i=1}^{n} Ni}, \quad (9.1.1)$$

$$\%W = \frac{100W_i}{\sum_{i=1}^{n} Wi}, \quad (9.1.2)$$

$$\%FO = \frac{100FO_i}{\sum_{i=1}^{n} FOi'} \quad (9.1.3)$$

$$\%IRI = 100 \times IRI_i \sum_{i=1}^{n} IRI_i, \quad (9.1.4)$$

where n is the number of prey categories identified for a sub-population, *Wi* and *Ni* are the total wet mass and number of individuals of prey *i* in a sub-population, respectively, *FOi* is the number of stomach contents containing prey *i* in a sub-population divided by the total number of individuals sampled in a sub-population, and *IRIi* = %*FOi*(%*Wi* + %*Ni*). Gravimetric measures of prey closely approximate volumetric measurements, and it is a preferred method of measurement for many invertebrate taxa with chitinous exoskeletons that tend to float, such as insects (Garnett 1985).

9.1.3.7 Turtles, Gastropods, and Herbivorous/Omnivorous Fish

Since gastric lavage of live specimens is rarely successful on turtles, we employed non-invasive fecal material analysis (i.e., scat analysis). Following capture, body measurements, and tissue collection, we placed individual turtles into appropriately sized plastic storage containers containing a few inches of ambient water free of particulates and/or small organisms overnight for approximately 12 hours. Following this time period, the water and any scat passed by each individual was sieved using 300 µm mesh, preserved in 10 % buffered formalin, and transferred to 70 % ethanol for storage. We subsequently released individuals at the site of capture. We calculated %IRI for prey and resource groups to draw comparisons among species.

We removed the contents from the stomachs of certain herbivorous/omnivorous, preserved the collected material, and examined it for presence and absence of primary producer groups (i.e., macroalgae, diatoms, macrophytes) as well as prey items. We quantified diets using %IRI as described for predatory fish and alligators.

9.1.3.8 Statistical Methods

To examine differences in stable isotope values among primary producers, we first grouped data from all river regions into three broad categories (algae, emergent macrophytes, and submerged macrophytes) representing the dominant resource pools available to primary consumers. The isotopic data from less common and/or unique taxa that were excluded from broad autotroph groupings are discussed separately. To draw more in-depth comparisons and determine how to delineate resource pools for use in isotopic mixing model analyses, we further categorized autotrophs based on river region, taxonomy, and growth form. To assess the potential effects of these factors on isotopic and elemental composition we performed separate ANOVAs for each dependent variable of interest (i.e., $\delta^{15}N$, $\delta^{13}C$, and C:N) and tested for interactions among predictor variables. If significant effects were detected, we performed post-hoc pairwise comparisons (Tukey HSD, $\alpha = 0.05$) to further examine significant differences among the groups being compared. Relationships between body size of consumers and isotopic composition were assessed using Pearson's correlation test. All significant differences were evaluated at $\alpha = 0.05$. All statistical analyses were performed in R 3.1.1 (R Core Team 2014). Stable isotope values are presented as mean ± 1 standard deviation (SD) unless otherwise noted.

9.1.4 RESULTS

9.1.4.1 Stable Isotope Ratios and Elemental Composition of Primary Producers

We conducted numerous field expeditions to Silver River and Alexander Springs Creek from 08-06-2014 to 06-02-2016 to collect tissue samples from resident primary producers. Although we collected and processed a total of 242 composite samples from approximately 42 autotroph taxa (this includes some broader classifications, unknown species, and mixed species groups), the data here represent only the results from 160 samples analyzed from Silver River (Appendix 9.1.1) and 15 samples from Alexander Spring Creek (Appendix 9.1.4).

In general, $\delta^{13}C$ values in algal taxa (n = 91, -37.4 ‰ ± 6.3) were lower in comparison to submerged (n = 39, -34.7 ‰ ± 3.7) and emergent macrophytes (n = 30, -30.3 ‰ ± 2.0) (Figure 9.1.5). Mean $\delta^{13}C$ values of broad primary producer groups significantly differed from one another ($F_{2,150}$ = 21.69, p-value < 0.001), but they were not significantly different among river regions ($F_{2,150}$ = 1.4, p-value = 0.25) nor was there a significant interaction between group and river region ($F_{4,150}$ = 0.6, p-value = 0.66). Post-hoc analysis indicated mean $\delta^{13}C$ values between all autotroph groups were significantly different from one another. Although relative differences in $\delta^{13}C$ values among primary producer groups were statistically equal across the three river regions, $\delta^{13}C$ values of algae were more positive and closer to those of submerged macrophytes in the mid river (Table 9.1.2 and Figure 9.1.6).

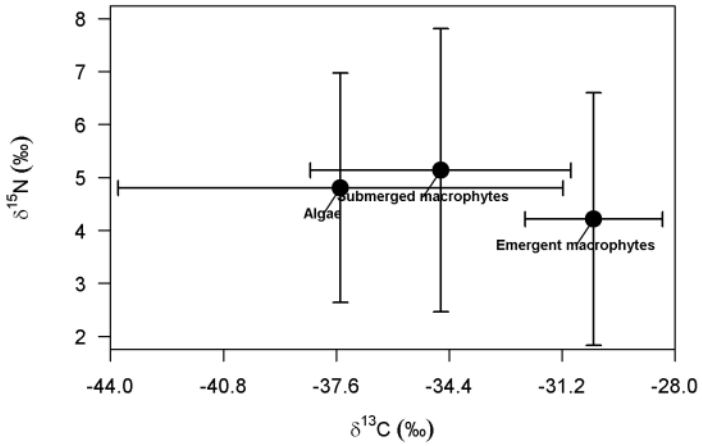

Figure 9.1.5. Stable carbon and nitrogen isotope composition of broad autotroph groups from Silver River. Points are means and error bars are ± 1 standard deviation (SD).

Table 9.1.2. Stable isotope composition ($\delta^{15}N$ and $\delta^{13}C$) and elemental ratios (C:N) of broadly characterized primary producer groups from Silver River as a function of river region. For each group, overall values are calculated across all river regions, i.e. upper, mid and lower.

		$\delta^{15}N$ (‰)		$\delta^{13}C$ (‰)		C:N	
Group and region	**n**	**mean**	**SD**	**mean**	**SD**	**mean**	**SD**
Algae (ALG)	91	4.8	2.2	-37.4	6.3	9.1	1.9
upper	46	3.8	2.1	-37.6	6.0	9.1	2.1
mid	29	5.1	1.7	-36.0	7.6	9.4	2.0
lower	16	7.0	1.4	-39.6	4.1	8.8	1.1
Emergent vegetation (EMG)	30	4.2	2.4	-30.3	2.0	14.4	3.7
upper	13	4.1	2.6	-30.5	2.5	13.4	3.0
mid	13	4.5	2.4	-30.4	1.5	15.5	4.4
lower	4	3.7	2.1	-29.4	1.3	13.9	2.9
Submerged aquatic vegetation (SAV)	39	5.2	2.7	-34.7	3.7	13.1	3.0
upper	22	4.4	2.9	-35.1	4.3	13.7	3.5
mid	11	5.3	1.9	-34.2	2.9	11.9	1.7
lower	6	7.8	1.2	-34.4	2.9	13.1	3.0

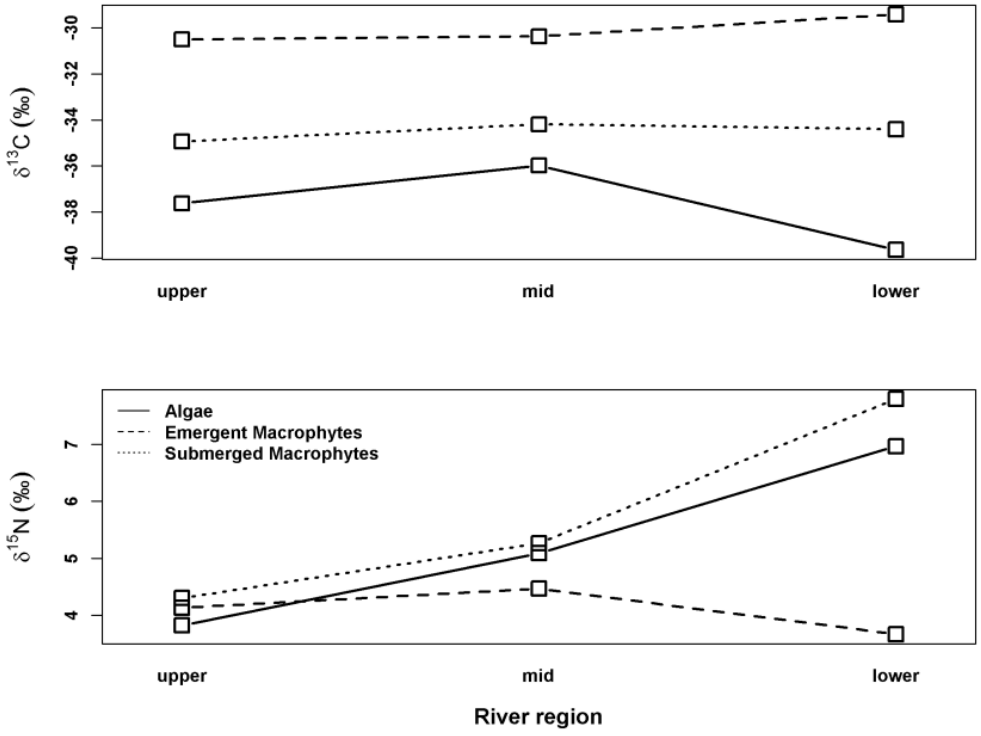

Figure 9.1.6. Interaction plots of the combined effects of group and river region on $\delta^{13}C$ (top panel) and $\delta^{15}N$ (bottom panel) values of dominant autotrophs. Symbols represent mean values.

The range in mean $\delta^{15}N$ values was narrower than for $\delta^{13}C$ values, ranging from +4.2 ‰ ± 2.4 for emergent **macrophytes** to +5.2 ‰ ± 2.7 for submerged macrophytes. We found $\delta^{15}N$ values were not significantly different among autotrophic groups ($F_{2,150}$ = 1.6, p-value = 0.20) or combinations of group and river region ($F_{4,150}$ = 2.0, p-value = 0.09), but they were significantly different among river regions ($F_{2,150}$ = 16.1, p-value < 0.001). $\delta^{15}N$ values significantly differed among all river regions, with $\delta^{15}N$ values increasing with distance from the main spring boil.

We found mean C:N ratios of autotrophs differed significantly among groups ($F_{2,150}$ = 57.1, p-value < 0.001), and they did not differ significantly among river regions ($F_{2,150}$ = 0.36, p-value = 0.70) or among combinations of groups and river regions ($F_{4,150}$ = 2.1, p-value = 0.08). Post-hoc analysis indicated mean C:N significantly differed between submerged macrophytes and algae, and emergent macrophytes and algae, while submerged and emergent macrophyte C:N values were not significantly different. Tissue C:N was highest for emergent macrophytes, slightly lower for submerged macrophytes, and lowest for algal taxa (Table 9.1.2).

Within our broad autotrophic groups, we investigated the effects of taxonomy and growth form to gain further insight into sources of isotopic variation within each resource pool. Algae within Silver River represent a diverse assemblage of organisms including diatoms, cyanobacteria, chlorophytes (green algae), rhodophytes (red algae), and xanthophytes (yellow-green algae). We separated data for algae based on growth form: epiphytic (found attached to surface of submerged macrophytes), benthic (found growing directly from or resting on the benthic substrate, hereafter referred to as nuisance algae), or unattached (found free in the water column or gently resting on macrophytes). The most commonly observed nuisance algae were *Vaucheria* (Xanthophyta) and *Lyngbya* (cyanobacteria); other filamentous taxa such as *Dichotomosiphon* (Chlorophyta) and *Compsopogon* (Rhodophyta) were found on occasion in benthic algal mats in the upper and mid river. The most commonly encountered unattached algae were chlorophytes including *Spirogyra*, *Ulothrix*, and *Rhizoclonium*. The epiphytic community included a variety of chlorophytes (e.g., *Cladophora*, *Mougeotia*, *Stigeoclonium*, and *Ulothrix*), the rhodophyte *Compsopogon*, and numerous pennate and centric diatoms (for detailed list of diatom genera and other algal taxa present at Silver River see Odum 1957a and Quinlan et al. 2008). It should be noted that all samples of filamentous algae likely contained a marginal number of diatoms and microscopic bacteria in addition to the dominant filamentous taxa. In addition to the presence of diatoms, benthic and epiphytic algal samples often contained two or more filamentous algae (Jacoby et al. 2007).

Among primary producers, algal taxa demonstrated the greatest range in stable carbon isotope composition. We found $\delta^{13}C$ values measured in individual algal samples ranged from -45.9 ‰ in the nuisance algae *Vaucheria* to -14.8 ‰ in the epiphytic algae *Cladophora* (Appendix 9.1.1). $\delta^{13}C$ and $\delta^{15}N$ values of algae were significantly different among growth forms ($F_{2,82}$ = 23.2, p-value < 0.001 and $F_{2,82}$ = 9.6, p-value < 0.001, for $\delta^{13}C$ and $\delta^{15}N$, respectively), while only $\delta^{15}N$ values were significantly different among river regions ($F_{2,82}$ = 2.6, p-value = 0.08 and $F_{2,82}$ = 21.2, p-value < 0.001, for $\delta^{13}C$ and $\delta^{15}N$, respectively). We found a significant interaction between algal growth form and river region for $\delta^{13}C$ ($F_{4,82}$ = 2.8, p-value = 0.03), but not for $\delta^{15}N$ ($F_{4,82}$ = 1.6, p-value = 0.17). Post-hoc analysis indicated that stable carbon isotope compositions of all algal growth forms were significantly different from one another. $\delta^{15}N$ values

were significantly greater for unattached algae than for nuisance and epiphytic forms (Table 9.1.3 and Figure 9.1.7). Similar to the overall pattern found for macrophytes, $\delta^{15}N$ values measured in algae increased with distance down river (Figure 9.1.8).

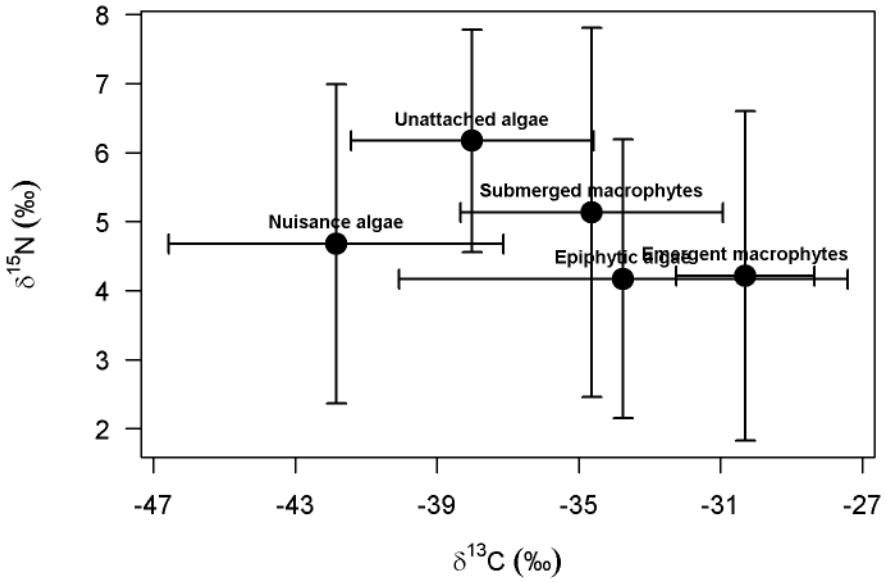

Figure 9.1.7. Carbon and nitrogen isotope composition of dominant autotroph groups and algal growth forms. Points are means and error bars are ± 1 standard deviation (SD).

Table 9.1.3. Stable isotope composition ($\delta^{15}N$ and $\delta^{13}C$) and elemental ratios (C:N) of algal growth forms from Silver River.

	$\delta^{15}N$ (‰)		$\delta^{13}C$ (‰)		C:N	
Growth form	**mean**	**SD**	**mean**	**SD**	**mean**	**SD**
Epiphytic	4.2	2.0	-33.7	6.3	9.5	2.1
Unattached	6.2	1.6	-38.0	3.4	9.6	2.1
Nuisance	4.7	2.3	-41.8	4.7	8.3	1.3

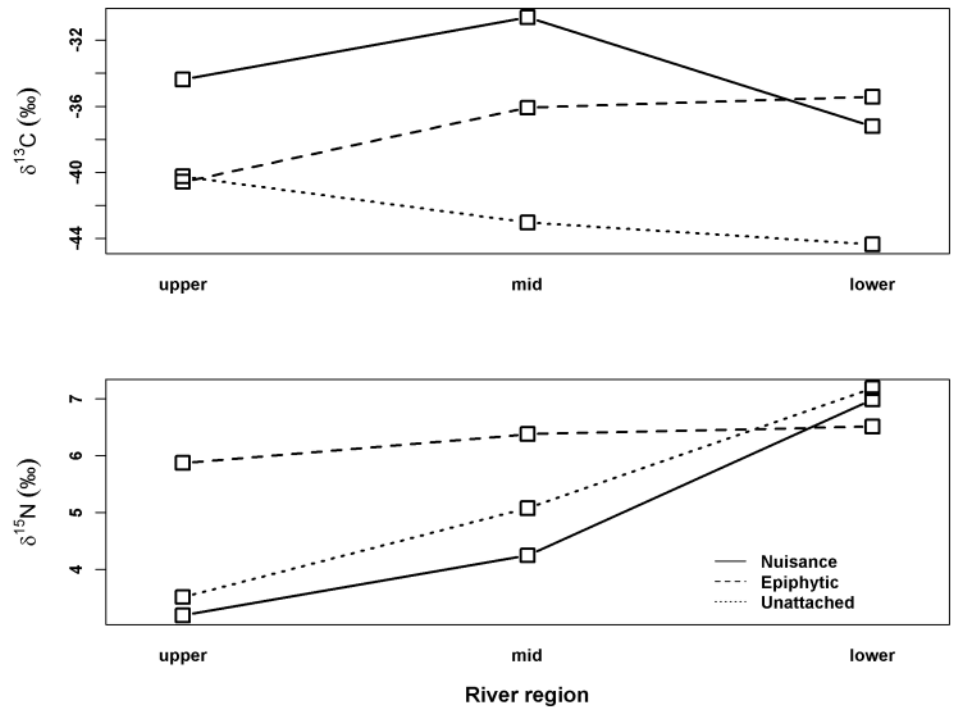

Figure 9.1.8. Interaction plots of the combined effects of growth form and river region on $\delta^{13}C$ (top panel) and $\delta^{15}N$ (bottom panel) values of algal taxa. Symbols represent mean values. Note the interaction of algal growth form and river region was not significant for $\delta^{15}N$.

We found mean C:N of algae differed significantly among growth forms ($F_{2,82} = 5.3$, p-value = 0.007) but not among river regions ($F_{2,82} = 0.7$, p-value = 0.49) or combinations of growth forms and regions ($F_{4,82} = 0.3$, p-value = 0.86). Post-hoc analysis indicated no significant differences between mean C:N of epiphytic and unattached algae, however, C:N of both epiphytic and unattached algae were found to be significantly greater than C:N of nuisance algae (Table 9.1.3).

By far the most abundant submerged macrophyte in Silver River is *Sagittaria kurziana*; however, a number of other macrophytes were frequently encountered throughout the study area (Appendix 9.1.1). While our sample sizes were small, we found significant differences among taxa for $\delta^{13}C$ values ($F_{4,33} = 7.7$, p-value < 0.001) and C:N ratios ($F_{4,33} = 5.0$, p-value = 0.003). Post-hoc analysis revealed $\delta^{13}C$ values of *S. kurziana* were significantly greater than *Ceratophyllum demersum* and *Hydrilla verticillata*, while $\delta^{13}C$ values of *Vallisneria americana* were significantly greater than *C. demersum*, with all other pair-wise differences being non-significant. Qualitatively, $\delta^{13}C$ values of submerged macrophytes seemed to fall into two major groupings, with *S. kurziana* and *V. americana* being more similar to each other than to *H. verticillata*, *Najas guadalupensis*, or *C. demersum* (Figure 9.1.9). In terms of C:N, we found the only significant pair-wise difference was between *V. americana* and *C. demersum,* with *V. americana* having higher C:N ratios (p-value = 0.002). Stable nitrogen isotope ratios did not vary significantly among submerged macrophytes ($F_{4,33} = 2.2$, p-value = 0.08).

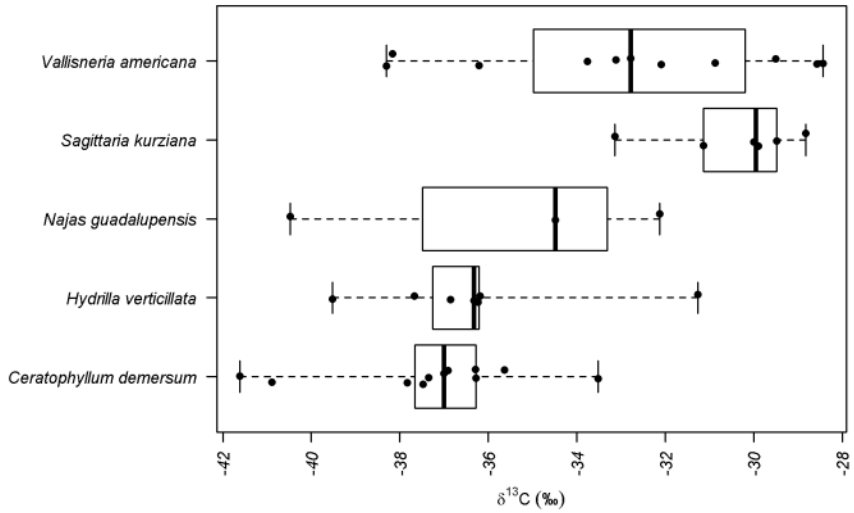

Figure 9.1.9. Box plot of $\delta^{13}C$ values measured in submerged macrophyte taxa. Center bars denote the median, box constrains the first and third quartiles, whiskers extend to data extremes, and points are individual sample values.

The emergent macrophyte assemblage present at Silver River comprise numerous species ranging from small plants such as duckweed (*Lemna* spp.) and floating fern (*Salvinia* spp.) to dense stands of large rooted plants, chiefly *Nuphar advena* (spatterdock) and *Pontederia cordata* (pickerel weed). In general, the $\delta^{13}C$ values of emergent macrophytes were more positive than submerged macrophytes and algae, with values ranging from -35.7 to -26.8 ‰, measured in *Nasturtium floridanus* (watercress) and *N. advena*, respectively. $\delta^{15}N$ values were also variable, and they ranged from 0 to +8.6 ‰, measured in *N. floridanus* and *P. cordata*, respectively. While we measured the stable isotope composition of a variety of emergent and floating autotrophs (Appendix 9.1.1), for the purposes of this study we concentrated on isotopic composition of the dominant taxa *N. advena* and *P. cordata* since these species comprised the majority of emergent macrophyte biomass and structure. Stable carbon isotope composition of *N. advena* (-28.5 ‰ ± 1.7) and *P. cordata* (-29.3 ‰ ± 0.7) were similarly positive, and they did not differ significantly (Welch t-test: t = 1.17, df = 9.7, p-value = 0.26). However, mean $\delta^{15}N$ of *P. cordata* (6.3 ‰ ± 1.4) was found to be significantly greater than *N. advena* (2.8 ‰ ± 1.5) (t = -4.6, df = 11.4, p-value < 0.001).

Stable isotope values of primary producer taxa collected from Alexander Spring Creek were in general more positive for $\delta^{13}C$ and similar for $\delta^{15}N$ as compared to samples collected from Silver River (Appendix 9.1.4). $\delta^{13}C$ values measured for SAV collected from Alexander Spring Creek averaged -23.6 ‰ ± 0.8 (n = 3) and $\delta^{15}N$ values averaged 1.7 ‰ ± 3.2. $\delta^{13}C$ values of green filamentous algae, represented by *Spirogyra* and an identified taxon, averaged -18.9 ‰ ± 2.8 (n =2) and $\delta^{15}N$ averaged 3.2 ‰ ± 1.5. We found that $\delta^{13}C$ values of benthic filamentous algae (*Lyngbya*, n = 4) collected from Alexander Spring Creek averaged -28.0 ‰ ± 2.0 and $\delta^{15}N$ values averaged 4.3 ‰ ±0.7.

9.1.4.2 Stable Isotope Composition of Less Common and Unique Autotrophs

To assess the potential for incorporation of terrestrial leaf litter into the detrital resource pool for the aquatic food web, we measured the isotopic composition of the dominant tree species along the river margins, *Taxodium distichum* (Bald cypress). The stable isotope composition of *T. distichum* was similar to that of emergent macrophytes; $\delta^{13}C$ measured for *T. distichum* was -29.6 ‰ ± 0.2 and $\delta^{15}N$ was 1.8 ‰ ± 1.6 (n = 2). We also measured the stable isotopic composition of a number unique autotrophs that could potentially contribute to basal resource pools, including *Tillandsia usneoides* (Spanish moss), *Utricularia* sp. (bladderwort), *Fontinalis* sp. (water moss), and lichen. The isotopic composition of *T. usneoides* was quite distinctive in that $\delta^{15}N$ values measured for this plant were extremely negative (-9.5 ‰) and $\delta^{13}C$ values (-17.2 ‰) were considerably higher than the majority of autotrophs. Bladderwort, water moss, and lichen were found to have similar $\delta^{13}C$ and $\delta^{15}N$ values to algal taxa. $\delta^{13}C$ values for these taxa ranged from -41.0 to -36.0 ‰, measured in water moss and bladderwort, respectively. $\delta^{15}N$ values for these taxa ranged from +3.5 to +7.0 ‰, measured in lichen and water moss, respectively.

9.1.4.3 Stable Isotope Composition of Consumers

We analyzed a total 989 consumer samples for stable carbon and nitrogen isotope composition (Appendix 9.1.2 and 9.1.3). Samples analyzed include 219 macroinvertebrates, 649 fish, 57 turtles, and 64 alligators.

In general, we found the stable isotope composition of consumers to follow well known patterns of isotopic discrimination within food webs (Figure 9.1.10). Specifically, we found enrichment of both ^{13}C and ^{15}N with increasing trophic position (i.e., primary producers to top predators); however, there was substantial variation in isotopic composition among taxa with similar trophic ecology (i.e., herbivore, predator, etc.), within taxa related to body size and life history stage, and in some cases, among river regions.

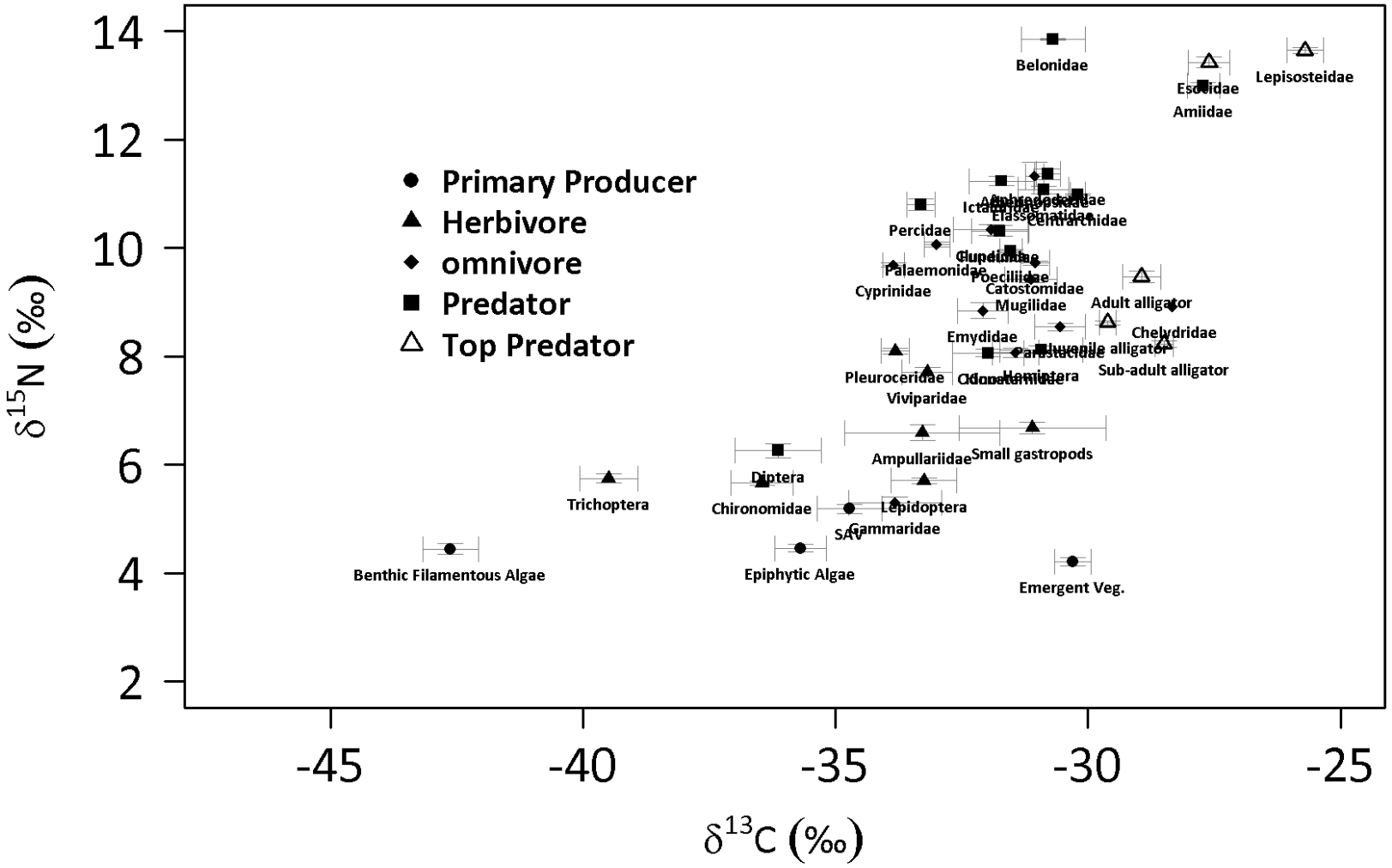

Figure 9.1.10. Scatter plot of $\delta^{13}C$ and $\delta^{15}N$ values measured in all food web constituents. Symbols represent means and error bars are ± Standard Error (SE). Resource group and consumer taxon are labeled under each symbol.

9.1.4.4 Stable Isotope Composition of Herbivores and Omnivores

Florida springs are home to a diverse assemblage of herbivores and omnivores that have the potential to directly utilize algal and macrophytic production. Species range in size from minute insect larvae such as chironomids (non-biting midges) to large-bodied fish (e.g., striped mullet, and lake chubsucker [*Erimyzon sucetta*]). The gastropod assemblage present in springs and spring-run streams was of particular interest as these organisms can be remarkably abundant, comprising the majority of macroinvertebrate biomass in macrophyte beds and benthic algal mats, and they are key herbivorous grazers in spring-run streams (Heffernan et al. 2010b; Liebowitz 2013). The gastropod assemblage present in Florida springs contains taxa from six families, Ampullariidae, Hydrobiidae, Physidae, Planorbidae, Pleuroceridae and Viviparidae.

In terms of the gastropod assemblage present in Silver River, the largest gastropod is the ampullarid *Pomacea paludosa* (Florida apple snail), whereas the smallest are various species of hydrobiids and physids. The most frequently encountered gastropods in submerged macrophytes beds were the pleurocerid *Elimia floridensis* (rasp elimia), various planorbids, and the viviparid, *Viviparus georgianus* (banded mystery snail).

The stable carbon isotope signatures of gastropods ranged widely, i.e. -39.1 to -20.0 ‰, whereas the stable nitrogen isotope signatures exhibited less variation, i.e. +5.0 to +10.4 ‰. To assess taxon specific differences in gastropod isotopic composition, isotopic data were grouped at the family-level; however, a few samples classified as families Planorbidae and Hydrobiidae contained individuals from the family Physidae due to processing errors. The stable carbon isotope composition of ampullariids (-33.3 ‰ ± 4.1), represented by the single species *P. paludosa*, was on average similar to pleurocerids and viviparids; whereas, $\delta^{13}C$ values of planorbids and hydrobiids were more positive near -30.0 ‰ (Table 9.1.4). We found a significant difference among taxa for $\delta^{13}C$ values ($F_{4,43} = 3.2$, p-value= 0.02); however, we did not detect a significant difference among river regions ($F_{4,43} = 1.3$, p-value = 0.28) or combinations of taxa and river regions ($F_{7,43} = 1.5$, p-value = 0.17; Figure 9.1.11).

Table 9.1.4. Stable isotope composition ($\delta^{15}N$ and $\delta^{13}C$) of gastropods.

		$\delta^{15}N$ (‰)		$\delta^{13}C$ (‰)	
Taxa	**n**	**mean**	**SD**	**Mean**	**SD**
Ampullariidae	13	7.4	1.7	-33.3	3.0
Hydrobiidae	6	7.0	1.6	-30.8	5.7
Planorbidae	6	6.9	0.9	-30.3	3.1
Pleuroceridae	16	8.0	0.7	-34.0	0.8
Viviparidae	16	7.9	1.2	-33.1	1.8

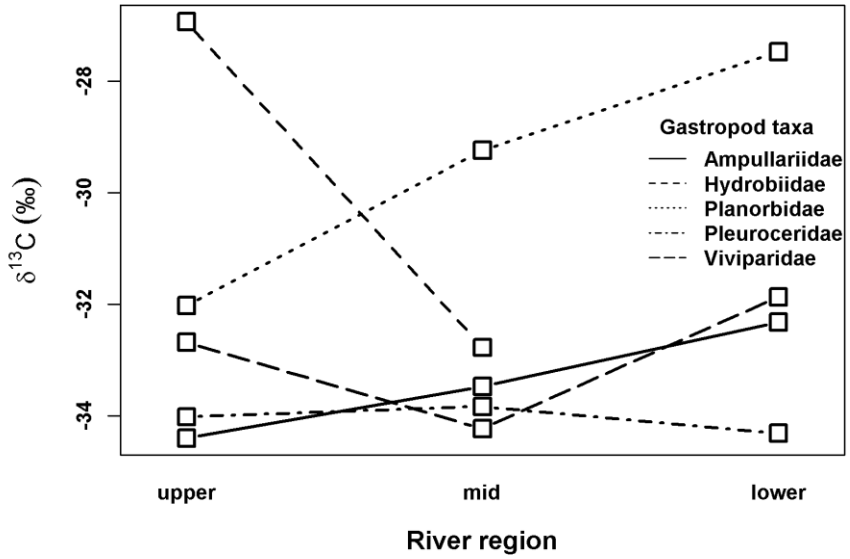

Figure 9.1.11. Interaction plot of the combined effects of taxon and river region on $\delta^{13}C$ values of gastropod taxa. Symbols represent mean values.

The stable nitrogen isotope composition of gastropods did not differ significantly among taxa ($F_{4,43}$ = 2.3, p-value = 0.07) or combinations of taxa and river regions ($F_{7,43}$ = 0.9, p-value = 0.52), but it did differ significantly among river regions ($F_{2,43}$ = 17.5, p-value < 0.001). Mean $\delta^{15}N$ values measured in all gastropod taxa were similar, differing by only 1.1‰ across families (Table 9.1.4 and Figure 9.1.12). As expected from patterns observed for primary producers, $\delta^{15}N$ values of gastropods were significantly elevated in the lower river relative to the mid (p-value < 0.001) and upper regions (p-value < 0.001, Figure 9.1.13), while $\delta^{15}N$ values did not differ among samples collected in the mid and upper regions.

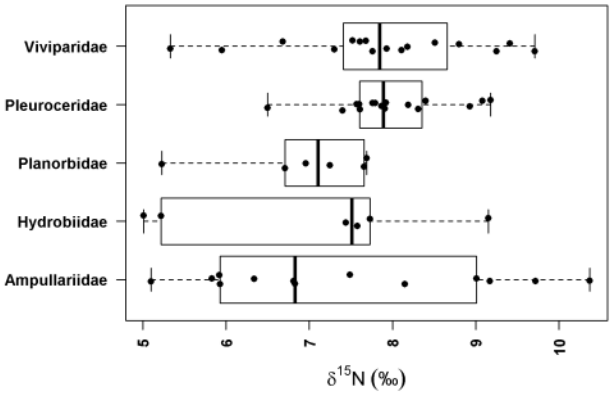

Figure 9.1.12. Box plot of $\delta^{15}N$ values measured for gastropods. Center bars denote the median, box constrains the first and third quartiles, whiskers extend to data extremes, and points are individual sample values.

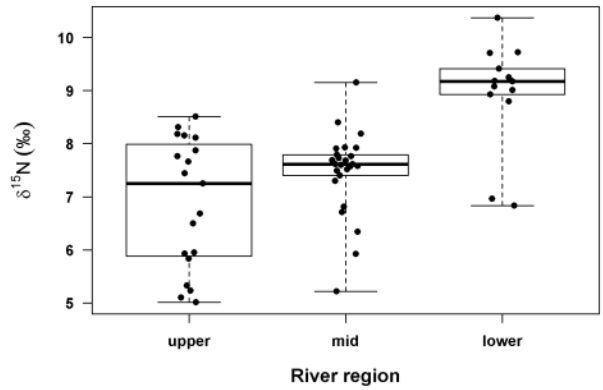

Figure 9.1.13. Box plot of $\delta^{15}N$ values measured for gastropods from different river regions. Center bars denote the median, box constrains the first and third quartiles, whiskers extend to data extremes, and points are individual sample values.

Many bivalves are long-lived, non-mobile filter feeders and their $\delta^{15}N$ values often are used as baselines for estimating the trophic position of higher order consumers in aquatic ecosystems (Post 2002). In springs, unionid mussels provide an integrated representation of the isotopic composition of particulate organic matter (POM) and planktonic organisms. Along the entire length of Silver River the $\delta^{13}C$ and $\delta^{15}N$ values of unionid mussels showed little variation (n = 9, $\delta^{15}N$ = 8.3 ‰ ± 0.6 and $\delta^{13}C$ = -32.9 ‰ ± 0.5). In relation to the isotopic composition of gastropods, the isotopic composition of unionids was highly similar to the isotopic composition observed for *Viviparous georgianus* (banded mystery snail); a taxon known to employ a pseudo-filter feeding technique known as ctenidial suspension feeding (Strong et al. 2008).

In addition to gastropods and bivalves, the macroinvertebrate community inhabiting Silver River includes aquatic insects (larvae and adults) and crustaceans. The feeding habits of larval insects can vary tremendously even by species, thus we acknowledge isotopic variation within broad taxonomic groups may be driven largely by interspecific differences in foraging ecology. Trichopteran larvae (caddisflies), predominantly hydroptilids (purse caddisflies), were commonly encountered on submerged macrophytes and within macroalgae in the upper and mid river sampling sites; however, we were unsuccessful in locating trichopterans at lower river sites. $\delta^{13}C$ values measured in trichopterans (-39.5 ‰ ± 2.4) were the most negative of any primary consumer or omnivore. $\delta^{15}N$ values of trichopterans were low (+5.7 ‰ ± 1.5) in the upper river relative to the mid-river. Larval chironomids were highly abundant in the epiphyton of macrophytes as well as within benthic algal mats. While more negative than most primary consumers, $\delta^{13}C$ values measured in chironomids (-36.4 ‰ ± 2.5) were highly variable. $\delta^{15}N$ values of chironomids were less variable and consistently low (5.6 ‰ ± 0.7). Isotopic composition of other more omnivorous dipteran larvae (i.e., Athericidiae, Stratiomyidae) was highly variable among taxa (n = 4, range $\delta^{13}C$ = -35.5 to -28.4 ‰; range $\delta^{15}N$ = 6.0 to 9.0 ‰). Larvae of multiple crambid and pyralid species (Lepidoptera; aquatic moths) were abundant on submerged macrophyte blades. Mean $\delta^{13}C$ values of crambids and pyralids (-33.2 ‰ ± 2.9) were more positive than other aquatic insects; however, there was a considerable range among individual samples (n = 20, range $\delta^{13}C$ = -35.5 to -26.6 ‰). Overall $\delta^{15}N$ values of crambids and pyralids were low (5.7 ‰ ± 1.5).

Isotopic compositions of herbivorous aquatic insects did differ significantly. We found significant differences among taxa ($F_{2,50}$ = 28.1, p-value < 0.001) and river regions ($F_{2,50}$ = 2.8, p-value = 0.05) for $\delta^{13}C$ values; however, the interaction of taxon and river region was not significant ($F_{3,50}$ = 0.4, p-value = 0.72). Post-hoc analysis indicated $\delta^{13}C$ significantly differed among all groups of herbivorous insects (Figure 9.1.14). $\delta^{15}N$ values of herbivorous insects did not differ significantly among taxa ($F_{2,50}$ = 0.01, p-value = 0.98), but the main effect of river region ($F_{2,50}$ = 17.9, p-value < 0.001) and the interaction of taxon and river region were significant ($F_{3,48}$ = 3.4, p-value = 0.02, Figure 9.1.15).

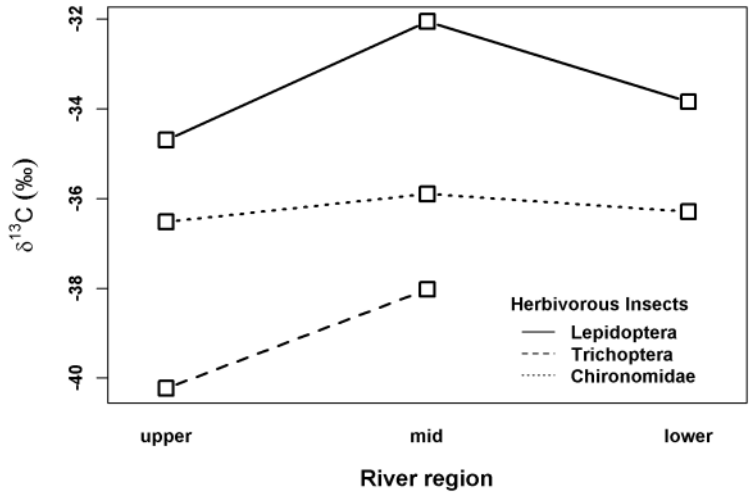

Figure 9.1.14. Interaction plot of the combined effects of taxon and river region on $\delta^{13}C$ values of aquatic herbivorous insects. Symbols represent mean values.

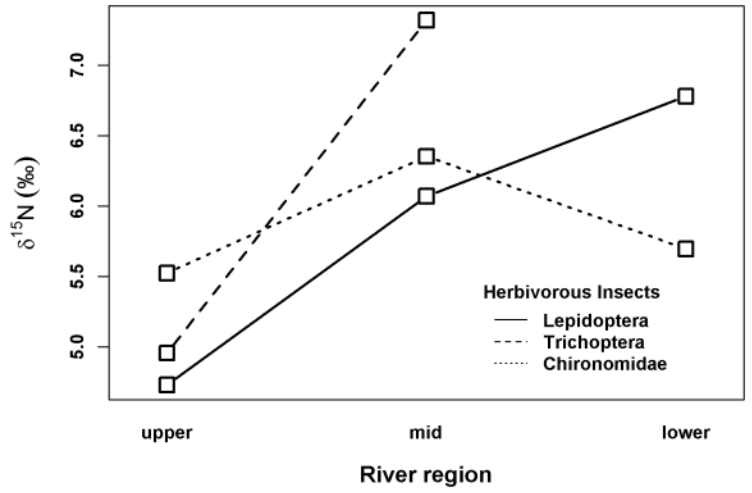

Figure 9.1.15. Interaction plot of the combined effects of taxon and river region on $\delta^{15}N$ values of aquatic herbivorous insect taxa. Symbols represent mean values.

We measured stable isotope composition in species from three crustacean families, Gammaridae (amphipods), Palaemonidae (grass shrimp), and Parastacidae (crayfish). The stable carbon isotope composition of crustaceans differed significantly among taxa ($F_{2,37}$ = 9.2, p-value < 0.001), and it was not significantly different among river regions ($F_{2,50}$ = 2.1, p-value = 0.14) or combinations of taxon and region ($F_{4,37}$ = 0.8, p-value = 0.56). Post-hoc analysis indicated $\delta^{13}C$ values measured in crayfish (-30.6 ‰ ± 2.1) were significantly greater than grass shrimp (p-value = 0.02) and amphipods (p-value < 0.001, Figure 9.1.16). Stable nitrogen isotope composition of omnivorous crustaceans only differed significantly among taxa ($F_{2,37}$ = 77.8, p-value < 0.001), with no significant differences among rivers region ($F_{2,37}$ = 1.6, p-value = 0.22) or combinations of taxa and regions ($F_{4,37}$ = 2.1, p-value = 0.09). Post-hoc analysis indicated $\delta^{15}N$ values of all taxa were significantly different from one another. $\delta^{15}N$ values were lowest in amphipods (5.4 ‰ ± 1.3), higher in crayfish (8.5 ‰ ± 1.2), and highest in grass shrimp (10.1 ‰ ± 0.6).

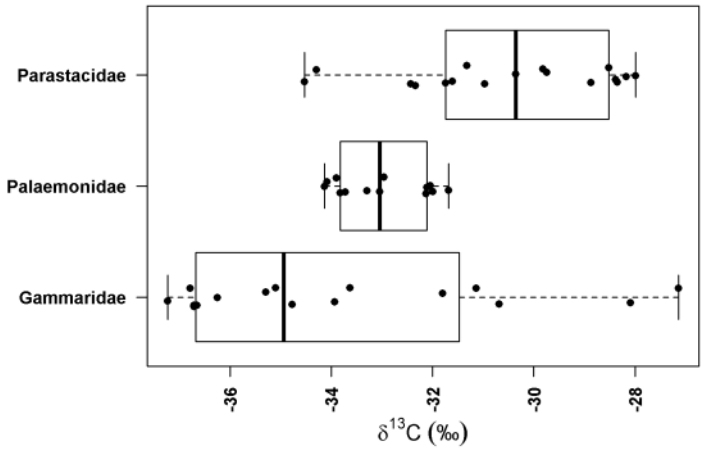

Figure 9.1.16. Boxplot of $\delta^{13}C$ values measured in omnivorous crustaceans. Center bars denote the median, box constrains the first and third quartiles, whiskers extend to data extremes, and points are individual sample values.

There are a number of fishes that are potentially important consumers of algal production in Florida springs and spring-fed rivers. While historically reported as one of the most abundant herbivorous fish in Silver River, striped mullet are now present in lower numbers (Odum 1957a). Both stable carbon and nitrogen isotope composition of striped mullet fin tissue were highly variable. From the 19 striped mullet samples analyzed, $\delta^{13}C$ values ranged from -35.3 to -26.6 ‰ and $\delta^{15}N$ values from +7.7 to +11.6 ‰. Other omnivorous fish included individuals from 6 families; silver sides (Atherniodidae), suckers (Catostomidae), shad (Clupeidae), shiners (Cyprinidae), Percidae (darters), and Poeciliidae (live-bearers). Mean $\delta^{13}C$ values measured in omnivorous fish ranged from -33.7 to -30.9 ‰ and mean $\delta^{15}N$ from +9.4 to 11.3 ‰. While groups differed in the amount of variation surrounding mean $\delta^{13}C$ values, values for silver sides (*Menidia* sp.), striped mullet, gizzard shad (*Dorosoma cepedianum*), and lake chubsucker (*Erimyzon sucetta*) were around -31 ‰, while mean $\delta^{13}C$ of shiners (*Notemigonus crysoleucas*-golden shiner, *Notropis petersoni*-coastal shiner, and *Pteronotropis hypselopterus*-sailfin shiner) and black banded darter (*Percina nigrofasciata*) were more negative (n = 30, -33.8 ‰ ± 1.3 for

shiners; n = 7, -33.3 ‰ ± 1.1 for darters; Figure 9.1.17). Mean $\delta^{15}N$ values were lowest for shiners (+9.4 ‰ ± 1.3) and highest for silver sides (11.3 ‰ ± 1.8, Figure 9.1.18).

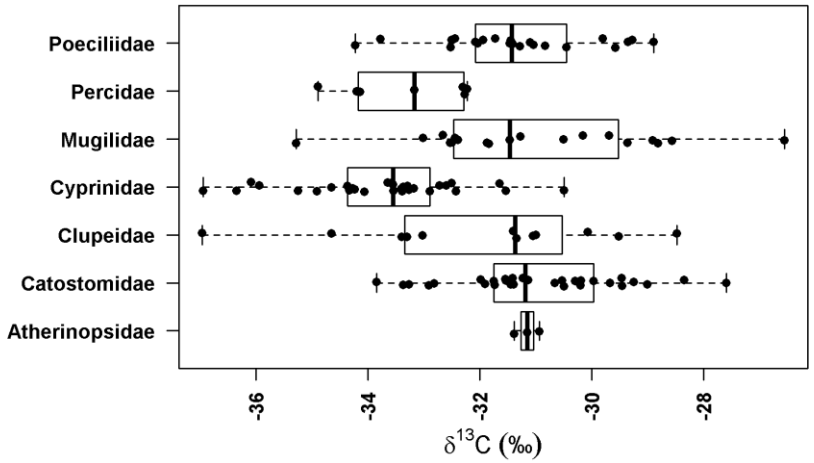

Figure 9.1.17. Boxplot of $\delta^{13}C$ values measured in families of herbivorous and omnivorous fish. Center bars denote the median, box constrains the first and third quartiles, whiskers extend to data extremes, and points are individual sample values.

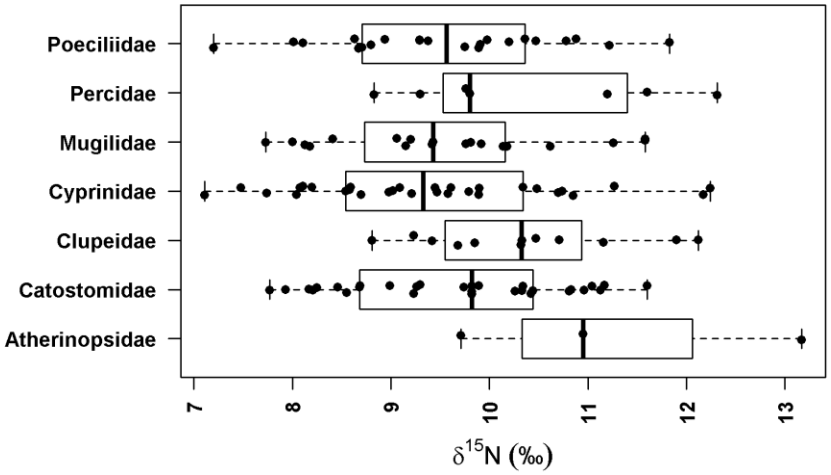

Figure 9.1.18. Boxplot of $\delta^{15}N$ values measured in families of herbivorous and omnivorous fish. Center bars denote the median, box constrains the first and third quartiles, whiskers extend to data extremes, and points are individual sample values.

We analyzed isotopic data for five omnivorous fish species that were encountered in all river regions (Catostomidae-*E. sucetta*, Cyprinidae-*N. petersoni*, Percidae-*Percina nigrofasciata*, Poeciliidae-*Gambusia affinis* and *Poecilia latipinna*). $\delta^{13}C$ values varied significantly among

taxa and river region ($F_{4,53}$ = 12.4, p-value < 0.001, for taxa; $F_{2,53}$ = 3.5, p-value = 0.04, for river region), but the interaction between taxa and river region was not significant ($F_{8,53}$ = 1.2, p-value = 0.34). Post-hoc comparisons yielded five significant pair-wise differences in $\delta^{13}C$ values among taxa, three involving *N. petersoni* and two involving *Percina nigrofasciata*. We found $\delta^{13}C$ values of *N. petersoni* were significantly less than *P. latipinna* (p-value = 0.05), *G. affinis* (p-value < 0.001), and *E. sucetta* (p-value < 0.001). We found $\delta^{13}C$ values of *P. nigrofasciata* to be significantly less than *G. affinis* (p-value = 0.007) and *E. sucetta* (p-value < 0.001). $\delta^{15}N$ values of omnivorous fish were not found to be significantly different among taxa ($F_{3,49}$ = 2.2, p-value = 0.10); however, we found significant differences among river regions ($F_{2,49}$ = 17.0, p-value < 0.001) and the interaction of taxa and river regions was significant ($F_{6,49}$ = 4.4, p-value = 0.001). Overall, $\delta^{15}N$ values of omnivorous fish in the lower river were significantly higher than in the mid (p-value < 0.001) and upper (p-value < 0.001) river, while $\delta^{15}N$ values of fish captured in the mid and upper river were similar and lower. This pattern held for all species except *E. sucetta* whose $\delta^{15}N$ values decreased from the upper to lower regions (Figure 9.1.19).

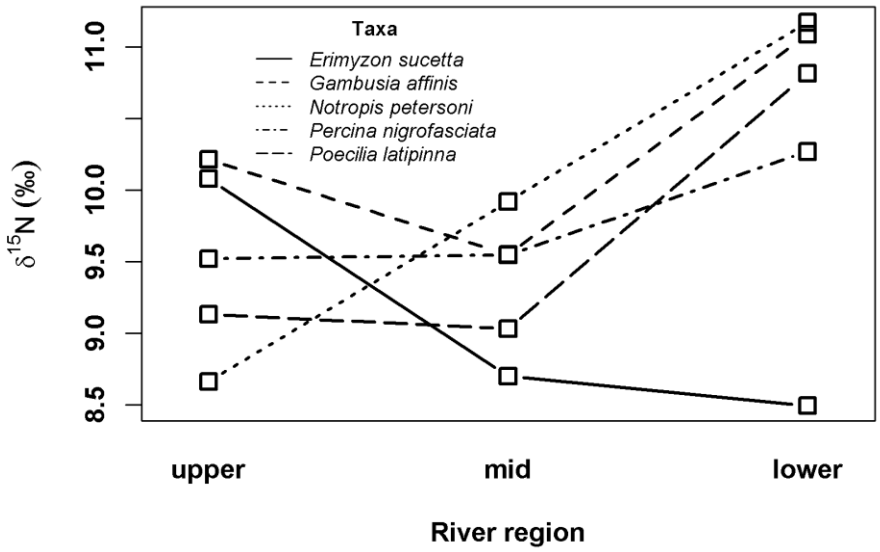

Figure 9.1.19. Interaction plot $\delta^{15}N$ values measured in omnivorous fish taxa across river regions. Symbols are mean values.

Florida springs and associated rivers are home to a number of omnivorous turtles. Turtles within the genus *Pseudemys* (River cooters) and the common snapping turtle (*Chelydra serpentina*) are known to consume SAV and macroalgae as well as infaunal organisms and carrion (Aresco et al. 2015). In Silver River, we obtained tissue samples from 38 individuals across four species, *Pseudemys nelsoni* (n = 13, Florida redbelly cooter), *P. peninsularis* (n = 8, Peninsular cooter), *P. suwanniensis* (n = 13, Suwannee cooter), and *C. serpentina* (n = 4). $\delta^{13}C$ values determined for these species ranged from -35.7 to -24.5 ‰, which were measured in *P. suwanniensis* and *P. peninsularis*, respectively. The composition of stable nitrogen isotopes spanned a 7 ‰ range, from +6.0 ‰ measured in *P. suwanniensis* to +13.2 ‰ measured in *P. nelsoni*. Stable carbon isotope composition of omnivorous turtles differed significantly among taxa ($F_{3,34}$ = 9.9, p-value < 0.001, Figure 9.1.20). Post-hoc comparisons yielded three significant pairwise differences in

$\delta^{13}C$ values among omnivorous turtle species, all of which included *P. suwanniensis*. We found $\delta^{13}C$ values of *P. suwanniensis* were significantly more negative than *P. nelsoni* (p-value = 0.01), *P. peninsularis* (p-value = 0.003), and *C. serpentina* (p-value < 0.001). Similarly, we found significant differences in $\delta^{15}N$ values among species ($F_{3,34}$ = 11.5, p-value < 0.001, Figure 9.1.21). Post-hoc comparisons detected two significant pair-wise differences, *P. suwanniensis* $\delta^{15}N$ values were found to be significantly less than $\delta^{15}N$ values of *C. serpentina* (p-value < 0.001) and *P. nelsoni* (p-value < 0.001).

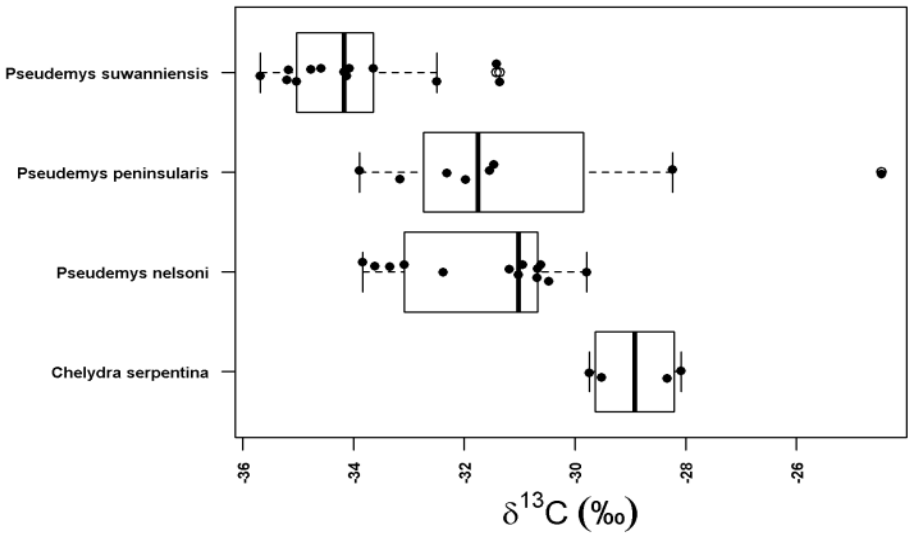

Figure 9.1.20. Boxplot of $\delta^{13}C$ values measured for omnivorous turtle species. Center bars denote the median, box constrains the first and third quartiles, whiskers extend to data extremes, and points are individual sample values.

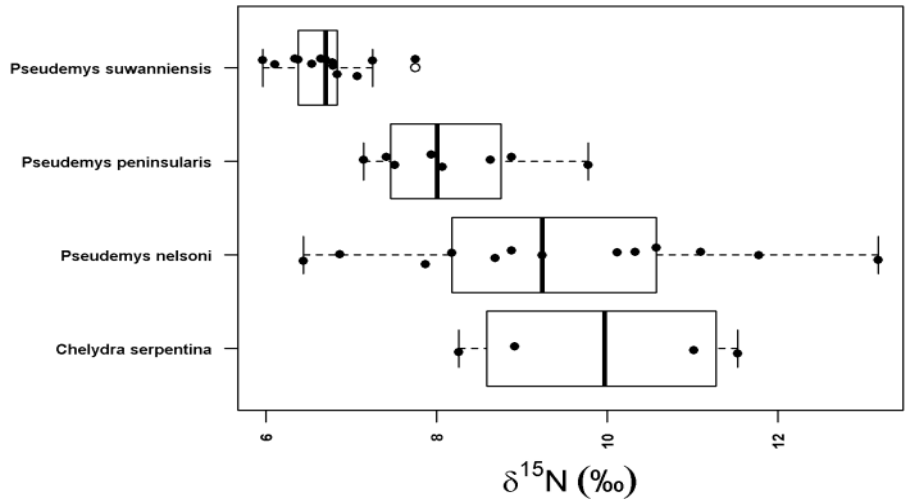

Figure 9.1.21. Boxplot of $\delta^{15}N$ values measured for omnivorous turtle species. Center bars denote the median, box constrains the first and third quartiles, whiskers extend to data extremes, and points are individual sample values.

We analyzed 12 samples of herbivore and omnivore taxa collected from Alexander Spring Creek (Appendix 9.1.4). In general, $\delta^{13}C$ values of taxa collected from Alexander Springs Creek were more positive then similar taxa collected in Silver River. $\delta^{13}C$ values ranged from -20.7 ‰, measured in *Viviparus georgianus*, to -26.4 ‰ measured in grass shrimp (*Palaemonetes* sp.) and averaged -23.5 ‰ ± 2.1 across all taxa.

9.1.4.5 Stable Isotope Composition of Secondary Consumers

Secondary consumers in Florida springs include larval and adult predaceous insects (i.e., hemiptera, odonota, diptera), snakes, turtles, and numerous predatory fishes. From our sampling efforts, we have analyzed a robust set of predatory fish samples (n = 247); however, we have analyzed only a relatively small sample set of predaceous insects (n = 27), carnivorous turtles (n = 19), and three snake species (n = 5).

The stable isotope composition of predaceous insects was highly variable and taxon dependent (Appendix 9.1.2). Hemipterans (true bugs,) and odonate larvae (damselflies and dragon flies) were found to have more positive $\delta^{13}C$ values (-30.3 ‰ ± 2.8 and -31.1 ‰ ± 2.7, for hemipterans and odonates, respectively) than predaceous dipterans (-36.1 ‰ ± 2.1). $\delta^{15}N$ values of hemipterans (8.1 ‰ ± 0.7) and odonates (8.6 ‰ ± 1.1) were more positive than dipterans (6.3 ‰ ± 0.8).

We collected stable isotope samples from nine families of predatory fish ranging from minute elassomatids (pygmy sunfish) to centrarchids (sunfish) and large lepisosteids (gar) (Appendix 9.1.3). Mean stable carbon isotope composition of predatory fish families ranged from -30.2 to -25.7 ‰ measured for Elassomatidae and Lepisosteidae, respectively (Figure 9.1.22). Mean $\delta^{15}N$ values of predatory fish families ranged from +9.7 to +13.6 ‰ measured for Fundulidae and Lepisosteidae, respectively (Figure 9.1.23).

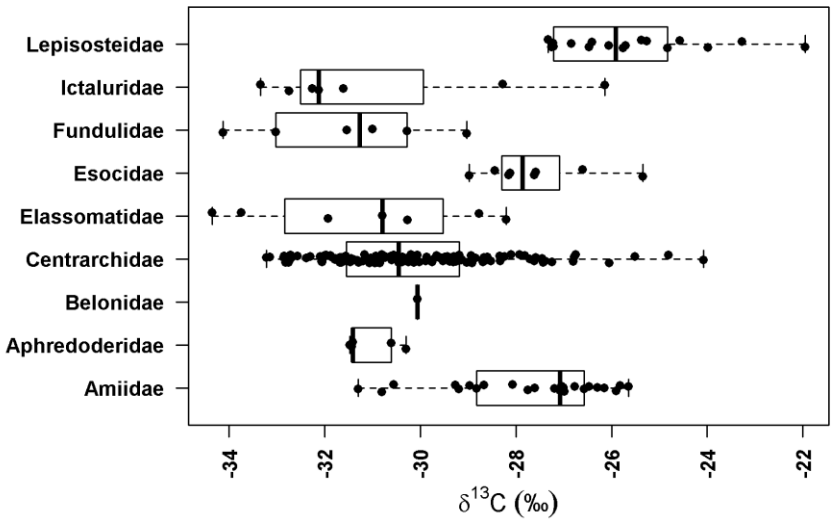

Figure 9.1.22. Boxplot of $\delta^{13}C$ values measured in families of predatory fish. Center bars denote the median, box constrains the first and third quartiles, whiskers extend to data extremes, and points are individual sample values.

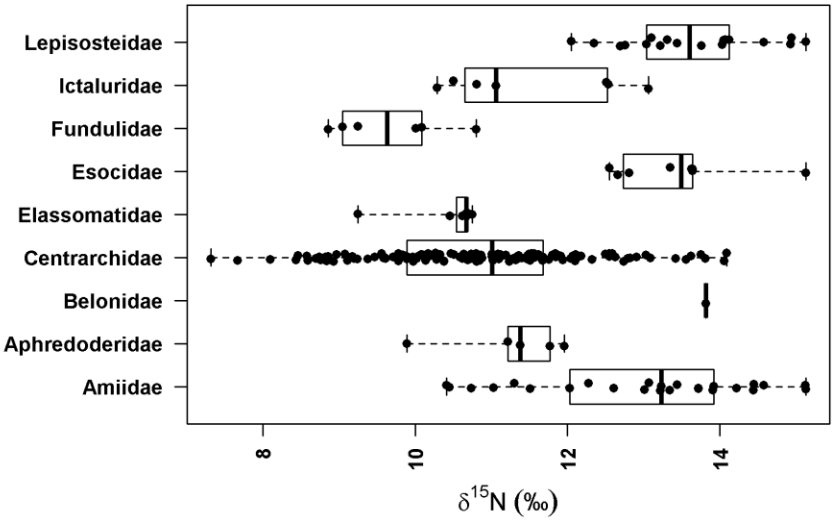

Figure 9.1.23. Boxplot of $\delta^{15}N$ values measured in families of predatory fish. Center bars denote the median, box constrains the first and third quartiles, whiskers extend to data extremes, and points are individual sample values.

For the five predatory fish families that were sampled in all river regions (n = 170, eight species), we found significant differences among mean values for $\delta^{13}C$ and $\delta^{15}N$ related to taxa ($F_{7,146}$ = 27.3, p-value < 0.001; $F_{7,146}$ = 51.7, p-value < 0.001, for $\delta^{13}C$ and $\delta^{15}N$, respectively), river region ($F_{2,146}$ = 4.6, p-value = 0.01; $F_{2,146}$ = 41.0, p-value < 0.001; Figure 9.1.24), and combinations of taxa and river region ($\delta^{13}C$, $F_{14,146}$ = 2.0, p-value = 0.02 and $\delta^{15}N$, $F_{14,146}$ = 1.9, p-value = 0.04). Post-hoc analysis indicated 14 significant pair-wise differences in $\delta^{13}C$ values among predatory fish taxa and 17 significant pair-wise differences in $\delta^{15}N$ values. In general, both $\delta^{13}C$ and $\delta^{15}N$ values of predaceous fish species increased with increasing distance downstream from the spring boil; however, a few taxa did not follow this pattern. We found significant positive correlations between both $\delta^{13}C$ and $\delta^{15}N$ values and body size (TL) of predatory fish (r = 0.70, p-value < 0.001 for $\delta^{13}C$ and r = 0.69, p-value < 0.001 for $\delta^{15}N$; Figure 9.1.25).

Silver River is home to three species of predaceous turtle from two families (Kinosternidae-musk turtles and Trionychidae-softshell turtles). We successfully collected samples from two species of kinosternids (*Sternotherus minor*-loggerhead musk and *S. odoratus*-common musk). In total, we have analyzed the stable isotope composition of 19 individuals (n = 16, *S. minor* and n = 3, *S. odoratus*). In general, mean isotopic compositions of *S. minor* and *S. odoratus* were similar and variation in both $\delta^{13}C$ and $\delta^{15}N$ was low (n = 19, $\delta^{13}C$ = -30.9 ‰ ± 1.6 and $\delta^{15}N$ = 8.3 ‰ ± 0.6).

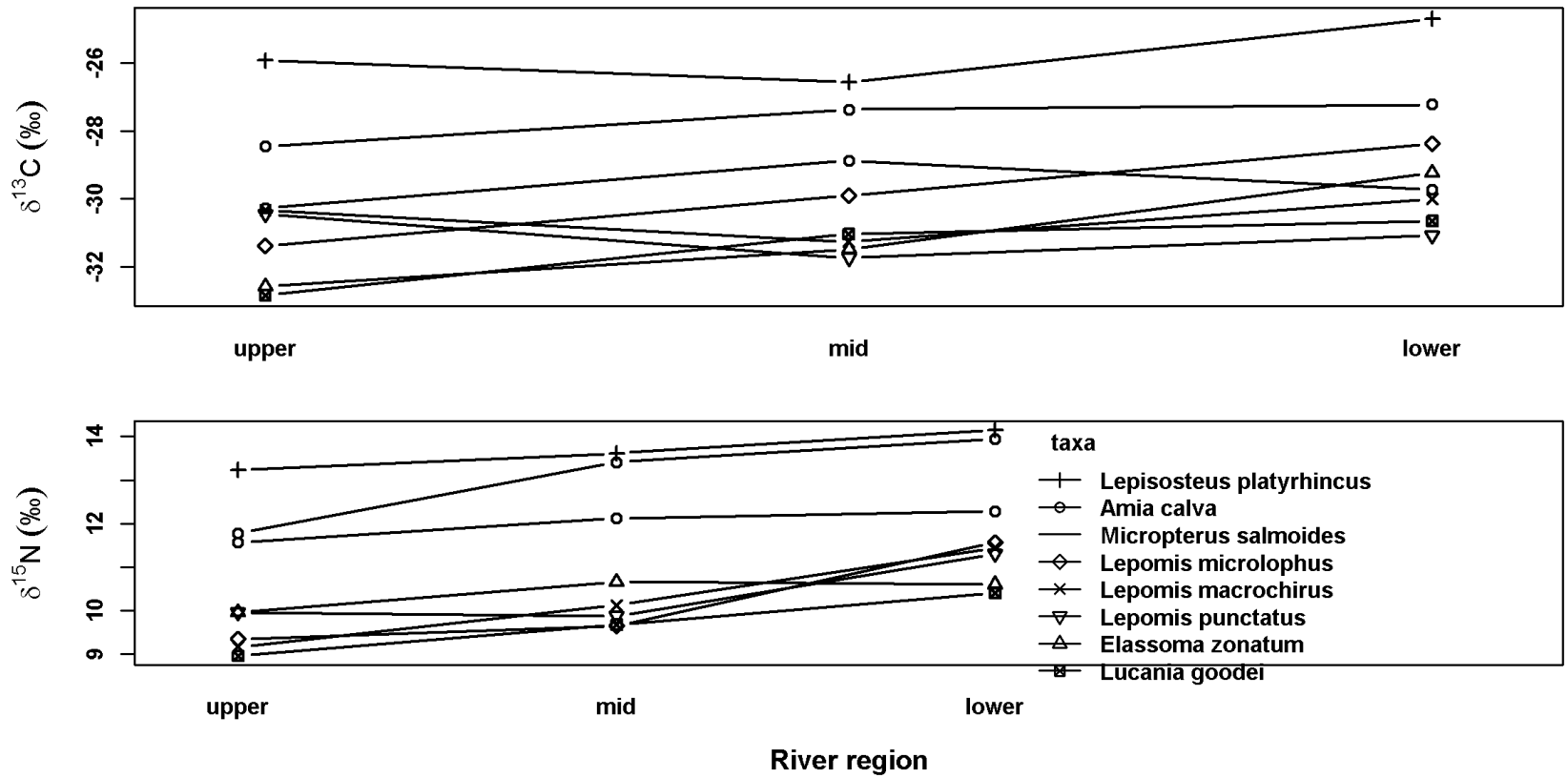

Figure 9.1.24. Interaction plot of the combined effects of taxon and river region on predatory fish isotopic composition. Top panel $\delta^{13}C$ values and bottom panel $\delta^{15}N$ values. Symbols represent mean values.

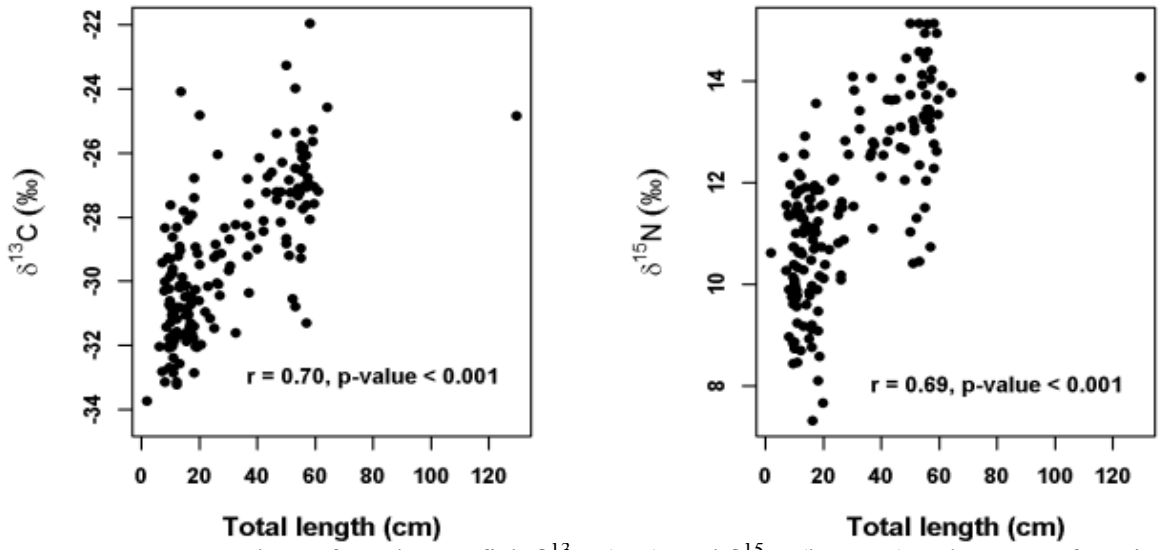

Figure 9.1.25. Scatterplots of predatory fish $\delta^{13}C$ (top) and $\delta^{15}N$ (bottom) values as a function of total length (cm). Correlation coefficient (r) and p-value for Pearson's Correlation Test are displayed on the plot.

9.1.4.6 Stable Isotope Composition of Parasitic Organisms

Consumers in spring ecosystems are host to a variety of parasitic organisms. We measured the stable isotope composition of two types of organisms, leeches (subclass: Hirudinea) and aquatic mites (order: Trombidiformes), known to parasitize gastropods and turtles. Since parasites are often host specific the isotopic composition of parasitic organisms may provide insight into the host's dietary patterns. $\delta^{13}C$ values measured in leeches (n = 2, -35.5 ‰ ± 1.7) and water mites (n = 3, -35.4 ‰ ± 0.8) were slightly more negative than their gastropod hosts/prey (see Table 9.1.4). Parasite $\delta^{15}N$ values (+8.1 ‰ ± 1.2 for leeches and +7.6 ‰ ± 0.5 for water mites) were similar to viviparid and pleurocerid snails and slightly higher than planorbid, hydrobiid, and ampullariid snails.

9.1.4.7 Stable Isotope Composition of Top and Apex Predators

The top predator assemblage in Florida springs and spring-fed rivers is presumed to comprise large predatory fish and alligators. Florida springs are, in fact, home to multiple species of fish that can attain large body sizes (TL > 40 cm) and are known to feed on larger prey, such as fish.

We analyzed a total of 43 individuals from three fish families represented by four species: pickerel (Esocidae, *Esox niger*-chain pickerel), sunfish (Centrarchidae, *Micropterus salmoides*-largemouth bass, TL > 30 cm) and two gar species (Lepisosteidae, *Lepisosteus osseus*-longnose gar and *L. platyrhincus*-Florida gar). $\delta^{13}C$ values of large predatory fish (n = 43, -27.3 ‰ ± 2.0) were the most positive of any fully aquatic consumer, ranging from -22.0 to -30.8 ‰. Likewise, $\delta^{15}N$ values (n = 43, +13.1 ‰ ± 1.1) were uniformly high for this assemblage. The maximum $\delta^{13}C$ found in higher order consumers (-22.0 ‰) was measured in fin tissues of a 58 cm TL *L. platyrhincus*. The maximum $\delta^{15}N$ values measured in this study (+15.1 ‰) were from fin tissues of a 53.0 cm TL *E. niger* and a 50.0 cm TL *L. platyrhincus*. Both $\delta^{13}C$ and $\delta^{15}N$ values differed significantly among predatory fish taxa ($F_{3,39}$ = 15.1, p-value < 0.001, for $\delta^{13}C$; $F_{3,39}$ = 5.3, p-

value = 0.004). Post-hoc analysis indicated one significant pair-wise difference among taxa for $\delta^{13}C$; wherein, *L. platyrhincus* $\delta^{13}C$ values were significantly greater than *M. salmoides* (p-value < 0.001). Similarly, the only pair-wise significant difference among $\delta^{15}N$ values was between *L. platyrhincus* and *M. salmoides* (p-value = 0.004), with *L. platyrhincus* having significantly higher $\delta^{15}N$ values (Figure 9.1.26).

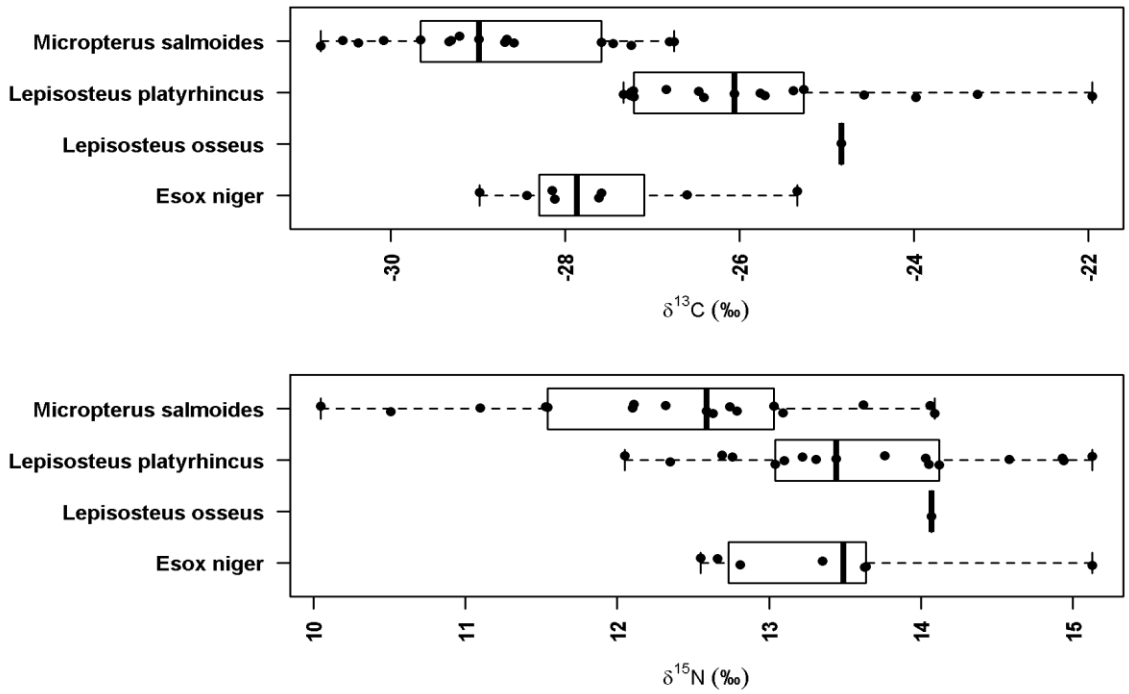

Figure 9.1.26. Boxplots of top predator fish taxa $\delta^{13}C$ (top) and $\delta^{15}N$ (bottom) values. Center bars denote the median, box constrains the first and third quartiles, whiskers extend to data extremes, and points are individual sample values.

We captured 64 *Alligator mississippiensis* (American alligator) ranging from 26.5 to 261.5 cm TL, representing the full range of *A. mississippiensis* size/age classes from young juveniles (TL < 75 cm) to adult males and females (TL > 175 cm, Figure 9.1.27). Despite extreme values contributing to the moderately large range in $\delta^{13}C$ (range = -31.4 to -26.3 ‰) and $\delta^{15}N$ (range = +3.7 to +10.9 ‰); overall, we found low variation (i.e., standard deviation [SD]) in the compositions of both stable carbon and nitrogen isotopes (n = 64, $\delta^{13}C_{SD}$ = 1.1‰ and $\delta^{15}N_{SD}$ = 1.2‰). Excluding values of individuals captured from a single pod of yearlings (n = 13) and two individuals of undetermined sex, we tested for significant differences in $\delta^{13}C$ and $\delta^{15}N$ values among sexes and size classes. Carbon isotope composition was found to be similar for sexes ($F_{1,43}$ = 0.3, p-value = 0.59) and size classes ($F_{2,43}$ = 1.2, p-value = 0.51), with no significant interaction ($F_{2,43}$ = 1.7, p-value = 0.20). Stable nitrogen isotope composition, however, was found to be significantly different among sexes ($F_{1,43}$ = 3.9, p-value = 0.05) and size classes ($F_{2,43}$ = 5.9, p-value = 0.005); however, the interaction was not significant (F2,43 = 2.6, p-value = 0.09). Post-hoc analysis indicated female alligators maintained significantly higher $\delta^{15}N$ values than males (p-value = 0.05). Furthermore, we found $\delta^{15}N$ values of adults were significantly greater than values for sub-adults (p-value = 0.005) and juveniles (p-value = 0.05), while sub-adult and juvenile $\delta^{15}N$ values were similar (Figure 9.1.28).

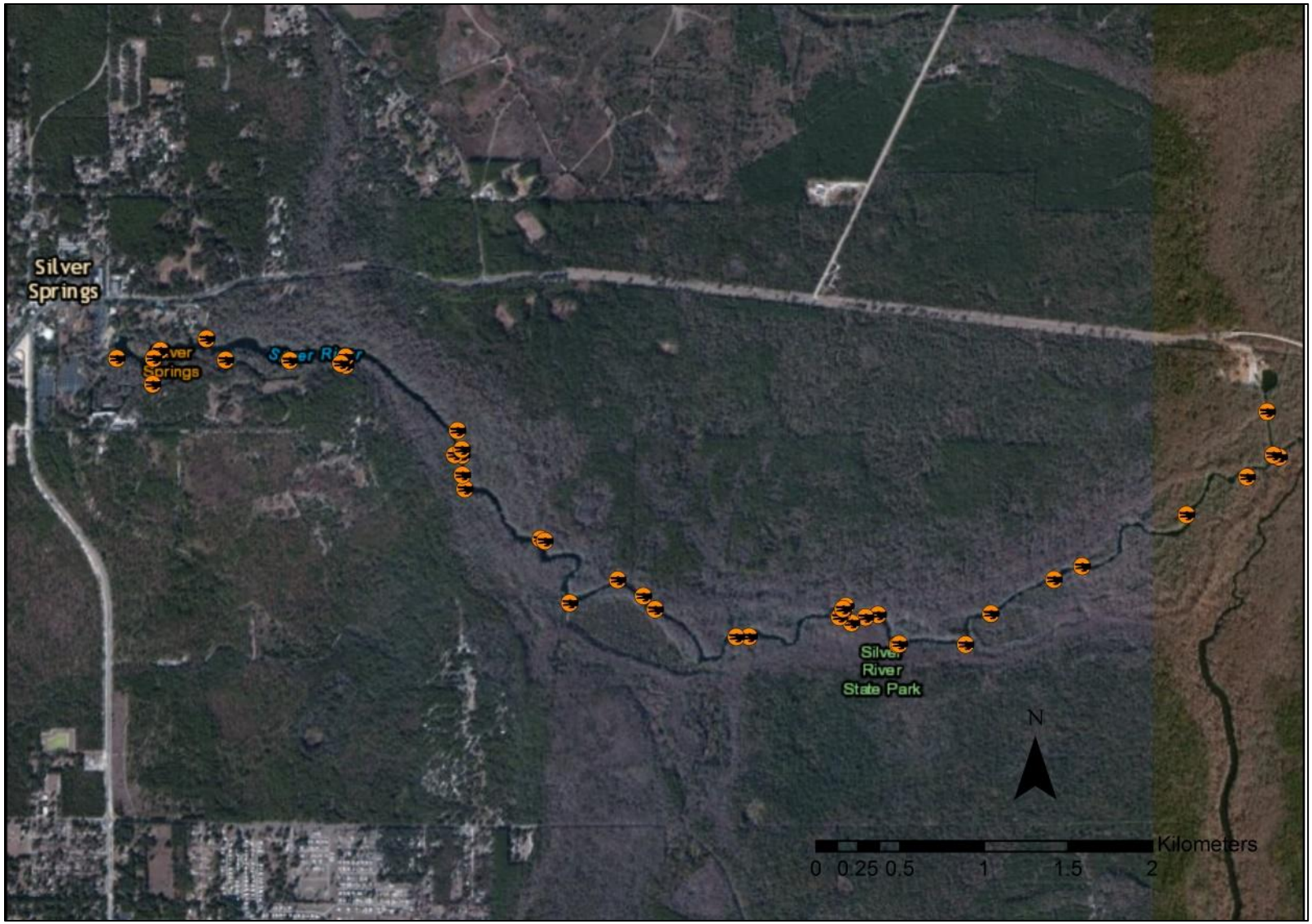

Figure 9.1.27. Map of American alligator capture locations along Silver River, Florida. Symbols are individual capture locations.

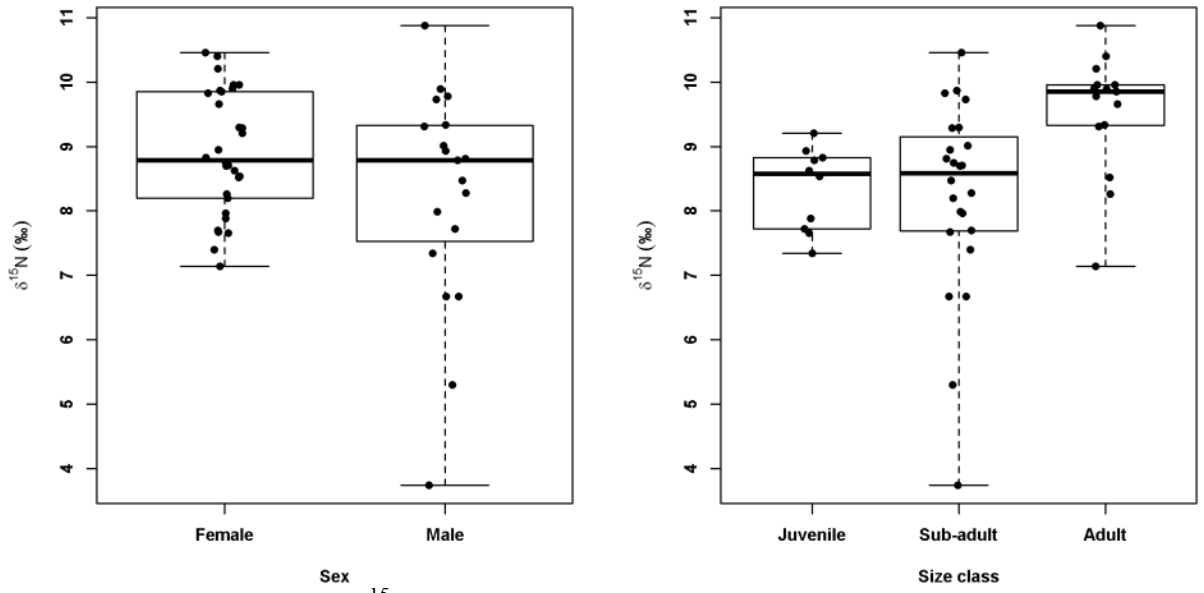

Figure 9.1.28. Boxplot of $\delta^{15}N$ values measured in American alligator sexes (left) and size classes (right). Center bars denote the median, box constrains the first and third quartiles, whiskers extend to data extremes, and points are individual sample values.

9.1.4.8 Isotopic Niche Area (SEA_B) for Herbivores and Omnivores

Using stable isotope composition data we calculated the isotopic niche area (SEA_B,) occupied by herbivorous and omnivorous taxa using Bayesian inference (Jackson et al. 2011). Median predictions for SEA_B ranged widely from 0.7 to 16.0 ‰^{2} estimated for the sessile filter feeding bivalve *Elliptio buckleyi* and the herbivorous gastropod *Pomaca paludosa*, respectively (Table 9.1.5). The isotopic niche area of taxa within the gastropod assemblage of Silver River was quite variable (median SEA_B range = 1.8–16.0 ‰^{2}, Figure 9.1.29). The pleurocerid *Elimia floridensis* maintained the smallest SEA_B of any gastropod taxon (median = 1.8 ‰^{2}, 95 % Bayesian Credible Interval [BCI] = 1.0–2.8). While less variable than predictions for gastropods, median predictions for herbivorous insects also ranged widely from 5.8 to 10.7 ‰^{2}, estimated for chironomid and lepidopteran larvae, respectively (Figure 9.1.30). The isotopic niche area occupied by omnivorous crustaceans was highly taxon dependent. Median SEA_B estimated for *Palaemonetes paludosus* was 6-times smaller than estimates for amphipods and 5-times smaller than estimates for *Procambarus fallax* (Figure 9.1.31). Estimated SEA_B of herbivorous and omnivorous fish taxa were much more constrained, ranging from 1.2 to 7.6 ‰^{2} estimated for *Pteronotropis hypselopterus* and *Mugil cephalus*, respectively. In general, the central locations (i.e., isotopic means) for various fish's SEA_{Bs} were similar, though the particular shape and size of each SEA_B differed substantially (Figure 9.1.32). The isotopic niche area occupied by herbivorous and omnivorous turtle taxa ranged in size from 1.9 to 8.9‰^{2}, estimated for *Pseudemys suwanniensis* (and *P. peninsularis*, respectively. Unlike the fish assemblage, herbivorous and omnivorous turtles demonstrated little overlap among niche areas (Figure 9.1.33).

Table 9.1.5. Stable carbon and nitrogen isotope ratios and statistics for SEA_B estimates for herbivorous and omnivorous taxa from Silver River.

Taxa (common name)	n	$\delta^{13}C$ (‰) mean ± SD	$\delta^{15}N$ (‰) mean ± SD	SEA_B (‰^{2}) median	99 % BCI	95 % BCI	50 % BCI
Invertebrates							
Amphipoda (*Gammarus* sp.)	16	-33.9 ± 3.2	+5.3 ± 1.3	9.8	4.9–19.0	5.6–15.6	7.6–10.8
Chironomidae (midge larvae)	20	-36.3 ± 2.5	+5.7 ± 0.8	5.8	3.1–10.3	3.5–8.8	4.6–6.3
Elliptio buckleyi (Florida shiney spike)	9	-32.9 ± 0.5	+8.3 ± 0.6	0.7	0.3–1.6	0.3–1.2	0.5–0.7
Lepidoptera (moth larvae)	20	-33.2 ± 2.9	+5.7 ± 1.2	10.7	5.6–19.0	6.4–16.1	8.6–11.7
Palaemonetes paludosa (grass shrimp)	13	-33.0 ± 0.9	+10.1 ± 0.6	1.6	0.7–3.3	0.8–2.6	1.2–1.7
Elimia floridensis (rasp elimia)	16	-33.9 ± 0.9	+8.0 ± 0.7	1.8	0.9–3.4	1.0–2.8	1.4–1.9
Pomacea paludosa (Florida apple snail)	13	-33.3 ± 3.0	+7.4 ± 1.7	16.0	7.2–33.5	8.5–26.9	12.0–17.7
Procambarus fallax (deceitful crayfish)	17	-30.5 ± 2.1	+8.5 ± 1.2	8.3	4.3–15.5	4.9–12.9	6.6–9.2
Rhagionidae (crane fly larvae)	6	-36.1 ± 2.1	+6.3 ± 0.8	4.1	1.2–13.0	1.5–8.9	2.5–4.5
Gastropods (families Hydrobiidae, Planorbidae, and Physidae)	6	-30.3 ± 3.1	+6.9 ± 0.9	6.7	1.9–21.2	2.4–14.6	4.1–7.4
Trichoptera (caddisfly larvae)	18	-39.4 ± 2.4	+5.7 ± 1.5	9.6	4.8–17.7	5.6–14.8	7.7–10.6
Viviparus georgianus (banded mystery snail)	16	-33.3 ± 1.8	+7.9 ± 1.2	5.3	2.6–10.2	3.0–8.4	4.1–5.8
Osteichthyes (bony fish)							
Dorosoma cepedianum (gizzard shad)	12	-32.0 ± 2.4	+10.3 ± 1.0	7.4	3.2–16.1	3.8–12.7	5.5–8.2
Erimyzon sucetta (lake chubsucker)	32	-31.1 ± 1.6	9.8 ± 1.2	6.1	3.7–9.6	4.1–8.4	5.2–6.6
Gambusia affinus (mosquito fish)	8	-31.2 ± 1.7	+9.7 ± 0.6	3.1	1.1–8.3	1.4–6.1	2.1–3.5
Heterandria formosa (least killifish)	9	-31.0 ± 1.5	+10.3 ± 1.4	6.6	2.4–16.5	3.0–12.3	4.6–7.4
Pterygoplichthys disjunctivus (vermiculated sailfin catfish)	6	-32.4 ± 0.6	+10.0 ± 1.0	1.9	0.6–6.1	0.7–4.2	1.2–2.1
Menidia beryllina (inland silverside)	6	-31.0 ± 0.4	+11.5 ± 1.2	1.4	0.4–4.4	0.5–3.1	0.9–1.6
Mugil cephalus (striped mullet)	16	-31.3 ± 2.1	+9.4 ± 1.1	7.6	3.7–14.7	4.3–12.1	6.0–8.4
Notemigonus crysoleucas (golden shiner)	16	-34.3 ± 1.8	+8.9 ± 1.2	7.1	3.5–13.9	4.1–11.4	5.6–7.9
Notropis petersoni (coastal shiner)	24	-33.6 ± 0.9	+10.4 ± 1.2	3.3	1.9–5.5	2.1–4.8	2.7–3.6
Percina nigrofasciata (black banded darter)	12	-33.2 ± 1.1	+10.9 ± 1.4	4.4	1.9–9.5	2.3–7.6	3.2–4.9
Poecilia latipinna (sailfin molly)	8	-31.9 ± 1.1	+9.1 ± 1.3	3.9	1.4–10.4	1.7–7.7	2.6–4.4
Pteronotropis hypselopterus (sailfin shiner)	6	-33.1 ± 0.4	+10.9 ± 0.9	1.2	0.4–3.8	0.4–2.6	0.7–1.3
Testudines (turtles)							
Chelydra serpentina (common snapping turtle)	4	-28.9 ± 0.8	+9.9 ± 1.6	3.1	0.6–13.9	0.9–8.4	1.6–3.4
Pseudemys nelsoni (Florida redbelly cooter)	13	-31.7 ± 1.4	+9.5 ± 1.9	7.2	3.2–15.1	3.8–12.0	5.4–7.9
Pseudemys peninsularis (peninsular cooter)	8	-30.9 ± 3.1	+8.2 ± 0.9	8.9	3.1–23.3	3.8–17.3	6.0–9.9
Pseudemys suwanniensis (suwannee cooter)	13	-34.0 ± 1.4	+6.7 ± 0.5	1.9	0.9–4.0	1.0–3.2	1.4–2.1

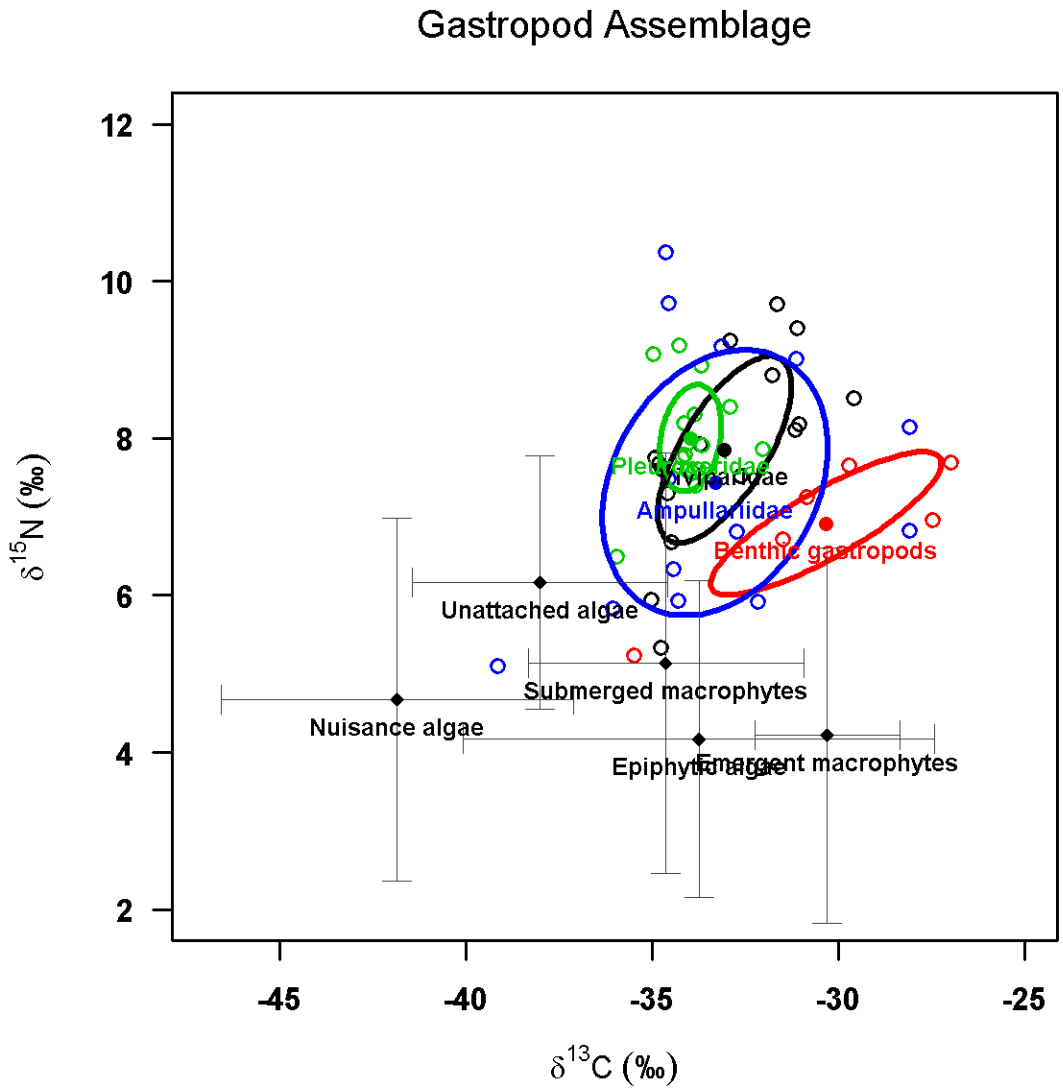

Figure 9.1.29. Isotopic bi-plot of SEA's (Standard Ellipse Areas) calculated for gastropod taxa. Filled symbols are mean values. Open symbols are individual data points. Autotroph data added for reference. Error bars are ± 1 SD.

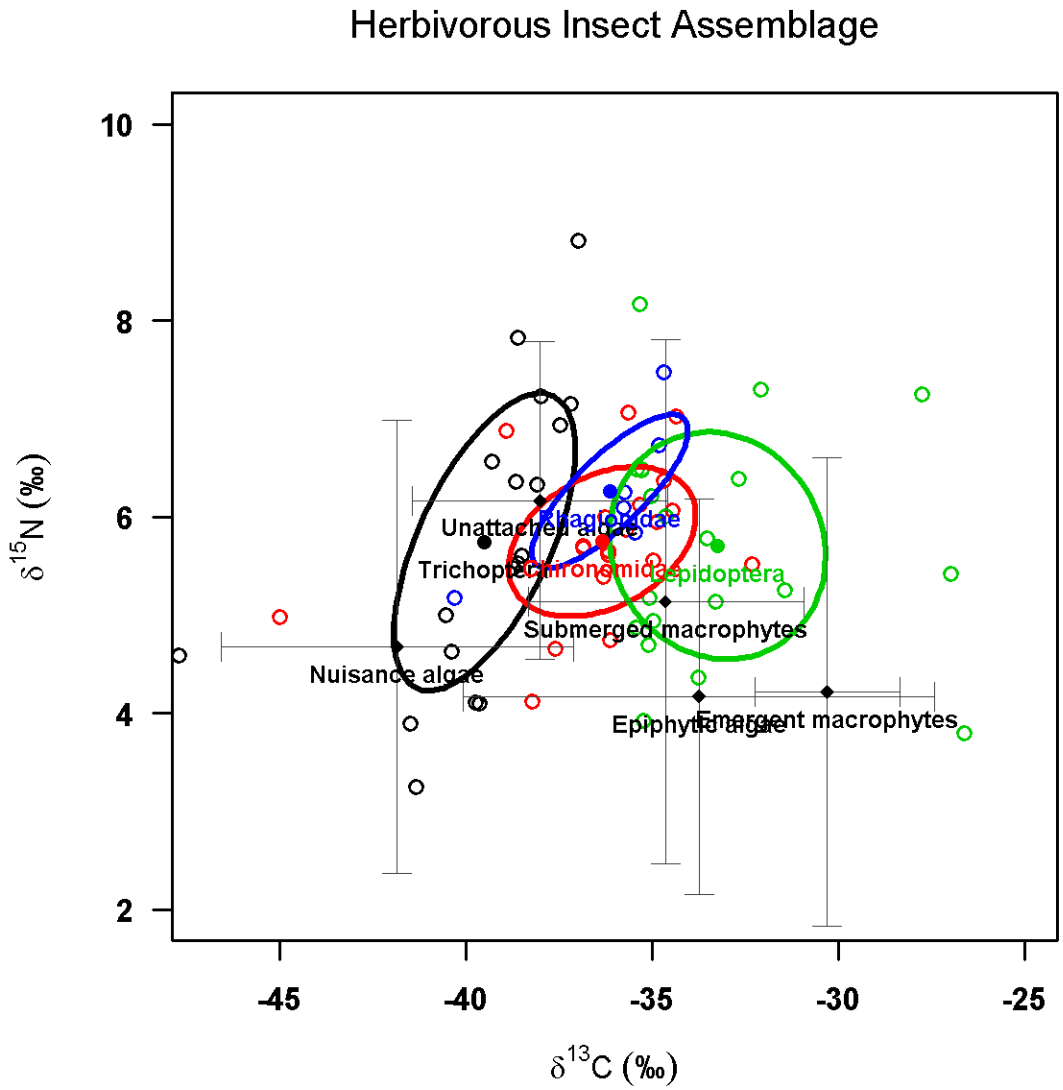

Figure 9.1.30. Isotopic bi-plot of SEA's (Standard Ellipse Areas) calculated for herbivorous insect taxa. Filled symbols are mean values. Open symbols are individual data points. Autotroph data added for reference. Error bars are ± 1 SD.

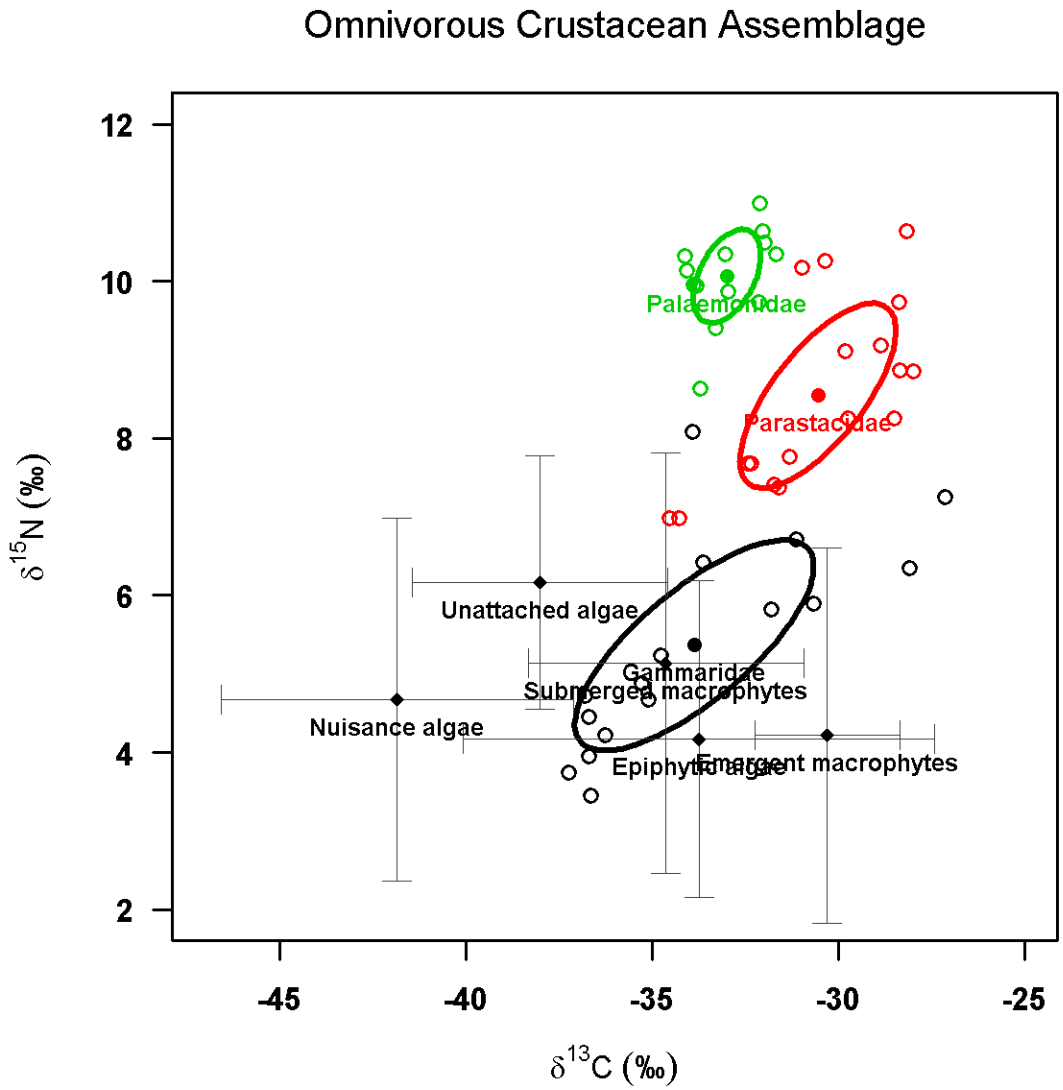

Figure 9.1.31. Isotopic bi-plot of SEA's (Standard Ellipse Areas) calculated for omnivorous crustaceans. Filled symbols are mean values. Open symbols are individual data points. Autotroph data added for reference. Error bars are ± 1 SD.

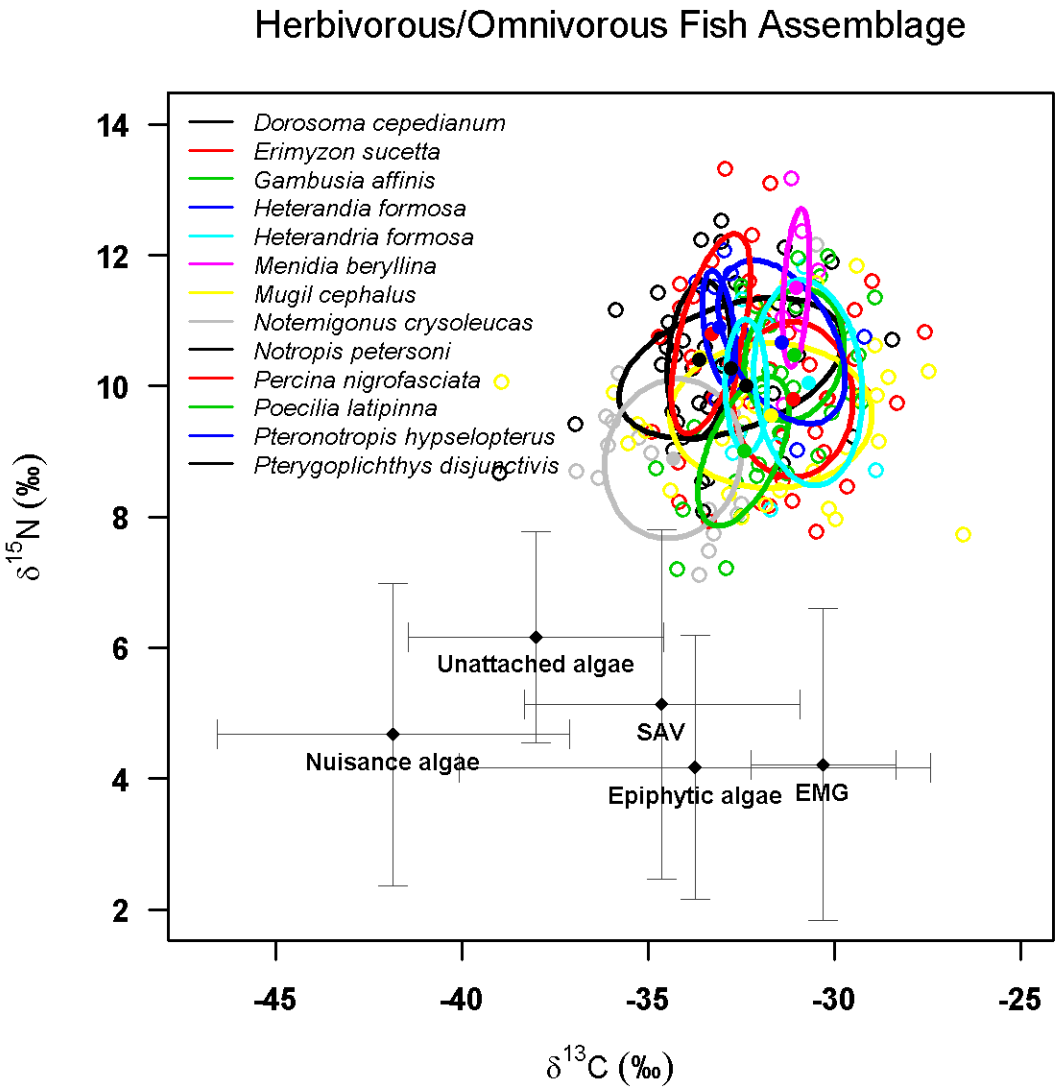

Figure 9.1.32. Isotopic bi-plot of SEA's (Standard Ellipse Areas) calculated for herbivorous omnivorous fish taxa. Filled symbols are mean values. Open symbols are individual data points. Autotroph data added for reference. Error bars are ± 1 SD.

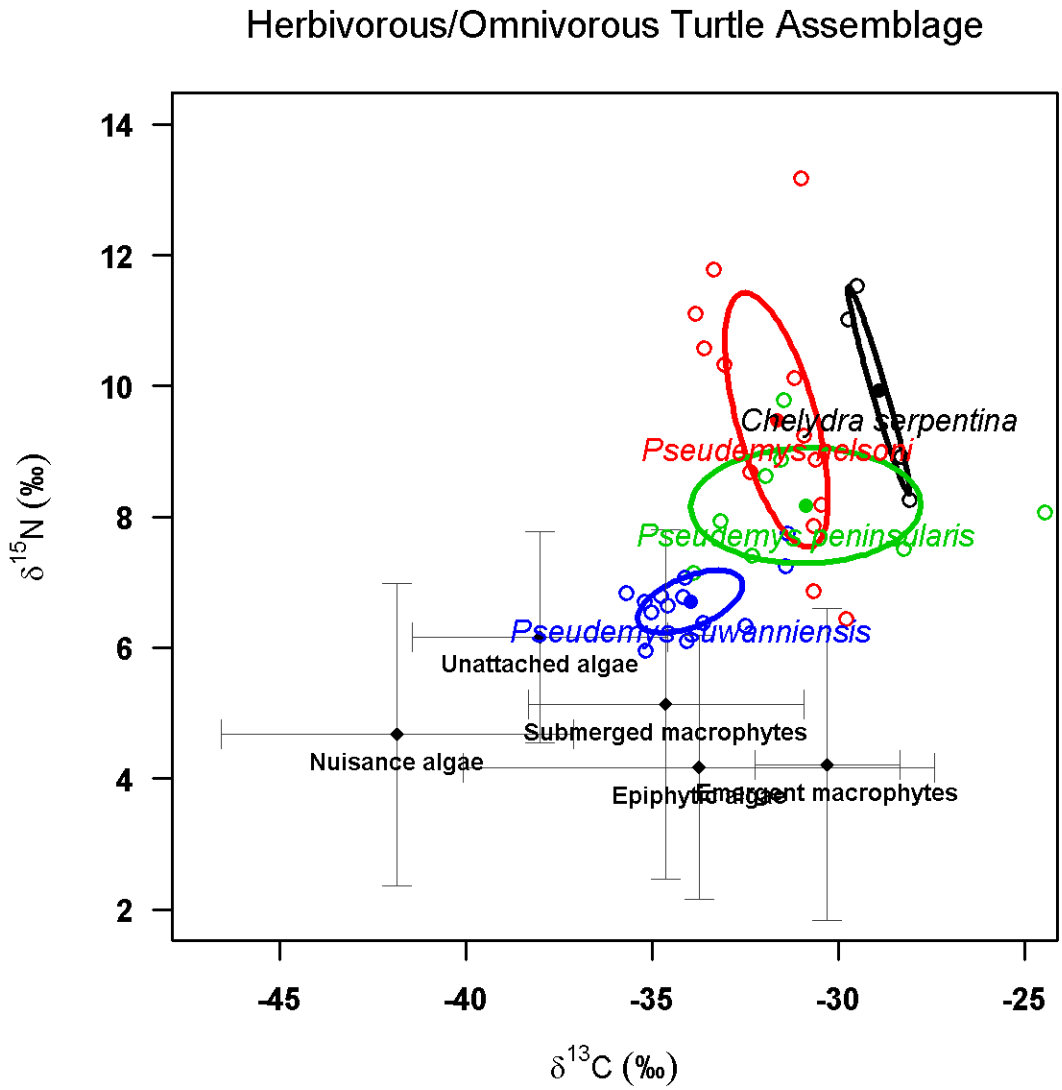

Figure 9.1.33. Isotopic bi-plot of SEA's (Standard Ellipse Areas) calculated for herbivorous omnivorous turtle taxa. Filled symbols are mean values. Open symbols are individual data points. Autotroph data added for reference. Error bars are ± 1 SD.

9.1.4.9 Isotopic Mixing Models and Niche Specialization Indices (ε)

We used a Bayesian isotopic mixing model (SIAR, Parnell et al 2010) to estimate the proportional contributions of primary producer groups and potential prey to the diet of resident herbivore and omnivore taxa within Silver River. We used a four end-member mixing model to examine the diets of strict herbivores (i.e., gastropods, trichopterans, lepidopterans, etc.) and omnivores, aggregating primary producer taxa into broader end-member groupings based on results of ANOVA tests and subsequent post-hoc comparisons (Section 9.1.5.1). Data from submerged macrophytes (SAV) and epiphytic algae were aggregated while data from emergent macrophytes, unattached algae, and nuisance algae remained separate.

Using a four end-member mixing model (i.e., primary producers only), across all herbivorous and omnivorous taxa, median predictions for the proportional contribution of nuisance algae to consumers' diets ranged from 0.04 to 0.74, estimated for the omnivorous turtle *Pseudemys nelsoni* and herbivorous trichopterans (Figure 9.1.34), respectively (Table 9.1.6). Taxa that demonstrated a strong reliance on nuisance algae as a food source included trichopterans (median = 0.74, 95 % BCI = 0.55–0.89), amphipods (median = 0.31, 95 % BCI = 0.08–0.50), chironomids (median = 0.51, 95 % BCI = 0.33–0.67), rhagionids (median = 0.36, 95 % BCI = 0.13–0.58), *Notemigonus crysoleucas* (golden shiner, median = 0.39, 95 % BCI = 0.22–0.55), *Notropis petersoni* (coastal shiner, median = 0.30, 95 % BCI = 0.11–0.44), *Percina nigrofasciata* (black banded darter, median = 0.31, 95 % BCI = 0.09–0.49), and *Pteronotropis hypselopterus* (median = 0.30, 95 % BCI = 0.05–0.51). We found the median proportional contribution of nuisance algae to the diets of all other taxa to be less 0.30. It should be noted that the turtle *Pseudemys suwanniensis* was estimated to rely on nuisance algae to a higher degree than all other turtles (median = 0.16, 95 % BCI = 0.03–0.29) and the diet of larval lepidopterans was estimated to be 29 % nuisance algae. We found unattached algae to contributed substantially to the diet of a number of taxa (median proportional estimates > 0.30 for 15 of 28 taxa), median estimates ranged from 0.06 to 0.52 for lepidopterans and *N. petersoni*, respectively. Chief consumers of unattached algae included *Elliptio buckleyi, Palaemonetes paludosa*, *Elimia floridensis*, *Viviparus georgianus*, *Dorosoma cepedianum*, *Erimyzon sucetta*, *Gambusia affinis*, *Heterandria formosa*, *Pterygoplichthys disjunctivis*, *Mugil cephalus*, *N. crysoleucas*, *P. nigrofasciata*, *Poecilia latipinna*, and *P. hypselopterus*. It should be noted that *Pseudemys peninsularis* was estimated to rely the more heavily on unattached algae than any other turtle species (median = 0.29, 95 % BCI = 0.03–0.53). We found median proportional contributions of the combined resource category SAV and epiphytic algae to range from 0.08 to 0.29 for trichopterans and small gastropod taxa, respectively. While we did not find the diet of any taxa to be predominantly comprised of SAV and epiphytic algae, the diets of 11 of the 28 taxa were found to be comprised of greater than 20% SAV and epiphytic algae (Table 9.1.6). These resuls included three of the four turtle species examined here (Figure 9.1.35). We found emergent macrophytes contributed significantly to the diets of certain taxa and very little to the diets of others. Median proportional contributions for emergent macrophytes ranged from 0.04 (for trichopterans) to 0.65 (for *P. nelson*). In addition to *P. nelsoni,* emergent macrophytes contributed heavily to the diet of the crayfish *Procambarus fallax* (median = 0.54, 95 % BCI = 0.30–0.75).

Table 9.1.6. Summary of posterior distributions from four end-member SIAR mixing model simulations and niche specialization index (ε) calculated for herbivore and omnivore taxa.

	Emergent macrophytes		Unattached algae		Nusiance algae		SAV + epiphytic algae		Epsilon (ε)
Taxa (common name)	**median**	**95% BCI**	**median**	**95% BCI**	**median**	**95% BCI**	**median**	**95% BCI**	**mean ± SD**
Invertebrates									
Amphipoda	0.29	0.06–0.50	0.11	0.00–0.40	0.31	0.08–0.50	0.27	0.02–0.57	0.29 ± 0.11
Chironomidae (midge larvae)	0.13	0.01–0.32	0.11	0.01–0.39	0.51	0.33–0.67	0.21	0.01–0.47	0.41 ± 0.09
Elliptio buckleyi (Florida shiney spike)	0.35	0.17–0.51	0.33	0.12–0.52	0.14	0.02–0.30	0.18	0.02–0.38	0.27 ± 0.10
Nymphulinae (moth larvae)	0.35	0.15–0.56	0.06	0.00–0.32	0.29	0.08–0.46	0.27	0.02–0.56	0.32 ± 0.11
Palaemonetes *paludosa* (grass shrimp)†	0.36	0.20–0.51	0.33	0.12–0.54	0.14	0.01–0.30	0.16	0.01–0.36	0.29 ± 0.10
Elimia floridensis (rasp elimia)	0.29	0.15–0.40	0.35	0.20–0.52	0.19	0.02–0.33	0.17	0.02–0.33	0.22 ± 0.09
Pomacea paludosa (Florida apple snail)	0.29	0.06–0.50	0.22	0.01–0.50	0.22	0.02–0.43	0.28	0.02–0.57	0.27 ± 0.11
Procambarus fallax (deceitful crayfish)†	0.54	0.30–0.75	0.19	0.02–0.42	0.04	0.00–0.16	0.21	0.01–0.49	0.47 ± 0.10
Rhagionidae (snipe fly larvae)†	0.16	0.01–0.39	0.24	0.02–0.50	0.36	0.13–0.58	0.23	0.01–0.49	0.30 ± 0.11
Small gastropods*	0.37	0.10–0.66	0.18	0.01–0.44	0.13	0.01–0.38	0.29	0.03–0.56	0.33 ± 0.13
Trichoptera (caddisfly larvae)	0.04	0.00–0.16	0.10	0.01–0.33	0.74	0.55–0.89	0.08	0.00–0.28	0.66 ± 0.10
Viviparus georgianus (banded mystery snail)	0.33	0.17–0.48	0.31	0.09–0.52	0.14	0.02–0.31	0.21	0.02–0.41	0.26 ± 0.10
Osteichthyes (bony fish)									
Dorosoma cepedianum (gizzard shad)†	0.14	0.01–0.35	0.43	0.12–0.80	0.20	0.01–0.43	0.19	0.01–0.45	0.36 ± 0.17
Erimyzon sucetta (lake chubsucker)†	0.27	0.12–0.39	0.49	0.27–0.68	0.11	0.01–0.27	0.12	0.01–0.32	0.37 ± 0.13
Gambusia affinis (mosquito fish)†	0.25	0.04–0.43	0.35	0.11–0.62	0.19	0.02–0.39	0.20	0.01–0.43	0.27 ± 0.12
Heterandria formosa (least killifish)†	0.28	0.06–0.46	0.32	0.08–0.61	0.19	0.02–0.38	0.20	0.01–0.43	0.26 ± 0.12
Pterygoplichthys disjunctivus (vermiculated sailfin catfish)	0.20	0.02–0.39	0.34	0.08–0.64	0.26	0.04–0.46	0.19	0.01–0.44	0.28 ± 0.12
Menidia beryllina (inland silverside)†	0.30	0.07–0.49	0.30	0.05–0.56	0.21	0.02–0.40	0.20	0.01–0.43	0.25 ± 0.11
Mugil cephalus (striped mullet)	0.23	0.05–0.40	0.38	0.14–0.65	0.18	0.02–0.37	0.20	0.01–0.43	0.29 ± 0.13
Notemigonus crysoleucas (golden shiner)	0.06	0.00–0.19	0.40	0.16–0.62	0.39	0.22–0.55	0.14	0.01–0.37	0.39 ± 0.09
Notropis petersoni (coastal shiner)	0.06	0.00–0.19	0.52	0.30–0.77	0.30	0.11–0.44	0.11	0.01–0.28	0.44 ± 0.12
Percina nigrofasciata (black banded darter)†	0.12	0.01–0.29	0.39	0.15–0.70	0.31	0.09–0.49	0.16	0.01–0.38	0.33 ± 0.12
Poecilia latipinna (sailfin molly)†	0.24	0.04–0.41	0.32	0.08–0.57	0.25	0.05–0.42	0.20	0.01–0.42	0.24 ± 0.11
Pteronotropis hypselopterus (sailfin shiner)	0.15	0.01–0.36	0.34	0.07–0.66	0.30	0.05–0.51	0.19	0.01–0.44	0.29 ± 0.12

Table 9.1.6. continued.

Taxa (common name)	Emergent macrophytes		Unattached algae		Nusiance algae		SAV + epiphytic algae		Epsilon (ε)
	median	95% BCI	median	95% BCI	median	95% BCI	median	95% BCI	mean ± SD
Testudines (Turtles)									
Chelydra serpentina (common snapping turtle)†	0.34	0.04–0.80	0.22	0.01–0.54	0.13	0.00–0.44	0.26	0.02–0.57	0.36 ± 0.16
Pseudemys nelsoni (Florida redbelly cooter)†	0.65	0.40–0.80	0.15	0.01–0.32	0.04	0.00–0.15	0.14	0.01–0.42	0.55 ± 0.10
Pseudemys peninsularis (peninsular cooter)†	0.37	0.09–0.67	0.29	0.03–0.53	0.07	0.00–0.31	0.25	0.02–0.54	0.35 ± 0.12
Pseudemys suwanniensis (Suwannee cooter)†	0.40	0.26–0.55	0.21	0.04–0.38	0.16	0.03–0.29	0.24	0.04–0.41	0.27 ± 0.08

*Includes data from the gastropod families: Hydrobiidae, Planorbidae, and Physidae.
†Omnivorous taxa.

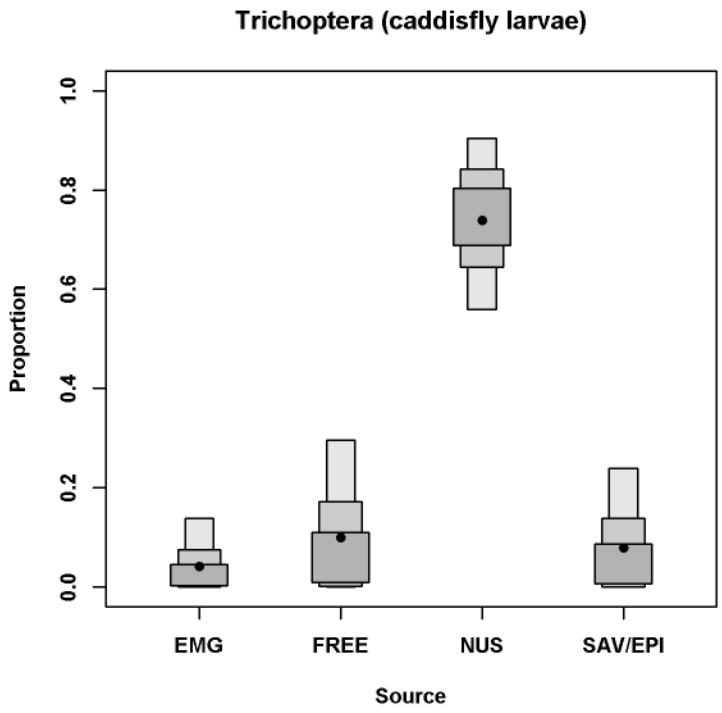

Figure 9.1.34. Boxplot of SIAR posterior distributions for the proportional contribution of resource groups to the diet of trichopterans using four end-member model. The outer light gray boxes enclose the 95% BCI, the slightly larger and darker boxes enclose the 75 % BCI, and the center box encloses the 50 % BCI. Points are median estimates. Source labels are as follows: EMG-emergent macrophytes, FREE-unattached algae, NUS-nuisance algae, SAV/EPI-submerged macrophytes + epiphytic algae.

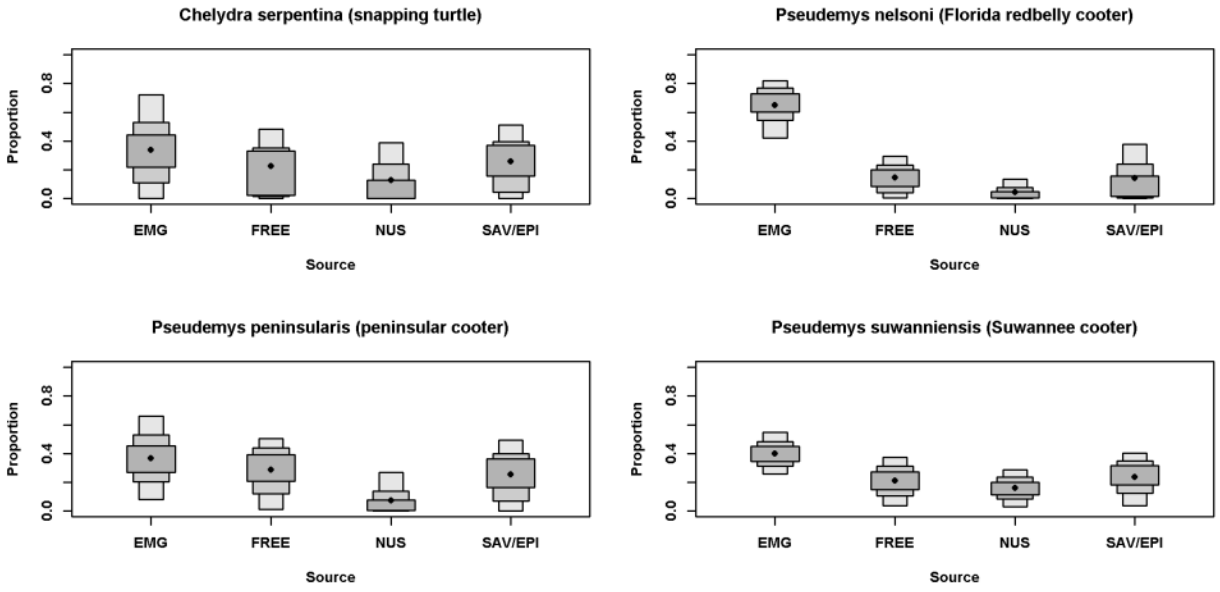

Figure 9.1.35. Boxplots of SIAR posterior distributions for the proportional contribution of resource groups to the diet of turtles using four end-member model. The outer light gray boxes enclose the 95 % BCI, the slightly larger and darker boxes enclose the 75% BCI, and the center box encloses the 50 % BCI. Points are median estimates. Source labels are as follows: EMG-emergent macrophytes, FREE-unattached algae, NUS-nuisance algae, SAV/EPI-submerged macrophytes + epiphytic algae.

Using the posterior distributions comprised of resource-to-diet proportional contribution vectors produced by SIAR analyses, we calculated the niche specialization index (ε). Values of ε range from 0 to 1 (unitless), with values approaching zero representing extreme dietary generalization (i.e., consumers feed on all available resource categories in equal proportions) and values approaching one representing extreme dietary specialization (i.e., consumers feed on a narrow subset of available resources). Mean niche specialization indices calculated for 28 herbivore and omnivore taxa ranged from 0.22 to 0.66 for *Elimia floridensis* and trichopterans, respectively (Table 9.1.6). Overall, ε averaged 0.33 across all taxa, suggesting the majority of consumer taxa are dietary generalists, consuming all resource categories to some degree. In addition to trichopterans, mean ε exceeded 0.50 for the omnivorous turtle *Pseudemys nelsoni*, and it was greater than 0.40 for chironomids (mean ± SD, 0.41 ± 0.09), *Procambarus fallax* (0.47 ± 0.10), and *Notropis petersoni* (0.44 ± 0.12); which suggests these taxa exhibit greater dietary specialization.

9.1.4.10 Analysis of Stomach Contents and Scat

In total, we analyzed stomach contents recovered from 45 *Alligator mississippiensis* ranging in size (TL) from 45.3 to 248.0 cm. For simplicity, we combined data on prey species into nine categories: Aves (birds), coleopterans (larval and adult beetles), fish, gastropods (single species, *Pomacea paludosa*), aquatic insects (larval and adult), decapod crustaceans (grass shrimp and crayfish), mammals, snakes, and turtles (Figure 9.1.36, Table 9.1.7). We assessed and compared *A. mississippiensis* diet at the size class level (juvenile, sub-adult, and adult). The diet of juveniles mainly consisted of decapod crustaceans (%IRI ≈ 61 %), aquatic insects (%IRI ≈ 17 %), and coleopterans (%IRI ≈ 17 %), with gastropods, fish, turtles, and mammals contributing very little to the importance index (combined %IRI ≈ 5 %). No remains of birds or snakes were recovered from juvenile stomach contents (Table 9.1.7). The diet of sub-adult individuals predominantly consisted of decapods (%IRI ≈ 55 %) and gastropods (%IRI ≈ 36 %); while of minor overall importance, coleopterans, fish, turtles, mammals, snakes, and birds (combined %IRI ≈ 9 %) were of slightly higher importance to sub-adults relative to juveniles. The diet of adult individuals overwhelmingly comprised gastropods (%IRI ≈ 54 %), decapods (%IRI ≈ 26 %), and fish (%IRI ≈ 14 %). Similar to the diet of sub-adults, coleopterans, turtles, mammals, snakes, and birds were consumed, but they contributed little to the diet of adults (combined %IRI ≈ 6 %).

Table 9.1.7. Percent Index of Relative Importance (%IRI) values for nine prey categories determined for *Alligator mississippiensis* size classes.

Prey group	Juvenile	Sub-adult	Adult
Aves	0.0	0.2	0.2
Coleoptera	17.3	4.2	1.1
Fish	0.9	1.2	13.6
Gastropoda	3.7	36.3	53.9
Aquatic insect	17.1	0.6	2.6
Decapoda	60.6	55.0	26.2
Mammal	0.0	0.5	0.8
Snake	0.0	0.1	1.1
Turtle	0.4	2.0	0.5

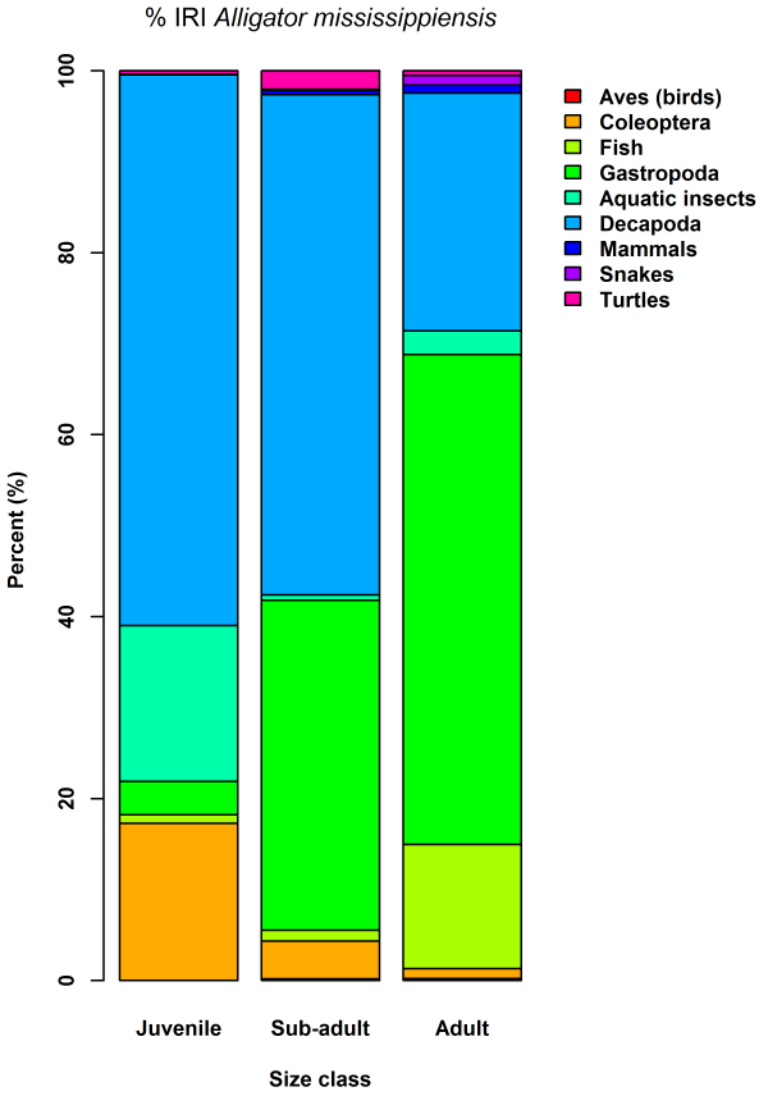

Figure 9.1.36. Bar charts of %IRI calculated for *Alligator mississippiensis* size classes. Color designation for prey categories are listed in the legend.

In total, we analyzed the stomach contents recovered from 291 individuals across 19 species of fish, with the number of individuals per species ranging from 1 to 69 (Table 9.1.8). Similar to the analysis of alligator stomach contents, we aggregated prey items into 11 broad categories: nuisance algae, epiphytic algae, diatoms, vegetation, chironomids, trichopterans, coleopterans, aquatic insects, crustaceans, gastropods, and fish. We decided to separate chironomids and trichopterans from other aquatic insect taxa since our SIAR results indicated these taxa rely more heavily on nuisance algae.

Table 9.1.8. Number of individuals examined for stomach content analysis of fish species.

Species (common name)	**n**
Amia calva (bowfin)	16
Aphredoderus sayanus (pirate perch)	2
Erimyzon sucetta (lake chubsucker)	8
Gambusia affinus (mosquito fish)	5
Heterandria formosa (least killifish)	1
Lepisosteus platyrhincus (Florida gar)	9
Lepomis auritus (redbreasted sunfish)	2
Lepomis gulosus (warmouth)	8
Lepomis macrochirus (bluegill)	35
Lepomis marginatus (dollar sunfish)	1
Lepomis microlophus (redear sunfish)	31
Lepomis punctatus (spotted sunfish)	69
Menidia sp. (silverside)	3
Micropterus salmoides (Florida largemouth bass)	48
Mugil cephalus (striped mullet)	3
Notemigonus crysoleucas (golden shiner)	12
Notropis petersoni (coastal shiner)	44
Percina nigrofasciata (darter)	5
Strongylura marina (Atlatic needlefish)	1

Excluding two species (*Percina nigrofasciata* and *Menidia* sp.), we found the diets of herbivorous and omnivorous fish taxa to be dominated by algae (chiefly diatoms) and macrophytes; however, certain species were also found to consume various fish and invertebrate taxa (Figure 9.1.37). The diet of the herbivorous *Mugil cephalus* solely comprised vegetation, with diatoms being the dominant item consumed (%IRI ≈ 72 %) followed by nuisance algae (%IRI ≈ 14 %), SAV (% RI ≈ 11 %), and filamentous epiphytic algae (%IRI ≈ 4 %). *Mugil cephalus* and *Erimyzon sucetta* were the only species in this assemblage identified as consumers of nuisance algae (nuisance algae %IRI ≈ 14 % for *M. cephalus* and 2% for *E. sucetta*). In addition to nuisance algae, the diet of *E. sucetta* chiefly comprised various crustaceans (%IRI ≈ 50%), chironomids (%IRI ≈ 21 %), diatoms (%IRI ≈ 15 %), aquatic insects (%IRI ≈ 7 %), and SAV (%IRI ≈ 6 %). The diets of the two species of shiners examined in this study, *Notemigonus crysoleucas* and *Notropis petersoni*, chiefly comprised diatoms (%IRI ≈ 70 % for *N. crysoleucas* and 79% for *N. petersoni*) and filamentous epiphytic algae (%IRI ≈ 25 % for *N. crysoleucas* and 18% for *N. petersoni*). *Notropis petersoni* also was found to consume various aquatic insects (including trichopterans and chironomids) and invertebrates (i.e., ostracods and water mites). The diet of the omnivore *Gambusia affinis* mainly comprised diatoms (%IRI ≈ 77 %), but it also contained various aquatic insects, including but not limited to trichopterans and chironomids (combined aquatic insect %IRI ≈ 16 %). The stomach contents of *Percina nigrofasciata* (black banded darter) and *Menidia* sp. (silverside) contained no evidence that these species consume vegetation (Figure 9.1.37). While we were only able to examine the stomach contents of one

Strongylura marina (Atlantic needlefish) and one *Heterandria formosa* (least killifish), we found both these species consumed macrophytes (likely incidental by-catch) and *S. marina* consumed fish as well.

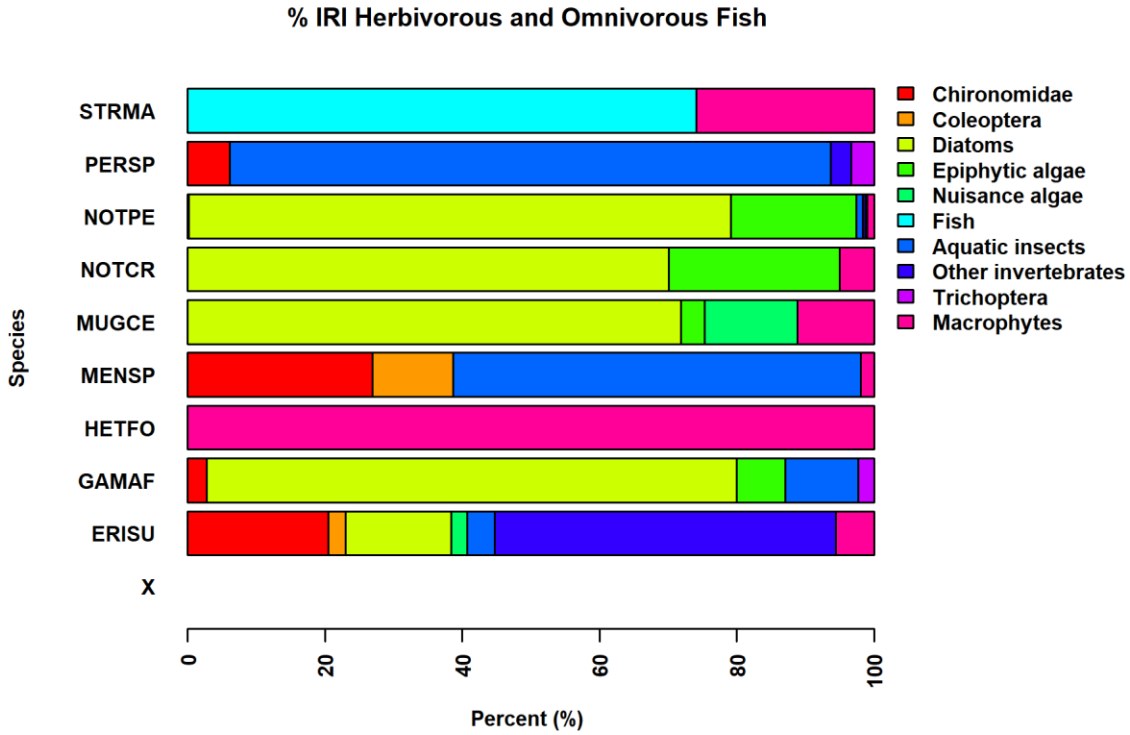

Figure 9.1.37. Bar charts of %IRI calculated for herbivorous and omnivorous fish taxa. The species abbreviation is the first three letters of the genus and first two letters of the species epithet, for example the abbreviation for *Amia calva* (bowfin) is AMICA (refer to Table 9.1.8 for list of species). If the five letter species codes matched for any two species than a third letter from the species epithet was added.

The diets of most predatory fish taxa predominantly comprised decapods, amphipods, aquatic insects, and fish (Figure 9.1.38). We identified four taxa that consumed gastropods (*Amia calva*, *Lepomis macrochirus*, *L. microlophus*, and *L. punctatus*); however, gastropods were a major dietary component only for *L. microlophus* (%IRI ≈ 99 %). The diet of *A. calva* chiefly consisted of decapod crustaceans (%IRI ≈ 81 %) and SAV (%IRI ≈ 16 %, likely secondarily consumed during prey capture). The stomach contents of two *Aphredoderus sayanus* (pirate perch) contained only aquatic insect larvae. While we were only able to collect contents from two *L. auritus* (redbreasted sunfish), we found their diet to primarily comprise chironomids (%IRI ≈ 48 %) and trichopterans (%IRI ≈ 28 %). Similarly, stomach contents from one *L. marginatus* (dollar sunfish) contained mostly chironomids (%IRI ≈ 56 %) and trichopterans (%IRI ≈ 38 %). The most heavily sampled species, *L. punctatus* (n = 69), was found to maintain the most diverse diet, with evidence it consumed all prey categories (Figure 9.1.38). However, the main components of *L. punctatus* diets were aquatic insects (other than chironomids and trichopterans, %IRI ≈ 27 %) and crustaceans (%IRI ≈ 45 %). Similarly, we found evidence of consumption for

10 of the 11 prey categories in the stomach contents of *L. macrochirus* (bluegill). The diet of *L. macrochirus* was representative of a generalist consumer, wherein, each prey category was consumed in similar proportions. The diets of the two top predator species *Lepisosteus platyrhincus* (Florida gar) and *Micropterus salmoides* (Florida largemouth bass) were similar; although, *L. platyrhincus* appeared to be more piscivorous than *M. salmoides* (fish %IRI ≈ 75 % for *L. platyrhincus* and 49 % for *M. salmoides*). The diet of both *L. platyrhincus* and *M. salmoides* contained decapod crustaceans, but for *L. platyrhincus* we suspect these occurrences may have been the result of secondary ingestion.

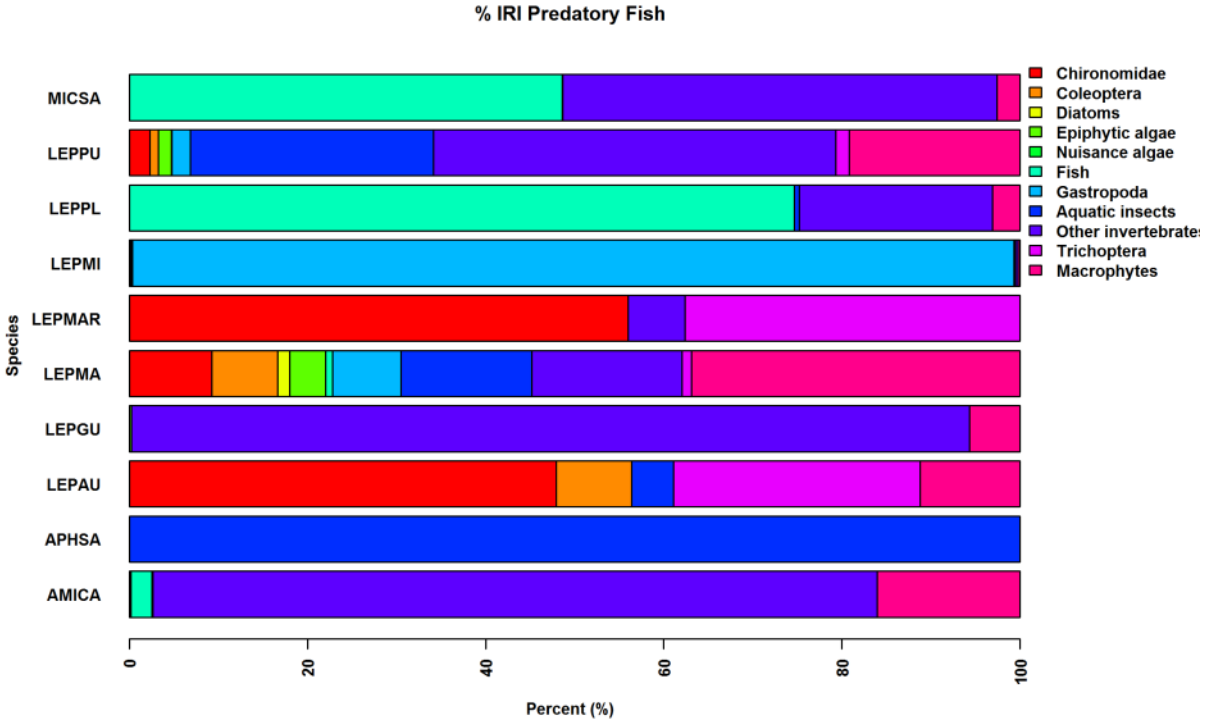

Figure 9.1.38. Bar charts of %IRI calculated for predatory fish taxa. The species abbreviation is the first three letters of the genus and first two letters of the species epithet, for example the abbreviation for *Amia calva* (bowfin) is AMICA (refer to Table 9.1.8 for list of species names). If the five letter species codes matched for any two species than a third letter from the species epithet was added (e.g., LEPMAR and LEPMA).

In total, we collected and analyzed scat from 29 individuals from five species (Table 9.1.9). To quantify the diets of turtles, we used 15 categories: nuisance algae, epiphytic algae (filamentous algae and diatoms), *Ceratophyllum demersum*, *Hydrilla verticillata*, *Sagittaria kurziana*, SAV (unidentified taxon), floating macrophytes (*Lemna* sp.-duckweed and *Salvinia* sp.-floating fern), emergent macrophytes, other vegetation (coarse woody debris-CWD, particulate organic matter, and seeds), chironomids, trichopterans, coleopterans, aquatic insects, crustaceans, and gastropods.

Table 9.1.9. Number of individual turtles that have been analyzed for composition of scat.

Species (common name)	**n**
Pseudemys nelsoni (Florida redbelly cooter)	7
Pseudemys peninsularis (peninsular cooter)	3
Pseudemys suwanniensis (Suwannee cooter)	4
Sternotherus minor (loggerhead musk turtle)	12
Sternotherus odoratus (common musk turtle)	3

From scat samples analyzed and observations at the time of sampling, there is a clear demarcation of dietary preferences among turtle taxa (Figure 9.1.39). The diets of the three species of cooter (genus *Pseudemys*) predominantly comprised macrophytes and macroalgae; however, dietary preferences for certain vegetation types and propensity to consume invertebrate prey differ among species. Of the three *Pseudemys* species, vegetation was most important to the diet of *P. nelsoni* (combined vegetation %IRI ≈ 77 %), with unidentified SAV (%IRI ≈ 21 %) and epiphytic algae (%IRI ≈ 32 %) also contributing to the importance indices for this species. Furthermore, *P. nelsoni* maintained the most diverse diet in terms of vegetation types (consumed all 8 vegetation types), and it was the only turtle species that consumed nuisance algae. In terms of animal prey, *P. nelsoni* primarily ate crustaceans and gastropods. Similar to *P. nelsoni*, the diet of *P. suwanniensis* consisted largely of epiphytic algae and SAV (combined vegetation %IRI ≈ 63 %) and crustaceans (%IRI ≈ 25 %); however, the diet of *P. suwanniensis* also contained trichopterans (%IRI ≈ 7 %) and other aquatic insects. The diet of *P. peninsularis* while still predominantly composed of vegetation in the form of SAV and epiphytic algae (combined vegetation %IRI ≈ 67 %), differed from the diets of *P. peninsularis* and *P. nelsoni* by containing a greater amount of aquatic insects (%IRI ≈ 22 %) relative to crustaceans (%IRI ≈ 11%, Figure 9.1.39). Scat of the two species of kinosternids (*Stenotherous minor* and *S. odoratus*) contained large numbers (range = 1–130 individuals) of smaller bodied gastropods (including planorbids, physids, hydrobids, and juvenile pleurocerids, %IRI ≈ 94 % for *S. minor* and 99 % for *S. odoratus*), small crustaceans (i.e., amphipods, ostracods, and decapods), and various aquatic insect taxa (e.g., hemipterans, trichopterans, and lepidopterans. Scat from the common snapping turtle (*Chelydra serpentina*) was found to be a mix of submerged macrophytes, detritus including coarse woody debris, and crayfish; however, scat was collected from only two individuals, limiting quantitative analysis of *C. serpentina* diets.

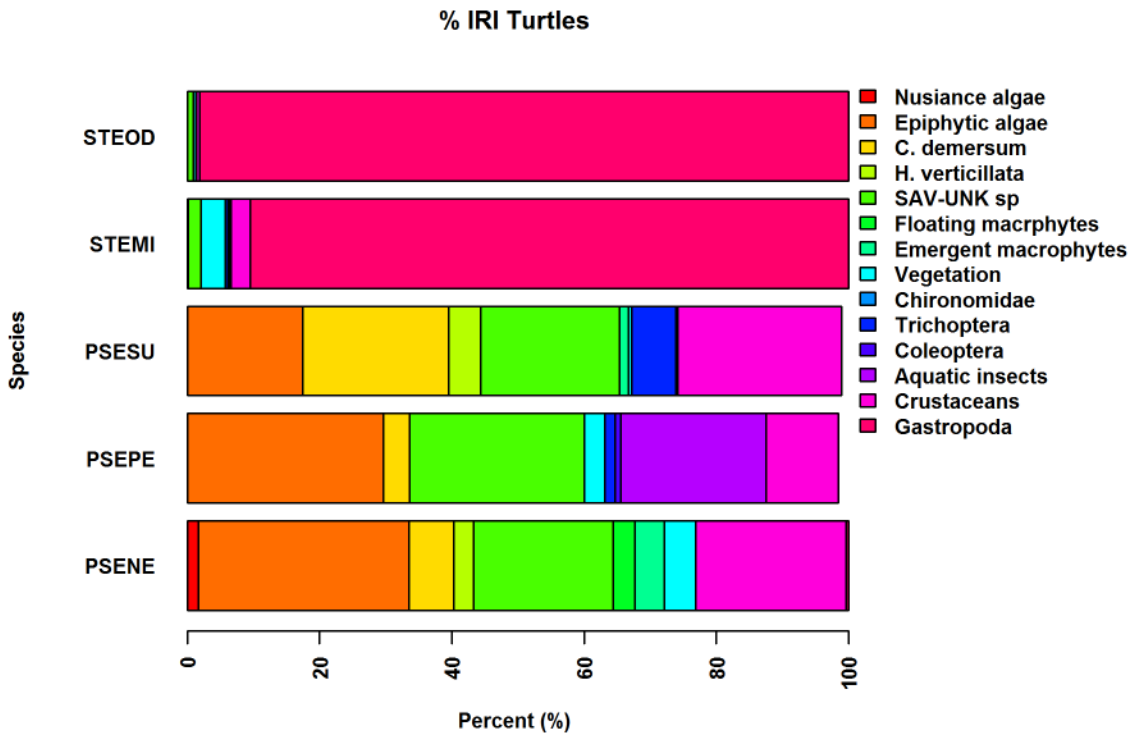

Figure 9.1.39. Percent Index of Relative Importance (%IRI) calculated for turtle taxa. The species abbreviation is the first three letters of the genus and first two letters of the species epithet (see Table 9.1.9 for species information).

9.1.5 DISCUSSION

9.1.5.1 What is the fate of nutrients and energy sequestered by nuisance algae?

Overall, results from preliminary stable isotope, isotopic mixing model, and diet analyses indicate a functional and diverse food web in Silver River (Figure 9.1.10); however, we found little evidence that many organisms consumed nuisance algae. We detected significant differences in composition of stable carbon and nitrogen isotopes among broad primary producer groups and among growth forms of macroalgae (Figure 9.1.7). The discriminatory ability of isotopic mixing models (including SIAR) hinges on sufficient differences in the isotopic composition of resource pools used as end-members (Phillips et al. 2014). Using our findings, we applied isotopic mixing models (SIARs) to four end-members, focused on estimating the proportional contribution of various autotrophic resources to the diets of dominant herbivores and omnivores (Table 9.1.6). Our results clearly indicate the majority of energy transferred within the aquatic food web present in Silver River originates from epiphytic algae (i.e., diatoms and filamentous algae) and macrophytes (i.e., SAV and emergent macrophytes; Table 9.1.6). Moreover, we found nuisance algae to be an insignificant dietary component for the majority of herbivores and omnivores. We estimated that the diets of only 8 of the 28 herbivores and omnivores (i.e., trichopterans, chironomids, amphipods, lepidopterans, 3 species of shiners, and darters) comprised greater than 30 % nuisance algae (Table 9.1.6). Furthermore, stomach contents and scat of larger-bodied herbivorous and omnivorous taxa provided little evidence that nuisance algae is consumed by fish and turtles. We did, however, observe a number of

omnivores and secondary consumers (i.e., fishes and turtles) that consumed grazers on nuisance algae, such as trichopterans, chironomids and lepidopterans, although these prey were of less importance in the overall diet. Combined, these results suggest the majority of nuisance algal production is exported to the terrestrial food web by emergent insects (i.e., trichopterans, chironomids, and lepidopterans) or translocated downstream rather than being transmitted through the aquatic food web.

We found the isotopic values of consumers to vary both among and within taxa due to location, body size and life history stage. More in-depth analyses of taxon-level differences in isotopic composition may elucidate the ecological relevance of this variation and determine the degree to which it changes predictions from isotopic mixing models. Through longitudinal sampling of the Silver River, from the main spring boil to the confluence with the Ocklawaha River, we found evidence of increasing $\delta^{15}N$ values throughout the food web. Downstream enrichment of ^{15}N (higher $\delta^{15}N$ values) is indicative of the preferential uptake of lighter ^{14}N in upstream reaches (Brabandere et al. 2007), and it is important to consider when establishing isotopic baselines for food web models and estimating trophic position (Post 2002, Phillips et al. 2014). Here, we did not estimate trophic position for consumers and variation in $\delta^{13}C$ values among potential food resources was the main influence on the discriminatory ability of our isotopic mixing model. Furthermore, developing an understanding of how the isotopic composition of major resource pools varies spatially helps to increase the discriminatory ability of isotopic mixing models. While we have not incorporated longitudinal differences in isotopic composition of primary producers and consumers into our mixing model analyses, we speculate that incorporating such variation would reduce uncertainty in our model predictions but not change the overall patterns in resource use.

9.1.5.2 Which consumers forage on nuisance algae and to what degree?

Results from isotopic mixing models suggest that few taxa exclusively exploit nuisance algae and most taxa rely heavily upon epiphytic algae and macrophytes (Table 9.1.6). The isotopic compositions of larval trichopterans (caddisfly) and chironomids (non-biting midges) were the most suggestive of a diet that relied heavily on nuisance algae. This conclusion was substantiated by the results of SIAR mixing models; wherein, the median % contribution of nuisance algae to diets was estimated to be 74 % (95 % BCI = 55–89 %) for trichopterans and 51 % (95 % BCI = 33–67 %) for chironomids. These two taxa also demonstrated relatively high degrees of niche specialization ($\varepsilon = 0.66 \pm 0.10$ and 0.41 ± 0.09, for trichopterans and chironomids, respectively) suggesting these taxa likely specialize on nuisance algae relative to other autotrophic resources. Mixing models also indicated that the diets of the majority of herbivores and omnivores predominantly comprised SAV and epiphytic algae, emergent macrophytes, and unattached algae; however the relative importance of these resources varied among taxa (Table 9.1.6).

Isotopic variation within the gastropod assemblage of Silver River suggests a wide range in dietary preferences. Given what is known of the dietary preferences and distribution of *Elimia floridensis* and *Viviparus georgianus*, their isotope values are suggestive of similar foraging patterns, both likely relying on epiphytic and unattached algae. Conversely, small gastropods (i.e., hydrobids, physids, and planorbids) appeared to be more closely associated with macrophyte-derived, detrital resources. Results from our SIAR models aligned with these predictions for the most part; however, we found unattached algae to be a significant dietary

component (> 30%) for small gastropods, *V. georgianus*, and *E. floridensis*. Additionally, our mixing model results indicated *V. georgianus* relied heavily on detritus derived from emergent macrophytes, most likely flocculent materials. The isotope composition of the ampullariid, *Pomacea paludosa* was highly variable (Figure 9.1.29), suggesting *P. paludosa* demonstrates a greater degree of dietary variability among individuals and a highly generalized diet. These results translated into *P. paludosa* occupying the largest isotopic niche area (SEA_B) of any herbivore or omnivore (median SEA_B = 16.0, Table 9.1.5) and demonstrating a low degree of niche specialization ($\varepsilon = 0.27 \pm 0.11$, Table 9.1.6).

Crustaceans also displayed stark differentiation in isotopic values among taxa. Amphipods showed a large amount of variation in both stable carbon and nitrogen isotopes suggesting assimilation of a wide range of food items, while the isotopic composition of *Palaemonetes paludosus* (grass shrimp) varied little so they are likely to be more specialized foragers (Figure 9.1.31). SIAR results indicated the diet of *P. paludosus* was predominantly a mixture of emergent macrophyte detritus (median % contribution = 36 %) and unattached algae (33 %); however, these patterns could change if ^{15}N enriched prey items are incorporated into the model framework. The isotopic composition of the parastacid, *Procambarus fallax* (deceitful crayfish), was somewhat variable, but more indicative of a stronger reliance on detritus derived from emergent macrophytes as opposed to algal resources. This finding was supported by SIAR results, wherein, we estimated the diet of *P. fallax* to comprise 30–75 % (95 % BCI) emergent macrophytes (Table 9.1.6).

The stable carbon isotopic composition of certain herbivorous (i.e., *Mugil cephalus*) and omnivorous fish (particularly *Dorosoma cepedianum*, *Erimyzon sucetta*, and several species of shiners) were suggestive of assimilation of algal resources either through direct ingestion or incidental ingestion during predation on macroinvertebrate algal grazers. While we found very little direct evidence of nuisance algae in the stomachs of fish (Figure 9.1.37), SIAR results indicated that the diets of the golden shiner (*Notemigonus crysoleucas*), coastal shiner (*Notropis petersoni*), black banded darter (*Percina nigrofasciata*), and sailfin shiner (*Pteronotropis hypselopterus*) comprised greater than 30% nuisance algae (Table 9.1.6). Relative to nuisance algae, epiphytic algae/SAV, unattached algae and detritus from emergent macrophytes seem to be of greater importance in the diets of *M. cephalus*, *E. sucetta,* and *D. cepedianum*.

Stable isotope data and findings from analyses of scat indicate turtles within the genus *Pseudemys* are important grazers of SAV, epiphytic algae and emergent macrophytes rather than nuisance algae (Table 9.1.6 and Figure 9.1.39). While we only found nuisance algae in the scat of *Pseudemys nelsoni*, our SIAR results indicated the diet of *P. suwanniensis* likely included 16% nuisance algae. However, we did observe large amounts of the SAV species *Ceratophyllum demersum* in the scat of *P. suwanniensis*, which we found to maintain a more negative $\delta^{13}C$ value than most other SAV taxa. The presence of this species may have biased predictions in favor of a higher contribution of nuisance algae to the diet of *P. suwanniensis*.

9.1.5.3 Which predators are major consumers of grazers?

The isotopic values of omnivores and secondary consumers varied markedly among taxa (Appendix 9.1.3 and Figure 9.1.10) and within a particular taxon due, in large part, to differences in body size, sex, and life history stage (Figure 9.1.28). Given the time constraints of this project and the primary focus on dietary interactions among lower trophic levels, we have not extended isotopic mixing models to diets of secondary consumers or other higher order consumers (i.e., top predators). In light of this, we draw conclusions based solely on the assessment of stomach contents and scat.

Fish displayed fairly diverse diets. We found trichopterans to be of greatest importance in the diets of two fish taxa, *Lepomis marginatus* (dollar sunfish, %IRI ≈ 38 %, n = 1) and *L. auritus* (redbreast sunfish, %IRI ≈ 28 %, n = 2); however, these taxa were encountered infrequently during sampling events and our sample sizes are too small to draw firm conclusions. Furthermore, isotopic compositions of these two species are not suggestive of heavy exploitation of trichopterans (Appendix 9.1.3). A greater number of fish species were found to consume chironomids (Figure 9.1.38) and larvae of other herbivorous and omnivorous aquatic insects (i.e., lepidopterans, dipterans, and ephemeropterans). Crustaceans (i.e., amphipods, decapods, and ostracods) along with other invertebrate taxa (e.g., water mites) were highly important to the diets of many omnivorous and predatory fishes. We found the diet of one fish, *L. microlophus* (redear sunfish), to almost exclusively comprise gastropods (predominantly from the families Hydrobiidae, Physidae, and Planorbidae; combined gastropod %IRI ≈ 99 %).

One interesting finding was the diet of all *Alligator mississippiensis* sub-populations relative to other taxa typically classified as top predators, such as gar, pickerel, and adult largemouth bass (Figure 9.1.10). Stomach contents of *A. mississippiensis* indicate that all life-history stages heavily rely on both crustaceans and gastropod prey (Table 9.1.7); however, the importance of crustaceans decreases and the importance of gastropods increases through ontogeny (Figure 9.1.36). The phenomena of a large-bodied predator foraging on small-bodied organisms from low trophic levels truncates food webs, and it should be considered when modeling energy flow in this ecosystem. The one species of gastropod consumed by *A. mississippiensis* was the apple snail (*Pomacea paludosa*), and this species has been demonstrated to be a major component of *A. mississippiensis* diets wherever their native ranges overlap (Rosenblatt et al. 2015).

Using scat content analysis, we identified two other key predators of gastropods, *Sternotherus minor* (loggerhead musk turtle) and *S. odoratus* (common musk turtle, Figure 9.1.39). Unlike alligators, *S. minor* and *S. odoratus* chiefly consumed smaller-bodied gastropods that are known to inhabit benthic substrata, such as hydrobiids, planorbids, and juvenile viviparids and pleurocerids.

9.1.5.4 Future Research Directions

Pronounced variation in the stable isotope composition of dominant primary producers in Silver River afforded a unique opportunity to apply mixing models to characterize the transfer of carbon and nitrogen to higher trophic levels, especially herbivores and omnivores. A logical extension of this approach is the incorporation of data specific to higher-order consumers. Strengths of consumer-resource interactions (that are provided as model outputs) when coupled with information on abundance and production can yield a better understanding of energy flow in

the Silver River system. In fact, ecosystem network models could be constructed to examine changes in energy flow under various environmental and management scenarios (Lau et al. 2015).

The stable carbon isotope composition of nuisance algae (mean $\delta^{13}C$ = -41.8 ‰) in the Silver River suggests uptake of methane-derived CO_2. $\delta^{13}C$ values for similar algal taxa in Alexander Springs are more positive (mean $\delta^{13}C$ = -28.0 ‰, Appendix 9.1.4) and call into question the generality of a methane-derived uptake path. With that said, variation in the stable isotope values of algae among systems is likely to yield important insights into the biogeochemical processes that promote and sustain the production of nuisance species within a broad suite of springs and their downstream receiving waters. To do so, however, will require extensive sampling and analysis of stable isotope values of food web constituents within and among spring systems.

9.1.6 CONCLUSIONS AND RECOMMENDATIONS

Measures of stable carbon and nitrogen isotopes provide new and important insights into energy flow and material transport in the Silver River ecosystem. Regarding primary producers present in the Silver River, $\delta^{13}C$ and $\delta^{15}N$ values together with predictions from our models clearly indicate macrophytes (SAV and emergent) and their associated epiphytes fuel much of the secondary production that, in turn, supports a diverse assemblage of organisms that occupy higher trophic levels. These findings are congruent with earlier studies performed by Odum (1957a) and suggest that while filamentous algae has proliferated within the system (Quinlan et al. 2008), the overall flow of energy through the aquatic food web has not changed. Of particular importance is the finding that nuisance algae do not contribute substantially to the diet of key consumers, such as gastropods and large herbivorous fish. Instead, it appears that a small number of herbivorous insect larvae (i.e., trichopterans and chironomids), amphipods, and small omnivorous fish (i.e., shiners and darters) exploit nuisance algae as a food source (proportion of diet > 30%). Because nuisance algal production is consumed predominantly by emergent insects, it is likely that much of this production is exported to the surrounding terrestrial environment. In essence, nuisance algal mats in Silver River, and likely other spring systems, may be decoupled from the broader aquatic food web. This is a dynamic that merits further investigation as it may fundamentally impact energy flow and material transport at the watershed scale.

Stable isotope analysis coupled with data from stomach contents and scat data indicates clearly that redear sunfish and kinosternid turtles are primary predators on the gastropods that have demonstrated any potential to control nuisance algal growth (Dormsjo 2008; Liebowitz et al. 2014). These predator-prey interactions have received little attention, but they merit further study as they are likely to have a profound influence on ecosystem function.

Finally, we note that alligators in the Silver River rely heavily on gastropods and crustaceans to support metabolism and growth. This finding has profound implications for any effort to model the Silver River food web. Previous food web models have considered alligators to be top/apex predators that mainly consume fish and other vertebrates occupying higher trophic levels. In other ecosystems, alligators are known to both directly and indirectly affect key ecosystem processes through their interactions with prey and the environment (Nifong and Silliman 2013, Rosenblatt et al. 2013). Integration of these novel data into spring food webs will help to refine

our understanding of how predation and top-down pressures influence community dynamics within these complex ecosystems.

9.1.7 REFERENCES

Albertin, A. R. 2009. Nutrient dynamics in florida springs and relationships to algal. Ph. D. Dissertation. University of Florida. 157 pp.

Albertin, A., Sickman, J., Pinowska, A. and Stevenson, R. 2012. Identification of nitrogen sources and transformations within karst springs using isotope tracers of nitrogen. Biogeochemistry 108: 219–232.

Ansari, A. A., Gill, S. S. and Khan, F. A. 2010a. Eutrophication: Threat to Aquatic Ecosystems. Pages 143–170 Eutrophication: causes, consequences and control. Springer Netherlands, Dordrecht.

Ansari, A. A., Khan, F. A. Gill, S. S. and Varshney, J. 2010b. Aquatic Plant Diversity in Eutrophic Ecosystems. Pages 247–263 Eutrophication: causes, consequences and control. Springer Netherlands, Dordrecht.

Aresco, M. J., Travis, J. and MacRae, P. S. D. 2015. Trophic Interactions of Turtles in a North Florida Lake Food Web: Prevalence of Omnivory. Copeia 103: 343–356.

Bonn, M., and Bell, F. 2003. Economic impact of selected Florida springs on surrounding local areas. Florida Department of Enviornmental Protection, Tallahassee, FL. 99 pp.

Brabandere, L. D., Frazer, T. K. and Montoya, J. P. 2007. Stable nitrogen isotope ratios of macrophytes and associated periphyton along a nitrate gradient in two subtropical, spring-fed streams. Freshwater Biology 52: 1564–1575.

Borisova, T., Hodges, A. W. and Stevens, T. J. 2014. Economic contributions and ecosystem services of Springs in the Lower Suwannee and Santa Fe River Basins of North-Central Florida. University of Florida, Gainesville, FL. 44 pp.

Brown, M., Reiss, K., Cohen, M., Evans, J., Reddy, K., Inglett, P., Inglett, K., Frazer, T.. Jacoby, C., Phlips, E., Knight, R., Notestein, S. and McKee, K. 2008. Summary and synthesis of the available literature on the effects of nutrients on spring organisms and systems. University of Florida Water Institute, Gainesville, FL. 350 pp.

Caffrey, J. M. 2004. Factors Controlling Net Ecosystem Metabolism in U.S. Estuaries. Estuaries 27: 90–101.

Camp, E. V, Gwinn, D. C., Pine, W. E. and Frazer, T. K. 2012. Changes in submersed aquatic vegetation affect predation risk of a common prey fish Lucania parva (Cyprinodontiformes: Fundulidae) in a spring-fed coastal river. Fisheries Management and Ecology 19: 245–251.

Camp, E. V, Staudhammer, C. L., Pine, W. E., Tetzlaff, J. C., and Frazer, T. K. 2014. Replacement of rooted macrophytes by filamentous macroalgae: Effects on small fishes and macroinvertebrates. Hydrobiologia 722: 159–170.

Canfield, D. E., and Hoyer, M. V. 1988. Influence of Nutrient Enrichment and Light Availability on the Abundance of Aquatic Macrophytes in Florida Streams. Canadian Journal of Fisheries and Aquatic Sciences 45: 1467-1472.

Carpenter, S. R., Kitchell, J. F., and Hodgson, J. R. 1985. Cascading trophic interactions and lake productivity. BioScience 35: 634–639.

Carpenter, S. R. and Lodge, D. M. 1986. Effects of submersed macrophytes on ecosystem processes. Aquatic Botany 26: 341–370.

Carpenter, S. R., Stanley, E. H. and Vander Zanden, M. J. 2011. State of the World's Freshwater Ecosystems: Physical, Chemical, and Biological Changes. Annual Review of Environment and Resources 36: 75–99.

Caut, S., Angulo, E. and Courchamp, F. 2009. Variation in discrimination factors (Δ 15 N and Δ 13 C): the effect of diet isotopic values and applications for diet reconstruction. Journal of Applied Ecology 46: 443–453.

Collins, W. D. and Howard, C. S. 1928. Chemical Character of Waters of Florida. U.S. Geological Survey Water-Supply Paper 596-G. 60 pp

Copeland, R. 2003. Florida Spring Classification System and Spring Glossary. Florida Geological Survey Special Publication No. 52, Tallahassee, FL. vi, 18 pp.

Cortés, E. 1997. A critical review of methods of studying fish feeding based on analysis of stomach contents: application to elasmobranch fishes. Canadian Journal of Fisheries and Aquatic Sciences 54: 726–738.

Cowell, B. C., and Botts, P. S. 1994. Factors influencing the distribution, abundance and growth of *Lyngbya wollei* in central Florida. Aquatic Botany 49: 1–17.

Cowell, B. C. and Dawes, C. J. 2004. Growth and nitrate-nitrogen uptake by the cyanobacterium *Lyngbya wollei*. Journal of Aquatic Plant Management 42: 69-71.

Cowell, B. C., and Dawes, C. J. 2008. Seasonal Comparisons of the Phytoplankton and Decline in Water Transparency in the Spring-Fed Rainbow River, Florida. Journal of Freshwater Ecology 23: 169–177.

Deniro, M., and Epstein. S. 1981. Influence of diet on the distribution of nitrogen isotopes in animals. Geochimica et Cosmochimica Acta 45: 341–351.

Deniro, M. J., and Epstein. S. 1978. Influence of diet on the distribution of carbon isotopes in animals. Geochimica et Cosmochimica Acta 42: 495–506.

Dial, Cordy and Associates. 2008. Submerged Aquatic Vegetation Communities in Selected Springs and Spring Runs in the Middle St. Johns River Basin. Report submitted to the St. Johns River Water Management District, Palatka, FL. iii, 13 pp., Appendices.

Dodds, W. K. 2006. Eutrophication and trophic state in rivers and streams 51:671–680.

Dodds, W. K., Bouska, W. W., Eitzmann, J. L., Pilger, T. J., Pitts, K. L., Riley, A. J.. Schloesser, J. T. and Thornbrugh, D. J. 2009. Eutrophication of U. S. freshwaters: Analysis of potential economic damages. Environmental Science and Technology 43: 12–19.

Dormsjo, K. 2008. Oxygen mediated grazing impacts in Florida springs. M.S. Thesis. University of Florida, Gainesville, FL. 69 pp.

Duarte, C. M. 1995. Submerged aquatic vegetation in relation to different nutrient regimes. Ophelia 41: 87–112.

Duarte, C. M., and Agustí, S. 1998. The CO_2 balance of unproductive aquatic ecosystems.

Duarte, C. M., and Canfield, D. E. 1991. Macrophyte standing crop and primary productivity in some Florida spring-runs. Water Resources Bulletin 26: 927–934.

Duffy, E. J., Richardson, P. J. and Canuel, E. A. 2003. Grazer diversity effects on ecosystem functioning in seagrass beds. Ecology Letters 6: 637–645.

Duraiappah, A. K.,Naeem, S., Agardy, T., Ash,N. J., Cooper, H. D., Díaz, S., Faith, D. P., Mace, G., McNeely, J. A., Mooney, H. A., Alfred. S., Oteng-Yeboah, A., Polasky, H. M. P., Prip, C., Reid, W. V., Samper, C., Schei, P. J., Scholes, R., Schutyser, F.,Van Jaarsve, A. and Millennium Ecosystem Assessment. 2005. Ecosystems and human well-being: Synthesis. Ecosystems.

Evans, J. M. 2007. Algae, exotics, and management reponse in two Florida srpings: Competing conceptions of ecological change in a time of nutrient enrichment. Ph. D. Dissertation. University of Florida. 168 pp.

Fitzgerald, L. A. 1989. An evaluation of stomach flushing techniques for crocodilians. Journal of Herpetology 23: 170–172.

Fry, B. 2006. Stable Isotope Ecology. 1st edition. Springer, New York, NY.

Garnett, S. 1985. The consequences of slow chitin digestion on crocodilian diet analyses. Journal of Herpetology 19: 303–304.

Hartnett, F. M., and Stevenson, J. 2000. Florida's Springs: Strategies for Protection & Restoration. Florida Department of Environmental Protection. Tallahassee, FL.63 pp

Heffernan, J.B., Liebowitz, D. M., Frazer, T. K., Evans, J. M. and Cohen, M. J. 2010. Algal blooms and the nitrogen enrichment hypothesis in Florida springs: evidence, alternatives, and adaptive management. Ecological Applications 20: 816–829.

Heffernan, J. B., Cohen, M. J., Frazer, T. K., Thomas, R. G., Rayfield, T. J., Gulley, J., Martin, J. B., Delfino, J. J. and Graham, W. D. 2010. Hydrologic and biotic influences on nitrate removal in a subtropical spring-fed river. Limnology and Oceanography 55: 249–263.

Hensley, R. T., and Cohen, M. J. 2012. Controls on solute transport in large spring-fed karst rivers. Limnology and Oceanography 57: 912–924.

Hicks, R. and Holland, K. 2012. Nutrient TMDL for Silver Springs, Silver Springs Group, and Upper Silver River (WBIDs 2772A, 2772C, and 2772E). Division of Environmental Assessment and Restoration, Florida Department of Environmental Protection, Tallahassee, FL. 112 pp.

Hudon, C., De Sève, M., and Cattaneo, A. 2014. Increasing occurrence of the benthic filamentous cyanobacterium *Lyngbya wollei*: a symptom of freshwater ecosystem degradation. Freshwater Science 33: 606–618.

Hughes, B. B., Eby, R., Van Dyke, E., Tinker, M. T., Marks, C. I., Johnson, K. S. and Wasson, K. 2013. Recovery of a top predator mediates negative eutrophic effects on seagrass. Proceedings of the National Academy of Sciences of the United States of America 110: 15313–15318.

Jackson, A. L., Inger, R., Parnell, A. C. and Bearhop, S. 2011. Comparing isotopic niche widths among and within communities: SIBER - Stable Isotope Bayesian Ellipses in R. The Journal of animal ecology 80: 595–602.

Jacoby, C. A., Frazer, T. K., Swett, R. A., Keller, S. R. and Notestein, S. K. 2007. Kings Bay vegetation evaluation. Final Report. Southwest Florida Water Management District, Brooksville, Florida. 166 pp.

Jiang, C., Zhu, L., Hu, X., Cheng, J. and Xie, M. 2010. Reasons and Control of Eutrophication in New Reservoirs. Pages 325–340 Eutrophication: causes, consequences and control. Springer Netherlands, Dordrecht.

Kadoya, T., Osada, Y. and Takimoto, G. 2012. IsoWeb: a bayesian isotope mixing model for diet analysis of the whole food web. PloS one 7:e41057.

Katz, B. G., Böhlke, J. K. and Hornsby, H. D. 2001. Timescales for nitrate contamination of spring waters, northern Florida, USA. Chemical Geology 179: 167–186.

King, S. A., Heffernan, J. B. and Cohen, M. J.. 2014. Nutrient flux, uptake, and autotrophic limitation in streams and rivers. Freshwater Science 33: 85–98.

Knight, R. L. 1980. Energy basis of control in aquatic ecosystems. Ph. D. Dissertation. University of Florida. 221 pp

Lau, M. K., Borrett, S. R. and Singh, P. 2015. Ecosystem Network Analysis with R : A guide for using enaR:1–45. http://CRAN.R-project.org/package=enaR.

Layman, C. A., Araujo, M. S., Boucek, R., Hammerschlag-Peyer, C. M., Harrison, E., Jud, Z. R., Matich, P., Rosenblatt, A. E., Vaudo, J. J., Yeager, L. A., Post, D. M. and Bearhop, S. 2012. Applying stable isotopes to examine food-web structure: an overview of analytical tools. Biological Reviews 87: 545–562.

Layman, C. A., Arrington, D. A., Monta a , C. G. and Post, D. M. 2007. Can stable isotope ratios provide for community-wide measures of trophic structure? Ecology 88: 42–48.

Liao, H., Pierce, C. L. and Larscheid, J. G. 2001. Empirical Assessment of Indices of Prey Importance in the Diets of Predacious Fish. Transactions of the American Fisheries Society 130: 583–591.

Liebowitz, D. M. 2013. Environmentally mediated consumer control of algae proliferation in Florida springs. Ph. D. Dissertation. University of Florida. 122 pp.

Liebowitz, D. M., Cohen, M. J., Heffernan, J. B., Korhnak, L. V., and Frazer, T. K. 2014. Environmentally-mediated consumer control of algal proliferation in Florida springs. Freshwater Biology 59: 2009–2023.

Mattson, R. A., Epler, J. H. and Hein, M. K.. 1995. Description of benthic communities in karst, spring-fed streams of north central Florida. Journal of the Kansas Entomological Society 68: 18–41.

McCutchan, J. H., Lewis, W. M., Kendall, C. and McGrath, C. C. 2003. Variation in trophic shift for stable isotope ratios of carbon, nitrogen, and sulfur. Oikos 102: 378–390.

McKinsey, D., and Chapman, L. 1998. Dissolved oxygen and fish distribution in a Florida spring. Environmental Biology of Fishes 53: 211–223.

Mumma, M. T., Cichra, C. E. and Sowards, J. T. 1996. Effects of recreation on the submersed aquatic plant community of Rainbow River, Florida. Journal of Aquatic Plant Management 34: 53–56.

Munch, D. A., Toth, D. J., Huang, C., Davis, J. B., Fortich, C. M., Osburn, W. L., Phlips, E. J., Quinlan, E. L., Allen, M. S., Woods, M. J., Cooney, P., Knight, R. L., Clarke, R. A., and Kinght, S. L. 2006. Fifty-Year Retrospective Study of the Ecology of Silver Springs, Florida. St. Johns River Water Management District Special Publication SJ2007-SP4. pp. variously numbered. Appendices.

Newsome, S. D., Martinez Del Rio, C., Bearhop, S. and Phillips, D. L. 2007. A niche for isotopic ecology. Frontiers in Ecology and the Environment 5: 429–436.

Newsome, S. D., Yeakel, J. D., Wheatley, P. V. and Tinker, M. T.. 2012. Tools for quantifying isotopic niche space and dietary variation at the individual and population level. Journal of Mammalogy 93: 329–341.

Nifong, J. C., and Silliman, B. 2013. Impacts of a large-bodied, apex predator (Alligator mississippiensis Daudin 1801) on salt marsh food webs. Journal of Experimental Marine Biology and Ecology 440: 185–191.

Nifong, R. L., Cohen, M. J. and Cropper, W. P. 2014. Homeostasis and nutrient limitation of benthic autotrophs in natural chemostats. Limnology and Oceanography 59: 2101–2111.

Nifong, R. L. 2017. Experimental effects of grazers on autotrophic species assemblages across a nitrate gradient in Florida springs. Aquatic Botany 139: 57–64.

Notestein, S. K., Frazer, T. K., Hoyer, M. V and Canfield, D. E. 2003. Nutrient Limitation of Periphyton in a Spring-Fed, Coastal Stream in Florida, USA. Journal of Aquatic Plant Management 41: 57–60.

O'Leary, J. K., and McClanahan, T. R. 2010. Trophic cascades result in large-scale coralline algae loss through differential grazer effects. Ecology 91: 3584–3597.

Odum, H. T. 1957a. Trophic structure and productivity of Silver Springs, Florida. Ecological monographs 27: 55–112.

Odum, H. T. 1957b. Primary production measurements in eleven Florida springs and a marine turtle-grass community. Limnology and Oceanography 2: 85–97.

Oulhote, Y., Le Bot, B., Deguen, S. and Glorennec, P. 2011. Using and interpreting isotope data for source identification. TrAC Trends in Analytical Chemistry 30: 302–312.

Paerl, H. W., and Otten, T. G. 2013. Harmful Cyanobacterial Blooms: Causes, Consequences, and Controls. Microbial Ecology 65: 995–1010.

Parnell, A., and Jackson, A. 2013. siar: Stable Isotope Analysis in R. R package version 4.2. http://CRAN.R-project.org/package=siar

Parnell, A. C., Inger, R., Bearhop, S. and Jackson, A. L. 2010. Source partitioning using stable isotopes: coping with too much variation. PloS one 5:e9672.

Peterson, B., and Fry, B. 1987. Stable isotopes in ecosystem studies. Annual Review of Ecology and Systematics 18:293–320.

Phillips, D. L., Inger, R., Bearhop, S., Jackson, A. L., Moore, J. W., Parnell, A. C., Semmens, B. X., and Ward, E. J. 2014. Best practices for use of stable isotope mixing models in food-web studies 835:823–835.

Post, D. M. 2002. Using stable isotopes to estimate trophic position: models, methods, and assumptions. Ecology 83: 703–718.

Post, D. M., Layman, C., Arrington, D., Takimoto, G., Quattrochi, J. and Montana, C. G. 2007. Getting to the fat of the matter: models, methods and assumptions for dealing with lipids in stable isotope analyses. Oecologia 152: 179–189.

Power, M., and Matthews, W. 1985. Grazing minnows, piscivorous bass, and stream algae: dynamics of a strong interaction. Ecology 66:1448–1456.

Quiblier, C., Wood, S., Echenique Subiabre, I., Heath, M., Villeneuve, A. and Humbert, J. F. 2013. A review of current knowledge on toxic benthic freshwater cyanobacteria - Ecology, toxin production and risk management. Water Research 47:5464–5479.

Quinlan, E. L., Phlips, E. J., Donnelly, K. A., Jett, C. H., Sleszynski, P. and Keller, S. 2008. Primary producers and nutrient loading in Silver Springs, FL, USA. Aquatic Botany 88: 247–255.

Radloff, F. G. T., Hobson, K. A. and Leslie, A. J. 2012. Characterising ontogenetic niche shifts in Nile crocodile using stable isotope ($\delta^{13}C$, $\delta^{15}N$) analyses of scute keratin. Isotopes in Environmental and Health Studies 48: 439–56.

Rosenau, J. C., Faulkner, G. L., Hendry, Jr., C. W. and Hull, R. W. 1977. Springs of Florida. Florida Department of Natural Resources Bureau of Geology Bulletin No. 31 (Revised). 461 pp.

Rosenblatt, A. E., and Heithaus, M. R. 2013. Slow isotope turnover rates and low discrimination values in the American alligator: implications for interpretation of ectotherm stable isotope data. Physiological and Biochemical Zoology 86: 137–48.

Rosenblatt, A. E., Nifong, J. C., Heithaus, M. R., Mazzotti, F. J., Cherkiss, M. S., Jeffery, B. M., Elsey, R. M., Decker, R. A., Silliman, B. R., Guillette, L. J., Lowers, R. H. and Larson, J. C. 2015. Factors affecting individual foraging specialization and temporal diet stability across the range of a large "generalist" apex predator. Oecologia 178:5–16.

Sanders, H. L. 1969. Benthic marine diversity and the stability-time hypothesis. Pp. 71-81 IN: Diversity and Stability in Ecological Systems, Brookhaven Symposia in Biology, No. 22. Brookhaven National Laboratory, Upton, NY.

Sanderson, B. L., Tran, C. D., Coe, H. J., Pelekis, V., Steel, E. A. and Reichert, W. L. 2009. Nonlethal Sampling of Fish Caudal Fins Yields Valuable Stable Isotope Data for Threatened and Endangered Fishes. Transactions of the American Fisheries Society 138: 1166–1177.

Scott, T. M., Means, G. H., Means, R. C. and Meegan, R. P. 2002. First Magnitude Springs of Florida. Florida Geological Survey Open File Report No. 85. Florida Geological Survey, Tallahassee, Florida. 138 pp.

Scott, T. M., Means, G. H., Meegan, R. P., Means, R. C., Upchurch, S. B., Copeland, R. E., Jones, J., Roberts, T. and Willet, A. 2004. Springs of Florida. Florida Geological Survey Open File Report No. 66. Florida Geological Survey, Tallahassee, Florida. 677 pp.

Sickman, J. O., Albertin, A., Anderson, M. W., Pinowska, A. and Stevenson, R. J. 2009. A Comparison of Internal and External Supply of Nutrients to Algal Mats in Two First Magnitude Springs in Florida. Journal of Aquatic Plant Management 47: 135–144.

Silliman, B. R., McCoy, M. W., Angelini, C., Holt, R. D., Griffin, J. N., and van de Koppel, J. 2013. Consumer Fronts, Global Change, and Runaway Collapse in Ecosystems. Annual Review of Ecology, Evolution, and Systematics 44: 503–538.

Stevenson, R. J., Pan, Y. and Van Dam, H. 2010. Assessing environmental conditions in rivers and streams with diatoms. The diatoms: Applications for the Environmental and Earth Sciences (2nd ed.): 57–85.

Stevenson, R. J., Pinowska, A.and Wang, Y. 2004. Ecological Condition of Algae and Nutrients in Florida Springs. Florida Department of Environmental Protection, Tallahassee, FL. 205 pp.

Stevenson, R., Pinowska, A., Albertin, A. and Sickman, J. 2007. Ecological condition of algae and nutrients in Florida springs: The synthesis report. Florida Department of Environmental Protection, Tallahassee, FL. 58 pp.

Strong, W. 2004. Temporal water chemistry trends within individual springs and within a population of Florida Springs: 1–54.

Strong, E. E., Gargominy, O., Ponder, W. F. & Bouchet, P. 2008. Global diversity of gastropods (Gastropoda; Mollusca) in freshwater. Hydrobiologia 595, 149–166.

Wetland Solutions, Inc. 2010. An Ecosystem-Level Study of Florida's Springs. FWC Project Agreement No. 08010. Report submitted to the Florida Fish and Wildlife Conservation Commission, Tallahassee, FL. Pp. variously numbered.

Wilson, M. A., and Carpenter, S. R. 1999. Economic Valuation of Freshwater Ecosystem Services in the United States: 1971-1997. Ecological Applications 9:772.

Woodruff, A. 1993. Florida springs chemical classification and aquatic biological communities. M.S. Thesis. University of Florida, Gainesville, FL. 117 pp.

Wynn, S., Borisova, T. and Hodges, A. 2014. Economic Value of the Services Provided by Florida Springs and Other Water Bodies : A Summary of Existing Studies 1 What the Literature Says about the Economic Value of Florida Springs:1–8.

Vander Zanden, M. J., and Rasmussen, J. B. 2001. Variation in $\delta^{15}N$ and $\delta^{13}C$ trophic fractionation: Implications for aquatic food web studies. Limnology and Oceanography 46:2061–2066.

9.2 GRAZING RATES FOR HERBIVORES FEEDING ON MACROPHYTES AND MACROALGAE

9.2.1 INTRODUCTION

Across diverse ecosystems worldwide, grazing by herbivorous and omnivorous consumers is recognized as an important mechanism that regulates autotrophic growth and production; furthermore, grazing often impacts the structure of autotrophic communities, which can alter ecosystem function and provision of ecological services (Power and Matthews 1985; Lodge 1991; Mumby et al. 2006; Silliman et al. 2013). Given the current state of the autotrophic communities in many of Florida's spring ecosystems (i.e., replacement of submerged macrophytes by benthic macroalgae and proliferation of epiphytic algae), quantifying consumption of macroalgae by resident herbivorous and omnivorous taxa to consume is essential to designing and implementing management and restoration strategies.

In spring ecosystems of Florida, two previous studies (Knight 1980; Liebowitz et al. 2014) provide evidence that a common, yet patchily distributed gastropod, *Elimia floridensis* (rasp elimia) can decrease colonization and proliferation of certain macroalgal taxa considered to be nuisance species (i.e., *Lyngbya* and *Vaucheria*); however, the consumption of mature algal tissues by *E. floridensis* has yet to be characterized and/or quantified. Additionally, correlative evidence suggests the distribution and activity of *E. floridensis* is tightly associated with dissolved oxygen (DO) concentrations (Liebowitz 2013; Liebowitz et al. 2014), which may limit the spatial and temporal extent of grazing by *E. floridensis* and its impact on nuisance algae. In addition to *E. floridensis*, there are resident herbivorous and omnivorous taxa that have been shown to be important grazers in other ecosystems, such as other gastropods and crustaceans (Lodge 1991; Silliman et al. 2013). For example, in Atlantic saltmarshes, Silliman and Zieman (2001) experimentally demonstrated that the gastropod *Littoraria irrorata* (periwinkle snail) can exert strong top-down control on growth and production of *Spartina alterniflora* (salt-marsh cordgrass); additionally, they demonstrated top-down control was magnified by increased nutrient concentrations. Later, Silliman and colleagues (2005) concluded that decreased predation on *L. irrorata* together with drought stress triggered widespread loss of saltmarsh habitat and conversion of these areas from once lush and complex vegetative matrices to barren mudflats that did not provide the same ecological services. While little research has been performed on the grazing capacity of resident taxa within Florida's spring ecosystems, results from stable isotope analyses suggest the diets of certain taxa (i.e., trichopterans and chironomids) include nuisance algae (Section 9.1 of this report). Identifying grazers with a higher capacity to consume *Lyngbya* is of particular importance since this taxon was avoided by amphipods in feeding trials (Camacho and Thacker 2006), is widely distributed and locally abundant, and is capable of producing noxious chemicals that may deter grazers (Hudon et al. 2014).

Here we assess the capacity of six abundant grazer taxa (*Elimia floridensis*, *Viviparus georgianus*, *Pomacea paludosa*, *Planorbella scalaris*, *Palaemonetes paludosus*, and *Procambarus fallax*) to consume six macroalgae (*Lyngbya*, *Vaucheria*, *Spirogyra*, *Rhizoclonium*, *Cladophora*, and mixed *Rhizoclonium* + *Cladophora*) and five submerged macrophytes (*Hydrilla verticillata*, *Ceratophyllum demersum*, *Sagittaria kurziana*, *Vallisneria americana*, and *Najas guadalupensis*) from the Silver River ecosystem.

9.2.2 DESIGN OF THE EXPERIMENTS

9.2.2.1 Laboratory Enclosures and Flow-through Systems

Three stand-alone flow-through systems were constructed to carry out laboratory grazing trials (Figure 9.2.1). Each flow-through system consisted of three shelves housing nine 2.25 L clear polycarbonate tanks, totaling 27 tanks per stand-alone system (n = 3). We maintained water (sourced from a well in the University of Florida Fisheries and Aquatic Sciences compound) at a volume of 1.5 L by filling each tank from the top and permitting draining via standpipe with a filter. Systems were recirculating, with effluent from each tank entering a reservoir below the system before it was pumped upwards (15 L per minute, NH-50PX Pentair, Manchester, United Kingdom) and distributed to each tank using irrigation tubing with in-line valves to regulate discharge rates. We cleaned systems between each trail with mild bleach solution and filled them with well water filtered through three successive filters with 1-µm, 0.5-µm, and 0.5-µm mesh.

Figure 9.2.1. Photographs (left-all three systems and right-single system) of the laboratory flow-through systems used to house study organisms during grazing trials.

9.2.2.2 Collection, Breeding and Housing of Organisms

We collected organisms for brood stock and direct use in grazing trials from Silver River, Florida, at six transects sampled for stable isotope analyses (Figure 9.1.4). We collected live individuals by-hand, using dip nets, or sieves. We placed captured individuals in 5-gallon, plastic buckets filled with ambient river water and vegetative material. We outfitted holding buckets with aeration systems and changed the water prior to departure to ensure adequate oxygen supply and decrease the potential for temperature shock. In addition to live individuals of *Pomaca paludosa*, we collected egg masses and reared young in the laboratory. Furthermore, we often collected gravid female *Palaemonetes paludosus* and *Procambrus fallax*, which we isolated from the brood stock in small aquaria until their eggs hatched. We then reared juveniles until they were large enough to introduce into the brood colony. Fortuitously, *Planorbella scalaris* was a prolific breeder that readily laid eggs. We maintained colonies of *P. paludosa*, *Elimia floridensis*, *Viviparous georgianus*, and *P. fallax* in cylindrical, 200 L fiberglass tanks outfitted with

recirculating bio-filtration systems to maintain water quality. We populated each tank with various macrophytes and macroalgae to provide organisms with abundant refugia and a diverse assortment of food. Additionally, we supplemented natural food with manufactured flakes formulated for omnivorous diets (Tropical Flakes, TetraMin, Blacksburg, Virginia). To decrease aggression among *P. fallax* we provided a large number of 4 cm to 10 cm sections of PCV piping (variable diameter) for individuals to inhabit. We maintained *P. scalaris* and *P. paludosus* in smaller glass aquaria (5–20 gallon) outfitted with either air-driven, gravel bed filtration systems or side mounted aquarium filters (Quiet Flow 10 Power Filter, Aqueon, Franklin, Wisconsin), and we stocked the aquaria with various macrophytes and macroalgae. Temperature was maintained by warming or cooling the entire room using an air conditioning/heating unit (UMatch, Gree, Zhuhai, China).

9.2.3 METHODS AND MATERIALS

9.2.3.1 Sourcing, Cleaning and Processing Macrophytes and Macroalgae

Macroalgae were collected from Silver River by hand. After collecting, we transferred large clumps of live vegetation into 1 gallon, plastic freezer bags that were filled with ambient river water. We placed bags on ice for the return to the laboratory and further processing. Upon return, we carefully removed any organisms and unwanted material (i.e., organic debris and sediment) and then transferred algae to 15 L, plastic bins filled with 10 L of filtered well water and outfitted with air stones. We maintained algae under four, 32-watt florescent lightbulbs (5000K, F32T8/TL850/ALTO, Phillips, Amsterdam, Netherland) that were on for 12 hours per day. To provide nutritional support, we added 1 mL of a concentrated macronutrient and micronutrient solution every other day (Table 9.2.1). We maintained 10 L of water in the tanks by adding filtered well water as needed.

Table 9.2.1. Concentrations of macronutrients and micronutrients in concentrated solution (stock) used to provide nutritional support to algae colonies (1 mL dose) and the expected nutrient concentrations (end) in 10 L colony tanks.

Nutrient	[stock] (mg L^{-1})	[end] (mg L^{-1})
Macronutrients		
KH_2PO_4	1,500.00	0.15
KNO_3	16,500.00	1.65
$MgSO_4$	10,000.00	1.00
K_2SO_4	14,500.00	1.45
Micronutrients		
Mg	300.00	0.03
Chelated Cu	20.00	0.00
Chelated Fe	1,400.00	0.14
Mo	12.00	0.00
Zn	80.00	0.01
B	8.00	0.00
Mn	400.00	0.04
EDTA	11,000.00	1.10

Macrophytes were either sourced directly from Silver River or gathered from outdoor stock collections maintained by the UF/IFAS Center for Aquatic Weeds and Invasive Plants (Gainesville, Florida). Specimens collected from Silver River were maintained in cylindrical, 200-L fiberglass tanks outfitted with recirculating bio-filtration systems and lit for 12 hours per day by the same type of bulbs used to illuminate macroalgae.

Prior to weighing, all macroalgal and macrophytic material was thoroughly inspected with the aid of a dissecting microscope (10–45X) for dead plant material, invertebrates, and other macroalgal or macrophytic taxa. We removed all unwanted materials by hand using forceps. To weigh cuttings, we placed wet vegetative material into the upper compartment of a two-part, 50-mL centrifuge tube that had the upper compartment separated from the lower by a 10-µm filter built into the ventral surface (Corning, Corning, New York). To remove excess water, tubes containing wet vegetation were centrifuged at 1,000 rpm for 5 minutes. We then removed the vegetation and measured its mass to the nearest 0.0001 g using a digital scale (XS204DR, Mettler Toledo, Columbus, Ohio). To secure vegetation during experiments we placed a single cutting on a glass microscope slide and wrapped a single silicon rubber band around the vegetation and slide (Figure 9.2.2).

Figure 9.2.2. Photograph of microscope slides used to offer vegetation cuttings to grazers during experimental trials.

9.2.3.2 Grazing Experiments

All trials were three days in duration. We attempted to replicate each grazer species-vegetation taxa combination a minimum of 8 times. This was not always possible given mortality and other constraining factors. Control treatments (three per grazer-vegetation combination) consisted of vegetation treated in the same manner as material introduced into tanks containing grazers, and

they were assigned to tanks using a random number generator (R Core Development Team 2013). To accustom organisms to the experimental tanks, we isolated them with no food for 24 hours prior to introducing vegetation. Prior to and following trials, we measured the wet mass of grazers to the nearest 0.01 g using a digital scale (PGL 2002, Adam Equipment Inc., Oxford, Connecticut) after blotting individuals with paper towels to remove excess water. If individuals suffered mortality during the 3-day trial, we used the mass of the remaining live individuals as the final grazer mass when calculating per capita gain/loss rates of macroalgae (g algae g grazer^{-1} d^{-1}, hereafter per capita consumption rate). We calculated per capita consumption rate as follows:

$$\text{Per capita consumption rate} = \frac{\frac{final\ algae\ mass - initial\ algae\ mass}{final\ grazer\ mass}}{3\ days} \qquad (9.2.1)$$

With this formulation of per capita consumption, more negative values indicate a greater rate of consumption (loss) and positive values represent increases in vegetation mass (gain).

9.2.3.3 Statistical Methods

We applied generalized linear models with Gaussian (normal) error distributions using the 'glm' function within the 'base' package of R statistical program (version 3.1.1) to examine differences in per capita consumption rates related to grazer taxa, autotrophic taxa, and their interactions (R Core Development Team 2013). We assessed the effects of location within the experimental set-up (flow-through unit [A, B, or C] and shelf-level [bottom, middle, or top]) as random effects in our best fit model (main effects only model) using the 'glmer' function of the R package 'lme4' (Bates et al. 2015). To select the most informative model we calculated Akaike's second-order information criterion (AICc, small sample AIC), ΔAIC, Akaike weight (*w*), and relative likelihood. We selected the best model or implemented model averaging, using the R package 'MuMIn' (Barton, 2016). If the Akaike weight (w) of the top performing model was < 0.90, we implemented model averaging to estimate parameters and predict effects for all candidate models with ΔAICc ≤ 2.0 (Burnham and Anderson 2002; Grueber et al. 2011). To compare the importance of each covariate, we calculated the Relative Importance of model covariates occurring in all candidate models (when model averaging was applied), which was calculated as the sum of the Akaike weights (w) from all the models in which the covariate appeared (Barton, 2016). We assessed the effect of body size (mass) on per capita consumption rate using linear regression. All significant differences were evaluated at $\alpha = 0.05$.

9.2.4 RESULTS

9.2.4.1 Macroalgal Trials

Our best performing model (lowest AICc) explaining variation in per capita consumption of macroalgae included the main effects of grazer taxon, macroalgal taxon, and their interaction (Table 9.2.2). The inclusion of location within the experimental set-up did not improve model performance and the amounts of variance explained by all random effect parameters were indistinguishable from zero; therefore, we chose to make predictions based on the model containing main effects only.

Table 9.2.2. Log-likelihood, number of parameters (*k*), Akaike's second-order information criterion (AICc), ΔAICc, and Akaike weight (*w*) for candidate generalized linear models of per capita consumption rate (g algae g grazer^{-1} d^{-1}) of macroalgae during 3-day trials.

Model*	Number of parameters (k)	Log-likelihood	AICc	Δ AICc	Akaike weight (*w*)
Grazer.taxon + Alg.taxon + (Grazer.taxon * Alg.taxon)	39	675.9	-1,265.2	0.0	1.0
Grazer.taxon + Alg.taxon	13	540.6	-1,054.2	211.0	0.0
Grazer.taxon	8	508.8	-1,001.2	264.0	0.0
Alg.taxon	7	495.9	-977.5	287.7	0.0
Intercept only (null)	2	468.4	-932.7	332.4	0.0

*Grazer.taxon: categorical variable with 5 levels (*Elimia floridensis*, *Viviparus georgianus*, *Pomacea paludosa*, *Planorbella scalaris*, *Palaemonetes paludosus*, and *Procambarus fallax*); Alg.taxon: categorical variable with 6 levels (*Lyngbya*, *Vaucheria*, *Spirogyra*, *Rhizoclonium*, *Cladophora*, and mixed *Rhizoclonium* + *Cladophora*).

Using our experimental design, it appears few of the grazer species demonstrated a significant capacity to consume macroalgal taxa (Figure 9.2.3). In terms of the effect of grazer taxon on per capita consumption, *Palaemonetes paludosus* (grass shrimp) maintained per capita consumption rates that were 7 to 114 times as high as other grazers (mean [95 % Confidence Interval-CI] = -0.11 [-0.08 – -0.15] g algae g grazer^{-1} d^{-1}, Table 9.2.3), and it was the only taxon whose 95 % CI did not include zero or positive values (i.e., algae mass gain). Similarly, the effect of macroalgae taxon was driven by one taxon (Figure 9.2.4); wherein, per capita consumption was highest for *Vaucheria* (mean [95 % CI] = -0.08 [-0.05 – -0.10] g algae g grazer^{-1} d^{-1}, Table 9.2.4), which was 6 to 73 times higher than the rate of consumption for other macroalgal taxa.

Table 9.2.3. Predicted β coefficient estimates and 95% Confidence Intervals based on our best fit GLM for per capita consumption rate of macroalgae as affected by grazer taxa.

Taxon	mean β (g algae g grazer^{-1} d^{-1})	95 % CI lower	95 % CI upper
Procambarus fallax	-0.017	0.016	-0.049
Elimia floridensis	-0.006	0.020	-0.032
Planorbella scalaris	-0.016	0.011	-0.043
Pomacea paludosa	-0.017	0.010	-0.044
Palaemonetes paludosus	-0.113	-0.082	-0.145
Viviparus georgianus	-0.001	0.025	-0.027

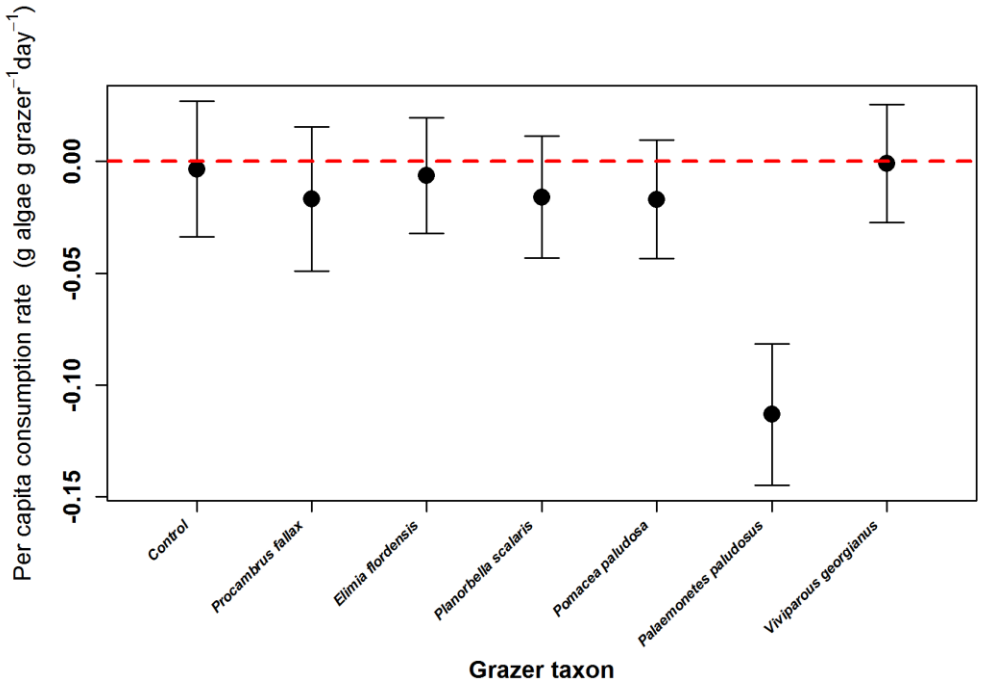

Figure 9.2.3. Predicted effects of grazer taxon on per capita consumption rate. Filled circles are mean values and error bars delineate the 95 % CI. The red dashed line represents zero change in macroalgae biomass during trials.

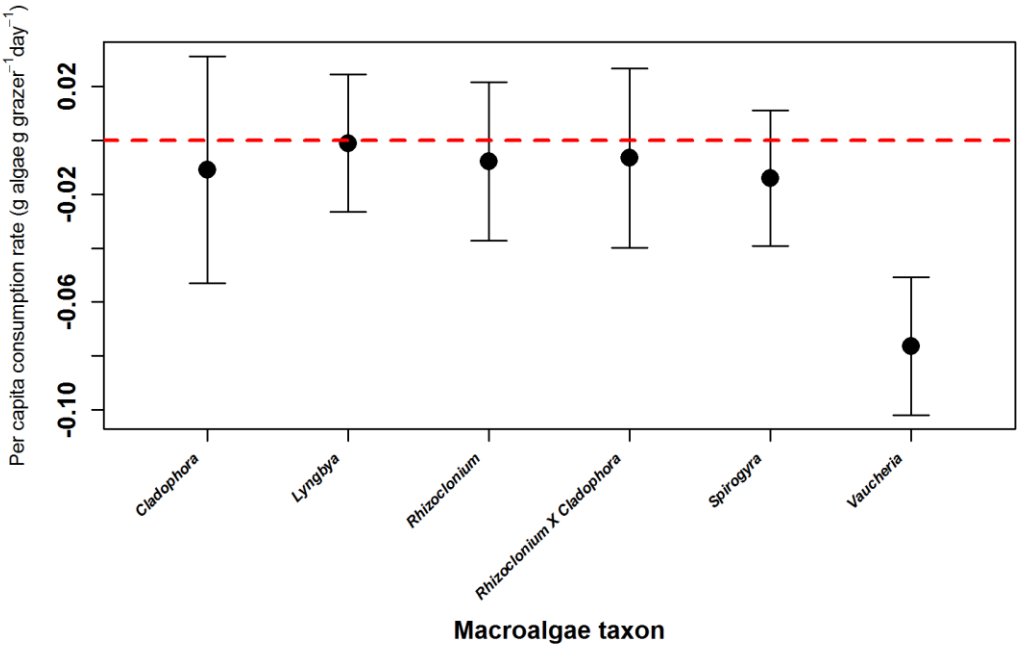

Figure 9.2.4. Predicted effects of macroalgae taxon on per capita consumption rate. Filled circles are mean values and error bars delineate the 95 % CI. The red dashed line represents zero change in macroalgae biomass during trials.

Table 9.2.4. Predicted β coefficient estimates and 95 % Confidence Intervals based on our best fit GLM for per capita consumption rate of macroalgae as affected by macroalgae taxa.

Taxon	mean β (g algae g grazer^{-1} d^{-1})	95 % CI lower	95 % CI upper
Cladophora	-0.011	0.031	-0.053
Lyngbya	-0.001	0.024	-0.027
Rhizoclonium	-0.008	0.022	-0.037
Rhizoclonium X Cladophora	-0.006	0.027	-0.040
Spirogyra	-0.014	0.011	-0.039
Vaucheria	-0.076	-0.051	-0.102

The interactive effect of grazer and macroalgae taxon on per capita consumption indicated per capita consumption rate was highest for *Palaemonetes paludosa* foraging on *Vaucheria* (mean [95 % CI] = -0.36 [-0.33 – -0.39] g algae g grazer^{-1} d $^{-1}$, Figure 9.2.5 and Table 9.2.5).

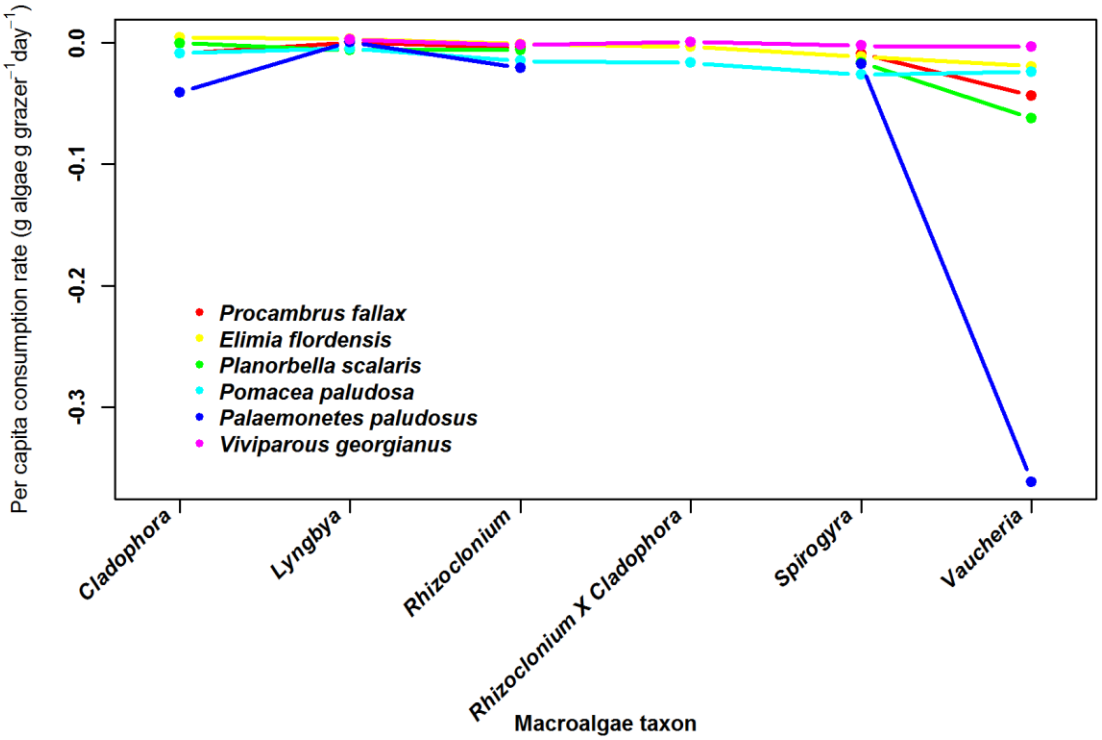

Figure 9.2.5. Interaction plot of per capita consumption rate as a function of grazer and macroalgae taxon. Symbols are predicted mean values. Error bars are not included for simplicity.

Table 9.2.5. Predicted β coefficient estimates and 95 % Confidence Intervals based on our best fit GLM for per capita consumption rate (g algae g grazer^{-1} d^{-1}) of macroalgae as affected by the interaction of grazer and macroalgae taxon. (–) denotes the grazer taxon is unchanged from row above.

Grazer taxon	Macrophyte taxon	mean β	95 % CI lower	95 % CI upper
Elimia floridensis	*Cladophora*	0.005	-0.038	0.047
–	*Lyngbya*	0.003	-0.021	0.026
–	*Rhizoclonium*	-0.001	-0.026	0.024
–	*Rhizoclonium X Cladophora*	-0.003	-0.037	0.030
–	*Spirogyra*	-0.012	-0.034	0.011
–	*Vaucheria*	-0.019	-0.043	0.004
Planorbella scalaris	*Cladophora*	0.000	-0.043	0.042
–	*Lyngbya*	-0.006	-0.029	0.017
–	*Rhizoclonium*	-0.006	-0.031	0.019
–	*Spirogyra*	-0.016	-0.043	0.010
–	*Vaucheria*	-0.062	-0.096	-0.029
Pomacea paludosa	*Cladophora*	-0.009	-0.051	0.034
–	*Lyngbya*	-0.005	-0.029	0.020
–	*Rhizoclonium*	-0.015	-0.041	0.011
–	*Rhizoclonium X Cladophora*	-0.017	-0.050	0.017
–	*Spirogyra*	-0.026	-0.050	-0.003
–	*Vaucheria*	-0.024	-0.047	0.000
Viviparous georgianus	*Lyngbya*	0.003	-0.021	0.026
–	*Rhizoclonium*	-0.002	-0.037	0.034
–	*Rhizoclonium X Cladophora*	0.001	-0.033	0.034
–	*Spirogyra*	-0.003	-0.027	0.022
–	*Vaucheria*	-0.004	-0.027	0.020
Palaemonetes paludosus	*Cladophora*	-0.041	-0.083	0.001
–	*Lyngbya*	0.001	-0.033	0.034
–	*Rhizoclonium*	-0.021	-0.060	0.017
–	*Spirogyra*	-0.017	-0.045	0.010
–	*Vaucheria*	-0.361	-0.388	-0.334
Procambarus fallax	*Cladophora*	-0.009	-0.051	0.033
–	*Lyngbya*	0.000	-0.033	0.033
–	*Rhizoclonium*	-0.004	-0.046	0.038
–	*Spirogyra*	-0.009	-0.038	0.019
–	*Vaucheria*	-0.044	-0.071	-0.017

Using pooled data from all grazers, we found a significant negative relationship between final biomass of individual grazers (i.e., final total grazer biomass divided by number of individuals) and per capita consumption rate ($F_{1,350}$ = 5.51, mean β = 0.003, R^2 = 0.02, p-value = 0.02, Figure 9.2.6). While our simple linear regression (i.e., y = ax + b) was significant, individual grazer biomass explained only 2 % of the variation in per capita consumption rate. We improved the explanatory power of our regression model by using a logarithmic functional response ($F_{1,342}$ = 48.0, R^2 = 0.12, p-value < 0.001, Figure 9.2.6).

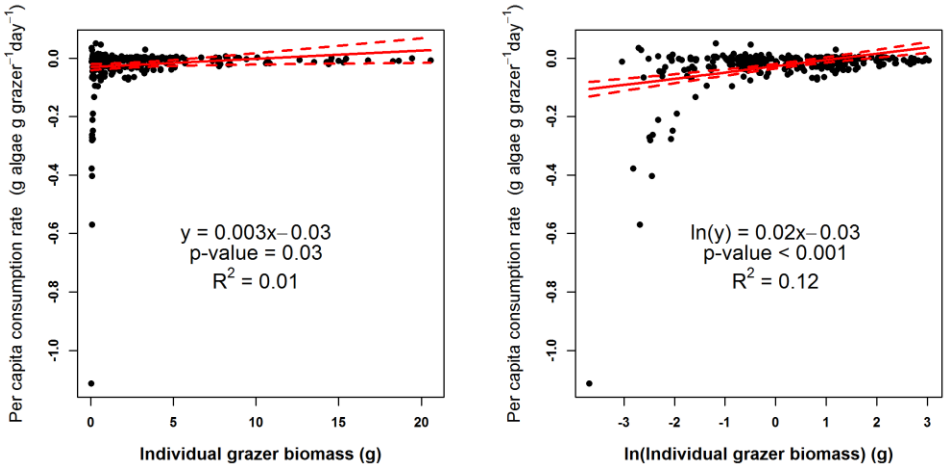

Figure 9.2.6. Scatterplot of per capita macroalgae consumption rate as a function of grazer biomass (data combined for all taxa), left-simple linear model (y = ax + b) and right-logarithmic model (y = ln(x)). Points are raw data. Solid red line is the regression line and dashed red lines enclose the 95 % CI. Note x-axis on the right graph is in log form.

To assess which grazers were predominantly driving this pattern, we performed linear regressions with data generated by each taxon independently. We found significant negative linear relationships between individual grazer biomass and per capita consumption for three of the six grazer taxa (*Pomacea paludosa*, *Palaemonetes paludosus*, and *Viviparous georgianus*, Figure 9.2.7). For all three taxa, the relationship of biomass and per capita consumption was best explained by a logarithmic functional response, indicating the relationship between biomass and per capita consumption rate is non-linear.

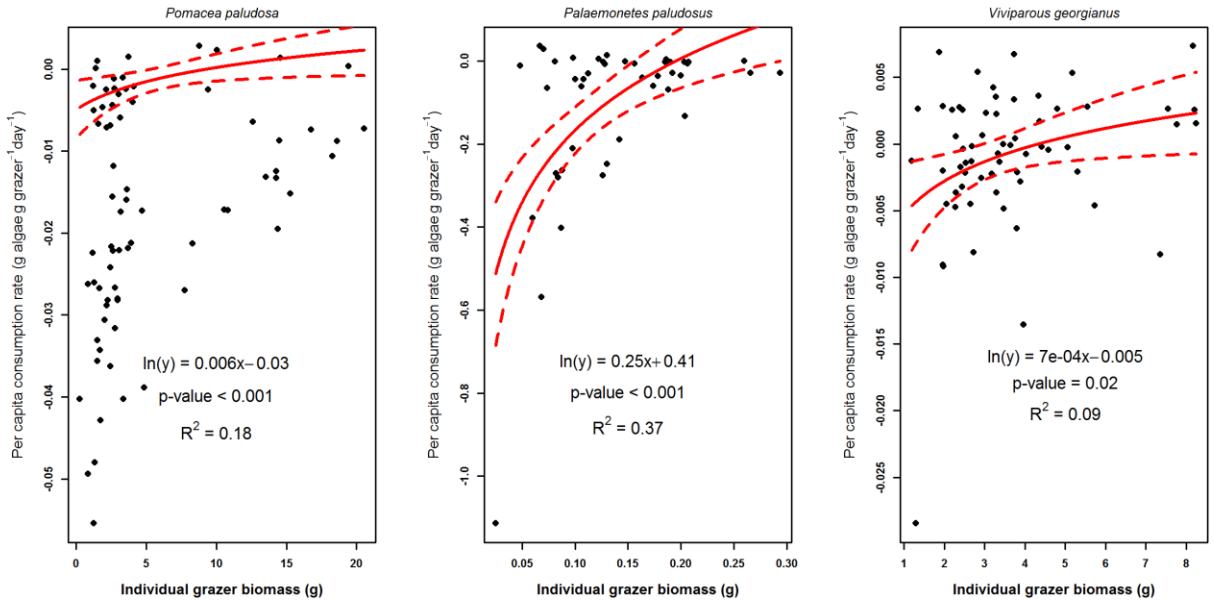

Figure 9.2.7. Scatterplot of per capita consumption rate as a function of grazer biomass. Points are raw data from taxa reported above the plot. Solid red line is the regression line and dashed red lines enclose the 95 % CI.

9.2.4.2 Macrophyte Trials

Due to the low rates of macroalgal consumption by *Viviparous georgianus*, we decided to exclude this taxon from macrophyte feeding trials. Similar to macroalgal trials, our best fit model explaining variation in per capita consumption of macrophytes included the main effects of grazer taxon, macrophyte taxon, and their interaction (Table 9.2.6). The inclusion of location within the experimental set-up did not improve model performance, and the amount of variance explained by all random effects was indistinguishable from zero. In terms of the main effect of grazer taxon, *Procambarus fallax* maintained the highest per capita consumption rate (estimated mean = -0.04 g macrophyte g grazer^{-1} d^{-1}), ranging from 2.5 to 61 times higher than the rates of other grazer taxa (Table 9.2.7). Furthermore, the predicted 95 % CI for *P. fallax* per capita consumption rate was the only 95 % CI that did not include zero (Figure 9.2.8). The gastropod *Elimia floridensis* maintained the lowest per capita consumption rate of macrophytes. In terms of the main effect of macrophytes, per capita consumption was highest for *Najas guadalupensis* (estimated mean = -0.05 g macrophyte g grazer^{-1} d^{-1}), ranging from 1.4 to 5.6 times higher than consumption rates for other macrophytic taxa (Table 9.2.8).

Table 9.2.6. Log-likelihood, number of parameters (*k*), Akaike's second-order information criterion (AICc), ΔAICc, and Akaike weight (*w*), for candidate generalized linear models of per capita consumption rate (g macrophyte g grazer^{-1} d^{-1}) of macrophytes during 3-day trials.

Model*	Number of parameters (k)	Log-likelihood	AICc	Δ AICc	Akaike weight (*w*)
Grazer.taxon + Macro.taxon + (Grazer.taxon *Macro.taxon)	31	724.0	-1380.2	0.0	1.0
Grazer.taxon + Macro.taxon	11	687.9	-1353.1	27.1	0.0
Macro.taxon	6	668.6	-1325.0	55.2	0.0
Grazer.taxon	7	655.6	-1296.9	83.3	0.0
Intercept only (null)	2	633.7	-1263.4	116.8	0.0

*Grazer.taxon: categorical variable with five levels (*Elimia floridensis*, *Pomacea paludosa*, *Planorbella scalaris*, *Palaemonetes paludosus*, and *Procambarus fallax*); Macro.taxon: categorical with five levels (*Ceratophyllum demersum*, *Hydrilla verticillata*, *Najas guadalupensis*, *Sagittaria kurziana*, and *Vallisneria americana*)

Table 9.2.7. Predicted β coefficient estimates and 95 % Confidence Intervals based on our best fit GLM for per capita consumption rate of macrophytes as affected by grazer taxa.

Taxon	mean β (g macrophyte g grazer^{-1} d^{-1})	95 % CI lower	95 % CI upper
Procambarus fallax	-0.044	-0.062	-0.026
Elimia floridensis	-0.001	-0.021	0.019
Planorbella scalaris	-0.014	-0.033	0.006
Pomacea paludosa	-0.013	-0.041	0.016
Palaemonetes paludosus	-0.018	-0.040	0.005

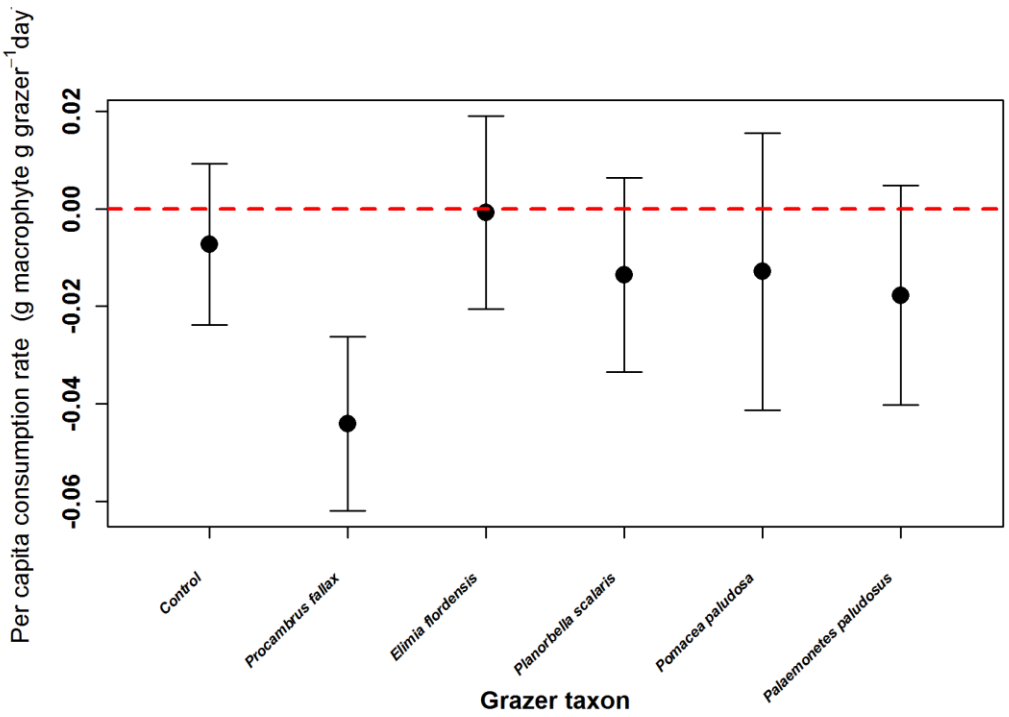

Figure 9.2.8. Predicted effects of grazer taxon on per capita consumption rate. Filled circles are mean values and error bars delineate the 95 % CI. The red dashed line represents zero change in macroalgae biomass during trials.

Table 9.2.8. Predicted β coefficient estimates and 95 % Confidence Intervals based on our best fit GLM for per capita consumption rate of macrophytes as affected by macrophyte taxa.

Taxon	mean β (g macrophyte g grazer^{-1} d^{-1})	95 % CI lower	95 % CI upper
Ceratophyllum demersum	-0.032	-0.051	-0.014
Hydrilla verticillata	-0.013	-0.035	0.009
Najas guadalupensis	-0.046	-0.069	-0.023
Sagittaria kurziana	0.000	-0.023	0.023
Vallisneria americana	-0.008	-0.027	0.011

The interaction effect of grazer and macrophytic taxa primarily was driven by the high per capita consumption rate of *Procambarus fallax* feeding on *Najas guadalupensis* (Figure 9.2.9). Estimated per capita consumption for *P. fallax* feeding on *N. guadalupensis* averaged -0.12 g macrophyte g grazer^{-1} d^{-1}, and it ranged from 2 to 274 times the estimated mean consumption rate for any other grazer-macrophyte combination (Table 9.2.9). Estimated per capita consumption was similarly high when *Palaemonetes paludosus* feed on *Ceratophyllum demersum* (mean β [95 % CI] = -0.06 [-0.08 – -0.04]) and when *Pomacea paludosa* fed on *Hydrilla verticillata* (mean β [95 % CI] = -0.03 [-0.06 – -0.01]).

Table 9.2.9. Predicted β coefficient estimates and 95 % Confidence Intervals based on our best fit GLM for per capita consumption rate (g macrophyte g grazer^{-1} d^{-1}) of macrophytes as affected by the interaction of grazer and macrophyte taxon. (–) denotes the grazer taxon is unchanged from row above.

Grazer taxon	Macrophyte taxon	β	95% CI lower	95% CI upper
Elimia floridensis	*Ceratophyllum demersum*	-0.005	-0.027	0.018
–	*Hydrilla verticillata*	-0.001	-0.023	0.020
–	*Najas guadalupensis*	-0.015	-0.037	0.008
–	*Sagittaria kurziana*	0.000	-0.023	0.022
–	*Vallisneria americana*	0.008	-0.008	0.023
Planorbella scalaris	*Ceratophyllum demersum*	-0.012	-0.033	0.010
–	*Hydrilla verticillata*	-0.006	-0.028	0.017
–	*Najas guadalupensis*	-0.030	-0.052	-0.009
–	*Sagittaria kurziana*	-0.002	-0.024	0.019
–	*Vallisneria americana*	-0.016	-0.032	0.000
Pomacea paludosa	*Ceratophyllum demersum*	-0.015	-0.047	0.017
–	*Hydrilla verticillata*	-0.035	-0.059	-0.011
–	*Najas guadalupensis*	-0.018	-0.050	0.014
–	*Sagittaria kurziana*	0.021	-0.011	0.053
–	*Vallisneria americana*	-0.003	-0.030	0.024
Palaemonetes paludosus	*Ceratophyllum demersum*	-0.061	-0.086	-0.036
–	*Hydrilla verticillata*	-0.009	-0.031	0.012
–	*Najas guadalupensis*	-0.031	-0.052	-0.009
–	*Sagittaria kurziana*	0.001	-0.022	0.023
–	*Vallisneria americana*	0.003	-0.019	0.026
Procambarus fallax	*Ceratophyllum demersum*	-0.043	-0.056	-0.031
–	*Hydrilla verticillata*	-0.016	-0.037	0.006
–	*Najas guadalupensis*	-0.124	-0.147	-0.102
–	*Sagittaria kurziana*	-0.006	-0.028	0.015
–	*Vallisneria americana*	-0.039	-0.061	-0.018

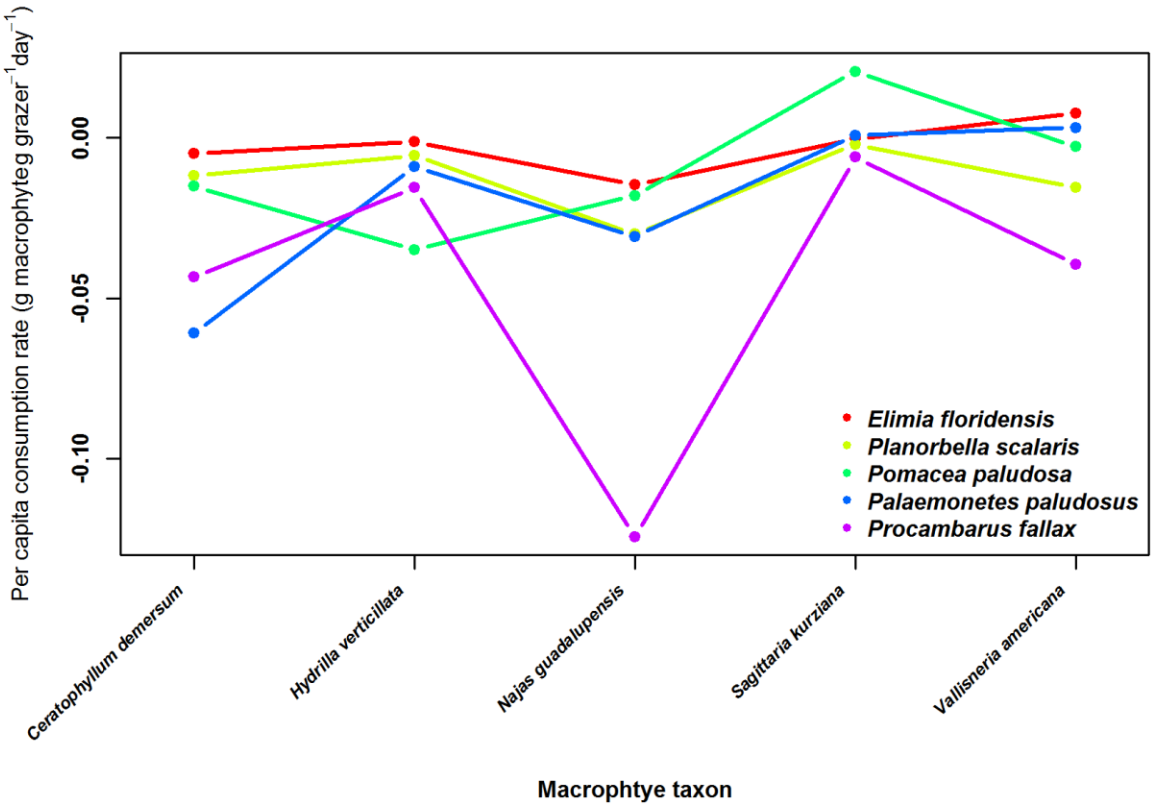

Figure 9.2.9. Interaction plot of estimated per capita consumption rate as a function of grazer and macrophyte taxon. Symbols are predicted mean values. Error bars are not included for simplicity.

When data from all grazers were combined, we found no significant linear relationship between individual grazer mass and per capita consumption rate (simple linear regression: $F_{1, 279} = 0.13$, p-value = 0.71; logarithmic response: $F_{1, 279} = 1.76$, p-value = 0.19). We suspected the low consumption rates for certain grazers contributed to the non-significant linear relationship, so we performed separate linear regressions for each taxon. Taxon-specific linear regressions yielded significant relationships for the decapod *Procambarus fallax* and the gastropod *Planorbella scalaris*, with logarithmic functional responses performing better (lower AICc) than simple linear responses, which suggest the relationship between biomass and per capita consumption rates is non-linear (Figure 9.2.10).

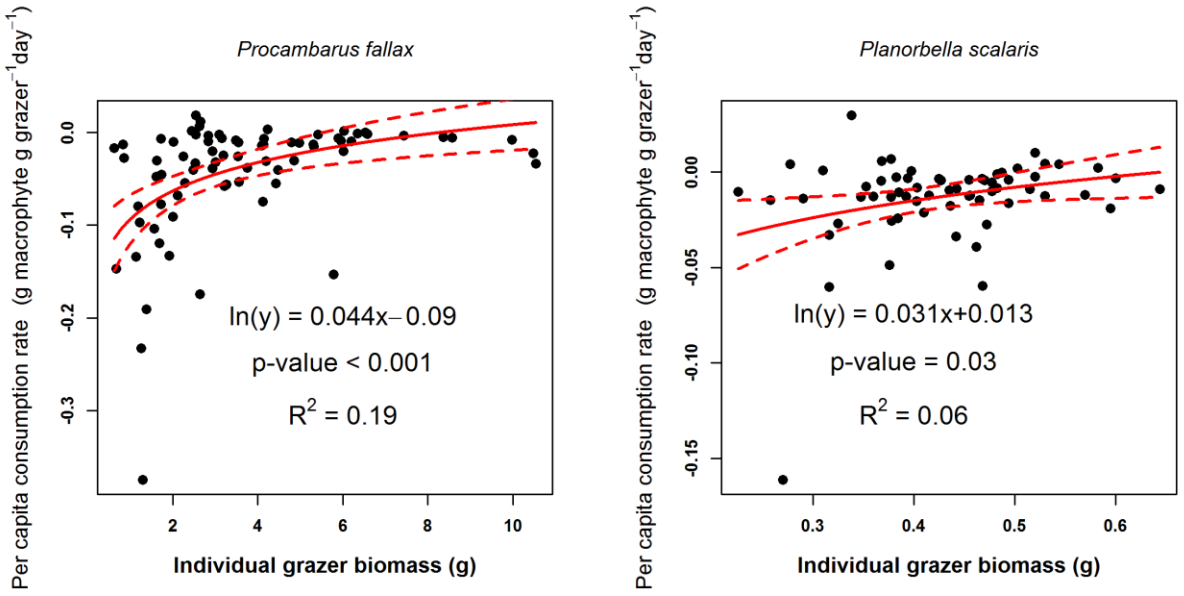

Figure 9.2.10. Scatterplot of per capita consumption rate of macrophyte material as a function of grazer biomass. Points are raw data from taxa reported above the plot.. Solid red line is the regression line and dashed red lines enclose the 95 % CI.

9.2.5 DISCUSSION

9.2.5.1 What grazers have the capacity to eat macroalgae?

Previous studies reported *Elimia floridensis* has the potential to curb the proliferation of the benthic filamentous macroalgae considered to be nuisance taxa, i.e., *Lyngbya* and *Vaucheria,* (Knight 1980; Liebowitz 2013; Liebowitz et. al. 2014). In addition, findings from field enclosure experiments indicate the presence of gastropod grazers enhances macrophytic standing stocks, and in their absence, macroalgal standing stock increases (Nifong 2017). However, few laboratory trials have specifically examined the consumption of macroalgal taxa by dominant grazers resident in Florida spring ecosystems, including *E. floridensis*.

Here, we assessed the per capita consumption rate of five macroalgal taxa (*Lyngbya*, *Vaucheria*, *Spirogyra*, *Rhizoclonium*, and *Cladophora*) and one combination of taxa (*Rhizoclonium* and *Cladophora*) by six grazer taxa (*Elimia floridensis*, *Viviparus georgianus*, *Pomacea paludosa*, *Planorbella scalaris*, *Palaemonetes paludosus*, and *Procambarus fallax*) abundant in Florida spring ecosystems. We selected macroalgal taxa representative of macroalgal groups used in isotopic mixing model analyses in Section 9.1 of this report. Benthic filamentous algae, a.k.a. nuisance algae, represented by the taxa *Lyngbya* and *Vaucheria*, unattached algae represented by *Spirogyra*, and epiphytic algae represented by the taxa *Rhizoclonium* and *Cladophora*.

Using multiple regression analysis (GLM), we determined that per capita consumption rates varied significantly among grazer and macroalgal taxa, and variation in per capita consumption was best explained by specific combinations of grazer and macroalgal taxa (Figure 9.2.5). Across all macroalgal taxa, per capita consumption was highest for *Palaemonetes paludosus,* followed by *Pomacea paludosa, Procambarus fallax, Planorbella scalaris, Elimia floridensis,* and

Viviparus georgianus (Figure 9.2.3 and Table 9.2.3). Across all grazers, per capita consumption was highest for *Vaucheria*, followed by *Spirogyra, Cladophora, Rhizoclonium,* the mixed colony of *Rhizoclonium* and *Cladophora,* and *Lyngbya* (Figure 9.2.4 and Table 9.2.4). When the interaction of grazer and macroalgal taxa was considered, the highest (most negative) per capita consumption rates were estimated for *P. paludosus* consuming *Vaucheria* followed by *P. scalaris* and *P. fallax* feeding on *Vaucheria* (Figure 9.2.5 and Table 9.2.5). Overall, estimated consumption of *Vaucheria* by all grazers, except *V. georgianus*, ranked in the top 10 of 32 combinations; however, only for the top six pairs did the estimated 95 % CI's for per capita consumption exclude zero. Consumption rates of *Lyngbya* ranked in the bottom 50 % of rates estimated for all grazer-macroalgae pairs, and mean consumption rates were estimated to be negative (indicating loss of algal biomass) only for two gastropod grazers, *P. scalaris* and *P. paludosa*; however, the 95 % CI's for all estimates included zero (Table 9.2.5).

Consumption rates of the unattached macroalgae *Spirogyra* ranked in the top 50 % of estimated rates for all grazer-macroalgae pairs. *Pomacea paludosa* feeding on *Spirogyra* yielded the 5th highest consumption rate, which narrowly exceeded the consumption rate when this snail fed on *Vaucheria*. Consumption of epiphytic algae, *Rhizoclonium* and *Cladophora*, were highly variable among grazers. For example, estimated consumption rates for *Cladophora* ranked last (32nd out of 32 pairs) for *Elimia floridensis* and 4th for *Palaemonetes paludosus*.

The gastropod *Viviparous georgianus*, while abundant in Silver River and other Florida spring-run streams, performed poorly in all macroalgal feeding trials. Based on natural history observations and feeding studies, Duch (1976) concluded *V. georgianus* primarily feed upon diatoms and suspended flocculant material (i.e., detritus, diatoms, algae fragments, etc.), and it is known to employ a pseudo-filter feeding technique known as ctenidial suspension feeding (Strong et al. 2008). Our findings corroborate previous studies and provide confirmation that *V. georgianus* has limited capacity to consume filamentous macroalgae. Considering these findings *V. georgianus* was not included in macrophyte feeding trials, since it is unlikely *V. georgianus* would consume their more structurally complex tissues.

The gastropod *Elimia floridensis* demonstrated limited capacity to consume both taxa of nuisance algae (*Vaucheria* and *Lyngbya*). While *E. floridensis* consumption of *Vaucheria* was the highest relative to rates for all other macroalgae, the predicted 95 % CI included zero. The predicted consumption rate for *E. floridensis* was next to last among rates estimated for all grazer-macroalgae pairs. These findings are contradictory to previous in-situ experimental studies that suggest *E. floridensis* has the potential to curtail nuisance algal growth and proliferation (Knight 1980; Liebowitz 2013; Liebowitz et. al. 2014). We hypothesize that our contradictory findings result from differences between *Lyngbya* growth stages considered in past studies and the growth stage used here. In our study, we offered clumps of fully mature *Lyngbya* filaments to all grazers. In previous in-situ field studies, macroalgae colonies formed on clean surfaces and young macroalgal filaments were available to *E. floridensis*. As a cyanobacterium, mature filaments of *Lyngbya* develop a polysaccharide sheath and produce various toxins and volatile organic compounds, which defend against grazing (Camacho and Thacker 2006; Hudon et al. 2014). Our findings suggest the chemical and structural defense strategies employed by *Lyngbya* effectively limit grazing by multiple gastropod and decapod taxa resident in Florida spring ecosystems.

In our isotopic mixing model and diet analyses (Section 9.1 this report), we found little evidence that nuisance algae were consumed, including *Vaucheria*. When presented in isolation, however, *Vaucheria* seems to be highly palatable for both gastropod and decapod grazers. One possible explanation for this mismatch between field and laboratory results is the absence of predators. Camp et. al. (2014) found the risk of predation for small fish and macroinvertebrates was significantly elevated when individuals were in beds of benthic macroalgae as compared to structurally complex stands of macrophytes. When abundant, *Vaucheria* forms large homogenous mats that offer little refuge from patrolling predators. Thus, grazers have the capacity to consume *Vaucheria* at high rates relative to other macroalgae, but actual grazing pressure in the field may be limited by the risk of predation.

9.2.5.2 What grazers have the capacity to eat macrophytes?

Similar to macroalgae, few studies have examined the capacity of resident grazers in Florida spring-run streams to consume dominant macrophyes. Here, we examined the per capita consumption rate for combinations of five macrophytic taxa (*Ceratophyllum demersum, Hydrilla verticillata, Najas guadalupensis, Sagittaria kurziana,* and *Vallisneria americana*) and five grazers (*Elimia floridensis, Pomacea paludosa, Planorbella scalaris, Palaemonetes paludosus,* and *Procambarus fallax*).

Using multiple regression analysis, we found variation in per capita consumption of macrophytic biomass was best explained by the main effects of grazer and macrophyte taxon as well as the interaction between grazer and macrophytic taxon (Table 9.2.6). With data from all macrophytes combined, we estimated per capita consumption was highest for *Procambarus fallax*, followed by *Palaemonetes paludosus*, *Pomacea paludosa*, *Planorbella scalaris*, and *Elimia floridensis*. Across all grazer taxa, per capita consumption rates were highest for *Najas guadalupensis*, followed by *Ceratophyllum demersum*, *Hydrilla verticillata,* and finally *Sagittaria kurziana* and *Vallisneria americana*.

When grazer and macrophyte combinations were considered separately, per capita consumption was highest for *Procambarus fallax* feeding on *Najas guadalupensis,* followed by *Palaemonetes paludosus* and *P. fallax* feeding on *Ceratophyllum demersum*, *P. fallax* feeding on *Vallisneria americana*, and *Pomacea paludosa* feeding on *Hydrilla verticillata*. The hardened mouthparts and specialized appendages maintained by the decapods *P. fallax* and *P. paludosus* are better adapted to shredding macrophyte tissues than the radula and soft mouth tissues of gastropods. Our data generally support this notion, apart from the gastropod *P. paludosa,* which attain large body sizes and seem well equipped to consume most macrophytes. Consumption rates determined for both the native *P. paludosa* and the non-native *P. insularum* (island apple snail) consuming blatterwort *Utricularia* and the macrophyte *Bacopa caroliniana* were much higher than the rates observed here (Morrison and Hay 2011).

Consumption rates for *N. guadalupensis* ranked in the top 50 % of rates for all combinations of grazer and macrophyte, and only one of the predicted 95 % CI's contained zero. The high palatability of *N. guadalupensis* for both gastropod and decapod grazers, may help to explain its low abundance and patchy distribution in spring-run streams.

Elimia floridensis maintained low rates of consumption on all macrophytes, and all 95 % CIs contained zero. Thus, we conclude that *E. floridensis* should be considered a strict algivore, with a diet consisting of diatoms and filamentous macroalgae.

9.2.5.3 Future Research Directions

Laboratory feeding trials are useful, perhaps most notably for providing estimates of maximal feeding rates for consumers that are removed from external stressors and environmental variation. However, in nature, consumers interact with multiple sources of stress (e.g., competitors, predators, hydrology, etc.), and they experience some degree of variation in environmental conditions. As such, there is often a mismatch between what we expect to see given results from laboratory trials and what we observe in nature. For example, in our feeding trials we found the nuisance macroalgae *Vaucheria* was readily consumed by both gastropod and decapod grazers (Figure 9.2.5 and Table 9.2.5). Contrary to this, our stomach content and stable isotope study (Section 9.1 of this report) indicated that nuisance macroalgae, such as *Vaucheria,* contribute little (< 30 %) to the diet of most herbivorous and omnivorous taxa (diets of 20 out of 28 consumers were estimated to contain < 30 % nuisance algae, Table 9.1.6). To identify the factors potentially contributing to this mismatch, we suggest using in-situ field experiments that isolate the effects of specific drivers (i.e., predators, competitors, etc.) or compare in-situ grazing rates across environmental gradients (e.g., concentrations of dissolved oxygen, nitrate concentrations, etc.). In Section 9.3 of this report, we test the hypothesis that top-down control by predators limits herbivore abundance and grazing intensity. Future studies should concentrate on other factors that could help explain differences between field and laboratory studies.

Our design allowed us to assess grazing without a choice of food; specifically, only one macroalga or macrophyte was presented during each trial. In nature, however, grazers are presented with many options for foraging that vary with the relative abundance and diversity of available macrophytes and macroalgae. Perhaps, grazer selectivity and preference help define in-situ foraging patterns. To examine this possibility, a logical next step would be to perform choice assays; wherein, several macrophytic and macroalgal taxa are presented to grazers in each trial.

In this study, we assessed the capacity of six grazer taxa, commonly found in Florida spring-run ecosystems, to consume various members of the vegetative community. These six taxa are not the only herbivorous and omnivorous taxa common in Florida spring-run ecosystems. In the future, quantifying the capacity of other grazers, such as emergent insects, fish, and turtles, may help to advance our understanding of how grazing pressure affects the structure and function of vegetative communities within Florida's spring-run ecosystems.

9.2.6 CONCLUSIONS AND RECOMMENDATIONS

Our results indicate decapod crustaceans demonstrate a greater capacity to consume both macroalgae and macrophytes than gastropod taxa. In terms of macroalgal consumption, *Vaucheria* was readily consumed by most grazers and at the highest rate by *Palaemonetes paludosus*. Similarly, macrophytic consumption was highest for *Procambarus fallax*, including consumption of the exotic macrophyte *Hydrilla verticillata* (second to the rate *Pomacea paludosa* consumed *Hydrilla verticillata*). Given these findings, it is likely that any efforts to

bolster populations of decapod crustaceans in springs-run ecosystems would likely increase grazing pressures on nuisance macroalgae as well as exotic macrophytes.

Contrary to previous claims, we found that grazers demonstrated a weak capacity to consume the nuisance algae *Lyngbya*. Therefore, we conclude that increasing grazing pressure by gastropods alone may not be a suitable option for reducing *Lyngbya* proliferation in the field. Perhaps, other options, such as mechanical removal, should be considered during the planning of restoration and removal efforts.

9.2.7 REFERENCES

Barton, K. 2016. MuMIn: Multi-Model Inference (R package version 1.15.6). Available at https://cran.r-project.org/package=MuMIn.

Bates, D., Maechler, M., Bolker, B., and Walker, S. 2015. Fitting Linear Mixed-Effects Models Using lme4. Journal of Statistical Software, 67(1): 1-48.

Burnham, K. P., and Anderson, D. R. 2002. Model Selection and Multimodel Inference: A Practical Information-Theoretic Approach. Springer-Verlag New York, Inc., New York, 515 pp.

Camacho, F. A., and Thacker, R. W. 2006. Amphipod herbivory on the freshwater cyanobacterium *Lyngbya wollei* : Chemical stimulants and morphological defenses. Limnology and Oceanography 51: 1870–1875.

Camp, E. V, Staudhammer, C. L., Pine, W. E., Tetzlaff, J. C., and Frazer, T. K. 2014. Replacement of rooted macrophytes by filamentous macroalgae: Effects on small fishes and macroinvertebrates. Hydrobiologia 722: 159–170.

Duch, T. M. 1976. Aspects of the feeding habits of *Viviparous georgianus*. The Nautilus 90(1): 7–10.

Grueber, C. E., Nakagawa, S., Laws, R. J., and Jamieson, I. G. 2011. Multimodel inference in ecology and evolution: Challenges and solutions. Journal of Evolutionary Biology 24: 699–711.

Hudon, C., De Sève, M., and Cattaneo, A. 2014. Increasing occurrence of the benthic filamentous cyanobacterium *Lyngbya wollei*: a symptom of freshwater ecosystem degradation. Freshwater Science 33:606–618.

Knight, R. L. 1980. Energy basis of control in aquatic ecosystems. Ph. D. Dissertation. University of Florida. 221 pp.

Liebowitz, D. M. 2013. Environmentally mediated consumer control of algae proliferation in Florida springs. Ph. D. Dissertation. University of Florida. 122 pp.

Liebowitz, D. M., Cohen, M. J., Heffernan, J. B., Korhnak, L. V. and Frazer, T. K.. 2014. Environmentally-mediated consumer control of algal proliferation in Florida springs. Freshwater Biology 59:2009–2023.

Lodge, D. M. 1991. Herbivory on freshwater macrophytes. Aquatic Botany 41:195–224.

Mumby, P. J., Dahlgren, C. P., Harborne, A. R., Kappel, C. V., Micheli, F., Brumbaugh, D. R., Holmes, K. E., Mendes, J. M., Broad, K., Sanchirico, J. N., Buch, K., Box, S., Stoffle, R. W. and Gill, A. B. 2006. Fishing, trophic cascades, and the process of grazing on coral reefs. Science 311: 98–101.

Nifong, R. L. 2017. Experimental effects of grazers on autotrophic species assemblages across a nitrate gradient in Florida springs. Aquatic Botany 139: 57–64.

Power, M., and Matthews, W. 1985. Grazing minnows, piscivorous bass, and stream algae: dynamics of a strong interaction. Ecology 66:1448–1456.

R Core Development Team. 2013. R: A Language and Environment for Statistical Computing. http://www.r-project.org/.

Silliman, B. R., Van De Koppel, J., Bertness, M. D. Stanton, L. E. and Mendelssohn, I. A. 2005. Drought, snails, and large-scale die-off of southern US salt marshes. Science 310: 1803–1806.

Silliman, B. R., McCoy, M. W., Angelini, C., Holt, R. D., Griffin, J. N. and van de Koppel, J. 2013. Consumer Fronts, Global Change, and Runaway Collapse in Ecosystems. Annual Review of Ecology, Evolution, and Systematics 44: 503–538.

Silliman, B., and Zieman, J. C. 2001. Top-down control of Spartina alterniflora production by periwinkle grazing in a Virginia salt marsh. Ecology 82: 2830–2845.

Strong, E. E., Gargominy, O., Ponder, W. F. and Bouchet, P. 2008. Global diversity of gastropods (Gastropoda; Mollusca) in freshwater. Hydrobiologia 595: 149–166.

Venables, W. N., and Ripley, B. D. 2002. Modern Applied Statistics with S. Fourth. Springer, New York, New York.

9.3 ASSESSING TOP-DOWN (CONSUMER) CONTROL OF KEY GRAZERS

9.3.1 INTRODUCTION

Predators influence the structure and function of food webs through both consumptive and non-consumptive interactions with their prey (e.g., Pace et al. 1999, Schmitz et al. 2000, Silliman and Bertness 2002, Schmitz et al. 2004). The indirect effects of predation can be profound and are often manifested most visibly at the base of a food web. Trophic cascades, for example, are common in aquatic ecosystems (Strong 1992) and can occur when reduced predation on grazers results in a compensatory response of increased grazing pressure on primary producers, either due to increased grazer abundance or increased rates of consumption (Hairston et al. 1960). The extent to which predator-induced trophic cascades may be operating in Florida's spring ecosystems is not known, but this ecological phenemonom may, in fact, help to explain the recent proliferation and persistence of nuisance algae in Florida's springs.

In Florida's spring-run streams, several grazers (chiefly gastropods) are hypothesized to have the capacity to control benthic filamentous algae (i.e., nuisance algae) through consumption (Knight 1980, Dormsjo 2008, Leibowitz 2013, Leibowitz et al. 2014). Experimental demonstration of such control in Florida springs is limited, however, to a single inclusion study (Nifong 2017). Across a gradient in nitrate concentrations in Florida spring-run streams, Nifong (2017) measured the response of macrophytic and nuisance algal biomass and net production in the presence and absence of gastropod grazers. Nifong (2017) reported 3X higher biomass of nuisance algae in the absence of gastropods. While encouraging, these findings are focused on the effects of a single group of grazers, i.e. gastropods, and do not capture the influence of other potentially important grazing organisms. There is, in fact, a diverse suite of macroinvertebrate grazers present in Florida's springs that may might be expected to play an important role in the control and regulation of algae in these ecosystems (Mattson et al. 1995).

Over the past 50 years, in addition to nuisance algae, the abundance of epiphytic algae has dramatically increased in many of Florida's spring-runs (Quinlan et al. 2008). Increased epiphytic loads on leaves of macrophytes have the potential to negatively impact macrophytic growth and production by reducing available light (i.e., shading) and rates of nutrient uptake, as well as increasing drag forces. When combined, the effects of heavy epiphytic loads likely limit macrophytic growth and increase stress.

In Section 9.2 of this report, we examined consumption rates of different macroinvertebrates (in isolation) on a variety of algae (including nuisance species and epiphytic forms) and macrophytes. These laboratory studies demonstrated that a number of grazers are capable of and readily consumed several different types of filamentous macroalgae (excluding the nuisance algae *Lyngbya*). Our field studies (Section 9.1 of this report), on the other hand, indicated limited consumption of filamentous algae, particularly nuisance species. Thus, we hypothesized that predation or risk of predation may play a role in limiting grazing. To test this hypothesis, we employed an in-situ predator exclusion experiment that attempted to answer the following questions related to the role of predation in Florida spring-run streams: 1) Does the absence of predation lead to decreased epiphytic loads on macrophytes? 2) Do growth and standing crop

(biomass) of macrophytes respond to changes in epiphytic loads? And, finally, 3) What is the effect of excluding predators on macroinvertebrates, including grazers?

9.3.2 EXPERIMENTAL DESIGN

We conducted this experiment in the upper and middle regions of Silver River, Florida (see Section 9.1.2 of this report for a detailed site description), at 10 sites (five upper and five mid-river locations; Figure 9.3.1). The sites were chosen to be near sampling locations used by other CRISPS working groups and to avoid damage to SAV beds caused by recreational boaters following recommendations from managers of Silver River State Park. In addition, we selected sites similar in depth, proximity to shoreline, and vegetative cover (100 % SAV); however, sites differed in the relative abundance of dominant SAV taxa (*Vallisneria americana* vs. *Sagittaria kurziana*). Within each site the configuration of the experimental array was randomized, and experimental plots (total three within each array) were separated by three to five meters (Figure 9.3.2).

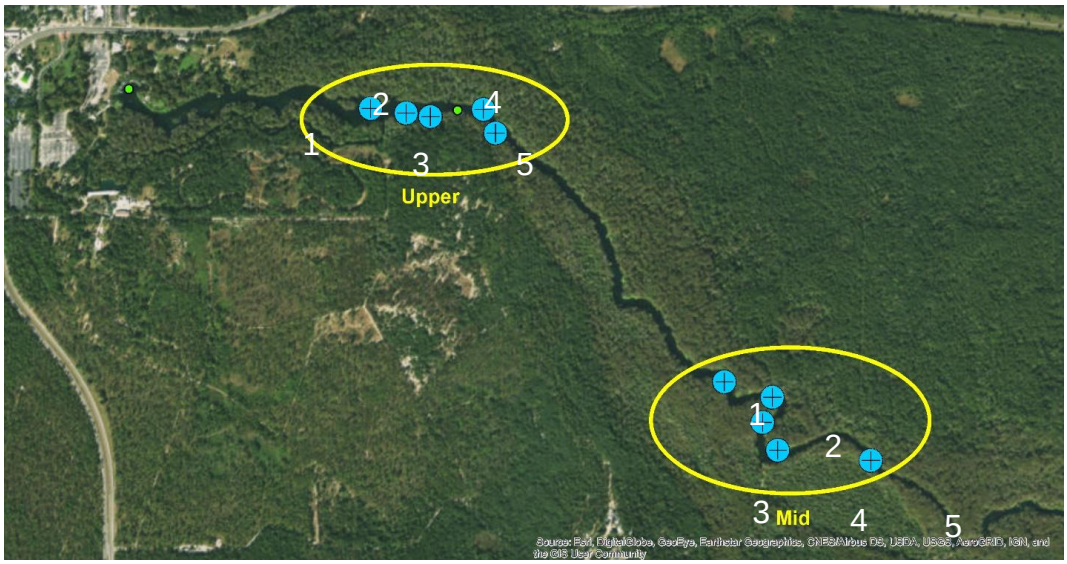

Figure 9.3.1. Map of study area and location of experimental arrays. Green circles denote locations of Mammoth Spring (head spring) and the downstream 1,200 m station.

Figure 9.3.2. Photographs of experimental cages in situ. Cage tops fully exposed (right) and fully submerged cage (left).

9.3.3 MATERIALS AND METHODS

9.3.3.1 Exclusion Cages

We used a cylindrical cage design (1.0 m in diameter by 1.2 m in height) to decrease fouling by drifting vegetation and other debris. We constructed exclusion cages by securing vinyl coated galvanized steel mesh (2.5 cm hexagonal openings) to a welded steel frame (0.625 cm diameter galvanized steel rods), and we enclosed the tops of cages using a piece of coated steel mesh and shock cords (Figure 9.3.2). For our cage control treatment, we removed two quarter panels of mesh (opposite one another) for the entire height of the cage and placed the mesh covered sides perpendicular to flow. This enabled consumers unrestricted access to the plot, while simulating the effects of exclusion cages on flow and light. Once deployed, we visually inspected cages weekly and removed any accumulated debris and algae by hand or using a boat brush. Finally, we established at fixed-locations in each study site control plots that were free of any cage material.

9.3.3.2 Aboveground Growth of Macrophytes

During the final month of the experiment, we assessed macrophyte growth using the "punch-method," as described by Hauxwell et al. (2007). Briefly, five shoots were randomly selected in each plot. Once selected, all leaves growing from a shoot were arranged in a single stack and an 18-gauge needle was used to punch two holes through all leaves at approximately 5 cm above the sediment. We marked punched-shoots with a brightly colored plastic straw attached to each shoot using a single small zip-tie so they could be identified for later collection. We allowed punched shoots to remain in-place for one week and subsequently collected them for processing. Samples were immediately placed on ice for transport and subsequently transferred to a -10 °C freezer in the laboratory. Leaves associated with individual shoots of both *Sagittaria kurziana* and *V. americana* demonstrate differential growth depending on the age of the leaf. Older senescing leaves, located toward the outside of the shoot, grow very little; plants allocate energy and materials instead to younger leaves located in the interior portion of a particular shoot. We quantified leaf growth of young leaves by measuring the displacement of the punched holes (mm) relative to the stationary position of reference holes punched in older, non-growing leaves. In addition, we measured the maximum and minimum widths and total lengths of all leaves to

calculate growth in units of surface area gained per day ($cm^2\ d^{-1}$). We then converted from units of surface area to dry mass ($g\ d^{-1}$), by applying the conversion factor of 0.0034 $g\ cm^{-2}$ for *V. americana* (Hauxwell et al. 2004) and 0.0032 $g\ cm^{-2}$ for *S. kurziana* (Hoyer and Canfield 1986).

9.3.3.3 Biomass and Leaf Areas of Macrophytes

At the beginning (October 2016) and end of the experiment (May 2017), we randomly placed a 25 cm by 25 cm quadrat (0.0625 m^{-2} area) near the center of each plot within an array and collected all aboveground vegetation and macroinvertebrates within the enclosed area. To sample aboveground vegetation within each quadrat, SCUBA divers enclosed the distal ends of all vegetation within the quadrat in an open, 9.5 L zip-lock bag, cut all rooted vegetation at the sediment-water interface using scissors, and packed the cut blades into the bag before closing it. Immediately following sampling, we carefully removed excess water from each sample by gently squeezing the sample bag and allowing only water to escape through a narrow opening. Samples were immediately placed on ice for transport and subsequently transferred to a -10 °C freezer in the laboratory.

For the two dominant rooted macrophytes, *Sagittaria kurziana* and *Vallisneria americana*, we enumerated all leaves, measured key aspects of leaf morphology (maximum width, minimum width, and total length), recorded wet weight, and obtained dry weight after placing samples in a drying oven at 60 °C for at least 48 hours. Prior to any mass measurements, we removed all epiphytic material by gently scraping leaves with the edge of a glass microscope slide and rinsing with deionized water. For less abundant macrophytes (i.e., *Hydrilla verticillata*, *Najas guadalupensis*, *Ceratophyllum demersum*, etc.), we obtained wet and dry mass without removing epiphytes.

9.3.3.4 Biomass of Epiphytic Algae

We determined epiphytic algal biomass using a subsampling protocol for epiphytic material obtained from the 0.0625 m^{-2} quadrats. We first randomly selected 10 *Sagittaria kurziana* and *Vallisneria americana* leaf blades from each sample (if 10 leaves of both taxa were not present, we included all leaves of the less abundant taxon). We then removed and collected all epiphytic material from the randomly selected leaves using a microscope slide. We further processed epiphytic material from the subsamples by removing all non-vegetative material and any organisms using a dissecting microscope (10–25X magnification) and forceps. We reserved all macroinvertebrates for community composition and biomass analyses. To remove excess water from epiphytic material, we placed it on a 300-µm mesh sieve and allowed water to drain out. Once excess water was drained, we recorded the wet mass measure. We subsequently dried the samples at 60 °C for at least 48 hours and then recorded the dry mass measure. We then placed dried samples in a muffle furnace (500 °C) for two hours and measured the mass of the remaining material (ash dry mass). We calculated ash-free dry mass (AFDM) as the difference between dry mass and ash dry mass.

Collection, transport, and thawing dislodged some epiphytic material from the macrophyte blades. To account for this, we subsampled the dislodged epiphytic material based on volume. First, all water and epiphytic material remaining in the sample bag after leaves had been removed was collected on a 300 µm mesh sieve. We placed the material into a graduated cylinder and adjusted the total volume to 50 mL by adding water. To subsample, we vigorously agitated the

water-epiphytic material slurry and immediately poured 12.5 mL (25 %) into a dish. We then removed all non-vegetative material (retaining the macroinvertebrates), obtained wet mass, and dried samples at 60 °C for at least 48 hours before obtaining a dry mass. We then obtained ash dry mass following combustion in a muffle furnace at 500 °C for two hours and calculated AFDM. We also obtained wet, dry, and ash dry mass for the remaining dislodged epiphytic material (47.5 mL, 75 %); however, we did not remove non-vegetative material prior to processing.

We scaled the epiphytic biomass from the 10–20 macrophyte leaves to g m^{-2} by first dividing epiphytic mass recovered from 10–20 leaf blades by the surface area (cm^{-2}) of all leaves in the subsample, then multiplying by the surface area of all leaves in the 0.065 m^{-2} quadrat and a factor of 16. We scaled the 25 % dislodged epiphytic material subsample to g m^{-2} by multiplying by a factor of 64.

9.3.3.5 Abundance, Biomass, and Community Composition for Macroinvertebrates

We estimated macroinvertebrate abundance and community composition using a combination of subsampling techniques from the 0.0625 m^{-2} quadrat samples. It should be noted that in addition to aboveground vegetation, we also collected all macroinvertebrates residing on the surface of the benthos within the quadrats. First, we removed, identified, enumerated, and measured the dry mass of all larger-bodied organisms such as adult gastropods, bivalves, and decapods after placing organisms in a drying oven (60 °C) for at least 48 hours. Smaller organisms present in the epiphytic sample material obtained by subsampling 10 to 20 leaves of the dominant rooted macrophytes and 25 % of the dislodged epiphytic material in the sample were similarly identified, enumerated, dried, and weighed. We identified most taxa to Order and others to family using field guides and dichotomous keys developed for invertebrate taxa of Florida. We scaled abundances and biomasses to 1.0 m^{-2} by multiplying the results for the 25 % subsample of dislodged epiphytic material by 64, and we divided abundances and biomasses of macroinvertebrates removed from leaves by the total leaf area sampled, with those results multiplied by the product of total surface area of all leaves within the 0.0625 m^{-2} quadrat sample and a factor of 16.

9.3.3.6 Statistical Analyses

We applied generalized linear models (GLM) with Gaussian (normal) error distributions using the 'glm' function within the 'base' package of the R statistical program (version 3.1.1) to assess the effects of treatment type, macrophyte taxon, river region, and their interactions on estimates of aboveground growth rates and all biomass metrics (i.e., macrophytes, epiphytic algae, and macroinvertebrates). For macroinvertebrate abundance, we used GLM with a negative binomial error distribution, as count data are often overdispersed. To select the most informative model, we calculated Akaike's second-order information criterion (AICc, small sample AIC), ΔAIC, Akaike weight (*w*), and relative likelihood. We selected the best model or implemented model averaging, using the R package 'MuMIn' (Barton, 2016). If the Akaike weight (w) of the top performing model was < 0.90, we implemented model averaging to estimate parameters and predict effects for all candidate models with $\Delta AICc \leq 2.0$ (Burnham and Anderson 2002; Grueber et al. 2011). To compare the importance of each covariate, we calculated the Relative Importance of model covariates when model averaging was applied, which was calculated as the

sum of the Akaike weights (w) from all the models in which the covariate appeared (Barton, 2016).

To examine differences in macroinvertebrate community composition among river regions and experimental treatments, we performed non-metric multidimensional scaling (nMDS) using the 'vegan' package (version 2.4-3) of the R statistical program (Oksanen et al. 2017). We performed separate nMDS analyses for abundance and biomass data. While nMDS allows to assess differences in the overall community composition, it does not allow for testing of hypotheses regarding the influence of predictor variables on community composition. To assess if community composition was significantly different among river regions, experimental treatments, and combinations of region and treatment, we employed a GLM framework developed for multivariate species abundance data within the 'mvabund' package in R (Wang et al. 2012). The model fitting function 'manyglm' within the 'mvabund' package fits an overall multivariate GLM using abundances of all taxa, as well as separate univariate GLMs to each taxon present in the community (p-values adjusted for multiple comparisons), and it considers correlations between taxa. We used a negative binomial error distribution and untransformed abundance data to construct our matrix.

9.3.4 RESULTS

9.3.4.1 Aboveground Growth of Macrophytes

We successfully recovered all but two of the 150 punched shoots. We were unable to recover one marked shoot from the cage control (CC) plot at mid river site 1 and one marked shoot from the exclusion treatment plot at upper river site 5 (Figure 9.3.1). Total number of leaf blades per shoot averaged 9.7 for *Sagittaria kurziana* (range = 4–18) and 7.6 for *Vallisneria americana* (range = 4–16). Shoots collected in the mid river region had slightly more blades per shoot (~ 1 blade) than shoots in the upper region for both *S. kurziana* and *V. americana*. Overall, we randomly selected similar numbers of shoots from both dominant macrophytes for growth assays (45.3 % versus 54.7 %, for *S. kurziana* and *V. americana*, respectfully). However, we observed a shift in the relative proportion of taxa in river regions; *S. kurziana* was most prevalent in the mid region and *V. americana* in the upper region (Table 9.3.1).

Table 9.3.1. Prevalence of macrophyte taxa randomly selected to perform growth assays in each river region.

Region	Macrophyte taxon	shoots (n)	Percent by region (%)
Mid	*S. kurziana*	43	58.1
Mid	*V. americana*	31	41.9
Upper	*S. kurziana*	24	32.4
Upper	*V. americana*	50	67.6

As detailed in section 9.3.4.2, leaves associated with shoots for both macrophytes studied here express differential growth depending on their ages. Energy and nutrients essential for growth are primarily routed to younger leaves located at or near the center of shoot, while older leaves at

or near the outside of the shoot experience minimal to no growth before senescencing. The average number of young leaves present in each plot (i.e., the total from four to five shoots) was 8.6, with a range of 4 to 14 young leaves plot^{-1}. This translated to an average of 1.9 leaves shoot^{-1} and we used this value for estimating and comparing aboveground growth rates.

Using our model selection process, we found the top performing models (ΔAICc $\leq$ 4) explaining variation in aboveground growth rates included the main effects of river region, macrophyte taxon, and treatment type, as well as interactions of river region with both macrophyte taxon and treatment type (Table 9.3.2). We employed model averaging across all top models to estimate β coefficients and 95 % confidence intervals (95 % CIs, Table 9.3.3), and we used the resulting coefficients to predict and compare the effects of model parameters (predictor variables) on aboveground growth rates.

Table 9.3.2. Model structure, number of parameters (*k*), log-likelihood, Akaike's second-order information criterion (AICc), ΔAICc, and Akaike weight (*w*), for candidate generalized linear models explaining variation in aboveground growth rates (g d^{-1}).

Model	Number of parameters (k)	Log-likelihood	AICc	Δ AICc	Akaike weight (*w*)
region + taxon + ttt + region*taxon + region*ttt	9	595.4	-1171.4	0.0	0.6
region + taxon + region*taxon	5	589.8	-1169.1	2.3	0.2
region + taxon + ttt + region*taxon	7	591.9	-1169.0	2.5	0.2

*region: categorical variable with two levels (upper and mid); taxon: categorical variable with two levels (*Sagittaria kurziana* and *Vallisneria americana*); ttt: treatment type, a categorical variable with three levels (control-C, cage control-CC, and exclusion-E).

Table 9.3.3. Model averaged β coefficient estimates and 95 % CI's based on our top performing candidate models explaining variation in aboveground macrophyte growth rates.

Parameter	mean β (g d^{-1})	β SE	95 % CI lower	95 % CI upper
(Intercept)	0.0037	0.0008	0.0021	0.0053
region(Upper)	-0.0013	0.0013	-0.0039	0.0012
taxon(VAL)	0.0042	0.0008	0.0026	0.0057
ttt(CC)	-0.0019	0.0014	-0.0045	-0.0001
ttt(E)	-0.0002	0.0008	-0.0021	0.0015
region(Upper):taxon(VAL)	-0.0029	0.0011	-0.0052	-0.0007
region(Upper):ttt(CC)	0.0021	0.0019	0.0008	0.0058
region(Upper):ttt(E)	0.0008	0.0012	-0.0013	0.0040

*Estimates are relative to reference conditions (Intercept). For river region reference condition is mid river, for taxon reference condition is *S. kurziana* (SAG), and for treatment type reference condition is control (C). The intercept is the mean across data within all reference conditions.

Using coefficients from averaged models to predict responses, we found mean aboveground growth was slightly greater in the mid river (mean ± SE = 0.0046 g d^{-1} ± 0.0008) as compared to the upper region (0.0035 g d^{-1} ± 0.0007, Figure 9.3.3); however, the confidence interval surrounding the estimated coefficient for river region contained zero so we have little evidence of a true difference. Comparing growth rates among macrophyte taxa, we found aboveground growth was 1.7 times greater for *Vallisneria americana* (0.0050 g d^{-1} ± 0.0008) as compared to *Sagittaria kurziana* (0.0029 g d^{-1} ± 0.0008, Figure 9.3.3). The confidence interval for the effect of macrophyte taxon did not contain zero, indicating taxon specific differences in aboveground growth rates. In terms of experimental treatments, mean aboveground growth was highest in the exclusion (E) treatment, slightly less in the control (C), and lowest in cage control (CC) treatment (Figure 9.3.4). On average, growth rates in the E treatment (0.0043 g d^{-1} ± 0.0007) were 1.04 times greater than the C treatment (0.00042 g d^{-1} ± 0.0008) and 1.21 times greater than the CC treatment (0.0036 g d^{-1} ± 0.0008). However, confidence intervals for estimated coefficients for both exclusion treatments and cage controls contained zero (Table 9.3.4), and 95 % CIs surrounding predicted means overlapped. Consequently, we have little evidence of a strong effect of treatment type on aboveground growth rates.

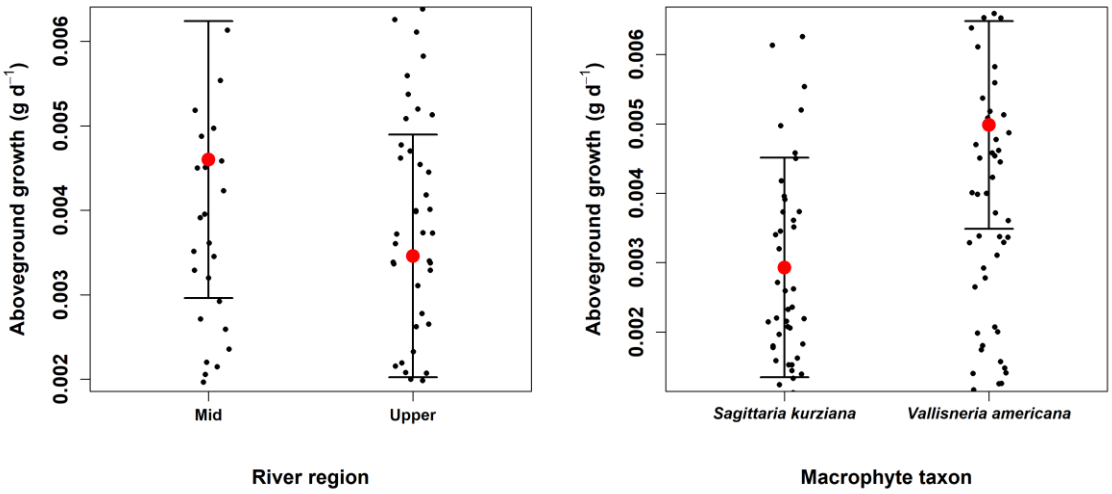

Figure 9.3.3. Predicted effects of river region (left) and macrophyte taxon (right) on macrophyte aboveground growth rates. Filled red circles are mean values and error bars delineate the 95 % CI.

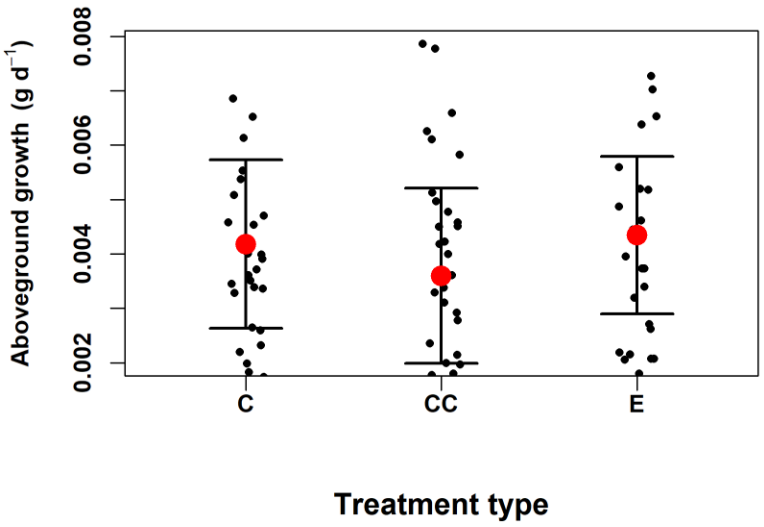

Figure 9.3.4. Predicted effects of experimental treatments on macrophyte aboveground growth rates.

The interaction between river region and macrophyte taxon was primarily driven by higher growth rates of *Vallisneria americana* in the mid river (0.0071 g d^{-1} ± 0.0009; Figure 9.3.5), and the fact that predicted growth rates for *Sagittaria kurziana* were similar among river regions and lower than growth rates for *V. americana* in both river regions. The interaction between river region and treatment type was more complex (Figure 9.3.6). In C and E treatments, growth rates were elevated in the mid river relative to the upper region, while growth rates in CC treatment were higher in the upper river relative to the mid. The relative ranking of growth rates estimated for treatments alternated depending on river region. In the mid river, the C treatment maintained the highest growth rate, followed by E and CC. Conversely, in the upper river growth rates in the E and CC treatments were similar, and both were higher than growth rates in the C treatment.

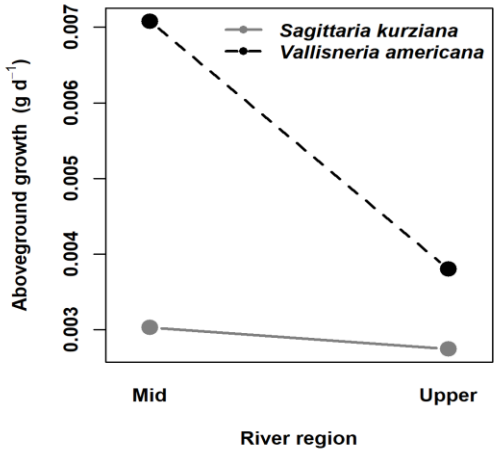

Figure 9.3.5. Interaction plot of mean aboveground growth rates as a function of the interaction between river region and macrophyte taxon. Error bars are not plotted for simplicity.

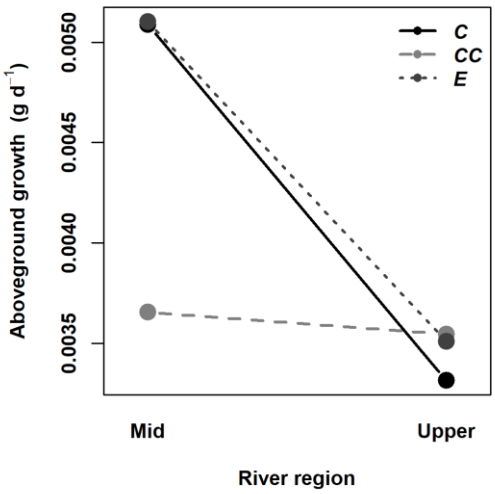

Figure 9.3.6. Interaction plot of mean aboveground growth rates as a function of the interaction between river region and treatment type. Error bars are not plotted for simplicity.

9.3.4.2 Aboveground Biomass of Macrophytes

Density of leaves within each 0.0625 m^{-2} quadrat ranged from 1 to 53 (16–848 blades m^{-2}), and densities averaged 12 blades per quadrat (194 blades m^{-2}). Overall, mean blade density of *Vallisneria americana* (209 blades m^{-2}) was greater than *Sagittaria kurziana* (179 blades m^{-2}). Collectively, aboveground macrophytic biomass (dry mass) ranged from 78.0 to 655.6 g m^{-2} across all plots, and averaged 269.5 g m^{-2}. Biomass was composed primarily of the two dominant macrophytes, *S. kurziana* and *V. americana*, with each contributing 47.4 % and 49.5 % to the total biomass, respectively. Three minor contributors to aboveground biomass were *Najas guadalupensis* (1.8 %), *Ceratophyllum demersum* (1.3 %), and *Hydrilla verticillata* (<1 %).

Our model selection process yielded two top performing models (ΔAICc $\leq$ 4.0; Table 9.3.4). The top performing model was the null or intercept only model and the next best model included the main effect of river region. As the addition of parameters to the null model did not reduce model deviance, data are better viewed as exhibiting random variation rather than meaningful trends. Given this actuality, we suggest caution when interpreting differences in aboveground macrophyte biomass.

Table 9.3.4. Model structure, Model structure, number of parameters (*k*), log-likelihood, Akaike's second-order information criterion (AICc), ΔAICc, and Akaike weight (*w*), for all candidate GLMs explaining variation in aboveground macrophyte biomass.

Model	Number of parameters (k)	Log-likelihood	AICc	ΔAICc	Akaike weight (*w*)
(Intercept)	2	-182.8	370.1	0.0	0.7
region	3	-182.8	372.6	2.5	0.2
ttt	4	-182.5	374.6	4.5	0.1
region + ttt	5	-182.5	377.5	7.4	0.0
region + ttt + region*ttt	7	-182.4	383.9	13.8	0.0

Using the coefficient estimates from the second best performing model, we predicted mean aboveground macrophyte biomass in the mid river and upper river to be nearly equal, with both being highly variable (i.e., large 95 % CIs, Figure 9.3.7). For comparative purposes, since treatment type was not present in our top performing models (ΔAICc $\leq$ 4.0), we simply summarize macrophytic biomass for treatment types (Figure 9.3.8). Based on these data, mean aboveground macrophyte biomass was highest and most variable in exclusion (E) treatments (291.1 g m^{-2} ± 158.8 [SD]). Mean biomass in controls (261.4 g m^{-2} ± 66.1) and cage controls (255.9 g m^{-2} ± 89.4) was lower and less variable. Given the amount of variability and similar central tendencies among treatments, we found little evidence of consistent and ecologically meaningful differences in aboveground biomass among treatments.

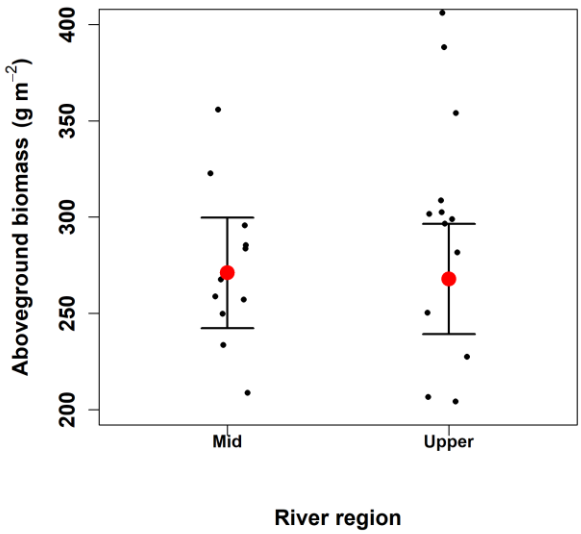

Figure 9.3.7. Predicted mean aboveground biomass across river regions. Large red circles are mean values and error bars are ± standard error (SE). Small black circles are empirical data.

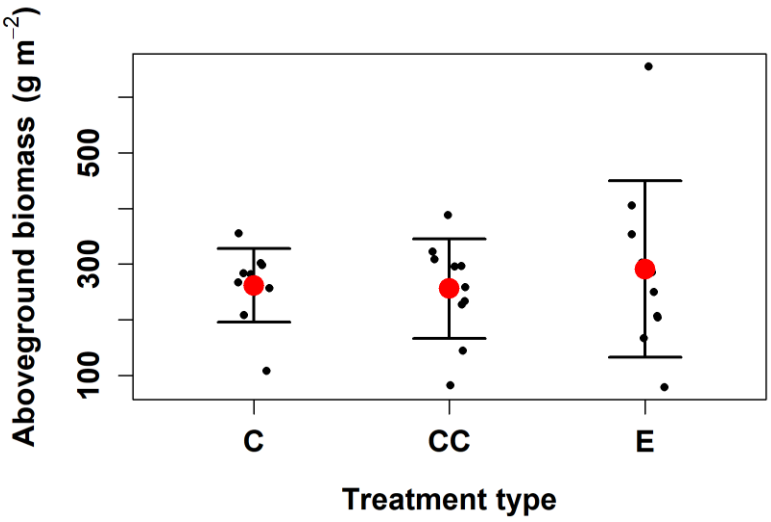

Figure 9.3.8. Macrophyte aboveground biomass measured in treatment plots. Large red circles are mean values and error bars are ± standard error (SE). Small black circles are empirical data.

9.3.4.3 Biomass of Epiphytic Algae

Epiphytic algal biomass (measured as AFDM) associated with 10–20 randomly sampled leaves and 25 % of dislodged epiphytic material, ranged from 1.03 to 204.71 g m^{-2}, with an average of 16.79 g m^{-2} ± 40.55 (SD). Our top performing models (ΔAICc ≤ 4.0) included the main effect of treatment type and region (Table 9.3.5). However, the null model (intercept only) ranked first. The fully parameterized model (global model) was not included in our set of top performing

models. Consequently, there is little indication that the interaction of region and treatment type influenced variation in epiphytic algal biomass. Based on coefficients averaged across models (Table 9.3.6), mean epiphytic biomass was lowest in the CC (11.45 g m^{-2} ± 12.41 [SE]) and E (12.10 g m^{-2} ± 12.10) treatments and greatest in the C (26.81 g m^{-2} ± 15.47) treatment. In other words, predicted mean epiphytic biomass was 2.3X greater in controls as compared to cage controls treatment and 2.2X greater when compared to exclusion treatments (Figure 9.3.9).

Table 9.3.5. Model structure, number of parameters (*k*), log-likelihood, Akaike's second-order information criterion (AICc), ΔAICc, and Akaike weight (*w*), for top performing candidate GLMs explaining variation in epiphytic algae biomass.

Model	Number of parameters (k)	Log-likelihood	AICc	Δ AICc	Akaike weight (*w*)
(Intercept)	2	-153.14	310.70	0.00	0.39
ttt	4	-150.69	311.00	0.25	0.34
region	3	-152.80	312.50	1.80	0.16
ttt + region	5	-150.29	313.10	2.36	0.12

Table 9.3.6. Model averaged β coefficient estimates and 95 % CIs based on our top performing candidate GLMs explaining variation in epiphytic algae biomass.

Parameter	mean β (g m^{-2})	SE	95 % CI lower	95 % CI upper
(Intercept)	25.17	15.53	-5.94	56.29
ttt (CC)	-15.36	20.42	-69.13	2.09
ttt (E)	-14.71	19.84	-67.72	3.50
region (Upper)	3.27	9.33	-18.08	41.87

*Estimates are relative to reference conditions (Intercept). For river region reference condition is mid river and for treatment type reference condition is control (C). The intercept is the mean across data within all reference conditions.

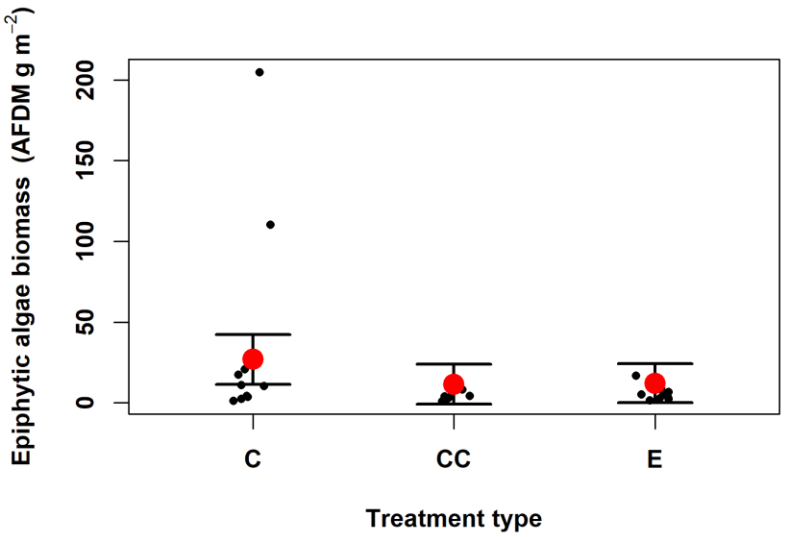

Figure 9.3.9. Predicted epiphytic biomass as a function of treatment type based on model averaged coefficients. Large red circles are mean values and error bars are ± standard error (SE). Small black circles are empirical data.

Based on coefficients averaged across models, we predicted epiphytic algal biomass to be slightly greater in the upper river (18.42 g m^{-2} ± 13.33 [SE]) relative to the mid river (15.15 g m^{-2} ± 13.32); however, differences were small and both regions displayed high degrees of variation (Figure 9.3.10). The 95 % CI's estimated for both regions contained zero, and they overlapped. Therefore, we have little evidence that epiphytic biomass differed consistently among regions.

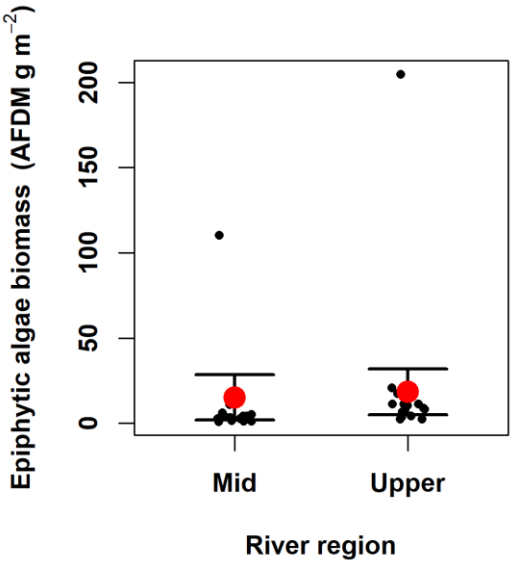

Figure 9.3.10. Predicted effects of river region on epiphytic algae biomass. Large Red circles are estimated means and error bars are ± standard error (SE). Small black circles are empirical data.

9.3.4.4 Abundance, Biomass, and Community Composition for Macroinvertebrates

Total macroinvertebrate biomass, associated with 10–20 randomly sampled leaves and 25 % of dislodged epiphytic material, ranged from 0.47 to 8.74 g m^{-2}, with an average of 2.04 g m^{-2} across all sample plots. Our model selection process yielded three top performing models, and the best performing model included the main effect of region, the second-best model included the main effects of both region and treatment type, and null model performed the worst (Table 9.3.7).

Table 9.3.7. Model structure, number of parameters (*k*), log-likelihood, Akaike's second-order information criterion (AICc), ΔAICc, and Akaike weight (*w*), for all candidate generalized linear models explaining variation in total macroinvertebrate biomass.

Model	Number of parameters (k)	Log-likelihood	AICc	ΔAICc	Akaike weight (*w*)
region	3	-59.7	126.2	0.0	0.7
region + ttt	5	-58.0	128.4	2.2	0.2
(Intercept)	2	-62.9	130.2	3.9	0.1

Table 9.3.8. Model averaged β coefficient estimates and 95 % CIs based on our top performing candidate models explaining variation in total macroinvertebrate biomass.

Parameter	mean β (g m^{-2})	SE	95 % CI lower	95 % CI upper
(Intercept)	1.43	0.63	0.17	2.70
region (Upper)	1.56	0.81	0.36	3.09
ttt (CC)	-0.32	0.70	-3.06	0.24
ttt (E)	-0.18	0.50	-2.44	0.86

*Estimates are relative to reference conditions (Intercept). For river region reference condition is mid river and for treatment type reference condition is control (C). The intercept is the mean across data within all reference conditions.

Using coefficients averaged across models, we predicted mean macroinvertebrate biomass to be 2.2X greater in the upper river (2.83 g m^{-2} ± 0.62[SE]) as compared to the mid river (1.27 g m^{-2} ± 0.62; Figure 9.3.11). We also predicted total macroinvertebrate biomass to be highest in the C treatment (2.21 g m^{-2} ± 0.65), followed by the E treatment (2.03 g m^{-2} ± 0.57), and the CC treatment (1.89 g m^{-2} ± 0.64; Figure 9.3.12).

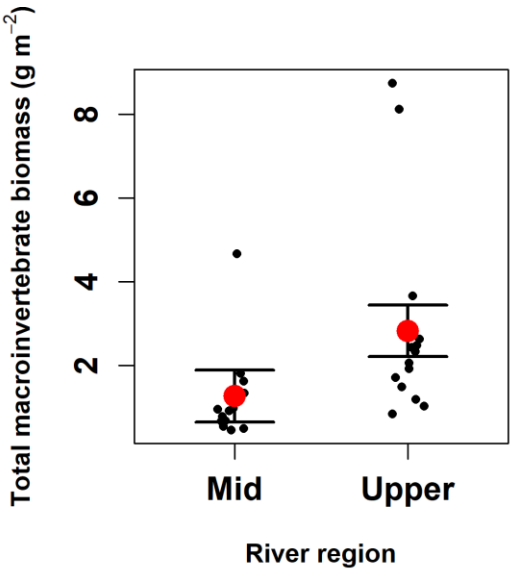

Figure 9.3.11. Predicted effects of region on total macroinvertebrate biomass. Large red circles are mean values and error bars are ± standard error (SE). Small black circles are empirical data.

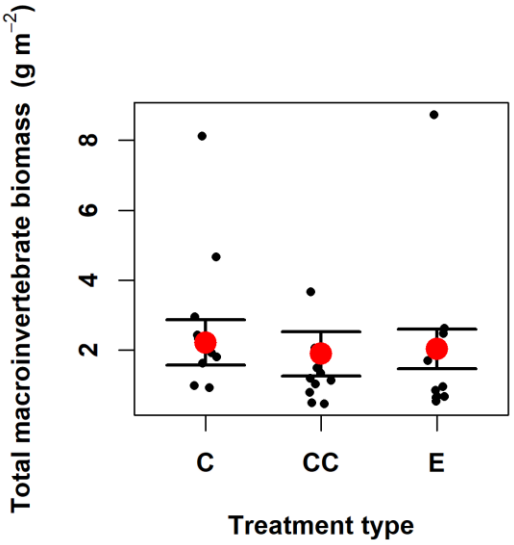

Figure 9.3.12. Predicted effects of treatment type on total macroinvertebrate biomass. Large red circles are mean values and error bars are ± standard error (SE). Small black circles are empirical data.

The macroinvertebrate community within our samples comprised taxa occupying several trophic guilds including grazers, omnivores, predators, and parasites. To investigate whether the biomass of trophic guilds differed among river regions and treatments, we performed GLM selection and calculated predicted responses separately for each trophic guild. Overall, grazers represented 87

% of the total macroinvertebrate biomass, omnivores and predators contributed 5.3 % and 4.7 %, respectively, and parasites contributed only 2.9 %.

The biomass of macroinvertebrate grazers ranged from 0.28 to 7.57 g m^{-2}, with an average of 1.67 g m^{-2} ± 1.79 (SD) across all plots. Our top performing models included the main effects of region and treatment type (Table 9.3.9). Using coefficients averaged across models, we predicted mean grazer biomass was 2.8X greater in the upper river (2.46 g m^{-2} ± 0.53 [SE]) as compared to the mid river (0.88 g m^{-2} ± 0.53; Table 9.3.10 and Figure 9.3.13). We estimated mean grazer biomass to be highest in the C treatment (1.87 g m^{-2} ± 0.57), followed by the E treatment (1.64 g m^{-2} ± 0.47), and than the CC treatment (1.50 g m^{-2} ± 0.54); however, differences among treatments were slight and predictions had a high degree of uncertainty.

Table 9.3.9. Model structure, number of parameters (*k*), log-likelihood, Akaike's second-order information criterion (AICc), ΔAICc, and Akaike weight (*w*), for top performing candidate GLMs explaining variation in macroinvertebrate grazer biomass.

Model	Number of parameters (k)	Log-likelihood	AICc	ΔAICc	Akaike weight (*w*)
region	3	-56.1	119.2	0.0	0.7
region + ttt	5	-54.3	121.0	1.9	0.3

Table 9.3.10. Model averaged β coefficient estimates and 95 % CIs based on our top performing candidate GLMs explaining variation in macroinvertebrate grazer biomass.

Parameter	mean β (g m^{-2})	SE	95 % CI lower	95 % CI upper
(Intercept)	1.08	0.57	-0.07	2.23
region (Upper)	1.58	0.59	0.37	2.79
ttt (CC)	-0.37	0.70	-2.76	0.16
ttt (E)	-0.24	0.53	-2.29	0.63

*Estimates are relative to reference conditions (Intercept). For river region reference condition is mid river and for treatment type reference condition is control (C). The intercept is the mean across data within all reference conditions.

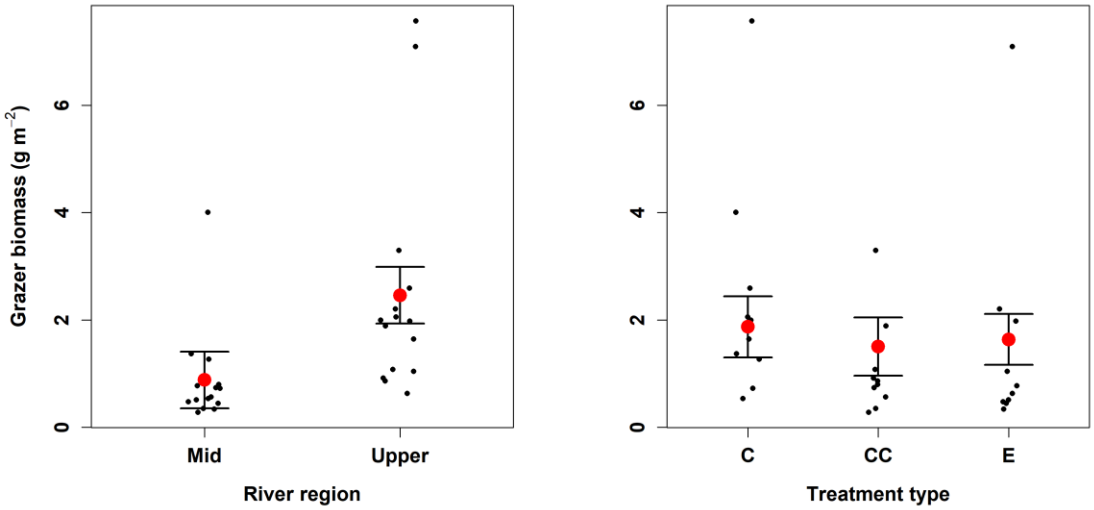

Figure 9.3.13. Predicted effects of river region (left) and treatment type (right) on macroinvertebrate grazer biomass. Large red circles are mean values and error bars are ± standard error (SE). Small black circles are empirical data.

Biomass of macroinvertebrate omnivores ranged from 0.01 to 0.46 g m^{-2}, with an average of 0.10 g m^{-2} ± 0.10 (SD) across all plots. Our top performing models included the main effects of region and treatment type (Table 9.3.11). Using coefficients averaged across models, we predicted mean omnivore biomass was 2.6X greater in the upper river (0.15 g m^{-2} ± 0.03[SE]) as compared to the mid river (0.06 g m^{-2} ± 0.03; Table 9.3.12 and Figure 9.3.14). Similar to grazer biomass, predicted mean omnivore biomass was highest in the C treatment (0.12 g m^{-2} ± 0.03), followed by the E treatment (0.10 g m^{-2} ± 0.03), and than the CC treatment (0.09 g m^{-2} ± 0.03); however, differences among treatments were small and predictions had a high degree of uncertainty.

Table 9.3.11. Model structure, number of parameters (*k*), log-likelihood, Akaike's second-order information criterion (AICc), ΔAICc, and Akaike weight (*w*), for all candidate generalized linear models explaining variation in macroinvertebrate omnivore biomass.

Model	Number of parameters (k)	Log-likelihood	AICc	ΔAICc	Akaike weight (*w*)
region	3	31.1	-55.3	0.0	0.7
region + ttt	5	33.2	-53.9	1.3	0.3

Table 9.3.12. Model averaged β coefficient estimates and 95 % CIs based on our top performing candidate models explaining variation in macroinvertebrate omnivore biomass.

Parameter	mean β (g m^{-2})	SE	95 % CI lower	95 % CI upper
(Intercept)	0.07	0.03	0.01	0.14
region (Upper)	0.09	0.03	0.02	0.15
ttt (CC)	-0.03	0.04	-0.15	0.00
ttt (E)	-0.02	0.03	-0.13	0.03

*Estimates are relative to reference conditions (Intercept). For river region reference condition is mid river and for treatment type reference condition is control (C). The intercept is the mean across data within all reference conditions.

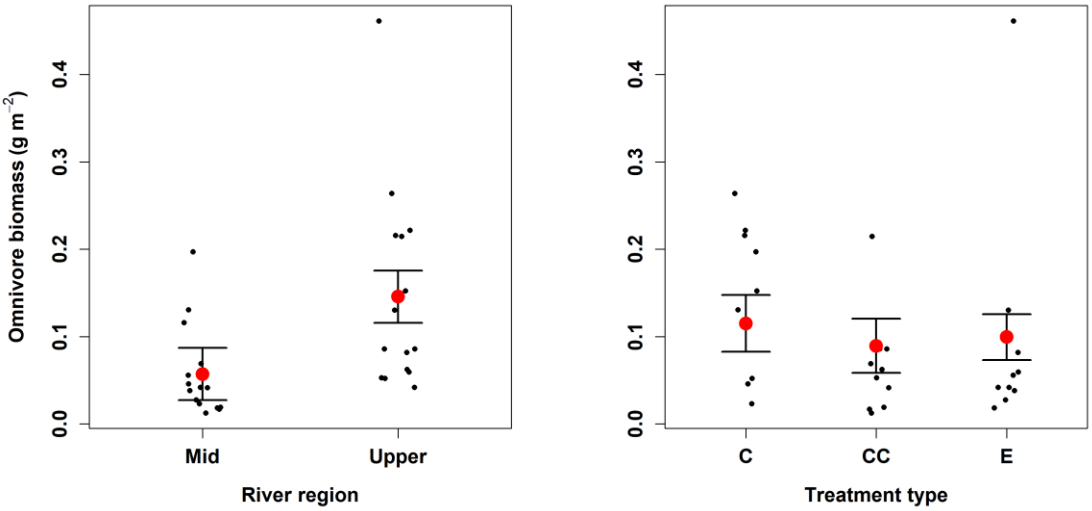

Figure 9.3.14. Predicted effects of river region (left) and treatment type (right) on macroinvertebrate omnivore biomass. Large red circles are mean values and error bars are ± standard error (SE). Small black circles are empirical data.

Biomass of macroinvertebrate predators ranged from 0.006 to 1.232 g m^{-2}, with an average of 0.093 g m^{-2} ± 0.223 (SD) across all plots. Our top performing models included the main effects of region and treatment type (Table 9.3.13). Using coefficients averaged across models, we predicted mean omnivore biomass was marginally greater in the upper river (0.106 g m^{-2} ± 0.057 [SE]) than mid river (0.081 g m^{-2} ± 0.058; Table 9.3.14 and Figure 9.3.15). Predicted mean biomass of predators was highest in the E treatment (0.104 g m^{-2} ± 0.062), followed by the C treatment (0.092 g m^{-2} ± 0.055), and than the CC treatment (0.086 g m^{-2} ± 0.058); however, the 95 % CIs surrounding estimated mean coefficients contained zero for all treatments, which suggests differences were not consistent.

Table 9.3.13. Model structure, number of parameters (*k*), log-likelihood, Akaike's second-order information criterion (AICc), ΔAICc, and Akaike weight (*w*), for top performing candidate GLMs explaining variation in macroinvertebrate predator biomass.

Model	Number of parameters (k)	Log-likelihood	AICc	ΔAICc	Akaike weight (*w*)
(Intercept)	2	2.9	-1.4	0.0	0.6
region	3	3.5	0.0	1.4	0.3
ttt	4	3.9	1.8	3.2	0.1

Table 9.3.14. Model averaged β coefficient estimates and 95 % CIs based on our top performing candidate models explaining variation in macroinvertebrate predator biomass.

Parameter	mean β (g m^{-2})	SE	95 % CI lower	95 % CI upper
(Intercept)	0.08	0.05	-0.03	0.19
region (Upper)	0.02	0.06	-0.09	0.25
ttt (CC)	-0.01	0.04	-0.25	0.16
ttt (E)	0.01	0.05	-0.12	0.30

*Estimates are relative to reference conditions (Intercept). For river region reference condition is mid river and for treatment type reference condition is control (C). The intercept is the mean across data within all reference conditions.

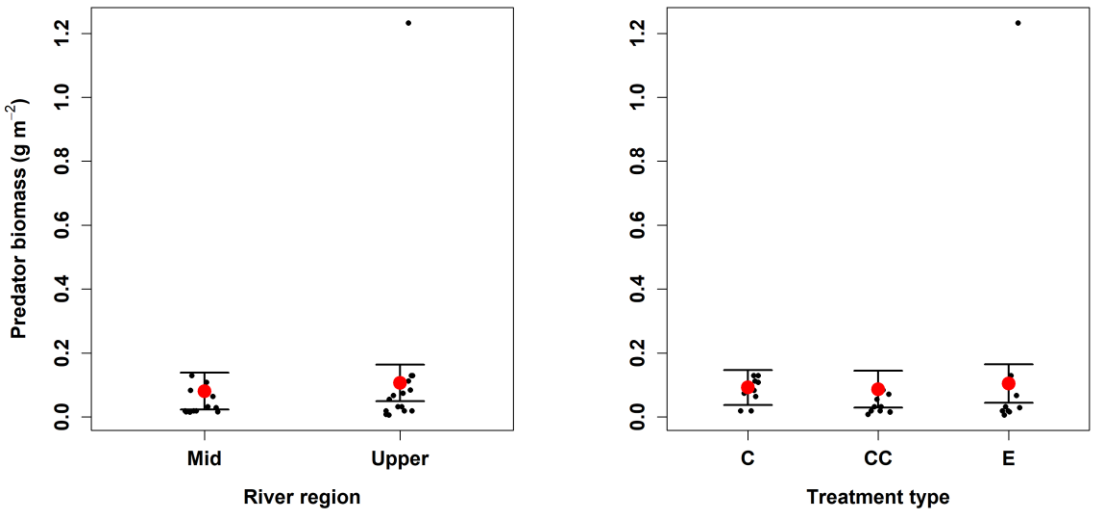

Figure 9.3.15. Predicted effects of river region (left) and treatment type (right) on macroinvertebrate predator biomass. Large red circles are mean values and error bars are ± standard error (SE). Small black circles are empirical data.

Biomass of macroinvertebrate parasites ranged from 0.008 to 0.208 g m^{-2}, with an average of 0.054 g m^{-2} ± 0.054 (SD) across all plots. There were two top performing models, with the best model containing the main effect of region and the second best model being the null or intercept only model (Table 9.3.15 and 9.3.16). Following a similar trend to other trophic guilds, we predicted mean parasite biomass to be 2X greater in the upper river (0.072 g m^{-2} ± 0.015 [SE]) as compared to the mid river (0.036 g m^{-2} ± 0.015; Figure 9.3.16).

Table 9.3.15. Model structure, number of parameters (*k*), log-likelihood, Akaike's second-order information criterion (AICc), ΔAICc, and Akaike weight (*w*), for top performing candidate GLMs explaining variation in macroinvertebrate parasite biomass.

Model	Number of parameters (k)	Log-likelihood	AICc	ΔAICc	Akaike weight (*w*)
region	3	48.1	-89.3	0.0	0.8
(Intercept)	2	45.4	-86.3	2.9	0.2

Table 9.3.16. Model averaged β coefficient estimates and 95 % CIs based on our top performing candidate models explaining variation in macroinvertebrate parasite biomass.

Parameter	mean β (g m^{-2})	SE	95 % CI lower	95 % CI upper
(Intercept)	0.04	0.02	0.01	0.07
region (Upper)	0.04	0.02	0.01	0.08

*Estimates are relative to reference conditions (Intercept). For river region reference condition is mid river and for treatment type reference condition is control (C). The intercept is the mean across data within all reference conditions.

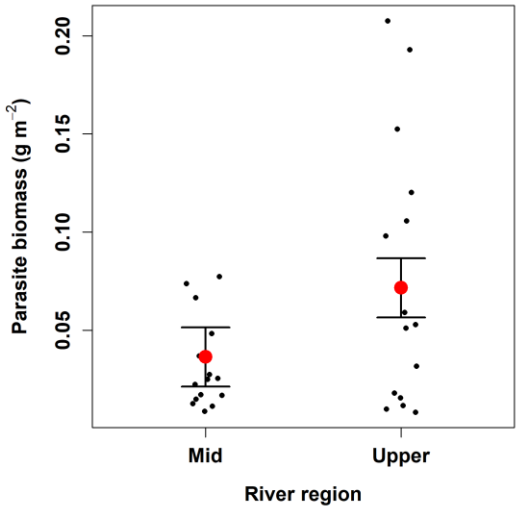

Figure 9.3.16. Predicted effects of river region on macroinvertebrate parasite biomass. Large red circles are mean values and error bars are ± standard error (SE). Small black circles are empirical data.

Total abundance of macroinvertebrates in experimental plots ranged from 16,450 to 366,400 individuals m^{-2}, with an average of 113,300 individuals m^{-2} ± 95,413 (SD). Our top performing models contained the main effects of river region and treatment type (Table 9.3.17). Based on coefficients averaged across models (Table 9.3.18), we predicted mean abundance of macroinvertebrates was 1.2X greater in the upper river (123, 413 individuals m^{-2} ± 28,679 [SE]) relative to the mid river (104, 319 individuals m^{-2} ± 24,042; Figure 9.3.17). However, the 95 % CI for the effect of river region contained zero, thus we consider river region a minor influence on variation in abundance of macroinvertebrates. Predicted mean abundance was highest in the C treatment (192,838 individuals m^{-2} ± 44,686), 2.4X less in the CC treatment and 2.8X less in the E treatment. While the estimated 95 % CIs for effect sizes related to treatments were sizeable, they did not contain zero (Table 9.3.18), so the patterns among treatments were consistent.

Table 9.3.17. Model structure, number of parameters (*k*), log-likelihood, Akaike's second-order information criterion (AICc), ΔAICc, and Akaike weight (*w*), for top performing candidate GLMs explaining variation in macroinvertebrate abundance.

Model	Number of parameters (k)	Log-likelihood	AICc	ΔAICc	Akaike weight (*w*)
ttt	4	-370.4	750.5	0.0	0.5
region + ttt	5	-369.2	750.8	0.4	0.5

Table 9.3.18. Model averaged β coefficient estimates and 95 % CIs based on our top performing candidate models explaining variation in macroinvertebrate abundance. Coefficient estimates are not transformed.

Parameter	mean β	SE	95 % CI lower	95 % CI upper
(Intercept)	12.08	0.23	11.61	12.54
ttt (CC)	-0.88	0.28	-1.45	-0.30
ttt (E)	-1.04	0.28	-1.61	-0.46
region (Upper)	0.17	0.24	-0.09	0.83

*Estimates are relative to reference conditions (Intercept). For river region reference condition is mid river and for treatment type reference condition is control (C). The intercept is the mean across data within all reference conditions.

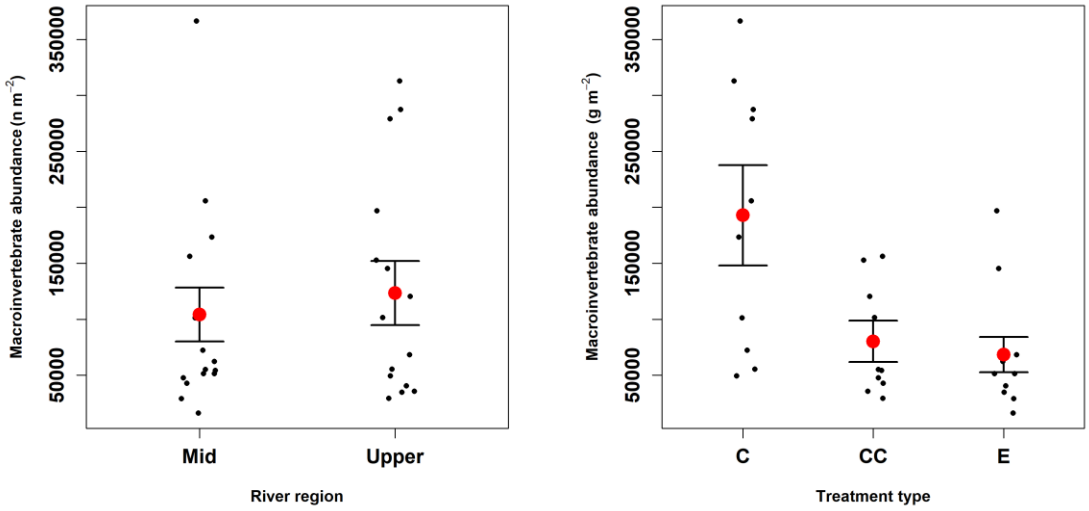

Figure 9.3.17. Predicted effects of river region (left) and treatment type (right) on macroinvertebrate abundance. Large red circles are mean values and error bars are ± standard error (SE). Small black circles are empirical data.

The relative contribution of trophic guilds to total abundance of macroinvertebrates differed slightly from their contributions to total biomass. Grazers, predominantly chironomids and trichopterans, comprised 82 % of all macroinvertebrates, followed by omnivores (9 %), parasites (8 %), and predators (< 1 %).

Variation in abundances of grazers closely matched patterns in total abundance, which was expected given that their contribution to total biomass far exceeded that of any other group. Our top performing GLMs contained the main effects of region and treatment type (Table 9.319). Based on coefficients averaged across models (Table 9.3.20), abundances of grazers were predicted to be marginally higher in the upper river (80,557 individuals m^{-2} ± 17,909 [SE]) relative to the mid river (Figure 9.3.18). Differences among treatments were more pronounced (Figure 9.3.18), with mean abundance in C treatments (138,585 individuals m^{-2} ± 30,633) predicted to be 2.7X higher than abundances in CC treatments and 3X higher than abundances in E treatments.

Table 9.3.19. Model structure, number of parameters (*k*), log-likelihood, Akaike's second-order information criterion (AICc), ΔAICc, and Akaike weight (*w*), for top performing candidate GLMs explaining variation in macroinvertebrate grazer abundance.

Model	Number of parameters (k)	Log-likelihood	AICc	ΔAICc	Akaike weight (*w*)
ttt	4	-359.5	728.7	0.0	0.8
region + ttt	5	-359.2	731.0	2.3	0.2

Table 9.3.20. Model averaged β coefficient estimates and 95 % CIs based on our top performing candidate models explaining variation in macroinvertebrate grazer abundance. Coefficient estimates are not transformed.

Parameter	mean β	SE	95 % CI lower	95 % CI upper
(Intercept)	11.81	0.22	11.36	12.27
ttt (CC)	-0.99	0.29	-1.60	-0.39
ttt (E)	-1.10	0.30	-1.70	-0.49
region (Upper)	0.05	0.14	-0.30	0.68

*Estimates are relative to reference conditions (Intercept). For river region reference condition is mid river and for treatment type reference condition is control (C). The intercept is the mean across data within all reference conditions.

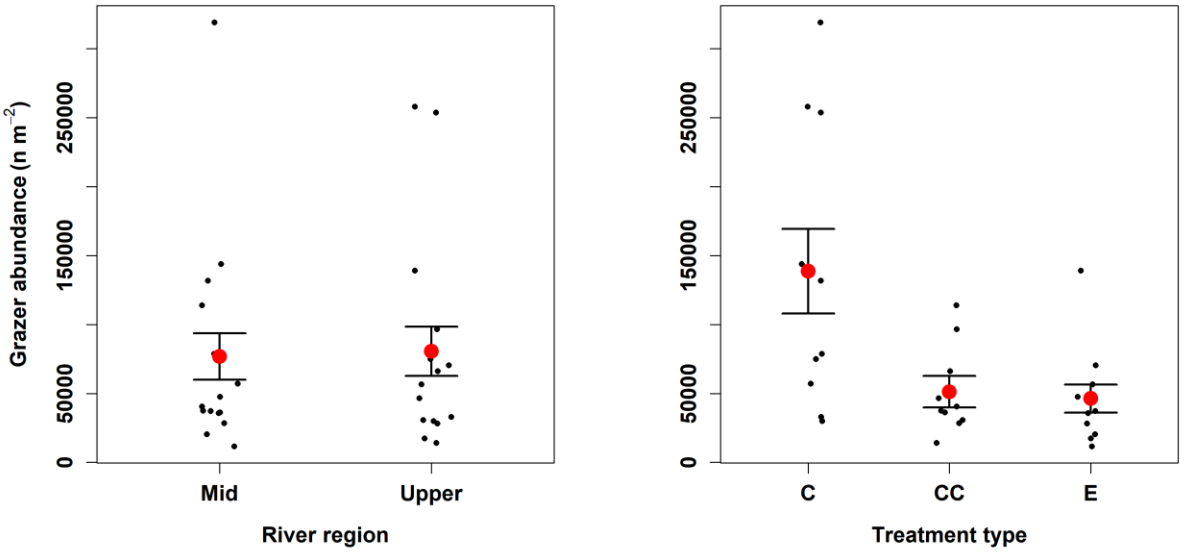

Figure 9.3.18. Predicted effects of river region (left) and treatment type (right) on macroinvertebrate grazer abundance. Large red circles are mean values and error bars are ± standard error (SE). Small black circles are empirical data.

Abundances of omnivores ranged from 600 to 193,072 individuals m^{-2}, with an average of 8,840 individuals m^{-2} ± 34,854 (SD) across all plots. Our top performing model included the main effects of river region and treatment in addition to the interaction between region and treatment (Table 9.3.21). Similar to abundances of grazers, mean abundances of omnivores were predicted to be considerably higher (8.6X) in the upper river (15,830 individuals m^{-2} ± 5,688 [SE]) as compared to the mid river (Table 9.3.22 and Figure 9.3.19). Mean abundances of omnivores in C treatments (22,772 individuals m^{-2} ± 8,183) were predicted to be 12.5X higher than abundances in CC treatments and 11.8X higher than abundances in E treatments. Mean abundances among combinations of river region and treatment were highest for C treatments in the upper river. Differences among river regions and treatment types were heavily influenced by an extreme datum estimated for the control treatment plot at site 2 in the upper river (U02C). This datum was 5.3 SD away from mean abundances of omnivores across all plots.

Table 9.3.21. Model structure, number of parameters (*k*), log-likelihood, Akaike's second-order information criterion (AICc), ΔAICc, and Akaike weight (*w*), for the top performing GLM explaining variation in macroinvertebrate omnivore abundance.

Model	Number of parameters (k)	Log-likelihood	AICc	ΔAICc	Akaike weight (*w*)
region + ttt + region*ttt	7	-271.3	561.8	0.0	1.0

Table 9.3.22. Model averaged β coefficient estimates and 95 % CIs based on our top performing candidate models explaining variation in macroinvertebrate omnivore abundance. Coefficient estimates are not transformed.

Parameter	mean β	SE	95 % CI lower	95 % CI upper
(Intercept)	7.84	0.36	7.21	8.64
region (Upper)	2.83	0.51	1.81	3.84
ttt (CC)	-0.57	0.51	-1.59	0.45
ttt (E)	-0.48	0.51	-1.50	0.53
region (Upper):ttt (CC)	-2.41	0.72	-3.84	-0.99
region (Upper):ttt (E)	-2.44	0.72	-3.86	-1.02

*Estimates are relative to reference conditions (Intercept). For river region reference condition is mid river and for treatment type reference condition is control (C). The intercept is the mean across data within all reference conditions.

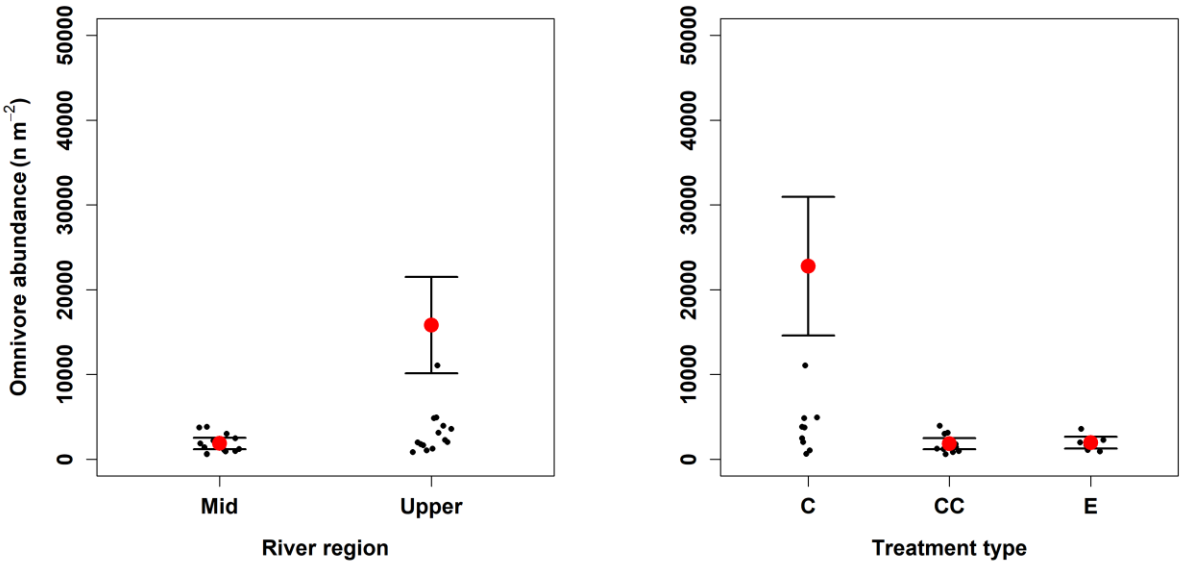

Figure 9.3.19. Predicted effects of river region (left) and treatment type (right) on macroinvertebrate omnivore abundance. Large red circles are mean values and error bars are ± standard error (SE). Small black circles are empirical data. Single extreme data point (see text) is removed to retain appropriate scale for presentation.

Abundances of macroinvertebrate predators ranged from 128 to 2605 individuals m^{-2}, with an average of 598 individuals m^{-2} ± 550 (SD). Our top performing models included the intercept only, singular main effects of treatment type and river region, as well as the interaction of treatment and region (Table 9.2.23). The best model (lowest AICc) included the main effect of treatment, and it performed marginally better than the intercept only model. Predicted mean abundances of predators were slightly higher in the mid river compared to the upper river (Figure 9.3.20); however, the 95 % CI for river region contained zero and the datasets overlapped considerably (Table 9.3.24). Following trends in overall abundances, predator abundances were predicted to be highest in C treatments and lower and similar in CC and E treatments (Figure 9.3.20); however, the 95 % CIs for treatements contained zero so the pattern was not very consistent.

Table 9.3.23. Model structure, number of parameters (*k*), log-likelihood, Akaike's second-order information criterion (AICc), ΔAICc, and Akaike weight (*w*), for all candidate GLMs explaining variation in macroinvertebrate predator abundance.

Model	Number of parameters (k)	Log-likelihood	AICc	ΔAICc	Akaike weight (*w*)
ttt	4	-209.0	427.6	0.0	0.5
(Intercept)	2	-212.1	428.7	1.1	0.3
ttt + region	5	-208.9	430.5	2.9	0.1
region	3	-212.0	430.9	3.4	0.1

Table 9.3.24. Model averaged β coefficient estimates and 95 % CIs based on our top performing candidate models explaining variation in macroinvertebrate predator abundance. Coefficient estimates are not transformed.

Parameter	mean β	SE	95 % CI lower	95 % CI upper
(Intercept)	6.64	0.27	6.10	7.18
ttt (CC)	-0.38	0.38	-1.24	0.02
ttt (E)	-0.48	0.45	-1.42	-0.12
region (Upper)	-0.01	0.13	-0.61	0.55

*Estimates are relative to reference conditions (Intercept). For river region reference condition is mid river and for treatment type reference condition is control (C). The intercept is the mean across data within all reference conditions.

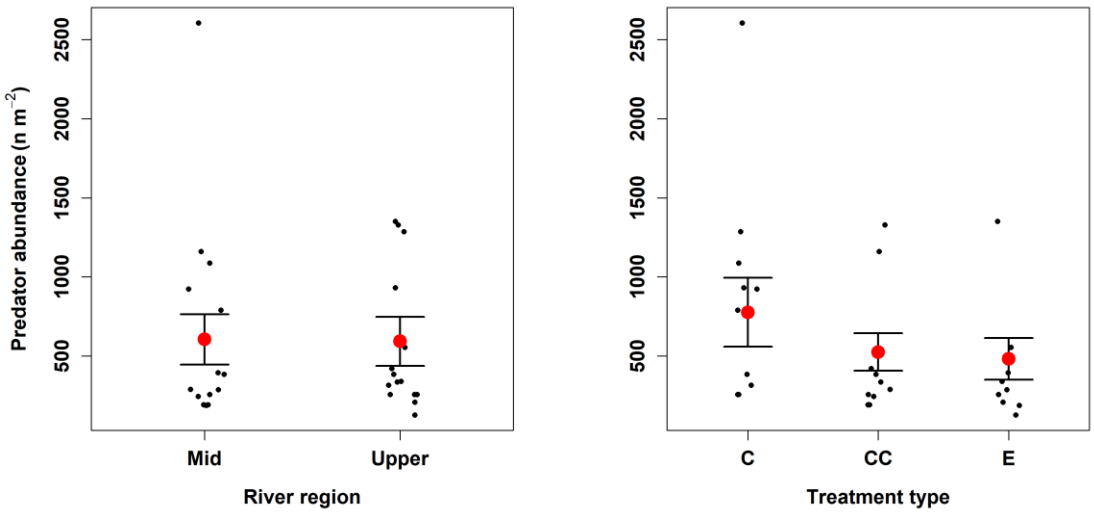

Figure 9.3.20. Predicted effects of river region (left) and treatment type (right) on macroinvertebrate predator abundance. Large red circles are mean values and error bars are ± standard error (SE). Small black circles are empirical data.

Abundance of macroinvertebrate parasites ranged from 1,188 to 22,322 individuals m^{-2}, with an average of 7838 individual m^{-2} ± 5,450 (SD). Our top performing models included the main effects of river region and treatment type (Table 9.3.25). Our candidate set also included the intercept only model, which performed slightly better than the poorest performing model that included the main effects of both river region and treatment type. Using coefficients averaged across models (Table 9.3.26), we predicted mean abundances of parasites to be 1.5X higher in the upper river relative to the mid river (Figure 9.3.21). Differences among predicted mean abundances of parasites across treatment types were negligible, and 95 % CIs for the relevant effect sizes contained zero.

Table 9.3.25. Model structure, number of parameters (*k*), log-likelihood, Akaike's second-order information criterion (AICc), ΔAICc, and Akaike weight (*w*), for top performing candidate GLMs explaining variation in macroinvertebrate parasite abundance.

Model	Number of parameters (k)	Log-likelihood	AICc	ΔAICc	Akaike weight (*w*)
region	3	-293.8	594.4	0.0	0.6
(Intercept)	2	-295.8	596.0	1.6	0.3
region + ttt	5	-292.2	596.8	2.4	0.2

Table 9.3.26. Model averaged β coefficient estimates and 95 % CIs based on our top performing candidate models explaining variation in macroinvertebrate parasite abundance. Coefficient estimates are not transformed.

Parameter	mean β	SE	95 % CI lower	95 % CI upper
(Intercept)	8.79	0.22	8.34	9.24
region (Upper)	0.39	0.31	0.02	1.02
ttt (CC)	-0.05	0.17	-0.91	0.28
ttt (E)	-0.09	0.23	-1.12	0.07

*Estimates are relative to reference conditions (Intercept). For river region reference condition is mid river and for treatment type reference condition is control (C). The intercept is the mean across data within all reference conditions.

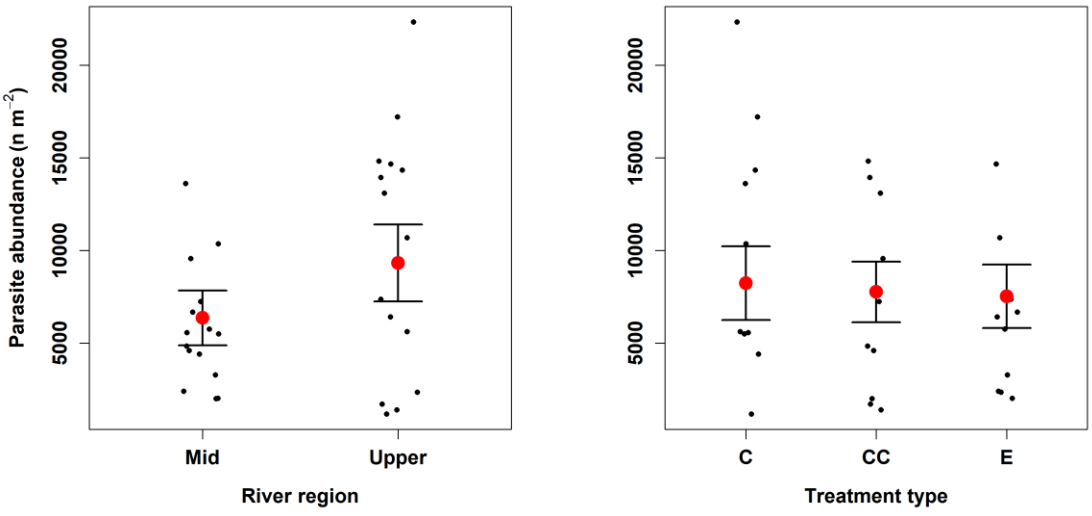

Figure 9.3.21. Predicted effects of river region (left) and treatment type (right) on macroinvertebrate parasite abundance. Large red circles are mean values and error bars are ± standard error (SE). Small black circles are empirical data.

The macroinvertebrate community comprised 16 Orders and other higher-level taxonomic classifications, which included typical taxa present in Florida spring-run streams (Mattson et al. 1995; Table 9.3.27). In terms of proportional contributions to abundance and biomass of macroinvertebrates, four taxa, dipterans (predominantly chironomids), ostracods, Acari (water mites), and trichopterans collectively comprised greater than 95 % of total abundance and greater than 70% of total biomass within experimental treatments. Dipterans were by far the most abundant taxa (comprising 62–65 % of total abundance across all treatments), and trichopterans contributed the most to biomass (comprising 46–57 % of the total biomass across all treatments). While the relative contribution of macroinvertebrate taxa to community composition was similar across treatments, river regions exhibited a few differences (Table 9.3.28). Most notably, the relative contribution of dipterans was ~20 % higher in the mid river in terms of abundance and ~15 % higher in terms of biomass. Conversely, the relative contributions of trichopterans and ostracods were higher in the upper river.

Table 9.3.27. Community composition (% abundance and % mass) of macroinvertebrates as a function of experimental treatments based on empirical data.

	Control		Cage control		Exclusion	
Taxon	**% n**	**% mass**	**% n**	**% mass**	**% n**	**% mass**
Acari	5.78%	1.53%	11.21%	4.33%	9.94%	2.03%
Amphipoda	0.70%	3.84%	2.05%	10.89%	1.28%	4.38%
Araneae	0.00%	0.00%	0.01%	0.12%	0.00%	0.00%
Coleoptera	0.03%	0.76%	0.11%	1.01%	0.08%	2.27%
Copepoda	0.26%	0.16%	0.04%	0.20%	0.38%	0.14%
Decapoda	0.00%	0.00%	0.13%	0.04%	0.01%	0.02%
Diptera	61.78%	22.08%	63.99%	21.93%	65.22%	28.51%
Ephemeroptera	0.28%	0.76%	0.66%	1.79%	0.58%	1.20%
Gastropoda	0.95%	8.09%	0.86%	8.66%	0.84%	10.03%
Hirudinea	0.04%	0.29%	0.15%	0.39%	0.04%	0.10%
Isopoda	0.02%	0.16%	0.02%	0.31%	0.02%	0.07%
Lepidoptera	0.28%	3.10%	0.53%	3.51%	0.33%	2.15%
Megaloptera	0.00%	0.00%	0.00%	0.00%	0.01%	0.02%
Odonata	0.11%	1.06%	0.15%	0.51%	0.17%	1.29%
Ostracoda	11.34%	1.10%	1.19%	0.78%	1.14%	0.84%
Trichoptera	18.43%	57.06%	18.90%	45.53%	19.97%	46.94%

Table 9.3.28. Community composition (% abundance and % mass) of macroinvertebrates as a function of river region based on empirical data.

	Mid		Upper	
Taxon	**% n**	**% mass**	**% n**	**% mass**
Acari	6.61%	2.65%	8.72%	2.16%
Amphipoda	0.24%	1.48%	1.73%	6.90%
Araneae	0.00%	0.00%	0.00%	0.03%
Coleoptera	0.01%	0.16%	0.09%	1.73%
Copepoda	0.28%	0.32%	0.21%	0.11%
Decapoda	0.00%	0.00%	0.05%	0.02%
Diptera	73.90%	34.01%	55.29%	20.83%
Ephemeroptera	0.41%	1.80%	0.44%	0.89%
Gastropoda	1.05%	6.02%	0.81%	9.86%
Hirudinea	0.05%	0.44%	0.08%	0.18%
Isopoda	0.00%	0.09%	0.03%	0.19%
Lepidoptera	0.27%	4.25%	0.39%	2.38%
Megaloptera	0.00%	0.03%	0.00%	0.00%
Odonata	0.21%	1.42%	0.08%	0.89%
Ostracoda	1.14%	1.10%	11.07%	0.89%
Trichoptera	15.81%	46.23%	21.02%	52.94%

We employed non-metric multidimensional scaling (nMDS) to examine dissimilarities in the composition of macroinvertebrate communities among experimental treatments and river regions. We used scaled abundances (individuals m^{-2}) for 16 taxa to construct our community matrix. We log-transformed abundance data (i.e., log[abundance + 1]) prior to performing nMDS. We used the Bray-Curtis dissimilarity index to estimate distances among samples within ordination space. nMDS performed relatively well in two dimensions (stress = 0.15); however, samples remained aggregated (Figure 9.3.22), which suggests similar compositions. Experimental treatments overlapped considerably in ordination space (Figure 9.3.23), with cage controls (CC) positioned near both control (C) and exclusion (E) treatments River regions overlapped less, suggesting that abundances of macroinvertebrates in the upper and mid river plots differed (Figure 9.3.23).

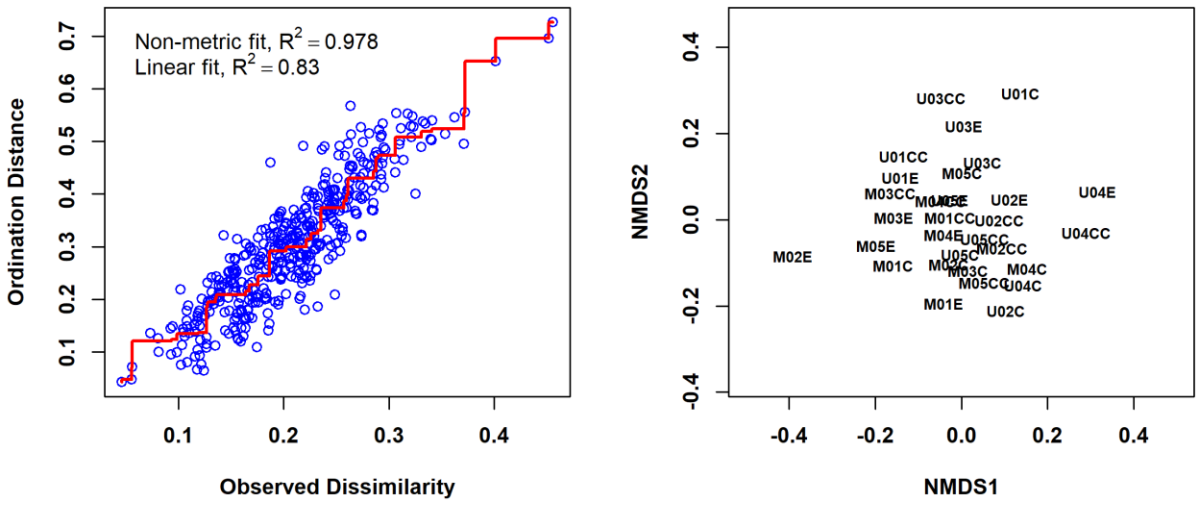

Figure 9.3.22. Shepard (left) and ordination plots of the first and second axes (right) resulting from nMDS analysis of macroinvertebrate community composition based on abundance data. Location of each plot within ordination space is labeled by site code, which denotes river region (mid [M] and upper [U] river), site number (1–5), and experimental treatment (control [C], cage control [CC], and exclusion [E]).

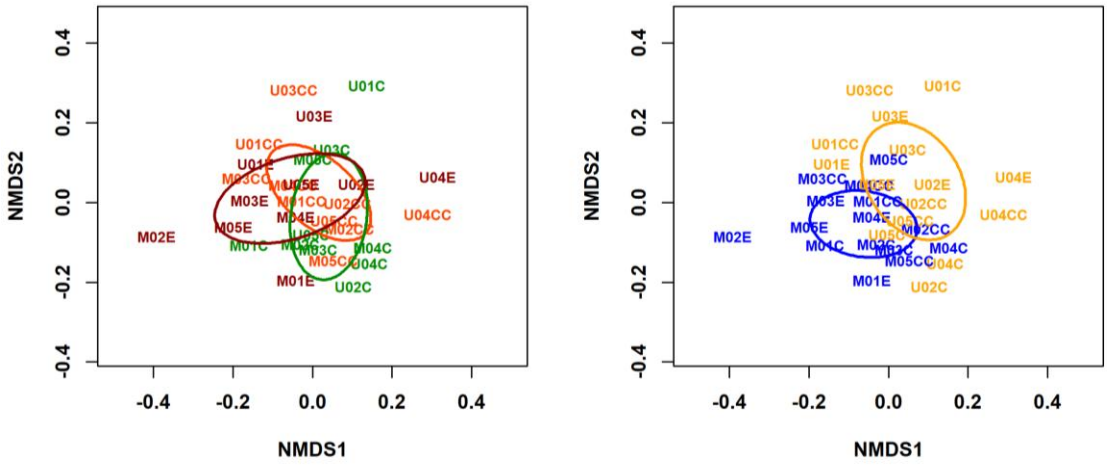

Figure 9.3.23. Ordination plots of the first and second axes from nMDS analysis of macroinvertebrate community composition, grouping site scores by treatment type (left) and river region (right) based on abundance data. Ellipses delineate the minimum bounds of the standard deviation for all ordination scores for communities within each corresponding group (color of ellipse contours matches the text color of communities within each group). Location of each plot within ordination space is labeled by site code, which denotes river region (mid [M] and upper [U] river), site number (1–5), and experimental treatment (control [C], cage control [CC], and exclusion [E]).

Ordination analysis (nMDS) based on untransformed biomass data performed better in two dimensions (stress = 0.08; Figure 9.3.24). Thise results exhibited further separation of river regions but little change in the differentiation of experimental treatments (Figure 9.3.25).

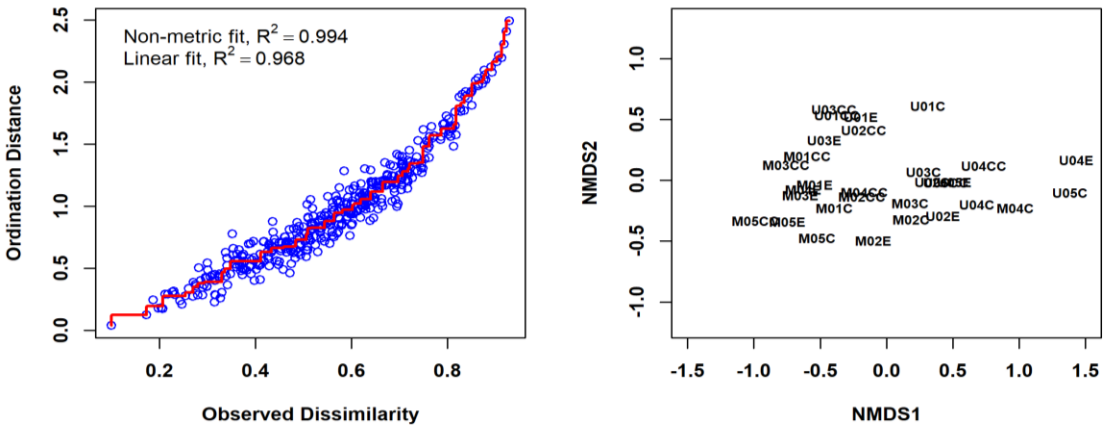

Figure 9.3.24. Shepard (left) and ordination plots of the first and second axes (right) resulting from nMDS analysis of macroinvertebrate community composition based on biomass data. Location of each plot within ordination space is labeled by site code, which denotes river region (mid [M] and upper [U] river), site number (1–5), and experimental treatment (control [C], cage control [CC], and exclusion [E]).

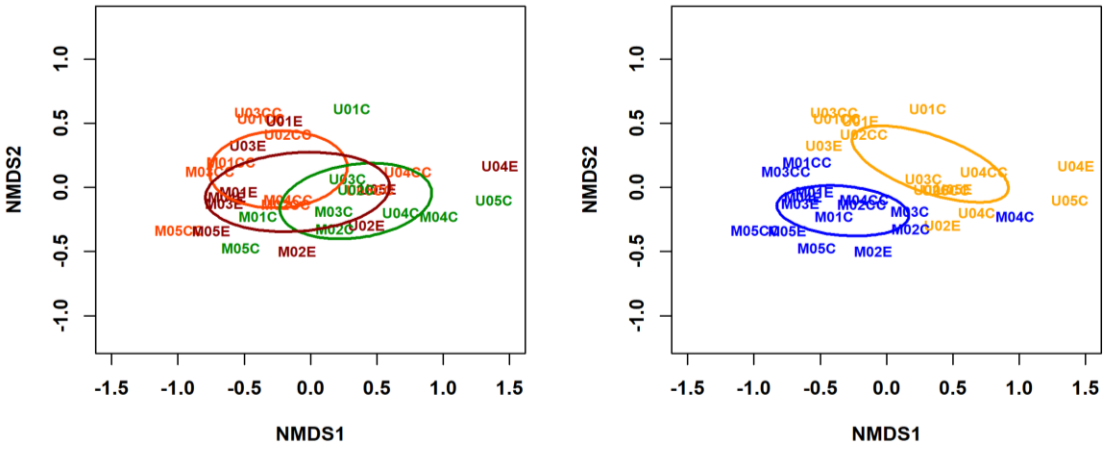

Figure 9.3.25. Ordination plots of the first and second axes from nMDS analysis of macroinvertebrate community composition, grouping site scores by treatment type (left) and river region (right) based on biomass data. Ellipses delineate the minimum bounds of the standard deviation for all ordination scores for communities within each corresponding group (color of ellipse contours matches the text color of communities within each group). Location of each plot within ordination space is labeled by site code, which denotes river region (mid [M] and upper [U] river), site number (1–5), and experimental treatment (control [C], cage control [CC], and exclusion [E]).

We employed a GLM framework to evaluate differences in macroinvertebrate community composition (multivariate tests) and abundances of individual taxa (univariate tests) among river regions and experimental treatments. Our multivariate test indicated significant differences among river regions (Deviance = 66.8, p-value = 0.005) and experimental treatments (Deviance = 47.23, p-value = 0.035); however, the interaction of region and treatment was non-significant (Deviance = 34.19, p-value = 0.225). Univariate tests yielded few significant results when p-values were adjusted for multiple comparisons. Specifically, we detected significant differences in abundances of amphipods among river regions (Deviance = 15.91, p-value = 0.004) and marginally significant differences in abundances of dipterans (chiefly chironomids, Deviance = 11.71, p-value = 0.071) and ostracods (Deviance = 23.98, p-value = 0.071 among treatments).

9.3.5 DISCUSSION

The exclusion of small-bodied to large-bodied predators (i.e., fish, turtles, alligators, birds, etc.) from submersed macrophyte beds in two regions of Silver River (upper and mid river) did not result in marked effects on macrophyte growth rates or biomass. Likewise, there was little indication that variation in the epiphytic loads on dominant macrophytes was substantially reduced as a consequence of predator exclusion. These findings, in combination, provide little support for a strong top-down influence on plant and algal dynamics in this spring-fed ecosystem. We note also that the abundance of macroinvertebrates (grazers in particular) was greatest in Control treatment plots. We expected, however, to document a compensatory increase in grazer abundance in the predator exclusion plots consistent with a trophic cascade model (Hairston et al. 1960).

It is possible that the short duration of the experiment failed to capture fully the expected longer-term responses of the lower trophic levels, i.e. primary producers and consumers, to the change in predator presence. For example, a difference in the mean growth rate of *Vallisneria americana* was evident between the upper river and mid river sites and macrophytes in the predator exclusion plots in the upper river exhibited qualitatively greater growth rates than those in control plots. Similarly, epiphytic loads on macrophytes were, in some cases, strikingly reduced in predator exclusion plots relative to control plots. Reduced epiphytic loads that result in increased light availability to host macrophytes are expected, of course, to result in improved plant performance, i.e., faster growth. These qualitative observations, though directionally consistent with the mechanistic link described above and also the expectation of top-down driven influences on grazing activity and primary production, are far from compelling and reflect an understanding of the system that is far from complete.

As indicated above, we expected macroinvertebrate abundance and biomass to increase in the absence of predation. We observed the opposite effect, i.e., macroinvertebrates (grazers specifically) were most abundant in the control treatment plots. We posit two mechanisms that might give rise to this finding. First, removal of larger-bodied predators may have released top-down pressure on smaller meso-predators, such as larval odonates and predaceous leeches. These smaller, meso-predators are able to freely move through the mesh in the exclusion cages to prey upon other macroinvertebrates and reduce their abundances. If this were true, however, we might have expected to detect an elevated abundance (or biomass) of macroinvertebrate predators

(meso-predators) in the predator exclusion plots. We did not. The second mechanism to explain the greater numbers of grazers in control plots is as follows: abundances of macroinvertebrates simply may be linked more tightly to the amount of available food than to predation. We note that epiphytic algal biomass, although highly variable and influenced by several extreme data points, was often appreciably higher in our control plots. This finding is consistent with the idea that the abundance and biomass or macroinvertebrates (dominated by grazers) tracks biomass of epiphytic algae, i.e. more food equals more consumers in the controls.

9.3.6 CONCLUSIONS AND RECOMMENDATIONS

Previous sections of this report characterize the food web in Silver River and quantify the grazing potential of numerically abundant and presumably important herbivores. Findings yielded new and important insights into energy flow and material transport and also pointed to the potential for grazer control of nuisance macroalgae in Silver River and other spring-fed systems. As a logical transition, we employed a manipulative field experiment (predator exclusion approach) to determine whether small and large-bodied predators in Silver directly influence the abundance of grazers and, in so doing, affect indirectly the primary producer community. Our findings, however, provided little evidence of a predator mediated influence on plant and algal dynamics in Silver River; i.e., strong top-down influences were not apparent. Given this finding, it is not likely that resource managers have the option to manipulate the abundance of higher-order predators in this spring-fed system to affect a desirable change in the primary producer community.

9.3.7 REFERENCES

Barton, K. 2016. MuMIn: Multi-Model Inference (R package version 1.15.6). Available at https://cran.r-project.org/package=MuMIn.

Burnham, K. P., and Anderson, D. R. 2002. Model Selection and Multimodel Inference: A Practical Information-Theoretic Approach. Springer-Verlag New York, Inc., New York, 515 pp.

Camacho, F. A., and Thacker, R. W. 2006. Amphipod herbivory on the freshwater cyanobacterium *Lyngbya wollei*: Chemical stimulants and morphological defenses. Limnology and Oceanography 51: 1870–1875.

Dormsjo, K. 2008. Oxygen mediated grazing impacts in Florida springs. Thesis. University of Florida. 69 pp.

Grueber, C. E., Nakagawa, S., Laws, R. J., and Jamieson, I. G. 2011. Multimodel inference in ecology and evolution: Challenges and solutions. Journal of Evolutionary Biology 24: 699–711.

Hairston, N., Smith, F. E. and Slobodkin, L. B.. 1960. Community structure, population control, and competition. The American Naturalist 94:421-425.

Hauxwell, J., Frazer, T. K., and Osenberg, C. W. 2007. An annual cycle of biomass and productivity of *Vallisneria americana* in a subtropical spring-fed estuary. Aquatic Botany 87: 61–68.

Hauxwell, J., Osenberg, C. W., and Frazer, T. K. 2004. Conflicting Management Goals: Manatees and Invasive Competitors Inhibit Restoration of a Native Macrophyte. Ecological Applications 14:571–586.

Hoyer, M. V., and D. E. Canfield, Jr. 1986. Surface area of aquatic macrophytes. Aquatics 8: 26–27

Knight, R. L. 1980. Energy basis of control in aquatic ecosystems. Ph. D. Dissertation. University of Florida. 221 pp.

Liebowitz, D. M. 2013. Environmentally mediated consumer control of algae proliferation in Florida springs. Ph. D. Dissertation. University of Florida. 122 pp.

Liebowitz, D. M., Cohen, M. J., Heffernan, J. B., Korhnak, L. V. and Frazer, T. K.. 2014. Environmentally-mediated consumer control of algal proliferation in Florida springs. Freshwater Biology 59:2009–2023.

Mattson, R. A., Epler, J. H. and Hein, M. K. 1995. Description of benthic communities in karst, spring-fed streams of north central Florida. Journal of the Kansas Entomological Society 68: 18–41.

Nifong, R. L. 2017. Experimental effects of grazers on autotrophic species assemblages across a nitrate gradient in Florida springs. Aquatic Botany 139: 57–64.

Oksanen, J., Blanchet, F. G., Friendly, M., Kindt, R., Legendre, P., McGlinn, D., Minchin, P. R., O'Hara, R. B., Simpson, G. L., Solymos, P., Stevens, M. H. H., Szoecs, E. and Wagner, H. 2017. vegan: Community Ecology Package. R package version 2.4-3. https://cran.r-project.org/package=vegan.

Pace, M. L., Cole, J. J., Carpenter, S. R., and Kitchell, J. F. 1999. Trophic cascades revealed in diverse ecosystems. Science 14:483–488.

Quinlan, E. L., Phlips, E. J., Donnelly, K. A., Jett, C. H., Sleszynski, P. and Keller, S. 2008. Primary producers and nutrient loading in Silver Springs, FL, USA. Aquatic Botany 88: 247–255.

Schmitz, O., Hambäck, P., and Beckerman, A. 2000. Trophic Cascades in Terrestrial Systems: A Review of the Effects of Carnivore Removals on Plants. The American Naturalist 155:141–153.

Schmitz, O. J., V. Krivan, and O. Ovadia. 2004. Trophic cascades: the primacy of trait-mediated indirect interactions. Ecology Letters 7:153–163.

Silliman, B. R., and Bertness, M. D. 2002. A trophic cascade regulates salt marsh primary production. Proceedings of the National Academy of Sciences of the United States of America 99:10500–10505.

Strong, D. 1992. Are trophic cascades all wet? Differentiation and donor-control in speciose ecosystems. Ecology 73:747–754.

Wang, Y., Naumann, U., Wright, S. T. and Warton, D. I. 2012. Mvabund- an R package for model-based analysis of multivariate abundance data. Methods in Ecology and Evolution 3:471–474.

APPENDICES

Appendix 5.1.1. BTC data.

Location	Date and Time	Rhodmaine Concentration Adjusted Concentration (ppb)
Spring Bowl ISCO	3/4/15 18:00	-0.061630859
Spring Bowl ISCO	3/4/15 18:30	93.15714589
Spring Bowl ISCO	3/4/15 19:00	66.21165902
Spring Bowl ISCO	3/4/15 19:30	26.85093745
Spring Bowl ISCO	3/4/15 20:00	10.41305477
Spring Bowl ISCO	3/4/15 20:30	4.09104542
Spring Bowl ISCO	3/4/15 21:00	1.406536894
Spring Bowl ISCO	3/4/15 21:30	0.639534458
Spring Bowl ISCO	3/4/15 22:00	0.219822825
Spring Bowl ISCO	3/4/15 22:30	0.073335235
Spring Bowl ISCO	3/4/15 23:00	-0.023774515
Spring Bowl ISCO	3/4/15 23:30	-0.028712299
Spring Bowl ISCO	3/5/15 0:00	-0.055047147
Spring Bowl ISCO	3/5/15 0:30	-0.028712299
Spring Bowl ISCO	3/5/15 1:00	-0.06821457
Spring Bowl ISCO	3/5/15 1:30	-0.058339003
Spring Bowl ISCO	3/5/15 2:00	-0.027066371
Spring Bowl ISCO	3/5/15 2:30	-0.046817507
Spring Bowl ISCO	3/5/15 3:00	-0.09290349
Spring Bowl ISCO	3/5/15 3:30	-0.114300554
Spring Bowl ISCO	3/5/15 4:00	-0.12582205
Spring Bowl ISCO	3/5/15 4:30	-0.134051689
Spring Bowl ISCO	3/5/15 5:00	-0.051755291
Spring Bowl ISCO	3/5/15 5:30	-0.035296011
Main Channel ISCO	3/4/15 18:00	0.03712482
Main Channel ISCO	3/4/15 19:00	22.35426222
Main Channel ISCO	3/4/15 20:00	40.84132523
Main Channel ISCO	3/4/15 21:00	11.97174856
Main Channel ISCO	3/4/15 22:00	2.32825656
Main Channel ISCO	3/4/15 23:00	0.567113628
Main Channel ISCO	3/5/15 0:00	0.213239113
Main Channel ISCO	3/5/15 1:00	0.068397451
Main Channel ISCO	3/5/15 2:00	0.033832964
Main Channel ISCO	3/5/15 3:00	-0.107716842
Main Channel ISCO	3/5/15 4:00	0.02066554
Main Channel ISCO	3/5/15 5:00	-0.036941939
Main Channel ISCO	3/5/15 6:00	-0.035296011
Main Channel ISCO	3/5/15 7:00	0.00420626
Main Channel ISCO	3/5/15 8:00	-0.041879723
Main Channel ISCO	3/5/15 9:00	0.130942714
Main Channel ISCO	3/5/15 10:00	0.107899723
Main Channel ISCO	3/5/15 11:00	0.030541108
Main Channel ISCO	3/5/15 12:00	0.070043379
Back Channel ISCO	3/4/15 18:00	-0.097841274

Location	Date and Time	Rhodmaine Concentration Adjusted Concentration (ppb)
Back Channel ISCO	3/4/15 19:00	-0.104424986
Back Channel ISCO	3/4/15 20:00	-0.173553961
Back Channel ISCO	3/4/15 21:00	-0.163678393
Back Channel ISCO	3/4/15 22:00	21.83744084
Back Channel ISCO	3/4/15 23:00	20.21290993
Back Channel ISCO	3/5/15 0:00	8.972867792
Back Channel ISCO	3/5/15 1:00	5.063788853
Back Channel ISCO	3/5/15 2:00	5.717222259
Back Channel ISCO	3/5/15 3:00	5.743557106
Back Channel ISCO	3/5/15 4:00	4.642431292
Back Channel ISCO	3/5/15 5:00	3.325688912
Back Channel ISCO	3/5/15 6:00	2.825326808
Back Channel ISCO	3/5/15 7:00	1.956276838
Back Channel ISCO	3/5/15 8:00	1.27980044
Back Channel ISCO	3/5/15 9:00	1.004930469
Back Channel ISCO	3/5/15 10:00	0.624721107
Back Channel ISCO	3/5/15 11:00	0.51608986
Back Channel ISCO	3/5/15 12:00	0.433793462
Back Channel ISCO	3/5/15 13:00	0.170444986
1,200 m Sattion Flurometer	3/4/15 8:08	1.297
1,200 m Sattion Flurometer	3/4/15 8:09	1.585
1,200 m Sattion Flurometer	3/4/15 8:10	1.257
1,200 m Sattion Flurometer	3/4/15 8:11	1.33
1,200 m Sattion Flurometer	3/4/15 8:12	1.364
1,200 m Sattion Flurometer	3/4/15 8:13	1.449
1,200 m Sattion Flurometer	3/4/15 8:14	1.19
1,200 m Sattion Flurometer	3/4/15 8:15	1.467
1,200 m Sattion Flurometer	3/4/15 8:16	1.105
1,200 m Sattion Flurometer	3/4/15 9:06	11.9
1,200 m Sattion Flurometer	3/4/15 9:07	12.26
1,200 m Sattion Flurometer	3/4/15 16:48	-0.017
1,200 m Sattion Flurometer	3/4/15 16:49	0.411
1,200 m Sattion Flurometer	3/4/15 16:50	-0.143
1,200 m Sattion Flurometer	3/4/15 16:51	-0.449
1,200 m Sattion Flurometer	3/4/15 16:52	-0.39
1,200 m Sattion Flurometer	3/4/15 16:53	10.8
1,200 m Sattion Flurometer	3/4/15 16:54	10.44
1,200 m Sattion Flurometer	3/4/15 16:55	11.58
1,200 m Sattion Flurometer	3/4/15 16:56	11.18
1,200 m Sattion Flurometer	3/4/15 16:57	10.72
1,200 m Sattion Flurometer	3/4/15 16:58	10.59
1,200 m Sattion Flurometer	3/4/15 16:59	0.167
1,200 m Sattion Flurometer	3/4/15 17:00	-0.39
1,200 m Sattion Flurometer	3/4/15 17:01	0.004
1,200 m Sattion Flurometer	3/4/15 17:02	-0.401
1,200 m Sattion Flurometer	3/4/15 17:03	0.097

Location	Date and Time	Rhodmaine Concentration Adjusted Concentration (ppb)
1,200 m Sattion Flurometer	3/4/15 17:04	-0.364
1,200 m Sattion Flurometer	3/4/15 17:05	-0.353
1,200 m Sattion Flurometer	3/4/15 17:06	-0.209
1,200 m Sattion Flurometer	3/4/15 17:07	-0.231
1,200 m Sattion Flurometer	3/4/15 17:08	-0.523
1,200 m Sattion Flurometer	3/4/15 17:09	-0.505
1,200 m Sattion Flurometer	3/4/15 17:10	-0.143
1,200 m Sattion Flurometer	3/4/15 17:11	-0.095
1,200 m Sattion Flurometer	3/4/15 17:12	-0.091
1,200 m Sattion Flurometer	3/4/15 17:13	-0.024
1,200 m Sattion Flurometer	3/4/15 17:14	-0.261
1,200 m Sattion Flurometer	3/4/15 17:15	-0.161
1,200 m Sattion Flurometer	3/4/15 17:16	-0.157
1,200 m Sattion Flurometer	3/4/15 17:17	-0.486
1,200 m Sattion Flurometer	3/4/15 17:18	-0.375
1,200 m Sattion Flurometer	3/4/15 17:19	-0.364
1,200 m Sattion Flurometer	3/4/15 17:20	1.142
1,200 m Sattion Flurometer	3/4/15 17:21	-0.106
1,200 m Sattion Flurometer	3/4/15 17:22	0.115
1,200 m Sattion Flurometer	3/4/15 17:23	-0.257
1,200 m Sattion Flurometer	3/4/15 17:24	0.954
1,200 m Sattion Flurometer	3/4/15 17:25	-0.198
1,200 m Sattion Flurometer	3/4/15 17:26	1.039
1,200 m Sattion Flurometer	3/4/15 17:27	0.093
1,200 m Sattion Flurometer	3/4/15 17:28	-0.013
1,200 m Sattion Flurometer	3/4/15 17:29	-0.076
1,200 m Sattion Flurometer	3/4/15 17:30	-0.128
1,200 m Sattion Flurometer	3/4/15 17:31	0.085
1,200 m Sattion Flurometer	3/4/15 17:32	0.824
1,200 m Sattion Flurometer	3/4/15 17:33	0.943
1,200 m Sattion Flurometer	3/4/15 17:34	0.1
1,200 m Sattion Flurometer	3/4/15 17:35	0.946
1,200 m Sattion Flurometer	3/4/15 17:36	1.29
1,200 m Sattion Flurometer	3/4/15 17:37	-0.021
1,200 m Sattion Flurometer	3/4/15 17:38	0.133
1,200 m Sattion Flurometer	3/4/15 17:39	1.028
1,200 m Sattion Flurometer	3/4/15 17:40	-0.265
1,200 m Sattion Flurometer	3/4/15 17:41	0.052
1,200 m Sattion Flurometer	3/4/15 17:42	1.29
1,200 m Sattion Flurometer	3/4/15 17:43	-0.132
1,200 m Sattion Flurometer	3/4/15 17:44	0.684
1,200 m Sattion Flurometer	3/4/15 17:45	0.152
1,200 m Sattion Flurometer	3/4/15 17:46	-0.054
1,200 m Sattion Flurometer	3/4/15 17:47	1.031
1,200 m Sattion Flurometer	3/4/15 17:48	-0.42
1,200 m Sattion Flurometer	3/4/15 17:49	-0.039

Location	Date and Time	Rhodmaine Concentration Adjusted Concentration (ppb)
1,200 m Sattion Flurometer	3/4/15 17:50	-0.084
1,200 m Sattion Flurometer	3/4/15 17:51	0.019
1,200 m Sattion Flurometer	3/4/15 17:52	0.241
1,200 m Sattion Flurometer	3/4/15 17:53	0.019
1,200 m Sattion Flurometer	3/4/15 17:54	0.289
1,200 m Sattion Flurometer	3/4/15 17:55	0.994
1,200 m Sattion Flurometer	3/4/15 17:56	-0.146
1,200 m Sattion Flurometer	3/4/15 17:57	0.226
1,200 m Sattion Flurometer	3/4/15 17:58	0.048
1,200 m Sattion Flurometer	3/4/15 17:59	0.156
1,200 m Sattion Flurometer	3/4/15 18:00	0.215
1,200 m Sattion Flurometer	3/4/15 18:01	0.004
1,200 m Sattion Flurometer	3/4/15 18:02	-0.231
1,200 m Sattion Flurometer	3/4/15 18:03	0.163
1,200 m Sattion Flurometer	3/4/15 18:04	0.285
1,200 m Sattion Flurometer	3/4/15 18:05	0.928
1,200 m Sattion Flurometer	3/4/15 18:06	-0.013
1,200 m Sattion Flurometer	3/4/15 18:07	0.928
1,200 m Sattion Flurometer	3/4/15 18:08	0.496
1,200 m Sattion Flurometer	3/4/15 18:09	0.015
1,200 m Sattion Flurometer	3/4/15 18:10	-0.165
1,200 m Sattion Flurometer	3/4/15 18:11	-0.261
1,200 m Sattion Flurometer	3/4/15 18:12	0.078
1,200 m Sattion Flurometer	3/4/15 18:13	0.034
1,200 m Sattion Flurometer	3/4/15 18:14	0.137
1,200 m Sattion Flurometer	3/4/15 18:15	-0.076
1,200 m Sattion Flurometer	3/4/15 18:16	-0.065
1,200 m Sattion Flurometer	3/4/15 18:17	0.366
1,200 m Sattion Flurometer	3/4/15 18:18	-0.168
1,200 m Sattion Flurometer	3/4/15 18:19	0.048
1,200 m Sattion Flurometer	3/4/15 18:20	-0.12
1,200 m Sattion Flurometer	3/4/15 18:21	0.115
1,200 m Sattion Flurometer	3/4/15 18:22	1.172
1,200 m Sattion Flurometer	3/4/15 18:23	0.211
1,200 m Sattion Flurometer	3/4/15 18:24	0.167
1,200 m Sattion Flurometer	3/4/15 18:25	-0.124
1,200 m Sattion Flurometer	3/4/15 18:26	0.045
1,200 m Sattion Flurometer	3/4/15 18:27	0.126
1,200 m Sattion Flurometer	3/4/15 18:28	0.259
1,200 m Sattion Flurometer	3/4/15 18:29	0.111
1,200 m Sattion Flurometer	3/4/15 18:30	-0.128
1,200 m Sattion Flurometer	3/4/15 18:31	0.189
1,200 m Sattion Flurometer	3/4/15 18:32	1.057
1,200 m Sattion Flurometer	3/4/15 18:33	-0.043
1,200 m Sattion Flurometer	3/4/15 18:34	-0.098
1,200 m Sattion Flurometer	3/4/15 18:35	1.227

Location	Date and Time	Rhodmaine Concentration Adjusted Concentration (ppb)
1,200 m Sattion Flurometer	3/4/15 18:36	-0.338
1,200 m Sattion Flurometer	3/4/15 18:37	0.041
1,200 m Sattion Flurometer	3/4/15 18:38	-0.047
1,200 m Sattion Flurometer	3/4/15 18:39	0.085
1,200 m Sattion Flurometer	3/4/15 18:40	-0.106
1,200 m Sattion Flurometer	3/4/15 18:41	0.333
1,200 m Sattion Flurometer	3/4/15 18:42	0.159
1,200 m Sattion Flurometer	3/4/15 18:43	0.636
1,200 m Sattion Flurometer	3/4/15 18:44	0.484
1,200 m Sattion Flurometer	3/4/15 18:45	0.252
1,200 m Sattion Flurometer	3/4/15 18:46	0.259
1,200 m Sattion Flurometer	3/4/15 18:47	0.222
1,200 m Sattion Flurometer	3/4/15 18:48	0.093
1,200 m Sattion Flurometer	3/4/15 18:49	0.082
1,200 m Sattion Flurometer	3/4/15 18:50	1.016
1,200 m Sattion Flurometer	3/4/15 18:51	1.216
1,200 m Sattion Flurometer	3/4/15 18:52	-0.006
1,200 m Sattion Flurometer	3/4/15 18:53	0.263
1,200 m Sattion Flurometer	3/4/15 18:54	0.097
1,200 m Sattion Flurometer	3/4/15 18:55	0.233
1,200 m Sattion Flurometer	3/4/15 18:56	0.296
1,200 m Sattion Flurometer	3/4/15 18:57	0.374
1,200 m Sattion Flurometer	3/4/15 18:58	-0.01
1,200 m Sattion Flurometer	3/4/15 18:59	-0.065
1,200 m Sattion Flurometer	3/4/15 19:00	0.133
1,200 m Sattion Flurometer	3/4/15 19:01	0.88
1,200 m Sattion Flurometer	3/4/15 19:02	-0.165
1,200 m Sattion Flurometer	3/4/15 19:03	0.159
1,200 m Sattion Flurometer	3/4/15 19:04	0.163
1,200 m Sattion Flurometer	3/4/15 19:05	-0.087
1,200 m Sattion Flurometer	3/4/15 19:06	0.222
1,200 m Sattion Flurometer	3/4/15 19:07	-0.006
1,200 m Sattion Flurometer	3/4/15 19:08	1.186
1,200 m Sattion Flurometer	3/4/15 19:09	-0.209
1,200 m Sattion Flurometer	3/4/15 19:10	-0.028
1,200 m Sattion Flurometer	3/4/15 19:11	-0.154
1,200 m Sattion Flurometer	3/4/15 19:12	-0.024
1,200 m Sattion Flurometer	3/4/15 19:13	1.286
1,200 m Sattion Flurometer	3/4/15 19:14	0.444
1,200 m Sattion Flurometer	3/4/15 19:15	0.233
1,200 m Sattion Flurometer	3/4/15 19:16	0.041
1,200 m Sattion Flurometer	3/4/15 19:17	0.322
1,200 m Sattion Flurometer	3/4/15 19:18	0.108
1,200 m Sattion Flurometer	3/4/15 19:19	-0.102
1,200 m Sattion Flurometer	3/4/15 19:20	0.902
1,200 m Sattion Flurometer	3/4/15 19:21	-0.157

Location	Date and Time	Rhodmaine Concentration Adjusted Concentration (ppb)
1,200 m Sattion Flurometer	3/4/15 19:22	-0.076
1,200 m Sattion Flurometer	3/4/15 19:23	0.355
1,200 m Sattion Flurometer	3/4/15 19:24	0.266
1,200 m Sattion Flurometer	3/4/15 19:25	0.418
1,200 m Sattion Flurometer	3/4/15 19:26	0.111
1,200 m Sattion Flurometer	3/4/15 19:27	-0.072
1,200 m Sattion Flurometer	3/4/15 19:28	0.063
1,200 m Sattion Flurometer	3/4/15 19:29	0.207
1,200 m Sattion Flurometer	3/4/15 19:30	1.279
1,200 m Sattion Flurometer	3/4/15 19:31	-0.05
1,200 m Sattion Flurometer	3/4/15 19:32	-0.183
1,200 m Sattion Flurometer	3/4/15 19:33	0.34
1,200 m Sattion Flurometer	3/4/15 19:34	0.082
1,200 m Sattion Flurometer	3/4/15 19:35	0.13
1,200 m Sattion Flurometer	3/4/15 19:36	1.216
1,200 m Sattion Flurometer	3/4/15 19:37	0.2
1,200 m Sattion Flurometer	3/4/15 19:38	1.094
1,200 m Sattion Flurometer	3/4/15 19:39	0.337
1,200 m Sattion Flurometer	3/4/15 19:40	0.913
1,200 m Sattion Flurometer	3/4/15 19:41	-0.021
1,200 m Sattion Flurometer	3/4/15 19:42	1.257
1,200 m Sattion Flurometer	3/4/15 19:43	0.089
1,200 m Sattion Flurometer	3/4/15 19:44	0.163
1,200 m Sattion Flurometer	3/4/15 19:45	-0.028
1,200 m Sattion Flurometer	3/4/15 19:46	0.266
1,200 m Sattion Flurometer	3/4/15 19:47	0.137
1,200 m Sattion Flurometer	3/4/15 19:48	0.263
1,200 m Sattion Flurometer	3/4/15 19:49	-0.242
1,200 m Sattion Flurometer	3/4/15 19:50	0.074
1,200 m Sattion Flurometer	3/4/15 19:51	0.078
1,200 m Sattion Flurometer	3/4/15 19:52	0.097
1,200 m Sattion Flurometer	3/4/15 19:53	-0.12
1,200 m Sattion Flurometer	3/4/15 19:54	0.174
1,200 m Sattion Flurometer	3/4/15 19:55	-0.198
1,200 m Sattion Flurometer	3/4/15 19:56	0.976
1,200 m Sattion Flurometer	3/4/15 19:57	1.253
1,200 m Sattion Flurometer	3/4/15 19:58	0.2
1,200 m Sattion Flurometer	3/4/15 19:59	0.133
1,200 m Sattion Flurometer	3/4/15 20:00	0.979
1,200 m Sattion Flurometer	3/4/15 20:01	0.152
1,200 m Sattion Flurometer	3/4/15 20:02	-0.087
1,200 m Sattion Flurometer	3/4/15 20:03	0.008
1,200 m Sattion Flurometer	3/4/15 20:04	0.163
1,200 m Sattion Flurometer	3/4/15 20:05	0.226
1,200 m Sattion Flurometer	3/4/15 20:06	0.473
1,200 m Sattion Flurometer	3/4/15 20:07	0.617

Location	Date and Time	Rhodmaine Concentration Adjusted Concentration (ppb)
1,200 m Sattion Flurometer	3/4/15 20:08	0.558
1,200 m Sattion Flurometer	3/4/15 20:09	0.322
1,200 m Sattion Flurometer	3/4/15 20:10	0.329
1,200 m Sattion Flurometer	3/4/15 20:11	0.854
1,200 m Sattion Flurometer	3/4/15 20:12	0.266
1,200 m Sattion Flurometer	3/4/15 20:13	0.717
1,200 m Sattion Flurometer	3/4/15 20:14	0.832
1,200 m Sattion Flurometer	3/4/15 20:15	1.142
1,200 m Sattion Flurometer	3/4/15 20:16	1.375
1,200 m Sattion Flurometer	3/4/15 20:17	0.883
1,200 m Sattion Flurometer	3/4/15 20:18	1.264
1,200 m Sattion Flurometer	3/4/15 20:19	1.5
1,200 m Sattion Flurometer	3/4/15 20:20	2.771
1,200 m Sattion Flurometer	3/4/15 20:21	1.53
1,200 m Sattion Flurometer	3/4/15 20:22	1.737
1,200 m Sattion Flurometer	3/4/15 20:23	1.844
1,200 m Sattion Flurometer	3/4/15 20:24	2.121
1,200 m Sattion Flurometer	3/4/15 20:25	2.128
1,200 m Sattion Flurometer	3/4/15 20:26	2.527
1,200 m Sattion Flurometer	3/4/15 20:27	3.248
1,200 m Sattion Flurometer	3/4/15 20:28	3.163
1,200 m Sattion Flurometer	3/4/15 20:29	2.934
1,200 m Sattion Flurometer	3/4/15 20:30	3.307
1,200 m Sattion Flurometer	3/4/15 20:31	4.109
1,200 m Sattion Flurometer	3/4/15 20:32	2.834
1,200 m Sattion Flurometer	3/4/15 20:33	4.057
1,200 m Sattion Flurometer	3/4/15 20:34	3.543
1,200 m Sattion Flurometer	3/4/15 20:35	4.944
1,200 m Sattion Flurometer	3/4/15 20:36	3.806
1,200 m Sattion Flurometer	3/4/15 20:37	4.131
1,200 m Sattion Flurometer	3/4/15 20:38	3.998
1,200 m Sattion Flurometer	3/4/15 20:39	4.508
1,200 m Sattion Flurometer	3/4/15 20:40	4.404
1,200 m Sattion Flurometer	3/4/15 20:41	4.973
1,200 m Sattion Flurometer	3/4/15 20:42	4.674
1,200 m Sattion Flurometer	3/4/15 20:43	5.113
1,200 m Sattion Flurometer	3/4/15 20:44	5.394
1,200 m Sattion Flurometer	3/4/15 20:45	4.822
1,200 m Sattion Flurometer	3/4/15 20:46	4.633
1,200 m Sattion Flurometer	3/4/15 20:47	5.173
1,200 m Sattion Flurometer	3/4/15 20:48	5.627
1,200 m Sattion Flurometer	3/4/15 20:49	6.636
1,200 m Sattion Flurometer	3/4/15 20:50	5.945
1,200 m Sattion Flurometer	3/4/15 20:51	6.019
1,200 m Sattion Flurometer	3/4/15 20:52	6.347
1,200 m Sattion Flurometer	3/4/15 20:53	6.159

Location	Date and Time	Rhodmaine Concentration Adjusted Concentration (ppb)
1,200 m Sattion Flurometer	3/4/15 20:54	7.615
1,200 m Sattion Flurometer	3/4/15 20:55	6.735
1,200 m Sattion Flurometer	3/4/15 20:56	6.684
1,200 m Sattion Flurometer	3/4/15 20:57	6.791
1,200 m Sattion Flurometer	3/4/15 20:58	6.466
1,200 m Sattion Flurometer	3/4/15 20:59	6.624
1,200 m Sattion Flurometer	3/4/15 21:00	6.728
1,200 m Sattion Flurometer	3/4/15 21:01	6.868
1,200 m Sattion Flurometer	3/4/15 21:02	6.676
1,200 m Sattion Flurometer	3/4/15 21:03	7.777
1,200 m Sattion Flurometer	3/4/15 21:04	6.728
1,200 m Sattion Flurometer	3/4/15 21:05	6.979
1,200 m Sattion Flurometer	3/4/15 21:06	6.687
1,200 m Sattion Flurometer	3/4/15 21:07	6.695
1,200 m Sattion Flurometer	3/4/15 21:08	6.621
1,200 m Sattion Flurometer	3/4/15 21:09	6.691
1,200 m Sattion Flurometer	3/4/15 21:10	6.857
1,200 m Sattion Flurometer	3/4/15 21:11	7.06
1,200 m Sattion Flurometer	3/4/15 21:12	6.961
1,200 m Sattion Flurometer	3/4/15 21:13	7.223
1,200 m Sattion Flurometer	3/4/15 21:14	6.868
1,200 m Sattion Flurometer	3/4/15 21:15	7.101
1,200 m Sattion Flurometer	3/4/15 21:16	6.562
1,200 m Sattion Flurometer	3/4/15 21:17	6.95
1,200 m Sattion Flurometer	3/4/15 21:18	5.952
1,200 m Sattion Flurometer	3/4/15 21:19	6.865
1,200 m Sattion Flurometer	3/4/15 21:20	6.669
1,200 m Sattion Flurometer	3/4/15 21:21	6.092
1,200 m Sattion Flurometer	3/4/15 21:22	6.658
1,200 m Sattion Flurometer	3/4/15 21:23	6.639
1,200 m Sattion Flurometer	3/4/15 21:24	6.251
1,200 m Sattion Flurometer	3/4/15 21:25	6.606
1,200 m Sattion Flurometer	3/4/15 21:26	6.351
1,200 m Sattion Flurometer	3/4/15 21:27	6.307
1,200 m Sattion Flurometer	3/4/15 21:28	6.358
1,200 m Sattion Flurometer	3/4/15 21:29	6.111
1,200 m Sattion Flurometer	3/4/15 21:30	6.052
1,200 m Sattion Flurometer	3/4/15 21:31	6.381
1,200 m Sattion Flurometer	3/4/15 21:32	5.974
1,200 m Sattion Flurometer	3/4/15 21:33	5.982
1,200 m Sattion Flurometer	3/4/15 21:34	6.288
1,200 m Sattion Flurometer	3/4/15 21:35	6
1,200 m Sattion Flurometer	3/4/15 21:36	5.993
1,200 m Sattion Flurometer	3/4/15 21:37	5.686
1,200 m Sattion Flurometer	3/4/15 21:38	6.17
1,200 m Sattion Flurometer	3/4/15 21:39	6.044

Location	Date and Time	Rhodmaine Concentration Adjusted Concentration (ppb)
1,200 m Sattion Flurometer	3/4/15 21:40	5.535
1,200 m Sattion Flurometer	3/4/15 21:41	5.727
1,200 m Sattion Flurometer	3/4/15 21:42	5.657
1,200 m Sattion Flurometer	3/4/15 21:43	5.402
1,200 m Sattion Flurometer	3/4/15 21:44	6.222
1,200 m Sattion Flurometer	3/4/15 21:45	5.206
1,200 m Sattion Flurometer	3/4/15 21:46	5.139
1,200 m Sattion Flurometer	3/4/15 21:47	5.405
1,200 m Sattion Flurometer	3/4/15 21:48	4.98
1,200 m Sattion Flurometer	3/4/15 21:49	5.317
1,200 m Sattion Flurometer	3/4/15 21:50	4.984
1,200 m Sattion Flurometer	3/4/15 21:51	5.228
1,200 m Sattion Flurometer	3/4/15 21:52	6.37
1,200 m Sattion Flurometer	3/4/15 21:53	5.054
1,200 m Sattion Flurometer	3/4/15 21:54	5.025
1,200 m Sattion Flurometer	3/4/15 21:55	5.232
1,200 m Sattion Flurometer	3/4/15 21:56	4.87
1,200 m Sattion Flurometer	3/4/15 21:57	4.744
1,200 m Sattion Flurometer	3/4/15 21:58	4.674
1,200 m Sattion Flurometer	3/4/15 21:59	4.836
1,200 m Sattion Flurometer	3/4/15 22:00	5.801
1,200 m Sattion Flurometer	3/4/15 22:01	5.479
1,200 m Sattion Flurometer	3/4/15 22:02	4.907
1,200 m Sattion Flurometer	3/4/15 22:03	4.415
1,200 m Sattion Flurometer	3/4/15 22:04	4.744
1,200 m Sattion Flurometer	3/4/15 22:05	5.734
1,200 m Sattion Flurometer	3/4/15 22:06	4.537
1,200 m Sattion Flurometer	3/4/15 22:07	4.537
1,200 m Sattion Flurometer	3/4/15 22:08	4.519
1,200 m Sattion Flurometer	3/4/15 22:09	5.971
1,200 m Sattion Flurometer	3/4/15 22:10	4.593
1,200 m Sattion Flurometer	3/4/15 22:11	5.043
1,200 m Sattion Flurometer	3/4/15 22:12	4.497
1,200 m Sattion Flurometer	3/4/15 22:13	5.069
1,200 m Sattion Flurometer	3/4/15 22:14	6.536
1,200 m Sattion Flurometer	3/4/15 22:15	5.102
1,200 m Sattion Flurometer	3/4/15 22:16	5.298
1,200 m Sattion Flurometer	3/4/15 22:17	5.387
1,200 m Sattion Flurometer	3/4/15 22:18	5.756
1,200 m Sattion Flurometer	3/4/15 22:19	5.886
1,200 m Sattion Flurometer	3/4/15 22:20	5.778
1,200 m Sattion Flurometer	3/4/15 22:21	5.778
1,200 m Sattion Flurometer	3/4/15 22:22	6.144
1,200 m Sattion Flurometer	3/4/15 22:23	5.908
1,200 m Sattion Flurometer	3/4/15 22:24	6.817
1,200 m Sattion Flurometer	3/4/15 22:25	7.204

Location	Date and Time	Rhodmaine Concentration Adjusted Concentration (ppb)
1,200 m Sattion Flurometer	3/4/15 22:26	6.761
1,200 m Sattion Flurometer	3/4/15 22:27	6.894
1,200 m Sattion Flurometer	3/4/15 22:28	7.389
1,200 m Sattion Flurometer	3/4/15 22:29	7.567
1,200 m Sattion Flurometer	3/4/15 22:30	8.56
1,200 m Sattion Flurometer	3/4/15 22:31	7.94
1,200 m Sattion Flurometer	3/4/15 22:32	8.715
1,200 m Sattion Flurometer	3/4/15 22:33	8.335
1,200 m Sattion Flurometer	3/4/15 22:34	8.723
1,200 m Sattion Flurometer	3/4/15 22:35	9.007
1,200 m Sattion Flurometer	3/4/15 22:36	9.007
1,200 m Sattion Flurometer	3/4/15 22:37	9.066
1,200 m Sattion Flurometer	3/4/15 22:38	10.4
1,200 m Sattion Flurometer	3/4/15 22:39	9.879
1,200 m Sattion Flurometer	3/4/15 22:40	9.861
1,200 m Sattion Flurometer	3/4/15 22:41	10.44
1,200 m Sattion Flurometer	3/4/15 22:42	11.78
1,200 m Sattion Flurometer	3/4/15 22:43	10.83
1,200 m Sattion Flurometer	3/4/15 22:44	10.6
1,200 m Sattion Flurometer	3/4/15 22:45	11.03
1,200 m Sattion Flurometer	3/4/15 22:46	11.92
1,200 m Sattion Flurometer	3/4/15 22:47	11.96
1,200 m Sattion Flurometer	3/4/15 22:48	12.32
1,200 m Sattion Flurometer	3/4/15 22:49	12.69
1,200 m Sattion Flurometer	3/4/15 22:50	12.21
1,200 m Sattion Flurometer	3/4/15 22:51	13.81
1,200 m Sattion Flurometer	3/4/15 22:52	12.47
1,200 m Sattion Flurometer	3/4/15 22:53	12.95
1,200 m Sattion Flurometer	3/4/15 22:54	13.21
1,200 m Sattion Flurometer	3/4/15 22:55	13.46
1,200 m Sattion Flurometer	3/4/15 22:56	13.56
1,200 m Sattion Flurometer	3/4/15 22:57	14.21
1,200 m Sattion Flurometer	3/4/15 22:58	14.86
1,200 m Sattion Flurometer	3/4/15 22:59	13.94
1,200 m Sattion Flurometer	3/4/15 23:00	14.48
1,200 m Sattion Flurometer	3/4/15 23:01	14.31
1,200 m Sattion Flurometer	3/4/15 23:02	14.58
1,200 m Sattion Flurometer	3/4/15 23:03	14.65
1,200 m Sattion Flurometer	3/4/15 23:04	14.73
1,200 m Sattion Flurometer	3/4/15 23:05	15.94
1,200 m Sattion Flurometer	3/4/15 23:06	15.32
1,200 m Sattion Flurometer	3/4/15 23:07	15.71
1,200 m Sattion Flurometer	3/4/15 23:08	15.01
1,200 m Sattion Flurometer	3/4/15 23:09	16.22
1,200 m Sattion Flurometer	3/4/15 23:10	16.69
1,200 m Sattion Flurometer	3/4/15 23:11	15.62

Location	Date and Time	Rhodmaine Concentration Adjusted Concentration (ppb)
1,200 m Sattion Flurometer	3/4/15 23:12	16.06
1,200 m Sattion Flurometer	3/4/15 23:13	15.97
1,200 m Sattion Flurometer	3/4/15 23:14	17.05
1,200 m Sattion Flurometer	3/4/15 23:15	15.87
1,200 m Sattion Flurometer	3/4/15 23:16	16.01
1,200 m Sattion Flurometer	3/4/15 23:17	16.07
1,200 m Sattion Flurometer	3/4/15 23:18	16.3
1,200 m Sattion Flurometer	3/4/15 23:19	15.96
1,200 m Sattion Flurometer	3/4/15 23:20	17.27
1,200 m Sattion Flurometer	3/4/15 23:21	15.88
1,200 m Sattion Flurometer	3/4/15 23:22	16.28
1,200 m Sattion Flurometer	3/4/15 23:23	16.09
1,200 m Sattion Flurometer	3/4/15 23:24	16.27
1,200 m Sattion Flurometer	3/4/15 23:25	16.12
1,200 m Sattion Flurometer	3/4/15 23:26	16.14
1,200 m Sattion Flurometer	3/4/15 23:27	16.33
1,200 m Sattion Flurometer	3/4/15 23:28	16.24
1,200 m Sattion Flurometer	3/4/15 23:29	16.36
1,200 m Sattion Flurometer	3/4/15 23:30	16.18
1,200 m Sattion Flurometer	3/4/15 23:31	16.38
1,200 m Sattion Flurometer	3/4/15 23:32	16.31
1,200 m Sattion Flurometer	3/4/15 23:33	17.09
1,200 m Sattion Flurometer	3/4/15 23:34	16.28
1,200 m Sattion Flurometer	3/4/15 23:35	16.06
1,200 m Sattion Flurometer	3/4/15 23:36	16.06
1,200 m Sattion Flurometer	3/4/15 23:37	16.11
1,200 m Sattion Flurometer	3/4/15 23:38	15.82
1,200 m Sattion Flurometer	3/4/15 23:39	16.09
1,200 m Sattion Flurometer	3/4/15 23:40	15.83
1,200 m Sattion Flurometer	3/4/15 23:41	16.69
1,200 m Sattion Flurometer	3/4/15 23:42	16.1
1,200 m Sattion Flurometer	3/4/15 23:43	15.66
1,200 m Sattion Flurometer	3/4/15 23:44	15.07
1,200 m Sattion Flurometer	3/4/15 23:45	16.75
1,200 m Sattion Flurometer	3/4/15 23:46	15.29
1,200 m Sattion Flurometer	3/4/15 23:47	15.34
1,200 m Sattion Flurometer	3/4/15 23:48	15.27
1,200 m Sattion Flurometer	3/4/15 23:49	14.97
1,200 m Sattion Flurometer	3/4/15 23:50	14.77
1,200 m Sattion Flurometer	3/4/15 23:51	14.73
1,200 m Sattion Flurometer	3/4/15 23:52	16.68
1,200 m Sattion Flurometer	3/4/15 23:53	14.74
1,200 m Sattion Flurometer	3/4/15 23:54	15.13
1,200 m Sattion Flurometer	3/4/15 23:55	14.61
1,200 m Sattion Flurometer	3/4/15 23:56	14.36
1,200 m Sattion Flurometer	3/4/15 23:57	14.57

Location	Date and Time	Rhodmaine Concentration Adjusted Concentration (ppb)
1,200 m Sattion Flurometer	3/4/15 23:58	14.28
1,200 m Sattion Flurometer	3/4/15 23:59	14.29
1,200 m Sattion Flurometer	3/5/15 0:00	14.02
1,200 m Sattion Flurometer	3/5/15 0:01	13.86
1,200 m Sattion Flurometer	3/5/15 0:02	15.32
1,200 m Sattion Flurometer	3/5/15 0:03	14.23
1,200 m Sattion Flurometer	3/5/15 0:04	15.04
1,200 m Sattion Flurometer	3/5/15 0:05	13.95
1,200 m Sattion Flurometer	3/5/15 0:06	13.65
1,200 m Sattion Flurometer	3/5/15 0:07	13.49
1,200 m Sattion Flurometer	3/5/15 0:08	13.19
1,200 m Sattion Flurometer	3/5/15 0:09	13.62
1,200 m Sattion Flurometer	3/5/15 0:10	13.53
1,200 m Sattion Flurometer	3/5/15 0:11	13.62
1,200 m Sattion Flurometer	3/5/15 0:12	15.92
1,200 m Sattion Flurometer	3/5/15 0:13	13.07
1,200 m Sattion Flurometer	3/5/15 0:14	12.92
1,200 m Sattion Flurometer	3/5/15 0:15	12.4
1,200 m Sattion Flurometer	3/5/15 0:16	16.58
1,200 m Sattion Flurometer	3/5/15 0:17	12.73
1,200 m Sattion Flurometer	3/5/15 0:18	12.56
1,200 m Sattion Flurometer	3/5/15 0:19	12.39
1,200 m Sattion Flurometer	3/5/15 0:20	13.33
1,200 m Sattion Flurometer	3/5/15 0:21	12.37
1,200 m Sattion Flurometer	3/5/15 0:22	11.82
1,200 m Sattion Flurometer	3/5/15 0:23	13.19
1,200 m Sattion Flurometer	3/5/15 0:24	11.95
1,200 m Sattion Flurometer	3/5/15 0:25	12.22
1,200 m Sattion Flurometer	3/5/15 0:26	11.61
1,200 m Sattion Flurometer	3/5/15 0:27	11.81
1,200 m Sattion Flurometer	3/5/15 0:28	11.25
1,200 m Sattion Flurometer	3/5/15 0:29	11.31
1,200 m Sattion Flurometer	3/5/15 0:30	11.67
1,200 m Sattion Flurometer	3/5/15 0:31	13.87
1,200 m Sattion Flurometer	3/5/15 0:32	11.93
1,200 m Sattion Flurometer	3/5/15 0:33	13.68
1,200 m Sattion Flurometer	3/5/15 0:34	11.71
1,200 m Sattion Flurometer	3/5/15 0:35	10.24
1,200 m Sattion Flurometer	3/5/15 0:36	11.47
1,200 m Sattion Flurometer	3/5/15 0:37	10.58
1,200 m Sattion Flurometer	3/5/15 0:38	10.72
1,200 m Sattion Flurometer	3/5/15 0:39	10.4
1,200 m Sattion Flurometer	3/5/15 0:40	10.21
1,200 m Sattion Flurometer	3/5/15 0:41	10.13
1,200 m Sattion Flurometer	3/5/15 0:42	10.17
1,200 m Sattion Flurometer	3/5/15 0:43	10.19

Location	Date and Time	Rhodmaine Concentration Adjusted Concentration (ppb)
1,200 m Sattion Flurometer	3/5/15 0:44	10.98
1,200 m Sattion Flurometer	3/5/15 0:45	9.007
1,200 m Sattion Flurometer	3/5/15 0:46	10.31
1,200 m Sattion Flurometer	3/5/15 0:47	9.078
1,200 m Sattion Flurometer	3/5/15 0:48	8.882
1,200 m Sattion Flurometer	3/5/15 0:49	9.011
1,200 m Sattion Flurometer	3/5/15 0:50	8.608
1,200 m Sattion Flurometer	3/5/15 0:51	8.66
1,200 m Sattion Flurometer	3/5/15 0:52	9.731
1,200 m Sattion Flurometer	3/5/15 0:53	8.605
1,200 m Sattion Flurometer	3/5/15 0:54	9.654
1,200 m Sattion Flurometer	3/5/15 0:55	8.339
1,200 m Sattion Flurometer	3/5/15 0:56	8.468
1,200 m Sattion Flurometer	3/5/15 0:57	7.991
1,200 m Sattion Flurometer	3/5/15 0:58	8.276
1,200 m Sattion Flurometer	3/5/15 0:59	8.361
1,200 m Sattion Flurometer	3/5/15 1:00	8.232
1,200 m Sattion Flurometer	3/5/15 1:01	8.132
1,200 m Sattion Flurometer	3/5/15 1:02	7.607
1,200 m Sattion Flurometer	3/5/15 1:03	8.697
1,200 m Sattion Flurometer	3/5/15 1:04	7.729
1,200 m Sattion Flurometer	3/5/15 1:05	7.999
1,200 m Sattion Flurometer	3/5/15 1:06	7.504
1,200 m Sattion Flurometer	3/5/15 1:07	8.254
1,200 m Sattion Flurometer	3/5/15 1:08	8.416
1,200 m Sattion Flurometer	3/5/15 1:09	7.315
1,200 m Sattion Flurometer	3/5/15 1:10	7.171
1,200 m Sattion Flurometer	3/5/15 1:11	7.116
1,200 m Sattion Flurometer	3/5/15 1:12	7.149
1,200 m Sattion Flurometer	3/5/15 1:13	6.961
1,200 m Sattion Flurometer	3/5/15 1:14	6.828
1,200 m Sattion Flurometer	3/5/15 1:15	7.991
1,200 m Sattion Flurometer	3/5/15 1:16	6.82
1,200 m Sattion Flurometer	3/5/15 1:17	6.95
1,200 m Sattion Flurometer	3/5/15 1:18	7.903
1,200 m Sattion Flurometer	3/5/15 1:19	7.393
1,200 m Sattion Flurometer	3/5/15 1:20	6.721
1,200 m Sattion Flurometer	3/5/15 1:21	6.528
1,200 m Sattion Flurometer	3/5/15 1:22	6.495
1,200 m Sattion Flurometer	3/5/15 1:23	6.307
1,200 m Sattion Flurometer	3/5/15 1:24	6.388
1,200 m Sattion Flurometer	3/5/15 1:25	6.447
1,200 m Sattion Flurometer	3/5/15 1:26	7.204
1,200 m Sattion Flurometer	3/5/15 1:27	7.005
1,200 m Sattion Flurometer	3/5/15 1:28	5.908
1,200 m Sattion Flurometer	3/5/15 1:29	6.384

Location	Date and Time	Rhodmaine Concentration Adjusted Concentration (ppb)
1,200 m Sattion Flurometer	3/5/15 1:30	5.967
1,200 m Sattion Flurometer	3/5/15 1:31	5.996
1,200 m Sattion Flurometer	3/5/15 1:32	5.974
1,200 m Sattion Flurometer	3/5/15 1:33	6.118
1,200 m Sattion Flurometer	3/5/15 1:34	5.93
1,200 m Sattion Flurometer	3/5/15 1:35	5.664
1,200 m Sattion Flurometer	3/5/15 1:36	6.673
1,200 m Sattion Flurometer	3/5/15 1:37	5.856
1,200 m Sattion Flurometer	3/5/15 1:38	5.886
1,200 m Sattion Flurometer	3/5/15 1:39	5.793
1,200 m Sattion Flurometer	3/5/15 1:40	5.645
1,200 m Sattion Flurometer	3/5/15 1:41	5.908
1,200 m Sattion Flurometer	3/5/15 1:42	6.602
1,200 m Sattion Flurometer	3/5/15 1:43	5.416
1,200 m Sattion Flurometer	3/5/15 1:44	5.505
1,200 m Sattion Flurometer	3/5/15 1:45	6.569
1,200 m Sattion Flurometer	3/5/15 1:46	6.499
1,200 m Sattion Flurometer	3/5/15 1:47	5.383
1,200 m Sattion Flurometer	3/5/15 1:48	5.627
1,200 m Sattion Flurometer	3/5/15 1:49	5.032
1,200 m Sattion Flurometer	3/5/15 1:50	6.628
1,200 m Sattion Flurometer	3/5/15 1:51	5.235
1,200 m Sattion Flurometer	3/5/15 1:52	6.554
1,200 m Sattion Flurometer	3/5/15 1:53	6.58
1,200 m Sattion Flurometer	3/5/15 1:54	5.128
1,200 m Sattion Flurometer	3/5/15 1:55	5.125
1,200 m Sattion Flurometer	3/5/15 1:56	5.287
1,200 m Sattion Flurometer	3/5/15 1:57	5.427
1,200 m Sattion Flurometer	3/5/15 1:58	6.281
1,200 m Sattion Flurometer	3/5/15 1:59	5.298
1,200 m Sattion Flurometer	3/5/15 2:00	5.52
1,200 m Sattion Flurometer	3/5/15 2:01	5.498
1,200 m Sattion Flurometer	3/5/15 2:02	5.029
1,200 m Sattion Flurometer	3/5/15 2:03	5.335
1,200 m Sattion Flurometer	3/5/15 2:04	4.803
1,200 m Sattion Flurometer	3/5/15 2:05	6.096
1,200 m Sattion Flurometer	3/5/15 2:06	5.435
1,200 m Sattion Flurometer	3/5/15 2:07	6.362
1,200 m Sattion Flurometer	3/5/15 2:08	5.102
1,200 m Sattion Flurometer	3/5/15 2:09	5.431
1,200 m Sattion Flurometer	3/5/15 2:10	4.992
1,200 m Sattion Flurometer	3/5/15 2:11	5.125
1,200 m Sattion Flurometer	3/5/15 2:12	5.354
1,200 m Sattion Flurometer	3/5/15 2:13	6.137
1,200 m Sattion Flurometer	3/5/15 2:14	5.309
1,200 m Sattion Flurometer	3/5/15 2:15	5.213

Location	Date and Time	Rhodmaine Concentration Adjusted Concentration (ppb)
1,200 m Sattion Flurometer	3/5/15 2:16	5.254
1,200 m Sattion Flurometer	3/5/15 2:17	5.25
1,200 m Sattion Flurometer	3/5/15 2:18	4.918
1,200 m Sattion Flurometer	3/5/15 2:19	5.464
1,200 m Sattion Flurometer	3/5/15 2:20	5.143
1,200 m Sattion Flurometer	3/5/15 2:21	5.099
1,200 m Sattion Flurometer	3/5/15 2:22	4.884
1,200 m Sattion Flurometer	3/5/15 2:23	5.457
1,200 m Sattion Flurometer	3/5/15 2:24	5.043
1,200 m Sattion Flurometer	3/5/15 2:25	6.237
1,200 m Sattion Flurometer	3/5/15 2:26	5.165
1,200 m Sattion Flurometer	3/5/15 2:27	5.11
1,200 m Sattion Flurometer	3/5/15 2:28	5.317
1,200 m Sattion Flurometer	3/5/15 2:29	4.814
1,200 m Sattion Flurometer	3/5/15 2:30	5.136
1,200 m Sattion Flurometer	3/5/15 2:31	5.217
1,200 m Sattion Flurometer	3/5/15 2:32	5.642
1,200 m Sattion Flurometer	3/5/15 2:33	4.774
1,200 m Sattion Flurometer	3/5/15 2:34	4.929
1,200 m Sattion Flurometer	3/5/15 2:35	5.572
1,200 m Sattion Flurometer	3/5/15 2:36	4.951
1,200 m Sattion Flurometer	3/5/15 2:37	5.446
1,200 m Sattion Flurometer	3/5/15 2:38	5.158
1,200 m Sattion Flurometer	3/5/15 2:39	5.15
1,200 m Sattion Flurometer	3/5/15 2:40	5.535
1,200 m Sattion Flurometer	3/5/15 2:41	4.984
1,200 m Sattion Flurometer	3/5/15 2:42	5.302
1,200 m Sattion Flurometer	3/5/15 2:43	5.287
1,200 m Sattion Flurometer	3/5/15 2:44	4.977
1,200 m Sattion Flurometer	3/5/15 2:45	6.244
1,200 m Sattion Flurometer	3/5/15 2:46	6.081
1,200 m Sattion Flurometer	3/5/15 2:47	5.531
1,200 m Sattion Flurometer	3/5/15 2:48	5.243
1,200 m Sattion Flurometer	3/5/15 2:49	5.427
1,200 m Sattion Flurometer	3/5/15 2:50	5.176
1,200 m Sattion Flurometer	3/5/15 2:51	5.239
1,200 m Sattion Flurometer	3/5/15 2:52	6.31
1,200 m Sattion Flurometer	3/5/15 2:53	5.258
1,200 m Sattion Flurometer	3/5/15 2:54	6.288
1,200 m Sattion Flurometer	3/5/15 2:55	5.128
1,200 m Sattion Flurometer	3/5/15 2:56	4.881
1,200 m Sattion Flurometer	3/5/15 2:57	5.195
1,200 m Sattion Flurometer	3/5/15 2:58	5.239
1,200 m Sattion Flurometer	3/5/15 2:59	5.195
1,200 m Sattion Flurometer	3/5/15 3:00	5.184
1,200 m Sattion Flurometer	3/5/15 3:01	5.165

Location	Date and Time	Rhodmaine Concentration Adjusted Concentration (ppb)
1,200 m Sattion Flurometer	3/5/15 3:02	5.088
1,200 m Sattion Flurometer	3/5/15 3:03	6.27
1,200 m Sattion Flurometer	3/5/15 3:04	4.999
1,200 m Sattion Flurometer	3/5/15 3:05	5.287
1,200 m Sattion Flurometer	3/5/15 3:06	5.021
1,200 m Sattion Flurometer	3/5/15 3:07	5.117
1,200 m Sattion Flurometer	3/5/15 3:08	5.121
1,200 m Sattion Flurometer	3/5/15 3:09	4.903
1,200 m Sattion Flurometer	3/5/15 3:10	5.368
1,200 m Sattion Flurometer	3/5/15 3:11	5.335
1,200 m Sattion Flurometer	3/5/15 3:12	5.258
1,200 m Sattion Flurometer	3/5/15 3:13	4.77
1,200 m Sattion Flurometer	3/5/15 3:14	5.121
1,200 m Sattion Flurometer	3/5/15 3:15	5.276
1,200 m Sattion Flurometer	3/5/15 3:16	5.671
1,200 m Sattion Flurometer	3/5/15 3:17	4.921
1,200 m Sattion Flurometer	3/5/15 3:18	5.235
1,200 m Sattion Flurometer	3/5/15 3:19	5.221
1,200 m Sattion Flurometer	3/5/15 3:20	5.306
1,200 m Sattion Flurometer	3/5/15 3:21	5.154
1,200 m Sattion Flurometer	3/5/15 3:22	5.335
1,200 m Sattion Flurometer	3/5/15 3:23	5.154
1,200 m Sattion Flurometer	3/5/15 3:24	5.394
1,200 m Sattion Flurometer	3/5/15 3:25	6.362
1,200 m Sattion Flurometer	3/5/15 3:26	5.25
1,200 m Sattion Flurometer	3/5/15 3:27	5.206
1,200 m Sattion Flurometer	3/5/15 3:28	5.254
1,200 m Sattion Flurometer	3/5/15 3:29	5.187
1,200 m Sattion Flurometer	3/5/15 3:30	5.125
1,200 m Sattion Flurometer	3/5/15 3:31	6.288
1,200 m Sattion Flurometer	3/5/15 3:32	5.176
1,200 m Sattion Flurometer	3/5/15 3:33	5.616
1,200 m Sattion Flurometer	3/5/15 3:34	5.354
1,200 m Sattion Flurometer	3/5/15 3:35	5.494
1,200 m Sattion Flurometer	3/5/15 3:36	4.921
1,200 m Sattion Flurometer	3/5/15 3:37	5.265
1,200 m Sattion Flurometer	3/5/15 3:38	5.176
1,200 m Sattion Flurometer	3/5/15 3:39	6.181
1,200 m Sattion Flurometer	3/5/15 3:40	5.512
1,200 m Sattion Flurometer	3/5/15 3:41	5.069
1,200 m Sattion Flurometer	3/5/15 3:42	4.995
1,200 m Sattion Flurometer	3/5/15 3:43	5.136
1,200 m Sattion Flurometer	3/5/15 3:44	4.98
1,200 m Sattion Flurometer	3/5/15 3:45	5.213
1,200 m Sattion Flurometer	3/5/15 3:46	5.162
1,200 m Sattion Flurometer	3/5/15 3:47	5.062

Location	Date and Time	Rhodmaine Concentration Adjusted Concentration (ppb)
1,200 m Sattion Flurometer	3/5/15 3:48	6.129
1,200 m Sattion Flurometer	3/5/15 3:49	5.091
1,200 m Sattion Flurometer	3/5/15 3:50	5.017
1,200 m Sattion Flurometer	3/5/15 3:51	5.239
1,200 m Sattion Flurometer	3/5/15 3:52	4.914
1,200 m Sattion Flurometer	3/5/15 3:53	4.951
1,200 m Sattion Flurometer	3/5/15 3:54	4.792
1,200 m Sattion Flurometer	3/5/15 3:55	5.52
1,200 m Sattion Flurometer	3/5/15 3:56	4.955
1,200 m Sattion Flurometer	3/5/15 3:57	5.043
1,200 m Sattion Flurometer	3/5/15 3:58	4.94
1,200 m Sattion Flurometer	3/5/15 3:59	5.989
1,200 m Sattion Flurometer	3/5/15 4:00	5.017
1,200 m Sattion Flurometer	3/5/15 4:01	5.213
1,200 m Sattion Flurometer	3/5/15 4:02	5.014
1,200 m Sattion Flurometer	3/5/15 4:03	5.948
1,200 m Sattion Flurometer	3/5/15 4:04	4.881
1,200 m Sattion Flurometer	3/5/15 4:05	4.932
1,200 m Sattion Flurometer	3/5/15 4:06	5.014
1,200 m Sattion Flurometer	3/5/15 4:07	4.98
1,200 m Sattion Flurometer	3/5/15 4:08	4.977
1,200 m Sattion Flurometer	3/5/15 4:09	5.106
1,200 m Sattion Flurometer	3/5/15 4:10	4.955
1,200 m Sattion Flurometer	3/5/15 4:11	4.785
1,200 m Sattion Flurometer	3/5/15 4:12	5.069
1,200 m Sattion Flurometer	3/5/15 4:13	4.94
1,200 m Sattion Flurometer	3/5/15 4:14	5.915
1,200 m Sattion Flurometer	3/5/15 4:15	6.011
1,200 m Sattion Flurometer	3/5/15 4:16	4.833
1,200 m Sattion Flurometer	3/5/15 4:17	4.777
1,200 m Sattion Flurometer	3/5/15 4:18	4.892
1,200 m Sattion Flurometer	3/5/15 4:19	4.836
1,200 m Sattion Flurometer	3/5/15 4:20	4.733
1,200 m Sattion Flurometer	3/5/15 4:21	4.711
1,200 m Sattion Flurometer	3/5/15 4:22	4.792
1,200 m Sattion Flurometer	3/5/15 4:23	4.718
1,200 m Sattion Flurometer	3/5/15 4:24	4.596
1,200 m Sattion Flurometer	3/5/15 4:25	4.585
1,200 m Sattion Flurometer	3/5/15 4:26	4.589
1,200 m Sattion Flurometer	3/5/15 4:27	4.559
1,200 m Sattion Flurometer	3/5/15 4:28	4.988
1,200 m Sattion Flurometer	3/5/15 4:29	4.884
1,200 m Sattion Flurometer	3/5/15 4:30	4.729
1,200 m Sattion Flurometer	3/5/15 4:31	4.282
1,200 m Sattion Flurometer	3/5/15 4:32	4.493
1,200 m Sattion Flurometer	3/5/15 4:33	4.511

Location	Date and Time	Rhodmaine Concentration Adjusted Concentration (ppb)
1,200 m Sattion Flurometer	3/5/15 4:34	5.797
1,200 m Sattion Flurometer	3/5/15 4:35	4.526
1,200 m Sattion Flurometer	3/5/15 4:36	5.671
1,200 m Sattion Flurometer	3/5/15 4:37	4.201
1,200 m Sattion Flurometer	3/5/15 4:38	4.615
1,200 m Sattion Flurometer	3/5/15 4:39	4.493
1,200 m Sattion Flurometer	3/5/15 4:40	4.478
1,200 m Sattion Flurometer	3/5/15 4:41	4.515
1,200 m Sattion Flurometer	3/5/15 4:42	5.391
1,200 m Sattion Flurometer	3/5/15 4:43	4.596
1,200 m Sattion Flurometer	3/5/15 4:44	5.427
1,200 m Sattion Flurometer	3/5/15 4:45	4.467
1,200 m Sattion Flurometer	3/5/15 4:46	4.714
1,200 m Sattion Flurometer	3/5/15 4:47	4.448
1,200 m Sattion Flurometer	3/5/15 4:48	4.607
1,200 m Sattion Flurometer	3/5/15 4:49	4.371
1,200 m Sattion Flurometer	3/5/15 4:50	4.319
1,200 m Sattion Flurometer	3/5/15 4:51	4.63
1,200 m Sattion Flurometer	3/5/15 4:52	4.315
1,200 m Sattion Flurometer	3/5/15 4:53	4.386
1,200 m Sattion Flurometer	3/5/15 4:54	4.482
1,200 m Sattion Flurometer	3/5/15 4:55	4.415
1,200 m Sattion Flurometer	3/5/15 4:56	4.423
1,200 m Sattion Flurometer	3/5/15 4:57	4.389
1,200 m Sattion Flurometer	3/5/15 4:58	4.36
1,200 m Sattion Flurometer	3/5/15 4:59	4.637
1,200 m Sattion Flurometer	3/5/15 5:00	4.452
1,200 m Sattion Flurometer	3/5/15 5:01	4.426
1,200 m Sattion Flurometer	3/5/15 5:02	5.18
1,200 m Sattion Flurometer	3/5/15 5:03	4.253
1,200 m Sattion Flurometer	3/5/15 5:04	5.56
1,200 m Sattion Flurometer	3/5/15 5:05	4.179
1,200 m Sattion Flurometer	3/5/15 5:06	5.147
1,200 m Sattion Flurometer	3/5/15 5:07	4.112
1,200 m Sattion Flurometer	3/5/15 5:08	4.471
1,200 m Sattion Flurometer	3/5/15 5:09	4.264
1,200 m Sattion Flurometer	3/5/15 5:10	3.691
1,200 m Sattion Flurometer	3/5/15 5:11	3.88
1,200 m Sattion Flurometer	3/5/15 5:12	4.079
1,200 m Sattion Flurometer	3/5/15 5:13	4.168
1,200 m Sattion Flurometer	3/5/15 5:14	4.168
1,200 m Sattion Flurometer	3/5/15 5:15	5.191
1,200 m Sattion Flurometer	3/5/15 5:16	4.12
1,200 m Sattion Flurometer	3/5/15 5:17	3.88
1,200 m Sattion Flurometer	3/5/15 5:18	4.267
1,200 m Sattion Flurometer	3/5/15 5:19	3.983

Location	Date and Time	Rhodmaine Concentration Adjusted Concentration (ppb)
1,200 m Sattion Flurometer	3/5/15 5:20	3.998
1,200 m Sattion Flurometer	3/5/15 5:21	4.027
1,200 m Sattion Flurometer	3/5/15 5:22	4.146
1,200 m Sattion Flurometer	3/5/15 5:23	3.983
1,200 m Sattion Flurometer	3/5/15 5:24	4.072
1,200 m Sattion Flurometer	3/5/15 5:25	3.983
1,200 m Sattion Flurometer	3/5/15 5:26	3.961
1,200 m Sattion Flurometer	3/5/15 5:27	3.754
1,200 m Sattion Flurometer	3/5/15 5:28	5.051
1,200 m Sattion Flurometer	3/5/15 5:29	4.87
1,200 m Sattion Flurometer	3/5/15 5:30	3.902
1,200 m Sattion Flurometer	3/5/15 5:31	3.946
1,200 m Sattion Flurometer	3/5/15 5:32	4.349
1,200 m Sattion Flurometer	3/5/15 5:33	3.887
1,200 m Sattion Flurometer	3/5/15 5:34	3.935
1,200 m Sattion Flurometer	3/5/15 5:35	3.536
1,200 m Sattion Flurometer	3/5/15 5:36	3.761
1,200 m Sattion Flurometer	3/5/15 5:37	3.591
1,200 m Sattion Flurometer	3/5/15 5:38	4.652
1,200 m Sattion Flurometer	3/5/15 5:39	3.772
1,200 m Sattion Flurometer	3/5/15 5:40	4.707
1,200 m Sattion Flurometer	3/5/15 5:41	3.75
1,200 m Sattion Flurometer	3/5/15 5:42	4.622
1,200 m Sattion Flurometer	3/5/15 5:43	3.676
1,200 m Sattion Flurometer	3/5/15 5:44	3.965
1,200 m Sattion Flurometer	3/5/15 5:45	4.086
1,200 m Sattion Flurometer	3/5/15 5:46	4.596
1,200 m Sattion Flurometer	3/5/15 5:47	3.931
1,200 m Sattion Flurometer	3/5/15 5:48	3.917
1,200 m Sattion Flurometer	3/5/15 5:49	3.458
1,200 m Sattion Flurometer	3/5/15 5:50	3.61
1,200 m Sattion Flurometer	3/5/15 5:51	3.602
1,200 m Sattion Flurometer	3/5/15 5:52	3.894
1,200 m Sattion Flurometer	3/5/15 5:53	3.499
1,200 m Sattion Flurometer	3/5/15 5:54	3.658
1,200 m Sattion Flurometer	3/5/15 5:55	4.474
1,200 m Sattion Flurometer	3/5/15 5:56	3.54
1,200 m Sattion Flurometer	3/5/15 5:57	3.133
1,200 m Sattion Flurometer	3/5/15 5:58	3.599
1,200 m Sattion Flurometer	3/5/15 5:59	3.58
1,200 m Sattion Flurometer	3/5/15 6:00	3.529
1,200 m Sattion Flurometer	3/5/15 6:01	3.17
1,200 m Sattion Flurometer	3/5/15 6:02	3.532
1,200 m Sattion Flurometer	3/5/15 6:03	3.503
1,200 m Sattion Flurometer	3/5/15 6:04	3.606
1,200 m Sattion Flurometer	3/5/15 6:05	2.993

Location	Date and Time	Rhodmaine Concentration Adjusted Concentration (ppb)
1,200 m Sattion Flurometer	3/5/15 6:06	3.226
1,200 m Sattion Flurometer	3/5/15 6:07	3.732
1,200 m Sattion Flurometer	3/5/15 6:08	4.763
1,200 m Sattion Flurometer	3/5/15 6:09	3.2
1,200 m Sattion Flurometer	3/5/15 6:10	3.418
1,200 m Sattion Flurometer	3/5/15 6:11	3.333
1,200 m Sattion Flurometer	3/5/15 6:12	3.181
1,200 m Sattion Flurometer	3/5/15 6:13	3.44
1,200 m Sattion Flurometer	3/5/15 6:14	4.157
1,200 m Sattion Flurometer	3/5/15 6:15	3.255
1,200 m Sattion Flurometer	3/5/15 6:16	3.318
1,200 m Sattion Flurometer	3/5/15 6:17	3.602
1,200 m Sattion Flurometer	3/5/15 6:18	3.089
1,200 m Sattion Flurometer	3/5/15 6:19	3.185
1,200 m Sattion Flurometer	3/5/15 6:20	3.115
1,200 m Sattion Flurometer	3/5/15 6:21	3.425
1,200 m Sattion Flurometer	3/5/15 6:22	3.518
1,200 m Sattion Flurometer	3/5/15 6:23	3.056
1,200 m Sattion Flurometer	3/5/15 6:24	3.233
1,200 m Sattion Flurometer	3/5/15 6:25	3.115
1,200 m Sattion Flurometer	3/5/15 6:26	2.963
1,200 m Sattion Flurometer	3/5/15 6:27	4.057
1,200 m Sattion Flurometer	3/5/15 6:28	3.192
1,200 m Sattion Flurometer	3/5/15 6:29	2.827
1,200 m Sattion Flurometer	3/5/15 6:30	4.16
1,200 m Sattion Flurometer	3/5/15 6:31	2.771
1,200 m Sattion Flurometer	3/5/15 6:32	3.022
1,200 m Sattion Flurometer	3/5/15 6:33	3.126
1,200 m Sattion Flurometer	3/5/15 6:34	2.882
1,200 m Sattion Flurometer	3/5/15 6:35	3.252
1,200 m Sattion Flurometer	3/5/15 6:36	4.075
1,200 m Sattion Flurometer	3/5/15 6:37	3.296
1,200 m Sattion Flurometer	3/5/15 6:38	3.019
1,200 m Sattion Flurometer	3/5/15 6:39	4.19
1,200 m Sattion Flurometer	3/5/15 6:40	2.93
1,200 m Sattion Flurometer	3/5/15 6:41	3.174
1,200 m Sattion Flurometer	3/5/15 6:42	3.566
1,200 m Sattion Flurometer	3/5/15 6:43	3.03
1,200 m Sattion Flurometer	3/5/15 6:44	2.753
1,200 m Sattion Flurometer	3/5/15 6:45	2.889
1,200 m Sattion Flurometer	3/5/15 6:46	2.967
1,200 m Sattion Flurometer	3/5/15 6:47	3.133
1,200 m Sattion Flurometer	3/5/15 6:48	3.026
1,200 m Sattion Flurometer	3/5/15 6:49	2.723
1,200 m Sattion Flurometer	3/5/15 6:50	2.635
1,200 m Sattion Flurometer	3/5/15 6:51	2.779

Location	Date and Time	Rhodmaine Concentration Adjusted Concentration (ppb)
1,200 m Sattion Flurometer	3/5/15 6:52	2.635
1,200 m Sattion Flurometer	3/5/15 6:53	2.749
1,200 m Sattion Flurometer	3/5/15 6:54	2.997
1,200 m Sattion Flurometer	3/5/15 6:55	2.997
1,200 m Sattion Flurometer	3/5/15 6:56	2.683
1,200 m Sattion Flurometer	3/5/15 6:57	2.705
1,200 m Sattion Flurometer	3/5/15 6:58	2.823
1,200 m Sattion Flurometer	3/5/15 6:59	2.812
1,200 m Sattion Flurometer	3/5/15 7:00	2.893
1,200 m Sattion Flurometer	3/5/15 7:01	3.787
1,200 m Sattion Flurometer	3/5/15 7:02	2.557
1,200 m Sattion Flurometer	3/5/15 7:03	2.853
1,200 m Sattion Flurometer	3/5/15 7:04	2.546
1,200 m Sattion Flurometer	3/5/15 7:05	2.723
1,200 m Sattion Flurometer	3/5/15 7:06	2.723
1,200 m Sattion Flurometer	3/5/15 7:07	2.768
1,200 m Sattion Flurometer	3/5/15 7:08	2.793
1,200 m Sattion Flurometer	3/5/15 7:09	2.967
1,200 m Sattion Flurometer	3/5/15 7:10	2.816
1,200 m Sattion Flurometer	3/5/15 7:11	2.531
1,200 m Sattion Flurometer	3/5/15 7:12	2.775
1,200 m Sattion Flurometer	3/5/15 7:13	3.795
1,200 m Sattion Flurometer	3/5/15 7:14	2.668
1,200 m Sattion Flurometer	3/5/15 7:15	2.716
1,200 m Sattion Flurometer	3/5/15 7:16	2.745
1,200 m Sattion Flurometer	3/5/15 7:17	2.224
1,200 m Sattion Flurometer	3/5/15 7:18	2.756
1,200 m Sattion Flurometer	3/5/15 7:19	2.45
1,200 m Sattion Flurometer	3/5/15 7:20	2.86
1,200 m Sattion Flurometer	3/5/15 7:21	2.72
1,200 m Sattion Flurometer	3/5/15 7:22	2.668
1,200 m Sattion Flurometer	3/5/15 7:23	2.413
1,200 m Sattion Flurometer	3/5/15 7:24	2.45
1,200 m Sattion Flurometer	3/5/15 7:25	2.465
1,200 m Sattion Flurometer	3/5/15 7:26	2.398
1,200 m Sattion Flurometer	3/5/15 7:27	3.359
1,200 m Sattion Flurometer	3/5/15 7:28	2.79
1,200 m Sattion Flurometer	3/5/15 7:29	3.44
1,200 m Sattion Flurometer	3/5/15 7:30	2.306
1,200 m Sattion Flurometer	3/5/15 7:31	2.779
1,200 m Sattion Flurometer	3/5/15 7:32	2.413
1,200 m Sattion Flurometer	3/5/15 7:33	2.738
1,200 m Sattion Flurometer	3/5/15 7:34	4.005
1,200 m Sattion Flurometer	3/5/15 7:35	3.843
1,200 m Sattion Flurometer	3/5/15 7:36	2.731
1,200 m Sattion Flurometer	3/5/15 7:37	3.894

Location	Date and Time	Rhodmaine Concentration Adjusted Concentration (ppb)
1,200 m Sattion Flurometer	3/5/15 7:38	2.646
1,200 m Sattion Flurometer	3/5/15 7:39	2.298
1,200 m Sattion Flurometer	3/5/15 7:40	2.454
1,200 m Sattion Flurometer	3/5/15 7:41	2.59
1,200 m Sattion Flurometer	3/5/15 7:42	2.723
1,200 m Sattion Flurometer	3/5/15 7:43	2.609
1,200 m Sattion Flurometer	3/5/15 7:44	2.494
1,200 m Sattion Flurometer	3/5/15 7:45	3.639
1,200 m Sattion Flurometer	3/5/15 7:46	2.413
1,200 m Sattion Flurometer	3/5/15 7:47	2.723
1,200 m Sattion Flurometer	3/5/15 7:48	1.947
1,200 m Sattion Flurometer	3/5/15 7:49	2.461
1,200 m Sattion Flurometer	3/5/15 7:50	3.665
1,200 m Sattion Flurometer	3/5/15 7:51	2.816
1,200 m Sattion Flurometer	3/5/15 7:52	2.579
1,200 m Sattion Flurometer	3/5/15 7:53	2.317
1,200 m Sattion Flurometer	3/5/15 7:54	2.114
1,200 m Sattion Flurometer	3/5/15 7:55	2.531
1,200 m Sattion Flurometer	3/5/15 7:56	2.535
1,200 m Sattion Flurometer	3/5/15 7:57	2.498
1,200 m Sattion Flurometer	3/5/15 7:58	2.465
1,200 m Sattion Flurometer	3/5/15 7:59	3.928
1,200 m Sattion Flurometer	3/5/15 8:00	3.093
1,200 m Sattion Flurometer	3/5/15 8:01	2.516
1,200 m Sattion Flurometer	3/5/15 8:02	2.114
1,200 m Sattion Flurometer	3/5/15 8:03	2.424
1,200 m Sattion Flurometer	3/5/15 8:04	2.114
1,200 m Sattion Flurometer	3/5/15 8:05	2.11
1,200 m Sattion Flurometer	3/5/15 8:06	1.888
1,200 m Sattion Flurometer	3/5/15 8:07	2.158
1,200 m Sattion Flurometer	3/5/15 8:08	2.003
1,200 m Sattion Flurometer	3/5/15 8:09	2.062
1,200 m Sattion Flurometer	3/5/15 8:10	2.169
1,200 m Sattion Flurometer	3/5/15 8:11	3.019
1,200 m Sattion Flurometer	3/5/15 8:12	2.176
1,200 m Sattion Flurometer	3/5/15 8:13	1.822
1,200 m Sattion Flurometer	3/5/15 8:14	2.439
1,200 m Sattion Flurometer	3/5/15 8:15	2.066
1,200 m Sattion Flurometer	3/5/15 8:16	2.066
1,200 m Sattion Flurometer	3/5/15 8:17	2.069
1,200 m Sattion Flurometer	3/5/15 8:18	2.062
1,200 m Sattion Flurometer	3/5/15 8:19	1.999
1,200 m Sattion Flurometer	3/5/15 8:20	1.733
1,200 m Sattion Flurometer	3/5/15 8:21	2.284
1,200 m Sattion Flurometer	3/5/15 8:22	2.088
1,200 m Sattion Flurometer	3/5/15 8:23	1.8

Location	Date and Time	Rhodmaine Concentration Adjusted Concentration (ppb)
1,200 m Sattion Flurometer	3/5/15 8:24	1.984
1,200 m Sattion Flurometer	3/5/15 8:25	2.945
1,200 m Sattion Flurometer	3/5/15 8:26	1.825
1,200 m Sattion Flurometer	3/5/15 8:27	2.014
1,200 m Sattion Flurometer	3/5/15 8:28	1.91
1,200 m Sattion Flurometer	3/5/15 8:29	3.026
1,200 m Sattion Flurometer	3/5/15 8:30	2.088
1,200 m Sattion Flurometer	3/5/15 8:31	1.855
1,200 m Sattion Flurometer	3/5/15 8:32	2.457
1,200 m Sattion Flurometer	3/5/15 8:33	1.981
1,200 m Sattion Flurometer	3/5/15 8:34	1.936
1,200 m Sattion Flurometer	3/5/15 8:35	1.94
1,200 m Sattion Flurometer	3/5/15 8:36	2.04
1,200 m Sattion Flurometer	3/5/15 8:37	1.648
1,200 m Sattion Flurometer	3/5/15 8:38	2.121
1,200 m Sattion Flurometer	3/5/15 8:39	1.984
1,200 m Sattion Flurometer	3/5/15 8:40	1.323
1,200 m Sattion Flurometer	3/5/15 8:41	2.568
1,200 m Sattion Flurometer	3/5/15 8:42	1.567
1,200 m Sattion Flurometer	3/5/15 8:43	1.829
1,200 m Sattion Flurometer	3/5/15 8:44	2.671
1,200 m Sattion Flurometer	3/5/15 8:45	1.519
1,200 m Sattion Flurometer	3/5/15 8:46	1.637
1,200 m Sattion Flurometer	3/5/15 8:47	2.679
1,200 m Sattion Flurometer	3/5/15 8:48	1.888
1,200 m Sattion Flurometer	3/5/15 8:49	1.678
1,200 m Sattion Flurometer	3/5/15 8:50	1.962
1,200 m Sattion Flurometer	3/5/15 8:51	1.744
1,200 m Sattion Flurometer	3/5/15 8:52	1.77
1,200 m Sattion Flurometer	3/5/15 8:53	1.885
1,200 m Sattion Flurometer	3/5/15 8:54	1.885
1,200 m Sattion Flurometer	3/5/15 8:55	1.829
1,200 m Sattion Flurometer	3/5/15 8:56	1.777
1,200 m Sattion Flurometer	3/5/15 8:57	1.678
1,200 m Sattion Flurometer	3/5/15 8:58	3.004
1,200 m Sattion Flurometer	3/5/15 8:59	1.209
1,200 m Sattion Flurometer	3/5/15 9:00	1.585
1,200 m Sattion Flurometer	3/5/15 9:01	2.564
1,200 m Sattion Flurometer	3/5/15 9:02	1.859
1,200 m Sattion Flurometer	3/5/15 9:03	1.486
1,200 m Sattion Flurometer	3/5/15 9:04	1.781
1,200 m Sattion Flurometer	3/5/15 9:05	1.763
1,200 m Sattion Flurometer	3/5/15 9:06	1.733
1,200 m Sattion Flurometer	3/5/15 9:07	1.692
1,200 m Sattion Flurometer	3/5/15 9:08	1.364
1,200 m Sattion Flurometer	3/5/15 9:09	1.523

Location	Date and Time	Rhodmaine Concentration Adjusted Concentration (ppb)
1,200 m Sattion Flurometer	3/5/15 9:10	1.755
1,200 m Sattion Flurometer	3/5/15 9:11	1.504
1,200 m Sattion Flurometer	3/5/15 9:12	2.594
1,200 m Sattion Flurometer	3/5/15 9:13	1.766
1,200 m Sattion Flurometer	3/5/15 9:14	1.622
1,200 m Sattion Flurometer	3/5/15 9:15	1.323
1,200 m Sattion Flurometer	3/5/15 9:16	1.09
1,200 m Sattion Flurometer	3/5/15 9:17	1.796
1,200 m Sattion Flurometer	3/5/15 9:18	1.467
1,200 m Sattion Flurometer	3/5/15 9:19	2.066
1,200 m Sattion Flurometer	3/5/15 9:20	1.704
1,200 m Sattion Flurometer	3/5/15 9:21	1.19
1,200 m Sattion Flurometer	3/5/15 9:22	2.731
1,200 m Sattion Flurometer	3/5/15 9:23	1.345
1,200 m Sattion Flurometer	3/5/15 9:24	1.611
1,200 m Sattion Flurometer	3/5/15 9:25	1.364
1,200 m Sattion Flurometer	3/5/15 9:26	2.498
1,200 m Sattion Flurometer	3/5/15 9:27	1.818
1,200 m Sattion Flurometer	3/5/15 9:28	2.21
1,200 m Sattion Flurometer	3/5/15 9:29	1.641
1,200 m Sattion Flurometer	3/5/15 9:30	1.548
1,200 m Sattion Flurometer	3/5/15 9:31	1.227
1,200 m Sattion Flurometer	3/5/15 9:32	1.692
1,200 m Sattion Flurometer	3/5/15 9:33	1.523
1,200 m Sattion Flurometer	3/5/15 9:34	1.305
1,200 m Sattion Flurometer	3/5/15 9:35	1.364
1,200 m Sattion Flurometer	3/5/15 9:36	1.563
1,200 m Sattion Flurometer	3/5/15 9:37	1.452
1,200 m Sattion Flurometer	3/5/15 9:38	1.205
1,200 m Sattion Flurometer	3/5/15 9:39	1.681
1,200 m Sattion Flurometer	3/5/15 9:40	1.644
1,200 m Sattion Flurometer	3/5/15 9:41	1.526
1,200 m Sattion Flurometer	3/5/15 9:42	1.415
1,200 m Sattion Flurometer	3/5/15 9:43	1.386
1,200 m Sattion Flurometer	3/5/15 9:44	1.467
1,200 m Sattion Flurometer	3/5/15 9:45	1.5
1,200 m Sattion Flurometer	3/5/15 9:46	1.257
1,200 m Sattion Flurometer	3/5/15 9:47	1.353
1,200 m Sattion Flurometer	3/5/15 9:48	1.334
1,200 m Sattion Flurometer	3/5/15 9:49	1.039
1,200 m Sattion Flurometer	3/5/15 9:50	1.877
1,200 m Sattion Flurometer	3/5/15 9:51	1.415
1,200 m Sattion Flurometer	3/5/15 9:52	0.946
1,200 m Sattion Flurometer	3/5/15 9:53	1.404
1,200 m Sattion Flurometer	3/5/15 9:54	1.489
1,200 m Sattion Flurometer	3/5/15 9:55	1.231

Location	Date and Time	Rhodmaine Concentration Adjusted Concentration (ppb)
1,200 m Sattion Flurometer	3/5/15 9:56	1.131
1,200 m Sattion Flurometer	3/5/15 9:57	1.696
1,200 m Sattion Flurometer	3/5/15 9:58	1.475
1,200 m Sattion Flurometer	3/5/15 9:59	0.909
1,200 m Sattion Flurometer	3/5/15 10:00	1.172
1,200 m Sattion Flurometer	3/5/15 10:01	1.234
1,200 m Sattion Flurometer	3/5/15 10:02	1.482
1,200 m Sattion Flurometer	3/5/15 10:03	1.072
1,200 m Sattion Flurometer	3/5/15 10:04	1.297
1,200 m Sattion Flurometer	3/5/15 10:05	2.04
1,200 m Sattion Flurometer	3/5/15 10:06	1.253
1,200 m Sattion Flurometer	3/5/15 10:07	1.571
1,200 m Sattion Flurometer	3/5/15 10:08	1.282
1,200 m Sattion Flurometer	3/5/15 10:09	0.972
1,200 m Sattion Flurometer	3/5/15 10:10	1.105
1,200 m Sattion Flurometer	3/5/15 10:11	2.202
1,200 m Sattion Flurometer	3/5/15 10:12	0.843
1,200 m Sattion Flurometer	3/5/15 10:13	2.487
1,200 m Sattion Flurometer	3/5/15 10:14	0.577
1,200 m Sattion Flurometer	3/5/15 10:15	1.556
1,200 m Sattion Flurometer	3/5/15 10:16	2.28
1,200 m Sattion Flurometer	3/5/15 10:17	1.186
1,200 m Sattion Flurometer	3/5/15 10:18	0.791
1,200 m Sattion Flurometer	3/5/15 10:19	1.903
1,200 m Sattion Flurometer	3/5/15 10:20	1.408
1,200 m Sattion Flurometer	3/5/15 10:21	1.393
1,200 m Sattion Flurometer	3/5/15 10:22	0.968
1,200 m Sattion Flurometer	3/5/15 10:23	1.386
1,200 m Sattion Flurometer	3/5/15 10:24	1.29
1,200 m Sattion Flurometer	3/5/15 10:25	1.367
1,200 m Sattion Flurometer	3/5/15 10:26	1.375
1,200 m Sattion Flurometer	3/5/15 10:27	1.161
1,200 m Sattion Flurometer	3/5/15 10:28	0.972
1,200 m Sattion Flurometer	3/5/15 10:29	0.887
1,200 m Sattion Flurometer	3/5/15 10:30	1.249
1,200 m Sattion Flurometer	3/5/15 10:31	0.979
1,200 m Sattion Flurometer	3/5/15 10:32	1.076
1,200 m Sattion Flurometer	3/5/15 10:33	1.112
1,200 m Sattion Flurometer	3/5/15 10:34	1.009
1,200 m Sattion Flurometer	3/5/15 10:35	0.987
1,200 m Sattion Flurometer	3/5/15 10:36	1.744
1,200 m Sattion Flurometer	3/5/15 10:37	1.36
1,200 m Sattion Flurometer	3/5/15 10:38	2.232
1,200 m Sattion Flurometer	3/5/15 10:39	2.176
1,200 m Sattion Flurometer	3/5/15 10:40	0.769
1,200 m Sattion Flurometer	3/5/15 10:41	1.316

Location	Date and Time	Rhodmaine Concentration Adjusted Concentration (ppb)
1,200 m Sattion Flurometer	3/5/15 10:42	1.057
1,200 m Sattion Flurometer	3/5/15 10:43	1.024
1,200 m Sattion Flurometer	3/5/15 10:44	0.839
1,200 m Sattion Flurometer	3/5/15 10:45	0.577
1,200 m Sattion Flurometer	3/5/15 10:46	0.769
1,200 m Sattion Flurometer	3/5/15 10:47	0.846
1,200 m Sattion Flurometer	3/5/15 10:48	0.902
1,200 m Sattion Flurometer	3/5/15 10:49	1.33
1,200 m Sattion Flurometer	3/5/15 10:50	0.75
1,200 m Sattion Flurometer	3/5/15 10:51	1.024
1,200 m Sattion Flurometer	3/5/15 10:52	1.083
1,200 m Sattion Flurometer	3/5/15 10:53	1.316
1,200 m Sattion Flurometer	3/5/15 10:54	1.209
1,200 m Sattion Flurometer	3/5/15 10:55	2.025
1,200 m Sattion Flurometer	3/5/15 10:56	1.434
1,200 m Sattion Flurometer	3/5/15 10:57	0.994
1,200 m Sattion Flurometer	3/5/15 10:58	1.238
1,200 m Sattion Flurometer	3/5/15 10:59	1.035
1,200 m Sattion Flurometer	3/5/15 11:00	1.046
1,200 m Sattion Flurometer	3/5/15 11:01	1.079
1,200 m Sattion Flurometer	3/5/15 11:02	1.083
1,200 m Sattion Flurometer	3/5/15 11:03	0.651
1,200 m Sattion Flurometer	3/5/15 11:04	1.175
1,200 m Sattion Flurometer	3/5/15 11:05	1.042
1,200 m Sattion Flurometer	3/5/15 11:06	1.02
1,200 m Sattion Flurometer	3/5/15 11:07	0.617
1,200 m Sattion Flurometer	3/5/15 11:08	0.961
1,200 m Sattion Flurometer	3/5/15 11:09	0.643
1,200 m Sattion Flurometer	3/5/15 11:10	0.865
1,200 m Sattion Flurometer	3/5/15 11:11	0.802
1,200 m Sattion Flurometer	3/5/15 11:12	2.058
1,200 m Sattion Flurometer	3/5/15 11:13	0.754
1,200 m Sattion Flurometer	3/5/15 11:14	1.231
1,200 m Sattion Flurometer	3/5/15 11:15	0.351
1,200 m Sattion Flurometer	3/5/15 11:16	0.946
1,200 m Sattion Flurometer	3/5/15 11:17	0.887
1,200 m Sattion Flurometer	3/5/15 11:18	2.243
1,200 m Sattion Flurometer	3/5/15 11:19	0.854
1,200 m Sattion Flurometer	3/5/15 11:20	0.769
1,200 m Sattion Flurometer	3/5/15 11:21	1.914
1,200 m Sattion Flurometer	3/5/15 11:22	0.928
1,200 m Sattion Flurometer	3/5/15 11:23	1.009
1,200 m Sattion Flurometer	3/5/15 11:24	2.047
1,200 m Sattion Flurometer	3/5/15 11:25	0.991
1,200 m Sattion Flurometer	3/5/15 11:26	1.715
1,200 m Sattion Flurometer	3/5/15 11:27	1.874

Location	Date and Time	Rhodmaine Concentration Adjusted Concentration (ppb)
1,200 m Sattion Flurometer	3/5/15 11:28	1.951
1,200 m Sattion Flurometer	3/5/15 11:29	1.781
1,200 m Sattion Flurometer	3/5/15 11:30	1.881
1,200 m Sattion Flurometer	3/5/15 11:31	1.789
1,200 m Sattion Flurometer	3/5/15 11:32	1.722
1,200 m Sattion Flurometer	3/5/15 11:33	0.828
1,200 m Sattion Flurometer	3/5/15 11:34	0.909
1,200 m Sattion Flurometer	3/5/15 11:35	0.529
1,200 m Sattion Flurometer	3/5/15 11:36	1.918
1,200 m Sattion Flurometer	3/5/15 11:37	0.994
1,200 m Sattion Flurometer	3/5/15 11:38	0.858
1,200 m Sattion Flurometer	3/5/15 11:39	1.094
1,200 m Sattion Flurometer	3/5/15 11:40	1.984
1,200 m Sattion Flurometer	3/5/15 11:41	0.562
1,200 m Sattion Flurometer	3/5/15 11:42	0.88
1,200 m Sattion Flurometer	3/5/15 11:43	0.544
1,200 m Sattion Flurometer	3/5/15 11:44	1.164
1,200 m Sattion Flurometer	3/5/15 11:45	0.943
1,200 m Sattion Flurometer	3/5/15 11:46	0.858
1,200 m Sattion Flurometer	3/5/15 11:47	0.924
1,200 m Sattion Flurometer	3/5/15 11:48	0.762
1,200 m Sattion Flurometer	3/5/15 11:49	0.673
1,200 m Sattion Flurometer	3/5/15 11:50	0.429
1,200 m Sattion Flurometer	3/5/15 11:51	0.765
1,200 m Sattion Flurometer	3/5/15 11:52	0.972
1,200 m Sattion Flurometer	3/5/15 11:53	0.584
1,200 m Sattion Flurometer	3/5/15 11:54	0.695
1,200 m Sattion Flurometer	3/5/15 11:55	0.78
1,200 m Sattion Flurometer	3/5/15 11:56	0.946
1,200 m Sattion Flurometer	3/5/15 11:57	0.525
1,200 m Sattion Flurometer	3/5/15 11:58	1.792
1,200 m Sattion Flurometer	3/5/15 11:59	0.473
1,200 m Sattion Flurometer	3/5/15 12:00	1.752
1,200 m Sattion Flurometer	3/5/15 12:01	1.153
1,200 m Sattion Flurometer	3/5/15 12:02	0.854
1,200 m Sattion Flurometer	3/5/15 12:03	1.161
1,200 m Sattion Flurometer	3/5/15 12:04	0.954
1,200 m Sattion Flurometer	3/5/15 12:05	0.895
1,200 m Sattion Flurometer	3/5/15 12:06	0.813
1,200 m Sattion Flurometer	3/5/15 12:07	1.042
1,200 m Sattion Flurometer	3/5/15 12:08	1.862
1,200 m Sattion Flurometer	3/5/15 12:09	1.637
1,200 m Sattion Flurometer	3/5/15 12:10	0.518
1,200 m Sattion Flurometer	3/5/15 12:11	1.153
1,200 m Sattion Flurometer	3/5/15 12:12	1.5
1,200 m Sattion Flurometer	3/5/15 12:13	0.821

Location	Date and Time	Rhodmaine Concentration Adjusted Concentration (ppb)
1,200 m Sattion Flurometer	3/5/15 12:14	0.311
1,200 m Sattion Flurometer	3/5/15 12:15	0.167
1,200 m Sattion Flurometer	3/5/15 12:16	0.606
1,200 m Sattion Flurometer	3/5/15 12:17	1.741
1,200 m Sattion Flurometer	3/5/15 12:18	0.455
1,200 m Sattion Flurometer	3/5/15 12:19	0.61
1,200 m Sattion Flurometer	3/5/15 12:20	1.789
1,200 m Sattion Flurometer	3/5/15 12:21	0.791
1,200 m Sattion Flurometer	3/5/15 12:22	1.615
1,200 m Sattion Flurometer	3/5/15 12:23	1.46
1,200 m Sattion Flurometer	3/5/15 12:24	1.364
1,200 m Sattion Flurometer	3/5/15 12:25	0.647
1,200 m Sattion Flurometer	3/5/15 12:26	0.883
1,200 m Sattion Flurometer	3/5/15 12:27	0.532
1,200 m Sattion Flurometer	3/5/15 12:28	1.016
1,200 m Sattion Flurometer	3/5/15 12:29	0.795
1,200 m Sattion Flurometer	3/5/15 12:30	1.811
1,200 m Sattion Flurometer	3/5/15 12:31	0.566
1,200 m Sattion Flurometer	3/5/15 12:32	0.872
1,200 m Sattion Flurometer	3/5/15 12:33	0.651
1,200 m Sattion Flurometer	3/5/15 12:34	1.6
1,200 m Sattion Flurometer	3/5/15 12:35	0.422
1,200 m Sattion Flurometer	3/5/15 12:36	0.355
1,200 m Sattion Flurometer	3/5/15 12:37	0.58
1,200 m Sattion Flurometer	3/5/15 12:38	1.53
1,200 m Sattion Flurometer	3/5/15 12:39	0.555
1,200 m Sattion Flurometer	3/5/15 12:40	0.266
1,200 m Sattion Flurometer	3/5/15 12:41	0.318
1,200 m Sattion Flurometer	3/5/15 12:42	0.363
1,200 m Sattion Flurometer	3/5/15 12:43	1.478
1,200 m Sattion Flurometer	3/5/15 12:44	0.684
1,200 m Sattion Flurometer	3/5/15 12:45	1.77
1,200 m Sattion Flurometer	3/5/15 12:46	1.707
1,200 m Sattion Flurometer	3/5/15 12:47	0.595
1,200 m Sattion Flurometer	3/5/15 12:48	0.58
1,200 m Sattion Flurometer	3/5/15 12:49	0.425
1,200 m Sattion Flurometer	3/5/15 12:50	0.473
1,200 m Sattion Flurometer	3/5/15 12:51	0.311
1,200 m Sattion Flurometer	3/5/15 12:52	0.252
1,200 m Sattion Flurometer	3/5/15 12:53	0.422
1,200 m Sattion Flurometer	3/5/15 12:54	0.27
1,200 m Sattion Flurometer	3/5/15 12:55	0.507
1,200 m Sattion Flurometer	3/5/15 12:56	0.758
1,200 m Sattion Flurometer	3/5/15 12:57	0.736
1,200 m Sattion Flurometer	3/5/15 12:58	1.076
1,200 m Sattion Flurometer	3/5/15 12:59	0.381

Location	Date and Time	Rhodmaine Concentration Adjusted Concentration (ppb)
1,200 m Sattion Flurometer	3/5/15 13:00	1.039
1,200 m Sattion Flurometer	3/5/15 13:01	0.163
1,200 m Sattion Flurometer	3/5/15 13:02	0.817
1,200 m Sattion Flurometer	3/5/15 13:03	0.089
1,200 m Sattion Flurometer	3/5/15 13:04	0.307
1,200 m Sattion Flurometer	3/5/15 13:05	1.641
1,200 m Sattion Flurometer	3/5/15 13:06	0.739
1,200 m Sattion Flurometer	3/5/15 13:07	0.562
1,200 m Sattion Flurometer	3/5/15 13:08	0.152
1,200 m Sattion Flurometer	3/5/15 13:09	0.717
1,200 m Sattion Flurometer	3/5/15 13:10	0.614
1,200 m Sattion Flurometer	3/5/15 13:11	1.696
1,200 m Sattion Flurometer	3/5/15 13:12	0.126
1,200 m Sattion Flurometer	3/5/15 13:13	0.333
1,200 m Sattion Flurometer	3/5/15 13:14	0.23
1,200 m Sattion Flurometer	3/5/15 13:15	0.281
1,200 m Sattion Flurometer	3/5/15 13:16	0.965
1,200 m Sattion Flurometer	3/5/15 13:17	0.189
1,200 m Sattion Flurometer	3/5/15 13:18	0.529
1,200 m Sattion Flurometer	3/5/15 13:19	0.326
1,200 m Sattion Flurometer	3/5/15 13:20	1.404
1,200 m Sattion Flurometer	3/5/15 13:21	0.632
1,200 m Sattion Flurometer	3/5/15 13:22	0.359
1,200 m Sattion Flurometer	3/5/15 13:23	0.392
1,200 m Sattion Flurometer	3/5/15 13:24	1.585
1,200 m Sattion Flurometer	3/5/15 13:25	1.401
1,200 m Sattion Flurometer	3/5/15 13:26	0.425
1,200 m Sattion Flurometer	3/5/15 13:27	0.303
1,200 m Sattion Flurometer	3/5/15 13:28	0.193
1,200 m Sattion Flurometer	3/5/15 13:29	1.345
1,200 m Sattion Flurometer	3/5/15 13:30	0.484
1,200 m Sattion Flurometer	3/5/15 13:31	0.669
1,200 m Sattion Flurometer	3/5/15 13:32	0.414
1,200 m Sattion Flurometer	3/5/15 13:33	0.292
1,200 m Sattion Flurometer	3/5/15 13:34	0.555
1,200 m Sattion Flurometer	3/5/15 13:35	0.344
1,200 m Sattion Flurometer	3/5/15 13:36	0.266
1,200 m Sattion Flurometer	3/5/15 13:37	0.702
1,200 m Sattion Flurometer	3/5/15 13:38	1.231
1,200 m Sattion Flurometer	3/5/15 13:39	0.303
1,200 m Sattion Flurometer	3/5/15 13:40	0.913
1,200 m Sattion Flurometer	3/5/15 13:41	1.567
1,200 m Sattion Flurometer	3/5/15 13:42	0.403
1,200 m Sattion Flurometer	3/5/15 13:43	0
1,200 m Sattion Flurometer	3/5/15 13:44	0.414
1,200 m Sattion Flurometer	3/5/15 13:45	0.241

Location	Date and Time	Rhodmaine Concentration Adjusted Concentration (ppb)
1,200 m Sattion Flurometer	3/5/15 13:46	0.64
1,200 m Sattion Flurometer	3/5/15 13:47	7.707
1,200 m Sattion Flurometer	3/5/15 16:13	13.72
1,200 m ISCO	3/4/15 17:00	0.259325096
1,200 m ISCO	3/4/15 18:00	0.058521884
1,200 m ISCO	3/4/15 19:00	-0.007315235
1,200 m ISCO	3/4/15 20:00	0.29718144
1,200 m ISCO	3/4/15 21:00	7.083342477
1,200 m ISCO	3/4/15 22:00	4.449857719
1,200 m ISCO	3/4/15 23:00	14.30238257
1,200 m ISCO	3/5/15 0:00	13.81847975
1,200 m ISCO	3/5/15 1:00	8.052794054
1,200 m ISCO	3/5/15 2:00	5.081894061
1,200 m ISCO	3/5/15 3:00	5.470333063
1,200 m ISCO	3/5/15 4:00	4.51404891
1,200 m ISCO	3/5/15 5:00	3.901763703
1,200 m ISCO	3/5/15 6:00	3.332272624
1,200 m ISCO	3/5/15 7:00	2.558686476
1,200 m ISCO	3/5/15 8:00	1.71103357
1,200 m ISCO	3/5/15 9:00	1.66988537
1,200 m ISCO	3/5/15 10:00	1.500354789
1,200 m ISCO	3/5/15 11:00	1.233714457
1,200 m ISCO	3/5/15 12:00	1.156355842
1,200 m ISCO	3/5/15 13:00	0.868318447
Mid Point Flurometer	3/4/2015 9:01	0
Mid Point Flurometer	3/4/2015 9:02	0
Mid Point Flurometer	3/4/2015 9:03	0
Mid Point Flurometer	3/4/2015 9:04	0
Mid Point Flurometer	3/4/2015 9:05	0
Mid Point Flurometer	3/4/2015 9:06	0
Mid Point Flurometer	3/4/2015 9:07	0
Mid Point Flurometer	3/4/2015 9:08	0
Mid Point Flurometer	3/4/2015 9:09	0
Mid Point Flurometer	3/4/2015 9:10	0
Mid Point Flurometer	3/4/2015 9:11	0
Mid Point Flurometer	3/4/2015 9:12	0
Mid Point Flurometer	3/4/2015 9:13	0
Mid Point Flurometer	3/4/2015 9:14	0
Mid Point Flurometer	3/4/2015 9:15	0
Mid Point Flurometer	3/4/2015 9:16	0
Mid Point Flurometer	3/4/2015 9:17	0
Mid Point Flurometer	3/4/2015 9:18	0
Mid Point Flurometer	3/4/2015 9:19	0
Mid Point Flurometer	3/4/2015 9:20	0
Mid Point Flurometer	3/4/2015 9:21	0
Mid Point Flurometer	3/4/2015 9:22	0

Location	Date and Time	Rhodmaine Concentration Adjusted Concentration (ppb)
Mid Point Flurometer	3/4/2015 9:23	0
Mid Point Flurometer	3/4/2015 9:24	0
Mid Point Flurometer	3/4/2015 9:25	0
Mid Point Flurometer	3/4/2015 9:26	0
Mid Point Flurometer	3/4/2015 9:27	0
Mid Point Flurometer	3/4/2015 9:28	0
Mid Point Flurometer	3/4/2015 9:29	0
Mid Point Flurometer	3/4/2015 9:30	0
Mid Point Flurometer	3/4/2015 9:31	0
Mid Point Flurometer	3/4/2015 9:32	0
Mid Point Flurometer	3/4/2015 9:33	0
Mid Point Flurometer	3/4/2015 9:34	0
Mid Point Flurometer	3/4/2015 9:35	0
Mid Point Flurometer	3/4/2015 9:36	0
Mid Point Flurometer	3/4/2015 9:37	0
Mid Point Flurometer	3/4/2015 9:38	0
Mid Point Flurometer	3/4/2015 9:39	0
Mid Point Flurometer	3/4/2015 9:40	0
Mid Point Flurometer	3/4/2015 9:41	0
Mid Point Flurometer	3/4/2015 9:42	0
Mid Point Flurometer	3/4/2015 9:43	0
Mid Point Flurometer	3/4/2015 9:44	0
Mid Point Flurometer	3/4/2015 9:45	0
Mid Point Flurometer	3/4/2015 9:46	0
Mid Point Flurometer	3/4/2015 9:47	0
Mid Point Flurometer	3/4/2015 9:48	0
Mid Point Flurometer	3/4/2015 9:49	0
Mid Point Flurometer	3/4/2015 9:50	0
Mid Point Flurometer	3/4/2015 9:51	0
Mid Point Flurometer	3/4/2015 9:52	0
Mid Point Flurometer	3/4/2015 9:53	0
Mid Point Flurometer	3/4/2015 9:54	0
Mid Point Flurometer	3/4/2015 9:55	0
Mid Point Flurometer	3/4/2015 9:56	0
Mid Point Flurometer	3/4/2015 9:57	0
Mid Point Flurometer	3/4/2015 9:58	0
Mid Point Flurometer	3/4/2015 9:59	0
Mid Point Flurometer	3/4/2015 10:00	0
Mid Point Flurometer	3/4/2015 10:01	0
Mid Point Flurometer	3/4/2015 10:02	0
Mid Point Flurometer	3/4/2015 10:03	0
Mid Point Flurometer	3/4/2015 10:04	0
Mid Point Flurometer	3/4/2015 10:05	0
Mid Point Flurometer	3/4/2015 10:06	0
Mid Point Flurometer	3/4/2015 10:07	0
Mid Point Flurometer	3/4/2015 10:08	0

Location	Date and Time	Rhodmaine Concentration Adjusted Concentration (ppb)
Mid Point Flurometer	3/4/2015 10:09	0
Mid Point Flurometer	3/4/2015 10:10	0
Mid Point Flurometer	3/4/2015 10:11	0
Mid Point Flurometer	3/4/2015 10:12	0
Mid Point Flurometer	3/4/2015 10:13	0
Mid Point Flurometer	3/4/2015 10:14	0
Mid Point Flurometer	3/4/2015 10:15	0
Mid Point Flurometer	3/4/2015 10:16	0
Mid Point Flurometer	3/4/2015 10:17	0
Mid Point Flurometer	3/4/2015 10:18	0
Mid Point Flurometer	3/4/2015 10:19	0
Mid Point Flurometer	3/4/2015 10:20	0
Mid Point Flurometer	3/4/2015 10:21	0
Mid Point Flurometer	3/4/2015 10:22	0
Mid Point Flurometer	3/4/2015 10:23	0
Mid Point Flurometer	3/4/2015 10:24	0
Mid Point Flurometer	3/4/2015 10:25	0
Mid Point Flurometer	3/4/2015 10:26	0
Mid Point Flurometer	3/4/2015 10:27	0
Mid Point Flurometer	3/4/2015 10:28	0
Mid Point Flurometer	3/4/2015 10:29	0
Mid Point Flurometer	3/4/2015 10:30	0
Mid Point Flurometer	3/4/2015 10:31	0
Mid Point Flurometer	3/4/2015 10:32	0
Mid Point Flurometer	3/4/2015 10:33	0
Mid Point Flurometer	3/4/2015 10:34	0
Mid Point Flurometer	3/4/2015 10:35	0
Mid Point Flurometer	3/4/2015 10:36	0
Mid Point Flurometer	3/4/2015 10:37	0
Mid Point Flurometer	3/4/2015 10:38	0
Mid Point Flurometer	3/4/2015 10:39	0
Mid Point Flurometer	3/4/2015 10:40	0
Mid Point Flurometer	3/4/2015 10:41	0
Mid Point Flurometer	3/4/2015 10:42	0
Mid Point Flurometer	3/4/2015 10:43	0
Mid Point Flurometer	3/4/2015 10:44	0
Mid Point Flurometer	3/4/2015 10:45	0
Mid Point Flurometer	3/4/2015 10:46	0
Mid Point Flurometer	3/4/2015 10:47	0
Mid Point Flurometer	3/4/2015 10:48	0
Mid Point Flurometer	3/4/2015 10:49	0
Mid Point Flurometer	3/4/2015 10:50	0
Mid Point Flurometer	3/4/2015 10:51	0
Mid Point Flurometer	3/4/2015 10:52	0
Mid Point Flurometer	3/4/2015 10:53	0
Mid Point Flurometer	3/4/2015 10:54	0

Location	Date and Time	Rhodmaine Concentration Adjusted Concentration (ppb)
Mid Point Flurometer	3/4/2015 10:55	0
Mid Point Flurometer	3/4/2015 10:56	0
Mid Point Flurometer	3/4/2015 10:57	0
Mid Point Flurometer	3/4/2015 10:58	0
Mid Point Flurometer	3/4/2015 10:59	0
Mid Point Flurometer	3/4/2015 11:00	0
Mid Point Flurometer	3/4/2015 11:01	0
Mid Point Flurometer	3/4/2015 11:02	0
Mid Point Flurometer	3/4/2015 11:03	0
Mid Point Flurometer	3/4/2015 11:04	0
Mid Point Flurometer	3/4/2015 11:05	0
Mid Point Flurometer	3/4/2015 11:06	0
Mid Point Flurometer	3/4/2015 11:07	0
Mid Point Flurometer	3/4/2015 11:08	0
Mid Point Flurometer	3/4/2015 11:09	0
Mid Point Flurometer	3/4/2015 11:10	0
Mid Point Flurometer	3/4/2015 11:11	0
Mid Point Flurometer	3/4/2015 11:12	0
Mid Point Flurometer	3/4/2015 11:13	0
Mid Point Flurometer	3/4/2015 11:14	0
Mid Point Flurometer	3/4/2015 11:15	0
Mid Point Flurometer	3/4/2015 11:16	0
Mid Point Flurometer	3/4/2015 11:17	0
Mid Point Flurometer	3/4/2015 11:18	0
Mid Point Flurometer	3/4/2015 11:19	0
Mid Point Flurometer	3/4/2015 11:20	0
Mid Point Flurometer	3/4/2015 11:21	0
Mid Point Flurometer	3/4/2015 11:22	0
Mid Point Flurometer	3/4/2015 11:23	0
Mid Point Flurometer	3/4/2015 11:24	0
Mid Point Flurometer	3/4/2015 11:25	0
Mid Point Flurometer	3/4/2015 11:26	0
Mid Point Flurometer	3/4/2015 11:27	0
Mid Point Flurometer	3/4/2015 11:28	0
Mid Point Flurometer	3/4/2015 11:29	0
Mid Point Flurometer	3/4/2015 11:30	0
Mid Point Flurometer	3/4/2015 11:31	0
Mid Point Flurometer	3/4/2015 11:32	0
Mid Point Flurometer	3/4/2015 11:33	0
Mid Point Flurometer	3/4/2015 11:34	0
Mid Point Flurometer	3/4/2015 11:35	0
Mid Point Flurometer	3/4/2015 11:36	0
Mid Point Flurometer	3/4/2015 11:37	0
Mid Point Flurometer	3/4/2015 11:38	0
Mid Point Flurometer	3/4/2015 11:39	0
Mid Point Flurometer	3/4/2015 11:40	0

Location	Date and Time	Rhodmaine Concentration Adjusted Concentration (ppb)
Mid Point Flurometer	3/4/2015 11:41	0
Mid Point Flurometer	3/4/2015 11:42	0
Mid Point Flurometer	3/4/2015 11:43	0
Mid Point Flurometer	3/4/2015 11:44	0
Mid Point Flurometer	3/4/2015 11:45	0
Mid Point Flurometer	3/4/2015 11:46	0
Mid Point Flurometer	3/4/2015 11:47	0
Mid Point Flurometer	3/4/2015 11:48	0
Mid Point Flurometer	3/4/2015 11:49	0
Mid Point Flurometer	3/4/2015 11:50	0
Mid Point Flurometer	3/4/2015 11:51	0
Mid Point Flurometer	3/4/2015 11:52	0
Mid Point Flurometer	3/4/2015 11:53	0
Mid Point Flurometer	3/4/2015 11:54	0
Mid Point Flurometer	3/4/2015 11:55	0
Mid Point Flurometer	3/4/2015 11:56	0
Mid Point Flurometer	3/4/2015 11:57	0
Mid Point Flurometer	3/4/2015 11:58	0
Mid Point Flurometer	3/4/2015 11:59	0
Mid Point Flurometer	3/4/2015 12:00	0
Mid Point Flurometer	3/4/2015 12:01	0
Mid Point Flurometer	3/4/2015 12:02	0
Mid Point Flurometer	3/4/2015 12:03	0
Mid Point Flurometer	3/4/2015 12:04	0
Mid Point Flurometer	3/4/2015 12:05	0
Mid Point Flurometer	3/4/2015 12:06	0
Mid Point Flurometer	3/4/2015 12:07	0
Mid Point Flurometer	3/4/2015 12:08	0
Mid Point Flurometer	3/4/2015 12:09	0
Mid Point Flurometer	3/4/2015 12:10	0
Mid Point Flurometer	3/4/2015 12:11	0
Mid Point Flurometer	3/4/2015 12:12	0
Mid Point Flurometer	3/4/2015 12:13	0
Mid Point Flurometer	3/4/2015 12:14	0
Mid Point Flurometer	3/4/2015 12:15	0
Mid Point Flurometer	3/4/2015 12:16	0
Mid Point Flurometer	3/4/2015 12:17	0
Mid Point Flurometer	3/4/2015 12:18	0
Mid Point Flurometer	3/4/2015 12:19	0
Mid Point Flurometer	3/4/2015 12:20	0
Mid Point Flurometer	3/4/2015 12:21	0
Mid Point Flurometer	3/4/2015 12:22	0
Mid Point Flurometer	3/4/2015 12:23	0
Mid Point Flurometer	3/4/2015 12:24	0
Mid Point Flurometer	3/4/2015 12:25	0
Mid Point Flurometer	3/4/2015 12:26	0

Location	Date and Time	Rhodmaine Concentration Adjusted Concentration (ppb)
Mid Point Flurometer	3/4/2015 12:27	0
Mid Point Flurometer	3/4/2015 12:28	0
Mid Point Flurometer	3/4/2015 12:29	0
Mid Point Flurometer	3/4/2015 12:30	0
Mid Point Flurometer	3/4/2015 12:31	0
Mid Point Flurometer	3/4/2015 12:32	0
Mid Point Flurometer	3/4/2015 12:33	0
Mid Point Flurometer	3/4/2015 12:34	0
Mid Point Flurometer	3/4/2015 12:35	0
Mid Point Flurometer	3/4/2015 12:36	0
Mid Point Flurometer	3/4/2015 12:37	0
Mid Point Flurometer	3/4/2015 12:38	0
Mid Point Flurometer	3/4/2015 12:39	0
Mid Point Flurometer	3/4/2015 12:40	0
Mid Point Flurometer	3/4/2015 12:41	0
Mid Point Flurometer	3/4/2015 12:42	0
Mid Point Flurometer	3/4/2015 12:43	0
Mid Point Flurometer	3/4/2015 12:44	0
Mid Point Flurometer	3/4/2015 12:45	0
Mid Point Flurometer	3/4/2015 12:46	0.52
Mid Point Flurometer	3/4/2015 12:47	0
Mid Point Flurometer	3/4/2015 12:48	0
Mid Point Flurometer	3/4/2015 12:49	0
Mid Point Flurometer	3/4/2015 12:50	0
Mid Point Flurometer	3/4/2015 12:51	0
Mid Point Flurometer	3/4/2015 12:52	0
Mid Point Flurometer	3/4/2015 12:53	0
Mid Point Flurometer	3/4/2015 12:54	0
Mid Point Flurometer	3/4/2015 12:55	0
Mid Point Flurometer	3/4/2015 12:56	0
Mid Point Flurometer	3/4/2015 12:57	0
Mid Point Flurometer	3/4/2015 12:58	0
Mid Point Flurometer	3/4/2015 12:59	0
Mid Point Flurometer	3/4/2015 13:00	0
Mid Point Flurometer	3/4/2015 13:01	0
Mid Point Flurometer	3/4/2015 13:02	0
Mid Point Flurometer	3/4/2015 13:03	0
Mid Point Flurometer	3/4/2015 13:04	0
Mid Point Flurometer	3/4/2015 13:05	0
Mid Point Flurometer	3/4/2015 13:06	0
Mid Point Flurometer	3/4/2015 13:07	0
Mid Point Flurometer	3/4/2015 13:08	0
Mid Point Flurometer	3/4/2015 13:09	0
Mid Point Flurometer	3/4/2015 13:10	0
Mid Point Flurometer	3/4/2015 13:11	0
Mid Point Flurometer	3/4/2015 13:12	0

Location	Date and Time	Rhodmaine Concentration Adjusted Concentration (ppb)
Mid Point Flurometer	3/4/2015 13:13	0
Mid Point Flurometer	3/4/2015 13:14	0
Mid Point Flurometer	3/4/2015 13:15	0
Mid Point Flurometer	3/4/2015 13:16	0
Mid Point Flurometer	3/4/2015 13:17	0
Mid Point Flurometer	3/4/2015 13:18	0
Mid Point Flurometer	3/4/2015 13:19	0
Mid Point Flurometer	3/4/2015 13:20	0
Mid Point Flurometer	3/4/2015 13:21	0
Mid Point Flurometer	3/4/2015 13:22	0
Mid Point Flurometer	3/4/2015 13:23	0
Mid Point Flurometer	3/4/2015 13:24	0
Mid Point Flurometer	3/4/2015 13:25	0
Mid Point Flurometer	3/4/2015 13:26	1.7
Mid Point Flurometer	3/4/2015 13:27	0.03
Mid Point Flurometer	3/4/2015 13:28	0
Mid Point Flurometer	3/4/2015 13:29	0
Mid Point Flurometer	3/4/2015 13:30	0
Mid Point Flurometer	3/4/2015 13:31	0
Mid Point Flurometer	3/4/2015 13:32	0
Mid Point Flurometer	3/4/2015 13:33	0
Mid Point Flurometer	3/4/2015 13:34	0
Mid Point Flurometer	3/4/2015 13:35	0
Mid Point Flurometer	3/4/2015 13:36	0
Mid Point Flurometer	3/4/2015 13:37	0
Mid Point Flurometer	3/4/2015 13:38	0
Mid Point Flurometer	3/4/2015 13:39	0
Mid Point Flurometer	3/4/2015 13:40	0
Mid Point Flurometer	3/4/2015 13:41	0
Mid Point Flurometer	3/4/2015 13:42	0
Mid Point Flurometer	3/4/2015 13:43	0
Mid Point Flurometer	3/4/2015 13:44	0
Mid Point Flurometer	3/4/2015 13:45	0
Mid Point Flurometer	3/4/2015 13:46	0
Mid Point Flurometer	3/4/2015 13:47	0
Mid Point Flurometer	3/4/2015 13:48	0
Mid Point Flurometer	3/4/2015 13:49	0
Mid Point Flurometer	3/4/2015 13:50	0
Mid Point Flurometer	3/4/2015 13:51	0
Mid Point Flurometer	3/4/2015 13:52	0
Mid Point Flurometer	3/4/2015 13:53	0
Mid Point Flurometer	3/4/2015 13:54	0
Mid Point Flurometer	3/4/2015 13:55	0
Mid Point Flurometer	3/4/2015 13:56	0
Mid Point Flurometer	3/4/2015 13:57	0
Mid Point Flurometer	3/4/2015 13:58	0

Location	Date and Time	Rhodmaine Concentration Adjusted Concentration (ppb)
Mid Point Flurometer	3/4/2015 13:59	0
Mid Point Flurometer	3/4/2015 14:00	0
Mid Point Flurometer	3/4/2015 14:01	0
Mid Point Flurometer	3/4/2015 14:02	0
Mid Point Flurometer	3/4/2015 14:03	0
Mid Point Flurometer	3/4/2015 14:04	0
Mid Point Flurometer	3/4/2015 14:05	0
Mid Point Flurometer	3/4/2015 14:06	0
Mid Point Flurometer	3/4/2015 14:07	0
Mid Point Flurometer	3/4/2015 14:08	0
Mid Point Flurometer	3/4/2015 14:09	0
Mid Point Flurometer	3/4/2015 14:10	0
Mid Point Flurometer	3/4/2015 14:11	0
Mid Point Flurometer	3/4/2015 14:12	0
Mid Point Flurometer	3/4/2015 14:13	0
Mid Point Flurometer	3/4/2015 14:14	0.02
Mid Point Flurometer	3/4/2015 14:15	0
Mid Point Flurometer	3/4/2015 14:16	0
Mid Point Flurometer	3/4/2015 14:17	0
Mid Point Flurometer	3/4/2015 14:18	0
Mid Point Flurometer	3/4/2015 14:19	0
Mid Point Flurometer	3/4/2015 14:20	0
Mid Point Flurometer	3/4/2015 14:21	0
Mid Point Flurometer	3/4/2015 14:22	0
Mid Point Flurometer	3/4/2015 14:23	0
Mid Point Flurometer	3/4/2015 14:24	0
Mid Point Flurometer	3/4/2015 14:25	0
Mid Point Flurometer	3/4/2015 14:26	0
Mid Point Flurometer	3/4/2015 14:27	0
Mid Point Flurometer	3/4/2015 14:28	0
Mid Point Flurometer	3/4/2015 14:29	0
Mid Point Flurometer	3/4/2015 14:30	0
Mid Point Flurometer	3/4/2015 14:31	0
Mid Point Flurometer	3/4/2015 14:32	0
Mid Point Flurometer	3/4/2015 14:33	0
Mid Point Flurometer	3/4/2015 14:34	0
Mid Point Flurometer	3/4/2015 14:35	0
Mid Point Flurometer	3/4/2015 14:36	0
Mid Point Flurometer	3/4/2015 14:37	0
Mid Point Flurometer	3/4/2015 14:38	0
Mid Point Flurometer	3/4/2015 14:39	0
Mid Point Flurometer	3/4/2015 14:40	0
Mid Point Flurometer	3/4/2015 14:41	0
Mid Point Flurometer	3/4/2015 14:42	0
Mid Point Flurometer	3/4/2015 14:43	0
Mid Point Flurometer	3/4/2015 14:44	0

Location	Date and Time	Rhodmaine Concentration Adjusted Concentration (ppb)
Mid Point Flurometer	3/4/2015 14:45	0
Mid Point Flurometer	3/4/2015 14:46	0
Mid Point Flurometer	3/4/2015 14:47	0
Mid Point Flurometer	3/4/2015 14:48	0
Mid Point Flurometer	3/4/2015 14:49	0
Mid Point Flurometer	3/4/2015 14:50	0
Mid Point Flurometer	3/4/2015 14:51	0
Mid Point Flurometer	3/4/2015 14:52	0
Mid Point Flurometer	3/4/2015 14:53	0
Mid Point Flurometer	3/4/2015 14:54	0
Mid Point Flurometer	3/4/2015 14:55	0
Mid Point Flurometer	3/4/2015 14:56	0
Mid Point Flurometer	3/4/2015 14:57	0
Mid Point Flurometer	3/4/2015 14:58	0
Mid Point Flurometer	3/4/2015 14:59	0
Mid Point Flurometer	3/4/2015 15:00	0
Mid Point Flurometer	3/4/2015 15:01	0
Mid Point Flurometer	3/4/2015 15:02	0
Mid Point Flurometer	3/4/2015 15:03	0
Mid Point Flurometer	3/4/2015 15:04	0
Mid Point Flurometer	3/4/2015 15:05	0
Mid Point Flurometer	3/4/2015 15:06	0
Mid Point Flurometer	3/4/2015 15:07	0
Mid Point Flurometer	3/4/2015 15:08	0
Mid Point Flurometer	3/4/2015 15:09	0
Mid Point Flurometer	3/4/2015 15:10	0
Mid Point Flurometer	3/4/2015 15:11	0
Mid Point Flurometer	3/4/2015 15:12	0
Mid Point Flurometer	3/4/2015 15:13	0
Mid Point Flurometer	3/4/2015 15:14	0
Mid Point Flurometer	3/4/2015 15:15	0
Mid Point Flurometer	3/4/2015 15:16	0
Mid Point Flurometer	3/4/2015 15:17	0
Mid Point Flurometer	3/4/2015 15:18	0
Mid Point Flurometer	3/4/2015 15:19	0.04
Mid Point Flurometer	3/4/2015 15:20	0
Mid Point Flurometer	3/4/2015 15:21	0
Mid Point Flurometer	3/4/2015 15:22	0
Mid Point Flurometer	3/4/2015 15:23	0
Mid Point Flurometer	3/4/2015 15:24	0
Mid Point Flurometer	3/4/2015 15:25	0
Mid Point Flurometer	3/4/2015 15:26	0
Mid Point Flurometer	3/4/2015 15:27	0
Mid Point Flurometer	3/4/2015 15:28	0
Mid Point Flurometer	3/4/2015 15:29	0
Mid Point Flurometer	3/4/2015 15:30	0

Location	Date and Time	Rhodmaine Concentration Adjusted Concentration (ppb)
Mid Point Flurometer	3/4/2015 15:31	0
Mid Point Flurometer	3/4/2015 15:32	0
Mid Point Flurometer	3/4/2015 15:33	0
Mid Point Flurometer	3/4/2015 15:34	0
Mid Point Flurometer	3/4/2015 15:35	0
Mid Point Flurometer	3/4/2015 15:36	0
Mid Point Flurometer	3/4/2015 15:37	0
Mid Point Flurometer	3/4/2015 15:38	0
Mid Point Flurometer	3/4/2015 15:39	0
Mid Point Flurometer	3/4/2015 15:40	0
Mid Point Flurometer	3/4/2015 15:41	0
Mid Point Flurometer	3/4/2015 15:42	0
Mid Point Flurometer	3/4/2015 15:43	0
Mid Point Flurometer	3/4/2015 15:44	0
Mid Point Flurometer	3/4/2015 15:45	0
Mid Point Flurometer	3/4/2015 15:46	0
Mid Point Flurometer	3/4/2015 15:47	0
Mid Point Flurometer	3/4/2015 15:48	0
Mid Point Flurometer	3/4/2015 15:49	0
Mid Point Flurometer	3/4/2015 15:50	0
Mid Point Flurometer	3/4/2015 15:51	0
Mid Point Flurometer	3/4/2015 15:52	0
Mid Point Flurometer	3/4/2015 15:53	0
Mid Point Flurometer	3/4/2015 15:54	0
Mid Point Flurometer	3/4/2015 15:55	0
Mid Point Flurometer	3/4/2015 15:56	0
Mid Point Flurometer	3/4/2015 15:57	0
Mid Point Flurometer	3/4/2015 15:58	0
Mid Point Flurometer	3/4/2015 15:59	0
Mid Point Flurometer	3/4/2015 16:00	0
Mid Point Flurometer	3/4/2015 16:01	0
Mid Point Flurometer	3/4/2015 16:02	0
Mid Point Flurometer	3/4/2015 16:03	0
Mid Point Flurometer	3/4/2015 16:04	0
Mid Point Flurometer	3/4/2015 16:05	0
Mid Point Flurometer	3/4/2015 16:06	0
Mid Point Flurometer	3/4/2015 16:07	0
Mid Point Flurometer	3/4/2015 16:08	0
Mid Point Flurometer	3/4/2015 16:09	0
Mid Point Flurometer	3/4/2015 16:10	0
Mid Point Flurometer	3/4/2015 16:11	0
Mid Point Flurometer	3/4/2015 16:12	0
Mid Point Flurometer	3/4/2015 16:13	0
Mid Point Flurometer	3/4/2015 16:14	0
Mid Point Flurometer	3/4/2015 16:15	0
Mid Point Flurometer	3/4/2015 16:16	0

Location	Date and Time	Rhodmaine Concentration Adjusted Concentration (ppb)
Mid Point Flurometer	3/4/2015 16:17	0
Mid Point Flurometer	3/4/2015 16:18	0
Mid Point Flurometer	3/4/2015 16:19	0
Mid Point Flurometer	3/4/2015 16:20	0
Mid Point Flurometer	3/4/2015 16:21	0
Mid Point Flurometer	3/4/2015 16:22	0
Mid Point Flurometer	3/4/2015 16:23	0
Mid Point Flurometer	3/4/2015 16:24	0
Mid Point Flurometer	3/4/2015 16:25	0
Mid Point Flurometer	3/4/2015 16:26	0
Mid Point Flurometer	3/4/2015 16:27	0
Mid Point Flurometer	3/4/2015 16:28	0
Mid Point Flurometer	3/4/2015 16:29	0
Mid Point Flurometer	3/4/2015 16:30	0
Mid Point Flurometer	3/4/2015 16:31	0
Mid Point Flurometer	3/4/2015 16:32	0
Mid Point Flurometer	3/4/2015 16:33	0
Mid Point Flurometer	3/4/2015 16:34	0
Mid Point Flurometer	3/4/2015 16:35	0
Mid Point Flurometer	3/4/2015 16:36	0
Mid Point Flurometer	3/4/2015 16:37	0
Mid Point Flurometer	3/4/2015 16:38	0
Mid Point Flurometer	3/4/2015 16:39	0
Mid Point Flurometer	3/4/2015 16:40	0
Mid Point Flurometer	3/4/2015 16:41	0
Mid Point Flurometer	3/4/2015 16:42	0
Mid Point Flurometer	3/4/2015 16:43	0
Mid Point Flurometer	3/4/2015 16:44	0
Mid Point Flurometer	3/4/2015 16:45	0
Mid Point Flurometer	3/4/2015 16:46	0
Mid Point Flurometer	3/4/2015 16:47	0
Mid Point Flurometer	3/4/2015 16:48	0
Mid Point Flurometer	3/4/2015 16:49	0.17
Mid Point Flurometer	3/4/2015 16:50	0
Mid Point Flurometer	3/4/2015 16:51	0
Mid Point Flurometer	3/4/2015 16:52	0
Mid Point Flurometer	3/4/2015 16:53	0
Mid Point Flurometer	3/4/2015 16:54	0
Mid Point Flurometer	3/4/2015 16:55	0
Mid Point Flurometer	3/4/2015 16:56	0
Mid Point Flurometer	3/4/2015 16:57	0
Mid Point Flurometer	3/4/2015 16:58	0
Mid Point Flurometer	3/4/2015 16:59	0
Mid Point Flurometer	3/4/2015 17:00	0
Mid Point Flurometer	3/4/2015 17:01	0
Mid Point Flurometer	3/4/2015 17:02	0

Location	Date and Time	Rhodmaine Concentration Adjusted Concentration (ppb)
Mid Point Flurometer	3/4/2015 17:03	0
Mid Point Flurometer	3/4/2015 17:04	0
Mid Point Flurometer	3/4/2015 17:05	0
Mid Point Flurometer	3/4/2015 17:06	0
Mid Point Flurometer	3/4/2015 17:07	0
Mid Point Flurometer	3/4/2015 17:08	0
Mid Point Flurometer	3/4/2015 17:09	0
Mid Point Flurometer	3/4/2015 17:10	0
Mid Point Flurometer	3/4/2015 17:11	0
Mid Point Flurometer	3/4/2015 17:12	0
Mid Point Flurometer	3/4/2015 17:13	0
Mid Point Flurometer	3/4/2015 17:14	0
Mid Point Flurometer	3/4/2015 17:15	0
Mid Point Flurometer	3/4/2015 17:16	0
Mid Point Flurometer	3/4/2015 17:17	0
Mid Point Flurometer	3/4/2015 17:18	0
Mid Point Flurometer	3/4/2015 17:19	0
Mid Point Flurometer	3/4/2015 17:20	0
Mid Point Flurometer	3/4/2015 17:21	0
Mid Point Flurometer	3/4/2015 17:22	0
Mid Point Flurometer	3/4/2015 17:23	0
Mid Point Flurometer	3/4/2015 17:24	0
Mid Point Flurometer	3/4/2015 17:25	0
Mid Point Flurometer	3/4/2015 17:26	0
Mid Point Flurometer	3/4/2015 17:27	0
Mid Point Flurometer	3/4/2015 17:28	0
Mid Point Flurometer	3/4/2015 17:29	0
Mid Point Flurometer	3/4/2015 17:30	0
Mid Point Flurometer	3/4/2015 17:31	0
Mid Point Flurometer	3/4/2015 17:32	0
Mid Point Flurometer	3/4/2015 17:33	0
Mid Point Flurometer	3/4/2015 17:34	0
Mid Point Flurometer	3/4/2015 17:35	0
Mid Point Flurometer	3/4/2015 17:36	0
Mid Point Flurometer	3/4/2015 17:37	0
Mid Point Flurometer	3/4/2015 17:38	0
Mid Point Flurometer	3/4/2015 17:39	0
Mid Point Flurometer	3/4/2015 17:40	0
Mid Point Flurometer	3/4/2015 17:41	0
Mid Point Flurometer	3/4/2015 17:42	0
Mid Point Flurometer	3/4/2015 17:43	0
Mid Point Flurometer	3/4/2015 17:44	0
Mid Point Flurometer	3/4/2015 17:45	0
Mid Point Flurometer	3/4/2015 17:46	0
Mid Point Flurometer	3/4/2015 17:47	0
Mid Point Flurometer	3/4/2015 17:48	0

Location	Date and Time	Rhodmaine Concentration Adjusted Concentration (ppb)
Mid Point Flurometer	3/4/2015 17:49	0
Mid Point Flurometer	3/4/2015 17:50	0
Mid Point Flurometer	3/4/2015 17:51	0
Mid Point Flurometer	3/4/2015 17:52	0
Mid Point Flurometer	3/4/2015 17:53	0
Mid Point Flurometer	3/4/2015 17:54	0
Mid Point Flurometer	3/4/2015 17:55	0
Mid Point Flurometer	3/4/2015 17:56	0
Mid Point Flurometer	3/4/2015 17:57	0
Mid Point Flurometer	3/4/2015 17:58	0
Mid Point Flurometer	3/4/2015 17:59	0
Mid Point Flurometer	3/4/2015 18:00	0
Mid Point Flurometer	3/4/2015 18:01	0
Mid Point Flurometer	3/4/2015 18:02	0
Mid Point Flurometer	3/4/2015 18:03	0
Mid Point Flurometer	3/4/2015 18:04	0
Mid Point Flurometer	3/4/2015 18:05	0
Mid Point Flurometer	3/4/2015 18:06	0
Mid Point Flurometer	3/4/2015 18:07	0
Mid Point Flurometer	3/4/2015 18:08	0
Mid Point Flurometer	3/4/2015 18:09	0
Mid Point Flurometer	3/4/2015 18:10	0
Mid Point Flurometer	3/4/2015 18:11	0
Mid Point Flurometer	3/4/2015 18:12	0
Mid Point Flurometer	3/4/2015 18:13	0
Mid Point Flurometer	3/4/2015 18:14	0.12
Mid Point Flurometer	3/4/2015 18:15	0
Mid Point Flurometer	3/4/2015 18:16	0
Mid Point Flurometer	3/4/2015 18:17	0
Mid Point Flurometer	3/4/2015 18:18	0
Mid Point Flurometer	3/4/2015 18:19	0
Mid Point Flurometer	3/4/2015 18:20	0
Mid Point Flurometer	3/4/2015 18:21	0
Mid Point Flurometer	3/4/2015 18:22	0
Mid Point Flurometer	3/4/2015 18:23	0
Mid Point Flurometer	3/4/2015 18:24	0
Mid Point Flurometer	3/4/2015 18:25	0
Mid Point Flurometer	3/4/2015 18:26	0
Mid Point Flurometer	3/4/2015 18:27	0
Mid Point Flurometer	3/4/2015 18:28	0
Mid Point Flurometer	3/4/2015 18:29	0
Mid Point Flurometer	3/4/2015 18:30	0
Mid Point Flurometer	3/4/2015 18:31	0
Mid Point Flurometer	3/4/2015 18:32	0
Mid Point Flurometer	3/4/2015 18:33	0
Mid Point Flurometer	3/4/2015 18:34	0.01

Location	Date and Time	Rhodmaine Concentration Adjusted Concentration (ppb)
Mid Point Flurometer	3/4/2015 18:35	0
Mid Point Flurometer	3/4/2015 18:36	0
Mid Point Flurometer	3/4/2015 18:37	0
Mid Point Flurometer	3/4/2015 18:38	0
Mid Point Flurometer	3/4/2015 18:39	0
Mid Point Flurometer	3/4/2015 18:40	0
Mid Point Flurometer	3/4/2015 18:41	0
Mid Point Flurometer	3/4/2015 18:42	0
Mid Point Flurometer	3/4/2015 18:43	0
Mid Point Flurometer	3/4/2015 18:44	0
Mid Point Flurometer	3/4/2015 18:45	0
Mid Point Flurometer	3/4/2015 18:46	0
Mid Point Flurometer	3/4/2015 18:47	0
Mid Point Flurometer	3/4/2015 18:48	0
Mid Point Flurometer	3/4/2015 18:49	0
Mid Point Flurometer	3/4/2015 18:50	0
Mid Point Flurometer	3/4/2015 18:51	0
Mid Point Flurometer	3/4/2015 18:52	0
Mid Point Flurometer	3/4/2015 18:53	0
Mid Point Flurometer	3/4/2015 18:54	0
Mid Point Flurometer	3/4/2015 18:55	0
Mid Point Flurometer	3/4/2015 18:56	0
Mid Point Flurometer	3/4/2015 18:57	0
Mid Point Flurometer	3/4/2015 18:58	0
Mid Point Flurometer	3/4/2015 18:59	0
Mid Point Flurometer	3/4/2015 19:00	0
Mid Point Flurometer	3/4/2015 19:01	0
Mid Point Flurometer	3/4/2015 19:02	0
Mid Point Flurometer	3/4/2015 19:03	0
Mid Point Flurometer	3/4/2015 19:04	0
Mid Point Flurometer	3/4/2015 19:05	0
Mid Point Flurometer	3/4/2015 19:06	0
Mid Point Flurometer	3/4/2015 19:07	0
Mid Point Flurometer	3/4/2015 19:08	0
Mid Point Flurometer	3/4/2015 19:09	0
Mid Point Flurometer	3/4/2015 19:10	0
Mid Point Flurometer	3/4/2015 19:11	0
Mid Point Flurometer	3/4/2015 19:12	0
Mid Point Flurometer	3/4/2015 19:13	0
Mid Point Flurometer	3/4/2015 19:14	0
Mid Point Flurometer	3/4/2015 19:15	0
Mid Point Flurometer	3/4/2015 19:16	0
Mid Point Flurometer	3/4/2015 19:17	0
Mid Point Flurometer	3/4/2015 19:18	0
Mid Point Flurometer	3/4/2015 19:19	0
Mid Point Flurometer	3/4/2015 19:20	0

Location	Date and Time	Rhodmaine Concentration Adjusted Concentration (ppb)
Mid Point Flurometer	3/4/2015 19:21	0
Mid Point Flurometer	3/4/2015 19:22	0
Mid Point Flurometer	3/4/2015 19:23	0
Mid Point Flurometer	3/4/2015 19:24	0
Mid Point Flurometer	3/4/2015 19:25	0
Mid Point Flurometer	3/4/2015 19:26	0
Mid Point Flurometer	3/4/2015 19:27	0
Mid Point Flurometer	3/4/2015 19:28	0
Mid Point Flurometer	3/4/2015 19:29	0
Mid Point Flurometer	3/4/2015 19:30	0
Mid Point Flurometer	3/4/2015 19:31	0
Mid Point Flurometer	3/4/2015 19:32	0
Mid Point Flurometer	3/4/2015 19:33	0
Mid Point Flurometer	3/4/2015 19:34	0
Mid Point Flurometer	3/4/2015 19:35	0
Mid Point Flurometer	3/4/2015 19:36	0
Mid Point Flurometer	3/4/2015 19:37	0
Mid Point Flurometer	3/4/2015 19:38	0
Mid Point Flurometer	3/4/2015 19:39	0
Mid Point Flurometer	3/4/2015 19:40	0
Mid Point Flurometer	3/4/2015 19:41	0
Mid Point Flurometer	3/4/2015 19:42	0
Mid Point Flurometer	3/4/2015 19:43	0
Mid Point Flurometer	3/4/2015 19:44	0
Mid Point Flurometer	3/4/2015 19:45	0
Mid Point Flurometer	3/4/2015 19:46	0
Mid Point Flurometer	3/4/2015 19:47	0
Mid Point Flurometer	3/4/2015 19:48	0
Mid Point Flurometer	3/4/2015 19:49	0
Mid Point Flurometer	3/4/2015 19:50	0
Mid Point Flurometer	3/4/2015 19:51	0
Mid Point Flurometer	3/4/2015 19:52	0
Mid Point Flurometer	3/4/2015 19:53	0
Mid Point Flurometer	3/4/2015 19:54	0
Mid Point Flurometer	3/4/2015 19:55	0
Mid Point Flurometer	3/4/2015 19:56	0
Mid Point Flurometer	3/4/2015 19:57	0
Mid Point Flurometer	3/4/2015 19:58	0
Mid Point Flurometer	3/4/2015 19:59	0
Mid Point Flurometer	3/4/2015 20:00	0
Mid Point Flurometer	3/4/2015 20:01	0
Mid Point Flurometer	3/4/2015 20:02	0
Mid Point Flurometer	3/4/2015 20:03	0
Mid Point Flurometer	3/4/2015 20:04	0
Mid Point Flurometer	3/4/2015 20:05	0
Mid Point Flurometer	3/4/2015 20:06	0

Location	Date and Time	Rhodmaine Concentration Adjusted Concentration (ppb)
Mid Point Flurometer	3/4/2015 20:07	0
Mid Point Flurometer	3/4/2015 20:08	0
Mid Point Flurometer	3/4/2015 20:09	0
Mid Point Flurometer	3/4/2015 20:10	0
Mid Point Flurometer	3/4/2015 20:11	0
Mid Point Flurometer	3/4/2015 20:12	0
Mid Point Flurometer	3/4/2015 20:13	0
Mid Point Flurometer	3/4/2015 20:14	0
Mid Point Flurometer	3/4/2015 20:15	0
Mid Point Flurometer	3/4/2015 20:16	0
Mid Point Flurometer	3/4/2015 20:17	0.03
Mid Point Flurometer	3/4/2015 20:18	0
Mid Point Flurometer	3/4/2015 20:19	0
Mid Point Flurometer	3/4/2015 20:20	0
Mid Point Flurometer	3/4/2015 20:21	0
Mid Point Flurometer	3/4/2015 20:22	0
Mid Point Flurometer	3/4/2015 20:23	0
Mid Point Flurometer	3/4/2015 20:24	0
Mid Point Flurometer	3/4/2015 20:25	0
Mid Point Flurometer	3/4/2015 20:26	0
Mid Point Flurometer	3/4/2015 20:27	0
Mid Point Flurometer	3/4/2015 20:28	0
Mid Point Flurometer	3/4/2015 20:29	0
Mid Point Flurometer	3/4/2015 20:30	0
Mid Point Flurometer	3/4/2015 20:31	0
Mid Point Flurometer	3/4/2015 20:32	0
Mid Point Flurometer	3/4/2015 20:33	0
Mid Point Flurometer	3/4/2015 20:34	0
Mid Point Flurometer	3/4/2015 20:35	0
Mid Point Flurometer	3/4/2015 20:36	0
Mid Point Flurometer	3/4/2015 20:37	0
Mid Point Flurometer	3/4/2015 20:38	0
Mid Point Flurometer	3/4/2015 20:39	0
Mid Point Flurometer	3/4/2015 20:40	0
Mid Point Flurometer	3/4/2015 20:41	0
Mid Point Flurometer	3/4/2015 20:42	0
Mid Point Flurometer	3/4/2015 20:43	0
Mid Point Flurometer	3/4/2015 20:44	0
Mid Point Flurometer	3/4/2015 20:45	0
Mid Point Flurometer	3/4/2015 20:46	0
Mid Point Flurometer	3/4/2015 20:47	0
Mid Point Flurometer	3/4/2015 20:48	0
Mid Point Flurometer	3/4/2015 20:49	0
Mid Point Flurometer	3/4/2015 20:50	0
Mid Point Flurometer	3/4/2015 20:51	0
Mid Point Flurometer	3/4/2015 20:52	0

Location	Date and Time	Rhodmaine Concentration Adjusted Concentration (ppb)
Mid Point Flurometer	3/4/2015 20:53	0
Mid Point Flurometer	3/4/2015 20:54	0
Mid Point Flurometer	3/4/2015 20:55	0
Mid Point Flurometer	3/4/2015 20:56	0
Mid Point Flurometer	3/4/2015 20:57	0
Mid Point Flurometer	3/4/2015 20:58	0
Mid Point Flurometer	3/4/2015 20:59	0
Mid Point Flurometer	3/4/2015 21:00	0
Mid Point Flurometer	3/4/2015 21:01	0
Mid Point Flurometer	3/4/2015 21:02	0
Mid Point Flurometer	3/4/2015 21:03	0
Mid Point Flurometer	3/4/2015 21:04	0
Mid Point Flurometer	3/4/2015 21:05	0
Mid Point Flurometer	3/4/2015 21:06	0
Mid Point Flurometer	3/4/2015 21:07	0
Mid Point Flurometer	3/4/2015 21:08	0
Mid Point Flurometer	3/4/2015 21:09	0
Mid Point Flurometer	3/4/2015 21:10	0
Mid Point Flurometer	3/4/2015 21:11	0
Mid Point Flurometer	3/4/2015 21:12	0
Mid Point Flurometer	3/4/2015 21:13	0
Mid Point Flurometer	3/4/2015 21:14	0
Mid Point Flurometer	3/4/2015 21:15	0.03
Mid Point Flurometer	3/4/2015 21:16	0.03
Mid Point Flurometer	3/4/2015 21:17	0.05
Mid Point Flurometer	3/4/2015 21:18	0.07
Mid Point Flurometer	3/4/2015 21:19	0.09
Mid Point Flurometer	3/4/2015 21:20	0.17
Mid Point Flurometer	3/4/2015 21:21	0.16
Mid Point Flurometer	3/4/2015 21:22	0.2
Mid Point Flurometer	3/4/2015 21:23	0.24
Mid Point Flurometer	3/4/2015 21:24	0.27
Mid Point Flurometer	3/4/2015 21:25	0.36
Mid Point Flurometer	3/4/2015 21:26	0.39
Mid Point Flurometer	3/4/2015 21:27	0.48
Mid Point Flurometer	3/4/2015 21:28	0.55
Mid Point Flurometer	3/4/2015 21:29	0.57
Mid Point Flurometer	3/4/2015 21:30	0.66
Mid Point Flurometer	3/4/2015 21:31	0.8
Mid Point Flurometer	3/4/2015 21:32	0.86
Mid Point Flurometer	3/4/2015 21:33	1.01
Mid Point Flurometer	3/4/2015 21:34	1.07
Mid Point Flurometer	3/4/2015 21:35	1.12
Mid Point Flurometer	3/4/2015 21:36	1.22
Mid Point Flurometer	3/4/2015 21:37	1.38
Mid Point Flurometer	3/4/2015 21:38	1.48

Location	Date and Time	Rhodmaine Concentration Adjusted Concentration (ppb)
Mid Point Flurometer	3/4/2015 21:39	1.59
Mid Point Flurometer	3/4/2015 21:40	1.73
Mid Point Flurometer	3/4/2015 21:41	1.95
Mid Point Flurometer	3/4/2015 21:42	1.96
Mid Point Flurometer	3/4/2015 21:43	2.15
Mid Point Flurometer	3/4/2015 21:44	2.24
Mid Point Flurometer	3/4/2015 21:45	2.41
Mid Point Flurometer	3/4/2015 21:46	2.75
Mid Point Flurometer	3/4/2015 21:47	3.02
Mid Point Flurometer	3/4/2015 21:48	3.18
Mid Point Flurometer	3/4/2015 21:49	3.16
Mid Point Flurometer	3/4/2015 21:50	3.51
Mid Point Flurometer	3/4/2015 21:51	3.69
Mid Point Flurometer	3/4/2015 21:52	3.74
Mid Point Flurometer	3/4/2015 21:53	4.01
Mid Point Flurometer	3/4/2015 21:54	4.19
Mid Point Flurometer	3/4/2015 21:55	4.46
Mid Point Flurometer	3/4/2015 21:56	4.62
Mid Point Flurometer	3/4/2015 21:57	4.98
Mid Point Flurometer	3/4/2015 21:58	5.25
Mid Point Flurometer	3/4/2015 21:59	5.47
Mid Point Flurometer	3/4/2015 22:00	5.42
Mid Point Flurometer	3/4/2015 22:01	6.03
Mid Point Flurometer	3/4/2015 22:02	6.13
Mid Point Flurometer	3/4/2015 22:03	6.32
Mid Point Flurometer	3/4/2015 22:04	6.41
Mid Point Flurometer	3/4/2015 22:05	6.43
Mid Point Flurometer	3/4/2015 22:06	6.52
Mid Point Flurometer	3/4/2015 22:07	6.74
Mid Point Flurometer	3/4/2015 22:08	6.97
Mid Point Flurometer	3/4/2015 22:09	7.19
Mid Point Flurometer	3/4/2015 22:10	7.47
Mid Point Flurometer	3/4/2015 22:11	7.77
Mid Point Flurometer	3/4/2015 22:12	7.98
Mid Point Flurometer	3/4/2015 22:13	8.06
Mid Point Flurometer	3/4/2015 22:14	8.33
Mid Point Flurometer	3/4/2015 22:15	8.47
Mid Point Flurometer	3/4/2015 22:16	8.56
Mid Point Flurometer	3/4/2015 22:17	8.46
Mid Point Flurometer	3/4/2015 22:18	8.69
Mid Point Flurometer	3/4/2015 22:19	9.02
Mid Point Flurometer	3/4/2015 22:20	9.32
Mid Point Flurometer	3/4/2015 22:21	9.47
Mid Point Flurometer	3/4/2015 22:22	9.57
Mid Point Flurometer	3/4/2015 22:23	9.61
Mid Point Flurometer	3/4/2015 22:24	9.73

Location	Date and Time	Rhodmaine Concentration Adjusted Concentration (ppb)
Mid Point Flurometer	3/4/2015 22:25	9.7
Mid Point Flurometer	3/4/2015 22:26	9.99
Mid Point Flurometer	3/4/2015 22:27	10.15
Mid Point Flurometer	3/4/2015 22:28	10.27
Mid Point Flurometer	3/4/2015 22:29	10.3
Mid Point Flurometer	3/4/2015 22:30	10.26
Mid Point Flurometer	3/4/2015 22:31	10.55
Mid Point Flurometer	3/4/2015 22:32	10.68
Mid Point Flurometer	3/4/2015 22:33	10.7
Mid Point Flurometer	3/4/2015 22:34	10.52
Mid Point Flurometer	3/4/2015 22:35	10.61
Mid Point Flurometer	3/4/2015 22:36	10.73
Mid Point Flurometer	3/4/2015 22:37	10.87
Mid Point Flurometer	3/4/2015 22:38	10.93
Mid Point Flurometer	3/4/2015 22:39	10.95
Mid Point Flurometer	3/4/2015 22:40	11.01
Mid Point Flurometer	3/4/2015 22:41	10.99
Mid Point Flurometer	3/4/2015 22:42	11.03
Mid Point Flurometer	3/4/2015 22:43	11.06
Mid Point Flurometer	3/4/2015 22:44	11.1
Mid Point Flurometer	3/4/2015 22:45	11.13
Mid Point Flurometer	3/4/2015 22:46	11.12
Mid Point Flurometer	3/4/2015 22:47	11.12
Mid Point Flurometer	3/4/2015 22:48	11.15
Mid Point Flurometer	3/4/2015 22:49	11.11
Mid Point Flurometer	3/4/2015 22:50	11.15
Mid Point Flurometer	3/4/2015 22:51	11.12
Mid Point Flurometer	3/4/2015 22:52	11.1
Mid Point Flurometer	3/4/2015 22:53	11.1
Mid Point Flurometer	3/4/2015 22:54	11.05
Mid Point Flurometer	3/4/2015 22:55	11.05
Mid Point Flurometer	3/4/2015 22:56	11.01
Mid Point Flurometer	3/4/2015 22:57	10.97
Mid Point Flurometer	3/4/2015 22:58	10.91
Mid Point Flurometer	3/4/2015 22:59	10.91
Mid Point Flurometer	3/4/2015 23:00	10.9
Mid Point Flurometer	3/4/2015 23:01	10.87
Mid Point Flurometer	3/4/2015 23:02	10.81
Mid Point Flurometer	3/4/2015 23:03	10.74
Mid Point Flurometer	3/4/2015 23:04	10.7
Mid Point Flurometer	3/4/2015 23:05	10.63
Mid Point Flurometer	3/4/2015 23:06	10.57
Mid Point Flurometer	3/4/2015 23:07	10.51
Mid Point Flurometer	3/4/2015 23:08	10.45
Mid Point Flurometer	3/4/2015 23:09	10.41
Mid Point Flurometer	3/4/2015 23:10	10.34

Location	Date and Time	Rhodmaine Concentration Adjusted Concentration (ppb)
Mid Point Flurometer	3/4/2015 23:11	10.33
Mid Point Flurometer	3/4/2015 23:12	10.22
Mid Point Flurometer	3/4/2015 23:13	10.16
Mid Point Flurometer	3/4/2015 23:14	10.18
Mid Point Flurometer	3/4/2015 23:15	10.05
Mid Point Flurometer	3/4/2015 23:16	10.02
Mid Point Flurometer	3/4/2015 23:17	9.88
Mid Point Flurometer	3/4/2015 23:18	9.78
Mid Point Flurometer	3/4/2015 23:19	9.73
Mid Point Flurometer	3/4/2015 23:20	9.63
Mid Point Flurometer	3/4/2015 23:21	9.57
Mid Point Flurometer	3/4/2015 23:22	9.51
Mid Point Flurometer	3/4/2015 23:23	9.54
Mid Point Flurometer	3/4/2015 23:24	9.4
Mid Point Flurometer	3/4/2015 23:25	9.27
Mid Point Flurometer	3/4/2015 23:26	9.15
Mid Point Flurometer	3/4/2015 23:27	9.16
Mid Point Flurometer	3/4/2015 23:28	9.08
Mid Point Flurometer	3/4/2015 23:29	8.97
Mid Point Flurometer	3/4/2015 23:30	8.9
Mid Point Flurometer	3/4/2015 23:31	8.87
Mid Point Flurometer	3/4/2015 23:32	8.82
Mid Point Flurometer	3/4/2015 23:33	8.76
Mid Point Flurometer	3/4/2015 23:34	8.67
Mid Point Flurometer	3/4/2015 23:35	8.52
Mid Point Flurometer	3/4/2015 23:36	8.5
Mid Point Flurometer	3/4/2015 23:37	8.42
Mid Point Flurometer	3/4/2015 23:38	8.33
Mid Point Flurometer	3/4/2015 23:39	8.2
Mid Point Flurometer	3/4/2015 23:40	8.14
Mid Point Flurometer	3/4/2015 23:41	8.1
Mid Point Flurometer	3/4/2015 23:42	8.06
Mid Point Flurometer	3/4/2015 23:43	8.02
Mid Point Flurometer	3/4/2015 23:44	7.99
Mid Point Flurometer	3/4/2015 23:45	7.87
Mid Point Flurometer	3/4/2015 23:46	7.8
Mid Point Flurometer	3/4/2015 23:47	7.83
Mid Point Flurometer	3/4/2015 23:48	7.71
Mid Point Flurometer	3/4/2015 23:49	7.7
Mid Point Flurometer	3/4/2015 23:50	7.5
Mid Point Flurometer	3/4/2015 23:51	7.51
Mid Point Flurometer	3/4/2015 23:52	7.46
Mid Point Flurometer	3/4/2015 23:53	7.38
Mid Point Flurometer	3/4/2015 23:54	7.33
Mid Point Flurometer	3/4/2015 23:55	7.24
Mid Point Flurometer	3/4/2015 23:56	7.19

Location	Date and Time	Rhodmaine Concentration Adjusted Concentration (ppb)
Mid Point Flurometer	3/4/2015 23:57	7.1
Mid Point Flurometer	3/4/2015 23:58	7.06
Mid Point Flurometer	3/4/2015 23:59	7.01
Mid Point Flurometer	3/5/2015 0:00	6.94
Mid Point Flurometer	3/5/2015 0:01	6.91
Mid Point Flurometer	3/5/2015 0:02	6.85
Mid Point Flurometer	3/5/2015 0:03	6.78
Mid Point Flurometer	3/5/2015 0:04	6.72
Mid Point Flurometer	3/5/2015 0:05	6.7
Mid Point Flurometer	3/5/2015 0:06	6.7
Mid Point Flurometer	3/5/2015 0:07	7.02
Mid Point Flurometer	3/5/2015 0:08	6.51
Mid Point Flurometer	3/5/2015 0:09	6.49
Mid Point Flurometer	3/5/2015 0:10	6.49
Mid Point Flurometer	3/5/2015 0:11	6.46
Mid Point Flurometer	3/5/2015 0:12	6.41
Mid Point Flurometer	3/5/2015 0:13	6.33
Mid Point Flurometer	3/5/2015 0:14	6.32
Mid Point Flurometer	3/5/2015 0:15	6.3
Mid Point Flurometer	3/5/2015 0:16	6.18
Mid Point Flurometer	3/5/2015 0:17	6.19
Mid Point Flurometer	3/5/2015 0:18	6.15
Mid Point Flurometer	3/5/2015 0:19	6.15
Mid Point Flurometer	3/5/2015 0:20	6.08
Mid Point Flurometer	3/5/2015 0:21	6.11
Mid Point Flurometer	3/5/2015 0:22	6.09
Mid Point Flurometer	3/5/2015 0:23	6.05
Mid Point Flurometer	3/5/2015 0:24	5.98
Mid Point Flurometer	3/5/2015 0:25	5.96
Mid Point Flurometer	3/5/2015 0:26	5.88
Mid Point Flurometer	3/5/2015 0:27	5.88
Mid Point Flurometer	3/5/2015 0:28	5.83
Mid Point Flurometer	3/5/2015 0:29	5.82
Mid Point Flurometer	3/5/2015 0:30	5.77
Mid Point Flurometer	3/5/2015 0:31	5.77
Mid Point Flurometer	3/5/2015 0:32	5.75
Mid Point Flurometer	3/5/2015 0:33	5.69
Mid Point Flurometer	3/5/2015 0:34	5.69
Mid Point Flurometer	3/5/2015 0:35	5.65
Mid Point Flurometer	3/5/2015 0:36	5.63
Mid Point Flurometer	3/5/2015 0:37	5.63
Mid Point Flurometer	3/5/2015 0:38	5.61
Mid Point Flurometer	3/5/2015 0:39	5.59
Mid Point Flurometer	3/5/2015 0:40	5.55
Mid Point Flurometer	3/5/2015 0:41	5.53
Mid Point Flurometer	3/5/2015 0:42	5.5

Location	Date and Time	Rhodmaine Concentration Adjusted Concentration (ppb)
Mid Point Flurometer	3/5/2015 0:43	5.48
Mid Point Flurometer	3/5/2015 0:44	5.45
Mid Point Flurometer	3/5/2015 0:45	5.45
Mid Point Flurometer	3/5/2015 0:46	5.39
Mid Point Flurometer	3/5/2015 0:47	5.37
Mid Point Flurometer	3/5/2015 0:48	5.35
Mid Point Flurometer	3/5/2015 0:49	5.35
Mid Point Flurometer	3/5/2015 0:50	5.29
Mid Point Flurometer	3/5/2015 0:51	5.29
Mid Point Flurometer	3/5/2015 0:52	5.3
Mid Point Flurometer	3/5/2015 0:53	5.29
Mid Point Flurometer	3/5/2015 0:54	5.2
Mid Point Flurometer	3/5/2015 0:55	5.23
Mid Point Flurometer	3/5/2015 0:56	5.19
Mid Point Flurometer	3/5/2015 0:57	5.19
Mid Point Flurometer	3/5/2015 0:58	5.1
Mid Point Flurometer	3/5/2015 0:59	5.1
Mid Point Flurometer	3/5/2015 1:00	5.06
Mid Point Flurometer	3/5/2015 1:01	5.07
Mid Point Flurometer	3/5/2015 1:02	5.07
Mid Point Flurometer	3/5/2015 1:03	5.05
Mid Point Flurometer	3/5/2015 1:04	5.03
Mid Point Flurometer	3/5/2015 1:05	5.02
Mid Point Flurometer	3/5/2015 1:06	4.98
Mid Point Flurometer	3/5/2015 1:07	4.98
Mid Point Flurometer	3/5/2015 1:08	4.93
Mid Point Flurometer	3/5/2015 1:09	4.91
Mid Point Flurometer	3/5/2015 1:10	4.9
Mid Point Flurometer	3/5/2015 1:11	4.86
Mid Point Flurometer	3/5/2015 1:12	4.87
Mid Point Flurometer	3/5/2015 1:13	4.83
Mid Point Flurometer	3/5/2015 1:14	4.78
Mid Point Flurometer	3/5/2015 1:15	4.76
Mid Point Flurometer	3/5/2015 1:16	4.74
Mid Point Flurometer	3/5/2015 1:17	4.73
Mid Point Flurometer	3/5/2015 1:18	4.71
Mid Point Flurometer	3/5/2015 1:19	4.67
Mid Point Flurometer	3/5/2015 1:20	4.65
Mid Point Flurometer	3/5/2015 1:21	4.65
Mid Point Flurometer	3/5/2015 1:22	4.62
Mid Point Flurometer	3/5/2015 1:23	4.64
Mid Point Flurometer	3/5/2015 1:24	4.59
Mid Point Flurometer	3/5/2015 1:25	4.56
Mid Point Flurometer	3/5/2015 1:26	4.53
Mid Point Flurometer	3/5/2015 1:27	4.5
Mid Point Flurometer	3/5/2015 1:28	4.49

Location	Date and Time	Rhodmaine Concentration Adjusted Concentration (ppb)
Mid Point Flurometer	3/5/2015 1:29	4.46
Mid Point Flurometer	3/5/2015 1:30	4.44
Mid Point Flurometer	3/5/2015 1:31	4.41
Mid Point Flurometer	3/5/2015 1:32	4.41
Mid Point Flurometer	3/5/2015 1:33	4.37
Mid Point Flurometer	3/5/2015 1:34	4.34
Mid Point Flurometer	3/5/2015 1:35	4.33
Mid Point Flurometer	3/5/2015 1:36	4.29
Mid Point Flurometer	3/5/2015 1:37	4.27
Mid Point Flurometer	3/5/2015 1:38	4.27
Mid Point Flurometer	3/5/2015 1:39	4.21
Mid Point Flurometer	3/5/2015 1:40	4.21
Mid Point Flurometer	3/5/2015 1:41	4.19
Mid Point Flurometer	3/5/2015 1:42	4.16
Mid Point Flurometer	3/5/2015 1:43	4.14
Mid Point Flurometer	3/5/2015 1:44	4.11
Mid Point Flurometer	3/5/2015 1:45	4.07
Mid Point Flurometer	3/5/2015 1:46	4.07
Mid Point Flurometer	3/5/2015 1:47	4.03
Mid Point Flurometer	3/5/2015 1:48	4.04
Mid Point Flurometer	3/5/2015 1:49	4.01
Mid Point Flurometer	3/5/2015 1:50	3.97
Mid Point Flurometer	3/5/2015 1:51	3.96
Mid Point Flurometer	3/5/2015 1:52	3.94
Mid Point Flurometer	3/5/2015 1:53	3.93
Mid Point Flurometer	3/5/2015 1:54	3.91
Mid Point Flurometer	3/5/2015 1:55	3.88
Mid Point Flurometer	3/5/2015 1:56	3.86
Mid Point Flurometer	3/5/2015 1:57	3.87
Mid Point Flurometer	3/5/2015 1:58	3.82
Mid Point Flurometer	3/5/2015 1:59	3.78
Mid Point Flurometer	3/5/2015 2:00	3.76
Mid Point Flurometer	3/5/2015 2:01	3.71
Mid Point Flurometer	3/5/2015 2:02	3.72
Mid Point Flurometer	3/5/2015 2:03	3.67
Mid Point Flurometer	3/5/2015 2:04	3.67
Mid Point Flurometer	3/5/2015 2:05	3.65
Mid Point Flurometer	3/5/2015 2:06	3.64
Mid Point Flurometer	3/5/2015 2:07	3.59
Mid Point Flurometer	3/5/2015 2:08	3.54
Mid Point Flurometer	3/5/2015 2:09	3.52
Mid Point Flurometer	3/5/2015 2:10	3.53
Mid Point Flurometer	3/5/2015 2:11	3.5
Mid Point Flurometer	3/5/2015 2:12	3.5
Mid Point Flurometer	3/5/2015 2:13	3.46
Mid Point Flurometer	3/5/2015 2:14	3.4

Location	Date and Time	Rhodmaine Concentration Adjusted Concentration (ppb)
Mid Point Flurometer	3/5/2015 2:15	3.4
Mid Point Flurometer	3/5/2015 2:16	3.36
Mid Point Flurometer	3/5/2015 2:17	3.35
Mid Point Flurometer	3/5/2015 2:18	3.34
Mid Point Flurometer	3/5/2015 2:19	3.33
Mid Point Flurometer	3/5/2015 2:20	3.32
Mid Point Flurometer	3/5/2015 2:21	3.28
Mid Point Flurometer	3/5/2015 2:22	3.23
Mid Point Flurometer	3/5/2015 2:23	3.22
Mid Point Flurometer	3/5/2015 2:24	3.19
Mid Point Flurometer	3/5/2015 2:25	3.17
Mid Point Flurometer	3/5/2015 2:26	3.19
Mid Point Flurometer	3/5/2015 2:27	3.16
Mid Point Flurometer	3/5/2015 2:28	3.11
Mid Point Flurometer	3/5/2015 2:29	3.08
Mid Point Flurometer	3/5/2015 2:30	3.05
Mid Point Flurometer	3/5/2015 2:31	3.04
Mid Point Flurometer	3/5/2015 2:32	3.01
Mid Point Flurometer	3/5/2015 2:33	2.99
Mid Point Flurometer	3/5/2015 2:34	2.98
Mid Point Flurometer	3/5/2015 2:35	2.92
Mid Point Flurometer	3/5/2015 2:36	2.92
Mid Point Flurometer	3/5/2015 2:37	2.89
Mid Point Flurometer	3/5/2015 2:38	2.87
Mid Point Flurometer	3/5/2015 2:39	2.85
Mid Point Flurometer	3/5/2015 2:40	2.83
Mid Point Flurometer	3/5/2015 2:41	2.81
Mid Point Flurometer	3/5/2015 2:42	2.78
Mid Point Flurometer	3/5/2015 2:43	2.83
Mid Point Flurometer	3/5/2015 2:44	2.76
Mid Point Flurometer	3/5/2015 2:45	2.71
Mid Point Flurometer	3/5/2015 2:46	2.7
Mid Point Flurometer	3/5/2015 2:47	2.7
Mid Point Flurometer	3/5/2015 2:48	2.66
Mid Point Flurometer	3/5/2015 2:49	2.67
Mid Point Flurometer	3/5/2015 2:50	2.61
Mid Point Flurometer	3/5/2015 2:51	2.6
Mid Point Flurometer	3/5/2015 2:52	2.57
Mid Point Flurometer	3/5/2015 2:53	2.58
Mid Point Flurometer	3/5/2015 2:54	2.55
Mid Point Flurometer	3/5/2015 2:55	2.53
Mid Point Flurometer	3/5/2015 2:56	2.52
Mid Point Flurometer	3/5/2015 2:57	2.5
Mid Point Flurometer	3/5/2015 2:58	2.47
Mid Point Flurometer	3/5/2015 2:59	2.46
Mid Point Flurometer	3/5/2015 3:00	2.44

Location	Date and Time	Rhodmaine Concentration Adjusted Concentration (ppb)
Mid Point Flurometer	3/5/2015 3:01	2.41
Mid Point Flurometer	3/5/2015 3:02	2.4
Mid Point Flurometer	3/5/2015 3:03	2.4
Mid Point Flurometer	3/5/2015 3:04	2.38
Mid Point Flurometer	3/5/2015 3:05	2.36
Mid Point Flurometer	3/5/2015 3:06	2.44
Mid Point Flurometer	3/5/2015 3:07	2.31
Mid Point Flurometer	3/5/2015 3:08	2.3
Mid Point Flurometer	3/5/2015 3:09	2.31
Mid Point Flurometer	3/5/2015 3:10	2.28
Mid Point Flurometer	3/5/2015 3:11	2.25
Mid Point Flurometer	3/5/2015 3:12	2.22
Mid Point Flurometer	3/5/2015 3:13	2.21
Mid Point Flurometer	3/5/2015 3:14	2.21
Mid Point Flurometer	3/5/2015 3:15	2.19
Mid Point Flurometer	3/5/2015 3:16	2.15
Mid Point Flurometer	3/5/2015 3:17	2.13
Mid Point Flurometer	3/5/2015 3:18	2.12
Mid Point Flurometer	3/5/2015 3:19	2.13
Mid Point Flurometer	3/5/2015 3:20	2.13
Mid Point Flurometer	3/5/2015 3:21	2.09
Mid Point Flurometer	3/5/2015 3:22	2.1
Mid Point Flurometer	3/5/2015 3:23	2.08
Mid Point Flurometer	3/5/2015 3:24	2.06
Mid Point Flurometer	3/5/2015 3:25	2.05
Mid Point Flurometer	3/5/2015 3:26	2.02
Mid Point Flurometer	3/5/2015 3:27	2.03
Mid Point Flurometer	3/5/2015 3:28	2.01
Mid Point Flurometer	3/5/2015 3:29	1.99
Mid Point Flurometer	3/5/2015 3:30	2.01
Mid Point Flurometer	3/5/2015 3:31	1.97
Mid Point Flurometer	3/5/2015 3:32	1.97
Mid Point Flurometer	3/5/2015 3:33	1.94
Mid Point Flurometer	3/5/2015 3:34	1.9
Mid Point Flurometer	3/5/2015 3:35	1.91
Mid Point Flurometer	3/5/2015 3:36	1.92
Mid Point Flurometer	3/5/2015 3:37	1.89
Mid Point Flurometer	3/5/2015 3:38	1.91
Mid Point Flurometer	3/5/2015 3:39	1.86
Mid Point Flurometer	3/5/2015 3:40	1.84
Mid Point Flurometer	3/5/2015 3:41	1.82
Mid Point Flurometer	3/5/2015 3:42	1.83
Mid Point Flurometer	3/5/2015 3:43	1.84
Mid Point Flurometer	3/5/2015 3:44	1.79
Mid Point Flurometer	3/5/2015 3:45	1.79
Mid Point Flurometer	3/5/2015 3:46	1.77

Location	Date and Time	Rhodmaine Concentration Adjusted Concentration (ppb)
Mid Point Flurometer	3/5/2015 3:47	1.77
Mid Point Flurometer	3/5/2015 3:48	1.78
Mid Point Flurometer	3/5/2015 3:49	1.75
Mid Point Flurometer	3/5/2015 3:50	1.77
Mid Point Flurometer	3/5/2015 3:51	1.73
Mid Point Flurometer	3/5/2015 3:52	1.72
Mid Point Flurometer	3/5/2015 3:53	1.7
Mid Point Flurometer	3/5/2015 3:54	1.7
Mid Point Flurometer	3/5/2015 3:55	1.69
Mid Point Flurometer	3/5/2015 3:56	1.7
Mid Point Flurometer	3/5/2015 3:57	1.7
Mid Point Flurometer	3/5/2015 3:58	1.67
Mid Point Flurometer	3/5/2015 3:59	1.67
Mid Point Flurometer	3/5/2015 4:00	1.65
Mid Point Flurometer	3/5/2015 4:01	1.64
Mid Point Flurometer	3/5/2015 4:02	1.65
Mid Point Flurometer	3/5/2015 4:03	1.63
Mid Point Flurometer	3/5/2015 4:04	1.63
Mid Point Flurometer	3/5/2015 4:05	1.62
Mid Point Flurometer	3/5/2015 4:06	1.6
Mid Point Flurometer	3/5/2015 4:07	1.6
Mid Point Flurometer	3/5/2015 4:08	1.58
Mid Point Flurometer	3/5/2015 4:09	1.59
Mid Point Flurometer	3/5/2015 4:10	1.59
Mid Point Flurometer	3/5/2015 4:11	1.58
Mid Point Flurometer	3/5/2015 4:12	1.56
Mid Point Flurometer	3/5/2015 4:13	1.56
Mid Point Flurometer	3/5/2015 4:14	1.53
Mid Point Flurometer	3/5/2015 4:15	1.53
Mid Point Flurometer	3/5/2015 4:16	1.55
Mid Point Flurometer	3/5/2015 4:17	1.53
Mid Point Flurometer	3/5/2015 4:18	1.53
Mid Point Flurometer	3/5/2015 4:19	1.51
Mid Point Flurometer	3/5/2015 4:20	1.5
Mid Point Flurometer	3/5/2015 4:21	1.55
Mid Point Flurometer	3/5/2015 4:22	1.51
Mid Point Flurometer	3/5/2015 4:23	1.5
Mid Point Flurometer	3/5/2015 4:24	1.51
Mid Point Flurometer	3/5/2015 4:25	1.47
Mid Point Flurometer	3/5/2015 4:26	1.47
Mid Point Flurometer	3/5/2015 4:27	1.47
Mid Point Flurometer	3/5/2015 4:28	1.46
Mid Point Flurometer	3/5/2015 4:29	1.46
Mid Point Flurometer	3/5/2015 4:30	1.47
Mid Point Flurometer	3/5/2015 4:31	1.47
Mid Point Flurometer	3/5/2015 4:32	1.43

Location	Date and Time	Rhodmaine Concentration Adjusted Concentration (ppb)
Mid Point Flurometer	3/5/2015 4:33	1.52
Mid Point Flurometer	3/5/2015 4:34	1.43
Mid Point Flurometer	3/5/2015 4:35	1.42
Mid Point Flurometer	3/5/2015 4:36	1.43
Mid Point Flurometer	3/5/2015 4:37	1.42
Mid Point Flurometer	3/5/2015 4:38	1.42
Mid Point Flurometer	3/5/2015 4:39	1.4
Mid Point Flurometer	3/5/2015 4:40	1.41
Mid Point Flurometer	3/5/2015 4:41	1.43
Mid Point Flurometer	3/5/2015 4:42	1.4
Mid Point Flurometer	3/5/2015 4:43	1.4
Mid Point Flurometer	3/5/2015 4:44	1.37
Mid Point Flurometer	3/5/2015 4:45	1.38
Mid Point Flurometer	3/5/2015 4:46	1.39
Mid Point Flurometer	3/5/2015 4:47	1.38
Mid Point Flurometer	3/5/2015 4:48	1.36
Mid Point Flurometer	3/5/2015 4:49	1.37
Mid Point Flurometer	3/5/2015 4:50	1.35
Mid Point Flurometer	3/5/2015 4:51	1.36
Mid Point Flurometer	3/5/2015 4:52	1.35
Mid Point Flurometer	3/5/2015 4:53	1.35
Mid Point Flurometer	3/5/2015 4:54	1.35
Mid Point Flurometer	3/5/2015 4:55	1.33
Mid Point Flurometer	3/5/2015 4:56	1.34
Mid Point Flurometer	3/5/2015 4:57	1.29
Mid Point Flurometer	3/5/2015 4:58	1.34
Mid Point Flurometer	3/5/2015 4:59	1.3
Mid Point Flurometer	3/5/2015 5:00	1.34
Mid Point Flurometer	3/5/2015 5:01	1.3
Mid Point Flurometer	3/5/2015 5:02	1.29
Mid Point Flurometer	3/5/2015 5:03	1.31
Mid Point Flurometer	3/5/2015 5:04	1.3
Mid Point Flurometer	3/5/2015 5:05	1.29
Mid Point Flurometer	3/5/2015 5:06	1.3
Mid Point Flurometer	3/5/2015 5:07	1.28
Mid Point Flurometer	3/5/2015 5:08	1.27
Mid Point Flurometer	3/5/2015 5:09	1.3
Mid Point Flurometer	3/5/2015 5:10	1.27
Mid Point Flurometer	3/5/2015 5:11	1.29
Mid Point Flurometer	3/5/2015 5:12	1.27
Mid Point Flurometer	3/5/2015 5:13	1.25
Mid Point Flurometer	3/5/2015 5:14	1.24
Mid Point Flurometer	3/5/2015 5:15	1.24
Mid Point Flurometer	3/5/2015 5:16	1.25
Mid Point Flurometer	3/5/2015 5:17	1.26
Mid Point Flurometer	3/5/2015 5:18	1.22

Location	Date and Time	Rhodmaine Concentration Adjusted Concentration (ppb)
Mid Point Flurometer	3/5/2015 5:19	1.22
Mid Point Flurometer	3/5/2015 5:20	1.24
Mid Point Flurometer	3/5/2015 5:21	1.22
Mid Point Flurometer	3/5/2015 5:22	1.23
Mid Point Flurometer	3/5/2015 5:23	1.24
Mid Point Flurometer	3/5/2015 5:24	1.21
Mid Point Flurometer	3/5/2015 5:25	1.22
Mid Point Flurometer	3/5/2015 5:26	1.21
Mid Point Flurometer	3/5/2015 5:27	1.23
Mid Point Flurometer	3/5/2015 5:28	1.19
Mid Point Flurometer	3/5/2015 5:29	1.19
Mid Point Flurometer	3/5/2015 5:30	1.19
Mid Point Flurometer	3/5/2015 5:31	1.21
Mid Point Flurometer	3/5/2015 5:32	1.24
Mid Point Flurometer	3/5/2015 5:33	1.18
Mid Point Flurometer	3/5/2015 5:34	1.2
Mid Point Flurometer	3/5/2015 5:35	1.18
Mid Point Flurometer	3/5/2015 5:36	1.19
Mid Point Flurometer	3/5/2015 5:37	1.15
Mid Point Flurometer	3/5/2015 5:38	1.16
Mid Point Flurometer	3/5/2015 5:39	1.16
Mid Point Flurometer	3/5/2015 5:40	1.17
Mid Point Flurometer	3/5/2015 5:41	1.16
Mid Point Flurometer	3/5/2015 5:42	1.15
Mid Point Flurometer	3/5/2015 5:43	1.15
Mid Point Flurometer	3/5/2015 5:44	1.14
Mid Point Flurometer	3/5/2015 5:45	1.15
Mid Point Flurometer	3/5/2015 5:46	1.13
Mid Point Flurometer	3/5/2015 5:47	1.14
Mid Point Flurometer	3/5/2015 5:48	1.12
Mid Point Flurometer	3/5/2015 5:49	1.14
Mid Point Flurometer	3/5/2015 5:50	1.16
Mid Point Flurometer	3/5/2015 5:51	1.13
Mid Point Flurometer	3/5/2015 5:52	1.13
Mid Point Flurometer	3/5/2015 5:53	1.13
Mid Point Flurometer	3/5/2015 5:54	1.11
Mid Point Flurometer	3/5/2015 5:55	1.12
Mid Point Flurometer	3/5/2015 5:56	1.1
Mid Point Flurometer	3/5/2015 5:57	1.11
Mid Point Flurometer	3/5/2015 5:58	1.14
Mid Point Flurometer	3/5/2015 5:59	1.12
Mid Point Flurometer	3/5/2015 6:00	1.09
Mid Point Flurometer	3/5/2015 6:01	1.11
Mid Point Flurometer	3/5/2015 6:02	1.17
Mid Point Flurometer	3/5/2015 6:03	1.11
Mid Point Flurometer	3/5/2015 6:04	1.08

Location	Date and Time	Rhodmaine Concentration Adjusted Concentration (ppb)
Mid Point Flurometer	3/5/2015 6:05	1.16
Mid Point Flurometer	3/5/2015 6:06	1.07
Mid Point Flurometer	3/5/2015 6:07	1.07
Mid Point Flurometer	3/5/2015 6:08	1.13
Mid Point Flurometer	3/5/2015 6:09	1.07
Mid Point Flurometer	3/5/2015 6:10	1.06
Mid Point Flurometer	3/5/2015 6:11	1.06
Mid Point Flurometer	3/5/2015 6:12	1.05
Mid Point Flurometer	3/5/2015 6:13	1.04
Mid Point Flurometer	3/5/2015 6:14	1.04
Mid Point Flurometer	3/5/2015 6:15	1.04
Mid Point Flurometer	3/5/2015 6:16	1.04
Mid Point Flurometer	3/5/2015 6:17	1.04
Mid Point Flurometer	3/5/2015 6:18	1.03
Mid Point Flurometer	3/5/2015 6:19	1.13
Mid Point Flurometer	3/5/2015 6:20	1.05
Mid Point Flurometer	3/5/2015 6:21	1.04
Mid Point Flurometer	3/5/2015 6:22	1.03
Mid Point Flurometer	3/5/2015 6:23	1.01
Mid Point Flurometer	3/5/2015 6:24	1.03
Mid Point Flurometer	3/5/2015 6:25	1.04
Mid Point Flurometer	3/5/2015 6:26	1.03
Mid Point Flurometer	3/5/2015 6:27	1
Mid Point Flurometer	3/5/2015 6:28	1
Mid Point Flurometer	3/5/2015 6:29	1.03
Mid Point Flurometer	3/5/2015 6:30	1.01
Mid Point Flurometer	3/5/2015 6:31	1
Mid Point Flurometer	3/5/2015 6:32	1
Mid Point Flurometer	3/5/2015 6:33	1.03
Mid Point Flurometer	3/5/2015 6:34	0.99
Mid Point Flurometer	3/5/2015 6:35	0.98
Mid Point Flurometer	3/5/2015 6:36	0.98
Mid Point Flurometer	3/5/2015 6:37	0.97
Mid Point Flurometer	3/5/2015 6:38	0.99
Mid Point Flurometer	3/5/2015 6:39	0.99
Mid Point Flurometer	3/5/2015 6:40	0.99
Mid Point Flurometer	3/5/2015 6:41	0.95
Mid Point Flurometer	3/5/2015 6:42	0.98
Mid Point Flurometer	3/5/2015 6:43	0.98
Mid Point Flurometer	3/5/2015 6:44	0.94
Mid Point Flurometer	3/5/2015 6:45	0.96
Mid Point Flurometer	3/5/2015 6:46	0.93
Mid Point Flurometer	3/5/2015 6:47	0.93
Mid Point Flurometer	3/5/2015 6:48	0.93
Mid Point Flurometer	3/5/2015 6:49	0.94
Mid Point Flurometer	3/5/2015 6:50	0.93

Location	Date and Time	Rhodmaine Concentration Adjusted Concentration (ppb)
Mid Point Flurometer	3/5/2015 6:51	0.93
Mid Point Flurometer	3/5/2015 6:52	0.99
Mid Point Flurometer	3/5/2015 6:53	0.92
Mid Point Flurometer	3/5/2015 6:54	0.91
Mid Point Flurometer	3/5/2015 6:55	0.9
Mid Point Flurometer	3/5/2015 6:56	0.92
Mid Point Flurometer	3/5/2015 6:57	0.91
Mid Point Flurometer	3/5/2015 6:58	0.92
Mid Point Flurometer	3/5/2015 6:59	0.91
Mid Point Flurometer	3/5/2015 7:00	0.94
Mid Point Flurometer	3/5/2015 7:01	0.91
Mid Point Flurometer	3/5/2015 7:02	0.91
Mid Point Flurometer	3/5/2015 7:03	0.9
Mid Point Flurometer	3/5/2015 7:04	0.9
Mid Point Flurometer	3/5/2015 7:05	0.88
Mid Point Flurometer	3/5/2015 7:06	0.88
Mid Point Flurometer	3/5/2015 7:07	0.89
Mid Point Flurometer	3/5/2015 7:08	0.89
Mid Point Flurometer	3/5/2015 7:09	0.9
Mid Point Flurometer	3/5/2015 7:10	0.89
Mid Point Flurometer	3/5/2015 7:11	0.88
Mid Point Flurometer	3/5/2015 7:12	0.87
Mid Point Flurometer	3/5/2015 7:13	0.86
Mid Point Flurometer	3/5/2015 7:14	0.87
Mid Point Flurometer	3/5/2015 7:15	0.91
Mid Point Flurometer	3/5/2015 7:16	0.87
Mid Point Flurometer	3/5/2015 7:17	0.84
Mid Point Flurometer	3/5/2015 7:18	0.85
Mid Point Flurometer	3/5/2015 7:19	0.86
Mid Point Flurometer	3/5/2015 7:20	0.82
Mid Point Flurometer	3/5/2015 7:21	0.84
Mid Point Flurometer	3/5/2015 7:22	0.87
Mid Point Flurometer	3/5/2015 7:23	0.85
Mid Point Flurometer	3/5/2015 7:24	0.84
Mid Point Flurometer	3/5/2015 7:25	0.81
Mid Point Flurometer	3/5/2015 7:26	0.83
Mid Point Flurometer	3/5/2015 7:27	0.81
Mid Point Flurometer	3/5/2015 7:28	0.82
Mid Point Flurometer	3/5/2015 7:29	0.83
Mid Point Flurometer	3/5/2015 7:30	0.81
Mid Point Flurometer	3/5/2015 7:31	0.82
Mid Point Flurometer	3/5/2015 7:32	0.82
Mid Point Flurometer	3/5/2015 7:33	0.79
Mid Point Flurometer	3/5/2015 7:34	0.79
Mid Point Flurometer	3/5/2015 7:35	0.75
Mid Point Flurometer	3/5/2015 7:36	0.83

Location	Date and Time	Rhodmaine Concentration Adjusted Concentration (ppb)
Mid Point Flurometer	3/5/2015 7:37	0.81
Mid Point Flurometer	3/5/2015 7:38	0.81
Mid Point Flurometer	3/5/2015 7:39	0.79
Mid Point Flurometer	3/5/2015 7:40	0.78
Mid Point Flurometer	3/5/2015 7:41	0.83
Mid Point Flurometer	3/5/2015 7:42	0.79
Mid Point Flurometer	3/5/2015 7:43	0.76
Mid Point Flurometer	3/5/2015 7:44	0.73
Mid Point Flurometer	3/5/2015 7:45	0.75
Mid Point Flurometer	3/5/2015 7:46	0.8
Mid Point Flurometer	3/5/2015 7:47	0.74
Mid Point Flurometer	3/5/2015 7:48	0.76
Mid Point Flurometer	3/5/2015 7:49	0.74
Mid Point Flurometer	3/5/2015 7:50	0.73
Mid Point Flurometer	3/5/2015 7:51	0.78
Mid Point Flurometer	3/5/2015 7:52	0.73
Mid Point Flurometer	3/5/2015 7:53	0.71
Mid Point Flurometer	3/5/2015 7:54	0.73
Mid Point Flurometer	3/5/2015 7:55	0.7
Mid Point Flurometer	3/5/2015 7:56	0.69
Mid Point Flurometer	3/5/2015 7:57	0.71
Mid Point Flurometer	3/5/2015 7:58	0.73
Mid Point Flurometer	3/5/2015 7:59	0.7
Mid Point Flurometer	3/5/2015 8:00	0.71
Mid Point Flurometer	3/5/2015 8:01	0.72
Mid Point Flurometer	3/5/2015 8:02	0.75
Mid Point Flurometer	3/5/2015 8:03	0.7
Mid Point Flurometer	3/5/2015 8:04	0.68
Mid Point Flurometer	3/5/2015 8:05	0.68
Mid Point Flurometer	3/5/2015 8:06	0.67
Mid Point Flurometer	3/5/2015 8:07	0.67
Mid Point Flurometer	3/5/2015 8:08	0.7
Mid Point Flurometer	3/5/2015 8:09	0.68
Mid Point Flurometer	3/5/2015 8:10	0.71
Mid Point Flurometer	3/5/2015 8:11	0.67
Mid Point Flurometer	3/5/2015 8:12	0.7
Mid Point Flurometer	3/5/2015 8:13	0.69
Mid Point Flurometer	3/5/2015 8:14	0.66
Mid Point Flurometer	3/5/2015 8:15	0.67
Mid Point Flurometer	3/5/2015 8:16	0.65
Mid Point Flurometer	3/5/2015 8:17	0.68
Mid Point Flurometer	3/5/2015 8:18	0.66
Mid Point Flurometer	3/5/2015 8:19	0.66
Mid Point Flurometer	3/5/2015 8:20	0.69
Mid Point Flurometer	3/5/2015 8:21	0.66
Mid Point Flurometer	3/5/2015 8:22	0.63

Location	Date and Time	Rhodmaine Concentration Adjusted Concentration (ppb)
Mid Point Flurometer	3/5/2015 8:23	0.64
Mid Point Flurometer	3/5/2015 8:24	0.62
Mid Point Flurometer	3/5/2015 8:25	0.62
Mid Point Flurometer	3/5/2015 8:26	0.61
Mid Point Flurometer	3/5/2015 8:27	0.61
Mid Point Flurometer	3/5/2015 8:28	0.63
Mid Point Flurometer	3/5/2015 8:29	0.63
Mid Point Flurometer	3/5/2015 8:30	0.6
Mid Point Flurometer	3/5/2015 8:31	0.61
Mid Point Flurometer	3/5/2015 8:32	0.64
Mid Point Flurometer	3/5/2015 8:33	0.61
Mid Point Flurometer	3/5/2015 8:34	0.6
Mid Point Flurometer	3/5/2015 8:35	0.59
Mid Point Flurometer	3/5/2015 8:36	0.61
Mid Point Flurometer	3/5/2015 8:37	0.62
Mid Point Flurometer	3/5/2015 8:38	0.59
Mid Point Flurometer	3/5/2015 8:39	0.59
Mid Point Flurometer	3/5/2015 8:40	0.63
Mid Point Flurometer	3/5/2015 8:41	0.6
Mid Point Flurometer	3/5/2015 8:42	0.57
Mid Point Flurometer	3/5/2015 8:43	0.58
Mid Point Flurometer	3/5/2015 8:44	0.57
Mid Point Flurometer	3/5/2015 8:45	0.6
Mid Point Flurometer	3/5/2015 8:46	0.59
Mid Point Flurometer	3/5/2015 8:47	0.58
Mid Point Flurometer	3/5/2015 8:48	0.56
Mid Point Flurometer	3/5/2015 8:49	0.58
Mid Point Flurometer	3/5/2015 8:50	0.55
Mid Point Flurometer	3/5/2015 8:51	0.57
Mid Point Flurometer	3/5/2015 8:52	0.55
Mid Point Flurometer	3/5/2015 8:53	0.56
Mid Point Flurometer	3/5/2015 8:54	0.54
Mid Point Flurometer	3/5/2015 8:55	0.56
Mid Point Flurometer	3/5/2015 8:56	0.57
Mid Point Flurometer	3/5/2015 8:57	0.56
Mid Point Flurometer	3/5/2015 8:58	0.52
Mid Point Flurometer	3/5/2015 8:59	0.54
Mid Point Flurometer	3/5/2015 9:00	0.54
Mid Point Flurometer	3/5/2015 9:01	0.56
Mid Point Flurometer	3/5/2015 9:02	0.54
Mid Point Flurometer	3/5/2015 9:03	0.53
Mid Point Flurometer	3/5/2015 9:04	0.5
Mid Point Flurometer	3/5/2015 9:05	0.54
Mid Point Flurometer	3/5/2015 9:06	0.54
Mid Point Flurometer	3/5/2015 9:07	0.5
Mid Point Flurometer	3/5/2015 9:08	0.52

Location	Date and Time	Rhodmaine Concentration Adjusted Concentration (ppb)
Mid Point Flurometer	3/5/2015 9:09	0.48
Mid Point Flurometer	3/5/2015 9:10	0.54
Mid Point Flurometer	3/5/2015 9:11	0.52
Mid Point Flurometer	3/5/2015 9:12	0.5
Mid Point Flurometer	3/5/2015 9:13	0.51
Mid Point Flurometer	3/5/2015 9:14	0.5
Mid Point Flurometer	3/5/2015 9:15	0.48
Mid Point Flurometer	3/5/2015 9:16	0.5
Mid Point Flurometer	3/5/2015 9:17	0.49
Mid Point Flurometer	3/5/2015 9:18	0.5
Mid Point Flurometer	3/5/2015 9:19	0.49
Mid Point Flurometer	3/5/2015 9:20	0.5
Mid Point Flurometer	3/5/2015 9:21	0.47
Mid Point Flurometer	3/5/2015 9:22	0.45
Mid Point Flurometer	3/5/2015 9:23	0.46
Mid Point Flurometer	3/5/2015 9:24	0.47
Mid Point Flurometer	3/5/2015 9:25	0.46
Mid Point Flurometer	3/5/2015 9:26	0.47
Mid Point Flurometer	3/5/2015 9:27	0.48
Mid Point Flurometer	3/5/2015 9:28	0.44
Mid Point Flurometer	3/5/2015 9:29	0.45
Mid Point Flurometer	3/5/2015 9:30	0.47
Mid Point Flurometer	3/5/2015 9:31	0.48
Mid Point Flurometer	3/5/2015 9:32	0.48
Mid Point Flurometer	3/5/2015 9:33	0.42
Mid Point Flurometer	3/5/2015 9:34	0.43
Mid Point Flurometer	3/5/2015 9:35	0.43
Mid Point Flurometer	3/5/2015 9:36	0.43
Mid Point Flurometer	3/5/2015 9:37	0.44
Mid Point Flurometer	3/5/2015 9:38	0.46
Mid Point Flurometer	3/5/2015 9:39	0.46
Mid Point Flurometer	3/5/2015 9:40	0.43
Mid Point Flurometer	3/5/2015 9:41	0.52
Mid Point Flurometer	3/5/2015 9:42	0.47
Mid Point Flurometer	3/5/2015 9:43	0.4
Mid Point Flurometer	3/5/2015 9:44	0.41
Mid Point Flurometer	3/5/2015 9:45	0.41
Mid Point Flurometer	3/5/2015 9:46	0.41
Mid Point Flurometer	3/5/2015 9:47	0.38
Mid Point Flurometer	3/5/2015 9:48	0.41
Mid Point Flurometer	3/5/2015 9:49	0.37
Mid Point Flurometer	3/5/2015 9:50	0.46
Mid Point Flurometer	3/5/2015 9:51	0.4
Mid Point Flurometer	3/5/2015 9:52	0.4
Mid Point Flurometer	3/5/2015 9:53	0.42
Mid Point Flurometer	3/5/2015 9:54	0.43

Location	Date and Time	Rhodmaine Concentration Adjusted Concentration (ppb)
Mid Point Flurometer	3/5/2015 9:55	0.4
Mid Point Flurometer	3/5/2015 9:56	0.43
Mid Point Flurometer	3/5/2015 9:57	0.38
Mid Point Flurometer	3/5/2015 9:58	0.39
Mid Point Flurometer	3/5/2015 9:59	0.39
Mid Point Flurometer	3/5/2015 10:00	0.43
Mid Point Flurometer	3/5/2015 10:01	0.38
Mid Point Flurometer	3/5/2015 10:02	0.41
Mid Point Flurometer	3/5/2015 10:03	0.47
Mid Point Flurometer	3/5/2015 10:04	0.36
Mid Point Flurometer	3/5/2015 10:05	0.38
Mid Point Flurometer	3/5/2015 10:06	0.39
Mid Point Flurometer	3/5/2015 10:07	0.38
Mid Point Flurometer	3/5/2015 10:08	0.37
Mid Point Flurometer	3/5/2015 10:09	0.36
Mid Point Flurometer	3/5/2015 10:10	0.37
Mid Point Flurometer	3/5/2015 10:11	0.37
Mid Point Flurometer	3/5/2015 10:12	0.35
Mid Point Flurometer	3/5/2015 10:13	0.38
Mid Point Flurometer	3/5/2015 10:14	0.33
Mid Point Flurometer	3/5/2015 10:15	0.35
Mid Point Flurometer	3/5/2015 10:16	0.37
Mid Point Flurometer	3/5/2015 10:17	0.33
Mid Point Flurometer	3/5/2015 10:18	0.33
Mid Point Flurometer	3/5/2015 10:19	0.37
Mid Point Flurometer	3/5/2015 10:20	0.38
Mid Point Flurometer	3/5/2015 10:21	0.36
Mid Point Flurometer	3/5/2015 10:22	0.34
Mid Point Flurometer	3/5/2015 10:23	0.32
Mid Point Flurometer	3/5/2015 10:24	0.34
Mid Point Flurometer	3/5/2015 10:25	0.34
Mid Point Flurometer	3/5/2015 10:26	0.34
Mid Point Flurometer	3/5/2015 10:27	0.34
Mid Point Flurometer	3/5/2015 10:28	0.32
Mid Point Flurometer	3/5/2015 10:29	0.35
Mid Point Flurometer	3/5/2015 10:30	0.33
Mid Point Flurometer	3/5/2015 10:31	0.36
Mid Point Flurometer	3/5/2015 10:32	0.29
Mid Point Flurometer	3/5/2015 10:33	0.35
Mid Point Flurometer	3/5/2015 10:34	0.34
Mid Point Flurometer	3/5/2015 10:35	0.31
Mid Point Flurometer	3/5/2015 10:36	0.31
Mid Point Flurometer	3/5/2015 10:37	0.34
Mid Point Flurometer	3/5/2015 10:38	0.3
Mid Point Flurometer	3/5/2015 10:39	0.33
Mid Point Flurometer	3/5/2015 10:40	0.3

Location	Date and Time	Rhodmaine Concentration Adjusted Concentration (ppb)
Mid Point Flurometer	3/5/2015 10:41	0.31
Mid Point Flurometer	3/5/2015 10:42	0.32
Mid Point Flurometer	3/5/2015 10:43	0.32
Mid Point Flurometer	3/5/2015 10:44	0.28
Mid Point Flurometer	3/5/2015 10:45	0.31
Mid Point Flurometer	3/5/2015 10:46	0.28
Mid Point Flurometer	3/5/2015 10:47	0.31
Mid Point Flurometer	3/5/2015 10:48	0.26
Mid Point Flurometer	3/5/2015 10:49	0.27
Mid Point Flurometer	3/5/2015 10:50	0.32
Mid Point Flurometer	3/5/2015 10:51	0.3
Mid Point Flurometer	3/5/2015 10:52	0.28
Mid Point Flurometer	3/5/2015 10:53	0.3
Mid Point Flurometer	3/5/2015 10:54	0.28
Mid Point Flurometer	3/5/2015 10:55	0.29
Mid Point Flurometer	3/5/2015 10:56	0.26
Mid Point Flurometer	3/5/2015 10:57	0.31
Mid Point Flurometer	3/5/2015 10:58	0.29
Mid Point Flurometer	3/5/2015 10:59	0.34
Mid Point Flurometer	3/5/2015 11:00	0.32
Mid Point Flurometer	3/5/2015 11:01	0.29
Mid Point Flurometer	3/5/2015 11:02	0.28
Mid Point Flurometer	3/5/2015 11:03	0.36
Mid Point Flurometer	3/5/2015 11:04	0.26
Mid Point Flurometer	3/5/2015 11:05	0.29
Mid Point Flurometer	3/5/2015 11:06	0.27
Mid Point Flurometer	3/5/2015 11:07	0.25
Mid Point Flurometer	3/5/2015 11:08	0.25
Mid Point Flurometer	3/5/2015 11:09	0.25
Mid Point Flurometer	3/5/2015 11:10	0.27
Mid Point Flurometer	3/5/2015 11:11	0.28
Mid Point Flurometer	3/5/2015 11:12	0.24
Mid Point Flurometer	3/5/2015 11:13	0.31
Mid Point Flurometer	3/5/2015 11:14	0.26
Mid Point Flurometer	3/5/2015 11:15	0.25
Mid Point Flurometer	3/5/2015 11:16	0.25
Mid Point Flurometer	3/5/2015 11:17	0.25
Mid Point Flurometer	3/5/2015 11:18	0.24
Mid Point Flurometer	3/5/2015 11:19	0.25
Mid Point Flurometer	3/5/2015 11:20	0.24
Mid Point Flurometer	3/5/2015 11:21	0.28
Mid Point Flurometer	3/5/2015 11:22	0.25
Mid Point Flurometer	3/5/2015 11:23	0.24
Mid Point Flurometer	3/5/2015 11:24	0.26
Mid Point Flurometer	3/5/2015 11:25	0.26
Mid Point Flurometer	3/5/2015 11:26	0.21

Location	Date and Time	Rhodmaine Concentration Adjusted Concentration (ppb)
Mid Point Flurometer	3/5/2015 11:27	0.28
Mid Point Flurometer	3/5/2015 11:28	0.22
Mid Point Flurometer	3/5/2015 11:29	0.23
Mid Point Flurometer	3/5/2015 11:30	0.23
Mid Point Flurometer	3/5/2015 11:31	0.27
Mid Point Flurometer	3/5/2015 11:32	0.23
Mid Point Flurometer	3/5/2015 11:33	0.19
Mid Point Flurometer	3/5/2015 11:34	0.3
Mid Point Flurometer	3/5/2015 11:35	0.22
Mid Point Flurometer	3/5/2015 11:36	0.19
Mid Point Flurometer	3/5/2015 11:37	0.22
Mid Point Flurometer	3/5/2015 11:38	0.23
Mid Point Flurometer	3/5/2015 11:39	0.24
Mid Point Flurometer	3/5/2015 11:40	0.2
Mid Point Flurometer	3/5/2015 11:41	0.2
Mid Point Flurometer	3/5/2015 11:42	0.2
Mid Point Flurometer	3/5/2015 11:43	0.24
Mid Point Flurometer	3/5/2015 11:44	0.24
Mid Point Flurometer	3/5/2015 11:45	0.19
Mid Point Flurometer	3/5/2015 11:46	0.25
Mid Point Flurometer	3/5/2015 11:47	0.22
Mid Point Flurometer	3/5/2015 11:48	0.19
Mid Point Flurometer	3/5/2015 11:49	0.2
Mid Point Flurometer	3/5/2015 11:50	0.21
Mid Point Flurometer	3/5/2015 11:51	0.21
Mid Point Flurometer	3/5/2015 11:52	0.17
Mid Point Flurometer	3/5/2015 11:53	0.21
Mid Point Flurometer	3/5/2015 11:54	0.22
Mid Point Flurometer	3/5/2015 11:55	0.2
Mid Point Flurometer	3/5/2015 11:56	0.23
Mid Point Flurometer	3/5/2015 11:57	0.2
Mid Point Flurometer	3/5/2015 11:58	0.26
Mid Point Flurometer	3/5/2015 11:59	0.2
Mid Point Flurometer	3/5/2015 12:00	0.18
Mid Point Flurometer	3/5/2015 12:01	0.18
Mid Point Flurometer	3/5/2015 12:02	0.18
Mid Point Flurometer	3/5/2015 12:03	0.18
Mid Point Flurometer	3/5/2015 12:04	0.19
Mid Point Flurometer	3/5/2015 12:05	0.15
Mid Point Flurometer	3/5/2015 12:06	0.22
Mid Point Flurometer	3/5/2015 12:07	0.18
Mid Point Flurometer	3/5/2015 12:08	0.17
Mid Point Flurometer	3/5/2015 12:09	0.16
Mid Point Flurometer	3/5/2015 12:10	0.17
Mid Point Flurometer	3/5/2015 12:11	0.17
Mid Point Flurometer	3/5/2015 12:12	0.2

Location	Date and Time	Rhodmaine Concentration Adjusted Concentration (ppb)
Mid Point Flurometer	3/5/2015 12:13	0.18
Mid Point Flurometer	3/5/2015 12:14	0.17
Mid Point Flurometer	3/5/2015 12:15	0.19
Mid Point Flurometer	3/5/2015 12:16	0.2
Mid Point Flurometer	3/5/2015 12:17	0.15
Mid Point Flurometer	3/5/2015 12:18	0.2
Mid Point Flurometer	3/5/2015 12:19	0.16
Mid Point Flurometer	3/5/2015 12:20	0.17
Mid Point Flurometer	3/5/2015 12:21	0.19
Mid Point Flurometer	3/5/2015 12:22	0.16
Mid Point Flurometer	3/5/2015 12:23	0.19
Mid Point Flurometer	3/5/2015 12:24	0.17
Mid Point Flurometer	3/5/2015 12:25	0.14
Mid Point Flurometer	3/5/2015 12:26	0.18
Mid Point Flurometer	3/5/2015 12:27	0.15
Mid Point Flurometer	3/5/2015 12:28	0.16
Mid Point Flurometer	3/5/2015 12:29	0.18
Mid Point Flurometer	3/5/2015 12:30	0.13
Mid Point Flurometer	3/5/2015 12:31	0.15
Mid Point Flurometer	3/5/2015 12:32	0.16
Mid Point Flurometer	3/5/2015 12:33	0.16
Mid Point Flurometer	3/5/2015 12:34	0.12
Mid Point Flurometer	3/5/2015 12:35	0.19
Mid Point Flurometer	3/5/2015 12:36	0.13
Mid Point Flurometer	3/5/2015 12:37	0.13
Mid Point Flurometer	3/5/2015 12:38	0.16
Mid Point Flurometer	3/5/2015 12:39	0.15
Mid Point Flurometer	3/5/2015 12:40	0.12
Mid Point Flurometer	3/5/2015 12:41	0.13
Mid Point Flurometer	3/5/2015 12:42	0.13
Mid Point Flurometer	3/5/2015 12:43	0.15
Mid Point Flurometer	3/5/2015 12:44	0.15
Mid Point Flurometer	3/5/2015 12:45	0.61
Mid Point Flurometer	3/5/2015 12:46	0.13
Mid Point Flurometer	3/5/2015 12:47	0.17
Mid Point Flurometer	3/5/2015 12:48	0.11
Mid Point Flurometer	3/5/2015 12:49	0.13
Mid Point Flurometer	3/5/2015 12:50	0.12
Mid Point Flurometer	3/5/2015 12:51	0.14
Mid Point Flurometer	3/5/2015 12:52	0.11
Mid Point Flurometer	3/5/2015 12:53	0.13
Mid Point Flurometer	3/5/2015 12:54	0.14
Mid Point Flurometer	3/5/2015 12:55	0.13
Mid Point Flurometer	3/5/2015 12:56	0.16
Mid Point Flurometer	3/5/2015 12:57	0.13
Mid Point Flurometer	3/5/2015 12:58	0.14

Location	Date and Time	Rhodmaine Concentration Adjusted Concentration (ppb)
Mid Point Flurometer	3/5/2015 12:59	0.11
Mid Point Flurometer	3/5/2015 13:00	0.14
Mid Point Flurometer	3/5/2015 13:01	0.16
Mid Point Flurometer	3/5/2015 13:02	0.16
Mid Point Flurometer	3/5/2015 13:03	0.12
Mid Point Flurometer	3/5/2015 13:04	0.14
Mid Point Flurometer	3/5/2015 13:05	0.12
Mid Point Flurometer	3/5/2015 13:06	0.11
Mid Point Flurometer	3/5/2015 13:07	0.1
Mid Point Flurometer	3/5/2015 13:08	0.16
Mid Point Flurometer	3/5/2015 13:09	0.12
Mid Point Flurometer	3/5/2015 13:10	0.12
Mid Point Flurometer	3/5/2015 13:11	0.13
Mid Point Flurometer	3/5/2015 13:12	0.11
Mid Point Flurometer	3/5/2015 13:13	0.39
Mid Point Flurometer	3/5/2015 13:14	0.12
Mid Point Flurometer	3/5/2015 13:15	0.1
Mid Point Flurometer	3/5/2015 13:16	0.11
Mid Point Flurometer	3/5/2015 13:17	0.13
Mid Point Flurometer	3/5/2015 13:18	0.14
Mid Point Flurometer	3/5/2015 13:19	0.13
Mid Point Flurometer	3/5/2015 13:20	0.24
Mid Point Flurometer	3/5/2015 13:21	0.11
Mid Point Flurometer	3/5/2015 13:22	0.1
Mid Point Flurometer	3/5/2015 13:23	0.15
Mid Point Flurometer	3/5/2015 13:24	0.12
Mid Point Flurometer	3/5/2015 13:25	0.31
Mid Point Flurometer	3/5/2015 13:26	0.1
Mid Point Flurometer	3/5/2015 13:27	0.13
Mid Point Flurometer	3/5/2015 13:28	0.1
Mid Point Flurometer	3/5/2015 13:29	0.12
Mid Point Flurometer	3/5/2015 13:30	0.14
Mid Point Flurometer	3/5/2015 13:31	0.1
Mid Point Flurometer	3/5/2015 13:32	0.1
Mid Point Flurometer	3/5/2015 13:33	0.13
Mid Point Flurometer	3/5/2015 13:34	0.16
Mid Point Flurometer	3/5/2015 13:35	0.13
Mid Point Flurometer	3/5/2015 13:36	0.11
Mid Point Flurometer	3/5/2015 13:37	0.14
Mid Point Flurometer	3/5/2015 13:38	0.14
Mid Point Flurometer	3/5/2015 13:39	0.08
Mid Point Flurometer	3/5/2015 13:40	0.16
Mid Point Flurometer	3/5/2015 13:41	0.07
Mid Point Flurometer	3/5/2015 13:42	0.09
Mid Point Flurometer	3/5/2015 13:43	0.08
Mid Point Flurometer	3/5/2015 13:44	0.1

Location	Date and Time	Rhodmaine Concentration Adjusted Concentration (ppb)
Mid Point Flurometer	3/5/2015 13:45	0.19
Mid Point Flurometer	3/5/2015 13:46	0.09
Mid Point Flurometer	3/5/2015 13:47	0.09
Mid Point Flurometer	3/5/2015 13:48	0.11
Mid Point Flurometer	3/5/2015 13:49	0.15
Mid Point Flurometer	3/5/2015 13:50	0.09
Mid Point Flurometer	3/5/2015 13:51	0.17
Mid Point Flurometer	3/5/2015 13:52	0.09
Mid Point Flurometer	3/5/2015 13:53	0.08
Mid Point Flurometer	3/5/2015 13:54	0.08
Mid Point Flurometer	3/5/2015 13:55	0.18
Mid Point Flurometer	3/5/2015 13:56	0.07
Mid Point Flurometer	3/5/2015 13:57	0.12
Mid Point Flurometer	3/5/2015 13:58	0.09
Mid Point Flurometer	3/5/2015 13:59	0.11
Mid Point Flurometer	3/5/2015 14:00	0.08
Mid Point Flurometer	3/5/2015 14:01	0.07
Mid Point Flurometer	3/5/2015 14:02	0.07
Mid Point Flurometer	3/5/2015 14:03	0.09
Mid Point Flurometer	3/5/2015 14:04	0.05
Mid Point Flurometer	3/5/2015 14:05	0.07
Mid Point Flurometer	3/5/2015 14:06	0.06
Mid Point Flurometer	3/5/2015 14:07	0.07
Mid Point Flurometer	3/5/2015 14:08	0.09
Mid Point Flurometer	3/5/2015 14:09	0.07
Mid Point Flurometer	3/5/2015 14:10	0.16
Mid Point Flurometer	3/5/2015 14:11	0.28
Mid Point Flurometer	3/5/2015 14:12	0.11
Mid Point Flurometer	3/5/2015 14:13	0.09
Mid Point Flurometer	3/5/2015 14:14	0.05
Mid Point Flurometer	3/5/2015 14:15	0.17
Mid Point Flurometer	3/5/2015 14:16	0.08
Mid Point Flurometer	3/5/2015 14:17	0.07
Mid Point Flurometer	3/5/2015 14:18	0.1
Mid Point Flurometer	3/5/2015 14:19	0.08
Mid Point Flurometer	3/5/2015 14:20	0.07
Mid Point Flurometer	3/5/2015 14:21	0.06
Mid Point Flurometer	3/5/2015 14:22	0.1
Mid Point Flurometer	3/5/2015 14:23	0.04
Mid Point Flurometer	3/5/2015 14:24	0.07
Mid Point Flurometer	3/5/2015 14:25	0.05
Mid Point Flurometer	3/5/2015 14:26	0.06
Mid Point Flurometer	3/5/2015 14:27	0.18
Mid Point Flurometer	3/5/2015 14:28	0.06
Mid Point Flurometer	3/5/2015 14:29	0.07
Mid Point Flurometer	3/5/2015 14:30	0.07

Location	Date and Time	Rhodmaine Concentration Adjusted Concentration (ppb)
Mid Point Flurometer	3/5/2015 14:31	0.05
Mid Point Flurometer	3/5/2015 14:32	0.09
Mid Point Flurometer	3/5/2015 14:33	0.06
Mid Point Flurometer	3/5/2015 14:34	0.05
Mid Point Flurometer	3/5/2015 14:35	0.04
Mid Point Flurometer	3/5/2015 14:36	0.05
Mid Point Flurometer	3/5/2015 14:37	0.05
Mid Point Flurometer	3/5/2015 14:38	0.03
Mid Point Flurometer	3/5/2015 14:39	0.04
Mid Point Flurometer	3/5/2015 14:40	0.05
Mid Point Flurometer	3/5/2015 14:41	0.06
Mid Point Flurometer	3/5/2015 14:42	0.04
Mid Point Flurometer	3/5/2015 14:43	0.06
Mid Point Flurometer	3/5/2015 14:44	0.08
Mid Point Flurometer	3/5/2015 14:45	0.02
Mid Point Flurometer	3/5/2015 14:46	0.04
Mid Point Flurometer	3/5/2015 14:47	0.96
Mid Point Flurometer	3/5/2015 14:48	0.02
Mid Point Flurometer	3/5/2015 14:49	0.05
Mid Point Flurometer	3/5/2015 14:50	0.03
Mid Point Flurometer	3/5/2015 14:51	0.08
Mid Point Flurometer	3/5/2015 14:52	0.09
Mid Point Flurometer	3/5/2015 14:53	0.07
Mid Point Flurometer	3/5/2015 14:54	0.03
Mid Point Flurometer	3/5/2015 14:55	0.02
Mid Point Flurometer	3/5/2015 14:56	0.04
Mid Point Flurometer	3/5/2015 14:57	0.04
Mid Point Flurometer	3/5/2015 14:58	0.05
Mid Point Flurometer	3/5/2015 14:59	0.06
Mid Point Flurometer	3/5/2015 15:00	0.01
Mid Point Flurometer	3/5/2015 15:01	0.06
Mid Point Flurometer	3/5/2015 15:02	0.04
Mid Point Flurometer	3/5/2015 15:03	0.07
Mid Point Flurometer	3/5/2015 15:04	0.08
Mid Point Flurometer	3/5/2015 15:05	0.03
Mid Point Flurometer	3/5/2015 15:06	0.04
Mid Point Flurometer	3/5/2015 15:07	0.03
Mid Point Flurometer	3/5/2015 15:08	0.06
Mid Point Flurometer	3/5/2015 15:09	0.04
Mid Point Flurometer	3/5/2015 15:10	0.06
Mid Point Flurometer	3/5/2015 15:11	0.04
Mid Point Flurometer	3/5/2015 15:12	0.04
Mid Point Flurometer	3/5/2015 15:13	0.06
Mid Point Flurometer	3/5/2015 15:14	0.04
Mid Point Flurometer	3/5/2015 15:15	0.03
Mid Point Flurometer	3/5/2015 15:16	0.03

Location	Date and Time	Rhodmaine Concentration Adjusted Concentration (ppb)
Mid Point Flurometer	3/5/2015 15:17	0.02
Mid Point Flurometer	3/5/2015 15:18	0.05
Mid Point Flurometer	3/5/2015 15:19	0.1
Mid Point Flurometer	3/5/2015 15:20	0.06
Mid Point Flurometer	3/5/2015 15:21	0.04
Mid Point Flurometer	3/5/2015 15:22	0.07
Mid Point Flurometer	3/5/2015 15:23	0.06
Mid Point Flurometer	3/5/2015 15:24	0.13
Mid Point Flurometer	3/5/2015 15:25	0.09
Mid Point Flurometer	3/5/2015 15:26	0.07
Mid Point Flurometer	3/5/2015 15:27	0.09
Mid Point Flurometer	3/5/2015 15:28	0.1
Mid Point Flurometer	3/5/2015 15:29	0.07
Mid Point Flurometer	3/5/2015 15:30	0.12
Mid Point Flurometer	3/5/2015 15:31	0.02
Mid Point Flurometer	3/5/2015 15:32	0.01
Mid Point Flurometer	3/5/2015 15:33	0.04
Mid Point Flurometer	3/5/2015 15:34	0.03
Mid Point Flurometer	3/5/2015 15:35	0.11
Mid Point Flurometer	3/5/2015 15:36	0.03
Mid Point Flurometer	3/5/2015 15:37	0.05
Mid Point Flurometer	3/5/2015 15:38	0.03
Mid Point Flurometer	3/5/2015 15:39	0.04
Mid Point Flurometer	3/5/2015 15:40	0.04
Mid Point Flurometer	3/5/2015 15:41	0.03
Mid Point Flurometer	3/5/2015 15:42	0.02
Mid Point Flurometer	3/5/2015 15:43	0.13
Mid Point Flurometer	3/5/2015 15:44	0.04
Mid Point Flurometer	3/5/2015 15:45	0.03
Mid Point Flurometer	3/5/2015 15:46	0.01
Mid Point Flurometer	3/5/2015 15:47	0.04
Mid Point Flurometer	3/5/2015 15:48	0.02
Mid Point Flurometer	3/5/2015 15:49	0.02
Mid Point Flurometer	3/5/2015 15:50	0.04
Mid Point Flurometer	3/5/2015 15:51	0.03
Mid Point Flurometer	3/5/2015 15:52	0.1
Mid Point Flurometer	3/5/2015 15:53	0.04
Mid Point Flurometer	3/5/2015 15:54	0.04
Mid Point Flurometer	3/5/2015 15:55	0.03
Mid Point Flurometer	3/5/2015 15:56	0
Mid Point Flurometer	3/5/2015 15:57	0.02
Mid Point Flurometer	3/5/2015 15:58	0.02
Mid Point Flurometer	3/5/2015 15:59	0.04
Mid Point Flurometer	3/5/2015 16:00	0.02
Mid Point Flurometer	3/5/2015 16:01	0.05
Mid Point Flurometer	3/5/2015 16:02	0.02

Location	Date and Time	Rhodmaine Concentration Adjusted Concentration (ppb)
Mid Point Flurometer	3/5/2015 16:03	0.05
Mid Point Flurometer	3/5/2015 16:04	0.04
Mid Point Flurometer	3/5/2015 16:05	3.85
Mid Point Flurometer	3/5/2015 16:06	0.34
Mid Point Flurometer	3/5/2015 16:07	0.06
Mid Point Flurometer	3/5/2015 16:08	0
Mid Point Flurometer	3/5/2015 16:09	0.15
Mid Point Flurometer	3/5/2015 16:10	0.07
Mid Point Flurometer	3/5/2015 16:11	1.14
Mid Point Flurometer	3/5/2015 16:12	0.24
Mid Point Flurometer	3/5/2015 16:13	0.2
Mid Point Flurometer	3/5/2015 16:14	0.11
Mid Point Flurometer	3/5/2015 16:15	1.76
Mid Point Flurometer	3/5/2015 16:16	0.97
Mid Point Flurometer	3/5/2015 16:17	0.07
Mid Point Flurometer	3/5/2015 16:18	0.03
Mid Point Flurometer	3/5/2015 16:19	0.12
Mid Point Flurometer	3/5/2015 16:20	2.42
Mid Point Flurometer	3/5/2015 16:21	0.03
Mid Point Flurometer	3/5/2015 16:22	1.72
Mid Point Flurometer	3/5/2015 16:23	0.12
Mid Point Flurometer	3/5/2015 16:24	4.87
Mid Point Flurometer	3/5/2015 16:25	0.04
Mid Point Flurometer	3/5/2015 16:26	0.4
Mid Point Flurometer	3/5/2015 16:27	0.98
Mid Point Flurometer	3/5/2015 16:28	0.04
Mid Point Flurometer	3/5/2015 16:29	0.32
Mid Point Flurometer	3/5/2015 16:30	0.12
Mid Point Flurometer	3/5/2015 16:31	0.1
Mid Point Flurometer	3/5/2015 16:32	0.35
Mid Point Flurometer	3/5/2015 16:33	0.08
Mid Point Flurometer	3/5/2015 16:34	0.06
Mid Point Flurometer	3/5/2015 16:35	0.07
Mid Point Flurometer	3/5/2015 16:36	0.35
Mid Point Flurometer	3/5/2015 16:37	0.12
Mid Point Flurometer	3/5/2015 16:38	0.21
Mid Point Flurometer	3/5/2015 16:39	0.21
Mid Point Flurometer	3/5/2015 16:40	0.11
Mid Point Flurometer	3/5/2015 16:41	0.02
Mid Point Flurometer	3/5/2015 16:42	3.76
Mid Point Flurometer	3/5/2015 16:43	0.86
Mid Point Flurometer	3/5/2015 16:44	0.44
Mid Point Flurometer	3/5/2015 16:45	0.04
Mid Point Flurometer	3/5/2015 16:46	0.32
Mid Point Flurometer	3/5/2015 16:47	0.07
Mid Point Flurometer	3/5/2015 16:48	1.51

Location	Date and Time	Rhodmaine Concentration Adjusted Concentration (ppb)
Mid Point Flurometer	3/5/2015 16:49	0.02
Mid Point Flurometer	3/5/2015 16:50	0.26
Mid Point Flurometer	3/5/2015 16:51	0.07
Mid Point Flurometer	3/5/2015 16:52	0.23
Mid Point Flurometer	3/5/2015 16:53	0.7
Mid Point Flurometer	3/5/2015 16:54	1.81
Mid Point Flurometer	3/5/2015 16:55	0.23
Mid Point Flurometer	3/5/2015 16:56	0.53
Mid Point Flurometer	3/5/2015 16:57	0.02
Mid Point Flurometer	3/5/2015 16:58	0.06
Mid Point Flurometer	3/5/2015 16:59	0.44
Mid Point Flurometer	3/5/2015 17:00	0.51
Mid Point Flurometer	3/5/2015 17:01	0.28
Mid Point Flurometer	3/5/2015 17:02	0.05
Mid Point Flurometer	3/5/2015 17:03	0.04
Mid Point Flurometer	3/5/2015 17:04	2.54
Mid Point Flurometer	3/5/2015 17:05	0.21
Mid Point Flurometer	3/5/2015 17:06	0.15
Mid Point Flurometer	3/5/2015 17:07	0.17
Mid Point Flurometer	3/5/2015 17:08	0.32
Mid Point Flurometer	3/5/2015 17:09	0.09
Mid Point Flurometer	3/5/2015 17:10	0.29
Mid Point Flurometer	3/5/2015 17:11	0
Mid Point Flurometer	3/5/2015 17:12	1.11
Mid Point Flurometer	3/5/2015 17:13	0.03
Mid Point Flurometer	3/5/2015 17:14	0.09
Mid Point Flurometer	3/5/2015 17:15	0.06
Mid Point Flurometer	3/5/2015 17:16	2.14
Mid Point Flurometer	3/5/2015 17:17	0
Mid Point Flurometer	3/5/2015 17:18	1.51
Mid Point Flurometer	3/5/2015 17:19	0.87
Mid Point Flurometer	3/5/2015 17:20	2.48
Mid Point Flurometer	3/5/2015 17:21	1.68
Mid Point Flurometer	3/5/2015 17:22	0.08
Mid Point Flurometer	3/5/2015 17:23	1.66
Mid Point Flurometer	3/5/2015 17:24	0.54
Mid Point Flurometer	3/5/2015 17:25	0.87
Mid Point Flurometer	3/5/2015 17:26	0.09
Mid Point Flurometer	3/5/2015 17:27	0.08
Mid Point Flurometer	3/5/2015 17:28	0.26
Mid Point Flurometer	3/5/2015 17:29	0.65
Mid Point Flurometer	3/5/2015 17:30	0.22
Mid Point Flurometer	3/5/2015 17:31	3.78
Mid Point Flurometer	3/5/2015 17:32	0.06
Mid Point Flurometer	3/5/2015 17:33	0.21
Mid Point Flurometer	3/5/2015 17:34	0.03

Location	Date and Time	Rhodmaine Concentration Adjusted Concentration (ppb)
Mid Point Flurometer	3/5/2015 17:35	0.07
Mid Point Flurometer	3/5/2015 17:36	0.07
Mid Point Flurometer	3/5/2015 17:37	2.49
Mid Point Flurometer	3/5/2015 17:38	1.27
Mid Point Flurometer	3/5/2015 17:39	0.15
Mid Point Flurometer	3/5/2015 17:40	0.11
Mid Point Flurometer	3/5/2015 17:41	3.95
Mid Point Flurometer	3/5/2015 17:42	0.06
Mid Point Flurometer	3/5/2015 17:43	0.08
Mid Point Flurometer	3/5/2015 17:44	0.75
Mid Point Flurometer	3/5/2015 17:45	0.07
Mid Point Flurometer	3/5/2015 17:46	2.96
Mid Point Flurometer	3/5/2015 17:47	0.05
Mid Point Flurometer	3/5/2015 17:48	0.14
Mid Point Flurometer	3/5/2015 17:49	0.48
Mid Point Flurometer	3/5/2015 17:50	0.66
Mid Point Flurometer	3/5/2015 17:51	0.02
Mid Point Flurometer	3/5/2015 17:52	0.14
Mid Point Flurometer	3/5/2015 17:53	0.25
Mid Point Flurometer	3/5/2015 17:54	0.12
Mid Point Flurometer	3/5/2015 17:55	0.6
Mid Point Flurometer	3/5/2015 17:56	0.22
Mid Point Flurometer	3/5/2015 17:57	2.58
Mid Point Flurometer	3/5/2015 17:58	3.75
Mid Point Flurometer	3/5/2015 17:59	0.07
Mid Point Flurometer	3/5/2015 18:00	0.03
Mid Point Flurometer	3/5/2015 18:01	0.06
Mid Point Flurometer	3/5/2015 18:02	0.07
Mid Point Flurometer	3/5/2015 18:03	0.02
Mid Point Flurometer	3/5/2015 18:04	0.13
Mid Point Flurometer	3/5/2015 18:05	0.02
Mid Point Flurometer	3/5/2015 18:06	7.56
Mid Point Flurometer	3/5/2015 18:07	0.08
Mid Point Flurometer	3/5/2015 18:08	0.05
Mid Point Flurometer	3/5/2015 18:09	0.02
Mid Point Flurometer	3/5/2015 18:10	0.12
Mid Point Flurometer	3/5/2015 18:11	0.27
Mid Point Flurometer	3/5/2015 18:12	0.09
Mid Point Flurometer	3/5/2015 18:13	0.26
Mid Point Flurometer	3/5/2015 18:14	0.03
Mid Point Flurometer	3/5/2015 18:15	1
Mid Point Flurometer	3/5/2015 18:16	0.11
Mid Point Flurometer	3/5/2015 18:17	0.53
Mid Point Flurometer	3/5/2015 18:18	0.2
Mid Point Flurometer	3/5/2015 18:19	1.13
Mid Point Flurometer	3/5/2015 18:20	0.06

Location	Date and Time	Rhodmaine Concentration Adjusted Concentration (ppb)
Mid Point Flurometer	3/5/2015 18:21	0.38
Mid Point Flurometer	3/5/2015 18:22	1.39
Mid Point Flurometer	3/5/2015 18:23	0.03
Mid Point Flurometer	3/5/2015 18:24	0.05
Mid Point Flurometer	3/5/2015 18:25	0.2
Mid Point Flurometer	3/5/2015 18:26	0.11
Mid Point Flurometer	3/5/2015 18:27	0.04
Mid Point Flurometer	3/5/2015 18:28	0.45
Mid Point Flurometer	3/5/2015 18:29	1.97
Mid Point Flurometer	3/5/2015 18:30	0.82
Mid Point Flurometer	3/5/2015 18:31	0.08
Mid Point Flurometer	3/5/2015 18:32	0.16
Mid Point Flurometer	3/5/2015 18:33	2.88
Mid Point Flurometer	3/5/2015 18:34	0.05
Mid Point Flurometer	3/5/2015 18:35	0.01
Mid Point Flurometer	3/5/2015 18:36	0.84
Mid Point Flurometer	3/5/2015 18:37	0.49
Mid Point Flurometer	3/5/2015 18:38	0.14
Mid Point Flurometer	3/5/2015 18:39	0.81
Mid Point Flurometer	3/5/2015 18:40	0.1
Mid Point Flurometer	3/5/2015 18:41	0.11
Mid Point Flurometer	3/5/2015 18:42	0.11
Mid Point Flurometer	3/5/2015 18:43	0.07
Mid Point Flurometer	3/5/2015 18:44	0.47
Mid Point Flurometer	3/5/2015 18:45	0.79
Mid Point Flurometer	3/5/2015 18:46	0.1
Mid Point Flurometer	3/5/2015 18:47	0.04
Mid Point Flurometer	3/5/2015 18:48	5.31
Mid Point Flurometer	3/5/2015 18:49	0.11
Mid Point Flurometer	3/5/2015 18:50	1.87
Mid Point Flurometer	3/5/2015 18:51	0.93
Mid Point Flurometer	3/5/2015 18:52	0.76
Mid Point Flurometer	3/5/2015 18:53	0.3
Mid Point Flurometer	3/5/2015 18:54	0.13
Mid Point Flurometer	3/5/2015 18:55	0.07
Mid Point Flurometer	3/5/2015 18:56	0.05
Mid Point Flurometer	3/5/2015 18:57	0.11
Mid Point Flurometer	3/5/2015 18:58	4.15
Mid Point Flurometer	3/5/2015 18:59	0.26
Mid Point Flurometer	3/5/2015 19:00	0.37
Mid Point Flurometer	3/5/2015 19:01	0.24
Mid Point Flurometer	3/5/2015 19:02	0.13
Mid Point Flurometer	3/5/2015 19:03	2.65
Mid Point Flurometer	3/5/2015 19:04	0.43
Mid Point Flurometer	3/5/2015 19:05	0.24
Mid Point Flurometer	3/5/2015 19:06	1.01

Location	Date and Time	Rhodmaine Concentration Adjusted Concentration (ppb)
Mid Point Flurometer	3/5/2015 19:07	3.25
Mid Point Flurometer	3/5/2015 19:08	0.47
Mid Point Flurometer	3/5/2015 19:09	0.12
Mid Point Flurometer	3/5/2015 19:10	0.16
Mid Point Flurometer	3/5/2015 19:11	0.1
Mid Point Flurometer	3/5/2015 19:12	0.09
Mid Point Flurometer	3/5/2015 19:13	0.13
Mid Point Flurometer	3/5/2015 19:14	0.09
Mid Point Flurometer	3/5/2015 19:15	2.6
Mid Point Flurometer	3/5/2015 19:16	0.06
Mid Point Flurometer	3/5/2015 19:17	0.56
Mid Point Flurometer	3/5/2015 19:18	0.76
Mid Point Flurometer	3/5/2015 19:19	0.89
Mid Point Flurometer	3/5/2015 19:20	0.05
Mid Point Flurometer	3/5/2015 19:21	0
Mid Point Flurometer	3/5/2015 19:22	0.1
Mid Point Flurometer	3/5/2015 19:23	0.02
Mid Point Flurometer	3/5/2015 19:24	0.11
Mid Point Flurometer	3/5/2015 19:25	0.15
Mid Point Flurometer	3/5/2015 19:26	1.26
Mid Point Flurometer	3/5/2015 19:27	0.03
Mid Point Flurometer	3/5/2015 19:28	0.08
Mid Point Flurometer	3/5/2015 19:29	3.02
Mid Point Flurometer	3/5/2015 19:30	0.05
Mid Point Flurometer	3/5/2015 19:31	0.35
Mid Point Flurometer	3/5/2015 19:32	0.05
Mid Point Flurometer	3/5/2015 19:33	0
Mid Point Flurometer	3/5/2015 19:34	0.32
Mid Point Flurometer	3/5/2015 19:35	0.02
Mid Point Flurometer	3/5/2015 19:36	0.05
Mid Point Flurometer	3/5/2015 19:37	2.51
Mid Point Flurometer	3/5/2015 19:38	0.02
Mid Point Flurometer	3/5/2015 19:39	8.46
Mid Point Flurometer	3/5/2015 19:40	0.11
Mid Point Flurometer	3/5/2015 19:41	0
Mid Point Flurometer	3/5/2015 19:42	0.05
Mid Point Flurometer	3/5/2015 19:43	0.19
Mid Point Flurometer	3/5/2015 19:44	0.15
Mid Point Flurometer	3/5/2015 19:45	0.01
Mid Point Flurometer	3/5/2015 19:46	0.12
Mid Point Flurometer	3/5/2015 19:47	0.23
Mid Point Flurometer	3/5/2015 19:48	0.56
Mid Point Flurometer	3/5/2015 19:49	0.41
Mid Point Flurometer	3/5/2015 19:50	0.01
Mid Point Flurometer	3/5/2015 19:51	0.02
Mid Point Flurometer	3/5/2015 19:52	0.05

Location	Date and Time	Rhodmaine Concentration Adjusted Concentration (ppb)
Mid Point Flurometer	3/5/2015 19:53	1.21
Mid Point Flurometer	3/5/2015 19:54	0.15
Mid Point Flurometer	3/5/2015 19:55	4.9
Mid Point Flurometer	3/5/2015 19:56	0.45
Mid Point Flurometer	3/5/2015 19:57	0.35
Mid Point Flurometer	3/5/2015 19:58	0.03
Mid Point Flurometer	3/5/2015 19:59	0.05
Mid Point Flurometer	3/5/2015 20:00	0.77
Mid Point Flurometer	3/5/2015 20:01	0.93
Mid Point Flurometer	3/5/2015 20:02	0.12
Mid Point Flurometer	3/5/2015 20:03	0.11
Mid Point Flurometer	3/5/2015 20:04	0.41
Mid Point Flurometer	3/5/2015 20:05	0.69
Mid Point Flurometer	3/5/2015 20:06	0.06
Mid Point Flurometer	3/5/2015 20:07	0.08
Mid Point Flurometer	3/5/2015 20:08	0.12
Mid Point Flurometer	3/5/2015 20:09	4.57
Mid Point Flurometer	3/5/2015 20:10	0.41
Mid Point Flurometer	3/5/2015 20:11	0.04
Mid Point Flurometer	3/5/2015 20:12	1.45
Mid Point Flurometer	3/5/2015 20:13	0.02
Mid Point Flurometer	3/5/2015 20:14	0.04
Mid Point Flurometer	3/5/2015 20:15	0.12
Mid Point Flurometer	3/5/2015 20:16	0.16
Mid Point Flurometer	3/5/2015 20:17	0.31
Mid Point Flurometer	3/5/2015 20:18	7.26
Mid Point Flurometer	3/5/2015 20:19	2.91
Mid Point Flurometer	3/5/2015 20:20	0.61
Mid Point Flurometer	3/5/2015 20:21	0.1
Mid Point Flurometer	3/5/2015 20:22	0.91
Mid Point Flurometer	3/5/2015 20:23	1.23
Mid Point Flurometer	3/5/2015 20:24	1.08
Mid Point Flurometer	3/5/2015 20:25	0.17
Mid Point Flurometer	3/5/2015 20:26	0.05
Mid Point Flurometer	3/5/2015 20:27	0.75
Mid Point Flurometer	3/5/2015 20:28	0.06
Mid Point Flurometer	3/5/2015 20:29	0.23
Mid Point Flurometer	3/5/2015 20:30	0.09
Mid Point Flurometer	3/5/2015 20:31	1.35
Mid Point Flurometer	3/5/2015 20:32	0.06
Mid Point Flurometer	3/5/2015 20:33	0.25
Mid Point Flurometer	3/5/2015 20:34	3.39
Mid Point Flurometer	3/5/2015 20:35	0.04
Mid Point Flurometer	3/5/2015 20:36	0.31
Mid Point Flurometer	3/5/2015 20:37	0.08
Mid Point Flurometer	3/5/2015 20:38	1.61

Location	Date and Time	Rhodmaine Concentration Adjusted Concentration (ppb)
Mid Point Flurometer	3/5/2015 20:39	2.01
Mid Point Flurometer	3/5/2015 20:40	0
Mid Point Flurometer	3/5/2015 20:41	0.22
Mid Point Flurometer	3/5/2015 20:42	0.74
Mid Point Flurometer	3/5/2015 20:43	0.05
Mid Point Flurometer	3/5/2015 20:44	0.1
Mid Point Flurometer	3/5/2015 20:45	0.16
Mid Point Flurometer	3/5/2015 20:46	0.05
Mid Point Flurometer	3/5/2015 20:47	0.03
Mid Point Flurometer	3/5/2015 20:48	0.26
Mid Point Flurometer	3/5/2015 20:49	0.02
Mid Point Flurometer	3/5/2015 20:50	0.05
Mid Point Flurometer	3/5/2015 20:51	1.95
Mid Point Flurometer	3/5/2015 20:52	2.4
Mid Point Flurometer	3/5/2015 20:53	0.26
Mid Point Flurometer	3/5/2015 20:54	0.35
Mid Point Flurometer	3/5/2015 20:55	1.21
Mid Point Flurometer	3/5/2015 20:56	0.92
Mid Point Flurometer	3/5/2015 20:57	0.08
Mid Point Flurometer	3/5/2015 20:58	0.14
Mid Point Flurometer	3/5/2015 20:59	0.24
Mid Point Flurometer	3/5/2015 21:00	0.16
Mid Point Flurometer	3/5/2015 21:01	1.59
Mid Point Flurometer	3/5/2015 21:02	0.02
Mid Point Flurometer	3/5/2015 21:03	0.19
Mid Point Flurometer	3/5/2015 21:04	0.3
Mid Point Flurometer	3/5/2015 21:05	0.18
Mid Point Flurometer	3/5/2015 21:06	0.08
Mid Point Flurometer	3/5/2015 21:07	0.08
Mid Point Flurometer	3/5/2015 21:08	0.39
Mid Point Flurometer	3/5/2015 21:09	0.15
Mid Point Flurometer	3/5/2015 21:10	0.03
Mid Point Flurometer	3/5/2015 21:11	0.07
Mid Point Flurometer	3/5/2015 21:12	0.25
Mid Point Flurometer	3/5/2015 21:13	0
Mid Point Flurometer	3/5/2015 21:14	2
Mid Point Flurometer	3/5/2015 21:15	0.07
Mid Point Flurometer	3/5/2015 21:16	0.12
Mid Point Flurometer	3/5/2015 21:17	0.06
Mid Point Flurometer	3/5/2015 21:18	0.09
Mid Point Flurometer	3/5/2015 21:19	0.04
Mid Point Flurometer	3/5/2015 21:20	2.57
Mid Point Flurometer	3/5/2015 21:21	0.49
Mid Point Flurometer	3/5/2015 21:22	0.03
Mid Point Flurometer	3/5/2015 21:23	0.1
Mid Point Flurometer	3/5/2015 21:24	0.11

Location	Date and Time	Rhodmaine Concentration Adjusted Concentration (ppb)
Mid Point Flurometer	3/5/2015 21:25	0.27
Mid Point Flurometer	3/5/2015 21:26	0.09
Mid Point Flurometer	3/5/2015 21:27	0.12
Mid Point Flurometer	3/5/2015 21:28	4.49
Mid Point Flurometer	3/5/2015 21:29	0.36
Mid Point Flurometer	3/5/2015 21:30	0.11
Mid Point Flurometer	3/5/2015 21:31	0.66
Mid Point Flurometer	3/5/2015 21:32	1.07
Mid Point Flurometer	3/5/2015 21:33	1.03
Mid Point Flurometer	3/5/2015 21:34	1.53
Mid Point Flurometer	3/5/2015 21:35	0.02
Mid Point Flurometer	3/5/2015 21:36	1
Mid Point Flurometer	3/5/2015 21:37	0.04
Mid Point Flurometer	3/5/2015 21:38	0.32
Mid Point Flurometer	3/5/2015 21:39	0.2
Mid Point Flurometer	3/5/2015 21:40	0.15
Mid Point Flurometer	3/5/2015 21:41	0.88
Mid Point Flurometer	3/5/2015 21:42	0.03
Mid Point Flurometer	3/5/2015 21:43	1.1
Mid Point Flurometer	3/5/2015 21:44	0.04
Mid Point Flurometer	3/5/2015 21:45	0.35
Mid Point Flurometer	3/5/2015 21:46	0.17
Mid Point Flurometer	3/5/2015 21:47	2.03
Mid Point Flurometer	3/5/2015 21:48	0
Mid Point Flurometer	3/5/2015 21:49	0.09
Mid Point Flurometer	3/5/2015 21:50	0.1
Mid Point Flurometer	3/5/2015 21:51	1.24
Mid Point Flurometer	3/5/2015 21:52	0.11
Mid Point Flurometer	3/5/2015 21:53	0.49
Mid Point Flurometer	3/5/2015 21:54	0.07
Mid Point Flurometer	3/5/2015 21:55	0.4
Mid Point Flurometer	3/5/2015 21:56	0.13
Mid Point Flurometer	3/5/2015 21:57	2.09
Mid Point Flurometer	3/5/2015 21:58	0.09
Mid Point Flurometer	3/5/2015 21:59	0.03
Mid Point Flurometer	3/5/2015 22:00	0.01
Mid Point Flurometer	3/5/2015 22:01	0.14
Mid Point Flurometer	3/5/2015 22:02	0.81
Mid Point Flurometer	3/5/2015 22:03	0.21
Mid Point Flurometer	3/5/2015 22:04	0.14
Mid Point Flurometer	3/5/2015 22:05	0.82
Mid Point Flurometer	3/5/2015 22:06	0.96
Mid Point Flurometer	3/5/2015 22:07	1.81
Mid Point Flurometer	3/5/2015 22:08	0.1
Mid Point Flurometer	3/5/2015 22:09	0.41
Mid Point Flurometer	3/5/2015 22:10	0.15

Location	Date and Time	Rhodmaine Concentration Adjusted Concentration (ppb)
Mid Point Flurometer	3/5/2015 22:11	0.59
Mid Point Flurometer	3/5/2015 22:12	2.7
Mid Point Flurometer	3/5/2015 22:13	1.35
Mid Point Flurometer	3/5/2015 22:14	0.06
Mid Point Flurometer	3/5/2015 22:15	0.1
Mid Point Flurometer	3/5/2015 22:16	0
Mid Point Flurometer	3/5/2015 22:17	0.3
Mid Point Flurometer	3/5/2015 22:18	0.02
Mid Point Flurometer	3/5/2015 22:19	0.6
Mid Point Flurometer	3/5/2015 22:20	0.67
Mid Point Flurometer	3/5/2015 22:21	1.01
Mid Point Flurometer	3/5/2015 22:22	1.4
Mid Point Flurometer	3/5/2015 22:23	0.35
Mid Point Flurometer	3/5/2015 22:24	0.12
Mid Point Flurometer	3/5/2015 22:25	0.09
Mid Point Flurometer	3/5/2015 22:26	1.64
Mid Point Flurometer	3/5/2015 22:27	1.48
Mid Point Flurometer	3/5/2015 22:28	2.08
Mid Point Flurometer	3/5/2015 22:29	0.09
Mid Point Flurometer	3/5/2015 22:30	0.27
Mid Point Flurometer	3/5/2015 22:31	0.01
Mid Point Flurometer	3/5/2015 22:32	0
Mid Point Flurometer	3/5/2015 22:33	2.74
Mid Point Flurometer	3/5/2015 22:34	0.12
Mid Point Flurometer	3/5/2015 22:35	0.18
Mid Point Flurometer	3/5/2015 22:36	0.1
Mid Point Flurometer	3/5/2015 22:37	0.74
Mid Point Flurometer	3/5/2015 22:38	0.15
Mid Point Flurometer	3/5/2015 22:39	0.69
Mid Point Flurometer	3/5/2015 22:40	0
Mid Point Flurometer	3/5/2015 22:41	0.13
Mid Point Flurometer	3/5/2015 22:42	0.04
Mid Point Flurometer	3/5/2015 22:43	1.85
Mid Point Flurometer	3/5/2015 22:44	0.51
Mid Point Flurometer	3/5/2015 22:45	0.16
Mid Point Flurometer	3/5/2015 22:46	0
Mid Point Flurometer	3/5/2015 22:47	0.01
Mid Point Flurometer	3/5/2015 22:48	0.05
Mid Point Flurometer	3/5/2015 22:49	0.02
Mid Point Flurometer	3/5/2015 22:50	0.02
Mid Point Flurometer	3/5/2015 22:51	1.03
Mid Point Flurometer	3/5/2015 22:52	0.03
Mid Point Flurometer	3/5/2015 22:53	0.5
Mid Point Flurometer	3/5/2015 22:54	0.2
Mid Point Flurometer	3/5/2015 22:55	1.32
Mid Point Flurometer	3/5/2015 22:56	1.66

Location	Date and Time	Rhodmaine Concentration Adjusted Concentration (ppb)
Mid Point Flurometer	3/5/2015 22:57	0.27
Mid Point Flurometer	3/5/2015 22:58	0.16
Mid Point Flurometer	3/5/2015 22:59	0.14
Mid Point Flurometer	3/5/2015 23:00	0.28
Mid Point Flurometer	3/5/2015 23:01	0.1
Mid Point Flurometer	3/5/2015 23:02	0.62
Mid Point Flurometer	3/5/2015 23:03	0.61
Mid Point Flurometer	3/5/2015 23:04	0.16
Mid Point Flurometer	3/5/2015 23:05	0.18
Mid Point Flurometer	3/5/2015 23:06	0.82
Mid Point Flurometer	3/5/2015 23:07	0
Mid Point Flurometer	3/5/2015 23:08	0.02
Mid Point Flurometer	3/5/2015 23:09	0.01
Mid Point Flurometer	3/5/2015 23:10	0.3
Mid Point Flurometer	3/5/2015 23:11	1.06
Mid Point Flurometer	3/5/2015 23:12	1.71
Mid Point Flurometer	3/5/2015 23:13	0.08
Mid Point Flurometer	3/5/2015 23:14	0.1
Mid Point Flurometer	3/5/2015 23:15	0.01
Mid Point Flurometer	3/5/2015 23:16	0.23
Mid Point Flurometer	3/5/2015 23:17	0.04
Mid Point Flurometer	3/5/2015 23:18	1.38
Mid Point Flurometer	3/5/2015 23:19	0.1
Mid Point Flurometer	3/5/2015 23:20	0.02
Mid Point Flurometer	3/5/2015 23:21	0.93
Mid Point Flurometer	3/5/2015 23:22	0.09
Mid Point Flurometer	3/5/2015 23:23	1.2
Mid Point Flurometer	3/5/2015 23:24	4.6
Mid Point Flurometer	3/5/2015 23:25	0.42
Mid Point Flurometer	3/5/2015 23:26	3.07
Mid Point Flurometer	3/5/2015 23:27	0.19
Mid Point Flurometer	3/5/2015 23:28	0.05
Mid Point Flurometer	3/5/2015 23:29	0
Mid Point Flurometer	3/5/2015 23:30	0.9
Mid Point Flurometer	3/5/2015 23:31	0.74
Mid Point Flurometer	3/5/2015 23:32	0.06
Mid Point Flurometer	3/5/2015 23:33	3.27
Mid Point Flurometer	3/5/2015 23:34	0.09
Mid Point Flurometer	3/5/2015 23:35	0.12
Mid Point Flurometer	3/5/2015 23:36	0.41
Mid Point Flurometer	3/5/2015 23:37	0.1
Mid Point Flurometer	3/5/2015 23:38	0.09
Mid Point Flurometer	3/5/2015 23:39	0.06
Mid Point Flurometer	3/5/2015 23:40	2.4
Mid Point Flurometer	3/5/2015 23:41	0.38
Mid Point Flurometer	3/5/2015 23:42	0.1

Location	Date and Time	Rhodmaine Concentration Adjusted Concentration (ppb)
Mid Point Flurometer	3/5/2015 23:43	0.56
Mid Point Flurometer	3/5/2015 23:44	1.4
Mid Point Flurometer	3/5/2015 23:45	1.64
Mid Point Flurometer	3/5/2015 23:46	0.07
Mid Point Flurometer	3/5/2015 23:47	0.08
Mid Point Flurometer	3/5/2015 23:48	0.06
Mid Point Flurometer	3/5/2015 23:49	0.02
Mid Point Flurometer	3/5/2015 23:50	0.51
Mid Point Flurometer	3/5/2015 23:51	0.05
Mid Point Flurometer	3/5/2015 23:52	0.05
Mid Point Flurometer	3/5/2015 23:53	2.85
Mid Point Flurometer	3/5/2015 23:54	0.07
Mid Point Flurometer	3/5/2015 23:55	0.11
Mid Point Flurometer	3/5/2015 23:56	0.12
Mid Point Flurometer	3/5/2015 23:57	0.03
Mid Point Flurometer	3/5/2015 23:58	0.06
Mid Point Flurometer	3/5/2015 23:59	0
Mid Point Flurometer	3/6/2015 0:00	0.42
Mid Point Flurometer	3/6/2015 0:01	1.74
Mid Point Flurometer	3/6/2015 0:02	0.13
Mid Point Flurometer	3/6/2015 0:03	1.23
Mid Point Flurometer	3/6/2015 0:04	0.12
Mid Point Flurometer	3/6/2015 0:05	0.38
Mid Point Flurometer	3/6/2015 0:06	6.31
Mid Point Flurometer	3/6/2015 0:07	0.06
Mid Point Flurometer	3/6/2015 0:08	0.02
Mid Point Flurometer	3/6/2015 0:09	1.09
Mid Point Flurometer	3/6/2015 0:10	0
Mid Point Flurometer	3/6/2015 0:11	0.48
Mid Point Flurometer	3/6/2015 0:12	0.01
Mid Point Flurometer	3/6/2015 0:13	0.35
Mid Point Flurometer	3/6/2015 0:14	0
Mid Point Flurometer	3/6/2015 0:15	0.18
Mid Point Flurometer	3/6/2015 0:16	0.02
Mid Point Flurometer	3/6/2015 0:17	0.12
Mid Point Flurometer	3/6/2015 0:18	0.07
Mid Point Flurometer	3/6/2015 0:19	0.08
Mid Point Flurometer	3/6/2015 0:20	0.25
Mid Point Flurometer	3/6/2015 0:21	0.05
Mid Point Flurometer	3/6/2015 0:22	0.03
Mid Point Flurometer	3/6/2015 0:23	3.5
Mid Point Flurometer	3/6/2015 0:24	0.05
Mid Point Flurometer	3/6/2015 0:25	6.32
Mid Point Flurometer	3/6/2015 0:26	0.35
Mid Point Flurometer	3/6/2015 0:27	0.04
Mid Point Flurometer	3/6/2015 0:28	0.2

Location	Date and Time	Rhodmaine Concentration Adjusted Concentration (ppb)
Mid Point Flurometer	3/6/2015 0:29	0
Mid Point Flurometer	3/6/2015 0:30	0.18
Mid Point Flurometer	3/6/2015 0:31	0.03
Mid Point Flurometer	3/6/2015 0:32	0.05
Mid Point Flurometer	3/6/2015 0:33	1.41
Mid Point Flurometer	3/6/2015 0:34	0.06
Mid Point Flurometer	3/6/2015 0:35	0.08
Mid Point Flurometer	3/6/2015 0:36	0.28
Mid Point Flurometer	3/6/2015 0:37	3.5
Mid Point Flurometer	3/6/2015 0:38	0.14
Mid Point Flurometer	3/6/2015 0:39	1.51
Mid Point Flurometer	3/6/2015 0:40	0.24
Mid Point Flurometer	3/6/2015 0:41	0.28
Mid Point Flurometer	3/6/2015 0:42	0.03
Mid Point Flurometer	3/6/2015 0:43	0.1
Mid Point Flurometer	3/6/2015 0:44	0.36
Mid Point Flurometer	3/6/2015 0:45	1.25
Mid Point Flurometer	3/6/2015 0:46	0.12
Mid Point Flurometer	3/6/2015 0:47	0.05
Mid Point Flurometer	3/6/2015 0:48	0.1
Mid Point Flurometer	3/6/2015 0:49	0.43
Mid Point Flurometer	3/6/2015 0:50	0.04
Mid Point Flurometer	3/6/2015 0:51	0.77
Mid Point Flurometer	3/6/2015 0:52	0.1
Mid Point Flurometer	3/6/2015 0:53	0.02
Mid Point Flurometer	3/6/2015 0:54	0.91
Mid Point Flurometer	3/6/2015 0:55	0.02
Mid Point Flurometer	3/6/2015 0:56	0.06
Mid Point Flurometer	3/6/2015 0:57	0.04
Mid Point Flurometer	3/6/2015 0:58	1.86
Mid Point Flurometer	3/6/2015 0:59	0.16
Mid Point Flurometer	3/6/2015 1:00	0.42
Mid Point Flurometer	3/6/2015 1:01	0.11
Mid Point Flurometer	3/6/2015 1:02	8.36
Mid Point Flurometer	3/6/2015 1:03	0.11
Mid Point Flurometer	3/6/2015 1:04	0.67
Mid Point Flurometer	3/6/2015 1:05	0
Mid Point Flurometer	3/6/2015 1:06	0.67
Mid Point Flurometer	3/6/2015 1:07	1.27
Mid Point Flurometer	3/6/2015 1:08	0.03
Mid Point Flurometer	3/6/2015 1:09	0.11
Mid Point Flurometer	3/6/2015 1:10	0.11
Mid Point Flurometer	3/6/2015 1:11	0.1
Mid Point Flurometer	3/6/2015 1:12	0.03
Mid Point Flurometer	3/6/2015 1:13	0
Mid Point Flurometer	3/6/2015 1:14	0.12

Location	Date and Time	Rhodmaine Concentration Adjusted Concentration (ppb)
Mid Point Flurometer	3/6/2015 1:15	0.23
Mid Point Flurometer	3/6/2015 1:16	1.51
Mid Point Flurometer	3/6/2015 1:17	0.05
Mid Point Flurometer	3/6/2015 1:18	0.05
Mid Point Flurometer	3/6/2015 1:19	1.6
Mid Point Flurometer	3/6/2015 1:20	0.2
Mid Point Flurometer	3/6/2015 1:21	0.02
Mid Point Flurometer	3/6/2015 1:22	0.01
Mid Point Flurometer	3/6/2015 1:23	0.04
Mid Point Flurometer	3/6/2015 1:24	0.65
Mid Point Flurometer	3/6/2015 1:25	0.08
Mid Point Flurometer	3/6/2015 1:26	0.32
Mid Point Flurometer	3/6/2015 1:27	1.71
Mid Point Flurometer	3/6/2015 1:28	0.12
Mid Point Flurometer	3/6/2015 1:29	0
Mid Point Flurometer	3/6/2015 1:30	0.15
Mid Point Flurometer	3/6/2015 1:31	0.14
Mid Point Flurometer	3/6/2015 1:32	0.3
Mid Point Flurometer	3/6/2015 1:33	0.05
Mid Point Flurometer	3/6/2015 1:34	0.06
Mid Point Flurometer	3/6/2015 1:35	0.09
Mid Point Flurometer	3/6/2015 1:36	0.05
Mid Point Flurometer	3/6/2015 1:37	0.45
Mid Point Flurometer	3/6/2015 1:38	0.05
Mid Point Flurometer	3/6/2015 1:39	0.09
Mid Point Flurometer	3/6/2015 1:40	0.12
Mid Point Flurometer	3/6/2015 1:41	0.02
Mid Point Flurometer	3/6/2015 1:42	0.02
Mid Point Flurometer	3/6/2015 1:43	0.07
Mid Point Flurometer	3/6/2015 1:44	0.32
Mid Point Flurometer	3/6/2015 1:45	0.04
Mid Point Flurometer	3/6/2015 1:46	0.11
Mid Point Flurometer	3/6/2015 1:47	0.05
Mid Point Flurometer	3/6/2015 1:48	0.21
Mid Point Flurometer	3/6/2015 1:49	0.03
Mid Point Flurometer	3/6/2015 1:50	0.14
Mid Point Flurometer	3/6/2015 1:51	1
Mid Point Flurometer	3/6/2015 1:52	0.01
Mid Point Flurometer	3/6/2015 1:53	0.14
Mid Point Flurometer	3/6/2015 1:54	0.05
Mid Point Flurometer	3/6/2015 1:55	0
Mid Point Flurometer	3/6/2015 1:56	0.08
Mid Point Flurometer	3/6/2015 1:57	0.07
Mid Point Flurometer	3/6/2015 1:58	0.12
Mid Point Flurometer	3/6/2015 1:59	0.02
Mid Point Flurometer	3/6/2015 2:00	0.02

Location	Date and Time	Rhodmaine Concentration Adjusted Concentration (ppb)
Mid Point Flurometer	3/6/2015 2:01	0.04
Mid Point Flurometer	3/6/2015 2:02	0.03
Mid Point Flurometer	3/6/2015 2:03	0.13
Mid Point Flurometer	3/6/2015 2:04	0.1
Mid Point Flurometer	3/6/2015 2:05	0.01
Mid Point Flurometer	3/6/2015 2:06	0.06
Mid Point Flurometer	3/6/2015 2:07	0.01
Mid Point Flurometer	3/6/2015 2:08	0.01
Mid Point Flurometer	3/6/2015 2:09	0.04
Mid Point Flurometer	3/6/2015 2:10	0.02
Mid Point Flurometer	3/6/2015 2:11	0.01
Mid Point Flurometer	3/6/2015 2:12	0.05
Mid Point Flurometer	3/6/2015 2:13	0.09
Mid Point Flurometer	3/6/2015 2:14	0.07
Mid Point Flurometer	3/6/2015 2:15	0.02
Mid Point Flurometer	3/6/2015 2:16	0
Mid Point Flurometer	3/6/2015 2:17	0.2
Mid Point Flurometer	3/6/2015 2:18	0.41
Mid Point Flurometer	3/6/2015 2:19	0.01
Mid Point Flurometer	3/6/2015 2:20	0.14
Mid Point Flurometer	3/6/2015 2:21	0
Mid Point Flurometer	3/6/2015 2:22	0.16
Mid Point Flurometer	3/6/2015 2:23	0.02
Mid Point Flurometer	3/6/2015 2:24	0.1
Mid Point Flurometer	3/6/2015 2:25	0.04
Mid Point Flurometer	3/6/2015 2:26	0.01
Mid Point Flurometer	3/6/2015 2:27	0.1
Mid Point Flurometer	3/6/2015 2:28	0.06
Mid Point Flurometer	3/6/2015 2:29	0.04
Mid Point Flurometer	3/6/2015 2:30	0.07
Mid Point Flurometer	3/6/2015 2:31	0
Mid Point Flurometer	3/6/2015 2:32	0.37
Mid Point Flurometer	3/6/2015 2:33	0.08
Mid Point Flurometer	3/6/2015 2:34	0.19
Mid Point Flurometer	3/6/2015 2:35	0.03
Mid Point Flurometer	3/6/2015 2:36	0.05
Mid Point Flurometer	3/6/2015 2:37	0.04
Mid Point Flurometer	3/6/2015 2:38	2.49
Mid Point Flurometer	3/6/2015 2:39	0
Mid Point Flurometer	3/6/2015 2:40	0.04
Mid Point Flurometer	3/6/2015 2:41	0.05
Mid Point Flurometer	3/6/2015 2:42	0.26
Mid Point Flurometer	3/6/2015 2:43	0.29
Mid Point Flurometer	3/6/2015 2:44	0.07
Mid Point Flurometer	3/6/2015 2:45	0.04
Mid Point Flurometer	3/6/2015 2:46	0.16

Location	Date and Time	Rhodmaine Concentration Adjusted Concentration (ppb)
Mid Point Flurometer	3/6/2015 2:47	0.02
Mid Point Flurometer	3/6/2015 2:48	0.09
Mid Point Flurometer	3/6/2015 2:49	0.11
Mid Point Flurometer	3/6/2015 2:50	0.03
Mid Point Flurometer	3/6/2015 2:51	1.14
Mid Point Flurometer	3/6/2015 2:52	0
Mid Point Flurometer	3/6/2015 2:53	0.04
Mid Point Flurometer	3/6/2015 2:54	0.15
Mid Point Flurometer	3/6/2015 2:55	0.25
Mid Point Flurometer	3/6/2015 2:56	0.05
Mid Point Flurometer	3/6/2015 2:57	0
Mid Point Flurometer	3/6/2015 2:58	0
Mid Point Flurometer	3/6/2015 2:59	0.09
Mid Point Flurometer	3/6/2015 3:00	0.02
Mid Point Flurometer	3/6/2015 3:01	0.03
Mid Point Flurometer	3/6/2015 3:02	0.01
Mid Point Flurometer	3/6/2015 3:03	0.03
Mid Point Flurometer	3/6/2015 3:04	0.06
Mid Point Flurometer	3/6/2015 3:05	1.58
Mid Point Flurometer	3/6/2015 3:06	0.03
Mid Point Flurometer	3/6/2015 3:07	0.06
Mid Point Flurometer	3/6/2015 3:08	0.17
Mid Point Flurometer	3/6/2015 3:09	0.1
Mid Point Flurometer	3/6/2015 3:10	0.06
Mid Point Flurometer	3/6/2015 3:11	0.18
Mid Point Flurometer	3/6/2015 3:12	0.05
Mid Point Flurometer	3/6/2015 3:13	2.37
Mid Point Flurometer	3/6/2015 3:14	0.07
Mid Point Flurometer	3/6/2015 3:15	0.05
Mid Point Flurometer	3/6/2015 3:16	0.07
Mid Point Flurometer	3/6/2015 3:17	0
Mid Point Flurometer	3/6/2015 3:18	0.63
Mid Point Flurometer	3/6/2015 3:19	0.04
Mid Point Flurometer	3/6/2015 3:20	0.1
Mid Point Flurometer	3/6/2015 3:21	0.16
Mid Point Flurometer	3/6/2015 3:22	0.05
Mid Point Flurometer	3/6/2015 3:23	0.03
Mid Point Flurometer	3/6/2015 3:24	0.05
Mid Point Flurometer	3/6/2015 3:25	0.08
Mid Point Flurometer	3/6/2015 3:26	0.1
Mid Point Flurometer	3/6/2015 3:27	0.08
Mid Point Flurometer	3/6/2015 3:28	0.04
Mid Point Flurometer	3/6/2015 3:29	0.06
Mid Point Flurometer	3/6/2015 3:30	1.08
Mid Point Flurometer	3/6/2015 3:31	0
Mid Point Flurometer	3/6/2015 3:32	0.28

Location	Date and Time	Rhodmaine Concentration Adjusted Concentration (ppb)
Mid Point Flurometer	3/6/2015 3:33	0.72
Mid Point Flurometer	3/6/2015 3:34	0.19
Mid Point Flurometer	3/6/2015 3:35	0.12
Mid Point Flurometer	3/6/2015 3:36	0.07
Mid Point Flurometer	3/6/2015 3:37	0.12
Mid Point Flurometer	3/6/2015 3:38	0.12
Mid Point Flurometer	3/6/2015 3:39	0.17
Mid Point Flurometer	3/6/2015 3:40	0.2
Mid Point Flurometer	3/6/2015 3:41	0.04
Mid Point Flurometer	3/6/2015 3:42	0.01
Mid Point Flurometer	3/6/2015 3:43	0.03
Mid Point Flurometer	3/6/2015 3:44	0.09
Mid Point Flurometer	3/6/2015 3:45	0.07
Mid Point Flurometer	3/6/2015 3:46	0.03
Mid Point Flurometer	3/6/2015 3:47	0.03
Mid Point Flurometer	3/6/2015 3:48	0.09
Mid Point Flurometer	3/6/2015 3:49	0.05
Mid Point Flurometer	3/6/2015 3:50	0.07
Mid Point Flurometer	3/6/2015 3:51	0.08
Mid Point Flurometer	3/6/2015 3:52	0.05
Mid Point Flurometer	3/6/2015 3:53	0.18
Mid Point Flurometer	3/6/2015 3:54	0.12
Mid Point Flurometer	3/6/2015 3:55	0.04
Mid Point Flurometer	3/6/2015 3:56	0.35
Mid Point Flurometer	3/6/2015 3:57	0.09
Mid Point Flurometer	3/6/2015 3:58	0.07
Mid Point Flurometer	3/6/2015 3:59	0.04
Mid Point Flurometer	3/6/2015 4:00	0.56
Mid Point Flurometer	3/6/2015 4:01	0.07
Mid Point Flurometer	3/6/2015 4:02	0.07
Mid Point Flurometer	3/6/2015 4:03	0.21
Mid Point Flurometer	3/6/2015 4:04	3.33
Mid Point Flurometer	3/6/2015 4:05	0.12
Mid Point Flurometer	3/6/2015 4:06	0.01
Mid Point Flurometer	3/6/2015 4:07	0.01
Mid Point Flurometer	3/6/2015 4:08	0.05
Mid Point Flurometer	3/6/2015 4:09	0.26
Mid Point Flurometer	3/6/2015 4:10	0.06
Mid Point Flurometer	3/6/2015 4:11	0.04
Mid Point Flurometer	3/6/2015 4:12	0
Mid Point Flurometer	3/6/2015 4:13	0.01
Mid Point Flurometer	3/6/2015 4:14	0.54
Mid Point Flurometer	3/6/2015 4:15	0.11
Mid Point Flurometer	3/6/2015 4:16	0.06
Mid Point Flurometer	3/6/2015 4:17	0.11
Mid Point Flurometer	3/6/2015 4:18	0.02

Location	Date and Time	Rhodmaine Concentration Adjusted Concentration (ppb)
Mid Point Flurometer	3/6/2015 4:19	0.2
Mid Point Flurometer	3/6/2015 4:20	0.1
Mid Point Flurometer	3/6/2015 4:21	0.05
Mid Point Flurometer	3/6/2015 4:22	2.69
Mid Point Flurometer	3/6/2015 4:23	0.14
Mid Point Flurometer	3/6/2015 4:24	0.14
Mid Point Flurometer	3/6/2015 4:25	0.12
Mid Point Flurometer	3/6/2015 4:26	0
Mid Point Flurometer	3/6/2015 4:27	0.5
Mid Point Flurometer	3/6/2015 4:28	0.04
Mid Point Flurometer	3/6/2015 4:29	0
Mid Point Flurometer	3/6/2015 4:30	0.1
Mid Point Flurometer	3/6/2015 4:31	0.04
Mid Point Flurometer	3/6/2015 4:32	0.15
Mid Point Flurometer	3/6/2015 4:33	0.12
Mid Point Flurometer	3/6/2015 4:34	0.09
Mid Point Flurometer	3/6/2015 4:35	0.09
Mid Point Flurometer	3/6/2015 4:36	0.04
Mid Point Flurometer	3/6/2015 4:37	0.03
Mid Point Flurometer	3/6/2015 4:38	0.09
Mid Point Flurometer	3/6/2015 4:39	0.13
Mid Point Flurometer	3/6/2015 4:40	0.1
Mid Point Flurometer	3/6/2015 4:41	0.06
Mid Point Flurometer	3/6/2015 4:42	0.14
Mid Point Flurometer	3/6/2015 4:43	0.73
Mid Point Flurometer	3/6/2015 4:44	0.06
Mid Point Flurometer	3/6/2015 4:45	0.04
Mid Point Flurometer	3/6/2015 4:46	1.01
Mid Point Flurometer	3/6/2015 4:47	0.06
Mid Point Flurometer	3/6/2015 4:48	0.71
Mid Point Flurometer	3/6/2015 4:49	0.1
Mid Point Flurometer	3/6/2015 4:50	0.02
Mid Point Flurometer	3/6/2015 4:51	0.05
Mid Point Flurometer	3/6/2015 4:52	0.12
Mid Point Flurometer	3/6/2015 4:53	0.09
Mid Point Flurometer	3/6/2015 4:54	0.06
Mid Point Flurometer	3/6/2015 4:55	0.16
Mid Point Flurometer	3/6/2015 4:56	0.08
Mid Point Flurometer	3/6/2015 4:57	0.04
Mid Point Flurometer	3/6/2015 4:58	0.01
Mid Point Flurometer	3/6/2015 4:59	0.05
Mid Point Flurometer	3/6/2015 5:00	0.05
Mid Point Flurometer	3/6/2015 5:01	0.04
Mid Point Flurometer	3/6/2015 5:02	8.21
Mid Point Flurometer	3/6/2015 5:03	0.13
Mid Point Flurometer	3/6/2015 5:04	0.02

Location	Date and Time	Rhodmaine Concentration Adjusted Concentration (ppb)
Mid Point Flurometer	3/6/2015 5:05	0.12
Mid Point Flurometer	3/6/2015 5:06	0.07
Mid Point Flurometer	3/6/2015 5:07	0.13
Mid Point Flurometer	3/6/2015 5:08	0.03
Mid Point Flurometer	3/6/2015 5:09	0.14
Mid Point Flurometer	3/6/2015 5:10	0.06
Mid Point Flurometer	3/6/2015 5:11	0.03
Mid Point Flurometer	3/6/2015 5:12	0.1
Mid Point Flurometer	3/6/2015 5:13	0.1
Mid Point Flurometer	3/6/2015 5:14	0
Mid Point Flurometer	3/6/2015 5:15	0.05
Mid Point Flurometer	3/6/2015 5:16	0.09
Mid Point Flurometer	3/6/2015 5:17	0.02
Mid Point Flurometer	3/6/2015 5:18	0.13
Mid Point Flurometer	3/6/2015 5:19	0.13
Mid Point Flurometer	3/6/2015 5:20	0.09
Mid Point Flurometer	3/6/2015 5:21	0.07
Mid Point Flurometer	3/6/2015 5:22	0.71
Mid Point Flurometer	3/6/2015 5:23	0.11
Mid Point Flurometer	3/6/2015 5:24	0.09
Mid Point Flurometer	3/6/2015 5:25	0.96
Mid Point Flurometer	3/6/2015 5:26	0.41
Mid Point Flurometer	3/6/2015 5:27	0.06
Mid Point Flurometer	3/6/2015 5:28	1.68
Mid Point Flurometer	3/6/2015 5:29	0.04
Mid Point Flurometer	3/6/2015 5:30	0.09
Mid Point Flurometer	3/6/2015 5:31	0
Mid Point Flurometer	3/6/2015 5:32	0.2
Mid Point Flurometer	3/6/2015 5:33	0.09
Mid Point Flurometer	3/6/2015 5:34	0.08
Mid Point Flurometer	3/6/2015 5:35	0.07
Mid Point Flurometer	3/6/2015 5:36	0.07
Mid Point Flurometer	3/6/2015 5:37	0.15
Mid Point Flurometer	3/6/2015 5:38	0.12
Mid Point Flurometer	3/6/2015 5:39	0.08
Mid Point Flurometer	3/6/2015 5:40	0.34
Mid Point Flurometer	3/6/2015 5:41	0.3
Mid Point Flurometer	3/6/2015 5:42	0.24
Mid Point Flurometer	3/6/2015 5:43	0.18
Mid Point Flurometer	3/6/2015 5:44	0.06
Mid Point Flurometer	3/6/2015 5:45	0.06
Mid Point Flurometer	3/6/2015 5:46	0.13
Mid Point Flurometer	3/6/2015 5:47	0.11
Mid Point Flurometer	3/6/2015 5:48	0
Mid Point Flurometer	3/6/2015 5:49	0.19
Mid Point Flurometer	3/6/2015 5:50	0.22

Location	Date and Time	Rhodmaine Concentration Adjusted Concentration (ppb)
Mid Point Flurometer	3/6/2015 5:51	0.3
Mid Point Flurometer	3/6/2015 5:52	0.07
Mid Point Flurometer	3/6/2015 5:53	0.1
Mid Point Flurometer	3/6/2015 5:54	0.31
Mid Point Flurometer	3/6/2015 5:55	0.09
Mid Point Flurometer	3/6/2015 5:56	0.48
Mid Point Flurometer	3/6/2015 5:57	0.19
Mid Point Flurometer	3/6/2015 5:58	0.04
Mid Point Flurometer	3/6/2015 5:59	0.04
Mid Point Flurometer	3/6/2015 6:00	8.42
Mid Point Flurometer	3/6/2015 6:01	0.09
Mid Point Flurometer	3/6/2015 6:02	0.07
Mid Point Flurometer	3/6/2015 6:03	0.1
Mid Point Flurometer	3/6/2015 6:04	0.08
Mid Point Flurometer	3/6/2015 6:05	0.08
Mid Point Flurometer	3/6/2015 6:06	0.09
Mid Point Flurometer	3/6/2015 6:07	0.08
Mid Point Flurometer	3/6/2015 6:08	0.04
Mid Point Flurometer	3/6/2015 6:09	0.38
Mid Point Flurometer	3/6/2015 6:10	0.25
Mid Point Flurometer	3/6/2015 6:11	0.17
Mid Point Flurometer	3/6/2015 6:12	0.11
Mid Point Flurometer	3/6/2015 6:13	0.02
Mid Point Flurometer	3/6/2015 6:14	0.11
Mid Point Flurometer	3/6/2015 6:15	0.09
Mid Point Flurometer	3/6/2015 6:16	0.18
Mid Point Flurometer	3/6/2015 6:17	0.08
Mid Point Flurometer	3/6/2015 6:18	0.17
Mid Point Flurometer	3/6/2015 6:19	0.13
Mid Point Flurometer	3/6/2015 6:20	0.07
Mid Point Flurometer	3/6/2015 6:21	0.16
Mid Point Flurometer	3/6/2015 6:22	0.13
Mid Point Flurometer	3/6/2015 6:23	0.19
Mid Point Flurometer	3/6/2015 6:24	0.23
Mid Point Flurometer	3/6/2015 6:25	0.01
Mid Point Flurometer	3/6/2015 6:26	0.07
Mid Point Flurometer	3/6/2015 6:27	0.12
Mid Point Flurometer	3/6/2015 6:28	0.15
Mid Point Flurometer	3/6/2015 6:29	0.17
Mid Point Flurometer	3/6/2015 6:30	0.95
Mid Point Flurometer	3/6/2015 6:31	0.18
Mid Point Flurometer	3/6/2015 6:32	0.82
Mid Point Flurometer	3/6/2015 6:33	0.43
Mid Point Flurometer	3/6/2015 6:34	0.17
Mid Point Flurometer	3/6/2015 6:35	0.09
Mid Point Flurometer	3/6/2015 6:36	0.08

Location	Date and Time	Rhodmaine Concentration Adjusted Concentration (ppb)
Mid Point Flurometer	3/6/2015 6:37	0.24
Mid Point Flurometer	3/6/2015 6:38	0.27
Mid Point Flurometer	3/6/2015 6:39	0.03
Mid Point Flurometer	3/6/2015 6:40	0.09
Mid Point Flurometer	3/6/2015 6:41	0.19
Mid Point Flurometer	3/6/2015 6:42	0.07
Mid Point Flurometer	3/6/2015 6:43	0.1
Mid Point Flurometer	3/6/2015 6:44	0.06
Mid Point Flurometer	3/6/2015 6:45	0.24
Mid Point Flurometer	3/6/2015 6:46	0.31
Mid Point Flurometer	3/6/2015 6:47	0.81
Mid Point Flurometer	3/6/2015 6:48	0.03
Mid Point Flurometer	3/6/2015 6:49	0.12
Mid Point Flurometer	3/6/2015 6:50	0.13
Mid Point Flurometer	3/6/2015 6:51	0.13
Mid Point Flurometer	3/6/2015 6:52	0.15
Mid Point Flurometer	3/6/2015 6:53	0.19
Mid Point Flurometer	3/6/2015 6:54	2.25
Mid Point Flurometer	3/6/2015 6:55	0.15
Mid Point Flurometer	3/6/2015 6:56	0.11
Mid Point Flurometer	3/6/2015 6:57	0.05
Mid Point Flurometer	3/6/2015 6:58	0.3
Mid Point Flurometer	3/6/2015 6:59	0.1
Mid Point Flurometer	3/6/2015 7:00	0.12
Mid Point Flurometer	3/6/2015 7:01	0.13
Mid Point Flurometer	3/6/2015 7:02	0.17
Mid Point Flurometer	3/6/2015 7:03	0.16
Mid Point Flurometer	3/6/2015 7:04	0.08
Mid Point Flurometer	3/6/2015 7:05	0.14
Mid Point Flurometer	3/6/2015 7:06	1.81
Mid Point Flurometer	3/6/2015 7:07	0.34
Mid Point Flurometer	3/6/2015 7:08	0.25
Mid Point Flurometer	3/6/2015 7:09	0.19
Mid Point Flurometer	3/6/2015 7:10	0.59
Mid Point Flurometer	3/6/2015 7:11	0.42
Mid Point Flurometer	3/6/2015 7:12	0.08
Mid Point Flurometer	3/6/2015 7:13	0.19
Mid Point Flurometer	3/6/2015 7:14	0.11
Mid Point Flurometer	3/6/2015 7:15	0.87
Mid Point Flurometer	3/6/2015 7:16	0.04
Mid Point Flurometer	3/6/2015 7:17	0.1
Mid Point Flurometer	3/6/2015 7:18	0.12
Mid Point Flurometer	3/6/2015 7:19	0.42
Mid Point Flurometer	3/6/2015 7:20	0
Mid Point Flurometer	3/6/2015 7:21	0
Mid Point Flurometer	3/6/2015 7:22	0

Location	Date and Time	Rhodmaine Concentration Adjusted Concentration (ppb)
Mid Point Flurometer	3/6/2015 7:23	0
Mid Point Flurometer	3/6/2015 7:24	0
Mid Point Flurometer	3/6/2015 7:25	0
Mid Point Flurometer	3/6/2015 7:26	0.04
Mid Point Flurometer	3/6/2015 7:27	1.37
Mid Point Flurometer	3/6/2015 7:28	0
Mid Point Flurometer	3/6/2015 7:29	0
Mid Point Flurometer	3/6/2015 7:30	0
Mid Point Flurometer	3/6/2015 7:31	0
Mid Point Flurometer	3/6/2015 7:32	0
Mid Point Flurometer	3/6/2015 7:33	0
Mid Point Flurometer	3/6/2015 7:34	0
Mid Point Flurometer	3/6/2015 7:35	0
Mid Point Flurometer	3/6/2015 7:36	0
Mid Point Flurometer	3/6/2015 7:37	0
Mid Point Flurometer	3/6/2015 7:38	0
Mid Point Flurometer	3/6/2015 7:39	0.01
Mid Point Flurometer	3/6/2015 7:40	0.01
Mid Point Flurometer	3/6/2015 7:41	0.03
Mid Point Flurometer	3/6/2015 7:42	0.03
Mid Point Flurometer	3/6/2015 7:43	0
Mid Point Flurometer	3/6/2015 7:44	0
Mid Point Flurometer	3/6/2015 7:45	0
Mid Point Flurometer	3/6/2015 7:46	0.05
Mid Point Flurometer	3/6/2015 7:47	0
Mid Point Flurometer	3/6/2015 7:48	0
Mid Point Flurometer	3/6/2015 7:49	0.01
Mid Point Flurometer	3/6/2015 7:50	0
Mid Point Flurometer	3/6/2015 7:51	0.03
Mid Point Flurometer	3/6/2015 7:52	0
Mid Point Flurometer	3/6/2015 7:53	0.03
Mid Point Flurometer	3/6/2015 7:54	0.03
Mid Point Flurometer	3/6/2015 7:55	0.04
Mid Point Flurometer	3/6/2015 7:56	0.09
Mid Point Flurometer	3/6/2015 7:57	0.01
Mid Point Flurometer	3/6/2015 7:58	0
Mid Point Flurometer	3/6/2015 7:59	0.05
Mid Point Flurometer	3/6/2015 8:00	0.05
Mid Point Flurometer	3/6/2015 8:01	0
Mid Point Flurometer	3/6/2015 8:02	0
Mid Point Flurometer	3/6/2015 8:03	0
Mid Point Flurometer	3/6/2015 8:04	0.07
Mid Point Flurometer	3/6/2015 8:05	0
Mid Point Flurometer	3/6/2015 8:06	0
Mid Point Flurometer	3/6/2015 8:07	0
Mid Point Flurometer	3/6/2015 8:08	0.02

Location	Date and Time	Rhodmaine Concentration Adjusted Concentration (ppb)
Mid Point Flurometer	3/6/2015 8:09	0
Mid Point Flurometer	3/6/2015 8:10	0.06
Mid Point Flurometer	3/6/2015 8:11	0.01
Mid Point Flurometer	3/6/2015 8:12	0
Mid Point Flurometer	3/6/2015 8:13	0
Mid Point Flurometer	3/6/2015 8:14	0
Mid Point Flurometer	3/6/2015 8:15	0.18
Mid Point Flurometer	3/6/2015 8:16	0.04
Mid Point Flurometer	3/6/2015 8:17	0.06
Mid Point Flurometer	3/6/2015 8:18	0
Mid Point Flurometer	3/6/2015 8:19	0.05
Mid Point Flurometer	3/6/2015 8:20	0
Mid Point Flurometer	3/6/2015 8:21	0.01
Mid Point Flurometer	3/6/2015 8:22	0.03
Mid Point Flurometer	3/6/2015 8:23	0.11
Mid Point Flurometer	3/6/2015 8:24	0.06
Mid Point Flurometer	3/6/2015 8:25	0
Mid Point Flurometer	3/6/2015 8:26	0
Mid Point Flurometer	3/6/2015 8:27	0
Mid Point Flurometer	3/6/2015 8:28	0
Mid Point Flurometer	3/6/2015 8:29	0
Mid Point Flurometer	3/6/2015 8:30	0
Mid Point Flurometer	3/6/2015 8:31	0
Mid Point Flurometer	3/6/2015 8:32	0
Mid Point Flurometer	3/6/2015 8:33	0.27
Mid Point Flurometer	3/6/2015 8:34	0
Mid Point Flurometer	3/6/2015 8:35	0
Mid Point Flurometer	3/6/2015 8:36	0
Mid Point Flurometer	3/6/2015 8:37	0
Mid Point Flurometer	3/6/2015 8:38	0.03
Mid Point Flurometer	3/6/2015 8:39	0
Mid Point Flurometer	3/6/2015 8:40	0
Mid Point Flurometer	3/6/2015 8:41	0
Mid Point Flurometer	3/6/2015 8:42	0.01
Mid Point Flurometer	3/6/2015 8:43	0.46
Mid Point Flurometer	3/6/2015 8:44	0.01
Mid Point Flurometer	3/6/2015 8:45	0
Mid Point Flurometer	3/6/2015 8:46	0.09
Mid Point Flurometer	3/6/2015 8:47	0
Mid Point Flurometer	3/6/2015 8:48	0.04
Mid Point Flurometer	3/6/2015 8:49	0
Mid Point Flurometer	3/6/2015 8:50	0.15
Mid Point Flurometer	3/6/2015 8:51	0.01
Mid Point Flurometer	3/6/2015 8:52	0.26
Mid Point Flurometer	3/6/2015 8:53	0.02
Mid Point Flurometer	3/6/2015 8:54	0.05

Location	Date and Time	Rhodmaine Concentration Adjusted Concentration (ppb)
Mid Point Flurometer	3/6/2015 8:55	0
Mid Point Flurometer	3/6/2015 8:56	0
Mid Point Flurometer	3/6/2015 8:57	0.07
Mid Point Flurometer	3/6/2015 8:58	0.71
Mid Point Flurometer	3/6/2015 8:59	0.03
Mid Point Flurometer	3/6/2015 9:00	0
Mid Point Flurometer	3/6/2015 9:01	0
Mid Point Flurometer	3/6/2015 9:02	0
Mid Point Flurometer	3/6/2015 9:03	0.07
Mid Point Flurometer	3/6/2015 9:04	0
Mid Point Flurometer	3/6/2015 9:05	0
Mid Point Flurometer	3/6/2015 9:06	0
Mid Point Flurometer	3/6/2015 9:07	0
Mid Point Flurometer	3/6/2015 9:08	0
Mid Point Flurometer	3/6/2015 9:09	0
Mid Point Flurometer	3/6/2015 9:10	0.01
Mid Point Flurometer	3/6/2015 9:11	0
Mid Point Flurometer	3/6/2015 9:12	0
Mid Point Flurometer	3/6/2015 9:13	0.1
Mid Point Flurometer	3/6/2015 9:14	0.02
Mid Point Flurometer	3/6/2015 9:15	0
Mid Point Flurometer	3/6/2015 9:16	0.02
Mid Point Flurometer	3/6/2015 9:17	0
Mid Point Flurometer	3/6/2015 9:18	0
Mid Point Flurometer	3/6/2015 9:19	0.02
Mid Point Flurometer	3/6/2015 9:20	0
Mid Point Flurometer	3/6/2015 9:21	0.06
Mid Point Flurometer	3/6/2015 9:22	0
Mid Point Flurometer	3/6/2015 9:23	0
Mid Point Flurometer	3/6/2015 9:24	0
Mid Point Flurometer	3/6/2015 9:25	0
Mid Point Flurometer	3/6/2015 9:26	0.24
Mid Point Flurometer	3/6/2015 9:27	0
Mid Point Flurometer	3/6/2015 9:28	0
Mid Point Flurometer	3/6/2015 9:29	0
Mid Point Flurometer	3/6/2015 9:30	0
Mid Point Flurometer	3/6/2015 9:31	0
Mid Point Flurometer	3/6/2015 9:32	0
Mid Point Flurometer	3/6/2015 9:33	0.09
Mid Point Flurometer	3/6/2015 9:34	0.02
Mid Point Flurometer	3/6/2015 9:35	0.3
Mid Point Flurometer	3/6/2015 9:36	0
Mid Point Flurometer	3/6/2015 9:37	0
Mid Point Flurometer	3/6/2015 9:38	0
Mid Point Flurometer	3/6/2015 9:39	0
Mid Point Flurometer	3/6/2015 9:40	0.04

Location	Date and Time	Rhodmaine Concentration Adjusted Concentration (ppb)
Mid Point Flurometer	3/6/2015 9:41	0.03
Mid Point Flurometer	3/6/2015 9:42	0.06
Mid Point Flurometer	3/6/2015 9:43	0.02
Mid Point Flurometer	3/6/2015 9:44	0
Mid Point Flurometer	3/6/2015 9:45	0
Mid Point Flurometer	3/6/2015 9:46	0
Mid Point Flurometer	3/6/2015 9:47	0.07
Mid Point Flurometer	3/6/2015 9:48	0
Mid Point Flurometer	3/6/2015 9:49	0
Mid Point Flurometer	3/6/2015 9:50	0.06
Mid Point Flurometer	3/6/2015 9:51	0
Mid Point Flurometer	3/6/2015 9:52	0.03
Mid Point Flurometer	3/6/2015 9:53	0.01
Mid Point Flurometer	3/6/2015 9:54	0.05
Mid Point Flurometer	3/6/2015 9:55	0
Mid Point Flurometer	3/6/2015 9:56	0
Mid Point Flurometer	3/6/2015 9:57	0
Mid Point Flurometer	3/6/2015 9:58	0
Mid Point Flurometer	3/6/2015 9:59	0
Mid Point Flurometer	3/6/2015 10:00	0.15
Mid Point Flurometer	3/6/2015 10:01	0
Mid Point Flurometer	3/6/2015 10:02	0.1
Mid Point Flurometer	3/6/2015 10:03	0.01
Mid Point Flurometer	3/6/2015 10:04	0
Mid Point Flurometer	3/6/2015 10:05	0
Mid Point Flurometer	3/6/2015 10:06	0.01
Mid Point Flurometer	3/6/2015 10:07	0
Mid Point Flurometer	3/6/2015 10:08	0
Mid Point Flurometer	3/6/2015 10:09	0
Mid Point Flurometer	3/6/2015 10:10	0.05
Mid Point Flurometer	3/6/2015 10:11	0
Mid Point Flurometer	3/6/2015 10:12	0
Mid Point Flurometer	3/6/2015 10:13	0.05
Mid Point Flurometer	3/6/2015 10:14	0.1
Mid Point Flurometer	3/6/2015 10:15	0.05
Mid Point Flurometer	3/6/2015 10:16	0
Mid Point Flurometer	3/6/2015 10:17	0
Mid Point Flurometer	3/6/2015 10:18	0.06
Mid Point Flurometer	3/6/2015 10:19	0
Mid Point Flurometer	3/6/2015 10:20	0
Mid Point Flurometer	3/6/2015 10:21	0
Mid Point Flurometer	3/6/2015 10:22	0.04
Mid Point Flurometer	3/6/2015 10:23	0
Mid Point Flurometer	3/6/2015 10:24	0
Mid Point Flurometer	3/6/2015 10:25	0
Mid Point Flurometer	3/6/2015 10:26	0.32

Location	Date and Time	Rhodmaine Concentration Adjusted Concentration (ppb)
Mid Point Flurometer	3/6/2015 10:27	0
Mid Point Flurometer	3/6/2015 10:28	0
Mid Point Flurometer	3/6/2015 10:29	0
Mid Point Flurometer	3/6/2015 10:30	0.02
Mid Point Flurometer	3/6/2015 10:31	0.01
Mid Point Flurometer	3/6/2015 10:32	0.06
Mid Point Flurometer	3/6/2015 10:33	0
Mid Point Flurometer	3/6/2015 10:34	0
Mid Point Flurometer	3/6/2015 10:35	0.04
Mid Point Flurometer	3/6/2015 10:36	0.05
Mid Point Flurometer	3/6/2015 10:37	0.21
Mid Point Flurometer	3/6/2015 10:38	0.03
Mid Point Flurometer	3/6/2015 10:39	0.09
Mid Point Flurometer	3/6/2015 10:40	0.09
Mid Point Flurometer	3/6/2015 10:41	0.04
Mid Point Flurometer	3/6/2015 10:42	0.01
Mid Point Flurometer	3/6/2015 10:43	0
Mid Point Flurometer	3/6/2015 10:44	0
Mid Point Flurometer	3/6/2015 10:45	0
Mid Point Flurometer	3/6/2015 10:46	0
Mid Point Flurometer	3/6/2015 10:47	0
Mid Point Flurometer	3/6/2015 10:48	0.07
Mid Point Flurometer	3/6/2015 10:49	0
Mid Point Flurometer	3/6/2015 10:50	0
Mid Point Flurometer	3/6/2015 10:51	0
Mid Point Flurometer	3/6/2015 10:52	0.01
Mid Point Flurometer	3/6/2015 10:53	0
Mid Point Flurometer	3/6/2015 10:54	0
Mid Point Flurometer	3/6/2015 10:55	0
Mid Point Flurometer	3/6/2015 10:56	0
Mid Point Flurometer	3/6/2015 10:57	0
Mid Point Flurometer	3/6/2015 10:58	0.01
Mid Point Flurometer	3/6/2015 10:59	0
Mid Point Flurometer	3/6/2015 11:00	0
Mid Point Flurometer	3/6/2015 11:01	0
Mid Point Flurometer	3/6/2015 11:02	0.09
Mid Point Flurometer	3/6/2015 11:03	0.01
Mid Point Flurometer	3/6/2015 11:04	0
Mid Point Flurometer	3/6/2015 11:05	0.04
Mid Point Flurometer	3/6/2015 11:06	0.01
Mid Point Flurometer	3/6/2015 11:07	0
Mid Point Flurometer	3/6/2015 11:08	0
Mid Point Flurometer	3/6/2015 11:09	0.05
Mid Point Flurometer	3/6/2015 11:10	0.05
Mid Point Flurometer	3/6/2015 11:11	0
Mid Point Flurometer	3/6/2015 11:12	0

Location	Date and Time	Rhodmaine Concentration Adjusted Concentration (ppb)
Mid Point Flurometer	3/6/2015 11:13	0.02
Mid Point Flurometer	3/6/2015 11:14	0
Mid Point Flurometer	3/6/2015 11:15	0.04
Mid Point Flurometer	3/6/2015 11:16	0
Mid Point Flurometer	3/6/2015 11:17	0
Mid Point Flurometer	3/6/2015 11:18	0.01
Mid Point Flurometer	3/6/2015 11:19	0.05
Mid Point Flurometer	3/6/2015 11:20	0
Mid Point Flurometer	3/6/2015 11:21	0.01
Mid Point Flurometer	3/6/2015 11:22	0
Mid Point Flurometer	3/6/2015 11:23	0
Mid Point Flurometer	3/6/2015 11:24	0
Mid Point Flurometer	3/6/2015 11:25	0
Mid Point Flurometer	3/6/2015 11:26	0
Mid Point Flurometer	3/6/2015 11:27	0.11
Mid Point Flurometer	3/6/2015 11:28	0.02
Mid Point Flurometer	3/6/2015 11:29	0.01
Mid Point Flurometer	3/6/2015 11:30	0.03
Mid Point Flurometer	3/6/2015 11:31	0
Mid Point Flurometer	3/6/2015 11:32	0.02
Mid Point Flurometer	3/6/2015 11:33	0
Mid Point Flurometer	3/6/2015 11:34	0.06
Mid Point Flurometer	3/6/2015 11:35	0
Mid Point Flurometer	3/6/2015 11:36	0.06
Mid Point Flurometer	3/6/2015 11:37	0.01
Mid Point Flurometer	3/6/2015 11:38	0
Mid Point Flurometer	3/6/2015 11:39	0
Mid Point Flurometer	3/6/2015 11:40	0
Mid Point Flurometer	3/6/2015 11:41	0
Mid Point Flurometer	3/6/2015 11:42	0
Mid Point Flurometer	3/6/2015 11:43	0
Mid Point Flurometer	3/6/2015 11:44	0
Mid Point Flurometer	3/6/2015 11:45	0
Mid Point Flurometer	3/6/2015 11:46	0
Mid Point Flurometer	3/6/2015 11:47	0
Mid Point Flurometer	3/6/2015 11:48	0
Mid Point Flurometer	3/6/2015 11:49	0.01
Mid Point Flurometer	3/6/2015 11:50	0.03
Mid Point Flurometer	3/6/2015 11:51	0.02
Mid Point Flurometer	3/6/2015 11:52	0
Mid Point Flurometer	3/6/2015 11:53	0
Mid Point Flurometer	3/6/2015 11:54	0
Mid Point Flurometer	3/6/2015 11:55	0.01
Mid Point Flurometer	3/6/2015 11:56	0
Mid Point Flurometer	3/6/2015 11:57	0.02
Mid Point Flurometer	3/6/2015 11:58	0.06

Location	Date and Time	Rhodmaine Concentration Adjusted Concentration (ppb)
Mid Point Flurometer	3/6/2015 11:59	0.11
Mid Point Flurometer	3/6/2015 12:00	0
Mid Point Flurometer	3/6/2015 12:01	0
Mid Point Flurometer	3/6/2015 12:02	0.02
Mid Point Flurometer	3/6/2015 12:03	0.02
Mid Point Flurometer	3/6/2015 12:04	0
Mid Point Flurometer	3/6/2015 12:05	0.04
Mid Point Flurometer	3/6/2015 12:06	0
Mid Point Flurometer	3/6/2015 12:07	0.51
Mid Point Flurometer	3/6/2015 12:08	0.1
Mid Point Flurometer	3/6/2015 12:09	0.17
Mid Point Flurometer	3/6/2015 12:10	0.11
Mid Point Flurometer	3/6/2015 12:11	0
Mid Point Flurometer	3/6/2015 12:12	0.18
Mid Point Flurometer	3/6/2015 12:13	0.12
Mid Point Flurometer	3/6/2015 12:14	0.18
Mid Point Flurometer	3/6/2015 12:15	0
Mid Point Flurometer	3/6/2015 12:16	0.07
Mid Point Flurometer	3/6/2015 12:17	0
Mid Point Flurometer	3/6/2015 12:18	0.03
Mid Point Flurometer	3/6/2015 12:19	0.06
Mid Point Flurometer	3/6/2015 12:20	0.08
Mid Point Flurometer	3/6/2015 12:21	0.11
Mid Point Flurometer	3/6/2015 12:22	0.03
Mid Point Flurometer	3/6/2015 12:23	0.17
Mid Point Flurometer	3/6/2015 12:24	0.1
Mid Point Flurometer	3/6/2015 12:25	0.03
Mid Point Flurometer	3/6/2015 12:26	0
Mid Point Flurometer	3/6/2015 12:27	0.02
Mid Point Flurometer	3/6/2015 12:28	0.08
Mid Point Flurometer	3/6/2015 12:29	0.18
Mid Point Flurometer	3/6/2015 12:30	0.06
Mid Point Flurometer	3/6/2015 12:31	0.08
Mid Point Flurometer	3/6/2015 12:32	0.1
Mid Point Flurometer	3/6/2015 12:33	0.22
Mid Point Flurometer	3/6/2015 12:34	0.1
Mid Point Flurometer	3/6/2015 12:35	0.14
Mid Point Flurometer	3/6/2015 12:36	0.01
Mid Point Flurometer	3/6/2015 12:37	0.58
Mid Point Flurometer	3/6/2015 12:38	0.04
Mid Point Flurometer	3/6/2015 12:39	0.17
Mid Point Flurometer	3/6/2015 12:40	0.03
Mid Point Flurometer	3/6/2015 12:41	0.26
Mid Point Flurometer	3/6/2015 12:42	0
Mid Point Flurometer	3/6/2015 12:43	0.18
Mid Point Flurometer	3/6/2015 12:44	0.11

Location	Date and Time	Rhodmaine Concentration Adjusted Concentration (ppb)
Mid Point Flurometer	3/6/2015 12:45	0.01
Mid Point Flurometer	3/6/2015 12:46	0.05
Mid Point Flurometer	3/6/2015 12:47	0
Mid Point Flurometer	3/6/2015 12:48	0.11
Mid Point Flurometer	3/6/2015 12:49	0
Mid Point Flurometer	3/6/2015 12:50	0.09
Mid Point Flurometer	3/6/2015 12:51	0.04
Mid Point Flurometer	3/6/2015 12:52	0.1
Mid Point Flurometer	3/6/2015 12:53	0.01
Mid Point Flurometer	3/6/2015 12:54	0.02
Mid Point Flurometer	3/6/2015 12:55	0.01
Mid Point Flurometer	3/6/2015 12:56	0
Mid Point Flurometer	3/6/2015 12:57	0.04
Mid Point Flurometer	3/6/2015 12:58	0.01
Mid Point Flurometer	3/6/2015 12:59	0.05
Mid Point Flurometer	3/6/2015 13:00	0
Mid Point Flurometer	3/6/2015 13:01	0.02
Mid Point Flurometer	3/6/2015 13:02	0.04
Mid Point Flurometer	3/6/2015 13:03	0.22
Mid Point Flurometer	3/6/2015 13:04	0.1
Mid Point Flurometer	3/6/2015 13:05	0
Mid Point Flurometer	3/6/2015 13:06	0.07
Mid Point Flurometer	3/6/2015 13:07	0.27
Mid Point Flurometer	3/6/2015 13:08	0.04
Mid Point Flurometer	3/6/2015 13:09	0
Mid Point Flurometer	3/6/2015 13:10	0
Mid Point Flurometer	3/6/2015 13:11	0
Mid Point Flurometer	3/6/2015 13:12	0.05
Mid Point Flurometer	3/6/2015 13:13	0
Mid Point Flurometer	3/6/2015 13:14	0.19
Mid Point Flurometer	3/6/2015 13:15	0
Mid Point Flurometer	3/6/2015 13:16	0.04
Mid Point Flurometer	3/6/2015 13:17	0.04
Mid Point Flurometer	3/6/2015 13:18	0.04
Mid Point Flurometer	3/6/2015 13:19	0.03
Mid Point Flurometer	3/6/2015 13:20	0.09
Mid Point Flurometer	3/6/2015 13:21	0.27
Mid Point Flurometer	3/6/2015 13:22	0.5
Mid Point Flurometer	3/6/2015 13:23	0.36
Mid Point Flurometer	3/6/2015 13:24	0.22
Mid Point Flurometer	3/6/2015 13:25	0.14
Mid Point Flurometer	3/6/2015 13:26	0.08
Mid Point Flurometer	3/6/2015 13:27	0
Mid Point Flurometer	3/6/2015 13:28	0.06
Mid Point Flurometer	3/6/2015 13:29	0
Mid Point Flurometer	3/6/2015 13:30	0

Location	Date and Time	Rhodmaine Concentration Adjusted Concentration (ppb)
Mid Point Flurometer	3/6/2015 13:31	0
Mid Point Flurometer	3/6/2015 13:32	0
Mid Point Flurometer	3/6/2015 13:33	0
Mid Point Flurometer	3/6/2015 13:34	0
Mid Point Flurometer	3/6/2015 13:35	0
Mid Point Flurometer	3/6/2015 13:36	0
Mid Point Flurometer	3/6/2015 13:37	0
Mid Point Flurometer	3/6/2015 13:38	0
Mid Point Flurometer	3/6/2015 13:39	0
Mid Point Flurometer	3/6/2015 13:40	0
Mid Point Flurometer	3/6/2015 13:41	0
Mid Point Flurometer	3/6/2015 13:42	0
Mid Point Flurometer	3/6/2015 13:43	0
Mid Point Flurometer	3/6/2015 13:44	0
Mid Point Flurometer	3/6/2015 13:45	0
Mid Point Flurometer	3/6/2015 13:46	0
Mid Point Flurometer	3/6/2015 13:47	0
Mid Point Flurometer	3/6/2015 13:48	0
Mid Point Flurometer	3/6/2015 13:49	0
Mid Point Flurometer	3/6/2015 13:50	0
Mid Point Flurometer	3/6/2015 13:51	0
Mid Point Flurometer	3/6/2015 13:52	0
Mid Point Flurometer	3/6/2015 13:53	0
Mid Point Flurometer	3/6/2015 13:54	0
Mid Point Flurometer	3/6/2015 13:55	0
Mid Point Flurometer	3/6/2015 13:56	0
Mid Point Flurometer	3/6/2015 13:57	0
Mid Point Flurometer	3/6/2015 13:58	0
Mid Point Flurometer	3/6/2015 13:59	0
Mid Point Flurometer	3/6/2015 14:00	0
Mid Point Flurometer	3/6/2015 14:01	0
Mid Point Flurometer	3/6/2015 14:02	0
Mid Point Flurometer	3/6/2015 14:03	0
Mid Point Flurometer	3/6/2015 14:04	0
Mid Point Flurometer	3/6/2015 14:05	0
Mid Point Flurometer	3/6/2015 14:06	0
Mid Point Flurometer	3/6/2015 14:07	0
Mid Point Flurometer	3/6/2015 14:08	0
Mid Point Flurometer	3/6/2015 14:09	0
Mid Point Flurometer	3/6/2015 14:10	0
Mid Point Flurometer	3/6/2015 14:11	0
Mid Point Flurometer	3/6/2015 14:12	0
Mid Point Flurometer	3/6/2015 14:13	0
Mid Point Flurometer	3/6/2015 14:14	0
Mid Point Flurometer	3/6/2015 14:15	0
Mid Point Flurometer	3/6/2015 14:16	0

Location	Date and Time	Rhodmaine Concentration Adjusted Concentration (ppb)
Mid Point Flurometer	3/6/2015 14:17	0
Mid Point Flurometer	3/6/2015 14:18	0
Mid Point Flurometer	3/6/2015 14:19	0
Mid Point Flurometer	3/6/2015 14:20	0
Mid Point Flurometer	3/6/2015 14:21	0
Mid Point Flurometer	3/6/2015 14:22	0
Mid Point Flurometer	3/6/2015 14:23	0
Mid Point Flurometer	3/6/2015 14:24	0
Mid Point Flurometer	3/6/2015 14:25	0
Mid Point Flurometer	3/6/2015 14:26	0
Mid Point Flurometer	3/6/2015 14:27	0
Mid Point Flurometer	3/6/2015 14:28	0
Mid Point Flurometer	3/6/2015 14:29	0
Mid Point Flurometer	3/6/2015 14:30	0
Mid Point Flurometer	3/6/2015 14:31	0
Mid Point Flurometer	3/6/2015 14:32	0
Mid Point Flurometer	3/6/2015 14:33	0
Mid Point Flurometer	3/6/2015 14:34	0
Mid Point Flurometer	3/6/2015 14:35	0
Mid Point Flurometer	3/6/2015 14:36	0
Mid Point Flurometer	3/6/2015 14:37	0
Mid Point Flurometer	3/6/2015 14:38	0
Mid Point Flurometer	3/6/2015 14:39	0
Mid Point Flurometer	3/6/2015 14:40	0
Mid Point Flurometer	3/6/2015 14:41	0
Mid Point Flurometer	3/6/2015 14:42	0
Mid Point Flurometer	3/6/2015 14:43	0
Mid Point Flurometer	3/6/2015 14:44	0
Mid Point Flurometer	3/6/2015 14:45	0
Mid Point Flurometer	3/6/2015 14:46	0
Mid Point Flurometer	3/6/2015 14:47	0
Mid Point Flurometer	3/6/2015 14:48	0
Mid Point Flurometer	3/6/2015 14:49	0
Mid Point Flurometer	3/6/2015 14:50	0
Mid Point Flurometer	3/6/2015 14:51	0
Mid Point Flurometer	3/6/2015 14:52	0
Mid Point Flurometer	3/6/2015 14:53	0
Mid Point Flurometer	3/6/2015 14:54	0
Mid Point Flurometer	3/6/2015 14:55	0
Mid Point Flurometer	3/6/2015 14:56	0
Mid Point Flurometer	3/6/2015 14:57	0
Mid Point Flurometer	3/6/2015 14:58	0
Mid Point Flurometer	3/6/2015 14:59	0
Mid Point Flurometer	3/6/2015 15:00	0
Mid Point Flurometer	3/6/2015 15:01	0
Mid Point Flurometer	3/6/2015 15:02	0

Location	Date and Time	Rhodmaine Concentration Adjusted Concentration (ppb)
Mid Point Flurometer	3/6/2015 15:03	0
Mid Point Flurometer	3/6/2015 15:04	0
Mid Point Flurometer	3/6/2015 15:05	0
Mid Point Flurometer	3/6/2015 15:06	0
Mid Point Flurometer	3/6/2015 15:07	0
Mid Point Flurometer	3/6/2015 15:08	0
Mid Point Flurometer	3/6/2015 15:09	0
Mid Point Flurometer	3/6/2015 15:10	0
Mid Point Flurometer	3/6/2015 15:11	0
Mid Point Flurometer	3/6/2015 15:12	0
Mid Point Flurometer	3/6/2015 15:13	0
Mid Point Flurometer	3/6/2015 15:14	0
Mid Point Flurometer	3/6/2015 15:15	0
Mid Point Flurometer	3/6/2015 15:16	0
Mid Point Flurometer	3/6/2015 15:17	0
Mid Point Flurometer	3/6/2015 15:18	0
Mid Point Flurometer	3/6/2015 15:19	0
Mid Point Flurometer	3/6/2015 15:20	0
Mid Point Flurometer	3/6/2015 15:21	0
Mid Point Flurometer	3/6/2015 15:22	0
Mid Point Flurometer	3/6/2015 15:23	0
Mid Point Flurometer	3/6/2015 15:24	0
Mid Point Flurometer	3/6/2015 15:25	0
Mid Point Flurometer	3/6/2015 15:26	0
Mid Point Flurometer	3/6/2015 15:27	0
Mid Point Flurometer	3/6/2015 15:28	0
Mid Point Flurometer	3/6/2015 15:29	0
Mid Point Flurometer	3/6/2015 15:30	0
Mid Point Flurometer	3/6/2015 15:31	0
Mid Point Flurometer	3/6/2015 15:32	0
Mid Point Flurometer	3/6/2015 15:33	0
Mid Point Flurometer	3/6/2015 15:34	0
Mid Point Flurometer	3/6/2015 15:35	0
Mid Point Flurometer	3/6/2015 15:36	0
Mid Point Flurometer	3/6/2015 15:37	0
Mid Point Flurometer	3/6/2015 15:38	0
Mid Point Flurometer	3/6/2015 15:39	0
Mid Point Flurometer	3/6/2015 15:40	0
Mid Point Flurometer	3/6/2015 15:41	0
Mid Point Flurometer	3/6/2015 15:42	0
Mid Point Flurometer	3/6/2015 15:43	0
Mid Point Flurometer	3/6/2015 15:44	0
Mid Point Flurometer	3/6/2015 15:45	0
Mid Point Flurometer	3/6/2015 15:46	0
Mid Point Flurometer	3/6/2015 15:47	0
Mid Point Flurometer	3/6/2015 15:48	0

Location	Date and Time	Rhodmaine Concentration Adjusted Concentration (ppb)
Mid Point Flurometer	3/6/2015 15:49	0
Mid Point Flurometer	3/6/2015 15:50	0
Mid Point Flurometer	3/6/2015 15:51	0
Mid Point Flurometer	3/6/2015 15:52	0
Mid Point Flurometer	3/6/2015 15:53	0
Mid Point Flurometer	3/6/2015 15:54	0
Mid Point Flurometer	3/6/2015 15:55	0
Mid Point Flurometer	3/6/2015 15:56	0
Mid Point ISCO	3/4/15 16:00	0.162215346
Mid Point ISCO	3/4/15 17:00	0.224760609
Mid Point ISCO	3/4/15 18:00	0.117775291
Mid Point ISCO	3/4/15 19:00	0.145756066
Mid Point ISCO	3/4/15 20:00	0.048646316
Mid Point ISCO	3/4/15 21:00	0.068397451
Mid Point ISCO	3/4/15 22:00	6.823285857
Mid Point ISCO	3/4/15 23:00	11.86970103
Mid Point ISCO	3/5/15 0:00	7.511283751
Mid Point ISCO	3/5/15 1:00	5.957527743
Mid Point ISCO	3/5/15 2:00	4.621034228
Mid Point ISCO	3/5/15 3:00	2.715049634
Mid Point ISCO	3/5/15 4:00	2.204811962
Mid Point ISCO	3/5/15 5:00	1.714325426
Mid Point ISCO	3/5/15 6:00	1.66988537
Mid Point ISCO	3/5/15 7:00	1.269924873
Mid Point ISCO	3/5/15 8:00	1.15800177
Mid Point ISCO	3/5/15 9:00	0.937447422
Mid Point ISCO	3/5/15 10:00	0.371248199
Mid Point ISCO	3/5/15 11:00	0.51608986
Mid Point ISCO	3/5/15 12:00	0.420626038
Mid Point ISCO	3/5/15 13:00	0.221468753
Mid Point ISCO	3/5/15 14:00	0.311994792
Lower Flurometer	3/4/2015 9:53	0.44
Lower Flurometer	3/4/2015 9:54	0.37
Lower Flurometer	3/4/2015 9:55	0.35
Lower Flurometer	3/4/2015 9:56	0.4
Lower Flurometer	3/4/2015 9:57	0.38
Lower Flurometer	3/4/2015 9:58	0.43
Lower Flurometer	3/4/2015 9:59	0.31
Lower Flurometer	3/4/2015 10:00	0.39
Lower Flurometer	3/4/2015 10:01	0.43
Lower Flurometer	3/4/2015 10:02	0.39
Lower Flurometer	3/4/2015 10:03	0.43
Lower Flurometer	3/4/2015 10:04	0.37
Lower Flurometer	3/4/2015 10:05	0.43
Lower Flurometer	3/4/2015 10:06	0.38
Lower Flurometer	3/4/2015 10:07	0.37

Location	Date and Time	Rhodmaine Concentration Adjusted Concentration (ppb)
Lower Flurometer	3/4/2015 10:08	0.45
Lower Flurometer	3/4/2015 10:09	0.41
Lower Flurometer	3/4/2015 10:10	0.38
Lower Flurometer	3/4/2015 10:11	0.32
Lower Flurometer	3/4/2015 10:12	0.34
Lower Flurometer	3/4/2015 10:13	0.38
Lower Flurometer	3/4/2015 10:14	0.38
Lower Flurometer	3/4/2015 10:15	0.41
Lower Flurometer	3/4/2015 10:16	0.34
Lower Flurometer	3/4/2015 10:17	0.43
Lower Flurometer	3/4/2015 10:18	0.38
Lower Flurometer	3/4/2015 10:19	0.34
Lower Flurometer	3/4/2015 10:20	0.39
Lower Flurometer	3/4/2015 10:21	0.36
Lower Flurometer	3/4/2015 10:22	0.33
Lower Flurometer	3/4/2015 10:23	0.44
Lower Flurometer	3/4/2015 10:24	0.38
Lower Flurometer	3/4/2015 10:25	0.36
Lower Flurometer	3/4/2015 10:26	0.42
Lower Flurometer	3/4/2015 10:27	0.42
Lower Flurometer	3/4/2015 10:28	0.35
Lower Flurometer	3/4/2015 10:29	0.4
Lower Flurometer	3/4/2015 10:30	0.4
Lower Flurometer	3/4/2015 10:31	0.39
Lower Flurometer	3/4/2015 10:32	0.42
Lower Flurometer	3/4/2015 10:33	0.34
Lower Flurometer	3/4/2015 10:34	0.43
Lower Flurometer	3/4/2015 10:35	0.45
Lower Flurometer	3/4/2015 10:36	0.39
Lower Flurometer	3/4/2015 10:37	0.33
Lower Flurometer	3/4/2015 10:38	0.39
Lower Flurometer	3/4/2015 10:39	0.39
Lower Flurometer	3/4/2015 10:40	0.43
Lower Flurometer	3/4/2015 10:41	0.37
Lower Flurometer	3/4/2015 10:42	0.35
Lower Flurometer	3/4/2015 10:43	0.41
Lower Flurometer	3/4/2015 10:44	0.46
Lower Flurometer	3/4/2015 10:45	0.38
Lower Flurometer	3/4/2015 10:46	0.44
Lower Flurometer	3/4/2015 10:47	0.35
Lower Flurometer	3/4/2015 10:48	0.39
Lower Flurometer	3/4/2015 10:49	0.44
Lower Flurometer	3/4/2015 10:50	0.44
Lower Flurometer	3/4/2015 10:51	0.45
Lower Flurometer	3/4/2015 10:52	0.42
Lower Flurometer	3/4/2015 10:53	0.4

Location	Date and Time	Rhodmaine Concentration Adjusted Concentration (ppb)
Lower Flurometer	3/4/2015 10:54	0.34
Lower Flurometer	3/4/2015 10:55	0.34
Lower Flurometer	3/4/2015 10:56	0.38
Lower Flurometer	3/4/2015 10:57	0.31
Lower Flurometer	3/4/2015 10:58	0.34
Lower Flurometer	3/4/2015 10:59	0.34
Lower Flurometer	3/4/2015 11:00	0.45
Lower Flurometer	3/4/2015 11:01	0.44
Lower Flurometer	3/4/2015 11:02	0.34
Lower Flurometer	3/4/2015 11:03	0.38
Lower Flurometer	3/4/2015 11:04	0.43
Lower Flurometer	3/4/2015 11:05	0.31
Lower Flurometer	3/4/2015 11:06	0.43
Lower Flurometer	3/4/2015 11:07	0.34
Lower Flurometer	3/4/2015 11:08	0.36
Lower Flurometer	3/4/2015 11:09	0.33
Lower Flurometer	3/4/2015 11:10	0.39
Lower Flurometer	3/4/2015 11:11	0.33
Lower Flurometer	3/4/2015 11:12	0.38
Lower Flurometer	3/4/2015 11:13	0.4
Lower Flurometer	3/4/2015 11:14	0.44
Lower Flurometer	3/4/2015 11:15	0.4
Lower Flurometer	3/4/2015 11:16	0.37
Lower Flurometer	3/4/2015 11:17	0.37
Lower Flurometer	3/4/2015 11:18	0.44
Lower Flurometer	3/4/2015 11:19	0.35
Lower Flurometer	3/4/2015 11:20	0.33
Lower Flurometer	3/4/2015 11:21	0.33
Lower Flurometer	3/4/2015 11:22	0.43
Lower Flurometer	3/4/2015 11:23	0.43
Lower Flurometer	3/4/2015 11:24	0.35
Lower Flurometer	3/4/2015 11:25	0.36
Lower Flurometer	3/4/2015 11:26	0.43
Lower Flurometer	3/4/2015 11:27	0.35
Lower Flurometer	3/4/2015 11:28	0.37
Lower Flurometer	3/4/2015 11:29	0.36
Lower Flurometer	3/4/2015 11:30	0.36
Lower Flurometer	3/4/2015 11:31	0.36
Lower Flurometer	3/4/2015 11:32	0.38
Lower Flurometer	3/4/2015 11:33	0.35
Lower Flurometer	3/4/2015 11:34	0.4
Lower Flurometer	3/4/2015 11:35	0.43
Lower Flurometer	3/4/2015 11:36	0.34
Lower Flurometer	3/4/2015 11:37	0.36
Lower Flurometer	3/4/2015 11:38	0.33
Lower Flurometer	3/4/2015 11:39	0.36

Location	Date and Time	Rhodmaine Concentration Adjusted Concentration (ppb)
Lower Flurometer	3/4/2015 11:40	0.41
Lower Flurometer	3/4/2015 11:41	0.33
Lower Flurometer	3/4/2015 11:42	0.33
Lower Flurometer	3/4/2015 11:43	0.35
Lower Flurometer	3/4/2015 11:44	0.33
Lower Flurometer	3/4/2015 11:45	0.32
Lower Flurometer	3/4/2015 11:46	0.27
Lower Flurometer	3/4/2015 11:47	0.3
Lower Flurometer	3/4/2015 11:48	0.27
Lower Flurometer	3/4/2015 11:49	0.35
Lower Flurometer	3/4/2015 11:50	0.33
Lower Flurometer	3/4/2015 11:51	0.25
Lower Flurometer	3/4/2015 11:52	0.21
Lower Flurometer	3/4/2015 11:53	0.26
Lower Flurometer	3/4/2015 11:54	0.26
Lower Flurometer	3/4/2015 11:55	0.26
Lower Flurometer	3/4/2015 11:56	0.27
Lower Flurometer	3/4/2015 11:57	0.25
Lower Flurometer	3/4/2015 11:58	0.24
Lower Flurometer	3/4/2015 11:59	0.34
Lower Flurometer	3/4/2015 12:00	0.29
Lower Flurometer	3/4/2015 12:01	0
Lower Flurometer	3/4/2015 12:02	0.29
Lower Flurometer	3/4/2015 12:03	0.33
Lower Flurometer	3/4/2015 12:04	0.31
Lower Flurometer	3/4/2015 12:05	0
Lower Flurometer	3/4/2015 12:06	0
Lower Flurometer	3/4/2015 12:07	0
Lower Flurometer	3/4/2015 12:08	0
Lower Flurometer	3/4/2015 12:09	0
Lower Flurometer	3/4/2015 12:10	0
Lower Flurometer	3/4/2015 12:11	0
Lower Flurometer	3/4/2015 12:12	0
Lower Flurometer	3/4/2015 12:13	0
Lower Flurometer	3/4/2015 12:14	0
Lower Flurometer	3/4/2015 12:15	0
Lower Flurometer	3/4/2015 12:16	0
Lower Flurometer	3/4/2015 12:17	0
Lower Flurometer	3/4/2015 12:18	0
Lower Flurometer	3/4/2015 12:19	0
Lower Flurometer	3/4/2015 12:20	0
Lower Flurometer	3/4/2015 12:21	0
Lower Flurometer	3/4/2015 12:22	0
Lower Flurometer	3/4/2015 12:23	0
Lower Flurometer	3/4/2015 12:24	0
Lower Flurometer	3/4/2015 12:25	0

Location	Date and Time	Rhodmaine Concentration Adjusted Concentration (ppb)
Lower Flurometer	3/4/2015 12:26	0
Lower Flurometer	3/4/2015 12:27	0
Lower Flurometer	3/4/2015 12:28	0
Lower Flurometer	3/4/2015 12:29	0
Lower Flurometer	3/4/2015 12:30	0
Lower Flurometer	3/4/2015 12:31	0
Lower Flurometer	3/4/2015 12:32	0
Lower Flurometer	3/4/2015 12:33	0
Lower Flurometer	3/4/2015 12:34	0
Lower Flurometer	3/4/2015 12:35	0
Lower Flurometer	3/4/2015 12:36	0
Lower Flurometer	3/4/2015 12:37	0
Lower Flurometer	3/4/2015 12:38	0
Lower Flurometer	3/4/2015 12:39	0
Lower Flurometer	3/4/2015 12:40	0
Lower Flurometer	3/4/2015 12:41	0
Lower Flurometer	3/4/2015 12:42	0
Lower Flurometer	3/4/2015 12:43	0
Lower Flurometer	3/4/2015 12:44	0
Lower Flurometer	3/4/2015 12:45	0
Lower Flurometer	3/4/2015 12:46	0
Lower Flurometer	3/4/2015 12:47	0
Lower Flurometer	3/4/2015 12:48	0
Lower Flurometer	3/4/2015 12:49	0
Lower Flurometer	3/4/2015 12:50	0
Lower Flurometer	3/4/2015 12:51	0
Lower Flurometer	3/4/2015 12:52	0
Lower Flurometer	3/4/2015 12:53	0
Lower Flurometer	3/4/2015 12:54	0
Lower Flurometer	3/4/2015 12:55	0
Lower Flurometer	3/4/2015 12:56	0
Lower Flurometer	3/4/2015 12:57	0
Lower Flurometer	3/4/2015 12:58	0
Lower Flurometer	3/4/2015 12:59	0
Lower Flurometer	3/4/2015 13:00	0
Lower Flurometer	3/4/2015 13:01	0
Lower Flurometer	3/4/2015 13:02	0
Lower Flurometer	3/4/2015 13:03	0
Lower Flurometer	3/4/2015 13:04	0
Lower Flurometer	3/4/2015 13:05	0
Lower Flurometer	3/4/2015 13:06	0
Lower Flurometer	3/4/2015 13:07	0
Lower Flurometer	3/4/2015 13:08	0
Lower Flurometer	3/4/2015 13:09	0
Lower Flurometer	3/4/2015 13:10	0
Lower Flurometer	3/4/2015 13:11	0

Location	Date and Time	Rhodmaine Concentration Adjusted Concentration (ppb)
Lower Flurometer	3/4/2015 13:12	0
Lower Flurometer	3/4/2015 13:13	0
Lower Flurometer	3/4/2015 13:14	0
Lower Flurometer	3/4/2015 13:15	0
Lower Flurometer	3/4/2015 13:16	0
Lower Flurometer	3/4/2015 13:17	0
Lower Flurometer	3/4/2015 13:18	0
Lower Flurometer	3/4/2015 13:19	0
Lower Flurometer	3/4/2015 13:20	0
Lower Flurometer	3/4/2015 13:21	0
Lower Flurometer	3/4/2015 13:22	0
Lower Flurometer	3/4/2015 13:23	0
Lower Flurometer	3/4/2015 13:24	0
Lower Flurometer	3/4/2015 13:25	0.05
Lower Flurometer	3/4/2015 13:26	0
Lower Flurometer	3/4/2015 13:27	0
Lower Flurometer	3/4/2015 13:28	0
Lower Flurometer	3/4/2015 13:29	0
Lower Flurometer	3/4/2015 13:30	0
Lower Flurometer	3/4/2015 13:31	0
Lower Flurometer	3/4/2015 13:32	0
Lower Flurometer	3/4/2015 13:33	0
Lower Flurometer	3/4/2015 13:34	0
Lower Flurometer	3/4/2015 13:35	0
Lower Flurometer	3/4/2015 13:36	0
Lower Flurometer	3/4/2015 13:37	0
Lower Flurometer	3/4/2015 13:38	0
Lower Flurometer	3/4/2015 13:39	0
Lower Flurometer	3/4/2015 13:40	0
Lower Flurometer	3/4/2015 13:41	0
Lower Flurometer	3/4/2015 13:42	0
Lower Flurometer	3/4/2015 13:43	0
Lower Flurometer	3/4/2015 13:44	0
Lower Flurometer	3/4/2015 13:45	0
Lower Flurometer	3/4/2015 13:46	0
Lower Flurometer	3/4/2015 13:47	0
Lower Flurometer	3/4/2015 13:48	0
Lower Flurometer	3/4/2015 13:49	0
Lower Flurometer	3/4/2015 13:50	0
Lower Flurometer	3/4/2015 13:51	0
Lower Flurometer	3/4/2015 13:52	0
Lower Flurometer	3/4/2015 13:53	0
Lower Flurometer	3/4/2015 13:54	0
Lower Flurometer	3/4/2015 13:55	0
Lower Flurometer	3/4/2015 13:56	0
Lower Flurometer	3/4/2015 13:57	0

Location	Date and Time	Rhodmaine Concentration Adjusted Concentration (ppb)
Lower Flurometer	3/4/2015 13:58	0
Lower Flurometer	3/4/2015 13:59	0
Lower Flurometer	3/4/2015 14:00	0
Lower Flurometer	3/4/2015 14:01	0
Lower Flurometer	3/4/2015 14:02	0
Lower Flurometer	3/4/2015 14:03	0
Lower Flurometer	3/4/2015 14:04	0
Lower Flurometer	3/4/2015 14:05	0
Lower Flurometer	3/4/2015 14:06	0
Lower Flurometer	3/4/2015 14:07	0
Lower Flurometer	3/4/2015 14:08	0
Lower Flurometer	3/4/2015 14:09	0
Lower Flurometer	3/4/2015 14:10	5.04
Lower Flurometer	3/4/2015 14:11	0
Lower Flurometer	3/4/2015 14:12	0
Lower Flurometer	3/4/2015 14:13	0
Lower Flurometer	3/4/2015 14:14	0
Lower Flurometer	3/4/2015 14:15	0
Lower Flurometer	3/4/2015 14:16	0
Lower Flurometer	3/4/2015 14:17	0
Lower Flurometer	3/4/2015 14:18	0
Lower Flurometer	3/4/2015 14:19	0
Lower Flurometer	3/4/2015 14:20	0
Lower Flurometer	3/4/2015 14:21	0
Lower Flurometer	3/4/2015 14:22	0
Lower Flurometer	3/4/2015 14:23	0
Lower Flurometer	3/4/2015 14:24	0
Lower Flurometer	3/4/2015 14:25	0
Lower Flurometer	3/4/2015 14:26	0
Lower Flurometer	3/4/2015 14:27	0
Lower Flurometer	3/4/2015 14:28	0
Lower Flurometer	3/4/2015 14:29	0
Lower Flurometer	3/4/2015 14:30	0
Lower Flurometer	3/4/2015 14:31	0
Lower Flurometer	3/4/2015 14:32	0
Lower Flurometer	3/4/2015 14:33	0
Lower Flurometer	3/4/2015 14:34	0
Lower Flurometer	3/4/2015 14:35	0
Lower Flurometer	3/4/2015 14:36	0
Lower Flurometer	3/4/2015 14:37	0
Lower Flurometer	3/4/2015 14:38	0
Lower Flurometer	3/4/2015 14:39	0
Lower Flurometer	3/4/2015 14:40	0
Lower Flurometer	3/4/2015 14:41	0
Lower Flurometer	3/4/2015 14:42	0
Lower Flurometer	3/4/2015 14:43	0

Location	Date and Time	Rhodmaine Concentration Adjusted Concentration (ppb)
Lower Flurometer	3/4/2015 14:44	0
Lower Flurometer	3/4/2015 14:45	0
Lower Flurometer	3/4/2015 14:46	0
Lower Flurometer	3/4/2015 14:47	0
Lower Flurometer	3/4/2015 14:48	0
Lower Flurometer	3/4/2015 14:49	0
Lower Flurometer	3/4/2015 14:50	0
Lower Flurometer	3/4/2015 14:51	0
Lower Flurometer	3/4/2015 14:52	0
Lower Flurometer	3/4/2015 14:53	0
Lower Flurometer	3/4/2015 14:54	0
Lower Flurometer	3/4/2015 14:55	0
Lower Flurometer	3/4/2015 14:56	0
Lower Flurometer	3/4/2015 14:57	0
Lower Flurometer	3/4/2015 14:58	0
Lower Flurometer	3/4/2015 14:59	0
Lower Flurometer	3/4/2015 15:00	0
Lower Flurometer	3/4/2015 15:01	0
Lower Flurometer	3/4/2015 15:02	0
Lower Flurometer	3/4/2015 15:03	0
Lower Flurometer	3/4/2015 15:04	0
Lower Flurometer	3/4/2015 15:05	0
Lower Flurometer	3/4/2015 15:06	0
Lower Flurometer	3/4/2015 15:07	0
Lower Flurometer	3/4/2015 15:08	0
Lower Flurometer	3/4/2015 15:09	0
Lower Flurometer	3/4/2015 15:10	0
Lower Flurometer	3/4/2015 15:11	0
Lower Flurometer	3/4/2015 15:12	0
Lower Flurometer	3/4/2015 15:13	0
Lower Flurometer	3/4/2015 15:14	0
Lower Flurometer	3/4/2015 15:15	0
Lower Flurometer	3/4/2015 15:16	0
Lower Flurometer	3/4/2015 15:17	0
Lower Flurometer	3/4/2015 15:18	0
Lower Flurometer	3/4/2015 15:19	0
Lower Flurometer	3/4/2015 15:20	0
Lower Flurometer	3/4/2015 15:21	0
Lower Flurometer	3/4/2015 15:22	0
Lower Flurometer	3/4/2015 15:23	0
Lower Flurometer	3/4/2015 15:24	0
Lower Flurometer	3/4/2015 15:25	0
Lower Flurometer	3/4/2015 15:26	0
Lower Flurometer	3/4/2015 15:27	0
Lower Flurometer	3/4/2015 15:28	0
Lower Flurometer	3/4/2015 15:29	0

Location	Date and Time	Rhodmaine Concentration Adjusted Concentration (ppb)
Lower Flurometer	3/4/2015 15:30	0
Lower Flurometer	3/4/2015 15:31	0
Lower Flurometer	3/4/2015 15:32	0
Lower Flurometer	3/4/2015 15:33	0
Lower Flurometer	3/4/2015 15:34	0
Lower Flurometer	3/4/2015 15:35	0
Lower Flurometer	3/4/2015 15:36	0
Lower Flurometer	3/4/2015 15:37	0
Lower Flurometer	3/4/2015 15:38	0
Lower Flurometer	3/4/2015 15:39	0
Lower Flurometer	3/4/2015 15:40	0
Lower Flurometer	3/4/2015 15:41	0
Lower Flurometer	3/4/2015 15:42	0
Lower Flurometer	3/4/2015 15:43	0
Lower Flurometer	3/4/2015 15:44	0
Lower Flurometer	3/4/2015 15:45	0
Lower Flurometer	3/4/2015 15:46	0
Lower Flurometer	3/4/2015 15:47	0
Lower Flurometer	3/4/2015 15:48	0
Lower Flurometer	3/4/2015 15:49	0
Lower Flurometer	3/4/2015 15:50	0
Lower Flurometer	3/4/2015 15:51	0
Lower Flurometer	3/4/2015 15:52	0
Lower Flurometer	3/4/2015 15:53	0
Lower Flurometer	3/4/2015 15:54	0
Lower Flurometer	3/4/2015 15:55	0
Lower Flurometer	3/4/2015 15:56	0.03
Lower Flurometer	3/4/2015 15:57	0
Lower Flurometer	3/4/2015 15:58	0
Lower Flurometer	3/4/2015 15:59	0
Lower Flurometer	3/4/2015 16:00	0
Lower Flurometer	3/4/2015 16:01	0
Lower Flurometer	3/4/2015 16:02	0
Lower Flurometer	3/4/2015 16:03	0
Lower Flurometer	3/4/2015 16:04	0
Lower Flurometer	3/4/2015 16:05	0
Lower Flurometer	3/4/2015 16:06	0
Lower Flurometer	3/4/2015 16:07	0
Lower Flurometer	3/4/2015 16:08	0
Lower Flurometer	3/4/2015 16:09	0
Lower Flurometer	3/4/2015 16:10	0
Lower Flurometer	3/4/2015 16:11	0
Lower Flurometer	3/4/2015 16:12	0
Lower Flurometer	3/4/2015 16:13	0
Lower Flurometer	3/4/2015 16:14	6.27
Lower Flurometer	3/4/2015 16:15	0

Location	Date and Time	Rhodmaine Concentration Adjusted Concentration (ppb)
Lower Flurometer	3/4/2015 16:16	0
Lower Flurometer	3/4/2015 16:17	0
Lower Flurometer	3/4/2015 16:18	0
Lower Flurometer	3/4/2015 16:19	0
Lower Flurometer	3/4/2015 16:20	0
Lower Flurometer	3/4/2015 16:21	0
Lower Flurometer	3/4/2015 16:22	0
Lower Flurometer	3/4/2015 16:23	0
Lower Flurometer	3/4/2015 16:24	0
Lower Flurometer	3/4/2015 16:25	0
Lower Flurometer	3/4/2015 16:26	0
Lower Flurometer	3/4/2015 16:27	0
Lower Flurometer	3/4/2015 16:28	0
Lower Flurometer	3/4/2015 16:29	0
Lower Flurometer	3/4/2015 16:30	0
Lower Flurometer	3/4/2015 16:31	0
Lower Flurometer	3/4/2015 16:32	0
Lower Flurometer	3/4/2015 16:33	0
Lower Flurometer	3/4/2015 16:34	0
Lower Flurometer	3/4/2015 16:35	0
Lower Flurometer	3/4/2015 16:36	0
Lower Flurometer	3/4/2015 16:37	0
Lower Flurometer	3/4/2015 16:38	0
Lower Flurometer	3/4/2015 16:39	0
Lower Flurometer	3/4/2015 16:40	0
Lower Flurometer	3/4/2015 16:41	0
Lower Flurometer	3/4/2015 16:42	0
Lower Flurometer	3/4/2015 16:43	0
Lower Flurometer	3/4/2015 16:44	0
Lower Flurometer	3/4/2015 16:45	0
Lower Flurometer	3/4/2015 16:46	0
Lower Flurometer	3/4/2015 16:47	0
Lower Flurometer	3/4/2015 16:48	0
Lower Flurometer	3/4/2015 16:49	0
Lower Flurometer	3/4/2015 16:50	0
Lower Flurometer	3/4/2015 16:51	0
Lower Flurometer	3/4/2015 16:52	0
Lower Flurometer	3/4/2015 16:53	0
Lower Flurometer	3/4/2015 16:54	0
Lower Flurometer	3/4/2015 16:55	0
Lower Flurometer	3/4/2015 16:56	0
Lower Flurometer	3/4/2015 16:57	0
Lower Flurometer	3/4/2015 16:58	0
Lower Flurometer	3/4/2015 16:59	0
Lower Flurometer	3/4/2015 17:00	0
Lower Flurometer	3/4/2015 17:01	0

Location	Date and Time	Rhodmaine Concentration Adjusted Concentration (ppb)
Lower Flurometer	3/4/2015 17:02	0
Lower Flurometer	3/4/2015 17:03	0
Lower Flurometer	3/4/2015 17:04	0
Lower Flurometer	3/4/2015 17:05	0
Lower Flurometer	3/4/2015 17:06	0
Lower Flurometer	3/4/2015 17:07	0
Lower Flurometer	3/4/2015 17:08	0
Lower Flurometer	3/4/2015 17:09	0
Lower Flurometer	3/4/2015 17:10	0
Lower Flurometer	3/4/2015 17:11	0
Lower Flurometer	3/4/2015 17:12	0
Lower Flurometer	3/4/2015 17:13	0
Lower Flurometer	3/4/2015 17:14	0
Lower Flurometer	3/4/2015 17:15	0
Lower Flurometer	3/4/2015 17:16	0
Lower Flurometer	3/4/2015 17:17	0
Lower Flurometer	3/4/2015 17:18	0
Lower Flurometer	3/4/2015 17:19	0
Lower Flurometer	3/4/2015 17:20	0
Lower Flurometer	3/4/2015 17:21	0
Lower Flurometer	3/4/2015 17:22	0
Lower Flurometer	3/4/2015 17:23	0
Lower Flurometer	3/4/2015 17:24	0
Lower Flurometer	3/4/2015 17:25	0
Lower Flurometer	3/4/2015 17:26	0
Lower Flurometer	3/4/2015 17:27	0
Lower Flurometer	3/4/2015 17:28	0
Lower Flurometer	3/4/2015 17:29	0
Lower Flurometer	3/4/2015 17:30	0
Lower Flurometer	3/4/2015 17:31	0
Lower Flurometer	3/4/2015 17:32	0
Lower Flurometer	3/4/2015 17:33	0
Lower Flurometer	3/4/2015 17:34	0
Lower Flurometer	3/4/2015 17:35	0
Lower Flurometer	3/4/2015 17:36	0
Lower Flurometer	3/4/2015 17:37	0
Lower Flurometer	3/4/2015 17:38	0
Lower Flurometer	3/4/2015 17:39	0
Lower Flurometer	3/4/2015 17:40	0
Lower Flurometer	3/4/2015 17:41	0
Lower Flurometer	3/4/2015 17:42	0
Lower Flurometer	3/4/2015 17:43	0
Lower Flurometer	3/4/2015 17:44	0
Lower Flurometer	3/4/2015 17:45	0
Lower Flurometer	3/4/2015 17:46	0
Lower Flurometer	3/4/2015 17:47	0

Location	Date and Time	Rhodmaine Concentration Adjusted Concentration (ppb)
Lower Flurometer	3/4/2015 17:48	0
Lower Flurometer	3/4/2015 17:49	0
Lower Flurometer	3/4/2015 17:50	0
Lower Flurometer	3/4/2015 17:51	0
Lower Flurometer	3/4/2015 17:52	0
Lower Flurometer	3/4/2015 17:53	0
Lower Flurometer	3/4/2015 17:54	0
Lower Flurometer	3/4/2015 17:55	0
Lower Flurometer	3/4/2015 17:56	0
Lower Flurometer	3/4/2015 17:57	0
Lower Flurometer	3/4/2015 17:58	0
Lower Flurometer	3/4/2015 17:59	0
Lower Flurometer	3/4/2015 18:00	0
Lower Flurometer	3/4/2015 18:01	0
Lower Flurometer	3/4/2015 18:02	0
Lower Flurometer	3/4/2015 18:03	0
Lower Flurometer	3/4/2015 18:04	0
Lower Flurometer	3/4/2015 18:05	0
Lower Flurometer	3/4/2015 18:06	0
Lower Flurometer	3/4/2015 18:07	0
Lower Flurometer	3/4/2015 18:08	0
Lower Flurometer	3/4/2015 18:09	0
Lower Flurometer	3/4/2015 18:10	0
Lower Flurometer	3/4/2015 18:11	0
Lower Flurometer	3/4/2015 18:12	0
Lower Flurometer	3/4/2015 18:13	0
Lower Flurometer	3/4/2015 18:14	0
Lower Flurometer	3/4/2015 18:15	0
Lower Flurometer	3/4/2015 18:16	0
Lower Flurometer	3/4/2015 18:17	0
Lower Flurometer	3/4/2015 18:18	0
Lower Flurometer	3/4/2015 18:19	0
Lower Flurometer	3/4/2015 18:20	0
Lower Flurometer	3/4/2015 18:21	0
Lower Flurometer	3/4/2015 18:22	0
Lower Flurometer	3/4/2015 18:23	0
Lower Flurometer	3/4/2015 18:24	0
Lower Flurometer	3/4/2015 18:25	0
Lower Flurometer	3/4/2015 18:26	0
Lower Flurometer	3/4/2015 18:27	0
Lower Flurometer	3/4/2015 18:28	0
Lower Flurometer	3/4/2015 18:29	0
Lower Flurometer	3/4/2015 18:30	0
Lower Flurometer	3/4/2015 18:31	0
Lower Flurometer	3/4/2015 18:32	0
Lower Flurometer	3/4/2015 18:33	0

Location	Date and Time	Rhodmaine Concentration Adjusted Concentration (ppb)
Lower Flurometer	3/4/2015 18:34	0
Lower Flurometer	3/4/2015 18:35	0
Lower Flurometer	3/4/2015 18:36	0
Lower Flurometer	3/4/2015 18:37	0
Lower Flurometer	3/4/2015 18:38	0
Lower Flurometer	3/4/2015 18:39	0
Lower Flurometer	3/4/2015 18:40	0
Lower Flurometer	3/4/2015 18:41	0
Lower Flurometer	3/4/2015 18:42	0
Lower Flurometer	3/4/2015 18:43	0
Lower Flurometer	3/4/2015 18:44	0
Lower Flurometer	3/4/2015 18:45	0
Lower Flurometer	3/4/2015 18:46	0
Lower Flurometer	3/4/2015 18:47	0
Lower Flurometer	3/4/2015 18:48	0
Lower Flurometer	3/4/2015 18:49	0
Lower Flurometer	3/4/2015 18:50	0
Lower Flurometer	3/4/2015 18:51	0
Lower Flurometer	3/4/2015 18:52	0
Lower Flurometer	3/4/2015 18:53	0
Lower Flurometer	3/4/2015 18:54	0
Lower Flurometer	3/4/2015 18:55	0
Lower Flurometer	3/4/2015 18:56	0
Lower Flurometer	3/4/2015 18:57	0
Lower Flurometer	3/4/2015 18:58	0
Lower Flurometer	3/4/2015 18:59	0
Lower Flurometer	3/4/2015 19:00	0
Lower Flurometer	3/4/2015 19:01	0
Lower Flurometer	3/4/2015 19:02	0
Lower Flurometer	3/4/2015 19:03	0
Lower Flurometer	3/4/2015 19:04	0
Lower Flurometer	3/4/2015 19:05	0
Lower Flurometer	3/4/2015 19:06	0
Lower Flurometer	3/4/2015 19:07	0
Lower Flurometer	3/4/2015 19:08	0
Lower Flurometer	3/4/2015 19:09	0
Lower Flurometer	3/4/2015 19:10	0
Lower Flurometer	3/4/2015 19:11	0
Lower Flurometer	3/4/2015 19:12	0
Lower Flurometer	3/4/2015 19:13	0
Lower Flurometer	3/4/2015 19:14	0
Lower Flurometer	3/4/2015 19:15	0
Lower Flurometer	3/4/2015 19:16	0
Lower Flurometer	3/4/2015 19:17	0
Lower Flurometer	3/4/2015 19:18	0
Lower Flurometer	3/4/2015 19:19	0

Location	Date and Time	Rhodmaine Concentration Adjusted Concentration (ppb)
Lower Flurometer	3/4/2015 19:20	0
Lower Flurometer	3/4/2015 19:21	0
Lower Flurometer	3/4/2015 19:22	0
Lower Flurometer	3/4/2015 19:23	0
Lower Flurometer	3/4/2015 19:24	0
Lower Flurometer	3/4/2015 19:25	0
Lower Flurometer	3/4/2015 19:26	0
Lower Flurometer	3/4/2015 19:27	0
Lower Flurometer	3/4/2015 19:28	0
Lower Flurometer	3/4/2015 19:29	0
Lower Flurometer	3/4/2015 19:30	0
Lower Flurometer	3/4/2015 19:31	0
Lower Flurometer	3/4/2015 19:32	0
Lower Flurometer	3/4/2015 19:33	0
Lower Flurometer	3/4/2015 19:34	0
Lower Flurometer	3/4/2015 19:35	0
Lower Flurometer	3/4/2015 19:36	0
Lower Flurometer	3/4/2015 19:37	0
Lower Flurometer	3/4/2015 19:38	0
Lower Flurometer	3/4/2015 19:39	0
Lower Flurometer	3/4/2015 19:40	0
Lower Flurometer	3/4/2015 19:41	0
Lower Flurometer	3/4/2015 19:42	0
Lower Flurometer	3/4/2015 19:43	0
Lower Flurometer	3/4/2015 19:44	0
Lower Flurometer	3/4/2015 19:45	0
Lower Flurometer	3/4/2015 19:46	0
Lower Flurometer	3/4/2015 19:47	0
Lower Flurometer	3/4/2015 19:48	0
Lower Flurometer	3/4/2015 19:49	0
Lower Flurometer	3/4/2015 19:50	0
Lower Flurometer	3/4/2015 19:51	0
Lower Flurometer	3/4/2015 19:52	0
Lower Flurometer	3/4/2015 19:53	0
Lower Flurometer	3/4/2015 19:54	0
Lower Flurometer	3/4/2015 19:55	0
Lower Flurometer	3/4/2015 19:56	0
Lower Flurometer	3/4/2015 19:57	0
Lower Flurometer	3/4/2015 19:58	0
Lower Flurometer	3/4/2015 19:59	0
Lower Flurometer	3/4/2015 20:00	0
Lower Flurometer	3/4/2015 20:01	0
Lower Flurometer	3/4/2015 20:02	0
Lower Flurometer	3/4/2015 20:03	0
Lower Flurometer	3/4/2015 20:04	0
Lower Flurometer	3/4/2015 20:05	0

Location	Date and Time	Rhodmaine Concentration Adjusted Concentration (ppb)
Lower Flurometer	3/4/2015 20:06	0
Lower Flurometer	3/4/2015 20:07	0
Lower Flurometer	3/4/2015 20:08	0
Lower Flurometer	3/4/2015 20:09	0
Lower Flurometer	3/4/2015 20:10	0
Lower Flurometer	3/4/2015 20:11	0
Lower Flurometer	3/4/2015 20:12	0
Lower Flurometer	3/4/2015 20:13	0
Lower Flurometer	3/4/2015 20:14	0
Lower Flurometer	3/4/2015 20:15	0
Lower Flurometer	3/4/2015 20:16	0
Lower Flurometer	3/4/2015 20:17	0
Lower Flurometer	3/4/2015 20:18	0
Lower Flurometer	3/4/2015 20:19	0
Lower Flurometer	3/4/2015 20:20	0
Lower Flurometer	3/4/2015 20:21	0
Lower Flurometer	3/4/2015 20:22	0
Lower Flurometer	3/4/2015 20:23	0
Lower Flurometer	3/4/2015 20:24	0
Lower Flurometer	3/4/2015 20:25	0
Lower Flurometer	3/4/2015 20:26	0
Lower Flurometer	3/4/2015 20:27	0
Lower Flurometer	3/4/2015 20:28	0
Lower Flurometer	3/4/2015 20:29	0
Lower Flurometer	3/4/2015 20:30	0
Lower Flurometer	3/4/2015 20:31	0
Lower Flurometer	3/4/2015 20:32	0
Lower Flurometer	3/4/2015 20:33	0
Lower Flurometer	3/4/2015 20:34	0
Lower Flurometer	3/4/2015 20:35	0
Lower Flurometer	3/4/2015 20:36	0
Lower Flurometer	3/4/2015 20:37	0
Lower Flurometer	3/4/2015 20:38	0
Lower Flurometer	3/4/2015 20:39	0
Lower Flurometer	3/4/2015 20:40	0
Lower Flurometer	3/4/2015 20:41	0
Lower Flurometer	3/4/2015 20:42	0
Lower Flurometer	3/4/2015 20:43	0
Lower Flurometer	3/4/2015 20:44	0
Lower Flurometer	3/4/2015 20:45	0
Lower Flurometer	3/4/2015 20:46	0
Lower Flurometer	3/4/2015 20:47	0
Lower Flurometer	3/4/2015 20:48	0
Lower Flurometer	3/4/2015 20:49	0
Lower Flurometer	3/4/2015 20:50	0
Lower Flurometer	3/4/2015 20:51	0

Location	Date and Time	Rhodmaine Concentration Adjusted Concentration (ppb)
Lower Flurometer	3/4/2015 20:52	0
Lower Flurometer	3/4/2015 20:53	0
Lower Flurometer	3/4/2015 20:54	0
Lower Flurometer	3/4/2015 20:55	0
Lower Flurometer	3/4/2015 20:56	0
Lower Flurometer	3/4/2015 20:57	0
Lower Flurometer	3/4/2015 20:58	0
Lower Flurometer	3/4/2015 20:59	0
Lower Flurometer	3/4/2015 21:00	0
Lower Flurometer	3/4/2015 21:01	0
Lower Flurometer	3/4/2015 21:02	0
Lower Flurometer	3/4/2015 21:03	0
Lower Flurometer	3/4/2015 21:04	0
Lower Flurometer	3/4/2015 21:05	0
Lower Flurometer	3/4/2015 21:06	0
Lower Flurometer	3/4/2015 21:07	0
Lower Flurometer	3/4/2015 21:08	0
Lower Flurometer	3/4/2015 21:09	0
Lower Flurometer	3/4/2015 21:10	0
Lower Flurometer	3/4/2015 21:11	0
Lower Flurometer	3/4/2015 21:12	0
Lower Flurometer	3/4/2015 21:13	0
Lower Flurometer	3/4/2015 21:14	0
Lower Flurometer	3/4/2015 21:15	0
Lower Flurometer	3/4/2015 21:16	0
Lower Flurometer	3/4/2015 21:17	0
Lower Flurometer	3/4/2015 21:18	0
Lower Flurometer	3/4/2015 21:19	0
Lower Flurometer	3/4/2015 21:20	0
Lower Flurometer	3/4/2015 21:21	0
Lower Flurometer	3/4/2015 21:22	0
Lower Flurometer	3/4/2015 21:23	0
Lower Flurometer	3/4/2015 21:24	0
Lower Flurometer	3/4/2015 21:25	0
Lower Flurometer	3/4/2015 21:26	0.1
Lower Flurometer	3/4/2015 21:27	0
Lower Flurometer	3/4/2015 21:28	0
Lower Flurometer	3/4/2015 21:29	0
Lower Flurometer	3/4/2015 21:30	0
Lower Flurometer	3/4/2015 21:31	0
Lower Flurometer	3/4/2015 21:32	0
Lower Flurometer	3/4/2015 21:33	0
Lower Flurometer	3/4/2015 21:34	0
Lower Flurometer	3/4/2015 21:35	0
Lower Flurometer	3/4/2015 21:36	0
Lower Flurometer	3/4/2015 21:37	0

Location	Date and Time	Rhodmaine Concentration Adjusted Concentration (ppb)
Lower Flurometer	3/4/2015 21:38	0
Lower Flurometer	3/4/2015 21:39	0
Lower Flurometer	3/4/2015 21:40	0
Lower Flurometer	3/4/2015 21:41	0
Lower Flurometer	3/4/2015 21:42	0
Lower Flurometer	3/4/2015 21:43	0
Lower Flurometer	3/4/2015 21:44	0
Lower Flurometer	3/4/2015 21:45	0
Lower Flurometer	3/4/2015 21:46	0
Lower Flurometer	3/4/2015 21:47	0
Lower Flurometer	3/4/2015 21:48	0
Lower Flurometer	3/4/2015 21:49	0
Lower Flurometer	3/4/2015 21:50	0
Lower Flurometer	3/4/2015 21:51	0
Lower Flurometer	3/4/2015 21:52	0
Lower Flurometer	3/4/2015 21:53	0
Lower Flurometer	3/4/2015 21:54	0
Lower Flurometer	3/4/2015 21:55	0
Lower Flurometer	3/4/2015 21:56	0
Lower Flurometer	3/4/2015 21:57	0
Lower Flurometer	3/4/2015 21:58	0
Lower Flurometer	3/4/2015 21:59	0
Lower Flurometer	3/4/2015 22:00	0
Lower Flurometer	3/4/2015 22:01	0
Lower Flurometer	3/4/2015 22:02	0
Lower Flurometer	3/4/2015 22:03	0
Lower Flurometer	3/4/2015 22:04	0
Lower Flurometer	3/4/2015 22:05	0
Lower Flurometer	3/4/2015 22:06	0
Lower Flurometer	3/4/2015 22:07	0
Lower Flurometer	3/4/2015 22:08	0
Lower Flurometer	3/4/2015 22:09	0
Lower Flurometer	3/4/2015 22:10	0
Lower Flurometer	3/4/2015 22:11	0
Lower Flurometer	3/4/2015 22:12	0
Lower Flurometer	3/4/2015 22:13	0
Lower Flurometer	3/4/2015 22:14	0
Lower Flurometer	3/4/2015 22:15	0
Lower Flurometer	3/4/2015 22:16	0
Lower Flurometer	3/4/2015 22:17	0
Lower Flurometer	3/4/2015 22:18	0
Lower Flurometer	3/4/2015 22:19	0
Lower Flurometer	3/4/2015 22:20	0
Lower Flurometer	3/4/2015 22:21	0
Lower Flurometer	3/4/2015 22:22	0
Lower Flurometer	3/4/2015 22:23	0

Location	Date and Time	Rhodmaine Concentration Adjusted Concentration (ppb)
Lower Flurometer	3/4/2015 22:24	0
Lower Flurometer	3/4/2015 22:25	0
Lower Flurometer	3/4/2015 22:26	0
Lower Flurometer	3/4/2015 22:27	0
Lower Flurometer	3/4/2015 22:28	0
Lower Flurometer	3/4/2015 22:29	0
Lower Flurometer	3/4/2015 22:30	0
Lower Flurometer	3/4/2015 22:31	0
Lower Flurometer	3/4/2015 22:32	0
Lower Flurometer	3/4/2015 22:33	0
Lower Flurometer	3/4/2015 22:34	0
Lower Flurometer	3/4/2015 22:35	0
Lower Flurometer	3/4/2015 22:36	0
Lower Flurometer	3/4/2015 22:37	0
Lower Flurometer	3/4/2015 22:38	0
Lower Flurometer	3/4/2015 22:39	0
Lower Flurometer	3/4/2015 22:40	0
Lower Flurometer	3/4/2015 22:41	0
Lower Flurometer	3/4/2015 22:42	0
Lower Flurometer	3/4/2015 22:43	0
Lower Flurometer	3/4/2015 22:44	0
Lower Flurometer	3/4/2015 22:45	0
Lower Flurometer	3/4/2015 22:46	0
Lower Flurometer	3/4/2015 22:47	0
Lower Flurometer	3/4/2015 22:48	0
Lower Flurometer	3/4/2015 22:49	0
Lower Flurometer	3/4/2015 22:50	0
Lower Flurometer	3/4/2015 22:51	0
Lower Flurometer	3/4/2015 22:52	0
Lower Flurometer	3/4/2015 22:53	0
Lower Flurometer	3/4/2015 22:54	0
Lower Flurometer	3/4/2015 22:55	0
Lower Flurometer	3/4/2015 22:56	0
Lower Flurometer	3/4/2015 22:57	0
Lower Flurometer	3/4/2015 22:58	0
Lower Flurometer	3/4/2015 22:59	0
Lower Flurometer	3/4/2015 23:00	0
Lower Flurometer	3/4/2015 23:01	0
Lower Flurometer	3/4/2015 23:02	0
Lower Flurometer	3/4/2015 23:03	0
Lower Flurometer	3/4/2015 23:04	0
Lower Flurometer	3/4/2015 23:05	0
Lower Flurometer	3/4/2015 23:06	0
Lower Flurometer	3/4/2015 23:07	0
Lower Flurometer	3/4/2015 23:08	0
Lower Flurometer	3/4/2015 23:09	0

Location	Date and Time	Rhodmaine Concentration Adjusted Concentration (ppb)
Lower Flurometer	3/4/2015 23:10	0
Lower Flurometer	3/4/2015 23:11	0
Lower Flurometer	3/4/2015 23:12	0
Lower Flurometer	3/4/2015 23:13	0
Lower Flurometer	3/4/2015 23:14	0
Lower Flurometer	3/4/2015 23:15	0
Lower Flurometer	3/4/2015 23:16	0
Lower Flurometer	3/4/2015 23:17	0
Lower Flurometer	3/4/2015 23:18	0
Lower Flurometer	3/4/2015 23:19	0
Lower Flurometer	3/4/2015 23:20	0
Lower Flurometer	3/4/2015 23:21	0
Lower Flurometer	3/4/2015 23:22	0
Lower Flurometer	3/4/2015 23:23	0
Lower Flurometer	3/4/2015 23:24	0
Lower Flurometer	3/4/2015 23:25	0
Lower Flurometer	3/4/2015 23:26	0
Lower Flurometer	3/4/2015 23:27	0
Lower Flurometer	3/4/2015 23:28	0
Lower Flurometer	3/4/2015 23:29	0
Lower Flurometer	3/4/2015 23:30	0
Lower Flurometer	3/4/2015 23:31	0
Lower Flurometer	3/4/2015 23:32	0
Lower Flurometer	3/4/2015 23:33	0
Lower Flurometer	3/4/2015 23:34	0
Lower Flurometer	3/4/2015 23:35	0
Lower Flurometer	3/4/2015 23:36	0
Lower Flurometer	3/4/2015 23:37	0
Lower Flurometer	3/4/2015 23:38	0
Lower Flurometer	3/4/2015 23:39	0
Lower Flurometer	3/4/2015 23:40	0
Lower Flurometer	3/4/2015 23:41	0
Lower Flurometer	3/4/2015 23:42	0
Lower Flurometer	3/4/2015 23:43	0
Lower Flurometer	3/4/2015 23:44	0
Lower Flurometer	3/4/2015 23:45	0
Lower Flurometer	3/4/2015 23:46	0
Lower Flurometer	3/4/2015 23:47	0
Lower Flurometer	3/4/2015 23:48	0
Lower Flurometer	3/4/2015 23:49	0
Lower Flurometer	3/4/2015 23:50	0
Lower Flurometer	3/4/2015 23:51	0
Lower Flurometer	3/4/2015 23:52	0
Lower Flurometer	3/4/2015 23:53	0
Lower Flurometer	3/4/2015 23:54	0
Lower Flurometer	3/4/2015 23:55	0

Location	Date and Time	Rhodmaine Concentration Adjusted Concentration (ppb)
Lower Flurometer	3/4/2015 23:56	0
Lower Flurometer	3/4/2015 23:57	0
Lower Flurometer	3/4/2015 23:58	0
Lower Flurometer	3/4/2015 23:59	0
Lower Flurometer	3/5/2015 0:00	0
Lower Flurometer	3/5/2015 0:01	0
Lower Flurometer	3/5/2015 0:02	0
Lower Flurometer	3/5/2015 0:03	0
Lower Flurometer	3/5/2015 0:04	0
Lower Flurometer	3/5/2015 0:05	0
Lower Flurometer	3/5/2015 0:06	0
Lower Flurometer	3/5/2015 0:07	0
Lower Flurometer	3/5/2015 0:08	0
Lower Flurometer	3/5/2015 0:09	0
Lower Flurometer	3/5/2015 0:10	0
Lower Flurometer	3/5/2015 0:11	0
Lower Flurometer	3/5/2015 0:12	0
Lower Flurometer	3/5/2015 0:13	0
Lower Flurometer	3/5/2015 0:14	0
Lower Flurometer	3/5/2015 0:15	0
Lower Flurometer	3/5/2015 0:16	0
Lower Flurometer	3/5/2015 0:17	0
Lower Flurometer	3/5/2015 0:18	0
Lower Flurometer	3/5/2015 0:19	0
Lower Flurometer	3/5/2015 0:20	0
Lower Flurometer	3/5/2015 0:21	0
Lower Flurometer	3/5/2015 0:22	0
Lower Flurometer	3/5/2015 0:23	0
Lower Flurometer	3/5/2015 0:24	0
Lower Flurometer	3/5/2015 0:25	0
Lower Flurometer	3/5/2015 0:26	0
Lower Flurometer	3/5/2015 0:27	0
Lower Flurometer	3/5/2015 0:28	0
Lower Flurometer	3/5/2015 0:29	0
Lower Flurometer	3/5/2015 0:30	0
Lower Flurometer	3/5/2015 0:31	0
Lower Flurometer	3/5/2015 0:32	0
Lower Flurometer	3/5/2015 0:33	0
Lower Flurometer	3/5/2015 0:34	0
Lower Flurometer	3/5/2015 0:35	0
Lower Flurometer	3/5/2015 0:36	0
Lower Flurometer	3/5/2015 0:37	0
Lower Flurometer	3/5/2015 0:38	0
Lower Flurometer	3/5/2015 0:39	0
Lower Flurometer	3/5/2015 0:40	0
Lower Flurometer	3/5/2015 0:41	0

Location	Date and Time	Rhodmaine Concentration Adjusted Concentration (ppb)
Lower Flurometer	3/5/2015 0:42	0
Lower Flurometer	3/5/2015 0:43	0
Lower Flurometer	3/5/2015 0:44	0
Lower Flurometer	3/5/2015 0:45	0
Lower Flurometer	3/5/2015 0:46	0
Lower Flurometer	3/5/2015 0:47	0
Lower Flurometer	3/5/2015 0:48	0
Lower Flurometer	3/5/2015 0:49	0
Lower Flurometer	3/5/2015 0:50	0
Lower Flurometer	3/5/2015 0:51	0
Lower Flurometer	3/5/2015 0:52	0
Lower Flurometer	3/5/2015 0:53	0
Lower Flurometer	3/5/2015 0:54	0
Lower Flurometer	3/5/2015 0:55	0
Lower Flurometer	3/5/2015 0:56	0
Lower Flurometer	3/5/2015 0:57	0
Lower Flurometer	3/5/2015 0:58	0
Lower Flurometer	3/5/2015 0:59	0
Lower Flurometer	3/5/2015 1:00	0
Lower Flurometer	3/5/2015 1:01	0
Lower Flurometer	3/5/2015 1:02	0
Lower Flurometer	3/5/2015 1:03	0
Lower Flurometer	3/5/2015 1:04	0
Lower Flurometer	3/5/2015 1:05	0
Lower Flurometer	3/5/2015 1:06	0
Lower Flurometer	3/5/2015 1:07	0
Lower Flurometer	3/5/2015 1:08	0
Lower Flurometer	3/5/2015 1:09	0
Lower Flurometer	3/5/2015 1:10	0
Lower Flurometer	3/5/2015 1:11	0
Lower Flurometer	3/5/2015 1:12	0
Lower Flurometer	3/5/2015 1:13	0.21
Lower Flurometer	3/5/2015 1:14	0
Lower Flurometer	3/5/2015 1:15	0
Lower Flurometer	3/5/2015 1:16	0
Lower Flurometer	3/5/2015 1:17	0
Lower Flurometer	3/5/2015 1:18	0
Lower Flurometer	3/5/2015 1:19	0
Lower Flurometer	3/5/2015 1:20	0
Lower Flurometer	3/5/2015 1:21	0
Lower Flurometer	3/5/2015 1:22	0
Lower Flurometer	3/5/2015 1:23	0
Lower Flurometer	3/5/2015 1:24	0
Lower Flurometer	3/5/2015 1:25	0
Lower Flurometer	3/5/2015 1:26	0
Lower Flurometer	3/5/2015 1:27	0

Location	Date and Time	Rhodmaine Concentration Adjusted Concentration (ppb)
Lower Flurometer	3/5/2015 1:28	0
Lower Flurometer	3/5/2015 1:29	0
Lower Flurometer	3/5/2015 1:30	0
Lower Flurometer	3/5/2015 1:31	0
Lower Flurometer	3/5/2015 1:32	0
Lower Flurometer	3/5/2015 1:33	0
Lower Flurometer	3/5/2015 1:34	0
Lower Flurometer	3/5/2015 1:35	0
Lower Flurometer	3/5/2015 1:36	0
Lower Flurometer	3/5/2015 1:37	0
Lower Flurometer	3/5/2015 1:38	0
Lower Flurometer	3/5/2015 1:39	0
Lower Flurometer	3/5/2015 1:40	0
Lower Flurometer	3/5/2015 1:41	0
Lower Flurometer	3/5/2015 1:42	0
Lower Flurometer	3/5/2015 1:43	0
Lower Flurometer	3/5/2015 1:44	0
Lower Flurometer	3/5/2015 1:45	0
Lower Flurometer	3/5/2015 1:46	0
Lower Flurometer	3/5/2015 1:47	0
Lower Flurometer	3/5/2015 1:48	0
Lower Flurometer	3/5/2015 1:49	0
Lower Flurometer	3/5/2015 1:50	0
Lower Flurometer	3/5/2015 1:51	0
Lower Flurometer	3/5/2015 1:52	0
Lower Flurometer	3/5/2015 1:53	0
Lower Flurometer	3/5/2015 1:54	0
Lower Flurometer	3/5/2015 1:55	0
Lower Flurometer	3/5/2015 1:56	0
Lower Flurometer	3/5/2015 1:57	0
Lower Flurometer	3/5/2015 1:58	0
Lower Flurometer	3/5/2015 1:59	0
Lower Flurometer	3/5/2015 2:00	0
Lower Flurometer	3/5/2015 2:01	0
Lower Flurometer	3/5/2015 2:02	0
Lower Flurometer	3/5/2015 2:03	0
Lower Flurometer	3/5/2015 2:04	0
Lower Flurometer	3/5/2015 2:05	0
Lower Flurometer	3/5/2015 2:06	0
Lower Flurometer	3/5/2015 2:07	0
Lower Flurometer	3/5/2015 2:08	0
Lower Flurometer	3/5/2015 2:09	0
Lower Flurometer	3/5/2015 2:10	0
Lower Flurometer	3/5/2015 2:11	0
Lower Flurometer	3/5/2015 2:12	0
Lower Flurometer	3/5/2015 2:13	0

Location	Date and Time	Rhodmaine Concentration Adjusted Concentration (ppb)
Lower Flurometer	3/5/2015 2:14	0
Lower Flurometer	3/5/2015 2:15	0
Lower Flurometer	3/5/2015 2:16	0
Lower Flurometer	3/5/2015 2:17	0
Lower Flurometer	3/5/2015 2:18	0
Lower Flurometer	3/5/2015 2:19	0
Lower Flurometer	3/5/2015 2:20	0
Lower Flurometer	3/5/2015 2:21	0
Lower Flurometer	3/5/2015 2:22	0
Lower Flurometer	3/5/2015 2:23	0
Lower Flurometer	3/5/2015 2:24	0
Lower Flurometer	3/5/2015 2:25	0
Lower Flurometer	3/5/2015 2:26	0
Lower Flurometer	3/5/2015 2:27	0
Lower Flurometer	3/5/2015 2:28	0
Lower Flurometer	3/5/2015 2:29	0
Lower Flurometer	3/5/2015 2:30	0
Lower Flurometer	3/5/2015 2:31	0
Lower Flurometer	3/5/2015 2:32	0
Lower Flurometer	3/5/2015 2:33	0
Lower Flurometer	3/5/2015 2:34	0
Lower Flurometer	3/5/2015 2:35	0
Lower Flurometer	3/5/2015 2:36	0
Lower Flurometer	3/5/2015 2:37	0
Lower Flurometer	3/5/2015 2:38	0
Lower Flurometer	3/5/2015 2:39	0
Lower Flurometer	3/5/2015 2:40	0
Lower Flurometer	3/5/2015 2:41	0
Lower Flurometer	3/5/2015 2:42	0
Lower Flurometer	3/5/2015 2:43	0
Lower Flurometer	3/5/2015 2:44	0
Lower Flurometer	3/5/2015 2:45	0
Lower Flurometer	3/5/2015 2:46	0
Lower Flurometer	3/5/2015 2:47	0
Lower Flurometer	3/5/2015 2:48	0.07
Lower Flurometer	3/5/2015 2:49	0
Lower Flurometer	3/5/2015 2:50	0.04
Lower Flurometer	3/5/2015 2:51	0
Lower Flurometer	3/5/2015 2:52	0.04
Lower Flurometer	3/5/2015 2:53	0.06
Lower Flurometer	3/5/2015 2:54	0.1
Lower Flurometer	3/5/2015 2:55	0.08
Lower Flurometer	3/5/2015 2:56	0.06
Lower Flurometer	3/5/2015 2:57	0.08
Lower Flurometer	3/5/2015 2:58	0.12
Lower Flurometer	3/5/2015 2:59	0.16

Location	Date and Time	Rhodmaine Concentration Adjusted Concentration (ppb)
Lower Flurometer	3/5/2015 3:00	0.15
Lower Flurometer	3/5/2015 3:01	0.15
Lower Flurometer	3/5/2015 3:02	1.69
Lower Flurometer	3/5/2015 3:03	0.23
Lower Flurometer	3/5/2015 3:04	0.2
Lower Flurometer	3/5/2015 3:05	0.19
Lower Flurometer	3/5/2015 3:06	0.28
Lower Flurometer	3/5/2015 3:07	0.3
Lower Flurometer	3/5/2015 3:08	0.3
Lower Flurometer	3/5/2015 3:09	0.39
Lower Flurometer	3/5/2015 3:10	0.42
Lower Flurometer	3/5/2015 3:11	0.41
Lower Flurometer	3/5/2015 3:12	0.43
Lower Flurometer	3/5/2015 3:13	0.46
Lower Flurometer	3/5/2015 3:14	0.45
Lower Flurometer	3/5/2015 3:15	0.52
Lower Flurometer	3/5/2015 3:16	0.6
Lower Flurometer	3/5/2015 3:17	0.57
Lower Flurometer	3/5/2015 3:18	0.62
Lower Flurometer	3/5/2015 3:19	0.62
Lower Flurometer	3/5/2015 3:20	0.7
Lower Flurometer	3/5/2015 3:21	0.7
Lower Flurometer	3/5/2015 3:22	0.76
Lower Flurometer	3/5/2015 3:23	0.77
Lower Flurometer	3/5/2015 3:24	0.77
Lower Flurometer	3/5/2015 3:25	0.83
Lower Flurometer	3/5/2015 3:26	0.84
Lower Flurometer	3/5/2015 3:27	0.92
Lower Flurometer	3/5/2015 3:28	1.02
Lower Flurometer	3/5/2015 3:29	1.07
Lower Flurometer	3/5/2015 3:30	1.11
Lower Flurometer	3/5/2015 3:31	1.11
Lower Flurometer	3/5/2015 3:32	1.14
Lower Flurometer	3/5/2015 3:33	1.29
Lower Flurometer	3/5/2015 3:34	1.16
Lower Flurometer	3/5/2015 3:35	1.28
Lower Flurometer	3/5/2015 3:36	1.26
Lower Flurometer	3/5/2015 3:37	1.35
Lower Flurometer	3/5/2015 3:38	1.46
Lower Flurometer	3/5/2015 3:39	1.49
Lower Flurometer	3/5/2015 3:40	1.48
Lower Flurometer	3/5/2015 3:41	1.56
Lower Flurometer	3/5/2015 3:42	1.56
Lower Flurometer	3/5/2015 3:43	1.6
Lower Flurometer	3/5/2015 3:44	1.79
Lower Flurometer	3/5/2015 3:45	1.77

Location	Date and Time	Rhodmaine Concentration Adjusted Concentration (ppb)
Lower Flurometer	3/5/2015 3:46	1.92
Lower Flurometer	3/5/2015 3:47	1.87
Lower Flurometer	3/5/2015 3:48	2.01
Lower Flurometer	3/5/2015 3:49	2.01
Lower Flurometer	3/5/2015 3:50	2.08
Lower Flurometer	3/5/2015 3:51	2.14
Lower Flurometer	3/5/2015 3:52	2.24
Lower Flurometer	3/5/2015 3:53	2.3
Lower Flurometer	3/5/2015 3:54	2.31
Lower Flurometer	3/5/2015 3:55	2.29
Lower Flurometer	3/5/2015 3:56	2.37
Lower Flurometer	3/5/2015 3:57	2.56
Lower Flurometer	3/5/2015 3:58	2.56
Lower Flurometer	3/5/2015 3:59	2.59
Lower Flurometer	3/5/2015 4:00	2.64
Lower Flurometer	3/5/2015 4:01	2.64
Lower Flurometer	3/5/2015 4:02	2.73
Lower Flurometer	3/5/2015 4:03	2.85
Lower Flurometer	3/5/2015 4:04	2.98
Lower Flurometer	3/5/2015 4:05	2.96
Lower Flurometer	3/5/2015 4:06	3.02
Lower Flurometer	3/5/2015 4:07	3.02
Lower Flurometer	3/5/2015 4:08	3.16
Lower Flurometer	3/5/2015 4:09	3.2
Lower Flurometer	3/5/2015 4:10	3.28
Lower Flurometer	3/5/2015 4:11	3.3
Lower Flurometer	3/5/2015 4:12	3.41
Lower Flurometer	3/5/2015 4:13	3.45
Lower Flurometer	3/5/2015 4:14	3.5
Lower Flurometer	3/5/2015 4:15	3.49
Lower Flurometer	3/5/2015 4:16	3.68
Lower Flurometer	3/5/2015 4:17	3.66
Lower Flurometer	3/5/2015 4:18	3.81
Lower Flurometer	3/5/2015 4:19	3.89
Lower Flurometer	3/5/2015 4:20	3.96
Lower Flurometer	3/5/2015 4:21	3.96
Lower Flurometer	3/5/2015 4:22	4.09
Lower Flurometer	3/5/2015 4:23	4.06
Lower Flurometer	3/5/2015 4:24	4.09
Lower Flurometer	3/5/2015 4:25	4.16
Lower Flurometer	3/5/2015 4:26	4.24
Lower Flurometer	3/5/2015 4:27	4.31
Lower Flurometer	3/5/2015 4:28	4.31
Lower Flurometer	3/5/2015 4:29	4.35
Lower Flurometer	3/5/2015 4:30	4.37
Lower Flurometer	3/5/2015 4:31	4.5

Location	Date and Time	Rhodmaine Concentration Adjusted Concentration (ppb)
Lower Flurometer	3/5/2015 4:32	4.95
Lower Flurometer	3/5/2015 4:33	4.57
Lower Flurometer	3/5/2015 4:34	4.63
Lower Flurometer	3/5/2015 4:35	4.79
Lower Flurometer	3/5/2015 4:36	4.79
Lower Flurometer	3/5/2015 4:37	4.87
Lower Flurometer	3/5/2015 4:38	4.93
Lower Flurometer	3/5/2015 4:39	4.97
Lower Flurometer	3/5/2015 4:40	5.05
Lower Flurometer	3/5/2015 4:41	4.98
Lower Flurometer	3/5/2015 4:42	5
Lower Flurometer	3/5/2015 4:43	5.12
Lower Flurometer	3/5/2015 4:44	5.15
Lower Flurometer	3/5/2015 4:45	5.27
Lower Flurometer	3/5/2015 4:46	5.33
Lower Flurometer	3/5/2015 4:47	5.26
Lower Flurometer	3/5/2015 4:48	5.29
Lower Flurometer	3/5/2015 4:49	5.3
Lower Flurometer	3/5/2015 4:50	5.33
Lower Flurometer	3/5/2015 4:51	5.4
Lower Flurometer	3/5/2015 4:52	5.52
Lower Flurometer	3/5/2015 4:53	5.59
Lower Flurometer	3/5/2015 4:54	5.62
Lower Flurometer	3/5/2015 4:55	5.56
Lower Flurometer	3/5/2015 4:56	5.6
Lower Flurometer	3/5/2015 4:57	5.69
Lower Flurometer	3/5/2015 4:58	5.65
Lower Flurometer	3/5/2015 4:59	5.67
Lower Flurometer	3/5/2015 5:00	5.76
Lower Flurometer	3/5/2015 5:01	5.73
Lower Flurometer	3/5/2015 5:02	5.75
Lower Flurometer	3/5/2015 5:03	5.79
Lower Flurometer	3/5/2015 5:04	5.88
Lower Flurometer	3/5/2015 5:05	5.96
Lower Flurometer	3/5/2015 5:06	5.9
Lower Flurometer	3/5/2015 5:07	6.03
Lower Flurometer	3/5/2015 5:08	6.06
Lower Flurometer	3/5/2015 5:09	6.07
Lower Flurometer	3/5/2015 5:10	6.02
Lower Flurometer	3/5/2015 5:11	6.11
Lower Flurometer	3/5/2015 5:12	6.1
Lower Flurometer	3/5/2015 5:13	6.12
Lower Flurometer	3/5/2015 5:14	6.14
Lower Flurometer	3/5/2015 5:15	6.19
Lower Flurometer	3/5/2015 5:16	6.25
Lower Flurometer	3/5/2015 5:17	6.19

Location	Date and Time	Rhodmaine Concentration Adjusted Concentration (ppb)
Lower Flurometer	3/5/2015 5:18	6.23
Lower Flurometer	3/5/2015 5:19	6.25
Lower Flurometer	3/5/2015 5:20	6.27
Lower Flurometer	3/5/2015 5:21	6.28
Lower Flurometer	3/5/2015 5:22	6.35
Lower Flurometer	3/5/2015 5:23	6.3
Lower Flurometer	3/5/2015 5:24	6.36
Lower Flurometer	3/5/2015 5:25	6.36
Lower Flurometer	3/5/2015 5:26	6.36
Lower Flurometer	3/5/2015 5:27	6.36
Lower Flurometer	3/5/2015 5:28	6.42
Lower Flurometer	3/5/2015 5:29	6.43
Lower Flurometer	3/5/2015 5:30	6.39
Lower Flurometer	3/5/2015 5:31	6.4
Lower Flurometer	3/5/2015 5:32	6.45
Lower Flurometer	3/5/2015 5:33	6.44
Lower Flurometer	3/5/2015 5:34	6.46
Lower Flurometer	3/5/2015 5:35	6.41
Lower Flurometer	3/5/2015 5:36	6.45
Lower Flurometer	3/5/2015 5:37	6.48
Lower Flurometer	3/5/2015 5:38	6.4
Lower Flurometer	3/5/2015 5:39	6.43
Lower Flurometer	3/5/2015 5:40	6.46
Lower Flurometer	3/5/2015 5:41	6.5
Lower Flurometer	3/5/2015 5:42	6.43
Lower Flurometer	3/5/2015 5:43	6.46
Lower Flurometer	3/5/2015 5:44	6.49
Lower Flurometer	3/5/2015 5:45	6.53
Lower Flurometer	3/5/2015 5:46	6.47
Lower Flurometer	3/5/2015 5:47	6.45
Lower Flurometer	3/5/2015 5:48	6.5
Lower Flurometer	3/5/2015 5:49	6.46
Lower Flurometer	3/5/2015 5:50	6.43
Lower Flurometer	3/5/2015 5:51	6.48
Lower Flurometer	3/5/2015 5:52	6.41
Lower Flurometer	3/5/2015 5:53	6.44
Lower Flurometer	3/5/2015 5:54	6.44
Lower Flurometer	3/5/2015 5:55	6.45
Lower Flurometer	3/5/2015 5:56	6.45
Lower Flurometer	3/5/2015 5:57	6.46
Lower Flurometer	3/5/2015 5:58	6.44
Lower Flurometer	3/5/2015 5:59	6.41
Lower Flurometer	3/5/2015 6:00	6.41
Lower Flurometer	3/5/2015 6:01	6.45
Lower Flurometer	3/5/2015 6:02	6.39
Lower Flurometer	3/5/2015 6:03	6.39

Location	Date and Time	Rhodmaine Concentration Adjusted Concentration (ppb)
Lower Flurometer	3/5/2015 6:04	6.39
Lower Flurometer	3/5/2015 6:05	6.4
Lower Flurometer	3/5/2015 6:06	6.36
Lower Flurometer	3/5/2015 6:07	6.39
Lower Flurometer	3/5/2015 6:08	6.34
Lower Flurometer	3/5/2015 6:09	6.4
Lower Flurometer	3/5/2015 6:10	6.36
Lower Flurometer	3/5/2015 6:11	6.32
Lower Flurometer	3/5/2015 6:12	6.34
Lower Flurometer	3/5/2015 6:13	6.3
Lower Flurometer	3/5/2015 6:14	6.33
Lower Flurometer	3/5/2015 6:15	6.25
Lower Flurometer	3/5/2015 6:16	6.26
Lower Flurometer	3/5/2015 6:17	6.25
Lower Flurometer	3/5/2015 6:18	6.23
Lower Flurometer	3/5/2015 6:19	6.28
Lower Flurometer	3/5/2015 6:20	6.2
Lower Flurometer	3/5/2015 6:21	6.22
Lower Flurometer	3/5/2015 6:22	6.26
Lower Flurometer	3/5/2015 6:23	6.18
Lower Flurometer	3/5/2015 6:24	6.19
Lower Flurometer	3/5/2015 6:25	6.24
Lower Flurometer	3/5/2015 6:26	6.19
Lower Flurometer	3/5/2015 6:27	6.2
Lower Flurometer	3/5/2015 6:28	6.12
Lower Flurometer	3/5/2015 6:29	6.14
Lower Flurometer	3/5/2015 6:30	6.11
Lower Flurometer	3/5/2015 6:31	6.12
Lower Flurometer	3/5/2015 6:32	6.09
Lower Flurometer	3/5/2015 6:33	6.1
Lower Flurometer	3/5/2015 6:34	6.05
Lower Flurometer	3/5/2015 6:35	6.06
Lower Flurometer	3/5/2015 6:36	6.05
Lower Flurometer	3/5/2015 6:37	6.06
Lower Flurometer	3/5/2015 6:38	6.06
Lower Flurometer	3/5/2015 6:39	5.97
Lower Flurometer	3/5/2015 6:40	6.08
Lower Flurometer	3/5/2015 6:41	6.04
Lower Flurometer	3/5/2015 6:42	5.97
Lower Flurometer	3/5/2015 6:43	5.91
Lower Flurometer	3/5/2015 6:44	5.94
Lower Flurometer	3/5/2015 6:45	5.92
Lower Flurometer	3/5/2015 6:46	5.9
Lower Flurometer	3/5/2015 6:47	5.9
Lower Flurometer	3/5/2015 6:48	5.86
Lower Flurometer	3/5/2015 6:49	5.87

Location	Date and Time	Rhodmaine Concentration Adjusted Concentration (ppb)
Lower Flurometer	3/5/2015 6:50	5.86
Lower Flurometer	3/5/2015 6:51	5.81
Lower Flurometer	3/5/2015 6:52	5.87
Lower Flurometer	3/5/2015 6:53	5.83
Lower Flurometer	3/5/2015 6:54	5.82
Lower Flurometer	3/5/2015 6:55	5.81
Lower Flurometer	3/5/2015 6:56	5.7
Lower Flurometer	3/5/2015 6:57	5.75
Lower Flurometer	3/5/2015 6:58	5.75
Lower Flurometer	3/5/2015 6:59	5.73
Lower Flurometer	3/5/2015 7:00	5.75
Lower Flurometer	3/5/2015 7:01	5.72
Lower Flurometer	3/5/2015 7:02	5.7
Lower Flurometer	3/5/2015 7:03	5.67
Lower Flurometer	3/5/2015 7:04	5.65
Lower Flurometer	3/5/2015 7:05	5.56
Lower Flurometer	3/5/2015 7:06	5.61
Lower Flurometer	3/5/2015 7:07	5.61
Lower Flurometer	3/5/2015 7:08	5.57
Lower Flurometer	3/5/2015 7:09	5.6
Lower Flurometer	3/5/2015 7:10	5.56
Lower Flurometer	3/5/2015 7:11	5.6
Lower Flurometer	3/5/2015 7:12	5.52
Lower Flurometer	3/5/2015 7:13	5.52
Lower Flurometer	3/5/2015 7:14	5.5
Lower Flurometer	3/5/2015 7:15	5.52
Lower Flurometer	3/5/2015 7:16	5.45
Lower Flurometer	3/5/2015 7:17	5.49
Lower Flurometer	3/5/2015 7:18	5.38
Lower Flurometer	3/5/2015 7:19	5.49
Lower Flurometer	3/5/2015 7:20	5.36
Lower Flurometer	3/5/2015 7:21	5.43
Lower Flurometer	3/5/2015 7:22	5.38
Lower Flurometer	3/5/2015 7:23	5.33
Lower Flurometer	3/5/2015 7:24	5.37
Lower Flurometer	3/5/2015 7:25	5.37
Lower Flurometer	3/5/2015 7:26	5.31
Lower Flurometer	3/5/2015 7:27	5.31
Lower Flurometer	3/5/2015 7:28	5.34
Lower Flurometer	3/5/2015 7:29	5.3
Lower Flurometer	3/5/2015 7:30	5.28
Lower Flurometer	3/5/2015 7:31	5.2
Lower Flurometer	3/5/2015 7:32	5.25
Lower Flurometer	3/5/2015 7:33	5.16
Lower Flurometer	3/5/2015 7:34	5.18
Lower Flurometer	3/5/2015 7:35	5.2

Location	Date and Time	Rhodmaine Concentration Adjusted Concentration (ppb)
Lower Flurometer	3/5/2015 7:36	5.12
Lower Flurometer	3/5/2015 7:37	5.13
Lower Flurometer	3/5/2015 7:38	5.12
Lower Flurometer	3/5/2015 7:39	5.14
Lower Flurometer	3/5/2015 7:40	5.13
Lower Flurometer	3/5/2015 7:41	5.12
Lower Flurometer	3/5/2015 7:42	5.09
Lower Flurometer	3/5/2015 7:43	5.03
Lower Flurometer	3/5/2015 7:44	5
Lower Flurometer	3/5/2015 7:45	5
Lower Flurometer	3/5/2015 7:46	5.03
Lower Flurometer	3/5/2015 7:47	4.97
Lower Flurometer	3/5/2015 7:48	4.95
Lower Flurometer	3/5/2015 7:49	4.99
Lower Flurometer	3/5/2015 7:50	5.01
Lower Flurometer	3/5/2015 7:51	4.95
Lower Flurometer	3/5/2015 7:52	4.99
Lower Flurometer	3/5/2015 7:53	4.89
Lower Flurometer	3/5/2015 7:54	4.88
Lower Flurometer	3/5/2015 7:55	4.86
Lower Flurometer	3/5/2015 7:56	4.89
Lower Flurometer	3/5/2015 7:57	4.84
Lower Flurometer	3/5/2015 7:58	4.82
Lower Flurometer	3/5/2015 7:59	4.82
Lower Flurometer	3/5/2015 8:00	4.8
Lower Flurometer	3/5/2015 8:01	4.87
Lower Flurometer	3/5/2015 8:02	4.73
Lower Flurometer	3/5/2015 8:03	4.77
Lower Flurometer	3/5/2015 8:04	4.75
Lower Flurometer	3/5/2015 8:05	4.74
Lower Flurometer	3/5/2015 8:06	4.71
Lower Flurometer	3/5/2015 8:07	4.69
Lower Flurometer	3/5/2015 8:08	4.6
Lower Flurometer	3/5/2015 8:09	4.63
Lower Flurometer	3/5/2015 8:10	4.65
Lower Flurometer	3/5/2015 8:11	4.62
Lower Flurometer	3/5/2015 8:12	4.59
Lower Flurometer	3/5/2015 8:13	4.59
Lower Flurometer	3/5/2015 8:14	4.65
Lower Flurometer	3/5/2015 8:15	4.57
Lower Flurometer	3/5/2015 8:16	4.52
Lower Flurometer	3/5/2015 8:17	4.55
Lower Flurometer	3/5/2015 8:18	4.63
Lower Flurometer	3/5/2015 8:19	4.51
Lower Flurometer	3/5/2015 8:20	4.49
Lower Flurometer	3/5/2015 8:21	4.47

Location	Date and Time	Rhodmaine Concentration Adjusted Concentration (ppb)
Lower Flurometer	3/5/2015 8:22	4.45
Lower Flurometer	3/5/2015 8:23	4.45
Lower Flurometer	3/5/2015 8:24	4.39
Lower Flurometer	3/5/2015 8:25	4.44
Lower Flurometer	3/5/2015 8:26	4.39
Lower Flurometer	3/5/2015 8:27	4.36
Lower Flurometer	3/5/2015 8:28	4.39
Lower Flurometer	3/5/2015 8:29	4.35
Lower Flurometer	3/5/2015 8:30	4.31
Lower Flurometer	3/5/2015 8:31	4.31
Lower Flurometer	3/5/2015 8:32	4.29
Lower Flurometer	3/5/2015 8:33	4.33
Lower Flurometer	3/5/2015 8:34	4.28
Lower Flurometer	3/5/2015 8:35	4.24
Lower Flurometer	3/5/2015 8:36	4.22
Lower Flurometer	3/5/2015 8:37	4.2
Lower Flurometer	3/5/2015 8:38	4.18
Lower Flurometer	3/5/2015 8:39	4.2
Lower Flurometer	3/5/2015 8:40	4.14
Lower Flurometer	3/5/2015 8:41	4.18
Lower Flurometer	3/5/2015 8:42	4.19
Lower Flurometer	3/5/2015 8:43	4.12
Lower Flurometer	3/5/2015 8:44	4.09
Lower Flurometer	3/5/2015 8:45	4.08
Lower Flurometer	3/5/2015 8:46	4.07
Lower Flurometer	3/5/2015 8:47	4.1
Lower Flurometer	3/5/2015 8:48	4.07
Lower Flurometer	3/5/2015 8:49	4.06
Lower Flurometer	3/5/2015 8:50	3.99
Lower Flurometer	3/5/2015 8:51	4
Lower Flurometer	3/5/2015 8:52	3.96
Lower Flurometer	3/5/2015 8:53	4.01
Lower Flurometer	3/5/2015 8:54	3.98
Lower Flurometer	3/5/2015 8:55	3.91
Lower Flurometer	3/5/2015 8:56	3.93
Lower Flurometer	3/5/2015 8:57	3.92
Lower Flurometer	3/5/2015 8:58	3.87
Lower Flurometer	3/5/2015 8:59	3.86
Lower Flurometer	3/5/2015 9:00	3.92
Lower Flurometer	3/5/2015 9:01	3.89
Lower Flurometer	3/5/2015 9:02	3.88
Lower Flurometer	3/5/2015 9:03	3.83
Lower Flurometer	3/5/2015 9:04	3.77
Lower Flurometer	3/5/2015 9:05	3.79
Lower Flurometer	3/5/2015 9:06	3.77
Lower Flurometer	3/5/2015 9:07	3.74

Location	Date and Time	Rhodmaine Concentration Adjusted Concentration (ppb)
Lower Flurometer	3/5/2015 9:08	3.77
Lower Flurometer	3/5/2015 9:09	3.76
Lower Flurometer	3/5/2015 9:10	3.75
Lower Flurometer	3/5/2015 9:11	3.7
Lower Flurometer	3/5/2015 9:12	3.75
Lower Flurometer	3/5/2015 9:13	3.78
Lower Flurometer	3/5/2015 9:14	3.64
Lower Flurometer	3/5/2015 9:15	3.65
Lower Flurometer	3/5/2015 9:16	3.58
Lower Flurometer	3/5/2015 9:17	3.64
Lower Flurometer	3/5/2015 9:18	3.64
Lower Flurometer	3/5/2015 9:19	3.56
Lower Flurometer	3/5/2015 9:20	3.6
Lower Flurometer	3/5/2015 9:21	3.54
Lower Flurometer	3/5/2015 9:22	3.52
Lower Flurometer	3/5/2015 9:23	3.56
Lower Flurometer	3/5/2015 9:24	3.54
Lower Flurometer	3/5/2015 9:25	3.56
Lower Flurometer	3/5/2015 9:26	3.55
Lower Flurometer	3/5/2015 9:27	3.49
Lower Flurometer	3/5/2015 9:28	3.5
Lower Flurometer	3/5/2015 9:29	3.43
Lower Flurometer	3/5/2015 9:30	3.44
Lower Flurometer	3/5/2015 9:31	3.46
Lower Flurometer	3/5/2015 9:32	3.44
Lower Flurometer	3/5/2015 9:33	3.45
Lower Flurometer	3/5/2015 9:34	3.43
Lower Flurometer	3/5/2015 9:35	3.38
Lower Flurometer	3/5/2015 9:36	3.38
Lower Flurometer	3/5/2015 9:37	3.39
Lower Flurometer	3/5/2015 9:38	3.36
Lower Flurometer	3/5/2015 9:39	3.33
Lower Flurometer	3/5/2015 9:40	3.35
Lower Flurometer	3/5/2015 9:41	3.34
Lower Flurometer	3/5/2015 9:42	3.32
Lower Flurometer	3/5/2015 9:43	3.29
Lower Flurometer	3/5/2015 9:44	3.3
Lower Flurometer	3/5/2015 9:45	3.3
Lower Flurometer	3/5/2015 9:46	3.27
Lower Flurometer	3/5/2015 9:47	3.26
Lower Flurometer	3/5/2015 9:48	3.25
Lower Flurometer	3/5/2015 9:49	3.25
Lower Flurometer	3/5/2015 9:50	3.22
Lower Flurometer	3/5/2015 9:51	3.2
Lower Flurometer	3/5/2015 9:52	3.21
Lower Flurometer	3/5/2015 9:53	3.16

Location	Date and Time	Rhodmaine Concentration Adjusted Concentration (ppb)
Lower Flurometer	3/5/2015 9:54	3.15
Lower Flurometer	3/5/2015 9:55	3.18
Lower Flurometer	3/5/2015 9:56	3.14
Lower Flurometer	3/5/2015 9:57	3.19
Lower Flurometer	3/5/2015 9:58	4.4
Lower Flurometer	3/5/2015 9:59	3.17
Lower Flurometer	3/5/2015 10:00	3.11
Lower Flurometer	3/5/2015 10:01	3.06
Lower Flurometer	3/5/2015 10:02	3.08
Lower Flurometer	3/5/2015 10:03	3.02
Lower Flurometer	3/5/2015 10:04	3.07
Lower Flurometer	3/5/2015 10:05	3.02
Lower Flurometer	3/5/2015 10:06	3.06
Lower Flurometer	3/5/2015 10:07	3
Lower Flurometer	3/5/2015 10:08	3.06
Lower Flurometer	3/5/2015 10:09	3.01
Lower Flurometer	3/5/2015 10:10	3
Lower Flurometer	3/5/2015 10:11	2.98
Lower Flurometer	3/5/2015 10:12	2.97
Lower Flurometer	3/5/2015 10:13	2.99
Lower Flurometer	3/5/2015 10:14	2.9
Lower Flurometer	3/5/2015 10:15	2.91
Lower Flurometer	3/5/2015 10:16	2.96
Lower Flurometer	3/5/2015 10:17	2.89
Lower Flurometer	3/5/2015 10:18	2.85
Lower Flurometer	3/5/2015 10:19	2.9
Lower Flurometer	3/5/2015 10:20	2.94
Lower Flurometer	3/5/2015 10:21	2.82
Lower Flurometer	3/5/2015 10:22	2.89
Lower Flurometer	3/5/2015 10:23	2.84
Lower Flurometer	3/5/2015 10:24	2.83
Lower Flurometer	3/5/2015 10:25	2.81
Lower Flurometer	3/5/2015 10:26	2.83
Lower Flurometer	3/5/2015 10:27	2.79
Lower Flurometer	3/5/2015 10:28	2.81
Lower Flurometer	3/5/2015 10:29	2.79
Lower Flurometer	3/5/2015 10:30	2.79
Lower Flurometer	3/5/2015 10:31	2.76
Lower Flurometer	3/5/2015 10:32	2.77
Lower Flurometer	3/5/2015 10:33	2.74
Lower Flurometer	3/5/2015 10:34	2.75
Lower Flurometer	3/5/2015 10:35	2.78
Lower Flurometer	3/5/2015 10:36	2.72
Lower Flurometer	3/5/2015 10:37	2.73
Lower Flurometer	3/5/2015 10:38	2.77
Lower Flurometer	3/5/2015 10:39	2.66

Location	Date and Time	Rhodmaine Concentration Adjusted Concentration (ppb)
Lower Flurometer	3/5/2015 10:40	2.79
Lower Flurometer	3/5/2015 10:41	2.75
Lower Flurometer	3/5/2015 10:42	2.69
Lower Flurometer	3/5/2015 10:43	2.69
Lower Flurometer	3/5/2015 10:44	2.67
Lower Flurometer	3/5/2015 10:45	2.66
Lower Flurometer	3/5/2015 10:46	2.69
Lower Flurometer	3/5/2015 10:47	2.66
Lower Flurometer	3/5/2015 10:48	2.65
Lower Flurometer	3/5/2015 10:49	2.61
Lower Flurometer	3/5/2015 10:50	2.65
Lower Flurometer	3/5/2015 10:51	2.62
Lower Flurometer	3/5/2015 10:52	2.6
Lower Flurometer	3/5/2015 10:53	2.56
Lower Flurometer	3/5/2015 10:54	2.58
Lower Flurometer	3/5/2015 10:55	2.57
Lower Flurometer	3/5/2015 10:56	2.51
Lower Flurometer	3/5/2015 10:57	2.5
Lower Flurometer	3/5/2015 10:58	2.52
Lower Flurometer	3/5/2015 10:59	2.5
Lower Flurometer	3/5/2015 11:00	2.52
Lower Flurometer	3/5/2015 11:01	2.47
Lower Flurometer	3/5/2015 11:02	2.52
Lower Flurometer	3/5/2015 11:03	2.63
Lower Flurometer	3/5/2015 11:04	2.5
Lower Flurometer	3/5/2015 11:05	2.47
Lower Flurometer	3/5/2015 11:06	2.46
Lower Flurometer	3/5/2015 11:07	2.48
Lower Flurometer	3/5/2015 11:08	2.48
Lower Flurometer	3/5/2015 11:09	2.46
Lower Flurometer	3/5/2015 11:10	2.45
Lower Flurometer	3/5/2015 11:11	2.42
Lower Flurometer	3/5/2015 11:12	2.46
Lower Flurometer	3/5/2015 11:13	2.43
Lower Flurometer	3/5/2015 11:14	2.39
Lower Flurometer	3/5/2015 11:15	2.37
Lower Flurometer	3/5/2015 11:16	2.39
Lower Flurometer	3/5/2015 11:17	2.36
Lower Flurometer	3/5/2015 11:18	2.33
Lower Flurometer	3/5/2015 11:19	2.38
Lower Flurometer	3/5/2015 11:20	2.38
Lower Flurometer	3/5/2015 11:21	2.37
Lower Flurometer	3/5/2015 11:22	2.38
Lower Flurometer	3/5/2015 11:23	2.34
Lower Flurometer	3/5/2015 11:24	2.33
Lower Flurometer	3/5/2015 11:25	2.36

Location	Date and Time	Rhodmaine Concentration Adjusted Concentration (ppb)
Lower Flurometer	3/5/2015 11:26	2.36
Lower Flurometer	3/5/2015 11:27	2.29
Lower Flurometer	3/5/2015 11:28	2.35
Lower Flurometer	3/5/2015 11:29	2.28
Lower Flurometer	3/5/2015 11:30	2.3
Lower Flurometer	3/5/2015 11:31	2.24
Lower Flurometer	3/5/2015 11:32	2.34
Lower Flurometer	3/5/2015 11:33	2.29
Lower Flurometer	3/5/2015 11:34	2.24
Lower Flurometer	3/5/2015 11:35	2.22
Lower Flurometer	3/5/2015 11:36	2.23
Lower Flurometer	3/5/2015 11:37	2.34
Lower Flurometer	3/5/2015 11:38	2.2
Lower Flurometer	3/5/2015 11:39	2.3
Lower Flurometer	3/5/2015 11:40	2.2
Lower Flurometer	3/5/2015 11:41	2.19
Lower Flurometer	3/5/2015 11:42	2.21
Lower Flurometer	3/5/2015 11:43	2.18
Lower Flurometer	3/5/2015 11:44	2.17
Lower Flurometer	3/5/2015 11:45	2.22
Lower Flurometer	3/5/2015 11:46	2.17
Lower Flurometer	3/5/2015 11:47	2.14
Lower Flurometer	3/5/2015 11:48	2.12
Lower Flurometer	3/5/2015 11:49	2.2
Lower Flurometer	3/5/2015 11:50	2.12
Lower Flurometer	3/5/2015 11:51	2.17
Lower Flurometer	3/5/2015 11:52	2.21
Lower Flurometer	3/5/2015 11:53	2.12
Lower Flurometer	3/5/2015 11:54	2.12
Lower Flurometer	3/5/2015 11:55	2.16
Lower Flurometer	3/5/2015 11:56	2.09
Lower Flurometer	3/5/2015 11:57	2.13
Lower Flurometer	3/5/2015 11:58	2.12
Lower Flurometer	3/5/2015 11:59	2.09
Lower Flurometer	3/5/2015 12:00	2.09
Lower Flurometer	3/5/2015 12:01	2.09
Lower Flurometer	3/5/2015 12:02	2.11
Lower Flurometer	3/5/2015 12:03	2.09
Lower Flurometer	3/5/2015 12:04	2.07
Lower Flurometer	3/5/2015 12:05	2.08
Lower Flurometer	3/5/2015 12:06	2.08
Lower Flurometer	3/5/2015 12:07	2.06
Lower Flurometer	3/5/2015 12:08	2.03
Lower Flurometer	3/5/2015 12:09	2.05
Lower Flurometer	3/5/2015 12:10	2.05
Lower Flurometer	3/5/2015 12:11	2.05

Location	Date and Time	Rhodmaine Concentration Adjusted Concentration (ppb)
Lower Flurometer	3/5/2015 12:12	2.05
Lower Flurometer	3/5/2015 12:13	2.01
Lower Flurometer	3/5/2015 12:14	1.99
Lower Flurometer	3/5/2015 12:15	2.04
Lower Flurometer	3/5/2015 12:16	2.03
Lower Flurometer	3/5/2015 12:17	1.93
Lower Flurometer	3/5/2015 12:18	2.02
Lower Flurometer	3/5/2015 12:19	1.97
Lower Flurometer	3/5/2015 12:20	2.09
Lower Flurometer	3/5/2015 12:21	1.99
Lower Flurometer	3/5/2015 12:22	1.99
Lower Flurometer	3/5/2015 12:23	1.96
Lower Flurometer	3/5/2015 12:24	1.95
Lower Flurometer	3/5/2015 12:25	1.91
Lower Flurometer	3/5/2015 12:26	1.9
Lower Flurometer	3/5/2015 12:27	1.95
Lower Flurometer	3/5/2015 12:28	1.95
Lower Flurometer	3/5/2015 12:29	1.9
Lower Flurometer	3/5/2015 12:30	1.88
Lower Flurometer	3/5/2015 12:31	1.88
Lower Flurometer	3/5/2015 12:32	1.86
Lower Flurometer	3/5/2015 12:33	1.89
Lower Flurometer	3/5/2015 12:34	1.88
Lower Flurometer	3/5/2015 12:35	1.89
Lower Flurometer	3/5/2015 12:36	1.9
Lower Flurometer	3/5/2015 12:37	1.88
Lower Flurometer	3/5/2015 12:38	1.88
Lower Flurometer	3/5/2015 12:39	1.89
Lower Flurometer	3/5/2015 12:40	1.85
Lower Flurometer	3/5/2015 12:41	1.88
Lower Flurometer	3/5/2015 12:42	1.85
Lower Flurometer	3/5/2015 12:43	1.81
Lower Flurometer	3/5/2015 12:44	1.83
Lower Flurometer	3/5/2015 12:45	1.79
Lower Flurometer	3/5/2015 12:46	1.8
Lower Flurometer	3/5/2015 12:47	1.82
Lower Flurometer	3/5/2015 12:48	1.87
Lower Flurometer	3/5/2015 12:49	1.82
Lower Flurometer	3/5/2015 12:50	1.77
Lower Flurometer	3/5/2015 12:51	1.78
Lower Flurometer	3/5/2015 12:52	1.81
Lower Flurometer	3/5/2015 12:53	1.77
Lower Flurometer	3/5/2015 12:54	1.79
Lower Flurometer	3/5/2015 12:55	1.79
Lower Flurometer	3/5/2015 12:56	1.78
Lower Flurometer	3/5/2015 12:57	1.78

Location	Date and Time	Rhodmaine Concentration Adjusted Concentration (ppb)
Lower Flurometer	3/5/2015 12:58	1.72
Lower Flurometer	3/5/2015 12:59	1.76
Lower Flurometer	3/5/2015 13:00	1.74
Lower Flurometer	3/5/2015 13:01	1.75
Lower Flurometer	3/5/2015 13:02	1.71
Lower Flurometer	3/5/2015 13:03	1.73
Lower Flurometer	3/5/2015 13:04	1.7
Lower Flurometer	3/5/2015 13:05	1.73
Lower Flurometer	3/5/2015 13:06	1.67
Lower Flurometer	3/5/2015 13:07	1.69
Lower Flurometer	3/5/2015 13:08	1.7
Lower Flurometer	3/5/2015 13:09	1.7
Lower Flurometer	3/5/2015 13:10	1.65
Lower Flurometer	3/5/2015 13:11	1.69
Lower Flurometer	3/5/2015 13:12	1.67
Lower Flurometer	3/5/2015 13:13	1.65
Lower Flurometer	3/5/2015 13:14	1.7
Lower Flurometer	3/5/2015 13:15	1.63
Lower Flurometer	3/5/2015 13:16	1.65
Lower Flurometer	3/5/2015 13:17	1.67
Lower Flurometer	3/5/2015 13:18	1.66
Lower Flurometer	3/5/2015 13:19	1.62
Lower Flurometer	3/5/2015 13:20	1.58
Lower Flurometer	3/5/2015 13:21	1.62
Lower Flurometer	3/5/2015 13:22	1.64
Lower Flurometer	3/5/2015 13:23	1.62
Lower Flurometer	3/5/2015 13:24	1.58
Lower Flurometer	3/5/2015 13:25	1.62
Lower Flurometer	3/5/2015 13:26	1.57
Lower Flurometer	3/5/2015 13:27	1.57
Lower Flurometer	3/5/2015 13:28	1.61
Lower Flurometer	3/5/2015 13:29	1.62
Lower Flurometer	3/5/2015 13:30	1.63
Lower Flurometer	3/5/2015 13:31	1.55
Lower Flurometer	3/5/2015 13:32	1.54
Lower Flurometer	3/5/2015 13:33	1.62
Lower Flurometer	3/5/2015 13:34	1.57
Lower Flurometer	3/5/2015 13:35	1.6
Lower Flurometer	3/5/2015 13:36	1.5
Lower Flurometer	3/5/2015 13:37	1.51
Lower Flurometer	3/5/2015 13:38	1.54
Lower Flurometer	3/5/2015 13:39	1.49
Lower Flurometer	3/5/2015 13:40	1.48
Lower Flurometer	3/5/2015 13:41	1.54
Lower Flurometer	3/5/2015 13:42	1.51
Lower Flurometer	3/5/2015 13:43	1.51

Location	Date and Time	Rhodmaine Concentration Adjusted Concentration (ppb)
Lower Flurometer	3/5/2015 13:44	1.48
Lower Flurometer	3/5/2015 13:45	1.52
Lower Flurometer	3/5/2015 13:46	1.49
Lower Flurometer	3/5/2015 13:47	1.5
Lower Flurometer	3/5/2015 13:48	1.51
Lower Flurometer	3/5/2015 13:49	1.47
Lower Flurometer	3/5/2015 13:50	1.51
Lower Flurometer	3/5/2015 13:51	1.51
Lower Flurometer	3/5/2015 13:52	1.47
Lower Flurometer	3/5/2015 13:53	1.47
Lower Flurometer	3/5/2015 13:54	1.52
Lower Flurometer	3/5/2015 13:55	1.43
Lower Flurometer	3/5/2015 13:56	1.47
Lower Flurometer	3/5/2015 13:57	1.52
Lower Flurometer	3/5/2015 13:58	1.39
Lower Flurometer	3/5/2015 13:59	1.45
Lower Flurometer	3/5/2015 14:00	1.46
Lower Flurometer	3/5/2015 14:01	1.43
Lower Flurometer	3/5/2015 14:02	1.39
Lower Flurometer	3/5/2015 14:03	1.43
Lower Flurometer	3/5/2015 14:04	1.4
Lower Flurometer	3/5/2015 14:05	1.38
Lower Flurometer	3/5/2015 14:06	1.39
Lower Flurometer	3/5/2015 14:07	1.33
Lower Flurometer	3/5/2015 14:08	1.33
Lower Flurometer	3/5/2015 14:09	1.35
Lower Flurometer	3/5/2015 14:10	1.36
Lower Flurometer	3/5/2015 14:11	1.36
Lower Flurometer	3/5/2015 14:12	1.32
Lower Flurometer	3/5/2015 14:13	1.35
Lower Flurometer	3/5/2015 14:14	1.32
Lower Flurometer	3/5/2015 14:15	1.33
Lower Flurometer	3/5/2015 14:16	1.38
Lower Flurometer	3/5/2015 14:17	1.33
Lower Flurometer	3/5/2015 14:18	1.35
Lower Flurometer	3/5/2015 14:19	1.32
Lower Flurometer	3/5/2015 14:20	1.39
Lower Flurometer	3/5/2015 14:21	1.31
Lower Flurometer	3/5/2015 14:22	1.36
Lower Flurometer	3/5/2015 14:23	1.31
Lower Flurometer	3/5/2015 14:24	1.32
Lower Flurometer	3/5/2015 14:25	1.28
Lower Flurometer	3/5/2015 14:26	1.3
Lower Flurometer	3/5/2015 14:27	1.27
Lower Flurometer	3/5/2015 14:28	1.27
Lower Flurometer	3/5/2015 14:29	1.27

Location	Date and Time	Rhodmaine Concentration Adjusted Concentration (ppb)
Lower Flurometer	3/5/2015 14:30	1.26
Lower Flurometer	3/5/2015 14:31	1.23
Lower Flurometer	3/5/2015 14:32	1.29
Lower Flurometer	3/5/2015 14:33	1.28
Lower Flurometer	3/5/2015 14:34	1.24
Lower Flurometer	3/5/2015 14:35	1.26
Lower Flurometer	3/5/2015 14:36	1.23
Lower Flurometer	3/5/2015 14:37	1.26
Lower Flurometer	3/5/2015 14:38	1.29
Lower Flurometer	3/5/2015 14:39	1.24
Lower Flurometer	3/5/2015 14:40	1.23
Lower Flurometer	3/5/2015 14:41	1.24
Lower Flurometer	3/5/2015 14:42	1.22
Lower Flurometer	3/5/2015 14:43	1.23
Lower Flurometer	3/5/2015 14:44	1.24
Lower Flurometer	3/5/2015 14:45	1.23
Lower Flurometer	3/5/2015 14:46	1.25
Lower Flurometer	3/5/2015 14:47	1.23
Lower Flurometer	3/5/2015 14:48	1.19
Lower Flurometer	3/5/2015 14:49	1.18
Lower Flurometer	3/5/2015 14:50	1.22
Lower Flurometer	3/5/2015 14:51	1.2
Lower Flurometer	3/5/2015 14:52	1.19
Lower Flurometer	3/5/2015 14:53	1.16
Lower Flurometer	3/5/2015 14:54	1.19
Lower Flurometer	3/5/2015 14:55	1.18
Lower Flurometer	3/5/2015 14:56	1.16
Lower Flurometer	3/5/2015 14:57	1.13
Lower Flurometer	3/5/2015 14:58	1.14
Lower Flurometer	3/5/2015 14:59	1.09
Lower Flurometer	3/5/2015 15:00	1.15
Lower Flurometer	3/5/2015 15:01	1.18
Lower Flurometer	3/5/2015 15:02	1.11
Lower Flurometer	3/5/2015 15:03	1.14
Lower Flurometer	3/5/2015 15:04	1.09
Lower Flurometer	3/5/2015 15:05	1.12
Lower Flurometer	3/5/2015 15:06	1.07
Lower Flurometer	3/5/2015 15:07	1.11
Lower Flurometer	3/5/2015 15:08	1.12
Lower Flurometer	3/5/2015 15:09	1.15
Lower Flurometer	3/5/2015 15:10	1.12
Lower Flurometer	3/5/2015 15:11	1.12
Lower Flurometer	3/5/2015 15:12	1.11
Lower Flurometer	3/5/2015 15:13	1.12
Lower Flurometer	3/5/2015 15:14	1.12
Lower Flurometer	3/5/2015 15:15	1.1

Location	Date and Time	Rhodmaine Concentration Adjusted Concentration (ppb)
Lower Flurometer	3/5/2015 15:16	1.07
Lower Flurometer	3/5/2015 15:17	1.11
Lower Flurometer	3/5/2015 15:18	1.02
Lower Flurometer	3/5/2015 15:19	1.05
Lower Flurometer	3/5/2015 15:20	1.06
Lower Flurometer	3/5/2015 15:21	1.06
Lower Flurometer	3/5/2015 15:22	1.06
Lower Flurometer	3/5/2015 15:23	1.02
Lower Flurometer	3/5/2015 15:24	1.01
Lower Flurometer	3/5/2015 15:25	1.04
Lower Flurometer	3/5/2015 15:26	1.05
Lower Flurometer	3/5/2015 15:27	1.02
Lower Flurometer	3/5/2015 15:28	1.01
Lower Flurometer	3/5/2015 15:29	1.03
Lower Flurometer	3/5/2015 15:30	1.03
Lower Flurometer	3/5/2015 15:31	1.02
Lower Flurometer	3/5/2015 15:32	1.01
Lower Flurometer	3/5/2015 15:33	1.03
Lower Flurometer	3/5/2015 15:34	1
Lower Flurometer	3/5/2015 15:35	0.98
Lower Flurometer	3/5/2015 15:36	1
Lower Flurometer	3/5/2015 15:37	0.99
Lower Flurometer	3/5/2015 15:38	1.02
Lower Flurometer	3/5/2015 15:39	1
Lower Flurometer	3/5/2015 15:40	0.99
Lower Flurometer	3/5/2015 15:41	0.97
Lower Flurometer	3/5/2015 15:42	0.99
Lower Flurometer	3/5/2015 15:43	0.93
Lower Flurometer	3/5/2015 15:44	0.98
Lower Flurometer	3/5/2015 15:45	0.98
Lower Flurometer	3/5/2015 15:46	0.97
Lower Flurometer	3/5/2015 15:47	0.97
Lower Flurometer	3/5/2015 15:48	0.92
Lower Flurometer	3/5/2015 15:49	0.97
Lower Flurometer	3/5/2015 15:50	0.95
Lower Flurometer	3/5/2015 15:51	1.05
Lower Flurometer	3/5/2015 15:52	0.94
Lower Flurometer	3/5/2015 15:53	0.94
Lower Flurometer	3/5/2015 15:54	0.94
Lower Flurometer	3/5/2015 15:55	0.98
Lower Flurometer	3/5/2015 15:56	0.89
Lower Flurometer	3/5/2015 15:57	0.95
Lower Flurometer	3/5/2015 15:58	0.91
Lower Flurometer	3/5/2015 15:59	0.93
Lower Flurometer	3/5/2015 16:00	0.88
Lower Flurometer	3/5/2015 16:01	0.97

Location	Date and Time	Rhodmaine Concentration Adjusted Concentration (ppb)
Lower Flurometer	3/5/2015 16:02	0.87
Lower Flurometer	3/5/2015 16:03	0.98
Lower Flurometer	3/5/2015 16:04	0.89
Lower Flurometer	3/5/2015 16:05	0.91
Lower Flurometer	3/5/2015 16:06	0.92
Lower Flurometer	3/5/2015 16:07	0.89
Lower Flurometer	3/5/2015 16:08	0.88
Lower Flurometer	3/5/2015 16:09	0.88
Lower Flurometer	3/5/2015 16:10	0.87
Lower Flurometer	3/5/2015 16:11	0.87
Lower Flurometer	3/5/2015 16:12	0.9
Lower Flurometer	3/5/2015 16:13	0.84
Lower Flurometer	3/5/2015 16:14	0.86
Lower Flurometer	3/5/2015 16:15	0.88
Lower Flurometer	3/5/2015 16:16	0.9
Lower Flurometer	3/5/2015 16:17	0.87
Lower Flurometer	3/5/2015 16:18	0.87
Lower Flurometer	3/5/2015 16:19	0.84
Lower Flurometer	3/5/2015 16:20	0.85
Lower Flurometer	3/5/2015 16:21	0.82
Lower Flurometer	3/5/2015 16:22	0.82
Lower Flurometer	3/5/2015 16:23	0.8
Lower Flurometer	3/5/2015 16:24	0.8
Lower Flurometer	3/5/2015 16:25	0.79
Lower Flurometer	3/5/2015 16:26	0.83
Lower Flurometer	3/5/2015 16:27	0.81
Lower Flurometer	3/5/2015 16:28	0.84
Lower Flurometer	3/5/2015 16:29	0.82
Lower Flurometer	3/5/2015 16:30	0.78
Lower Flurometer	3/5/2015 16:31	0.79
Lower Flurometer	3/5/2015 16:32	0.78
Lower Flurometer	3/5/2015 16:33	0.76
Lower Flurometer	3/5/2015 16:34	0.84
Lower Flurometer	3/5/2015 16:35	0.79
Lower Flurometer	3/5/2015 16:36	0.79
Lower Flurometer	3/5/2015 16:37	0.8
Lower Flurometer	3/5/2015 16:38	0.79
Lower Flurometer	3/5/2015 16:39	0.77
Lower Flurometer	3/5/2015 16:40	0.85
Lower Flurometer	3/5/2015 16:41	0.84
Lower Flurometer	3/5/2015 16:42	0.8
Lower Flurometer	3/5/2015 16:43	0.75
Lower Flurometer	3/5/2015 16:44	0.73
Lower Flurometer	3/5/2015 16:45	0.78
Lower Flurometer	3/5/2015 16:46	0.72
Lower Flurometer	3/5/2015 16:47	2.68

Location	Date and Time	Rhodmaine Concentration Adjusted Concentration (ppb)
Lower Flurometer	3/5/2015 16:48	0.76
Lower Flurometer	3/5/2015 16:49	0.79
Lower Flurometer	3/5/2015 16:50	0.72
Lower Flurometer	3/5/2015 16:51	0.75
Lower Flurometer	3/5/2015 16:52	0.7
Lower Flurometer	3/5/2015 16:53	0.72
Lower Flurometer	3/5/2015 16:54	0.78
Lower Flurometer	3/5/2015 16:55	0.74
Lower Flurometer	3/5/2015 16:56	0.79
Lower Flurometer	3/5/2015 16:57	0.69
Lower Flurometer	3/5/2015 16:58	0.72
Lower Flurometer	3/5/2015 16:59	0.71
Lower Flurometer	3/5/2015 17:00	0.75
Lower Flurometer	3/5/2015 17:01	0.73
Lower Flurometer	3/5/2015 17:02	0.68
Lower Flurometer	3/5/2015 17:03	0.72
Lower Flurometer	3/5/2015 17:04	0.74
Lower Flurometer	3/5/2015 17:05	0.7
Lower Flurometer	3/5/2015 17:06	0.7
Lower Flurometer	3/5/2015 17:07	0.71
Lower Flurometer	3/5/2015 17:08	0.67
Lower Flurometer	3/5/2015 17:09	0.69
Lower Flurometer	3/5/2015 17:10	0.72
Lower Flurometer	3/5/2015 17:11	0.66
Lower Flurometer	3/5/2015 17:12	0.67
Lower Flurometer	3/5/2015 17:13	0.66
Lower Flurometer	3/5/2015 17:14	0.66
Lower Flurometer	3/5/2015 17:15	0.69
Lower Flurometer	3/5/2015 17:16	0.67
Lower Flurometer	3/5/2015 17:17	0.7
Lower Flurometer	3/5/2015 17:18	0.71
Lower Flurometer	3/5/2015 17:19	0.66
Lower Flurometer	3/5/2015 17:20	0.66
Lower Flurometer	3/5/2015 17:21	0.65
Lower Flurometer	3/5/2015 17:22	0.68
Lower Flurometer	3/5/2015 17:23	0.65
Lower Flurometer	3/5/2015 17:24	0.66
Lower Flurometer	3/5/2015 17:25	0.65
Lower Flurometer	3/5/2015 17:26	0.64
Lower Flurometer	3/5/2015 17:27	0.66
Lower Flurometer	3/5/2015 17:28	0.62
Lower Flurometer	3/5/2015 17:29	0.64
Lower Flurometer	3/5/2015 17:30	0.62
Lower Flurometer	3/5/2015 17:31	0.65
Lower Flurometer	3/5/2015 17:32	0.64
Lower Flurometer	3/5/2015 17:33	0.59

Location	Date and Time	Rhodmaine Concentration Adjusted Concentration (ppb)
Lower Flurometer	3/5/2015 17:34	0.62
Lower Flurometer	3/5/2015 17:35	0.63
Lower Flurometer	3/5/2015 17:36	0.63
Lower Flurometer	3/5/2015 17:37	0.59
Lower Flurometer	3/5/2015 17:38	0.59
Lower Flurometer	3/5/2015 17:39	0.64
Lower Flurometer	3/5/2015 17:40	0.58
Lower Flurometer	3/5/2015 17:41	0.61
Lower Flurometer	3/5/2015 17:42	0.64
Lower Flurometer	3/5/2015 17:43	0.58
Lower Flurometer	3/5/2015 17:44	0.57
Lower Flurometer	3/5/2015 17:45	0.64
Lower Flurometer	3/5/2015 17:46	0.61
Lower Flurometer	3/5/2015 17:47	0.62
Lower Flurometer	3/5/2015 17:48	0.59
Lower Flurometer	3/5/2015 17:49	0.6
Lower Flurometer	3/5/2015 17:50	0.59
Lower Flurometer	3/5/2015 17:51	0.58
Lower Flurometer	3/5/2015 17:52	0.57
Lower Flurometer	3/5/2015 17:53	0.56
Lower Flurometer	3/5/2015 17:54	0.57
Lower Flurometer	3/5/2015 17:55	0.58
Lower Flurometer	3/5/2015 17:56	0.56
Lower Flurometer	3/5/2015 17:57	0.53
Lower Flurometer	3/5/2015 17:58	0.54
Lower Flurometer	3/5/2015 17:59	0.58
Lower Flurometer	3/5/2015 18:00	0.56
Lower Flurometer	3/5/2015 18:01	0.56
Lower Flurometer	3/5/2015 18:02	0.54
Lower Flurometer	3/5/2015 18:03	0.57
Lower Flurometer	3/5/2015 18:04	0.54
Lower Flurometer	3/5/2015 18:05	0.57
Lower Flurometer	3/5/2015 18:06	0.57
Lower Flurometer	3/5/2015 18:07	0.56
Lower Flurometer	3/5/2015 18:08	0.54
Lower Flurometer	3/5/2015 18:09	0.57
Lower Flurometer	3/5/2015 18:10	0.53
Lower Flurometer	3/5/2015 18:11	0.52
Lower Flurometer	3/5/2015 18:12	0.54
Lower Flurometer	3/5/2015 18:13	0.51
Lower Flurometer	3/5/2015 18:14	0.51
Lower Flurometer	3/5/2015 18:15	0.5
Lower Flurometer	3/5/2015 18:16	0.55
Lower Flurometer	3/5/2015 18:17	0.56
Lower Flurometer	3/5/2015 18:18	0.53
Lower Flurometer	3/5/2015 18:19	0.54

Location	Date and Time	Rhodmaine Concentration Adjusted Concentration (ppb)
Lower Flurometer	3/5/2015 18:20	0.52
Lower Flurometer	3/5/2015 18:21	0.49
Lower Flurometer	3/5/2015 18:22	0.55
Lower Flurometer	3/5/2015 18:23	0.52
Lower Flurometer	3/5/2015 18:24	0.54
Lower Flurometer	3/5/2015 18:25	0.49
Lower Flurometer	3/5/2015 18:26	0.49
Lower Flurometer	3/5/2015 18:27	0.49
Lower Flurometer	3/5/2015 18:28	0.45
Lower Flurometer	3/5/2015 18:29	0.58
Lower Flurometer	3/5/2015 18:30	0.5
Lower Flurometer	3/5/2015 18:31	0.49
Lower Flurometer	3/5/2015 18:32	0.48
Lower Flurometer	3/5/2015 18:33	0.52
Lower Flurometer	3/5/2015 18:34	0.51
Lower Flurometer	3/5/2015 18:35	0.53
Lower Flurometer	3/5/2015 18:36	0.47
Lower Flurometer	3/5/2015 18:37	0.5
Lower Flurometer	3/5/2015 18:38	0.5
Lower Flurometer	3/5/2015 18:39	0.5
Lower Flurometer	3/5/2015 18:40	0.46
Lower Flurometer	3/5/2015 18:41	0.45
Lower Flurometer	3/5/2015 18:42	0.48
Lower Flurometer	3/5/2015 18:43	0.55
Lower Flurometer	3/5/2015 18:44	0.44
Lower Flurometer	3/5/2015 18:45	0.44
Lower Flurometer	3/5/2015 18:46	0.48
Lower Flurometer	3/5/2015 18:47	0.44
Lower Flurometer	3/5/2015 18:48	0.45
Lower Flurometer	3/5/2015 18:49	0.46
Lower Flurometer	3/5/2015 18:50	0.43
Lower Flurometer	3/5/2015 18:51	0.44
Lower Flurometer	3/5/2015 18:52	0.42
Lower Flurometer	3/5/2015 18:53	0.47
Lower Flurometer	3/5/2015 18:54	0.45
Lower Flurometer	3/5/2015 18:55	0.44
Lower Flurometer	3/5/2015 18:56	0.43
Lower Flurometer	3/5/2015 18:57	0.43
Lower Flurometer	3/5/2015 18:58	0.44
Lower Flurometer	3/5/2015 18:59	0.42
Lower Flurometer	3/5/2015 19:00	0.44
Lower Flurometer	3/5/2015 19:01	0.45
Lower Flurometer	3/5/2015 19:02	0.45
Lower Flurometer	3/5/2015 19:03	0.45
Lower Flurometer	3/5/2015 19:04	0.4
Lower Flurometer	3/5/2015 19:05	0.44

Location	Date and Time	Rhodmaine Concentration Adjusted Concentration (ppb)
Lower Flurometer	3/5/2015 19:06	0.44
Lower Flurometer	3/5/2015 19:07	0.46
Lower Flurometer	3/5/2015 19:08	0.4
Lower Flurometer	3/5/2015 19:09	0.46
Lower Flurometer	3/5/2015 19:10	0.44
Lower Flurometer	3/5/2015 19:11	0.43
Lower Flurometer	3/5/2015 19:12	0.39
Lower Flurometer	3/5/2015 19:13	0.44
Lower Flurometer	3/5/2015 19:14	0.4
Lower Flurometer	3/5/2015 19:15	0.45
Lower Flurometer	3/5/2015 19:16	0.39
Lower Flurometer	3/5/2015 19:17	0.41
Lower Flurometer	3/5/2015 19:18	0.39
Lower Flurometer	3/5/2015 19:19	0.38
Lower Flurometer	3/5/2015 19:20	0.4
Lower Flurometer	3/5/2015 19:21	0.37
Lower Flurometer	3/5/2015 19:22	0.42
Lower Flurometer	3/5/2015 19:23	0.39
Lower Flurometer	3/5/2015 19:24	0.44
Lower Flurometer	3/5/2015 19:25	0.38
Lower Flurometer	3/5/2015 19:26	0.49
Lower Flurometer	3/5/2015 19:27	0.42
Lower Flurometer	3/5/2015 19:28	0.38
Lower Flurometer	3/5/2015 19:29	0.41
Lower Flurometer	3/5/2015 19:30	0.37
Lower Flurometer	3/5/2015 19:31	0.37
Lower Flurometer	3/5/2015 19:32	0.42
Lower Flurometer	3/5/2015 19:33	0.37
Lower Flurometer	3/5/2015 19:34	0.36
Lower Flurometer	3/5/2015 19:35	0.36
Lower Flurometer	3/5/2015 19:36	0.4
Lower Flurometer	3/5/2015 19:37	0.36
Lower Flurometer	3/5/2015 19:38	0.36
Lower Flurometer	3/5/2015 19:39	0.4
Lower Flurometer	3/5/2015 19:40	0.37
Lower Flurometer	3/5/2015 19:41	0.36
Lower Flurometer	3/5/2015 19:42	0.38
Lower Flurometer	3/5/2015 19:43	0.36
Lower Flurometer	3/5/2015 19:44	0.37
Lower Flurometer	3/5/2015 19:45	0.39
Lower Flurometer	3/5/2015 19:46	0.37
Lower Flurometer	3/5/2015 19:47	0.38
Lower Flurometer	3/5/2015 19:48	0.37
Lower Flurometer	3/5/2015 19:49	0.41
Lower Flurometer	3/5/2015 19:50	0.39
Lower Flurometer	3/5/2015 19:51	0.38

Location	Date and Time	Rhodmaine Concentration Adjusted Concentration (ppb)
Lower Flurometer	3/5/2015 19:52	0.37
Lower Flurometer	3/5/2015 19:53	0.33
Lower Flurometer	3/5/2015 19:54	0.37
Lower Flurometer	3/5/2015 19:55	0.36
Lower Flurometer	3/5/2015 19:56	0.32
Lower Flurometer	3/5/2015 19:57	0.3
Lower Flurometer	3/5/2015 19:58	0.33
Lower Flurometer	3/5/2015 19:59	0.37
Lower Flurometer	3/5/2015 20:00	0.35
Lower Flurometer	3/5/2015 20:01	0.35
Lower Flurometer	3/5/2015 20:02	0.36
Lower Flurometer	3/5/2015 20:03	0.31
Lower Flurometer	3/5/2015 20:04	0.35
Lower Flurometer	3/5/2015 20:05	0.35
Lower Flurometer	3/5/2015 20:06	0.33
Lower Flurometer	3/5/2015 20:07	0.33
Lower Flurometer	3/5/2015 20:08	0.35
Lower Flurometer	3/5/2015 20:09	0.29
Lower Flurometer	3/5/2015 20:10	0.36
Lower Flurometer	3/5/2015 20:11	0.3
Lower Flurometer	3/5/2015 20:12	0.33
Lower Flurometer	3/5/2015 20:13	0.31
Lower Flurometer	3/5/2015 20:14	0.31
Lower Flurometer	3/5/2015 20:15	0.3
Lower Flurometer	3/5/2015 20:16	0.33
Lower Flurometer	3/5/2015 20:17	0.31
Lower Flurometer	3/5/2015 20:18	0.29
Lower Flurometer	3/5/2015 20:19	0.32
Lower Flurometer	3/5/2015 20:20	0.32
Lower Flurometer	3/5/2015 20:21	0.29
Lower Flurometer	3/5/2015 20:22	0.29
Lower Flurometer	3/5/2015 20:23	0.28
Lower Flurometer	3/5/2015 20:24	0.3
Lower Flurometer	3/5/2015 20:25	0.3
Lower Flurometer	3/5/2015 20:26	0.3
Lower Flurometer	3/5/2015 20:27	0.28
Lower Flurometer	3/5/2015 20:28	0.32
Lower Flurometer	3/5/2015 20:29	0.28
Lower Flurometer	3/5/2015 20:30	0.27
Lower Flurometer	3/5/2015 20:31	0.27
Lower Flurometer	3/5/2015 20:32	0.29
Lower Flurometer	3/5/2015 20:33	0.27
Lower Flurometer	3/5/2015 20:34	0.29
Lower Flurometer	3/5/2015 20:35	0.27
Lower Flurometer	3/5/2015 20:36	0.26
Lower Flurometer	3/5/2015 20:37	0.31

Location	Date and Time	Rhodmaine Concentration Adjusted Concentration (ppb)
Lower Flurometer	3/5/2015 20:38	0.33
Lower Flurometer	3/5/2015 20:39	0.31
Lower Flurometer	3/5/2015 20:40	0.32
Lower Flurometer	3/5/2015 20:41	0.29
Lower Flurometer	3/5/2015 20:42	0.25
Lower Flurometer	3/5/2015 20:43	0.3
Lower Flurometer	3/5/2015 20:44	0.26
Lower Flurometer	3/5/2015 20:45	0.26
Lower Flurometer	3/5/2015 20:46	0.26
Lower Flurometer	3/5/2015 20:47	0.29
Lower Flurometer	3/5/2015 20:48	0.28
Lower Flurometer	3/5/2015 20:49	0.25
Lower Flurometer	3/5/2015 20:50	0.26
Lower Flurometer	3/5/2015 20:51	0.25
Lower Flurometer	3/5/2015 20:52	0.26
Lower Flurometer	3/5/2015 20:53	0.29
Lower Flurometer	3/5/2015 20:54	0.29
Lower Flurometer	3/5/2015 20:55	0.28
Lower Flurometer	3/5/2015 20:56	0.27
Lower Flurometer	3/5/2015 20:57	0.23
Lower Flurometer	3/5/2015 20:58	0.29
Lower Flurometer	3/5/2015 20:59	0.28
Lower Flurometer	3/5/2015 21:00	0.25
Lower Flurometer	3/5/2015 21:01	0.25
Lower Flurometer	3/5/2015 21:02	0.22
Lower Flurometer	3/5/2015 21:03	0.27
Lower Flurometer	3/5/2015 21:04	0.28
Lower Flurometer	3/5/2015 21:05	0.27
Lower Flurometer	3/5/2015 21:06	0.21
Lower Flurometer	3/5/2015 21:07	0.26
Lower Flurometer	3/5/2015 21:08	0.27
Lower Flurometer	3/5/2015 21:09	0.23
Lower Flurometer	3/5/2015 21:10	0.27
Lower Flurometer	3/5/2015 21:11	0.23
Lower Flurometer	3/5/2015 21:12	0.23
Lower Flurometer	3/5/2015 21:13	0.24
Lower Flurometer	3/5/2015 21:14	0.22
Lower Flurometer	3/5/2015 21:15	0.21
Lower Flurometer	3/5/2015 21:16	0.22
Lower Flurometer	3/5/2015 21:17	0.25
Lower Flurometer	3/5/2015 21:18	0.25
Lower Flurometer	3/5/2015 21:19	0.25
Lower Flurometer	3/5/2015 21:20	0.22
Lower Flurometer	3/5/2015 21:21	0.22
Lower Flurometer	3/5/2015 21:22	0.2
Lower Flurometer	3/5/2015 21:23	0.19

Location	Date and Time	Rhodmaine Concentration Adjusted Concentration (ppb)
Lower Flurometer	3/5/2015 21:24	0.25
Lower Flurometer	3/5/2015 21:25	0.24
Lower Flurometer	3/5/2015 21:26	0.19
Lower Flurometer	3/5/2015 21:27	0.24
Lower Flurometer	3/5/2015 21:28	0.19
Lower Flurometer	3/5/2015 21:29	0.2
Lower Flurometer	3/5/2015 21:30	0.38
Lower Flurometer	3/5/2015 21:31	0.2
Lower Flurometer	3/5/2015 21:32	0.25
Lower Flurometer	3/5/2015 21:33	0.22
Lower Flurometer	3/5/2015 21:34	0.27
Lower Flurometer	3/5/2015 21:35	0.22
Lower Flurometer	3/5/2015 21:36	0.24
Lower Flurometer	3/5/2015 21:37	0.24
Lower Flurometer	3/5/2015 21:38	0.24
Lower Flurometer	3/5/2015 21:39	0.24
Lower Flurometer	3/5/2015 21:40	0.24
Lower Flurometer	3/5/2015 21:41	0.21
Lower Flurometer	3/5/2015 21:42	0.21
Lower Flurometer	3/5/2015 21:43	0.2
Lower Flurometer	3/5/2015 21:44	0.2
Lower Flurometer	3/5/2015 21:45	0.19
Lower Flurometer	3/5/2015 21:46	0.21
Lower Flurometer	3/5/2015 21:47	0.2
Lower Flurometer	3/5/2015 21:48	0.22
Lower Flurometer	3/5/2015 21:49	0.23
Lower Flurometer	3/5/2015 21:50	0.21
Lower Flurometer	3/5/2015 21:51	0.19
Lower Flurometer	3/5/2015 21:52	0.22
Lower Flurometer	3/5/2015 21:53	0.17
Lower Flurometer	3/5/2015 21:54	0.17
Lower Flurometer	3/5/2015 21:55	0.2
Lower Flurometer	3/5/2015 21:56	0.17
Lower Flurometer	3/5/2015 21:57	0.17
Lower Flurometer	3/5/2015 21:58	0.17
Lower Flurometer	3/5/2015 21:59	0.22
Lower Flurometer	3/5/2015 22:00	0.17
Lower Flurometer	3/5/2015 22:01	0.19
Lower Flurometer	3/5/2015 22:02	0.16
Lower Flurometer	3/5/2015 22:03	0.18
Lower Flurometer	3/5/2015 22:04	0.22
Lower Flurometer	3/5/2015 22:05	0.22
Lower Flurometer	3/5/2015 22:06	0.16
Lower Flurometer	3/5/2015 22:07	0.21
Lower Flurometer	3/5/2015 22:08	0.19
Lower Flurometer	3/5/2015 22:09	0.19

Location	Date and Time	Rhodmaine Concentration Adjusted Concentration (ppb)
Lower Flurometer	3/5/2015 22:10	0.16
Lower Flurometer	3/5/2015 22:11	0.19
Lower Flurometer	3/5/2015 22:12	0.19
Lower Flurometer	3/5/2015 22:13	0.18
Lower Flurometer	3/5/2015 22:14	0.18
Lower Flurometer	3/5/2015 22:15	0.17
Lower Flurometer	3/5/2015 22:16	0.17
Lower Flurometer	3/5/2015 22:17	0.21
Lower Flurometer	3/5/2015 22:18	0.19
Lower Flurometer	3/5/2015 22:19	0.19
Lower Flurometer	3/5/2015 22:20	0.18
Lower Flurometer	3/5/2015 22:21	0.19
Lower Flurometer	3/5/2015 22:22	0.15
Lower Flurometer	3/5/2015 22:23	0.15
Lower Flurometer	3/5/2015 22:24	0.18
Lower Flurometer	3/5/2015 22:25	0.15
Lower Flurometer	3/5/2015 22:26	0.14
Lower Flurometer	3/5/2015 22:27	0.13
Lower Flurometer	3/5/2015 22:28	0.19
Lower Flurometer	3/5/2015 22:29	0.17
Lower Flurometer	3/5/2015 22:30	0.15
Lower Flurometer	3/5/2015 22:31	0.14
Lower Flurometer	3/5/2015 22:32	0.13
Lower Flurometer	3/5/2015 22:33	0.15
Lower Flurometer	3/5/2015 22:34	0.17
Lower Flurometer	3/5/2015 22:35	0.15
Lower Flurometer	3/5/2015 22:36	0.22
Lower Flurometer	3/5/2015 22:37	0.12
Lower Flurometer	3/5/2015 22:38	0.17
Lower Flurometer	3/5/2015 22:39	0.13
Lower Flurometer	3/5/2015 22:40	0.17
Lower Flurometer	3/5/2015 22:41	0.13
Lower Flurometer	3/5/2015 22:42	0.13
Lower Flurometer	3/5/2015 22:43	0.14
Lower Flurometer	3/5/2015 22:44	0.15
Lower Flurometer	3/5/2015 22:45	0.12
Lower Flurometer	3/5/2015 22:46	0.13
Lower Flurometer	3/5/2015 22:47	0.17
Lower Flurometer	3/5/2015 22:48	0.14
Lower Flurometer	3/5/2015 22:49	0.11
Lower Flurometer	3/5/2015 22:50	0.17
Lower Flurometer	3/5/2015 22:51	0.13
Lower Flurometer	3/5/2015 22:52	0.13
Lower Flurometer	3/5/2015 22:53	0.11
Lower Flurometer	3/5/2015 22:54	0.13
Lower Flurometer	3/5/2015 22:55	0.12

Location	Date and Time	Rhodmaine Concentration Adjusted Concentration (ppb)
Lower Flurometer	3/5/2015 22:56	0.16
Lower Flurometer	3/5/2015 22:57	0.13
Lower Flurometer	3/5/2015 22:58	0.16
Lower Flurometer	3/5/2015 22:59	0.11
Lower Flurometer	3/5/2015 23:00	0.17
Lower Flurometer	3/5/2015 23:01	0.13
Lower Flurometer	3/5/2015 23:02	0.12
Lower Flurometer	3/5/2015 23:03	0.13
Lower Flurometer	3/5/2015 23:04	0.11
Lower Flurometer	3/5/2015 23:05	0.15
Lower Flurometer	3/5/2015 23:06	0.12
Lower Flurometer	3/5/2015 23:07	0.15
Lower Flurometer	3/5/2015 23:08	0.12
Lower Flurometer	3/5/2015 23:09	0.18
Lower Flurometer	3/5/2015 23:10	0.12
Lower Flurometer	3/5/2015 23:11	0.14
Lower Flurometer	3/5/2015 23:12	0.12
Lower Flurometer	3/5/2015 23:13	0.14
Lower Flurometer	3/5/2015 23:14	0.1
Lower Flurometer	3/5/2015 23:15	0.16
Lower Flurometer	3/5/2015 23:16	0.11
Lower Flurometer	3/5/2015 23:17	0.1
Lower Flurometer	3/5/2015 23:18	0.12
Lower Flurometer	3/5/2015 23:19	0.11
Lower Flurometer	3/5/2015 23:20	0.09
Lower Flurometer	3/5/2015 23:21	0.14
Lower Flurometer	3/5/2015 23:22	0.13
Lower Flurometer	3/5/2015 23:23	0.13
Lower Flurometer	3/5/2015 23:24	0.12
Lower Flurometer	3/5/2015 23:25	0.11
Lower Flurometer	3/5/2015 23:26	0.09
Lower Flurometer	3/5/2015 23:27	0.1
Lower Flurometer	3/5/2015 23:28	0.09
Lower Flurometer	3/5/2015 23:29	0.13
Lower Flurometer	3/5/2015 23:30	0.14
Lower Flurometer	3/5/2015 23:31	0.08
Lower Flurometer	3/5/2015 23:32	0.09
Lower Flurometer	3/5/2015 23:33	0.13
Lower Flurometer	3/5/2015 23:34	0.11
Lower Flurometer	3/5/2015 23:35	0.12
Lower Flurometer	3/5/2015 23:36	0.14
Lower Flurometer	3/5/2015 23:37	0.09
Lower Flurometer	3/5/2015 23:38	0.12
Lower Flurometer	3/5/2015 23:39	0.1
Lower Flurometer	3/5/2015 23:40	0.11
Lower Flurometer	3/5/2015 23:41	0.09

Location	Date and Time	Rhodmaine Concentration Adjusted Concentration (ppb)
Lower Flurometer	3/5/2015 23:42	0.11
Lower Flurometer	3/5/2015 23:43	0.09
Lower Flurometer	3/5/2015 23:44	0.09
Lower Flurometer	3/5/2015 23:45	0.13
Lower Flurometer	3/5/2015 23:46	0.1
Lower Flurometer	3/5/2015 23:47	0.12
Lower Flurometer	3/5/2015 23:48	0.12
Lower Flurometer	3/5/2015 23:49	0.12
Lower Flurometer	3/5/2015 23:50	0.1
Lower Flurometer	3/5/2015 23:51	0.12
Lower Flurometer	3/5/2015 23:52	0.09
Lower Flurometer	3/5/2015 23:53	0.07
Lower Flurometer	3/5/2015 23:54	0.09
Lower Flurometer	3/5/2015 23:55	0.07
Lower Flurometer	3/5/2015 23:56	0.08
Lower Flurometer	3/5/2015 23:57	0.12
Lower Flurometer	3/5/2015 23:58	0.07
Lower Flurometer	3/5/2015 23:59	0.11
Lower Flurometer	3/6/2015 0:00	0.1
Lower Flurometer	3/6/2015 0:01	0.12
Lower Flurometer	3/6/2015 0:02	0.08
Lower Flurometer	3/6/2015 0:03	0.1
Lower Flurometer	3/6/2015 0:04	0.09
Lower Flurometer	3/6/2015 0:05	0.09
Lower Flurometer	3/6/2015 0:06	0.1
Lower Flurometer	3/6/2015 0:07	0.07
Lower Flurometer	3/6/2015 0:08	0.09
Lower Flurometer	3/6/2015 0:09	0.11
Lower Flurometer	3/6/2015 0:10	0.08
Lower Flurometer	3/6/2015 0:11	0.07
Lower Flurometer	3/6/2015 0:12	0.08
Lower Flurometer	3/6/2015 0:13	0.1
Lower Flurometer	3/6/2015 0:14	0.11
Lower Flurometer	3/6/2015 0:15	0.06
Lower Flurometer	3/6/2015 0:16	0.15
Lower Flurometer	3/6/2015 0:17	0.06
Lower Flurometer	3/6/2015 0:18	0.12
Lower Flurometer	3/6/2015 0:19	0.06
Lower Flurometer	3/6/2015 0:20	0.06
Lower Flurometer	3/6/2015 0:21	0.07
Lower Flurometer	3/6/2015 0:22	0.08
Lower Flurometer	3/6/2015 0:23	0.1
Lower Flurometer	3/6/2015 0:24	0.1
Lower Flurometer	3/6/2015 0:25	0.09
Lower Flurometer	3/6/2015 0:26	0.07
Lower Flurometer	3/6/2015 0:27	0.08

Location	Date and Time	Rhodmaine Concentration Adjusted Concentration (ppb)
Lower Flurometer	3/6/2015 0:28	0.05
Lower Flurometer	3/6/2015 0:29	0.07
Lower Flurometer	3/6/2015 0:30	0.1
Lower Flurometer	3/6/2015 0:31	0.09
Lower Flurometer	3/6/2015 0:32	0.06
Lower Flurometer	3/6/2015 0:33	0.09
Lower Flurometer	3/6/2015 0:34	0.04
Lower Flurometer	3/6/2015 0:35	0.05
Lower Flurometer	3/6/2015 0:36	0.04
Lower Flurometer	3/6/2015 0:37	0.08
Lower Flurometer	3/6/2015 0:38	0.07
Lower Flurometer	3/6/2015 0:39	0.06
Lower Flurometer	3/6/2015 0:40	0.08
Lower Flurometer	3/6/2015 0:41	0.04
Lower Flurometer	3/6/2015 0:42	0.09
Lower Flurometer	3/6/2015 0:43	0.09
Lower Flurometer	3/6/2015 0:44	0.08
Lower Flurometer	3/6/2015 0:45	0.04
Lower Flurometer	3/6/2015 0:46	0.05
Lower Flurometer	3/6/2015 0:47	0.04
Lower Flurometer	3/6/2015 0:48	0.06
Lower Flurometer	3/6/2015 0:49	0.09
Lower Flurometer	3/6/2015 0:50	0.07
Lower Flurometer	3/6/2015 0:51	0.04
Lower Flurometer	3/6/2015 0:52	0.11
Lower Flurometer	3/6/2015 0:53	0.04
Lower Flurometer	3/6/2015 0:54	0.05
Lower Flurometer	3/6/2015 0:55	0.05
Lower Flurometer	3/6/2015 0:56	0.03
Lower Flurometer	3/6/2015 0:57	0.09
Lower Flurometer	3/6/2015 0:58	0.05
Lower Flurometer	3/6/2015 0:59	0.06
Lower Flurometer	3/6/2015 1:00	0.03
Lower Flurometer	3/6/2015 1:01	0.07
Lower Flurometer	3/6/2015 1:02	0.07
Lower Flurometer	3/6/2015 1:03	0.06
Lower Flurometer	3/6/2015 1:04	0.07
Lower Flurometer	3/6/2015 1:05	0.04
Lower Flurometer	3/6/2015 1:06	0.07
Lower Flurometer	3/6/2015 1:07	0.03
Lower Flurometer	3/6/2015 1:08	0.05
Lower Flurometer	3/6/2015 1:09	0.09
Lower Flurometer	3/6/2015 1:10	0.04
Lower Flurometer	3/6/2015 1:11	0.07
Lower Flurometer	3/6/2015 1:12	0.08
Lower Flurometer	3/6/2015 1:13	0.03

Location	Date and Time	Rhodmaine Concentration Adjusted Concentration (ppb)
Lower Flurometer	3/6/2015 1:14	0.05
Lower Flurometer	3/6/2015 1:15	0.04
Lower Flurometer	3/6/2015 1:16	0.02
Lower Flurometer	3/6/2015 1:17	0.05
Lower Flurometer	3/6/2015 1:18	0.06
Lower Flurometer	3/6/2015 1:19	0.05
Lower Flurometer	3/6/2015 1:20	0.04
Lower Flurometer	3/6/2015 1:21	0.06
Lower Flurometer	3/6/2015 1:22	0.03
Lower Flurometer	3/6/2015 1:23	0.06
Lower Flurometer	3/6/2015 1:24	0.06
Lower Flurometer	3/6/2015 1:25	0.06
Lower Flurometer	3/6/2015 1:26	0.05
Lower Flurometer	3/6/2015 1:27	0.06
Lower Flurometer	3/6/2015 1:28	0.07
Lower Flurometer	3/6/2015 1:29	0.08
Lower Flurometer	3/6/2015 1:30	0.15
Lower Flurometer	3/6/2015 1:31	0.04
Lower Flurometer	3/6/2015 1:32	0.03
Lower Flurometer	3/6/2015 1:33	0.02
Lower Flurometer	3/6/2015 1:34	0.03
Lower Flurometer	3/6/2015 1:35	0.02
Lower Flurometer	3/6/2015 1:36	0.03
Lower Flurometer	3/6/2015 1:37	0.05
Lower Flurometer	3/6/2015 1:38	0.03
Lower Flurometer	3/6/2015 1:39	0.07
Lower Flurometer	3/6/2015 1:40	0.02
Lower Flurometer	3/6/2015 1:41	0.07
Lower Flurometer	3/6/2015 1:42	0.05
Lower Flurometer	3/6/2015 1:43	0.04
Lower Flurometer	3/6/2015 1:44	0.07
Lower Flurometer	3/6/2015 1:45	0.04
Lower Flurometer	3/6/2015 1:46	0.01
Lower Flurometer	3/6/2015 1:47	0.06
Lower Flurometer	3/6/2015 1:48	0
Lower Flurometer	3/6/2015 1:49	0.01
Lower Flurometer	3/6/2015 1:50	0.06
Lower Flurometer	3/6/2015 1:51	0.05
Lower Flurometer	3/6/2015 1:52	0.04
Lower Flurometer	3/6/2015 1:53	0.04
Lower Flurometer	3/6/2015 1:54	0.04
Lower Flurometer	3/6/2015 1:55	0.04
Lower Flurometer	3/6/2015 1:56	0.03
Lower Flurometer	3/6/2015 1:57	0.03
Lower Flurometer	3/6/2015 1:58	0.03
Lower Flurometer	3/6/2015 1:59	0

Location	Date and Time	Rhodmaine Concentration Adjusted Concentration (ppb)
Lower Flurometer	3/6/2015 2:00	0.02
Lower Flurometer	3/6/2015 2:01	0.04
Lower Flurometer	3/6/2015 2:02	0.03
Lower Flurometer	3/6/2015 2:03	0.03
Lower Flurometer	3/6/2015 2:04	0.05
Lower Flurometer	3/6/2015 2:05	0.02
Lower Flurometer	3/6/2015 2:06	0.03
Lower Flurometer	3/6/2015 2:07	0.01
Lower Flurometer	3/6/2015 2:08	0.05
Lower Flurometer	3/6/2015 2:09	0.04
Lower Flurometer	3/6/2015 2:10	0
Lower Flurometer	3/6/2015 2:11	0.04
Lower Flurometer	3/6/2015 2:12	0
Lower Flurometer	3/6/2015 2:13	0.01
Lower Flurometer	3/6/2015 2:14	0.01
Lower Flurometer	3/6/2015 2:15	0.04
Lower Flurometer	3/6/2015 2:16	0.04
Lower Flurometer	3/6/2015 2:17	0.02
Lower Flurometer	3/6/2015 2:18	0
Lower Flurometer	3/6/2015 2:19	0.04
Lower Flurometer	3/6/2015 2:20	0.09
Lower Flurometer	3/6/2015 2:21	0
Lower Flurometer	3/6/2015 2:22	0.05
Lower Flurometer	3/6/2015 2:23	0.03
Lower Flurometer	3/6/2015 2:24	0.04
Lower Flurometer	3/6/2015 2:25	0
Lower Flurometer	3/6/2015 2:26	0.02
Lower Flurometer	3/6/2015 2:27	0
Lower Flurometer	3/6/2015 2:28	0.01
Lower Flurometer	3/6/2015 2:29	0.01
Lower Flurometer	3/6/2015 2:30	0.01
Lower Flurometer	3/6/2015 2:31	0
Lower Flurometer	3/6/2015 2:32	0.05
Lower Flurometer	3/6/2015 2:33	0.19
Lower Flurometer	3/6/2015 2:34	0.04
Lower Flurometer	3/6/2015 2:35	0.03
Lower Flurometer	3/6/2015 2:36	0.04
Lower Flurometer	3/6/2015 2:37	0.04
Lower Flurometer	3/6/2015 2:38	0.03
Lower Flurometer	3/6/2015 2:39	0.04
Lower Flurometer	3/6/2015 2:40	0.04
Lower Flurometer	3/6/2015 2:41	0
Lower Flurometer	3/6/2015 2:42	0.04
Lower Flurometer	3/6/2015 2:43	0.01
Lower Flurometer	3/6/2015 2:44	0
Lower Flurometer	3/6/2015 2:45	0

Location	Date and Time	Rhodmaine Concentration Adjusted Concentration (ppb)
Lower Flurometer	3/6/2015 2:46	0.03
Lower Flurometer	3/6/2015 2:47	0.05
Lower Flurometer	3/6/2015 2:48	0
Lower Flurometer	3/6/2015 2:49	0
Lower Flurometer	3/6/2015 2:50	0.07
Lower Flurometer	3/6/2015 2:51	0.04
Lower Flurometer	3/6/2015 2:52	0
Lower Flurometer	3/6/2015 2:53	0.03
Lower Flurometer	3/6/2015 2:54	0
Lower Flurometer	3/6/2015 2:55	0.03
Lower Flurometer	3/6/2015 2:56	0
Lower Flurometer	3/6/2015 2:57	0.04
Lower Flurometer	3/6/2015 2:58	0
Lower Flurometer	3/6/2015 2:59	0.01
Lower Flurometer	3/6/2015 3:00	0.02
Lower Flurometer	3/6/2015 3:01	0.05
Lower Flurometer	3/6/2015 3:02	0
Lower Flurometer	3/6/2015 3:03	0.01
Lower Flurometer	3/6/2015 3:04	0
Lower Flurometer	3/6/2015 3:05	0
Lower Flurometer	3/6/2015 3:06	0
Lower Flurometer	3/6/2015 3:07	0.01
Lower Flurometer	3/6/2015 3:08	0.06
Lower Flurometer	3/6/2015 3:09	0.02
Lower Flurometer	3/6/2015 3:10	0.02
Lower Flurometer	3/6/2015 3:11	0
Lower Flurometer	3/6/2015 3:12	0.03
Lower Flurometer	3/6/2015 3:13	0.02
Lower Flurometer	3/6/2015 3:14	0.05
Lower Flurometer	3/6/2015 3:15	0.03
Lower Flurometer	3/6/2015 3:16	0
Lower Flurometer	3/6/2015 3:17	0
Lower Flurometer	3/6/2015 3:18	0.01
Lower Flurometer	3/6/2015 3:19	0
Lower Flurometer	3/6/2015 3:20	0
Lower Flurometer	3/6/2015 3:21	0
Lower Flurometer	3/6/2015 3:22	0
Lower Flurometer	3/6/2015 3:23	0.01
Lower Flurometer	3/6/2015 3:24	0.03
Lower Flurometer	3/6/2015 3:25	0
Lower Flurometer	3/6/2015 3:26	0
Lower Flurometer	3/6/2015 3:27	0
Lower Flurometer	3/6/2015 3:28	0.01
Lower Flurometer	3/6/2015 3:29	0
Lower Flurometer	3/6/2015 3:30	0
Lower Flurometer	3/6/2015 3:31	0.02

Location	Date and Time	Rhodmaine Concentration Adjusted Concentration (ppb)
Lower Flurometer	3/6/2015 3:32	0
Lower Flurometer	3/6/2015 3:33	0
Lower Flurometer	3/6/2015 3:34	0.01
Lower Flurometer	3/6/2015 3:35	0.01
Lower Flurometer	3/6/2015 3:36	0
Lower Flurometer	3/6/2015 3:37	0.04
Lower Flurometer	3/6/2015 3:38	0.02
Lower Flurometer	3/6/2015 3:39	0
Lower Flurometer	3/6/2015 3:40	0
Lower Flurometer	3/6/2015 3:41	0
Lower Flurometer	3/6/2015 3:42	0
Lower Flurometer	3/6/2015 3:43	0.02
Lower Flurometer	3/6/2015 3:44	0.01
Lower Flurometer	3/6/2015 3:45	0.36
Lower Flurometer	3/6/2015 3:46	0.03
Lower Flurometer	3/6/2015 3:47	0.01
Lower Flurometer	3/6/2015 3:48	0.01
Lower Flurometer	3/6/2015 3:49	0
Lower Flurometer	3/6/2015 3:50	0
Lower Flurometer	3/6/2015 3:51	0
Lower Flurometer	3/6/2015 3:52	0
Lower Flurometer	3/6/2015 3:53	0.01
Lower Flurometer	3/6/2015 3:54	0
Lower Flurometer	3/6/2015 3:55	0
Lower Flurometer	3/6/2015 3:56	0.03
Lower Flurometer	3/6/2015 3:57	0
Lower Flurometer	3/6/2015 3:58	0
Lower Flurometer	3/6/2015 3:59	0
Lower Flurometer	3/6/2015 4:00	0
Lower Flurometer	3/6/2015 4:01	0
Lower Flurometer	3/6/2015 4:02	0.01
Lower Flurometer	3/6/2015 4:03	0.01
Lower Flurometer	3/6/2015 4:04	0.03
Lower Flurometer	3/6/2015 4:05	0
Lower Flurometer	3/6/2015 4:06	0
Lower Flurometer	3/6/2015 4:07	0
Lower Flurometer	3/6/2015 4:08	0
Lower Flurometer	3/6/2015 4:09	0.02
Lower Flurometer	3/6/2015 4:10	0
Lower Flurometer	3/6/2015 4:11	0.01
Lower Flurometer	3/6/2015 4:12	0
Lower Flurometer	3/6/2015 4:13	0.02
Lower Flurometer	3/6/2015 4:14	0.01
Lower Flurometer	3/6/2015 4:15	0
Lower Flurometer	3/6/2015 4:16	0
Lower Flurometer	3/6/2015 4:17	0.01

Location	Date and Time	Rhodmaine Concentration Adjusted Concentration (ppb)
Lower Flurometer	3/6/2015 4:18	0
Lower Flurometer	3/6/2015 4:19	0
Lower Flurometer	3/6/2015 4:20	0
Lower Flurometer	3/6/2015 4:21	0
Lower Flurometer	3/6/2015 4:22	0
Lower Flurometer	3/6/2015 4:23	0
Lower Flurometer	3/6/2015 4:24	0
Lower Flurometer	3/6/2015 4:25	0
Lower Flurometer	3/6/2015 4:26	0
Lower Flurometer	3/6/2015 4:27	0
Lower Flurometer	3/6/2015 4:28	0.02
Lower Flurometer	3/6/2015 4:29	0
Lower Flurometer	3/6/2015 4:30	0
Lower Flurometer	3/6/2015 4:31	0
Lower Flurometer	3/6/2015 4:32	0
Lower Flurometer	3/6/2015 4:33	0
Lower Flurometer	3/6/2015 4:34	0.01
Lower Flurometer	3/6/2015 4:35	0
Lower Flurometer	3/6/2015 4:36	0
Lower Flurometer	3/6/2015 4:37	0
Lower Flurometer	3/6/2015 4:38	0.02
Lower Flurometer	3/6/2015 4:39	0
Lower Flurometer	3/6/2015 4:40	0
Lower Flurometer	3/6/2015 4:41	0
Lower Flurometer	3/6/2015 4:42	0
Lower Flurometer	3/6/2015 4:43	0.01
Lower Flurometer	3/6/2015 4:44	0
Lower Flurometer	3/6/2015 4:45	0
Lower Flurometer	3/6/2015 4:46	0
Lower Flurometer	3/6/2015 4:47	0
Lower Flurometer	3/6/2015 4:48	0
Lower Flurometer	3/6/2015 4:49	0
Lower Flurometer	3/6/2015 4:50	0
Lower Flurometer	3/6/2015 4:51	0
Lower Flurometer	3/6/2015 4:52	0
Lower Flurometer	3/6/2015 4:53	0
Lower Flurometer	3/6/2015 4:54	0
Lower Flurometer	3/6/2015 4:55	0
Lower Flurometer	3/6/2015 4:56	0
Lower Flurometer	3/6/2015 4:57	0
Lower Flurometer	3/6/2015 4:58	0
Lower Flurometer	3/6/2015 4:59	0
Lower Flurometer	3/6/2015 5:00	0
Lower Flurometer	3/6/2015 5:01	0
Lower Flurometer	3/6/2015 5:02	0
Lower Flurometer	3/6/2015 5:03	0

Location	Date and Time	Rhodmaine Concentration Adjusted Concentration (ppb)
Lower Flurometer	3/6/2015 5:04	0
Lower Flurometer	3/6/2015 5:05	0
Lower Flurometer	3/6/2015 5:06	0
Lower Flurometer	3/6/2015 5:07	0
Lower Flurometer	3/6/2015 5:08	0
Lower Flurometer	3/6/2015 5:09	0
Lower Flurometer	3/6/2015 5:10	0
Lower Flurometer	3/6/2015 5:11	0
Lower Flurometer	3/6/2015 5:12	0
Lower Flurometer	3/6/2015 5:13	0
Lower Flurometer	3/6/2015 5:14	0
Lower Flurometer	3/6/2015 5:15	0
Lower Flurometer	3/6/2015 5:16	0
Lower Flurometer	3/6/2015 5:17	0
Lower Flurometer	3/6/2015 5:18	0
Lower Flurometer	3/6/2015 5:19	0
Lower Flurometer	3/6/2015 5:20	0
Lower Flurometer	3/6/2015 5:21	0
Lower Flurometer	3/6/2015 5:22	0
Lower Flurometer	3/6/2015 5:23	0
Lower Flurometer	3/6/2015 5:24	0
Lower Flurometer	3/6/2015 5:25	0
Lower Flurometer	3/6/2015 5:26	0
Lower Flurometer	3/6/2015 5:27	0.12
Lower Flurometer	3/6/2015 5:28	0
Lower Flurometer	3/6/2015 5:29	0
Lower Flurometer	3/6/2015 5:30	0
Lower Flurometer	3/6/2015 5:31	0
Lower Flurometer	3/6/2015 5:32	0
Lower Flurometer	3/6/2015 5:33	0
Lower Flurometer	3/6/2015 5:34	0
Lower Flurometer	3/6/2015 5:35	0
Lower Flurometer	3/6/2015 5:36	0
Lower Flurometer	3/6/2015 5:37	0
Lower Flurometer	3/6/2015 5:38	0.01
Lower Flurometer	3/6/2015 5:39	0
Lower Flurometer	3/6/2015 5:40	0
Lower Flurometer	3/6/2015 5:41	0
Lower Flurometer	3/6/2015 5:42	0
Lower Flurometer	3/6/2015 5:43	0
Lower Flurometer	3/6/2015 5:44	0
Lower Flurometer	3/6/2015 5:45	0
Lower Flurometer	3/6/2015 5:46	0
Lower Flurometer	3/6/2015 5:47	0
Lower Flurometer	3/6/2015 5:48	0
Lower Flurometer	3/6/2015 5:49	0

Location	Date and Time	Rhodmaine Concentration Adjusted Concentration (ppb)
Lower Flurometer	3/6/2015 5:50	0
Lower Flurometer	3/6/2015 5:51	0.02
Lower Flurometer	3/6/2015 5:52	0
Lower Flurometer	3/6/2015 5:53	0
Lower Flurometer	3/6/2015 5:54	0
Lower Flurometer	3/6/2015 5:55	0
Lower Flurometer	3/6/2015 5:56	0
Lower Flurometer	3/6/2015 5:57	0
Lower Flurometer	3/6/2015 5:58	0
Lower Flurometer	3/6/2015 5:59	0
Lower Flurometer	3/6/2015 6:00	0
Lower Flurometer	3/6/2015 6:01	0
Lower Flurometer	3/6/2015 6:02	0
Lower Flurometer	3/6/2015 6:03	0
Lower Flurometer	3/6/2015 6:04	0
Lower Flurometer	3/6/2015 6:05	0
Lower Flurometer	3/6/2015 6:06	0
Lower Flurometer	3/6/2015 6:07	0
Lower Flurometer	3/6/2015 6:08	0
Lower Flurometer	3/6/2015 6:09	0
Lower Flurometer	3/6/2015 6:10	0
Lower Flurometer	3/6/2015 6:11	0
Lower Flurometer	3/6/2015 6:12	0
Lower Flurometer	3/6/2015 6:13	0
Lower Flurometer	3/6/2015 6:14	0
Lower Flurometer	3/6/2015 6:15	0
Lower Flurometer	3/6/2015 6:16	0
Lower Flurometer	3/6/2015 6:17	0
Lower Flurometer	3/6/2015 6:18	0
Lower Flurometer	3/6/2015 6:19	0
Lower Flurometer	3/6/2015 6:20	0
Lower Flurometer	3/6/2015 6:21	0
Lower Flurometer	3/6/2015 6:22	0
Lower Flurometer	3/6/2015 6:23	0.01
Lower Flurometer	3/6/2015 6:24	0
Lower Flurometer	3/6/2015 6:25	0
Lower Flurometer	3/6/2015 6:26	0
Lower Flurometer	3/6/2015 6:27	0
Lower Flurometer	3/6/2015 6:28	0
Lower Flurometer	3/6/2015 6:29	0
Lower Flurometer	3/6/2015 6:30	0
Lower Flurometer	3/6/2015 6:31	0
Lower Flurometer	3/6/2015 6:32	0
Lower Flurometer	3/6/2015 6:33	0
Lower Flurometer	3/6/2015 6:34	0
Lower Flurometer	3/6/2015 6:35	0

Location	Date and Time	Rhodmaine Concentration Adjusted Concentration (ppb)
Lower Flurometer	3/6/2015 6:36	0
Lower Flurometer	3/6/2015 6:37	0
Lower Flurometer	3/6/2015 6:38	0
Lower Flurometer	3/6/2015 6:39	0
Lower Flurometer	3/6/2015 6:40	0
Lower Flurometer	3/6/2015 6:41	0
Lower Flurometer	3/6/2015 6:42	0
Lower Flurometer	3/6/2015 6:43	0
Lower Flurometer	3/6/2015 6:44	0
Lower Flurometer	3/6/2015 6:45	0
Lower Flurometer	3/6/2015 6:46	0
Lower Flurometer	3/6/2015 6:47	0
Lower Flurometer	3/6/2015 6:48	0.02
Lower Flurometer	3/6/2015 6:49	0
Lower Flurometer	3/6/2015 6:50	0
Lower Flurometer	3/6/2015 6:51	0
Lower Flurometer	3/6/2015 6:52	0
Lower Flurometer	3/6/2015 6:53	0
Lower Flurometer	3/6/2015 6:54	0
Lower Flurometer	3/6/2015 6:55	0
Lower Flurometer	3/6/2015 6:56	0
Lower Flurometer	3/6/2015 6:57	0
Lower Flurometer	3/6/2015 6:58	0
Lower Flurometer	3/6/2015 6:59	0
Lower Flurometer	3/6/2015 7:00	0
Lower Flurometer	3/6/2015 7:01	0
Lower Flurometer	3/6/2015 7:02	0
Lower Flurometer	3/6/2015 7:03	0
Lower Flurometer	3/6/2015 7:04	0
Lower Flurometer	3/6/2015 7:05	0
Lower Flurometer	3/6/2015 7:06	0
Lower Flurometer	3/6/2015 7:07	0.02
Lower Flurometer	3/6/2015 7:08	0
Lower Flurometer	3/6/2015 7:09	0
Lower Flurometer	3/6/2015 7:10	0
Lower Flurometer	3/6/2015 7:11	0
Lower Flurometer	3/6/2015 7:12	0
Lower Flurometer	3/6/2015 7:13	0
Lower Flurometer	3/6/2015 7:14	0
Lower Flurometer	3/6/2015 7:15	0
Lower Flurometer	3/6/2015 7:16	0
Lower Flurometer	3/6/2015 7:17	0
Lower Flurometer	3/6/2015 7:18	0
Lower Flurometer	3/6/2015 7:19	0
Lower Flurometer	3/6/2015 7:20	0
Lower Flurometer	3/6/2015 7:21	0

Location	Date and Time	Rhodmaine Concentration Adjusted Concentration (ppb)
Lower Flurometer	3/6/2015 7:22	0.23
Lower Flurometer	3/6/2015 7:23	0
Lower Flurometer	3/6/2015 7:24	0
Lower Flurometer	3/6/2015 7:25	0
Lower Flurometer	3/6/2015 7:26	0
Lower Flurometer	3/6/2015 7:27	0
Lower Flurometer	3/6/2015 7:28	0
Lower Flurometer	3/6/2015 7:29	0
Lower Flurometer	3/6/2015 7:30	0
Lower Flurometer	3/6/2015 7:31	0
Lower Flurometer	3/6/2015 7:32	0
Lower Flurometer	3/6/2015 7:33	0
Lower Flurometer	3/6/2015 7:34	0
Lower Flurometer	3/6/2015 7:35	0
Lower Flurometer	3/6/2015 7:36	0
Lower Flurometer	3/6/2015 7:37	0
Lower Flurometer	3/6/2015 7:38	0
Lower Flurometer	3/6/2015 7:39	0
Lower Flurometer	3/6/2015 7:40	0
Lower Flurometer	3/6/2015 7:41	0
Lower Flurometer	3/6/2015 7:42	0
Lower Flurometer	3/6/2015 7:43	0
Lower Flurometer	3/6/2015 7:44	0
Lower Flurometer	3/6/2015 7:45	0
Lower Flurometer	3/6/2015 7:46	0
Lower Flurometer	3/6/2015 7:47	0
Lower Flurometer	3/6/2015 7:48	0
Lower Flurometer	3/6/2015 7:49	0
Lower Flurometer	3/6/2015 7:50	0
Lower Flurometer	3/6/2015 7:51	0
Lower Flurometer	3/6/2015 7:52	0
Lower Flurometer	3/6/2015 7:53	0
Lower Flurometer	3/6/2015 7:54	0
Lower Flurometer	3/6/2015 7:55	0
Lower Flurometer	3/6/2015 7:56	0
Lower Flurometer	3/6/2015 7:57	0
Lower Flurometer	3/6/2015 7:58	0
Lower Flurometer	3/6/2015 7:59	0.02
Lower Flurometer	3/6/2015 8:00	0
Lower Flurometer	3/6/2015 8:01	0
Lower Flurometer	3/6/2015 8:02	0
Lower Flurometer	3/6/2015 8:03	0
Lower Flurometer	3/6/2015 8:04	0
Lower Flurometer	3/6/2015 8:05	0
Lower Flurometer	3/6/2015 8:06	0.06
Lower Flurometer	3/6/2015 8:07	0

Location	Date and Time	Rhodmaine Concentration Adjusted Concentration (ppb)
Lower Flurometer	3/6/2015 8:08	0
Lower Flurometer	3/6/2015 8:09	0.05
Lower Flurometer	3/6/2015 8:10	0
Lower Flurometer	3/6/2015 8:11	0
Lower Flurometer	3/6/2015 8:12	0
Lower Flurometer	3/6/2015 8:13	0
Lower Flurometer	3/6/2015 8:14	0
Lower Flurometer	3/6/2015 8:15	0
Lower Flurometer	3/6/2015 8:16	0
Lower Flurometer	3/6/2015 8:17	0
Lower Flurometer	3/6/2015 8:18	0
Lower Flurometer	3/6/2015 8:19	0
Lower Flurometer	3/6/2015 8:20	0
Lower Flurometer	3/6/2015 8:21	0
Lower Flurometer	3/6/2015 8:22	0.03
Lower Flurometer	3/6/2015 8:23	0
Lower Flurometer	3/6/2015 8:24	0
Lower Flurometer	3/6/2015 8:25	0
Lower Flurometer	3/6/2015 8:26	0
Lower Flurometer	3/6/2015 8:27	0
Lower Flurometer	3/6/2015 8:28	0.12
Lower Flurometer	3/6/2015 8:29	0
Lower Flurometer	3/6/2015 8:30	0
Lower Flurometer	3/6/2015 8:31	0
Lower Flurometer	3/6/2015 8:32	0
Lower Flurometer	3/6/2015 8:33	0
Lower Flurometer	3/6/2015 8:34	0
Lower Flurometer	3/6/2015 8:35	0
Lower Flurometer	3/6/2015 8:36	0
Lower Flurometer	3/6/2015 8:37	0
Lower Flurometer	3/6/2015 8:38	0
Lower Flurometer	3/6/2015 8:39	0
Lower Flurometer	3/6/2015 8:40	0
Lower Flurometer	3/6/2015 8:41	0
Lower Flurometer	3/6/2015 8:42	0
Lower Flurometer	3/6/2015 8:43	0
Lower Flurometer	3/6/2015 8:44	0
Lower Flurometer	3/6/2015 8:45	0
Lower Flurometer	3/6/2015 8:46	0
Lower Flurometer	3/6/2015 8:47	0
Lower Flurometer	3/6/2015 8:48	0
Lower Flurometer	3/6/2015 8:49	0
Lower Flurometer	3/6/2015 8:50	0
Lower Flurometer	3/6/2015 8:51	0
Lower Flurometer	3/6/2015 8:52	0.13
Lower Flurometer	3/6/2015 8:53	0

Location	Date and Time	Rhodmaine Concentration Adjusted Concentration (ppb)
Lower Flurometer	3/6/2015 8:54	0
Lower Flurometer	3/6/2015 8:55	0
Lower Flurometer	3/6/2015 8:56	0
Lower Flurometer	3/6/2015 8:57	0
Lower Flurometer	3/6/2015 8:58	0
Lower Flurometer	3/6/2015 8:59	0
Lower Flurometer	3/6/2015 9:00	0
Lower Flurometer	3/6/2015 9:01	0
Lower Flurometer	3/6/2015 9:02	0
Lower Flurometer	3/6/2015 9:03	0
Lower Flurometer	3/6/2015 9:04	0.08
Lower Flurometer	3/6/2015 9:05	0
Lower Flurometer	3/6/2015 9:06	0
Lower Flurometer	3/6/2015 9:07	0
Lower Flurometer	3/6/2015 9:08	0.36
Lower Flurometer	3/6/2015 9:09	0
Lower Flurometer	3/6/2015 9:10	0
Lower Flurometer	3/6/2015 9:11	0
Lower Flurometer	3/6/2015 9:12	0
Lower Flurometer	3/6/2015 9:13	0
Lower Flurometer	3/6/2015 9:14	0
Lower Flurometer	3/6/2015 9:15	0
Lower Flurometer	3/6/2015 9:16	0
Lower Flurometer	3/6/2015 9:17	0
Lower Flurometer	3/6/2015 9:18	0
Lower Flurometer	3/6/2015 9:19	0
Lower Flurometer	3/6/2015 9:20	0.1
Lower Flurometer	3/6/2015 9:21	0.03
Lower Flurometer	3/6/2015 9:22	0
Lower Flurometer	3/6/2015 9:23	0
Lower Flurometer	3/6/2015 9:24	0.12
Lower Flurometer	3/6/2015 9:25	0
Lower Flurometer	3/6/2015 9:26	0.01
Lower Flurometer	3/6/2015 9:27	0
Lower Flurometer	3/6/2015 9:28	0
Lower Flurometer	3/6/2015 9:29	0
Lower Flurometer	3/6/2015 9:30	0
Lower Flurometer	3/6/2015 9:31	0
Lower Flurometer	3/6/2015 9:32	0
Lower Flurometer	3/6/2015 9:33	0
Lower Flurometer	3/6/2015 9:34	0
Lower Flurometer	3/6/2015 9:35	0
Lower Flurometer	3/6/2015 9:36	0
Lower Flurometer	3/6/2015 9:37	0
Lower Flurometer	3/6/2015 9:38	0
Lower Flurometer	3/6/2015 9:39	0

Location	Date and Time	Rhodmaine Concentration Adjusted Concentration (ppb)
Lower Flurometer	3/6/2015 9:40	0
Lower Flurometer	3/6/2015 9:41	0
Lower Flurometer	3/6/2015 9:42	0
Lower Flurometer	3/6/2015 9:43	0
Lower Flurometer	3/6/2015 9:44	0
Lower Flurometer	3/6/2015 9:45	0
Lower Flurometer	3/6/2015 9:46	0
Lower Flurometer	3/6/2015 9:47	0.01
Lower Flurometer	3/6/2015 9:48	0
Lower Flurometer	3/6/2015 9:49	0
Lower Flurometer	3/6/2015 9:50	0
Lower Flurometer	3/6/2015 9:51	0
Lower Flurometer	3/6/2015 9:52	0
Lower Flurometer	3/6/2015 9:53	0
Lower Flurometer	3/6/2015 9:54	0
Lower Flurometer	3/6/2015 9:55	0
Lower Flurometer	3/6/2015 9:56	0
Lower Flurometer	3/6/2015 9:57	0
Lower Flurometer	3/6/2015 9:58	0
Lower Flurometer	3/6/2015 9:59	0
Lower Flurometer	3/6/2015 10:00	0
Lower Flurometer	3/6/2015 10:01	0
Lower Flurometer	3/6/2015 10:02	0
Lower Flurometer	3/6/2015 10:03	0.01
Lower Flurometer	3/6/2015 10:04	0
Lower Flurometer	3/6/2015 10:05	0
Lower Flurometer	3/6/2015 10:06	0
Lower Flurometer	3/6/2015 10:07	0
Lower Flurometer	3/6/2015 10:08	0
Lower Flurometer	3/6/2015 10:09	0
Lower Flurometer	3/6/2015 10:10	0
Lower Flurometer	3/6/2015 10:11	0
Lower Flurometer	3/6/2015 10:12	0
Lower Flurometer	3/6/2015 10:13	0
Lower Flurometer	3/6/2015 10:14	0
Lower Flurometer	3/6/2015 10:15	0.01
Lower Flurometer	3/6/2015 10:16	0
Lower Flurometer	3/6/2015 10:17	0
Lower Flurometer	3/6/2015 10:18	0
Lower Flurometer	3/6/2015 10:19	0
Lower Flurometer	3/6/2015 10:20	0
Lower Flurometer	3/6/2015 10:21	0
Lower Flurometer	3/6/2015 10:22	0
Lower Flurometer	3/6/2015 10:23	0
Lower Flurometer	3/6/2015 10:24	0
Lower Flurometer	3/6/2015 10:25	0

Location	Date and Time	Rhodmaine Concentration Adjusted Concentration (ppb)
Lower Flurometer	3/6/2015 10:26	0.02
Lower Flurometer	3/6/2015 10:27	0
Lower Flurometer	3/6/2015 10:28	0
Lower Flurometer	3/6/2015 10:29	0
Lower Flurometer	3/6/2015 10:30	0
Lower Flurometer	3/6/2015 10:31	0
Lower Flurometer	3/6/2015 10:32	0
Lower Flurometer	3/6/2015 10:33	0
Lower Flurometer	3/6/2015 10:34	0
Lower Flurometer	3/6/2015 10:35	0
Lower Flurometer	3/6/2015 10:36	0
Lower Flurometer	3/6/2015 10:37	0
Lower Flurometer	3/6/2015 10:38	0
Lower Flurometer	3/6/2015 10:39	0
Lower Flurometer	3/6/2015 10:40	0
Lower Flurometer	3/6/2015 10:41	0
Lower Flurometer	3/6/2015 10:42	0
Lower Flurometer	3/6/2015 10:43	0
Lower Flurometer	3/6/2015 10:44	0
Lower Flurometer	3/6/2015 10:45	0
Lower Flurometer	3/6/2015 10:46	0
Lower Flurometer	3/6/2015 10:47	0
Lower Flurometer	3/6/2015 10:48	0
Lower Flurometer	3/6/2015 10:49	0
Lower Flurometer	3/6/2015 10:50	0.01
Lower Flurometer	3/6/2015 10:51	0
Lower Flurometer	3/6/2015 10:52	0
Lower Flurometer	3/6/2015 10:53	0
Lower Flurometer	3/6/2015 10:54	0
Lower Flurometer	3/6/2015 10:55	0
Lower Flurometer	3/6/2015 10:56	0
Lower Flurometer	3/6/2015 10:57	0
Lower Flurometer	3/6/2015 10:58	0
Lower Flurometer	3/6/2015 10:59	0
Lower Flurometer	3/6/2015 11:00	0
Lower Flurometer	3/6/2015 11:01	0
Lower Flurometer	3/6/2015 11:02	0
Lower Flurometer	3/6/2015 11:03	0
Lower Flurometer	3/6/2015 11:04	0
Lower Flurometer	3/6/2015 11:05	0
Lower Flurometer	3/6/2015 11:06	0
Lower Flurometer	3/6/2015 11:07	0
Lower Flurometer	3/6/2015 11:08	0
Lower Flurometer	3/6/2015 11:09	0
Lower Flurometer	3/6/2015 11:10	0
Lower Flurometer	3/6/2015 11:11	0

Location	Date and Time	Rhodmaine Concentration Adjusted Concentration (ppb)
Lower Flurometer	3/6/2015 11:12	0
Lower Flurometer	3/6/2015 11:13	0
Lower Flurometer	3/6/2015 11:14	0
Lower Flurometer	3/6/2015 11:15	0
Lower Flurometer	3/6/2015 11:16	0
Lower Flurometer	3/6/2015 11:17	0
Lower Flurometer	3/6/2015 11:18	0
Lower Flurometer	3/6/2015 11:19	0
Lower Flurometer	3/6/2015 11:20	0
Lower Flurometer	3/6/2015 11:21	0
Lower Flurometer	3/6/2015 11:22	0
Lower Flurometer	3/6/2015 11:23	0
Lower Flurometer	3/6/2015 11:24	0
Lower Flurometer	3/6/2015 11:25	0
Lower Flurometer	3/6/2015 11:26	0
Lower Flurometer	3/6/2015 11:27	0
Lower Flurometer	3/6/2015 11:28	0
Lower Flurometer	3/6/2015 11:29	0.01
Lower Flurometer	3/6/2015 11:30	0
Lower Flurometer	3/6/2015 11:31	0
Lower Flurometer	3/6/2015 11:32	0
Lower Flurometer	3/6/2015 11:33	0
Lower Flurometer	3/6/2015 11:34	0
Lower Flurometer	3/6/2015 11:35	0
Lower Flurometer	3/6/2015 11:36	0
Lower Flurometer	3/6/2015 11:37	0
Lower Flurometer	3/6/2015 11:38	0
Lower Flurometer	3/6/2015 11:39	0
Lower Flurometer	3/6/2015 11:40	0
Lower Flurometer	3/6/2015 11:41	0
Lower Flurometer	3/6/2015 11:42	0
Lower Flurometer	3/6/2015 11:43	0
Lower Flurometer	3/6/2015 11:44	0
Lower Flurometer	3/6/2015 11:45	0
Lower Flurometer	3/6/2015 11:46	0
Lower Flurometer	3/6/2015 11:47	0
Lower Flurometer	3/6/2015 11:48	0
Lower Flurometer	3/6/2015 11:49	0
Lower Flurometer	3/6/2015 11:50	0
Lower Flurometer	3/6/2015 11:51	0
Lower Flurometer	3/6/2015 11:52	0
Lower Flurometer	3/6/2015 11:53	0
Lower Flurometer	3/6/2015 11:54	0
Lower Flurometer	3/6/2015 11:55	0
Lower Flurometer	3/6/2015 11:56	0
Lower Flurometer	3/6/2015 11:57	0

Location	Date and Time	Rhodmaine Concentration Adjusted Concentration (ppb)
Lower Flurometer	3/6/2015 11:58	0
Lower Flurometer	3/6/2015 11:59	0
Lower Flurometer	3/6/2015 12:00	0
Lower Flurometer	3/6/2015 12:01	0
Lower Flurometer	3/6/2015 12:02	0
Lower Flurometer	3/6/2015 12:03	0
Lower Flurometer	3/6/2015 12:04	0
Lower Flurometer	3/6/2015 12:05	0
Lower Flurometer	3/6/2015 12:06	0
Lower Flurometer	3/6/2015 12:07	0
Lower Flurometer	3/6/2015 12:08	0
Lower Flurometer	3/6/2015 12:09	0
Lower Flurometer	3/6/2015 12:10	0
Lower Flurometer	3/6/2015 12:11	0
Lower Flurometer	3/6/2015 12:12	0
Lower Flurometer	3/6/2015 12:13	0
Lower Flurometer	3/6/2015 12:14	0
Lower Flurometer	3/6/2015 12:15	0
Lower Flurometer	3/6/2015 12:16	0
Lower Flurometer	3/6/2015 12:17	0.04
Lower Flurometer	3/6/2015 12:18	0
Lower Flurometer	3/6/2015 12:19	0.21
Lower Flurometer	3/6/2015 12:20	0
Lower Flurometer	3/6/2015 12:21	0
Lower Flurometer	3/6/2015 12:22	0
Lower Flurometer	3/6/2015 12:23	0
Lower Flurometer	3/6/2015 12:24	0
Lower Flurometer	3/6/2015 12:25	0.04
Lower Flurometer	3/6/2015 12:26	0
Lower Flurometer	3/6/2015 12:27	0
Lower Flurometer	3/6/2015 12:28	0
Lower Flurometer	3/6/2015 12:29	0
Lower Flurometer	3/6/2015 12:30	0
Lower Flurometer	3/6/2015 12:31	0
Lower Flurometer	3/6/2015 12:32	0
Lower Flurometer	3/6/2015 12:33	0
Lower Flurometer	3/6/2015 12:34	0
Lower Flurometer	3/6/2015 12:35	0
Lower Flurometer	3/6/2015 12:36	0
Lower Flurometer	3/6/2015 12:37	0.02
Lower Flurometer	3/6/2015 12:38	0
Lower Flurometer	3/6/2015 12:39	0
Lower Flurometer	3/6/2015 12:40	0
Lower Flurometer	3/6/2015 12:41	0
Lower Flurometer	3/6/2015 12:42	0
Lower Flurometer	3/6/2015 12:43	0

Location	Date and Time	Rhodmaine Concentration Adjusted Concentration (ppb)
Lower Flurometer	3/6/2015 12:44	0
Lower Flurometer	3/6/2015 12:45	0
Lower Flurometer	3/6/2015 12:46	0
Lower Flurometer	3/6/2015 12:47	0
Lower Flurometer	3/6/2015 12:48	0
Lower Flurometer	3/6/2015 12:49	0
Lower Flurometer	3/6/2015 12:50	0
Lower Flurometer	3/6/2015 12:51	0
Lower Flurometer	3/6/2015 12:52	0.04
Lower Flurometer	3/6/2015 12:53	0
Lower Flurometer	3/6/2015 12:54	0.04
Lower Flurometer	3/6/2015 12:55	0
Lower Flurometer	3/6/2015 12:56	0
Lower Flurometer	3/6/2015 12:57	0
Lower Flurometer	3/6/2015 12:58	0
Lower Flurometer	3/6/2015 12:59	0
Lower Flurometer	3/6/2015 13:00	0
Lower Flurometer	3/6/2015 13:01	0
Lower Flurometer	3/6/2015 13:02	0.1
Lower Flurometer	3/6/2015 13:03	0
Lower Flurometer	3/6/2015 13:04	0
Lower Flurometer	3/6/2015 13:05	0
Lower Flurometer	3/6/2015 13:06	0
Lower Flurometer	3/6/2015 13:07	0
Lower Flurometer	3/6/2015 13:08	0
Lower Flurometer	3/6/2015 13:09	0
Lower Flurometer	3/6/2015 13:10	0
Lower Flurometer	3/6/2015 13:11	0.02
Lower Flurometer	3/6/2015 13:12	0
Lower Flurometer	3/6/2015 13:13	0
Lower Flurometer	3/6/2015 13:14	0
Lower Flurometer	3/6/2015 13:15	0.04
Lower Flurometer	3/6/2015 13:16	0
Lower Flurometer	3/6/2015 13:17	0
Lower Flurometer	3/6/2015 13:18	0
Lower Flurometer	3/6/2015 13:19	0.02
Lower Flurometer	3/6/2015 13:20	0
Lower Flurometer	3/6/2015 13:21	0
Lower Flurometer	3/6/2015 13:22	0
Lower Flurometer	3/6/2015 13:23	0
Lower Flurometer	3/6/2015 13:24	0
Lower Flurometer	3/6/2015 13:25	0
Lower Flurometer	3/6/2015 13:26	0
Lower Flurometer	3/6/2015 13:27	0
Lower Flurometer	3/6/2015 13:28	0
Lower Flurometer	3/6/2015 13:29	0.06

Location	Date and Time	Rhodmaine Concentration Adjusted Concentration (ppb)
Lower Flurometer	3/6/2015 13:30	0
Lower Flurometer	3/6/2015 13:31	0
Lower Flurometer	3/6/2015 13:32	0
Lower Flurometer	3/6/2015 13:33	0
Lower Flurometer	3/6/2015 13:34	0
Lower Flurometer	3/6/2015 13:35	0
Lower Flurometer	3/6/2015 13:36	0
Lower Flurometer	3/6/2015 13:37	0
Lower Flurometer	3/6/2015 13:38	0
Lower Flurometer	3/6/2015 13:39	0.02
Lower Flurometer	3/6/2015 13:40	0
Lower Flurometer	3/6/2015 13:41	0
Lower Flurometer	3/6/2015 13:42	0
Lower Flurometer	3/6/2015 13:43	0.02
Lower Flurometer	3/6/2015 13:44	0
Lower Flurometer	3/6/2015 13:45	0.13
Lower Flurometer	3/6/2015 13:46	0
Lower Flurometer	3/6/2015 13:47	0
Lower Flurometer	3/6/2015 13:48	0
Lower Flurometer	3/6/2015 13:49	0
Lower Flurometer	3/6/2015 13:50	0
Lower Flurometer	3/6/2015 13:51	0
Lower Flurometer	3/6/2015 13:52	0
Lower Flurometer	3/6/2015 13:53	0
Lower Flurometer	3/6/2015 13:54	0
Lower Flurometer	3/6/2015 13:55	0
Lower Flurometer	3/6/2015 13:56	0
Lower Flurometer	3/6/2015 13:57	0
Lower Flurometer	3/6/2015 13:58	0
Lower Flurometer	3/6/2015 13:59	0
Lower Flurometer	3/6/2015 14:00	0
Lower Flurometer	3/6/2015 14:01	0
Lower Flurometer	3/6/2015 14:02	0
Lower Flurometer	3/6/2015 14:03	0
Lower Flurometer	3/6/2015 14:04	0
Lower Flurometer	3/6/2015 14:05	0
Lower Flurometer	3/6/2015 14:06	0
Lower Flurometer	3/6/2015 14:07	0
Lower Flurometer	3/6/2015 14:08	0
Lower Flurometer	3/6/2015 14:09	0
Lower Flurometer	3/6/2015 14:10	0
Lower Flurometer	3/6/2015 14:11	0
Lower Flurometer	3/6/2015 14:12	0
Lower Flurometer	3/6/2015 14:13	0
Lower Flurometer	3/6/2015 14:14	0
Lower Flurometer	3/6/2015 14:15	0

Location	Date and Time	Rhodmaine Concentration Adjusted Concentration (ppb)
Lower Flurometer	3/6/2015 14:16	0
Lower Flurometer	3/6/2015 14:17	0.01
Lower Flurometer	3/6/2015 14:18	0
Lower Flurometer	3/6/2015 14:19	0
Lower Flurometer	3/6/2015 14:20	0
Lower Flurometer	3/6/2015 14:21	0
Lower Flurometer	3/6/2015 14:22	0
Lower Flurometer	3/6/2015 14:23	0.04
Lower Flurometer	3/6/2015 14:24	0.09
Lower Flurometer	3/6/2015 14:25	0.09
Lower Flurometer	3/6/2015 14:26	0.04
Lower Flurometer	3/6/2015 14:27	0.08
Lower Flurometer	3/6/2015 14:28	0.04
Lower Flurometer	3/6/2015 14:29	0
Lower Flurometer	3/6/2015 14:30	0.12
Lower Flurometer	3/6/2015 14:31	0.11
Lower Flurometer	3/6/2015 14:32	0.04
Lower Flurometer	3/6/2015 14:33	0.13
Lower Flurometer	3/6/2015 14:34	0.13
Lower Flurometer	3/6/2015 14:35	0.11
Lower Flurometer	3/6/2015 14:36	0.1
Lower Flurometer	3/6/2015 14:37	0.12
Lower Flurometer	3/6/2015 14:38	0.13
Lower Flurometer	3/6/2015 14:39	0.14
Lower Flurometer	3/6/2015 14:40	0.1
Lower Flurometer	3/6/2015 14:41	0.1
Lower Flurometer	3/6/2015 14:42	0.14
Lower Flurometer	3/6/2015 14:43	0.12
Lower Flurometer	3/6/2015 14:44	0.1
Lower Flurometer	3/6/2015 14:45	0.18
Lower Flurometer	3/6/2015 14:46	0.12
Lower Flurometer	3/6/2015 14:47	0.13
Lower Flurometer	3/6/2015 14:48	0.14
Lower Flurometer	3/6/2015 14:49	0.16
Lower Flurometer	3/6/2015 14:50	0.19
Lower Flurometer	3/6/2015 14:51	0.16
Lower Flurometer	3/6/2015 14:52	0.1
Lower Flurometer	3/6/2015 14:53	0.18
Lower Flurometer	3/6/2015 14:54	0.18
Lower Flurometer	3/6/2015 14:55	0.1
Lower Flurometer	3/6/2015 14:56	0.18
Lower Flurometer	3/6/2015 14:57	0.13
Lower Flurometer	3/6/2015 14:58	0.1
Lower Flurometer	3/6/2015 14:59	0.14
Lower Flurometer	3/6/2015 15:00	0.1
Lower Flurometer	3/6/2015 15:01	0.1

Location	Date and Time	Rhodmaine Concentration Adjusted Concentration (ppb)
Lower Flurometer	3/6/2015 15:02	0.18
Lower Flurometer	3/6/2015 15:03	0.17
Lower Flurometer	3/6/2015 15:04	0.15
Lower Flurometer	3/6/2015 15:05	0.08
Lower Flurometer	3/6/2015 15:06	0.17
Lower Flurometer	3/6/2015 15:07	0.12
Lower Flurometer	3/6/2015 15:08	0.15
Lower Flurometer	3/6/2015 15:09	0.09
Lower Flurometer	3/6/2015 15:10	0.1
Lower Flurometer	3/6/2015 15:11	0.14
Lower Flurometer	3/6/2015 15:12	0.1
Lower Flurometer	3/6/2015 15:13	0.12
Lower Flurometer	3/6/2015 15:14	0.17
Lower Flurometer	3/6/2015 15:15	0.17
Lower Flurometer	3/6/2015 15:16	0.1
Lower Flurometer	3/6/2015 15:17	0.15
Lower Flurometer	3/6/2015 15:18	0.07
Lower Flurometer	3/6/2015 15:19	0.17
Lower Flurometer	3/6/2015 15:20	0.14
Lower Flurometer	3/6/2015 15:21	0.13
Lower Flurometer	3/6/2015 15:22	0.1
Lower Flurometer	3/6/2015 15:23	0.11
Lower Flurometer	3/6/2015 15:24	0.09
Lower Flurometer	3/6/2015 15:25	0.1
Lower Flurometer	3/6/2015 15:26	0.12
Lower Flurometer	3/6/2015 15:27	0.09
Lower Flurometer	3/6/2015 15:28	0.14
Lower Flurometer	3/6/2015 15:29	0.08
Lower Flurometer	3/6/2015 15:30	0.13
Lower Flurometer	3/6/2015 15:31	0.13
Lower Flurometer	3/6/2015 15:32	0.08
Lower Flurometer	3/6/2015 15:33	0.1
Lower Flurometer	3/6/2015 15:34	0.08
Lower Flurometer	3/6/2015 15:35	0.06
Lower Flurometer	3/6/2015 15:36	0.13
Lower Flurometer	3/6/2015 15:37	0.07
Lower Flurometer	3/6/2015 15:38	0.14
Lower Flurometer	3/6/2015 15:39	0.14
Lower Flurometer	3/6/2015 15:40	0.06
Lower Flurometer	3/6/2015 15:41	0.12
Lower Flurometer	3/6/2015 15:42	0.13
Lower Flurometer	3/6/2015 15:43	0.04
Lower Flurometer	3/6/2015 15:44	0.08
Lower Flurometer	3/6/2015 15:45	0.04
Lower Flurometer	3/6/2015 15:46	0.05
Lower Flurometer	3/6/2015 15:47	0.11

Location	Date and Time	Rhodmaine Concentration Adjusted Concentration (ppb)
Lower Flurometer	3/6/2015 15:48	0.09
Lower Flurometer	3/6/2015 15:49	0.06
Lower Flurometer	3/6/2015 15:50	0.1
Lower Flurometer	3/6/2015 15:51	0.03
Lower Flurometer	3/6/2015 15:52	0.02
Lower Flurometer	3/6/2015 15:53	0.03
Lower Flurometer	3/6/2015 15:54	0
Lower Flurometer	3/6/2015 15:55	0.01
Lower Flurometer	3/6/2015 15:56	0.1
Lower Flurometer	3/6/2015 15:57	0.02
Lower Flurometer	3/6/2015 15:58	0.06
Lower Flurometer	3/6/2015 15:59	0
Lower Flurometer	3/6/2015 16:00	0.01
Lower Flurometer	3/6/2015 16:01	0.06
Lower Flurometer	3/6/2015 16:02	0.02
Lower ISCO	3/4/15 16:00	-0.091257562
Lower ISCO	3/4/15 17:00	-0.043525651
Lower ISCO	3/4/15 18:00	0.04535446
Lower ISCO	3/4/15 19:00	-0.11759241
Lower ISCO	3/4/15 20:00	-0.12582205
Lower ISCO	3/4/15 21:00	-0.143927257
Lower ISCO	3/4/15 22:00	-0.073152354
Lower ISCO	3/4/15 23:00	-0.048463435
Lower ISCO	3/5/15 0:00	-0.083027922
Lower ISCO	3/5/15 1:00	-0.06821457
Lower ISCO	3/5/15 2:00	-0.061630859
Lower ISCO	3/5/15 3:00	0.173736842
Lower ISCO	3/5/15 4:00	1.901961215
Lower ISCO	3/5/15 5:00	4.273743425
Lower ISCO	3/5/15 6:00	5.317261761
Lower ISCO	3/5/15 7:00	4.668766139
Lower ISCO	3/5/15 8:00	4.168404035
Lower ISCO	3/5/15 9:00	3.312521489
Lower ISCO	3/5/15 10:00	2.746322265
Lower ISCO	3/5/15 11:00	2.254189801
Lower ISCO	3/5/15 12:00	1.905253071
Lower ISCO	3/5/15 13:00	1.633674955
Lower ISCO	3/5/15 14:00	1.227130745
Lower ISCO	3/5/15 15:00	1.046078668
Lower ISCO	3/5/15 16:00	0.968720053
Lower ISCO	3/5/15 17:00	0.838691743
Lower ISCO	3/5/15 18:00	0.621429251
Lower ISCO	3/5/15 19:00	0.519381716
Lower ISCO	3/5/15 20:00	0.433793462
Lower ISCO	3/5/15 21:00	0.307057008
Lower ISCO	3/5/15 22:00	0.29718144

Location	Date and Time	Rhodmaine Concentration Adjusted Concentration (ppb)
Lower ISCO	3/5/15 23:00	0.213239113
Lower ISCO	3/6/15 0:00	0.224760609
Lower ISCO	3/6/15 1:00	0.137526426
Lower ISCO	3/6/15 2:00	0.160569418
Lower ISCO	3/6/15 3:00	0.157277562
Lower ISCO	3/6/15 4:00	0.260971024
Lower ISCO	3/6/15 5:00	0.114483435
Lower ISCO	3/6/15 6:00	0.096378227
Lower ISCO	3/6/15 7:00	0.060167812
Lower ISCO	3/6/15 8:00	0.084856731
Lower ISCO	3/6/15 9:00	0.035478892
Lower ISCO	3/6/15 10:00	0.009144044
Lower ISCO	3/6/15 11:00	0.047000388
Lower ISCO	3/6/15 12:00	0.02066554
Lower ISCO	3/6/15 13:00	-0.018836731
Lower ISCO	3/6/15 14:00	0.027249252

Appendix 5.3.1. Discrete velocity measurements were taken on 10/3, 10/6, and 10/8/2014.

Date	Transect	Distance from Left Bank (m)	Depth (m)	Velocity (m s^{-1}) (up to 4 repeated measures)					Depth to top of Vegetation (m)
				1	2	3	4	Avg.	
10/3/2014	3	0	0.690	0.010				0.010	n/a
10/3/2014	3	0	0.610	0.240				0.240	n/a
10/3/2014	3	0	0.560	0.060				0.060	n/a
10/3/2014	3	0	0.440	0.020				0.020	n/a
10/3/2014	3	0	0.290	0.080	0.070			0.075	n/a
10/3/2014	3	0	0.210	0.090	0.070			0.080	n/a
10/3/2014	3	0	0.140	0.090	0.080	0.140		0.103	n/a
10/3/2014	3	0	0.050	0.120	0.090	0.140		0.117	n/a
10/3/2014	3	1	0.800	0.000	0.000	0.000		0.000	n/a
10/3/2014	3	1	0.690	0.000	0.070	0.050		0.040	n/a
10/3/2014	3	1	0.640	0.070	0.060	0.060		0.063	n/a
10/3/2014	3	1	0.590	0.090	0.040	0.060		0.063	n/a
10/3/2014	3	1	0.480	0.060	0.060	0.060		0.060	n/a
10/3/2014	3	1	0.420	0.050	0.060	0.070		0.060	n/a
10/3/2014	3	1	0.320	0.070	0.070	0.060		0.067	n/a
10/3/2014	3	1	0.220	0.040	0.040	0.050		0.043	n/a
10/3/2014	3	1	0.100	0.040	0.040	0.050		0.043	n/a
10/3/2014	3	1	0.070	0.100	0.090	0.070		0.087	n/a
10/3/2014	3	2	0.880	0.000	0.000	0.000		0.000	0.05
10/3/2014	3	2	0.760	0.030	0.020	0.030		0.027	0.05
10/3/2014	3	2	0.610	0.020	0.030	0.020		0.023	0.05
10/3/2014	3	2	0.520	0.060	0.060	0.050		0.057	0.05
10/3/2014	3	2	0.440	0.040	0.030	0.040		0.037	0.05
10/3/2014	3	2	0.340	0.050	0.150	0.100		0.100	0.05
10/3/2014	3	2	0.280	0.050	0.050	0.040		0.047	0.05
10/3/2014	3	2	0.140	0.110	0.100	0.110		0.107	0.05
10/3/2014	3	2	0.040	0.080	0.220	0.130	0.170	0.150	0.05
10/3/2014	3	3	1.250	0.008	0.008	0.010		0.009	0.298
10/3/2014	3	3	0.995	0.024	0.026	0.036		0.029	0.298
10/3/2014	3	3	0.813	0.063	0.041	0.059		0.054	0.298
10/3/2014	3	3	0.651	0.050	0.029	0.047		0.042	0.298
10/3/2014	3	3	0.447	0.041	0.069	0.228	0.090	0.107	0.298
10/3/2014	3	3	0.325	0.141	0.150	0.060		0.117	0.298
10/3/2014	3	3	0.230	0.191	0.308	0.308		0.269	0.298
10/3/2014	3	3	0.156	0.100	0.209	0.162		0.157	0.298
10/3/2014	3	3	0.067	0.178	0.266	0.279		0.241	0.298
10/3/2014	3	4	2.429	0.040	0.033	0.058		0.044	1.5
10/3/2014	3	4	2.146	0.154	0.204	0.230		0.196	1.5
10/3/2014	3	4	1.878	0.196	0.079	0.221	0.204	0.175	1.5
10/3/2014	3	4	1.683	0.144	0.132	0.198		0.158	1.5
10/3/2014	3	4	1.461	0.194	0.127	0.186		0.169	1.5
10/3/2014	3	4	1.251	0.310	0.345	0.259		0.305	1.5
10/3/2014	3	4	1.020	0.233	0.275	0.236		0.248	1.5

Date	Transect	Distance from Left Bank (m)	Depth (m)	Velocity (m s^{-1}) (up to 4 repeated measures)					Depth to top of Vegetation (m)
				1	2	3	4	Avg.	
10/3/2014	3	4	0.785	0.259	0.213	0.362	0.428	0.316	1.5
10/3/2014	3	4	0.545	0.280	0.315	0.375		0.323	1.5
10/3/2014	3	4	0.241	0.337	0.391	0.285		0.338	1.5
10/3/2014	3	4	0.090	0.251	0.295	0.353		0.300	1.5
10/6/2014	3	6	3.628	0.052	0.019	0.049		0.040	n/a
10/6/2014	3	6	3.237	0.188	0.140	0.067		0.132	n/a
10/6/2014	3	6	2.849	0.331	0.257	0.298		0.295	n/a
10/6/2014	3	6	2.380	0.252	0.204	0.133		0.196	n/a
10/6/2014	3	6	2.010	0.337	0.342	0.367		0.349	n/a
10/6/2014	3	6	1.594	0.498	0.432	0.527		0.486	n/a
10/6/2014	3	6	1.220	0.526	0.375	0.483		0.461	n/a
10/6/2014	3	6	0.853	0.565	0.449	0.409		0.474	n/a
10/6/2014	3	6	0.413	0.345	0.339	0.371		0.352	n/a
10/6/2014	3	6	0.125	0.451	0.505	0.433		0.463	n/a
10/3/2014	3	7	4.240	0.048	0.028	0.023		0.033	n/a
10/3/2014	3	7	3.674	0.347	0.303	0.229		0.293	n/a
10/3/2014	3	7	3.286	0.407	0.442	0.371		0.407	n/a
10/3/2014	3	7	2.600	0.394	0.390	0.423		0.402	n/a
10/3/2014	3	7	2.121	0.560	0.430	0.462		0.484	n/a
10/3/2014	3	7	1.645	0.555	0.482	0.560		0.532	n/a
10/3/2014	3	7	1.076	0.597	0.568	0.586		0.584	n/a
10/3/2014	3	7	0.660	0.515	0.522	0.547		0.528	n/a
10/3/2014	3	7	0.365	0.494	0.532	0.578		0.535	n/a
10/6/2014	3	8	4.250	0.085	0.018	0.089		0.064	n/a
10/6/2014	3	8	3.725	0.228	0.297	0.366		0.297	n/a
10/6/2014	3	8	3.301	0.387	0.362	0.376		0.375	n/a
10/6/2014	3	8	2.795	0.298	0.470	0.445		0.404	n/a
10/6/2014	3	8	2.381	0.515	0.478	0.489		0.494	n/a
10/6/2014	3	8	1.970	0.411	0.469	0.468		0.449	n/a
10/6/2014	3	8	1.565	0.512	0.507	0.490		0.503	n/a
10/6/2014	3	8	1.155	0.469	0.561	0.562		0.531	n/a
10/6/2014	3	8	0.722	0.635	0.546	0.535		0.572	n/a
10/6/2014	3	8	0.375	0.447	0.459	0.467		0.458	n/a
10/6/2014	3	8	0.095	0.455	0.335	0.452		0.414	n/a
10/6/2014	3	9	4.320	0.016	0.020	0.016		0.017	n/a
10/6/2014	3	9	3.864	0.319	0.264	0.284		0.289	n/a
10/6/2014	3	9	3.407	0.227	0.265	0.269		0.254	n/a
10/6/2014	3	9	3.072	0.378	0.344	0.286		0.336	n/a
10/6/2014	3	9	2.585	0.356	0.483	0.476		0.438	n/a
10/6/2014	3	9	2.218	0.394	0.435	0.517		0.449	n/a
10/6/2014	3	9	1.842	0.341	0.441	0.460		0.414	n/a
10/6/2014	3	9	1.343	0.401	0.494	0.494		0.463	n/a
10/6/2014	3	9	0.922	0.441	0.432	0.449		0.441	n/a
10/6/2014	3	9	0.900	0.518	0.491	0.417		0.475	n/a
10/6/2014	3	10	4.300	0.016	0.005	0.011		0.011	n/a
10/6/2014	3	10	3.863	0.209	0.133	0.134		0.159	n/a

Date	Transect	Distance from Left Bank (m)	Depth (m)	Velocity (m s^{-1}) (up to 4 repeated measures)					Depth to top of Vegetation (m)
				1	2	3	4	Avg.	
10/6/2014	3	10	3.364	0.219	0.195	0.091		0.168	n/a
10/6/2014	3	10	2.888	0.295	0.394	0.430		0.373	n/a
10/6/2014	3	10	2.435	0.248	0.345	0.282		0.292	n/a
10/6/2014	3	10	2.002	0.409	0.480	0.459		0.449	n/a
10/6/2014	3	10	1.523	0.442	0.358	0.355		0.385	n/a
10/6/2014	3	10	1.219	0.380	0.380	0.337		0.366	n/a
10/6/2014	3	10	0.818	0.370	0.333	0.356		0.353	n/a
10/6/2014	3	10	0.297	0.359	0.346	0.337		0.347	n/a
10/6/2014	3	11	4.112	0.034	0.046	0.014		0.031	n/a
10/6/2014	3	11	3.664	0.033	0.120	0.087		0.080	n/a
10/6/2014	3	11	3.184	0.113	0.115	0.152		0.127	n/a
10/6/2014	3	11	2.849	0.190	0.189	0.175		0.185	n/a
10/6/2014	3	11	2.462	0.181	0.296	0.168		0.215	n/a
10/6/2014	3	11	1.955	0.193	0.179	0.303		0.225	n/a
10/6/2014	3	11	1.572	0.286	0.303	0.396		0.328	n/a
10/6/2014	3	11	1.163	0.316	0.226	0.343		0.295	n/a
10/6/2014	3	11	0.729	0.290	0.296	0.309		0.298	n/a
10/6/2014	3	11	0.202	0.344	0.351	0.394		0.363	n/a
10/6/2014	3	12	3.702	0.020	0.015	0.046		0.027	n/a
10/6/2014	3	12	3.243	0.057	0.090	0.071		0.073	n/a
10/6/2014	3	12	2.963	0.129	0.128	0.136		0.131	n/a
10/6/2014	3	12	2.571	0.273	0.264	0.194		0.244	n/a
10/6/2014	3	12	2.101	0.121	0.105	0.208		0.145	n/a
10/6/2014	3	12	1.647	0.204	0.234	0.158		0.199	n/a
10/6/2014	3	12	1.207	0.297	0.246	0.189		0.244	n/a
10/6/2014	3	12	0.773	0.251	0.293	0.277		0.274	n/a
10/6/2014	3	12	0.416	0.339	0.360	0.307		0.335	n/a
10/6/2014	3	12	0.132	0.309	0.340	0.307		0.319	n/a
10/6/2014	3	13	3.243	0.003	0.002	0.002		0.002	n/a
10/6/2014	3	13	2.825	0.073	0.115	0.131		0.106	n/a
10/6/2014	3	13	2.417	0.112	0.125	0.221		0.153	n/a
10/6/2014	3	13	2.025	0.191	0.171	0.163		0.175	n/a
10/6/2014	3	13	1.622	0.156	0.198	0.217		0.190	n/a
10/6/2014	3	13	1.228	0.256	0.298	0.275		0.276	n/a
10/6/2014	3	13	0.881	0.177	0.284	0.272		0.244	n/a
10/6/2014	3	13	0.499	0.233	0.287	0.280		0.267	n/a
10/6/2014	3	13	0.153	0.277	0.280	0.238		0.265	n/a
10/6/2014	3	14	2.530	0.005	0.011	0.021		0.012	n/a
10/6/2014	3	14	2.225	0.056	0.063	0.031		0.050	n/a
10/6/2014	3	14	2.021	0.044	0.048	0.047		0.046	n/a
10/6/2014	3	14	1.758	0.012	0.016	0.021		0.016	n/a
10/6/2014	3	14	1.503	0.023	0.023	0.009		0.018	n/a
10/6/2014	3	14	1.273	0.052	0.015	0.096		0.054	n/a
10/6/2014	3	14	1.010	0.130	0.109	0.128		0.122	n/a
10/6/2014	3	14	0.752	0.214	0.210	0.343		0.256	n/a
10/6/2014	3	14	0.514	0.286	0.252	0.302		0.280	n/a

Date	Transect	Distance from Left Bank (m)	Depth (m)	Velocity (m s^{-1}) (up to 4 repeated measures)					Depth to top of Vegetation (m)
				1	2	3	4	Avg.	
10/6/2014	3	14	0.112	0.369	0.270	0.193		0.277	n/a
10/6/2014	3	15	2.001	0.008	0.013	0.015		0.012	1.17
10/6/2014	3	15	1.860	0.038	0.033	0.010		0.027	1.17
10/6/2014	3	15	1.597	0.038	0.020	0.038		0.032	1.17
10/6/2014	3	15	1.376	0.155	0.024	0.048		0.076	1.17
10/6/2014	3	15	1.178	0.072	0.154	0.084		0.103	1.17
10/6/2014	3	15	0.977	0.154	0.181	0.153		0.163	1.17
10/6/2014	3	15	0.771	0.101	0.178	0.195		0.158	1.17
10/6/2014	3	15	0.603	0.249	0.159	0.148		0.185	1.17
10/6/2014	3	15	0.377	0.063	0.163	0.182		0.136	1.17
10/6/2014	3	15	0.070	0.134	0.242	0.195		0.190	1.17
10/6/2014	3	16	1.230	0.016	0.000	0.005		0.007	0.902
10/6/2014	3	16	1.085	0.020	0.034	0.049		0.034	0.902
10/6/2014	3	16	0.863	0.157	0.051	0.014		0.074	0.902
10/6/2014	3	16	0.741	0.082	0.086	0.163		0.110	0.902
10/6/2014	3	16	0.575	0.092	0.038	0.111		0.080	0.902
10/6/2014	3	16	0.456	0.166	0.115	0.179		0.153	0.902
10/6/2014	3	16	0.318	0.271	0.201	0.172		0.215	0.902
10/6/2014	3	16	0.185	0.222	0.098	0.090		0.137	0.902
10/6/2014	3	16	0.101	0.136	0.202	0.201		0.180	0.902
10/6/2014	3	16	0.051	0.236	0.254	0.048		0.179	0.902
10/6/2014	3	17	1.035	0.002	0.000	0.000		0.001	0.692
10/6/2014	3	17	0.897	0.001	0.017	0.001		0.006	0.692
10/6/2014	3	17	0.826	0.014	0.039	0.013		0.022	0.692
10/6/2014	3	17	0.706	0.030	0.037	0.014		0.027	0.692
10/6/2014	3	17	0.583	0.078	0.038	0.033		0.050	0.692
10/6/2014	3	17	0.515	0.006	0.098	0.141		0.082	0.692
10/6/2014	3	17	0.373	0.132	0.100	0.102		0.111	0.692
10/6/2014	3	17	0.293	0.104	0.116	0.083		0.101	0.692
10/6/2014	3	17	0.189	0.095	0.113	0.128		0.112	0.692
10/6/2014	3	17	0.062	0.128	0.277	0.111		0.172	0.692
10/6/2014	3	18	0.780	0.015	0.027	0.020		0.021	n/a
10/6/2014	3	18	0.681	0.037	0.063	0.053		0.051	n/a
10/6/2014	3	18	0.575	0.121	0.076	0.001		0.066	n/a
10/6/2014	3	18	0.555	0.054	0.002	0.067		0.041	n/a
10/6/2014	3	18	0.481	0.071	0.092	0.063		0.075	n/a
10/6/2014	3	18	0.435	0.007	0.033	0.035		0.025	n/a
10/6/2014	3	18	0.381	0.079	0.066	0.056		0.067	n/a
10/6/2014	3	18	0.286	0.059	0.039	0.069		0.056	n/a
10/6/2014	3	18	0.148	0.055	0.017	0.069		0.047	n/a
10/6/2014	3	18	0.058	0.068	0.094	0.110		0.091	n/a
10/6/2014	3	19	0.670	0.006	0.006	0.005		0.006	n/a
10/6/2014	3	19	0.537	0.011	0.032	0.032		0.025	n/a
10/6/2014	3	19	0.479	0.040	0.008	0.028		0.025	n/a
10/6/2014	3	19	0.415	0.046	0.034	0.042		0.041	n/a
10/6/2014	3	19	0.378	0.054	0.031	0.045		0.043	n/a

Date	Transect	Distance from Left Bank (m)	Depth (m)	Velocity (m s^{-1}) (up to 4 repeated measures)					Depth to top of Vegetation (m)
				1	2	3	4	Avg.	
10/6/2014	3	19	0.280	0.027	0.063	0.069		0.053	n/a
10/6/2014	3	19	0.202	0.027	0.060	0.043		0.043	n/a
10/6/2014	3	19	0.165	0.023	0.047	0.070		0.047	n/a
10/6/2014	3	19	0.091	0.091	0.050	0.060		0.067	n/a
10/6/2014	3	19	0.062	0.046	0.061	0.048		0.052	n/a
10/8/2015	7	0	1.105	0.003	0.001	0.005		0.003	n/a
10/8/2015	7	0	0.951	0.035	0.035	0.035		0.035	n/a
10/8/2015	7	0	0.895	0.029	0.038	0.042		0.036	n/a
10/8/2015	7	0	0.805	0.067	0.067	0.061		0.065	n/a
10/8/2015	7	0	0.710	0.059	0.057	0.057		0.058	n/a
10/8/2015	7	0	0.609	0.071	0.068	0.068		0.069	n/a
10/8/2015	7	0	0.502	0.060	0.058	0.058		0.059	n/a
10/8/2015	7	0	0.403	0.063	0.063	0.063		0.063	n/a
10/8/2015	7	0	0.307	0.056	0.070	0.070		0.065	n/a
10/8/2015	7	0	0.209	0.048	0.051	0.051		0.050	n/a
10/8/2015	7	0	0.105	0.052	0.046	0.046		0.048	n/a
10/8/2015	7	2	1.372	0.000	0.000	0.000		0.000	0.570
10/8/2015	7	2	1.230	0.000	0.000	0.000		0.000	0.570
10/8/2015	7	2	1.086	0.061	0.061	0.063		0.062	0.570
10/8/2015	7	2	0.936	0.065	0.084	0.084		0.078	0.570
10/8/2015	7	2	0.783	0.087	0.086	0.086		0.086	0.570
10/8/2015	7	2	0.654	0.088	0.088	0.088		0.088	0.570
10/8/2015	7	2	0.516	0.114	0.114	0.114		0.114	0.570
10/8/2015	7	2	0.384	0.096	0.096	0.100		0.097	0.570
10/8/2015	7	2	0.156	0.102	0.102	0.119		0.108	0.570
10/8/2015	7	2	0.059	0.054	0.054	0.054		0.054	0.570
10/8/2015	7	4	1.348	0.004	0.000	0.011		0.005	0.702
10/8/2015	7	4	1.201	0.026	0.026	0.009		0.020	0.702
10/8/2015	7	4	1.084	0.039	0.030	0.030		0.033	0.702
10/8/2015	7	4	0.948	0.044	0.030	0.030		0.035	0.702
10/8/2015	7	4	0.815	0.018	0.018	0.018		0.018	0.702
10/8/2015	7	4	0.653	0.059	0.059	0.056		0.058	0.702
10/8/2015	7	4	0.409	0.098	0.098	0.107		0.101	0.702
10/8/2015	7	4	0.277	0.109	0.109	0.109		0.109	0.702
10/8/2015	7	4	0.133	0.134	0.098	0.098		0.110	0.702
10/8/2015	7	4	0.057	0.060	0.060	0.060		0.060	0.702
10/8/2015	7	6	1.535	0.000	0.000	0.000		0.000	0.830
10/8/2015	7	6	1.372	0.005	0.000	0.000		0.002	0.830
10/8/2015	7	6	1.211	0.013	0.012	0.012		0.012	0.830
10/8/2015	7	6	1.057	0.025	0.025	0.025		0.025	0.830
10/8/2015	7	6	0.874	0.057	0.057	0.057		0.057	0.830
10/8/2015	7	6	0.723	0.099	0.099	0.099		0.099	0.830
10/8/2015	7	6	0.580	0.131	0.131	0.125		0.129	0.830
10/8/2015	7	6	0.378	0.141	0.127	0.127		0.132	0.830
10/8/2015	7	6	0.140	0.109	0.122	0.122		0.118	0.830
10/8/2015	7	6	0.067	0.024	0.024	0.024		0.024	0.830

Date	Transect	Distance from Left Bank (m)	Depth (m)	Velocity (m s^{-1}) (up to 4 repeated measures)					Depth to top of Vegetation (m)
				1	2	3	4	Avg.	
10/8/2015	7	8	1.574	0.000	0.000	0.000		0.000	0.825
10/8/2015	7	8	1.410	0.030	0.030	0.008		0.023	0.825
10/8/2015	7	8	1.254	0.031	0.031	0.027		0.030	0.825
10/8/2015	7	8	1.012	0.070	0.070	0.070		0.070	0.825
10/8/2015	7	8	0.844	0.030	0.030	0.030		0.030	0.825
10/8/2015	7	8	0.687	0.112	0.112	0.112		0.112	0.825
10/8/2015	7	8	0.539	0.160	0.160	0.164		0.161	0.825
10/8/2015	7	8	0.302	0.210	0.210	0.210		0.210	0.825
10/8/2015	7	8	0.133	0.150	0.154	0.154		0.153	0.825
10/8/2015	7	8	0.081	0.000	0.213	0.213		0.142	0.825
10/8/2015	7	10	1.830	0.001	0.001	0.001		0.001	1.118
10/8/2015	7	10	1.596	0.004	0.004	0.004		0.004	1.118
10/8/2015	7	10	1.430	0.068	0.022	0.022		0.037	1.118
10/8/2015	7	10	1.257	0.008	0.008	0.030		0.015	1.118
10/8/2015	7	10	1.097	0.157	0.157	0.069		0.128	1.118
10/8/2015	7	10	0.801	0.165	0.165	0.134		0.155	1.118
10/8/2015	7	10	0.614	0.180	0.182	0.182		0.181	1.118
10/8/2015	7	10	0.435	0.176	0.176	0.176		0.176	1.118
10/8/2015	7	10	0.232	0.158	0.186	0.186		0.177	1.118
10/8/2015	7	10	0.092	0.211	0.211	0.211		0.211	1.118
10/8/2015	7	12	1.979	0.000	0.000	0.000		0.000	1.155
10/8/2015	7	12	1.696	0.000	0.000	0.000		0.000	1.155
10/8/2015	7	12	1.490	0.012	0.009	0.009		0.010	1.155
10/8/2015	7	12	1.276	0.116	0.116	0.116		0.116	1.155
10/8/2015	7	12	1.080	0.074	0.074	0.074		0.074	1.155
10/8/2015	7	12	0.901	0.196	0.196	0.196		0.196	1.155
10/8/2015	7	12	0.690	0.159	0.169	0.169		0.166	1.155
10/8/2015	7	12	0.466	0.195	0.156	0.156		0.169	1.155
10/8/2015	7	12	0.268	0.226	0.226	0.226		0.226	1.155
10/8/2015	7	12	0.095	0.301	0.301	0.219		0.274	1.155
10/8/2015	7	14	2.175	0.001	0.000	0.000		0.000	0.976
10/8/2015	7	14	1.877	0.025	0.025	0.012		0.021	0.976
10/8/2015	7	14	1.650	0.035	0.042	0.042		0.040	0.976
10/8/2015	7	14	1.478	0.017	0.017	0.022		0.019	0.976
10/8/2015	7	14	1.268	0.056	0.087	0.087		0.077	0.976
10/8/2015	7	14	1.062	0.177	0.158	0.158		0.164	0.976
10/8/2015	7	14	0.818	0.258	0.207	0.207		0.224	0.976
10/8/2015	7	14	0.500	0.225	0.225	0.221		0.224	0.976
10/8/2015	7	14	0.242	0.212	0.200	0.200		0.204	0.976
10/8/2015	7	14	0.067	0.389	0.389	0.356		0.378	0.976
10/8/2015	7	16	2.490	0.001	0.006	0.006		0.004	1.416
10/8/2015	7	16	2.200	0.000	0.000	0.000		0.000	1.416
10/8/2015	7	16	1.928	0.017	0.019	0.019		0.018	1.416
10/8/2015	7	16	1.748	0.027	0.040	0.040		0.036	1.416
10/8/2015	7	16	1.436	0.157	0.157	0.057		0.124	1.416
10/8/2015	7	16	1.153	0.036	0.127	0.127		0.097	1.416

Date	Transect	Distance from Left Bank (m)	Depth (m)	Velocity (m s^{-1}) (up to 4 repeated measures)					Depth to top of Vegetation (m)
				1	2	3	4	Avg.	
10/8/2015	7	16	0.881	0.055	0.216	0.216		0.162	1.416
10/8/2015	7	16	0.654	0.288	0.216	0.216		0.240	1.416
10/8/2015	7	16	0.358	0.202	0.219	0.219		0.213	1.416
10/8/2015	7	16	0.069	0.293	0.293	0.293		0.293	1.416
10/8/2015	7	18	2.525	0.001	0.000	0.000		0.000	1.260
10/8/2015	7	18	2.254	0.004	0.004	0.001		0.003	1.260
10/8/2015	7	18	2.076	0.019	0.019	0.036		0.025	1.260
10/8/2015	7	18	1.716	0.051	0.051	0.051		0.051	1.260
10/8/2015	7	18	1.503	0.047	0.047	0.074		0.056	1.260
10/8/2015	7	18	1.288	0.145	0.145	0.093		0.128	1.260
10/8/2015	7	18	0.909	0.172	0.172	0.159		0.168	1.260
10/8/2015	7	18	0.687	0.233	0.233	0.222		0.229	1.260
10/8/2015	7	18	0.304	0.209	0.237	0.237		0.228	1.260
10/8/2015	7	18	0.087	0.199	0.199	0.199		0.199	1.260
10/8/2015	7	20	3.041	0.000	0.000	0.000		0.000	1.667
10/8/2015	7	20	2.596	0.032	0.032	0.025		0.030	1.667
10/8/2015	7	20	2.329	0.043	0.043	0.043		0.043	1.667
10/8/2015	7	20	2.051	0.067	0.067	0.085		0.073	1.667
10/8/2015	7	20	1.720	0.145	0.055	0.036		0.079	1.667
10/8/2015	7	20	1.365	0.168	0.231	0.231		0.210	1.667
10/8/2015	7	20	1.025	0.193	0.193	0.193		0.193	1.667
10/8/2015	7	20	0.680	0.232	0.232	0.227		0.230	1.667
10/8/2015	7	20	0.315	0.265	0.231	0.231		0.242	1.667
10/8/2015	7	20	0.071	0.218	0.218	0.280		0.239	1.667
10/8/2015	7	22	3.541	0.000	0.000	0.000		0.000	1.997
10/8/2015	7	22	3.130	0.000	0.000	0.000		0.000	1.997
10/8/2015	7	22	2.777	0.039	0.018	0.018		0.025	1.997
10/8/2015	7	22	2.301	0.027	0.106	0.075		0.069	1.997
10/8/2015	7	22	1.905	0.099	0.157	0.181		0.146	1.997
10/8/2015	7	22	1.545	0.239	0.231	0.207		0.226	1.997
10/8/2015	7	22	1.112	0.249	0.243	0.237		0.243	1.997
10/8/2015	7	22	0.695	0.279	0.266	0.231		0.259	1.997
10/8/2015	7	22	0.298	0.263	0.220	0.206		0.230	1.997
10/8/2015	7	22	0.056	0.206	0.289	0.223		0.239	1.997
10/8/2015	7	24	3.687	0.008	0.008	0.007		0.008	2.865
10/8/2015	7	24	3.209	0.002	0.002	0.002		0.002	2.865
10/8/2015	7	24	2.876	0.051	0.122	0.122		0.098	2.865
10/8/2015	7	24	2.458	0.194	0.232	0.232		0.219	2.865
10/8/2015	7	24	2.063	0.268	0.257	0.257		0.261	2.865
10/8/2015	7	24	1.755	0.284	0.276	0.257		0.272	2.865
10/8/2015	7	24	1.394	0.210	0.161	0.161		0.177	2.865
10/8/2015	7	24	1.040	0.276	0.276	0.276		0.276	2.865
10/8/2015	7	24	0.686	0.257	0.196	0.196		0.216	2.865
10/8/2015	7	24	0.134	0.230	0.230	0.230		0.230	2.865
10/8/2015	7	26	3.785	0.005	0.003	0.003		0.004	3.144
10/8/2015	7	26	3.199	0.046	0.094	0.094		0.078	3.144

Date	Transect	Distance from Left Bank (m)	Depth (m)	Velocity (m s^{-1}) (up to 4 repeated measures)					Depth to top of Vegetation (m)
				1	2	3	4	Avg.	
10/8/2015	7	26	2.852	0.220	0.220	0.220		0.220	3.144
10/8/2015	7	26	2.425	0.313	0.294	0.294		0.300	3.144
10/8/2015	7	26	2.027	0.332	0.265	0.265		0.287	3.144
10/8/2015	7	26	1.650	0.301	0.301	0.260		0.287	3.144
10/8/2015	7	26	1.255	0.277	0.254	0.254		0.262	3.144
10/8/2015	7	26	0.896	0.257	0.257	0.255		0.256	3.144
10/8/2015	7	26	0.412	0.250	0.250	0.258		0.253	3.144
10/8/2015	7	26	0.055	0.281	0.281	0.281		0.281	3.144
10/8/2015	7	28	3.738	0.000	0.007	0.007		0.005	2.900
10/8/2015	7	28	3.246	0.034	0.034	0.061		0.043	2.900
10/8/2015	7	28	2.776	0.266	0.266	0.144		0.225	2.900
10/8/2015	7	28	2.357	0.174	0.174	0.287		0.212	2.900
10/8/2015	7	28	1.880	0.321	0.292	0.292		0.302	2.900
10/8/2015	7	28	1.367	0.279	0.322	0.322		0.308	2.900
10/8/2015	7	28	0.868	0.272	0.267	0.267		0.269	2.900
10/8/2015	7	28	0.600	0.310	0.310	0.277		0.299	2.900
10/8/2015	7	28	0.215	0.278	0.278	0.272		0.276	2.900
10/8/2015	7	28	0.063	0.316	0.316	0.231		0.288	2.900
10/8/2015	7	30	3.440	0.024	0.024	0.041		0.030	3.018
10/8/2015	7	30	2.960	0.129	0.129	0.161		0.140	3.018
10/8/2015	7	30	2.527	0.204	0.221	0.221		0.215	3.018
10/8/2015	7	30	2.175	0.305	0.342	0.342		0.330	3.018
10/8/2015	7	30	1.755	0.291	0.318	0.318		0.309	3.018
10/8/2015	7	30	1.305	0.359	0.322	0.322		0.334	3.018
10/8/2015	7	30	1.068	0.275	0.275	0.249		0.266	3.018
10/8/2015	7	30	0.670	0.295	0.352	0.352		0.333	3.018
10/8/2015	7	30	0.302	0.283	0.283	0.273		0.280	3.018
10/8/2015	7	30	0.067	0.255	0.255	0.311		0.274	3.018
10/8/2015	7	32	3.245	0.023	0.023	0.063		0.036	3.140
10/8/2015	7	32	2.816	0.014	0.014	0.140		0.056	3.140
10/8/2015	7	32	2.440	0.247	0.247	0.300		0.265	3.140
10/8/2015	7	32	2.040	0.347	0.347	0.347		0.347	3.140
10/8/2015	7	32	1.733	0.406	0.406	0.352		0.388	3.140
10/8/2015	7	32	1.308	0.289	0.289	0.325		0.301	3.140
10/8/2015	7	32	1.081	0.379	0.379	0.354		0.371	3.140
10/8/2015	7	32	0.764	0.304	0.304	0.279		0.296	3.140
10/8/2015	7	32	0.386	0.327	0.327	0.260		0.305	3.140
10/8/2015	7	32	0.123	0.372	0.265	0.265		0.301	3.140
10/8/2015	7	39	2.560	0.023	0.023	0.023		0.023	1.680
10/8/2015	7	39	2.297	0.038	0.038	0.033		0.036	1.680
10/8/2015	7	39	2.107	0.015	0.010	0.010		0.012	1.680
10/8/2015	7	39	1.772	0.035	0.035	0.023		0.031	1.680
10/8/2015	7	39	1.518	0.084	0.084	0.099		0.089	1.680
10/8/2015	7	39	1.219	0.054	0.039	0.039		0.044	1.680
10/8/2015	7	39	0.920	0.113	0.113	0.180		0.135	1.680
10/8/2015	7	39	0.719	0.201	0.189	0.189		0.193	1.680

Date	Transect	Distance from Left Bank (m)	Depth (m)	Velocity (m s^{-1}) (up to 4 repeated measures)					Depth to top of Vegetation (m)
				1	2	3	4	Avg.	
10/8/2015	7	39	0.344	0.173	0.173	0.141		0.162	1.680
10/8/2015	7	39	0.101	0.096	0.235	0.235		0.189	1.680
10/8/2015	7	44	1.698	0.000	0.000	0.000		0.000	1.240
10/8/2015	7	44	1.505	0.000	0.000	0.000		0.000	1.240
10/8/2015	7	44	1.397	0.010	0.010	0.000		0.007	1.240
10/8/2015	7	44	1.275	0.044	0.044	0.033		0.040	1.240
10/8/2015	7	44	1.137	0.008	0.008	0.008		0.008	1.240
10/8/2015	7	44	0.962	0.018	0.018	0.012		0.016	1.240
10/8/2015	7	44	0.787	0.066	0.066	0.061		0.064	1.240
10/8/2015	7	44	0.629	0.039	0.034	0.034		0.036	1.240
10/8/2015	7	44	0.336	0.069	0.069	0.069		0.069	1.240
10/8/2015	7	44	0.175	0.020	0.020	0.630		0.223	1.240

Appendix 6.1 Nutrient limitation assays were deployed at 28 locations that spanned longitudinally across Silver River (Note: In order of deployment, not longitudinal location).

#	Latitude (N)	Longitude (W)
1	29.207034	81.996546
2	29.215222	82.041441
3	29.215222	82.041441
4	29.215062	82.044703
5	29.215069	82.044699
6	29.211968	82.035284
7	29.205928	82.028676
8	29.202438	82.016842
9	29.203147	82.014248
10	29.202143	82.010566
11	29.207038	81.997353
12	29.208000	81.995850
13	29.202030	82.010270
14	29.202000	82.011417
15	29.202116	82.018116
16	29.202100	82.020250
17	29.204150	82.025166
18	29.204283	82.027783
19	29.206050	82.029800
20	29.207900	82.032767
21	29.211070	82.035250
22	29.213020	82.036670
23	29.215210	82.041600
24	29.215220	82.041570
25	29.215220	82.041570
26	29.206996	81.997591
27	29.207300	81.996733
28	29.205440	82.002230

Appendix 6.2. Site characteristics.

Table 6.2.1. Site characteristics (mean ± standard deviation) at Silver River.

Site	1	2	3	4	5	6	7	8
Water Depth (m)	0.9 ± 0.05	0.78 ± 0.05	0.93 ± 0	0.92 ± 0.03	0.79 ± 0.07	0.73 ± 0.02	0.87 ± 0.14	0.6 ± 0.07
Flow Velocity (m/s)	0 ± 0	0.15 ± 0.07	0.25 ± 0	0.16 ± 0.06	0.19 ± 0.02	0.1 ± 0.02	0.34 ± 0.06	0.1 ± 0.01
Incident Light (W/m^2)	88.57 ± 45.45	133.7 ± 35.27	128.85 ± 20.6	101.77 ± 26.9	85.41 ± 26.04	119.57 ± 23.69	42.04 ± 29.27	46.29 ± 17.66
Canopy Cover (%)	57.45 ± 19.16	34.96 ± 10.75	44.36 ± 0	51.63 ± 8.65	58.06 ± 9.91	41.82 ± 10.84	77.76 ± 15.26	76.2 ± 10.39
Algal Cover (Braun-Blanquet)	5 ± 1	1 ± 0	5 ± 0	5 ± 1	1 ± 1	5 ± 0	2 ± 1	5 ± 1
Sediment Organic Matter (%)	32.71 ± 13.56	41.4 ± 0	15.8 ± 0	23.05 ± 7.31	20.65 ± 5.2	10.48 ± 6.89	5.27 ± 1.34	20.98 ± 5.35
Water Column Ca (mg/L)	88.12 ± 2.32	80.05 ± 0	80.39 ± 0	80.4 ± 0.66	80.48 ± 1.1	82.68 ± 3.46	80.71 ± 1.47	80.45 ± 1.07
Water Column Cl (mg/L)	12.04 ± 0.44	11.72 ± 0	11.6 ± 0	11.94 ± 0.23	11.79 ± 0.08	11.8 ± 0.57	11.77 ± 0.21	11.85 ± 0.44
Water Column NH_3-N (mg/L)	0.17 ± 0.08	0.23 ± 0	0.24 ± 0	0.15 ± 0.05	0.14 ± 0.06	0.3 ± 0.53	0.17 ± 0.04	0.2 ± 0.07
Water Column NO_x-N (mg/L)	1.94 ± 0.3	1.73 ± 0	1.49 ± 0	1.35 ± 0.08	1.33 ± 0.07	1.28 ± 0.17	1.24 ± 0.04	1.39 ± 0.09
Water Column OrthoP (µg/L)	49.58 ± 13.08	36.48 ± 0	38.35 ± 0	35.48 ± 3.02	31.39 ± 4.46	57.65 ± 60.15	43.12 ± 18.23	40.82 ± 11.9
Porewater Ca (mg/L)	93.25 ± 5.2	68.24 ± 0	112.63 ± 0	112.47 ± 14.5	97.11 ± 24.2	94.57 ± 25.45	99.87 ± 12.96	104 ± 29.59
Porewater Cl (mg/L)	11.48 ± 0.85	12.34 ± 0	12.24 ± 0	14.83 ± 1.32	14.39 ± 5.19	14.72 ± 5.15	14.19 ± 1.19	15.69 ± 4.74
Porewater NH_3-N (mg/L)	0.47 ± 0.2	0.19 ± 0	0.51 ± 0	0.73 ± 0.48	0.54 ± 0.26	0.05 ± 0	0.21 ± 0.02	0.41 ± 0.12
Porewater NO_x-N (mg/L)	0.77 ± 0.19	0.53 ± 0	0.28 ± 0	0.57 ± 0.17	1.54 ± 0.47	0.75 ± 0.35	0.56 ± 0.37	0.6 ± 0.47
Porewater OrthoP (µg/L)	115.6 ± 24.5	27.6 ± 0	189.2 ± 0	1687 ± 827.7	21.7 ± 11.5	224.4 ± 152.5	167.9 ± 107.4	119.8 ± 38.7
Sediment P (mg/kg)	13.81 ± 6.66	58.59 ± 0	3.46 ± 0	12.46 ± 1.23	1.85 ± 1.68	7.53 ± 3.55	13.34 ± 6.41	12.61 ± 0.27
Sediment K (mg/kg)	17.0 ± 14.1	43.5 ± 0	12.3 ± 0	33.1 ± 10.8	23.0 ± 3.0	20.4 ± 17.0	20.8 ± 15.8	35.2 ± 3.2
Sediment Ca (mg/kg)	6211.0 ± 509.5	4127.3 ± 0	6262.9 ± 0	6206.3 ± 415	2736.3 ± 2358.5	6673.8 ± 570.9	6570.0 ± 388.3	6472.2 ± 309.5
Sediment Mg (mg/kg)	441.1 ± 139.2	541.1 ± 0	224.2 ± 0	248.2 ± 5.7	116.7 ± 116.8	198.3 ± 42.1	167.6 ± 53.3	303.9 ± 15.4
Sediment Mn (mg/kg)	BDL	BDL	BDL	0.05 ± 0.05	0.02 ± 0.06	0 ± 0.01	0.3 ± 0.19	0.44 ± 0.25
Sediment Fe (mg/kg)	BDL	BDL	BDL	BDL	BDL	BDL	BDL	BDL
Sediment %C	22.98 ± 7.53	40.62 ± 0	16.35 ± 0	16.08 ± 0.97	17.67 ± 1.58	14.43 ± 1.01	13.4 ± 0.43	17.73 ± 1.06
Sediment %N	0.98 ± 0.43	2.26 ± 0	0.42 ± 0	0.61 ± 0.09	1.03 ± 0.25	0.47 ± 0.14	0.27 ± 0.08	0.98 ± 0.18
Sediment %S	0.46 ± 0	2.49 ± 0	0.23 ± 0	0.53 ± 0	0.55 ± 0	0.24 ± 0	0.07 ± 0	0.65 ± 0
Shallow Redox Potential (mV)	-	-	-	-	-	-	-	-289.5 ± 0
Medium Redox Potential (mV)	-	-	-	-	-	-	-	-303.7 ± 0
Deep Redox Potential (mV)	-	-	-	-	-	-	-	-326.6 ± 0

Table 6.2.1. continued.

Site	9	10	11	12	13	14	15	16
Water Depth (m)	0.68 ± 0.06	0.48 ± 0.06	0.62 ± 0.09	0.55 ± 0.05	0.32 ± 0.04	0.39 ± 0.09	0.78 ± 0.24	0.36 ± 0.1
Flow Velocity (m/s)	0.37 ± 0.02	0.13 ± 0.02	0.29 ± 0.01	0.15 ± 0.07	0.09 ± 0.02	0.08 ± 0.02	0.24 ± 0.01	0.06 ± 0.03
Incident Light (W/m²)	127.98 ± 30.13	56.93 ± 26.31	62.39 ± 10.62	55.77 ± 43.26	153.6 ± 38.41	169.01 ± 51.29	30.78 ± 12.28	38.2 ± 25.91
Canopy Cover (%)	35.35 ± 20.74	69.82 ± 16.55	70.45 ± 5.7	72.84 ± 17.6	26.32 ± 4.25	19.57 ± 8.17	85.02 ± 4.27	79.12 ± 17.7
Algal Cover (Braun-Blanquet)	2 ± 1	2 ± 1	4 ± 1	2 ± 1	1 ± 1	4 ± 1	4 ± 1	2 ± 1
Sediment Organic Matter (%)	5.51 ± 1.23	5.05 ± 2.16	4.16 ± 1.49	18.27 ± 10.54	15.24 ± 6.52	10.44 ± 3	19.36 ± 8.22	17.09 ± 4.47
Water Column Ca (mg/L)	79.97 ± 1.48	79.83 ± 1.49	79.89 ± 1.53	79.94 ± 1.49	79.5 ± 0.88	80.83 ± 1.04	81.47 ± 0.65	80.01 ± 2.2
Water Column Cl (mg/L)	11.7 ± 0.15	11.54 ± 0.2	11.57 ± 0.24	11.91 ± 0.16	10.84 ± 0.76	11.78 ± 0.37	11.64 ± 0.17	13.55 ± 2.02
Water Column NH_3-N (mg/L)	0.14 ± 0.07	0.14 ± 0.06	0.14 ± 0.07	0.11 ± 0.06	0.16 ± 0.07	0.13 ± 0.05	0.14 ± 0.05	0.11 ± 0.06
Water Column NO_x-N (mg/L)	1.27 ± 0.1	1.19 ± 0.09	1.22 ± 0.08	1.25 ± 0.08	1.24 ± 0	1.35 ± 0.11	1.29 ± 0.08	1.27 ± 0.19
Water Column OrthoP (µg/L)	28.26 ± 6.24	28.05 ± 8.33	27.07 ± 1.28	29.25 ± 3.69	47.96 ± 12.32	35.38 ± 4.56	32.53 ± 1.21	20.84 ± 11.78
Porewater Ca (mg/L)	98.39 ± 12.88	84.94 ± 2.36	84.2 ± 2.85	105.03 ± 22.81	89.44 ± 5.41	91.75 ± 7.35	89.95 ± 4.24	107.84 ± 24.58
Porewater Cl (mg/L)	13.51 ± 3.39	13.57 ± 0.62	12.12 ± 0.18	13.34 ± 0.65	12.69 ± 0.23	14.92 ± 1.58	12.57 ± 0.64	16.78 ± 5
Porewater NH_3-N (mg/L)	0.05 ± 0.01	0.21 ± 0.1	0.14 ± 0.06	0.11 ± 0.03	0.07 ± 0.01	0.67 ± 0.21	0.05 ± 0	0.05 ± 0.01
Porewater NO_x-N (mg/L)	0.65 ± 0.33	0.89 ± 0.15	1.11 ± 0.08	0.64 ± 0.53	0.95 ± 0.12	1.18 ± 0	0.47 ± 0.3	0.56 ± 0.41
Porewater OrthoP (µg/L)	145.5 ± 77.2	108.2 ± 45.6	20.0 ± 14.1	359.7 ± 302.2	56.1 ± 7.9	126.3 ± 62.8	265.8 ± 102.3	537.3 ± 457.5
Sediment P (mg/kg)	6.81 ± 1	7.86 ± 0.01	6.77 ± 1.64	20.82 ± 4.86	19.03 ± 2.71	10.28 ± 2.55	16.08 ± 2.56	15.95 ± 1.28
Sediment K (mg/kg)	21.1 ± 5.5	15.5 ± 2.8	12.2 ± 0.5	40.6 ± 21.8	30.1 ± 5.3	22.5 ± 6.1	24.9 ± 7.1	28.0 ± 11.2
Sediment Ca (mg/kg)	6750.2 ± 605	6691.5 ± 498.3	6883.3 ± 576.4	6748.5 ± 358.8	6569.2 ± 290.9	6429.2 ± 294	5517.7 ± 855.8	6447.0 ± 312
Sediment Mg (mg/kg)	134.2 ± 16.9	158.4 ± 24.0	136.4 ± 25.1	244.45 ± 56.8	226.9 ± 49.8	183.6 ± 30.3	289.6 ± 72.4	251.8 ± 29.5
Sediment Mn (mg/kg)	0.19 ± 0.05	0.38 ± 0.05	0.48 ± 0.34	0.59 ± 0.09	0.32 ± 0.03	0.35 ± 0.1	0.65 ± 0.06	0.86 ± 0.38
Sediment Fe (mg/kg)	BDL	BDL	BDL	BDL	BDL	BDL	BDL	BDL
Sediment %C	11.43 ± 0.58	14.51 ± 1.09	12.48 ± 0.6	16.75 ± 4.31	14.05 ± 2.67	14.91 ± 1.63	17.39 ± 2.05	16.15 ± 0.81
Sediment %N	0.26 ± 0.02	0.3 ± 0.1	0.22 ± 0.07	0.68 ± 0.32	0.62 ± 0.2	0.47 ± 0.16	0.8 ± 0.28	0.65 ± 0.09
Sediment %S	0.11 ± 0	0.09 ± 0	0.05 ± 0	0.82 ± 0	0.54 ± 0	0.14 ± 0	0.7 ± 0	0.71 ± 0
Shallow Redox Potential (mV)	204.39 ± 0	-277.8 ± 0	29.02 ± 0	-64.56 ± 0	-190.1 ± 0	-237.76 ± 0	-	-100.30 ± 0
Medium Redox Potential (mV)	197.77 ± 0	-298.7 ± 0	-58.54 ± 0	-79.61 ± 0	-96.9 ± 0	-195.73 ± 0	-	-23.50 ± 0
Deep Redox Potential (mV)	114.36 ± 0	-292.4 ± 0	-83.85 ± 0	-201.3 ± 0	-212.4 ± 0	-248.65 ± 0	-	-152.80 ± 0

Table 6.2.2. Site characteristics (mean ± standard deviation) at Alexander Springs Creek.

Site	1	2	3	4	5	6	7	8
Water Depth (m)	0.83 ± 0.04	0.61 ± 0.03	0.73 ± 0	0.75 ± 0.09	0.46 ± 0.08	0.48 ± 0.02	0.76 ± 0.05	0.6 ± 0.01
Flow Velocity (m/s)	0.03 ± 0	0.2 ± 0.02	0.17 ± 0	0.15 ± 0.03	0.09 ± 0.03	0.09 ± 0.04	0.15 ± 0	0.06 ± 0.03
Incident Light (W/m^2)	173.97 ± 29.14	117.11 ± 31.69	205.77 ± 25.89	114.75 ± 27.31	157.48 ± 35.46	166.41 ± 30.85	223.57 ± 38.59	37.61 ± 33.51
Canopy Cover (%)	22.52 ± 0	48.76 ± 10.34	14.72 ± 0	48.78 ± 8.88	31.46 ± 7.96	27.37 ± 4.29	2.24 ± 1.06	81.34 ± 18.97
Algal Cover (Braun-Blanquet)	5 ± 1	4 ± 1	5 ± 0	2 ± 1	4 ± 1	4 ± 2	5 ± 0	5 ± 1
Sediment Organic Matter (%)	9.16 ± 10.79	11.08 ± 6.62	8 ± 0	41.86 ± 20.7	9.97 ± 7.82	10.83 ± 6.37	8.88 ± 5.94	13.08 ± 6.85
Water Column Ca (mg/L)	49.16 ± 0	49.49 ± 0	48.15 ± 0	52.72 ± 0	48.03 ± 0	48.11 ± 0	48.01 ± 0	49.91 ± 0
Water Column Cl (mg/L)	260.27 ± 0	266.43 ± 0	268.98 ± 0	260.6 ± 0	263.77 ± 0	274.48 ± 0	265.1 ± 0	279.76 ± 0
Water Column NH_3-N (mg/L)	0.05 ± 0	0.04 ± 0	0.04 ± 0	0.05 ± 0	0.03 ± 0	0.05 ± 0	0.03 ± 0	0.03 ± 0
Water Column NO_x-N (mg/L)	0.42 ± 0	0.17 ± 0	0.14 ± 0	0.08 ± 0	0.38 ± 0	0.15 ± 0	0.12 ± 0	0.08 ± 0
Water Column OrthoP (µg/L)	34.53 ± 0	37.24 ± 0	28.6 ± 0	22.38 ± 0	39.65 ± 0	34.56 ± 0	39.77 ± 0	37.01 ± 0
Porewater Ca (mg/L)	48.52 ± 0	48.87 ± 0	95.87 ± 0	50.91 ± 0	50.1 ± 0	49.19 ± 0	50.43 ± 0	51.15 ± 0
Porewater Cl (mg/L)	278.95 ± 0	289.34 ± 0	286.85 ± 0	286.62 ± 0	232.24 ± 0	276.85 ± 0	276.98 ± 0	310.43 ± 0
Porewater NH_3-N (mg/L)	0.05 ± 0	0.35 ± 0	2.93 ± 0	0.05 ± 0	0.17 ± 0	0.03 ± 0	0.04 ± 0	0.06 ± 0
Porewater NO_x-N (mg/L)	0.09 ± 0	0.11 ± 0	0.12 ± 0	0.1 ± 0	0.42 ± 0	0.14 ± 0	0.13 ± 0	0.11 ± 0
Porewater OrthoP (µg/L)	42.08 ± 0	12.7 ± 0	29.51 ± 0	36.61 ± 0	106.77 ± 0	41.45 ± 0	88.45 ± 0	31.76 ± 0
Sediment P (mg/kg)	22.8 ± 17.6	563.1 ± 117.7	797.6 ± 0	110.6 ± 68.8	333.9 ± 112.4	226.3 ± 165.4	285.7 ± 0	158 ± 30.9
Sediment K (mg/kg)	119.1 ± 179.1	32.0 ± 19.7	7.8 ± 0	32.7 ± 1.8	23.7 ± 5.6	39.4 ± 10.2	79.9 ± 0	19.4 ± 2.9
Sediment Ca (mg/kg)	6497.9 ± 772.9	3766.4 ± 150.1	2804.9 ± 0	4624.3 ± 69.3	3965.9 ± 258.9	5426.1 ± 928.6	5503.3 ± 0	3688.2 ± 155.8
Sediment Mg (mg/kg)	401.2 ± 145.7	480.3 ± 100.6	88.7 ± 0	977.6 ± 53.2	537.5 ± 170.8	1122.6 ± 311.9	494.4 ± 0	598.7 ± 59.7
Sediment Mn (mg/kg)	0 ± 0.01	0.64 ± 0.14	0.81 ± 0	0.42 ± 0.17	0.84 ± 0.12	0.06 ± 0.19	0.89 ± 0	1.01 ± 0.08
Sediment Fe (mg/kg)	BDL	14.11 ± 3.67	6.79 ± 0	17.8 ± 6.61	18.01 ± 7.16	0.61 ± 2.08	33.84 ± 0	32.54 ± 10.91
Sediment %C	8.77 ± 3.89	3.99 ± 1.55	0.37 ± 0	12.53 ± 9.25	17.91 ± 9.36	14 ± 9.57	6.55 ± 0.04	4.7 ± 1.66
Sediment %N	0.5 ± 0.34	0.27 ± 0.11	0.03 ± 0	0.82 ± 0.6	1.05 ± 0.66	0.67 ± 0.45	0.39 ± 0.08	0.25 ± 0.09
Sediment %S	0.79 ± 0	0.05 ± 0	BDL	BDL	1.96 ± 0	0.06 ± 0	0.51 ± 0	0.12 ± 0
Shallow Redox Potential (mV)	-190.09 ± 0	-66.13 ± 0	-	-109.73 ± 0	-58.82 ± 0	-58.82 ± 0	-	-223.04 ± 0
Medium Redox Potential (mV)	-252.57 ± 0	-132.49 ± 0	-	-163.14 ± 0	-223.93 ± 0	-223.93 ± 0	-	-242.55 ± 0
Deep Redox Potential (mV)	-244.24 ± 0	-187.37 ± 0	-	-115.54 ± 0	-168.52 ± 0	-168.52 ± 0	-	-239.99 ± 0

Table 6.2.2. continued.

Site	9	10	11	12	13	14	15	16
Water Depth (m)	0.66 ± 0.01	0.42 ± 0.05	0.66 ± 0.03	0.56 ± 0.05	0.68 ± 0.06	0.56 ± 0.11	0.57 ± 0.05	0.52 ± 0.07
Flow Velocity (m/s)	0.07 ± 0.01	0.09 ± 0.05	0.05 ± 0.02	0.15 ± 0.01	0.17 ± 0.01	0.03 ± 0	0.23 ± 0.05	0.04 ± 0
Incident Light (W/m^2)	87.61 ± 16.18	104.55 ± 30.46	134.2 ± 55.86	208.42 ± 45.4	231.83 ± 39.23	117.3 ± 32.56	130.95 ± 60.58	219.51 ± 39.52
Canopy Cover (%)	62.4 ± 1.37	54.66 ± 8.8	43.24 ± 20.18	10.68 ± 10.23	0.16 ± 0	48.21 ± 10.47	40.14 ± 24.34	3.14 ± 2.53
Algal Cover (Braun-Blanquet)	5 ± 0	5 ± 0	3 ± 1	3 ± 2	2 ± 1	2 ± 1	2 ± 1	4 ± 1
Sediment Organic Matter (%)	6.1 ± 3.54	10.26 ± 4.09	5.52 ± 1.98	12.05 ± 11.19	20.02 ± 14.35	12.72 ± 8.18	1.94 ± 0.21	35 ± 10.24
Water Column Ca (mg/L)	48.15 ± 0	48.16 ± 0	49.61 ± 3.95	108.44 ± 0	46.05 ± 0	47.35 ± 0	53.98 ± 0	46.97 ± 0
Water Column Cl (mg/L)	272.74 ± 0	269.9 ± 0	279.24 ± 0	767.22 ± 0	265.32 ± 0	276.11 ± 0	335.47 ± 0	256.74 ± 0
Water Column NH_3-N (mg/L)	0.03 ± 0	0.03 ± 0	0.03 ± 0	0.04 ± 0	0.03 ± 0	0.03 ± 0	0.04 ± 0	0.03 ± 0
Water Column NO_x-N (mg/L)	0.1 ± 0	0.09 ± 0	0.1 ± 0	0.11 ± 0	0.09 ± 0	0.1 ± 0	0.05 ± 0	0.05 ± 0
Water Column OrthoP (µg/L)	36.83 ± 0	34.53 ± 0	35.32 ± 0	31.23 ± 0	40.38 ± 0	40.95 ± 0	48.56 ± 0	51.21 ± 0
Porewater Ca (mg/L)	80.27 ± 0	75.34 ± 0	47.07 ± 4.99	48.31 ± 0	87.73 ± 0	81.94 ± 0	46.11 ± 0	136.65 ± 0
Porewater Cl (mg/L)	454.39 ± 0	290.36 ± 0	258.39 ± 0	293.35 ± 0	492.86 ± 0	601.86 ± 0	246.74 ± 0	954.08 ± 0
Porewater NH_3-N (mg/L)	1.26 ± 0	0.05 ± 0	0.03 ± 0	0.04 ± 0	0.68 ± 0	0.31 ± 0	0.09 ± 0	0.04 ± 0
Porewater NO_x-N (mg/L)	0.13 ± 0	0.1 ± 0	0.12 ± 0.01	0.05 ± 0	0.09 ± 0	0.1 ± 0	0.09 ± 0	0.11 ± 0
Porewater OrthoP (µg/L)	135.84 ± 0	340.28 ± 0	75.57 ± 0	138.25 ± 0	124.38 ± 0	161.09 ± 0	141.08 ± 0	73.04 ± 0
Sediment P (mg/kg)	333.7 ± 37.5	46.4 ± 10	480.6 ± 57.7	111.6 ± 4.9	197.8 ± 22.8	146.3 ± 34.7	15.5 ± 3.4	113.9 ± 8.4
Sediment K (mg/kg)	37.5 ± 4.0	37.6 ± 13.4	15.0 ± 2.4	68.8 ± 15.1	261 ± 71.0	70.4 ± 8.2	6.5 ± 0.4	178.1 ± 49.2
Sediment Ca (mg/kg)	5493.9 ± 430.3	4271.6 ± 1576.3	2780.8 ± 304.9	5400.1 ± 760.3	5517.8 ± 843.7	4986.1 ± 321.3	773.8 ± 60.6	5151.3 ± 1091.8
Sediment Mg (mg/kg)	718.3 ± 48.1	829.2 ± 329.4	290.3 ± 28.5	1247.4 ± 248.3	1452.8 ± 345.8	1195.1 ± 155.3	123.4 ± 16.2	1616.9 ± 444.3
Sediment Mn (mg/kg)	0.97 ± 0.07	0.98 ± 0.5	0.63 ± 0.12	0.03 ± 0.09	0.02 ± 0.06	0.67 ± 0.03	0.02 ± 0.04	0.01 ± 0.02
Sediment Fe (mg/kg)	7.37 ± 0.74	12.42 ± 0.11	11.44 ± 1.9	0.81 ± 2.87	1.09 ± 3.86	0.2 ± 0.41	5.63 ± 1.13	1.96 ± 6.35
Sediment %C	10.18 ± 7.41	17.02 ± 8.58	4.68 ± 0.92	11.75 ± 11.06	10.24 ± 9	6.07 ± 4.15	1.26 ± 0.31	17.92 ± 5.16
Sediment %N	0.45 ± 0.29	0.83 ± 0.37	0.3 ± 0.06	0.65 ± 0.62	0.72 ± 0.68	0.4 ± 0.25	0.08 ± 0.01	1.2 ± 0.34
Sediment %S	0.13 ± 0	0.66 ± 0	0.23 ± 0	0.06 ± 0	0.13 ± 0	0.14 ± 0	0.07 ± 0	BDL
Shallow Redox Potential (mV)	-211.39 ± 0	-158.37 ± 0	-192.18 ± 0	-123.74 ± 0	-210.77 ± 0	-155.95 ± 0	-175.45 ± 0	-180.71 ± 0
Medium Redox Potential (mV)	38.97 ± 0	3.52 ± 0	-116.96 ± 0	-197.86 ± 0	-236.86 ± 0	-150.12 ± 0	-102.56 ± 0	-177.35 ± 0
Deep Redox Potential (mV)	-267.41 ± 0	-61.83 ± 0	-155.41 ± 0	-131.34 ± 0	-237.04 ± 0	-171.17 ± 0	-179.48 ± 0	-133.38 ± 0

Appendix 8.1. Sediment chemical composition

Site	Depth below SWI (cm)	TN (wt%)	TC (wt%)	$CaCO_3$ (wt%)	TIC (wt%)	TOC (wt%)	TP (wt%)	C:N	$\delta^{13}C_{org}$ (‰)	$\delta^{13}N_{org}$ (‰)
RM0.7	1	1.50	24.07	39.37	4.72	19.35	0.08	15.05	-26.98	3.56
	5	1.51	23.23	41.28	4.95	18.28	0.08	14.13	-28.31	3.33
	10	1.71	26.32	38.73	4.65	21.67	0.08	14.79	-28.27	3.38
	15	1.62	25.34	37.25	4.47	20.87	0.07	15.03	-28.09	3.22
	20	1.69	27.58	39.61	4.75	22.83	0.09	15.76	-27.71	3.20
	25	1.64	26.02	36.16	4.34	21.68	0.08	15.43	-28.35	3.20
	30	1.28	23.45	18.34	2.20	21.25	0.24	19.37	-23.42	1.66
	35	1.66	33.59	21.02	2.52	31.07	0.12	21.84	-23.79	1.40
	40	0.87	23.28	26.69	3.20	20.08	0.17	26.93	-23.96	1.29
	45	1.54	41.20	15.72	1.89	39.31	0.07	29.79	-25.51	-0.62
	50	2.07	41.29	11.69	1.40	39.89	0.10	22.49	-26.84	0.86
	60	1.85	48.98	0.21	0.03	48.95	0.13	30.88	-27.76	1.83
	70	2.73	44.56	0.95	0.11	44.45	0.17	19.00	-30.94	2.64
	80	2.58	45.55	1.11	0.13	45.42	0.10	20.54	-28.70	2.49
	90	2.69	46.81	0.44	0.05	46.76	0.21	20.28	-29.16	2.77
	100	1.17	30.22	20.53	2.46	27.76	0.25	27.69	-27.15	1.21
	110	1.89	32.43	30.07	3.61	28.82	0.09	17.80	-29.93	2.99
	120	1.46	26.11	44.35	5.32	20.79	0.08	16.62	-28.30	2.07
	130	1.16	23.17	56.54	6.78	16.39	0.09	16.49	-27.67	1.70
	140	1.02	22.53	63.23	7.59	14.94	0.08	17.09	-27.82	1.66
	150	0.34	15.56	87.14	10.46	5.10	0.05	17.51	-27.96	1.66
	160	0.66	18.69	78.96	9.48	9.21	0.07	16.28	-29.69	2.09
	170	0.26	14.48	90.19	10.82	3.66	0.01	16.43	-28.76	1.66
	180	0.18	14.07	91.19	10.94	3.13	0.04	20.29	-29.02	1.77
	190	0.20	14.16	91.07	10.93	3.23	0.07	18.85	-26.67	0.72
	200	0.28	13.84	89.60	10.75	3.09	0.16	12.88	-25.49	1.95
	210	0.21	14.14	89.78	10.77	3.37	0.12	18.73	-23.80	0.98
	220	0.18	13.95	91.17	10.94	3.01	0.01	19.52	-23.43	0.73
	230	0.12	13.23	88.12	10.57	2.66	0.01	25.87	-23.36	0.20
	240	0.15	13.44	91.84	11.02	2.42	0.01	18.83	-24.18	0.26
	250	0.19	14.03	89.41	10.73	3.30	0.01	20.27	-23.80	0.55
	260	0.20	13.98	89.72	10.77	3.21	0.03	18.75	-24.22	0.25
	270	0.22	14.51	88.54	10.62	3.89	0.04	20.61	-23.01	0.55

Site	Depth below SWI (cm)	TN (wt%)	TC (wt%)	$CaCO_3$ (wt%)	TIC (wt%)	TOC (wt%)	TP (wt%)	C:N	$\delta^{13}C_{org}$ (‰)	$\delta^{13}N_{org}$ (‰)
	280	0.48	17.41	81.18	9.74	7.67	0.05	18.64	-24.45	0.90
	290	0.36	16.12	83.92	10.07	6.05	0.09	19.61	-27.46	1.58
	300	0.90	21.71	65.75	7.89	13.82	0.06	17.92	-34.59	3.42
	310	0.61	18.06	75.45	9.05	9.01	0.03	17.24	-34.39	3.44
	320	0.69	18.73	74.20	8.90	9.83	0.03	16.63	-34.96	3.60
	330	0.82	20.83	23.50	2.82	18.01	0.13	25.63	-30.02	1.40
	339	2.05	33.40	34.75	4.17	29.23	0.13	16.64	-34.01	3.80
MFL7	1	0.71	17.38	61.54	7.39	9.99	0.48	16.43	-31.32	2.81
	5	1.01	20.83	57.90	6.95	13.88	0.49	16.04	-31.01	2.79
	10	0.79	17.71	53.58	6.43	11.28	0.51	16.66	-31.40	2.73
	15	1.09	21.33	49.29	5.92	15.41	0.50	16.50	-31.35	2.84
	20	1.18	22.40	45.17	5.42	16.98	0.94	16.79	-31.04	2.98
	25	1.06	20.25	53.19	6.38	13.87	0.61	15.27	-31.93	3.05
	30	0.74	14.43	45.54	5.47	8.96	0.50	14.14	-30.79	2.72
	35	0.60	14.42	58.17	6.98	7.44	0.93	14.47	-31.49	2.80
	40	0.71	17.57	68.16	8.18	9.39	0.92	15.43	-31.15	3.01
	45	0.66	17.95	67.65	8.12	9.83	0.70	17.38	-31.53	2.99
	50	1.27	22.78	48.88	5.87	16.91	0.53	15.54	-31.74	3.35
	60	0.74	18.80	67.53	8.10	10.70	0.36	16.87	-31.65	2.94
	70	0.67	17.10	63.14	7.58	9.52	0.41	16.59	-32.22	2.70
	80	0.51	16.32	74.81	8.98	7.34	0.93	16.80	-32.19	2.89
	90	0.53	16.75	72.74	8.73	8.02	0.30	17.66	-32.69	3.09
	100	0.75	19.34	62.00	7.44	11.90	0.73	18.52	-31.69	3.17
	110	0.69	17.80	65.56	7.87	9.93	0.36	16.80	-32.66	3.27
	120	0.60	16.45	65.97	7.92	8.53	0.72	16.60	-32.99	3.12
	130	0.50	16.59	76.17	9.14	7.45	0.53	17.39	-32.87	3.76
	140	0.07	11.02	85.32	10.24	0.78	0.44	13.03	-30.99	3.43
	150	0.13	12.09	84.49	10.14	1.95	0.66	17.51	-30.80	3.66
	160	0.09	12.33	92.25	11.07	1.26	0.08	16.33	-30.92	4.04
	170	0.04	6.56	29.56	3.55	3.01	0.54	87.89	-31.27	2.42
	180	0.25	14.59	82.66	9.92	4.67	0.56	21.80	-31.19	3.58
	190	0.48	16.30	75.59	9.07	7.23	0.53	17.58	-32.86	3.50
	200	0.04	6.93	53.58	6.43	0.50	0.57	14.59	-31.70	2.97

Site	Depth below SWI (cm)	TN (wt%)	TC (wt%)	$CaCO_3$ (wt%)	TIC (wt%)	TOC (wt%)	TP (wt%)	C:N	$\delta^{13}C_{org}$ (‰)	$\delta^{13}N_{org}$ (‰)
	210	0.36	14.07	73.52	8.82	5.25	0.56	17.01	-33.50	3.04
	220	0.81	18.70	57.83	6.94	11.76	0.69	16.94	-33.79	3.66
	230	0.49	15.51	74.37	8.92	6.59	0.39	15.68	-33.63	3.18
	240	0.49	15.70	73.25	8.79	6.91	0.35	16.46	-33.05	3.29
	250	0.66	18.27	73.74	8.85	9.42	0.25	16.66	-33.01	3.35
	260	0.48	15.73	75.05	9.01	6.72	0.21	16.35	-32.37	3.79
	270	0.30	11.42	59.08	7.09	4.33	0.28	16.84	-33.43	3.12
	280	1.27	23.58	46.48	5.58	18.00	0.36	16.54	-33.49	4.28
	290	0.71	17.25	54.53	6.54	10.71	0.42	17.60	-33.85	4.11
	300	0.67	15.22	51.74	6.21	9.01	0.50	15.70	-33.91	3.99
	310	0.60	14.79	56.57	6.79	8.00	0.44	15.56	-32.51	3.80
	320	0.11	10.52	71.73	8.61	1.91	0.11	20.29	-32.85	3.90
	330	0.07	4.57	25.14	3.02	1.55	0.14	25.89	-33.09	4.40
	340	0.31	14.05	65.99	7.92	6.13	0.12	23.08	-32.08	4.72
	350	0.15	9.03	50.38	6.05	2.98	0.20	23.22	-32.45	4.60
	360	0.50	15.69	58.54	7.03	8.66	0.18	20.22	-32.50	4.65
	370	0.02	4.84	33.61	4.03	0.81	0.74	47.06	-29.40	1.88
	380	0.05	10.35	78.79	9.46	0.89	0.11	20.89	-28.98	2.91
	390	0.03	7.89	60.75	7.29	0.60	0.06	23.33	-29.52	1.07
	400	0.02	8.12	55.69	6.68	1.44	0.09	83.85	-29.43	0.46
	410	0.12	11.69	81.93	9.83	1.86	0.69	18.07	-29.00	3.95
	417	0.14	11.33	67.46	8.10	3.23	0.77	26.96	-31.16	4.14
MFL6	1	0.75	17.66	61.83	7.42	10.24	0.41	15.93		
	5	0.82	18.15	65.96	7.92	10.23	0.27	14.57		
	10	0.95	19.33	61.84	7.42	11.91	0.27	14.63		
	15	1.06	21.03	58.21	6.99	14.04	0.74	15.46		
	20	1.57	26.56	43.68	5.24	21.32	0.64	15.85		
	25	1.04	21.04	57.44	6.89	14.15	0.28	15.87		
	30	0.39	14.88	76.08	9.13	5.75	0.14	17.21		
	35	0.56	16.81	72.26	8.67	8.14	0.19	16.96		
	40	0.74	18.18	63.20	7.58	10.60	0.25	16.71		
	45	0.67	17.35	66.41	7.97	9.38	0.72	16.34		
	50	0.39	14.46	73.00	8.76	5.70	0.16	17.06		
	60	0.50	15.44	70.97	8.52	6.92	0.21	16.16		

Site	Depth below SWI (cm)	TN (wt%)	TC (wt%)	$CaCO_3$ (wt%)	TIC (wt%)	TOC (wt%)	TP (wt%)	C:N	$\delta^{13}C_{org}$ (‰)	$\delta^{13}N_{org}$ (‰)
	70	0.70	17.67	56.82	6.82	10.85	0.22	18.09		
	80	0.94	20.39	63.79	7.66	12.73	0.27	15.81		
	90	0.99	20.58	58.01	6.96	13.62	0.79	16.05		
	100	1.13	22.39	48.29	5.80	16.59	0.33	17.14		
	110	0.66	17.43	62.78	7.53	9.90	0.22	17.50		
	120	0.51	15.31	59.48	7.14	8.17	0.27	18.70		
	130	0.65	17.99	63.20	7.58	10.41	0.21	18.68		
	140	0.96	21.02	52.56	6.31	14.71	0.24	17.88		
	150	0.64	18.11	64.74	7.77	10.34	0.18	18.86		
	160	1.06	22.59	55.35	6.64	15.95	0.29	17.56		
	170	0.89	20.43	58.98	7.08	13.35	0.22	17.51		
	180	0.75	18.41	60.82	7.30	11.11	0.23	17.29		
	190	0.61	17.26	66.04	7.93	9.33	0.19	17.86		
	200	0.32	12.95	68.35	8.20	4.75	0.09	17.31		
	210	0.03	6.64	56.39	6.77	-0.13	0.10	0.00		
	220	0.33	13.78	68.21	8.19	5.59	0.10	19.78		
	230	0.06	8.92	71.24	8.55	0.37	0.86	7.22		
	240	0.13	11.05	76.53	9.18	1.87	0.11	16.75		
MFL3	1	1.32	24.53	34.78	4.17	20.36	0.13	18.00	-29.42	4.88
	5	1.30	23.79	39.10	4.69	19.10	0.36	17.15	-29.71	4.72
	10	1.18	21.74	45.42	5.45	16.29	0.12	16.11	-29.44	4.48
	15	1.03	20.54	47.34	5.68	14.86	0.14	16.84	-29.32	4.46
	20	1.04	20.56	52.61	6.31	14.25	0.10	15.99	-29.14	4.25
	25	0.49	16.74	67.16	8.06	8.68	0.07	20.67	-28.48	3.64
	30	0.36	14.88	81.54	9.78	5.10	0.06	16.53	-28.28	2.12
	35	0.38	15.23	81.57	9.79	5.44	0.06	16.71	-27.63	2.32
	40	0.42	15.94	78.71	9.45	6.49	0.06	18.03	-27.81	2.00
	45	0.54	16.80	71.97	8.64	8.16	0.07	17.64	-29.10	2.61
	50	0.23	13.54	84.29	10.11	3.43	0.05	17.40	-28.22	2.44
	60	0.21	13.21	82.88	9.95	3.26	0.07	18.12	-28.17	2.33
	70	0.23	13.12	81.51	9.78	3.34	0.08	16.95	-28.64	2.26
	80	0.27	13.62	80.27	9.63	3.99	0.07	17.25	-28.25	2.12
	90	0.18	12.86	81.58	9.79	3.07	0.07	19.90	-28.27	2.40
	100	0.19	13.05	82.51	9.90	3.15	0.07	19.35	-28.34	2.36

Site	Depth below SWI (cm)	TN (wt%)	TC (wt%)	$CaCO_3$ (wt%)	TIC (wt%)	TOC (wt%)	TP (wt%)	C:N	$\delta^{13}C_{org}$ (‰)	$\delta^{13}N_{org}$ (‰)
	110	0.21	12.86	81.33	9.76	3.10	0.07	17.23	-28.33	2.16
	120	0.21	12.94	80.94	9.71	3.23	0.07	17.95	-28.33	2.35
	130	0.29	13.94	79.26	9.51	4.43	0.08	17.83	-28.34	2.07
	140	0.27	13.54	79.76	9.57	3.97	0.07	17.16	-27.92	2.23
	150	0.24	13.37	81.46	9.78	3.59	0.07	17.46	-28.12	2.45
	160	0.28	13.38	76.72	9.21	4.17	0.08	17.38	-28.43	2.46
	170	0.32	14.02	78.14	9.38	4.64	0.08	16.92	-28.26	2.11
	180	0.26	13.11	79.41	9.53	3.58	0.07	16.07	-28.16	2.29
	190	0.24	13.34	79.19	9.50	3.84	0.08	18.67	-27.85	2.43
	200	0.26	13.13	78.49	9.42	3.71	0.07	16.65	-28.24	2.34
	210	0.23	13.09	80.90	9.71	3.38	0.07	17.15	-28.01	2.48

Appendix 8.2. Sediment pore water chemistry

Site/Date	Depth below SWI (cm)	F (mM)	Cl (mM)	SO_4 (mM)	Na (mM)	K (mM)	Mg (mM)	Ca (mM)	H_2S (mg L^{-1})	NO_3 (µg L^{-1})	SRP (µg L^{-1})	NH_4 (µg L^{-1})	SiO_2 (µg L^{-1})	Fe (ppb)	Mn (ppb)
CL5	WC	0.006	0.33	0.48	0.30	0.02	0.44	1.90	-1.15	1,186	23	11	3,594	0.78	0.05
8/4/2016	1	0.011	0.74	0.37	0.32	0.04	0.42	2.10	-1.15	931	91	169	7,374	4.14	2.52
	3	0.015	0.34	0.42	0.31	0.03	0.42	2.09	-0.76	808	73	209	5,838	11.97	2.30
	5	0.020	0.34	0.45	0.34	0.03	0.43	2.08	-0.54	833	83	320	9,286	2.85	2.77
	7	0.023	0.34	0.21	0.34	0.02	0.48	1.90	9.13	261	85	762	10,552	22.26	2.60
	9	0.015	0.34	0.23	0.33	0.02	0.46	1.88	5.57	361	101	931	9,945	28.51	2.32
	11	0.044	0.36	0.07	0.34	0.03	0.45	1.80	11.33	264	94	1,096	8,566	33.48	2.51
	13	n.a.	0.34	0.12	0.33	0.02	0.42	1.61	11.91	13	72	605	9,574	34.08	1.21
	15	0.009	0.71	0.09	0.31	0.02	0.42	1.65	13.16	-3	64	688	5,926	5.38	1.19
	18	0.021	0.32	0.04	0.31	0.02	0.41	1.68	6.67	19	97	694	12,644	18.07	2.03
	21	0.026	0.33	0.07	0.30	0.02	0.40	1.64	6.74	33	80	466	8,483	18.33	1.63
	24	0.080	0.38	0.10	0.36	0.05	0.41	1.69	5.21	332	114	796	11,147	15.58	8.09
	27	0.008	0.32	0.06	0.30	0.02	0.41	1.67	13.31	28	109	1,028	12,292	7.81	2.59
	30	0.052	0.35	0.09	0.34	0.04	0.40	1.67	4.73	56	110	1,440	11,814	15.04	1.76
	33	0.011	0.34	0.05	0.30	0.02	0.39	1.60	8.41	16	111	1,496	12,138	7.98	1.71
RM0.7	WC	0.009	0.33	0.46	0.30	0.02	0.42	1.80	-0.04	772	13	19	2,604	0.15	0.22
5/22/2015	2	0.010	0.45	0.27	0.39	0.03	0.45	2.04	1.15	682	346	5,481	10,716	30.69	34.97
	4	0.008	0.39	0.06	0.33	0.05	0.51	2.68	12.31	50	863	8,010	15,583	38.93	67.26
	6	0.009	0.32	0.07	0.33	0.04	0.52	2.61	12.17	-26	1,040	7,947	24,892	9.25	47.28
	8	0.008	0.43	0.07	0.36	0.06	0.62	3.23	12.09	2	800	10,387	19,599	55.51	38.50
	10	0.006	0.47	0.06	0.38	0.06	0.68	3.64	22.57	-38	773	10,692	23,418	6.14	13.59
	12	0.006	0.52	0.07	0.40	0.06	0.72	3.81	26.20	-25	763	10,339	26,304	8.21	13.07
	14	0.007	0.49	0.07	0.39	0.06	0.70	3.74	23.87	-14	768	8,758	29,675	4.74	12.30

Site/Date	Depth below SWI (cm)	F (mM)	Cl (mM)	SO_4 (mM)	Na (mM)	K (mM)	Mg (mM)	Ca (mM)	H_2S (mg L^{-1})	NO_3 (µg L^{-1})	SRP (µg L^{-1})	NH_4 (µg L^{-1})	SiO_2 (µg L^{-1})	Fe (ppb)	Mn (ppb)
	17	0.005	0.51	0.07	0.40	0.05	0.69	3.74	29.55	9	670	9,335	15,551	2.09	9.89
	20	0.006	0.52	0.08	0.40	0.05	0.68	3.73	28.44	-41	619	7,101	23,575	1.62	9.98
	23	n.a.	0.52	0.06	0.40	0.05	0.68	3.69	29.48	-48	513	7,595	19,911	3.65	9.42
	26	n.a.	0.52	0.07	0.39	0.04	0.65	3.58	27.16	-35	450	7,132	17,125	1.76	9.40
	29	0.006	0.51	0.07	0.39	0.04	0.63	3.49	29.43	-36	301	5,081	10,881	0.79	8.85
	32	0.007	0.49	0.17	0.38	0.04	0.62	3.39	25.52	-28	359	6,273	18,703	2.91	7.96
	35	0.007	0.39	0.34	0.37	0.03	0.56	3.08	24.44	-57	323	5,827	16,866	1.18	5.84
	155	0.005	0.46	0.25	0.49	0.02	0.40	1.45	16.10	78	18	1,833	1,962	8.19	9.00
	210	0.008	0.35	0.43	0.32	0.02	0.39	1.37	14.04	78	34	2,396	717	3.20	2.07
	272	0.007	0.38	0.14	0.40	0.02	0.37	1.32	16.23	14	18	1,466	5,604	7.22	10.48
MFL7	WC	0.007	0.33	0.47	0.30	0.02	0.43	1.88	-0.29	726	15	21	2,157	1.03	-0.32
1/12/2016	1	0.009	0.34	0.12	0.32	0.04	0.48	2.51	6.69	347	2,987	9,147	17,883	4.03	17.88
	3	n.a.	0.34	0.05	0.33	0.06	0.59	3.24	7.40	121	4,666	18,580	20,395	3.47	25.18
	5	n.a.	0.33	0.04	0.34	0.07	0.62	3.46	7.35	36	4,974	17,955	24,997	3.68	26.76
	7	n.a.	0.34	0.04	0.34	0.07	0.65	3.66	6.85	29	5,111	21,809	36,174	4.58	28.85
	9	n.a.	0.29	0.03	0.34	0.07	0.66	3.74	7.02	-2	5,148	20,555	31,630	4.07	27.94
	11	n.a.	0.33	0.04	0.34	0.08	0.67	3.81	7.77	35	4,824	25,581	29,984	3.91	25.30
	13	0.005	0.27	0.03	0.34	0.08	0.69	3.89	7.31	1	4,762	22,195	28,084	17.68	25.84
	15	n.a.	0.33	0.03	0.34	0.08	0.70	4.02	8.96	24	4,860	28,394	27,964	3.26	23.15
	18	0.010	0.34	0.03	0.34	0.09	0.71	4.07	8.32	45	4,066	26,848	27,525	3.92	19.68
	21	0.011	0.34	0.04	0.34	0.09	0.70	4.04	8.68	51	4,978	27,809	30,241	4.22	20.42
	24	0.005	0.35	0.04	0.34	0.08	0.71	4.15	11.40	8	3,265	27,440	30,267	6.17	18.22
	27	0.014	0.34	0.04	0.34	0.09	0.71	4.18	11.53	49	2,701	25,164	28,316	5.09	17.38

Site/Date	Depth below SWI (cm)	F (mM)	Cl (mM)	SO_4 (mM)	Na (mM)	K (mM)	Mg (mM)	Ca (mM)	H_2S (mg L^{-1})	NO_3 (µg L^{-1})	SRP (µg L^{-1})	NH_4 (µg L^{-1})	SiO_2 (µg L^{-1})	Fe (ppb)	Mn (ppb)
	30	n.a.	0.34	0.04	0.34	0.08	0.71	4.19	11.03	39	4,526	26,841	26,525	2.26	18.54
	33	n.a.	0.34	0.04	0.33	0.08	0.71	4.21	10.25	23	2,600	21,871	26,427	1.80	20.27
3/8/2016	WC	0.008	0.33	0.48	0.30	0.02	0.44	1.87	-0.62	1,044	17	22	2,645	1.84	0.63
	180	0.004	0.78	0.26	0.69	0.03	1.03	4.29	34.18	22	137	12,861	2,372	53.39	152.20
MFL6	WC	0.009	0.34	0.47	0.30	0.02	0.43	1.89	-0.28	1312	9	15	1,832	0.94	-0.20
1/12/2016	1	0.006	0.36	0.44	0.32	0.02	0.44	1.96	0.14	479	1,736	373	11,247	8.09	14.94
	3	0.006	0.35	0.38	0.31	0.02	0.44	2.10	0.80	273	1,884	228	14,640	4.53	8.95
	5	0.005	0.37	0.34	0.33	0.02	0.46	2.30	2.88	291	1,419	569	14,002	7.26	7.14
	7				0.34	0.02	0.49	2.52	4.69	169	1,515	1077	18,146	4.98	7.72
	9	0.012	0.34	n.a.	0.32	0.02	0.46	2.46	3.77	107	1,461	429	16,625	9.15	4.86
	11	n.a.	0.38	0.20	0.33	0.02	0.47	2.62	5.79	60	1,388	650	15,942	9.39	5.40
	13	n.a.	0.41	0.14	0.34	0.02	0.49	2.82	12.12	66	1,593	1,229	18,340	7.05	6.15
	15	0.004	0.40	0.61	0.33	0.02	0.48	2.75	8.81	53	1,618	1,024	17,262	6.47	6.10
	18	n.a.	0.41	0.09	0.35	0.02	0.51	3.01	15.27	39	1,576	1,227	20,595	5.03	6.55
	21	0.017	0.45	0.07	0.36	0.03	0.52	3.17	13.80	36	1,558	1,601	23,181	8.81	8.23
	24	n.a.	0.47	0.05	0.38	0.03	0.53	3.31	17.44	39	1,624	2,088	23,752	8.22	10.24
	27	0.015	0.47	0.05	0.39	0.03	0.54	3.45	16.03	40	1,531	2,596	19,672	4.57	11.30
	30	n.a.	0.48	0.06	0.39	0.03	0.54	3.54	16.35	26	1,610	2,873	23,361	6.25	12.57
	33	n.a.	0.55	0.05	0.41	0.03	0.55	3.64	20.24	8	1,492	2,652	19,579	5.26	13.86
3/8/2016	WC	0.010	0.33	0.48	0.31	0.02	0.43	1.88	-0.38	1,451	21	18	1,519	1.47	0.33
	215	0.007	0.54	0.06	0.43	0.02	0.59	3.41	32.07	26	280	6,440	2,433	15.78	15.48
CL10	WC	0.006	0.34	0.47	0.31	0.02	0.44	1.89	-0.71	1,210	25	6	1,235	1.37	0.41
4/27/2016	1	0.009	0.38	0.38	0.32	0.03	0.52	1.89	-0.73	582	524	713	12,192	24.71	13.12

Site/Date	Depth below SWI (cm)	F (mM)	Cl (mM)	SO_4 (mM)	Na (mM)	K (mM)	Mg (mM)	Ca (mM)	H_2S (mg L^{-1})	NO_3 (µg L^{-1})	SRP (µg L^{-1})	NH_4 (µg L^{-1})	SiO_2 (µg L^{-1})	Fe (ppb)	Mn (ppb)
	3	0.006	0.37	0.31	0.32	0.03	0.43	1.99	-0.73	110	625	570	16,259	17.02	11.23
	5	0.013	0.36	0.23	0.31	0.03	0.43	2.08	-0.67	67	387	896	13,600	16.82	5.41
	7	0.007	0.35	0.04	0.32	0.03	0.42	2.45	1.55	45	291	1,431	11,786	10.79	3.92
	9	0.007	0.35	0.04	0.32	0.04	0.41	2.49	1.46	25	249	1,755	10,448	6.95	4.50
	11	0.007	0.36	0.04	0.34	0.04	0.42	2.55	2.24	53	271	2,022	9,156	6.61	4.30
	13	0.007	0.34	0.01	0.35	0.04	0.42	2.56	6.42	13	332	3,255	8,288	4.51	2.81
	15	0.010	0.34	0.18	0.31	0.04	0.41	2.68	9.41	14	318	3,358	8,931	6.14	3.82
	18	0.007	0.38	0.13	0.33	0.04	0.46	3.03	6.10	38	403	4,611	16,524	6.54	5.56
	21	0.006	0.32	0.02	0.32	0.04	0.46	3.17	6.21	44	391	5,221	18,873	8.18	6.16
	24	0.009	0.34	0.03	0.31	0.04	0.48	3.33	10.06	27	446	6,767	12,957	5.70	5.70
	27	0.009	0.35	0.05	0.30	0.04	0.48	3.48	10.78	28	496	7,590	12,507	4.05	6.45
	30	0.022	0.37	0.05	0.34	0.05	0.50	3.61	8.35	81	533	8,441	12,234	4.78	9.13
MFL3	WC	0.004	0.32	0.43	0.29	0.02	0.41	1.79	-0.27	1128	20	18	3,517	1.69	1.38
8/6/2015	1	0.010	0.37	0.31	0.32	0.03	0.35	2.07	1.84	281	481	1,738	9,507	6.82	8.72
	3	0.007	0.34	0.34	0.30	0.02	0.34	2.04	0.69	198	590	1,695	8,146	7.89	4.79
	5	0.021	0.36	0.37	0.33	0.03	0.36	1.93	-0.26	142	343	1,168	7,452	9.23	5.46
	7	0.019	0.37	0.05	0.31	0.05	0.51	3.10	9.11	19	760	5,780	27,499	4.36	5.36
	9	0.034	0.39	0.03	0.33	0.06	0.58	3.63	8.56	23	559	6,532	29,646	8.46	4.70
	11	0.015	0.35	0.02	0.30	0.05	0.59	3.65	7.65	25	427	8,689	27,570	4.53	4.36
	13	0.005	0.33	0.01	0.28	0.05	0.64	4.05	8.65	0	418	7,900	31,146	2.93	4.49
	15	0.028	0.36	0.01	0.30	0.05	0.64	4.10	7.30	24	903	6,267	28,364	3.39	4.50
	18	0.005	0.34	0.01	0.29	0.06	0.66	4.22	9.42	10	727	7,621	23,588	2.08	4.70
	21	0.005	0.31	0.01	0.28	0.05	0.65	4.25	10.64	-5	897	6,255	26,368	3.92	5.06

Site/Date	Depth below SWI (cm)	F (mM)	Cl (mM)	SO_4 (mM)	Na (mM)	K (mM)	Mg (mM)	Ca (mM)	H_2S (mg L^{-1})	NO_3 (µg L^{-1})	SRP (µg L^{-1})	NH_4 (µg L^{-1})	SiO_2 (µg L^{-1})	Fe (ppb)	Mn (ppb)
	24	n.a.	0.32	0.01	0.27	0.05	0.66	4.28	11.68	-14	1,451	5,671	21,919	2.27	5.94
	27	0.006	0.33	0.01	0.28	0.05	0.65	4.27	12.80	1	1,795	5,167	28,235	3.28	6.81
	30	0.012	0.48	0.03	0.28	0.05	0.65	4.24	11.64	-6	1,414	4,110	22,183	4.58	7.75
	33								7.48	44	2,215		28,316		
2/27/2015	WC	0.008	0.33	0.48	0.30	0.02	0.43	1.89		56	-1	2		2.69	0.28
	35	0.009	0.26	0.04	0.19	0.04	0.72	4.67		14	13	224		21.14	11.77
	120	0.007	0.33	0.08	0.25	0.03	0.58	3.81		-6	30	333		14.84	29.00
	150	0.008	0.35	0.07	0.27	0.03	0.55	3.50		-6	33	296		26.34	26.66
	190	0.008	0.39	0.22	0.31	0.03	0.54	3.05		-5	44	482		7.56	16.38
CL12	WC	0.006	0.34	0.47	0.31	0.02	0.44	1.88	-0.73	933	21	18	1,391	0.79	0.24
4/27/2016	1	0.009	0.40	0.71	0.39	0.07	0.42	2.32	-0.72	161	155	239	12,244	41.38	13.72
	3	0.006	0.35	0.59	0.32	0.06	0.39	2.06	-0.76	468	210	320	7,168	3.10	8.22
	5	0.008	0.35	0.53	0.32	0.07	0.45	2.41	-0.62	91	203	666	10,722	3.72	6.45
	7	0.005	0.35	0.39	0.33	0.06	0.46	2.53	0.86	38	133	737	21,557	2.27	5.76
	9	0.006	0.35	0.17	0.32	0.06	0.43	2.35	1.10	52	200	1,014	19,325	3.17	5.60
	11	0.008	0.34	0.18	0.32	0.06	0.43	2.37	3.50	23	161	1,030	18,082	2.96	5.42
	13	0.009	0.35	0.15	0.32	0.06	0.43	2.35	2.23	42	195	1,263	18,309	3.45	5.55
	15	0.006	0.35	0.07	0.32	0.06	0.43	2.34	4.60	129	211	1,618	16,170	5.26	6.29
	18	0.007	0.36	0.04	0.32	0.06	0.43	2.35	3.74	393	244	1,963	16,717	4.65	5.18
	21	0.009	0.34	0.03	0.31	0.05	0.42	2.36	5.00	26	214	2,334	15,131	3.06	4.84
	24	0.013	0.34	0.04	0.31	0.05	0.42	2.37	2.94	41	265	2,518	16,140	4.53	6.10
	27	0.007	0.35	0.04	0.32	0.05	0.42	2.38	2.96	53	263	2,687	15,440	16.84	5.73
	30	0.011	0.34	0.04	0.31	0.05	0.42	2.44	4.72	41	290	3,177	14,712	4.76	6.67

Site/Date	Depth below SWI (cm)	F (mM)	Cl (mM)	SO_4 (mM)	Na (mM)	K (mM)	Mg (mM)	Ca (mM)	H_2S (mg L^{-1})	NO_3 (µg L^{-1})	SRP (µg L^{-1})	NH_4 (µg L^{-1})	SiO_2 (µg L^{-1})	Fe (ppb)	Mn (ppb)
	33	0.006	0.34	0.04	0.33	0.05	0.42	2.46	7.23	57	261	3,362	18,954	3.66	4.67

Appendix 8.3. Sediment age dating data (gamma-counting)

Core ID	Depth (cm)	Cs-137 Activity (dpm g^{-1})	Cs-137 Error ± (dpm g^{-1})	Pb-210 Activity (dpm g^{-1})	Pb-210 Error ± (dpm g^{-1})	Ra-226 Activity (dpm g^{-1})	Ra-226 Error ± (dpm g^{-1})
RM0.7	0-3	ND	--	19.92	0.74	1.51	0.17
	3-6	ND	--	20.22	0.54	1.05	0.11
	6-9	ND	--	19.66	0.68	0.92	0.13
	9-12	ND	--	20.73	0.63	1.14	0.12
	12-15	ND	--	18.15	0.54	0.94	0.11
	15-18	ND	--	16.56	0.61	0.97	0.12
	18-21	ND	--	16.55	0.51	1.11	0.11
	21-24	ND	--	17.15	0.51	0.89	0.10
	24-27	ND	--	16.84	0.56	1.29	0.12
	27-30	ND	--	8.37	0.42	1.54	0.12
MFL7	0-3	ND	--	4.64	0.22	1.14	0.06
	3-6	ND	--	2.11	0.20	1.08	0.07
	6-9	ND	--	1.19	0.22	0.87	0.08
	9-12	ND	--	1.19	0.19	0.73	0.07
	12-15	ND	--	1.09	0.16	0.79	0.06
	15-18	ND	--	0.96	0.16	0.80	0.06
	18-21	ND	--	1.09	0.21	0.93	0.08
	21-24	ND	--	0.82	0.13	0.57	0.05
	24-27	ND	--	1.02	0.15	0.68	0.06
	27-30	ND	--	0.90	0.19	0.69	0.06
MFL6	0-3	ND	--	7.51	0.35	0.98	0.08
	3-6	ND	--	3.81	0.30	1.07	0.09
	6-9	ND	--	1.43	0.19	1.17	0.07
	9-12	ND	--	1.87	0.23	1.09	0.08
	12-15	ND	--	1.44	0.20	1.05	0.07
	15-18	ND	--	1.48	0.15	1.16	0.05
	18-21	ND	--	1.29	0.20	1.05	0.07
	21-24	ND	--	1.44	0.18	0.91	0.06
	24-27	ND	--	1.30	0.18	0.84	0.06
	27-30	ND	--	1.01	0.16	0.66	0.05
MFL3	0-3	ND	--	19.94	0.61	1.03	0.11
	3-6	ND	--	19.03	0.65	1.19	0.12
	6-9	0.10	0.05	12.08	0.39	1.23	0.09

Core ID	Depth (cm)	Cs-137 Activity (dpm g^{-1})	Cs-137 Error ± (dpm g^{-1})	Pb-210 Activity (dpm g^{-1})	Pb-210 Error ± (dpm g^{-1})	Ra-226 Activity (dpm g^{-1})	Ra-226 Error ± (dpm g^{-1})
	9-12	ND	--	8.02	0.33	0.89	0.07
	18-21	ND	--	2.39	0.22	0.88	0.06
	21-24	ND	--	2.42	0.24	0.88	0.07
	24-27	ND	--	1.82	0.22	1.04	0.08
	27-30	0.06	0.02	1.58	0.15	1.08	0.05

Appendix 8.4. Manual water level measurements used for CTD head data calibration

Date	Site	GW depth from top of piezometer (cm)	River water depth from top of piezometer (cm)	Head difference (cm)
2/27/2015	MFL3	53.5	54.2	0.7
4/17/2015	RM0.7	99	100.2	1.2
	MFL7	117.5	118.5	1
	MFL6	96	96.5	0.5
	MFL3	65.7	66	0.3
5/22/2015	RM0.7	105.9	106.8	0.9
	MFL7	124.1	125	0.9
	MFL6	103.7	104.1	0.4
	MFL3	77.5	77.7	0.2
8/6/2015	RM0.7	98.1	98.8	0.7
	MFL7	114.7	115.4	0.7
	MFL6	90.6	91.1	0.5
	MFL3	55.3	55.9	0.6
10/22/2015	RM0.7	91.7	92.2	0.5
	MFL7	112.4	112.8	0.4
	MFL6	91.4	91.8	0.4
	MFL3	63.5	63.4	-0.1
12/8/2015	RM0.7	105.2	106.1	0.9
	MFL7	127.4	128.3	0.9
	MFL6	106.6	107.5	0.9
	MFL3	77.9	78.4	0.5
3/8/2016	RM0.7	115.4	115.8	0.4
	MFL7	134.7	135.3	0.6
	MFL6	111.8	112.3	0.5
	MFL3	81.8	82.1	0.3
6/30/2016	RM0.7	124.7	125.2	0.5
	MFL7	143.6	144.6	1
	MFL6	120.3	120.7	0.4
	MFL3	100.9	101.9	1
8/4/2016	RM0.7	125.8	126.1	0.3
	MFL7	144.6	145.4	0.8

Date	Site	GW depth from top of piezometer (cm)	River water depth from top of piezometer (cm)	Head difference (cm)
	MFL6	121.1	121.4	0.3
	MFL3	104.4	104.9	0.5
10/20/2016	RM0.7	108.4	109.2	0.8
	MFL7	127.7	128.5	0.8
	MFL6	105.3	105.8	0.5
	MFL3	90.2	90.7	0.5
12/21/2016	RM0.7	124.8	125.7	0.9
	MFL7	145	145.6	0.6
	MFL6	123.9	124.3	0.4
	MFL3	103.8	104.2	0.4

Appendix 9.1.1

Taxa	n	$\delta^{15}N$ (‰)		$\delta^{13}C$ (‰)		C:N	
		Mean	SD	Mean	SD	Mean	SD
Angiosperm	71	4.4	3.1	-32.4	4.1	15.4	9.6
Emergent	21	4.2	2.4	-30.3	2.0	14.4	3.7
Cicuta mexicana (water hemlock)	1	7.3	-	-31.3	-	11.2	-
Nasturtium floridanum (water cress)	3	3.0	4.4	-32.9	2.6	10.4	0.2
Nuphar advena (spatterdock)	8	2.8	1.5	-28.5	1.7	11.3	1.6
Pontederia cordata (pickerel weed)	6	6.4	1.4	-29.3	0.7	16.9	2.0
Sagittaria lancifolia (duck potato)	2	3.0	3.2	-31.0	0.2	13.2	1.2
Zizania aquatica (wild rice)	1	7.7	-	-33.3	-	23.9	-
Floating	8	3.9	1.6	-31.1	1.1	16.0	2.6
Hydrocotyle (dollarweed)	3	3.1	0.7	-30.6	1.1	14.7	2.5
Pistia stratiotes (Water lettuce)	5	4.1	2.1	-31.7	0.9	15.9	2.1
Salvinia (floating fern)	1	5.4	-	-30.0	-	20.0	-
Submerged	38	5.1	2.7	-34.6	3.7	13.1	3.1
Ceratophyllum demersum (coontail)	11	3.6	3.1	-37.3	2.3	10.9	1.7
Hydrilla verticillata (Hydrilla)	7	6.6	2.4	-36.3	2.5	12.8	2.6
Naja guadalupensis (southern waternymph)	3	7.2	4.2	-35.7	4.3	11.6	2.6
Sagittaria kurziana (strap-leaf sagittaria)	6	4.5	1.8	-30.4	1.5	14.0	1.2
Vallisneria americana (eel grass)	11	5.5	1.6	-32.9	3.5	15.5	3.5
Terrestrial	3	-1.9	6.6	-25.5	7.2	55.5	17.4
Taxodium distichum (bald cypress)	2	1.9	1.6	-29.7	0.2	45.6	3.9
Tillandsia usneoides (spanish moss)	1	-9.5	-	-17.2	-	75.3	-
Bacillariophyta (epiphytic diatoms)	8	4.4	1.1	-28.7	5.6	9.4	1.4
Bryophyta (*Fontinalis*, water moss)	2	6.1	1.3	-42.6	2.2	19.9	7.1
Chlorophyta	47	4.9	2.2	-36.8	5.8	9.6	1.9
Benthic	4	3.6	0.7	-42.4	2.9	9.9	2.0

Taxa	n	$\delta^{15}N$ (‰)		$\delta^{13}C$ (‰)		C:N	
		Mean	SD	Mean	SD	Mean	SD
Dichotomosiphon	4	3.6	0.7	-42.4	2.9	9.9	2.0
Epiphytic	23	3.9	2.2	-34.8	7.0	9.6	1.9
Cladophora	11	4.8	2.5	-33.1	9.1	10.4	1.9
Mougeotia+Spirogyra	1	2.5	-	-41.4	-	-	-
Unknown branched	3	3.7	1.4	-35.9	4.9	8.6	1.5
Unknown filamentous+Diatoms	1	2.6	-	-31.9	-	8.6	-
Unknown filamentous	6	2.8	1.9	-36.4	4.3	9.7	1.8
Unknown branched+Diatoms	1	4.9	-	-36.8	-	6.6	-
Unattached	20	6.2	1.6	-38.0	3.4	9.6	2.1
Rhizoclonium (green filamentous)	7	5.7	1.3	-36.6	2.3	8.3	0.5
Spirogyra (green filamentous)	9	6.4	1.5	-38.5	3.7	10.1	2.1
Unknown (green filamentous)	2	4.7	2.8	-41.2	3.1	9.0	0.2
Ulothrix (green filamentous)	2	8.0	0.8	-37.6	5.8	10.3	4.5
Cyanobacteria	4	4.7	2.6	-33.6	9.9	7.8	1.5
Lyngbya (benthic cyanobacteria)	5	3.8	3.0	-34.9	9.0	7.8	1.5
Lentibulariaceae (*Utricularia*, blatterwort)	1	5.5	-	-35.9	-	11.3	-
Xanthophycea	15	3.9	1.6	-42.9	2.0	9.0	1.4
Vaucheria (benthic yellow algae)	11	4.3	2.4	-43.3	1.0	8.2	0.8
Rhodophyta (red algae)	3	5.4	0.9	-42.6	0.2	-	-
Compsopogon	3	5.4	0.9	-42.6	0.2	-	-
Multiple Algal	14	4.9	2.4	-38.5	4.4	8.2	0.7
Benthic	6	5.6	2.3	-43.9	1.2	7.7	0.4
Vaucheria+Unknown filamentous	1	6.4	-	-43.9	-	7.5	-
Vaucheria+Cladophora	1	5.7	-	-43.6	-	7.5	-
Vaucheria+Diatoms	1	6.3	-	-43.6	-	-	-
Vaucheria+Lyngbya	3	5.1	3.5	-44.0	1.8	7.9	0.5
Epiphytic	9	4.5	2.3	-35.5	1.5	8.5	0.6

Taxa	n	δ^{15}N (‰)		δ^{13}C (‰)		C:N	
		Mean	SD	Mean	SD	Mean	SD
Unknown branched and filamentous+*Spyrogira*+Diatoms	1	5.7	-	-36.5	-	8.5	-
Cladophora+*Vaucheria*+Diatoms	2	2.5	0.4	-34.1	1.7	8.7	0.6
Cladophora+Unknown filamentous+Diatoms	1	2.3	-	-35.3	-	8.9	-
Unknown filamentous+Diatoms	1	4.5	-	-35.1	-	8.2	-
Unknown branched+Diatoms	2	5.8	3.9	-36.0	2.8	7.6	0.2
Unknown branched+Unknown filamentous+ *Vaucheria*+Diatoms	1	3.9	-	-35.2	-	9.2	-
Unknown filamentous+*Vaucheria*	1	7.6	-	-37.2	-	8.9	-
Lichen	1	3.5	-	-38.3	-	10.3	-

Appendix 9.1.2.

Trophic status	Taxa	n	$\delta^{15}N$ (‰)		$\delta^{13}C$ (‰)	
			Mean	SD	Mean	SD
Filter feeder						
	Unionidae (*Elliptio buckleyi*, Florida shiny spike)	9	8.3	0.6	-32.9	0.5
Herbivore						
	Ampullariidae (*Pomacea paludosa,* Florida apple snail)	13	7.4	1.7	-33.3	3.0
	Hydrobiidae	5	6.6	1.4	-31.2	6.2
	Physidae + Hydrobiidae	1	7.7	-	-34.1	-
	Physidae + Planorbidae	1	5.2	-	-35.5	-
	Planorbidae (*Planorbella scalaris*-rams horn snail)	4	7.2	0.4	-29.2	2.3
	Pleuroceridae (*Elimia floridensis*, rasp elimia)	16	8.0	0.7	-34.0	0.8
	Pleuroceridae (*Tarebia granifera*, quilted melania)					
	Viviparidae (*Viviparus georgianus*, banded mysterysnail)	16	7.9	1.2	-33.1	1.8
	Coleoptera	3	5.8	1.3	-35.1	1.3
	Diptera (Chironomidae)	20	5.7	0.8	-36.3	2.5
	Ephemeroptera	1	5.5	-	-35.9	-
	Lepidoptera	20	5.7	1.2	-33.2	2.9
	Trichoptera	18	5.7	1.5	-39.5	2.4
Omnivore						
	Coleoptera	1	6.1	-	-32.3	-
	Diptera (Athericidae)	4	7.4	1.1	-31.5	3.8
	Diptera (Stratiomyidae)	2	7.0	0.0	-28.4	2.0
	Diptera (Unknown)	1	6.7	-	-35.5	-

Trophic status	Taxa	n	$\delta^{15}N$ (‰)		$\delta^{13}C$ (‰)	
			Mean	SD	Mean	SD
	Amphipoda (Gammaridae)	16	5.4	1.3	-33.9	3.2
	Palaemonidae (*Palaemonetes* sp.)	13	10.1	0.6	-33.0	0.9
	Parastacidae (*Procambarus speculifer*)	17	8.5	1.2	-30.6	2.1
Parasite						
	Trombidiformes	4	6.3	2.7	-37.0	3.4
	Clitellata	2	8.2	1.2	-35.5	1.7
Predator						
	Insecta	25	7.7	1.0	-32.4	3.1
	Diptera (Rhagionidae)	6	6.3	0.8	-36.1	2.1
	Hemiptera	10	8.1	0.7	-30.9	2.6
	Belostomidae	7	7.9	0.5	-28.6	1.5
	Gerridae	3	8.3	0.5	-33.6	2.6
	Naucoridae	1	8.3	-	-29.2	-
	Nepidae	1	9.3	-	-32.7	-
	Odonata	9	8.3	0.9	-30.8	2.4

Appendix 9.1.3.

Trophic status	Taxa	n	$\delta^{15}N$ (‰)		$\delta^{13}C$ (‰)	
			Mean	SD	Mean	SD
Omnivore/herbivore						
	Atherinopsidae (*Menidia* sp., silver side)	3	11.3	1.8	-31.2	0.2
	Catostomidae (*Erimyzon sucetta*, lake chubsucker)	30	9.7	1.1	-30.9	1.5
	Clupeidae (*Dorosoma cepedianum*, gizzard shad)	12	10.3	1.0	-32.0	2.4
	Cyprinidae	30	9.4	1.3	-33.7	1.4
	Notemigonus crysoleucas (Golden Shiner)	14	8.7	1.2	-34.1	1.8
	Notropis petersoni (Coastal Shiner)	13	9.9	1.2	-33.5	1.0
	Pteronotropis hypselopterus (Sailfin Shiner)	3	10.2	0.6	-33.0	0.5
	Hypostominae (*Pterygoplichthys disjunctivus*,vermiculated sailfin catfish)	3	9.7	1.1	-32.0	0.6
	Mugilidae (*Mugil cephalus*, striped mullet)	17	9.4	1.1	-31.1	2.1
	Percidae (*Percina* sp. , darter)	7	10.4	1.3	-33.3	1.1
	Poeciliidae (live bearers)	22	9.6	1.1	-31.3	1.4
	Poecilia latipinna (sailfin molly)	7	9.0	1.3	-31.9	1.2
	Gambusia affinis (mosquito fish)	11	9.8	0.6	-31.1	1.5
	Heterandria formosa (least killifish)	4	9.9	1.7	-31.0	1.5
	Chelydridae (*Chelydra serpentina*, common snapping turtle)	4	9.9	1.6	-28.9	0.8
	Emydidae	34	8.1	1.8	-32.4	2.3
	Pseudemys nelsoni (Florida redbelly)	13	9.5	1.9	-31.7	1.4

Trophic status	Taxa	n	δ^{15}N (‰)		δ^{13}C (‰)	
			Mean	SD	Mean	SD
	Pseudemys peninsularis (Peninsular cooter)	8	8.2	0.9	-30.9	3.1
	Pseudemys suwanniensis (Suwannee cooter)	13	6.7	0.5	-34.0	1.4
Secondary consumer						
	Amiidae (*Amia calva*, bowfin)	25	13.0	1.4	-27.7	1.6
	Aphredoderidae (*Aphredoderus sayanus*, pirate perch)	5	11.2	0.8	-31.0	0.5
	Belonidae (Strongylura marina, Atlantic needlefish)	1	13.8	-	-30.1	-
	Centrarchidae	133	10.9	1.4	-30.2	1.8
	Lepomis auritus (redbreast sunfish)	7	10.0	1.5	-30.5	3.1
	Lepomis gulosus (warmouth)	7	11.0	0.6	-30.3	1.6
	Lepomis macrochirus (bluegill)	31	10.3	1.2	-30.5	1.6
	Lepomis marginatus (dollar sunfish)	1	11.2	-	-27.7	-
	Lepomis microlophus (redear sunfish)	18	10.2	1.5	-29.9	1.8
	Lepomis punctatus (spotted sunfish)	27	10.3	1.0	-31.1	1.4
	Micropterus salmoides (largemouth bass)	39	12.0	0.9	-29.5	1.7
	Pomoxis nigromaculatus (black crappie)	3	13.7	0.2	-29.4	1.1
	Elassomatidae (*Elassoma zonatum*, Banded Pygmy Sunfish)	7	10.4	0.5	-31.2	2.3
	Fundulidae (*Lucania goodei*, bluefin killifish)	6	9.7	0.7	-31.5	1.8
	Ictaluridae (catfish)	7	11.5	1.1	-30.9	2.7
	Ameriurus sp. (juvenile catfish)	2	10.6	0.4	-32.2	0.1

Trophic status	Taxa	n	$\delta^{15}N$ (‰)		$\delta^{13}C$ (‰)	
			Mean	SD	Mean	SD
	Ameriurus natalis (yellow bullhead catfish)	3	12.2	1.0	-30.4	3.8
	Ameriurus nebulosus (brown bullhead catfish)	1	12.5	-	-28.3	-
	Noturus leptacanthus (speckled madtom)	1	10.5	-	-32.7	-
	Percidae (*Percina* sp., darter)	12	11.0	1.4	-33.2	1.1
	Poeciliidae	26	9.8	1.2	-31.3	1.3
	Gambusia affinus (mosquitofish)	13	10.1	0.9	-31.2	1.3
	Heterandia formosa (least killifish)	5	10.7	1.1	-31.1	1.7
	Poecilia latipinna (sailfin molly)	8	9.1	1.3	-31.9	1.1
	Kinosternidae	19	8.3	0.6	-30.9	1.6
	Sternotherus minor (loggerhead musk turtle)	16	8.4	0.5	-30.6	1.5
	Sternotherus odoratus (common musk turtle)	3	7.7	1.0	-31.9	1.6
Top predator						
	Esocidae (*Esox niger*, Chain pickerel)	8	13.4	0.8	-27.6	1.2
	Lepisosteidae	19	13.6	0.9	-25.7	1.5
	Lepisosteus osseus (Longnose Gar)	1	14.1	-	-24.8	-
	Lepisosteus platyrhincus (Florida Gar)	18	13.6	0.9	-25.8	1.6
	Alligatoridae (*Alligator mississippiensis*, American alligator)	64	8.7	1.2	-29.1	1.1
	Hatchling	14	8.8	0.6	-29.9	0.1
	Juvenile	11	8.5	0.7	-28.6	1.0

Trophic status	Taxa	n	$\delta^{15}N$ (‰)		$\delta^{13}C$ (‰)	
			Mean	SD	Mean	SD
	Sub-adult	24	8.2	1.5	-28.7	1.0
	Adult	15	9.5	0.9	-29.1	1.3

Appendix 9.1.4.

Trophic status	Taxa	n	$\delta^{15}N$ (‰)		$\delta^{13}C$ (‰)		C:N	
			Mean	SD	Mean	SD	Mean	SD
Primary producer								
	Angiosperm							
	Submerged	3	1.7	3.2	-23.6	0.8	15.9	3.9
	Naja guadalupensis (southern waternymph)	2	0.1	2.3	-23.8	1.0	15.9	5.5
	Vallisneria americana (eel grass)	1	4.9	-	-23.3	-	15.9	-
	Chlorophyta	2	3.2	1.5	-18.9	2.8	9.5	1.1
	Spirogyra (green filamentous)	1	4.3	-	-20.9	-	8.7	-
	unknown taxa (green filamentous)	1	2.1	-	-16.9	-	10.2	-
	Cyanobacteria	4	4.3	0.7	-28.0	2.0	6.1	0.4
	Lyngbya (benthic cyanobacteria)	2	4.3	1.3	-28.3	3.3	5.8	0.2
Herbivore	*Lyngbya* + Diatoms	2	4.2	0.1	-27.7	0.4	6.4	0.2
	Ampullariidae (*Pomacea paludosa,* Florida apple snail)	1	6.2	-	-24.2	-	4.4	-
	Planorbidae (*Planorbella scalaris,* rams horn snail)	1	6.1	-	-24.9	-	4.7	-
	Viviparidae (*Viviparus georgianus*, banded mysterysnail)	2	6.8	1.4	-20.7	1.5	4.1	0.1
	Ephemeroptera (mayfly larvae)	1	3.4	-	-20.8	-	5.5	-
	Lepidoptera (moth larvae)	1	7.1	-	-25.0	-	4.8	-
Omnivore								
	Amphipoda (Gammaridae)	3	4.8	0.6	-21.3	1.6	5.4	0.4
	Clitellata (round worm)	1	7.6	-	-22.8	-	5.7	-
	Palaemonidae (*Palaemonetes* sp., grass shrimp)	1	9.8	-	-26.4	-	3.2	-
	Parastacidae (*Procambarus* sp., crayfish)	1	7.1	-	-25.2	-	3.1	-